

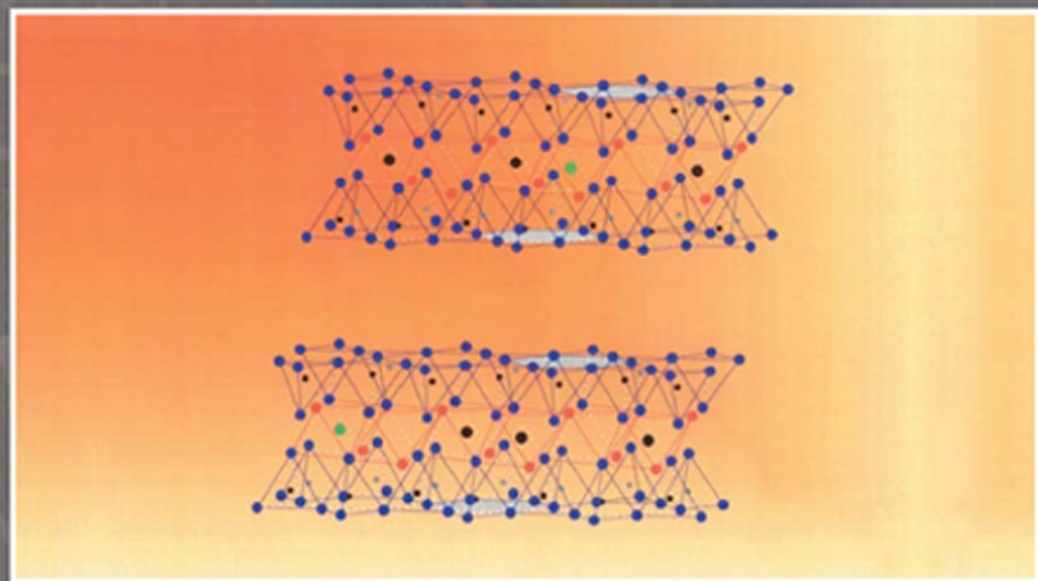


DEVELOPMENTS IN CLAY SCIENCE

1

# HANDBOOK OF CLAY SCIENCE

EDITED BY  
F. BERGAYA,  
B.K.G. THENG  
AND G. LAGALY





*Developments in Clay Science, 1*

# HANDBOOK OF CLAY SCIENCE

*Région*



*Centre*

*Dans le Centre, c'est vous le centre*

This page intentionally left blank



*Developments in Clay Science, 1*

# HANDBOOK OF CLAY SCIENCE

Edited by

**FAÏZA BERGAYA**

CRMD, CNRS-Université d'Orléans  
Orléans  
France

**BENNY K.G. THENG**

Landcare Research  
Palmerston North  
New Zealand

**GERHARD LAGALY**

Institute für Anorganische Chemie  
Universität Kiel, Kiel  
Germany



ELSEVIER

Amsterdam • Boston • Heidelberg • London • New York • Oxford  
Paris • San Diego • San Francisco • Singapore • Sydney • Tokyo



Elsevier

The Boulevard, Langford Lane, Kidlington, Oxford OX5 1GB, UK  
Radarweg 29, PO Box 211, 1000 AE Amsterdam, The Netherlands

First edition 2006

Copyright © 2006 Elsevier Ltd. All rights reserved

No part of this publication may be reproduced, stored in a retrieval system or transmitted in any form or by any means electronic, mechanical, photocopying, recording or otherwise without the prior written permission of the publisher

Permissions may be sought directly from Elsevier's Science & Technology Rights Department in Oxford, UK: phone (+44) (0) 1865 843830; fax (+44) (0) 1865 853333; email: [permissions@elsevier.com](mailto:permissions@elsevier.com). Alternatively you can submit your request online by visiting the Elsevier web site at <http://elsevier.com/locate/permissions>, and selecting *Obtaining permission to use Elsevier material*

#### Notice

No responsibility is assumed by the publisher for any injury and/or damage to persons or property as a matter of products liability, negligence or otherwise, or from any use or operation of any methods, products, instructions or ideas contained in the material herein. Because of rapid advances in the medical sciences, in particular, independent verification of diagnoses and drug dosages should be made

#### British Library Cataloguing in Publication Data

A catalogue record for this book is available from the British Library

#### Library of Congress Cataloguing-in-Publication Data

A catalogue record for this book is available from the British Library of Congress

ISBN-13: 978-0-08-044183-2

ISBN-10: 0-08-044183-1

ISSN: 1572-4352

For information on all Elsevier publications  
visit our website at [books.elsevier.com](http://books.elsevier.com)

Printed and bound in The Netherlands

06 07 08 09 10 10 9 8 7 6 5 4 3 2 1

Working together to grow  
libraries in developing countries

[www.elsevier.com](http://www.elsevier.com) | [www.bookaid.org](http://www.bookaid.org) | [www.sabre.org](http://www.sabre.org)

ELSEVIER

BOOK AID  
International

Sabre Foundation

## **DEDICATION**

To my mother, to my father  
And to my two wonderful daughters Sonia and Rym and their beloved father

Faïza Annabi-Bergaya

This page intentionally left blank

## CONTENTS

List of Contributors by Country of Residence. . . . .	xi
Acknowledgements. . . . .	xiii
Contributing Authors. . . . .	xv
Foreword . . . . .	xix
<i>R. Kühnel</i>	
Chapter 1. General Introduction: Clays, Clay Minerals, and Clay Science. . . . .	1
<i>F. Bergaya and G. Lagaly</i>	
Chapter 2. Structures and Mineralogy of Clay Minerals . . . . .	19
<i>M.F. Brigatti, E. Galan and B.K.G. Theng</i>	
Chapter 3. Surface and Interface Chemistry of Clay Minerals . . . . .	87
<i>R.A. Schoonheydt and C.T. Johnston</i>	
Chapter 4. Synthetic Clay Minerals and Purification of Natural Clays . . . . .	115
<i>K.A. Carrado, A. Decarreau, S. Petit, F. Bergaya and G. Lagaly</i>	
Chapter 5. Colloid Clay Science . . . . .	141
<i>G. Lagaly</i>	
Chapter 6. Mechanical Properties of Clays and Clay Minerals. . . . .	247
<i>R. Pusch</i>	
Chapter 7. Modified Clays and Clay Minerals . . . . .	261
<i>F. Bergaya, B.K.G. Theng and G. Lagaly</i>	
Chapter 7.1. Acid Activation of Clay Minerals . . . . .	263
<i>P. Komadel and J. Madejová</i>	
Chapter 7.2. Thermally Modified Clay Minerals . . . . .	289
<i>L. Heller-Kallai</i>	
Chapter 7.3. Clay Mineral Organic Interactions . . . . .	309
<i>G. Lagaly, M. Ogawa and I. Dékány</i>	
Chapter 7.4. Clay Minerals and the Origin of Life. . . . .	379
<i>A. Brack</i>	
Chapter 7.5. Pillared Clays and Clay Minerals . . . . .	393
<i>F. Bergaya, A. Aouad and T. Mandalia</i>	
Chapter 8. Properties and Behavior of Iron in Clay Minerals. . . . .	423
<i>J.W. Stucki</i>	

Chapter 9.	Clays, Microorganisms, and Biomineralization . . . . .	477
	<i>K. Tazaki</i>	
Chapter 10.	Clays in Industry . . . . .	499
	<i>F. Bergaya, B.K.G. Theng and G. Lagaly</i>	
Chapter 10.1.	Conventional Applications . . . . .	501
	<i>C.C. Harvey and G. Lagaly</i>	
Chapter 10.2.	Clay Minerals as Catalysts . . . . .	541
	<i>J.M. Adams and R.W. McCabe</i>	
Chapter 10.3.	Clay Mineral– and Organoclay–Polymer Nanocomposite. . . . .	583
	<i>E. Ruiz-Hitzky and A. Van Meerbeek</i>	
Chapter 11.	Clays, Environment and Health. . . . .	623
	<i>F. Bergaya, B.K.G. Theng and G. Lagaly</i>	
Chapter 11.1.	Clays and Clay Minerals for Pollution Control. . . . .	625
	<i>G.J. Churchman, W.P. Gates, B.K.G. Theng and G. Yuan</i>	
Chapter 11.2.	Clays and Pesticides . . . . .	677
	<i>S. Nir, Y. El-Nahhal, T. Undabeytia, G. Rytwo, T. Polubesova, Y. Mishael, O. Rabinovitz and B. Rubin</i>	
Chapter 11.3.	Clay Liners and Waste Disposal . . . . .	693
	<i>K. Czurda</i>	
Chapter 11.4.	Clays and Nuclear Waste Management . . . . .	703
	<i>R. Pusch</i>	
Chapter 11.5.	Clays and Human Health . . . . .	717
	<i>M.I. Carretero, C.S.F. Gomes and F. Tateo</i>	
Chapter 11.6.	Clays and Clay Minerals as Drugs. . . . .	743
	<i>M.T. Droy-Lefaix and F. Tateo</i>	
Chapter 12.	Critical Assessment of Some Analytical Techniques. . . . .	753
	<i>F. Bergaya, B.K.G. Theng and G. Lagaly</i>	
Chapter 12.1.	Mössbauer Spectroscopy of Clays and Clay Minerals . . . . .	755
	<i>E. Murad</i>	
Chapter 12.2.	Identification and Quantitative Analysis of Clay Minerals . . . . .	765
	<i>J. Šrodoň</i>	
Chapter 12.3.	X-ray Absorption Spectroscopy. . . . .	789
	<i>W.P. Gates</i>	
Chapter 12.4.	X-ray Photoelectron Spectroscopy . . . . .	865
	<i>H. Seyama, M. Soma and B.K.G. Theng</i>	

Chapter 12.5.	Small-angle Scattering Techniques . . . . .	879
	<i>D. Tchoubar and N. Cohaut</i>	
Chapter 12.6.	Fourier Transform Infrared Spectroscopy . . . . .	909
	<i>S. Petit</i>	
Chapter 12.7.	Nuclear Magnetic Resonance Spectroscopy . . . . .	919
	<i>J. Sanz</i>	
Chapter 12.8.	Transmission Electron Microscopy . . . . .	939
	<i>F. Elsass</i>	
Chapter 12.9.	Surface Area and Porosity . . . . .	965
	<i>L.J. Michot and F. Villieras</i>	
Chapter 12.10.	Cation and Anion Exchange . . . . .	979
	<i>F. Bergaya, G. Lagaly and M. Vayer</i>	
Chapter 12.11.	Thermal Analysis . . . . .	1003
	<i>F. Rouquerol, J. Rouquerol and P. Llewellyn</i>	
Chapter 13.	Some Other Materials Related to Clays . . . . .	1019
	<i>F. Bergaya, B.K.G. Theng and G. Lagaly</i>	
Chapter 13.1.	Layered Double Hydroxides . . . . .	1021
	<i>C. Forano, T. Hibino, F. Leroux and C. Taviot-Guého</i>	
Chapter 13.2.	Parallels and Distinctions between Clay Minerals and Zeolites . . . . .	1097
	<i>D.L. Bish</i>	
Chapter 13.3.	Cement Hydrates . . . . .	1113
	<i>H. Van Damme and A. Gmira</i>	
Chapter 14.	Genesis of Clay Minerals . . . . .	1129
	<i>E. Galín</i>	
Chapter 15.	History of Clay Science: A Young Discipline . . . . .	1163
	<i>F. Bergaya, G. Lagaly and K. Beneke</i>	
Chapter 16.	Teaching Clay Science: A Great Perspective . . . . .	1183
	<i>R. Berry, F. Bergaya and G. Lagaly</i>	
Subject Index . . . . .		1197

This page intentionally left blank

## LIST OF CONTRIBUTORS BY COUNTRY OF RESIDENCE

<b>AUSTRALIA</b>	G. Jock Churchman, Will P. Gates
<b>BELGIUM</b>	Robert A. Schoonheydt, André Van Meerbeek
<b>FRANCE</b>	Amina Aouad, Faïza Bergaya, André Brack, Nathalie Cohaut, Alain Decarreau, Marie Thérèse Droy-Lefaix, Françoise Elsass, Claude Forano, Ahmed Gmira, Fabrice Leroux, Philip L. Llewellyn, Tushar Mandalia, Laurent J. Michot, Sabine Petit, Françoise Rouquérol, Jean Rouquérol, Christine Taviot-Guého, Denise Tchoubar, Henri Van Damme, Marylène Vayer, Frédéric Villiéras
<b>GERMANY</b>	Klaus Beneke, Kurt Czurda, Gerhard Lagaly, Enver Murad
<b>HUNGARY</b>	Imre Dékány
<b>ISRAEL</b>	Lisa Heller-Kallai, Yael Mishael, Shlomo Nir, Tamara Polubesova, Onn Rabinovitz, Baruch Rubin, Giora Rytwo
<b>ITALY</b>	Maria Franca Brigatti, Fabio Tateo
<b>JAPAN</b>	Toshiyuki Hibino, Makoto Ogawa, Haruhiko Seyama, Mitsuyuki Soma, Kazue Tazaki
<b>THE NETHERLANDS</b>	Radko A. Kühnel
<b>NEW ZEALAND</b>	Colin C. Harvey, Benny K.G. Theng, Guodong Yuan
<b>PALESTINIAN NATIONAL AUTHORITY</b>	Yasser El-Nahhal
<b>POLAND</b>	Jan Środoń
<b>PORTUGAL</b>	Celso de Sousa Figueiredo Gomez
<b>SLOVAKIA</b>	Peter Komadel, Jana Madejová
<b>SPAIN</b>	Maria Isabel Carretero, Emilio Galán, Eduardo Ruiz-Hitzky, Jesus Sanz, Tomas Undabeytia
<b>SWEDEN</b>	Roland Pusch
<b>UNITED KINGDOM</b>	John M. Adams, Richard W. McCabe
<b>UNITED STATES OF AMERICA</b>	Richard W. Berry, David L. Bish, Kathleen A. Carrado, Cliff T. Johnston, Joseph W. Stucki



This page intentionally left blank

## ACKNOWLEDGEMENTS

The editors acknowledge all the people who have helped them to realise this handbook, especially the contributing authors. Without their cooperation, enthusiasm, and dedication, this handbook would not have been possible. The editors are grateful for their patience and forbearance, and acknowledge their great efforts in condensing and summarising the vast amount of information in their individual fields of expertise.

F. Bergaya wishes to acknowledge the “Conseil Régional du Centre” for their financial support without which this project would not have started. She thanks all the contributing authors of this book. She is especially grateful to Benny Theng and Gerhard Lagaly for accepting her proposal to share the task of editing this book, and to Elsevier for their agreement to publish. Finally, she is deeply grateful to her husband, Badreddine, whose patience and encouragement were invaluable since the beginning of this project, particularly during the last three years.

B.K.G. Theng acknowledges the efforts made by Faïza Bergaya in obtaining funds for him to spend 12 months, spread over three leave periods during 2001–2003, in her laboratory (CRMD, CNRS-Université d’Orléans). He is grateful to Landcare Research New Zealand for providing office space and associated facilities as well as some financial assistance, and to the Royal Society of New Zealand for their support under the ISAT Linkages Fund. He also thanks the following people from Landcare Research: Nicolette Faville and Janie Jansen for drawing up figures, and Anne Austin for editorial assistance. Lastly, he is grateful to his wife, Judith Theng, for encouragement and support.

G. Lagaly thanks Faïza Bergaya for the invitation to participate in editing this handbook, and the kind hospitality provided by her family during his several visits to Orléans. He is also very grateful to Klaus Beneke for furnishing literature references, and to Mrs. Britta Bahn for editorial assistance.

The author(s) of certain chapters wish to acknowledge the following persons and agencies:

Part of the time for writing Chapter 4 was provided under the auspices of the U.S. Department of Energy under contract #W-31-109-ENG-38 (to K.A.C.).

The author of Chapter 7.4 is very grateful to Professor J.P. Ferris for his helpful comments.

The author of Chapter 8 expresses his thanks to the following agencies for their recent financial support of his research: The International Arid Lands Consortium, Grant No. 03R-15; BARD, The United States-Israel Binational Agricultural Research and Development Fund, Research Grant Award No. AG IS-3162-99R; the National Science Foundation, Division of Petrology and Geochemistry, Grant No.

EAR 01-26308; and the Natural and Accelerated Bioremediation Research (NABIR) Program, Biological and Environmental Research (BER), U.S. Department of Energy, Grant No. DE-FG02-00ER62986, subcontract FSU F48792.

The authors of Chapter 10.3 are indebted to P. Aranda for her critical review of the manuscript and to S. Letaïef for editorial assistance. One of the authors (E. Ruiz-Hitzky) thanks the CICYT, Spain, for financial support.

In Chapter 11.2, the research was supported by Grant G-641.106.8/1999 from G.I.F., the German-Israeli Foundation for Research and Development.

The authors of Chapter 11.5 are grateful to E. Galán (Seville University, Spain) for helpful discussions and critical review of the manuscript. They also thank F. Veniale (Pavia University, Italy) for useful suggestions, and L. Cima and F. Cozzi (Padua University, Italy) for their comments on some aspects of this chapter.

One of the authors (F. Tateo) of Chapter 11.6 is grateful to L. Cima and F. Cozzi (Padua University, Italy) for helpful discussions.

The author of Chapter 12.2 thanks W. Gates and B.K.G. Theng for their critical comments and language corrections.

The author of Chapter 12.3 is grateful to F. Bergaya, G. Lagaly, and B.K.G. Theng for inviting him to submit this contribution, and to A. Manceau and J.W. Stucki for providing the extended X-ray absorption fine structure spectroscopy (EXAFS) data used to illustrate spectral analyses.

The author of Chapter 14 thanks R.E. Ferrell (Louisiana State University, USA) for his critical reading, discussion, and numerous suggestions, leading to considerable improvement of the manuscript, and for his assistance with style corrections. He also thanks P. Aparicio (Seville University, Spain) for her helpful comments and editorial assistance, as well as G.J. Churchman (University of Adelaide, Australia) for his collaboration in the final version and editing. He would also like to thank the editors, F. Bergaya, G. Lagaly, and B.K.G. Theng, for giving him an opportunity to contribute to this handbook.

F. Bergaya, B.K.G. Theng and G. Lagaly  
*June 2005*

## CONTRIBUTING AUTHORS

J.M. ADAMS

*School of Engineering, University of Exeter, Harrison Building, North Park Road, Exeter, Devon EX4 4QF, UK*

A. AOUAD

*CRMD, CNRS-Université d'Orléans, F-45071 Orléans Cedex 2, France*

K. BENEKE

*Institut für Anorganische Chemie, Universität Kiel, D-24118 Kiel, Germany*

F. BERGAYA

*CRMD, CNRS-Université d'Orléans, F-45071 Orléans Cedex 2, France*

R.W. BERRY

*Department of Geological Sciences, San Diego State University, San Diego, CA 92182-1020, USA*

D.L. BISH

*Department of Geological Science, Indiana University, Bloomington, IN 47405-1405, USA*

A. BRACK

*Centre de Biophysique Moléculaire, CNRS, F-45071 Orléans Cedex 2, France*

M.F. BRIGATTI

*Dipartimento di Scienze della Terra, Università di Modena, I-41100 Modena, Italy*

K.A. CARRADO

*Chemistry Division, CHM 200, Argonne National Laboratory, Argonne, IL60439-4837, USA*

M.I. CARRETERO

*Departamento de Cristalografía, Mineralogía y Química Agrícola, Facultad de Química, Universidad de Sevilla, ES-41071 Sevilla, Spain*

G.J. CHURCHMAN

*School of Earth and Environmental Sciences, University of Adelaide, Glen Osmond, S.A. 5064, Australia*

N. COHAUT

*CRMD, CNRS-Université d'Orléans, F-45071 Orléans Cedex 2, France*

K. CZURDA

*Angewandte Geologie, Universität Karlsruhe, D-76128 Karlsruhe, Germany*

A. DECARREAU

*UMR 6532, HydrASA, F-8602 Poitiers Cedex, France*

I. DÉKÁNI

*Department of Colloid Chemistry and Nanostructured Materials Research Group of the Hungarian Academy of Sciences, University of Szeged, H-6720 Szeged, Hungary*

M.T. DROY-LEFAIX

*Beaufour-IPSEN, F-75016 Paris, France*

Y. EL NAHHAL

*Environmental Protection and Research Institute (EPRI), PO Box 1175, Gaza, PNA (Palestinian National Authority)*

F. ELSASS

*INRA, Unité de Science du Sol, Centre Versailles-Grignon, F-78026 Versailles, France*

*Present address: CNRS, Centre de Geochimie de la Surface, 1 rue Blessig, F-67084 Strasbourg, France.*

C. FORANO

*Laboratoire de Matériaux Inorganiques, CNRS UMR 6002, Université Blaise Pascal, F-63177 Aubière Cedex, France*

E. GALÁN

*Departamento de Cristalografía, Mineralogía y Química Agrícola, Facultad de Química, Universidad de Sevilla, ES-41071 Sevilla, Spain*

W.P. GATES

*Centre for Green Chemistry, School of Chemistry, Monash University, Clayton, VIC 6800, Australia*

A. GMIRA

*CRMD, CNRS-Université d'Orléans, F-45071 Orléans Cedex 2, France*

C.S.F. GOMES

*Departamento de Geociências, Universidade de Aveiro, P-3810-193 Aveiro, Portugal*

C.C. HARVEY

*Institute of Geological and Nuclear Sciences, Wairakei Research Centre, Private Bag 2000, Taupo, New Zealand*

L. HELLER-KALLAI

*Institute of Earth Sciences, The Hebrew University of Jerusalem, IL-91904 Jerusalem, Israel*

T. HIBINO

*Ecological Materials Group, AIST, 16-1 Onogawa, Tsukuba 305-8569, Japan*

C.T. JOHNSTON

*Department of Soil and Environmental Sciences, Purdue University, West Lafayette, IN 47907-1150, USA*

P. KOMADEL

*Institute of Inorganic Chemistry, Slovak Academy of Sciences, SK-845 36 Bratislava, Slovakia*

R.A. KÜHNEL

*Burg. Merkusstraat 5, NL-2645 NJ Delfgauw, The Netherlands*

G. LAGALY

*Institut für Anorganische Chemie, Universität Kiel, D-24118 Kiel, Germany*

F. LEROUX

*Laboratoire de Matériaux Inorganiques, CNRS UMR 6002, Université Blaise Pascal, F-63177, Aubière Cedex, France*

P.L. LLEWELLYN

*Laboratoire MADIREL, UMR CNRS-Université de Provence Centre de St Jérôme, 13397 Marseille Cedex 20, France*

J. MADEJOVÁ

*Institute of Inorganic Chemistry, Slovak Academy of Sciences, SK-845 36 Bratislava, Slovakia*

T. MANDALIA

*CRMD, CNRS-Université d'Orléans, F-45071 Orléans, Cedex 2, France*

R.W. McCABE

*Center for Materials Science, University of Central Lancashire, Preston PR1 2HE, United Kingdom*

L.J. MICHOT

*Laboratoire Environnement et Minéralurgie, BP 40, F-54501 Vandoeuvre Cedex, France*

Y. MISHAEL

*Faculty of Agricultural, Food and Environmental Quality Sciences, The Hebrew University of Jerusalem, PO Box 12, IL-76100 Rehovot, Israel*

E. MURAD

*Bayerisches Landesamt für Umwelt, D-95603 Marktredwitz, Germany*

S. NIR

*Faculty of Agricultural, Food and Environmental Quality Sciences, The Hebrew University of Jerusalem, PO Box 12, IL-76100 Rehovot, Israel*

M. OGAWA

*Department of Earth Sciences, Waseda University, Nishiwaseda 1-6-1, Shinjuku-ku, Tokyo 169-8050, Japan*

S. PETIT

*UMR 6532, HydrASA, F-86022 Poitiers Cédex, France*

T. POLUBESOVA

*Faculty of Agricultural, Food and Environmental Quality Sciences, The Hebrew University of Jerusalem, PO Box 12, IL-76100 Rehovot, Israel*

R. PUSCH

*Geodevelopment AB, Ideon, S-22370 Lund, Sweden*

O. RABINOVITZ

*Faculty of Agricultural, Food and Environmental Quality Sciences, The Hebrew University of Jerusalem, PO Box 12, IL-76100 Rehovot, Israel*

F. ROUQUEROL

*Laboratoire MADIREL, UMR CNRS-Université de Provence Centre de St Jérôme, 13397 Marseille Cedex 20, France*

J. ROUQUEROL

*Laboratoire MADIREL, UMR CNRS-Université de Provence Centre de St Jérôme, 13397 Marseille Cedex 20, France*

B. RUBIN

*Faculty of Agricultural, Food and Environmental Quality Sciences, The Hebrew University of Jerusalem, PO Box 12, IL-76100 Rehovot, Israel*

E. RUIZ-HITZKY

*Instituto de Ciencia de Materiales de Madrid, Campus de Cantoblanco, CSIC, ES-28049 Madrid, Spain*

**G. RYTWO**

*Tel Hai Academic College, Biotechnology and Environmental Sciences Department, Upper Galilee  
IL-12210, Israel*

**J. SANZ**

*Instituto de Ciencia de Materiales de Madrid, CSIC, Campus de Cantoblanco, ES-28049 Madrid,  
Spain*

**R.A. SCHOONHEYDT**

*Center for Surface Chemistry and Catalysis, Kuleuven, B-3001 Leuven, Belgium*

**H. SEYAMA**

*Environmental Chemistry Division, National Institute for Environmental Studies, 16-2 Onogawa, Tsukuba,  
Ibaraki 305-8506, Japan*

**M. SOMA**

*Institute for Environmental Sciences, University of Shizuoka, 52-1 Yada, Shizuoka, Shizuoka 422-8526,  
Japan*

*Present address: 6-8 Tsutsujigaoka, Aoba-ku, Yokohama 227-0055, Japan*

**J. ŚRODOŃ**

*Institute of Geological Sciences, PAN, PL-31-002 Krakow, Poland*

**J. STUCKI**

*Department of Natural Resources and Environmental Sciences, University of Illinois, W-321 Turner Hall,  
1102 S. Goodwin Ave, Urbana, IL 61801-4798, USA*

**F. TATEO**

*Istituto di Ricerca sulle Argille, CNR, I-85050 Tito Scalo (PZ), Italy*

**C. TAVIOT-GUÉHO**

*Laboratoire de Matériaux Inorganiques, CNRS UMR 6002, Université Blaise Pascal, F-63177 Aubière  
Cedex, France*

**K. TAZAKI**

*Department of Earth Sciences, Kanazawa University, Kanazawa, Ishikawa 920-1192, Japan*

**D. TCHOUBAR**

*Expert CRT-Plasma Laser, Orléans, F-45160 Olivet, France*

**B.K.G. THENG**

*Landcare Research, Palmerston North, New Zealand*

**T. UNDABEYTIA**

*Instituto de Recursos Naturales y Agrobiología, CSIS, Apdo 1052, ES-41080 Sevilla, Spain*

**H. VAN DAMME**

*Ecole Supérieure de de Physique et de Chimie Industrielle (ESPCI-PPMD), F-75231 Paris Cedex, France*

**A. VAN MEERBEEK**

*Advanced Elastomer Systems SA, B-1140 Bruxelles, Belgium*

**M. VAYER**

*CRMD, CNRS-Université d'Orléans, 1b Rue de la Férollerie, F-45071 Orléans Cedex 2, France*

**F. VILLIÉRAS**

*Laboratoire Environnement et Minéralurgie, BP 40, F-54501 Vandoeuvre Cedex, France*

**G. YUAN**

*Landcare Research, Palmerston North, New Zealand*

## FOREWORD

Clay science has emerged after a few millennia of clay use and a century-long accumulation of written information about clays and clay minerals. No other minerals currently attract so great an interest, or are being subjected to such an intensive examination as clays. The focus of clay research has long been on the geological, geotechnical, and mineralogical aspects of clays. It is only relatively recently that clay science has assumed a physico-chemical orientation. The rapid development of clay science over the past few decades is attested to by the voluminous literature on clays. It is also reflected by the establishment of clay groups and societies in many countries. New information is regularly communicated in a variety of journals and through numerous national, regional, and international conferences and symposia as well as by dissertations, lecture notes, technical reports, and patents. At a rough estimate, several hundred scientific communications on clays and clay minerals are published annually.

The two main features that evoke interest in clays are: (1) their common availability, and (2) their extraordinary properties. Archaeological research has indicated that the first use of clays by humans coincided with ancient agrarian settlements. As humans sowed the first grain seeds, they also began to make bricks, utensils, and artistic objects from clay. Pottery developed into an important and respected profession, the associated skills and experiences being handed down from one generation to the next. Likewise, the technological improvements were transmitted from decade to decade. Over time, empirical technology has been systematically converted into scientific procedure based on sound theoretical principles.

Clays and clay minerals represent the youngest members of the family of minerals in the Earth's crust. Being formed from different parent rocks under variable conditions, clay minerals vary in chemical composition, structure, and modes of occurrence. Clay minerals are irregularly distributed in the lithosphere, while their concentration steadily increases due to weathering and/or hydrothermal alteration. Clay minerals in nature also undergo spontaneous modification and transformation as environmental conditions change. These processes are driven by physical, chemical, and biological forces, including anthropogenic effects.

Natural clays are highly heterogeneous in composition and, almost invariably, contain 'impurities' in the form of associated minerals and X-ray amorphous materials. The mineralogical composition of clays is also influenced by particle size, the smaller the size the larger the contribution of X-ray amorphous material. The fineness of clays predetermines both their vulnerability and reactivity. By the same token, clay particles are sensitive to mechanical and chemical treatments. These features raise the question of scale. A small sample of material examined



under laboratory conditions may react and behave differently from its bulky counterpart. Issues of heterogeneity aside, minor constituents in clays and the scale and conditions of testing can give rise to discrepancies in the results of measurements carried out in different laboratories. A variety of spectroscopic and instrumental techniques have been used to analyse and characterize clays and clay minerals. Improvements in sensitivity, selectivity, and accuracy are constantly being sought. The development of new techniques and the refinement of old ones create a complex, multidimensional problem. Verification of the reproducibility of results, obtained in different laboratories, is not an option but a necessity. The chemical and mineral composition of clays is more difficult to quantify than other hard rocks. Differences in clay mineral populations, structural imperfections, variations in crystallinity, and the presence of impurities are problems that are specifically associated with the identification and quantitative analysis of clays.

Experimenting with artificial mixtures of clay minerals is popular in soil and geotechnical testing. Mixtures of clay minerals of different origin would be expected to behave like natural, multiphase clay material. However, it is difficult, if not impossible, to simulate the natural fabric and the intimacy of contact between neighbouring particles formed over geological periods of interaction. Likewise, computer modelling has become important over the past decade or so. This approach to research can be rewarding if the model is properly validated, and not used to justify or prove a preconceived notion.

The different aspects of clays mentioned above reflect the unique nature of clays and clay minerals. No other group of inorganic materials have so many species, show such a wide range of reactivity and propensity for modification, or enjoy such a diversity of practical applications as clay minerals. In addition to their conventional uses, as in ceramics and paper coating, clays have found many novel applications. Clay minerals are naturally occurring nanomaterials, abundant, inexpensive, and environmental friendly. As such, they have a huge potential for the synthesis of clay-polymer nanocomposites with superior mechanical and thermal properties. The optimization of adsorption properties, swelling behaviour, colloidal and rheological properties, and the design of new types of organo-clays also open prospects of using clay minerals for pollution control and environmental protection. Many clay scientists and geotechnical engineers are also aware of the negative side of clays as manifested in the form of landslides, mudflows, and the deterioration of clay-based construction materials. In so far as it is impossible to control nature, prevention, and remediation are the only practical ways of responding to such destructive natural processes.

Clay science is a multidisciplinary endeavour, combining geology, mineralogy, crystallography with physics, geotechnology, and soil mechanics together with inorganic, organic, physical, and colloid chemistry. The contributions to clay science of the biological, medical, and pharmaceutical sciences are increasing, and this trend will continue.

These considerations reveal the strong need for bringing together the scattered literature on the many and varied disciplines that make up clay science. The *Handbook of Clay Science* fulfils these requirements. Leading scientists covering a wide field of expertise have given much of their time and energy to write critical accounts of the current state of knowledge. All manuscripts have been carefully edited and coordinated. Besides being a reference text and a source of information on clays and clay minerals, the *Handbook of Clay Science* provides a point of first entry into a unique and very important field of materials science for research scientists, university teachers, industrial chemists, physicists, graduate students as well as the environmental engineers and technologists, including people with political responsibility.

Radko A. Kühnel

This page intentionally left blank

## *Chapter 1*

# **GENERAL INTRODUCTION: CLAYS, CLAY MINERALS, AND CLAY SCIENCE**

**F. BERGAYA<sup>a</sup> AND G. LAGALY<sup>b</sup>**

<sup>a</sup>*CRMD, CNRS-Université d'Orléans, F-45071 Orléans Cedex 2, France*

<sup>b</sup>*Institut für Anorganische Chemie, Universität Kiel, D-24118 Kiel, Germany*

The authors believe that clays and clay minerals, either as such or after modification, will be recognized as the materials of the 21st century because they are abundant, inexpensive, and environment friendly. With that in view, this *Handbook of Clay Science* has assembled core information on the varied and diverse aspects that make up the discipline of clay science, ranging from the fundamental structure and surface properties of clays and clay minerals to their industrial and environmental applications.

Clay has been known to, and used by, humans since antiquity. Indeed, clay has been implicated in the prebiotic synthesis of biomolecules, and the very origins of life on earth. Clay has also become indispensable to modern living. It is the material of many kinds of ceramics, such as porcelain, bricks, tiles, and sanitary ware as well as an essential constituent of plastics, paints, paper, rubber, and cosmetics. Clay is non-polluting and can be used as a depolluting agent. Of great importance for the near future is the potential of some clays to be dispersed as nanometer-size unit particles in a polymer phase, forming novel nanocomposite materials with superior thermo-mechanical properties. The diversity of structures and properties of clays, and their wide-ranging applications, make it difficult to compile a comprehensive reference text on clay science.

## **1.1. AIM AND SCOPE**

If the general knowledge and usage of clay have ancient roots, the scientific study of clay (i.e., 'clay science') is a relatively recent discipline, dating back only to the mid-1930s, following on the emergence and general acceptance of the 'clay mineral concept'. According to this concept, clays are essentially composed of micro-crystalline particles of a small group of minerals, referred to as the clay minerals

(Grim, 1968). Since then, clay science or ‘argillology’ (Konta, 2000) has become an autonomous, multi-faceted discipline.

Since people who work with clay come from diverse backgrounds and have diverse interests, there are probably as many concepts and views of clay as there are clay mineral species. It is not surprising, therefore, that clay scientists have varied trainings, including geology, mineralogy, chemistry, physics, and biology, and hold different perspectives. The multi-disciplinary nature of clay science is indicated by the scope, contents, and multi-authorship of this handbook. It is also reflected in the wide range and variety of scientific journals where papers on clays and clay minerals are published. At the same time, individuals or groups who investigate and use clay—whether they be in academe or industry—often fail to realize that they share a common interest, or worse, are ignorant of one another’s existence. Similarly, information about clay is dispersed in many scientific conferences and symposia whose themes (e.g., nanotechnology, rheology, and heterogeneous catalysis) often make no reference to the experimental material used. Indeed, the word ‘clay’ in many publications is often subsumed into such terms as ‘microporous solid’ or ‘layered material’. This is probably because in the mind of many people, clay is associated with soil (dirt) and mud. By the same token, clay science is not generally considered to be intellectually challenging. If clay science features at all in the syllabus or curriculum of a university degree course, the focus is usually on the mineralogy of clay, while its colloidal and physico-chemical aspects are glanced over, if not ignored. The teaching of clay science also varies from school to school within a given country, and from one country to another.

The first two textbooks by Grim, *Clay Mineralogy* and *Applied Clay Mineralogy*, were published some 4–5 decades ago (Grim, 1953, 1962, 1968). Since then a great deal of information on clays and clay minerals has accumulated. Also, many advanced analytical and instrumental techniques have been developed as well as novel industrial and environmental applications. Yet, no general reference text on clay science in the English language has been published to date, although a number of books on particular aspects are available (e.g., Weaver and Pollard, 1973; Farmer, 1974; Theng, 1974, 1979; van Olphen, 1977; Brindley and Brown, 1980; Chamley, 1989; Wilson, 1994; Velde, 1995; Moore and Reynolds, 1997).

The *Handbook of Clay Science* aims to provide up-to-date information on the fundamental structural and surface properties of clay minerals, their industrial and environmental applications as well as analytical techniques, and the teaching and history of clay science. The book is intended to be a critical review and not just a compilation of the published literature. To our knowledge, this holistic multi-disciplinary approach does not exist in any other clay book. Here, we describe some generally held concepts and working definitions of clay and clay mineral that might be acceptable to most disciplines and practitioners of clay science.

The structures of clays and clay minerals together with their surface-chemical properties are summarized in Chapters 2 and 3. Synthetic clay minerals and clay purification are described in Chapter 4, while Chapter 5 deals with the colloid chemistry of clays,

and Chapter 6 with their mechanical properties. Chapter 7 describes modifications of clays and clay minerals by acid activation (Chapter 7.1), thermal treatment (Chapter 7.2), and pillaring (Chapter 7.5), and has subchapters on the clay-organic interaction (Chapter 7.3), and the possible involvement of clay in the origins of life (Chapter 7.4). The properties and behaviour of iron in clay minerals are discussed in Chapter 8, while Chapter 9 reviews the role of clays in biomineralization. Chapter 10 deals with clays in industry with subchapters on the conventional applications of clays (Chapter 10.1), catalysis by clay minerals (Chapter 10.2), and the formation and properties of clay-polymer nanocomposites (Chapter 10.3). The role of clays in environmental and human health protection is discussed in Chapter 11 with six subchapters covering a wide range of topics from pollution control to clays as drugs. The eleven subchapters of Chapter 12 give a critical assessment of spectroscopic and analytical techniques commonly used in clay studies. The handbook also contains in subchapters of Chapter 13, reviews on layered double hydroxides (LDH) (Chapter 13.1), zeolites (Chapter 13.2), and cement hydrates (Chapter 13.3) because these materials are related to smectite clays in structure and certain properties. Clay mineral formation and the genesis of the principal clay deposits are described in Chapter 14, while the last two chapters are concerned with the history (Chapter 15), and teaching (Chapter 16) of clay science.

This handbook will therefore provide a point of first entry into the clay science literature for research scientists, university teachers, postgraduate students, industrial chemists as well as people in agriculture, environmental engineering, industry, and waste disposal, who need to know about clays and clay minerals. This book will also be useful to commercial users of clays.

## 1.2. CLAY

There is, as yet, no uniform nomenclature for clay and clay material. Nonetheless, we do not seek a consensus<sup>1</sup> about the meaning of the terms ‘clay’, ‘clays’, and ‘clay minerals’ (Table 1.1). Indeed, the quest for a unifying terminology that is acceptable to all disciplines, users, and producers would be a fruitless exercise (R.A. Kühnel, personal communication). Rather, here we aim to highlight the common meaning of these terms, and the impact of these materials on our actual daily life together with their potential for the ever-growing number of practical applications (Kühnel, 1990; Murray, 1999).

Georgius Agricola (1494–1555), the founder of geology, was apparently the first to have formalized a definition of clay (Guggenheim and Martin, 1995). The latest effort in this direction was made nearly five centuries later by the joint nomenclature

---

<sup>1</sup>One of the authors (FB) is a member of the AIPEA nomenclature committee dealing with definitions of clay and clay mineral. However, the views expressed here are the entire responsibility of the authors and do not necessarily reflect those of the nomenclature committee.

Table 1.1. Current names of clays

Current names of clays	Origin <sup>a</sup>	Main clay mineral constituents	Remarks
Ball clay	Sedimentary	Kaolinite	Highly plastic, white burning (Grim, 1962)
Bentonite	Volcanic rock alteration or authigenic	Montmorillonite	
Bleaching earth	Acid-activated bentonite	Decomposed montmorillonite	
Common clay	Sedimentary or by weathering	Various, often illite/smectite mixed-layer minerals	General for ceramics excluding porcelain
China clay	Hydrothermal	Kaolinite	Kaolins from Cornwall plastic, white burning
Fire clay	Sedimentary	Kaolinite	Plastic, high refractoriness (Grim, 1962)
Flint clay	Sedimentary with subsequent diagenesis	Kaolinite	Non-slaking, not plastic, used for refractories (Grim, 1962; Keller, 1978, 1981, 1982)
Fuller's earth	Sedimentary, residual, or hydrothermal	Montmorillonite, sometimes palygorskite, sepiolite	
Primary kaolin	Residual or by hydrothermal alteration	Kaolinite	
Secondary kaolin	Authigenic sedimentary	Kaolinite	
Refractory clay	Authigenic sedimentary	Kaolinite	With low levels of iron, alkali and alkali earth cations for refractories (Grim, 1962)
Laponite	Synthetic	Hectorite-type smectite	
Nanoclay		Mostly montmorillonite	Superfluous term for clays used for nanocomposites

<sup>a</sup>See Chapter 14 for more details.

committees (JNCs) of the Association Internationale pour l'Etude des Argiles (AIPEA) and the Clay Minerals Society (CMS). The JNCs have defined 'clay' as "... a *naturally occurring* material composed primarily of *fine-grained* minerals, which is generally *plastic* at appropriate water contents and will *harden* with (*sic*) dried or

fired” (Guggenheim and Martin, 1995). (The authors have italicized some words to alert the reader, and indicate that these words will be commented on below). By this definition synthetic clays and clay-like materials are not regarded as clay even though they may be fine grained, and display the attributes of plasticity and hardening on drying and firing.

Although particle size is a key parameter in all definitions of clay, there is no generally accepted upper limit. Some disciplines and professions, however, have conventionally set a maximum size of clay particles. In pedology, for example, the ‘clay fraction’ refers to a class of materials whose particles are smaller than  $2\text{ }\mu\text{m}$  in equivalent spherical diameter (e.s.d.). In geology, sedimentology, and geo-engineering the size limit is commonly set at  $<4\text{ }\mu\text{m}$  e.s.d. (Moore and Reynolds, 1997), while in colloid science the value of  $<1\text{ }\mu\text{m}$  is generally accepted. Indeed, Weaver (1989) has suggested that the term ‘clay’ should only be used in the textural sense to indicate material that is finer than  $4\text{ }\mu\text{m}$ .

Although plasticity is a part of the JNCs’ definition, some non-plastic clays (e.g., ‘flint clays’) are still regarded as ‘clay’ because of past usage.

The JNCs also state that the plastic properties of clay do not need quantification since plasticity is affected by many factors, including chemical composition and particle aggregation. Operationally, ‘plasticity’ may be defined as the ability (of a clay material) to be moulded into a certain shape without rupturing when stress is applied, and for this shape to be retained after the stress is removed. However, in the ceramics industry, plasticity is commonly measured in terms of the ‘water of plasticity’ (liquid and plastic limits) (see Chapter 5). In engineering, plasticity is measured or expressed in terms of the ‘plasticity index’ (PI), that is, the difference in water content between the liquid and plastic limits of the clay material. As a rule of thumb, a clay with a  $\text{PI} > 25\%$  would tend to expand or swell when wet.

In industrial applications of clays one distinguishes four types of clays: (i) bentonites with montmorillonite as the principal clay mineral constituent, (ii) kaolins containing kaolinite, (iii) palygorskite and sepiolite, and (iv) ‘common clays’ which often contain illite/smectite mixed-layer minerals, and are largely used for ceramics (see Chapter 10.1).

### 1.3. CLAY MINERAL

Likewise, the term ‘clay mineral’ is difficult to define. As a first approximation, the term signifies a class of hydrated phyllosilicates (Tables 1.2 and 1.3) making up the fine-grained fraction of rocks, sediments, and soils. The definition that the JNCs have proposed is “... phyllosilicate minerals and minerals which impart plasticity to clay and which harden upon drying or firing” (Guggenheim and Martin, 1995). Since the origin of the material is not part of the definition, clay mineral (unlike clay) may be synthetic.



Table 1.2. Classification of planar hydrous phyllosilicates

Interlayer material <sup>a</sup>	Group	Octahedral character <sup>b</sup>	Species
<i>1:1 Clay minerals</i>			
None or H <sub>2</sub> O only, $\xi \sim 0$	Serpentine-kaolin	Tri	Amesite, berthierine, brindleyite, cronstedtite, fraipontite, kellyite, lizardite, nepouite
		Di	Dickite, halloysite (planar), kaolinite, nacrite
		Di-tri	Odinite
<i>2:1 Clay minerals</i>			
None, $\xi \sim 0$	Talc-pyrophyllite	Tri Di	Kerolite, pimelite, talc, willemsite Ferripyrophyllite, pyrophyllite
Hydrated exchangeable cations, $\xi \sim 0.2\text{--}0.6$	Smectite	Tri	Hectorite, saponite, sauconite, stevensite, swinefordite
		Di	Beidellite, montmorillonite, nontronite, volkonskoite
Hydrated exchangeable cations, $\xi \sim 0.6\text{--}0.9$	Vermiculite	Tri	Trioctahedral vermiculite
		Di	Diocahedral vermiculite
Non-hydrated monovalent cations, $\xi \sim 0.6\text{--}1.0$	True (flexible) mica	Tri	Biotite, lepidolite, phlogopite, etc.
		Di	Celadonite, illite, glauconite, muscovite, paragonite, etc.
Non-hydrated divalent cations, $\xi \sim 1.8\text{--}2.0$	Brittle mica	Tri	Anandite, bityite, clintonite, kinoshitalite
		Di	Margarite
Hydroxide sheet, $\xi$ variable	Chlorite	Tri	Baileychlore, chamosite, clinochlore, nimite, pennantite
		Di	Donbassite
		Di-tri	Cookeite, sudoite
<i>Regularly interstratified 2:1 clay minerals</i>			
$\xi$ Variable		Tri	Aliettite, corrensite, hydrobiotite, kulkeite
		Di	Rectorite, tosudite

Source: Adapted from [Martin et al. \(1991\)](#).

<sup>a</sup> $\xi$  = net layer charge per formula unit.

<sup>b</sup>tri = trioctahedral, di = dioctahedral.

Nor does grain size feature as a criterion in the JNCs' definition of clay mineral. Accordingly, phyllosilicates of any size, such as macroscopic mica, vermiculite, and chlorite may be regarded as clay minerals. Indeed, much of our basic and detailed understanding of clay mineral structures is derived from X-ray diffraction analysis of

Table 1.3. Classification of non-planar hydrous phyllosilicates

Modulated component	Linkage configuration	Unit layer $c \sin \beta$ value	Traditional affiliation	Species
<i>1:1 Minerals with modulated structures</i>				
Tetrahedral sheet	Strips	0.7 nm	Serpentine	Antigorite, bementite
	Islands	0.7 nm	Serpentine	Caryopillite, ferropyrrosmalite, friedelite, greenalite, manganpyrosmalite, mcgillite, nelenite, pyrosmalite, schallerite
	Other		None	None
<i>2:1 Minerals with modulated structures</i>				
Tetrahedral sheet	Strips	0.95 nm 1.25 nm	Talc Mica	Minnesotaite Eggletonite, ganophyllite
	Islands	0.96–1.25 nm	Mica/complex	Ferristilpnomelane, ferrostilpnomelane, lennilenapeite, parsettensite, stilpnomelane, zussmanite
	Other	1.23 nm 1.4 nm	None Chlorite	Bannisterite Gonyerite
Octahedral sheet	Strips	1.27–1.34 nm	Pyribole	Falcondoite, loughlinite, palygorskite, sepiolite, yofortierite
<i>1:1 Minerals with rolled and spheroidal structures</i>				
None	Trioctahedral		Serpentine	Chrysotile, percoraite
	Diocahedral		Kaolin	Halloysite (nonplanar)

Source: Adapted from [Martin et al. \(1991\)](#).

macrocrystalline forms, notably the micas and vermiculites (see Chapter 2). A similar concept was advocated by [Weaver \(1989\)](#) who suggested the term ‘physils’ for the whole family of phyllosilicates (including palygorskite and sepiolite) irrespective of grain size.

The JNCs have further proposed that non-phyllosilicate minerals would qualify as clay minerals if they impart plasticity to clay, and harden on drying or firing.

1.4. DISTINCTION BETWEEN CLAY AND CLAY MINERAL

In commenting on the joint report, [Moore \(1996\)](#) has pointed out that ‘clay’ is used as a mineral term (as well as a size term and a rock term). However, we would agree with the JNCs that clay should not be used as a mineral term, and that a clear distinction must be made between clay and clay mineral ([Guggenheim and Martin, 1995](#)). The position of the JNCs on using clay as a rock term is still indeterminate. On the basis of past usage, we would agree with [Moore \(1996\)](#) that the term ‘clay’ can signify a rock, a sedimentary deposit, and the alteration (weathering) products of primary silicate minerals. It is in one or other of these senses that the terms ‘ball clay’, ‘fire clay’, ‘bentonite’, ‘bleaching earth’, and ‘fuller’s earth’ have been used in the literature ([Grim, 1962](#); [Weaver and Pollard, 1973, Table 1.1](#)).

The distinction between clay and clay mineral must always be kept in mind, as the criteria mentioned above are different ([Table 1.4](#)). Nevertheless, the literature often uses the term ‘clay’ for ‘clay mineral’ because the former is shorter and less cumbersome. This handbook is primarily concerned with clay minerals rather than clays.

1.5. CLAY MINERAL PROPERTIES

- Clay minerals are characterized by certain properties, including
1. a layer structure with one dimension in the nanometer range; the thickness of the 1:1 (TO) layer is about 0.7 nm, and that of the 2:1 (TOT) layer is about 1 nm,
  2. the anisotropy of the layers or particles,
  3. the existence of several types of surfaces: external basal (planar) and edge surfaces as well as internal (interlayer) surfaces (e.g., [Annabi-Bergaya et al., 1979](#)),
  4. the ease with which the external, and often also the internal, surface can be modified (by adsorption, ion exchange, or grafting),
  5. plasticity, and
  6. hardening on drying or firing; this applies to most (but not all) clay minerals.

Table 1.4. Distinction between clay and clay mineral

Clay	Clay mineral
Natural	Natural and synthetic
Fine-grained (<2 μm or <4 μm)	No size criterion
Phyllosilicates as principal constituents	May include non-phyllosilicates
Plastic <sup>a</sup>	Plastic
Hardens on drying or firing	Hardens on drying or firing

<sup>a</sup>With some exceptions like flint clays.

Many people associate clay minerals with smectites, which have the following properties:

- particles of colloidal size,
- high degree of layer stacking disorder,
- high specific surface area,
- moderate layer charge (Table 1.2),
- large cation exchange capacity that is little dependent on ambient pH,
- small pH-dependent anion exchange capacity,
- variable interlayer separation, depending on ambient humidity,
- propensity for intercalating<sup>2</sup> extraneous substances, including organic compounds and macromolecules, and
- ability of some members (e.g., Li<sup>+</sup> - and Na<sup>+</sup> -exchanged forms) to show extensive interlayer swelling in water; under optimum conditions, the layers can completely dissociate (delaminate).

## 1.6. ASSOCIATED MINERALS

The clay fraction of soils and sediments (having particles of either  $<2\mu\text{m}$  or  $<4\mu\text{m}$ ) often contains non-phyllsilicate minerals, such as carbonates, feldspars, and quartz together with the (hydr)oxides of iron and aluminium. Since these minerals do not impart plasticity to clay, they have been referred to as ‘non-clay constituents’ or ‘accessory minerals’ (Greenland and Hayes, 1978; Brown, 1980; Hall, 1987). However, following the recommendation of the JNCs (Guggenheim and Martin, 1995), we would prefer to call them ‘associated minerals’, a detailed description of which has been given by Dixon and Schulze (2002). As the name suggests, these minerals are closely associated with the phyllsilicate component of clay, and hence interfere with its identification. The presence of associated minerals in natural clay deposits also reduces the commercial value of the resource. For these reasons, much effort has been expended in purifying raw clays and in synthesizing ‘pure’ clay minerals. Although associated minerals exert a strong influence on the behaviour of soil and sediment (Dixon and Weed, 1989), a discussion of their nature and properties lies beyond the scope of the present book.

## 1.7. ASSOCIATED PHASES

Non-crystalline or X-ray amorphous materials (sometimes also considered as gels), including organic matter, are referred to by the JNCs as ‘associated phases’ whether or not they impart plasticity to clay. Accordingly, allophane would qualify

---

<sup>2</sup>The term ‘intercalation’ denotes both interlayer adsorption and interlayer ion exchange reactions.

as an associated phase since this group of hydrated aluminosilicates lacks long-range order; that is, its structural regularity does not extend much beyond  $\sim 1$  nm (Parfitt, 1990). Nevertheless, we propose that allophane be regarded as a clay mineral because of past usage. The same applies to imogolite, an aluminosilicate with long-range order in one direction (Wada, 1989). Chapter 2 gives more detail about allophane and imogolite.

## 1.8. OTHER SOLIDS WITH SIMILAR PROPERTIES

In this context, we should mention the existence of other types of solids that have similar properties to the phyllosilicates in terms of layer structure, charge characteristics, and potential for intercalation but are not components of clay. In other words, these layered materials are neither associated minerals nor associated phases of the fine-grained fraction of soil and sediment.

Some notable examples are the alkali silicates, crystalline silicic acids, niobates, phosphates, titanates, and LDH (Lagaly and Beneke, 1991; Schwieger and Lagaly, 2004). Only LDH are included in this handbook (Chapter 13.1). This is partly because of space limitation, and partly because LDH have been referred to as ‘anionic clays’. Further, LDH have attracted a great deal of attention for their actual and potential applications in catalysis and environmental protection (Newman and Jones, 1998; Tichit and Vaccari, 1998; Basile et al., 2001).

According to the definition of ‘clay’, proposed by the JNCs (Guggenheim and Martin, 1995), LDH should not be considered as clay because of their synthetic origin. On the other hand, hydrotalcite, the naturally occurring analogue of LDH, would clearly qualify as clay. The term ‘anionic clays’ may also cause confusion since the layers of LDH are positively charged, and hence are cationic (the *anionic* designation being a reference to the anion exchange property of LDH). Another name for LDH, used in the literature, is ‘hydrotalcite-like compounds’ but this term seems less descriptive and more cumbersome than ‘layered double hydroxides’. Similarly, the term ‘cationic clays’ to denote the (conventional) phyllosilicates with a negative layer charge (Tables 1.2 and 1.3) is not advocated. As already mentioned, the term ‘clay mineral’, as defined by the JNCs (Guggenheim and Martin, 1995), may encompass non-phyllosilicates (if they impart plasticity to clay). This would open the way for the inclusion of natural and synthetic minerals, such as LDH in the clay mineral family although synthetic LDH are not part of common clay material. This issue needs to be clarified (and resolved).

Clay minerals are often confused with zeolites because they tend to occur together and share many attributes (Chapter 13.2). Both groups of materials can be synthesized, modified, and tailored by chemical, physical, and thermal treatments.

Other materials with properties related to phyllosilicates, notably smectites, are cement and concrete (Chapter 13.3).

## 1.9. CLAY MINERAL PARTICLES AND AGGREGATES

According to the JNCs definition ‘clay minerals’ may be either natural or synthetic, phyllosilicates or non-phyllosilicates, and have no size connotation. The structures of phyllosilicates are all based on a tetrahedral (T) and an octahedral (O) sheet that may condense in either a 1:1 or 2:1 proportion to form an anisotropic TO or TOT layer. The structure of LDH (‘anionic clay minerals’) is based on an octahedral sheet (O). The layers or sheets may be negatively charged (as for the majority of clay minerals), positively charged (as in LDH), or essentially uncharged (as in talc and pyrophyllite; Table 1.2). The layer charge density and the nature of the compensating (charge-balancing) cation determine many important surface and colloidal properties.

For simplicity sake, we refer to an assembly of layers as a ‘particle’,<sup>3</sup> and an assembly of particles as an ‘aggregate’. Accordingly we may distinguish between interlayer, interparticle, and interaggregate pores (Fig. 1.1). The arrangement of the particles or aggregates leads to different morphologies, such as plates, tubules, laths, and fibres (Fig. 1.2). All phyllosilicates are therefore porous, containing pores of varied size and shape.

## 1.10. CLAY MINERALS AND ENVIRONMENT

As clay scientists, we are interested not only in the material itself but also in its interaction with extraneous substances (i.e., in the environment). This interaction is influenced by many factors, such as the acid–basic character (pH and ionic strength), and thermodynamic conditions (pressure and temperature) of the surrounding medium. As we need to know the properties of the clay mineral in question, and those of the interacting compound (water, polymer, iron, organic/inorganic molecule), research into the clay–environment interaction requires collaboration between several disciplines. Moreover, the interaction between clay minerals and other compounds in the environment can occur at different states of matter (solid, melted solid, liquid, gas, and plasma). Its study would therefore involve the classical disciplines of solid/liquid physics and chemistry as well as the developing disciplines of melted- and plasma-state science. Fig. 1.3 shows the variety of parameters influencing the clay mineral–compound interaction, and the importance of relating ‘microscopic’ properties to ‘macroscopic’ behaviour.

---

<sup>3</sup>In the clay science literature the term ‘particle’, as defined here, is often referred to as ‘crystallite’ (or even ‘crystal’). For consistency, we have used ‘particle’ throughout the handbook.

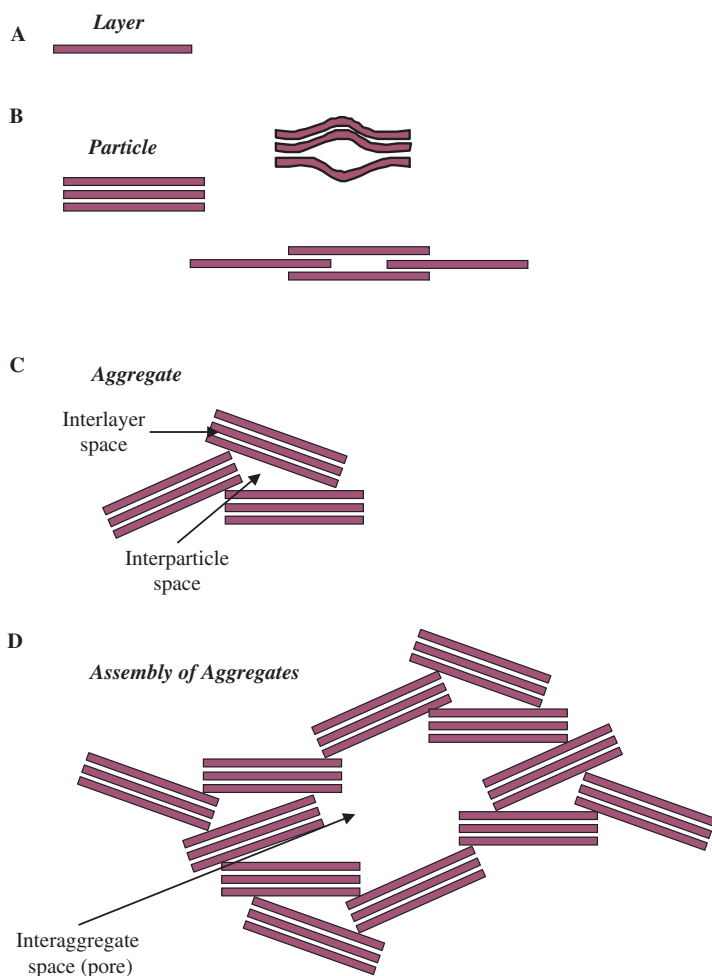


Fig. 1.1. Diagram showing (A) a clay mineral layer; (B) a particle, made up of stacked layers; layer translation and deformation can give rise to a lenticular pore; (C) an aggregate, showing an interlayer space and an interparticle space; and (D) an assembly of aggregates, enclosing an interaggregate space (pore).

### 1.11. ALTERNATIVE CONCEPTS OF CLAY MINERALS

Clay minerals are traditionally classified under 'silicates' but since their formulae (chemical compositions) have more oxygen than Si, Al, or Mg (Table 1.5), these minerals may arguably be considered as (hydr)oxides of silicon, aluminium, or magnesium. By the same token, LDH may be regarded as (hydr)oxides of metal ions.

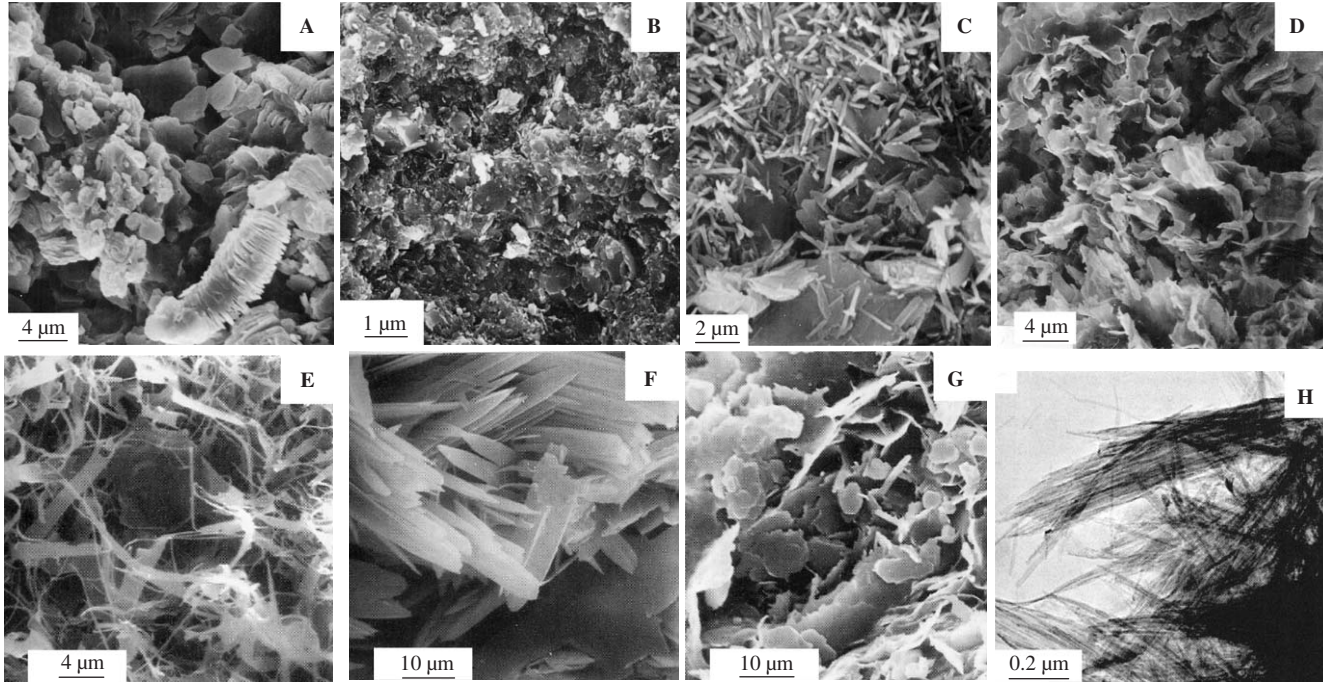


Fig. 1.2. Transmission electron micrographs of some clay minerals with varied particle morphology: (A) kaolinite from Sasso (Italy) showing typical books of particles; (B) high-quality flint clay from Gasconade County, Missouri, USA; (C) tubular halloysite particles alongside kaolinite plates from Sasso, Italy; (D) smectite or illite/smectite from Sasso, Italy; (E) filamentous illite from sandstones in offshore Netherlands; (F) lath-shaped illite from sandstones in offshore Netherlands; (G) pseudo-hexagonal illite particles from sandstones in offshore Netherlands; (H) fibrous palygorskite from Southern Georgia (USA). (A), (C), and (D) are taken from Lombardi et al., (1987); (B) is taken from Keller and Stevens (1983); E, F, and G are taken from Lanson et al., (2002); and (H) is taken from Krekeler (2004).



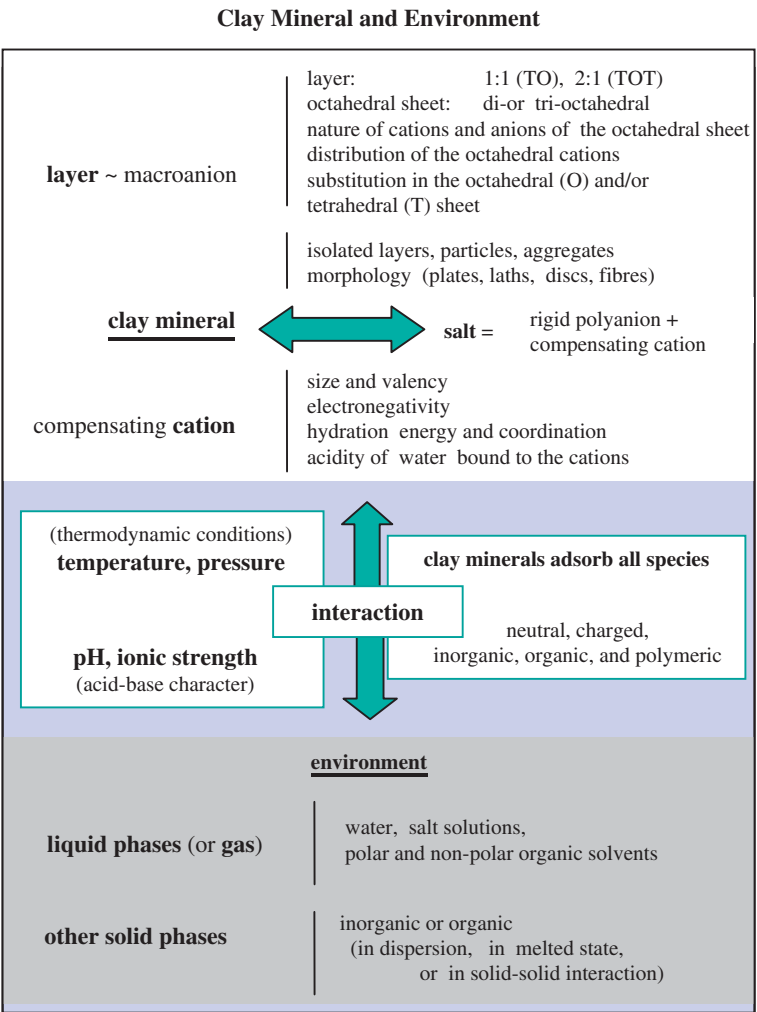


Fig. 1.3. Diagram showing the interactions of clay minerals with the environment.

Thus clay minerals and related layer materials (see Section 1.8) may be referred to as *porous layered (hydr)oxides*.

Clay minerals may also be considered as *salts* of rigid (two-dimensional) polyanions with infinite radius and their compensating (exchangeable) cations (Fig. 1.3), or as *inorganic polymers* where the continuous octahedral sheet is based on a repetition of an octahedron monomer. The other basic monomer is the silica tetrahedron, which is bound on one or both sides to the octahedral sheet.

Table 1.5. Layer charge and idealized formulae (chemical compositions) of some representative 1:1 and 2:1 clay minerals

Charge/ formula unit	Di octahedral species	Tri octahedral species
<i>Serpentine-kaolin group</i>		
~0	Kaolinite (Si <sub>2</sub> ) <sup>IV</sup> (Al <sub>2</sub> ) <sup>VI</sup> O <sub>5</sub> (OH) <sub>4</sub>	Serpentine (Si <sub>2</sub> ) <sup>IV</sup> (Mg <sub>3</sub> ) <sup>VI</sup> O <sub>5</sub> (OH) <sub>4</sub>
<i>Talc-pyrophyllite group</i>		
~0	Pyrophyllite (Si <sub>4</sub> ) <sup>IV</sup> (Al <sub>2</sub> ) <sup>VI</sup> O <sub>10</sub> (OH) <sub>2</sub>	Talc (Si <sub>4</sub> ) <sup>IV</sup> (Mg <sub>3</sub> ) <sup>VI</sup> O <sub>10</sub> (OH) <sub>2</sub>
<i>Smectite group</i>		
~0.2–0.6	Montmorillonite (Si <sub>4</sub> ) <sup>IV</sup> (Al <sub>2–y</sub> Mg <sub>y</sub> ) <sup>VI</sup> O <sub>10</sub> (OH) <sub>2</sub> , yM <sup>+</sup> .nH <sub>2</sub> O Beidellite (Si <sub>4–x</sub> Al <sub>x</sub> ) <sup>IV</sup> (Al <sub>2</sub> ) <sup>VI</sup> O <sub>10</sub> (OH) <sub>2</sub> , xM <sup>+</sup> .nH <sub>2</sub> O	Hectorite (Si <sub>4</sub> ) <sup>IV</sup> (Mg <sub>3–y</sub> Li <sub>y</sub> ) <sup>VI</sup> O <sub>10</sub> (OH) <sub>2</sub> , yM <sup>+</sup> .nH <sub>2</sub> O Saponite (Si <sub>4–x</sub> Al <sub>x</sub> ) <sup>IV</sup> (Mg <sub>3</sub> ) <sup>VI</sup> O <sub>10</sub> (OH) <sub>2</sub> , xM <sup>+</sup> .nH <sub>2</sub> O
<i>Vermiculite group</i>		
~0.6–0.9	Vermiculite (Si <sub>4–x</sub> Al <sub>x</sub> ) <sup>IV</sup> (Al <sub>2–y</sub> Mg <sub>y</sub> ) <sup>VI</sup> O <sub>10</sub> (OH) <sub>2</sub> , (x + y)M <sup>+</sup>	Vermiculite (Si <sub>4–x</sub> Al <sub>x</sub> ) <sup>IV</sup> (Mg <sub>3–y</sub> M <sub>y</sub> <sup>3+</sup> ) <sup>VI</sup> O <sub>10</sub> (OH) <sub>2</sub> , (x – y)/2 Mg <sup>2+</sup>
<i>True (flexible) mica group<sup>a</sup></i>		
~0.9–1.0	Celadonite (Si <sub>4–x</sub> Al <sub>x</sub> ) <sup>IV</sup> (Fe <sub>2–y</sub> Mg <sub>y</sub> ) <sup>VI</sup> O <sub>10</sub> (OH) <sub>2</sub> , (x + y)K <sup>+</sup> Muscovite (Si <sub>3</sub> Al) <sup>IV</sup> (Al <sub>2</sub> ) <sup>VI</sup> O <sub>10</sub> (OH) <sub>2</sub> , K <sup>+</sup>	Lepidolite (Si <sub>4–x</sub> Al <sub>x</sub> ) <sup>IV</sup> (Mg <sub>3–y</sub> Li <sub>y</sub> ) <sup>VI</sup> O <sub>10</sub> (OH) <sub>2</sub> , (x + y)K <sup>+</sup> Phlogopite (Si <sub>3</sub> Al) <sup>IV</sup> (Mg <sub>3</sub> ) <sup>VI</sup> O <sub>10</sub> (OH) <sub>2</sub> , K <sup>+</sup>
<i>Brittle mica group</i>		
2.0	Margarite (Si <sub>2</sub> Al <sub>2</sub> ) <sup>IV</sup> (Al <sub>2</sub> ) <sup>VI</sup> O <sub>10</sub> (OH) <sub>2</sub> , Ca <sup>2+</sup>	Clintonite (Si Al <sub>3</sub> ) <sup>IV</sup> (Mg <sub>2</sub> Al) <sup>VI</sup> O <sub>10</sub> (OH) <sub>2</sub> , Ca <sup>2+</sup>

<sup>a</sup>Illite is the subject of controversy in the literature. In Table 1.2, illite is classified as a species in the true mica group. However, illite is also considered to be a separate group of clay-size, dioctahedral mica-type minerals (Meunier and Velde, 2004). The general formula for illite group may be written as (Si<sub>4–x</sub> Al<sub>x</sub>)<sup>IV</sup>(Al<sub>2–y</sub> Mg<sub>y</sub>)<sup>VI</sup> O<sub>10</sub> (OH)<sub>2</sub>, (x + y)K<sup>+</sup> with a charge of 0.9 per O<sub>10</sub> (OH)<sub>2</sub>, although the existence of Na<sup>+</sup>–illite (brammalite) (Bannister, 1943) and NH<sub>4</sub><sup>+</sup>–illite (tobellite) (Šucha et al., 1994) has been documented.

These concepts may promote clay science by attracting an increasing number of chemists and physicists besides the large number of earth and soil scientists, as is traditionally the case.

## 1.12. CLAY SCIENCE

Clay minerals are probably unique in the sense that these materials are studied by, and used in, many disciplines for fundamental and applied research. The *multi-disciplinary* approach is at the frontier between materials science and colloid science, while the *multi-scale* approach linking nano-, micro- and macro-scale studies is a challenge for the future of clay science.

Studying the same sample by several techniques simultaneously (Annabi-Bergaya et al., 1981, 1996) is a method that is seldom followed by researchers. We would recommend this approach in future investigations as it can provide valuable and insightful information.

Clay research is being actively pursued by many people and in many countries, and the future of clay science looks bright, exciting, and promising.

## 1.13. CONCLUDING REMARKS

The aim of this handbook is to attract the attention of clay scientists in academe and industry as well as in politics (as research needs funding), and to stress the importance of clay science to society and the quality of life. The economic benefits seem evident because clays are abundant, widespread, and inexpensive compared with other raw materials.

The table of contents of this handbook indicates the industrial and environmental importance of clays and clay minerals. The great variety of physical, chemical, and thermal treatments that may be used to modify clays and clay minerals provide unlimited scope for future applications, particularly in terms of protecting our environment.

Because of the multi-disciplinary nature of clay science, its teaching is another challenging task. By learning about the mineralogical, physico-chemical, and industrial aspects of clay science, students would not only gain an appreciation of the 'scientific method' and the physical environment but also find suitable employment and a fulfilling career.

## REFERENCES

- Annabi-Bergaya, F., Cruz, M.I., Gatinneau, L., Fripiat, J.J., 1979. Adsorption of alcohols by smectites. I. Distinction between internal and external surfaces. *Clay Minerals* 14, 249–258.

- Annabi-Bergaya, F., Cruz, M.I., Gatinéau, L., Fripiat, J.J., 1981. Adsorption of alcohols by smectites. IV. Models. *Clay Minerals* 16, 115–122.
- Annabi-Bergaya, F., Estrade-Szwarcckopf, H., Van Damme, H., 1996. Dehydration of Cu—Hectorite: water isotherm, XRD, and EPR studies. *Journal of Physical Chemistry* 100, 4120–4126.
- Bannister, F.A., 1943. Brammalite (sodium illite), a new mineral from Llandebie, South Wales. *Mineralogical Magazine* 26, 304–307.
- Basile, F., Campanati, M., Serwicka, E.M., Vaccari, A. (Eds.), 2001. Special Issue. Hydrotalcites '99. *Applied Clay Science* 18, 1–110.
- Brindley, G.W., Brown, G. (Eds.), 1980. *Crystal Structures of Clay Minerals and their X-ray Identification*. Mineralogical Society, London.
- Brown, G., 1980. Associated minerals. In: Brindley, G.W., Brown, G. (Eds.), *Crystal Structures of Clay Minerals and their X-ray Identification*. Mineralogical Society, London, pp. 361–410.
- Chamley, H., 1989. *Clay Sedimentology*. Springer, Berlin.
- Dixon, J.B., Schulze, D.G. (Eds.), 2002. *Soil Mineralogy with Environmental Applications*. Soil Science Society of America, Madison, WI.
- Dixon, J.B., Weed, S.B. (Eds.), 1989. *Minerals in Soil Environments*, 2nd edition. Soil Science Society of America, Madison, WI.
- Farmer, V.C. (Ed.), 1974. *The Infrared Spectra of Minerals*. Mineralogical Society, London.
- Greenland, D.J., Hayes, M.H.B. (Eds.), 1978. *The Chemistry of Soil Constituents*. Wiley, Chichester.
- Grim, R.E., 1953. *Clay Mineralogy*. McGraw-Hill, New York.
- Grim, R.E., 1962. *Applied Clay Mineralogy*. McGraw-Hill, New York.
- Grim, R.E., 1968. *Clay Mineralogy*, 2nd edition. McGraw-Hill, New York.
- Guggenheim, S., Martin, R.T., 1995. Definition of clay and clay mineral: joint report of the AIPEA nomenclature and CMS nomenclature committees. *Clays and Clay Minerals* 43, 255–256 and *Clay Minerals* 30, 257–259.
- Hall, P.L., 1987. Clays: their significance, properties, origins and uses. In: Wilson, M.J. (Ed.), *A Handbook of Determinative Methods in Clay Mineralogy*. Blackie, Glasgow, pp. 1–25.
- Keller, W.D., 1978. Flint-clay facies illustrated within one deposit of refractory clay. *Clays and Clay Minerals* 26, 237–243.
- Keller, W.D., 1981. The sedimentology of flint clay. *Journal of Sedimentary Petrology* 51, 233–244.
- Keller, W.D., 1982. Kaolin—a most diverse rock in genesis, texture, physical properties, and uses. *Geological Society of America Bulletin* 93, 27–36.
- Keller, W.D., Stevens, R.P., 1983. Physical arrangement of high-alumina clay types in a Missouri clay deposit and implications for their genesis. *Clays and Clay Minerals* 31, 422–434.
- Konta, J., 2000. Clay science at the threshold of the new millennium: a look at the history and present trends. *Acta Universitatis Carolinae—Geologica* 44, 11–48.
- Krekeler, M.P., 2004. Improved constraints on sedimentary environments of palygorskite deposits of the Hawthorne formation, Southern Georgia, from a detailed study of a core. *Clays and Clay Minerals* 52, 253–262.
- Kühnel, R.A., 1990. The modern days of clays. *Applied Clay Science* 5, 135–143.
- Lagaly, G., Beneke, K., 1991. Intercalation and exchange reactions of clay minerals and non-clay layer compounds. *Colloid and Polymer Science* 269, 1198–1211.

- Lanson, B., Beaufort, D., Berger, G., Bauer, A., Cassagnabère, A., Meunier, A., 2002. Authigenic kaolin and illitic minerals during burial diagenesis of sandstones: a review. *Clay Minerals* 37, 1–22.
- Lombardi, G., Russell, J.D., Keller, W.D., 1987. Compositional and structural variations in the size fractions of a sedimentary and a hydrothermal kaolin. *Clays and Clay Minerals* 35, 321–335.
- Martin, R.T., Bailey, S.W., Eberl, D.D., Fanning, D.S., Guggenheim, S., Kodama, H., Pevear, D.R., Środoń, J., Wicks, F.J., 1991. Report on the Clay Minerals Society nomenclature committee: revised classification of clay minerals. *Clays and Clay Minerals* 39, 333–335.
- Meunier, A., Velde, B., 2004. *Illite. Origins, Evolution and Metamorphism*. Springer, Berlin.
- Moore, D.M., 1996. Comment on: definition of clay and clay mineral: joint report of the AIPEA nomenclature and CMS nomenclature committees. *Clays and Clay Minerals* 44, 710–712.
- Moore, D.M., Reynolds, R.C. Jr., 1997. *X-ray Diffraction and the Identification and Analysis of Clay Minerals*, 2nd edition. Oxford University Press, Oxford.
- Murray, H., 1999. Clays for our future. In: Kodama, H., Mermut, A.R., Torrance, J.K. (Eds.), *Clays for Our Future*. Proceedings of the 11th International Clay Conference, Ottawa, Canada, 1997. ICC97 Organizing Committee, Ottawa, pp. 3–11.
- Newman, S.P., Jones, W., 1998. Synthesis, characterization and applications of layered double hydroxides containing organic guests. *New Journal of Chemistry* 22, 105–115.
- Parfitt, R.L., 1990. Allophane in New Zealand—a review. *Australian Journal of Soil Research* 28, 343–360.
- Schwieger, W., Lagaly, G., 2004. Alkali silicates and crystalline silicic acids. In: Auerbach, S.M., Carrado, K.A., Dutta, P.K. (Eds.), *Handbook of Layered Materials*. Marcel Dekker, New York, pp. 541–629.
- Šucha, V., Kraus, I., Madejová, J., 1994. Ammonium illite from anchimetamorphic shales associated with anthracite in the Zemplinicum of the western Carpathians. *Clay Minerals* 29, 69–77.
- Theng, B.K.G., 1974. *The Chemistry of Clay-Organic Reactions*. Adam Hilger, London.
- Theng, B.K.G., 1979. *Formation and Properties of Clay-Polymer Complexes*. Elsevier, Amsterdam.
- Tichit, D., Vaccari, A. (Eds.), 1998. Recent catalytic applications of hydrotalcite-type anionic clays (layered double hydroxides). *Applied Clay Science* 13 (Special Issue), 311–518.
- van Olphen, H., 1977. *An Introduction to Clay Colloid Chemistry*, 2nd edition. Wiley, New York.
- Velde, B. (Ed.), 1995. *Origin and Mineralogy of Clays*. Springer, Berlin.
- Wada, K., 1989. Allophane and imogolite. In: Dixon, J.B., Weed, S.B. (Eds.), *Minerals in Soil Environments*, 2nd edition. Soil Science Society of America, Madison, WI, pp. 1051–1087.
- Weaver, C.E., 1989. *Clays, Muds, and Shales*. Elsevier, Amsterdam.
- Weaver, C.E., Pollard, L.D., 1973. *The Chemistry of Clay Minerals*. Developments in Sedimentology 15. Elsevier, Amsterdam.
- Wilson, M.J. (Ed.), 1994. *Clay Mineralogy: Spectroscopic and Chemical Determinative Methods*. Chapman & Hall, London.

## Chapter 2

# STRUCTURES AND MINERALOGY OF CLAY MINERALS

M.F. BRIGATTI<sup>a</sup>, E. GALAN<sup>b</sup> AND B.K.G. THENG<sup>c</sup>

<sup>a</sup>*Dipartimento di Scienze della Terra, Università di Modena, I-41100 Modena, Italy*

<sup>b</sup>*Departamento de Cristalografía, Mineralogía y Química Agrícola, Facultad de Química, Universidad de Sevilla, ES-41071 Sevilla, Spain*

<sup>c</sup>*Landcare Research, Palmerston North, New Zealand*

## 2.1. GENERAL STRUCTURAL INFORMATION

Phyllosilicates considered in this section ideally contain a continuous tetrahedral sheet. Each tetrahedron consists of a cation, T, coordinated to four oxygen atoms, and linked to adjacent tetrahedra by sharing three corners (the basal oxygen atoms, O<sub>b</sub>) to form an infinite two-dimensional 'hexagonal' mesh pattern along the *a*, *b* crystallographic directions (Fig. 2.1). In the octahedral sheet, connections between each octahedron, M, to neighbouring octahedra are made by sharing edges. The edge-shared octahedra form sheets of hexagonal or pseudo-hexagonal symmetry (Fig. 2.2). Common tetrahedral cations are Si<sup>4+</sup>, Al<sup>3+</sup>, and Fe<sup>3+</sup>. Octahedral cations are usually Al<sup>3+</sup>, Fe<sup>3+</sup>, Mg<sup>2+</sup>, and Fe<sup>2+</sup>, but other cations, such as Li<sup>+</sup>, Mn<sup>2+</sup>, Co<sup>2+</sup>, Ni<sup>2+</sup>, Cu<sup>2+</sup>, Zn<sup>2+</sup>, V<sup>3+</sup>, Cr<sup>3+</sup>, and Ti<sup>4+</sup> were identified. Octahedra show two different topologies related to (OH) position, i.e., the *cis*- and the *trans*-orientation (Fig. 2.2).

The free corners (the tetrahedral apical oxygen atoms, O<sub>a</sub>) of all tetrahedra point to the same side of the sheet and connect the tetrahedral and octahedral sheets to form a common plane with octahedral anionic position O<sub>oct</sub> (O<sub>oct</sub> = OH, F, Cl, O) (Fig. 2.3). O<sub>oct</sub> anions lie near to the centre of each tetrahedral 6-fold ring, but are not shared with tetrahedra. The 1:1 layer structure consists of the repetition of one tetrahedral and one octahedral sheet, while in the 2:1 layer structure one octahedral sheet is sandwiched between two tetrahedral sheets (Fig. 2.3).

In the 1:1 layer structure, the unit cell includes six octahedral sites (i.e., four *cis*- and two *trans*-oriented octahedral) and four tetrahedral sites. Six octahedral sites and eight tetrahedral sites characterize the 2:1 layer unit cell. Structures with all the six octahedral sites occupied are known as trioctahedral (Fig. 2.4a). If only four of the six octahedra are occupied, the structure is referred to as dioctahedral (Fig. 2.4b). The structural formula is often reported on the basis of the half unit-cell content, i.e., it is based on three octahedral sites.

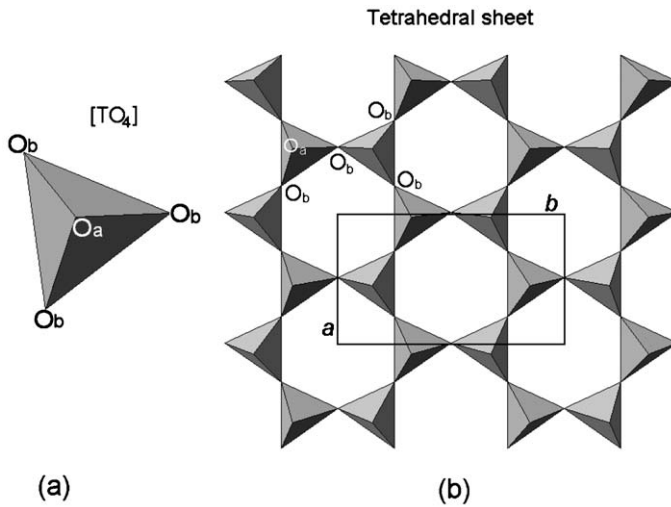


Fig. 2.1. (a) Tetrahedron  $[TO_4]$ ; (b) tetrahedral sheet.  $O_a$  and  $O_b$  refer to apical and basal oxygen atoms, respectively.  $a$  and  $b$  refer to unit-cell parameters.

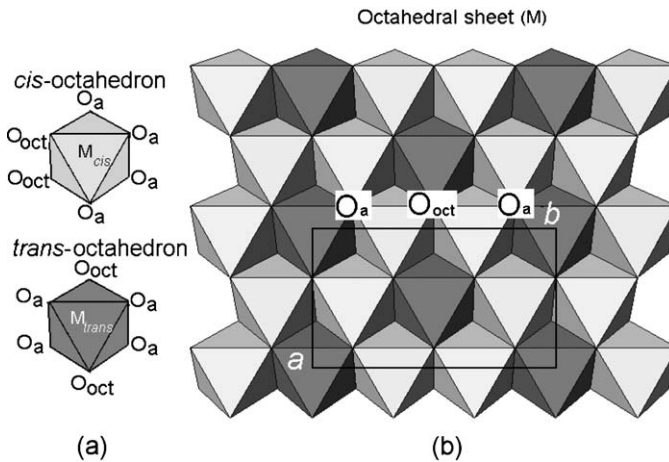


Fig. 2.2. (a)  $O_{oct}$  (OH, F, Cl) orientation in *cis*-octahedron and *trans*-octahedron; (b) location of *cis*- and *trans*-sites in the octahedral sheet.  $O_a$  and  $O_b$  refer to apical and basal oxygen atoms, respectively.  $a$  and  $b$  refer to unit cell parameters.

In the 1:1 or TM phyllosilicates (e.g., dioctahedral kaolinite and trioctahedral serpentine) each layer is about 0.7 nm thick (Fig. 2.5a). One surface of the layer consists entirely of oxygen atoms ( $O_b$ ) belonging to the tetrahedral sheet, while the other surface is composed of  $O_{oct}$  (mostly OH groups) from the octahedral sheet (Fig. 2.3). In the 2:1 or TMT layer the tetrahedral sheets are inverted and two-thirds of the octahedral

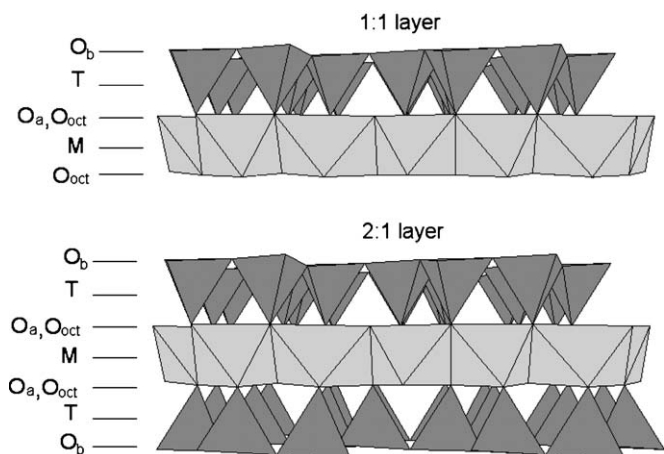


Fig. 2.3. Models of a 1:1 and 2:1 layer structure.  $O_a$ ,  $O_b$ , and  $O_{oct}$  refer to tetrahedral basal, tetrahedral apical, and octahedral anionic position, respectively. M and T indicate the octahedral and tetrahedral cation, respectively.

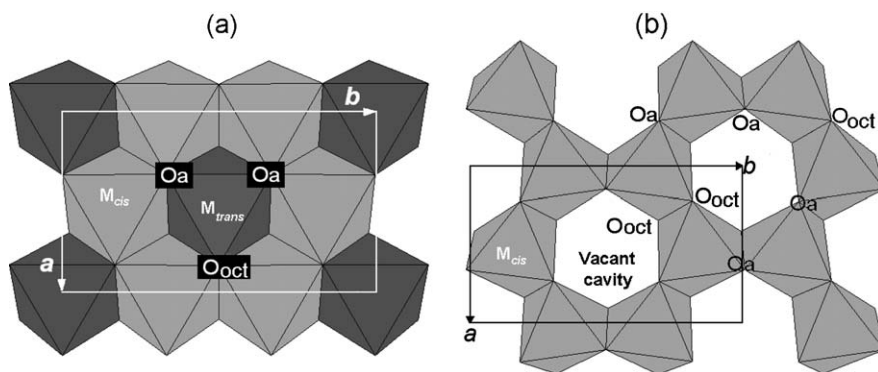


Fig. 2.4. (a) trioctahedral sheet; (b) dioctahedral sheet.  $O_a$  represents the apical oxygen atoms shared with tetrahedra, and  $O_{oct}$  is the anionic site shared between adjacent octahedra.  $a$  and  $b$  are unit-cell parameters.

hydroxyl groups are replaced by tetrahedral apical oxygen atoms (Fig. 2.3). Both surfaces of such a layer consist of tetrahedral basal oxygen atoms  $O_b$ . The periodicity along the  $c$ -axis varies from 0.91–0.95 nm in talc and pyrophyllite (Fig. 2.5b) to 1.40–1.45 nm in chlorite (Fig. 2.5e). The higher values for chlorite are due to interlayer occupancy. In talc, the interlayer space is empty, whereas in mica and illite (Fig. 2.5c) it is occupied by anhydrous alkaline and alkaline-earth cations (layer periodicity  $\approx 1.0$  nm). The interlayer space of smectite and vermiculite (Fig. 2.5d) contains alkaline or alkaline-earth cations together with water molecules (layer periodicity is about



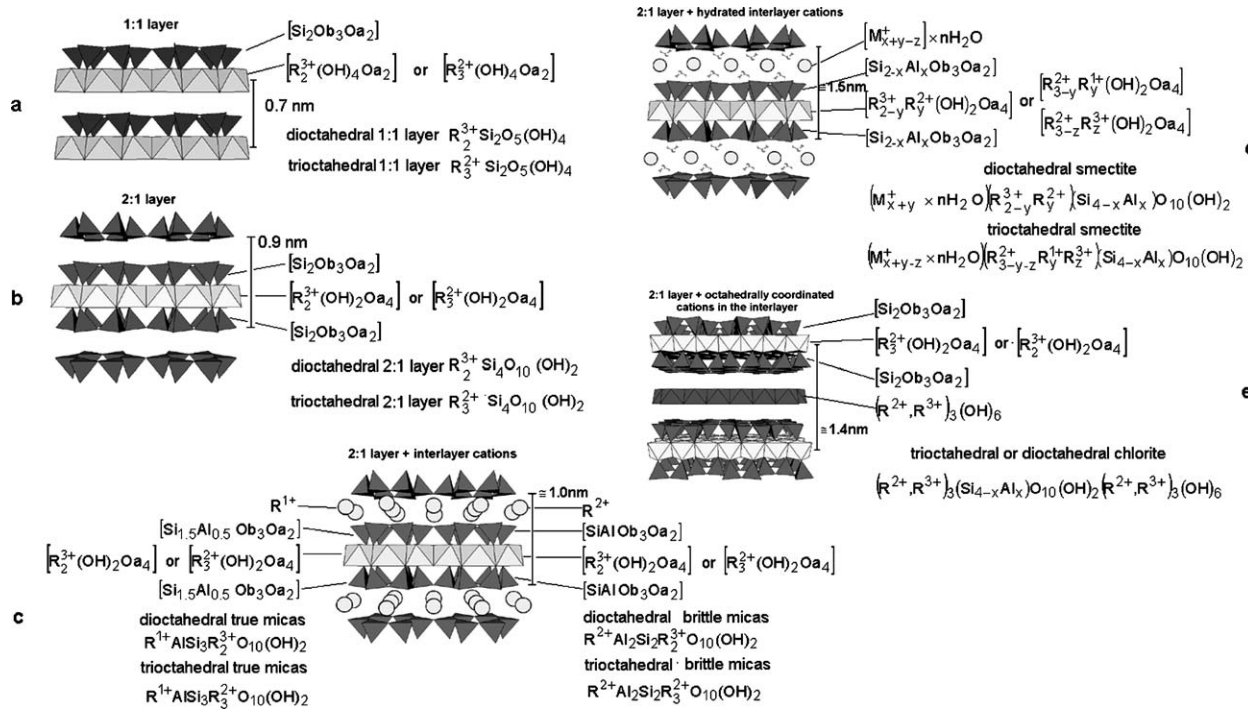


Fig. 2.5. Different layer structures: (a) 1:1 layer (i.e., kaolinite- and serpentine-like layer); (b) 2:1 layer (i.e., pyrophyllite- and talc-like layer); (c) 2:1 layer with anhydrous interlayer cations (i.e., the mica-like layer); (d) 2:1 layer with hydrated interlayer cations (i.e., smectite- and vermiculite-like layer); (e) 2:1 layer with octahedrally coordinated interlayer cations (i.e., chlorite-like layer).

1.2 nm when the interlayer position is occupied by cations with low-field strength and water molecules, about 1.5 nm when the interlayer is occupied by high-field strength cations and water molecules, and more than 1.5 nm when water molecules are exchanged by different polar molecules). On the contrary, in chlorite (Fig. 2.5e) the interlayer is occupied by a continuous octahedral sheet, thus showing a  $\text{TMTM}_{\text{int}}$  sequence (where  $\text{M}_{\text{int}}$  is the octahedral interlayer sheet).

The lateral dimension of the tetrahedral sheet is usually greater than that of the octahedral sheet. The lateral misfit between the two sheets requires an adjustment in one or both sheets, causing the layer structure to deviate from ideal hexagonal symmetry. Layer distortion, following from the matching of tetrahedral and octahedral lateral dimensions, usually follows three different mechanisms: (i) the rotation of adjacent tetrahedral as evaluated by the angle  $\alpha$  (i.e., the deviation from  $120^\circ$  of each angle in the ring (Fig. 2.6a); (ii) the increase in thickness of the tetrahedral sheet, thereby reducing the basal area of each tetrahedron as evaluated by the angle  $\tau$  (i.e., the deviation from  $109^\circ 28'$  of  $\text{O}_a\text{--T--O}_b$  triads, Fig. 2.6b); and (iii) the tilting of the tetrahedral basal oxygen plane as evaluated by the  $\Delta z$  parameter (Fig. 2.6c). More

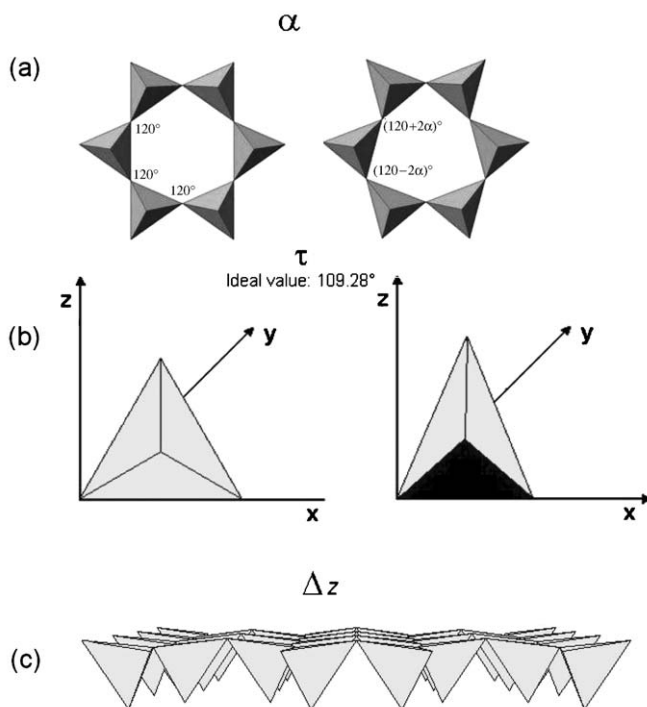


Fig. 2.6. Individual tetrahedra and tetrahedral sheet adjustments in order to accommodate the tetrahedral sheet to the octahedral sheet. (a) tetrahedral ring rotation,  $\alpha$  parameter; (b) tetrahedral flattening,  $\tau$  parameter; (c) tetrahedral tilting,  $\Delta z$  parameter.

details are provided by Brindley and Brown (1980), Bailey (1988a), de la Calle and Suquet (1988), Evans and Guggenheim (1988), Giese (1988), Güven (1988), Wicks and O'Hanley (1988), Moore and Reynolds (1989), Brigatti and Guggenheim (2002).

## 2.2. LAYER CHARGE ( $X$ )

When the tetrahedral and octahedral sheets are joined in a layer, the resulting structure can be either electrically neutral or negatively charged. Electrical neutrality exists if (i) the octahedral sheet contains trivalent cations ( $R^{3+}$ ) in two octahedral sites (usually  $Al^{3+}$  and  $Fe^{3+}$ ), with a vacancy ( $\square$ ) in the third octahedron [ $R_2^{3+}(OH)_6$ ]; (ii) divalent cations ( $R^{2+}$ , usually  $Fe^{2+}$ ,  $Mg^{2+}$ ,  $Mn^{2+}$ ) occupy all the octahedral sites [ $R_3^{2+}(OH)_6$ ]; and (iii) the tetrahedral sheet contains  $Si^{4+}$  in all tetrahedra. A negative layer charge arises from (i) substitution of  $Al^{3+}$  for  $Si^{4+}$  in tetrahedral sites; (ii) substitution of  $Al^{3+}$  or  $Mg^{2+}$  for lower charge cations in octahedral sites, and (iii) the presence of vacancies. This charge variability is recognized as one of the most important features of 2:1 phyllosilicates and micas, because it induces occupancy of the interlayer space by exchangeable cations. In 2:1 phyllosilicates the (negative) layer charge ranges from 0.2 in montmorillonite and hectorite to 2.0 in brittle micas, calculated on the basis of their structural formulae (i.e., half unit-cell content). In 1:1 phyllosilicates the layer charge is usually close to zero.

## 2.3. POLYTYPISM

A compound is polytypic if it occurs in several different structural modifications for which layers of identical structure and composition are stacked in different ways. In a polytypic series the two-dimensional translations within the layers are (essentially) preserved. The periodicity normal to the layers varies between polytypes according to the number of layers involved in the stacking sequence. Thus, small deviations from stoichiometry (up to 0.20 atoms per formula unit) within a same polytypic series are admissible in the case of phyllosilicates. The theoretical principles of polytypism have been reviewed by Baronnet (1978), Bailey (1988a), Takeda and Ross (1995), Āuroviĉ (1997, 1999), and Nespolo et al. (1997) and will not be further discussed. Polytypism will only be mentioned when we describe relevant features of clay mineral structures.

## 2.4. MIXED-LAYER STRUCTURES

Mixed-layer phyllosilicates or interstratified phyllosilicates can be built up by two or more different components. Structures with more than two components are less common, possibly because it is difficult to recognize all the different layers. Interstratified clay minerals can have (i) ordered or regular mixed-layer structures if different layers

alternate along the  $c^*$  direction in a periodic pattern (e.g., the stacking of generic type A and type B layers can be ... ABABAB ... or ... AABAABAA ... or ... AAAABAAAAB ... etc.) and (ii) disordered or irregular mixed-layer structures, if the stacking along the  $c^*$  direction of type A and B layers is random (e.g., ... AB-BABAA ... or ... AAABABBAAAAABABA ...). Fig. 2.7 shows an example of interstratification between 2:1 anhydrous layers with periodicity of about 1 nm and 2:1 hydrated layers with periodicity of about 1.4 nm. Regular sequences are identified by special names. For example, the name ‘rectorite’ is attributed to a regular interstratification of dioctahedral mica and dioctahedral smectite; ‘tosudite’ is a regular interstratification of dioctahedral chlorite and dioctahedral smectite; ‘corrensite’ represents a regular interstratification of trioctahedral vermiculite with trioctahedral chlorite; ‘aliettite’ is a regular interstratification of talc and trioctahedral smectite (saponite or vermiculite) (Bailey, 1982). The criterion adopted by the AIPEA Nomenclature Committee to attribute special names to regular 1:1 interstratification is that the sequence gives rational reflections. A test of rationality for the diffraction pattern is provided by calculating the coefficient of variability ( $CV$ ) applied to at least ten 00/ reflections

$$CV = 100 \left[ \sum_{i=1}^n \frac{(X_i - \bar{X})^2}{(n-1)} \right]^{1/2} \frac{1}{\bar{X}}$$

where  $X_i = l \times d_{(001)}$  and  $\bar{X} = \sum_{i=1}^n X_i / n < 0.75$  (Bailey, 1982)

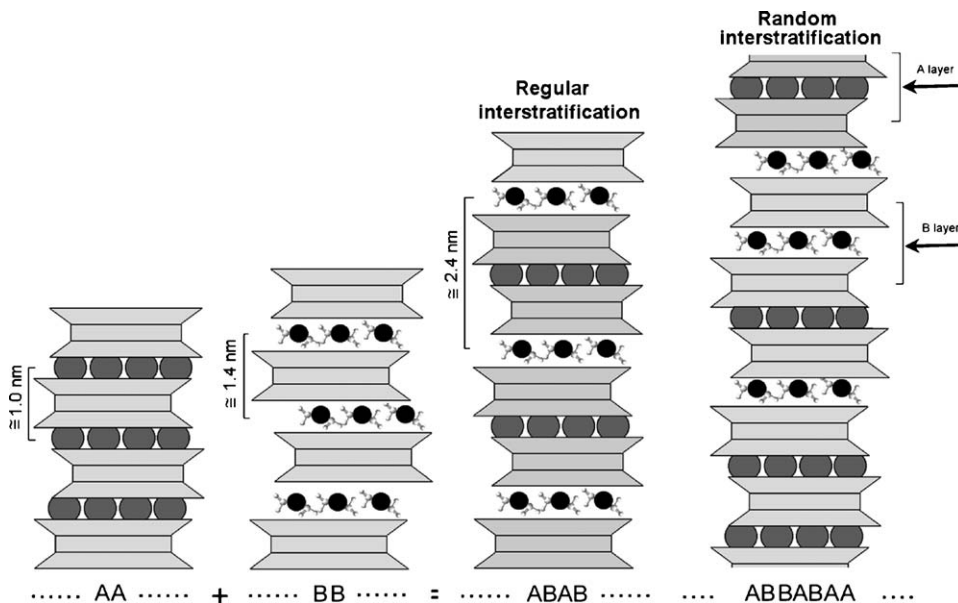


Fig. 2.7. Regularly and randomly interstratified phyllosilicates. A and B are layers with different periodicity along the  $c$  direction.

If a two-component type having different  $d(001)$  periodicity is randomly interstratified, the mineral is identified by using the name of the components such as illite–smectite, illite–chlorite, illite–vermiculite, and kaolinite–smectite. In randomly stacked mixed layer structures, layer sequence can be ‘completely different’. Examples are the irregular stacking of (i) illite (1 nm) and smectite (1.4 nm), (ii) integral multiples of serpentine (0.7 nm) and chlorite (1.4 nm), or (iii) layers with similar basal spacing but with different local structure such as the random stacking of *trans*-vacant and *cis*-vacant illite layers (Drits, 1997). A ‘completely different’  $d_{(001)}$  distance is measured by X-ray diffraction (XRD). The basal reflections  $d(00l)$  form a succession that does not correspond to a series of rational and integral values of  $l$  indices. This deviation from the Bragg rule arises from the random variation of the basal periodicity along  $c^*$  and can be a good criterion to identify the presence of irregular interstratified structures (Drits and Tchoubar, 1990). When the interstratified material is made up from sequences of different layers with the same thickness, or a thickness that is an integer multiple of the other (e.g., chlorite–serpentine), the XRD pattern looks like that of a regular phase.

Recognition of the interstratified character of a sequence requires a precise analysis of the position intensity and of the profile width of basal reflections, in conjunction with high-resolution transmission electron microscopy (HRTEM) (Moore and Reynolds, 1989; Banfield and Bailey, 1996). Finally, the analysis of XRD patterns can provide useful guidance even in the case of equal layer distance of the component. For example, the sequence of *cis*- and *trans*-vacant sites in adjacent illite layers, produces displacements along the  $a$  direction, yielding  $d(110)$  reflections that violate the individual layer symmetry.

Useful references to the application of statistical methods to the interpretation and prediction of interstratified mineral structures have been provided by Nadeau et al. (1984, 1985), Reynolds (1988), Drits and Tchoubar (1990), Baronnet (1992), Veblen (1992), and Drits (1997).

## 2.5. THE 1:1 LAYER

### 2.5.1. Dioctahedral 1:1 Minerals: The Kaolin Group

The clay minerals in the kaolin group consist of dioctahedral 1:1 layer structures with a general composition of  $\text{Al}_2\text{Si}_2\text{O}_5(\text{OH})_4$ . Kaolinite, dickite, and nacrite are polytypes. The kaolinite stacking sequence consists of identical layers with an interlayer shift of  $2a/3$ . Dickite and nacrite have a two-layer stacking sequence where the vacant site of the octahedral sheet alternates between two distinct sites (Brindley and Brown, 1980). Halloysite is a hydrated polymorph of kaolinite with curved layers and a basal spacing of 1 nm that decreases to about 0.7 nm on dehydration. The composition of the kaolin group minerals is characterized by a predominance of  $\text{Al}^{3+}$  in octahedral sites, although some isomorphous substitution of  $\text{Mg}^{2+}$ ,  $\text{Fe}^{3+}$ ,  $\text{Ti}^{4+}$ , and  $\text{V}^{3+}$  for  $\text{Al}^{3+}$  can occur.

### A. Kaolinite

Pauling (1930) was the first to outline the crystal structure of kaolinite using models based on idealized polyhedra. Gruner (1932b) reported the first structural interpretation of the kaolinite powder XRD pattern. He indicated that the mineral belonged to the monoclinic  $Cc$  symmetry with  $d(001) = 1.43$  nm, corresponding to a two-layer structure. This was subsequently confirmed by Hendricks (1938b). Brindley and Robinson (1945, 1946) found that many reflections in the powder pattern could not be indexed correctly on the basis of a monoclinic structure, and suggested a lowering of layer symmetry to the triclinic  $C1$ . This symmetry is consistent with a 1:1 layer structure built up by stacking of identical layers with a translation of  $-a/3$ . Kaolinite, dickite, and nacrite consist of sequences with different position of octahedral vacancies in adjacent layers. Bailey (1963) has demonstrated that both kaolinite and dickite have a  $1M$  stacking sequence of layers. Octahedral site vacancies alternate in dickite, whereas in kaolinite the location of the vacancy is the same in adjacent layers. Three polytypes, all based on a  $1M$  structure, are found for 1:1 dioctahedral phyllosilicates. The  $1M$  structure presents three possible locations for the vacant octahedral site, commonly referred as A, B, or C site vacancy (Adams, 1983; Thompson and Withers, 1987; Bish and Von Dreele, 1989; Bukin et al., 1989; Smrčok et al., 1990; Bish, 1993). The structure is chiral if the vacant site is B or C, and achiral if the vacant site is A. All naturally occurring kaolinites are chiral (Fig. 2.8).

Hobbs et al. (1997) have modelled the kaolinite structure by an all-atom ab initio energy minimization method. Their results confirm the space group  $C1$ , and predict significantly different Si–O bond lengths for the basal and apical tetrahedral oxygen atoms. A low-temperature neutron powder diffraction study by Bish (1993) indicates that low temperatures influence the interlayer separation but has little effect on tetrahedral and octahedral parameters. The structure refinement, derived by Neder et al. (1999) from single-crystal synchrotron data, confirms the  $C1$  symmetry and provides

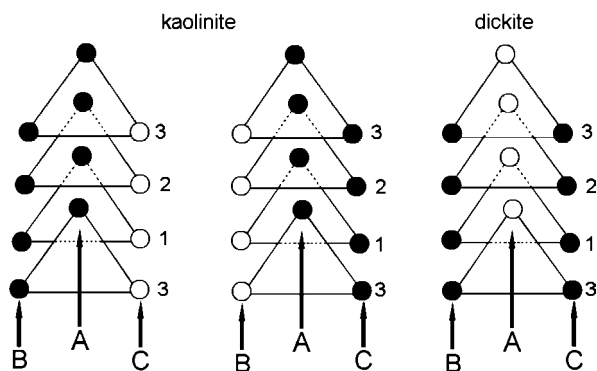


Fig. 2.8. Projection on the (001) plane of the octahedral sites in kaolinite and dickite showing the possible placement of the vacant octahedral site (open circles). Closed circles represent  $\text{Al}^{3+}$  octahedra. Modified after Bailey (1963).

the following unit-cell parameters:  $a = 0.5154(9)$  nm,  $b = 0.8942(4)$  nm,  $c = 0.7401(10)$  nm,  $\alpha = 91.69(9)^\circ$ ,  $\beta = 104.61(5)^\circ$ , and  $\gamma = 89.82(4)^\circ$ . Except for the slight difference in  $\beta$ -angle, these values are very similar to those obtained by Bish and Von Dreele (1989), using X-ray and neutron powder diffraction, i.e.,  $a = 0.5156(1)$  nm,  $b = 0.89446(2)$  nm,  $c = 0.740485(2)$  nm,  $\alpha = 91.697(2)^\circ$ ,  $\beta = 104.862(2)^\circ$ , and  $\gamma = 89.823(2)^\circ$ . The refinement indicates that tetrahedra are significantly distorted with the Si–O<sub>a</sub> bond shorter by 0.0013 nm than the average Si–O bond distances. On the other hand, the octahedral Al–O<sub>a</sub> bonds are significantly longer than the Al–O<sub>oct</sub> (i.e., Al–OH) bonds.

The interlayer OH vectors associated with H-bonding are nearly normal to (001), forming three interlayer hydrogen bonds as shown in Fig. 2.9. Previous studies generally agreed on the position of the Si, Al, and O atoms. However, some uncertainties remain as to the position of the OH groups. The kaolinite layer is essentially neutral and any two contiguous layers are linked through –Al–O–H···O–Si– hydrogen bonding. The primitive unit cell contains four crystallographically distinct O–H groups. Three of them (labelled OH<sub>2</sub>, OH<sub>3</sub>, OH<sub>4</sub>) are located at the inner surface and one (labelled OH<sub>1</sub>) is inside the layer as shown in Fig. 2.9a. These hydroxyl groups form strong hydrogen bonds if they are oriented nearly perpendicular to the layer but are not involved in H-bonding if they are parallel to the layer (Fig. 2.9). The extensive research into OH group orientation has been reviewed by Giese (1988). The crystal structure refinement of a deuterated kaolinite (Akiba et al., 1997) confirms that the three inner OD vectors point toward the tetrahedral sheet, and form H-bonding with basal oxygen atoms of the adjacent kaolinite layer. One of these three, however, differs from the other two in bond angle, thus, suggesting a different orientation of the bond. Benco et al. (2001a–c) have explained interlayer

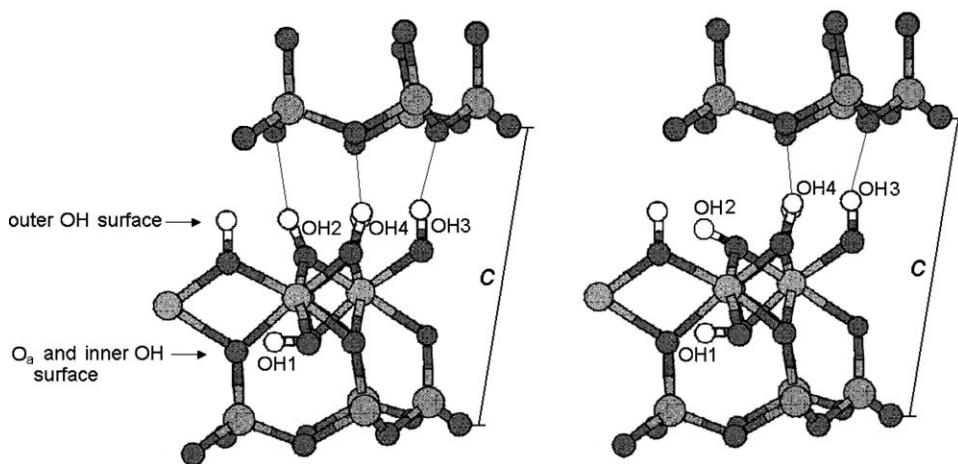


Fig. 2.9. Different OH orientations on the octahedral surface of kaolinite. Modified after (Benco et al., 2001a).

H-bonding in kaolinite by ab initio molecular dynamic simulations of a hypothetical isolated layer. They identify four distinct OH groups, two of which (OH<sub>3</sub> and OH<sub>4</sub>) form weak H bonds with O—H···O distances between 0.18 and 0.26 nm, while the other two (OH<sub>1</sub> and OH<sub>2</sub>) do not participate in H bonding (Fig. 2.9b).

The poor structural order commonly observed in kaolin minerals may be explained in terms of a series of stacking faults or defects in the *ab* plane and along the *c*-axis. This feature accounts for the well-known tendency of kaolin minerals to form a wide variety of ordered and disordered polytypes as well as twins (Dornberger-Schiff and Đurovič, 1975; Plançon et al., 1989; Zvyagin and Drits, 1996). The diffraction patterns of ordered kaolinite are significantly different from those of disordered kaolinite. Ordered kaolinite shows sharp and narrow peaks, while its disordered counterpart gives less well-defined, broad, and asymmetrical peaks. The *hkl* reflections with  $k = 3n$  (where *n* is an integer) are generally less affected than those with  $k \neq 3n$  (Brindley and Robinson, 1946; Murray, 1954). In extreme cases, peaks lose their identity and merge to form a two-dimensional modulated band of diffracted intensity.

Structural order/disorder in kaolinite can be assessed by different tests. The most widely used (Fig. 2.10) are those based on changes in two groups of XRD

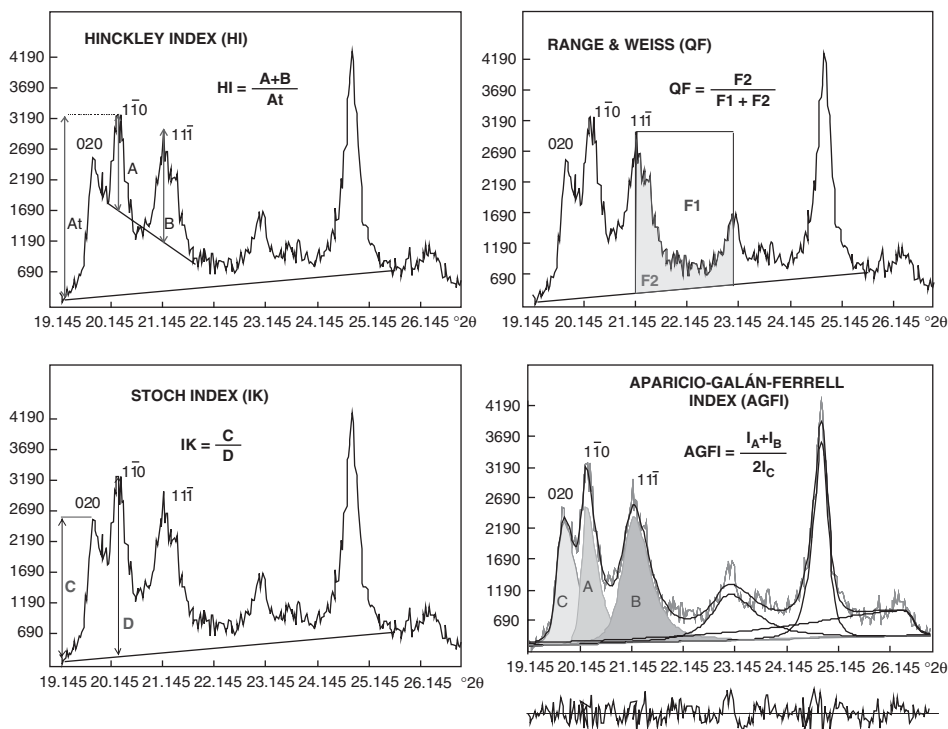


Fig. 2.10. XRD-based methods for assessing the degree of structural order in kaolinite. The  $2\theta$  values refer to  $\text{CuK}\alpha$  radiation.



reflections: (i) the 02/ and 11/ sequences ( $20\text{--}23^\circ 2\theta$  using Cu  $K\alpha$ ) that are sensitive to arbitrary and special interlayer displacements (such as  $b/3$ ) and (ii) the 13/ and 20/ sequences ( $35\text{--}40^\circ 2\theta$  using Cu  $K\alpha$ ) that are affected by arbitrary displacements (Cases et al., 1982). Some of these tests are (i) the Hinckley index (HI) (Hinckley, 1963) and Range–Weiss index (QF) (Range and Weiss, 1969); (ii) the Stoch index (IK) (Stoch, 1974), measured in the same zone as the previous two indices but is less sensitive to the presence of quartz; and (iii) the Liétard index (R2) (Liétard, 1977) that is sensitive to the presence of arbitrary defects only (Cases et al., 1982). Aparicio and Galán (1999) have investigated the influence of mineral and amorphous phases, associated with kaolin and kaolinitic rock, on kaolinite order–disorder measurements by XRD. Both the Hinckley and Range–Weiss indices appear to be influenced by quartz, feldspar, iron gels, illite, smectite, and halloysite. On the other hand, the Stoch index can be used in the presence of quartz, feldspar, iron, and silica gels, while the Liétard index is not affected by phases other than halloysite. As a result, Aparicio et al. (1999) have proposed the Aparicio–Galán–Ferrell index. Derived from the intensity of reflections in the 02/ and 11/ sequence, and obtained by pattern fitting, this index is less influenced by peak overlap (Aparicio et al., 2001).

On the other hand, Plançon and Zacharie (1990) have proposed ‘an expert system’ that runs on a compatible PC and describes the structural defects of kaolinite based on direct measurements of the diffraction pattern. The results of this system are acceptably consistent with the theoretical and experimental diffractograms for kaolinite. The expert system describes kaolinite defects and provides a global abundance of translation defects, but cannot distinguish between the  $t_0$  translation (roughly  $t_1 - b/3$ ) and the  $t_2$  translation (roughly  $t_1 + b/3$ ). It gives the number of different phases in the sample (1 or 2 phases). For bi-phase samples, it establishes the percentage of low-defect or well-crystallized phases (%wp). In the case of single-phase samples, it fixes the amount of the  $C$  layers ( $W_C$ ), the variation of interlayer translations about the mean values ( $\delta$ ), the proportion of translation defects ( $p$ ), and the mean number of layers ( $M$ ).

Aparicio and Galán (1999) have suggested that the expert system of Plançon and Zacharie (1990) is the best method for determining the degree of order–disorder in kaolinite, although it is highly affected by the presence of other phases, particularly when more than 25% of well-crystallized kaolinite is present. However, the system can be used with single-phase kaolinite (disordered kaolinite), which is not affected by the presence of phases other than halloysite, thus seemingly increasing the amount of translation defects. In any case, the expert system should not be used with kaolinite of medium order–disorder because the well-ordered phase is present in a low amount ( $<10\%$ ).

### *B. Dickite*

Gruner (1932a) was the first to propose a structural refinement for dickite (general formula  $\text{Al}_2\text{Si}_2\text{O}_5(\text{OH})_4$ ). Subsequent refinements were proposed by Hendricks (1938b), Newnham and Brindley (1956), and Newnham (1960). On the basis of these

refinements, the crystal structure of dickite belongs to the monoclinic space group *Cc* with the vacant cavity alternating in adjacent layers between B and C sites (Fig. 2.8). Symmetry requirements (site A of Fig. 2.8) are met by placing the vacant cavity at the *trans*-site (Bailey, 1963). The cell parameters are as follows:  $a = 0.5138(1)$  nm,  $b = 0.8918(2)$  nm,  $c = 1.4389(2)$  nm,  $\beta = 96.74(2)^\circ$  (Joswig and Drits, 1986). As with kaolinite, the vector orientation of inner and outer OH groups, and the strength of interlayer H-bonding, have attracted much attention (Giese and Datta, 1973; Adams and Hewat, 1981; Rozhdestvenskaya et al., 1982; Sen Gupta et al., 1984; Joswig and Drits, 1986; Giese, 1988; Bukin et al., 1989; Johnston et al., 1990).

Using polarized single-crystal Fourier-transform infrared microscopy, Johnston et al. (1990) have deduced that the angle between the inner OH<sub>1</sub> vector and the *b*-axis is  $47^\circ$ , while the inner-surface OH-group vectors are oriented at different angles with respect to the *b*-axis (OH<sub>3</sub> =  $22^\circ$ ; OH<sub>2</sub> and OH<sub>4</sub> =  $45^\circ$ ). Benco et al. (2001a–c) have assessed the orientation of OH vectors using *ab initio* molecular dynamics and total energy calculations. They suggest that the inner hydroxyl and one inner-surface hydroxyl are horizontally oriented, while the other two hydroxyls are involved in interlayer bonding. Bish and Johnston (1993) have provided a low-temperature structural refinement for dickite. The structure is the same as that deduced previously from room temperature measurements, except for the orientation of OH vectors. In particular, the inner hydroxyl group is almost parallel to (001), inclined by  $1.3^\circ$  towards the tetrahedral sheet. The internuclear O–H<sub>3</sub>···O distance increases as well as the Al–OH<sub>1</sub>–Al. The two-dimensional crystal structure refinement at  $535^\circ\text{C}$  suggests that the OH groups on the surface are completely removed.

### C. Nacrite

The first crystal structure refinement of nacrite was reported by Hendricks (1939) who suggested the space group *Cc*. The structure is made up by stacking six layers, closely approaching rhombohedral symmetry with a pseudo-space group *R3c*. Blount et al. (1969) have confirmed that the ideal structure of nacrite is based on a *6R* stacking sequence of kaolinite layers (TM layers), in which each successive layer is shifted relative to the layer below by  $-1/3$  of the 0.89 nm lateral repeat direction. This direction is referred to as *x* in nacrite, contrary to the usual convention for layer silicates, because of the positioning of the (010) symmetry planes normal to the 0.51 nm repeat direction. Alternate layers are also rotated by  $180^\circ$ . The pattern of vacant octahedral sites reduces the symmetry to *Cc* and permits description of the structure as a two-layer form with an inclined *z*-axis. Adjacent tetrahedra are twisted by  $7.3^\circ$  in opposite directions so that the basal oxygen atoms are nearer to both the Al<sup>3+</sup> cations in the same layer and the surface hydroxyls of the layer below. Interlocking corrugations in the oxygen and hydroxyl surfaces of adjacent layers run alternately parallel to the [110] and  $[\bar{1}\bar{1}0]$  axes in the adjacent layers. The upper and lower O–Al–O groups in each Al octahedron are rotated by  $5.4^\circ$  and  $7.0^\circ$  in opposite directions resulting in the shortening of shared edges. Nacrite has a greater interlayer separation and smaller lateral dimensions than dickite and kaolinite, and the

observed  $\beta$ -angle deviates by 11–12° from the ideal value. These features, and the overall lower stability, of nacrite are ascribed to the less-favourable positioning of the basal  $O_b$  atoms relative to the directed interlayer H-bonds. The nacrite crystal structure, refined by Zvyagin et al. (1972, 1979) using high-voltage electron diffraction (ED), is very similar to that proposed by Blount et al. (1969). However, the tetrahedral rotation angle in the structure of Zvyagin et al. (1972, 1979) is smaller. Zheng and Bailey (1994) have confirmed the crystal structure reported by Blount et al. (1969), giving the following unit-cell parameters:  $a = 0.8906(2)$  nm,  $b = 0.5146(1)$  nm,  $c = 1.5664(3)$  nm, and  $\beta = 113.58(3)^\circ$ . The location of hydrogen atoms is deduced from different electron density maps. The inner  $OH_1$  vector points exactly towards the vacant octahedron and is depressed by  $-18.6^\circ$  away from the level of the octahedral cations. All three surface OH groups have OH vectors at  $50$ – $66^\circ$  to (001), although  $OH_2$  may not participate in interlayer hydrogen bonding. All three interlayer OH–OH contacts (between 0.294 and 0.312 nm) are bent at angles between  $132$  and  $141^\circ$ .

Ben Haj Amara et al. (1997, 1998) have described the structure of hydrated and dehydrated nacrite. The hydrated form is characterized by a basal distance of 0.842 nm, containing one water molecule per  $Si_2Al_2O_5(OH)_4$  in the interlayer space. The interlayer water molecule is placed above the vacant octahedral site of the layer and is embedded in the ditrigonal cavity of the tetrahedral sheet of the upper layer.

#### *D. Halloysite*

Halloysite may be regarded as a hydrated kaolinite phase. Hofmann et al. (1934) showed by XRD that water was present in the interlayer space, giving a general formula of  $Si_2Al_2O_5(OH)_4 \times 2H_2O$ . As hydrated halloysite has a layer periodicity (basal spacing) close to 1 nm ( $10 \text{ \AA}$ ) (Brindley and Robinson, 1948), it is often denoted as ‘halloysite-(10  $\text{\AA}$ )’. The interlayer water in halloysite can be easily removed. The resultant dehydrated form with a basal spacing close to 0.72 nm ( $7.2 \text{ \AA}$ ) is referred to as ‘halloysite-(7  $\text{\AA}$ )’ although the name ‘metahalloysite’ is sometimes used. The particles of halloysite can adopt different morphologies, such as spheres, tubes, plates, and laths (e.g., Churchman and Theng, 1984). More often than not, the long tubular forms are relatively well crystallized. In most cases the direction of particle orientation coincides with the  $b$ -axis (Zvyagin et al., 1966).

The interlayer water in halloysite can be irreversibly removed by heating (Zvyagin et al., 1966). Costanzo and Giese (1985) have suggested a continuous sequence of hydration states, ranging from fully hydrated through partially hydrated to dehydrated halloysite. Costanzo et al. (1984) have identified two types of interlayer  $H_2O$ : (i) ‘hole’  $H_2O$  located in the ditrigonal cavities of the tetrahedral sheet and (ii) ‘associated’  $H_2O$  forming a discontinuous layer of mobile molecules. The 0.84 and 0.86 nm hydrates have only ‘hole’  $H_2O$ , whereas the 1 nm hydrates and natural halloysite contain both ‘hole’ and ‘associated’  $H_2O$ . Hole water is H-bonded to the basal oxygen atoms of the tetrahedral sheet. Associated water forms intermolecular

H-bonds approximately equal in strength to that in liquid water, and is less strongly bonded to the clay surface than hole water.

The dehydration of halloysite has been discussed by Bhattacharjee (1973) and Mizuki et al. (1985) who indicated dehydration at 70–100 °C and collapse of the structure at approximately 400 °C. Okada and Ossaka (1983) suggested that the halloysite layer periodicity changed coherently from 1 to 0.7 nm and that dehydration progressed perpendicular to the layers of each particle.

Kohyama et al. (1978) have determined the unit-cell parameters for 1 nm- and 0.7 nm-halloysites, both of which have a two-layer structure in the space group *Cc* with unit-cell parameters  $a = 0.514(4)$  nm,  $b = 0.890(4)$  nm,  $c = 2.07(1)$  nm,  $\beta = 99.7^\circ$  and  $a = 0.514(4)$  nm,  $b = 0.890(4)$  nm,  $c = 1.49(1)$  nm,  $\beta = 101.9^\circ$ . Bayliss (1989) has refined the halloysite unit-cell parameters in the hexagonal system.

#### *E. Hisingerite*

Hisingerite, first described in 1810, has been variously regarded as a non-crystalline silicate, a ferric allophane, a ferric halloysite, and a poorly crystallized nontronite. On the basis of TEM data, Frost et al. (1997) and Eggleton and Tilley (1998) have interpreted hisingerite to be the iron analogue of spherical halloysite.

#### 2.5.2. *Trioctahedral 1:1 Minerals: The Serpentine Group*

The trioctahedral 1:1 layer silicates have been investigated by many authors (e.g., Wicks and O'Hanley, 1988) using well-crystallized phases similar to those found in the clay fraction of soils and sediments.

Lizardite, antigorite, and chrysotile are Mg-rich 1:1 trioctahedral layer minerals with an ideal composition of  $\text{Mg}_3\text{Si}_2\text{O}_5(\text{OH})_4$ . Although chemically simple, they are structurally complex. Lizardite has an ideal layer topology, whereas antigorite is modulated and chrysotile is bent (Wicks and Whittaker, 1975; Wicks and O'Hanley, 1988; Veblen and Wylie, 1993).

These structural differences are recognized by the AIPEA Nomenclature Committee (Martin et al., 1991). Like lizardite, the trioctahedral 1:1 minerals berthierine, amesite, cronstedtite, nepouite, kellyite, fraipontite, and brindleyite have been classified as serpentine minerals with a planar structure. Other minerals, traditionally referred to as serpentine, show a modulated layer structure. They are subdivided into minerals with tetrahedral sheet strips such as antigorite and bementite, or with tetrahedral sheet islands such as greenalite, caryopilite, pyrosmalite, manganypyrosmalite, ferropyrosmalite, friedelite, mcgillite, schallerite, and nelenite.

Suitable crystals of Mg-rich serpentine minerals for high-quality three-dimensional structural studies were not available until 1980. Since then, however, Mellini and co-workers (Mellini, 1982; Mellini and Zanazzi, 1989; Mellini and Viti, 1994) have performed a structural study on two polytypes of lizardite:  $1T$  and  $2H_1$  in the space group  $P31m$ , whereas  $2H_1$  polytype structure belongs to the space group  $P6_3cm$  (Mellini and Zanazzi, 1987). Brigatti et al. (1997) examined the  $2H_2$  form of

lizardite in the space group  $C2/c$ . The effect of pressure on the structure of  $1T$  lizardite has been determined by Mellini and Zanazzi (1989). Guggenheim and Zhan (1998) reported a high-temperature study on both  $1T$  and  $2H_1$  lizardite crystals. The overall structure of lizardite consists of two submodules: the 1:1 layer itself and the empty space where two adjacent 1:1 layers meet through interfacing hexagonally close-packed oxygen atoms. The internal dimension of 1:1 layer shows only minor changes after chemical substitutions, increasing pressure or temperature. On the contrary, the interlayer thickness varies significantly with composition (Chernoski, 1975) or when the pressure increases (Mellini and Zanazzi, 1989). As the interlayer thickness decreases, the ditrigonalization of the tetrahedral sheet increases either in a positive or in a negative way. In the  $1T$  polytype the ditrigonal ring distortion changes from  $-1.5^\circ$  to approximately  $0^\circ$  when the temperature changes from 20 to  $480^\circ\text{C}$ . In the  $2H_1$  polytype this structural parameter changes from  $1.8^\circ$  to  $1.3^\circ$  at  $300^\circ\text{C}$  and remains unchanged up to  $475^\circ\text{C}$ . For the  $2H_1$  polytype the O–O distance in the interlayer O–H $\cdots$ O bond increases linearly from 0.308 to 0.315 nm as the temperature increases from 20 to  $475^\circ\text{C}$ . On the contrary, for the  $1T$  polytype this distance remains nearly constant up to  $360^\circ\text{C}$ . Above this temperature the O–O distance increases slightly. Thus, the  $2H_1$  polytype appears to have weaker hydrogen bonding than the  $1T$  polytype (Guggenheim and Zhan, 1998).

Antigorite is characterized by a large superstructure along the  $[100]$  direction. On the basis of X-ray and optical diffraction, Zussman (1954) has suggested that the superstructure is a result of a repeating wave structure. The structure has been subsequently studied by Kunze (1956, 1958, 1959), who identified the super-cell unit as ' $A$ ' and the sub-cell unit as ' $a$ '. Aruja (1945) derived a value of about 0.455 nm for the  $A$  parameter. Uehara and Shirozu (1985) defined the superstructure in terms of the number ( $M$ ) of sub-cells ( $a = 0.544$  nm) along the  $x$ -axis, with  $M = A/a$ . They also suggested that samples of antigorite might be classified into three structural types. In the first type  $M = n$  (where  $n$  is an integer); in the second type  $M = (2n + 1)/2$ ; and in the third type  $M$  is different from  $n/2$ . The first type contains an odd number of tetrahedra ( $n$ ) and an even number of octahedra ( $n - 1$ ) in the superstructure period  $A$  (space group  $Pm$ ). The structure of the second type derives from that of the first type but is different from the structure proposed by Kunze (1959), where  $M$  is an even number in the space group  $P2/m$ . The model based on  $M = (2n + 1)/2$  is obtained by shifting Kunze's model at each wave limit along the  $y$  direction by  $b/2$  (resulting in lattice  $C$ -centered). The model contains an even number of tetrahedra ( $m$ ) and an odd number of octahedra ( $m - 1$ ). The third structure, with  $M$  different from  $n/2$ , is a mixture of the two structures described above in coherent domains. This structure is commonly found in poorly crystallized disordered materials (Uehara, 1987).

Difficulties in studying single crystals of chrysotile can be related to fibre intergrowth, polygonalization of the layer, polytype intergrowth, and crystal bending.

Amesite with an ideal composition of  $(\text{Mg}_2\text{Al})(\text{SiAl})\text{O}_5(\text{OH})_4$  can have an ordered or disordered cation distribution in the 1:1 layer. Thus, differences in both polytypic arrangements and ordering patterns inside the same polytype can occur. Four

regular polytypes ( $2H_1$ ,  $2H_2$ ,  $6R_1$ , and  $6R_2$ ) as well as random stacking polytypes have been determined (Steinfink and Brunton, 1956; Hall and Bailey, 1976; Anderson and Bailey, 1981; Wiewióra et al., 1991; Zheng and Bailey, 1997). Since cations of different size and charge occur both in tetrahedral and octahedral sites, there is a very strong tendency for ordering. All amesites are therefore presumed to be ordered. As a result, the hexagonal or rhombohedral symmetry of the ideal polytypes is reduced to triclinic symmetry with complete cation disorder, and the  $\beta$  unit-cell angle deviates slightly from  $90^\circ$  ( $90.2 \leq \beta \leq 90.3^\circ$ ).

Carlosturanite, an octahedrally modulated structure (Compagnoni et al., 1985), has the general formula of  $M_{21}[T_{12}O_{28}(OH)_4](OH)_{30} \times H_2O$  where M is predominantly  $Mg^{2+}$  with small amounts of  $Fe^{3+}$ ,  $Mn^{3+}$ ,  $Ti^{4+}$ ,  $Cr^{3+}$ , and T is  $Si^{4+}$ ,  $Al^{3+}$ . The unit-cell parameters are  $a = 1.670$  nm,  $b = 0.941$  nm,  $c = 0.7291$  nm,  $\beta = 101.1^\circ$ , and the space group is  $Cm$ . The model structure consists of a continuous planar octahedral sheet and a discontinuous 'tetrahedral sheet'. The latter is modified to strips, six tetrahedra in width, running parallel to the  $b$ -axis.

Greenalite is a 1:1 structure having the tetrahedral sheet completely occupied by  $Si^{4+}$ , and the octahedral sheet mostly occupied by  $Fe^{2+}$ , with a significant substitution of  $Mg^{2+}$  for  $Fe^{3+}$  (Floran and Papike, 1975). The greenalite structure has been investigated by Guggenheim et al. (1982) using ED, HRTEM, and optical imaging techniques. They have suggested that the tetrahedral sheet is made up of 'islands' of six-member tetrahedral rings, with four and three-members ring at the island borders. More detailed information on greenalite can be found in the review by Guggenheim and Eggleton (1998).

## 2.6. THE 2:1 LAYER

The layer of 2:1 phyllosilicates consists of an octahedral sheet sandwiched between two opposing tetrahedral sheets. In pyrophyllite (dioctahedral) and talc (trioctahedral), the layer is electrically neutral. In the other 2:1 phyllosilicates (e.g., smectite, vermiculite, mica, chlorite), the layer is usually negatively charged. The magnitude of the layer charge ( $X$ ) measures the deviation of charge from neutrality. For true micas  $X$  is close to  $-1$ , while for brittle micas it is approximately equal to  $-2$ ; in both cases the space between two adjacent layers is occupied by anhydrous cations. Illite is a micaceous clay mineral that occurs widely in soils and sediments. A fractional value for layer charge and the presence of hydrated cations in the interlayer space characterize the most common 2:1 clay minerals, such as smectites and vermiculites. In smectites, the negative charge per half-unit-cell ranges from 0.2 to 0.6, while in vermiculites this value is between 0.6 and 0.9. In chlorite, the negative layer charge is neutralized by the presence of a positively charged octahedral sheet in the interlayer space. Most chlorites are trioctahedral; dioctahedral chlorites, and intermediate forms with alternating dioctahedral and trioctahedral sheets, are rare. As in 1:1 phyllosilicates, the 2:1 layer structure can be non-planar. For example,



minnesotaite (traditionally considered as a variety of talc) has a modulated structure with tetrahedral strips. Other 2:1 layer silicates, such as sepiolite, palygorskite, and loughlinite also show a modulated structure but the strips are made up of octahedral sheets (Martin et al., 1991).

### 2.6.1. Pyrophyllite, Talc, and Related Minerals

The ideal layer structure of pyrophyllite (dioctahedral) and talc (trioctahedral) is electrically neutral, and hence no charge-balancing cation is present in the interlayer space. Contiguous layers are held together by van der Waals interactions. This affects both the mechanical properties of the minerals and the quality of crystals for structural investigation.

Pyrophyllite with an ideal structural formula of  $\text{Al}_2\text{Si}_4\text{O}_{10}(\text{OH})_2$ , is not known to vary greatly in composition. Only limited substitution of  $\text{Al}^{3+}$  for  $\text{Si}^{4+}$  and minor amounts of  $\text{Fe}^{2+}$ ,  $\text{Fe}^{3+}$ ,  $\text{Mg}^{2+}$ , and  $\text{Ti}^{4+}$  have so far been found. Although structural investigations of this mineral are complicated by its small size and irregular layer stacking, polytypism in pyrophyllite has been identified by several authors (Zvyagin et al., 1968; Shitov and Zvyagin, 1972; Evans and Guggenheim, 1988). There are two dominant polytypes, a two-layer monoclinic (2M), and a one-layer triclinic (1Tc). Investigations into the pyrophyllite structure date back to Gruner (1934), Hendricks (1938a). Rayner and Brown (1966) have proposed the space group  $C2/c$  and  $Cc$  with  $a = 0.517 \text{ nm}$ ,  $b = 0.892 \text{ nm}$ ,  $c = 1.866 \text{ nm}$ ,  $\beta = 99.8^\circ$  as unit-cell parameters. Brindley and Wardle (1970) determined the XRD powder patterns of pyrophyllite samples from different localities, and showed the existence of both one-layer triclinic and two-layer monoclinic forms. Some samples were mixtures of the two forms, while others were so disordered, either naturally or by mesh grinding, that differentiation was not possible. The powder pattern of the best-crystallized sample gave the following parameters:  $a = 0.5173 \text{ nm}$ ,  $b = 0.8960 \text{ nm}$ ,  $c = 0.9360 \text{ nm}$ ,  $\alpha = 91.2^\circ$ ,  $\beta = 100.4^\circ$ ,  $\gamma = 90^\circ$  for the triclinic form; and  $a = 0.5172 \text{ nm}$ ,  $b = 0.8958 \text{ nm}$ ,  $c = 1.867 \text{ nm}$ ,  $\beta = 100.0^\circ$  for the monoclinic form. The corresponding anhydrous phases gave the following parameters:  $a = 0.5140 \text{ nm}$ ,  $b = 0.9116 \text{ nm}$ ,  $c = 0.9504 \text{ nm}$ ,  $\alpha = 91.2^\circ$ ,  $\beta = 100.2^\circ$ ,  $\gamma = 90^\circ$  for the triclinic form, and  $a = 0.5173 \text{ nm}$ ,  $b = 0.9114 \text{ nm}$ ,  $c = 1.899 \text{ nm}$ ,  $\beta = 100.0^\circ$  for the monoclinic form. The expansion of the  $b$  parameter was attributed to a relaxation of the twisted Si–O network. After dehydroxylation, the  $\text{Al}^{3+}$  ion coordination appeared to change only slightly, possibly causing the structures to be constrained in the  $a$  direction (Wardle and Brindley, 1972).

The first three-dimensional crystal structure refinement of pyrophyllite (polytype 1Tc, space group symmetry  $C\bar{1}$ ) has been carried out by Lee and Guggenheim (1981). The mean tetrahedral cation-oxygen bond length (0.1618 nm) is consistent with the lack of significant  $\text{Al}^{3+}$  for  $\text{Si}^{4+}$  substitutions. Similarly, the octahedral cation-oxygen distance (0.1912 nm) indicates a nearly complete Al occupancy. The OH vector points away from the (001) plane and forms an angle of about  $26^\circ$  (Giese, 1973). This

value is much higher than that commonly found for muscovite containing  $K^+$  in the interlayer space. This feature is explained in terms of the sole contribution of  $Al^{3+}$  cations to the attainment of a theoretical equilibrium position. Molecular dynamic modelling by Teppen et al. (1997) gives results that are in good agreement with experimentally derived values, although the OH vector is predicted to be less inclined than what is observed. Since van der Waals interactions are primarily involved in keeping adjacent 2:1 layers together, interlayer cohesion is weak.

Isomorphous substitution in pyrophyllite has been suggested by Kodama (1959). A pale blue sample containing  $V^{3+}$  (44–190 ppm),  $Cr^{3+}$  (30–80 ppm),  $Sn^{4+}$  (20–50 ppm),  $Ni^{2+}$ ,  $Co^{2+}$ ,  $Pb^{2+}$ , and  $Ga^{3+}$  shows the following unit-cell parameters:  $a = 0.517$  nm,  $b = 0.895$  nm,  $c = 1.864$  nm,  $\beta = 99.8^\circ$ .

Substitution in the octahedral sheet of pyrophyllite has also been indicated by theoretical ab initio calculations.  $Mg^{2+}$  for  $Al^{3+}$  substitutions tend to be distributed in the octahedral sheet, whereas  $Fe^{3+}$  for  $Al^{3+}$  substitutions tends to be clustered (Sainz-Diaz et al., 2002).

Even if pyrophyllite is characterized by the near absence of layer charge, the mineral can react with heavy metals in solution. For instance, Scheidegger et al. (1997) found that pyrophyllite can adsorb  $Ni^{2+}$  from aqueous solution using X-ray absorption fine structure (XAFS). Their data suggest the formation of multinuclear  $Ni^{2+}$  complexes after a reaction time of few minutes. The size of these complexes increases with time. Ni–Ni bond distances (0.299–0.303 nm) are similar to those in mixed Ni–Al hydroxides, but distinctively shorter than in  $Ni(OH)_2$ .

The thermal transformation of pyrophyllite, analysed by different techniques ( $^{27}Al$  and  $^{29}Si$  MAS-NMR, thermal analysis DTA-TG, dilatometry, and XRD), suggests that dehydroxylation occurs above  $800^\circ C$ . The  $^{27}Al$  NMR obtained on the mineral after heating at  $800^\circ C$  suggests the occurrence of Al in a distorted five-fold coordination. At  $1000^\circ C$ , the tetrahedral sheet breaks down and a partial segregation of amorphous  $SiO_2$  occurs. This process is consistent with the rearrangement of aluminium ions, favouring the formation of small disordered nuclei of mullite and cristobalite. The formation of  $[AlO_5]$  polyhedra during pyrophyllite dehydroxylation has also been detected by Klevtsov et al. (1987).

Recently, the structure of brinrobertsite, an ordered, mixed-layered, dioctahedral pyrophyllite–smectite, has been modelled from TEM data. TEM images show sequences of dominant 2.4 nm periodicity, produced by 2:1 layers with alternate pyrophyllite-like (low-charge) and smectite-like (high-charge) interlayers.

The chemical composition of talc-like minerals does not usually differ significantly from that of the end-member ( $Mg_3Si_4O_{10}(OH)_2$ ), even if limited substitution of  $Al^{3+}$  or  $Fe^{3+}$  for  $Mg^{2+}$  occurs. Charge balance is usually achieved by tetrahedral  $^{IV}Al^{3+}$  for  $^{IV}Si^{4+}$  substitutions and/or by insertion of vacancies in octahedral position. Talc-like minerals are kerolite (hydrated variety), minnesotaite (Fe-rich variety), and willemseite (Ni-rich variety). Different polytypic sequences have been derived by Weiss and Đurovič (1984) who found ten non-equivalent polytypes but only seven of these may actually be distinguished by XRD.



### 2.6.2. True and Brittle Micas

Brigatti and Guggenheim (2002) have discussed the structural and chemical features of more than 200 mica crystals. Most of these are true micas, belonging to the  $1M$ ,  $2M_1$ ,  $3T$ ,  $2M_2$ , and  $2O$  polytypes. The dominant polytype in trioctahedral true micas is  $1M$ , whereas in dioctahedral micas, the most common stacking sequence is  $2M_1$ . The structure refinements of brittle micas confirm that the  $1M$  polytype is generally trioctahedral whereas the  $2M_1$  polytype is dioctahedral. The  $2O$  structure has been found for the trioctahedral brittle mica anandite (Giuseppetti and Tadini, 1972; Filut et al., 1985) and recently for a phlogopite from the Kola Peninsula (Ferraris et al., 2000).

In some naturally occurring true micas,  $\text{Si}^{4+}$  nearly fills all of the tetrahedral sites (e.g., polyolithionite, tainiolite, norrishite, and celadonite), whereas in the most common mica species (muscovite and phlogopite)  $\text{Al}^{3+}$  substitutes for  $\text{Si}^{4+}$  in a ratio close to 1:3. In some true micas and brittle micas, the  $\text{Al}^{3+}$  for  $\text{Si}^{4+}$  substitution corresponds to a ratio of  $\text{Al}:\text{Si} = 1:1$  (e.g., ephesite, preiswerkite, siderophyllite, margarite, and kinoshitalite) whereas the trioctahedral brittle mica, clintonite, has an unusually high  $\text{Al}^{3+}$  content with a ratio of  $\text{Al}:\text{Si} = 3:1$  (Bailey, 1984a–c). Evidence of  $\text{Fe}^{3+}$  tetrahedral substitution was reported on the basis of optical observations (Farmer and Boettcher, 1981; Neal and Taylor, 1989), spectroscopic studies (Dyar, 1990; Rancourt et al., 1992; Cruciani et al., 1995), and crystal-structure refinements (Guggenheim and Kato, 1984; Joswig et al., 1986; Cruciani and Zanazzi, 1994; Medici, 1996; Brigatti et al., 1996a; Brigatti et al., 1999). In tetra-ferriphlogopite, tetra-ferri-annite, and anandite  $\text{Fe}^{3+}$  is the only  $\text{Si}^{4+}$ -substituting cation, with a  $\text{Fe}:\text{Si}$  ratio of about 1:3 (Giuseppetti and Tadini, 1972; Semenova et al., 1977; Hazen et al., 1981; Filut et al., 1985; Brigatti et al., 1996a, b; Mellini et al., 1996; Brigatti et al., 1999). Two mica end-members contain boron (boromuscovite) (Liang et al., 1995) and berillium (bityite) (Lin and Guggenheim, 1983), and some synthetic micas contain Ge in the tetrahedral sheet (Toraya et al., 1978a, b; Toraya and Marumo, 1981). Most mica structures show a disordered distribution of tetrahedral cations, with the exception of some brittle mica species, such as margarite (Guggenheim and Bailey, 1975, 1978; Kassner et al., 1993), anandite (Giuseppetti and Tadini, 1972; Filut et al., 1985), bityite (Lin and Guggenheim, 1983), and a few true micas, e.g., polyolithionite-3T (Brown, 1978) and muscovite-3T (Güven and Burnham, 1967).

As already mentioned, the dimensions of an ideal octahedral sheet in the (001) plane are commonly less than those of an ideal and unconstrained tetrahedral sheet. In order to obtain congruence, the difference in size between the octahedral and tetrahedral sheets is adjusted by mechanisms involving both sheets (Mathieson and Walker, 1954; Newnham and Brindley, 1956; Zvyagin, 1957; Bradley, 1959; Radoslovich, 1961; Radoslovich and Norrish, 1962; Brown and Bailey, 1963; Donay et al., 1964; Lee and Guggenheim, 1981; Bailey, 1984b).

Three translationally independent octahedral cation sites characterize the 2:1 layer. One site, called M(1), is *trans*-coordinated by OH (or F and/or Cl, but rarely by S).

Both the remaining two sites are *cis*-coordinated and are referred to as M(2) if a relevant symmetry plane exists in the layer. Otherwise, the two *cis*-sites are labelled M(2) and M(3), respectively. In dioctahedral micas, M(1) is usually vacant, whereas in trioctahedral micas all three octahedral sites are occupied. The cation distribution in octahedral sites may be summarized as (i) all octahedra are occupied by the same kind of ‘crystallographic entity’, i.e., the same kind of ion or a statistical average of different kinds of ions, including voids (homo-octahedral micas; Đurović (1981, 1994)); (ii) two octahedra are occupied by the same kind of ‘crystallographic entity’ and the third by a different entity in an ordered way (meso-octahedral micas); or (iii) each of the three sites is occupied by a different ‘crystallographic entity’ in an ordered way (hetero-octahedral micas). Several phlogopite and tetra-ferriphlogopite crystals (space group  $C2/m$ ) show the same kind of cations (or a disordered cation distribution) in M(1) and M(2) octahedra. Some Li-rich micas (space group  $C2$ ) have different cation ordering in M(1), M(2), and M(3) sites, e.g., zinnwaldite-1M (Guggenheim and Bailey, 1977), lepidolite-1M (Backhaus, 1983), zinnwaldite-2M1 (Rieder et al., 1998), ferroan polyolithionite-1M, and lithian siderophyllite-1M (Brigatti et al., 2000).

#### A. Illite

A recent review on illite has been provided by Brigatti and Guggenheim (2002). Illite is a dioctahedral 2:1 phyllosilicate of common occurrence in soils and sedimentary rocks. The term ‘illite’ is used for 2:1 minerals with a non-expandable layer and a wide variety of chemical compositions. For this reason, Rieder et al. (1998) have suggested that ‘illite’ be used as a series name. The composition of illite differs from that of dioctahedral mica muscovite,  $[\text{XII}] \text{K}^{[\text{VI}]} \text{Al}_2^{[\text{VI}]} (\text{Si}_3\text{Al}) \text{O}_{10} (\text{OH})_2$  in having heterovalent substitutions of the type  $^{[\text{IV}]} \text{Si}_{-1}^{4+[\text{VI}]} \text{Al}_{3+}^{[\text{IV}]} \text{Al}_{-1}^{3+[\text{VI}]} (\text{Fe}_{2+}, \text{Mg}_{2+})$  and  $^{[\text{IV}]} \text{Si}_{-1}^{4+[\text{VI}]} \text{Al}_{3+}^{[\text{XII}]} (\square, \text{H}_2\text{O})^{[\text{XII}]} \text{K}_{-1}$ , homovalent substitution of the type  $^{[\text{VI}]} \text{Fe}_{3+}^{[\text{VI}]} \text{Al}_{-1}^{3+}$ , and a layer charge between  $-0.6$  and  $-0.9$  (Bailey, 1986).

Different chemical compositions have been found for samples from diverse genetic environments, such as hydrothermally altered igneous rocks (Środoń et al., 1992), shales, and mudstones (Lindgreen et al., 1991). Zöller and Brockamp (1997) have also reported different chemical compositions for co-existing 1M and 2M<sub>1</sub> illites.

A high-quality three-dimensional structure refinement for illite is still missing, even if some models show a good fit with (thermal gravimetric analysis) TGA and XRD data. Drits et al. (1984, 1993) have suggested a statistical distribution of cations over all three octahedral sites. Bailey (1984a) and Drits et al. (1984) have established a relationship between the intralayer shift (i.e. the displacement along parameter  $a$  between two adjacent 2:1 layers) and octahedral site size (Bailey, 1984a). This intralayer shift is larger than the theoretical value ( $1/3 a$ ) for *trans*-vacant illite and smaller for *cis*-vacant illite, allowing the *trans*- or *cis*-vacant structure to be identified by XRD.

A great deal of research has been carried out on the variation of the (001) XRD reflection in different illitic materials. The half-height-width value of this reflection,

known as the 'Kübler index', is measured using the  $<2\text{ }\mu\text{m}$  fraction of air-dried illite and Cu K $\alpha$  radiation (Kübler, 1964, 1967; Kübler and Goy-Eggenberger, 2001). The 'Kübler index', expressed as small changes in the Bragg angle ( $\Delta 2\theta$ ), has been used to identify the diagenesis-archizone and archizone-epizone metamorphic boundaries (Antonelli et al., 2003). Standardization of sample preparation and instrumental-measuring conditions have been discussed. Besides being influenced by experimental conditions and sample preparation, the Kübler index is affected by (i) the mean size of domains that scatter X-rays coherently; (ii) lattice strain; and (iii) the amount of swelling part in the interstratified component. Nevertheless, this index can serve as a useful indicator of diagenesis and low-temperature metamorphism in different geotectonic environments (Guggenheim et al., 2002 and references therein). Other indices using illite features to indicate the grade of diagenesis and incipient metamorphism of clastic rocks are the 'Weaver index' (Weaver, 1960), the 'Weber index' (Weber, 1972), the 'Flehmig index' (Flehmig, 1973), and the 'Watanabe index' (Watanabe, 1988).

Zöller and Brockamp (1997) have observed that  $1M$ - and  $2M_1$ -illite polytypes are distinct in composition, and hence should be considered as different mineral phases. Peacor et al. (2002) have reported that dioctahedral clay minerals, including illite-montmorillonite and illite, proceed from a partially disordered  $1M_d$  stacking to a  $2M_1$  type during normal prograde diagenetic and low-grade metamorphic sequence, and that  $1M$  does not normally occur as an intermediate polytype.

Extended X-ray absorption fine structure spectroscopy (EXAFS) studies have suggested that the  $\text{Fe}^{2+}$  cations in the octahedral sheet of Fe-rich illites preferentially occupy the *cis*-sites, giving rise to domains of different size (Drits et al., 1997a, b). Sainz-Diaz et al. (2002) have confirmed the clustering of  $\text{Fe}^{2+}$  atoms in the octahedral sheet by theoretical calculations. Furthermore, illites with *cis*-vacant (cv) 2:1 layers have higher dehydroxylation temperatures than those with *trans*-vacant (tv) 2:1 layers (Drits et al., 1996).

The phase changes that take place when Fe-rich illites are heated have been discussed by Murad and Wagner (1996).  $\text{Fe}^{2+}$  is completely oxidized at  $250\text{ }^\circ\text{C}$ , and the layer gradually dehydroxylates between about  $350$  and  $900\text{ }^\circ\text{C}$ . At  $900\text{ }^\circ\text{C}$  the illite structure breaks down, and hematite clusters appear.

The stability of illite in natural environments is the subject of much controversy. Evidence for the metastability of 'illite' with respect to ideal muscovite plus pyrophyllite has been discussed by Rosenberg (2002).

### 2.6.3. Smectites

Smectites are 2:1 phyllosilicates with a total (negative) layer charge between 0.2 and 0.6 per half unit cell. Except for the layer charge and hydration of the interlayer cations, their structure is similar to that of other 2:1 phyllosilicates already described. The octahedral sheet may either be dominantly occupied by trivalent cations (dioctahedral smectites) or divalent cations (trioctahedral smectites). The general formula for

dioctahedral smectites is  $(M_{x+y}^+ \times nH_2O)(R_{2-y}^{3+}R_y^{2+})(Si_{4-x}^{4+}Al_x^{3+})O_{10}(OH)_2$  and that for trioctahedral species (e.g., saponite) is  $(M_x^+ \times nH_2O)(R_{3-y}^{2+}R_y^{3+})(Si_{4-x-y}Al_{x+y})O_{10}(OH)_2$  where  $x$  and  $y$  indicate the layer charge resulting from substitutions in tetrahedral and octahedral sites, respectively;  $R^{2+}$  and  $R^{3+}$  refer to a generic divalent and trivalent octahedral cation, respectively;  $M^+$  refers to a generic monovalent interlayer cation (equivalent numbers of cations of different valency may be indicated by  $M_{x+y/n}^{n+}$ ).

A wide range of cations can occupy tetrahedral, octahedral, and interlayer positions. Commonly  $Si^{4+}$ ,  $Al^{3+}$ , and  $Fe^{3+}$  are found in tetrahedral sites. Substitution of  $R^{3+}$  for  $Si^{4+}$  in tetrahedral sites creates an excess of negative charge on the three basal oxygens and the apical oxygen. This affects the total charge of the 2:1 layer as well as the local negative charge at the layer surface.  $Al^{3+}$ ,  $Fe^{3+}$ ,  $Fe^{2+}$ ,  $Mg^{2+}$ ,  $Ni^{2+}$ ,  $Zn^{2+}$ , and  $Li^+$  generally occupy octahedral sites. In dioctahedral smectites, substitution of divalent cations for trivalent cations creates an excess of negative layer charge, whereas substitution of trivalent for divalent cations in trioctahedral smectites generates an excess of positive charge. These events have implications for many physical properties of smectites such as swelling and rheological behaviour.

Most of the technological uses of smectite are related to reactions that take place in the interlayer space.  $Na^+$ ,  $K^+$ ,  $Ca^{2+}$ , and  $Mg^{2+}$ , which balance the negative 2:1 layer charge, are commonly hydrated and exchangeable. Smectites contain water in several forms. The water held in pores may be removed by drying under ambient conditions. Water may also be associated with layer surfaces and in interlayer spaces (Güven, 1992). Usually, three modes of hydration (recognized as pH-dependent) are distinguished: (i) interlayer hydration (of internal surfaces) of primary clay mineral particles; (ii) continuous hydration relating to an unlimited adsorption of water on internal and external surfaces; and (iii) capillary condensation of free water in micropores. The main elements of interlayer hydration are (i) hydration of interlayer cations, (ii) interaction of clay surfaces with water molecules and interlayer cations, and (iii) water activity in the clay-water system.

A voluminous literature exists on the hydration of interlayer cations (Hendricks et al., 1940; Mooney et al., 1952; Norrish, 1954; van Olphen, 1965, 1969; Suquet et al., 1975, 1977; MacEwan and Wilson, 1980; Suquet and Pezerat, 1987). The interlayer hydration complexes of smectites, arising from intercalation of a discrete number of water layers, can be distinguished by X-ray or neutron diffraction. This number ranges from zero to three, corresponding to the formation of zero-, one-, two- or three-layer hydrates. The main factors affecting the interlayer hydration of smectites are: (i) hydration energy of the interlayer cation; (ii) polarization of water molecules by interlayer cations; (iii) variation of electrostatic surface potentials because of differences in layer charge location; (iv) activity of water; (v) size and morphology of smectite particles. Two types of hydration complexes can form in the interlayer space: 'inner-sphere' and 'outer sphere' complexes. In the former case the cation is directly bound to the clay surface on one side and to a number of water molecules on the other side, whereas in outer sphere hydration complexes, the interlayer cation is completely surrounded by water molecules and interacts with the clay mineral

surface through its water ligands. The interactions between clay minerals and water molecules are further described in Chapter 3, while the reviews by McEwan and Wilson (1980), Sposito and Prost (1982), Parker (1986), Newman (1987), McBride (1989), Güven (1992) and Brown et al. (1995) should be consulted for more details.

Swelling of smectites occurs in a stepwise fashion, through the sequential formation of integer-layer hydrates (Norrish, 1954), and hence may be viewed as a series of phase transitions between such hydrates (Laird, 1994). At total water contents intermediate between phases, a two-phase coexistence is observed in the form of interstratified or mixed layer hydrates (Cases et al., 1997). Many theoretical approaches, such as Monte Carlo simulation, have been applied to investigating the interlayer cation-water interaction. In  $\text{Na}^+$ -exchanged smectites each  $\text{Na}^+$  ion is surrounded by five water molecules, while its position depends on the layer charge location. In montmorillonite,  $\text{Na}^+$  is located above the hexagonal cavity just over the octahedron where  $\text{Mg}^{2+}$  substitutes for  $\text{Al}^{3+}$ , whereas in beidellite,  $\text{Na}^+$  is located near the  $\text{Al}^{3+}$ -substituted tetrahedron (Chatterjee et al., 1999). Water shows a strong preference to forming an intermolecular hydrogen-bonded network, while the hydrogen bonds to the aluminosilicate surface are weak and short-lived (Boek and Sprik, 2003).

The location of isomorphous substitution in the layer (i.e., whether the layer charge derives from substitution in the tetrahedral or octahedral sheet) is an important factor affecting smectite hydration. In electrically neutral layers the basal oxygen atoms act as a weak Lewis base (electron donor), forming weak hydrogen bonds with water molecules. When isomorphous substitution occurs, the basal oxygen atoms have an excess of negative charge, and their electron-donating capacity increases. Sposito (1984) has shown that H-bonding between water molecules and basal oxygens is stronger for tetrahedral than for octahedral sheet substitution. The surface charge density ( $\delta$ ) of a smectite with layer charge  $x_j$  (in electrons) can be computed by the equation:  $\sigma = x_j/a \times b$  where  $a$  and  $b$  denote the unit-cell parameters.

Another type of surface having variable charge develops along the edges of clay mineral particles where Si–O–Si and Al–O–Al bonds are ‘broken’ and may convert into Si–OH and Al–OH groups (Güven, 1992). The surface potential ( $\psi_0$ ) at these edges is related to the pH of the ambient solution, and the proton concentration at the point of zero charge (PZC) of the edge surface.

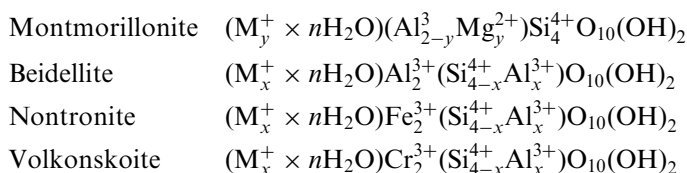
The propensity of smectites for sorbing cationic species from solution is given as the cation exchange capacity (CEC) (see Chapter 12.9). CEC values are expressed in centimole of positive charge per kilogram of dry clay mineral ( $\text{cmol}(+)/\text{kg}$ ) which is numerically equal to the traditional unit of milliequivalents per 100 g clay ( $\text{meq}/100\text{g}$ ). The exchange between cations balancing the negative layer charge and cations in solution shows the following general features: (i) it is reversible; (ii) it is diffusion-controlled (the rate-limiting step being the diffusion of one charge-balancing ion against another); (iii) it is stoichiometric; and (iv) in most cases there is selectivity of one cation over another (Gast, 1977).

Polymeric hydr(oxides) of aluminium, iron, chromium, zinc, and titanium can intercalate into smectites by cation exchange. After heating, these ‘pillared clays’ show a

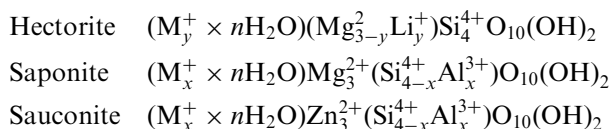
large surface area and porosity, high acidity, and catalytic properties (see Chapters 7.5 and 10.2). Likewise, cationic organic molecules (e.g., aliphatic and aromatic amines, pyridines, methylene blue) may replace the inorganic exchangeable cations in the interlayer space, while non-ionic polar organic molecules may replace adsorbed water on external surfaces and in the interlayer space. As a result, the surface of smectite particles becomes hydrophobic, losing its tendency to bind water (see Chapter 7.3).

Species of smectites may be differentiated according to the following criteria: (i) dioctahedral or trioctahedral nature of the octahedral sheet; (ii) predominant octahedral cation; and (iii) density and location of the layer charge.

The most important end-members of dioctahedral smectites have the following general compositions:



The most important species of trioctahedral smectites are:



Intermediate compositions can occur as swinefordite, a dioctahedral-trioctahedral lithium-rich species (Tien et al., 1975). Moreover, significant differences in chemical composition with respect to end-members occur for both dioctahedral and trioctahedral smectites.

#### 2.6.4. Vermiculite

Vermiculite is generally trioctahedral. As in smectite the 2:1 layers are separated by hydrated cations occupying the interlayer space. However, the (negative) layer charge of vermiculite ( $>0.6$  per formula unit), arising mostly from substitution of  $Al^{3+}$  for  $Si^{4+}$  in tetrahedral sites, is larger than that of smectite. Furthermore, vermiculite particles ('crystals') are often large enough for detailed structural studies to be performed. Stacking disorder produces 'streaking' in the diffraction pattern parallel to  $c^*$  for  $0kl$  reflections where  $k \neq 3n$ . This feature, involving semi-random layer displacement of  $\pm b/3$ , is always found in  $Mg^{2+}$ -vermiculite (Shirozu and Bailey, 1966; Slade et al., 1985). For the 2-layer hydrates of  $Na^+$ - and  $Ca^{2+}$ -vermiculites that develop at a relative humidity ( $P/P_0$ )  $> 0.5$ , sharp diffraction patterns can be obtained, indicative of a high degree of stacking order. In this instance, the ditrigonal cavities of adjacent silicate layers face each other across the interlayer (Slade et al., 1987; de la Calle and Suquet, 1988). This arrangement



(of adjacent silicate layers) contrasts with that found in natural semi-ordered  $\text{Mg}^{2+}$ -vermiculite (Mathieson and Walker, 1954; Shirozu and Bailey, 1966; Alcover and Gatinneau, 1980), where tetrahedral bases of a given silicate layer can lie opposite ditrigonal cavities of an adjacent silicate layer. This leads to a structure in which the interlayer  $\text{Mg}^{2+}$  ions are positioned between the bases of aluminium tetrahedra. In the two-layer hydrates of  $\text{Na}^+$ - and  $\text{Ca}^{2+}$ -vermiculites,  $\text{Na}^+$  and  $\text{Ca}^{2+}$  cations have a high probability of occurring between the bases of silicon tetrahedra, but  $\text{Ca}^{2+}$  ions also occur between ditrigonal cavities (Slade et al., 1985). The nature of the interlayer cation and the relative position of adjacent silicate layers influence the organization of the interlayer water molecules. In general, these molecules show an ordered arrangement, although they are somewhat mobile. The oldest structural study on vermiculite was carried out by Gruner (1934). The results of many investigations that followed have been reviewed (e.g., de la Calle and Suquet, 1988). Here, we focus on more recent contributions that are of general interest.

The structure of vermiculite from Santa Olalla, Spain, intercalated with different organic cations, such as tetramethylammonium ( $\text{TMA}^+$ ), monomethylammonium ( $\text{MMA}^+$ ), dimethylammonium ( $\text{DMA}^+$ ) and tetramethylphosphonium ( $\text{TMP}^+$ ), has been investigated by Vahedi-Faridi and Guggenheim (1997, 1999a, b). In  $\text{MMA}^+$ -exchanged vermiculite, the interlayer  $\text{MMA}^+$  ion occupies two distinct sites (i) where the N–C axis is perpendicular to the basal oxygen plane, and the N atom being offset from the centre of the interlayer by 0.104 nm and (ii) where the N atom is at the centre of the interlayer between adjacent 2:1 layers, and the N–C axis presumably lying parallel to the basal oxygen plane. Similarly, the C–N–C plane of the  $\text{DMA}^+$  ion in  $\text{DMA}^+$ -vermiculite shows two different orientations with respect to the (001) plane.  $\text{TMA}^+$ -vermiculite shows a near-perfect three-dimensional stacking order with the  $\text{TMA}^+$  ion offset from the centre plane between two silicate layers (Vahedi-Faridi and Guggenheim, 1997).

Earlier, Slade et al. (1987) investigated the structure of a vermiculite-anilinium interlayer complex. Intercalation increases the stacking order of adjacent silicate layers, giving rise to sharp single-crystal reflections in the XRD pattern. Apparently, the packing of the intercalated organic cations produces a superstructure and bonding from layer to layer, promoting ordered layer stacking. The principal axes of the anilinium ions, i.e., N–C(1)–C(4), are nearly perpendicular to the silicate layers, while the planes of the aromatic rings are about  $\pm 30^\circ$  to the  $a$ -axis of the unit cell.

### 2.6.5. Chlorite

The structure of chlorite is made up of a regularly stacked, negatively charged 2:1 layers and a single, positively charged interlayer octahedral sheet that are linked to each other by H bonds. The simplest structural unit of chlorite, therefore, consists of the repetition of a 2:1 layer along  $c^*$  and an octahedral interlayer sheet with a periodicity along  $c$  of about 1.4 nm.

Chlorites are usually trioctahedral with  $\text{Mg}^{2+}$ ,  $\text{Al}^{3+}$ , and  $\text{Fe}^{2+}$ ,  $\text{Fe}^{3+}$  in octahedral sites. More rarely octahedra are occupied by  $\text{Cr}^{3+}$ ,  $\text{Mn}^{3+}$ ,  $\text{Ni}^{2+}$ ,  $\text{V}^{3+}$ ,  $\text{Cu}^{2+}$ ,  $\text{Zn}^{2+}$ , and  $\text{Li}^{+}$ . Tetrahedral cations are  $\text{Si}^{4+}$  and  $\text{Al}^{3+}$  (0.4–1.8 atoms per four tetrahedral positions).  $\text{Si}^{4+}$  can occasionally be substituted by  $\text{Fe}^{3+}$ ,  $\text{Zn}^{2+}$ ,  $\text{Be}^{2+}$ , or  $\text{B}^{3+}$ .

Bailey (1980) has divided chlorites in four sub-groups: (i) trioctahedral chlorites, the most common, where both the interlayer and the 2:1 octahedral sheets are trioctahedral; (ii) dioctahedral chlorites, where both the interlayer and the 2:1 octahedral sheets are dioctahedral (e.g., donbassite); (iii) di-trioctahedral chlorites, where the 2:1 octahedral sheet is dioctahedral and the interlayer sheet is trioctahedral (e.g., cookeite and sudoite); and (iv) tri-dioctahedral chlorites, where the interlayer sheet is dioctahedral and the 2:1 octahedral sheet is trioctahedral (the only mineral with a similar arrangement is franklinfurnaceite, which also contains  $\text{Ca}^{2+}$  ions, and should be considered as intermediate in structure between chlorites and brittle micas).

Bayliss (1975) introduced a nomenclature for trioctahedral chlorites based on five end-members:

Clinochlore	$(\text{Mg}_5^{2+}\text{Al}^{3+}) (\text{Si}_3^{4+}\text{Al}^{3+}) \text{O}_{10}(\text{OH})_8$
Chamosite	$(\text{Fe}_5^{2+}\text{Al}^{3+}) (\text{Si}_3^{4+}\text{Al}^{3+}) \text{O}_{10}(\text{OH})_8$
Pennantite	$(\text{Mn}_5^{2+}\text{Al}^{3+}) (\text{Si}_3^{4+}\text{Al}^{3+}) \text{O}_{10}(\text{OH})_8$
Nimite	$(\text{Ni}_5^{2+}\text{Al}^{3+}) (\text{Si}_3^{4+}\text{Al}^{3+}) \text{O}_{10}(\text{OH})_8$
Baileychlore	$(\text{Zn}_5^{2+}\text{Al}^{3+}) (\text{Si}_3^{4+}\text{Al}^{3+}) \text{O}_{10}(\text{OH})_8$

Intermediate compositions and the presence of other cations are identified by adding a prefix or suffix to the end-member name. For example, the name ‘kämmererite’ in the old nomenclature for a magnesian chlorite with chromium substitution, should now be changed to ‘chromian clinochlore’.

Wiewióra and Weiss (1990) have proposed a different chemical classification based on the values of the following variables: (i)  $\text{R}^{3+}$ , representing the sum of higher charge cations such as  $\text{Al}^{3+}$ ,  $\text{Fe}^{3+}$ , and  $\text{Cr}^{3+}$ ; (ii)  $\text{R}^{2+}$ , representing the content of divalent cations, such as  $\text{Mg}^{2+}$ ,  $\text{Fe}^{2+}$ ,  $\text{Mn}^{2+}$ , and  $\text{Ni}^{2+}$ ; (iii)  $\square$ , representing octahedral vacancies; and (iv)  $\text{Si}_{(4-x)}$ , where  $x$  represents the number of trivalent cations substituting for Si. The structural chemical formula of chlorites may thus be given as  $(\text{R}_u^{2+}\text{R}_y^{3+}\text{W}_z)(\text{Si}_{4-x}^{4+}\text{Al}_x^{3+}) \text{O}_{10}(\text{OH})_8$  where  $u + y + z = 6$  and  $z = (y - x)/2$ . However, this classification has so far not been accepted by the IMA Commission.

The ideal composition of the 2:1 chlorite layer is  $(\text{R}^{2+}, \text{R}^{3+})_3(\text{Si}_{4-x}\text{Al}_x)\text{O}_{10}(\text{OH})_2$ , and that of the interlayer octahedral sheet is  $(\text{R}^{2+}, \text{R}^{3+})_3(\text{OH})_6$ . The positive charge of the interlayer octahedral sheet commonly balances the negative charge of the 2:1 layer arising from substitution of  $\text{Al}^{3+}$  for  $\text{Si}^{4+}$ . Sometimes, the octahedral sheet in the 2:1 layer contributes to balancing the tetrahedral charge. The charge of the octahedral sheet in the 2:1 layer is positive if the overall tetrahedral charge is  $< -1$ , and usually negative when the tetrahedral charge is  $> -1$ . Thus, the stable chlorite



configuration is characterized by a total charge of  $-1$  for the 2:1 layer and a total charge of  $+1$  for the interlayer sheet.

The main chemical substitutions in chlorite have been summarized by Bailey (1988b) as

$^{[VI]}\text{Fe}^{2+}$   $^{[VI]}\text{Mg}^{2+}$   
 $^{[IV]}\text{Si}^{4+}$   $^{[VI]}\text{R}^{2+}$   $^{[IV]}\text{Al}^{3+}$   $^{[VI]}\text{Al}^{3+}$  (Al-Tschermak)  
 $^{[IV]}\text{Si}^{4+}$   $^{[VI]}\text{R}^{2+}$   $^{[IV]}\text{Al}^{3+}$   $^{[VI]}\text{Cr}^{3+}$  and  $^{[IV]}\text{Si}^{4+}$   $^{[VI]}\text{R}^{2+}$   $^{[IV]}\text{Al}^{3+}$   $^{[VI]}\text{Ti}^{4+}$   
 $^{[VI]}\text{(Mg}^{2+}, \text{Fe}^{2+})_{-3}$   $^{[VI]}\text{Al}_2^{3+}$   $^{[VI]}\square$   
 $^{[IV]}\text{Si}^{4+}$   $^{[VI]}\text{Mg}^{2+}$   $^{[IV]}\text{Al}^{3+}$   $^{[VI]}\text{Al}^{3+}$  (common in clinocllore)  
 $^{[VI]}\text{Fe}^{2+}$   $(\text{OH})_{-1}$   $^{[VI]}\text{Fe}^{3+}$   $\text{O}_2$  and  $^{[IV]}\text{Si}^{4+}$   $^{[VI]}\text{Fe}^{2+}$   $^{[IV]}\text{Al}^{3+}$   $^{[VI]}\text{Al}^{3+}$  (common in chamosite)

Brown and Bailey (1963) have studied possible polytypism in a 1.4 nm sequence. In the 2:1 layer, each superior tetrahedral sheet is displaced by  $a/3$  with respect to the inferior, due to the presence of the octahedral sheet. This displacement can be either positive or negative. The interlayer octahedral sheet can be oriented in two different ways with respect to the 2:1 layer, referred to as type I and type II. In type I, the octahedra in both the interlayer and the 2:1 layer are oriented in the same way as shown in Fig. 2.11. On the other hand, type II is characterized by an opposite orientation of octahedra in the interlayer and 2:1 layer (Fig. 2.12).

The interlayer sheet, in either type I or type II orientation, needs to match the 2:1 layer to form H-bonds between basal oxygen atoms and OH groups of the octahedral interlayer. This requirement is satisfied by six different geometrical arrangements that can be divided into two sets (A and B), composed of three equivalent positions. In set A, one of the three interlayer cations, if projected on the basal plane, overlaps with the H placed at the centre of the hexagonal ring in the matching tetrahedral sheet of the 2:1 layer. In set B, the interlayer sheet is displaced by  $a/3$  and thus, the projection of the octahedral cation on the basal plane matches the H

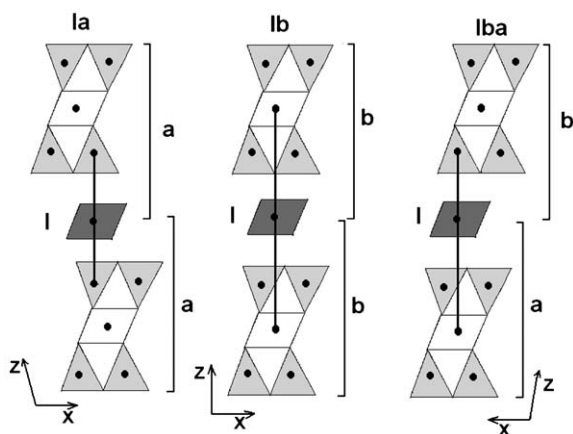


Fig. 2.11. Relationships between the 2:1 layer and the octahedral sheet in I chlorite polytype.

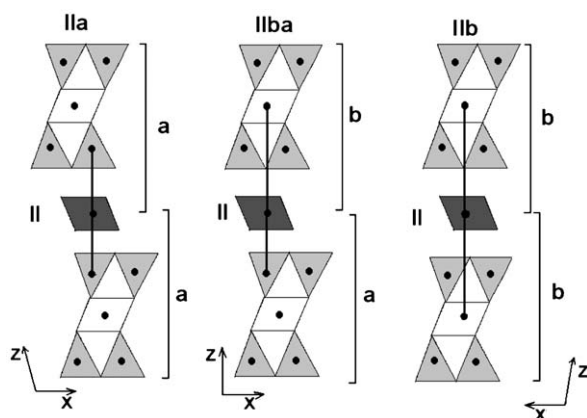


Fig. 2.12. Relationships between the 2:1 layer and octahedral sheet in II chlorite polytype.

position in the adjacent 2:1 layer on the tetrahedral sheet below (Figs. 2.11 and 2.12). These arrangements are referred to as Ia, Ib, IIa, and IIb. Moreover, the overlapping of another 2:1 layer creates six other different orientations. Combination with the four previously derived gives rise to 24 polytypes although only 12 of which are effectively different (Brown and Bailey, 1963). Different notations for chlorite polytypes have been introduced by Bailey (1988a), Zvyagin (1963), and Zvyagin and Mishchenko (1965). The polytypic notation for sequences at 2.8 nm has been proposed by Lister and Bailey (1967) and Drits and Karavan (1969).

Chlorites from clay environments usually present random or semi-random sequences. Random stacking can be identified from the analysis of reflections with  $k = 3n$ , which are well defined. Broad and very weak reflections, however, characterize spots with  $k \neq 3n$ .

Single-crystal studies on chlorites have recently been performed (Nelson and Guggenheim, 1993; Smyth et al., 1997; Welch and Marshall, 2001; Kleppe et al., 2003) both at room temperature and at high temperature and pressure. The greatest number of structural refinements pertains to clinochlore.

## 2.7. ILLITE–SMECTITE AND OTHER INTERSTRATIFICATIONS BETWEEN DIOCTAHEDRAL NON-EXPANDABLE AND EXPANDABLE 2:1 LAYERS

Interstratifications between non-expandable layers of illite and expandable layers of smectite have attracted the attention of many researchers because of their properties (Środoń, 1989), petrogenetic significance (Velde and Köster, 1992), and application in the oil industry (Drits et al., 1997b). In addition to time, temperature, pressure, and  $K^+$  content,  $Al^{3+}$  for  $Si^{4+}$  substitution and interlayer dehydration are

the main crystal chemical parameters controlling the smectite-to-illite transformation (Środoń and Eberl, 1984; Lindgreen et al., 1991; Huang, 1992; Drits, 1997). The dynamics of this process have been investigated using a wide range of approaches, notably HRTEM and modelling (Bethke and Altaner, 1986).

In the model, developed by Altaner and Ylagan (1997) the crystal structure of illite-smectite (I–S) is interpreted in terms of a non-polar and a polar 2:1 layer. In the non-polar model, individual 2:1 layers are chemically homogeneous, whereas 2:1 layers in the polar model can have a smectite charge on one side and an illite charge on the other. Assuming a polar 2:1 layer model for I–S, the reaction mechanisms required for smectite illitization are (i) solid-state transformation (SST); (ii) dissolution and crystallization (DC); and (iii) Ostwald ripening (OR). SST features the replacement of smectite interlayers by illite interlayers, leading to gradual changes in interlayer ordering, polytype, chemical and isotopic composition, crystal size and shape. Several SST models are possible depending on the nature of the reaction site (framework cations, polyhedra, or interlayers). In contrast, DC models allow for abrupt changes in the structure, composition, and texture of I–S as illitization proceeds. Several DC models are possible depending on the nature of the rate-controlling step, i.e., diffusional transport or surface reactions during crystal growth. The OR model represents the coarsening of a single mineral where the smallest crystals dissolve and nucleate onto existing larger crystals, allowing for evolution in the overgrowth but not in the template crystal. An SST mechanism, involving either reacting polyhedra or reacting interlayers, seems to provide the best model of illitization in rock-dominated systems such as bentonite, while a DC mechanism seems best in describing illitization in fluid-dominated systems such as sandstone and hydrothermal environments. Both DC and SST mechanisms can occur in shale. Differences in reaction mechanism may be related to permeability. The OR model poorly describes illitization because of the progressive mineralogical and chemical changes involved.

In rectorite, there is regular interstratification of one layer of illite and one layer of smectite (... ISIS ...), while regular interstratification of one smectite and three illite layers (... IISIIS ...) gives rise to tarasovite.

Other interstratified minerals composed of non-expandable and expandable 2:1 layers are leucophyllite–smectite (Sokolova, 1982), glauconite–nontronite (Odom, 1984) and celadonite–nontronite (Lipkina et al., 1987).

## 2.8. ALLOPHANE AND IMOGOLITE

Allophane and imogolite are clay-size hydrous aluminosilicates of short-range order. Although, these minerals have been found in soils of different origins and environments, they are especially abundant in soils derived from volcanic ash and weathered pumice. Not all allophanes, however, are associated with soil environments. A prime example is the type that occurs as a deposit on a stream bed near Silica Springs, New Zealand. The literature also mentions ‘proto-imogolite’, which is a

synthetic alumino-silicate sol formed from the interaction of hydroxyaluminium species and orthosilicic acid in dilute aqueous solutions of  $\text{pH} < 5$  (Farmer et al., 1979). The natural analogue of proto-imogolite that occurs in soil is sometimes referred to as 'allophane-like constituents' (Wada, 1995). For more details about the nature, occurrence, and properties of allophane and imogolite, the reader is referred to the reviews by Fieldes and Claridge (1975), Wada (1989), Parfitt (1990), and Harsh (2000).

Since allophane gives broad, diffuse peaks in its XRD pattern (Fig. 2.13), this mineral has often been described as amorphous. HRTEM, however, has consistently shown (Henmi and Wada, 1976; Wada and Wada, 1977; Hall et al., 1985) that the unit particles of allophane consist of nanometre-size hollow spherules, forming micro-aggregates (clusters) of varied size and shape (Fig. 2.14). On this basis, the term

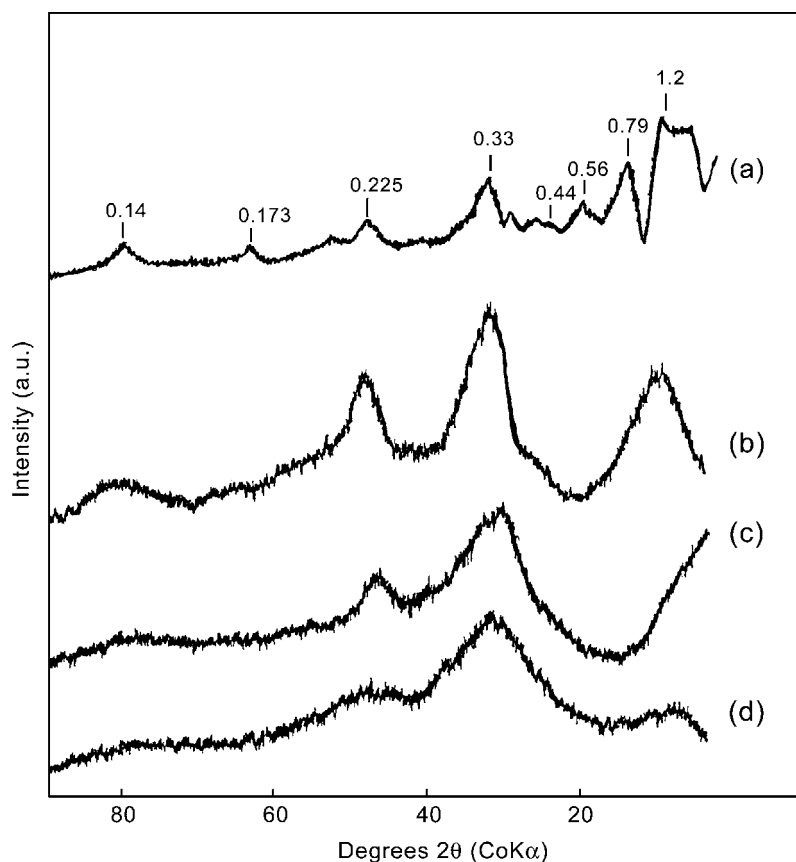


Fig. 2.13. XRD patterns of imogolite and some allophanes: (a) imogolite from soil; (b) imogolite-like allophane ( $\text{Al/Si} = 2.3$ ) from soil; (c) halloysite-like allophane ( $\text{Al/Si} = 1.1$ ) from soil; (d) Silica Springs allophane ( $\text{Al/Si} = 1.7$ ). Adapted from Brown et al. (1978); Childs et al. (1990); Parfitt (1990).

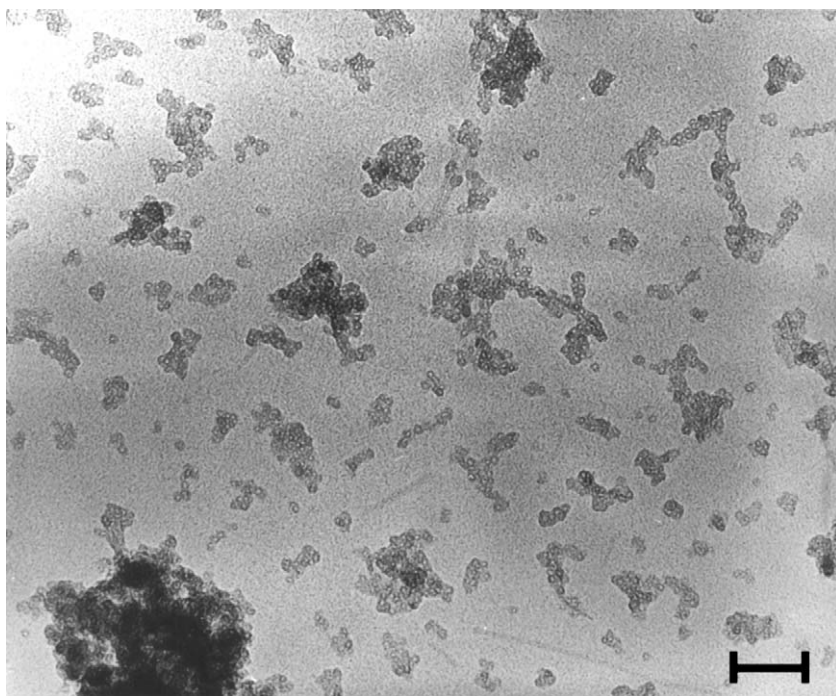


Fig. 2.14. High-resolution transmission electron micrograph of allophane separated from the Kitakami pumice ( $200\,000\times$  magnification; bar = 50 nm). Courtesy: S.-I. Wada, Kyushu University, Japan.

‘short-range order’ seems more appropriate than, and preferable to, ‘amorphous’. Thus, allophane may be defined as ‘...a group of clay-size minerals with short-range order which contain silica, alumina, and water in chemical combination’ (Parfitt, 1990).

When examined by HRTEM (Fig. 2.15), imogolite appears as slender, hollow tubules forming 10–30 nm thick bundles of several micrometres in length (Henmi and Wada, 1976; Wada, 1989). Further, the XRD pattern of imogolite shows a series of bands (Fig. 2.13) that can be assigned to ( $hk$ ) indices. Similarly, the ring reflections in its ED pattern may be indexed as ( $kl$ ) (Wada, 1995). In having long-range order in one dimension (with a repeat distance of 0.84 nm along the tubule axis), imogolite has been described as para-crystalline. However, there is as yet no generally acceptable terminology to denote the crystalline state of allophane, imogolite, and related minerals. Besides ‘short-range order’ and ‘para-crystalline’, the terms ‘poorly crystalline’, ‘non-crystalline’, ‘sub-crystalline’, and ‘disordered’ have been used in the literature (Brown et al., 1978; Wada, 1995).

Fig. 2.16 shows a cross section of an individual tubule of imogolite as deduced by Cradwick et al. (1972) from chemical, infrared spectroscopic, XRD, and ED analyses.



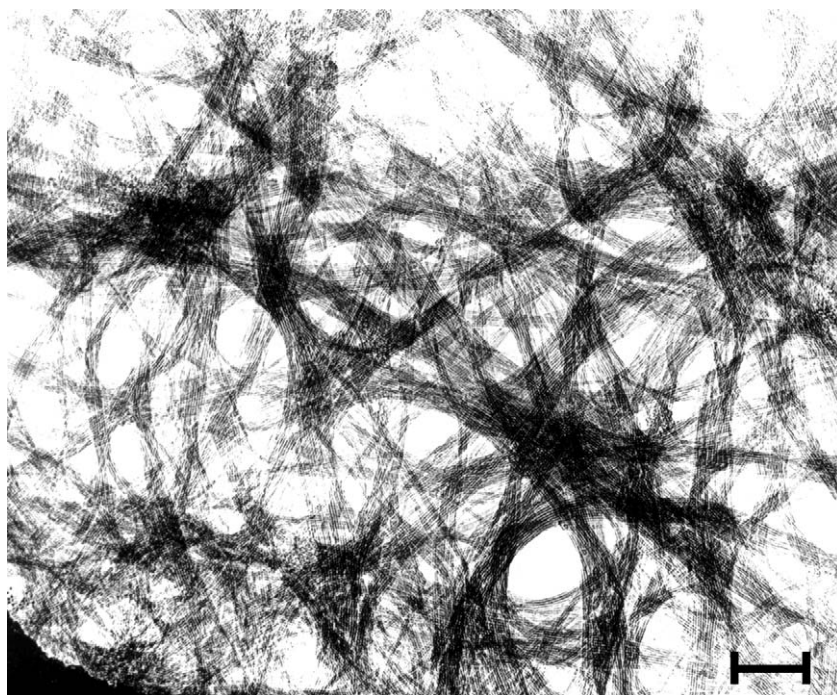


Fig. 2.15. High-resolution transmission electron micrograph of imogolite separated from a gel film of the Kitakami pumice bed ( $200\,000\times$  magnification; bar = 50 nm). Courtesy: N. Yoshinaga, Ehime University, Japan.

Here, each hollow tubule is depicted as having an outer diameter of 2.14 nm, inner diameter of 0.64 nm, and ten unit cells. The atom positions of two unit cells are shown in detail in [Brown et al. \(1978\)](#). The ideal unit formula of imogolite may thus be written as  $\text{SiO}_2 \cdot \text{Al}_2\text{O}_3 \cdot 2\text{H}_2\text{O}$ . The commonly used notation for imogolite, however, is  $(\text{OH})_3\text{Al}_2\text{O}_3\text{SiOH}$  giving the sequence of ions from the periphery to the centre of the tubule, and indicating that the orthosilicate group shares three oxygens with aluminium. [Fig. 2.16](#) also gives the structure of gibbsite, drawn to the same scale, to illustrate the similarity between imogolite and gibbsite in terms of atomic arrangement and unit-cell dimensions.

Unlike imogolite, allophane has a variable composition. Although, the Al/Si ratio of some specimens may be as high as four, the vast majority of allophanes have Al/Si ratios between 1 and 2 ([Wada, 1989](#); [Parfitt, 1990](#)). Irrespective of chemical composition and origin, however, the unit particle of allophane is a hollow spherule with an outer diameter of 3.5–5.5 nm, and a wall thickness of 0.7–1.0 nm ([Fig. 2.17](#)). Because of its similarity in composition to that of imogolite, the Al-rich end-member of allophane (Al/Si~2) has been referred to as either ‘proto-imogilite allophane’ ([Farmer et al., 1979](#)) or ‘imogolite-like allophane’ ([Parfitt and Wilson, 1985](#)). IR

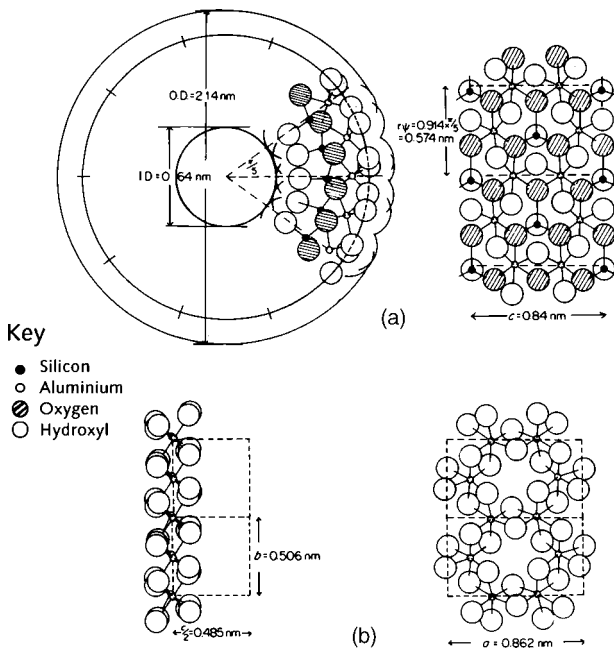


Fig. 2.16. Diagram comparing the structure and unit cell dimensions of imogolite with those of gibbsite. (a) the structure of imogolite viewed down the tubule axis showing the atomic arrangement for two of the 10 unit cells (left); the same projected on a cylinder surface through the centres of the outer hydroxyl groups (right); (b) the structure of a gibbsite sheet showing linked alumina octahedra (left), and projected on the  $ab$  plane (right). Note that the repeat distance along the tubule axis of imogolite ( $c = 0.84$  nm) is close to the  $a$  dimension of gibbsite ( $= 0.862$  nm); OD = outer diameter; ID = inner diameter. From Brown et al. (1978).

(Fig. 2.18) and NMR spectroscopic measurements (Table 2.1) further indicate that this type of allophane is composed of fragments having the imogolite structure over a short range (Parfitt and Henmi, 1980).

By analogy with imogolite (Fig. 2.16), the spherule wall of imogolite-like allophane is apparently composed of an outer gibbsitic sheet to which  $(\text{O}_3\text{SiOH})$  groups are attached on the inside. Unlike the situation in imogolite, however, the layer structure contains vacancies, particularly in the octahedral sheet. Clusters of such 'defects' give rise to discontinuities or perforations of  $\sim 0.3$  nm in diameter along the spherule wall, allowing small extraneous molecules, notably water, to enter in the spherule void space (Fig. 2.17). Depending on the ambient solution pH, the  $(\text{OH})\text{Al}(\text{OH}_2)$  groups, exposed at wall perforations, can either acquire or lose protons. Besides being at the source of the pH-dependent charge characteristics, these groups control the reactivity of allophane toward extraneous ionic species, such as phosphate, humic acid, and amino acids. The anion adsorption data further indicate that the wall of individual

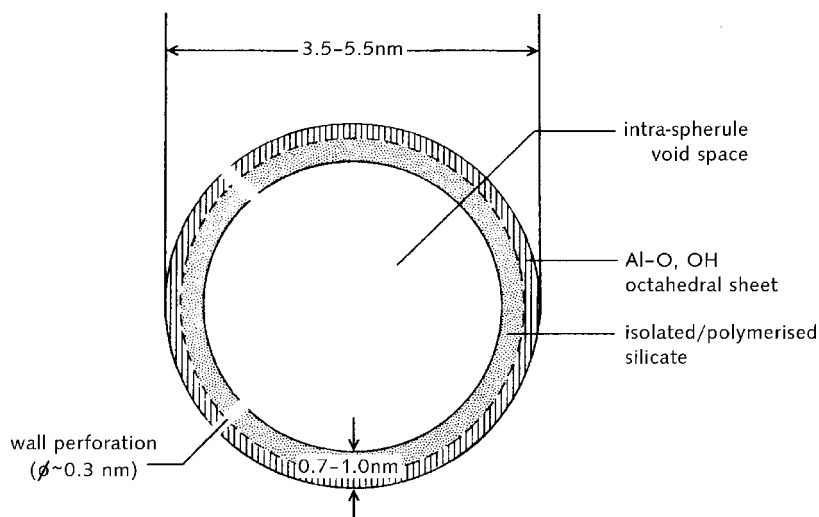


Fig. 2.17. Diagram of a soil allophane unit particle or hollow spherule showing the probable structure of the spherule wall, the intra-spherule void space, and wall perforations. Modified from Wada and Wada (1977).

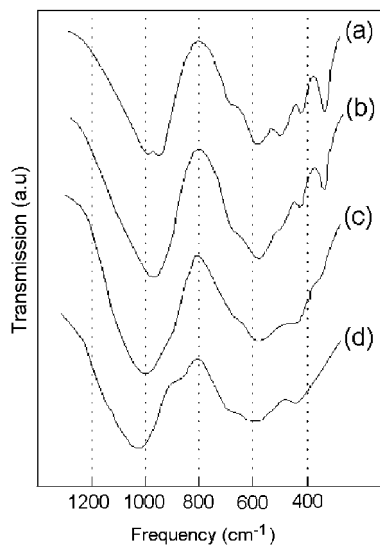


Fig. 2.18. Infrared spectra of imogolite and some allophanes: (a) imogolite from soil; (b) imogolite-like allophane ( $\text{Al/Si} = 2$ ) from soil; (c) halloysite-like allophane ( $\text{Al/Si} = 1.1$ ) from soil; (d) Silica Springs allophane ( $\text{Al/Si} = 1.5$ ). Adapted from Parfitt (1990).



allophane spherules may contain as many as eight perforations (Theng et al., 1982; Hashizume and Theng, 1999; Yuan et al., 2000; Hashizume et al., 2002).

The Si-rich end-member of allophane with an Al/Si ratio of  $\sim 1$  has been referred to as either ‘defect-kaolin allophane’ or ‘halloysite-like allophane’ (Yoshinaga, 1986). Although some orthosilicate may still be present, the  $^{29}\text{Si}$  NMR spectroscopy (Goodman et al., 1985; Shimizu et al., 1988) indicates that in this type of allophane the silicate group is polymerized with some  $\text{Al}^{3+}$  substituting for  $\text{Si}^{4+}$  in tetrahedral sites (Table 2.1). The IR spectrum shows an intense Si–O stretching band near  $1020\text{ cm}^{-1}$  while the peak at  $348\text{ cm}^{-1}$ , characteristic of proto-imogolite, imogolite, and imogolite-like allophane, is hardly detectable (Fig. 2.18).

The question arises whether the octahedral Al sheet still provides the structural framework in halloysite-like allophane as Parfitt (1990) proposed. A variant, suggested by MacKenzie et al. (1991), has the (isolated) orthosilicate groups penetrating the inner silica tetrahedral sheet through defect structures (‘holes’) in this sheet. Nevertheless, the possibility that the Si- or Si(Al)- tetrahedral sheet serves as the framework structure cannot be ruled out (van der Gaast et al., 1985). In any case, samples with Al/Si ratios between 1 and 2 are likely to be mixtures of halloysite- and imogolite-like allophanes. These mixtures may be of unit particles or of structures within particles (Parfitt, 1990).

On the other hand, there is little doubt that a curved halloysite-like layer structure constitutes the framework of ‘stream-deposit allophane’ from Silica Springs, New

Table 2.1. Types and structural features of allophane and imogolite (modified from Parfitt, 1990)

Features	Imogolite	Imogolite-like allophane (soil) <sup>a</sup>	Halloysite-like allophane (soil) <sup>b</sup>	Silica Springs allophane <sup>c</sup>
Al/Si ratio	2	$\sim 2$	$\sim 1$	1.1–1.9
Infrared bands ( $\text{cm}^{-1}$ )	1000, 950, 700, 570, 500, 428, 348	975, 690, 570, 500, 428, 348	1020, 680, 580, 450	1020, 880, 670, 610, 450
$^{29}\text{Si}$ NMR chemical shift (ppm) <sup>d</sup>	–78 (isolated orthosilicate)	–78 (isolated orthosilicate)	–90 (polymerized silicate) –78 (isolated orthosilicate)	–86 (sheet silicate)
$^{27}\text{Al}$ NMR chemical shift (ppm) <sup>e</sup>	5 ( $\text{Al}^{\text{VI}}$ )	5 ( $\text{Al}^{\text{VI}}$ )	5 ( $\text{Al}^{\text{VI}}$ ) 60 ( $\text{Al}^{\text{IV}}$ )	3 ( $\text{Al}^{\text{VI}}$ ) 51 ( $\text{Al}^{\text{IV}}$ )

<sup>a</sup>Also known as ‘Al-rich allophane’ or ‘proto-imogolite allophane’.

<sup>b</sup>Also known as ‘Si-rich allophane’ or ‘defect-kaolin allophane’.

<sup>c</sup>Also known as ‘stream-deposit allophane’ or ‘hydrous feldspathoid allophane’.

<sup>d</sup>Relative to tetramethylsilane.

<sup>e</sup>Relative to  $\text{Al}(\text{H}_2\text{O})_6^{3+}$ .

Zealand (Wells et al., 1977). The XRD pattern of a Silica Springs allophane sample is shown in Fig. 2.13 and its IR spectrum in Fig. 2.18. The Al/Si ratio of Silica Springs allophanes varies between 1.1 and 1.9. As this ratio increases, the  $^{[IV]}Al/^{[VI]}Al$  ratio decreases but the  $^{[IV]}Al/^{[IV]}Si$  ratio remains invariant at 1/3. These observations led Childs et al. (1990) to suggest that a more or less complete tetrahedral sheet (containing one  $Al^{3+}$  for every three  $Si^{4+}$ ) forms the outer, convex surface of the spherule wall while the inner  $^{[VI]}Al^{3+}$  octahedral sheet is incomplete and fragmented (Fig. 2.19). These non-soil allophanes have also been referred to as hydrous feldspathoids (Farmer et al., 1979; Farmer and Russell, 1990).

X-ray photoelectron spectroscopy (XPS) of Silica Springs allophane (Childs et al., 1997) indicates that the binding energies of Al, Si, and O electrons are similar to those for kaolinite, in agreement with the findings by He et al. (1995). The values are also closely similar to those measured for some framework silicates (feldspars) having 4-coordinate  $Al^{3+}$ . Atomic Al/Si, C/Si, and N/Si ratios by XPS further indicate that the surfaces of Silica Springs allophanes are enriched in Al, C, and N (Childs et al., 1997). The surface enrichment by Al may be explained in terms of the presence of Al-octahedral fragments (Fig. 2.18) at the surface of the allophane aggregates. Similarly, the surface enrichment by C and N may be ascribed to surface-adsorbed organic structures. Application of  $^{27}Al$  NMR spectroscopy with high magnetic field strength, and fast MAS, has further revealed the presence of 5-coordinate  $Al^{3+}$  in Silica Springs allophanes (Childs et al., 1999). This Al species may be associated with the edges of octahedral sheet fragments. The presence of  $^{[IV]}Al^{3+}$  in Si-rich soil allophanes is yet to be established.

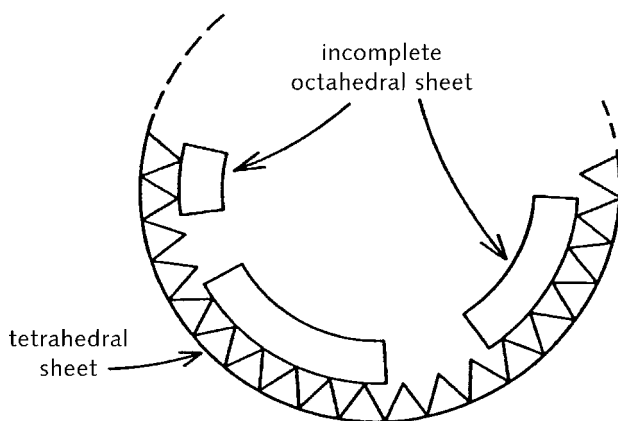


Fig. 2.19. Proposed structural model for the unit particle of Silica Springs allophane showing part of a hollow spherule with an outer diameter of 2–3 nm. Here the outer Si(Al)-tetrahedral sheet serves as the framework and the inner Al-octahedral sheet is incomplete (fragmented). From Childs et al. (1990).

## 2.9. Palygorskite and Sepiolite

Palygorskite and sepiolite are phyllosilicates inasmuch as they contain a continuous two-dimensional tetrahedral sheet; however, they differ from other layer silicates in that they lack continuous octahedral sheets. Their structure can be considered to contain ribbons of a 2:1 phyllosilicate structure, each ribbon being linked to the next inversion of  $\text{SiO}_4$  tetrahedra along a set of Si–O bonds. Thus, tetrahedral apices point in opposite directions in adjacent ribbons. These ribbons extend parallel to the *X*-axis and have an average width along *Y* of three linked pyroxene-like single chains in sepiolite and two linked chains in palygorskite (Fig. 2.20); in this framework, rectangular channels run parallel to the *X*-axis between opposing 2:1 ribbons. As the octahedral sheet is discontinuous at each inversion of the tetrahedra, oxygen atoms in the octahedra at the edge of the ribbons are coordinated to cations on the ribbon side only, while coordination and charge balance are completed along the channels by protons, coordinated water and a small number of exchangeable cations. Furthermore, the channels contain a variable amount of zeolitic water (Galán, 1996).

Chain phyllosilicates have a fibrous habit (Fig. 2.21) with channels running parallel to the fibre length. Fibre sizes vary widely but generally range from about 10 to about 30 nm in width, and from about 5 to about 10 nm in thickness (Jones and Galán, 1988; Galán, 1996).

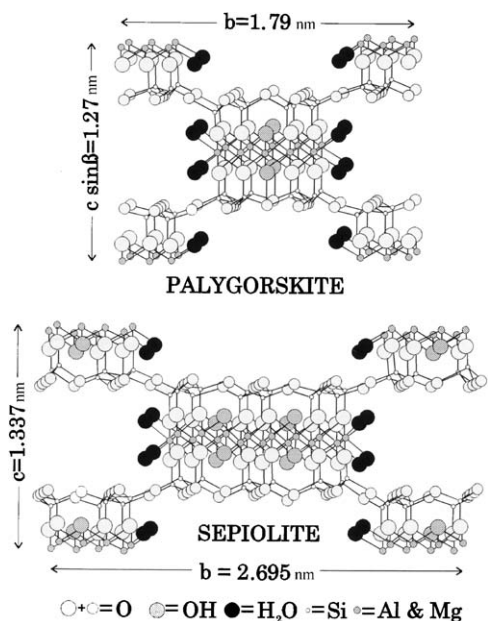


Fig. 2.20. Schematic structure of palygorskite (after Bradley (1940)) and sepiolite (after (Brauner and Preisinger, 1956; Jones and Galán, 1988)).

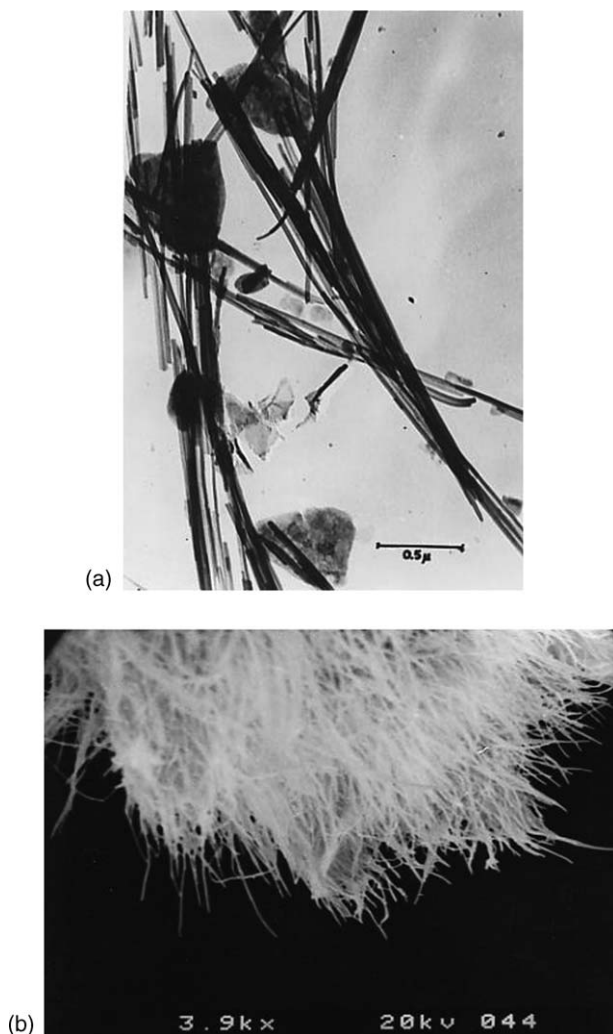


Fig. 2.21. (a) transmission electron micrograph of palygorskite (Torrejón, Spain); (b), scanning electron micrograph of sepiolite (Vallecas, Spain).

Early attempts at determining the sepiolite structure were carried out by Migeon (1936), Longchambon and Migeon (1936), Longchambon (1937), and Caillère (1951). The first structural pattern for sepiolite was proposed by Nagy and Bradley (1955) who suggested the  $C2/m$  ( $A2/m$ ) space group as being the most appropriate (Table 2.2). However, their interpretation from X-ray fibre photographs (using  $0kl$  reflections) was not very conclusive.

Table 2.2. Some crystallographic data for sepiolite and palygorskite (Jones and Galán, 1988)

	<i>a</i> (nm)	<i>b</i> (nm)	<i>c</i> or <i>c</i> sin $\beta$ (nm)	$\beta$ (°)	Space group
<i>Sepiolite</i>					
Nagy and Bradley (1955)	0.530	2.70	1.34	?	<i>A2/m</i>
Brauner and Preisinger (1956)	0.528	2.680	1.340	90°	<i>Pnan</i>
Brindley (1959)	0.525	2.696	1.350	90°	—
Zvyagin et al. (1963)	0.524	2.72	1.34	90°	<i>Pnan</i>
Bailey (1980) (average)	0.528	2.695	1.337	90°	<i>Pnan</i>
Galán (unpublished, Vallecas sepiolite)	0.523	2.677	1.343	90°	<i>Pnan</i>
<i>Palygorskite</i>					
Bradley (1940)	0.52	1.80	1.29	?	<i>A2/m</i>
Zvyagin et al. (1963)	0.522	1.806	1.275	95.83°	<i>P2/a</i>
Christ et al. (1969) (Sapillo)	0.524	1.787	1.272	90°	<i>Pn</i>
Christ et al. (1969)	0.524	1.783	1.278	95.78°	<i>P2/a</i>
Drits and Sokolova (1971)	0.515	1.785	1.314	107°	<i>A2/m</i>
Bailey (1980) (average)	0.520	1.790	1.270	90°, 96°, 107°	

Later, Brauner and Preisinger (1956) and Preisinger (1959) proposed another model for sepiolite with space group *Pnan* (Fig. 2.20, Table 2.3). The fundamental difference between both models lies in whether the tetrahedral inversion at the edge of the ribbons occurs along the middle of the zig-zag Si–O–Si chains (Nagy and Bradley, 1955) or along their edges (Brauner and Preisinger, 1956). In the Brauner and Preisinger (1956) model, adjacent inverted ribbons are joined by a single basal oxygen (instead of two as in the Nagy–Bradley model), and there are eight octahedral sites in a ribbon (instead of nine), four OH (instead of six), and eight zeolitic water molecules (instead of six).

ED patterns from single fibres by Brindley (1959), Zvyagin (1967), and Gard and Follet (1968) have confirmed that the extinctions are in agreement with the space group *Pnan*. The Brauner–Preisinger model for sepiolite has also been confirmed and refined by Rautureau et al. (1972), Rautureau and Tchoubar (1974), Rautureau (1974), and Yucel et al. (1981).

The unit-cell parameters determined for sepiolite are:  $a = 0.528$  nm,  $b = 2.695$  nm,  $c = 1.33$  nm,  $\beta = 90^\circ$  (Table 2.2). Channels in the structure are  $0.37$  nm  $\times$   $1.06$  nm in dimension.

Regarding the palygorskite structure, Bradley (1940) proposed a model with a probable *A2/m* space group (Table 2.2). The main difference from the sepiolite model is the shorter  $b$  dimension because only two linked pyroxene-like single chains are in the ribbon. Later, Drits and Sokolova (1971) confirmed the Bradley model and measured a  $\beta$ -angle of  $107^\circ$ . It would therefore appear that for both sepiolite and palygorskite, the linkage by two oxygens can be excluded.

Table 2.3. Octahedral and tetrahedral occupancy ranges for bulk and EDX analyses of sepiolite and palygorskite (in bracket mean value) (Galán and Carretero, 1999).

		Bulk analyses	EDX analyses by (Paquet et al., 1987)	Other EDX analyses from literature	EDX analyses by (Galán and Carretero, 1999)
<i>Sepiolite</i>	<sup>VI</sup> R	6.95–8.11 (7.72)	6.93–8.5	7.61–7.87 (7.74)	7.93–7.98 (7.95)
	<sup>VI</sup> Mg	4.96–8.1 (7.36)	5.6–8.5	6.05–7.73 (7.11)	7.93–7.98 (7.95)
	<sup>VI</sup> (R <sup>2</sup> + R <sup>3</sup> )	0–2.28 (0.32)	0–1.8	0–1.8 (0.62)	0
	<sup>IV</sup> (Al + Fe <sup>3+</sup> )	0–0.72 (0.19)	—	0–0.2 (0.10)	0
<i>Palygorskite</i>	<sup>VI</sup> R	3.45–4.33 (3.96)	2.63–4.63	3.36–4.17 (3.88)	3.95–4.09 (4.00)
	<sup>VI</sup> Mg	1.12–2.82 (2.00)	0.83–3.08	1.32–2.60 (1.97)	1.71–2.10 (1.96)
	<sup>VI</sup> (R <sup>2</sup> + R <sup>3</sup> )	1.12–2.50 (1.96)	1.5–2.66	1.46–2.41 (1.91)	1.87–2.24 (2.04)
	<sup>IV</sup> (Al + Fe <sup>3+</sup> )	0–0.67 (0.29)	—	0.07–0.49 (0.30)	0–0.29 (0.14)

<sup>VI</sup>R = all octahedral cations.

<sup>VI</sup>(R<sup>2</sup> + R<sup>3</sup>) = octahedral cations other than Mg. They are mainly Al and Fe<sup>3+</sup>.

Preisinger (1963) reported an orthorhombic model for palygorskite similar to the orthorhombic sepiolite of Brauner and Preisinger (1956) except for the ribbon width. Christ et al. (1969) studied five palygorskite samples by XRD and found three orthorhombic (Pn) and two different monoclinic cells. Although there are not sufficient data to define exactly the difference between them, it is clear that at least two symmetries are possible for palygorskite, one orthorhombic and another monoclinic. Monoclinic structures have an *n*-glide plane parallel to (1 0 0) (Table 2.2). One of the monoclinic symmetries is similar to the one proposed by Zvyagin et al. (1963) (*P*2/*a*,  $\beta = 95.83^\circ$ ). The other, with the *Z*-axis as the monoclinic axis and  $\gamma = 92.23^\circ$  for the monoclinic angle, has no structural interpretation up to the present time.

More recently, Chisholm (1992) analysed the structural models given by Christ et al. (1969) and other authors, and found two palygorskite structures, one orthorhombic (Pbmn $\equiv$ Pnmb) and another monoclinic (C2/*m* $\equiv$ A/2*m*). Most palygorskite samples appear to contain both forms. There are samples of pure or nearly pure monoclinic palygorskite but there is no pure orthorhombic palygorskite. The co-existence of both structures lies behind the confusion that arises from indexing XRD patterns in terms of a single phase, and using different unit cells and space groups for palygorskite. The two structures determined by Chisholm (1992) agree with those

proposed by [Drits and Sokolova \(1971\)](#) for the monoclinic form ( $\beta$  about  $105.2^\circ$ , is not far from [Drits and Sokolova's](#) value of  $107^\circ$ ), and that by [Preisinger \(1963\)](#) for the orthorhombic form.

Each form has some reflections (with  $l \neq 0$ ) that are not shown by the other; these can be used for discrimination ([Figs. 2.22 and 2.23](#)). For example, the lines at 0.425 nm (121), 0.309 nm (123), and 0.2536 nm (161) indicate the presence of orthorhombic palygorskite, while those at 0.436 nm (120) and 0.251 nm (162, overlapping with 200) are indicative of monoclinic palygorskite. Two lines near 0.320 nm also indicate the presence of the monoclinic form, while a single line at 0.319 nm is expected for the orthorhombic forms. The  $d$ -values for monoclinic palygorskite depend on  $\beta$ , even in the narrow range of  $106$ – $108^\circ$  ([Figs. 2.22 and 2.23](#)).

One palygorskite structure must be considered as orthorhombic: Pnmb ([Preisinger, 1963](#)) and another as monoclinic:  $A2/m$  ([Bradley, 1940](#); [Drits and Sokolova, 1971](#)). Monoclinic cells proposed by [Zvyagin et al. \(1963\)](#) and [Christ et al. \(1969\)](#) with smaller values of  $\beta$  may represent alternative choices of axes in the monoclinic system, as noted by [Bailey \(1980\)](#) who also gave the following unit-cell parameters:  $a = 0.52$  nm,  $b = 1.79$  nm,  $c \sin \beta = 1.27$  nm,  $\beta = 90, 96$  or  $107^\circ$ . Channels in the structure are  $0.37 \times 0.64$  nm in dimension and run parallel to the fibre length. Powder XRD patterns of palygorskite and sepiolite are shown in [Figs. 2.24 and 2.25](#).

[Zoltai \(1981\)](#) has described the palygorskite and sepiolite structures as biopyriboles (bio = biotite, pyr = pyroxenes, iboles = amphiboles) built of tri-di-octahedral modules, the tri-module being  $M_3A_2Si_4O_{10}$ , and di-module  $M_2A_2Si_4O_{10}$ . M is the octahedral cation and A is the anion not bonded to Si within to module; it can be oxygen when bonded to Si and is (OH) when bonded to more than one M cations. One half of each A anion is  $H_2O$  molecule when the anion bonded to only one M cation. The width of these modules is one tetrahedral chain, and their height ( $t$ ) is four times the height of an ideal polyhedral layer. Combinations of these modules can give rise to complete crystal structures with a vertical displacement between the modules equal to  $n \times t$  (with  $n = 0, 1/2, 3/4$ ). If  $n = 0$ , the major layer silicates are produced. A sequence of  $n = 0$  and  $3/4$  between modules produces palygorskite, and the sequence 0, 0, and  $3/4$  gives the sepiolite structure ([Fig. 2.26](#)). Symbol 0 is relative to the orientation of tetrahedral chains, indicating that the faces of adjacent tetrahedra point in opposite directions ('0' chains).

Although the crystallographic description by [Zoltai \(1981\)](#) is attractive, palygorskite and sepiolite should be considered as phyllosilicates (see above) with special features rather than as biopyriboles. This is because the physicochemical properties and genetic environments of palygorskite and sepiolite are akin to those of clay minerals. In common with many other phyllosilicates, a detailed single-crystal structure of sepiolite and palygorskite is still wanting. IR studies combined with powdered diffraction EM and TA have provided insight into the nature of the water in sepiolite and palygorskite, and the structural changes that occur after heating/dehydration ([Hayashi et al., 1969](#); [Serna et al., 1975, 1977](#); [Mifsud et al., 1978](#); [Van Scoyoc et al., 1979](#); [Blanco et al., 1988](#)).

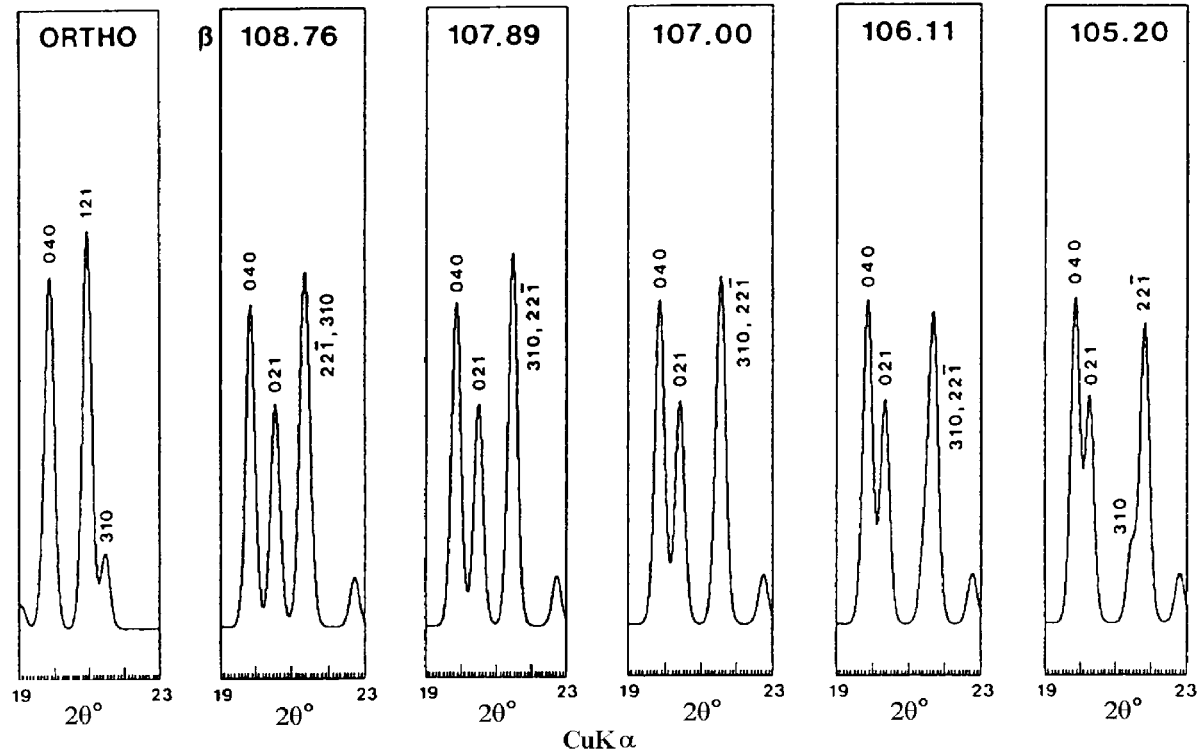


Fig. 2.22. XRD powder patterns in the  $19$ – $23^\circ$  range of  $2\theta$  (Cu K $\alpha$  radiation), showing the  $0.40$ – $0.45$  nm diagnostic region calculated for idealized orthorhombic and monoclinic palygorskites. The  $121$  reflection is characteristic of the orthorhombic form, while the  $021$  and strong  $22\bar{1}$  reflections are characteristic of the monoclinic form. After [Chisholm \(1992\)](#).



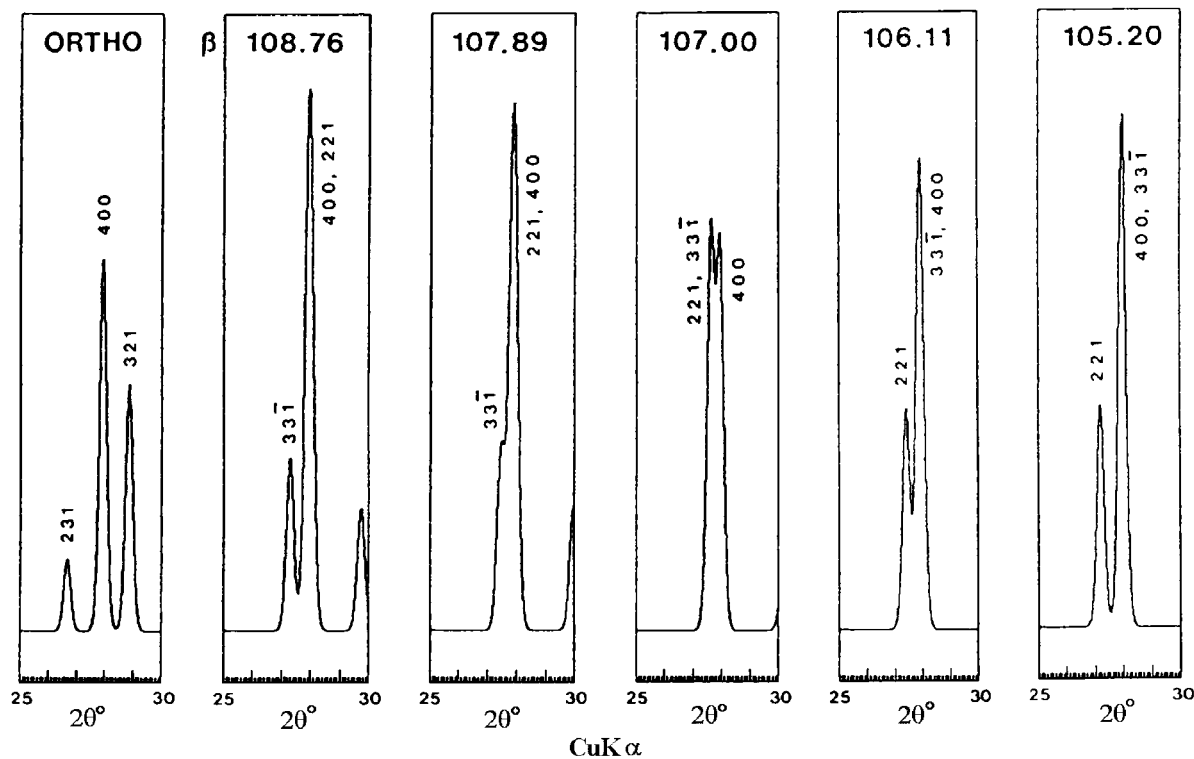


Fig. 2.23. XRD powder patterns in the 25–30° range of  $2\theta$  (Cu  $K\alpha$  radiation), showing the 0.305–0.33 nm diagnostic region calculated for idealized orthorhombic and monoclinic palygorskites. The 321 line is characteristic of the orthorhombic form. The appearance of two lines close together near 400 indicate the presence of the monoclinic form; the exact position of these lines is sensitive to the value of  $\beta$  in the range 106–108°. After Chisholm (1992).

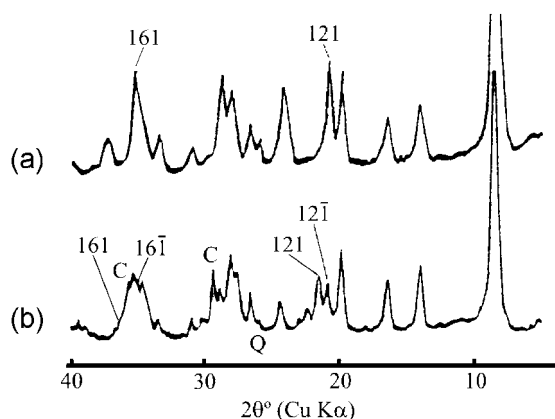


Fig. 2.24. XRD pattern of the orthorhombic form (a) and monoclinic form (b) of palygorskite (C = calcite, Q = quartz). After Christ et al. (1969). Indices for the monoclinic form are taken from Chisholm (1992).

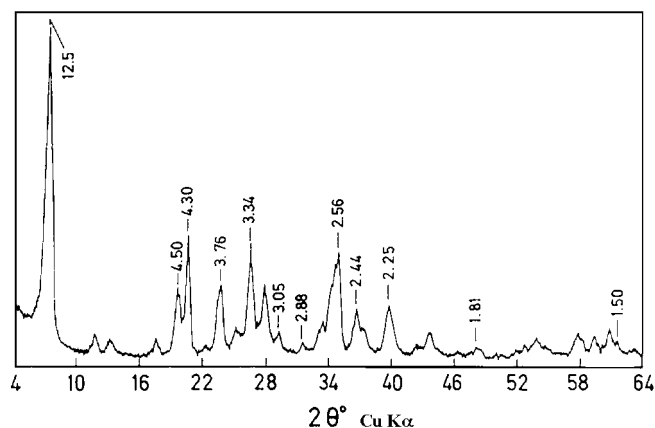


Fig. 2.25. XRD diagram of sepiolite from Vallecas. The numbers at the top of each peak refer to Ångstrom units ( $1 \text{ \AA} = 0.1 \text{ nm}$ ). After Pérez-Rodríguez and Galán (1994).

A more recent study by McKeown et al. (2002), using polarized Raman and FTIR spectroscopy, indicates that the Si–O stretching and O–Si–O bending force constants for palygorskite are similar to the corresponding values previously calculated for other phyllosilicates. However, the values for Mg–O stretching are about half of those obtained for the Al–O and Mg–O stretching force constants in other phyllosilicates (i.e., the octahedral sheets in micas). This finding suggests that the respective interatomic bonds within the octahedral ribbons of palygorskite and sepiolite are weaker than those in a continuous octahedral sheet.

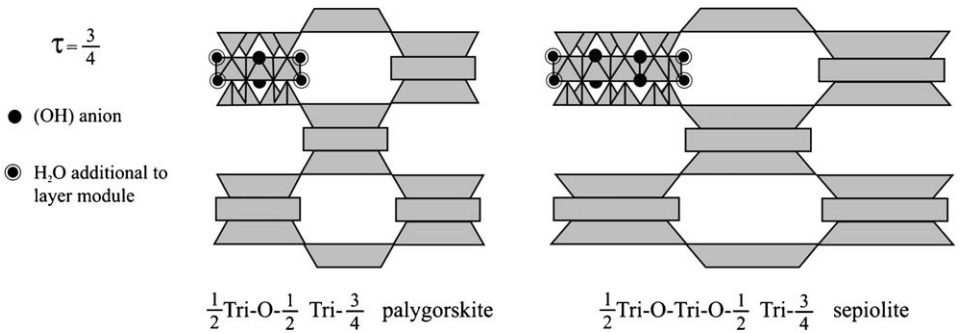


Fig. 2.26. Palygorskite and sepiolite structures. After Zoltai (1981). ( $\tau$  = displacement between a pair of 1/2 Tri modules; 1/2 indicates that only half of the extra trioctahedral sites are occupied, that is, those sites between the two linked modules.)

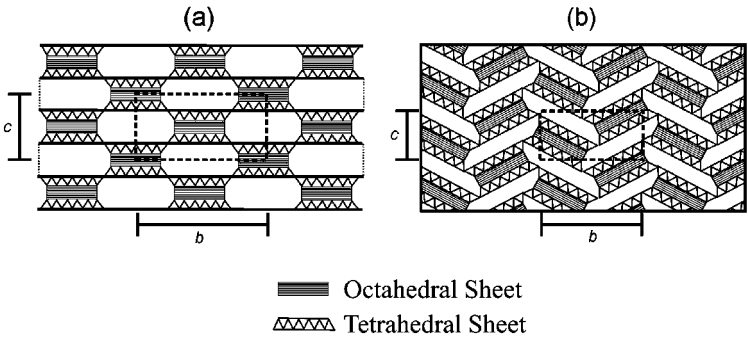


Fig. 2.27. General scheme for an unfolded (a) and folded (b) fibrous clay mineral. After Jones and Galán, 1988).

Four water molecules (zeolitic water) are present in the channels, and four others are bound to the octahedral edge inside the channels. Accordingly, the DTA curves can be divided into three parts: (i) the low-temperature region ( $< 300^\circ\text{C}$ ) where the minerals lose water adsorbed on outer surfaces and zeolitic water (peak at  $120\text{--}150^\circ\text{C}$ ); (ii) the central region ( $300\text{--}600^\circ\text{C}$ ), where two endothermic peaks occur at about  $350^\circ\text{C}$  and  $500\text{--}550^\circ\text{C}$  for sepiolite, but only one (about  $450\text{--}500^\circ\text{C}$ ) for palygorskite; and (iii) the high-temperature region ( $> 600^\circ\text{C}$ ) where an endothermic effect (at about  $800^\circ\text{C}$ ) is immediately followed by an exothermic maximum.

In sepiolite, the first endotherm in the central region is narrower and more intense than the second one (Fig. 2.27). The first endothermic peak is ascribed to the loss of the first two water molecules coordinated to the inner octahedral edge, causing rotation of alternate ribbons and particle folding (Nagata et al., 1974; Serna et al., 1975; Van Scoyoc et al., 1979). The second central endotherm in sepiolite is due to the loss of the other two edge-coordinated water molecules that are ‘trapped’ inside

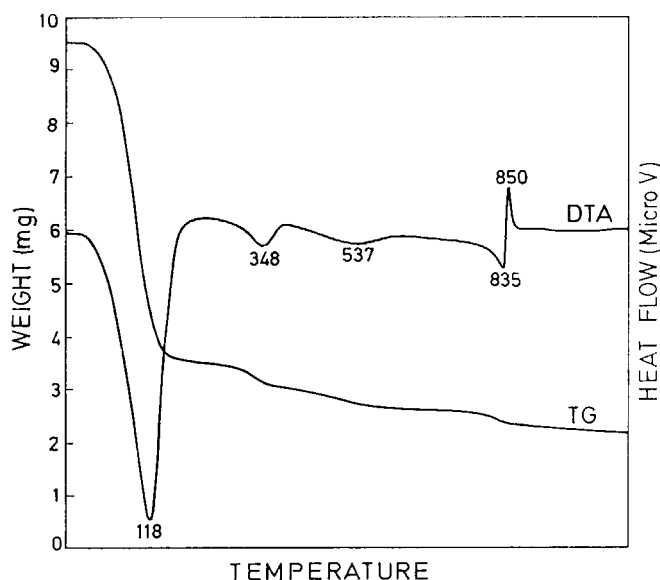


Fig. 2.28. DTA and TG curves of sepiolite from Vallecas. (temperature in  $^{\circ}\text{C}$ , weight sample = 42 mg, heating rate =  $12^{\circ}\text{min}^{-1}$ , ambient conditions). After Pérez-Rodríguez and Galán (1994).

the collapsed channels (Pérez-Rodríguez and Galán, 1994). In palygorskite, coordination water is gradually lost through the whole interval, starting when zeolitic water is lost and ending when dehydroxylation begins (Mifsud et al., 1978). The high-temperature endotherm represents dehydroxylation of the structure, and the exothermic peak that follows is due to the formation of clinoenstatite. Typical DTA–TG curves for sepiolite are shown in Fig. 2.28.

The structural changes that occur on heating also lead to a decrease in the intensity of the principal XRD peaks. For instance, in sepiolite (Fig. 2.29) the reflections at 1.2, 0.45, 0.38, and 0.34 nm decrease when the mineral is heated at  $250^{\circ}\text{C}$  for 1 h, while new reflections appear at 1.04 and 0.82 nm. Further heating to  $450^{\circ}\text{C}$  increases the intensity of these new reflections, which persist up to  $700^{\circ}\text{C}$  (Hayashi et al., 1969; Fernández Álvarez, 1970; Nagata et al., 1974). In palygorskite, the intensity of the reflections at 1.05, 0.45, and 0.323 nm decreases on heating, and new peaks appear at 0.92 and 0.47 nm. On heating to  $325^{\circ}\text{C}$ , these changes become more marked. Heating to  $600^{\circ}\text{C}$  completely eliminates the 1.05 nm reflection. At the same time, the 0.92 nm peak becomes less intense (Hayashi et al., 1969) and shifts to 0.87 nm. At  $700^{\circ}\text{C}$ , palygorskite is practically X-ray amorphous.

The decrease in intensity of the principal reflection occurs because structural disorder produced by heating is more prominent along the principal cleavage face (011) and less along the (040) plane (Lokanatha and Bhattacharjee, 1984). In the  $200\text{--}300^{\circ}\text{C}$  range, the particle size of palygorskite slightly increases as water

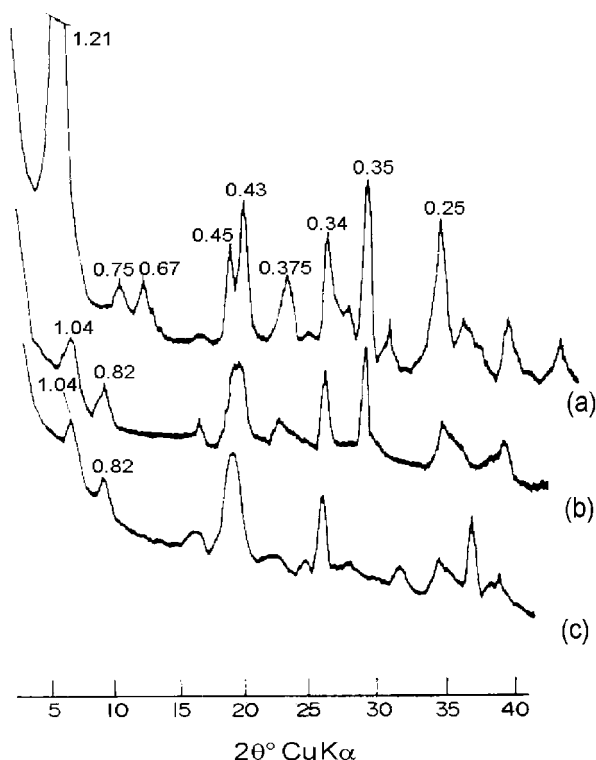


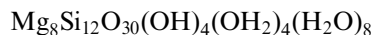
Fig. 2.29. XRD diffraction pattern of sepiolite recorded under vacuum at 25 °C, 4 h (a); 200 °C, 4 h (b); 530 °C, 6 h (c). After Serna et al. (1975).

molecules are expelled from the channels, but decreases markedly at 600 °C when the anhydrous stage is reached. As particle size decreases, the parameter  $a$  along the fibre axis increases until the structure collapses. Both palygorskite and sepiolite can rehydrate following particle folding. However, rehydration is difficult once the anhydrous state is reached when new interparticle bonds are formed.

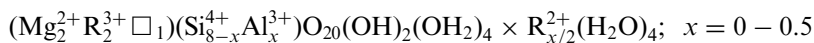
From an historical point of view, the chemical analysis of sepiolite (in the form of a 'meerscham' pipe from Turkey) was first attempted in the second half of the 18th century by Johann Christian Wiegler. In 1794, Martin Heinrich Klaproth made a chemical analysis of a sepiolite from Eskişehir, Turkey. Since then most papers on sepiolite and palygorskite have information about their respective chemical compositions.

However, published analytical data mostly refer to bulk samples. As such, they are affected by both crystallochemical variations and admixed contaminants (other clay minerals and associated minerals). The most frequent admixtures in sepiolite and palygorskite are smectite, illite, chlorite, quartz, feldspars, carbonates, zeolites, iron, and silica gels.

Galán and Carretero (1999) have reviewed the literature on chemical analyses, including bulk chemical analyses, and EDX analyses of selected individual particles and pure samples. Their assessment indicates that sepiolite is a true trioctahedral mineral with eight octahedral positions filled by  $\text{Mg}^{2+}$  (Table 2.3) and negligible structural substitutions. A very pure (near end-member) specimen has close to the theoretical formula of



Palygorskite is intermediate between di- and tri-octahedral. The octahedral sheet contains mainly  $\text{Mg}^{2+}$ ,  $\text{Al}^{3+}$ , and  $\text{Fe}^{3+}$ , with an  $\text{R}^{2+}/\text{R}^{3+}$  ratio close to 1, and has four of the five structural positions occupied (Table 2.3). The theoretical formula is



The proposed formula is very close to that given by Smith and Norem (1986) for very pure palygorskite samples obtained by electron-microprobe analysis.

Figs. 2.30 and 2.31 indicate that the compositions of sepiolite and palygorskite are more limited than previously reported. The two minerals show no compositional gap if bulk analytical data are plotted on the Martin-Vivaldi and Cano (1956) diagram

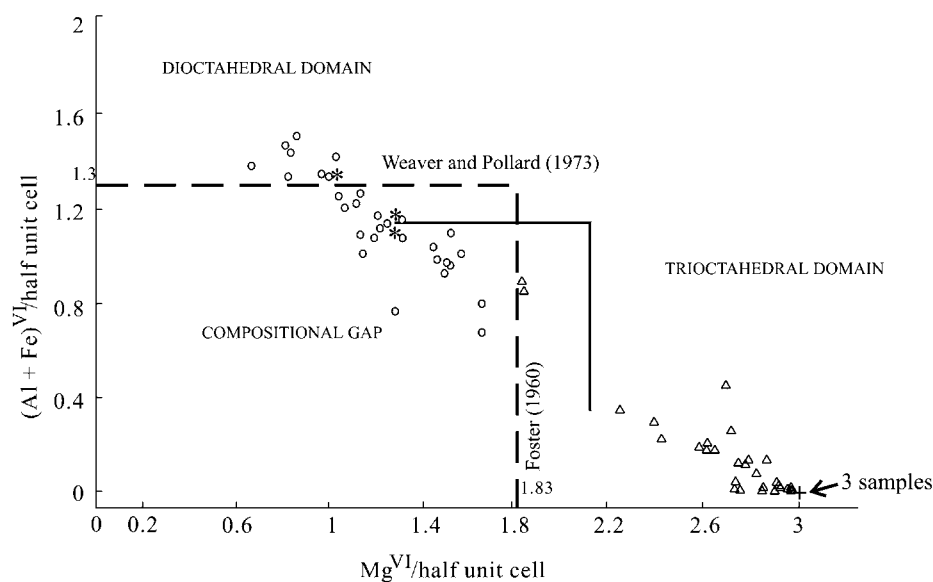


Fig. 2.30. Selected bulk analysis data for sepiolite and palygorskite, plotted as the content of 6-coordinate Mg atoms per half unit cell against the content of 6-coordinate (Al + Fe) atoms per half unit cell. (○): data for palygorskite from the literature; (△): data for sepiolite from the literature. The EDX results for palygorskite (\*) and sepiolite (+) from Galán and Carretero (1999) are also included. Broken line represents the conventional plot; solid line denotes the relationship proposed by Paquet et al. (1987).

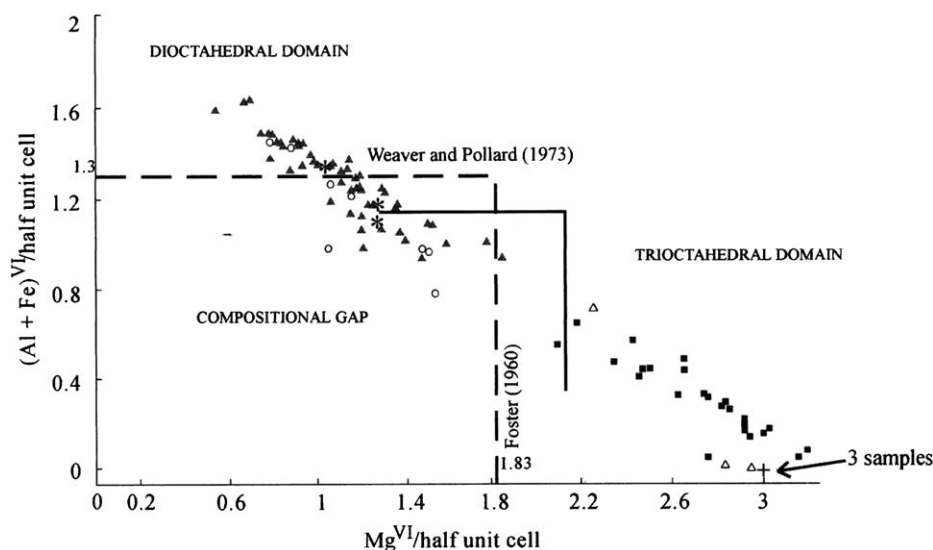


Fig. 2.31. EDX analysis data for sepiolite and palygorskite. ○: data for palygorskite from the literature; △: data for sepiolite from the literature. The results for palygorskite (\*) and sepiolite (+) from Galán and Carretero (1999) are also included. Broken line represents the conventional plot; solid line denotes the relationship proposed by Paquet et al. (1987) from their sepiolite (■) and palygorskite (▲) data.

(Fig. 2.32). On the contrary, a gap can be recognized if the EDX results alone are considered.

On the basis of trace elements content, sepiolite is a more 'restricted' mineral than palygorskite. According to Torres-Ruiz et al. (1994), sepiolite contains three or four times more trace elements than palygorskite. Both minerals are rich in  $F^-$  and  $Li^+$ . Sepiolite can contain up to 1.5%  $F^-$ , and 800 ppm  $Li^+$  (Leguey et al., 1995; Torres-Ruiz et al., 1994). Inherited minerals have higher values of REE and transition-metal elements, and lower values of  $F^-$  and  $Li^+$ , than those formed by chemical precipitation in depositional basins (Torres-Ruiz et al., 1994; López-Galindo et al., 1996).

The CEC of both minerals is quite low, ranging from 4 to 40 cmol/kg; higher values are probably related to impurities (Galán, 1996).

In some sepiolites cations other than  $Mg^{2+}$  may occur in octahedral positions. If  $Ni^{2+} > Mg^{2+}$  the species is known as falcondoite (Springer, 1976). Iron- and aluminium-rich varieties are named  $Fe^{3+}$ -sepiolite and  $Al^{3+}$ -sepiolite, respectively. Loughlinite is  $Na^+$ -sepiolite where two  $Na^+$  substitute for two  $Mg^{2+}$ , and two  $Na^+$  are in the channels (Fahey and Axelrod, 1948; Echle, 1978). Since it is very difficult to conceive of a stable sepiolite structure containing octahedral  $Na^+$ , Jones and Galán (1988) have suggested that the occurrence of loughlinite as a different mineral from sepiolite is still to be conclusively demonstrated. Other varieties of sepiolite are

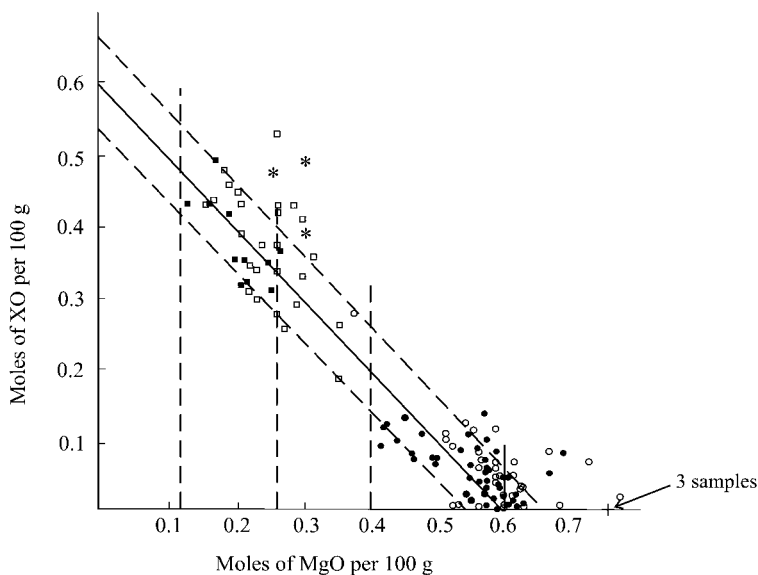


Fig. 2.32. Bulk analysis data for sepiolite and palygorskite, taken from the literature unless specified otherwise, plotted as moles of MgO per 100 g against moles of XO per 100 g where  $XO = Al_2O_3 + Fe_2O_3 + FeO + MnO$ .  $\square$  = palygorskite;  $\circ$  = sepiolite;  $\blacksquare$  = palygorskite from Martín-Vivaldi and Cano (1956);  $\bullet$  = sepiolite from Martín-Vivaldi and Cano (1956). EDX results for palygorskite (\*) and sepiolite (+) are taken from Galán and Carretero (1999).

$Al^{3+}$ -sepiolite (Rogers et al., 1956; Firman, 1966),  $Mn^{2+}$ -sepiolite, and  $Mn^{2+}$ - $Fe^{2+}$ -sepiolite (Semenov, 1969).

Among palygorskite varieties,  $Mn^{2+}$ -palygorskite and  $Mn^{2+}$ -ferropalygorskite are worthy of note (Semenov, 1969). Two new minerals, yofortierite (Perrault et al., 1975) and tuperssuatsiaite (Karup-Møller and Petersen, 1984), have been accepted as belonging to the palygorskite group. The former contains a high percentage of  $Mn^{2+}$  and a definite quantity of  $Zn^{2+}$  substituting for  $Al^{3+}$ . The latter can be considered a  $Na^+$ - $Fe^{3+}$ -palygorskite.

The name attapulgite (for palygorskite), still widely used in industry and for deposits, was given by de Lapparent (1935) to a clay mineral found in fuller's earth from Attapulgis, Georgia, USA, and Mormoiron, France. Although 'attapulgite' is well established in industrial and trade circles because of the commercially available 'attapulgite clays' from the USA, the name 'palygorskite' has priority and should be used in preference (Bailey et al., 1971).

## REFERENCES

Adams, J.M., 1983. Hydrogen atom positions in kaolinite by neutron profile refinement. *Clays and Clay Minerals* 31, 352–356.



- Adams, J.M., Hewat, A.W., 1981. Hydrogen atom positions in dickite. *Clays and Clay Minerals* 29, 316–319.
- Akiba, E., Hayakawa, H., Hayashi, S., Miyawaki, R., Tomura, S., Shibasaki, Y., Izumi, F., Asano, H., Kamiyama, T., 1997. Structure refinement of synthetic deuterated kaolinite by Rietveld analysis using time-of-flight neutron powder diffraction data. *Clays and Clay Minerals* 45, 781–788.
- Alcover, J.F., Gatineau, L., 1980. Structure de l'espace interlamellaire de la vermiculite Mg bicouche. *Clay Minerals* 15, 25–35.
- Altaner, S.P., Ylagan, R.E., 1997. Comparison of structural models of mixed layer illite/smectite and reactions mechanisms of smectite illitization. *Clays and Clay Minerals* 45, 517–533.
- Anderson, C.S., Bailey, S.W., 1981. A new cation-ordering pattern in amesite-2H<sub>2</sub>. *American Mineralogist* 66, 185–195.
- Antonelli, F., Zane, A., Sassi, R., Lazzarini, L., Árkai, P., 2003. Illite Kübler index and chlorite “crystallinity” of marbles as indicators of metamorphic grade. *Geophysical Research Abstracts* 5, 21–42.
- Aparicio, P., Ferrell, E., Galán, E., 1999. A new kaolinite crystallinity index from mathematical modeling of XRD data. Euroclay'99, Kraków, Program with Abstracts, p. 57.
- Aparicio, P., Ferrell, E., Galán, E., 2001. Aplicación de la modelización matemática a los diagramas de DRX de la caolinita para mejorar el cálculo de índices de cristalinidad. In: Pascual Cosp, J., Zapatero Arenzana, J., Ramírez del Valle, A.J., Moya García, M.V. (Eds.), Integración de Ciencia-Tecnología de las arcillas en el Contexto Tecnológico-Social del Nuevo Milenio. Sociedad Española de Arcillas, Málaga, Spain, pp. 21–29.
- Aparicio, P., Galán, E., 1999. Mineralogical interference on kaolinite crystallinity index measurements. *Clays and Clay Minerals* 47, 12–27.
- Aruja, E., 1945. An X-ray study of the crystal structure of antigorite. *Mineralogical Magazine* 27, 65–74.
- Backhaus, K.O., 1983. Structure refinement of a lepidolite-1M. *Crystal Research and Technology* 18, 1253–1260.
- Bailey, S.W., 1963. Polymorphism of the kaolin minerals. *American Mineralogist* 48, 1196–1209.
- Bailey, S.W., 1980. Structure of layer silicates. In: Brindley, G.W., Brown, G. (Eds.), *Crystal Structures of Clay Minerals and Their X-ray Identification*. Mineralogical Society, London, pp. 1–123.
- Bailey, S.W., 1982. Nomenclature for regular interstratification. *American Mineralogist* 67, 394–398.
- Bailey, S.W., 1984a. Classification and structures of the micas. In: Bailey, S.W. (Ed.), *Micas. Reviews in Mineralogy*, vol. 13. Mineralogical Society of America, Washington, DC, pp. 1–12.
- Bailey, S.W., 1984b. Crystal chemistry of the true micas. In: Bailey, S.W. (Ed.), *Micas. Reviews in Mineralogy*, vol. 13. Mineralogical Society of America, Washington, DC, pp. 13–60.
- Bailey, S.W., 1984c. Review of cation ordering in micas. *Clays and Clay Minerals* 32, 81–92.
- Bailey, S.W., 1986. Report of the AIPEA Nomenclature Committee (illite, glauconite and volkonskoite). Supplement to the AIPEA Newsletter 22, 1–3.

- Bailey, S.W., 1988a. Structure and composition of other trioctahedral 1:1 phyllosilicates. In: Bailey, S.W. (Ed.), *Hydrous Phyllosilicates (Exclusive of Micas)*. Reviews in Mineralogy, vol.19. Mineralogical Society of America, Washington, DC, pp. 169–186.
- Bailey, S.W., 1988b. Chlorites: structures and crystal chemistry. In: Bailey, S.W. (Ed.), *Hydrous Phyllosilicates (Exclusive of Micas)*. Reviews in Mineralogy, vol. 19. Mineralogical Society of America, Washington, DC, pp. 347–403.
- Bailey, S.W., Brindley, G.W., Johns, W.D., Martín, R.T., Ross, M., 1971. Clay minerals society report of nomenclature committee 1969–1970. *Clays and Clay Minerals* 19, 132–133.
- Banfield, J.F., Bailey, S.W., 1996. Formation of regularly interstratified serpentine-chlorite minerals by inversion in long-period serpentine polytypes. *American Mineralogist* 81, 79–91.
- Baronnet, A., 1978. Some aspects of polytypism in crystals. In: *Progress in Crystal Growth Characterization*, vol. 1. Pergamon Press, Oxford, pp. 111–151.
- Baronnet, A., 1992. Polytypism and stacking disorder. In: Buseck, P.R. (Ed.), *Minerals and Reactions at the Atomic Scale: Transmission Electron Microscopy*. Reviews in Mineralogy, vol. 27. Mineralogical Society of America, Washington, DC, pp. 231–282.
- Bayliss, P., 1975. Nomenclature of the trioctahedral chlorites. *Canadian Mineralogist* 13, 178–180.
- Bayliss, P., 1989. Unit-cell dimensions of two-dimensional clay minerals. *Powder Diffractions* 4, 19–20.
- Ben Haj Amara, A., Ben Brahim, J., Plançon, A., Ben Rhaïem, H., 1998. The structure of 8.4 Å hydrated and dehydrated nacrite determined by X-ray diffraction. *Journal of Applied Crystallography* 31, 654–662.
- Ben Haj Amara, A., Ben Brahim, J., Plançon, A., Ben Rhaïem, H., Besson, G., 1997. Etude structurale d'une nacrite Tunisienne. *Journal of Applied Crystallography* 30, 338–344.
- Benco, L., Tunega, D., Hafner, J., Lischka, H., 2001a. Orientation of OH groups in kaolinite and dickite: ab initio molecular dynamics study. *American Mineralogist* 86, 1057–1065.
- Benco, L., Tunega, D., Hafner, J., Lischka, H., 2001b. Upper limit of the O–H–O hydrogen bond. Ab initio study of the kaolinite structure. *Journal of Physical Chemistry B* 105, 10812–10817.
- Benco, L., Tunega, D., Hafner, J., Lischka, H., 2001c. Ab initio density functional theory applied to the structure and proton dynamics of clays. *Chemical Physics Letters* 333, 479–484.
- Bethke, C.M., Altaner, S.P., 1986. Layer-by-layer mechanism of smectite illitization and application to a new rate law. *Clays and Clay Minerals* 34, 136–145.
- Bhattacharjee, S., 1973. Dehydration transformation in metahalloysite. *Proceedings of the Indian National Science Academy, Part A*, vol. 39, pp. 54–61 (abstract).
- Bish, D.L., 1993. Rietveld refinement of the kaolinite structure at 1.5 K. *Clays and Clay Minerals* 41, 738–744.
- Bish, D.L., Johnston, C.T., 1993. Rietveld refinement and Fourier-transform infrared spectroscopic study of the dickite structure at low temperature. *Clays and Clay Minerals* 41, 297–304.
- Bish, D.L., Von Dreele, R.B., 1989. Rietveld refinement of non-hydrogen atom position in kaolinite. *Clays and Clay Minerals* 37, 289–296.
- Blanco, C., Herrero, J., Mendioroz, S., Pajares, J.A., 1988. Infrared studies of surface acidity and reversible folding in palygorskite. *Clays and Clay Minerals* 36, 364–368.

- Blount, A.M., Threadgold, I.M., Bailey, S.W., 1969. Refinement of the crystal structure of nacrite. *Clays and Clay Minerals* 17, 185–194.
- Boek, E.S., Sprik, M., 2003. Ab initio molecular dynamics study of the hydration of a sodium smectite clay. *Journal of Physical Chemistry B* 107, 3251–3256.
- Bradley, W.F., 1940. The structural scheme of attapulgite. *American Mineralogist* 25, 405–410.
- Bradley, W.F., 1959. Current progress in silicate structures. *Clays and Clay Minerals* 6, 18–25.
- Brauner, K., Preisinger, A., 1956. Struktur und Entstehung des Sepioliths. *Tschermaks Mineralogische und Petrographische Mitteilungen* 6, 120–140.
- Brigatti, M.F., Galli, E., Medici, L., Poppi, L., 1997. Crystal structure refinement of aluminian lizardite-2H<sub>2</sub>. *American Mineralogist* 82, 931–935.
- Brigatti, M.F., Guggenheim, S., 2002. Mica crystal chemistry and the influence of pressure, temperature, and solid solution on atomistic models. In: Mottana, A., Sassi, F.P., Thompson, J.B., Guggenheim, S. (Eds.), *Micas: Crystal Chemistry and Metamorphic Petrology. Reviews in Mineralogy and Geochemistry*, vol. 46. Mineralogical Society of America, Washington, DC, pp. 1–97.
- Brigatti, M.F., Lalonde, A.E., Medici, L., 1999. Crystal chemistry of IVFe<sup>3+</sup>-rich phlogopites: a combined single-crystal X-ray and Mössbauer study. In: Kodama, H., Mermut, A.R., Torrance, J.K. (Eds.), *Clays for our Future. Proceedings of the 11th International Clay Conference*, Ottawa, pp. 317–327.
- Brigatti, M.F., Lugli, C., Poppi, L., Foord, E.E., Kile, D.E., 2000. Crystal chemical variations in Li- and Fe-rich micas from Pikes Peak Batholith (central Colorado). *American Mineralogist* 85, 1275–1286.
- Brigatti, M.F., Medici, L., Poppi, L., 1996b. Refinement of the structure of natural ferriphlogopite. *Clays and Clay Minerals* 44, 540–545.
- Brigatti, M.F., Medici, L., Saccani, E., Vaccaro, C., 1996a. Crystal chemistry and petrologic significance of Fe<sup>3+</sup>-rich phlogopite from the Tapira carbonatite complex, Brazil. *American Mineralogist* 81, 913–927.
- Brindley, G.W., 1959. X-ray and electron diffraction data for sepiolite. *American Mineralogist* 44, 495–500.
- Brindley, G.W., Brown, G. (Eds.), 1980. *Crystal Structures of Clay minerals and Their X-ray Identification*. Mineralogical Society, London.
- Brindley, G.W., Robinson, K., 1945. Structure of kaolinite. *Nature* 156, 661–663.
- Brindley, G.W., Robinson, K., 1946. The structure of kaolinite. *Mineralogical Magazine* 27, 242–253.
- Brindley, G.W., Robinson, K., 1948. X-ray studies of halloysite and metahalloysite, I. The structure of metahalloysite, an example of random layer lattice. *Mineralogical Magazine* 28, 393–406.
- Brindley, G.W., Wardle, R., 1970. Monoclinic and triclinic forms of pyrophyllite and pyrophyllite anhydride. *American Mineralogist* 55, 1259–1272.
- Brown, B.E., 1978. The crystal structure of 3T lepidolite. *American Mineralogist* 63, 332–336.
- Brown, B.E., Bailey, S.W., 1963. Chlorite polytypism, II. Crystal structure of one layer Cr-chlorite. *American Mineralogist* 48, 42–61.

- Brown, G., Newman, A.C.D., Rayner, J.H., Weir, A.H., 1978. The structures and chemistry of soil clay minerals. In: Greenland, D.J., Hayes, M.H.B. (Eds.), *The Chemistry of Soil Constituents*. Wiley, Chichester, pp. 29–178.
- Brown, G.E., Parks, G.A., O'Day, P.A., 1995. Sorption at mineral-water interfaces: macroscopic and microscopic perspectives. In: Vaughan, D.J., Pattrick, R.A.D. (Eds.), *Mineral Surfaces*. Mineralogical Society, Series 5. Chapman & Hall, London, pp. 129–183.
- Bukin, A.S., Drits, V.A., Plançon, A., Tchoubar, C., 1989. Stacking faults in kaolin-group minerals in light of real structural features. *Clays and Clay Minerals* 37, 297–307.
- Caillère, S., 1951. Sepiolite. In: Brindley, G.W. (Ed.), *X-ray Identification and Structures of Clay Minerals*. Mineralogical Society, London, pp. 224–233.
- Cases, J.M., Liétard, O., Yvon, J., Delon, J.F., 1982. Étude des propriétés cristallochimiques, morphologiques, superficielles de kaolinites désordonnées. *Bulletin de Minéralogie* 105, 439–455.
- Cases, J.M., Bèrend, I., François, M., Uriot, J.P., Michot, L.J., Thomas, F., 1997. Mechanisms of adsorption and desorption of water vapor by homoionic montmorillonite: 3. The  $\text{Mg}^{2+}$ ,  $\text{Ca}^{2+}$ ,  $\text{Sr}^{2+}$ , and  $\text{Ba}^{2+}$  exchanged forms. *Clays and Clay Minerals* 45, 8–22.
- Chatterjee, A., Iwasaki, T., Ebina, T., Miyamoto, A., 1999. A DFT study on clay–cation–water interaction in montmorillonite and beidellite. *Computational Materials Science* 14, 119–124.
- Chernoski, J.V., 1975. Aggregate refractive indices and unit cell parameters of synthetic serpentine in the system  $\text{MgO}-\text{Al}_2\text{O}_3-\text{SiO}_2-\text{H}_2\text{O}$ . *American Mineralogist* 60, 2000–2008.
- Childs, C.W., Hayashi, S., Newman, R.H., 1999. Five-coordinate aluminum in allophane. *Clays and Clay Minerals* 47, 64–69.
- Childs, C.W., Inoue, K., Seyama, H., Soma, M., Theng, B.K.G., Yuan, G., 1997. X-ray photoelectron spectroscopic characterization of Silica Springs allophane. *Clay Minerals* 32, 565–572.
- Childs, C.W., Parfitt, R.L., Newman, R.H., 1990. Structural studies of Silica Springs allophane. *Clay Minerals* 25, 329–341.
- Chisholm, J.E., 1992. Powder diffraction patterns and structural models for palygorskite. *Canadian Mineralogist* 30, 61–73.
- Christ, C.L., Hathaway, J.C., Hostetler, P.B., Shepard, A.O., 1969. Palygorskite: new X-ray data. *American Mineralogist* 54, 198–205.
- Churchman, G.J., Theng, B.K.G., 1984. Interactions of halloysites with amides: mineralogical factors affecting complex formation. *Clay Minerals* 19, 161–175.
- Compagnoni, R., Ferraris, G., Mellini, M., 1985. Carlosturanite, a new asbestiform rock-forming silicate from Val Variata, Italy. *American Mineralogist* 70, 767–772.
- Costanzo, P.M., Giese, R.F. Jr., 1985. Dehydration of synthetic hydrated kaolinites: a model for the dehydration of halloysite (10 Å). *Clays and Clay Minerals* 33, 415–423.
- Costanzo, P.M., Giese, R.F. Jr., Lipsicas, M., 1984. Static and dynamic structure of water in hydrated kaolinites, I. The static structure. *Clays and Clay Minerals* 32, 419–428.
- Cradwick, P.D.G., Farmer, V.C., Russell, J.D., Masson, C.R., Wada, K., Yoshinaga, N., 1972. Imogolite, a hydrated aluminium silicate of tubular structure. *Nature Physical Science* 240, 187–189.
- Cruciani, G., Zanazzi, P.F., 1994. Cation partitioning and substitution mechanism in 1M-phlogopite: a crystal chemical study. *American Mineralogist* 78, 289–301.

- Cruciani, G., Zanazzi, P.F., Quartieri, S., 1995. Tetrahedral ferric iron in phlogopite. XANES and Mössbauer comparison to single-crystal X-ray data. *European Journal of Mineralogy* 7, 255–265.
- de la Calle, C., Suquet, H., 1988. Vermiculite. In: Bailey, S.W. (Ed.), *Hydrous Phyllosilicates (Exclusive of Micas)*. Reviews in Mineralogy, vol. 19. Mineralogical Society of America, Washington, DC, pp. 455–492.
- de Lapparent, J., 1935. Sur un constituant essentiel des terres a foulon. *Comptes Rendues de l'Académie des Sciences, Paris*, vol. 201, pp. 481–482.
- Donnay, G., Morimoto, N., Takeda, H., Donnay, J.D.H., 1964. Trioctahedral one-layer micas, I. Crystal structure of a synthetic iron mica. *Acta Crystallographica* 17, 1369–1373.
- Dornberger-Schiff, K., Đurovič, S., 1975. OD [order–disorder]-interpretation of kaolinite-type structures. I. Symmetry of kaolinite packets and their stacking possibilities. *Clays and Clay Minerals* 23, 219–229.
- Drits, V.A., 1997. Mixed layer minerals. In: Merlino, S. (Ed.), *Modular Aspects of Minerals*, EMU Notes in Mineralogy, vol. 1. Eötvös University Press, Budapest, pp. 153–190.
- Drits, V.A., Besson, G., Muller, F., 1996. X-ray diffraction study of structural transformations of aluminous 2:1 layer silicates during dehydroxylation. *Journal de Physique IV* 6 (C4, Rayons X et Matière), 91–102.
- Drits, V.A., Dainyak, L.G., Muller, F., Besson, G., Manceau, A., 1997a. Isomorphous cation distribution in celadonites, glauconites and Fe-illites determined by infrared, Mossbauer and EXAFS spectroscopies. *Clay Minerals* 32, 153–179.
- Drits, V.A., Karavan, Yu, V., 1969. Polytypes of the two-packet chlorites. *Acta Crystallographica B* 25, 632–639.
- Drits, V.A., Lindgreen, H., Salyn, A.L., 1997b. Determination by XRD of content and distribution of fixed ammonium in illite-smectite. Application to North Sea illite-smectite. *American Mineralogist* 82, 80–88.
- Drits, V.A., Plançon, A., Sakharov, B.A., Besson, G., Tshipursky, S.I., Tchoubar, C., 1984. Diffraction effects calculated for structural models of K-saturated montmorillonite containing different types of defects. *Clay Minerals* 19, 541–561.
- Drits, V.A., Sokolova, G.V., 1971. Structure of palygorskite. *Soviet Physics, Crystallography* 16, 183–185.
- Drits, V.A., Tchoubar, C., 1990. X-ray diffraction by disordered lamellar structures. Theory and application to microdivided silicates and carbons. Springer, Berlin.
- Drits, V.A., Weber, F., Salyn, A.L., Tshipursky, S.I., 1993. X-ray identification of one-layer illite varieties; Application to the study of illite around uranium deposits of Canada. *Clays and Clay Minerals* 41, 389–398.
- Đurovič, S., 1981. OD-caracter, Polytypie und Identifikation von Schichtsilikaten. *Forschritte der Mineralogie* 59, 191–226.
- Đurovič, S., 1994. Classification of phyllosilicates according to the symmetry of their octahedral sheets. *Ceramics—Silikáty* 38, 81–84.
- Đurovič, S., 1997. Fundamentals of OD theory. In: Merlino, S. (Ed.), *Modular Aspects of Minerals*, EMU Notes in Mineralogy, vol. 1. Eötvös University Press, Budapest, pp. 1–28.
- Đurovič, S., 1999. Layer stacking in general polytypic structures. Section 9.2.2. In: Wilson, A.C.J., Prince, E. (Eds.), *International Tables for Crystallography*, vol. C. Kluwer Academic Publishers, Dordrecht, pp. 752–765.

- Dyar, M.D., 1990. Mössbauer spectra of biotite from metapelites. *American Mineralogist* 75, 656–666.
- Echle, W., 1978. The transformation sepiolite-loughlinite: experiments and field observations. *Neues Jahrbuch für Mineralogie, Abhandlungen* 133, 303–321.
- Eggleton, R.A., Tilley, D.B., 1998. Hisingerite a ferric kaolin mineral with curved morphology. *Clays and Clay Minerals* 46, 400–413.
- Evans, B.W., Guggenheim, S., 1988. Talc, phyrophyllite, and related minerals. In: Bailey, S.W. (Ed.), *Hydrous Phyllosilicates (Exclusive of Micas)*. Reviews in Mineralogy, vol. 19. Mineralogical Society of America, Washington, DC, pp. 225–280.
- Fahey, J.J., Axelrod, J.M., 1948. Loughlinite, a new hydrous magnesium silicate. *American Mineralogist* 33, 195.
- Farmer, L.G., Boettcher, A.I., 1981. Petrologic and crystal chemical significance of some deep-seated phlogopites. *American Mineralogist* 66, 1154–1163.
- Farmer, V.C., Fraser, A.R., Tait, J.M., 1979. Characterization of the chemical structures of natural and synthetic aluminosilicate gels and sols by infrared spectroscopy. *Geochimica et Cosmochimica Acta* 43, 1417–1420.
- Farmer, V.C., Russell, J.D., 1990. The structure and genesis of allophanes and imogolite: their distribution in non-volcanic soils. In: De Boedt, M.F., Hayes, M.H.B., Herbillon, A. (Eds.), *Soil Colloids and Their Associations in Aggregates*. Proceedings NATO Advanced Studies Workshop, Ghent 1985. Plenum Press, New York, pp. 165–178.
- Fernández Álvarez, T., 1970. Superficie específica y estructura de poro de la sepiolita calentada a diferentes temperaturas. Proceedings Reunión Hispano-Belga de Minerales de la Arcilla, Madrid, 202–209.
- Ferraris, G., Gula, A., Ivaldi, G., Nespolo, M., Soboleva, E., Khomyakov, A.P., Uvarova, Yu., 2000. First structural determination of a truly-polytypic mica-2O. In: *Advances on Micas (Problems, Methods, Applications in Geodynamics)*. Accademia Nazionale dei Lincei, Roma, pp. 205–209.
- Fielde, M., Claridge, G.G.C., 1975. Allophane. In: Gieseking, J.E. (Ed.), *Soil Components, Inorganic Components*, vol. 2. Springer, New York, pp. 351–393.
- Filut, A.M., Rule, A.C., Bailey, S.W., 1985. Crystal structure refinement of anandite 2Or, a barium- and sulfur-bearing trioctahedral mica. *American Mineralogist* 70, 1298–1308.
- Firman, R.J., 1966. Sepiolite from the Malvern Hill. *Mercian Geologist* 1, 247–253.
- Flehmig, W., 1973. Kristallinität und Infrarotspektroskopie natürlicher dioktaedrischer illite. *Neues Jahrbuch für Mineralogie—Monatshefte*, pp. 351–361.
- Floran, R.J., Papike, J.J., 1975. Petrology of the low-grades rocks of the Gunflint iron-Formation, Ontario-Minnesota. *Geological Society of America Bulletin* 86, 1169–1190.
- Frost, R.L., Rintoul, L., Eggleton, R.A., 1997. Structural aspects of hisingerite: a vibrational spectroscopic study. In: Kodama, H., Mermut, A.R., Torrance, J.K. (Eds.), *Clays for Our Future*. Proceedings of the 11th International Clay Conference, Ottawa, 1997, pp. 409–412.
- Galán, E., 1996. Properties and applications of palygorskite-sepiolite clays. *Clay Minerals* 31, 443–453.
- Galán, E., Carretero, M.I., 1999. A new approach to compositional limits for sepiolite and palygorskite. *Clays and Clay Minerals* 47, 399–409.
- Gard, J.A., Follet, E.A., 1968. A structural scheme for palygorskite. *Clay Minerals* 7, 367–369.

- Gast, R.G., 1977. Surface and colloid chemistry. In: Dixon, J.B., Weed, S.B. (Eds.), *Minerals in Soil Environments*. Soil Science Society of America, Madison, WI, pp. 27–73.
- Giese, R.F. Jr., 1973. Hydroxyl Orientation in Pyrophyllite. *Nature Physical Science* 241, 151.
- Giese, R.F., 1988. Kaolin minerals: structures and stabilities. In: Bailey, S.W. (Ed.), *Hydrous Phyllosilicates (Exclusive of Micas)*. Reviews in Mineralogy, vol. 19. Mineralogical Society of America, Washington, DC, pp. 29–66.
- Giese, R.F. Jr., Datta, P., 1973. Hydroxyl orientation in kaolinite, dickite, and nacrite. *American Mineralogist* 58, 471–479.
- Giuseppetti, G., Tadini, C., 1972. The crystal structure of 2O brittle mica: anandite. *Tschermaks Mineralogische und Petrographische Mitteilungen* 18, 169–184.
- Goodman, B.A., Russell, J.D., Montez, B., Oldfield, E., Kirkpatrick, R.J., 1985. Structural studies of imogolite and allophanes by aluminium-27 and silicon-29 nuclear magnetic resonance spectroscopy. *Physics and Chemistry of Minerals* 12, 342–346.
- Gruner, J.W., 1932a. The crystal structure of dickite. *Zeitschrift für Kristallographie, Kristallgeometrie, Kristallphysik, Kristallchemie* 83, 394–404.
- Gruner, J.W., 1932b. The crystal structure of kaolinite. *Zeitschrift für Kristallographie, Kristallgeometrie, Kristallphysik, Kristallchemie* 83, 75–80.
- Gruner, J.W., 1934. The crystal structure of talc and pyrophyllite. *Zeitschrift für Kristallographie, Kristallgeometrie, Kristallphysik, Kristallchemie* 88, 412–419.
- Guggenheim, S., Bailey, S.W., 1975. Refinement of the margarite structure in subgroup symmetry. *American Mineralogist* 60, 1023–1029.
- Guggenheim, S., Bailey, S.W., 1977. The refinement of zinnwaldite-1M in subgroup symmetry. *American Mineralogist* 62, 1158–1167.
- Guggenheim, S., Bailey, S.W., 1978. Refinement of the margarite structure in subgroup symmetry: correction, further refinement, and comments. *American Mineralogist* 63, 186–187.
- Guggenheim, S., Bailey, S.W., Eggleton, R.A., Wikes, P., 1982. Structural aspect of greenalite and related minerals. *Canadian Mineralogist* 20, 1–18.
- Guggenheim, S., Bain, D.C., Bergaya, F., Brigatti, M.F., Drits, V.A., Eberl, D.D., Formoso, M.L.L., Galán, E., Merriman, R.J., Peacor, D.R., Stanjek, H., Watanabe, T., 2002. Report of the Association Internationale Pour l'Étude des Argiles (AIPEA). Nomenclature Committee for 2001: order, disorder and crystallinity in phyllosilicates and the use of the crystallinity index. *Clays and Clay Minerals* 50, 406–409.
- Guggenheim, S., Eggleton, R.A., 1998. The crystal structure of greenalite and caryopilite. *Canadian Mineralogist* 36, 163–179.
- Guggenheim, S., Kato, T., 1984. Kinoshitalite and Mn phlogopites: trial refinements in subgroup symmetry and further refinement in ideal symmetry. *Mineralogical Journal* 12, 1–5.
- Guggenheim, S., Zhan, W., 1998. Effect of temperature on the structures of lizardite-1T and lizardite-2H<sub>1</sub>. *Canadian Mineralogist* 36, 1587–1594.
- Güven, N., 1988. Smectites. In: Bailey, S.W. (Ed.), *Hydrous Phyllosilicates (Exclusive of Micas)*, Reviews in Mineralogy, vol. 19. Mineralogical Society of America, Washington, DC, pp. 497–559.
- Güven, N., 1992. Molecular aspects of clay-water interactions. In: Güven, N., Pollastro, R.M. (Eds.), *Clay–Water Interface and its Rheological Implications*, CMS Workshop Lectures, vol. 4. The Clay Minerals Society, Boulder, CO, pp. 1–80.
- Güven, N., Burnham, C.W., 1967. The crystal structure of 3T muscovite. *Zeitschrift für Kristallographie* 125, 163–183.

- Hall, P.L., Churchman, G.J., Theng, B.K.G., 1985. Size distribution of allophane unit particles in aqueous suspensions. *Clays and Clay Minerals* 33, 345–349.
- Hall, S.H., Bailey, S.W., 1976. Amesite from Antarctica. *American Mineralogist* 61, 497–499.
- Harsh, J., 2000. Poorly crystalline aluminosilicate clays. In: Sumner, M.E. (Ed.), *Handbook of Soil Science*. CRC Press, Boca Raton, FL, F-169–F-182.
- Hashizume, H., Theng, B.K.G., 1999. Adsorption of DL-alanine by allophane: effect of pH and unit particle aggregation. *Clay Minerals* 34, 233–238.
- Hashizume, H., Theng, B.K.G., Yamagishi, A., 2002. Adsorption and discrimination of alanine and alanyl-alanine enantiomers by allophane. *Clay Minerals* 37, 551–557.
- Hayashi, H., Otsuka, R., Imai, N., 1969. Infrared study of sepiolite and palygorskite on heating. *American Mineralogist* 53, 1613–1624.
- Hazen, R.M., Finger, L.W., Velde, D., 1981. Crystal structure of a silica- and alkali-rich trioctahedral mica. *American Mineralogist* 66, 586–591.
- He, H., Barr, T.L., Klinowski, J., 1995. ESCA and solid-state NMR studies of allophane. *Clay Minerals* 30, 201–209.
- Hendricks, S.B., 1938a. The crystal structure of talc and pyrophyllite. *Zeitschrift für Kristallographie* 99, 264–274.
- Hendricks, S.B., 1938b. The crystal structure of the clay minerals: dickite, halloysite and hydrated halloysite. *American Mineralogist* 23, 295–301.
- Hendricks, S.B., 1939. The crystal structure of nacrite,  $\text{Al}_2\text{O}_3 \cdot 2\text{SiO}_2 \cdot 2\text{H}_2\text{O}$ , and the polymorphism of the kaolin minerals. *Zeitschrift für Kristallographie* 100, 509–518.
- Hendricks, S.B., Nelson, R.A., Alexander, L.T., 1940. Hydration mechanism of the clay mineral montmorillonite saturated with various cations. *Journal of the American Chemical Society* 62, 1457–1464.
- Henmi, T., Wada, K., 1976. Morphology and composition of allophane. *American Mineralogist* 61, 379–390.
- Hinckley, D., 1963. Variability in crystallinity values among the kaolin deposits of the Coastal Plain of Georgia and South Carolina. *Clays and Clay Minerals* 11, 229–235.
- Hobbs, J.D., Cygan, R.T., Nagy, K.L., Schultz, P.A., Sears, M.P., 1997. All-atom ab initio energy minimization of the kaolinite crystal structure. *American Mineralogist* 82, 657–662.
- Hofmann, U., Endell, K., Wilm, D., 1934. X-ray and colloid-chemical studies of clay. *Angewandte Chemie* 47, 539–547.
- Huang, W.L., 1992. Illitic clay formation during experimental diagenesis of arkoses. In: Houseknecht, D.W., Pittman, E.D. (Eds.), *Origin, Diagenesis, and Petrophysics of Clay Minerals in Sandstones*. SEPM Special Publication. vol. 47, pp. 49–63.
- Johnston, C.T., Agnew, S.F., Bish, D.L., 1990. Polarized single-crystal Fourier-transform infrared microscopy of Ouray dickite and Keokuk kaolinite. *Clays and Clay Minerals* 38, 573–583.
- Jones, B.F., Galán, E., 1988. Sepiolite and palygorskite. In: Bailey, S.W. (Ed.), *Hydrous Phyllosilicates (Exclusive of Micas)*. Reviews in Mineralogy, vol. 19. Mineralogical Society of America, Washington, DC, pp. 631–674.
- Joswig, W., Amthauer, G., Takéuchi, Y., 1986. Neutron diffraction and Mössbauer spectroscopic study of clintonite (xanthophyllite). *American Mineralogist* 71, 1194–1197.
- Joswig, W., Drits, V.A., 1986. The orientation of the hydroxyl groups in dickite by X-ray diffraction. *Neues Jahrbuch für Mineralogie—Monatshefte*, 19–22.



- Karup-Møller, S., Petersen, O.V., 1984. Tuperssuatsiaite, a new mineral species from the Ilimaussaq intrusion in South Greenland. *Neues Jahrbuch für Mineralogie—Monatshefte* 11, 501–512.
- Kassner, D., Baur, W.H., Joswig, W., Eichhorn, K., Wendschuh-Jostier, M., Kupčík, V., 1993. A test of the importance of weak reflections in resolving a space-group ambiguity involving the presence or absence of an inversion centre. *Acta Crystallographica B* 49, 646–654.
- Kleppe, A.K., Jephcoat, A.P., Welch, M.D., 2003. The effect of pressure upon hydrogen bonding in chlorite: a Raman spectroscopic study of clinochlore to 26.5 GPa. *American Mineralogist* 88, 567–573.
- Klevtsov, D.P., Krivoruchko, O.P., Mastikhin, V.M., Buyanov, R.A., Zolotovskii, B.P., Paramzin, S.M., 1987. Formation of  $[AlO_5]$  polyhedra during the dehydroxylation of layered compounds. *Doklady Akademii Nauk SSSR* 295, 381–384.
- Kodama, H., 1959. Crystallo-chemical studies on pyrophyllite. *Nendo Kagaku* 1, 13–27.
- Kohyama, N., Fukushima, K., Fukami, A., 1978. Observation of the hydrated form of tubular halloysite by an electron microscope equipped with an environmental cell. *Clays and Clay Minerals* 26, 25–40.
- Kübler, B., 1964. Les argiles, indicateurs de métamorphisme. *Revue de l'Institut Français du Pétrole* 19, 1093–1112.
- Kübler, B., 1967. La cristallinité de l'illite et les zones tout à fait supérieures du métamorphisme. In: *Etages tectoniques. Colloque de Neuchâtel, 1966*. Editions de la Baconnière, Neuchâtel, pp. 105–121.
- Kübler, B., Goy-Eggenberger, D., 2001. The crystallinity of illite revisited: a review of knowledge acquired. *Clay Minerals* 36, 143–157.
- Kunze, G., 1956. Die gewellte Struktur des Antigorits, I. *Zeitschrift für Kristallographie* 108, 82–107.
- Kunze, G., 1958. Die gewellte Struktur des Antigorits, II. *Zeitschrift für Kristallographie* 110, 282–320.
- Kunze, G., 1959. Fehlordnungen des Antigorits. *Zeitschrift für Kristallographie* 111, 190–212.
- Laird, D.A., 1994. Evaluation of structural formulae and alkylammonium methods of determining layer charge. In: Mermut, A.R. (Ed.), *Layer Charge Characteristics of 2:1 Silicate Clay Minerals. CMS Workshop Lectures*. vol. 6, pp. 79–104.
- Lee, H.-L., Guggenheim, S., 1981. Single crystal refinement of pyrophyllite-1Tc. *American Mineralogist* 66, 350–357.
- Leguey, S., Martín Rubi, J.A., Casas, J., Marta, J., Cuevas, J., Álvarez, A., Median, J.A., 1995. Diagenetic evolution and mineral fabric in sepiolite materials from the Vicálvaro deposit (Madrid basin). In: Churchman, G.J., Fitzpatrick, R.W., Eggleton, R.A. (Eds.), *Clays Controlling the Environment. Proceedings of the 10th International Clay Conference, Adelaide, 1993*. CSIRO Publishing, Melbourne, pp. 383–392.
- Liang, J.-J., Hawthorne, F.C., Novák, M., Černý, P., Ottolini, L., 1995. Crystal-structure refinement of boromuscovite polytypes using a coupled Rietveld-static-structure energy-minimization method. *Canadian Mineralogist* 33, 859–865.
- Liétard, O., 1977. Contribution à l'étude des propriétés physicochimiques, cristallographiques et morphologiques des kaolins. PhD thesis. University of Nancy, France, p. 322 (in French).

- Lin, J.-C., Guggenheim, S., 1983. The crystal structure of a Li, Be-rich brittle mica: a dioctahedral-trioctahedral intermediate. *American Mineralogist* 68, 130–142.
- Lindgreen, H., Hansen, P.L., Jakobsen, H.J., 1991. Diagenetic structural transformation in North Sea Jurassic illite/smectite. *Clays and Clay Minerals* 39, 54–69.
- Lipkina, M.I., Drits, V.A., Tsipurskii, S.I., Ustinov, V.I., Strizhev, V.P., Yakusheva, I.N., Cherkashin, V.I., 1987. Dioctahedral Fe-rich layer silicates from hydrothermal rocks and sediments of volcanogenic mountains of Japan Sea. *Izvestiya Akademii Nauk SSSR, seriya geologia* 10, 92–111 (in Russian).
- Lister, J.S., Bailey, S.W., 1967. Chlorite polytypism, IV. Regular two-layer structures. *American Mineralogist* 52, 1614–1631.
- Lokanatha, S., Bhattacharjee, S., 1984. Structure defects in palygorskite. *Clay Minerals* 19, 253–255.
- Longchambon, H., 1937. Thermal properties of sepiolites. *Bulletin de la Société française de Minéralogie et de Cristallographie* 60, 232–276.
- Longchambon, H., Migeon, G., 1936. Sepiolite. *Comptes Rendues de l'Académie des Sciences, Paris*, vol. 203, pp. 431–433.
- López-Galindo, A., Ben Abound, A., Fenoll Hach-Ali, P., Casas Ruiz, J., 1996. Mineralogical and geochemical characterization of palygorskite from Gabasa (NE Spain). Evidence of a detrital precursor. *Clay Minerals* 31, 33–44.
- MacEwan, D.M.C., Wilson, M.J., 1980. Interlayer and intercalation complexes of clay minerals. In: Brindley, G.W., Brown, G. (Eds.), *Crystal Structures of Clay Minerals and Their X-ray Identification*. Mineralogical Society, London, pp. 197–248.
- MacKenzie, K.J.D., Bowden, M.E., Meinhold, R.H., 1991. The structure and thermal transformations of allophanes studied by  $^{29}\text{Si}$  and  $^{27}\text{Al}$  high resolution solid-state NMR. *Clays and Clay Minerals* 39, 337–346.
- Martín-Vivaldi, J.L., Cano, J., 1956. Contribution to the study of sepiolite, II. Some considerations regarding the mineralogical formula. *Clays and Clay Minerals* 4, 173–176.
- Martin, R.T., Bailey, S.W., Eberl, D.D., Fanning, D.S., Guggenheim, S., Kodama, H., Pev-ear, D.R., Środoń, J., Wicks, F.J., 1991. Report of the Clay Minerals Society Nomenclature Committee: revised classification of clay materials. *Clays and Clay Minerals* 39, 333–335.
- Mathieson, A.McL., Walker, G.F., 1954. Crystal structure of magnesium vermiculite. *American Mineralogist* 39, 231–255.
- McBride, M.B., 1989. Surface chemistry of soil minerals. In: Dixon, J.B., Weed, S.B. (Eds.), *Minerals in Soil Environments*, 2nd edition. Soil Science Society of America, Madison, WI, pp. 35–88.
- McKeown, D.A., Post, J.E., Etz, E.S., 2002. Vibrational analysis of palygorskite and sepiolite. *Clays and Clay Minerals* 50, 537–684.
- Medici, L., 1996. *Cristallochimica delle miche di Tapira (Brasile)*. PhD. thesis. University of Modena and Reggio Emilia, 140pp. (in Italian).
- Mellini, M., 1982. The crystal structure of lizardite 1T: hydrogen bonds and polytypism. *American Mineralogist* 67, 587–598.
- Mellini, M., Viti, C., 1994. Crystal structure of lizardite-1T from Elba, Italy. *American Mineralogist* 79, 1194–1198.
- Mellini, M., Weiss, Z., Rieder, M., Drábek, M., 1996. Cs-ferriannite as a possible host for waste cesium: crystal structure and synthesis. *European Journal of Mineralogy* 8, 1265–1271.

- Mellini, M., Zanazzi, P.F., 1987. Crystal structures of lizardite-1T and lizardite-2H1 from Coli, Italy. *American Mineralogist* 72, 943–948.
- Mellini, M., Zanazzi, P.F., 1989. Effects of pressure on the structure of lizardite-1T. *European Journal of Mineralogy* 1, 13–19.
- Mifsud, A., Rautureau, M., Fornes, V., 1978. Etude de l'eau dans la palygorskite à l'aide des analyses thermiques. *Clay Minerals* 13, 367–374.
- Migeon, G., 1936. Sepiolites. *Bulletin de la Société française de Minéralogie et de Cristallographie* 59, 6–134.
- Mizuki, K., Suzuki, M., Akiyama, H., 1985. Transformation of structure in heating of clay minerals. *Kanzei Chuo Bunsekishoho* 25, 49–57 (in Japanese, English abstract).
- Mooney, R.W., Keenan, A.G., Wood, L.A., 1952. Adsorption of water vapor by montmorillonite, II Effect of exchangeable ions and lattice swelling as measured by X-ray diffraction. *Journal of the American Chemical Society* 74, 1371–1374.
- Moore, D.M., Reynolds, R.C. Jr., 1989. *X-Ray Diffraction and the Identification and Analysis of Clay Minerals*. Oxford University Press, New York.
- Murad, E., Wagner, U., 1996. The thermal behavior of an Fe-rich illite. *Clay Minerals* 31, 45–52.
- Murray, H.H., 1954. Structural variations in some kaolinites in relation to dehydrated halloysite. *American Mineralogist* 39, 97–108.
- Nadeau, P.H., Wilson, M.J., McHardy, W.J., Tait, J.M., 1984. Interstratified clays as fundamental particles. *Science* 225, 923–925.
- Nadeau, P.H., Wilson, M.J., McHardy, W.J., Tait, M.J., 1985. The conversion of smectite to illite during diagenesis: Evidence from some illitic clays from bentonites and sandstones. *Mineralogical Magazine* 49, 393–400.
- Nagata, M., Shimoda, S., Sudo, T., 1974. On dehydration of bound water of sepiolite. *Clays and Clay Minerals* 22, 285–293.
- Nagy, B., Bradley, W.F., 1955. Structure of sepiolite. *American Mineralogist* 40, 885–892.
- Neal, C.R., Taylor, L.A., 1989. The petrography and composition of phlogopite micas from the Blue Ball kimberlite, Arkansas: a record of chemical evolution during crystallization. *Mineralogy and Petrology* 40, 207–224.
- Neder, R.B., Burghammer, M., Grasl, Th., Schulz, H., Bram, A., Fiedler, S., 1999. Refinement of the kaolinite structure from single-crystal synchrotron data. *Clays and Clay Minerals* 47, 487–494.
- Nelson, D.O., Guggenheim, S., 1993. Inferred limitations to the oxidation of Fe in chlorite: a high-temperature single-crystal X-ray study. *American Mineralogist* 78, 1197–1207.
- Nespolo, M., Takeda, H., Ferraris, G., 1997. Crystallography of mica polytypes. In: Merlino, S. (Ed.), *Modular Aspects of Minerals*, EMU Notes in Mineralogy, vol. 1. Eötvös University Press, Budapest, pp. 81–118.
- Newman, A.C.D., 1987. The interaction of water with clay mineral surfaces. In: Newman, A.C.D. (Ed.), *Chemistry of Clays and Clay Minerals*, Mineralogical Society, Monograph 6. Wiley, New York, pp. 237–274.
- Newnham, R.E., 1960. A refinement of the dickite structure and some remarks on polymorphism in kaolin minerals. *Mineralogical Magazine* 32, 683–704.
- Newnham, R.E., Brindley, G.W., 1956. The crystal structure of dickite. *Acta Crystallographica* 9, 759–764.
- Norrish, K., 1954. The swelling of montmorillonite. *Discussions of the Faraday Society*, No 18, 120–133.

- Odom, I.E., 1984. Glauconite and celadonite minerals. In: Bailey, S.W. (Ed.), *Micas. Reviews in Mineralogy*, vol. 13. Mineralogical Society of America, Washington, DC, pp. 545–572.
- Okada, K., Ossaka, J., 1983. Dehydration reaction of interlayer water of halloysite by heating. Faculty of Engineering, Tokyo Institute of Technology. *Nendo Kagaku* 23, 27–31.
- Paquet, H., Duplay, J., Valleron-Blanc, M.M., Millot, G., 1987. Octahedral composition of individual particles in smectite-palygorskite and smectite-sepiolite assemblages. In: Schultz, L.G., van Olphen, H., Mumpton, F.A. (Eds.), *Proceedings of the International Clay Conference*, Denver, 1985. The Clay Minerals Society, Bloomington, IN, pp. 73–77.
- Parfitt, R.L., 1990. Allophane in New Zealand—A review. *Australian Journal of Soil Research* 28, 343–360.
- Parfitt, R.L., Henmi, T., 1980. Structure of some allophanes from New Zealand. *Clays and Clay Minerals* 28, 285–294.
- Parfitt, R.L., Wilson, A.D., 1985. Estimation of allophane and halloysite in three sequences of volcanic soils, New Zealand. *Catena Supplement* 7, 1–8.
- Parker, J.C., 1986. Hydrostatics of water in porous media. In: Sparks, D.L. (Ed.), *Soil Physical Chemistry*. CRC Press, Boca Raton, FL, pp. 209–296.
- Pauling, L., 1930. The structures of the micas and related minerals. *Proceedings of the National Academy of Sciences of the United States of America* 16, 123–129.
- Peacor, D.R., Bauluz, B., Dong, H., Tillick, D., Yan, Y., 2002. Transmission and analytical electron microscopy evidence for high Mg contents of 1M illite: absence of 1M polytypism in normal prograde diagenetic sequences of pelitic rocks. *Clays and Clay Minerals* 50, 757–765.
- Pérez-Rodríguez, J.L., Galán, E., 1994. Determination of impurity in sepiolite by thermal analysis. *Journal of Thermal Analysis* 42, 131–141.
- Perrault, G., Harvey, J., Pertsowwsky, R., 1975. La yofortierite, un nouveau silicate de manganese de St. Hilaire. *Canadian Mineralogist* 13, 68–74.
- Plançon, A., Zacharie, C., 1990. An expert system for the structural characterization of kaolinites. *Clay Minerals* 25, 249–260.
- Plançon, A., Giese, R.F. Jr., Snyder, R., Drits, V.A., Bukin, A.S., 1989. Stacking faults in the kaolin-group minerals: defect structures of kaolinite. *Clays and Clay Minerals* 37, 203–210.
- Preisinger, A., 1959. X-ray study of the structure of sepiolite. *Clays and Clay Minerals* 6, 61–67.
- Preisinger, A., 1963. Sepiolite and related compounds: its stability and application. *Clays and Clay Minerals* 10, 365–371.
- Radoslovich, E.W., 1961. Surface symmetry and cell dimensions of layer lattice silicates. *Nature* 191, 67–68.
- Radoslovich, E.W., Norrish, K., 1962. The cell dimensions and symmetry of layer-lattice silicates, I. Some structural considerations. *American Mineralogist* 47, 599–616.
- Rancourt, D.G., Dang, M.Z., Lalonde, A.E., 1992. Mössbauer spectroscopy of tetrahedral Fe<sup>3+</sup> in trioctahedral micas. *American Mineralogist* 77, 34–93.
- Range, K.J., Weiss, A., 1969. Über das Verhalten von kaolinitit bei hohen Drücken. *Deutsche Keramische Gesellschaft* 46, 231–288.
- Rautureau, M., 1974. Analyse structurale de la sepiolite par microdiffraction electronique. Thesis. University of Orléans, France, 89pp.

- Rautureau, M., Tchoubar, C., 1974. Precisions concernant l'analyse structurale de la sepiolite par microdiffraction electronique. *Comptes Rendues de l'Académie des Sciences, Paris* 278, 25–28.
- Rautureau, M., Tchoubar, C., Méring, J., 1972. Analyse structurale de la sepiolite par microdiffraction electronique. *Comptes Rendues de l'Académie des Sciences, Paris*, vol. 274, pp. 269–271.
- Rayner, J.H., Brown, G., 1966. Structure of pyrophyllite. *Clays and Clay Minerals* 14, 73–84.
- Reynolds, R.C., 1988. Mixed layer chlorite minerals. In: Bailey, S.W. (Ed.), *Hydrous Phyllosilicates (Exclusive of Micas)*. *Reviews in Mineralogy*, vol. 19. Mineralogical Society of America, Washington, DC, pp. 601–629.
- Rieder, M., Cavazzini, G., D'yakonov, Y.S., Frank-Kamenetskii, V.A., Gottardi, G., Guggenheim, S., Koval, P.V., Müller, G., Neiva, A.M.R., Radoslovich, E.W., Robert, J.-L., Sassi, F.P., Takeda, H., Weiss, Z., Wones, D.R., 1998. Nomenclature of the Micas. *Clays and Clay Minerals* 46, 586–595.
- Rogers, L.E., Quirk, J.P., Norrish, K., 1956. Occurrence of an aluminium-sepiolite in a soil having unusual water relationships. *Journal of Soil Science* 7, 177–184.
- Rosenberg, P.E., 2002. The nature, formation, and stability of end-member illite: a hypothesis. *American Mineralogist* 87, 103–107.
- Rozhdestvenskaya, I.V., Bukin, A.S., Drits, V.A., Fin'ko, V.I., 1982. Proton position and structural features of dickite according to X-ray diffraction analysis data. *Mineralogicheskii Zhurnal* 4, 52–58.
- Sainz-Diaz, C.I., Timon, V., Botella, V., Artacho, E., Hernandez-Laguna, A., 2002. Quantum mechanical calculations of dioctahedral 2:1 phyllosilicates: effect of octahedral cation distributions in pyrophyllite, illite, and smectite. *American Mineralogist* 87, 958–965.
- Scheidegger, A.M., Lamble, G.M., Sparks, D.L., 1997. The kinetics of nickel sorption on pyrophyllite as monitored by X-ray absorption fine structure (XAFS) spectroscopy. *Journal de Physique IV*, 7 (C2, X-Ray Absorption Fine Structure, vol. 2), 773–775.
- Semenov, E.I., 1969. Mineralogy of the Ilimaussaq Alkaline Massif, Southern Greenland. *Inst. Mineral. Geokhim. Krystallokhim. Redk Elementov*, Izdat. “Nauka” 1969, 164pp. (in Russian).
- Semenova, T.F., Rozhdestvenskaya, I.V., Frank-Kamenetskii, V.A., 1977. Refinement of the crystal structure of tetraferriphlogopite. *Soviet Physics, Crystallography* 22, 680–683.
- Sen Gupta, P.K., Schlemper, E.O., Johns, W.D., Ross, F., 1984. Hydrogen positions in dickite. *Clays and Clay Minerals* 32, 483–485.
- Serna, C., Ahlrichs, J.L., Serratos, J.M., 1975. Folding in sepiolite crystals. *Clays and Clay Minerals* 23, 452–457.
- Serna, C., Van Scoyoc, G.E., Ahlrichs, J.L., 1977. Hydroxyl groups and water in palygorskite. *American Mineralogist* 62, 784–792.
- Shimizu, H., Watanabe, T., Henmi, T., Masuda, A., Saito, H., 1988. Studies on allophane and imogolite by high-resolution solid-state  $^{29}\text{Si}$ - and  $^{27}\text{Al}$ -NMR and ESR. *Geochemical Journal* 22, 23–31.
- Shirozu, H., Bailey, S.W., 1966. Crystal structure of a two-layer Mg-vermiculite. *American Mineralogist* 51, 1124–1143.
- Shitov, V.A., Zvyagin, B.B., 1972. Relative stability of polytypal modifications of micalike minerals. *Kristallografiya* 17, 1162–1165.

- Slade, P.G., Dean, C., Schultz, P.K., Self, P.G., 1987. Crystal structure of a vermiculite-anilinium intercalate. *Clays and Clay Minerals* 35, 177–188.
- Slade, P.G., Stone, P.A., Radoslovich, E.W., 1985. Interlayer structures of the two layer hydrates of Na- and Ca-vermiculites. *Clays and Clay Minerals* 33, 51–61.
- Smith, D.G.W., Norem, D., 1986. The electron-microprobe analysis of palygorskite. *Canadian Mineralogist* 24, 499–511.
- Smrčok, L., Gyepesová, D., Chmielová, M., 1990. New X-ray Rietveld refinement of kaolinite from Keokuk, Iowa. *Crystal Research and Technology* 25, 105–110.
- Smyth, J.R., Dyar, M.D., May, H.M., Bricker, O.P., Acker, J.G., 1997. Crystal structure refinement and Mössbauer spectroscopy of an ordered, triclinic clinocllore. *Clays and Clay Minerals* 45, 544–550.
- Sokolova, T.N., 1982. Authigenic formation of silicate minerals of various salinization stages. Nauka, Moskva, 163pp. (in Russian).
- Sposito, G., 1984. *The Surface Chemistry of Soils*. Oxford University Press, New York.
- Sposito, G., Prost, R., 1982. Structure of water adsorbed on smectites. *Chemical Reviews* 82, 553–573.
- Springer, G., 1976. Falcondoite, a nickel analogue of sepiolite. *Canadian Mineralogist* 14, 407–409.
- Środoń, J., 1989. Illite-smectite in the rock cycle. In: Perez-Rodriguez, J.L., Galan, E. (Eds.), *Lectures-Conferencias, Euroclay'87, Sevilla*. Sociedad Espanola de Arcillas, pp. 137–151.
- Środoń, J., Eberl, D.D., 1984. Illite. In: Bailey, S.W., (Ed.), *Micas*, Mineralogical Society of America, *Reviews in Mineralogy* 13, pp. 495–544.
- Środoń, J., Elsass, F., McHardy, W.J., Morgan, D.J., 1992. Chemistry of illite-smectite inferred from TEM measurements of fundamental particle. *Clay Minerals* 27, 137–158.
- Steinfink, H., Brunton, G., 1956. The crystal structure of amesite. *Acta Crystallographica* 9, 487–492.
- Stoch, L., 1974. *Mineralny Ilaste (Clay Minerals)*. Geological Publishers, Warsaw, 186–193.
- Suquet, H., de la Calle, C., Pezerat, H., 1975. Swelling and structural organization of saponite. *Clays and Clay Minerals* 23, 1–9.
- Suquet, H., Iiyama, J.T., Kodama, H., Pezerat, H., 1977. Sythesis and swelling properties of saponite with increasing layer charge. *Clays and Clay Minerals* 25, 231–242.
- Suquet, H., Pezerat, H., 1987. Parameters influencing layer stacking types in saponite and vermiculite: a review. *Clays and Clay Minerals* 35, 353–362.
- Takeda, H., Ross, M., 1995. Mica polytypism: identification and origin. *American Mineralogist* 80, 715–724.
- Teppen, B.J., Rasmussen, K., Bertsch, P.M., Miller, D.M., Schaefer, L., 1997. Molecular dynamics modeling of clay minerals, 1. Gibbsite, kaolinite, pyrophyllite, and beidellite. *Journal of Physical Chemistry* 101, 1579–1587.
- Theng, B.K.G., Russell, M., Churchman, G.J., Parfitt, R.L., 1982. Surface properties of allophane, halloysite, and imogolite. *Clays and Clay Minerals* 30, 143–149.
- Thompson, J.G., Withers, R.L., 1987. A transmission electron microscopy contribution to the structure of kaolinite. *Clays and Clay Minerals* 35, 237–239.
- Tien, P.-L., Leavens, P.B., Nelen, J.A., 1975. Swinefordite, a dioctahedral-trioctahedral lithium-rich member of the smectite group from Kings Mountain, North Carolina. *American Mineralogist* 60, 540–547.

- Toraya, H., Iwai, S., Marumo, F., Hirao, M., 1978a. The crystal structures of germanate micas  $\text{KMg}_{2.5}\text{Ge}_4\text{O}_{10}\text{F}_2$  and  $\text{KLiMg}_2\text{Ge}_4\text{O}_{10}\text{F}_2$ . *Zeitschrift für Kristallographie* 148, 65–81.
- Toraya, H., Iwai, S., Marumo, F., Hirao, M., 1978b. The crystal structure of germanate micas  $\text{KMg}_3\text{Ge}_3\text{AlO}_{10}\text{F}_2$ . *Mineralogical Journal* 9, 221–230.
- Toraya, H., Marumo, F., 1981. Structure variation with octahedral cation substitution in the system of germanate micas  $\text{KMg}_{3-x}\text{Mn}_x\text{Ge}_3\text{AlO}_{10}\text{F}_2$ . *Mineralogical Journal* 10, 396–407.
- Torres-Ruiz, J., López-Galindo, A., González-López, J.M., Delgado, A., 1994. Geochemistry of Spanish sepiolite-palygorskite deposits: genetic considerations based on trace elements and isotopes. *Chemical Geology* 112, 221–245.
- Uehara, S., 1987. Serpentine minerals from Sasaguri area, Fukuoka Prefecture, Japan. *Journal of the Japanese Association of Mineralogists, Petrologists and Economic Geologists* 82, 106–118 (in Japanese, English abstract).
- Uehara, S., Shirozu, H., 1985. Variations in chemical composition and structural properties of antigorites. *Mineralogical Journal* 12, 299–318.
- Vahedi-Faridi, A., Guggenheim, S., 1997. Crystal structure of tetramethylammonium-exchanged vermiculite. *Clays and Clay Minerals* 45, 859–866.
- Vahedi-Faridi, A., Guggenheim, S., 1999a. Structural study of TMP-exchanged vermiculite. *Clays and Clay Minerals* 47, 219–225.
- Vahedi-Faridi, A., Guggenheim, S., 1999b. Structural study of monomethylammonium and dimethylammonium-exchanged vermiculite. *Clays and Clay Minerals* 47, 338–347.
- van der Gaast, S.J., Wada, K., Wada, S.-I., Kakuto, Y., 1985. Small-angle X-ray powder diffraction, morphology, and structure of allophane and imogolite. *Clays and Clay Minerals* 33, 237–243.
- van Olphen, H., 1965. Thermodynamics of interlayer adsorption of water in clays, I Sodium vermiculite. *Journal of Colloid Science* 20, 822–837.
- van Olphen, H., 1969. Thermodynamics of interlayer adsorption of water in clays, II Magnesian vermiculite. In: *Proceedings of the 3rd International Clay Conference*, Tokyo. Israel University Press, Jerusalem, vol. 1, pp. 649–657.
- Van Scoyoc, G.E., Serna, C., Ahlrichs, J.L., 1979. Structural changes in palygorskite during dehydration and dehydroxylation. *American Mineralogist* 64, 216–223.
- Veblen, D.R., 1992. Electron microscopy applied to nonstoichiometry, polysomatism, and replacement reactions in minerals. In: Buseck, P.R. (Ed.), *Minerals and Reactions at the Atomic Scale: transmission Electron Microscopy*. *Reviews in Mineralogy* vol. 27, pp. 181–223.
- Veblen, D.R., Wylie, A.G., 1993. Mineralogy of amphiboles and 1:1 layer silicates. In: Guthrie, G.D. Jr., Mossman, B. (Eds.), *Health Effects of Mineral Dusts*. *Reviews in Mineralogy*, vol. 28. Mineralogical Society of America, Washington, DC, pp. 61–131.
- Velde, B., Köster, H.M., 1992. A kinetic model of the smectite-to-illite transformation based on diagenetic mineral series. *American Mineralogist* 77, 967–976.
- Wada, K., 1989. Allophane and imogolite. In: Dixon, J.B., Weed, S.B. (Eds.), *Minerals in Soil Environments*, 2nd edition. Soil Science Society of America, Madison, WI, pp. 1051–1087.
- Wada, K., 1995. Structure and formation of non- and para-crystalline aluminosilicate clay minerals: a review. In: Churchman, G.J., Fitzpatrick, R.W., Eggleton, R.A. (Eds.), *Clays: Controlling the Environment*, *Proceedings of the 10th International Conference*, Adelaide, 1993. CSIRO Publishing, Melbourne, pp. 443–448.
- Wada, S.-I., Wada, K., 1977. Density and structure of allophane. *Clay Minerals* 12, 289–298.

- Wardle, R., Brindley, G.W., 1972. Crystal structures of pyrophyllite, 1Tc, and of its dehydroxylate. *American Mineralogist* 57, 732–750.
- Watanabe, T., 1988. The structural model of illite/smectite interstratified minerals and the diagram for its identifications. *Clay Science* 7, 97–114.
- Weaver, C.E., 1960. Possible uses of clay minerals in search for oil. *American Association of Petroleum Geologists Bulletin* 44, 1505–1518.
- Weber, K., 1972. Notes on the determination of illite crystallinity. *Neues Jahrbuch für Mineralogie—Monatshefte*, 267–276.
- Weiss, Z., Đurovič, S., 1984. Polytypism of pyrophyllite and talc. *Silikáty* 28, 289–309.
- Welch, M.D., Marshall, W.G., 2001. High-pressure behavior of clinocllore. *American Mineralogist* 86, 1380–1386.
- Wells, N., Childs, C.W., Downes, C.J., 1977. Silica Springs, Tongariro National Park, New Zealand—analysis of the spring water and characterization of the alumino-silicate deposit. *Geochimica et Cosmochimica Acta* 41, 1497–1506.
- Wicks, F.J., O'Hanley, D.S., 1988. Serpentine minerals: structure and petrology. In: Bailey, S.W. (Ed.), *Hydrous Phyllosilicates (Exclusive of Micas)* Reviews in Mineralogy, vol. 19. Mineralogical Society of America, Washington, DC, pp. 91–159.
- Wicks, F.J., Whittaker, E.J.W., 1975. A reappraisal of the structures of the serpentine minerals. *Canadian Mineralogist* 13, 227–243.
- Wiewióra, A., Rausell-Colom, J.A., García-González, T., 1991. The crystal structure of amesite from Mount Sobotka: a nonstandard polytype. *American Mineralogist* 76, 647–652.
- Wiewióra, A., Weiss, Z., 1990. Crystallochemical classifications of phyllosilicates based on the unified system of projection of chemical composition, II. The chlorite group. *Clay Minerals* 25, 83–92.
- Yoshinaga, N., 1986. Recent clay mineralogical studies of Ando soils—a review. *Nendo Kagaku* 26 (4), 281–291.
- Yuan, G., Theng, B.K.G., Parfitt, R.L., Percival, H.J., 2000. Interactions of allophane with humic acid and cations. *European Journal of Soil Science* 51, 35–41.
- Yucel, A.M., Rautureau, M., Tchoubar, D., Tchoubar, C., 1981. Calculation of the X-ray powder reflection profiles of very small needle-like crystal, II. Quantitative results on Eskischir sepiolite fibers. *Journal of Applied Crystallography* 14, 431–454.
- Zheng, H., Bailey, S.W., 1994. Refinement of the nacrite structure. *Clays and Clay Minerals* 42, 46–52.
- Zheng, H., Bailey, S.W., 1997. Refinement of an amesite—2H<sub>1</sub> polytype from Postmasburg, South Africa. *Clays and Clay Minerals* 45, 301–310.
- Zöller, M., Brockamp, O., 1997. 1M- and 2M1-illites: different minerals and not polytypes. Results from single-crystal investigations at the transmission electron microscope (TEM). *European Journal of Mineralogy* 9, 821–827.
- Zoltai, T., 1981. Amphibole asbestos mineralogy. In: Veblen, D.R. (Ed.), *Amphiboles and Other Hydrous Pyriboles*. Reviews in Mineralogy, vol. 9. Mineralogical Society of America, Washington, DC, pp. 237–278.
- Zussman, J., 1954. Investigation of the crystal structure of antigorite. *Mineralogical Magazine* 30, 498–512.
- Zvyagin, B.B., 1957. Determination of the structure of celadonite by electron diffraction. *Soviet Physics, Crystallography* 2, 388–394.



- Zvyagin, B.B., 1963. The theory of polymorphism in chlorite. *Kristallografiya* 8, 32–38 (abstract).
- Zvyagin, B.B., 1967. *Electron Diffraction Analysis of Clay Mineral Structures*. Plenum Press, New York.
- Zvyagin, B.B., Berkhin, S.I., Gorshkov, A.I., 1966. Structural characteristics of halloysite based on X-ray and electron-diffraction patterns. *Akademii Nauk SSSR*, 69–93 (in Russian, English abstract).
- Zvyagin, B.B., Drits, V.A., 1996. Interrelated features of structure and stacking of kaolin mineral layers. *Clays and Clay Minerals* 44, 297–303.
- Zvyagin, B.B., Mishchenko, K.S., 1965. Diagnostics of one-stacking semirandom polymorphic modifications of chlorites. *Kristallografiya* 10, 555–557 (abstract).
- Zvyagin, B.B., Mishchenko, K.S., Shitov, V.A., 1963. Electron diffraction data on the structures of sepiolite and palygorskite. *Soviet Physics, Crystallography* 8, 148–153.
- Zvyagin, B.B., Mishchenko, K.S., Soboleva, S.V., 1968. Structures of pyrophyllite and talc in the light of the multiplicity of types of mica-like. *Kristallografiya* 13, 599–604.
- Zvyagin, B.B., Soboleva, S.V., Fedotov, A.F., 1972. Refinement of nacrite structure by a high-voltage electron-diffraction method. *Kristallografiya* 17, 514–520.
- Zvyagin, B.B., Soboleva, S.V., Fedotov, A.F., 1979. Determination of the crystal structures of layer silicates, 4. Crystal structure of nacrite. In: Drits, V.A. (Ed.), *Vysokovol'tnaya Elektronogr. Issled. Sloistyykh Miner.* vol. 171–177. Izd. Nauka, Moscow, pp. 216–223.

### *Chapter 3*

## **SURFACE AND INTERFACE CHEMISTRY OF CLAY MINERALS**

**R.A. SCHOONHEYDT<sup>a</sup> AND C.T. JOHNSTON<sup>b</sup>**

<sup>a</sup>*Center for Surface Chemistry and Catalysis, Kuleuven, B-3001 Leuven, Belgium*

<sup>b</sup>*Department of Soil and Environmental Sciences, Purdue University, West Lafayette, IN 47907-1150, USA*

The surface properties of clay minerals depend on many factors including chemical composition, nature of the surface atoms (mainly oxygen and hydrogen), extent and type of defect sites, layer charge and the type of exchangeable cation(s) (see Chapter 2). One distinguishes between the edge surface and the planar surface, edges being usually associated with defect sites and pH-dependent charges (see also Chapter 5). Here we start with a description of the surface atoms and surfaces of clay minerals and continue with the interaction between the surface atoms and adsorbed molecules with special attention to water. This is followed by a discussion of the surface chemistry of smectites in aqueous suspension, leading to the exciting recent research on clay mineral nanofilms. The general principles are given and illustrated with specific examples. Experimental data are mainly derived from spectroscopic studies.

### **3.1. SURFACE ATOMS**

The basal surface atoms of a 2:1 clay mineral are the oxygen atoms of the Si-tetrahedra; for 1:1 minerals the surface is constituted by the same type of oxygen atoms on the Si-side of the layer and by OH groups from Al-octahedra (kaolinite) and Mg-octahedra (serpentine) on the Al- or Mg-side of the layer. These basal surface oxygen atoms and hydrogen atoms are chemically similar but are crystallographically different.

Permanent charge is introduced onto the siloxane surface of clay minerals as a result of isomorphous substitution. Common examples are Al for Si in the tetrahedral sheet and Mg for Al in the octahedral sheet. When Al substitutes for Si in the tetrahedral sheet, local distortions occur because of the difference between the Si–O and Al–O bond lengths, respectively, 0.162 and 0.177 nm (Nemecz, 1981). The bridging oxygen, Si–O–Al, is similar to the bridging oxygen in zeolites (Sauer, 1989).

The most important structural-chemical information about the surface oxygens can be obtained from simple considerations of the Pauling electronegativity of the atoms of the crystallographic unit cell (Table 3.1).

As the ionicity of a bond is proportional to the difference in electronegativities of the atoms, involved in the bond, it follows that the ionicity of the bonds in clay minerals follows the order:

$$\text{H-O} < \text{Si-O} < \text{Al}_{\text{subind}} : -\text{O} < \text{Mg}_{\text{subind}} : -\text{O} < \text{Li-O}$$

As a consequence, the charge on the oxygen is expected to increase in the same order (i.e., Si < Al < Mg < Li). Although these considerations are oversimplified because they do not take into account the structure and chemical composition of the clay mineral, nor the coordination of the cations, they provide the correct qualitative differences between these structural cations. Sanderson’s (1976) electronegativity equalisation principle states that the electron flow in a molecule or solid in the ground state is such that, at equilibrium, the electronegativities of all the atoms are equal. The electronegativity of molecules and solids is then calculated as the geometric mean of the electronegativities of the constituent atoms (Table 3.1). The calculated electronegativity values of selected clay minerals are given in Table 3.2.

Table 3.1. Electronegativity of the most common atoms in clay minerals<sup>a</sup>

Atom	χ (Pauling)	χ (Sanderson)
O	3.44	3.46
Si	1.90	1.74
Al	1.61	1.54
Mg	1.31	1.42
Li	0.98	0.86
H	2.2	2.31

<sup>a</sup>From Huheey (1978).

Table 3.2. Sanderson’s electronegativity values of typical clay minerals

Clay	Idealised chemical formula	χ (Sanderson)	χ (EEM)
Hectorite	Si <sub>3</sub> Mg <sub>5.25</sub> Li <sub>0.75</sub> O <sub>20</sub> (OH) <sub>4</sub>	2.760	
Beidellite	Si <sub>7.25</sub> Al <sub>0.75</sub> Al <sub>4</sub> O <sub>20</sub> (OH) <sub>4</sub>	2.928	
Montmorillonite	Si <sub>8</sub> Al <sub>3.5</sub> Mg <sub>0.5</sub> O <sub>20</sub> (OH) <sub>4</sub>	2.927	5.11
Kaolinite	Si <sub>4</sub> Al <sub>4</sub> O <sub>10</sub> (OH) <sub>8</sub>	2.895	3.27

Table 3.3. Charges on surface atoms, obtained by EEM

Structure	Atom	Electronic charge
Kaolinite	H(inner)	0.152
	H(surface)	0.219
Montmorillonite	O(no cation)	−0.522 to −0.741 <sup>a</sup>
	O(K <sup>+</sup> )	−0.800 to −0.867 <sup>a</sup>

<sup>a</sup>The charge depends on the crystallographic position.

Using the semi-empirical electronegativity equalisation method (EEM), (Mortier, 1987) the structure of the clay minerals can also be taken into account in the calculations. This has been done for kaolinite and K<sup>+</sup>-montmorillonite (Nulens et al., 1998). These numbers are also given in Table 3.2.

The data show that beidellite with tetrahedral Al in the structure is the most electronegative 2:1 clay mineral and is predicted to have the most reactive surface.

Besides these overall chemical properties of clay minerals, special attention must be given to the surface atoms: oxygen and hydrogen. When one compares the charges on the atoms calculated with the EEM method (Nulens et al., 1998), two trends are immediately clear. The charge on the surface hydrogen atoms of kaolinite is higher than on the inner hydrogen atoms; and the charge on the oxygen atoms in contact with an exchangeable cation is higher than in the absence of exchangeable cations. In other words, the cations (represented as point charges) polarise the oxygen atoms with which they are in contact (Table 3.3).

One comes then to the following general conclusions about the surface properties of clay minerals. In the absence of isomorphous substitution and defect sites, the clay–mineral surface is composed of oxygen atoms involved in Si–O bonds. The latter have considerable covalent character and the surface is hydrophobic. Hydrophilicity is introduced by isomorphous substitution inducing the presence of exchangeable cations, which are hydrophilic and which polarise the surface oxygen atoms (Nulens et al., 1998). Hydrophilicity may also arise from the presence of hydroxyl groups at the surface such as in kaolinite and from defect sites.

## 3.2. SURFACE STRUCTURES AND PROPERTIES

### 3.2.1. The Neutral Siloxane Surface

The least reactive surface found on clay minerals under ambient conditions is the neutral siloxane surface that occurs on 2:1 phyllosilicates where no isomorphous substitution has occurred (e.g., talc and pyrophyllite), and on the Si-tetrahedral side

of 1:1 kaolin group (Yariv, 1992; Giese and van Oss, 1993; Michot et al., 1994; Charnay et al., 2001).

The external oxygen atoms on the siloxane surface are relatively weak electron donors (Lewis bases) and are not capable of having strong interactions with water molecules. Minerals dominated by the neutral siloxane surface (e.g., talc and pyrophyllite) are hydrophobic as evidenced by contact angle and flotation measurements (Giese et al., 1990; Schrader and Yariv, 1990; Michot et al., 1994; Malandrini et al., 1997). These surfaces are non-polar and are not capable of forming hydrogen bonds with water molecules. Recent theoretical studies have shown that the neutral siloxane surface interacts only weakly with water molecules (Nulens et al., 1998). With this type of surface, the water molecules interact predominantly with each other and not with the surface. Additional support comes from a recent *ab initio* molecular dynamics study of the water–siloxane surface interactions (Tunega et al., 2002) where very weak hydrogen bonds are spontaneously broken and created by the movement of water molecules.

### 3.2.2. Constant Charge Sites (*Siloxane Surface with Permanent Charge*)

Many of the chemical and physical surface properties of 2:1 phyllosilicates are influenced by the extent and location of isomorphous substitution in the clay mineral structure. When substitution occurs in the octahedral sheet, the negative charge is more delocalised and the Lewis base character of the siloxane surface is enhanced (Sposito, 1984).

Depending on the extent of isomorphous substitution, these negatively charged sites are separated by distances ranging from 0.7 to 2 nm on the basal surface. The negative charge that results from isomorphous substitution is balanced by the presence of exchangeable cations of which  $\text{Ca}^{2+}$ ,  $\text{Mg}^{2+}$ ,  $\text{K}^{+}$  and  $\text{Na}^{+}$  ions are the most common. The chemical nature of these exchangeable cations (i.e., effective ionic radius, hydration energy, hydrolysis constant) determines many of the important chemical and physical properties of clay minerals. A common feature to these cations is that they all have appreciable enthalpies of hydration, with values ranging from  $-300$  to  $-1500 \text{ kJ mol}^{-1}$  (Atkins and de Paula, 2002). As a result, these cations are capable of acquiring complete or partial hydration shells, the effect of which is to impart an overall hydrophilic nature to the clay mineral. Furthermore, the water molecules surrounding these cations have chemical and physical properties that are distinct from those of bulk water because of their close proximity to the metal cation. Their mobility is more restricted due to polarisation effects by the cation and depends on the nature of the interlayer cation. The water molecules coordinated to the cations can be considerably more acidic than the bulk water. There is increased interest in the swelling mechanisms of clay minerals and the interplay between the hydrophobic and hydrophilic character of clay minerals (Chang et al., 1998; Great-house and Sposito, 1998; Swenson et al., 2000; Sutton and Sposito, 2001; Hensen and Smit, 2002).

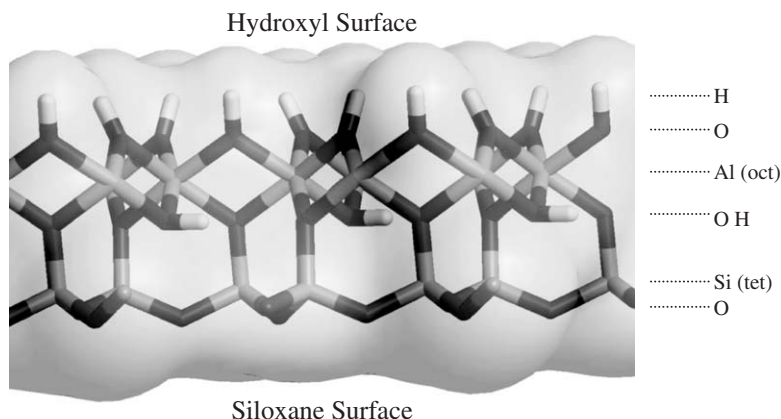


Fig. 3.1. Hydroxyl and siloxane surface of kaolinite.

### 3.2.3. The Hydroxyl Surface

Another type of surface that clay minerals and related hydroxides possess is the hydroxyl surface. An example is the Al-octahedral surface of kaolinite, shown in Fig. 3.1. This surface is found on 1:1 (kaolin group minerals, halloysite, serpentine) and 2:1:1 (e.g., chlorite) phyllosilicates and also on hydroxides such as gibbsite and brucite.

In the case of kaolinite, the two surfaces (hydroxyl and siloxane) have very different structures and corresponding surface chemistries. This was shown recently in an *ab initio* molecular dynamics study of water interacting with both types of surfaces (Tunega et al., 2002). Unlike the siloxane surface, which interacts very weakly with interfacial water molecules, the hydroxyl surface interacts strongly with water. This is shown in Figs. 3.2 and 3.3 where the closest  $O_{\text{surface}}$  to  $O_{\text{water}}$  distances are plotted over the time course of the molecular dynamics study. The average O...O distances for two different surface oxygen atoms in the tetrahedral sheet are 0.445 and 0.427 nm, respectively. In contrast, the corresponding  $O_{\text{surface}}$  to  $O_{\text{water}}$  distances for the oxygen atoms in the hydroxyl plane are 0.263 nm. The considerably shorter distance for the octahedral oxygen atoms reflects the fact that water molecules are hydrogen bonded to the hydroxyl surface. The hydroxyl groups on the basal surfaces of gibbsite and 1:1 phyllosilicates, as well as goethite and other oxides, are coordinated to metal atoms whose coordination environment is complete, and hence are considered to have minimal chemical reactivity.

Hydroxyl groups located at broken edges, steps and related defects of clay minerals and oxides are different, however, and are called ‘terminal OH groups’. These OH groups are under-coordinated and carry either a positive or negative charge depending on the type of metal ion and the pH of the ambient aqueous solution (Fig. 3.4). The pH value where the net surface charge is zero is referred to as the

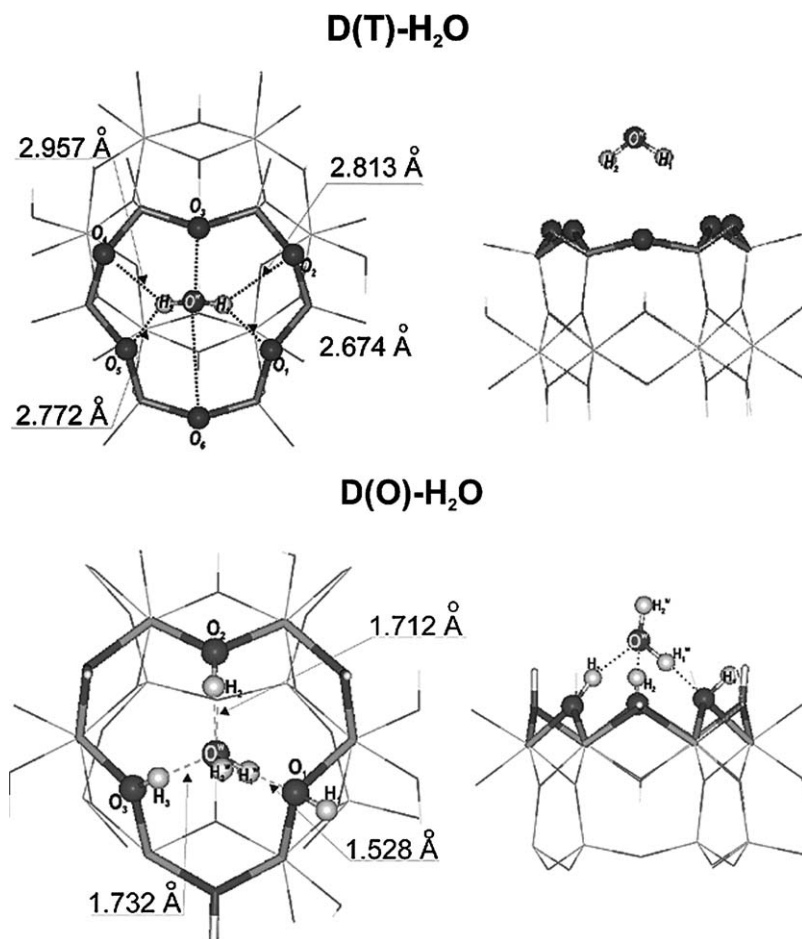


Fig. 3.2. Two views on the H<sub>2</sub>O molecule interacting with the octahedral side of the kaolinite layer. The lengths of hydrogen bonds obtained from static relaxations are given in the figure.

point of zero charge (p.z.c.). At pH values higher than the p.z.c of a mineral, the surface will have a net negative charge and will tend to accumulate cationic species. Similarly, the edge surface will have a net positive charge when the ambient pH is lower than the p.z.c. These terminal OH groups also have the potential to chemisorb (also referred to as specific adsorption) certain types of ions, regardless of the pH value. An example is the high affinity of both terminal Al–OH and Fe–OH groups for the phosphate ion. Because these (under-coordinated) terminal OH groups have either a partial positive or partial negative charge, these sites are more reactive than the charge-neutral OH groups on basal surfaces.

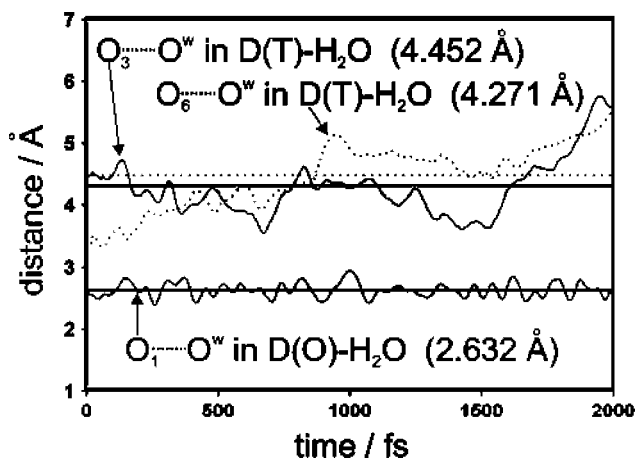


Fig. 3.3. The time evolution of the distances between the water oxygen atom and two-basal surface atoms ( $O_3$  and  $O_6$ ) in the  $D(T)\text{-H}_2\text{O}$  system (two upper curves). The bottom curve represents the time evolution of the  $O_1\cdots O_w$  distance in the  $D(O)\text{-H}_2\text{O}$  system. Horizontal lines indicate mean values and correspond to the numbers given in the figure.

Gibbsite - edge view

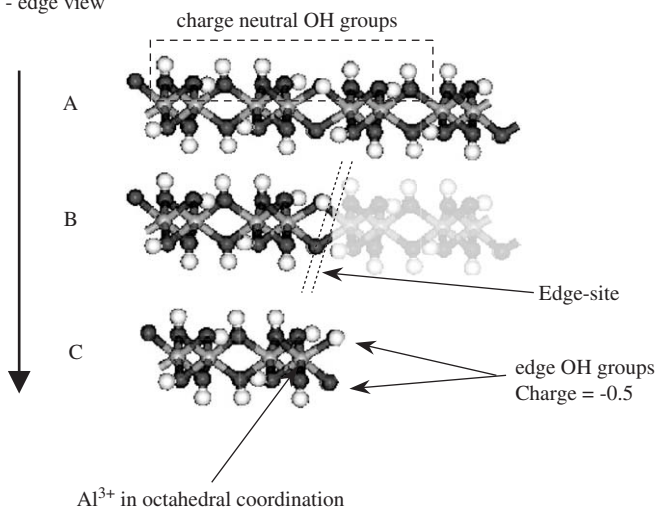


Fig. 3.4. Edge sites of kaolinite.



### 3.2.4. Hydrophobic–Hydrophilic Character of Clay Mineral Surfaces

The neutral siloxane surfaces found on kaolinite, talc and pyrophyllite have an overall hydrophobic character (Yariv, 1992; Giese and van Oss, 1993; Michot et al., 1994; Charnay et al., 2001). These clay minerals have little, if any, isomorphous substitution, and there is no permanent charge or dipole moment associated with their basal surfaces. Although polar molecules, including water and aqueous electrolytes have a low affinity for the neutral siloxane surface (Michot et al., 1994), non-polar organic solutes (van Oss et al., 1992; Giese and van Oss, 1993), and the non-polar portion of larger biological molecules, such as proteins and enzymes (Servagent-Noinville et al., 2000), can interact with the siloxane-type of surface.

On a more restricted spatial scale, this type of surface also occurs between hydrated cations sites on the basal surface of smectites and vermiculites (Fig. 3.5). The accessibility of non-polar compounds to these sites is controlled by the surface charge density of the clay mineral, and the nature of the exchangeable cation and its

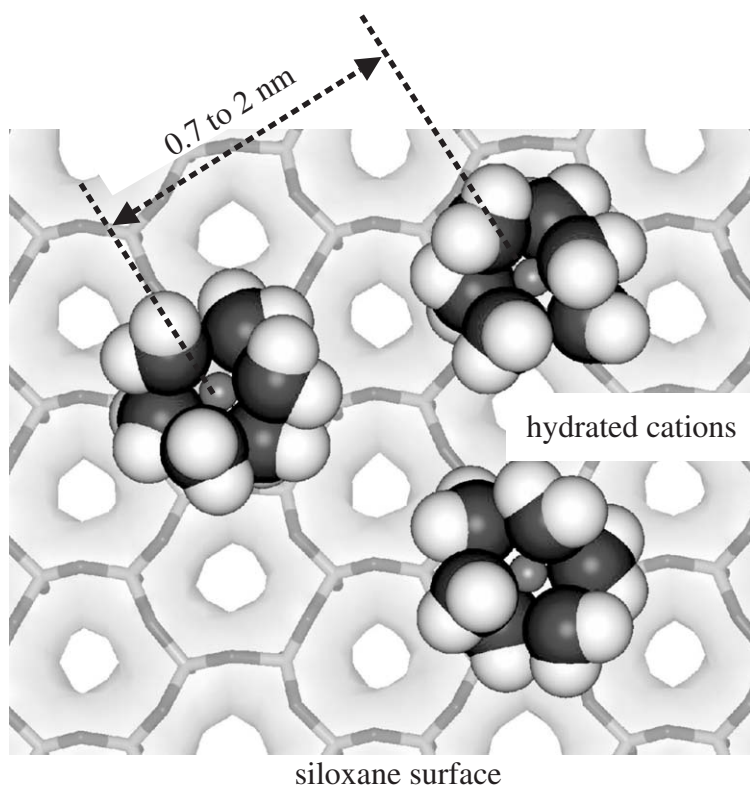


Fig. 3.5. Sites at siloxane surface.

corresponding enthalpy of hydration. For smectites with relatively low surface charge density and containing weakly hydrated exchangeable inorganic cations (e.g.,  $K^+$  and  $Cs^+$ ), the interaction of organic molecules with these surface sites can be significant. Current evidence has shown that these non-polar regions between isomorphous substitution sites have some hydrophobic character. Jaynes and Boyd (1991) and Boyd and Jaynes (1994) have examined the hydrophobicity of clay minerals containing these types of surface sites by measuring the adsorption of aromatic hydrocarbons from water by smectites exchanged with inorganic and organic cations. When alkali and alkaline earth cations are present at exchange sites, little, if any, hydrocarbon sorption occurs because the hydrated cations obscure the hydrophobic regions. However, when the inorganic cations are replaced by the relatively small trimethyl phenylammonium (TPMA) cation, significant sorption takes place. Since the 'footprint' (i.e., cross-sectional area) of this cation is relatively small, a portion of the siloxane surface is accessible to organic solutes. The sharp increase in organic sorption for these organically modified smectites is attributed, in part, to hydrophobic surface interactions between the organic solute and the siloxane surface.

Additional evidence comes from the work by Laird et al. (1992) on the sorption of atrazine from water on 13 different types of  $Ca^{2+}$ -exchanged smectites, ranging from low- to high-layer charge. As shown in Fig. 3.6, the Freundlich sorption coefficients range from  $<0.01$  to 1330. This is remarkable since all of the sorbents are  $Ca^{2+}$ -smectites. With smectites of low-charge densities, surface charge density of the clay is

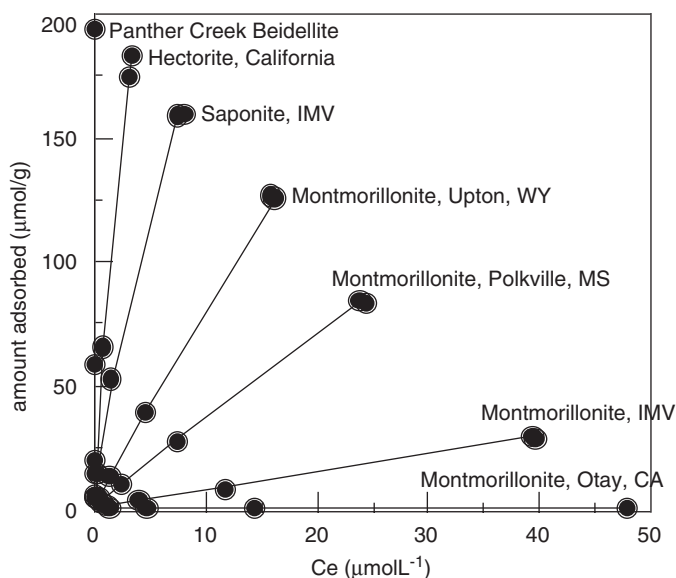


Fig. 3.6. Adsorption of atrazine by  $Ca^{2+}$ -smectites.

the most important determinant of its affinity for atrazine. In both examples, as charge density decreases, the size of the adsorptive region between neighbouring exchangeable cations increases. As a result, the siloxane surface becomes more accessible to atrazine (and other aromatic hydrocarbons). In the case of  $\text{Ca}^{2+}$ -smectites, the greater separation of exchangeable cations allowed atrazine sorption (up to 100% of that added) even though the presence of hydration water around  $\text{Ca}^{2+}$  would obscure some of the siloxane surface. These studies clearly established the importance of surface charge density to the adsorptive capabilities of smectites for non-polar organic compounds (NOCs). These experimental findings are supported by theoretical studies. For example, in a theoretical study of water molecules clustered near the siloxane surface of kaolinite, the water molecules had a tendency to avoid this surface consistent with its hydrophobic character (Nulens et al., 1998).

In contrast, the presence of hydrated cations, such as  $\text{Na}^+$ ,  $\text{K}^+$ ,  $\text{Mg}^{2+}$  and  $\text{Ca}^{2+}$ , in the interlayer region of smectites and vermiculites impart an overall hydrophilic nature to these clay minerals. The hydration dynamics of these cations, and the interaction of water with these metal ions underlie many of the important processes associated with clay minerals including their ability to swell in water. Expandable clay minerals are known to be strongly hydrophilic and this is largely attributed to the hydration of certain inorganic cations (Sposito and Prost, 1982; Jouany and Chassin, 1987; Johnston et al., 1992; Xu et al., 2000). In addition, the hydroxylated surface of gibbsite, and the gibbsite-like surface of kaolinite have some hydrophilic character (Nulens et al., 1998). Central to these processes are the clay–water interactions and this will be reviewed in the next section.

### 3.3. CLAY–WATER INTERACTIONS

Since the first reported infrared study of clay–water interactions by Buswell et al. (1937), water has been used to probe the clay–water interface. The chemical and physical properties of clay minerals are integrally linked to some aspect of how water interacts with the clay surface. Examples include essentially all of the adsorptive, catalytic and cationic exchange reactions. In fact, many of the interesting features of clay–water interactions are observable at the macroscopic level, including such properties as shrink–swell phenomena, water sorption, plasticity and catalysis.

Smectites, for example, have exceptional water sorption characteristics. Mooney et al. (1952a, 1952b) were among the first authors to show that smectites were able to sorb up to half of their mass in water and that the water sorption behaviour is strongly dependent on the nature of the exchangeable cation. The mechanisms underlying these interactions have been the subject of intense studies in recent years using a broad spectrum of sophisticated experimental and computational approaches. Examples include infrared and Raman spectroscopy, a wide range of nuclear magnetic resonance (e.g.,  $^2\text{H}$ ,  $^{29}\text{Si}$ ,  $^{27}\text{Al}$ ,  $^{23}\text{Na}$ ,  $^7\text{Li}$ ), electron spin resonance,

neutron scattering, neutron and X-ray diffraction and dielectric relaxation. Recognising that each of these experimental methods has a time scale associated with it, the structural information was grouped into two categories: vibrationally averaged structure ('V structure') is measured at a short-time scale, while diffusionally averaged structure ('D structure') is obtained over a long-time scale, both contributing to our knowledge about the structure and behaviour of water. For example, the time scale associated with nuclear magnetic resonance spectroscopy is generally between  $10^{-10}$  and  $10^{-3}$  s, whereas infrared and Raman spectroscopies measure vibrational transitions that occur over a much shorter time frame of  $10^{-15}$  to  $10^{-12}$  s (see Chapter 12.6).

For the purposes of our discussion, we will consider clay–water interactions from two different perspectives. First, the influence of the clay surface on the structure and properties of water will be examined. Most of the work on clay–water interactions has focused on this topic and has been the subject of several reviews (e.g. [Sposito and Prost, 1982](#)). Second, recent studies have demonstrated that the clay structure itself is influenced by changes in water content. Also, appropriate experimental methods have to be selected to provide information about the exchangeable cation itself.

### 3.3.1. Structure and Properties of Water Sorbed to Clay Mineral Surfaces

Because of their unique expansive nature, smectites and vermiculites are the most important clay minerals related to clay–water interactions. For these clay minerals, the initial sorption of water and related polar solvents, such as methanol, is influenced mainly by the hydration of exchangeable cations. These cations have substantial single-ion enthalpies and serve as strong hydrophilic sites for water and solvent sorption ([Annabi-Bergaya et al., 1980a, 1980b](#); [Cancela et al., 1997](#)). Numerous spectroscopic studies have shown that the properties of sorbed water are different from those of bulk water, especially when less than three layers of water are present in the interlayer region. Water sorption on clay surfaces often shows significant hysteresis because of differences in water adsorption and desorption mechanisms. Adsorption of water proceeds by initial solvation of the exchangeable cations, followed by the occupancy of remaining interlayer space. In the case of desorption, physisorbed water molecules in interparticle or interaggregate pores, and sorbed on external surfaces, are removed first followed by the desorption of the more strongly bonded water molecules coordinated to the exchangeable cations.

Water molecules coordinated to exchangeable cations have chemical and physical properties that are different from those of bulk water. NMR and dielectric relaxation studies have shown that these water molecules have fewer intermolecular interactions and actually rotate faster about the  $C_2$  axis as compared with bulk water. Infrared spectroscopy provides a direct means of studying water molecules and their interaction with other water molecules, solutes and surfaces. [Russell and Farmer \(1964\)](#) were among the first to show that water molecules coordinated to exchangeable cations were more strongly polarised than bulk water. More recently, [Johnston et al.](#)

(1992) measured the molar absorptivity of water molecules coordinated to different exchangeable cations in smectites as a function of water content. They found that the molar absorptivity of the  $\nu_2$  mode of water (i.e., the H–O–H bending mode) was up to three times greater than that of bulk water. Upon lowering the water content of the clay–water system, the position of the  $\nu_2$  band shifted to lower energy, indicating that the water molecules coordinated to exchangeable cations were less strongly hydrogen bonded compared with bulk water (Pimentel and McClellan, 1960; Poinsignon et al., 1978; Xu et al., 2000). By contrast, water molecules on polar surfaces tend to be more strongly hydrogen bonded at low water content.

The combined spectral data reveal that water molecules coordinated to exchangeable cations in the interlayer region are clustered around, and strongly polarised by, the exchangeable cation (Sposito and Prost, 1982). These water molecules apparently interact more strongly with the exchangeable cation and less strongly with each other. A similar behaviour has been reported for methanol interactions with montmorillonite exchanged with different cations (Annabi-Bergaya et al., 1980a, 1980b). One of the advantages of using a solvent molecule such as methanol is that it contains only one hydroxyl group, which simplifies spectral interpretation. A study of water sorption on talc suggested that the siloxane surface has some local hydrophilic character although the overall surface is strongly hydrophobic (Michot et al., 1994). Exchangeable cations control the sorption of water on clay surfaces at low water content but the influence of siloxane surfaces on water cannot be neglected, especially at high water content.

### 3.3.2. Influence of Water on Clay Mineral Structure

For many years, the presence of guest species, including water, in the interlayer space of 1:1 clay minerals (kaolin group of minerals) has been known to influence the inner-surface OH groups (Theng, 1974) and not only the surface hydroxyl groups.

Halloysite is a naturally occurring hydrated form of kaolinite intercalated with a monolayer of water molecules, giving a basal ( $d_{001}$ ) spacing of 1.0 nm ( $\sim 0.7$  nm for kaolinite plus  $\sim 0.3$  nm for water). Its structural formula is  $\text{Si}_4\text{Al}_4\text{O}_{10}(\text{OH})_8 \cdot 4\text{H}_2\text{O}$ . Costanzo et al. (1980, 1982) and Costanzo and Giese (1990) prepared partially hydrated kaolinite complexes with  $d$ -spacings of 0.84 and 0.92 nm. Infrared studies of these hydrated kaolinite complexes have shown that the inner OH groups of kaolinite are perturbed because of the partial collapse of the hydrated structure and keying of water molecules into the kaolinite structure (Costanzo et al., 1982). In addition to water, other small, polar molecules (e.g., hydrazine) could penetrate the ditrigonal cavities of the kaolinite and perturb the inner OH groups (Johnston and Stone, 1990; Johnston et al., 2000).

Similar mechanisms have also been shown to occur on expandable 2:1 clay minerals. For example, the  $\nu(\text{OH})$  band of trioctahedral vermiculite was perturbed by the presence of interlayer cations at different water contents (Fernandez et al., 1970). When  $\text{Na}^+$ -vermiculite is dehydrated, the interlayer cations migrate from the centre

of the interlayer space into the siloxane ditrigonal cavity and perturb the hydroxyl groups located at the base of this cavity. This has also been shown for other cations, including butylammonium (Serratosa et al., 1984). In an infrared study of reduced-charged smectites, the intensity of the hydroxyl deformation bands (e.g., Al–O(OH)–Al bending) is strongly reduced at low water content. This is attributed to the dehydration-induced movement of the exchangeable cations into the ditrigonal cavities (Sposito et al., 1983). Xu et al. (2000) have shown that the molar absorptivities of both the  $\nu(\text{OH})$  and  $\delta(\text{MOH})$  bands decrease upon lowering the water content.

There has been some speculation that in smectites the oxygen atoms of the siloxane surface interact directly with water molecules. In support of this hypothesis, the  $\nu(\text{Si–O})$  modes are coupled to the vibrational modes of water (Yan et al., 1996). In an aqueous suspension of smectite, this coupling is due to a change in particle orientation as the water content decreases (Johnston and Premachandra, 2001).

### 3.4. SURFACE CHEMISTRY IN AQUEOUS DISPERSIONS

Clay minerals often occur in an aqueous environment. Depending on the conditions they may be present as single layers, particles or aggregates (see Fig. 1.1). The ideal dispersion consists of individual layers that are randomly oriented and constantly moving. In 2:1 phyllosilicates, the surface consists of the planar siloxane surfaces and the edge surfaces.

To achieve this condition, very dilute aqueous dispersions of smectites, exchanged with small monovalent cations such as  $\text{Li}^+$  and  $\text{Na}^+$ , have to be prepared. A very sensitive molecule is used to probe these clay surfaces in an aqueous environment when there is an excess of water. Such a molecule must be selectively adsorbed, and be easily detectable at trace amounts by a spectroscopic technique, for example. Cationic dyes fulfil this requirement because they are very selectively ion-exchanged. At the same time, they are easily detected in trace amounts by visible spectroscopy due to their large extinction coefficients. This subject has been recently reviewed by Yariv and Cross (2002). Only the fundamental principles are considered in the following section.

#### 3.4.1. Preliminary Considerations

Table 3.4 lists the absorption maxima of the monomers of the most commonly used dyes on the clay mineral surface.

When these cationic dyes are ion-exchanged on the surface of smectites in dilute aqueous suspension, the clay mineral particles become hydrophobic. The clay–dye complexes form flocs and precipitate. To avoid this precipitation, the loading cannot exceed some threshold value, usually 10–15% of the cation exchange capacity (CEC) of the smectite. This loading can be increased using a very small size fraction

Table 3.4. Band positions of monomers of dye molecules in water and on the clay mineral surface

Cationic dye	$\lambda_{\text{max}}$ (nm) in water	$\lambda_{\text{max}}$ (nm) on clay mineral surface
Methylene blue	664	670, 652
Rhodamine 6G	526	533
Rhodamine B	555	562
Crystal violet	595	610
Thionine	595	621
Acridine orange	490	500

of the clay mineral ( $<0.5\mu\text{m}$ ). With Laponite with an average size of 20 nm (Thompson and Butterworth, 1992) loadings of up to 100% of the CEC can be achieved without precipitation.

In the absence of any other specific interactions, the ion exchange of cationic dyes leads to a concentration of the dye molecules around the elementary clay layers. Similarly, increasing the concentration of dyes in aqueous solution gives rise to dimers and aggregates, which have their own spectroscopic signatures. The same behaviour occurs in the clay mineral suspension.

However, the environment of the dye molecules at the clay surface is different from that in pure water. Two situations can be envisaged. Firstly, the dye molecule is adsorbed and as a result, the water molecules in the first coordination sphere of the dye are partially replaced by oxygen atoms of the clay mineral surface. Secondly, the adsorbed dye molecule remains completely surrounded by water molecules and there is no replacement of water molecules by surface oxygen atoms. In both cases, the environment of the adsorbed dye molecules is different from that of its counterpart in bulk water. Therefore, the absorption maxima of the dye molecules adsorbed on the clay mineral surfaces are expected to shift from those in water. These shifts can be towards longer wavelengths or towards shorter wavelengths, as explained below.

### 3.4.2. Spectroscopy

All dye molecules of Table 3.4 have a dipole moment of the ground state and a dipole moment of the electronically excited state. These dipoles interact with the solvent molecules (water) and with surface oxygen atoms. The position of the band maximum of the electronic transition is then influenced by these interactions. This is schematically shown in Fig. 3.7. Thus, if the solvent–molecule interaction is stronger in the excited state than in the ground state a red shift of the band position of the monomer is expected and the reverse is true for a weaker solvent–molecule interaction in the excited state. In most cases a red shift is observed, indicating a stronger interaction of the excited dye molecules with water and surface oxygen atoms than



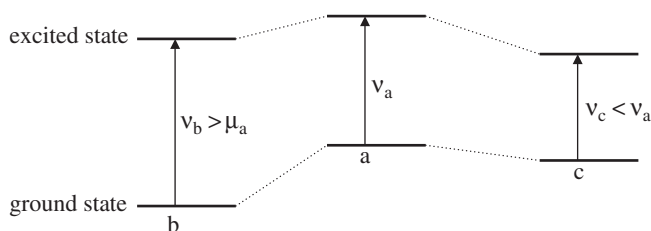


Fig. 3.7. Ground state and excited state of a dye molecule (a) in vacuo; (b) the solvent interacts more strongly with the ground state than with the excited state and (c) the solvent interacts more strongly with the excited state than with the ground state.

the dye molecules in their ground state. If the solvent is more polar than water a red shift of the band maximum of the electronic transition will be observed and a blue shift for a less polar solvent than water.

#### A. Monomers, Dimers and Aggregates

One observes a red shift for the dyes upon transfer from aqueous solution to aqueous clay suspension, indicating that the environment of the clay-adsorbed dye is more polar than that of the dye in aqueous solution (Table 3.4). In the case of methylene blue (MB) and very small loadings (0.1% of the CEC) two monomer bands are observed, one is blue shifted (652 nm) and the other red-shifted (670 nm) with respect to the band position in aqueous suspension (664 nm). The relative intensity of these bands depends on the type of clay mineral, as shown in Fig. 3.8. This is indicative of two different environments for the MB molecules: one is less polar (652 nm), while the other is more polar (670 nm), than water (Cenens and Schoonheydt, 1988). The time of contact as well as the type of clay, and more specifically the site of isomorphous substitution, are important factors influencing the band position of the monomer (Jacobs and Schoonheydt, 1999). Isomorphous substitution in the tetrahedral sheet gives rise to localised charges at the clay mineral surface and this results in a strong MB-surface interaction. The dye molecule is predominantly in direct contact with the surface and the absorption maximum of the monomer is at 670 nm. For clay minerals with isomorphous substitution in the octahedral sheet, the negative layer charge is diffuse and the MB-surface interaction is weak. The dye molecule remains in the water phase near the siloxane surface. The band maximum of the monomer is at 652 nm.

Fig. 3.8 also shows a third type of monomer, the protonated MB ( $\text{MBH}^{2+}$ ) with its main absorption band at 760 nm. It is the only species present in the Barasym suspension at a loading of 0.1% of the CEC and it is present in trace amounts in the other clay suspensions. Thus all clay minerals in aqueous suspension contain trace concentrations of acid sites (ranging from about 0.1 to  $0.5 \mu\text{mol g}^{-1}$ ), probably located at the edges and strong enough to protonate MB ( $\text{pK}_a$  is about zero).



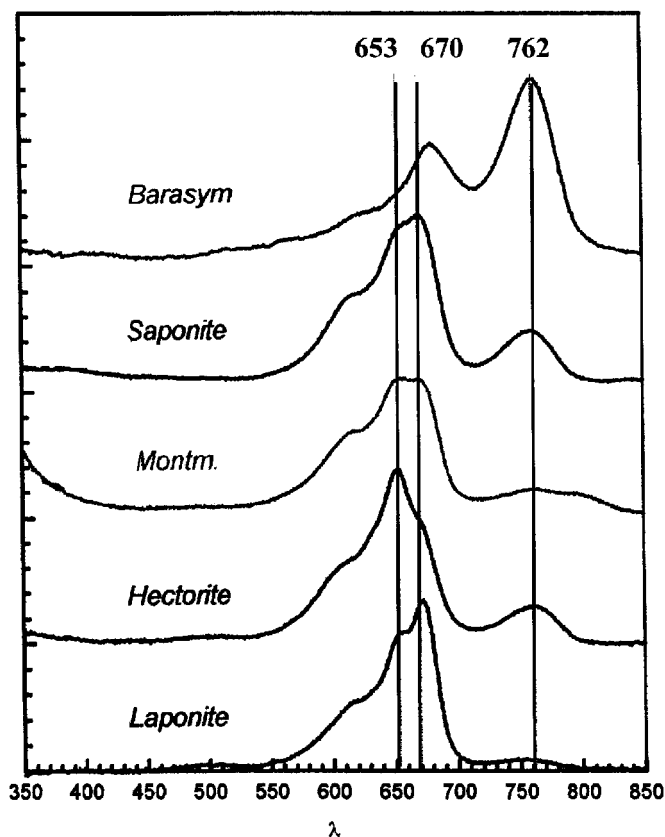


Fig. 3.8. Spectra of MB on smectites in aqueous suspension; the loading of MB is 0.1% of the CEC at 0.1 wt% clay in the suspension.

As the loading increases, more MB molecules reach the surface of the clay minerals and the dominant absorption maximum of the monomer is at 670 nm, irrespective of the type of smectite. In addition, the dye molecules are not randomly distributed over the surface. They preferentially form dimers and aggregates: the H-dimer is characterised by parallel transition dipole moments and absorbs around 600 nm; the J-dimer has antiparallel transition dipole moments and absorbs at 720 nm; and the H-aggregates absorb around 575 nm. Typical spectra of MB are given in Fig. 3.9. The relative intensity of these dimer and aggregate bands depends on the loading (the higher the loading the more intense the band of the H-aggregates); the type of exchangeable cation ( $\text{Cs}^+$ -smectites have more monomers than aggregates than  $\text{Na}^+$ -smectites); the type of clay mineral (particle size, CEC, isomorphous substitution) and time (indeed, clay-dye suspensions are not

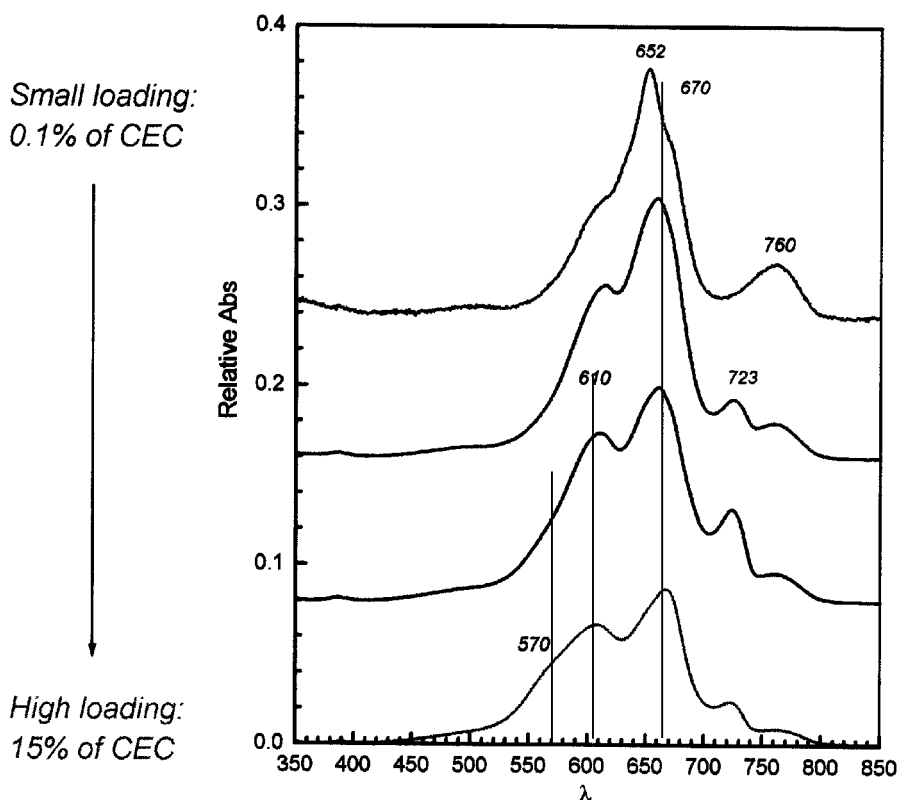


Fig. 3.9. Spectra of MB on hectorite in aqueous suspension; the amount of hectorite in the suspension is 0.1 wt%.

in a thermodynamic equilibrium, but may change slightly with time over weeks and months) (Jacobs and Schoonheydt, 2001).

In any case, clay–dye suspensions are complex systems, resulting from the balance of different interacting forces. The main forces are the dye–dye and dye–surface interactions.

In this discussion we have not specified interactions between the dye molecules and the surface oxygen atoms. Yariv and Cross (2002) have suggested that the  $\pi$ -electrons of the dye interact with the hybridised orbitals of the surface oxygen atoms, leading to a stabilisation of the  $\pi$ -orbitals and destabilisation of the  $\pi^*$ -orbitals. This gives rise to a blue shift of the absorption band of the adsorbed monomer.

When  $\text{Al}^{3+}$  substitutes for  $\text{Si}^{4+}$  in the tetrahedral sheet, the basicity of the surface oxygen atoms increases and so is the interaction with the  $\pi$ -orbitals. Thus, the blue shift of the monomer band of the adsorbed dye with respect to the monomer band in aqueous solution, due to the dye–surface interaction, reflects the basicity of the surface oxygen atoms.

This alternative explanation meets several difficulties. Indeed, as explained above, it is not evident that the monomer in an aqueous suspension, is in direct contact with the surface, in order to have the surface–dye interaction. In the case of MB, monomers in direct contact with the surface oxygen atoms absorb at 670 nm. This is a red shift of 8 nm with respect to the monomer absorption maximum in water, and contrary to the blue shift expected on the basis of the theory of Yariv and Cross (2002). Also, the removal of water (e.g., by air-drying) increases the interaction between the siloxane surface and the MB molecules and leads to a breakdown of the aggregates into monomers.

In summary, the organisation of the dye molecules at the clay mineral surface in aqueous suspensions is subjected to a sensitive balance of forces: molecule–molecule interactions, molecule–surface interactions, molecule–solvent and solvent–surface interactions. One would like to have control over the system, i.e., organise the molecules at the surface in the way we want. This requires quantitative knowledge of the different types of interactions. We are still far from that. In the mean time, the problem can be tackled experimentally and this is the subject of the next section.

### 3.5. ORGANISATION OF CLAY MINERAL PARTICLES AND MOLECULES

There are several ways of organising clay mineral particles: casting, spin coating, self-assembling, also called fuzzy-assembling or layer-by-layer deposition and application of the Langmuir–Blodgett (LB) technique. With all these techniques the goal is to obtain films, formed by continuous non-overlapping clay mineral layers. This ultimate goal can be attained to a large extent by self-assembling and by the LB technique. We limit the discussion to these techniques. These nanofilms are ideal samples for crystal-chemical studies of clay minerals, for studies of the adsorbed molecules and their organisation at the clay mineral surface, and for development of high-tech devices.

#### 3.5.1. Self-Assembling

Self-assembling, fuzzy-assembling or layer-by-layer deposition refers to the alternate deposition of sheets of positively charged molecules and layers of smectite on a suitable substrate, such as glass and mica. The deposition is done from dilute aqueous solutions of cationic polymers and from dilute aqueous clay dispersions. After each deposition the excess material is washed away, and the films are gently dried before a new deposition is made. The process of film formation has been studied by van Duffel et al. (1999) and Kotov (2001).

Atomic force microscopy (AFM) shows that each clay layer is not fully covered with clay mineral particles and contains appreciable amounts of empty spaces between the particles. It is therefore a sub-monolayer of randomly oriented partially overlapping clay layers. Although a linear increase of film thickness with number of

depositions has been observed, the partial overlap of randomly oriented clay layers in the film has two consequences: the extrapolation of film thickness to zero layers does not go exactly through the origin and the roughness of the films (measured as the standard deviation of the film height from the average along a straight line over the film) increases with the number of layers, and is proportional to the concentration of cationic polymer. For film thicknesses of approximately 80 nm the roughness attains values of 4–5 nm in the case of Laponite and 10–12 nm in the case of hectorite. If the cationic polymer is deposited in large amounts, it induces aggregation of clay mineral particles in the film and roughness is increased. A simple model has been developed describing the development of roughness as a function of the degree of coverage of each clay layer by the clay particles. Since Laponite has very small layer sizes, overlapping of layers in a particle does not occur. Surface coverages of 90% or more can be attained, leading to relatively smooth films. Being composed of particles with different sizes and shapes, hectorite gives surface coverages of 60–65% and more pronounced roughness than Laponite (van Duffel et al., 1999).

If functional films are to be prepared, the desired functionality has to be introduced. Several attempts have been published in the open literature. Thus, Kleinfeld and Ferguson (1994) have developed films with water-sensing properties, based on the layer-by-layer deposition of polydimethyl diallyl (PDDA) and smectite layers. van Duffel et al. (2001) have prepared films of smectite/PDDA/NAMO on glass substrate, with non-linear optical properties where NAMO is 4-[4-(*n*-allyl, *N*-methylamino) phenylazo] benzenesulphonic acid. When this film is illuminated with a Nd:YAG laser at 1064 nm, light at 532 nm is generated, the intensity of which depends on the type of clay mineral and the amount of PDDA in the film. The organisation of the positively charged PDDA polymers determines the organisation of the NAMO anions and in this case, an optimum configuration for the second harmonic light generation is obtained.

Films with magnetic properties have been prepared by Mamedov and Kotov (2000) and Mamedov et al. (2000). Here Fe<sub>2</sub>O<sub>3</sub> nanoparticles are organised in films together with the cationic polymer PDDA and smectite layers. The latter clearly serve for strengthening the films. Finally, the development of clay-based biosensors must be mentioned such as urease (de Melo et al., 2002) and polyphenol oxidase (Coche-Guérente et al., 1999) on Laponite; layer-by-layer deposition of clay mineral–polymer–protein (Lvov et al., 1996) and hydrogenase biosensor (Qian et al., 2002). Heme–protein–clay mineral films have also been used for electrochemical catalysis (Zhou et al., 2002). This field is under intense investigation and major developments can be expected in the future.

### 3.5.2. Langmuir–Blodgett Technique

A highly organised layer-by-layer deposition of elementary clay mineral particles can be achieved with the LB technique. In the early days of development, hydrophobic clay minerals are dispersed in a volatile organophilic solvent such as chloroform.

This dilute suspension is spread over the water surface in a LB trough, the chloroform evaporates, and the film of hydrophobic clay minerals is compressed and transferred on to a substrate (Kotov et al., 1994; Hotta et al., 1997a, 1997b).

A more elegant method is to spread the amphiphilic cations on the water surface of a dilute aqueous dispersion. The dispersion has been prepared at least 24 h before use so as to ensure complete swelling and delamination. The amphiphilic cations, dissolved in chloroform or chloroform–methanol mixture, are spread over the air–water interface of the dilute clay suspension in the LB trough. An instantaneous ion-exchange reaction with the amphiphilic cations takes place at the air–water interface, giving a monolayer of elementary clay layers covered with amphiphilic cations. The monolayer can be compressed and then transferred to a substrate by vertical upstroke or horizontal deposition. If the substrate is hydrophilic, vertical deposition is preferred; if it is hydrophobic, one can perform the horizontal deposition. In the first case the sequence is substrate/clay/amphiphilic cation; in the second case it is substrate/amphiphilic cation/clay. By repetition of the procedure multilayers are obtained. The film thickness and the amount of amphiphiles have been checked in the case of horizontal deposition. Both have been found to increase linearly with the number of layers deposited, indicating that the overall composition of the layers is identical (Umemura et al., 2001a, 2001b).

From the scientific point of view the LB films are also useful for crystal-chemical studies of the elementary clay mineral layers and for studies on the organisation of the amphiphilic cations at the clay mineral surface. Molecules with desired functionality have to be used for the fabrication of functional films.

Atomic force microscopy reveals beyond any doubt that the LB films contain elementary clay mineral layers. Further, if deposition is performed at a low surface pressure (in any case below the critical pressure of film destruction), a monolayer is formed, covering more than 90% of the surface of the substrate. Occasionally, particles of elementary clay mineral layers are found. Spectroscopy with polarised light is used to study the films that are horizontally deposited. Fig. 3.10 shows the spectra of the Si–O vibrations and the structural O–H vibrations of saponite. The band positions and dichroic ratios are given in Table 3.5.

These data confirm that the elementary clay mineral layers are lying flat on the surface of the ZnSe substrate, used to deposit the film. For the first time highly resolved spectra of the in-plane and out-of-plane Si–O vibrations have been obtained. It is confirmed that the structural OH groups of the trioctahedral saponite are vibrating almost perpendicular to the planar surface and those of the dioctahedral Wyoming bentonite almost horizontally to the surface of the clay minerals. The OH bending vibrations of Wyoming bentonite have slightly different dichroic ratios, suggesting that the orientation of these OH groups depends on the cationic composition of the octahedral sheet:  $\text{AlAlOH}$  ( $919\text{ cm}^{-1}$ ),  $\text{AlFeOH}$  ( $885\text{ cm}^{-1}$ ) and  $\text{AlMgOH}$  ( $846\text{ cm}^{-1}$ ) (Ras et al., 2003).

There are several spectroscopic techniques available to study the amphiphilic molecules adsorbed in mono- and multilayers, the most popular being FTIR and

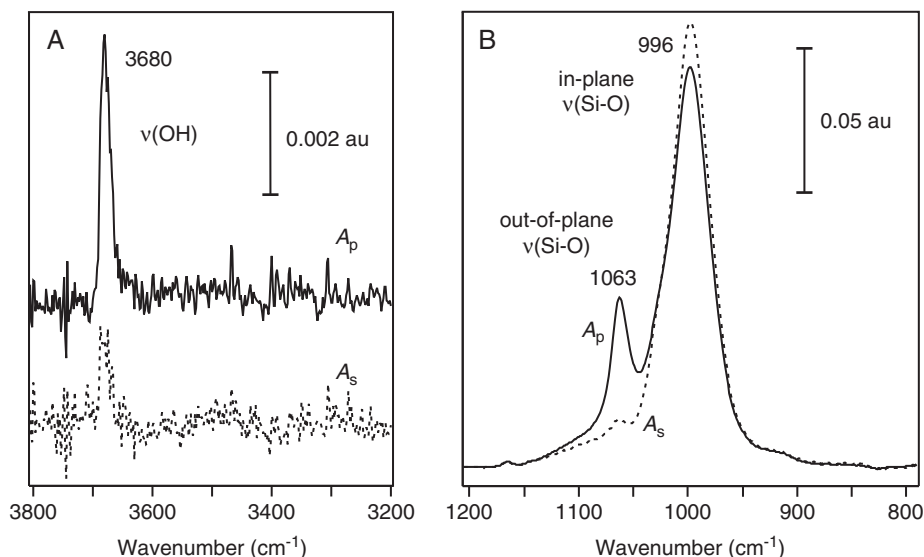


Fig. 3.10. Polarised ATR-FTIR spectra of a hybrid LB monolayer of SapCa-1 saponite and dioctadecyl thiacyanine surfactant prepared on a  $50 \text{ mg dm}^{-3}$  clay dispersion, deposited on ZnSe at a surface pressure of  $5 \text{ mN m}^{-1}$ : (A)  $\nu(\text{OH})$  region and (B)  $\nu(\text{Si-O})$  region.

Table 3.5. Band positions ( $\text{cm}^{-1}$ ) and dichroic ratios  $R$  ( $A_s/A_p$ )<sup>a</sup> of Si-O and O-H vibrations

Vibration	Saponite	Dichroic ratio	Wyoming bentonite	Dichroic ratio
In plane Si-O	996	1.11	1024	1.11
Out-of-plane Si-O	1063	0.23	1085	0.12
Stretching O-H	3680	0.33	3628	1.08
Bending O-H	<sup>b</sup>		919	1.18
			885	1.13
			846	1.31

<sup>a</sup> $A_s$  and  $A_p$  are, respectively, the absorption of in-plane and out-of-plane polarised light.

<sup>b</sup>Not detectable with ZnSe as substrate.

UV-VIS spectroscopy. With octadecylammonium (ODA) as the amphiphilic cation, the organisation of the alkyl chains is dependent on the concentration of the clay mineral in the suspension of the LB trough. At low concentration ( $< 10 \text{ ppm}$ ) the alkyl chains are highly ordered, similar to a crystalline ordering. This is reflected in the position of the  $\text{CH}_2$  stretching vibration at  $2925 \text{ cm}^{-1}$ . At higher clay concentration ( $> 10 \text{ ppm}$ ) the alkyl chains are disordered as evidenced from the  $2917 \text{ cm}^{-1}$  position of the  $\text{CH}_2$  stretch (Ras, 2003).

This difference in ordering has also been observed by Umemura et al. (2003). It indicates that at low clay concentration the ODA cations are organised at the air–water interface of the LB trough into two-dimensional crystalline aggregates to which the clay mineral particles are attached. At high clay concentration the clay mineral particles are attached to the ODA cations at the air–water interface before the latter have time to form the two-dimensional crystalline aggregates. In any case, the alkyl chains are oriented largely perpendicular to the surface (Ras, 2003; Umemura et al., 2003). In multilayered films the amount of ODA cations per layer is the same. This can be deduced from the linear increase of the intensity of the antisymmetric  $\text{CH}_2$  vibrations with the number of layers (Umemura et al., 2001a, 2001b). This observation has also been made for other amphiphilic cations such as  $[\text{Ru}(\text{phen})_2(\text{dcC12bpy})]$  where phen is 1,10-phenanthroline and dcC12bpy is 4,4'-carboxyl-2,2'-bipyridyl didodecyl ester (Umemura et al., 2002). The monolayer films of clay mineral particles and ODA cations, deposited on ZnSe by upstroke vertical deposition, do not contain water (Ras, 2003). This means that in the configuration of ZnSe/clay/ODA there is no water at both ZnSe/clay mineral and clay mineral/ODA interfaces, indicating that there are no residual  $\text{Na}^+$  cations and that the dense ODA layer is completely hydrophobic.

We end this discussion of the ODA-clay films with two remarks: (1) the ammonium group of the molecule is oxidised to the corresponding carbamate in the presence of dissolved  $\text{CO}_2$  and methanol. The latter is present in the chloroform solution, used to spread ODA cations on the surface of water (Ras, 2003); and (2) short-chain, water-soluble alkylammonium cations can also be used for construction of hybrid clay mineral/alkylammonium films (Umemura et al., 2001a, 2001b). This means that under suitable conditions the alkylammonium cations are captured by the clay particles at the air–water interface before they are solubilised in the water of the sub-phase.

Research has been started to produce functional LB films with clay minerals. Thus, films with non-linear optical properties have been produced (Umemura et al., 2002) with the above mentioned  $[\text{Ru}((\text{phen})_2(\text{dcC12bpy}))]$  complex, which is non-centrosymmetric and chiral. A second harmonic generation (SHG) signal is produced only in the presence of ODA cations. The configuration of the films is then hydrophobic glass/ $[\text{Ru}(\text{phen})_2(\text{dcC12bpy})]$ /clay mineral/ODA/ $[\text{Ru}(\text{phen})_2(\text{dcC12bpy})]$ . It is suggested that in the presence of ODA, the Ru complexes are all oriented in the same direction in the film. This is not the case in the absence of ODA, i.e., when the Ru complexes are in direct contact with the hydrophilic surface of the clay mineral. In other words, the organisation of amphiphilic cations may be controlled by the hydrophobic/hydrophilic balance of the surface.

A hybrid film hydrophobic glass/ODA/clay mineral/ $\text{Fe}(\text{phen})_3^{2+}$  has also been assembled by Umemura (2002) that generates a SHG signal. This indicates again that the  $\text{Fe}(\text{phen})_3^{2+}$  complexes are organised at the clay surface in a non-centrosymmetric fashion. However, prior deposition of ODA cations is not necessary to give the required hydrophobic/hydrophilic balance at the clay mineral surface,

whereas this is the case for Ru. Both the Ru- and Fe-complexes are supposed to be adsorbed on the clay mineral surfaces by cation exchange, possibly leaving some residual  $\text{Na}^+$  ions. This is contrary to the conclusion drawn from the ODA/clay mineral films. These results raise several questions: (i) what is the mobility of the amphiphilic cations at the clay mineral particle surface; (ii) can they diffuse from one siloxane surface to the opposite siloxane surface of the same particle or between particles and (iii) what is the dependence of the orientation of these cations on the hydrophobic/hydrophilic balance of the clay mineral surface? Further research is needed to resolve these questions, and clarify other points of discussion.

## REFERENCES

- Annabi-Bergaya, F., Cruz, M.I., Gatinéau, L., Fripiat, J.J., 1980a. Adsorption of alcohols by smectites. 2. Role of the exchangeable cations. *Clay Minerals* 15, 219–223.
- Annabi-Bergaya, F., Cruz, M.I., Gatinéau, L., Fripiat, J.J., 1980b. Adsorption of alcohols by smectites. 3. Nature of the bonds. *Clay Minerals* 15, 225–237.
- Atkins, P., de Paula, J., 2002. *Physical Chemistry*, 7th edition. Oxford University Press, Oxford, p. 1084.
- Boyd, S.A., Jaynes, W.F., 1994. Role of layer charge in organic contaminant sorption by organo-clays. In: Mermut, A.R. (Ed.), *Layer Charge Characteristics of 2:1 Silicate Clay Minerals*. CMS Workshop Lectures, vol. 6. Clay Minerals Society, Boulder, CO, pp. 48–77.
- Buswell, A.M., Krebs, K., Rodebush, W.H., 1937. Infrared studies. III. Absorption bands of hydrogels between 2.5 and 3.5 micrometers. *Journal of the American Chemical Society* 59, 2603–2605.
- Cancela, G.D., Huertas, F.J., Taboada, E.R., Sanchez Rasero, F., Laguna, A.H., 1997. Adsorption of water vapor by homoionic montmorillonites. Heats of adsorption and desorption. *Journal of Colloid and Interface Science* 185, 343–354.
- Cenens, J., Schoonheydt, R.A., 1988. Visible spectroscopy of methylene blue on hectorite, Laponite B and barasym. *Clays and Clay Minerals* 36, 214–224.
- Chang, F.C., Skipper, N.T., Sposito, G., 1998. Monte Carlo and molecular dynamics simulations of electrical double-layer structure in potassium-montmorillonite hydrates. *Langmuir* 14, 1201–1207.
- Charnay, C., Lagerge, S., Partyka, S., 2001. Assessment of the surface heterogeneity of talc materials. *Journal of Colloid and Interface Science* 233, 250–258.
- Coche-Guérente, L., Desprez, V., Labbé, P., Therias, S., 1999. Amplification of amperometric biosensor responses by electrochemical substrate recycling. Part II. Experimental study of the catechol–polyphenol oxidase system immobilized in a laponite clay matrix. *Journal of Electroanalytical Chemistry* 470, 61–69.
- Costanzo, P.M., Clemency, C.V., Giese, R.F., 1980. Low temperature synthesis of a 10-Å hydrate of kaolinite using dimethylsulfoxide and ammonium fluoride. *Clays and Clay Minerals* 28, 155–156.
- Costanzo, P.M., Giese, R.F., 1990. Ordered and disordered organic intercalates of 8.4-Å synthetically hydrated kaolinite. *Clays and Clay Minerals* 38, 160–170.
- Costanzo, P.M., Giese, R.F., Lipsicas, M., Straley, C., 1982. Synthesis of a quasi-stable kaolinite and heat-capacity of interlayer water. *Nature* 296, 549–551.



- de Melo, P.M., Cosnier, S., Mousty, C., Martelet, C., Jaffrezic-Renault, N., 2002. Urea biosensors based on immobilization of urease into two oppositely charged clays (Laponite and Zn-Al layered double hydroxides). *Analytical Chemistry* 74, 4037–4043.
- Fernandez, M., Serratosa, J.M., Johns, W.D., 1970. Perturbation of the stretching vibration of OH groups in phyllosilicates by the interlayer cations. *Reunion Hispano-Belga de Minerales de la Arcilla* 163–167.
- Giese, R.F., van Oss, C.J., 1993. The surface thermodynamic properties of silicates and their interactions with biological materials. In: Guthrie, C.D., Mossman, B.T. (Eds.), *Health Effects of Mineral Dusts. Reviews in Mineralogy*, vol. 28. Mineralogical Society of America, Washington, DC, pp. 327–346.
- Giese, R.F., van Oss, C.J., Norris, J., Costanzo, P.M., 1990. Surface energies of some smectite clay minerals. In: Farmer, V.C., Tardy, Y. (Eds.), *Proceedings of the 9th International Clay Conference, Strasbourg, 1989. Sciences Géologiques, Mémoire No. 86*, pp. 33–41.
- Greathouse, J., Sposito, G., 1998. Monte-Carlo and molecular dynamics studies of interlayer structure in  $\text{Li}(\text{H}_2\text{O})_3$ -smectites. *The Journal of Physical Chemistry B* 102, 2406–2414.
- Hensen, E.J.M., Smit, B., 2002. Why clays swell. *The Journal of Physical Chemistry B* 106, 12664–12667.
- Hotta, Y., Inukai, K., Taniguchi, M., Yamagishi, A., 1997a. Electrochemical behaviour of hexa-ammineruthenium(II) cations in clay-modified electrodes prepared by the Langmuir–Blodgett method. *Journal of Electroanalytical Chemistry* 429, 107–114.
- Hotta, Y., Taniguchi, M., Yamagishi, A., 1997b. A clay self-assembled on a gold surface as studied by atomic force microscopy. *Journal of Colloid and Interface Science* 188, 404–408.
- Huheey, J.E., 1978. *Inorganic Chemistry: Principles of Structure and Reactivity*, 2nd edition. Harper & Row, New York.
- Jacobs, K.Y., Schoonheydt, R.A., 1999. Spectroscopy of methylene blue-smectite suspensions. *Journal of Colloid and Interface Science* 220, 103–111.
- Jacobs, K.Y., Schoonheydt, R.A., 2001. Time dependence of the spectra of methylene blue-clay mineral suspensions. *Langmuir* 17, 5150–5155.
- Jaynes, W.F., Boyd, S.A., 1991. Hydrophobicity of siloxane surfaces in smectites as revealed by aromatic hydrocarbon adsorption from water. *Clays and Clay Minerals* 39, 428–436.
- Johnston, C.T., Bish, D.L., Eckert, J., Brown, L.A., 2000. Infrared and inelastic neutron scattering study of the 1.03- and 0.95-nm kaolinite-hydrazine intercalation complexes. *The Journal of Physical Chemistry B* 104, 8080–8088.
- Johnston, C.T., Premachandra, G.S., 2001. Polarized ATR-FTIR study of smectite in aqueous suspension. *Langmuir* 17, 3712–3718.
- Johnston, C.T., Sposito, G., Erickson, C., 1992. Vibrational probe studies of water interactions with montmorillonite. *Clays and Clay Minerals* 40, 722–730.
- Johnston, C.T., Stone, D.A., 1990. Influence of hydrazine on the vibrational modes of kaolinite. *Clays and Clay Minerals* 38, 121–128.
- Jouany, C., Chassin, P., 1987. Determination of the surface-energy of clay-organic complexes by contact-angle measurements. *Colloids and Surfaces* 27, 289–303.
- Kleinfeld, E.R., Ferguson, G.S., 1994. Stepwise formation of multilayered nanostructural films from macromolecular precursors. *Science* 265, 370–373.
- Kotov, N.A., 2001. Ordered layered assemblies of nanoparticles. *Materials Research Bulletin* 26, 992–997.

- Kotov, N.A., Meldrum, F., Wu, C., Fendler, J.H., 1994. Monoparticulate layer and Langmuir–Blodgett type multiparticulate layers of size-quantized cadmium sulfide clusters—a colloid-chemical approach to superlattice construction. *The Journal of Physical Chemistry* 98, 2735–2738.
- Laird, D.A., Barriuso, E., Dowdy, R.H., Koskinen, W.C., 1992. Adsorption of atrazine on smectites. *Soil Science Society of America Journal* 56, 62–67.
- Lvov, Y., Arija, K., Ichinose, I., Tunitake, T., 1996. Molecular film assembly via layer-by-layer adsorption of oppositely charged molecules (biopolymer, protein, clay) and concanavalin A and glycogen. *Thin Solid Films* 284, 797–801.
- Malandrini, H., Clauss, F., Partyka, S., Douillard, J.M., 1997. Interactions between talc particles and water and organic solvents. *Journal of Colloid and Interface Science* 194, 183–193.
- Mamedov, A.A., Kotov, N.A., 2000. Free standing layer-by-layer assembled films of magnetite nanoparticles. *Langmuir* 16, 5530–5533.
- Mamedov, A.A., Ostrander, J., Aliev, F., Kotov, N.A., 2000. Stratified assemblies of magnetite nanoparticles and montmorillonite prepared by the layer-by-layer assembly. *Langmuir* 16, 3941–3949.
- Michot, L.J., Villieras, F., Francois, M., Yvon, J., LeDred, R., Cases, J.M., 1994. The structural microscopic hydrophilicity of talc. *Langmuir* 10, 3765–3773.
- Mooney, R.W., Keenan, A.G., Wood, L.A., 1952a. Adsorption of water vapor by montmorillonite. I. Heat of desorption and application of BET theory. *Journal of the American Chemical Society* 74, 1367–1374.
- Mooney, R.W., Keenan, A.G., Wood, L.A., 1952b. Adsorption of water vapor by montmorillonite. II. Effect of exchangeable ions and lattice swelling as measured by X-ray diffraction. *Journal of the American Chemical Society* 74, 1371–1374.
- Mortier, W.J., 1987. Electronegativity equalization and its applications. *Structure and Bonding* 66, 125–143.
- Nemecz, E., 1981. *Clay Minerals*. Akademiai Kiado, Budapest.
- Nulens, K.H.L., Toufar, H., Janssens, G.O.A., Schoonheydt, R.A., Johnston, C.T., 1998. Clay minerals and clay mineral–water interactions: a combined EEM–Monte Carlo study. In: Yamagishi, A., Aramata, A., Taniguchi, M. (Eds.), *The Latest Frontiers of the Clay Chemistry. Proceedings of the Sapporo Conference on the Chemistry of Clays and Clay Minerals*, 1996. The Smectite Forum of Japan, Sendai, pp. 116–133.
- Pimentel, G.C., McClellan, A.B., 1960. *The Hydrogen Bond*, 1st edition. W.H. Freeman, San Francisco.
- Poinsignon, C., Cases, J.M., Fripiat, J.J., 1978. Electrical-polarization of water molecules adsorbed by smectites. An infrared study. *The Journal of Physical Chemistry* 82, 1855–1860.
- Qian, D.-J., Nakamura, C., Wenk, S.-O., Ishikawa, H., Zorin, N., Miyake, J., 2002. A hydrogen biosensor made of clay, poly(butylviologen) and hydrogenase sandwiched on a glass carbon electrode. *Biosensors and Bioelectronics* 17, 789–796.
- Ras, R.H.A., 2003. *Molecular and Particulate Organization in Organo-Clay Monolayers*. Ph.D. thesis. K.U. Leuven, p. 139.
- Ras, R.H.A., Johnston, C.T., Franses, E.I., Ramaekers, R., Maes, G., Foubert, P., De Schryver, F.C., Schoonheydt, R.A., 2003. Polarized infrared study of hybrid Langmuir–Blodgett monolayers containing clay mineral nanoparticles. *Langmuir* 19, 4295–4302.

- Russell, J.D., Farmer, V.C., 1964. Infra-red spectroscopic study of the dehydration of montmorillonite and saponite. *Clay Minerals Bulletin* 5, 443–464.
- Sanderson, R.T., 1976. *Chemical Bonds and Bond Energy*, 2nd edition. Academic Press, New York.
- Sauer, J., 1989. Molecular models in ab initio studies of solids and surfaces: from ionic crystals and semiconductors to catalysts. *Chemical Reviews* 89, 199–255.
- Schrader, M.E., Yariv, S., 1990. Wettability of clay minerals. *Journal of Colloid and Interface Science* 136, 85–94.
- Serratos, J.M., Rausell-Colom, J.A., Sanz, J., 1984. Charge density and its distribution in phyllosilicates: effect on the arrangement and reactivity of adsorbed species. *Journal of Molecular Catalysis* 27, 225–234.
- Servagent-Noinville, S., Revault, M., Quiquampoix, H., Baron, M.H., 2000. Conformational changes of bovine serum albumin induced by adsorption on different clay surfaces: FTIR analysis. *Journal of Colloid and Interface Science* 221, 273–283.
- Sposito, G., 1984. *The Surface Chemistry of Soils*. Oxford University Press, New York.
- Sposito, G., Prost, R., 1982. Structure of water adsorbed on smectites. *Chemical Reviews* 82, 553–573.
- Sposito, G., Prost, R., Gaultier, J.P., 1983. Infrared spectroscopic study of adsorbed water on reduced-charge Na/Li montmorillonites. *Clays and Clay Minerals* 31, 9–16.
- Sutton, R., Sposito, G., 2001. Molecular simulation of interlayer structure and dynamics in 12.4 angstrom Cs-smectite hydrates. *Journal of Colloid and Interface Science* 237, 174–184.
- Swenson, J., Bergman, R., Howells, W.S., 2000. Quasielastic neutron scattering of two-dimensional water in a vermiculite clay. *Journal of Chemical Physics* 113, 2873–2879.
- Theng, B.K.G., 1974. *The Chemistry of Clay-Organic Reactions*. Wiley, New York.
- Thompson, D.W., Butterworth, J.T., 1992. The nature of laponite and its aqueous dispersions. *Journal of Colloid and Interface Science* 151, 236–243.
- Tunega, D., Benco, L., Haberhauer, G., Gerzabek, M.H., Lischka, H., 2002. Ab initio molecular dynamics study of adsorption sites on the (001) surfaces of 1:1 dioctahedral clay minerals. *The Journal of Physical Chemistry B* 106, 11515–11525.
- Umemura, Y., 2002. Hybrid films of a clay mineral and an iron(II) complex cation prepared by a combined method of the Langmuir–Blodgett and self-assembly techniques. *The Journal of Physical Chemistry B* 106, 11168–11171.
- Umemura, Y., Onodera, Y., Yamagishi, A., 2003. Layered structure of hybrid films of an alkylammonium cation and a clay mineral as prepared by the Langmuir–Blodgett method. *Thin Solid Films* 426, 216–220.
- Umemura, Y., Yamagishi, A., Schoonheydt, R.A., Persoons, A., De Schryver, F.C., 2001a. Fabrication of hybrid films of alkylammonium cations ( $C_nH_{2n+1}NH_3^+$ ;  $n = 4–18$ ) and a smectite clay by the Langmuir–Blodgett method. *Langmuir* 17, 449–455.
- Umemura, Y., Yamagishi, A., Schoonheydt, R.A., Persoons, A., De Schryver, F.C., 2001b. Formation of hybrid monolayers of alkylammonium cations and a clay mineral at the air-water interface: clay as an inorganic stabilizer for water-soluble amphiphiles. *Thin Solid Films* 388, 5–8.
- Umemura, Y., Yamagishi, A., Schoonheydt, R.A., Persoons, A., De Schryver, F.C., 2002. Langmuir–Blodgett films of a clay mineral and ruthenium(II) complexes with a non-centrosymmetric structure. *Journal of the American Chemical Society* 124, 992–997.
- van Duffel, B., Schoonheydt, R.A., Grim, C.P.M., De Schryver, F.C., 1999. Multilayered clay films: atomic force microscopy study and molecular modeling. *Langmuir* 15, 7520–7529.

- van Duffel, B., Verbiest, T., Van Elshocht, T., Persoons, A., Schoonheydt, R.A., 2001. Fuzzy assembly and second harmonic generation of clay-polymer-dye monolayer films. *Langmuir* 17, 1243–1249.
- van Oss, C.J., Giese, R.F., Li, Z., Murphy, K., Norris, J., Charudhury, M.K., Good, R.J., 1992. Determination of contact angles and pore sizes of porous-media by column and thin-layer wicking. *Journal of Adhesion Science and Technology* 6, 413–428.
- Xu, W., Johnston, C.T., Parker, P., Agnew, S.F., 2000. Infrared study of water sorption on Na-, Li-, Ca- and Mg-exchanged (SWy-1 and SAz-1) montmorillonite. *Clays and Clay Minerals* 48, 120–131.
- Yan, L., Roth, C.B., Low, P.F., 1996. Changes in the Si-O vibrations of smectite layers accompanying the sorption of interlayer water. *Langmuir* 12, 4421–4429.
- Yariv, S., 1992. Wettability of clay minerals. In: Schrader, M.E., Loeb, G. (Eds.), *Modern Approaches to Wettability: Theory and Applications*. Plenum Press, New York, pp. 279–326.
- Yariv, S., Cross, H. (Eds.) 2002. *Organo-Clay Complexes and Interactions*. Marcel Dekker, New York.
- Zhou, Y., Hu, N., Zeng, Y., Rusling, J.F., 2002. Heme-protein-clay films: direct electrochemistry and electrochemical catalysis. *Langmuir* 18, 211–219.

This page intentionally left blank

## *Chapter 4*

# **SYNTHETIC CLAY MINERALS AND PURIFICATION OF NATURAL CLAYS**

**K.A. CARRADO<sup>a</sup>, A. DECARREAU<sup>b</sup>, S. PETIT<sup>b</sup>, F. BERGAYA<sup>c</sup>  
AND G. LAGALY<sup>d</sup>**

<sup>a</sup>*Chemistry Division, Argonne National Laboratory, Argonne, IL 60439-4837, USA*

<sup>b</sup>*UMR 6532, HydrASA, F-8602 Poitiers Cedex, France*

<sup>c</sup>*CRMD, CNRS-Université d'Orléans, F-45071 Orléans Cedex 2, France*

<sup>d</sup>*Institut für Anorganische Chemie, Universität Kiel, D-24118 Kiel, Germany*

Salient points on the synthesis of clay minerals are summarized in this chapter, focusing on specific clay mineral types. Further, methods of clay purification are described.

A subjective differentiation can be made between the formation of clay minerals in their natural, geologic environment such as in soils, and the synthesis of pure minerals in a controlled, laboratory environment. The former point would be of interest to the geochemist, soil scientist, or mineralogist, whereas the latter materials are prepared to exploit a clay mineral's unique structure and/or surface chemistry for some particular application. Among recent reviews on the geological aspects of clay mineral synthesis, that by [Wilson \(1999\)](#) makes the distinction between 'transformation' and 'neotransformation' in natural environments. The present review is concerned with the laboratory synthesis of clay minerals.

## **4.1. METHODOLOGY**

More often than not, the main objective of producing synthetic clay minerals is to obtain pure samples in a short time and at the lowest possible temperature. These two parameters are important for geologists whose aim is to reproduce in the laboratory clay mineral formation under hydrothermal and diagenetic conditions (weathering, sedimentary neoformation) that prevail at the earth's surface. These parameters are equally important for chemists and physicists who aim to minimize the energy needed for clay synthesis.

Clay mineral synthesis can be viewed as a heterogeneous chemical reaction in an aqueous phase. The global kinetics of such a reaction are given by the classical

Arrhenius equation:

$$K_{(T)} = Ae^{-E_a/RT} \quad (1)$$

where  $K_{(T)}$  is the rate constant of the reaction;  $A$  the pre-exponential factor;  $E_a$  the activation energy;  $R$  the gas constant; and  $T$  the absolute temperature.

The duration of clay mineral synthesis can therefore be minimized by an increase of  $T$  and/or a decrease of  $E_a$ . Many different varieties of clay minerals have been synthesized as described in the next section. Some general variables of clay mineral synthesis, with an emphasis on starting materials and hydrothermal conditions, are presented.

#### 4.1.1. Synthesis from Very Dilute Solutions

This method, developed by Caillère et al. (1953, 1954) and used later by Harder (1972, 1978), is based on two assumptions: (i) that clay minerals are formed from dilute solutions in natural (weathering) processes (Milot, 1965) and (ii) that clay minerals can grow by silicification of  $Mg(OH)_2$  (brucite-) or  $Al(OH)_3$  (gibbsite-) like sheets (Caillère et al., 1956). The salt solutions used are very dilute (10–30 mg/L) and  $SiO_2$  concentrations are less than 100 mg/L so as to prevent polymerization of silicic monomers. Since this method yields very small quantities of clay minerals that are difficult to characterize, it is no longer used.

#### 4.1.2. Solid-State Reactions

In this process, three kinds of solids can be used as starting materials: minerals or rocks, glasses, and gels.

When minerals or rocks are used, they are of igneous origin such as feldspars, olivines, pyroxenes, basalts, and rhyolites (Fiore et al., 2001). This approach is interesting for geochemists because it involves hydrothermal alteration of primary minerals or rocks into clay minerals. However, the kinetics involved are generally slow as shown below, and clay minerals are often mixed with other phases. It is preferable, therefore, to use starting materials with a similar chemistry to that of clay minerals.

Glasses are easily obtained by the melting of salts (or oxides) mixed in the proper ratios. However, melting requires high temperatures (900 °C and above) and, if a salt flux is not added (such as  $Na_2CO_3$ ), then demixing can occur (e.g., formation of hematite in the presence of Fe ions). For this reason, glasses also are not often used as starting materials.

The most commonly used starting materials are gels that can be prepared by one of the three methods: (i) using only organic salts tetraethoxysilane (TEOS), triisopropyl aluminate, iron acetylacetonate, etc. (De Kimpe et al., 1981); (ii) using TEOS and  $Mg^{2+}$ -,  $Al^{3+}$ -, or  $Fe^{3+}$ -nitrates, and heating the gels at 800 °C for

complete dehydration (Roy and Tuttle, 1956; Klopogge and Vogel, 1995); and (iii) using sodium metasilicate and  $\text{Mg}^{2+}$ -,  $\text{Al}^{3+}$ -, or  $\text{Fe}^{3+}$ -chlorides or sulphates (Decarreau, 1980). Applying all three methods, Iriarte-Lecumberri (2003) obtained 21 starting gels for the synthesis of smectites with variable ratios of  $\text{Fe}^{3+}$ ,  $\text{Al}^{3+}$ , and  $\text{Mg}^{2+}$  ions. With the first method, the dissolution of magnesium ethylate is difficult, the dehydration of gels is long (480 h at 30 °C), and the gels are heterogeneous showing macroscopic segregation of elements. With the second method, the gels obtained are macroscopically homogeneous but the clay mineral compositions are significantly different from expectation, with an excess of  $\text{Al}^{3+}$ ,  $\text{Fe}^{3+}$ ,  $\text{Mg}^{2+}$ , and a deficit of  $\text{Si}^{4+}$ . At the TEM-AEM scale, the gels are heterogeneous with small dark nodules of high iron concentrations. Gels obtained by the third method are homogeneous at the TEM-AEM scale, and their compositions are close to expectation. These gels appear to form 2:1 clay minerals when they contain  $\text{Mg}^{2+}$ , and protoferrihydrite when they contain  $\text{Fe}^{3+}$  (Decarreau, 1980, 1981; Decarreau and Bonnin, 1986; Decarreau et al., 1987). Iriarte-Lecumberri (2003) concluded that gels obtained by this last method are more suitable for the synthesis of clay minerals having a complex chemistry, such as smectites. In all cases, the gels must be dried at a low temperature (30–60 °C) to prevent possible partial demixing and crystallization.

#### 4.1.3. Hydrothermal Synthesis

Hydrothermal treatment can induce the germination and crystal growth of clay minerals. The important controlling parameters are temperature ( $T$ ), duration of treatment ( $t$ ) and solution chemistry, notably pH.

##### A. Germination Process

To ensure that germination of clay minerals occurs, the concentration of ions in solution ( $\text{Si}^{4+}$ ,  $\text{Al}^{3+}$ ,  $\text{Mg}^{2+}$ ,  $\text{Fe}^{3+}$ , etc.) must be high enough to reach critical oversaturation ( $S^*$ ). This condition is easily reached when the starting materials are gels or glasses because they are highly soluble and have compositions similar to those of the required clay minerals.  $S^*$  is more difficult to reach when the starting materials are minerals or rocks. For a given rate of nucleation (one seed per second per  $\text{cm}^3$ ) the value of  $S^*$  is given by Eq. (2) (Stumm and Morgan, 1981):

$$\log S^* = \left[ C \frac{\gamma^3}{T^3} \right]^{1/2} \quad (2)$$

where  $C$  includes the Boltzmann constant and parameters depending on the kind of clay mineral,  $T$  is the temperature, and  $\gamma$  is the clay/solution interface tension.

This simplified expression of  $S^*$  shows that elevated temperatures will act to decrease  $S^*$  values. Also, the value of  $\gamma$  is inversely related to the solubility product of the clay minerals ( $K_s$ ). Trioctahedral clay minerals have high  $K_s$  values as compared with their dioctahedral counterparts with  $\log K_s = 31.6$  for chrysolite and  $\log$



$K_s = 7.43$  for kaolinite ( $K_s$  values given for  $T = 298$  K and  $P = 1$  b) (Fritz, 1981). Therefore, germination of trioctahedral clay minerals requires lower  $S^*$  values, and these minerals are easier to crystallize. In fact, explosive germination occurs for trioctahedral clay minerals after the co-precipitation reaction during gel preparation (Decarreau, 1980). This may explain the role of magnesium in the synthesis of dioctahedral aluminous clays since the presence of magnesium, even in low amounts, is essential for the formation of smectites (Kloprogge et al., 1999).

### B. Crystal Growth

The rate of crystal growth ( $v$ ) at a given temperature ( $T$ ) is given by Eq. (3) (Steefel and Van Capellen, 1990):

$$v = k_{(T)} S [(Q/K_s)^n - 1]^m \quad (3)$$

where  $k_{(T)}$  is the rate constant of clay mineral precipitation;  $S$  is the external surface area of the mineral;  $K_s$  is the solubility product;  $(Q/K_s - 1)$  is the index of  $S^*$  of the solution;  $m$  and  $n$  are experimental constants.

*Role of temperature.* The kinetics of clay mineral growth are strongly dependent on temperature, through  $k_{(T)}$  and Eq. (1). Therefore, syntheses performed at low temperatures often do not succeed. For example, Rayner (1962) calculated a half-reaction time of  $16 \times 10^4$  years for kaolinite synthesis at  $20^\circ\text{C}$ . At  $T > 500^\circ\text{C}$ , other silicate or oxide phases become more stable than clay minerals. As a result, most clay mineral syntheses are performed in the range of  $100$ – $500^\circ\text{C}$ .

*Role of pH.* Data from numerous studies, described in the next section, show that the type of synthetic clay mineral produced depends on the pH of solutions at the end of hydrothermal treatment ( $\text{pH}_f$ ). Especially for systems containing  $\text{Al}^{3+}$  and/or  $\text{Fe}^{3+}$ , low  $\text{pH}_f$  (2–6) favours the formation of 1:1 clay minerals such as kaolinite, more or less mixed with oxides. Medium  $\text{pH}_f$  (7–10 for  $\text{Al}^{3+}$ , up to 12 for  $\text{Fe}^{3+}$ ) favours 2:1 clay minerals such as smectites and micas. High  $\text{pH}_f$  favours zeolite (with  $\text{Al}^{3+}$ ) or aegerine (with  $\text{Fe}^{3+}$ ) minerals (Frank-Kamenetskii et al., 1973; Kloprogge et al., 1990; Huertas et al., 1999, 2000; Nagase et al., 1999; Decarreau et al., 2004). Fig. 4.1, from Grauby et al. (1993), demonstrates these phenomena. One of the major reasons for the higher dependence on  $\text{pH}_f$  than the Si/Al ratio is probably related to the thermodynamic stability fields of clay minerals (Bowers et al., 1984). Frank-Kamenetskii et al. (1973) have also suggested that the synthesis of tetrahedrally substituted ( $\text{Si}^{4+}$ – $\text{M}^{3+}$ ) 2:1 clay minerals is favoured at alkaline  $\text{pH}_f$ .

Since the type of synthetic clay is dependent on  $\text{pH}_f$ , it is necessary to follow the evolution of pH during synthesis. Appropriate starting gels have their own buffering power; although a drop of several pH units can occur after only a few minutes, this process may extend up to a few days at  $25^\circ\text{C}$ . The decrease in pH is most likely due to surface reactions between the solution and the oxo- or hydroxo-complexes present

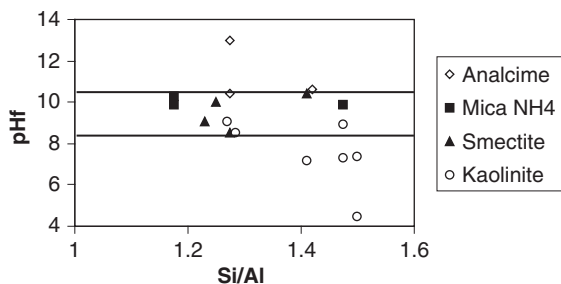


Fig. 4.1. Synthesized clay minerals in the system Si/Al/Na/H<sub>2</sub>O at 200 °C. pH<sub>f</sub> = final pH (end of synthesis), Si/Al = atomic ratio. 2:1 clay minerals are synthesized at pH<sub>f</sub> values between 8.2 and 10.3.

at gel/solution interfaces (Decarreau, 1980; Huertas et al., 1999). Therefore, in constraining the pH<sub>f</sub> for a given clay mineral synthesis the initial pH must be adjusted so that the buffering power of the gel does not contribute (Iriarte-Lecumberri, 2003).

*Role of time: crystallization versus crystallinity.* With increasing synthesis time the amount of starting material that is transformed into clay minerals increases. Thermal gravimetric analysis (TGA) is the method most often used to quantify the crystallization rate. Dehydroxylation of clay minerals occurs at relatively well-defined temperatures (Mackenzie, 1970; Smykatz-Kloss and Warne, 1991; Drits et al., 1995; Emmerich and Kahr, 2001). For poorly crystallized clay minerals, dehydroxylation occurs at lower temperatures. For example, in synthetic kaolinites the temperature shifts from 550 to 420 °C (Petit and Decarreau, 1990). For all types of clay minerals, the experimental rate of crystallization follows a similar pattern given by the relation:

$$\% \text{clay} = 1 - e^{-kt}$$

The value of  $k$  is dependent on experimental conditions, notably temperature (Huertas et al., 1999, 2000). Depending on the nature of the synthetic clay mineral, and for temperatures in the range 150–300 °C, crystallization reaches a plateau after a few days to a few months. These results can be explained by the kinetic law of Eq. (3). At the beginning, large amounts of starting materials dissolve and concentrations of ions in solution are high. At this point,  $Q/K_s \gg 1$  and the rate of crystal growth is fast. Gradually  $Q \approx K_s$  with time ( $t$ ), and the kinetics of crystal growth tend to be very slow. At this point, additional time has no effect on crystallization.

As synthesis time increases, the crystallinity of clay minerals generally increases. Traditionally, ‘crystallinity’ is quantified by measuring the width of reflections in XRD patterns (mean crystal size coherency obtained using the Scherrer equation), or specific measurements such as the Hinckley (1963) index for kaolinites (Aparicio and Galan, 1999) (see Chapter 2). Crystallinity enhancement in the layer planes of clay minerals was measured for synthesized smectites and chrysotile using the width of

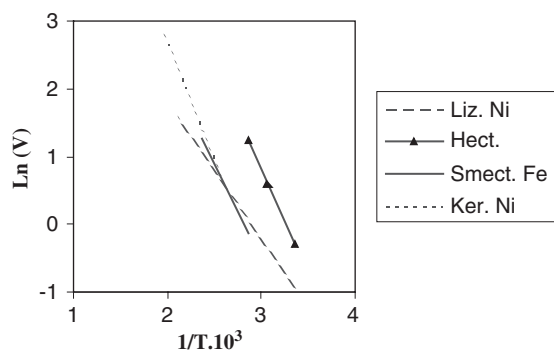


Fig. 4.2. Arrhenius scheme for the crystal growth of clay minerals synthesized from co-precipitated gels at neutral to alkaline pH<sub>f</sub>. V = linear speed of domain size increase in the plane of layers (Ångstroms/day) where Liz.Ni = Ni-lizardite; Hect. = hectorite; Smect.Fe = iron smectite; Ker.Ni = Ni-kerolite.

(060,330) reflections in the XRD patterns. It appears that an increase in ‘crystallinity’ is strongly dependent on temperature, pH, and is similar for all kinds of clay minerals as will be seen in the following section (Fig. 4.2).

*C. Intermediate phases.* Intermediate phases commonly appear during synthesis. Most of these are hydroxides or pseudo-hydroxides such as the pseudo-boehmite observed during the synthesis of kaolinite (Fialips et al., 2000). These phases are generally of low crystallinity and/or are non-stoichiometric (siliceous hematite is an example) and are difficult to identify using classical techniques such as XRD, DTA-TGA, and FTIR.

The occurrence of these phases suggests that clay mineral synthesis is a complex heterogeneous reaction. Numerous authors suggest that the key step in smectite synthesis is the formation of pseudo-hydroxides of the octahedral cations, to which silica species are attached forming clay mineral nuclei (Kloprogge et al., 1999; Huertas et al., 2000). In a more complex system, the clay mineral itself can act as an intermediate phase. Grauby et al. (1993) have synthesized a metastable di-trioctahedral smectite that evolves by demixing (with increasing time and temperature) into extended dioctahedral (with Al<sup>3+</sup>) and trioctahedral (with Mg<sup>2+</sup>) domains in 2:1 layers. Huertas et al. (2000) have shown that smectites appear as intermediate phases during kaolinite synthesis. In summary, clay minerals may occur as metastable phases during synthesis. Therefore, one has to be certain that the reactions have been completed.

#### 4.1.4. Characterization of Synthetic Clay Minerals

The characterization of synthetic clay minerals is often not adequate. For example, Nagase et al. (1999) have synthesized a smectite from a gel with a Si<sup>4+</sup>/Fe<sup>3+</sup>/Mg<sup>2+</sup>

ratio of 4/1.7/0.3 at 200 °C. On the basis of XRD data alone, they concluded that the synthesized smectite was a  $\text{Fe}^{3+}$ -montmorillonite. However, [Grauby et al. \(1994\)](#) using similar synthesis conditions concluded from XRD before and after the Hofmann–Klemen test, FTIR, and TEM-AEM that the product was actually an Fe-beidellite.

The following set of characterization techniques should at least be used: (i) XRD of both powder and oriented samples, including all the classical tests for swelling. The Rietveld approach is useful for quantifying the amount of mixed phases and the occurrence of disordered phases; (ii) TEM-AEM for a precise measurement of clay mineral particle morphologies; and (iii) appropriate spectroscopic techniques such as EXAFS, NMR, Mössbauer, FTIR, ESR, for obtaining independent crystal-chemical data. These data are essential to characterize clay minerals with tetrahedral and/or octahedral substitutions. In particular, FTIR can readily provide much information on the structural composition, crystal chemistry, and crystallinity of the product ([Farmer, 1974](#); [Petit et al., 1998, 1999](#); [Petit, 2004](#)).

## 4.2. SYNTHESIS OF SPECIFIC CLAY MINERALS

### 4.2.1. *Micas*

The literature concerning micas, including their synthesis, is so vast that only some points will be highlighted here. For further information the reader is referred to the recent monograph by [Mottana et al. \(2002\)](#). The vast majority of mica minerals are assumed to be ‘inherited’ i.e., derived from pre-existing parent rock or weathered materials. This occurs under pressure and temperature conditions different from those that exist at the earth’s surface ([Fanning et al., 1989](#); [Wilson, 1999](#)). The few cases of apparently neoformed micas have been discussed recently. An iron-rich sample with perfect platy hexagonal morphology is an example ([Norrish and Pickering, 1983](#)). The low-grade metamorphism (or transformation) of phyllosilicates to micas has been reviewed by [Arkai \(2002\)](#). Weathering processes that form the rare trioctahedral micas have been summarized by [Wilson \(1999\)](#).

Laboratory syntheses of micas from as early as 1887 up to 1955 have been summarized by [Cipriani \(2002\)](#). He also points out that after this time micas have continued to be synthesized for one of two reasons: (i) verification of the geological conditions of formation with the goal of using micas as geothermometer or geobarometer indicators (mineral-petrogenic goal) or (ii) investigation of compositional variations including rare elements such as Ge or Rb (a crystallo-chemical goal). Early reports on hydrothermal synthetic micas include paragonite obtained at 420 °C ([Barrer and White, 1952](#)), ammonium mica at 300 °C ([Levinson and Day, 1968](#)), and muscovite at 500–700 °C ([Rosenberg, 1987](#)). [Robert et al. \(1993\)](#) have examined the distribution of fluorine versus hydroxyl in a synthetic tetra-silicic magnesium mica series. These synthetic micas have been characterized by X-ray crystallography

(Toraya et al., 1978),  $^{27}\text{Al}$  and  $^{29}\text{Si}$  MAS NMR (Komarneni et al., 1999), and XANES (Mottana et al., 1997).

A high-charge sodium fluoro-phlogopite mica, called 'Na-4-mica', has been synthesized via sol-gel hydrothermal techniques (Paulus et al., 1992) as is a K-fluorophlogopite (Duldulao and Burlitch, 1991). This procedure has been simplified by using a solid-state method where the precursors in powder form are mixed and heated at high temperatures (Franklin and Lee, 1996; Komarneni et al., 1998; Kodama et al., 2000, 2001a). A 'Na-2-mica' has also been prepared by the latter method (Kodama et al., 2001b). An expandable fluorine-containing mica has been synthesized via solid-state method from talc and sodium fluorosilicate precursors (Tateyama et al., 1992).

Examples of micas synthesized with isomorphous layer substitutions include octahedral  $\text{Ni}^{2+}$ - and  $\text{Ga}^{3+}$ -phlogopite (Klingsberg and Roy, 1957), tetrahedral beta-phlogopite and muscovite (Stubican and Roy, 1962),  $\text{Sr}^{2+}$ -mica (Barrer and Marshall, 1964),  $\text{Zn}^{2+}$ -mica (Barrer and Sieber, 1977), and  $\text{Rb}^{+}$ -muscovite (Voncken et al., 1987). Some of these lead to partial layer substitution, while others containing rare elements form complete mica analogues. In other words, layer substitution can range from partial to full replacement of  $\text{Si}^{4+}$  or  $\text{Al}^{3+}$  by the rare element.

#### 4.2.2. Smectites

The small particle size and highly variable composition of naturally occurring smectites led to considerable uncertainty regarding their origin and thermodynamic stability. Borchardt (1989) reviewed the natural formation of smectite minerals. He described the strong evidence for their detrital origin, a stage in the weathering of micas and chlorites to kaolinite and gibbsite. He also suggested that the phases are not thermodynamically stable, although at least some of the end-member phases may form authigenically in sediments under ambient conditions. Wilson (1999) also discussed the origin and formation of smectites in soils.

Because natural smectite-rich clays contain impurities and mixed phases, questions about their formation and stability are best addressed by studying synthetic, single-phase clay minerals that are more amenable to detailed structural characterization. Comprehensive reviews of smectite synthetic methods were provided by Kloprogge (1998) and Kloprogge et al. (1999). These include information on beidellite, hectorite, montmorillonite, nontronite, saponite, saucanite, and stevensite. In summary, synthetic conditions include (i) ambient pressure and temperature  $< 100^\circ\text{C}$ ; (ii) moderate hydrothermal conditions  $100\text{--}1000^\circ\text{C}$ , pressures to several kbars; (iii) extreme hydrothermal conditions with  $T > 1000^\circ\text{C}$  or pressures  $> 10$  kb; and iv) using fluoride ions as a flux. The mild hydrothermal approach is used most often because it yields the greatest amounts of high-purity smectites. This is especially true for beidellite and transition metal smectites. Montmorillonite remains the most difficult mineral to crystallize in high purity. This may be due, at least in part, to its low magnesium content.

Some additional studies regarding smectite synthesis have recently been published. One review (Manning, 2003), which is concerned with clay mineral occurrence and distribution in sedimentary rocks, discusses thermodynamic stability and reaction kinetics for kaolin, illite, smectite, and chlorite. It also includes the principles involved in experimental design of clay–mineral reactions. Another report concerns the synthesis of smectite from igneous rocks in NaOH at 100 °C, atmospheric pressure, and dilute suspensions (Tomita and Kawano, 2002). Huertas et al. (2000) have reported that kaolinite, formed from a gel by hydrothermal treatment, can transform through an intermediate phase to di- and trioctahedral smectites. Hectorite particles of approximately 0.3–0.5  $\mu\text{m}$  have been obtained hydrothermally using TEOS, brucite, and LiF (Carrado et al., 2001). A high-temperature, high-pressure study has yielded large ( $> 10 \mu\text{m}$ ) smectite ‘crystals’ with a homogenous charge distribution capable of stepwise hydration (Tamura et al., 2000).

Various metal-substituted smectites (e.g.,  $\text{Zn}^{2+}$ ,  $\text{Co}^{2+}$ ,  $\text{Ni}^{2+}$ ) have been synthesized by Shirai et al. (2001) and Higashi et al. (2002) and their catalytic activity has been investigated by Bhanage et al. (2002).

Of relatively new interest is the introduction of mesoporosity during the synthesis of smectite-based materials, including (i) hectorites derived from an excess of silica sol (Carrado et al., 2002) and (ii)  $\text{Mg}^{2+}$ - or  $\text{Co}^{2+}$ -based trioctahedral minerals that are talc-like (Shirai et al., 2000, 2002). These methods employ hydrothermal crystallization under mild conditions with catalytic applications in mind.

Another area of interest concerns the synthesis of hybrid smectite-organic nanocomposites. Some examples include (i) clay organic microspheres (talc-like) with either bubbled or entirely hollow interiors (Muthusamy et al., 2002); (ii) phenyl-grafted synthetic hectorite layers (Carrado et al., 2001); and (iii) alternating smectite-organo-siloxane layers where the talc-like layers are grafted with alkylammonium-derived molecules (Fujii et al., 2003).

#### 4.2.3. Kaolinite

Wilson (1999) summarized the literature regarding the origin and formation of kaolin minerals in soils. Soil kaolinites are usually smaller in particle size, more disordered, more likely to be interstratified with smectites, and more likely to contain isomorphous  $\text{Fe}^{3+}$  than kaolinites in geological deposits.

Roy and Osborn (1954) were the first to investigate the initial phase equilibrium for kaolinite. Since then, numerous reports on laboratory-scale preparations of kaolin minerals have been published. Synthesis at low or room temperature requires low-to-neutral pH and six-fold coordinated Al (Harder, 1970; Linares and Huertas, 1971). La Iglesia and Van Oosterwyck-Gastuche (1978) and Van Oosterwyck-Gastuche and La Iglesia (1978) discussed the low-temperature (60 °C) synthesis of kaolinite including the thermodynamics and rates involved.

The use of aluminosilicate gels as starting materials is quite common, and the Si/Al ratio is important in hydrothermal systems. In some methods, gel precipitation

is dependent on pH. The gels are then washed to eliminate excess ions. For example, kaolinite formed from amorphous gels ( $\text{Si}/\text{Al} < 2$ ) persists up to 405 °C. The formation of b-axis ordered kaolinite is favoured over the disordered form at lower Si/Al ratios and higher temperatures (Eberl and Hower, 1975). These authors also reported that contamination by alkali ions inhibits crystallization. However, De Vijnck (1973, 1975, 1976) published a series of papers on the formation of kaolinite from aluminosilicate sols containing  $\text{Li}^+$  or  $\text{K}^+$ . Miyawaki et al. (1991) examined in detail the effects of solution chemistry by reacting  $\text{Al}_2\text{O}_3\text{--SiO}_2\text{--H}_2\text{O}$  gels at 220 °C and autogenous pressure for 5 days. They found that (i) the inhibitory effect of monovalent  $\text{Li}^+$ ,  $\text{Na}^+$ , and  $\text{K}^+$  ions is less than that of divalent  $\text{Mg}^{2+}$  and  $\text{Ca}^{2+}$  ions; (ii) trivalent  $\text{Fe}^{3+}$  and excess  $\text{Al}^{3+}$  significantly interfere with crystallization; (iii) chloride and nitrate salts are better than sulfate and acetate salts; and (iv)  $\text{Li}^+$  ions give just a slight improvement in crystallinity, especially with respect to the 001 peak.

In other methods, gels are formed by hydrolysis of tetraethylorthosilicate and aluminium isopropoxide (De Vijnck, 1973; De Kimpe et al., 1981; De Kimpe and Kodama, 1984), sometimes followed by a thermal treatment (Tomura et al., 1983; Petit and Decarreau, 1990).

Tomura et al. (1985a, 1985b) produced kaolinites of spherical morphology through hydrothermal treatment of aluminosilicate gels. In ceramic technology, such materials improve some of the properties of the products. In addition, pure kaolinite of spherical morphology was synthesized at 150–200 °C, and platy kaolinite at 250 °C in hydrothermal experiments at autogenous pressure (Tomura et al., 1983). Solid-state  $^{27}\text{Al}$  and  $^{29}\text{Si}$  NMR investigations showed that the coordination number of aluminium in these minerals changes from a mixture of four- and six-fold to full six-fold coordination, and the spherical morphology is transformed to a platy one with time (Miyawaki et al., 1992). Satokawa et al. (1994) examined the importance of the silica-alumina gel structure. The spherical morphology develops when the gel, consisting of silica and alumina tetrahedra and some alumina octahedra, is precipitated at pH 9.6. The platy morphology with an allophane-like structure arises from a gel precipitated at pH 4.2. Using the co-hydrolysis method, Huertas et al. (1993a) reported a 65% yield of spherical kaolinite. Nearly perfect crystals are obtained from gels with Si/Al ratios lower than those of kaolinite.

The process of kaolinite formation via the co-hydrolysis method was studied by applying a two-stage kinetic model, with separate calculated rate constants and activation energies (Huertas et al., 1993b). The first step involves transformation of the amorphous gel into an intermediate product, with an activation energy of 86–118 kJ/mol depending on gel composition. The second step is the transformation of the intermediate phase to kaolinite, with an activation energy of 66 kJ/mol independent of gel composition.

Fialips et al. (2000) suggested that the hydrothermal formation of kaolinite from metakaolinite involves two processes that depend on pH and the type of metakaolinite. The kaolinite obtained is less ordered when the  $\text{pH} = 4\text{--}6$  than when the



pH = 1. The first process involves dissolution of the metakaolinite followed by crystallization of either thin prismatic or dendritic kaolinite particles that curl due to surface tension. The second process involves the rapid formation of small, pseudo-hexagonal kaolinite particles that aggregate and coalesce to form larger particles.

Using seeds of dickite at 200–250 °C for 1–9 days, Tomura et al. (1990) obtained good yields of kaolinite. Petit and Decarreau (1990) obtained iron-rich kaolinites from glasses by hydrothermal synthesis at 200 °C. Some of these kaolinites show relatively good crystallinity as determined by IR spectroscopy.

The synthesis of a mixed kaolinite–smectite mineral was reported by Środoń (1980). He obtained a mixed-layer mineral with 40–90% kaolinite layers, depending on the concentration of  $\text{Al}^{3+}$ , by reacting a Wyoming smectite in  $\text{Al}^{3+}/\text{K}^{+}$  or  $\text{Al}^{3+}/\text{Ca}^{2+}$  salt solutions at 150 °C for 4 months.

#### 4.2.4. Sepiolite

Few references exist concerning the laboratory synthesis of sepiolite and palygorskite. This is because sepiolite is (i) unstable at hydrothermal conditions ( $> 300$  °C) (Frank-Kamenetskii et al., 1972; Otsuka et al., 1974; Güven and Carney, 1979; Komarneni, 1989); (ii) unstable in both acidic and alkaline solutions at elevated temperatures (Golden et al., 1985); and (iii) usually dominated by smectites that crystallize more readily from magnesium silicate gels at high pH. Although the synthesis of sepiolite was successful, the yields are low (Hast, 1956; Wiegmann and Horte, 1960; Siffert and Wey, 1962; Wollast et al., 1968; Nesterchuk and Makarova, 1973; Abtahi, 1985). Mizutani et al. (1991) successfully obtained sepiolite with the potential for greater yields by adding seed particles of sepiolite to a magnesium silicate gel at 150–200 °C, and subjecting the mixture to hydrothermal treatment. Under these conditions, the formation is determined primarily by the hydrothermal stability of sepiolite itself.

Recently, Birsoy (2002) calculated equilibrium activity diagrams for a seven-component system, pointing out that the most common formation mechanism of natural sepiolite–palygorskite minerals involves crystallization from solution. Some highlights from this detailed thermodynamic study are (i) the formation of these minerals is more favoured in the presence of amorphous silica than of quartz and (ii) the activity of aluminium affects the type of minerals formed.

### 4.3. PURIFICATION OF CLAYS

With the possible exception of vermiculites and micas, clay minerals are found mixed or associated with other minerals and/or amorphous materials. In many applications the clays, in particular bentonites, are used as mined from the deposit without separation or enrichment of the clay minerals. In the case of kaolins, a certain fractionation is required to enrich the kaolinite and to remove other



unwanted clay minerals, especially montmorillonites (Jepson, 1984). However, the increased application of clay minerals in the manufacture of advanced materials raises the need for purification and enrichment.

Identification of clay minerals in a raw clay or soil always requires a purification step. This is because the presence of carbonates, iron oxides, or organic materials interferes with the identification procedure. Purification is also required for studying the properties of clay minerals. A common method for obtaining purified clay minerals is fractionation by sedimentation after removal of carbonates, (hydr)oxides,<sup>1</sup> and organic materials. However, complete (100%) enrichment of a clay mineral may only be achieved at the laboratory scale rather than at an industrial scale. Even then, no more than 90% enrichment is usually achievable.

Size fractionation of purified clays and identification of the clay minerals in different fractions often provide more precise information than could be obtained by analysis of the whole unfractionated purified clay. Size fractionation is especially recommended for soil clays because they usually contain different types and proportions of clay minerals (Tributh, 1976; Tributh and Lagaly, 1986b). Size fractions of several clay mineral standards differ in the type and amount of admixed phases, and in the structures of the clay minerals (Köster, 1996). For example, the finest fraction of kaolins contains montmorillonite, an unwanted phase in many ceramic applications (Jepson, 1984). Enrichment of clay minerals involves two steps (i) removal of unwanted materials by physical or chemical treatment and (ii) fractionation by sedimentation to facilitate the removal of the remaining larger than clay-size impurities (such as quartz) that could be trapped between the non-exfoliated aggregates.

#### 4.3.1. Purification Procedures

These procedures consist of the decomposition of carbonates, the dissolution of (hydr)oxides and silica (Tributh and Lagaly, 1986a, 1986b), and the oxidation of organic materials.

Carbonates must be decomposed, especially when the purified clays are to be used in colloid chemical studies. This is because the calcium and magnesium ions in carbonates impede complete peptization of the clay minerals and the delamination of smectites.

Similarly, the presence of (hydr)oxides prevents optimal dispersion of the clay minerals and successful fractionation, because trivalent cations released by the (hydr)oxides cause strong coagulation. In addition, pH-dependent interactions of (hydr)oxides with clay minerals lead to aggregation. Such inorganic impurities also interfere with the X-ray identification of the clay minerals.

Likewise, organic materials must be removed because high amounts of humic materials, mainly associated with soil clays, can render X-ray identification difficult.

---

<sup>1</sup>The term (hydr)oxides indicates that the oxidic admixtures comprise oxides, hydroxides, and oxide hydroxides.

Organic materials, even in small amounts, can also exert a strong influence on the mechanical properties, stability, and flow behaviour of clay mineral dispersions.

Moreover, the presence of amorphous silica, acting as a cementing agent, impedes swelling and dispersion.

#### *A. Decomposition of Carbonates*

Carbonates are decomposed by the addition of dilute hydrochloric acid, taking care that the pH does not drop below 4.5 to avoid any attack on the clay mineral structure. Decomposition of high carbonate concentrations requires significant time (up to 2 days). A less drastic procedure is to treat the clay with acetate buffer (Tributh and Lagaly, 1986a) or complex the divalent cations with ethylenediamine tetraacetate (EDTA) (Köster et al., 1973; Köster, 1996, 1997). Treatment with EDTA solutions is also recommended when other  $\text{Ca}^{2+}$ - and  $\text{Mg}^{2+}$ -containing minerals (such as members of the apatite group) are present. Since EDTA adsorbs at clay mineral edges, the negative edge charge density increases. This influences the colloid chemical behaviour, and especially the rheological properties, of clay mineral dispersions. On the other hand, this effect can be of advantage in some other applications.

*Recommended procedure.* Disperse 10–15 g clay in 100 mL water, add 2 M HCl dropwise. The pH must not decrease below 4.5, control with a glass electrode is not always reliable because the electrode often does not indicate correct pH values in the presence of clays. Indicator strips are more reliable (Keller and Matlack, 1990). Recommended is an acetate buffer solution of pH = 4.8 (2 M sodium acetate + 2 M acetic acid) instead of hydrochloric acid. EDTA solutions can also be used to complex the divalent cations: either 0.1 mol/L  $\text{Na}_2\text{H}_2\text{EDTA}^{2-}$  solution of pH = 4.5, or 0.1 mol/L  $\text{Na}_3\text{HEDTA}$  solution of pH = 8. After the decomposition of carbonates the sample should be washed to remove the dissolved or complexed cations.

#### *B. Dissolution of (Hydr)oxides*

Iron (hydr)oxides (as also aluminium and manganese (hydr)oxides) are removed by complexing the multivalent cations with citrate. Fe(III) must be reduced with sodium dithionite to Fe(II) which forms a stable citrate complex (Mehra and Jackson, 1960; Holmgren, 1967). Stul and van Leemput (1982) have modified the procedure for bentonites to avoid the formation of (small amounts) of iron sulphides. The small amount of organic materials, commonly present in bentonites, is oxidized with  $\text{H}_2\text{O}_2$  following reduction with dithionite.

The oxidation and reduction processes may change the layer charge. Although modest in the case of smectites, these changes are detectable (Rengasamy et al., 1976; Lagaly, 1981, 1994; Stul and van Leemput, 1982). Reduction of smectites increases the cation exchange capacity (CEC) in proportion to the  $\text{Fe}^{2+}$  content. Re-oxidation

---

<sup>2</sup>Both forms of EDTA are commercially available.

reduces the CEC which, however, remains somewhat higher than that of the starting material. This difference is dependent on the type of smectite (Stucki et al., 1984a, 1984b).

The CEC of high-charge clay minerals (vermiculites, micas) is distinctly enhanced by reduction (Roth et al., 1969). Subsequent oxidation does not reduce the CEC although the amounts of Fe(III) increase. The decrease in layer charge due to oxidation of Fe(II) is largely compensated by the dissociation of protons from structural OH groups. Ryan and Gschwend (1991) recommended extraction of iron and aluminium (hydr)oxides with the strongly reducing agent  $\text{TiCl}_3$  in the presence of EDTA. These reagents remove the iron (hydr)oxides more effectively and more selectively than dithionite. Some  $\text{TiO}_2$  particles are formed by hydrolysis of  $\text{Ti}^{4+}$ .

Iron and aluminium (hydr)oxides can also be removed by treating the clays with acidified sodium oxalate solution (1 M NaCl + 0.1 M  $\text{Na}_2\text{C}_2\text{O}_4$  + 0.1 M HCl) for a few minutes, then washing several times with 1 M NaCl + 0.1 M  $\text{Na}_2\text{C}_2\text{O}_4$  (Janek et al., 1997). As mentioned above, oxalate is adsorbed at the edges and changes the edge charge density. Calcium ions, when still present after the first treatment, are precipitated as  $\text{CaC}_2\text{O}_4^3$ , representing a permanent source of calcium ions.

*Recommended procedure.* Add 50 mL of 0.3 M sodium citrate solution and 10 mL of 1 M sodium hydrogen carbonate to the clay dispersion, heat to 75–80 °C. Add 3 g (solid) sodium dithionite. The colour should change from brown to blue; if not, add more dithionite. Hold at 75–80 °C for about 30 min and wash four times with 2 M NaCl. Washing with water is not possible because the clay begins to disperse. For bentonites, disperse 15 g of the clay in 250 mL water, and 200 mL buffer solution (a solution containing 0.3 M sodium citrate + 1 M sodium hydrogen carbonate + 1.2 M HCl), heat to 75 °C and add 4 g sodium dithionite (Stul and van Leemput, 1982). After about 30 min wash twice with 200 mL 0.05 M HCl. Repeat the reduction, wash with a mixture of 200 mL 0.5 M NaCl and 200 mL 0.5 M sodium acetate. Then oxidize the organic material by adding 1000 mL  $\text{H}_2\text{O}_2$  solution (250 mL 30%  $\text{H}_2\text{O}_2$  + 750 mL 0.5 M sodium acetate), holding for 30 min at 70 °C, washing twice with 200 mL of 0.5 M NaCl, and dialysing.

### C. Oxidation of Organic Materials

The organic materials can be oxidized with hydrogen peroxide, sodium hypochlorite (Anderson, 1963), bromine in water (Pérez-Rodríguez and Wilson, 1969; Mitchell and Smith, 1974), and peroxodisulphate in the presence of a buffer such as sodium hydrogen carbonate, sodium tetraborate, or sodium hydrogen phosphate (Meier and Menegatti, 1997; Menegatti et al., 1999). Sodium hypochlorite is more effective than  $\text{H}_2\text{O}_2$  while bromine and peroxodisulphate are even more effective (van Langeveld et al., 1978; Meier and Menegatti, 1997). Oxidation of organic materials to  $\text{CO}_2$  using hydrogen peroxide is seldom complete (Theng et al., 1999) and several low

---

<sup>3</sup>Calcium oxalate is insoluble in solutions acidified with acetic acid but is dissolved with stronger acids.

molecular weight compounds, especially oxalate, are formed (Pérez-Rodriguez and Wilson, 1969). Since some of this oxalate are adsorbed at clay mineral edges by complexing to aluminium ions in the structure (Siffert and Espinasse, 1980; Permien and Lagaly, 1994), only a portion can be removed by washing (Farmer and Mitchell, 1963). Oxidation with peroxodisulphate (in great excess, about 40 g  $\text{Na}_2\text{S}_2\text{O}_8$  per g sample), with  $\text{NaHCO}_3$  as buffer, is performed at about 80 °C. The procedure does not appear to cause any significant damage to clay mineral, such as kaolinite, montmorillonite, and illite.

*Recommended procedure.* Following removal of carbonates, add small amounts of 10%  $\text{H}_2\text{O}_2$  to the wet sediment. The reaction can be vehement when large amounts of organic materials are present. Heat to 60–70 °C and add further amounts of about 50 mL  $\text{H}_2\text{O}_2$  as long as any reaction (foaming) is observed. To avoid vigorous reactions, wash the sediment with water. If some clay is dispersed, add small volumes of 2 M NaCl solution (never  $\text{CaCl}_2$ ) to coagulate the dispersion.

#### D. Dissolution of Silica

Amorphous silica is dissolved in a boiling solution of 5% (w/w) sodium carbonate. Because this reaction makes the dissolution of the metal (hydr)oxides more difficult, it should be used when all the above treatments have been completed (Stul and van Leemput, 1982). Allophanes are rapidly dissolved in boiling 0.5 M NaOH or KOH (Hashimoto and Jackson, 1960; Alexiades and Jackson, 1966). However, this method is not recommended because it attacks other clay minerals. The preferred method is treatment with acid oxalate solution at pH 3.5 in the dark (Parfitt, 1989).

#### 4.3.2. Removal of Remaining Salt by Dialysis and Fractionation

The clay dispersions obtained after the treatments described above contain considerable amounts of salts, mainly NaCl. Excess salts are normally removed by washing with large amounts of water. However, repeated washing with water causes peptization of the clay mineral particles. In terms of separating the solids, filtration is impractical because of the formation of very thin but almost impermeable filter cakes, while centrifugation requires strong centrifugal fields and long running times. In practice, excess salt is removed by dialysis. This process takes several days but it should not be unnecessarily prolonged because this can lead to coagulation of the clay mineral particles, especially when the pH decreases below 7. Removal of  $\text{Na}^+$  and  $\text{Cl}^-$  promotes edge(+)/face(−) coagulation.

Because clay mineral particles begin to coagulate below pH of about 6, the pH of the water outside of the dialysis bags must be held at pH = 7.5–8 by adding small amounts of dilute sodium hydroxide. Dialysis is complete when no traces of chloride are detected by a test with silver nitrate or when the conductivity of the water outside the dialysis bags is  $\leq 30 \mu\text{S}/\text{cm}$ . Optimal dispersion is obtained after removal of the salts. The dispersion may be dried in several ways. However, drying in air

produces a hard mass that is difficult to re-disperse. Similarly, spray-drying gives rise to materials that are not completely re-dispersible. Thus, freeze-drying is normally recommended. A certain amount of water may be removed beforehand in a rotary evaporator.

#### 4.3.3. *A Simplified 'Gentle' Purification Method*

Raw clays from identified geological deposits may be purified without applying the treatments to remove carbonates, hydr(oxides), and organic material. This classical 'gentle' purification method (van Olphen, 1963) consists of replacing the exchangeable cations with  $\text{Na}^+$  followed by washing with water. Washing removes excess salts as described before and also enables fine impurities to be separated (Annabi-Bergaya, 1978; Benna et al., 1999).

##### *A. $\text{Na}^+$ -exchange*

The raw clay is carefully dispersed in 1 M NaCl solution by shaking for about 12 h, and separated by centrifugation. This procedure is repeated several times (at least 5 times for  $\text{Ca}^{2+}$ -saturated clays).

##### *B. Washing*

The sediment of the  $\text{Na}^+$ -exchanged clay mineral is washed with water. As long as the clay minerals can be separated by centrifugation, the 'visually' clear supernatant is decanted. After each centrifugation, the fine fraction on the top of the sediment is collected with a spatula and separated from the coarse fractions. The procedure may be repeated until the clay mineral forms a stable colloidal dispersion. Then the dispersion and the re-dispersed fine fractions of the sediments are dialysed until free of chloride. The very dilute dispersion (1%) is then allowed to stand and the  $<2\ \mu\text{m}$  fraction is collected according to Stokes law. The bulk of the water is removed by oven drying at  $60^\circ\text{C}$ , while the remaining purified clay mineral slurry is freeze-dried.

*Recommended procedure.* The raw clay (180 g) is placed in 6 centrifuge bottles ( $6 \times 30\ \text{g}$ ) and 400 mL of 1 M NaCl is added to each bottle. The bottles are shaken in a rotary shaker overnight and then centrifuged at 3000 rpm for 2 h. This cycle of agitation/centrifugation is repeated 6 times to achieve close to 99% exchange. The washing procedure is the same as that for the  $\text{Na}^+$ -exchange (3–4 agitation/centrifugation cycles) but more drastic centrifugation (7000 rpm for 3 h) is used because the stability of the colloidal dispersion has increased. The final 'washing' is performed by dialysis (about 7 days). After evaporating the bulk of the water in an oven at  $60^\circ\text{C}$  (1 day), the concentrated purified slurry is freeze-dried (2 weeks). The amount of clay mineral recovered is about one third of the initial weight. This method is also suitable for clay mineral identification but it is time-consuming and yields are low. However, a highly purified clay mineral can be obtained without damage to the initial structure and fabric.

#### 4.3.4. A Pilot Purification Technique

To save time and increase yield, a pilot-scale purification technique was developed. Here the  $\text{Na}^+$ -exchange step is carried out by continuous circulation of 1 M NaCl through the clay mineral suspension (180 g in about 10 L) in a multi-channel membrane. The exchange takes 3 h to complete. The  $\text{Na}^+$ -exchanged clay is then washed by passing water continuously through a series of dialysis columns for about 12 h to reach the conductivity of deionized water. The technique is user-friendly, largely automatic, and easy to extend to an industrial scale. At the same time, a two-fold increase in yield is achieved within a fraction of the time required in the conventional method (2 days versus 1 month).

#### 4.3.5. Conclusions

A complete purification cycle is time-consuming. However, not all the purification steps described above are always necessary. Which steps can be omitted depend on the purpose of the investigation. In contrast to soil clays, clays from geological deposits (such as bentonites, kaolins) commonly contain only small amounts of organic materials. As such, oxidation with  $\text{H}_2\text{O}_2$  or peroxodisulphate may not be required and the simplified ('gentle') procedure may be satisfactory. Similarly, silica does not always act as a cementing agent, and can be removed without chemical treatment.

It should be stressed, however, that even small amounts of carbonates, (hydr)oxides, and organic materials can strongly influence the colloidal and rheological properties of clay pastes, slips, and dispersions. The chemical reactions involved in clay mineral purification may also cause changes to the clay mineral structure. In selecting a given purification procedure, the effect of different reactions must be duly considered.

## REFERENCES

- Abtahi, A., 1985. Synthesis of sepiolite at room temperature from silica and magnesium chloride solution. *Clay Minerals* 20, 521–523.
- Alexiades, C.A., Jackson, M.L., 1966. Quantitative clay mineralogical analysis of soils and sediments. *Clays and Clay Minerals* 164, 35–52.
- Anderson, J.U., 1963. An improved treatment for mineralogical analysis of samples containing organic matter. *Clays and Clay Minerals* 10, 380–388.
- Annabi-Bergaya, F., 1978. Adsorption du Méthanol par la Montmorillonite. Ph.D. thesis. University of Orléans, France.
- Aparicio, P., Galan, E., 1999. Mineralogical interference on kaolinite crystallinity index measurements. *Clays and Clay Minerals* 47, 12–27.
- Arkai, P., 2002. Phyllosilicates in very low-grade metamorphism: transformation to micas. In: Mottana, A., Sassi, F.P., Thompson, J.B., Guggenheim, S. (Eds.), *Micas: Crystal*

- Chemistry and Metamorphic Petrology. Reviews in Mineralogy & Geochemistry, vol. 46. Mineralogical Society of America, Washington, DC, pp. 463–478.
- Barrer, R.M., Marshall, D.J., 1964. Hydrothermal chemistry of silicates. Part XII. Synthetic strontium aluminosilicates. *Journal of the Chemical Society*, 485–497.
- Barrer, R.M., Sieber, W., 1977. Evidence for the replacement of silicon by a divalent cation: synthesis of a novel zinc mica,  $K_2H_2Zn_5[ZnSi_7O_{20}](OH)_4$ . *Journal of the Chemical Society, Chemical Communications*, 905.
- Barrer, R.M., White, E.A.D., 1952. The hydrothermal chemistry of silicates. Part II. Synthetic crystalline sodium aluminosilicates. *Journal of the Chemical Society*, 1561–1571.
- Benna, M., Kbir-Ariguib, N., Magnin, A., Bergaya, F., 1999. Effect of pH on rheological properties of purified sodium bentonite suspensions. *Journal of Colloid and Interface Science* 218, 442–455.
- Bhanage, B.M., Fujita, S., He, Y., Ikushima, Y., Shirai, M., Torii, K., Arai, M., 2002. Concurrent synthesis of dimethyl carbonate and ethylene glycol via transesterification of ethylene carbonate and methanol using smectite catalysts containing Mg and/or Ni. *Catalysis Letters* 83, 137–141.
- Birsoy, R., 2002. Formation of sepiolite–palygorskite and related minerals from solution. *Clays and Clay Minerals* 50, 736–745.
- Borchardt, G., 1989. Smectites. In: Dixon, J.B., Weed, S.B. (Eds.), *Minerals in Soil Environments*. Soil Science Society of America, Madison, WI, pp. 675–727.
- Bowers, T.S., Jackson, K.J., Helgeson, H.C., 1984. *Equilibrium Activity Diagrams: for Co-existing Minerals and Aqueous Solutions at Temperature and Pressures up to 5 Kb and 600 °C*. Springer, Berlin.
- Caillère, S., Hénin, S., Esquevin, J., 1953. Synthèses à basse température de phyllites ferrifères. *Comptes Rendus de l'Académie des Sciences, Paris* 237, 1724–1726.
- Caillère, S., Hénin, S., Esquevin, J., 1956. Etude expérimentale du mécanisme de la formation des antigorites nickellifères. *Bulletin de Société Française de Minéralogie et Cristallographie* 79, 408–421.
- Caillère, S., Oberlin, A., Hénin, S., 1954. Etude au microscope électronique de quelques silicates phylliteux obtenus par synthèses à basse température. *Clay Minerals Bulletin* 2, 146–156.
- Carrado, K.A., Csencsits, R., Thiagarajan, P., Seifert, S., Macha, S.M., Harwood, J.S., 2002. Crystallization and textural porosity of synthetic clay minerals. *Journal of Materials Chemistry* 12, 3228–3237.
- Carrado, K.A., Xu, L., Csencsits, R., Muntean, J.V., 2001. The use of organo- and alkoxy-silanes in the synthesis of grafted and pristine clays. *Chemistry of Materials* 13, 3766–3773.
- Cipriani, C., 2002. Micas: historical perspective. In: Mottana, A., Sassi, F.P., Thompson, J.B., Guggenheim, S. (Eds.), *Micas: Crystal Chemistry & Metamorphic Petrology*. Reviews in Mineralogy, vol. 46. Mineralogical Society of America, Washington, DC, pp. 479–499.
- Decarreau, A., 1980. Cristallogénèse expérimentale des smectites magnésiennes: hectotite, stévensite. *Bulletin de Minéralogie* 103, 579–590.
- Decarreau, A., 1981. Cristallogénèse à basse température de smectites trioctaédriques par vieillissement de coprécipités silicométalliques. *Comptes Rendus de l'Académie des Sciences, Paris* 292, 61–64.
- Decarreau, A., Bonnin, D., 1986. Synthesis and crystallogeneses at low temperature of  $Fe^{3+}$  smectites by evolution of coprecipitated gels: experiments in partly reducing conditions. *Clay Minerals* 21, 861–877.

- Decarreau, A., Bonnin, D., Badaut-Trauth, D., Couty, R., Kaiser, P., 1987. Synthesis and crystallogenesi s of ferric smectite by evolution of Si-Fe coprecipitates in oxidizing conditions. *Clay Minerals* 22, 207–223.
- Decarreau, A., Petit, S., Viellard, Ph., Dabert, N., 2004. Hydrothermal synthesis of aegirine at 200 °C. *European Journal of Mineralogy* 16, 85–90.
- De Kimpe, C.R., Kodama, H., 1984. Transformation of aluminosilicate gels into pre-kaolinitic and pre-zeolitic structure: effects of the solution media. *Clay Minerals* 19, 237–242.
- De Kimpe, C.R., Kodama, H., Rivard, R., 1981. Hydrothermal formation of a kaolinite-like product from noncrystalline aluminosilicate gels. *Clays and Clay Minerals* 29, 446–450.
- De Vijnck, Y.A., 1973. Etude des phases cristallines appartenant au système  $\text{Al}_2\text{O}_3\text{-SiO}_2\text{-H}_2\text{O}$  formées par traitement hydrothermal de gels obtenus par coprécipitation d' $\text{Al}(\text{OH})_3$  et de  $\text{Si}(\text{OH})_4$ . *Silicates Industriels* 38, 193–209.
- De Vijnck, Y.A., 1975. Action des ions alcalins sur la transformation hydrothermale de gels silico-alumineux. I. Influence de l'ion  $\text{Li}^+$ . *Silicates Industriels* 40, 259–272.
- De Vijnck, Y.A., 1976. Action des ions alcalins sur la transformation hydrothermale de gels silico-alumineux. II. Influence de l'ion  $\text{K}^+$ . *Silicates Industriels* 41, 67–81.
- Drits, V.A., Besson, G., Muller, F., 1995. An improved model for structural transformations of heat-treated aluminous dioctahedral 2:1 layer silicates. *Clays and Clay Minerals* 43, 718–731.
- Duldulao, F.D., Burlitch, J.M., 1991. Multistep sol-gel synthesis of a layered silicate, potassium fluorophlogopite. *Chemistry of Materials* 3, 772–775.
- Eberl, D., Hower, J., 1975. Kaolinite synthesis. The role of the silicon-aluminum ratio and alkali-hydrogen ion ratio in hydrothermal systems. *Clays and Clay Minerals* 23, 301–309.
- Emmerich, K., Kahr, G., 2001. The cis- and trans-vacant variety of a montmorillonite: an attempt to create a model smectite. *Applied Clay Science* 20, 119–127.
- Fanning, D.S., Keramid as, V.Z., El-Desoky, M.A., 1989. Micas. In: Dixon, J.B., Weed, S.B. (Eds.), *Minerals in Soil Environments*. Soil Science Society of America, Madison, WI, pp. 551–634.
- Farmer, V.C., 1974. The layer silicates. In: Farmer, V.C. (Ed.), *The Infrared Spectra of Minerals*. Mineralogical Society, London, pp. 331–365.
- Farmer, V.C., Mitchell, B.D., 1963. Occurrence of oxalates in soil clays following hydrogen peroxide treatment. *Soil Science* 96, 221–229.
- Fialips, C.-I., Petit, S., Decarreau, A., 2000. Hydrothermal formation of kaolinite from various metakaolins. *Clay Minerals* 35, 559–572.
- Fiore, S., Huertas, F.J., Huertas, F., Linares, J., 2001. Smectite formation in rhyolitic obsidian as inferred by microscopic (SEM-TEM-AEM) investigations. *Clay Minerals* 36, 489–500.
- Frank-Kamenetskii, V.A., Kotov, N.V., Klochkova, G.N., 1972. Phase and structural changes in sepiolite and palygorskite under hydrothermal conditions in the presence of KCl and NaCl. *Geokhimiya* 10, 1227–1235.
- Frank-Kamenetskii, V.A., Kotov, N.V., Tomashenko, A.N., 1973. Role of Al(IV) and Al(VI) in transformation and synthesis of layer silicates. *Kristall und Technik* 8, 425–435.
- Franklin, K.R., Lee, E., 1996. Synthesis and ion-exchange properties of Na-4-mica. *Journal of Materials Chemistry* 6, 109–115.
- Fritz, B., 1981. Etudes Thermodynamiques et Modélisation des Réactions Hydrothermales et Diagenétiques. *Sciences Géologiques, Mémoire* 65, 197.



- Fujii, K., Hayashi, S., Kodama, H., 2003. Synthesis of an alkylammonium/magnesium phyllosilicate hybrid nanocomposite consisting of a smectite-like layer and organosiloxane layers. *Chemistry of Materials* 15, 1189–1197.
- Golden, D.C., Dixon, J.B., Shadfan, H., Kippenberger, L.A., 1985. Palygorskite and sepiolite alteration to smectite under alkaline conditions. *Clays and Clay Minerals* 33, 44–50.
- Grauby, O., Petit, S., Decarreau, A., Baronnet, A., 1993. The beidellite–saponite solid-solution: an experimental approach. *European Journal of Mineralogy* 5, 623–635.
- Grauby, O., Petit, S., Decarreau, A., Baronnet, A., 1994. The nontronite–saponite series: an experimental approach. *European Journal of Mineralogy* 6, 99–112.
- Güven, N., Carney, L.L., 1979. The hydrothermal transformation of sepiolite to stevensite and the effect of added chlorides and hydroxides. *Clays and Clay Minerals* 27, 253–260.
- Harder, H., 1970. Kaolinit-Synthese bei niedrigen Temperaturen. *Naturwissenschaften* 4, 193.
- Harder, H., 1972. The role of magnesium in the formation of smectite minerals. *Chemical Geology* 10, 31–39.
- Harder, H., 1978. Synthesis of iron layer silicate minerals under natural conditions. *Clays and Clay Minerals* 26, 65–72.
- Hashimoto, J., Jackson, M.L., 1960. Rapid dissolution of allophane and kaolinite–halloysite after dehydration. *Clays and Clay Minerals* 7, 102–113.
- Hast, N., 1956. A reaction between silica and some magnesium compounds at room temperature and at +37 °C. *Arkiv för Kemi* 9, 343–360.
- Higashi, S., Miki, K., Komarneni, S., 2002. Hydrothermal synthesis of Zn-smectite. *Clays and Clay Minerals* 50, 299–305.
- Hinckley, D.N., 1963. Variability in “crystallinity” values among the kaolin deposits of the coastal plain of Georgia and South Carolina. *Clays and Clay Minerals* 11, 229–235.
- Holmgren, G.G.S., 1967. A rapid citrate–dithionite extractable iron procedure. *Soil Science Society of America Proceedings* 31, 210–211.
- Huertas, F.J., Cuadros, J., Huertas, F., Linares, J., 2000. Experimental study of the hydrothermal formation of smectite in the beidellite–saponite series. *American Journal of Science* 300, 504–527.
- Huertas, F.J., Fiore, S., Huertas, F., Linares, J., 1999. Experimental study of the hydrothermal formation of kaolinite.. *Chemical Geology* 156, 171–190.
- Huertas, F.J., Huertas, F., Linares, J., 1993a. Hydrothermal synthesis of kaolinite: method and characterization of synthetic materials. *Applied Clay Science* 7, 345–356.
- Huertas, F.J., Huertas, F., Linares, J., 1993b. A new approach to kinetics of kaolinite synthesis. In: Cuney, M., Cathelineau, M. (Eds.), *Proceedings of the 4th International Symposium on Hydrothermal Reactions*. Nancy, France, pp. 87–90.
- Iriarte-Lecumberri, I., 2003. Synthèse de minéraux argileux dans le système  $\text{SiO}_2\text{--Al}_2\text{O}_3\text{--Fe}_2\text{O}_3\text{--Na}_2\text{O--H}_2\text{O}$ . Ph.D. thesis. Universities of Poitiers, France and Granada, Spain, p. 2.
- Janek, M., Komadel, P., Lagaly, G., 1997. Effect of autotransformation on the layer charge of smectites determined by the alkylammonium method. *Clay Minerals* 32, 623–632.
- Jepson, W.B., 1984. Kaolins: their properties and uses. *Philosophical Transactions of the Royal Society, London, A* 311, 411–432.
- Keller, W.D., Matlack, K., 1990. The pH of clay suspensions in the field and laboratory, and methods of measurement of their pH. *Applied Clay Science* 5, 123–133.
- Klingsberg, C., Roy, R., 1957. Synthesis, stability and polytypism of nickel and gallium phlogopite. *American Mineralogist* 42, 629–634.

- Kloprogge, J.T., 1998. Synthesis of smectites and porous pillared clay catalysts: a review. *Journal of Porous Materials* 5, 5–41.
- Kloprogge, J.T., Jansen, J.B., Geus, J.W., 1990. Characterization of synthetic Na-beidellite. *Clays and Clay Minerals* 38, 409–414.
- Kloprogge, J.T., Komarneni, S., Amonette, J.E., 1999. Synthesis of smectite clay minerals: a critical review. *Clays and Clay Minerals* 47, 529–554.
- Kloprogge, J.T., Vogels, R.J., 1995. Hydrothermal synthesis of ammonium-beidellite. *Clays and Clay Minerals* 43, 135–137.
- Kodama, T., Harada, Y., Ueda, M., Shimizu, K., Shuto, K., Komarneni, S., Hoffbauer, W., Schneider, H., 2001a. Crystal-size control and characterization of Na-4-mica prepared from kaolinite. *Journal of Materials Chemistry* 11, 1222–1227.
- Kodama, T., Higuchi, T., Shimizu, T., Shimizu, K., Komarneni, S., Hoffbauer, W., Schneider, H., 2001b. Synthesis of Na-2-mica from metakaolin and its cation exchange properties. *Journal of Materials Chemistry* 11, 2072–2077.
- Kodama, T., Komarneni, S., Hoffbauer, W., Schneider, H., 2000. Na-4-mica: simplified synthesis from kaolinite, characterization and Zn, Cd, Pb, Cu and Ba uptake kinetics. *Journal of Materials Chemistry* 10, 1649–1653.
- Komarneni, S., 1989. Mechanisms of palygorskite and sepiolite alteration as deduced from solid-state  $^{27}\text{Al}$  and  $^{29}\text{Si}$  NMR. *Clays and Clay Minerals* 37, 469–473.
- Komarneni, S., Pidugu, R., Amonette, J.E., 1998. Synthesis of Na-4-mica from metakaolinite and MgO: characterization and  $\text{Sr}^{2+}$  uptake kinetics. *Journal of Materials Chemistry* 8, 205–208.
- Komarneni, S., Pidugu, R., Hoffbauer, W., Schneider, H., 1999. A synthetic Na-rich mica: synthesis and characterization by  $^{27}\text{Al}$  and  $^{29}\text{Si}$  magic angle spinning nuclear magnetic resonance spectroscopy. *Clays and Clay Minerals* 47, 410–416.
- Köster, H.M., 1996. Mineralogical and chemical heterogeneity of three standard clay mineral samples. *Clay Minerals* 31, 417–422.
- Köster, H.M., 1997. Methoden und kritische Anmerkungen zur Aufbereitung von Karbonatgesteinen und zur Analyse der schwerlöslichen Gesteinsbestandteile und der Carbonate. *Zentralblatt für Geologie und Paläontologie I* 1033–1043.
- Köster, H.M., Kohler, E.E., Krah, J., Kröger, J., Vogt, K., 1973. Veränderungen am Montmorillonit durch Einwirkung von 0,1 m AeDTE-Lösungen, 1 n NaCl-Lösung und 0,1 n Salzsäure. *Neues Jahrbuch für Mineralogie. Abhandlungen* 119, 8–100.
- La Iglesia, A., Van Oosterwyck-Gastuche, M.C., 1978. Kaolinite synthesis. I. Crystallization conditions at low temperatures and calculation of thermodynamic equilibria. Applications to laboratory and field observations. *Clays and Clay Minerals* 26, 397–408.
- Lagaly, G., 1981. Characterization of clays by organic compounds. *Clay Minerals* 16, 1–21.
- Lagaly, G., 1994. Layer charge determination by alkylammonium ions. In: Mermut, A. (Ed.), *Charge Characteristics of 2:1 Clay Minerals. CMS Workshop Lectures*, vol. 6. The Clay Minerals Society, Boulder, CO, pp. 1–46.
- Levinson, A.A., Day, J.J., 1968. Low-temperature hydrothermal synthesis of montmorillonite, ammonium-micas, and ammonium-zeolites. *Earth and Planetary Science Letters* 5, 52–54.
- Linares, J., Huertas, F., 1971. Kaolinite: synthesis at room temperature. *Science* 171, 896–897.
- Mackenzie, R. C. (Ed.), 1970. *Differential Thermal Analysis*. In: *Fundamental Aspects*, vol. 1. Academic Press, London.

- Manning, D.A.C., 2003. Experimental studies of clay mineral occurrence. In: Worden, R., Morad, S. (Eds.), *Clay Mineral Cements in Sandstones*. Special Publication of the International Association of Sedimentologists 34. Blackwell Science, Oxford, pp. 177–190.
- Mehra, O.P., Jackson, M.L., 1960. Iron oxide removal from soils and clays by a dithionite-citrate system buffered with sodium bicarbonate. *Clays and Clay Minerals* 7, 317–327.
- Meier, L.P., Menegatti, A.P., 1997. A new, efficient, one-step method for the removal of organic matter from clay-containing sediments. *Clay Minerals* 32, 557–563.
- Menegatti, A.P., Früh-Green, G.L., Stille, P., 1999. Removal of organic matter by disodium peroxodisulphate: effects on mineral structure, chemical composition, and physicochemical properties of some clay minerals. *Clay Minerals* 34, 247–257.
- Millot, G., 1965. *Géologie des Argiles*. Masson, Paris (Section C).
- Mitchell, B.D., Smith, B.F.L., 1974. The removal of organic matter from soil extracts by bromine oxidation. *Journal of Soil Science* 25, 239–241.
- Miyawaki, R., Tomura, S., Inukai, K., Shibasaki, Y., Okazaki, M., Samejima, S., Satokawa, S., 1992. Formation process of kaolinite from the amorphous mixture of silica and alumina. *Clay Science* 8, 273–284.
- Miyawaki, R., Tomura, S., Samejima, S., Okazaki, M., Mizuta, H., Maruyama, S.-I., Shibasaki, Y., 1991. Effects of solution chemistry on the hydrothermal synthesis of kaolinite. *Clays and Clay Minerals* 39, 498–508.
- Mizutani, T., Fukushima, Y., Okada, A., Kamigaito, O., 1991. Hydrothermal synthesis of sepiolite. *Clay Minerals* 26, 441–445.
- Mottana, A., Robert, J.-L., Marcelli, A., Giuli, G., Della Ventura, G., Paris, E., Wu, Z., 1997. Octahedral vs tetrahedral coordination of Al in synthetic micas determined by XANES. *American Mineralogist* 82, 497–502.
- Mottana, A., Sassi, F. P., Thompson, J. B., Guggenheim, S. (Eds.), 2002. *Micas: Crystal Chemistry and Metamorphic Petrology*. In: *Reviews in Mineralogy & Geochemistry*, vol. 46. Mineralogical Society of America, Washington, DC.
- Muthusamy, E., Walsh, D., Mann, S., 2002. Morphosynthesis of organoclay microspheres with sponge-like or hollow interiors. *Advanced Materials* 14, 969–972.
- Nagase, T., Iwasaki, T., Ebina, T., Hayashi, H., Onodera, Y., Dutta, N.C., 1999. Hydrothermal synthesis of Fe-montmorillonite in Si-Fe-Mg system. *Chemistry Letters* 28, 303–304.
- Nesterchuk, N.I., Makarova, T.A., 1973. Hydrothermal synthesis of sepiolite. *Zapisky Vsesoyuznogo Mineralogicheskogo Obshchestva* 102, 232–242.
- Norrish, K., Pickering, J.G., 1983. Clay minerals. In: *Soils: an Australian Viewpoint*. CSIRO, Melbourne/Academic Press, London, pp. 281–308.
- Otsuka, R., Sakamoto, T., Hara, Y., 1974. Phase transformations of sepiolite under hydrothermal conditions. *Journal of the Clay Science Society of Japan* 14, 8–19.
- Parfitt, R.L., 1989. Optimum conditions for extraction of Al, Fe and Si from soils with acid oxalate. *Communications in Soil Science and Plant Analysis* 20, 801–806.
- Paulus, W.J., Komarneni, S., Roy, R., 1992. Bulk synthesis and selective exchange of strontium ions in  $\text{Na}_4\text{Mg}_6\text{Al}_4\text{Si}_4\text{O}_{20}\text{F}_4$  mica. *Nature* 357, 571–573.
- Pérez-Rodríguez, J.L., Wilson, M.J., 1969. Effects of pretreatment on a 14 Å swelling mineral from Gartly, Aberdeenshire. *Clay Minerals* 8, 39–45.
- Permien, T., Lagaly, G., 1994. The rheological and colloidal properties of bentonite dispersions in the presence of organic compounds. IV. Sodium montmorillonites and acids. *Applied Clay Science* 9, 251–263.

- Petit, S., 2004. Crystal-chemistry of talcs: a NIR and MIR spectroscopic approach. In: Klopogge, J.T. (Ed.), *Vibrational Spectroscopies. CMS Workshop Lectures*. vol. 13. The Clay Minerals Society, Aurora, CO., in press.
- Petit, S., Decarreau, A., 1990. Hydrothermal (200 °C) synthesis and crystal chemistry of iron-rich kaolinites. *Clay Minerals* 25, 181–196.
- Petit, S., Righi, D., Madejova, I., Decarreau, A., 1998. Layer charge estimation of smectites using infrared spectroscopy. *Clay Minerals* 33, 579–591.
- Petit, S., Righi, D., Madejova, I., Decarreau, A., 1999. Interpretation of the infrared  $\text{NH}_4^+$  spectrum of the  $\text{NH}_4^+$ -clays: application to the evaluation of the layer charge. *Clay Minerals* 34, 543–549.
- Rengasamy, P., van Assche, J.B., Uytterhoeven, J.B., 1976. Particle size of Wyoming bentonite and its relation to the cation exchange capacity and the homogeneity of the charge density. *Journal of the Chemical Society, Faraday Transactions I* 72, 376–381.
- Rayner, J.H., 1962. An examination of the rate of formation of kaolinite from a co-precipitated silica gel. *Colloques Internationaux du CNRS*, 105, Genese et Synthèse des Argiles, pp. 124–127.
- Robert, J.-L., Beny, J.-M., Della Ventura, G., Hardy, M., 1993. Fluorine in micas: crystal-chemical control of the OH–F distribution between trioctahedral and dioctahedral sites. *European Journal of Mineralogy* 5, 7–18.
- Rosenberg, P.E., 1987. Synthetic muscovite solid solutions in the system  $\text{K}_2\text{O}-\text{Al}_2\text{O}_3-\text{SiO}_2-\text{H}_2\text{O}$ . *American Mineralogist* 72, 716–723.
- Roth, C.B., Jackson, M.L., Syers, J.K., 1969. Deferration effect on structural ferrous–ferric iron ratio and cec of vermiculites and soils. *Clays and Clay Minerals* 17, 2.
- Roy, R., Osborn, E.F., 1954. The system  $\text{Al}_2\text{O}_3-\text{SiO}_2-\text{H}_2\text{O}$ . *American Mineralogist* 39, 853–885.
- Roy, R., Tuttle, O.F., 1956. Investigations under hydrothermal conditions. *Physics and Chemistry of the Earth* 1, 138–180.
- Ryan, J.N., Gschwend, P.M., 1991. Extraction of iron oxides from sediments using reductive dissolution by titanium(III). *Clays and Clay Minerals* 39, 509–518.
- Satokawa, S., Osaki, Y., Samejima, S., Miyawaki, R., Tomura, S., Shibasaki, Y., Sugahara, Y., 1994. Effects of the structure of silica-alumina gel on the hydrothermal synthesis of kaolinite. *Clays and Clay Minerals* 42, 288–297.
- Shirai, M., Aoki, K., Arai, M., 2002. Control of mesopore structure of smectite-type materials synthesized with a hydrothermal method. *Studies in Surface Science and Catalysis* 141, 281–288.
- Shirai, M., Aoki, K., Torii, K., Arai, M., 2001. In situ EXAFS study on the formation of smectite-type clays containing cobalt cations in lattice. *Journal of Synchrotron Radiation* 8, 743–745.
- Shirai, M., Torii, K., Arai, M., 2000. Synthesis and size-selective application of palladium metal particles intercalated in mesopore-size controlled smectite. *Molecular Crystals and Liquid Crystals* 341, 1125–1130.
- Siffert, B., Espinasse, P., 1980. Adsorption of organic diacids and sodium polyacrylate onto montmorillonite. *Clays and Clay Minerals* 28, 381–387.
- Siffert, B., Wey, R., 1962. Synthèse d'une sepiolite a temperature ordinaire. *Comptes Rendus de l'Académie des Sciences* 254, 1460–1464.
- Smykatz-Kloss, W., Warne, S. St. J., 1991. Thermal analysis in the geosciences. *Lecture Notes in Earth Sciences*, vol. 38. Springer, Berlin.

- Srodon, J., 1980. Synthesis of mixed-layer kaolinite/smectite. *Clays and Clay Minerals* 28, 419–424.
- Steeffel, C.I., Van Capellen, P., 1990. A new kinetic approach to modeling the water-rock interaction: the role of nucleation, precursors and Ostwald ripening. *Geochimica et Cosmochimica Acta* 54, 2657–2677.
- Stubican, V., Roy, R., 1962. Boron substitution in synthetic micas and clays. *American Mineralogist* 47, 1166–1173.
- Stucki, J.W., Golden, D.C., Roth, C.B., 1984a. Effects of reduction and reoxidation of structural iron on the surface charge and dissolution of dioctahedral smectites. *Clays and Clay Minerals* 32, 350–356.
- Stucki, J.W., Low, P., Roth, C.B., Golden, D.C., 1984b. Effects of oxidation state of octahedral iron on clay swelling. *Clays and Clay Minerals* 32, 357–362.
- Stul, M.S., van Leemput, L., 1982. Particle-size distribution, cation exchange capacity and charge density of deferrated montmorillonites. *Clay Minerals* 17, 209–215.
- Stumm, W., Morgan, J.J., 1981. *Aquatic Chemistry*, 2nd edition. Wiley, New York.
- Tamura, K., Yamada, H., Nakazawa, H., 2000. Stepwise hydration of high-quality synthetic smectite with various cations. *Clays and Clay Minerals* 48, 400–404.
- Tateyama, H., Hishimura, S., Tsunematsu, K., Jinnai, K., Adachi, Y., Kimura, M., 1992. Synthesis of expandable fluorine mica from talc. *Clays and Clay Minerals* 40, 180–185.
- Theng, B.K.G., Ristori, G.G., Santi, C.A., Percival, H.J., 1999. An improved method for determining the specific surface areas of topsoils with varied organic matter content, texture and clay mineral composition. *European Journal of Soil Science* 50, 309–316.
- Tomita, K., Kawano, M., 2002. Synthesis of smectite from igneous rocks at atmospheric pressure. *Clay Science* 11, 585–599.
- Tomura, S., Shibasaki, Y., Mizuta, H., Kitamura, M., 1983. Spherical kaolinite: synthesis and mineralogical properties. *Clays and Clay Minerals* 31, 413–421.
- Tomura, S., Shibasaki, Y., Mizuta, H., Kitamura, M., 1985a. Growth conditions and genesis of spherical and play kaolinite. *Clays and Clay Minerals* 33, 200–206.
- Tomura, S., Shibasaki, Y., Mizuta, H., Sunagawa, I., 1985b. Origin of morphology of spherical kaolinite. *Clay Science* 6, 159–166.
- Tomura, S., Shibasaki, Y., Miyawaki, R., Mizuta, H., Yamashita, Y., 1990. Synthesis of kaolinite with dickite seed: a study by the experimental design method. *Clay Science* 7, 315–323.
- Toraya, H., Iwai, S., Marumo, F., Hishikawa, T., Hirao, M., 1978. The crystal structure of synthetic mica,  $\text{KMg}_2.75\text{Si}_3.5\text{AlO}_5\text{O}_{10}\text{F}_2$ . *Mineralogical Journal* 9, 210–220.
- Tributh, H., 1976. Die Umwandlung der glimmerartigen Schichtsilikate zu aufweitbaren Dreischicht-Tonmineralen. *Zeitschrift für Pflanzenernährung und Bodenkunde* 1, 7–25.
- Tributh, H., Lagaly, G., 1986a. Aufbereitung und Identifizierung von Boden- und Lagerstättentonen. I. Aufbereitung der Proben um Labor. *GIT-Fachzeitschrift für das Laboratorium* 30, 524–529.
- Tributh, H., Lagaly, G., 1986b. Aufbereitung und Identifizierung von Boden- und Lagerstättentonen. II. Korngrößenanalyse und Gewinnung von Tonsubfraktionen. *GIT-Fachzeitschrift für das Laboratorium* 30, 771–776.
- van Langeveld, A.D., van der Gaast, S.J., Eisma, D., 1978. A comparison of the effectiveness of eight methods for the removal of organic matter from clay. *Clays and Clay Minerals* 26, 361–364.

- van Olphen, H., 1963. *An Introduction to Clay Colloid Chemistry*, 2nd edition. Wiley, New York.
- Van Oosterwyck-Gastuche, M.C., La Iglesia, A., 1978. Kaolinite synthesis. II. A review and discussion of the factors influencing the rate process. *Clays and Clay Minerals* 26, 409–417.
- Voncken, J.H.L., van der Eerden, M.J., Jansen, J.B.H., 1987. Synthesis of a Rb analogue of 2M1 muscovite. *American Mineralogist* 72, 551–554.
- Wiegmann, J., Horte, C.H., 1960. Eigenschaften und thermische Reaktionen gefällter Magnesiumsilikate. *Silikattechnik* 11, 380–384.
- Wilson, M.J., 1999. The origin and formation of clay minerals in soils: past, present and future perspectives. *Clay Minerals* 34, 7–25.
- Wollast, R., Mackenzie, F.T., Bricker, O.P., 1968. Experimental precipitation and genesis of sepiolite at earth-surface conditions. *American Mineralogist* 53, 1645–1662.

This page intentionally left blank

## *Chapter 5*

# COLLOID CLAY SCIENCE

## G. LAGALY

*Institut für Anorganische Chemie, Universität Kiel, D-24118 Kiel, Germany*

Clay minerals are distinguished from other colloidal materials by the highly anisometric and often irregular particle shape, the broad particle size distribution, the different types of charges (permanent charges on the faces, pH-dependent charges at the edges), the heterogeneity of the layer charges, the pronounced cation exchange capacity (CEC), the disarticulation (in case of smectites), the flexibility of the layers, and the different modes of aggregation (see Chapter 1) (van Olphen, 1977; Lagaly, 1993, 2005; Jasmund and Lagaly, 1993; Lagaly et al., 1997).

### 5.1. CLAY MINERAL PARTICLES

#### *5.1.1. Particle and Aggregate Structure*

Clay mineral particles, in particular those of smectites, are never crystals in the strict sense (Brindley and Brown, 1980; Moore and Reynolds, 1997; Plançon, 2001). Many crystallographers are dismayed at the particles clay scientists often call ‘crystals’. In fact, a smectite ‘crystal’ is more equivalent to an assemblage of silicate layers than to a true crystal (Fig. 5.1). Montmorillonite particles seen in the electron microscope never have the regular shape of real crystals but look like paper torn into irregular pieces. Instructive pictures of smectite particles were published by Vali and Köster (1986). The core of the particles is surrounded by disordered and bent silicate layers with frayed edges. Layers or thin particles of a few layers protrude from the packets and enclose wedge-shape pores. The particles reveal many points of weak contacts between the stacks of the layers. At these ‘breaking points’ the particles may easily disintegrate during interlayer reactions, or as a result of mechanical forces that influence rheological behaviour.

In particles of  $\text{Ca}^{2+}$ -smectite only a few layers form coherent domains in which all silicate layers have the same distance, for instance, corresponding to two layers of water. These domains are separated by zones composed of silicate layers with different distances because of the presence of one, three, four, or even more water



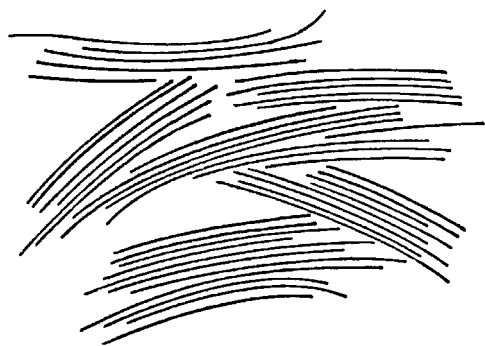


Fig. 5.1. A schematic view of montmorillonite particles. From Lagaly and Malberg (1990).

layers. This structure could clearly be observed by TEM inspection (Chenu and Jaunet, 1990). A few of the units composed of coherent domains and zones of differently spaced silicate layers are aggregated with almost parallel orientation. These particles are arranged in a network with pores of different sizes, thus constituting the whole aggregate (following the nomenclature given in Chapter 1). The pore structure is very complex with lenticular pores between parallel oriented layers together with pores within the network of particles and between the aggregates (see electron micrographs in (Touret et al., 1990)). The texture of synthetic hectorites was recently derived from small-angle X-ray scattering (SAXS) (Koschel et al., 2000; Gille et al., 2002). It seems possible to estimate the volumes of the different types of pores from the kinetics of water uptake (Touret et al., 1990). Nomenclature for the different levels of organisation is still lacking; a simplified one is suggested in Chapter 1.

The electrostatic attractions between the layers and the interlayer cations increase the stacking order in more highly charged 2:1 clay minerals. The domains with equally spaced layers become thicker and the influence of the defects on the shape and position of the (001) reflections decreases. Defects of unequally spaced silicate layers due to different degrees of hydration (probably a consequence of charge inhomogeneity) are still observable by delicate analysis of the X-ray reflection profiles of  $\text{Na}^+$ -beidellite with water monolayers (Ben Brahim et al., 1986). The different types of layer stacking in vermiculites were reviewed by Suquet and Pézérat (1987). Generally micas are considered as true crystals, and many polymorphs were described (see Chapter 2).

### 5.1.2. Layer and Edge Charges

In the general formula for 2:1 clay minerals, the average charge of the silicate layers is indicated by  $(x+y)$  per formula unit. The unit cell of the clay mineral lattice contains two formula units  $(\text{Si,Al})_4\text{O}_{10}$  and has the dimensions  $a$  and  $b$  in the plane

of the layer. The surface charge density ( $\sigma_0$ ), expressed as C/m<sup>2</sup>, is given by

$$\sigma_0 = 1.602 \times 10^{-19}(x + y)/ab$$

where  $1.602 \times 10^{-19}$  C is the elementary charge of one electron.

Typical surface charge densities are listed in Table 5.1. The average layer charge of montmorillonites varies between 0.2 and 0.4 eq/formula unit (Si,Al)<sub>4</sub>O<sub>10</sub>, but most montmorillonites have layer charges around 0.3 eq/formula unit corresponding to a surface charge density of 0.10 C/m<sup>2</sup> (Jasmund and Lagaly, 1993; Lagaly, 1993, 2005). On the basis of the high layer charge densities one calculates high surface potentials for isolated particles, e.g., ~200 mV, at a salt concentration of 10<sup>-3</sup> mol/L and a surface charge density of 0.10 C/m<sup>2</sup> (Verwey and Overbeek, 1948; van Olphen, 1977; Lagaly et al., 1997).

Sign and density of the charges at the crystal edges depend on the pH of the dispersion. Some clay scientists still use the term ‘broken bonds’ that colloid scientists never used. The charging arises from adsorption or dissociation of protons as in the case of oxides (Fig. 5.2). In an acidic medium an excess of protons creates positive edge charges, the density of which decreases with rising pH. Negative charges are produced by the dissociation of silanol and aluminol groups (Tournassat et al., 2003a, 2003b). On the acidity of the silanol and aluminol groups see Wanner et al. (1994), Janek and Lagaly (2001), and Jozefaciuk (2002).

The interesting question concerns the condition that leads to virtually uncharged edges. When alkylammonium ions were exchanged at pH 6.5, the total amount of ions bound by Wyoming montmorillonite was 1.07 meq/g silicate (Lagaly, 1993, 2005). As the interlayer CEC was 0.78 meq/g silicate, the remaining 0.29 meq alkylammonium ions (= 27% of the total CEC) were bound at the edges. A very similar

Table 5.1. Layer charge ( $x + y$ ), surface charge density  $\sigma_0$  and equivalent area\*  $A_c$  of clay minerals

Mineral	$M^\dagger$	$(x + y)$ (charges/formula unit)	$\sigma_0$ (Cm <sup>-2</sup> )	$ab$ (nm <sup>2</sup> )	$A_c$ (nm <sup>2</sup> /charge)
Biotite	455	1	0.326	0.492	0.246
Muscovite	390	1	0.343	0.467	0.234
Vermiculites	390	0.8	0.259	0.495	0.309
		0.6	0.194	0.495	0.412
Beidellite	360	0.5	0.172	0.466	0.466
Montmorillonites	362	0.4	0.137	0.466	0.583
		0.3	0.103	0.466	0.777
		0.2	0.069	0.466	1.165
Hectorite	380	0.23	0.076	0.482	1.048

\*The equivalent area is the area per monovalent interlayer cation :  $A_c = ab/2(x + y)$ .

<sup>†</sup>Mean molecular mass of the formula unit (Si<sub>4</sub>O<sub>10</sub> (OH)<sub>2</sub>) without interlayer cations and water calculated for typical compositions (Jasmund and Lagaly, 1993).

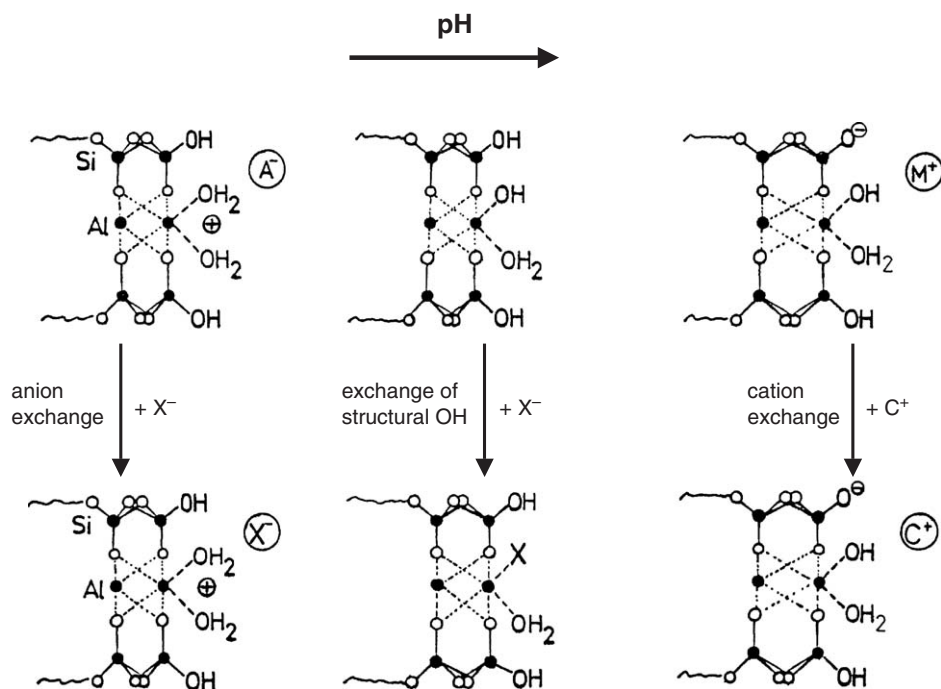


Fig. 5.2. The pH-dependent ion and ligand exchange reactions at the edges of the clay mineral layers, shown for 2:1 clay minerals. From Lagaly (1993).

result was obtained by surface charge measurements using a particle charge detector. This simple instrument indicates the point at which all charges of a colloidal particle are compensated by macro-ions, or in our case by alkylammonium ions. The amount of alkylammonium ions required to uncharge the particles, increased rapidly with pH because in an acidic medium protons compete with alkylammonium ions even in the interlayer space. At pH 6–8, a plateau was reached and, in agreement with the analytical data, a dose of 1.03 meq alkylammonium ions/g montmorillonite uncharged the particles of montmorillonite. The increase at higher pH was caused by the presence of alkylamine molecules, which were strongly adsorbed by the alkylammonium montmorillonite.

The total amount of alkylammonium ions bound by 2:1 clay minerals is often slightly higher than the total CEC determined by other methods (Bain and Smith, 1987; Jasmund and Lagaly, 1993). This is a consequence of the charge regulation at the edges. Adsorption of surface active agents on oxidic surfaces increases the surface charge density by adsorption (anionic surfactants) or desorption (cationic surfactants) of protons (Böhmer and Koopal, 1992; Schmidt and Lagaly, 1999). Thus, adsorption of alkylammonium ions in excess of the CEC is accompanied by

desorption of protons from surface OH groups. The analytical data clearly reveal that, at pH 6.5, a considerable amount of alkylammonium ions are bound at the edges.

The flow behaviour of  $\text{Na}^+$ -montmorillonite dispersions in water or in dilute NaCl solutions shows characteristic changes with pH (Section 5.6.1). The shear stress decreases steeply at  $\text{pH} > 4$  (see Fig. 5.26). This reduction of viscosity is generally attributed to the destruction of the card-house when the amount of positive edge charges becomes too small to stabilise the card-house by edge(+)/face(−) contacts (Brandenburg and Lagaly, 1988; Lagaly, 1989). Thus, rheological measurements indicate an apparent point of zero charge (p.z.c.) of the edges at pH somewhat above 5. The titration experiments of Wanner et al. (1994) revealed the point of zero net proton charge (p.z.n.p.c.) at pH 6.1 for montmorillonite (from bentonite MX-80, American Colloid Co.). Electrokinetic measurements led to strikingly different values, between  $\text{pH} \sim 3.5$  and 8.5, probably near  $\text{pH} \sim 7$  (Section 5.2.4). The p.z.c. at the edges of colloidal pyrophyllite particles ( $x + y \sim 0$ ) was found at pH 4.2 by titrations at various indifferent electrolyte concentrations (Keren and Sparks, 1995).

Exchangeable cations balancing negative charges due to isomorphous substitution within the kaolinite particles are located at the external surface, generally on the basal surfaces or near the edges. Weiss and Russow (1963) deduced from several independent measurements (exchange of tetraalkylammonium ions, TEM observation after adsorption of positively charged colloidal silver iodide particles, adsorption of dyes, exchange of radioactive  $^{63}\text{Ni}^{2+}$  ions, fluoride decomposition at  $\text{pH} \sim 7$ ) that only the external tetrahedral basal planes show isomorphous substitutions that are balanced by exchangeable cations. Not all kaolinite particles are characterised by different external basal planes. Particles with two identical surfaces were found as the consequence of layer inversion within the particles.

In comparing model cation exchange curves with experimental data, Bolland et al. (1980) derived charge densities between 1 and  $1.3 \times 10^{-10}$  eq/cm<sup>2</sup> corresponding to 0.10–0.12 C/m<sup>2</sup>, and concluded that kaolinite particles possessed permanent charges. They noted that the negative surface charges on the kaolinites could be mistakenly attributed to a pH-dependent, oxide-like charge (Ferris and Jepson, 1975) if the dissolution of  $\text{Al}^{3+}$  species and formation of gel-like coatings during the titration experiments are not considered.

In common with other clay minerals, kaolinite particles possess variable charges. Apparently, permanent charges cannot be assessed from potentiometric titration experiments alone (Herrington et al., 1992; Ganor et al., 2003; Tournassat et al., 2003a, 2003b). Schroth and Sposito (1997) determined the permanent structural charge density ( $\sigma_0$ ) by measuring the surface excess of  $\text{Cs}^+$  ions, which are highly selective to permanent charge sites. The net proton surface charge density ( $\sigma_{\text{H}}$ ) was measured as a function of pH by potentiometric titrations. The values of  $\sigma_0$  for the Georgia kaolinites KGa-1 (well-crystallised; Washington County) and KGa-2 (poorly crystallised; Warren County), both from the Clay Minerals Society, were given as −6.3 and

−13.6 mmol/kg. The specific surface areas were given as 10.0 and 23.5 m<sup>2</sup>/g (van Olphen and Fripiat, 1979). Assuming a homogeneous distribution of the charges, one calculates a permanent surface charge density of 0.06 C/m<sup>2</sup> for both kaolinites. Thus, the density of the permanent charges corresponds to low-charged smectites.

Because of their importance to colloidal behaviour, the p.z.c. are mentioned (Schroth and Sposito, 1997). The point of zero net charge (p.z.n.c.) was found at pH ~3.6 for both kaolinites, whereas the p.z.n.p.c. were at pH 5.0 (KGa-1) and 5.4 (KGa-2). The authors also observed that the p.z.n.p.c. changed with time due to dissolution effects. Siffert and Kim (1992) deduced an isoelectric point (i.e.p.) of the edges of kaolinite particles (Brittany, France) at pH 4.9. Dollimore and Horridge (1973) derived the point of zero edge charge ( $\equiv$ p.z.n.p.c) at pH 5.8 from flocculation experiments with polyacrylamide. Studying the coagulation kinetics of kaolinite at different pH in the presence of humic acid, Kretzschmar et al. (1998) also found the point of zero edge charge at pH 5.8 (see this paper for further references).

## 5.2. CLAY MINERALS IN WATER

### 5.2.1. Hydrates of 2:1 Clay Minerals

The 2:1 clay minerals form hydrates with one, two, three, or four pseudo-layers of water molecules between the silicate layers. The state of hydration changes with the water vapour pressure, the water content, and in salt solutions with the type and concentration of salts, and is dependent on the layer charge and the interlayer cation density. Typical basal spacings are: 1.18–1.24 nm (water pseudo-monolayer), 1.45–1.55 nm (water pseudo-bilayer), and 1.9–2.0 nm (four water pseudo-layers). The term ‘water layer’ is often used instead of ‘pseudo-layer’, even if the ‘layer’ is not always close-packed (see Chapter 13.2). The number of water pseudo-layers is simply derived from the layer separation and the thickness of a water layer in close-packed water molecules (about 0.25 nm).

The dotted fields in Fig. 5.3 comprise the spacings of a large collection of smectites and vermiculites. Na<sup>+</sup>-smectites change from a state indicated by a basal spacing  $\rightarrow \infty$  into hydrates with four, and at higher salt concentration two layers of water (Slade et al., 1991); vermiculites persist in the two-layer hydrate over the whole range of concentrations. Potassium ions in higher concentrations restrict the interlayer expansion of smectites to water monolayers. The hydration of vermiculites is virtually impeded by KCl solutions at concentrations above 0.01 M. In the presence of calcium ions the four-layer hydrate of smectites and the two-layer hydrate of vermiculites persist over a wide range of concentrations.

The variation of the basal spacings with salt concentration (Fig. 5.3) is of great interest to colloid scientists. To explain the reversibility of salt coagulation for many colloidal dispersions, Frens and Overbeek (1972) and Overbeek (1977) introduced the concept of the ‘distance of closest approach’. They postulated that the particles

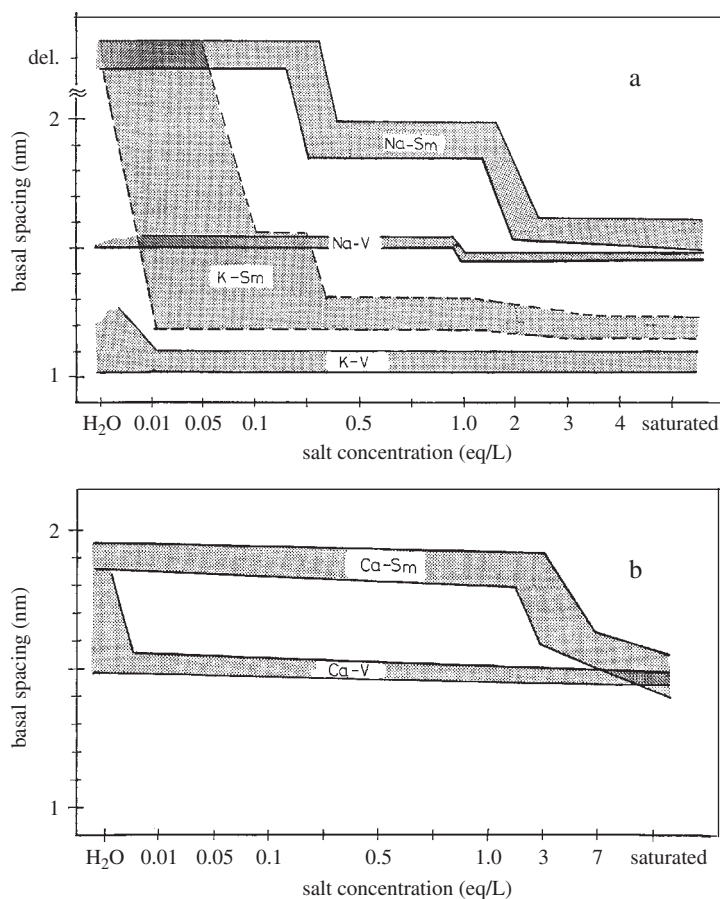


Fig. 5.3. Basal spacing of 2:1 clay minerals as a function of salt concentration. Na-Sm,  $\text{Na}^+$ -smectites and NaCl; K-Sm,  $\text{K}^+$ -smectites and KCl; Ca-Sm,  $\text{Ca}^{2+}$ -smectites and  $\text{CaCl}_2$ ; Na-V,  $\text{Na}^+$ -vermiculites and NaCl; K-V,  $\text{K}^+$ -vermiculites and KCl; and Ca-V,  $\text{Ca}^{2+}$ -vermiculites and  $\text{CaCl}_2$ , del = delamination. From Lagaly and Fahn (1983).

are not in direct contact at the onset of coagulation but remain separated by a certain distance. Through a number of calculations, a value of 0.4 nm corresponding to two water layers was derived for the most probable minimum separation. That a distance of closest approach really exists is clearly seen by the behaviour of  $\text{Na}^+$ - and  $\text{Ca}^{2+}$ -smectites as well as  $\text{Na}^+$ - and  $\text{Ca}^{2+}$ -vermiculites in NaCl and  $\text{CaCl}_2$  solution. Even far above the critical coagulation concentrations and up to concentrations as high as 5 M NaCl, the silicate layers remain separated by two pseudo-water layers. The water layers are displaced from between the surfaces only when the exchangeable cations, such as  $\text{K}^+$ , are attracted to the surface by specific interactions. The 'fixation' of  $\text{K}^+$  ions (and  $\text{Cs}^+$  and  $\text{Rb}^+$  ions) is well known to clay scientists and is





range (NMR measurements). The number of water layers influenced by the surface forces is 3–4, i.e. a water film of  $\sim 1$  nm thickness. In contrast, [Mulla and Low \(1983\)](#) concluded that the molecular dynamics of vicinal water as seen by IR spectroscopy is affected by the particle surface to an appreciable distance of about 4 nm.

Another question concerns the basicity of the oxygen atoms, i.e. their ability to bind protons (see Chapter 3.3.). Tetrahedral substitution of  $\text{Al}^{3+}$  for  $\text{Si}^{4+}$  increases the basic strength of the siloxane groups. The reason is the influence of aluminium atoms on the  $\text{d}_\pi\text{-p}_\pi$  bonds to oxygen. As a consequence, three types of water have to be distinguished: (i) the water hydrating the interlayer cations; (ii) an ordered layer of water at the flat oxygen plane; and (iii) less ordered water molecules between regions (i) and (ii). The structure of (ii) depends on the basicity of the siloxane groups. In the absence of tetrahedral substitution, the siloxane groups are really hydrophobic (which is also known from the silica surface) and the water molecules are closely linked one to another by hydrogen bonds. With increasing tetrahedral substitution the hydrophilic character of the oxygen plane increases and the interaction between the water molecules and the surface oxygen atoms increases ([Yariv, 1992](#); [Garfinkel-Shweky and Yariv, 1997](#)). Adsorption studies of binary liquids also reveal the hydrophilic/hydrophobic character (see Chapter 7.3).

Molecular dynamics simulations of the montmorillonite hydrates mainly confirm the experimental results on the position of the interlayer cations and the interlayer water structure. Interlayer  $\text{Li}^+$  ions partly form inner-sphere surface complexes (i.e. the  $\text{Li}^+$  ions are directly co-ordinated to the surface oxygen atoms). Expansion of the interlayer space is accompanied by the conversion of outer-sphere surface complexes into diffuse double-layer species as a result of the strong  $\text{Li}^+$ –water interactions. However, some of the  $\text{Li}^+$  ions persist as inner-sphere surface complexes although they can readily exchange with  $\text{Li}^+$  ions in the diffuse double-layer ([Chang et al., 1997](#)).  $\text{Na}^+$  and  $\text{K}^+$  ions also have a significant co-ordination with surface oxygen atoms and exist in inner- and outer-sphere surface complexes ([Delville and Laszlo, 1989](#); [Chang et al., 1995, 1998](#); [Skipper et al., 1995](#)). Increasing tetrahedral substitution shows a trend of direct binding between  $\text{Na}^+$  and surface oxygen atoms and a corresponding dissimilarity with the co-ordination structure in bulk solution. The co-ordination structure of water molecules around  $\text{K}^+$  ions as expected for this water-structure breaking cation ([Lagaly et al., 1997](#)) is not nearly so well defined as it is for  $\text{Li}^+$  and  $\text{Na}^+$  ions. Magnesium cations on montmorillonite reside at the midplane of the interlayer space. Non-solvating water molecules move freely on planes above and below the midplane. In the case of beidellites, the motion of water molecules is more hindered because of the presence of negative charge sites close to the surface ([Greathouse et al., 2000](#)). The co-ordination number of calcium ions in the interlayer space is a subject of ongoing debate. Monte Carlo simulations by [Greathouse and Storm \(2002\)](#) indicated an eight-fold water hydration shell. Surface energy studies by contact angle measurements also indicated that divalent cations are shielded from the silicate surface by water molecules whereas monovalent cations can be in direct contact with the surface oxygen atoms ([Norris et al., 1993](#)).



Results of simulation studies on the dynamics of water molecules and cations in the interlayer space cannot be directly compared with experimental values, e.g., obtained from tracer measurements. The experimental diffusion coefficients are distinctly lower than the calculated ones, especially in the case of caesium ions (Marry et al., 2002), not only because of the different timescale (nanoseconds in the simulation techniques) but also because of the influence of the macroscopic structure of the clay mineral particles.

### 5.2.3. Colloidal Dispersions

An outstanding property of dispersed montmorillonite particles is delamination into individual silicate layers or thin packets of them when the exchangeable cations are alkali cations, preferentially  $\text{Li}^+$  and  $\text{Na}^+$ , and the salt concentration is sufficiently small ( $<0.2 \text{ mol/L}$  for  $\text{Na}^+$  ions) (Fig. 5.4) (Norrish, 1954; Norrish and Rausell-Colom, 1963; Cebula et al., 1980; Schramm and Kwak, 1982a; Nadeau, 1985; Avery and Ramsay, 1986; Sposito, 1992; Jasmund and Lagaly, 1993; Lagaly, 1993, 2005; Sposito and Grasso, 1999). The thickness and width of the individual layers and thin particles or packets of layers, produced by the disarticulation of a large variety of smectites and I/S mixed-layer particles were determined by TEM and X-ray techniques (Nadeau, 1985; Śröder et al., 2000; Dudek et al., 2002) (see Section 5.3.5). The interlayer cations are in the diffuse double layers around the silicate layers and thin particles. The presence of these units that do not interact strongly and flow independently was proved by light and small-angle neutron scattering (Schramm and Kwak, 1982a, 1982b; Avery and Ramsay, 1986). This state is sometimes called ‘osmotic swelling’ by clay scientists (not by colloid scientists!).

The average interparticle distance (obtained from small-angle scattering) responds to the addition of sodium salts in an almost linear decrease with  $2/\sqrt{c}$  ( $c$  = salt concentration) until, at  $c \approx 0.2 \text{ mol/L}$ , particle rearrangement occurs and the basal spacing abruptly decreases from about 4 to 2 nm (Norrish, 1954; Odom, 1984; Kraehenbuehl et al., 1987) (see Chapter 13.2).

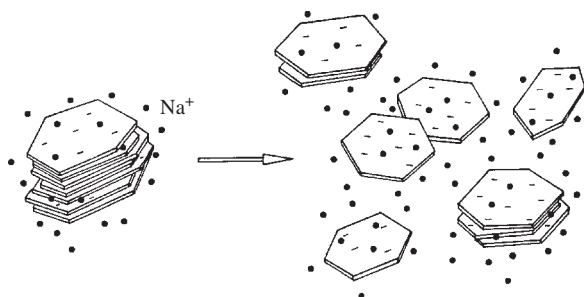


Fig. 5.4. Disarticulation (delamination) of alkali smectite particles in aqueous dispersions. From Jasmund and Lagaly (1993).

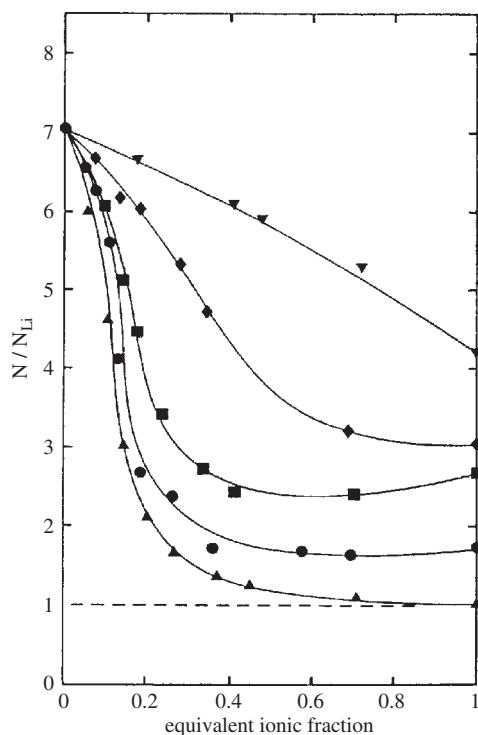


Fig. 5.5. Relative number of layers per particle,  $N/N_{\text{Li}}$  ( $N_{\text{Li}} = 1$ ) as a function of surface coverage when the  $\text{Ca}^{2+}$  ions are exchanged by  $\text{Li}^+$  (▲),  $\text{Na}^+$  (●),  $\text{K}^+$  (■),  $\text{Cs}^+$  (◆), and  $\text{Mg}^{2+}$  (▼) ions (Schramm and Kwak, 1982a). From (Jasmund and Lagaly, 1993).

With cations other than  $\text{Li}^+$  and  $\text{Na}^+$  the distances separating individual layers are no longer equal but vary around a mean value. Particles<sup>1</sup> are formed by a columnar-like superposition of a few silicate layers at equal distances. The distances between these particles are larger than within these units. Fig. 5.5 shows the relative number  $N/N_{\text{Li}}$  of layers per particle ( $N_{\text{Li}} = 1$  for  $\text{Li}^+$  as the exchangeable cation) when the  $\text{Ca}^{2+}$  ions are progressively replaced by alkali and  $\text{Mg}^{2+}$  ions (Schramm and Kwak, 1982a, 1982b). In the presence of  $\text{Ca}^{2+}$  ions the particles contain about seven silicate layers. Even small amounts ( $\leq 0.2$  equivalent fractions) of alkali metal ions reduce the size of the particles to one to three layers.

From SANS measurements Cebula et al. (1980) inferred that a considerable part of the layers is aggregated to units consisting of two silicate layers (potassium montmorillonite) or three silicate layers (caesium montmorillonite) interleaved with bimolecular water layers.

<sup>1</sup>In the literature, particles with large separations between the silicate layers are often called 'tactoids'.

Delamination of smectite particles into thinner particles or single silicate layers is an important process during soda-activation of bentonites. However, optimal delamination is only attained when the exchangeable cations are  $\text{Na}^+$  (or  $\text{Li}^+$ ) and all multivalent cations are removed. Ancillary minerals, in particular carbonates, have also to be removed or decomposed because they act as reservoirs of multivalent cations. Amorphous silica and organic materials can also reduce or even impede delamination. Thus, optimal delamination is only achieved when the bentonites are purified and fractionated (see Section 5.3.1). The technical soda-activation process does not proceed to complete delamination. Rather, the adjustment (often instinctively) of a certain degree of delamination is helpful in optimising the properties of a bentonite dispersion for a particular application.

#### 5.2.4. Electrokinetic Properties

The electrokinetic mobility of colloidal particles is related to their movement in an electrical field (Hunter, 1993; Lyklema, 1995; Lagaly et al., 1997). The potential at the shearing plane is referred to as the 'zeta potential', and is usually derived from the mobility by the Henry or Helmholtz–Smoluchowski equation. However, the relation between the mobility and the zeta potential is much more complicated because of relaxation and retardation effects and the influence of surface conduction. Surface conduction arises from counterions that are not immobile below the shear plane but migrate in directions tangential to the surface in the electrical field<sup>2</sup>, reducing the mobility of the particles (O'Brien and White, 1978; Mangelsdorf and White, 1990; Hunter, 1993; Rowlands and O'Brien, 1995; Lyklema, 1995; Lagaly et al., 1997). If the moving particles are aggregates and contain pores, the effect of liquid transport in the pores must be considered (Miller et al., 1992).

The non-spherical shape of clay mineral particles provides a further complication because no mathematical formulations could be derived for the relation between mobility and zeta potential. In an acidic medium the presence of positive edge charges complicates the electrokinetic behaviour. The zeta potential of clay mineral particles (calculated from mobility data by the Helmholtz–Smoluchowski equation, as often reported in the literature) indicates nothing more than the sign of the external charge of the particles, and only provides a value proportional to the electrophoretic mobility. Thus, the reporting of mobility rather than zeta potential values is strongly recommended.

The electrophoretic properties of clay mineral particles received much attention (Thomas et al., 1999, and references therein; Li et al., 2003). Typical mobility data<sup>3</sup> are in the range of  $-2$  to  $-3 \times 10^{-8}$  [ $\text{m}^2/\text{sV}$ ] and no i.e.p. is observed in the pH range of 2–12 (except for chlorite with an i.e.p. at pH  $\sim 5$ ). Similarly, kaolinite particles do

---

<sup>2</sup>This phenomenon is sometimes called 'anomalous' surface conduction but this term should be avoided.

<sup>3</sup>Mobility has no sign. Nevertheless, signs are used to indicate the sign of the shear plane potential.

not show positive mobility even at pH approaching zero (Siffert and Kim, 1992; Galassi et al., 2001). Due to the spillover effect (see Section 5.4.1) which reduces the influence of the positive edge charges, the aspect ratio (diameter/thickness ratio) of the particles must be considered. Face/face aggregation of the silicate layers (thicker particles) can reduce mobility because of the stronger influence of the positive edge charges in acidic medium whereas a higher extent of delamination will increase the mobility. This effect was clearly observed for dispersed saponites (Thomas et al., 1999).

The mobility of smectite particles is almost constant over a wide pH range around the neutral point (Benna et al., 1999; Thomas et al., 1999; Li et al., 2003). Only very highly charged saponites show a strong pH-dependent mobility because of the strong influence of the positive edge charges and increased aggregation (Thomas et al., 1999). The independence of the mobility over a wide pH range was modelled by Tombácz et al. (1990) (see Section 5.4.10) and Avena and de Pauli (1998). Despite the pH-dependent  $\text{Na}^+/\text{H}^+$  exchange, the amount of screened structural charge, i.e. the amount of cations below the shear plane, seems to remain constant at this pH range. Indifferent electrolytes with the same valence as the exchangeable cation induce only little, if any, variation of mobility, while divalent cations reduce the mobility more than monovalent cations. Trivalent cations can cause charge reversal (see Section 5.4.8).

The electrophoretic mobility (in a moderately acidic medium) is not much influenced by the layer charge (Thomas et al., 1999). This is because a high layer charge promotes Stern-layer adsorption, and the zeta potential does not increase in direct response to the layer charge. We should also mention that the surface charge density is not proportional to the surface potential but to the hyperbolic sine of the potential (van Olphen, 1977; Hunter, 1993; Lyklema, 1995; Lagaly et al., 1997). As the tetrahedral charge also increases Stern-layer adsorption, the mobility of saponites is smaller than that of montmorillonites of similar charge (Thomas et al., 1999).

Since many factors determine the mobility of clay mineral particles, the p.z.n.p.c. of the edges can only be deduced from mobility data with a certain arbitrariness. Thus, Thomas et al. (1999) concluded that the charge of the edges is negative at  $\text{pH} \geq 3.5$ . On the other hand, Benna et al. (1999) suggested that  $\text{pH} \sim 7$  is a more probable value, while Avena and de Pauli (1998) reported  $\text{pH} \geq 8.5$ .

In very diluted dispersions (5 mg/L) imogolite fibres showed a mobility that decreased from  $+3 \times 10^{-8} \text{ m}^2/\text{s V}$  at  $\text{pH} \sim 5$  to  $-1.5 \times 10^{-8} \text{ m}^2/\text{s V}$  at  $\text{pH} \sim 10$ . In dispersions of 100 mg/L, the mobility decreased from pH 4 to 7 but became zero at  $\text{pH} > 7$ . Dispersed imogolite easily flocculates under alkaline conditions, and the zero mobility value indicates formation of large immobile aggregates (Karube et al., 1992).

Electrokinetic measurements are required to detect charge reversal of colloidal particles by adsorption of multivalent cations or organic cations, such as alkylammonium ions and organic dye cations (Pashley 1985; Hunter and James, 1992; Schramm et al., 1997; Penner and Lagaly, 2000).

The interaction of clay mineral particles with polymers influences the mobility in a subtle way. Adsorption of neutral macromolecules often shifts the position of the shear plane so that the mobility changes despite constant charge densities (Theng, 1979). As an example, poly(vinylpyrrolidone), PVP, with a molecular weight of  $\sim 400,000$  decreased the mobility of  $\text{Li}^+$  montmorillonite particles more strongly than low molecular weight PVP. The high molecular weight PVP is adsorbed in loops that shift the shear plane away from the particle surface in direction to the solution, i.e. to smaller potentials. PVP with a molecular weight of 5000 is mainly adsorbed in trains, and the influence of the shear plane position is distinctly smaller (Séguaris et al., 2002).

Adsorption of polycations usually causes charge reversal when a certain amount is adsorbed. However, the amount of polymer charges at the i.e.p. is often distinctly below the CEC of the clay mineral because accumulation of the positive charges at the external surfaces is decisive. Soft particles where a hard core is surrounded by an envelope of macro-ions show a highly complex relation between the mobility and the properties and charges of the polyelectrolyte envelope (Ohshima, 1995; Lagaly et al., 1997).

Dynamic mobility measurements using electroacoustic instruments became more and more common in colloid science, even if the theoretical background is still in development (Hunter, 1998). This method shows the important advantage that concentrated dispersions, often needed in applications, can directly be measured whereas all other electrophoretic measurements require highly dilute dispersions.

Electroacoustic investigation of kaolinite and montmorillonite dispersions revealed the presence of a high surface conductance that complicates the interpretation of the dynamic mobility spectrum (O'Brien and Rowlands, 1993; Rowlands and O'Brien, 1995; Rasmusson et al., 1997).

### 5.3. PREPARATION OF COLLOIDAL DISPERSIONS

#### 5.3.1. Fractionation of Clay Dispersions

Clay minerals with a certain degree of purity can be separated from raw clay samples by sedimentation techniques. The first step consists of removal of iron oxides and organic materials. These materials not only affect the properties of colloidal dispersions but also prevent optimal peptisation of clay particles and successful fractionation by sedimentation. To prepare colloidal dispersions it is important to remove carbonates and silica (see Chapter 4). Carbonates can release calcium or magnesium ions into solution, reducing the degree of peptisation. Amorphous silica can act as a cementing agent between the particles.

In contrast to their counterparts from soils, kaolins and bentonites from geologic deposits contain only small amounts of organic materials. However, since they can

contain appreciable amounts of iron oxides, purification is needed to obtain colloidal dispersions with an optimal degree of delamination.

A decisive step in preparing a stable clay dispersion is the replacement of divalent exchangeable cations by  $\text{Na}^+$  (or  $\text{Li}^+$ ) ions. Following the procedure described by Stul and van Leemput (1982) and Tributh and Lagaly (1986), the final dispersion obtained by dialysis and adjusted to pH 7.5 is stable, containing particles in an optimal degree of dispersion. Addition of deflocculating agents such as phosphates and polyphosphates is not required to attain the colloidal distribution (Lagaly, 1993).

The stable dispersion of clay minerals in homoionic form is fractionated by gravity sedimentation or, for particle sizes of  $<2\text{ }\mu\text{m}$ , by centrifugation. To reduce particle/particle interaction during sedimentation, the volume fraction of the particles should be in the range of  $1\text{--}2 \times 10^{-3}$  (about 5 g clay/1000 mL water). The pH should not decrease below 6.5. Note that the pH of water in contact with the atmosphere is usually  $<6$ .

Fractionation by sedimentation belongs to the established industrial separation procedures and is used at a technical scale for kaolin processing. It is the most important procedure to obtain relatively pure clay minerals in the laboratory.

The particle size of the fractions is expressed in Stokes equivalent spherical diameters<sup>4</sup>. The particles of a dispersion settle with a constant velocity  $v$ , which is determined by the gravitation force  $mg = \rho Vg$  minus the buoyancy  $\rho_0 Vg$  and the Stokes' friction force  $3\pi\eta vd$ :

$$V(\rho - \rho_0)g = 3\pi\eta vd \quad (1)$$

$V = (\pi d^3/6)$  is the particle volume;  $\rho$  is the particle density;  $\rho_0$  is the density of the solvent;  $g$  is the gravitational acceleration ( $= 9.81\text{ m/s}^2$ );  $\eta$  is the solvent viscosity; and  $d$  is the particle diameter. The settling velocity  $v$  ( $= h/t$ ) of a particle is therefore:

$$v = \frac{h}{t} = \frac{(\rho - \rho_0)g}{18\eta} d^2 \quad (2)$$

The time ( $t$ ) needed for a particle to settle within a given distance ( $h$ ) is given by

$$t = \frac{18\eta}{(\rho - \rho_0)g} \frac{h}{d^2} \quad (3)$$

A quartz particle (density  $2.65 \times 10^3\text{ kg/m}^3$ ) with a diameter of  $20\text{ }\mu\text{m}$  needs 3 min 58 s to settle in water at  $25^\circ\text{C}$  within a distance of 0.1 m. Particles with 10, 2, and  $1\text{ }\mu\text{m}$  need 15 min 51 s, 6 h 36 min, and 26 h 25 min. Since viscosity increases with decreasing temperature, the corresponding sedimentation times at  $20^\circ\text{C}$  are distinctly longer: 4 min 38 s ( $20\text{ }\mu\text{m}$ ), 18 min 33 s ( $10\text{ }\mu\text{m}$ ), 7 h 44 min ( $2\text{ }\mu\text{m}$ ), and 30 h

<sup>4</sup>The conditions of the validity of Stokes' law were fully discussed by von Hahn (1928).

55 min ( $1\text{ }\mu\text{m}$ ) (the density of water at 20 and  $25^\circ\text{C}$  is  $998.00$  and  $997.05\text{ kg/m}^3$ , respectively, while the viscosity is  $1.002 \times 10^{-3}$  and  $0.8904 \times 10^{-3}\text{ kg/ms}$ , respectively).

Fractionation of particles with diameters  $<1\text{ }\mu\text{m}$  would require very long sedimentation times. For  $0.2\text{ }\mu\text{m}$  particles one calculates  $t = 660\text{ h } 33\text{ min}$  at  $25^\circ\text{C}$  and  $h = 0.1\text{ m}$ . For still smaller particles the Brownian movement hinders sedimentation. Fractionation then requires the stronger centrifugal fields. In this case the gravitational acceleration,  $g$ , has to be replaced by the acceleration  $4\pi^2\omega^2r$  where  $\omega$  is rotations per second, and  $r$  is distance of the particle from the rotational axis (Fig. 5.6).

As acceleration depends on  $r$ , the sedimentation velocity  $dh/dt$  also depends on  $r$ . The time  $dt$  for a particle to move through a distance  $dh$  at the position  $r$  is given by

$$dt = \frac{18\eta}{(\rho - \rho_0)4\pi^2\omega^2r} \frac{dh}{d^2} \quad (4)$$

Integration gives the time for the particles to move from  $r_0$  to  $r = r_0 + h$  (Fig. 5.6):

$$t = \frac{18\eta}{(\rho - \rho_0)4\pi^2\omega^2d^2} \int_{r_0}^r \frac{dr}{r} = \frac{18\eta}{(\rho - \rho_0)4\pi^2\omega^2d^2} \ln \frac{r}{r_0} \quad (5)$$

By way of illustration, Table 5.2 gives the sedimentation times for quartz. The separation of increasingly smaller particles requires higher centrifugal forces, i.e. an enhancement of the rotation velocity. Separation of the  $<0.2\text{ }\mu\text{m}$  fraction needs a running time of 17 min, while that of the  $<0.02\text{ }\mu\text{m}$  fraction requires 4 h.

The choice of particle density provides a certain problem because not only the densities of the species among the different clay mineral groups vary but the density of the species within a group can also vary due to differences in chemical composition and hydration state. The variation is small for kaolinites ( $2600\text{--}2680\text{ kg/m}^3$ ), and somewhat larger for muscovite ( $2760\text{--}3000\text{ kg/m}^3$ ) and biotite ( $2700\text{--}3100\text{ kg/m}^3$ ) (Grim, 1968). Dry illites may have a density of about  $2650\text{ kg/m}^3$  but due to the

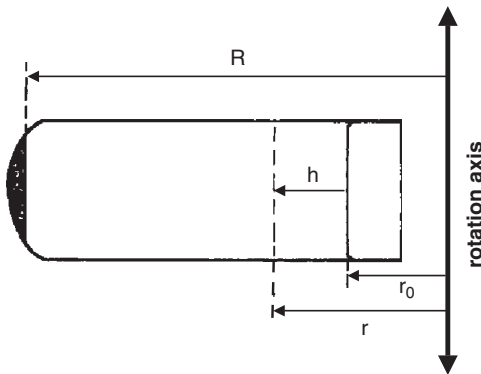


Fig. 5.6. Fractionation by centrifugation.

Table 5.2. Sedimentation in the centrifugal field; for  $r_0$ ,  $r$ ,  $h$  see Fig. 5.6. Quartz particles (density 2650 kg/m<sup>3</sup>) in water (density ~1000 kg/m<sup>3</sup>) at 20 °C

$r_0^*$ (m)	$r$ (m)	$h$ (m)	Rotations/min	Diameter (μm)	Sedimentation time		
					hours	min	s
0.104	0.124	0.02	1000	0.6	—	8	7
0.112	0.132	0.02	2000	0.2	—	17	4
0.120	0.140	0.02	4000	0.06	—	44	28
0.128	0.148	0.02	5000	0.02	4	1	11

\*The increasing values of  $r_0$  are related to the decreasing volume of the dispersion after removal of about 10 mL of the dispersion after each step for particle size analysis (see Section 5.3.5).

relative small particle sizes, adsorbed water decreases the density of the particles in the dispersion.

Smectites are an extreme case. Dehydrated montmorillonites may have densities between 2500 kg/m<sup>3</sup> at low and 2700 kg/m<sup>3</sup> at high iron contents (Grim, 1968). Zerwer and Santamarina (1994) reported the density (in kg/m<sup>3</sup>) for pyrometamorphosed bentonite of 2600 (room temperature), 2670 (200 °C), 2680 (400 °C), and 2730 (600 °C). During dispersion the particles delaminate. The thin particles or single silicate layers are surrounded by a few water layers that move with the settling particles. It is very likely that at least two layers of water remain attached to the particles. Assuming an average mass of 750 g/mol unit cell with a basal plane surface area of 0.465 nm<sup>2</sup>, and bimolecular water layers (density ~1000 kg/m<sup>3</sup>) attached to the basal plane surfaces, one estimates a density for a hydrated single layer of 2250 kg/m<sup>3</sup>. This value is recommended for calculating the sedimentation times of dispersed montmorillonite particles.

The density of I/S mixed-layer particles will also be somewhat lower than 2650 kg/m<sup>3</sup> but the real value depends on the size of the fundamental particles (see Section 5.3.3) formed in the dispersion.

Grim (1968) reported densities of montmorillonites, illites, and kaolinites when the particles were equilibrated at relative humidity between 0 and 1. However, the small values at high humidity are certainly not the real densities of the dispersed particles but are caused by condensation of water in the pores of the aggregated particles.

Usually, the density of quartz (2650 kg/m<sup>3</sup>) is used in calculating sedimentation times of clay dispersions. For bentonites a density of 2250 kg/m<sup>3</sup> may be more appropriate.

The different densities are not a serious obstacle in separating size fractions. It must be remembered that the diameters related to the sedimentation times are not real particle dimensions but are the diameters of the Stokes' equivalent spheres.

For fractionation (Atterberg procedure) the dispersion of the purified clays can be directly used without dialysis because of the enormous dilution during the procedure.



The dispersion is transferred to one or more cylindrical vessels and well dispersed. After a calculated sedimentation time, the upper part with a depth  $h$  (= sedimentation distance) is withdrawn by careful suction or siphoning. For instance, when  $h = 0.2\text{ m}$  and  $t = 52\text{ h } 50\text{ min}$ , this part of the dispersion only contains particles  $\leq 1\text{ }\mu\text{m}$ . However, the lower part of the dispersion and the sediment still contain  $\leq 1\text{ }\mu\text{m}$  particles. The withdrawn dispersion volume has to be replaced by water. After intense mixing the same volume of the dispersion is again removed after the same time period. This procedure is repeated until all  $\leq 1\text{ }\mu\text{m}$  particles are separated, i.e. the upper part of the dispersion after the selected sedimentation time remains completely clear and free of particles. The next step is the separation of the next larger fraction, which may be the fraction  $1\text{--}2\text{ }\mu\text{m}$  using the sedimentation time for  $2\text{ }\mu\text{m}$  particles.

The choice of the size fractions was often discussed. A modified Atterberg scale is recommended (Tributh and Lagaly, 1986):  $> 63$ ,  $63\text{--}20$ ,  $29\text{--}6.3$ ,  $6.3\text{--}2$ ,  $2\text{--}0.6$ ,  $0.6\text{--}0.2$ , and  $< 0.2\text{ }\mu\text{m}$ . (This is fractionation in a logarithmic scale because the logarithm decreases by 0.5 in every step).

An important condition for a clear separation is a sufficiently low particle concentration that allows the particles to settle independently (granular or free sedimentation). Clay mineral dispersions often show a combination of free and structural sedimentation when the particle concentration is too high. In this case not all particles settle and form a sediment (see Section 5.6.3).

### 5.3.2. Dispersions of Kaolins

The width of kaolinite particles varies from about  $0.1$  to  $20\text{ }\mu\text{m}$  (Jepson, 1984). The content of ancillary minerals (feldspars, quartz, mica, smectites) in kaolins varies with particle size. Pure kaolinite can often be obtained from kaolins by selecting the appropriate particle size fractions. In fractions  $< 0.1\text{ }\mu\text{m}$ , smectites are enriched; in fractions  $> 1\text{ }\mu\text{m}$ , quartz, feldspars, and micas become abundant (Jepson, 1984). However, the variation of the composition with particle size depends on the deposit, and pure kaolinite cannot be obtained in any case by fractionation.

When the hydrogen bonds and the dipole interactions that hold together the silicate layers of kaolinite particles are weakened by intercalation of suitable organic molecules, the particles can be separated into thinner ones under the action of mechanical forces. This reaction was used by Chinese ceramists to improve the quality of porcelain (Weiss, 1963). Colloidal dispersions of kaolinite can be prepared when kaolinite is treated with DMSO and ammonium fluoride (Lahav, 1990; Chekin, 1992). The fluoride ions replace some  $\text{OH}^-$  groups and reduce the number of hydrogen bonds and the bonding energy between the layers (Costanzo et al., 1984).

### 5.3.3. Dispersions of Smectites and Vermiculites

Smectite particles may be as large as  $2\text{ }\mu\text{m}$  and as small as  $0.1\text{ }\mu\text{m}$ , with average sizes of about  $0.5\text{ }\mu\text{m}$  (Grim and Güven, 1978; Odom, 1984). The morphology of

individual particles ranges from platy to lath-shape; some are even fibrous but mostly the particles are of irregular shape. Aggregates may be compact, foliated, or reticulated (Keller, 1985; Keller et al., 1986).

The unique fractionation procedure for smectites distinguishes smectites from all other clay minerals. Pre-treatment reactions and saturation with  $\text{Na}^+$  ions enhance delamination, i.e., the particles disarticulate into individual silicate layers during sedimentation. Those particles with equivalent diameters measured by sedimentation are artefacts, and not the same particles that are originally present in the bentonite. Nevertheless, fractionation is a sensitive tool for detecting differences between bentonites of different origin. A bentonite consisting of particles with varied thickness and plate width may be fractionated by sedimentation at conditions where all particles are delaminated. The mass content of the different particle-size fractions is then representative of the number of silicate layers with a given diameter (mean equivalent spherical diameter) that were originally aggregated into thicker particles. Naturally, nothing can be said about the thickness of the original particles. Thus, the particle size distribution obtained by fractionation represents the plate width distribution in the parent bentonite. A bentonite that produces fractions of very fine particles must contain particles of small diameters. In fact, bentonites of various deposits differ mainly in the particle size distribution below  $2\text{ }\mu\text{m}$ . Again, it should be noted that the diameter derived from the sedimentation process is the diameter of the Stokes' equivalent sphere and not any real particle diameter.

As many montmorillonites are formed by alteration and weathering processes, particles of different size may not have the same layer charge. However, the mean layer charge of the particles of various fractions often changes only slightly (Lagaly, 1994). For instance, the layer charge of Wyoming montmorillonite only increased from 0.27 charges/formula unit ( $<0.06\text{ }\mu\text{m}$  fraction) to 0.28 charges/formula unit ( $2\text{--}63\text{ }\mu\text{m}$  fraction). The Bavarian montmorillonite (bentonite from Niederschönbuch) showed similar changes: 0.27 charges/formula unit for  $<0.06\text{ }\mu\text{m}$  particles and 0.29 charges/formula unit for  $2\text{--}63\text{ }\mu\text{m}$  particles. However, distinct changes of the charge distribution curves were observed. During peptisation and fractionation, the particles are completely disarticulated. Afterwards the layers are re-aggregated by coagulation, and the sequence of the differently charged layers (as a consequence of charge heterogeneity) is not the same as in the parent material (see Section 5.4.2). Dialysis can also change the charge distribution to some extent, not only because of the disaggregation/re-aggregation mechanism but also because of the increased risk of chemical attack on the thin silicate layers (Lagaly, 1994).

As a consequence of the disarticulation of smectite particles into individual silicate layers, I/S mixed-layer particles can disintegrate at the low-charged interlayer space. The type of fundamental particles obtained depends on the charge distribution, i.e. the variation of the cation density from interlayer space to interlayer space (Fig. 5.7). The particles break up only at interlayer spaces with cation densities typical of smectites.

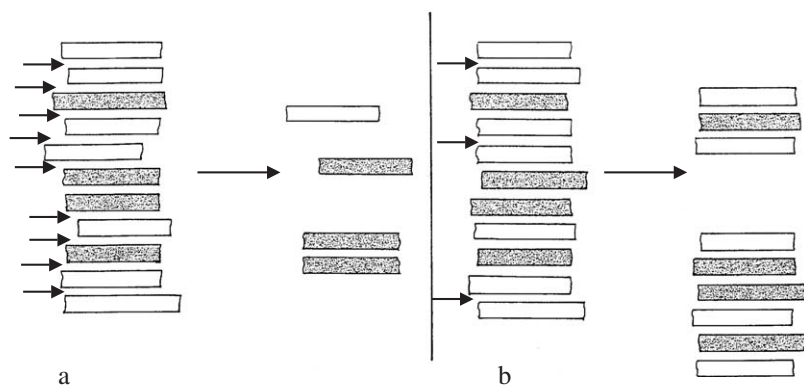


Fig. 5.7. Delamination of I/S mixed-layer particles. Different types of fundamental particles form depending on the variation of the interlayer cation density, i.e. the charge distribution. (a) Low mean layer charge: the particles split (arrows) between the low-charged layers and the low and more highly charged layers (dotted) but not between the highly charged layers. (b) Higher mean layer charge: the particles split only between the low-charged layers.

The way in which the I/S mixed-layer particles delaminate has technical consequences because many common clays contain I/S materials. The different types of particles produced by the break-up of the mixed-layer particles of soda-activated clays determine the flow behaviour of these dispersed clays (Lagaly, 1989).

Submicron vermiculite particles could be prepared from macroscopic vermiculite flakes by ultrasound treatment (Pérez-Maqueda et al., 2001; Wiewiora et al., 2003).

#### 5.3.4. $H^+$ -Saturated Smectites

It is sometimes desirable to prepare dispersions of  $H^+$ -saturated smectites. Leaching of smectites with acids results in a high degree of  $H^+$  saturation and is accompanied by a severe chemical decomposition of the layers. Since the  $Al^{3+}$  ions (also  $Mg^{2+}$  and other divalent ions) released during decomposition are preferentially adsorbed, the structure progressively transforms into the  $Al^{3+}$  form (Janek et al., 1997; Janek and Lagaly, 2001). The dispersion is stable for a certain time (Schwertmann, 1969) but as decomposition progresses, the  $Al^{3+}$  ions released from the structure cause coagulation. Barshad (1969) recommended passing a  $Na^+$ -smectite dispersion (1–2%) rapidly (200 mL within 1–5 min) through a series of three exchange resin columns arranged in the order:  $H^+$  resin  $\rightarrow$   $HO^-$  resin  $\rightarrow$   $H^+$  resin. By this means, a  $H^+$ -saturated, highly peptised smectite dispersion is obtained that remains stable for some time.

#### 5.3.5. Determination of Particle Size and Shape in Colloidal Clay Dispersions

It is difficult to evaluate the size and shape of dispersed particles. The oldest method for assessing the size of dispersed clay mineral particles is the sedimentation

procedure, giving particle size in terms of Stokes' equivalent diameters (Section 5.3.1). The application of the pipette method (von Hahn, 1928; Andreasen, 1931, 1935) in the gravitational and centrifugal field was optimised by Tributh and Lagaly (1986). During sedimentation of dispersed particles a certain volume of the dispersion is removed by a pipette at a given height after calculated time intervals. The mass of the particles in this volume is determined by weighing after slow evaporation of the water. It is important that the volume ratio particles/water does not exceed  $2 \times 10^{-3}$  to ensure free sedimentation of the particles (Section 5.6.3). This ratio should not be  $< 10^{-3}$  to have enough material for weighing. Thus, about 5 g clay ( $< 2 \mu\text{m}$ ) are recommended for 1000 mL water.

The specific surface area of the dispersed particles in contact with water can be directly determined by the co-ion exclusion (Chan et al., 1984). As very small concentration changes have to be measured, the method yields reliable values only for dispersed smectites.

XRD is a common technique to determine the size of crystalline colloidal particles. The technique is based on the peak profile analysis of periodic structures, i.e. the effect of interstratification has to be excluded. A simple but useful method to derive the size of coherent scattering domains is based on the Scherrer equation. The Bertaut-Warren-Averbach (BWA) method is the most universal method. It allows the mean size, the size distribution, and the effect of strain (fluctuations of  $d$ -values) to be evaluated (Dudek et al., 2002). SAXS was employed to determine the specific surface area and fractal dimensions of soil particles (Borkovec et al., 1993).

The different methods of particle-size determination in colloidal dispersions (sedimentation, turbidity measurements, static and dynamic light scattering, streaming methods, flow field flow fractionation (Allen, 1997)) are based on the assumption of spherical particles. In all cases the information obtained is the mean equivalent spherical diameter and never the real dimension. When different methods are applied, different size-dependent properties are measured. Because of the non-spherical shape of the clay mineral particles, the application of different characterisation methods is a prerequisite to obtain information on the size and shape of colloidal particles. To compare different investigation methods, one has to consider that different methods give different average values, e.g., microscopic methods give the number-weighted particle diameter, and dynamic light scattering (photon correlation spectroscopy, PCS) the intensity-weighted diameter (Lagaly et al., 1997). Plaschke et al. (2001) investigated smectite particles from a low-mineralised groundwater by AFM, PCS, flow field flow fractionation (FFFF), and laser-induced breakdown detection (LIBD). AFM revealed particles (aspect ratio  $\sim 0.1$ ) with a broad distribution and a number-weighted average diameter of 73 nm. LIBD indicated an average value of 63 nm. The maximum of the number size distribution was found by FFFF at 70 nm. PCS gave an intensity-weighted average hydrodynamic diameter of 235 nm corresponding to the maximum of the number-weighted distribution at 138 nm. Mackinnon et al. (1993) found reasonable agreement between size determination of kaolinite particles by sedimentation, electron microscopy, image

analysis, and laser scattering when the particle sizes were calculated from the scattering data by the Mie theory.

The relation between the real dimensions of rods and discs and the measured equivalent spherical diameter depends on the type of measurement (Jennings and Parslow, 1988; Lagaly et al., 1997). As shown by Jennings and co-workers (Oakley and Jennings, 1982; Jennings and Parslow, 1988; Jennings, 1993; Hinds et al., 1996) and Slepetyts and Cleland (1993), the ratio diameter/length (for rods) or diameter/thickness (aspect ratio of discs) can be estimated from the equivalent diameters measured by two different methods, giving distinctly different equivalent diameters. For example, when kaolinite dispersions were analysed by rotary diffusion (electro-optic and magneto-optic experiments) or light scattering as against sedimentation (Jennings, 1993; Slepetyts and Cleland, 1993).

Microscopic observations (TEM, SEM, ESEM, AFM, etc.) are useful for investigating clay minerals as they directly provide shape and geometric dimensions within the inherent instrumental uncertainties. However, the transfer of particles from the dispersion to the sample holder of the electron microscope can strongly change the appearance of the particles and their size. In many cases the microscope methods may not be statistically satisfactory (Dudek et al., 2002). The modern technique of jet-freezing allows particles in colloidal dispersions, and also the structure of emulsions and microemulsions to be determined (Lagaly et al., 1997). Reliable information about the state of montmorillonite particles in dispersion and formation of band-type and card-house structures was obtained (Vali and Bachmann, 1988; Benna et al., 2001a, 2001b).

## 5.4. COAGULATION OF COLLOIDAL CLAY MINERAL DISPERSIONS AND MECHANISMS OF COAGULATION

### 5.4.1. Coagulation by Inorganic Salts

Since the colloidal state of dispersed clay minerals is decisive in many practical applications, the coagulation of kaolinite and montmorillonite dispersions was investigated for many decades (Jenny and Reitemeier, 1935; Kahn, 1958). Unlike other colloidal dispersions, well-dispersed clay minerals (kaolinites, smectites, illites, palygorskite) in the sodium form may be coagulated by very low concentrations of inorganic salts. The critical coagulation concentration,  $c_K$ , of sodium chloride varies between 3 and 20 mmol/L. The data assembled in Table 5.3 also reveal the modest influence of different types of montmorillonites, even illites, beidellites and Laponites in that all give similar  $c_K$  values. For palygorskite see Section 5.4.2.

The very strong influence of the valence of the counterions is typical of electrostatically stabilised dispersions. The 0.025%  $\text{Na}^+$ -montmorillonite dispersions were coagulated by 5 mmol/L sodium chloride, 0.4 mmol/L calcium chloride, and 0.08 mmol/L aluminium chloride (Table 5.4) (Penner and Lagaly, 2000). Oster

et al. (1980) reported a  $c_K$  of 0.125 mmol/L  $\text{CaCl}_2$  for 0.1% dispersions of  $\text{Na}^+$ -montmorillonite (Wyoming) and illite (Fithian, Montana). As expected,  $\text{K}^+$  ions were strong coagulants for illites. Hesterberg and Page (1990b) reported  $c_K$  values of  $\text{KClO}_4$  for 0.05% dispersions of  $\text{K}^+$  illite:  $c_K = 2.5$  mmol/L (pH= 6); 3 mmol/L (pH= 6.6); 8 mmol/L (pH= 7.2); 11 mmol/L (pH= 9.3); and 14 mmol/L (pH= 10).  $\text{NaCl}$  coagulated  $\text{Na}^+$ -illite dispersions at concentrations between 6.5 and 48 mmol/L at pH 6–10 (Table 5.3).

As a function of pH, the  $c_K$  value of  $\text{Na}^+$ -montmorillonite showed a plateau between pH 4 and pH 6–7, and increased at higher pH (Perkins et al., 1974; Swartzen-Allen and Matijević, 1976; Keren et al., 1988; Goldberg and Forster, 1990). The dispersion coagulated spontaneously at pH < 3.5 and was destabilised by the base necessary to raise the pH above 10.5. The  $c_K$  value of Laponite increased linearly with pH. A step-wise increase was also found for  $\text{Na}^+$ -kaolinite and  $\text{NaNO}_3$ .

Dynamic light scattering was indicated that the kaolinite (KGa-2) dispersions show fast coagulation kinetics (stability factor  $W = 1$ ) below pH 5.8 (point of zero edge charge), regardless of the ionic strength ( $10^{-3}$ –1 mol/L  $\text{NaClO}_4$ ). Above pH  $\sim 5.8$  the dispersions were charge-stabilised and the coagulation rate strongly depended on pH and ionic strength (Kretzschmar et al., 1998).

The  $c_K$  value increased with solid content (Williams and Drover, 1967). The 0.5% dispersions of  $\text{Na}^+$ -montmorillonite (Wyoming) were coagulated by 20 mmol/L sodium chloride, 3 mmol/L calcium chloride, and 1.5 mmol/L aluminium chloride (test-tube tests) (Table 5.4) (Penner and Lagaly, 2000; Lagaly and Ziesmer, 2003).

The values of  $c_K$  also depended on the type of anion (Table 5.5). Nitrate instead of chloride increased  $c_K$  from 5 to 16 mmol/L and sodium sulphate to 18 mmol/L (0.025% dispersion). The influence of certain phosphates can be extremely strong (Lagaly, 1989; Manfredini et al., 1990; Penner and Lagaly, 2001). Thus,  $\text{Na}_2\text{HPO}_4$  and  $\text{NaH}_2\text{PO}_4$  coagulated the 0.025% dispersion at 1100 and 460 mmol/L, respectively. Sodium diphosphate ( $\text{Na}_4\text{P}_2\text{O}_7$ ) up to its solubility limit ( $\sim 130$  mmol/L) did not coagulate the dispersion. In contrast, sodium phosphate ( $\text{Na}_3\text{PO}_4$ ) showed the very low coagulation concentration of 25 mmol/L because the dispersion was highly alkaline (pH 11.5–12) at the point of coagulation.  $\text{NaOH}$  also coagulated at 20 mmol/L. In contrast to the influence of chlorides and nitrates, the  $c_K$  of  $\text{NaH}_2\text{PO}_4$  and  $\text{NaH}_2\text{PO}_4$  decreased with increasing solid content (Table 5.5).

The effect of phosphate was also seen when the montmorillonite dispersion was coagulated with  $\text{NaCl}$  in the presence of sodium diphosphate. Even an addition of 0.1 mmol/L  $\text{Na}_4\text{P}_2\text{O}_7$  increased the  $c_K$  of  $\text{NaCl}$  from 5 to 195 mmol/L (Permien and Lagaly, 1994c). Larger quantities of this phosphate raised the  $c_K$  to about 300 mmol/L  $\text{NaCl}$  (Table 5.6). This effect was also observed for a 0.1% pyrophyllite dispersion at pH 5.3 which was coagulated by 0.4 mmol/L sodium nitrate but 100 mmol/L of this salt was required in the presence of 0.16 mmol/L sodium hexametaphosphate  $\text{Na}_6\text{P}_6\text{O}_{18}$ .

The critical coagulation concentration of 5–10 mmol/L  $\text{Na}^+$  ions for  $\text{Na}^+$ -clay mineral dispersions is extremely low compared with the usual values between 25 and

Table 5.3. Reliable critical coagulation concentrations  $c_K$  of sodium chloride for clay mineral dispersions

Origin	$c_K$ (mmol/L)	Conditions of coagulation*	Reference
<b>Kaolinites</b>			
Benson deposit, Troy, USA	7–12	$\leq 1\%$ , $< 10 \mu\text{m}$ , pH = 7.1	Hsi and Clifton (1962)
Not identified	16–40	0.025%, pH = 4–10	Swartzen-Allen and Matijević (1976)
<b>Montmorillonites</b>			
Wyoming, USA	3.5	0.025–0.8%	Kahn (1958)
Upton, Wyoming	13	0.025%, $< 0.1 \mu\text{m}$ , pH = 6–7	Frey and Lagaly (1979b)
	10–15	0.025%, $0.1\text{--}2 \mu\text{m}$ , pH = 6–7	
Upton, Wyoming	12	0.1%, $< 2 \mu\text{m}$ ,	Oster et al. (1980)
Upton, Wyoming	10, 13, 31, 44	0.1%, $< 2 \mu\text{m}$ , pH = 5, 7.5, 8.5, 9.8	Keren et al. (1988)
Crook County, Wyoming	10–33	0.1%, $< 0.2 \mu\text{m}$ ; pH = 6.3–9	Hetzel and Doner (1993)
Crook County, Wyoming	13.3; 50	0.1%, $< 2 \mu\text{m}$ , pH = 7.6, 10.7	Neaman and Singer (1999)
Otay, California, USA	7–13	0.1%, $< 0.2 \mu\text{m}$ , pH = 6–9.3	Hetzel and Doner (1993)
Chambers, Arizona, USA	1–10	0.025%, pH = 4–10	Swartzen-Allen and Matijević (1976)
Cheto, Arizona	15, 24, 29, 32	0.07%, $< 2 \mu\text{m}$ , pH = 6.4, 6.7, 8, 9	Goldberg and Forster (1990)
Cyprus	8–12	0.025%, $0.1\text{--}2 \mu\text{m}$ , pH = 6–7	Frey and Lagaly (1979b)
Cerro Bandera, Argentina	8	0.09%, pH = 7.4	Helmy and Ferreiro (1974)
<b>Beidellites</b>			
Unterrupsroth, Germany	7	0.025%, $< 0.1 \mu\text{m}$ , pH = 6–7	Frey and Lagaly (1979)
	5–7	0.025%, $0.1\text{--}2 \mu\text{m}$ , pH = 6–7	
Silver City, Idaho, USA	4–5, 28–52	0.1%, $< 0.2 \mu\text{m}$ , pH = 6.1–7.2; 8.3–9.3	Hetzel and Doner (1993)

(continued on next page)

Table 5.3. (Continued)

Origin	$c_K$ (mmol/L)	Conditions of coagulation*	Reference
<b>Laponites</b>			
Laponite CP.	10 2–20	2% (!), pH = 8.5 (?) 0.2%, pH = 7–12	Neumann and Sansom (1971) Perkins et al. (1974)
<b>Illites</b>			
Fithian, Illinois, USA	55	0.1%, <2 $\mu\text{m}$	Oster et al. (1980)
Silver Hill, Montana, USA	5.5, 6.5, 29, 36, 48, 57.5 <sup>†</sup>	0.05%, <0.2 $\mu\text{m}$ , pH = 5.8, 6, 7.5, 9, 10, 10.6	Hesterberg and Page (1990a, 1990b)
<b>Palygorskites</b>			
Mt. Grainger (Australia)	2.5, 25	0.1%, <2 $\mu\text{m}$ , pH = 6.7; 10.6	Neaman and Singer (1999)
Mt. Flinders (Australia)	0.2, 25	0.1%, <2 $\mu\text{m}$ , pH = 7.3, 10.9	Neaman and Singer (1999)
Yucatan (Mexico)	1, 25	0.1%, <2 $\mu\text{m}$ , pH = 7.1, 10.6	Neaman and Singer (1999)
Florida (USA)	2.5, 25	0.1%, <2 $\mu\text{m}$ , pH = 7.4, 10.6	Neaman and Singer (1999)

\*Solid content of the dispersion, size fraction, pH.

<sup>†</sup>Coagulation with NaClO<sub>4</sub>.



Table 5.4.  $C_K$  of  $\text{Na}^+$ ,  $\text{Ca}^{2+}$ , and  $\text{Al}^{3+}$  chloride for  $\text{Na}^+$ -montmorillonite dispersions (0.025, 0.5, 1.0% w/w solid content) at pH  $\sim 6.5$  ( $\text{Na}^+$ ,  $\text{Ca}^{2+}$ ) (test-tube tests). Montmorillonite from Wyoming (M 40A) (Penner and Lagaly, 2000)

Exchangeable cation	$c_K(\text{mmol/L})$		
	0.025%	0.5%	1%
$\text{Na}^+$	5	15	20
$\text{Ca}^{2+}$	0.4	2	3
$\text{Al}^{3+}$	0.08	1	1.5

Table 5.5.  $C_K$  of sodium salts for 0.025 and 2% dispersions of  $\text{Na}^+$ -montmorillonite (Wyoming M 40A) (Penner and Lagaly, 2001)

	$c_K(\text{mmol/L})$		pH		$c_K(\text{mmol/L})$		pH
	0.025%	2%			0.025%	2%	
NaCl	5	30	6.5	$\text{Na}_2\text{HPO}_4$	1100	80	9
$\text{NaNO}_3$	16	12	6.5	$\text{NaH}_2\text{PO}_4$	460	40	$\sim 5$
$\text{Na}_2\text{SO}_4$	18	35	6.5	$\text{Na}_3\text{PO}_4$	25	$35^\dagger$	11.5
$\text{NaHSO}_4$	4	4	$\sim 5$	$\text{Na}_4\text{P}_2\text{O}_7$	—*	—*	10
				NaOH	20	$30^*$	11.5, 12

\*No coagulation up to the solubility limit of  $\sim 130$  mmol/L.

$^\dagger$ 0.5% dispersion.

500 mmol/L (Verwey and Overbeek, 1948; Matijević, 1973; Overbeek, 1982; Lagaly et al., 1997). Decades ago, this observation was explained by the interaction of positive edge charges with negative basal surface charges producing T-type contacts and card-house type aggregation (Hofmann, 1961, 1962, 1964; van Olphen, 1977). However, pH  $\approx 6.5$  is near or, more likely, above the p.z.c. of the edges, i.e. positive edge charges are no longer present or their number is very small.

An additional effect increases the negative field at the edges (Secor and Radke, 1985; Chou Chang and Sposito, 1994, 1996; Sposito and Grasso, 1999): The edge thickness of montmorillonite particles is small relative to the Debye-Hückel length at the critical salt concentration. The negative double layer extending from the basal plane surfaces spills over into the edge region. Even for an edge charge density of  $+0.1 \text{ C/m}^2$  (which is very high!) and a face charge density of  $-0.1 \text{ C/m}^2$  (typical of montmorillonite), the influence of the negative face charges is still significant at sodium salt concentrations  $\leq 10^{-3} \text{ M}$  (Secor and Radke, 1985). Coagulation therefore occurs between edges (–) and faces (–) (Fig. 5.8). The importance of the edge surface in the coagulation process also follows from the coagulation experiments of Keren and Sparks (1995) with colloidal pyrophyllite particles.

Table 5.6.  $C_K$  of NaCl in the presence of phosphates: 1.  $\text{Na}^+$ -montmorillonite dispersion (Wyoming) and sodium polyphosphates  $(\text{NaPO}_3)_n$  (Oster et al., 1980); 2.  $\text{Na}^+$ -beidellite (Unterruproth, Germany, fraction 0.1–2  $\mu\text{m}$ , 0.025% dispersion) and sodium diphosphate  $\text{Na}_4\text{P}_2\text{O}_7$  (Frey and Lagaly, 1979b)

Phosphate	Phosphate concentration (mmol/L)	$c_K$ mmol/L	pH
<b><math>\text{Na}^+</math>-montmorillonite</b>			
$(\text{NaPO}_3)_n$	0	12	
	0.01	20	
	0.1	80	
	1	120	
<b><math>\text{Na}^+</math>-beidellite</b>			
$\text{Na}_4\text{P}_2\text{O}_7$	0	6	6
	1.25*	230	6
	5	250	8.3
	10	270	9
	12.5	280	9.3
	25	310	9.7

\* $\text{Na}^+$ -montmorillonite dispersion at 0.1 mmol/L  $\text{Na}_4\text{P}_2\text{O}_7$ :  $c_K = 195$  mmol/L NaCl (Permien and Lagaly, 1994c).

Coagulation by salts, pH > 6

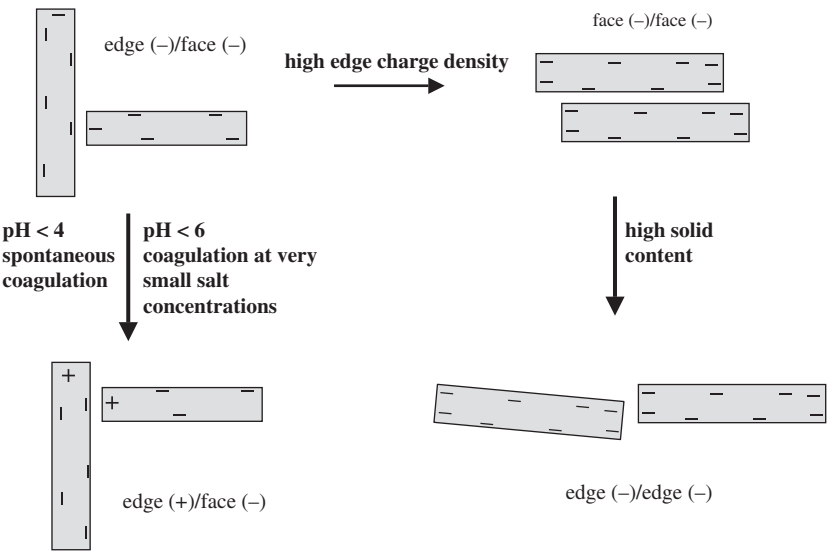


Fig. 5.8. The different modes of coagulation of clay mineral particles. From Lagaly and Ziesmer (2003).

As the negative edge charge density is very small, coagulation requires low sodium salt concentrations. [Pierre \(1992\)](#) calculated the electrostatic repulsion between an edge (–) and a face (–) on the basis of the DLVO theory. Assuming that the value of the charge density at the edges and the faces is identical, this repulsion is distinctly smaller than between faces. Because of the edge(–)/face(–) coagulation in dilute dispersions, the  $c_K$  values of Laponite, montmorillonites, beidellites, and illites are very similar ([Table 5.3](#)). The increased Stern-layer adsorption at high layer charges reduces the potential of the diffuse layer. As a result, both the electrostatic repulsion and the colloid stability are not distinctly enhanced.

Kaolinites have a surface charge density (see [Section 5.1.2](#)) that is comparable to that of montmorillonites ([Table 5.1](#)), and hence similar coagulation concentrations are expected.

As explained by the DLVO theory ([Verwey and Overbeek, 1948](#); [Overbeek, 1977, 1980, 1982](#)), the critical coagulation concentration of  $\text{Ca}^{2+}$  (0.4 mmol/L) and  $\text{Al}^{3+}$  counterions (0.08 mmol/L), is distinctly smaller than that of  $\text{Na}^+$  ions. The relationship between the  $c_K$  values is

$$c_K(\text{Na}^+) \approx 12c_K(\text{Ca}^{2+}) \approx 63c_K(\text{Al}^{3+})$$

while the DLVO theory predicts:

$$c_K(\text{Me}^+) = (4 - 64)c_K(\text{Me}^{2+}) = (9 - 729)c_K(\text{Me}^{3+})$$

where Me denotes a metal ion. The range of the predicted  $c_K$  values is related to different diffuse layer potentials. The smaller value corresponds to potentials  $\leq 50$  mV, the larger value to  $\geq 150$  mV. The observed ratios are near the values for lower potentials and indicate the pronounced effect of Stern-layer adsorption of the di- and trivalent cations on clay mineral surfaces ([Chan et al., 1984](#); [Goldberg, 1992](#); [Quirk and Marčelja, 1997](#); [Permien and Lagaly, 1994a, 1994b](#); [Sridharan and Satayamurty, 1996](#)). The aggregation of clay mineral layers in the presence of multivalent cations is enhanced by ion-ion correlation forces ([Kjellander et al., 1988](#); [Kjellander, 1996](#)).

The strong Stern-layer adsorption is also indicated by the increase in  $c_K$  values with solid content ([Tables 5.4 and 5.5](#)). When the salts solely regulate the thickness of the diffuse ionic layer,  $c_K$  is independent of the solid content of the dispersion. However,  $c_K$  increases with solid content when the counterions are adsorbed at the surface, as they are in the Stern layer ([Stumm et al., 1970](#); [de Rooy et al., 1980](#)).

The slightly increased coagulation concentration of  $\text{NaNO}_3$  in comparison with  $\text{NaCl}$  may be due to the water structure breaking effect of nitrate ions. As a result, the hydration of the cation increases, and its adsorption in the Stern layer decreases. Coagulation then requires a slightly higher salt concentration. This effect was also observed in coagulation experiments with latex dispersions ([Zimehl and Lagaly, 1986](#); [Lagaly et al., 1997](#)).

The 'liquefying' property<sup>5</sup> of phosphates is related to two effects. Phosphate anions are strongly adsorbed on oxide surfaces, and also on the edges of the silicate layers. They replace structural OH groups by ligand exchange (Muljadi et al., 1966; Parfitt, 1978; Jasmund and Lagaly, 1993; Lagaly 1993, 2005). By acting as multivalent anions phosphate increases the negative edge charge density, and hence the salt stability. As the electrostatic repulsive force is strongly dependent on the surface potential as long as this value is low (Verwey and Overbeek, 1948; Lagaly, 1986; Lagaly et al., 1997) a weak increase of the edge charge density by phosphate adsorption can strongly increase the repulsive force and the  $c_K$  value.

The second effect is the transition of edge(-)/face(-) coagulation into face(-)/face(-) coagulation (Fig. 5.8). When the increased salt concentration required for edge(-)/face(-) coagulation approximates the salt concentration for face(-)/face(-) aggregation, the dispersion coagulates face-to-face because the area between two faces is larger than between an edge and a face. Keren and co-workers (Keren et al., 1988; Heller and Keren, 2001) suggested that face/face aggregation between two layers or particles might be initiated at surface regions with lower than average charge density because of layer charge heterogeneity.

Transition from edge(-)/face(-) to face(-)/face(-) coagulation, in particular at somewhat higher particle concentration, is promoted by the following effect. As discussed by Tateyama et al. (1988), edge(-)/face(-) attraction depends on the angle between the two particles and particle thickness. This potential is very small for delaminated montmorillonite because the layers are only 1 nm thick. Attraction becomes strong enough only for an almost perpendicular orientation of the two particles. Such contacts are only formed at low particle concentrations. At higher concentrations, the strong repulsion between the faces disrupts the edge/face contacts more easily and the attraction must be enhanced to reach the face/face coagulation condition.

A striking effect is the pronounced decrease in the critical coagulation concentration of sodium hydrogen phosphates at higher montmorillonite contents (Table 5.5). In dispersions with high clay mineral contents and a high negative edge charge density of the particles, the strong repulsion between the faces forces the particles into adopting a certain parallel orientation (Section 5.6.1), promoting edge(-)/edge(-) coagulation (Fig. 5.8) (Pierre, 1992, 1996). This is less likely to occur in dilute dispersions. Coagulation is then initiated when the interaction between the edges(-) becomes attractive. This process may include a certain overlapping of silicate layers forming band-type fragments. This type of coagulation requires lower concentrations than those initiated by face(-)/face(-) coagulation.

---

<sup>5</sup>Liquefaction describes the decrease in the viscosity of dispersions by certain agents, e.g., of kaolin dispersions by phosphate addition (Lagaly, 1989; Manfredini et al., 1990; Penner and Lagaly, 2001), which is very important for ceramic masses and paper coating. Phosphates also decrease the viscosity of bentonite dispersions although an increase in viscosity was observed under certain conditions (Penner and Lagaly, 2001).

In comparison with sodium hydrogen phosphates ( $\text{Na}_2\text{HPO}_4$ ,  $\text{NaH}_2\text{PO}_4$ ) and sodium diphosphate ( $\text{Na}_4\text{P}_2\text{O}_7$ ), sodium phosphate ( $\text{Na}_3\text{PO}_4$ ) shows a very weak liquefying effect. The critical  $\text{Na}^+$  concentration is  $3 \times 25 = 75 \text{ meq Na}^+/\text{L}$  and therefore higher than for  $\text{NaCl}$ ,  $\text{NaNO}_3$ , and  $\text{NaOH}$ , but distinctly lower than for sodium hydrogen phosphates. This is because the high pH (11.5) reduces the adsorption of phosphate by ligand exchange (Muljadi et al., 1966; Parfitt, 1978). Model calculations for the homologous anion arsenate showed a distinct adsorption maximum at  $\text{pH} \sim 7$  (Manning and Goldberg, 1996). The increase in negative edge charge density as a result of the high pH and modest adsorption of phosphate raises the  $c_K$  value for edge(-)/face(-) coagulation but the increase is not sufficiently high to initiate face(-)/face(-) coagulation.

A modest liquefying effect is also observed with sulphate anions. The critical  $\text{Na}^+$  concentration is  $36 \text{ mmol Na}^+/\text{L}$  for  $\text{Na}_2\text{SO}_4$  which is somewhat higher than for sodium chloride and sodium nitrate. Wendelbo and Rosenqvist (1987) suggested that sulphate in soils from rain or industrial effluents could promote the dispersion of clays in soils.

#### 5.4.2. Coagulation of Mixed Clay Mineral Dispersions

An interesting question concerns the coagulation of dispersions containing two different clay minerals. Goldberg and Glaubig (1987) measured the critical coagulation concentration of  $\text{NaCl}$  for mixtures of  $\text{Na}^+$ -montmorillonite and  $\text{Na}^+$ -kaolinite, and of  $\text{CaCl}_2$  for mixtures of the corresponding  $\text{Ca}^{2+}$ -clay minerals (Table 5.7a). The addition of only 25% (w/w) montmorillonite to the kaolinite dispersion caused the  $c_K$  value of the mixed dispersion to approach that of the pure montmorillonite dispersion. The flocs contained both clay minerals with the kaolinite particles probably being incorporated into the montmorillonite particles (cf. footnote 1). These particles were coagulated when the salt concentration approximated the critical coagulation concentration for the montmorillonite dispersion. The stronger coagulation power of calcium cations impeded this effect. Thus, even small amounts of montmorillonite can deflocculate kaolinite dispersions at low salt concentrations. This effect was long known (Schofield and Samson, 1954) and explained by the attachment of the thinner and smaller montmorillonite layers to the positive edges of the large kaolinite particles.

Mixing palygorskite needles with montmorillonite presents an example of coagulation of dispersions containing particles with different shapes. Dispersions of palygorskite at neutral pH were coagulated by very low concentrations of  $\text{NaCl}$  (0.2 and 2.5 mmol/L) depending on the origin of the samples (Table 5.7b). The  $c_K$  values of the four samples increased strongly with pH and reached 25 mmol/L at pH 10–11 (Neaman and Singer, 1999).

Because of the low rate of isomorphous substitution in palygorskite, the negative surface charge density is small and the dispersions are sensitive to salt addition. The pronounced anisometric shape of the particles may also contribute to the low critical

Table 5.7a.  $C_K$  of mixed dispersions of  $\text{Na}^+$ -montmorillonite and  $\text{Na}^+$ -kaolinite (Goldberg and Glaubig, 1987)

% (w/w) montmorillonite	$c_K$ (mmol/L NaCl)	pH
0	<0.2	5.8
10	2.3	5.7
25	11.4	5.9
50	13.2	6.2
100	14.0	6.4

Table 5.7b.  $C_K$  of mixed dispersions of montmorillonite and palygorskite at neutral pH. Palygorskite: *A* Mount Flinders (Australia), *B* Yucatan (Mexico), *C* Florida (USA), *D* Mount Grainger (Australia) (Neaman and Singer, 1999)

% (w/w) montmorillonite	$c_K$ (mmol/L NaCl)			
	A	B	C	D
0	0.2	1.0	2.5	2.5
10	1.0	2.5	5.0	5.0
20	2.5	5.0	5.0	5.0
40	5.0	7.5	7.5	13.3
50	5.0	13.3	9.2	13.3
60	13.3	13.3	13.3	13.3
100	13.3	13.3	13.3	13.3

coagulation concentration. The variation in  $c_K$  values for different samples is likely to relate to different charge densities. The stronger increase of  $c_K$  with pH in comparison with montmorillonite is a consequence of the different surface structure.

In combination with montmorillonite, the  $c_K$  values show the same trend as for kaolinite/montmorillonite dispersions, i.e. they approach the values for the montmorillonite dispersion. The higher repulsion between montmorillonite particles probably impedes aggregation of the palygorskite needles.

A particular case is the coagulation of dispersions containing two smectites. When a dispersion of delaminated low- and high-charge smectites is coagulated by the addition of sodium chloride, the particles can aggregate in different ways (Fig. 5.9). When selective coagulation occurs, one type of particles is formed first, and hence the coagulate consists of a mixture of particles that contain the same layers as the starting particles (but may differ in size). When low- and high-charge layers aggregate within individual particles, mixed-layer particles grow with random, regular, or zonal (segregation) layer sequences. The problem is to analyse the coagulate and find which type of aggregation is predominant. The analysis is further complicated as the charge density within the individual particles of the parent smectites varies to some

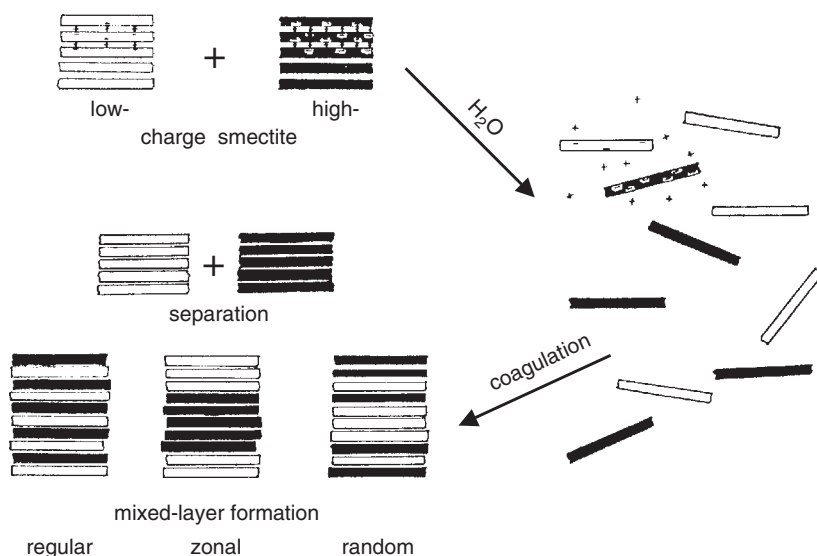


Fig. 5.9. Disarticulation of two Na<sup>+</sup>-smectites in water; formation of a mixed colloidal dispersion and re-aggregation by coagulation (surface charges and interlayer cations not entirely shown). From Frey and Lagaly (1979b).

extent (charge heterogeneity). Only the alkylammonium method allows a clear distinction to be made between selective coagulation and random or regular mixed-layer formation (Frey and Lagaly, 1979a, 1979b; Lagaly, 1981, 1994).

Two differently charged smectites were used: a montmorillonite (Upton, Wyoming) with a mean surface charge density  $\sigma_0$  of 0.096 C/m<sup>2</sup> (mean interlayer cation density  $\bar{\xi} = 0.192$  C/m<sup>2</sup>), and a beidellite (Unterrupsroth, Germany) with  $\sigma_0$  of 0.13 C/m<sup>2</sup> ( $\bar{\xi} = 0.26$  C/m<sup>2</sup>). The cation density in the interlayer space of the montmorillonite varied from 0.17 to 0.25 C/m<sup>2</sup> and of the beidellite from 0.20 to 0.35 C/m<sup>2</sup> (Fig. 5.10).

The homoionic Na<sup>+</sup>-smectites were dispersed in 0.01 M sodium diphosphate solution at pH > 7 to give dispersions with a mass content of 250 mg/L. Equal volumes of these colloidal dispersions were mixed and coagulated under different experimental conditions. Aggregation type was determined by particle size. Larger particles (0.1–2 μm fraction) were selectively coagulated. Two different experimental conditions were used to separate beidellite from montmorillonite: (i) slow coagulation by adding NaCl solution gradually to raise the Na<sup>+</sup> concentration to 0.28 M at pH 9. The coagulate consisted mostly of beidellite-like particles while the remaining dispersion contained montmorillonite; (ii) rapid coagulation by fast addition of NaCl to give a final concentration of 0.5 M NaCl. The coagulate contained a mixture of low- and high-charge particles. As discussed in Section 5.4.1, the beidellite coagulated at a lower salt concentration. The particles composed of low- or

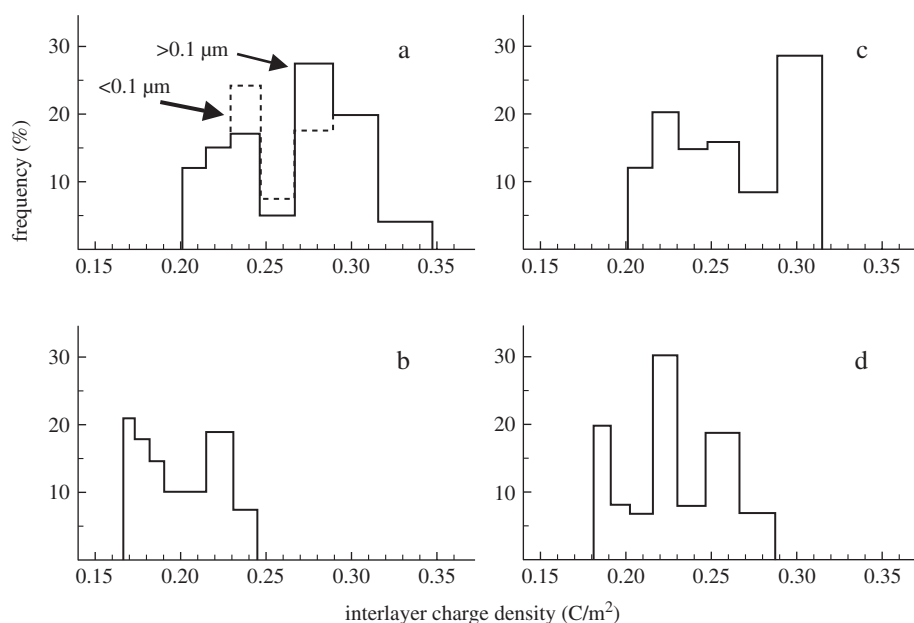


Fig. 5.10. Formation of mixed-layer particles by coagulation of dispersions containing two smectites. (a) Pure beidellite (Unterrupsroth, Germany; particle size fraction  $<0.1\ \mu\text{m}$  and  $0.1\text{--}2\ \mu\text{m}$ ). (b) Pure montmorillonite (Wyoming, USA; particle size fraction  $<2\ \mu\text{m}$ ). (c) Coagulated material from the mixed colloidal dispersion, particle size fraction  $0.1\text{--}2\ \mu\text{m}$ . (d) Coagulated material from the mixed colloidal dispersion, particle size fraction  $<0.1\ \mu\text{m}$ . From Frey and G. Lagaly (1979b).

high-charge layers were not identical with the particles of the starting materials. The charge distribution curve of the high-charge particles (Fig. 5.10c) was substantially different from that of the starting beidellite particles (Fig. 5.10a).

When the particles were smaller than  $0.1\ \mu\text{m}$ , the coagulate consisted of mixed-layer particles. The charge distribution curve (Fig. 5.10d) clearly showed a succession of low- and high-charge layers within the same particle. The layer sequence was not completely random; swelling tests revealed a certain amount of segregated layers (Frey and Lagaly, 1979a).

The delamination and re-aggregation of I/S mixed-layer particles were thoroughly investigated by Nadeau (1985) and Środoń et al. (2000). At conditions of delamination, only the smectitic interlayer spaces show extensive expansion; the particles break into ‘fundamental particles’ consisting of one, two, or a few illitic layers (Fig. 5.7, see Section 5.3.3). The physical dimensions of the fundamental particles were determined by TEM. Once the clay minerals had been fully disarticulated, mixed colloidal dispersions could be prepared. Re-aggregation produced I/S mixed-layer particles that were substantially different from the starting materials. Aggregation



may be performed not only by coagulation but also by simple air-, spray-, or freeze-drying. Some possible applications are directed to the design of special heterogeneous catalysts and the preparation of very thin films and coatings (Nadeau, 1987; Lagaly, 1987a).

#### 5.4.3. Influence of Alcohols

Addition of methanol, ethanol and propanol decreased the critical coagulation concentration of 0.025%  $\text{Na}^+$ -montmorillonite dispersion from 8 to 3.6 mmol/L NaCl (with 70% v/v methanol), to 1.2 mmol/L NaCl (with 70% v/v ethanol), and to 0.8 mmol/L NaCl (with 60% v/v propanol) (Permien and Lagaly, 1994c). This effect was even more pronounced in the presence of 0.1 mmol/L sodium diphosphate. The  $c_K$  value then decreased from 195 to 7.5 mmol/L NaCl (with 70% methanol), to 2.5 mmol/L NaCl (with 70% ethanol), and to 5 mmol/L NaCl (with 60% propanol).

The adsorption of counterions at the particle surface generally increases when organic solvents are added to the aqueous dispersion. Several examples were reported by de Rooy et al. (1980). Similarly, the  $c_K$  of NaCl for  $\text{Na}^+$ -montmorillonite dispersions decreases after addition of methanol, ethanol, and propanol. The effect is very strong for the phosphate-stabilised dispersions where  $c_K$  is reduced from 195 mmol/L NaCl to  $\leq 7.5$  mmol/L NaCl.

#### 5.4.4. Influence of Surface Active Agents on Salt Coagulation

It was surprising that small amounts ( $< 1$  mmol/L) of hexadecylpyridinium chloride (cetylpyridinium chloride, CPC) raised the critical coagulation concentration of NaCl from 8 to 16 mmol/L (Table 5.8). At higher CPC concentrations, the dispersion was coagulated by the surfactant itself. The addition of sodium dodecylsulphate (SDS) increased the  $c_K$  value of NaCl even more strongly. In the presence of 100 mmol/L SDS, a salt concentration of 136 mmol/L was required to coagulate the 0.025% dispersion (Permien and Lagaly, 1995).

Adsorption of hexadecyl pyridinium ions presumably modifies the distribution of the  $\text{Na}^+$  ions between the Stern layer and the diffuse ionic layer. The hydrophobic chains near the surface also influence the water structure in a certain region (Lagaly et al., 1983), pushing the  $\text{Na}^+$  ions away from the surface. The resulting weak increase in the Stern potential enhances  $c_K$  from 8 to 16 mmol/L.

The stabilising effect of dodecylsulphate anions is stronger. At pH  $\sim 6.5$  a few surfactant anions can adsorb at sporadically occurring positive edge sites. These anions can then act as nuclei around which additional surfactant molecules can cluster (Rupprecht and Gu, 1991). As a result, the negative edge charge density and the salt stability increase. It would be interesting to determine the salt stability as a function of sodium dodecylsulphate adsorbed. However, the adsorption of small amounts of anionic surfactants at pH  $> 4$  is difficult to measure because of the pronounced volume exclusion effect for anions (Chan et al., 1984; Chou Chang and Sposito, 1996).

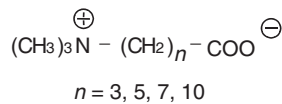
Table 5.8.  $c_K$  of NaCl for 0.025% dispersions of  $\text{Na}^+$ -montmorillonite (Wyoming, M 40) at pH  $\sim 6.5$  in the presence of cetyl pyridinium chloride (CPC) and sodium dodecylsulphate (SDS) (Permien and Lagaly, 1995)

Surfactant concentration mmol/L	$c_K(\text{mmol/L})$	
	CPC	SDS
0	8	8
$5 \times 10^{-4}$	9.5	
$10^{-3}$	9	10
$10^{-2}$	7	10
$2 \times 10^{-2}$	11	
$10^{-1}$	13	10
$2 \times 10^{-1}$	16	
1	*	12
10	*	81
100	*	136

\*Coagulation by CPC itself.

5.4.5. Stabilisation by Betaines

Betaines as surface-modifying agents



were synthesised to prepare organic derivatives that delaminate when dispersed in water. The quaternary ammonium groups replace the interlayer cations, whereas the negative charges at the opposite end and their compensating cations initiate the separation of the silicate layers: Colloidal dispersions of single silicate layers with attached betaines are formed (Schmidt and Lagaly, 1999). In contrast to the dispersions of  $\text{Li}^+$ - and  $\text{Na}^+$ -montmorillonite with yield values of  $\sim 400$  mPa the betaine-montmorillonite dispersion showed Newtonian flow, and the viscosity of the dispersion (solid content 1.5% w/w, pH 7) approximated the viscosity of water.

LiCl coagulated the dispersion of  $\text{Li}^+$ - and betaine-montmorillonite ( $n = 3$ ) at a concentration of 8 mmol/L. The  $c_K$  value increased with  $n$  to a maximum of 60 mmol/L LiCl at  $n = 7$ , then decreased slightly at  $n = 10$  (Table 5.9). The strong influence of small amounts of diphosphate was again noted: A maximum  $c_K$  value of 1320 mmol/L LiCl was reached for  $n = 7$ .

Surface modification with betaines reduced the stability of the montmorillonite dispersions in water-alcohol solutions. Whereas the colloidal dispersions of  $\text{Li}^+$ - and

Table 5.9. Critical LiCl concentration for the coagulation of 0.05% dispersions of  $\text{Li}^+$  - and betaine-montmorillonite (Wyoming M 40) in water and in the presence of 0.1 mmol/L  $\text{Na}_4\text{P}_2\text{O}_7$  Schmidt and Lagaly (1999)

Cation	$c_K(\text{mmol/L})$	
	in water	with phosphate
$\text{Li}^+$	8	570
Betaine		
$n = 3$	8	505
$n = 5$	17	835
$n = 7$	60	1320
$n = 10$	50	1180

betaine-montmorillonite (in the absence of any salt) were stable up to a methanol molar fraction  $\chi = 0.7$ , dispersions of the long-chain derivatives ( $n = 7, 10$ ) coagulated at  $\chi = 0.1$ , i.e. were only stable in water. In water/propanol mixtures,  $\text{Li}^+$  and betaine montmorillonite ( $n = 3$ ) as well as betaine-montmorillonite ( $n = 10$ ) were stable up to a molar fraction of propanol  $\chi = 0.3$ , and the samples with  $n = 5, 7$  up to  $\chi = 0.5$  and 0.4.

Adsorbed betaines show a pronounced stabilisation effect when the negative edge charge density is sufficiently increased by phosphate adsorption (Table 5.9). As the number of betaine molecules corresponds to the CEC (Schmidt and Lagaly, 1999), the total number of negative betaine end groups is identical with the number of layer charges (Fig. 5.11), and the enhanced stability cannot arise from an increased charge density. Nor is it very probable that steric stabilisation occurs because the chains are too short to make this mechanism effective. As the negative charges are shifted away from the particle surface, the electrostatic interaction occurs over a smaller distance than the van der Waals interaction. This would increase salt stability. However, the decisive effect seems to be the formation of lyospheres composed of betaine and water molecules around the particles (Fig. 5.11a) (Ottewill and Walker, 1968). As the lyospheres incorporate large amounts of water, the Hamaker constant of the envelope approximates the value for of the dispersion medium (water), and the van der Waals interaction weakens (Verwey and Overbeek, 1948; Vincent, 1973). The dominance of the electrostatic repulsion then increases the salt stability. For the short chain betaine ( $n = 3$ ), the lyospheres (if ever formed) are too thin to reduce the van der Waals interaction.

In the absence of phosphate a few betaine molecules can bridge between the surface charges and the sporadically occurring positive edge charges (Fig. 5.11b). Since betaines with  $n < 7$  are too short to form bridges, the above-mentioned shift of the charges may slightly enhance salt stability.

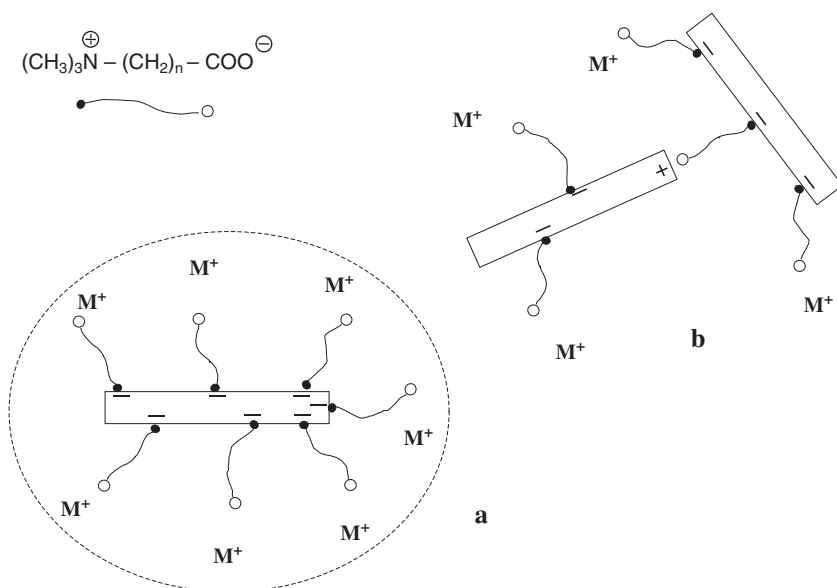
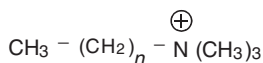


Fig. 5.11. Stabilisation by adsorbed betaine molecules. (a) Lyospheres composed of water and betaine molecules surround the particles. (b) Betaine molecules bridge between surface charges and positive edge charges of neighbouring particles. From [Lagaly and Ziesmer \(2003\)](#).

Replacement of water by organic solvents in the lyospheres can increase the van der Waals attraction, and hence reduce the stability of the (salt-free) dispersions ([Machula et al., 1993](#); [Király et al., 1996b](#)). However, the Hamaker constants for water and the alcohols are not very different (water  $3.7 \times 10^{-20}$  J, ethanol  $4.2 \times 10^{-20}$  J) ([Israelachvili, 1994](#)), and this effect will only be weak. Thus, the decisive effect of alcohol addition is the compression of the diffuse double layer ([de Rooy et al., 1980](#)) causing the betaine-montmorillonite complex to coagulate at a critical alcohol concentration.

#### 5.4.6. Coagulation by Organic Cations

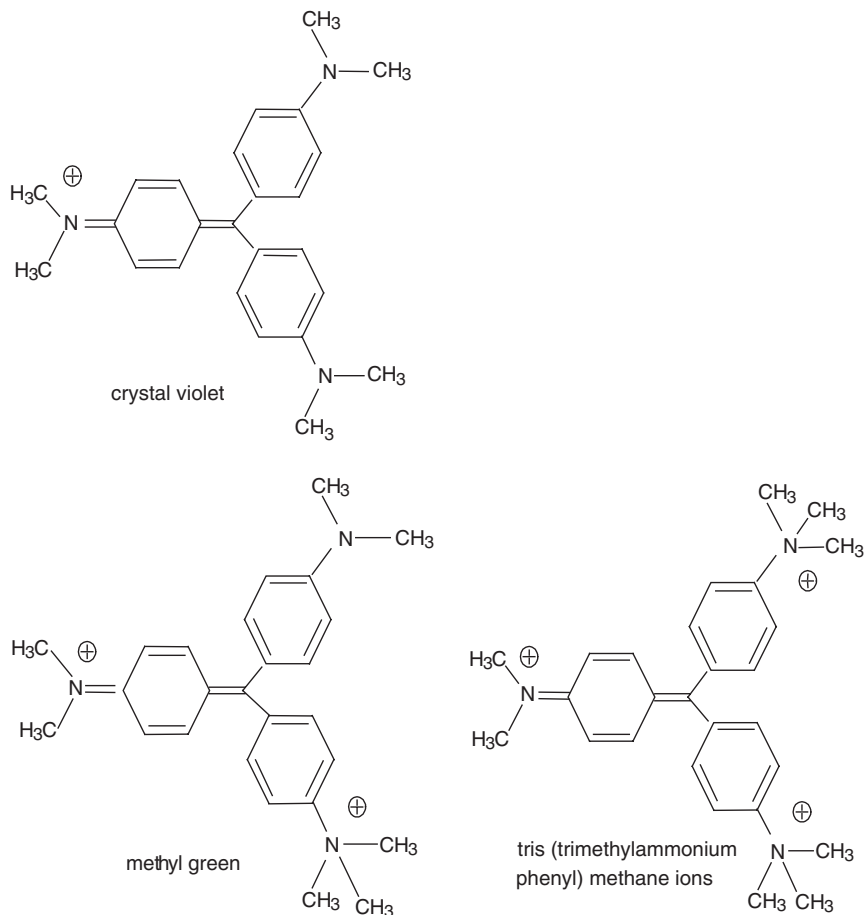
Tetramethylammonium chloride coagulated a  $\text{Na}^+$ -montmorillonite (Wyoming) dispersion at the same concentration (5 mmol/L) as NaCl ([Penner and Lagaly, 2000](#)). Monovalent long-chain cations such as



trimethyl alkylammonium ions

trimethyl alkylammonium ions coagulated at very low concentrations,  $c_K \leq 0.3$  mmol/L (Table 5.10). Restabilisation was observed when larger amounts of surface-active agents (above the CEC) were added.

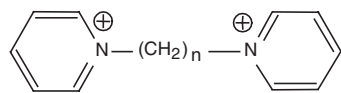
Very small coagulation concentrations were also observed with large organic cations such as monovalent crystal violet (0.1 mmol/L), divalent methyl green (0.2 mmol/L), and trivalent TTP, tris(trimethylammonium phenyl) methane chloride, (0.05 mmol/L). Dispersions coagulated by crystal violet were restabilised by addition of CV in amounts  $> 1.5$  mmol/g montmorillonite.



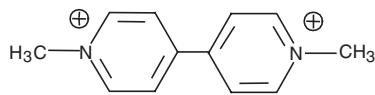
Divalent paraquat and diquat cations were also strongly coagulating with  $c_K$  values of  $\sim 0.1$  mmol/L. The divalent long-chain hexyl- and dodecyl-bispyridinium cations showed coagulation concentrations similar to trimethyl alkylammonium (Table 5.10). The valence of the organic cations was not as dominant as for inorganic cations. In all cases the  $c_K$  value increased with the montmorillonite content of the dispersion.

Table 5.10. Coagulation of Na<sup>+</sup>-montmorillonite dispersions by organic cations. *c<sub>K</sub>* of the 0.025% dispersions by test-tube tests, of the 0.5% (w/w) dispersions from rheological measurements, pH ~6.5. Montmorillonite from Wyoming (Penner and Lagaly, 2000)

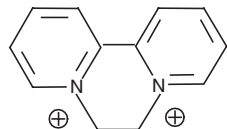
Cation	Valency	<i>c<sub>K</sub></i> (mmol/L)	
		0.025%	0.5%
Tetramethylammonium	1	5	5.8
Hexyl trimethylammonium	1	0.3	2
Dodecyl trimethylammonium	1	0.15	0.76
Hexadecyl trimethylammonium	1	0.09	0.35
Methyl bispyridinium	2	0.2	0.85
Hexyl bispyridinium	2	0.2	0.62
Dodecyl bispyridinium	2	0.1	0.18
Crystal violet	1	0.1	0.9
Methyl green	2	0.2	0.9
Tris(trimethylammonium phenyl)methane	3	0.05	0.09
Paraquat	2	0.08	0.4
Diquat	2	0.1	0.45



alkyl bispyridinium ions



paraquat



diquat

The reduced salt stability and the dependence of *c<sub>K</sub>* on the solid content as a consequence of the specific adsorption of the counterions (as defined by Lyklema (1984, 1989)) is very pronounced for large organic cations. The *c<sub>K</sub>* of long chain cations generally decreases with chain length (Table 5.10). The adsorption of organic cations can obscure the influence of counterion valence. As evident from Table 5.10, increasing valence does not reduce *c<sub>K</sub>* as it does with inorganic counterions. The adsorption of organic cations is not only regulated by electrostatic forces but is enhanced by van der Waals interactions between the organic cations and the surface.

In addition, the influence of the cations on surface properties, notably the increase in hydrophobicity with increasing chain length (Lagaly et al., 1983) has to be considered. The disturbance of the water structure enhances the adsorption of counterions and decreases the Stern potential and the electrostatic repulsion.

In a case of strong counterion adsorption, the amount of salt at the point of coagulation can approximate the total amount of adsorption sites on the particles ('equivalent coagulation' (de Rooy et al., 1980)). Because of particle formation in montmorillonite dispersions the amount of organic cations is similar in magnitude to the amount of surface charges but not identical with it (Penner and Lagaly, 2000).

It is difficult to explain the smaller  $c_K$  of the monovalent crystal violet (CV) compared with the divalent methyl green (MG). A reason may be the different orientation of the cations on the surface. The plane of the CV cations is inclined to the silicate layer, whereas that of the MG cations is parallel to the montmorillonite surface (Rytwo et al., 1995). The van der Waals contact is probably enhanced between the inclined CV cations of two adjacent montmorillonite layers, promoting coagulation. The higher yield value of CV-containing montmorillonite dispersions compared with the corresponding dispersions with MG was explained in a similar way (Penner and Lagaly, 2000).

#### 5.4.7. Coagulation by Acids

Acids like HCl, HNO<sub>3</sub>, H<sub>2</sub>SO<sub>4</sub>, and H<sub>3</sub>PO<sub>4</sub> coagulated a 0.025% Na<sup>+</sup>-montmorillonite (Wyoming) dispersion (pH ~2) at concentrations similar to the corresponding salts:  $c_K(\text{HCl, HNO}_3) = 5.5 \text{ mmol/L}$ ,  $c_K(\text{H}_2\text{SO}_4) = 12.5 \text{ mmol/L}$ , and  $c_K(\text{H}_3\text{PO}_4) = 32 \text{ mmol/L}$ .

In acidic medium (pH < 5) the edges of clay mineral particles are positively charged, promoting coagulation by edge(+)/face(-) contacts and formation of house-of-card aggregates (Fig. 5.8). Because of this heterocoagulation process acidic dispersions are very sensitive to salts. Indeed, Na<sup>+</sup>-montmorillonite dispersions coagulate spontaneously at pH < 3.5. The  $c_K$  value of NaCl increased from about 1 mmol/L at pH ~3.5 to a plateau of ~2 mmol/L; with the transition into edge(-)/face(-) coagulation at pH ≥ 6 this value increased to 10 mmol/L (Swartzen-Allen and Matijević, 1976). The pH-dependent colloidal stability was explained on the basis of an ionisation model and the DLVO theory (Tombácz et al., 1990).

Acids, such as HCl and HNO<sub>3</sub>, coagulate at 5.5 mmol/L. The concentration for coagulation apparently corresponds to the proton concentration (solution pH ~2.3) at which the positive edge charge density is high enough to initiate edge(+)/face(-) coagulation. In the presence of sulphuric and phosphoric acids the stabilising effect is also evident. When these acids or their anions (e.g., H<sub>2</sub>PO<sub>4</sub><sup>-</sup>, HPO<sub>4</sub><sup>2-</sup>) are adsorbed at the edges, higher proton concentrations are required to recharge the edges. Therefore, the critical proton concentration increases from 5.5 meq/L for HCl and HNO<sub>3</sub> to 25 meq/L for H<sub>2</sub>SO<sub>4</sub> and 32 meq/L for H<sub>3</sub>PO<sub>4</sub> (which dissociates only one proton in weakly acidic medium; pK<sub>a</sub> values: 2.1; 7.2; 12.7).

The reaction with acids not only consists of protonating the edges. Protons also replace interlayer cations, and initiate a slow decomposition of the silicate layers by liberating octahedral cations (Jasmund and Lagaly, 1993; Janek et al., 1997; Janek and Lagaly, 2001). Since this process is much slower than edge protonation, the reported  $c_K$  values of acids may be in the right order of magnitude.

#### 5.4.8. Influence of Poly(hydroxo metal) Cations

Trivalent cations are highly effective coagulating agents as expressed by the Hardy–Schulze rule (Section 5.4.1). Several trivalent cations ( $\text{Al}^{3+}$ ,  $\text{Fe}^{3+}$ , but not  $\text{La}^{3+}$ ) can also induce the dissociation of water molecules in their hydration shell to produce protons (hydronium ions):



Thus, an aluminium salt solution ( $\text{p}K_a = 4.8$ ) is as acidic as a solution of acetic acid ( $\text{p}K_a = 4.75$ ). Solutions of iron salts are even more acidic ( $\text{p}K_a = 2.2$ ). A pH shift must therefore be considered when these salts are added to dispersions. In relation to their coagulating power the consecutive reactions are more important. The hexaquo aluminium ions are only present at  $\text{pH} \leq 3$ . The formation of the hydroxopentaquo complex at higher pH initiates polycondensation and formation of high-charge polynuclear cations (poly(hydroxo aluminium) cations) (Bottero et al., 1980, 1987; Bertram et al., 1985). One of these is the Keggin cation  $[\text{Al}_{13}\text{O}_4(\text{OH})_{24}(\text{H}_2\text{O})_{12}]^{7+}$  which plays an important role in the preparation of Al-pillared clay minerals (see Chapter 7.5). Basic aluminium salt solutions ('aluminum chlorohydrate') are widely used in the production of anti-transpirants. They contain chain-like poly(hydroxo aluminium) cations with a low degree of crosslinking, and probably form sheet-like aggregates.

The polycondensation of the hydrated iron ions starts at  $\text{pH} < 3.5$  (Dousma and de Bruyn, 1976; Khoe and Robins, 1989). In contrast to the chain-like poly(hydroxo aluminium) ions the polynuclear iron species form more complex, sphere-like macroions (Bottero et al., 1991; Tchoubar et al., 1991; Hagen, 1992).

The formation of colloidal particles during ageing, even in very acidic solutions, is characteristic of poly(hydroxo metal) complexes and other hydrated multivalent cations, such as  $\text{Cr}^{3+}$  and  $\text{Ti}^{4+}$ . For example, hematite ( $\alpha\text{-Fe}_2\text{O}_3$ ) and akaganeite ( $\beta\text{-FeO}(\text{OH})$ ) form at  $\text{pH} \sim 1$ . Diaspore ( $\gamma\text{-Al}_2\text{O}_3$ ) forms at  $\text{pH} 2\text{--}2.5$  (Matijević, 1977). The crystal modification is not only determined by concentration, pH, and temperature but also by the type of anions present.

The potential for interaction between colloidal particles in the presence of polycations is controlled by a number of factors in a very subtle way (Matijević, 1981). As a function of pH and aluminium concentration the phase diagrams reveal fields of destabilisation and restabilisation. On oxidic surfaces poly(hydroxo metal) cations are more strongly adsorbed than monomeric hexaquo complexes (Matijević, 1977).



Re-charging of negative colloidal particles by multivalent cations was explained by Matijević (1973) on the basis of the adsorption of poly(hydroxo metal) cations. Charge reversal of montmorillonite particles by such  $\text{Al}^{3+}$  complexes was reported (Penner and Lagaly, 2000). Kaolinite particles were also re-charged by adsorption of  $\text{Co}^{2+}$ ,  $\text{Cd}^{2+}$ , and  $\text{Cu}^{2+}$  (Hunter and James, 1992).

An anomalous stability of aqueous boehmite ( $\gamma\text{-AlO}(\text{OH})$ ) dispersions at high electrolyte concentrations (!) was reported by several authors (van Bruggen et al., 1999 and references therein). This might be because the polymeric cations shift the (apparent) plane of surface charges away from the bare particle surface into the solution. The electrostatic repulsion then operates over a shorter distance between two particles than the van der Waals attraction. When pH is too low, smaller oligomers or even  $\text{Al}^{3+}$  cations are formed that are not large enough to overcome the van der Waals attraction. When the pH is too high, polycondensation of the hydroxo complexes leads to the formation of individual colloidal particles without providing any stabilisation. Only at a certain range of pH values is the shift of the apparent plane of positive charges large enough for repulsion to overcome the van der Waals attraction.

Frenkel and Shainberg (1980) reported a certain re-stabilisation of montmorillonite dispersions by poly(hydroxo metal) cations, the iron cations being stronger than the aluminium cations. Evidently, the poly(hydroxo metal) complexes of different metal cations can influence dispersion stability in different ways. Polymer morphology is certainly an important factor (Oades, 1984).

#### 5.4.9. Clay Mineral-Oxide Interactions

The interaction between clay minerals and colloidal (hydr)oxides<sup>6</sup> is very important in soil science. Goldberg and Glaubig (1987) observed a reduction of the  $c_K$  values of NaCl and  $\text{CaCl}_2$  for dispersions of  $\text{Na}^+$ -montmorillonite and sodium kaolinite in the presence of 2 and 10% amorphous aluminium and iron (hydr)oxides.

The colloidal behaviour of clay-oxide dispersions is much more complicated than it appears at first sight. Dispersed oxides usually show a p.z.c. at a particular pH. Below this value the particles are positively charged while above this pH they are negatively charged. The colloid stability of oxide dispersions therefore decreases with increasing pH to a minimum (spontaneous coagulation), then increases again (Fig. 5.12). Below the p.z.c. anions are the counterions, and  $c_K$  is strongly dependent on the valence of the anions. At pH above the p.z.c., the valence of the cations determines the critical coagulation concentration. We should stress that the p.z.c. of oxides not only depends on the chemical composition but also on the crystal structure and modification and the way the particles were prepared and aged. Also, adsorption of solutes, especially anions, can strongly influence the position of the

<sup>6</sup>(Hydr)oxide is used as a general term for hydroxides like  $\text{Al}(\text{OH})_3$ , oxyhydroxides such as  $\text{FeO}(\text{OH})$ , and oxides. Most amorphous samples are oxyhydroxides.

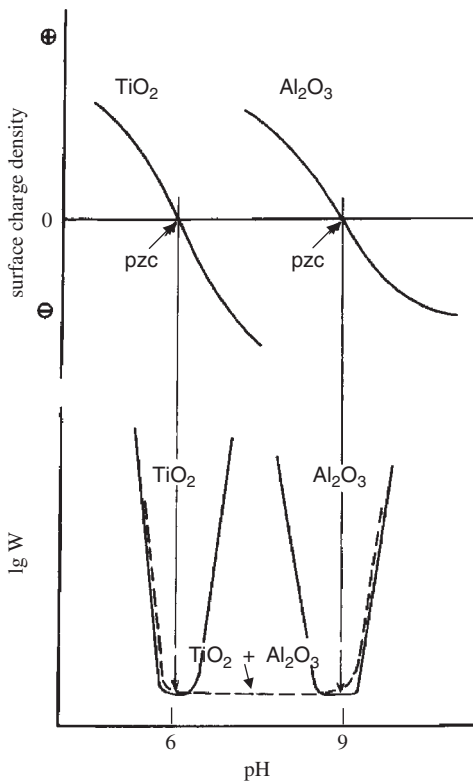


Fig. 5.12. Heterocoagulation between two oxides, e.g.  $\text{TiO}_2$  and  $\text{Al}_2\text{O}_3$ . Surface charge density  $\sigma$  of the oxides and stability factor  $W$  as a function of pH. The mixture of both oxides should coagulate spontaneously between  $\text{pH} = 6$  and  $\text{pH} = 9$  (---). Adapted from Healy et al. (1973). From Lagaly et al. (1997).

p.z.c. It is essential in coagulation studies to determine the p.z.c. This is mostly done by measuring the electrokinetic mobility as a function of salt concentration and pH (Lyklema, 1984, 1995).

Assuming a p.z.c. of about 6 of the oxide, heterocoagulation can occur between the positively charged oxide particles and clay mineral particles at  $\text{pH} < 6$ . When aluminium and iron (hydr)oxides were precipitated in the presence of kaolinite alternating stabilisation and re-stabilisation domains were observed as a function of pH (Arias et al., 1995). The coagulation process and the type of coagulate depend on the mass ratio between the oxide and the clay mineral. A certain amount of the heterocoagulate may be formed spontaneously, but salt addition is needed to coagulate the remaining part of dispersed particles.

At the p.z.c. of the (hydr)oxide, selective coagulation of the (hydr)oxide particles may be observed. Above the p.z.c. the oxide particles and the edges and faces of clay

minerals are negatively charged. If the  $c_K$  values of the pure components (oxide and clay mineral) are distinctly different, selective coagulation may occur; if not, the critical coagulation concentration will be intermediate between the  $c_K$  values of the components. It is therefore imperative to observe very carefully the coagulation process.

Several additional effects have to be considered in clay-oxide interactions:

- (i) since the solubility of the (hydr)oxides is pH-dependent, multivalent cations released into the solution not only act as coagulating species but also adsorb on the surface of clay mineral particles, changing the surface charge density;
- (ii) in mixed oxide dispersions the more soluble oxide can cover the other particles forming core shell particles. This behaviour is well known for alumina (p.z.c.  $\sim 8.8$ ) and titania (p.z.c.  $\sim 6$ ) particles (Healy et al., 1973). When dispersions of  $Al_2O_3$  and  $TiO_2$  were mixed and immediately coagulated, the dispersion became unstable between the p.z.c. values of the components (broken line in Fig. 5.12). When the mixed dispersions were coagulated a few hours later, all particles of the mixed dispersion behaved like alumina particles because of the formation of alumina shells around the  $TiO_2$  particles. In a similar way, the surface structure of clay minerals could be changed by the deposition of aluminium (hydr)oxide species;
- (iii) an important factor is the relative size of the different particles. The smaller particles can be coagulated or attached to the surface of the larger particles and change the colloidal behaviour of the larger particles (see also Section 5.4.2). McAtee and Wells (1967) observed the adsorption of gibbsite particles on the edges of kaolinite and the basal surfaces of montmorillonite particles by TEM. Evidently, the gibbsite particles re-charged the montmorillonite particles. Similar observations were reported for iron (hydr)oxides and kaolinite. The influence of surface charge, however, was strongly dependent on the type of hydroxide (Greenland, 1975). Bridging of iron (hydr)oxide aggregates by montmorillonite particles was described by Ferreiro et al. (1995);
- (iv) if (hydr)oxides are precipitated in the presence of colloidal particles, complexes between metal ions and  $OH^-$  can be formed at the surface of the particles under conditions that did not cause metal hydroxide precipitation in homogeneous solutions (surface precipitation). In dispersions of clay minerals and (hydr)oxides dissolution and surface precipitation can therefore strongly change the surface structure of the clay mineral particles;
- (v) an interesting effect is the interaction between particles having surfaces with distinctly different charge densities but of the same sign. In this case the repulsion can change into attraction (Lagaly et al., 1972, 1997; Usui, 1973; Gregory, 1975; McCormack et al., 1995). This effect promotes the mixing of differently charged particles during re-aggregation (Sections 5.4.2 and 5.4.10).
- (vi) the properties of a clay-oxide dispersion can be strongly influenced by the way the particles were brought into contact (Yong and Ohtsubo, 1987). Due to edge(+) / face(-) contacts, a 9%  $Na^+$ -kaolinite dispersion showed a high value

of yield stress at pH  $\sim 3$  (Fig. 5.13). When ferrihydrite was added at pH 3, the hydroxide was preferentially adsorbed on the faces of the kaolinite particles and re-charged them (edge(+)/face(+)) so that the yield stress disappeared. With increasing pH, the edges of the kaolinite particles became negative, and edge(-)/face(+) contacts formed a network of particles with a broad maximum of yield stress at pH  $\sim 7$ . The initial re-charging of the ferrihydrite reduced the positive face charge density, causing the network to disintegrate, and the yield stress to approach zero at pH  $\sim 10$ . If the ferrihydrite was added at pH 9.5, all particles were negatively charged, and a yield value was not observed. Decreasing pH increased the positive charge of the ferrihydrite, which then bridged the negative kaolinite particles, and the yield value increased to a sharp and high maximum. The very high positive charge density of the hydroxide at still lower pH promoted adsorption of ferrihydrite on the basal plane surfaces of the kaolinite particles, and the kaolinite(-)/ferrihydrite(+)/kaolinite(-) network collapsed, as indicated by the strong decrease in yield value;

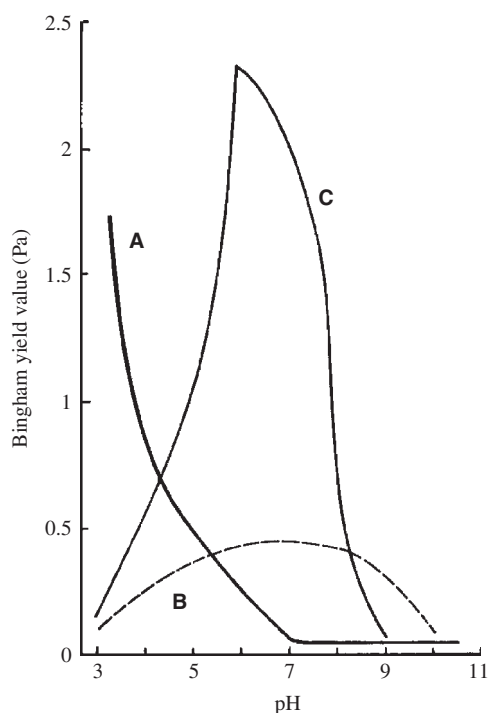


Fig. 5.13. Bingham yield value of a 9% (w/w)  $\text{Na}^+$ -kaolinite (Georgia) dispersion (A), yield value when a synthetic ferrihydrite (1 g ferrihydrite per 19 g kaolinite) was added at pH = 3 (B) or at pH = 9.5 (C). Adapted from (Yong and Ohtsubo, 1987). From (Jasmund and Lagaly, 1993).

- (vii) the presence of (hydr)oxides, especially in amorphous form, can reduce the mechanical swelling of the clay minerals. This may be ascribed to cementation of the clay mineral particles by shells of (hydr)oxides, and penetration of poly(hydroxo metal) ions, such as poly(hydroxo aluminium) and poly(hydroxo iron) ions, between the layers. The permeability can be influenced in two ways. If the particles form larger individual aggregates, the permeability may increase. It decreases when the (hydr)oxides act as cementing agents (Deshpande et al., 1964; El Rayah and Rowell, 1973; Blackmore, 1973; Greenland, 1975; Alperovitch et al., 1985). The conclusion is that the behaviour of such systems depends very much on the very nature of the (hydr)oxides and the way they react with the clay mineral.

#### 5.4.10. Calculation of Interaction Energies

The interaction between dispersed clay mineral particles or individual silicate layers may be described by the DLVO theory (Barclay and Ottewill, 1970; Ottewill, 1977; van Olphen, 1977; Sposito, 1992; Güven, 1992a; Sposito and Grasso, 1999) even though other types of interactions (Sun et al., 1986; Low, 1987; van Oss et al., 1990) and long-range Coulombic attraction (McBride, 1997) may be operative. As the charge density of the faces is determined by isomorphous substitution and defects within the layer, the calculations are carried out on the assumption that the charge density of the faces remains constant when the salt concentration is varied (Usui, 1973; Gregory, 1975; van Olphen, 1977).

A pronounced Stern-layer adsorption is characteristic (Chan et al., 1984; Sridharan and Satayamurty, 1996). The surface potential calculated by the DLVO theory for montmorillonite layers (surface charge density  $\sim 0.10 \text{ C/m}^2$ ) would be 308, 206, and 88 mV at NaCl concentrations of  $10^{-5}$ ,  $10^{-3}$ , and  $10^{-1} \text{ mol/L}$ , respectively. Such high surface potentials are not determinative of colloid stability because they lead to a strong Stern-layer adsorption. Chan et al. (1984) derived distinctly smaller values from anion exclusion measurements (Section 5.3.5). The distribution of cations between the Stern layer, the diffuse double layer, and the solution can be calculated by a model developed by Nir et al. (1986, 1994) and Hirsch et al. (1989). An advantage of this model is that complex formation of the counterions in solution can be considered.

For an Opalinus clay Madsen and Müller-Vonmoos (1985) found good agreement between the swelling pressure calculated by the DLVO theory and that measured experimentally. Lubetkin et al. (1984) measured the pressure created by several alkali montmorillonites and beidellites as a function of the distance between the plates (calculated from the mass content of smectite on the assumption that the particles were completely delaminated) (Fig. 5.14a). At separations  $> 5 \text{ nm}$  the repulsive pressure arose solely from electrostatic repulsion. On the basis of diffuse layer interactions, reasonably good agreement between theory and experiment was obtained (Fig. 5.14b). The effect of particle formation (see Section 5.2.3) is clearly seen in Fig. 5.14a. In the

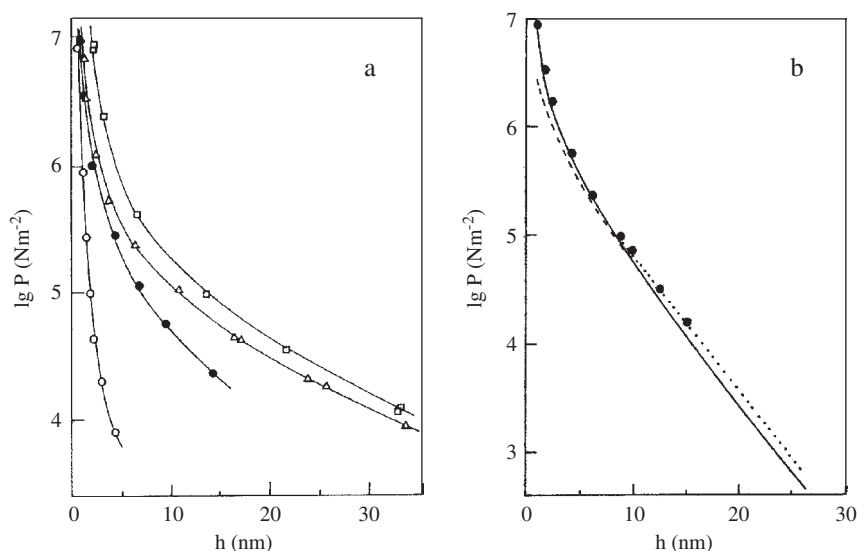


Fig. 5.14. Pressure against plate distance  $h$  for Wyoming montmorillonite. (a) In  $10^{-4}$  M salt solutions of various counterions:  $\square$ ,  $\text{Li}^+$ ;  $\triangle$ ,  $\text{Na}^+$ ;  $\bullet$ ,  $\text{K}^+$ ;  $\circ$ ,  $\text{Cs}^+$ . (b) Experimental data for  $\text{Li}^+$  montmorillonite in  $10^{-2}$  M LiCl ( $\bullet$ ), and calculated curves for the constant potential model (---), constant surface charge model (—), and by approximation (....). From Lubetkin et al. (1984).

presence of alkali metal ions, other than  $\text{Li}^+$  and  $\text{Na}^+$  ions, the distances between the silicate layers are no longer equal. As these distances are smaller within than between particles, the pressure decreases more strongly in the presence of  $\text{K}^+$  and  $\text{Cs}^+$  ions than when  $\text{Li}^+$  and  $\text{Na}^+$  ions are present.

Ottewill (1977) noted that the theory should be corrected because a partition of the counterions between the clay dispersion and the external finite reservoir has to be considered due to the finite volume of the dispersion. At separations of about 1 nm there is a discontinuous decrease in basal spacing, indicating transition into the quasi-crystalline structure. It is then no longer reasonable to calculate the interaction forces on the basis of the simple DLVO model. As discussed in Section 5.2.2 the distribution of interlayer cations deviates considerably from that of two interacting double layers. The hydration shells around the interlayer cations resist further compression of the interlayer space (see Israelachvili (1994) for a discussion of hydration forces).

Huerta et al. (1992) considered the effect of counterions and co-ions of unequal size and calculated the swelling pressure by the modified Gouy-Chapman theory for constant surface charge density. The influence of co-ion size was only important at surface charge densities distinctly below  $0.10 \text{ C/m}^2$ .

By considering  $\text{H}^+$ -saturated montmorillonite as a solid acid with ionisable surface groups, Tombácz et al. (1990) calculated the density of these groups (sites) and

their intrinsic ionisation constants from potentiometric and conductometric titrations. Two types of ionisable sites with intrinsic ionisation constants  $pK_{s1} = 2.6$  and  $pK_{s2} = 6.4$  were distinguished. The total number of sites,  $N_1 + N_2 = 4.8 \times 10^{17}$  (sites/m<sup>2</sup>), was calculated from the CEC of 0.59 meq/g (montmorillonite of Kuzmice). The ratio of weak and strong acid groups was  $N_2/N_1 = 0.41$ , i.e. 29% of all sites were weak acidic centres. The most acidic sites were the  $H_3O^+$  ions replacing exchangeable  $Na^+$  ions (Janek and Lagaly, 2001). The surface potential as a function of pH was calculated from the charge densities. At  $10^{-3}$  M NaCl and above pH  $\sim 4$ , the surface potential showed a plateau at 185 mV. This value decreased to 70 mV in  $10^{-1}$  M NaCl and to 30 mV in 1 M NaCl, and the plateau extended to pH  $\approx 6$ . On the basis of these surface potentials, the total interaction curves (Hamaker constant  $A = 0.5 \times 10^{-20}$  J) were hypothetical at small distances (see remark above), but they clearly showed that the maximum of the total interaction energy disappears at about 0.1 M NaCl (pH = 2), 0.3 M NaCl (pH = 4), and 0.4 M NaCl (pH = 8). These results agree with the experimental data for samples treated with sodium hexametaphosphate (0.1, 0.2–0.25, and 0.35–0.40 M at pH = 2, 4, and 8, respectively (Tombácz et al., 1990)) and diphosphate (0.36–0.44 M at pH = 9, Frey and Lagaly, 1979b).

A quite different (and, for a colloid scientist, strange) view was put forward by Low and co-workers (Sun et al., 1986; Low, 1987; Miller and Low, 1990) on the basis of extensive studies on the clay–water system. They suggested that hydration of the clay mineral surface was the primary cause of swelling. This ‘non-specific interaction of water’ (undefined term) with the clay surface could not be fully explained. Hydration of the interlayer cations was assumed to be of minor importance. However, Delville and Laszlo (1989) showed that the Poisson-Boltzmann formalism correctly reproduces the relation between interlayer distance and swelling pressure. The driving force is the stabilisation of water molecules within the interlayer force field. In all cases, the Poisson-Boltzmann approximation, modified to incorporate ion/polyion-excluded volume effects, led to a concentration profile in agreement with Monte Carlo calculations. Quirk and Marčelja (1997) examined published data on the extensive swelling of  $Li^+$ -montmorillonite as revealed by  $d_{(001)}$  spacings over the pressure 0.05–0.9 MPa and  $1\text{--}10^{-4}$  M LiCl. Both the Poisson-Boltzmann and DLVO double layer theories satisfactorily predict surface separations over the range 1.8–12.0 nm. The DLVO theory with a 0.55 nm-thick Stern layer indicated Stern potentials of  $-58$  to  $-224$  mV (for  $1\text{--}10^{-4}$  M LiCl) and a constant Gouy plane charge of  $0.038$  C/m<sup>2</sup> (about 30% of the layer charge). There was no additional pressure contributing to hydration forces (Israelachvili, 1994) for surface separations of about 1.8 nm or larger. (The hydration force was considerable for muscovite, with a surface charge density about three times that of montmorillonite (Pashley and Quirk, 1984)).

In the presence of  $Ca^{2+}$  (and other di- and trivalent metal) ions, the particles remain coagulated and cannot be dispersed even in pure water. Fitzsimmons et al. (1970) showed that, just after contact of  $Na^+$ -montmorillonite dispersions with calcium-saturated exchange resins,  $Ca^{2+}$ -montmorillonite exists as single layers like the

sodium form. With time the individual silicate layers aggregated by overlapping of the edges, forming large, flat sheets (band-type aggregation; Section 5.6.1). The basal spacings (Fig. 5.3) indicate that calcium ions maintain the 'quasi-crystalline' structure. These ions are located in the middle of the interlayer space, restricting the interlayer distance to 1 nm (basal spacing 2 nm), and impeding transition into the structure with diffuse ionic layers.

Kleijn and Oster (1982) were the first to explain the attractive interactions in the presence of calcium ions in terms of the DLVO theory. The cations located between the layers are assumed to be in equilibrium with the bulk solution (see also Dufrêche et al., 2001) so their charge density was slightly different in magnitude from the charge density of the layers. The electrostatic contribution to the Gibbs energy was calculated for constant surface charge density (van Olphen, 1977). The Gibbs energy was positive (peptisation) over a wide range of salt concentrations ( $c_s$ ) and surface charge densities ( $\sigma_0$ ) when the exchangeable cations were monovalent.  $\text{Na}^+$ -montmorillonite particles were coagulated by salt concentrations slightly above 0.1 M as long as the surface charge density remained below  $0.1 \text{ C/m}^2$  (Table 5.1) and by salt concentrations slightly below 0.1 M for  $\sigma_0 = 0.1 - 0.15 \text{ C/m}^2$ . For more highly charged clay minerals (vermiculites, micas) the Gibbs energy was negative even at very low salt concentrations, and formation of colloidal dispersions was not expected. In the presence of divalent cations the colloidal dispersions became unstable at  $c_s \leq 10^{-3} \text{ M}$  and  $\sigma_0 > 0.07 \text{ C/m}^2$ .

Kjellander et al. (1988) used an advanced statistical mechanical method to calculate the diffuse double-layer interaction. This model gives strongly attractive double-layer interactions for divalent ions (Fig. 5.15) in contrast to what the simple Poisson-Boltzmann theory predicts. The position of the minimum is in reasonable agreement with basal spacing measurements by XRD. The most important reason for the occurrence of the potential minimum is the attraction due to the ion-ion correlation. In the Gouy-Chapman model of the diffuse ionic layer, this correlation is entirely neglected, i.e. the ion density in the neighbourhood of each ion is assumed to be unaffected by this ion. This neglect of the ion-ion correlation is a reasonable approximation when both the electrolyte concentration and the surface charge density are sufficiently low. However, if either condition is violated, the ion-ion correlation must be taken into account. This would lead to attractive double layer interactions between equally charged particles at short separations (Kjellander, 1996). The correlation influences the interaction by two different mechanisms: (i) by changing the ion concentration in the middle of the interlayer space; and (ii) by contributing to an attractive electrostatic fluctuation force (Kjellander, 1996).

An interesting aspect of the coagulation of clay mineral particles by salts should be mentioned. Frens and Overbeek (1972), Overbeek (1977) and Frens (1978) introduced the 'distance-of-closest-approach' concept to explain the reversibility of coagulation. The existence of such a limiting distance of about two water layers ( $\sim 0.5 \text{ nm}$ ) is clearly proved by the behaviour of montmorillonite. Even in concentrated NaCl solutions the basal spacing of  $\text{Na}^+$ -montmorillonite does not decrease



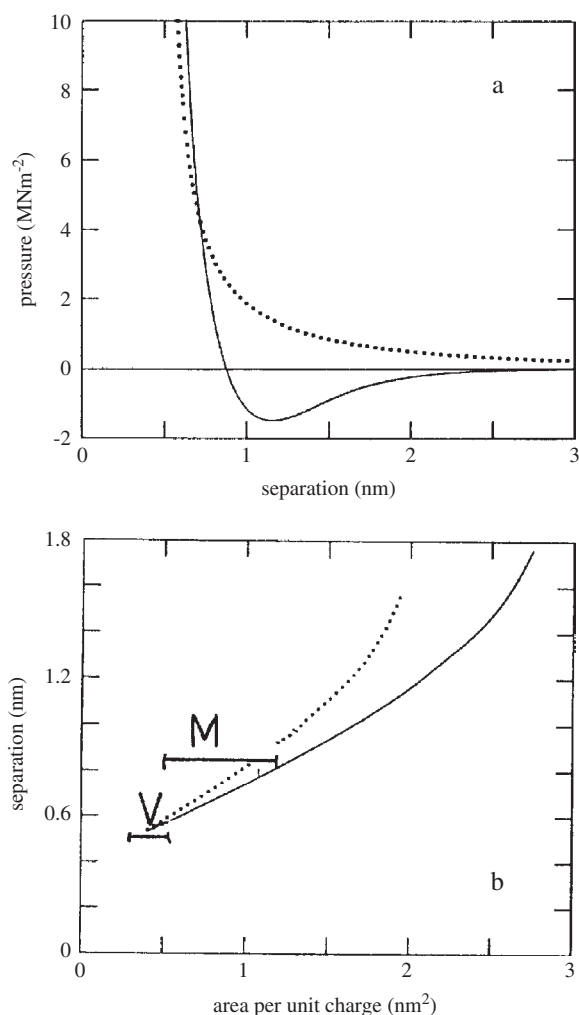


Fig. 5.15. Calculation of the pressure between two silicate layers of  $\text{Ca}^{2+}$ -montmorillonite and vermiculite. (a) total pressure, calculated for montmorillonite with a surface charge density  $\sigma_0 = 0.12 \text{ C/m}^2$  (full line); results of the DLVO theory shown as dotted line. (b) Position of the potential minimum as a function of the area per unit charge. Solid line: the total net pressure; dotted line: pressure without van der Waals interaction included. (M), montmorillonites; (V), vermiculites Kjellander et al. (1988). From Jasmund and Lagaly (1993).

below 1.4–1.5 nm, i.e. two layers of water are maintained between the coagulating silicate layers (Fig. 5.3) (Jasmund and Lagaly, 1993; Lagaly, 1993, 2005; Lagaly et al., 1997). This water is only displaced when, in addition to the electrostatic forces, specific interactions, as defined by Lyklema (1984, 1989, 1995), become important.

A well-known example is the collapse of more highly charged silicate layers in the presence of potassium ions (van Olphen, 1977; Jasmund and Lagaly, 1993).

Fig. 5.16 illustrates the coagulation of mixed dispersions of two smectites (Section 5.4.2). Only very small particles were mixed during coagulation. The maximum total interaction energy  $V_{t,m}$  is calculated for particles of  $10^2$  and  $10^4 \text{ nm}^2$  and surface charge densities of 0.069, 0.096, and  $0.12 \text{ C/m}^2$ . The total interaction curves are obtained by the linear superposition approximation for constant surface charge density (van Olphen, 1977). The curves terminate at a layer separation of 1 nm because at smaller distances DLVO calculations are no longer appropriate. At 0.3 M NaCl,  $V_{t,m}$  is about 5 kT/particle for the small particles and  $\sigma_0 = 0.069 \text{ C/m}^2$ , and increases to 17 kT/particle for  $\sigma_0 = 0.096 \text{ C/m}^2$  (Fig. 5.16a). An increase of concentration to 0.38 M NaCl leads to  $V_{t,m} \approx 1 \text{ kT/particle}$  for  $\sigma_0 = 0.069 \text{ C/m}^2$  and 10 kT/particle for  $\sigma_0 = 0.096 \text{ C/m}^2$ . Thus, mixing of both types of layer is highly probable during coagulation. The curves calculated for larger particles (Fig. 5.16b) clearly

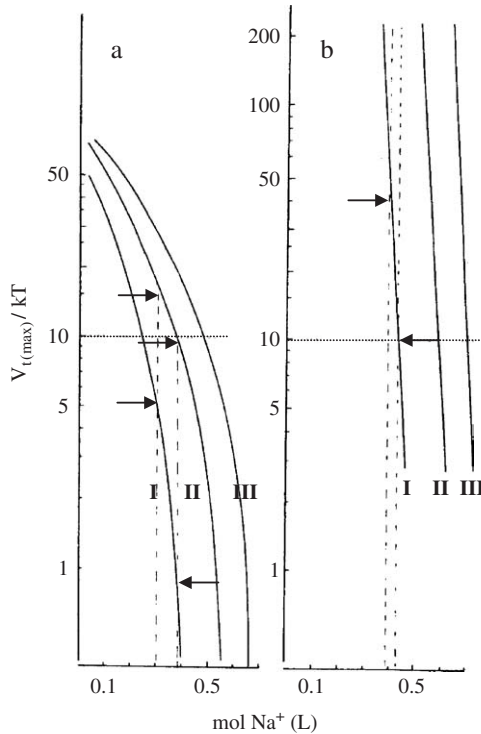


Fig. 5.16. Maximum interaction energy (in  $kT/\text{plate}$ ) as a function of  $\text{Na}^+$  concentration for particles  $10 \times 10 \text{ nm}^2$  (a) and  $100 \times 100 \text{ nm}^2$  (b) Surface charge densities: I, 0.069; II, 0.096; III,  $0.120 \text{ C/m}^2$ ; calculated for constant charge density, Hamaker value  $5 \times 10^{-20} \text{ J}$ . From Frey and Lagaly (1979b).

show that at a salt concentration of about 0.4 M only the low-charge layers are coagulated.  $V_{t,m}$  of the high-charge layers remains so large as to prevent coagulation.

It is interesting to consider the depth of the secondary minimum. For larger layers with low charge density the depth is about 50 kT/particle, and  $\approx 20$  kT/particle for the high-charge layers. Thus, aggregation of the low-charge layers is initiated by preliminary demixing in the secondary minimum.

In more sophisticated calculations, the total interaction energies have to be calculated between differently charged plates. This reduces  $V_{t,m}$  and makes the mixing of the small particles still more probable (Lagaly et al., 1972; Usui, 1973; Gregory, 1975; Derjaguin et al., 1987). For large particles, the differences of  $V_{t,m}$  remain large enough to prevent the layers from mixing during coagulation. The effect of particle size on the simultaneous coagulation of differently charged particles is also evident from the calculations by Pugh and Kitchener (1971).

## 5.5. FLOCCULATION AND STABILISATION BY POLYMERS

### 5.5.1. Flocculation and Stabilisation Mechanisms

Macromolecules can flocculate colloidal dispersions by two different mechanisms: bridging between the particles and charge neutralisation (Fig. 5.17) (Theng, 1979; Chaplain et al., 1995; Lagaly et al., 1997).

Bridging requires that the macromolecules can attach to the surface of two approaching particles and that the bridging part of the macromolecules is compatible with the solvent (the solvent has to be a better-than- $\theta$  solvent). In aqueous dispersions a certain low salt concentration is often needed to bring the particles in distances that can be spanned by the macromolecules.

Charge neutralisation occurs when the charges on the particle surface and the polymer are opposite in sign. The polyions can then compensate the surface charges (Fig. 5.17b, c). However, site-by-site compensation only occurs at suitable geometrical conditions. A general model is flocculation by patch-charge interactions (Gregory, 1973; Mabire et al., 1984). For example, polycations are adsorbed in patches, giving rise to an excess of positive charges. This excess is compensated by negative charges of patches that are not covered by the polycations. An attractive force operates between one or more cationic patches of one particle and domains of negative surface charges of a neighbouring particle. These contacts can be broken and re-established under shearing forces. The formation of polymer patches on charged colloidal particles was observed by AFM (Akari et al., 1996).

Since flocculation is often irreversible, the amount adsorbed and the properties of the flocs depend on the manner by which the macromolecules were added to the dispersion. The formation of flocs can retard equilibration when adsorption sites within the flocs are difficult to access by the macromolecules (see Section 5.5.3). The amount adsorbed and the type of aggregation are therefore critically sensitive to the

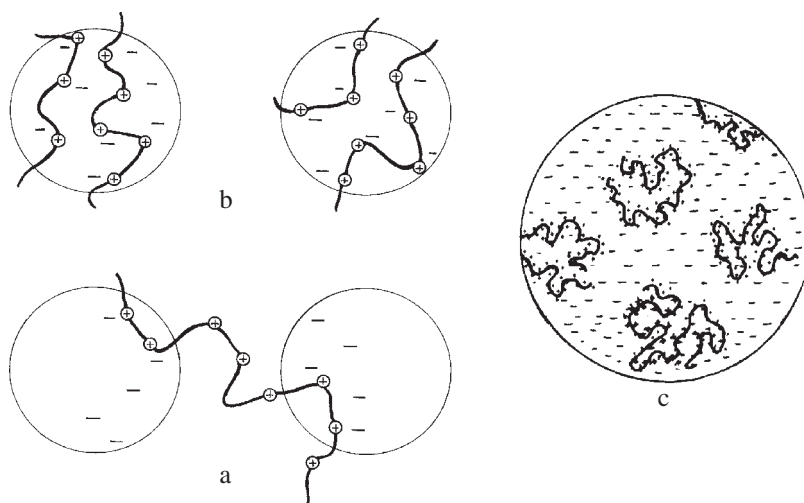


Fig. 5.17. Destabilisation of colloidal dispersions by (a) bridging flocculation, (b) charge neutralisation, and (c) patch-charge interaction. From Lagaly et al. (1997).

details of the mixing and stirring procedure, giving rise to non-reproducible experimental results (Chaplain et al., 1995). The amount adsorbed usually decreases as the solid/liquid ratio increases (Lee et al., 1991). Polymer adsorption and the influence of polymers on dispersion stability are strongly dependent on the true nature of the polymer. For example, polyacrylamides may be neutral (uncharged) polymers, anionic (hydrolysed) products, cationic derivatives, or copolymers (of acrylic acid and acrolein derivatives).

Many polymers flocculate a dispersion at very low concentration but re-stabilise at higher concentration. The latter is an osmotic process, referred to as 'steric stabilisation' (Napper, 1983; Lagaly et al., 1997). When the macromolecules of two approaching particles begin to interpenetrate, the segment density between the particles becomes larger than outside of the interpenetrating domain. Solvent penetrates between the particles, and the particles remain separated (Fig. 5.18). The influence of volume restriction is related to the loss of conformational entropy, and only comes into play at high particle concentrations or near the theta point.

The most important condition for steric stabilisation is that the solvent is a better-than-theta solvent in relation to the macromolecular segments remaining in the solvent. Examples are poly(ethylene oxides), poly(vinyl alcohol), and polyacrylates in water. The polymer must have anchor segments with a high affinity for the particle surface if it is to become attached to the particles. Thus, di-block copolymers are often very suitable.

Steric stabilisation provides a high stability to the dispersion. Destabilisation requires the reduction of the solvency. The particles flocculate when the theta

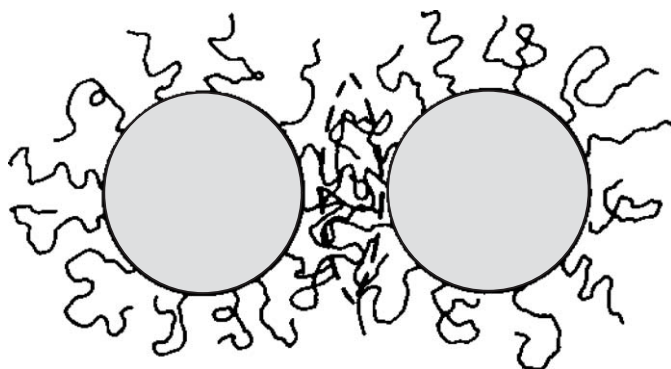


Fig. 5.18. Steric stabilisation as the consequence of the osmotic effect due to the high concentration of segments in the region within the dashed lines. From [Overbeek \(1982\)](#).

condition is reached by the addition of another solvent or a solute. An important advantage is that destabilisation is completely reversible: increasing the solvency or changing the temperature re-stabilise the dispersion. A pronounced influence of temperature is noted in contrast to electrostatically stabilised dispersions. Depending on the thermodynamic functions, the dispersions can be destabilised with increasing but also with decreasing temperature.

A prerequisite for steric stabilisation is the attachment of the macromolecules at the particle surfaces. Macromolecules enriched in the solvent cause destabilisation by the depletion effect ([Napper, 1983](#); [Vincent, 1990](#); [Lagaly et al., 1997](#)).

### 5.5.2. Flocculation by Polyanions

Polymers are extensively used as flocculating agents for clay dispersions. In practical applications, polyanions are more effective in flocculating clay dispersions than polycations. Polyanions are attached to the particles at a few sites, and larger parts of the macromolecules remain free in solution to form bridges between neighbouring particles.

Several studies are reported on the adsorption of polyacrylates and polyacrylamides by montmorillonite ([Stutzmann and Siffert, 1977](#); [Siffert and Espinasse, 1980](#); [Bottero et al., 1988](#); [Heller and Keren, 2002, 2003](#)) and on kaolinite ([Hollander et al., 1981](#); [Pefferkorn et al., 1985, 1987](#); [Nabzar and Pefferkorn, 1985](#); [Stenius et al., 1990](#); [Lee et al., 1991](#)).

Neutral polyacrylamide is adsorbed at the edges and faces of kaolinite particles. The amount adsorbed was independent on salinity (NaCl) and pH between 3.5 and 10, then decreased above pH 10. The adsorption density on the lateral surfaces was distinctly higher than on the basal surface. The adsorption of anionic polyamide<sup>7</sup>

<sup>7</sup>Technical “non-ionic” polyacrylamides also contain about 2–6 mol% carboxyl groups!

also occurred preferentially at the edges. Adsorption decreased strongly with increasing pH (increasing negative charge density of the edges) but increased with NaCl concentration (up to 3.3 mol/L) due to charge screening (Lee et al., 1991).

Adsorption of polyacrylamide on the basal surface of kaolinite occurs mainly on the aluminium hydroxide surface, being driven by van der Waals interactions and an entropy contribution when adsorbed water molecules are displaced by the macromolecules (Lee et al., 1991). At the edges, polyacrylamides are mainly bound by hydrogen bonds between the amide groups and aluminol and silanol groups. Formation of these hydrogen bonds seems to be competitive with hydrogen bond formation between neighbouring aluminol and silanol groups. Hydrogen bonding to silanol groups as anchoring sites is promoted in acidic medium when neighbouring aluminol groups are protonated. Bonding to aluminol groups is favoured in alkaline medium when the neighbouring silanol groups are dissociated. In agreement with this model the adsorption of a statistical copolymer (acrylamide-acrolein) showed a minimum at pH 6–8 (Pefferkorn et al., 1985, 1987). In the case of smectites, amide groups can be protonated by the increased acidity of the interlayer water molecules and then bound by electrostatic forces (Stutzmann and Siffert, 1977).

Polyacrylates and anionic (hydrolysed) polyacrylamides are adsorbed by complex formation between the carboxyl groups of the polyanion and aluminium ions exposed at the edges. Thus, adsorption of polyacrylate by montmorillonite reached a maximum at pH  $\sim 7$  (Siffert and Espinasse, 1980). A further consequence is that adsorption increased with the degree of hydrolysis (increased number of carboxyl groups) (Stutzmann and Siffert, 1977).

Bottero et al. (1988) studied the effect of polyacrylamide on dispersions of  $\text{Na}^+$ -montmorillonite. The polyacrylamide did not flocculate montmorillonite particles but influenced the structure of the particles. Similarly, Heller and Keren (2002) observed that in electrolyte-free dispersions only polymers with high molecular weight form a three-dimensional structure of the clay mineral particles. The effectiveness of polyacrylamides in bridging flocculation increased with decreasing degree of hydrolysis.

The addition of polyacrylamide to  $\text{Na}^+$ -kaolinite dispersions (2% by mass) initiated different types of aggregation (Nabzar et al., 1984). The fraction of flocculated kaolinite first decreased to a minimum, and then increased to a maximum (Fig. 5.19). Polyacrylamide adsorbed at the edges broke up edge(+)/face(−) contacts and increased the dispersibility of the kaolinite particles (B  $\rightarrow$  C in Fig. 5.19). Pronounced adsorption of polyacrylamides on the edges of kaolinite particles was observed by Lee et al. (1991). Bridging of the particles occurred at somewhat higher levels of polyacrylamide addition (C  $\rightarrow$  D), increasing the amount of flocculated kaolinite. At high dosages of polymer, flocculation was reduced by steric stabilisation (D  $\rightarrow$  E). Floc density (determined from the volume and weight of sediment after freeze-drying) was inversely related to the amount flocculated. The presence of a few macromolecules on

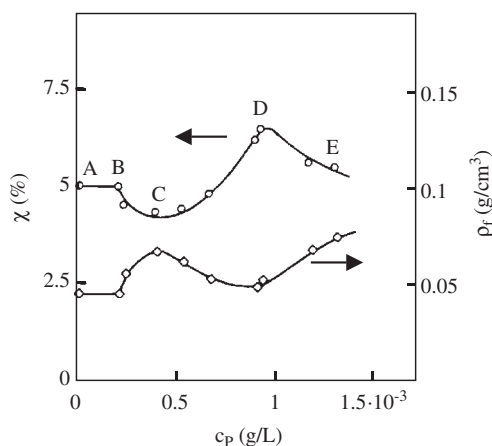


Fig. 5.19. Flocculation of  $\text{Na}^+$ -kaolinite dispersions (2% by weight) with polyacrylamide ( $M = 1.2 \times 10^6$ ) (concentration  $c_P$ ) in  $10^{-4}$  M NaCl at pH = 3.7.  $\circ$ , fraction  $\chi$  of kaolinite flocculated;  $\diamond$ , density  $\rho_f$  of the flocs (Nabzar et al., 1984). From (Jasmund and Lagaly, 1993).

the edges of the particles prevented formation of extended networks during sedimentation, giving rise to densely packed particles (C in Fig. 5.19). Bridging produced relatively loosely packed flocs (E in Fig. 5.19). The increase in floc density at E indicated that the most loosely packed aggregates were the first to be redispersed by steric stabilisation.

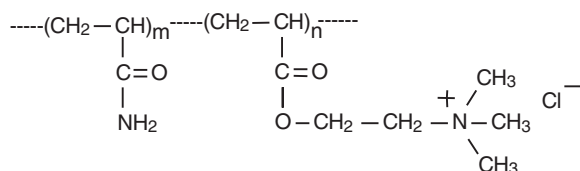
### 5.5.3. Flocculation by Polycations

Polycations are strongly adsorbed by clay mineral particles. Since a large proportion of the segments become attached to the negatively charged surface, bridging between particles does not occur as easily as with polyanions. In many cases flocculation occurs as a consequence of charge neutralisation (Theng, 1979).

Cationic polymers generally flocculate a clay dispersion at a narrow polymer concentration. Even slightly higher polymer concentrations cause re-dispersion. Flocculation, therefore, often requires a sophisticated adjustment of clay, polymer, and salt concentrations as well as pH (Kim et al., 1983). In the domain of re-dispersion the clay mineral-polymer complexes can be flocculated by addition of anionic surfactants but again optimal flocculation is achieved at narrow surfactant concentrations that depend on the amount of polycations added (Magdassi and Rodel, 1996).

Durand-Piana et al. (1987) examined the effect of cationic groups attached to polyacrylamide on the flocculation of  $\text{Na}^+$ -montmorillonite dispersions. Random copolymers consisting of  $m$  units acrylamide (AM) and  $n$  units  $N,N,N$ -trimethyl

aminoethyl chloride acrylate (CMA) were synthesised:



The ‘cationicity’  $\tau = n/(n + m)$  was varied between 0 and 1. At low cationicity the weakly charged polyelectrolytes caused flocculation by interparticle bridging. The optimal flocculation concentration decreased with increasing molecular mass, and for  $\tau \geq 0.01$  with increasing cationicity. Above  $\tau \approx 0.2$  flocculation apparently occurred by charge neutralisation, and the optimal flocculation concentration became independent of molecular mass (Fig. 5.20). The saturation value of adsorption decreased when the solid content of montmorillonite exceeded 2 g/L. Polymer-induced aggregation of montmorillonite platelets can be so extensive as to limit the number of surface sites available for polymer adsorption.

Parazak et al. (1988) studied the flocculation of dispersed montmorillonite, kaolinite, illite, and silica by three types of polycations: poly(dimethylamine epichlorohydrin), poly(dimethyl diallylammonium chloride), and poly(1,2-dimethyl-5-vinylpyridinium chloride). They interpreted the results in terms of ‘hydrophobic interactions’ although patch-charge interactions seem more appropriate.

Since the charges on polycations and clay mineral particles are opposite in sign, polycations can penetrate the interlayer space of smectites to a certain extent.

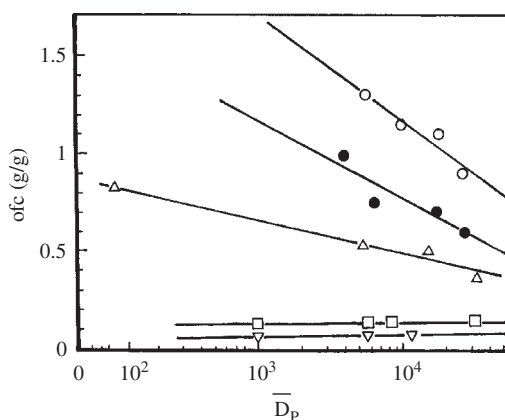


Fig. 5.20. Optimal flocculation concentration (ofc, g/g  $\text{Na}^+$ -montmorillonite) vs. degree of polymerisation,  $\bar{D}_p$ , for polycations (see formula) of various cationicities  $\tau$ :  $\circ$ ,  $\tau = 0.01$ ;  $\bullet$ ,  $\tau = 0.05$ ;  $\triangle$ ,  $\tau = 0.13$ ;  $\square$ ,  $\tau = 0.30$ ;  $\nabla$ ,  $\tau = 1.0$  Durand-Piana et al. (1987). From Jasmund and Lagaly (1993).



However, as the number of contacts between polymer and surface increases, interlayer diffusion of the polycation is retarded and eventually ceases. Complete coverage of the interlayer surfaces by polycations may be achieved by a disaggregation-reaggregation process as proposed for the adsorption of lysozyme by  $\text{Na}^+$ -montmorillonite (Larsson and Siffert, 1983). When a particle with its external faces saturated by polycations collides with another with no polycations on its faces, strong interactions between the polymer-covered face and the bare face can cause an individual layer to peel off either tactoid. This would expose two fresh surfaces for further interaction with polycations. Eventually, all layers are interleaved with polycations, and thick particles are formed (Breen et al., 1996; Billingham et al., 1997; Breen, 1999).

In papermaking, cationic lattices ('polymer microparticles') are used as flocculants to improve retention, drainage, and formation ('retention aids') (Xiao et al., 1999). In the presence of polycations such as cationic polyacrylamides and poly(ethylene imines), the microparticles are flocculated by patch-charge interactions. Being shear-sensitive, these flocs can de-agglomerate under the influence of the high shear forces used in paper machines. Bridging of these particles by montmorillonite particles makes the flocs shear-resistant (Fig. 5.21) (Horn, 2001/2002). However, bridging by montmorillonite is not always effective. In certain two-component microparticle

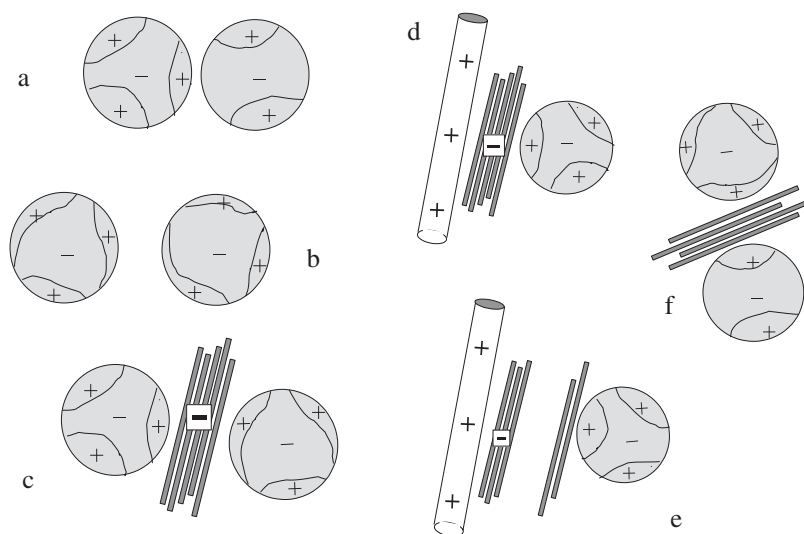


Fig. 5.21. Patchwise coagulation of latex particles and bridging by montmorillonite particles. (a) Flocculation by patch-charge interaction of latex particles covered by polycations, (b) de-agglomeration by shear forces and re-distribution of the adsorbed polycations, (c) bridging of the latex particles by montmorillonite lamellae forming shear-resistant flocculates, (d) attachment of latex particles on the fibres by montmorillonite particles, (e) detachment of the particles by delamination of the clay mineral during shearing, (f) agglomeration of these particles.

retention systems, cationic polyacrylamide and bentonite particles induce the deposition of calcium carbonate particles on the fibre surface. The montmorillonite particles form bridges between the fibre and calcium carbonate particles, both of which are covered with polycations. However, delamination of thicker montmorillonite particles by shearing can lead to detachment and subsequent flocculation of the polyamide-coated carbonate particles (Alince et al., 2001). The shear resistivity of bridging clay mineral particles and particle-fibre agglomerates depends, therefore, on the shear stability of the montmorillonite particles. Thick montmorillonite particles with many breaking points will be less shear-resistant than thin particles consisting of large coherent domains.

#### 5.5.4. Peptisation (Deflocculation) of Clay Dispersions by Macromolecules

As seen in the previous section, optimal flocculation is reached at a distinct polymer concentration. When this concentration is exceeded, restabilisation occurs, and the amount of flocculated clay decreases. Restabilisation is accompanied by an increased salt stability. An instructive example was reported by van Olphen (1977) (Fig. 5.22). Addition of CMC (sodium carboxy methylcellulose) to a  $\text{Na}^+$ -bentonite dispersion

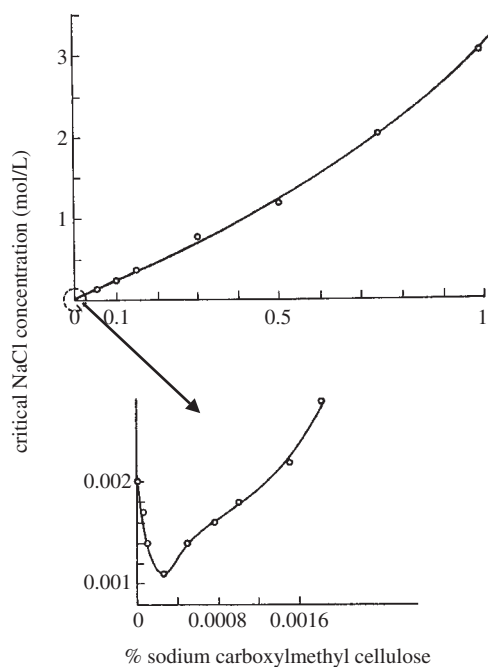


Fig. 5.22. Effect of sodium carboxy methylcellulose on the salt stability of  $\text{Na}^+$ -bentonite dispersions (van Olphen, 1977). From Jasmund and Lagaly (1993).

first decreased the critical NaCl concentration from 20 to 10 mmol/L at 0.0003% CMC (sensitising action of CMC). The colloidal stability then increased strongly up to 3.1 mol/L at 0.1% CMC. Steric stabilisation is the main cause of the enhanced salt stability.

The effect of polymer addition, shown in Fig. 5.22, is basically different from the action of several other polyanions like natural tannates (Fig. 5.23a). Addition of small amounts of Quebracho tannate, a common additive in drilling muds, caused a steep increase in the critical salt concentration reaching a plateau at 270 meq/L NaCl. The Quebracho polyanion does not exert steric stabilisation but simply acts by recharging the edges. Because tannate is added as the sodium salt, the total amount of  $\text{Na}^+$  ions in the dispersion increases to 430 meq/L at the highest dosage of tannate (broken line in Fig. 5.23a). This range of critical cation concentrations is typical of face/face aggregation of clay mineral particles (see Section 5.4.1).

Polyphosphate ions belong to the most important deflocculants in practical applications. In the presence of polyphosphate, the critical coagulation concentration of NaCl increased to a maximum and decreased with further addition of the

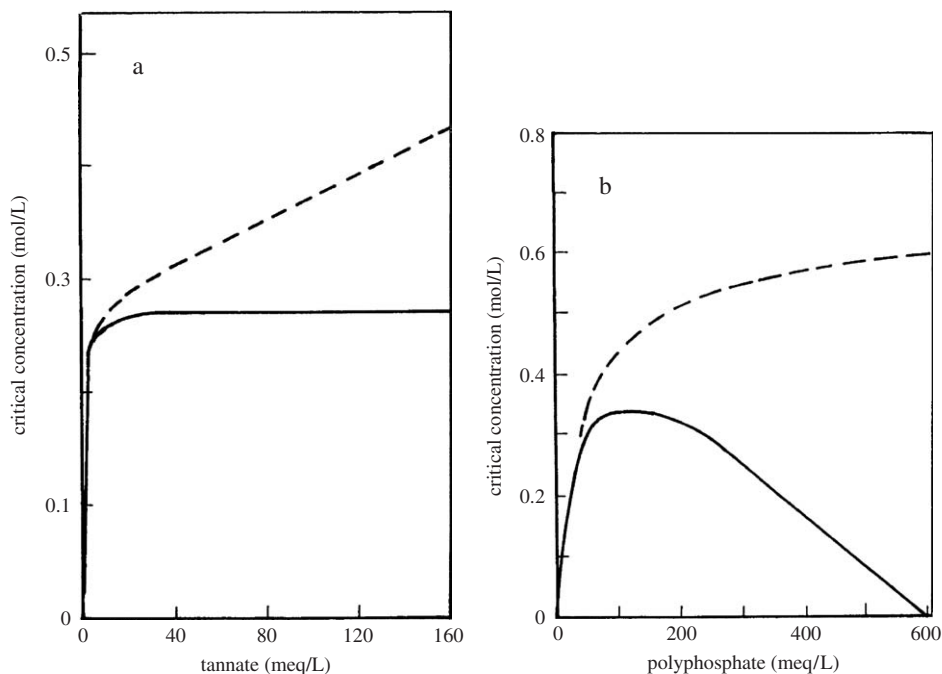


Fig. 5.23. Effect of polyanions on the salt stability of  $\text{Na}^+$ -bentonite dispersions. Solid line critical NaCl concentration to attain coagulation broken line total  $\text{Na}^+$  concentration at the point of coagulation. (a) Quebracho tannate (sodium salt), (b) sodium polyphosphate. From Lagaly (1993).

polyanion (Fig. 5.23b). However, the total concentration of  $\text{Na}^+$  ions increased only slightly at higher amounts of polyphosphate ( $\geq 200$  meq/L) and is, again, typical of face/face aggregation. Polyacrylates are important dispersants for kaolinites in the paper industry. They stabilise dispersions by increasing the absolute value of the (negative) surface potential (Li et al., 2001) and steric stabilisation.

Using dynamic light-scattering, Kretzschmar et al. (1998) showed that under acidic conditions humic acid markedly increased the stability of kaolinite dispersions, primarily by reversing the charge of the edge surface. However, at high-electrolyte concentrations, steric stabilisation by adsorbed humic substances became effective.

## 5.6. AGGREGATION OF CLAY MINERAL PARTICLES AND GELATION

### 5.6.1. Modes of Aggregation

The most well-known mode of aggregation is the house-of-cards model where the clay mineral particles are held together by edge/face contacts (Fig. 5.24a) (Hofmann, 1961, 1962, 1964). This type of network only forms when the edges are positively charged, or in a slightly alkaline medium above the critical salt concentration. Formation of edge/face contacts below  $\text{pH} \approx 6$  is due to heterocoagulation between the positive edges and the negative faces of the particles or silicate layers.<sup>8</sup> House-of-cards aggregation is characterised by non-Newtonian flow<sup>9</sup> of the dispersions, and the development of yield stresses in acidic medium (Figs. 5.25 and 5.26). Note the yield value at  $\text{pH} 4.5$  increased with temperature.

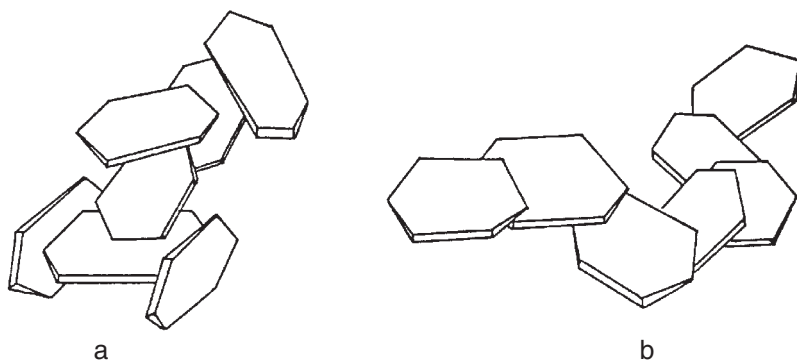


Fig. 5.24. Aggregation of clay mineral layers in (a) card-house and (b) band-type networks by edge/face and face/face contacts.

<sup>8</sup>Card-house type edge(+)/face(−) aggregation was also observed for gibbsite particles,  $\gamma\text{-AlO}(\text{OH})$ , with isoelectric points at  $\text{pH} \sim 7$  (edges) and  $\text{pH} \sim 10$  (faces) Wierenga et al. (1998).

<sup>9</sup>For a review on the flow behaviour of colloidal dispersions see Güven (1992b).

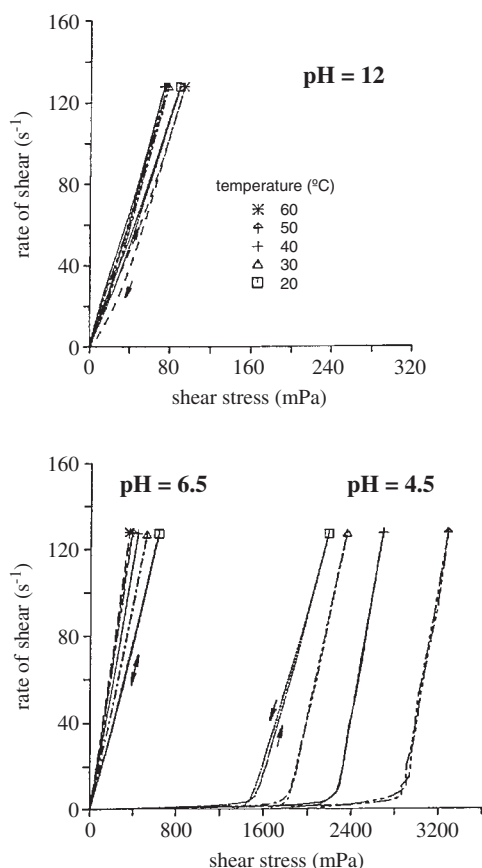


Fig. 5.25. Flow curves (shear rate vs. shear stress) for Na<sup>+</sup>-montmorillonite dispersions (Wyoming, 4% by weight) at various pH and different temperatures (pH adjusted by addition of HCl or NaOH).

With increasing pH the network composed of edge/face contacts breaks down and the shear stress  $\tau$  (at a given rate of shear,  $\dot{\gamma}$ ) of the Na<sup>+</sup>-montmorillonite dispersion decreases to a sharp minimum (Fig. 5.26). The increase in shear stress at pH > 5 results from the higher degree of delamination and therefore from the higher number of particles in the dispersion. Raising the pH above 7 by increased addition of NaOH reduces the degree of delamination and the electroviscous effect (see below). As a result, the shear stress again decreases (Permien and Lagaly, 1995).

Weiss and Frank (1961) and Weiss (1962) were the first to stress the importance of face/face contacts and the possible formation of three-dimensional band-type networks ('Bänderstrukturen') (Fig. 5.24b). The band-type network of Ca<sup>2+</sup>-kaolinite

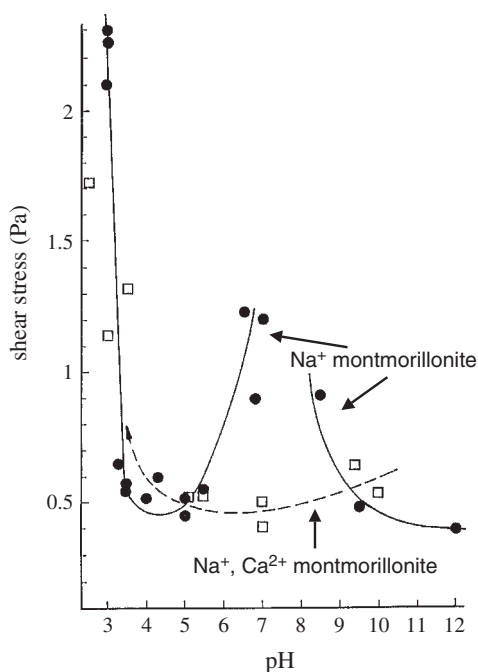


Fig. 5.26. Dependence of the shear stress (at a rate of shear of  $94.5 \text{ s}^{-1}$ ) on the pH value for the dispersion of  $\text{Na}^+$ -montmorillonite ( $\bullet$  —) and of the parent ( $\text{Na}^+$ ,  $\text{Ca}^{2+}$ )-bentonite ( $\square$  - - -) (from Wyoming). The pH values were determined with indicator sticks just before the rheological measurements. From [Permien and Lagaly \(1995\)](#).

showed some elasticity in contrast to the more rigid card-house structure. Face/face aggregation and formation of band-type structures were clearly observed by TEM ([Vali and Bachmann, 1988](#); [Benna et al., 2001a, 2001b](#)).

The effect of salt addition on the aggregation of clay mineral particles in dilute ( $<2\%$  w/w) dispersions, and the resulting rheological properties are schematically shown in [Fig. 5.27](#). Both the yield value and the viscosity are low when salt is absent. They decrease even further after the addition of modest amounts of salt ( $10^{-3}$ – $10^{-2}$  mol/L NaCl) ([Permien and Lagaly, 1995](#)), then increase steeply. High salt concentrations can reduce viscosity and yield value again.

The minimum at low salt concentration is a consequence of the secondary electroviscous effect. In the absence of salt or at very low salt concentrations, single silicate layers, or packets of them, are surrounded by diffuse layers of cations, repelling each other by electrostatic forces ([van Olphen, 1977](#); [Güven and Pollastro, 1992](#); [Jasmund and Lagaly, 1993](#); [Lagaly et al., 1997](#); [Quirk and Marčelja, 1997](#)). When the particle concentration is sufficiently high ( $\geq 1\%$  w/w for many  $\text{Na}^+$ -montmorillonite dispersions), the diffuse ionic layers around the silicate layers, or

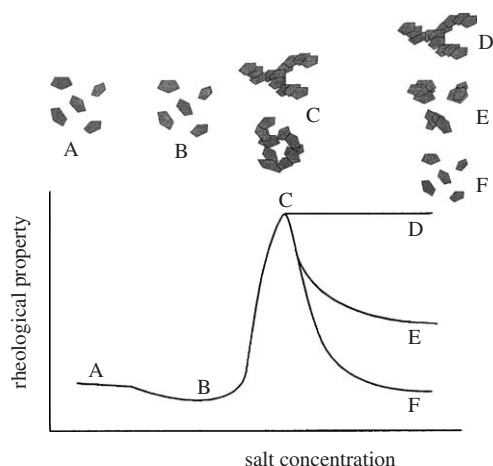


Fig. 5.27. Influence of 1:1 electrolytes on the flow behaviour of diluted clay dispersions. (A, B) isolated particles (B) minimum of rheological properties (viscosity, yield value) due to the electroviscous effect (C, D) aggregation in the form of networks (E, F) fragmentation of the networks at high salt concentrations.

particles restrict the translational and rotational motion of these units. As a result, the viscosity increases and a small yield value is observed (Norris, 1954; Callaghan and Ottewill, 1974; Rand et al., 1980; Permien and Lagaly, 1994a). Addition of salt reduces the thickness of the diffuse ionic layer, increases the translational and rotational freedom of the particles, and reduces viscosity and yield value (Fig. 5.28). The thin shape together with the high aspect (diameter/thickness) ratio of these units are critical factors determining the appearance of the electroviscous effect (Adachi et al., 1998) which induces a certain parallel orientation of the platelets (Fukushima, 1984; Ramsay et al., 1990; Mourchid et al., 1995; Mongondry et al., 2005; Tateyama et al., 1997; Abend and Lagaly, 2000). As the repulsive force strongly decreases when the particle orientation deviates from the exact parallel position (Anandarajah, 1997), the particles arrange in a certain zig-zag structure as indicated in Fig. 5.28.

The sharp increase in rheological parameters at moderately high salt concentrations corresponds to the coagulation of the particles forming a volume-spanning network. This network may resist further salt addition but in most cases the influence of the van der Waals attraction at high salt concentrations contracts the bands into smaller aggregates (Fig. 5.27, E), or even to particle-like assemblages, disrupting the network structure (Fig. 5.27, F).

Addition of calcium ions has a pronounced effect on the type of aggregation. Small additions can strongly increase the yield value of  $\text{Na}^+$ -montmorillonite dispersions but high amounts of  $\text{Ca}^{2+}$  ions reduce this value considerably (Permien and

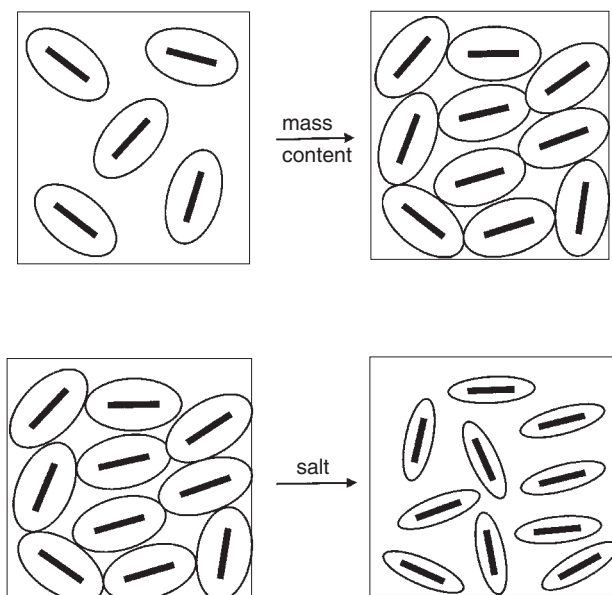


Fig. 5.28. The electroviscous effect: (above) Sufficiently high particle concentration reduces the mobility of the particles. (below) When the thickness of the diffuse ionic layers decreases at higher salt concentration, the particles again become more mobile. From [Permien and Lagaly \(1994a\)](#).

[Lagaly, 1994b](#)). The maximum of the shear stress at pH  $\sim 7$  disappears in the presence of even small amounts of calcium ions (see also [Permien and Lagaly, 1995](#); [Benna et al., 1999](#)). As discussed in Sections 5.2.1 and 5.4.10, calcium ions held together the silicate layers at a maximum distance of 1 nm (basal spacing 2 nm). Even small amounts of calcium ions nucleate face/face contacts and build up band-type networks. The flow behaviour of  $\text{Ca}^{2+}/\text{Na}^{+}$ -bentonite dispersions is therefore complex, and is sensitive to the ratio of  $\text{Ca}^{2+}/\text{Na}^{+}$  in the dispersion ([Tombácz et al., 1989](#)). Small amounts of calcium ions added to a  $\text{Na}^{+}$ -montmorillonite dispersion promote face/face contacts and stabilise band-type networks (Fig. 5.29b). At large amounts of calcium ions, the bands contract to form small aggregates, and eventually particle-like assemblages, and the network falls apart (Fig. 5.29c). Homoionic  $\text{Ca}^{2+}$ -smectites thus show only a modest tendency for forming band-type networks.

It may be assumed that calcium ions held between the negative charges at the edges and faces of two approaching particles act in a similar way as in the interlayer space and limit the particle distance to 2 nm. Stable edge  $(-)/\text{Ca}^{2+}/\text{face}(-)$  contacts would then be created that would build up a stable card-house network. However, this behaviour seems very unlikely. Calcium ions lying at the edges of particles with



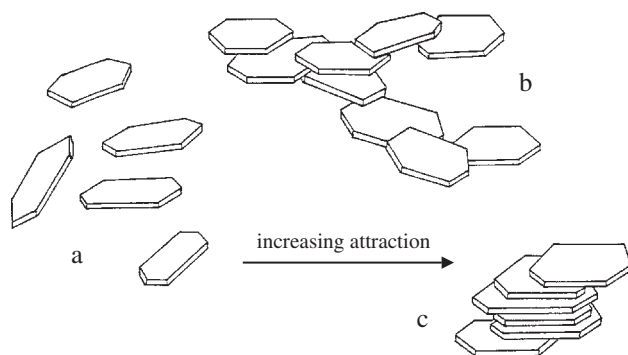


Fig. 5.29. Aggregation of the clay mineral layers with increasing attraction: (a) single layers, (b) band-type aggregates, (c) compact particles. From [Permien and Lagaly \(1994a\)](#).

very irregular contour lines are in a quite different force field than between the planar silicate layers in the interlayer space. The modest importance of the edge(-)/ $\text{Ca}^{2+}$ /face(-) contacts is expressed by the low shear stresses of the  $\text{Ca}^{2+}$ -montmorillonite dispersions in alkaline medium.

### 5.6.2. Plasticity

Plasticity is a very important property of ceramic masses (but also of metals, alloys, polymers, and plastics). “It may be defined as the property of a material which permits it to be deformed under stress without rupturing and to retain the shape produced after the stress is removed. It is the property that permits the material to be shaped by the application of a force. Clay materials in general develop plasticity when they are mixed with relatively small amounts of water” (cited from [Grim, 1962](#)). The plasticity of ceramic masses strongly depends on water content. The Atterberg method ([Atterberg, 1911, 1912](#); [Grim, 1962](#)) determines the water content needed to develop optimum plasticity (see also [Lagaly, 1989](#)). Usually, there is a defined amount of water at which the clay is easily mouldable. With less moisture the mass cracks when moulded. The plastic limit is the lowest water content (expressed in percentage by weight of the clay dried at  $120^\circ\text{C}$ ) at which the mass can be rolled into threads without breaking. The Atterberg liquid limit is the water content at which the mass begins to flow. The difference between both values is called the ‘plasticity index’. [Table 5.11](#) shows these values for kaolinite, illite and montmorillonite. Different methods of shear-strain measurements of clay bodies as a function of the water content are also used to find optimum plasticity.

The plastic deformation of a given clay mass not only depends on the water content but also on the time needed for the clay to adjust so that shaping proceeds without rupturing. The rate of application of the stress is therefore important in the shaping process.

Table 5.11. Atterberg limits (percentage per mass of dried (120 °C) clays). Data from Müller-Vonmoos, see Lagaly (1989)

Clay	Cation	Liquid limit	Plastic limit	Plasticity index
Kaolin, KGa-2,	Na <sup>+</sup>	69	31	38
Warren County,	Ca <sup>2+</sup>	74	31	43
Georgia, USA	Na <sup>+</sup> *	33	24	9
Illite, Bassin du	Na <sup>+</sup>	76	29	47
Velay, Massif	Ca <sup>2+</sup>	93	32	61
Central, France	Na <sup>+</sup> *	54	29	25
Montmorillonite,	Na <sup>+</sup>	431	48	383
SAz-1, Arizona, USA	Ca <sup>2+</sup>	190	50	140

\*In the presence of 0.5 g Na<sub>4</sub>P<sub>2</sub>O<sub>7</sub> · 10 H<sub>2</sub>O/100 g clay.

Hofmann (1961, 1962) explained the cause of plasticity in terms of the card-house model (Fig. 5.30a).<sup>10</sup> When mechanical force is applied to the clay body, the T-type contacts between two particles may be broken but the particles can easily shift into neighbouring contact positions so cohesion between the particles is never lost as long as the water content is not too large. In the case of band-type structures, the particles may not only change positions, the network can also be deformed by rotation of the particles (Fig. 5.30b).

Bentonites are used very extensively in binding foundry-moulding sands (Grim, 1962; Odom, 1984), because the thin flexible layers of montmorillonite wrap up/envelop the quartz particles, and the band-type arrangement of the silicate layers provides the necessary plasticity to the sand (Fig. 5.31) (Hofmann, 1961, 1962).

### 5.6.3. Sedimentation and Filtration

In many practical applications, the process of sedimentation, the type of sediments, and conditions of destabilisation are important.

Two types of sedimentation may be distinguished (Fig. 5.32). If the solid content of the dispersion is low and the forces between the particles are not attractive, the particles settle independently from each other and accumulate at the bottom of the vessel forming a sediment the height of which increases with time (free or granular sedimentation). Usually, a sharp interface between the accumulated sediment and the dispersion is observed. The settling behaviour is described by Stokes' law (see

<sup>10</sup>The term "house-of-cards" was first used by Le Chatelier to explain the plasticity of clay masses. His idea was that the platy clay mineral particles adhere together as playing cards do when they are thrown on a table (Salmang, 1927). This picture describes band-type aggregates whereas Hofmann used this term for the 3-dimensional edge-face aggregation.

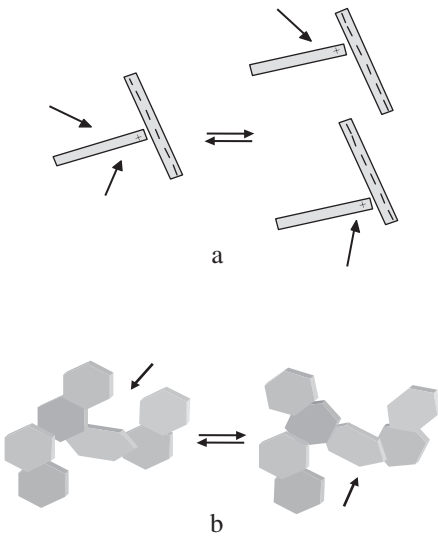


Fig. 5.30. Plasticity of ceramic masses is caused by particle movement from one contact into a neighbouring position (a) or by particle rotation (b).

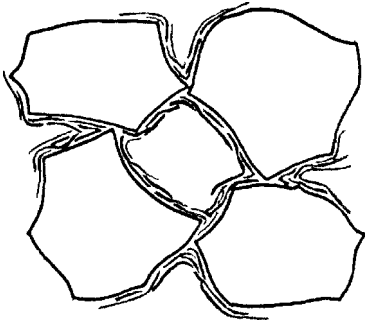


Fig. 5.31. Montmorillonite particles between quartz particles in foundry moulding sands Hofmann (1961). From Jasmund and Lagaly (1993).

Section 5.3.1). Free sedimentation is a pre-requisite for the size-fractionation of clays.

When attractive forces are operative, the particles no longer settle independently. At the upper end of the column the dispersion separates into a thin clear supernatant liquid and a sediment of apparently uniform visual characteristics. With time this interface slowly moves down. Structural sedimentation can also be observed when repulsive interparticle forces operating at high particle concentrations cause a certain ordering of the particles. This effect is pronounced for particles of anisotropic shape, which assume a preferred orientation (see Sections 5.6.1 and 5.6.4). Mixed types of

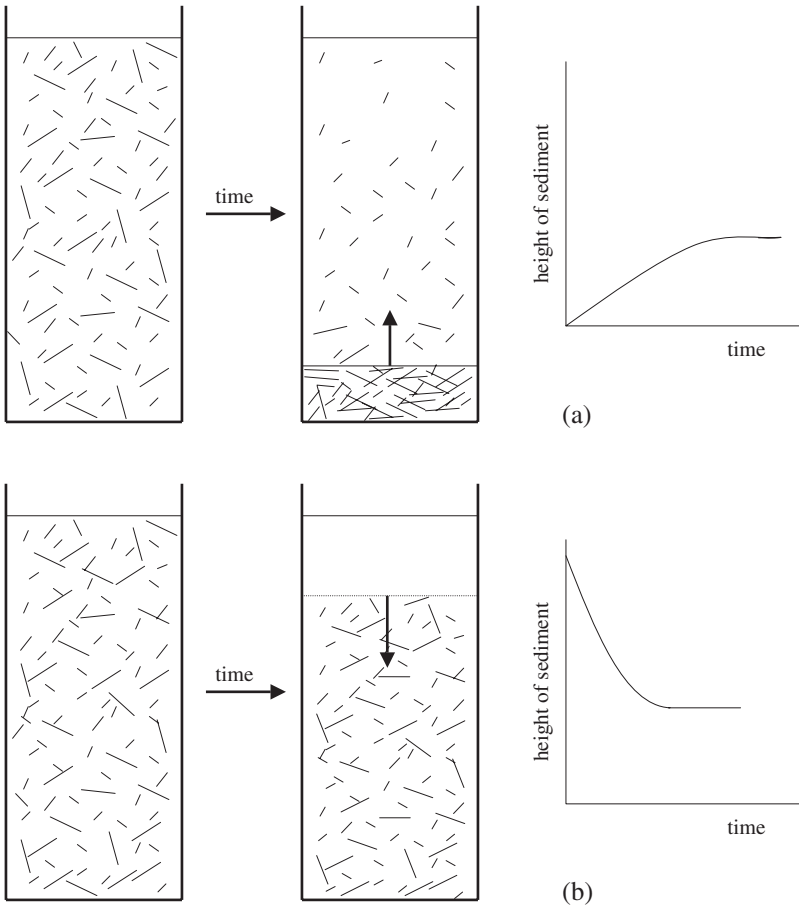


Fig. 5.32. Free (a) and structural (b) sedimentation.

sedimentation were also observed when a sediment grows on the bottom of the vessel and simultaneously a sediment separates at the top of the vessel.

Dispersions of  $\text{Ca}^{2+}$  and  $\text{Mn}^{2+}$  montmorillonite particles in the presence of 7 mmol/L  $\text{CaCl}_2$  and 3 mmol/L  $\text{MnCl}_2$  show a combination of free and structural sedimentation. In the first stage of an induction period, the dispersion occupies the entire volume of the column and only small amounts of particles settle. This is followed by a period of rapid sedimentation and finally by a stage of slow settling (Lapides and Heller-Kallai, 2002). The interaction between the particles causes several interesting phenomena including horizontal lenticular stratification during sedimentation, the dependence on the particle concentration, and the geometrical dimensions (diameter and height) of the columns. It seems that a weak interaction

between the particles stabilises the dispersion against sedimentation during the induction period. When the disturbance of the network of weakly connected particles during the induction period reaches a certain degree, the network falls apart, and the particles settle more rapidly.

Different types of sedimentation were observed with montmorillonite and kaolinite particles (treated with sodium diphosphate) in the presence of  $\text{FeCl}_3$  solutions (newly prepared and aged solutions) and iron (hydr)oxide particles at different pHs (Pierre and Ma, 1997). The kaolinite dispersions showed a structural sedimentation at  $\text{pH} < 4$  due to the formation of edge(+)/face(-) contacts and free sedimentation at higher pHs (Fig. 5.33). At  $\text{FeCl}_3$  contents  $\geq 3 \text{ mmol/L}$  the coagulated particles settled independently. At lower  $\text{FeCl}_3$  concentrations structural sedimentation at  $\text{pH} < 4$  changed into mixed-type sedimentation and free sedimentation with increasing pH. Ageing of the iron chloride solution changed the phase diagram, and the domain of structural sedimentation at  $\text{FeCl}_3$  concentrations  $< 3 \text{ mmol/L}$  was extended to high pH as a consequence of the formation of iron (hydr)oxide particles. A detailed discussion is difficult because even unaged  $\text{FeCl}_3$  solutions form poly(hydroxo iron) species and colloidal iron (hydr)oxide particles such as goethite,  $\alpha\text{-FeO(OH)}$ , or akaganeite,  $\beta\text{-FeO(OH)}$  (Sections 5.4.8 and 5.4.9). The strong interaction between the iron ions and phosphate adsorbed at the edges should also be considered. In the presence of aluminium ions, structural sedimentation was observed at  $\text{pH} < 11$  at all aluminium concentrations. No significant difference was found between aged and unaged aluminium salt solutions (Pierre and Ma, 1999).

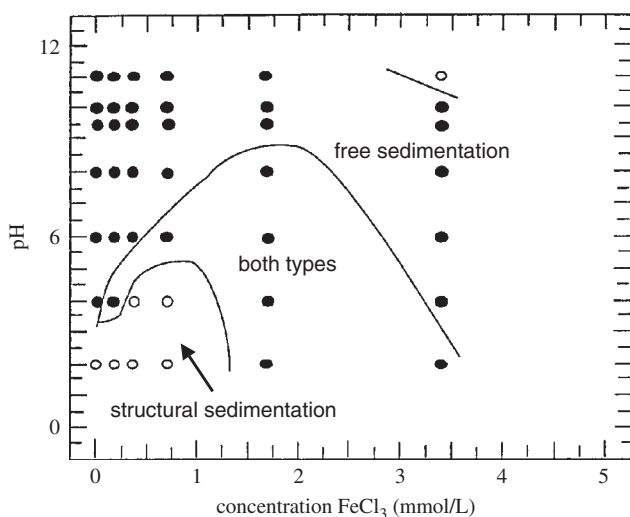


Fig. 5.33. Sedimentation behaviour of 0.5% dispersions of  $\text{Na}^+$ -kaolinite (Hydrite UF, Georgia Kaolin Comp., USA, treated with  $\text{Na}_4\text{P}_2\text{O}_7$ ) in the presence of freshly prepared  $\text{FeCl}_3$  solutions (Pierre and Ma (1997)).

The  $\text{Na}^+$ -montmorillonite particles of a 0.5% dispersion settled independently at  $4 \leq \text{pH} \leq 10$  in the absence of  $\text{FeCl}_3$ . Structural sedimentation was observed at  $\text{pH} < 4$  because of the formation of edge(+)/face(-) contacts between the particles. Addition of  $\text{FeCl}_3$  or  $\text{AlCl}_3$  solutions caused structural sedimentation at all pH values (Pierre and Ma, 1997, 1999).

The structure of the sediments was studied by SEM after supercritical drying with liquid  $\text{CO}_2$  (Pierre, 1996). At low  $\text{FeCl}_3$  concentrations some edge/face associations of kaolinite particles were observed but more typical was the agglomeration of small particles close to the edges of very larger particles. The montmorillonite particles looked like potato chips in a bag: while the accumulated sediments roughly maintained a uniform packing over longer distances, the other sediment types mostly comprised flocs with an increasingly open structure when going away from the centre of a floc. The accumulated sediments made at high  $\text{FeCl}_3$  concentrations showed extensive face/face association so the sedimented particles had a preferred orientation.

The importance of sediment type to practical applications is illustrated in Fig. 5.34, which shows highly dispersed clay mineral layers and two types of aggregates. The sediments or filter cakes formed from these two types of dispersions are substantially different. Highly peptised dispersions of individual platelets (or silicate layers) form virtually impermeable filter cakes and compact, dense sediments that are difficult to stir. Formation of dense filter cakes finds applications in sealing operations, causes the plastering effect of drilling muds, and is of great importance to producing ceramic casts (see Chapter 10.1).

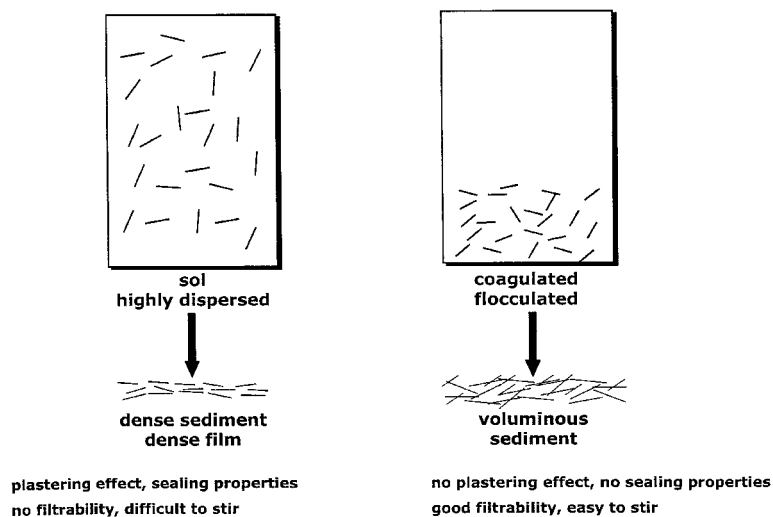


Fig. 5.34. Structure and properties of sediments formed from well dispersed (left) and aggregated (right) particles.

When the particle–particle interaction becomes attractive, the particles aggregate to some extent, and voluminous sediments are formed with large pores between the clay mineral plates. These sediments are easy to re-disperse by stirring and show no plastering effect. The simplest way of inducing the particles to settle, and changing the properties of the sediment, is to adjust the  $\text{Na}^+/\text{Ca}^{2+}$  ratio.

The influence of the different types of aggregation of montmorillonite particles (edge/face, face/face) on the filtration behaviour and the properties of the filter cakes obtained at two pressures ( $1.5$  and  $5.7 \cdot 10^5 \text{ Pa}$ ) and three pH values was evaluated by [Benna et al. \(2001a, 2001b\)](#) (Fig. 5.35). At the lower applied pressure, the filter cake obtained from the acidic dispersion was thinner and less permeable than the filter

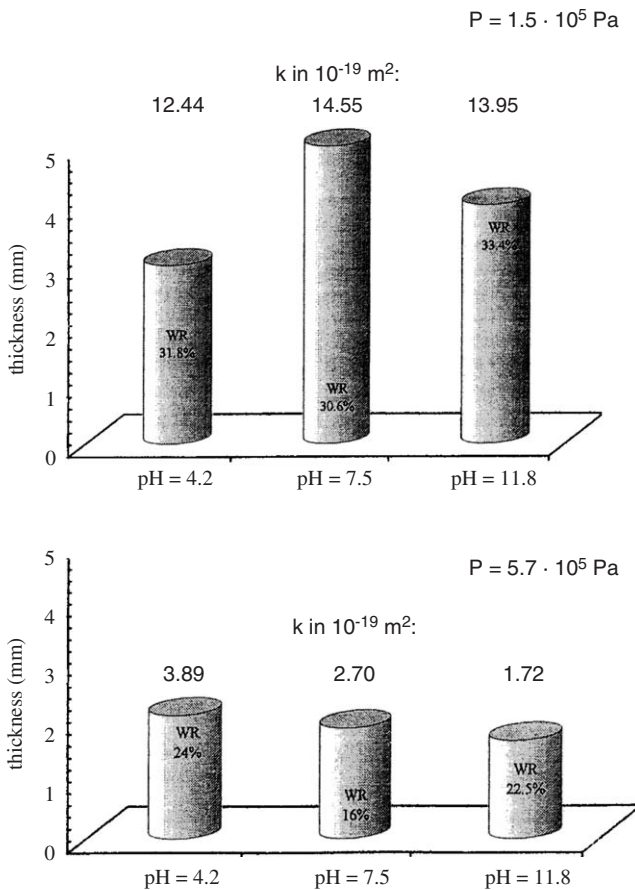


Fig. 5.35. Volume, water retention (WR in percentage of the water content before filtration), and permeability (Darcy's law) of filter cakes obtained from  $\text{Na}^+$ -bentonite (Wyoming) dispersions at three pH and two filtration pressures. From [Benna et al. \(2001b\)](#).

cakes from dispersions at pH 7.5 and 11.8. The largest cake volume and the highest permeability were observed at pH 7.5. In contrast to the edge(+) / face(−) network at acidic pH, the electrostatic repulsion between the faces increased cake volume and permeability. A certain degree of elasticity of the band-type structure in comparison with the card-house structure (Weiss and Frank, 1961; Weiss, 1962) may also contribute to the larger cake volume when band-type networks are formed at  $\text{pH} > 4.2$ . A somewhat stronger aggregation occurs at higher pH and electrolyte concentrations, reducing the volume and permeability. The higher applied pressure may overcome the double layer repulsion, and the cake volume and permeability at  $\text{pH} > 4.2$  became smaller than for the acidic cake. The calculated and observed swelling pressure for plate–plate distances of 10 nm and 5 nm is  $10^5$  Pa and  $5 \times 10^5$  Pa, respectively (Lubetkin et al., 1984; Huerta et al., 1992).

The settling behaviour of dispersed palygorskite is important in practical applications. Whereas the particles settle in dispersions with palygorskite contents  $\leq 0.1\%$ , settling is not observed at higher solid contents. Even if the force between the particles below  $c_K$  is repulsive, the highly anisometric particles form a network structure throughout the mass of the suspension. This is another example of repulsive gels (see Section 5.6.4).

The relation between polymer flocculation, sedimentation and filtration rate, and sediment volume was studied much earlier for kaolinite and neutral polyacrylamide (Dollimore and Horridge, 1973). The maximum sedimentation and filtration rates were always observed at  $\text{pH} \sim 5.8$ , irrespective of polymer concentration. The authors concluded that  $\text{pH} \sim 5.8$  is the point of zero edge charge, and the kaolinite particles form card-house type aggregates. The sediment volume was high at  $\text{pH} < 5.8$ , and increased weakly with pH. At  $\text{pH} > 5.8$  face(−) / face(−) aggregation began to form, and sediment volume decreased steeply with rising pH. Thus, sediment permeability was highest at  $\text{pH} \sim 5.8$ .

As montmorillonite is easily coagulated by salts or flocculated by polymers, this clay mineral can be used as a clarifying agent, especially when added to streams that naturally have a low concentration of dispersed particles.

#### 5.6.4. Sol–Gel Transition

Transition from a sol into a gel and vice versa is very important in many practical applications because this phenomenon strongly influences flow behaviour, sedimentation, agitation, and filtration (Benna et al., 2001a), and lies behind time-dependent rheological behaviour. Gels are usually described as dispersed systems that show a degree of stiffness. That is, the vessel containing the dispersion can be upturned without the dispersion flowing out. Gels also show a degree of elasticity, and creeping measurements may be used to distinguish between sol and gel (Abend and Lagaly, 2000).

The experiment is briefly explained in Fig. 5.36. When a constant shear stress  $\tau_0$  is applied to the dispersion within time  $t_e$ , the strain increases as shown. At  $t = t_e$  the



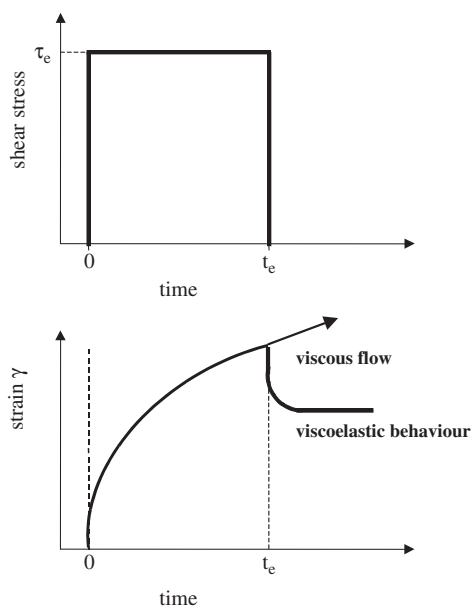


Fig. 5.36. Creeping experiments: The strain (relative deformation)  $\gamma$  is shown as a function of time  $t$ . During the time  $t_e$  the sample is deformed by applying the constant shear stress  $\tau_e$ . At  $t = t_e$   $\tau$  is set to zero and the sample relaxes (viscoelastic behaviour, full line) or flows further (viscous fluid, dotted line).

shear stress is set to zero, the sample relaxes, and in case of a viscoelastic behaviour, the strain decreases to a plateau. If the dispersion is a viscous fluid, the strain increases further. The reversible part of the compliance ( $J = \gamma/\tau_0$ ) is  $J_{\text{rev}} = 100 (J_0 + J_R)/(J_0 + J_R + J_N)$ . The position of the plateau gives the elastic ( $J_0 + J_R$ ) and viscous ( $J_N$ ) contributions to the compliance. A sol shows  $J_{\text{rev}} = 0$ , a gel  $J_{\text{rev}} > 0$ .

Fig. 5.37 shows the reversible compliance of  $\text{Na}^+$ -montmorillonite dispersion as a function of the NaCl concentration.  $J_{\text{rev}} > 0$  indicates gel formation at low and high salt concentrations. Due to the electroviscous effect (Fig. 5.28), the dispersion stiffens at low salt concentrations and high montmorillonite contents (above 3–3.5% w/w). This type of gel is called a ‘repulsive gel’ although this is incorrect because it is not the gel but the interparticle force that is repulsive (Norris, 1954; Callaghan and Ottewill, 1974; Rand et al., 1980; Ramsay, 1986; Sohm and Tadros, 1989; Ramsay and Lindner, 1993; Mourchid et al., 1995; Lott et al., 1996; Kroon et al., 1998; Mongondry et al., 2005). Addition of salt reduces the thickness of the diffuse ionic layer, the particles become more mobile again, and the gel turns into a sol. In a similar way, colloidal rod-like boehmite particles ( $\gamma\text{-AlO(OH)}$ ) form repulsive gels at solid contents of 0.67% in solutions containing less than  $10^{-4}$  mol/L NaCl. Despite

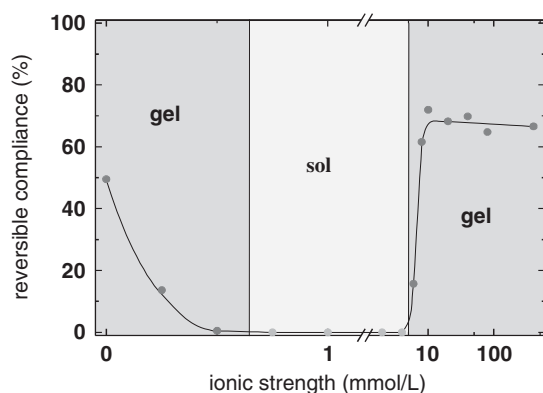


Fig. 5.37. Reversible compliance as a function of the NaCl concentration. 4% (w/w) dispersion of  $\text{Na}^+$ -montmorillonite (M 50, Ordu Turkey). From [Abend and Lagaly \(2000\)](#).

the repulsive forces, the particles are immobilised in a preferred orientation as indicated by birefringence measurements ([Buining et al., 1994](#)).

Temperature-dependent changes of  $\text{Na}^+$ -smectite gels were investigated using synchrotron-based small-angle scattering ([Pons et al., 1981](#)). A gel containing 17% (w/w)  $\text{Na}^+$ -montmorillonite (Wyoming) was studied before and after several cooling–heating cycles between  $-70^\circ\text{C}$  and room temperature. Below  $-10^\circ\text{C}$  the silicate layers were aggregated into 500–600 nm thick particles composed of domains of 4–5 silicate layers with two water layers between them. These domains were separated by zones of one or two silicate layers spaced less regularly by one, three or four layers of water. During heating to room temperature the interlayer spaces took up water molecules to form discrete hydrates with up to four water layers. This process proceeded slowly and could be followed by the changes in scattering patterns. Intercalation of more than four water layers was accompanied by a large expansion of the interlayer space, giving rise to a gel in which assemblages of (on average) 4–5 almost parallel silicate layers were still retained. Isolated and no longer parallel silicate layers filled the space between these units. About 25% of the layers were distributed as single layers. An interesting point is that the domains of 4–5 layers (in distances of about 8 nm) reflected the structure of the particle in the frozen gels. As the changes during cooling–heating cycles were nearly reversible, the deviation of the silicate layers from parallel orientation during heating must be modest, say, by no more than  $15^\circ$ . Several causes of this peculiar behaviour were mentioned ([Pons et al., 1982](#)). The influence of layer charge distribution was noted for beidellite gels where the layers constituting the domains remained at spacings of 1.54 nm and did not move in distances of 7–8 nm, as in montmorillonite, saponite, and hectorite ([Pons et al., 1982](#)). Organisation of the layers at different levels was also observed in TEM and SAXS studies ([Hetzel et al., 1994](#); [Faisander et al., 1998](#)).

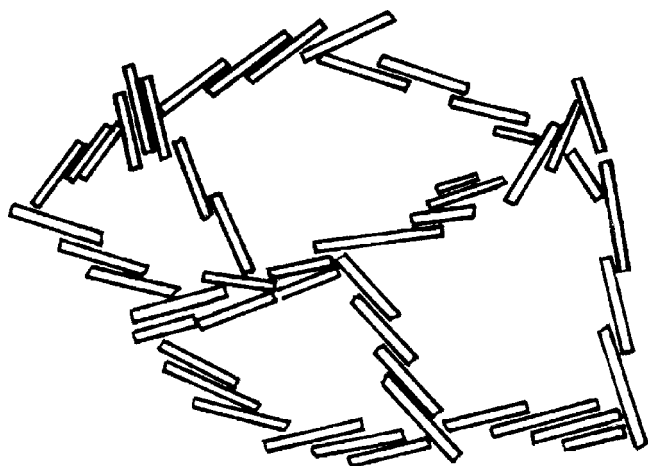


Fig. 5.38. Transition between band-type and card-house aggregation: formation of card-house contacts in band-type assemblages. Adapted from O'Brien (1971). From Lagaly et al. (1997).

Gel formation at salt concentrations above the critical coagulation concentration is caused by attractive forces between the particles when the van der Waals attraction dominates the electrostatic repulsion ('attractive gel'). At lower salt concentration the interaction is attractive between edges(−) and edges(−) and between edges(−) and faces(−); at higher salt concentrations it becomes attractive between the faces. It is likely there is a continuous transition from the edge(−)/face(−) (card-house) to the face(−)/face(−) aggregation (band-type structure) (Fig. 5.38). If the forces between the faces are strongly attractive at high salt concentration, the network contracts and disintegrates (Fig. 5.29b, c). Distinct particles form, the dispersion destabilises forming flocs that settle into a sediment.

The domains of sol, repulsive gel, attractive gel, and flocs are clearly seen in the phase diagrams (Fig. 5.39). The large domain of sol separates the two gel types. As expected, the repulsive gel forms only when the particle concentration is  $> 3\%$  (w/w) and  $3.5\%$  (w/w), respectively. The salt concentration at which the gel liquefies into the sol increases with particle concentration because more densely packed particles require thinner diffuse ionic layers to become mobile again. If there is attraction between the particles, the attractive gel also has smaller solid contents because band-type aggregates can span a distinctly larger volume. Flocs are formed only at the highest salt concentration and moderately high particle concentrations. When  $\text{Na}^+$  ions are replaced by  $\text{K}^+$  and  $\text{Cs}^+$  ions, the attraction between the particles becomes stronger because these cations are more strongly adsorbed in the Stern layer. The band-type aggregates are more stable resisting floc formation. A  $2\%$  (w/w)  $\text{Na}^+$ -montmorillonite dispersion does not coagulate into flocs, even at the highest KCl and

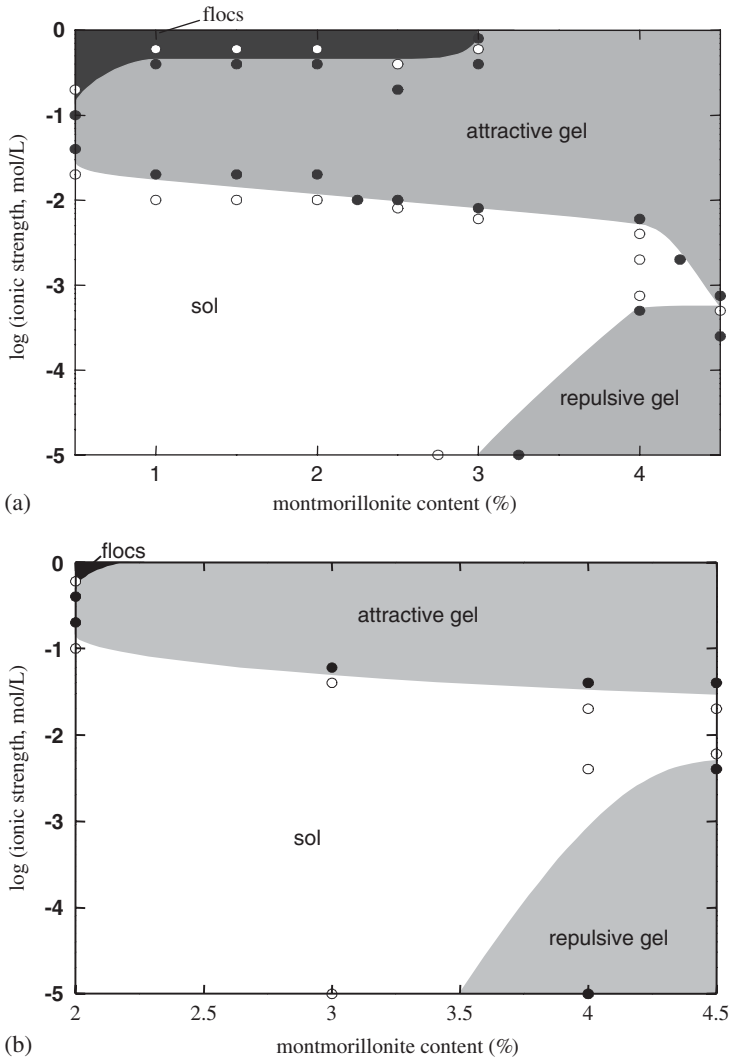


Fig. 5.39. Sol-gel diagram for  $\text{Na}^+$ -montmorillonite and NaCl. (a) Montmorillonite of Ordu, Turkey (M50); (b) montmorillonite of Wyoming (M 40A). From [Abend and Lagaly \(2000\)](#).

CsCl concentration, but remains in the gel state (Fig. 5.40). The liquefying action of phosphate addition ([Penner and Lagaly, 2001](#)) is also seen in the sol-gel diagram.

The difference between Laponite and montmorillonite is also seen in the phase diagram reported by ([Mourchid et al., 1995](#); [Mongondry et al., 2005](#)). In Laponite

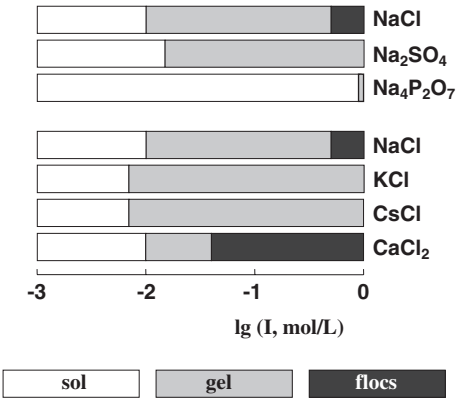


Fig. 5.40. Effect of salts on the transitions sol-gel and gel-flocs. 2% (w/w) Na<sup>+</sup>-montmorillonite (Ordu, Turkey, M 50),  $I$  = ionic strength. From [Abend and Lagaly \(2000\)](#).

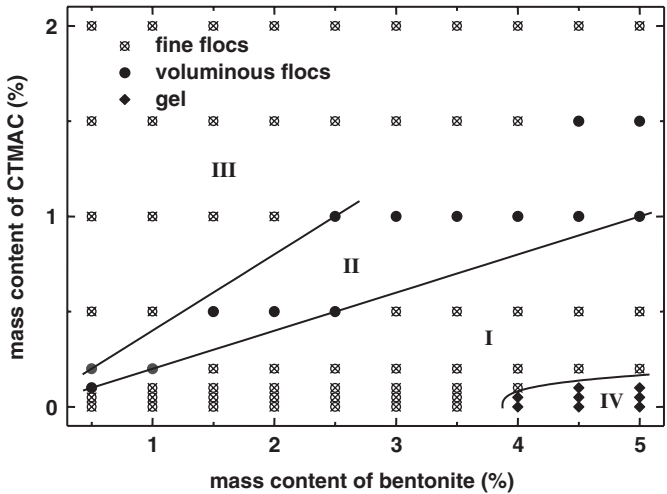


Fig. 5.41. Phase diagram of bentonite dispersions (Wyoming) in the presence of hexadecyl trimethylammonium chloride. From [Janek and Lagaly \(2002\)](#).

the gel domain extends to lower solid contents at higher salt concentrations, distinctly different from the sol-gel diagrams of montmorillonites ([Fig. 5.39](#)).

The addition of cationic surfactants impedes gel formation. Gels only form at low surfactant concentrations and high montmorillonite contents ([Fig. 5.41](#)). Outside the gel domain three types of dispersions were observed ([Tahani et al., 1999](#); [Janek and Lagaly, 2002](#); [Kuwaharada et al., 2002](#)). In domain I the dispersion consisted of fine flocs that separated into a voluminous sediment and a clear supernatant. When the

addition of the surfactant corresponded to the CEC of the bentonite, the particles showed maximum hydrophobicity, forming voluminous flocs that hardly settled (domain II), and the sediment volume reached its maximum value (Kuwaharada et al., 2002). At surfactant additions corresponding to twice the CEC, all particles were re-charged and again formed fine flocs (domain III). However, these fine flocs settled to distinctly thinner sediments than the fine flocs of domain I because the flocs were more densely packed, immobilising smaller volumes of water.

Different types of dispersions showed different flow behaviour: shear thinning flow and Bingham flow in domain I, plastic flow at the I/II transition, and Newtonian flow in domain III (Janek and Lagaly, 2002).

#### 5.6.5. Thixotropy

Attractive gels often show thixotropic behaviour. In this case the gel is liquefied by shaking, stirring, or pouring but stiffens again with time. Stiffening and liquefaction are reversible. When mechanical energy is applied to a network of weakly adhering particles, contacts are broken, and the network disintegrates into fragments. During resting, the fragments driven by Brownian motion of the solvent molecules came into contact, an extended network reforms, and the liquefied dispersion becomes gel-like (Hofmann, 1952). This reversible process requires moderately attractive particle-particle interactions. Thixotropy is a very important property in many practical applications of clay, kaolin, and bentonite dispersions.

Thixotropic behaviour and the resting time required for gelation are highly dependent on the solid content of the dispersion. In simple experiments Hofmann (1952) determined the solid content required to form a gel that liquefied by shaking. The gel point was reached when the tubes could be turned without the dispersion flowing out. In modern viscometers, thixotropy (and antithixotropy) is indicated by the hysteresis between the up and down curves in shear stress-shear rate diagrams (see e.g., Lagaly, 1989). Dispersions of allophane show thixotropic behaviour (Wells and Theng, 1985).

Antithixotropic behaviour is not uncommon for clay dispersions. In this case the dispersions stiffen by (in most cases modest) shaking, inducing the particles to move into contact positions. It is therefore often observed that the up and down curves cross at a certain shear rate (Brandenburg and Lagaly, 1988).

Dispersions of Laponite, a synthetic hectorite-like mineral, often show an unusual thixotropic behaviour, limiting the practical uses of such materials. After cessation of shearing, the viscosity increases over a long period. Willenbacher (1996) observed a monotonic increase of the complex viscosity,  $|\eta|^* = \omega^{-1}(G'^2 + G''^2)^{1/2}$ , of 1–3% (w/w) Laponite RD dispersions. An equilibrium value was not reached even after 16 days. The re-organisation is a co-operative, self-delaying process where the increasing rigidity of the network increasingly retards the mobility and orientation of the particles. This effect is probably related to the reduced anisotropy of the Laponite particles compared with montmorillonite, and hence the particles cannot align over

long distances as in montmorillonite gels. The sol–gel transition involves the formation of oriented micro-domains of particles (Mourchid et al., 1995).

#### 5.6.6. Hydrogels of Organo-Clays

Garret and Walker (1962) described formation of gels of low-charge vermiculites in water after replacing the inorganic exchangeable cations by butylammonium ions. The gels are formed by delamination of the butylammonium vermiculite particles (Rausell-Colom, 1964; Smalley et al., 1989, 2001; Braganza et al., 1990; Hat-harasinghe et al., 2000). This very peculiar behaviour seems to be related to the organisation of the water molecules between the alkyl chains (Lagaly, 1987b). The swelling of butylammonium vermiculites cannot be described by the DLVO theory because hydrophobic interactions have also to be considered. Smalley and co-workers (Smalley et al., 1989; Smalley, 1994a, 1994b) proposed a model for the swelling and gel formation of butylammonium vermiculite based on the Coulombic attraction theory (Sogami theory), postulating the existence of long-range attraction between the vermiculite layers.

Rausell-Colom and Salvador (1971a, 1971b) described gel formation of vermiculites in solutions of amino acids such as  $\gamma$ -aminobutyric acid,  $\omega$ -aminocaproic acid, and ornithine. Repulsion between the carboxylate groups, accumulated in the interlayer space, promotes particle delamination. The gels are composed of independently diffracting large particles of silicate layers (19 layers spaced around  $d = 13.5$  nm; Santa Ollala vermiculite in the presence of  $2 \times 10^{-2}$  mol/L ornithine, confined by a pressure of  $99.4$  g/cm<sup>2</sup>). These particles have an average thickness of 260 nm and are completely separated from each other by the solution phase. Within the particles, ordered coherent domains (with about 6 silicate layers at equal distances of 13.1 nm) are separated by layers also in parallel orientation but less regularly spaced (Rausell-Colom et al., 1989).

Stable colloidal dispersions of fully delaminated montmorillonites were obtained by exchanging the inorganic interlayer cations by betaines  $(\text{CH}_3)_3 \text{N}^+ - (\text{CH}_2)_n - \text{CO}_2^-$   $\text{Li}^+$  ( $\text{Na}^+$ ). These dispersions were more stable against salts than  $\text{Li}^+$  and  $\text{Na}^+$  montmorillonites (Section 5.4.5).

#### 5.6.7. Gelation in Organic Solvents

Thickening of organic solvents by hydrophobised bentonites (in a few cases also by hydrophobised clays and kaolins) is needed in many practical applications (Jones, 1983; Jasmund and Lagaly, 1993). Gelation of these dispersions often requires small amounts of polar additives (water, ethanol) to increase gel strength (Granquist and McAtee, 1963; Jasmund and Lagaly, 1993; Gherardi et al., 1996; Moraru, 2001).

The influence of small amounts of alkanols on gel formation of an industrial organo-bentonite in butyl acetate is shown in Fig. 5.42. A content of 11% (w/w) bentonite was required to form a gel. Addition of methanol reduced the solid content

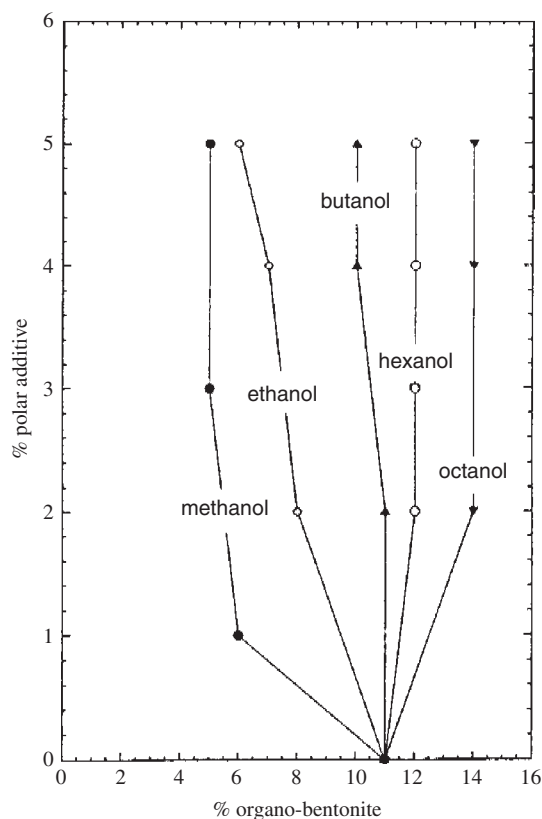


Fig. 5.42. Sol-gel diagram of an industrial organo-bentonite in butyl acetate in the presence of alcohols as polar additives. From Gherardi et al. (1996).

to about 5%. As the chain length of the alcohol increases, the phase boundary moved to higher solid contents, even above 11%. Hexanol and octanol no longer acted as stiffening agents but produced a liquefying effect (Gherardi et al., 1996).

The influence of polar additives was explained by the strong orientation of the adsorbed water molecules, giving rise to giant dipole moments on, and hydrogen bonding between, the particles (Moraru, 2001). Beyond a certain chain length alcohols evidently interfere with the formation of the network of hydrogen bonds between adjacent dispersed particles.

In referring to practical applications, the following effect is noted. Organophilic bentonites are usually prepared at an industrial scale by reacting the bentonite with quaternary alkylammonium ions without removing the excess cationic surfactants. The presence of excess alkylammonium ions can strongly influence the flow behaviour of dispersions in organic solvents (Fig. 5.43). A 1% dispersion of a technical



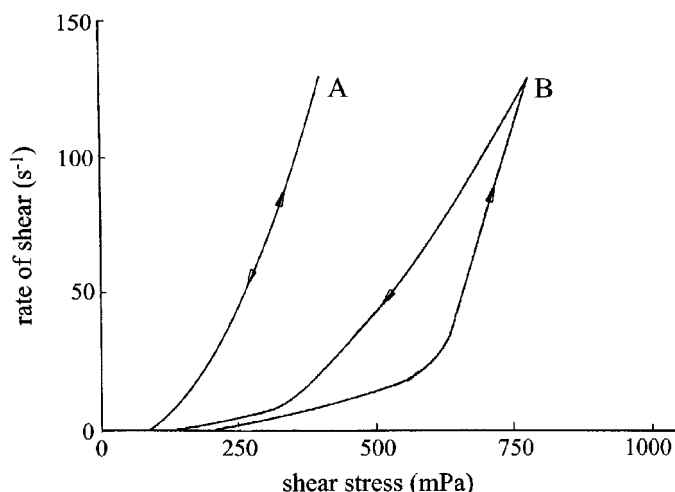


Fig. 5.43. Flow behaviour (rate of shear against shear stress) of 1% (w/w) dispersions of dioctadecyl dimethylammonium bentonite in xylene containing 0.2% ethanol and 0.02% water. (A) Organo bentonite as obtained with an excess of the alkylammonium salt (1.22 mmol N/g bentonite); (B) after washing out the excess of the alkylammonium salt (1.02 mmol N/g bentonite).

dioctadecyl dimethylammonium bentonite in xylene (activated with 0.2% ethanol and 0.02% water) showed low shear stress values. The excess surfactant cations i.e. the amount not bound by cation exchange but adsorbed together with the exchangeable cations, enhanced electrostatic repulsion by acting as a lubricant between the particles. When these cations were removed by washing, the dispersion stiffened and showed pronounced thixotropy. This example shows that even small changes in surfactant/bentonite ratio can markedly change flow properties and thixotropic (or antithixotropic) behaviour.

## 5.7. LAYER-BY-LAYER AGGREGATION: CLAY HYBRID FILMS

The formation and properties of hybrid films of clay minerals bridge clay colloid science and materials science. If appropriate conditions are selected, clay mineral platelets settle to form a sediment where the platelets preferentially adopt a parallel orientation (see Section 5.6.3). Drying produces oriented films that are often used in spectroscopic investigations and X-ray diffraction and are considered for possible new applications of clay minerals (Fitch et al., 1998; Fendler, 2001). Such films can also be prepared using the established methods of spin coating.

Possible applications require functionalisation of the films by introducing active compounds with the desired properties (optical, photochemical, electrochemical,

redox, acid/base properties). The diversity of designs is largely extended by building up hybrid films. Such films are constructed by the layer-by-layer techniques producing layers of clay mineral platelets that alternate with layers of organic materials, mainly long-chain compounds and polymers. Two methods were used.

Decher and co-workers (Decher and Schmitt, 1992; Lvov et al., 1993) studied the layer-by-layer superposition of polyanions and polycations on a substrate. These hybrid films are sometimes called “fuzzy assemblies” because of the lack of order in the film. Replacing the layers of the polyanions by layers of clay mineral platelets leads to clay-polymer hybrid films (Lvov et al., 1996; Kotov et al., 1997). The properties of these films, in particular their non-linear optical properties, are influenced by the textural organisation. AFM shows that these films never have a smooth surface (van Duffel et al., 1999, 2001; Schoonheydt, 2002).

The second method is based on the Langmuir–Blodgett technique. Kuhn and co-workers (Kuhn and Möbius, 1971; Kuhn, 1981; see also Möbius, 1978) studied the energy transfer between donor and acceptor molecules across layers of highly ordered alkyl chains. Langmuir–Blodgett films containing clay mineral particles can be prepared in two ways. The clay mineral is dispersed in the water subphase in the Langmuir trough and the water surface is covered with a chloroform solution of surfactant cations. The clay mineral platelets adsorb the cations and arrange in a floating film at the chloroform/water interface from where they can be picked up on to glass plates using the Langmuir–Blodgett technique (Umemura et al., 2001, 2002; Schoonheydt, 2002) (see Chapter 3). In a variant method, hydrophobised clay mineral platelets are dispersed in chloroform, spread over the water surface in the trough, and picked up on to hydrophobised glass plates (Kotov et al., 1994; Hotta et al., 1997).

Because of their optical and photochemical functionality the clay hybrid films so produced constitute interesting new materials for non-linear optics and sensors (Eckle and Decher, G., 2001; Fendler, 2001; van Duffel et al., 2001; Schoonheydt, 2002; Umemura et al., 2002) (see Chapter 3).

## 5.8. NANOPARTICLE GROWTH IN CLAYS<sup>11</sup>

Clay mineral particles provide confined volumes for the formation of colloidal particles, in particular of nano-size dimensions. The preparation of nanoparticles received a great deal of attention in the past few years because of their potential applications as nanostructured catalysts. As the growing nanoparticles have to be stabilised against aggregation, it is important to choose a suitable stabilising agent and process. The most commonly used stabilising agents are surfactants and polymers (Mayer and Antonietti, 1998). Colloid particles of controlled size were

---

<sup>11</sup>In co-operation with I. Dékány.

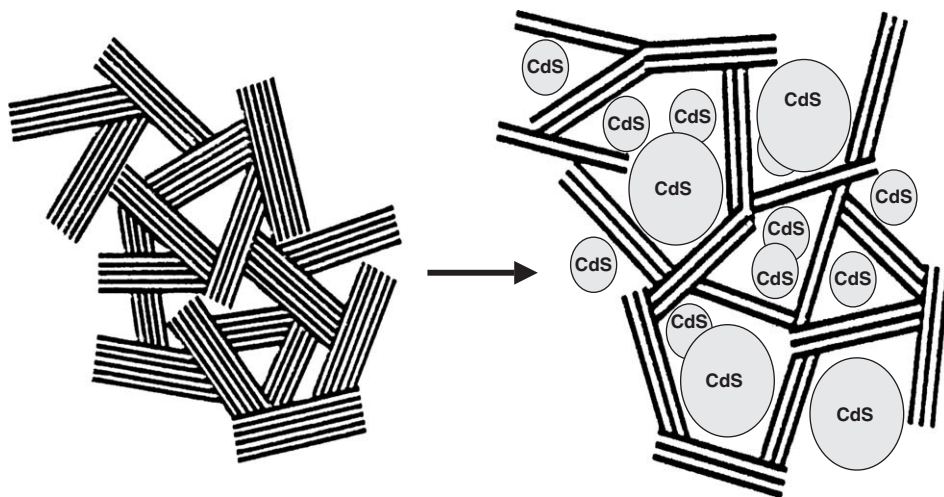


Fig. 5.44. Schematic illustration of nanophase reactors formed by aggregating clay mineral particles. CdS particles were nucleated in the methanol/cyclohexane adsorption layer around hexadecylpyridinium montmorillonite layers and particles [Dékány et al. \(1995\)](#).

generated within the internal space of micelles and microemulsions ([Chen et al., 1999](#); [Chiang, 2001](#); [Ingelsten et al., 2001](#)).

Another concept of recent development is to use the confined space between particles or layers of clay minerals as a nanoreactor, i.e. nanoparticle growth is limited by the clay mineral particles or layers surrounding the nanoparticles ([Fig. 5.44](#)).

Formation of colloidal metal particles was observed decades ago during the oxidation of octahedral  $\text{Fe}^{2+}$  ions in micas by interlayer silver cations. The silver atoms aggregated to  $\text{Ag}^0$  particles outside the interlayer spaces ([Sayin et al., 1979](#)). [Giannelis et al. \(1988\)](#) described the diffusion of ruthenium atoms and clusters out of the interlayer space and aggregation between the clay mineral layers. [Dékány and co-workers \(Dékány, 1996; Király et al., 1996a; Szűcs et al., 1998; Dékány et al., 1999\)](#) reported the formation and properties of noble metal nanoparticles in great detail. Under appropriate experimental conditions metal particles are also observed between the silicate layers. The corresponding salts are usually dissolved in the confined volume of the interlayer space of intercalated clay minerals or between aggregated layers, and the absorbed metal ions are then reduced. In a typical experiment, montmorillonite modified by cationic surfactants (alkylammonium and alkylpyridinium ions) was first swollen in toluene. Palladium acetate (highly soluble in the aromatic solvent) was then adsorbed in the interlayer space of the organophilic montmorillonite and reduced to  $\text{Pd}^0$  particles by ethanol at room temperature.

Nanosized palladium and silver particles were also prepared between kaolinite layers ([Figs. 5.45 and 5.46](#)). The large specific surface area necessary for the growth

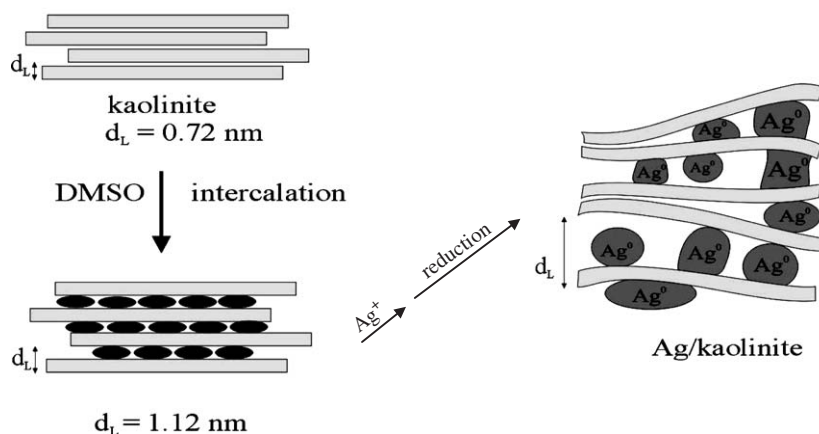


Fig. 5.45. Formation of silver nanoparticles between kaolinite particles.

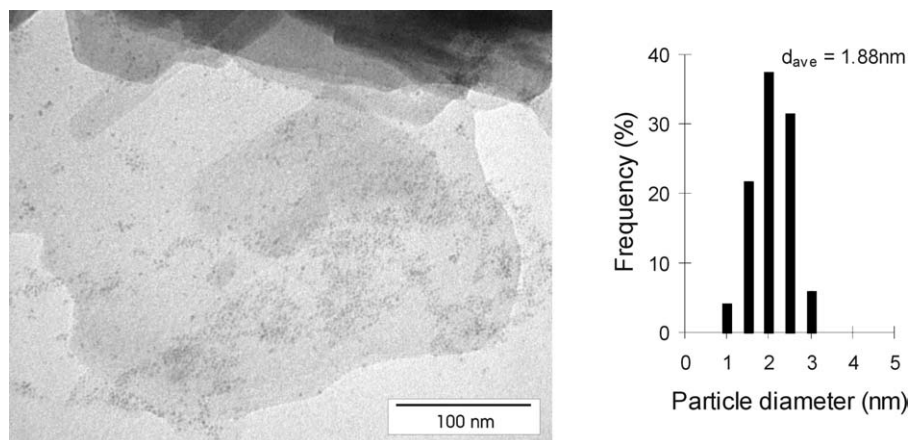


Fig. 5.46. Transmission electron micrograph of silver nanoparticles in kaolinite.

of the nanoparticles was created by intercalation of hydrazine, DMSO, and potassium acetate.

Several semiconductor and transition metal sulphides and oxides such as CdS, ZnS, FeS,  $\text{Fe}_2\text{O}_3$ , and  $\text{TiO}_2$  were prepared by precipitation (e.g.,  $\text{Cd}^{2+}$  and  $\text{Zn}^{2+}$  cations with  $\text{H}_2\text{S}$ ), or hydrolysis in the limited volume between the layers of hydrophobised or pillared montmorillonite and layered double hydroxides (Fig. 5.44). These sulphide(oxide)/clay mineral nanocomposites provide new types of catalysts (Dékány, 1996; Dékány et al., 1995, 1996, 1999). Iron oxide nanoparticles on the

montmorillonite surface probably act as the nuclei for the formation of carbon nanotubes by decomposition of acetylene (Gournis et al., 2002).

In another procedure, the surface of the support is not hydrophobised by long alkyl chains before nanoparticle preparation, in contrast to the procedures described before. This simplifies the interpretation of catalytic processes because they are not influenced by the presence of alkyl chains. The preparation consists of two steps. First, the precursor ions are adsorbed on the surface of a dispersed clay mineral, e.g., on montmorillonite and saponite dispersed in toluene. Adsorption conditions have to be selected to ensure complete adsorption of the added precursor ions by the clay mineral. In the second step, the precursor ions in the adsorption layer are reduced. This is achieved by adding a reducing agent such as ethanol that is preferentially adsorbed by the clay mineral surface, as shown by test experiments. The important requirement is that no particles are formed in the bulk phase (dispersion medium). The size of such particles would significantly exceed the size of nanostructured materials (1–50 nm). Clay minerals are especially suitable because the adsorption of the precursor as well as the subsequent nanoparticle formation and growth proceed within the interlayer space (as nanophase reactor).

Polymers such as poly(vinyl pyrrolidone) and poly(diallyl dimethylammonium chloride) in combination with clay minerals were also used in the synthesis of nanoparticles (Papp and Dékány, 2003). For instance, Pd<sup>0</sup> particles were prepared in the presence of these polymers and well crystallised kaolinite intercalated with DMSO. The interlayer formation of nanoparticles is indicated by X-ray measurements. The presence of nanoparticles is also verified by TEM.

## REFERENCES

- Abend, S., Lagaly, G., 2000. Sol–gel transitions of sodium montmorillonite dispersions. *Applied Clay Science* 16, 201–227.
- Adachi, Y., Nakaishi, K., Tamaki, M., 1998. Viscosity of a dilute suspension of sodium montmorillonite in an electrostatically stable condition. *Journal of Colloid and Interface Science* 198, 100–105.
- Akari, S., Schrepp, W., Horn, D., 1996. Imaging of single polyethyleneimine polymers adsorbed on negatively charged latex spheres by chemical force microscopy. *Langmuir* 12, 857–860.
- Alinec, B., Bednar, F., van de Ven, T.G.M., 2001. Deposition of calcium carbonate particles on fiber surfaces induced by cationic polyelectrolyte and bentonite. *Colloids and Surfaces A* 190, 71–80.
- Allen, T., 1997. Particle Size Measurement, vols. 1 and 2. Chapman & Hall, London.
- Alperovitch, N., Shainberg, I., Keren, R., Singer, M.J., 1985. Effect of clay mineralogy and aluminum and iron oxides on the hydraulic conductivity of clay–sand mixtures. *Clays and Clay Minerals* 33, 443–450.
- Anandarajah, A., 1997. Influence of particle orientation on one-dimensional compression of montmorillonite. *Journal of Colloid and Interface Science* 194, 44–52.

- Andreasen, A.H.M., 1931. Einige Beiträge zur Erörterung der Feinheitsanalyse und ihrer Resultate. *Archiv für Pflanzenbau*. p. 245, see also *Angewandte Chemie*, 1935, p. 283.
- Andreasen, A.H.M., 1935. Beispiele der Verwendung der Pipettenmethode bei der Feinheitsanalyse unter besonderer Berücksichtigung von Mineralfarben. *Angewandte Chemie* 48, 283–285.
- Arias, M., Barral, M.T., Diaz-Fierros, F., 1995. Effects of iron and aluminium oxides on the colloidal and surface properties of kaolin. *Clays and Clay Minerals* 43, 406–416.
- Atterberg, A., 1911. Die Plastizität der Tone. *Internationale Mitteilungen der Bodenkunde* I, 4–37.
- Atterberg, A., 1912. Die Konsistenz und Bindigkeit der Boden. *Interne Mitteilungen der Bodenkunde*. II.
- Avena, M.J., de Pauli, C.P., 1998. Proton adsorption and electrokinetics of an Argentinian montmorillonite. *Journal of Colloid and Interface Science* 202, 195–204.
- Avery, R.G., Ramsay, J.D.F., 1986. Colloidal properties of synthetic hectorite clay dispersions. III. Light and small angle neutron scattering. *Journal of Colloid and Interface Science* 109, 448–454.
- Bain, D.C., Smith, B.F.L., 1987. Chemical analysis. In: Wilson, M.J. (Ed.), *A Handbook of Determinative Methods in Clay Mineralogy*. Blackie, Glasgow, pp. 248–274.
- Barclay, L.M., Ottewill, R.H., 1970. Measurement of forces between colloidal particles. *Special Discussions of the Faraday Society*, 138–147.
- Barshad, I., 1969. Preparation of H saturated montmorillonite. *Soil Science* 108, 38–42.
- Ben Brahim, J., Armağan, N., Besson, G., Tchoubar, C., 1986. Methode diffractometrique de caracterisation des etats d'hydratation des smectites stabilité relative des couches eau insérées. *Clay Minerals* 21, 111–124.
- Benna, M., Kbir-Ariguib, N., Clinard, C., Bergaya, F., 2001a. Static filtration of purified bentonite clay suspensions. Effect of clay content. *Applied Clay Science* 19, 103–120.
- Benna, M., Kbir-Ariguib, N., Clinard, C., Bergaya, F., 2001b. Card-house microstructure of purified sodium montmorillonite gels evidenced by filtration properties at different pH. *Progress in Colloid and Polymer Science* 117, 204–210.
- Benna, M., Kbir-Ariguib, N., Magnin, A., Bergaya, F., 1999. Effect of pH on rheological properties of purified sodium bentonite suspensions. *Journal of Colloid and Interface Science* 218, 442–455.
- Bergman, R., Swenson, J., Börjesson, L., Jacobsson, P., 2000. Dielectric study of supercooled 2D water in a vermiculite clay. *Journal of Chemical Physics* 113, 357–363.
- Bertram, R., Gessner, W., Müller, D., Görz, H., Schönherr, S., 1985. Zur Art der Al-Kationen in hochbasischen, hochkonzentrierten Aluminiumchloridlösungen. *Zeitschrift für Anorganische und Allgemeine Chemie* 525, 14–22.
- Besson, G., Mifsud, C., Tchoubar, D.D., Mering, J., 1974. Order and disorder relations in the distribution of the substitutions in smectites, illites and vermiculites. *Clays and Clay Minerals* 22, 379–384.
- Beyer, J., Graf von Reichenbach, H., 2002. An extended revision of the interlayer structures of one- and two-layer hydrates of Na-vermiculite. *Clay Minerals* 37, 157–168.
- Billingham, J., Breen, C., Rawson, J.O., Yarwood, J., Mann, B.E., 1997. Adsorption of polycations on clays: a comparative in situ study using  $^{133}\text{Cs}$  and  $^{23}\text{Na}$  solution phase NMR. *Journal of Colloid and Interface Science* 193, 183–189.

- Blackmore, A.V., 1973. Aggregation of clay by the products of iron(III) hydrolysis. *Australian Journal of Soil Research* 11, 75–82.
- Böhmer, M.R., Koopal, L.K., 1992. Adsorption of ionic surfactants on variable-charge surfaces. 1. Charge effects and structure of the adsorbed layer. *Langmuir* 8, 2649–2665.
- Bolland, M.D.A., Posner, A.M., Quirk, J.P., 1980. pH-independent and pH-dependent surface charges on kaolinite. *Clays and Clay Minerals* 28, 412–418.
- Borkovec, M., Wu, A., Degavics, G., Laggner, P., Sticher, H., 1993. Surface area and size distributions of soil particles. *Colloids Surfaces A* 73, 65–76.
- Bottero, J.Y., Axelos, M., Tchoubar, D., Cases, J.M., Fripiat, J.J., Fiessinger, F., 1987. Mechanism of formation of aluminum trihydroxide from Keggin  $Al_{13}$  polymers. *Journal of Colloid and Interface Science* 117, 47–57.
- Bottero, J.Y., Bruant, M., Cases, J.M., Canet, D., Fiessinger, F., 1988. Adsorption of non-ionic polyacrylate on sodium montmorillonite. *Journal of Colloid and Interface Science* 124, 515–527.
- Bottero, J.Y., Cases, J.M., Fiessinger, F., Poirier, J.E., 1980. Studies of hydrolyzed aluminum chloride solutions. 1. Nature of aluminum species and composition of aqueous solutions. *Journal of Physical Chemistry* 84, 2933–2939.
- Bottero, J.Y., Tchoubar, D., Arnaud, M., Quienne, P., 1991. Partial hydrolysis of ferric nitrate salt. Structural investigation by dynamic light scattering and small-angle X-ray scattering. *Langmuir* 7, 1365–1369.
- Braganza, L.F., Crawford, R.J., Smalley, M.V., Thomas, R.K., 1990. Swelling of butylammonium vermiculite in water. *Clays and Clay Minerals* 38, 90–96.
- Brandenburg, U., Lagaly, G., 1988. Rheological properties of sodium montmorillonite dispersions. *Applied Clay Science* 3, 263–279.
- Breen, C., 1999. The characterisation and use of poly cation-exchanged bentonites. *Applied Clay Science* 15, 187–219.
- Breen, C., Rawson, J.O., Mann, B.E., 1996. Adsorption of polycations on clays: an in situ study using  $^{133}\text{Cs}$  solution-phase NMR. *Journal of Materials Chemistry* 6, 253–260.
- Brindley, G.W., Brown, G. (Eds.), 1980. *Crystal Structures of Clay Minerals and their X-ray Identification*. Mineralogical Society, London.
- Buining, P.A., Philipse, A.P., Lekkerkerker, H.N.W., 1994. Phase behavior of aqueous dispersions of colloidal boehmite rods. *Langmuir* 10, 2106–2114.
- Cady, S.S., Pinnavaia, T.J., 1978. Porphyrin intercalation in mica-type silicates. *Inorganic Chemistry* 17, 1501–1507.
- Callaghan, I.C., Ottewill, R.H., 1974. Interparticle forces in montmorillonite gels. *Faraday Discussions* 57, 110–118.
- Cebula, J.D., Thomas, R.K., White, J.W., 1980. Small angle neutron scattering from dilute aqueous dispersions of clay. *Journal of the Chemical Society, Faraday I* 76, 314–321.
- Chan, D.Y.C., Pashley, R.M., Quirk, J.P., 1984. Surface potentials derived from co-ion exclusion measurements on homoionic montmorillonite and illite. *Clays and Clay Minerals* 32, 131–138.
- Chang, F.R.C., Skipper, N.T., Sposito, G., 1997. Monte Carlo and molecular dynamics simulations of interfacial structure in lithium-montmorillonite hydrates. *Langmuir* 13, 2074–2082.

- Chang, F.R.C., Skipper, N.T., Sposito, G., 1995. Computer simulation of interlayer molecular structure in sodium montmorillonite hydrates. *Langmuir* 11, 2734–2741.
- Chang, F.R.C., Skipper, N.T., Sposito, G., 1998. Monte Carlo and molecular dynamics simulations of electrical double-layer structures in potassium-montmorillonite hydrates. *Langmuir* 14, 1201–1207.
- Chaplain, V., Janex, M.L., Lafuma, F., Graillat, C., Audebert, R., 1995. Coupling between polymer adsorption and colloidal particle aggregation. *Colloid and Polymer Science* 273, 984–993.
- Chekin, S.S., 1992. Swelling of kaolinite crystals in polar organic liquids. *Clays and Clay Minerals* 40, 740–741.
- Chen, D., Wang, C., Huang, T., 1999. Preparation of palladium ultrafine particles in reverse micelles. *Journal of Colloid and Interface Science* 210, 123–129.
- Chenu, C., Jaunet, A.M., 1990. Modification de l'organisation texturale d'une montmorillonite calcique liées à l'adsorption d'un polysaccharide. *Comptes Rendues de l' Académie Française des Sciences, Paris, Series 2*, 30, 975–980.
- Chiang, C.L., 2001. Controlled growth of gold nanoparticles in AOT/C12E4/isooctane mixed reverse micelles. *Journal of Colloid and Interface Science* 239, 334–341.
- Chou Chang, F.R., Sposito, G., 1994. The electrical double layer of a disk-shaped clay mineral particle: effect of particle size. *Journal of Colloid and Interface Science* 163, 19–27.
- Chou Chang, F.R., Sposito, G., 1996. The electrical double layer of a disk-shaped clay mineral particle: effect of electrolyte properties and surface charge density. *Journal of Colloid and Interface Science* 178, 555–564.
- Costanzo, P.M., Giese, R.F., Clemency, C.V., 1984. Synthesis of a 10-Å hydrated kaolinite. *Clays and Clay Minerals* 32, 29–35.
- de Rooy, J.N., de Bruyn, P.L., Overbeek, J.T.G., 1980. Stability of dispersions in polar organic media. I. Electrostatic stabilization. *Journal of Colloid and Interface Science* 75, 542–554.
- Decher, G., Schmitt, J., 1992. Fine-tuning of the film thickness of ultrathin multilayer films composed of consecutively alternating layers of anionic and cationic polyelectrolytes. *Progress in Colloid and Polymer Science* 89, 160–164.
- Dékány, I., 1996. Preparation of nanoparticles in the interfacial layer of solid supports. In: Fendler, J.H., Dékány, I. (Eds.), *Nanoparticles in Solids and Solutions*. Nato ASI Series, High Technology, vol. 18. Kluwer Academic Publishers, Dordrecht, pp. 293–322.
- Dékány, I., Túri, L., Galbács, Fendler, J.H., 1999. Cadmium ion adsorption controls the growth of CdS nanoparticles on layered montmorillonite and calumite surfaces. *Applied Clay Science* 15, 221–239.
- Dékány, I., Turi, L., Tombácz, E., Fendler, J.H., 1995. Preparation of size-quantised CdS and ZnS particles in nanophase reactors provided by binary liquid adsorption at layered silicates. *Langmuir* 11, 2285–2292.
- Dékány, I., Túri, L., Vankó, Gy., Juhász, G., Vérts, A., Burger, K., 1996. Preparation and characterisation of FeS and Fe<sub>2</sub>O<sub>3</sub> nanoparticles. In: Fendler, J.H., Dékány, I. (Eds.), *Nanoparticles in Solids and Solutions*. Nato ASI Series, High Technology, vol. 18. Kluwer Academic Publishers, Dordrecht, pp. 555–568.
- Delville, A., Laszlo, P., 1989. Simple results on cohesive energies of clays from a Monte Carlo calculation. *New Journal of Chemistry* 13, 481–491.



- Derjaguin, B.V., Churaev, N.V., Müller, V.M., 1987. *Surface Forces*. Consultants Bureau, New York.
- Deshpande, T.L., Greenland, D.J., Quirk, J.P., 1964. Role of iron oxides in the bonding of soil particles. *Nature* 201, 107–108.
- Di Leo, P., Cuadros, J., 2003.  $^{113}\text{Cd}$ ,  $^1\text{H}$  MAS and FTIR analysis of  $\text{Cd}^{2+}$  adsorption on dioctahedral and trioctahedral smectite. *Clays and Clay Minerals* 51, 403–414.
- Dollimore, D., Horridge, T.A., 1973. The dependence of the flocculation behavior of China clay-polyacrylamide suspensions on the suspension pH. *Journal of Colloid and Interface Science* 42, 581–588.
- Dousma, J., de Bruyn, P.L., 1976. Hydrolysis-precipitation studies of iron solutions I. Model for hydrolysis and precipitation from  $\text{Fe(III)}$  nitrate solutions. *Journal of Colloid and Interface Science* 56, 527–539.
- Dudek, T., Środoń, J., Eberl, D.D., Elsass, F., Uhlik, P., 2002. Thickness distribution of illite crystals in shales. I: X-ray diffraction vs. high-resolution transmission electron microscopy measurements. *Clays and Clay Minerals* 50, 562–577.
- Dufrêche, J.F., Marry, V., Bernard, O., Turq, P., 2001. Models for electrokinetic phenomena in montmorillonite. *Colloids and Surfaces A* 195, 171–180.
- Durand-Piana, G., Lafuma, F., Audebert, R., 1987. Flocculation and adsorption properties of cationic polyelectrolytes toward Na-montmorillonite dilute suspensions. *Journal of Colloid and Interface Science* 119, 474–480.
- Eckle, M., Decher, G., 2001. Tuning the performance of layer-by-layer assembled organic light emitting diodes by controlling the position of isolating clay barrier sheets. *Nano Letters* 1, 45–49.
- El Rayah, H.M.E., Rowell, D.L., 1973. The influence of iron and aluminum hydroxides on the swelling of Na-montmorillonite and the permeability of a Na-soil. *Journal of Soil Science* 24, 137–144.
- Faisander, K., Pons, C.H., Tchoubar, D., Thomas, F., 1998. Structural organization of Na- and K-montmorillonite suspensions in response to osmotic and thermal stresses. *Clays and Clay Minerals* 46, 636–648.
- Fendler, J.H., 2001. Chemical self-assembly for electronic applications. *Chemistry of Materials* 13, 3196–3210.
- Ferreiro, E.A., Helmy, A.K., de Bussetti, S.G., 1995. Interaction of Fe-oxyhydroxide colloidal particles with montmorillonite. *Clay Minerals* 30, 195–200.
- Ferris, A.P., Jepson, W.B., 1975. The exchange capacities of kaolinite and the preparation of homoionic clays. *Journal of Colloid and Interface Science* 51, 245–259.
- Fitch, A., Wang, Y., Park, S., Joo, P., 1998. Intelligent design of thin clay films: transport and tailoring. In: Yamagishi, A., Aramata, A., Taniguchi, M. (Eds.), *The Latest Frontiers of Clay Chemistry*. Proceedings of Sapporo Conference on the Chemistry of Clays and Clay Minerals, 1996. The Smectite Forum of Japan, Sendai, pp. 1–15.
- Fitzsimmons, R.D., Posner, A.M., Quirk, J.P., 1970. Electron microscopic and kinetic study of the flocculation of calcium montmorillonite. *Israel Journal of Chemistry* 8, 301–314.
- Frenkel, H., Shainberg, I., 1980. The effect of hydroxy-Al and hydroxy-Fe on montmorillonite particle size. *Soil Science Society of America Journal* 44, 626–629.
- Frens, G., 1978. On coagulation in the primary minimum. *Faraday Discussions of the Chemical Society* 65, 146–155.

- Frens, G., Overbeek, J.T.G., 1972. Repeptization and the theory of electrostatic colloids. *Journal of Colloid and Interface Science* 38, 376–387.
- Frey, E., Lagaly, G., 1979a. Selective coagulation and mixed-layer formation from sodium smectite solutions. In: Mortland, M.M., Farmer, V.C. (Eds.), *International Clay Conference 1978. Developments in Sedimentology* 27. Elsevier, Amsterdam, pp. 131–140.
- Frey, E., Lagaly, G., 1979b. Selective coagulation in mixed colloidal suspensions. *Journal of Colloid and Interface Science* 70, 46–55.
- Fripiat, J.J., Cases, J., Francois, M., Letellier, M., 1982. Thermodynamic and microdynamic behavior of water in clay suspensions and gels. *Journal of Colloid and Interface Science* 89, 378–400.
- Fripiat, J.J., Letellier, M., Levitz, P., 1984. Interactions of water with clay surfaces. *Philosophical Transaction of the Royal Society, London, A* 311, 287–299.
- Fukushima, Y., 1984. X-ray diffraction study of aqueous montmorillonite emulsions. *Clays and Clay Minerals* 32, 320–326.
- Galassi, C., Costa, A.L., Pozzi, P., 2001. Influence of ionic environment and pH on the electrokinetic properties of Ball Clays. *Clays and Clay Minerals* 49, 263–269.
- Ganor, J., Cama, J., Metz, V., 2003. Surface protonation data of kaolinite-reevaluation based on dissolution experiments. *Journal of Colloid and Interface Science* 264, 67–75.
- Garret, W.G., Walker, G.F., 1962. Swelling of some vermiculite-organic complexes in water. *Clays and Clay Minerals* 9, 557–567.
- Garfinkel-Shweky, D., Yariv, S., 1997. The determination of surface basicity of the oxygen planes of expanding clay minerals by acridine orange. *Journal of Colloid and Interface Science* 188, 168–175.
- Gherardi, B., Tahani, A., Levitz, P., Bergaya, F., 1996. Sol/gel phase diagrams of industrial organo-bentonites in organic media. *Applied Clay Science* 11, 163–170.
- Giannelis, E.P., Rightor, E.G., Pinnavaia, T.J., 1988. Reaction of metal-cluster carbonyls in pillared clay galleries: surface coordination chemistry and Fischer–Tropsch catalysis. *Journal of the American Chemical Society* 110, 3880–3885.
- Giese, R.F., Fripiat, J.J., 1979. Water molecule positions, orientations, and motions in the dihydrates of Mg and Na vermiculites. *Journal of Colloid and Interface Science* 71, 441–450.
- Gille, W., Koschel, B., Schwieger, W., 2002. The morphology of isomorphous substituted hectorites. *Colloid and Polymer Science* 280, 471–478.
- Glaeser, R., Mantin, I., Mering, J., 1967. Observation sur la beidellite. *Bulletin du Groupe Français des Argiles* 19, 125–130.
- Goldberg, S., 1992. Use of surface complexation models in soil chemical systems. *Advances in Agronomy* 47, 233–329.
- Goldberg, S., Forster, H.S., 1990. Flocculation of reference clays and arid-zone soil clays. *Soil Science Society of America Journal* 54, 714–718.
- Goldberg, S., Glaubig, R.A., 1987. Effect of saturating cation, pH, and aluminum and iron oxide on the flocculation of kaolinite and montmorillonite. *Clays and Clay Minerals* 35, 220–227.
- Gournis, D., Karakassides, M.A., Baka, T., Boukos, N., Petridis, D., 2002. Catalytic synthesis of carbon nanotubes on clay minerals. *Carbon* 40, 2641–2646.
- Grandjean, I., Laszlo, P., 1989. Deuterium nuclear magnetic resonance studies of water molecules restrained by their proximity to a clay surface. *Clays and Clay Minerals* 37, 403–408.

- Granquist, W.T., McAtee, J., 1963. The gelation of hydrocarbons by montmorillonite organic complexes. *Journal of Colloid Science* 18, 409–420.
- Greathouse, J.A., Refson, K., Sposito, G., 2000. Molecular dynamics simulation of water mobility in magnesium-smectite hydrates. *Journal of the American Chemical Society* 122, 11459–11464.
- Greathouse, J.A., Storm, E.W., 2002. Calcium hydration on montmorillonite clay surfaces studied by Monte Carlo simulations. *Molecular Simulation* 28, 633–647.
- Greenland, D.J., 1975. Charge characteristics of some kaolinite-iron hydroxide complexes. *Clay Minerals* 10, 407–416.
- Gregory, J., 1973. Rates of flocculation of latex particles by cationic polymers. *Journal of Colloid and Interface Science* 42, 448–456.
- Gregory, J., 1975. Interaction of unequal double layers at constant charge. *Journal of Colloid and Interface Science* 51, 44–51.
- Grim, R.E., 1962. *Applied Clay Mineralogy*. McGraw-Hill, New York.
- Grim, R.E., 1968. *Clay Mineralogy*, 2nd edition. McGraw-Hill, New York.
- Grim, R.E., Güven, N., 1978. *Bentonites, Geology, Mineralogy and Uses*. Elsevier, New York.
- Güven, N., 1992a. Molecular aspects of clay-water interactions. In: Güven, N., Pollastro, R.M. (Eds.), *Clay–Water Interface and its Rheological Implications. CMS Workshop Lectures*, vol. 4. The Clay Minerals Society, Boulder, CO, pp. 2–79.
- Güven, N., 1992b. Rheological aspects of aqueous smectite suspensions. In: Güven, N., Pollastro, R.M. (Eds.), *Clay–Water Interface and its Rheological Implications. CMS Workshop Lectures*, vol. 4. The Clay Minerals Society, Boulder, CO, pp. 82–125.
- Güven, N., Pollastro, R.M. (Eds.), 1992. *Clay–Water Interface and its Rheological Implications. CMS Workshop Lectures*, vol. 4. The Clay Minerals Society, Boulder, CO.
- Hagen, K.S., 1992. Modellverbindungen für die Eisen-Sauerstoff-Aggregation und die Bio-mineralisation. *Angewandte Chemie* 104, 1036.
- Hatharasinghe, H.L.M., Smalley, M.V., Swenson, J., Hannon, A.C., King, S.M., 2000. Freezing experiments on clay gels. *Langmuir* 16, 5562–5567.
- Healy, T.W., Wiese, G.R., Yates, D.E., Kavanagh, B.V., 1973. Heterocoagulation in mixed oxide colloidal dispersions. *Journal Colloid Interface Science* 42, 647–649.
- Heller, H., Keren, R., 2001. Rheology of Na-rich montmorillonite suspension as affected by electrolyte concentration and shear rate. *Clays and Clay Minerals* 49, 286–291.
- Heller, H., Keren, R., 2002. Anionic polyacrylamide polymers effect on rheological behavior of sodium montmorillonite suspensions. *Soil Science Society of America Journal* 66, 19–25.
- Heller, H., Keren, R., 2003. Anionic polyacrylamide polymer adsorption by pyrophyllite and montmorillonite. *Clays and Clay Minerals* 51, 334–339.
- Helmy, A.K., Ferreiro, E.A., 1974. Flocculation of  $\text{NH}_4$ -montmorillonite by electrolytes. *Electroanalytical Chemistry and Interface Electrochemistry* 57, 103–112.
- Herrington, T.M., Clarke, A.Q., Watts, J.C., 1992. The surface charge of kaolin. *Colloids and Surfaces* 68, 161–169.
- Hesterberg, D., Page, A.L., 1990a. Flocculation series test yielding time-invariant critical coagulation concentrations of sodium illite. *Soil Science Society of America Journal* 54, 729–735.
- Hesterberg, D., Page, A.L., 1990b. Critical coagulation concentrations of sodium and potassium illite as affected by pH. *Soil Science Society of America Journal* 54, 735–739.

- Hetzel, F., Doner, H.E., 1993. Some colloidal properties of beidellite: comparison with low and high charge montmorillonites. *Clays and Clay Minerals* 41, 453–460.
- Hetzel, F., Tessier, D., Jaunet, A.M., Doner, H., 1994. The microstructure of three  $\text{Na}^+$  smectites: the importance of particle geometry on dehydration and rehydration. *Clays and Clay Minerals* 42, 242–248.
- Hinds, I.C., Ridler, P.J., Jennings, B.R., 1996. Electric birefringence for monitoring size changes in clay suspensions. *Clay Minerals* 31, 549–556.
- Hirsch, D., Nir, S., Banin, A., 1989. Prediction of cadmium complexation in solution and adsorption to montmorillonite. *Soil Science Society of America Journal* 53, 716–721.
- Hofmann, U., 1952. Neue Erkenntnisse auf dem Gebiete der Thixotropie, insbesondere bei tonhaltigen Gelen. *Kolloid-Zeitschrift* 125, 86–99.
- Hofmann, U., 1961. Geheimnisse des Tons. *Berichte der Deutschen Keramischen Gesellschaft* 38, 201–207.
- Hofmann, U., 1962. Die Tonminerale und die Plastizität des Tons. *Keramische Zeitschrift* 14, 14–19.
- Hofmann, U., 1964. Oberflächenladung und Rheologie der Tonminerale. *Berichte der Deutschen Keramischen Gesellschaft* 41, 680–686.
- Hollander, A.F., Somasundaran, P., Gryte, C.C., 1981. Adsorption of polyacrylamide and sulfonated polyacrylamide on Na-kaolinite. In: Tewari, P.H. (Ed.), *Adsorption from Aqueous Solution*. Plenum Press, New York, pp. 143–162.
- Horn, D., 2001/2002. Vorstoß in die Nanowelt der Grenzflächen bei der Papierherstellung und -veredelung. *Wochenblatt für Papierfabrikation* 129/130, 3–15.
- Hotta, Y., Taniguchi, M., Inukai, K., Yamagishi, A., 1997. Clay-modified electrodes prepared by the Langmuir-Blodgett method. *Clay Minerals* 32, 79–88.
- Hougardy, J., Stone, W.E.E., Fripiat, J.J., 1976. NMR study of adsorbed water. I. Molecular orientation and protonic motions in the two-layer hydrate of a Na vermiculite. *The Journal of Physical Chemistry* 64, 3840–3851.
- Hsi, H.R., Clifton, D.F., 1962. Flocculation of selected clays by various electrolytes. *Clays and Clay Minerals* 9, 269–275.
- Huerta, M.M., Curry, J.E., McQuarrie, D.A., 1992. The effect of unequal ionic size on the swelling pressure in clays. *Clays and Clay Minerals* 40, 491–500.
- Hunter, R.J., 1993. *Introduction to Modern Colloid Science*. Oxford University Press, Oxford.
- Hunter, R.J., 1998. Recent developments in the electroacoustic characterisation of colloidal suspensions and emulsions. *Colloids and Surfaces A* 141, 37–65.
- Hunter, R.J., James, M., 1992. Charge reversal of kaolinite by hydrolyzable metal ions: an electroacoustic study. *Clays and Clay Minerals* 40, 644–649.
- Ingelsten, H.H., Bagve, R., Palmqvist, A., Skoglundh, M., Svanberg, C., Holmberg, K., Shah, D.O., 2001. Kinetics of formation of nano-sized platinum particles in water-in-oil micro-emulsions. *Journal of Colloid and Interface Science* 241, 104–111.
- Israelachvili, J.N., 1994. *Intermolecular and Surface Forces*. Academic Press, London.
- Janek, M., Komadel, P., Lagaly, G., 1997. Effect of autotransformation on the layer charge of smectites determined by the alkylammonium method. *Clay Minerals* 32, 623–632.
- Janek, M., Lagaly, G., 2001. Proton saturation and rheological properties of smectite dispersions. *Applied Clay Science* 19, 121–130.

- Janek, M., Lagaly, G., 2002. Interaction of a cationic surfactant with bentonite, a colloid chemistry study. *Colloid and Polymer Science* 281, 293–301.
- Jasmund, K., Lagaly, G. (Eds.), 1993. *Tonminerale und Tone, Struktur, Eigenschaften, Anwendung und Einsatz in Industrie und Umwelt*. Steinkopff Verlag, Darmstadt.
- Jennings, B.R., 1993. Size and thickness measurement of polydisperse clay samples. *Clay Minerals* 28, 485–494.
- Jennings, B.R., Parslow, K., 1988. Particle size measurement: the equivalent spherical diameter. *Proceedings of the Royal Society, London, A* 419, 137–149.
- Jenny, H., Reitemeier, R.F., 1935. Ionic exchange in relation to the stability of colloidal systems. *Journal of Physical Chemistry* 39, 593–604.
- Jepson, W.B., 1984. Kaolins: their properties and uses. *Philosophical Transactions of the Royal Society, London, A* 311, 411–432.
- Johnston, C.T., Sposito, G., Erickson, C., 1992. Vibrational probe studies of water interactions with montmorillonite. *Clays and Clay Minerals* 40, 722–730.
- Jones, T.R., 1983. The properties and uses of clays which swell in organic solvents. *Clay Minerals* 18, 399–410.
- Jozefaciuk, G., 2002. Effect of acid and alkali treatments on surface-charge properties of selected minerals. *Clays and Clay Minerals* 50, 647–656.
- Kahn, A.J., 1958. The flocculation of sodium montmorillonite by electrolytes. *Journal of Colloid Science* 13, 51–60.
- Karube, J., Nakaoshi, K., Sugimoto, H., Fujihira, M., 1992. Electrophoretic behavior of imogolite under alkaline conditions. *Clays and Clay Minerals* 40, 625–628.
- Keller, W.D., 1985. The nascence of clay minerals. *Clays and Clay Minerals* 33, 161–172.
- Keller, W.D., Reynolds, R.C., Inoue, A., 1986. Morphology of clay minerals in the smectite-to-illite conversion series by scanning electron microscopy. *Clays and Clay Minerals* 34, 187–197.
- Keren, R., Shainberg, I., Klein, E., 1988. Settling and flocculation value of sodium–montmorillonite particles in aqueous media. *Soil Science Society of America Journal* 52, 76–80.
- Keren, R., Sparks, D.L., 1995. The role of edge surfaces in flocculation of 2:1 clay minerals. *Soil Science Society of America Journal* 59, 430–435.
- Khoe, G.H., Robins, R.G., 1989. Polymerization reactions in hydrolyzed iron (III) solutions. *Journal of Colloid and Interface Science* 133, 244–252.
- Kim, H.S., Lamarche, C., Verdier, A., 1983. Étude des interactions entre une polyélectrolyte cationique de type ammonium tertiaire et une suspension de bentonite aqueuse. *Colloid and Polymer Science* 261, 64–69.
- Király, Z., Dékány, I., Mastalir, Á., Bartók, M., 1996a. In situ generation of palladium nanoparticles in smectite clays. *Journal of Catalysis* 161, 401–408.
- Király, Z., Turi, L., Dékány, I., Bean, K., Vincent, B., 1996b. Van der Waals attraction between Stöber silica particles in a binary solvent system. *Colloid and Polymer Science* 274, 779–787.
- Kjellander, R., 1996. Ion-ion correlations and effective charges in electrolyte and macroion systems. *Berichte der Bunsengesellschaft für Physikalische Chemie* 100, 894–904.
- Kjellander, R., Marčelja, S., Quirk, J.P., 1988. Attractive double layer interactions between calcium clay particles. *Journal of Colloid and Interface Science* 126, 194–211.
- Kleijn, W.B., Oster, J.D., 1982. A model of clay swelling and tactoid formation. *Clays and Clay Minerals* 30, 383–390.
- Koschel, B., Gille, W., Schwieger, W., Janowski, F., 2000. Analysis of the morphology of hectorite by use of small-angle X-ray scattering. *Colloid and Polymer Science* 278, 805–809.

- Kotov, N.A., Haraszti, T., Turi, L., Zavala, G., Geer, R.E., Dékány, I., Fendler, J.H., 1997. Mechanism of and defect formation in the self-assembly of polymeric polycation-montmorillonite ultrathin films. *Journal of the American Chemical Society* 119, 6821–6832.
- Kotov, N.A., Meldrum, F.C., Fendler, J.H., Tombácz, E., Dékány, I., 1994. Spreading of clay organocomplexes on aqueous solutions: construction of Langmuir-Blodgett clay organo-complex multilayer films. *Langmuir* 10, 3797–3804.
- Kraehenbuehl, F., Stoeckli, H.F., Brunner, F., Kahr, G., Müller-Vonmoos, M., 1987. Study of the water bentonite system by vapour adsorption, immersion calorimetry and X-ray techniques. *Clay Minerals* 22, 1–9.
- Kretschmar, R., Holthoff, H., Sticher, H., 1998. Influence of pH and humic acid on coagulation kinetics of kaolinite. A dynamic light scattering study. *Journal of Colloid and Interface Science* 202, 95–103.
- Kroon, M., Vos, W.L., Wegdam, G.H., 1998. Structure and formation of a gel of colloidal disks. *Physical Review E* 57, 1962–1970.
- Kuhn, H., 1981. Information, electron and energy transfer in surface layers. *Pure and Applied Chemistry* 53, 2105–2122.
- Kuhn, H., Möbius, D., 1971. Systeme aus monomolekularen Schichten – Zusammenbau und physikalisch-chemisches Verhalten. *Angewandte Chemie* 83, 672–690.
- Kuwaharada, S., Tateyama, H., Nishimura, S., Hirose, H., 2002. Smectite quasicrystals in aqueous solutions as a function of cationic surfactant concentration. *Clays and Clay Minerals* 50, 18–24.
- Lagaly, G., 1981. Characterization of clays by organic compounds. *Clay Minerals* 16, 1–21.
- Lagaly, G., 1986. Colloids. *Ullmann's Encyclopedia of Industrial Chemistry*, vol. A7. VCH, Weinheim, pp. 341–367.
- Lagaly, G., 1987a. Surface chemistry and catalysis. In: Pérez-Rodríguez, J.L., Galán, E. (Eds.), *Lectures Conferencias. Euroclay '87*. Sociedad Española de Arcillas, Sevilla, pp. 97–115.
- Lagaly, G., 1987b. Water and solvents on surfaces bristling with alkyl chains. In: Kleeberg, H. (Ed.), *Interaction of Water in Ionic and Nonionic Hydrates*. Springer-Verlag, Berlin, pp. 229–240.
- Lagaly, G., 1989. Principles of flow of kaolin and bentonite dispersions. *Applied Clay Science* 4, 105–123.
- Lagaly, G., 1993. From clay mineral crystals to colloidal clay mineral dispersions. In: Dobias, B. (Ed.), *Coagulation and Flocculation. Theory and Applications*. Marcel Dekker, New York, pp. 427–494.
- Lagaly, G., 1994. Layer charge determination by alkylammonium ions. In: Mermut, A. (Ed.), *Charge Characteristics of 2:1 Clay Minerals. CMS Workshop Lectures*, vol. 6. The Clay Minerals Society, Boulder, CO, pp. 1–46.
- Lagaly, G., 2005. From clay minerals to clay mineral dispersions. In: Stechemesser, H., Dobias, B. (Eds.), *Coagulation and Flocculation*, 2nd edition. Taylor and Francis, Boca Raton, pp. 519–600.
- Lagaly, G., Fahn, R., 1983. Ton und Tonminerale. In: *Ullmann's Encyclopedia of Technical Chemistry*, 4th ed., vol. 23. Verlag Chemie, Weinheim, pp. 311–326.
- Lagaly, G., Malberg, R., 1990. Disaggregation of alkylammonium montmorillonites in organic solvents. *Colloids and Surfaces* 49, 11–27.

- Lagaly, G., Schön, G., Weiss, A., 1972. Über den Einfluß einer unsymmetrischen Ladungsverteilung auf die Wechselwirkung zwischen plättchenförmigen Kolloidteilchen. *Kolloid-Zeitschrift und Zeitschrift für Polymere* 250, 667–674.
- Lagaly, G., Schulz, O., Zimehl, R., 1997. Dispersionen und Emulsionen. Eine Einführung in die Kolloidik feinverteilter Stoffe einschließlich der Tonminerale. Mit einem historischen Beitrag über Kolloidwissenschaftler von Klaus Beneke. Steinkopff Verlag, Darmstadt.
- Lagaly, G., Witter, R., Sander, H., 1983. Water on hydrophobic surfaces. In: Ottewill, R.H., Rochester, C.H., Smith, A.L. (Eds.), *Adsorption from Solution*. Academic Press, London, pp. 65–77.
- Lagaly, G., Ziesmer, S., 2003. Colloid chemistry of clay minerals: the coagulation of montmorillonite dispersions. *Advances in Colloid and Interface Science* 100–102, 105–128.
- Lahav, N., 1990. Preparation of stable suspensions of delaminated kaolinite by combined dimethylsulfoxide–ammonium fluoride treatment. *Clays and Clay Minerals* 38, 219–222.
- Lapides, I., Heller-Kallai, L., 2002. Novel features of smectite settling. *Colloid and Polymer Science* 280, 554–561.
- Larsson, N., Siffert, B., 1983. Formation of lysozyme-containing crystals of montmorillonite. *Journal of Colloid and Interface Science* 93, 424–431.
- Lee, L.T., Rahbari, R., Lecourtier, J., Chauveteau, G., 1991. Adsorption of polyacrylamides on the different faces of kaolinites. *Journal of Colloid and Interface Science* 147, 351–357.
- Li, J., Tanguy, P.A., Carreau, P.J., Moan, M., 2001. Effect of thickener structure on paper-coating color properties. *Colloid and Polymer Science* 279, 865–871.
- Li, H., Wei, S., Qing, C., Yang, J., 2003. Discussion on the position of the shear plane. *Journal of Colloid and Interface science* 258, 40–44.
- Lott, M.P., Williams, D.J.A., Williams, P.R., 1996. The elastic properties of sodium montmorillonite suspensions. *Colloid and Polymer Science* 274, 43–48.
- Low, P.F., 1987. The clay–water interface. In: Schultz, L.G., van Olphen, H., Mumpton, F.A. (Eds.), *Proceedings of the International Clay Conference Denver 1985*. The Clay Minerals Society, Bloomington, IN, pp. 247–256.
- Lubetkin, S.D., Middleton, S.R., Ottewill, R.H., 1984. Some properties of clay water dispersions. *Philosophical Transactions of the Royal Society, London, A* 311, 353–368.
- Lvov, Y., Ariga, K., Ichinose, I., Kunitake, T., 1996. Formation of ultrathin multilayer and hydrated gel from montmorillonite and linear polycations. *Langmuir* 12, 3038–3044.
- Lvov, Y., Haas, H., Decher, G., Möhwald, H., Kalachev, A., 1993. Assembly of polyelectrolyte molecular films onto plasma-treated glass. *Journal of Chemical Physics* 97, 12835–12841.
- Lyklema, J., 1984. Points of zero charge in the presence of specific adsorption. *Journal of Colloid and Interface Science* 99, 109–177.
- Lyklema, J., 1989. Discrimination between physical and chemical adsorption of ions on oxides. *Colloids and Surfaces* 37, 197–204.
- Lyklema, J., 1995. *Fundamentals of Interface and Colloid Science. Volume II: Solid-Liquid Interfaces*. Academic Press, London.
- Mabire, F., Audebert, R., Quivoron, C., 1984. Flocculation properties of water-soluble cationic copolymers towards silica suspension: a semiquantitative interpretation of the role of molecular weight and cationicity through a “patchwork” model. *Journal of Colloid and Interface Science* 97, 120–136.
- Machula, G., Dékány, I., Nagy, L.G., 1993. The properties of the adsorption layer and the stability of aerosil dispersions in binary liquids. *Colloids and Surfaces A* 71, 241–254.

- Mackinnon, I.D.R., Uwins, P.J.R., Yago, A., Page, D., 1993. Kaolinite particle sizes in the  $<2\text{ }\mu\text{m}$  range using laser scattering. *Clays and Clay Minerals* 41, 613–623.
- Madsen, F.T., Müller-Vonmoos, M., 1985. Swelling pressure calculated from mineralogical properties of a Jurassic Opalinum shale, Switzerland. *Clays and Clay Minerals* 33, 501–509.
- Magdassi, S., Rodel, B.Z., 1996. Flocculation of montmorillonite dispersions based on surfactant-polymer interactions. *Colloids and Surfaces A* 119, 51–56.
- Mamy, J., Gaultier, J.P., 1975. Étude de l'évolution de l'ordre cristallin dans la montmorillonite en relation avec la diminution d'échangeabilité de potassium. In: Bailey, S.W. (Ed.), *Proceedings of the International Clay Conference 1975*. Applied Publishing Ltd., Wilmette, IL, pp. 149–155.
- Manfredini, T., Pellacani, G.C., Pozzi, P., Corradi, A.B., 1990. Monomeric and oligomeric phosphates as deflocculants of concentrated aqueous clay suspensions. *Applied Clay Science* 5, 193–201.
- Mangelsdorf, C.S., White, L.R., 1990. Effect of Stern-layer conductance on electrokinetic transport properties of colloidal particles. *Journal of the Chemical Society Faraday Transactions* 86, 2859–2870.
- Manning, B.A., Goldberg, S., 1996. Modeling arsenate competitive adsorption on kaolinite, montmorillonite and illite. *Clays and Clay Minerals* 44, 609–623.
- Marry, V., Turq, P., Cartailier, T., Levesque, D., 2002. Microscopic simulation of structure and dynamics of water and counterions in a monohydrated montmorillonite. *Journal of Chemical Physics* 117, 3454–3463.
- Matijević, E., 1973. Colloid stability and complex chemistry. *Journal of Colloid and Interface Science* 43, 217–245.
- Matijević, E., 1977. The role of chemical complexing in the formation and stability of colloidal dispersions. *Journal of Colloid and Interface Science* 58, 374–389.
- Matijević, E., 1981. Interactions in mixed colloidal systems (heterocoagulation, adhesion, microflotation). *Pure and Applied Chemistry* 53, 2167–2179.
- Mayer, A., Antonietti, M., 1998. Investigation of polymer-protected noble metal nanoparticles by transmission electron microscopy: control of particle morphology and shape. *Colloid and Polymer Science* 276, 769–779.
- McAtee, J.L., Wells, L.M., 1967. Mutual adsorption of clay minerals and colloidal aluminum oxide—an electron microscopy investigation. *Journal of Colloid and Interface Science* 24, 203–210.
- McBride, M.B., 1997. A critic of the diffuse double layer models applied to colloid and surface chemistry. *Clays and Clay Minerals* 45, 598–608.
- McCormack, D., Carnie, S.L., Chan, D.Y.C., 1995. Calculation of electric double-layer force and interaction free energy between dissimilar surfaces. *Journal of Colloid and Interface Science* 169, 177–196.
- Miller, N.P., Berg, J.C., O'Brien, R.W., 1992. The electrophoretic mobility of a porous aggregate. *Journal of Colloid and Interface Science* 153, 237–243.
- Miller, S.E., Low, P.F., 1990. Characterization of the electrical double layer of montmorillonite. *Langmuir* 6, 572–578.
- Möbius, D., 1978. Designed monolayer assemblies. *Berichte der Bunsengesellschaft für Physikalische Chemie* 82, 848–858.
- Mongondry, P., Tassin, J.F., Nicolai, T., 2005. Revised state diagram of Laponite dispersions. *Journal of Colloid and Interface Science* 283, 397–405.



- Moore, D.M., Reynolds, R.C. Jr., 1997. X-ray Diffraction and the Identification and Analysis of Clay Minerals, 2nd edition. Oxford University Press, Oxford.
- Moraru, V.N., 2001. Structure formation of alkylammonium montmorillonites in organic media. *Applied Clay Science* 19, 11–26.
- Mortland, M.M., Raman, K.V., 1968. Surface acidity of smectites in relation to hydration, exchangeable cation, and structure. *Clays and Clay Minerals* 16, 393–398.
- Mourchid, A., Delville, A., Lambard, J., Lécolier, E., Levitz, P., 1995. Phase diagram of colloidal dispersions of anisotropic charged particles: equilibrium properties, structure, and rheology of Laponite suspensions. *Langmuir* 11, 1942–1950.
- Muljadi, D., Posner, A.M., Quirk, J.P., 1966. The mechanism of phosphate adsorption by kaolinite, gibbsite and pseudoboehmite. *Journal of Soil Science* 17, 212–229.
- Mulla, D.J., Low, P.F.J., 1983. The molar absorptivity of interparticle water in clay–water systems. *Journal of Colloid and Interface Science* 95, 51–60.
- Nabzar, L., Pefferkorn, E., 1985. An experimental study of kaolinite crystal edge-polyacrylamide interactions in dilute suspensions. *Journal of Colloid and Interface Science* 108, 243–248.
- Nabzar, L., Pefferkorn, E., Varoqui, R., 1984. Polyacrylamide-sodium kaolinite interactions: flocculation behavior of polymer clay suspensions. *Journal of Colloid and Interface Science* 102, 380–388.
- Nadeau, P., 1985. The physical dimensions of fundamental particles. *Clay Minerals* 20, 499–514.
- Nadeau, P., 1987. Clay particle engineering: a potential new technology with diverse applications. *Applied Clay Science* 2, 83–93.
- Napper, D.H., 1983. *Polymeric Stabilization of Colloidal Dispersions*. Academic Press, London.
- Neaman, A., Singer, A., 1999. Flocculation of homoionic sodium palygorskite, palygorskite-montmorillonite mixtures and palygorskite containing soil clays. *Soil Science* 164, 914–921.
- Neumann, B.S., Sansom, K.G., 1971. The rheological properties of dispersions of Laponite, a synthetic hectorite-like clay, in electrolyte solutions. *Clay Minerals* 9, 231–243.
- Nir, S., Hirsch, D., Navrot, J., Banin, A., 1986. Specific adsorption of lithium, sodium, potassium, and strontium to montmorillonite: observations and predictions. *Soil Science Society of America Journal* 50, 40–45.
- Nir, S., Rytwo, G., Yermiyahu, U., Margulies, L., 1994. A model for cation adsorption to clays and membranes. *Colloid and Polymer Science* 272, 619–632.
- Norris, J., Giese, R.F., Costanzo, P.M., van Oss, C., 1993. The surface energies of cation substituted laponite. *Clay Minerals* 28, 1–11.
- Norrish, K., 1954. The swelling of montmorillonite. *Discussions of the Faraday Society* 18, 120–134.
- Norrish, K., Rausell-Colom, J.A., 1963. Low-angle X-ray diffraction studies of the swelling of montmorillonite and vermiculite. In: Shineford, A., Franks, P.C. (Eds.), *Clays and Clay Minerals, Proceedings of the 10th National Conference*. Austin, Texas. Pergamon Press, New York, pp. 123–149.
- Oades, J.M., 1984. Interactions of polycations of aluminum and iron with clays. *Clays and Clay Minerals* 32, 49–57.
- Oakley, D.M., Jennings, B.R., 1982. Clay particle sizing by electrically induced birefringence. *Clay Minerals* 17, 313–325.

- O'Brien, N.R., 1971. Fabric of kaolinite and illite floccules. *Clays and Clay Minerals* 19, 353–359.
- O'Brien, R.W., Rowlands, W.N., 1993. Measuring the surface conductance of kaolinite particles. *Journal of Colloid and Interface Science* 159, 471–476.
- O'Brien, R.W., White, L.R., 1978. Electrophoretic mobility of a spherical colloidal particle. *Journal of the Chemical Society Faraday Transactions 2* (74), 1607–1626.
- Odom, I.E., 1984. Smectite clay minerals: properties and uses. *Philosophical Transactions of the Royal Society, London, A* 311, 391–409.
- Ohshima, H., 1995. Electrophoretic mobility of soft particles. *Electrophoresis* 16, 1360–1363.
- Oster, J.D., Shainberg, I., Wood, J.D., 1980. Flocculation value and gel structure of sodium/calcium montmorillonite and illite suspensions. *Soil Science Society of America Journal* 44, 955–959.
- Ottewill, R.H., 1977. Stability and instability in disperse systems. *Journal of Colloid and Interface Science* 58, 357–373.
- Ottewill, R.H., Walker, T., 1968. The influence of nonionic surface active agents on the stability of polystyrene latex dispersions. *Kolloid Zeitschrift und Zeitschrift für Polymere* 227, 108–116.
- Overbeek, J.T.G., 1977. Recent developments in the understanding of colloid stability. *Journal of Colloid and Interface Science* 58, 408–422.
- Overbeek, J.T.G., 1980. The rule of Schulze and Hardy. *Pure and Applied Chemistry* 52, 1151–1161.
- Overbeek, J.T.G., 1982. Strong and weak points in the interpretation of colloid stability. *Advances in Colloid and Interface Science* 16, 17–30.
- Papp, S., Dékány, I., 2003. Stabilization of palladium nanoparticles by polymers and layer silicates. *Colloid and Polymer Science* 281, 727–737.
- Parazak, D.P., Burkhardt, C.W., McCarthy, K.J., Stehlin, M.P., 1988. Hydrophobic flocculation. *Journal of Colloid and Interface Science* 123, 59–72.
- Parfitt, R.L., 1978. Anion adsorption by soils and soil materials. *Advances in Agronomy* 30, 1–50.
- Pashley, R.M., 1985. Electromobility of mica particles dispersed in aqueous solutions. *Clays and Clay Minerals* 33, 193–199.
- Pashley, R.M., Quirk, J.P., 1984. The effect of cation valency on DLVO and hydration forces between macroscopic sheets of muscovite mica in relation to clay swelling. *Colloids and Surfaces* 9, 1–17.
- Pefferkorn, E., Nabzar, I., Carroy, A., 1985. Adsorption of polyacrylamide to Na-kaolinite: correlation between clay structure and surface properties. *Journal of Colloid and Interface Science* 106, 94–103.
- Pefferkorn, E., Nabzar, L., Varoqui, R., 1987. Polyacrylamide Na-kaolinite interactions: effect of electrolyte concentration on polymer adsorption. *Colloid and Polymer Science* 265, 889–896.
- Penner, D., Lagaly, G., 2000. Influence of organic and inorganic salts on the aggregation of montmorillonite dispersions. *Clays and Clay Minerals* 48, 246–255.
- Penner, D., Lagaly, G., 2001. Influence of anions on the rheological properties of clay mineral dispersions. *Applied Clay Science* 19, 131–142.
- Pérez-Maqueda, L.A., Caneo, O.B., Poyato, J., Pérez-Rodríguez, J.L., 2001. Preparation and characterization of micron and submicron-sized vermiculite. *Physical Chemistry of Minerals* 28, 61–66.

- Perkins, R., Brace, R., Matijević, E., 1974. Colloidal and surface properties of clay suspensions. I. Laponite CP. *Journal of Colloid and Interface Science* 48, 417–426.
- Permien, T., Lagaly, G., 1994a. The rheological and colloidal properties of bentonite dispersions in the presence of organic compounds. I. Flow behaviour of sodium montmorillonite in water-alcohol. *Clay Minerals* 29, 751–760.
- Permien, T., Lagaly, G., 1994b. The rheological and colloidal properties of bentonite dispersions in the presence of organic compounds. II. Flow behaviour of Wyoming bentonite in water-alcohol. *Clay Minerals* 29, 761–766.
- Permien, T., Lagaly, G., 1994c. The rheological and colloidal properties of bentonite dispersions in the presence of organic compounds. III. The effect of alcohols on the coagulation of sodium montmorillonite. *Colloid and Polymer Science* 272, 1306–1312.
- Permien, T., Lagaly, G., 1995. The rheological and colloidal properties of bentonite dispersions in the presence of organic compounds. V. Bentonite and sodium montmorillonite and surfactants. *Clays and Clay Minerals* 43, 229–236.
- Pierre, A.C., 1992. The gelation of colloidal platelike particles. *Journal of the Canadian Ceramic Society* 61, 135–138.
- Pierre, A.C., 1996. Structure of gels comprised of platelike particles. Case of boehmite, montmorillonite and kaolinite. *Journal de Chimie et Physique* 93, 1065–1079.
- Pierre, A.C., Ma, K., 1997. Sedimentation behaviour of kaolinite and montmorillonite mixed with iron additives, as a function of their zeta potential. *Journal of Materials Science* 32, 2937–2947.
- Pierre, A.C., Ma, K., 1999. DLVO theory and clay aggregate architectures formed with  $\text{AlCl}_3$ . *Journal of the European Ceramic Society* 19, 1615–1622.
- Plançon, A., 2001. Order–disorder in clay mineral structures. *Clay Minerals* 36, 1–14.
- Plaschke, M., Schäfer, T., Bundschuh, T., Ngo Manh, T., Knopp, R., Geckeis, H., Kim, J.I., 2001. Size characterization of bentonite colloids by different methods. *Analytical Chemistry* 73, 4338–4347.
- Poinsignon, C., Cases, J.M., Fripiat, J.J., 1978. Electrical polarization of water molecules adsorbed by smectites. An infrared study. *The Journal of Physical Chemistry* 82, 1855–1860.
- Pons, C.H., Rousseaux, E., Tchoubar, D., 1981. Utilisation du rayonnement synchrotron en diffusion aux petits angles pour l'étude du gonflement des smectites: Étude du système eau–montmorillonite–Na en fonction de la température. *Clay Minerals* 16, 23–42.
- Pons, C.H., Rousseaux, E., Tchoubar, D., 1982. Utilisation du rayonnement synchrotron en diffusion aux petits angles pour l'étude du gonflement des smectites: II. Étude de différents systèmes eau–smectites en fonction de la température. *Clay Minerals* 17, 327–338.
- Pugh, R.J., Kitchener, J.A., 1971. Theory of selective coagulation in mixed colloidal systems. *Journal of Colloid and Interface Science* 35, 656–664.
- Quirk, J.P., Marčelja, S., 1997. Application of double-layer theories to the extensive crystalline swelling of Li-montmorillonite. *Langmuir* 13, 6241–6248.
- Ramsay, J.D.F., 1986. Colloidal properties of synthetic hectorite clay dispersions. *Journal of Colloid and Interface Science* 109, 441–447.
- Ramsay, J.D.F., Lindner, P., 1993. Small-angle neutron scattering investigations of the structure of thixotropic dispersions of smectite clay colloids. *Journal of the Chemical Society Faraday Transactions* 89, 4207–4217.

- Ramsay, J.D.F., Swanton, S.W., Bunce, J., 1990. Swelling and dispersion of smectite clay colloids: determination of structure by neutron diffraction and small-angle neutron scattering. *Journal of the Chemical Society Faraday Transactions* 86, 3919–3926.
- Rand, B., Pekenć, E., Goodwin, J.W., Smith, R.W., 1980. Investigation into the existence of edge-face coagulated structures in Na-montmorillonite suspensions. *Journal of the Chemical Society Faraday I* 76, 225–235.
- Rasmusson, M., Rowlands, W., O'Brien, R.W., Hunter, R.J., 1997. The dynamic mobility and dielectric response of sodium bentonite. *Journal of Colloid and Interface Science* 189, 92–100.
- Rausell-Colom, J.A., 1964. Small-angle X-ray diffraction study of the swelling of butylammonium-vermiculite. *Transactions of the Faraday Society* 60, 190–201.
- Rausell-Colom, J.A., Saez-Auñón, J., Pons, C.H., 1989. Vermiculite gelation: structural and textural properties. *Clay Minerals* 24, 459–478.
- Rausell-Colom, J.A., Salvador, P.S., 1971a. Complexes vermiculite-aminoacides. *Clay Minerals* 9, 139–149.
- Rausell-Colom, J.A., Salvador, P.S., 1971b. Gélification de vermiculite dans des solutions d'acide  $\gamma$ -amino butyrique. *Clay Minerals* 9, 193–208.
- Rowlands, W.N., O'Brien, R.W., 1995. The dynamic mobility and dielectric response of kaolinite particles. *Journal of Colloid and Interface Science* 175, 190–200.
- Rupprecht, H., Gu, T., 1991. The structure of the adsorption layers of ionic surfactants at the solid/liquid interface. *Colloid and Polymer Science* 269, 506–522.
- Rytwo, G., Nir, S., Margulies, L., 1995. Interactions of monovalent organic cations with montmorillonite: adsorption studies and model calculations. *Soil Science Society of America Journal* 59, 554–564.
- Salmang, H., 1927. Die Ursachen der Bildsamkeit der Tone. *Zeitschrift für Anorganische und Allgemeine Chemie* 162, 115–126.
- Sayin, M., Beyme, B., Graf von Reichenbach, H., 1979. Formation of metallic silver as related to iron oxidation in K-depleted micas. In: Mortland, M.M., Farmer, V.C. (Eds.), *International Clay Conference 1978. Developments in Sedimentology* 27. Elsevier, Amsterdam, pp. 177–186.
- Schmidt, C.U., Lagaly, G., 1999. Surface modification of bentonites. I. Betaine montmorillonites and their rheological and colloidal properties. *Clay Minerals* 34, 447–458.
- Schofield, R.K., Samson, H.R., 1954. Flocculation of kaolinite due to the attraction of oppositely charged crystal faces. *Discussions of the Faraday Society* 18, 135–145.
- Schoonheydt, R.A., 2002. Smectite-type clay minerals as nanomaterials. *Clays and Clay Minerals* 50, 411–420.
- Schramm, L.L., Kwak, J.C.T., 1982a. Influence of exchangeable cation composition on the size and shape of montmorillonite particles in dilute suspension. *Clays and Clay Minerals* 30, 40–48.
- Schramm, L.L., Kwak, J.C.T., 1982b. Interactions in clay suspensions: the distribution of ions in suspension and the influence of tactoid formation. *Colloids and Surfaces* 3, 43–60.
- Schramm, L.L., Yariv, S., Ghosh, D.K., Hepler, L.G., 1997. Electrokinetic study of the adsorption of ethyl violet and crystal violet by montmorillonite clay particles. *Canadian Journal of Chemistry* 75, 1868–1877.
- Schroth, B.K., Sposito, G., 1997. Surface charge properties of kaolinite. *Clays and Clay Minerals* 45, 85–91.

- Schwertmann, U., 1969. Aggregation of aged hydrogen clays. In: Heller, L. (Ed.), *Proceedings of the International Clay Conference*, Tokyo, 1969. Israel University Press, Jerusalem, pp. 683–690.
- Secor, R.B., Radke, C.J., 1985. Spillover of the diffuse double layer on montmorillonite particles. *Journal of Colloid and Interface Science* 103, 237–244.
- Séquaris, J.M., Camara Decimavilla, S., Correales Ortega, J.A., 2002. Polyvinylpyrrolidone adsorption and structural studies on homoionic Li-, Na-, K-, and Cs-montmorillonite colloidal solutions. *Journal of Colloid and Interface Science* 252, 93–101.
- Siffert, B., Espinasse, P., 1980. Adsorption of organic diacids and sodium polyacrylate onto montmorillonite. *Clays and Clay Minerals* 28, 381–387.
- Siffert, B., Kim, K.B., 1992. Study of surface ionization of kaolinite in water by zetametry – influence on the rheological properties of kaolinite suspension. *Applied Clay Science* 6, 369–382.
- Skipper, N.T., Sposito, G., Chang, F.R.C., 1995. Monte Carlo simulation of interlayer molecular structure in swelling clay minerals. 2. Monolayer hydrates. *Clays and Clay Minerals* 43, 294–303.
- Slade, P.G., Quirk, J.P., Norrish, K., 1991. Crystalline swelling of smectite samples in concentrated NaCl solutions in relation to layer charge. *Clays and Clay Minerals* 39, 234–238.
- Slepetys, R.A., Cleland, A.J., 1993. Determination of shape of kaolin pigment particles. *Clay Minerals* 28, 495–508.
- Smalley, M.V., 1994a. Electrical theory of clay swelling. *Langmuir* 10, 2884–2891.
- Smalley, M.V., 1994b. One-phase and two-phase regions of colloid stability. *Progress in Colloid and Polymer Science* 97, 59–64.
- Smalley, M.V., Hathrasinghe, H.L.M., Osborne, I., Swenson, J., King, S.M., 2001. Bridging flocculation in vermiculite-PEO mixtures. *Langmuir* 17, 3800–3812.
- Smalley, M.V., Thomas, R.K., Braganza, L.F., Matsuo, T., 1989. Effects of hydrostatic pressure on the swelling of butylammonium vermiculite. *Clays and Clay Minerals* 37, 474–478.
- Sohm, R., Tadros, T.F., 1989. Viscoelastic properties of sodium montmorillonite (gelwhite H) suspensions. *Journal of Colloid and Interface Science* 132, 62–71.
- Sposito, G., 1992. The diffuse-ion swarm near smectitic particles suspended in 1:1 electrolyte solutions: modified Gouy-Chapman theory and quasicrystal formation. In: Güven, N., Pollastro, R.M. (Eds.), *Clay-Water Interface and its Rheological Implications. CMS Workshop Lectures*, vol. 4. The Clay Minerals Society, Boulder, CO, pp. 128–155.
- Sposito, G., Grasso, D., 1999. Electrical double layer structure, forces, and fields at the clay water interface. In: Hsu, J.P. (Ed.), *Interfacial Forces and Fields: Theory and Applications*. Marcel Dekker, New York, pp. 207–249.
- Sridharan, A., Satayamurty, P.V., 1996. Potential-distance relationships of clay–water systems considering the Stern theory. *Clays and Clay Minerals* 44, 479–484.
- Środoń, J., Eberl, D.D., Drits, V.A., 2000. Evolution of fundamental-particle size during illitization of smectite and implications for reaction mechanism. *Clays and Clay Minerals* 48, 446–458.
- Stenius, P., Järnström, L., Rigdahl, M., 1990. Aggregation in concentrated kaolin suspensions stabilized by polyacrylate. *Colloids and Surfaces* 51, 219–238.
- Stul, M.S., van Leemput, L., 1982. Particle-size distribution, cation exchange capacity and charge density of deferrated montmorillonites. *Clay Minerals* 17, 209–215.

- Stumm, W., Huang, C.P., Jenkins, S.R., 1970. Specific chemical interaction affecting the stability of dispersed systems. *Croatica Chemica Acta* 42, 233–244.
- Stutzmann, T., Siffert, B., 1977. Contribution to the adsorption mechanism of acetamide and polyacrylamide onto clays. *Clays and Clay Minerals* 25, 392–406.
- Sun, Y., Lin, H., Low, P.F., 1986. The nonspecific interaction of water with the surfaces of clay minerals. *Journal of Colloid and Interface Science* 112, 556–564.
- Suquet, H., de la Calle, C., Pézérat, H., 1975. Swelling and structural organization of saponite. *Clays and Clay Minerals* 23, 1–9.
- Suquet, H., Pézérat, H., 1987. Parameters influencing layer stacking types in saponite and vermiculite: a review. *Clays and Clay Minerals* 35, 353–362.
- Swartzen-Allen, L.S., Matijević, E., 1976. Colloid and surface properties of clay suspensions. III. Stability of montmorillonite and kaolinite. *Journal of Colloid and Interface Science* 56, 159–167.
- Swenson, J., Bergman, R., Bowron, D.T., Longeville, S., 2002. Water structure and dynamics in a fully hydrated sodium vermiculite clay. *Philosophical Magazine B* 82, 497–506.
- Swenson, J., Bergman, R., Longeville, S., 2001. A neutron spin-echo study of confined water. *Journal of Chemical Physics* 115, 11299–11305.
- Szűcs, A., Király, Z., Berger, F., Dékány, I., 1998. Preparation and hydrogen sorption of Pd nanoparticles on  $\text{Al}_2\text{O}_3$ -pillared clays. *Colloids and Surfaces A* 139, 109–118.
- Tahani, A., Karroua, M., Van Damme, H., Levitz, P., Bergaya, F., 1999. Adsorption of a cationic surface on Na-montmorillonite: inspection of adsorption layer by X-ray and fluorescence spectroscopies. *Journal of Colloid and Interface Science* 216, 242–249.
- Tateyama, H., Hirose, H., Nishimura, S., Tsunematsu, K., Jinnai, K., Imagawa, K., 1988. Theoretical aspects of interaction between colloidal particles with various shapes in liquid. In: Mackenzie, J.D., Ulrich, D.R. (Eds.), *Ultrastructure Processing of Advanced Ceramics*. John Wiley & Sons, New York, pp. 453–461.
- Tateyama, H., Scales, P.J., Ooi, M., Nishimura, S., Rees, K., Healy, T.W., 1997. X-ray diffraction and rheology study of highly ordered clay platelet alignment in aqueous solutions of sodium tripolyphosphate. *Langmuir* 13, 2440–2446.
- Tchoubar, D., Bottero, J.Y., Quenne, P., Arnaud, M., 1991. Partial hydrolysis of ferric chloride salt. Structural investigation by photon-correlation spectroscopy and small-angle X-ray scattering. *Langmuir* 7, 398–402.
- Theng, B.K.G., 1979. *Formation and Properties of Clay-Polymer Complexes*. Elsevier, Amsterdam.
- Thomas, F., Michot, L.J., Vantelon, D., Montargès, E., Prélôt, B., Cruchaudet, M., Delon, J.F., 1999. Layer charge and electrophoretic mobility of smectites. *Colloids and Surfaces A* 159, 351–358.
- Tombácz, E., Ábrahám, I., Gilde, M., Szántó, F., 1990. The pH-dependent colloidal stability of aqueous montmorillonite suspensions. *Colloids and Surfaces* 49, 71–80.
- Tombácz, E., Balázs, I., Lakatos, J., Szántó, F., 1989. Influence of exchangeable cations on stability and rheological properties of montmorillonite suspensions. *Colloid and Polymer Science* 267, 1016–1025.
- Touillaux, P., Salvador, P., Vandermeersche, C., Fripiat, J.J., 1968. Study of water layers adsorbed on Na- and Ca-montmorillonite by the pulsed nuclear magnetic resonance technique. *Israel Journal of Chemistry* 6, 337–348.

- Touret, O., Pons, C.H., Tessier, D., Tardy, Y., 1990. Étude de la repartition de l'eau dans des argiles saturées  $Mg^{2+}$  aux fortes teneurs en eau. *Clay Minerals* 25, 217–233.
- Tournassat, C., Grenèche, J.-M., Tisserant, D., Charlet, L., 2003a. The titration of clay minerals. I. Discontinuous backtitration technique combined with CEC measurements. *Journal of Colloid and Interface Science* 273, 224–233.
- Tournassat, C., Ferrage, E., Poinssignon, C., Charlet, L., 2003b. The titration of clay minerals. II. Structure-based model and implications for clay reactivity. *Journal of Colloid and Interface Science* 273, 234–246.
- Tributh, H., Lagaly, G., 1986. Aufbereitung und Identifizierung von Boden- und Lagerstättentonen. *GIT-Fachzeitschrift für das Laboratorium* 30, 524–529, 771–776.
- Umemura, Y., Yamagishi, A., Schoonheydt, R.A., Persoons, A., de Schryver, F., 2001. Fabrication of hybrid films of alkylammonium cations ( $C_nH_{2n+1}NH_3^+$ ;  $n = 4-18$ ) and a smectite clay by the Langmuir-Blodgett method. *Langmuir* 17, 449–455.
- Umemura, Y., Yamagishi, A., Schoonheydt, R.A., Persoons, A., de Schryver, F., 2002. Langmuir-Blodgett films of a clay mineral and ruthenium(II) complexes with a noncentrosymmetric structure. *Journal of the American Chemical Society* 124, 992–997.
- Usui, S., 1973. Interaction of electrical double layers at constant surface charge. *Journal of Colloid and Interface Science* 44, 107–113.
- Vali, H., Bachmann, L., 1988. Ultrastructure and flow behavior of colloidal smectite dispersions. *Journal of Colloid and Interface Science* 126, 278–291.
- Vali, H., Köster, H.M., 1986. Expanding behaviour, structural disorder, regular and random irregular interstratification of 2:1 layer-silicates studied by high-resolution images of transmission electron microscopy. *Clay Minerals* 21, 827–859.
- van Bruggen, M.P.B., Donker, M., Lekkerkerker, H.N.W., Hughes, T.L., 1999. Anomalous stability of aqueous boehmite dispersions induced by hydrolyzed aluminium poly cations. *Colloids and Surfaces A* 150, 115–128.
- van Duffel, B., Schoonheydt, R.A., Grim, C.P.M., de Schryver, F.C., 1999. Multilayered clay films: atomic force microscopy study and modeling. *Langmuir* 15, 7520–7529.
- van Duffel, B., Verbies, T., Elshocht, S.V., Persoons, A., De Schryver, F.C., Schoonheydt, R.A., 2001. Fuzzy assembly and second harmonic generation of clay/polymer/dye monolayer films. *Langmuir* 17, 1243–1249.
- van Olphen, H., 1977. *An Introduction to Clay Colloid Chemistry*, 2nd edition. Wiley, New York.
- van Olphen, H., Fripiat, J.J., 1979. *Data Handbook for Clay Materials and other Non-Metallic Minerals*. Pergamon Press, Oxford.
- van Oss, C.J., Giese, R.F., Costanzo, P.M., 1990. DLVO and non-DLVO interactions in hectorite. *Clays and Clay Minerals* 38, 151–159.
- Verwey, E.J.W., Overbeek, J.T.G., 1948. *Theory of the Stability of Lyophobic Colloids*. Elsevier, Amsterdam.
- Vincent, B., 1973. The van der Waals attraction between colloid particles having adsorbed layers. II. Calculation of interaction curves. *Journal of Colloid and Interface Science* 42, 270–285.
- Vincent, B., 1990. The calculation of depletion layer thickness as a function of bulk polymer concentration. *Colloids and Surfaces* 50, 241–249.

- von Hahn, F.-V., 1928, Dispersoidanalyse. Die Methoden der Teilchengrößenbestimmung und ihre theoretischen Grundlagen. Ostwald, Wolfgang (Ed.) Handbuch der Kolloidwissenschaft, Band III. Verlag Theodor Steinkopff, Dresden und Leipzig.
- Wanner, H., Albinsson, Y., Karnland, O., Wieland, E., Wersin, P., Charlet, L., 1994. The acid/base chemistry of montmorillonite. *Radiochimica Acta* 66/67, 157–162.
- Weiss, A., 1962. Neuere Untersuchungen über die Struktur thixotroper Gele. *Rheologica Acta* 2, 292–304.
- Weiss, A., 1963. Ein Geheimnis des chinesischen Porzellans. *Angewandte Chemie* 72, 755–762.
- Weiss, A., Frank, R., 1961. Über den Bau der Gerüste in thixotropen Gelen. *Zeitschrift für Naturforschung* 16b, 141–142.
- Weiss, A., Häbisch, A., Weiss, A., 1964. Einige Eigenschaften der 1. bis 4. Wasserschicht in quellungsfähigen Schichtsilicaten. *Berichte der Deutschen Keramischen Gesellschaft* 41, 687–690.
- Weiss A., Russow, J., 1963. Über die Lage der austauschbaren Kationen bei Kaolinit. In: *Proceedings of the International Clay Conference Stockholm*, vol. 1, pp. 203–213.
- Wendelbo, R., Rosenqvist, I.T., 1987. Effects of anion adsorption on mechanical properties of clay–water systems. In: Schultz, L.G., van Olphen, H., Mumpton, F.A. (Eds.), *Proceedings of the International Clay Conference Denver 1985*. The Clay Minerals Society, Bloomington, IN, pp. 422–426.
- Wells, N., Theng, B.K.G., 1985. Factors affecting the flow behaviour of soil allophane suspensions under low shear rates. *Journal of Colloid and Interface Science* 104, 398–408.
- Wierenga, A.M., Lenstra, T.A.J., Philipse, A.P., 1998. Aqueous dispersions of colloidal gibbsite platelets: synthesis, characterisation and intrinsic viscosity measurements. *Colloids and Surfaces A* 134, 359–371.
- Wiewiora, A., Pérez-Rodríguez, J.L., Pérez-Maqueda, L.A., Drapala, J., 2003. Particle size distribution in sonicated high- and low-charge vermiculites. *Applied Clay Science* 24, 51–58.
- Willenbacher, N., 1996. Unusual thixotropic properties of aqueous dispersions of Laponite RD. *Journal of Colloid and Interface Science* 182, 501–510.
- Williams, B.G., Drover, S.P., 1967. Factors in gel formation in soil suspensions. *Soil Science* 104, 326–331.
- Xiao, H., Lui, Z., Wiseman, N., 1999. Synergetic effect of cationic polymer microparticles and anionic polymer on fine clay flocculation. *Journal of Colloid and Interface Science* 216, 409–417.
- Yariv, S., 1992. The effect of tetrahedral substitution of Si by Al on the surface acidity of the oxygen plane of clay minerals. *International Reviews on Physical Chemistry* 11, 345–375.
- Yong, R.N., Ohtsubo, M., 1987. Interparticle action and rheology of kaolinite–amorphous iron hydroxide (ferrihydrite) complexes. *Applied Clay Science* 2, 63–81.
- Zerwer, A., Santamarina, J.C., 1994. Double layers in pyrometamorphosed bentonite: index properties and complex permittivity. *Applied Clay Science* 9, 283–291.
- Zimehl, R., Lagaly, G., 1986. Coagulation of latex dispersions by inorganic salts: structural effects. *Progress in Colloid and Polymer Science* 72, 28–36.



This page intentionally left blank

*Chapter 6*

## **MECHANICAL PROPERTIES OF CLAYS AND CLAY MINERALS**

**R. PUSCH**

*Geodevelopment AB, Ideon, S-22370 Lund, Sweden*

Probably a glossary is needed to explain the different terms used by people working on soil mechanics and by clay scientists from other different disciplines (physico-chemists, for example). The terminology used in clay science to denote the same concepts is often different.

In civil engineering, the relationship between the visual mechanical behaviour of clays and the properties of clay minerals at the nano- and meso-scales (usually referred to as “micro-scale”) is now well recognised. Investigating the properties at these scales would allow predictions to be made of macroscopic behaviour.

Among the most important properties of clays in the fields of soil mechanics are hydraulic conductivity, gas conductivity, ion diffusion capacity, swelling potential, compressibility and rheological properties. All these properties depend on the type and content of clay minerals in, and the bulk density of, the soils.

### **6.1. PHYSICO-CHEMICAL BEHAVIOUR OF CLAY MINERALS**

This section summarises some basic physico-chemical properties of clays that are important to the understanding of their behaviour.

#### *6.1.1. General*

The electrical charge and colloidal size of clay mineral particles make them hydrate and interact so that their hydraulic conductivity and stress/strain properties are quite different from those of sandy soils. This is particularly important for smectites because they can absorb much water. The very fine, tortuous pore systems of clay materials, particularly of smectitic clays, offer considerable resistance to water and gas flow. This is especially true at high densities, and such compacted clays exert a suction (negative pressure) of water. The resultant soil–water potentials are of fundamental importance to the performance of such soils.

### 6.1.2. Clay Mineral– Water Interaction

Kaolinite and smectites represent the extremes of hydration and gel-forming capacity potentials, while illites and chlorites are intermediate in these respects.

Mostly smectites are considered here because they exhibit the clearest relationship between the hydration state, micro-structural constitution and bulk physical properties. The energy state of the clay mineral water system governs the development of “matric” and “osmotic” forces responsible for hydration and dehydration. In general one can explain clay water suction that is measured by tensiometers, for example, as the net effect of the following thermodynamic terms (Yong and Mohamed, 1992):

$\Psi_m$  = matric potential,

$\Psi_s = ncRT$  is the osmotic potential, i.e. solution potential (referring to the interaction between solute and water molecules) where  $n$  is the number of mol ions per mol salt = 2 for NaCl, or 3 for  $\text{CaCl}_2$ ,  $R$  is the universal gas constant,  $T$  is the absolute temperature and  $c$  is the molar concentration of salt,

$\Psi_g$  = gravitational potential,

$\Psi_a$  = pneumatic air pressure,

$\Psi_p$  = external pressure transmitted to the particles through the fluid phase.

Considering clay as a soil–water continuum, the swelling pressure at different basal spacings corresponding to the interlayer water content can be calculated. For  $\text{Na}^+$ -montmorillonite saturated with 0.003 mol. NaCl solution (Fig. 6.1) a very good fit is obtained between the calculated swelling pressure and measured values from high-pressure consolidation tests. Since there is good agreement between theories and experiments, the compression-swelling performance can be considered as

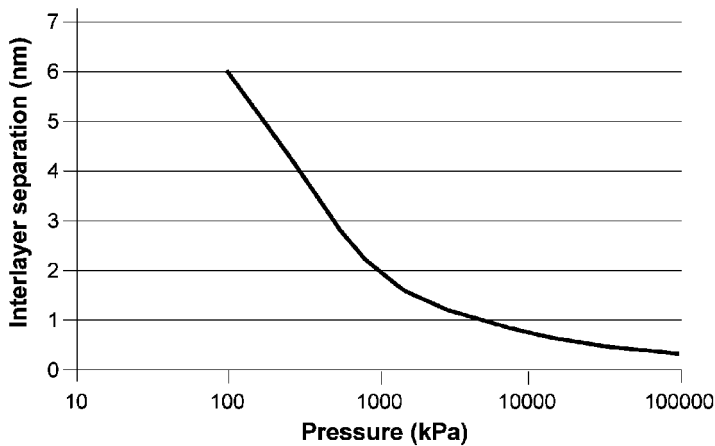


Fig. 6.1. Interlayer separation versus swelling pressure for  $\text{Na}^+$ -montmorillonite in 0.003 molar NaCl.

dependent on the osmotic ( $\Psi_s$ ) water potential, and on the matric potential ( $\Psi_m = 0$  at complete fluid saturation). However, these potentials are average values; basal spacing and density variations at the micro-structural scale need to be taken into account to define the real thermodynamic conditions in the clay matrix.

It is generally accepted that no more than 3 discrete pseudo-layers of water can occur in the interlayer space of most smectites (Chapters 3 and 5). At basal distances corresponding to 3, 2 and 1 water layers, the bulk densities are high. Under these conditions, the arrangement of layers is approximately plane-parallel. This arrangement is quite different at lower swelling pressures, and the energy state of the water in the different pores is consequently not similar. For lower bulk densities, a large part of the total pore space contains “free” water i.e. in the space located between particles and aggregates. The observed interlayer spacing represents some average of the distance between aggregates and the distance between particles.

The type of exchangeable cations influences the thickness of the particles. Divalent and polyvalent cations lead to larger particles;  $\text{Ca}^{2+}$ -montmorillonite is often considered to consist of about 10 layers per particle compared to  $\text{Na}^+$ -montmorillonite with 3–5 layers or even less. The interlayer distance in  $\text{Na}^+$ -montmorillonite is much larger than for  $\text{Ca}^{2+}$ -montmorillonite implying that the latter has less interlayer water at low and medium bulk densities.

Fig. 6.2 shows the amounts of interlayer water as a percentage of total pore water (Pusch, 1994) for montmorillonite-rich bentonite in the  $\text{Na}^+$ - and  $\text{Ca}^{2+}$ -exchanged forms. At moderate and high densities the larger part of all pore water in smectite is apparently associated with the mineral surface, whereas in illite and kaolinite this is

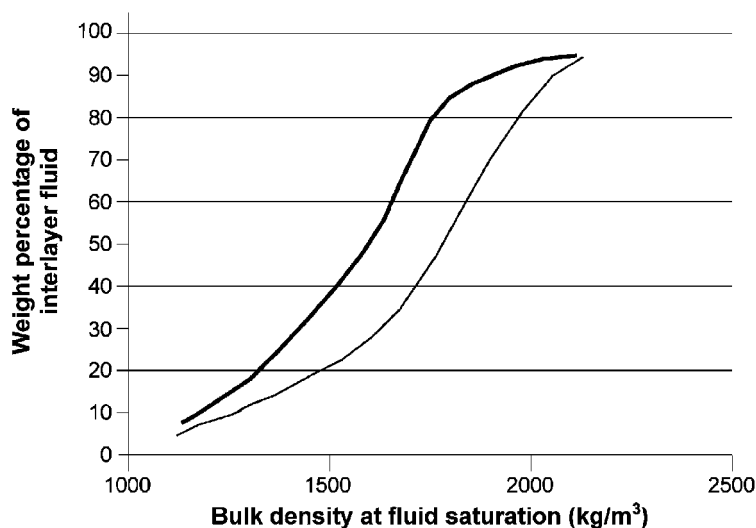


Fig. 6.2. Theoretical fraction of total pore water in interlayer spaces. Upper curve represents  $\text{Na}^+$ -montmorillonite and the lower curve  $\text{Ca}^{2+}$ -montmorillonite.

the case for only a small fraction of the pore water. The interlayer water is strongly adsorbed and appears to be “immobile” at normal hydraulic gradients. As a result, the hydraulic conductivity of dense smectites is very low, irrespective of the type of exchangeable cation. This means that consolidation under an applied external load, and expansion under a reduced load, are very slow.

Swelling beyond complete interlayer saturation is associated with double-layer interactions between external surfaces of particles, and hence is an osmotic phenomenon. The extension of the double-layers is less under marine than under fresh-water conditions. Thus, the clay mineral expands to larger volume in the latter case.

At high densities, the space between clay particles and aggregates is smaller and the repulsion between the negatively charged surface is greater. As a result, the swelling pressure increases.

At low and moderate densities, the electrolyte concentration has a substantial influence on the distance between particles. The particles forming a network with rather much free space can coagulate at high electrolyte concentration. The effect of changes in pore water composition on the micro-structural constitution is obvious. When a  $\text{Na}^+$ -smectite is put in contact with water rich in  $\text{Ca}^{2+}$  ions, partial interlayer dehydration takes place because the stacks of layers contract and the pore spaces between the particles become larger and more continuous. This leads to a drop in shear strength and swelling pressure under constant bulk volume conditions, and to an increased hydraulic conductivity.

Fig. 6.3 shows the relationship between pore water salinity, bulk density and swelling pressure for  $\text{Na}^+$ - and  $\text{Ca}^{2+}$ -smectites. For  $\text{Ca}^{2+}$ -smectite, the influence of the salt content on the swelling pressure is appreciably smaller than for the  $\text{Na}^+$ -smectite particularly at low and intermediate bulk densities ( $< 1800 \text{ kg/m}^3$ ). The difference in swelling behaviour between the two smectites may be explained in terms of their microstructure; there are few contacts between thicker particles of  $\text{Ca}^{2+}$ -smectite than between thin ones of  $\text{Na}^+$ -smectite.

Like natural clays, artificially “prepared” clays maintain a significant degree of micro-structural heterogeneity. The softer parts of the clay matrix, i.e. the gels in the

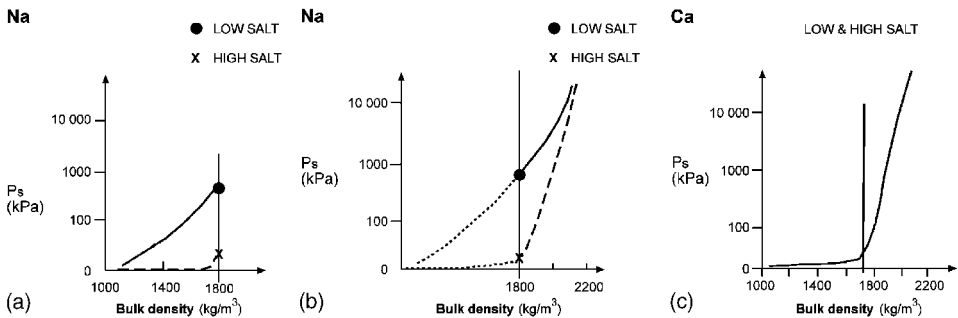


Fig. 6.3. Relationship between swelling pressure and density, at water saturation, at low and high salt concentrations for  $\text{Na}^+$ -montmorillonite (a and b) and  $\text{Ca}^{2+}$ -montmorillonite (c).

pore spaces between stable and dense particles or aggregates, are particularly sensitive to pore water chemistry.

### 6.1.3. Hydraulic Conductivity

Bulk density and swelling pressure have a direct effect on hydraulic conductivity. High density and low electrolyte content of the clay mineral give rise to a very low conductivity for  $\text{Na}^+$ -smectite. The conductivity of  $\text{Ca}^{2+}$ -smectite is only slightly higher because of the dense particle arrangement. However the difference between the two becomes obvious at low densities. Indeed, for densities lower than  $1600\text{--}1800\text{ kg/m}^3$   $\text{Ca}^{2+}$ -smectite becomes very conductive because of the lack of micro-structural continuity and coherence.

A general picture of the importance of the mineralogical composition of clays to hydraulic conductivity is shown in Fig. 6.4, illustrating the dependence of hydraulic conductivity on density at fluid saturation for different clay minerals.

Fig. 6.5 shows the approximate relationship between the smectite content and the hydraulic conductivity for mechanically undisturbed clay with a high percentage of clay-sized particles, low-electrolyte pore water and a bulk density at saturation of about  $2000\text{ kg/m}^3$ . The conductivity is very low even when the smectite content drops to a few percent.

If the hydraulic gradient is high, as in many laboratory oedometer tests, the particles can also move and this affects the hydraulic conductivity. Thus, particles and aggregates that are set free can be transported by flowing pore water to narrow parts of the pore spaces and cause clogging (Hansbo, 1960).

### 6.1.4. Gas Penetrability

Permeation of gas through clay is a phenomenon of considerable practical importance for the clay sealing of underground facilities. It is equally important for the understanding of gas prospection and exploitation in areas like the North Sea. However, it is not yet fully understood.

In practice one can assume gas conductivity to be about a thousand times higher than that of water. Once gas has made its way through buffer clay and further out through even more permeable geological units, its rate of flow is more dependent on the availability of pressurized gas than on the gas conductivity. Therefore, the gas pressure that yields penetration through the buffer clay, i.e. the “critical gas pressure”, is the most important factor. The solubility of the gas such as air, hydrogen or organic gases is also important. The bubbles of temporarily stagnant gas contained in pore water of the clay shrink and the dissolved gas diffuses out of the system.

According to current hypotheses micro-structural heterogeneity has a decisive influence on the critical gas pressure. Gas makes its way along continuous channels of neighbouring larger spaces, where it finds least resistance. Here capillary retention is at minimum and the bonds between adjacent particles are overcome (Pusch, 1994;

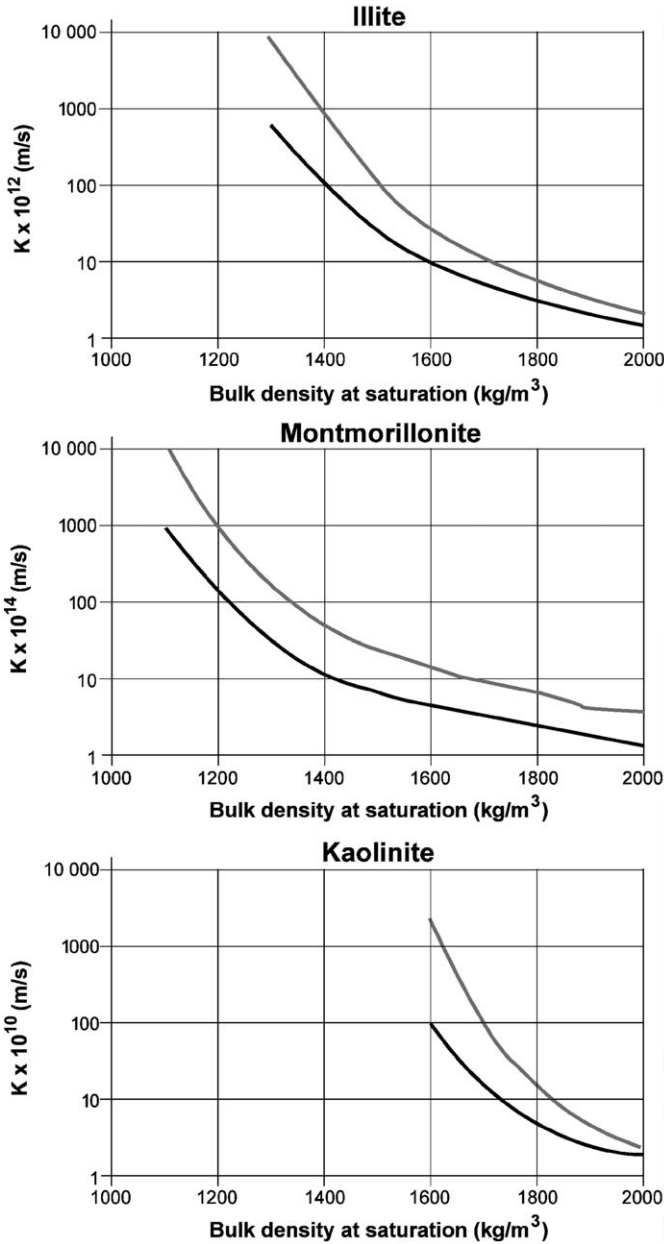


Fig. 6.4. Hydraulic conductivity  $K$  of artificially prepared mono-mineral clays as a function of density at fluid saturation (literature survey). The upper curve in each diagram represents saline (ocean-type) pore water, while the lower represents saturation and percolation with distilled water (Pusch, 1994).

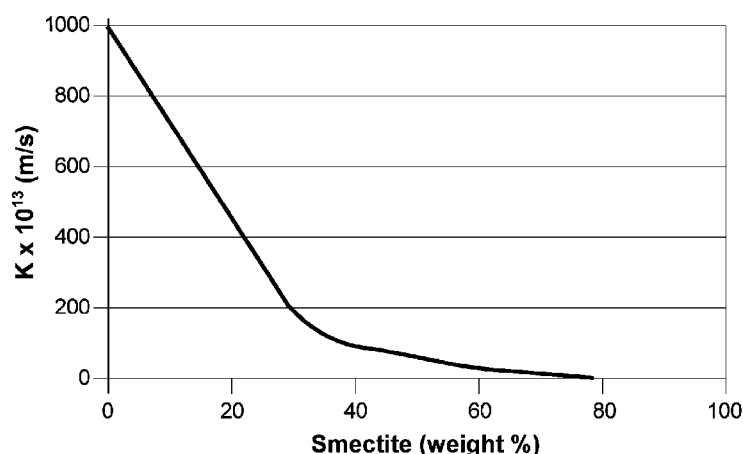


Fig. 6.5. Approximate relationship between the content in weight percent of smectite clay minerals and the hydraulic conductivity  $K$  for natural, mechanically undisturbed clay with a high percentage of clay-sized particles, mostly illite and chlorite, and saturated and permeated by low-electrolyte pore water.

Horseman and Harrington, 1997). These hypotheses imply that the critical gas pressure is of the same order of magnitude as the prevailing effective pressure.

#### 6.1.5. Ion Diffusivity

The transport rate of dissolved ions and molecules in clays depends on their diffusivity under the influence of concentration gradients. Diffusion transport capacity is expressed by the “effective” diffusion coefficient. This parameter refers to the actual “effective” porosity and gives information on the ion transport at the micro-structural level. On the other hand, the “apparent” diffusion coefficient derives directly from recording of the concentration profile in the clay. Thus, the importance of porosity is emphasised by the fact that cation diffusion takes place in several ways: in continuous water-filled voids, along particle surfaces with electrical double-layers, and through the interlayer space in smectites. The latter two mechanisms involve ion-exchange for which a sorption parameter,  $K_d$ , is used.

In practice, the ion transport capacity can be predicted by applying Fick’s law, using the relevant values for the coefficient  $D_e$  of the density-related “effective” diffusion. Table 6.1 gives typical literature-derived data on this parameter for montmorillonite-rich bentonite with a density at saturation of  $2000 \text{ kg/m}^3$ , which represents the approximate density of clay embedding canisters with highly radioactive waste.

The density of the clay plays a rather important role in ion diffusion except for clays exchanged with monovalent cations. Fig. 6.6 implies that the  $D_e$  of the anion



Table 6.1. Effective diffusion coefficient  $D_e$  for elements migrating in MX-80 bentonite with a density at saturation of about 2000 kg/m<sup>3</sup> (Brandberg and Skagius, 1991)

Species	$D_e$ , m <sup>2</sup> /s
C-14	$10^{-10}$
I-129	$2 \cdot 10^{-12}$
Sr-90	$2 \cdot 10^{-8}$
Cs-137	$2 \cdot 10^{-9}$
Na-22	$2 \cdot 10^{-9}$
Pu-238	$10^{-10}$
Am-243	$10^{-10}$

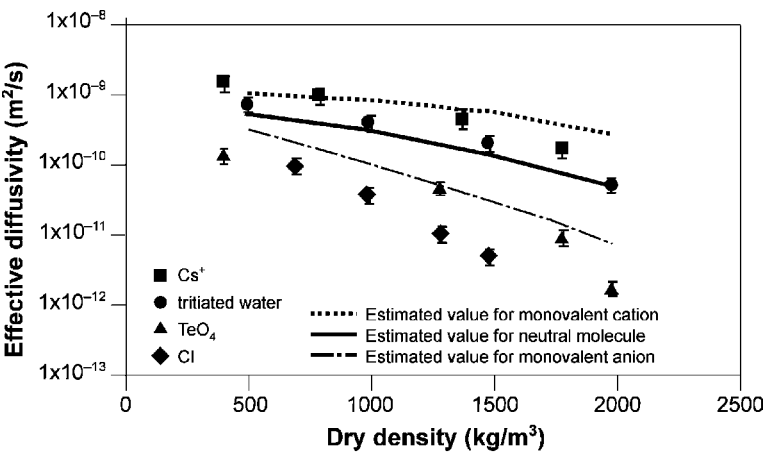


Fig. 6.6. Measured and calculated effective diffusivities for smectite-rich clay (Kato et al., 1995).

chloride becomes one order of magnitude lower if the dry density is increased from 500 to 1500 kg/m<sup>3</sup>. At fluid saturation the density is 1950 kg/m<sup>3</sup> and  $D_e$  is  $10^{-11}$  m<sup>2</sup>/s. The curve for neutral molecules is also approximately valid for water.

The diffusive anion transport capacity is proportional to the pore space/smectite particles ratio since the anions are excluded from the interlayer space by the Donnan effect. With increasing density there is a strong reduction of the available space for migration, causing the diffusion coefficient of anions to drop significantly. Many cations move by both pore and surface diffusion. This includes respectively the interlayer space and the vicinity of the particles where electrical double-layers with dominant cationic population are present. Hence, increasing the density has a small effect on retarding the diffusion of cations, especially for monovalent ions.

6.2. MECHANICAL CHARACTERISTICS OF CLAYS

Textbooks on soil mechanics specify the parameters used in applied foundation engineering and the ways of determining them in the laboratory and under field conditions. The physico-chemical background, with special reference to processes at the micro-structural level is usually not a major issue in applied engineering geology, but is the focus of this section.

6.2.1. Swelling and Consolidation Properties

Smectitic soils give a clear picture of the physical performance of clay minerals, and the following is focused on such clay materials. The expandability of clay is best expressed in terms of swelling pressure, which is strongly dependent on density and, at low densities, on the salinity and major type of exchangeable cation.

Density is the major factor, as illustrated in Fig. 6.7, which refers to MX-80 ( $\text{Na}^+$ -bentonite) and a commercial  $\text{Ca}^{2+}$ -bentonite from Moosburg, Germany (Süd-Chemie). The difference in swelling pressure between the two clays is due to different

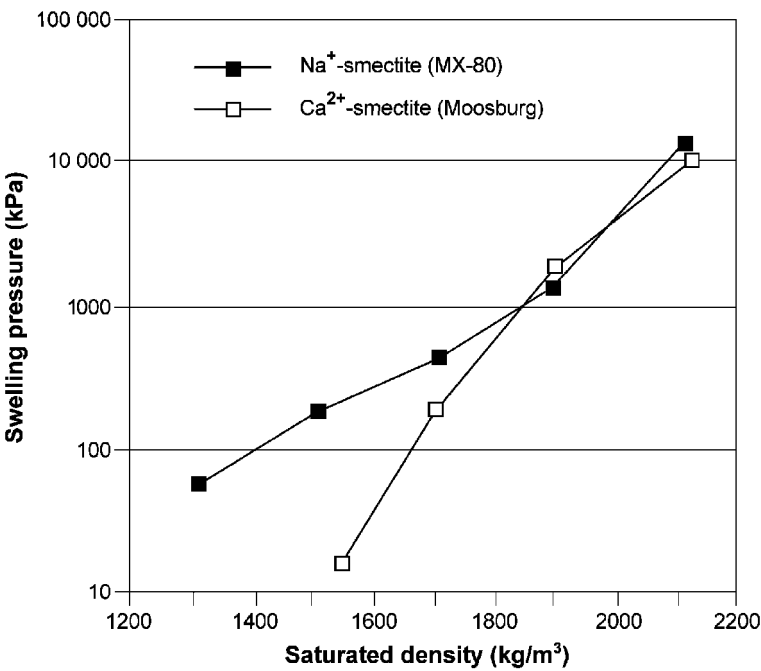


Fig. 6.7. Generalized diagram showing swelling pressure versus density at saturation, with distilled water of a  $\text{Na}^+$ -bentonite (MX-80) and a  $\text{Ca}^{2+}$ -bentonite with similar smectite content (bentonite from Bavaria, Germany) (Pusch, 1994).

microstructures and is negligible at densities higher than about  $2000 \text{ kg/m}^3$ . Under these conditions, the particles have been forced together so that their micro-structural patterns are similar.

Fig. 6.8 shows the relationship between swelling pressure and the smectite content of mechanically undisturbed clays. Saturation is made with low-electrolyte pore water, and bulk density at fluid saturation is about  $2000 \text{ kg/m}^3$ . This figure indicates that the influence on the expandability, and particularly on the swelling pressure, of the content of expandable minerals becomes significant when this content exceeds about 30%. At lower bulk densities most of the expandable minerals consist of relatively soft gels in pore spaces between non-expandable minerals. When the content exceeds about 70%, which is typical for many commercially exploited bentonites, the expandable minerals form a continuous matrix with a density similar to the bulk density. For densities below 1800 and  $1900 \text{ kg/m}^3$ , clay with illite as the dominant clay mineral has a swelling pressure of 5–20% of that of smectites. At higher densities this percentage can be much larger. Common sedimentary clays of pre-Ordovician age have low smectite contents and the swelling pressure is therefore not significant.

Consolidation–expansion of smectite-rich clays are almost reversible at least over a limited density range since the process depends primarily on the hydration potential. Some hysteresis is involved but in principle the same swelling pressure is obtained by compression of soft smectite clay to a certain density as when a dense clay of this type is allowed to expand to this same density. This is not the case for non-expandable clays because the change in micro-structure induced by

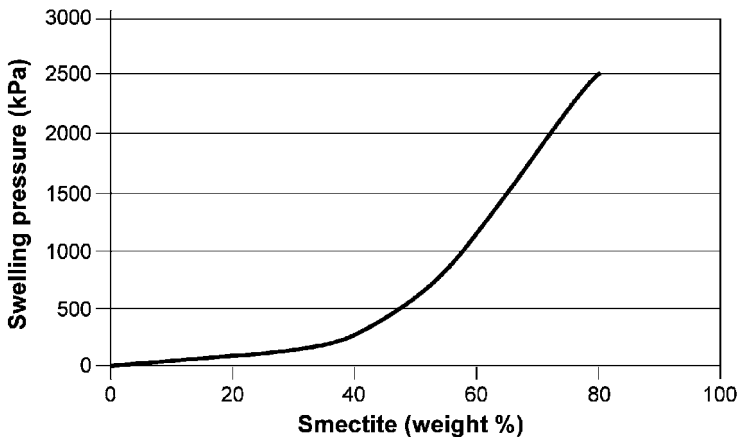


Fig. 6.8. Approximate relationship between the content in weight percent of smectite minerals and the swelling pressure for natural, mechanically undisturbed clay with a high percentage of clay-sized particles, mostly illite and chlorite, and saturated and permeated by distilled water. The bulk density at saturation is around  $2000 \text{ kg/m}^3$  (Pusch et al., 1987).

consolidation is largely permanent. Thus, when the consolidation pressure of a typical soft natural illitic clay is exceeded, larger pores become compressed first, resulting in shearing of weak aggregates in the clay matrix. Further increase in effective pressure also starts compression of smaller pores and the shear-strain of the clay matrix becomes significant.

The effect of unloading after consolidation of strongly compressed illitic clay is similar to that of smectitic clays. Expansion occurs when compressed, and partly dehydrated, particles are rehydrated. This expansion is much smaller for illitic than for smectitic clays, because the number of restored hydrated layers in smectite is greater. The compressed pore spaces in illite are not re-established.

### 6.2.2. Rheological Properties

The rheological properties of clays are expressed in the form of parameters defining stress- and time-dependent strain. The maximum shear stress that clay can resist under defined boundary conditions is referred to as “strength”. This can be expressed in terms of the unconfined, undrained compressive strength and a number of traditional strength and strain parameters. These parameters are determined in the laboratory using ordinary laboratory compression devices such as triaxial test equipment or a simple uniaxial compression machine. A typical picture of the stress/strain behaviour of natural dense bentonite clay is shown in Fig. 6.9. Because of slight cementation in nature, this material is somewhat stronger than an artificially altered clay. Failure occurs at an axial strain of about 3% for a compressive stress of 2.5 MPa.

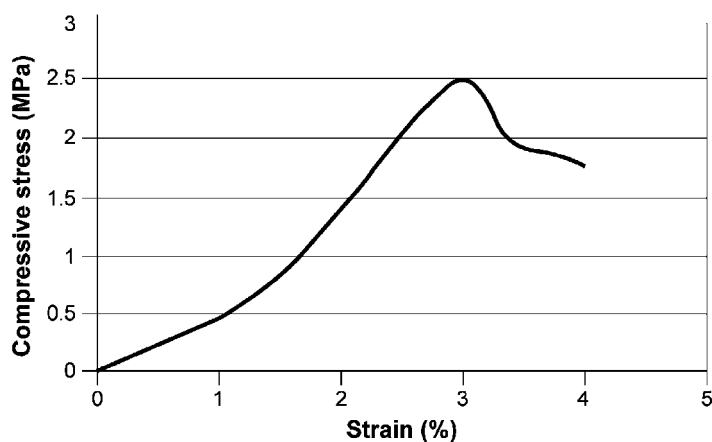


Fig. 6.9. Example of uniaxial testing of natural bentonite clay from Burgsvik, Sweden. The density of the saturated clay is about  $2100 \text{ kg/m}^3$ .

Equation 6.1 gives a generalized expression of the shear strength,  $q$ , as a function of the mean effective stress,  $p$ :

$$q = ap^b \tag{1}$$

where  $a = q$  for  $p = 1$  kPa; and  $b$  is the slope of  $\log p/\log q$  curve (Fig. 6.10). The key parameter,  $a$ , is a particularly good measure of how shear strength depends on the microstructure. Thus the value of  $a$ , is much higher for coarse- than fine-grained clays. This is illustrated by the facts that this value is twice higher for  $\text{Ca}^{2+}$  than for  $\text{Na}^{+}$ -smectite, and that strengthening by coagulation is induced by salt water.

Creep is the expression for time-dependent strain and is caused by shearing at the micro-structural level both in consolidation (compression under drained conditions) and by macro-strain under undrained conditions.

Based on a conceptual model that takes strain processes at the micro-structural level into consideration, and applying thermodynamics and stochastic mechanics

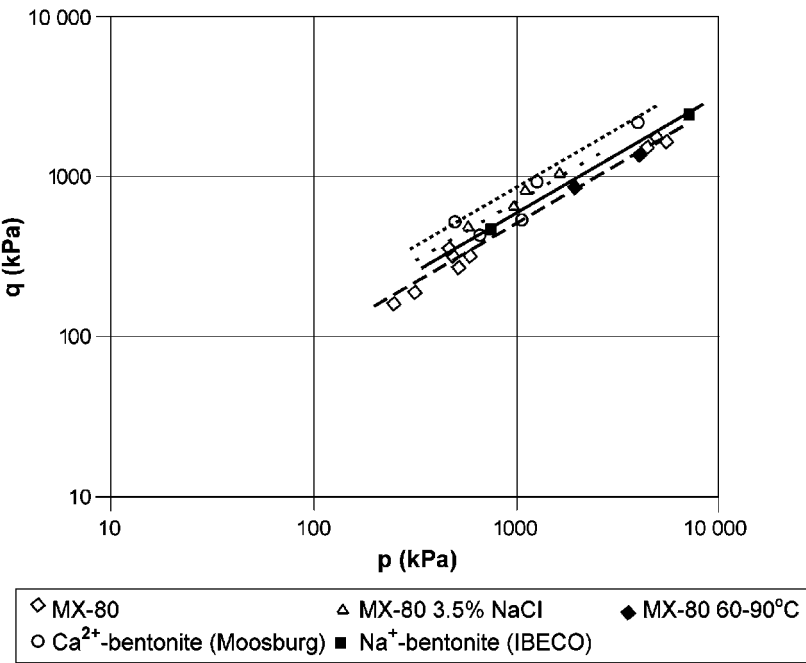


Fig. 6.10. Triaxial tests on bentonite as buffer materials (Börgesson and Hernelind, 1999).  $q$  = shear stress,  $p$  = average effective normal stress.

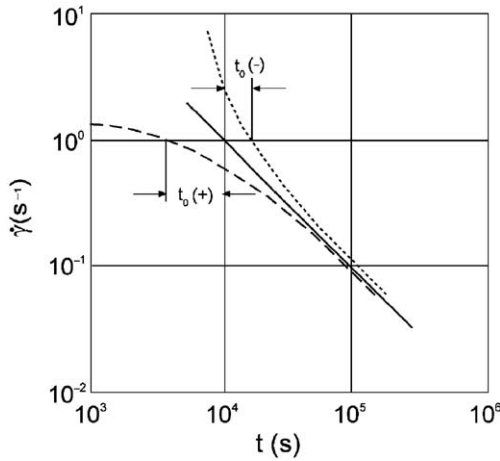


Fig. 6.11. Typical clay creep curves. The term  $t_0$  describes the form of the creep onset, i.e. the initial part of the creep strain rate  $\dot{\gamma}$  at stress application, assuming that  $\dot{\gamma}$  is ultimately proportional to log time. Negative  $t_0$  indicates cementation of the clay matrix by precipitated matter.

(Pusch and Adey, 1999), the impact of time,  $t$ , on the shear strain can be expressed by Equation 6.2:

$$d\gamma/dt = \beta T D \ln(t) \quad (2)$$

where  $\gamma$  is the angular strain;  $\beta$  is a strain parameter evaluated from undrained triaxial tests ( $3 \cdot 10^{-10}$  to  $2 \cdot 10^{-8}$  kPa for the density range of 1900–2100 kg/m<sup>3</sup> for MX-80);  $D$  is the deviator stress ( $\sigma_1 - \sigma_3$ ) in kPa and  $T$  is the absolute temperature in Kelvin.

Typical generalised curves for primary creep, implying strain attenuation, are shown in Fig. 6.11. This type of creep usually prevails when bulk shear stress is in the interval 1/3–2/3 of the conventionally determined shear strength. For lower stresses the attenuation is stronger; for higher stresses failure cannot be avoided (secondary creep). Creep will occur when critical strain has been reached, i.e. when comprehensive breakdown of the microstructure has taken place.

## REFERENCES

- Börjesson, L., Hernelind, J., 1999. Coupled thermo-hydro-mechanical calculations of the water saturation phase of a KBS-3 deposition hole. SKB Technical Report TR-99-41. SKB, Stockholm.
- Brandberg, F., Skagius, K., 1991. Porosity, sorption and diffusivity data compiled for the SKB 91 study. SKB Technical Report TR 91-16, SKB, Stockholm.

- Hansbo, S., 1960. Consolidation of clay with special reference to influence of vertical sand drains. Study in connection with full-scale investigations at Skå-Edeby. Swedish Geotechnical Institute, Proceeding No 18.
- Horseman, S. T., Harrington, J. F., 1997. Study of gas migration in MX-80 buffer bentonite. National Environmental Research Council, British Geological Survey. Report WE/97/7.
- Kato, H., Muroi M., Yamada, N., Ishida, H., Sato, H., 1995. Estimation of effective diffusivity in compacted bentonite. In: Murakami, T., Ewing, R. C. (Eds). Scientific Basis for Nuclear Waste Management XVIII. Materials Research Society Symposium Proceedings 353, 277–284.
- Pusch, R., 1994. Waste disposal in rock. Developments in Geotechnical Engineering, 76. Elsevier Amsterdam.
- Pusch, R., Adey, R., 1999. Creep in buffer clay. SKB Technical Report TR-99-32. SKB, Stockholm.
- Pusch, R., Børgesson, L., Erlström, M., 1987. Alteration of isolating properties of dense smectite clay in repository environment as exemplified by seven pre-Quaternary clays. SKB Technical Report TR 87-29. SKB, Stockholm.
- Yong, R. N., Mohamed, A.M.O., 1992. A study of particle interaction energies in wetting of unsaturated expansive clays. Canadian Geotechnical Journal 29, 1060–1070.

*Chapter 7*

## **MODIFIED CLAYS AND CLAY MINERALS**

**F. BERGAYA<sup>a</sup>, B.K.G. THENG<sup>b</sup> AND G. LAGALY<sup>c</sup>**

<sup>a</sup>*CRMD, CNRS-Université d'Orléans, 1F-45071 Orleans Cedex 2, France*

<sup>b</sup>*Landcare Research, Palmerston North, New Zealand*

<sup>c</sup>*Institut für Anorganische Chemie, Universität Kiel, D-24118 Kiel, Germany*

This composite chapter deals with the physical and chemical modification of clays and clay minerals in the broad sense. Acid activation and thermal treatment (heating), described in Chapters 7.1 and 7.2, have long been used to produce materials for certain practical applications. The surface properties and reactivity of clay minerals may also be modified by adsorption and intercalation of small and polymeric organic species. Chapter 7.3 reviews the important topic of clay mineral–organic interactions. Clay minerals have been implicated in the abiotic origins of life on earth because of their ability to adsorb, protect, concentrate, and transform biomolecules. On this basis, the possible role of clay minerals in life's origins is included here (Chapter 7.4). In relation to acid activation and thermal treatment, the pillaring of clay minerals (Chapter 7.5) is a recent method of modification. As the term suggests, the process commonly involves intercalation of cationic species acting as 'pillars' to prop the mineral layers apart. Subsequent heating gives rise to a permanently porous material, useful for organic catalysis and other environmental applications.



This page intentionally left blank

*Chapter 7.1*

## ACID ACTIVATION OF CLAY MINERALS

P. KOMADEL AND J. MADEJOVÁ

*Institute of Inorganic Chemistry, Slovak Academy of Sciences, SK-845 36 Bratislava, Slovakia*

One of the most common chemical modifications of clays, used for both industrial and scientific purposes, is their acid activation. This consists of the treatment of clay with a mineral acid solution, usually HCl or H<sub>2</sub>SO<sub>4</sub>. The main task is to obtain partly dissolved material of increased specific surface area, porosity and surface acidity (Komadel, 2003). The manufactured materials are widely available, relatively inexpensive solid sources of protons, effective in a number of industrially significant reactions and processes. Acid attack on clays also occurs naturally, e.g., in the interaction of acid mine drainage with clay minerals (Galán et al., 1999; Dubíková et al., 2002). Mining waste containing sulphides is the most common and greatest anthropogenic source of acidity. Progressive oxidation leads to the production of protons and sulphates in leaching waters, which generally also mobilize large amount of metals by dissolution of minerals. These waters influence the composition of surface waters but also have an impact on surrounding soils and terrestrial ecosystems.

From the industrial point of view, the term ‘acid-activated clays’ was reserved mainly for acid-treated bentonites. Bentonite has always had a multitude of markets and acid-activated bentonite was a traditional product for many decades. It is usually a Ca<sup>2+</sup>-bentonite that was treated with inorganic acids to replace divalent calcium ions with monovalent hydrogen ions and to leach out ferric, ferrous, aluminium and magnesium ions thus altering the layers of smectite and increasing the specific surface area and porosity. This results in the production of bleaching earths, clays suitable for a range of bleaching or decolourising applications, in which they compete against natural bleaching earths (Siddiqui, 1968; Kendall, 1996).

This chapter mainly reviews acid treatment of smectites, the dominant minerals in bentonites. Other products include environmentally benign catalysts or their supports, which are used in various chemical reactions such as Friedel-Crafts alkylation and acylation, dimerisation and polymerisation of unsaturated hydrocarbons, etc. (Adams, 1987; Brown, 1994; see also Chapter 10.2), or colour developers in carbonless copying papers (Fahn and Fenderl, 1983). Acid-treated clays pillared with

oxyhydroxyaluminium species are used to prepare clay-modified electrodes (Falaras et al., 2000a), as adsorbents for oil clarification (Mokaya et al., 1993; Falaras et al., 2000b; Pagano et al., 2001) and as catalysts (Mokaya and Jones, 1994; Bovey and Jones, 1995; Bovey et al., 1996).

#### 7.1.1.1. PROPERTIES AND AUTO-TRANSFORMATION OF $H^+$ -EXCHANGED CLAY MINERALS

The acidity of acid-untreated smectites has two sources: (i) the compensating cations; these may have a strong polarizing effect on coordinating water molecules, most of which are in the interlayer spaces and may not be easily accessible; and (ii) specific sites at the layer edges, where unsaturated “broken” bonds occur; these may be compensated by OH groups formation, leading to Brønsted acid sites such as Si–OH and also coordinately unsaturated  $Al^{3+}$  and  $Mg^{2+}$  easily formed at the edges, behave as Lewis acid sites (Lambert and Poncelet, 1997).

The first step in acid treatment is that the protons replace the exchangeable cations and then they attack the layers (Čičel and Komadel, 1994). The exchange reaction is fast if there is good contact between acid and smectite, and the quantity of available protons is sufficient. The substitution rate is independent of the smectite if the mineral contains only swelling layers. In contrast to smectites saturated with metal cations, proton-saturated smectites are unstable. The layers are attacked by surface and interlayer hydrated protons, even after drying the separated activated smectite, similar to what occurs in solution. This process, known as ‘auto-transformation’, spontaneously changes  $H^+$ -smectites to their ( $Al^{3+}$ ,  $Fe^{3+}$ ,  $Mg^{2+}$ ) -forms on ageing (Barshad and Foscolos, 1970). In aqueous dispersion at 90 °C the process is completed within 4 days (Janek and Komadel, 1999).

To study the properties of  $H^+$ -clays, maximal saturation by protons and stability of the product are required. Various preparation methods were tested. The best results are obtained by passing the clay suspension through a succession of  $H^+$ –OH<sup>–</sup>– $H^+$  ion-exchange resins.  $H^+$ -forms of <2 μm fractions of bentonites with varied  $Fe^{3+}$  contents are prepared by this method. Potentiometric titrations of proton-saturated fine fractions of bentonites have been used to characterize the acid sites at the smectite–water interface in dispersions. The titration curves have revealed that the number of strong acid sites varies and accounts for 60–95% of the total acidity in the freshly prepared  $H^+$ -forms (Janek et al., 1997). Layer-charge distributions of all samples are inhomogeneous. This distribution is changed after oxalate pretreatment of the samples, due to the removal of readily soluble phases that might have blocked exchange sites. After auto-transformation, the alkylammonium exchange method (Lagaly, 1994) reveals inhomogeneous charge density distributions; the fraction of layers of the highest charge decreases. Comparison of cation exchange capacity (CEC) obtained from potentiometric curves and the CEC calculated from the mean layer charge has confirmed that the attack of protons occurs from particle edges.

However, for several samples the structural attack may also occur from the inter-layer space. Autotransformation of the  $H^+$ -smectites also decreases the mean layer charge. Protons preferentially attack the octahedral  $Mg^{2+}$  during the auto-transformation. A number of strong acid sites decreases and the number of weak acid sites increases on ageing.

The titration data obtained are used in a thermodynamic calculation of proton affinity distribution. Numerical solving of an integral adsorption equation reveals a continuous distribution of proton interaction sites. Proton affinity distributions clearly detected up to five different proton interaction sites in all the smectite–water systems, within accessible experimental range of pHs between 2 and 12. The amount of the strongest acid sites decreases on ageing, while the amount of all weaker acid sites increases with the progress of autotransformation. The strongest acid sites are connected with free protons present in the dispersion while the weaker acid sites are connected with the titration of released structural  $Al^{3+}$ ,  $Fe^{3+}$ ,  $Mg^{2+}$  cations and/or their hydrolysed species, and deprotonation of SiOH groups. These results indicate the sources of acidity in acid activated bentonites (Janek and Komadel, 1993). Hydrated aluminium ions in freshly proton-saturated dispersions contribute to a group of weak acid sites, which also include oligomeric hydroxoaluminium cations. The amount of these sites increases during auto-transformation. The freshly prepared proton-saturated dispersions show low pH values and the particles interact by edge-to-face contacts. This increases the viscosity in comparison with the sodium forms at pH close to 7 (Janek and Lagaly, 2001). A kinetic study of proton-promoted dissolution of  $K^+$ -montmorillonite in solutions with constant KCl concentrations, using both titration and batch equilibration experiments, shows that adsorption of  $H^+$  and dissolution of  $Al^{3+}$  occur (Zysset and Schindler, 1996).

Different clay minerals are treated with HCl or NaOH at room temperature for 2 weeks to obtain information on variable surface charge. Both treatments lead to an increase of variable surface charge, while the actual charge value increases and decreases depending on the mineral and the treatment. The heterogeneity of charge-generating surface groups is observed in natural minerals. During acid treatment, the number of weakly acidic surface functional groups increases, while the number of groups of stronger acidic character decreases. Dissolution of  $Al^{3+}$  prevails over  $Si^{4+}$  in acid treatments. Illite and kaolinite are most resistant to acid attack. The surface areas of the minerals computed from both water and nitrogen adsorption isotherms increase with acid and alkali treatments. The effects of acid and alkali attacks are controlled by the individual character of the minerals (Jozefaciuk, 2002; Jozefaciuk and Bowanko, 2002).

### 7.1.2. METHODS OF INVESTIGATION

The methods being employed to characterize acid-activated silicates include chemical analysis, XRD, Mössbauer, Fourier transform infrared (FTIR), and

MAS-NMR spectroscopies; Scanning electron microscopy, transmission electron microscopy (TEM) and high resolution transmission electron microscopy (HRTEM); acidity, surface area and pore size measurements, etc. Usually a combination of several methods is needed for sufficient characterization of the materials obtained (Čičel and Komadel, 1994; Vicente et al., 1994; Breen et al., 1995b; Komadel et al., 1996b; 1995a; 1995b, 1996b; Gates et al., 2002).

Chemical analysis of solid and/or liquid reaction products, infrared spectroscopy (IR) and MAS-NMR spectroscopies are very sensitive to the nature and content of the octahedral atoms and thus, also to the changes that occur in different stages of acid attack (Breen et al., 1995a, 1995b).

IR spectroscopy has been used for identification of the main mineral and the admixtures in the fine fractions of bentonites (Farmer, 1974; Madejová et al., 1992, 1995 Russell and Fraser, 1994; Madejová and Komadel, 2001). It is also a routine characterization technique for acid-treated clays, very sensitive to modifications of the clay structure resulting from acid treatment. As protons penetrate into the clay layers and attack the OH groups, the resulting dehydroxylation connected with successive release of the octahedral atoms can be readily followed by changes in the characteristic absorption bands attributed to vibrations of OH groups and/or octahedral cations. Comparative IR studies of acid-treated smectites (Madejová et al., 1998) as well as saponites, sepiolite and palygorskite (Vicente et al., 1996a) have been published.

Changes in the IR spectra of SWy-1 montmorillonite (with quartz admixture) after treatment with 6 M HCl (Figure 7.1.1) demonstrate the alteration of the chemical bonds in the structure.

The spectrum of the untreated sample shows an intensive band at  $1048\text{ cm}^{-1}$  attributed to the Si–O stretching vibrations, and bands at  $524$  and  $466\text{ cm}^{-1}$  assigned to Al–O–Si (octahedral Al) and Si–O–Si bending vibrations, respectively. Three peaks in the hydroxyl bending region at  $917\text{ cm}^{-1}$  for  $\text{Al}_2\text{OH}$ ,  $886\text{ cm}^{-1}$  for  $\text{AlFeOH}$ , and  $850\text{ cm}^{-1}$  for  $\text{AlMgOH}$  reflect that octahedral  $\text{Al}^{3+}$  is partially replaced by  $\text{Fe}^{3+}$  and  $\text{Mg}^{2+}$ . The doublet at  $799$  and  $779\text{ cm}^{-1}$  indicates the presence of quartz impurity in the sample, which has been confirmed by XRD.  $^{29}\text{Si}$  MAS-NMR shows that 12% of total  $\text{Si}^{4+}$  is associated with quartz (Tkáč et al., 1994; Madejová et al., 1998).

After 8 h of HCl treatment, no significant changes are seen in the IR spectra of SWy-1 montmorillonite except for a slight upward shift of the Si–O stretching band ( $\Delta\nu = 6\text{ cm}^{-1}$ ) together with a weak decrease in the intensities of the OH and Al–O–Si bending bands. This reflects the partially diminishing content of octahedral cations due to acid attack.

As the treatment time progresses, a more pronounced decrease is observed in the intensities of the bands related to octahedral cations. Changes in the  $\text{Si}^{4+}$  environment with prolonged acid treatment are reflected in both the position and the shape of the Si–O stretching band. In addition to the tetrahedral Si–O band near  $1058\text{ cm}^{-1}$ , the IR spectrum of the sample treated for 12 h shows a pronounced

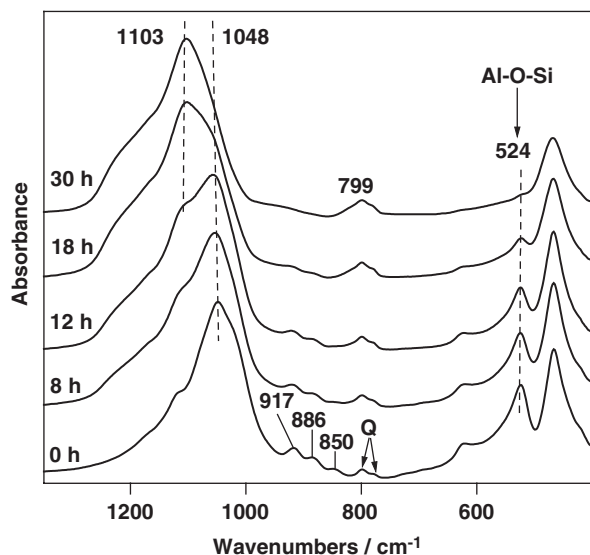


Fig. 7.1.1. IR spectra of SWy-1 montmorillonite treated with 6 M HCl at 95 °C for 0, 8, 12, 18 and 30 h. Q is quartz. (From [Madejová et al., 1998](#).)

absorption near  $1100\text{ cm}^{-1}$ . This absorption band is assigned to Si-O vibrations of amorphous silica with a three-dimensional framework formed during acid treatment.

The spectrum of the sample treated for 18 h confirms a high degree of structural decomposition. The Si-O band of amorphous silica at  $1103\text{ cm}^{-1}$  dominates the Si-O stretching region and only inflections related to OH bending bands are present in the  $950\text{--}800\text{ cm}^{-1}$  region. Another characteristic band of amorphous silica near  $800\text{ cm}^{-1}$  increases in intensity with treatment time and gradually overlaps the doublet of quartz. The band near  $524\text{ cm}^{-1}$ , which is most sensitive to the presence of residual  $\text{Al}^{3+}$  in the octahedral sheets, decreases stepwise in intensity with increasing layer decomposition.

After 30 h of treatment, the small band near  $524\text{ cm}^{-1}$  in the spectrum of the 18 h treated sample, is changed to an inflection. This reflects a very high, but yet incomplete dissolution of montmorillonite in 6 M HCl ([Madejová et al., 1998](#)).

### 7.1.3. ACID DISSOLUTION OF SMECTITES

Treatment of clays with strong inorganic acids is frequently called “acid dissolution” or “acid activation” of clays. Depending on the extent of acid activation, the resulting solid product also contains unaltered layers and amorphous three-dimensional cross-linked silica, while the ambient acid solution contains ions according to the chemical composition of the smectite and acid used.

Early acid-dissolution studies of dioctahedral smectites in HCl by Osthaus (1954, 1956), based on solution analysis, indicated faster dissolution of octahedral than tetrahedral sheets. Assays of solid reaction products employing advanced spectroscopic techniques provided experimental evidence that acid treatments dissolve central atoms from the tetrahedral and octahedral sheets at similar rates (Luca and MacLachlan, 1992; Tkáč et al., 1994).

Luca and MacLachlan (1992) studied the dissolution in 10% HCl of two nontronites from Garfield and Hohen-Hagen, by Mössbauer spectroscopy. They fit the spectra either with two octahedral  $\text{Fe}^{3+}$  doublets or with two octahedral and one tetrahedral  $\text{Fe}^{3+}$  doublet. Isomer shift and quadrupole splitting values obtained from the two-doublet models correspond to octahedral  $\text{Fe}^{3+}$  and not to tetrahedral  $\text{Fe}^{3+}$  as Osthaus (1954) has suggested. When a tetrahedral  $\text{Fe}^{3+}$  doublet is included in the model used to fit the Mössbauer spectra of acid-treated Garfield nontronite samples, a slight increase in the intensity of that doublet occurs with increasing dissolution. This is much lower than Osthaus (1954) indicated. No trend in the intensity of the tetrahedral  $\text{Fe}^{3+}$  doublet is observed for acid-treated Hohen-Hagen nontronite samples. Therefore, acid treatment appears to remove octahedral and tetrahedral  $\text{Fe}^{3+}$  from the nontronite structure at about the same rate. Mössbauer and IR spectroscopies, and XRD indicate that the undissolved part of nontronite remaining after acid treatment is structurally similar to the untreated nontronite.  $^{27}\text{Al}$  and  $^{29}\text{Si}$  MAS NMR spectroscopic studies on removal of tetrahedral and octahedral  $\text{Al}^{3+}$  from montmorillonite by 6 M HCl, yield very similar conclusions (Tkáč et al., 1994). The rates of dissolution of tetrahedral and octahedral  $\text{Al}^{3+}$  are also comparable for montmorillonite. Three different types of structural units have been identified in acid-treated samples, including  $(\text{SiO})_3\text{SiOH}$  units, remaining as a result of poor-ordering of the framework without the possibility of cross-linking.

The extent of the dissolution reaction depends on both clay mineral type and reaction conditions, such as the acid/clay ratio, acid concentration, time and temperature of the reaction. The composition of the clay layers substantially affects their stability against acid attack; trioctahedral layers dissolve much faster than their dioctahedral counterparts (Vicente et al., 1994, 1995b; Breen et al., 1995a; Komadel et al., 1996b). Higher substitutions of  $\text{Mg}^{2+}$  and/or  $\text{Fe}^{3+}$  for  $\text{Al}^{3+}$  in dioctahedral smectites increase their dissolution rate in acids (Breen et al., 1995b). For 15 dioctahedral smectites, there is a good correlation of the  $\text{Mg}^{2+}$  and  $\text{Fe}^{3+}$  contents with the half time of dissolution in 6 M HCl at 96 °C (Novák and Čičel, 1978). Effects of smectite type, acid concentration and temperature on the half time of dissolution in 0.2 L HCl/g smectite acid/clay ratio in closed systems (no substances being added or removed) are summarized in Table 7.1.1.

The rate of dissolution of various atoms, obtained from chemical analysis of the liquid reaction products, indicates the presence of different phases in bentonite. Readily soluble octahedral and tetrahedral constituents, and “insoluble” portions of constituent atoms can be calculated from the dissolution curves. This provides information on the distribution of atoms in the sample (Čičel and Komadel, 1994).

Table 7.1.1. Effects of smectite type, acid concentration and temperature on half time of dissolution in 0.2L HCl/g smectite in closed systems

Smectite	HCl (M)	$T(^{\circ}\text{C})$	$t_{0.5}$ (h)
<i>Effect of smectite type</i>			
Nontronite	6.0	95	0.16
Mg-rich montmorillonite	6.0	95	6.2
Al-rich montmorillonite	6.0	95	8.0
<i>Effect of acid concentration</i>			
Hectorite	0.25	20	4.6
Hectorite	0.50	20	2.6
Hectorite	1.00	20	1.7
<i>Effect of temperature</i>			
$\text{Fe}^{3+}$ -beidellite	6.0	50	12.0
$\text{Fe}^{3+}$ -beidellite	6.0	60	6.0

Readily soluble portions include exchangeable cations and easily soluble admixtures such as goethite (Komadel et al., 1993) and calcite (Komadel et al., 1996b). The most common “insoluble” phases found in the fine fractions of bentonites include kaolinite, quartz, anatase and volcanic glass. Halloysite is the most decomposed mineral after treatment in sulphuric acid of different concentrations, followed by montmorillonite, pyrophyllite and kaolinite (Kato et al., 1966). Low octahedral substitution is one reason for the observed low dissolution rate of pyrophyllite compared with montmorillonite. The other reason is the presence of collapsed, non-swelling interlayers in pyrophyllite.

A series of reduced-charge montmorillonites is prepared via  $\text{Li}^+$  fixation at elevated temperatures (Hofmann–Klemen effect) to explore how the expandability of the interlayer spaces influences the extent of dissolution. As the negative layer charge of these samples decreases substantially, pyrophyllite-like features appear in both IR (Madejová et al., 1996) and  $^{29}\text{Si}$  MAS NMR (Gates et al., 2000) spectra. The increased content of non-swelling interlayer spaces is confirmed by both XRD and HRTEM images (Komadel et al., 1996a). The dissolution of reduced-charge montmorillonites in HCl indicates that pyrophyllite-like layers surrounded by non-swelling interlayer spaces dissolve much more slowly than montmorillonite layers of similar chemical composition located between swelling interlayer spaces (Figure 7.1.2). This clearly shows that protons attack the layers not only from the particle edges but also from the swollen interlayer spaces. Non-swelling illite and kaolinite are also more resistant to HCl attack than montmorillonite or vermiculite (Jozefaciuk and Bowanko, 2002).

IR spectroscopy in both middle and near regions was applied for the investigation of acid dissolution of reduced-charge montmorillonites. Reduction of the layer



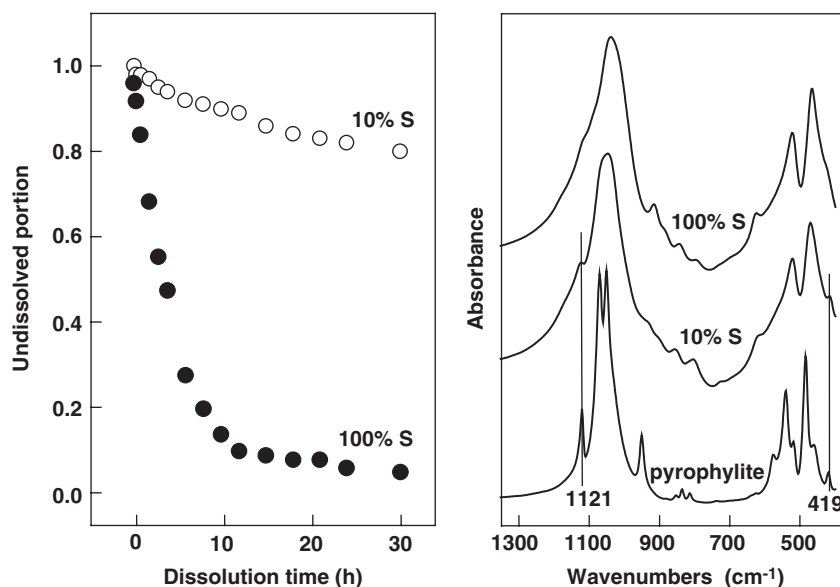


Fig. 7.1.2.  $\text{Ca}^{2+}$ -saturated 100% smectite and a reduced-charge smectite with about 10% swelling interlayers. Left: dissolution of  $\text{Al}^{3+}$  in 6 M HCl at 95 °C; Right: pyrophyllite-like features in the IR spectra. From Komadel et al. (1996a).

charge connected with development of non-swelling interlayer spaces substantially decreases the extent of the dissolution of SAz-1 montmorillonite in HCl. New bands at 3744 and 7314  $\text{cm}^{-1}$  are assigned to the vibrations of Si–OH groups formed by acid treatment. These bands are indicative of the extent of acid attack, even when no differences are observed in the 1300–400  $\text{cm}^{-1}$  spectral region, commonly used to follow this process. Both the IR spectra and solution analysis reveal that non-swelling interlayers develop on heating, causing a marked reduction in dissolution rate. The results obtained confirm that acid attack of the smectite structure occurs at both interlayer surfaces and edges. However, if the accessibility of the layers to protons is low, due to non-swelling interlayer spaces, the dissolution is reduced and takes place mainly from the particle edges (Pálková et al., 2003).

An in situ observation by AFM shows that the dissolution of hectorite and nontronite particles in acid solutions occurs inward from the edges; the basal surfaces appear to be unreactive during the timescale of the experiments. The hectorite (0 1 0) faces appear to dissolve about six times more slowly than the lath ends, usually involving “broken” bonds at the edge surfaces. The edges visibly dissolve on all sides, and appear to roughen somewhat. On the other hand, the (0 1 0), (1 1 0), and (1  $\bar{1}$  0) faces on nontronite particles are exceptionally stable. Thus, dissolution fronts originating at broken edges or defects would quickly become fixed along these faces, after which no more dissolution is observable. These observations can be explained

in terms of different oxygen sites connecting the octahedral and tetrahedral sheets. All the oxygens on the nontronite stable edge faces are saturated, whereas the connecting oxygens on all hectorite edge faces and nontronite broken edges are coordinatively unsaturated. This difference in reactivity of these particle faces suggests that the rate-limiting step of the dissolution process is breaking the bonds of connecting O atoms (Bickmore et al., 2001).

Mg-rich clay minerals, such as trioctahedral smectites (hectorites, saponites, etc.) are much less stable in inorganic acids than their Al-rich counterparts. Therefore, the activation of the former minerals requires low temperatures and acid concentrations. For example, a hectorite can be completely dissolved in 0.25 M HCl at 30 °C for 8 h whereas Wyoming montmorillonite requires 6 M acid at 95 °C for > 30 h (Madejová et al., 1998).

$\text{Li}^+$  dissolves slightly faster than  $\text{Mg}^{2+}$  from hectorite layers at low acid concentrations (Komadel et al., 1996b). Thus, protons are preferentially attracted to sites close to  $\text{Li}^+$  (in the octahedral sheet) that are more negative compared to sites adjacent to  $\text{Mg}^{2+}$ . This difference disappears at high acid concentrations when the reaction rates are high. Similarly, octahedrally coordinated  $\text{Mg}^{2+}$  are preferentially released by HCl in comparison with  $\text{Fe}^{3+}$  and  $\text{Al}^{3+}$  (Christidis et al., 1997; Gates et al., 2002). The effect of acid anion on dissolution of hectorite is complex and remains uncertain (Komadel et al., 1996b; Van Rompaey et al., 2002).

Two saponites and a ferrous saponite (griffithite) were treated by up to 2.5% HCl at 25 °C for periods up to 48 h. Most of the octahedral sheets of the minerals are dissolved. This is indicated by the high removal of  $\text{Mg}^{2+}$ , the changes in the IR spectra and the thermal gravimetric analysis-differential thermal analysis (TGA-DTA) curves of the activated saponites. Destruction of the saponite structure gives rise to free silica, and the specific surface area of the saponites is doubled even after mild acid activation (Vicente et al., 1996b; Suárez Barrios et al., 2001). The specific surface areas of griffithite samples increase greatly after activation, with values up to 10 times higher than the surface area of the untreated sample. The creation of microporosity has a substantial influence on surface area. Likewise, the free silica has a very important contribution to the surface area of leached samples (Vicente et al., 1995b). The high surface area (197 m<sup>2</sup>/g) of a natural saponite is related to the very small particle size because of its sedimentary origin. Treatment of the sedimentary saponites at room temperature by 0.62 wt% HCl for times up to 48 h or by 1.25 wt% HCl solutions for times up to 6 h gives rise to a partial dissolution of the saponite structures. A mixture of unaltered saponite and free silica is obtained. The latter treatment (1.25 wt% HCl for over 6 h) leads to an almost total dissolution of the clay mineral structure. The solid products consist mainly of some delaminated saponite layers, free silica and insoluble impurities. The surface area is 462 m<sup>2</sup>/g and the number of acid centres is 0.98 mmol H<sup>+</sup>/g (Prieto et al., 1999).

A new short-time synthesis route for preparation of mesoporous materials (Folded Sheet Materials, FSMs) have been developed from HCl-leached saponite samples. The acid treatment is performed under stirring for 24 h at 25 °C and 100 °C

Table 7.1.2. Effect of acid concentration on BET surface areas and pore volumes (PV) of mesoporous FSM materials prepared from saponite samples leached by HCl at 25 and 100 °C

<i>Acid leaching at 25 °C</i>					
HCl (mol.dm <sup>3</sup> )	6	7	8	9	10
S <sub>BET</sub> (m <sup>2</sup> /g)	643	726	900	785	478
PV (cm <sup>3</sup> /g)	0.44	0.54	0.61	0.54	0.37
<i>Acid leaching at 100 °C</i>					
HCl (mol.dm <sup>3</sup> )	3	4	5		
S <sub>BET</sub> (m <sup>2</sup> /g)	521	539	575		
PV (cm <sup>3</sup> /g)	0.50	0.45	0.98		

[Data from Linssen et al. (2002)]

in 6–10 and 3–7 M HCl aqueous solutions, respectively. The leached silicate powders are washed, suspended in hexadecyl trimethylammonium bromide solution as a structure-directing agent, with stirring at pH = 12.3 for 3 h at 70 °C and afterwards at pH = 8.5 for an additional 3 h at room temperature, and finally calcined at 550 °C to obtain the mesoporous materials. As could be expected, the intensity of the treatment increases with acid concentration and temperature. General improvement of the mesoporous FSM structure is obtained when a filtration step is added to the synthesis route after the dissolution at pH = 12.3, by removing all dissolved silicates and thus, preventing the formation of amorphous silica. The material synthesized after acid leaching by 8 M HCl at ambient temperature has the most condensed structure, the highest unit-cell dimensions, surface area and pore volume, and the narrowest pore-size distribution (Linssen et al., 2002). The properties of the FMS prepared from differently HCl-treated saponite samples are reported in Table 7.1.2. For most preparations obtained at 25 °C, the Brunauer Emmett and Teller (BET) specific surface areas are much higher and more sensitive to the acid concentrations than for the materials prepared at 100 °C. On the other hand, the material obtained after leaching with 5 M HCl at 100 °C has the highest pore volume.

#### 7.1.4. FINAL SOLID REACTION PRODUCT

For industrial uses, complete decomposition of the parent mineral is rarely wanted. The bleaching earths contain substantial amounts of parent smectite, exhibiting an increased surface area and porosity. The final reaction product of various acid-treated clay minerals is always the same. For several silicates, such as hectorite (Komadel et al., 1996b), saponite (Vicente et al., 1995b), dioctahedral smectites (Komadel et al., 1990; Tkáč et al., 1994; He et al., 2002), illite–smectite (Schmidt et al., 1990), sepiolite (Vicente et al., 1995a) and palygorskite (Suárez Barrios et al., 1995) this product consists of amorphous, porous, protonated and hydrated silica with a three-dimensional cross-linked structure (Komadel, 1999).

Only  $\text{SiO}_2$  remained after leaching of phlogopite powder in nitric acid. At high temperatures, the reaction rate is fast and the resulting specific surface area of the porous silica product increases at each activation temperature. The porous silica maintains its original platy particle shape. The  $^{29}\text{Si}$  MAS-NMR spectra of the products, however, reveal that the layered type structure of  $\text{SiO}_4$  tetrahedra in the original phlogopite is converted into a framework type. A porous silica product with micropores of  $\sim 0.7$  nm, mesopores of  $\sim 4$  nm, and a maximum specific surface area of  $532 \text{ m}^2/\text{g}$  is obtained. The pore size of the products, ranging from 0.7 to 4 nm, reaches 6 nm with increased leaching time (Okada et al., 2002).

### 7.1.5. OPTIMUM ACTIVATION CONDITIONS

Acid activation of bentonites with HCl results in a substantial increase of the surface area of the raw materials. As mentioned above, activation is generally characterized by destruction of the original smectite structure, removal of octahedral cations, uptake of  $\text{OH}^-$  and formation of an amorphous Si-rich phase. Mg-rich montmorillonites are more easily activated than other forms because Mg is the most readily removed element.

Optimum conditions for activation can be achieved by combining different acid strengths and reaction times. The activated materials are suitable for the bleaching of rapeseed oil through removal of  $\beta$ -carotene. The optimum bleaching capacity is not associated with maximum surface area (Christidis et al., 1997). The difference in the bleaching efficiency of cottonseed oil is related to differences in physical and chemical properties of the activated clay minerals. The oil acid value is not affected by the bleaching procedure but a slight shift in the absorption maximum of the bleached cottonseed oil is observed. A progressive decrease in CEC values is found when  $\text{Ca}^{2+}$ -montmorillonite is treated with sulphuric acid solutions. Elemental analysis shows that with moderate activation only 25–30% of the octahedral cations are removed. At the same time, the total surface area and the clay acidity increase. Moderate activation of the clay is most effective in bleaching cottonseed oil, resulting in the best colour index and the lowest peroxide value. A linear dependence of the bleaching efficiency on the clay surface area and acidity is observed (Falaras et al., 1999).

### 7.1.6. ACID-ACTIVATION AND PORE STRUCTURES

Acid activation of a  $\text{Ca}^{2+}$ -montmorillonite by treatment with sulphuric-acid solutions and subsequent pillaring (intercalation of oligomeric Al (hydr)oxides, 'Keggin ions', and calcination at temperatures to  $500^\circ\text{C}$ ) produce new materials for bleaching of cottonseed oil. These materials have bleaching properties dependent on the extent of activation of the clay mineral prior to pillaring. The pillared

acid-activated montmorillonites possess a higher bleaching efficiency compared with the pillared non-activated clay minerals usually called ‘pillared interlayered clays’ or ‘pillared interlayered clay’ (PILC) (see Chapter 7.5). Mild activation of the montmorillonite followed by pillaring produces materials with the best fractional degree of bleaching (Falaras, 2000b).

Detailed study of preparation and characterisation of Al PILC materials derived from an acid-treated montmorillonite shows that careful selection of the level of acid treatment is necessary to optimise the surface area, pore volume, surface acidity and thermal stability of the final pillared clay. The optimum level of acid treatment corresponds to the removal of between 19 and 35% of the octahedral cations. However, these values depend on the clay mineral. The pillared acid activated clay minerals have significantly higher pore volume and acidity than conventional PILC, but similar basal spacings, surface areas and thermal stability. Higher acidity is mainly due to an increase in intrinsic Brønsted acid sites arising from acid treatment before pillaring procedure. The higher acidity of the pillared acid activated clay mineral is reflected in better catalytic activity for the acid-catalysed reactions as compared with PILC (Mokaya and Jones, 1995).

Falaras et al. (2000a) have investigated the effect of acid activation of montmorillonite before pillaring and of calcination temperature on the efficiency of Al-pillared acid-activated clay-modified electrodes. The electrochemical behaviour of PILC has been compared with that of two pillared acid-activated montmorillonites. The pillared acid-activated montmorillonite-modified electrodes present better electro-activity than the modified electrodes of the conventional PILC for cationic and anionic redox active species. The same conditions as mentioned before (mild acid activation and calcination up to 500 °C) lead to modified materials that efficiently concentrate the cationic species. Lower calcination temperatures reverse the electrode activity. For anionic redox-active species the best electro-activity is observed for pillared acid-activated montmorillonite films corresponding to a medium acid activation. In that case, dependence of the electro-chemical response on the pH is confirmed. The mechanism responsible for the observed cationic electro-activity was investigated. The behaviour of the Al-pillared acid-activated montmorillonite-modified electrodes is attributed to the specific structure, the increase in surface area due to mesopores and the acidity of the clay films (Falaras et al., 2000a).

Porous clay heterostructures with enhanced acidity may be prepared from suitably acid-activated montmorillonites. The high acidity arises from Brønsted acid sites (Pichowicz and Mokaya, 2001). The ion-exchange properties of  $\text{Na}^+$ -montmorillonite and its derivative PILC were investigated in electrolyte solutions containing KCl. The pH curves of the two clay materials indicate anion and cation uptake as a function of the solution pH. In highly acidic medium, the surface area and micropore volume decrease significantly, and a considerable amount of  $\text{Al}^{3+}$  is leached from the pillars. The alumina pillars are attacked during this treatment, leading to partial destruction or dissolution of the pillars (Ahenach et al., 1998).

### 7.1.7. ACID ACTIVATION OF OTHER CLAY MINERALS

#### A. Kaolinite and Metakaolinite

Dissolution rates of natural kaolinites of different origin, and of halloysite and illitic clays in sulphuric and hydrochloric acids were determined by measuring the release rate of aluminium. The dissolution rate of kaolinite in 0.5 M sulphuric acid at 25 °C is approximately three times higher than in hydrochloric acid of equivalent proton concentration. The dissolution in 5 M sulphuric acid was eight times faster when the solid phase is periodically separated from the acid solution, washed by distilled water and dried. The aluminium release rate decreases as the amount of clay-size micas in kaolinitic clays increases. The rate is also significantly influenced by the crystallinity of the clay mineral (Hradil et al., 2002).

The three kaolin polytypes—kaolinite, dickite and nacrite—can be identified with great certainty by examining the hydroxyl-stretching region of the IR spectra of the samples before and after treatment with hydrofluoric acid (HF). SEM observations suggest that the rate of dissolution of kaolinite is largely dependent on particle size. In general, dickite and nacrite tend to occur in the coarser clay fractions, and for this reason the finer grained kaolinite is preferentially dissolved by the HF treatment. However, in the Keokuk kaolinite, which occurs in exceptionally large particles, it is still possible to concentrate a dickite fraction by HF treatment. This suggests that in some cases kaolinite may be more susceptible to HF dissolution for reasons other than particle size. Kaolinite and dickite components of disordered kaolinite dissolve at the same rate in HF, supporting the idea that disordered kaolinite consists of an intimate association of randomly stacked dickite-and kaolinite-like components (Fraser et al., 2002).

Proton adsorption or desorption may be computed from potentiometric titration data at pH 2–12 using surface complexation models. The surface behaviour is explained in terms of the formation of four active sites. The pH of zero proton charge is close to 5.5. The positive charge that develops below pH 5.5 is due to proton adsorption on aluminium sites of the octahedral sheet. The external hydroxyls of the octahedral sheet are the first to be protonated, whereas the second protonation may take place either at the inner hydroxyls or at the edge aluminol groups. Above pH 5.5, the kaolinite surface undergoes two successive deprotonations, the first occurs at pH about 5.5 and the second at pH about 9 (Huertas et al., 1998). The dissolution mechanism of kaolinite is mainly controlled by aluminol surface sites (external and internal structural hydroxyls, and aluminol at the particle edges) under both acidic and alkaline conditions (Huertas et al., 1999).

Devidal et al. (1997) described dissolution and crystallization rates of kaolinite at both acidic and alkaline pH, over the full range of chemical affinity and aqueous  $\text{Al}^{3+}$  and  $\text{Si}^{4+}$  concentrations. Kaolinite dissolution rates were obtained based on the release of  $\text{Al}^{3+}$  and  $\text{Si}^{4+}$  at steady state conditions. In general, dissolution rate increases with temperature and decreases with pH (Cama et al., 2002).

Kaolinite dissolution rates at pH 2–4 and temperatures of 25–70 °C were obtained using stirred and non-stirred flow-through reactors. The rates increase with increasing

stirring speed and the stirring effect is reversible. The effect of stirring speed on kaolinite dissolution rate is higher at 25 °C than at 50 and 70 °C and at pH 4 than at pH 2 and 3. Stirring induces spalling or abrasion of kaolinite giving rise to the formation of fine particles. As a result the ratio of reactive surface area to specific surface area increases, and the dissolution rate of kaolinite is enhanced. A balance between the production and dissolution of the fine particles explains the reversibility as well as the temperature and the pH dependence of the stirring effect (Metz and Ganor, 2001).

Wieland and Stumm (1992) investigated the acid/base properties of the terminal OH<sup>-</sup> groups and ion exchange reactions occurring at the kaolinite surface and interpret the dissolution of kaolinite in terms of the surface complexation model. A three-site model, incorporating solid-solution equilibria at aluminol groups of the edge and basal surfaces and at negatively charged groups of the siloxane surfaces, accounts for the protonation of kaolinite in acidic solutions. The dissolution kinetics of kaolinite at 25 °C was studied as a function of solution pH. The dissolution of kaolinite is non-stoichiometric in the pH range 2–6.5 with a preferential release of Si<sup>4+</sup>. Stoichiometry of the dissolution reaction is observed in the presence of oxalate as Al<sup>3+</sup>-complexing ligand. The detachment of Al<sup>3+</sup> from the layer structure of kaolinite surface and its readsorption on distinct surface sites occur simultaneously during the dissolution process. This accounts for the experimentally observed non-stoichiometry of the process. Although oxalate and salicylate form surface complexes only with Al<sup>3+</sup> sites, they promote the release of both Al<sup>3+</sup> and Si<sup>4+</sup> during dissolution. The detachment of Al<sup>3+</sup> is considered as the rate-limiting step. The proton-promoted dissolution of kaolinite occurs at the edge surface at pH < 6.5 and the basal surface at pH < 4. The pH-dependence of the dissolution rate reflects sequential protonation of terminal OH<sup>-</sup> groups on both surfaces.

Surface characteristics and dissolution behaviour of well-crystallized kaolinite KGa-1b and poorly crystallized kaolinite KGa-2 were compared. Particles of KGa-1b generally have hexagonal micro-morphology and crystallographically controlled micro-topographic features. Particles of KGa-2 are also hexagonal, but their micro-morphology is more rounded and their basal-plane surfaces are more irregular with fewer clearly crystallographically controlled features. KGa-1b particles are larger in diameter and thicker than those of KGa-2. Dissolution experiments were conducted in oxalic acid and inorganic acids at pH 3. Dissolution in oxalic acid is approximately twice as fast for KGa-2 as for KGa-1b, while it is similar in HNO<sub>3</sub>. The comparable dissolution rates for these two sedimentary kaolinites suggest that the fundamental structure of kaolinite has a larger influence on dissolution kinetics than specific surface details. For dissolution in 10<sup>-3</sup> M oxalate, Al<sup>3+</sup>-oxalates complexes are observed almost exclusively in agreement with the results of equilibrium speciation calculations. For dissolution in HNO<sub>3</sub>, uncomplexed Al<sup>3+</sup> species are identified (Sutheimer et al., 1999).

Pyridine adsorption data indicate that the strong acid sites on activated kaolinite are of the Lewis type (Tabak and Afsin, 2001). This also applies to the adsorption of NH<sub>3</sub>. Acid activation increases the protonated species on a kaolinite surface at the expense of coordinately bound NH<sub>3</sub>. The presence of NH<sub>4</sub><sup>+</sup> ions on an activated



sample is not a proof of the presence of protonic acid sites alone, since the added proton may come from the residual water in the interlayer space. Progressive dehydration of the surface results in a strong increase in chemisorbed  $\text{NH}_3$ .

A natural kaolinitic clay is metakaolinized at  $550^\circ\text{C}$  and activated separately with  $\text{H}_2\text{SO}_4$ ,  $\text{HNO}_3$  and  $\text{HClO}_4$  of varying concentrations (Sabu et al., 1999). Silica/alumina molar ratio, surface area and the number of strong acid sites increase when the concentration of acid used for activation increases. Metakaolinite activated with 4 M  $\text{HNO}_3$  has the highest surface area and surface acidity.

### *B. Sepiolite and Palygorskite*

After dissolution of sepiolite samples in  $\text{HCl}$ , the free silica produced has little influence on the properties of the mildly acid treated solids. However, the influence of this silica becomes very important when solids are obtained by more intense acid treatments (Vicente et al., 1995a). As the amount of  $\text{Fe}^{3+}$  and  $\text{Al}^{3+}$  extracted from sepiolite by acid treatment increases, the specific surface area of the mineral increases from 195 to  $306\text{ m}^2/\text{g}$  and the original microporous structure becomes mesoporous.

The CEC of sepiolite may be fully eliminated by acid treatment, during which the mineral structure is progressively transformed into amorphous silica-alumina (Dékány et al., 1999). The BET surface area of the original sepiolite increases from 148 to  $263\text{ m}^2/\text{g}$ , after which it decreases. Approximately 16% of the total volume is in the micropores. Acid activation restricts particle deformation during thermal treatment. The micropore volume increases by 20% and the BET surface area reaches values  $> 500\text{ m}^2/\text{g}$  for the acid-treated samples (Balci, 1999).

When sepiolite and palygorskite are activated by  $\text{HCl}$ , there is progressive dissolution of the octahedral layers. Silica contents increase and octahedral cations decrease with the intensity of the acid attack. In both cases, fibrous free silica is obtained. Sepiolite decomposes more rapidly than palygorskite because its octahedral sheet contains more  $\text{Mg}^{2+}$  and the structural microchannels are larger. The removal of the cations and disaggregation of the particles as well as the increase in the micropore volume cause an increase in specific surface area (Myriam et al., 1998). A substantial increase in the specific surface area is also observed for  $\text{HCl}$ -treated palygorskite. The free silica obtained has the fibrous morphology of natural palygorskite and no microporosity is detected (Suárez Barrios et al., 1995).

## 7.1.8. CATALYTIC PROPERTIES OF ACID ACTIVATED CLAY MINERALS

### *A. Smectites*

Acid-activated clays are well established as both solid acid catalysts and catalyst supports. Measurements of heats of adsorption of ammonia were carried out with a K10 catalyst in the acid and  $\text{Na}^+$ -forms. This is performed in a flow calorimeter



linked to a thermal conductivity detector. Ammonia is used as a probe because it interacts with acid sites. The irreversibly adsorbed ammonia is mobile on the catalyst. Molar heats of adsorption as surface coverage increases are recorded. The results show that the sites first covered do not necessarily correspond to those with the highest heats of adsorption. This illustrates that the flow technique provides important information on the relative accessibilities of acid sites as well as on their strengths (Brown and Groszek, 2000).

The nature of the exchangeable cations substantially affects the acidity of clay catalysts due to possible formation of strong acid sites resulting from their polarising power. The high catalytic activity of  $\text{Al}^{3+}$ -exchanged montmorillonites was attributed to the enhanced polarization of water molecules in the primary coordination sphere of the  $\text{Al}^{3+}$  cation, giving rise to strong Brønsted acidity (Varma, 2002; Jankovič and Komadel, 2003b).

$\text{H}^+$ -saturated montmorillonites of considerable catalytic activity can be prepared by means of thermal decomposition of ammonium clays (Jankovič and Komadel, 2000, 2003a); however, a more typical way is through acid activation with a mineral acid. Acid-activated clays are of interest in their role as high surface area supports for environmentally benign catalysts. Commercial products are normally treated with a fixed amount of acid, sufficient to remove the required number of octahedral cations to optimise the surface area and Brønsted acidity for a particular application. Consequently, systematic appraisals of how the extent of acid decomposition of the parent mineral contributes to the catalytic activity are not very frequent.

Several catalytic studies illustrate the application of commercial acid-activated montmorillonites, K-catalysts. Flessner et al., (2001) investigated the surface acidity of a series K-catalysts using a wide range of complementary experimental techniques. The different methods applied allow a rather complete characterization of the surface acidity. The strength and abundance (density) of Brønsted acid sites are correlated with the trend in iso-butene conversion.

The catalytic activity of acid-treated montmorillonite towards Brønsted acid catalysed reactions is highly dependent on the degree of acid treatment. Two contrasting model reactions have been used.

The first, involving highly polar reactants, is the acid-catalysed addition of 3,4-dihydropyran to methanol. The dihydropyran molecule is protonated to give a stabilized carbocation that reacts with methanol to form tetrahydropyranyl ether as the only product.

The second reaction, involving a non-polar, hydrophobic reactant is the acid-catalysed rearrangement of  $\alpha$ -pinene to camphene. The optimum treatment conditions for an acid-treated clay catalyst also depend upon the type of reaction being catalysed (Rhodes and Brown, 1994).

Acid treatment of  $\text{Ca}^{2+}$ -montmorillonite increases significantly its effectiveness as a support for  $\text{ZnCl}_2$  Friedel–Crafts alkylation catalysts; optimum treatment conditions are established and there is evidence for a synergistic interaction between adsorbed salt and acid-activated clay (Rhodes et al., 1991). Maximum activity is

associated with long acid treatment times. Structural characterization by XRD,  $^{29}\text{Si}$  MA-NMR spectroscopy, and elemental analysis suggest there is little residual clay mineral in the most active supports (Rhodes and Brown, 1992).

A series of progressively acid-treated montmorillonites and a range of porous silicas were tested for their effectiveness as supports for  $\text{ZnCl}_2$  alkylation catalysts. The highest catalytic activities are associated with significant pores of 10–12 nm in diameter (Rhodes and Brown, 1993). Supports exhibiting pore diameters below this range produce catalysts with very low activities. The fall in catalytic activity associated with larger pore diameter supports is less dramatic.

Different clay minerals with different contents of octahedral cations, such as magnesium- or aluminium-rich montmorillonites, a ferruginous smectite, an iron-rich beidellite and a hectorite, have been leached with  $\text{H}_2\text{SO}_4$  or  $\text{HCl}$ . The acid concentrations and treatment temperatures are selected to control the extent of activation. The elemental composition of the starting materials makes no significant contribution to the catalytic activity of 2,3-dihydropyran with methanol reaction to yield the tetrahydropyranyl ether. But the composition plays a key role in controlling the conditions required for the optimization of catalytic activity. The Brønsted acidity and catalytic activity of the resulting materials are highest for the samples prepared with the mild acid treatments but decreases as more octahedral cations are removed. The acid sites formed in the acid-treated montmorillonite are strong enough to produce tetrahydropyranyl ether in 80% yield. However, the acid-treated hectorite shows no catalytic activity. FTIR spectroscopy is as sensitive to structural acid attack as  $^{29}\text{Si}$  MAS NMR. The octahedral depletion correlates well with the acidity (determined from thermal desorption of cyclohexylamine) and the catalytic activity for the chosen test reaction (Breen et al., 1995a, 1995b 1997b; Komadel et al., 1997).

Catalytic activity of montmorillonite in dimerization of oleic acid increases upon mild activation in  $\text{HCl}$ . However, the activity of a catalyst with about 50% of octahedral  $\text{Al}^{3+}$  removed is comparable to that of the untreated clay mineral (Čičel et al., 1992).

Acid-activated smectites can convert the alkenes from the thermal decomposition of high-density polyethylene into light gases and aromatic species. Total conversion increases with both the extent of acid treatment and the temperature. The proportion of aromatic products is greatest for catalysts prepared using short acid-treatment times (Breen et al., 2000).

Acid-activated natural bentonite (and kaolin) can debutylate 2-tert-butylphenol and shows varying debutylation vs isomerization selectivity. The resulting catalytic activity of these samples is dependent on the type of acid used. Samples treated with acetic acid shows relatively low conversions, whereas those treated with hydrochloric or phosphoric acid are very active (Mahmoud and Saleh, 1999).

### *B. Metakaolinite*

The solid acid-activated metakaolinites are promising as adsorbents and catalyst supports (Belter et al., 2002). The ability of these products to transform the waste

gases from the conversion of waste plastics into aromatic hydrocarbons was evaluated. The amount of adsorbed water and the number of acid sites increase with the severity of acid treatment. Both Brønsted and Lewis acid sites are present until 425 °C. Pyridine bonded to the Lewis acid sites is more thermally stable than that associated with Brønsted sites. The materials are all selective to the production of toluene with respectable, but lesser, amounts of xylenes and trimethylbenzenes (Breen et al., 2002).

All the activated metakaolinites are active catalysts for the alkylation of benzene with benzyl chloride at reflux, giving above 75% conversion of the alkylating agent. Metakaolinite activated with 4 M HNO<sub>3</sub> gives 87% conversion of benzyl chloride into diphenylmethane with 100% selectivity within 30 min of reaction time. This may be correlated with the greater surface acidity of this sample. Extremely efficient solid catalysts of remarkable acidic properties can be produced by the activation of metakaolinite with H<sub>2</sub>SO<sub>4</sub>, HNO<sub>3</sub> and HClO<sub>4</sub> (Sabu et al., 1999). Metakaolinites were also prepared by calcination of natural kaolinites at 600–900 °C and are more reactive than the parent kaolinite after acid activation, with 6 M HCl at 90 °C under reflux conditions. Treatment for 6 h leads to the removal of most of the octahedral Al<sup>3+</sup> cations and the formation of an amorphous silica phase with high specific surface area. Acid treatment for 24 h also removes the octahedral cations, but leads to the formation of amorphous silica with much lower specific surface area. The metakaolinite prepared by calcination at 900 °C shows a lower reactivity than the materials obtained at lower temperatures (Belver et al., 2002).

### C. Modified Clay Minerals

The hydrophilic aluminosilicate surface of smectites can be rendered hydrophobic by exchanging the naturally occurring inorganic cations with organic cations. Acid activation of tetralkylammonium-exchanged smectites produces hybrid catalysts for the isomerisation of alpha-pinene to camphene. This catalytic activity is attributed to the enhanced hydrophobicity of the organo-clay. Acid-activated tetramethylammonium-exchanged smectites are the most active and give 60–90% conversion based on alpha-pinene. The yields are comparable with those obtained with other solid catalysts such as zeolites and PILC. The iron-substituted smectites are more active than the aluminium counterparts. The dodecyl trimethylammonium- and octadecyl trimethylammonium- exchanged smectites are generally less active (Breen et al., 1997a).

SWy-2 and SAz-1 montmorillonites loaded with increasing amounts of the polycation magnafloc 206 were acid-treated with 6 M HCl at 95 °C. The acid-treated polycation-exchanged smectites are active catalysts for the isomerisation of alpha-pinene to camphene and limonene. The conversion by the polycation-exchanged SAz-1 samples is greater than by the unloaded activated counterpart, because the former material is more hydrophobic. In the case of SWy-2 the yields in the absence and presence of polycation are similar suggesting good dispersion of both samples in

the non-polar alpha-pinene. The yields, based on alpha-pinene, for the most active catalysts are between 80 and 90%. These yields are directly comparable with those obtained by others using zeolites and PILC although the acid-activated polycation-treated clays are marginally less selective towards camphene (Breen and Watson, 1998).

Two montmorillonites STx-1 and SWy-2 were activated with different amounts of 12 M HCl and then exchanged with a fixed amount of 1 M tetramethylammonium ( $\text{TMA}^+$ ) chloride solution at room temperature, giving rise to  $\text{H}^+/\text{TMA}^+$  samples. In addition,  $\text{TMA}^+/\text{H}^+$  samples were obtained by acid-activation of  $\text{TMA}^+$ -exchanged samples. The BET surface area of these samples is determined by  $\text{N}_2$  adsorption, the acidity by adsorption of cyclohexylamine and the catalytic activity by the isomerization of 1-butene at 300 °C (to yield *cis*- and *trans*-2-butene). The total conversion for the isomerization of 1-butene is higher for the  $\text{TMA}^+/\text{H}^+$ -samples than for the  $\text{H}^+/\text{TMA}^+$ -samples.  $\text{TMA}^+$  cations adsorbed on the clays are extremely resistant to exchange by protons, but protons are easily displaced by  $\text{TMA}^+$  cations (Moronta et al., 2002).

The preparation and characterization of Ti-pillared acid-activated clays and conventional Ti-pillared clays were described by Bovey et al. (1996). These materials have good catalytic properties for the dehydration of pentanol compared with PILC.

## 7.1.9. CONCLUSION

Acid activation of clays and clay minerals was used for decades both in laboratories for basic and applied research and in industrial production for many applications. Even so, it still remains one of the most common chemical modifications of clays for the future of clay science and applications.

## REFERENCES

- Adams, J.M., 1987. Synthetic organic chemistry using pillared, cation-exchanged and acid-treated montmorillonite catalysts—a review. *Applied Clay Science* 2, 309–342.
- Ahenach, J., Cool, P., Vansant, E.F., 1998. Acid/base treatment of Al-PILC in KCl solution. *Microporous and Mesoporous Materials* 25, 185–192.
- Balci, S., 1999. Effect of heating and acid pre-treatment on pore size distribution of sepiolite. *Clay Minerals* 34, 647–655.
- Barshad, I., Foscolos, A.E., 1970. Factors affecting the rate of interchange reaction of adsorbed  $\text{H}^+$  on the 2:1 clay minerals. *Soil Science* 110, 52–60.
- Belver, C., Bñares Muñ, M.A., Vicente, M.A., 2002. Chemical activation of a kaolinite under acid and alkaline conditions. *Chemistry of Materials* 14, 501–506.
- Bickmore, B.R., Bosbach, D., Hochella, M.F., Charlet, L., Rufe, E., 2001. In situ atomic force microscopy study of hectorite and nontronite dissolution: implications for phyllosilicate edge surface structures and dissolution mechanisms. *American Mineralogist* 86, 411–423.

- Bovey, J., Jones, W., 1995. Characterisation of Al-pillared acid-activated clay catalysts. *Journal of Materials Chemistry* 5, 2027–2035.
- Bovey, J., Kooli, F., Jones, W., 1996. Preparation and characterization of Ti-pillared acid-activated clay catalyst. *Clay Minerals* 31, 501–506.
- Breen, C., Last, P.M., Taylor, S., Komadel, P., 2000. Synergic chemical analysis—the coupling of TG with FTIR, MS and GC-MS 2. Catalytic transformation of the gases evolved during the thermal decomposition of HDPE using acid-activated clays. *Thermochimica Acta* 363, 93–104.
- Breen, C., Madejová, J., Komadel, P., 1995a. Correlation of catalytic activity with infrared-red,  $^{29}\text{Si}$  MAS NMR and acidity data for HCl-treated fine fractions of montmorillonites. *Applied Clay Science* 10, 219–230.
- Breen, C., Madejová, J., Komadel, P., 1995b. Characterisation of moderately acid-treated, size-fractionated montmorillonites using IR and MAS NMR spectroscopy and thermal analysis. *Journal of Materials Chemistry* 5, 469–474.
- Breen, C., Taylor, S., Burguin, E., Centeno, M., 2002. Preparation and characterization of dealuminated metakaolin and its use in the transformation of waste plastics to aromatic hydrocarbons. *Journal of Colloid and Interface Science* 247, 246–250.
- Breen, C., Watson, R., 1998. Acid-activated organoclays: preparation, characterisation and catalytic activity of polycation-treated bentonites. *Applied Clay Science* 12, 479–494.
- Breen, C., Watson, R., Madejová, J., Komadel, P., Klapýta, Z., 1997a. Acid-activated organoclays: Preparation, characterisation and catalytic activity of acid-treated tetra-alkyl-ammonium exchanged smectites. *Langmuir* 13, 6473–6479.
- Breen, C., Zahoor, F.D., Madejová, J., Komadel, P., 1997b. Characterisation and catalytic activity of acid treated, size fractionated smectites. *Journal of Physical Chemistry B* 101, 5324–5331.
- Brown, D.R., 1994. Review: clays as catalyst and reagent support. *Geologica Carpathica. Series Clays* 45, 45–56.
- Brown, D.R., Groszek, A.J., 2000. Heats of adsorption of ammonia on a zeolite catalyst and an acid-activated clay catalyst determined by flow adsorption microcalorimetry. *Langmuir* 16, 4207–4212.
- Cama, J., Metz, V., Ganor, J., 2002. The effect of pH and temperature on kaolinite dissolution rate under acidic conditions. *Geochimica et Cosmochimica Acta* 66, 3913–3926.
- Christidis, G.E., Scott, P.W., Dunham, A.C., 1997. Acid activation and bleaching capacity of bentonites from the islands of Milos and Chios, Aegean, Greece. *Applied Clay Science* 12, 329–347.
- Čičel, B., Komadel, P., 1994. Structural formulae of layer silicates. In: Amonette, J.E., Zelazny, L.W. (Eds.), *Quantitative Methods in Soil Mineralogy*. Soil Science Society of America Soil Science Society of America. Miscellaneous Publication, Madison, WI, pp. 114–136.
- Čičel, B., Komadel, P., Nigrin, M., 1992. Catalytic activity of smectites on dimerization of oleic acid. *Collection of Czechoslovak Chemical Communications* 57, 1666–1671.
- Dékány, I., Turi, L., Fonseca, A., Nagy, J.B., 1999. The structure of acid treated sepiolites: small-angle X-ray scattering and multi MAS-NMR investigations. *Applied Clay Science* 14, 141–160.
- Devidal, J.L., Schott, J., Dandurand, J.L., 1997. An experimental study of kaolinite dissolution and precipitation kinetics as a function of chemical affinity and solution composition at 150 °C, 40 bars, and pH 2, 6.8, and 7.8. *Geochimica et Cosmochimica Acta* 61, 5165–5186.

- Dubíková, M., Cambier, P., Šucha, V., Čaplovičová, M., 2002. Experimental soil acidification. *Applied Geochemistry* 17, 245–257.
- Fahn, R., Fenderl, K., 1983. Reaction products of organic dye molecules with acid-treated montmorillonite. *Clay Minerals* 18, 447–458.
- Falaras, P., Kovanis, I., Lezou, F., Seiragakis, G., 1999. Cottonseed oil bleaching by acid-activated montmorillonite. *Clays and Clay Minerals* 34, 221–232.
- Falaras, P., Lezou, F., Pomonis, P., Ladavos, A., 2000a. Al-pillared acid-activated montmorillonite modified electrodes. *Journal of Electroanalytical Chemistry* 486, 156–165.
- Falaras, P., Lezou, F., Seiragakis, G., Petrakis, D., 2000b. Bleaching properties of alumina-pillared acid-activated montmorillonite. *Clays and Clay Minerals* 48, 549–556.
- Farmer, V.C., 1974. The layer silicates. In: Farmer, V.C. (Ed.), *The Infrared Spectra of Minerals*. The Mineralogical Society, London, pp. 331–363.
- Flessner, U., Jones, D.J., Roziere, J., Zajac, J., Storaro, L., Lenarda, M., Pavan, M., Jimenez-Lopez, A., Rodriguez-Castellon, E., Trombetta, M., Busca, G., 2001. A study of the surface acidity of acid-treated montmorillonite clay catalysts. *Journal of Molecular Catalysis A: Chemical* 168, 247–256.
- Fraser, A.R., Wilson, M.J., Roe, M.J., Shen, Z.Y., 2002. Use of hydrofluoric acid dissolution for the concentration of dickite and nacrite from kaolin deposits: an FTIR study. *Clay Minerals* 37, 559–570.
- Galán, E., Carretero, M.I., Fernandez-Caliani, J.C., 1999. Effects of acid mine drainage on clay minerals suspended in the Tinto River (Rio Tinto, Spain). An experimental approach. *Clay Minerals* 34, 99–108.
- Gates, W.P., Anderson, J.S., Raven, M.D., Churchman, G.J., 2002. Mineralogy of a bentonite from Miles, Queensland, Australia and characterisation of its acid activation products. *Applied Clay Science* 20, 189–197.
- Gates, W.P., Komadel, P., Madejová, J., Bujdák, J., Stucki, J.W., Kirkpatrick, R.J., 2000. Electronic and structural properties of reduced-charge montmorillonites. *Applied Clay Science* 16, 257–271.
- He, H.P., Guo, J.G., Xie, X.D., Lin, H.F., Li, L.Y., 2002. A microstructural study of acid-activated montmorillonite from Choushan, China. *Clay Minerals* 37, 337–344.
- Hradil, D., Hostomský, J., Soukupová, J., 2002. Aluminium release rates from acidified clay structures: comparative kinetic study. *Geologica Carpathica* 53, 117–121.
- Huertas, F.J., Chou, L., Wollast, R., 1998. Mechanism of kaolinite dissolution at room temperature and pressure: Part I: Surface speciation. *Geochimica et Cosmochimica Acta* 62, 417–431.
- Huertas, F.J., Chou, L., Wollast, R., 1999. Mechanism of kaolinite dissolution at room temperature and pressure: Part II: Kinetic study. *Geochimica et Cosmochimica Acta* 63, 3261–3275.
- Janek, M., Komadel, P., 1993. Autotransformation of H-smectites in aqueous solution. Effect of octahedral iron content. *Geologica Carpathica. Series Clays* 44, 59–64.
- Janek, M., Komadel, P., 1999. Acidity of proton saturated and autotransformed smectites characterised with proton affinity distribution. *Geologica Carpathica* 50, 373–378.
- Janek, M., Komadel, P., Lagaly, G., 1997. Effect of autotransformation on the layer charge of smectites determined by the alkylammonium method. *Clay Minerals* 32, 623–632.
- Janek, M., Lagaly, G., 2001. Proton saturation and rheological properties of smectite dispersions. *Applied Clay Science* 19, 121–130.

- Jankovič, Ľ., Komadel, P., 2000. Catalytic properties of a heated ammonium-saturated dioctahedral smectite. *Collection of Czechoslovak Chemical Communications* 65, 1527–1536.
- Jankovič, Ľ., Komadel, P., 2003a. Microwave assisted synthesis of substituted indoles using montmorillonite as catalyst. *Solid State Phenomena* 90–91, 481–486.
- Jankovič, Ľ., Komadel, P., 2003b. Metal cation-exchanged montmorillonite catalysed protection of aromatic aldehydes with  $\text{Ac}_2\text{O}$ . *Journal of Catalysis* 218, 227–233.
- Jozefaciuk, G., 2002. Effect of acid and alkali treatments on surface-charge properties of selected minerals. *Clays and Clay Minerals* 50, 647–656.
- Jozefaciuk, G., Bowanko, G., 2002. Effect of acid and alkali treatments on surface areas and adsorption energies of selected minerals. *Clays and Clay Minerals* 50, 771–783.
- Kato, C., Suzuki, T., Fujiwara, T., 1966. Decomposition and structural change of clay minerals by acid. *Memories of the School of Science & Engineering, Waseda University*, 13–24.
- Kendall, T., 1996. Smectite clays. In: Kendall, T. (Ed.), *Industrial Clays*. Industrial Minerals Information Ltd, London, pp. 1–12.
- Komadel, P., 1999. Structure and chemical characteristics of modified clays. In: Micalides, P., Macásek, F., Pinnavaia, T.J., Colella, C. (Eds.), *Natural Microporous Materials in Environmental Technology*. Kluwer, The Netherlands, pp. 3–18.
- Komadel, P., 2003. Chemically modified smectites. *Clay Minerals* 38, 127–138.
- Komadel, P., Bujdák, J., Madejová, J., Šucha, V., Elsass, F., 1996a. Effect of non-swelling layers on the dissolution of reduced-charge montmorillonite in hydrochloric acid. *Clay Minerals* 31, 333–345.
- Komadel, P., Janek, M., Madejová, J., Weekes, A., Breen, C., 1997. Acidity and catalytic activity of mildly acid-treated Mg-rich montmorillonite and hectorite. *Journal of the Chemical Society, Faraday Transactions* 93, 4207–4210.
- Komadel, P., Madejová, J., Janek, M., Gates, W.P., Kirkpatrick, R.J., Stucki, J.W., 1996b. Dissolution of hectorite in inorganic acids. *Clays and Clay Minerals* 44, 228–236.
- Komadel, P., Schmidt, D., Madejová, J., Čičel, B., 1990. Alteration of smectites by treatments with hydrochloric acid and sodium carbonate solutions. *Applied Clay Science* 5, 113–122.
- Komadel, P., Stucki, J.W., Čičel, B., 1993. Readily HCl-soluble iron in the fine fractions of some Czech bentonites. *Geologica Carpathica. Series Clays* 44, 11–16.
- Lagaly, G., 1994. Layer charge determination by alkylammonium ions. *Layer Charge Characteristics of 2:1 Silicate Clay Minerals*. In: Mermut, A.R. (Ed.), *Clay Minerals Society Workshop Lectures 6*. Boulder, CO, USA, pp. 1–46.
- Lambert, J.-F., Poncelet, G., 1997. Acidity in pillared clays: origin and catalytic manifestations. *Topics in Catalysis* 4, 43–56.
- Linssen, T., Cool, P., Baroudi, M., Cassiers, K., Vansant, E.F., Lebedev, O., Van Landuyt, J., 2002. Leached natural saponite as the silicate source in the synthesis of aluminosilicate hexagonal mesoporous materials. *Journal of Physical Chemistry B* 106, 4470–4476.
- Luca, V., MacLachlan, D.J., 1992. Site occupancy in nontronite studied by acid dissolution and Mössbauer spectroscopy. *Clays and Clay Minerals* 40, 1–7.
- Madejová, J., Bujdák, J., Gates, W.P., Komadel, P., 1996. Preparation and infrared spectroscopic characterization of reduced-charge montmorillonite with various Li contents. *Clay Minerals* 31, 233–241.

- Madejová, J., Bujdák, J., Janek, M., Komadel, P., 1998. Comparative FT-IR study of the structural modifications during acid treatment of dioctahedral smectites and hectorite. *Spectrochimica Acta A* 54, 1397–1406.
- Madejová, J., Komadel, P., 2001. Baseline studies of the Clay Minerals Society Source Clays: Infrared methods. *Clays and Clay Minerals* 49, 410–432.
- Madejová, J., Komadel, P., Čičel, B., 1992. Infrared spectra of some Czech and Slovak smectites and their correlation with structural formulas. *Geologica Carpathica. Series Clays* 43, 9–12.
- Madejová, J., Kraus, I., Komadel, P., 1995. Fourier transform infrared spectroscopic characterization of dioctahedral smectites and illites from the main Slovak deposits. *Geologica Carpathica. Series Clays* 46, 23–32.
- Mahmoud, S., Saleh, S., 1999. Effect of acid activation on the de-tert-butylation activity of some Jordanian clays. *Clays and Clay Minerals* 47, 481–486.
- Metz, V., Ganor, J., 2001. Stirring effect on kaolinite dissolution rate. *Geochimica et Cosmochimica Acta* 65, 3475–3490.
- Mokaya, R., Jones, W., 1994. Pillared acid-activated clay catalysts. *Journal of the Chemical Society, Chemical Communications* 929–930.
- Mokaya, R., Jones, W., 1995. Pillared clays and pillared acid-activated clay: a comparative study of physical, acidic and catalytic properties. *Journal of Catalysis* 153, 76–85.
- Mokaya, R., Jones, W., Davies, W., Whittle, M.E., 1993. Preparation of alumina-pillared acid-activated clays and their use as chlorophyll adsorbents. *Journal of Materials Chemistry* 3, 381–387.
- Moronta, A., Ferrer, V., Quero, J., Arteaga, G., Choren, E., 2002. Influence of preparation method on the catalytic properties of acid-activated tetramethylammonium-exchanged clays. *Applied Catalysis A—General* 230, 127–135.
- Myriam, M., Suarez, M., Martin-Pozas, J.M., 1998. Structural and textural modifications of palygorskite and sepiolite under acid treatment. *Clays and Clay Minerals* 46, 225–231.
- Novák, I., Čičel, B., 1978. Dissolution of smectites in hydrochloric acid: II. Dissolution rate as a function of crystallochemical composition. *Clays and Clay Minerals* 26, 341–344.
- Okada, K., Nakazawa, N., Kameshima, Y., Yasumori, A., Temuujin, J., MacKenzie, K.J.D., Smith, M.E., 2002. Preparation and porous properties of materials prepared by selective leaching of phlogopite. *Clays and Clay Minerals* 50, 624–632.
- Osthaus, B.B., 1954. Chemical determination of tetrahedral ions in nontronite and montmorillonite. *Clays and Clay Minerals* 2, 404–417.
- Osthaus, B.B., 1956. Kinetic studies on montmorillonite and nontronite by the acid dissolution technique. *Clays and Clay Minerals* 4, 301–321.
- Pagano, T., Sergio, M., Glisenti, L., Diano, W., Grompone, M.A., 2001. Use of pillared montmorillonites to eliminate chlorophyll from rice bran oil. *Ingenieria Quimica*, 11–19.
- Pálková, H., Madejová, J., Righi, D., 2003. Acid dissolution of reduced-charge Li- and Ni-montmorillonites. *Clays and Clay Minerals* 51, 133–142.
- Pichowicz, M., Mokaya, R. 2001. Porous clay heterostructures with enhanced acidity obtained from acid-activated clays. *Journal of the Chemical Society, Chemical Communications* 2100–2101.
- Prieto, O., Vicente, M.A., Bañares-Muñoz, M.A., 1999. Study of the porous solids obtained by acid treatment of a high surface area saponite. *Journal of Porous Materials* 6, 335–344.



- Rhodes, C.N., Brown, D.R., 1992. Structural characterization and optimization of acid-treated montmorillonite and high-porosity silica supports for  $\text{ZnCl}_2$  alkylation catalysts. *Journal of the Chemical Society, Faraday Transactions* 88, 2269–2274.
- Rhodes, C.N., Brown, D.R., 1993. Surface properties and porosities of silica and acid-treated montmorillonite catalyst support—influence on activities of supported  $\text{ZnCl}_2$  alkylation catalysts. *Journal of the Chemical Society, Faraday Transactions* 89, 1387–1391.
- Rhodes, C.N., Brown, D.R., 1994. Catalytic activity of acid-treated montmorillonite in polar and nonpolar reaction media. *Catalysis Letters* 24, 285–291.
- Rhodes, C.N., Franks, M., Parkes, G.M.B., Brown, D.R., 1991. The effect of acid treatment on the activity of clay supports for  $\text{ZnCl}_2$  alkylation catalysts. *Journal of the Chemical Society, Chemical Communications* 804–807.
- Russell, J.D., Fraser, A.R., 1994. Infrared methods. In: Wilson, M.J. (Ed.), *Clay Mineralogy: Spectroscopic and Chemical Determinative Methods*. Chapman & Hall, London, pp. 11–67.
- Sabu, K.R., Sukumar, R., Rekha, R., Lalithambika, M., 1999. A comparative study on  $\text{H}_2\text{SO}_4$ ,  $\text{HNO}_3$  and  $\text{HClO}_4$  treated metakaolinite of a natural kaolinite as Friedel–Crafts alkylation catalyst. *Catalysis Today* 49, 321–326.
- Schmidt, D., Komadel, P., Madejová, J., Čičel, B., 1990. Veränderungen im Illit-Smektit-Ton von Friedland (DDR) bei Behandlung mit  $\text{HCl}$ - und  $\text{Na}_2\text{CO}_3$ -Lösungen. *Silikattechnik* 41, 347–349.
- Siddiqui, M.H.K., 1968. *Bleaching Earths*. Pergamon Press, London, 86pp.
- Suárez Barrios, M., Flores González, L.V., Vicente, M.A., Martín Pozas, J.M., 1995. Acid activation of palygorskite with  $\text{HCl}$ : Development of physico-chemical textural and surface properties. *Applied Clay Science* 10, 247–258.
- Suárez Barrios, M., Buey, C.S., Garcia Romero, E., Martín Pozas, J.M., 2001. Textural and structural modifications of saponite from Cerro del Aguila by acid treatment. *Clay Minerals* 36, 483–488.
- Sutheimer, S.H., Maurice, P.A., Zhou, Q.H., 1999. Dissolution of well and poorly crystallized kaolinites: Al speciation and effects of surface characteristics. *American Mineralogist* 84, 620–628.
- Tabak, A., Afsin, B., 2001. Firmly adsorbed ammonia and pyridine species at activated kaolinite surfaces. *Adsorption Science and Technology* 19, 673–679.
- Tkáč, I., Komadel, P., Müller, D., 1994. Acid-treated montmorillonites—a study by  $^{29}\text{Si}$  and  $^{27}\text{Al}$  MAS-NMR. *Clay Minerals* 29, 11–19.
- Van Rompaey, K., Van Ranst, E., De Coninck, F., Vindevogel, N., 2002. Dissolution characteristics of hectorite in inorganic acids. *Applied Clay Science* 21, 241–256.
- Varma, R.S., 2002. Clay and clay-supported reagents in organic synthesis. *Tetrahedron* 58, 1235–1255.
- Vicente, M.A., Lopez-González, J.D., Bañares-Muñoz, M.A., 1995a. Influence of the free silica generated during acid activation of a sepiolite on adsorbent and textural properties of the resulting solids. *Journal of Materials Chemistry* 5, 127–132.
- Vicente, M.A., López González, J.D., Bañares Muñoz, M.A., 1995b. Preparation of microporous solids by acid treatment of a saponite. *Microporous Materials* 4, 251–264.
- Vicente, M.A., Suárez, M., Bañares Muñoz, M.A., López González, J.D., 1996a. Comparative FT-IR study of the removal of octahedral cations and structural modifications during acid treatment of several silicates. *Spectrochimica Acta A* 52, 1685–1694.

- Vicente, M.A., Suárez Barrios, M., López González, J.D., Bañares Muñoz, M.A., 1996b. Characterization, surface area, and porosity analyses of the solids obtained by acid leaching of a saponite. *Langmuir* 12, 566–572.
- Vicente, M.A., Suárez Barrios, M., López-González, J.D., Bañares-Muñoz, M.A., 1994. Acid activation of a ferrous saponite (griffithite): Physicochemical characterization and surface area of the products obtained. *Clays and Clay Minerals* 42, 724–730.
- Wieland, E., Stumm, W., 1992. Dissolution kinetics of kaolinite in acidic aqueous solutions at 25 °C. *Geochimica et Cosmochimica Acta* 56, 3339–3355.
- Zysset, M., Schindler, W., 1996. The proton promoted dissolution kinetics of K-montmorillonite. *Geochimica et Cosmochimica Acta* 60, 921–931.

This page intentionally left blank

*Chapter 7.2*

## **THERMALLY MODIFIED CLAY MINERALS**

### **L. HELLER-KALLAI**

*Institute of Earth Sciences, The Hebrew University of Jerusalem, IL-91904 Jerusalem, Israel*

The structure and composition of clay minerals are modified by heating. The concomitant changes in properties can be exploited for practical purposes. The actual temperatures at which changes occur vary greatly from one clay mineral group to another, and even for different specimens within a given group. These temperatures also depend on the particle size and on the heating regime. Four principal temperature ranges in which significant changes occur in the structures of clay minerals may be distinguished.

- (1) Temperatures sufficiently low to cause partial freezing of clay suspensions or pastes ( $-5^{\circ}\text{C}$ ): in this temperature range some of the water is converted into ice. However, even at a temperature as low as  $-60^{\circ}\text{C}$  a significant amount of water remains in a liquid or semi-liquid state, forming a film that separates the mineral surface from the ice.
- (2) Temperatures above dehydration but below dehydroxylation: when the temperature is raised from ambient to that of the onset of dehydroxylation, clays lose adsorbed and hydration water. As a result, the interlayer spaces collapse, while pore space is changed, and the acidity of the clay mineral surfaces and interlayers is substantially altered.
- (3) Temperatures above dehydroxylation, but below those leading to complete destruction of the structure: the changes occurring in this temperature range vary for different clay mineral groups. Dehydroxylation destroys the layer structure of trioctahedral, 2:1 type (T-O-T) minerals, whereas that of their dioctahedral counterparts is preserved. Kaolinite group minerals become amorphous to X-rays although some features of the structural framework are preserved.
- (4) Temperatures at which new phases crystallise: dehydroxylated clays that do not turn amorphous to X-rays may become so on further heating, before high-temperature phases crystallise. With trioctahedral clay minerals and palygorskite the interval between stages (3) and (4) is very short. Thus, intermediate phases, if formed, may escape detection. When new phases crystallise, clay minerals lose

their original identity although the crystallographic orientation of the products is frequently related to that of the starting material.

Clay minerals can be heated in different forms: (i) without any admixtures or pretreatment; (ii) mixed with various reagents before heating; (iii) after pretreatment such as acid-activation; and (iv) after preheating and pretreatment, for example, by acid-activation, and subsequent reheating.

In view of the great variety of starting materials and the many variables involved in the heating regime, a range of options is available for the thermal modification of clays. The ubiquitous impurities in natural clays may also play a part. The pre-activation temperatures required to develop desirable properties, or prevent undesirable properties from developing, vary with different clay minerals. Some minerals are preferably used in the dehydrated, others in the dehydroxylated form. The following discussion is concerned with some properties of clay minerals that are changed or modified by thermal treatment.

### 7.2.1. FREEZING OF CLAY MINERALS

Freezing affects pore water and water adsorbed on clay mineral surfaces, in the interlayer spaces, and in channels. Not all the water is converted into ice. Some remains in a mobile semi-liquid or liquid state, coating the surfaces (Anderson and Tice, 1971).

#### *A. Effect of Freeze-Drying on the Texture of Clay Minerals*

On freeze-drying, water is expelled from the frozen mineral (under vacuum) by evaporation of liquid water and sublimation of ice. This affects the texture of the clay mineral. Freeze-drying tends to promote edge-to-face association resulting in the formation of aggregates with more macropores than in air-dried samples (Lagaly, 1987) (Fig. 7.2.1). Freeze-drying may either increase or decrease the BET surface area, depending on the original clay mineral (de Carvalho et al., 1996).

#### *B. Changes in Acidity*

The effect of freezing on the acidity of smectite interlayers is similar to that of drying. As some of the hydration water is removed the interlayer spaces become more acidic (see Section 7.2.2.C). The proportion of water that is frozen depends upon the temperature. Changes in acidity in the interlayer spaces are clearly demonstrated by the colour of a benzidine–montmorillonite assemblage, which depends upon the  $H^+$ -ion concentration. On cooling from  $-5$  to  $-15^\circ C$  and below, the colour changes from the original blue of the monovalent semiquinone to green or bluish-green. The green colour is produced by a mixture of the blue monomer and the yellow dimer that is formed at low pH (Lahav and Anderson, 1973).

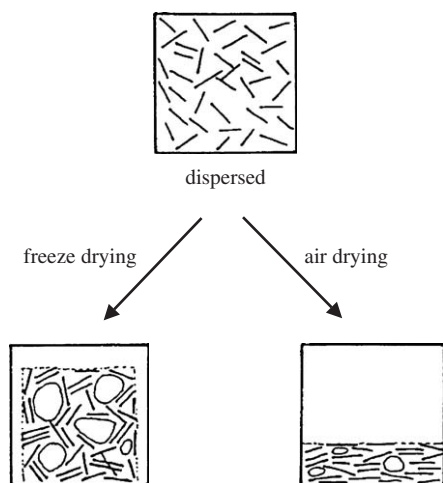


Fig. 7.2.1. Effect of freeze-drying on the aggregation of clay mineral particles (Lagaly, 1987).

### C. Changes in Mechanical and Rheological Properties

Freezing of water in pores and fissures causes expansion, which leads to cracking and changes in the mechanical properties of the clay mineral. Repeated freezing–thawing cycles exacerbate this condition. The effect of freezing on clay mineral properties is of considerable importance to the behaviour of soils in cold climates.

Freezing and thawing has long-lasting effects on the rheological properties of 2:1 type clay minerals. Schwinka and Mortel (1999), for example, have found that the viscosity and plasticity of illite suspensions are increased by freezing and thawing. The effects are enhanced by the addition of small amounts of  $\text{Na}_2\text{SiO}_3$ , but reduced by addition of divalent cations. Freezing and thawing also increase weight loss on dehydration. These phenomena are attributed to the formation of water layers bound to the clay mineral surface but are not observed with kaolins. The effects of freezing–thawing cycles on the illite slurries are persistent. They extend up to the sintering process and even influence the texture and mechanical strength of the ceramic material obtained from the slurries.

## 7.2.2. DEHYDRATION OF CLAY MINERALS

On heating, all clay minerals pass through a temperature range in which they are dehydrated to various degrees. In the upper region of this temperature range dehydration and dehydroxylation may overlap. Dehydration causes changes that can be controlled and utilised. Loss of adsorbed water alters the macro- and microporosity of the clay mineral as well as its plasticity. Interlayer spaces collapse and CEC

is reduced. Partial loss of adsorbed and hydration water increases hydrophilicity and surface acidity. The actual and potential applications of these modifications of clay mineral properties at relatively low temperatures have been investigated.

### *A. Changes in Porosity*

Porous materials, and especially those that are thermally stable, are in great demand as adsorbents, catalysts, and catalyst supports. Clay mineral systems have macro-, meso-, and micropores. Macro- and mesopores arise from particle-to-particle interactions, while micropores occur in the interlayer spaces of pillared phyllosilicates, in channels of sepiolite or palygorskite, and also between interconnected fibres or layers of clay minerals.

The porosity of clay mineral aggregates is closely linked to their water content. On heating, water is driven off and the porosity changes. Acid treatment also increases the porosity. This property can therefore be manipulated by a combination of acid attack and heat treatment.

The porosity of smectites has mostly been investigated for acid-treated or pillared samples (see Chapters 7.1 and 7.5). Complex changes in surface properties occur when untreated smectites are heated. This is because different hydration states co-exist at any particular vapour pressure. Mesoporosity in  $\text{Na}^+$ -montmorillonite is attributed to interparticle associations, while microporosity is due to irregular stacking of layers of different lateral dimensions within a particle. On dehydration, water is first lost from external surfaces and meso-pores. As the vapour pressure decreases, the hydration state of the interlayer spaces changes stepwise from a three- to a two- and then a one-layer structure, with some overlap. At a relative vapour pressure of 0.05 the interlayer spaces are completely collapsed.  $\text{Na}^+$ -montmorillonite shows a strong hysteresis effect of surface properties on de- and re-hydration (Cases et al., 1992). Exchange of the interlayer cations affects the texture of smectites both before and after heating.

Changes in surface area and pore size distribution of sepiolite and palygorskite on heating were extensively investigated. Three temperature regions can be distinguished in which loss of hydration water and concomitant changes in porosity occur. In the first stage adsorbed and zeolitic water is lost, in the second two of the four molecules of coordination water are driven off, causing the structure to fold, and in the third the remaining two water molecules are eliminated (Nagata et al., 1974; Van Scoyoc et al., 1979). The actual temperature ranges in which these changes occur depend on the sample, the pretreatment, and the thermal regime. Sepiolite loses zeolitic water below 100 °C, two of the four water molecules coordinating  $\text{Mg}^{2+}$  in the channels below 300–380 °C, and the remaining coordination water below about 650 °C. Dehydroxylation occurs at higher temperatures. The corresponding temperature ranges for palygorskite are about 100 °C lower and dehydroxylation overlaps the final dehydration.

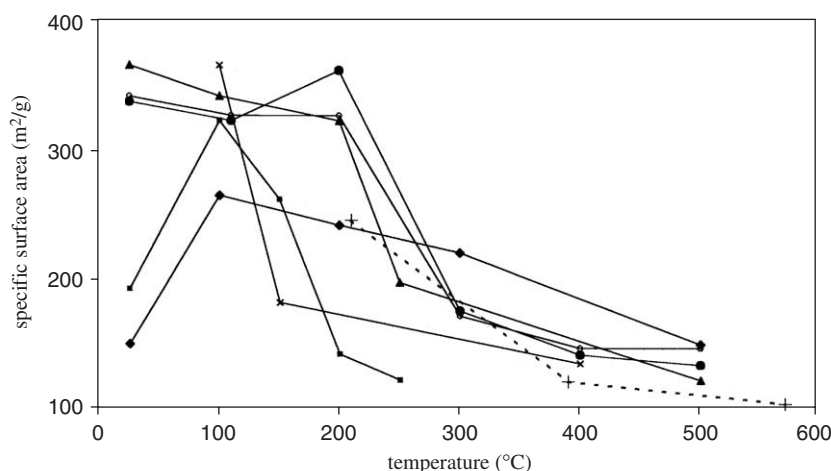


Fig. 7.2.2. Changes in the BET surface area ( $N_2$ ) of sepiolite with temperature. Data from Dandy and Nadiye-Tabbiruka (1975) ( $\times$ ); Fernandez Alvarez (1970, 1978) ( $\blacksquare$ ); Jimenez-Lopez et al. (1978) ( $\bullet$ ); Grillet et al. (1988) ( $\blacktriangle$ ); Ruiz et al. (1996) (dotted line—few data points); Balci (1999) ( $\blacklozenge$ ); and Caturla et al. (1999) (o).

Fig. 7.2.2 shows the effect of heating on total surface area ( $S_{\text{total}}$ ), determined by  $N_2$  adsorption, obtained in different studies.  $S_{\text{total}}$  comprises the total external surface area and the pore surfaces that are accessible to  $N_2$  molecule. The graphs show some common features, but also significant differences. In the first stage of heating, below  $100^\circ\text{C}$ , an increase in  $S_{\text{total}}$  is observed in some instances, and a slight decrease in others. A drastic decrease occurs at higher temperatures when the structure folds (Serna et al., 1975) and pores are blocked. This reversible collapse commences at different temperatures in the various studies. On further heating, more water is expelled, and  $S_{\text{total}}$  of all the samples gradually decreases. In this temperature range the remaining coordination water is lost, the channels collapse irreversibly, sepiolite becomes hydrophobic, and sintering occurs.

The  $S_{\text{total}}$  of sepiolite can be increased, and its thermal stability improved, by acid pretreatment. In a systematic study of activation with  $\text{HNO}_3$  of increasing acid strength and subsequent heating, the surface area of the sepiolite sample attained a maximum after pretreatment with  $0.5\text{ N HNO}_3$  and outgassing at  $200^\circ\text{C}$ .  $S_{\text{total}}$  decreased at higher temperatures, but the extent of reduction is less than for the untreated sample (Lopez-Gonzales et al., 1981).

Several investigations deal with changes in micro- and mesoporosity, as distinct from  $S_{\text{total}}$ . Because of the different definitions employed, however, it is difficult to compare the results. Micropores in the range of  $0.015\text{--}1.0\text{ }\mu\text{m}$  are preserved almost unchanged up to  $900^\circ\text{C}$  and in one, impure, sample even up to  $1100^\circ\text{C}$  (Goktas et al., 1997). Balci (1999) defines micropores as pores with diameter  $<6.7\text{ nm}$ ,



observing an initial increase in microporosity as zeolitic water is lost from the channels. Further heating leads to a progressive decrease in microporosity although about 60% of the original microporosity is retained up to 900 °C. [Fernandez Alvarez \(1978\)](#) restricts the size of micropores to pores with diameter <1.6–2 nm. These disappear after heating at 250 °C. [Grillet et al. \(1988\)](#) differentiate between structural micropores (cross-sectional area  $1.34 \times 0.67 \text{ nm}^2$ ) and interfibre micropores (diameter 2–30 nm). After outgassing at 350 °C structural micropores disappear entirely, while interparticle microporosity is reduced from 0.031 to 0.026 cm<sup>3</sup>/g, but persists to 500 °C. [Molina-Sabio et al. \(2001\)](#) have derived the micropore volume and non-microporous surface area of a sepiolite from adsorption isotherms of various gases by application of the Dubinin–Radushkevich and BET equations. They define microporosity as the porosity that is lost between 110 and 500 °C. This amounts to ~0.11 cm<sup>3</sup>/g. Whereas this micropore volume is independent of the adsorbate used (N<sub>2</sub>, CO<sub>2</sub>, NH<sub>3</sub>, or H<sub>2</sub>O), the external surface area derived from the adsorption isotherms varies. The differences are attributed to the presence of specific adsorption sites on the surface.

Valid comparison of the results, obtained in investigations using different samples of sepiolite, would require similar pretreatment and identical thermal regimes. Even then, however, it would only be possible to establish general trends because the actual values of  $S_{\text{total}}$  and of the various porosities must be determined for individual samples.

Exfoliated vermiculite provides an extreme example of the changes in void volume that can occur when a clay mineral is heated. When the temperature is gradually raised, stepwise dehydration occurs. However, when vermiculite is flash-heated to temperatures of about 870–900 °C ([Justo et al., 1989](#)), or even up to 1500 °C ([Lagaly, 1993](#)) and then rapidly cooled, the mineral exfoliates in a direction approximately perpendicular to the layers. As a result, its volume increases to more than 20 times the original value, giving rise to a very porous, lightweight material with good absorptive and thermo-insulating properties. Exfoliation is attributed to the action of steam, which develops explosively between the layers, pushing them apart, while layer dehydroxylation (at the high prevailing temperatures) is restrained by rapid cooling. The degree of exfoliation depends upon the particle size. The smaller the particles, the easier it is for interlayer water to escape, and the less extensive is the exfoliation. [Justo et al. \(1989\)](#) reported that vermiculite samples containing mica or interstratified mica/vermiculite exfoliate more than pure vermiculite. They, therefore, consider that the sudden release of interlayer water is not the only factor controlling exfoliation. Impurities in, and the chemical composition or partial dehydroxylation of, the vermiculite may also play a part. No completely satisfactory explanation for the unique behaviour of vermiculite was yet offered. The phenomenon probably requires an appropriate balance between the amount of interlayer water and particle size. The latter controls the ease of diffusion of interlayer water and the stability of the T-O-T layers, as evidenced by the high dehydroxylation temperature. In view of the economic importance of exfoliated vermiculite, surprisingly few scientific papers

were published on this topic although many technical reports are available. This is an interesting challenge for further study.

### *B. De- and Re-Adsorption of Water*

For the majority of clay minerals partial de- and re-hydration occurs very readily, but the temperatures required vary with clay mineral species.

Repeated wetting–drying cycles of  $K^+$ -smectites cause ordering of layer stacking, accompanied by  $K^+$  fixation (Gaultier and Mamy, 1979). These effects are more evident as the total layer charge of the smectite increases (Schultz, 1969; Eberl et al., 1986). Wetting–drying cycles in the presence of soluble salts cause some deprotonation, and effectively increase the layer charge (Heller-Kallai and Eberl, 1999).

Because dehydration is an endothermic and, conversely, re-hydration is an exothermic process, clay minerals can, in principle, be used for energy storage and as heat exchangers. Allophane and imogolite lose adsorbed water on mild heating. The total heat of re-hydration after preheating to 80–100 °C compares favourably with that of either Mg A-type zeolite or with B-type silica gel, which serve as standards (Suzuki et al., 2001a, 2001b). Montmorillonite requires higher temperatures for dehydration. Sadek and Mekhamer (2000, 2001) reported efficient energy storage with  $Na^+$ - and  $Ca^{2+}$ -montmorillonites preheated at 200 and 250 °C, respectively, for extended periods. At these temperatures surface-adsorbed and interlayer water is lost, but is subsequently re-adsorbed exothermally on cooling in the presence of water vapour.

The reversibility of the dehydration process can also be exploited for humidity control. Attempts at using clays for this purpose have mostly focused on sepiolite. After prolonged outgassing at room temperature or heating up to 200 °C, when the micropores are still accessible and  $S_{total}$  is unchanged, sepiolite is very sensitive to changes in humidity. Even diurnal fluctuations can change the amount of water adsorbed, particularly at high relative humidities. These changes are attributed to differences in humidity rather than to variations in temperature (Caturla et al., 1999).

### *C. Changes in Surface Acidity on Dehydration*

Clay mineral surfaces have both Brønsted and Lewis acid sites. The total acidity and the ratio of Brønsted to Lewis sites change with the hydration state of the mineral. Exposed  $Si^{4+}$  and tetrahedrally or octahedrally coordinated  $Al^{3+}$  and  $Fe^{3+}$  ions, when hydrated, are weak Brønsted acids. As in zeolites and silica–alumina catalysts, Si–OH–Al groups are much stronger Brønsted acids than either Si–OH–Si or Al–OH–Al groups. The acidity of Si–OH–Al groups may be greatly increased by drying, whereby these Brønsted sites are converted into Lewis acid sites. Incompletely coordinated  $Al^{3+}$  and  $Fe^{3+}$  ions, exposed at the edges, act as Lewis acids. Exposed  $Mg^{2+}$  ions, when hydrated, are basic (Yariv and Michaelian, 2002).

In smectites, strong Brønsted acidity derives from dissociation of water that is directly coordinated to interlayer cations. The acid strength increases with the polarising power of the cations, i.e. with decreasing size and increasing charge. The smaller the amount of hydration water present, the greater the polarisation of the remaining water molecules and hence their ability to donate protons. Dehydrated interlayer cations also act as Lewis acids. (For a review of methods of determining the surface acidity of smectites, see [Heller-Kallai, 2002](#).)

Quantitative measurements of changes in total surface acidity and in the ratio of Brønsted to Lewis acid sites, induced by heating, were mostly performed on acid-activated smectites because of their importance as catalysts for organic reactions. Using IR spectroscopy with pyridine as a molecular probe, [Cseri et al. \(1995\)](#) determined the Brønsted and Lewis acidity of a series of monoionic samples of K10 (a commercially available, acid-activated montmorillonite) after drying at 120 °C or calcining at 500 °C. Both Brønsted and Lewis acidity vary greatly with the nature of the interlayer cation. Brønsted acidity is much higher at 120 °C than at 500 °C. Lewis acidity is also reduced at the higher temperature, but not as much as Brønsted acidity. Similarly, [Brown and Rhodes \(1997\)](#) measured changes in surface acidity with preheating temperature of another commercially available acid-activated montmorillonite, Fulcat 40, by determining the rate constants of the Brønsted acid-catalyzed rearrangement of  $\alpha$ -pinene to camphene, and of the Lewis acid-catalysed rearrangement of camphene hydrochloride to isobornyl chloride. IR studies using pyridine as a probe give results that are broadly consistent with those based on relative catalytic activities. Irrespective of the type of interlayer cation, maximum Brønsted activity is attained at about 150 °C and tends to zero on further heating. Maximum Lewis acidity is generated after thermal activation at 250–300 °C and does not change appreciably up to 500 °C.

The results for  $\text{Fe}^{2+}$ - and  $\text{Zn}^{2+}$ -saturated samples, used in the two studies, are shown in [Fig. 7.2.3](#). It is evident that there are significant differences between them. In both cases, Lewis sites predominate over Brønsted sites at high activation temperatures. However, the changes that occur in the number of Lewis sites with increasing temperatures are quite different. Whereas [Brown and Rhodes \(1997\)](#) measure higher Lewis acidity at higher temperatures, [Cseri et al. \(1995\)](#) report lower Lewis acidity after calcining at 500 °C than after drying at 120 °C. This applies to all nine monoionic samples examined. The ratio of Brønsted to Lewis acidity in the samples at any given temperature is also appreciably different in the two studies. It is difficult to determine the reasons for these discrepancies. Differences in thermal activation procedures (with Cseri et al. using a heating rate of 1 K/min in air, and Brown and Rhodes calcining for 1 h in dry air at the specified temperature) may account for some, but not all, of the differences. Other factors, such as specific features of the starting material, must also be considered. It would, therefore, appear that quantitative results obtained in any investigation are only valid for the particular system studied, and only overall trends can presently be generalised.

[Brown and Rhodes \(1997\)](#) also remarked that when heated,  $\text{Na}^+$ -exchanged clay minerals have very low acid activity, concluding that both Brønsted and Lewis

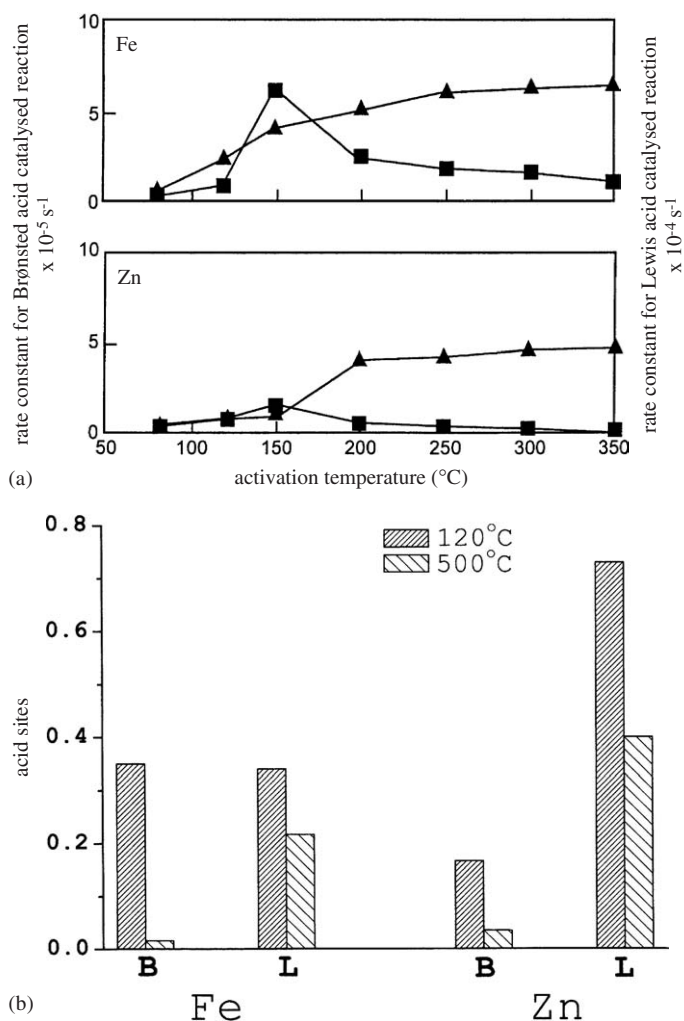


Fig. 7.2.3. Changes in acidity with temperature of Fe and Zn saturated acid-activated montmorillonite. (a) Activity in the Brønsted acid-catalysed rearrangement of  $\alpha$ -pinene (■) and the Lewis acid-catalysed rearrangement of camphene hydrochloride (▲). Adapted from Brown and Rhodes (1997). (b) Brønsted (B) and Lewis (L) acid sites determined by pyridine adsorption at 120 and 500 °C. Data from Cseri et al. (1995).

acidity derive mostly from the interlayer cations. Acid sites known to be present elsewhere on the mineral may be too weak to be effective in the reactions studied.

Thermally activated acid-treated smectites are widely used as catalysts in organic syntheses (Balogh and Laszlo, 1993).

#### D. The Hofmann–Klemen Effect

This effect refers to the reduction in negative layer charge, CEC and expansibility of octahedrally charged smectites saturated with small cations (e.g.  $\text{Li}^+$ ,  $\text{Mg}^{2+}$ ,  $\text{Cu}^{2+}$ ) following thermal treatment (Hofmann and Klemen, 1950; Quirk and Theng, 1960; Russell and Farmer, 1964; McBride and Mortland, 1974; Emmerich et al., 1999; Stackhouse and Coveney, 2002; Komadel et al., 2003). The common explanation of this effect is that heating induces the small cations to migrate from their interlayer positions into the layer structure where they become essentially non-exchangeable. In the case of  $\text{Li}^+$ -montmorillonite, heating induces the  $\text{Li}^+$  ions to migrate from the interlayer space into the vacant octahedral sites (Hofmann and Klemen, 1950), or into the hexagonal holes of the tetrahedral sheets (Tettenhorst, 1962; Theng et al., 1997), or both. The appearance of an  $\text{AlMgLiOH}$  stretching band near  $3670\text{ cm}^{-1}$  in the IR spectrum of montmorillonites and some features of the near-IR region are indicative of the presence of  $\text{Li}^+$  in the octahedral sheets (Madejová et al., 2000a, 2000b). The amount of ‘fixed’  $\text{Li}^+$  increases as the temperature is increased, up to about  $250^\circ\text{C}$ . A series of reduced-charge smectites can thus be prepared from the same parent mineral. A high  $\text{Mg}^{2+}$  for  $\text{Al}^{3+}$  substitution and a high ratio of octahedral to tetrahedral charge are conducive to extensive negative-charge reduction. Low  $\text{Li}^+$  fixation is observed for heated minerals with a relatively high fraction of tetrahedral charge (Madejová et al., 2000a; Hrobáriková and Komadel, 2002).

$\text{Li}^+$  fixation decreases the layer charge density, CEC, the amount of water and ethylene glycol monoethyl ether sorbed, as well as swelling (in water) of the smectite. Since the layer charge density controls the distribution of cations in the interlayer spaces, the interlayer spacing of alkylammonium–montmorillonite complexes is affected (Bujdák et al., 1992). Likewise, layer charge reduction affects the distance separating adsorbed dye cations (e.g. methylene blue). As a result, the colour of the clay mineral–dye complexes is modified because colour is determined by the type and extent of molecular aggregation (Bujdák et al., 2001). The presence of non-expanding layers in reduced-charge montmorillonite reduces its solubility in  $\text{HCl}$  (Komadel et al., 1996).

Heating in the presence of proton acceptors leads to partial deprotonation of structural hydroxyl groups, thus facilitating penetration of small divalent cations into the octahedral sheets (Heller-Kallai, 2001).

### 7.2.3. DEHYDROXYLATED PHASES

#### A. Kaolinite Group

When kaolinite is heated beyond the temperature of the dehydroxylation endotherm, metakaolinite is formed. Between  $500$  and  $900^\circ\text{C}$ , this is the main product obtained. The exact temperature range depends on the starting kaolinite and on the heating regime. At higher temperatures a spinel-type phase is formed together with

amorphous silica, after which mullite and cristobalite appear. Nacrite and halloysite resemble kaolinite in their dehydroxylation reactions. Dickite forms a 1.4 nm superstructure before complete dehydroxylation occurs (Brindley and Lemaitre, 1987).

Brindley and Nakahira (1959) pioneered the study of the kaolinite-to-mullite reaction sequence. Since then numerous publications on this topic appeared, and only the salient points will be mentioned here.

As metakaolinite is amorphous to X-rays, alternative methods were used for structure determination, including IR spectroscopy (Stubican and Roy, 1961; Pampuch, 1966), X-ray fluorescence (XRF) spectrometry (Gastuche et al., 1963), radial distribution function (RDF) (Gualtieri and Bellotto, 1998), NMR spectroscopy (Komarneni et al., 1985; Watanabe et al., 1987; Sanz et al., 1988; Lambert et al., 1989; Rocha and Klinowski, 1990; Lussier, 1991; Massiot et al., 1995), and conductometry (Murat and Driouche, 1988). The results indicate that in metakaolinite the  $\text{SiO}_4$  sheets persist but in a distorted form, while the octahedral sheets are profoundly altered although some short-range order is preserved. A TEM study (Bergaya et al., 1996), which includes selected area diffraction and lattice imaging, shows that metakaolinite has a layer structure, composed of very distorted  $\text{SiO}_4$  sheets and Al-polyhedra. The particles are a few layers thick. Metakaolinite can be completely rehydroxylated, restoring the kaolinite particles with edges parallel to those of the original material (Rocha and Klinowski, 1991).

The structure of metakaolinite changes on heating. Solid-state NMR spectroscopy (Massiot et al., 1995) showed that, as the temperature is increased, the coordination number of Al atoms is reduced from 6 to 5 and 4, with  $\text{Al}^{\text{V}}$  and  $\text{Al}^{\text{IV}}$  developing simultaneously. At high temperatures, when new phases begin to crystallise,  $\text{Al}^{\text{VI}}$  reappears, some  $\text{Al}^{\text{IV}}$  persists, but  $\text{Al}^{\text{V}}$  disappears. The reactivity of metakaolinite is at a maximum when the content of  $\text{Al}^{\text{VI}}$  is at a minimum. This is illustrated in Fig. 7.2.4, which compares changes in Al coordination (determined by NMR, for a kaolinite calcined in air for 1 h in the range 400–1000 °C at 50 °C intervals) with the changes in some properties of kaolinites. Although these properties are assessed by different investigators, using different samples of kaolinite and under different thermal regimes, the trend of increasing reactivity of metakaolinite with decreasing content of 6-coordinated Al is common to all.

The chemical properties of metakaolinite differ greatly from those of the parent material. Whereas kaolinite is fairly stable towards acids, metakaolinite is easily attacked. Better ordered kaolinite is transformed into less-reactive metakaolinite (Kakali et al., 2001). A decrease in Al-coordination number renders the Al sheets prone to acid extraction, leaving a very porous material. Metakaolinite with the highest content of 5-coordinated Al is also the most acid-reactive (Lussier, 1991). The tetrahedral sheets of the microporous products retain some structural features of kaolinite and do not resemble the structure of silica gel (Okada et al., 1998).

Kaolinite and metakaolinite have globular pores with a mean diameter of 10.5 nm. Dealumination of metakaolinite by acid attack enhances the globular pore volume and also creates slit-shaped pores (Vollet et al., 1994). The total surface area

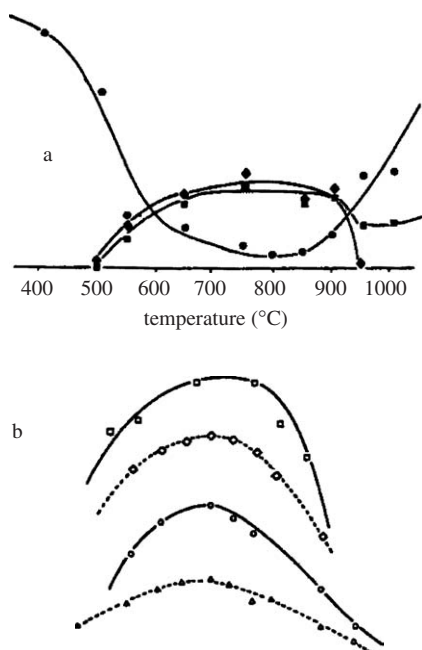


Fig. 7.2.4. Changes in kaolinite heated at different temperatures: (a) population of 6-(●), 5-(◆), and 4-(■) coordinated Al; (b) compressive strength of mixture of metakaolinite and  $\text{Ca}(\text{OH})_2$  ( $\Delta$ ); IR-disorder index of the 460–470/cm band (○); dissolution enthalpy in HF ( $\diamond$ ); and yield of zeolite X synthesis ( $\square$ ). Adapted from Rocha and Klinowski (1990).

and the microporosity of kaolinite increase with calcination temperature, up to a maximum of about 850–875 °C. Above that temperature non-microporous solids are obtained (Duarte et al., 1995).

Dealuminated metakaolinite has both Lewis and Brønsted acid sites. The total number of sites, the ratio of Lewis to Brønsted sites, and their relative strengths depend on the calcination temperature, the acid used, the severity of acid treatment, and the washing procedure. A judicious choice of porosity and acidity can produce efficient, selective catalysts (Macedo and Duarte, 1995; Perissinotto et al., 1997; Sabu et al., 1999; Breen et al., 2002). Indeed, Macedo et al. (1994) claimed that calcined, partially dealuminated metakaolinites may act as superacids, capable of catalysing cumene cracking. This was attributed to synergism between Brønsted and Lewis acidity, associated with 4- and 5-coordinated Al, respectively.

Acid-activated metakaolinite has a higher CEC than the parent clay mineral, and can be used to scavenge hazardous metal ions, such as  $\text{Cd}^{2+}$  and  $\text{Cu}^{2+}$  (Suraj et al., 1998).

Metakaolinite combines rapidly with lime at ambient temperatures to develop cementing properties. Ever since its incorporation into the Jupia Dam, Brazil in 1962, metakaolinite has been used to supplement or replace cement in mortar or



concrete. The extensive literature on the pozzolanic properties of metakaolinite has recently been reviewed by [Sabir et al. \(2001\)](#). At the high pH prevalent in cement, some Al is dissolved from metakaolinite and forms an Al-rich calcium silicate hydrate gel (C–S–A–H). In the presence of water, crystalline calcium aluminate hydrates and calcium silicate aluminate hydrates develop, the composition of which depends on the  $AS_2/CH$  ratio and the thermal regime. Gypsum enhances the pozzolanic reactivity of metakaolinite ([Kurdowski and Pomadovski, 2001](#)). Partial replacement of cement by metakaolinite in cement pastes reduces the pore volume and shifts the distribution towards smaller values. A good correlation is obtained between porosity and degree of hydration of the pastes ([Frias and Cabrera, 2000](#)). Use of less porous metakaolinite-blended cements in mortar or concrete increases their strength and durability as well as their resistance to aggressive solutions, such as sulphate ([Vu et al., 2001](#)) or chloride ([Gruber et al., 2001](#)).

Metakaolinite was long used as a starting material for zeolite synthesis. In recent years the ever-increasing demand for zeolites provided a new impetus for further research, giving rise to an extensive literature. Zeolites are formed when metakaolinite is hydrothermally reacted with NaOH or KOH solutions. The synthesis occurs most readily when the content of 4- and 5-coordinated Al is at a maximum, while the population of 6-coordinated Al is at a minimum ([Madani et al., 1990](#); [Rocha et al., 1991](#)).

When kaolinite is heated in the presence of salts of alkali metals, alkali ions are incorporated into the structure during the course of dehydroxylation. The greater the solubility of the salt in hot water, the further the reaction proceeds under given experimental conditions ([Heller-Kallai, 1978](#); [Heller-Kallai and Frenkel, 1979](#)). X-ray amorphous products with an  $SiAlO_4$  tetrahedral framework are formed when kaolinite– $K_2CO_3$  mixtures are calcined at about 500 °C. This amorphous phase, with a composition of  $KAlSiO_4$ , is converted into crystalline kaliophilite at about 700 °C, far below the temperature at which metakaolinite is transformed to high-temperature phases. Attempts at synthesising zeolite from the amorphous phase gave promising results ([Heller-Kallai and Lapides, 2003](#)).

### *B. Serpentine*

With serpentines, the trioctahedral analogues of kaolinite, the interval between dehydroxylation and crystallisation of new phases is small. Several reaction mechanisms were proposed for the dehydroxylation of chrysotile ([Ball and Taylor, 1963](#); [MacKenzie and Meinhold, 1994a](#)). Solid-state NMR spectroscopy provided evidence for the existence of two dehydroxylates. Dehydroxylate I appears at the onset of dehydroxylation, at about 650–700 °C, when some of the original chrysotile is still present. Dehydroxylate I is a Mg-rich, X-ray amorphous phase with  $Mg^{2+}$  in octahedral coordination. It transforms to forsterite on further heating. Simultaneously, at about 800 °C, the remaining chrysotile forms dehydroxylate II. This phase contains less  $Mg^{2+}$  than dehydroxylate I, and transforms to enstatite at higher



temperatures. The two reaction pathways may be ascribed to the presence of different amounts of water in the outer and inner regions of the chrysotile fibrils. Water diffuses readily from the outer regions, whereas quasi-hydrothermal conditions prevail on the inside, where dehydroxylate II is formed. If this interpretation is correct, the particle size and heating regime would be expected to have a drastic effect on the relative amounts of the two dehydroxylates formed. This point needs to be checked.

### C. T-O-T Minerals

Dehydroxylation disrupts the structure of trioctahedral minerals, such as talc (Ball and Taylor, 1963) and hectorite (MacKenzie and Meinhold, 1994b). On the other hand, the layer structure of pyrophyllite and other dioctahedral T-O-T minerals is preserved on dehydroxylation. However, the interlayer spaces collapse, the CEC approaches zero, and the surface area and porosity decrease. The XRD patterns of these dehydroxylates are diffuse but distinct.

The differential thermal analysis (DTA) curves of dioctahedral smectites and of finely divided micas show that dehydroxylation occurs at different temperatures, giving rise to single peaks at either  $\sim 700^\circ\text{C}$  or at  $\sim 500^\circ\text{C}$ , or to a doublet between 500 and  $700^\circ\text{C}$ . Beidellites, nontronites, and volkhonskoites dehydroxylate at about  $500^\circ\text{C}$  (Greene-Kelly, 1957).

Drits et al. (1995) were able to relate the dehydroxylation temperature to the structure of the octahedral sheets of the phyllosilicates. In dioctahedral structures, octahedral cations occupy either two *cis* sites (*tv*), or one *cis* and one *trans* site (*cv*) (see Chapter 2). On dehydroxylation, cations that originally occupy *cis* sites become 5-coordinated, while those occupying *trans* positions become 6-coordinated. Structures with  $\text{Al}^{3+}$  in distorted hexagonal sites are unstable and these ions migrate to vacant 5-coordinated sites. Thus, the dehydroxylates derived from samples that are originally of the *cv* type are similar to those obtained from the *tv* type, with all former *cis* sites occupied. Dehydroxylation of *cv* structures is a two-stage process, which is completed at higher temperatures than dehydroxylation of *tv* structures.

Al-rich dioctahedral clay minerals rehydroxylate readily (Grim and Bradley, 1948; Heller et al., 1962) and *cv* montmorillonite even spontaneously (Emmerich, 2000). The rehydroxylates are of the *tv* type, whatever the cation distribution is in the original structure. In contrast, dehydroxylation of glauconite and celadonite is accompanied by migration of cations from *cis* to formerly vacant *trans* sites. They hydroxylate to predominantly *cv* structures (Muller et al., 2000).

#### 7.2.4. HIGH-TEMPERATURE PHASES

When clay minerals are heated to sufficiently high temperatures, new phases crystallise. These are of great industrial importance, and play a significant role in natural processes.

Diocahedral clay minerals generally show a temperature interval between the breakdown of the dehydroxylated phase (whether this be crystalline or amorphous to X-rays) and the crystallisation of new phases. In the case of trioctahedral clay minerals, on the other hand, the breakdown of the dehydroxylate and the crystallisation of high-temperature phases tend to coincide.

The compositions of the high-temperature products frequently differ from those of the dehydroxylates, although they are necessarily limited by the chemical composition of the starting clay mineral. The Al-rich members of the kaolinite group, as well as allophane, pyrophyllite, and montmorillonites of the Wyoming-type ultimately produce mullite and cristobalite. Talc forms enstatite and cristobalite. Apart from having minor amounts of an Al-containing phase, the high-temperature products of saponite are similar to those of talc. The high-temperature reactions of serpentines, in particular those of chrysotile fibres, were studied in considerable detail (see MacKenzie and Meinhold, 1994a and references therein). Mixtures of forsterite, enstatite, and silica are first obtained. On further heating, forsterite reacts with silica to form more enstatite.

The chemical composition of the starting materials is not the only factor that determines the nature of the high-temperature products. Thus, montmorillonites of the Cheto-type, which contain more  $Mg^{2+}$  in octahedral positions than montmorillonites of the Wyoming-type, form cordierite, instead of mullite, at high temperatures. However, addition of  $Mg^{2+}$  to the Wyoming-type montmorillonite does not inhibit mullite formation, nor does leaching of  $Mg^{2+}$  from the octahedral sheets of the Cheto-type montmorillonite promote its formation (Grim and Kulbicki, 1961).

In many instances, the crystalline products that form at high temperatures are topotactically related to the starting clay. This was long regarded as an indication of structural inheritance in solid-state reactions. It is possible, however, that the original structures do break down, and that nucleation of the products occurs in orientations that reduce the misfit between old and new phases (Brindley and Lemaitre, 1987). The two mechanisms may not be mutually exclusive but perhaps operate either separately or simultaneously in different systems.

## REFERENCES

- Anderson, D.M., Tice, A.T., 1971. Low-temperature phases of interfacial water in clay-water systems. *Soil Science Society of America Proceedings* 35, 47–54.
- Balci, S., 1999. Effect of heating and acid pre-treatment on pore size distribution of sepiolite. *Clay Minerals* 34, 647–655.
- Ball, M.C., Taylor, H.F.W., 1963. The dehydroxylation of chrysotile in air and under hydrothermal conditions. *Mineralogical Magazine* 33, 467–482.
- Balogh, M., Laszlo, P., 1993. *Organic Chemistry Using Clay*. Springer, Berlin.
- Bergaya, F., Dion, P., Alcover, J.F., Clinard, C., Tchoubar, D., 1996. TEM study of kaolinite thermal decomposition by controlled-rate thermal analysis. *Journal of Materials Science* 31, 5069–5075.

- Breen, C., Taylor, S., Burguin, E., Centeno, M., 2002. Preparation and characterization of dealuminated metakaolin and its use in the transformation of waste plastics to aromatic hydrocarbons. *Journal of Colloid and Interface Science* 247, 246–250.
- Brindley, G., Lemaître, J., 1987. Thermal, oxidation and reduction reactions of clay minerals. In: Newman, A.C.D. (Ed.), *Chemistry of Clays and Clay Minerals*, Monograph No. 6. Mineralogical Society, London, pp. 319–370.
- Brindley, G.W., Nakahira, M., 1959. The kaolinite–mullite reaction series: I. Survey of outstanding problems. II. Metakaolin. III. The high-temperature phases. *Journal of the American Ceramic Society* 42, 311–324.
- Brown, D.R., Rhodes, C.N., 1997. Brønsted and Lewis acid catalysis with ion-exchanged clays. *Catalysis Letters* 45, 35–40.
- Bujdák, J., Janek, M., Madejová, J., Komadel, P., 2001. Methylene blue interactions with reduced charge smectites. *Clays and Clay Minerals* 49, 244–254.
- Bujdák, J., Slosiariková, H., Čičel, B., 1992. Interaction of long chain alkylammonium cations with reduced charge montmorillonite. *Journal of Inclusion Phenomena and Molecular Recognition* 13, 321–327.
- Cases, J.M., Berend, I., Besson, G., François, M., Uriot, J.P., Thomas, F., Poirier, J.E., 1992. Mechanism of adsorption and desorption of water-vapor by homoionic montmorillonite. 1. The sodium-exchanged form. *Langmuir* 8, 2730–2739.
- Caturla, F., Molina-Sabio, M., Rodriguez-Reinoso, F., 1999. Adsorption-desorption of water vapor by natural and heat-treated sepiolite in ambient air. *Applied Clay Science* 15, 367–380.
- Cseri, T., Bekassy, S., Figueras, F., Rizner, S., 1995. Benzylation of aromatics on ion-exchanged clays. *Journal of Molecular Catalysis A: Chemical* 98, 101–107.
- Dandy, A.J., Nadiye-Tabbiruka, M.S., 1975. The effect of heating in vacuo on the micro-porosity of sepiolite. *Clays and Clay Minerals* 23, 428–430.
- de Carvalho, M.B., Pires, J., Carvalho, A.P., 1996. Characterisation of clays and aluminium pillared clays by adsorption of probe molecules. *Microporous Materials* 6, 65–77.
- Drits, V.A., Besson, G., Muller, F., 1995. An improved model for structural transformations of heat-treated aluminous dioctahedral 2:1 layer silicates. *Clays and Clay Minerals* 43, 718–731.
- Duarte, M.A.I., Macedo, J.C.D., Alves, D.B., 1995. Generation of pores in metakaolin by acid dealumination. In: Churchman, G.J., Fitzpatrick, R.W., Eggleton, R.A. (Eds.), *Clays: Controlling the Environment. Proceedings of the 10th International Clay Conference*, Adelaide, Australia, 1993. CSIRO, pp. 112–115.
- Eberl, D.D., Šrodoň, J., Northrop, H.R., 1986. Potassium fixation in smectites by wetting and drying. In: Davis, A., Hayes, K.F. (Eds.), *Geochemical Processes at Mineral Surfaces*, ACS Symposium Series 323. American Chemical Society, Washington, DC, pp. 296–326.
- Emmerich, K., 2000. Spontaneous rehydroxylation of a dehydroxylated cis-vacant montmorillonite. *Clays and Clay Minerals* 48, 405–408.
- Emmerich, K., Madsen, F.T., Kahr, G., 1999. Dehydroxylation behaviour of heat-treated and steam-treated homoionic cis-vacant montmorillonite. *Clays and Clay Minerals* 47, 591–604.
- Fernandez Alvarez, T., 1970. Superficie específica y estructura de poro de la sepiolita calentada a diferentes temperaturas. In: Serratosa, J.M. (Ed.), *Reunion Hispano-Belga de Minerales de la Arcilla*, Madrid. Consejo Superior de Investigaciones Científicas, Madrid, pp. 202–209.

- Fernandez Alvarez, T., 1978. Efecto de la deshidratacion sobre las propiedades adsorbentes de la palygorskita y sepiolita. *Clay Minerals* 13, 325–335.
- Frias, M., Cabrera, J., 2000. Pore size distribution and degree of hydration of metakaolin-cement pastes. *Cement and Concrete Research* 30, 561–569.
- Gastuche, M.C., Toussaint, F., Fripiat, J.J., Touilleaux, R., van Meersche, M., 1963. Study of intermediate stages in the kaolin–metakaolin transformation. *Clay Minerals Bulletin* 5, 227–236.
- Gaultier, J.P., Mamy, J., 1979. Evolution of exchange properties and crystallographic characteristics of bionic K–Ca montmorillonite submitted to alternate wetting and drying. In: Mortland, M.M., Farmer, V.C. (Eds.), *International Clay Conference 1978*. Elsevier, Amsterdam, pp. 167–175.
- Goktas, A.A., Misirli, Z., Baykara, T., 1997. Sintering behaviour of sepiolite. *Ceramics International* 23, 305–311.
- Greene-Kelly, R., 1957. The montmorillonite minerals (smectites). In: Mackenzie, R.C. (Ed.), *The Differential Thermal Investigations of Clays*. Mineralogical Society, London, pp. 140–164.
- Grillet, Y., Cases, J.M., François, M., Rouquérol, J., Poirier, J.E., 1988. Modification of the porous structure and surface area of sepiolite under vacuum thermal treatment. *Clays and Clay Minerals* 36, 233–242.
- Grim, R.E., Bradley, W.F., 1948. Rehydration and dehydration of the clay minerals. *American Mineralogist* 33, 50–59.
- Grim, R.E., Kulbicki, G., 1961. Montmorillonite: high temperature reactions and classification. *American Mineralogist* 46, 1329–1369.
- Gruber, K.A., Ramlochan, T., Boddy, A., Hooton, R.D., Thomas, M.D.A., 2001. Increasing concrete durability with high-reactivity metakaolin. *Cement and Concrete Composites* 23, 479–484.
- Gualtieri, A., Bellotto, M., 1998. Modelling the structure of the metastable phases in the reaction sequence kaolinite–mullite by X-ray scattering experiments. *Physics and Chemistry of Minerals* 25, 442–452.
- Heller, L., Farmer, V.C., Mackenzie, R.C., Mitchell, B.D., Taylor, H.F.W., 1962. The dehydroxylation and rehydroxylation of triphormic dioctahedral clay minerals. *Clay Minerals Bulletin* 5, 56–72.
- Heller-Kallai, L., 1978. Reactions of salts with kaolinite at elevated temperatures. 1. *Clay Minerals* 13, 221–235.
- Heller-Kallai, L., 2001. Protonation–deprotonation of dioctahedral smectites. *Applied Clay Science* 20, 27–38.
- Heller-Kallai, L., 2002. Clay catalysis in reactions of organic matter. In: Yariv, S., Cross, H. (Eds.), *Organo-Clay Complexes and Interactions*. Marcel Dekker, New York, pp. 567–613.
- Heller-Kallai, L., Eberl, D.D., 1999. Potassium fixation by smectites in wetting–drying cycles with different anions. In: Kodama, H., Mermut, A.R., Torrance, J.K. (Eds.), *Clays for our Future. Proceedings of the 11th International Clay Conference*, Ottawa, Canada. ICC97 Organizing Committee, Ottawa, pp. 561–567.
- Heller-Kallai, L., Frenkel, M., 1979. Reactions of salts with kaolinite at elevated temperatures—Part 2. In: Mortland, M.M., Farmer, V.C. (Eds.), *International Clay Conference 1978*. Elsevier, Amsterdam, pp. 629–637.
- Heller-Kallai, L., Lapidés, I., 2003. Thermal reactions of kaolinite with potassium carbonate. *Journal of Thermal Analysis and Calorimetry* 71, 689–698.

- Hofmann, U., Klemen, R., 1950. Verlust der Austauschfähigkeit von Lithiumionen an Bentonit durch Erhitzung. *Zeitschrift für anorganische und allgemeine Chemie* 262, 95–99.
- Hrobáriková, J., Komadel, P., 2002. Sorption properties of reduced-charge montmorillonites. *Geologica Carpathica* 53, 93–98.
- Jimenez-Lopez, A., Lopez-Gonzales, J.D., Ramirez-Saenz, A., Rodriguez-Reinoso, F., Valenzuela-Calahorra, C., Zurita-Herrera, L., 1978. Evolution of surface area in a sepiolite as a function of acid and heat treatments. *Clay Minerals* 13, 375–385.
- Justo, A., Maqueda, C., Perez-Rodriguez, J.L., Morillo, E., 1989. Expansibility of some vermiculites. *Applied Clay Science* 4, 509–519.
- Kakali, G., Perraki, T., Tsvilis, S., Badogiannis, E., 2001. Thermal treatment of kaolin: the effect of mineralogy on the pozzolanic activity. *Applied Clay Science* 20, 73–80.
- Komadel, P., Bujdák, J., Madejová, J., Šucha, V., Elsass, F., 1996. Effect of non-swelling layers on the dissolution of reduced-charge montmorillonite in hydrochloric acid. *Clay Minerals* 31, 333–345.
- Komadel, P., Madejová, J., Hrobáriková, J., Janek, M., Bujdák, J., 2003. Fixation of  $\text{Li}^+$  cations in montmorillonite upon heating. *Solid State Phenomena* 90/91, 497–502.
- Komarneni, S., Fyfe, C.A., Kennedy, G.J., 1985. Order–disorder in 1:1 type clay minerals by solid-state  $^{27}\text{Al}$  and  $^{29}\text{Si}$  magic-angle-spinning NMR spectroscopy. *Clay Minerals* 20, 327–334.
- Kurdowski, W., Pomadovski, H., 2001. Influence of Portland cement composition on pozzolanic reactivity of metakaolin. *Silicates Industriels* 66, 85–90.
- Lagaly, G., 1987. Surface chemistry and catalysis. The 6th Meeting of the European Clay Groups, Seville, Spain, pp. 97–115.
- Lagaly, G., 1993. Praktische Verwendung und Einsatzmöglichkeiten von Tonen. In: Jasmund, K., Lagaly, G. (Eds.), *Tonminerale und Tone*. Steinkopff Verlag, Darmstadt, pp. 358–427.
- Lahav, N., Anderson, D.M., 1973. Montmorillonite–benzidine reactions in the frozen and dry states. *Clays and Clay Minerals* 21, 137–139.
- Lambert, J.F., Millman, W.S., Fripiat, J.J., 1989. Revisiting kaolinite dehydroxylation: a  $^{29}\text{Si}$  and  $^{27}\text{Al}$  MAS NMR study. *Journal of the American Chemical Society* 111, 3517–3522.
- Lopez-Gonzales, J.deD., Ramirez-Saenz, A., Rodriguez-Reinoso, F., Valenzuela-Calahorra, C., Zurita-Herrera, L., 1981. Activation de una sepiolita con disoluciones diluidas de  $\text{NO}_3\text{H}$  y posteriores tratamientos termicos: I Estudio de la superficie especifica. *Clay Minerals* 16, 103–113.
- Lussier, R.J., 1991. A novel clay-based catalytic material—preparation and properties. *Journal of Catalysis* 129, 225–237.
- Macedo, J.C.D., Duarte, M., 1995. Alternative methods for synthesis of catalyst matrices. 1. Silica–alumina from metakaolinite. *Quimica Nova* 18, 26–29.
- Macedo, J.C.D., Mota, C.J.A., de Menezes, S.M.C., Camorim, V., 1994. NMR and acidity studies of dealuminated metakaolin and their correlation with cumene cracking. *Applied Clay Science* 8, 321–330.
- MacKenzie, K.J.D., Meinhold, R.H., 1994a. Thermal reactions of chrysotile revisited: a  $^{29}\text{Si}$  and  $^{25}\text{Mg}$  MAS NMR study. *American Mineralogist* 79, 43–50.
- Mackenzie, K.J.D., Meinhold, R.H., 1994b. The thermal reactions of synthetic hectorite studied by  $^{29}\text{Si}$ ,  $^{25}\text{Mg}$  and  $^7\text{Li}$  magic angle spinning nuclear magnetic resonance. *Thermochimica Acta* 232, 85–94.

- Madani, A., Aznar, A., Sanz, J., Serratos, J.M., 1990.  $^{29}\text{Si}$  and  $^{27}\text{Al}$  NMR study of zeolite formation from alkali-leached kaolinites. Influence of thermal preactivation. *Journal of Physical Chemistry* 94, 760–765.
- Madejová, J., Bujdák, J., Petit, S., Komadel, P., 2000a. Effect of chemical composition and temperature of heating on the infrared spectra of Li-saturated dioctahedral smectites. (I) Mid-infrared region. *Clay Minerals* 35, 739–751.
- Madejová, J., Bujdák, J., Petit, S., Komadel, P., 2000b. Effect of chemical composition and temperature of heating on the infrared spectra of Li-saturated dioctahedral smectites. (II) Near-infrared region. *Clay Minerals* 35, 753–761.
- Massiot, D., Dion, P., Alcover, J.F., Bergaya, F., 1995. Al-27 and Si-29 MAS NMR-study of kaolinite thermal decomposition by controlled rate thermal-analysis. *Journal of the American Ceramic Society* 78, 2940–2944.
- McBride, M.B., Mortland, M.M., 1974. Copper(II) interactions with montmorillonite: evidence from physical methods. *Soil Science Society of America Proceedings* 38, 408–415.
- Molina-Sabio, M., Caturla, F., Rodriguez-Reinoso, F., Kharitonova, G.V., 2001. Porous structure of a sepiolite as deduced from the adsorption of  $\text{N}_2$ ,  $\text{CO}_2$ ,  $\text{NH}_3$  and  $\text{H}_2\text{O}$ . *Microporous and Mesoporous Materials* 47, 389–396.
- Muller, F., Drits, V., Plançon, A., Robert, J.-L., 2000. Structural transformation of 2:1 dioctahedral layer silicates during dehydroxylation–rehydroxylation reactions. *Clays and Clay Minerals* 48, 572–585.
- Murat, M., Driouche, M., 1988. Conductometric investigations on the dissolution of metakaolinite in dilute hydrofluoric acid. Structural implications. *Clay Minerals* 23, 55–67.
- Nagata, H., Shimoda, S., Sudo, T., 1974. On dehydration of bound water of sepiolite. *Clays and Clay Minerals* 22, 285–293.
- Okada, K., Shimai, A., Takei, T., Hayashi, S., Yasumori, A., MacKenzie, K.J.D., 1998. Preparation of microporous silica from metakaolinite by selective leaching method. *Microporous and Mesoporous Materials* 21, 289–296.
- Pampuch, R., 1966. Infrared study of thermal transformations of kaolinite and the structure of metakaolin (in Polish). *Polska Akademia Nauk, Prace Mineralogiczne* 6, 53–70.
- Perissinotto, M., Lenarda, M., Storaro, L., Ganzerla, R., 1997. Solid acid catalysts from clays: acid-leached metakaolin as isopropanol dehydration and 1-butene isomerization catalyst. *Journal of Molecular Catalysis A-Chemical* 121, 103–109.
- Quirk, J.P., Theng, B.K.G., 1960. Effect of surface density of charge on the physical swelling of lithium montmorillonite. *Nature* 187, 967–968.
- Rocha, J., Klinowski, J., 1990. Solid-state NMR studies of the structure and reactivity of metakaolinite. *Angewandte Chemie International Edition (in english)* 29, 553–554.
- Rocha, J., Klinowski, J., 1991. The rehydration of metakaolinite to kaolinite. *Journal of the Chemical Society—Chemical Communications* 8, 582–584.
- Rocha, J., Klinowski, J., Adams, J.M., 1991. Synthesis of zeolite Na-A from metakaolinite revisited. *Journal of the Chemical Society, Faraday Transactions* 87, 3091–3097.
- Ruiz, R., del Moral, J.C., Pesquera, C., Benito, I., Gonzalez, F., 1996. Reversible folding in sepiolite: study by thermal and textural analysis. *Thermochimica Acta* 279, 103–110.
- Russell, J.D., Farmer, V.C., 1964. Infrared spectroscopic study of the dehydration of montmorillonite and saponite. *Clay Minerals Bulletin* 5, 443–464.
- Sabir, B.B., Wild, S., Bai, J., 2001. Metakaolin and calcined clays as pozzolans for concrete: a review. *Cement and Concrete Composites* 23, 441–454.

- Sabu, K.R., Sukumar, R., Rekha, R., Lalithambika, M., 1999. A comparative study on  $\text{H}_2\text{SO}_4$ ,  $\text{HNO}_3$  and  $\text{HClO}_4$  treated metakaolinite of a natural kaolinite as Friedel-Crafts alkylation catalyst. *Catalysis Today* 49, 321–326.
- Sadek, O.M., Mekhamer, W.K., 2000. Ca-montmorillonite clay as thermal energy storage material. *Thermochimica Acta* 363, 47–54.
- Sadek, O.M., Mekhamer, W.K., 2001. Na-montmorillonite clay as thermal energy storage material. *Thermochimica Acta* 370, 57–63.
- Sanz, J., Madani, A., Serratos, J.M., Moya, J.S., Aza, S., 1988. Aluminum-27 and silicon-29 magic angle spinning nuclear magnetic resonance study of the kaolinite–mullite transformation. *Journal of the American Ceramic Society* 71, C418–C421.
- Schultz, L.G., 1969. Lithium and potassium absorption, dehydroxylation temperature and structural water content of aluminous smectites. *Clays and Clay Minerals* 17, 115–149.
- Schwinka, V., Mortel, H., 1999. Physico-chemical properties of illite suspensions after cycles of freezing and thawing. *Clays and Clay Minerals* 47, 718–725.
- Serna, C., Ahlrichs, J.L., Serratos, J.M., 1975. Folding in sepiolite crystals. *Clays and Clay Minerals* 23, 452–457.
- Stackhouse, S., Coveney, P.V., 2002. Study of thermally treated lithium montmorillonite by Ab Initio methods. *Journal of Physical Chemistry B* 106, 12470–12477.
- Stubican, V., Roy, R., 1961. Proton retention in heated 1:1 clays studied by infrared spectroscopy, weight loss and deuterium uptake. *Journal of Physical Chemistry* 65, 1348–1351.
- Suraj, G., Iyer, C.S.P., Lalithambika, M., 1998. Adsorption of cadmium and copper by modified kaolinite. *Applied Clay Science* 13, 293–306.
- Suzuki, M., Ohashi, F., Inukai, K., Maeda, M., Tomura, S., Mizota, T., 2001a. Hydration enthalpy measurement and evaluation as heat exchangers of allophane and imogolite (in Japanese). *Journal of the Ceramic Society of Japan* 109, 681–685 (abstract ISI Web of Science).
- Suzuki, M., Suzuki, S., Maeda, M., Tomura, S., Mizota, T., 2001b. Hydration rate of allophane and imogolite by hydration heat measurement—using as heat exchange absorbents for lower temperature heat source and speedy drying desiccant (in Japanese). *Journal of the Ceramic Society of Japan* 109, 874–881 (abstract ISI Web of Science).
- Tettenhorst, R., 1962. Cation migration in montmorillonites. *American Mineralogist* 47, 769–773.
- Theng, B.K.G., Hayashi, S., Soma, M., Seyama, H., 1997. Nuclear magnetic resonance and X-ray photoelectron spectroscopic investigation of lithium migration in montmorillonite. *Clays and Clay Minerals* 45, 718–723.
- Van Scoyoc, G.E., Serna, C.J., Ahlrichs, J.L., 1979. Structural changes in palygorskite during dehydration and dehydroxylation. *American Mineralogist* 64, 215–223.
- Vollet, D.R., Macedo, J.C.D., Mascarenhas, Y.P., 1994. Pore structure characterization of kaolin, metakaolin, and their acid treated products using small-angle X-ray scattering. *Applied Clay Science* 8, 397–404.
- Vu, D.D., Stroeven, P., Bui, V.B., 2001. Strength and durability aspects of calcined kaolin-blended Portland cement mortar and concrete. *Cement and Concrete Composites* 23, 471–478.
- Watanabe, T., Shimizu, H., Nagasawa, K., Masuda, A., Saito, H., 1987.  $^{29}\text{Si}$  and  $^{27}\text{Al}$ -MAS/NMR study of the thermal transformations of kaolinite. *Clay Minerals* 22, 37–48.
- Yariv, S., Michaelian, K.H., 2002. Structure and surface acidity of clay minerals. In: Yariv, S., Cross, H. (Eds.), *Organo-Clay Complexes and Interactions*. Marcel Dekker, New York, pp. 1–38.

*Chapter 7.3*

## CLAY MINERAL ORGANIC INTERACTIONS

G. LAGALY<sup>a</sup>, M. OGAWA<sup>b</sup> AND I. DÉKÁNY<sup>c</sup>

<sup>a</sup>*Institut für Anorganische Chemie, Universität Kiel, D-24118 Kiel, Germany*

<sup>b</sup>*Department of Earth Sciences, Waseda University, Nishiwaseda 1-6-1, Shinjuku-ku, Tokyo 169-8050, Japan*

<sup>c</sup>*Department of Colloid Chemistry and Nanostructured Materials Research Group of the Hungarian Academy of Sciences, University of Szeged, H-6720 Szeged, Hungary*

Clay minerals can react with different types of organic compounds in particular ways (Fig. 7.3.1). Kaolin species (kaolinite, nacrite, and dickite) adsorb particular types of neutral organic compounds between the layers. The penetration of organic molecules into the interlayer space of clay minerals is called intercalation. Intercalated guest molecules can be displaced by other suitable molecules.

A broader diversity of reactions characterises the behaviour of 2:1 clay minerals. Water molecules in the interlayer space of smectites and vermiculites can be displaced by many polar organic molecules. Neutral organic ligands can form complexes with the interlayer cations. The interlayer cations can be exchanged by various types of organic cations. Alkylammonium ions, in industrial applications mainly quaternary alkylammonium ions, are widely used in modifying bentonites. The other important group of organic compounds are cationic dyes and cationic complexes. The interaction of clay minerals with different types of polymers including polypeptides and proteins was intensely studied many decades ago and recently seems to revive.

Grafting reactions, i.e. forming covalent bonds between reactive surface groups and organic species is an important step to hydrophobise the surface of clay mineral particles. The 2:1 clay minerals provide the silanol and aluminol groups on the edge surface for grafting reactions. The hydroxyl groups on the interlayer surface of kaolinite are accessible to the grafting agents when the interlayer space is expanded by intercalation.

Clay mineral–organic reactions are used to identify kaolinites and 2:1 clay mineral, to modify the surface character of clay mineral particles and the colloidal behaviour of clay dispersions in industrial applications. The organic derivatives are suitable adsorbents and useful in pollution control. Clay mineral–dye interactions, clay mineral–hybrid film formation, and clay polymer nanocomposites are actual



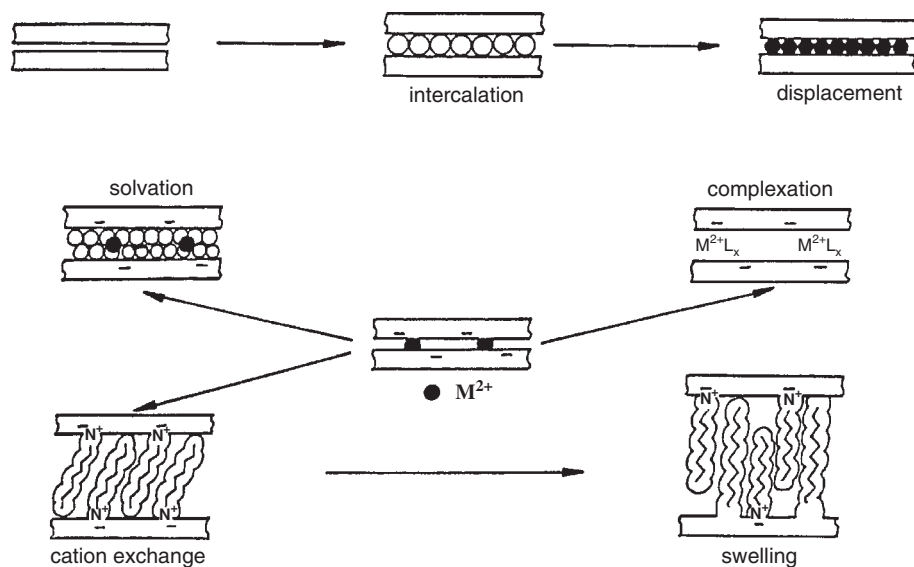


Fig. 7.3.1. Interlayer reactions of 1:1 and 2:1 clay minerals. From [Jasmund and Lagaly \(1993\)](#).

topics in material science. These aspects of clay–organic interaction are discussed in more detail in Chapters 5, 10.1, 10.2, 10.3, 11.1 and 11.2.

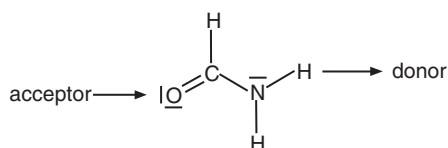
### 7.3.1. INTERCALATION REACTIONS OF KAOLINITES

Among 1:1 clay minerals only the kaolin species intercalate various organic molecules ([Fig. 7.3.1](#)); serpentines are non-reactive.

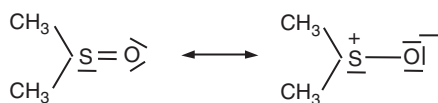
#### A. Type of Guest Compounds

As the layers in kaolinite and its polytypes are held together by hydrogen bonds and dipole–dipole interactions in addition to the van der Waals forces, the organic guest compounds that are directly intercalated are divided into three groups ([Weiss, 1961](#); [Weiss et al., 1963a, 1963b, 1966](#); [Olejnik et al., 1970](#)):

1. Compounds that form hydrogen bonds like hydrazine, urea, and formamide. To break the hydrogen bonds between the layers, the guest molecules must contain two separated groups to accept and donate hydrogen bonds, like acid, amides, and urea ([Scheme I](#)): the carbonyl group accepts and the amide group donates hydrogen bonds. Alcohol molecules are not directly intercalated because the OH group combines donor and acceptor properties.



Scheme I.



Scheme II.

2. Compounds with high-dipole moments like dimethyl sulfoxide (DMSO) and pyridine-*N*-oxide (Scheme II).

3. Potassium, rubidium, caesium, and ammonium salts of short-chain fatty acids (acetates, propionates, butyrates, and isovalerates) (Wada, 1961; Weiss et al., 1966). The reason for this reaction is still unclear. The intercalation of cadmium cysteine complexes into a low-ordered kaolinite may belong to this group of reactions (Benincasa et al., 2002).

Compounds with bulky substituents are not intercalated, but many are intercalated by displacement or entraining reactions.

Intercalation reactions were also reported for nacrite and dickite (Weiss and Orth, 1973; Weiss et al., 1973; Adams and Jefferson, 1976b; Adams 1978b; Adams, 1979; Ben Haj Amara et al., 1995).

Most intercalated guest compounds are easily desorbed by washing with water or by heating. As the state with the maximum number of intercalated molecules is only achieved in the presence of an excess of guest molecules (outside of the interlayer space), the analytical composition of many intercalates can only be approximately determined. Removing the excess of guest molecules (by washing or heating) is accompanied by desorption of a certain amount of intercalated molecules. High temperature X-ray studies of dimethyl sulfoxide–kaolinite indicated the thermal desorption of the sulfoxide occurred over several stages up to 300 °C (Franco and Ruiz-Cruz, 2002). The potassium acetate–kaolinite complex was stable up to 298 °C. At this temperature the intercalated potassium acetate melted. The following decomposition took place in two stages at 430 °C and 480 °C. Dehydroxylation occurred at a lower temperature than for the pure kaolinite (Gábor et al., 1995).

### B. Mechanism of Intercalation

Intercalation compounds are usually prepared by reacting the kaolinite with the guest molecules in the form of liquids, melts, or concentrated solutions, often at about 60–80 °C. Intercalation is a slow process that often requires several days

(Table 7.3.1; Fig. 7.3.2). The reaction rate depends not only on the type of guest compound, temperature, and concentration (if solutions are used) but also on the type of kaolinite and the particle size. It can also depend on the host–guest mass ratio.

The degree of reaction is calculated from the intensities of the (00 *l*) reflections of the unreacted kaolinite,  $I_K$ , and the intercalation compound,  $I_I$ :

$$\alpha = I_I / (I_K + I_I)$$

Table 7.3.1. Reaction conditions and basal spacing of a few kaolinite intercalation compounds

Guest compound	Basal spacing (nm)	Reaction conditions
None	0.71	
Formamide	1.01	4 days, 60 °C
Hydrazine hydrate	1.04	1 day, 60 °C
Urea*	1.07	8 days, 60–110 °C
<i>N</i> -methylformamide	1.08	2 days, 60 °C
Dimethyl sulphoxide	1.12	30 h, 50 °C
	1.12	20 min, 150 °C*
Potassium acetate*	1.40	1 day, 65 °C, pH = 8
Ammonium acetate*	1.41	20 days, 20 °C, pH = 8–9

From Weiss et al. (1966); Weiss and Orth (1973); Vempati et al. (1996)

\*In saturated aqueous solutions.

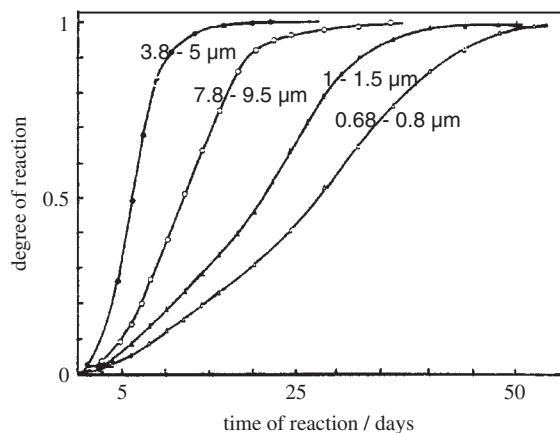


Fig. 7.3.2. Intercalation of urea (saturated aqueous solution at 65 °C) into kaolinites of different particle sizes (Weiss et al., 1970). From Jasmund and Lagaly (1993).

The degree of reaction defined in this way can differ from the effective degree of reaction because the influence of the Lorentz and Polarization factor, the possible effects of distortion of the layers (see below), and interstratification are not considered.

The degree of reaction as a function of time often increases in the form of an S-shaped curve, and the reaction rate obeys the Avrami–Erofeev equation for a two-dimensional phase boundary reaction and can eventually change into a two-dimensional diffusion controlled reaction (Fenoll Hach Ali and Weiss, 1969). Many kaolinites do not reach quantitative reaction, i.e.  $\alpha = 1$ .

Weiss and co-workers concluded from neutron scattering data that the reaction is started by the migration of protons or re-orientation of OH groups under the influence of the dipole moment of the guest molecules adsorbed at the external basal plane surfaces (Weiss et al., 1981; see also Lagaly, 1984, 1986a). This causes an elastic deformation of the kaolinite layer near the basal plane that opens the interlayer space. Electron resonance spectroscopy revealed that the kaolinite layer is deformed by the intercalated guest compounds (Lipsicas et al., 1986). The effect was stronger for DMSO than for *N*-methylformamide. A certain deformation and disorder of the layers was retained after desorption of the guest molecules.

After nucleation, intercalation proceeds as a co-operative process (Fenoll Hach-Ali and Weiss, 1969). The first guest molecules can only penetrate between the silicate layers when one or both layers begin to curl (Fig. 7.3.3). This creates a zone of deformation the extent of which depends on the elastic properties of the silicate layer. After the nucleation step (*N* in Fig. 7.3.3) the layer rolls up and promotes the penetration of guest molecules at the neighbouring sites along the edge *N*. Thus, cooperativity is caused by the process in which a few molecules succeed in rolling up the layer so that a large number of guest molecules can rapidly penetrate between layers, and the reaction front moves to the centre of the particle. The reaction front moving

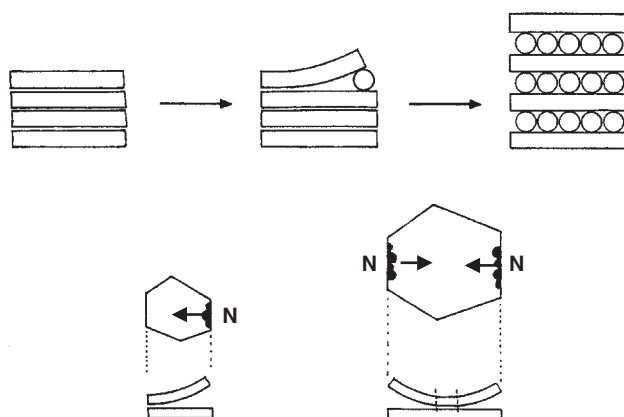


Fig. 7.3.3. Mechanism of intercalation. N nucleation sites, arrow: moving reaction front.

in the direction of the arrow (Fig. 7.3.3) exerts a geometrical constraint to nucleation at other sites. Only when the distance of edges from the reaction front starting at N exceeds a critical value (which depends on the elasticity moduli of the layer) can nucleation start at these edges simultaneously with nucleation at edge N. Thus, nucleation at any site of small crystals cannot occur independently of the nucleation at other sites. In contrast, nucleation at large crystals can start simultaneously at several edges. As a consequence, smaller particles react more slowly than larger ones, contrary to the general rule in solid-state chemistry (Fig. 7.3.2). More recently, Uwins et al. (1993) observed that the intercalation of *N*-methyl formamide into kaolinites was strongly reduced for particles  $< 0.4 \mu\text{m}$  and concluded that particle size is a more significant controlling factor for intercalation than defect distributions.

Cooperativity was also observed with other types of layer compounds (see also Section 7.3.8) (Lagaly, 1986a). For instance, cation-exchange reactions of micas revealed cooperative effects (Mortland and Lawton, 1961; Graf von Reichenbach and Rich, 1969; Sawhney, 1972; Graf von Reichenbach, 1973; Ross and Rich, 1973). While formation of superstructures (regular interstratification) by cation-exchange reactions can be related to (negative) cooperativity it may also be produced by unsymmetrical charge distributions (Lagaly, 1986a).

The rate of intercalation can be strongly dependent on the liquid structure of the guest molecules (Olejnik et al., 1970), for example, on the mass ratio of DMSO to kaolinite. Intercalation rate is at maximum when the amount of DMSO corresponds to a monomolecular layer on the external surface. The self-preservation of the strongly organised liquid DMSO retards the entry of the DMSO molecules between the layers. Therefore, soluble salts that change the liquid structure can influence the reaction rate (see also Section 7.3.6).

Desorption of the intercalated guest molecules can be a complex process. A two-dimensional contracting-circle mechanism was consistent with the results of the thermal desorption of dimethyl sulphoxide, provided the nucleation process was not instantaneous (Adams and Walth, 1980). The activation rate was very high ( $\sim 105 \text{ kJ/mol}$  dimethyl sulphoxide), indicating that the rate-determining step is complex and cannot be interpreted by assuming that single guest molecules are desorbed as in the case of *N*-methylformamide-kaolinite (Adams, 1978a).

Intercalation into kaolin minerals can split larger particles into thinner lamellae. The extreme stability of Chinese eggshell porcelain results from delamination of the kaolinite particles by urea (Weiss, 1963a). Even weak mechanical forces can delaminate the particles of intercalated kaolinite to such an extent that the lamellae roll up forming halloysite-type structures (Weiss and Russow, 1963; Poyato-Ferrera et al., 1977; Gardolinski and Lagaly, 2005b). Colloidal dispersions of finest kaolinite particles were prepared by the reaction of kaolinite with DMSO in the presence of ammonium fluoride (Lahav, 1990; Chekin, 1992). A certain exchange of hydroxyl ions by fluoride ions reduces the number of hydrogen bonds and promotes delamination.

Kaolinitic claystones (tonsteins, flint clays) are difficult to disaggregate. Immersion in hydrazine hydrate disaggregates most claystones as a consequence of

the swelling pressure developed during intercalation. Hydrazine hydrate works more quickly and efficiently than DMSO (Weiss and Range, 1970; Triplehorn et al., 2002).

### C. Structure of Intercalation Complexes

Infrared, Raman, and NMR studies are useful to derive the arrangement and orientation of guest molecules between the silicate layers (Johnston et al., 1984; Duer and Rocha, 1992; Duer et al., 1992; Hayashi, 1995, 1997; Frost et al., 1997, 1998a, 1998b). The intensity of the OH stretching modes of the inner surface hydroxyl groups might serve as a quantitative measure of the number of the interlayer OH groups interacting with the guest molecules (Frost et al., 1998c). X-ray diffraction studies and one-dimensional Fourier projections were reported for kaolinite intercalated with dimethyl sulphoxide, *N*-methylformamide, imidazole, pyridine-*N*-oxide, picoline-*N*-oxide (Weiss et al., 1963a, 1963b, 1966, 1973; Weiss and Orth, 1973). The first three-dimensional crystal structure was solved for dickite intercalated with formamide and *N*-methylformamide (Adams and Jefferson, 1976b; Adams 1978b, 1979). A neutron powder diffraction study revealed the hydrogen bonding system in formamide-kaolinite (Adams et al., 1976a).

### D. Displacement Reactions

Almost all intercalated molecules can be displaced by other polar molecules, even by molecules that are not directly intercalated. A large number of intercalation compounds were prepared in this way (Weiss et al., 1966; Olejnik et al., 1970; Gardolinski et al., 2000; Kelleher and O'Dwyer, 2002). Suitable starting materials are DMSO and ammonium acetate kaolinite. For example, ammonium acetate was displaced by *N,N*-dimethyl formamide, *N,N*-dimethyl urea, and pyridine (Weiss et al., 1966). Long-chain alkylamines were intercalated by displacement of ammonium acetate, and considerably increased the basal spacing (2.2 nm for butylamine, 5.8 nm for octadecylamine) (Weiss et al., 1966). Intercalated ammonium propionate obtained by the displacement of ammonium acetate combined in the interlayer space with diaminoethane to the corresponding amide (Seto et al., 1978a, 1978b). Acrylamide intercalated by displacement of *N*-methylformamide was polymerised by heating to 300 °C for 1 h (Komori et al., 1999). Poly( $\beta$ -alanine)-kaolinite was prepared by the polycondensation of intercalated  $\beta$ -alanine, with ammonium acetate-kaolinite as the precursor material (Itagaki et al., 2001).

The kaolinite methanol complex is a highly versatile intermediate/intermediary for displacement reactions (Komori et al., 1999). The methanol intercalate itself is prepared by displacement of *N*-methylformamide. As an example, methanol was displaced by ortho- and para-nitroaniline (not by the meta-isomer!). These intercalates may be of interest for future research because they exhibit second-harmonic generation (Takenawa et al., 2001).

Several guest molecules intercalated into kaolinite can be replaced by water molecules (basal spacing 1.0 nm), simply by washing with water (Wada, 1965). A part of the water molecules are keyed into the ditrigonal holes, while the remaining water molecules are more mobile (Costanzo et al., 1984; Lipsicas et al., 1985). The hydrates of different types of kaolinites differ in stability and not all types of kaolinites form hydrates (Range et al., 1968, 1969; Bartz and Range, 1979; Lipsicas et al., 1985). In many but not all kaolinites the water molecules can be replaced by other guest compounds (Costanzo and Giese, 1990). Wada (1959a, 1959b, 1964) earlier reported the penetration of salts into the interlayer space of halloysite.

### *E. Entraining Reactions*

Many non-reactive compounds are intercalated in the presence of guest molecules that directly penetrate into the interlayer space. Weiss et al. (1963a) studied the intercalation of several potassium salts of organic acids. As long as hydrazine hydrate was present, the basal spacing of the kaolinite was similar to the hydrazine intercalation compound (1.04 nm). When hydrazine was removed by desorption in air, the spacing typical of the entrained compounds developed, often distinctly higher than 1.04 nm.

This type of reaction is distinguished from the displacement reaction. Entraining occurs when reactive guest molecules open the interlayer space so that non-reactive compounds simultaneously penetrate between the layers.

### *F. Intercalation of Alkali Halogenides*

An interesting group of reactions is the intercalation of alkali halogenides (Wada, 1964). One possible way to intercalate inorganic salts is the displacement of DMSO or ammonium acetate by the salts (Weiss et al., 1966; Yariv et al., 2000). CsCl and CsBr intercalated kaolinite was also prepared by grinding the kaolinite-salt mixtures with a limited amount of water or by evaporating dispersions of kaolinite in aqueous caesium salt solutions, followed by ageing in humid air (Michaelian et al., 1991a, 1991b; Yariv et al., 1991, 1994; Thompson et al., 1993; Lapidés et al., 1994, 1995).

### *G. Grafting Reactions*

Grafting reactions, i.e. attachment of organic groups by covalent bonds, is an important step to make clay minerals compatible with organic polymers (van Meerbeek and Ruiz-Hitzky, 1979). For practical applications, kaolinites are modified, for instance, with alkoxy aluminium acrylates and alkoxy titanium acrylates (Solomon and Hawthorne, 1983). In these cases, only the silanol groups at the crystal edges react with the organic agents.

Grafting reactions between the layers require the formation of an intercalation complex as the intermediate step (Gardolinski and Lagaly, 2005a). Dimethyl

sulphoxide–kaolinite and *N*-methylformamide–kaolinite reacted with methanol at 150–270 °C and yielded products in that every third OH group of the interlayer aluminol groups was replaced by methoxy groups (Tunney and Detellier, 1996).

Displacement of DMSO by ethylene glycol yields an ethylene glycol intercalate with a basal spacing of 1.08 nm. Refluxing the dimethyl sulphoxide–kaolinite with dry ethylene glycol yielded a well-ordered, thermally robust derivative with a basal spacing of 0.94 nm where the glycol was grafted to the interlayer aluminol groups (Tunney and Detellier, 1994).

Phenylphosphonium acid underwent a topotactic reaction with the aluminol groups of kaolinite and halloysite during refluxing in water-acetone at 70 °C (Breen et al., 2002). In an acidic medium, phosphates, especially in the presence of potassium ions, decompose clay minerals through the formation of aluminium phosphates like taranakite (Weiss et al., 1995). The reaction with several organo-phosphates like trimethyl phosphate or phenyl phosphonates did not yield the intercalation compound, but decomposed the kaolinite structure under formation of metal organo-phosphonates (Sánchez-Camazano and Sánchez-Martín, 1994; Guimarães et al., 1998; Trobajo et al., 2001; Wypych et al., 2003; Gardolinski et al., 2004).

#### H. Differentiation of Kaolinites

Many kaolinites do not react quantitatively with reactive guest molecules such as DMSO or hydrazine, and the (001) reflection of non-reacted kaolinite remains visible, i.e.  $\alpha < 1$ , even after prolonged reaction periods (Fig. 7.3.4). A possible explanation is that these kaolinites are mixtures (or zonal structures) of kaolinites of different reactivity. Three types of kaolinites are classified (Fig. 7.3.4) (Range et al., 1968, 1969; Fernandez-Gonzales et al., 1976; Lagaly, 1981a):

*Type A* is the most reactive species. It intercalates dimethyl sulphoxide, urea, and many other compounds.

*Type B* reacts with DMSO but not with urea.

*Type C* is non-reactive.

Measuring the degree of reaction with DMSO and urea allows the determination of the mass fractions of the three types that make up the investigated kaolin sample.

Many kaolins are in fact composed of different kaolinites (Keller and Haenni, 1978; de Luca and Slaughter, 1985; Lombardi et al., 1987; Plançon et al., 1988). However, different reactivity may be related to defects like the presence of a few interlayer cations compensating sporadically occurring charges of the silicate layers (Range et al., 1969). The difficulty of intercalation of a kaolinite from Birdwood, South Australia, was related to a highly disordered kaolinite coating the particles of highly ordered kaolinite (Frost et al., 2002). All types of kaolinites are expanded by hydrazine-DMSO after they were ground with dried CsCl (Jackson and Abdel-Kader, 1978; Calvert, 1984).

The lattice expansion with DMSO (or hydrazine hydrate), if necessary after grinding with CsCl, is used for X-ray identification of kaolinites and to distinguish



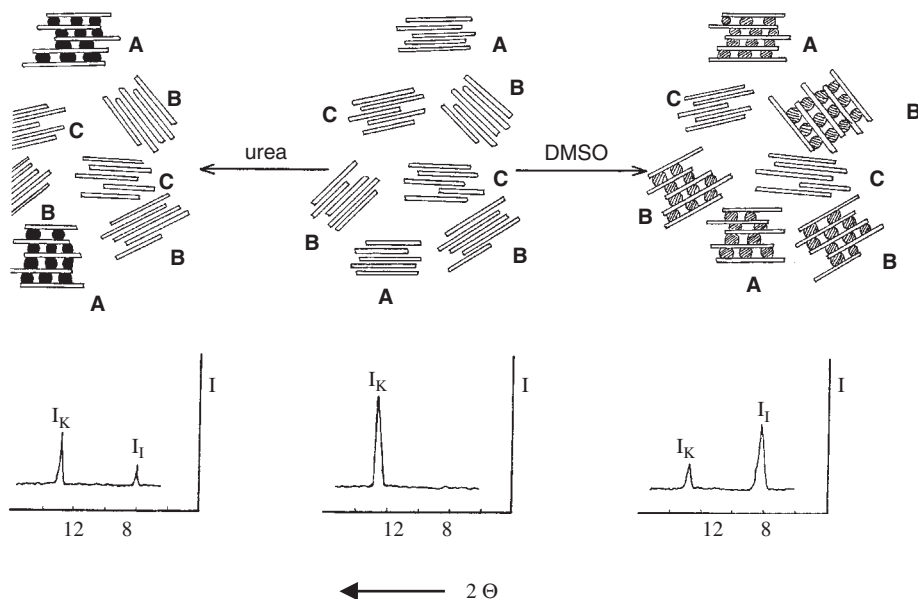


Fig. 7.3.4. Reaction of a kaolin sample consisting of three types of kaolinites (reaction types A, B, and C) with dimethyl sulphoxide (DMSO) and urea (see text). [Fernandez-Gonzales et al. \(1976\)](#).

them from chlorites that show the (002) reflection at 0.71 nm. Dehydrated halloysite and kaolinite are distinguished by the rate of reaction with formamide. Halloysite reacts within about 1 h, kaolinite expands after 4 hs. This reaction can also be used to determine the halloysite content ([Churchman et al., 1984](#); [Theng et al., 1984](#); [Churchman, 1990](#)). Halloysite may also be identified by the reaction with ethylene glycol. The response to ethylene glycol solvation involves a decrease in the intensity of the 0.72 nm reflection but an increase in the intensity of the peak at  $\sim 0.358$  nm (MacEwan effect) and is related to an interstratification effect ([Hillier and Ryan, 2002](#)).

### 7.3.2. REACTIONS OF 2:1 CLAY MINERALS

The adsorption of neutral molecules on smectites is driven by various chemical interactions: hydrogen bonds, ion–dipole interaction, co-ordination bonds, acid–base reactions, charge-transfer, and van der Waals forces ([Weiss, 1963b](#); [Theng, 1974](#); [Lagaly, 1984, 1987a](#); [Jasmund and Lagaly, 1993](#); [Yariv and Cross, 2002](#)). Polar molecules such as alcohols, amines, amides, ketones, aldehydes, and nitriles form intercalation complexes with smectites. Even acids are intercalated ([Brindley and Moll, 1965](#); [Yariv and Shoval, 1982](#); [Ogawa et al., 1992c](#)). Guest compounds can be intercalated from the vapour, liquid, and solid state. When intercalated from solutions, solvent molecules are generally coadsorbed in the interlayer space.

Guest molecules may be intercalated in dried clay minerals or may displace the water molecules of hydrated smectites and vermiculites. The displacement of interlayer water molecules depends on the HSAB character<sup>1</sup> of the interlayer cations and the interacting groups of the guest molecules. Water molecules around hard cations like  $\text{Na}^+$ ,  $\text{Mg}^{2+}$ , and  $\text{Ca}^{2+}$  are displaced only by  $\text{HO}-$  or  $\text{O} =$  containing compounds but not by amines. In contrast, amines as soft bases displace water molecules from soft interlayer cations like  $\text{Cu}^{2+}$  and  $\text{Zn}^{2+}$ .

Intercalation of neutral compounds into dried montmorillonites and vermiculites is not necessarily accompanied by cation movement midway between the silicate layers (outer-surface complexes). The cations can remain in contact with one silicate layer, i.e. the oxygen atoms of the silicate surface occupy the coordination sites of the cations (inner-surface complexes). However, little relationship was found between the intercalation and bulk properties of the liquid guest molecules (Berkheiser and Mortland, 1975).

Many large molecules are not directly intercalated, but can be introduced by stepwise expansion of the interlayer space (propping-open procedure). For instance, the ethanol intercalation complex of  $\text{Ca}^{2+}$  montmorillonite was used as a starting material to prepare the butanol and hexanol intercalates. The hexanol complex was then used as a base to intercalate longer chain alkanols up to octadecanol (Brindley and Ray, 1964). Fatty acids up to 18 carbon atoms were intercalated into  $\text{Ca}^{2+}$  montmorillonite starting from the hexanol or octanol intercalates. Shorter chain fatty acids with less than 10 carbon atoms could be directly intercalated because they expanded only to basal spacings  $< 1.7$  nm (Brindley and Moll, 1965).

Colour often changes when clay minerals with transition metal ions on exchange positions react with aromatic ligands. UV-Vis, IR, and ESR spectroscopic techniques are useful tools to investigate the cation–ligand interactions (Farmer and Russell, 1967; Yariv and Cross, 2002). The relationship between the infrared absorption frequency and the polarisation by the interlayer cations confirms the importance of the ion–dipole interactions. As an example, the frequency shift of the CN stretching vibration of acrylonitrile indicates the strength of the cation–nitrile interactions (Yamanaka et al., 1974). Unlike other ligands the CN stretching vibration of benzonitrile shifted to larger wave numbers when the polarising power of the interlayer cations increased (Serratos, 1968).

The solid–solid reaction between 2,2'-bipyridine and montmorillonite yielded metal-(2,2'-bipyridine) complexes in the interlayer space. The products were identical to those prepared by cation-exchange reactions of montmorillonite with pre-formed complex cations (Ogawa et al., 1991).

A few complexes that were not stable in homogeneous solution were found to be stable in the interlayer space. Benzene vapour reacts with copper(II)-montmorillonite and hectorite by displacing a part of the hydration water. In these yellow

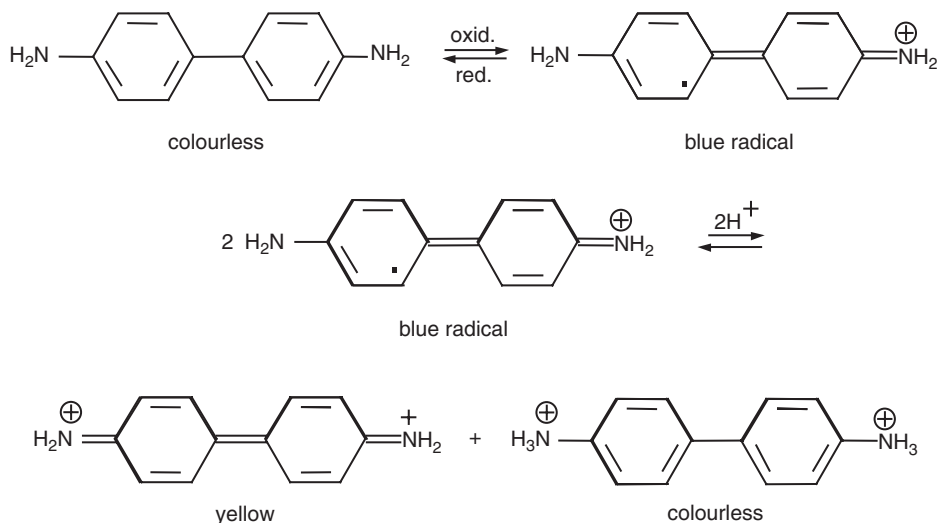
---

<sup>1</sup>Concept of hard and soft acid and bases, see Textbooks of Inorganic Chemistry (see also (Auboiroux et al., 1998)).

complexes, the  $\pi$  electrons of benzene interact with the copper ions. Complete removal of the interlayer water yields red benzene complexes by one-electron transfer from benzene to the interlayer cation, and the aromaticity of benzene is lost. Such complexes were also formed with a few other aromatic compounds and also with  $\text{Fe}^{3+}$  and  $\text{VO}^{2+}$  interlayer cations (Doner and Mortland, 1969; Pinnavaia and Mortland, 1971; Rupert, 1973; Pinnavaia et al., 1974; see also Lagaly, 1984).

Other well-known species that undergo charge transfer reactions with the clay mineral layers are benzidine and strongly electron-accepting species like tetracyanoethylene. Electron transfer from the diamine to the clay mineral produces the blue monovalent radical cation (Scheme III) (Theng, 1971). The electron acceptors are Lewis acid sites, mainly  $\text{Fe}^{3+}$  ions in structure. Octahedrally coordinated aluminium ions at the edges only act as Lewis acid sites when coordinated OH or  $\text{OH}_2$  groups are desorbed in the form of water (see discussion below). The radical cation, which is unstable in a homogeneous solution, is stabilised by  $\pi$  electron interactions with the oxygen atoms of the silicate layer (Yariv et al., 1976). When pH of the dispersion is below  $\sim 2$ , the blue radical cation disproportionates into the yellow divalent radical cation and the colourless benzidinium dication (Lahav, 1972; Furukawa and Brindley, 1973; Soma and Soma, 1988). Hendricks and Alexander (1940) proposed this colour reaction as a qualitative test of montmorillonites.

Another blue dye–clay mineral complex is the famous Maya blue. It can be prepared by a solid–state reaction between indigo and sepiolite or palygorskite with subsequent heating to  $120^\circ\text{C}$  (sepiolite) and  $150^\circ\text{C}$  (palygorskite). The indigo molecules are attached at the openings of the tunnels and are anchored by hydrogen bonds to the silanol groups projecting out from the edges of the tunnels (van Olphen,



Scheme III.

1966; Hubbard et al., 2003). The unusually radiant colour of the ancient Maya blue is probably related to the presence of iron and iron oxide nanoparticles (Polette et al., 2002).

The arrangement and orientation of the intercalated molecules depend not only on the type of bonding (un-directed for ion–dipole interactions, directed for all types of coordination bonds), the polarisation power of the cations, i.e. the size and charge of the cations, the properties of the guest molecules, but also on the association tendencies of the guest molecules and their van der Waals interaction with the silicate layer. The structure of the intercalation compounds is often derived by considering the size and shape of the guest molecules and the basal spacing. The orientation of several intercalated species was derived from anisotropic infrared spectra, for instance of pyridine (Serratosa, 1966) and benzonitrile (Serratosa, 1968). More precise information is obtained from one-dimensional electron density projections (Fourier analysis of the  $(00l)$  reflections). Oriented films are often used in such studies.

Studying homologous series of adsorptives such as alkanols and alkylamines allows the arrangement of the intercalated molecules to be derived from the changes of the basal spacing with the alkyl chain length. A linear increase of the basal spacing with the alkyl chain length, for instance observed for *n*-alcohols and *n*-alkylamines, is interpreted by assuming paraffin-type mono- or bi-layer arrangements, and the mean tilting angle is derived from the increase of the basal spacing per C–C bond (Brindley and Ray, 1964; Brindley and Moll, 1965; Brindley, 1965). The derived model is correct when a good agreement between the calculated and observed basal spacings is reached by considering the position of the polar end groups and the van der Waals distance between the CH<sub>3</sub> groups and the silicate layer (for monolayers) or between the methyl end groups midway in the interlayer space (for bilayers). Neglecting these distances can lead to unrealistic models.

The arrangement and orientation of intercalated long chain compounds is therefore decisively dependent on the van der Waals energy between the alkyl chains (Sections 7.3.3, and 7.3.6). This strong interaction can shift the polar end groups out of the positions for optimal hydrogen bond formation. As a consequence, the orientation of guest molecules with short alkyl chains is mainly determined by the interactions of the polar groups with the silicate layer, whereas the increased van der Waals energy forces longer chain compounds into paraffin-type arrangements. An example is the transition from flat-lying fatty acids into the paraffin-type structure when the number of carbon atoms exceeds nine (Brindley and Moll, 1965).

The interlamellar adsorption of methanol on Li<sup>+</sup>- and Ca<sup>2+</sup>-montmorillonite illustrates the interplay of the ion–dipole interaction between the alcohol molecules and the interlayer cations with the association tendency of the guest molecules (Annabi-Bergaya et al., 1981). In the presence of lithium ions, the arrangement of methanol molecules in zigzag chains is similar in structure to solid methanol (Fig. 7.3.5). The strong polarising power of calcium ions impedes the association of the methanol molecules and leads to the formation of a strong solvation shell around the cations.

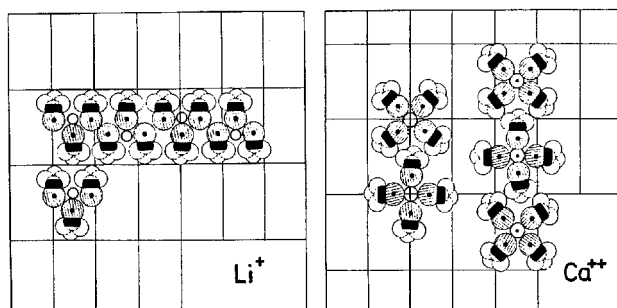


Fig. 7.3.5. Idealised arrangement of methanol molecules in the interlayer space of  $\text{Li}^+$ -montmorillonite and  $\text{Ca}^{2+}$ -montmorillonite. From Annabi-Bergaya et al. (1981).

Intercalation of ethylene glycol (1,2-ethanediol) and glycerol (1,2,3-propanetriol) in expanding 2:1 clay minerals is widely used for routine identification of montmorillonite and vermiculite (Bradley, 1945; MacEwan, 1946; Walker 1958; Reynolds, 1965; Brindley, 1966). Smectites show basal spacings of 1.70–1.77 nm (Table 7.3.2), which correspond to the bilayer arrangement of the intercalated molecules. Vermiculite can form either mono- or bilayer complexes depending on the type of the interlayer cation and the layer charge. However, clear differentiation of montmorillonite and vermiculite is difficult and requires the determination of the layer charge, for instance by the alkylammonium method (see below). The specific surface area of montmorillonite (internal and external) was measured by glycol adsorption (Moore and Dixon, 1970; Madsen, 1977). The retention of the adsorbed molecules is dependent on the polarising power of the interlayer cations. Multivalent cations with their strong electrostatic field retain larger amounts of the organic compounds than alkali and ammonium ions (Brindley, 1966).

The intercalation of macrocyclic polyethers into smectites was investigated by Ruiz-Hitzky and co-workers (Ruiz-Hitzky and Casal, 1978; Aranda et al., 1994; Ruiz-Hitzky et al., 2001). These intercalation compounds may be used as solid-electrolytes and ion selective membranes. The interaction between the interlayer cations and the ligands caused different arrangements of the polyether molecules (Fig. 7.3.6).

Aliphatic and aromatic amines can be directly coordinated to the interlayer cations (Scheme IVa) or bound by water bridges (Scheme IVb) (Farmer and Mortland, 1966; Yariv and Heller, 1970; Heller and Yariv, 1970; Cloos et al., 1975; Laura and Cloos, 1975). The type of bonding is mainly determined by the hardness or softness of the cations due to the HSAB concept. While soft cations such as  $\text{Zn}^{2+}$ ,  $\text{Cd}^{2+}$ ,  $\text{Cu}^{2+}$ , and  $\text{Ag}^+$  bind amines directly, water bridges are formed between amines and hard cations (alkali and earth alkali ions,  $\text{Al}^{3+}$ ).<sup>2</sup> For instance, pyridine is directly

<sup>2</sup>These cations do not form stable amino complexes in water.

Table 7.3.2. Basal spacing (nm) of 2:1 clay minerals after solvation with ethylene glycol and glycerol (Brindley, 1966; Malla and Douglas, 1987). On the influence of humidity see Hsieh (1989)

Cation	Montmorillonite	Beidellite	Vermiculite	
	$\zeta = 0.3^*$	$\zeta = 0.45$	$\zeta = 0.55$	$\zeta \geq 0.7$
<i>Ethylene glycol</i>				
Lithium	1.69–1.71		1.62	1.60
Sodium	1.69–1.71	1.69	1.63	1.48 <sup>†</sup>
Potassium	1.69–1.71	1.35		1.04
Magnesium	1.69–1.71	1.69	1.63	1.40–1.43
Calcium	1.69–1.71	1.69	1.62	1.56 <sup>†</sup>
Strontium	1.69–1.71		1.61	1.56 <sup>†</sup>
Barium	1.69–1.71		1.62	1.60
<i>Glycerol</i>				
Lithium	1.68–1.78		1.42	1.43
Sodium	1.64–1.78	1.77	1.48	1.43–1.48
Potassium	1.32–1.42		~1.4	1.04
Magnesium	1.76–1.81	1.76–1.79	1.43	1.42–1.46 <sup>‡</sup>
Calcium	1.68–1.78	1.76–1.78	1.76	1.43
Strontium	1.70–1.78		1.76	1.43
Barium	1.72–1.78		1.76	1.43

\*Mean layer charge (eq/formula unit).

<sup>†</sup>Non-integral (00 $l$ ) reflections.

<sup>‡</sup>Dioctahedral vermiculites from soils ( $\zeta \geq 0.6$ ) also showed basal spacings of 1.79–1.86 nm (Malla and Douglas, 1987).

coordinated to copper ions, but bound by water bridges to magnesium and calcium interlayer cations (Farmer and Mortland, 1966).

In addition to the coordination bonds, ionic bonds are often observed, especially in aqueous dispersions when the base is protonated due to acidic solution pH (Ainsworth et al., 1987; Slide et al., 1987) or to the increased acidity of interlayer water molecules (Scheme V) (see Chapter 5):

Pyridine molecules in Na<sup>+</sup> montmorillonite are oriented about perpendicular to the silicate layers with the nitrogen atom pointing to the sodium ions. Three different states with basal spacings of 1.48, 1.94, and 2.33 nm were observed in the presence of water (Adams and Breen, 1982). In contrast, pyridinium cations were arranged flat between the layers (Serratos, 1966; van Olphen, 1968). The amount of protonated base was determined by DTG or temperature programmed desorption (Ballantine et al., 1987; Breen et al., 1987).

The ratio of protonated base to unprotonated base in the interlayer space differs from the ratio in homogeneous solution (Karickhoff and Bailey, 1976). An important reason is the increased acidity of interlamellar water. In addition, protonation is

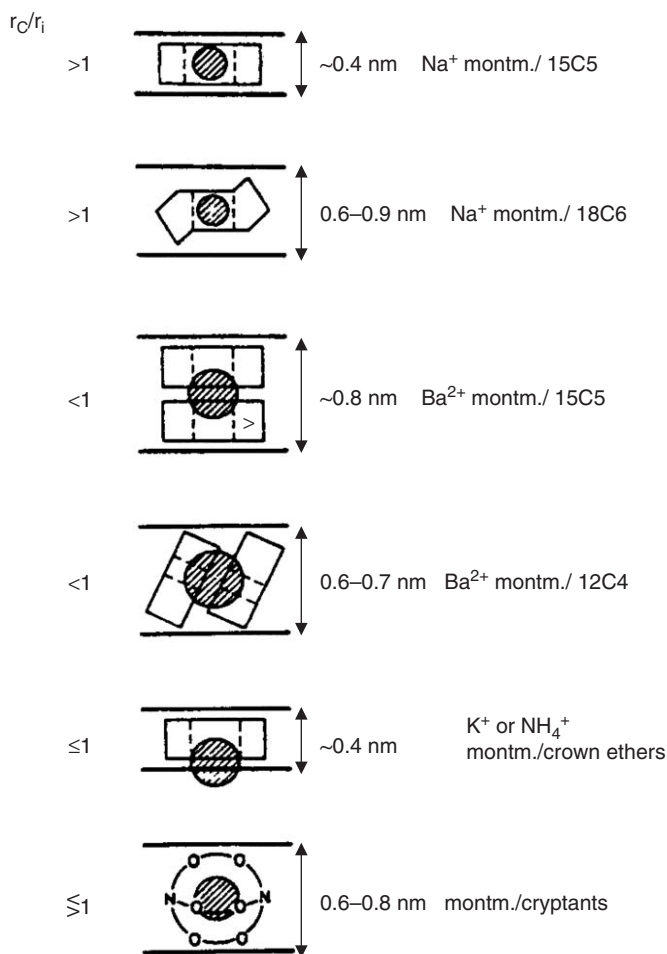
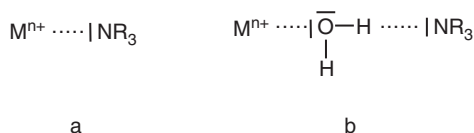


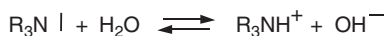
Fig. 7.3.6. Interlamellar arrangement of crown ether and cryptant molecules in homoionic smectites. From Ruiz-Hitzky et al. (2001).

enhanced by the ability of the negatively charged clay mineral surface to lower the chemical potential of the protonated form of the base relative to the neutral form (Feldkamp and White, 1979). Often, acid–base pairs (Scheme VI) are formed in a certain pH range around neutral.

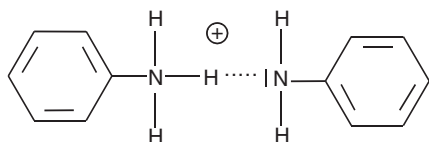
Bases are often used to measure the amount of acidic sites of clay minerals and to distinguish between Brønsted and Lewis acid sites. Brønsted acidity mainly arises from interlamellar water (see Chapter 5) (Yariv, 1992) as silanol groups at the edges are only weak-acidic centres. The simplest method for determining the Brønsted acidity strength is the use of Hammett indicators (Benesi, 1957; Benesi and Winquist,



Scheme IV.



Scheme V.



Scheme VI.

1978; Solomon and Hawthorne, 1983). However, these indicators only measure the acidity of the external surfaces. Yermiyahu et al. (2003) proposed the use of Congo red as an indicator in the study of surface acidity of smectites in aqueous dispersions.

Lewis acidic sites on clay mineral surfaces are usually coordinately unsaturated  $\text{Al}^{3+}$  ions that can accept electron pairs from donor molecules. Such sites can be formed by aluminium atoms at the edges or of adsorbed oligomeric hydroxo aluminium ions. In the presence of water the Lewis acidic species are hydrated and their Lewis acidity is masked. As the electron pair of nitrogen groups cannot displace water molecules from  $\text{Al}^{3+}$  ions, Lewis acidity of these  $\text{Al}^{3+}$  ions only develop after thermal decomposition of the water molecule, i.e. when the heated clay mineral is reacted with a base in the absence of water.

The protonated (Brønsted) and coordinated (Lewis) amines are distinguished by spectroscopic measurements, in some cases also by temperature programmed desorption (Solomon and Hawthorne, 1983; Breen et al., 1987; Carvalho et al., 2003).

Amino acids are bound by cation exchange and/or complexation (Theng, 1974, 1979; Siffert and Kessaissia, 1978). The charge of these molecules depends on the solution pH. With increasing pH the charge changes from positive to the neutral zwitter ion and, at still higher pH, to the anionic form. The isoelectric point varies between pH = 5 and 10 (cysteine 5.1 and glycine, alanine 6.1, histidine 7.6, and lysine 9.6).

Most studies of the adsorption of amino acids were carried out in a medium (mostly acidic) where the cationic forms of the acids were bound by cation exchange. A further mechanism is the complexation of the interlayer cations by the carboxylate groups of the zwitter ion and the anionic form. The degree of ion exchange and complexation in an acidic medium depends on the interlayer cation. Generally, the formation of complexes is stronger with transition metal cations than with alkali and



earth alkali cations. Di Leo (2000) compared the intercalation of glycine into  $\text{Ca}^{2+}$  and  $\text{Cd}^{2+}$  montmorillonite. The exchange reaction was dominant for  $\text{Ca}^{2+}$  montmorillonite. Once glycine molecules in the zwitter ionic form penetrated the interlayer space, the molecules were fully protonated due to the enhanced acidity of interlayer water molecules. Complexation was preferred by  $\text{Cd}^{2+}$  ions. The interesting observation that  $\text{Cd}^{2+}$  ions on the external surface were not complexed was related to the formation of inner-surface complexes between these  $\text{Cd}^{2+}$  ions and the surface oxygen atoms. Aspartic acid in the anionic form (isoelectric point at  $\text{pH} = 3$ ) was weakly bound in the interlayer space of montmorillonite and easily extractable with KCl solutions (Naidja and Huang, 1994). The authors assumed the carboxylate groups were coordinated to the interlayer calcium ions by water bridges. The intercalation of several amino acids (cysteine, lysine, and proline) can be accompanied by polycondensation (Siffert and Kessaissia, 1978).

When vermiculite was reacted with  $\gamma$ -amino butyric acid,  $\omega$ -amino caproic acid, or ornithine (Rausell-Colom and Fornés, 1974; Raupach et al., 1975; Raupach and Janik, 1976), the vermiculite particles delaminated in water and formed hydrogels (see Chapter 5). The exchange of the inorganic interlayer cations by 11-carboxy undecylammonium ions (the protonated form of  $\omega$ -amino undecanoic acid) allowed the intercalation and polymerisation of  $\epsilon$ -caprolactam (see Chapter 10.3).

The study of amino acid–clay mineral interactions was promoted by the possibility that a clay mineral may discriminate between optical isomers of amino acids. This possibility attracted much interest as well as controversy (see Hashizume et al., 2002). Kaolinite with other than triclinic stacking of the layers exhibits two inverse forms, and a stereoselective adsorption of optically active molecules may be understandable. The reports in the literature are contradictory (Siffert and Naidja, 1992). In contrast, montmorillonite particles do not exhibit “structural asymmetry”. However, structural chirality may be induced by the different packing modes of adsorbed enantiomers or DL pairs as proposed by Yamagishi (see Section 7.3.5). In fact, Siffert and Naidja (1992), studying the adsorption and deamination of glutaminic and aspartic acid, found a certain preference for the L forms and a higher degree of deamination of these enantiomers. More recently, Hashizume et al. (2002) reported a preference of certain allophanes for the L form of alanyl alanine, but no clear preference was developed for D- or L-alanine.

The adsorption of organic molecules with more highly complicated structures depends on the type of the clay mineral, the degree of purification (see Chapter 4), the interlayer cation, the mean layer charge, concentration (or vapour pressure) of the adsorptive, pH value, and temperature, but also on the fine structure of the clay mineral (type and degree of substitutions, especially  $\text{Al}^{3+}/\text{Si}^{4+}$ , layer charge distribution), particle size, degree of dispersion, ionic strength (Narine and Guy, 1981), type of salts present, and possible association equilibria in the solution. The adsorption of nuclein bases (adenine, cytosine, thymine, and uracil) on montmorillonite not only depended on the salts present and the mean layer charge but also on the charge distribution (Lagaly, 1984; Samii and Lagaly, 1987). Exchange of the sodium

and calcium ions by several diammonium cations showed a certain selectivity strongly influenced by the solvent (Mizutani et al., 1995).

Synergism effects were observed in co-adsorption experiments (Lailach and Brindley, 1969). Corresponding to the base pairing in DNA, the adsorption of thymine and uracil was enhanced in the presence of adenine (Lagaly, 1984, 1987a; Samii and Lagaly, 1987). Another example was the adsorption of adenosine monophosphate (AMP), which was increased by addition of adenosine triphosphate (ATP) whereas the adsorption of ATP was not influenced by AMP. As the adenosine phosphates are bound at the edges, their adsorption depends on the degree of dispersion (and, therefore, on the exact procedure of purification and fractionation, see Chapters 4 and 5) and the particle size (Graf and Lagaly, 1980; Herrmann and Lagaly, 1985).

Competitive adsorption (see Section 7.3.7) and co-adsorption phenomena must be considered when clays are applied as adsorbents. A model for calculating co-adsorption processes of cations was developed by Margulies et al. (1988).

### 7.3.3. ALKYLAMMONIUM DERIVATIVES

The interlayer cations of smectites and vermiculites can be exchanged by organic and organometallic cations in solution and in the solid state. Cation exchange reactions are performed by mixing aqueous dispersions of clay mineral and a solution of organoammonium salt. The products are separated by centrifugation or filtration and washed repeatedly. When the solubility of the guest species is low, water–alcohol mixtures are often used as solvents. Quantitative exchange requires a certain excess of alkylammonium salts in relation to the cation-exchange capacity (Lagaly, 1981a, 1994a). The alkylammonium derivatives in contact with the alkylammonium salt solutions not only intercalate water molecules but also some amounts of alkylammonium ions together with the anion, i.e. as ion pairs (Lagaly, 1981a; Klapys et al., 2001; Lee and Kim, 2002; Kuwaharada et al., 2002; Janek and Lagaly, 2003). The pure alkylammonium derivatives needed for layer charge determination are obtained after washing and careful drying (Rühlicke and Kohler, 1981; Lagaly, 1994a). For solid-state reactions the clay mineral and solid organoammonium salt are mixed without solvent and ground in a mortar (Ogawa et al., 1990).

Thermodynamic excess functions were derived for the exchange of Laponite with primary, secondary, and ternary amines and indicated the importance of the van der Waals interaction (Vansant and Peeters, 1978).

Quantitative exchange of the interlayer cations of smectites by alkylammonium ions provides a method for characterisation of smectites and vermiculites and determination of their layer charge (Lagaly, 1981a, 1994a; Mermut and Lagaly, 2001). The arrangement of the intercalated surfactant cations depends on the layer charge and the alkyl chain length (Figs. 7.3.7 and 7.3.8). Short chain alkylammonium ions are arranged in monolayers, longer chain alkylammonium ions in bilayers with the alkyl chain axes parallel to the silicate layers. The monolayer has a basal spacing of  $\sim 1.4$  nm, the bilayer

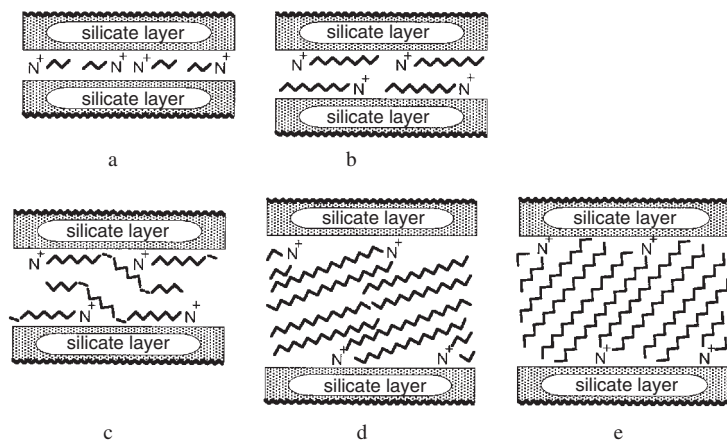


Fig. 7.3.7. Arrangement of alkylammonium ions in the interlayer space of smectites: (a) monolayers, (b) bilayers, (c) *pseudo*-trimolecular layers, and (d, e) paraffin-type arrangements of dialkylammonium ions with different tilting angles of the alkyl chains.

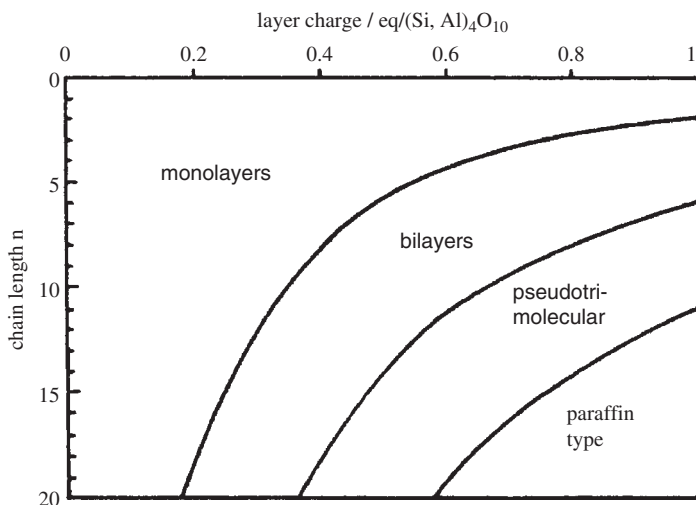


Fig. 7.3.8. Influence of layer charge and alkyl chain length on the arrangement of alkylammonium ions.  $n$  = number of carbon atoms in the  $n$ -alkyl chains. From Lagaly, (1986b).

of  $\sim 1.8$  nm. The monolayer rearranges into the bilayer when the area of the flat-lying alkylammonium ions becomes larger than the equivalent area. The monolayer/bilayer transition is used to measure the charge distribution and the mean layer charge.

Three-layer structures of kinked alkyl chains (see Section 7.3.8) are observed with highly charged smectites and/or long surfactant cations. This pseudotrimolecular

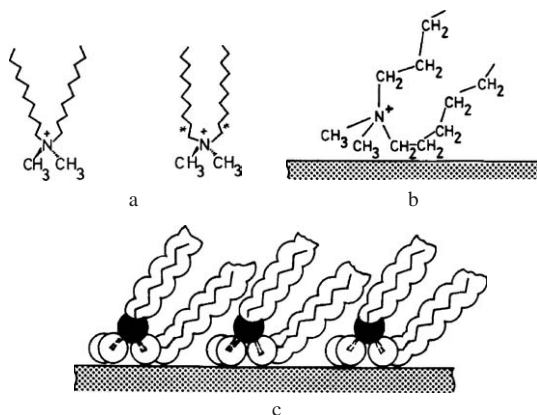


Fig. 7.3.9. (a–c) Conformation of dialkylammonium ions with and without *gauche* bonds (\*) near the ammonium group.

arrangement exhibits a basal spacing of  $\sim 2.2$  nm. The term *pseudo* is used because the positive surfactant groups are attached on the silicate layers whereas the alkyl chains assume a trimolecular arrangement by formation of kinks (Fig. 7.3.7).

Paraffin-type arrangements (Fig. 7.3.7d,e) in the interlayer space of smectites are formed by quaternary alkylammonium ions with two or more long alkyl chains. If all C–C bonds are in *trans*-conformation, the dialkylammonium ions are V-shaped. An almost parallel orientation of the chains is attained by formation of *gauche*-bonds near the ammonium group (Fig. 7.3.9). This conformation allows a denser packing of these surfactants in mono- and bimolecular films (Lagaly et al., 1975; Favre and Lagaly, 1991).

The alkylammonium ions in more highly charged vermiculites (mean layer charge  $\geq 0.8$  eq/(Si, Al) $_4$ O $_{10}$ ) form paraffin-type monolayers. The basal spacing increases linearly with the alkyl chain length and the layer charge is derived from the mean increase of the basal spacing (Lagaly, 1982; Ghabru et al., 1989; Mermut, 1994; Mermut and Lagaly, 2001). Low-charged vermiculites (mean layer charge  $\leq 0.6$  eq/(Si, Al) $_4$ O $_{10}$ ) intercalate alkylammonium ions in monolayers, bilayers, and pseudo-trimolecular arrangements, and the basal spacing increases in steps. These arrangements of flat-lying alkyl chains alternate with paraffin-type structures in medium-charged vermiculites. In these cases the layer charge is best derived by comparison with theoretical diagrams (Lagaly, 1982).

Paraffin-type arrangements are also observed in several types of layered materials with high-layer charge density such as M(IV) phosphates, niobyl phosphate, titanates, niobates, molybdates (Lagaly, 1981b; 1986b; Lagaly and Beneke, 1991).

Orientation and mobility of the intercalated organoammonium cations were examined by infrared (Stevens and Anderson, 1996a, 1996b; Parker and Frost, 1996; Yariv, 1996) and  $^{13}\text{C}$ -nuclear magnetic resonance spectroscopy (Pratum, 1992).

High-resolution transmission electron microscopy revealed the paraffin-type arrangement of alkylammonium ions in  $\text{Ba}^{2+}$  exchanged biotites (Marcks et al., 1989). This method of investigation of alkylammonium exchanged samples is a sensitive tool to visualise the organisation of smectite particles (see Chapter 5) (Vali and Köster, 1986; Lee and Kim, 2002) and to detect different types of interlayer spaces, especially of illite/smectite mixed-layer minerals (Rühlicke and Niederbudde, 1985; Bell, 1986; Klimentidis and Mackinnon, 1986; Ghabru et al., 1989; Vali et al., 1991; Cetin and Huff, 1995).

### 7.3.4. INTERACTIONS WITH CATIONIC DYES

#### *A. Aggregation of the Adsorbed Dyes*

The interaction of cationic dyes with clay mineral surfaces changes the spectroscopic properties of the dye molecules (see Chapter 3). An example of the influence of surface acidity on the colour of adsorbed dyes was reported for Congo red (Yerminahu et al., 2003). The adsorbed dyes often exhibit unique spectroscopic and photochemical properties. Orientation and aggregation of the intercalated dye molecules can be derived from absorption and luminescence spectra, in steady-state mode or time-resolved. The study of photo-processes also gives information about the distribution and mobility of adsorbed photoactive species (Ogawa and Kuroda, 1995; Garfinkel-Shweky and Yariv, 1999).

Metachromasy is a deviation from Beer's law caused by the aggregation of the dye molecules. The principal band in the visible region is gradually replaced by a band at a shorter (or longer) wavelength (Ogawa and Kuroda, 1995; Garfinkel-Shweky and Yariv, 1999; Yariv and Cross, 2002).

The adsorption of methylene blue (and other cationic dyes) from aqueous solution is often used to measure the cation-exchange capacity and specific surface area of clay minerals. However, spectroscopic studies of aqueous dispersions indicated the distribution of the dye cations on the surface of smectites is determined not only by electrostatic interactions, but also by dye-dye interactions (Cenens and Schoonheydt, 1988; Bujdák et al., 1998, 2003; Jacobs and Schoonheydt, 2001). Simply measuring the maximum amount adsorbed of methylene blue provides only approximate values, and modification of this procedure is required (Hang and Brindley, 1970; Rytwo et al., 1991; Kahr and Madsen, 1995; see also Avena et al., 2001).

That methylene blue adsorption occurs initially on the external surfaces of montmorillonite particles was discussed by several researchers. The concentration of dye in this area increases considerably and induces the formation of MB aggregates (Breen and Loughlin, 1994; Breen and Rock, 1994; Neumann et al., 2002). The dye molecules then migrate from the external surface to the interlayer region. The endothermic reaction of montmorillonite with methylene blue at loadings smaller than the cation-exchange capacity (Rytwo and Ruiz-Hitzky, 2003) supports this hypothesis. The reaction changed

to exothermic at higher loadings when interactions between the methylene blue cations became more dominant. Due to the stronger aggregation of crystal violet cations the reaction of montmorillonite with this dye was exothermic even at small amounts adsorbed. The more pronounced intermolecular interactions of the crystal violet cations also caused the larger yield value of crystal violet containing montmorillonite dispersions in comparison with methylene blue (Penner and Lagaly, 2000).

If the intercalation is really a two-step process, the re-arrangement will depend on particle size and texture (see Fig. 5.1, Chapter 5), the layer charge and charge distribution. Due to the strong electrostatic interactions, formation of aggregates should be promoted by a favourable distribution of the electrostatically anchored methylene blue cations; i.e. the aggregation is influenced by the distribution of the charges in the silicate layer (Bujdák et al., 1998). Methylene blue cations competed effectively with cationic surfactants but were also solubilised in the surfactant clusters on the clay mineral surface (Breen and Loughlin, 1994).

Because of their biological, catalytic, conductive, and photoactive properties, porphins and phthalocyanines were intercalated. Porphins undergo reversible protonation–deprotonation reactions and can be used as probes for the Brønsted acidity of the interlayer environment. Cady and Pinnavaia (1978) reported on the reaction of *meso*-tetraphenylporphyrine (TPPH<sub>2</sub>) with the interlayer cations of montmorillonite. The acidity of the hydrated interlayer cations affected the adsorption state of TPPH<sub>2</sub>. The strongly acidic aquo complexes of Fe<sup>3+</sup> and VO<sup>2+</sup> protonated the porphyrines quantitatively, and the cations were arranged in monolayers in the interlayer space. Hydrated Na<sup>+</sup> and Mg<sup>2+</sup> yielded only trace amounts of TPPH<sub>4</sub><sup>2+</sup>. The reaction of (n-C<sub>3</sub>H<sub>7</sub>)<sub>4</sub>N<sup>+</sup>-, Co<sup>2+</sup>-, Cu<sup>2+</sup>-, and Zn<sup>2+</sup>- montmorillonite with TPPH<sub>4</sub><sup>2+</sup> mainly yielded the proton-exchanged form of the montmorillonite, and the metalloporphyrine was displaced into solution. Formation of porphyrine from aldehyde and pyrrole was catalysed by the Brønsted acidity of the hydrated cations (Cady and Pinnavaia, 1978).

Abdo et al. (1980) described metallation–demetallation reactions of tin tetra(4-pyridyl) porphyrine in Na<sup>+</sup>- hectorite. The UV–Vis and luminescence spectra revealed that the adsorbed complex was demetallated, forming the tetra(4-pyridyl) porphyrine dication when the clay mineral was dehydrated. This process was reversible, indicating that the Sn<sup>4+</sup> ions remained in the vicinity of the porphyrine after demetallation.

Photoluminescence is a powerful tool to obtain information on the composition, structure and dynamics of the surrounding medium. The luminescence parameters (decay, quantum efficiency, and polarisation) are sensitive to changes in the microenvironment of the probe. Quenching, sensitisation, and energy transfer observed by adding a second component or changing the microenvironment also provide information, especially on dynamics.

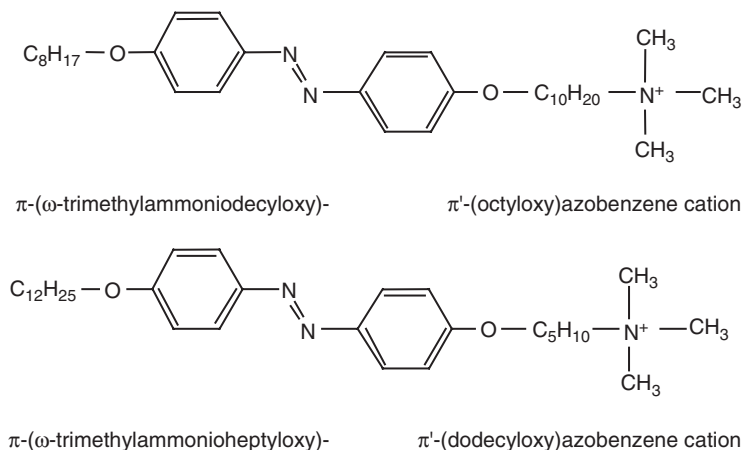
Aromatic hydrocarbons like pyrene and anthracene were applied as luminescence probes in a variety of assemblies. The vibronic fine structure of the pyrene monomer is sensitive to the polarity of the surrounding molecules. When pyrene molecules are

forced into close proximity or are present at high concentrations, excited state dimers (excimers) are observed. The intensity ratio of excimer to monomer fluorescence is often considered as a measure of pyrene mobility and proximity. The luminescence properties of cationic pyrene derivatives like (1-pyrenyl) trimethylammonium ions indicated the distribution of the adsorbed ions was determined by the surrounding medium as well as by the distribution of negative adsorption sites. The bonding between the positive probe and negative surface sites was not strong enough to inhibit diffusion of the adsorbed ions on the surface (Viane et al., 1988).

### B. Orientation of Intercalated Dye Molecules

In addition to one-dimensional Fourier analysis, the orientation of intercalated dye molecules can be derived from the spectroscopic anisotropy. As an example, the orientation of cationic amphiphilic azobenzene derivatives (Scheme VII) in the interlayer space was derived from the spectral shifts and the basal spacings (Ogawa and Ishikawa, 1998). The spectral shifts reflect the orientation of the dipoles in the aggregates; smaller red shifts are expected for dipole orientations with larger tilting angles.

The orientation of Co(II) tetrakis-(1-methyl-4-pyridyl) porphyrine in the interlayer space of  $\text{Na}^+$  hectorite and synthetic  $\text{Li}^+$  fluorhectorite was studied by X-ray diffraction and anisotropic ESR spectroscopy of oriented thin films (Ukrainczyk et al., 1994). It depended on the layer charge. When intercalated in hectorite, the porphyrine ring was oriented with its molecular plane parallel to the silicate layer and did not coordinate water molecules in the axial direction. In the more highly charged fluorhectorite, the porphyrine ring was tilted at  $27^\circ$  to the silicate layer, with



Scheme VII.



water molecules coordinated to Co(II). Dehydration in vacuum decreased the basal spacing from 1.96 to 1.76 nm, causing a rearrangement of the intercalated porphyrine into a staggered bilayer with no axial water bound to Co(II).

The electric linear dichroism (ELD), which measures the change in the absorption of light linearly polarised in the directions parallel and perpendicular to the applied electric field (Fig. 7.3.10), is a further powerful tool to determine the orientation of the guest molecules. For 2- and 4-[4-(dimethylamino)styryl]-1-ethylpyridinium cations on saponite, the tilting angles were determined by the amount of the intercalated dye as well as its molecular structure (the position of cationic site within the dye) (Sasai et al., 2000b).

Regioselective photocycloaddition of stilbazolium cations intercalated in the interlayer space of saponite was reported by Usami et al. (1990). Four photochemical reaction paths have to be considered for the stilbazolium ion (Scheme VIII). During irradiation of the dispersed stilbazolium saponite by UV light, *syn*-head-to-tail dimers were predominantly formed at the expense of *cis*-*trans* isomerisation, which is the major path in homogeneous solution. The selective formation of head-to-tail dimers suggests the intercalation occurs in an anti-parallel mode (Fig. 7.3.11). As the yield of dimers was barely dependent on the amount of the guest ions added, one has to assume the cations formed aggregates with alternating anti-parallel orientation, even at very low loading (e.g. 1% of the cation-exchange capacity). The preferential formation of *syn*-head-to-tail dimers reveals the influence of the van der Waals interaction between the adsorbed ions. Co-adsorption of alkylammonium ions affected the photoreactivity of the intercalated stilbazolium ions (Usami et al.,

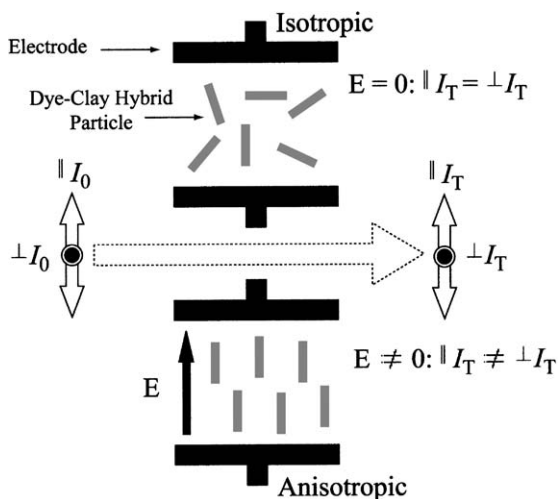
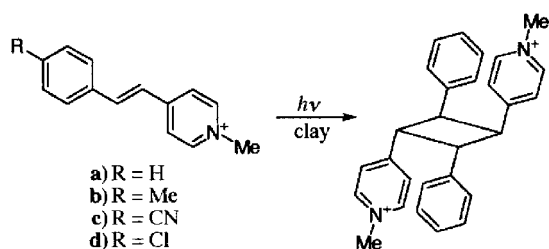


Fig. 7.3.10. Principles of electric dichroism in clay mineral-dye systems From Sasai et al. (2000b).





Scheme VIII.

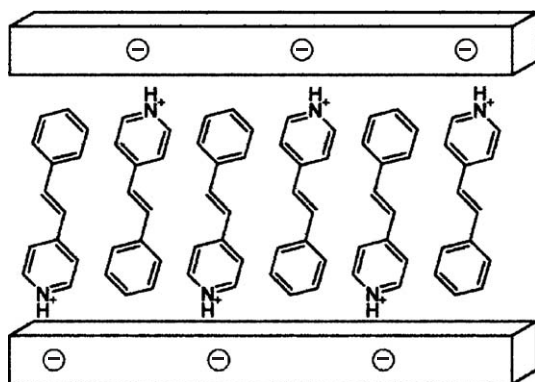


Fig. 7.3.11. Packing of stilbazolium cations in the interlayer space of saponite. From Usami et al. (1990).

1990). When the co-adsorbed alkylammonium ion was longer than the stilbazolium ion, the dominant photoreaction changed from cyclodimerization to *cis-trans* isomerization and the excimer emission of the intercalated stilbazolium ions was strongly reduced.

### 7.3.5. REACTION WITH CATIONIC COMPLEXES

Cationic organometallic complexes are intercalated by cation exchange or formed by in situ complexation in the interlayer space. The catalytic application of clay minerals with intercalated heavy metal complexes was studied some time ago (Pinnaia, 1983). The tris (2,2'-bipyridine) ruthenium(II) complex  $(\text{Ru}(\text{bpy})_3)^{2+}$ , abbreviated as Ru(II), is widely used as a luminescence probe (Kalyanasundaram, 1992). The shift of metal-to-ligand charge transfer bands and the  $\pi-\pi^*$  transitions of bipyridine as well as Raman and XPS studies indicated the bipyridine ligands were slightly distorted by the steric constraints when Ru(II) was adsorbed on montmorillonite. Partial oxidation of Ru(II) was also reported (Habti et al., 1984).

Ru(II) complexes are adsorbed at the edges, the external basal plane surfaces and between the silicate layers (DellaGuardie and Thomas, 1983; Schoonheydt et al., 1984). The occupancy of edge sites for the planar sites increased with decreasing particle size (Thomas, 1988). The Ru(II) and  $\text{Na}^+$  ions were segregated in the interlayer space of montmorillonite, yielding high local concentrations of the complex ions in the interlayer space even when the concentration of Ru(II) added was only 1–2% of the cation-exchange capacity (Ghosh and Bard, 1984). When  $(\text{Zn}(\text{bpy})_3)^{2+}$  was co-adsorbed with Ru(II) on hectorite, the effective self-quenching rate was largely reduced, presumably due to surface dilution of the Ru(II) cations. The origin of the segregation process is unclear. The non-uniform charge distribution of the silicate layers or interactions between the Ru(II) complexes may be involved.

The decay profiles indicated the quenching effect of iron ions in the clay mineral structure and the essentially immobile character of adsorbed Ru(II) cations in the time-scale of microseconds (Habt et al., 1984). The total quenching probability for a particular probe was determined by the quencher concentration in the solid and by the number of solid particles in contact with the probe.

Yamagishi (1987, 1993) observed differences in the adsorption of the enantiomers and racemic pairs of ruthenium and iron polypyridine and 1,10-phenanthroline (phen) complexes on montmorillonite. When a racemic mixture of  $[\text{Fe}(\text{phen})_3]^{3+}$  was added to a montmorillonite dispersion, racemic pairs rather than optical isomers in random distribution were adsorbed. Enantiomeric  $[\text{Fe}(\text{phen})_3]^{3+}$  cations were adsorbed in excess of the cation-exchange capacity. When the tris(phen) complex is oriented with its threefold symmetry axis perpendicular to the silicate surface, the base of the complex forms a regular triangle with a side length of about 0.65 nm. Since this distance is close to the distance of 0.55 nm between the centres of the hexagonal holes of the silicate layer, the three hydrogen atoms of the ligands can be buried in the silicate surface, and the chelate is rigidly fixed on the surface at a definite orientation. It was concluded from molecular model considerations that racemic adsorption by metal chelates on a solid surface is preferential when (i) the density of the adsorbed chelated cations allows lateral interactions and (ii) the surface is capable of fixing the complexes at a definite orientation. When bound by cation exchange, a divalent complex cation should have a molecular radius larger than 0.5 nm. Breu and Catlow (1995) pointed out that observed chiral recognition phenomena are related to the lateral interactions between the guest complexes that are modified by the corrugation of the silicate layer. The clay mineral controls the orientation and relative positions of the complexes in the interlayer space, i.e. the geometrical fit between host and guest shapes is important.

Cationic imine and amine complexes with 2:1 type clay minerals were used in preparing clay-modified electrodes (Fitch, 1990).

Synthetic fluorhectorites modified with  $[\text{Co}(\text{en})_3]^{3+}$  cations showed pronounced differences in rates of gas uptake at 77.3 and 90.2 K.  $\text{H}_2$ ,  $\text{D}_2$ ,  $\text{O}_2$ , and Ne were much more rapidly adsorbed than  $\text{N}_2$ , Ar, and  $\text{CH}_4$ . Similar effects were observed with certain zeolites (Barrer, 1986).

### 7.3.6. ADSORPTIVE PROPERTIES OF ALKYLAMMONIUM CLAY MINERALS

Replacement of the inorganic interlayer cations by cationic surfactants changes the hydrophilic silicate surface into hydrophobic (Jordan, 1950; Jones, 1983; Lagaly et al., 1983). The hydrophilic/hydrophobic balance depends on the length and packing density of the alkyl chains (Weiss, 1966; Lagaly, 1984, 1987b). Organophilic clays are used as rheological additives in paints, greases, and cosmetic formulations (see Chapter 10.1) (Jones, 1983).

The adsorptive properties of the organoammonium clay minerals were already been recognised (Barrer, 1978; 1989a, 1989b). Adsorption from aqueous solutions is usually studied by adding a solution of the organic compound to the dispersed clay mineral, shaking for 12–24 h, centrifuging, and determining the amount of the organic compound remaining in solution (often by ultraviolet spectroscopy and gas chromatography). Depletion of the organic compound measured in this way does not give the real amount adsorbed but rather the specific surface excess (see Section 7.3.7). Adsorption from the vapour phase is measured by gravimetric or volumetric methods.

As long as the alkylammonium ions lie flat between the silicate layers, small molecules like short chain alcohols, formamide, dimethyl sulphoxide, and water are adsorbed in the pores between the alkylammonium ions with none or only a modest increase of the basal spacing (by a few 0.01 nm). Longer alkylammonium ions  $C_{n_C}H_{2n_C+1}NH_3^+$ , typical  $n_C > 8$  (Malberg et al., 1989) move from flat into perpendicular orientation so that the volume accessible to the adsorptive increases strongly. Short-chain alcohols  $C_{n_A}H_{2n_A+1}OH$  ( $n_A < 8$ ) fill the space between the perpendicular alkylammonium ions arranged in monolayers (Fig. 7.3.12). Longer chain alkanols form interlayer bimolecular films composed of alkanol molecules and alkylammonium ions. When  $n_A = n_C$ , the bilayers are densely packed but contain vacancies for  $n_A \neq n_C$ . These bilayers are stable in spite of relatively high amounts of vacancies (Lagaly, 1976). Too large vacant volumes are reduced by formation of kinks (see Section 7.3.8).

The numerical values of the exothermic heats of immersion decreased strongly with  $n_C$ , which illustrates the importance of the enthalpy required to move the alkyl chains from close contacts with the surface oxygen atoms in perpendicular orientation. The gain of adsorption enthalpy due to the increased adsorption volume is largely consumed to overcome the van der Waals energy between the surface and the alkyl chains lying flat in close contacts with the surface oxygen atoms. The energy required is about  $+5.7 \text{ kJ/mol} - \text{CH}_2$  – for  $n_C = 6$ –10 and above  $+3.8 \text{ kJ/mol} - \text{CH}_2$  – for  $n_C > 10$ . The decrease is related to the different interlayer packing density of the alkyl chains because the flat-lying alkyl chains in bilayers ( $n_C > 10$ ) are not as tightly fixed between the silicate layers as in monolayers (Malberg et al., 1989; Lagaly and Malberg, 1990). In the bilayer structures at  $n_A \sim n_C$  the van der Waals energy between the long alkyl chains is decisive. It is about  $2.5 \text{ kJ/mol} - \text{CH}_2$  – and smaller than in

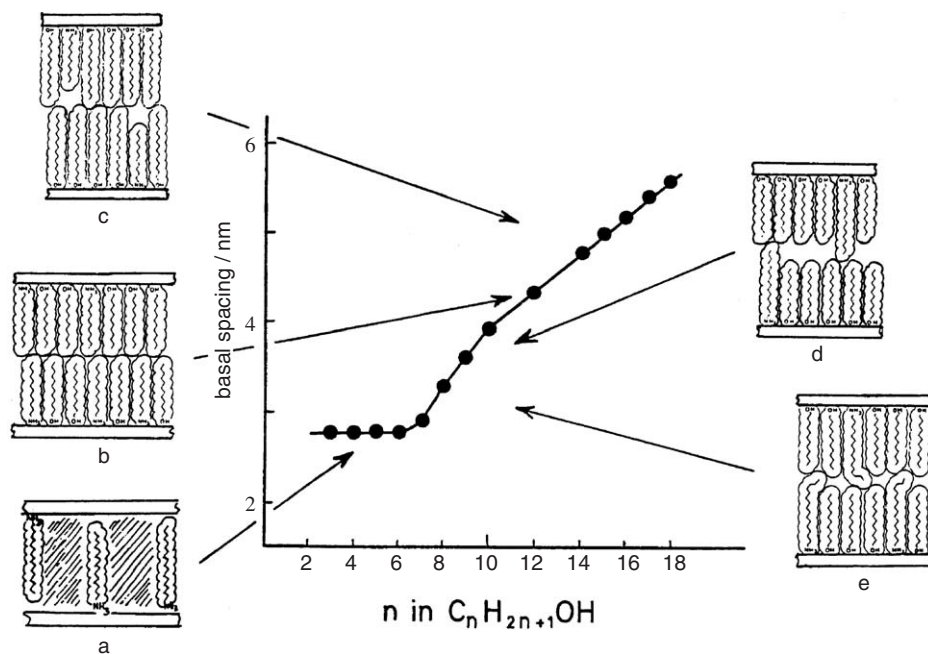


Fig. 7.3.12. Interlayer arrangements of alkylammonium ions and alkanol molecules. As an example: dodecylammonium montmorillonite and  $n$ -alkanols. (a) zeolitic uptake of short chain alcohol molecules, (b) dense bimolecular films for equal chain lengths, (c, d) vacancies in case of differently long chains, and (e) shortening of longer chains by kinks. From Jasmund and Lagaly (1993).

the crystalline long-chain compounds (about  $5.8 \text{ kJ/mol} - \text{CH}_2 -$ ) because the chains in the interlayer space are more loosely packed (Lagaly and Weiss, 1969). Owing to the high van der Waals energy between the alkyl chains, the bilayer structures tolerate relatively large vacancies. In addition, the distribution of vacancies and, in some cases, kinks represent an important entropy contribution.

Smaller molecules like formamide, dimethyl formamide, DMSO increase the spacing of the alkylammonium montmorillonites and vermiculites at least to separations corresponding to monomolecular films of perpendicular alkyl chains. Salts soluble in the organic solvent strongly influence the adsorption of the solvent and the basal spacing. They can increase or decrease the layer separation. The effects are more strongly influenced by the salt cations, less by the anions. In comparison with water, cations in organic liquids are more strongly solvated than anions. The structure-breaking influence of potassium iodide exerted a strong effect on the swelling of tetradecylammonium montmorillonite in DMSO. Even concentrations as low as  $0.01 \text{ M}$  impeded the intercalation of solvent molecules (Lagaly et al., 1983; Lagaly, 1987b).

Swelling of the alkylammonium derivatives in polar liquids was discussed on the basis of formation of solvent clusters between the alkyl chains (Lagaly and Witter, 1982; Lagaly et al., 1983). If this were true, salts should exert a strong effect on the swelling in water. The basal spacings of alkylammonium beidellites (not of alkylammonium vermiculites) dispersed in water were distinctly below the spacings produced by the organic liquids. However, they were considerably enhanced by addition of modest amounts of salts (concentrations  $> 0.01$  mol/L), especially by structure breaking salts like KSCN (Fig. 7.3.13) (Lagaly et al., 1983; Lagaly, 1987b).

An interesting question, even for practical applications, concerns the possibility of delamination of alkylammonium clay minerals in organic solvents. Owing to the strong van der Waals interaction between the chains and the chains and solvent molecules, basal spacings exceeding the bilayer arrangement were seldom observed. A certain but not complete disaggregation was observed in nitrobenzene (Lagaly and Malberg, 1990). The impossibility of delamination in organic liquids is a serious obstacle in preparing clay-polymer nanocomposites (see Chapter 10.3). It is therefore still surprising that the butylammonium derivative of low-charged vermiculites delaminates in water and forms hydrogels (see Chapter 7.6).

Mortland et al. (1986) determined the adsorption isotherms of phenol, 3-chlorophenol, 3,5-dichloropheno, and 3,4,5-trichlorophenol from water on hexadecyl

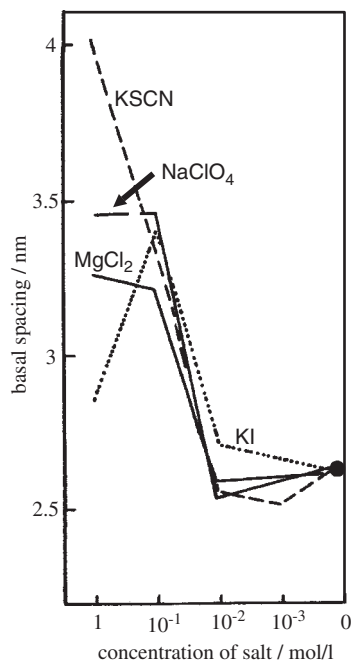


Fig. 7.3.13. Salt effects on interlayer water: basal spacing of tetradecylammonium montmorillonite in aqueous salt solutions. From Lagaly (1987b).

trimethylammonium smectite. The amount adsorbed increased with the number of chlorine atoms on the benzene ring. In contrast, similar amounts of phenol and 3,4,5-trichlorophenol were adsorbed from *n*-hexane. This different behaviour was ascribed to the influence of adsorptive-solvent and adsorptive-surface interactions on the partitioning of the adsorptive between solvent and surface (see Chapter 11.1). Compared with the long-chain derivatives, rigid interlayer cations like tetramethylammonium ions (Lee et al., 1989, 1990; Jaynes and Boyd, 1991) or tetraphenylphosphonium ions (Meier et al., 2001) can improve the adsorption properties towards certain organic compounds (see Chapter 11.1). Infrared studies of water adsorption on tetramethylammonium and triethyl phenylammonium montmorillonite revealed that water preferentially hydrates the organic ions but not the siloxane surface of montmorillonite (Stevens and Anderson, 1996a, 1996b). The orientation of the cations determines the siloxane surface area accessible to the adsorptive and whether the phenyl ring can interact with the aromatic groups of the adsorptive. A further example of the importance of the phenyl ring orientation on the adsorption of aromatic compounds was reported by Nir and co-workers (see Chapter 11.2).

In comparison with the tetramethylammonium smectite, the tetraphenylphosphonium derivative was a better adsorbent of aromatic and chlorinated hydrocarbons from water. The reason is seen in the lower degree of hydration of the tetraphenylphosphonium cations (Kukkadapu and Boyd, 1995). Compared with smectites modified with flexible organic cations, the tetraphenylphosphonium derivatives of low-charged smectites also revealed an enhanced adsorption of 2-chlorophenol, especially at low-pollutant concentrations (Meier et al., 2001).

Organo bentonites retained considerable amounts of heavy metal ions (together with the counterions) from aqueous solutions. The adsorption increased in mixtures of water with organic solvents. Synergetic effects were observed: addition of the organic solvent enhanced the heavy metal adsorption and the metal ions enhanced the adsorption of the organic component (Stockmeyer and Kruse, 1991; Lagaly, 1994b, 1995).

The adsorption of anions by alkylammonium bentonites is probably mediated by the particular arrangement of the water molecules around the alkyl chains (Lagaly, 1995). Adsorption of radioiodide by organo bentonites may be of practical interest (Bors, 1990; Bors and Gorny, 1992).

### 7.3.7. ADSORPTION FROM BINARY SOLUTIONS AND THE HYDROPHILIC/HYDROPHOBIC CHARACTER OF CLAY MINERAL SURFACES

Hydrophobisation of clay minerals by adsorption of surfactants and macromolecules is an important step in modifying clays. This step is needed for many technical applications when the clay minerals are dispersed in less polar solvents or polymers

or are tailored to improve gas and liquid adsorption properties (see Chapters 10.1 and 10.3). A quantitative description of the surface modification requires evaluation of the mosaic structure of the surface. Liquid sorption and immersionsal wetting experiments (mostly by microcalorimetry) open the way for a quantitative characterisation of surface hydrophobisation and for describing the effects of surface modification on the properties of the clay minerals.

The solid–liquid interaction can be derived from the adsorption excess isotherms in liquid mixtures and the heat of immersion in pure liquids, mixtures, or solutions (Everett, 1964, 1965; Kipling, 1965). Further information is obtained if the amount of liquid adsorbed on the surface is related to the heat of immersion. A further benefit of the adsorption excess isotherms is the possibility of calculating the free enthalpy of adsorption as a function of the composition (Dékány, 1992; Regdon et al., 1998).

#### A. Adsorption Excess Isotherms

When solid particles are immersed in a liquid medium, solid/liquid interfacial interactions lead to formation of an adsorption layer. The material content of the adsorption layer is the adsorption capacity of the solid particle and can be derived from the so-called adsorption excess isotherms of binary liquid mixtures (Everett, 1964, 1965). Adsorption changes the composition of the liquid mixture from  $x_1^0$  to the equilibrium concentration  $x_1$ . The value  $\Delta x_1 = x_1^0 - x_1$  is analytically determined. The relationship between the specific adsorption excess amount  $n_1^{\sigma(n)} = n^0(x_1^0 - x_1)$  calculated from  $\Delta x_1$  and the material content of the interfacial layer is given by the Ostwald–de Izaguirre equation (Kipling, 1965):

$$n_1^{\sigma(n)} = n^0(x_1^0 - x_1) = n_1^s - n^s x_1 = n^s(x_1^s - x_1) \quad (1)$$

where  $n^0$  is the total amount of adsorptive molecules (e.g. in mmol/g),  $n^s = n_1^s + n_2^s$  is the mass content of the interfacial phase, and  $x_1^s = n_1^s/n^s$  is the molar fraction of component 1 in the interfacial phase. According to Eq. (1), the excess isotherm  $n_1^{\sigma(n)} = f(x_1)$  represents the combination of the individual isotherms  $n_1^s = f(x_1)$  and  $n_2^s = f(x_1)$ .

The volume occupied by the components adsorbed on the solid surface is  $V^s = n_1^s V_{m,1} + n_2^s V_{m,2}$  where  $n_1^s$  and  $V_{m,1}$  are the amount and the partial molar volume of the components in the adsorption layer. The volume fraction of component 1 in the adsorption layer is calculated from the excess isotherm:

$$\phi_1^s = \frac{n_1^s}{n_{1,0}^s} = \phi_1 + \frac{r n_1^{\sigma(n)} V_{m,1}}{V^s(x_1 + r x_2)} \quad (2)$$

The adsorption capacity of the pure component 1 is  $n_{1,0}^s = n_1^s + r n_2^s = n^s x_1^s + r n^s x_2^s$  where  $r = V_{m,2}/V_{m,1} = n_{1,0}^s/n_{2,0}^s$ . It can be determined by the Everett–Schay method



(Everett, 1964, 1965; Kipling, 1965):

$$\frac{x_1 x_2}{n_1^{\sigma(n)}} = \frac{1}{n_{1,0}^s} \left[ \frac{r}{S-1} + \frac{S-r}{S-1} x_1 \right] \quad (3)$$

where  $S$  is constant for ideal adsorption from ideal solutions (Kipling, 1965). The value of  $n_{1,0}^s$  is derived from the linear relation between  $x_1 x_2 / n_1^{\sigma(n)}$  and  $x_1$ .

Since in liquid adsorption processes the surface of the adsorbent is always completely covered, the equivalent specific surface area  $a_{\text{eq}}^s$  is related to the cross-sectional areas of the components,  $a_{m,1}$  and  $a_{m,2}$ , which are calculated from the molar volumes of the components (Dékány et al., 1985a):

$$n_1^s a_{m,1} + n_2^s a_{m,2} = a_{\text{eq}}^s \quad (4)$$

Thus, the specific surface area of the adsorbent can be calculated from the adsorption capacities and the cross-sectional areas. The specific surface area determined in this way for many non-swelling and dis-aggregating adsorbents was in good agreement with the areas obtained by gas adsorption measurements (Dékány et al., 1985a).

The liquid adsorption capacity can be expressed as a function of surface modification  $\Theta_2 = n_2^s a_{m,2} / a^s$ , where  $n_2^s a_{m,2}$  is the hydrophobic surface area and  $a^s$  is the total surface area of the adsorbent (Dékány et al., 1985a).

### B. Heat of Wetting

Immersion microcalorimetry is a simple and straightforward method for quantifying the solid/liquid interfacial interaction. The solid material previously heated in vacuum is brought into contact with the pure liquid (Dékány, 1992, 1993). It is advisable to choose liquids of different polarity so that the hydrophobic/hydrophilic balance of the surface can be estimated from the heats of wetting. Wetting a hydrophilic surface by a polar liquid liberates a large enthalpy, while wetting a hydrophobic surface yields a smaller exothermic heat. When a solid adsorbent is immersed in a binary mixture, the heat of wetting is intermediate between the values  $\Delta_w H_1^0$  and  $\Delta_w H_2^0$  measured in the pure components. This immersion technique gives direct information on the strength of the solid/liquid interactions. According to Everett's adsorption layer model (1965; Kipling, 1965; Everett, 1964; Dékány, 1993) the heat of immersional wetting,  $\Delta_w H_t$ , can be calculated when the molar adsorption enthalpies of the components,  $(h_1^s - h_1)$  and  $(h_2^s - h_2)$ , of the system are known. Introducing the volume fractions  $\phi_1^s$  and  $\phi_2^s$ , the heat of wetting is determined as

$$\Delta_w H_t = \phi_1^s \Delta_w H_1^0 + \phi_2^s \Delta_w H_2^0 + H^{\text{se}}(x_1^s) \quad (6)$$

$H^{\text{se}}(x_1^s)$  is an excess enthalpy of the adsorption layer due to deviation from ideality.



### C. Examples

When the components of a binary mixture largely differ in polarity, for instance methanol and benzene, the shape of the excess isotherms and the azeotropic composition are related to the polarity of the surface. As an example, adsorption excess isotherms were determined on hydrophilic and partially hydrophobic illites in methanol–benzene mixtures (Fig. 7.3.14). The adsorption capacities were obtained by the Schay–Nagy extrapolation and the adsorption space-filling model. The amount of methanol in the adsorption layer,  $1-\Theta_2$ , decreased with increasing coverage of the illite surface by hexadecylpyridinium cations (Table 7.3.3). The free energy of adsorption  $\Delta_{21}G = f(x_1)$  was derived from the excess isotherms (Fig. 7.3.15) (Dékány, 1992; Regdon et al., 1998).

The enthalpy of wetting as a function of the molar fraction of methanol in the equilibrium solution was large for  $\text{Na}^+$  illite because of the preferential adsorption of methanol (Fig. 7.3.16). It decreased after hydrophobisation and became even endothermic at  $x_1 > 0.5$ . The molar wetting enthalpy decreased with increasing hydrophobicity (Table 7.3.3).

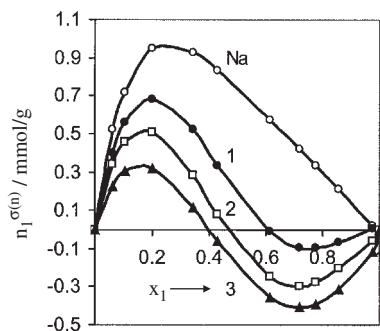


Fig. 7.3.14. Adsorption excess isotherms for  $\text{Na}^+$  illite (Na) and hexadecylpyridinium illites (1,2,3: increasing amounts of hexadecylpyridinium ions, see Table 7.3.3) in methanol(1)-benzene(2).

Table 7.3.3. Adsorption of methanol(1)-benzene(2) mixtures on  $\text{Na}^+$  illite and hexadecylpyridinium illites

Adsorbent	$n_{1,0}^s$ (mmol/g)	$a_{\text{eq}}^s$ ( $\text{m}^2/\text{g}$ )	$\Theta_2^*$	$-\Delta_{2,1}H_t$ (J/g)	$-(h_1^s - h_2^s/r)$ (kJ/mol)
$\text{Na}^+$ illite	0.84	51	0.11	11.10	13.65
HDP $^+$ illite <b>1</b> <sup>†</sup>	1.25	57	0.52	1.70	4.32
HDP $^+$ illite <b>2</b>	1.30	78	0.66	1.35	3.21
HDP $^+$ illite <b>3</b>	1.42	85	0.78	0.85	2.27

\* $\Theta_2 = n_2^s a_{m,2} / a^s$ : Surface hydrophobicity.

<sup>†</sup>Content of hexadecylpyridinium ions: **1** 0.097, **2** 0.139, **3** 0.233 mmol/g.

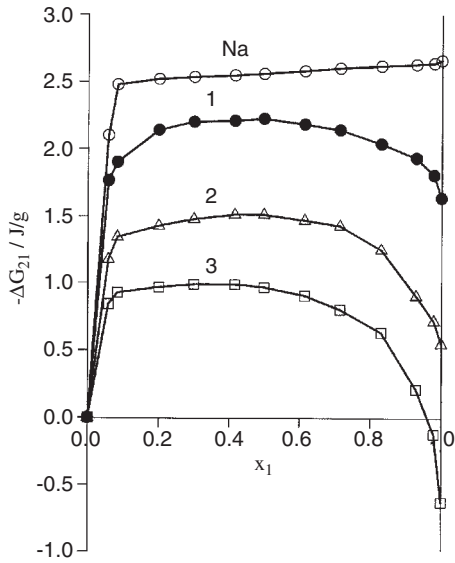


Fig. 7.3.15. Free enthalpy of adsorption,  $\Delta_{21}G$ , of methanol(1)-benzene(2) on  $\text{Na}^+$  illite (Na) and hexadecylpyridinium illites (1, 2, 3: see Table 7.3.3).

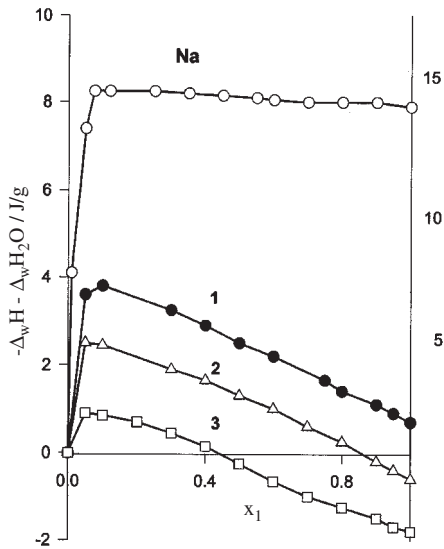


Fig. 7.3.16. Immersional wetting enthalpy of  $\text{Na}^+$  illite ( $\circ$ ) and illites modified with hexadecylpyridinium ions ( $\bullet$ 1,  $\Delta$  2;  $\square$  3, see Table 7.3.3) in methanol (1)-benzene (2).

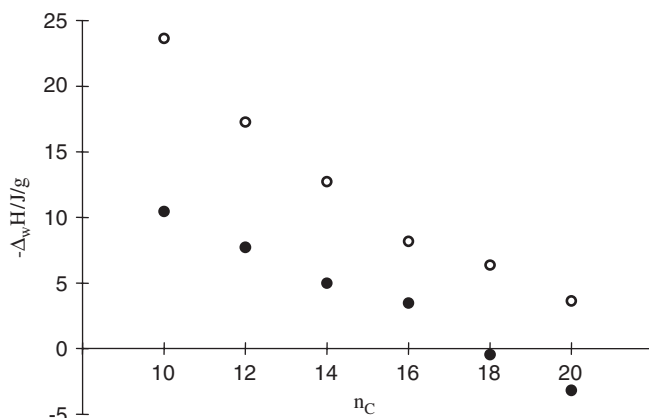


Fig. 7.3.17. Immersional wetting enthalpy as a function of the chain length of alkylammonium illites in methanol ( $\circ$ ) and toluene ( $\bullet$ ).

The heat of immersion of hydrophobised montmorillonite in methanol decreased almost exponentially with increasing alkyl chain length (Fig. 7.3.17). The decrease in toluene was surprising because the increased organophilicity of the surface should be associated with an increase of the enthalpy of immersional wetting as measured in the case of non-swelling hexadecylpyridinium illites. The immersional wetting of hydrophobised montmorillonites in methanol, toluene, and their mixtures gave rise to three types of detector signals (Fig. 7.3.18). The heat of immersion of hexadecylpyridinium montmorillonite in methanol was exothermic, whereas in toluene a sharp endothermic signal was followed by an exothermic peak. The first endothermic signal is caused by the opening of the interlayer space. This step consumes enthalpy because the alkyl chains in bilayers move from close contacts with the surface oxygen atoms into upright positions (see Section 7.3.6), which allows the exothermic solvation of the chains and the silicate surface by toluene. The importance of the endothermic re-arrangement of the alkyl chains is illustrated in Fig. 7.3.18c. The large enthalpy required for the re-orientation of the octadecyl chains is not compensated by the solvation enthalpy of the chains (mainly by toluene) and the surface (mainly by methanol) (Dékány et al., 1985b, 1986; Regdon et al., 1998), and the total process becomes endothermic. Thus, entropy effects are very important in swelling processes of hydrophobised clay minerals. A considerable part of the entropy increase is related to the increased conformational freedom when the chains move in upright position.

### 7.3.8. PHASE TRANSITIONS

The interlayer bilayers composed of long-chain alkylammonium ions and alkanol molecules show a series of thermal phase transitions, indicated by basal spacings stepwise decreasing with increasing temperature (Fig. 7.3.19). The small steps of

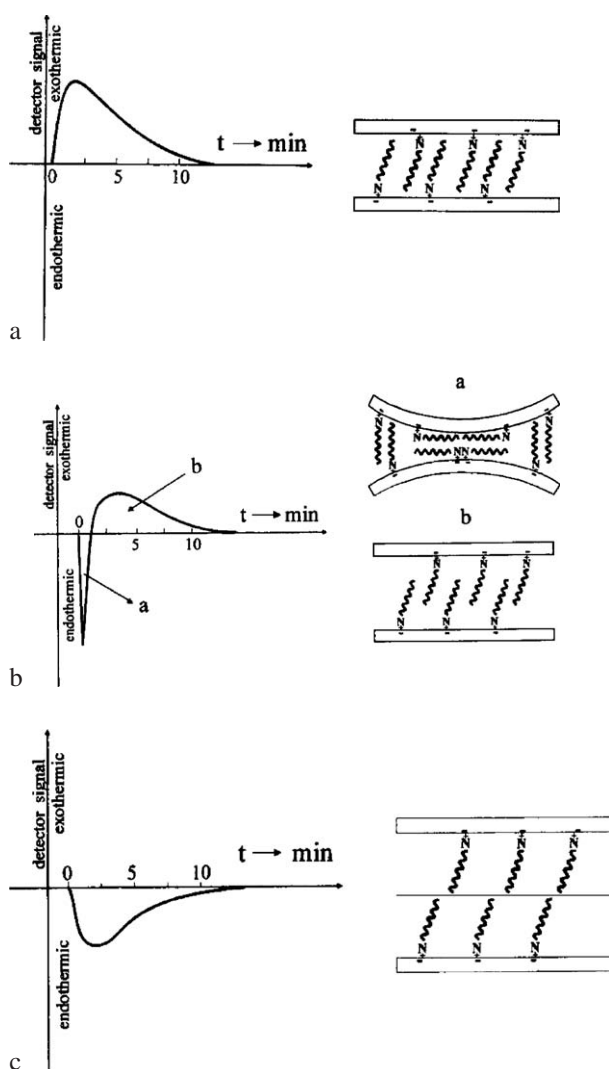


Fig. 7.3.18. Heat effects during immersion of organo montmorillonites in organic solvents (a) exothermic signals for hexadecylammonium montmorillonite in methanol (basal spacing 3.2 nm), (b) endothermic and exothermic heat effects for hexadecylammonium montmorillonite in toluene (basal spacing 3.8 nm), (c) endothermic signal for octadecylammonium montmorillonite in methanol-toluene (molar fraction of methanol 0.05, basal spacing 4.6 nm).

about 0.11 nm are related to the formation of kink-blocks, whereas the larger decrease at higher temperature (between 45 °C and 100 °C, depending on the alkyl chain lengths) is caused by the re-arrangement of the kink-blocks into gauche-blocks (Baur, 1975; Stohrer and Noack, 1975; Lagaly, 1976, 1981b; Pechhold et al., 1976).

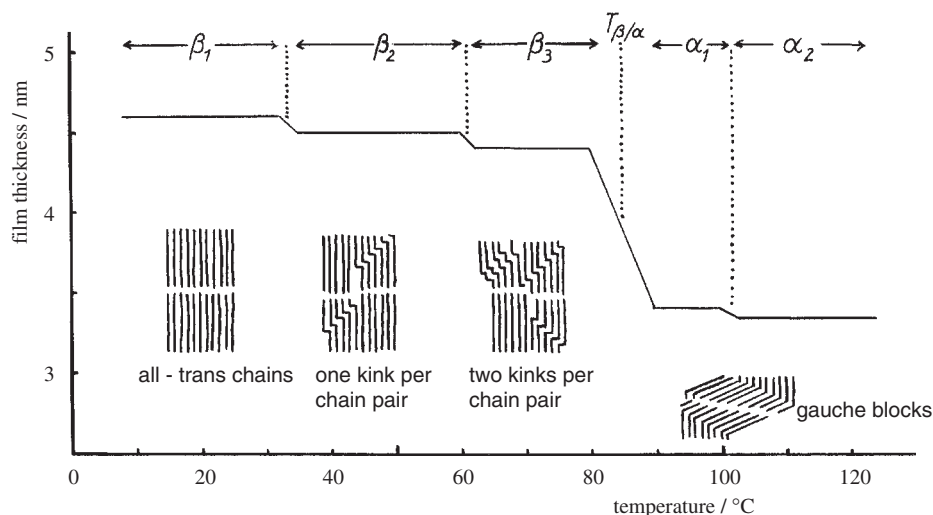


Fig. 7.3.19. Phase changes (schematic) of interlayer bimolecular films, for instance of bilayers of alkanol and alkylammonium ions in 2:1 clay minerals. From Lagaly et al. (1976).

Kink-block formation is a consequence of conformational changes of the alkyl chains. Transition of the sequence of three *trans* C–C bonds into a *gauche*(+)*–trans–gauche*(–) conformation is called a kink (Fig. 7.3.20). Gauche-blocks are formed due to the desorption of a certain amount of interlayer alcohol. The chains in these structures contain isolated gauche bonds or, more likely, *gauche*(+)*–trans–gauche*(+) conformations, and both chain sections are no longer parallel but form an angle.

Kink and gauche-block formation were also reported for alkylammonium montmorillonites with intercalated poly(ethylene oxides) (Platikanov et al., 1977) and the alkanol derivatives of alkali and earth alkali clay minerals (Pfaffmann et al., 1973). Many other layered materials with intercalated long-chain compounds show these thermal phase transitions (Lagaly et al., 1975; Lagaly, 1981b; Rösner and Lagaly, 1984).

Kinks are typical defects in films of self-aggregating long chain compounds. In a lamella of alkyl chains the probability of kink formation in a chain depends on the state of neighbouring chains. Steric effects play a fundamental role in this process. The geometric conditions in the alkanol-alkylammonium smectites and vermiculites appear to be optimal for kink-block formation. If a kink is formed in one alkyl chain (nucleation step), the displaced part of the chain thrusts against the neighbouring chains, which give way in a formation of kinks (growth step), and an ordered kink-block forms (Fig. 7.3.21). If the packing density is too high (as in the uranyl vanadate uvanite), the nucleation of kinks is rendered more difficult and the basal spacing remains constant up to the transition into gauche-blocks. The different lateral symmetry in uranium micas leads to random formation of kinks (Lagaly, 1981b).

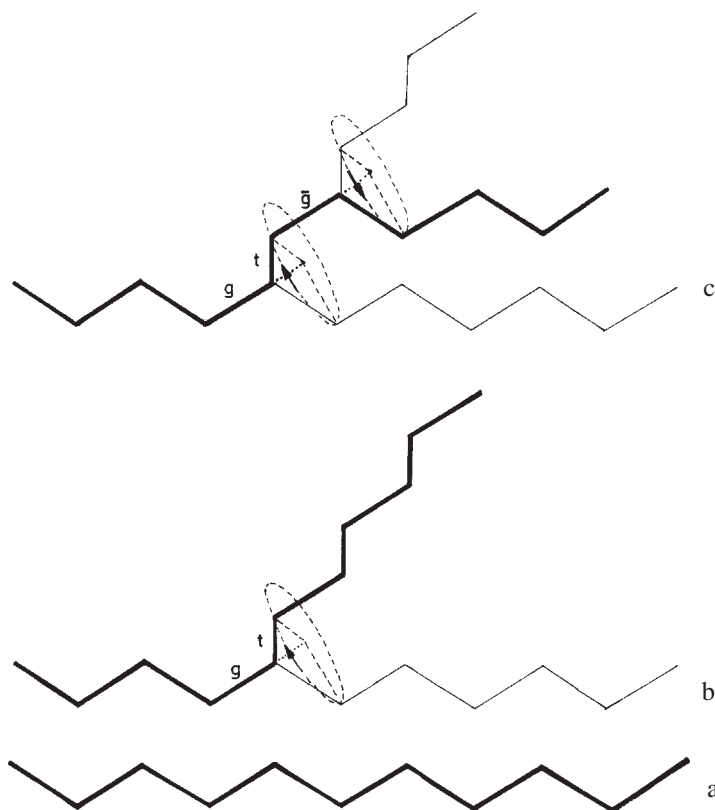


Fig. 7.3.20. Formation of kinks in alkyl chains (a) all-trans chain, (b) insertion of one *gauche* bond, (c) insertion of a second *gauche* bond and formation of the kink. From [Lagaly \(1976\)](#).

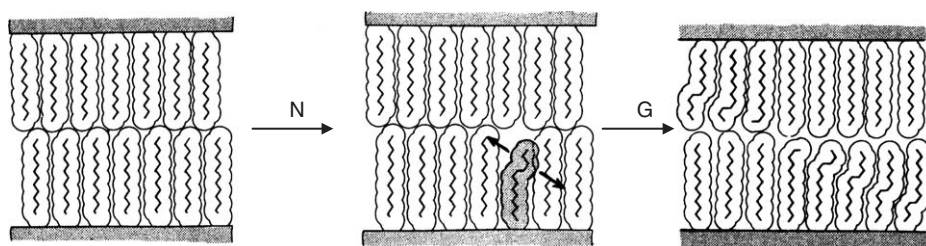


Fig. 7.3.21. Formation of kink-blocks as a co-operative reaction. N, G nucleation and growth step. From [Lagaly \(1976\)](#).

The alkanol-alkylammonium clay minerals and their phase transitions provide useful models of possible conformational changes of alkyl chains in mono- and bi-layer films. Unsaturated chains with *cis*- double bonds are important components in biomembranes. It was shown that they can be incorporated in lipid films when the

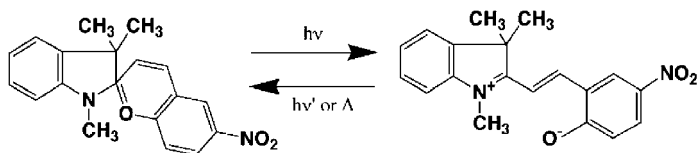
chains assume conformations like *cis-trans-gauche* (Lagaly, 1976; Lagaly et al., 1976). The transition into *gauche*-blocks is related to the “chain melting” or crystalline/liquid-crystalline phase transitions of lipids. The possibility of conformational changes of interlayer alkyl chains is an important condition in preparing nanocomposites.

Phase transitions induced by conformational changes of the alkyl chains were also observed for dialkyl dimethylammonium clay minerals (Okahata and Shimizu, 1989). The phase transition affects the permeation properties and intra- and intermolecular reaction kinetics of the adsorbed species. An example is the photoinduced thermal isomerisation of merocyanine (MC) into spiropyran (SP) (Scheme IX) in dioctadecyl dimethylammonium montmorillonite (Seki and Ichimura, 1990). The decoloration reaction rate is dependent on the mobility of the surrounding chains and is influenced by the phase transition. The reaction rate abruptly increased near the gel to liquid-crystal phase transition temperature at 54 °C.

The phase transition was also investigated by luminescence measurements with 1,3-di(1-pyrenyl)propane and pyrene (Ahmadi and Rusling, 1995). The first molecule provided a better probe molecule than pyrene because of the two pyrene groups and formed intramolecular excimers at extremely low concentrations. In the gel state at lower temperature, the hydrocarbon chains in *trans* conformation were more rigid than in the liquid crystalline state when the alkyl chains contained many *gauche* conformations and kinks. Above the phase transition the relative intensity of the excimer peak increased gradually with increasing temperature and indicated the increased mobility of the alkyl chains. The phase transitions of the dialkyl dimethylammonium silicates were also indicated by the temperature dependence of the pyrene fluorescence as well as by the photochromism of azobenzene. The phase transition temperatures reported for the dioctadecyl dimethylammonium clay minerals are listed in Table 7.3.4 (Ogawa et al., 1999).

### 7.3.9. INTERCALATION OF POLYMERS AND PROTEINS

The interaction of clay minerals with organic macromolecules received a considerable amount of attention because of the use of clays and polymers in many industrial applications and in soil conditioning (see Chapter 10) (Theng, 1970, 1979, 1982). In many cases the polymers are adsorbed on the external surface and are not intercalated. The adsorption of macromolecules and the influence of polymers on the



Scheme IX.

Table 7.3.4. Basal spacings and phase transition temperatures of silicates modified with dioctadecyl dimethylammonium ions

Silicate	Phase transition temperature (K)	Basal spacing (nm)	Technique	Reference
Montmorillonite*	327	4.24	Thermal decoloration of photomerocyanine to spiropyran	<a href="#">Seki and Ichimura (1990)</a>
Montmorillonite*	327	4.83	Permeation of a fluorescence probe <sup>‡</sup> and DSC	<a href="#">Okahata and Shimizu (1989)</a>
Bentonite	326	4.3	Pyrene luminescence	<a href="#">Ahmadi and Rusling (1995)</a>
Bentonite	327		Electrochemical reduction of trichloro acetic acid	<a href="#">Hu and Rusling (1991)</a>
TSM <sup>†</sup>	328	3.4	Photochromism of azobenzene	<a href="#">Ogawa et al. (1999)</a>

\*Kunipia G, Kunimine Industries Co.

<sup>†</sup>Sodium fluorotetrasilicic mica, ideal composition  $\text{NaMg}_{2.5}\text{Si}_4\text{O}_{10}\text{F}_2$ , Topy Industries Co.

<sup>‡</sup>1-(1,3,4,5-Tetrahydroxy cyclohexane carboxyamido) naphthalene.

colloidal properties of clay dispersions are described in Chapter 5. The discussion in this chapter refers to the intercalation of polymers.

Many linear non-ionic polymers penetrate into the interlayer space when the clay mineral is dispersed in aqueous or organic solvents of the polymers. Several types of macromolecules of technical importance are intercalated from aqueous solutions ([Table 7.3.5](#)). Even alkylammonium montmorillonites intercalate poly(ethylene oxides) from aqueous solutions.

Many polymers are intercalated in extended conformation and in strong contact with one (bilayers of macromolecules) or two silicate layers (monolayers) ([Table 7.3.5](#)). The unfolding of polylysine and polyglutamic acid during intercalation into montmorillonite was recently described by [Gougeon et al. \(2003\)](#). The reason for the preference of trains over loops is the van der Waals interaction between the polymer segments and the surface oxygen atoms and the reduced importance of the solvent in the interlayer space. A good geometrical fit is often achieved between the macromolecules and the surface, which increases the van der Waals interaction considerably. As a result, the amount of solvent in the interlayer space is determined by the volume available between the macromolecules constrained between the silicate layers. Loops as a consequence of good solvency are generally not formed and the expansion



Table 7.3.5. Intercalation of neutral polymers into Na<sup>+</sup> and Ca<sup>2+</sup>-montmorillonite

Polymer	Cation	Basal spacing (nm)		Reference
		in solution	dried	
Poly(vinyl alcohol)	Na <sup>+</sup>	Diffuse	1.36, at 65 °C	Lagaly, 1986a
	Ca <sup>2+</sup>	1.9–2.0	1.48, at 70 °C	Greenland, 1963
Poly(vinyl alcohol)*	Na <sup>+</sup>	Diffuse	4.0, at 65 °C	Lagaly, 1986a
Poly(ethylene oxide)	Na <sup>+</sup>		1.74, Air-dried	Parfitt and Greenland, 1970a, 1970b
	Ca <sup>2+</sup>	1.7–2.2	1.73, 10% R. H.	Parfitt and Greenland, 1970a, 1970b
	Na <sup>+</sup>	1.46 + 1.86		Billingham et al., 1997
	Na <sup>+</sup>		1.75, at 70 °C	Aranda and Ruiz-Hitzky, 1999
	Na <sup>+</sup> †	1.78–1.87		Bujdák et al., 2000
Poly(ethylene-propylene oxide)	Na <sup>+</sup>	1.83‡	1.37, at 200 °C	Breen et al., 1998
Poly(ethylene oxide)-10-cetyl ether (Brij 56)	Ca <sup>2+</sup>		1.73, Air-dried	Deng et al., 2003
Poly(ethylene oxide)-12-nonylphenyl ether (Igepal CO 720)	Ca <sup>2+</sup>		1.65, Air-dried	Deng et al., 2003
Poly(vinyl pyrrolidone)	Na <sup>+</sup>	Diffuse§	2.45–2.85, Air-dried	Levy and Francis, 1975a, 1975b
	Ca <sup>2+</sup>	1.88–1.96§	1.70–1.92, Air-dried	Levy and Francis, 1975a, 1975b
Dextran	Na <sup>+</sup>		1.76, Air-dried	Olness and Clapp, 1973
	Ca <sup>2+</sup>		1.43, Air-dried	Olness and Clapp, 1973
Polysaccharides	Na <sup>+</sup>	1.6	1.47, P <sub>4</sub> O <sub>10</sub>	Parfitt and Greenland, 1970c
	Ca <sup>2+</sup>	1.4	1.37, P <sub>4</sub> O <sub>10</sub>	Parfitt and Greenland, 1970c

\*In the presence of boric acid.

†With reduced charge montmorillonites.

‡Stable up to 150 °C.

§In contact with 1% PVP ethanol solutions and different amounts of water.

||Reflections rather diffuse.

of the interlayer space is modest, often corresponding to the thickness of the linear macromolecules (for monolayers) or twice this value (for bilayers). Thus, large basal spacings up to delamination are generally not observed. This structure distinguishes intercalated polymers from polymers adsorbed on freely accessible surfaces.

In contrast to polymer adsorption on external surfaces, interlayer adsorption can lead to a preference for smaller macromolecules. Simon et al. (2002) observed the preference of montmorillonite for hydroxyethyl cellulose molecules of lower molecular weight.

The single silicate layers often aggregate when a polymer is added to highly dispersed and delaminated sodium smectites. Examples are poly(vinyl pyrrolidone) (PVP) (Levy and Francis, 1975a, 1975b), poly(ethylene oxides) (Ogata et al., 1997a), and poly(L-lactide) (Ogata et al., 1997b). In other cases, e.g. with non-ionic polyacrylamide, the colloidal distribution of the silicate layers is retained but the tactoid size increases (Bottero et al., 1988). Larger amounts of macromolecules can impede parallel orientation of the silicate layers as observed for sodium montmorillonite and poly(vinyl alcohol). When this polymer is added to a sodium montmorillonite dispersion, the silicate layers remain in colloidal distribution (Ogata et al., 1997a). During the desorption of water by drying, steric constraints by some macromolecules attached to the silicate layers impede re-aggregation of a certain number of layers so that not all silicate layers can re-aggregate forming ordered domains (Fig. 7.3.22) (Lagaly, 1986a). Wide-angle X-ray powder diffraction diagrams pretend fully ordered materials but small-angle scattering reveals the presence of additional disordered domains.

A few macromolecules assume helical conformations in the interlayer space: poly(vinyl alcohol) intercalated in sodium montmorillonite in the presence of boric acid (Table 7.3.5) (Lagaly, 1986a) and poly(ethylene oxides) intercalated in clay

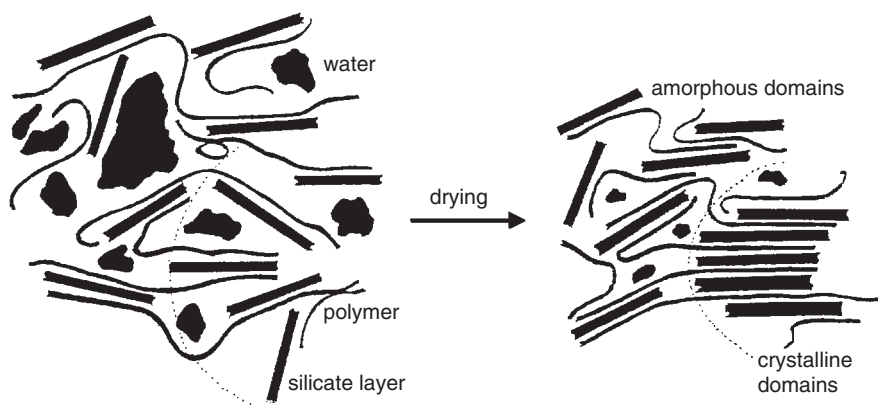


Fig. 7.3.22. Single silicate layers embedded in poly(vinyl alcohol)-water. The geometrical constraint exerted by a part of the macromolecules impedes re-aggregation of a certain number of silicate layers into ordered domains during drying. From Jasmund and Lagaly (1993).

minerals (Aranda and Ruiz-Hitzky, 1999) and layered dichalcogenides (Hernán et al., 1998).

The effect of the nanometer confinement on the short-time dynamics of intercalated polymers was studied by molecular dynamics simulation for poly(ethylene oxides) (Kuppa and Manias, 2003).

Strawhecker and Manias (2003) studied the crystallisation of poly(ethylene oxides) in the presence of sodium montmorillonite with differential scanning calorimetry and cross-polarisation optical microscopy. The coordination of poly(ethylene oxide) to the surface sodium ions promoted the miscibility of montmorillonite and polymer, but favoured the amorphous structure of poly(ethylene oxide) on the montmorillonite surface so that formation of crystal nuclei in the vicinity of the clay mineral was inhibited.

Complex macromolecules cannot penetrate into the interlayer space. One possible way to enhance polymer adsorption is the propping-open procedure (see Section 7.3.1). Observations during the alkylammonium exchange of Andalusian black soils were explained by the presence of natural macromolecules (of unknown identity) that penetrated into the interlayer space when it was opened by alkylammonium ions (Fernandez-Gonzales et al., 1976). The disaggregation–reaggregation mechanism provides a further way of enhanced polymer adsorption (Larsson and Siffert, 1983). When clay mineral particles came into contact with the protein lysozyme, they aggregated forming an interlayer space filled with the protein (Fig. 7.3.23a). Stirring this dispersion created fresh surfaces that again adsorbed lysozyme molecules and aggregated. In this way complete saturation with lysozyme was achieved by alternating disaggregation and reaggregation processes. In a similar way, sodium montmorillonite reacted with polyvanadic acid forming montmorillonite–vanadium oxide hydrogels. Drying yielded non-dispersible xerogels of the lamellar solids (Anaissi et al., 2001).

The particles may not require to be split under mechanical forces. As described for polycations (see Chapter 5), the strong interaction between a polymer-coated face and the bare face of two particles can peel off one silicate layer of each particle so that two fresh surfaces can again adsorb the macromolecules. Eventually, all layers are aggregated and separated by the polymer (Fig. 7.3.23b) (Breen et al., 1996; Billingham et al., 1997).

Cationic polymers strongly interact with clay minerals and penetrate between the layers if their segments are not too bulky. Displacement of the interlayer cations and covering of the internal surface are often not quantitative. As penetration proceeds, the increasing number of contacts reduces the mobility of the polycations so they cannot occupy the whole interlayer space, but accumulate near the edges.

The adsorption of polycations reduces the cation-exchange capacity of the clay mineral and can provide the clay mineral a certain anion-exchange capacity as a consequence of positive charges not balanced by surface charges (Ueda and Harada, 1968). These authors attributed the anion-exchange capacity to the loops and tails of the polycations. With denser surface coverage, the proportion of loops and tails increased relative to the train segments and the anion-exchange capacity gradually raised while the cation-exchange capacity was reduced. However, this effect was

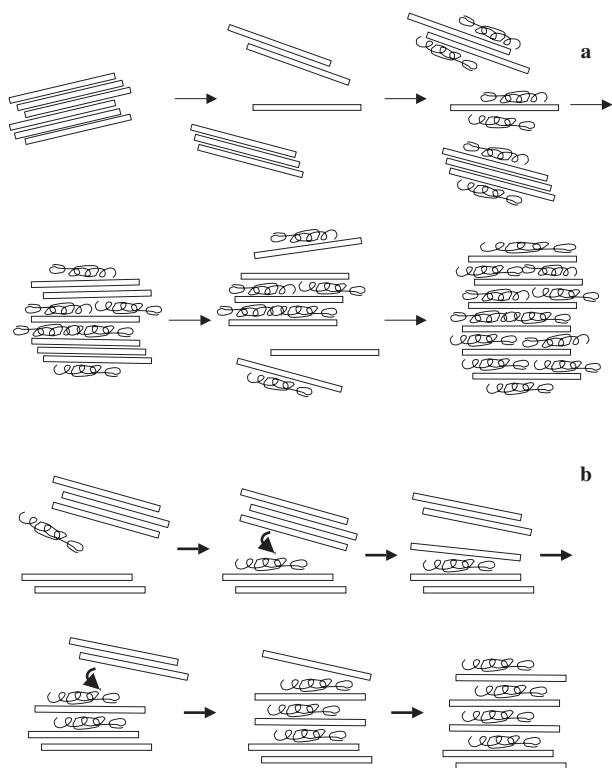
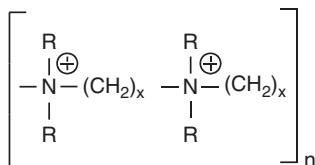


Fig. 7.3.23. Formation of intercalated montmorillonite-polymer hybrids by the dis-aggregation/re-aggregation mechanism proposed for lysozyme intercalation (Larsson and Siffert, 1983) (a) and (b) the “peal-off mechanism” proposed for polycations (Breen et al., 1996; Billingham et al., 1997).



Scheme X.

scarcely been studied. A recent study revealed the anion-exchange capacity of chitosane–montmorillonite (Ruiz-Hitzky et al., 2001).

The adsorption of polyionenes (Scheme X) was studied in detail and illustrated the combined effects of electrostatic interaction and steric factors (Lagaly, 1986a). The electrostatic interaction of the charges is important but by no means exclusively

decisive. An optimal geometrical fit between the macromolecules and the surface atoms has great influence and can overcome the electrostatic interactions. The high van der Waals energy at optimum geometrical fit can even lead to the adsorption of macroions at surfaces with the same sign of charges (Norde, 1983, 1986).

Polyimines are important technical products, for example used in paper making as retention aids. The technical polyimines are not simple linear polycations but are branched and cross-linked polymers. Nevertheless, they penetrate to some extent into the interlayer space of montmorillonite. The interplay between disaggregation and reaggregation of montmorillonite particles by polyimines or other polymers may be useful in optimising retention aids in the paper industry (see Chapter 5).

Polyanions do not penetrate into the interlayer space but considerable amounts can be enriched at the edges of clay mineral particles. The edges provide strong adsorption sites for many polyanions so that these compounds are very useful as flocculants (see Chapter 5).

The pronounced aggregation of delaminated smectites in the presence of polymers is a serious obstacle in preparing clay-polymer nanocomposites (see Chapter 10.3). A promising way is intercalation of melted polymers, for instance poly(ethylene oxides) (Vaia et al., 1993, 1995, 1997) or polystyrene (Vaia et al., 1993, 1996). When melted poly(ethylene oxide) was intercalated, the macromolecules penetrated completely between the layers whereas poly(ethylene oxide) molecules from aqueous solutions penetrated only to some extent between the silicate layers, a consequence of the good solvency of water for poly(ethylene oxides) (better-than-theta condition).

The study of protein adsorption began many decades ago. Proteins of minor complexity that can unfold penetrate between the silicate layers (Ensminger and Gieseking, 1939; Talibudeen, 1954; Weiss, 1963b; Armstrong and Chesters, 1964). Large size and high complexity (inability to unfold) prevent most proteins from penetrating between the silicate layers. However, many proteins are tightly adsorbed at the edges. The wedge-shaped opening of the interlayer spaces favours the adsorption of complex molecules.

Protein adsorption often goes through a maximum near the isoelectric point of the protein. The adsorption maximum indicates the protonation of the protein is not the only effect of pH changes. Progressive unfolding with increasing distance from the isoelectric point can decrease the adsorption. The protein is still adsorbed at higher pH where the net protein charge is negative. As mentioned above, strong van der Waals interactions can overcome the electrostatic repulsion (an effect well-known to colloid scientists).

Adsorption and activity of enzymes were studied in detail by Quiquampoix and co-workers using  $\beta$ -D-glucosidase and bovine serum albumin (Quiquampoix, 1987a, 1987b; Quiquampoix and Ratcliffe, 1992; Quiquampoix et al., 1989, 1993). Owing to the irreversible adsorption of these enzymes, the activity of an adsorbed enzyme at a given pH depended on the pH at which adsorption took place. Three domains are distinguishable:

- At pH below the isoelectric point, the electrostatic interaction between the enzyme and the surface is strong and causes conformational changes of the enzyme with a reduction or loss of the catalytic activity.

- At pH near the isoelectric point, the enzyme is adsorbed by non-electrostatic forces (hydrogen bonds, van der Waals forces, and hydrophobic interaction), which in many cases are too weak to modify the protein structure.
- At pH above the isoelectric point, adsorption of the enzyme at low-ionic strength is reduced or absent but occurs at high-ionic strength.

In displacement reactions, [Quiquampoix \(1987b\)](#) observed small cations like pentylammonium were displaced by  $\beta$ -D-glucosidase regardless of the enzyme charge. Adsorbed poly(ethylene oxides) were displaced when the enzyme was positively charged. Positively charged lysozyme was not displaced by glucosidase.

As a consequence of the clay mineral–enzyme interaction, the effect of pH on the activity of an enzyme in soils differs from that in solution. In other words, at a given pH in the soil, enzymes excreted by microorganisms or plant roots can show an activity different from that in solution ([Quiquampoix and Ratcliffe, 1992](#); [Quiquampoix et al., 1993](#)).

Recently, [Baron et al. \(1999\)](#) studied the interaction of  $\alpha$ -chymotrysin with montmorillonite (in D<sub>2</sub>O). At pD = 4.5–10 (pD = pH + 0.4) adsorption only perturbed some peripheral domains of the protein compared to the solution. The inactivation of the catalytic activity of the adsorbed enzyme at pD = 5–7 was due mainly to the steric hindrance when three essential imino/amino groups were oriented to the clay mineral surface. When these functional groups lost their positive charge at higher pD values, the enzyme changed the orientation and recovered an activity similar to that in solution at equivalent pH.

### 7.3.10. POLYMERISATION IN THE INTERLAYER SPACE

Interlayer polymerisation and polycondensation reactions were described for many monomers. The reaction is usually started by initiator molecules, e.g. polymerisation of acrylonitrile by initiation with benzoyl peroxide ([Kato et al., 1979a, 1979b](#); [Bergaya and Kooli, 1991](#)), or by enhanced temperature, e.g.  $\epsilon$ -caprolactam into poly 6-amide at 250 °C ([Fukushima et al., 1988](#)) and acrylonitrile in kaolinite ([Sugahara et al., 1988](#)). In a few cases, e.g. diazomethane ([Bart et al., 1979](#)) or 4-vinylpyridine ([Friedlander, 1963](#)), spontaneous polymerisation was observed, probably initiated by the enhanced acidity of the interlayer water molecules. Potential initiation sites are also Lewis acid sites and redox centres ([Solomon and Loft, 1968](#)). Polymerisation of benzene to poly(*p*-phenylene) on Cu<sup>2+</sup>-smectites is initiated by the loss of aromaticity of benzene by charge transfer from benzene to the Cu<sup>2+</sup> ions ([Stoessel et al., 1977](#); [Walter et al., 1990](#); [Eastman et al., 1996](#)).

If the monomers are hydrophobic molecules such as styrene, the clay mineral has to be made hydrophobic by the reaction with alkylammonium ions ([Kato et al., 1981](#)). [Fukushima and Inagaki \(1987\)](#) and [Fukushima et al. \(1988\)](#) modified montmorillonite with 11-carboxy undecylammonium cations (protonated  $\omega$ -amino undecanoic acid) before  $\epsilon$ -caprolactam was intercalated and polymerised into poly 6-amide: the study of clay mineral–polymer nanocomposites came into vogue.

Polyimide clay hybrids were prepared by interlayer polymerisation of diamino diphenyl ether and pyromellitic dianhydride yielding of poly(amic acid) which was transformed into the polyimide by decomposition of water at 300 °C (Yano et al., 1997).

Weimer et al. (1999) described the anchoring of living polymerisation initiator molecules inside the interlayer space.

As discussed in Section 7.3.8, adsorption of polymers by clay minerals, even after modification, usually does not lead to delamination, which is a basic requirement for preparing clay mineral–polymer nanocomposites for technical applications. The most promising way is the interlayer polymerisation. The enthalpy evolved during the interlayer polymerisation provides an essential contribution to the exfoliation (Lan et al., 1995). A variety of interlayer polymerisation or polycondensation reactions were studied (Kelly et al., 1994; Lan and Pinnavaia, 1994; Messersmith and Giannelis, 1994; Lan et al., 1995; LeBaron et al., 1999; Triantafillidis et al., 2002). Interlayer polycondensation of polyols and diisocyanates yielded polyurethane–clay mineral nanocomposites (Wang and Pinnavaia, 1998; LeBaron et al., 1999; Zilg et al., 1999).

### 7.3.11. ADVANCED APPLICATIONS OF CLAY MINERAL-ORGANIC COMPLEXES

Organic modification of clay minerals is a decisive step in preparing very different types of advanced materials. Actual interests are directed to the tailoring of clay minerals for the use of adsorbents, thickening and thixotropic agents, for preparing nanocomposites (see Chapter 10.3), and to create new materials with catalytic (Hu and Rusling, 1991), optical (Ogawa and Kuroda, 1997), and electronic functions (switches and sensors) (Fitch, 1990; Fitch et al., 1998; Fendler, 2001). Bentonites modified by organic cations provide colloidal adsorbents for improved pesticide formulations with reduced leaching (see Chapter 11.2). The dispersion of organoammonium clays in organic solvents and polymers is an important step in many practical applications (see Chapters 5, 10.1, and 10.3). The enhanced thermal stability of the organo phosphonium derivatives compared with the alkylammonium derivatives may be of advantage for melting processing of clay mineral nanocomposites (Xie et al., 2002). Preparation of pellets of clays and clay–organic intercalation compounds for chromatographic applications was reported by several authors (Bondarenko et al., 1982; Nakamura et al., 1988; Klopogge et al., 1997).

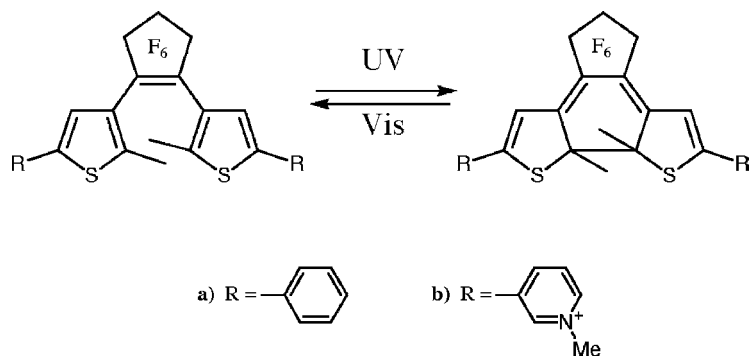
The organoammonium ions not only provide hydrophobic interlayer spaces but also control the states of the adsorbed species. An example is the intercalation of aromatic molecules in long-chain quaternary alkylammonium smectites by solid-state reactions (Ogawa et al., 1992a, 1993). Fluorescence spectra of the intercalated arenes and X-ray diffraction indicated the influence of the arrangement of the alkylammonium ions on the adsorption state of the guest species. When, for instance,

the alkylammonium ions were arranged parallel to the silicate layers, the intercalated pyrene molecules were aggregated, but were more evenly distributed when the interlayer alkylammonium ions assumed a paraffin-type arrangement. Thus, one can create various reaction environments by selecting alkylammonium ions of different size and differently charged clay minerals.

To develop advanced materials, a wide variety of photochromic reactions in clay-organic systems were studied (Seki and Ichimura, 1990; Takagi et al., 1991; Tomioka and Itoh, 1991; Ogawa and Ishikawa 1998; Ogawa et al., 1999). The photochromism of an intercalated cationic diarylethene, 1,2-bis(2-methyl-3thiophenyl) perfluorocyclopentene bearing two pyridinium substituents at each thiophenyl ring, was recently reported (Scheme XI) (Sasai et al., 2000a). Oriented films of the intercalation compound were prepared by casting so that the dye orientation could be derived from the basal spacing and the spectra of polarised light. The photochromic reaction was efficient and smooth but efficiency decreased with repeated irradiation. The decrease was attributed to the formation of photoinactive species. Degradation was suppressed by co-adsorption of dodecylpyridinium cations.

The optical properties of pseudoisocyanine dyes are under extensive investigation. Important properties of molecular assemblies of these dyes in head-to-tail arrangement (J-type aggregates) are non-linear optical behaviour and spectral hole burning, which is potentially used as a new type of memory storage. The pseudoisocyanine dyes mostly form H-aggregates (head-to-head aggregation) in aqueous solutions. Formation of J- and H-aggregates was observed in dispersions of montmorillonite. Evidently, the cationic dyes formed domains with J- or H-type aggregation. Spectral bleaching of the dyes was also observed in these systems (Bujdák et al., 2002).

Ogawa et al. (1992b) described the photochemical hole burning (PHB) of tetramethylammonium saponite with intercalated quinizarine. PHB was induced by resonant laser light irradiation at cryogenic temperatures. The site-selective and persistent photobleaching was indicated by the decreased absorption (hole) at the wavelength of the laser within the broadened absorption band. PHB attracted



Scheme XI.



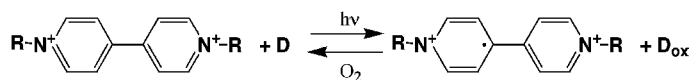
increasing attention due to its possible application for optical storage at the high-density frequency domain. The PHB characteristics depend significantly on the nature of host–guest interactions. The PHB reaction of quinizarine is related to the break of one or more internal hydrogen bonds and the subsequent formation of external hydrogen bonds to proton acceptors in the matrix. The quinizarine molecules were incorporated into the tetramethylammonium saponite at monomolecular level without aggregation, a pre-requisite for effective PHB.

Miyata *et al.* (1987) reported the photochromism of viologens (1,1'-dialkyl-4,4'-bipyridinium ions) intercalated into montmorillonite together with PVP. The viologens were reversibly photoreduced in the presence of an electron donor, forming blue radical cations with absorption bands at 610 and 400 nm (Scheme XII). The co-intercalated PVP was assumed to act as an electron donor for the reduction of the viologens. Colour-fading of the blue radical cations required a longer time period than in the matrix of pure PVP because the contacts between the viologen radical cations and the oxidising agents were reduced.

Stabilisation of dyes by intercalation was applied in the production of carbon-less copying paper and for thermal dye transfer printing (Ito *et al.*, 1996). During this type of printing, the dye migrates from an ink layer (a colour ribbon) to the clay particles dispersed in a receiver layer. Tetra-*n*-decylammonium or dioctadecyl dimethylammonium montmorillonite was used as a component in the receiving layer for cationic dyes like Rhodamine 6G and an oxazine dye. The image fixation occurred by cation exchange. The counter anions of the dye in the ink layer and the interlayer cations of the clay mineral in the receiving layer influenced the printing speed.

Preparation of ultraviolet radiation filters was based on the absorption properties of dye–clay mineral hybrids (Vicente *et al.*, 1989; Del Hoyo *et al.*, 2001). Further studies are needed to optimise the UV absorption and to reduce desorption of the intercalated dye molecules.

Application of clay minerals in advanced materials will increasingly require oriented films. Smectites can be fabricated as thin films on substrates or self-supporting films by casting the aqueous dispersions. Long-chain alkylammonium smectites swell in organic solvents, while the tetramethylammonium smectites swell in water. By simply casting the dispersions in organic solvents or water, thin films are formed with the *ab* planes of elementary platelets oriented parallel to the substrate. The driving force for the orientation is gravity. Spin and dip coating of clay dispersions on substrates are further ways to prepare thin films with thicknesses of ~10 nm to a few hundreds of nm. Films with precisely controlled thickness are prepared by the Langmuir–Blodgett technique (see Chapter 5).



Scheme XII.

## REFERENCES

- Abdo, S., Cruze, M.I., Fripiat, J.J., 1980. Metallation–demetallation reaction of tin tetra(4-pyridyl)porphyrin in Na-hectorite. *Clays and Clay Minerals* 28, 125–129.
- Adams, J.M., 1978a. Differential scanning calorimetric study of the kaolinite: *N*-methylformamide intercalate. *Clays and Clay Minerals* 26, 169–172.
- Adams, J.M., 1978b. Unifying features relating to the 3D structures of some intercalates of kaolinite. *Clays and Clay Minerals* 26, 291–295.
- Adams, J.M., 1979. The crystal structure of a dickite: *N*-methylformamide intercalate. *Acta Crystallographica B* 35, 1084–1087.
- Adams, J.M., Breen, C., 1982. The temperature stability of the  $\geq 19.4 \text{ \AA}$  intercalates of the  $\text{Na}^+$ -montmorillonite: pyridine/water systems and the rate of their conversion to the  $14.8 \text{ \AA}$  intercalate. *Journal of Colloid and Interface Science* 89, 272–289.
- Adams, J.M., Jefferson, D.A., 1976b. The crystal structure of a dickite: formamide intercalate  $\text{Al}_2\text{Si}_2\text{O}_5(\text{OH})_4 \cdot \text{HCONH}_2$ . *Acta Crystallographica* 32, 1180–1183.
- Adams, J.M., Reid, P.I., Thomas, J.M., Walters, M.J., 1976a. On the hydrogen atom positions in a kaolinite: formamide intercalate. *Clays and Clay Minerals* 24, 267–269.
- Adams, J.M., Walzl, G., 1980. Thermal decomposition of a kaolinite: dimethyl sulfoxide intercalate. *Clays and Clay Minerals* 28, 130–134.
- Ahmadi, M., Rusling, J., 1995. Fluorescence studies of solute microenvironment in composite clay–surfactant films. *Langmuir* 11, 94–100.
- Ainsworth, C.C., Zachara, J.M., Schmidt, R.L., 1987. Quinoline sorption on Na montmorillonite: contributions of the protonated and neutral species. *Clays and Clay Minerals* 35, 121–128.
- Anaissi, F.J., Demets, G.J.F., Toma, H.E., Dovidauskas, S., Coelho, A.C.V., 2001. Characterization and properties of mixed bentonite–vanadium(V) oxide xerogels. *Materials Research Bulletin* 36, 289–306.
- Annabi-Bergaya, F., Cruz, I.M., Gatineau, L., Fripiat, J.J., 1981. Adsorption of alcohols by smectites. *Clay Minerals* 16, 115–122.
- Aranda, P., Casal, B., Fripiat, J.J., Ruiz-Hitzky, E., 1994. Intercalation of macrocyclic compounds (crown ethers and cryptands) into 2:1 type phyllosilicates. Stability and calorimetric study. *Langmuir* 10, 1207–1212.
- Aranda, P., Ruiz-Hitzky, E., 1999. Poly(ethylene oxide)/ $\text{NH}_4^+$ -smectite nanocomposites. *Applied Clay Science* 15, 119–135.
- Armstrong, D.E., Chesters, G., 1964. Properties of protein-bentonite complexes as influenced by equilibration conditions. *Journal of Soil Science* 98, 39–52.
- Auboiroux, M., Melou, F., Bergaya, F., Touray, J.C., 1998. Hard and soft acid-base model applied to bivalent cation selectivity on a 2:1 clay mineral. *Clays and Clay Minerals* 46, 546–555.
- Avena, M.J., Valenti, L.E., Pfaffen, V., De Pauli, C.P., 2001. Methylene blue dimerization does not interfere in surface-area measurements of kaolinites and soils. *Clays and Clay Minerals* 49, 167–173.
- Ballantine, J.A., Graham, P., Patel, I., Purnell, J.H., Williams, K.J., Thomas, J.M., 1987. New differential thermogravimetric method using cyclohexylamine for measuring the concentration of interlamellar protons in clay catalysts. In: Schultz, L.G., van Olphen, H., Mumpton, F.A. (Eds.), *Proceedings of the International Clay Conference*, Denver, 1985. The Clay Minerals Society, Bloomington, IN, pp. 311–318.

- Baron, M.H., Revault, M., Servagent-Noinville, S., Abadie, J., Quiquampoix, H., 1999. Chymotrypsin adsorption on montmorillonite: enzymatic activity and kinetic FTIR structural analysis. *Journal of Colloid and Interface Science* 214, 319–332.
- Barrer, B.M., 1978. *Zeolites and Clay Minerals as Sorbents and Molecular Sieves*. Academic Press, London.
- Barrer, R.M., 1986. Expanded clay minerals: a major class of molecular sieves. *Journal of Inclusion Compounds* 4, 109–119.
- Barrer, R.M., 1989a. Clay minerals as selective and shape-selective sorbents. *Pure and Applied Chemistry* 61, 1903–1912.
- Barrer, R.M., 1989b. Shape-selective sorbents based on clay minerals: a review. *Clays and Clay Minerals* 37, 385–395.
- Bart, J.C., Cariati, F., Erre, L., Gessa, C., Mecera, G., Piu, P., 1979. Formation of polymeric species in the interlayer of bentonite. *Clays and Clay Minerals* 27, 429–432.
- Bartz, P., Range, K.J., 1979. Bildung von Wasser-Intercalationskomplexen nach mechanischer Beanspruchung von Kaolinit. *Zeitschrift für Naturforschung* 34b, 766–767.
- Baur, H., 1975. Zur Defektttheorie des ein-phasigen Vorschmelzens von *n*-Paraffinen, Teil II: Quasi-Chemische Näherung; Lagaly-Fitz-Weiss-Effekt. *Progress in Colloid and Polymer Science* 58, 1–18.
- Bell, T.E., 1986. Microstructure in mixed-layer illite/smectite and its relationship to the reaction of smectite to illite. *Clays and Clay Minerals* 34, 146–154.
- Ben Haj Amara, A., Ben Brahim, J., Besson, G., Pons, C.H., 1995. Etude d'une nacrite intercalée par du dimethylsulfoxyde et *N*-methylacetamide. *Clay Minerals* 30, 295–306.
- Benesi, H.A., 1957. Acidity of catalyst surfaces. II. Amine titration using Hammett indicators. *The Journal of Physical Chemistry* 61, 970–973.
- Benesi, H.A., Winquist, B.H.C., 1978. Surface acidity of solid catalysts. In: Eley, D.D., Pines, H., Weisz, P.B. (Eds.), *Advances in Catalysis*, vol. 27. Academic Press, New York, pp. 97–181.
- Benincasa, E., Brigatti, M.F., Malferrari, D., Medici, L., Poppi, L., 2002. Sorption of Cd-cysteine complexes by kaolinite. *Applied Clay Science* 21, 191–201.
- Bergaya, F., Kooli, F., 1991. Acrylonitrile-smectite complexes. *Clay Minerals* 26, 33–41.
- Berkheiser, V., Mortland, M.M., 1975. Variability in exchange ion position in smectite: dependence on interlayer solvent. *Clays and Clay Minerals* 23, 404–410.
- Billingham, J., Breen, C., Yarwood, J., 1997. Adsorption of polyamine, polyacrylic acid and polyethylene glycol on montmorillonite: an in situ study using ATR-FTIR. *Vibrational Spectroscopy* 14, 19–34.
- Bondarenko, S.V., Zhukova, A.I., Tarasevich, Y.I., 1982. Evaluation of the selectivity of some organo-substituted layer silicates. *Journal of Chromatography* 241, 281–286.
- Bors, J., 1990. Sorption of radioiodine in organo-clays and soils. *Radiochimica Acta* 51, 139–143.
- Bors, J., Gorny, A., 1992. Studies on the interactions of HDPY-vermiculite with radioiodine. *Applied Clay Science* 7, 245–250.
- Bottero, I.Y., Bruant, M., Cases, I.M., Canet, D., Fiessinger, F., 1988. Adsorption of nonionic polyacrylate on sodium montmorillonite. *Journal of Colloid Interface Science* 124, 515–527.
- Bradley, W.F., 1945. Diagnostic criteria. *American Mineralogist* 30, 704–713.
- Breen, C., Deane, A.R., Flynn, J.J., 1987. The acidity of trivalent cation-exchanged montmorillonite. Temperature-programmed desorption and infrared studies of pyridine and *n*-butylamine. *Clay Minerals* 22, 169–178.

- Breen, C., D'Mello, N., Yarwood, J., 2002. The thermal stability of mixed phenylphosphonic acid/water intercalates of kaolin and halloysite. A TG-EGA and VT-DRIFTS study. *Journal of Materials Chemistry* 12, 273–278.
- Breen, C., Loughlin, H., 1994. The competitive adsorption of methylene blue to Na-montmorillonite from binary solution with *n*-alkyltrimethylammonium surfactants. *Clay Minerals* 29, 775–783.
- Breen, C., Rawson, J.O., Mann, B.E., 1996. Adsorption of polycations on clays: an in situ study using  $^{133}\text{Cs}$  solution-phase NMR. *Journal of Materials Science* 6, 253–260.
- Breen, C., Rawson, J.O., Mann, B.E., Aston, M., 1998. In situ  $^{133}\text{Cs}$  and  $^1\text{H}$  solution-phase NMR, thermoanalytical and X-ray diffraction studies of the adsorption of polyalkylene-glycol on Texas bentonite. *Colloids and Surfaces A* 132, 17–30.
- Breen, C., Rock, B., 1994. The competitive adsorption of methylene blue on to montmorillonite from binary solution with thioflavin T, proflavin and acridine yellow. Steady-state and dynamic studies. *Clay Minerals* 29, 179–189.
- Breu, J., Catlow, C.R.A., 1995. Chiral recognition among tris(diimine)-metal complexes. 4. Atomistic computer modeling of a monolayer of  $[\text{Ru}(\text{bpyr})_3]^{2+}$  intercalated into a smectite clay. *Inorganic Chemistry* 34, 4504–4510.
- Brindley, G.W., 1965. Clay-organic studies. X. Complexes of primary amines with montmorillonite and vermiculite. *Clay Minerals* 6, 91–96.
- Brindley, G.W., 1966. Ethylene glycol and glycerol complexes of smectites and vermiculites. *Clay Minerals* 6, 237–259.
- Brindley, G.W., Moll, W.F., 1965. Complexes of natural and synthetic Ca-montmorillonites with fatty acids (clay-organic studies-IX). *American Mineralogist* 50, 1355–1370.
- Brindley, G.W., Ray, S., 1964. Complexes of Ca-montmorillonite with primary monohydric alcohols (clay-organic studies-VIII). *American Mineralogist* 49, 106–115.
- Bujdák, J., Hackett, E., Giannelis, E.P., 2000. Effect of layer charge on the intercalation of poly(ethylene oxide) in layered silicates: implications on nanocomposite polymer electrolytes. *Chemistry of Materials* 12, 2168–2174.
- Bujdák, J., Iyi, N., Hrobáriková, J., Fujita, T., 2002. Aggregation and decomposition of a pseudoisocyanine dye in dispersions of layered silicates. *Journal of Colloid and Interface Science* 247, 494–503.
- Bujdák, J., Iyi, N., Kaneko, Y., Sasi, R., 2003. Molecular orientation of methylene blue cations adsorbed on clay surfaces. *Clay Minerals* 38, 561–573.
- Bujdák, J., Janek, M., Madejová, J., Komadel, P., 1998. Influence of the layer charge density of smectites on the interaction with methylene blue. *Journal of the Chemical Society, Faraday Transactions* 94, 3487–3492.
- Cady, S.S., Pinnavaia, T.J., 1978. Porphyrin intercalation in mica-type silicates. *Inorganic Chemistry* 17, 1501–1507.
- Calvert, C.S., 1984. Simplified complete CsCl-hydrazine-dimethylsulfoxide intercalation of kaolinite. *Clays and Clay Minerals* 32, 125–130.
- Carvalho, A.P., Martins, A., Silva, J.M., Pires, J., Vasques, H., Brotas de Carvalho, M., 2003. Characterization of the acidity of Al- and Zr-pillared clays. *Clays and Clay Minerals* 51, 340–349.
- Cenens, J., Schoonheydt, R.A., 1988. Visible spectroscopy of methylene blue on hectorite, laponite B and barasym in aqueous suspension. *Clays and Clay Minerals* 36, 214–224.

- Cetin, K., Huff, W.D., 1995. Characterization of untreated and alkylammonium ion exchanged illite/smectite by high-resolution transmission electron microscopy. *Clays and Clay Minerals* 43, 337–345.
- Chekin, S.S., 1992. Swelling of kaolinite crystals in polar organic liquids. *Clays and Clay Minerals* 40, 740–741.
- Churchman, G.J., 1990. Relevance of different intercalation tests for distinguishing halloysite from kaolinite in soils. *Clays and Clay Minerals* 38, 591–599.
- Churchman, G.J., Whitton, J.S., Claridge, G.G.C., Theng, B.K.G., 1984. Intercalation method using formamide for differentiating halloysite from kaolinite. *Clays and Clay Minerals* 32, 241–248.
- Cloos, P., Laura, R.D., Badot, C., 1975. Adsorption of ethylene diamine on montmorillonite saturated with different cations—V: Ammonium- and triethylammonium-montmorillonite: ion exchange, protonation and hydrogen-bonding. *Clays and Clay Minerals* 23, 417–423.
- Costanzo, P.M., Giese, R.F., 1990. Ordered and disordered organic intercalates of 8.4-Å, synthetically hydrated kaolinite. *Clays and Clay Minerals* 38, 160–170.
- Costanzo, P.M., Giese, R.F., Lipsicas, M., 1984. Static and dynamic structure of water in hydrated kaolinites I. The static structure. *Clays and Clay Minerals* 32, 419–428.
- Dékány, I., 1992. Liquid adsorption and immersional wetting on hydrophilic/hydrophobic solid surfaces. *Pure and Applied Chemistry* 64, 1499–1509.
- Dékány, I., 1993. Thermodynamic properties of the S/L interfacial layer: stabilization of the colloidal system in binary liquids. *Pure and Applied Chemistry* 65, 901–906.
- de Luca, S., Slaughter, M., 1985. Existence of multiple kaolinite phases and their relationship to disorder in kaolin minerals. *American Mineralogist* 70, 149–164.
- Dékány, I., Szántó, F., Nagy, L.G., 1985a. Sorption and immersional wetting on clay minerals having modified surface. *Journal of Colloid and Interface Science* 103, 321–331.
- Dékány, I., Szántó, F., Weiss, A., Lagaly, G., 1985b. Interlamellar liquid sorption on hydrophobic silicates. *Berichte der Bunsengesellschaft für Physikalische Chemie* 89, 62–67.
- Dékány, I., Szántó, F., Weiss, A., Lagaly, G., 1986. Interactions of hydrophobic layer silicates with alcohol–benzene mixtures. *Berichte der Bunsengesellschaft für Physikalische Chemie* 90, 422–431.
- Del Hoyo, C., Vicente, M.A., Rives, V., 2001. Preparation of drug-montmorillonite UV-radiation protection compounds by gas–solid adsorption. *Clay Minerals* 36, 541–546.
- DellaGuardie, R.A., Thomas, J.K., 1983. Photoprocesses on colloidal clay systems. Tris(2,2'-bipyridinium)ruthenium(II) bound to colloidal kaolin and montmorillonite. *The Journal of Physical Chemistry* 87, 990–998.
- Deng, Y., Dixon, J.B., White, G.N., 2003. Intercalation and surface modification of smectite by two non-ionic surfactants. *Clays and Clay Minerals* 51, 150–161.
- Di Leo, P., 2000. A nuclear magnetic resonance (NMR) and Fourier-transform infrared (FTIR) study of glycine specification on a Cd-rich montmorillonite. *Clays and Clay Minerals* 48, 495–502.
- Doner, H.E., Mortland, M.M., 1969. Benzene complexes with Cu(II)-montmorillonite. *Science* 66, 1406–1407.
- Duer, M.J., Rocha, J., 1992. A two-dimensional solid-state  $^2\text{H}$  exchange NMR study of the molecular motion in the kaolinite: DMSO intercalation compound. *Journal of Magnetic Resonance* 98, 524–533.

- Duer, M.J., Rocha, J., Klinowski, J., 1992. Solid-state NMR studies of the molecular motion in the kaolinite: DMSO intercalate. *Journal of the American Chemical Society* 114, 6867–6874.
- Eastman, M.P., Hagerman, M.E., Attuso, J.W., Bain, E.D., Porter, T.L., 1996. Polymerization of benzene and aniline on Cu(II)-exchanged hectorite clay films: a scanning force microscope study. *Clays Clay Minerals* 44, 769–773.
- Ensminger, L.E., Gieseking, J.E., 1939. The adsorption of proteins by montmorillonitic clays. *Soil Science* 48, 467–474.
- Everett, D.H., 1964. Thermodynamics of adsorption from solution. Part 1. Perfect systems. *Transactions of the Faraday Society* 60, 1803–1813.
- Everett, D.H., 1965. Thermodynamics of adsorption from solution. Part 2. Imperfect systems. *Transactions of the Faraday Society* 61, 2478–2495.
- Farmer, V.C., Mortland, M.M., 1966. An infrared study of the coordination of pyridine and water to exchangeable cations in montmorillonite and saponite. *Journal of the Chemical Society A*, 344–351.
- Farmer, V.C., Russell, J.D., 1967. Infrared absorption spectrometry in clay studies. *Clays and Clay Minerals* 15, 121–142.
- Favre, H., Lagaly, G., 1991. Organo-bentonites with quaternary alkylammonium ions. *Clay Minerals* 26, 19–32.
- Feldkamp, J.R., White, J.L., 1979. Acid-base equilibria in clay suspension. *Journal of Colloid and Interface Science* 69, 97–106.
- Fendler, J.H., 2001. Chemical self-assembly for electronic applications. *Chemistry of Materials* 13, 3196–3210.
- Fenoll Hach-Ali, P.F., Weiss, A., 1969. Estudio de la reaccion de caolinita y *N*-metilformamida. *Quimica* LXV, 769–790.
- Fernandez-Gonzales, M., Weiss, A., Lagaly, G., 1976. Über das Verhalten nordwest-spanischer Kaoline bei der Bildung von Einlagerungsverbindungen. *Keramische Zeitschrift* 28, 55–58.
- Fitch, A., 1990. Clay-modified electrode: a review. *Clays and Clay Minerals* 38, 391–400.
- Fitch, A., Wang, Y., Park, S., Joo, P., 1998. Intelligent design of thin clay films: transport and tailoring. *The Latest Frontiers of Clay Chemistry*. In: Yamagishi, A., Aramata, A., Tanguchi, M. (Eds.), *Proceedings of the Sapporo Conference on the Chemistry of Clays and Clay Minerals*, Sapporo 1996. The Smectite Forum of Japan, Sendai, Japan, pp. 1–15.
- Franco, F., Ruiz Cruz, M.D., 2002. High-temperature X-ray diffraction, differential thermal analysis and thermogravimetry of the kaolinite-dimethylsulfoxide intercalation complex. *Clays and Clay Minerals* 50, 47–55.
- Friedlander, H.Z., 1963. Spontaneous polymerization in and on clay. *American Chemical Society, Division of Polymer Chemistry Reprints* 4, 300–306.
- Frost, R.L., Kristof, J., Paroz, G.N., Klopogge, J.T., 1998a. Role of water in the intercalation of kaolinite with hydrazine. *Journal of Colloid and Interface Science* 208, 216–225.
- Frost, R.L., Kristof, J., Paroz, G.N., Klopogge, J.T., 1998b. Modification of the kaolinite hydroxyl surfaces through intercalation with potassium acetate under pressure. *Journal of Colloid and Interface Science* 208, 478–486.
- Frost, R.L., Kristof, J., Paroz, G.N., Klopogge, J.T., 1998c. Molecular structure of dimethyl sulfoxide intercalated kaolinites. *The Journal of Physical Chemistry* 102, 8519–8532.

- Frost, R.L., Tran, T.H., Kristof, J., 1997. The structure of an intercalated ordered kaolinite—a Raman microscopy study. *Clay Minerals* 32, 587–596.
- Frost, R.L., van der Gaast, S.J., Zbik, M., Klopogge, J.T., Paroz, G.N., 2002. Birdwood kaolinite: a highly ordered kaolinite that is difficult to intercalate—an XRD, SEM and Raman spectroscopic study. *Applied Clay Science* 20, 177–187.
- Fukushima, Y., Inagaki, S., 1987. Synthesis of an intercalated compound of montmorillonite and 6-polyamide. *Journal of Inclusion Phenomena* 5, 473–482.
- Fukushima, Y., Okada, A., Kawasumi, M., Kurauchi, T., Kamigaito, O., 1988. Swelling behaviour of montmorillonite by poly 6-amide. *Clay Minerals* 23, 27–34.
- Furukawa, T., Brindley, G.W., 1973. Adsorption and oxidation of benzidine and aniline by montmorillonite and hectorite. *Clays and Clay Minerals* 21, 279–288.
- Gábor, M., Tóth, M., Krisof, J., Komáromi-Hiller, G., 1995. Thermal behavior and decomposition of intercalated kaolinite. *Clays and Clay Minerals* 43, 223–228.
- Gardolinski, J.E.F.C., Lagaly, G., Czank, M., 2004. On the destruction of kaolinite and gibbsite by phenylphosphonic, phenylphosphinic and phenylarsonic acids: evidence for the formation of new Al compounds. *Clay Minerals* 39, 391–404.
- Gardolinski, J.E.F.C., Lagaly, G., 2005a. Grafted organic derivatives of kaolinite: I. Synthesis, chemical and rheological characterization. *Clay Minerals* 40, 499–548.
- Gardolinski, J.E.F.C., Lagaly, G., 2005b. Grafted organic derivatives of kaolinite: I. Intercalation of primary n-alkylamines and delamination. *Clay Minerals* 40, 549–558.
- Gardolinski, J.E., Ramos, L.P., Pinto de Souza, G., Wypych, F., 2000. Intercalation of benzamide into kaolinite. *Journal of Colloid and Interface Science* 221, 284–290.
- Garfinkel-Shweky, D., Yariv, S., 1999. Metachromasy in clay dye systems: the adsorption of acridine orange by Na-beidellite. *Clay Minerals* 34, 459–467.
- Ghabru, S.K., Mermut, A., Arnoud, R.J.S., 1989. Layer charge and cation-exchange characteristics of vermiculite (weathered biotite) isolated from a gray luvisol in northeastern Saskatchewan. *Clays and Clay Minerals* 37, 1–11.
- Ghosh, P.K., Bard, A.J., 1984. Photochemistry of tris(2,2'-bipyridine)ruthenium(II) in colloidal clay suspension. *The Journal of Physical Chemistry* 88, 5519.
- Gougeon, R.D., Soulard, M., Reinholdt, M., Miché-Brendlé, J., Chézeau, J.M., Le Dred, R., Marchal, R., Jeandet, P., 2003. Polypeptide adsorption on a synthetic montmorillonite: a combined solid-state NMR spectroscopy, X-ray diffraction, thermal analysis and N<sub>2</sub> adsorption study. *European Journal of Inorganic Chemistry*, 1366–1372.
- Graf, G., Lagaly, G., 1980. Interactions of clay minerals with adenosine-5-phosphates. *Clay and Clay Minerals* 28, 12–18.
- Graf von Reichenbach, H., 1973. Exchange equilibria of interlayer cations in different particle size fractions of biotite and phlogopite. In: Serratos, J.M. (Ed.), *Proceedings of the International Clay Conference, Madrid, 1972*. Division of Ciencias C.S.I.C. Madrid, pp. 457–479.
- Graf von Reichenbach, H., Rich, C.I., 1969. Potassium release from muscovite as influenced by particle size. *Clays and Clay Minerals* 17, 23–29.
- Greenland, D.J., 1963. Adsorption of polyvinyl alcohols by montmorillonite. *Journal of Colloid Science* 18, 647–664.
- Guimarães, J.L., Peralta-Zamora, P., Wypych, F., 1998. Covalent grafting of phenylphosphate groups onto the interlamellar aluminol surface of kaolinite. *Journal of Colloid and Interface Science* 206, 281–287.

- Habti, A., Keravis, D., Levitz, P., Van Damme, H., 1984. Influence of surface heterogeneity on the luminescence decay of probe molecules in heterogeneous systems;  $\text{Ru}(\text{bpy})_3^{2+}$  on clays. *Journal of the Chemical Society, Faraday Transaction 2* 80, 67–83.
- Hang, P.T., Brindley, G.W., 1970. Methylene blue absorption by clay minerals. Determination of surface areas and cation exchange capacities (clay-organic studies XVIII). *Clays and Clay Minerals* 18, 203–212.
- Hashizume, H., Theng, B.K.G., Yamagishi, A., 2002. Adsorption and discrimination of alanine and alanyl-alanine enantiomers by allophane. *Clay Minerals* 37, 551–557.
- Hayashi, S., 1995. NMR study of dynamics of dimethyl sulfoxide molecules in kaolinite/dimethyl sulfoxide intercalation compound. *The Journal Physical Chemistry* 99, 7120–7129.
- Hayashi, S., 1997. NMR study of dynamics and evolution of guest molecules in kaolinite/dimethyl sulfoxide intercalation compound. *Clays and Clay Minerals* 45, 724–732.
- Heller, L., Yariv, S., 1970. Anilinium montmorillonites and the formation of ammonium/amine associations. *Israel Journal of Chemistry* 8, 391–397.
- Hendricks, S.B., Alexander, L.T., 1940. A qualitative test for the montmorillonite type clay minerals. *Journal of the American Society of Agronomy* 32, 455–458.
- Hernán, L., Morales, J., Santos, J., 1998. Synthesis and characterization of poly(ethylene oxide) nanocomposites of misfit layer chalcogenides. *Journal of Solid State Chemistry* 141, 323–329.
- Herrmann, H., Lagaly, G., 1985. ATP–clay interactions. In: Konta, J. (Ed.), 5th Meeting of the European Clay Groups, Prague 1985. Charles University Prague, pp. 269–277.
- Hillier, S., Ryan, P.C., 2002. Identification of halloysite (7 Å) by ethylene glycol solvation: the “MacEwan effect”. *Clay Minerals* 37, 487–496.
- Hsieh, Y.P., 1989. Effects of relative humidity on the basal expansion of Mg-smectite equilibrated with ethylene glycol at low vapor pressure. *Clays and Clay Minerals* 37, 459–463.
- Hu, N., Rusling, J.F., 1991. Surfactant-intercalated clay films for electrochemical catalysis. Reduction of trichloroacetic acid. *Analytical Chemistry* 63, 2163–2168.
- Hubbard, B., Kuang, W., Moser, A., Facey, G.A., Detellier, C., 2003. Structural study of Maya blue: textural, thermal and solid-state multinuclear magnetic resonance characterization of the palygorskite-indigo and sepiolite-indigo adducts. *Clays and Clay Minerals* 51, 318–326.
- Itagaki, T., Komori, Y., Sugahara, Y., Kuroda, K., 2001. Synthesis of a kaolinite-poly( $\beta$ -alanine) intercalation compound. *Journal of Materials Chemistry* 11, 3291–3295.
- Ito, K., Kuwabara, M., Fukunishi, K., Fujiwara, Y., 1996. Application of clay-cationic dye intercalation to image fixation in thermal dye transfer printing. *Journal of Imaging Science and Technology* 40, 275–280.
- Jackson, M.L., Abdel-Kader, F.H., 1978. Kaolinite intercalation procedure for all sizes and types with XRD spacing distinctive from other phyllosilicates. *Clays and Clay Minerals* 26, 81–87.
- Jacobs, K.Y., Schoonheydt, R.A., 2001. Time dependence of the spectra of methylene blue-clay mineral suspensions. *Langmuir* 17, 5150–5155.
- Janek, M., Lagaly, G., 2003. Interaction of a cationic surfactant with bentonite: a colloid chemistry study. *Colloid and Polymer Science* 281, 293–301.
- Jasmund, K., Lagaly, G., 1993. Tonminerale und Tone. Struktur, Eigenschaften, Anwendung und Einsatz in Industrie und Umwelt, Steinkopff Verlag, Darmstadt.



- Jaynes, W.F., Boyd, S.A., 1991. Hydrophobicity of siloxane surfaces in smectites as revealed by aromatic hydrocarbon adsorption from water. *Clays and Clay Minerals* 39, 428–436.
- Johnston, C.T., Sposito, G., Bocian, D.F., Birge, R.R., 1984. Vibrational spectroscopic study of the interlamellar kaolinite-dimethyl sulfoxide complex. *The Journal of Physical Chemistry* 88, 5959–5964.
- Jones, T.R., 1983. The properties and uses of clays which swell in organic solvents. *Clay Minerals* 18, 399–410.
- Jordan, J.W., 1950. Organophilic bentonites 1. Swelling in organic liquids. *The Journal of Physical and Colloid Chemistry* 54, 294–306.
- Kahr, G., Madsen, F.T., 1995. Determination of the cation exchange capacity and the surface area of bentonite, illite, and kaolinite by methylene blue adsorption. *Applied Clay Science* 9, 327–336.
- Kalyanasundaram, K., 1992. *Photochemistry of Polypyridine and Porphyrin Complexes*. Academic Press, London.
- Karickhoff, S.W., Bailey, G.W., 1976. Protonation of organic bases in clay–water systems. *Clays and Clay Minerals* 24, 170–176.
- Kato, C., Kuroda, K., Hasegawa, K., 1979a. Electrical conductivity of a montmorillonite-organic complex. *Clay Minerals* 14, 13–20.
- Kato, C., Kuroda, K., Misawa, K., 1979b. Preparation of montmorillonite–nylon complexes and their thermal properties. *Clays and Clay Minerals* 27, 129–136.
- Kato, C., Kuroda, K., Takahara, H., 1981. Preparation and electrical properties of quaternary ammonium montmorillonite–polystyrene complexes. *Clays and Clay Minerals* 29, 294–298.
- Kelleher, B.P., O'Dwyer, T.F., 2002. Intercalation of benzamide into expanded kaolinite under ambient environmental conditions. *Clays and Clay Minerals* 50, 331–335.
- Keller, W.D., Haenni, R.P., 1978. Effects of micro-sized mixtures of kaolin minerals on properties of kaolinites. *Clays and Clay Minerals* 26, 384–396.
- Kelly, P., Akelah, A., Qutubuddin, S., Moet, A., 1994. Reduction of residual stress in montmorillonite/epoxy compounds. *Journal of Material Science* 29, 2274–2280.
- Kipling, J.J., 1965. *Adsorption from Solutions of Non-Electrolytes*. Academic Press, London.
- Klapyta, Z., Fujita, T., Iyi, N., 2001. Adsorption of dodecyl- and octadecyltrimethylammonium ions on a smectite and synthetic micas. *Applied Clay Science* 19, 5–10.
- Klimentidis, R.E., Mackinnon, I.D.R., 1986. High-resolution imaging of ordered mixed-layer clays. *Clays and Clay Minerals* 34, 155–164.
- Klopprogge, J.T., Korbijn, L., Koster, T.P.M., 1997. Head-space gas-chromatography, a quick and simple method to screen adsorption capabilities of porous materials: adsorption of chlorobenzene on modified montmorillonite. *Applied Clay Science* 12, 85–91.
- Komori, Y., Sugahara, Y., Kuroda, K., 1999. Thermal transformation of a kaolinite-poly(acrylamide) intercalation compound. *Journal of Materials Chemistry* 9, 3081–3085.
- Kukkadapu, R.K., Boyd, S.A., 1995. Tetramethyl phosphonium- and tetramethylammonium-smectites as adsorbents of aromatic and chlorinated hydrocarbons: effect of water on adsorption efficiency. *Clays and Clay Minerals* 43, 318–323.
- Kuppa, V., Manias, E., 2003. Dynamics of poly(ethylene oxide) in nanoscale confinements: a computer simulation perspective. *Journal of Chemical Physics* 118, 3421–3429.
- Kuwaharada, S., Tateyama, H., Nishimura, S., Hirose, H., 2002. Smectite quasicrystals in aqueous solutions as a function of cationic surfactant concentration. *Clays and Clay Minerals* 50, 18–24.

- Lagaly, G., 1976. Kink-block and gauche-block structures of bimolecular films. *Angewandte Chemie International Edition in English* 15, 575–586.
- Lagaly, G., 1981a. Characterization of clays by organic compounds. *Clay Minerals* 16, 1–21.
- Lagaly, G., 1981b. Inorganic layer compounds. Phenomena of interface reactions with organic compounds. *Naturwissenschaften* 68, 82–88.
- Lagaly, G., 1982. Layer charge heterogeneity in vermiculites. *Clays and Clay Minerals* 30, 215–222.
- Lagaly, G., 1984. Clay–organic interactions. *Philosophical Transactions of the Royal Society of London* 311, 315–332.
- Lagaly, G., 1986a. Smectitic clays as ionic macromolecules. In: Wilson, A.D., Prosser, H.J. (Eds.), *Developments of Ionic Polymers*, vol. 2. Elsevier, London, pp. 77–140.
- Lagaly, G., 1986b. Interaction of alkylamines with different types of layered compounds. *Solid State Ionics* 22, 43–51.
- Lagaly, G., 1987a. Clay–organic interactions: problems and recent results. In: Schultz, L.G., van Olphen, H., Mumpton, F.A. (Eds.), *Proceedings of the International Clay Conference*, Denver, 1985. The Clay Minerals Society, Bloomington, IN, pp. 343–351.
- Lagaly, G., 1987b. Water and solvents on surfaces bristling with alkyl chains. In: Kleeberg, H. (Ed.), *Interactions of Water in Ionic and Nonionic Hydrates*. Springer, Berlin, pp. 229–240.
- Lagaly, G., 1994a. Layer charge determination by alkylammonium ions. In: Mermut, A.R. (Ed.), *Layer Charge Characteristics of Clays*, CMC Workshop Lectures, vol. 6. The Clay Minerals Society, Boulder, CO, pp. 1–46.
- Lagaly, G., 1994b. Bentonites: adsorbents of toxic substances. *Progress in Colloid and Polymer Science* 95, 61–72.
- Lagaly, G., 1995. Surface and interlayer reactions: bentonites as adsorbents. In: Churchman, G.J., Fitzpatrick, R.W., Eggleton, R.A. (Eds.), *Clays: Controlling the Environment*, Proceedings of the 10th International Clay Conference, Adelaide Australia 1993. CSIRO Publishing, Melbourne, pp. 137–144.
- Lagaly, G., Beneke, K., 1991. Intercalation and exchange reactions of clay minerals and non-clay compounds. *Colloid and Polymer Science* 269, 1198–1211.
- Lagaly, G., Beneke, K., Weiss, A., 1975. Magadiite and H-magadiite: I. Sodium magadiite and some of its derivatives. *American Mineralogist* 60, 642–649.
- Lagaly, G., Malberg, R., 1990. Disaggregation of alkylammonium montmorillonites in organic solvents. *Colloids and Surfaces* 49, 11–27.
- Lagaly, G., Stuke, E., Weiss, A., 1976. Der Einfluß von *cis*-Doppelbindungen auf die Struktur bimolekularer Filme. *Colloid and Polymer Science* 60, 102–107.
- Lagaly, G., Weiss, A., 1969. Zur van-der-Waals-Wechselwirkung in n-Dodecylammonium-Schichtsilicaten. *Zeitschrift für Naturforschung* 24b, 1057–1058.
- Lagaly, G., Witter, R., 1982. Clustering of liquid molecules on solid surfaces. *Berichte der Bunsengesellschaft für Physikalische Chemie* 86, 74–80.
- Lagaly, G., Witter, R., Sander, H., 1983. Water on hydrophobic surfaces. In: Ottewill, R.H., Rochester, C.H. (Eds.), *Adsorption from Solution*. Academic Press, London, pp. 65–77.
- Lahav, N., 1972. Interaction between montmorillonite and benzidine in aqueous solutions III. The color reaction in the air dry state. *Israel Journal of Chemistry* 10, 925–934.
- Lahav, N., 1990. Preparation of stable suspensions of delaminated kaolinite by combined dimethylsulfoxide-ammonium fluoride treatment. *Clays and Clay Minerals* 38, 219–222.

- Lailach, G., Brindley, G.W., 1969. Specific co-adsorption of purines and pyrimidines by montmorillonite. *Clays and Clay Minerals* 17, 95–100.
- Lan, T., Kaviratna, P.D., Pinnavaia, T.J., 1995. Mechanism of clay tactoid exfoliation in epoxy-clay nanocomposites. *Chemistry of Materials* 7, 2144–2150.
- Lan, T., Pinnavaia, T.J., 1994. Clay-reinforced epoxy nanocomposites. *Chemistry of Materials* 6, 2216–2219.
- Lapides, I., Yariv, S., Lahav, N., 1994. Interaction between kaolinite and caesium halides. Comparison between intercalated samples obtained from aqueous suspensions and by mechanochemical techniques. *International Journal of Mechanochemistry and Mechanical Alloying* 1, 79–91.
- Lapides, I., Yariv, S., Lahav, N., 1995. The intercalation of CsF in kaolinite. *Clay Minerals* 30, 287–294.
- Larsson, N., Siffert, B., 1983. Formation of lysozyme-containing crystals of montmorillonite. *Journal of Colloid Interface Science* 93, 424–431.
- Laura, R.D., Cloos, P., 1975. Adsorption of ethylene diamine on montmorillonite saturated with different cations—IV: Al-, Ca-, and Mg-montmorillonite: protonation, ion exchange, co-ordination and hydrogen-bonding. *Clays and Clay Minerals* 23, 343–348.
- LeBaron, P.C., Wang, Z., Pinnavaia, T.J., 1999. Polymer-layered silicate nanocomposites: an overview. *Applied Clay Science* 15, 11–29.
- Lee, J.F., Mortland, M.M., Boyd, S.A., 1989. Shape-selective adsorption of aromatic molecules from water by tetramethylammonium-smectite. *Journal of the Chemical Society, Faraday Transactions 1* 85, 2953–2962.
- Lee, J.F., Mortland, M.M., Chiou, C.T., Kile, D.E., Boyd, S.A., 1990. Adsorption of benzene, toluene, and xylene by two tetramethylammonium-smectites having different charge densities. *Clays and Clay Minerals* 38, 113–120.
- Lee, S.Y., Kim, S.J., 2002. Expansion of smectites by hexadecyltrimethylammonium. *Clays and Clay Minerals* 50, 435–445.
- Levy, R., Francis, C.W., 1975a. Interlayer adsorption of polyvinylpyrrolidone on montmorillonite. *Journal of Colloid and Interface Science* 50, 442–450.
- Levy, R., Francis, C.W., 1975b. A quantitative method for the determination of montmorillonite in soils. *Clays and Clay Minerals* 23, 85–89.
- Lipsicas, M., Raythatha, R., Giese, R.F., Costanzo, P.M., 1986. Molecular motions, surface interactions, and stacking disorder in kaolinite intercalates. *Clays and Clay Minerals* 34, 635–644.
- Lipsicas, M., Straley, C., Costanzo, P.M., Giese, R.F., 1985. Static and dynamic structure of water in hydrated kaolinites. II. The dynamic structure. *Journal of Colloid and Interface Science* 107, 221–230.
- Lombardi, G., Russel, J.D., Keller, W.D., 1987. Compositional and structural variations in size fractions of a sedimentary and a hydrothermal kaolin. *Clays and Clay Minerals* 35, 321–335.
- MacEwan, D.M.C., 1946. The identification and estimation of the montmorillonite group of clay minerals, with special reference to soil clays. *Journal of the Society of the Chemical Industries (London)* 65, 298–305.
- Madsen, F., 1977. Surface area measurements of clay minerals by glycerol sorption on a thermobalance. *Thermochimica Acta* 21, 89–93.

- Malberg, R., Dékány, I., Lagaly, G., 1989. Short-chain alkylammonium montmorillonites and alcohols: gas adsorption and immersionsal wetting. *Clay Minerals* 24, 631–647.
- Malla, P.B., Douglas, L.A., 1987. Identification of expanding layer silicates: layer charge vs expansion properties. In: Schultz, L.G., van Olphen, H., Mumpton, F.A. (Eds.), *Proceedings of the International Clay Conference, Denver 1985*. The Clay Minerals Society, Bloomington, IN, pp. 277–283.
- Marcks, C.H., Wachsmuth, H., Graf von Reichenbach, H., 1989. Preparation of vermiculite for HRTEM. *Clay Minerals* 24, 23–32.
- Margulies, L., Rozen, H., Nir, S., 1988. Model for competitive adsorption of organic cations on clays. *Clays and Clay Minerals* 36, 270–276.
- Meier, L.P., Nuesch, R., Madsen, F.T., 2001. Organic pillared clays. *Journal of Colloid and Interface Science* 238, 24–32.
- Mermut, A.R., 1994. Problems associated with layer charge characterization of phyllosilicates. In: Mermut, A.R. (Ed.), *Layer Charge Characteristics of Clays, CMC Workshop Lectures*, vol. 6. The Clay Minerals Society, Boulder, CO, pp. 106–122.
- Mermut, A.R., Lagaly, G., 2001. Baseline studies of the Clay Minerals Society Source Clays: layer-charge determination and characteristics of those minerals containing 2.1 layers. *Clays and Clay Minerals* 49, 393–397.
- Messersmith, P.B., Giannelis, E.P., 1994. Synthesis and characterization of layered silicate-epoxy nanocomposites. *Chemistry of Materials* 6, 1719–1725.
- Michaelian, K.H., Friesen, W.I., Yariv, S., Nasser, A., 1991b. Diffuse reflectance infrared spectra of kaolinite and kaolinite/alkali halide mixtures. Curve-fitting of the OH stretching region. *Canadian Journal of Chemistry* 69, 1786–1790.
- Michaelian, K.H., Yariv, S., Nasser, A., 1991a. Study of the interactions between caesium bromide and kaolinite by photoacoustic and diffuse reflectance infrared spectroscopy. *Canadian Journal of Chemistry* 69, 749–754.
- Miyata, H., Sugahara, Y., Kuroda, K., Kato, C., 1987. Synthesis of montmorillonite-viologen intercalation compounds and their photochromic behaviour. *Journal of the Chemical Society, Faraday Transition* 1, 83, 1851–1858.
- Mizutani, T., Takano, T., Ogoshi, H., 1995. Selective adsorption of organic ammonium ions onto smectite clays. *Langmuir* 11, 880–884.
- Moore, D.E., Dixon, J.B., 1970. Glycerol vapor adsorption on clay minerals and montmorillonite soil clays. *Soil Science Society of America Proceedings* 34, 816–822.
- Mortland, M.M., Lawton, K., 1961. Relationships between particle size and potassium release from biotite and its analogues. *Soil Science Society American Proceedings* 25, 473–476.
- Mortland, M.M., Shaobai, S., Boyd, S.A., 1986. Clay-organic complexes as adsorbents for phenol and chlorophenols. *Clays and Clay Minerals* 34, 581–585.
- Naidja, A., Huang, P.M., 1994. Aspartic acid interaction with Ca-montmorillonite: adsorption, desorption and thermal stability. *Applied Clay Science* 9, 265–281.
- Nakamura, Y., Yamagishi, A., Iwamoto, T., Kaga, M., 1988. Adsorption properties of montmorillonite and synthetic saponite as packing materials in liquid-column chromatography. *Clays and Clay Minerals* 36, 530–536.
- Narine, D.R., Guy, R.D., 1981. Interaction of some large organic cations with bentonite in dilute aqueous systems. *Clays and Clay Minerals* 29, 205–212.

- Neumann, M.G., Gessner, F., Schmitt, C.C., Sartori, R., 2002. Influence of the layer charge and clay particle size on the interactions between the cationic dye methylene blue and clays in aqueous suspension. *Journal of Colloid and Interface Science* 255, 254–259.
- Norde, W., 1983. The role of charged groups in the adsorption of proteins at solid surfaces. *Croatica Chemica Acta* 56, 705–720.
- Norde, W., 1986. Adsorption of proteins from solution at the solid-liquid interface. *Advances in Colloid and Interface Science* 25, 267–340.
- Ogata, N., Jimenez, G., Kawai, H., Ogihara, T., 1997b. Structure and thermal/mechanical properties of poly(L-lactide)-clay blend. *Journal of Polymer Science, Part B: Polymer Physics* 35, 389–396.
- Ogata, N., Kawakage, S., Ogihara, T., 1997a. Poly(vinyl alcohol)-clay and poly(ethylene oxide)-clay blends prepared using water as solvent. *Journal of Applied Polymer Science* 66, 573–581.
- Ogawa, M., Aono, T., Kuroda, K., Kato, C., 1993. Photophysical probe study of alkylammonium-montmorillonites. *Langmuir* 9, 1529–1533.
- Ogawa, M., Hama, M., Kuroda, K., 1999. Photochromism of azobenzene in the hydrophobic interlayer spaces of dialkyldimethylammonium-fluor-tetrasilicic mica films. *Clay Minerals* 34, 213–220.
- Ogawa, M., Handa, T., Kuroda, K., Kato, C., 1990. Formation of organoammonium-montmorillonites by solid–solid reactions. *Chemistry Letters* 19, 71–74.
- Ogawa, M., Handa, T., Kuroda, K., Kato, C., Tani, T., 1992b. Photochemical hole burning of 1,4-dihydroxyanthraquinone intercalated in a pillared layered clay mineral. *The Journal of Physical Chemistry* 96, 8116–8119.
- Ogawa, M., Hashizume, T., Kuroda, K., Kato, C., 1991. Intercalation of 2,2'-bipyridine and complex formation in the interlayer space of montmorillonite by solid–solid reactions. *Inorganic Chemistry* 30, 584–585.
- Ogawa, M., Hirata, M., Kuroda, K., Kato, C., 1992c. Selective solid-state intercalation of cis–trans isomers into montmorillonite. *Chemistry Letters* 21, 365–368.
- Ogawa, M., Ishikawa, A., 1998. Controlled microstructures of the amphiphilic cationic azobenzene-montmorillonite intercalation compounds. *Journal of Materials Chemistry* 8, 463–467.
- Ogawa, M., Kuroda, K., 1995. Photofunctions of intercalation compounds. *Chemical Reviews* 95, 399–438.
- Ogawa, M., Kuroda, K., 1997. Preparation of inorganic–organic nanocomposites through intercalation of organoammonium ions into layered silicates. *Bulletin of the Chemical Society of Japan* 70, 2593–2618.
- Ogawa, M., Shirai, H., Kuroda, K., Kato, C., 1992a. Solid-state intercalation of naphthalene and anthracene into alkylammonium-montmorillonites. *Clays and Clay Minerals* 40, 485–490.
- Okahata, Y., Shimizu, A., 1989. Preparation of bilayer-intercalated clay films and permeation control responding to temperature, electric field, and ambient pH changes. *Langmuir* 5, 954–959.
- Olejnik, S., Posner, A.M., Quirk, J.P., 1970. The intercalation of polar organic compounds into kaolinite. *Clay Minerals* 8, 421–434.
- Olness, A., Clapp, C.E., 1973. Occurrence of collapsed and expanded crystals in montmorillonite-dextran complexes. *Clays and Clay Minerals* 21, 289–293.

- Parfitt, R.L., Greenland, D.J., 1970a. The adsorption of poly(ethylene glycols) on clay minerals. *Clay Minerals* 8, 305–315.
- Parfitt, R.L., Greenland, D.J., 1970b. Adsorption of water by montmorillonite-poly(ethylene glycol) adsorption products. *Clay Minerals* 8, 317–323.
- Parfitt, R.L., Greenland, D.J., 1970c. Adsorption of polysaccharides by montmorillonite. *Soil Science Society of America Proceedings* 34, 862–866.
- Parker, R.W., Frost, R.L., 1996. The application of drift spectroscopy to the multicomponent analysis of organic chemicals adsorbed on montmorillonite. *Clays and Clay Minerals* 44, 32–40.
- Pechhold, W., Liska, E., Grossmann, H.P., Hägele, P.C., 1976. On present theories of the condensed polymer state. *Pure and Applied Chemistry* 46, 127–134.
- Penner, D., Lagaly, G., 2000. Influence of organic and inorganic salts on the coagulation of montmorillonite dispersions. *Clays and Clay Minerals* 48, 246–255.
- Pfirrmann, G., Lagaly, G., Weiss, A., 1973. Phase transitions in complexes of nontronite with *n*-alkanols. *Clays and Clay Minerals* 21, 239–247.
- Pinnavaia, T.J., 1983. Intercalated clay catalysts. *Science* 220, 365–371.
- Pinnavaia, T.J., Hall, P.L., Cady, S.S., Mortland, M.M., 1974. Aromatic radical cation formation on the intracrystal surfaces of transition metal layer lattice silicates. *The Journal of Physical Chemistry* 78, 994–999.
- Pinnavaia, T.J., Mortland, M.M., 1971. Interlamellar metal complexes of layer silicates. I. Copper(II)-arene complexes on montmorillonite. *The Journal of Physical Chemistry* 75, 3957–3962.
- Plançon, A., Giese, R.F., Snyder, R., 1988. The Hinckley index for kaolinites. *Clay Minerals* 23, 249–260.
- Platikanov, D., Weiss, A., Lagaly, G., 1977. Orientation of nonionic surfactants on solid surfaces: *n*-alkyl polyglycol ethers on montmorillonite. *Colloid and Polymer Science* 255, 907–915.
- Polette, L.A., Meitzner, G., Jose-Yacaman, M., Chianelli, R.R., 2002. Maya blue: application of XAS and HRTEM to materials science in art and archaeology. *Microchemical Journal* 71, 167–174.
- Poyato-Ferrera, J., Becker, H.O., Weiss, A., 1977. Phase changes in kaolinite-amine-complexes. In: Rosenquist, J. F. (Ed.), *Proceedings of the Third European Clay Conference*, Oslo. Nordic Society for Clay Research, pp. 148–150.
- Pratum, T.K., 1992. A solid-state  $^{13}\text{C}$  NMR study of tetraalkylammonium/clay complexes. *The Journal of Physical Chemistry* 96, 4567–4571.
- Quiquampoix, H., 1987a. A stepwise approach to the understanding of extracellular enzyme activity in soil I. Effect of electrostatic interaction on the conformation of a  $\beta$ -D-glucosidase adsorbed on different mineral surfaces. *Biochimie* 69, 753–763.
- Quiquampoix, H., 1987b. A stepwise approach to the understanding of extracellular enzyme activity in soil II. Competitive effects on the adsorption of a  $\beta$ -D-glucosidase in mixed mineral or organo-mineral systems. *Biochimie* 69, 765–771.
- Quiquampoix, H., Chassin, P., Ratcliffe, R.G., 1989. Enzyme activity and cation exchange as tools for the study of the conformation of proteins adsorbed on mineral surfaces. *Progress in Colloid & Polymer Science* 79, 59–63.
- Quiquampoix, H., Ratcliffe, R.G., 1992. A  $^{31}\text{P}$  NMR study of the adsorption of bovine serum albumin on montmorillonite using phosphate and the paramagnetic cation  $\text{Mn}^{2+}$ : modification of conformation with pH. *Journal of Colloid and Interface Science* 148, 343–352.

- Quiquampoix, H., Staunton, S., Baron, M.H., Ratcliffe, R.G., 1993. Interpretation of the pH dependence of protein adsorption on clay mineral surfaces and its relevance to the understanding of extracellular enzyme activity in soil. *Colloids and Surfaces* 75, 85–93.
- Range, K.J., Range, A., Weiss, A., 1968. Zur Existenz von Kaolinithydraten. *Zeitschrift für Naturforschung* 23b, 1144–1147.
- Range, K.J., Range, A., Weiss, A., 1969. Fire-clay type kaolinite or fire-clay mineral? Experimental classification of kaolinite-halloysite minerals. In: Heller, L. (Ed.), *Proceedings of the International Clay Conference, Tokyo, 1969*. Israel University Press, Jerusalem, pp. 3–13.
- Raupach, M., Janik, L.J., 1976. The orientation of ornithine and 6-aminohexanoic acid adsorbed on vermiculite from polarized I.R. ATR spectra. *Clays and Clay Minerals* 24, 127–133.
- Raupach, M., Slade, P.G., Radoslovich, E.W., 1975. A polarized infrared and X-ray study of lysine-vermiculite. *Clays and Clay Minerals* 23, 181–186.
- Rausell-Colom, J.A., Fornés, V., 1974. Monodimensional Fourier analysis of some vermiculite-L-ornithine complexes. *American Mineralogist* 59, 790–798.
- Regdon, I., Király, Z., Dékány, I., Lagaly, G., 1998. Microcalorimetric studies of S/L interfacial layers: thermodynamic parameters of the adsorption of butanol-water on hydrophobized clay minerals. *Progress in Colloid & Polymer Science* 109, 214–220.
- Reynolds, R.C., 1965. An X-ray study of an ethylene glycol-montmorillonite complex. *American Mineralogist* 50, 990–1001.
- Rösner, C., Lagaly, G., 1984. Interlayer reactions of the silver molybdate  $\text{Ag}_6\text{Mo}_{10}\text{O}_{33}$ . *Journal of Solid State Chemistry* 53, 92–100.
- Ross, G.J., Rich, C.I., 1973. Effect of particle thickness on potassium exchange from phlogopite. *Clays and Clay Minerals* 21, 77–81.
- Rühlicke, G., Kohler, E.E., 1981. A simplified procedure for determining layer charge by the n-alkylammonium method. *Clay Minerals* 16, 305–307.
- Rühlicke, G., Niederbudde, E.A., 1985. Determination of layer charge density of expandable 2:1 clay minerals in soils and loess sediments using the alkylammonium method. *Clay Minerals* 20, 291–300.
- Ruiz-Hitzky, E., Casal, B., 1978. Crown ether intercalations with phyllosilicates. *Nature* 276, 596–597.
- Ruiz-Hitzky, E., Casal, B., Aranda, P., Galvan, J.C., 2001. Inorganic-organic nanocomposite materials based on macrocyclic compounds. *Reviews in Inorganic Chemistry* 21, 125–159.
- Rupert, J.P., 1973. Electron spin resonance spectra of interlamellar copper(II)-arene complexes on montmorillonite. *The Journal of Physical Chemistry* 77, 784–790.
- Rytwo, G., Ruiz-Hitzky, E., 2003. Enthalpies of adsorption of methylene blue and crystal violet to montmorillonite. *Journal of Thermal Analysis and Calorimetry* 71, 751–759.
- Rytwo, G., Serban, C., Nir, S., Margulies, L., 1991. Use of methylene blue and crystal violet for determination of exchangeable cations in montmorillonite. *Clays and Clay Minerals* 39, 551–555.
- Samii, A.M., Lagaly, G., 1987. Adsorption of nuclein bases on smectites. In: Schultz, L.G., van Olphen, H., Mumpton, F.A. (Eds.), *Proceedings of the International Clay Conference, Denver, 1985*. The Clay Minerals Society, Bloomington, IN, pp. 363–369.
- Sánchez-Camazano, M., Sánchez-Martín, M.J., 1994. Trimethyl phosphate induced decomposition of kaolinite. *Clays and Clay Minerals* 42, 221–225.

- Sasai, R., Ogiso, H., Shindachi, I., Shichi, T., Takagi, K., 2000a. Photochromism in oriented thin films prepared by the hybridization of diarylethenes in clay interlayers. *Tetrahedron* 56, 6979–6984.
- Sasai, R., Shichi, T., Gekko, K., Takagi, K., 2000b. Continuously changing the conformational dependence of saponite hybrid materials on the intercalation degree: electric linear dichroism of stilbazolium derivatives intercalated in saponite clay. *Bulletin of the Chemical Society of Japan* 73, 1925–1931.
- Sawhney, B.L., 1972. Selective sorption and fixation of cations by clay minerals: a review. *Clays and Clay Minerals* 20, 93–100.
- Schoonheydt, R.A., de Pauw, P., Vliers, D., de Schryver, F.C., 1984. Luminescence of tris(2,2'-bipyridine)ruthenium(II) in aqueous clay mineral suspensions. *The Journal of Physical Chemistry* 88, 5113–5118.
- Seki, T., Ichimura, K., 1990. Thermal isomerization behaviors of a spiropyran in bilayers immobilized with a linear polymer and a smectic clay. *Macromolecules* 23, 31–35.
- Serratosa, J.M., 1966. Infrared analysis of the orientation of pyridine molecules in clay complexes. *Clays and Clay Minerals* 14, 385–391.
- Serratosa, J.M., 1968. Infrared study of benzonitrile–montmorillonite complexes. *American Mineralogist* 53, 1244–1251.
- Seto, H., Cruz-Cumplido, M.I., Fripiat, J.J., 1978a. Reactivity of a long-spacing ammonium-propionate-kaolinite intercalate toward diol, diamines and quaternary ammonium salts. *Clay Minerals* 13, 309–323.
- Seto, H., Cruz, M.I., Fripiat, J.J., 1978b. Long-range organization in the ammonium propionate intercalation complex of kaolinite. *American Mineralogist* 63, 572–583.
- Siffert, B., Kessaissia, S., 1978. Contribution au mécanisme d'adsorption des  $\alpha$ -amino-acids par la montmorillonite. *Clay Minerals* 13, 255–270.
- Siffert, B., Naidja, A., 1992. Stereoselectivity of montmorillonite in the adsorption and deamination of some amino acids. *Clay Minerals* 27, 109–118.
- Simon, S., Le Cerf, D., Picton, L., Muller, G., 2002. Adsorption of cellulose derivatives onto montmorillonite: a SEC-MALLS study of molar masses influence. *Colloids and Surfaces* 203, 77–86.
- Slade, P.G., Dean, C., Schultz, P.K., Self, P.G., 1987. Crystal structure of a vermiculite-anilinium intercalate. *Clays and Clay Minerals* 35, 177–188.
- Solomon, D.H., Hawthorne, D.G., 1983. *Chemistry of Pigments and Fillers*. Wiley, New York.
- Solomon, D.H., Loft, B.C., 1968. The mechanism of spontaneous interlamellar polymerization in aluminosilicates. *Journal of Applied Polymer Science* 12, 1253–1262.
- Soma, Y., Soma, M., 1988. Adsorption of benzidines and anilines on Cu- and Fe-montmorillonites studied by Resonance Raman Spectroscopy. *Clay Minerals* 23, 1–12.
- Stevens, J.J., Anderson, S.J., 1996a. Orientation of trimethylphenylammonium (TMPA) on Wyoming montmorillonite: implications for sorption of aromatic compounds. *Clays and Clay Minerals* 44, 132–141.
- Stevens, J.J., Anderson, S.J., 1996b. An FTIR study of water sorption on TMA- and TMPA-montmorillonites. *Clays and Clay Minerals* 44, 142–150.
- Stockmeyer, M., Kruse, K., 1991. Adsorption of zinc and nickel ions and phenol and diethylketone by bentonites of different organophilicities. *Clay Minerals* 26, 431–434.
- Stoessel, F., Guth, J.L., Wey, R., 1977. Polymerisation de benzene en polyparaphénylene dans une montmorillonite cuivrique. *Clay Minerals* 12, 255–259.



- Stohrer, M., Noack, F., 1975. Magnetische Relaxationsspektroskopie an gequollenem Beidellit, einer Paraffin-Modellsubstanz. *Progress in Colloid and Polymer Science* 57, 61–68.
- Strawhecker, K.E., Manias, E., 2003. Crystallization behavior of poly(ethylene oxide) in the presence of  $\text{Na}^+$  montmorillonite fillers. *Chemistry of Materials* 15, 844–849.
- Sugahara, Y., Satokawa, S., Kuroda, K., Kato, C., 1988. Evidence for the formation of interlayer polyacrylonitrile in kaolinite. *Clays and Clay Minerals* 36, 343–348.
- Takagi, K., Kurematsu, T., Sawaki, Y., 1991. Intercalation and photochromism of spiropyrans on clay interlayers. *Journal of the Chemical Society, Perkin Transactions 2*, 1517–1522.
- Takenawa, R., Komori, Y., Hayashi, S., Kawamata, J., Kuroda, K., 2001. Intercalation of nitroanilines into kaolinite and second harmonic generation. *Chemistry of Materials* 13, 3741–3746.
- Talibudeen, O., 1954. Complex formation between montmorillonoid clays and amino-acids and proteins. *Transactions of the Faraday Society* 51, 582–590.
- Thomas, J.K., 1988. Photophysical and photochemical processes on clay surfaces. *Accounts of Chemical Research* 21, 275–280.
- Theng, B.K.G., 1971. Mechanisms of formation of colored clay–organic complexes. A review. *Clays and Clay Minerals* 19, 383–390.
- Theng, B.K.G., 1974. *The Chemistry of Clay–Organic Reactions*. Adam Hilger, London.
- Theng, B.K.G., 1979. *Formation and Properties of Clay–Polymer Complexes*. Elsevier, Amsterdam.
- Theng, B.K.G., 1982. Clay-polymer interactions: summary and perspectives. *Clays and Clay Minerals* 30, 1–10.
- Theng, B.K.G., Churchman, G.J., Whitton, J.S., Claridge, G.G.C., 1984. Comparison of intercalation methods for differentiating halloysite from kaolinite. *Clays and Clay Minerals* 32, 249–258.
- Theng, B.K.G., 1970. Interactions of clay minerals with organic polymers. Some practical applications. *Clays and Clay Minerals* 18, 357–362.
- Thompson, J.G., Gabbittas, N., Uwins, P.J.R., 1993. The intercalation of kaolinite by alkali halides in the solid state: a systematic study of the intercalates and their derivatives. *Clays and Clay Minerals* 41, 73–86.
- Tomioka, H., Itoh, T., 1991. Photochromism of spiropyrans in organized molecular assemblies. Formation of J- and H-aggregates of photomerocyanines in bilayer-clay matrices. *Journal of the Chemical Society, Chemical Communications*, 532–533.
- Triantafillidis, C.S., LeBaron, P.C., Pinnavaia, T.J., 2002. Thermoset epoxy-clay nanocomposites: the dual role of  $\alpha$ ,  $\omega$ -diamines as clay surface modifiers and polymer curing agents. *Journal of Solid State Chemistry* 167, 354–362.
- Triplehorn, D.M., Bohor, B.F., Betterton, W.J., 2002. Chemical disaggregation of kaolinitic claystones (tonsteins and flintclays). *Clays and Clay Minerals* 50, 766–770.
- Trobajo, C., Khainakov, S.A., Espina, A., Garcia, J.R., 2001. Synthesis of a mineral-organic hybrid by treatment of phlogopite with phenylphosphonic acid. *Chemistry of Materials* 13, 4457–4462.
- Tunney, J.J., Detellier, C., 1994. Preparation and characterization of two distinct ethylene glycol derivatives of kaolinite. *Clays and Clay Minerals* 42, 552–560.
- Tunney, J.J., Detellier, C., 1996. Chemically modified kaolinite. Grafting of methoxy groups on the interlamellar aluminol surface of kaolinite. *Journal of Materials Chemistry* 6, 1679–1685.

- Ueda, T., Harada, S., 1968. Adsorption of cationic polysulfone on bentonite. *Journal of Applied Polymer Science* 12, 2395–2401.
- Ukrainczyk, L., Chibwe, M., Pinnavaia, T.J., Boyd, S.A., 1994. ESR Study of cobalt(II) tetrakis (*N*-methyl-4-pyridiniumyl) porphyrin and cobalt(II) tetrasulfophthalocyanine intercalated in layered aluminosilicates and a layered double hydroxide. *The Journal of Physical Chemistry* 98, 2668–2676.
- Usami, H., Takagi, K., Sawaki, Y., 1990. Controlled photocycloaddition of stilbazolium ions intercalated in saponite clay layers. *Journal of Chemical Society, Perkin Transactions 2*, 1723–1728.
- Uwins, P.J.R., Mackinnon, I.D.R., Thompson, J.G., Yago, A.J.E., 1993. Kaolinite: NMF intercalates. *Clays and Clay Minerals* 41, 707–717.
- Vaia, R.A., Ishii, H., Giannelis, E.P., 1993. Synthesis and properties of two-dimensional nanostructures by direct intercalation of polymer melts in layered silicates. *Chemistry of Materials* 5, 1694–1696.
- Vaia, R.A., Jandt, K.D., Kramer, E.J., Giannelis, E.P., 1996. Microstructural evolution of melt intercalated polymer-organically modified layered silicates nanocomposites. *Chemistry of Materials* 8, 2628–2635.
- Vaia, R.A., Sauer, B.B., Oliver, K.T., Giannelis, E.P., 1997. Relaxation of confined chains in polymer nanocomposites: glass transition properties of poly(ethylene oxide) intercalated in montmorillonite. *Journal of Polymer Science, Part B. Polymer Physics* 35, 59–67.
- Vaia, R.A., Vasudevan, S., Krawiec, W., Scanlon, L.G., Giannelis, E.P., 1995. New polymer electrolyte nanocomposites: melt intercalation of poly(ethylene oxide) in mica-type silicates. *Advanced Materials* 7, 154–156.
- Vali, H., Hesse, R., Kohler, E.E., 1991. Combined freeze-etched replicas and HRTEM images as tools to study fundamental-particles and multi-phase nature of 2:1 layer silicates. *American Mineralogist* 76, 1973–1984.
- Vali, H., Köster, H.M., 1986. Expanding behaviour, structural disorder, regular and random irregular interstratification of 2:1 layer silicates studied by high-resolution images of transmission electron microscopy. *Clay Minerals* 21, 827–859.
- van Meerbeek, A., Ruiz-Hitzky, E., 1979. Mechanism of grafting of organosilanes on mineral surfaces. *Colloid and Polymer Science* 257, 178–181.
- van Olphen, H., 1966. Maya blue: a clay mineral-organic pigment? *Science* 154, 645–646.
- van Olphen, H., 1968. Modification of the clay surface by pyridine-type compounds. *Journal of Colloid and Interface Science* 28, 370–375.
- Vansant, E.F., Peeters, G., 1978. The exchange of alkylammonium ions on Na-Laponite. *Clays and Clay Minerals* 26, 279–284.
- Vempati, R.K., Mollah, M.Y.A., Reddy, G.R., Cocke, D.L., Lauer, H.V., 1996. Intercalation of kaolinite under hydrothermal conditions. *Journal of Materials Science* 31, 1255–1259.
- Viane, K., Schoonheydt, R.A., Crutzen, M., Kunyama, B., Schryver, F.C., 1988. Study of the adsorption of clay particles by means of fluorescence probes. *Langmuir* 4, 749–754.
- Vicente, M.A., Sánchez-Camazano, M., Sánchez-Martín, M.J., DelArco, M., Martín, C., Rives, V., Vicente-Hernández, J., 1989. Adsorption and desorption of *N*-methyl-8-hydroxy quinoline methyl sulfate on the smectites and the potential use of the clay-organic product as an ultraviolet radiation collector. *Clays and Clay Minerals* 37, 157–163.
- Wada, K., 1959a. Oriented penetration of ionic compounds between the silicate layers of halloysite. *American Mineralogist* 44, 153–165.

- Wada, K., 1959b. An interlayer complex of halloysite with ammonium chloride. *American Mineralogist* 44, 1237–1247.
- Wada, K., 1961. Lattice expansion of kaolin minerals by treatment with potassium acetate. *American Mineralogist* 46, 78–91.
- Wada, K., 1964. Ammonium chloride-kaolin complexes. *Clay Science (Tokyo)* 2, 43–56.
- Wada, K., 1965. Intercalation of water in kaolin minerals. *American Mineralogist* 50, 924–941.
- Walker, G.F., 1958. Reactions of expanding-lattice clay minerals with glycerol and ethylene glycol. *Clay Minerals Bulletin* 3, 302–313.
- Walter, D., Saehr, D., Wey, R., 1990. Les complexes montmorillonite-Cu(II)-benzene: une contribution. *Clay Minerals* 25, 343–354.
- Wang, Z., Pinnavaia, T.J., 1998. Nanolayer reinforcement of elastomeric polyurethane. *Chemistry of Materials* 10, 3769–3773.
- Weimer, M.W., Chen, H., Giannelis, E.P., Sogah, Y.D., 1999. Direct synthesis of dispersed nanocomposites by in situ living free radical polymerization using a silicate-anchored initiator. *Journal of the American Chemical Society* 121, 1615–1616.
- Weiss, A., 1961. Eine Schichteinschlußverbindung von Kaolinit mit Harnstoff. *Angewandte Chemie* 73, 736–737.
- Weiss, A., 1963a. Secret of Chinese porcelain manufacture. *Angewandte Chemie, International Edition in English* 2, 697–703.
- Weiss, A., 1963b. Organische Derivate der glimmerartigen Schichtsilicate. *Angewandte Chemie* 75, 113–122.
- Weiss, A., 1966. Modellversuche zur Hydrophobierung hydrophiler Grenzflächen von Schichtsilicaten. *Kolloid-Zeitschrift und Zeitschrift für Polymere* 211, 94–97.
- Weiss, A., Becker, H.O., Orth, H., Mai, G., Lechner, H., Range, K.J., 1970. Particle size effect and reaction mechanism of the intercalation into kaolinite. In: Heller, L. (Ed.), *Proceedings of the International Clay Conference, Tokyo, 1969*, vol. 2. Israel University Press, Jerusalem, pp. 180–184.
- Weiss, A., Choy, J.H., Meyer, H., Becker, H.O., 1981. Hydrogen reorientation, a primary step of intercalation reactions into kaolinite. In: *Proceedings of the International Clay Conference, Bologna, Pavia, Abstracts* p. 331.
- Weiss, A., Gossner, U., Robl, C., 1995. Transformation of clay minerals into taranakite and the crystal structure of taranakite. In: Churchman, G.J., Filzpatrick, R.W., Eggleton, R.A. (Eds.), *Clays: Controlling the Environment, Proceedings of the 10th International Clay Conference, Adelaide Australia, 1993*. CSIRO Publishing Melbourne, pp. 253–259.
- Weiss, A., Orth, H., 1973. Zur Kenntnis der Intercalationsverbindungen von Kaolinit, Nakrit, Dickit und Halloysit mit Pyridin-*N*-oxid und Picolin-*N*-oxid. *Zeitschrift für Naturforschung* 28b, 252–254.
- Weiss, A., Range, K.J., 1970. Superiority of hydrazine over potassium acetate in the formation of kaolinite intercalation complexes. In: Heller, L. (Ed.), *Proceedings of the International Clay Conference, Tokyo 1969*, vol. 2. Israel University Press, Jerusalem 1970, pp. 185–186.
- Weiss, A., Russow, J., 1963. Über das Einrollen von Kaolinitkristallen zu halloysitähnlichen Röhren und einen Unterschied zu Halloysit und röhrenförmigem Kaolinit. *Proceedings of the International Clay Conference, Stockholm*, vol. 1, pp. 69–74.
- Weiss, A., Ruthard, R., Orth, H., 1973. Neue Einlagerungsverbindungen von Kaolinit, Nakrit, Dickit, Halloysit und Titandisulfid mit Imidazol und Methylimidazol. *Zeitschrift für Naturforschung* 28b, 446–449.

- Weiss, A., Thielepape, W., Göring, G., Ritter, W., Schäfer, H., 1963a. Kaolinit-Einlagerungs-Verbindungen Rosenquist, T., Graff-Pettersen, P. (Eds). Proceedings of the International Clay Conference, Stockholm, vol. 1, pp. 287–305.
- Weiss, A., Thielepape, W., Orth, H., 1966. Neue Kaolinit-Einlagerungsverbindungen Rosenquist, T., Graff-Pettersen, P. (Eds). Proceedings of the International Clay Conference, Jerusalem, vol. 1, pp. 277–293.
- Weiss, A., Thielepape, W., Ritter, W., Schäfer, H., Göring, G., 1963b. Zur Kenntnis von Hydrazin-Kaolinit. *Zeitschrift für anorganische und allgemeine Chemie* 320, 183–204.
- Wypych, F., Schreiner, W.H., Mattoso, N., Mosca, D.H., Marangoni, R., da S. Bento, C.A., 2003. Covalent grafting of phenylphosphonate groups onto layered silica derived from in situ leached chrysotile fibers. *Journal of Materials Chemistry* 13, 304–307.
- Xie, W., Xie, R., Pan, W.P., Hunter, D., Koene, B., Tan, L.S., Vaia, R., 2002. Thermal stability of quaternary phosphonium modified montmorillonites. *Chemistry of Materials* 14, 4837–4845.
- Yamagishi, A., 1987. Optical resolution and asymmetric syntheses by use of adsorption on clay minerals. *Journal of Coordination Chemistry* 16, 131–211.
- Yamagishi, A., 1993. Chirality recognition by a clay surface modified with an optically active metal chelate. In: Kenzi Tamura (Ed.), *Dynamic Processes on Solid Surfaces*. Plenum Press, New York, pp. 307–347.
- Yamanaka, S., Kanamaru, K., Koizumi, M., 1974. Role of interlayer cations in the formation of acrylonitrile–montmorillonite complexes. *The Journal of Physical Chemistry* 78, 42–44.
- Yano, K., Usuki, A., Okada, A., 1997. Synthesis and properties of polyimide–clay hybrid films. *Journal Polymer Science, Part A–Polymer Chemistry* 35, 2289–2294.
- Yariv, S., 1992. The effect of tetrahedral substitution of Si by Al on the surface acidity of the oxygen plane of clay minerals. *International Reviews in Physical Chemistry* 11, 345–375.
- Yariv, S., 1996. Thermo-IR-spectroscopy analysis of interactions between organic pollutants and clay minerals. *Thermochimica Acta* 274, 1–35.
- Yariv, S., Cross, H. (Eds.), 2002. *Organo-Clay Complexes and Interactions*. Marcel Dekker, New York.
- Yariv, S., Heller, L., 1970. Sorption of cyclohexylamine by montmorillonites. *Israel Journal of Chemistry* 8, 935–945.
- Yariv, S., Lahav, N., Lacher, M., 1976. On the mechanism of staining montmorillonite by benzidine. *Clays and Clay Minerals* 24, 51–52.
- Yariv, S., Lapides, I., Nasser, A., Lahav, N., Brodsky, I., Michaelian, K.H., 2000. Infrared study of the intercalation of potassium halides in kaolinite. *Clays and Clay Minerals* 48, 10–18.
- Yariv, S., Nasser, A., Deutsch, Y., Michaelian, K.H., 1991. Study of the interaction between caesium bromide and kaolinite by differential thermal analysis. *Journal of Thermal Analysis* 37, 1373–1388.
- Yariv, S., Nasser, A., Michaelian, K.H., Lapides, I., Deutsch, Y., Lahav, N., 1994. Thermal treatment of the kaolinite/CsCl/H<sub>2</sub>O intercalation complex. *Thermochimica Acta* 234, 275–285.
- Yariv, S., Shoval, S., 1982. The effects of thermal treatment on associations between fatty acids and montmorillonite. *Israel Journal of Chemistry* 22, 259–265.
- Yerminahu, Z., Lapides, I., Yariv, S., 2003. Visible adsorption spectroscopy study of the adsorption of Congo red by montmorillonite. *Clay Minerals* 38, 483–500.
- Zilg, C., Thomann, R., Mülhaupt, R., Finter, J., 1999. Polyurethane nanocomposites containing laminated anisotropic nanoparticles derived from organophilic layered silicates. *Advanced Materials* 11, 49–52.

This page intentionally left blank

## *Chapter 7.4*

# **CLAY MINERALS AND THE ORIGIN OF LIFE**

## **A. BRACK**

*Centre de Biophysique Moléculaire, CNRS, F-45071 Orléans Cedex 2, France*

It is difficult to define what is meant by the word “life”. One generally considers living as an open chemical system able, *a minima*, to transfer its molecular information via self-reproduction, and also able to evolve. The concept of evolution implies that the system normally transfers its information fairly faithfully but makes a few random errors, leading potentially to a higher efficiency and to a better adaptation to environmental stresses.

Schematically, the premises of primitive life can be compared to parts of chemical assemblages. By chance, some parts self-assemble to generate assemblages capable of bringing other parts together to form identical assemblages. Sometimes, a minor error in the building generates more efficient assemblages that become the dominant species. By analogy with contemporary life, it is generally believed that the parts are made of organic matter, i.e. carbon skeletons flanked by H, O, N, S atoms.

As parts of an open system, the constituents must have been able to diffuse at a reasonable rate. A solid-state life is generally discarded, the constituents being unable to migrate and be easily exchanged. A gaseous phase would allow fast diffusion of the parts, but the limited inventory of stable volatile organic molecules would constitute a severe handicap. Ocean (liquid) water offers the best environment for the diffusion and exchange of organic molecules. However, the diffusion within the oceans must have been somewhat limited to allow the self-organization of the first living assemblages.

The key role of clay minerals in the origins of life was first suggested by J.D. Bernal (1949). For Bernal, the advantageous features of clays are (i) their ordered arrangement, (ii) their large adsorption capacity, (iii) their shielding against sunlight (ultraviolet radiation), (iv) their ability to concentrate organic chemicals, and (v) their ability to serve as polymerization templates.

### **7.4.1. CLAY MINERALS AS POSSIBLE GENETIC MATERIAL**

Most clay minerals are formed by aqueous alteration of silicate minerals (see Chapter 14). As soon as liquid water is permanently present on the surface of the

earth, clay minerals accumulate and become dispersed in the water reservoir. Since this seminal hypothesis of Bernal (1949), many prebiotic scenarios involving clays were written and many prebiotic experiments used clays.

Any scientist who observed the crystallization of minerals, initiated by the addition of seeds to a supersaturated solution, is tempted to associate life with mineral crystals. Schneider (1977), for example, has suggested that complex dislocation networks encountered in crystals could, in some cases, follow the criteria of living units and lead to a crystalline physiology. He also discussed the places of possible natural occurrence of such kinds of physiology as terrestrial and extraterrestrial rocks, interplanetary dust, white dwarfs and neutron stars.

According to Cairns-Smith (1982), there is no compelling reason necessarily to relate the last common ancestor made of organic molecules with first life. Although the easy accessibility of numerous organic building blocks of life was demonstrated experimentally, the dominant use of these molecules in living organisms can be seen as a result of evolution, rather than a prerequisite for its initiation. Cairns-Smith (1982) proposed that the first living systems, and the chemical evolution preceding them, could have been based on a chemistry different from that which we know. The structurally and functionally complex genetic system of modern life arises secondarily in a living organism using a less efficient primary system with a much higher probability of spontaneous assembly. This author advocated, as genetic candidates, crystalline inorganic materials presenting suitable properties, such as the ability to store and replicate information in the form of defaults, dislocations and substitutions. Clay minerals, such as kaolinite, are particularly attractive because they crystallize at ambient temperatures from aqueous solutions of silicate rock weathering products. The following ‘genetic take-over’ scenario was proposed by Cairns-Smith (1982) for the mineral origins of life. Certain clays, having properties that favour their synthesis, proliferate and their replication defects, likewise, become more common.

In certain lines, the development of crude photochemical machinery favours the synthesis of some non-clay species, such as polyphosphates and small organic compounds. Natural selection favours these lines of clays since the organic compounds they produce can catalyse clay formation. Multiple step pathways of high specificity, including chiral stereoselection, arise through specific adsorption, followed by the appearance of polymers of specified sequence, at first serving only structural roles. Base-paired polynucleotides replicate, giving rise to a secondary and minor genetic material. This secondary material proves to be useful in the alignment of amino acids for polymerization. Concomitant with the ability to produce sequence-specific polypeptides and proteins, comes the ability to produce specific enzymes. More efficient pathways of organic synthesis ensue, and finally the clay machinery is dispensed with in favour of a polynucleotide-based replication–translation system. Although each step of the hypothetical sequence of events is developed in detail, the scenario was not supported by experimental facts.

About the same period, Armin Weiss (1981) at the Institute of Inorganic Chemistry in Munich, published a paper that appeared, at that time, to provide

experimental support to Cairns-Smith's scenario. He selected and purified a 'matrix' montmorillonite having an excess charge of  $0.28\text{ e}^-/\text{formula ((Si,Al)}_4\text{O}_{10})$  unit. An aliquot of the matrix clay mineral is added to a breeding solution containing  $\text{Na}^+$ ,  $\text{K}^+$ ,  $\text{Mg}^{2+}$ ,  $\text{Al}^{3+}$  and  $\text{Si(OH)}_4$ . The concentration of the breeding solution is such that homogeneous nucleation in the absence of matrix layers yields montmorillonites with isomorphous substitution of  $0.42\text{ e}^-/\text{formula unit}$ . The  $\text{D}_1$ -daughter first generation montmorillonite exhibits a charge density of  $0.28\text{ e}^-/\text{formula unit}$ . This  $\text{D}_1$ -generation is then used as a matrix for the analogous synthesis of the  $\text{D}_2$ -generation. Up to the 10th generation, the spread is low, the main products being clays with a charge density of  $0.28\text{ e}^-/\text{formula unit}$ . From the 16th to the 18th generation, the number of errors increases rapidly. In the generation of  $\text{D}_{20}$ , almost no material with the original value of  $0.28\text{ e}^-/\text{formula unit}$  remains. Although a rapid decay in replication quality is observed at the 20th generation, the experiments demonstrate that clay minerals are capable of replicating. Unfortunately, this publication itself does not undergo replication. To duplicate these experiments, several requests for experimental details are addressed to the author. Since no satisfactory answers could be obtained, the clay-mediated replication cannot be considered as established.

Other mineral surfaces were tested to understand how exceedingly complicated molecules and connections, such as the protein biosynthesis via DNA and RNA required for living systems, could have evolved from the chemical systems that lack these molecules. The most promising avenue was opened by Wächtershäuser (1988, 1998). According to this author, the starting materials are simple inorganic molecules, such as  $\text{CO}_2$ ,  $\text{H}_2\text{S}$ ,  $\text{N}_2$  in contact with the sulphur on metallic surfaces of Fe, Ni, Co. The energy source required to reduce  $\text{CO}_2$  is provided by the oxidative formation of pyrite ( $\text{FeS}_2$ ) from troilite ( $\text{FeS}$ ) and hydrogen sulphide. The surface of pyrite is positively charged and capable of binding the products of carbon dioxide reduction. This gives rise to a two-dimensional reaction system, a 'surface metabolism,' which later on, includes autocatalytic cycles. Experimental laboratory work has already legitimized the first steps of this new hypothesis (Heinen and Lauwers, 1996; Huber and Wächtershäuser, 1997, 1998).

#### 7.4.2. CLAY MINERALS AND THE ORIGIN OF BIOLOGICAL ONE-HANDEDNESS

Common clay minerals, such as kaolinite and montmorillonite, have no intrinsic chirality associated with their structures and thus are not expected to develop stereoselective interactions with chiral prebiotic molecules. Nevertheless, both clay minerals were claimed to exhibit asymmetric effects. Degens et al. (1970) reported that kaolinite catalyses the stereo-selective polymerization of L-aspartic acid eight times faster than the corresponding D-enantiomer. These claims were repeated by Jackson (1971), who reports further that kaolinite preferentially adsorbs L- rather than D-phenylalanine, the edge faces of kaolinite crystals being responsible for the



stereo-selective effects. Using a variety of analytical techniques, Bonner and Flores (1973) found no differences in the adsorption of L- vs. D-phenylalanine on kaolinite. In Bonner's hands, kaolinite also fails to promote the asymmetric polymerization of aspartic acid (Flores and Bonner, 1974; Bonner and Flores, 1975). Bondy and Harrington (1979) incubated very dilute  $10^{-8}$  M solutions of D- and L-enantiomers of  $^3\text{H}$ -labelled leucine, aspartic acid and glucose with small quantities of montmorillonite and assayed the clay samples for adsorbed radioactivity. They claim that the natural L-enantiomers are bound about 10 times more effectively than the mirror images, and suggest that primordial clays may have been responsible for the pre-biotic selection of L-amino acids and D-sugars. In experiments carefully designed to eliminate artefacts, Youatt and Brown (1981) showed that there is no stereo-selective binding of L-amino acids by the clay, the results of Bondy and Harrington being attributed to the adsorption of the decomposition products of the radioactive substrates. Similarly, Friebele et al. (1981) failed to observe stereo-selective adsorption when exposing several racemic amino acids in solutions of pH 3, 7 and 10 to  $\text{Na}^+$ -montmorillonite. Siffert and Naidja (1992) observed a stereo-selectivity of montmorillonite in the adsorption and deamination of aspartic and glutamic acids. L-glutamic acid and D-aspartic acid were found to be more adsorbed than the enantiomeric or the racemic forms. As for deamination, the amounts of ammonia released from the L-enantiomers of glutamic and aspartic acids are clearly higher than those obtained from the D- or racemic forms. These results are somehow contradictory. To confirm the data, it would be helpful to repeat the experiments with synthetic clays devoid of any organic contaminants or imprints.

It was recently reported that an allophane sample from New Zealand, a clay-size mineral with short-range order composed of silica, alumina and water, shows a clear preference for L-alanyl-L-alanine over the D-enantiomer. The size, intra-molecular charge separation, and surface orientation of L-alanyl-L-alanine are suggested to confer a 'structural chirality' to the complex. The allophane sample was extracted from a weathered, 150,000 years old, volcanic ash bed. Although the clay was carefully purified before use, some original organic contamination and/or imprinting cannot be ruled out. Here again, synthetic allophane with varied Al/Si ratios and devoid of any organic contaminant or imprint needs to be prepared in order to confirm and quantify the enantiomeric preference (Hashizume et al., 2002).

By means of a self-consistent field method, Julg (1988) calculated that two identified enantiomeric forms of kaolinite exhibit different energies owing to the nuclear weak interactions. The kaolinite form, whose trihedron (vectors a, b, c) is direct, is more stable and should, consequently, be more abundant in nature. He then calculates that the adsorption energy of L-amino acids on the preferred kaolinite structure is greater than that of the D-forms by 0.14 and 0.04 kJ/mol for the amino acid positive ion and the zwitterion, respectively (Julg et al., 1989). Julg (1987) also calculated that the addition of cyanide ions to ethyliminium cations adsorbed on the preferred enantiomeric form of a kaolinite could lead to an excess of L-alanine at the expense of the D-form by 0.36 kcal/mol. Consequently, he advocates that kaolinite

could have been one of the causes of the L-homochirality of the protein amino acids. Nevertheless, quoting [Bonner \(1991\)](#): “it should be emphasized that none of Julg’s speculations and conjectures is supported by a single shred of experimental evidence”.

It must be noted that the stimulating hypotheses of [Cairns-Smith \(1982\)](#) emphasizing the role of clays in the origin of life do not account for the crucial one-handedness of biopolymers required to ensure the survival of self-replicating organic systems ([Avetisov et al., 1991](#)).

Obviously, the possibility that clays can discriminate between optical isomers of amino acids attracted a great deal of interest and hopes but at the same time generated much controversy about false positives. No doubt is attached to results obtained when clay minerals are coated with chiral adducts, such as phenanthroline tris-chelated nickel ions ([Yamagishi, 1985](#)). For non-coated clay minerals, there is always a serious risk of biological contamination or imprinting by bacteria or biofilms. Even if the purification is pushed to the extreme, biological imprinting of the clay during its geochemical formation is still possible. Repeating the experiments with artificial clay minerals appears to be the best way to legitimate the data.

#### 7.4.3. CLAYS AS PREBIOTIC CATALYSTS

By analogy with contemporary living systems, primitive life is often considered to have emerged as a cellular species, requiring boundary molecules able to isolate the system from the aqueous environment (membrane). Also needed would have been catalytic molecules to provide the basic chemical work of the cell (enzymes) and information-retaining molecules that allow the storage and the transfer of the information needed for replication (nucleic acids).

Formally, the synthesis of polymers of nucleotide and amino acids appears simple. The condensation reaction consists of eliminating water molecules between monomer units, thus linking them together. However, the formation of either proteins or nucleic acids from their monomers in water is not energetically favoured. For example, the peptide bond of proteins is thermodynamically unstable in water, so energy is required to link two amino acids together in an aqueous media; and for example, the free energy needed for two amino acids to form the dipeptide in water is about 4 kcal/mol at 37 °C and pH 7. The equilibrium constant of the reaction is only about  $10^{-3}$ , and the equilibrium concentration of the dipeptide for 1 M solution of the free amino acids is only slightly above  $10^{-3}$  M. The thermodynamic barrier is very large for the formation of a long-chain polypeptide. [Dixon and Webb \(1958\)](#) pointed out that 1 M solution in each of the 20 proteinaceous amino acids would yield at equilibrium a  $10^{-99}$  M concentration for a 12,000 Dalton protein. The volume of this solution would have to be  $10^{50}$  times the volume of the Earth to yield one molecule of protein at equilibrium. So energy input, such as heat or chemical activation, is necessary to have made nucleic acids and polypeptides on the primitive Earth.

Polymers can be prepared in the presence of water if chemical condensing agents are added or if activating groups are bound to the reacting monomers to provide the requisite free energy for bond formation. In both cases, it is important to limit the competing hydrolysis of the activating groups. Polymer formation on clays is a solution to this problem.

#### 7.4.4. CLAY-CATALYSED SYNTHESIS OF RNA

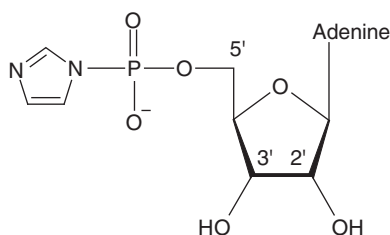
There is general consensus that RNA is the most important biopolymer in early life on Earth (the RNA world), since even modern peptide bond formation (protein biosynthesis) in the ribosome was found to be catalysed by RNA and not by protein enzymes (Ban et al., 2000). DNA is believed to have appeared after RNA and to have later derived from RNA for the following reasons:

- (i) The ribose structural unit present in RNA monomers is probably formed from formaldehyde or an oligomer of formaldehyde. The prebiotic synthesis of the deoxyribose of DNA requires the reaction of a mix of starting materials.
- (ii) The modern biosynthesis of DNA triphosphates proceeds from RNA triphosphates using an unusual enzyme that apparently evolved after RNA formed.
- (iii) RNA, in contrast to DNA, exhibits catalytic activity as well as information storage, and thus could have served both as a catalyst and storehouse of genetic information in the first life (Zaug and Cech, 1986).

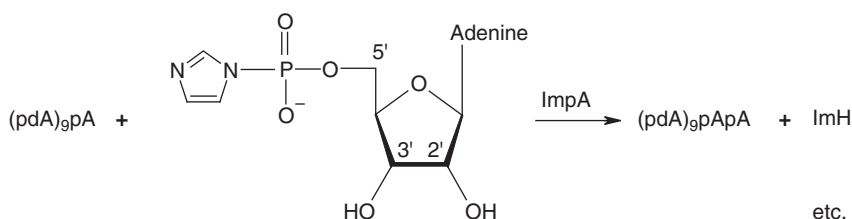
Initial attempts to form RNA by heating monomers or by using condensing agents does not yield long oligomers. Polymerization studies, which use activated monomers, were the most successful and these will be reviewed here, keeping in mind that, in most instances, potential prebiotic sources of the activated monomers remains to be discovered.

One of the successful applications of Bernal's (1949) proposal is the observation that oligomers containing 6 to 14 monomer units are formed when RNA monomers ImpA (Scheme I) activated on the phosphate with an imidazole group condense in the presence of montmorillonite (Ferris and Ertem, 1993).

The formation of oligomers was generalized to the other nucleotide bases, cytosine, guanine, inosine and uracil. Catalysis has the potential for limiting the number of isomers formed. For example, the natural 3',5'-linked phosphodiester bond is favoured in the reaction of purine nucleotides on montmorillonite. The 2', 5'-link is favoured in the absence of catalysis and in the clay-catalysed reactions of pyrimidine nucleotides. Analysis of the dimers formed in the reaction of mixtures of two or more activated nucleotides demonstrate strong sequence selectivity of the dimers formed (Ertem and Ferris, 2000). The 5'-purine-pyrimidine sequence is favoured over the 5'-pyrimidine-purine sequence at the end of the polymer chain by a factor of about 20. In addition, five 5'-sequences (A-C, A-U, G-C, A-A and GA) are formed in significantly larger amounts (73% total yield) than the eleven others in the reaction



Scheme I. RNA activated monomer ImpA with the 2', 3' and 5' positions for the phosphodiester links.



Scheme II. Elongation of a decanucleotide by reaction with ImpA.

of mixtures of the four activated monomers of the nucleotides A, C, G and U. The formation of short RNA oligomers by montmorillonite catalysis is the first step in the preparation of the RNAs needed for the initiation of the RNA world. In the second step, it was shown that it is possible to generate longer RNAs by elongation of short oligomers (Scheme II) using the “feeding” protocol (Ferris et al., 1996; Ferris, 2002).

The decanucleotide (pdA)<sub>9</sub>pA bound to Na<sup>+</sup>-montmorillonite is fed with ImpA and the reaction mixture is allowed to stand for one day at 25 °C. The suspension is then centrifuged to remove the aqueous phase from the montmorillonite. Fresh ImpA solution is added to the clay-oligomer complex and the reaction allowed to proceed for another day. Polyadenylates containing more than 20-mers are formed after feeding twice with ImpA, with the main products being 11–14-mers. Polynucleotides containing more than 50-mers are formed after 14 feedings, with the principal oligomeric products containing 20–40 monomer units. 25–30-mers are obtained with the corresponding uridine activated monomer (Ferris, 2002).

The reaction of D,L-ImpA shows partial inhibition by the monomer unit of the opposite handedness. The longest oligomer formed is an 8-mer, while the longest oligomer formed from one enantiomer is a 10-mer (Joshi et al., 2000; Urata et al., 2001). The linear dimers formed from racemic mixtures of ImpA and ImpU exhibit a 60:40 ratio of the D–D and L–L dimers to D–L and L–D dimers formed (Joshi et al., 2000).

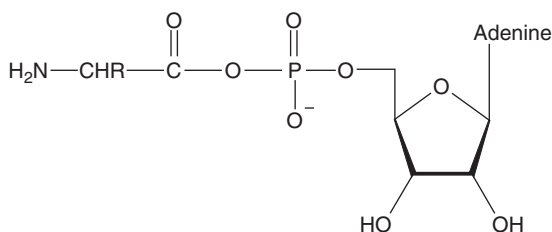
## 7.4.5. POLYPEPTIDE FORMATION ON CLAY MINERALS

Clays can also be used to condense amino acids in water using chemical activation, temperature/moisture cycles or both of them. A model for the prebiotic formation of polypeptides is based on the contemporary biosynthesis of proteins, which proceeds via the chemically activated monomer aminoacyladenylate (Scheme III).

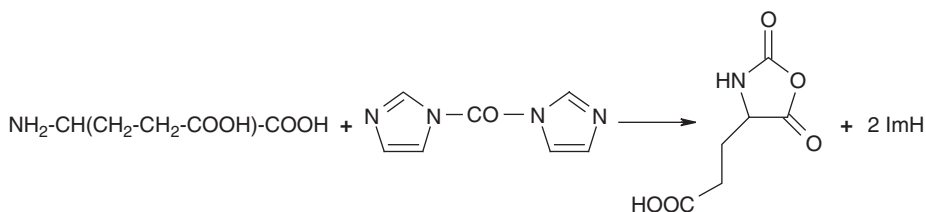
The aminoacylphosphate derivatives of 5'-AMP condense to polypeptides on montmorillonite (Paecht-Horowitz et al., 1970; Paecht-Horowitz and Eirich, 1988). The products are polypeptides as long as 56-mers in which the C-terminal group of the peptide is attached to the 2'- and/or 3'-hydroxyl group of 5'-AMP. In a homogeneous aqueous solution, mixed anhydride alanyladenylate condense partially up to heptaalanine but deactivation via hydrolysis remains the main pathway. It was initially reported that aminoacyladenylates are formed by the reaction of amino acids with ATP in the presence of a zeolite, but it is not possible to reproduce this synthesis (Warden et al., 1974).

Glutamic acid, an acidic amino acid containing an additional carboxylic acid group on the side-chain, was subjected to the feeding protocol using the condensing agent, carbonyldiimidazole (Scheme IV). The activation proceeds via the intermediary formation of an *N*-carboxyanhydride (Ehler and Orgel, 1976; Brack, 1987).

Illite was incubated with the amino acid and carbonyl diimidazole until short oligomers are formed. The solid is separated by centrifugation and fresh monomer and activating agent are added. The process is repeated as often as necessary for the



Scheme III. Aminoacyladenylate.



Scheme IV. Formation of the *N*-carboxyanhydride of glutamic acid with carbonyl diimidazole.

production of oligomers of lengths of 40-mers or more. In the absence of clay, oligomers up to the 10-mer are detected, but the majority of the products are shorter than the 5-mer. In the presence of illite, the shorter oligomers remain in the supernatant while the longer oligomers adsorb to the clay mineral. After 50 feedings, oligomers up to at least 55-mer are detected, the bulk of the adsorbed product being in the 30–50 size range (Ferris et al., 1996; Hill et al., 1998). Illite failed to produce substantial amounts of aspartic acid, the other acidic amino acid (Hill et al., 1998). The feeding protocol is not restricted to negatively charged amino acids. Oligoarginines are accumulated on the surface of illite using carbonyl diimidazole. In the absence of a mineral, the longest detectable oligomer is the 6-mer. In the presence of illite, oligomers up to the 12-mer were detected after 10 cycles (Liu and Orgel, 1998). The formation of long polypeptide chains from neutral amino acids (ones that are neither acidic nor basic) was not yet accomplished.

Fluctuating moisture and temperature cycles are used to polymerize amino acids in the presence of clays. Lahav et al. (1978) subjected mixtures of glycine and  $\text{Na}^+$ -kaolinite or  $\text{Na}^+$ -bentonite to wet-dry and temperature fluctuations (25–94 °C) and observes the formation of oligopeptides up to five glycine residues in length. Only trace amounts of diglycine form without clays. White and Erickson (1980) studied the effects of the dipeptide histidyl–histidine in the polymerization of glycine during fluctuating moisture and temperature cycles on kaolinite. A turnover of 52 is observed, i.e. each molecule of dipeptide helps the polymerization of 52 molecules of glycine. The drying/wetting cycles at 80 °C are extended to alanine in the presence of smectites (montmorillonite and hectorite) (Bujdák and Rode, 1997). Only 0.1% of alanine dimerizes on hectorite and no reaction proceeds on montmorillonite. Clay minerals more efficiently catalyse peptide chain elongation than amino acid dimerization. The reaction yields of tripeptides from diglycine and cyclic diglycine reached about 0.3% on montmorillonite and 1% on hectorite.

Different amino acids thioesters were polymerized as shown in the following equation, in the presence of montmorillonite (Bertrand et al., 2001)



Thioesters represent a moderate, prebiotically plausible, amino acid activation (Weber and Orgel, 1979; Weber, 1998) and have been shown to adsorb onto montmorillonite. They easily form in warm, acid and sulphur-rich environments. They play a key role in modern metabolisms, e.g., acetyl-coenzyme A, and could be the origin of a prebiotic energy transfer (De Duve, 1998). In the presence of clay, the formation of the cyclic dipeptide, the main product formed in the control reaction, is totally inhibited. However, no oligomer longer than the tetrapeptide could be obtained. It is likely that thioesters remain inserted in the clay mineral layers since they could not be detected in the supernatant. Leu–Set subjected to wetting-drying and temperature (25–80 °C) cycles, polymerizes up to the heptapeptide in the presence of montmorillonite.

#### 7.4.6. UNRESOLVED QUESTIONS AND CONCLUSIONS

Since Bernal's suggestion that clays could have participated in the processes leading to primordial life, mineral surfaces were endowed with exceptional virtues such as the possibility of hosting a primitive mineral life or of having generated the biological one-handedness. So far, these exceptional virtues were not legitimized by any experimental data.

On the contrary, clay minerals were shown to be excellent catalysts promoting the formation of biopolymers of the first life in an aqueous environment, as demonstrated by the remarkable experiments run by the group of Orgel at the Salk Institute in San Diego, California (Hill et al., 1998; Liu and Orgel, 1998; Joyce and Orgel, 1999) and by the group of Ferris at the Rensselaer Polytechnic Institute in Troy, New York (Ferris and Ertem, 1993; Ferris et al., 1996; Ferris, 2002). The elongation of RNA to chains longer than 40-mers could have provided the RNAs that initiated the RNA world. It was proposed that such RNAs with chain lengths greater than 40-mers would have been able to replicate by template-directed synthesis with sufficient fidelity to maintain the core information content of their sequences (Joyce and Orgel, 1999). In addition, it was postulated that a 40-mer is the minimum chain length required for RNA to catalyse the reactions of other RNA molecules (Joyce and Orgel, 1999; Szostak and Ellington, 1993). The longest chains of both polynucleotides and polypeptides are obtained by using the feeding protocol that represents a plausible model for prebiotic polymerization, simulating rocks that are in constant contact with low concentrations of activated monomers, or that are episodically washed with higher concentrations.

#### REFERENCES

- Avetisov, V.A., Goldanskii, V.I., Kuz'min, V.V., 1991. Handedness, origin of life and evolution. *Physics Today* 44, 33–42.
- Ban, N., Nissen, P., Hansen, J., Moore, P.B., Steitz, T.A., 2000. The complete atomic structure of the large ribosomal subunit at 2.4 Å resolution. *Science* 289, 905–920.
- Bernal, J.D., 1949. The physical basis of life. *The Proceedings of the Physical Society Section A* 62, 537–558.
- Bertrand, M., Bure, C., Fleury, F., Brack, A., 2001. Prebiotic polymerisation of amino acid thioesters on mineral surfaces. In: Nakashima, S., Maruyama, S., Brack, A., Windley, B.F. (Eds.), *Geochemistry and the Origin of Life*. Universal Academy Press, Tokyo, pp. 51–60.
- Bondy, S.C., Harrington, M.E., 1979. L-amino acids and D-glucose bind stereospecifically to a colloidal clay. *Science* 203, 1243–1244.
- Bonner, W.A., 1991. The origin and amplification of biomolecular chirality. *Origins of Life and Evolution of the Biosphere* 21, 59–111.
- Bonner, W.A., Flores, J.J., 1973. On the asymmetric adsorption of phenylalanine enantiomers by kaolin. *Currents in Modern Biology* 5, 103–113.

- Bonner, W.A., Flores, J.J., 1975. Experiments on the origins of optical activity. *Origins of Life* 6, 187–194.
- Brack, A., 1987. Selective emergence and survival of early polypeptides in water. *Origins of Life* 17, 367–379.
- Bujdák, J., Rode, B.M., 1997. Silica, alumina and clay-catalyzed alanine peptide bond formation. *Journal of Molecular Evolution* 45, 457–466.
- Cairns-Smith, A.G., 1982. *Genetic Takeover*. Cambridge University Press, Cambridge.
- De Duve, C., 1998. Possible starts for primitive life. Clues from present-day biology: the thioester world. In: Brack, A. (Ed.), *The Molecular Origins of Life: Assembling Pieces of the Puzzle*. Cambridge University Press, Cambridge, pp. 219–236.
- Degens, E.T., Matheja, J., Jackson, T., 1970. Template catalysis: asymmetric polymerization of amino-acids on clay minerals. *Nature* 227, 492–493.
- Dixon, M.A., Webb, E.C., 1958. *Enzymes*. Academic Press, New York.
- Ehler, K.W., Orgel, E.L., 1976. N,N'-carbonyldiimidazole-induced peptide formation in aqueous solution. *Biochimica et Biophysica Acta* 434, 233–243.
- Ertem, G., Ferris, J.P., 2000. Sequence- and regio-selectivity in the montmorillonite-catalyzed synthesis of RNA. *Origins of Life and Evolution of the Biosphere* 30, 411–422.
- Ferris, J.P., 2002. Montmorillonite catalysis of 30-50 mer oligonucleotides: laboratory demonstration of potential steps in the origin of the RNA world. *Origins of Life and Evolution of the Biosphere* 32, 311–322.
- Ferris, J.P., Ertem, G., 1993. Montmorillonite catalysis of RNA oligomer formation in aqueous solution. A model for the prebiotic formation of RNA. *Journal of the American Chemical Society* 115, 12270–12275.
- Ferris, J.P., Hill, A.R. Jr., Liu, R., Orgel, L.E., 1996. Synthesis of long prebiotic oligomers on mineral surfaces. *Nature* 381, 59–61.
- Flores, J.J., Bonner, W.A., 1974. On the asymmetric polymerization of aspartic acid enantiomers by kaolin. *Journal of Molecular Evolution* 3, 49–56.
- Friebele, E., Shimoyama, A., Hare, P.E., Ponnampereuma, C., 1981. Adsorption of amino acid enantiomers by Na-montmorillonite. *Origins of Life* 11, 173–184.
- Hashizume, H., Theng, B.K.G., Yamagishi, A., 2002. Adsorption and discrimination of alanine and alanyl-alanine enantiomers by allophane. *Clay Minerals* 37, 551–557.
- Heinen, W., Lauwers, A.M., 1996. Sulfur compounds resulting from the interaction of iron sulfide, hydrogen sulfide and carbon dioxide in an anaerobic aqueous environment. *Origins of Life and Evolution of the Biosphere* 26, 131–150.
- Hill, A.R. Jr., Böhrer, C., Orgel, L.E., 1998. Polymerization on the rocks: negatively charged  $\alpha$ -amino acids. *Origins of Life and Evolution of the Biosphere* 28, 235–243.
- Huber, C., Wächtershäuser, G., 1997. Activated acetic acid by carbon fixation on (Fe, Ni)S under primordial conditions. *Science* 276, 245–247.
- Huber, C., Wächtershäuser, G., 1998. Peptides by activation of amino acids with CO on (Ni, Fe)S surfaces: implications for the origin of life. *Science* 281, 670–672.
- Jackson, T.A., 1971. Evidence for selective adsorption and polymerization of the L-optical isomers on the edge faces of kaolinite. *Experientia* 27, 242–243.
- Joshi, P.C., Pitsch, S., Ferris, J.P., 2000. Homochiral selection in the montmorillonite-catalyzed and uncatalyzed prebiotic synthesis of RNA. *Chemical Communications Part* 24, 2497–2498.



- Joyce, G.F., Orgel, L.E., 1999. Prospects for understanding the origin of the RNA world. In: Gesteland, R.F., Cech, T.R., Atkins, J.F. (Eds.), *The RNA World*, 2nd edition. Cold Spring Harbor Laboratory Press, New York, pp. 49–79.
- Julg, A., 1987. Synthèse asymétrique sur la kaolinite de l' $\alpha$ -aminopropionitrile, précurseur de l'alanine et homochiralité des acides aminés des protéines. *Comptes Rendus de l'Académie des Sciences, Série II* 305, 563–565.
- Julg, A., 1988. Stabilité relative des deux formes inverses de la kaolinite. Application à l'homochiralité L des acides aminés des protéines. *Comptes Rendus de l'Académie des Sciences, Série II* 306, 1153–1156.
- Julg, A., Favier, A., Ozias, Y., 1989. A theoretical study of the difference in the behavior of L- and D-alanine toward the two forms of kaolinite. *Structural Chemistry* 1, 137–141.
- Lahav, N., White, D.H., Chang, S., 1978. Peptide formation in the prebiotic era: thermal condensation of glycine in fluctuating clay environment. *Science* 201, 67–69.
- Liu, R., Orgel, L.E., 1998. Polymerization on the rocks:  $\beta$ -amino acids and arginine. *Origins of Life and Evolution of the Biosphere* 28, 245–257.
- Paecht-Horowitz, M., Berger, J., Katchalsky, A., 1970. Prebiotic synthesis of polypeptides by heterogeneous polycondensation of amino-acid adenylates. *Nature* 228, 636–639.
- Paecht-Horowitz, M., Eirich, F.R., 1988. The polymerization of amino acid adenylates on sodium-montmorillonite with preadsorbed peptides. *Origins of Life and Evolution of the Biosphere* 18, 359–387.
- Schneider, J., 1977. A model for a non-chemical form of life: crystalline physiology. *Origins of Life* 8, 33–38.
- Siffert, B., Naidja, A., 1992. Stereoselectivity of montmorillonite in the adsorption and deamination of some amino acids. *Clay Minerals* 27, 109–118.
- Szostak, J.W., Ellington, A.D., 1993. In vitro selection of functional RNA sequences. In: Gesteland, R.F., Atkins, J.F. (Eds.), *The RNA World*, 1st edition. Cold Spring Harbor Laboratory Press, New York, pp. 511–534.
- Urata, H., Aono, C., Ohmoto, N., Shimamoto, Y., Kobayashi, Y., Akaga, M., 2001. Efficient and homochiral selective oligomerization of racemic ribonucleotides on mineral surface. *Chemistry Letters* 30, 324–325.
- Wächtershäuser, G., 1988. Before enzymes and templates: theory of surface metabolism. *Microbiological Reviews* 52, 452–484.
- Wächtershäuser, G., 1998. Origin of life in an iron-sulfur world. In: Brack, A. (Ed.), *The Molecular Origins of Life: Assembling Pieces of the Puzzle*. Cambridge University Press, Cambridge, pp. 206–218.
- Warden, J.T., McCullough, J.J., Lemmon, R.M., Calvin, M., 1974. A re-examination of the zeolite-promoted, clay-mediated peptide synthesis. *Journal of Molecular Evolution* 4, 189–194.
- Weber, A.L., 1998. Prebiotic amino acid thioester synthesis: thiol-dependent amino acid synthesis from formose substrates (formaldehyde and glycolaldehyde) and ammonia. *Origins of Life and Evolution of the Biosphere* 28, 259–270.
- Weber, A.L., Orgel, L.E., 1979. The formation of peptides from glycine thioesters. *Journal of Molecular Evolution* 13, 193–202.
- Weiss, A., 1981. Replication and evolution in inorganic systems. *Angewandte Chemie, International Edition in English* 20, 850–860.

- White, D.H., Erickson, J.D., 1980. Catalysis of peptide bond formation by histidyl-histidine in a fluctuating clay environment. *Journal of Molecular Evolution* 16, 279–290.
- Yamagishi, A., 1985. Chromatographic resolution of enantiomers having aromatic groups by an optically active clay-chelate adduct. *Journal of the American Chemical Society* 107, 732–734.
- Youatt, J.B., Brown, R.D., 1981. Origins of chirality in Nature: a reassessment of the postulated role of bentonite. *Science* 212, 1145–1146.
- Zaug, A.J., Cech, T.R., 1986. The intervening sequence RNA of *Tetrahymena* is an enzyme. *Science* 231, 470–475.

This page intentionally left blank

## *Chapter 7.5*

# **PILLARED CLAYS AND CLAY MINERALS**

**F. BERGAYA, A. AOUAD AND T. MANDALIA**

*CRMD, CNRS-Université d'Orléans, F-45071 Orléans Cedex 2, France*

## **7.5.1. PILLARING CONCEPT**

The term 'pillaring' is often associated with the formation and preparation of catalytically active microporous materials. Thus, many reviews devoted to 'pillared interlayered clays' (PILC<sup>1</sup>) are published in catalysis journals (Pinnavaia, 1984; Burch, 1988; Figueras, 1988; Fripiat, 1997; Gil et al., 2000a) although some recent summaries appeared in journals on porous materials (Kloprogge, 1998; Gil et al., 2000b; Ding et al., 2001), and as chapters or subchapters in books on clay minerals (Bergaya, 1990; Konta, 2001). Most of these publications deal with the history, synthesis, properties, and applications of the PILC.

The pillaring concept was extended to other layered materials (Vaughan, 1988a; Mitchell, 1990), such as manganese oxide (Wong and Cheng, 1993) and LDH (see Chapter 13.1). This chapter is an attempt to summarize the vast volume of literature on (cationic) clay minerals that has accumulated over the past 30 years.

## **7.5.2. PILLARED CLAY MINERALS AND CATALYSIS**

That clays can function as catalysts was known for a very long time (Robertson, 1986). For example, Gurvich (1915) used attapulgite (palygorskite) and montmorillonites to polymerize pinene. The most widely known application of clay catalysis is the French Houdry cracking process developed in the 1930s (Houdry et al., 1938). By the 1960s, clays were replaced by synthetic zeolites (Breck, 1980) because the latter show better activity and selectivity for cracking. However, PILC (which may be considered as two-dimensional zeolite-like materials) began to compete with zeolites in the 1970s. Intensive research into the synthesis of suitable cracking catalysts for heavy petroleum was stimulated by the 'oil shock' of 1973. This is because

---

<sup>1</sup>The term 'PILC' is not strictly correct. Since it is the clay mineral that is pillared, the term 'PILCM' (for pillared interlayered clay mineral) should be used. However, by analogy with using 'clay' for 'clay mineral' (see Chapter 1), PILC will continue to be used on the basis of past usage.

zeolites catalysts have a limited micropore size, and are rapidly poisoned by metals in the heavy oil fractions.

Since the first announcement of the commercial availability of PILC (Vaughan et al., 1979), their use in petroleum cracking alone exceeded that of other catalysts (Adams, 1987). PILC also found applications in environmental protection and as molecular sieves, selective adsorbents (Karamanis et al., 1997), thermal insulators, and electrochemical and optical devices (Mitchell, 1990).

Research into the synthesis of PILC builds on the pioneering work by Barrer and McLeod (1955) who obtained microporous materials by replacing the interlayer exchangeable cations in smectites with tetraalkylammonium ions (Barrer, 1986). The synthesis of the first organic pillared clay minerals with an interlayer distance of 0.5–0.6 nm and a permanent porosity was independently reported by Mortland and Berkheiser (1976) and Shabtai et al. (1976). However, organic pillared clay minerals of this type are thermally unstable at high temperatures ( $> 250^{\circ}\text{C}$ ) when interlayer collapse occurs as in pristine (unmodified) clay minerals. However, below the decomposition temperature organic pillared clays can usefully serve as molecular sieves, selective adsorbents, and catalysts.

Clay minerals intercalated with inorganic species retain their micro- (and meso-) porosity after heating at  $\geq 300^{\circ}\text{C}$ . Although polymeric (hydr)oxymetal cations were used as pillaring agents for clay minerals since the late 1960s (Sawhney, 1968), the paper by Brindley and Sempels (1977) is regarded as the first account on the preparation of an inorganic pillared clay mineral. The procedure consists of exchanging the  $\text{Na}^{+}$  ions in the pristine smectite with oligomeric (hydr)oxy aluminum cations which are then converted by heat treatment into Al-oxides. By propping the smectite layers permanently apart, these Al-oxide species act as ‘pillars’ in the interlayer space.

Here we give the recent IUPAC<sup>2</sup> definition, followed by a brief summary of the fundamental principles of pillaring. These include a description of the different clay minerals used, the pillaring species, the properties of the PILC products, and possible modes of bonding between pillar and clay mineral surface. The numerous applications of PILC are not described here. For their industrial and environmental applications, see Chapters 10.2, 11.1 and 11.2.

### 7.5.3. IUPAC DEFINITION OF PILLARING AND PILLARED CLAY MINERALS

Bergaya (1990) suggested that three criteria must be met for successful pillaring: (i) a preliminary step of quasi-reversible intercalation of various species (charged and/or uncharged, organic or inorganic) causing up to a 5-fold increase in basal ( $d_{001}$ ) spacing of the clay mineral by XRD; (ii) after heating at high temperatures,

---

<sup>2</sup>IUPAC: International Union of Pure Applied Chemistry.

this spacing may decrease slightly but must not collapse, and its final value must be maintained; and (iii) the last and fundamental criterion is that the product must have an accessible porosity, that is, the intercalated species must not fill the entire interlayer space as in chlorite. However, subsequent research into the pillaring of different layered materials, and for different applications, led Bergaya (1994) to modify the above conditions slightly. The three new criteria for pillaring are: (i) intercalation, generally by exchanging the interlayer inorganic cations with cationic pillars, increasing the  $d_{001}$  spacing by at least 0.7 nm (yielding a structure with properties resembling those of zeolites in their applications); (ii) a free height (which is not always correctly evaluated by porosity measurements (Bergaya et al., 1993a; Bergaya, 1995); and (iii) the basal spacing and free height do not change when the material is heated to at least 200 °C and in some cases up to 700–800 °C, under anhydrous or hydrothermal atmosphere, or when the pH is varied (placed in acidic or basic solutions). The latest technical report of the IUPAC (Schoonheydt et al., 1999) gives a similar definition of pillared clays (enlarged to pillared layered solids): “... pillaring is a process by which a layered compound is transformed in a thermally stable micro- and/or mesoporous material with retention of the layer structure”. The report adds that “a pillaring agent is any compound which maintains the spacing between adjacent layers upon removal of the solvent and which induces an experimentally observable pore structure between the layers called ‘interlayer region’ accessible to molecules at least as large as  $N_2$ ”. Thus, a ‘pillared material’ must fulfill at least three criteria: (i) chemical and thermal stability (without further specifying the chemical or temperature conditions); (ii) a certain layer ordering that enables at least a  $d_{001}$  spacing to be determined (although a rational series of basal reflections is not necessary); and (iii) accessibility of the interlayer space to molecules at least as large as  $N_2$  (thus,  $N_2$  adsorption–desorption isotherms must be determined, and analyzed via  $t$ - and  $\alpha$ -plots; however, no order in the pillars and consequently in the pores is required).

We should also add that different abbreviations were used to denote pillared materials, in particular pillared clay minerals. The most widely used are PILC (for ‘pillared interLayered clays’) and PLS (for the more general ‘pillared layered structures’). CLS (for ‘cross-linked smectites’) was also used (Lahav et al., 1978; Pinnavaia et al., 1985; Sterte and Shabtai, 1987) when the authors propose some chemical bonding between the pillars and the clay mineral layers. Other abbreviations that occur in the literature are ‘ELS’ (for expanded layered structures) and ‘MELS’ (for molecularly engineered layered structures). The technical report of the IUPAC (Schoonheydt et al., 1999) accepted (with some restrictions) ELS as denoting pillared compounds, and MELS for pillared derivatives. The IUPAC report also recommends the term pillared ‘LDH’ (for layered double hydroxides) rather than pillared ‘anionic clays’ (see Chapter 13.1).

The number of layered materials, including clay minerals and LDH (Vaccari, 1998), that can be pillared, is very large. This chapter is limited to the phyllosilicates. The main factors influencing the intercalating/pillaring process are directly related to

the nature of the clay mineral host, the pillar guest (intercalated species), and experimental conditions.

#### 7.5.4. HOST CLAY MINERALS

The nature of the clay mineral host (or parent material) is very important since this determines layer composition and charge as well as the site of isomorphous substitution (in the octahedral and/or tetrahedral sheet). The dimension and shape of the clay mineral layers and the different arrangements of particles and aggregates are also influential. These arrangements are related to the initial concentration of the aqueous clay dispersion. Single layers and particles can occur in very dilute dispersions, while aggregates are formed in concentrated suspensions. Natural swelling clay minerals (montmorillonite, hectorite, beidellite, saponite) and synthetic smectites (saponite and Laponite) were mostly used as hosts because the first step in pillaring is the intercalation of the pillaring agent by cation exchange. Vermiculite (Suquet et al., 1991), phlogopite (del Rey-Perez-Caballero and Poncelet, 2000), talc (Urabe et al., 1991), F-tetrasilic mica (Sakurai et al., 1990), rectorite, which is a regularly interstratified pyrophyllite-beidellite (Brody and Johnson, 1990; Occelli, 1991; Guan and Pinnavaia, 1994) and any other interstratified clay mineral-smectite (Jie et al., 1986; Sterte, 1990) also featured as mineral hosts.

Another important factor is the nature of the exchangeable cation, initially present.  $\text{Na}^+$ -exchanged smectites were used in the majority of cases because they are dispersible in water, facilitating intercalation of the pillaring agents by cation exchange. In some instances, the clay minerals are purified, or organically modified, prior to intercalating the pillars.

Since impurities associated with naturally occurring clays may give rise to inhomogeneous particle distribution, and prior purification of such clays is laborious and time consuming, synthetic clay minerals of high purity were used as hosts (Kloprogge, 1998). Then direct synthesis of pillared clay minerals from synthetic layer silicates is an alternative approach to obtaining PILC.

#### 7.5.5. PILLARING SPECIES

Bergaya (1990) set out the different metal ions that were studied as pillaring agents in the form of a 'Periodic Table of elements'. An updated version of this is shown in Table 7.5.1. The vacant squares in this table denote the number of elements that have yet to be investigated. Although the hydrolysis behaviour of metal cations (Baes and Mesmer, 1976) is generally understood, that of aluminium is more fully known. For this reason, Al-pillared clay minerals were the first to be prepared, and extensively documented.

Table 7.5.1. The different elements that were used as pillars (underlined elements) or co-pillars (and/or by post-exchange or by impregnation of the PILC) shown as the Periodic Table

Be											B		
Mg											Al	Si	P
	Ti	V	Cr	Mn	Fe	Co	Ni	Cu	Zn		Ga	Ge	
	Y	Zr	Nb	Mo	Ru	Rh	Pd <sub>(i)</sub>					Sn	
	La		Ta		Os		Pt <sub>(i)</sub>						Bi
			Ce	Pr	Nd								
					U								

Notes: Al is surrounded by a bold square, because it is the first and most studied element. Some elements are only used for impregnation of PILC denoted by subscript (i).

A.  $(Al_{13})^{7+}$ -Pillaring Agent

Hydrolysis Products

The composition of the Al-pillaring solutions strongly depends on the preparation conditions. The degree of hydrolysis or basicity ( $OH_{base}/Al_{salt}$  ratio) is an important factor controlling solution pH, and hence the nature of the Al species. The controlled hydrolysis of Al salts gives rise to a number of species, such as  $[Al(H_2O)_6]^{3+}$  monomers and different polymers. Even so, the  $[Al^{IV}Al^{VI}_{12}O_4(OH)_{24}(H_2O)_{12}]^{7+}$  cation denoted as ‘Al<sub>13</sub>’ (Fig. 7.5.1) is assumed to be the pillaring species. Its pseudospherical structure was deduced from X-ray crystallography using a well-crystallized Al<sub>13</sub> sulphate (Johansson, 1960, 1962). The geometrical ( $M^{IV}M^{VI}_{12}O_{40}$ ) structure was already deduced from XRD patterns by Keggin (1934) whose name is attached to this structure. However, the first ‘Keggin’ structure was ammonium 12-molybdophosphate, an anionic metal–oxygen cluster synthesized by Berzelius in 1826 (Ohler and Bell, 2002).

<sup>27</sup>Al-NMR spectroscopy was helpful in determining the Al environment in Al Keggin ions both in solution and in the solid state (Akitt et al., 1972; Akitt and Farthing, 1978; Pinnavaia et al., 1984). The structure of Al<sub>13</sub> was also analyzed by other methods, including SAXS, Raman spectroscopy, and light scattering. SEM photographs of Al<sub>13</sub> crystals show a tetrahedral symmetrical structure of the tridecamers (Furrer et al., 1992). Using <sup>27</sup>Al-NMR spectroscopy, Parker and Kiricsi (1995) reported a facile, reproducible method, and the optimal experimental conditions, for the preparation of thermally stable Al Keggin cations. The decomposition kinetics of Al<sub>13</sub> indicates the formation of ‘defective’ Al<sub>13</sub> dimers (Al<sub>24</sub>O<sub>72</sub>), which become the main active pillaring intercalant after lengthy thermal ageing. Under some particular conditions (NH<sub>3</sub>), Al Keggin cations can be stabilized by self-polymerization leading to the formation of Al<sub>26</sub> (Vaughan, 1988b).



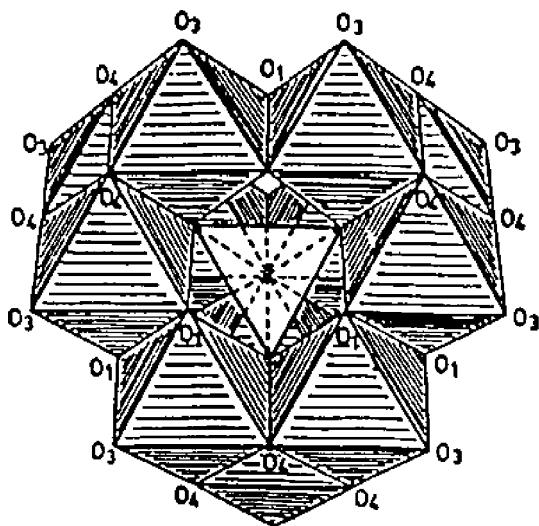


Fig. 7.5.1. The structure of Al<sub>13</sub> (Keggin cation).

#### *Procedures for Obtaining Al<sub>13</sub>*

Al<sub>13</sub> precursors can be obtained by three main methods. The widely used method is hydrolysis of aqueous Al salt solutions (often 1 M) with a base (NaOH solution or solid Na<sub>2</sub>CO<sub>3</sub>). Al<sub>13</sub> is the dominant species in AlCl<sub>3</sub> solutions of 10<sup>-1</sup>–10<sup>-3</sup> M and an Al/OH ratio of 2–2.2 (Bottero et al., 1980, 1982). Al salts with anions other than chloride (Akitt and Farthing, 1981a), and M<sub>2</sub>CO<sub>3</sub> as base where M is not Na<sup>+</sup>, was also used (Akitt and Farthing, 1978). The second method involves dissolution of Al metal (Akitt and Farthing, 1981b) in HCl or in aqueous AlCl<sub>3</sub> solution, which is acidic because of the dissociation of water molecules induced by the high-polarizing power of the small Al<sup>3+</sup> cation. The second method has the advantage of excluding interfering ions, and is preferred for the industrial preparation of commercial Al chlorohydrates<sup>3</sup> (Jones, 1988). The third method involves electrolysis of AlCl<sub>3</sub> solution, yielding pure Al<sub>13</sub> with an OH/Al ratio of 2.4 (Akitt and Farthing, 1981c).

#### *Factors Influencing Al<sub>13</sub> Formation*

Although the method of preparation is clearly of prime importance, many other factors influence the formation of pure Al<sub>13</sub> in solution, such as the nature and initial concentration of the reagents used, the degree of hydrolysis (OH/Al ratio), the rate of adding the reactants, the temperature, and the time and temperature of ageing the hydrolyzed solutions.

<sup>3</sup>Chlorhydrol (abbreviated as ACH) from Chemical Reheis Company. Locron L from Hoechst.

### B. Other Pillaring Agents

The solution chemistry of other elements (M), like Zr, Cr, and Fe that are potentially capable of acting as pillaring agents was reviewed in a special volume of *Catalysis Today*, edited by Burch (1988). References related to other elements such as Be, Mg, Ti, Nb, Ta, Mo, Ni, Cu, B, Si, and Bi pillaring species were mentioned in the review by Bergaya (1990).

During the last 15 years, a large volume of literature appeared on the above elements as well as new ones like Ga, Sn, and V. Since Al and Ga have very similar chemical properties, the  $\text{Ga}_{13}$  ion appears to be isostructural with  $\text{Al}_{13}$  (Bellaloui et al., 1990; Bradley et al., 1990a, 1990b; Bradley and Kydd, 1991; Tang et al., 1993). Sn was used as metal complex precursor (Palinko et al., 1993; Bodman et al., 2002). When a vanadium precursor in the form of  $\text{VOCl}_3$  is refluxed with a  $\text{H}^+$ -montmorillonite in benzene, the corresponding pillared clay mineral is obtained (Choudary et al., 1990).

The theses by Molinard (1994) and Montargès (1997) also contain a bibliography about Al and the above-mentioned elements.

There are also numerous patents from many countries, some of which are mentioned by Burch (1988) and Konta (2001). Since the patent literature is not easily accessible, this is not referred to in this chapter.

### C. Mixed Al–M and M–M' Pillaring Agents

The intercalation/pillaring of clay minerals with solutions containing two different cations was investigated since the 1980s. One of the pillaring cation is usually Al. The second inorganic cation is then added in various molar fractions to improve the thermal, adsorptive, and catalytic properties of the pillared products (Gil et al., 2000a; Konta, 2001).

Incorporation of Zr, Ga, transition metal elements like Cr, Fe, Cu, Mo, Ru, and lanthanides into Al-pillaring solutions was reported. Such mixed pillaring agents were widely used over the past two decades as the following references indicate:

- mixed Al–Zr: Ocelli (1986), Ocelli and Finseth (1986), Moreno et al. (1999);
- mixed Al–Ga: Vieira Coelho and Poncelet (1990, 1991), Bradley et al. (1990a, 1990b, 1990c, 1992), Gonzalez et al. (1991, 1992), Bradley and Kydd (1991, 1993), Tang et al. (1993, 1995), Bagshaw and Cooney (1995), Pesquera et al. (1995), Hernando et al. (1996a,b), Benito et al. (1999);
- mixed Al–Ge: Lee et al. (2001);
- mixed Al–Cr: Carrado et al. (1986a, 1986b), Skoularikis et al. (1988), Zhao et al. (1995), Storaro et al. (1997), Toranzo et al. (1997);
- mixed Al–Fe: Barrault et al. (1988, 1992), Lee et al. (1989), Bergaya and Barrault (1990), Rightor et al. (1991), Bergaya et al. (1991, 1993b), Zhao et al. (1993a), Bakas et al. (1994), Lenarda et al. (1994), Storaro et al. (1995, 1996), Ladavos et al. (1996), Mandalia et al. (1998);

- mixed Al–Cu: Frini et al. (1997), Barrault et al. (1998);
- mixed Al–Mo: Gil and Montes (1997);
- mixed Al–Ru: Lenarda et al. (1994), Storaro et al. (1995);
- mixed Al–La: Sterte (1991), Trillo et al. (1991, 1993a, 1993b), Zhao et al. (1993b);
- mixed Al–Ce, Pires et al. (1998).

Sterte (1991) prepared mixed solutions of Al not only with La and with Ce, but also with Pr and Nd. In contrast to La and Ce, the two last lanthanides fail to give a pillared product. Moreover, Dominguez et al. (1998) compared the experimental results with theoretical calculations using mixed solutions of Al–Ga, Al–La, and Al–Ce.

The rapid growth in the use of mixed pillared solutions is due to demand for improvement in specific properties. In particular, the heat stability of AlMPILC is greater than that of the classical Al pillared clay minerals.

Sometimes, elements as Pt and Pd act not as co-pillars, but are specifically used for impregnation of the PILC (Table 7.5.1). Moreover, a great number of MPILC is often used as support to other combination of elements (see, for example, Fe and Cr supported on TiPILC (Cheng et al., 1996).

The use of Al-free, mixed Fe–Cr (Akçay, 2004), Fe–Zr (Heylen and Vansant, 1997), and Cr–Zr (Toranzo et al., 1998) pillaring solutions was also reported. Again, the aim here is to produce pillared clay minerals with improved properties for specific applications.

#### *D. Pillaring Agents with More Than Two Cations*

The use of mixed pillaring solutions containing more than two metal cations was also reported:

- for Al–La–Ce by Gonzalez et al. (1992), Mendioroz et al. (1993), Booij et al. (1996a,b);
- for Cr–Fe–Zr by Jamis et al. (1995a, 1995b).

#### *E. New Pillaring Agents*

The literature also mentions the use of metal complexes as pillaring agents. Many of these involve the chlorides of transition metals like niobium, tantalum, and molybdenum (Christiano et al., 1985; Christiano and Pinnavaia, 1986), and tin (Palinko et al., 1993).

Pillared clay minerals obtained from inorgano-organo pillaring agents were also been described. Coordination compounds, organometallic complexes, surfactants, and/or polymers are the source of the organic carbon in the pillaring agents (Gil et al., 2000a).

The early papers by Loeppert et al. (1979) and Pinnavaia (1983) on the preparation of clay minerals pillared with organometallic complexes indicate that the

thermal stability is not high, because the C–C bonds decompose at about 400 °C. The PILC can swell in water and the intercalated complexes remain exchangeable.

However, organometallic precursors based on Si complexes (Endo et al., 1980, 1981) are converted into silica pillars when heated at 500 °C. Tetraethoxysilane (TEOS) is often used in Al–Si pillaring agents (Wada and Wada, 1980; Sterte and Shabtai, 1987; Figueras, 1988; Zhao et al., 1992; Fetter et al., 1995; Gil et al., 1995).

Other organometallic precursors based on iron complexes (Yamanaka et al., 1984; Doff et al., 1988; Martin-Luengo et al., 1989; Maes and Vansant, 1995) are converted into iron oxide pillars when heated at 350 °C. Heating clay minerals intercalated with organo-inorgano binuclear oxobridged Fe complexes (Dick and Weiss, 1998) gives rise to zeolite-like channels in the products that show interesting properties depending on the ligands used.

Direct intercalation of metal oxide sols (DIMOS) precursors in the presence of silica and/or alumina or other aqueous oxide sols leads to basal spacings of more than twice the thickness of the host clay mineral layer (see references in Pinnavaia, 1992; Cool and Vansant, 1998).

Some cases are more complex. For example, intercalated mixed organometal complexes are converted into oxide sol particles on calcination (Yamanaka and Takahama, 1993). This leads to pillars formed by clusters of SiO<sub>2</sub> particles covered by TiO<sub>2</sub> on their surface. However, by intercalating the sols of the two oxides simultaneously with an organic structure-directing agent, and burning the latter off, mixed SiO<sub>2</sub> and TiO<sub>2</sub> pillars are obtained.

The intercalation of imogolite (a tubular alumino-silicate) into montmorillonite (a layered alumino-silicate) gives rise to a tubular silicate-layered silicate (TSLS) nanocomposite (Pinnavaia and Johnson, 1986).

Co-intercalation of Al (and/or La) pillaring species and a cationic surfactant as precursors (Srinivasan and Fogler, 1990a, 1990b) produces a cheap organo-inorgano clay mineral with better adsorptive properties than classical activated carbon. Co-intercalation of Al<sub>13</sub> cations and a non-ionic surfactant (Michot and Pinnavaia, 1991; Michot et al., 1992, 1993) gives a pillared clay with enhanced capacity for adsorbing toxic pollutants.

The pillaring of acid-activated clays was investigated since the early 1990s (Mokaya et al., 1991; Mokaya, 1992) coinciding with research into pillaring processes with mixed agents.

## 7.5.6. PILLARING METHODS

### *A. Pillaring in Dilute Dispersions*

The classical pillaring method involves two successive steps. The first is the intercalation of the pillaring agent. This is done by adding a dilute solution of the precursor slowly to an already prepared dilute clay mineral dispersion (Fig. 7.5.2).

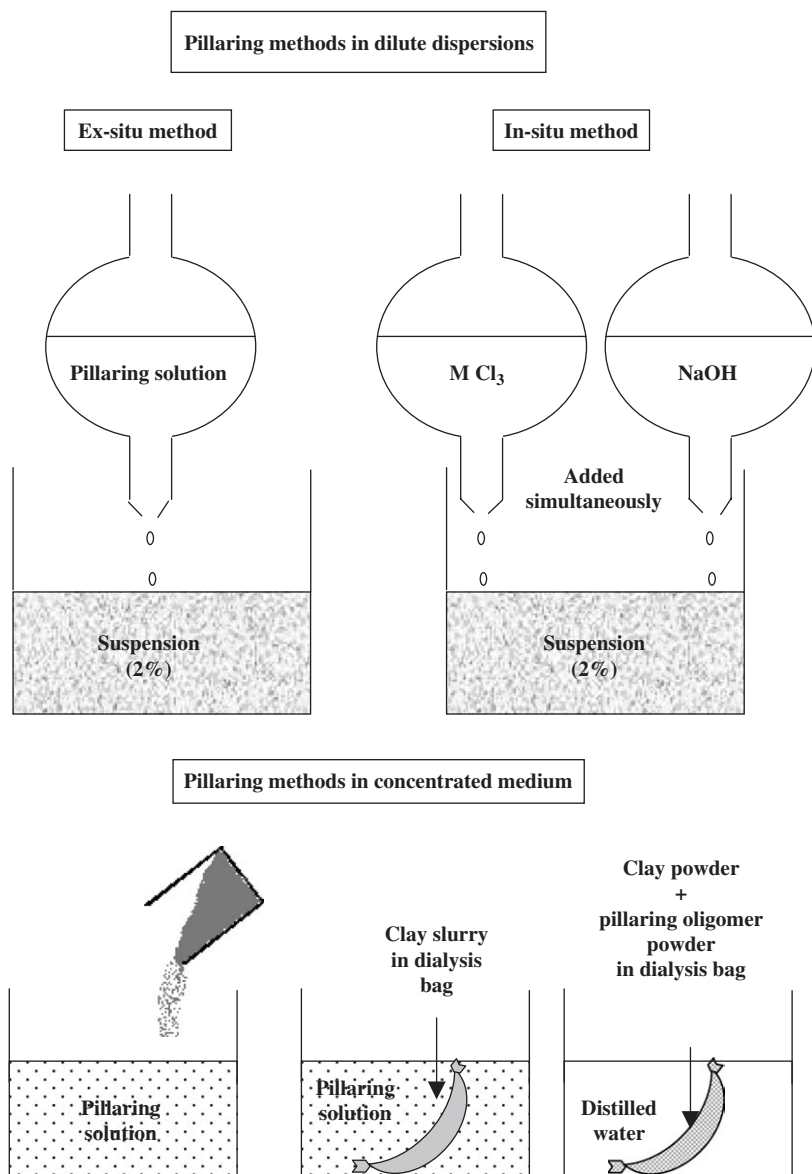


Fig. 7.5.2. Comparison of different pillaring methods.

The property of the intercalated clay mineral is dependent on the nature of the metallic cation, hydrolysis conditions, and type of clay mineral. Ageing time, with or without stirring, temperature, mode of washing (filtration and/or by dialysis), drying (at room temperature, or at low temperature in an oven, or by freeze-drying) are also

important parameters (Pinnavaia et al., 1984). The second step consists of heating the intercalated clay mineral. Here, the heating temperature (in air or in a closed reactor with flowing gas) as well as the duration and rate of heating have a strong influence on the properties of the resultant PILC.

For the Al Keggin cation, the charge ( $7+$ ) in solution changes upon further hydrolysis, and after intercalation and heating. The final charge of the pillars is variable, but appears to be about  $4+$ . Since each of the parameters mentioned above is influential, data comparison is difficult. Different PILC are commonly characterized by their interlayer distance (by XRD), surface area, and porosity (see Section 7.5.7).

Variants of the classical method were described, but all these still consume large amounts of liquid. One variant involves the in-situ hydrolysis of the exchangeable cation in the interlayer space (Yamanaka and Brindley, 1978; Brindley and Kao, 1980). This method therefore requires pre-exchange of the clay mineral with a suitable cation and does not yield a satisfactory product. Another variant involves adding a dilute solution of both the metal salt and the base simultaneously to a dilute clay dispersion (Fig. 7.5.2). Here, the pillaring species is presumed to form directly in situ (in the clay dispersion). The rate of addition of the two solutions needs to be carefully controlled so that the final pH does not vary much with every added drop of the two constituents. This requires vigorous stirring of the clay suspension, which must remain clear during the whole course of addition, showing no sign of precipitation. The advantage of this latter in-situ method is less time-consuming than the former because the intercalant does not have to be prepared separately, and no pre-exchange of the starting clay mineral is required.

During intercalation at ambient temperature, ultrasonic treatment during 20 min of  $\text{Ca}^{2+}$ -montmorillonite with chlorhydrol leads to PILC with improved textural properties and higher stability (Katdare et al., 1997, 2000).

Microwave irradiation can be used as an adequate rapid procedure to reduce the time of intercalation required in traditional intercalation step (Fetter et al., 1996). However, the whole pillars are not completely affected by this treatment (de Andres et al., 1999).

### *B. Pillaring in Concentrated Medium*

Although pillared clay minerals attracted much attention over the past 30 years, particularly from industry, they were not yet used as commercial catalysts. A few kilograms of commercial PILC per batch (N.T.U.A., Athens) were produced at a small pilot scale level (Kaloidas et al., 1995). One reason is that the pillaring procedure, developed in the laboratory, is difficult to extend to an industrial scale. This method is time-consuming, needs a large volume of liquid and repeated separations of huge amounts of clay dispersions by centrifugation or filtration. To produce pillared clay minerals at an industrial scale, the above procedure must be simplified. In particular, the volume of all reagents needs to be greatly reduced. It is only in the

past decade that information on methods using concentrated reagents and/or dialysis bags is available. This is summarized in Table 7.5.2 (Aouad et al., 2005).

Vaughan (1988b) was the first to report the successful pillaring of clay minerals by adding the mineral as a powder to the pillaring solution to give a slurry of up to 40%. At this high concentration, the clay mineral does not delaminate or gellify. Ex-situ pillaring (Fig. 7.5.2) can also be achieved by placing a concentrated clay suspension, contained in a dialysis bag, in a dilute pillaring solution (Schoonheydt and Leeman, 1992; Frini et al., 1997; Sanchez and Montes, 1998). Using a range of concentrated clay suspensions, Schoonheydt et al. (1993) found other unidentified Al species besides the Keggin ions.

Frini et al. (1997) compared the results obtained from a classical method with 'dilute dispersion' with the methods using 'clay powder' and also a 'concentrated clay slurry in dialysis bag'. After repeated washing and centrifuging of the intercalated clay mineral dispersions, and heating the precipitate, the PILC prepared by the two last methods are easier to grind than the product obtained by the classical method.

The use of concentrated dispersions or pastes, and dialysis, facilitates the recovery of the intercalated suspensions (Molina et al., 1992; Del Riego et al., 1994; Schoonheydt et al., 1994). At the same time the number of washing cycles is reduced. However, all these procedures still use dilute pillaring solutions and large amounts of liquid.

In the pilot scale production (> 1 kg per run) at N.T.U.A. (Athens) and Tolsa (Madrid) pilot, the dry clay mineral powder was added to a dilute commercial pillaring solution (chlorhydrol), and the dispersion was washed in a filter-press (Moreno et al., 1997). PILC prepared at the laboratory scale (g), at a batch level (100 g), and at a pilot scale shown similar catalytic activities. Commercially available concentrated Al-pillaring solutions (50% w/w chlorhydrol) were used with concentrated 50% w/w aqueous or acetone clay mineral dispersions (Storaro et al., 1996). The suspensions in acetone are less sticky and easier to handle than their aqueous counterparts. By this means, up to 500 g of PILC can be obtained. Storaro et al. (1998) made further improvements by mixing solid chlorhydrol with different clay minerals in acetone. A similar procedure was used by Salerno and Mendoroz (2002) by mixing a suspension of raw clay in acetone with Locron (a commercial Al hydroxychloride containing 47% Keggin cations). The method proposed by Fetter et al. (1997) consists of mixing a highly concentrated chlorhydrol solution (50% w/w, 2.5 M) with a concentrated 50% w/w clay mineral suspension, and microwave irradiation for the intercalation step.

Recently, Vicente and Lambert (2003) reported a new synthetic route of pillaring by putting 1 g clay in powder form in a dialysis tube with 10 ml very concentrated solutions (40 times smaller volume than in classical pillaring) of Al poly(hydroxo cations). This compound is obtained by reacting alumina with a chloride salt, but its nature was not elucidated. The mixture is immediately washed five times by dialysis, centrifuged, and heated. However, the method at the highest clay content with a minimum expenditure of time and water is that of Aouad et al. (2005). At the same time, this method offers the potential for extension to an industrial scale. Here, 1 g of raw clay powder and solid  $\text{Al}_{13}$  is dialyzed five times against 5 ml of water

Table 7.5.2. Experimental conditions used in the pillaring method using concentrated dispersions, or solid powders

Reference	1	2	3	4	5	6	7	8	9	10	11	12	13	14
Clay	Mt	Mt	Ht, Sap	Ht, Sap Lap	Sap	Mt	Mt Illite- Sm	Mt	Mt	Mt Sap	Mt, Lap Sap, Bd	Mt	Sap	Mt
OH/Al	1.6	2	2.4	1 and 2	1 and 2	2	2	Not defined	2	1.9	Not defined	Not defined	Not defined	2.4
[Al] <sub>f</sub> (M)	0.1	0.1	0.07	0.8	0.5	Not defined	Al-Cu		Chlorhyd.S 50% hydr.chlor.)	Chlorhyd.S 50% 2.5 M	0.068 or chlorhyd.S 0.07			
Chlorhyd.P	Locron (Al-													
Clay/water	40% in DB	10% in DB	1% in DB	Different Cc	P	P and 10%	P and 33%in DB	50% in water in acetone	10, 15, 20 40, 50%	P or suspension	50% in acetone	50% in acetone	P in DB	P in DB
Al meq/g clay	25, 50, 75, 100	20, 40, 60, 70	Not defined	Not defined	23	9	30, 60	30	15	11.4	30	5, 10, 30	Not defined	18
Time of exchange	24 h 48 h	1, 3 7 days	48 h	24 h	1 night under reflux	24 h	48 h	17	7 min in microwave	12 h	24 h	2 h	0 h	0 h
W/D	2 D	1 D	D until Cl <sup>-</sup> free	W until Cl <sup>-</sup> free	5 W	4 W	5 D	4 W	W until Cl <sup>-</sup> free	Filter-press	4 W	D until Cl <sup>-</sup> free	5 D	5 D

Notes:

- 1: Molina et al. (1992)
- 2: Del Riego et al. (1994)
- 3: Schoonheydt et al. (1994)
- 4: Schoonheydt et al. (1993)
- 5: Schoonheydt and Leeman (1992)
- 6: Sanchez and Montes (1998)
- 7: Frini et al. (1997)
- 8: Storaro et al. (1996)
- 9: Fetter et al. (1997)
- 10: Moreno et al. (1997)
- 11: Storaro et al. (1998)
- 12: Salerno and Mendioroz (2002)
- 13: Vicente and Lambert (2003)
- 14: Aouad et al. (2005)

Bd: Beidellite  
 Ht: Hectorite  
 Il: Illite  
 Lap: Laponite  
 Mt: Montmorillonite  
 Sap: Saponite  
 Sm: Smectite  
 Cc: Concentrations  
 Chlorhyd: Chlorhydrol  
 D: Dialysis  
 DB: Dialysis bags  
 P: Powder  
 W: Washing  
 S: Solution



(Fig. 7.5.2). Such a truly solid–solid reaction was not reached till now. The dialysis step seems crucial for pre-pillaring. More fundamental research is needed to understand the reactions and mechanisms involved.

### 7.5.7. MAIN PILC CHARACTERISTICS FOR DIFFERENT APPLICATIONS

The first common characteristic of PILC is the distance ( $\Delta d$ ) separating contiguous layers after heating the intercalated clay minerals. Thus, PILC have a permanent porosity and a higher accessible specific surface area (SSA) than the pristine clay. The basal spacing of smectite intercalated with Al Keggin cations is about 1.8 nm, corresponding to  $\Delta d$  of 0.9 nm (Fig. 7.5.3). If a smaller  $\Delta d$  value is observed, pillaring is not regarded to be achieved. A basal spacing of about 2.7 nm was reported for Al PILC (Singh and Kodama, 1988) and for Ti PILC (Sterte, 1986). However, Singh and Kodama showed by Fourier transform analysis of the XRD basal reflections that a regular interstratified structure of 0.96 nm and 1.8 nm occurred. Pillaring occurs between each two-layers of montmorillonite. Still higher interlayer distances (up to 7 nm) were observed by Mandalia et al. (1998) for a series

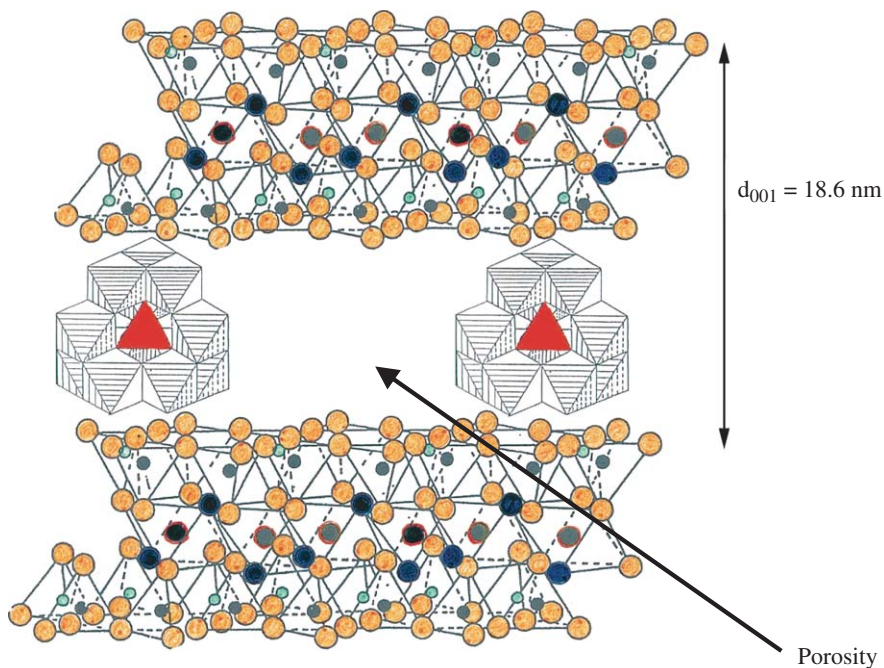


Fig. 7.5.3. AlPILC structure.

of Al–Fe PILC. However, a TEM image analysis performed on one of these samples (Clinard et al., 2003) shows that this value refers to a correlation distance for Fe particles present between clay mineral particles, each of which is composed of 4–5 layers. In this case, pillaring occurs between particles rather than between individual layers.

Moreover this interlayer distance, PILC are also characterized by interpillar distance (as shown in Fig. 7.5.3), which is more difficult to determine (Gil and Gandia, 2003).

The important property is the accessible porosity leading to a higher SSA than the pristine (parent) clay mineral. A smectite with completely exfoliated layers has an SSA of about 800 m<sup>2</sup>/g. The highest SSA recorded for PILC is 600 m<sup>2</sup>/g with a total pore volume of 0.6 cm<sup>3</sup>/g (Vaughan et al., 1979). This porosity is due to pores of different size, although micropores (< 2 nm) are usually obtained by Al pillaring. In some instances, such as the mixed Al–Fe PILC, mesopores (2–50 nm) are observed (Mandalia et al., 1998). Macropores (> 50 nm) are also obtained with delaminated pillared Laponites (Butruille and Pinnavaia, 1996).

The acidity of PILC is important for catalytic applications. This property arises from both the clay mineral and the pillar. In comparing a number of pillared bentonites, Zonghui and Guida (1985) found that the Ti PILC are the most acidic (Table 7.5.3). The nature, number, and strength of acid sites in PILC can be controlled by competitive ion exchange during the intercalation step, or by ion exchange of the residual cations after the pillaring step, or by steaming the PILC (Figueras et al., 1990; Tichit et al., 1991).

The structure of the Al Keggin cation, the most used intercalant for PILC, was established by instrumental techniques, particularly NMR spectroscopy, but that of other metal intercalants is less understood. Some of these, such as Ga<sub>13</sub>, are assumed to be similar in structure to Al<sub>13</sub> (Bradley and Kydd, 1990a, 1990b). In other cases, hypothetical structures were proposed for Zr and Si pillars, as reported in some

Table 7.5.3. Comparative acidities of different pillared bentonites as measured by titration with an ammonia adsorption differential thermal method developed in China

Samples	Acidity (μV)
Al-CLB	425–442
Zr-CLB	570
Ti-CLB	620
Fe-CLB	340
Ni-CLB	228
Al–Zr-CLB	390
Al–Fe-CLB	340
Na–B	86

Notes: The unit of acidity is expressed in μV. From Zonghui and Guida (1985). B: bentonite; CLB: cross-linked bentonite.

reviews (Figueras, 1988; Klopprogge, 1998; Konta, 2001), while the structures of the metal intercalant in Cr and Sn PILC have yet to be determined (Bodman et al., 2002).

#### 7.5.8. INTERCALANT STABILITY BEFORE AND AFTER PILLARING

The stability of the intercalant species before and after pillaring is of primary importance to using PILC in different applications.

The stability of  $\text{Al}_{13}^{7+}$  sulfate hydrate was investigated by Klopprogge et al. (1992) who shows that the water adsorbed in excess is lost at 80 °C. On further heating, the oligomer gradually decomposes losing its 12 water molecules and 24 hydroxyl groups, becoming finally X-ray amorphous at 360 °C. Above this temperature, the Al oxide is formed till 950 °C.

The required thermal stability of the PILC is generally difficult to define, because it is application dependent. Of course, heating of the intercalated clay mineral is supposed to stabilize the structure of PILC. Except for Zr PILC, however, both intercalated and pillared clay minerals are chemically modified when stored in air (Chevalier et al., 1992). According to Schoonheydt et al. (1993), the increase in basal spacing alone is not a sufficient criterion for thermal stability, the line width of the (001) reflection must also be taken into account.

The most important question is whether the structure of the intercalated oligomers is maintained after heating, or whether the intercalant species are transformed into oxide pillars, as proposed by Vaughan et al. (1979). The available data are scattered and contradictory. If the intercalant is transformed into classical oxides, why does the basal spacing remain almost unchanged in the PILC? Many NMR studies showed that the  $\text{Al}_{13}$  structure is maintained till 500 °C, except for pillared beidellite (Plée et al., 1985). This might be because the water of hydration of the intercalant is lost by heating, and dehydroxylation occurs in the 300–400 °C range (Schutz et al., 1987). At higher temperatures, oxide pillars with a  $\gamma$ -alumina structure are presumed to form in the interlayer space (Tennakoon et al., 1986). A recent NMR and microcalorimetry study (Occelli et al., 2000) of Al-pillared montmorillonite shows that heating the Keggin ion at 500 °C in the intercalated clay leads to the formation of blocks of 13 Al atoms containing Al (IV and VI) as well as new Al (V). The  $\text{Al}_{13}$  structure is no longer maintained at this temperature, but  $\gamma$ -alumina is also not detected by XRD. Moreover, a thermo-XRD study (Aceman et al., 2000) of Al-pillared smectites shows that the added Keggin ion first dissociates into smaller hydroxy- and/or chloro-Al oligomers, which increase in size after water addition (thorough washing or dialysis) in the interlayer space. At 600 °C, these Al oxocations adsorbed by the smectites, condensed with the silicate sheet, preventing further swelling in water. However, the exact nature of the obtained alumina clusters that form the pillars in  $\text{Al}_{13}$ -PILC still remains a subject of discussion.

### 7.5.9. LINKAGE BETWEEN PILLARS AND CLAY MINERAL LAYERS

Many hypotheses were proposed about the manner in which the pillars are linked to the interlayer surface of the clay mineral, but the precise mechanism is not well understood.

When  $\text{Al}_{13}$  is heated, protons and water are simultaneously released, and condensation takes place between the OH groups of the oligomeric ion and lattice hydroxyls of the silicate layer. One suggestion is that the resultant Al oxide pillar is linked via oxygen to the cation of the octahedral sheet (Tennakoon et al., 1986), giving rise to a rigid cross-linked structure and loss of expansion. This hypothesis, however, was not widely accepted because it is difficult to visualize how such a link can form with the tetrahedral sheet acting as a barrier.

There is no generally accepted mechanism that can account for the stable linkage that exists between pillar and clay mineral surface, especially at high temperatures.

Cross-linking between pillars and silica tetrahedra that become inverted after calcination, was proposed by Fripiat (1988) on the basis of NMR studies. Tetrahedral inversion is influenced by the origin of the layer charge as in the case of beidellite or synthetic saponite where the (substituted) Al tetrahedra invert after calcination (Pl  e et al., 1985; Lambert et al., 1994; Klopprogge et al., 1994; Lambert and Poncelet, 1997). It would also depend on the composition of the octahedral sheet. For example, in fluorohectorite the presence of electronegative fluorine ions stabilizes the Si–O bond, promoting coupling between inverted Si tetrahedra and the  $\text{Al}_{13}$  pillars on calcination (Pinnavaia et al., 1985). In case of synthetic saponite, a covalent Si–(OH)–Al<sub>pillar</sub> bond was suggested. The silanol groups result from the attack of the Si–O groups on the surface of the tetrahedral sheet, by the protons released during calcination (Sterte and Shabtai, 1987; Jones, 1988; Bukka et al., 1992; Li et al., 1993; Klopprogge, 1998; Aceman et al., 1999; Occelli et al., 2000).

### 7.5.10. CONCLUSIONS

A lot of fundamental work was realized in these three past decades on PILC, particularly with Al-pillared smectites. Surprisingly, all the available data open the way to numerous questions and to the need of better understanding the hydrolysis of cations, even for the Al ion as the most studied one.

Many other metal ions can act as pillaring species. For example, a few papers are published on Ti PILC (Valverde et al., 2002, 2003') despite their high thermal stability and high acidity. The challenge will be to pillar modified kaolinite or sepiolite to take profit about its particular texture.

To be of useful interest, these PILC must be used in some industrial or environmental applications. For this reason, one has to pay more attention to the

fundamental point of view toward the pillaring in concentrated clay dispersions. Solid–solid state reaction remains a challenge for the future.

In spite of the knowledge actually accumulated on PILC, two main questions remain (i) the real structure of the intercalated species before and after heating, and (ii) the type of bonds formed between the clay mineral host and the pillar guest that maintains the stability of the pillared clays minerals.

## REFERENCES

- Aceman, S., Lahav, N., Yariv, S., 1999. A thermo-FTIR-spectroscopy analysis of Al-pillared smectites differing in source of charge in KBr disks. *Thermochimica Acta* 340–341, 349–366.
- Aceman, S., Lahav, N., Yariv, S., 2000. A thermo-XRD-study of Al-pillared smectites differing in source of charge, obtained in dialyzed, non-dialyzed and washed systems. *Applied Clay Science* 17, 99–126.
- Adams, J.M., 1987. Synthetic organic chemistry using pillared, cation-exchanged and acid-treated montmorillonite catalysts. A review. *Applied Clay Science* 2, 309–342.
- Akçay, M., 2004. The catalytic acylation of alcohols with acetic acid by using Lewis acid character pillared clays. *Applied Catalysis A: General* 269, 157–160.
- Akitt, J.W., Farthing, A., 1978. New  $^{27}\text{Al}$  NMR studies of the hydrolysis of the aluminium (III) cation. *Journal of Magnetic Resonance* 32, 345–352.
- Akitt, J.W., Farthing, A., 1981a. Aluminium-27 nuclear magnetic resonance studies of the hydrolysis of Aluminium (III). Part 4. Hydrolysis using sodium carbonate. *Journal of the Chemical Society, Dalton Transactions* 7, 1617–1623.
- Akitt, J.W., Farthing, A., 1981b. Aluminium-27 nuclear magnetic resonance studies of the hydrolysis of aluminium III. Part 5. Slow hydrolyse using aluminium metal. *Journal of the Chemical Society, Dalton Transactions* 7, 1624–1628.
- Akitt, J.W., Farthing, A., 1981c. Aluminium-27 nuclear magnetic resonance studies of the hydrolysis of aluminium III. Part 2. Gel-permeation chromatography. *Journal of the Chemical Society, Dalton Transactions* 7, 1606–1608.
- Akitt, J.W., Greenwood, N.N., Khandelwal, B.L., Lester, G.D., 1972.  $^{27}\text{Al}$  nuclear magnetic resonance studies of the hydrolysis and polymerisation of the hexa-aquo-aluminium (III) cation. *Journal of the Chemical Society, Dalton Transactions* 5, 604–610.
- Aouad, A., Mandalia, T., Bergaya, F., 2005. A novel method of Al-pillared montmorillonite preparation for potential industrial up-scaling. *Applied Clay Science* 19, 175–182.
- Baes, C.F. Jr., Mesmer, R.E. (Eds.), 1976. *The Hydrolysis of Cations*. Wiley, New York.
- Bagshaw, S.A., Cooney, R.P., 1995. Preparation and characterization of a highly stable pillared clay. *Chemistry Materials* 7, 1384–1389.
- Bakas, T., Moukarika, A., Papaefthymiou, V., Ladavos, A., 1994. Redox treatment of an Fe/Al pillared montmorillonite. A Mössbauer study. *Clays and Clay Minerals* 42, 634–642.
- Barrault, J., Zivkov, C., Bergaya, F., Gatinéau, L., Hassoun, N., Van Damme, H., Mari, D., 1988. Iron-doped pillared laponites as catalysts for the selective conversion of syngas into light alkenes. *Journal of the Chemical Society, Chemical Communications* 21, 1403–1404.
- Barrault, J., Gatinéau, L., Hassoun, N., Bergaya, F., 1992. Selective syngas conversion over mixed Al–Fe pillared laponite clay. *Energy and Fuels* 6, 760–763.

- Barraut, J., Bouchoule, C., Echachoui, K., Frini-Srasra, N., Trabelsi, M., Bergaya, F., 1998. Catalytic wet peroxide oxidation (CWPO) of phenol over mixed (Al–Cu)-pillared clays. *Applied Catalysis B: Environmental* 15, 269–274.
- Barrer, R.M., 1986. Expanded clay minerals: a major class of molecular sieves. *Journal of Inclusion Phenomena* 4, 109–119.
- Barrer, R.M., MacLeod, D.M., 1955. Activation of montmorillonite by ion exchange and sorption complexes of tetra-alkylammonium montmorillonites. *Transactions of the Faraday Society* 51, 1290–1300.
- Bellaloui, A., Plee, D., Meriaudeau, P., 1990. Gallium containing pillared interlayer clays: preparation, characterization and catalytic properties. *Applied Catalysis*, vol. 63. Elsevier, Amsterdam, pp. L7–L10.
- Benito, I., del Riego, A., Martínez, M., Blanco, C., Pesquera, C., González, F., 1999. Toluene methylation on  $\text{Al}_{13}$ - and  $\text{GaAl}_{12}$ -pillared clay catalysts. *Applied Catalysis A: General* 180, 175–182.
- Bergaya, F., 1990. Argiles à pilers. In: Decarreau, A. (Ed.), *Matériaux Argileux. Structures, Propriétés et Applications*, Chapter II. Société Française de Minéralogie et de Cristallographie et Groupe Français des Argiles, Paris, pp. 513–537.
- Bergaya, F., 1994. Focus on mixed pillaring and mixed  $\text{Al}_{3-x}\text{Fe}_x$  PILCs clays. *Concerted European Action-Pillared Layered Structures, Newsletter* 7, 11–12.
- Bergaya, F., 1995. The meaning surface area and porosity measurements of clays and pillared clays. *Journal of Porous Materials* 2, 91–96.
- Bergaya, F., Barraut, J., 1990. Mixed Al–Fe pillared laponites: preparation, characterization and their catalytic properties in syngas conversion. In: Mitchell, I.V. (Ed.), *Pillared Layered Structures. Current Trends and Applications*. Elsevier Applied Science, London, pp. 167–184.
- Bergaya, F., Hassoun, N., Gatineau, L., Barraut, J., 1991. Mixed Al–Fe pillared laponites: preparation, characterization and catalytic properties in syngas conversion. In: Poncelet, G., Jacobs, P.A., Grange, P., Delmon, B. (Eds.), *Preparation of Catalysts V*. Elsevier, Amsterdam, pp. 329–336.
- Bergaya, F., Gatineau, L., Van Damme, H., 1993a. About surface area and porosity measurements in pillared clays. In: Sequeira, C.A.C., Hudson, M.J. (Eds.), *Multifunctional Mesoporous Inorganic Solids*. NATO ASI Series. Kluwer Academic Publishers, Dordrecht, pp. 19–26.
- Bergaya, F., Hassoun, N., Barraut, J., Gatineau, L., 1993b. Pillaring of synthetic hectorite by mixed ( $\text{Al}_{13-x}\text{Fe}_x$ ) pillars. *Clay Minerals* 28, 109–122.
- Bodman, S.D., Mc Whinnie, W.R., Begon, V., Suelves, I., Lazaro, M.-J., Morgan, T.J., Herod, A.A., Kandiyoti, R., 2002. Metal-ion pillared clays as hydrocracking catalysts (I): catalyst preparation and assessment of performance at short contact times. *Fuel* 81, 449–459.
- Booij, E., Klopogge, J.T., van Veen, J.A.R., 1996a. Preparation, structural characteristics and catalytic properties of large-pore rare earth element (Ce, La)/Al-pillared smectites. *Clays and Clay Minerals* 44, 774–782.
- Booij, E., Klopogge, J.T., van Veen, J.A.R., 1996b. Large pore REE/Al pillared bentonites: preparation, structural aspects and catalytic properties. *Applied Clay Science* 11, 155–162.
- Bottero, J.Y., Cases, J.M., Fiessinger, F., Poirier, J.E., 1980. Studies of the hydrolysed aluminium chloride solutions. 1. Nature of aluminium species and composition of aqueous solution. *Journal of Physical Chemistry* 84, 2933–2939.

- Bottero, J.Y., Tchoubar, D., Cases, J.M., Fiessinger, F., 1982. Investigation of the hydrolysis of aqueous solutions of aluminium chloride. 2. Nature and structure by small-angle X-ray scattering. *Journal of Physical Chemistry* 86, 3667–3673.
- Bradley, S.M., Kydd, R.A., 1991. A comparison of the thermal stabilities of Ga13, GaAl12 and Al13-pillared clay minerals. *Catalysis Letters* 8, 185–192.
- Bradley, S.M., Kydd, R.A., 1993. Ga13, GaAl12, and chromium-pillared montmorillonites: acidity and reactivity for cumene conversion. *Journal of Catalysis* 141, 239–249.
- Bradley, S.M., Kydd, R.A., Yamdagni, R., 1990a. Detection of a new polymeric species formed through the hydrolysis of gallium (III) salt solutions. *Journal of the Chemical Society, Dalton Transactions*, 413–417.
- Bradley, S.M., Kydd, R.A., Yamdagni, R., 1990b. Comparison of the hydrolysis of gallium (III) and aluminium (III) solutions by nuclear magnetic resonance spectroscopy. *Journal of the Chemical Society, Dalton Transactions* 9, 2653–2656.
- Bradley, S.M., Kydd, R.A., Yamdagni, R., 1990c. Study of the hydrolysis of combined  $\text{Al}^{3+}$  and  $\text{Ga}^{3+}$ . Aqueous solutions: formation of an extremely stable  $\text{GaO}_4\text{Al}_{12}(\text{OH})_{24}(\text{H}_2\text{O})_{12}^{+7}$  polyoxycation. *Magnetic Resonance in Chemistry* 28, 746–750.
- Bradley, S.M., Kydd, R.A., Fyfe, C.A., 1992. Characterization of the  $\text{GaO}_4\text{Al}_{12}(\text{OH})_{24}(\text{H}_2\text{O})_{12}^{+7}$  polyoxocation by MAS NMR and infrared spectroscopies and powder X-ray diffraction. *Inorganic Chemistry* 31, 1181–1185.
- Breck, D.W., 1980. Potential uses of natural and synthetic zeolites in industry. In: Towsend, R.P. (Ed.), *The Properties and Applications of Zeolites*. The Chemical Society, London, pp. 391–422.
- Brindley, G.W., Sempels, R.E., 1977. Preparation and properties of some hydroxy-aluminium beidellites. *Clay Minerals* 12, 229–236.
- Brindley, G.W., Kao, C.C., 1980. Formation, composition and properties of hydroxy-Al and hydroxy-Mg-montmorillonite. *Clays and Clay Minerals* 28, 435–443.
- Brody, J.F., Johnson, J.W., 1990. Utilization of novel materials component and synthetic techniques. In: Corcoran, E.W., Ledoux, M.J. (Eds.), *Proceeding of the Symposium: Synthesis and Properties of New catalysts: Fall Meeting of the Materials Research Society*, Boston, p. 65.
- Bukka, K., Miller, J.D., Shabtai, J., 1992. FTIR study of deuterated montmorillonites: structural features relevant to pillared clay stability. *Clays and Clay Minerals* 40, 92–102.
- Burch, R. (Ed.), 1988. Pillared clays, *Catalysis Today* 2, 185–367.
- Butruille, J.R., Pinnavaia, T.J., 1996. Alumina pillared clays. In: Albert, G., Bein, T. (Eds.), *Comprehensive Supramolecular Chemistry*, vol. 7. Solid-state Supramolecular Chemistry: Two and Three dimensional Inorganic Networks. Pergamon Press, New York, pp. 219–250.
- Carrado, K.A., Kostapapas, A., Suib, S.L., Coughlin, R.W., 1986a. Physical and chemical stabilities of pillared clays containing transitional metal ions. *Solid State Ionics* 22, 117–125.
- Carrado, K.A., Suib, S.L., Skoularikis, N.D., 1986b. Chromium (III)-doped pillared clays (PILC's). *Inorganic Chemistry* 25, 4217–4221.
- Cheng, L.S., Yang, R.T., Chen, N., 1996. Iron oxide and chromia supported on titania-pillared clay for selective catalytic reduction of nitric oxide with ammonia. *Journal of Catalysis* 164, 70–81.
- Chevalier, S., Franck, R., Lambert, J.-F., Barthoneuf, D., Suquet, H., 1992. Stability of Al-pillared saponites: evidence for disorganization during storage in air. *Clay Minerals* 27, 245–248.

- Choudary, B.M., Valli, V.L.K., Prasad, A.D., 1990. A new vanadium-pillared montmorillonite catalyst for the regioselective epoxidation of allylic alcohols. *Journal of the Chemical Society, Chemical Communications* 9, 721–722.
- Christiano, S.P., Pinnavaia, T.J., 1986. Intercalation in montmorillonite of molybdenum cations containing the  $\text{Mo}_6\text{Cl}_8$  cluster core. *Journal of Solid State Chemistry* 64, 232–239.
- Christiano, S.P., Wang, J., Pinnavaia, T.J., 1985. Intercalation of niobium and tantalum  $\text{M}_6\text{Cl}_{12n+}$  in montmorillonite: a new route to pillared clays. *Inorganic Chemistry* 24, 1222–1227.
- Clinard, C., Tchoubar, D., Mandalia, T., Bergaya, F., 2003. HRTEM image filtration: nanostructural analysis of a pillared clay. *Clays and Clay Minerals* 52, 421–429.
- Cool, P., Vansant, E.F., 1998. Pillared clays: preparation, characterization and applications. *Molecular Sieves* 1, 265–288.
- De Andres, A.M., Merino, J., Galvan, J.C., Ruiz-Hitzky, E., 1999. Synthesis of pillared clays assisted by microwaves. *Materials Research Bulletin* 34, 641–651.
- Del Rey-Perez-Caballero, F., Poncelet, G., 2000. Preparation and characterization of 18 Å Al-pillared structures from natural phlogopite micas. *Microporous and Mesoporous Materials* 41, 169–181.
- del Riego, A., Herrero, I., Pesquera, C., Blanco, C., Benito, I., González, F., 1994. Preparation of PILC-Al through dialysis bags: a comparative study. *Applied Clay Science* 9, 189–197.
- Dick, S., Weiss, A., 1998. Reactions of smectites with binuclear oxobridge iron complexes of *N*-alkyl-*N,N*-bis(2-pyridylmethyl)-amines. *Clay Minerals* 33, 35–42.
- Ding, Z., Klopogge, J.T., Frost, R.L., Lu, G.Q., Zhu, H.Y., 2001. Porous clays and pillared clays-based catalysts. Part 2: a review of the catalytic and molecular sieve applications. *Journal of Porous Materials* 8, 273–293.
- Doff, D.H., Gangas, N.H.J., Allan, J.E.M., Coey, J.M.D., 1988. Preparation and characterization of the iron oxide pillared montmorillonites. *Clay Minerals* 23, 367–377.
- Dominguez, J.M., Botello-Pozos, J.C., López-Ortega, A., Ramírez, M.T., Sandoval-Flores, G., Rojas-Hernández, A., 1998. Study of pillar precursors [Ga(III)–Al(III), In(III)–Al(III), Zr(IV)] for hydrothermally stable pillared clays. *Catalysis Today* 43, 69–77.
- Endo, T., Mortland, M.M., Pinnavaia, T.J., 1980. Intercalation of silica in smectites. *Clays and Clay Minerals* 28, 105–110.
- Endo, T., Mortland, M.M., Pinnavaia, T.J., 1981. Properties of silica intercalated smectites. *Clays and Clay Minerals* 29, 153–156.
- Fetter, G., Tchit, D., de Menorval, L.C., Figueras, F., 1995. Synthesis and characterization of pillared clays containing both Si and Al pillars. *Applied Catalysis A: General* 126, 165–176.
- Fetter, G., Heredia, G., Maubert, A.M., Bosch, P., 1996. Synthesis of Al-intercalated montmorillonites using microwave irradiation. *Journal of Materials Chemistry* 6, 1857–1858.
- Fetter, G., Heredia, G., Velazquez, L.A., Maubert, A.M., Bosch, P., 1997. Synthesis of aluminium-pillared montmorillonites using highly concentrated clay suspensions. *Applied Catalysis A: General* 62, 42–45.
- Figueras, F., 1988. Pillared clays as catalysts. *Catalysis Reviews: Science and Engineering* 30, 457–499.
- Figueras, F., Klapys, Z., Massiani, P., Mountassir, Z., Tichit, D., Fajula, D., Gueguen, C., Bousquet, J., Auroux, A., 1990. Use of competitive ion exchange for intercalation of montmorillonite with hydroxy-aluminum species. *Clays and Clay Minerals* 38, 257–264.



- Frini, N., Crespin, M., Trabelsi, M., Messad, D., Van Damme, H., Bergaya, F., 1997. Preliminary results on the properties of pillared clays by mixed Al-Cu solutions. *Applied Clay Science* 12, 281–292.
- Fripiat, J.J., 1988. High resolution solid state NMR study of pillared clays. In: Burch, R. (Ed.), *Catalysis Today* 2–3, 281–295.
- Fripiat, J.J., 1997. Pillared clays. In: Ertl, G., Knözinger, H., Weitkamp, J. (Eds.), *Handbook of Heterogeneous Catalysis*, vol. 1. Wiley, New York, pp. 387–403.
- Furrer, G., Ludwig, C., Schindler, P.W., 1992. On the chemistry of the Keggin  $\text{Al}_{13}$  polymer I- Acid-base properties. *Journal of Colloid and Interface Science* 149, 56–67.
- Gil, A., Gandia, L.M., 2003. Microstructure and quantitative estimation of the micropore-size distribution of an alumina-pillared clay from nitrogen adsorption at 77 K and carbon dioxide adsorption at 273 K. *Chemical Engineering Science* 58, 3059–3075.
- Gil, A., Montes, M., 1997. Metathesis of propene on molybdenum-alumina-pillared montmorillonite. *Industrial and Engineering Chemistry Research* 36, 1431–1443.
- Gil, A., Guieu, G., Grange, P., Montes, M., 1995. Preparation and characterization of microporosity and acidity of silica-aluminum pillared clays. *Journal of Physical Chemistry* 99, 301–312.
- Gil, A., Gandia, L.M., Vicente, M.A., 2000a. Recent advances in the synthesis and catalytic applications of pillared clays. *Catalysis Reviews: Science and Engineering* 42, 145–212.
- Gil, A., Vicente, M.A., Gandia, L.M., 2000b. Main factors controlling the texture of zirconia and alumina pillared clays. *Microporous and Mesoporous Materials* 34, 115–125.
- Gonzalez, F., Pesquera, C., Benito, I., Mendioroz, S., 1991. Aluminum-gallium pillared montmorillonite with high thermal stability. *Journal of the Chemical Society, Chemical Communications*, 587–588.
- Gonzalez, F., Pesquera, C., Blanco, C., Benito, I., Mendioroz, S., 1992. Synthesis and characterization of aluminum-gallium pillared clays with high thermal and hydrothermal stability. *Inorganic Chemistry* 31, 727–731.
- Guan, J., Pinnavaia, T.J., 1994. A pillared rectorite clay with highly stable supergalleries. *Materials Science Forum* 152–153, 109–114.
- Gurvich, L., 1915. Attapulgit, also natural and activated montmorillonite, polymerise pinene. *Russian Chemical Society* 47, 827–830.
- Hernando, M.J., Pesquera, C., Blanco, C., Benito, I., González, F., 1996a. Differences in structural, textural and catalytic properties of montmorillonite pillared with  $(\text{GaAl}_2)$  and  $(\text{AlAl}_2)$  polyoxocations. *Chemistry of Materials* 8, 76–82.
- Hernando, M.J., Pesquera, C., Blanco, C., Benito, I., González, F., 1996b. Effect of Ce on catalytic properties of pillared montmorillonite with Al- and GaAl-polyoxocations. *Applied Catalysis A: General* 141, 175–183.
- Heylen, I., Vansant, E.F., 1997. The difference in adsorption capacity between Fe-PILCs and modified Fe-BuA- and Fe-Zr-PILCs. *Microporous Materials* 10, 41–50.
- Houdry, E., Burt, W.F., Pew, A.E., Peters, W.A. Jr., 1938. Catalytic processing by the Houdry process. *National Petroleum News*, R570–R580.
- Jamieson, J., Drljaca, A., Spiccia, L., Smith, T.D., 1995a. Infrared spectroscopic study of the occupation of hydrogen cyanide receptor sites of metallo-oxide pillared clays by hydrocarbons. *Chemistry of Materials* 7, 2078–2085.

- Jamis, J., Drljaca, A., Spiccia, L., Smith, T.D., 1995b. FTIR spectroscopic study of the occupation of hydrogen cyanide receptor sites metallo-oxide pillared clays by hydrocarbons. *Chemistry of Materials* 7, 2086–2089.
- Jie, G.J., Ze, M.E., Zhiqing, Y. 1986. A class of pillared interlayered clay molecular sieve products with regularly interstratified mineral structure. European Patent 0 197 012.
- Johansson, G., 1960. On the crystal structure of some basic aluminium salts. *Acta Chemica Scandinavia* 14, 771–773.
- Johansson, G., 1962. The crystal structure of  $[\text{Al}_2(\text{OH})_2(\text{H}_2\text{O})_8](\text{SO}_4)_2 \cdot 2\text{H}_2\text{O}$  and  $[\text{Al}_2(\text{OH})_2(\text{H}_2\text{O})_8](\text{SeO}_4)_2 \cdot 2\text{H}_2\text{O}$ . *Acta Chemica Scandinavia* 16, 403–420.
- Jones, S.L. (Ed.), 1988. The preparation and solution chemistry of Al (III) and Zr (IV) pillaring species, In: Burch, R. (Ed.), *Catalysis Today* 2, 209–217.
- Kaloidas, V., Koufopoulos, C.A., Gangas, N.H., Papayannakos, N.G., 1995. Scale-up studies for the preparation of pillared layered clays at 1 kg per batch level. *Microporous Materials* 5, 97–106.
- Karamanis, D.T., Aslanoglou, X.A., Assimakopoulos, P.A., Gangas, N.H., Pakou, A.A., Papayannakos, N.G., 1997. An aluminum pillared montmorillonite with fast uptake of strontium and cesium from aqueous solutions. *Clays and Clay Minerals* 45, 709–717.
- Katdare, S.P., Ramaswamy, V., Ramaswamy, A.V., 1997. Intercalation of Al oligomers into  $\text{Ca}^{2+}$ -montmorillonite using ultrasonics. *Journal of Materials Chemistry* 7, 2197–2199.
- Katdare, S.P., Ramaswamy, V., Ramaswamy, A.V., 2000. Factors affecting the preparation of alumina pillared montmorillonite employing ultrasonics. *Microporous and Mesoporous Materials* 37, 329–336.
- Keggin, J.F., 1934. The structure and formula of 12-phosphotungstic acid. *Proceedings of the Royal Society of London* 144, 75–100.
- Kloprogge, J.T., 1998. Synthesis of smectites and porous pillared clay catalysts: a review. *Journal of Porous Materials* 5, 5–41.
- Kloprogge, J.T., Geus, J.W., Jansen, J.B.H., Seykens, D., 1992. Thermal stability of basic aluminium sulfate. *Thermochimica Acta* 209, 265–276.
- Kloprogge, J.T., Booi, E., Jansen, J.B.H., Geus, J.W., 1994. The effect of thermal treatment on the properties of hydroxy-Al and hydroxy-Ga pillared montmorillonite and beidellite. *Clay Minerals* 29, 153–167.
- Konta, J., 2001. Pillared clays with hydroxy-R (III) or (IV) cations as molecular sieves and catalysts in: theoretical argillology for the applications of sealing, sorbent and catalytic clays. *Incontri Scientifica* 3, 104–118.
- Ladavos, A.K., Trikalitis, P.N., Pomonis, P.J., 1996. Surface characteristics and catalytic activity of Al-pillared (AZA) and Fe-Al-pillared (FAZA) clays for isopropanol decomposition. *Journal of Molecular Catalysis A: Chemical* 106, 241–254.
- Lahav, N., Shani, U., Shabtai, J., 1978. Cross-linked smectites: I. Synthesis and properties of hydroxy-aluminium montmorillonite. *Clays and Clay Minerals* 26, 107–115.
- Lambert, J.F., Poncelet, G., 1997. Acidity in pillared clays origin and catalytic manifestations. *Topics in Catalysis* 4, 43–56.
- Lambert, J.-F., Chevalier, S., Franck, R., Suquet, H., Barthomeuf, D., 1994. Al pillared saponites Part 2-NMR studies. *Journal of the Chemical Society, Faraday Transactions* 90, 675–682.
- Lee, W.Y., Raythatha, R.H., Tatarchuck, B.J., 1989. Pillared-clay catalysts containing mixed-metal complexes: I. Preparation and characterization. *Journal of Catalysis* 115, 159–179.

- Lee, A.P., Phillips, B.L., Olmstead, M.M., Casey, W.H., 2001. Synthesis and characterization of the  $\text{GeO}_4\text{Al}_{12}(\text{OH})_{24}(\text{OH}_2)_{12}^{8+}$  polyoxocation. *Inorganic Chemistry* 40, 4485–4487.
- Lenarda, M., Gazerla, R., Storaro, L., Enzo, S., Zandoni, R., 1994. Bifunctional catalysts from pillared clays: vapour phase conversion of propane to acetone catalysed by iron and ruthenium containing aluminum pillared bentonites. *Journal of Molecular Catalysis* 92, 201–213.
- Li, L., Liu, X., Ge, Y., Xu, R., Rocha, J., Klinowski, J., 1993. Structural studies of pillared saponite. *Journal of Physical Chemistry* 97, 10389–10393.
- Loeppert, R.H. Jr., Mortland, M.M., Pinnavaia, T.J., 1979. Synthesis and properties of heat-stable expanded smectite and vermiculite. *Clays and Clay Minerals* 27, 201–208.
- Maes, N., Vansant, E.F., 1995. Study of  $\text{Fe}_2\text{O}_3$ -pillared clays synthesized using the trinuclear  $\text{Fe(III)}$ -acetato complex as pillaring precursor. *Microporous Materials* 4, 43–51.
- Mandalia, T., Crespin, M., Messad, D., Bergaya, F., 1998. Large interlayer repeat distance observed for montmorillonites treated by mixed Al–Fe pillaring solutions. *Chemical Communications* 19, 2111–2112.
- Martin-Luengo, M.A., Martins-Carvalho, H., Ladriere, J., Grange, P., 1989.  $\text{Fe(III)}$ -pillared montmorillonites: preparation and characterization. *Clay Minerals* 24, 495–504.
- McCauley, J.R., 1988. Stable intercalated clays and preparation method. International Patent Application PCT/US88/00567.
- Mendioroz, S., Gonzalez, F., Pesquera, C., Benito, I., Blanco, C., Poncelet, G., 1993. Preparation of thermal stable pillared clays. *Studies in Surface Science and Catalysis* 75, 1637–1640.
- Michot, L.J., Pinnavaia, T.J., 1991. Adsorption of chlorinated phenols from aqueous solutions by surfactant-modified pillared clays. *Clays and Clay Minerals* 39, 634–641.
- Michot, L.J., Barres, O., Hegg, E.L., Pinnavaia, T.J., 1992. Improved synthesis of alumina pillared montmorillonite by surfactant modification. *Chemical Materials* 4, 1433–1437.
- Michot, L.J., Barres, O., Hegg, E.L., Pinnavaia, T.J., 1993. Co-intercalation of  $\text{Al}_{13}$  poly-cations and non-ionic surfactants in montmorillonite clay. *Langmuir* 9, 1794–1800.
- Mitchell, I.V. (Ed.), 1990. *Pillared Layered Structures, Current Trends and Applications*. Elsevier Applied Science, London.
- Mokaya, R., 1992. *Layered Materials as Selective Adsorbents*. Ph.D. thesis. Trinity College, Cambridge.
- Mokaya, R., Jones, W., Whittel, M.E., Davies, M.E., 1991. Synthesis and characterization of pillared acid-activated montmorillonites. *Material Research Society Symposium Proceedings* 223, 81–88.
- Molinar, A., 1994. *Physicochemical and Gas Adsorption Properties of Ion-exchanged Alumina-pillared Clays*. Ph.D. thesis. University of Antwerp (UIA).
- Molina, R., Vieira-Coelho, A., Poncelet, G., 1992. Hydroxy-Al pillaring of concentrated clay suspensions. *Clays and Clay Minerals* 40, 480–482.
- Montargès, E., 1997. *Synthèse et Caractérisation d'Argiles Intercalées par des Espèces Métalliques et Organiques. Application à l'Adsorption de Polluants en Phase Aqueuse*. Ph.D. thesis. University of Nancy.
- Moreno, S., Gutierrez, E., Alvarez, A., Papayannakos, N.G., Poncelet, G., 1997. Al-pillared clays: from lab synthesis to pilot scale production. Characterization and catalytic properties. *Applied Catalysis A: General* 165, 103–114.

- Moreno, S., Sun Kou, R., Molina, R., Poncelet, G., 1999. Al-, Al, Zr- and Zr-pillared montmorillonites and saponites: preparation, characterization and catalytic activity in heptane hydroconversion. *Journal of Catalysis* 182, 174–185.
- Mortland, M.M., Berkheiser, V., 1976. Triethylene diamine–clay complexes as matrices for adsorption and catalytic reactions. *Clays and Clay Minerals* 24, 60–63.
- Occelli, M.L., 1986. New routes to the preparation of pillared montmorillonite catalysts. *Journal of Molecular Catalysis* 35, 377–389.
- Occelli, M.L., 1991. Thermal stability, acidity and cracking properties of pillared rectorite catalysts. In: Poncelet, G., Jacobs, P.A., Grange, P., Delmond, B. (Eds.), *Scientific Basis for the Preparation of Heterogeneous Catalysts*, 5th International Symposium. Elsevier, Amsterdam, pp. 287–299.
- Occelli, M.L., Finseth, D.H., 1986. Preparation and characterization of pillared hectorite catalysts. *Journal of Catalysis* 99, 316–326.
- Occelli, M.L., Auroux, A., Ray, G.J., 2000. Physicochemical characterization of a Texas montmorillonite pillared with polyoxocations of aluminium. II. NMR and microcalorimetry results. *Microporous and Mesoporous Materials* 39, 43–56.
- Ohler, N., Bell, A.T., 2002. Properties and reactivity of Keggin structures. *Chemical Engineering*, 245: Catalysis, 1–16.
- Palinko, I., Kiricsi, I., Tasi, G., Varga, K., 1993. Thermal behaviour of montmorillonite pillared with different metal oxides. *Journal of Thermal Analysis* 39, 197–205.
- Parker, W.O. Jr., Kiricsi, I., 1995. Aluminum complexes in partially hydrolyzed aqueous  $\text{AlCl}_3$  solutions used to prepare pillared clay catalysts. *Applied Catalysis A: General* 121, L7–L11.
- Pesquera, C., Gonzalez, F., Hernando, M.J., Blanco, C., Benito, I., 1995. Selectivity in the conversion of *n*-heptane on an Al-PILC modified with Ga. *Reaction Kinetics and Catalysis Letters* 55, 267–274.
- Pinnavaia, T.J., 1983. Intercalated clay catalysts. *Science* 220, 365–371.
- Pinnavaia, T.J., 1984. Preparation and properties of pillared and delaminated clay catalysts. In: Shapiro, B.L. (Ed.), *Heterogeneous Catalysis*. Texas A&M University Press, College Station, pp. 142–164.
- Pinnavaia, T.J., 1992. Approaches to the synthesis of super gallery pillared clays. In: Occelli, M.L., Robson, H.E. (Eds.), *Expanded Clays and Other Microporous Solids*. Van Nostrand Reinhold, New York, pp. 1–12.
- Pinnavaia, T.J., Johnson, I.D., 1986. Pillared interlayered clays and method of preparation. US Patent 4 621 070.
- Pinnavaia, T.J., Tzou, M.S., Landau, S.D., Raythatha, R.J., 1984. On the pillaring and the delamination of smectite clay catalysts by polyoxocations of aluminum. *Journal of Molecular Catalysis* 27, 195–212.
- Pinnavaia, T.J., Landau, S.D., Tzou, M.S., Johnson, I.D., 1985. Layer cross-linking in pillared clays. *Journal of the American Chemical Society* 107, 7222–7224.
- Pires, J., Machado, M., Brotas de Carvalho, M., 1998. Porosity and thermal stability of PILCs prepared with clays from different origins and different metal-polyhydroxycationic species of Al and Al/Ce. *Journal of Materials Chemistry* 8, 1465–1469.
- Plée, D., Borg, F., Gatineau, L., Fripiat, J.J., 1985. High resolution solid state  $^{27}\text{Al}$  and  $^{29}\text{Si}$  nuclear magnetic resonance study of pillared clays. *Journal of the American Chemical Society* 107, 2362–2369.

- Rightor, E.G., Tzou, M.S., Pinnavaia, T.J., 1991. Iron oxide pillared clay with large gallery height: synthesis and properties as a Fischer-Tropsch catalyst. *Journal of Catalysis* 130, 29–40.
- Robertson, R.H.S., 1986. *Fuller's Earth A History of Calcium Montmorillonite*. Volturna Press, Hythe Kent.
- Sakurai, H., Urabe, K., Izumi, Y., 1990. Pillared tetrasilic mica catalysts modified by fixed interlayer cations. Classification of fixation mode by cations. *Bulletin of the Chemical Society of Japan* 63, 1389–1395.
- Salerno, P., Mendioroz, S., 2002. Preparation of Al-pillared montmorillonite from concentrated dispersions. *Applied Clay Science* 22, 115–123.
- Sanchez, A., Montes, M., 1998. Influence of the preparation parameters (particle size and aluminium concentration) on the textural properties of Al-pillared clays for a scale-up process. *Microporous and Mesoporous Materials* 21, 117–125.
- Sawhney, B.L., 1968. Aluminum interlayers in layer silicates: effect of OH/Al ratio of Al solution, time of reaction, and type of structure. *Clays and Clay Minerals* 16, 157–163.
- Schoonheydt, R.A., Leeman, H., 1992. Pillaring of saponite in concentrated medium. *Clay Minerals* 27, 249–252.
- Schoonheydt, R.A., Van Den Eynde, J., Tubbax, H., Leeman, H., Stuyckens, M., Lenotte, I., Stone, W.E.E., 1993. The aluminum pillaring of clays. Part I. Pillaring with dilute and concentrated aluminum solutions. *Clays and Clay Minerals* 41, 598–607.
- Schoonheydt, R.A., Leeman, H., Scorpion, A., Lenotte, I., Grobet, P., 1994. The Al pillaring of clays. Part II. Pillaring with  $\text{Al}_{13}\text{O}_4(\text{OH})_{24}(\text{H}_2\text{O})_{12}$ . *Clays and Clay Minerals* 42, 518–525.
- Schoonheydt, R.A., Pinnavaia, T., Lagaly, G., Gangas, N., 1999. Pillared clays and pillared layered solids. *Pure and Applied Chemistry* 71, 2367–2371.
- Schutz, A., Plée, D., Borg, F., Jacobs, P., Poncelet, G., Fripiat, J.J., 1987. Acidity and catalytic properties of pillared montmorillonite and beidellite. In: Schultz, L.G., van Olphen, H., Mumpton, F.A. (Eds.), *Proceedings of the International Clay Conference*, Denver, 1995, The Clay Minerals Society. Bloomington, IN, pp. 305–310.
- Shabtai, J., Frydman, N., Lazar, R., 1976. Synthetic and catalytic properties of a 1,4-diazabicyclo [2,2,2] octane–montmorillonite system—a novel type of molecular sieve. *Proceedings of the 6th International Congress on Catalysis*, vol. B5, pp. 660–666.
- Singh, S.S., Kodama, H., 1988. Reactions of polynuclear hydroxyaluminium cations with montmorillonite and the formation of a 28 Å-pillared complex. *Clays and Clay Minerals* 36, 397–402.
- Skoularikis, N.D., Coughlin, R.W., Kostapapas, A., Carrado, K., Suib, S.L., 1988. Catalytic performance of iron (III) and chromium (III) exchanged pillared clays. *Applied Catalysis* 39, 61–76.
- Srinivasan, K.R., Fogler, H.S., 1990a. Use of inorgano-organo clays in the removal of priority pollutants from industrial waste waters: structural aspects. *Clays and Clay Minerals* 38, 277–286.
- Srinivasan, K.R., Fogler, H.S., 1990b. Use of inorgano-organo clays in the removal of priority pollutants from industrial waste waters: adsorption of benzo(a)pyrene and chlorophenols from aqueous solutions. *Clays and Clay Minerals* 38, 287–293.
- Sterte, J., 1986. Synthesis and properties of titanium oxide crossed-linked montmorillonite. *Clays and Clay Minerals* 34, 658–664.

- Sterte, J., 1990. Preparation and properties pillared interstratified illite/smectites. *Clays and Clay Minerals* 38, 609–616.
- Sterte, J., 1991. Preparation and properties of large-pore La–Al-pillared montmorillonite. *Clays and Clay Minerals* 39, 167–173.
- Sterte, J., Shabtai, J., 1987. Cross-linked smectites. V. Synthesis and properties of hydroxy-silicoaluminum montmorillonites and fluorohectorites. *Clays and Clay Minerals* 35, 429–439.
- Storaro, L., Ganzerla, R., Lenarda, M., Zanoni, R., 1995. Vapour phase deep oxidation of chlorinated hydrocarbons catalyzed by pillared bentonites. *Journal of Molecular Catalysis A: Chemical* 97, 139–143.
- Storaro, L., Lenarda, M., Ganzerla, R., Rinaldi, A., 1996. Preparation of hydroxy Al and Al/Fe pillared bentonites from concentrated clay suspensions. *Microporous Materials* 6, 55–63.
- Storaro, L., Ganzerla, R., Lenarda, M., Zanoni, R., Antonio, J., Lopez, J., Olivera-Pastor, P., Castellon, E.R., 1997. Catalytic behavior of chromia and chromium-doped alumina pillared clay materials for the vapour phase deep oxidation of chlorinated hydrocarbons. *Journal of Molecular Catalysis A: Chemical* 115, 329–338.
- Storaro, L., Lenarda, M., Perissinotto, M., Lucchini, V., Ganzerla, R., 1998. Hydroxy-Al pillaring of concentrated suspensions of smectites clays. *Microporous and Mesoporous Materials* 20, 317–331.
- Suquet, H., Chevalier, S., Marcilly, C., Barthomeuf, D., 1991. Preparation of porous materials by chemical activation of the Liano vermiculite. *Clay Minerals* 26, 49–60.
- Tang, X., Xu, W.-Q., Shen, Y.-F., Suib, S.L., 1993. Synthesis and characterization of gallium pillared clay catalysts for aromatization of butane. *The American Chemical Society, Division of Petroleum Chemistry* 38, 516–517.
- Tang, X., Xu, W.-Q., Shen, Y.-F., Suib, S.L., 1995. Preparation and characterization of pillared gallium aluminum clays with enriched pillars. *Chemistry of Materials* 7, 102–110.
- Tennakoon, D.T.B., Jones, W., Thomas, J.M., 1986. Structural aspect of metal-oxide-pillared sheet silicates. *Journal of the Chemical Society, Faraday Transactions* 82, 3081–3095.
- Tichit, D., Mountassir, Z., Figueras, F., Auroux, A., 1991. Control of the acidity of montmorillonites pillared by Al-hydroxy cationic species. In: Poncelet, G., Jacobs, P.A., Grange, P., Delmon, B. (Eds.), *The Preparation of Catalysts V*. Elsevier, Amsterdam, pp. 345–353.
- Toranzo, R., Vicente, M.A., Banares-Munoz, M.A., 1997. Pillaring of a saponite with aluminum–chromium oligomers. Characterization of the solids obtained. *Chemistry of Materials* 9, 1829–1836.
- Toranzo, R., Vicente, M.A., Banares-Munoz, M.A., Gandia, L.M., Gil, A., 1998. Pillaring of saponite with zirconium oligomers. *Microporous and Mesoporous Materials* 173, 173–188.
- Trillo, J.M., Alba, M.D., Alvero, R., Castro, M.A., Poyato, J., Tobias, M.M., 1991. Effect of La(III) on the thermal stability of Al-pillared montmorillonite. In: Rodriguez-Reinoso, F., Rouquerol, J., Sing, K.S.W. (Eds.), *Characterization of Porous Solids II*. Elsevier, Amsterdam, pp. 607–613.
- Trillo, J.M., Alba, M.D., Alvero, R., Castro, M.A., Muñoz, A., Poyato, J., Tobias, M.M., Lagaly, G., 1993a. Montmorillonites intercalated with Al(III), La(III) and alumina pillars: structural aspects and reactivity. *Solid State Ionics* 63–65, 457–463.

- Trillo, J.M., Alba, M.D., Alvero, R., Castro, M.A., Poyato, J., Tobias, M.M., 1993b. Alumina pillared montmorillonite: effect of thermal and hydrothermal treatment on the accessible micropore volume. *Journal of Materials Science* 28, 373–378.
- Urabe, K., Kenmoku, I., Kawabe, K., Izumi, Y., 1991. Talc-derived pillared clay as an acidity tunable catalyst. *Journal of the Chemical Society, Chemical Communications* 13, 867–868.
- Vaccari, A., 1998. Preparation and catalytic properties of cationic and anionic clays. *Catalysis Today* 41, 53–71.
- Valverde, J.L., Sanchez, P., Dorado, F., Molina, C.B., Romero, A., 2002. Influence of the synthesis conditions on the preparation of titanium-pillared clays using hydrolysed titanium ethoxide as the pillaring agent. *Microporous and Mesoporous Materials* 54, 155–165.
- Valverde, J.L., de Lucas, A., Sanchez, P., Dorado, F., Romero, A., 2003. Cation exchanged and impregnated Ti-pillared clays for selective catalytic reduction of  $\text{NO}_x$  by propylene. *Applied Catalysis B: Environmental* 43, 43–56.
- Vaughan, D.E.W., 1988a. Recent developments in pillared interlayered clays. In: Flank, W.H., Whyte, Jr., T.E. (Eds.), *Perspective in Molecular Sieve Science*. American Chemical Society, Washington, DC, pp. 308–323.
- Vaughan, D.E.W., 1988b. Pillared clays—a historical perspective. In: Burch, R. (Ed.), *Catalysis Today* 2, 187–198.
- Vaughan, D.E.W., Lussier, R.J., Magee, S.J. Jr., 1979. Pillared interlayered clay materials useful as catalysts and sorbents. US Patent 4 176 090.
- Vicente, M.A., Lambert, J.-F., 2003. Al-Pillaring of saponite with the Al polycation  $[\text{Al}_{13}(\text{OH})_{24}(\text{H}_2\text{O})_{24}]^{15+}$  using a new synthetic route. *Clays and Clay Minerals* 51, 168–171.
- Vieira Coelho, A., Poncelet, G., 1990. Preparation, characterization and some catalytic properties of different smectites pillared with hydroxyaluminium and hydroxygallium solutions. Preliminary study—pillared layered structures. In: Mitchell, I.V. (Ed.), *Pillared Layered Structures. Current Trends and Applications*. Elsevier Applied Science, London, pp. 185–193.
- Vieira Coelho, A., Poncelet, G., 1991. Gallium, aluminium and mixed gallium–aluminium pillared montmorillonite: preparation and characterization. *Applied Catalysis* 77, 303–314.
- Wada, S.-I., Wada, K., 1980. Formation, composition and structure of hydroxy-aluminosilicate ions. *Journal of Soil Science* 31, 457–467.
- Wong, S.T., Cheng, S., 1993. Pillared layered manganese oxide. Synthesis and redox properties. *Journal of Thermal Analysis* 40, 1181–1192.
- Yamanaka, S., Brindley, G.W., 1978. Hydroxy-nickel interlayering in montmorillonites by titration method. *Clays and Clay Minerals* 26, 21–24.
- Yamanaka, S., Takahama, K., 1993. Micro- and mesoporous clays pillared with  $\text{SiO}_2$ – $\text{TiO}_2$  mixed oxide sols. In: Sequeira, C.A.C., Hudson, M.J. (Eds.), *Multifunctional Mesoporous Inorganic Solids*. Kluwer Academic Publishers, Dordrecht, pp. 237–258.
- Yamanaka, S., Doi, T., Sako, S., Hattori, M., 1984. High surface area solids obtained by intercalation of iron oxide pillars in montmorillonite. *Materials Research Bulletin* 19, 161–168.
- Zhao, D., Yang, Y., Guo, X., 1992. Preparation and characterization of hydroxysilicoaluminium pillared clays. *Inorganic Chemistry* 31, 4727–4732.

- Zhao, D., Wang, G., Yang, Y., Guo, X., Wang, Q., Ren, J., 1993a. Preparation and characterization of hydroxy-FeAl pillared clays. *Clays and Clay Minerals* 41, 317–327.
- Zhao, D., Wang, G., Yang, Y., Guo, X., Wang, Q., 1993b. Preparation and characterization of lanthanum-doped pillared clays. *Materials Research Bulletin* 28, 939–949.
- Zhao, D., Yang, Y., Guo, X., 1995. Synthesis and characterization of hydroxy-Cr–Al pillared clays. *Zeolites* 15, 58–66.
- Zonghui, L., Guida, S., 1985. Factors affecting acidity and basal spacing of crossed-linked smectites. In: Drzaj, B., Hocevar, S., Pejovnik, S. (Eds.), *Studies in Surface Science and Catalysis* 24. Zeolites. Elsevier, Amsterdam, pp. 493–500.



This page intentionally left blank

*Chapter 8*

## **PROPERTIES AND BEHAVIOUR OF IRON IN CLAY MINERALS**

**J.W. STUCKI**

*Department of Natural Resources and Environmental Sciences, University of Illinois, W-321 Turner Hall, 1102 S. Goodwin Ave, Urbana, IL 61801-4798, USA*

Because iron (Fe) is the fourth most abundant element in the Earth's crust (6% of mass), next to oxygen, silicon, and aluminium, its ubiquitous presence in clays and clay minerals should be no surprise. It is, in fact, an intimate part of many processes occurring in natural ecosystems. [Murad and Fischer \(1988\)](#) have reviewed many pools of iron that exist in nature and discussed the geobiochemical cycle of iron (summarised briefly in [Fig. 8.1](#)), illustrating how it is transformed from one pool to another. They have also pointed out the many connections within and between the mineral or inorganic phases of iron and its organic or biological phases in the environment. The number and complexity of these interactions are great, so a complete discussion of the significance of terrestrial iron would fill many volumes. In this chapter, emphasis is placed on a description of the phases in which iron occurs in clay minerals and the properties and behaviours it imparts to them by virtue of its susceptibility to oxidation and reduction (redox) reactions. As is evident from [Fig. 8.1](#), redox is a pathway that is common to several of the inter-pool transformations and thus exerts much influence on terrestrial ecosystems.

An expanded treatise on iron in soils and clay minerals was published by [Stucki et al. \(1988\)](#), who reviewed the chemistry, detection, and characterisation of iron in oxides, carbonates, sulphides and sulphates, phyllosilicates, agricultural soils, hydromorphic and lateritic soils, and pedogenic processes. The treatise also touched on the role of microorganisms in determining the fate of iron in soils and sediments. Since that work was published, much progress has been made in understanding and characterising structural iron in smectites, especially in relation to redox processes. Advances have also been made in the study of iron in other phyllosilicate minerals such as kaolinite and mica.

The effects of structural iron on clay mineral properties have been reviewed by [Stucki \(1988\)](#) and [Stucki and Lear \(1989\)](#). Since then little new information has come to light regarding the overall effect of structural iron on clay mineral properties, although much has been learned about the effects brought about by changes in the

## Pools of Iron in Soils

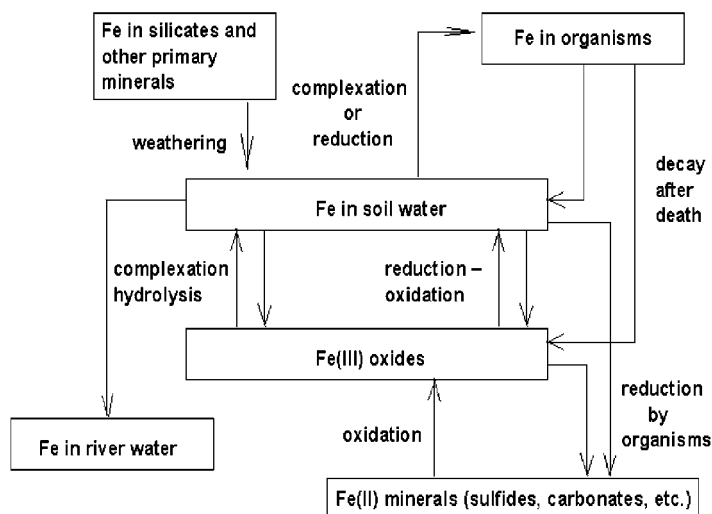


Fig. 8.1. Illustration of some of the forms of Fe that exist in the Earth's crust and how they interact. From Murad and Fischer (1988).

oxidation state of iron (Stucki et al., 2002). The current chapter will focus largely on the latter aspect.

### 8.1. PHASES OF IRON IN CLAY MINERALS

Iron-bearing clays are ubiquitous in nature; in fact, the presence of iron in the structure of smectites is clearly the rule rather than the exception. They may form through natural or synthetic processes (Stucki, 1988; Badraoui and Bloom, 1990; Aoki and Kohyama, 1991; Boiabid et al., 1991; Badaut et al., 1992; Decarreau et al., 1992; Martin et al., 1992, 1998; Grauby, 1993; Grauby et al., 1993, 1994; Petit et al., 1995; Giresse and Wiewiora, 2001). Stucki (1988) has illustrated the classification scheme for iron-bearing smectites, for which nontronite is the dioctahedral end member. A number of nontronites, varying in total iron contents and some fine detail of their properties, have been studied (Köster et al., 1999; Gates et al., 2002). The supply of many of these samples is dwindling, but a new source that is less limited was recently discovered in Australia (Keeling et al., 2000) and reports of its characteristics are now beginning to emerge (Frost et al., 2002a, 2002b; Gates et al., 2002). Montmorillonite also contains structural iron, but to an extent of about 3% by weight compared with about 20% or more for nontronite.

Iron may occur in both the octahedral and tetrahedral sheets of 1:1 and 2:1 clay minerals, and in the gibbsite/brucite sheet of 2:1:1 minerals. Iron can also exist as a compensating (charge-balancing) cation on clay mineral exchange complex (Diamant et al., 1982; Yamagishi, 1982; Helsen and Goodman, 1983; Johnston and Cardile, 1985; Coyne and Banin, 1986; Thompson and Tahir, 1991; Hirt et al., 1993; Choudary et al., 1994; Ebitani et al., 2002; Letaief et al., 2002), or as pillars between the 2:1 layers (Bergaya and Barrault, 1990; Bergaya et al., 1991; Rightor et al., 1991; Mody et al., 1993; Komadel et al., 1994; Mishra and Parida, 1998; Wasserman and Soderholm, 1998; Chirchi and Ghorbel, 2002). In natural soils, iron (hydr)oxides (usually  $\text{Fe}^{3+}$  forms) are commonly precipitated or adsorbed on clay mineral surfaces or admixed as a separate phase (Murad, 1987, 1988; Schwertmann, 1988a, 1988b). Minerals containing  $\text{Fe}^{2+}$  are also important, such as vivianite (Nembrini et al., 1983; Hansen and Poulsen, 1999), siderite (Loeppert, 1988), and pyrite (van Breemen, 1988b, 1988c). In sulphur-rich and oxidising environments, jarosite is commonly formed (van Breemen, 1988a, 1988b, 1988c). Green rust is a mixed-valent iron mineral that has attracted much recent interest (Murad and Taylor, 1984; Hansen, 1989; Cuttler et al., 1990; Koch and Morup, 1991; Schwertmann and Fechter, 1994; Genin et al., 1998; Erbs et al., 1999; Hansen and Poulsen, 1999; Lee and Batchelor, 2002) and appears to be a highly reactive iron phase in some soils and sediments. Characterising the distribution of iron among these various phases and crystallographic sites is both a challenging and a rewarding endeavour, warranting the expenditure of much effort and energy.

#### 8.1.1. Phase Identification

After reviewing many studies on the subject of iron-phase identification, one concludes that identifying the location of iron with respect to the general phases (e.g., oxide, phyllosilicate) is more readily accomplished than pin-pointing the exact site in which it is located (e.g., *cis*-, *trans*-octahedral, tetrahedral, exchanged). The mixing of iron (hydr)oxides with iron-bearing smectites is readily observed using Mössbauer spectroscopy (Fig. 8.2a). The iron (hydr)oxides are identified by the component peaks of a six-line pattern and the silicate iron is identified from the main central doublet at about 0.3 mm/sec and the additional feature located at about 2.2 mm/sec. The six-line features of the (hydr)oxides are readily distinguished from silicate structural  $\text{Fe}^{3+}$  and  $\text{Fe}^{2+}$ , especially if the Mössbauer spectra are obtained at the temperature of liquid He (4.2 K) when all iron oxides are magnetically ordered but the iron in the silicate is not. The Mössbauer spectrum may also be used to establish the identity of iron oxides that may be present by examining the Mössbauer hyperfine parameters (isomer shift, quadrupole shifting, and magnetic hyperfine field) (Murad, 1987, 1988, 1998; Murad et al., 1990; Rancourt, 1998).

The complete separation of these various phases as a pure component by either chemical or physical means is highly unlikely, if not impossible. The iron (hydr)oxide can, however, be effectively removed by the CBD reductive dissolution treatment

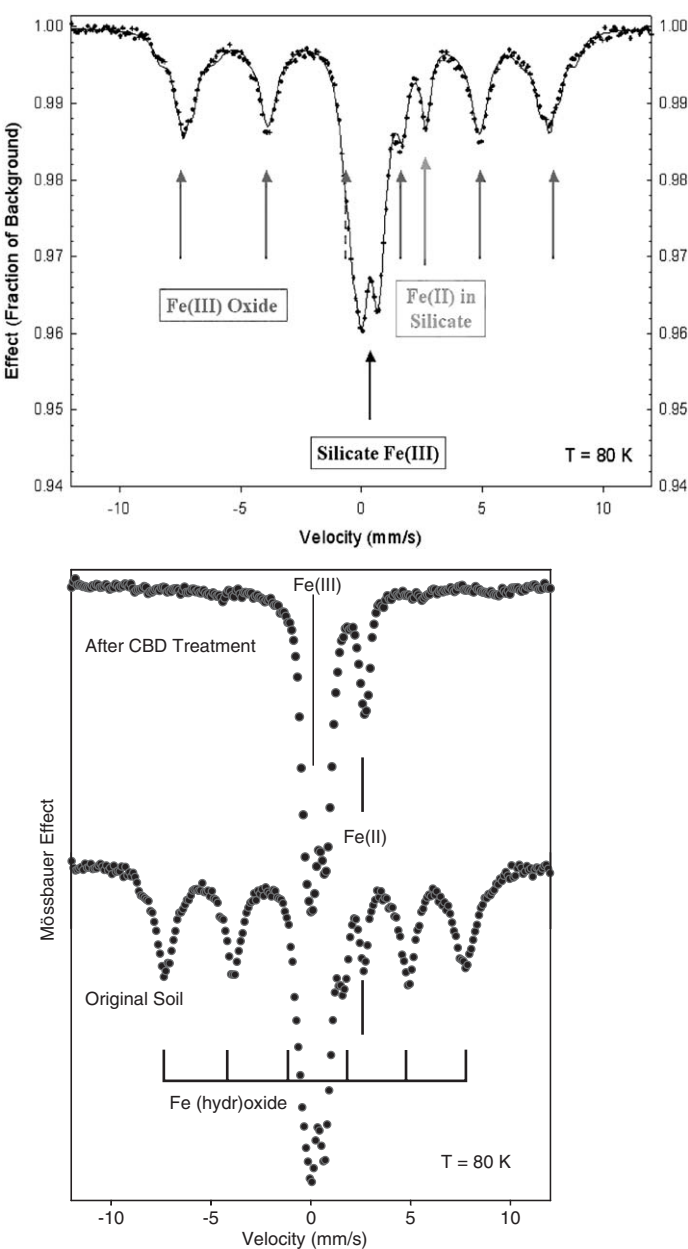


Fig. 8.2. (Top) Example Mössbauer spectrum of a saprolitic soil sample containing Fe in both oxides and silicates and in both Fe(III) and Fe(II) oxidation states. (Bottom) Mössbauer spectrum of the same saprolitic soil sample as in Fig. 8.2a, which was treated with citrate–bicarbonate–dithionite to remove the Fe oxide phases.

(citrate–bicarbonate–dithionite as described by Mehra and Jackson (1960)) as indicated by the disappearance of the six-line pattern from the Mössbauer spectrum (Fig. 8.2b). Removal of only the poorly crystalline, or more readily soluble, iron oxide phases can also be carried out using various methods such as ammonium oxalate or dilute HCl extractions (Borggaard, 1988). Complete separation or removal of the iron oxide phases by chemical means without in some way altering the remaining phases is, with current practice, unlikely. The importance of such cross-cutting effects on the other phases may be of limited significance compared with the advantages attained by removal of the iron. Alternatively, a certain level of refined physical separation can be accomplished by successive and repeated particle-size fractionations (Manceau et al., 2000a). The latter approach is non-specific for iron, so it also removes much of the other, non-iron phases such as quartz, which may have been present in a finely divided form. A possible disadvantage of this physical separation is that the resulting particle-size fraction of the recovered clay mineral phase is of limited range.

#### 8.1.2. Distribution between Octahedral and Tetrahedral Sites

Iron may be distributed randomly or clustered in the octahedral sheet, with the latter occurring normally in the iron-rich smectites. Theoretically, however, clustering could also occur in iron-poor smectites; but, magnetic susceptibility measurements (Schuette et al., 2000) of oxidised and reduced Upton montmorillonite (total iron = 3% by weight) only indicate paramagnetic ordering. This means that the iron ions are too far apart to interact with one another; and no intervalence electron transfer band is observed in partially reduced montmorillonite. On the other hand, strong interactions are observed in the iron-rich smectites. These two methods, i.e., magnetic susceptibility and visible absorption spectroscopy, combined with partial reduction of structural iron, provide a convenient method to determine the distribution of iron ions relative to one another.

A discussion about how iron is distributed between the *cis* (M2) and *trans* (M1) octahedral sites in 2:1 dioctahedral smectites has been going on for many years. Although it is continuing; some things are now more clear. A rule that continues to be generally accepted is that the more iron-rich the layer, the more vacant the M1 sites (centrosymmetric structure, sometimes referred to as *trans*-vacant); and, conversely, the more iron-poor, the more populated the M1 sites (non-centrosymmetric structure). In other words, nontronite and ferruginous smectite are largely, if not completely, *trans*-vacant, whereas montmorillonite contains some  $\text{Fe}^{3+}$  in the M1 sites. These conclusions are based on a variety of spectroscopic and structural measurements, including X-ray diffraction, selected area diffraction, Mössbauer, and infrared (Tsipursky et al., 1978; Bookin et al., 1979; Besson et al., 1981, 1983; Drits et al., 1981; Tsipursky and Drits, 1984; Dainyak et al., 1984a, 1984b, 1992; Dainyak and Drits, 1987; Muller et al., 1997).

The least reliable method for this purpose is Mössbauer spectroscopy. Soon after its advent as a tool in iron clay mineral chemistry, the curve fitting of its absorption spectrum almost always required two doublets for octahedral  $\text{Fe}^{3+}$  in order to obtain a proper match of experimental and theoretical spectra. The temptation was to assign these two doublets of slightly different quadrupole splitting to the *cis* and *trans* sites (e.g., Goodman et al. (1976); Rozenson and Heller-Kallai (1977); Goodman (1978); Russell et al. (1979); Heller-Kallai and Rozenson (1981)). This spectral interpretation has since been suggested to be a great over-simplification of a Mössbauer spectrum, and spectral fittings using a distribution of quadrupole splittings are now becoming the preferred practice. Rancourt and co-workers (Rancourt, 1989, 1994a, 1994b, 1998; Rancourt et al., 1993, 1994a, 1994b) have thoroughly discussed the analytical and experimental requirements if Mössbauer spectroscopy is to be used for the identification of specific site symmetries.

While the strictly centrosymmetric structure of oxidised (unaltered) nontronite is widely accepted, magnetic susceptibility measurements of a series of nontronites have raised some doubt regarding the complete absence of  $\text{Fe}^{3+}$  in M1 sites. Lear and Stucki (1990) and Schuette et al. (2000) reported magnetic susceptibility of five nontronites, ranging in total iron content from about 18 to 24% iron by weight. In every case, these nontronites exhibit frustrated anti-ferromagnetism, meaning that the inverse susceptibility versus temperature plots fail to reveal the characteristic cusp at the magnetic ordering temperature as seen with ferripyrophyllite (Coey et al., 1983), and instead continue downward as they do when magnetic frustration occurs (Ballet and Coey, 1982; Coey, 1988). The cusp is expected if the structure is strictly centrosymmetric. Manceau et al. (2000a) have offered alternative explanations for each of these nontronites that reconcile these aberrant data with the other structural observations. However, since the data are rather uniform and the explanations are non-uniform, further studies of the magnetic interactions in iron-bearing smectites appear to be warranted in order to understand these inconsistencies better.

The vibrational energy of structural OH groups reveals the presence of octahedral iron, as pointed out by Stubican and Roy (1961a, 1961b, 1961c) and Farmer and Russell (1964, 1966, 1967), and again more recently by Robert and Kodama (1988), Bishop et al. (2002), Madejová et al. (1992, 1994, 1995), and Petit et al. (1999). If  $\text{Fe}^{3+}$  is present, the shift is to lower frequency. Reduction of  $\text{Fe}^{3+}$  to  $\text{Fe}^{2+}$  causes an even further shift to lower frequency (Stucki and Roth, 1976; Fialips et al., 2002a, 2002b; Lee et al., 2006). If used in combination with other structural information, such as EXAFS (Manceau et al., 2000b; Li et al., 2003, 2005), and by extending the range of analysis to both the mid- and near-infrared regions of the spectrum, this method would add further detail that may be helpful in distinguishing local coordination symmetry for structural iron.

Much less is known about the amount, chemistry, and behaviour of tetrahedral iron than of octahedral iron in smectites. Tetrahedral iron evidently is always in the trivalent state, since no case of tetrahedral  $\text{Fe}^{2+}$  has been reported in phyllosilicates and its ionic radius is too large for that site. The historical or traditional approach

for calculating structural formulas first places excess  $\text{Al}^{3+}$  in the tetrahedral sheet, then  $\text{Fe}^{3+}$  if required to satisfy the  $\text{Si}^{4+}$  deficit. This assignment order is arbitrary (Luca and Cardile, 1989; Luca, 1991a, 1991b; Luca and Maclachlan, 1992; Manceau et al., 2000a; Gates et al., 2002) and creates the potential for underestimating the amount of tetrahedral iron; so, published formulas using this approach should be viewed skeptically insofar as the tetrahedral iron content is concerned.

Conclusive, quantitative evidence for the substitution of  $\text{Fe}^{3+}$  for  $\text{Si}^{4+}$  in tetrahedral sites continues to be rather elusive, but some progress has been made over the past two decades. An early strategy for measuring tetrahedral  $\text{Fe}^{3+}$  was proposed by Osthhaus (1953, 1956), based on the premise that the rate of dissolution of octahedral cations was greater than that of tetrahedral cations. He found two slopes in the plot of time versus the amount of iron released during HCl dissolution. Tetrahedral iron was estimated by extrapolating the lesser rate to time zero. Komadel and co-workers (Čičel et al., 1990; Komadel et al., 1993, 1996, 1998; Madejová et al., 1993, 1998; Tkáč Komadel, 1999), however, have found that the rates of dissolution of octahedral and tetrahedral cations are the same. Cardile (1989) and Luca and Maclachlan (1992) have also questioned the validity of Osthhaus' approach. The underlying premise for the selective dissolution method has, therefore, been discounted and alternative methods for assigning tetrahedral iron must be found.

Cardile (1989), Cardile and Slade (1987), Johnston and Cardile (1985, 1987), Luca (1991), and Luca and Cardile (1989) have proposed that Mössbauer spectroscopy can be used to identify tetrahedral iron by emphasizing the small shoulder on the low energy side of the main central peak in dioctahedral, iron-rich smectites. This is done by saturating the smectite with a high charge density cation such as  $\text{Ca}^{2+}$ , then dehydrating at  $300^\circ\text{C}$  to bring about an interaction between the interlayer cation and the tetrahedral iron. By this method, the tetrahedral  $\text{Fe}^{3+}$  content of Garfield nontronite has been estimated to be about 9% (Johnston and Cardile, 1985) and of ferruginous smectite (SWa-1) about 5% (Luca and Cardile, 1989). The author (J.W. Stucki, unpublished results) was able to reproduce Luca and Cardile's (1989) Mössbauer spectra for  $\text{Ca}^{2+}$ -exchanged, dehydrated ferruginous smectite SWa-1, but X-ray absorption near-edge spectroscopy (XANES) failed to verify that this sample contained tetrahedral iron (Manceau et al., 2000a). Of the four nontronites (ferruginous smectite, SWa-1; Panamint Valley; Garfield; and Hohen Hagen, NG-1) studied by Manceau et al. (2000a) using XANES, conclusive evidence for tetrahedral iron was found in only the NG-1 sample. Its level was very high at about 17% of total iron. In the case of the other two nontronites (Panamint Valley and Garfield), the Mössbauer (J. W. Stucki, unpublished data) and XANES results were consistent in indicating no tetrahedral iron. Other workers have also found XANES to be a useful method to help sort out the site occupancy questions of structural iron (Dyar et al., 2001, 2002).

Gates et al. (2002) performed an in-depth analysis of the tetrahedral  $\text{Fe}^{3+}$  content of 14 different nontronites and ferruginous smectites using near-infrared, XANES, polarised EXAFS, and XRD methods. They concluded that the tetrahedral  $\text{Fe}^{3+}$  contents for these respective samples were: (1) ferruginous smectites, none; (2)



Manito nontronite (API #33-b), 3%; (3) Bingham nontronite, 6.5%; (4) Garfield, ~3% (except the oriented powder method gave a value of 10.5%); (5) Hohen Hagen (NG-1), 16.5%; (6) Spokane, 15.3%; (7) Clausthal Zellerfeld, 19.8%, (8) NAu-1, 1.9%; (9) NAu-2, 7.6%; (10) Mountainville, Pennsylvania, 5.8%; and (11) Tasmania, 10.8%. As these results indicate, the amount of tetrahedral  $\text{Fe}^{3+}$  can be rather substantial. Using these data, calibrations of other methods, including Mössbauer spectroscopy, may be possible.

Sherman and Vergo (1988) have observed an  ${}^6\text{A}_1 \rightarrow {}^4\text{E}_1, {}^4\text{A}_1$  ( ${}^4\text{G}$ ) electronic transition for tetrahedrally coordinated  $\text{Fe}^{3+}$  in nontronites, occurring at 429–434 nm in the visible spectrum. Since this is a Laporte-allowed ligand-field transition, its absorption coefficient is 10–100 times that of octahedral  $\text{Fe}^{3+}$ , potentially making it an excellent indicator for even small amounts of tetrahedral iron. Surprisingly, this method for distinguishing tetrahedral  $\text{Fe}^{3+}$  has received no further attention; although, with the application of suitable curve-fitting techniques, it could very well provide a wealth of untapped information.

## 8.2. METHODS FOR IRON REDUCTION

Structural iron in the octahedral sheet of smectites is clearly more difficult to reduce than iron in hydr(oxides), because it is located at a distance of several Å from the point of closest approach (basal surfaces) by any reducing agent. How this gap is overcome is unknown and is at the source of understanding the electron transfer process. Many different reducing agents have been tried (summarised in Table 8.1), including hydrazine, hydrogen gas, and hydrogen sulphide, but the two most commonly used agents are dithionite and bacteria. Hydrazine may be effective in low-iron smectites, but it is a poor reductant of iron-rich smectites. The two most widely used methods are described in more detail below.

### 8.2.1. Dithionite

Most studies of the variable oxidation states of iron in smectites have focused on the use of sodium dithionite as the reducing agent in citrate–bicarbonate buffered suspensions. The dithionite method is based on the procedure of Mehra and Jackson (1960), devised to remove iron oxides from soils, as modified by Roth et al. (1968, 1969), Stucki and Roth (1977), and Stucki et al. (1984b) for smectites.

The method typically involves preparing the smectite suspension in an 8:1 (v/v) 0.3 M Na-citrate:1.0 M Na-bicarbonate buffered (C–B) solution in a septum-capped reaction tube, heating the suspension to 70 °C with continuous purge of  $\text{O}_2$ -free  $\text{N}_2$  gas, adding Na-dithionite as the salt (solid phase), and reacting for up to 4 h. The suspension is then cooled to room temperature and washed under inert-atmosphere conditions to remove excess dithionite and establish a background solute concentration. The temperature, time, and dithionite/smectite ratio all contribute to determining

Table 8.1. Summary of reducing agents used to reduce structural iron in phyllosilicates

Reducing agent	Reference*
Dithionite in citrate–bicarbonate buffer (CBD)	Stucki and Roth (1976, 1977), Anderson and Stucki (1979), Ericsson et al. (1984), Lear and Stucki (1985)
Dithionite without pH buffering	Rozenson and Heller-Kallai (1976a), Russell et al. (1979)
Hydrazine	Stucki et al. (1976), Rozenson and Heller-Kallai (1976a), Stucki and Roth (1977), Chen et al. (1979), Lerf et al. (2001)
Sulphide	Rozenson and Heller-Kallai (1976b)
Hydrogen sulphide	Kawasaki (1974)
Benzidine	Tennakoon et al. (1974), McBride (1979)
Hydrogen gas at high temperature (> 300 °C)	Kawasaki (1974), MacKenzie and Rogers (1977), Aronowitz et al. (1982), Vieira Coelho et al. (2000)
Electron irradiation	Drago et al. (1977)
Bacteria†	Stucki et al. (1987), Kostka et al. (1996)
Heating	Malysheva (1994)
Phenylenediamine	Lerf et al. (2001)
Thiourea	Bhattacharyya and Saha (1990)
Tetraphenyl boron	Hunter and Bertsch (1994), Hunter et al. (1998)

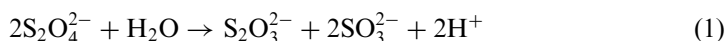
\*Not necessarily a comprehensive list, especially with respect to dithionite and bacteria.

†See Table 8.2 for a complete list.

the extent of reduction. If the amount of dithionite to be added becomes too large, it may overcome the buffering capacity of the C–B buffer. Amonette (2003) has calculated that the buffering capacity must be at least four protons per dithionite molecule. The N<sub>2</sub> purge greatly advances the level of reduction by removing the gaseous products from the otherwise closed reaction vessel (Komadel et al., 1990).

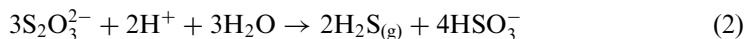
Inert-atmosphere conditions should include the removal of O<sub>2</sub> from exchange solutions by boiling while purging with O<sub>2</sub>-free N<sub>2</sub>, then exchanging solutions without exposing either the reaction system or the exchanger solution to the atmosphere. This is accomplished in the author's laboratory using a Controlled Atmosphere Liquid Exchanger—an updated version of that described by Stucki et al. (1984).

In aqueous solution the dithionite anion, S<sub>2</sub>O<sub>4</sub><sup>2-</sup>, undergoes two types of reaction. The first is the irreversible disproportionation into thiosulphate and sulphite according to the reaction (Amonette, 2003)



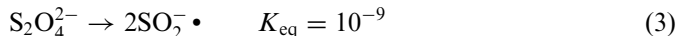
The reaction products are rather mild reductants and, in fact, are ineffective in reducing structural iron in smectite (Gan, Stucki, and Bailey, unpublished results).

Thiosulphate in acid solution further disproportionates to



where the hydrogen sulphide gas produces a pungent and easily recognisable odour. While these reactions are rather slow, they do render a solution of dithionite ineffective as a reductant of structural iron in smectite within a few hours (Gan et al., 1992). The decreased pH resulting from this reaction also creates an environment in which the smectite will dissolve, releasing  $\text{Fe}^{2+}$  ions into solution. The hydrogen sulphide will then react with  $\text{Fe}^{2+}$  to produce  $\text{FeS}$ , a black precipitate. These problems, along with the problem of dissipation of  $\text{S}_2\text{O}_4^{2-}$  reduction capacity with time in aqueous solution, are overcome by preparing the clay mineral in a pH-buffered solution including a chelate for  $\text{Fe}^{2+}$  (e.g., citrate) and by adding  $\text{S}_2\text{O}_4^{2-}$  as the solid salt rather than as a solution. The pH is thus maintained at a circum-neutral value while any dissolved  $\text{Fe}^{2+}$  is kept in solution and the reduction reaction is allowed to proceed before significant disproportionation occurs. Recent preliminary studies in the author's laboratory (Dottori and Stucki, unpublished results) indicate that the concentration of bicarbonate buffer typically used (1 M) may provide too much buffering capacity for the amount of dithionite used, so the pH can increase to  $>9$ . A proper balance between dithionite and buffer must, therefore, be considered.

The second reaction of  $\text{S}_2\text{O}_4^{2-}$  in water is the reversible breaking of the S-S bond to form two sulfoxylate free-radical anions (Rinker et al., 1964)



that are very reactive towards the reduction of structural  $\text{Fe}^{3+}$  in smectites. The sulfoxylate free radical becomes the actual reductant of structural iron in smectite, and is capable of reducing virtually all of the structural iron whereas no other reductant has yet been found that will accomplish the same. Gan et al. (1992) found a direct, linear correlation between the intensity of the EPR signal originating from the sulfoxylate unpaired electron and the level of iron reduction achieved in ferruginous smectite. They also showed that the free radical is labile with time, reinforcing the need to add the dithionite as the solid-phase salt rather than as a solution.

Dithionite has been used effectively to create spatially fixed reduced zones in sub-surface aquifers at the Hanford site, Washington, for the purpose of intercepting and chemically reducing contaminants such as  $\text{Cr}^{6+}$  and nitroaromatics (Amonette, 2003). The use of microorganisms as an alternative reductant has also proven effective.

### 8.2.2. Bacteria

Since the discovery in 1986 and 1987 by Stucki and co-workers (Stucki and Getty, 1986; Komadel et al., 1987; Stucki et al., 1987) that bacteria are able to reduce

structural  $\text{Fe}^{3+}$  in clay minerals, many studies have confirmed this finding and extended the range of possibilities for its exploitation. Wu et al. (1988) showed that bacteria in extracts from Chinese rice-paddy soils actively reduce structural iron in smectite, while Kostka et al. (1999a, 2002) and Cervini-Silva et al. (2003) reported that bacteria from a variety of origins, including well-drained and flooded soils, can reduce structural  $\text{Fe}^{3+}$  in smectite and change its physico-chemical properties.

The extent and rate of bacterial reduction vary depending on the bacterial system. The highest level of bacterial reduction of iron-rich smectite reported thus far is about 45% of the total octahedral iron. This is achieved either with an unidentified rice-paddy inoculum (Wu et al., 1988) or with the metal-reducing bacterium *Shewanella oneidensis* (*putrefaciens*) (Kostka et al., 1996). The rate of reduction is greatest with *Shewanella*, achieving the half-level of reduction in only 4 h. Other general types of bacteria known to reduce structural iron in clay minerals include *Geobacter* (reference), *Pseudomonas* (reference), and *Bacillus* (Stucki and Getty, 1986). The reduction of iron observed in rice-paddy soils presumably is also the product of bacterial activity (Boivin et al., 2002; Favre et al., 2002a, 2002b).

The basic method used for bacterial reduction will vary somewhat depending on the bacterium selected for the purpose. Some bacteria are facultative anaerobes whereas others are strict anaerobes, so the method of culture must be modified accordingly. *Shewanella*, the most often used bacteria (Gorby et al., 1994; Kostka et al., 1996), are facultative anaerobes and can be grown aerobically. However, in order to utilise  $\text{Fe}^{3+}$  as their electron acceptor, they must be cultured anaerobically in the presence of the clay mineral. In the method of Kostka et al. (1996), which uses *S. oneidensis*, the clay mineral suspension is prepared in an iron-free growth medium and sterilised (either by microwave or autoclave heating). The *Shewanella* bacteria are initially cultured aerobically in a separate vessel on a minimal  $\text{Fe}^{3+}$  medium, then an inoculum of growing cells is transferred to the sterilised smectite and incubated under anaerobic conditions. After the desired incubation time, the reaction is terminated and analyses are performed. Reaction termination can be either by sterilisation or washing with dilute NaCl solution. The former creates a sterile system in which no further bacterial activity occurs, whereas the latter simply dilutes the concentration of bacterial cells. Since the bacteria are still viable they will continue to grow slowly over time. While the presence of viable bacteria presents some problems with the stability of the reduction product, termination by washing is advantageous for samples with properties that are sensitive to the elevated temperatures of heat sterilisation (e.g., mineral-phase transformations). In this case, however, analyses would normally be carried out soon after washing and the presence of bacteria would be taken into consideration in interpreting the results.

Bacterial reduction of structural iron in phyllosilicates has now been employed in a number of studies (summarised in Table 8.2) and appears to be an area of increasing interest. These studies have focused on topics varying from the effects of bacterial reduction on clay mineral dissolution and mineral-phase transformation to effects on the transformation of chlorinated aliphatics and pesticides.

Table 8.2. Summary of studies performed in which structural  $\text{Fe}^{3+}$  in phyllosilicates was reduced by bacteria

Reference	Topic or general observation
Stucki et al. (1987)	Bacterial reduction of Fe in smectite by indigenous bacteria
Komadel et al. (1987)	<i>Pseudomonas</i> bacteria found to reduce Fe in smectite
Wu et al. (1988)	Rice-paddy bacteria reduce 41%
Gates et al. (1993)	Bacterial reduction affects clay swelling
Gorby et al. (1994)	Sub-surface bioremediation
Kostka et al. (1996)	Metal-reducing bacteria (FeRB) greatly increase rate
Lovley et al. (1998)	Humics promote rates of reduction
Gates et al. (1998)	Swelling and texture effects, TEM
Ernstsen et al. (1998)	Renewable source for <i>in situ</i> nitrate reduction
Kostka et al. (1999a)	CEC, surface area, organic cations, and UV-vis reflectance
Kostka et al. (1999b)	Bacterial Fe reduction coupled with respiration, Fe dissolution
Xu et al. (2001)	Pesticide degradation
Kostka et al. (2002)	Growth with smectite as sole electron acceptor
Favre et al. (2002a)	CEC of reduced Fe soil smectite
Favre et al. (2002b)	More CEC changes in soil clay
Dong et al. (2003a)	Dissolution, then reprecipitation of biogenic smectite and vivianite
Dong et al. (2003b)	AQDS necessary for bacterial reduction of illite
Cervini-Silva et al. (2003)	Degradation of chlorinated aliphatics
Kim et al. (2003)	Texture by Environmental Cell TEM, observed collapsed layers
Kim et al. (2004)	Dissolution of nontronite by <i>S. oneidensis</i> , reprecipitation of illite
Favre et al. (2004)	TEM, CEC, texture of reduced soil clays

### 8.3. SURFACE INTERACTIONS WITH WATER

Smectites are well known for their affinity for water (Low, 1961, 1979, 1980, 1987). Structural  $\text{Fe}^{3+}$  and  $\text{Fe}^{2+}$  both significantly affect the smectite–water interaction. Early studies (reviewed by Stucki, 1988) indicated that the swelling of smectite is influenced by the cationic composition of the mineral layer, and that the presence of octahedral  $\text{Fe}^{3+}$  has a modest but generally depressing effect on water retention capacity. A more pronounced effect is observed when the structural iron is reduced. This phenomenon was first observed by Foster (1953, 1955), who found that the blue-grey form of Wyoming montmorillonite swelled to about half the water volume as the olive-green form, while the  $\text{Fe}^{2+}/\text{Fe}^{3+}$  ratio of the blue-grey form was double that of the olive-green form. Both the  $\text{Fe}^{2+}$  content and the swelling volume of the blue-grey sample reverted to the olive-green values upon reoxidation. Nothing more was published on this subject until Egashira and Ohtsubo (1983) reported a depressing effect of structural  $\text{Fe}^{2+}$  on the swelling of smectites reclaimed from marine environments in Japan. Shortly thereafter, Stucki et al. (1984c) observed systematic changes in the swelling of several reference clay minerals reduced with

pH-buffered sodium dithionite in the laboratory (Fig. 8.3). Similar results have since been reported also by Lear and Stucki (1985), Yan and Stucki (1999, 2000), and Stucki et al. (2000) for dithionite-reduced smectites; and, by Gates et al. (1993) and Kostka et al. (1999a) for bacteria-reduced smectites.

Our understanding of the exact mechanism by which structural  $\text{Fe}^{2+}$  alters the hydration of clay mineral surfaces is still incomplete, but by combining the observations of Viani et al. (1983, 1985), Yan et al. (1996a, 1996b, 1996c, 1996d), Yan and Stucki (1999, 2000), Fialips et al. (2002a, 2002b), Wu et al. (1989), Cervini-Silva et al. (2000b), and Stucki and co-workers (Stucki and Roth, 1976, 1977; Stucki et al., 2000) some interesting conclusions can be made. These studies offer convincing and self-consistent evidence that interlayer  $\text{H}_2\text{O}$  molecules interact directly with the oxygen ions which comprise the basal surfaces of the clay mineral layers, and that this interaction is coupled with the vibrational energies of the Si–O groups in the smectite tetrahedral sheet. By virtue of this coupling at the clay mineral–water interface, forces affecting the structure of either the adsorbed  $\text{H}_2\text{O}$  or the Si–O tetrahedra will alter clay mineral swelling. Reduction of octahedral  $\text{Fe}^{3+}$  to  $\text{Fe}^{2+}$  does both, affecting  $\text{H}_2\text{O}$  by increasing the electron density and proton attraction at the surface oxygen atoms (as revealed by increased Brønsted basicity) (Cervini-Silva et al., 2000b) and the Si–O tetrahedra by disrupting the crystallographic structure (Stucki and Roth, 1976; Manceau et al., 2000b; Fialips et al., 2002a, 2002b).

Two examples that reveal the increasing strength of interaction between the basal oxygen atoms and interlayer  $\text{H}_2\text{O}$  as structural iron reduction increases are provided by the studies of Cervini-Silva et al. (2000b) and Yan and Stucki (1999, 2000). When pentachloroethane interacts with reduced smectite, it is rapidly degraded to tetrachloroethene through a base-catalysed dehydrochlorination reaction (Cervini-Silva

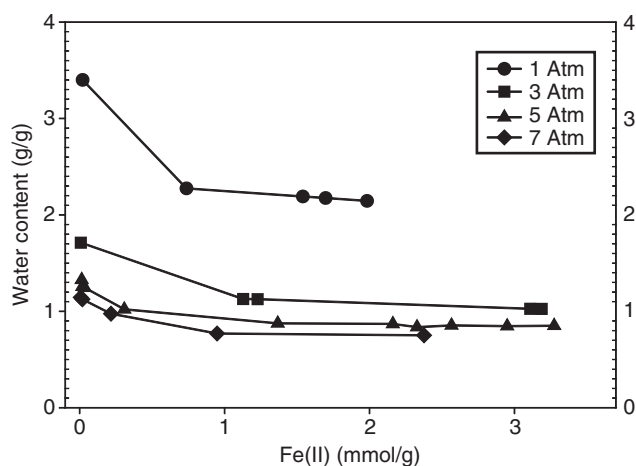


Fig. 8.3. Effects of Fe oxidation state on the swellability (equilibrium water content at a fixed applied swelling pressure) of Garfield nontronite. From Stucki et al. (1984c).

et al., 2000b). The rate of degradation increases linearly with the structural  $\text{Fe}^{2+}$  content of the smectite (Fig. 8.4). The proposed mechanism of interaction is illustrated in Fig. 8.5, showing that reduction increases the attraction of basal oxygen atoms for protons. This polarises interlayer  $\text{H}_2\text{O}$  and increases the electron density on the aqueous oxygen ion, which, in turn, promotes the abstraction of the proton from the pentachloroethane and the  $\alpha$ ,  $\gamma$  elimination of chlorine to yield tetrachloroethene. This reaction is direct evidence that the reduced clay mineral surface has a greater Brønsted basicity than the oxidised surface. Degradation of the pesticide oxamyl also appears to follow a similar hydrolysis pathway in the presence of reduced smectite (Zhang, 2002).

If the surface attracts interlayer  $\text{H}_2\text{O}$  more strongly in the reduced than in the oxidised state, this should be reflected in the vibrational energies of the interlayer  $\text{H}_2\text{O}$ . Indeed, Yan and Stucki (1999, 2000) observed an increase in the vibrational energy of the H–O–H bending mode for interlayer  $\text{H}_2\text{O}$  with increasing  $\text{Fe}^{2+}$  content of the clay mineral. An increase in the energy of this bending mode is consistent with a greater constraint being applied to the vibrational freedom of one or both of the hydrogen ions on the interlayer  $\text{H}_2\text{O}$ , which would be the case in the event of stronger interaction with the surface. Yan et al. (1996a, 1996b, 1996c, 1996d) and Yan and Stucki (1999, 2000) further observed that the vibrational energy of the interlayer  $\text{H}_2\text{O}$  molecules is coupled with the vibrational energy of the structural Si–O stretching bands (Fig. 8.6). This is a most remarkable observation and provides another key link in the puzzle for understanding how structural  $\text{Fe}^{2+}$  in the octahedral sheet has such a great effect on surface hydration and other surface properties.

The effects of structural iron reduction on the vibrational energy of Si–O bands was noted as early as 1976 by Stucki and Roth (1976), who observed a systematic

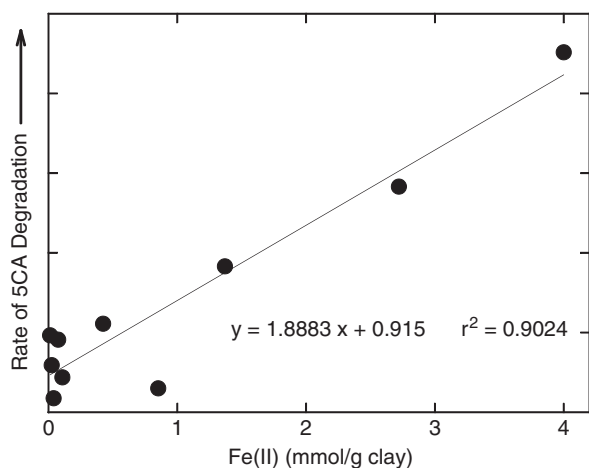


Fig. 8.4. Effects of structural Fe(II) in smectites on the rates of pentachloroethane transformation to tetrachloroethene. From Cervini-Silva et al. (2000b).

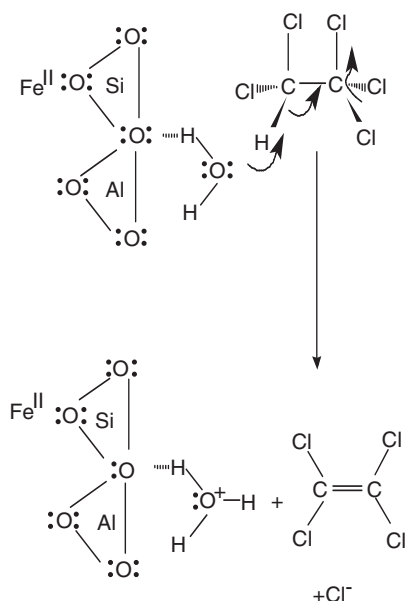


Fig. 8.5. Schematic illustration of Brønsted base catalyzed dehydrochlorination of pentachloroethane by reduced-Fe smectite. From [Cervini-Silva et al. \(2000b\)](#).

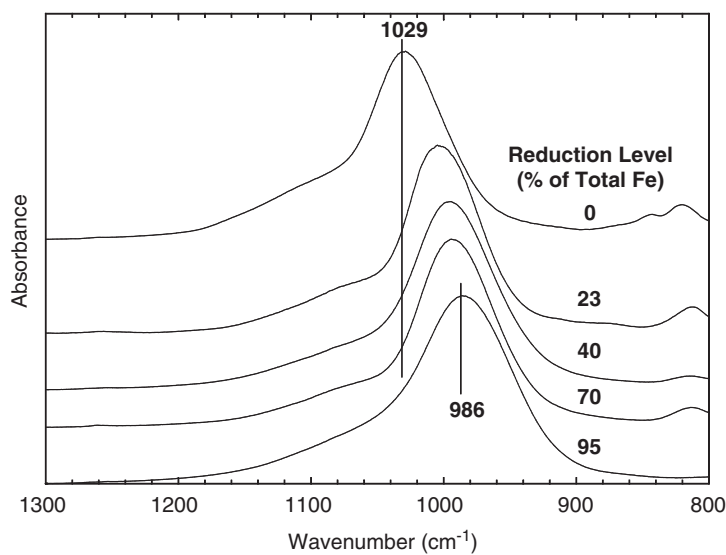


Fig. 8.6. Effect of structural Fe(II) on the Si-O vibrational frequencies in Garfield nontro-nite. From [Fialips et al. \(2002a\)](#).



downward shift in the Si–O vibrational energy as structural  $\text{Fe}^{2+}$  increased. This observation was confirmed and characterised more completely by Huo (1997), Yan and Stucki (1999, 2000), and Fialips et al. (2002a, 2002b) (Fig. 8.7). These shifts are consequences of rearrangements occurring in the octahedral sheet as the clay mineral particle attempts to compensate for the increased size of the octahedral  $\text{Fe}^{2+}$  ion compared to  $\text{Fe}^{3+}$  and to balance the increased negative charge due to iron reduction, such as by the models proposed by Manceau et al. (2000b) and Li et al. (2003, 2005). In summary, changes in iron oxidation state alter the structure of the clay mineral, which is reflected in the Si–O stretching vibrations which are coupled to the vibrational energy of interlayer  $\text{H}_2\text{O}$ . Through this coupling, the change in oxidation state induces a change in free energy of the interlayer  $\text{H}_2\text{O}$ , which in turn affects the swellability of the clay mineral, as described by the following discussion.

Clay mineral swelling or hydration occurs because the interaction between  $\text{H}_2\text{O}$  and the basal surface decreases the partial molar Gibbs free energy of bulk  $\text{H}_2\text{O}$  ( $\bar{G}_0$ ) as it approaches the solid clay mineral surface. The difference between the partial molar Gibbs free energy of clay mineral water ( $\bar{G}_{\text{H}_2\text{O}}$ ) and that of bulk water, given by  $\bar{G}_{\text{H}_2\text{O}} - \bar{G}_0$ , defines the potential for water to enter the interlayer from the bulk phase, i.e., the affinity of the clay mineral surface for water, and is measured by the swelling pressure,  $\Pi$ , of the clay mineral as represented by the equation (Low, 1951, 1980)

$$\bar{G}_{\text{H}_2\text{O}} - \bar{G}_0 = -\bar{V}\Pi \quad (4)$$

where  $\bar{V}$  is the partial molar volume of the water in the clay mineral–water system.

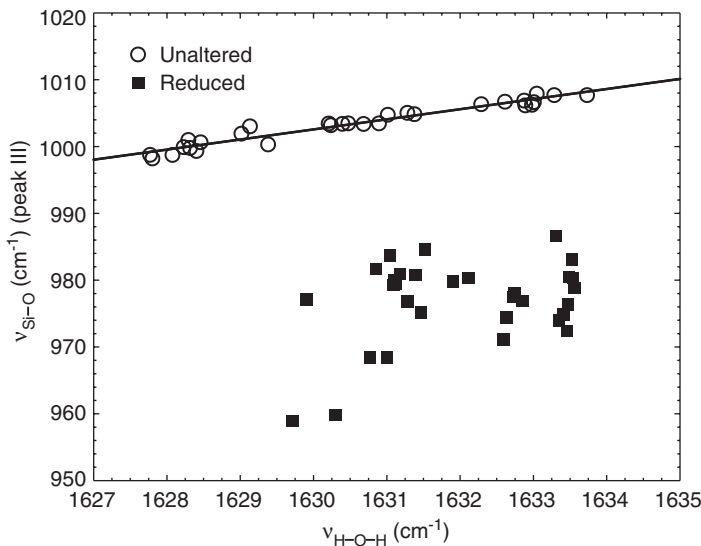


Fig. 8.7. Coupling between vibrational frequencies of structural Si–O and adsorbed H–O–H modes in Garfield nontronite. From Yan and Stucki (2000).

Since structural  $\text{Fe}^{2+}$  increases the interaction between  $\text{H}_2\text{O}$  and the clay mineral surface, these thermodynamic arguments predict that swelling in reduced smectite should be greater than in oxidised smectite. If this is true, then why are the observed effects just the opposite (Foster, 1953, 1955; Egashira and Ohtsubo, 1983; Stucki et al., 1984b, 2000; Lear and Stucki, 1985; Gates et al., 1993). The answer is found by comparing the studies of Viani et al. (1983) and Wu et al. (1989), who discovered that two types of interlayers are possible in swelling smectites: fully expanded and fully or partially collapsed. At any given swelling pressure, the distance between the fully expanding layers is the same, regardless of the water content of the clay mineral at that pressure. So the differences in water content for two clay minerals at the same swelling pressure occurs because of a difference in the fraction of layers that are fully expanded relative to the fraction that are partially or fully collapsed, rather than from the layers expanding to different distances. They described these relationships by the expression

$$\ln(\Pi + 1) = \ln \beta + \frac{\alpha}{\lambda} \quad (5)$$

where  $\alpha$  and  $\beta$  are constants and  $\lambda$  is the interlayer distance. Notice that the swelling pressure,  $\Pi$ , is a single-valued function of interlayer distance.

Reduction of octahedral  $\text{Fe}^{3+}$  causes more of the clay mineral layers to collapse compared to the oxidised state, thereby removing those layers from the pool of fully expanded layers (Wu et al., 1989). The overall capacity of the clay mineral to adsorb water on a mass basis is thus diminished. This observation compares well with other studies showing an increase in cation fixation as the reduced state of the clay mineral increases. Chen et al. (1987) observed an increase in K fixation in agricultural soils as the amount of structural  $\text{Fe}^{2+}$  in the constituent clay minerals increased, and Khaled and Stucki (1991), Lear and Stucki (1987), and Shen and Stucki (1994) confirmed this principle in standard reference clay minerals, indicating that layers are indeed collapsing around these cations. The extent of cation fixation by the reduced smectite depends inversely on the hydration energy of the cation (Khaled and Stucki, 1991).

Another consequence of the increased interaction between reduced smectite surfaces and interlayer  $\text{H}_2\text{O}$  is that the hydration energy of the surfaces exposed to  $\text{H}_2\text{O}$  should increase, even though the net water holding capacity can decrease for the reasons just explained. Stucki et al. (2000), in a study of the effects of organic cations on clay mineral swelling, demonstrated that this is indeed the case. The quaternary ammonium cation trimethylphenyl ammonium ( $\text{TMPA}^+$ ) was exchanged onto the oxidised and reduced smectites, then the water retention curve was obtained. Water retention curves were also obtained for the  $\text{Na}^+$ -exchanged analogues (Fig. 8.8). Remarkably, in comparing the water contents of  $\text{Na}^+$ -oxidised,  $\text{Na}^+$ -reduced,  $\text{TMPA}^+$ -oxidised, and  $\text{TMPA}^+$ -reduced smectites, all at the same applied swelling pressure, they found that the  $\text{TMPA}^+$ -reduced sample held the most water! How can this be, since  $\text{TMPA}^+$  is largely a hydrophobic cation (notice that it depresses the water content when the clay mineral is in the oxidised state)? A plausible explanation

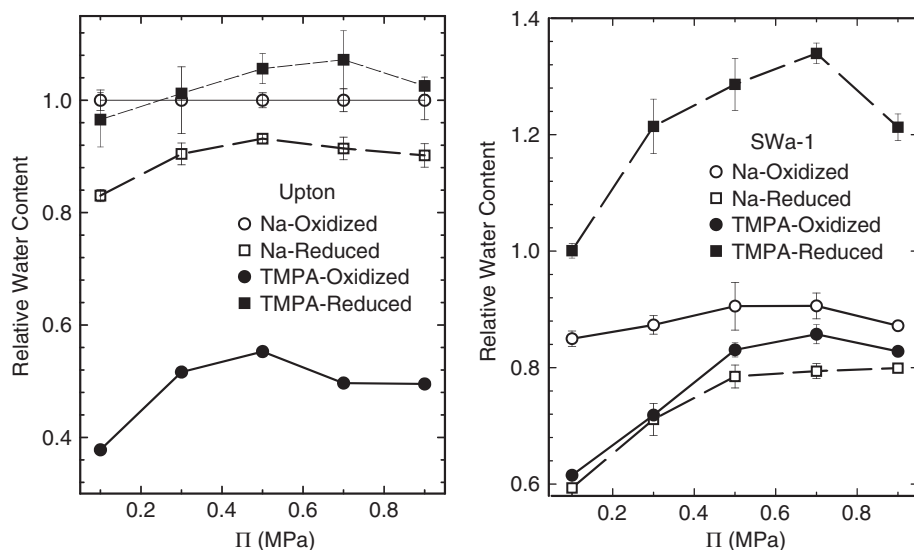


Fig. 8.8. Effects of the organic cation trimethylphenylammonium (TMPA) and structural Fe reduction on the swelling pressure curves of ferruginous smectite SWa-1. From [Stucki et al. \(2000\)](#).

is that this cation prevents the clay mineral layers from collapsing upon iron reduction, and thereby allows their surfaces to become hydrated and to participate in swelling, whereas with  $\text{Na}^+$  as the exchanged cation the collapse occurs and their swelling is precluded. The reduced clay mineral surface then is apparently much more attractive to  $\text{H}_2\text{O}$  than is the oxidised surface because its water content exceeds that of even the  $\text{Na}^+$ -oxidised form of the smectite (fully expanded state with no collapsed layers) leading to a conclusion that the hydration energy of the reduced surfaces far exceeds that of the oxidised surfaces, consistent with the enhanced interaction between basal oxygen atoms and adsorbed  $\text{H}_2\text{O}$ . The dominant hydrating force in the interlayer, moreover, is not the interlayer cation, but the clay mineral surface itself.

If the reduced clay mineral surface is more highly hydrated than the oxidised surface, or that its hydration energy is greater, one would expect the adsorbed water to be held with greater energy. [MacKenzie and Rogers \(1977\)](#), using differential thermal analysis (DTA), observed that the hydration energy of an  $\text{Fe}^{2+}$ -containing clay mineral is more complex than the oxidised analogue (also see discussion by [Stucki, 1988](#)). [Huo \(1997\)](#) and [Fialips et al. \(2002a, 2002b\)](#), using infrared spectroscopy, discovered in reduced smectite a  $\text{H}_2\text{O}$  phase that was more resistant to dehydration than in the oxidised smectite, and the intensity of the O–H stretching bands from this  $\text{H}_2\text{O}$  phase increased as the extent of structural  $\text{Fe}^{2+}$  increased ([Fig. 8.9](#)). These observations are consistent with more strongly bound  $\text{H}_2\text{O}$ .

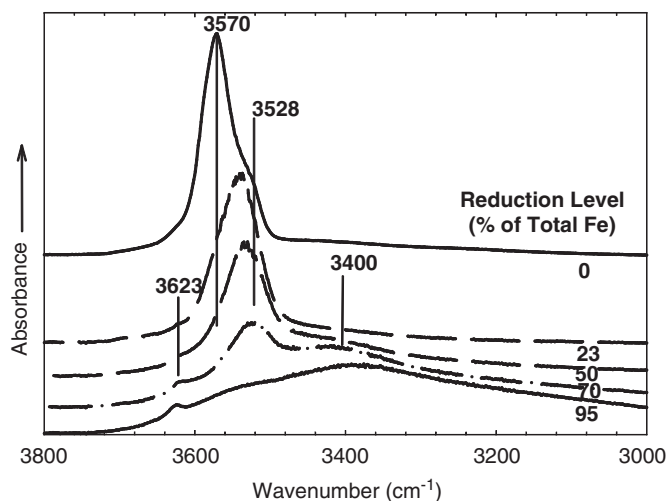


Fig. 8.9. Effect of structural Fe(II) on the structural O–H vibrational stretching frequencies in Garfield nontronite. From Fialips et al. (2002a).

Iron reduction also affects the hydraulic conductivity through a clay mineral–water paste. This is a property of compacted clay mineral that is related to both clay mineral–water interactions and to the texture or fabric of the clay mineral matrix, and studies have shown that it may either increase or decrease upon structural iron reduction, depending on the order in which the sample was reduced and compacted. Shen et al. (1992) observed a decrease in the hydraulic conductivity of reduced ferruginous smectite that was compacted onto a membrane filter, as compared to the unaltered or oxidised form. This decrease in hydraulic conductivity was attributed to the particles of the reduced smectite having a smaller aspect ratio (thicker and of more limited lateral extent) (see Stucki and Tessier, 1991), which enables them to form a denser matrix upon compaction.

If, however, the smectite is first compacted, then reduced by percolation of a pH-buffered dithionite solution, the hydraulic conductivity actually increases. Shen et al. (1992) explained this behaviour as being due to the strong interlayer attractive forces that are asserted when structural iron is reduced, causing the superimposed layers to collapse and, to a certain extent, rotate in the *a*–*b* plane to form a less turbostratic stacking order. The latter was reported previously by Stucki and Tessier (1991), who observed an increased order in the electron diffraction patterns upon structural iron reduction. When these actions of layer rotation and collapse occur in a previously compacted gel, the movement of particles creates voids between them that gives rise to meso pores with greater conductivity than the micropores in a highly compacted smectite. These studies were carried out using sodium dithionite as the reducing agent, but the phenomena of layer collapse and rotation have also been observed in

bacteria-reduced smectites (Kim et al., 2003), indicating that such processes affecting hydraulic conductivity could well be occurring in natural or engineered clay barriers.

#### 8.4. CLAY MINERAL–ORGANIC INTERACTIONS

The discovery that reduction of structural iron activates smectite surfaces with respect to chlorinated aliphatics (Gorby et al., 1994) and pesticides (Xu et al., 1996) has opened an exciting new area of investigation into clay mineral–organic interactions. Pesticides, chlorinated aliphatics, and nitroaromatics have thus far been investigated (Table 8.1). Pesticides studied include atrazine, alachlor, trifluralin, oxamyl, chloropicrin, dicamba, and 2,4-D. These studies are significant because they demonstrate that the interaction mechanism between the smectite and the pesticide involves much more than mere sorption to the clay mineral surface. The pesticides, with the exception of 2,4-D, react with reduced clay mineral surfaces much more extensively than with oxidised or reduced-reoxidised surfaces, and degradation products are observed (examples given in Figs. 8.10–8.12). Atrazine (Fig. 8.10), for example, partially degrades to hydroxyatrazine when reacted with reduced ferruginous smectite (Xu et al., 2001), but no products are observed by HPLC when it is reacted with the oxidised (unaltered) or reduced-reoxidised form of the same smectite. A similar phenomenon occurs with alachlor (Kocherginsky and Stucki, 2000; Xu et al., 2001), except the degradation products are many and have yet to be fully identified. Chloropicrin (trichloronitromethane) is transformed to the di- and monochloro forms (Cervini-Silva et al., 2000a) by reductive dechlorination (Fig. 8.11).

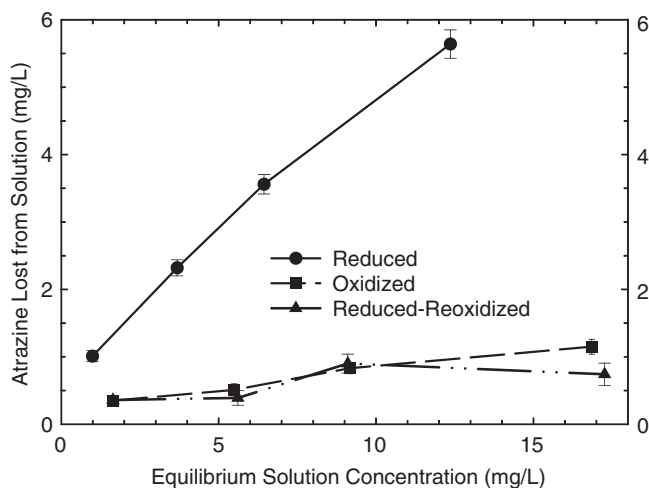


Fig. 8.10. Effect of structural Fe(II) on the degradation of atrazine by ferruginous smectite SWa-1. From Xu et al. (2001).

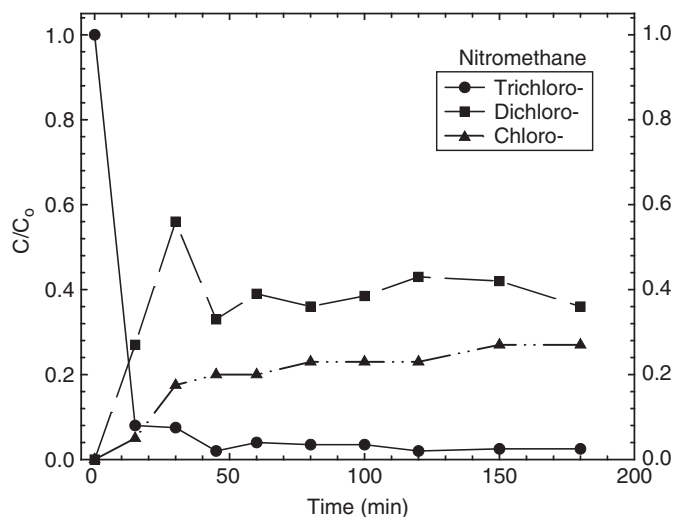


Fig. 8.11. Degradation of trimethylnitromethane (chloropicrin) by reduced-Fe ferruginous smectite SWa-1. From Cervini-Silva et al. (2000a).

Oxamyl converts into either the hydrolysis product, oxamyl oxime (OO), or to the reduction product, *N,N*-dimethyl-1-cyanoformamide (DMCF), depending on the solution pH. Smectites in any oxidation state will promote the hydrolysis product, but the rate of degradation is greatly accelerated by the reduced smectite (unpublished data by Dottori Dr. Fabiana in the author's laboratory). Specific degradation products from trifluralin (Fig. 8.12) and dicamba are still unidentified (Tor et al., 2000; Sorensen et al., 2003, 2004, 2005).

Clearly, the reduced smectite acts as a reducing agent with most of the pesticides studied, either eliminating  $-Cl$  or  $-NO_2$  groups. But in the case of oxamyl a hydrolysis product is also observed, indicating that reduced-clay mineral surfaces, in addition to catalysing redox activity, also promote pH-catalysed reactions. This is consistent with results from chlorinated alkanes (see below).

The extent to which the reduced smectite degrades the pesticide varies from one pesticide to the other. As mentioned above, 2,4-D seems to be unaffected by the smectite, regardless of oxidation state, and only a small fraction of alachlor (Kocherginsky and Stucki, 2000; Xu et al., 2001) and dicamba are affected. Oxamyl (unpublished data by Dr. Fabiana Dottori in the author's laboratory), chloropicrin (Cervini-Silva et al., 2000a), and trifluralin (Tor et al., 2000), on the other hand, are almost completely degraded by the reduced smectite (Figs. 8.11 and 8.12) but little affected by the oxidised smectite.

The effect of reduced smectites on organics is not limited to pesticides. Studies have reported the dechlorination of chlorinated aliphatics (Gorby et al., 1994; Rodriguez et al., 1999; Cervini-Silva et al., 2000a, 2000b, 2001, 2002, 2003;

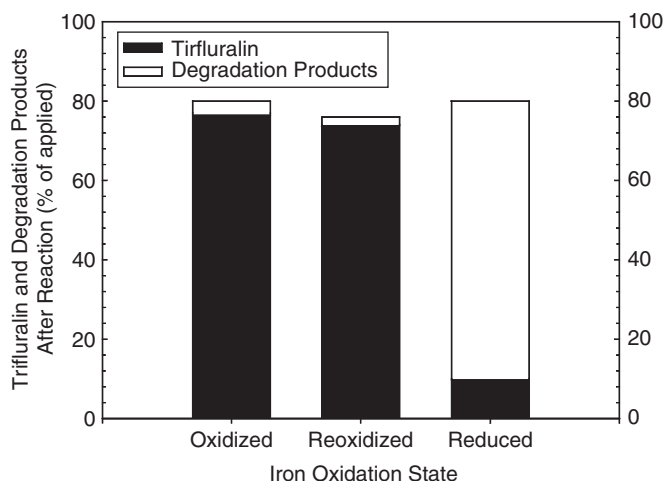


Fig. 8.12. Effects of structural Fe oxidation state on the degradation of trifluralin by ferrous smectite SWa-1. From [Tor et al. \(2000\)](#).

[Nzengung et al., 2001](#)) and the reduction of nitroaromatics ([Yan and Bailey, 2001](#); [Hofstetter et al., 2003](#)) by reduced smectites. [Gorby et al. \(1994\)](#) found that tetrachloromethane reacts with dithionite-reduced Panther Creek bentonite to yield tri- and dichloromethanes by step-wise hydrogenation. The reaction rate increased if Fe(0) was combined with the smectite. Whether the enhanced reaction rates can be attributed to structural  $\text{Fe}^{2+}$  in the smectite is, however, in question because: (1) when the sample was washed with HCl to remove sulphides and  $\text{Fe}^{2+}$ , its reactivity with  $\text{CCl}_4$  was greatly diminished, (2) reactivity of the clay mineral was restored if  $\text{Fe}^{2+}$  was added back as an exchanged cation, and (3) the interaction mechanism for admixing with Fe(0) is unknown. The authors stated that the products are consistent with other proposed reaction pathways ([Kriegman-King and Reinhard, 1994](#)) for degradation of polyhalogenated methanes by reduced-sulphur compounds. Similar results were found for degradation of trichloroethene. All of these tests apparently were conducted using a heterogeneous clay mineral system rather than with just the pure smectite.

[Nzengung et al. \(2001\)](#) also reported that dechlorination of trichloroethene is faster in a heterogeneous system than with pure reduced smectite. The heterogeneous system tested was smectite+dithionite. In the absence of dithionite the smectite failed to promote the dechlorination of trichloroethene, whereas dithionite alone at approximately the same pH was effective. The most effective combination, however, was dithionite combined with the smectite. Comparison of different smectites found the rate of dechlorination to be greater with montmorillonite than with ferruginous smectite. They attributed these differences in smectite behaviour to a difference in available interlayer surface area due to greater layer collapse in the ferruginous

sample, but more work is needed to clarify the relative roles of smectite and dithionite.

The observed lack of reactivity of the pure smectites with the chlorinated alkene may, on the other hand, be attributed to the fact that the primary mechanism for dechlorination of chlorinated aliphatics is hydrolysis or dehydrochlorination, which may be rather difficult with the trichloroethene, since it already possesses one double bond. Pentachloroethane can degrade either by a reductive dechlorination pathway, which produces trichloroethene, or by a dehydrochlorination pathway, which yields tetrachloroethene. When reacted with dithionite- or bacteria-reduced smectite, it degrades via the dehydrochlorination pathway rather than the reductive dechlorination pathway (Cervini-Silva et al., 2000b, 2003). No further degradation of the tetrachloroethene was observed. Other chlorinated alkanes also appear to follow this same pathway (Cervini-Silva et al., 2003) in the presence of pure smectite.

Nitroaromatic compounds (NAC), including nitrobenzene, acetylnitrobenzene, and trinitrotoluene can be reduced by chemically reduced smectite. Nitrobenzene is converted into aniline when reacted with reduced ferruginous smectite (SWa-1) or Upton montmorillonite (Yan and Bailey, 2001). Reaction kinetics revealed extensive conversion by SWa-1 within the first 40 h; then it levelled to a small non-zero slope and after 500 h reduction was still increasing slightly. The rate was slower with Upton and the extent of degradation was less. Adsorption of nitrobenzene to the clay mineral surfaces was unaffected by the iron oxidation state; but aniline adsorption was significantly depressed by iron reduction. Interestingly, the amount of structural  $\text{Fe}^{2+}$  actually participating in the reaction (as a fraction of total Fe) was rather low (<40% in SWa-1 and 10% in Upton). Perhaps the reaction occurs primarily at clay mineral layer edges.

Hofstetter et al. (2003) investigated the reactivity of different forms of iron in and on smectites for transforming acetylnitrobenzene to the corresponding aniline. The isomers 2- and 4-acetylnitrobenzene have different selectivities for the clay mineral interlayers, namely, the *para* (4-) isomer is planar and is easily sorbed between smectite layers, whereas the *cis* (2-) isomer sorbs only to the edge surfaces. These properties were exploited to probe the reactivities of structural  $\text{Fe}^{2+}$ , edge-complexed  $\text{Fe}^{2+}$ , and exchanged  $\text{Fe}^{2+}$  towards reductive amination to the corresponding anilines. Hectorite was used as the non-structural iron control. Results revealed that exchanged  $\text{Fe}^{2+}$  has no reactivity towards NAC reduction, but both edge-complexed and structural  $\text{Fe}^{2+}$  were effective in producing the aniline product. The observed fraction of total  $\text{Fe}^{2+}$  that participated in the process was similar to that of Yan and Bailey (2001), providing further indication that NAC reduction may occur primarily at the edge surfaces.

Further investigations of the reactions of redox-modified clay minerals with organic compounds are in progress and are greatly needed. Little is known about the reduction potential of reduced smectite, except that it must lie somewhere between the reduction potentials of chloropicrin and pentachloroethane, since it reduces the former but not the latter. Organic compounds may be effective probes of the surface



characteristics of the reduced smectite, revealing properties such as effective pH and reduction potentials. The specific site on the clay mineral surface, i.e., edge versus basal surface, where organic reactions take place is also an area that needs much further study.

The toxicity of pesticides to mammals, which are obviously non-target organisms for pesticides, can be greatly altered by exposing the pesticide to reduced-iron smectites. Sorensen et al. (2004, 2005) compared the mammalian toxicity of four different pesticides (alachlor, oxamyl, 2,4-D, and dicamba) before and after treatment with either oxidised or reduced smectite. They found that the oxidised smectite had no effect on toxicity, but the reduced smectite significantly decreased the toxicity of alachlor and oxamyl, increased the toxicity of dicamba, and had no effect on the toxicity of 2,4-D. The redox state of smectites, from either natural or imposed processes, may, therefore, be an important factor in determining or manipulating the risks associated with pesticides in the environment.

## 8.5. LAYER CHARGE, CATION EXCHANGE, AND CATION FIXATION

The layer charge of smectite clay minerals is susceptible to modification *in situ* by reduction of structural  $\text{Fe}^{3+}$  to  $\text{Fe}^{2+}$ . The isomorphous substitution of  $\text{Fe}^{3+}$  (for  $\text{Al}^{3+}$ ) in the octahedral sheet of phyllosilicates of course invokes no change in layer charge, and in the tetrahedral sheet it has the same effect on charge as does  $\text{Al}^{3+}$  substitution for  $\text{Si}^{4+}$ . However, reduction of  $\text{Fe}^{3+}$  to  $\text{Fe}^{2+}$  in a dioctahedral structure is reflected in an increase in the negative surface charge. Stucki et al. (1984a) found that the layer charge increases upon iron reduction; but the increase is less than predicted by the structural  $\text{Fe}^{2+}$  content. This difference in measured layer charge compared to the apparent number of electrons added to the clay mineral particle has led to further investigations of potential ancillary reactions, such as concomitant protonation or dehydroxylation. It has also motivated numerous discussions regarding the complete reduction mechanism as given in more detail in Section 8.6.

An increase in layer charge is accompanied by an increase in cation exchange capacity (CEC) as well as an increase in the ability of the smectite to fix interlayer cations. Stucki et al. (1984b) reported a steady increase in the CEC of nontronite as iron reduction progresses. This observation was confirmed by others for dithionite-reduced smectites (Lear and Stucki, 1985; Khaled and Stucki, 1991; Gates et al., 1996), bacteria-reduced smectites (Kostka et al., 1999b; Gates et al., 2000), and rice-cropped vertisols (Favre et al., 2002a, 2002b). Lear and Stucki (1985) further observed that a small fraction of the exchangeable  $\text{Na}^+$  becomes non-exchangeable (fixed) during the reduction process, probably because of the complete or partial collapse of smectite layers (Wu et al., 1989).

Heller-Kallai (1997) pointed out, however, that the layer charge in these studies might have been underestimated due to the explicit assumption that  $\text{Na}^+$  was the

only interlayer cation and accounted for all of the layer charge. She argued that, even though the citrate–bicarbonate buffer and dithionite-reducing solutions were comprised of only the Na salts, the documented dissolution of aluminium from the smectite (Stucki et al., 1984b; Leite et al., 2000) during the reduction process could have led to formation of complex Al-citrate cations. Perhaps, these cations could then be preferentially adsorbed by the mineral surface in place of some of the  $\text{Na}^+$ . The fact that the ratios of dissolved silicon, aluminium, and iron in solution after reduction differed from the ratios in the clay mineral structure was offered as potential evidence to support this hypothesis. She further suggested that cation fixation could occur by the complex Al-citrate cation blocking the exchange of  $\text{Na}^+$  and other interlayer cations, thus providing an alternative mechanism for cation fixation which does not require the complete collapse of superimposed clay mineral layers. Direct evidence establishing the existence of the complex Al-citrate cation and its potential to fix other interlayer cations, however, is still lacking. Recent observations of collapsed layers in bacteria-reduced smectites (Kim et al., 2003) indicate that such an alternative explanation for cation fixation may be unnecessary.

The effects of iron reduction on cation fixation have significant implications for soil fertility, mineral transformations in the soil, and the fate of redox-sensitive pollutants such as Cr (Taylor et al., 2000). Potassium is a key plant nutrient, but fertiliser recommendations for K are often inaccurate for reasons that are yet to be fully explained. Some soils exhibit K deficiencies even though the total K appears to be sufficient (Singh and Heffernan, 2002). Chen et al. (1987) most likely found the answer, however, when they discovered that structural iron reduction leads to extensive  $\text{K}^+$  fixation in smectitic soils. Khaled and Stucki (1991) and Shen and Stucki (1994) verified that structural  $\text{Fe}^{2+}$  reduction in smectites does, indeed, lead to a sharp increase in the fixation of  $\text{K}^+$ . They also observed that the amount of exchangeable  $\text{K}^+$  was similar in oxidised and reduced forms of the clay mineral (Fig. 8.13), and that the increased layer charge due to  $\text{Fe}^{3+}$  to  $\text{Fe}^{2+}$  reduction was manifested primarily in the pool of fixed K.

The potential for this process to remove large amounts of K from the plant-available pool in the soil is made dramatically apparent by the following calculation for a rather typical agricultural soil. Assumptions: (i) a soil with medium texture having 15% clay mineral content, of which 2/3 is smectite (10% of soil by weight is smectite); (ii) iron content of the smectite is 3% by weight (a typical montmorillonite); (iii) approximate weight of a hectare-furrow slice of soil is  $2 \times 10^6$  kg; (iv) extent of reduction is only 20% of total iron (generally consistent with Favre et al., 2002b); (v) K fixation in Upton montmorillonite at this level of reduction is about 0.1 meq/g clay mineral = 0.0047 kg  $\text{K}_2\text{O}$ /kg clay mineral (Shen and Stucki, 1994).

$$\text{K(fixed)} = \frac{0.0047 \text{ kg } \text{K}_2\text{O}}{\text{kg smectite}} \times \frac{1 \text{ kg smectite}}{10 \text{ kg soil}} \times \frac{2 \times 10^6 \text{ kg soil}}{\text{hectare-furrow slice}} = 940 \frac{\text{kg } \text{K}_2\text{O fixed}}{\text{hectare}}$$

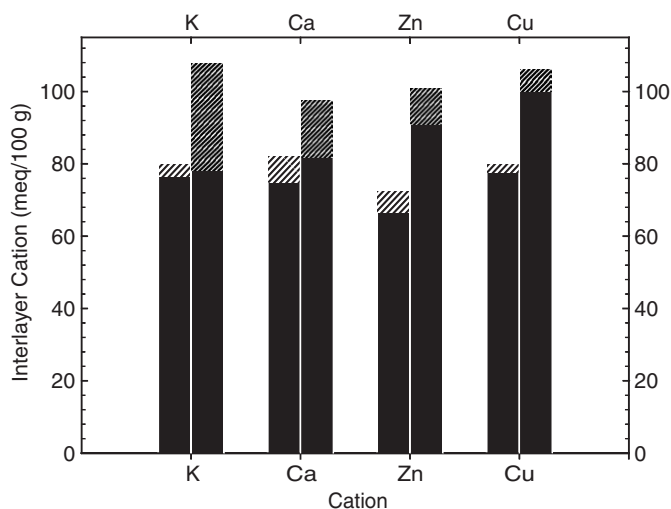


Fig. 8.13. Effect of structural Fe reduction on cation fixation in ferruginous smectite SWa-1. From [Khaled and Stucki \(1991\)](#).

This is an extremely large amount of K to cycle between the plant-available and the plant-non-available pools in the soil due to changing redox conditions. A typical fertiliser recommendation for K, based on conventional soil tests in the State of Illinois, is about 50–100 kg  $K_2O$ /hectare (Theodore R. Peck, personal communication). The very modest level of redox cycling used in the above calculation proves that the potential for K fixation due to iron reduction in the soil absolutely overwhelms the practical ability to amend the soil with K fertilisers. If the observations by [Favre et al. \(2002a, 2002b\)](#) and [Chen et al. \(1987\)](#), i.e., that the effects of redox processes in smectites on CEC are manifested in the field as well as in the laboratory, also apply to cation fixation, then the above calculation presents a significant understanding and a challenge for modifying soil management practices, especially under conditions where the soil experiences alternate flooding (reducing) and draining (oxidising) through rainfall or irrigation practices. These results of [Chen et al. \(1987\)](#) and [Favre et al. \(2002b\)](#) from soil clays and of [Shen and Stucki \(1994\)](#) from Wyoming montmorillonite confirm that  $K^+$  fixation due to iron reduction is a general phenomenon in smectites that extends beyond the iron-rich forms.

Cation fixation as a consequence of iron-reducing conditions may also affect other cationic nutrients in the soil such as  $Ca^{2+}$ ,  $Cu^{2+}$ ,  $Zn^{2+}$  ([Fig. 8.13](#)), and  $NH_4^+$  ([Scherer and Zhang, 2002](#)). Because the charge density of  $NH_4^+$  is similar to that of  $K^+$ , the behaviour of these two cations in smectites is often regarded as being similar. Ammonium should, therefore, also have a high susceptibility for fixation. Evangelou and co-workers ([Lumbanraja and Evangelou, 1990, 1992, 1994](#); [Evangelou et al., 1994](#); [Barbayannis et al., 1996](#)) found significant correlations

between the fixations of these two ions in agricultural soils, suggesting that their tendencies towards fixation are indeed similar. Scherer and Zhang (2002) subsequently identified a clear link between the amount of  $\text{NH}_4^+$  fixed in periodically flooded rice–paddy soils and the oxidation state of structural  $\text{Fe}^{2+}$  in the clay minerals. Shen and Stucki (unpublished results) observed that the behaviour of  $\text{NH}_4^+$  in redox-modified ferruginous smectite is in fact similar to that of  $\text{K}^+$  as illustrated in Fig. 8.14. The general trend appears to be that the extent of fixation is inversely proportional to the hydration energy of the cation (Khaled and Stucki, 1991).

The reversibility of the fixation process of these cations is an important factor in determining the fate of the nutrient and the nature of the clay mineral. If fixation is even partially irreversible, cycles of iron reduction and reoxidation could be an important mechanism for the sequestering of plant nutrients into a low-availability form and for the conversion of smectite into illite in natural environments (Eslinger et al., 1979). The feasibility for iron redox cycling to be a significant force in converting smectite into a more illitic form was investigated by Shen and Stucki (1994), who measured the amount of structural  $\text{Fe}^{2+}$  and fixed  $\text{K}^+$  remaining in the re-oxidised form of ferruginous smectite after passing through several redox cycles (Fig. 8.15). At the end of each successive cycle, i.e., when the clay mineral was in its oxidised or reoxidised state, the amount of  $\text{K}^+$  that remained fixed, in spite of reoxidation, increased over the level observed at the end of the previous cycle. Similarly, the amount of  $\text{Fe}^{2+}$  that resisted reoxidation increased after each cycle. These phenomena are absent when  $\text{Na}^+$  is the exchangeable cation during iron reduction. Surprisingly,  $\text{NH}_4^+$  seems to be released when the smectite is reoxidised and fails to accumulate over several redox cycles (Shen and Stucki, unpublished

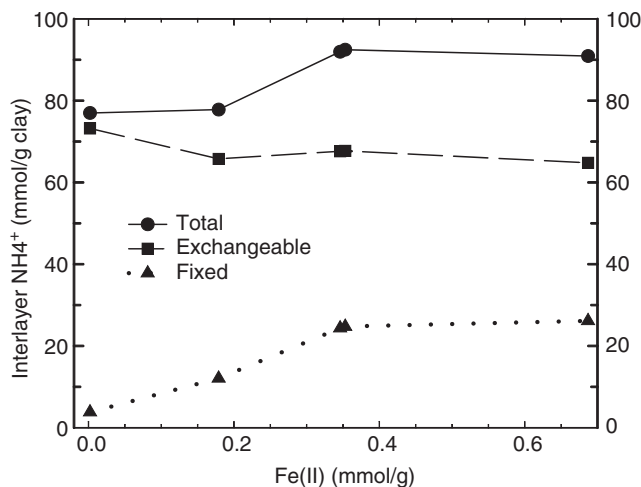


Fig. 8.14. Exchangeable and fixed  $\text{NH}_4^+$  in reduced Upton montmorillonite. From Shen and Stucki (1994).

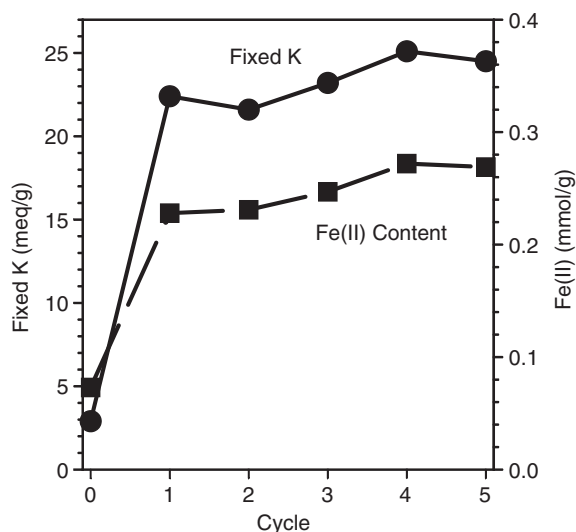


Fig. 8.15. Effects of redox cycles on structural Fe(II) content and the extent of residual fixation of  $K^+$  after reoxidation. From Shen and Stucki (1994).

results). In this sense,  $NH_4^+$  is different from  $K^+$ . This is only a preliminary result, however, and should be verified. Clearly the presence of  $K^+$  promotes the irreversible collapse of some smectite layers. As a result, access to the interlayer space by the oxidising agent (presumably  $O_2$  in this case) is diminished, and reoxidation of the octahedral  $Fe^{2+}$  is impeded.

The possibility that this process is active in natural soils and sediments has recently been established by the existence of collapsed layers in bacteria-reduced smectite, using an environmental cell transmission electron microscope (ED-TEM) (Kim et al., 2003). In a related study, the transformation of smectite to illite was also proposed as a result of bacterial reduction of structural iron (Kim et al., 2004). No overt assertion was made that layer collapse was influenced by the presence of  $K^+$  during structural iron reduction, and no redox cycling was performed; but, because the nutrient medium used in the bacterial culture contained significant amounts of  $K^+$  (Myers and Nealson, 1988), its influence on the process should not be overlooked and could well be contributing to the observed collapsing of layers. Projecting the synergy between redox cycling and cation fixation to geologic time, one would expect many thousands of these cycles to occur in natural soils and sediments, causing a large increase in the number of collapsed layers with the attendant increases in the amount of structural  $Fe^{2+}$  and fixed K. Such a process essentially defines the conversion of smectite into illite.

The ability of exchanged  $K^+$  to promote the irreversible collapse of smectite layers decreases the ability of the reduced smectite to react with redox-sensitive metals at the basal surfaces. Taylor et al. (2000) studied the reduction of  $Cr^{6+}$  to  $Cr^{3+}$  by reduced

smectite. The extent of  $\text{Cr}^{6+}$  reduction decreased by 35% if the exchanged cation on the smectite was K rather than Na. This is most likely related to a decrease in the available basal surface area due to an increase in the number of collapsed layers. A similar phenomenon may occur with other redox-sensitive pollutants.

## 8.6. REDUCTION POTENTIALS AND REACTION WITH REDOX-ACTIVE IONS

The soil environment is filled with a host of redox-active ions and compounds, so reactions between such species and redox-modified smectites is an extremely important process contributing to the fate of such species and to the behaviour of soils and sediments. The Eh of the soil in a rice-paddy field typically can cycle from a high of about 600 mV under well-aerated conditions to less than -150 mV during flooding (Boivin et al., 2002; Favre et al., 2002b). How this reduction potential is attributed to the minerals and the bacteria is undetermined, but clearly the oxidation state of structural iron in the constituent phyllosilicates is cycled between the oxidised and reduced states under these conditions. If formal and/or effective reduction potentials were known and understood for all of these species, effective models could be developed.

The exact reduction potential for  $\text{Fe}^{3+}$  in smectites is unknown, but Amonette (2002), using theoretical considerations, estimated it to be about 0.71 V. This value is highly dependent on iron-oxygen distances and other structural distortions. Knowledge of the reduction reaction mechanism, along with its associated structural changes, is crucial to the prediction of the true reduction potential. Since iron reduction undoubtedly alters the structure, estimating the surface reduction potential *a priori* is challenging to say the least. Empirical evidence does exist, however, with respect to redox reactions involving reduced smectites and redox-sensitive surface species. Among the ions or compounds that are known to engage in redox reactions with reduced structural iron in smectites are nitrate, chromium, and the pesticides (see above) chloropicrin and oxamyl. These reactions play a significant role in the fate of these compounds in the environment.

### 8.6.1. Redox Transformation of Nitrate

Nitrate in natural soil profiles is rapidly reduced at the boundary between the oxic and anoxic zones. The distribution of nitrate in several Danish soil profiles drops dramatically in the very narrow zone where the upper oxidised horizon meets the lower reduced formation (Ernstsen, 1996). Bacterial denitrification was ruled out as the mechanism controlling this process, but bacteria may play a catalytic role in restoring the reduced state of structural iron in the clay mineral after its oxidation by the nitrate reduction reaction (Ernstsen et al., 1998). On the basis of formal reduction potentials, structural  $\text{Fe}^{2+}$  in smectite should readily reduce nitrate; but,

experience has shown that the reaction is more complex than simply combining these two reactants (Ernstsen, Mulvaney, and Stucki, unpublished results). Since iron (hydr)oxides are also present in the Danish soils, the hypothesis is that they serve as a catalyst in promoting the reaction. Some, but not all, of the nitrate reduction could also be attributed to reaction with green rust (Hansen and Koch, 1998).

#### 8.6.2. Redox Transformation of $\text{Cr}^{6+}$

Reduced structural iron in smectites and other clay–mineral constituents of soils is an effective reductant for  $\text{Cr}^{6+}$  (Gan et al., 1996; Taylor et al., 2000), and possibly for other redox-sensitive metals of environmental concern such as  $\text{U}^{6+}$  and  $\text{Tc}^{7+}$ . Gan et al. (1996) were the first to report a redox reaction between reduced smectite and  $\text{Cr}^{6+}$ , and Brigatti et al. (2000) reported  $\text{Cr}^{6+}$  reduction by structural  $\text{Fe}^{2+}$  naturally present in chlorite and corrensite. No reduction occurred with unaltered (oxidised) montmorillonite. Taylor et al. (2000) found that reduced ferruginous smectite (sample SWa-1) reduces  $\text{Cr}^{6+}$  to  $\text{Cr}^{3+}$  with an efficiency of 79% of the idealised 1:3 ratio of  $\text{Cr}^{6+}$  reduced to structural  $\text{Fe}^{2+}$  oxidised. The amount of  $\text{Cr}^{3+}$  immobilised on the clay mineral surfaces was greatly increased if reduced smectite was used as the reductant rather than using the sequence of  $\text{Cr}^{6+}$  reduction in solution by dithionite followed by the addition of oxidised smectite, which confirms the important role of the reduced smectite in this process. The oxidation state of sorbed Cr was confirmed by XANES to be  $\text{Cr}^{3+}$ . The extent of  $\text{Cr}^{6+}$  reduction is greater if the exchanged cation in the reduced smectite is  $\text{Na}^+$  rather than  $\text{K}^+$ , indicating that the reaction occurs primarily at basal surfaces since the presence of exchanged  $\text{K}^+$  during structural iron reduction enhances layer collapse and decreases the amount of exposed basal surface area (Shen and Stucki, 1994).

Istok et al. (1999) investigated the possibility of reducing the iron in minerals comprising sub-surface horizons as a means for intercepting and remediating plumes of  $\text{Cr}^{6+}$ -contaminated waters. They injected a solution of dithionite and K-bicarbonate–carbonate into wells drilled into the subsurface formation, then monitored the Cr concentration and oxidation state of groundwater exiting from the formation. Analyses indicated that substantial  $\text{Fe}^{3+}$  was reduced to  $\text{Fe}^{2+}$  in the formation, and laboratory column studies revealed that the dithionite-treated sediment was capable of removing 2 mg/L  $\text{Cr}^{6+}$  from about 100 column pore volumes of synthetic groundwater. Although this experiment did not determine that the  $\text{Fe}^{2+}$  was in the structure of the constituent phyllosilicate minerals, it raised the possibility for this to be an effective in situ method for groundwater remediation.

### 8.7. MECHANISM FOR IRON REDUCTION

The mechanisms for structural  $\text{Fe}^{3+}$  reduction and reoxidation in smectites is only partially understood. Much progress has been made over the past two decades

in learning about changes in composition and structure that accompany redox processes, but the specific pathway by which electrons penetrate the 2:1 layer is still unknown. More investigations based on quantum chemical studies of phyllosilicates, such as those performed by Peterson et al. (1979), Aronowitz et al. (1982), Bleam and Hoffmann (1988a, 1988b), and Delville (1991), and on the theoretical discussions of Bleam (1993) and Amonette (2002) are critically needed. In fact, Bleam (1993) stated that “electron transport in transition-metal-containing phyllosilicates” is one of the major needs for future research.

Evidence seems to reject the hypothesis that structural iron reduction occurs only at the edge surfaces of the smectite layers, and is more consistent with reduction occurring primarily at the basal surfaces. The progression of the reduction reaction in iron-rich smectite suspensions can be followed by monitoring the absorption band for the  $\text{Fe}^{2+}$ – $\text{Fe}^{3+}$  intervalence electron transfer transition (IT) observed at about 730 nm in the visible spectrum (Lear and Stucki, 1987; Komadel et al., 1990). This band increases linearly (Fig. 8.16) until the reduction level reaches about 45% of total iron, at which point the intensity of the band levels off and then decreases. This behaviour is easily understood when one realises that the intensity of the band is actually a measure of the number of  $\text{Fe}^{2+}$ – $\text{O}$ – $\text{Fe}^{3+}$  entities in the octahedral sheet. In order for this band to appear, iron ions must occupy adjacent octahedral sites and be of different valence. The fact that the intensity of this band increases linearly with  $\text{Fe}^{2+}$  content is direct evidence that the number of adjacent  $\text{Fe}^{2+}$ – $\text{Fe}^{3+}$  ions also increases linearly; or, in other words, the reducing electron seeks out  $\text{Fe}^{3+}$  sites that are as far as possible from  $\text{Fe}^{2+}$  sites. Lear and Stucki (1987) described this as a random reduction with a next-nearest neighbour exclusion. This condition applies in Region I of Fig. 8.16.

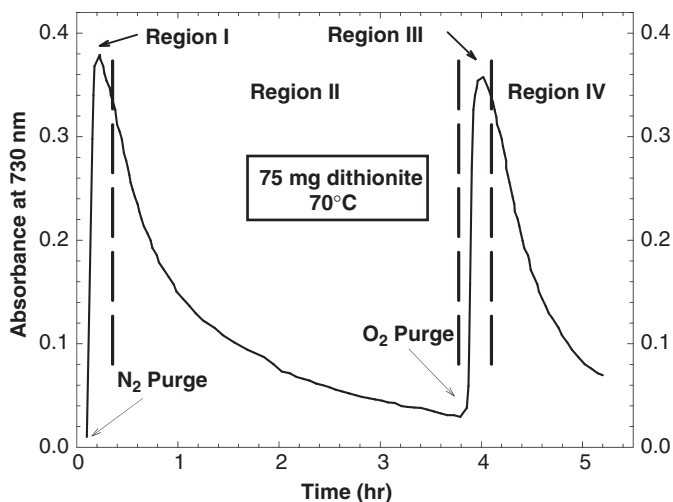


Fig. 8.16. Reduction kinetics of structural Fe in Hohen Hagen nontronite sample NG-1. From Komadel et al. (1990).



As the reduction reaction proceeds beyond the point where all possible  $\text{Fe}^{2+}\text{--O--Fe}^{3+}$  groupings have been established,  $\text{Fe}^{2+}\text{--O--Fe}^{2+}$  groups begin to form. This causes the intensity of the IT band to decrease as  $\text{Fe}^{2+}\text{--O--Fe}^{3+}$  is eliminated. When the reduction process is complete, the matrix is fully comprised of  $\text{Fe}^{2+}\text{--O--Fe}^{2+}$  groups and the IT band is gone. This phase of the process is observed in Region II of Fig. 8.16. These changes in the iron-rich smectite are easily visible to the eye also, as the colour of the sample changes in Region I from yellow to green, then blue-green; and in Region II from blue-green to blue-grey, then to grey.

When the fully reduced smectite is reoxidised by bubbling  $\text{O}_2$  gas through the suspension, the reoxidation process follows a similar pattern where  $\text{Fe}^{2+}$  is reoxidised to  $\text{Fe}^{3+}$  in a random pattern, with next-nearest neighbour exclusion. The intensity of the IT band increases due to formation of  $\text{Fe}^{2+}\text{--Fe}^{3+}$  pairs, only this time through oxidation, and the colour reverts from grey to blue-green in Region III of Fig. 8.16. In the final phase of the process, the IT band intensity decreases as the remaining  $\text{Fe}^{2+}\text{--Fe}^{3+}$  pairs are eliminated by complete oxidation, as indicated in Region IV of Fig. 8.16.

If reduction or reoxidation were occurring from the edge surfaces only, the semi-randomness observed in the distribution of  $\text{Fe}^{2+}$  in the octahedral sheet would require a very well ordered, two-dimensional network of octahedral iron sites through which an electron can easily pass. This possibility seems remote, although not impossible. Biotite is a phyllosilicate system in which octahedral iron is oxidised from the edges (Amonette and Scott, 1988). In that case, an oxidising front is observed, creating a zone of all  $\text{Fe}^{3+}$  and a zone of all  $\text{Fe}^{2+}$ , with a moving interface between the zones as oxidation proceeds. One might expect a similar model in smectites if reduction or reoxidation were occurring from the edges only, giving rise to oxidised and reduced zones with an inter-zonal interface having a relatively constant amount of mixed-valent iron sites and thus a relatively constant intensity for the IT band. This model fails to fit the observed changes in IT band intensity with  $\text{Fe}^{2+}$  content (Fig. 8.16). Redox reactions at the basal surfaces, on the other hand, would have better access to the iron sites towards the centre of the smectite layer and thereby produce a more random distribution of  $\text{Fe}^{2+}$  within the octahedral sheet.

Magnetic exchange interactions also reveal that iron reduction must occur in a somewhat random pattern rather than as a reducing front through the clay mineral particle. Schuette et al. (2000) observed that the iron in iron-rich smectites is antiferromagnetically ordered in the unaltered or oxidised state, but as iron is reduced to  $\text{Fe}^{2+}$  the exchange interaction changes to superparamagnetic or spin glass behaviour at the lowest temperatures. As temperature increases, the exchange interaction transforms to a ferromagnetic state in the reduced samples. The transition between superparamagnetic and ferromagnetic states is temperature-dependent and increases linearly with increasing  $\text{Fe}^{2+}$  content in the structure. This transition is also sensitive to isomorphous substitutions in the clay mineral structure.

Characterisations of changes in clay mineral structure accompanying iron reduction have been the focus of many studies, beginning with Addison and Sharp (1963).

They reduced structural iron by heating the nontronite in an  $H_2$  atmosphere at  $450^\circ C$  and proposed that the mechanism involved the protonation of both the apical oxygen ions and the structural OH groups, causing the latter to be released from the structure as  $H_2O$  and leaving  $Si-O-H$  behind. Roth and Tullock (1973), Stucki and Roth (1976), Huo (1997), and Fialips et al. (2002a, 2002b) conducted in-depth infrared studies of reduced and reduced-reoxidised nontronite and ferruginous smectite, and found significant changes in the vibrational energies of structural OH groups, confirming (at least in part) the proposition of Addison and Sharp that reduction destabilises the structural OH apparatus. To date no direct evidence has been reported that apical oxygen ions are protonated, but none of these studies has used the same reduction method as Addison and Sharp. Considerable evidence now exists, on the other hand, that structural OH groups are lost upon iron reduction by dithionite in aqueous solution.

Manceau et al. (2000b) noted, however, that this loss of hydroxyls occurs while the structural iron retains six-fold coordination. In order to accomplish this, while losing hydroxyls, they proposed a reorganisation in the octahedral sheet to form trioctahedral domains by the migration of iron from *cis* to *trans* sites (Fig. 8.17). The

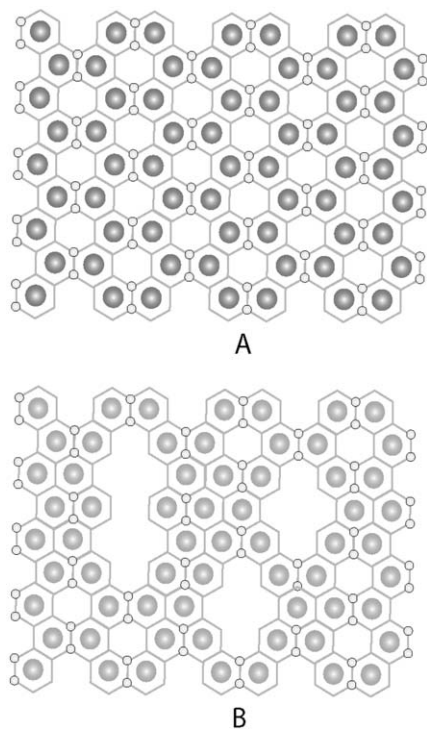
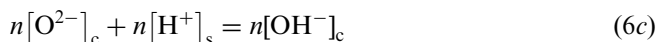
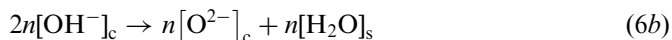
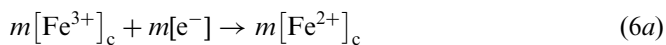


Fig. 8.17. Schematic illustration of changes in structure of the octahedral sheet of Garfield nontronite before (A) and after (B) reduction by dithionite. From Manceau et al. (2000b).

formation of a trioctahedral environment for structural OH may explain the appearance of the small peak at  $3622\text{ cm}^{-1}$  in the O–H stretching region of reduced nontronite (Fig. 8.9). A similar peak was observed in griffithite by Komadel et al. (2000), where Griffithite is a saponite with about 26% of octahedral sites being in trioctahedral configuration. Li et al. (2005) have offered an alternative interpretation of polarised EXAFS observations that allows for the protonation of structural OH by  $\text{H}^+$  in solution to form structural  $\text{H}_2\text{O}$ , which is also consistent with six-fold coordination and the infrared spectra.

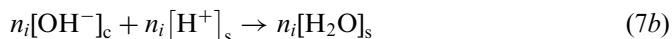
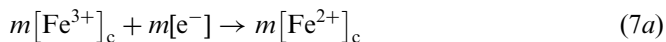
Drits and Manceau (2000) presented a mechanistic model that is consistent with the structural changes observed by Manceau et al. (2000b) and the observed changes in layer charge (Stucki and Roth, 1977; Lear and Stucki, 1985). It differs from the mechanism proposed by Stucki and Roth (1977) and Lear and Stucki (Lear and Stucki, 1985; Stucki and Lear, 1989) in the following ways (compare Eqs. (6) and (7)): (1) iron retains six-fold coordination in the reduced structure, instead of converting into five-fold; and (2) dehydroxylation of the structure as a result of iron reduction is initiated by the adsorption of protons by structural OH groups to form  $\text{H}_2\text{O}$ , which then diffuses into solution; rather than following the sequence presented by Stucki and Roth (1977) where two adjacent OH groups coalesce to form one  $\text{H}_2\text{O}$  molecule, which then diffuses into solution, leaving behind one  $\text{O}^{2-}$  in the structure. The  $\text{O}^{2-}$  is subsequently protonated by the solvent. The Drits and Manceau model takes into account the elimination of a *cis*-dihydroxide octahedral site during iron reduction, as proposed by Manceau et al. (2000b), due to the loss of its two hydroxyl groups, and the migration of  $\text{Fe}^{2+}$  into the *trans*-dihydroxide site. This migration preserves the six-fold coordination of the iron, but, as noted above, creates trioctahedral domains mixed with the defects in the crystal where the *cis* sites existed previously (Fig. 8.17).

These mechanisms are compared in Eqs. (6) and (7). The mechanism proposed by Stucki and Roth (1977) is given by



where subscripts c and s represent species in the clay mineral particle and the surrounding solution, respectively, and  $m$  and  $n$  are stoichiometry coefficients related by  $n = 0.32m$  (Lear and Stucki, 1985).

The mechanism of Drits and Manceau (2000) is given by



where  $n_i$  is the stoichiometry coefficient governing the protonation of structural OH groups from the solvent (and equivalently the amount of dehydroxylation). Notice that Eqs. (6a) and (7a) are identical, and the principal difference in these two mechanisms is the manner in which dehydroxylation occurs. [Drits and Manceau \(2000\)](#) found that  $n_i$  depends on  $m$ , but in a more complex manner than  $n$  ([Lear and Stucki, 1985](#)). This dependence on the extent of iron reduction is given by

$$n_i = \frac{K_0(m^2/m_{\text{tot}})}{1 + K_0(m/m_{\text{tot}})} \quad (8)$$

where  $m_{\text{tot}}$  is the total iron content of the clay mineral and  $K_0$ , a constant that depends on the clay mineral. The corresponding increase in layer charge in both mechanisms is given by the increased amount of interlayer cation that is measured ([Stucki et al., 1984a](#)), which was represented by [Drits and Manceau \(2000\)](#) by the symbol  $p$  and related to the total layer charge before and after reduction by the expression

$$w = w_0 + p \quad (9)$$

where  $w$  and  $w_0$  are the total layer charge of the reduced and unaltered (oxidised) smectites, respectively. They further expressed  $p$  as a function of the extent of reduction ( $m$ ) by the expression

$$p = \frac{m}{1 + K_0(m/m_{\text{tot}})} \quad (10)$$

Combining Eqs. (9) and (10) gives

$$w = w_0 + \frac{m}{1 + K_0(m/m_{\text{tot}})} \quad (11)$$

They found that by empirically optimising the value of  $K_0$  they could accurately predict from this equation the total layer charge observed by [Stucki et al. \(1984a\)](#) in reduced smectites as a function of  $m$ . If no ancillary reactions or structural changes occurred during the reduction process, the layer charge would be expected to increase by the same amount as the level of reduction, i.e.,  $p$  would be equal to  $m$ . If dehydroxylation occurs, however, the increased negative charge due to iron reduction will be partially compensated by the elimination of negatively charged structural OH groups, causing the value of  $p$  to decline by the amount of dehydroxylation, or  $n_i$ . This leads to the conclusion that

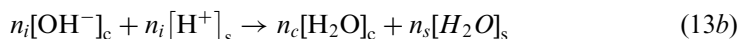
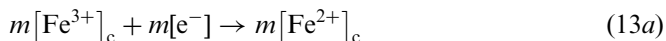
$$m = p + n_i \quad (12)$$

The [Drits and Manceau \(2000\)](#) model is self-consistent with this relationship.

While Eqs. (7)–(12) provide a meaningful mathematical model for predicting layer charge from the extent of reduction and total iron content of the clay mineral, efforts to give a physical explanation, especially in terms of the particular site occupancy of structural iron (*cis* versus *trans*), appear to have been less successful. The model

mineral system chosen by [Drits and Manceau \(2000\)](#), and the particular combinations of parameters used to glean further information from this term, yields the unintended consequence that the CEC of the smectite must decrease as the level of reduction increases. Since this is contrary to known measurements of CEC versus reduction level at the low to mid levels of reduction, any conclusions based on that model mineral system are questionable. This does not, however, invalidate their proposed reaction mechanism (Eqs. (7a) and (7b)).

Further refinements of the reduction mechanism may be found by removing the assumption that  $n_i$  represents both the amount of  $H^+$  adsorbed and the amount of  $OH^-$  lost. Some of the  $H_2O$  formed by  $H^+$  adsorption may, in fact, remain in the smectite structure at higher levels of iron reduction. Evidence for this is found in the infrared spectra of reduced smectites ([Huo, 1997](#); [Fialips et al., 2002a, 2002b](#)). As shown in [Fig. 8.9](#), there is a steady increase in the H–O–H stretching band at about  $3400\text{ cm}^{-1}$  with increasing levels of iron reduction. All samples were submitted to the same dehydration treatment, so increased persistence of this band suggests that it derives from  $H_2O$  molecules that are held more strongly in the clay mineral structure than those that are simply adsorbed to the outer surfaces, as appeared to be the case for the unreduced and lesser-reduced samples. One interpretation of this phenomenon is that the hydration energy of the reduced smectite surface is greater than the oxidised surface (see Section 8.5), but another equally valid interpretation is that the  $H_2O$  is actually part of the structure. Studies by [Roth and Tullock \(1973\)](#) and [Lear and Stucki \(1985\)](#) clearly showed that  $H^+$  in the solvent became incorporated into the smectite structure during reduction. This could well be in the form of  $H_2O$  instead of  $OH$ , as originally proposed by those authors. While the strict application of the Drits and Manceau mechanism would preclude this possibility, reverting to a process that involves protonation of structural  $OH$  groups without the subsequent dehydroxylation is a scenario that is consistent with the body of information currently available. In this case, the mechanism would be



where  $n_c$  and  $n_s$  are, respectively, the stoichiometry coefficients for the amount of  $H_2O$  that remains in the clay mineral structure and the amount that diffuses into solution to cause structural dehydroxylation. Notice that Eq. (13a) is identical to Eqs. (6a) and (7a), but Eq. (13b) allows the possibility for proton adsorption to evoke any degree of dehydroxylation up to  $n_i$ , where  $n_i = n_c + n_s$ . Since neutralisation of the increased negative charge due to iron reduction occurs when  $H^+$  is adsorbed, whether or not the resulting  $H_2O$  molecule diffuses out of the clay mineral structure, the expressions relating  $n_i$  to total layer charge and extent of reduction (Eqs. (8) and (11)) are also valid for this revised mechanism.

If  $n_c$  is non-zero, some of the *cis*-dihydroxide sites in the octahedral sheet will remain intact and the extent of iron migration from *cis* to *trans* sites will be lessened. Infrared spectra (Fig. 8.9) indicate that  $n_c$  could, in fact, account for a large fraction of  $n_i$ . If this is true, then the model proposed by Manceau et al. (2000b) may provide only one possible explanation for the observations by polarised EXAFS, and/or the extent of such radical alterations of the structure may be rather small. This model involves the destruction of *cis* sites via dehydroxylation, resulting in the creation of structural defects and trioctahedral domains.

The extent to which the structure can be reduced may depend on the site occupancy of iron in the octahedral sheet. For example, Komadel et al. (2000) have studied griffithite, a mixed di-tri-octahedral smectite having about 26% of the octahedra in trioctahedral domains. The extent of maximum reduction of octahedral  $\text{Fe}^{3+}$  in this clay mineral is only 60%, compared to almost 100% in ferruginous smectite. The pre-existence of  $\text{Fe}^{3+}$  in trioctahedral domains may either resist reduction because protonation of a fully bonded OH group may be energetically difficult and/or dehydroxylation would require the breakage of three instead of two bonds. This is direct evidence that reduction is impossible or very difficult without concomitant changes in clay mineral structure.

## 8.8. USE OF REDOX-MODIFIED SMECTITES IN CLAY-MODIFIED ELECTRODES

Cyclic voltammetry is a method that imposes oxidising and reducing conditions on the elements of a set of electrodes, and enables the study of a variety of systems in which electron transfer processes are active. The modification of these electrodes by coating them with smectites has been employed for a variety of purposes. With respect to studying the clay mineral itself, this method could become useful as a way to impose redox cycles on structural  $\text{Fe}^{3+}$  in the smectite or for characterising the effects of redox state in the clay mineral on surface and textural properties of the mineral. Fitch et al. (1995) found that coating the electrode with reduced smectite rather than with oxidised smectite increased the rate of transport of an electroactive species,  $\text{Fe}(\text{CN})_6^{3-}$ , through the clay mineral film in response to the cyclic current applied through the electrode. This observation may be related to the change in CEC of the smectite upon reduction. The key factor appears to be the change in redox status of the structural iron, since total iron content appears to have little or no influence on the transport of electroactive species (Xiang and Villemure, 1994).

Xiang and Villemure (1992, 1995) prepared clay-modified electrodes (CME) using reduced-iron smectites. They found that the oxidation of structural iron in the smectite might account for an increased intensity in the anodic (oxidative) peak when an electron transport shuttle or mediator was present, such as  $\text{Fe}^{2+}$  bipyridyl or  $\text{Ru}^{2+}$  hexamine. They also used CME to monitor the behaviour of synthetic smectites prepared with either iron or nickel as the transition metal cation in the

octahedral sheet. They found that the addition of nickel in the synthesis of an iron-bearing smectite enhanced both the cathodic (reductive) and anodic (oxidative) waves. This hybrid synthetic sample performed better than either the pure iron or pure nickel analogues. Changes in intensity of the 246 nm UV absorption band ( $O \rightarrow Fe^{3+}$  charge transfer (Karickhoff and Bailey, 1973; Sherman and Vergo, 1988)) were correlated with the initial reduction of structural iron followed by its oxidation as the potential was swept in the presence of  $Fe^{2+}$  bipyridyl or  $Ru^{2+}$  hexamine.

## 8.9. SUMMARY AND CONCLUSIONS

Because of their great abundance, high specific surface area, layer charge, laminar morphology, and chemical reactivity towards both neutral and charged species, clay minerals are of great importance to agriculture, industry, and the environment. The presence of iron in the structures of clay minerals infuses an additional facet into their importance. This is because the oxidation state of iron can be rather easily modified *in situ* and such a change can evoke profound differences in the surface-chemical and structural behaviour of the mineral. Examples of clay mineral properties that are greatly affected by changes in iron oxidation state are swelling in water, CEC, cation fixation capacity, surface area, clay mineral–organic interactions, surface pH, reduction potential, ability to transform chlorinated organic compounds, and ability to degrade pesticides and thereby alter their toxicity to mammals. Reduction of structural iron from  $Fe^{3+}$  to  $Fe^{2+}$  in smectites has been observed both in the laboratory and *in situ* in the field. Bacteria are second only to dithionite in their effectiveness to reduce structural iron in clay mineral and are the most important agent responsible for this phenomenon in natural soils and sediments.

Because the manipulation of the iron oxidation state causes such large changes in chemical and physical behaviour and because such changes can be invoked under field conditions, a great opportunity exists to exploit this phenomenon for a myriad of purposes beneficial to mankind. Although such exploitation has yet to occur to any large extent, it has found application in the remediation of subsurface soils contaminated with radioactive and other harmful metals. Studies are also beginning to emerge that recognise this as an important factor in sustaining the fertility and use of flooded soils. Clearly, other opportunities will arise for its use in creating designer minerals for industrial uses.

Challenges and many unanswered questions still face those who study redox processes of iron in clay minerals, especially with respect to the mechanisms governing the electron transfer and the linkages between  $Fe^{2+}$  and surface behaviour. How is the electron passed from the outer surfaces of the clay mineral layers into the octahedral sheet? What are the precise energies associated with this process? The exact surface forces altered by the redox process appear to be both coulombic and non-coulombic, but the precise nature of the latter is not well understood. What is the mechanism for electron transfer from bacteria to clay mineral layers—is it done



through a direct membrane contact or are electron shuttles or mediators utilised? Is the mechanism the same for all bacteria? Even though the phenomenon of iron redox in clay minerals has been studied for several decades, the number of scientists participating in such studies is still rather small. Interest in this field of inquiry is beginning to grow, however, and answers to these and other questions are anticipated to be forthcoming.

On a personal note, this author has been the beneficiary of many intriguing twists and turns along the path in the realm of iron redox chemistry, which has provided a most interesting, challenging, and rewarding perspective to his study of clay science. He has been awed by the intricacies of Nature as seen at such a seemingly insignificant level in the grand overall scheme of things, but which reveal such majestic order and complexity at the same time. His feelings about this are well captured in the words of the poet Elizabeth Barrett Browning (1937), who declared, "*Earth's crammed with heaven, and every common bush afire with God; only he who sees takes off his shoes.*" My shoes are off!

## REFERENCES

- Addison, W.E., Sharp, J.H., 1963. Redox behavior of iron in hydroxylated silicates. *Clays and Clay Minerals* 11, 95–104.
- Amonette, J.E., 2002. Iron redox chemistry of clays and oxides: environmental applications. In: Fitch, A. (Ed.), *Electrochemical Properties of Clays*. CMS Workshop Lectures, vol. 10. The Clay Minerals Society, Aurora, CO, pp. 89–148.
- Amonette, J.E., Scott, A.D., 1988. Iron in micas. In: Stucki, J.W., Goodman, B.A., Schwertmann, U. (Eds.), *Iron in Soils and Clay Minerals*. D. Reidel, Dordrecht, pp. 576–624.
- Anderson, W.L., Stucki, J.W., 1979. Effect of structural  $\text{Fe}^{2+}$  on visible absorption spectra of nontronite suspensions. In: Mortland, M.M., Farmer, V.C. (Eds.), *Proceedings International Clay Conference, 1978*, Oxford. Elsevier, Amsterdam, pp. 75–83.
- Aoki, S., Kohyama, N., 1991. Vertical change in clay mineral composition and chemical characteristics of smectite in sediment cores from the southern part of the Central Pacific Basin. *Marine Geology* 98, 41–49.
- Aronowitz, S., Coyne, L., Lawless, J., Rishpon, J., 1982. Quantum-chemical modeling of smectite clays. *Inorganic Chemistry* 21, 3589–3593.
- Badaut, D., Decarreau, A., Besson, G., 1992. Ferripyrophyllite and related  $\text{Fe}^{3+}$ -rich 2:1 clays in recent deposits of Atlantis II Deep, Red Sea. *Clay Minerals* 27, 227–244.
- Badraoui, M., Bloom, P.R., 1990. Iron-rich high-charge beidellite in vertisols and mollisols of the High Chaouia region of Morocco. *Soil Science Society of America Journal* 54, 267–274.
- Ballet, O., Coey, J.M.D., 1982. Magnetic properties of sheet silicates; 2:1 layer minerals. *Physics and Chemistry of Minerals* 8, 218–229.
- Barbayanis, N., Evangelou, V.P., Keramidas, V.C., 1996. Potassium–ammonium–calcium quantity/intensity studies in the binary and ternary modes in two soils of micaceous mineralogy of northern Greece. *Soil Science* 161, 716–724.
- Bergaya, F., Barrault, J., 1990. Mixed Al–Fe pillared laponites: preparation, characterization and their catalytic properties in syngas conversion. In: Mitchell, I.V. (Ed.), *Pillared Layered Structures. Current Trends and Applications*. Elsevier, Amsterdam, pp. 167–184.



- Bergaya, F., Hassoun, N., Gatinneau, L., Barrault, J., 1991. Mixed Al-Fe pillared laponites: preparation, characterization and catalytic properties in syngas conversion. In: Poncelet, G., Jacobs, P.A., Grange, P., Delmon, B. (Eds.), *Preparation of Catalysts V*. Elsevier, Amsterdam, pp. 329–336.
- Besson, G., Bookin, A.S., Dainyak, L.G., Rautureau, M., Tsipursky, S.I., Tchoubar, C., Drits, V.A., 1983. Use of diffraction and Mössbauer methods for the structural and crystallochemical characterization of nontronites. *Journal of Applied Crystallography* 16, 374–383.
- Besson, G., Dainyak, L.G., De la Calle, C., Tsipursky, S.I., Rautureau, M., Bookin, A.S., Tchoubar, C., Drits, V.A., 1981. Cation distribution pattern, nature, and concentration of stacking faults in the structure of potassium-saturated nontronite. *Mineralogicheskii Zhurnal* 36, 66–77.
- Bhattacharyya, J., Saha, S.K., 1990. Aqueous polymerization on clay surfaces. V. Role of lattice substituted iron in montmorillonite in polymerizing methyl methacrylate in the presence of thiourea. *Journal of Polymer Science A: Polymer Chemistry* 28, 2249–2254.
- Bishop, J., Murad, E., Dyar, M.D., 2002. Influence of octahedral and tetrahedral cation substitution on the structure of smectites and serpentines as observed through infrared spectroscopy. *Clay Minerals* 37, 617–628.
- Bleam, W.F., 1993. Atomic theories of phyllosilicates: quantum chemistry, statistical mechanics, electrostatic theory, and crystal chemistry. *Reviews of Geophysics* 31, 51–73.
- Bleam, W.F., Hoffmann, R., 1988a. Orbital interactions in phyllosilicates: perturbations of an idealized two-dimensional, infinite silicate frame. *Physics and Chemistry of Minerals* 15, 398–408.
- Bleam, W.F., Hoffmann, R., 1988b. Isomorphous substitution in phyllosilicates as an electronegativity perturbation: its effect on bonding and charge distribution. *Inorganic Chemistry* 27, 3180–3186.
- Boiabid, R., Badraoui, M., Bloom, P.R., 1991. Potassium fixation and charge characteristics of soil clays. *Soil Science Society of America Journal* 55, 1493–1498.
- Boivin, P., Favre, F., Hammecker, C., Maeght, J.L., Delarivière, J., Poussin, J.C., Wopereis, M.C.S., 2002. Processes driving soil solution chemistry in a flooded rice-cropped vertisol: analysis of long-time monitoring data. *Geoderma* 110, 87–107.
- Bookin, A.S., Dainyak, L.G., Drits, V.A., 1979. Interpretation of the Mössbauer spectra of iron(3+)-containing layered silicates based on structural modeling. *Kation Uporyadochenie V Strukturalakh Mineralov, Novosibirsk*, 23–41.
- Borggaard, O.K., 1988. Phase identification by selective dissolution techniques. In: Stucki, J.W., Goodman, B.A., Schwertmann, U. (Eds.), *Iron in Soils and Clay Minerals*. D. Reidel, Dordrecht, pp. 83–98.
- Brigatti, M.F., Lugli, C., Cibir, G., Marcelli, A.G.G., Paris, E., Mottana, A., Wu, Z., 2000. Reduction and sorption of chromium by Fe(II)-bearing phyllosilicates: chemical treatments and X-ray absorption spectroscopy (XAS) studies. *Clays and Clay Minerals* 48, 272–281.
- Browning, E.B., 1937. Quoted in Bartlett, J., *Familiar Quotations*. Little, Brown, and Company, Boston, p. 371.
- Cardile, C.M., 1989. Tetrahedral iron in smectite: a critical commentary. *Clays and Clay Minerals* 37, 185–188.
- Cardile, C.M., Slade, P.G., 1987. Structural study of a benzidine-vermiculite intercalate having a high tetrahedral-iron content by Fe<sup>57</sup> Mössbauer spectroscopy. *Clays and Clay Minerals* 35, 203–207.

- Cervini-Silva, J., Kostka, J.E., Larson, R.A., Stucki, J.W., Wu, J., 2003. Dehydrochlorination of 1,1,1 trichloroethane and pentachloroethane by microbially reduced ferruginous smectite. *Environmental Toxicology and Chemistry* 22, 1046–1050.
- Cervini-Silva, J., Larson, R.A., Wu, J., Stucki, J.W., 2001. Transformation of chlorinated aliphatic compounds by ferruginous smectite. *Environmental Science and Technology* 35, 805–809.
- Cervini-Silva, J., Larson, R.A., Wu, J., Stucki, J.W., 2002. Dechlorination of pentachloroethane by commercial Fe and ferruginous smectite. *Chemosphere* 47, 971–976.
- Cervini-Silva, J., Wu, J., Larson, R.A., Stucki, J.W., 2000a. Transformation of chloropicrin in the presence of iron-bearing clay minerals. *Environmental Science and Technology* 34, 915–917.
- Cervini-Silva, J., Wu, J., Stucki, J.W., Larson, R.A., 2000b. Adsorption kinetics of pentachloroethane in iron-bearing smectites. *Clays and Clay Minerals* 48, 132–138.
- Chen, S.Z., Low, P.F., Roth, C.B., 1987. Relation between potassium fixation and the oxidation rate of octahedral iron. *Soil Science Society of America Journal* 51, 82–86.
- Chen, Y., Shaked, D., Banin, A., 1979. The role of structural iron(III) in the UV absorption by smectites. *Clay Minerals* 14, 93–102.
- Chirchi, L., Ghorbel, A., 2002. Use of various Fe-modified montmorillonite samples for 4-nitrophenol degradation by  $H_2O_2$ . *Applied Clay Science* 21, 271–276.
- Choudary, B.M., Ravichandra Sarma, M., Vijaya Kumar, K., 1994.  $Fe^{3+}$  montmorillonite catalyst for selective nitration of chlorobenzene. *Journal of Molecular Catalysis* 87, 33–38.
- Cicel, B., Komadel, P., Hronsky, J., 1990. Dissolution of the fine fraction of Jelšov Potok bentonite by hydrochloric and sulphuric acids. *Ceramics Silikaty* 34, 41–48.
- Coey, J.M.D., 1988. Magnetic properties of iron in soil iron oxides and clay minerals. In: Stucki, J.W., Goodman, B.A., Schwertmann, U. (Eds.), *Iron in Soils and Clay Minerals*. D. Reidel, Dordrecht, pp. 397–466.
- Coey, J.M.D., Chukhrov, F.V., Zvyagin, B.B., 1983. Cation distribution, Mössbauer spectra, and magnetic properties of ferripyrophyllite. *Clays and Clay Minerals* 32, 198–204.
- Coyne, L.M., Banin, A., 1986. Effect of adsorbed iron on thermoluminescence and electron spin resonance spectra of Ca–Fe-exchanged montmorillonite. *Clays and Clay Minerals* 34, 645–650.
- Cuttler, A.H., Man, V., Cranshaw, T.E., Longworth, G., 1990. A Mössbauer study of green rust precipitates: I. Preparations from sulphate solutions. *Clay Minerals* 25, 289–302.
- Dainyak, L.G., Bookin, A.S., Drits, V.A., 1984a. Interpretation of Mössbauer spectra of dioctahedral iron(3+)–containing layered silicates. II. Nontronite. *Kristallografiya* 29, 304–311.
- Dainyak, L.G., Dainyak, B.A., Bookin, A.S., Drits, V.A., 1984b. Interpretation of Mössbauer spectra of dioctahedral iron(3+)–containing layered silicates. I. Calculation of electric field gradients and relative intensities. *Kristallografiya* 29, 94–100.
- Dainyak, L.G., Drits, V.A., 1987. Interpretation of Mössbauer spectra of nontronite, celadonite, and glauconite. *Clays and Clay Minerals* 35, 363–372.
- Dainyak, L.G., Drits, V.A., Heifits, L.M., 1992. Computer simulation of cation distribution in dioctahedral 2:1 layer silicates using IR data: application to Mössbauer spectroscopy of a glauconite sample. *Clays and Clay Minerals* 40, 470–479.
- Decarreau, A., Grauby, O., Petit, S., 1992. The actual distribution of octahedral cations in 2:1 clay minerals: results from clay synthesis. *Applied Clay Science* 7, 147–167.

- Delville, A., 1991. Modeling the clay–water interface. *Langmuir* 7, 547–555.
- Diamant, A., Pasternak, M., Banin, A., 1982. Characterization of adsorbed iron in montmorillonite by Mössbauer spectroscopy. *Clays and Clay Minerals* 30, 63–66.
- Dong, H., Kostka, J.E., Kim, J., 2003a. Microscopic evidence for microbial dissolution of smectite. *Clays and Clay Minerals* 51, 502–512.
- Dong, H.G., Kukkadapu, R.K., Frederickson, J.K., Zachara, J.M., Kennedy, D.W., Kostandarithes, H.M., 2003b. Microbial reduction of structural Fe(III) in Illite and Goethite. *Environmental Science and Technology* 37, 1268–1276.
- Drago, V., Saitovitch, E.B., Danon, J., 1977. Mössbauer spectroscopy of electron irradiated natural layered silicates. *Inorganic Nuclear Chemistry* 39, 973–979.
- Drits, V.A., Dainyak, L.G., Slonimskaya, M.V., 1981. Procedure for the calculation of crystal-chemical formulas of iron-containing sheet silicates. *Izvestiia Akademii Nauk SSSR, Serii Geologicheskaya* 12, 87–98.
- Drits, V.A., Manceau, A., 2000. A model for the mechanism of  $\text{Fe}^{3+}$  to  $\text{Fe}^{2+}$  reduction in dioctahedral smectites. *Clays and Clay Minerals* 48, 185–195.
- Dyar, M.D., Delaney, J.S., Sutton, S.R., 2001. Fe XANES spectra of iron-rich micas. *European Journal of Mineralogy* 13, 1079–1098.
- Dyar, M.D., Gunter, M., Delaney, J.S., Lanzarotti, A., Sutton, S.R., 2002. Systematics in the structure and XANES spectra of pyroxenes, amphiboles, and micas as derived from oriented single crystals. *Canadian Mineralogist* 40, 1375–1393.
- Ebitani, K., Ide, M., Mitsudome, T., Mizugaki, T., Kaneda, K., 2002. Creation of a chain-like cationic iron species in montmorillonite as a highly active heterogeneous catalyst for alkane oxygenations using hydrogen peroxide. *Chemical Communications* 2002, 690–691.
- Egashira, K., Ohtsubo, M., 1983. Swelling and mineralogy of smectites in paddy soils derived from marine alluvium, Japan. *Geoderma* 29, 119–127.
- Erbs, M., Hansen, H.C.B., Olsen, C.E., 1999. Reductive dechlorination of carbon tetrachloride using iron(II)–iron(III) hydroxide sulfate (green rust). *Environmental Science and Technology* 33, 307–311.
- Ericsson, T., Linares, J., Lotse, E., 1984. A Mössbauer study of the effect of dithionite/citrate/bicarbonate treatment on a vermiculite, smectite and a soil. *Clay Minerals* 19, 85–91.
- Ernstsen, V., 1996. Reduction of nitrate by  $\text{Fe}^{2+}$  in clay minerals. *Clays and Clay Minerals* 44, 599–608.
- Ernstsen, V., Gates, W.P., Stucki, J.W., 1998. Microbial reduction of structural iron in clays—A renewable source of reduction capacity. *Journal of Environmental Quality* 27, 761–766.
- Eslinger, E., Highsmith, P., Albers, D., deMayo, B., 1979. Role of iron reduction in the conversion of smectite to illite in bentonites in the Disturbed Belt, Montana. *Clays and Clay Minerals* 27, 327–338.
- Evangelou, V.P., Wang, J., Phillips, R.E., 1994. New developments and perspectives on soil potassium quantity/intensity relationships. *Advances in Agronomy* 52, 173–227.
- Farmer, V.C., Russell, J.D., 1964. The infra-red spectra of layer silicates. *Spectrochimica Acta* 20, 1149–1173.
- Farmer, V.C., Russell, J.D., 1966. Infrared absorption spectrometry in clay studies. *Clays and Clay Minerals* 15, 121–142.
- Farmer, V.C., Russell, J.D., 1967. Infrared absorption spectrometry in clay studies. *Clays and Clay Minerals* 15, 121–142.

- Favre, F., Ernsten, V., Tessier, D., Boivin, P., 2002a. Short scale changes in soil properties due to structural iron reduction. *Geochimica et Cosmochimica Acta*, Goldschmidt Conference Abstracts, A226.
- Favre, F., Tessier, D., Abdelmoula, M., Genin, J.M., Gates, W.P., Boivin, P., 2002b. Iron reduction and changes in cation exchange capacity in intermittently waterlogged soil. *European Journal of Soil Science* 53, 175–183.
- Fialips, C.-I., Huo, D., Yan, L., Wu, J., Stucki, J.W., 2002a. Infrared study of reduced and reduced-reoxidized ferruginous smectite. *Clays and Clay Minerals* 50, 455–469.
- Fialips, C.-I., Huo, D., Yan, L., Wu, J., Stucki, J.W., 2002b. Effect of iron oxidation state on the IR spectra of Garfield nontronite. *American Mineralogist* 87, 630–641.
- Fitch, A., Du, J., Gan, H., Stucki, J.W., 1995. Effect of clay charge on swelling: a clay-modified electrode study. *Clays and Clay Minerals* 43, 607–614.
- Foster, M.D., 1953. Geochemical studies of clay minerals: II. Relation between ionic substitution and swelling in montmorillonites. *American Mineralogist* 38, 994–1006.
- Foster, M.D., 1955. The relationship between composition and swelling in clays. *Clays and Clay Minerals* 3, 205–220.
- Frost, R.L., Klopogge, J.T., Ding, Z., 2002a. Garfield and Uley nontronites—an infrared spectroscopic comparison. *Spectrochimica Acta A* 58, 1881–1894.
- Frost, R.L., Klopogge, J.T., Ding, Z., 2002b. Near-infrared spectroscopic study of nontronites and ferruginous smectite. *Spectrochimica Acta A* 58, 1657–1668.
- Gan, H., Bailey, G.W., Yu, Y.S., 1996. Morphology of Lead(II) and Chromium(III) reaction products on phyllosilicate surfaces as determined by Atomic Force Microscopy. *Clays and Clay Minerals* 44, 734–743.
- Gan, H., Stucki, J.W., Bailey, G.W., 1992. Reduction of structural iron in ferruginous smectite by free radicals. *Clays and Clay Minerals* 40, 659–665.
- Gates, W.P., Jaunet, A.-M., Tessier, D., Cole, M.A., Wilkinson, H.T., Stucki, J.W., 1998. Swelling and texture of iron-bearing smectites reduced by bacteria. *Clays and Clay Minerals* 46, 487–497.
- Gates, W.P., Komadel, P., Madejová, J., Bujdák, J., Stucki, J.W., Kirkpatrick, R.J., 2000. Electronic and structural properties of reduced-charge montmorillonites. *Applied Clay Science* 16, 257–271.
- Gates, W.P., Slade, P.G., Manceau, A., Lanson, B., 2002. Site occupancies by iron in nontronites. *Clays and Clay Minerals* 50, 223–239.
- Gates, W.P., Stucki, J.W., Kirkpatrick, R.J., 1996. Structural properties of reduced Upton montmorillonite. *Physics and Chemistry of Minerals* 23, 535–541.
- Gates, W.P., Wilkinson, H.T., Stucki, J.W., 1993. Swelling properties of microbially reduced ferruginous smectite. *Clays and Clay Minerals* 41, 360–364.
- Genin, J.M.R., Bourrie, G., Trolard, F., Abdelmoula, M., Jaffrezic, A., Refait, P., Maitre, V., Humbert, B., Herbillon, A., 1998. Thermodynamic equilibria in aqueous suspensions of synthetic and natural Fe(II)–Fe(III) green rusts: occurrences of the mineral in hydromorphic soils. *Environmental Science and Technology* 32, 1058–1068.
- Giresse, P., Wiewiora, A., 2001. Stratigraphic condensed deposition and diagenetic evolution of green clay minerals in deep water sediments on the Ivory Coast-Ghana Ridge. *Marine Geology* 179, 51–70.
- Goodman, B.A., 1978. The Mössbauer spectra of nontronites: consideration of an alternative assignment. *Clays and Clay Minerals* 26, 176–177.

- Goodman, B.A., Russell, J.D., Fraser, A.R., Woodhams, F.D., 1976. A Mössbauer and IR spectroscopic study of the structure of nontronite. *Clays and Clay Minerals* 24, 53–59.
- Gorby, Y.A., Amonette, J.E., Fruchter, J.S., 1994. Remediation of contaminated subsurface materials by a metal-reducing bacterium. In: Gee, G.W., Wing, N.R. (Eds.), *Thirty-third Hanford Symposium on Health and the Environment*. Battelle Pacific Northwest National Laboratory, pp. 233–247.
- Grauby, O., 1993. Nature et etendue des solutions solides octaédriques argileuses. Approche par synthèse minérale. Thesis. University of Poitiers.
- Grauby, O., Petit, S., Decarreau, A., Baronnet, A., 1993. The beidellite–saponite series: an experimental approach. *European Journal of Mineralogy* 5, 623–635.
- Grauby, O., Petit, S., Decarreau, A., Baronnet, A., 1994. Nontronite–saponite series: an experimental approach. *European Journal of Mineralogy* 4, 99–112.
- Hansen, H.C.B., 1989. Composition, stabilization and light absorption of Fe(II)–Fe(III) hydroxy carbonate (“Green Rust”). *Clay Minerals* 24, 663–670.
- Hansen, H.C.B., Koch, C.B., 1998. Reduction of nitrate to ammonium by sulphate green rust: activation energy and reaction mechanism. *Clay Minerals* 33, 87–101.
- Hansen, H.C.B., Poulsen, I.F., 1999. Interaction of synthetic sulphate “Green Rust” with phosphate and the crystallization of vivianite. *Clays and Clay Minerals* 47, 312–318.
- Heller-Kallai, L., 1997. Reduction and reoxidation of nontronite: the data reassessed. *Clays and Clay Minerals* 45, 476–479.
- Heller-Kallai, L., Rozenson, I., 1981. The use of Mössbauer spectroscopy of iron in clay mineralogy. *Physics and Chemistry of Minerals* 7, 223–238.
- Helsen, J.A., Goodman, B.A., 1983. Characterization of iron(II)- and iron(III)-exchanged montmorillonite and hectorite using the Mössbauer effect. *Clay Minerals* 13, 117–125.
- Hirt, A.M., Banin, A., Gehring, A.U., 1993. Thermal generation of ferromagnetic minerals from iron-enriched smectites. *Geophysical Journal International* 115, 1161–1168.
- Hofstetter, T.B., Schwarzenbach, R.P., Haderlein, S.B., 2003. Reactivity of Fe(II) species associated with clay minerals. *Environmental Science and Technology* 37, 519–528.
- Hunter, D.B., Bertsch, P.M., 1994. *In situ* measurements of tetraphenylboron degradation kinetics on clay mineral surfaces by IR. *Environmental Science and Technology* 28, 686–691.
- Hunter, D.B., Gates, W.P., Bertsch, P.M., Kemner, K.M., 1998. Degradation of tetraphenylboron at hydrated smectite surfaces studies by time resolved IR and X-ray absorption spectroscopies. In: Sparks, D.L., Grundl, T.J. (Eds.), *Mineral–Water Interfacial Reactions*. American Chemical Society, Washington, DC, pp. 282–299.
- Huo, D., 1997. Infrared Study of Oxidized and Reduced Nontronite and Ca–K Competition in the Interlayer. Ph.D. dissertation, University of Illinois at Urbana-Champaign, Urbana, IL, p. 61801.
- Istok, J.D., Amonette, J.E., Cole, C.R., Fruchter, J.S., Humphrey, M.D., Szecsody, J.E., Teel, S.S., Vermeul, V.R., Williams, M.D., Yabusaki, S.B., 1999. *In situ* redox manipulation by dithionite injection: intermediate-scale laboratory experiments. *Ground Water* 37, 884–889.
- Johnston, J.H., Cardile, C.M., 1985. Iron sites in nontronite and the effect of interlayer cations from Mössbauer spectra. *Clays and Clay Minerals* 33, 21–30.
- Johnston, J.H., Cardile, C.M., 1987. Iron substitution in montmorillonite, illite, and glauconite by Fe<sub>57</sub> Mössbauer spectroscopy. *Clays and Clay Minerals* 35, 170–176.

- Karickhoff, S.W., Bailey, G.W., 1973. Optical absorption spectra of clay minerals. *Clays and Clay Minerals* 21, 59–70.
- Kawasaki, H., 1974. Change of ferric iron to ferrous iron in 2:1 type layer silicates by reduction. *Nippon Dojo Hiriyogaku Zasshi* 45, 318–320.
- Keeling, J., Raven, M., Gates, W.P., 2000. Geology and preliminary characterisation of two nontronites from Uley graphite mine, South Australia. *Clays and Clay Minerals* 48, 537–548.
- Khaled, E.M., Stucki, J.W., 1991. Fe oxidation state effects on cation fixation in smectites. *Soil Science Society of America Journal* 55, 550–554.
- Kim, J., Dong, H., Seabaugh, J., Newell, S.W., Eberl, D.D., 2004. Role of microbes in the smectite-to-illite reaction. *Science* 303, 830–832.
- Kim, J., Furukawa, Y., Daulton, T.E., Lavoie, D., Newell, S.W., 2003. Characterization of microbially Fe(III) reduced nontronite: environmental cell-transmission electron microscopy study. *Clays and Clay Minerals* 51, 382–389.
- Koch, C.B., Morup, S., 1991. Identification of green rust in an ochre sludge. *Clay Minerals* 26, 577–582.
- Kocherginsky, N.M., Stucki, J.W., 2000. Sorption, diffusion, and desorption of alachlor in oxidized and reduced smectite membranes. *Environmental Science and Technology* 34, 3574–3578.
- Komadel, P., 1999. Structure and chemical characteristics of modified clays. In: Misaelides, P., Macasek, F., Pinnavaia, T.J., Colella, C. (Eds.), *Natural Microporous Materials in Environmental Technology*. Kluwer Academic Publishers, Dordrecht, pp. 3–18.
- Komadel, P., Doff, D.H., Stucki, J.W., 1994. Chemical stability of aluminium–iron- and iron-pillared montmorillonite: extraction and reduction of iron. *Journal of the Chemical Society, Chemical Communications* 1994, 1243–1244.
- Komadel, P., Grygar, T., Mehner, H., 1998. Reductive dissolution and Mössbauer spectroscopic study of Fe forms in the fine fractions of Slovak Fe-rich bentonites. *Clay Minerals* 33, 593–599.
- Komadel, P., Lear, P.R., Stucki, J.W., 1990. Reduction and reoxidation of nontronite: extent of reduction and reaction rates. *Clays and Clay Minerals* 38, 203–208.
- Komadel, P., Madejová, J., Janek, M., Gates, W.P., Kirkpatrick, R.J., Stucki, J.W., 1996. Dissolution of hectorite in inorganic acids. *Clays and Clay Minerals* 44, 228–236.
- Komadel, P., Madejová, J., Laird, D.A., Xia, Y., Stucki, J.W., 2000. Reduction of Fe(III) in griffithite. *Clay Minerals* 35, 625–634.
- Komadel, P., Stucki, J.W., Cicel, B., 1993. Readily HCl-soluble iron in the fine fractions of some Czech bentonites. *Geologica Carpathica, Series Clays* 44, 11–16.
- Komadel, P., Stucki, J.W., Wilkinson, H.T., 1987. Reduction of structural iron in smectites by microorganisms. In: Galan, E. (Ed.), *The Sixth Meeting of the European Clay Groups*, Madrid, pp. 322–324.
- Köster, H.M., Ehrlicher, U., Gilg, H.A., Jordan, R., Murad, E., Onnich, K., 1999. Mineralogical and chemical characteristics of five nontronites and Fe-rich smectites. *Clay Minerals* 34, 579–600.
- Kostka, J.E., Dalton, D.D., Skelton, H., Dollhopf, S., Stucki, J.W., 2002. Growth of iron(III)-reducing bacteria on clay minerals as the sole electron acceptor and comparison of growth yields on a variety of oxidized iron forms. *Applied and Environmental Microbiology* 68, 6256–6262.

- Kostka, J.E., Haefele, E., Viehweger, R., Stucki, J.W., 1999b. Respiration and dissolution of Fe(III)-containing clay minerals by bacteria. *Environmental Science and Technology* 33, 3127–3133.
- Kostka, J.E., Stucki, J.W., Nealson, K.H., Wu, J., 1996. Reduction of structural Fe(III) in smectite by a pure culture of the Fe-reducing bacterium *Shewanella putrefaciens* strain MR-1. *Clays and Clay Minerals* 44, 522–529.
- Kostka, J.E., Wu, J., Nealson, K.H., Stucki, J.W., 1999a. Effects of microbial reduction on physical and chemical properties of clay minerals. *Geochimica et Cosmochimica Acta* 63, 3705–3713.
- Kriegman-King, M.R., Reinhard, M., 1994. Transformation of carbon tetrachloride by pyrite in aqueous solution. *Environmental Science and Technology* 28, 692–700.
- Lear, P.R., Stucki, J.W., 1985. The role of structural hydrogen in the reduction and reoxidation of iron in nontronite. *Clays and Clay Minerals* 33, 539–545.
- Lear, P.R., Stucki, J.W., 1987. Intervalence electron transfer and magnetic exchange in reduced nontronite. *Clays and Clay Minerals* 35, 373–378.
- Lear, P.R., Stucki, J.W., 1990. Magnetic properties and site occupancy of iron in nontronite. *Clay Minerals* 25, 3–13.
- Lee, W., Batchelor, B., 2002. Abiotic reductive dechlorination of chlorinated ethylenes by iron-bearing soil minerals. 2. Green Rust. *Environmental Science and Technology* 36, 5348–5354.
- Lee, K., Kostka, J.E., Stucki, J.W., 2006. Infrared spectra of bacteria-reduced smectite. *Clays and Clay Minerals* 54, submitted.
- Leite, S.Q.M., Colodete, C.H.A., Dieguez, L.C., 2000. Extração de ferro de esmectita brasileira com emprego do método ditionito-citrato-bicarbonato. *Química Nova* 23, 297–302.
- Lerf, A., Wagner, L.F., Poyato, J., 2001. Mössbauer spectroscopic investigation of redox reactions in vermiculites from Santa Olalla (Huelva, Spain). *Solid State Ionics* 141–142, 479–486.
- Letaief, S., Casal, B., Kbir-Ariguib, N., Trabelsi-Ayadi, M., Ruiz-Hitzky, E., 2002. Fe-rich smectites from Gafsa (Tunisia): characterization and pillaring behavior. *Clay Minerals* 37, 517–529.
- Li, O., Bleam, W.F., Kostka, J.E., Stucki, J.W., Lee, K., 2003. Polarized EXAFS studies of nontronite reduced by anaerobic bacteria. *Abstracts of Papers of the American Chemical Society, Abstracts*, 226, U492, 152-ENVR Part 1, September 2003.
- Loeppert, R.H., 1988. Chemistry of iron in calcareous systems. In: Stucki, J.W., Goodman, B.A., Schwertmann, U. (Eds.), *Iron in Soils and Clay Minerals*. D. Reidel, Dordrecht, pp. 689–713.
- Lovley, D.R., Fraga, J.L., Blunt-Harris, E.L., Hayes, L.A., Phillips, E.J.P., Coates, J.D., 1998. Humic substances as a mediator for microbially catalyzed metal reduction. *Acta Hydrochimica et Hydrobiologica* 26, 152–157.
- Low, P.F., 1951. Force fields and chemical equilibrium in heterogeneous systems with special reference to soils. *Soil Science* 71, 409–418.
- Low, P.F., 1961. Physical chemistry of clay–water interaction. *Advances in Agronomy* 13, 269–327.
- Low, P.F., 1979. Nature and properties of water in montmorillonite–water systems. *Soil Science Society of America Journal* 43, 651–658.

- Low, P.F., 1980. The swelling of clay. II. Montmorillonites. *Soil Science Society of America Journal* 44, 667–676.
- Low, P.F., 1987. Structural component of the swelling pressure of clays. *Langmuir* 3, 18–25.
- Luca, V., 1991a. Detection of tetrahedral  $\text{Fe}^{3+}$  site in nontronite and vermiculite by Mössbauer spectroscopy. *Clays and Clay Minerals* 39, 467–477.
- Luca, V., 1991b.  $^{57}\text{Fe}$  Mössbauer spectroscopic study of structural changes during dehydration of nontronite: effect of different exchangeable cations. *Clays and Clay Minerals* 39, 478–489.
- Luca, V., Cardile, C.M., 1989. Improved detection of tetrahedral  $\text{Fe}^{3+}$  in nontronite SWa-1 by Mössbauer spectroscopy. *Clay Minerals* 24, 555–560.
- Luca, V., MacLachlan, D.J., 1992. Site occupancy in nontronite studied by acid dissolution and Mössbauer spectroscopy. *Clays and Clay Minerals* 40, 1–7.
- Lumbanraja, J., Evangelou, V.P., 1990. Binary and ternary exchange behavior of potassium and ammonium on Kentucky subsoils. *Soil Science Society of America Journal* 54, 698–705.
- Lumbanraja, J., Evangelou, V.P., 1992. Potassium quantity–intensity relationships in the presence and absence of  $\text{NH}_4$  for three Kentucky soils. *Soil Science* 154, 366–376.
- Lumbanraja, J., Evangelou, V.P., 1994. Adsorption–desorption of potassium and ammonium at low cation concentrations in three Kentucky subsoils. *Soil Science* 157, 269–278.
- MacKenzie, K.J.D., Rogers, D.E., 1977. Thermal and Mössbauer studies of iron-containing hydrous silicates. I. Nontronite. *Thermochimica Acta* 18, 177–196.
- Madejová, J., Bednarikova, E., Komadel, P., Čičel, B., 1993. Structural study of acid-treated sectites by IR spectroscopy. *Eleventh Conference on Clay Mineralogy and Petrology*, C, Budejovice, pp. 267–271.
- Madejová, J., Bujdák, J., Janek, M., Komadel, P., 1998. Comparative FTIR study of structural modifications during acid treatment of dioctahedral smectites and hectorite. *Spectrochimica Acta, Part A* 54, 1397–1406.
- Madejová, J., Komadel, P., Čičel, B., 1992. Infrared spectra of some Czech and Slovak smectites and their correlation with structural formulas. *Geologica Carpathica, Series Clays* 1, 9–12.
- Madejová, J., Komadel, P., Čičel, B., 1994. Infrared study of octahedral site populations in smectites. *Clay Minerals* 29, 319–326.
- Madejová, J., Kraus, I., Komadel, P., 1995. Fourier transform infrared spectroscopic characterization of dioctahedral smectites and illites from the main Slovak deposits. *Geologica Carpathica, Series Clays* 4, 23–32.
- Malysheva, T.V., 1994. Mössbauer study of redox processes in the evolution of chondrites. *Mineralogical Magazine* 58, 151–158.
- Manceau, A., Lanson, B., Drits, V.A., Chateigner, D., Gates, W.P., Wu, J., Huo, D., Stucki, J.W., 2000a. Oxidation–reduction mechanism of iron in dioctahedral smectites. 1. Crystal chemistry of oxidized reference nontronites. *American Mineralogist* 85, 133–152.
- Manceau, A., Lanson, B., Drits, V.A., Chateigner, D., Wu, J., Huo, D., Gates, W.P., Stucki, J.W., 2000b. Oxidation–reduction mechanism of iron in dioctahedral smectites. 2. Structural chemistry of reduced Garfield nontronite. *American Mineralogist* 85, 153–172.
- Martin, F., Petit, M., Decarreau, A., Grauby, O., Hazemann, J.L., Noack, Y., 1992. Experimental study of Si–Ge tetrahedral solid solution in Ni–Co–Mg talcs. *Thin Solid Films* 222, 189–195.



- Martin, F., Petit, S., Decarreau, A., Ildefonse, P., Grauby, O., Beziat, D., Parseval, P.D., Noack, Y., 1998. Ga/Al substitutions in synthetic kaolinites and smectites. *Clay Minerals* 33, 231–241.
- McBride, M.B., 1979. Reactivity of adsorbed and structural iron in hectorite as indicated by oxidation of benzidine. *Clays and Clay Minerals* 27, 224–230.
- Mehra, O.P., Jackson, M.L., 1960. Iron oxide removal from soils and clays by a dithionite–citrate system buffered with sodium bicarbonate. In: Swineford, A. (Ed.), *Seventh National Conference on Clays and Clay Minerals*. National Research Council, Washington, DC, pp. 317–327.
- Mishra, T., Parida, K., 1998. Transition metal oxide pillared clay: 5. Synthesis, characterisation and catalytic activity of iron–chromium mixed oxide pillared montmorillonite. *Applied Catalysis A: General* 174, 91–98.
- Mody, H.M., Oza, P.M., Pandya, V.P., 1993. Thermally stable and acidic iron oxide pillared clay. *Journal of Indian Chemical Society* 70, 11–13.
- Muller, F., Besson, G., Manceau, A., Drits, V.A., 1997. Distribution of isomorphous cations within octahedral sheets in montmorillonite from Camp-Bertaux. *Physics and Chemistry of Minerals* 24, 159–166.
- Murad, E., 1987. Mössbauer spectra of nontronites: structural implications and characterization of associated iron oxides. *Zeitschrift für Pflanzenernährung und Bodenkunde* 150, 279–285.
- Murad, E., 1988. Properties and behavior of iron oxides as determined by Mössbauer spectroscopy. In: Stucki, J.W., Goodman, B.A., Schwertmann, U. (Eds.), *Iron in Soils and Clay Minerals*. D. Reidel, Dordrecht, pp. 309–350.
- Murad, E., 1998. Clays and clay minerals: what can Mössbauer spectroscopy do to help understand them? *Hyperfine Interactions* 117, 39–70.
- Murad, E., Cashion, J.D., Brown, L.J., 1990. Magnetic ordering in Garfield nontronite under applied magnetic fields. *Clay Minerals* 25, 261–265.
- Murad, E., Fischer, W.R., 1988. Geobiochemical cycle of iron. In: Stucki, J.W., Goodman, B.A., Schwertmann, U. (Eds.), *Iron in Soils and Clay Minerals*. D. Reidel, Dordrecht, pp. 1–18.
- Murad, E., Taylor, R.M., 1984. The Mössbauer spectra of hydroxycarbonate green rusts. *Clay Minerals* 19, 77–83.
- Myers, C.R., Nealson, K.H., 1988. Bacterial manganese reduction and growth with manganese oxide as the sole electron acceptor. *Science* 240, 1319–1321.
- Nembrini, G.P., Capobianco, J.A., View, M., Williams, A.F., 1983. A Mössbauer and chemical study of the formation of vivianite in sediments of Lago Maggiore (Italy). *Geochimica et Cosmochimica Acta* 47, 1459–1464.
- Nzengung, V.A., Castillo, R.M., Gates, W.P., Mills, G.L., 2001. Abiotic transformation of perchloroethylene in homogeneous dithionite solution and in suspension of dithionite-treated clay minerals. *Environmental Science and Technology* 35, 2244–2251.
- Osthaus, B.B., 1953. Chemical determination of tetrahedral ions in nontronite and montmorillonite. *Clays and Clay Minerals* 2, 404–417.
- Osthaus, B.B., 1956. Kinetic studies on montmorillonites and nontronites by the acid dissolution technique. *Clays and Clay Minerals* 4, 301–321.
- Peterson, R.C., Hill, R.J., Gibbs, G.V., 1979. A molecular-orbital study of distortions in the layer structures of brucite, gibbsite and serpentine. *Canadian Mineralogist* 17, 703–711.

- Petit, S., Madejová, J., Decarreau, A., Martin, F., 1999. Characterization of octahedral substitutions in kaolinites using near infrared spectroscopy. *Clays and Clay Minerals* 47, 103–108.
- Petit, S., Robert, J.L., Decarreau, A., Besson, G., Grauby, O., Martin, F., 1995. Contribution of spectroscopic methods to 2/1 clay characterization. *Bulletin des Centres de Recherches Exploration-Production Elf Aquitaine* 19, 119–147.
- Rancourt, D.G., 1989. Accurate site populations from Mössbauer spectroscopy. *Nuclear Instruments and Methods in Physics Research* 44, 199–210.
- Rancourt, D.G., 1994a. Mössbauer spectroscopy of minerals. I. Inadequacy of Lorentzian-line doublets in fitting spectra arising from quadrupole splitting distributions. *Physics and Chemistry of Minerals* 21, 244–249.
- Rancourt, D.G., 1994b. Mössbauer spectroscopy of minerals. II. Problem of resolving *cis* and *trans* octahedral  $\text{Fe}^{2+}$  sites. *Physics and Chemistry of Minerals* 21, 250–257.
- Rancourt, D.G., 1998. Mössbauer spectroscopy in clay science. *Hyperfine Interactions* 117, 3–38.
- Rancourt, D.G., Christie, I.A.D., Royer, M., Kodama, H., Robert, J.L., Lalonde, A.E., Murad, E., 1994b. Determination of accurate  $^{57}\text{Fe}^{3+}$ ,  $^{57}\text{Fe}^{3+}$ , and  $^{57}\text{Fe}^{2+}$  site populations in synthetic annite by Mössbauer spectroscopy. *American Mineralogist* 79, 51–62.
- Rancourt, D.G., McDonald, A.M., Lalonde, A.E., Ping, J.Y., 1993. Mössbauer absorber thicknesses for accurate site populations in Fe-bearing minerals. *American Mineralogist* 78, 1–7.
- Rancourt, D.G., Ping, J.Y., Berman, R.G., 1994a. Mössbauer spectroscopy of minerals. III. Octahedral-site  $\text{Fe}^{2+}$  quadrupole splitting distributions in the phlogopite–annite series. *Physics and Chemistry of Minerals* 21, 258–267.
- Rightor, E.G., Tzou, M.S., Pinnavaia, T.J., 1991. Iron oxide pillared clay with large gallery height: synthesis and properties as a Fischer–Tropsch catalyst. *Journal of Catalysis* 130, 29–40.
- Rinker, R.G., Gordon, T.P., Corcoran, W.H., 1964. Electron spin resonance studies of sodium dithionite and sodium formaldehyde sulfoxylate. *Inorganic Chemistry* 3, 1467–1469.
- Robert, J.L., Kodama, H., 1988. Generalization of the correlations between hydroxyl-stretching wavenumbers and composition of micas in the system  $\text{K}_2\text{O}$ – $\text{MgO}$ – $\text{Al}_2\text{O}_3$ – $\text{SiO}_2$ – $\text{H}_2\text{O}$ : a single model for trioctahedral and dioctahedral micas. *American Journal of Science* 288-A, 196–212.
- Rodriguez, E.A., Amonette, J.E., Divanfar, H.R., Marquez, J.F., 1999. Use of Fe(II) associated with layer silicates for remediation of groundwater contaminated by  $\text{CCl}_4$ , TCE, and TNT. Abstracts and Program, Environmental Molecular Sciences Symposia and First Users' Meeting, Pacific Northwest National Laboratory, Richland, pp. 41–42.
- Roth, C.B., Jackson, M.L., Lotse, E.G., Syers, J.K., 1968. Ferrous–ferric ratio and C. E. C. changes on deferration of weathered micaceous vermiculites. *Israel Journal of Chemistry* 6, 261–273.
- Roth, C.B., Jackson, M.L., Syers, J.K., 1969. Deferration effect on structural ferrous–ferric iron ratio and CEC of vermiculites and soils. *Clays and Clay Minerals* 17, 253–264.
- Roth, C.B., Tullock, R.J., 1973. Deprotonation of nontronite resulting from chemical reduction of structural ferric iron. In: Serratos, J.M. (Ed.), *Proceedings of the International Clay Conference, 1972, Madrid*. Division Ciencias C.S.I.C., Madrid, pp. 107–114.

- Rozenson, I., Heller-Kallai, L., 1976a. Reduction and oxidation of  $\text{Fe}^{3+}$  in dioctahedral smectite—1: reduction with hydrazine and dithionite. *Clays and Clay Minerals* 24, 271–282.
- Rozenson, I., Heller-Kallai, L., 1976b. Reduction and oxidation of  $\text{Fe}^{3+}$  in dioctahedral smectite—2: reduction with sodium sulphide solution. *Clays and Clay Minerals* 24, 283–288.
- Rozenson, I., Heller-Kallai, L., 1977. Mössbauer spectra of dioctahedral smectites. *Clays and Clay Minerals* 25, 94–101.
- Russell, J.D., Goodman, B.A., Fraser, A.R., 1979. Infrared and Mössbauer studies of reduced nontronites. *Clays and Clay Minerals* 27, 63–71.
- Scherer, H., Zhang, Y., 2002. Mechanisms of fixation and release of ammonium in paddy soils after flooding. III. Effect of the oxidation state of octahedral Fe on ammonium fixation. *Journal of Plant Nutrition and Soil Science* 165, 185–189.
- Schuette, R., Goodman, B.A., Stucki, J.W., 2000. Magnetic properties of oxidized and reduced smectites. *Physics and Chemistry of Minerals* 27, 251–257.
- Schwertmann, U., 1988a. Occurrence and formation of iron oxides in various pedoenvironments. In: Stucki, J.W., Goodman, B.A., Schwertmann, U. (Eds.), *Iron in Soils and Clay Minerals*. D. Reidel, Dordrecht, pp. 267–308.
- Schwertmann, U., 1988b. Some properties of soil and synthetic iron oxides. In: Stucki, J.W., Goodman, B.A., Schwertmann, U. (Eds.), *Iron in Soils and Clay Minerals*. D. Reidel, Dordrecht, pp. 203–250.
- Schwertmann, U., Fechter, H., 1994. The formation of green rust and its transformation to lepidocrocite. *Clay Minerals* 29, 87–92.
- Shen, S., Stucki, J.W., 1994. Effects of iron oxidation state on the fate and behavior of potassium in soils. In: Havlin, J.L., Jacobsen, J.S. (Eds.), *Soil Testing: Prospects for Improving Nutrient Recommendations*, SSSA Special Publication 40. Soil Science Society of America, Madison, WI, pp. 173–185.
- Shen, S., Stucki, J.W., Boast, C.W., 1992. Effects of structural iron reduction on the hydraulic conductivity of Na-smectite. *Clays and Clay Minerals* 40, 381–386.
- Sherman, D.M., Vergo, N., 1988. Optical (diffuse reflectance) and Mössbauer spectroscopic study of nontronite and related Fe-bearing smectites. *American Mineralogist* 73, 1346–1354.
- Singh, B., Hefferman, S., 2002. Layer charge characteristics of smectites from Vertosols (Vertisols) of New South Wales. *Australian Journal of Soil Research* 40, 1159–1170.
- Sorensen, K.C., Stucki, J.W., Plewa, M.J., 2003. Comparative quantitative analysis of agricultural chemicals using a microplate mammalian cell cytotoxicity assay. *Bulletin of Environmental Contamination and Toxicology* 70, 1083–1088.
- Sorensen, K.C., Stucki, J.W., Warner, R.E., Plewa, M.J., 2004. Alteration of mammalian-cell toxicity of pesticides by structural iron(II) in ferruginous smectite. *Environmental Science and Technology* 38, 4383–4389.
- Sorensen, K.C., Stucki, J.W., Warner, R.E., Wagner, E.D., Plewa, M.J., 2005. Modulation of the genotoxicity of pesticides reacted with redox-modified smectite clay. *Environmental and Molecular Mutagenesis* 46, 174–181.
- Stubican, V., Roy, R., 1961a. Infrared spectra of layer-structure silicates. *Journal of the American Ceramic Society* 44, 625–627.

- Stubican, V., Roy, R., 1961b. Isomorphous substitution and infrared spectra of the layer silicates. *American Mineralogist* 46, 32–51.
- Stubican, V., Roy, R., 1961c. A new approach to assignment of infrared absorption bands in layer-structure silicates. *Zeitschrift für Kristallografie* 115, 200–214.
- Stucki, J.W., 1988. Iron in smectites. In: Stucki, J.W., Goodman, B.A., Schwertmann, U. (Eds.), *Iron in Soils and Clay Minerals*. D. Reidel, Dordrecht, pp. 625–675.
- Stucki, J.W., Getty, P.J., 1986. Microbial reduction of iron in nontronite. *Agronomy Abstracts* 1986, 279.
- Stucki, J.W., Golden, D.C., Roth, C.B., 1984a. Effects of reduction and reoxidation of structural Fe on the surface charge and dissolution of dioctahedral smectites. *Clays and Clay Minerals* 32, 350–356.
- Stucki, J.W., Golden, D.C., Roth, C.B., 1984b. Preparation and handling of dithionite-reduced smectite suspensions. *Clays and Clay Minerals* 32, 191–197.
- Stucki, J.W., Goodman, B.A., Schwertmann, U. (Eds.), 1988. *Iron in Soils and Clay Minerals*. D. Reidel, Dordrecht, p. 893.
- Stucki, J.W., Komadel, P., Wilkinson, H.T., 1987. Microbial reduction of structural iron(III) in smectites. *Soil Science Society of America Journal* 51, 1663–1665.
- Stucki, J.W., Lear, P.R., 1989. Variable oxidation states of Fe in the crystal structure of smectite clay minerals. In: Coyne, L.M., McKee, S.W.S., Blake, D.E. (Eds.), *Spectroscopic Characterization of Minerals and their Surfaces*. American Chemical Society, Washington, DC, pp. 330–358.
- Stucki, J.W., Lee, K., Zhang, L., Larson, R.A., 2002. The effects of iron oxidation state on the surface and structural properties of smectites. *Pure and Applied Chemistry* 74, 2145–2158.
- Stucki, J.W., Low, P.F., Roth, C.B., Golden, D.C., 1984c. Effects of oxidation state of octahedral iron on clay swelling. *Clays and Clay Minerals* 32, 357–362.
- Stucki, J.W., Roth, C.B., 1976. Interpretation of infrared spectra of oxidized and reduced nontronite. *Clays and Clay Minerals* 24, 293–296.
- Stucki, J.W., Roth, C.B., 1977. Oxidation–reduction mechanism for structural iron in nontronite. *Soil Science Society of America Journal* 41, 808–814.
- Stucki, J.W., Roth, C.B., Baitinger, W.E., 1976. Analysis of iron-bearing clay minerals by electron spectroscopy for chemical analysis (ESCA). *Clays and Clay Minerals* 24, 289–292.
- Stucki, J.W., Tessier, D., 1991. Effects of iron oxidation state on the texture and structural order of Na-nontronite gels. *Clays and Clay Minerals* 39, 137–143.
- Stucki, J.W., Wu, J., Gan, H., Komadel, P., Banin, A., 2000. Effects of Fe oxidation state and organic cations on smectite hydration. *Clays and Clay Minerals* 48, 290–298.
- Taylor, R.W., Shen, S., Bleam, W.F., Tu, S.I., 2000. Chromate removal by dithionite-reduced clays: evidence from direct X-ray absorption near edge spectroscopy (XANES) of chromate reduction at clay surfaces. *Clays and Clay Minerals* 48, 648–654.
- Tennakoon, D.T.B., Thomas, J.M., Tricker, M.J., 1974. Surface and intercalate chemistry of layered silicates. Part II. An iron-57 Mössbauer study of the role of lattice-substituted iron in the benzidine blue reaction of montmorillonite. *Journal of the Chemical Society Dalton Transactions* 1974, 2207–2211.
- Thompson, D.W., Tahir, N.M., 1991. Influence of a smectite clay on the hydrolysis of iron(III). *Colloids and Surfaces* 60, 369–398.

- Tkáč, I., Komadel, P., Müller, D., 1993.  $^{29}\text{Si}$  and  $^{27}\text{Al}$  MAS-NMR study of acid leaching of montmorillonite. Eleventh Conference on Clay Mineralogy and Petrology, C, Budejovice, pp. 273–279.
- Tkac, I., Komadel, P., Muller, D., 1994. Acid-treated montmorillonites—a study by  $^{29}\text{Si}$  and  $^{27}\text{Al}$  MAS NMR. *Clay Minerals* 29, 11–19.
- Tor, J.M., Xu, C., Stucki, J.W., Wander, M.M., Sims, G.K., 2000. Trifluralin degradation under microbiologically induced nitrate and Fe(III) reduced conditions. *Environmental Science and Technology* 34, 3148–3152.
- Tsipursky, S.I., Drits, V.A., 1984. The distribution of octahedral cations in the 2:1 layers of dioctahedral smectites studied by oblique-texture electron diffraction. *Clay Minerals* 19, 177–193.
- Tsipursky, S.I., Drits, V.A., Checkin, S.S., 1978. Study of structural ordering of nontronite by oblique texture electron diffraction. *Investiya Akademii Nauk, SSSR, Seriya Geologicheskaya* 10, 105–113.
- van Breemen, N., 1988a. Effects of seasonal redox processes involving iron on the chemistry of periodically reduced soils. In: Stucki, J.W., Goodman, B.A., Schwertmann, U. (Eds.), *Iron in Soils and Clay Minerals*. D. Reidel, Dordrecht, pp. 797–809.
- van Breemen, N., 1988b. Long-term chemical, mineralogical, and morphological effects of iron-redox processes in periodically flooded soils. In: Stucki, J.W., Goodman, B.A., Schwertmann, U. (Eds.), *Iron in Soils and Clay Minerals*. D. Reidel, Dordrecht, pp. 810–823.
- van Breemen, N., 1988c. Redox processes of iron and sulfur involved in the formation of acid sulfate soils. In: Stucki, J.W., Goodman, B.A., Schwertmann, U. (Eds.), *Iron in Soils and Clay Minerals*. D. Reidel, Dordrecht, pp. 824–841.
- Viani, B.E., Low, P.F., Roth, C.B., 1983. Direct measurement of the relation between interlayer force and interlayer distance in the swelling of montmorillonites. *Journal of Colloid and Interface Science* 96, 229–244.
- Viani, B.E., Roth, C.B., Low, P.F., 1985. Direct measurement of the relation between swelling pressure and interlayer distance in Li-vermiculite. *Clays and Clay Minerals* 33, 244–250.
- Vieira Coelho, A.C., Ladrerie, J., Poncelet, G., 2000. Nickel, iron-containing clay minerals from Niquelândia deposit, Brazil. 2. Behavior under reducing conditions. *Applied Clay Science* 17, 183–204.
- Wasserman, S.R., Soderholm, L., 1998. Effect of surface modification on the interlayer chemistry of iron in a smectite clay. *Chemistry of Materials* 10, 559–566.
- Wu, J., Low, P.F., Roth, C.B., 1989. Effects of octahedral iron reduction and swelling pressure on interlayer distances in Na-nontronite. *Clays and Clay Minerals* 37, 211–218.
- Wu, J., Roth, C.B., Low, P.F., 1988. Biological reduction of structural Fe in sodium-nontronite. *Soil Science Society of America Journal* 52, 295–296.
- Xiang, Y., Villemure, G., 1992. Electron transport in clay-modified electrodes: study of electron transfer between electrochemically oxidized tris(2,2'-bipyridyl) iron cations and clay structural iron(II) sites. *Canadian Journal of Chemistry* 70, 1833–1837.
- Xiang, Y., Villemure, G., 1994. Influence of dissociation of tris(2,2'-bipyridyl) iron(II) cations on the time dependence of currents in clay-modified electrodes. *Journal of Electroanalytical Chemistry* 370, 53–58.

- Xiang, Y., Villemure, G., 1995. Electrodes modified with synthetic clay minerals: evidence of direct electron transfer from structural iron sites in the clay lattice. *Journal of Electroanalytical Chemistry* 381, 21–27.
- Xu, C., Kocherginsky, N.M., Stucki, J.W., Sims, G.K., 1996. Effect of soil oxidation state on the fate and behavior of agricultural chemicals. In: *Research on Agricultural Chemicals in Illinois Groundwater: Status and Future Directions*. VI. Proceedings of the Sixth Annual Conference. Illinois Groundwater Consortium, Carbondale, pp. 251–260.
- Xu, J.C., Sims, G.K., Kostka, J.E., Wu, J., Stucki, J.W., 2001. Fate of atrazine and alachlor in redox treated ferruginous smectite. *Environmental Toxicology and Chemistry* 20, 2717–2724.
- Yamagishi, A., 1982. Racemic adsorption of iron(II)tris(1,10-phenanthroline) chelate on a colloidal clay. *Journal of Physical Chemistry* 86, 2472–2479.
- Yan, L., Bailey, G.W., 2001. Sorption and abiotic redox transformation of nitrobenzene at the smectite–water interface. *Journal of Colloid and Interface Science* 241, 142–153.
- Yan, L., Low, P.F., Roth, C.B., 1996a. Enthalpy changes accompanying the collapse of montmorillonite layers and the penetration of electrolyte into interlayer space. *Journal of Colloid and Interface Science* 182, 417–424.
- Yan, L., Low, P.F., Roth, C.B., 1996b. Swelling pressure of montmorillonite layers versus H–O–H bending frequency of the interlayer water. *Clays and Clay Minerals* 44, 749–765.
- Yan, L., Roth, C.B., Low, P.F., 1996c. Changes in the Si–O vibrations of smectite layers accompanying the sorption of interlayer water. *Langmuir* 12, 4421–4429.
- Yan, L., Roth, C.B., Low, P.F., 1996d. Effects of monovalent, exchangeable cations and electrolytes on the infrared vibrations of smectite layers and interlayer water. *Journal of Colloid and Interface Science* 184, 663–670.
- Yan, L., Stucki, J.W., 1999. Effects of structural Fe oxidation state and hydration on layer Si–O stretching vibrations of montmorillonite. *Langmuir* 15, 4648–4657.
- Yan, L., Stucki, J.W., 2000. Structural perturbations in the solid–water interface of redox transformed nontronite. *Journal of Colloid and Interface Science* 225, 429–439.
- Zhang, L., 2002. Impact of iron and iron-containing smectites on the fate of organic contaminants. M.S. thesis. University of Illinois, Urbana, IL.

This page intentionally left blank

*Chapter 9*

## CLAYS, MICROORGANISMS, AND BIOMINERALIZATION

K. TAZAKI

*Department of Earth Sciences, Kanazawa University, Kanazawa, Ishikawa 920-1192, Japan*

Clays and microorganisms are ubiquitous on the Earth's surface and, more often than not, are closely associated with one another. Indeed, microorganisms in soil tend to gather at or near clay surfaces as these are enriched in ions, water, and organic matter relative to the bulk soil (Theng and Orchard, 1995). In other ecosystems the mineral–microbe interaction is reflected in the widespread occurrence of colorful microbial mats in river, hot springs, ponds, lakes, deep sea floor, and geothermal areas (Tazaki, 1999). The mineral component in these biomineral assemblages variously consists of carbonates, Fe–Mn oxides, hydrated phosphates, and sulfides as well as layer silicates (clay minerals). The type of assemblage formed is dependent on a number of biogeochemical factors, such as temperature, pH, redox potential (Eh), dissolved oxygen (DO) concentration, electrical conductivity (EC), and element supply (Tazaki, 1997a, 1997b). For example, the formation of intra- and extra-cellular magnetite by Fe(III)-reducing bacteria requires a suitable combination of Eh and pH together with a favourable rate of supply of Fe(II) and Fe(III) ions to the growing crystal (Mann et al., 1990; Schwertmann and Fitzpatrick, 1992). The bioformation of magnetite (and siderite) plays an important role in the cycling of iron and carbon as well as in carbon sequestration in natural environments (Roh et al., 2003). Biogenic iron-rich minerals may also serve as physical indicators of previous biological activities in modern and ancient geological settings.

'Biomineralization' is the process by which living organisms convert ions in solution into solid minerals. The process is the result of cellular activities that allow for certain physicochemical changes to occur (Simkiss and Wilbur, 1989). The number of minerals of biological origin currently exceeds 250. The most numerous biogenic minerals in terms of anion type are phosphates, followed by oxides, and carbonates. All the major groups of microorganisms have members that are capable of forming minerals. Here we focus on the ability of various bacteria to accumulate metallic ions from their external aquatic environments, and mediate the crystallization and precipitation of clay minerals (Tazaki et al., 2002). Such minerals were referred to as 'bio-clays' (Tazaki and Ishida, 1996; Tazaki and Asada, 2003) although according to



the proposed definitions for ‘clay’ and ‘clay mineral’ (Guggenheim and Martin, 1995, see Chapter 1), they should strictly be called ‘bio-clay minerals’.

## 9.1. EXPERIMENTAL ASPECTS

The study of biomineralization is a multi-disciplinary science involving geology, mineralogy, microbiology, and chemistry. Both field observations and laboratory measurements are required for an understanding of the underlying mechanisms.

### 9.1.1. Field Investigation

#### A. Geology

An appreciation of the geological environment in which bio-clays are formed is fundamental to their investigation. This is because microorganisms in microbial mats metabolize and use materials from the surrounding air, water, sediments, and rocks. For this reason, it is essential to record details not only of the mats but also of the terrain, basement petrology, soils, and hydrology. Depending on the situation, samples are taken of sediments, rocks, water, and other materials. Appropriate sampling and handling methods must be followed in collecting microbial mats.

#### B. Water Chemistry

Since microorganisms in microbial mats take in ions (into their cells) from the external solution, knowledge of the chemistry of the surrounding water is important in identifying the microbial species in question. Water temperature, pH, Eh, DO, and EC are measured in the field. Seasonal changes in these parameters should be taken into consideration.

#### C. Microbial Mats

The following information should be recorded: colour of mat; exposure to solar radiation; volume and flow rate of surrounding water; sediment and rock type; thickness, hardness, and any other physical characteristics of mat. In addition, photographs of the location and physical background are taken.

### 9.1.2. Laboratory Work

#### A. Sample Preparation

(a) *Thin sections.* Optical microscopy examination of thin sections is required to determine the spatial relationship between microorganisms and clay minerals in microbial mats. However, the preparation of thin sections can be problematic because microbial mats contain water and are often fragile. Breakage may be prevented by coating the samples with a resin. The following steps are commonly taken: drying in air at room temperature; embedding in cyanobond; coating with epoxy or

polyester resin; thin section preparation is completed in the same way as for ordinary rock and mineral preparation.

(b) *Ultra-thin sections.* Ultra-thin sections (80–100 nm in thickness) are used to observe the inner micro-texture of cells, and the distribution of minute mineral grains. The procedure for preparing ultra-thin sections is as follows: fixing with glutaraldehyde or a similar fixative (to preserve micro-texture); dehydration (to substitute water for a water-soluble synthetic resin); coating with a synthetic resin; cutting with an ultra-microtome; dyeing or coating (to increase contrast in Transmission Electron Microscopy (TEM) image).

### B. Optical Microscopy

(a) *Bright field image.* Observation by a bright field image in transmitted light is a standard first step in laboratory studies of microbial mats. This method is usually used in conjunction with stereoscopic and differential interference imagery distribution. Form, color, and texture of microorganisms and minerals, ranging in size from a few to several hundred microns, can be observed at the level of magnification of an optical microscope.

(b) *Polarizing microscope image.* Observation by a polarizing microscope with plane-polarized light, crossed Nicols, and conoscopic illumination is essential in identifying the minerals present in microbial mats.

(c) *Fluorescence and epifluorescence microscope images.* When exposed to ultraviolet (UV) radiation, some minerals and microorganisms in microbial mats show fluorescence and epifluorescence, which can be observed by means of a fluorescence and epifluorescence microscope. For example, the chlorophyll of bacteria exhibits red fluorescence. In some instances, fluorescence is observed before and after dyeing to help distinguish microorganisms from minerals. Nucleic acids (DNA and RNA) can combine with certain fluorescing dyes. Thus, DNA stained with 4',6-diamidino-2-phenylindole (DAPI) displays blue fluorescence when exposed to UV rays. Similarly, the RNA in cells can be specifically stained with acridine orange (AO), causing it to fluoresce on exposure to light at a wavelength of 436 or 490 nm. Indian ink, ruthenium red, and vinegar are used to indicate the existence of S-layers or extracellular polymers around microbial cells.

### C. X-ray Diffraction (XRD)

X-ray diffraction (XRD) remains the single, most useful method of identifying and quantifying clay minerals (Brindley, 1980; Moore and Reynolds, 1997). For XRD analysis of microbial mats, either a powdered sample of the mat or a piece of dry, intact mat is placed on a non-refracting glass slide.

#### *D. X-ray Fluorescence Spectroscopy (XRF)*

When an element is bombarded by hard X-rays, it emits X-rays at a wavelength characteristic of the element. The elements present in microbial mats can thus be determined qualitatively and quantitatively by XRF.

#### *E. Scanning Electron Microscopy (SEM)*

Microbial mats must be dried under high-vacuum conditions before observation by SEM. Where this is a problem, other methods such as freeze-drying or observation under low-vacuum conditions can be used.

#### *F. Transmission Electron Microscopy (TEM)*

Since microbial mats contain very fine mineral grains that are scarcely visible under an optical microscope, TEM is a very useful instrumental method of investigation. TEM images can be divided into bright-field (high-resolution images, crystal lattice images) and dark-field images. Electron diffraction patterns of selected areas (of mineral grains) can also be obtained from a TEM image.

#### *G. Energy Dispersive X-ray Spectrometry (EDX)*

EDX allows qualitative and quantitative analysis to be made of elements that are associated with specific sites/structures within the SEM or TEM image of the sample.

#### *H. Microorganism Culture Methods*

Field environmental conditions may be simulated by supplying water and sediments, collected from the field, to living microbial mats in the laboratory. This “natural” culture method also helps preserve the integrity of the mats. Other environmental parameters, such as pH, temperature, light, and partial pressure of oxygen can be controlled or modified during culture in the laboratory. However, problems can arise when microbial mats are cultured by such methods over a long period.

Alternatively, we may separate a particular species of microorganism from a microbial mat, and culture it in an artificial medium. This approach is especially useful for studying the behaviour and properties of individual microorganisms.

The applications of these experimental methods and instrumental techniques to characterizing microbial mats and bio-clays from various localities are summarized below.

## 9.2. BIOFORMATION OF X-RAY AMORPHOUS LAYER SILICATES

### *9.2.1. Microbial Mats in Ponds*

Red-brownish microbial mats, in solid or colloidal form, are found at various locations in Japan: over a cut cliff in the Omma Formation of sandstone, and in drains and settling ponds near the Kakuma campus of Kanazawa University ([Tazaki](#),

1997a, 1997b; Yoshizu and Tazaki, 1997). The pH of the water flowing through the Omma Formation into settling ponds ranges from weakly acidic to neutral (pH 6.4–7.1). The values of Eh (–40 to –80 mV) and DO (6.3–9.7 mg/L) are subjected to seasonal variations. The fresh water chemistry is as follows: Mn 1.03 ppm; Fe 2.50–10.00 ppm; Ca 76.00 ppm; K 18.00 ppm; pH 6.5–6.8; temperature 12–20 °C.

Optical and fluorescence microscopy revealed the presence of bacillus, spiral, and filamentous microbes associated with holdfast (Fig. 9.1A). SEM showed a doughnut-shaped structure with a capsule of *Siderocapsa* sp. in the centre (Figs. 9.1B, C). EDX analysis indicated that this structure was mainly composed of Al, Si, Ca, and Fe probably in layer silicate structures (Fig. 9.1D).

XRD patterns showed strong peaks for crystalline calcite (0.3 nm) and illite together with large amounts of X-ray amorphous (short-range order) layer silicates and/or organic matter. Natural culturing gave rise to Fe- and Mn-rich structures after ageing for 2 months. SEM of the holdfasts on the cover glass of slides showed successive formation of mixtures of layer silicates and hydrated Fe/Mn oxides. TEM also showed the doughnut-shaped holdfast with a hole in its center, containing coccus-type bacteria (arrows) (Fig. 9.2A). A close-up photograph of the bacteria revealed dense granular materials on the cell wall (Fig. 9.2B).

### 9.2.2. Microbial Mats in Hot Springs

The coccus and bacillus-type bacteria in microbial mats collected from hot springs (pH 6.8, 39 °C) in Laugarvatn, Iceland, indicated the incipient formation of granular layer silicates on the cell wall. TEM of an ultra-thin section of the cells clearly showed a distinct cell wall (a), surface array (b), capsule (c), and plasma membrane (d), covered by layer silicates of high density (Figs. 9.3A, B) (Tazaki and Ishida, 1996).

The XRD pattern of the bulk microbial mats showed a broad, diffuse band centering at 0.3–0.4 nm (Figs. 9.3A', B'). The TEM and EDX of thin-sections revealed the remains of bacterial cells with accumulation of Si, Al, and Fe.

## 9.3. BIOFORMATION OF HALLOYSITE, KAOLINITE AND IMOGOLITE

### 9.3.1. Bio-Halloysite from Feldspar in Kutani Glaze

Bio-weathering of K-feldspar was investigated using aqueous suspensions of Kutani glaze (“Kutani” is a distinctive ceramic ware from Kanazawa Prefecture, Japan). After 3 years standing in a brightly lit room, green microbial mats (Fig. 9.4A) formed in the container together with (solid) precipitates composed mainly of K-feldspar.

The pH of the water was 9.0–9.4 and the EC was 0.38–0.65 mS/cm. Major oxide analysis of the K-feldspar by XRF yielded the following composition: SiO<sub>2</sub> 69.03,

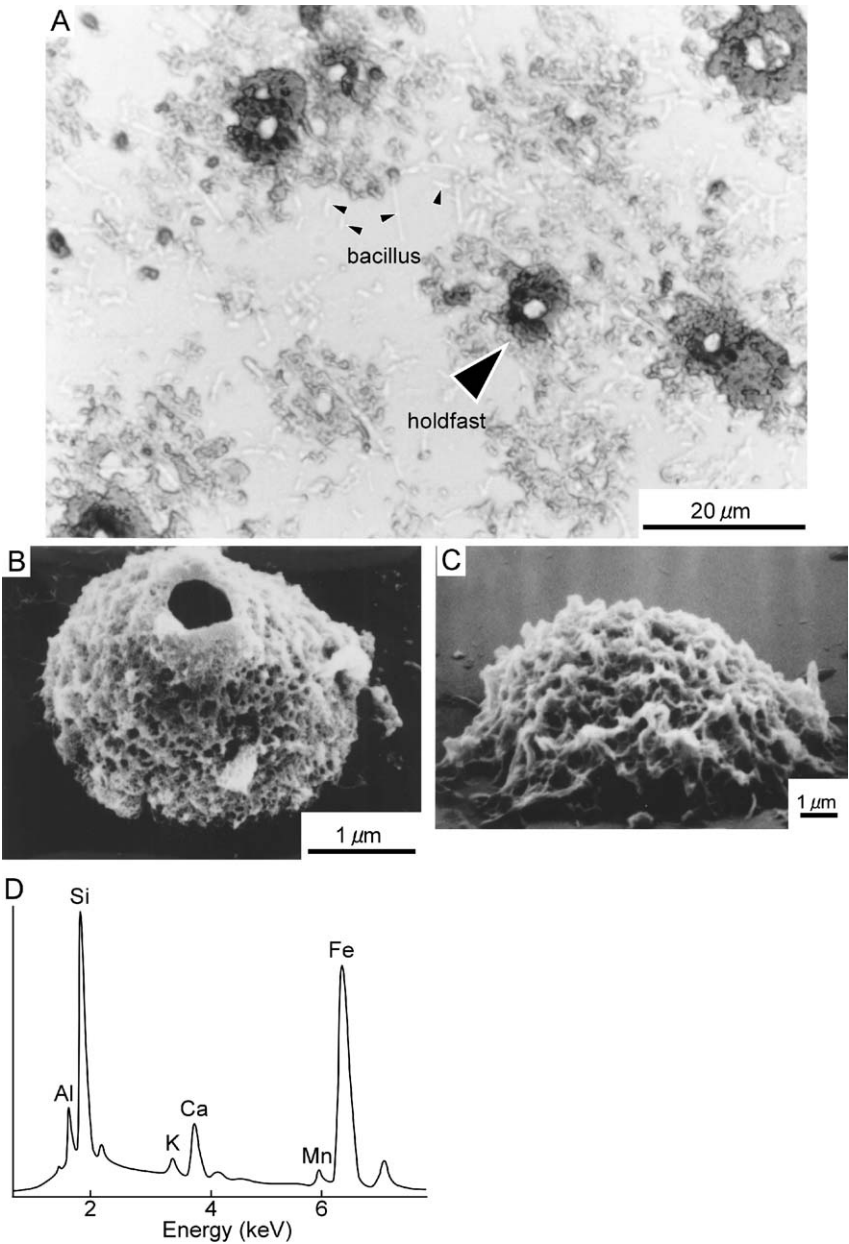


Fig. 9.1. Optical (A), SEM (B, C), and EDX (D) micrographs of the holdfasts and bacilli (arrows) on the slide cover glass showing successive formation of mixtures of layer silicates and Fe/Mn oxides. (From Tazaki, 1997a.)

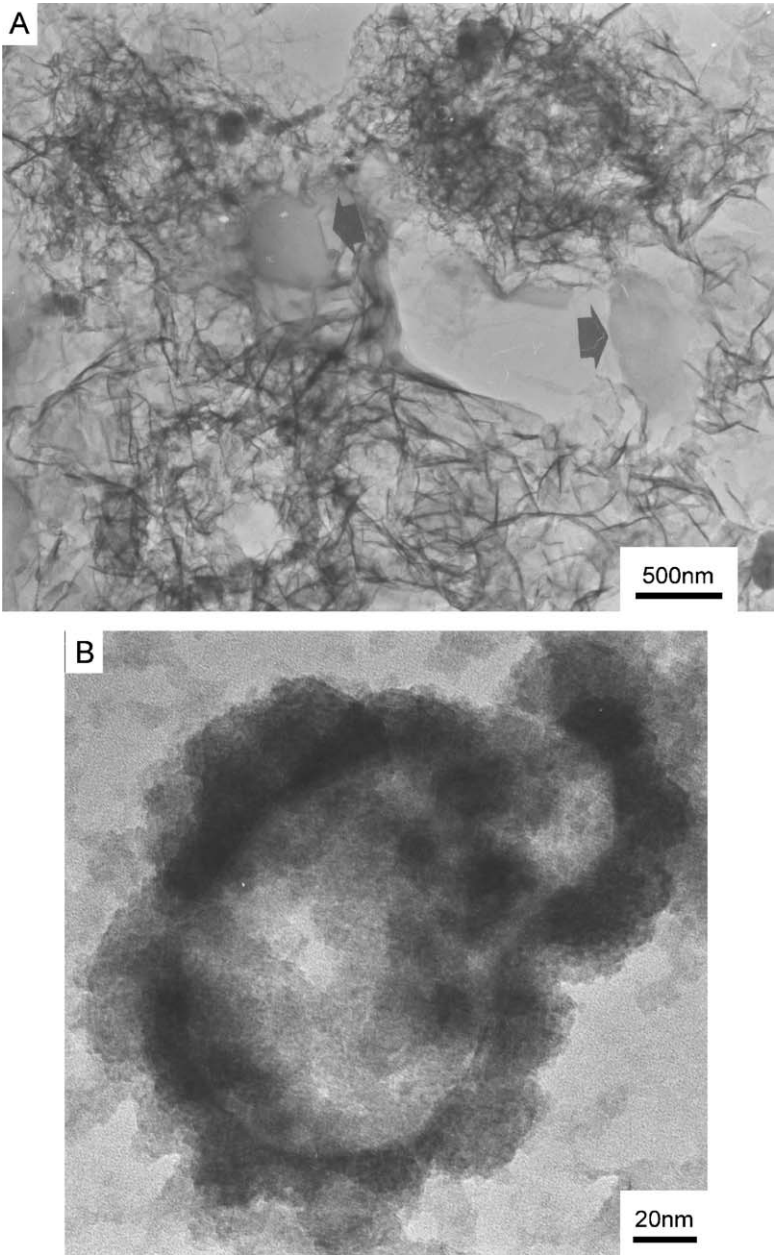


Fig. 9.2. TEM micrographs of clay films attached to doughnut-shaped holdfasts with bacilli and coccus bacteria (A, arrows), and of coccus bacteria with granular coating of X-ray amorphous materials (B). (From Tazaki, 1997a.)



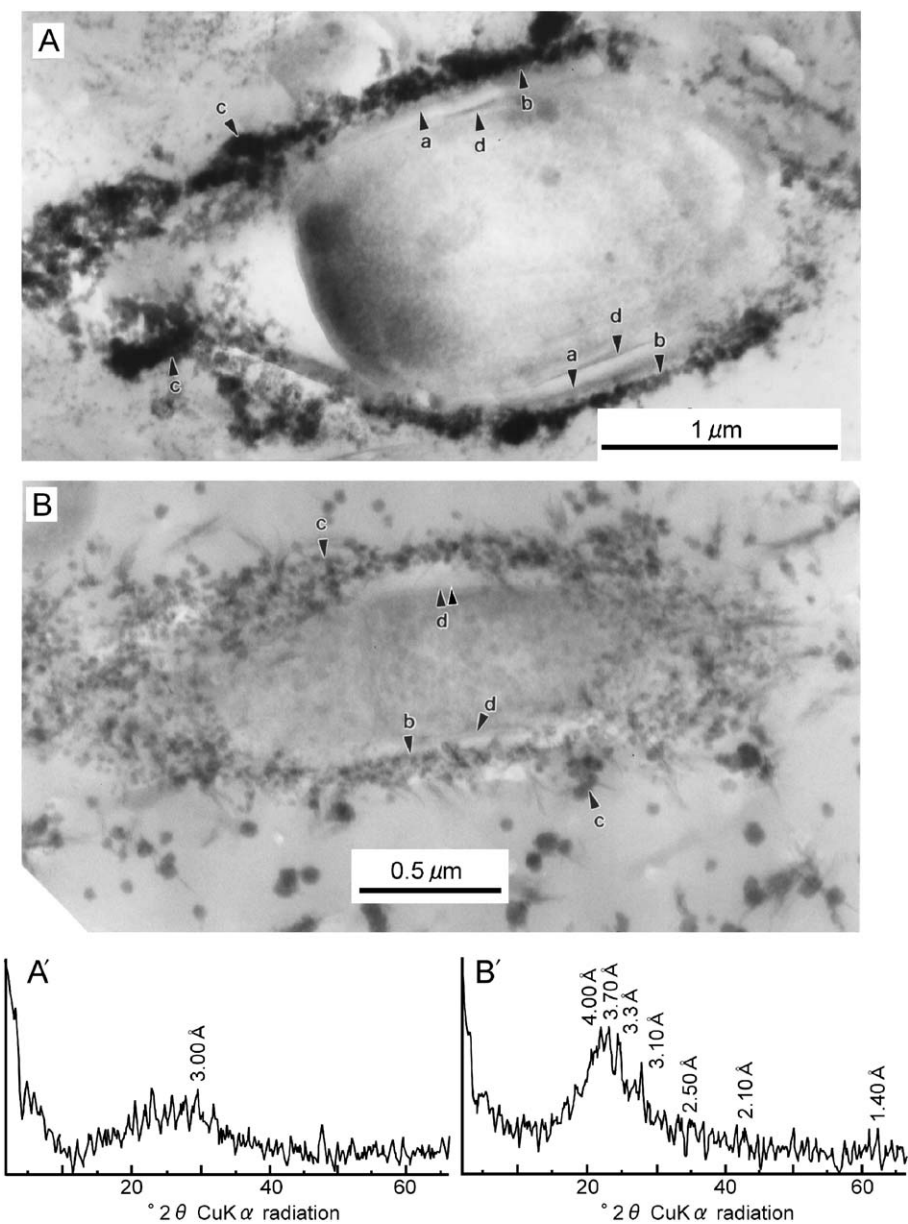


Fig. 9.3. TEM micrographs (ultra-thin section) of X-ray amorphous layer silicates. The spherules with high concentrations of Fe and Ca show internal cell structures: a, cell wall; b, surface array; c, capsule; d, plasma membrane. XRD patterns of A and B samples indicating presence of X-ray amorphous materials (A', B'). (From Tazaki and Ishida, 1996.)

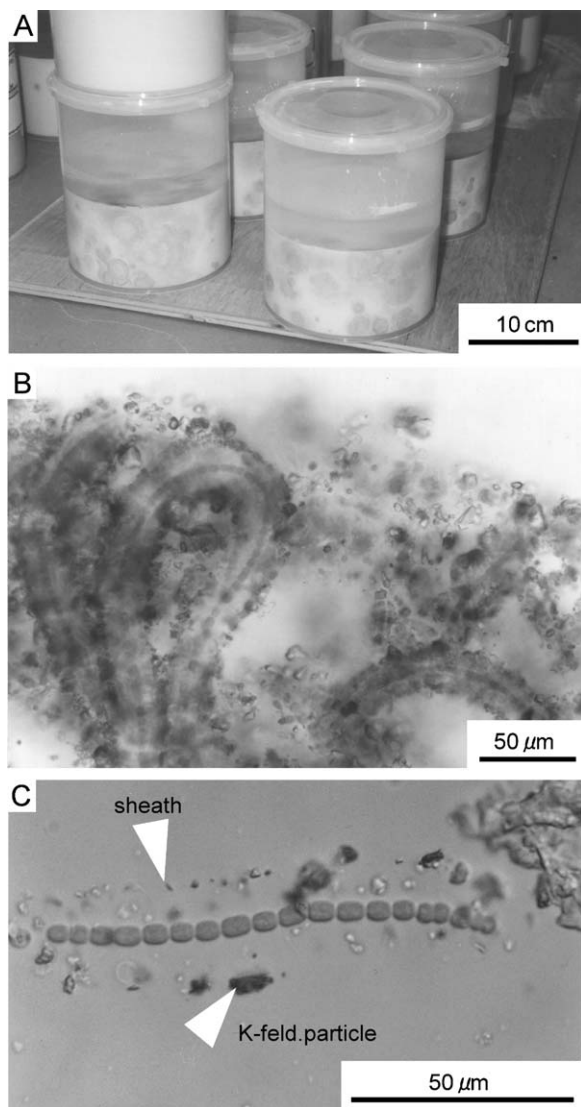


Fig. 9.4. Green microbial colonies in Kutani glaze solution (A) and optical micrographs of a green cyanobacterial colony (B) and  $K^+$ -feldspar particles (arrow in C) on the sheath (arrow in C) of cyanobacteria surrounding capsule. (From Ueshima and Tazaki, 1997.)

$Al_2O_3$  17.37,  $Fe_2O_3$  0.06,  $CaO$  0.89,  $MgO$  0.06,  $K_2O$  8.94,  $Na_2O$  3.33, loss on ignition 0.31 where the numbers denote wt% (Ueshima and Tazaki, 1997).

Optical microscopy of the green microbial mats showed chains of microbial cells with a capsule of fine- and coarse-grained particles surrounded by a sheath of



cyanobacteria (*Phormidium* sp.) (Figs. 9.4B, C). Microbial chlorophyll was indicated by the intense red auto-fluorescence.

The weak red pseudo-fluorescence may be ascribed to the presence of clay minerals. The green microbial mats, stained with Indian ink, indicated the existence of *Phormidium* sp. coated with extra-cellular polymers (Fig. 9.5A). After staining the cells with ruthenium red, the acidic polysaccharide polymers took on a pink colour (Fig. 9.5B).

SEM and TEM images also revealed the presence of adhesive materials and that of fine-grained particles, composed of Al, Si, and K. This would suggest the transformation of  $K^+$ -feldspar fragments to form halloysite in the layer of extracellular polymers on the cell surface of *Phormidium* sp. (Figs. 9.6A, B). The primitive clay precursors and halloysite formed contained Si and Al and trace amounts of K. The fragments of  $K^+$ -feldspar apparently derived from the surface of coarse-grained particles.

### 9.3.2. Bio-Halloysite Balls from Dam Sediments

Biomineralization was investigated in a solution containing natural dam sediments collected from Portalegre, Brazil (Asada and Tazaki, 2000; Tazaki and Asada, 2003). The microorganisms were cultured for a few months and up to 2 years at pH 6.0–7.4 in order to understand how microorganisms, living in microbial mats at room temperature, induce the formation of clay minerals. Fig. 9.7A shows a diagram of the cultivation system, and the formation of microbial films on a glass slide, container wall, and top surface of the sediments. Optical microscopy of cultured microbes, stained with DAPI, revealed the presence of spherical clays (Figs. 9.7B, C arrows).

Examination of the films by TEM clearly showed the close association of spherical halloysite particles with coccus- and bacillus-type bacteria (Fig. 9.8A). The electron diffraction pattern of the halloysite balls corresponded to reflections at 0.443, 0.256, 0.249, 0.222, and 0.148 nm (Fig. 9.8B). The films were composed of Al, Si, S, and Fe with traces of Mg, P, K, Ca, Ti, and Mn (Fig. 9.8C). XRD gave a  $d(001)$  spacing of 0.713 nm ascribed to (dehydrated) halloysite (Fig. 9.8D). Atomic force microscopy (AFM) using contact mode showed formation of bio-halloysite on the surface of bacterial cell walls. The halloysite particles formed clusters of 50–500 nm in width and 2–20 nm in thickness with an orientation along the same direction. The clusters developed into spherical halloysite through hollow halloysite ranging in diameter from 800 to 1000 nm (Tazaki and Asada, 2003).

### 9.3.3. Bio-Kaolinite and Bio-Imogolite from Weathered Feldspar

Bioweathering experiments were carried out by incubating granite in freshwater from the Omma Formation of sandstone, Ishikawa Prefecture, Japan. A thin section of granite with iron bacteria (*Toxothrix* sp. and *Gallionella* sp.) were observed. After 3–10 days microbial mats were formed on the surface of the granite. Cavities and

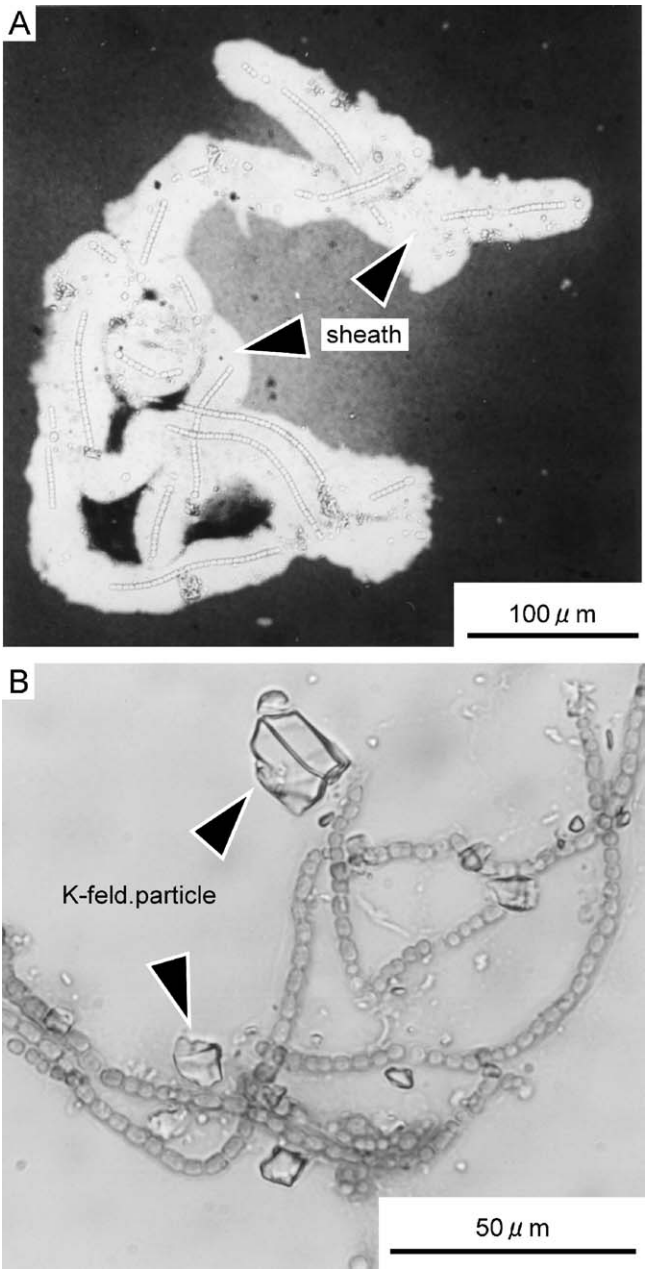


Fig. 9.5. Optical micrograph of *Phormidium* sp. in green microbial colony stained with Indian ink (A) and stained with ruthenium red (B), indicating the presence of sheath (arrows in A) and acidic polysaccharids on the cell walls together with  $K^+$ -feldspar particles (arrows in B).

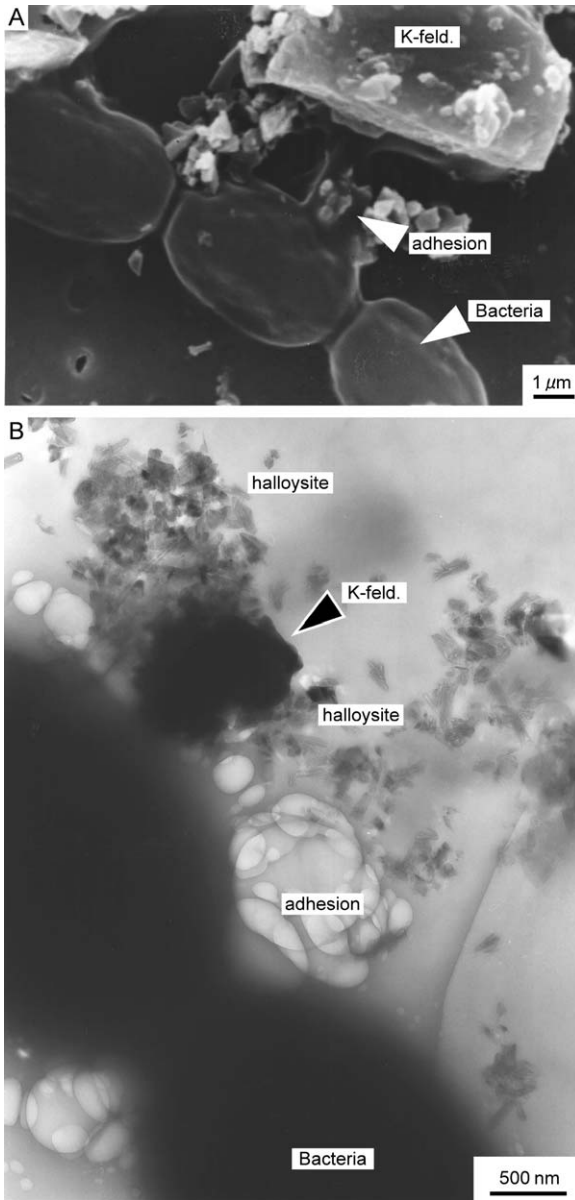


Fig. 9.6. SEM image of green colony showing the adhesive materials beside the bacteria (A) and TEM image of *Phormidium* sp. adhering to  $\text{K}^+$ -feldspar particles, forming halloysite beside the bacteria (B).

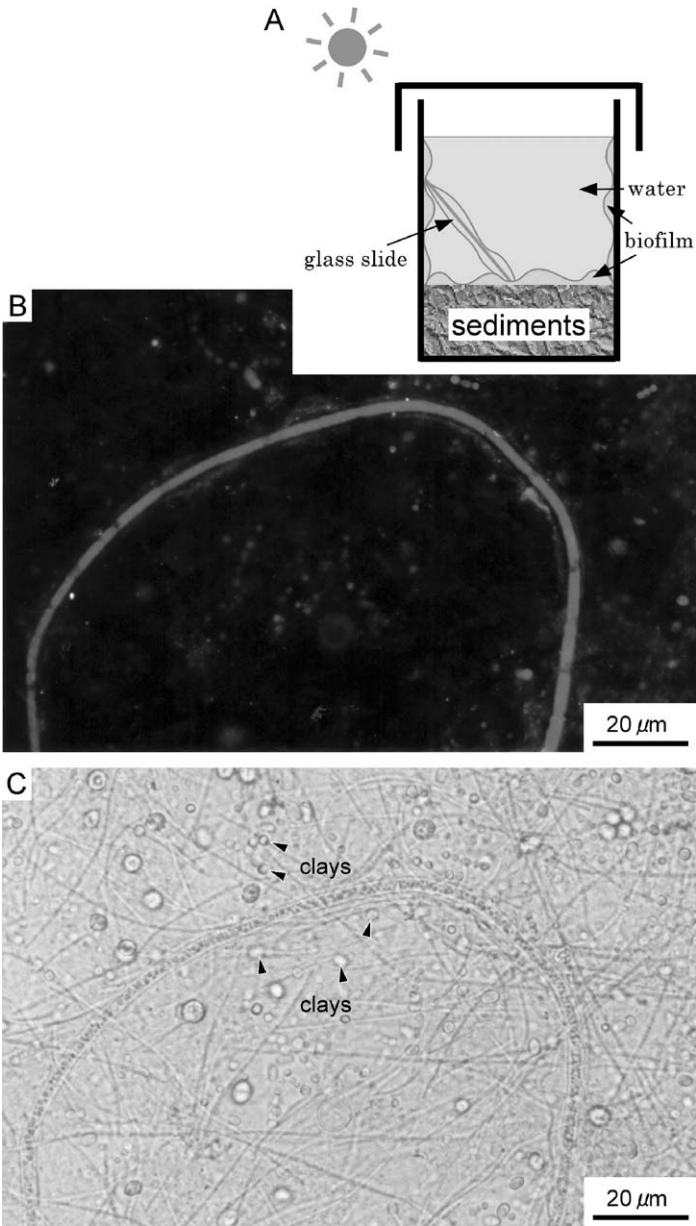


Fig. 9.7. Diagram of a natural cultivation system showing biofilm formation on a glass slide, wall of beaker, and upper surface of sediments (A); optical micrographs of DAPI-stained microorganisms associated with spherical clays (B, C arrows). (From Asada and Tazaki, 2000.)

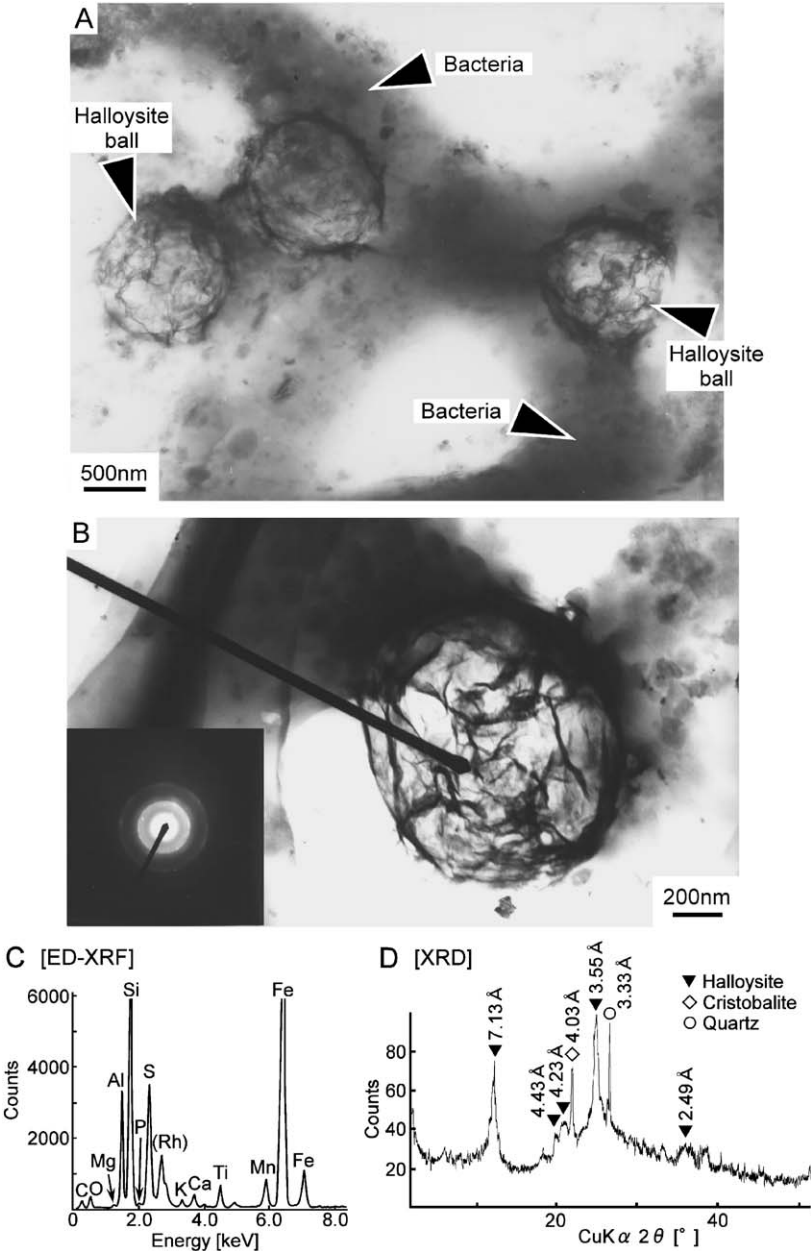


Fig. 9.8. TEM micrographs of bio-halloysite balls associated with bacillus type bacteria (A) with electron diffraction spots and rings (B inset). ED-XRF (C) and XRD (D) analyses of a cultured biofilm indicating presence of Al, Si, Fe, and formation of halloysite (0.713 nm). (From Tazaki and Asada, 2003.)

cracks filled with rod-like and filamentous bacteria were observed on the surface of feldspar particles in the granite. The Si content of flake materials (Si/Al ratio of the flakes equals 3/2), associated with bacilli on the surface of  $K^+$ -feldspar immersed in freshwater, was less than the value obtained with fresh  $K^+$ -feldspar. After 2 months of incubation,  $K^+$  and  $Si^{4+}$  ions were released from  $K^+$ -feldspar. TEM observation and electron diffraction analyses indicated the formation of kaolinite on the surface of  $K^+$ -feldspar (Ueshima and Tazaki, 1998).

The bioweathering of feldspar was also investigated by incubating granite with either water from the Kurobe River, Toyama Prefecture, Japan, or deionized water. The starting material was feldspar collected from the bank of the Kurobe river. The composition of the latter sample is given in Figs. 9.9A–F. The river and deionized waters have the following characteristics: pH = 7.3 (5.5); Eh = 313 (322) mV; EC = 84 (0.7)  $\mu$ S/cm; temperature = 20 (21) °C at the initial stage of the experiment. The numbers in brackets refer to deionized water. The river water contained Na 14.7, Mg 14.4, Al 1.6, Si 31.3, K 1.4, and Ca 36.8, all values being expressed as wt% (Morikawa, 2002). After 55 days of incubation (in both river and deionized water) a thin, adhesive film formed on the surface of feldspar together with a large number of microorganisms. The film is composed of Al and Si with trace concentrations of Na, P, S, K, and Ca (Figs. 9.9E, F). TEM of the adhesive film further showed a network of very slender threads, indicative of imogolite (Figs. 9.9C, F).

## 9.4. BIOFORMATION OF SMECTITES MINERALS

### 9.4.1. Bio-Nontronite from Iheya Deep-Sea Sediments

The Okinawa Trough lies northwest of Iheya-Jima Island, Okinawa Prefecture, Japan. It is one of the rear arc basins along the western part of the Eurasian plate, associated with the subduction of the Philippine Sea plate along the Ryukyu Trench. Hydrothermal smoking vents were observed at the Natsushima Sea mound in the Iheya basin of the middle Okinawa Trough. Black manganese oxide covers the mound and yellowish sediments are distributed along its ridge. These sediments are composed of iron (hydr)oxide, amorphous silica, and nontronite (Tawara et al., 1997).

The temperature of the discharge water is 2–3 °C higher than that of the ambient sea water. The pH of the discharged water was 5, the Eh –110 mV, and the EC 47 mS/cm. A 40-cm long thermometer, inserted into the mound, recorded temperatures ranging from 20 to 50 °C. Analysis of the water showed a methane concentration of about 200 mL/kg. Tubular and granular nontronite was identified by XRD, SEM-EDX, and TEM. The sediments were rich in Si and Fe. Tubular materials, collected from the vicinity of deep-sea smoking vents were uniformly coated with a film of nontronite (Fig. 9.10). After 3 minutes of ultrasonic treatment colonies of bacilli were observed. TEM of ultra thin sections showed thin flakes of nontronite

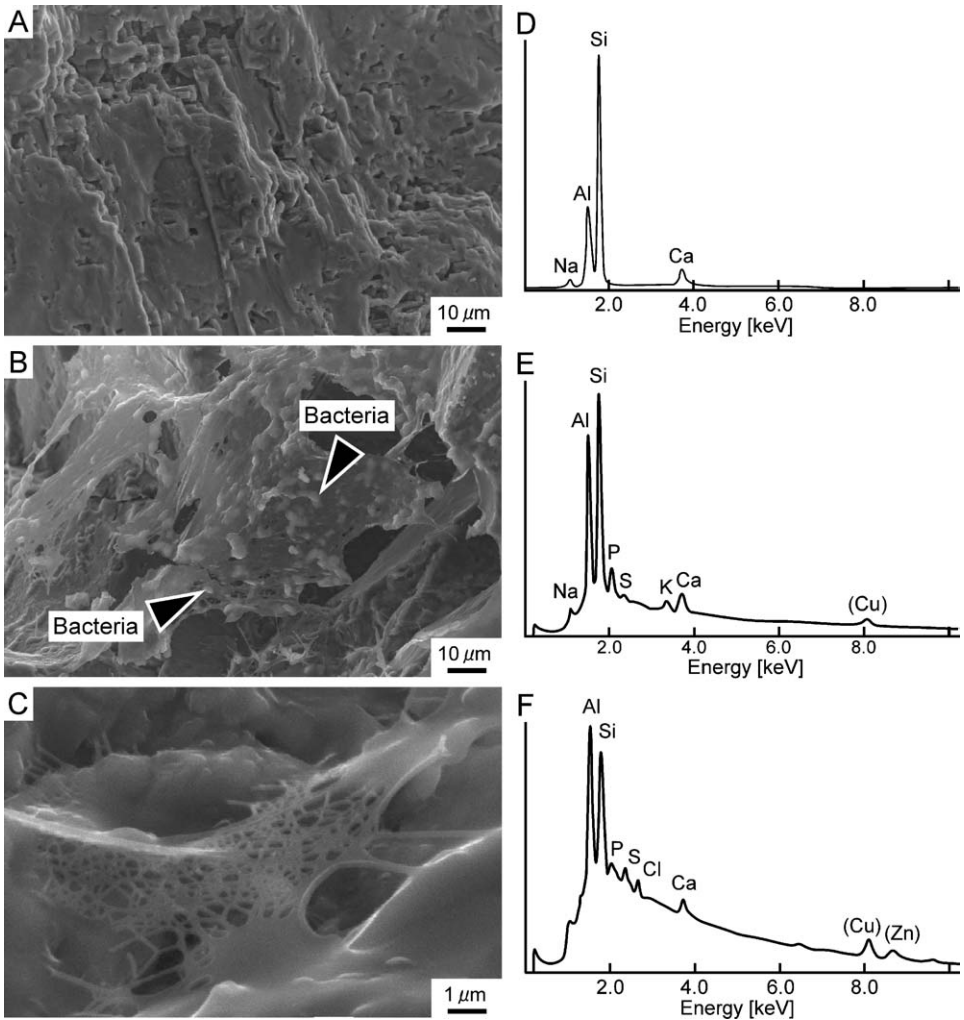


Fig. 9.9. SEM micrograph of bio-weathering of feldspar grain with etch pits at initial stage (A); weathered surface with biofilms associated with abundant bacteria (B, arrows); formation of imogolite network structure on the surface (C); and EDX analyses of initial stage (D) and imogolite network (E, F), showing an Al:Si ratio of about 1:1. (From Morikawa, 2002 unpublished.)

covered with living bacteria (Fig. 9.11). The nontronite particles were oriented in the same direction as the lipopolysaccharides exuded from surface of the bacterial cell wall. This would suggest that the extracellular lipopolysaccharides could accumulate Si and Fe from the ambient seawater, inducing nontronite crystallization on and along the polymer chain (Ueshima and Tazaki, 2001).

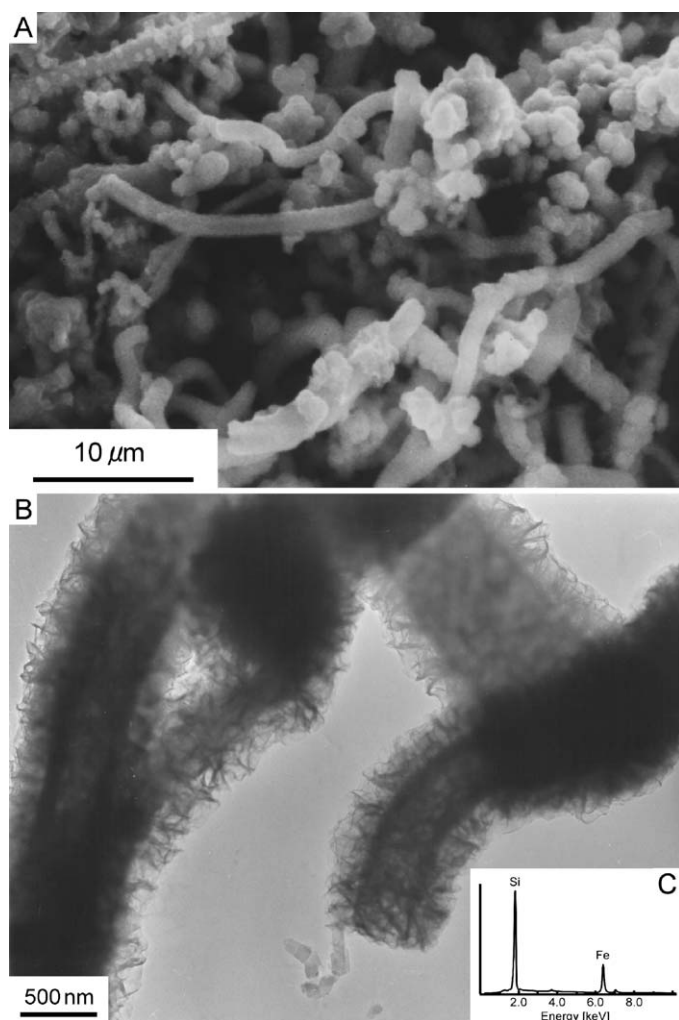


Fig. 9.10. SEM-EDX (A, C) and TEM (B) micrographs of filamentous bacteria collected from Iheya deep sea floor. The sediments are composed of Si and Fe; XRD pattern shows shift of 1.34 nm peak to 1.72 nm after treatment with ethylene glycol, indicative of nontronite. (From Ueshima and Tazaki, 2001.)

#### 9.4.2. Bio-Smectite from a Pond of Kasaoka Bentonite Mine

Bentonite is a clay that is largely made up of the clay mineral montmorillonite (smectite). Interaction between bentonite and microorganisms was observed in a floc collected from the pond of the Kasaoka bentonite mine, Okayama, Japan. The floc contained bentonite, algae, diatoms, and bacteria. The pond water had the following



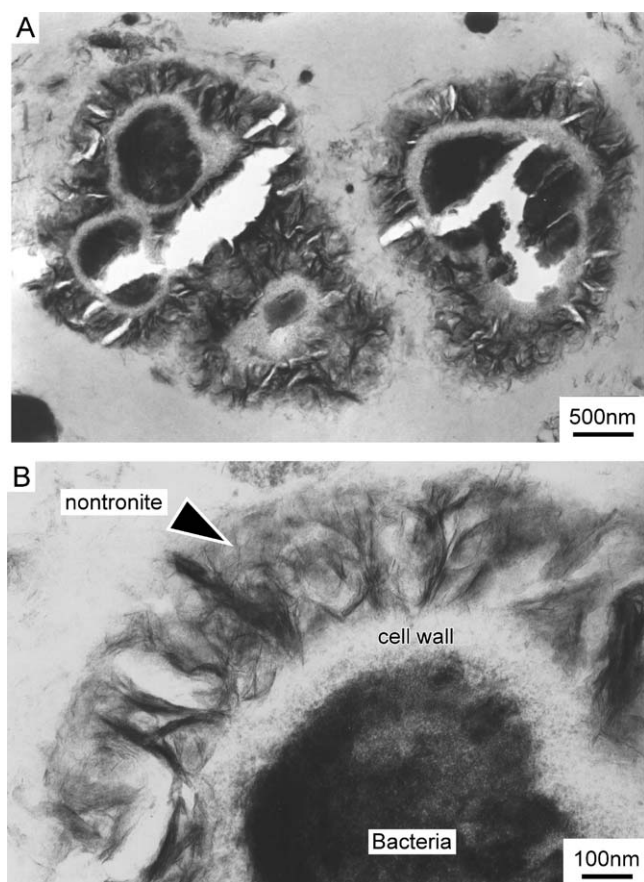


Fig. 9.11. TEM micrographs of ultra-thin section of nontronite collected from Iheya deep-sea floor sediment, showing filamentous bacteria (in cross section) surrounded by extra-cellular acidic polysaccharides, and covered with radially oriented nontronite particles (B arrow).

characteristics: pH = 7.7, EC = 120  $\mu$ S/cm, DO = 12 mg/L, temperature = 27 °C. The XRD pattern of the floc showed a strong peak at 1.53 nm. After treatment with ethylene glycol this peak was shifted to 1.72 nm, characteristic of smectite (Ueshima et al., 2000). Epifluorescence microscopy of a thin section of floc, stained with DAPI, showed the presence of bentonite (yellow), DNA (blue), and chlorophyll of living algae (red). SEM-EDX of the floc, following 30 min of ultrasonic treatment, showed the presence in the algae of Al and Si together with P, S, Cl, K, and Fe (Figs. 9.12A, B). The TEM image and the electron diffraction pattern of the algae (after ultrasonication) were also consistent with smectite (Fig. 9.12C and inset).

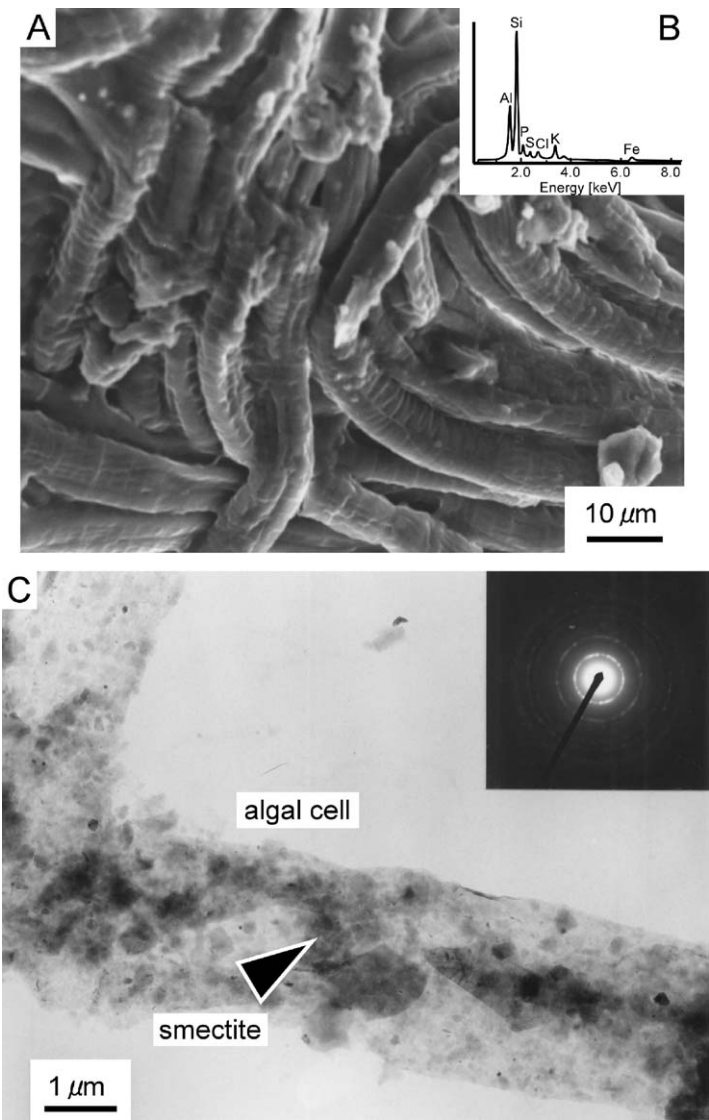


Fig. 9.12. SEM-EDX (A, B) and TEM (C) micrographs of a floc collected from the pond of Kasaoka bentonite mine, Okayama, Japan, showing bio-bentonite (after 30 minutes of ultrasonic treatment). The electron diffraction pattern of an algal cell in the floc corresponds to that of smectite (C, inset). (From [Ueshima et al., 2000.](#))

## 9.5. CONCLUSIONS

Microorganisms are ubiquitous on the Earth's surface. They are especially abundant in biofilms and microbial mats associated with ponds, hot springs, weathered feldspar, deep-sea floor vents, and mine drainage areas. In these environments microorganisms can synthesize many kinds of clay minerals, both inside and outside their living cells. The study of biomineralization and the processes involved requires a multidisciplinary approach and the application of a range of analytical and instrumental techniques. At the same time, the results can provide valuable background information with respect to environmental protection, such as bioremediation of polluted sites, as well as an insight into the sustainable development of new, clean energy sources, mineral resources, and biomedical technologies (Tazaki et al., 2002).

## REFERENCES

- Asada, R., Tazaki, K., 2000. Observation of bio-kaolinite clusters. *Journal of the Clay Science Society of Japan* 40, 24–37 (in Japanese with English abstract).
- Brindley, G.W., 1980. Quantitative analysis of clay mixtures. In: Brindley, G.W., Brown, G. (Eds.), *Crystal Structures of Clay Minerals and Their X-ray Identification*, Monograph 5. Mineralogical Society, London, pp. 411–438.
- Guggenheim, S., Martin, R.T., 1995. Definition of clay and clay mineral: joint report of the AIPEA nomenclature and CMS nomenclature committees. *Clays and Clay Minerals* 43, 255–256.
- Mann, S., Sparks, N.H.C., Wade, V.J., 1990. Crystallochemical control of iron oxide biomineralization. In: Skinner, H.C.W., Fitzpatrick, R.W. (Eds.), *Biomineralization Processes of Iron and Manganese—Modern and Ancient Environments*. Catena suppl. no. 21, pp. 21–49.
- Moore, D.M., Reynolds, R.C. Jr., 1997. *X-ray Diffraction and the Identification and Analysis of Clay Minerals*. Oxford University Press, Oxford.
- Morikawa, T., 2002. Bacterial Bio-Weathering of Feldspar at the Dam Reservoir. Graduate thesis. Kanazawa University, Japan (unpublished, in Japanese).
- Roh, Y., Zhang, C.L., Hali, H., Lauf, R.T., Zhou, J., Phelps, T.J., 2003. Biogeochemical and environmental factors in Fe biomineralization: magnetite and siderite formation. *Clays and Clay Minerals* 51, 83–95.
- Schwertmann, U., Fitzpatrick, R.W., 1992. Iron minerals in surface environments. In: Skinner, H.C.W., Fitzpatrick, R.W. (Eds.), *Biomineralization Processes of Iron and Manganese—Modern and Ancient Environments*. Catena suppl. no. 21, pp. 7–30.
- Simkiss, K., Wilbur, K.M., 1989. *Biomineralization, Cell Biology and Mineral Deposition*. Academic Press, London.
- Tawara, K., Yamamura, T., Tazaki, K., 1997. Microorganisms of hydrothermal vents at Iheya Ridge. *Journal of the Mineralogical Society of Japan* 26, 81–85 (in Japanese).
- Tazaki, K., 1997a. Biomineralization of layer silicates and hydrated Fe–Mn oxides in microbial mats: an electron microscopically studies. *Clays and Clay Minerals* 45, 203–212.

- Tazaki, K. (Ed.), 1997b. A new world in the science of biomineralization: Environmental biomineralization in microbial mats in Japan. *Science Reports of Kanazawa University*, XLII, 1–65.
- Tazaki, K., 1999. Architecture of biomats reveals history of geo-, aqua-, and bio-systems. *Episodes* 22, 21–25.
- Tazaki, K., Asada, R., 2003. Microbes associated with clay minerals: formation of bio-halloysite. In: Dominguez, E.A., Mas, G.R., Cravero, F. (Eds.), 2001. *A Clay Odyssey*, Proceedings of the 12th International Clay Conference, Bahia Blanca, Argentina. Elsevier, Amsterdam, pp. 569–576.
- Tazaki, K., Asada, R., Ikeda, Y., 2002. Quick occurrence of Fe-rich biofilms on the water surface. *Journal of the Clay Science Society of Japan* 42, 21–36 (in Japanese with English abstract).
- Tazaki, K., Ishida, H., 1996. Bacteria as nucleation sites for authigenic minerals. *Journal of the Geological Society of Japan* 102, 866–878.
- Theng, B.K.G., Orchard, V.A., 1995. Interactions of clays with microorganisms and bacterial survival in soil: A physicochemical perspective. In: Huang, P.M., Berthelin, J., Bollag, J-M., McGill, W.B., Page, A.L. (Eds.), *Environmental Impact of Soil Component Interactions*. Lewis Publishers, Boca Raton, FL, pp. 123–143.
- Ueshima, M., Mogi, K., Tazaki, K., 2000. Microbes associated with bentonite. *Journal of the Clay Science Society of Japan* 39, 171–183 (in Japanese with English abstract).
- Ueshima, M., Tazaki, K., 1997. Bacterial biomineralization of clay minerals. *Journal of the Mineralogical Society of Japan* 26, 87–92 (in Japanese with English abstract).
- Ueshima, M., Tazaki, K., 1998. Bacterial bioweathering of K-feldspar and biotite in granite. *Journal of the Clay Science Society of Japan* 38, 68–82 (in Japanese with English abstract).
- Ueshima, M., Tazaki, K., 2001. Possible role of microbial polysaccharides in nontronite formation. *Clays and Clay Minerals* 49, 292–299.
- Yoshizu, K., Tazaki, K., 1997. Role of microorganisms in iron and manganese mineral formation. *Journal of the Mineralogical Science Society of Japan* 26, 69–72 (in Japanese with English abstract).

This page intentionally left blank

*Chapter 10*

## CLAYS IN INDUSTRY

F. BERGAYA<sup>a</sup>, B.K.G. THENG<sup>b</sup> AND G. LAGALY<sup>c</sup>

<sup>a</sup>*CRMD, CNRS-Université d'Orléans, Orléans Cedex 2, France*

<sup>b</sup>*Landcare Research, Palmerston North, New Zealand*

<sup>c</sup>*Institut für Anorganische Chemie, Universität Kiel, D-24118 Kiel, Germany*

This composite chapter is concerned with the industrial applications of clays in general. Conventional applications, as in ceramics and paper coating, are described in Chapter 10.1. Catalysis by clay minerals, including their use as catalyst supports, has received much attention, and is discussed in Chapter 10.2. The versatility of clay minerals is also reflected by their usage in the formation and preparation of clay–polymer nanocomposites. As described in Chapter 10.3, these inorganic–organic hybrid materials are the subject of intensive research because of their huge potential for novel applications.

This page intentionally left blank

## *Chapter 10.1*

# CONVENTIONAL APPLICATIONS

C.C. HARVEY<sup>a</sup> AND G. LAGALY<sup>b</sup>

<sup>a</sup>*Institute of Geological and Nuclear Sciences, Wairakei Research Centre, Private Bag 2000, Taupo, New Zealand*

<sup>b</sup>*Institut für Anorganische Chemie, Universität Kiel, Otto-Hahn-Platz 6-7, D-24118 Kiel, Germany*

Clays and clay minerals are extensively used in a wide variety of industrial applications (Grim, 1962; van Olphen, 1977; Lagaly and Fahn, 1983; Jepson, 1984; Odom, 1984; Murray, 1986, 1999, 2000, 2003; Harvey and Murray, 1997). Their usages fall into two contrasting broad classes:

- Clays are used because of their inertness and stability. A large variety of industrial uses are also related to the unique rheological properties of clay and clay mineral dispersions.
- Clays are used because of their reactivity and catalytic activity.

In the following section the various families of clays are discussed in terms of their inert or reactive applications and their unique rheological properties. In many cases the different clay types are modified to meet required specifications.

Pure clays do not usually occur in nature. In terms of tonnage used, we may distinguish four classes of clay. The so-called ‘common clays’ enjoy the largest usage in numerous engineering applications. These clays contain mixtures of different clay minerals such as illite/smectites, kaolinites, smectites, micas and associated minerals. This is followed by ‘industrial kaolins’ that contain relatively high amounts of kaolinite (kaolins), and sometimes a small proportion of high-quality kaolin minerals. The third class is ‘bentonite’ with a high montmorillonite (smectite) content. The fourth class is the ‘palygorskite-sepiolite clays’ that have many similarities to bentonites and are specifically used because of their surface properties and reactivity.

The world production of processed kaolins is about 20 million tons/year and that of bentonites is 13 million tons/year, while palygorskite-sepiolite production is around 2 million tons/year. The amount of common clays used worldwide is difficult to estimate since there are no statistics. However, it is likely to exceed many hundreds of millions tons/year. There are also a few deposits of high-purity clays, such as halloysite (used in high-quality porcelain and catalysis) and hectorite (used in cosmetics and pharmaceuticals). Their peculiar properties classify them as



high-quality additives rather than bulk industrial minerals. In addition, some finely ground minerals with similar properties to some industrial clays are frequently included in industrial clay surveys. They include vermiculite, mica, talc and pyrophyllite. A brief summary of their uses is included here.

### 10.1.1. INDUSTRIAL USES

#### *A. Common Clays*

Although the technologies associated with the engineering properties of clays are not covered in this chapter, large tonnages of common clays are used in a wide variety of engineering applications including road construction, fill, dam construction and in waste containment. The mineralogy and particle size distribution determine their engineering properties.

Large tonnages of common clays are used in ceramic production (bricks, tiles, terracotta, earthenware, stoneware, sewer pipes, paving bricks, refractory bricks, etc.). Although these clays are typically impure, they contain sufficient clay minerals to cause them to develop plasticity and to produce adequate strength, porosity and other properties to justify their use. These raw materials may contain high amounts of mixed-layer clay minerals, notably illite/smectite. As illite/smectite particles can delaminate to a certain extent depending on their layer charge distribution (see Chapter 5), the type of illite/smectite may influence the ceramic properties of common clays, and their behaviour in dispersions (for casting processes, etc.). A small amount of smectite can be tolerated or is added to improve plasticity. Large amounts of smectite would give undesirable shrinkage and drying properties. The presence of kaolinite is not desirable in clays used for bricks and tiles because kaolinite would increase the firing temperature and a light burning colour is not required (Grim, 1962).

#### *B. Kaolins*

##### *Kaolins as Filler and Coating Particles*

Table 10.1.1 provides a general summary of the uses of clays as inert components in industrial systems (Murray, 1986, 1999, 2000; Harvey and Murray, 1997; Harvey, 1997). Amongst the earliest industrial uses of clays are water-based systems such as paper or water-based paints where the hydrophilic nature of clays enables them to readily disperse in such systems. However, kaolins were long used as fillers for plastics and rubber. To make the hydrophilic surface of the clay mineral compatible with the organic material, the surface is modified by reacting with organic compounds, in most cases by grafting (see Chapter 7.3). If the clay mineral particles are highly dispersed in the polymer matrix and the adhesion between the filler particles

Table 10.1.1. Uses of clay minerals as inert components

Clay family	Industry	Use
Kaolin	Paper, plastics, rubber	Filler
	Pesticides	Carrier, diluent
Vermiculite	Building industry	Heat insulation, sound dissipation
	Package industry	Shock proof materials, thermal protection, liquid absorption
	Foundries	thermal protection
Mica	Electrical industry	Insulation
	Paints	UV-, heat-stable and under-water paints
	Cosmetics	Nacreous pigments
	Coating	Corrosion proof, polymer coatings, underseal
Talcum, pyrophyllite	Plastics, rubber, paper industry	Filler
	cosmetics, pharmaceuticals	Powders, pastes, ointments, lotions
	refractory industry	Refractories
Palygorskite, sepiolite	Pesticides	Carrier for insecticides and herbicides
	Chemical industry	Catalyst carrier, filter material, anti-caking agent
	Cosmetics, plastics	Filler

and the matrix is good, the kaolinite particles act as active fillers, i.e., they improve certain mechanical properties of the polymers (Lagaly, 1999).

Modern developments in this field not only aim to increase the bonding strength between the filler particles and the polymer matrix but also to produce clay mineral–polymer nanocomposites where the fully delaminated mineral is dispersed in the matrix (see Chapter 10.3).

Kaolin, bentonite, palygorskite and sepiolite are used as carriers and diluents of pesticides (insecticides, fungicides, herbicides). Enhanced application of herbicides requires particular formulations based on modified clay minerals (see Chapter 11.2).

The largest amounts of processed kaolins (more than 60% of the world production) are used in the paper industry as fillers within the network of cellulose fibres and as coating particles. The technical requirements for filler clays are significantly less than for kaolinite particles in the coating colours. Gloss, brightness, opacity and smoothness generally improve with increasing coat mass and decreasing particle size. The  $\leq 2\mu\text{m}$  fraction is particularly important in coating kaolins and high-glossing paint kaolins. More than 70% (w/w) of the coating particles should be smaller than  $2\mu\text{m}$ . Very finely divided kaolins can cause technical problems. Filler clays typically

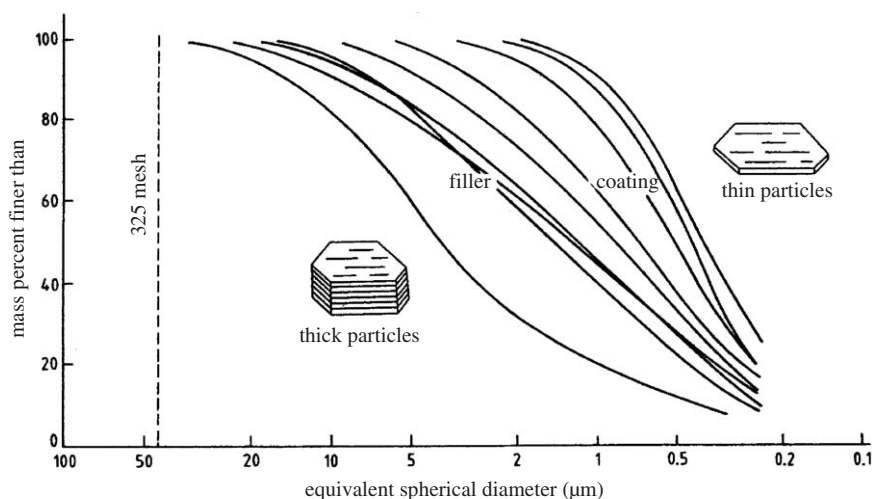


Fig. 10.1.1. Typical particle size distribution of filler and coating grade kaolins. From Murray (1986).

have 50–70% particles  $> 2\ \mu\text{m}$  (Jepson, 1984; Murray, 1986, 1999, 2000), the optimum particle size for lodging within paper fibres being 5–7  $\mu\text{m}$ . Typical particle size distributions of industrially processed filler and coating kaolins from the sedimentary kaolin deposits in Georgia (USA) are illustrated in Fig. 10.1.1.

Coating of paper is done at very high speeds (1200 m/min and even more), and using large machines (Bundy, 1993). As such, it requires an exact tuning of the rheological properties of the highly concentrated slurries. In blade coating the rate of shear can reach  $10^6\ \text{s}^{-1}$  along the line of contact of the blade with the paper. The relation between bulk kaolin properties and coating colour rheology is complex. Particle shape, size, size distribution and particle packing are critical factors. For the same clay content, dispersions of thin, large particles have higher viscosities than those of blocky particles. The more platy the particle shape, the lower is the shear rate at which shear thickening starts.

To prepare homogeneous slurries of kaolin with up to 70% (w/w) solids, anionic macromolecules, mainly polyphosphates and polyacrylates,<sup>1</sup> are added. This enhances the negative charge density at particle edges, providing steric stabilisation to the dispersion (see Chapter 5). It is necessary to select appropriate size fractions and particle shapes to obtain the required rheological properties (yield value, viscosity, thixotropy). One also has to consider the interaction of the coating particles with the thickeners (often carboxy methylcellulose and starch) as this plays a key role in controlling the rheological and dewatering properties (Li et al., 2001).

<sup>1</sup>Some polyphosphate containing kaolin slurries can form gels within a few hours if left undisturbed producing discharge problems. Gelation is retarded or impeded by adding sodium polyacrylates.

### *Kaolins in Ceramics*

A major use for high-purity kaolins is for ceramic products such as porcelain, bone china, vitreous sanitary ware and earthenware. Low-quality kaolins are also used as fillers in a wide range of ceramic products including brick, pipes and tiles. Refractory clays are dominantly composed of kaolins with low levels of iron, alkali and alkaline earth cations. High levels of such metals would reduce the fusion point.

Delamination of kaolinite particles<sup>2</sup> improves the quality of porcelain. This reaction was used by Chinese ceramists to produce very thin ('egg-shell') porcelain of high mechanical stability (see Chapter 7.3). Delamination was also used in the production of speciality paper clays. Delamination of large particle-size kaolin stacks can convert filler clay into high-surface area platelets with superior opacity in light-weight coatings (Bundy, 1993).

The presence of smectites in commercially exploited kaolin resources is undesirable for most industrial applications. The smectites may therefore have to be removed in order to meet the required specifications. As these minerals are generally concentrated in the finest size fractions ( $< 0.5 \mu\text{m}$ ) of kaolins (Fig. 10.1.2), size fractionation can help to reduce the smectite content. Chemical modification of the smectites was also proposed to reduce their negative effect (Jepson, 1984).

Historically, mainly in China and Eastern Asia, clays and kaolins for the production of fine ceramics were traditionally matured by placement in humid pits for several years. The improvement in properties is caused by the modification of particle size (and possibly composition) through the action of microorganisms. This

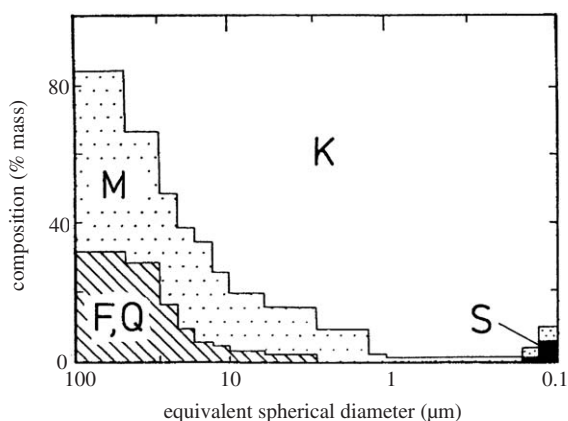


Fig. 10.1.2. Variation in mineral composition with particle size for Cornish kaolin. F = feldspar; Q = quartz; M = mica; S = smectite; K = kaolinite. From Jepson (1984).

<sup>2</sup>In a strength sense 'delamination' describes the disarticulation of the particles into single silicate layers (see Chapter 5). In industrial applications 'delamination' stands for the dissociation of aggregates into single particles or smaller aggregates.

beneficiation process is currently attracting the attention of scientists (Groudeva and Groudev, 1995; Lee et al., 2002).

Ceramic masses can be shaped because of the unique ability of clay mineral particles to form card-house or band-type networks (see Chapter 5). On the other hand, the ease with which clay mineral particles form stable colloidal dispersions also allows the production of ceramics by casting, especially porcelain and vitreous sanitary ware. The deflocculated slip (total solid content  $\geq 70\%$  (w/w) is poured into a porous plaster mould so that a filter cake builds up on the plaster surface. The mould is inverted, and the excess slip is allowed to drain. After de-watering in the mould, the cast is removed, and, after a few further steps, is sprayed with glaze and fired (Jepson, 1984). This technique needs fluid colloidal dispersions with clay contents as high as possible. Liquefaction requires the addition of sodium salts and a pH above 6. At the same water content, a sodium kaolinite dispersion can be fluid whereas calcium kaolinite forms a plastic mass (see Chapter 5). This behaviour was first described by Justus von Liebig (1865). Fine ceramics produced by slip casting commonly have a higher dry breaking strength than shaped ceramics. The filter cake built up during slip casting consists of kaolinite particles that are more densely packed in parallel orientation as compared with moulded plastic masses in the presence of calcium ions (Hofmann, 1962a).

In technical processes the charge on particle edges is changed from positive to negative by addition of multivalent anions, particularly oligo- and poly-phosphates as well as polyanions like polyacrylate and less well-defined macromolecular compounds such as humic substances. These additives often impart a certain amount of steric stabilization to the dispersion (see Chapter 5). One of the most effective dispersants for modern high-performance ceramics is oxidized fish oil (Böhnlein-Mauß et al., 1992). Liquefaction of a mass of 100 g kaolinite ('China clay') in 200 ml water by 1 g tetrasodium diphosphate ( $\text{Na}_4\text{P}_2\text{O}_7 \cdot 10 \text{H}_2\text{O}$ ) is illustrated in Fig. 10.1.3. The fluid dispersion can stiffen again by the addition of salts such as KCl (in this case 3 g/100 g clay), causing the clay mineral particles to coagulate (flocculate).

### C. Bentonites

World production tonnages for bentonites are very difficult to obtain. Our best estimate is 13 million tons and the major usages are iron ore pelletizing, foundry mouldings and oil well drilling (Fig. 10.1.4). However, the use of bentonite in numerous environmental applications is growing fast. Large volumes are needed for filtering, decolourizing and clarifying (mostly in form of bleaching earths), pelletising animal feed, as pet litter adsorbent,<sup>3</sup> pesticide carrier and oil and grease adsorbent. Smaller amounts of bentonites are needed for paints, pharmaceutical and cosmetic uses, waste disposal, lubricants, as additives for cement and mortar, as catalysts and

---

<sup>3</sup>The effectiveness of clays for pet litter may also be related to the deactivation of enzymes that convert urea to ammonia (W. P. Moll, personal communication, see Chapter 11.1).

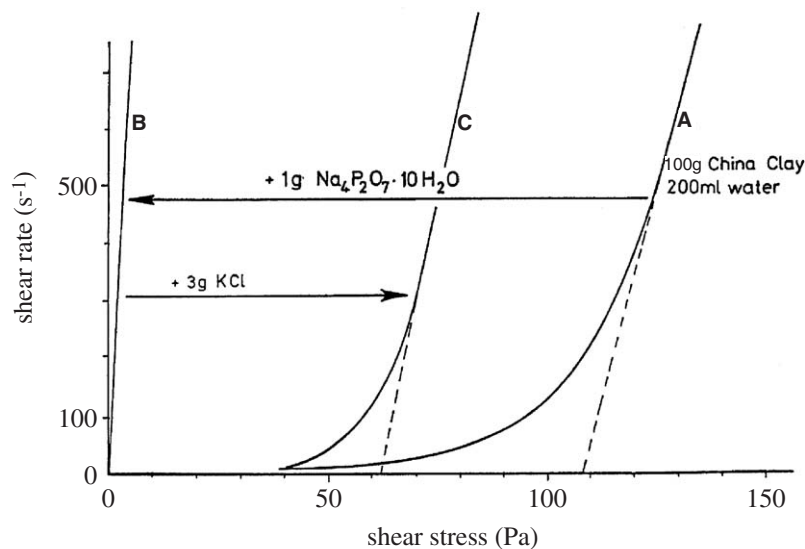


Fig. 10.1.3. Liquefaction of kaolin by tetrasodium diphosphate. A 100 g China Clay in 200 ml water. B Liquefaction by addition of 1 g  $\text{Na}_4\text{P}_2\text{O}_7 \cdot 10\text{H}_2\text{O}$ , C again stiffening by addition of 3 g KCl. Data from M. Müller-Vonmoos, ETH Zurich. From Jasmund and Lagaly (1993).

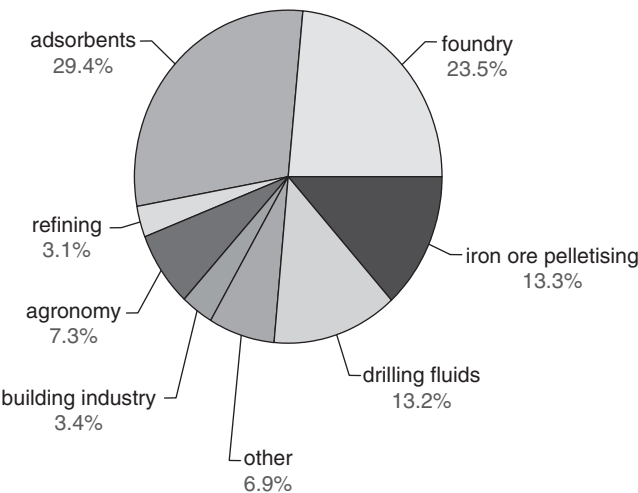


Fig. 10.1.4. Use of bentonite. World production may be 13 million tons in 1993 (Courtesy N. Schall, Süd-Chemie AG, Germany).

catalyst supports, water purification, fertilizers, ceramics and other miscellaneous applications such as additives in washing powders, for newspaper recycling, cleaning waste water from car washes and as flocculation aids, often together with soluble flocculating agents such as polyions, alum (aluminium sulphate) and iron chloride (Table 10.1.2a, b and 10.1.3) (Grim, 1962; Odom, 1984; Fahn and Schall, 1985; Schall, 1988; Murray, 1986, 1999, 2000; Harvey and Murray, 1997; Caine et al., 1999; Panpanit and Visvanathan, 2001; Philippakopoulou et al., 2003).

### *Bentonite as Binding Agents*

Bentonites are extensively used as binding agents in the pelletization of iron ore, other fine-grained solids and animal feed. The sands are prepared with about 2% bentonite. The montmorillonite layers ensure adhesion between the particles in a similar way as described for moulding sands (see below). Natural sodium and sodium-exchanged calcium bentonites are preferred for iron ore pelletising because of their high capacity for removing excess water from the powdered ore. In other cases, both sodium and calcium bentonites are used. Bentonite added to animal feeds can increase their nutritional benefit.

In foundry moulding sands the clay mineral particles have to make the sand plastic and cohesive so that the sand can be moulded around a pattern. The bentonite also gives the sand sufficient strength to resist the thermal stress of the molten metal. Green compression strength, dry compression strength, wet tensile strength, hot compression strength, flowability and durability (clay-bonded moulding sands are recycled many times) are crucial properties in foundry usage. Again, the  $\text{Na}^+/\text{Ca}^{2+}$  ratio is very important to adjusting these properties (Odom, 1984). Natural sodium bentonites have better durability and higher fusion temperature and are favoured for use in steel foundries. Bentonites containing  $\text{Ca}^{2+}$  ions are preferred for preparing moulds for iron casting. Many foundries use specified blends of specific types of sodium and calcium smectites to achieve the optimum moulding sand properties.

Table 10.1.2a. Uses of clay minerals based on their rheological properties

Clay family	Industry	Uses
Common clays	Ceramics	Tiles, bricks, earthenware, stoneware, sewer pipes, sanitary ware, refractory bricks
Kaolins	Paper Ceramics	Coating Porcelain, bone china, vitreous sanitary ware, earthenware
Bentonites Palygorskite, sepiolite	See Table 10.1.2b Paints, chemical and mineral oil industry	Thickening and thixotropic additive, dispersing and anti-settling agent, drilling fluids

Table 10.1.2b. Uses of bentonites based on their rheological properties

Area of applications	Uses	Activation*
Agriculture, horticulture	Soil improvement	r, s
Building industry	Supporting dispersions for cut-off diaphragma wall constructions, shield tunneling, subsoil sealing, antifriction agents for pipejacking and shaft sinking additions to concrete and mortar	r, s r, s
Ceramics	Plasticising of organic masses, improvement of strength, fluxing agents	r, a
Foundries	Binding agents for moulding and core sands	r, s
	binding agents for anhydrous casting sands	o
	thickening of blackwashes	o
Mineral oil industry	Drilling fluids	r, a, o
	thickening of greases	o
Paints, varnishes	Thickening, thixotroping, stabilising, anti-settling agents	s, o
	coating materials, sealing cement, additives for waxes and adhesives	s, o
Pharmaceutical industry, cosmetics	Bases of creams, ointments and cosmetics	r, a, s
	Stabilisation of emulsions	r, o
Tar exploitation	Emulsification and thixotroping of tar-water emulsions, tar and asphalt coatings, additives for bitumen	a, o

\*r: raw bentonite, a: acid-activated bentonite, s: soda-activated bentonite, o: organo-bentonite.

The importance of having sodium ions in the interlayer space was described by Hofmann and Endell (1935, 1936). Adding soda ash ( $\text{Na}_2\text{CO}_3$ ) to German bentonites that are not suited for foundry-moulding sands should be made such clays suitable for use as a moulding sand binder.

#### *Bentonite in Drilling Muds*

Oil well drilling fluids are colloidal dispersions of complex composition (van Olphen, 1977; Odom, 1984; Darley and Gray, 1991). First of all, the fluid acts as a lubricant to reduce the friction between the drilling string and the side of the hole. The drilling fluid is circulated to bring the drill cuttings from beneath the bit up to the separation site and to cool the bit. Therefore, drilling fluids must have a relatively high density to carry the fine cuttings. The drilling fluid builds up an impermeable filter cake of smectite (montmorillonite) particles on the side of the hole, preventing the loss of fluid into the permeable rock (see Chapter 5). It also prevents the inflow of fluids (oil, gas, or water) from permeable rocks. When the drilling operation is interrupted



Table 10.1.3. Uses of clay minerals based on their adsorption properties and reactivity

Clay family	Industry	Uses	Activation*
Kaolin	Fibre glass	Source of alumina	
	Petrochemicals	Catalyst support	
	Chemical industry	Zeolite synthesis	
	Building industry	Additive in cement	
Bentonite	Agriculture, horticulture	Soil improvement, composting	r, s
		adsorption of mycotoxins	o
		Sulphur production: refining, decolouration, bitumen extraction	r, a
		Catalysts	r, a, s
	Cleaning industry	Carriers for pesticides	r, a, s, o
		Dehydrating agents	r, a, s
		Adsorbents for radioactive materials	r, a, s, o
		Regeneration of organic fluids for dry cleaning	a
		Polish and dressings	r, s
		Additives for washing and cleaning agents and soap production	r, s
	Environmental technology	Forest and water conservation: fire extinguishing powders, binding agents for oil on water	r, a
		Animal husbandry, manure treatment, cat litter	r, s
		Water and waste water purification	r, s, a
		Sewage sludge pelletizing	r, a
	Food stuff industry	Barriers	r, s
		Refining, decolouration and stabilization of vegetable and animal oils and fats	r, a
		Fining of wine, juices, beer stabilisation, purification of saccharine juice and syrup	r, a, s
		Refining, decolouration, purification and stabilization of mineral oils, fats, waxes and paraffins	r, a
	Mineral oil industry	Refining, decolouration, purification and stabilization of mineral oils, fats, waxes and paraffins	r, a
		Pigment and colour developer for carbonless copying paper	a
		Adsorption of impurities in circulation water	r, a, s
		De-inking in waste-paper recycling	r, a, s
	Cosmetics, pharmaceuticals	Powders, tablets, drug carrier, odour control, liquid absorption	r, a, s, o
		Palygorskite, sepiolite	Adsorbent, carrier, bleaching,
		decolouration, anti-caking agent	
		Cigarette filters (sepiolite), cat box litter	

\*r: raw bentonite, a: acid-activated bentonite, s: soda-activated bentonite, o: organo-bentonite.

before the drill cuttings and sand were circulated out of the hole, the thixotropic stiffening (see Chapter 5) of the drilling fluid prevents settling of the fine material. In offshore drilling or drilling through salt domes the fluid must be protected against destabilization by salts.

Drilling fluids are mainly based on dispersed sodium bentonites. The particular requirements can only be fulfilled by components whose properties may in some cases be counteractive. For instance, the thixotropic property of the fluid requires conditions that are adverse to optimal plastering. When calcium and/or barium sulphate are added to enhance the density, or calcium and barium hydroxide are added to reduce the large increase of viscosity at the high temperatures in deeper holes, the divalent cations would cause coagulation of the dispersed particles. This effect is usually overcome by the addition of complexing macromolecular compounds that also impart a high degree of steric stabilization. A well-known additive is carboxymethyl cellulose (cf. Fig. 5.22). Other macromolecular compounds such as polyphosphates are less effective as steric stabilizers but they improve the salt stability by reversing the edges of the clay mineral particles from positive to negative, or increasing the negative edge charge density. The common Quebracho tannates in the red muds exert both effects (see Chapter 5).

#### *Bentonite in Engineering*

Bentonite dispersions are used in many civil engineering applications. Most impressive is the diaphragm-walling technique. A thixotropic bentonite dispersion is used as an intermediate supporting material, obviating the need for revetting (retaining wall) when the trench is excavated. In addition, the plastering effect (see Chapter 5) is important. The slurry penetrates only to some extent into the trench sides and forms an impermeable filter cake of clay mineral layers on the walls so that excessive loss of fluid to the surrounding formation is prevented. In the next step, the bentonite dispersion is displaced by the concrete (Fig. 10.1.5). Concrete walls about 100 m deep and 0.8–1.5 m thick are built up by this technique. (It is interesting to note that the stabilizing effect of bentonite dispersions was observed in the middle of the 19th century. The first patent was issued in 1912 but the technique was only widely applied since about 1950.)

In other applications bentonite dispersions are used to grout cracks and fissures in rocks, for soil injection, or to impede water and waste-water movement through soils, sand, or gravel. Examples are sealing waste deposits (see Chapter 11.3), sewage ponds or ornamental ponds. The dispersions are used as lubricants not only in drilling fluids but also to lubricate caissons (Fig. 10.1.6) and piles or cables as well as pipes for pulling through conduit. In shield tunnelling the thixotropic bentonite supports the soil in front of the shield until it is removed by the tools of the rotating shield. It also has to keep back ground water, and transport the excavated soil to a separation plant above ground.

Bentonite can be added to waterproof concrete walls and floors, or added to mortar to increase its plasticity (see also (Krøyer et al., 2003)). Bentonite also serves as an important additive in bitumen emulsions.

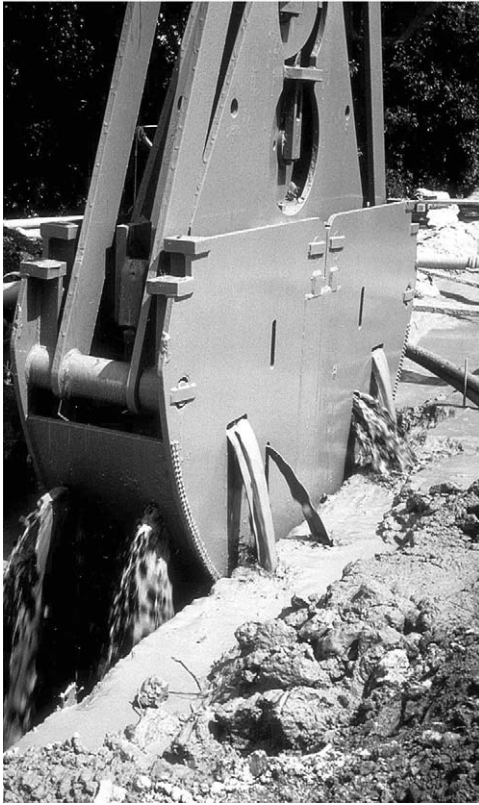


Fig. 10.1.5. Diaphragma walling. Excavation of a trench and its subsequent lining with a thixotropic bentonite slurry.

The properties of bentonite that are most significant in the above-mentioned civil engineering applications are viscosity, yield value, thixotropy, plastering ability and plasticity. Thus, only natural sodium bentonites and certain sodium-exchanged calcium (magnesium) bentonites are suited for the purpose.

#### *Bentonite as a Thickener*

Bentonites are added to paints and enamel paints not only as thickening agents and gellants but also to impart a certain degree of thixotropy to the dispersion and so impedes sagging of the paints (Jones, 1983) (Fig. 10.1.7). In non-polar systems the clay mineral particles have to be hydrophobized (see Chapter 7.3).

#### *Activated Bentonites, Fuller's Earth and Catalysis*

A large diversity of applications are related to the adsorption capacity and chemical reactivity of bentonites (Table 10.1.3). Their ability to adsorb proteins and high-molecular

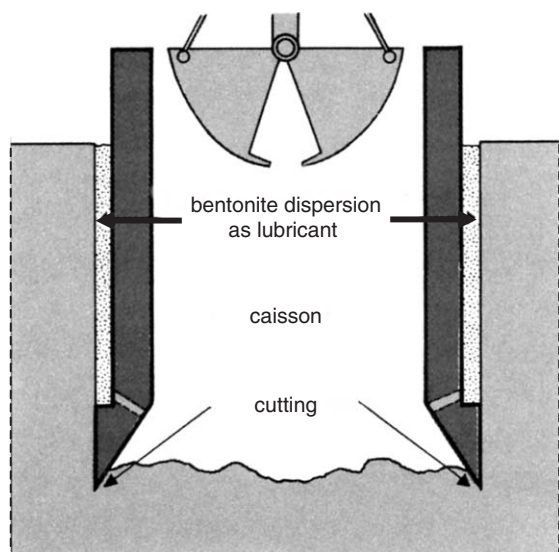


Fig. 10.1.6. During caisson sinking and pipe checking a highly viscous bentonite slurry reduces the friction between building structure and soil (outer light-shaded piece). Shown is the cutting face of the caisson to be sunk or the pipe to be checked.

compounds (see Chapters 5 and 7.3) is useful for stabilizing beer,<sup>4</sup> and improving the taste and quality of juices and even cheap wines (Rankine, 1995; Sarmiento et al., 2000). An up-coming important application is the use of modified bentonites as adsorbent of mycotoxins. These excretions of certain moulds on cereal grains and oil seeds are extremely toxic and enter the food chain of both animals and humans.

Most important is the use of acid-activated bentonites ('bleaching earths', see Chapter 7.1) for decolourizing vegetable and mineral oils (Fahn, 1963, 1973; Sarier and Güler, 1988; Srasra et al., 1989; Jovanović and Janačković, 1991; Mokaya et al., 1994; Theng and Wells, 1995; Erdoğan et al., 1996; Ravichandran and Sivasankar, 1997; Christidis et al., 1997, 2003; Falaras et al., 1999, 2000; Jozefaciuk and Bowanko, 2002). The removal of pigments not only decolourizes vegetable oils but also improves taste and stability.

Fuller's earth were used for centuries to remove fat from animal wool ('fulling'), and is a mixture of different clay minerals (palygorskite, sepiolite, smectites). The composition of fuller's earth varies between different localities. Fuller's earth was used for oil refining before the industrial production of acid-activated bentonites. The history of fuller's earths was described by Robertson (1986) and Beneke and Lagaly (2002).

Clays are used as catalysts and catalyst supports in many organic syntheses. Montmorillonite is the most important clay mineral for these uses. The acid forms

<sup>4</sup>When the proteins are not removed from beer, their decomposition makes the beer undrinkable.

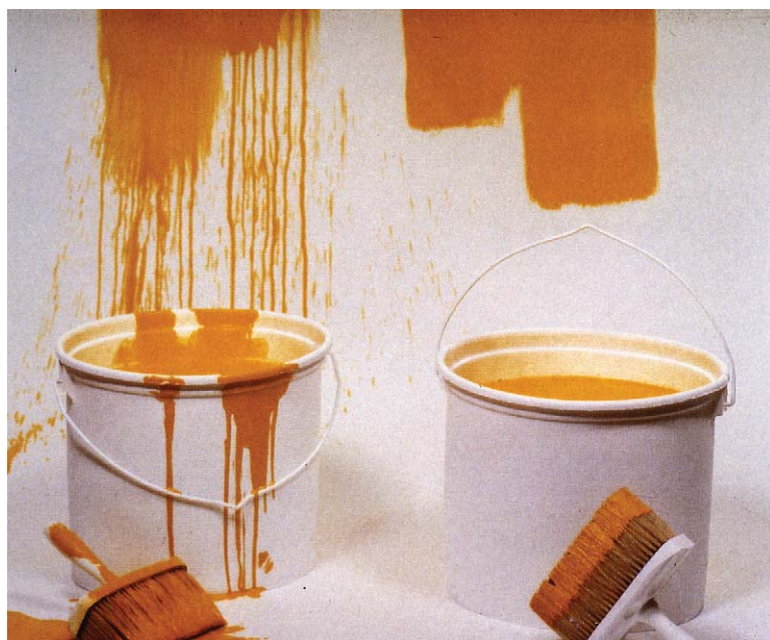


Fig. 10.1.7. Addition of a thixotropic agent impedes sagging of the paints. From Lagaly et al. (1997).

can provide environmental friendly alternatives to liquid Brønsted acids. ‘Clayfen’ and ‘Claycop’ are not catalysts but useful montmorillonite-supported reagents (see Chapter 10.2).

Carbonless copying papers are composed of paper sheets with different coatings on the back of the upper sheet (CB) and on the front of the lower sheet (CF) (Fig. 10.1.8). CB is coated with micro-capsules (1–10  $\mu\text{m}$ ) of gelatine or polyurethane. The capsules contain a solution of leuco dyes, commonly crystal violet lactone or *N*-benzoyl leuco methylene blue. CF is covered with a coating colour consisting of an acid-activated bentonite (adjusted to pH 9–10) together with water and binders. The pressure of a pencil or the stroke of a typewriter breaks the micro-capsules at the point of contact. As the solution is released, the dye is adsorbed on the coating colour of the CF front page, and the colour (crystal violet or methylene blue) develops at this point (Fahn and Fenderl, 1983).

#### *D. Vermiculites and Micas*

Vermiculites are commonly used in the form of expanded particles as shown in Fig. 10.1.9 (see Chapter 7.2). The vermiculite flakes are expanded by rapid heating from 250 to 1500  $^{\circ}\text{C}$  followed by immediate cooling to 400  $^{\circ}\text{C}$ . The evaporating water

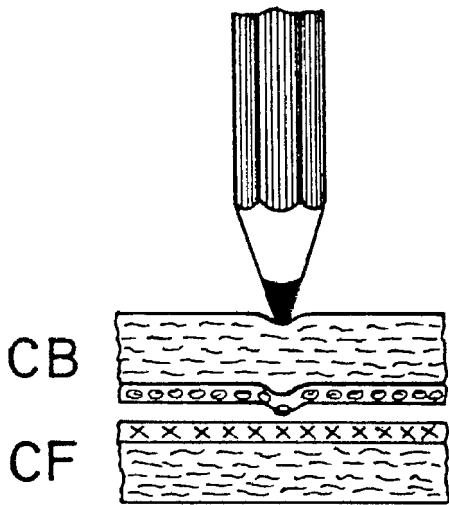


Fig. 10.1.8. Carbonless copying paper. The back of the upper sheet is coated with microcapsules containing the leuco dye, the front of the lower sheet is coated with an acid-activated bentonite. From [Fahn and Fenderl \(1983\)](#).



Fig. 10.1.9. Shock-heated expanded vermiculite flakes (Courtesy K. Beneke, University Kiel).



expands the particles in worm-like (vermiform) manner (Grim, 1968; Bergaya et al., 2001) and increases the volume by up to 1500 times. Extremely short heating periods are required to avoid the decomposition of structural OH groups (Klose, 1982).

Expanded vermiculite is used in the building industry for heat insulation and sound dissipation. In the packaging industry it is used as a thermal protecting and shock-proof-filling material for glass containers and vessels. The high liquid absorption capacity of expanded vermiculite reduces damage by breaking containers. In metallurgy the surface of molten metals is covered with vermiculite for thermal protection.

Wet or dry finely ground micas, typically with a particle size similar to that of filler clays, are found in heat-stable, UV-stable and under-water paints. Nacreous (pearlescent) pigments ('Perlglanzpigmente'), especially used in cosmetics, obtain their exceptional optical properties from parallel oriented mica particles. Ground micas are also used in corrosion-proof materials, polymer coatings, underseal and as an insulating material.

#### *E. Talc and Pyrophyllite*

Talc and pyrophyllite are important filler materials for polymer and rubber. Talc is also used extensively in cosmetic and pharmaceutical powders. In pharmaceutical technology talc is needed as an indispensable slip additive.

#### *F. Palygorskite and Sepiolite*

Sepiolite is used as a filler (cosmetics, polyester), a carrier (insecticides, herbicides, catalysts) and as filter material and anti-caking agent. It is also used as a dispersing, antisetling, thickening and thixotropic additive in paints and drilling fluids. The thickening effect mainly results from the fibrous shape of the particles, and hence is much less dependent on salt concentration and cations present than is the case with bentonites. Palygorskite<sup>5</sup> is used in similar applications. Sepiolite is further used as adsorbent, for instance in cigarette filters, and as a decolourant, sometimes after acid-activation (see Chapter 7.1). Sepiolite in the form of 'meerscham' is also made into pieces of jewellery and pipe bowls (Galan, 1996; Harvey and Murray, 1997).

#### *G. Industrial uses of Mixtures of Clay Types*

It is not unusual for single industrial users to utilise clays for both their inertness and reactivity. For example, in many ceramic applications kaolins may be used as an inert filler, while the reactive properties of bentonites or ball clays impart plasticity, unfired strength and perhaps critical fired properties.

Combinations of clay minerals, such as kaolinite, smectite, talc and palygorskite have long been in the preparation of pastes, ointments and lotions for external use.

---

<sup>5</sup>Technical reports still use the older term 'attapulgit'.

Cosmetic formulations also take advantage of the softness, dispersing, gelling, emulsifying and adsorption properties of clays. Talc is the basis of cosmetic and pharmaceutical powders, often combined with kaolins, bentonites and starch.

Solid particles, in particular combinations of bentonite and layered double hydroxides, are excellent stabilizers of emulsions. The important advantage is that such emulsions can remain stable in the absence of any organic surface-active agents (Abend *et al.*, 1998; Lagaly *et al.*, 1999a, 1999b; Abend and Lagaly, 2001).

Certain clays show a soapy appearance and, in fact, can be used for cleaning.<sup>6</sup> In Europe, soap-like materials containing high amounts of clays were used during the world wars and some time after. Clays were also used as shampoos, and not only by primitive people (Mahjoory, 1996). Actually, clay minerals find increasing use in hair cosmetics. Eating earth or clay is widespread throughout the world. Clays were used for centuries in therapeutic, intestinal and adsorbent preparations (see Chapters 11.5 and 11.6).

## 10.1.2. PROCESSING INDUSTRIAL CLAYS

### A. Purification and Fractionation

In most cases, relatively simple techniques are used to investigate the properties of clay mineral dispersions. Clay minerals having a certain degree of purity are separated from the non-clay minerals by sedimentation techniques. Particle size fractionation is necessary to separate the clay minerals from associated minerals and phases (see Chapter 1). Dry separation processes are effective down to sizes of about 7  $\mu\text{m}$ . However, wet processing is necessary for finer particle sizes or for raw materials requiring chemical treatment for such processes as chemical bleaching or magnetic separation. In wet processing, a decisive step preceding sedimentation is the preparation of a stable dispersion of the clay by replacing the divalent compensating (charge-balancing) cations with sodium ions. The pH of the dispersion must be maintained at 7–8 because the clay mineral particles aggregate at pH < 6.5. The stable dispersion of the clay minerals in homoionic form may then be fractionated by gravity sedimentation, or for particle sizes below 1  $\mu\text{m}$  this is usually done by centrifugation (see Chapters 4 and 5).

Naturally occurring clays are typically mixtures of clay minerals and non-clay minerals. Such clays may be cemented by metal hydr(oxides) or carbonates. Before any processing flow sheet can be designed it is recommended that the clay materials be disaggregated, the cements removed and the clay particles dispersed.

It is important to understand the nature of the cements and the composition of the total material, so that any processing flow sheet can be designed to remove the non-clay minerals. The following processes may be involved: (i) purification; (ii) wet versus dry processing; (iii) particle size separation (fractionation); (iv) bleaching and

---

<sup>6</sup>Saponite is derived from Latin *sapo*, meaning soap (Grim, 1968; Bergaya *et al.*, 2001).



magnetic separation; (v) flotation and selective flocculation; (vi) drying and calcination; and (vii) chemical modification and activation. A typical dry processing plant for kaolin or bentonite is shown in Fig. 10.1.10. Once the basic composition of a raw material was understood, a series of processing steps may be introduced. For high-quality clays the processing may be relatively complex.

### *B. Processing of Kaolins*

Common clays for production of tiles, bricks and ceramics are generally used without any processing. In some cases the largest particles are removed by simple sedimentation techniques without pre-purification to obtain homogeneous ceramic bodies. Antique ceramists used advanced processing of common clays to obtain the refined clays for shaping and the slips for decoration. The red/black decoration ('Glanzton' technique) of the famous Antique vases with the appealing gloss was produced by using clay masses and slurries with different contents of kaolinite and illite (Hofmann, 1962b; Noll, 1982, 1991).

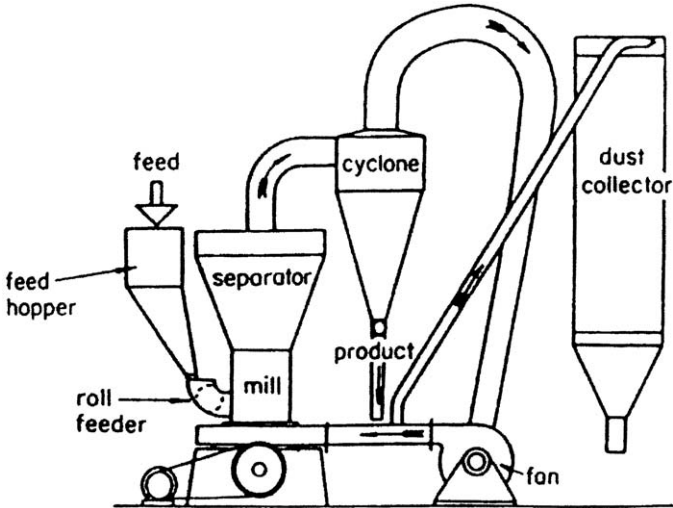
Kaolins for the paper industry now require sophisticated and extensive processing technologies (Table 10.1.4). Fig. 10.1.11 summarizes the applied technologies that may be used to refine and improve the industrial properties of kaolins. Fig. 10.1.12 shows a US kaolin mining and degrading operation from which the degraded kaolin is piped up to 40 km to a processing plant (Fig. 10.1.13) that may typically produce over 1 million tons of processed kaolin.

### *C. Raw and Activated Bentonites*

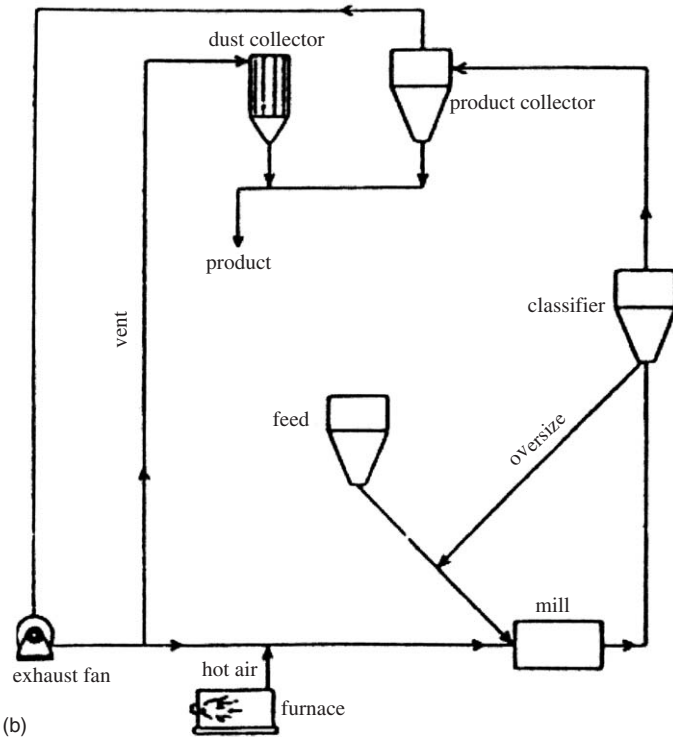
Bentonites are fine-sized materials, and hence are generally used without significant size fractionation (Figs. 10.1.14 and 10.1.15). As certain properties of bentonites can change between neighbouring pits or between individual layers within a pit, blending is commonly used to maintain a consistent product with standard properties.

Bentonites may be used in the raw form (as mined) or they may be activated (Tables 10.1.2b and 10.1.3). Alkali or soda-activation, using sodium carbonate ( $\text{Na}_2\text{CO}_3$ ), transforms the calcium (magnesium) bentonites into sodium-calcium forms. The bentonite with water contents of 35–40% (w/w) is usually kneaded or milled with 1–5% (w/w) sodium carbonate and homogenized (Fig. 10.1.16). This process of soda-activation was first proposed by Hofmann and Endell (1935). Fluid dispersions are usually avoided because sodium bentonite dispersions are extremely difficult to filter due to their high viscosities (see Chapter 5). Nevertheless, smaller amounts of high-quality sodium bentonites, or especially hectorites for certain applications, are produced in dispersions after careful selection of the raw bentonite. The quality of the products can be improved by special processing of the raw bentonite (fractionation or hydrocycloning, mechanical treatments, reaction with heated water vapour, etc.).

During soda-activation a large part of the interlayer calcium ions is precipitated as calcium carbonate. As the calcium ions are still present in the system when this



(a)



(b)

Fig. 10.1.10. Dry processing for kaolin or bentonite. (a) Mill, cyclone, and dust collection circuit, (b) hot air circuit for drying in grinding mill.

Table 10.1.4. Applied technologies used in kaolin processing

Delamination  
High gradient magnetic separation  
Selective flocculation  
Column flotation  
Ozone bleaching  
Ultrafine particle size separation  
Surface modification  
Calcination

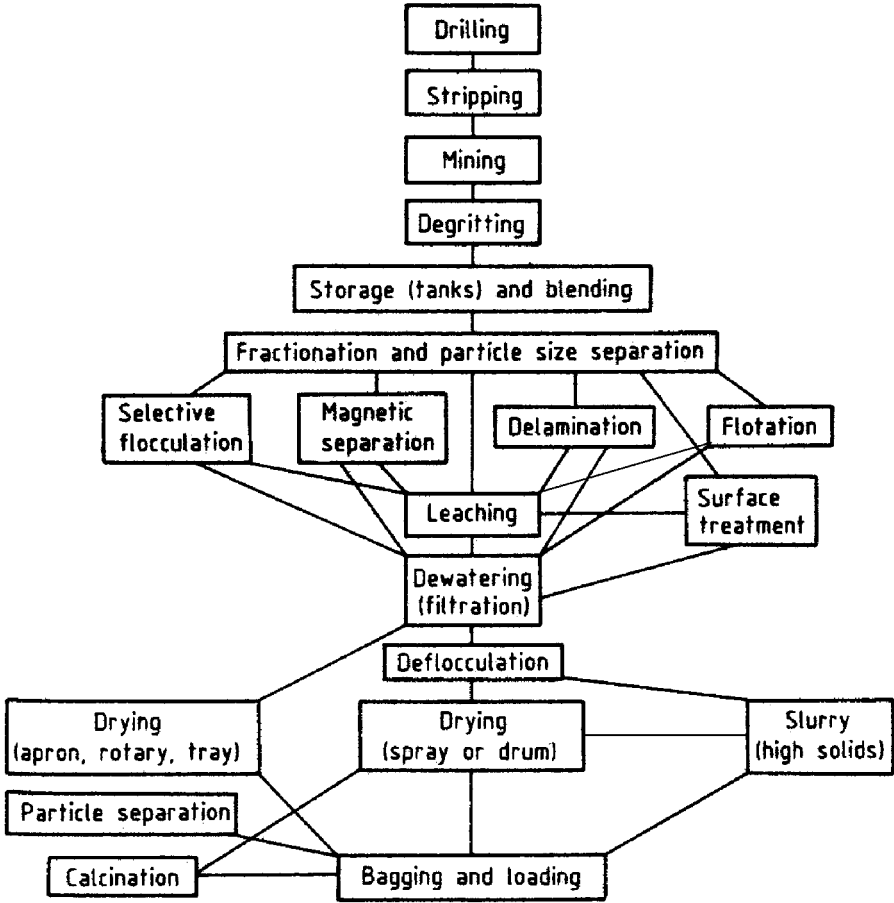


Fig. 10.1.11. Flow sheet showing the various stages and complexities in the modern wet processing of kaolin.



Fig. 10.1.12. Mining and degritting operation in a kaolin mine, Georgia USA.

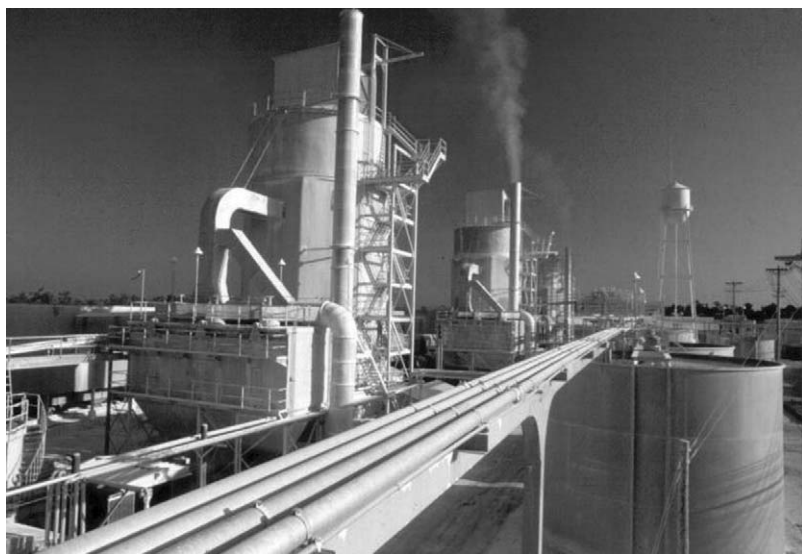


Fig. 10.1.13. A US kaolin processing plant, Georgia, USA.

bentonite is dispersed in water, the degree of delamination is not optimal, and the colloidal properties depend on the amount of soda added (Fig. 10.1.17) (see Chapters 4 and 5). The degree of thixotropy (hysteresis of the flow curves) reaches a maximum as a function of the amount of soda added. The yield value also increases to a



Fig. 10.1.14. Bentonite pit in Bavaria, Germany (Courtesy N. Schall, Süd-Chemie AG, Germany).

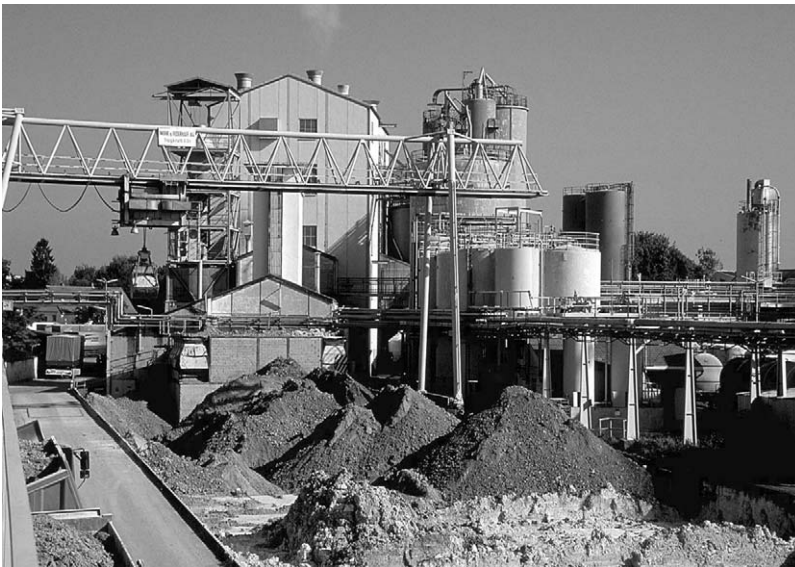


Fig. 10.1.15. Storage of raw bentonite (Courtesy N. Schall, Süd-Chemie AG, Germany).

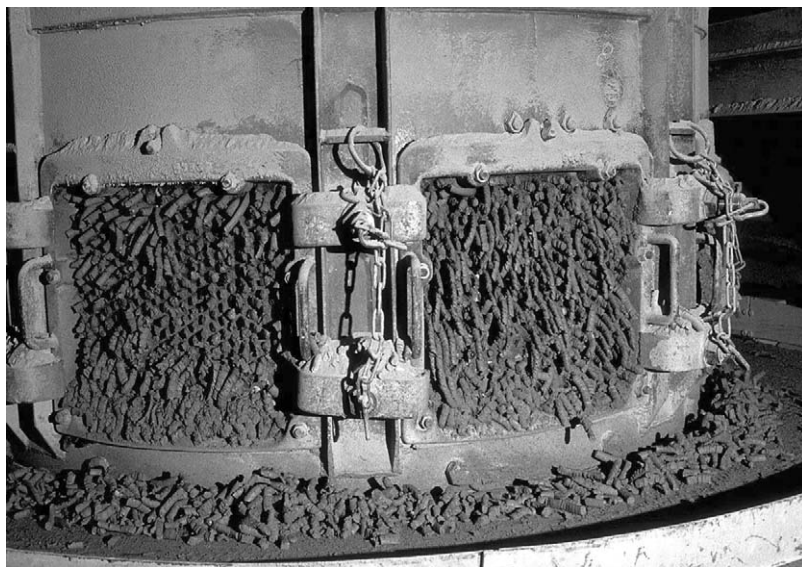
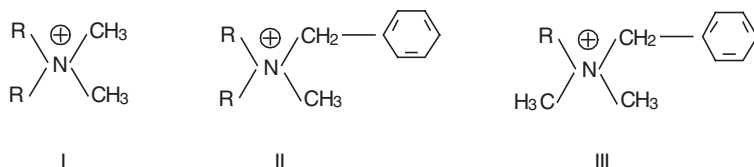


Fig. 10.1.16. Activation of bentonite by kneading with soda (Courtesy N. Schall, Süd-Chemie AG, Germany).

maximum at an optimum addition of soda (Fig. 10.1.18). The properties of bentonites respond differently to soda-activation. This is not only due to differences in particle size distribution between the raw bentonites but also because of differences in layer arrangement within individual montmorillonite particles (see Chapter 5). Domains of silicate layers with a certain degree of ordering are separated by areas of loose contacts ('breaking points'), denoted by arrows in Fig. 10.1.19. Depending on the distribution and the extent of these defects in the parent montmorillonite, soda-activation yields different size distributions of the delaminated particles.

The strong dependence of rheological properties on the  $\text{Na}^+/\text{Ca}^{2+}$  ratio is illustrated in Fig. 10.1.20 (see also Chapter 5). Varying the  $\text{Na}^+/\text{Ca}^{2+}$  ratio is, therefore, an important way to optimize and tailor the properties of soda-activated bentonites for the intended applications.

Many applications, listed in Tables 10.1.2b and 10.1.3, require hydrophobized bentonites. To this end, the bentonite is usually reacted with quaternary alkylammonium salts such as dialkyl dimethylammonium (I), dialkyl benzylmethylammonium (II), and alkyl benzyltrimethylammonium salts (III),



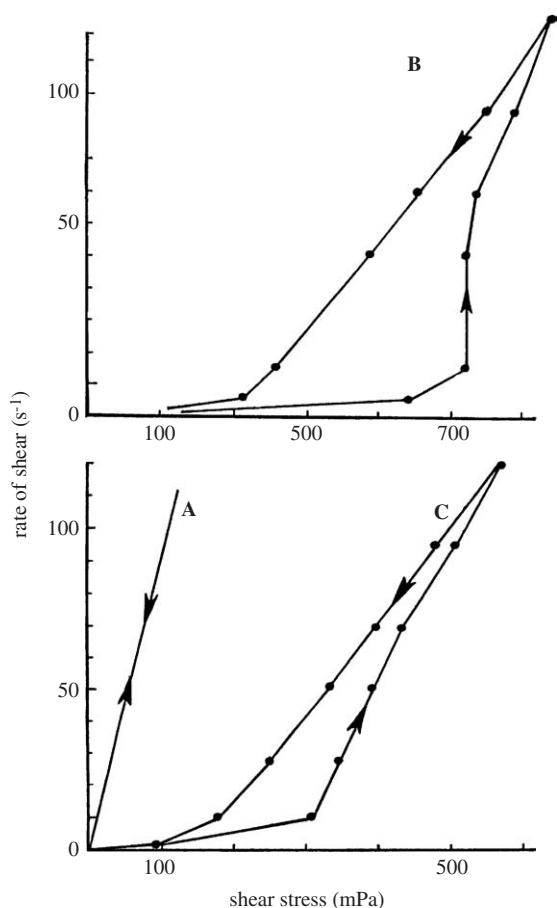


Fig. 10.1.17. Soda-activation of bentonites. Influence of soda addition on the flow behaviour (shear rate vs. shear stress) and thixotropy. 2% dispersions of Amory bentonite (Mississippi, API 22b, Wards). **A** 0.5 mmol Na<sub>2</sub>CO<sub>3</sub>/g bentonite, **B** 2.5 mmol Na<sub>2</sub>CO<sub>3</sub>/g bentonite, **C** 5 mmol Na<sub>2</sub>CO<sub>3</sub>/g bentonite.

The technical products contain alkyl chains (**R**) of different lengths. For instance, a technical dioctadecyl dimethylammonium chloride had the composition (% w/w): 1.5 C<sub>14</sub>, 0.8 C<sub>15</sub>, 27.5 C<sub>16</sub>, 2 C<sub>17</sub>, 67 C<sub>18</sub>, 1.2 C<sub>20</sub> (Favre and Lagaly, 1991). Ditalloyl ammonium salts (derived from by-products of cellulose production from deal and pine wood) are mixtures of dialkyl dimethylammonium surfactants with varied alkyl chain lengths, for instance ~65% C<sub>18</sub>, ~30% C<sub>16</sub> and ~5% C<sub>14</sub>.

The amount of alkylammonium ions added corresponds to the cation exchange capacity (CEC) of the clay, and the exchange is nearly quantitative. Products with smaller amounts of alkylammonium salts can also be obtained.



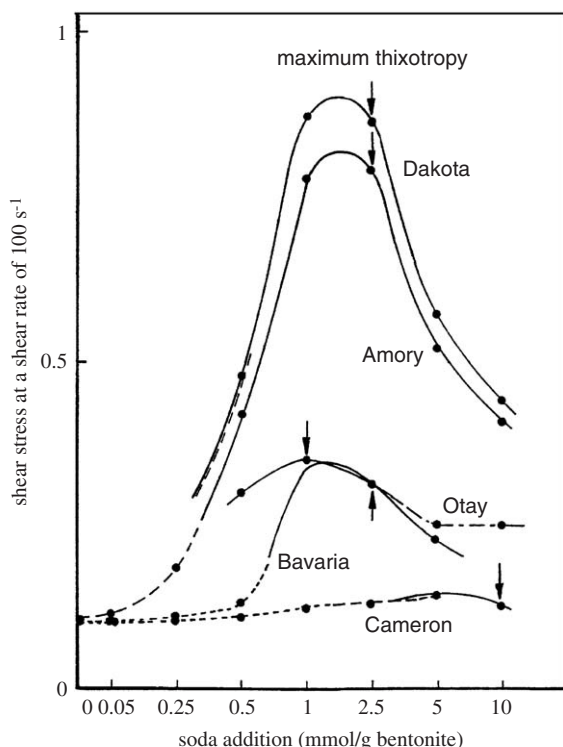


Fig. 10.1.18. Rheological properties of 2% dispersions of different bentonites. The curves show the effect of soda addition on shear stress measured at a rate of shear of  $100 \text{ s}^{-1}$ . Arrows: denote maximum thixotropy. . . . . Newtonian flow, - • - • - (pseudoplastic), — thixotropic, --- antithixotropic. Bentonite from Amory, Mississippi (API 22b, Wards); Bavaria (Schwaiba, Süd-Chemie, Germany); Cameron (Arizona, API 31); Dakota; Otay (California, API 24). From Jasmund and Lagaly (1993).

In most cases the products are not washed after cation exchange so that some free (unreacted) alkylammonium salts may still be present. These free salt influences the properties of the product such as ion-exchange and rheological behaviour (see Fig. 5.43, Chapter 5). The ratio alkylammonium salt/CEC and the treatment of the organo-bentonite after the exchange reaction are parameters that can be used to tailor these products.

Bleaching earths are obtained by treating bentonite with acids in such a way that the layer structure is largely decomposed (see Chapter 7.1). Typically, the bentonite is reacted with hydrochloric acid (up to  $17 \text{ mmol/g}$  bentonite) at  $90\text{--}100^\circ\text{C}$  for a few hours, then washed to reach  $\text{pH} \sim 4$ , dried, milled and sieved (Fig. 10.1.21). Concentration of the acid, temperature and activation time determine the properties of the product (Fahn, 1973). The specific surface area and bleaching activity usually



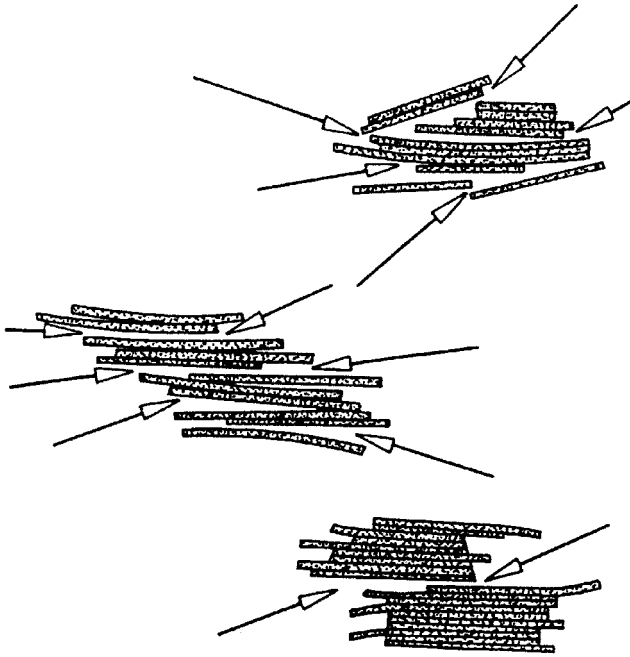


Fig. 10.1.19. Montmorillonite particles with inherent “breaking points” (arrows). From [Jas-mund and Lagaly \(1993\)](#).

show maximum values at distinct activation conditions whereas the pore volume and the silica content increase continuously ([Fig. 10.1.22](#)) ([Fahn, 1973](#); [Christidis et al., 1997](#)). The large volumes of acidic waste waters, containing aluminium salts, that are produced can give rise to environmental problems. Clays of certain localities exhibit similar adsorption properties without acid-activation. Before bleaching earths were produced at an industrial scale, fuller’s earth was used for oil bleaching ([Beneke and Lagaly, 2002](#)).

### 10.1.3. LABORATORY EVALUATION OF CLAY SAMPLES

Any clay material may be recognized by some plasticity in its raw state. Some clay materials may meet the required specifications for industrial uses with no processing or blending with other raw materials. Other clays may be components in simple or complex blends of various raw materials. Other clay raw materials require simple or complex processing to remove contaminants or non-clay minerals.

The assessment of an undeveloped clay resource requires a series of screening techniques by which the clay technician can progressively move towards the

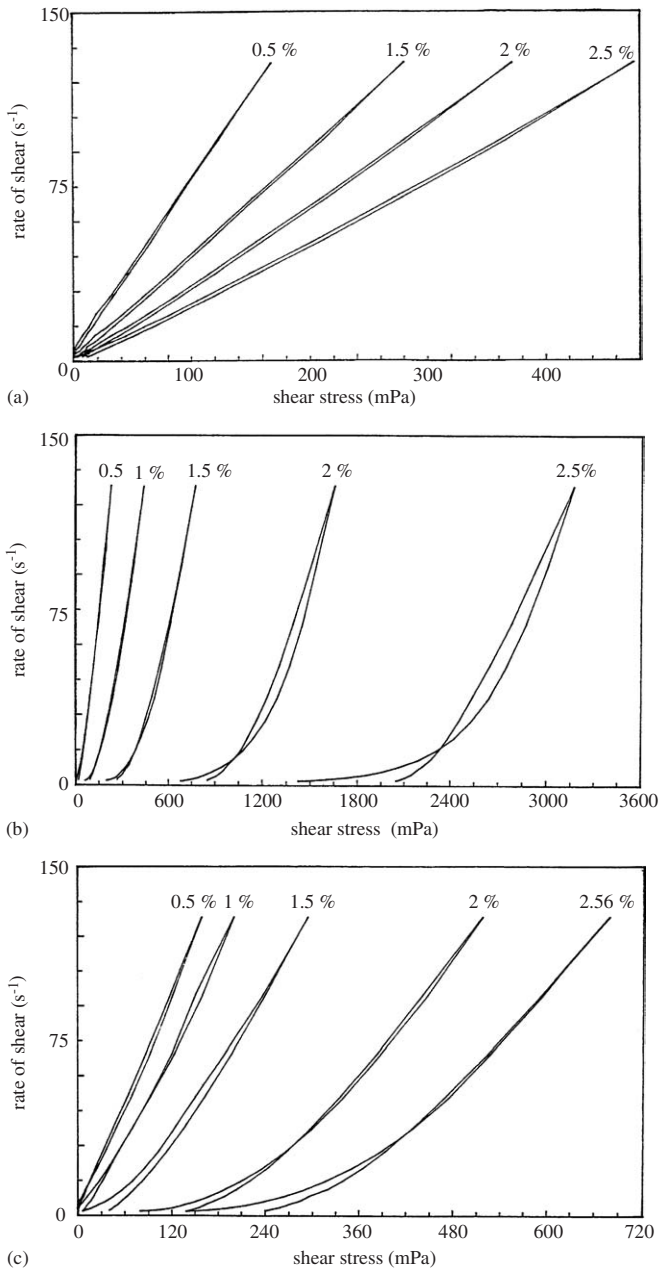


Fig. 10.1.20. Flow curves of sodium bentonite (Bavaria, Germany), (a) in water, (b) in 0.01 M  $CaCl_2$ , (c) in 0.025 M  $CaCl_2$ . Bentonite content 0.5–2.5% (w/w), pH = 6.5, 20 °C. From Permien and Lagaly (1994).



Fig. 10.1.21. Reaction vessels for acid-activation of bentonite (Courtesy N. Schall, Süd-Chemie AG, Germany).

identification of the most suitable uses for the material. The 3 stages involved are summarized below.

Stage 1: screening, consisting of the following steps.

- Step 1 colour
- Step 2 X-ray diffraction analysis
- Step 3 chemical analysis
- Step 4 mineralogical analysis
- Step 5 mineral distribution with particle size

Stage 2: initial testing of industrial properties

- Step 1 Table of industrial properties

Stage 3: Applied testing.

#### 10.1.4. CATEGORIZATION OF CLAY RESOURCES

With the continuing growth in global population, rising urbanization and expanding industrialization there is an ongoing and growing need throughout the world to develop resources of industrial clays. The development of resources in developed countries during the early to middle part of the 20th century typically began on a small scale from a low-technology base with the initial market focus

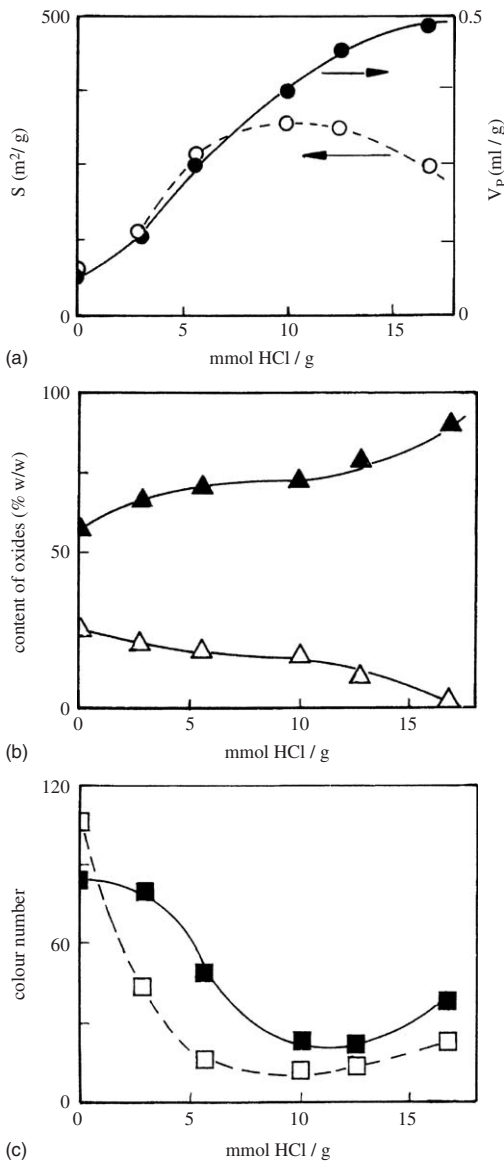


Fig. 10.1.22. Influence of the acid/bentonite ratio on the properties of bleaching earths. (a) Specific surface area  $S$  ( $\circ$ ), pore volume ( $\bullet$ ,  $< 80$  nm diameter), (b) chemical composition,  $\Delta$  content of  $\text{Al}_2\text{O}_3 + \text{Fe}_2\text{O}_3$ ,  $\blacktriangle$  content of  $\text{SiO}_2$ , (c) bleaching (Lovibond colour numbers) of soybean oil ( $\square$ ) and linseed oil ( $\blacksquare$ ). After Fahn (1973). From Jasmund and Lagaly (1993).

towards construction materials or relatively low-quality ceramic products. With increasing levels of industrialization, the level of technology and product sophistication increased with the ultimate objective of achieving high-quality products.

Over the past 20 years, the developed world has seen:

- the exhaustion of many natural resources
- the maturation of low-growth markets
- an increase in environmental constraints
- a rise in labour costs
- a general movement against mining in many countries.

This stimulated interest in the resources of, and encourage investment in, developing countries. In addition, the growth in the gross domestic product (GDP) of many developing nations provided investment capital for the development of their indigenous clay mineral resources.

On the basis of many studies on industrial clay mineral resources carried out in both developed and developing countries, the placement of industrial clays into one of four categories is a useful precursor to undertaking technical and economic evaluations of potential resources. Such categorization also benefits the explorer or developer since it:

- assists in identifying the most suitable development strategy
- provides a general estimate of the time required to move from greenfields development to production
- enables a work programme to be broadly defined
- permits provisional project cost estimates to be made.

#### *A. Categories of Industrial Clays*

Four categories are proposed for industrial clay resources.

- Category 1 clays. These are high-quality, high-technology clays requiring major investment for large tonnage production to supply both local and international markets.
- Category 2 clays. These are unique specialty clays requiring advanced technologies for small tonnage niche markets, locally and internationally.
- Category 3 clays. These include relatively low-technology clay of moderate quality that mainly supply local markets.
- Category 4 clays. These have variable quality. The low-quality materials may justify little or no processing but be suitable for large tonnage local markets. Some category 4 clays may be of moderate to high quality but for one or more reasons be considered non-economic. These reasons may include:
  - isolation from markets
  - politically or economically unstable locations
  - unfavourable legislative environment.

### *B. Examples of Different Categories*

*Category 1.* Currently there are three regions in which Category 1 kaolin clays are produced. These kaolin provinces are:

- (i) the sedimentary kaolins of South-east Georgia, USA
- (ii) the hydrothermal kaolins of Cornwall, England
- (iii) the sedimentary kaolins of the Amazon Basin, Brazil

The limited number of kaolin resources identified in this category confirms the rarity of Category 1 clays presently known on the world scene.

*Category 2.* There are also very few resources that might be classified under Category 2. These are relatively rare, unique resources of somewhat unusual, but valuable industrial clay minerals. Such deposits are typically of high purity and are found in somewhat unique geological settings. Examples include the halloysite deposits of Northland, New Zealand. These deposits of unusually pure halloysite were formed by low temperature hydrothermal alteration of volcanic ash (Harvey and Murray, 1993, Harvey, 1996). It is wet processed and supplied to a unique niche market for high-quality ceramics.

A second example is hectorite, a lithium-rich smectite (bentonite), formed by hydrothermal alteration of basaltic ash containing elevated concentrations of magnesium and lithium. It is wet or dry processed and used in a wide variety of industries (coatings, greases, adhesives and paints) because of its high viscosity, high gel strength and good temperature stability.

A third example is white bentonite which is very rare in nature and command high prices in colloid applications, detergents, pharmaceuticals and ceramics. For some specialty markets, these bentonites may be wet processed or surface-modified to achieve the high quality required for such applications.

*Category 3.* Resources are numerous and widespread. Their specifications are typically not rigid, and the level of processing is only moderate since the market quality requirements and pricing do not justify high processing costs. All of the known Category 1 resources around the world also contain large tonnages of Category 3 clays that are too impure to meet Category 1 requirements. Examples of large exploited resources of Category 3 clays associated with Category 1 clays are the filler kaolins of Georgia, USA and Cornwall, England. Other Category 3 resources contain few if any Category 1 component. These include the kaolin resources of the Czech Republic, Ukraine and Germany; the filler grade kaolins of Indonesia; and the bentonite resources of Wyoming and the southeastern USA.

An example of a Category 3 clay is the Belitung kaolins of Indonesia. During the 1960s and early 1970s these primary kaolins were mined as an adjunct to the associated, highly profitable, tin-mining operations. With the radical drop in tin prices during the 1970s and 1980s more emphasis was placed on the kaolin operations. These clays are currently exploited to supply large ceramic and filler clay markets

within Indonesia and they are also exported to adjacent Asian countries including Taiwan, Japan and Korea.

*Category 4.* Clays exist in all countries of the world and are typically used as mined.

### *C. Role of Categorization in Assessing Industrial Clay Resources*

In any assessment of an industrial clay resource the explorer or developer has to go through the various stages of resource assessment, raw material testing, assessment of product quality, market size and market demand. All these data must then be integrated into a feasibility study which will recommend that the project proceed or be abandoned.

An early classification of materials into one or more of the categories can prove to be a useful precursor to establishing development strategies and likely project costs. Such categorizations can provide a useful insight into the complexities of such studies because the different categories have different requirements with respect to the work programme needed and time frame to reach the feasibility study.

### *D. Relationship between Category and Annual Tonnage*

In any mineral processing operation the term 'benefits of scale' is used to denote that significant economic advantages can be obtained by having larger production volumes and using larger ships. Larger tonnage operations operate with fewer man-hours per ton while capital costs for larger machines are less than the multiples of their relative production capacities. In order to compete on world markets, Category 1 producers must consider the benefits of scale. For example, in the kaolin industry during the 1970s a 100,000 tons per year operation was considered to be a reasonable commercial operation. For the current developments in Brazil, a minimum plant size of 300,000 tons per year is being quoted.

For Category 2 clays the annual tonnage requirement is governed by market size rather than 'benefits of scale'. Annual productions from such processing operations typically fall between 10,000 and 100,000 tons per year. The sizes of Category 3 operations are typically governed by other factors such as market size or accessible market share.

### *E. Relationship between Category and Resource Confidence*

Based on the criteria defined above, the development of a Category 1 resource requires a very high level of confidence in the quality and quantity of the raw material. If a minimum resource life of 20 years is required at 300,000 tons per year, then the resource must be of sufficient size to produce 6 million tons of product. For Category 2 and Category 3 industrial clays the tonnage requirements may be significantly less and resource confidence may be less.

The various levels of resource certainty are internationally recognized in the classification of industrial mineral resources. For resources in Categories 1 and 2 it is essential that the knowledge be at the 'mineable proven resource' stage. For Category 3 resources the resource certainty may be much less, possibly at the 'inferred resource' level or lower.

#### *F. Relationship between Category and Value*

Category 1 kaolin products command the largest tonnage and high added value positions in the industry. Frequently, however, it is the Category 2 products that may command the highest unit value position, although their tonnages may be relatively small. Category 3 kaolins command an intermediate value between Category 1 and Category 4 kaolins.

#### *G. Relationship between Category and Pre-investment Capital*

Category 1 projects require significant pre-investment or 'risk' capital. The level of confidence in the resource and markets has to be very high, requiring a level of investment that may well exceed US\$1 million. The pay-back time for such investments may be at least 5 years, because of the time required to move from reconnaissance through to commissioning (Table 10.1.5). The pre-investment capital requirements for Categories 2, 3 and 4 become progressively lower as you move to the lower category clays.

#### *H. Relationship between Category and Investment Capital*

The investment capital required for large tonnage, high-complexity Category 1 kaolin projects is quoted to be as high as US\$ 300 per processed ton (Pleeth, 1997; Harvey, 1995). For Category 2 kaolins, investment capital costs would depend on the complexity of the process but might range between US\$ 100 and US\$ 500 per processed ton. For Category 3 kaolins, the investment level may be of the order of US \$50 per finished ton.

### 10.1.5. THE RESOURCE EVALUATION PROCESS

The assessor moves progressively through a series of progressively more detailed stages. He/she must first look at surface outcrops, and gain a general appreciation of the regional geology. The variability in the outcrops and any indications of the real extent and depth of the resource are then assessed. The credibility of the guide has also to be assessed at this time by asking the following questions:

- does the person have any idea of what he/she is dealing with?
- is he/she technically competent?



Table 10.1.5. Timetable of activities and investments

Activity	Category 1	Category 2	Category 3	Category 4
Stage I: Reconnaissance Geological reconnaissance, property surveys, testing, broad categorization of materials, market surveys and evaluation				
Decision to proceed	12 months	9 months	6 months	3 months
Stage II: Exploration (pre- feasibility) Property negotiation, drilling, testing, market surveys, precise material characterizations, process flow sheet development, resource calculations, economic studies and evaluation				
Pre-feasibility study and decision to proceed	18–24 months	9 months	9 months	6 months
Stage III: Delineation and feasibility Drilling, testing, market surveys, bulk samples, engineering studies, assessment of products in the marketplace, economic studies and evaluation				
Feasibility study	24 months	12 months	9 months	3 months
Stage IV: Decision to invest	4–5 years	2–2.5 years	2 years	1 year
Total elapsed time since project initiation				
Design, construction and commissioning	1–2 years	1 year	1 year	1 year
Typical overall project time	5–7 years	3–4 years	2–3 years	1 year

- is the quality of the material being overstated or exaggerated?
- based on the work that was done, what level of confidence can be placed on the quality and quantity of the resource.

Other questions that must be addressed are:

- what is the local infrastructure like?
- what local support services are available?

- what is the situation regarding land tenure? For example, In North Vietnam land tenure is relatively straight forward, while in South Vietnam it is a nightmare.
- is a trained workforce available locally?
- if qualified engineers, technologists and managers have to be brought in, could they and their families survive and be content?
- what are the local ground rules for joint ventures, taxation and moving profits offshore?
- All these questions may have a bearing on whether or not a project may be attractive or not.

If, however, the project does progress through to Stage II then the work programme becomes increasingly complex and more costly. It is beyond the scope of this review to discuss this in detail but the programme will include:

- property negotiations
- exploration drilling
- detailed testing (possibly at a site laboratory)
- resource estimates
- detailed market surveys
- product categorization
- preliminary plant design and engineering studies
- preliminary economic studies

All these data are combined into a 'pre-feasibility study' on which to base a decision on whether or not to proceed to Stage III, 'delineation and feasibility'. The Stage III programme includes:

- detailed drilling and delineation of the resource
- detailed testing and resource calculations
- extraction of bulk samples for detailed engineering studies
- pilot scale testing leading to process flow sheet design
- market surveys and market negotiations
- market product testing
- final negotiations for land, leases, joint ventures, etc.
- All these studies culminate in economic studies and a full 'feasibility study'.

#### 10.1.6. OTHER CONSIDERATIONS

##### *A. From Laboratory Scale Testing to Major Plant Scale*

The clay industry has many examples of insufficient scale up factors being applied to basic laboratory data. This ranges from basic recovery figures to assessments of product quality based on too few laboratory test data. For example, losses during commercial plant operations may be much higher than in small-scale laboratory test equipment. A conservative approach to both laboratory and pilot scale test data is essential.

### *B. Level of Applied Technology*

Almost anything can be done with a low-grade clay resource if a sufficient number of applied technologies is ‘thrown’ at it. For example, a wide selection of technologies can be applied to upgrade commercial kaolin resources (Fig. 10.1.11). However, when all the various processes are costed into the operation, the total costs (and process losses) may become prohibitive, effectively constraining development of the resource.

### *C. Losses Associated with Applied Processing Steps*

For each technology introduced into a process there will be process losses. These may range from 2% to much higher values. If, however, we generalize that each process step loses 4% of product, then the effects of multi-stage processing on recoveries may be very significant. Also such losses will be cumulative. For example, a raw material that perhaps has 40% recovery in the laboratory may have say 5 applied technologies incorporated in its process flow sheet. If each technology results in a 4% loss then:

- after technology 1 the recovery dropped from 40% to 38.4%,
- after technology 2, recovery drops to 36.9%;
- after technology 3, recovery drops to 35.4%;
- after technology 4, recovery drops to 34% and
- after technology 5 recovery drops to 32.6%.

Such losses may negatively affect mining costs and overall process profitability.

### *D. Time to Move from Commissioning to Full Production*

Industrial mineral users are often conservative by nature and do not readily accept new products. For example the paper industry is a complex technology and an industrial clay such as kaolin may be just one component in a complex formulation. Purchasing agents have to be convinced that the product is compatible with their formulations and further that the product quality and supply are going to be consistent.

The first stage is to convince a company to trial your product. To reach this stage it will be necessary to convince the company of both the quality, consistency and value of your product over and above the quality of his existing supplier. In such cases it may be necessary to compete on the basis of:

- higher quality
- lower price
- better continuity
- better technical support.

Even with such strengths, however, the new player in the marketplace still has to deal with buyer conservatism. Therefore the rate at which a product is accepted may be a combination of good fortune or even luck. For some products it may take years

to gain full market acceptance. For example, recent developments of Category 1 kaolin resources in Brazil (Pleeth, 1997) quote time intervals of at least 5 years to move from initial exploration through to commissioning.

#### *E. Reducing Risk during Development*

There are several techniques or procedures for minimizing risk and shortening the time necessary to establish Category 1 or Category 2 ventures:

- associate, or form a joint venture, with established producers in the industry
- associate, or form a joint venture, with major market users of the product
- engage specialist consultants for resource evaluation, market surveys, etc.
- develop resources adjacent to proven established resources.

### 10.1.7. CONCLUSIONS

This review of conventional applications of clay minerals illustrates the great diversity in compositions and properties of clay minerals and the even greater ranges of processes and products in which they may be used.

Clay minerals may be utilised in their as-mined state, as low-cost impure materials because of their engineering, physical and or chemical properties. Indeed, in archaeology, clay utilization became recognized as a means of identifying early human progress and development.

At the other end of the spectrum, refined high-purity clay minerals play an integral part in the highest technological achievements of man including space capsules, pharmaceuticals, medicine and catalysis.

### REFERENCES

- Abend, S., Bonnke, N., Gutschner, U., Lagaly, G., 1998. Stabilization of emulsions by heterocoagulation of clay minerals and layered double hydroxides. *Colloid and Polymer Science* 276, 730–737.
- Abend, S., Lagaly, G., 2001. Bentonite and double hydroxides as emulsifying agents. *Clay Minerals* 36, 557–570.
- Beneke, K., Lagaly, G., 2002. From fuller's earth to bleaching earth: a historical note. *ECGA Newsletter* 5, Verlag R. Knof, Nehnten, Germany, pp. 57–78.
- Bergaya, F., Beneke, K., Lagaly, G., 2001. History and perspectives of clay science. *ECGA Newsletter* 4, Verlag R. Knof, Nehnten, Germany, pp. 5–41.
- Böhnlein-Mauß, J., Sigmund, W., Wegner, G., Meyer, W.H., Heßel, F., Seitu, K., Roosen, A., 1992. The function of polymers in the tape casting of alumina. *Advanced Materials* 4, 73–81.
- Bundy, W.M., 1993. The diverse industrial applications of kaolin. In: Murray, H.H., Bundy, W.M., Harvey, C.C. (Eds.), *Kaolin Genesis and Utilization*, The Clay Minerals Society. Boulder, CO, pp. 43–73.

- Caine, M., Dyer, G., Holder, J.V., Osbourne, B.N., Mear, W.A., McCabe, R.W., Mobbs, D., Richardson, S., Wang, L., 1999. The use of clays as sorbents and catalysts. In: Misaelides, P., Macasek, F., Pinnavaia, T.J., Colella, C. (Eds.), *Natural Microporous Materials in Environmental Technology*. NATO Advanced Research Workshop, Smolenice Castle, Slovakia, 26–30 October 1998, NATO Science Series 362. Kluwer Academic Publishers, Dordrecht, 49–69.
- Christidis, G.E., Kosiari, S., 2003. Decolorization of vegetable oils: a study of the mechanism of adsorption of  $\beta$ -carotene by an acid-activated bentonite from Cyprus. *Clays and Clay Minerals* 51, 327–333.
- Christidis, G.E., Scott, P.W., Dunham, A.C., 1997. Acid activation and bleaching capacity of bentonites from the islands of Milos and Chios, Aegean, Greece. *Applied Clay Science* 12, 329–347.
- Darley, H.C.H., Gray, G.R., 1991. *Composition and Properties of Drilling and Completion Fluids*, 5th edition. Gulf Publishing Company, Houston.
- Erdoğan, B., Demirci, S., Akay, Y., 1996. Treatment of sugar beet juice with bentonite, sepiolite, diatomite and quartz to remove color and turbidity. *Applied Clay Science* 11, 55–67.
- Fahn, R., 1963. Innerkristalline Quellung und Farbstoffadsorption säurebehandelter Montmorillonite. *Kolloid-Zeitschrift und Zeitschrift für Polymere* 187, 120–127.
- Fahn, R., 1973. Einfluß der Struktur und der Morphologie von Bleicherden auf die Bleichwirkung bei Ölen und Fetten. *Fette, Seifen, Anstrichmittel* 75, 77–82.
- Fahn, R., Fenderl, K., 1983. Reaction products of organic dye molecules with acid-treated montmorillonite. *Clay Minerals* 18, 447–458.
- Fahn, R., Schall, N., 1985. Über die Verwendung von Bentoniten in Wasch- und Reinigungsmitteln. *Tenside Detergents* 22, 57–61.
- Falaras, P., Kovanis, I., Lezou, F., Seiragakis, G., 1999. Cottonseed oil bleaching by acid-activated montmorillonite. *Clay Minerals* 34, 221–232.
- Falaras, P., Lezou, F., Seiragakis, G., Petrakis, D., 2000. Bleaching properties of alumina-pillared acid-activated montmorillonite. *Clays and Clay Minerals* 48, 549–556.
- Favre, H., Lagaly, G., 1991. Organo-bentonites with quaternary alkylammonium ions. *Clay Minerals* 26, 19–32.
- Galán, E., 1996. Properties and applications of palygorskite-sepiolite clays. *Clay Minerals* 31, 443–453.
- Grim, R.E., 1962. *Applied Clay Mineralogy*. McGraw-Hill, New York.
- Grim, R.E., 1968. *Clay Mineralogy*, 2nd edition. McGraw-Hill, New York.
- Groudeva, V.I., Groudev, S.N., 1995. Microorganisms improve kaolin properties. *American Ceramic Society Bulletin* 74, 85–89.
- Harvey, C.C., Murray, H.H., 1993. The geology, mineralogy and exploitation of halloysite clays of Northland, New Zealand. In: Murray, H.H., Bundy, W.M., Harvey, C.C. (Eds.), *Kaolin Genesis and Utilization*. The Clay Minerals Society.
- Harvey, C.C., 1995. Kaolin resources of the United States and their industrial utilization. *Proceedings of the 1993 UN Workshop for Industrial Minerals Development in Asia and the Pacific*, vol. 8, pp. 252–265.
- Harvey, C.C., 1996. Halloysite for high quality ceramics. In: Kendall, T. (Ed.), *Industrial Clays*, 2nd edition. Industrial Minerals Information Ltd., London, pp. 71–73.

- Harvey, C.C., 1997. Kaolinite and halloysite ASEAN resources and trade. *Industrial Minerals* 356, 55–59.
- Harvey, C.C., Murray, H.H., 1997. Industrial clays in the 21st century: a perspective of exploration, technology and utilization. *Applied Clay Science* 11, 285–310.
- Hofmann, U., 1962a. Die chemischen Grundlagen der griechischen Vasenmalerei. *Angewandte Chemie* 74, 397–442.
- Hofmann, U., 1962b. Die Tonminerale und die Plastizität des Tons. *Keramische Zeitschrift* 14, 14–18.
- Hofmann, U., Endell, K., 1935. British Patent 447710.
- Hofmann, U., Endell, K., 1936. British Patent 458240.
- Jasmund, K., Lagaly, G. (Eds.), 1993. *Tonminerale und Tone. Struktur, Eigenschaften, Anwendung und Einsatz in Industrie und Umwelt*. Steinkopff Verlag, Darmstadt.
- Jepson, W.B., 1984. Kaolins: their properties and uses. *Philosophical Transactions of the Royal Society of London A* 311, 411–432.
- Jones, T.R., 1983. The properties and uses of clays which swell in organic solvents. *Clay Minerals* 18, 399–410.
- Jovanović, N., Janacković, J., 1991. Pore structure and adsorption properties of an acid-activated bentonite. *Applied Clay Science* 6, 59–68.
- Jozefaciuk, G., Bowanko, G., 2002. Effect of acid and alkali treatments on surface areas and adsorption energies of selected minerals. *Clays and Clay Minerals* 50, 771–783.
- Klose, D., 1982. *Natürliche Silikate*. Ullmanns Encyklopädie der technischen Chemie, vol. 21. Verlag Chemie, Weinheim, pp. 376–408.
- Krøyer, H., Lindgreen, H., Jakobsen, H.J., Skibsted, J., 2003. Hydration of Portland cement in the presence of clay minerals studied by  $^{29}\text{Si}$  and  $^{27}\text{Al}$  MAS NMR spectroscopy. *Advances in Cement Research* 15, 103–112.
- Lagaly, G., 1999. Introduction: from clay mineral-polymer interactions to clay mineral-polymer nanocomposites. *Applied Clay Science* 15, 1–9.
- Lagaly, G., Fahn, R., 1983. Tone und Tonminerale. In: *Ullmann's Encyclopedia of Technical Chemistry*. 4th edition. vol. 23. Verlag Chemie, Weinheim, pp. 311–326.
- Lagaly, G., Reese, M., Abend, S., 1999a. Smectites as colloidal stabilizers of emulsions I. Preparation and properties of emulsions with smectites and nonionic surfactants. *Applied Clay Science* 14, 83–103.
- Lagaly, G., Reese, M., Abend, S., 1999b. Smectites as colloidal stabilizers of emulsions II. Rheological properties of smectite-laden emulsions. *Applied Clay Science* 14, 279–298.
- Lagaly, G., Schulz, O., Zimehl, R., 1997. *Dispersionen und Emulsionen. Eine Einführung in die Kolloidik feinverteilter Stoffe einschließlich der Tonminerale*. Mit einem historischen Beitrag über Kolloidwissenschaftler von Klaus Beneke. Steinkopff Verlag, Darmstadt.
- Lee, E.Y., Cho, K.-S., Ryu, H.W., 2002. Microbial refinement of kaolin by iron-reducing bacteria. *Applied Clay Science* 22, 47–53.
- Li, J., Tanguy, P.A., Carreau, P.J., Moan, M., 2001. Effect of thickener structure on paper-coating color properties. *Colloid Polymer Science* 279, 865–871.
- Mahjoory, R.A., 1996. Occurrence and mineralogy of a deposit of shampoo-clay in southern Iran. *Applied Clay Science* 11, 69–76.
- Mokaya, R., Jones, W., Davies, M.E., Whittle, M.E., 1994. The mechanism of chlorophyll adsorption on acid-activated clays. *Journal of Solid State Chemistry* 111, 157–163.

- Murray, H.H., 1986. Clays. In: Ullmann's Encyclopedia of Industrial Chemistry, vol. A7. VCH, Weinheim, pp. 109–136.
- Murray, H.H., 1999. Applied clay mineralogy today and tomorrow. *Clay Minerals* 34, 39–49.
- Murray, H.H., 2000. Traditional and new applications for kaolin, smectite, and palygorskite: a general overview. *Applied Clay Science* 17, 207–221.
- Murray, H.H., 2003. Clays in industry. In: Dominguez, E.A., Mas, G.R., Cravero, F. (Eds.), 2001. *A Clay Odyssey*. Proceedings of the 12th International Clay Conference. Elsevier, Amsterdam, pp. 3–14.
- Noll, W., 1982. Antique ceramic decoration techniques. *Berichte der Deutschen Keramischen Gesellschaft* 59, 17–25.
- Noll, W., 1991. *Alte Keramiken und ihre Pigmente*. Schweizerbart'sche Verlagsbuchhandlung Nägeli und Obermiller, Stuttgart.
- Odom, E., 1984. Smectite clay minerals: properties and uses. *Philosophical Transactions of the Royal Society of London A* 311, 391–409.
- Panpanit, S., Visvanathan, C., 2001. The role of bentonite addition in UF flux enhancement mechanisms for oil/water emulsion. *Journal of Membrane Science* 184, 59–68.
- Permien, T., Lagaly, G., 1994. The rheological and colloidal properties of bentonite dispersions in the presence of organic compounds. II. Flow behaviour of Wyoming bentonite in water-alcohol. *Clay Minerals* 29, 761–766.
- Philippakopoulou, T., Simonetis, S., Economides, D., 2003. The use of bentonites in newspaper recycling. Part 2: Influence on wash deinked and post-bleached pulp optical properties. *Appita Journal* 56, 284–289.
- Pleeth, A., 1997. Forecasting for greenfield kaolin projects. *Industrial Minerals* 352, 59–63.
- Rankine, B., 1995. *Making Good Wine: A Manual of Winemaking Practices for Australia and New Zealand*. Sun Books, Melbourne.
- Ravichandran, J., Sivasankar, B., 1997. Properties and catalytic activity of acid-modified montmorillonite and vermiculite. *Clays and Clay Minerals* 45, 854–858.
- Robertson, R.H.S., 1986. *Fuller's Earth: A History of Calcium Montmorillonite*. Volturna Press, Hythe, Kent.
- Sarier, N., Güler, C., 1988. The mechanism of  $\beta$ -carotene adsorption on activated montmorillonite. *Journal of the American Oil Chemists' Society* 66, 917–923.
- Sarmiento, M.R., Oliveira, J.C., Boulton, R.B., 2000. Selection of low swelling materials for protein adsorption from white wines. *International Journal of Food Science and Technology* 35, 41–47.
- Schall, N., 1988. Bentonite. Wechselwirkungen von kationischen und anionischen Tensiden in Gegenwart von Bentonit. *Tenside Surfactants Detergents* 25, 14–20.
- Srasra, E., Bergaya, F., van Damme, H., Ariguib, N.K., 1989. Surface properties of an activated bentonite-decolorisation of rape-seed oils. *Applied Clay Science* 4, 411–421.
- Theng, B.K.G., Wells, N., 1995. Assessing the capacity of some New Zealand clays for decolourizing vegetable oil and butter. *Applied Clay Science* 9, 321–326.
- van Olphen, H., 1977. *An Introduction to Clay Colloid Chemistry*, 2nd edition. Wiley, New York.
- von Liebig, J., 1865. *Chemische Briefe*. 35. Brief, C. F. Winkler'sche Verlagshandlung, Leipzig.

*Chapter 10.2*

## CLAY MINERALS AS CATALYSTS

J.M. ADAMS<sup>a</sup> AND R.W. McCABE<sup>b</sup>

<sup>a</sup>*School of Engineering, University of Exeter, Harrison Building, North Park Road, Exeter, Devon, EX4 4QF, UK*

<sup>b</sup>*Center for Materials Science, University of Central Lancashire, Preston PR1 2HE, United Kingdom*

In most petrochemical processing, such as cracking, solid catalysts were used for decades. Originally, the catalysts were based on acid-treated clays (Franz *et al.*, 1959) but, for many years now, framework silicates (zeolites) proved more effective and selective.

Established manufacturing processes for other organic chemicals are, however, still largely based on stirred tank reactors and out-dated methods, employing volatile solvents, stoichiometric reagents and hazardous chemicals. The processes are often inefficient and produce large volumes of waste (commonly 10–50 times product). Heterogenisation is one of the most important of the new clean technologies, which are being developed to reduce waste in liquid phase organic reactions. If the catalyst or reagent stays in a separate, solid phase then a water quench phase (the source of much of the waste) is unnecessary. Additional benefits of this approach include avoiding solvent (a heterogeneous catalyst or reagent can act as a solid solvent) and enhancing selectivity (due to pore constraints).

In order to exploit this exciting, greener technology in organic chemical manufacturing, we need to produce highly effective catalysts in flexible physical forms to suit a multitude of chemical process technologies. Zeolites have attractions but are limited in the size of molecule they can accommodate in their limited-size pores. Mesoporous silicas, on the other hand, have suitable pore sizes, but lack chemical activity.

Clay minerals have a different and interesting set of properties. They are very effective catalysts for a wide variety of organic reactions, often displaying highly sought product-, regio- or shape-selectivity. In addition, however, “soft” dimensional



constraints are often displayed. They have significant potential in organic chemical processing. Their potential was not realised, we believe, because:

- (1) The variability of natural clays, the wide variety of clay mineral types and the range of possible treatments meant that a reliable set of data on which predictive capability can be based was not generated: there have been too many restricted studies which do not link together.
- (2) Not enough attention was given to the engineering of the clays into catalyst particles, pellets, membranes, etc. so that they can survive the rigorous conditions in a range of reactor types. The changes in interlayer spacing, which occur with exposure to reactants/solvents/products makes this particularly challenging, affecting the mechanical integrity of any catalyst “artefact”.

Here, we confirm the range of catalytic options provided by clay minerals. We hope that the phenomenal range of activity displayed will encourage dedicated study to overcome the issues above.

Previous reviews in the area included those by Theng (1974, 1982), Solomon and Hawthorne (1983), Laszlo (1986a), Adams (1987) and McCabe (1996).

Early work with clays concentrate either on acid treatment or on cation exchange to increase Brønsted or Lewis acidity. However, in the last few years, the reaction portfolio widened so that clay minerals are now recognised (McCabe, 1996) as effective for a range of other types of reaction including redox reactions, reactions involving reactive intermediates and cycloadditions (such as Diels–Alder reactions). The high surface area of clays also means that they can act as effective supports for (usually inorganic) reagents bringing the benefits of heterogeneous catalysis to several important reactions.

The benefit of previous reviews allows us to focus on material most relevant to green/clean technologies. This chapter focuses on smectites and their derivatives, which display by far the highest activity levels and range of reactions catalysed. After a short discussion of the origins of the activity of these clay minerals, the authors summarized the performance in different types of reaction. Finally, they covered the more important recent developments and commented on current utilisation of these clays in industrial processes and prospects for the future.

### 10.2.1. ORIGIN OF ACTIVITY

#### *A. Low Dimensionality*

Laszlo (1987) made the point elegantly that not only is the activity of clay minerals a consequence of their high surface area and chemical nature: there are two other closely related factors:

- (1) Local concentration effects—the act of adsorption on the solid surface increases the reactant concentrations.

- (2) Low dimensionality ( $<3$ ) of the clay minerals means that molecules on the surface are more likely to meet (drunkards walk) than they would be in three dimensions. Both factors lead to enhanced collision frequency and, hence, reactivity.

### B. Structural Characteristics Imparting Activity

Most of the reactions catalysed by smectites make use of the acidic nature of acid-treated or cation-exchanged clay minerals. Both Lewis and Brønsted activity are common, the former deriving from aluminium or iron species located at crystal edges (see Chapters 5 and 7.3) (Theng, 1974). The Brønsted activity, however, results either from free acid (in some acid-activated clays) or from the dissociation of interlayer water molecules coordinated to polarising interlayer cations ( $M^{m+}$ ). It was shown (see, e.g., Mortland and Raman, 1968) that acidity in the latter case increases at low water contents and is enhanced when using interlayer cations of high charge and small radius such as  $Al^{3+}$ ,  $Fe^{3+}$  or  $Cr^{3+}$ :



where B is water or an organic species in the interlayer space.  $H_3O^+$  or the protonated base are available for further reaction. Weiss (1981) suggested that interlayer  $H^+$  concentrations could be as high as 10 M in some cases.

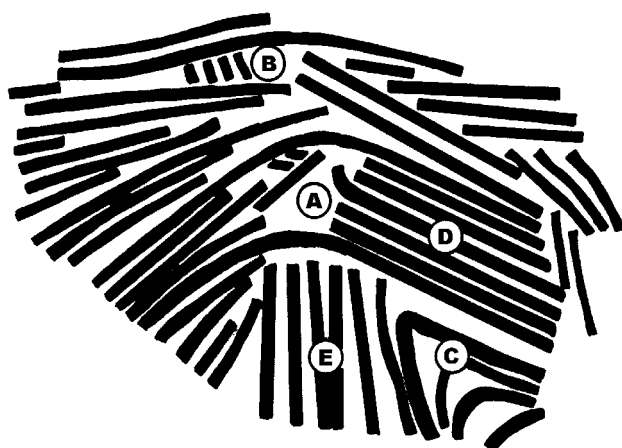
For acid-activated clays (see Chapter 7.1) a significant amount of the activity derives from  $Al^{3+}$  or  $Fe^{3+}$  ions which have been liberated from the octahedral sheet and relocated to crystal edges or into the interlayer region (Fahn and Fenderl, 1983). In this case, also, there is an enhancement of activity deriving from increased surface area (up to  $300\text{ m}^2\text{ g}^{-1}$ , Süd-Chemie, 1961).

Increases in Lewis acidity at room temperature were made by depositing Lewis acids such as  $ZnCl_2$  (clayzic) and  $AlCl_3$  onto clay mineral surfaces (Clark et al., 1994). Activity is enhanced by synergistic effects with the clay, and the Lewis acidity of the supported salt is often greater than would be expected (e.g., clayzic  $>$  clay/ $AlCl_3$ ).

Redox reactivity can be derived from either  $Fe^{2+}$  or  $Fe^{3+}$  in the octahedral sheet (Solomon et al., 1968), from exchange of redox-active cations such as  $Cu^{2+}$ ,  $Fe^{2+}$  or  $Fe^{3+}$  into the interlayer region (Caine, 1999) or by depositing anhydrous metal nitrates on the clay support (e.g., claycop and clayfen, Laszlo (1987)).

### C. Shape/Size Selectivity

Smectites ideally consist of regular, parallel layers. The reality is somewhat different (see Fig. 10.2.1 from Cebula et al., 1979). Nonetheless, if we consider the energy required to separate the “parallel” layers, it depends upon electrostatic and van der Waals components (Lee et al., 1987). For a given set of reaction conditions (reactant concentrations, solvent, temperature, etc.) the interlayer spacing will be set by the



**A = voids   B = edge to face stacking**  
**C = gross folding region**  
**D = ordered domain   E = disordered stacking**

Fig. 10.2.1. Schematic structure of a clay: water system.



Fig. 10.2.2. For intercalation to occur, the energy gain on intercalation  $\geq$  that required to separate layers.

balance between energy gained by intercalation (usually coordination around the interlayer cation) and that required to separate the layers (Fig. 10.2.2), thus giving, in effect, a soft constraint to reaction geometry. In principle, these clay minerals can accommodate larger molecules between their layers than do relatively rigid framework silicates (zeolites).

If catalytic properties of clays and zeolites are compared, the activity of acid-treated or cation-exchanged clays are relatively poor at temperatures above 150 °C, a result of dehydration and collapse of the clay layers. To overcome this problem, the so-called pillared clays were produced. These materials use inorganic cations to prop the layers apart (Vaughan et al., 1979; Pinnavaia, 1986; Poncelet and Schutz, 1986) and have the advantage that the pillar itself may be catalytically active (see, e.g., Suib et al., 1986). Pillaring also confers some degree of size/shape selectivity (e.g., Kikuchi and Matsuda, 1988).

### D. Catalysis of Inorganic Reactions

Clay minerals are well-known catalysts for organic reactions, but recently they were shown to catalyse the equation of  $[\text{Cr}(\text{H}_2\text{O})_4\text{Cl}_2]^+$  to  $[\text{Cr}(\text{H}_2\text{O})_5\text{Cl}]^{2+}$  and  $[\text{Cr}(\text{H}_2\text{O})_6]^{3+}$  (Caine et al., 1999). Normally, these reactions are quite slow (weeks), as the  $d^3$  chromium (III) cations have a half  $t_{2g}$  sub-shell and are substitutionally inert. However, intact (not acid activated) clays, along with alumina and zeolites, catalyse these reactions in a matter of minutes or hours. The catalytic reaction appears to be dissociative and aided by conjugate base formation, i.e.,  $S_N1CB$  (Mao, 2003). Thus, unusually, the clay minerals appear to be acting as *base* catalysts by exchanging protons from solution. Similar results are being found with other chromium (III) halide complexes and with even more inert Co(III) complexes ( $d^6$ -filled  $t_{2g}$  sub-shell). Improved yields of sodium or potassium *tris*-oxalatochromate(III) (3–4 fold) and *tris*-ethylenediaminechromium(III) chloride (1.5-fold) complexes were found using powdered Surrey bentonite (Mao, 2003).

### E. Clays as Supports for Reagents

Clays provide high surface area on which to support reactive compounds. They can also provide (see above) a variety of types of active sites, which can be co-active with the supported reagent. A surge of interest in the area in the 1990s used “claycop” and “clayfen” for selective oxidations (e.g., Cornelis and Laszlo, 1986). Very high acidities can be achieved by supporting superacids and heteropolyacids on clays (e.g., Knifton and Edwards, 1999).

## 10.2.2. PREPARATION/ACTIVATION OF CLAY CATALYSTS

To achieve the highest activity, the smectite component needs to be separated from the impurities in the mineral ore, usually by sedimentation/size fractionation (see Chapter 4).

Cation exchange of smectite is usually carried out by exposing the clay to an appropriate salt solution of  $\sim 0.5$ – $1$  M for 24 h. The clay can then be centrifuged and re-suspended repetitively to remove excess exchangeable cation before drying at  $40$ – $50^\circ\text{C}$  and fine grinding (see Chapter 4).

Commercial acid treatment is carried out using concentrated hydrochloric, sulphuric or phosphoric acids. The concentration of the acid and the treatment time varies between producers and products, as does the removal of excess acid or otherwise by washing (see Chapters 7.1 and 10.1). There is, therefore a great variety of products available (e.g., Fahn, 1979, and commercial literature such as that from Süd Chemie).

Ion exchange of montmorillonites with cations such as:  $\text{Al}^{3+}$ ,  $\text{Fe}^{3+}$ ,  $\text{Cu}^{2+}$ ,  $\text{Zn}^{2+}$ ,  $\text{Ni}^{2+}$ ,  $\text{Co}^{2+}$  and  $\text{Na}^+$  can modify the catalytic activities of the clay catalyst.

For example, the rearrangement of  $\alpha$ -pinene to camphene and the rearrangement of camphene hydrochloride to isobornyl chloride were used to determine the catalyst's Brønsted and Lewis acid strengths, respectively (Brown and Rhodes, 1997). Thermal activation of the catalyst is also important with maximum Brønsted acidity developing at approximately 150 °C and maximum Lewis acidity at 250–300 °C. Significantly,  $\text{Al}^{3+}$ -exchanged clay minerals demonstrate relatively low surface Lewis acidity. Metal oxide pillared clay (PILC) possesses several interesting properties, such as large surface area, high pore volume and tunable pore size (from micropore to mesopore), high thermal stability, strong surface acidity and catalytic active substrates/metal oxide pillars. These unique characteristics make PILC an attractive material in catalytic reactions (Klopprogge, 1998; Ding et al., 2001; Vansant and Cool, 2001). The activity and porosity of the PILC are highly dependent on the method of preparation (Salerno et al., 2001; Sapag and Mendioroz, 2001).

The surface acidity of alumina- and double-pillared montmorillonite and saponite was studied by ammonia TPD, *iso*-propanol conversion and *n*-butene skeletal isomerisation catalysis and by FTIR spectroscopy of the surface hydroxy-groups, and of adsorbed acetonitrile and pivalonitrile (Trombetta et al., 2000). The alumina pillars in montmorillonite carry stronger Lewis sites than those of pillared saponite. Stronger Brønsted sites occur on the montmorillonite layers and the pillared montmorillonite is more active in converting *iso*-propanol. However, it is too active in converting *n*-butene, giving rise to faster coking and more extensive cracking; thus, the pillared saponite was more selective for converting *n*-butene into *iso*-butene.

Heating cation-exchanged or acid-treated clay minerals leads to loss of inter-layer water. For clay minerals exchanged with monovalent cations, heating much above 100 °C leads to a decrease in interlayer spacing, after which re-expansion is difficult. For higher charged cations, the greater stability of the primary coordination sphere means that the layers do not collapse completely, even at 300 °C. Breen et al. (1987) showed that excessive heating can lead to a reduction in reactivity. PILCs are much more thermally stable and can be pre-conditioned at 500–600 °C if required.

Since the reactivity of smectites depends so critically on water content (Mortland and Raman, 1968) to attain reproducibility in the rate of reactions carried out at low temperatures, it is essential to equilibrate the clay at a known relative humidity before reaction (Adams, 1987). Finally, while solvents in clay-catalysed reactions are often chosen for their reflux temperature or for solubility reasons, it is known that even allowing for these factors, alteration of solvent can lead to extreme variation in reactivity (e.g., Adams et al., 1983a).

Three main strategies are employed with supported reagents/catalysts (McCabe, 1996): (a) deposition of a large excess of reagent from solution onto the clay; (b) heterogenisation of small amounts of expensive catalyst by sorption onto the clay; and (c) covalent bonding of the catalyst to the clay mineral surface.

### 10.2.3. SUMMARY OF CATALYTIC ACTIVITY

The diverse catalytic activity of clay minerals is derived mainly from four main sources, Brønsted acidity, Lewis acidity, presence of redox active species and introduction of catalytically active (mainly) transition metals or cations. Such activity can be either a natural property of the clay or can be introduced by cation exchange, acid activation or deposition of the co-catalyst onto the clay surface.

The expandable layers of clay minerals provide useful two-dimensional hosts, which facilitate introduction of catalytically active metal complexes by cation exchange and ligand exchange methods (Tao and Zou, 2002). Intercalation of metal complexes into the interlayer space of clay minerals is an excellent method for homogeneous catalyst heterogenisation. Metal complex catalysts intercalated into clay minerals display molecular-recognising catalysis, such as shape selectivity, stereoselectivity and regio-selectivity. The application of these heterogenised catalysts in asymmetric hydrogenation, regioselective hydrogenation, regioselective carbonylation and stereoselective arylation is described below. Metal complex catalysts intercalated into clay minerals exhibit sufficiently high activity and selectivity to make them competitive to the homogeneous catalysts.

#### *A. Brønsted Acid Catalysis*

The inherent Brønsted acidity of cation-exchanged clays can be used to catalyse a very large number of organic reactions (Table 10.2.1); they are often clean, high yielding and offer routes to products that are inaccessible or difficult to obtain by other, more conventional means. The reactivity arises from dissociation of interlayer water molecules and reaction in the interlayer space often leads to shape selectivity in terms of reactants or products.

Adams et al. (1983a) produced a set of guidelines concerning Brønsted reactivity of cation-exchanged clay minerals which covered:

- reaction site (interlayer space for unsaturated hydrocarbons; interlayer space and surface for polar, oxygenated species);
- effective interlayer cations ( $\text{Cr}^{3+}$  and  $\text{Fe}^{3+}$  most active and reproducible);
- solvent (in liquid phase, when low acidity is satisfactory, solvent should be chosen for miscibility; when higher acidity is required, a non-polar solvent is more efficacious); and
- type of carbocations involved (below 100 °C, tertiary or allylic; at 150–180 °C, primary or secondary carbocations could be involved).

Laszlo (1986b) subsequently pointed out that primary carbocations are probably not involved, and that by 150 °C benzyl carbocations probably would be involved, where relevant.

While interest in clay minerals for coupling amino acids to give polypeptides continues (Bujdák and Rode, 1996, 1997, 1999; Bujdák, et al., 1996; Rode, 1999; Rode et al., 1999; Porter et al., 2000, 2001), clay minerals were also implicated in the

Table 10.2.1. Types and examples of Brønsted acid-catalysed reactions on clay minerals

Reaction type	Example	Catalyst	Reference
Deuterium exchange	Deuteration of $\beta$ -ketoesters, $\beta$ -diketones, pyrrole, indoles	Clays containing interlayer D <sub>2</sub> O	Rao et al. (1989)
Ether formation and cleavage	Alkenes + primary alcohols	M <sup>3+</sup> -clays	Adams et al. (1983b), Ballantine et al. (1984a)
	Substituted alkenes, butadiene + alcohols	Cation-exchanged clays	Adams et al. (1983a)
	Isobutene + methanol to form MTBE	M <sup>3+</sup> -clays	Adams et al. (1981, 1982, 1986), Bylina et al. (1980)
	Primary alcohols to 1,1'-ethers	Al <sup>3+</sup> -or Fe <sup>3+</sup> -clays	Habib et al. (1988)
	Deprotection of tetrahydropyranyl ethers to give alcohols and phenols	K10 in methanol	Li et al. (1999)
Ester and lactone formation	Cholesteryl ethers from alcohols or phenols with cholesterol	K10	Lu et al. (1998)
	Preparation of silyl ethers from alcohols or phenols with hexamethyldisilazane and their desilylation	K10 then K10 methanol to remove	Zhang et al. (1998)
	Alkylene oxides + alcohols to form hydroxyalkylated ether products	Bentonites or Group 11 or 12 cation-exchanged clays	Kapustin et al. (1986), Fujita et al. (1987a)
	Alkenes, chloroalkanes or alcohols react with carboxylic acids to make esters	Acid-treated clays	Ballantine et al. (1984b), Gregory et al. (1983), Atkins (1986), BASF (1963)
	Ketenes + alcohols to esters	Acid activated clays	BASF (1971)
Formation of amides and peptides	Alcohols, phenols, thiols acetylated with acetic anhydride	K10 or KSF	Li and Li (1998)
	Isobutene + diethyl keto-malonate gives $\gamma$ -lactones (ene reaction)	Acid-treated clays	Roudier and Foucaud (1986)
	<i>Tert</i> -alcohols and nitriles form substituted amides (Ritter reaction)	Al <sup>3+</sup> -montmorillonite	O'Neil (1982)
	Amines are acetylated with acetic anhydride	K10 or KSF	Li and Li (1998)
	Esters and ammonia can give amides and nitriles	K10	Wali et al. (1998)
	Amino acid adenylates give polypeptides	Montmorillonites	Katchalsky and Ailam (1967), Paecht-Horowitz (1977), Paecht-Horowitz, et al. (1970)

(continued on next page)

Table 10.2.1 (Continued)

Reaction type	Example	Catalyst	Reference
Reactions dependent on protection, deprotection or activation of carbonyl groups	Acetal formation from carbonyls and alcohols	Cation-exchanged montmorillonites, Filtrol 24 or dodecatungstophosphoric acid on (K10, Süd Chemie)	Tateiwa et al. (1995), Li et al. (1997a), Yadav and Pujari (1999)
	Ketals (incl. cyclic) from 1,2-diols or epoxides	Acid-treated or cation-exchanged clays	Conan et al. (1976), Süd Chemie (1961)
	Diols and enol ethers form acetals and ketals	Montmorillonite	Vu Moc and Maitte (1979)
	Acetals and ketals from trialkylorthoformates and carbonyls	Acid-treated clay	Taylor and Chaing (1977)
	Dithianes, thioacetals, thioketals from ketones or aldehydes and thiols	Acid-treated clay (KSF, Süd Chemie)	Labiad and Villemin (1989)
	1,1'-Diacetates from aldehydes and acetic anhydride	H <sup>+</sup> or Zn <sup>2+</sup> -montmorillonite	Zhang et al. (1997a), Jankovic and Komadel (2000), Nagy et al. (2002)
	Deprotect 1,1'-diacetates	K10	Li et al. (1997b)
	Enamines from sec-amines and ketones	Acid-treated or cation-exchanged montmorillonites	Hünig et al. (1962), Dewan et al. (1995)
	Deprotection of acetals to aldehydes	K10	Li and Li (1997)
	Removal of acetal, silyl and 4,4'-dimethoxytrityl protecting groups from carbohydrate and nucleoside hydroxyl groups	Clay in aqueous methanol	Asakura et al. (1996)
	Oximes can be cleaved to aldehydes or ketones	Bentonite	Alvarez et al. (1987)
	Aldoximes can be dehydrated to nitriles	Acid-treated clay KSF	Meshram (1992)
	Semicarbazones can be cleaved to aldehydes or ketones	Bentonite + acid or supported reagents such as clayfen	Cano et al. (1988)
	$\alpha$ , $\omega$ -dicarboxylic acids can be converted to cyclic anhydrides under very mild conditions	M <sup>3+</sup> - montmorillonite or microwave plus acid-treated clay KSF	Graham et al. (1974), Villemin et al. (1993)
Cyclic anhydride formation			

(continued on next page)



Table 10.2.1 (Continued)

Reaction type	Example	Catalyst	Reference
Formation of heterocyclics	Primary amines + 1,4-diketones form pyrroles	Acid-treated clay (K10)	Texier-Boullet et al. (1986)
	Piperonyl alcohol gives trimethylenedioxyortho-cyclophane	A bentonitic earth, Tonsil Actisil FF	Miranda et al. (1999)
	Phenylhydrazine + ketones give 2-substituted indoles	Microwave plus acid-treated clay KSF	Villemin et al. (1989)
	Pyrrole + benzaldehyde give <i>meso</i> -tetraphenylporphyrin	Montmorillonite	Geier et al. (2000), Geier and Lindsey (2002)
	Tetrahydroquinolines from aromatic amines, aromatic aldehydes and cyclopentadiene	Bieliaca bentonite or KSF montmorillonite	Sartori et al. (2001), Ballini et al. (2000)
	Dihydropyrimidines from aldehydes, $\beta$ -dicarbonyls and urea	Solventless, KSF montmorillonite or in water	Ballini et al. (2000) Bigi et al. (1999)
	Chromenes	KSF montmorillonite	Ballini et al. (2000)
	Malononitriles and 1,2-aminoalcohol gives 2-oxazolines which on hydrolysis give 2,2-dialkyl-3-aminopropanoic acids	Natural kaolinitic clay	Jnaneshwara et al. (1998, 1999)
	Phenols and ketones or aldehydes give 2,2- or 2-substituted 1,3-benzodioxoles	montmorillonite KSF or K10	Li et al. (1998a)
	Pechmann condensation of phenols with ethyl acetoacetate give coumarins	montmorillonite	Li et al. (1998b)
	2-Methyl-8-ethylquinoline from ethylene glycol and excess 2-ethylaniline	In vapour phase over K10 montmorillonite	Campanati et al. (1997)

(continued on next page)

Table 10.2.1 (Continued)

Reaction type	Example	Catalyst	Reference
Rearrangement reactions	1,2-Diols undergo pinacol rearrangements to form 2-hydroxyketones rather than dehydration products	1,2-Diols intercalated in montmorillonite	Gutierrez and Ruiz-Hitzky (1987), Gutierrez et al. (1988)
	4,4-Dialkylcholest-5-enes undergo backbone rearrangement to (20R)- and (20R)-4,4-dialkyl-5 $\beta$ ,14 $\beta$ -dimethyl-18,19-dinor-8 $\alpha$ ,9 $\beta$ ,10-cholest-13(17)-enes	K10	Duan et al. (1999)
	Allyl phenyl ethers to <i>o</i> -allyl phenols	Montmorillonite	Dauben et al. (1990)
	Alkyl phenyl ethers to 4-alkyl phenols	Cation-exchanged montmorillonites	Tateiwa et al. (1994)
	Claisen orthoester rearrangements	Microwave plus acid-treated clay (KSF, Süd Chemie)	Huber and Jones (1992)
	$\alpha$ -Pinene rearranges to camphene, limonene and tricyclene	Acid-treated clays; cation-exchanged clays; polyaminocation-exchanged clay	Kullaj (1989), Besun et al. (2002), Breen and Moronta (2001), Breen (1999), Breen and Watson (1998)
	<i>N</i> -methyl- <i>N</i> -nitrosoaniline (I) undergoes Fischer rearrangement to <i>N</i> -methyl-4-nitrosoaniline	K10 or KSF montmorillonite	Kannan et al. (1997)
Electrophilic aromatic substitution reactions	2-(Trifluoromethyl)aniline gives dimers and oligomers	Cation-exchanged KSF or K10	Kowalska et al. (2001)
	Phenylacetylene reacts with <i>p</i> -toluidine or <i>p</i> -anisidine to give the corresponding 2,6- <i>bis</i> (1-phenylvinyl)anilines	KSF	Arienti et al. (1997)

pre-biotic synthesis of RNA type oligonucleotides from activated nucleotides (Tessis et al., 1995; Ding et al., 1996; Ertem and Ferris, 1997; Prabahar and Ferris, 1997; Sawai et al., 1997; Ertem and Ferris, 1998; Ferris, 1999; Kawamura and Ferris, 1999; Porter et al., 1999; Ertem et al., 2000; Wang and Ferris, 2001; Ferris, 2002).

Clay minerals (montmorillonite, beidellite, illite and vermiculite) were compared for the hydrolysis of five carbamate pesticides: carbofuran, carbofuran, aldicarb, pirimicarb and chlorpropham (Wei et al., 2001). Montmorillonite has the strongest influence on the hydrolysis of these carbamates. Similarly, the phosphorous containing pesticides chlorpyrifos-methyl, oxon, and paraoxon are hydrolysed by montmorillonite and kaolinite (Smolen and Stone, 1998).

The unusual product *p*-nitrosodiphenylamine is formed from *N*-phenylhydroxylamine in the presence of K10 or cation-exchanged K10 rather than the typical Bamberger products, aminophenols (Naicker et al., 1998).

### B. Lewis Acid Catalysis

It was shown, for example, by the thermal desorption of ammonia (Matsuda et al., 1988) and the changes in the IR spectrum of pyridine adsorbed on clay minerals (e.g., Breen et al., 1987) that as the clay mineral is dehydrated with increasing temperature, its Lewis acidity becomes more important than its Brønsted acidity. Several of the reactions listed below have complex mechanisms, but Lewis activity is thought to be crucial (Table 10.2.2).

In 1930, clays were first used as catalysts for cracking petroleum (Franz et al., 1959). At 300 °C, the efficiency and stability of montmorillonite catalysts was much improved by acid activation (Thomas et al., 1950). Nonetheless, there is a theme in reactions of this type for the catalysts not to be resistant enough to the hydrothermal treatment needed for oxidation of coke (catalyst regeneration) which builds up in catalyst pores (Ballantine, 1986). Thus there was a trend towards use of zeolites, though PILC derivatives are promising.

### C. Redox Reactions

Redox reactions are associated with transition metals either substituted in the octahedral or tetrahedral sheets of the clay mineral or those introduced as exchangeable cations between the clay mineral layers. We summarise the situation for oxidation reactions in Tables 10.2.3 and 10.2.4.

Several smectite-based materials were also been found to be efficacious for oxidation when used in concert with hydrogen peroxide, *t*-butyl hydroperoxide or iodosylbenzene.

Sodium hypochlorite or potassium persulphate epoxidise 1-hexene preferentially over cyclic alkenes when catalysed by M(salen) complexes (M = Mn(III), Ni(II); salen = *bis*-(salicylidene)ethylenediamine) adsorbed onto montmorillonite or zeolite Y (Chatterjee and Mitra, 1999). Iodosylbenzene and a chiral Mn(salen) complex on a

Table 10.2.2. Types and examples of Lewis acid catalysed reactions on clay minerals

Reaction type	Example	Catalyst	Reference
Catalytic cracking and isomerisation	Long-chain cracking to short-chain alkanes	Pillared clays	Lahav et al. (1978), Endo et al. (1980)
	Isomerisation of <i>n</i> -alkanes to <i>iso</i> -alkanes	TM-exchanged clays	See, e.g., Chevron Research (1972, 1973)
	Dehydration and isomerisation of alcohols, e.g., 1-hexanol to 2- and 3-hexenes	Clays	Musaev et al. (1986)
Methanol and Syn-gas conversions	Methanol to C <sub>2</sub> –C <sub>4</sub> alkenes	Ce-clays; Zr–PILC	Toyo Soda (1983), Burch and Warburton (1986)
	Methanol to methyl formate Syn gas to alkene/alkane mix (C <sub>5</sub> –C <sub>10</sub> )	Cu-TFSM TM-exchanged clays	Morikawa et al. (1982) NL Industries (1977)
Friedel-Crafts alkylation and acylation of aromatics	Phenol alkylation with alkenes, branched alkenes, substituted styrenes, cycloalkenes and polyalkenes	Cation-exchanged or acid-treated clays	Chivadze and Khakhnelidze (1987), Imanari et al. (1987), Takagi and Naruse (1989)
	Aniline alkylated by alkenes	Cation-exchanged or acid-treated montmorillonite, Ce-exchanged Al pillared SWy-2	Shigeshiro et al. (1987), Bacskai and Valerias (1988), Narayanan and Deshpande (2000)
	Unactivated aromatic and heteroaromatic hydrocarbons alkylated by halides, alcohols and alkenes	Cation-exchanged clays, K10 and PILCs.	Hassan et al. (1985), Laszlo and Mathy (1987), Natekar and Samant (1995), Narayanan and Deshpande (2000), Li et al. (1998) Clark and Mesher (1995)

(continued on next page)

Table 10.2.2 (*Continued*)

Reaction type	Example	Catalyst	Reference
Other electrophilic aromatic substitution reactions	Acylation of benzo-15-crown-5 ether with acetyl chloride gives 4'-acetyl-benzo-15-crown-5	Best with Sn exchanged K10	Biro et al. (2000)
	Acylation of aromatic hydrocarbons with carboxylic acids	Cation-exchanged montmorillonite	Chiche et al. (1987)
	Nitration of aromatics	Nitric acid and cation-exchanged clay	Bakke and Liaskan (1979), Sato et al. (1989)
	Chlorination of toluene	Clay	Pitchumani et al. (1993)
	Reduction of mutagenicity of benzopyrenes by methyl transfer	Acid-activated clay or pillared clay	Roy et al.(1999)
	Methylation of alkylnaphthalenes with hexamethylbenzene as a model for natural occurrence of methylnaphthalenes in crude oil	Al-montmorillonite	Bastow et al. (2000)
Rearrangements	Citronellal to menthone and isomenthone	Al/Fe-pillared clay at 80 °C	Cramarossa et al. (2001)
	Citronellal to pulegol and isopulegol	Al/Fe-pillared clay at room temperature	Cramarossa et al. (2001)

Table 10.2.3. Examples of clay-catalysed redox reactions

Substrate	(A)/(P)*	Product	Clay	Reference
Allylic alcohols	A	Ketones	Ni <sup>2+</sup> -F-containing synthetic mica	Fujita et al. (1987b)
2-propenyl aromatics	A	Acetophenones	Cr <sup>3+</sup> -Mica	Kondo et al. (1990)
Cyclohexene	A	Cyclohexanol and cyclohexanone	Co <sup>3+</sup> -clays	Hashimoto et al. (1988)
Ethanol and ether	P	n.r.	Uranyl-exchanged PILCs	Suib et al. (1986)

n.r. = not required.

\*A = aerobic oxidation; P = photooxidation.

Table 10.2.4. Examples of clay-catalysed redox reactions requiring a co-reactant

Substrate	Co-reagent	Product	Clay	Reference
Phenols and phenolic ethers	Hydrogen peroxide	Hydroxylated products	Al <sup>3+</sup> -beidellite	Constantini and Popa (1989)
Allyl alcohols	Hydrogen peroxide	Epoxides	V-PILC	Choudary et al. (1990)
Arylmethylenes	<i>t</i> -butyl peroxide	Monocarbonyl compounds	Cr-PILC	Choudary et al. (1992)
Styrene	Iodosylbenzene	1-Phenyl-1,2-dihydroxyethane	Mn(III)- or Fe(III)-exchanged clay	Boricha et al. (1999)

montmorillonite showed slightly decreased enantioselectivity compared to free solution epoxidation (Fraile et al., 1998).

Alkanethiols undergo facile anti-Markovnikov addition to styrene over K10-montmorillonite and cation-exchanged clay minerals by way of a radical mechanism to form sulphides (Kannan and Pitchumani, 1997). Surfactant PILC minerals were found to be remarkably selective at suppressing side reactions. Iron cations in mica or talc can produce a conducting polymer of anilinium dodecylbenzenesulphonate, which encapsulates the clay particle (Segal et al., 2000; Jia et al., 2002). The preparation of a zirconia-pillared montmorillonite was made more effective by ultrasonication during adsorption of the polyhydroxyzirconium cation (Awate et al., 2001). The Zr-PILC was very effective for the hydroxylation of phenol.

Few reduction reactions mediated by clay minerals alone were reported. One example is the acid-treated clay-catalysed reduction of nitroarenes to anilines with hydrazine

(Han and Jang, 1990); another is the reduction of ketones and aldehydes to hydrocarbons by triethylsilane and highly acidic clay minerals (Onaka et al., 1993).

Ghosh and Bard (1983) and Ghosh et al. (1984) first established the field of clay-modified electrodes in the mid-1980s. Since then understanding the nature of the clay mineral structural units and their impact on transport of a variety of electroactive probes (anions, neutrals, small cations, large cations and compounds with distributed charge) increased (Macha and Fitch, 1998). The nature of the layered material (i.e., size, charge, iron content, pillaring and organic tailoring) controls access to the interlayer sites. Alumina PILC films, made using preformed pillared structures, were constructed on graphite electrodes (Petridis et al., 1996). The films exhibit very good electroactivity when immersed in solutions containing redox active cationic species, e.g.,  $\text{Fe}(\text{bpy})_3^{2+}$ ,  $\text{Os}(\text{bpy})_3^{2+}$ ,  $\text{Ru}(\text{NH}_3)_6^{3+}$  and methyl viologen. Excellent catalytic activity was observed for the electroreduction of  $\text{H}_2\text{O}_2$  by a nontronite (SWa-1, ferruginous smectite) clay coating on a glassy carbon electrode with incorporated methyl viologen as mediator (Zen et al., 1996).

Electrochemical reduction of haemoglobin in assembled, stable films of alternating clay mineral haemoglobin layers on electrode surfaces was achieved (Zhou et al., 2002b). The films are deposited layer-by-layer on various solid substrates by alternate adsorption of negatively charged clay mineral particles from their aqueous dispersions and positively charged haemoglobin from pH 4.5 buffers. Similar clay mineral intercalated deposits of myoglobin, haemoglobin or horseradish peroxidase were examined as potential electrocatalytic sensors for pollutants (Hu, 2001). Oxygen, trichloroacetic acid, nitrite and hydrogen peroxide are catalytically reduced by all three proteins in clay mineral films (Zhou et al., 2002a). Hexacyanoferrate and vitamin B-12 hexacarboxylate intercalated into clay mineral-surfactant (cetyltrimethylammonium bromide) films on electrodes also show good electrocatalytic activity (Carrero and Leon, 2001).

Electro-inactive  $\text{Fe}(\text{bpy})_3^{2+}$  becomes electro-catalytic for the oxidation of guanine on binding to nontronite on a graphite surface (Ilangoan and Zen, 1999).  $\text{Mn}^{2+}$ -exchanged montmorillonite catalyses the production of hydrogen peroxide efficiently from dioxygen (or air) and hydroxylamine at pH 8.0 in aqueous solution (Hothi et al., 1997). Oxygen can be reduced electrocatalytically at clay-modified electrodes in the presence of tetraazamacrocyclic cobalt(III) complexes (Gobi and Ramaraj, 1998) or platinum particles (Premkumar and Ramaraj, 1997). The Faradaic yield and the rate of  $\text{H}_2\text{O}_2$  production are found to be higher at clay-coated electrodes than at Nafion<sup>®</sup>-coated electrodes. During photoelectrocatalytic reduction of oxygen at  $\text{Pt}/\text{H}^+$ -montmorillonite/ $[\text{Ru}(\text{bpy})_3]^{2+}$  electrodes, the amounts of  $\text{H}_2\text{O}_2$  produced increase by a factor of two under light irradiation when compared to dark.

#### D. Reactions via Reactive Intermediates

$\text{Na}^+$ -montmorillonite catalyses the condensation of glycolaldehyde to monosaccharides, apparently by an aldol process (Martil and Aragon de la Cruz, 1986).  $\text{Al}^{3+}$ -exchanged clay minerals catalyse the cross aldol-addition of silyl enol ethers to

carbonyl compounds or acetals (Kawai et al., 1986a, 1988a, 1988b). Similarly, silyl ketene acetals and carbonyls give 3-silylether esters (Onaka et al., 1987). Acetals and carbonyls can be allylated using the acid-activated clay, K10 (Kawai et al., 1986b).

Substituted salicylic aldehydes are synthesised in good yields and excellent selectivities by reaction of phenols with formaldehyde over montmorillonite KSF-triethylamine (Bigi et al., 2000). An intermediate 2-hydroxybenzaldehyde is formed initially and this undergoes Oppenauer oxidation with a further mole of formaldehyde to the salicylic aldehyde. In the absence of triethylamine the higher acidity of the clay mineral results in mainly acetal and diphenylmethane formation instead; while, the lower iron K10 gives just the 2-hydroxybenzaldehyde, suggesting that iron cations aid the oxidation. Aromatic amines adsorbed on kaolinite condense with formaldehyde to give the corresponding diaminodiphenylmethanes (Bahulayan et al., 1999). Triarylmethanes are synthesised in good to excellent yield via Baeyer condensation of aromatic aldehydes with *N,N*-dimethylaniline catalysed by montmorillonite K10 at 100 °C in the absence of solvent (Zhang, et al., 1997b). Cyclohexane and morpholine in the presence of KSF under azeotropic distillation give 1-morpholinocyclohexene which, when alkylated or acylated in situ without isolation of the enamine, give overall yields of better or equivalent than those obtained by isolation of the enamine (Hammadi and Villemain, 1996).

Dual catalysis of the Michael addition of  $\beta$ -diketones to  $\alpha,\beta$ -unsaturated ketones by  $\text{FeCl}_3$  and  $\text{NiBr}_2$ /clay was reported (Laszlo, et al., 1990). Michael adducts can also be obtained from  $\alpha,\beta$ -unsaturated esters or ketones with silyl ketene acetals or silyl enol ethers using clay catalysts (Kawai et al., 1987, 1988a, 1988b) or from 1,3-diketones using K10 or KSF (Soriente et al., 1999). The reactions are versatile and highly regiospecific. 3-Unsubstituted indoles add  $\alpha,\beta$ -unsaturated ketones and esters at the 3-position (Iqbal et al., 1988). 3-Methylindoles give 2-substituted products, while 3-benzylindoles give 2,3-migration of the benzyl group. Similar reactions on K10 are improved by addition of alcohols and nitromethane as solvent (Poupaert et al., 1999).

Synthesis of alkenes via the Knoevenagel reaction from aldehydes and C-acids (e.g., Meldrum's acid) (Thorat et al., 1987) or malonate derivatives (Foucaud and Bakouetila, 1987) was achieved using clays. Silylpropylethylenediamine modified montmorillonites are weakly basic and were used for the Knoevenagel reaction (Subba Rao and Choudary, 1991).

Certain transition metals and their cations are noted for their ability to coordinate alkenes and generate carbenes from diazoalkanes (Wulfsberg et al., 1976). These can be used for the cyclopropanation of alkenes and dienes.  $\text{Cu}^{2+}$ -montmorillonite is effective with ethyl diazoacetate at room temperature (Yamagishi, 1986). Stereo selectivity is not affected.

### E. Cycloaddition Reactions

Uncatalysed Diels–Alder reactions often require extended reaction times at elevated temperatures and pressures. Several different catalyst types shown to be effective,



including Brønsted and Lewis acids (Houk and Strozier, 1973), radical cations (Belville et al., 1981), use of aqueous solvents (Laszlo and Lucchetti, 1984a) and solventless reactions on K10 (Avalos et al., 1998a, 1998b). The latter reactions also show Michael addition products.

The most important (apparently) commercial Diels-Alder reaction catalysed by clays is the cyclo-dimerisation of oleic acids (Den Otter, 1970a, 1970b, 1970c; Newton, 1984). The reaction involves high temperatures to effect the preliminary dehydrogenation of the oleic acid. Thus it is possible that there is no catalysis of the Diels-Alder step. Many other reactions, clearly of Diels-Alder type were, however, been shown to be catalysed by smectite-based catalysts (Table 10.2.5).

Non-acid-activated transition metal-exchanged clay minerals give better control of stereoselectivity than do acid-activated catalysts (Martin, 1986; Adams et al., 1987a, 1994). Rates of reaction are much greater with  $M^{3+}$ -exchanged clay minerals than with  $M^{2+}$ -clay minerals, but the former produce a much greater proportion of endo-isomers.

The greater the layer charge, the smaller the interlayer spacing and the lower the rate of reaction. The endo/exo ratio also diminishes, suggesting that the less bulky

Table 10.2.5. Clay-catalysed Diels-Alder reactions

Substrate	Product	Clay	Reference
Butadiene	Vinyl cyclohexene	$Cu^{2+}$ -montmorillonite	Downing et al. (1978)
Butadiene, isoprene	Dimers	TM-exchanged clays	Adams and Clapp (1986), Adams et al. (1987b)
1,3-Hexadiene	Dimer	$Fe^{3+}$ -K10	Laszlo and Lucchetti (1984b)
Methyl vinyl ketone or acrolein with cyclopentadiene, furan or 2,5-dimethylfuran	Adducts	Cation-exchanged clay, hydroxy-chromium pillared clays	Laszlo and Lucchetti (1984c, 1984d), Laszlo and Moison (1989), Martin (1986), McCabe (1996)
6-Methylpyran-2( <i>H</i> )-ones with 1,4-naphthoquinone or <i>N</i> -phenylmaleimide	Adducts	Montmorillonite K10, fultrol-24 (best), bentonite or pyrophyllite (poor) clays or $AlCl_3$ , $ZnCl_2$ and $FeCl_3$ on montmorillonite or bentonite	Kamath and Samant (1999) Kamath et al. (2000)

transition state (which leads to the *exo*-isomer) is formed preferentially when the interlayer space is reduced (Adams et al., 1994).

A small number of other cycloaddition reactions were also demonstrated. For example, stilbazolium cations adsorbed on clays undergo efficient and selective photodimerisation to the cyclobutane dimer (Takagi et al., 1989). *Cis-trans* isomerisation of the double bond is suppressed between the clay mineral layers.

### F. Clays as Supports

In the 1990s, there was a surge in the use of supported reagents and catalysts as the use of heterogeneous systems simplifies the purification of reaction products. The benefits of this approach include low cost, high reactivity and the ease with which the reactions are carried out. Some examples are given below of the use of “Clayfen” and “Claycop” (Table 10.2.6) (Cornelis and Laszlo, 1986; Clark et al., 1994), iron(III) and copper(II) nitrates supported on acid-treated clay (K10 from Süd-Chemie). They all depend on the fact that the reagents are sources of nitrosonium ions.

Palladium chloride and tetraphenylphosphonium bromide intercalated clay mineral were used in the Heck reaction (coupling of aryl halides and styrenes to give stilbenes) (Varma et al., 1999f) and for Suzuki coupling (coupling of aryl halides with arylboronic acids to give biphenyls) (Varma and Naicker, 1999a, 1999b). The Heck coupling vinylation of halobenzenes with methyl acrylate was achieved with clay-supported palladium catalysts in *N*-methylpyrrolidone in the presence of triethylamine and/or sodium carbonate (Zhao et al., 2000). Significant amounts of palladium leach out into the solvent and these dissolved Pd species essentially catalyse the reaction; however, almost all the palladium species in the solution are re-deposited onto the surface of the supports after the reaction was completed (at 100% conversion of iodobenzene).

Alcohols were acylated efficiently using anhydrides/acetic acid and [*N,N'*-ethylene bis(salicylideneaminato)] manganese(III) chloride supported on a clay (Choudary et al., 2001).

Table 10.2.6. Stoichiometric oxidation reactions with iron(III) or copper(II) nitrates supported on K10

Reaction	Reference
Alkyl secondary alcohols oxidised to ketones	Cornelis and Laszlo (1980)
Aromatic primary alcohols oxidised to aldehydes	Cornelis and Laszlo (1980)
Thiols oxidised to disulphides	Cornelis et al. (1983)
Thioketones oxidised to ketones	Chalais et al. (1985)
Hydrazides converted to azides	Laszlo and Polla (1984)

Palladium(II) chloride/copper(II) chloride complex (Wacker catalyst) heterogenised on montmorillonite catalyses low-temperature oxidation of carbon monoxide, carbonylation in the synthesis of ibuprofen or naproxen, oxidative carbonylation for the synthesis of diphenyl carbonate and the functionalisation of methane (Park et al., 2000). There appears to be no significant change in the reaction mechanisms when the catalyst is transferred from solution to the solid surface.

Chirally modified hectorites (Laponite RD) are prepared by ion exchange with (*R*)- and (*S*)-*N*-alkyl-phenylethyl ammonium salts (Torok et al., 2000). Enantiodifferentiation is observed on using these chiral nanoreactors for a transition metal-catalysed hydrogenation reaction. A chiral rhodium complex intercalated into hectorite containing guest molecules shows drastic changes in catalytic properties for asymmetric hydrogenation depending on the orientation of the guests (Sento et al., 1998).

Cubooctahedral palladium particles deposited on montmorillonite from colloidal dispersion give particles ranging in size from 1.5 to 6.2 nm in mean diameter (Veisz et al., 2002). These catalysts hydrogenate styrene to ethylbenzene under mild conditions. Good correlation between the turnover frequencies and the defect site densities suggest that hydrogenation occurs on the defect sites and that terrace sites have only minimal catalytic activity or are inactive.

Anhydrous iron(III) chloride supported on K10 acts as a Lewis acid catalyst for the benzylolation of arenes with benzyl chloride (Natekar and Samant, 1995; Pai et al., 2000); the latter authors also report efficient reaction with aluminium(III) chloride and zinc(II) chloride on the same support. Anhydrous lanthanide salts supported on K10 act as good acylating agents for arenes with acid chlorides and anhydrides (Baudry-Barbier et al., 1999) and as arene alkylating agents (Baudry-Barbier et al., 1998). In both cases fairly activated substrates were used.

Zinc bromide supported on mesoporous silica or acid-activated montmorillonite is a fast, efficient, selective and reusable catalyst for the *para*-bromination of activated and moderately deactivated aromatic substrates (Clark et al., 1997).

Pillared clay minerals are being examined as catalysts for removal of NO<sub>x</sub> from exhaust fumes (Serwicka, 2001). Zirconium aquahydroxylation pillared clay minerals prepared from untreated or HCl-pretreated montmorillonite are promoted by adsorption of manganese and they show catalytic activity in the specific catalytic reduction of NO<sub>x</sub> (Grzybek et al., 2001). Thermally stable Al- and Zr-PILC loaded with copper and cobalt cations and silver nanoparticles are examined for their specificity for the catalytic reduction of NO<sub>x</sub> by propane, propylene and decane in excess of oxygen. Formation of adsorbed-NO<sub>x</sub>, nitroxyl-hydrocarbon C<sub>x</sub>H<sub>y</sub>NO<sub>2</sub> and isocyanate NCO intermediates is observed by ESR and IR spectroscopy (Konin et al., 2001).

### G. Organo-Clays as Phase Transfer Agents

Quaternary ammonium organo-clays were used as phase transfer catalysts for nucleophilic substitution (Cornelis and Laszlo, 1982; Lin and Pinnavia, 1991) reactions, including the formation of cyanides, thiocyanides and alcohols from benzyl bromides

and the corresponding aqueous sodium salts (Varma et al., 1999d), and azides from benzyl and alkyl bromides or  $\alpha$ -tosyloxyketones in organic solvents (Varma and Kumar, 1998; Varma and Naicker, 1998; Varma et al., 1999c) with sodium azide in water. 18-Crown-6-ether supported on a clay was also used as a phase transfer catalyst for the conversion of alkyl bromides to alkyl azides (Varma et al., 1999e).

Benzoic anhydride can be prepared from benzoyl chloride and sodium benzoate using clay-supported quaternary ammonium salts as phase transfer catalyst (Yadav and Naik, 2000).

#### 10.2.4. SIGNIFICANT RECENT DEVELOPMENTS

In line with the strong trends towards green chemistry over the last decade or so, clays were investigated as supports for many toxic reagents or as replacements for stoichiometric reagents that produce large volumes of pollutant by-products. Another trend in the same vein is the upsurge of “solventless” reactions initiated by microwave or ultrasound irradiation.

##### A. Supported Acids

Very high acidities can be achieved by supporting superacids and heteropoly acids on clay mineral surfaces. For example, trifluoromethanesulphonic acid supported on a montmorillonite gives a superacid sulphonic clay with a Hammett acidity function,  $H_0 < -12.75$ . The clay mineral activity has been evaluated in the solvolysis of propylene oxide with a series of alcohols, yielding high conversion (88.9 – 99.8%) and selectivity (27.6 – 80.8%) to monomer formation (Salmon et al., 1997).

The esterification of lactic acid with *iso*-propanol and maleic acid with ethanol catalysed by ion-exchange resins and 20% dodecatungstophosphoric acid supported on K10 at reflux were compared (Yadav and Kulkarni, 2000; Yadav and Thathagar, 2002). The ion-exchange resins produce somewhat better results.

Heteropoly acids, such as 12-tungstophosphoric acid and 12-molybdophosphoric acid, on HF-treated montmorillonites or mineral acid-activated clay minerals are very effective in the synthesis of methyl *tert*-butyl ether from methanol/*tert*-butanol (Knifton and Edwards, 1999) and for the formation of acetone and phenol from the cleavage of cumene hydroperoxide (Knifton and Sanderson, 1997), using continuous, plug-flow, reactor systems. Dodecatungstophosphoric acid supported on K10 is found to be a very efficient catalyst in comparison with several others for alkylation of hydroquinone with alkylating agents such as methyl *tert*-butyl ether (MTBE) and *tert*-butanol (Yadav and Doshi, 2000).

Palladium (1 wt%) supported on alumina pillared acid-activated montmorillonite or sulphated zirconium pillared sodium montmorillonite exhibits much higher activities and isomerisation selectivities for hydroisomerisation of hexanes and cyclohexanes than those obtained on a conventional pillared montmorillonite (Issaadi et al., 2001).

The sulphated zirconium pillared sodium montmorillonite catalyst is two to three times more active than the other catalysts and the reaction is thought to go through a protonated alkane intermediate.

### *B. Reactions Initiated by Microwave, Ultrasound or Gamma Irradiation*

A large number of the more traditional clay-catalysed or stoichiometric clay-supported reagent reactions were reported, usually under solvent-free conditions using microwave irradiation of the dry mixture followed by solvent extraction. Improved yields (often > 90%), much shortened reaction time (seconds to minutes), occasional improved selectivity and specificity for polar substrates are found. Varma (2002) and Loupy (1999) reviewed this growing field recently and a selection of the types of compounds examined is listed in Table 10.2.7.

The Beckman rearrangement of ketoximes to 2 amides on K10 (Gutierrez et al., 1989) and the pinacol to pinacolone rearrangement on  $\text{Al}^{3+}$ -exchanged K10 (Bosch et al., 1995) are readily promoted by microwave irradiation. Several heterocyclic systems were synthesised on acid-activated clays under microwave irradiation, including the following (Table 10.2.8):

1. The rates of formation of azides from benzyl and alkyl bromides or  $\alpha$ -tosyloxyketones in organic solvents (Varma and Kumar, 1998; Varma and Naicker, 1998; Varma et al., 1999c) and sodium azide in water are enhanced by ultrasound irradiation.
2. The rate of glucosylation of butanol and dodecanol in the presence of KSF/O as catalyst is increased by application of ultrasound (Brochette et al., 1997). In the case of dodecanol high yields of 1,6-polyglucose are obtained. Radiolysis of carboxylic acids adsorbed on clay minerals shows mainly decarboxylation in contrast to condensation/dimerisation reactions in free solution (Negron-Mendoza and Ramos-Bernal, 1998).

### *C. Clay Nanocomposites*

The catalytic properties of clay minerals were used to form a variety of clay-polymer nanocomposites with novel material properties (Carrado, 2000; see Chapter 10.3). Examples include: polybenzoxazine-montmorillonite (Shi et al., 2002) and formaldehyde with ethylenediamine on montmorillonite (Stackhouse et al., 2001).

## 10.2.5. INDUSTRIAL SITUATION

Acid-treated clay minerals continue to be used industrially (see Chapter 10.1). The Claycop and Clayfen type of supported reagents became “standard practice” in many laboratory situations and related catalysts, the so-called Envirocats (environmentally friendly catalysts) made some headway, marketed by Contract Chemicals.

Table 10.2.7. Microwave-initiated, clay-catalysed functional group modifications

Substrate	Co-substrate	Product	Clay	Reference
Aldehyde	Amine	Imine	K10 or Envirocat EPZG	Dewan et al. (1995), Varma and Dahiya (1997a)
Creatine	Aromatic aldehyde	Z-arylidene creatinines	Clay	Villemin and Martin (1995)
Diethyl or dimethyl malonate	Aldehydes	gem-bis(Alkoxy-carbonyl)alkenes	K10	Abdallahelayoubi and Texierboullet (1995)
Ketone	Amine	Enamine	K10 or Envirocat EPZG	Varma and Dahiya (1997a, 1997b), Varma et al. (1997), Rechsteiner et al. (1993)
Dialkyl sulphide	n.r.	Sulphoxide	Clayfen	Varma and Dahiya (1998a)
Alcohol	n.r.	Aldehyde or ketone	Clayfen	Varma and Dahiya (1997b)
Alcohol	Hydrogen peroxide	Aldehyde or ketone	Claycop	Varma and Dahiya (1998b)
Aldehyde	1° Amine	2° Amine	K10 then NaBH <sub>4</sub> /K10/water	Varma and Dahiya (1998c)
Aromatic Aldehyde	n.r.	Nitrile	NH <sub>2</sub> OH/K10	Varma et al. (1999a)
Semicarbazones or hydrazones	n.r.	Ketone	(NH <sub>4</sub> ) <sub>2</sub> S <sub>2</sub> O <sub>8</sub> on K10*	Varma and Meshram (1997)
Thioketones or dithioketals or dithioacetals	n.r.	Ketone or aldehyde	Clayfen or clayan (NH <sub>4</sub> NO <sub>3</sub> /K10)	Varma and Kumar (1999a), Varma and Saini (1997a)
Aldoximes	Tetrachloro-pyridine	Nitrile	Acid clay	Lingaiah and Narender (2002)
Aldehyde bisulfite addition products	n.r.	Aldehydes	Montmorillonite KSF	Mitra et al. (1999)

n.r. = not required.

\*Also promoted by ultrasound irradiation.

Table 10.2.8. Microwave-initiated, clay-catalysed formation of heterocyclic compounds

Substrate	Co-substrate	Product	Clay	Reference
$\alpha$ , $\beta$ -Dibromoester	1° Amine	Aziridine	Bentonite	Saoudi et al.(1996)
Orthoesters	<i>o</i> -Phenylene-diamine	Benzimidazoles	KSF	Villemin et al. (1996)
Ketone + amine	Then a 2-hydroxy-benzaldehyde	Isoflav-3-ene	K10 then + NH <sub>4</sub> OAc	Varma and Dahiya (1998d)
<i>o</i> -Hydroxydibenzoyl-methanes	n.r.	Flavone	K10	Varma et al. (1998)
2'-Aminochalcones	n.r.	Tetrahydroquinolones	K10	Varma and Saini (1997b)
Arylmethyl ketone + [hydroxyl(tosyloxy)iodo]-benzene	Thioamide	Thiazoles	K10	Varma et al. (1999b)
Arylmethyl ketone + [hydroxyl(tosyloxy)iodo]-benzene	Ethylenethiourea	Fused imidazothiazoles	K10	Varma et al. (1999b)
2-Amino pyridines, pyrimidines or pyrazines	Aldehydes then + isocyanide	Imidazo[1,2a]pyridine, pyrimidine or pyrazine	Clay	Varma and Kumar (1999b)
N-(carbotrifuoromethyl)-ortho-arylenediamines	n.r.	2-Trifluoromethyl-arylimidazoles	K10	Bougrin et al. (2001)

n.r. = not required.

There was some work in the 1970s and 1980s by Laporte aimed at pelletising clays with attapulgite in a similar manner to zeolites, with some success. In addition, some work was carried out in adapting some of the laboratory-based chemistry outlined above to refinery-based situations using acid-activated and PILC minerals. Examples include the direct addition of carboxylic acids to alkenes (Gregory et al., 1983; Ballantine et al., 1984b) and Friedel-Crafts alkylation with C3–C5 alkenes reducing the mutagenicity of refinery streams and coal tars containing polynuclear aromatic compounds (PACs) (Roy et al., 1999). However, smectite- (and other clay-) derived catalysts are rare in industry.

### 10.2.6. CONCLUSIONS

Generating activity from clay-based catalysts is not really the problem. The issues that remain are those set out at the beginning of this chapter, i.e.:

- (1) There remains too much “stamp collecting”. Fundamental work needs to be done on a set of carefully selected reactions using extremely well-characterised materials, to generate predictive capability.
- (2) Not enough attention was paid to engineering of clays into catalyst particles, pellets, membranes, etc. that can survive industrial processing conditions.

Both matters need addressing if engineers and other industrialists are to have confidence in clays as solutions to their real problems. A focussed, integrated project, concentrating on these issues could well be profitable.

## REFERENCES

- Abdallah-El Ayoubi, S., Texier-boullet, F., 1995. Clay-mediated synthesis of gem-bis(alkoxycarbonyl) alkenes under microwave irradiation. *Journal of Chemical Research-(S)* 5, 208–209.
- Adams, J.M., 1987. Synthetic organic chemistry using pillared, cation-exchanged and acid-treated montmorillonite catalysts—a review. *Applied Clay Science* 2, 309–342.
- Adams, J.M., Clapp, T.V., 1986. Reactions of the conjugated dienes butadiene and isoprene alone and with methanol over ion-exchanged montmorillonites. *Clays and Clay Minerals* 34, 287–294.
- Adams, J.M., Clapp, T.V., Clement, D.E., 1983a. Catalysis by montmorillonite. *Clay Minerals* 18, 411–421.
- Adams, J.M., Clement, D.E., Graham, S.H., 1981. Low-temperature reaction of alcohols to form *tert*-butyl ethers using clay catalysts. *Journal of Chemical Research-(S)*, pp. 254–255.
- Adams, J.M., Clement, D.E., Graham, S.H., 1982. Synthesis of methyl-*tert*-butyl ether from methanol and isobutene using a clay catalyst. *Clays and Clay Minerals* 30, 129–134.
- Adams, J.M., Clement, D.E., Graham, S.H., 1983b. Reactions of alcohols with alkenes over an aluminium-exchanged montmorillonite. *Clays and Clay Minerals* 31, 129–136.
- Adams, J.M., Dyer, S., Martin, K., Matear, A., McCabe, R.W., 1994. Diels-Alder reactions catalysed by cation-exchanged clay minerals. *Journal of the Chemical Society, Perkin Transactions Issue*, pp. 761–765.
- Adams, J.M., Martin, K., McCabe, R.W., 1987a. Clays as selective catalysts in organic synthesis. *Journal of Inclusion Phenomena* 5, 663–674.
- Adams, J.M., Martin, K., McCabe, R.W., 1987b. Catalysis of Diels-Alder reactions by transition metal exchanged clays. In: Schultz, L.G., van Olphen, H., Mumpton, F.A. (Eds.), *Proceedings of the International Clay Conference, Denver, 1985*. Clay Minerals Society, Bloomington, IN, pp. 324–328.
- Adams, J.M., Martin, K., McCabe, R.W., Murray, S., 1986. Methyl *t*-butyl ether formation: a comparison of montmorillonite-derived catalysts with an ion exchange resin. *Clay Minerals* 34, 587–603.
- Alvarez, C., Cano, A.C., Rivera, V., Marquez, C., 1987. Carbonyl-compounds regeneration with a Mexican bentonite. *Synthetic Communications*, pp. 279–282.
- Arienti, A., Bigi, F., Maggi, R., Marzi, E., Moggi, P., Rastelli, M., Sartori, G., Tarantola, F., 1997. Regioselective electrophilic alkylation of anilines with phenylacetylene in the presence of montmorillonite KSF. *Tetrahedron* 53, 3795–3804.
- Asakura, J., Robins, M.J., Asaka, Y., Kim, T.H., 1996. Removal of acetal, silyl, and 4,4'-dimethoxytrityl protecting groups from hydroxyl functions of carbohydrates and nucleosides with clay in aqueous methanol. *Journal of Organic Chemistry* 61, 9026–9027.
- Atkins, M.P., 1986. Process for the production of carboxylic acid esters. UK Patent, GB 2175300.
- Avalos, M., Babiano, R., Bravo, J.L., Cintas, P., Jimenez, J.L., Palacios, J.C., 1998a. Clay-catalyzed solventless addition reactions of furan with  $\alpha,\beta$ -unsaturated carbonyl compounds. *Tetrahedron Letters* 39, 9301–9304.



- Avalos, M., Babiano, R., Bravo, J.L., Cintas, P., Jimenez, J.L., Palacios, J.C., Ranu, B.C., 1998b. Cycloadditions with clays and alumina without solvents. *Tetrahedron Letters* 39, 2013–2016.
- Awate, S.V., Waghmode, S.B., Patil, K.R., Agashe, M.S., Joshi, P.N., 2001. Influence of preparation parameters on characteristics of zirconia-pillared clay using ultrasonic technique and its catalytic performance in phenol hydroxylation reaction. *Korean Journal of Chemical Engineering* 18, 257–262.
- Bacskai, R., Valerias, H.A., 1988. Process for the preparation of allylaniline using an aluminosilicate catalyst. European Patent, 265932.
- Bahulayan, D., Sukumar, R., Sabu, K.R., Lalithambika, M., 1999. An easy synthesis of 4,4'-di-aminodiphenylmethanes on natural kaolinites. *Green Chemistry* 1, 191–193.
- Bakke, J.M., Liaskan, J., 1979. Nitration of organic compounds. Patent, GB2000141.
- Ballantine, J.A., 1986. The reactions of clays and pillared clays. In: Setton, R. (Ed.), *Chemical Reactions in Organic and Inorganic Constrained Systems*. Reidel, New York, pp. 197–212.
- Ballantine, J.A., Davies, M., Patel, I., Purnell, J.H., Rayanakorn, M., Williams, K.J., Thomas, J.M., 1984a. Organic-reactions catalyzed by sheet silicates—ether formation by the intermolecular dehydration of alcohols and by addition of alcohols to alkenes. *Journal of Molecular Catalysis* 26, 37–56.
- Ballantine, J.A., Davies, M., O'Neil, R.M., Patel, I., Purnell, J.H., Rayanakorn, M., Williams, K.J., Thomas, J.M., 1984b. Organic-reactions catalyzed by sheet silicates—ester production by the direct addition of carboxylic-acids to alkenes. *Journal of Molecular Catalysis* 26, 57–77.
- Ballini, R., Bigi, F., Conforti, M.L., De Santis, D., Maggi, R., Oppici, G., Sartori, G., 2000. Multicomponent reactions under clay catalysis. *Catalysis Today* 60, 305–309.
- BASF, 1963. No Title, German Patent, 1211643.
- BASF, 1971. No Title, German Patent, 1643712.
- Bastow, T.P., Alexander, R., Fisher, S.J., Singh, R.K., van Aarssen, B.G.K., Kagi, R.I., 2000. Geosynthesis of organic compounds. Part V—methylation of alkynaphthalenes. *Organic Geochemistry* 31, 523–534.
- Baudry-Barbier, D., Dormond, A., Duriau-Montagne, F., 1998. Friedel-Crafts catalytic alkylations using rare earth based mineral supports. *Comptes Rendus de l'Académie des Sciences, Serie II Fascicule C-Chimie* 1, 41–48.
- Baudry-Barbier, D., Dormond, A., Duriau-Montagne, F., 1999. Catalytic activity of rare-earth-supported catalysts in Friedel-Crafts acylations. *Journal of Molecular Catalysis A-Chemistry* 149, 215–224.
- Belville, D.J., Wirth, D.D., Bauld, N.L., 1981. The cation-radical catalyzed Diels-Alder reaction. *Journal of the American Chemical Society* 103, 718–720.
- Besun, N., Ozkan, F., Gunduz, G., 2002. Alpha-pinene isomerization on acid-treated clays. *Applied Catalysis A-General* 224, 285–297.
- Bigi, F., Carloni, S., Frullanti, B., Maggi, R., Sartori, G., 1999. A revision of the Biginelli reaction under solid acid catalysis. Solvent-free synthesis of dihydropyrimidines over montmorillonite KSF. *Tetrahedron Letters* 40, 3465–3468.
- Bigi, F., Conforti, M.L., Maggi, R., Sartori, G., 2000. Trialkylamine controlled phenol-formaldehyde reaction over clay catalysts: selective and environmentally benign synthesis of salicylic aldehydes. *Tetrahedron* 56, 2709–2712.

- Biro, K., Bekassy, S., Agai, B., Figueras, F., 2000. Heterogeneous catalysis for the acetylation of benzo crown ethers. *Journal of Molecular Catalysis A-Chemistry* 151, 179–184.
- Boricha, A.B., Mody, H.M., Das, A., Bajaj, H.C., 1999. Facile dihydroxylation of styrene using clay based catalysts. *Applied Catalysis A-General* 179, 5–10.
- Bosch, A.I., de la Cruz, P., Diez-Barra, E., Loupy, A., Langa, F., 1995. Microwave-assisted Beckmann rearrangement of ketoximes in dry media. *Synthesis Letters*, pp. 1259–1260.
- Bougrin, K., Loupy, A., Petit, A., Daou, B., Soufiaoui, M., 2001. Novel synthesis of 2-trifluoromethylarylimidazoles on montmorillonite K10 in a 'dry medium' under microwave irradiation. *Tetrahedron* 57, 163–168.
- Breen, C., 1999. The characterisation and use of polycation-exchanged bentonites. *Applied Clay Science* 15, 187–219.
- Breen, C., Deane, A., Flynn, J.J., 1987. The acidity of trivalent cation-exchanged montmorillonite—temperature-programmed desorption and infrared studies of pyridine and *n*-butylamine. *Clays and Clay Minerals* 22, 169–178.
- Breen, C., Moronta, A.J., 2001. Influence of exchange cation and layer charge on the isomerization of  $\alpha$ -pinene over SWy-2, SAZ-1 and Sap-Ca. *Clay Minerals* 36, 467–472.
- Breen, C., Watson, R., 1998. Acid-activated organoclays: preparation, characterisation and catalytic activity of polycation-treated bentonites. *Applied Clay Science* 12, 479–494.
- Brochette, S., Descotes, G., Bouchu, A., Queneau, Y., Monnier, N., Petrier, C., 1997. Effect of ultrasound on KSF/O mediated glycosylations. *Journal of Molecular Catalysis A-Chemistry* 123, 123–130.
- Brown, D.R., Rhodes, C.N., 1997. Brønsted and Lewis acid catalysis with ion-exchanged clays. *Catalysis Letters* 45, 35–40.
- Bujdák, J., Rode, B.M., 1996. The effect of smectite composition on the catalysis of peptide bond formation. *Journal of Molecular Evolution* 43, 326–333.
- Bujdák, J., Rode, B.M., 1997. Silica, alumina, and clay-catalyzed alanine peptide bond formation. *Journal of Molecular Evolution* 45, 457–466.
- Bujdák, J., Rode, B.M., 1999. The effect of clay structure on peptide bond formation catalysis. *Journal of Molecular Catalysis A-Chemistry* 144, 129–136.
- Bujdák, J., LeSon, H., Yongyai, Y., Rode, B.M., 1996. The effect of reaction conditions on montmorillonite-catalysed peptide formation. *Catalysis Letters* 37, 267–272.
- Burch, R., Warburton, C.I., 1986. Pillared clays as demetallization catalysts. *Journal of Catalysis* 97, 511–515.
- Bylina, A., Adams, J.M., Graham, S.H., Thomas, J.M., 1980. Chemical conversions using sheet silicates: a simple method for producing methyl *t*-butyl ether (MTBE). *Journal of the Chemical Society, Chemical Communications*, pp. 1003–1004.
- Caine, M., Dyer, G., Holder, J.V., Osbourne, B.N., Mear, W.A., McCabe, R.W., Mobbs, D., Richardson, S., Wang, L., 1999. The use of clays as sorbents and catalysts. Natural microporous materials in environmental technology, In: Misaelides, P., Macasek, F., Pinnavaia, T.J., Colella, C. (Eds.), NATO Advanced Research Workshop, Smolenice Castle, Slovakia, 26–30 October 1998. NATO Science Series 362, Kluwer Academic Publishers, Dordrecht, Netherlands, pp. 49–69.
- Campanati, M., Savini, P., Tagliani, A., Vaccari, A., Piccolo, O., 1997. Environmentally friendly vapour phase synthesis of alkylquinolines. *Catalysis Letters* 47, 247–250.
- Cano, A.C., Cordoba, A.A., Marquez, C., Alvarez, C., 1988. Carbonyl-compounds regeneration with a Mexican bentonite. 2. *Synthetic Communications* 18, 2051–2053.

- Carrado, K.A., 2000. Synthetic organo- and polymer-clays: preparation, characterization, and materials applications. *Applied Clay Science* 17, 1–23.
- Carrero, H., Leon, L.E., 2001. Electrochemically active films of negatively charged molecules, surfactant and synthetic clays. *Electrochemical Communications* 3, 417–420.
- Cebula, D.J., Thomas, R.K., Middleton, S., Ottewill, R.H., White, J.W., 1979. Neutron diffraction from clay water systems. *Clays and Clay Minerals* 27, 39–52.
- Chalais, S., Cornelis, A., Laszlo, P., Mathy, A., 1985. Catalysis of the Knoevenagel reaction. *Tetrahedron Letters*, pp. 2327–2328.
- Chatterjee, D., Mitra, A., 1999. Olefin epoxidation catalysed by Schiff-base complexes of Mn and Ni in heterogenised-homogeneous systems. *Journal of Molecular Catalysis A-Chemistry* 144, 363–367.
- Chevron Research Co., 1972. Catalytic isomerization process. US Patent, 3655798.
- Chevron Research Co., 1973. Process for obtaining isopentane from butane hexane or mixtures thereof. US Patent, 3766292.
- Chiche, B., Finiels, A., Gauthier, C., Geneste, P., Graille, J., Pioch, D., 1987. Acylation over cation-exchanged montmorillonite. *Journal of Molecular Catalysis* 42, 229–235.
- Chivadze, G.O., Khakhnelidze, V.V., 1987. New catalysts based on aluminosilicates for alkylation of phenol by olefins. *Heterogeneous Catalysis* 6, 454–458.
- Choudary, B.M., Kantam, M.L., Bharathi, B., Reddy, C.R.V., 2001. Mn(III) salen complex: an efficient reusable acylation catalyst. *Journal of Molecular Catalysis A-Chemistry* 168, 69–73.
- Choudary, B.M., Prasad, A.D., Bhuma, V., Swapna, V., 1992. Chromium-pillared clay as a catalyst for benzylic oxidation and oxidative deprotection of benzyl ethers and benzylamines—a simple and convenient procedure. *Journal of Organic Chemistry* 57, 5841–5844.
- Choudary, B.M., Villi, V.L.K., Prasad, A.D., 1990. A new vanadium-pillared montmorillonite catalyst for the regioselective epoxidation of allylic alcohols. *Journal of the Chemical Society, Chemical Communications*, pp. 721–722.
- Clark, J.H., Cullen, S.R., Barlow, S.J., Bastock, T.W., 1994. Environmentally friendly chemistry using supported reagent catalysts—structure–property relationships for Clayzic. *Journal of the Chemical Society, Perkin Transactions* 2, 1117–1130.
- Clark, J.H., Ross, J.C., Macquarrie, D.J., Barlow, S.J., Bastock, T.W., 1997. Environmentally friendly catalysis using supported reagents: the fast and selective bromination of aromatic substrates using supported zinc bromide. *Chemical Communications* 13, 1203–1204.
- Clark, P.D., Mesher, S.T., 1995. Benzylolation of benzo[b]thiophene using ZnCl<sub>2</sub>-modified montmorillonite clay. *Phosphorus, Sulfur & Silicon & the Related Elements* 105, 157–162.
- Conan, J.Y., Natat, A., Privolet, D., 1976. Acid hydrolysis of some dioxaspirocyclanes. *Bulletin de la Société Chimique de France* 11–12 (pt 2), 1935–1940.
- Constantini, M., Popa, J.M., 1989. Process for hydroxylating phenols and phenol ethers. European Patent, EP0299893.
- Cornelis, A., Depaye, N., Gerstmans, A., Laszlo, P., 1983. Clay-supported reagents 4. A novel coupling of thiols into disulfides, via thionitrite intermediates using a clay-supported nitrosation reagent. *Tetrahedron Letters*, pp. 3103–3106.
- Cornelis, A., Laszlo, P., 1980. Oxidation of alcohols by clay-supported iron(III) nitrate; a new efficient oxidising agent. *Synthesis*, pp. 849–850.

- Cornelis A., Laszlo P., 1982. Clay-supported reagents 2. Quaternary ammonium-exchanged montmorillonite as catalyst in the phase-transfer preparation of symmetrical formaldehyde acetals. *Synthesis*, pp. 162–163.
- Cornelis, A., Laszlo, P., 1986. Preparative organic chemistry using clays. In: Setton, R. (Ed.), *Chemical Reactions in Organic and Inorganic Constrained Systems*. Reidel, New York, pp. 213–218.
- Cramarossa, M.R., Forti, L., Pagnoni, U.M., Vidali, M., 2001. Cyclization of citronellal to menthone and *iso*-menthone catalyzed by Al/Fe-pillared clays. *Synthesis* (1), pp. 52–54.
- Dauben, W.G., Cogen, J.M., Behar, V., 1990. Clay catalyzed rearrangement of substituted allyl phenyl ethers—synthesis of ortho-allyl phenols, chromans and coumarans. *Tetrahedron Letters* 31, 3241–3244.
- Den Otter, M.J.A.M., 1970a. The dimerization of oleic acid with a montmorillonite catalyst, I. Important process parameters; some main reactions. *Fette, Seifen, Anstrichmittel* 72, 667–673.
- Den Otter, M.J.A.M., 1970b. The dimerization of oleic acid with a montmorillonite catalyst, II. Glc analysis of the monomer; the structure of the dimer; a reaction model. *Fette, Seifen Anstrichmittel* 72, 875–883.
- Den Otter, M.J.A.M., 1970c. The dimerization of oleic acid with a montmorillonite catalyst, III. Test of the reaction model. *Fette, Seifen, Anstrichmittel* 72, 1056–1066.
- Dewan, S.K., Varma, U., Malik, S.D., 1995. Synthesis of enamines from cycloalkanones and secondary cyclic amines using K-10 montmorillonite clay. *Journal of Chemical Research* (1), 21.
- Ding, P.Z., Kawamura, K., Ferris, J.P., 1996. Oligomerization of uridine phosphorimidazolides on montmorillonite: a model for the prebiotic synthesis of RNA on minerals. *Origins of Life and Evolution of the Biosphere* 26, 151–171.
- Ding, Z., Klopogge, J.T., Frost, R.L., Lu, G.Q., Zhu, H.Y., 2001. Porous clays and pillared clay-based catalysts. Part 2: a review of the catalytic and molecular sieve applications. *Journal of Porous Materials* 8, 273–293.
- Downing, R.S., van Amstel, J., Joustra, A.H., 1978. Dimerization process catalyst. US Patent, 4125483.
- Duan, H.Y., Wang, J.X., Li, T.S., 1999. Montmorillonite clay catalysis. Part 15. Backbone rearrangement of 4,4-dialkylcholest-5-enes catalyzed by montmorillonite K-10. *Synthetic Communications* 29, 3197–3205.
- Endo, T., Mortland, M.M., Pinnavaia, T.J., 1980. Intercalation of silica in smectite. *Clays and Clay Minerals* 28, 105–110.
- Ertem, G., Ferris, J.P., 1997. Template-directed synthesis using the heterogeneous templates produced by montmorillonite catalysis. A possible bridge between the prebiotic and RNA worlds. *Journal of the American Chemical Society* 119, 7197–7201.
- Ertem, G., Ferris, J.P., 1998. Formation of RNA oligomers on montmorillonite: site of catalysis. *Origins of Life and Evolution of the Biosphere* 28, 485–499.
- Ertem, G., Prabakar, K.J., Joshi, P.C., Ferris, J.P., 2000. Bridging the prebiotic and RNA worlds: prebiotic RNA synthesis on clay. *Journal of Biomolecular Structure and Dynamics*, Special Issue S2, 207–210.
- Fahn, R., 1979. Acid-activated clays and their adsorption properties. SME-AIME Fall Meeting, Tucson, Arizona.

- Fahn, R., Fenderl, K., 1983. Reaction-products of organic-dye molecules with acid-treated montmorillonite. *Clay Minerals* 18, 447–458.
- Ferris, J.P., 2002. Montmorillonite catalysis of 30–50 mer oligonucleotides: laboratory demonstration of potential steps in the origin of the RNA world. *Origins of Life and Evolution of the Biosphere* 32, 311–332.
- Ferris, J.P., 1999. Prebiotic synthesis on minerals: bridging the prebiotic and RNA worlds. *Biological Bulletin* 196, 311–314.
- Ferris, J.P., 2002. Montmorillonite catalysis of 30–50 mer oligonucleotides: laboratory demonstration of potential steps in the origin of the RNA world. *Origins of Life and Evolution of the Biosphere* 32, 311–332.
- Foucaud, A., Bakouetila, M., 1987. Facile epoxidation of alumina-supported electrophilic alkenes and montmorillonite-supported electrophilic alkenes with sodium-hypochlorite. *Synthesis* 9, 854–856.
- Fraile, J.M., Garcia, J.I., Massam, J., Mayoral, J.A., 1998. Clay-supported non-chiral and chiral Mn(salen) complexes as catalysts for olefin epoxidation. *Journal of Molecular Catalysis A-Chemistry* 136, 47–57.
- Franz, W., Gunter, P., Hofstadt, C.E., 1959. Catalysis based on acid activated bentonites. *Erdöl und Kohle* 12, 335.
- Fujita, K., Ishida, Y., Suezawa, J., 1987a. Production of alkylene glycol monoalkyl ether. *Japanese Patent*, 62289537.
- Fujita, T., Mizuno, K., Saeli, K., 1987b. Oxidation of alcohols. *Japanese Patent*, 62142134 A2.
- Geier, G.R., Ciringh, Y., Li, F.R., Haynes, D.M., Lindsey, J.S., 2000. A survey of acid catalysts for use in two-step, one-flask syntheses of meso-substituted porphyrinic macrocycles. *Organic Letters* 2, 1745–1748.
- Geier, G.R., Lindsey, J.S., 2002. Effects of diverse acid catalysts on the reaction course in the two-step one-flask synthesis of meso-tetraphenylporphyrin. *Journal of Porphyrins and Phthalocyanines* 6 (3), 159–185.
- Ghosh, P.K., Bard, A.J., 1983. Clay-modified electrodes. *Journal of the American Chemical Society* 105, 5691–5693.
- Ghosh, P.K., Mau, A.W.H., Bard, A.J., 1984. Clay-modified electrodes. 2. Electrocatalysis at bis(2,2'-bipyridyl) (4,4'-dicarboxy-2,2'-bipyridyl)Ru(II)-dispersed ruthenium dioxide hectorite layers. *Journal of Electroanalytical Chemistry* 169, 315–317.
- Gobi, K.V., Ramaraj, R., 1998. Multistep one-electron photoelectrocatalytic reduction of oxygen at tris(2,2'-bipyridine)ruthenium(II)-incorporated Nafion (R)- and clay-coated electrodes in the presence of macrocyclic cobalt(III) complexes. *Journal of Electroanalytical Chemistry* 449, 81–89.
- Graham, A.R., McGrath, B.P., Yoemans, B., 1974. Maleic anhydride production. *GB Patent*, 1359113.
- Gregory, R., Smith, D.J.H., Westlake, D.J., 1983. The production of ethyl-acetate from ethylene and acetic-acid using clay catalysts. *Clay Minerals* 18, 431–435.
- Grzybek, T., Klinik, J., Olszewska, D., Papp, H., Smarzowski, J., 2001. The influence of montmorillonite treatment on structure, sorption properties and catalytic behaviour: part I. Zirconia-pillared clays modified with manganese as denox catalysts. *Polish Journal of Chemistry* 75, 857–868.
- Gutierrez, E., Aznar, A.J., Ruiz-Hitzky, E., 1988. Selectivity of the catalytic rearrangement of 1,2-glycols on acidic solids. *Studies in Surface Science and Catalysis* 41, 211–219.

- Gutierrez, E., Loupy, A., Bram, G., Ruiz-Hitzky, E., 1989. Inorganic solids in dry media—an efficient way for developing microwave irradiation-activated organic reactions. *Tetrahedron Letters* 30, 945–948.
- Gutierrez, E., Ruiz-Hitzky, E., 1987. Intracrystalline pinacol rearrangement in layer silicates. *Molecular Crystals and Liquid Crystals* 161B, 453–458.
- Habib, A.M., Saafan, A.A., Abou-Seif, A.K., Salem, M.A., 1988. Catalytic conversion of *n*-pentanol to 1,1-dialkyl ether by aluminum and iron exchanged montmorillonite catalyst. *Colloids and Surfaces* 29, 337–341.
- Hammadi, M., Villemin, D., 1996. Clay catalysis: Stork's alkylation and acylation of cyclohexanone without isolation of enamine. *Synthetic Communications* 26, 2901–2904.
- Han, B.H., Jang, D.G., 1990. Montmorillonite catalyzed reduction of nitroarenes with hydrazine. *Tetrahedron Letters* 31, 1181–1182.
- Hashimoto, K., Asahi, Y., Maki, T., 1988. Production of cyclohexanol and cyclohexanone. Japanese Patent, 63303936.
- Hassan, B.E.M., Sultan, E.A., Tawfik, F.M., Sappah, S.M., 1985. Catalytic alkylation of benzene in the vapor phase. *Egyptian Journal of Chemistry* 28, 93–98.
- Hothi, B., Lechene, V., Robinson, J., Sheriff, T.S., 1997. The production of hydrogen peroxide from dioxygen using hydroxylamine as substrate catalysed by  $Mn^{2+}$ -exchanged montmorillonite clay. *Polyhedron* 16, 1403–1406.
- Houk, K.N., Strozier, R.W., 1973. On Lewis acid catalysis of Diels-Alder reactions. *Journal of the American Chemical Society* 95, 4094–4096.
- Hu, N.F., 2001. Direct electrochemistry of redox proteins or enzymes at various film electrodes and their possible applications in monitoring some pollutants. *Pure and Applied Chemistry* 73, 1979–1991.
- Huber, R.S., Jones, G.B., 1992. Acceleration of the ortho ester Claisen rearrangement by clay-catalyzed microwave thermolysis—expeditious route to bicyclic lactones. *Journal of Organic Chemistry* 57, 5778–5780.
- Hünig, S., Hubner, K., Benzing, S.D., 1962. Synthesis with enamines VII. Addition of isocyanates and isothiocyanates to enamines. *Chemische Berichte* 95, 926–936.
- Ilangovan, G., Zen, J.M., 1999. First observation that electroinactive bound cations in clay can participate in electrocatalytic reaction. *Chemical Letters* 2, 153–154.
- Imanari, M., Iwane, H., Sugawara, T., 1987. Production of *tert*-amylphenol. Japanese Patent, 62153235.
- Iqbal, Z., Jackson, A.H., Rao, K.R.N., 1988. Reactions on solid supports. 4. Reactions of  $\alpha$ ,  $\beta$ -unsaturated carbonyl-compounds with indoles using clay as catalyst. *Tetrahedron Letters* 29, 2577–2580.
- Issaadi, R., Garin, F., Chitour, C.E., Maire, G., 2001. Catalytic behaviour of combined palladium-acid catalysts: use of Al and Zr-pillared montmorillonite as supports. Part I. Reactivity of linear, branched and cyclic hexane hydrocarbons. *Applied Catalysis A-General* 207, 323–332.
- Jankovic, E., Komadel, P., 2000. Catalytic properties of a heated ammonium-saturated dioctahedral smectite. *Collection of Czech Chemical Communications* 65, 1527–1536.
- Jia, W., Segal, E., Narkis, M., Siegmann, A., 2002. Polymerization of anilinium-DBSA in the presence of clay particles: kinetics and formation of core-shell structures. *Polymer Advanced Technology* 13, 16–24.

- Jnaneshwara, G.K., Deshpande, V.H., Bedekar, A.V., 1999. Clay-catalyzed conversion of 2,2-disubstituted malononitriles to 2-oxazolines: towards unnatural amino acids. *Journal of Chemical Research (S)* 4, 252–253.
- Jnaneshwara, G.K., Deshpande, V.H., Lalithambika, M., Ravindranathan, T., Bedekar, A.V., 1998. Natural kaolinitic clay-catalyzed conversion of nitriles to 2-oxazolines. *Tetrahedron Letters* 39, 459–462.
- Kamath, C.R., Samant, S.D., 1999. Diels-Alder reaction of pyran-2(H)-ones: part III—The Diels-Alder reactions of 4,6-disubstituted pyran-2(H)-ones with naphthoquinone and *N*-phenylmaleimide on montmorillonite K10, Engelhard Filtrol-24 and pyrophyllite clays. *Indian Journal of Chemistry Section B-Organic Chemistry Including Medicinal Chemistry* 38, 1214–1217.
- Kamath, C.R., Shinde, A.B., Samant, S.D., 2000. Diels-Alder reaction of Pyran-2(H)-ones: part V—Diels-Alder reaction of 4,6-disubstituted pyran-2(H)-ones with 1,4-naphthoquinone and *N*-phenylmaleimide under dry state adsorbed condition (DSAC) on montmorillonite K10, Filtrol-24, bentonite, pyrophyllite; and  $\text{Al}^{3+}$ ,  $\text{Zn}^{2+}$ ,  $\text{Fe}^{3+}$  exchanged montmorillonite K10 and bentonite. *Indian Journal of Chemistry Section B-Organic Chemistry Including Medicinal Chemistry* 39, 270–276.
- Kannan, P., Pitchumani, K., 1997. Clay-catalysed radical addition of aliphatic thiols to styrene. *Catalysis Letters* 45, 271–273.
- Kannan, P., Pitchumani, K., Rajagopal, S., Srinivasan, C., 1997. Sheet silicate catalysed demethylation and Fischer-Hepp rearrangement of *N*-methyl-*N*-nitrosoaniline. *Journal of Molecular Catalysis A-Chemistry* 118, 189–193.
- Kapustin, A.E., Shvets, V.F., Makarove, M.G., Simenido, A.V., Zeiberlikh, F.N., 1986. Hydroxyethylation of alcohols in the presence of bentonite. *Neftekhimiya* 26, 267–271.
- Katchalsky, A., Ailam, G., 1967. Polycondensation of amino acid phosphoanhydrides. I. Theoretical. *Biochimica et Biophysica Acta* 140, 1–13.
- Kawai, M., Onaka, M., Izumi, Y., 1986a. Clay montmorillonite-catalyzed aldol reactions of silyl enol ethers with aldehydes and acetals. *Chemical Letters* 9, 1581–1584.
- Kawai, M., Onaka, M., Izumi, Y., 1986b. Solid acid-catalyzed allylation of acetals and carbonyl-compounds with allylic silanes. *Chemical Letters* 9, 381–384.
- Kawai, M., Onaka, M., Izumi, Y., 1987. Clay montmorillonite-catalyzed Michael reactions of silyl ketene acetals and a silyl enol ether with unsaturated carbonyl-compounds. *Journal of the Chemical Society, Chemical Communications*, pp. 1203–1204.
- Kawai, M., Onaka, M., Izumi, Y., 1988a. New application of solid acid to carbon-carbon bond formation reactions—clay montmorillonite-catalyzed Aldol reactions of silyl enol ethers with aldehydes and acetals. *Bulletin of the Chemical Society of Japan* 61, 1237–1245.
- Kawai, M., Onaka, M., Izumi, Y., 1988b. Clay montmorillonite—an efficient, heterogeneous catalyst for Michael reactions of silyl ketene acetals and silyl enol ethers with  $\alpha,\beta$ -unsaturated carbonyl-compounds. *Bulletin of the Chemical Society of Japan* 61, 2157–2164.
- Kawamura, K., Ferris, J.P., 1999. Clay catalysis of oligonucleotide formation: kinetics of the reaction of the 5'-phosphorimidazolides of nucleotides with the non-basic heterocycles uracil and hypoxanthine. *Origins of Life and Evolution of the Biosphere* 29, 563–591.
- Kikuchi, E., Matsuda, T., 1988. Shape selective acid catalysis by pillared clays. *Catalysis Today* 2, 297–307.
- Klopprogge, J.T., 1998. Synthesis of smectites and porous pillared clay catalysts: a review. *Journal of Porous Materials* 5, 5–41.

- Knifton, J.F., Edwards, J.C., 1999. Methyl *tert*-butyl ether synthesis from *tert*-butanol via inorganic solid acid catalysis. *Applied Catalysis A-General* 183, 1–13.
- Knifton, J.F., Sanderson, J.R., 1997. Phenol/acetone cogeneration via solid acid catalysis. *Applied Catalysis A-General* 161, 199–211.
- Kondo, M., Tanaka, M., Taniguchi, K., 1990. Production of aromatic acetyl compound. Japanese Patent, 02115140.
- Konin, G.A., Il'ichev, A.N., Matyshak, V.A., Khomenko, T.I., Korchak, V.N., Sadykov, V.A., Doronin, V.P., Bunina, R.V., Alikina, G.M., Kuznetsova, T.G., Paukshtis, E.A., Fenelonov, V.B., Zaikovskii, V.I., Ivanova, A.S., Beloshapkin, S.A., Rozovskii, A.Y., Tretyakov, V.F., Ross, J.R.H., Breen, J.P., 2001. Cu, Co, Ag-containing pillared clays as catalysts for the selective reduction of NO<sub>x</sub> by hydrocarbons in an excess of oxygen. *Topics in Catalysis* 16, 193–197.
- Kowalska, M.W., Ortego, J.D., Jezierski, A., 2001. Transformation of 2-(trifluoromethyl)aniline over ion-exchanged montmorillonites: Formation of a dimer and cyclic trimer. *Applied Clay Science* 18, 233–243.
- Kullaj, S., 1989. Effect of the characteristics of activated clays on their ability to lead to isomerization of  $\alpha$ -pinene into camphene and tricyclene. *Buletini i Shkencave të Natyrës* 43, 81–85 (in Albanian).
- Labiad, B., Villemin, D., 1989. Clay catalysis—synthesis of organosulfur synthons. *Synthetic Communications* 19, 31–38.
- Lahav, N., Shani, U., Shabtai, J., 1978. Cross-linked smectites II. Flocculation and microfabric characteristics of hydroxyaluminium montmorillonite. *Clays and Clay Minerals* 26, 107–115.
- Laszlo, P., 1986a. Catalysis of organic reactions by inorganic solids. *Accounts of Chemical Research* 19, 121–127.
- Laszlo, P., 1986b. Personal communication.
- Laszlo, P., 1987. *Preparative Chemistry using Supported Reagents*. Academic Press, New York.
- Laszlo, P., Lucchetti, J., 1984a. Catalyse de la réaction de Diels et Alder. *L'Actualité Chimique* 42–44.
- Laszlo, P., Lucchetti, J., 1984b. Catalysis of the Diels-Alder reaction in the presence of clays. *Tetrahedron Letters* 25, 1567–1570.
- Laszlo, P., Lucchetti, J., 1984c. Acceleration of the Diels-Alder reaction by clays suspended in organic solvents. *Tetrahedron Letters* 25, 2147–2150.
- Laszlo, P., Lucchetti, J., 1984d. Easy formation of Diels-Alder cycloadducts between furans and  $\alpha$ ,  $\beta$ -unsaturated aldehydes and ketones at normal pressure. *Tetrahedron Letters* 25, 4387–4388.
- Laszlo, P., Mathy, A., 1987. Catalysis of Friedel-Crafts alkylation by a montmorillonite doped with transition-metal cations. *Helvetica Chimica Acta* 70, 577–586.
- Laszlo, P., Moison, H., 1989. Catalysis of Diels-Alder reactions with acrolein as dienophile by iron(III)-doped montmorillonite. *Chemical Letters* 6, 1031–1034.
- Laszlo, P., Montaufer, M.T., Randriamahefa, S.L., 1990. Dual catalysis of the Michael Reaction. *Tetrahedron Letters* 31, 4867–4870.
- Laszlo, P., Polla, E., 1984. Efficient conversion of hydrazines to azides with clay-supported ferric nitrate. *Tetrahedron Letters* 25, 3701–3704.
- Lee, V.S., Kim, H., Solin, S.A., Pinnavaia, T.J., 1987. Layer rigidity of clay intercalation compounds: [Me<sub>4</sub>N<sup>+</sup>]<sub>1-x</sub>[Me<sub>3</sub>NH<sup>+</sup>]<sub>x</sub>-vermiculite. In: Legrand, A.P., Flandrois, S. (Eds.), *NATO Advanced Study Institute on the Chemical Physics of Intercalation*, pp. 172, 497.



- Li, L.J., Lu, B., Li, T.S., Li, J.T., 1998. Montmorillonite clay catalysis. Part 8. Synthesis of arylcholestenes by Friedel-Crafts reaction catalysed by montmorillonite K-10. *Synthetic Communications* 28, 1439–1449.
- Li, T.S., Li, A.X., 1998. Montmorillonite clay catalysis. Part 10. K-10 and KSF-catalysed acylation of alcohols, phenols, thiols and amines: scope and limitation. *Journal of the Chemical Society, Perkin Transactions I* 12, 1913–1917.
- Li, T.S., Li, L.J., Lu, B., Yang, F., 1998a. Montmorillonite clay catalysis. Part 14. A facile synthesis of 2-substituted and 2,2-disubstituted 1,3-benzodioxoles. *Journal of the Chemical Society, Perkin Transactions I* 21, 3561–3564.
- Li, T.S., Li, S.H., 1997. Montmorillonite clay catalysis. 3. A new ready and high yield procedure for the cleavage of acetals catalysed by montmorillonite K10. *Synthetic Communications* 27, 2299–2303.
- Li, T.S., Li, S.H., Li, J.T., Li, H.Z., 1997a. Montmorillonite clay catalysis. 2. An efficient and convenient procedure for the preparation of acetals catalysed by montmorillonite K-10. *Journal of Chemical Research (S)*, (1), 26–27.
- Li, T.S., Zhang, Z.H., Fu, C.G., 1997b. Montmorillonite clay catalysis V: an efficient and facile procedure for deprotection of 1,1-diacetates. *Tetrahedron Letters* 38 (18), 3285–3288.
- Li, T.S., Zhang, Z.H., Jin, T.S., 1999. Montmorillonite clay catalysis IX: a mild and efficient method for removal of tetrahydropyranyl ethers. *Synthetic Communications* 29, 181–188.
- Li, T.S., Zhang, Z.H., Yang, F., Fu, C.G., 1998b. Montmorillonite clay catalysis. Part 7. An efficient and facile procedure for the synthesis of coumarins via Pechmann condensation of phenols with ethyl acetoacetate. *Journal of Chemical Research (S)*, (1), 38–39.
- Lin, C.L., Pinnavaia, T.J., 1991. Organo clay assemblies for triphase catalysis. *Chemistry of Materials* 3, 213–215.
- Lingaiah, N., Narender, R., 2002. Tetrachloropyridine: a new reagent for the dehydration of aldoximes under microwave. *Synthetic Communications* 32, 2391–2394.
- Loupy, A., 1999. Solvent-free reactions. *Topics in Current Chemistry* 206, 153–207.
- Lu, B., Li, L.J., Li, T.S., Li, J.T., 1998. Montmorillonite clay catalysis. Part 13. Etherification of cholesterol catalysed by montmorillonite K-10. *Journal of Chemical Research (S)*, (9), 604–605.
- Macha, S.M., Fitch, A., 1998. Clays as architectural units at modified-electrodes. *Mikrochimica Acta* 128 (1–2), 1–18.
- Mao, R., 2003. Heterogenous Catalysis of Inorganic Reactions. Ph.D. thesis. University of Central Lancashire.
- Martil, E.N., Aragon de la Cruz, F., 1986. Formation of monosaccharides from glycolaldehyde in a water suspension of  $\text{Na}^+$ -montmorillonite. *Anales de Quimica Serie B-Quimica Inorganica y Quimica Analytica* 82, 256–259.
- Martin, K., 1986. Clay Catalysed Organic Reactions. Ph.D. thesis. University College of Wales, Aberystwyth.
- Matsuda, T., Asanuma, M., Kikuchi, E., 1988. Effect of high-temperature treatment on the activity of montmorillonite pillared by alumina in the conversion of 1,2,4-trimethylbenzene. *Applied Catalysis* 38, 289–299.
- McCabe, R.W., 1996. Clay chemistry. In: Bruce, D.W., O'Hare, D. (Eds.), *Inorganic Materials*, 2nd ed. Wiley, Chichester, pp. 313–376.
- Meshram, H.M., 1992. Dehydration of aldoximes to nitriles with clay. *Synthesis*, pp. 943–944.

- Miranda, R., Escobar, A., Delgado, F., Salmon, M., Cabrera, A., 1999. Catalytic promotion of piperonyl alcohol to trimethylenedioxyorthocyclophane by bentonitic earth, or by hydrochloric acid. *Journal of Molecular Catalysis A-Chemistry* 150, 299–305.
- Mitra, A.K., De, A., Karchaudhuri, N., 1999. Regeneration of aldehydes from bisulfite addition products in the solid state using montmorillonite KSF clay under microwave irradiation. *Journal of Chemical Research (S)* 9, 560–561.
- Morikawa, Y., Goto, T., Moro-oka, Y., Ikawa, T., 1982. Conversion of methanol to low molecular weight hydrocarbons over Ti ion-exchanged form of layered silicate minerals. *Chemical Letters*, pp. 1667–1670.
- Mortland, M.M., Raman, K.V., 1968. Surface acidity of smectites in relation to hydration, exchangeable cation and structure. *Clays and Clay Minerals* 16, 393–398.
- Musaev, M.R., Mirzabekova, S.R., Alieva, L.I., Gasanov, A.G., Makhmudov, Kh.I., 1986. Isomerisation of hexenes on perlite in their formation from alcohols. *Azerbajdzhanskij Neftekhimiya Khozyajstve* 1, 44–46.
- Nagy, N.M., Jakab, M.A., Konya, J., Antus, S., 2002. Convenient preparation of 1,1-diacetates from aromatic aldehydes catalysed by zinc-montmorillonite. *Applied Clay Science* 21, 213–216.
- Naicker, K.P., Pitchumani, K., Varma, R.S., 1998. The catalytic influence of clays on Bamberger rearrangement: unexpected formation of *p*-nitrosodiphenyl amine from *N*-phenylhydroxylamine. *Catalysis Letters* 54 (3), 165–167.
- Narayanan, S., Deshpande, K., 2000. Alumina pillared montmorillonite: characterization and catalysis of toluene benzylation and aniline ethylation. *Applied Catalysis A-General* 193 (1–2), 17–27.
- Natekar, R.S., Samant, S.D., 1995. Catalysis of Friedel-Crafts alkylation using virgin and Lewis-acid doped bentonite K-10. *Indian Journal of Chemistry Section B-Organic Chemistry Including Medicinal Chemistry* 34, 257–260.
- Negron-Mendoza, A., Ramos-Bernal, S., 1998. Radiolysis of carboxylic acids adsorbed in clay minerals. *Radiation Physics and Chemistry* 52 (1–6), 395–399.
- Newton, L.S., 1984. Dimer acids and their derivatives—potential applications. *Speciality Chemicals* 17.
- NL Industries Inc., 1977. Catalyst useful in alkylation of aromatic hydrocarbons. US Patent, 4217295.
- O'Neil, R.M., 1982. Post doctoral report. University College Swansea.
- Onaka, M., Higuchi, K., Nanami, H., Izumi, Y., 1993. Reduction of carbonyl-compounds with hydrosilanes on solid acid and solid base. *Bulletin of the Society of Japan* 66, 2638–2645.
- Onaka, M., Ono, R., Kawai, M., Izumi, Y., 1987. Clay montmorillonite-catalyzed aldol reactions of silyl ketene acetals with carbonyl-compounds. *Bulletin of the Chemical Society of Japan* 60, 2689–2691.
- Paecht-Horowitz, M., 1977. The mechanism of clay catalysed polycondensation of amino acid adenylates. *Biosystems* 9, 93–98.
- Paecht-Horowitz, M., Berger, J., Katchalsky, A., 1970. Prebiotic synthesis of polypeptides by heterogeneous polycondensation of amino acid adenylates. *Nature* 228, 636–639.
- Pai, S.G., Bajpai, A.R., Deshpande, A.B., Samant, S.D., 2000. Benzylation of arenes in the presence of montmorillonite K10 modified using aqueous and acetonitrile solutions of FeCl<sub>3</sub>. *Journal of Molecular Catalysis A-Chemistry* 156, 233–243.

- Park, E.D., Lee, K.H., Lee, J.S., 2000. Easily separable molecular catalysis. *Catalysis Today* 63, 147–157.
- Petridis, D., Kaviratna, P.D., Pinnavaia, T.J., 1996. Electrochemistry of alumina pillared clay modified electrodes. *Journal of Electroanalytical Chemistry* 410, 93–99.
- Pinnavaia, T.J., 1986. Pillared clays: synthesis and structural features. In: Setton, R. (Ed.), *Chemical Reactions in Organic and Inorganic Constrained Systems*. Reidel, New York, pp. 151–164.
- Pitchumani, K., Baskar, P., Venkatachalapathy, C., 1993. Clay-catalyzed nitrodecarboxylation of aromatic-acids. *Catalysis Letters* 21, 157–163.
- Poncelet, G., Schutz, A., 1986. Pillared montmorillonite and beidellite. In: Setton, R. (Ed.), *Chemical Reactions in Organic and Inorganic Constrained Systems*. Reidel, New York, pp. 165–178.
- Prabakar, K.J., Ferris, J.P., 1997. Effect of dinucleoside pyrophosphates on the oligomerization of activated mononucleotides on  $\text{Na}^+$ -montmorillonite: reaction of 5'-phosphoro-4-(dimethylamino)pyridinium [4-( $\text{CH}_3$ )<sub>2</sub>NPYPA] with A(5') ppA. *Origins of Life and Evolution of the Biosphere* 27, 513–523.
- Premkumar, J., Ramaraj, R.J., 1997. Electrocatalytic reduction of dioxygen at platinum particles deposited on Nafion- and clay-coated electrodes. *Solid State Electrochemistry* 1, 172–179.
- Porter, T.L., Eastman, M.P., Bain, E., Begay, S., 2001. Analysis of peptides synthesized in the presence of Saz-1 montmorillonite and  $\text{Cu}^{2+}$  exchanged hectorite. *Biophysical Chemistry* 91, 115–124.
- Porter, T.L., Eastman, M.P., Whitehorse, R., Bain, E., Manygoats, K., 2000. The interaction of biological molecules with clay minerals: a scanning force microscopy study. *Scanning* 22, 1–5.
- Porter, T.L., Whitehorse, R., Eastman, M.P., Bain, E.D., 1999. Studies on the reaction of the 5'-phosphorimidazolide of adenosine with Cu(II)-exchanged hectorite. *Applied Physics Letters* 75, 2674–2676.
- Poupaert, J.H., Bukuru, J., Gozzo, A., 1999. Clay (montmorillonite K10) catalysis of the Michael addition of  $\alpha,\beta$  unsaturated carbonyl compounds to indoles: the beneficial role of alcohols. *Monatshefte für Chemie* 130, 929–932.
- Rao, K.R.N., Towill, R.C., Jackson, A.H., 1989. Reactions on solid supports. 3. Hydrogen isotope exchange-reactions catalyzed by montmorillonite clay. *Journal of the Indian Chemical Society* 66, 654–655.
- Rechsteiner, B., Texier-Boullet, F., Hamelin, J., 1993. Synthesis in dry media coupled with microwave irradiation—application to the preparation of enamino ketones. *Tetrahedron Letters* 34, 5071–5074.
- Rode, B.M., 1999. Peptides and the origin of life. *Peptides* 20, 773–786.
- Rode, B.M., Son, H.L., Suwannachot, Y., Bujdák, J., 1999. The combination of salt induced peptide formation reaction and clay catalysis: a way to higher peptides under primitive Earth conditions. *Origins of Life and Evolution of the Biosphere* 29, 273–286.
- Roudier, J.F., Foucaud, A., 1986. Clay catalysed ene reactions. Synthesis of  $\gamma$ -lactones. In: Setton, R. (Ed.), *Chemical Reactions in Organic and Inorganic Constrained Systems*. Reidel, New York, pp. 229–235.
- Roy, T.A., Blackburn, G.R., Mackerer, C.R., 1999. Processes for reducing the mutagenicity of refinery streams and coal tars via = C3-alkylation. *Polycyclic Aromatic Compounds* 14, 241–251.

- Salerno, P., Asenjo, M.B., Mendioroz, S., 2001. Influence of preparation method on thermal stability and acidity of Al-PILCs. *Thermochimica Acta* 379, 101–109.
- Salmon, M., Perez Luna, M., Lopez Franco, C., Hernandez, E., Alvarez Ramirez, R.A., Lopez Ortega, A., Dominguez, J.M., 1997. Catalytic conversion of propylene oxide on a super acid sulfonic clay (SASC) system. *Journal of Molecular Catalysis A-Chemistry* 122, 169–174.
- Saoudi, A., Hamelin, J., Benhaoua, H., 1996. A rapid synthesis of aziridine derivatives over bentonite in 'dry media'. *Journal of Chemical Research (S)* 11, 492–493.
- Sapag, K., Mendioroz, S., 2001. Synthesis and characterization of micro-mesoporous solids: pillared clays. *Colloids and Surfaces A-Physicochemical and Engineering Aspects* 187, 141–149.
- Sartori, G., Bigi, F., Maggi, R., Mazzacani, A., Oppici, G., 2001. Clay/water mixtures—a heterogeneous and ecologically efficient catalyst for the three-component stereoselective synthesis of tetrahydroquinolines. *European Journal of Organic Chemistry* 13, 2513–2518.
- Sato, H., Hirose, K., Nagai, K., Yoshiokai, H., Nagaoka, Y., 1989. Process for producing nitrobenzenes. European Patent, 343048.
- Sawai, H., Itoh, T., Kokaji, K., Shinozuka, K., 1997. An approach to prebiotic synthesis of alpha-oligoribonucleotides and description of their properties: selective advantage of beta-RNA over alpha-RNA. *Journal of Molecular Evolution* 45, 209–215.
- Segal, E., Aviel, O., Narkis, M., 2000. Polymerization of anilinium/DBSA in the presence of clay particles: catalysis and encapsulation. *Polymer Engineering and Science* 40, 1915–1920.
- Sento, T., Shimazu, S., Ichikuni, N., Uematsu, T., 1998. New clay-supported chiral rhodium complexes: interlayer modification with structural tuning guests and asymmetric hydrogenation. *Chemical Letters* 12, 1191–1192.
- Serwicka, E.M., 2001. Clays as catalysts for the removal of nitrogen oxides. *Polish Journal of Chemistry* 75, 307–328.
- Shi, Z.X., Yu, D.S., Wang, Y.Z., Xu, R.W., 2002. Investigation of isothermal curing behaviour during the synthesis of polybenzoxazine-layered silicate nanocomposites via cyclic monomer. *European Polymer Journal* 38, 727–733.
- Shigeshiro, Y., Oyoshi, H., Fujita, T., 1987. Production of *bis(p-aminocumyl)benzene* compound. Japanese Patent, 62155242.
- Smolen, J.M., Stone, A.T., 1998. Metal (hydr)oxide surface catalyzed hydrolysis of chlorpyrifos-methyl, chlorpyrifos-methyloxon, and paraoxon. *Soil Science Society of America Journal* 62, 636–643.
- Solomon, D.H., Hawthorne, D.G., 1983. *Chemistry of Pigments and Fillers*. Wiley, New York.
- Solomon, D.H., Loft, B.C., Swift, J.D., 1968. Reactions catalysed by minerals. IV. The mechanism of the benzidine blue reaction on silicate minerals. *Clay Minerals* 7, 389–397.
- Soriente, A., Arienzo, R., De Rosa, M., Palombi, L., Spinella, A., Scettri, A., 1999. K10 montmorillonite catalysis—C–C bond formation by catalyzed conjugate addition and alkoxyalkylation of 1,3-dicarbonyl compounds. *Green Chemistry* 1, 157–162.
- Stackhouse, S., Coveney, P.V., Sandre, E., 2001. Plane-wave density functional theoretic study of formation of clay-polymer nanocomposite materials by self-catalyzed in situ intercalative polymerisation. *Journal of the American Chemical Society* 123, 11764–11774.

- Subba Rao, Y.V., Choudary, B.M., 1991. Knoevenagel condensation catalyzed by new montmorillonite silylpropylethylenediamine. *Synthetic Communications* 21, 1163–1166.
- Süd-Chemie, A.G., 1961. Verfahren zur Herstellung von 1,3-Dioxolanen. German Patent, 1086241.
- Suib, S.L., Tanguy, J.F., Occelli, M.F., 1986. Comparison of the photochemical and photophysical properties of clays, pillared clays, and zeolites. *Journal of the American Chemical Society* 108, 6972–6977.
- Taylor, E.C., Chaing, C.-S., 1977. Trimethyl orthoformate adsorbed on montmorillonite clay K-10: an effective reagent for acetal formation. *Synthesis*, pp. 467–467.
- Takagi, K., Usami, H., Fukaya, H., Sawaki, Y., 1989. Spatially controlled photocycloaddition of a clay-intercalated stilbazolium cation. *Journal of the Chemical Society, Chemical Communications*, pp. 1174–1175.
- Takagi, K., Naruse, Y., 1989. Production of monoalkylated phenols. Japanese Patent, 1238549.
- Tao, L.X., Zou, D.X., 2002. Clay-intercalated metal complex catalysts and their molecular recognition catalysis. *Progress in Chemistry* 14, 200–206.
- Tateiwa, J., Nashimura, T., Horiuchi, H., Uemura, S., 1994. Rearrangement of alkyl phenyl ethers to alkylphenols in the presence of cation-exchanged montmorillonite ( $M^{n+}$ -mont). *Journal of the Chemical Society, Perkin Transactions*, pp. I 3367–3371.
- Tateiwa, J.I., Horiuchi, H., Uemura, S., 1995.  $Ce^{3+}$ -exchanged montmorillonite ( $Ce^{3+}$ -mont) as a useful substrate-selective acetalization catalyst. *Journal of Organic Chemistry* 60, 4039–4043.
- Tessis, A.C., Deamorim, H.S., Farina, M., Desouzabarras, F., Vieyra, A., 1995. Adsorption of 5'-amp and catalytic synthesis of 5'-ADP onto phosphate surfaces—correlation to solid-matrix structures. *Origins of Life and Evolution of the Biosphere* 25, 351–373.
- Texier-Boullet, F., Klein, B., Hamelin, J., 1986. Pyrrole and pyrazole ring-closure in heterogeneous media. *Synthesis*, pp. 409–411.
- Theng, B.K.G., 1974. *The Chemistry of Clay-Organic Reactions*. Adam Hilger, London.
- Theng, B.K.G., 1982. Clay-activated organic reactions. In: van Olphen, H., Veniale, F. (Eds.), *International Clay Conference 1981. Developments in Sedimentology*, Vol. 35. Elsevier, Amsterdam, pp. 197–238.
- Thomas, C.L., Hickey, J., Strecker, G., 1950. Clay cracking catalysts. *Industrial Engineering Chemistry* 42, 866–871.
- Thorat, M.T., Jagdale, M.H., Mane, R.B., Sadunkhe, M.M., Wadagaonkar, P.P., 1987. Clay-catalyzed Knoevenagel condensation. *Current Science, India* 56, 771–772.
- Torok, B., Balazsik, K., Dekany, I., Bartok, M., 2000. Preparation and characterization of new chirally modified laponites. *Molecular Crystals and Liquid Crystals* 341, 1143–1148.
- Toyo Soda, M.F.G., 1983. Preparation of hydrocarbon from methanol and/or dimethyl ether. Japanese Patent, 58083635.
- Trombetta, M., Busca, G., Lenarda, M., Storaro, L., Ganzerla, R., Piovesan, L., Lopez, A.J., Alcantara-Rodriguez, M., Rodriguez-Castellon, E., 2000. Solid acid catalysts from clays—evaluation of surface acidity of mono- and bi-pillared smectites by FT-IR spectroscopy measurements,  $NH_3$ -TPD and catalytic tests. *Applied Catalysis A-General* 193, 55–69.
- Vansant, E.F., Cool, P., 2001. Chemical modifications of oxide surfaces. *Colloids and Surfaces A-Physicochemical and Engineering Aspects* 179, 145–150.

- Varma, R.S., 2002. Clay and clay supported reagents in organic synthesis. *Tetrahedron* 58, 1235–1255.
- Varma, R.S., Dahiya, R., 1997a. Microwave-assisted facile synthesis of imines and enamines using envirocat EPZG(R) as a catalyst. *Synthesis Letters*, p. 1245.
- Varma, R.S., Dahiya, R., 1997b. Microwave-assisted oxidation of alcohols under solvent-free conditions using clayfen. *Tetrahedron Letters* 38, 2043–2044.
- Varma, R.S., Dahiya, R., 1998a. Microwave thermolysis with clayfen: solvent-free oxidation of sulfides to sulfoxides. *Synthetic Communications* 28, 4087–4095.
- Varma, R.S., Dahiya, R., 1998b. Copper(ii) nitrate on clay (claycop) hydrogen peroxide: selective and solvent-free oxidations using microwaves. *Tetrahedron Letters* 39, 1307–1308.
- Varma, R.S., Dahiya, R., 1998c. Sodium borohydride on wet clay: solvent-free reductive amination of carbonyl compounds using microwaves. *Tetrahedron* 54, 6293–6298.
- Varma, R.S., Dahiya, R., 1998d. An expeditious and solvent-free synthesis of 2-amino-substituted isoflav-3-enes using microwave irradiation. *Journal of Organic Chemistry* 63, 8038–8041.
- Varma, R.S., Dahiya, R., Kumar, S., 1997. Clay catalyzed synthesis of imines and enamines under solvent-free conditions using microwave irradiation. *Tetrahedron Letters* 38, 2039–2042.
- Varma, R.S., Kumar, D., 1998. Surfactant pillared clays as phase-transfer catalysts: a facile synthesis of  $\alpha$ -azidoketones from  $\alpha$ -tosyloxyketones and sodium azide. *Catalysis Letters* 53, 225–227.
- Varma, R.S., Kumar, D., 1999a. Solventless regeneration of ketones from thioketones using clay supported nitrate salts and microwave irradiation. *Synthetic Communications* 29, 1333–1340.
- Varma, R.S., Kumar, D., 1999b. Microwave-accelerated three-component condensation reaction on clay: solvent-free synthesis of imidazo[1,2-a] annulated pyridines, pyrazines and pyrimidines. *Tetrahedron Letters* 40, 7665–7669.
- Varma, R.S., Kumar, D., Liesen, P.J., 1999b. Solid state synthesis of 2-arylbenzo[b]furans, 1,3-thiazoles and 3-aryl-5,6-dihydroimidazo[2,1-b][1,3]thiazoles from  $\alpha$ -tosyloxyketones using microwave irradiation. *Journal of the Chemical Society, Perkin Transactions 1*, 4093–4096.
- Varma, R.S., Meshram, H.M., 1997. Solid state cleavage of semicarbazones and phenylhydrazones with ammonium persulfate clay using microwave or ultrasonic irradiation. *Tetrahedron Letters* 38, 7973–7976.
- Varma, R.S., Naicker, K.P., 1998. Surfactant pillared clays in phase transfer catalysis: a new route to alkyl azides from alkyl bromides and sodium azide. *Tetrahedron Letters* 39, 2915–2918.
- Varma, R.S., Naicker, K.P., 1999a. Palladium chloride tetraphenylphosphonium bromide intercalated clay: new catalyst for cross-coupling of aryl halides with arylboronic acids. *Tetrahedron Letters* 40, 439–442.
- Varma, R.S., Naicker, K.P., 1999b. Synthesis of allylbenzenes by cross-coupling of allyl bromide with arylboronic acids using a palladium chloride and tetraphenylphosphonium bromide intercalated clay catalyst. *Green Chemistry* 1, 247–249.
- Varma, R.S., Naicker, K.P., Aschberger, J., 1999e. A facile preparation of alkyl azides from alkyl bromides and sodium azide using 18-crown-6 ether doped clay. *Synthetic Communications* 9, 2823–2830.

- Varma, R.S., Naicker, K.P., Kumar, D., 1999c. Can ultrasound substitute for a phase-transfer catalyst? Triphase catalysis and sonochemical acceleration in nucleophilic substitution of alkyl halides and  $\alpha$ -tosyloxyketones: synthesis of alkyl azides and  $\alpha$ -azidoketone. *Journal of Molecular Catalysis A-Chemistry* 149, 153–160.
- Varma, R.S., Naicker, K.P., Kumar, D., Dahiya, R., Liesen, P.J., 1999a. Solvent-free organic transformations using supported reagents and microwave irradiation. *Journal of Microwave Power and Electromagnetic Energy* 34, 113–123.
- Varma, R.S., Naicker, K.P., Liesen, P.J., 1999f. Palladium chloride and tetraphenylphosphonium bromide intercalated clay as a new catalyst for the Heck reaction. *Tetrahedron Letters* 40, 2075–2078.
- Varma, R.S., Pitchumani, K., Naicker, K.P., 1999d. Triphasic catalyst systems based on surfactant/clay composites—facile synthesis of cyano, thiocyno and hydroxy compounds using a triphasic catalyst. *Green Chemistry* 1, 95–97.
- Varma, R.S., Saini, R.K., 1997a. Solid state dethioacetalization using clayfen. *Tetrahedron Letters* 38, 2623–2624.
- Varma, R.S., Saini, R.K., 1997b. Microwave-assisted isomerization of 2'-aminochalcones on clay: an easy route to 2-aryl-1,2,3,4-tetrahydro-4-quinolones. *Synthesis Letters*, pp. 857–857.
- Varma, R.S., Saini, R.K., Kumar, D., 1998. An expeditious synthesis of flavones on montmorillonite K10 clay with microwaves. *Journal of Chemical Research (S)*, pp. 348–348.
- Vaughan, D.E.W., Lussier, R.J., Magee, J.S., 1979. Pillared interlayer clay products useful as catalysts and sorbents. US Patent, 4176090.
- Veisz, B., Kiraly, Z., Toth, L., Pecz, B., 2002. Catalytic probe of the surface statistics of palladium crystallites deposited on montmorillonite. *Chemistry of Materials* 14, 2882–2888.
- Villemin, D., Hammadi, M., Martin, B., 1996. Clay catalysis: condensation of orthoesters with o-substituted aminoaromatics into heterocycles. *Synthetic Communications* 26, 2895–2899.
- Villemin, D., Labiad, B., Loupy, A., 1993. Clay catalysis—a convenient and rapid formation of anhydride from carboxylic-acid and isopropenyl acetate under microwave irradiation. *Synthetic Communications* 23, 419–424.
- Villemin, D., Labiad, B., Ouhilal, Y., 1989. One-pot synthesis of indoles catalyzed by montmorillonite under microwave irradiation. *Chemistry and Industry*, pp. 607–608.
- Villemin, D., Martin, B., 1995. Dry condensation of creatinine with aldehydes under focused microwave irradiation. *Synthetic Communications* 25, 3135–3140.
- Vu Moc Thuy, Maitte, P., 1979. Reaction of enol ethers with diols in the presence of montmorillonite: a convenient synthesis of cyclic acetals. *Bulletin de la Société Chimique de France* 15, 264–265.
- Wali, A., Unnikrishnan, S., Pillai, S.M., Kaushik, V.K., Satish, S., 1998. Montmorillonite clay catalysis: conversion of methyl benzoate and  $\text{NH}_3$  into benzonitrile and amides. *Journal of Catalysis* 173 (1), 84–94.
- Wang, K.J., Ferris, J.P., 2001. Effect of inhibitors on the montmorillonite clay-catalyzed formation of RNA: studies on the reaction pathway. *Origins of Life and Evolution of the Biosphere* 31, 381–402.
- Wei, J., Furrer, G., Kaufmann, S., Schulin, R., 2001. Influence of clay minerals on the hydrolysis of carbamate pesticides. *Environmental Science and Technology* 35, 2226–2232.

- Weiss, A., 1981. Replication and evolution in inorganic systems. *Angewandte Chemie, International Edition in English* 20, 850–860.
- Wulfsberg, D.S., McDaniel, R.S. Jr., Peace, B.W., 1976. Metal-salt catalysed carbenoids XIII. On the mechanisms of cyclopropanation and allylic C–H insertions by diazo esters in the presence of olefins and homogeneous copper catalysts. *Tetrahedron* 32, 1241–1251.
- Yadav, G.D., Doshi, N.S., 2000. Alkylation of hydroquinone with methyl *tert*-butyl-ether and *tert*-butanol. *Catalysis Today* 60, 263–273.
- Yadav, G.D., Kulkarni, H.B., 2000. Ion-exchange resin catalysis in the synthesis of isopropyl lactate. *Reactive and Functional Polymers* 44 (2), 153–165.
- Yadav, G.D., Naik, S.S., 2000. Clay-supported liquid-liquid-solid phase transfer catalysis: synthesis of benzoic anhydride. *Organic Process Research and Development* 4, 141–146.
- Yadav, G.D., Pujari, A.A., 1999. Kinetics of acetalization of perfumery aldehydes with alkanols over solid acid catalysts. *Canadian Journal of Chemical Engineering* 77, 489–496.
- Yadav, G.D., Thathagar, M.B., 2002. Esterification of maleic acid with ethanol over cation-exchange resin catalysts. *Reactive and Functional Polymers* 52, 99–110.
- Yamagishi, A., 1986. Method of resolving optical isomer. Japanese Patent, 61204138.
- Zen, J.M., Jeng, S.H., Chen, H.J., 1996. Catalysis of the electroreduction of hydrogen peroxide by nontronite clay coatings on glassy carbon electrodes. *Journal of Electroanalytical Chemistry* 408, 157–163.
- Zhang, Z.H., Li, T.S., Fu, C.G., 1997a. Montmorillonite clay catalysis 4. An efficient and convenient procedure for preparation of 1,1-diacetates from aldehydes. *Journal of Chemical Research (S)*, (5), 174–175.
- Zhang, Z.H., Li, T.S., Yang, F., Fu, C.G., 1998. Montmorillonite clay catalysis XI: protection and deprotection of hydroxyl group by formation and cleavage of trimethylsilyl ethers catalysed by montmorillonite K-10. *Synthetic Communications* 28, 3105–3114.
- Zhang, Z.H., Yang, F., Li, T.S., Fu, C.G., 1997b. Montmorillonite clay catalysis 6. Synthesis of triarylmethanes via Baeyer condensation of aromatic aldehydes with *N,N*-dimethylaniline catalysed by montmorillonite K-10. *Synthetic Communications* 27, 3823–3828.
- Zhao, F.Y., Bhanage, B.M., Shirai, M., Arai, M., 2000. Heck reactions of iodobenzene and methyl acrylate with conventional supported palladium catalysts in the presence of organic and/or inorganic bases without ligands. *Chemistry-A European Journal* 6, 843–848.
- Zhou, Y.L., Hu, N.F., Zeng, Y.H., Rusling, J.F., 2002a. Heme protein-clay films: direct electrochemistry and electrochemical catalysis. *Langmuir* 18, 211–219.
- Zhou, Y.L., Li, Z., Hu, N.F., Zeng, Y.H., Rusling, J.F., 2002b. Layer-by-layer assembly of ultrathin films of hemoglobin and clay nanoparticles with electrochemical and catalytic activity. *Langmuir* 18, 8573–8579.



This page intentionally left blank

Chapter 10.3

## CLAY MINERAL– AND ORGANOCLAY–POLYMER NANOCOMPOSITE<sup>☆</sup>

E. RUIZ-HITZKY<sup>a</sup> AND A. VAN MEERBEEK<sup>b</sup>

<sup>a</sup>*Instituto de Ciencia de Materiales de Madrid, Campus de Cantoblanco, CSIC,  
ES-28049 Madrid, Spain*

<sup>b</sup>*Advanced Elastomer Systems SA, B-1140 Bruxelles, Belgium*

The development of inorganic-organic hybrid materials was especially trendy in the last decade. This is attested by the ever growing number of symposia, books, and specialised journals that are devoted to this subject. They parallel the intensive research activity in complex systems at the atomic/molecular scale (nanometer scale) of organic species of diverse functionality with inorganic entities, generally based on silica or silicates. The application of the concepts of molecular engineering enables new materials with a wide range of predetermined properties to be obtained (Ruiz-Hitzky, 1988).

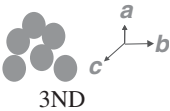


By definition, composite materials are solids resulting from the combination of two or more simple materials that develop a continuous phase (polymer, metal, ceramic, etc.), and a dispersed phase such as glass fibres, carbon particles, silica powder, clay minerals, etc. In addition they have properties that are essentially different from the components taken separately. Within the vast collection of inorganic-organic hybrid materials, nanocomposites are an emerging group that received a great deal of attention not only because of their potential in industrial applications but also from their fundamental point of view (Ruiz-Hitzky, 2003, 2004). Recent reviews on this topic were published by Alexandre and Dubois (2000) Sinha Ray and Okamoto (2003) and Ruiz-Hitzky et al. (2004).

A well-accepted definition of nanocomposites is that the dispersed particles have at least one dimension in the nanometer range (*nanofillers*). Although it could be confusing to the clay scientists, nanocomposites are usually classified according to the number of the nanodimensions of the filler (Table 10.3.1). Thus, in the case of phyllosilicates like smectites integrated into nanocomposites, the clay–polymer

---

<sup>☆</sup>“Polymer-clay nanocomposites” is more widely used than “clay-polymer nanocomposites” (and thereby “organic-inorganic hybrids” vs. “inorganic-organic-hybrids”) but the last term was retained in this Chapter for coherence with the book style.

Table 10.3.1. Definition of dimensionality in fine particles used as fillers in nanocomposites

Size/dimensionality	Scheme	Examples
$a, b, c: 1\text{--}100\text{ nm}$ 3-nano-dimensional	 3ND	silica nanoparticles carbon black fullerenes allophanes
$a, b: 1\text{--}100\text{ nm}$ $c > 100\text{ nm}$ 2-nano-dimensional	 2ND	nanowires (metals) nanofibers (sepiolite) nanotubes (carbon)
$c: 1\text{--}100\text{ nm}$ $a, b > 100\text{ nm}$ 1-nano-dimensional	 1ND	smectites, kaolinites layered double hydroxides (LDH)

nanocomposite could be considered as “one-nano-dimensional” (1ND) because the clay filler has one dimension at the nanometer scale, although the clay filler is two dimensional (2D) in the microscopic sense.

This chapter is not an exhaustive summary of the published literature on nanocomposites. Rather, the aim is to call the attention of clay scientists and engineers to the numerous opportunities that this type of new materials offer. Another aim of this contribution is to establish a base for further studies, rationalise and comment on the processes used to prepare those compounds, and finally to illustrate some properties of these materials such as thermal, mechanical, flammability, and conductivity.

### 10.3.1. EXFOLIATION OR INTERCALATION?

Many authors claim to achieved exfoliation (also called delamination) when preparing a nanocomposite. In fact only a fraction (often not quantified) of the clay mineral is truly exfoliated.

There is probably nothing to gain in entering into the futile debate of the classification of polymer-clay nanocomposites in intercalated or exfoliated compounds. It should suffice to say that there is a continuum of morphologies and physical/mechanical properties associated with either one or the other.

Purely exfoliated clay-polymer compounds are by definition those in which the clay mineral particles are individually dispersed in the polymer. Only a few examples of this type can be found in the literature, but many published microphotographs show small regions in a compound where complete exfoliation occurred. Consistent orientation of these particles during processing is certainly a challenge that was not

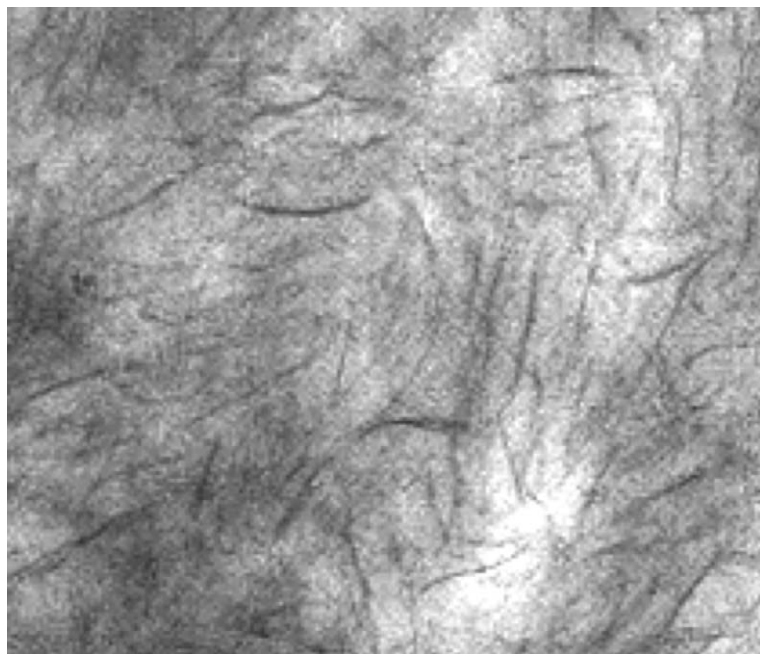


Fig. 10.3.1. Transmission electron microscopy (TEM) image of a section of a clay-polystyrene nanocomposite. From (Hoffmann et al., 2000).

addressed: the organoclay particles are folded during processing (Fig. 10.3.1). Perfectly exfoliated compounds constitute one end of the spectrum; the other end is represented by clay mineral–polymer compounds in which the polymer is intercalated as a monolayer into the clay mineral. The reality of nanocomposites is that even in cases where exfoliation appears to have taken place, little if any individual platelets can be found in the compound, and most often exfoliation only leads to one layer or few layers (Akelah, et al., 1994; Gilman et al., 2000; Bafna et al., 2003).

It is beneficial for the discussion, however, to agree and assign the most widely acceptable definitions to the different polymer nanocomposite types, and above all, to differentiate them clearly from the micro-composites. The latter are clay–polymer compounds wherein clay is predominantly present as large size aggregates (dimensions larger than 1  $\mu\text{m}$ ). For the nanocomposites, interesting sets of definitions were been proposed to which even clay mineral specialists may partially adhere as follows: (i) intercalated structures are formed when the polymer chains are inserted into the interlayer space; and (ii) a delaminated (or exfoliated) structure results when the silicate layers are no longer close enough to interact with each other.

Many authors proposed artificial limits to define the type of structure, based on the presence or absence of diffraction peaks in a X-ray diffraction (XRD) diagram. In particular, exfoliation was often hastily concluded from wide angle X-ray diffraction

(WXRd) or small angle X-ray scattering (SAXS) measurements of the interlayer spacing, overlooking the fact that interlayer expansion can occur without disaggregation of the mineral (Moet, 1990). XRD diagrams do not show reflections for intercalated structures having an interlayer space larger than 8 nm, corresponding to a few mono-layers of polymer in the interlayer space. Distinguishing between the two types of structures on the basis of their mechanical properties is often not possible as some interesting properties were found also for intercalated structures, and mechanical properties are not always improving with increasing interlayer expansion (Yano et al., 1993; Kodgire et al., 2000).

Further, exfoliated nanocomposites can return to the status of intercalated morphology under certain conditions (Manias et al., 2001). In the melt, mass transport of the polymer, entering the interlayer space is rapid, and the polymer chains exhibit a mobility similar to or faster than the polymer self-diffusion (Giannelis et al., 1999). If the thermodynamic conditions are favourable for intercalation, the polymer can crawl in and out of the interlayer space until equilibrium is reached. Changes in physical conditions (external pressure, temperature, shear, etc.) disturb this equilibrium, and the polymer may eventually leave the interlayer space. The mechanical and physical properties of nanocomposites, and the relation to their morphology will be discussed later.

### 10.3.2. CLAY MINERAL-POLYMER INTERACTIONS AND STRUCTURES

The interaction of phyllosilicates with polymers is an old theme (Theng, 1979), but it is only recently that innovative new uses of these materials emerged.

By the beginning of the 1960s (Blumstein, 1961), the ability of smectites to induce the polymerisation of certain unsaturated monomers in the interlayer space of clay minerals were already demonstrated (see Chapter 7.3). Once the polymer is formed, it remains strongly associated to the mineral substrate, and is clearly located in the interlayer space of the clay mineral. The resulting material displays a widely different behaviour from either the original clay mineral or the neat polymer. From this pioneering work to the recent commercialisation of TPO (modified polypropylene) nanocomposite rocker panels in the 2002 models of General Motors Safari and Astro vans, the clay–polymer interaction was intensively investigated in both basic research and technological aspects. These developments always require a high degree of creativity.

The most intense research devoted to clay–polymer nanocomposites concerns natural (montmorillonite, hectorite, saponite) or synthetic (Laponite, fluorohectorites) smectites. These 1D nanofillers have a layer thickness of the order of one nanometer. The other dimensions of the clay mineral (except for Laponite) are about 1000 times larger than the thickness, i.e. they are at the micrometer scale. The association of these clay minerals with polymers gives materials with different structures (Fig. 10.3.2). The dispersion of clay aggregates in polymer corresponds to

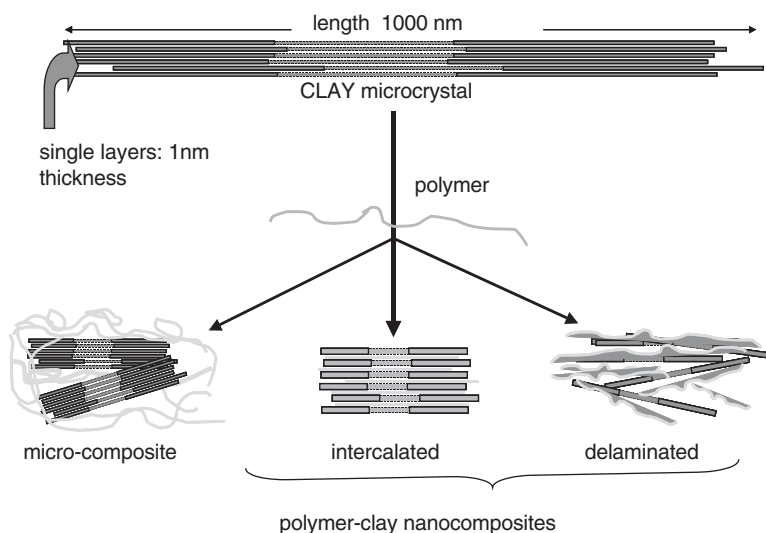


Fig. 10.3.2. Different structures proposed for clay-polymer materials arranged as nano- and micro-structured solids.

conventional filler-polymer micro-composites. On the other hand, in nanocomposites the single clay mineral layers or nanometer particles are dispersed in the polymer. If the layers are regularly intercalated with polymers the nanocomposites are called 'intercalated'. If the clay mineral layers or the particles are irregularly dispersed in the polymer, the nanocomposites are called 'delaminated' or 'exfoliated'. All these structures can be characterized by XRD and TEM.

In addition to smectites, other clay minerals such as sepiolite and kaolinite can be used to prepare nanocomposites. Polymers not only interact with the external surface of sepiolite, but it can also penetrate into the structural tunnels of the mineral (Inagaki et al., 1995; Sandi et al., 1999; Ruiz-Hitzky, 2001). Since these cavities are organised as nanostructured pores, the resulting materials are considered as clay-polymer nanocomposites. There are other cavities of nanometric dimensions along the fibre axis, mainly attributed to defects in particle growth that are accessible to organic species (Kuang et al., 2003). Kaolinite is also of interest in the preparation of clay-polymer nanocomposites (Tunney and Detellier, 1996).

### 10.3.3. PREPARATION OF CLAY MINERAL–POLYMER NANOCOMPOSITES

Smectites could form nanocomposites using one of the three preparation methods (i) direct incorporation of the polymers; (ii) in situ polymerisation of the monomers; and (iii) template synthesis of clay minerals.

The clay mineral selected to prepare nanocomposites can occur in different forms such as powder, films, colloidal dispersion in water or in other polar liquids. Depending on the polymer or monomer to be intercalated, the clay mineral can be used in the raw (untreated) state, or after specific modification.

#### *A. Direct Intercalation from Solution or Melt*

Polar polymers, like poly (vinyl alcohol) (PVA), poly (ethylene glycol) (PEG) (Parfitt and Greenland, 1970a, 1970b), poly (N-vinyl pyrrolidone) (PVP) (Levy and Francis, 1975), poly (ethylene oxide) (PEO) (Ruiz-Hitzky and Aranda, 1990; Aranda and Ruiz-Hitzky, 1992; Wu and Lerner, 1993; Aranda and Ruiz-Hitzky, 1994; Vaia et al., 1995; Aranda and Ruiz-Hitzky, 1999; Aranda et al., 2003), and chitosan (Darder et al., 2003; 2005) that can be directly intercalated into smectites from solutions of the polymers in polar solvents (water, alcohols, nitriles, etc.), and in some cases from the melt.

The mechanism of this interaction is based in each case on the formation of hydrogen bonds between the hydroxyl groups (in PVA, PEG), or the oxyethylene groups (in PEO, PEG), or nitrogen heteroatoms (in PVP), of the polymers with the mineral surface. This interaction occurs directly with the siloxane surface of the clay mineral layer or with the water molecules coordinated to the interlayer cations, through water bridges. Interactions of the ion-dipole type between the oxygen atoms of the oxyethylene ( $-\text{CH}_2-\text{CH}_2-\text{O}-$ ) groups and the interlayer cations were also proposed (Aranda and Ruiz-Hitzky, 1992, 1994; Ruiz-Hitzky and Aranda, 2000). The cation biopolymer chitosan is intercalated in homoionic smectites from solutions through a cation exchange mechanism giving nanocomposites with a monolayer of the polymer. At high concentration, a second layer of chitosan is intercalated by hydrogen bonding between the first layer of polymer and the clay mineral surface (Darder et al., 2003; 2005).

The synthesis of montmorillonite-PEO nanocomposites is a representative model of the direct adsorption method. These functional nanocomposites show an attractive ion-conducting behaviour as reported for the first time by Ruiz-Hitzky and Aranda (1990). PEO of different molecular mass in acetonitrile solutions or other polar solvents, are intercalated by smectites, forming stable interlayer coordination complexes with the exchangeable cations. XRD shows an increase of the interlayer distance ( $\Delta d$ ), of about 0.8 nm, compatible with two possible arrangements of PEO: (i) a bilayer of polymer chains in a planar zig-zag disposition or (ii) a monolayer of polymer with helical conformation. The latter arrangement occurs when  $\text{Li}^+$  or  $\text{Na}^+$  is the exchangeable cation (Fig. 10.3.3). This is also consistent with IR,  $^{13}\text{C}$  and  $^{23}\text{Na}$  NMR spectroscopic data indicating that the oxygen atoms of PEO interact with these cations (Aranda and Ruiz-Hitzky, 1992, 1994). Wu and Lerner (1993) described two phases for  $\text{Na}^+$ -montmorillonite-PEO nanocomposites prepared from aqueous dispersions of the clay minerals suggesting either a mono- or bi-layer arrangement of the polymer in zig-zag conformations. The arrangement of PEO in the

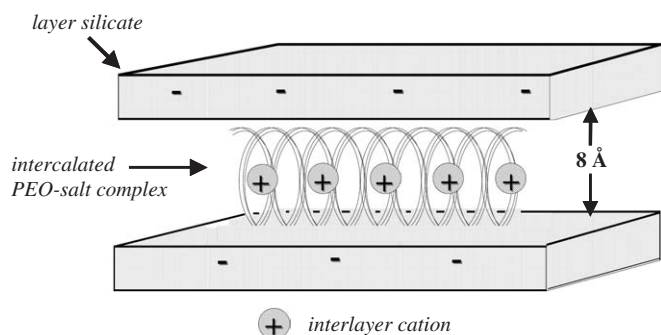


Fig. 10.3.3. Structural model of montmorillonite-PEO nanocomposites prepared from acetonitrile solutions. After Ruiz-Hitzky and Aranda (1990).

interlayer space depends on such factors as the nature of the exchangeable cation and the water content (Hackett et al., 2000).

The technique of melt intercalation (Vaia et al., 1993) of polymers into phyllosilicates, is considered as one of the major practical steps forward in the field of nanocomposite preparation. This procedure was successfully applied to prepare PEO nanocomposites (Vaia et al., 1995; Giannelis, 1996). PEO is intercalated in homionic alkaline cations exchanged montmorillonites after 6 h of treatment at 80 °C. This temperature is only about 10 °C above the melting point of PEO, but is apparently sufficient to ensure the mobility of the polymer chains so that they can migrate into the interlayer space of the clay mineral.

The effectiveness of melt intercalation could be further improved by using microwave (MW) irradiation. The energy is mainly absorbed by the water molecules coordinated to the interlayer cations. As a result the polymer and eventually the clay mineral are heated, promoting rapid entry of the polymer into the interlayer space of the montmorillonite. The MW-assisted melt intercalation procedure is successfully applied for the first time to the preparation of montmorillonite-PEO nanocomposites (Aranda et al., 1998, 2003), saving time and energy compared to the conventional method of oven-heating.

PEO is also adsorbed on sepiolite, either from a solution or from the melt by MW irradiation. Only preliminary results were published (Ruiz-Hitzky, 2001). The salient feature is that the polymer chains can partially penetrate into the structural tunnels of 0.4 by 1.1 nm. This process apparently involves the irreversible displacement of water molecules filling the tunnels of the natural sepiolite.

Until recently, the direct intercalation of polymers into kaolinite appears to be unfeasible (Sanz and Serratosa, 2002). However, if the kaolinite layers are previously expanded, using polar molecules like dimethylsulphoxide (DMSO), the interlayer space becomes accessible to polar polymers like PEG (Tunney and Detellier, 1996). The resulting kaolinite-PEG nanocomposites show  $\Delta d$  values of about 0.4 nm indicating that monolayers of polyoxyethylene chains in planar zig-zag conformation



were intercalated. In contrast, a distorted helical structure for PEG is observed in modified PEG intercalated in layered double hydroxides (LDH). This is attributed to strong interactions between surface hydroxyl groups of LDH and the oxygen atoms of the polymer (Leroux et al., 2003).

### *B. In Situ Polymerisation*

This process consists of the intercalation of monomers as precursor species, followed by their polymerisation inside the interlayer space of the pristine clay mineral.

The first polymerisation in the interlayer space of a clay mineral was reported by Blumstein (1961) who demonstrated the possibility of achieving the homopolymerisation of unsaturated monomers, such as acetonitrile and methyl methacrylate, previously intercalated in smectites. Numerous nanocomposite materials were prepared by the so-called ‘in situ intercalative polymerisation’ (Kanatzidis et al., 1986). For instance, the polymerisation of pyrrole and aniline in the interlayer space of a clay mineral was reported by Cloos and co-workers (Cloos et al., 1979; Moreale et al., 1985). In this process, interlayer exchangeable  $\text{Cu}^{2+}$  cations in smectites promote the formation of the aniline radical (by oxidation), inducing its polymerisation into polyaniline (PANI). The interaction of pyrrole with iron-rich smectites, containing structural Fe(III), exchangeable  $\text{Fe}^{3+}$  species or associated oxyhydroxyde Fe species, spontaneously gives clay mineral–PPy nanocomposites (Letaïef et al., 2005).

Other polar species like thiophene and its derivatives can also form nanocomposites by interlayer polymerisation induced by  $\text{Cu}^{2+}$  and other transition metal ions in smectites (Cloos et al., 1973; Soma et al., 1987). Not every polar monomer gives nanocomposites by this process. For example, vinylcarbazole gives clay–polymer compounds after treatment of a smectite by the monomer in benzene solution (or in presence of the molten polymer, at 65 °C) (Biswas and Ray, 1998). The authors indicate that the formation of the poly(N-vinylcarbazole) (PNVC) is directly induced by the action of the clay mineral involving cationic proton species, without any addition of polymerisation initiators. Similarly, Lewis or Brønsted acid sites in clay minerals such as montmorillonite and kaolinite can induce polymerisation of different vinyl monomers such as styrene (Solomon, 1968; Solomon et al., 1971; Hawthorne et al., 1974). These reactions occur by simply heating a blend of the clay mineral and the monomer in soft conditions, giving in this case non-intercalated clay mineral–polymer materials (micro-composites). Further, XRD shows a very weak peak at 1.46 nm assigned to the intercalated PNVC in addition to the peak at 1.0 nm characteristic of the pristine clay mineral. These results are not conclusive for the formation of true nanocomposites.

AN can also easily intercalate into smectites where it is directly associated with the interlayer cations such as  $\text{Li}^+$  or  $\text{Na}^+$ , forming complexes through  $-\text{C}\equiv\text{N}\cdots\text{cation}$  (ion-dipole) interactions (Blumstein et al., 1974; Bergaya and Kooli, 1991; Sanz and Serratos, 2002). Heat treatment or gamma-irradiation induces the polymerisation of AN in the interlayer space, giving PAN. Similarly, AN is incorporated into the

channels of sepiolite replacing zeolitic water and interacting with coordinated water molecules by hydrogen bonding (Fernández-Saavedra et al., 2004). In this case the polymerisation of AN to PAN is achieved using a radical initiator such as 2,2'-azobisisobutyronitrile.

In contrast to hydrophilic monomers, which polymerise in the interlayer space, low polarity monomers such as styrene, can only polymerise in the interlayer space if the clay mineral was previously modified. This will be discussed later in this chapter.

The preparation of sepiolite–polymer nanocomposites based on isoprene and styrene entering into the tunnels of this clay mineral was reported (Inagaki et al., 1995). On the basis of adsorption isotherms, the authors propose that the monomers are adsorbed on both the external surface and in the tunnels of the mineral. The strong Brønsted acid sites of sepiolite being assumed to catalyse the process of the in situ polymerisation. However, the occurrence of acid sites in sepiolite is uncertain because adsorbed basic species such as pyridine are not protonated (Ruiz-Hitzky, 2001; Kuang et al., 2003). The colour changes observed after adsorption of isoprene suggest instead that the transition metals such as iron, are involved in the polymerisation reaction.

Other molecules such as pyrrole and thiophene polymerise incompletely when adsorbed on sepiolite (Inagaki et al., 1995). The formation of polymers from such monomers, however, is of potential interest for the development of conducting nanowires, having the size and shape imposed by the geometry of the sepiolite. Under drastic conditions, it is possible, to polymerise unsaturated monomers such as ethylene in the tunnels of sepiolite (Sandi et al., 1999). If the sepiolite–PE nanocomposites are subsequently carbonised by pyrolysis, carbon nanofibres useful for solid-state lithium batteries, can be produced. Similarly, carbonisation of sepiolite–PAN nanocomposites can give rise to sepiolite-carbon materials useful as electro-active components in electrochemical devices. The elimination of the sepiolite moiety by treatment with HCl and HF acids gives rise to carbon nanofibres of ca. 1 µm by 20–30 nm (Fernández-Saavedra et al., 2004).

### C. Template Synthesis

This recent procedure (Carrado and Xu, 1998; Carrado, 2000; Carrado et al., 2000) is based on the in situ hydrothermal crystallisation of gels from a mixture of silica sol, magnesium hydroxide, LiF and selected water-soluble polymers in solution (Fig. 10.3.4). The synthetic clay mineral formed under these conditions is considered as a poorly ordered fluorohectorite.

By this method, polymers like PANI, PAN and PVP give hybrid materials with a controllable silicate/polymer ratio. This value determines both the structural arrangement and properties such as the electrical conductivity. The clay mineral–PANI nanocomposites prepared following this procedure are semi-delaminated, showing clay/polymer ratios smaller than those of their counterparts prepared by in situ polymerisation. One interesting characteristic of these nanocomposites prepared by

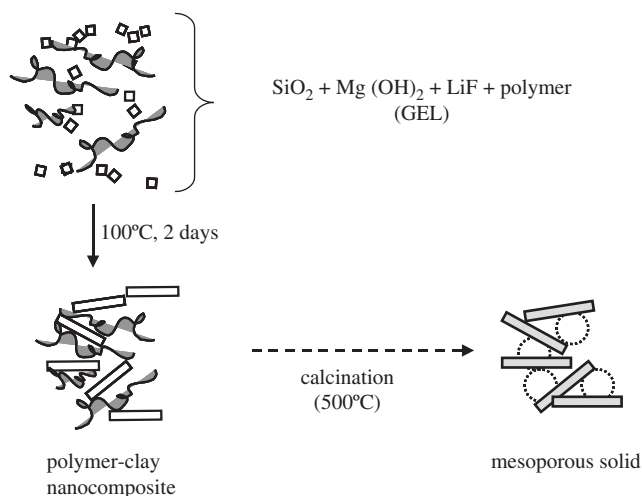


Fig. 10.3.4. Template synthesis of clay-polymer nanocomposites as intermediates for preparing mesoporous solids. After Carrado (2000).

this method is their ability to form well-dispersed systems in an aqueous medium without any loss of the polymer back into the solution (Carrado et al., 2000). Unfortunately, this method does not work with certain polymers such as PEO.

The compounds obtained by template synthesis are of great interest in view of the preparation of inorganic porous materials (Fig. 10.3.4). When the PVP is removed from the nanocomposite by calcination (at  $500^\circ\text{C}$  in air), the rearrangement of individual clay mineral layers gives nanoporous materials with a narrow distribution of mesopores in the range of 4 to 10 nm (Carrado, 2000); in general, the pore size of such materials is related to the MW of the polymer involved (Carrado and Xu, 1999). This is then a very interesting method to design inorganic materials with pre-determined mesoporous dimensions representing new applications of clay-polymer nanocomposites. An alternative approach to preparing of clay mineral-silica nanocomposites from organoclays uses the sol-gel processes involving the controlled hydrolysis of alkoxysilanes such as tetramethylorthosilicate (TMOS) (Lataïef and Ruiz-Hitzky, 2003). In this case the exfoliation of montmorillonite occurs as a consequence of the formation of silica, which is in fact an inorganic polymer.

#### 10.3.4. HOST-GUEST COMPATIBILITY

Most polar monomers or polymers can be intercalated in the pristine clay mineral. Because clays are hydrophilic, polymers of low polarity are in general incompatible with unmodified raw clays. The less polar compounds can be intercalated only if the clay minerals are previously modified by exchange with alkylammonium ions

(organoclays) or by grafting with suitable species. For intercalation of non-polar polymers, it is necessary to render the mineral surface organophilic, or modify the polymers.

### A. Organoclays

The principal method used to modify the interlayer space of smectites is based on cation exchange with alkylammonium ions (Jordan, 1949a, 1949b). Such a procedure, well known since several decades, was thoroughly investigated by numerous researchers (Theng, 1974; Lagaly, 1986; Raussell-Colom and Serratos, 1987; Yariv and Cross, 2002; Ruiz-Hitzky et al., 2004), and the resulting materials, the so-called organoclays, are used commercially in many industries under the generic name of ‘Bentones’. The alkylammonium species used to prepare organoclays are quaternary ammonium compounds containing alkyl, phenyl, benzyl and pyridyl groups (Table 10.3.2).

In some cases, a mixture of alkyl- and alkenylammonium ions is used. The most important application of these organoclays is to control the rheological behaviour of dispersions in organic solvents where they function as thickeners and thixotropic agents (Cody and Kemnetz, 1987; Finlayson et al., 1987).

Sepiolite has a much lower cation exchange capacity (CEC) than smectites (about 15 vs. about 100 cmol/kg). Nevertheless, treatment with quaternary ammonium salts also produce organophilic solids (Alvarez et al., 1987). As in the case of smectites additional surfactant ion pairs (cations plus the counterions) can be adsorbed (see Chapter 7.3). These types of materials also show an excellent compatibility with low polar organic media, and are used as paint thickeners and other industrial applications (Alvarez et al., 1984, 1985).

Several interlayer structures were proposed for alkylammonium-exchanged phyllosilicates, mainly smectites and vermiculites. The alkyl chains are generally lying flat on the clay mineral surface as mono- or bilayers. Other arrangements are the pseudo-trimolecular and paraffin-type arrangements (Lagaly, 1986; Ruiz-Hitzky et al., 2004). The factors controlling the interlayer arrangement of the alkyl chains

Table 10.3.2. Quaternary ammonium cations frequently used to prepare organoclays

Quaternary cation	Abbreviation	Formula
Tetramethylammonium	TMA	$(\text{CH}_3)_4\text{N}^+$
Trimethyl phenylammonium	TPMA	$\text{C}_6\text{H}_5\text{N}^+(\text{CH}_3)_3$
Benzyl trimethylammonium	BTMA	$\text{C}_6\text{H}_5\text{CH}_2\text{N}^+(\text{CH}_3)_3$
Hexadecylpyridinium	HDPY	$\text{C}_6\text{H}_5\text{N}^+(\text{C}_{16}\text{H}_{33})$
Benzyl dimethyl tetradecylammonium	BDTDA	$\text{C}_6\text{H}_5\text{CH}_2\text{N}^+(\text{C}_{14}\text{H}_{29})(\text{CH}_3)_2$
Hexadecyl trimethylammonium	HDTMA	$\text{C}_{16}\text{H}_{33}\text{N}^+(\text{CH}_3)_3$
Diocadecyl dimethylammonium	DODMA	$(\text{C}_{18}\text{H}_{37})_2\text{N}^+(\text{CH}_3)_2$

are discussed in detail in Chapter 7.3. The surface properties of the organoclays predetermine their potential uses.

The most important new application of organoclays today is the preparation of various types of nanocomposites. As shown above, PAN is not intercalated by untreated clay minerals but vermiculite exchanged with *n*-butylammonium is able to form nanocomposites after treatment with PAN in dimethylformamide (Aviles et al., 1993; Pérez-Rodríguez and Maqueda, 2002). Alternatively, this type of nanocomposite was prepared by intercalation of AN monomer into untreated clay mineral, followed by polymerisation using a radical initiator such as benzoyl peroxide at 50 °C during 24 h (Pérez-Rodríguez and Maqueda, 2002). As already indicated, PAN is a polymer of interest as it may form carbon fibres by an adequate thermal treatment. When heated, clay mineral-PAN nanocomposites give graphitised carbonaceous clay materials, which are transformed at high temperature into sialons, after carboreduction of the silica and other metal oxides composing the silicate (Aviles et al., 1993, 1994; Pérez-Rodríguez and Maqueda, 2002).

Low polarity polymers such as PS, in the molten state, can be directly intercalated in alkyl-ammonium-exchanged smectites. Typical experimental conditions (Vaia et al., 1993) require heating at 165 °C in vacuum for more than 24 h. The resulting organosmectite-PS nanocomposites show a basal spacing of 3.2 nm, which decreases to the value of the pristine organosmectite (2.52 nm) after toluene extraction. This type of nanocomposites displays a heterogeneous structure with well ordered intercalated layers and some disordered layers. This structure depends on processing conditions. Ultrasonication and other experimental procedures were proposed to obtain more homogeneous systems (Vaia et al., 1993).

Organoclay-PS materials have also been prepared by a novel procedure consisting of modifying the clay mineral ( $\text{Na}^+$ -montmorillonite) by ion-exchange with an ammonium salt containing a styrene group such as  $\text{CH}_2=\text{CH}-\text{C}_6\text{H}_4\text{CH}_2(\text{CH}_3)_3\text{N}^+\text{Cl}^-$  (Moet and Akelah, 1993). In this case, the PS remains partially attached to the exchangeable cations of the clay mineral, and only the excess polymer can be extracted with appropriate organic solvents. The insertion of grafted PS between the clay mineral layers is clearly monitored by XRD. The basal spacing of the exchanged clay mineral (1.5 nm) increases to 2.45 nm after reaction with styrene.

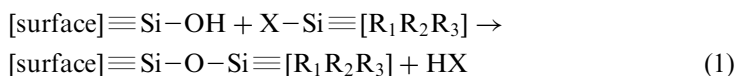
Clay mineral-nylon nanocomposites were prepared at the Toyota Central Research Laboratories (Fukushima and Inagaki, 1987; Fukushima et al., 1988; Usuki et al., 1993). The original method involves three steps: (i) ion exchange of  $\text{Na}^+$  for protonated 12-aminolauric acid  $^+\text{NH}_3-(\text{CH}_2)_{11}-\text{COOH}$ ; (ii) intercalation of epsilon-caprolactam into the modified clay mineral; and (iii) thermal polymerisation of the monomer, generating nylon-6 nanocomposites. These materials show interesting mechanical properties. Although they are not the first clay-polymer nanocomposite, they are the first to were used commercially. Since the first publication in 1993, the preparation method for clay-nylon nanocomposites was further improved by adding small amounts of 6-aminocaproic to accelerate the polymerisation process

(Usuki et al., 1993). Researchers at Toyota laboratory made various attempts to prevent the partial co-polymerisation of the epsilon-caprolactam with the intercalated 12-aminolauric acid. They found that the epsilon-caprolactam can be directly intercalated in the unmodified clay mineral at 200°C. The lactam is then reacted with the 6-aminocaproic acid, yielding also a nylon-6 nanocomposite (in situ polymerisation) (Kojima et al., 1993a).

Numerous papers were published, showing that the choice of the clay modifier is important in reaching optimum mechanical properties and nowadays, commercial nylon nanocomposites exist, wherein the 12-aminolauric acid was eventually replaced by alkylammonium cations (Vaia et al., 1993; Krishnamoorti et al., 1996; Fornes et al., 2002). Further, it was reported that clay-nylon nanocomposites can be synthesised in one step, instead of the original three steps process (Kojima et al., 1993b).

### B. Grafting of Clay Minerals

Silane coupling agents were extensively used to prepare micro-composites based on clays, silica, fibreglass, etc. These agents can also be used effectively to prepare nanocomposites, since they make the clay mineral surfaces organophilic. Organosilane coupling agents contain  $\equiv\text{Si-X}$  groups ( $\text{X} = \text{OR}, \text{Cl}$ ) and are able to react with silanol groups on the clay mineral surface, giving stable siloxane bridges.



Smectites and vermiculites have a low content in silanol groups because these groups only occur at particle edges. In contrast, sepiolite is rich in such reactive hydroxyls, due to the discontinuity of the silicate layers (Ahlrichs et al., 1975). The silanol groups located on the external surface, at the edges of the structural channels, are directly accessible to reagents. After grafting with organosilanes (Ruiz-Hitzky and Fripiat, 1976), the hydrophilic surface becomes organophilic, and sepiolite can be easily dispersed in low-polarity compounds including polymers (Ruiz-Hitzky, 1974). The stability of these organic derivatives is excellent; the attached groups are only eliminated after heating at elevated temperatures by combustion or pyrolysis, respectively in the presence or absence of oxygen.

Organosilanes containing unsaturated groups (vinyl and methacryloxi) or thiol functions (3-propylmercapto) give organic derivatives of sepiolite capable of further co-polymerisation reactions. Nanocomposites in which the polymer is covalently bonded to the modified clay mineral were prepared (Ruiz-Hitzky, 1974).

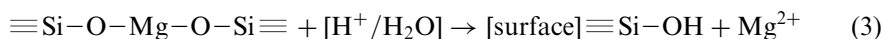
Direct reaction of organochlorosilanes with vermiculite gives essentially organosiloxanes where the silane is not grafted to the silicate (Aragón de la Cruz et al., 1973). In the absence of reactive silanol groups on the surface, the  $\equiv\text{Si-Cl}$  groups of

the reagent are quickly hydrolysed by the water molecules directly coordinated to the interlayer cations.



Unstable intermediates are formed which polycondense to siloxanes.

Nanocomposites were prepared by co-hydrolysis involving silicates, organosilanes and strong acids. The clay minerals involved are chrysotile, sepiolite, and vermiculite (Fripiat and Mendelovici, 1968; Zapata et al., 1972; Ruiz-Hitzky and Van Meerbeek, 1978; Van Meerbeek and Ruiz-Hitzky, 1979). The extraction of octahedral cations such as  $\text{Mg}^{2+}$  ions by acid attack yields silica containing fresh silanol groups,

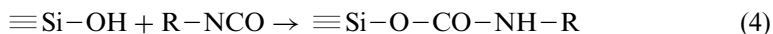


which reacts with the organosilanols produced by hydrolysis of the chloro- or alkoxy-organosilanes as shown in Eq. (1). Chrysotile and sepiolite preserve their morphology even after complete removal of the octahedral sheet. When this sheet is eliminated the particles disintegrate, and individual inorganic-organic micro- or even nanofibres are produced. When the surface was made compatible, nanocomposites can be prepared with many polymers.

Surface-grafting with vinylsilanes further allows co-polymerisation with various unsaturated monomers such as methylacrylate, methylmethacrylate, *n*-butylacrylate, vinylacetate and styrene (Zapata et al., 1973). The resulting nanocomposites show improved mechanical properties; for example, the dynamic modulus is nearly 100 times higher than the neat polymer (Zapata et al., 1973). These and other grafted phyllosilicates, and especially their blending with polymers merit thorough investigation.

After reaction of sepiolite with vinylsilanes, the unsaturated groups are homogeneously distributed. This is visualised by TEM by reacting the vinyl groups on the sepiolite with  $\text{OsO}_4$  (Barrios-Neira et al., 1974), confirming the arrangement of the grafted species to silanol sites along the edge of the structural channels.

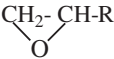
Clay minerals such as sepiolites and vermiculites can also be grafted using compounds of various functionalities such as isocyanates and epoxides (Table 10.3.3). Isocyanates react with silanol groups forming silyl-urethane bridges:



as demonstrated by IR spectroscopy (Fernández-Hernández and Ruiz-Hitzky, 1979).

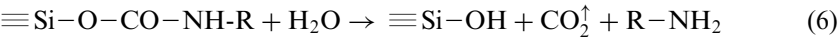
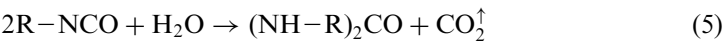
The stability of the grafted species depends on the nature of the alkyl groups (R), which stabilise the bridges by their positive inductive effect whereas phenyl groups

Table 10.3.3. Organic derivatives of silicates by grafting of isocyanates and epoxides

Function	Grafted groups	Reagent	Substrate
Isocyanates			
$R-C\equiv N=O$	$\equiv Si-O-CO-NH-R$	Butyl isocyanate	Sepiolite <sup>*,†</sup>
		Phenyl isocyanate	Sepiolite <sup>*,†</sup>
		Hexamethylene di-isocyanate	Sepiolite <sup>†</sup> Vermiculite <sup>‡</sup>
		2,4-Toluene di-isocyanate	Sepiolite <sup>†</sup> Vermiculite <sup>‡</sup>
Epoxides			
	$\equiv Si-O-CH(CH_2OH)-R$	1,2-Epoxybutan	Sepiolite <sup>§,¶,  </sup>
		1,2-Epoxyethyl benzene (epoxystyrene)	Sepiolite <sup>§,¶,  </sup>
		1-Allyloxy-2,3-epoxypropane (allylglycidyl ether)	Sepiolite <sup>§,¶,  </sup>
		2,3-Epoxypropyl methacrylate	Sepiolite <sup>  </sup>
		3-Vinyl-7-oxabicycle (4,1,0) heptane	Sepiolite

\*Fernández-Hernández and Ruiz-Hitzky (1979).  
†Ruiz-Hitzky et al. (1979).  
‡Siffert and Biava (1976).  
§Casal and Ruiz-Hitzky (1977).  
¶Casal and Ruiz-Hitzky (1984).  
||Casal et al. (1980).

give less stable bridges. A competitive reaction is the hydrolysis of both the isocyanate reagents and the silylurethane bridges.



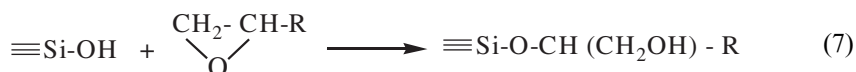
The formation of N,N'-disubstituted ureas (R-NH)<sub>2</sub>C=O, by reaction of isocyanates with water molecules adsorbed on the surface of clay minerals is a further process that predominates when R is a phenyl group. When sepiolite is reacted with phenyl isocyanate diphenyl urea is almost quantitatively formed (Fernández-Hernández and



Ruiz-Hitzky, 1979). By contrast, alkyl isocyanates, like butyl isocyanate, give stable grafted sepiolite compounds.

The reaction of di-isocyanates, such as hexamethylene di-isocyanate and 2,4-toluylene di-isocyanate, with vermiculite were also reported (Siffert and Biava, 1976). By heating the clay mineral to remove the associated water before starting the chemical reaction, urea formation is avoided. The yield of grafted species depends on the temperature of the pre-treatment. The potential interest of these grafted minerals is to introduce free  $-C\equiv N=O$  functions on the mineral, which are able to react further with polyols and polyesters in view of preparing inorganic-organic polycondensates. Nanocomposites of isocyanate grafted silicates and polyurethane foams have promising industrial applications (Casal et al., 1980).

Grafting of 1,2-epoxides to silanol groups present on mineral surfaces was well established by IR spectroscopy. The epoxy functions are opened at 80–100 °C, in vapour phase or in solution using aprotic solvents. The coupling reaction of the epoxide group with the  $\equiv Si-OH$  groups in sepiolite (Casal and Ruiz-Hitzky, 1977, 1984) is shown below:



In this case the organic R groups are linked to the surface through  $\equiv Si-O-C\equiv$  bonds. The reaction takes place only in the absence of physically adsorbed water. Vapour phase reactions can be made easily under dynamic vacuum. Reactions in solution are carried out after elimination of adsorbed water molecules, using a Dean-Stark system to separate the azeotrope during the grafting reactions.

IR and chemical analysis show that the extent of grafting, related to the same available surface area, is greater for sepiolite than for silica (Casal and Ruiz-Hitzky, 1977, 1984). This is attributed to the better ordering of  $\equiv Si-OH$  groups on the clay mineral compared to amorphous silica.

The reaction of allylglycidyl ether with sepiolite in organic solvents gives a monomolecular surface coverage even when the concentrations of the starting epoxide are low (Casal and Ruiz-Hitzky, 1977, 1984). The treatment of clays by epoxides with unsaturated groups such as allylglycidyl ether, 2,3-epoxypropyl methacrylate or 3-vinyl-7-oxabicyclo (4,1,0) heptane (Casal et al., 1980) give rise to materials that can be used as reinforcing fillers for elastomers and thermoplastics. The grafted groups are very stable, and are eliminated only by burning. However, the  $Si-O-C$  bonds could be hydrolysed by hot water. Secondary reactions giving carbonyl compounds by the catalytic activity of silico-alumina centres can be produced in the reactions of epoxides with clay minerals (Ruiz-Hitzky and Casal, 1985).

The opening of epoxy rings can be applied to forming smectite-polyether nanocomposites. This chemistry is therefore useful for the preparation of thermoset nanocomposites that have potential applications (Wang et al., 2000).

### C. Modified Polymers

For non-polar species, such as PP, the alkylammonium clay mineral has almost the same apolar character as the PP itself. Consequently, such systems are at “theta” conditions: there is no favourable excess enthalpy to promote the formation of the nanocomposite (Giannelis et al., 1999; Manias et al., 2001). Thus, the challenge with PP is to design a system wherein the clay–polymer interactions are more favourable than the surfactant–clay mineral interactions.

Improving the interactions between the polymer and the clay mineral can be achieved by PP functionalisation, introducing polar groups in the PP polymer. By far, the most popular method consists in modifying the polymer by grafting maleic anhydride. This is usually done in a twin-screw extruder and the grafting is initiated by peroxides.

Other methods to enhance the polarity of PP consist in making hydroxylated PP, grafting acrylic acid, or forming random and block copolymers using various polar monomers (Manias et al., 2001).

Another approach to compatibilise clay minerals and non-polar polymers consists of introducing cationic groups into the polymer, facilitating polymer intercalation by ion-exchange (10.3.4.A).

As mentioned before, organoclay–PS nanocomposites can be prepared by reacting the melted polymer with organoclays. Alternatively, the introduction of  $\text{-NH}_2$  functional groups which can be protonated, facilitates direct intercalation of the PS into untreated smectites (Hoffmann et al., 2000).

## 10.3.5. CLAY-POLYMER NANOCOMPOSITES: PROPERTIES AND APPLICATIONS

Clay mineral– and organoclay–polymer nanocomposites are still under development. They were successfully marketed because they fulfill at least two market needs: increased stiffness and increased resistance to the permeation of gases, at reasonable cost. For example organoclay–PP nanocomposites having a high modulus are suitable for use in automotive panels, whereas organoclay–nylon nanocomposites with low gas permeability can be used for packaging.

Toyota was the first to develop commercial clay–nylon nanocomposites. They patented almost every conceivable combination of clay mineral type and polymer, including the methods of preparation of nanocomposites.

Other potential improvements in properties were identified. This may drive new future developments, as shown in the web sites of the major “nanoclay” manufacturers: <http://www.nanocor.com>, <http://www.nanoclay.com>, <http://www.sued-chemie.com>.

There is an extensive literature on the polymer nanocomposites used for different applications, but this chapter only considers the properties of nanocomposites based

on polymers of current considerable commercial interest. However, some examples of nanocomposites involving different polymers that were not been commercialised such as PS, PMM, polysiloxanes or epoxy resins (Pinnavaia and Beall, 2000) will be mentioned to illustrate potential applications.

### *A. Mechanical Properties*

The design of new thermoplastic parts takes into account the mechanical properties of the raw material. Often, the most important mechanical property of plastic materials is the elastic modulus (measured both in tension and in compression). The modulus is in principle sufficient to calculate stresses and strains exerted by external forces, and to optimise new designs by computer simulations.

In general, the restricted mobility of polymers at the filler interface is the main cause of the high modulus of filler-loaded polymers (Lipatov, 1995). This also applies to clay-polymer nanocomposites. This mechanical property is very dependent on the structure of the nanocomposite such as the extent of exfoliation of the clay mineral. In turn, the structure is dependent on the physical properties of the clay mineral, such as its CEC, which can vary from one particle to another and from lot to lot of the clay (Quarmley and Rossi, 2001).

Other mechanical properties such as the modulus at high temperature, creep, chemical resistance, weathering resistance have to be evaluated. Properties at break such as impact resistance, tensile strength and elongation at break, indicate product quality, and resistance to harsh treatments, shocks, etc., during service life. Some of these parameters may sometimes be evaluated by specialist software.

### *Tensile Properties*

Clay-nylon nanocomposites can be obtained by melt blending organomodified clay with nylon. The data in Fig. 10.3.5 show selected mechanical properties of clay-nylon 6 nanocomposites (Cho and Paul, 2001).

Regardless of preparation method or type of clay, the modulus and strength of the nanocomposites are remarkably similar, and proportional to the content of clay mineral. The data suggest that the organoclay is much more efficient than other mineral fillers in increasing the mechanical properties of the polymer (Goettler and Recktenwald, 1998).

The extent of organoclay-polymer interaction in nylon nanocomposites, and therefore the level of modulus, yield strength, and elongation at break is in general a function of (i) the type and concentration of clay (Kojima et al., 1993c); (ii) the choice of adequate treatment of the clay (Kodgire et al., 2000; Fornes et al., 2002); (iii) the molecular weight of the nylon (Fornes et al., 2002); and (iv) the processing conditions (Davis et al., 2002).

The reinforcing effect of the clay mineral is further clarified (Fig. 10.3.6) by the evolution of the dynamic elastic modulus as a function of the temperature (Gloaguen and Lefebvre, 2000). This effect is clearly more pronounced above the glass

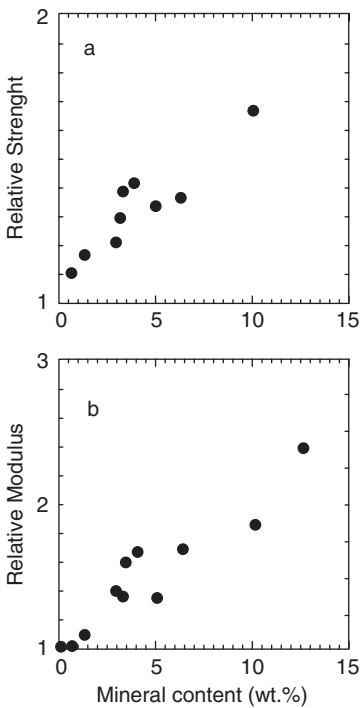


Fig. 10.3.5. Relative mechanical properties of various organoclay-nylon 6 nanocomposites as a function of the clay mineral content: (a) yield strength, (b) tensile modulus. From (Cho and Paul, 2001).

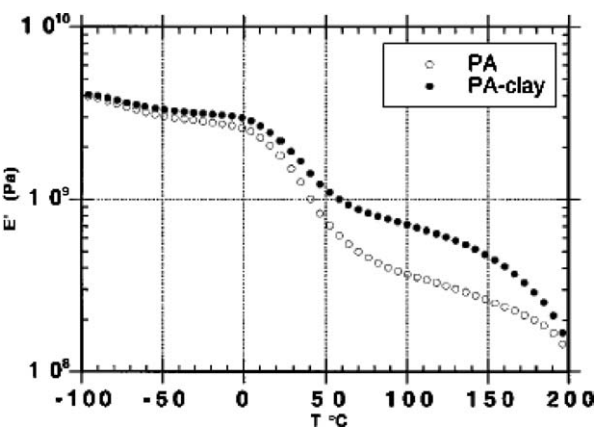


Fig. 10.3.6. Dynamic elastic modulus of an organoclay-nylon 6 nanocomposite as a function of temperature. From (Gloaguen and Lefebvre, 2000).

temperature,  $T_g$ . This indicates restricted mobility in the amorphous phase close to the clay mineral surface, at temperatures below the melting point. This effect occurs with many different polymers and types of synthetic or natural clay minerals. Not unexpectedly, further improvements of the modulus can be obtained by biaxial stretching (Worley et al., 2001).

The modulus and tensile strength in Nylon are known to be highly dependent on water content. In the literature, mechanical properties of organoclay-nylon nanocomposites are often evaluated on DAM (dry as moulded) specimens. Little attention was paid to evaluate mechanical properties after adequate equilibrium water absorption. In nanocomposites based on blends of Nylon and grafted PP, the data show that not only the rate but also the total water absorption is reduced for the nanocomposites (Liu et al., 2001). It is clear that the reduced water absorption may have a deleterious effect on the impact properties of the product (see next section Impact resistance and ductility).

Nanocomposites based on PP can be made only if both the clay mineral and the polymer are modified. Using unmodified PP and an organoclay (Hasegawa et al., 1998; Gloaguen and Lefebvre, 2000; Wang et al., 2001), the modulus increase (15–25%) is almost the same above and below  $T_g$ . It is assumed that in this case, PP interacts very little with the modified clay mineral (i.e., the polymer is not crawling into the interlayer space).

Manufacturing processes to make the nanocomposites normally involve preparing a masterbatch (made of organoclay intercalated by PP-g-MA), and diluting it into pure PP. The influence of MW and MA content in PP-g-MA was extensively studied, and published results are sometimes contradictory.

In general, modulus improvements for PP- based nanocomposites are lower than for their nylon counterparts. Intercalated nanocomposites containing 5% clay mineral show a 50% increase in tensile modulus and 10–15% increase in tensile strength, compared to pure PP (Wang et al., 2001). These properties are almost unaffected by the MA content (1.5–5.8%) and the MW (9,100–330,000) of PP-g-MA and its content (5–15%) in the nanocomposites.

However, the type of organoclay appears to be more important than the PP modification: Cloisite® 20A (dimethyl di-hydrogenated tallow ammonium modified clay) is claimed to give 20% higher tensile properties than the more heat-stable Nanomer® I.30 TC (octadecyl ammonium-modified clay mineral).

Interestingly, the partial substitution of the PP-g-MA for nylon, has a significant effect on the interlayer space. Nylon crawls into the interlayer space, (increasing significantly the basal spacing) but does not improve the mechanical properties.

The Toyota laboratory also studied the mechanical properties of PP/PP-g-MA nanocomposites based on octadecylammonium modified clay minerals. Tensile moduli of the nanocomposites are approximately 30% higher than the pure PP. Fig. 10.3.7 shows the relative dynamic storage modulus as a function of the temperature (Hasegawa et al., 1998). As in the case of nylon the increase in modulus is higher above than below the glass temperature of the PP phase. The maximum

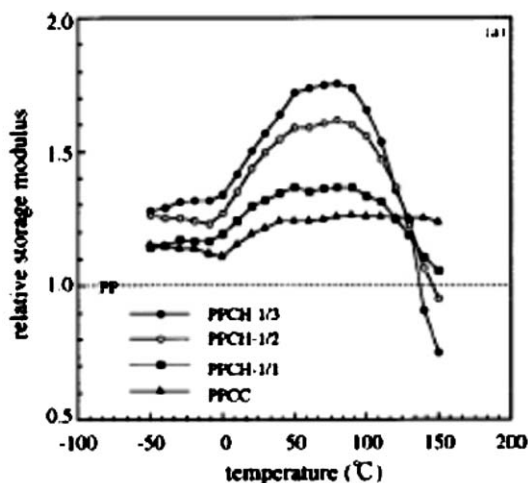


Fig. 10.3.7. Dynamic storage modulus of the organoclay-PP nanocomposites and clay-PP composite in relation to PP. From (Hasegawa et al., 1998).

reinforcement is obtained at 80°C. Above this temperature, the modulus is reduced due to the lower modulus of the PP-g-MA, compared to PP.

Modified routes to the melt intercalation to obtain PP nanocomposites were considered to improve the exfoliation of the clay mineral, such as swelling of the clay by a solvent that is subsequently volatilised during melt blending (Wolf et al., 1999). Other concepts were evaluated such as the use of random copolymers instead of PP-g-MA, or specific surfactants for the modification of the clay mineral, having less favourable interaction with the clay mineral than the PP itself (Manias, 2001). The modulus improvements obtained with these alternative methods are not significantly different than those reported for commonly used surfactants. However, the fluoro-organoclay-PP nanocomposites have almost the same elongation at break as pure PP, hence they have potentially a better impact resistance than other nanocomposites.

#### *Impact Resistance and Ductility*

Achieving a high impact resistance (sometimes called toughness) at low temperature for polymers such as nylon and PP was long considered a technical challenge. At ambient temperature, PP in particular, displays a relatively ductile behaviour but this degenerates below  $T_g$ . Compounding the polymer with rubber was successful in alleviating the brittleness of these materials, although stiffness is reduced. Some nanocomposites composed of nanoparticles of vulcanised rubber have however increased impact resistance with a minimal effect on the modulus (Zhang et al., 2002). Conversely, rigid fillers are commonly used to improve the modulus of the matrix, usually with the penalty of decreased toughness. Hence, optimal compounding of PP

is usually the result of a delicate balance of rubber and mineral fillers, to promote ductility at low temperature and adequate stiffness.

Organoclay-nylon nanocomposites have a slightly lower impact resistance than the neat polymer. The influence of the organoclay is shown in Fig. 10.3.8, where the Izod-impact strength is plotted against temperature. The data show that the ductile-brittle transition is simply moved towards higher temperatures with increasing content of organoclays, even though  $T_g$  does not change (Cho and Paul, 2001). This can be at least partially attributed to the reduced water absorption of the nanocomposites.

Fracture toughness results show that, in contrast to neat nylon, the nanocomposite at equilibrium water uptake (Section 10.3.5.D) does not show an elasto-plastic (super-tough) behaviour (Bureau et al., 2001). This may be due to the lower water content of the nanocomposite. Grafting the surfactant (hexamethylene diamine) to the polymer apparently makes the organoclay-nylon nanocomposite to have the same level of impact resistance as the neat polymer (Maul, 1999).

Nanocomposites obtained by reacting co-intercalated epoxy resin and quaternary ammonium into  $\text{Na}^+$ -montmorillonite with nylons, show higher impact strength than the neat polymer (Liu and Wu, 2002; Liu et al., 2003).

Nanofillers such as nano- $\text{CaCO}_3$ , are effective nucleating agents and improve the impact resistance of PP (Chan et al., 2002). This is due to the nanoparticles introducing a massive number of stress concentration sites, hence promoting cavitation during an impact test. The cavities release the plastic constraints and trigger large-scale plastic deformation of the matrix, which consume high fracture energy. This

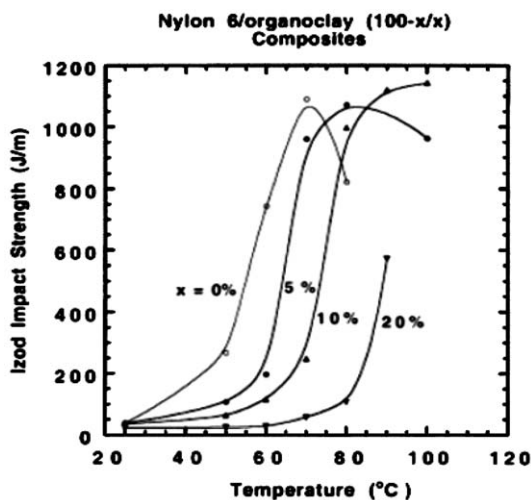


Fig. 10.3.8. Notched Izod impact strength for organoclay-nylon 6/nanocomposites as a function of temperature. From (Cho and Paul, 2001).

ideal scenario is unfortunately not found with organoclay-PP nanocomposites, which display systematically a lower impact resistance than the pure polymer.

### *B. Fire Retardancy and Thermal Properties*

#### *Fire Retardancy*

The cone calorimeter is one of the most effective bench-scale laboratory equipments for studying the flammability of materials. In evaluating new materials, the industry takes cone calorimeter results into consideration, but commercial products are normally evaluated against industry standards such as the UL94 tests. Although these tests are not necessarily better, nor more practical than the cone calorimeter, they are the industrial bench mark against which materials need to be evaluated. The most severe fire retardancy rating is referred to as UL94 V-0 (similar to EN/IEC 60695-11-10 Method B, VDE 0471 Part 11-10 Method B, CSA 22.2 Vertical Burning Test). The V-0 rating at a given thickness means essentially that under the conditions of the tests, the material must self-extinguish within a very short time, and must not drip. To achieve the status of UL94 V-0, polymers most often need to be compounded with fire retardant (FR) additives.

In general, FR additives have an effect either in the condensed phase or in the gas phase, by respectively creating an isolating char or preventing oxygen from reaching the burning material. Examples of additives producing char are phosphorous or melamine compounds; and those working through the gas phase are synergistic blends of decabromodiphenyl oxide and antimony sesquioxide.

Nylon can be easily compounded with FR additives (Gilman et al., 2000). Organoclay-nylon nanocomposites, containing 3.3% melamine and 5% organoclay produce a UL94 V-0 rating. In this case, some of the melamine is intercalated in a layered silicic acid salt (Inoue and Hosokawa, 1998). For reference, normally 6 to 10% melamine is needed to provide a V-0 rating to nylon neat polymer.

Polyolefins are the most difficult to be compounded for reduced flammability. In the flame, PP decomposes into small volatile fragments by chain scission resulting in a high pre-ignition zone and flame temperature, contributing to the high exothermic reaction in the flame.

Organoclay-PP nanocomposites based on PP-g-MA show 70 to 80% reduction in PHRR in the cone calorimeter, slowing down the combustion process significantly (Gilman et al., 2000). This behaviour is due to the formation of a powerful char induced by the clay mineral. At the end of the combustion process, almost all nanocomposites tested leave behind a layered carbonaceous silicate structure, which is polymer type-dependent.

Some nanocomposites with intercalated polymers in clay minerals show excellent fire retardancy. For other nanocomposites a minimum amount of delaminated clay particles is needed to provide good fire retardancy. However, an apparently well-exfoliated fluorohectorite-polymer nanocomposite has no fire retardant properties. No fundamental explanation was proposed to explain this surprising behaviour.



Organoclay-PP nanocomposites do not reach the UL 94 V-0 rating, but in a traditional V-0 rated PP compound, 25% of the FR additives such as a blend of decabromo diphenyl oxide and antimony sesquioxide, can be replaced by an organoclay in a ratio of almost 1:1 (Nanocor, 2003). The resulting nanocomposite has the same V-0 rating, a slightly lower specific gravity, and potentially higher mechanical properties than, the original compound.

ATH and MH are traditional FR additives for polyolefins. They have very desirable properties (non-toxic and halogen-free) but have many practical disadvantages, such as their low efficiency. Additions of up to 65% by weight (40% in volume) may be required to achieve UL 94 V-0 ratings. At these high filler levels, a marked deterioration in mechanical properties and significant viscosity increases, can limit the mechanical performance and their selection for more demanding applications. Hence, reducing filler level without compromising fire retardancy is needed. The use of modified forms of hydroxides, and their combination with alternative additives acting in a synergistic manner are the most promising ways to achieve this goal. In the very short list of effective additives that can be used to partially replace ATH, such as the extremely efficient PAN fibres (Myata and Imahashi, 1992), carbon powder, transition metal oxides, and zinc stannates and hydrostannates (Hornsby and Ahmadnia, 2002), organoclays should be considered as valid candidates.

Even though ATH is normally used for PE and EVA, Table 10.3.4 shows the results of the partial replacement of MH by an organoclay in a UL94 V-0 rated EVA compound. The data show that the organoclay is much more efficient than the hydroxide in providing flame retardancy. For the same V-0 rating, as the loading of magnesium hydroxide is lower, improved processing and mechanical properties are expected (Nanocor, 2003).

Other valuable but less known FR additives exist alongside organoclays to improve the fire resistance of polymers. For example, adding 15% lignin gives a 60% reduction in PHRR in the cone calorimeter; further reductions in PHRR are obtained in the presence of lignin with traditional char forming additives (De Chirico et al., 2003). However, organoclays appear to be unique in their ability to provide both increased modulus and fire resistance, but at the expense of the impact resistance.

Table 10.3.4. EVA compounds and clay mineral-EVA nanocomposites for UL94 V-0 rating (thickness: 3.2 mm) (from Nanocor)

	Traditional EVA nanocomposites		Clay mineral-EVA nanocomposites	
	% Weight	% Volume	% Weight	% Volume
EVA	40	63	47	69
Mg(OH) <sub>2</sub>	60	37	50	29
Clay mineral	0	0	3	2

### *Thermal Stability and Expansion*

One property of organoclay-PP nanocomposites is the increase (of up to 130 °C) in the onset of the degradation temperature in TGA experiments (Kodgire et al., 2000). Unfortunately, this is not an indication of an improvement in the resistance to ageing or oxidation of the nanocomposite, which in fact is reduced compared to that of the neat polymer (Tidjani and Wilkie, 2000; Chin and Solera, 2002). The increase in the degradation temperature is generally regarded as a consequence of the low permeability of the nanocomposites preventing oxygen to reach the polymer, and preventing the volatiles generated during the decomposition of the polymer to leave the nanocomposites (Gilman, 2000). Thus, the TGA experiment would appear to duplicate the observations from the cone calorimeter. However, organoclay-nylon and -polyimide nanocomposites do not have a higher degradation temperature in TGA experiments, but they nevertheless display interesting fire retardancy properties.

It is clear that each polymer may be a special case, and there is no general understanding of this clay mineral-polymer nanocomposite behaviour.

As expected the CLTE of nanocomposites based on HMW (high molecular weight) nylon is lower than that formed from LMW (low molecular weight) nylon (Yoon et al., 2002). The better behaviour of the organoclay-HMW nylon nanocomposite was attributed to its higher viscosity, inducing higher shear during processing and a higher degree of clay mineral exfoliation, eventually a higher orientation.

Organoclay-PP nanocomposites also have a lower CLTE than the neat polymer. This is a definite advantage in a number of automotive applications such as bodywork panels, because the decrease in CLTE allows the designer to reduce the gap between the body panels; this is of general benefit to the car design and aesthetics.

### *C. Electrical and Electrochemical Properties*

The electrical behaviour of nanocomposites based on clay minerals and related solids combined with various conducting polymers was intensively studied in the last decade (Ruiz-Hitzky, 1993; Ruiz-Hitzky and Aranda, 1997). Clay mineral-PEO nanocomposites based on homoionic montmorillonites and other smectites, are anisotropic solid electrolyte materials presenting ionic conductivity values several orders of magnitude higher than that of the parent silicate. The thermal stability of this class of materials is strongly enhanced in comparison with conventional salt-PEO complexes. Moreover, a salient feature of these clay mineral-polymer nanocomposites compared with electrolytes in solution, is that in the former case, the silicate layer acts as the anion. In theory, therefore, ionic conductivity should exclusively involve a cationic transport mechanism.

Recent results of solid-state polarisation (Ruiz-Hitzky et al., 2000; Aranda et al., 2003) using Na<sup>+</sup>-montmorillonite-PEO nanocomposites confirm this hypothesis, giving a transport number ( $t_+$ ) close to 0.99 compared to the theoretical value of 1 for an ideal pure cationic solid electrolyte. This unique behaviour can serve as a

model for ionic conductors; these nanocomposites have important potential applications as components in electrochemical devices, such as rechargeable solid-state batteries and electrochemical sensors. Intercalation of PEO into clay minerals can promote co-adsorption of other polymers, such as PMMA, improving further the ionic conductivity (Chen et al., 1999).

An electronic conducting polymer is formed during the intercalation of aniline into a  $\text{Cu}^{2+}$ -smectite giving PANI, by the conversion of the emeraldine base into the emeraldine salt (Fig. 10.3.9) by exposure to HCl vapours (Mehrota and Giannelis, 1991). Alternatively, if the clay mineral is ion-exchanged by treatment with aniline hydrochloride followed by oxidation with ammonium peroxodisulphate, the anilinium cations give after polymerisation the conductive emeraldine salt form of the polymer (Chang et al., 1992) (Fig. 10.3.10). This type of material exhibits interesting electrical properties, because the conducting polymer remains in the interlayer space of the clay mineral. The electrical conductivity shows, as expected, a highly anisotropic character; the value measured in the direction parallel to the basal layer silicate plane is in the order of  $10^{-3}$  S/cm.

Similarly, iodine doping of polypyrrole spontaneously formed from adsorbed pyrrole on transition-metal exchanged smectites, enhances dramatically the conductivity

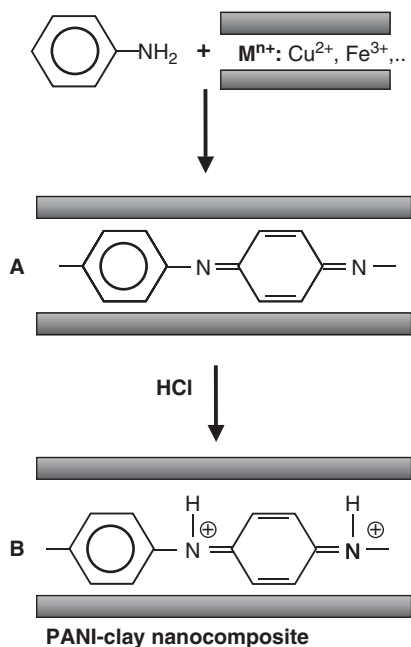


Fig. 10.3.9. Reactions of aniline in the formation of clay-PANI-nanocomposites from smectites exchanged with transition-metal ions. A) emeraldine-base formation; B) emeraldine-salt conducting polymer.

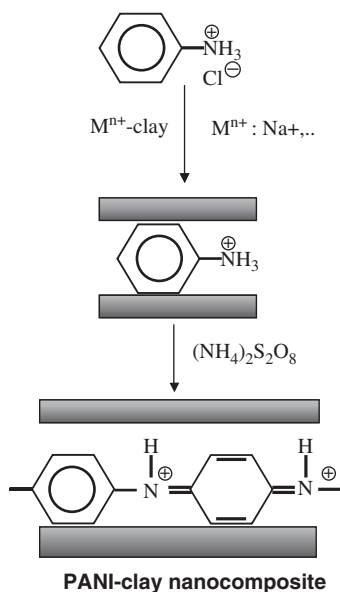


Fig. 10.3.10. Formation of  $\text{Na}^+$ -montmorillonite-PANI nanocomposites.

of this nanocomposite from about  $10^{-5}$  to  $10^{-2}$  S/cm (Mehrota and Giannelis, 1992). The effect of the Fe(III) localisation in iron-rich smectites on the electrical behaviour of clay mineral-PPy nanocomposites doped with  $\text{I}_2$  was recently reported (Letaïef et al., 2005). As expected, the electrical conductivity here also shows a highly anisotropic character imposed by the 2D geometry of the clay mineral particles.

The electrical conductivity of montmorillonite-PNVC systems (Biswas and Ray, 1998) is about  $10^{-6}$  S/cm, which is higher than that of pure PNVC but lower than that of montmorillonite alone. Nonetheless, future investigations should be carried out on the potential behaviour of clay mineral-PNVC nanocomposites as photoconductors based on charge transfer between these materials and electron acceptors such as 2,4,7-trinitro-9-fluorenone (Schaffert, 1971).

As indicated above, heating clay mineral-PAN nanocomposites gives rise to carbonaceous-clay materials which can be used as electrodes for electrochemical devices (Duclaux et al., 2000; Fernández-Saavedra et al., 2004). To clarify the mechanisms involved in the different steps of PAN transformation into graphitised materials was applied the in situ EIS technique has been applied simultaneously with FTIR and XRD analyses (Fernández-Saavedra et al., 2004). This will provide means of controlling the structural and textural characteristics of the resulting carbonaceous materials and their relationship with the electrical and electrochemical behaviour of the nanocomposites.

As shown above, the intercalation of chitosan in smectites gives clay mineral-bio-polymer nanocomposites having an anion-exchange capacity. Based on this property,

these materials could be used as active elements in electrochemical sensors for selective detection of ions in solution: they should easily discriminate monovalent from polyvalent species (Darder et al., 2005).

#### *D. Gas and Water Permeation*

Low gas permeation of nanocomposites was long considered as one of their most important technological advantages. The simple tortuous model (Nielsen, 1967) does explain many experimental results but many new models were recently developed, most of which can explain the low permeability, and the high modulus of nanocomposites. (Beall, 2001; Bonner et al., 2001; Swannack et al., 2002; Drozdov et al., 2003).

It is interesting to note that total exfoliation with random orientation of the individual clay mineral particles may not be favourable to low permeability; the more favourable morphology should be that of intercalated compounds, where the particles are well oriented, and remain parallel to each other, even in the final part.

The application of polymers in films, such as nylon in food packaging, where reduced permeability is valued, is a very complex subject, which cannot be simplified without missing important points. The mechanical properties of the finished film are an intricate function of the characteristics and processing history of the product.

For example, clay-nylon nanocomposites show improvements in transparency, gas barrier properties and modulus, but none in elongation at break and tear resistance compared with typical nylons used in such applications. If the nanocomposite film is made with a reduced film thickness (to take advantage of the higher modulus and lower gas permeability), the potential applications of this new product will be limited to the few cases, where its lower tear resistance will be acceptable. The permeability of nylon and organoclay-nylon nanocomposites is a function of crystallinity, and hence of the processing conditions. For example if colder than normal roller temperature have to be used during extrusion, the film will show sub-optimal permeability.

In two-layered films, organoclay-nylon nanocomposites may cause waviness and curling because the film is asymmetric, hence exacerbating the difference in properties between the two materials. These issues are not uncommon and can be easily resolved, but usually, the solutions reduce the advantages of the nanocomposites versus the neat polymer.

Besides the organoclay-EVOH nanocomposites (Lucciarini et al., 2002), and the patented butyl based coatings (Feeney, et al., 1998), the best barrier properties obtained so far with nanocomposites are with the aromatic-aliphatic polyamide nanocomposites (Imperm<sup>TM</sup>) (Bagrodia et al., 2001).

In one article by Bureau et al. (2001), an organoclay-polyamide 6 nanocomposite having a low vapour transmission rate, absorbs at equilibrium as much water as the neat polymer. This result, if not unexpected, is in contradiction with published data.

The permeability and the solvent uptake of organoclay-PP nanocomposites is lower than for the neat polymer (Manias et al., 2001). For example a PP nanocomposite

containing 6% organoclay shows about half the oxygen transmission rate of the neat PP (Qian et al., 2001).

### *E. Other Properties*

#### *Polymer Crystallization*

It is generally accepted, that the degree of crystallisation of organoclay–nylon 6 nanocomposites does not vary with organoclay content. However, the presence of the organoclay may change the crystal form, from alpha (normally present in neat nylon 6) to predominantly gamma (Kojima et al., 1993c). The organoclay has a strong nucleation effect, and increases the crystallisation rate (Liu et al., 1998). As a result, the melting point of the clay mineral–nylon nanocomposites is slightly reduced compared to the neat nylon, and the crystallisation temperature is increased. The reduction in melting temperature is usually associated with the smaller size of the crystallised nylon, whereas the higher crystallisation temperature is associated with the nucleation effect of the clay mineral. Stretching during processing promotes the formation of the alpha phase at all temperatures for organoclay–nylon 6 nanocomposites (Ergungor et al., 2002).

In microcomposites, the degree of crystallisation of PP decreases with increasing filler volume fractions, while some fillers such as talc are known to be powerful nucleating agents for PP (Varga and Schulek-Tóth, 1991). Organoclays apparently do not change the crystallinity of PP in the nanocomposites. Nevertheless, if PP normally forms spherulites, apparently PP nanocomposites form fibres at 142 °C, a temperature at which the PP alone does not crystallise (Kodgire et al., 2000).

By contrast, a significant reduction in the degree of crystallinity of organoclay–PE nanocomposites is observed, which tends to work against the reinforcement effect of the organoclay (Gopakumar et al., 2002).

#### *Degradation During Nanocomposite Processing*

A problem with clay–polymer nanocomposites is associated with degradation during processing. There is an obvious need for more studies regarding additional stabilisation of the polymers.

During melt blending of an organoclay–nylon 6 nanocomposite, in a twin screw at 240 °C, the organic modifier degrades to an extent correlated with the residence time in the extruder (Davis et al., 2002). Further, this nanocomposite significantly degrades during injection moulding, even if it was thoroughly dried. The authors conclude that small amounts of water adsorbed by the clay mineral are responsible for the degradation of the nanocomposite. Here again new stabilisation techniques need to be worked out.

Other issues are associated with the chemicals used to modify the clay: Hoffman degradation of the tetraalkylammonium ions in some organoclays is apparently responsible for the broadening of the polydispersity of the polymer matrix during processing (Gilman et al., 2000). It is interesting to note that the additive used for

compatibilising the clay mineral, may represent from 20 to almost 50% by weight relative to the clay (Usuki et al., 1996; Kodgire et al., 2000).

Clays are derived from natural products, thus containing impurities as organic matter from soils and oxyhydroxides mainly of iron or aluminium. These are normally eliminated by appropriate techniques during clay purification. These impurities and structural transition metals, such as iron, titanium, if not completely removed, are known to promote degradation of the organoclay-PP nanocomposite by UV, for example. Possible solutions include the use of adequate UV additives, or synthetic clay minerals, but the mechanical properties of the resulting nanocomposites are inferior to those prepared from natural clay (Wang and Pinnavaia, 1998).

In the majority of the organoclay-polymer nanocomposites described in the literature there is an ionic bond between the swelling agent and the clay mineral. If the swelling agent is accidentally released (in a reverse ion exchange reaction), the organoclay itself may separate from the polymer (Moet and Akelah, 1993; Messersmith and Giannelis, 1995).

Until now, little value was attached to organoclays as sole reinforcing agent. For example, the relatively high heat deformation temperatures characteristic of the nylon nanocomposites are largely insufficient compared to actual market requirements, especially in automotive applications. Organoclays can however partially replace other reinforcing agents, like glass fibre.

### 10.3.6. CONCLUSIONS

Clay minerals and polymers can be used to prepare almost tailor-made clay mineral-polymer nanocomposites, having interesting physical properties and, in some instances, commercial applications.

It is obvious that the information is extensive, but the quality of published papers is uneven. In such an emerging “new science”, much needs to be learned. Every step, every experiment takes the scientist into the exciting field of the unknown and unexpected innovation. Many statements are made that contradict previous ideas. These are sometimes partially “revisited”.

Even if the vast majority of people involved in clay mineral-polymer nanocomposite research rightfully believe in the future of these new materials, few products reached industrial application. In some papers on nanocomposites, the polymer science aspects are not well considered, but most often, it is the understanding of the peculiar properties of the clay minerals that is rather limited. Clearly, nanocomposite developments would benefit from a stronger cooperation between polymer and clay scientists.

Suggestions are made to explore new routes, such as using kaolinite and sepiolite as clay mineral components instead of the widely used montmorillonite. Similarly, the co-hydrolysis route to compatibilise the clay mineral with the polymer was not fully investigated, although the results are promising.

Current commercial nanocomposites were not really optimised, and their mechanical and functional performance could still be vastly improved. In this respect, knowledge of clay mineral properties, as well as clay mineral conditioning by controlled modification, and polymer chemistry should be more integrated into the fast-growing “nanofield” programs.

## REFERENCES

- Ahlich, J.L., Serna, C.J., Serratos, J.M., 1975. Structural hydroxyls in sepiolite. *Clays and Clay Minerals* 23, 119–124.
- Akelah, A., Salahuddin, N., Hiltner, A., Baer, E., Moet, A., 1994. Morphological hierarchy of butadieneacrylonitrile/montmorillonite nanocomposite. *Nanostructured Materials* 4, 965–978.
- Alexandre, M., Dubois, P., 2000. Polymer-layered silicate nanocomposites: preparation, properties and uses of a new class of materials. *Materials Science and Engineering Report* 28, 1–283.
- Alvarez, A., Casal, B., Fripiat, J.J., Pérez Castells, R., Ruiz-Hitzky, E., Santarén, J., 1984. Procedimiento de fabricación de arcillas fibrosas organofílicas. Spanish Patent 535, 316.
- Alvarez, A., Casal, B., Fripiat, J.J., Pérez Castells, R., Ruiz-Hitzky, E., Santarén, J., 1985. Process for manufacturing organophilic fibrous clays. European Patent Application, 85,830,264.9.
- Alvarez, A., Santarén, J., Pérez-Castells, R., Casal, B., Ruiz-Hitzky, E., Levitz, P., Fripiat, J.J., 1987. Surfactant adsorption and rheological behavior of surface-modified sepiolite. In: Schultz, L.G., van Olphen, H., Mumpton, F.A. (Eds.), *Proceedings of the International Clay Conference, Denver 1985*. The Clay Minerals Society. Bloomington, IN, pp. 370–374.
- Aragón de la Cruz, F., Esteban, F., Vitón, C., 1973. Intercalation of chlorosilanes with montmorillonite and vermiculite. In: Serratos, J.M. (Ed.), *Proceedings of the International Clay Conference, Madrid 1972*. División de Ciencias CSIC, Madrid, pp. 705–710.
- Aranda, P., Galván, J.C., Ruiz-Hitzky, E., 1998. Organic/inorganic hybrid materials. In: Laine, R.M., Sanchez, C., Brinker, C.J., Giannelis, E. (Eds.), *Materials Research Society (MRS) Symposium Proceedings*, vol. 519, Warrendale, PA, pp. 375–380.
- Aranda, P., Mosqueda, Y., Perez-Capote, E., Ruiz-Hitzky, E., 2003. Electrical characterization of PEO-clay nanocomposites prepared by microwave irradiation. *Journal of Polymer Science, Part B. Polymer Physics* 41, 3249–3263.
- Aranda, P., Ruiz-Hitzky, E., 1992. Poly(ethylene oxide)-silicate intercalation materials. *Chemistry of Materials* 4, 1395–1403.
- Aranda, P., Ruiz-Hitzky, E., 1994. New polyelectrolyte materials based on smectite polyoxyethylene intercalation compounds. *Acta Polymerica* 45, 59–67.
- Aranda, P., Ruiz-Hitzky, E., 1999. Poly(ethylene oxide)/NH<sub>4</sub><sup>+</sup> nanocomposites. *Applied Clay Science* 15, 119–135.
- Aviles, M.A., Justo, A., Sánchez-Soto, P.J., Pérez-Rodríguez, J.L., 1993. Synthesis of nitrogen ceramics from a new vermiculite-polyacrylonitrile intercalation compound by carbothermal reduction. *Journal of Materials Chemistry* 3, 223–224.



- Aviles, M.A., Sánchez-Soto, P.J., Justo, A., Pérez-Rodríguez, J.L., 1994. Compositional variation of sialon phase produced after carbothermal reduction and nitridation of a vermiculite-polyacrylonitrile intercalation compound. *Materials Research Bulletin* 29, 1085–1090.
- Bafna, A., Beaucage, G., Mirabella, F., Mehta, S., 2003. 3D hierarchical orientation in polymer-clay nanocomposite films. *Polymer* 44, 1103–1115.
- Bagrodia, S., Germinario, L.T., Gilmer, J.W., Tant, M.R., 2001. Structure-property relationships in Polyamide based nanocomposites. *Antec* 2001 2, 176–179.
- Barrios-Neira, J., Rodrique, L., Ruiz-Hitzky, E., 1974. Mise en évidence de groupements organiques insaturés greffés sur la sepiolite. *Journal de Microscopie et de Spectroscopie Electroniques* 20, 295–298.
- Beall, G.W., 2001. A new model for interpreting nanocomposite behavior. *Antec* 2001 2, 283–290.
- Bergaya, F., Kooli, F., 1991. Acrylonitrile-smectite complexes. *Clay Minerals* 26, 33–41.
- Biswas, M., Ray, S.S., 1998. Preparation and evaluation of composites from montmorillonite and some heterocyclic polymers—I—Poly(N-vinylcarbazole) montmorillonite nanocomposite system. *Polymer* 39, 6423–6428.
- Blumstein, A., 1961. Étude des polymérisations en couche adsorbée I. *Bulletin de la Société Chimique de France*, 899–906.
- Blumstein, R., Blumstein, A., Parikh, K., 1974. Polymerisation of monomolecular layers adsorbed on montmorillonite: cyclization in polyacrylonitrile and polymethacrylonitrile. *Applied Polymer Symposia* 25, 81–88.
- Bonner, S., Sabandith, D., Swannack, C., Zhou, W., 2001. Nanocomposite polymer film technology. *Antec* 2001 3, 1057–1061.
- Bureau, M.N., Denault, J., Glowacz, F., 2001. Mechanical behavior and crack propagation in injection molded polyamide 6/clay nanocomposites. *Antec* 2001 2, 620–624.
- Carrado K.A., Xu, L., Seifert, S., Csencsits, R., 2000. Polymer-clay nanocomposites from synthetic polymer-silicate Gels. In: Pinnavaia, T.J., Beall, G.W. (Eds.), *Polymer-clay nanocomposites*. Chapter 3, Wiley, West Sussex, pp. 47–63.
- Carrado, K.A., 2000. Synthetic organo- and polymer-clays: preparation, characterization, and materials applications. *Applied Clay Science* 17, 1–23.
- Carrado, K.A., Xu, L., 1998. In-situ synthesis of polymer-clay nanocomposites from Silicate gels. *Chemistry of Materials* 10, 1440–1445.
- Carrado, K.A., Xu, L., 1999. Materials with controlled mesoporosity derived from synthetic polyvinylpyrrolidone-clay composites. *Microporous and Mesoporous Materials* 27, 87–94.
- Casal, B., Ruiz-Hitzky, E., 1977. Reaction of Epoxides on Mineral Surfaces. Organic Derivatives of Sepiolite. In: Rosenqvist, I.Th. (Ed.), *Proceedings of the III European Clay Conference, Oslo 1977*, vol. I. Nordic Society for Clay Research, Oslo, pp. 35–37.
- Casal, B., Ruiz-Hitzky, E., 1984. Estudio por espectroscopia IR de la interaccion de epoxidos con grupos silanoles en superficies silícicas. *Anales de Química* 80, 315–320.
- Casal, B., Ruiz-Hitzky, E., Serratosa, J.M., 1980. Nuevo procedimiento de obtención de compuestos organo-minerales derivados del mineral sepiolita. *Spanish Patent* 480550 (1 April 1980).
- Chan, C.M., Wu, J., Li, J.X., Cheung, Y.K., 2002. Polypropylene/calcium carbonate nanocomposites. *Polymer* 43, 2981–2992.

- Chang, T.-C., Ho, S.-Y., Chao, K.-J., 1992. Intercalation of polyaniline in montmorillonite and zeolite. *Journal of the Chinese Chemical Society* 39, 209–212.
- Chen, W., Xu, Q., Yuan, R.Z., 1999. Modification of poly(ethylene oxide) with polymethylmethacrylate in polymer-layered silicate nanocomposites. *Journal of Materials Science Letters* 18, 711–713.
- Chin, H., Solera, P., 2002. Stabilization of polypropylene nanocomposites, *Nanocomposites* 2002, September 23–25, San Diego.
- Cho, J.W., Paul, D.R., 2001. Nylon 6 nanocomposites by melt compounding. *Polymer* 42, 1083–1094.
- Cloos, P., Moreale, A., Braers, C., Badot, C., 1979. Adsorption and oxidation of aniline and p-chloroaniline by montmorillonite. *Clay Minerals* 14, 307–321.
- Cloos, P., Vande Poel, D., Camerlynck, J.P., 1973. Thiophene complexes on montmorillonite saturated with different cations. *Nature. Physical Science (London)* 243, 54–55.
- Cody, C.A., Kemnetz, S.J., 1987. Improved organophilic clay gellant and process for preparing organophilic clay gellants. *European Patent Application*, 0312988.
- Darder, M., Colilla, M., Ruiz-Hitzky, E., 2003. Biopolymer-clay nanocomposites based on chitosan intercalated in montmorillonite. *Chemistry of Materials* 15, 3774–3780.
- Darder, M., Colilla, M., Ruiz-Hitzky, E., 2005. Chitosan-clay nanocomposites: application as electrochemical sensors. *Applied Clay Science* 28, 199–208.
- Davis, R.D., Gilman, W., VanderHart, D.L., 2002. Processing degradation of polyamide 6/montmorillonite clay nanocomposites and clay organic modifier. *Polymer Degradation and Stability* 79, 111–121.
- De Chirico, A., Armanini, M., Chini, P., Cioccolo, G., Provasoli, F., Audisio, G., 2003. Flame retardants for polypropylene based on lignin. *Polymer Degradation and Stability* 79, 139–145.
- Drozdov, A.D., Christiansen, J.deC., Gupta, R.K., Shah, A.P., 2003. Model for anomalous moisture diffusion through a polymer-clay nanocomposite. *Journal of Polymer Science, Part B. Polymer Physics* 41, 476–492.
- Duclaux, L., Frackowiak, E., Gibinski, T., Benoit, R., Béguin, F., 2000. Clay/carbon nanocomposites as precursors of electrode materials for lithium-ion batteries and supercapacitors. *Molecular Crystals and Liquid Crystals* 340, 449–454.
- Ergungor, Z., Cakmak, M., Batur, C., 2002. Basic studies on uniaxial deformation of nylon 6-clay nanocomposite films. *Antec* 2002 2, 602–606.
- Feeney, C.A., Farrel, M., Tannert, K., Goldberg, H.A., Lu, M., Grah, M.D., Steiner, W.G., Winston, P.B., 1998. Barrier coating of an elastomer and a dispersed layered filler in a liquid carrier, *U.S. Patent* 6,087,016.
- Fernández-Saavedra, R., Aranda, P., Ruiz-Hitzky, E., 2004. Templated synthesis of carbon nanofibers using sepiolite. *Advanced Functional Materials* 14, 77–82.
- Fernández-Hernández, M.N., Ruiz-Hitzky, E., 1979. Interacción de isocianatos con sepiolita. *Clay Minerals* 14, 295–305.
- Finlayson, C.M., Cody, C.A., Kemnetz, S.J., Reichert, W.W., Magauran, E. D., Johnson, J.R., 1987. Organophilic clay gellants and process for preparation. *U.S. Patent* 4,695,402.
- Fornes, T.D., Yoon, P.J., Hunter, D.L., Heskkula, H., Paul, D.R., 2002. Effect of organoclay structure on nylon 6 nanocomposite morphology and properties. *Polymer* 43 22, 5915–5933.
- Fripiat, J.J., Mendelovici, E., 1968. Dérivés organiques des silicates. I. Le dérivé méthylé du chrysotile. *Bulletin de la Société Chimique de France*, 483–492.

- Fukushima, Y., Inagaki, S., 1987. Synthesis of an intercalated compound of montmorillonite and 6-polyamide. *Journal of Inclusion Phenomena* 5, 473–482.
- Fukushima, Y., Okada, A., Kawasumi, M., Kurauchi, T., Kamigaito, O., 1988. Swelling behavior of montmorillonite by poly 6-amide. *Clay Minerals* 23, 27–34.
- Giannelis, E.P., 1996. Polymer layered silicate nanocomposites. *Advanced Materials* 8, 29–35.
- Giannelis, E.P., Krishnamoorti, R., Manias, E., 1999. Polymer-silicate nanocomposites: model systems for confined polymers and polymer brushes. In: Granick, S. (Ed.), *Advances in Polymer Science*, Springer, 138, pp. 107–147.
- Gilman, J.W., Jackson, C.L., Morgan, A.B., Harris, R., Manias, E., Giannelis, E.P., Wuthe-now, M., Hilton, D., Philips, S., 2000. Flammability properties of polymer layered silicate (clay) nanocomposites, Paper presented at “Flame retardants 2000”, Interscience Publishers, London, 49–68.
- Gloaguen, J.M., Lefebvre, J.M., 2000. Plastic deformation behavior of thermoplastic/clay nanocomposites. *Polymer* 42, 5841–5847.
- Goettler, L.A., Recktenwald, D.W., 1998. Nylon nanocomposites: performance attributes and potential applications. *Additives* 98, February 17, Orlando.
- Gopakumar, T.G., Lee, J.A., Kontopoulou, M., Parent, J.S., 2002. Influence of clay exfoliation on the physical properties of Montmorillonite /polyethylene composites. *Polymer* 43, 5483–5491.
- Hackett, E., Manias, E., Giannelis, E.P., 2000. Computer simulation studies of PEO/layer silicate nanocomposites. *Chemistry of Materials* 12, 2161–2167.
- Hasegawa, N., Kawasumi, M., Kato, M., Usuki, A., Okada, A., 1998. Preparation and mechanical properties of Polypropylene-clay hybrids using a maleic anhydride-modified polypropylene oligomer. *Journal of Applied Polymer Science* 67, 87–92.
- Hawthorne, D.G., Hodgkin, J.H., Loft, B.C., Solomon, D.H., 1974. Polymerization of vinyl monomers on mineral surfaces; a novel method of preparing reinforcing fillers. *Journal of Macromolecular Science-Chemistry A* 8, 649–657.
- Hoffmann, B., Dietrich, C., Thomann, R., Friedrich, C., Mülhaupt, R., 2000. Morphology and rheology of polystyrene nanocomposites based upon organoclays. *Macromolecular Rapid Communications* 21, 57–61.
- Hornsby, P.R., Ahmadnia, A., 2002. Synergistic effects in halogen free polymer compounds containing hydrated mineral fillers. *Antec* 2002 3, 58–62.
- Inagaki, S., Fukushima, Y., Miyata, M., 1995. Inclusion polymerization of isoprene in the channels of sepiolite. *Research on Chemical Intermediates* 21, 167–180.
- Inoue, H., Hosokawa, T., 1998. Silicate-triazine complex and flame retardant resin composite containing the same complex. *Japan Patent* 10 81,510 (98 81,510).
- Jordan, J.W., 1949a. Organophilic bentonites. I. Swelling in organic liquids. *Journal of Physical Chemistry* 53, 294–306.
- Jordan, J.W., 1949b. Alteration of the properties of bentonite by reaction with amines. *Mineralogical Magazine* 28, 598–605.
- Kanatidis, M.G., Tonge, L.M., Marks, T.J., Marcy, H.O., Kannewurf, C.R., 1986. In situ intercalative polymerization of pyrrole in FeOCl. A new class of layered, conducting polymer-inorganic hybrid materials. *Journal of the American Chemical Society* 109, 3797–3799.

- Kodgire, P., Kalgaonkar, R., Hambir, S., Bulakh, N., Jog, J.P., 2000. PP/clay nanocomposites: effect of clay treatment on morphology and dynamic mechanical properties. *Journal of Polymer Science* 81, 1786–1792.
- Kojima, Y., Usuki, A., Kawasumi, M., Okada, A., Kurauchi, T., Kamigaito, O., 1993a. Synthesis of nylon 6-clay hybrid by Montmorillonite intercalated with  $\epsilon$ -caprolactam. *Journal of Polymer Science, Part A* 31, 983–986.
- Kojima, Y., Usuki, A., Kawasumi, M., Okada, A., Kurauchi, T., Kamigaito, O., 1993b. One-pot synthesis of nylon 6-clay hybrid. *Journal of Polymer Science, Part A* 31, 1755–1758.
- Kojima, Y., Usuki, A., Kawasumi, M., Okada, A., Fukushima, Y., Kurauchi, T., Kamigaito, O., 1993c. Mechanical properties of nylon 6-clay hybrid. *Journal of Materials Research* 8 5, 1185–1189.
- Krishnamoorti, R., Vaia, R.A., Giannelis, E.P., 1996. Structure and Dynamics of Polymer-Layered Silicate Nanocomposites. *Chemistry of Materials* 8, 1733.
- Kuang, W., Facey, G.A., Detellier, C., Casal, B., Serratos, J.M., Ruiz-Hitzky, E., 2003. Nanostructured hybrid materials formed by sequestration of pyridine molecules in the tunnels of sepiolite. *Chemistry of Materials* 15, 4956–4967.
- Lagaly, G., 1986. Interaction of alkylamines with different types of layered compounds. *Solid State Ionics* 22, 43–51.
- Leroux, F., Aranda, P., Besse, J.P., Ruiz-Hitzky, E., 2003. Intercalation of poly(ethylene oxide) derivatives into layered double hydroxides. *European Journal of Inorganic Chemistry*, 1242–1251.
- Letaïef, S., Aranda, P., Ruiz-Hitzky, E., 2005. Influence of iron in the formation of conductive polypyrrole-clay nanocomposites. *Applied Clay Science* 28, 183–198.
- Lataïef, S., Ruiz-Hitzky, E., 2003. Silica-clay nanocomposites. *Chemical Communications*, 2956–2997.
- Levy, R., Francis, C.W., 1975. Interlayer adsorption of polyvinyl pyrrolidone on montmorillonite. *Journal of Colloid and Interface Science* 50, 442–450.
- Lipatov, Y.S., 1995. *Polymer Reinforcement*. ChemTech Publishing, Toronto.
- Liu, L., Qi, Z., Zhu, X., 1998. Studies on nylon 6/clay nanocomposites by melt intercalation process. *Journal of Applied Polymer Science* 71, 1133–1138.
- Liu, X., Wu, Q., Berglund, L.A., Fan, J.F., Qi, Z., 2001. Polyamide 6-clay nanocomposites/polypropylene-grafted-maleic anhydride alloys. *Polymer* 42, 8235–8239.
- Liu, X., Wu, Q., 2002. Polyamide 66/clay nanocomposites via melt co-intercalation. *Macromolecular Materials and Engineering* 287 3, 180–186.
- Liu, X., Wu, Q., Berglund, L.A., Lindberg, H., Fan, J., Qi, Z., 2003. Polyamide 6/clay nanocomposites using a co-intercalation organophilic clay via melt compounding. *Journal of Applied Polymer Science* 88, 953–958.
- Lucciarini, J.M., Ratto, J.A., Koene, B.E., Powell, B., 2002. Nanocomposites study of ethylene co-vinyl alcohol and montmorillonite clay. *Antec* 2002 2, 760–764.
- Manias, E., Touny, A., Wu, L., Strawhecker, K., Lu, B., Chung, T.C., 2001. Polypropylene/Montmorillonite nanocomposites. Review of the synthetic routes and material properties. *Chemistry of Materials* 13, 3516–3523.
- Massersmith, P.B., Giannelis, E.P., 1995. Synthesis and barrier properties of poly( $\epsilon$ -caprolactone) layered silicate nanocomposites. *Journal of Polymer Science, Part A* 33, 1047–1057.

- Maul, P., 1999. Plastic nanocomposites: the concept goes commercial. Paper presented at "Plastic fair", June 15–17, Rosemount.
- Mehrota, V., Giannelis, E.P., 1991. Metal-insulator molecular multilayers of electroactive polymers: intercalation of polyaniline in mica-type layered silicates. *Solid State Communications* 77, 155–158.
- Mehrota, V., Giannelis, E.P., 1992. Nanometer scale multilayers of electroactive polymers: intercalation of polypyrrole in mica-type silicates. *Solid State Ionics* 51, 115–122.
- Moet, A., 1990. Final report, The Edison Materials Technology Center, October, Dayton.
- Moet, A.S., Akelah, A., 1993. Polymer-clay nanocomposites-polystyrene grafted onto montmorillonite interlayers. *Materials Letters* 18, 97–102.
- Moreale, A., Cloos, P., Badot, C., 1985. Differential behaviour of Fe(III)- and Cu(II)-montmorillonite with aniline: I. suspensions with constant solid:liquid ratio. *Clay Minerals* 20, 29–37.
- Myata, S., Imahashi, T., 1992. Fire-retardant resin composition, US Patent 5,094,781.
- Nanocor, 2003. web site: [http://www.nanocor.com/tech\\_papers/FRAppsPlastic.asp](http://www.nanocor.com/tech_papers/FRAppsPlastic.asp).
- Nielsen, L.E., 1967. Models for the permeability of filled polymer system. *Journal of Macromolecular Science-Chemistry* A1, 929–942.
- Parfitt, R.L., Greenland, D.J., 1970a. The adsorption of poly(ethylene glycols) on clay minerals. *Clay Minerals* 8, 305–315.
- Parfitt, R.L., Greenland, D.J., 1970b. Adsorption of water by montmorillonite-poly(ethylene glycol) adsorption products. *Clay Minerals* 8, 317–323.
- Pérez-Rodríguez, J.L., Maqueda, C., 2002. Interactions of vermiculite with organic compounds. In: Yariv, S., Cross, H. (Eds.), *Organoclay Complexes and Interactions*. Marcel Dekker, New York, pp. 113–173.
- Pinnavaia, T.J., Beall, G.W. (Eds.), 2000. *Polymer-Clay Nanocomposites*. Wiley, West Sussex.
- Qian, G., Cho, J.W., Lan, T., 2001. Preparation and properties of polyolefin nanocomposites, *Polyolefins* 2001, February 25–28, Houston.
- Quarmley, J., Rossi, A., 2001. Nanoclays: opportunities in polymer compounds. *Industrial Minerals*, January, 47–53.
- Raussell-Colom, J.A., Serratos, J.M., 1987. Reactions of clays with organic substances. In: Newman, A.C.D. (Ed.), *Chemistry of Clays and Clay Minerals*. Longman Scientific & Technical, Essex, pp. 371–422.
- Ruiz-Hitzky, E., 1974. Contribution à l'étude des réactions de greffage de groupements organiques sur les surfaces minérales. Greffage de la sepiolite. Ph.D. thesis. Université Catholique de Louvain, Leuven, Belgium.
- Ruiz-Hitzky, E., 1988. Génie cristalline dans les solides organo-minéraux. *Molecular Crystals and Liquid Crystals* 161, 433–452.
- Ruiz-Hitzky, E., 1993. Conducting polymers intercalated in layered solids. *Advanced Materials* 5, 334–340.
- Ruiz-Hitzky, E., 2001. Molecular access to intracrystalline tunnels of sepiolite. *Journal of Materials Chemistry* 11, 86–91.
- Ruiz-Hitzky, E., 2003. Functionalizing inorganic solids: towards organic-inorganic nanostructured materials for intelligent and bio-inspired systems. *The Chemical Records* 3, 88–100.
- Ruiz-Hitzky, E., 2004. Organic-inorganic materials: from intercalations to devices. In: Gómez-Romero, P., Sánchez, C. (Eds.), *Functional Hybrid Materials*, Chapter 2. Wiley-VCH, Weinheim, pp. 15–49.

- Ruiz-Hitzky, E., Aranda, P., 1990. Polymer-salt intercalation complexes in layer silicates. *Advanced Materials* 2, 545–547.
- Ruiz-Hitzky, E., Aranda, P., 1997. Confinement of conductive polymers into inorganic solids. *Anales de Química, International Edition* 93, 197–212.
- Ruiz-Hitzky, E., Aranda, P., 2000. Electroactive polymers intercalated in clays and related solids. In: Pinnavaia, T.J., Beall, G.W. (Eds.), *Polymer-Clay Nanocomposites*, Chapter 2. Wiley, West Sussex, pp. 19–46.
- Ruiz-Hitzky, E., Aranda, P., Perez-Capote, E., Villanueva, A., Mosqueda Laffita, Y., 2000. Habilidad como conductor iónico del sistema montmorillonita/PEO. *Revista Cubana de Química* 12, 58–63.
- Ruiz-Hitzky, E., Aranda, P., Serratos, J.M., 2004. Clay organic interactions: organo-clay complexes and polymer-clay nanocomposites. In: Auerbach, S., Carrado, K.A., Dutta, P. (Eds.), *Handbook of Layered Materials*, chapter 3. Marcel Dekker, New York, pp. 91–154.
- Ruiz-Hitzky, E., Casal, B., 1985. Epoxide rearrangements on silicoalumina surfaces. *Journal of Catalysis* 92, 291–295.
- Ruiz-Hitzky, E., Fernandez-Hernandez, M.N., Serratos, J.M., 1979. Procedimiento de obtención de compuestos organo-minerales derivados de sílices y de silicates por tratamientos con isocianatos. Spanish Patent 479518.
- Ruiz-Hitzky, E., Fripiat, J.J., 1976. Organomineral derivatives obtained by reaction of organochlorosilanes with the surface of silicates in organic solvents. *Clays and Clay Minerals* 24, 25–30.
- Ruiz-Hitzky, E., Van Meerbeek, A., 1978. Mechanism of the grafting of organosilanes on mineral surfaces. I. Nature and role of the hydrolysis products of the methylvinylchlorosilane in the grafting of silicates in hydrochloric acid and isopropanol. *Colloid and Polymer Science* 256, 135–139.
- Sandi, G., Carrado, K.A., Winans, R.E., Johnson, C.S., Csencsits, R., 1999. Carbons for lithium battery applications prepared using sepiolite as an inorganic template. *Journal of the Electrochemical Society* 146, 3644–3648.
- Sanz, J., Serratos, J.M., 2002. Nuclear magnetic resonance spectroscopy of organoclay complexes. In: Yariv, S., Cross, H. (Eds.), *Organoclay Complexes and Interactions*. Marcel Dekker, New York, pp. 223–272.
- Schaffert, R.M., 1971. A new high-sensitivity organic photoconductor for electrophotography IBM. *Journal of Research and Development* 15, 75–89.
- Siffert, B., Biava, H., 1976. The surface reactivity of vermiculite towards hexamethylene diisocyanate (HMDI). *Clays and Clay Minerals* 24, 303–311.
- Sinha Ray, S., Okamoto, M., 2003. Polymer/layered nanocomposites: a review from preparation to processing. *Progress in Polymer Science* 28, 1539–1641.
- Solomon, D.H., 1968. Clay minerals as electron acceptors and/or electron donors in organic reactions. *Clays and Clay Minerals* 16, 31–39.
- Solomon, D.H., Swift, J.D., Murphy, A.J., 1971. The acidity of clay minerals in polymerization and related reactions. *Journal of Macromolecular Science-Chemistry A* A5, 587–601.
- Soma, T.Y., Soma, M., Furukawa, Y., Harada, I., 1987. Reactions of thiophene and methylthiophenes in the interlayer of transition-metal ion-exchanged montmorillonite studied by resonance Raman spectroscopy. *Clays and Clay Minerals* 35, 53–59.

- Swannack, C., Cox, C., Hirt, D., Liakos, A., 2002. Nanocomposite modeling and simulation. *Antec* 2002 3, 1201–1205.
- Theng, B.K.G., 1974. *The Chemistry of Clay-Organic Reactions*. Adam Hilger, London.
- Theng, B.K.G., 1979. *Formation and Properties of Clay-Polymer Complexes*. Elsevier, Amsterdam.
- Tidjani, A., Wilkie, C., 2000. Photo-oxidation of polymeric-inorganic nanocomposites: chemical, thermal stability and fire retardancy investigations. *Polymer Degradation and Stability* 74, 33–37.
- Tunney, J.J., Detellier, C., 1996. Aluminosilicate nanocomposite materials. Poly(ethylene glycol)-kaolinite intercalates. *Chemistry of Materials* 8, 927–935.
- Usuki, A., Kato, M., Okada, A., Kurauchi, T., 1996. Synthesis of polypropylene-clay hybrid. *Journal of Applied Polymer Science* 63, 137–139.
- Usuki, A., Kojima, Y., Kawasumi, M., Okada, A., Fukushima, Y., Kurauchi, T., Kamigaito, O., 1993. Synthesis of nylon 6-clay hybrid. *Journal of Materials Research* 8, 1179–1184.
- Vaia, R.A., Ishii, H., Giannelis, E.P., 1993. Synthesis and properties of two-dimensional nanostructures by direct intercalation of polymer melts in layered silicates. *Chemistry of Materials* 5, 1694–1696.
- Vaia, R.A., Vasudevan, S., Krawiec, W., Scanlon, L.G., Giannelis, E.P., 1995. New polymer electrolyte nanocomposites: melt intercalation of poly(ethylene oxide) in mica-type silicates. *Advanced Materials* 7, 154–156.
- Van Meerbeek, A., Ruiz-Hitzky, E., 1979. Mechanism of the grafting of organosilanes on mineral surfaces. II. Secondary reactions during the grafting of alkenylchlorosilanes. *Colloid and Polymer Science* 257, 178–181.
- Varga, J., Schulek-Tóth, F., 1991. Filled compounds of the beta-modification of polypropylene. *Angewandte Makromolekulare Chemie* 188, 11–25.
- Wang, H., Zeng, C., Svoboda, P., Lee, L.J., 2001. Preparation and properties of polypropylene nanocomposites. *Antec* 2, 226–230.
- Wang, Z., Massam, J., Pinnavaia, T.J., 2000. Epoxy-clay nanocomposites. In: Pinnavaia, T.J., Beall, G.W. (Eds.), *Polymer-Clay Nanocomposites*, chapter 7. Wiley, West Sussex, pp. 127–149.
- Wang, Z., Pinnavaia, T.J., 1998. Hybrid organic-inorganic nanocomposites: exfoliation of magadiite nanolayers in an elastomeric epoxy polymer. *Chemistry of Materials* 10, 1820–1826.
- Wolf, D., Fuchs, A., Wagenknecht, U., Kretschmar, B., Jehnichen, D., Häussler, L., 1999. Nanocomposites of polyolefin clay hybrids. *Proceedings of Eurofiller'99*, 6–9 September, Lyon.
- Worley, D.C., Akkapedi, M.K., Socci, E.P., 2001. Deformation and orientation of Polyamide 6 nanocomposite. *Antec* 2001 2, 708–712.
- Wu, J., Lerner, M.M., 1993. Structural, thermal, and electrical characterization of layered nanocomposites derived from Na-montmorillonite and polyethers. *Chemistry of Materials* 5, 835–838.
- Yano, K., Usuki, A., Okada, A., Kurauchi, T., Kamigaito, O., 1993. Synthesis and properties of Polyimide-clay hybrid. *Journal of Polymer Science, Part A* 31, 2493–2498.
- Yariv, S., Cross, H. (Eds.), 2002. *Organo-Clay Complexes and Interactions*. Marcel Dekker, New York.
- Yoon, P.J., Fornes, T.D., Paul, D.R., 2002. Thermal expansion behavior of nylon 6 nanocomposites. *Polymer* 43, 6727–6741.

- Zapata, L., Castelein, J., Mercier, J.P., Fripiat, J.J., 1972. Dérivés organiques des silicates. II. Les dérivés vinyliques et allyliques du chrysotile et de la vermiculite. *Bulletin de la Société Chimique de France*, 54–63.
- Zapata, L., Van Meerbeek, A., Fripiat, J.J., Della Faille, M., Van Russelt, M., Mercier, J.P., 1973. Synthesis and physical properties of graft copolymers derived from phyllosilicates: I. The chrysotile and vermiculite derivatives. *Journal of Polymer Science-Polymer Symposia* 42, 257–272.
- Zhang, M., Liu, Y., Zhang, X., Gao, J., Huang, F., Song, Z., Wei, G., Qiao, J., 2002. The effect of elastomeric nano-particles on the mechanical properties and crystallization behavior of polypropylene. *Polymer* 43, 5133–5138.



This page intentionally left blank

*Chapter 11*

## **CLAYS, ENVIRONMENT AND HEALTH**

**F. BERGAYA<sup>a</sup>, B.K.G. THENG<sup>b</sup> AND G. LAGALY<sup>c</sup>**

<sup>a</sup>*CRMD, CNRS-Université d'Orléans, F-45071 Orléans Cedex 2, France*

<sup>b</sup>*Landcare Research, Palmerston North, New Zealand*

<sup>c</sup>*Institut für Anorganische Chemie, Universität Kiel, D-24118 Kiel, Germany*

Because of their large propensity for adsorbing and immobilizing extraneous species, clays and clay minerals can serve as materials for pollution control (Chapter 11.1), carriers of pesticides (Chapter 11.2), liners in waste disposal (Chapter 11.3) and barriers in nuclear waste management (Chapter 11.4). The peculiar surface properties of clays, such as the large specific surface area, layer charge, and swelling capacity also make these materials generally beneficial to human health. The ability of clays and clay minerals to serve as active principles, or excipients, in pharmaceutical formulations, spas, and aesthetic medicine is described in Chapter 11.5. Being good adsorbents and mucostabilizers, clay minerals are also useful as drugs in the treatment of intestinal disorders (Chapter 11.6).

This page intentionally left blank

*Chapter 11.1*

## CLAYS AND CLAY MINERALS FOR POLLUTION CONTROL

G.J. CHURCHMAN<sup>a</sup>, W.P. GATES<sup>b</sup>, B.K.G. THENG<sup>c</sup> AND  
G. YUAN<sup>c</sup>

<sup>a</sup>*School of Earth and Environmental Sciences, University of Adelaide, Glen Osmond, S.A. 5064, Australia*

<sup>b</sup>*Centre for Green Chemistry, School of Chemistry, Monash University, Clayton, VIC 6800, Australia*

<sup>c</sup>*Landcare Research, Palmerston North, New Zealand*

A widespread recognition of the need to develop technologies for pollution control has arisen in only relatively recent times. This has been a result of increased awareness of the effects of pollution on the health and longevity of both human beings and the earth's fragile ecosystems. Therefore it is not surprising to find that clays were not used for environmental protection to any great extent until quite recently. Thus, such an authoritative volume on the practical applications of clays as Grim's *Applied Clay Mineralogy* (Grim, 1962) included only three uses that could be called 'environmental' among the 34 miscellaneous uses that he identified, and none among the 5 major uses that were enumerated. The uses of clays with arguably environmental aspects that Grim (1962) identified over four decades ago were those for radioactive waste disposal, floor adsorbents, and water clarification. The major uses that were identified for clays at that time were for ceramics, foundry-moulding sands, engineering properties, petroleum discovery and recovery, and the refining and preparation of organic materials.

Because of the ubiquitous and widespread occurrence of clays in soils and sediments, it is not surprising that clays were long used for the control of toxic materials albeit at a small scale or only locally. For example, 'Lemnian earth', known only by its location, was used medicinally in ancient Greece and Turkey to counter the effects of snake-bites and poisons, and to cure festering wounds (Robertson, 1986; see also Chapter 11.5). Likewise, Sudanese villagers along the Nile long used a local clay—recently identified as a bentonite—to purify the river's turbid water. As a consequence, these people suffer fewer gastrointestinal disturbances than other

communities nearby. Experiments showed that viruses (Lund and Nissen, 1986), parasites (Olsen, 1987) and many types of bacteria (Madsen and Schlundt, 1989) are removed from the water through addition of the clay, probably acting as both an adsorbent and a flocculant for the disease-bearing organisms.

The undoubted usefulness of clays for pollution control and environmental protection arises from many of the same characteristics that made them so useful industrially and otherwise in human societies for many centuries (e.g., Mackenzie, 1979; Robertson, 1986). Table 11.1.1 gives some of the particular or proposed applications of clays for pollution control and environmental protection, delineates properties of clays that make them useful for these applications, and outlines the requirements for pre-treatment that enhance their effectiveness in each case. Table 11.1.1 also refers to other sections of this chapter where further details of each application are given. Nonetheless, it is important to realise that categorisation, whether within sections of this chapter or into other parts of Chapter 11 is necessarily arbitrary. This is because those properties of clays that are important for pollution control *per se*, such as uptake capacity, also make clays most suitable for specific applications. These include their use for pesticide application and control of excess pesticides (see Chapter 11.2), in liners for waste disposal (see Chapter 11.3) and nuclear waste management (see Chapter 11.4) and also in their application for health (see Chapter 11.5) and to aid the delivery of drugs (see Chapter 11.6). This chapter will focus on the use of natural, mined clays, largely to the exclusion of 'synthetic' clay minerals (see Chapter 4).

Table 11.1.1 and the related detailed discussions specify certain technical characteristics of clays such as their charge, uptake abilities, high-surface areas, colloidal or swelling capacities, among others. Clays are also attractive in comparison with other environmental materials because they are widespread, generally easily mined, and relatively inexpensive. Clays are also naturally occurring materials, generally non-toxic, and have a considerable capacity to adsorb water. Hence, aside from their use for controlling contaminants, they are also useful as adsorbents for water in such modern, and generally urban, applications as in pet litter, although their function in that case may extend beyond that of the simple uptake of water.

#### 11.1.1. CONTROL OF HEAVY METAL CATIONS AND SIMPLE CATIONS

As cation exchangers, clays are effective for the control of cations in solution, although, where only ion exchange is involved, their effectiveness is dictated by the imperative of attaining equilibrium between ions in solution and those on exchange sites. However, clays are most useful for the control of cationic pollutants when the mechanism of uptake extends beyond that of just cation exchange. This is particularly the case for heavy metal ions, on which the following discussion is focussed. The control of heavy metal ions in anionic form is related to that for anions in general (see Section 11.1.4).

Table 11.1.1. Applications of clays for pollution control and environmental protection

Contaminants for control	Status (actual or potential use)	Pretreatments required	Relevant clay properties	Further description
Heavy metal cations and simple cations	Actual, mainly passive, use (e.g., in soils, liners)	Mostly none, some organic and inorganic modification	Charge, surface area, reactive surface groups	11.1.1
Organic and biological cations	Potential for water and wastewater treatment, pesticide control	Generally none, except cation saturation	Charge, surface area, especially interlayer	11.1.2, also 11.2
Non-ionic organic molecules	Actual, for water and wastewater treatment; potential, for pesticide control, waste liners	Cation saturation, organic or inorganic modification	Charge	11.1.3, also 11.2 and 11.3
Anions	Actual, for water and wastewater treatment; potential, for pesticide and nutrient leaching control	Appropriate organic modification	Charge	11.1.4, also 11.2
Turbidity and residual treatment chemicals	Actual, for treatment of potable water and some wastewaters and sewage	Generally none	Colloidal, from size and charge; charge, surface area	11.1.5
Leachates	Actual, for waste liners and radioactive waste storage	Generally none, except cation saturation	Swelling, charge, surface area, reactive surface groups	11.5 and 11.6

### A. Practical Applications

As liners in waste repositories clays are used for the control of heavy metal ions, often among other pollutants. Otherwise, clay minerals in soils, along with metal hydr(ox-ides) and organic matter, control the concentrations of heavy metal ions in surrounding and leaching solutions. The relative contribution of each of these soil components to heavy metal ion uptake can vary with the particular heavy metal ion (Elliott et al., 1986; Lumsdon et al., 1995; Tiller, 1996), and solution pH (Metwally et al., 1993;

Lumsdon et al., 1995), among other environmental factors. For example, organic materials removed more  $\text{Cu}^{2+}$  from solution than pedogenic oxides, and each of these removed more than a montmorillonite (McLaren et al., 1981) from concentrations similar to those in soil solution. By contrast, McLaren et al. (1986) found that a pedogenic oxide was much more effective than organic materials in removing  $\text{Co}^{2+}$  from solution, with a montmorillonite being the least effective. Furthermore, combinations of soil components, notably clay–organic matter complexes, can strongly influence heavy metal ion uptake (Lumsdon et al., 1995; Petrović et al., 1999). Similarly, heavy metal ion adsorption by clay minerals in soil may occur via hydr(oxides) and/or organic matter coating their surfaces (Swift and McLaren, 1991; Jackson, 1998).

### *B. Mechanisms of Heavy Metal Ion Uptake*

In summarising the uptake of trace and heavy metal ions by clay minerals, Tiller (1996) has concluded that these minerals have a stronger affinity for heavy metal ions than for alkali and alkaline earth cations. Adsorption of heavy metal ions by clays is a complex process, reflecting their strong tendency to form covalent bonds (Jackson, 1998). The extent of uptake is not simply a function of the cation exchange capacity (CEC) of the clay minerals. This is because heavy metal ion uptake involves a variety of processes, including surface complexation—which can be either direct ('inner-sphere') or indirect ('outer-sphere'), simple ion exchange, and surface precipitation (Swift and McLaren, 1991; Scheidegger and Sparks, 1996; Stumm and Morgan, 1996; Jackson, 1998). Some common types of complexes at the mineral/solution interface are illustrated in Fig. 11.1.1.

Surface complexation, constituting specific adsorption, occurs on edge sites. It involves the formation of direct bonds between the metal cations, and surface OH groups and O atoms, that are intermediate in strength between ionic and covalent bonds (McBride, 1991; Swift and McLaren, 1991; Jackson, 1998; Wu et al., 1999). The process is not completely reversible, although this may reflect kinetic effects rather than true irreversibility (McBride, 1991; Scheidegger and Sparks, 1996).

Adsorption of cationic heavy metal ions can occur at different sites on the aluminosilicate structure (Inskeep and Baham, 1983), and the site involved may vary with each particular heavy metal. Using models for adsorption–desorption of copper and cadmium by montmorillonite, Undabeytia et al. (1998, 2002) found that these metal ions can be adsorbed on both edge and interlayer sites. For each of the metal ions the preferred site may depend, in different ways and to different extents, on such factors as ionic strength, pH, and the anions that are present in solution. Cadmium is mostly adsorbed as the uncomplexed cation on planar (interlayer) sites over a wide range of concentrations, and also in potentially complexing chloride solutions (Undabeytia et al., 1998). On the other hand, adsorption of copper is affected by pH and by the presence of  $\text{Cl}^-$ , when  $\text{CuCl}^+$  could form (Undabeytia et al., 2002). Unlike that of  $\text{Cd}^{2+}$ , desorption of  $\text{Cu}^{2+}$  shows hysteresis. This would indicate that

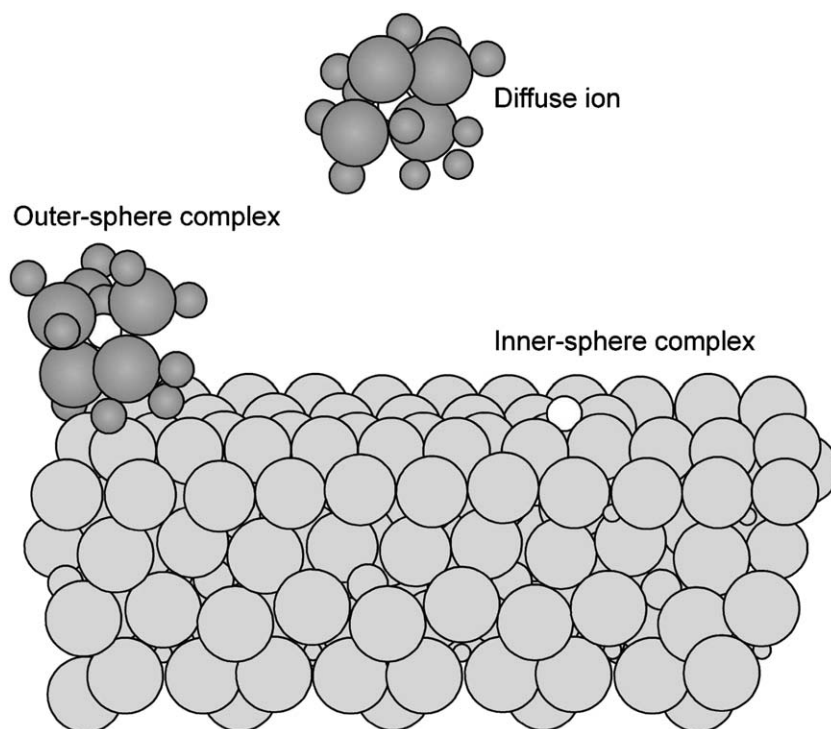


Fig. 11.1.1. The location of inner- and outer-sphere complexes and a diffuse ion relative to an aluminosilicate layer. From [Sposito \(1992\)](#).

adsorption occurs on both edge and planar sites, the former being relatively irreversible while the latter is reversible.

Metal ion hydroxide phases may form as precipitates on mineral surfaces especially when the concentrations of the heavy metal ion are higher than those found in most natural waters, and the pH is close to neutral or alkaline ([Jackson, 1998](#)). As [Tiller \(1996\)](#) has pointed out, however, it is difficult to explain the results of solid–solution interactions in terms of precipitation, rather than simple ion exchange, adsorption of the hydroxo-ion, hydrolysis of the simple ion in solution concomitant with its adsorption, or surface complexation. According to [McBride \(1991\)](#), many so-called adsorption isotherms combine the effects of chemisorption and precipitation with those of nucleation of metal hydroxides at surfaces, while [Scheidegger and Sparks \(1996\)](#) suggested that there is a continuum between surface complexation (understood as adsorption) and surface precipitation. The application of high-resolution electron microscopy (HRTEM) and X-ray absorption fine structure spectroscopy (EXAFS) has led [Scheidegger et al. \(1996\)](#) to conclude that  $\text{Ni}^{2+}$



preferentially forms a mixed hydroxo-Ni precipitate at the edge surface of pyrophyllite particles, even at low Ni concentrations.

The ambient pH often has a strong influence on the extent of adsorption because it affects the nature of the heavy metal cation (Jackson, 1998; Garcia Sanchez et al., 1999). Generally, high pH favours adsorption through the production of hydroxy cations (Jackson, 1998). For example, lead is only retained strongly by clays as long as the pH is high enough to ensure that precipitation of lead occurs (Yong et al., 1990) although in the case of mercury, an increase in pH causes uptake to decrease (Farrah and Pickering, 1978). High pHs can also result in greater specificity of clay minerals for heavy metal ions relative to alkaline earth ions, probably because of the much greater tendency of heavy metal ions to hydrolyse (McBride, 1991).

In the last several years, synchrotron-based studies aided our understanding of surface complexation and precipitation reactions (see Chapter 12.3). In particular, they shed light on the mechanisms by which surface-induced precipitation can result in the formation of more phases, including oxides, layered double hydroxides (LDHs), and new phyllosilicates (see Chapter 12.3).

### C. Relative Affinities of Clays for Different Heavy Metal Ions

The preference of bentonites for heavy metal ions that adsorb by cation exchange decreases in the order  $\text{Cu}^{2+} > \text{Pb}^{2+} > \text{Zn}^{2+} > \text{Cd}^{2+} > \text{Mn}^{2+}$  (Lagaly, 1995). From a survey of the literature prior to 1961, Tiller (1996) has deduced that the relative bonding energies to several minerals of some common heavy metals follows the sequence:  $\text{Cu}^{2+} > \text{Zn}^{2+} > \text{Co}^{2+} > \text{Ni}^{2+} \cong \text{Mn}^{2+}$  which approximates the hydrolysis constants of the metal cations. This suggests the important role played by hydroxo-cations in adsorption. However, Tiller (1996) has also observed that the order is not invariant in that  $\text{Co}^{2+}$  and  $\text{Ni}^{2+}$  could change places. In agreement with McBride (1991), Tiller (1996) concluded that the mechanism of uptake was far from certain. Jackson (1998) has summarised the literature on the relative affinities of different clay minerals for the same divalent cations, and given the following sequences:

montmorillonite	$\text{Ca}^{2+} > \text{Pb}^{2+} > \text{Cu}^{2+} > \text{Mg}^{2+} > \text{Cd}^{2+} > \text{Zn}^{2+}$
illite	$\text{Pb}^{2+} > \text{Cu}^{2+} > \text{Zn}^{2+} > \text{Ca}^{2+} > \text{Cd}^{2+} > \text{Mg}^{2+}$
kaolinite	$\text{Pb}^{2+} > \text{Ca}^{2+} > \text{Cu}^{2+} > \text{Mg}^{2+} > \text{Zn}^{2+} > \text{Cd}^{2+}$

As already noted, the adsorption capacity of different clay minerals for heavy metal ions does not necessarily follow that of their CEC. Furthermore, their relative affinities can vary with solution concentration of heavy metal ion. For example, illite is more effective than montmorillonite at high concentrations of  $\text{Cu}^{2+}$ , but the order reverses at low concentrations (Swift and McLaren, 1991). For a single montmorillonite, selectivities may also vary with saturating cation. According to Lagaly (1995), the selectivity of montmorillonite for cations generally depends on the

restriction of interlayer expansion, being minimal for sodium montmorillonites. Metwally et al. (1993) found palygorskite to be more effective than montmorillonite, and very much more effective than kaolinite, for the uptake of  $\text{Zn}^{2+}$ , at least under the conditions of their experiments (pH 4.5–7.0). Minerals were tailored to remove particular elements (e.g., radioactive species) quite specifically. By this means high affinities for  $\text{Cu}^{2+}$  and  $\text{Pb}^{2+}$  (Kodama and Komarneni, 1999),  $\text{Sr}^{2+}$  (of importance as  $^{90}\text{Sr}$  in radioactive wastes) (Komarneni et al., 2000), and radium ions (Komarneni et al., 2001) were obtained with  $\text{Na}^+$ -rich micas synthesised from kaolinite. Some natural clays can also show a high selectivity for particular cations, e.g., palygorskite (attapulgite) for radioactive  $\text{Cs}^+$  (Chandra, 1970).

In summary we can say that the laws governing the selective uptake and release of heavy metal ions by clays and clay minerals are so numerous and diverse that they probably cannot be reduced to a universally applicable predictive formula (Swift and McLaren, 1991). Furthermore, the operation of such factors as the inherent variability of natural minerals, the influence of surface coatings, the variety of surface-binding sites, and the variability of environmental conditions means that there are contradictions between experimental results of different investigators (Jackson, 1998). More fundamentally, Scheidegger and Sparks (1996) point out that many studies of adsorption processes were limited because they were carried out only at the macroscopic scale. They see considerable hope for future understanding arising from the increasingly common application of molecular and/or surface analytical techniques, including X-ray photoelectron spectroscopy (XPS), Auger electron spectroscopy (AES), secondary ion mass spectroscopy (SIMS), electron spin resonance (ESR), Fourier-transform infrared (FTIR) spectroscopy, nuclear magnetic resonance (NMR), X-ray absorption spectroscopy (XAS), scanning force microscopy (SFM), and HRTEM. These approaches, which are largely microscopic, already showed the great heterogeneity of mineral surfaces and the unique properties of both solid and liquid interfaces relative to their bulk (see Chapter 12.4). An instance of their power is the application of two of these microscopic techniques by Scheidegger et al. (1996) to show surface precipitates of  $\text{Ni}^{2+}$  on pyrophyllite, as already described.

#### *D. Ease of Displacement of Heavy Metal Ions from Clays*

The ease of desorption and the exchange of heavy metal ions, after their uptake by clays, are just as important as their adsorption or absorption. Managers of natural resources and waste depositories usually require materials that hold on to metal ions against desorption and exchange as effectively as is possible. The reviews by Swift and McLaren (1991), Scheidegger and Sparks (1996), and Jackson (1998) show that few studies dealt with the desorption of heavy metal ions from clays. Churchman (2002a) has found that heating a bentonite, following uptake of heavy metal cations, diminishes the ease of their desorption. The immobilisation of small cations (e.g.,  $\text{Cr}^{3+}$ ) on bentonite surfaces requires less heating (lower temperatures) as compared with the larger-adsorbed cations ( $\text{Pb}^{2+}$ ,  $\text{Cd}^{2+}$ ,  $\text{Ni}^{2+}$ ).

### *E. Effects of Clay Modification on Uptake of Heavy Metal Ions*

The ability of clays to attract and hold heavy metal ions can be enhanced by suitable modifications of, or at least additions to, the minerals. [Cremers et al. \(1979\)](#) patented a process whereby the addition of a polyamine to clay minerals enhances the removal of heavy metal cations from solution. Similarly, organically modified smectites such as dimethyl dioctadecylammonium (DMDOA)-bentonite can take up considerable amounts of heavy metal ions from aqueous solution ([Lagaly, 1995](#)). The amount of zinc ions adsorbed by DMDOA-bentonite is virtually trebled in the presence of phenol and diethyl ketone, while the uptake of these organic compounds increases synergetically ([Stockmeyer and Kruse, 1991](#)). Lead and chlorobenzene are adsorbed simultaneously by a bentonite that has been modified with hexadecyltrimethylammonium (HDTMA) ([Lee et al., 2002](#)). In recognition of the common association of heavy metal ions with some organic complexing agents, including natural organic compounds ([Krishnamurti et al., 1997](#)), studies were carried out on the uptake of  $\text{Cd}^{2+}$ -cysteine by montmorillonite and kaolinite. Complexation with cysteine aids the uptake of  $\text{Cd}^{2+}$  by montmorillonite ([Undabeytia et al., 1998](#)) and, perhaps more surprisingly, also by kaolinite ([Benincasa et al., 2002](#)). Indeed,  $\text{Cd}^{2+}$ -cysteine can intercalate into kaolinite to some extent, and more so into a less well-ordered than a well-ordered kaolinite. In a procedure developed for the clean-up of galvanic water, [Tarasevich and Klimova \(2001\)](#) showed that grafting polyphosphates on to the edges of kaolinite, metakaolinite, and  $\text{Al}^{3+}$  (hydr)oxides greatly increases the capacities of these materials to remove  $\text{Ni}^{2+}$ ,  $\text{Co}^{2+}$ , and  $\text{Cr}^{3+}$  from solutions through the formation of complexes with the phosphate groups.

Modification of smectites by interlayering with hydroxy-cations and pillaring (see Chapter 7.5) can markedly increase the uptake of heavy metal cations, especially certain specific metal ions. In studying the adsorption of  $\text{Cu}^{2+}$  on a poly(hydroxo aluminium) interlayered smectite between pH 4.5 and 6.5, [Harsh and Doner \(1984\)](#) found this adsorbent to be much more reactive towards  $\text{Cu}^{2+}$  than either montmorillonite itself or aluminium (hydr)oxides. Similarly, [Cooper et al. \(2002\)](#) observed that poly(hydroxo iron) or poly(hydroxo iron/aluminium)-interlayered montmorillonites have higher affinities for  $\text{Cd}^{2+}$ ,  $\text{Cu}^{2+}$ ,  $\text{Ni}^{2+}$ ,  $\text{Pb}^{2+}$  and  $\text{Zn}^{2+}$  than the corresponding poly(hydroxo aluminium) compounds.

In investigating the adsorption of some common heavy metal ions ( $\text{Cu}^{2+}$ ,  $\text{Zn}^{2+}$ ,  $\text{Cd}^{2+}$  and  $\text{Pb}^{2+}$ ) by 'clay-aluminium hydroxide complexes' (CALHO), [Keizer and Bruggenwert \(1991\)](#) found that the relative extent of adsorption was strongly affected by the hydroxy interlayering in a manner that particularly reflected pH. The adsorption of  $\text{Cu}^{2+}$  and  $\text{Zn}^{2+}$  by CALHO proceeded differently from that of  $\text{Cd}^{2+}$  and  $\text{Pb}^{2+}$ . CALHO showed an exceptionally strong affinity for  $\text{Cu}^{2+}$  and  $\text{Zn}^{2+}$ , especially at pH 6 (rather than pH 5), but not for  $\text{Cd}^{2+}$  and  $\text{Pb}^{2+}$ . Furthermore,  $\text{Cd}^{2+}$  and  $\text{Pb}^{2+}$  could be desorbed almost completely without affecting the interlayers, while complete desorption of  $\text{Cu}^{2+}$  and  $\text{Zn}^{2+}$  required dissolution of the interlayers. [Keizer and Bruggenwert \(1991\)](#) suggested that  $\text{Cu}^{2+}$  and  $\text{Zn}^{2+}$  became

incorporated in the poly(hydroxo aluminium) interlayers while the larger cations  $\text{Cd}^{2+}$  and  $\text{Pb}^{2+}$  were excluded from these high energy sites.

There was also a striking comparison to be made between the relative affinities of CALHO and hydrous aluminium oxides for the different heavy metals. Whereas the discrete oxides (of Al, and also Fe) took up the metal ions in the order:  $\text{Cu}^{2+} \cong \text{Pb}^{2+} \gg \text{Zn}^{2+} > \text{Cd}^{2+}$  (Kinniburgh et al., 1976), the order of preference for CALHO was  $\text{Cu}^{2+} > \text{Zn}^{2+} > \text{Pb}^{2+} > \text{Cd}^{2+}$ , especially at low pH and low concentrations of the heavy metal ions (Keizer and Bruggenwert, 1991). The latter trend was confirmed by Matthes et al. (1999) who studied the adsorption of the same four heavy metals by bentonite that had been interlayered with both poly(hydroxo aluminium) and poly(hydroxo zirconium) ions, and also pillared by calcination of the interlayered materials. On both interlayered and pillared clays, uptake of  $\text{Zn}^{2+}$ , in particular, increased markedly as the pH was raised from 4.9 to 6.9. Alone among the four heavy metals,  $\text{Zn}^{2+}$  was adsorbed in excess of the CEC of the various interlayered and pillared clays at pH 6.9. Matthes et al. (1999) attributed the higher and partially non-exchangeable uptake of  $\text{Zn}^{2+}$  at pH 6.9 to a dominance of surface complexation of  $\text{Zn}^{2+}$  ions with hydroxyl groups of the Al and Zr (poly)hydroxy cations and the interlayer pillars. The affinity of  $\text{Zn}^{2+}$  for the Al interlayer species was apparently higher than that for the Zr species. Since the specific adsorption of  $\text{Zn}^{2+}$  was little influenced by ionic strength, these interlayered clays could be useful for the removal of Zn from saline solutions, wastewaters, and leachates at neutral pH. The results led Matthes et al. (1999) to conclude that the binding of metal cations to oxide and hydroxide surfaces is a complex process, determined by the electrostatic and electron-sharing properties of both adsorbate and solvent.

In general, poly(hydroxy aluminium) smectite can be used to immobilise  $\text{Cu}^{2+}$ ,  $\text{Zn}^{2+}$ ,  $\text{Cd}^{2+}$ , and also  $\text{Ni}^{2+}$ , but not  $\text{Pb}^{2+}$  to any extent. For each metal ion, the most effective immobilisation occurs over a particular pH range: 6–8 for  $\text{Zn}^{2+}$  and  $\text{Ni}^{2+}$ ; 4–6 for  $\text{Cu}^{2+}$ ; and 7–9 for  $\text{Cd}^{2+}$  (Lothenbach et al., 1997). Vengris et al. (2001) devised a novel route for the production of polycation-modified clays. The clay, a mixture of 2:1 aluminosilicate minerals, is treated with concentrated HCl, and the products are neutralised with NaOH. This latter step results in the re-adsorption of Al, Fe and Mg on the acid-activated clay, giving a material with a high capacity to adsorb  $\text{Cu}^{2+}$ ,  $\text{Ni}^{2+}$  and  $\text{Zn}^{2+}$  from water.

### 11.1.2. CONTROL OF ORGANIC AND BIOLOGICAL CATIONS

Since the majority of clay minerals are negatively charged they would have a strong affinity for organic cations. Although the number of organic species that can acquire a positive charge or act as a base may be limited (Theng, 1974), some of these are important. For example, the pesticides paraquat and diquat present problems as pollutants whereas amines, especially alkylammonium cations, are useful for modifying clay properties, and amino acids, peptides and proteins are biologically

important. Waste proteins from food processing may also be important as pollutants, lending value to their affinity for clays.

### *A. Practical Applications*

The interactions of clays in soil with excess paraquat and diquat, enzymes, and other forms of protein received considerable attention (e.g., [Theng, 1979](#)) but only a limited amount of information is available on the active use of clays for the environmental control of these and other organic cations. [Stansfield \(1986\)](#) reported the contamination of river waters in England by diquat and paraquat, leaking out of plastic storage drums that had melted as a result of a fire. Bentonite was employed to constrain the leakages at their source. The use of bentonite clays to remove excess proteins from wine during its production is a well-established process in the wine industry ([Rankine, 1995](#)). However, this attractive interaction between clays and proteins has not been exploited in the wider environment. [Morris et al. \(2000\)](#) showed that a fine-grained marine sediment, containing kaolinite and montmorillonite, was able to adsorb microcystin-LR. This indicates the potential use of clays to remove this class of potent mammalian liver toxins from drinking waters. As a cyclic heptapeptide ([Moore et al., 1991](#)) microcystin-LR would be expected to adsorb on to clays, in general, provided that the pH of the infected waters are close to the pI of the peptide. [Holo et al. \(1973\)](#) patented a method for reducing the biochemical oxygen demand of sewage, and recovering the protein in sewage by using a clay (either bentonite or kaolin), along with aluminium sulphate and a co-polymer of acrylic acid and acrylic amide. Although the clay here may function partly as a flocculating agent, it is almost certainly responsible for the process of protein recovery within the overall method. [Landau et al. \(2002\)](#) have also experimented with a system for the recovery of protein from water by means of the addition of bentonite that is later removed by fractionation in foam. Similarly, [Churchman \(2002a\)](#) has shown that some bentonites can remove all the proteins from abattoir wastes which otherwise could cause eutrophication of aqueous systems. The use of natural clay by villagers along the Nile River in the Sudan to remove viruses from the river water ([Lund and Nissen, 1986](#)) has already been mentioned. This practice is based on the ability of clay minerals to adsorb viruses (nucleoproteins) in a similar way to proteins ([Theng, 1979](#)). The propensity of clays for taking-up viruses could be exploited further, as demonstrated by the laboratory use of clays for virus removal or concentration ([Barkley and Desjardins, 1977](#); [Simmonds et al., 1983](#); [Sobsey and Cromeans, 1985](#)).

### *B. Mechanisms of Uptake of Organic and Biological Cations by Clay Minerals*

[Theng \(1974\)](#) has summarised the early literature on the interactions of clay minerals with organic and biological cations, including compounds that can acquire a positive charge via acceptance of a proton in acidic solutions. While electrostatic attraction

leading to exchange for other, generally simple, cations, is perhaps the principal mechanism, other forces also influence the interaction. Even the adsorption by clay minerals of the fully ionised bipyridinium halides, paraquat and diquat, may involve charge transfer between these cations and the negatively charged silicate framework, in addition to the dominant cation exchange process. For larger organic cations such as members of the alkylammonium series, van der Waals attractive forces play a notable role in linking cations to clays. Both [Theng et al. \(1967\)](#) and [Vansant and Uytterhoeven \(1972\)](#) found that the affinity of alkylammonium cations for montmorillonite increases with an increase in the length of the alkyl chains, indicating an increased contribution of van der Waals forces to adsorption energy.

The charge characteristics of biologically important molecules, such as amino acids, peptides and proteins, vary with the pH of the surrounding solution. These molecules have a net positive charge (generally expressed on a nitrogen atom of the amino group) at pH values below their isoelectric point, pI. Early work on the uptake of these molecules by clay minerals ([Theng, 1979](#)) indicated that smectites adsorbed more of these cationic species than clays with lower negative layer charge (e.g., kaolinites). Further, these biological cations entered the interlayer spaces of smectites, and their uptake was enhanced by Na<sup>+</sup> saturation of the clays. Maximum uptake of proteins commonly occurred at a pH close to their pI, when the proteins are least soluble. At pI > pH proteins tend to be repelled by clays. At least for 'soft proteins' the extent of their spread over clay surfaces increases at pH < pI ([Quiquampoix et al., 1989, 1995, 2002](#); [Quiquampoix and Ratcliffe, 1992](#)). [Fig. 11.1.2](#) supports this mechanism by showing that below the pI the protein (bovine serum albumin) does not displace the exchangeable cations (Mn<sup>2+</sup>) from the mineral surface. The decrease in protein uptake below the pI indicates that the area of surface covered by each protein macromolecule increases with decreasing pH. Protein uptake tends to decrease quite rapidly with pH at pH > pI, when the positive charge on the protein diminishes. Nonetheless, some uptake can still occur at pHs far above the pI, thanks to the non-electrostatic interactions such as hydrogen bonding, van der Waals interactions, hydrophobic forces, and entropy effects ([Theng, 1979](#); [Quiquampoix et al., 1989, 1995](#); [Quiquampoix and Ratcliffe, 1992](#); [Staunton and Quiquampoix, 1994](#)). 'Hard proteins', such as  $\alpha$ -chymotrypsin, are less likely to show a conformational change on clay mineral surfaces with pH ([Quiquampoix et al., 2002](#)). Coatings of either natural organic matter (NOM) ([Quiquampoix et al., 1995](#)) or aluminium hydroxide ([Naidja et al., 1995](#); [Violante et al., 1995](#)) tend to decrease protein uptake compared with that by pure Na-saturated clay.

As another class of biologically important molecules, antibiotics may be basic (like paraquat and diquat), or amphoteric (like proteins). Basic antibiotics such as streptomycin, dihydrostreptomycin, neomycin and kanamycin, are taken up and strongly retained by clays. By the same token, amphoteric antibiotics, including bacitracin, auromycin and terramycin, interact strongly with clays at pH values near, or below, their pI ([Theng, 1974](#)). There do not appear to be any reports of the use of clays to control the spread of antibiotics in wastewaters (e.g., from clinics and hospitals), but their use for this purpose seems feasible. The effect of associations of

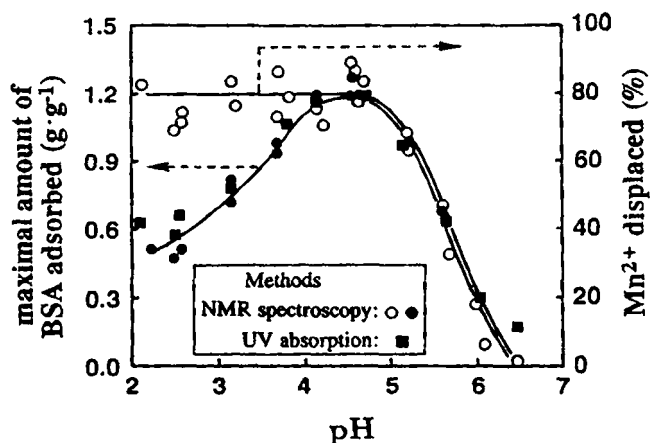


Fig. 11.1.2. Effect of pH on the maximal amount of bovine serum albumin ( $pI = 4.7$ ) adsorbed on montmorillonite and the release of  $Mn^{2+}$  displaced by the protein. From Quiquampoix et al. (2002).

enzymes, as proteins, with clays upon their catalytic activity has been discussed at length by Theng (1979) and Quiquampoix et al. (1995, 2002), and is of only indirect interest here. However, following the types of uses cited above, the usefulness of clays for pet litter may derive as much from the deactivation through uptake by the clay of the enzyme urease, which converts urea to ammonia, as by the adsorption of water by the clay (W.P. Moll, personal communication).

Most studies of the association of organic and biological cations with clay minerals focussed on montmorillonite, although early work on proteins also used kaolinite (e.g., McLaren, 1954) and halloysite (Mills and Creamer, 1971). Using sepiolite, Rytwo et al. (2002) showed that the mechanism and also extent of uptake can depend on the charge on the organic cation in a counterintuitive manner, that is, divalent cations are adsorbed less than monovalent cations. The divalent cations paraquat, diquat, and methyl green are adsorbed up to nearly the CEC of the sepiolite, with a maximum uptake being reached between 100% and 140% of the CEC. By contrast, monovalent cations such as methylene blue (Aznar et al., 1992), crystal violet (Rytwo et al., 1998), and TX100 (Alvarez et al., 1987) were adsorbed up to a maximum of 400% of the CEC of sepiolite. The difference is explained by the association of the monovalent cations on neutral sites of the clay mineral, whereas the more highly charged divalent cations do not associate.

### C. Ease of Displacement of Organic and Biological Cations

Ease of displacement of organic cations from clays appears to depend upon the size of the organic cation although factors such as clay type and cation shape also play a



role since these latter two factors affect the ease and extent of uptake (Theng, 1974). Thus, large organic cations such as DMDO and dimethyl benzylammonium ions (DMBL) are strongly retained once they are intercalated by smectites. Replacement by simple inorganic cations may not occur to any extent, but one organic cation may be able to replace another (Theng, 1974). Paraquat and diquat, as examples of relatively small organic cations, could be released from complexes with clays by exchange with simple inorganic cations, although their release was less easily achieved from complexes with montmorillonite than from those with kaolinite (Theng, 1974). Proteins could be released by kaolinite when the pH was raised (McLaren, 1954). By contrast, strong treatment with concentrated solutions of both mono- and divalent cations, including very high pH values and severe agitation (prolonged mechanical and ultrasonic), released little protein from proteinaceous complexes of bentonites in waste lees from winemaking (Churchman, 2002a). In general, little desorption of proteins is found to occur from clays (Theng, 1974). As is the case for large quaternary ammonium cations (QACs), it appears that the bonds that form between clays and proteins are not simply electrostatic. Although charge interactions play a large part in holding proteins to the clays, van der Waals interactions and favourable entropy changes contribute to the overall attraction (Theng, 1979; Staunton and Quiquampoix, 1994; Churchman, 2002a; Quiquampoix et al., 2002). Clays are useful for extracting proteins from wastewaters and sewage, for example, but it would be difficult to recycle the clays after usage and so minimise waste and capital costs. Nonetheless, chemical or photo-oxidative methods (Churchman, 2002a), as well as microbial agents, could be employed to destroy the adsorbed protein, without affecting the clay. In stark contrast, Armstrong and Chesters (1964) were able to remove 63% of the protein pepsin ( $pI = 2.8$ ) that had been adsorbed by a bentonite at pH 3.0. They achieved this simply by raising the pH to 5.2 with NaOH. Clearly the ease of protein removal from complexes with bentonite varies with the type of protein.

### 11.1.3. CONTROL OF NON-IONIC ORGANIC COMPOUNDS

Because of their charge characteristics, clays are naturally hydrophilic. Nevertheless, their high-surface areas and volume of fine pores enable them to adsorb significant amounts of non-ionic substances. There are records of the use of clays for 'fulling', i.e., cleaning grease from wool, that date back before 2000 BC, hence the term 'fuller's earth' (Robertson, 1986). Fuller's earth generally denotes calcium montmorillonite, although it is sometimes used to refer to palygorskite (attapulgite), especially in the USA. Today, clays are used quite widely to adsorb oil and grease, e.g. on floors of workshops (Grim, 1962). Coarser particles are preferred for this purpose, and palygorskite is particularly suitable, while montmorillonite that has been calcined to a sufficiently high temperature to prevent its break-up into small particles is also used. However, clays in their natural state usually effect little uptake



of small non-ionic organic compounds (NOCs) in the presence of water. Despite this drawback, their attractiveness for environmental applications as low-cost, generally non-toxic, high surface-area materials mean that much recent research has gone into the adaptation of clays for the removal of NOCs, which include many substances of concern to environmental and human health.

#### *A. Uptake of NOCs by Organically Unmodified Clay Minerals*

In principle, clays and clay minerals could be used to adsorb NOCs from either the vapour or the solution phase. In the absence of water, clay minerals can adsorb significant amounts of non-ionic gases, with amounts adsorbed depending on the surface areas of the clays (Jurinak, 1957; Lee et al., 1990; Sawhney, 1996). However, as NOCs cannot compete well with water, their adsorption as gas by clays diminishes as humidity rises, and only negligible amounts adsorb from aqueous solutions (Lee et al., 1990). Nonetheless, potassium-saturated smectites can show a greater, or at least, similar affinity as soil organic matter for some NOCs, including some pesticides (Sheng et al., 2001). Similarly, Boyd et al. (2001), Johnston et al. (2001), and Sheng et al. (2002) demonstrated that uptake of NOCs by expanding clay minerals was enhanced when the saturating cations are weakly hydrated, such as  $K^+$  and  $Cs^+$ , while the more strongly hydrated cations ( $Na^+$ ,  $Mg^{2+}$ ,  $Ca^{2+}$ ,  $Ba^{2+}$ ) have the opposite effect. Cations with weaker hydration, i.e., lower enthalpies of hydration: (i) provide larger adsorption domains (Sheng et al., 2001); (ii) form stronger interactions with the  $-NO_2$  groups that are common to many of the NOCs studied (Boyd et al., 2001; Johnston et al., 2001); and (iii) minimise swelling, thus enabling the NOCs to interact simultaneously with the opposing pairs of silicate layers, minimising contact with water (Johnston et al., 2001; Sheng et al., 2002). Using two dinitrophenol herbicides, Sheng et al. (2002) also showed that uptake of these NOCs increases as the layer charge of the clay mineral decreases.

#### *B. Organic Modification of Clays and Uptake of NOCs*

The capacity of clays to adsorb NOCs is greatly enhanced when the minerals are modified by the uptake of organic cations, rendering the clays hydrophobic and organophilic. QACs were found to be most useful for this purpose. Generally, QACs can easily replace the inorganic cations occupying exchange sites on clays (Xu et al., 1997). However, the degree of hydrophobicity that is attained and the efficiency of uptake of NOCs achieved by these so-called 'organo-clays' depend greatly on the nature of the QACs used, notably on the length of the carbon chains in the QACs.

#### *C. Uptake of NOCs from the Gas Phase by Organo-Clays*

Replacement of the inorganic cations in smectite by tetramethylammonium (TMA) and tetraethylammonium (TEA) allows appreciable uptake of gaseous organic

molecules, including hydrocarbons, to take place (Barrer and McLeod, 1955). The organo-clays adsorb organic molecules without the need for any threshold pressure, as is the case for adsorption of simple gases (e.g.,  $N_2$  and Ar), on clays or organo-clays. These authors proposed that the intercalation of these short-chain QACs caused the development of pores, creating a zeolite-like structure in the clay interlayer space where NOCs could adsorb. These organo-clays showed a selectivity for the uptake of hydrocarbons that appeared to relate to their molecular shape, a proposition that was confirmed by Lee et al. (1989a). Layer charge also affected uptake of a gaseous NOC (*o*-xylene) by complexes of smectites with TMA. Less of the NOC was adsorbed by the TMA derivative of a high-charge smectite than by the corresponding derivative of a low-charge smectite. This is because the density of packing of TMA cations in the smectite interlayer spaces was relatively low in the low-charge clay mineral, giving rise to more free pore space in its TMA complex than in the derivative of the high-charge clay mineral (Lee et al., 1990).

When a long-chain QAC such as DMDOA intercalates into the smectite, it fills a large proportion of the interlayer space. Nonetheless, the derivative is an effective adsorbent for gaseous NOCs when dry (Barrer and Kelsey, 1961). When a different long-chain QAC (hexadecyltrimethylammonium, HDTMA) replaces the inorganic cations on a smectite, partially at first, and then fully (i.e., to satisfy the CEC of the clay mineral), uptake of NOCs tends to increase with the amount of HDTMA (or organic C) in the derivative (Boyd et al., 1988b; Zhu and Su, 2002). In addition, the shape of the adsorption isotherm also changes with the content of HDTMA. At a low content (35% of the CEC) a type II isotherm in Brunauer's classification (Brunauer, 1944) is obtained (similar to that for the uptake of small NOC by  $Ca^{2+}$ -smectite), while at a HDTMA content corresponding to the CEC, the isotherm is essentially linear. Thus, NOC uptake by the derivative with a low-QAC content occurs, at least partly, by adsorption on to the interlayer surface, while in the fully exchanged HDTMA derivative adsorption takes place by partitioning into the QAC. An analogy is drawn between partitioning of NOCs into QACs in the derivatives with pure clay minerals and that into the organic matter in soils (Chiou et al., 1979, 1983).

#### *D. Uptake of NOCs from Aqueous Solutions by Organo-Clays*

Most interest has centred on the use of organo-clays for the control, by uptake, of NOCs occurring as pollutants in aqueous solution. Cowan and White (1962) made a systematic study of the uptake from water of phenol by complexes of montmorillonite with different quaternary ammonium cations. Derivatives with QACs having carbon chains from  $C = 2$  up to  $C = 18$  were effective adsorbents for phenol. In relation to chain length, uptake reached a maximum for  $C = 12$  (dodecylammonium bentonite). Street and White (1963) investigated the uptake from water of a variety of NOCs, although not including hydrocarbons, by dodecylammonium montmorillonite. All could be adsorbed, but to different extents. The implications of these

early findings, as well as those from later studies, for the mechanism of uptake will be discussed below.

Since the late 1980s, there has been a strong revival of interest in the use of clay minerals that were organically modified, mostly by exchange with QACs, but not exclusively. Much of this work has been carried out by Mortland, Boyd and co-workers at Michigan State University (see Xu et al., 1997). The major focus has been on the control by uptake of toxic pollutants that occur in fuel oils, comprising benzene, toluene, ethylbenzene and xylene ('BTEX'). Using phenol, trichlorophenol and pentachlorophenol (PCP), Mortland et al. (1986) and also Boyd et al. (1988c) found that smectites modified with long-chain QACs adsorb more of these NOCs from water than those modified with short-chain QACs. Furthermore, smectites reacted with short-chain QACs can show considerable selectivity of molecules for adsorption, as already noted for hydrocarbons from the gas phase. Molecular shape and size are the principal determinants of the ability of NOCs to be adsorbed by TMA-smectite and, in the extreme, larger molecules such as the herbicide lindane (hexachlorocyclohexane,  $\gamma$ -isomer) can be excluded from sites for adsorption on TMA-smectite (Lee et al., 1989a). There appears to be a distinct difference in mechanism of uptake between smectites modified with either short- or long-chain QACs. This is also reflected by their different effects on the adsorption of gases as discussed below.

While most research on the modification of clay minerals for non-ionic organic contaminant uptake has been carried out on smectites, some has shown the feasibility of this approach for a wide range of clay minerals. Indeed, the enhanced uptake of a number of NOCs by soils containing many different clay minerals besides smectites (Boyd et al., 1988a, 1988b, 1988c) suggested the universal applicability of this approach for clay minerals. A study of uptake of a range of hydrocarbons by the HDTMA derivatives of a variety of clay minerals (Jaynes and Boyd, 1991a) has confirmed the effectiveness of these organo-clays as adsorbents of hydrocarbons. A vermiculite, a high-charge smectite, and an illite each retained more ethylbenzene than a low-charge smectite and a kaolinite. Curiously, this was in spite of the low-charge smectite incorporating more HDTMA than the high-charge type. It would appear that the alignment of the HDTMA in the high-charge smectite is more favourable for partitioning NOCs than that in the low-charge mineral. Xu and Boyd (1995b) also found that HDTMA adsorption by swelling clays was more complex than that by non-swelling clays.

A further curiosity is that an illite incorporated more HDTMA than expected from its CEC, apparently because HDTMA can displace some interlayer  $K^+$  from the illite (Jaynes and Boyd, 1991a). Nonetheless, the uptake of ethylbenzene by the illite is less than that by the high-charge smectite. One possible explanation may arise from the observation that HDTMA-halide salts employed in the modification may be retained by the clay if washing is inadequate. Slade and Gates (2003) found that water-washed HDTMA montmorillonite had greater capacity for toluene uptake than its ethanol-washed counterpart, which contained no HDTMA-Br. The salt may be included in the close-packed structure of the interlayer (Slade and Gates, 2004).

Lee et al. (1989a) showed that TMA-illite could adsorb a large organic molecule (lindane) whereas the TMA-smectite had a much reduced capacity due to steric exclusion of the organic molecule from the interlayer spaces of TMA-smectite. Akcay and Yurdakoc (2000) also observed that smectite modified with a particular QAC was not necessarily superior for the adsorption of organic compounds, although not NOCs in this case. For example, a dodecylammonium-modified sepiolite effected more and stronger adsorption of a range of phenoxyalkanoic acid herbicides (2,4-D, 2,4-DP, 2,4-DB, 2,4,5-T) and MCPA than a smectite modified with the same QAC.

#### *E. Practical Applications of Organo-Clays for Control of NOCs*

The preparation of organo-clays formed by reacting clay minerals (generally smectites) with QACs (generally long-chain varieties) and their applications for the removal of organic pollutants from water were described in several patents (e.g., McBride and Mortland, 1973; Kokai, 1975; Beall, 1984, 1985a, 1985b, 1996; Alther, 1999). These organo-clays were used most widely for removing oil and grease from water. They are included in a patent for the specialised task of clearing spills of oil on water (Kemnetz and Cody, 1996). In potable water treatment, they may be used synergistically with more expensive activated carbon, in order to prolong the useful lifetime of the latter material (Alther, 1999). Their use for the removal of trihalomethanes has been proposed, but not established, to our knowledge at the time of writing. However, a recent patent (Gates and Slades, 2001) describes their use for the removal of microcystin toxins from cyanobacteria (blue-green algae) that accumulated in waterways and water storages. They may also be used to remove waste organic materials from industrial processes, such as tanneries (Cioffi et al., 2001a). Organo-clays were also proposed for use in waste containment barriers (Smith et al., 1990; Sheng et al., 1996a, 1996b). Modelling has shown that small amounts of these materials included in conventional clay barriers would enable effective containment of NOCs for > 100 years (Adu-Wusu et al., 1997). Organo-clays may also be used as adsorption (chemical) barriers in association with landfill liners, where they can increase the useful life of the associated liner by 5–10 years (Voudrias, 2002). They can also be employed as containment barriers for BTEX pollutants around petroleum storage tanks (Jaynes and Vance, 1996; Xu et al., 1997; Sharmasarkar et al., 2000; Lo and Yang, 2001).

Since clays are ubiquitous components of soils and many other earth materials (e.g., sediments and regolith), the knowledge gained from research on organo-clays has found application in the in situ modification of soils for taking-up and immobilising NOCs. Particular uses to which this technology can be put include the immobilisation of leachable pollutants in contaminated land (Boyd et al., 1988a, 1988b; Lee et al., 1989b; Brixie and Boyd, 1994; Xu et al., 1997). This approach can prevent the transport by leaching of pesticides into ground water. To this end, soils, subsoils and aquifer materials are treated with QACs to provide adsorptive zones for

the retardation of pesticide transport (Sheng et al., 1998). The primary concern is with highly water-soluble pesticides that are minimally adsorbed by soil particles and not readily degradable, and hence can move rapidly with infiltrating water. Both Zhao et al. (1996) and Carrizosa et al. (2001) showed that dicamba, a highly soluble herbicide, and so presents these concerns, can be adsorbed by QAC-modified clays. Similarly, Hermosin and Cornejo (1992) demonstrated the effectiveness of QAC-clay as an adsorbent for another soluble herbicide, 2,4-D. Sparingly soluble pesticides like malathion and butachlor are also strongly adsorbed by QAC-clays (Pal and Vanjara, 2001). However, it should be noted that uptake of contaminants may alter important properties of organo-clays. Considerable interlayer swelling of organo-clays can occur as a result of the uptake of both water-immiscible organic contaminants (Sheng et al., 1996b; Singh et al., 2003; Slade and Gates, 2003) and aqueous-miscible solvents (Nzengung et al., 1996; Gates, 2004). Gates et al. (2004) found that such adsorption induces swelling, and decreases the permeability of an organo-modified bentonite to aqueous-miscible solutions by more than three orders of magnitude. Adsorption of pollutants by organo-clays may nonetheless allow their biodegradation. Naphthalene adsorbed by HDTMA-smectite was available to some organisms for degradation directly from the adsorbed state (Crocker et al., 1995), as was the herbicide, fenamiphos, when adsorbed by the same type of organo-clay (Singh et al., 2003). Even when the organism used is unable to access the contaminant (naphthalene) directly, its rapid desorption from the organo-clay meant that biodegradation can occur (Crocker et al., 1995). By contrast, phenanthrene intercalated into a long-chain QAC derivative of montmorillonite is inaccessible to microorganisms. Since the interlayer phenanthrene does not appear to be desorbable, it is not biodegradable, at least within the period of incubation used (Theng et al., 2001). As Sheng et al. (1996a) pointed out, the coupling of immobilisation with in situ biodegradation provides a comprehensive restoration technology to remove target contaminants.

#### *F. Effect of Hydrocarbon Chain Length on Uptake of NOCs by Organo-Clays*

Alkylammonium cations are attracted to clays in amounts that increase with the charge on the clays. As noted above in relation to uptake of NOC gases by organo-clays, the influence of the amount of each particular QAC on uptake of NOCs from either aqueous solution or the gas phase, differs according to the length of the alkyl chain (number of C atoms). In the case of short-chain QACs such as TMA, an increase in concentration of QAC on a smectite with increasing layer charge on the mineral, leads to a decrease in the amount of NOC removed from solution (Lee et al., 1990). For long-chain QACs, such as HDTMA, a similar relationship is obtained between the concentration of adsorbed QAC and smectite layer charge but in this case, and in stark contrast, uptake of any particular NOC increases (Jaynes and Boyd, 1991a). Furthermore, adsorption of NOCs by short-chain QAC clay minerals show typical curvilinear isotherms, indicating both high- and low-energy sites (Lee et al.,

1990) (Fig. 11.1.3), whereas long-chain QAC derivatives give essentially linear isotherms, indicating that all sites are equal in energy (Boyd et al., 1988b) (Fig. 11.1.4). Mechanistically, the difference is that short-chain QACs form 'pillars' in the interlayer space, giving rise to pores for the adsorption of NOCs (Fig. 11.1.5), whereas long-chain QACs provide a microscopic organic phase into which NOCs are partitioned (Fig. 11.1.6); that is, they effectively act as a solvent in which NOCs become dissolved (Yariv, 2002). Jaynes and Boyd (1991a) made an extensive study of the retention of eight aromatic NOCs by HDTMA complexes with seven different clay minerals (vermiculites, illites, kaolinites, as well as smectites). They show that the organic matter-normalised adsorption coefficients ( $K_{OM}$ ), expressed as logarithms, for each adsorbent-adsorbate pair generally parallel the octanol-water partition coefficients ( $K_{OW}$ ) of the appropriate NOCs. This confirmed that partition is the dominant mechanism for uptake of the NOCs by derivatives of clay minerals with HDTMA.

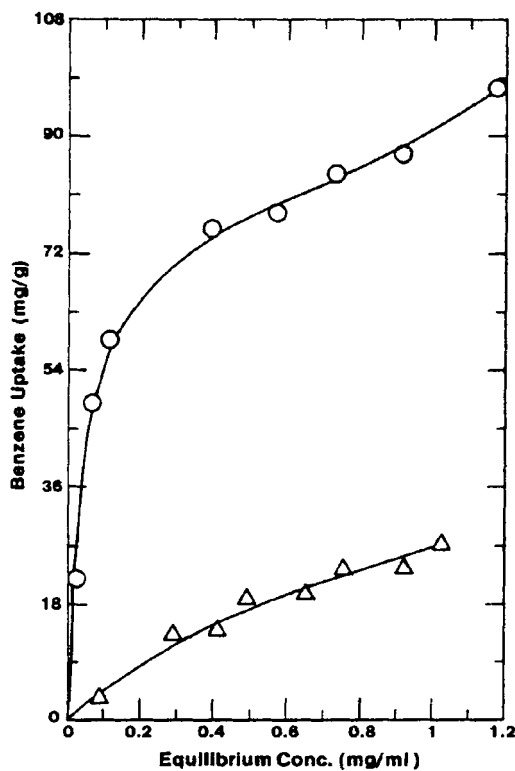


Fig. 11.1.3. Adsorption of benzene from aqueous solution by TMA derivatives of a high-charge smectite, SAz (triangles) and a low-charge smectite, SWy (circles). From Lee et al. (1990).

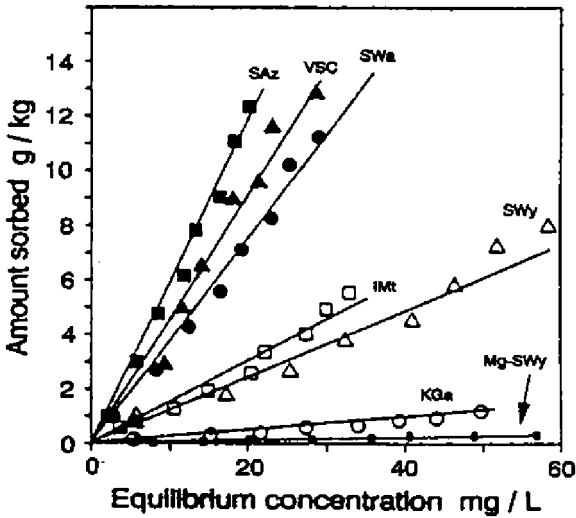


Fig. 11.1.4. Adsorption of ethylbenzene from aqueous solution by HDTMA derivatives of different clay minerals: SAz: high-charge smectite, CEC = 130 cmol(+)/kg; VSC: vermiculite, CEC = 80 cmol(+)/kg; SWa: high-charge smectite, CEC = 107 cmol(+)/kg; IMt: illite, CEC = 24 cmol(+)/kg; SWy: low-charge smectite, CEC = 87 cmol(+)/kg; KGa: kaolinite, CEC = 4 cmol(+)/kg. MG-SWy is the  $Mg^{2+}$ -saturated low-charge smectite. From Jaynes and Boyd (1991a).

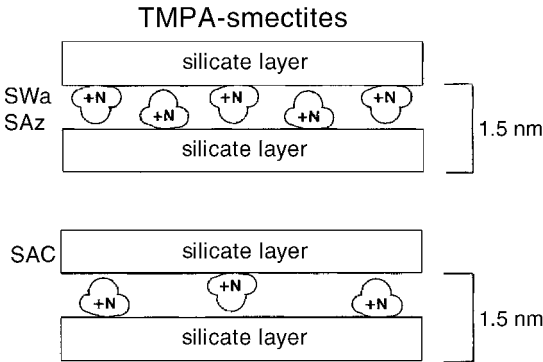


Fig. 11.1.5. Schematic diagram of short-chain QACs, such as TMPA in the interlayer spaces of high-charge smectites (SWa, SAz) and a low-charge smectite (SAC; CEC = 90 cmol(+)/kg). In both instances the basal spacing is about 15 nm. From Jaynes and Boyd (1991b).

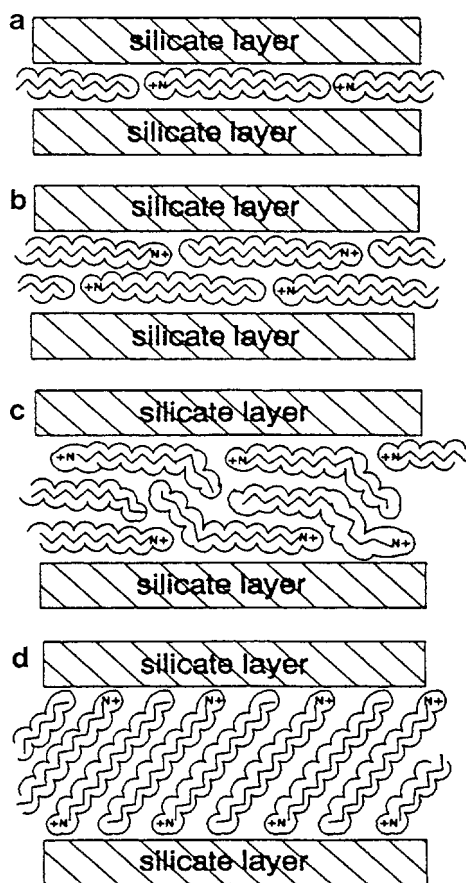


Fig. 11.1.6. Schematic diagram of different possible conformations of long-chain QACs, such as HDTMA in the interlayer space of an expansive clay mineral. (a) monolayer (basal spacing = 1.37 nm); (b) bilayer (basal spacing = 1.77 nm); (c) pseudotrimolecular layer (basal spacing = 2.17 nm); and (d) paraffin-type structure (basal spacing > 2.2 nm). From [Lagaly and Weiss \(1969\)](#); [Jaynes and Boyd \(1991a\)](#).

### G. Demarcation between Short-Chain and Long-Chain QACs

As a 'working hypothesis', we may say that the size (length) of the hydrocarbon chain in QACs tends to control whether uptake of NOCs by the corresponding clay mineral derivatives occurs by adsorption or partition. The study by [Smith et al. \(1990\)](#) confirms this view. Derivatives with QACs containing eight or fewer C atoms give rise to



adsorption, while those having more than 14 C atoms show partitioning. QACs containing hydrocarbon groups with between 9 and 13 C atoms were not examined although Jaynes and Vance (1996) showed that clay minerals modified by QACs with 12 C atoms in their hydrocarbon chain take up NOCs by a partitioning mechanism. Smith et al. (1990) also found that the adsorption mechanism (characterised by non-linear isotherms) leads to increased uptake as compared with partition. In the case of adsorption there is competitive adsorption when more than one NOC is present whereas the partition mechanism (giving linear isotherms) shows non-competitive adsorption. However, later work has suggested that the reality is a little more complex. As already noted, some trimethylphenylammonium (TMPA)-like cations, containing one or more aromatic groups, promote uptake by partition, albeit poorly, rather than by adsorption (Jaynes and Vance, 1999). Furthermore, uptake by partition in long-chain QACs can be supplemented by a solvation mechanism for some NOCs and certain clay minerals, causing the isotherm to deviate from linearity through a steadily increasing upward curvature with increasing solution concentration (Jaynes and Vance, 1996; Sheng et al., 1996a; Singh et al., 2003).

#### *H. Influence of Water on Uptake of NOCs by Organo-Clays*

For derivatives with short-chain QACs, the presence of water strongly affects their capacity as adsorbents, and especially their selectivity for different NOCs (Lee et al., 1989a). Water molecules shrink the pores in the interlayer spaces of smectites created by the intercalation of short-chain QACs. Depending on their molecular sizes and shapes, NOC molecules may or may not be able to enter these pores. Peaks shifts in the FTIR spectra indicate that in dry derivatives hydrocarbons interact with the QAC pillars, including TMPA and TMA. On the other hand, in aqueous systems water interacts with these pillars in place of the hydrocarbons (Stevens et al., 1996). Nonetheless, hydrocarbons can adsorb on siloxane surfaces in the aqueous systems (Stevens et al., 1996; Stevens and Anderson, 1996). Whether in the absence of water (for gaseous uptake by dry derivatives) or in its presence (for uptake from aqueous solutions), adsorption occurs because the siloxane surfaces of aluminosilicates, specifically those of smectites, are hydrophobic, according to Jaynes and Boyd (1991b). Even when only some, but not all, of the inorganic cations ( $\text{Ca}^{2+}$ ) on a smectite are replaced by TMPA, hydrocarbons are adsorbed by the organo-clay but to a lesser extent (Sheng and Boyd, 1998). It appears that TMPA and remaining  $\text{Ca}^{2+}$  ions are mixed together within the interlayer spaces, rather than segregated into separate layers. As a result of its exchange behaviour, TMPA does not only replace some  $\text{Ca}^{2+}$  ions, but also disrupts the network of water molecules associated with the inorganic cations. The 'exposure' of the siloxane surface by TMPA exchange appears to make the environment relatively hydrophobic. By contrast, prior to the introduction of TMPA the interlayer environment of smectite is hydrophilic because of the dominating influence of hydrated exchangeable cations.

*I. Cation Properties and Uptake of NOCs by Short-Chain QAC-Clays*

In using different QACs (TMPA and the larger trimethylammonium adamantine) and a series of QACs of increasing size from TMA to benzyltrimethylammonium (BTMA), TEA, and benzyltriethylammonium (BTEA), [Sharmasarkar et al. \(2000\)](#) and [Shen \(2002a\)](#) showed that the size of the pillaring organic cation determines the amount of each NOC adsorbed and also the selectivity for adsorption. In each of these studies, uptake of each particular NOC increases to a maximum, and then decreases, as the size of the QAC increases. A variety of aromatic organic cations that are otherwise similar in structure to TMPA are compared to one another and to TMPA as modifiers of hectorite for their efficiency in taking up a mixture of BTEX compounds ([Jaynes and Vance, 1999](#)). Hectorites reacted with the largest cations, and also a highly hydrated cation, are poor adsorbents of BTEX. Furthermore, such adsorption as occurred on these three derivatives occurs by partition, while adsorption prevails with the smaller and/or less strongly hydrated cations tested. Nonetheless, selectivity of adsorption may not depend on the size of the QAC alone. Furthermore, it is the interaction between adsorbent and adsorbate that governs uptake. [Nzengung et al. \(1996\)](#) compared the relative efficiencies of derivatives with TMA and TMPA for the uptake of naphthalene (having two aromatic rings) and diuron with a branched structure on the side of an aromatic ring. Naphthalene uptake is considerably greater on TMPA-clay than on TMA-clay. By contrast, diuron is taken up strongly by clay modified with either TMPA or TMA. In comparing the adsorption of phenols by derivatives of bentonite with TMA and TMPA, [Ceyhan et al. \(1999\)](#) observed that selectivities of adsorption varies with the pillaring QAC, suggesting that the energy of interaction between QAC and NOC affects uptake. [Kukkadapu and Boyd \(1995\)](#) compared the uptake of NOCs by smectite modified by TMA and that with its phosphorus analogue, trimethylphosphonium (TMP). Derivatives with the relatively small TMA cation are more effective adsorbents in the absence of water, while those with TMP are more effective in aqueous solutions. As TMP is less extensively hydrated than TMA, water associated with the organic pillars decreases the area of siloxane surface available for uptake. However, [Sheng and Boyd's \(1998\)](#) study of the effectiveness of only partially exchanged organo-smectites shows that uptake of NOCs actually decreases from a maximum with further addition of the QAC. This would indicate that the space available for NOCs tends to diminish with increasing occupancy of the surface by QAC.

*J. Nature of Exchangeable Cations and the Incorporation of Long-Chain QACs into Clays*

In the case of derivatives with long-chain QACs, increasing the organic cation content leads to an increasingly hydrophobic material ([Boyd et al., 1988b](#)). The nature of the inorganic cations originally occupying exchange sites affects the way that long-chain QACs are incorporated into expansible clays. Introduction of HDTMA

into a dispersed  $\text{Na}^+$ -smectite leads to mixing of  $\text{Na}^+$  and HDTMA cations in each layer. On the other hand, a non-dispersed  $\text{Ca}^{2+}$ -clay produces segregation of inorganic and organic cations into separate layers (Xu and Boyd, 1995b, 1995c). The nature of the exchangeable inorganic cations also influences the rate of uptake of HDTMA into smectite at low concentrations of the organic cation;  $\text{Na}^+$  enhances uptake, but there is no effect on the final amount of HDTMA adsorbed (Xu and Boyd, 1995a, 1995b, 1995c).

#### *K. Effect of Amount of Organic Cation on Uptake of NOCs by Long-Chain QAC-Clays*

For derivatives with long-chain QACs, the uptake of NOCs, by partitioning into the interlayer organic phase, increases as the extent of that phase increases. This effect may be achieved by increasing the amount of a particular QAC taken up (Boyd et al., 1988b), using high-charge clay minerals (Jaynes and Boyd, 1991a), or increasing the length of the hydrocarbon chain of the QAC (Cowan and White, 1962; Jaynes and Vance, 1996). In expansive clays (smectites and vermiculites), the packing and orientation of the large QACs in the interlayer spaces change with the layer charge on the clay mineral so as to accommodate the amount of organic cation needed to satisfy the CEC of the mineral (Lagaly and Weiss, 1969; Slade et al., 1978; Slade and Gates, 2003, 2004). These changes are reflected by the basal spacings of the organo-clays. In general, the intercalated organic cations tend to maximise their contact with the silicate surface, and hence the basal spacing increases as more QAC cations are accommodated in the interlayer regions (Xu et al., 1997). Thus, while QACs such as HDTMA may intercalate as a monolayer (basal spacing = 1.37 nm) in low-charge smectites, increases in layer charge see their arrangement change to a bilayer (spacing = 1.77 nm), and then a pseudotrimolecular layer (spacing = 2.17 nm) (Lagaly and Weiss, 1969; Jaynes and Boyd, 1991a). When the layer charge further increases, long-chain QACs form paraffin-like arrangements, comprising tightly packed layers inclined at a high angle to the interlayer surface with each QAC lying parallel to one another (spacing > 2.2 nm). Fig. 11.1.6 shows a schematic representation of the different packing and orientation of long-chain QACs in the interlayer spaces of expansive clay minerals.

#### *L. Size of Organic Cation and Uptake of NOCs by Long-Chain QAC-Clays*

Cowan and White (1962) showed that increases in the number of C atoms in the QAC tend to lead to increased uptake of a given NOC by the resulting clay derivative, up to a point at which the number of C atoms is so large as to decrease the amount of the QAC that is adsorbed by the clay. Following on Cowan and White (1962), Jaynes and Vance (1996) made derivatives from different expansive clay minerals with each of 5 QACs containing C atoms/molecule in the range from 15 (cyclododecyl trimethylammonium, CDTMA, molecular weight (Mw) = 226 and

dodecyl trimethylammonium, DTMA,  $M_w = 228$ ) to 38 (dioctadecyl trimethylammonium, DODMA,  $M_w = 551$ ). There was a general increase in uptake of BTEX hydrocarbons as the C content of the QAC increased. However, comparison of CDTMA and DTMA showed that the former QAC, having straight-chain alkyl groups, was much more effective in taking up BTEX than the latter, containing cyclic groups with the same number of C atoms and almost identical  $M_w$ . The derivative with QAC of  $M_w = 383$  (didodecyl dimethylammonium, DDDMA, 26 C atoms/molecule) was the most efficient adsorbent for BTEX molecules, while the derivative with the largest QAC (DODMA) was less efficient.

#### *M. Co-adsorption and Uptake of NOCs by Long-Chain QAC-Clays*

Jaynes and Vance (1996) also showed that NOCs, after adsorption, can increase the capacity of the organic phase for further molecules. In particular, they observe that the adsorption of individual BTEX components (from a mixture of BTEX compounds) is enhanced relative to that from solutions of the pure component. This process of co-adsorption, by which one or more NOCs generally produce a synergistic effect on the uptake of others, gives rise to an isotherm that curves upwards from a straight line. Similarly, Sheng et al. (1996a) reported that nitrobenzene and, to a lesser extent, carbon tetrachloride, enhance uptake of trichloroethylene (TCE) by an HDTMA-smectite. Likewise, chlorobenzene enhances the uptake of TCE and dichlorobenzenes (Sheng et al., 1996b; Sheng and Boyd, 2000), while Gao et al. (2001) found that the uptake of chlorobenzene by an HDTMA-soil is enhanced by the presence of nitrobenzene. Co-adsorption may be employed to increase uptake of NOCs generally, or else to encourage the uptake of particular NOCs (Jaynes and Vance, 1996). The adsorption of an organic compound can even enhance its own uptake. Isotherms for the uptake by HDTMA-clays of aromatic hydrocarbons and chlorohydrocarbons, as well as interlayer swelling shown by X-ray diffraction (XRD), suggested that, especially for high-charge smectites, the rate of uptake of these NOCs with increasing solution concentration is increased as a result of HDTMA solvation (Sheng et al., 1996b). Aromatic molecules, in particular, interact strongly with interlayer HDTMA, because of their planar shape and delocalised  $\pi$ -bonds. As a result, the alkyl chains of HDTMA adopt a more vertical orientation and the basal spacing increases. These changes occur more easily, although not exclusively, with high-charge smectites, creating space for the uptake of more of the aromatic molecules. Where enhancement of adsorption of one NOC by another occurs by co-adsorption, as described above, this may also occur as a result of solvation of the QAC by one of the co-adsorbates. For example, enhanced uptake of TCE in the presence of nitrobenzene (Sheng et al., 1996a) or chlorobenzene (Sheng et al., 1996b) could occur because these aromatic compounds solvate interlayer HDTMA, and thereby promote intercalation of HDTMA. Slade and Gates (2003) found that NOCs replace water on HDTMA, enhancing swelling. Although

carbon tetrachloride enhances the uptake of TCE by HDTMA-smectite this apparently affects only HDTMA located specifically on external surfaces and hence obtains to a lesser extent than for the aromatic benzenes (Sheng et al., 1996b). By way of exception, ethyl ether actually suppresses TCE uptake by the HDTMA-smectite, apparently by decreasing the capacity of HDTMA for TCE (Sheng et al., 1996a).

#### *N. Bonding Modes of Long-Chain QAC in Organo-Clays*

Although the bulk of a QAC may be held strongly by the aluminosilicate layer via electrostatic forces, a part of the organic cation may be held by van der Waals attraction (Sheng et al., 1998). One result of this van der Waals bonding is that, while QACs are generally very strongly retained by clay minerals, the fractions that are bound by van der Waals forces may be easily desorbable (Xu and Boyd, 1995a; Xu et al., 1997; Lee and Kim, 2002; Slade and Gates, 2003). These particular fractions usually only develop when the amount added exceeds the CEC of the minerals (Xu and Boyd, 1995a; Xu et al., 1997).

#### *O. Properties of NOCs and their Uptake by Organo-Clays*

The factors controlling the relative affinities of different NOCs for organo-clays were also investigated. We have seen earlier that QACs, acting as pillars, promote adsorption of NOCs. However, some NOCs may be prevented from entering the pores within the interlayer spaces because of the size and/or shape of the NOC. Apart from this 'gateway' condition, other factors that affect the affinities of NOCs for organo-clays, in general, include the solubility of the NOCs in the relevant solvent, specific interactions of the organo-clay with the solvent, the C content of the NOC, its structure, especially in relation to that of the QAC on the clay, and its polarity.

According to Street and White (1963), the solubility of NOCs in water has an over-riding influence on the extent of their adsorption by octadecyl trimethylammonium montmorillonite. The dissolved portions of the NOCs with the lowest solubility in water are taken up most completely by the organo-clay. Jaynes and Boyd (1991a) also found an inverse relationship between the solubility in water of eight different aromatic NOCs and their retention by HDTMA derivatives of a vermiculite, an illite, a kaolinite and smectites. These results show that the QAC phase and water compete for uptake of NOCs. In most studies, interest has focussed on uptake from water. However, in recognition that wastes to be controlled by organo-clay liners may contain substantial proportions of organic solvents, Nzengung et al. (1996) studied the uptake of two NOCs from mixed solutions of methanol and water. They found that the organo-clays swelled to different extents in methanol and that swelling enhanced uptake of the NOCs because the interlayer organic phase became both more organophilic and more accessible. In comparing TMPA- and TMA-montmorillonite for their ability to take up two molecules with contrasting aromaticities, Nzengung et al. (1996) suggested that the more aromatic molecule

(naphthalene) is more strongly attracted to TMPA-clay than to TMA-clay because TMPA contains a aromatic group, but not TMA. Similarities between the structures of QAC and NOCs appear to promote the uptake of the latter by clay minerals containing the former. The polarity of NOCs can also influence their uptake by clay minerals containing long-chain QACs (Sheng and Boyd, 2000). Generally, adsorption is enhanced by a high-solute polarity and the effect is most pronounced at large interlayer separations. Sheng and Boyd (2000) demonstrated the effect of polarity by comparing the uptake by HDTMA derivatives of a high- and low-charge smectite and an illite of *o*-, *m*- and *p*-dichlorobenzene (DCB) where the order of polarities was *o*-DCB > *m*-DCB > *p*-DCB. All were intercalated, leading to interlayer expansion, by the high-charge smectite derivative, but only the *o*- and *m*- forms were intercalated by the low-charge smectite derivative, and then only at high concentrations of the compounds. Intercalation led to a double-sigmoid isotherm, indicating two different mechanisms for uptake. The differences could be explained by solvation of HDTMA with the more polar forms, leading to interlayer expansion. This did not happen with the less polar forms, and hence the interlayer spaces were not expanded by these compounds.

#### *P. Mechanisms of Uptake of NOCs by Organo-Clays*

It is clear from the foregoing discussion that there are many factors affecting the uptake of different NOCs by derivatives of various clays with the range of QACs. As a result, a variety of mechanisms are involved. Indeed, for many studies these mechanisms cannot be deduced with certainty because of the possible combinations of adsorbate and adsorbent involving an enormous range of NOCs and a considerable range of QACs as well as the many subtleties of composition and structure that can affect clay behaviour. Table 11.1.2 provides a summary of the knowledge and understanding that we gleaned on the likely mechanisms for the uptake of NOCs by organo-clays.

#### *Q. NOC Uptake by Long-Chain QAC-Clays and Organic Matter*

Several workers have compared the effectiveness of organo-clays with soil organic matter for the uptake of NOCs. Lee et al. (1989b) showed that modification of two different subsoils, containing mainly vermiculite and illite, by addition of HDTMA, increased the uptake from aqueous solution of individual BTEX compounds by over two orders of magnitude. The relevant coefficients of adsorption for benzene and TCE were 5–10 times higher for HDTMA-smectite than common values obtained with soil organic matter (Boyd et al., 1988b). Smith et al. (1990) determined coefficients for the adsorption of tetrachloromethane (TCM) by a smectite that had been modified by five different long-chain QACs with different chain lengths, and with or without aromatic substituent groups. They found that QACs with 12, 14 and 16 C atoms in their hydrocarbon chain were actually less effective in adsorbing

Table 11.1.2. Summary of factors involved and the mechanisms proposed for the uptake of non-ionic compounds (NOCs) by derivatives of clays with quaternary ammonium cations (QACs)

Type of cation	Short-chain	Long-chain	Key References*
Hydrocarbon C atoms (number)	1–8 <sup>†</sup>	12 or more <sup>†</sup>	Smith et al. (1990) <sup>sc</sup> ; Jaynes and Vance (1996) <sup>lc</sup>
Influence of amount of QAC on NOC uptake	Increases to maximum, then decreases	Generally increases	Sheng and Boyd (1998) <sup>sc</sup> ; Boyd et al. (1988b) <sup>lc</sup>
Influence of QAC size on NOC uptake	Uptake decreases with increase in QAC size	Uptake increases with increase in QAC size	Jaynes and Vance (1999) <sup>sc</sup> ; Sharmasarkar et al. (2000) <sup>sc</sup> ; Jaynes and Vance (1996) <sup>lc</sup>
Effect of water on NOC uptake	Tends to decrease uptake	Appears to decrease uptake	Lee et al. (1990) <sup>sc</sup> ; Boyd et al. (1988b) <sup>lc</sup>
Effect of other NOCs	Competitive—decrease uptake	Most are synergistic—increase uptake	Smith et al. (1990) <sup>sc</sup> ; Jaynes and Vance (1996) <sup>lc</sup> ; Sheng et al. (1996a) <sup>lc</sup>
Influence of clay type	Apparently ineffective with non-expansible clays	Effective with all, most effective with expansible clays	Ceyhan et al. (1999) <sup>sc</sup> ; Jaynes and Boyd (1991a) <sup>lc</sup>
Influence of higher layer charge on clay	Can decrease uptake, depending on NOC size and shape	Increases uptake	Lee et al. (1990) <sup>sc</sup> ; Jaynes and Boyd (1991a) <sup>lc</sup>
Effect of NOC properties on uptake	Size and shape critical, to enable NOCs to fit	Enhanced by low solubility; high polarity, and similar groups as on QAC	Lee et al. (1990) <sup>sc</sup> ; Nzungu et al. (1996) <sup>sc</sup> ; Sheng and Boyd (2000) <sup>lc</sup>
Role of QAC	Pillaring between layers in expandible clays	Organophilic phase between layers or on edges	Lee et al. (1989a) <sup>sc</sup> ; Mortland et al. (1986) <sup>lc</sup>
Mechanism of NOC uptake	Adsorption on to siloxane surface	Partitioning into QAC, with possible solvation	Jaynes and Boyd (1991b) <sup>sc</sup> ; Boyd et al. (1988b) <sup>lc</sup> ; Sheng et al. (1996a) <sup>lc</sup>

\*References for short-chain QACs denoted by 'sc', those for long-chain QACs by 'lc'.

<sup>†</sup>Information lacking on QACs with hydrocarbon C from 9 to 12, to our knowledge.



TCM, in relation to percent C content, than was soil organic matter. However, 2 QACs with 12 and 16 C atoms containing an aromatic group could partition TCM as effectively as soil organic matter.

Of course, the usefulness of an organo-clay or a competing adsorbent in a particular situation is ultimately determined by its cost. A competitor that may not be as effective as an adsorbent may be preferred for its relatively low cost. Thus, shales that can adsorb appreciable amounts of two chlorohydrocarbons and a ketone but less than some QAC-bentonites, may be preferred as barrier materials because of their much lower cost (Gullick and Weber, 2001). On the other hand, organo-clays may be preferred over more effective adsorbents because they are cheaper. Activated carbon can adsorb much more benzene than a bentonite modified with either a short-chain QAC, BTEA, or HDTMA (Redding et al., 2002). Nevertheless, the organo-clays may be preferred to activated carbon as barriers for wastes involving organic liquids because organo-clays swell in non-polar liquids, and show low permeability (Gates et al., 2004). In addition, they are less likely to be saturated and 'poisoned' by adsorbates than activated carbon (Alther, 1999).

#### *R. Alternatives to QAC Clay Minerals for Control of NOCs*

In order to enhance their capacity for taking up NOCs, clays may be modified ('activated') by other methods besides the simple addition of quaternary ammonium cations (QACs). These include addition of (i) other organic cations; (ii) non-cationic organic materials; and (iii) inorganic (acids) and mixed inorganic/organic materials. Clays can also serve as carriers of catalysts to break down NOCs.

Among other cationic organic compounds that were used are positively charged polyelectrolytes or polycations (Breen and Watson, 1998; Breen, 1999, Churchman, 2002a, 2002b). The effectiveness of polycation-clay complexes in adsorbing NOCs depends on their structure and the degree of loading of the clay (Breen and Watson, 1998; Churchman, 2002b). The advantage of polycations over QACs is likely to be economic and also acceptability for human health, especially when used to help clean potable water. This is because polyelectrolytes such as poly(diallyldimethylammonium) chloride (poly DADMAC), are commonly used as coagulants for potable water treatment (Churchman, 2002b). Other organic cations that may be reacted with clays to enhance their uptake of NOCs include pyridinium ions, which affect clay properties in a similar fashion to QACs (Jaynes and Vance, 1999) and cationic dyes. Among the many cationic dyes in common use are methyl green, acraflavine, thioflavin-T, methylene blue, crystal violet, and rhodamine-B. Borisover et al. (2001) studied the latter two dyes as candidates for the modification of a smectite to enhance NOC uptake from aqueous solutions. The capacity of smectite modified with crystal violet CV or rhodamine-B for the uptake of naphthalene, phenol and the herbicide, atrazine was similar to that of some QAC-smectites. However, the isotherms were non-linear and adsorption was competitive from mixed NOC solutions,



suggesting adsorption rather than partition. This is consistent with the dye molecules forming rigid structures on the clay surface (see Chapter 12.3).

Shen (2001) has described the formation of organo-clays with high C contents using non-ionic surfactants that intercalate into smectite and are held by hydrogen bonding. To our knowledge, however, these materials were not tested for their uptake of NOCs. Cowan and White (1962) have prepared derivatives of clays with tertiary amines that could adsorb phenol to an extent depending on a balance between hydrophilicity and hydrophobicity. Khalil and Abdelhakim (2002) showed that fatty acids can become physically adsorbed by smectites, rendering the minerals organophilic, but tests of the adsorption of NOCs by these materials were apparently not carried out. Churchman and Anderson (2001) took out a patent for the use of the waste products (comprising organic materials mixed with clays and/or acid-activated clays) from food industries as adsorbents for fuel oil.

Acid-activated clays were long used industrially for decolourising or bleaching raw-cooking oils and animal fats to produce acceptable products for edible use (Anderson and Williams, 1962). Acid activation also increased the uptake of gases by smectites, as well as increasing their selectivity for some gases ( $\text{SO}_2$  and  $\text{CO}_2$ ) in relation to others ( $\text{CH}_4$  and  $\text{O}_2$ ) (Volzone and Ortiga, 2000; Venaruzzo et al., 2002). The capacity and selectivity of even kaolinite for gas adsorption can be improved by acid activation, followed by mechanical and thermal treatments (Churchman and Volzone, 2003). Treatment of smectites with hot concentrated acids greatly increases their surface acidity, surface areas, and volume of meso-pores (2–10 nm), while the materials become more siliceous (Anderson and Williams, 1962). Some naturally acidic clays can decolourise fats and oils, but not to the same extent as acid-activated clays (Theng and Wells, 1995). The decolourisation process involves the adsorption of large, generally polyaromatic, non-polar molecules, and carotenoids, especially  $\beta$ -carotene, but also xanthophylls, chlorophyll, pheophytin, tocopherols and gossypol and their degradation products, as well as phospholipids, soap and trace metals (Sarier and Güler, 1988; Christidis et al., 1997). Acid-activated clays are also used as adsorbents for neutral polyaromatic leuco dyes that become positively charged and coloured on adsorption, and are used in carbonless copying papers. The XRD patterns indicated that adsorption of leuco dyes led to a reordering of the aluminosilicate layers (Fahn and Fenderl, 1983). Acid-activated clays can serve as carriers for fungicides and insecticides, and can be used to regenerate organic fluids for dry cleaning. It seems surprising, therefore, that acid-activated clays are not used more widely as adsorbents for NOCs (Lagaly, 1995).

Modifying clays with hydr(oxides), and subsequent heating, can also provide materials ('pillared clays') with an enhanced capacity for taking-up NOCs. Zielke and Pinnavaia (1988) suggested that PCP was adsorbed on clays pillared with  $\text{Al}_2\text{O}_3$  (and  $\text{Cr}_2\text{O}_3$  but to a lesser extent), through direct association with the oxides rather than with the faces or edges of the aluminosilicate layers. The enhanced uptake of PCP by delaminated pillared clays apparently reflects a greater availability of oxide-treated surfaces. The inorganic pillars themselves appear to act as adsorbents for

NOCs whereas the silicate surface appears to be the main adsorbent for NOCs in organically pillared clays. Neither the hydroxy-interlayered nor oxide pillared clays adsorb as much PCP as organo-clays, let alone activated carbon. However, a poly(hydroxo aluminium) smectite was shown to be a powerful adsorbent for polychlorinated dibenzo dioxins (PCDDs) and polychlorinated biphenyls (PCBs) (Srinivasan et al., 1985), and was as effective as activated carbon for binding the more hydrophobic pollutants (Srinivasan and Fogler, 1986a, 1986b). Similarly, Matthes and Kahr (2000) found that Al- and Zr-hydroxy interlayered, and pillared smectites, could completely remove atrazine and chloranilines at ppm levels from water. Of these sorbents, the pillared smectites were more effective than the hydroxy-interlayered minerals and the Zr-pillared smectites were the most effective of all. They suggested that increased acidity of the intercalated species enhances the adsorption of organic bases. Like Zielke and Pinnavaia (1988), Nolan et al. (1989) suggested that the poly(hydroxo aluminium) material adsorbs dioxin through electrostatic forces.

Subsequently, a series of materials has been devised that constitute variations on pillaring, to produce a class of materials generally described as 'inorgano-organo-clays'. Srinivasan and Fogler (1990) produced a material of this kind by adsorbing a cationic surfactant (in particular, cetylpyridinium) on a smectite clay exchanged with polyvalent inorganic cations (either poly(hydroxo aluminium) cations, or  $\text{La}^{3+}$ ). This composite clay mineral can strongly adsorb highly hydrophobic molecules (PCP and benzo(a)pyrene) with the latter apparently being held more strongly than by activated carbon. The partition coefficients for these two essentially insoluble hydrophobic compounds into the inorgano-organo clay were at least two orders of magnitude greater than those for the organo-clay (cetylpyridinium-smectite) itself. A more water-soluble, hence less hydrophobic, compound (3,5-dichlorophenol) is adsorbed by the composite material but is not held any more strongly than by the cetylpyridinium-smectite. Another variant of an inorgano-organo-clay is obtained by incorporating a non-ionic surfactant during the synthesis of pillars in a smectite with aluminium hydroxide, but without calcination to produce oxides (Michot and Pinnavaia, 1991). Incorporation of surfactant around pillars in the interlayer increased the uptake of phenols and chlorinated phenols from aqueous solution. Notably there was much greater uptake of PCP by this material (recyclable by heating) than what Zielke and Pinnavaia (1988) obtained with alumina-pillared smectite. Bouras et al. (2001, 2002) used a similar approach, but with surfactants included in poly(hydroxo iron) smectites, for the removal of PCP from water. A further approach involves the addition to smectites of surfactants, both cationic and non-ionic, together with Si and/or Al in solution forms, followed by calcination, to produce the so-called 'porous clay heterostructures' (Galarneau et al., 1995). Although these materials were generally tailored to produce highly acidic catalysts, their large porosity and surface areas mean that they could be very useful as adsorbents (Zhu et al., 2002a).

Catalysts based on clays can also be used to control pollutants in both gas and aqueous phases, generally by enhancing their decomposition. A common approach

has been through the attachment to clays of titanium dioxide, which is pre-eminent as a catalyst for the photo-oxidation of refractory organic pollutants in water and air.  $\text{TiO}_2$  can be incorporated into clays either as a pillar by adding Ti as an acid sol-gel to a smectite with NaOH (Sun et al., 2002), or as solid dispersions with the clay formed by adding a Ti gel to a smectite in the presence of a polyethylene oxide surfactant (Zhu et al., 2002b). The resulting materials are effective catalysts for the photo-degradation of various dyes (Li et al., 2002; Sun et al., 2002; Zhu et al., 2002b) and phenol (Zhu et al., 2005) and also, in association with  $\text{V}_2\text{O}_5$ , for the reduction of NO by  $\text{NH}_3$  (Chae et al., 2001). As an alternative approach, emphasising prevention of pollution rather than its amelioration, Pinnavaia (1995) has suggested that clay minerals, principally smectites, modified by oxide pillaring or by the exchange with QACs, as well as LDH ('anionic clays'), could be used to promote 'green chemistry', a process that achieves complete conversion of reagents to products while avoiding the production of pollutant by-products.

#### 11.1.4. CONTROL OF ANIONS

##### *A. Uptake of Anions by Unmodified Clays*

As clay minerals are predominantly negatively charged, they have only a small capacity for taking-up anions. Anion exchange generally occurs on the edges of the aluminosilicate layers and is pH-dependent. The anion exchange capacity (AEC) of clays increases with decreasing pH but its magnitude is never high, being  $< 5$  cmol/kg for smectites (Borchardt, 1989) and apparently not more than 2 cmol/kg for kaolinites (Dixon, 1989). Some anions, notably phosphates, may be adsorbed, at least partially irreversibly, to layer silicates (Dixon, 1989; McLaren and Cameron, 1996). However, layer silicates may be modified to give materials that can take up substantial amounts of anions. Even though these materials tend to have much lower capacities for anions than many LDH, they may offer advantages from the point of view of economics because they can be prepared in situ from clays in soils or sediments, or because they are more stable in particular environments.

##### *B. Anion Uptake by Clays Modified with Organic Cations*

The studies by Bors and co-workers (Bors, 1990; Bors and Gorny, 1992; Dultz and Bors, 2000; Riebe et al., 2001) showed that iodide (which, as radioiodide, is a dangerous component of radioactive waste), and also pertechnetate ( $\text{TcO}_4^-$ ) can be adsorbed by clay minerals, particularly smectites, that were modified with long-chain QACs. The adsorption data are consistent with different types of binding of the QAC (generally hexadecylpyridinium, HDPy) for different levels of loading of the clay. The  $\text{HDPy}^+$  cation was dominant, in exchangeable form, at low loadings. At intermediate loadings, the chloride salt ( $\text{HDPyCl}$ ) became associated with the clay

mineral, while micelles were formed at high loadings. This suggests adsorption of the anions occurring by a variety of mechanisms. Nonetheless, caution is advised when interpreting uptake of simple anions by organo-modified clays, as large amounts of organo-salts can remain associated with the intercalate in aqueous solutions (Slade et al., 1978; Lee and Kim, 2002; Slade and Gates, 2003, 2004) (also see Section 11.1.3.D).

Li (1999) has shown that addition of HDTMA, in amounts sufficient to satisfy the plateau for adsorption, to a kaolinite, an illite and a smectite, enabled the uptake of chromate and nitrate anions from aqueous solutions. Krishna et al. (2001) showed that the adsorption of chromate by HDTMA-clays, which included montmorillonite, pillared montmorillonite, and kaolinite, was strongly dependent upon pH, the amount adsorbed decreasing from pH 1 to ~8, when it became negligible. This reflected the form of chromium in solution.

Undoubtedly, the development of positively charged areas on the clay is a prime requirement for the uptake of anions. Xu and Boyd (1995b) showed that the electrophoretic mobility of a  $\text{Na}^+$ -smectite, treated with HDTMA, changed abruptly from negative to positive as the CEC of the clay was exceeded. Since electrophoretic mobility reflects the charge on the external surfaces little, if any, of the QAC was found on these surfaces until the amount that satisfied the layer charge (CEC) was intercalated. Changes in zeta potential also occur as cationic polymers are added to clays. However, these appear to be more complex than shown by Xu and Boyd (1995b) for the addition of HDTMA to clay. Instead, a gradual decrease in the magnitude of the negative zeta potential occurs prior to the point at which a more abrupt change occurs to a positive value (Billingham et al., 1997; Churchman, 2002b) (Fig. 11.1.7). This reflects the adsorption of some polycation to external sites, as well as their incorporation into interlayer spaces, even at low concentrations of polyelectrolyte. Ueda and Harada (1968) found that the AEC of the product gradually increased while its CEC decreased as polycation was added to a smectite. They attributed the origin of the AEC to the loops and tails on the adsorbed cationic polymer. These extended away from the clay mineral surface while the trains of the polymer were held close to the surface. As the surface coverage of the polymer increased, the proportion of its loops and tails, the segments for anion uptake, increased relative to its train segments. Similarly, Kleinig et al. (2003) reported that more phosphate was adsorbed (at comparable concentrations) on a smectite when it was complexed with poly DADMAC of high-molecular weight than of one with low-molecular weight. They explained the difference by the higher proportions of loops on the high-molecular weight variant of the polycation. From an electrostatic interaction viewpoint, the mechanism by which associated polycations can enable clays to adsorb anions is thought to involve positive patches that are formed on clay surfaces because the centres of positive charge on the polycations are closer together than the centres of negative charge on the clays, so localities of excess positive charge develop (Durand-Piana et al., 1987; Denoyel et al., 1990; Breen and Watson, 1998). It seems probable that positively charged areas occur alongside negatively charged

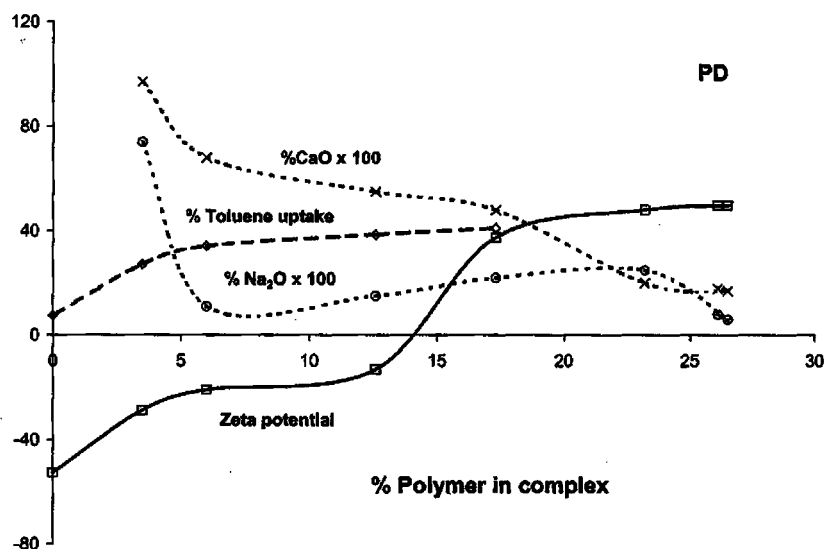


Fig. 11.1.7. Zeta potential, percentage removal of toluene from solution and percentages of both  $\text{Ca}^{2+}$  and  $\text{Na}^+$ , expressed as oxide (and multiplied by 100), plotted simultaneously against changes in the actual percentage of the polymer (polydiallyldimethylammonium chloride; poly DADMAC) in the polymer-smectite. From Churchman (2002b).

areas, so that adsorption of anions and of cations can occur together, as shown by Ueda and Harada (1968). For clays modified with long-chain QACs (Dultz and Bors, 2000; Riebe et al., 2001) as for polycation-modified clays (Billingham et al., 1997; Churchman, 2002b), exchangeable inorganic cations can remain while the net charge of the clay derivative has reversed and the material has become an adsorbent for anions.

### C. Alternative Methods of Modifying Clays for Anion Adsorption

Clays that are pillared with inorganic hydroxy cations can promote the adsorption of anions. Polubesova et al. (2000) demonstrated the effectiveness of hydroxy-Al pillared clay for the uptake of an anionic herbicide, sulfometron, as well as of sulphate, acetate, and chloride. They suggested that the association between the anions and the pillars was electrostatic. In a later paper, these authors compared a poly(hydroxo aluminium) pillared smectite and a positively charged derivative of the smectite with crystal violet (CV) for their relative abilities as adsorbents of the herbicide imazaquin, which is anionic under the experimental conditions used. Both materials are similarly effective, but desorption and also displacement by other anions are more difficult from the clay-CV derivative than from the pillared clay (Polubesova et al., 2002). Bouras et al.

(2002) showed that an inorgano-organo clay prepared from a smectite by the co-adsorption of the cationic surfactant hexadecyltrimethylammonium (i.e., HDTMA) chloride and poly(hydroxo titanium) cations can decolourise a solution containing the anionic textile dye, sulfacid brilliant pink.

#### 11.1.5. CONTROL OF TURBIDITY AND RESIDUAL TREATMENT CHEMICALS

##### *A. Control of Turbidity in Water Treatment*

The addition of clays, and particularly bentonite (i.e., smectite, as mined), as an aid to flocculation/coagulation during the treatment of water or wastewater is a well-established technology. Its historical use in the Sudan to clean pathogenic organisms from river water has already been observed. Bentonite was included, along with the soluble cationic polymeric flocculant, ferric chloride, and aluminium sulphate (alum) for use in a water filtration plant planned for Los Angeles (McBride et al., 1982). Bentonite can reduce the need for soluble flocculants by 1.5–2 times and has the added advantage of being non-toxic (Akhundov et al., 1983). It can also give a greater reduction of phosphate in water, when used in conjunction with aluminium sulphate, than either aluminium sulphate alone or calcium hydroxide (Jorgensen et al., 1973).

Dissolved NOM is one of the major causes of turbidity in drinking water. It is also a pollutant insofar as it produces poisonous trihalomethanes upon chlorination. Coagulation with cationic electrolytes can remove NOM but only partially unless suspended solids are present (Bolto et al., 2001). Apparently solids are required to adsorb NOM, with the solid-NOM combination being flocculated by the added polycation. Bolto et al. (2001) found that a high-surface area kaolinite, ball clay, was more effective than smectites for aiding NOM removal, while illite and palygorskite were also more effective than smectites for removing NOM. The superiority of kaolinite is consistent with its stronger affinity for humic acid as compared with smectite, and reflects the aluminous and less hydrated surface of kaolinite (Parazak et al., 1988). Curiously, bentonite is also used in a completely contrasting process proposed for the treatment of highly turbid waters, this time as a flotation aid with (QAC) surfactants (Grieves, 1967). Bentonite is also useful for removing mercury from water in treatment (Logsdon and Symons, 1973; Hatch, 1975) where it acts as an adsorbent that is itself coagulated with alum, ferric sulphate, or a polyelectrolyte.

##### *B. Control of Turbidity in Wastewater Treatment*

Clays, especially bentonite, proved to be particularly useful as flocculation aids in the treatment of effluent from pulp and paper mills. Additions of bentonite effected the removal from these effluents of starch (Gillespie et al., 1970), ammonium-base spent

sulphite liquor (Scherler, 1972), basic dyes (Mobius and Gunther, 1974), and colour and fines generally (Potskhershvili et al., 1977; Ciba-Geigy, 1978; Delaine, 1978), in processes that also involve coagulating agents such as alum, polymers, sulphuric acid and/or lime, usually in combinations. The bentonite could serve the dual roles of adsorbent and nucleation solid for flocculation in these processes. Dilek and Bese (2001) found that colour removal efficiency was improved over that from using alum alone when sepiolites, and  $\text{Ca}^{2+}$ - or  $\text{Na}^{+}$ -bentonites were added to wastewaters along with alum, as were the settling characteristics of the sludge produced. Compared with virgin  $\text{Na}^{+}$ -bentonite, acid-activated bentonite greatly improved the sludge settling characteristics.

Clays can also be used as flocculant/coagulant aids in some treatments of sewage designed to reduce their biological oxygen demand, principally by the removal of protein (Holo et al., 1973; Ogedengbe, 1976). Treatment of acid-cracked waste liquor from wool scouring can also be assisted by the addition of bentonite to aid flocculation (Heisey, 1975, 1977). Many different clays were more effective than either alum, polyaluminium chloride and 4 organic flocculants for the removal by flocculation of red-tide and brown-tide organisms (Sengco et al., 2001).

### *C. Control of Residual Treatment Chemicals*

Clays may further act as scavengers for chemicals used in certain wastewater treatments in order to remove these after the treatment is complete. For example, the presence of surfactants in water, whether cationic or non-ionic, and also polyelectrolytes, can result in the poisoning of marine organisms as many of these organic molecules are very toxic. However, addition of bentonite can remove both surfactants (Cary et al., 1987) and polyelectrolytes (Carberry et al., 1977) by adsorption (see Section 11.1.3.R). In some cases, treatment of sewage to remove pathogenic organisms is aided by dye-sensitisers, such as methylene blue. After treatment, bentonite can be added to adsorb the excess dye (Acher and Juven, 1977; Acher and Rosenthal, 1977).

## 11.1.6. CONCLUDING REMARKS AND FUTURE PROSPECTS

The use, and enhancement of the utility, of clays, for the control of each of the different classes of pollutants has reached its own particular stage of maturity or development. This point will be discussed, along with research which shows promise for new targets for the environmental use of clays and also for overcoming some of the problems raised in their environmental applications to date.

### *A. Heavy Metal Ions and Simple Cations*

Clays provide an in situ, or low-cost method of attenuating and/or immobilising heavy metal ions. Although their applicability was established decades ago, our



understanding of the mechanisms involved in the uptake of different heavy metal cations by clays is still incomplete. Modern, sophisticated surface analytical techniques are poised to greatly aid our understanding of the clay–heavy metal ion interaction. Even so, enough work has been done on various modification methods for the enhancement of heavy metal ion uptake to suggest that organic complexation as well as hydroxyl interlayering and pillaring can improve the adsorption capacity of clays for metal cations in general.

### *B. Organic and Biological Cations*

There has been interest for many years in the interactions of clays with both permanently charged organic cations and amphoteric molecules that are positively charged under ambient conditions. There is now enough knowledge to provide the basis for the use of clays as low cost, non-toxic adsorbents for the removal of waste proteins, biological toxins, antibiotics, and biological entities such as viruses, from water.

### *C. Non-Ionic Organic Molecules*

The late 1980s and the 1990s saw an explosion of scientific interest in the use of clays, and particularly organically modified clays, for the control of NOCs in the environment. Most of the research on this topic has concentrated on modifying clay minerals by exchange and intercalation of a few quaternary ammonium cations in order to exploit their large surfaces as organophilic adsorbents. Much is now known about the procedures involved, enabling organo-clays to be put to relevant environmental uses, such as water clean-up, in barriers, and for the prevention of leaching of contaminants to groundwater and sensitive surface water bodies. The procedure for producing organophilic clays *in situ* through the addition of an appropriate cation that is available as a surfactant or coagulant is particularly useful for the modification of soils for environmental protection.

As people become more sensitive to the probable toxicity of chemicals in everyday use, the protective use of appropriately treated clays on a personal, household, workplace or even vehicle scale may increase. There may be particular opportunities to extend the use of modified clays for the control of gas-phase pollutants and also to expand the scope of these. There may also be opportunities for cross- and interdisciplinary work, in which organic chemists and even biochemists associate with clay mineralogists in testing a wide range of organic and biological cations for modifying and tailoring clays for environmental protection and remediation. Cost will almost always remain a decisive factor influencing the use of modified clays and clay minerals. Further, public sensitivities to the use of synthetic chemicals, even when they are bound by clay, could force a re-think of the conventional approach to organo-clays. For these reasons, research that is aimed to re-use clay-based wastes may become particularly valuable. For example, spent bleaching earths constitute a



waste that is rich in clays. Although such clays are altered, their activation can actually enhance their adsorption qualities, as also may their association with organic compounds from the oil-bleaching process. It is an abundant waste material as the edible oil industry world-wide uses almost 1 million tonnes of clays annually (Crossley, 2001). Pollard et al. (1992) showed that spent bleaching earth could be chemically activated to produce a char that adsorbs phenols from water, while Tsai et al. (2002) demonstrated how this waste material could be activated by controlled heating to produce a mesoporous material that can adsorb paraquat.

#### *D. Anions*

It has long been known that the charge on clays can be reversed in sign by appropriate organic modification. However, the implications of charge reversal for the uptake and possible immobilisation of anions were hardly explored. Yet anions, in run-off and leaching water following the application of fertilizers and some pesticides, and also as dyes (e.g., in wool processing), are common environmental contaminants. Although positively charged organo- and polymer-clays may not be competitive with LDH in terms of their anion uptake capacity, the ability to produce such clays in situ means that they may have a cost advantage over LDH. Their main rivals among natural materials are hydr(oxides) particularly of ferric iron, as these are positively charged in weakly acidic environments such as those of natural waters. However, organo- and polymer-clays are likely to be more stable than either LDH in acidic environments, or ferric hydr(oxides) in reductive environments.

#### *E. Turbidity and Use of Colloidal Characteristics*

The well-established use of clays as flocculation aids offers prospects for future environmental uses because of the colloidal properties of certain clays. Recent work has shown that these properties may be exploited in such diverse applications as reducing fouling by oil of ultrafiltration membranes used to clean up wastewater from car washes (Panpanit and Visvanathan, 2001). Bentonite is effective in this application partly because it promotes aggregate formation, thereby enhancing the flux. This characteristic of bentonites can also be used in newspaper recycling to avoid ink speck formation (Philippakopoulou et al., 2002).

#### *F. Exploitation of Mixtures of Properties*

Organo-clays can be both hydrophilic and organophilic at the same time. They can therefore be tailored to retain some CEC while organic contaminants can be adsorbed on organophilic sites, as already discussed. Furthermore, the usefulness of organo-clays can be enhanced if their interaction with contaminants involves more than one useful characteristic of the clay derivative. For example, phenol could be removed from water through the application of a short-chain surfactant cation

(benzyltrimethylammonium) to the contaminated water containing pre-dispersed bentonite to bring about flocculation of the bentonite on complex formation through cation exchange (Shen, 2002b). Phenol may then be removed by a combination of adsorption and flocculation.

### *G. Waste Removal and Disposal*

Flocculation enables the pollutant, associated with the adsorbent, to be separated from water. However, since the clay materials often remain in suspension, the contaminant may be immobilised but is not removed from the system. In this case, other means of withdrawing the dispersed phase from the liquid phase need to be devised. Oliveira et al. (2003) proposed the use of magnetic clay-iron oxide composites for this purpose. These synthetic adsorbents are re-usable as Taylor and Churchman (1998) showed for magnetised alumina. Adsorbed contaminants may be degraded by microorganisms, as already discussed. However, if the adsorbed contaminants are not bioavailable, recalcitrant, or highly toxic, their leaching may be prevented through solidification in cements. This seems feasible in the case of clay minerals modified with quaternary ammonium ions (Montgomery et al., 1988; Lo, 1996; Cioffi et al., 2001b), whereas free organic matter in cements generally causes difficulties with hardening and strength.

## REFERENCES

- Acher, A.J., Juven, B.J., 1977. Destruction of coliforms in water and sewage water by dye-sensitized photooxidation. *Applied and Environmental Microbiology* 33, 1019–1022.
- Acher, A.J., Rosenthal, I., 1977. Dye-sensitized photo-oxidation—a new approach to the treatment of organic matter in sewage effluents. *Water Research* 11, 557–562.
- Adu-Wusu, K., Whang, J.M., McDevitt, M.F., 1997. Modification of clay-based waste containment materials. *Land Contamination & Reclamation* 5, 171–175.
- Akcay, G., Yurdakoc, K., 2000. Removal of various phenoxyalkanoic acid herbicides from water by organo-clays. *Acta Hydrochimica et Hydrobiologica* 28, 300–304.
- Akhundov, V.I., Akhundov, K.F., Mamedova, A.P., Dzafaron, S.M., Naumova, N.N., 1983. Hygienic evaluation of bentonitic clays and filtrating material from Azerbaijan deposits. 2nd communication: toxicologic and hygienic studies of the bentonitic clays from Agburun deposits (translated). *Izvestiya Akademii Nauk Azerbaydzhanskoy SSR Seriya Biologicheskikh Nauk* 2, 115–123 (*Water Resources Abstract* No. 8601257).
- Alther, G.R., 1999. Removal of oil from wastewater with organoclay. *International Water Irrigation Review* 19, 44.
- Alvarez, A., Santaren, J., Perez-Castells, R., Casal, B., Ruiz-Hitzky, E., Levitz, P., Fripiat, J.J., 1987. Surfactant adsorption and rheological behavior of surface modified sepiolite. In: Schultz, L.G., van Olphen, H., Mumpton, F.A. (Eds.), *Proceedings of the International Clay Conference, Denver, 1985*. The Clay Minerals Society, Bloomington, IN, pp. 370–374.
- Anderson, A.J.C., Williams, P.N., 1962. *Refining of Oils and Fats for Edible Purposes*, 2nd edition. Pergamon Press, New York.

- Armstrong, D.E., Chesters, G., 1964. Properties of protein–bentonite complexes as influenced by equilibration conditions. *Soil Science* 98, 39–52.
- Aznar, A.J., Casal, B., Ruiz-Hitzky, E., Lopez-Arbeloa, I., Lopez-Arbeloa, F., Santaren, J., Alvarez, A., 1992. Adsorption of methylene blue on sepiolite gels: spectroscopic and rheological studies. *Clay Minerals* 27, 101–108.
- Barkley, M.B., Desjardins, P.R., 1977. Simple, effective method for purifying the AS-1 cyanophage. *Applied and Environmental Microbiology* 33, 971–974.
- Barrer, R.M., Kelsey, K.E., 1961. Thermodynamics of interlamellar complexes. *Transactions of the Faraday Society* 57, 452–462.
- Barrer, R.M., McLeod, D.M., 1955. Activation of montmorillonite by ion exchange and sorption complexes of tetra-alkyl ammonium montmorillonites. *Transactions of the Faraday Society* 51, 1290–1300.
- Beall, G.W., 1984. Method of breaking emulsions; absorption of a quaternary ammonium exchanged clay in wastewater. U.S. Patent 4,470,912.
- Beall, G.W., 1985a. Process for treating organic contaminated water; organoclay absorption column followed by active carbon. U.S. Patent 4,517,094.
- Beall, G.W., 1985b. Method of removing organic contaminants from aqueous compositions; absorption with reaction product of clay and quaternary ammonium salt. U.S. Patent 4,549,590.
- Beall, G.W., 1996. Method of removing water-insoluble organic contaminants from an acidic aqueous stream. U.S. Patent 5,567,318.
- Benincasa, E., Brigatti, M.F., Malferrari, D., Medici, L., Poppi, L., 2002. Sorption of Cd-cysteine complexes by kaolinite. *Applied Clay Science* 21, 191–201.
- Billingham, J., Breen, C., Rawson, J.O., Yarwood, J., Mann, B.E., 1997. Adsorption of polycations on clays: a comparative in situ study using  $^{133}\text{Cs}$  and  $^{23}\text{Na}$  solution phase NMR. *Journal of Colloid and Interface Science* 193, 183–189.
- Bolto, B., Dixon, D., Eldridge, R., King, S., 2001. Cationic polymer and clay or metal oxide combinations for natural organic matter removal. *Water Research* 35, 2669–2676.
- Borchardt, G., 1989. Smectites. In: Dixon, J.B., Weed, S.B. (Eds.), *Minerals in Soil Environments*, 2nd edition. Soil Science Society of America, Madison, WI, pp. 675–727.
- Borisover, M., Graber, E.R., Bercovich, F., Gerstl, Z., 2001. Suitability of dye–clay complexes for removal of non-ionic organic compounds from aqueous solutions. *Chemosphere* 44, 1033–1040.
- Bors, J., 1990. Sorption of radioiodine in organo-clays and organo-soils. *Radiochimica Acta* 51, 139–143.
- Bors, J., Gorny, A., 1992. Studies on the interactions of HDPY-vermiculite with radioiodine. *Applied Clay Science* 7, 245–250.
- Bouras, O., Chami, T., Houari, M., Khalaf, H., Bollinger, J.C., Baudu, M., 2002. Removal of sulfacid brilliant pink from an aqueous stream by adsorption onto surfactant-modified Ti-pillared montmorillonite. *Environmental Technology* 23, 405–411.
- Bouras, O., Houari, M., Khalaf, H., 2001. Using of surfactant modified Fe-pillared bentonite for the removal of pentachlorophenol from aqueous stream. *Environmental Technology* 22, 69–74.
- Boyd, S.A., Lee, J.F., Mortland, M.M., 1988a. Attenuating organic contaminant mobility by soil modification. *Nature* 333, 345–347.

- Boyd, S.A., Mortland, M.M., Chiou, C.T., 1988b. Sorption characteristics of organic compounds on hexadecyltrimethylammonium-smectite. *Soil Science Society of America Journal* 52, 652–657.
- Boyd, S.A., Shaobai, S., Lee, J.F., Mortland, M.M., 1988c. Pentachlorophenol sorption by organo-clays. *Clays and Clay Minerals* 36, 125–130.
- Boyd, S.A., Sheng, G.Y., Teppen, B.J., Johnston, C.T., 2001. Mechanisms for the adsorption of substituted nitrobenzenes by smectite clays. *Environmental Science and Technology* 35, 4227–4234.
- Breen, C., 1999. The characterisation and use of polycation-exchanged bentonites. *Applied Clay Science* 15, 187–219.
- Breen, C., Watson, R., 1998. Polycation-exchanged clays as sorbents for organic pollutants. Influence of layer charge on sorption capacity. *Journal of Colloid and Interface Science* 208, 422–429.
- Brixie, J.M., Boyd, S.A., 1994. Treatment of contaminated soils with organoclays to reduce leachable pentachlorophenol. *Journal of Environmental Quality* 23, 1283–1290.
- Brunauer, S., 1944. *The Adsorption of Gases and Vapours*. Oxford University Press, Oxford.
- Carberry, J.G., Twardowski, C.J., Eberhart, D.K., 1977. Clay adsorption treatment of non-ionic surfactants in waste water. *Journal of the Water Pollution Control Federation* 49, 452–459.
- Carrizosa, M.J., Koskinen, W.C., Hermosin, M.C., Cornejo, J., 2001. Dicamba adsorption-desorption on organoclays. *Applied Clay Science* 18, 223–231.
- Cary, G.A., McMahon, J.A., Kuc, W.J., 1987. Effect of suspended solids and naturally occurring dissolved organics in reducing the acute toxicities of cationic polyelectrolytes to aquatic organisms. *Environmental Toxicology and Chemistry* 6, 469–474.
- Ceyhan, O., Guler, H., Guler, R., 1999. Adsorption mechanisms of phenol and methylphenols on organoclays. *Adsorption Science & Technology* 17, 469–477.
- Chae, K.J., Nam, I.S., Yang, H.S., Song, S.L., Dohur, I., 2001. Use of  $V_2O_5/Ti$ -PILC catalyst for the reduction of NO by  $NH_3$ . *Journal of Chemical Engineering, Japan* 34, 148–153.
- Chandra, U., 1970. Removal of radioisotopes from liquid wastes by sorption in local minerals. NTIS. BARC-454, 29pp. (Water Resources Abstract No. 7109517).
- Chiou, C.T., Peters, L.J., Freed, V.H., 1979. A physical concept of soil-water equilibria for nonionic organic compounds. *Science* 213, 684.
- Chiou, C.T., Porter, P.E., Schmedding, D.W., 1983. Partition equilibria of nonionic organic compounds between soil organic matter and water. *Environmental Science and Technology* 17, 227–231.
- Christidis, G.E., Scott, P.W., Dunham, A.C., 1997. Acid activation and bleaching capacity of bentonites from the islands of Milos and Chios, Aegean, Greece. *Applied Clay Science* 12, 329–347.
- Churchman, G.J., 2002a. The role of clays in the restoration of perturbed ecosystems. In: Violante, A., Huang, P.M., Bollag, J.-M., Gianfreda, L. (Eds.), *Soil Mineral–Organic Matter–Microorganism Interactions and Ecosystem Health. Development in Soil Science* 28A. Elsevier, Amsterdam, pp. 333–350.
- Churchman, G.J., 2002b. Formation of complexes between bentonite and different cationic polyelectrolytes and their use as sorbents for non-ionic and anionic pollutants. *Applied Clay Science* 21, 177–189.

- Churchman, G.J., Anderson, J.S., 2001. Use of solid waste material. Australian Patent No. PCT/AU01/00915.
- Churchman, G.J., Volzone, C., 2003. Activation of clays for environmental uses—can we improve on nature, and can it pay? In: Dominguez, E.A., Mas, G.R., Cravero, F. (Eds.), 2001. *A Clay Odyssey*. Proceedings of the 12th International Clay Conference. Elsevier, Amsterdam, pp. 31–38.
- Ciba-Geigy Ltd., 1978. Process for purifying aqueous industrial effluents. British Patent No. 1,499,387.
- Cioffi, R., Costanzo, S., Maffucci, L., Santoro, L., 2001a. Adsorption of the organic fraction of a tannery sludge by means of organophilic bentonite. *Environmental Technology* 22, 83–89.
- Cioffi, R., Maffucci, L., Santoro, L., Glasser, F.P., 2001b. Stabilization of chloro-organics using organophilic bentonite in a cement-blast furnace slag matrix. *Waste Management* 21, 651–660.
- Cooper, C., Jiang, J.Q., Ouki, S., 2002. Preliminary evaluation of polymeric Fe- and Al-modified clays as adsorbents for heavy metal removal in water treatment. *Journal of Chemical Technology and Biotechnology* 77, 546–551.
- Cowan, C.T., White, D., 1962. Adsorption by organo-clay complexes. *Clays and Clay Minerals* 9, 459–467.
- Cremers, A.E.J., Maes, A.P.A., Piegneur, P.G.L., 1979. Process for the removal of metals from solution. U.S. Patent 4,167,481.
- Crocker, F.H., Guerin, W.F., Boyd, S.A., 1995. Bioavailability of naphthalene sorbed to cationic surfactant-modified smectite clay. *Environmental Science and Technology* 29, 2953–2958.
- Crossley, P., 2001. Clear opportunities for bleaching and clarifying clays. *Industrial Minerals*, March, 69–75.
- Delaine, J., 1978. Papermill effluent turbidity removal—a new approach. *Effluent and Water Treatment Journal* 18, 219–221.
- Denoyel, R., Durand, G., Lafuma, F., Audebert, R., 1990. Adsorption of cationic polyelectrolytes on to montmorillonite and silica: microcalorimetric study of their conformation. *Journal of Colloid and Interface Science* 139, 281–290.
- Dilek, F.B., Bese, S., 2001. Treatment of pulping effluents by using alum and clay—colour removal and sludge characteristics. *Water SA* 27, 361–366.
- Dixon, J.B., 1989. Kaolin and serpentine group minerals. In: Dixon, J.B., Weed, S.B. (Eds.), *Minerals in Soil Environments*, 2nd edition. Soil Science Society of America, Madison, WI, pp. 467–525.
- Dultz, S., Bors, J., 2000. Organophilic bentonites as adsorbents for radionuclides: I. Adsorption of anionic and cationic fission products. *Applied Clay Science* 16, 15–29.
- Durand-Piana, G., Lafuma, F., Audebert, R., 1987. Flocculation and adsorption properties of cationic polyelectrolytes toward Na-montmorillonite dilute suspensions. *Journal of Colloid and Interface Science* 119, 474–480.
- Elliott, H.A., Liberati, M.R., Huang, C.P., 1986. Competitive adsorption of heavy metals by soils. *Journal of Environmental Quality* 15, 214–219.
- Fahn, R., Fenderl, K., 1983. Reaction products of organic dye molecules with acid-treated montmorillonite. *Clay Minerals* 18, 447–458.
- Farrah, H., Pickering, W.F., 1978. The sorption of mercury species by clay minerals. *Water, Air and Soil Pollution* 9, 23–31.

- Galarneau, A., Barodawalla, A., Pinnavaia, T.J., 1995. Porous clay heterostructures formed by gallery templated synthesis. *Nature* 374, 529.
- Gao, B., Wang, X., Zhao, J., Sheng, G.Y., 2001. Sorption and cosorption of organic contaminant on surfactant-modified soils. *Chemosphere* 43, 1095–1102.
- Garcia Sanchez, A., Alastuey, A., Querol, X., 1999. Heavy metal adsorption by different minerals: application to the remediation of polluted soils. *Science of the Total Environment* 242, 179–188.
- Gates, W.P., 2004. Crystalline swelling of organo-modified clays in ethanol–water solutions. *Applied Clay Science* 27, 1–12.
- Gates, W.P., Nefiodovas, A., Peter, P., 2004. Permeability of an organo-modified bentonite to ethanol–water solutions. *Clays and Clay Minerals* 52, 192–203.
- Gates, W.P., Slade, P.G., 2001. Removal of toxins from water. Australian Patent No. PCT/AU01/00586.
- Gillespie, W.J., Mazzola, C.A., Marshall, D.W., 1970. Review of starch problems as related to stream pollution. *Paper Trade Journal* 154, 29–32 (Water Resources Abstract No. 7203753).
- Grieves, R.B., 1967. Foam separation method for the clarification of natural waters. *Journal of the American Water Works Association* 59, 859–866.
- Grim, R.E., 1962. *Applied Clay Mineralogy*. McGraw-Hill, New York.
- Gullick, R.W., Weber, W.J. Jr., 2001. Evaluation of shale and organoclays as sorbent additives of low-permeability soil containment barriers. *Environmental Science and Technology* 35, 1523–1530.
- Harsh, J.B., Doner, H.E., 1984. Specific adsorption of copper on an hydroxy-aluminum-montmorillonite complex. *Soil Science Society of America Journal* 48, 1034–1039.
- Hatch, A.E., 1975. Removal of heavy metals from aqueous solutions. U.S. Patent 3,859,210.
- Heisey, W.A., 1975. Treatment of wool scouring wastes. U.S. Patent 3,909,407.
- Heisey, W.A., 1977. Process for treating wool scouring wastes. U.S. Patent 4,059,516.
- Hermosin, M.C., Cornejo, J., 1992. Removing 2,4-D from water by organo-clays. *Chemosphere* 24, 1493–1503.
- Holo, J., Toth, J., Zagyvai, I., 1973. Process for the reduction of the biochemical oxygen demand of sewage and for the recovery of the inherent protein. U.S. Patent 3,738, 933.
- Inskip, W.P., Baham, J., 1983. Adsorption of Cd(II) and Cu(II) by Na-montmorillonite at low surface coverage. *Soil Science Society of America Journal* 47, 660–665.
- Jackson, T.A., 1998. The biogeochemical and ecological significance of interactions between colloidal minerals and trace elements. In: Parker, A., Rae, J.E. (Eds.), *Environmental Interactions of Clays*. Springer-Verlag, Berlin, pp. 93–205.
- Jaynes, W.F., Boyd, S.A., 1991a. Clay mineral type and organic-compound sorption by hexadecyltrimethylammonium-exchanged clays. *Soil Science Society of America Journal* 55, 43–48.
- Jaynes, W.F., Boyd, S.A., 1991b. Hydrophobicity of siloxane surfaces in smectites as revealed by aromatic hydrocarbon adsorption from water. *Clays and Clay Minerals* 39, 428–436.
- Jaynes, W.F., Vance, G.F., 1996. BTEX sorption by organo-clays: cosorptive enhancement and equivalence of interlayer complexes. *Soil Science Society of America Journal* 60, 1742–1749.

- Jaynes, W.F., Vance, G.F., 1999. Sorption of benzene, toluene, ethylbenzene and xylene (BTEX) compounds by hectorite clays exchanged with aromatic organic cations. *Clays and Clay Minerals* 47, 358–365.
- Johnston, C.T., De Oliveira, M.F., Teppen, B.J., Sheng, G.Y., Boyd, S.A., 2001. Spectroscopic study of nitroaromatic-smectite sorption mechanisms. *Environmental Science and Technology* 35, 4767–4772.
- Jorgensen, S.E., Libor, O., Barkacs, K., 1973. Investigation of phosphorus removal from water. *Water Research* 7, 1885–1897.
- Jurinak, J.J., 1957. The effect of clay minerals and exchangeable cations on the adsorption of ethylene dibromide vapour. *Soil Science Society of America Proceedings* 21, 599–602.
- Keizer, P., Bruggenwert, M.G.M., 1991. Adsorption of heavy metals by clay–aluminum hydroxide complexes. In: Bolt, G.H., de Boodt, M.F., Hayes, M.H.B., McBride, M.B. (Eds.), *Interactions at the Soil Colloid–Soil Solution Interface*. Kluwer, Dordrecht, pp. 177–203.
- Kemnetz, S., Cody, C.A., 1996. Oil spill flocculating agent and method of remediating oil spills. U.S. Patent 5,558,777.
- Khalil, H.S.A., Abdelhakim, A.A., 2002. Adsorption studies of fatty acids on montmorillonite-based filler clay. *Journal of Applied Polymer Science* 86, 2574–2580.
- Kinniburgh, D.G., Jackson, M.L., Syers, J.K., 1976. Adsorption of alkaline earth, transition and heavy metal cations by hydrous gels of iron and aluminium. *Soil Science Society of America Journal* 40, 796–799.
- Kleinig, T., Churchman, G.J., Chittleborough, D.J., Saunders, B.R., 2003. A study of polymer–clay composite particles: preparation, properties and potential applications. *Plastics, Rubbers and Composites* 32, 224–229.
- Kodama, T., Komarneni, S., 1999. Selective  $\text{Cu}^{2+}$  and  $\text{Pb}^{2+}$  exchange with highly charged cation exchanger of Na-4-mica. *Separation Science and Technology* 34, 2275–2292.
- Kokai, T., 1975. Japanese Patent Application 25,489.
- Komarneni, S., Kodama, T., Paulus, W.J., Carlson, C., 2000. Synthetic clay excels in Sr-90 removal. *Journal of Materials Research* 15, 1254–1256.
- Komarneni, S., Kozai, N., Paulus, W.J., 2001. Superselective clay for radium uptake. *Nature* 410, 771.
- Krishna, B.S., Murty, D.S.R., Prakash, B.S.J., 2001. Surfactant-modified clay as adsorbent for chromate. *Applied Clay Science* 20, 65–71.
- Krishnamurti, G.S.R., Cielinski, G., Huang, P.M., Van Rees, K.C.J., 1997. Kinetics of cadmium release from soils as influenced by organic acids: implication in cadmium availability. *Journal of Environmental Quality* 26, 271–277.
- Kukkadapu, R.K., Boyd, S.A., 1995. Tetramethylphosphonium-smectite and tetramethylammonium-smectite as adsorbents of aromatic and chlorinated hydrocarbons—effect of water on adsorption efficiency. *Clays and Clay Minerals* 43, 318–323.
- Lagaly, G., 1995. Surface and interlayer reactions: bentonites as adsorbents. In: Churchman, G.J., Fitzpatrick, R.W., Eggleton, R.A. (Eds.), *Clays: Controlling the Environment*, Proceedings of the 10th International Clay Conference. Adelaide, Australia, 1993. CSIRO Publishing, Melbourne, pp. 137–144.
- Lagaly, G., Weiss, A., 1969. Determination of the layer charge in mica-type layer silicates. In: Heller, L. (Ed.), *Proceedings of the International Clay Conference*, Tokyo, 1969. Israel University Press, Jerusalem.

- Landau, M., Richard, C., Erstfeld, K., 2002. The effect of suspended clay on protein removal during foam fractionation. *North American Journal of Aquaculture* 64, 217–219.
- Lee, J.F., Crum, J.R., Boyd, S.A., 1989b. Enhanced retention of organic contaminants by soils exchanged with organic cations. *Environmental Science and Technology* 23, 1365–1372.
- Lee, J.F., Mortland, M.M., Boyd, S.A., Chiou, C.T., 1989a. Shape-selective adsorption of aromatic molecules from water by tetramethylammonium-smectite. *Journal of the Chemical Society, Faraday Transactions I* 8, 2953–2962.
- Lee, J.F., Mortland, M.M., Chiou, C.T., Kile, D.E., Boyd, S.A., 1990. Adsorption of benzene, toluene, and xylene by two tetramethylammonium-smectites having different charge densities. *Clays and Clay Minerals* 38, 113–120.
- Lee, J.J., Choi, J., Park, J.W., 2002. Simultaneous sorption of lead and chlorobenzene by organo-bentonite. *Chemosphere* 49, 1309–1315.
- Lee, S.Y., Kim, S.J., 2002. Expansion of smectite by hexadecyltrimethylammonium. *Clays and Clay Minerals* 50, 435–445.
- Li, J.Y., Chen, C.C., Zhao, J.C., Zhu, H.Y., Ding, Z., 2002. Photodegradation of dye pollutants on TiO<sub>2</sub> pillared bentonites after UV light irradiation. *Science in China Series B-Chemistry* 45, 445–448 (Abstract: ISI Web of Science).
- Li, Z., 1999. Oxyanion sorption and surface anion exchange by surfactant-modified clay minerals. *Journal of Environmental Quality* 28, 1457–1463.
- Lo, I.M.C., 1996. Solidification/stabilization of phenolic waste using organic-clay complex. *Journal of Environmental Engineering* 12, 850–855.
- Lo, I.M.C., Yang, X.Y., 2001. Laboratory investigation of the migration of hydrocarbons in organobentonite. *Environmental Science and Technology* 35, 620–625.
- Logsdon, G.S., Symons, J.M., 1973. Mercury removal by conventional water-treatment techniques. *Journal of the American Water Works Association* 65, 554–562.
- Lothenbach, B., Furrer, G., Schulín, R., 1997. Immobilization of heavy metals by polynuclear aluminium and montmorillonite compounds. *Environmental Science and Technology* 31, 1452–1462.
- Lumsdon, D.G., Evans, L.J., Bolton, K.A., 1995. The influence of pH and chloride on the retention of cadmium, lead, mercury and zinc by soils. *Journal of Soil Contamination* 4, 137–150.
- Lund, E., Nissen, B., 1986. Low technology water purification by bentonite clay flocculation as performed in Sudanese villages: virological examinations. *Water Research* 20, 37–43.
- Mackenzie, R.C., 1979. Clay mineralogy—whence and whither? In: Mortland, M.M., Farmer, V.C. (Eds.), *International Clay Conference 1978. Developments in Sedimentology* 27. Elsevier, Amsterdam, pp. 1–14.
- Madsen, M., Schlundt, J., 1989. Low technology water purification by bentonite clay flocculation as performed in Sudanese villages: bacteriological examinations. *Water Research* 23, 873–882.
- Matthes, W., Kahr, G., 2000. Sorption of organic compounds by Al- and Zr-hydroxy-intercalated and pillared bentonite. *Clays and Clay Minerals* 48, 593–602.
- Matthes, W., Madsen, F.T., Kahr, G., 1999. Sorption of heavy-metal cations by Al- and Zr-hydroxy-intercalated and pillared bentonite. *Clays and Clay Minerals* 47, 617–629.
- McBride, M.B., 1991. Processes of heavy and transition metal sorption by soil minerals. In: Bolt, G.H., de Boodt, M.F., Hayes, M.H.B., McBride, M.B. (Eds.), *Interactions at the Soil Colloid–Soil Solution Interface*. Kluwer, Dordrecht, pp. 149–175.



- McBride, M.B., Mortland, M.M., 1973. Segregation and exchange properties of alkylammonium ions in a smectite and vermiculite. *Clays and Clay Minerals* 21, 323–329.
- McBride, D.G., Prendiville, P.W., Hoover, M.G., 1982. Design of the Los Angeles aqueduct water filtration plant. *Public Works* 113, 36–38.
- McLaren, A.D., 1954. The adsorption and reactions of enzymes and proteins on kaolinite. I. *Journal of Physical Chemistry* 58, 129–137.
- McLaren, R.G., Cameron, K.C., 1996. *Soil Science*, 2nd edition. Oxford University Press, Auckland.
- McLaren, R.G., Lawson, D.M., Swift, R.S., 1986. Sorption and desorption of cobalt by soils and soil components. *Journal of Soil Science* 37, 413–426.
- McLaren, R.G., Swift, R.S., Williams, J.G., 1981. The adsorption of copper by soil minerals at low equilibrium solution concentrations. *Journal of Soil Science* 32, 247–256.
- Metwally, A.I., Mashhady, A.S., Falatah, A.M., Reda, M., 1993. Effect of pH on zinc adsorption and solubility in suspensions of different clays and soils. *Zeitschrift für Pflanzenernährung und Bodenkunde* 156, 131–135.
- Michot, L.J., Pinnavaia, T.J., 1991. Adsorption of chlorinated phenols from aqueous solution by surfactant-modified pillared clays. *Clays and Clay Minerals* 39, 634–641.
- Mills, O.E., Creamer, L.K., 1971. The binding of casein to halloysite. *New Zealand Journal of Dairy Science and Technology* 6, 61–65.
- Mobius, C.H., Gunther, T.H., 1974. Removal of dyes from paper mill effluents through treatment by the Flygtol process (translated). *Wochenblatt für Papierfabrikation* 102, 559–561 (Water Resources Abstract No. 7504963).
- Montgomery, D.M., Sollars, C.J., Sheriff, T.S., Perry, R., 1988. Organophilic clays for the successful stabilisation/solidification of problematic organic wastes. *Environmental Technology Letters* 9, 1403.
- Moore, R.E., Chen, J.L., Moore, B.S., Patterson, G.M.L., 1991. Biosynthesis of mycrocystin-LR. Origin of the carbons in the Adda and Masp units. *Journal of the American Chemical Society* 113, 5083–5084.
- Morris, R.J., Williams, D.E., Luu, H.A., Holmes, C.F.B., Andersen, R.J., Calvert, S.E., 2000. The adsorption of mycrocystin-LR by natural clay particles. *Toxicon* 38, 303–308.
- Mortland, M.M., Sun, Shaobai., Boyd, S.A., 1986. Clay–organic complexes as adsorbents for phenol and chlorophenols. *Clays and Clay Minerals* 34, 581–595.
- Naidja, A., Violante, A., Huang, P.M., 1995. Adsorption of tyrosinase onto montmorillonite as influenced by hydroxyaluminum coatings. *Clays and Clay Minerals* 43, 647–655.
- Nolan, T.F., Srinivasan, K.R., Fogler, H.S., 1989. Dioxin sorption by hydroxy-aluminum-treated clays. *Clays and Clay Minerals* 37, 487–494.
- Nzengung, V.A., Voudrias, E.A., Nkedi-Kizza, P., Wampler, J.M., Weaver, C.E., 1996. Organic cosolvent effects on sorption equilibrium of hydrophobic chemicals by organoclays. *Environmental Science and Technology* 30, 89–96.
- Ogedengbe, O., 1976. The performance-potential of polyelectrolytes and high velocity gradients in the treatment of wastewaters. *Effluent and Water Treatment Journal* 16, 289–292.
- Oliveira, L.C.A., Rios, R.V.R.A., Fabris, J.D., Sapag, K., Garg, V.K., Lago, R.M., 2003. Clay–iron oxide magnetic composites for the adsorption of contaminants in water. *Applied Clay Science* 22, 169–177.

- Olsen, A., 1987. Low technology water purification by bentonite clay and moringa oleifera seed flocculation as performed in Sudanese villages: effects on schistosoma mansoni cercariae. *Water Research* 21, 517–522.
- Pal, O.R., Vanjara, A.K., 2001. Removal of malathion and butachlor from aqueous solution by clays and organoclays. *Separation and Purification Technology* 24, 167–172.
- Panpanit, S., Visvanathan, C., 2001. The role of bentonite addition in UF flux enhancement mechanisms for oil/water emulsion. *Journal of Membrane Science* 184, 59–68.
- Parazak, D.P., Burkhardt, C.W., McCarthy, K.J., Stehlin, M.P., 1988. Hydrophobic flocculation. *Journal of Colloid and Interface Science* 123, 59–72.
- Petrović, M., Kaštelan-Macan, M., Horvat, A.J.M., 1999. Interactive sorption of metal ions and humic acids onto mineral particles. *Water, Air and Soil Pollution* 111, 41–56.
- Philippakopoulou, T.L., Simonetis, S.I., Perraki, T.S., Tsetsekou, A.C., Vlyssides, A.G., Economides, D.G., 2002. The use of bentonites in newspaper recycling. Part 1: bentonite properties and speck control efficiency. *Appita Journal* 55, 294 (Abstract: ISI Web of Science).
- Pinnavaia, T.J., 1995. Clay catalysts: opportunities for use in improving environmental quality. In: Churchman, G.J., Fitzpatrick, R.W., Eggleton, R.A. (Eds.), *Clays: Controlling the Environment*, Proceedings of the 10th International Clay Conference. Aldelaide, Australia, 1993. CSIRO Publishing, Melbourne, pp. 3–8.
- Pollard, S.J.T., Sollars, C.J., Perry, R., 1992. A clay–carbon adsorbent derived from spent bleaching earth—surface characterization and adsorption of chlorophenols from aqueous solution. *Carbon* 30, 639–645.
- Polubesova, T., Nir, S., Gerstl, Z., Borisover, M., Rubin, B., 2002. Imazaquin adsorbed on pillared clay and crystal violet-montmorillonite complexes for reducing leaching in soil. *Journal of Environmental Quality* 31, 1657–1664.
- Polubesova, T., Undabeytia, T., Nir, S., Chertova, L., Van Damme, H., Annabi-Bergaya, F., 2000. Adsorption of sulfameturon and other anions on pillared clay. *Journal of Environmental Quality* 29, 948–954.
- Potskshershvili, B.S., Murguliya, L.S., Dzvelaya, Z.S., 1977. Purification of effluents of paper mills processing waste paper (translation). *Bumazhnaya Promyshlennost* 9, 29–30.
- Quiquampoix, H., Abadie, J., Baron, M.H., Leprince, F., Matumoto-Pintro, P.T., Ratcliffe, R.G., Staunton, S., 1995. Mechanisms and consequences of protein adsorption on soil minerals surfaces. *ACS Symposium Series* 602, 321–333.
- Quiquampoix, H., Chasin, P., Ratcliffe, R.G., 1989. Enzyme activity and cation exchange as tools for the study of the conformation of proteins adsorbed on mineral surfaces. *Progress in Colloid and Polymer Science* 79, 59–63.
- Quiquampoix, H., Ratcliffe, R.G., 1992. A  $^{31}\text{P}$  NMR study of the adsorption of bovine serum albumin on montmorillonite using phosphate and the paramagnetic cation  $\text{Mn}^{2+}$ : modification of conformation with pH. *Journal of Colloid and Interface Science* 148, 343–352.
- Quiquampoix, H., Servagent-Noirville, S., Baron, M.H., 2002. Enzyme adsorption on soil mineral surfaces and consequences for the catalytic activity. In: Burns, R.G., Dick, R.P. (Eds.), *Enzymes in the Environment: Activity, Ecology, and Applications*. Marcel Dekker, New York, pp. 285–306.
- Rankine, B., 1995. *Making Good Wine: A Manual of Winemaking Practices for Australia and New Zealand*. Sun Books, Melbourne.

- Redding, A.Z., Burns, S.E., Upson, R.T., Andersen, E.F., 2002. Organoclay sorption of benzene as a function of total organic carbon content. *Journal of Colloid and Interface Science* 250, 261–264.
- Riebe, B., Bors, J., Dultz, S., 2001. Retardation capacity of organophilic bentonite for anionic fission products. *Journal of Contaminant Hydrology* 47, 255–264.
- Robertson, R.H.S., 1986. *Fuller's Earth: A History of Calcium Montmorillonite*. Volturna Press, Hythe, Kent.
- Rytwo, G., Nir, S., Margulies, L., Casal, B., Merino, J., Ruiz-Hitzky, E., Serratosa, J.M., 1998. Adsorption of monovalent organic cations to sepiolite: experimental results and model calculations. *Clays and Clay Minerals* 46, 340–348.
- Rytwo, G., Tropp, D., Serban, C., 2002. Adsorption of diquat, paraquat and methyl green on sepiolite: experimental results and model calculations. *Applied Clay Science* 20, 273–282.
- Sarier, N., Güler, C., 1988. The mechanism of  $\beta$ -carotene adsorption on activated montmorillonite. *Journal of the American Oil Chemists' Society* 66, 917–923.
- Sawhney, B.L., 1996. Sorption and desorption of organic contaminants by clays and soils. In: Sawhney, B.L. (Ed.), *Organic Pollutants in the Environment*. CMS Workshop Lectures, vol. 8. The Clay Minerals Society, Boulder, CO, pp. 45–68.
- Scheidegger, A.M., Fendorf, M., Sparks, D.L., 1996. Mechanisms of nickel sorption on pyrophyllite: macroscopic and microscopic approaches. *Soil Science Society of America Journal* 60, 1763–1772.
- Scheidegger, A.M., Sparks, D.L., 1996. A critical assessment of sorption–desorption mechanisms at the soil mineral/water interface. *Soil Science* 161, 813–831.
- Scherler, A., 1972. The purification of residual waste waters of the sulfite pulp industry (translation). *Das Papier* 26, 637–642.
- Sengco, M.R., Li, A.S., Tugend, K., Kulis, D., Anderson, D.M., 2001. Removal of red- and brown-tide cells using clay flocculation. I. Laboratory culture experiments with *Gymnodinium breve* and *Aureococcus anophagefferens*. *Marine Ecology Progress Series* 210, 41–53.
- Sharmasarkar, S., Jaynes, W.F., Vance, G.F., 2000. BTEX sorption by montmorillonite organo-clays: TMPA, ADAM, HDTMA. *Water, Air and Soil Pollution* 119, 257–273.
- Shen, Y.H., 2001. Preparations of organobentonite using nonionic surfactants. *Chemosphere* 44, 989–995.
- Shen, Y.H., 2002a. Sorption of benzene and naphthol to organobentonites intercalated with short chain cationic surfactants. *Journal of Environmental Science and Health, Part A – Toxic/Hazardous Substances and Environmental Engineering* 37, 43–54.
- Shen, Y.H., 2002b. Removal of phenol from water by adsorption–flocculation using organobentonite. *Water Research* 36, 1107–1114.
- Sheng, G.Y., Boyd, S.A., 1998. Relation of water and neutral organic compounds in the interlayers of mixed Ca/trimethylphenylammonium-smectites. *Clays and Clay Minerals* 46, 10–17.
- Sheng, G.Y., Boyd, S.A., 2000. Polarity effect on dichlorobenzene sorption by hexadecyltrimethylammonium-exchanged clays. *Clays and Clay Minerals* 48, 43–50.
- Sheng, G.Y., Johnston, C.T., Teppen, B.J., Boyd, S.A., 2001. Potential contributions of smectite clays and organic matter to pesticide retention in soils. *Journal of Agricultural and Food Chemistry* 49, 2899–2907.

- Sheng, G.Y., Johnston, C.T., Teppen, B.J., Boyd, S.A., 2002. Adsorption of dinitrophenol herbicides from water by montmorillonites. *Clays and Clay Minerals* 50, 25–34.
- Sheng, G.Y., Wang, X., Wu, S., Boyd, S.A., 1998. Enhanced sorption of organic contaminants by smectitic soils modified with a cationic surfactant. *Journal of Environmental Quality* 27, 806–814.
- Sheng, G.Y., Xu, S.H., Boyd, S.A., 1996a. Cosorption of organic contaminants from water by hexadecyltrimethylammonium-exchanged clays. *Water Research* 30, 1483–1489.
- Sheng, G.Y., Xu, S.H., Boyd, S.A., 1996b. Mechanism(s) controlling sorption of neutral organic contaminants by surfactant-derived and natural organic matter. *Environmental Science and Technology* 30, 1553–1557.
- Simmonds, R.S., Loutit, M.W., Austin, F.J., 1983. Enteric viruses in New Zealand wastewaters. *New Zealand Journal of Science* 26, 437–441.
- Singh, N., Megharaj, M., Gates, W.P., Churchman, G.J., Anderson, J., Kookana, R.S., Naidu, R., Chen, Z., Slade, P.G., Sethunathan, N., 2003. Bioavailability of an organophosphorus pesticide, fenamiphos, sorbed on an organo-clay. *Journal of Agricultural and Food Chemistry* 51, 2653–2658.
- Slade, P.G., Gates, W.P., 2003. The swelling of HDTMA smectites as influenced by their preparation and layer charge. *Applied Clay Science* 25, 93–101.
- Slade, P.G., Gates, W.P., 2004. The ordering of HDTMA in the interlayers of vermiculites and the influence of solvents. *Clays and Clay Minerals* 52, 204–210.
- Slade, P.G., Raupach, M., Emerson, W.W., 1978. The ordering of cetylperidinium bromide on vermiculite. *Clays and Clay Minerals* 26, 125–134.
- Smith, J.A., Jaffè, P.R., Chiou, C.T., 1990. Effect of ten quaternary ammonium cations on tetrachloromethane sorption to clay from water. *Environmental Science and Technology* 24, 1167–1172.
- Sobsey, M.D., Cromeans, T., 1985. Effects of bentonite clay solids on poliovirus concentration from water by microporous filter methods. *Applied and Environmental Microbiology* 49, 795–798.
- Sposito, G., 1992. The diffuse-ion swarm near smectite particles suspended in 1:1 electrolyte solutions: modified Gouy-Chapman theory and quasicrystal formation. In: Güven, N., Pollastro, R.M. (Eds.), *Clay Water Interface and its Rheological Implications*, CMS Workshop Lectures, vol. 4. The Clay Minerals Society, Boulder, CO, pp. 127–155.
- Srinivasan, K.R., Fogler, H.S., 1986a. Removal of trace levels of 2,3,7,8-TCDD from industrial wastewaters by sorption on clay-based sorbents: Part I. Preparation and characterisation of clay-based sorbents. In: Rappe, C., Choudhary, G., Keith, L.H. (Eds.), *Chlorinated Dioxins and Dibenzofurans in Perspective*. Lewis Publishers, Chelsea, MI, pp. 519–530.
- Srinivasan, K.R., Fogler, H.S., 1986b. Removal of trace levels of 2,3,7,8-TCDD from industrial wastewaters by sorption on clay-based sorbents: Part II. Binding of OCDD, 2,3,7,8-TCDD and HCB to clay-based sorbents. In: Rappe, C., Choudhary, G., Keith, L.H. (Eds.), *Chlorinated Dioxins and Dibenzofurans in Perspective*. Lewis Publishers, Chelsea, MI, pp. 531–539.
- Srinivasan, K.R., Fogler, H.S., 1990. Use of inorgano-organo-clays in the removal of priority pollutants from industrial wastewaters: adsorption of benzo(a)pyrene and chlorophenols from aqueous solutions. *Clays and Clay Minerals* 38, 287–293.
- Srinivasan, K.R., Fogler, H.S., Gulari, E.G., Nolan, T.F., Schultz, J.S., 1985. The removal of trace levels of dioxins from wastewater by sorption on modified clay. *Environmental Progress* 4, 239–245.

- Stansfield, R.A., 1986. The diquat incident at Woodkirk, Yorkshire. *European Water and Sewage* 90, 450–451.
- Staunton, S., Quiquampoix, H., 1994. Adsorption and conformation of bovine serum albumin on montmorillonite: modification of the balance between hydrophilic and electrostatic interactions by protein methylation and pH variation. *Journal of Colloid and Interface Science* 166, 89–94.
- Stevens, J.J., Anderson, S.J., 1996. An FTIR study of water sorption on TMA- and TMPA-montmorillonites. *Clays and Clay Minerals* 44, 142–150.
- Stevens, J.J., Anderson, S.J., Boyd, S.A., 1996. FTIR study of competitive water-arene sorption on tetramethylammonium- and trimethylammonium montmorillonites. *Clays and Clay Minerals* 44, 88–95.
- Stockmeyer, M., Kruse, K., 1991. Adsorption of zinc and nickel ions and phenol and diethylketone by bentonites of different organophilicities. *Clay Minerals* 26, 431–434.
- Street, G.B., White, D., 1963. Adsorption by organo-clay derivatives. *Journal of Applied Chemistry* 13, 288–291.
- Stumm, W., Morgan, J.J., 1996. *Aquatic Chemistry*. Wiley, New York.
- Sun, Z., Chen, Y., Ke, Q., Yang, Y., Yuan, J., 2002. Photocatalytic degradation of cationic azo dye by  $\text{TiO}_2$ /bentonite nanocomposite. *Journal of Photochemistry and Photobiology A, Chemistry* 149, 169–174.
- Swift, R.S., McLaren, R.G., 1991. Micronutrient adsorption by soils and soil colloids. In: Bolt, G.H., de Boodt, M.F., Hayes, M.H.B., McBride, M.B. (Eds.), *Interactions at the Soil Colloid–Soil Solution Interface*. Kluwer, Dordrecht, pp. 257–292.
- Tarasevich, Y.I., Klimova, G.M., 2001. Complex-forming adsorbents based on kaolinite, aluminium oxide and polyphosphates for the extraction and concentration of heavy metal ions from water solutions. *Applied Clay Science* 19, 95–101.
- Taylor, R.M., Churchman, G.J., 1998. Magnetised fine-grained minerals as reusable adsorbents for dissolved organic carbon. Abstract, Abstracts and Program, Humic Substances Downunder, 9th Conference of the International Humic Substances Society, 20–25 September, Adelaide, Australia.
- Theng, B.K.G., 1974. *The Chemistry of Clay–Organic Reactions*. Adam Hilger, London.
- Theng, B.K.G., 1979. *Formation and Properties of Clay–Polymer Complexes*. Elsevier, Amsterdam.
- Theng, B.K.G., Aislabie, J., Fraser, R., 2001. Bioavailability of phenanthrene intercalated into an alkylammonium-montmorillonite clay. *Soil Biology and Biochemistry* 33, 845–848.
- Theng, B.K.G., Greenland, D.J., Quirk, J.P., 1967. Adsorption of alkylammonium cations by montmorillonite. *Clay Minerals* 7, 1–17.
- Theng, B.K.G., Wells, N., 1995. Assessing the capacity of some New Zealand clays for decolourizing vegetable oil and butter. *Applied Clay Science* 9, 321–326.
- Tiller, K.G., 1996. Soil contamination issues: past, present and future, a personal perspective. In: Naidu, R., Kookana, R.S., Oliver, D.P., Rogers, S., McLaughlin, M.J. (Eds.), *Contaminants and the Soil Environment in the Australasia-Pacific Region*. Kluwer, Dordrecht, pp. 1–27.
- Tsai, W.T., Chen, C.H., Yang, J.M., 2002. Adsorption of paraquat on the physically activated bleaching earth waste from soybean oil processing plant. *Journal of Environmental Science and Health, Part B—Pesticides Food Contaminants and Agricultural Wastes* 37, 453–463.
- Ueda, T., Harada, S., 1968. Adsorption of cationic poly sulfone on bentonite. *Journal of Applied Polymer Science* 12, 2395–2401.

- Undabeytia, T., Nir, S., Rytwo, G., Morillo, E., Maqueda, C., 1998. Modeling adsorption-desorption processes of Cd on montmorillonite. *Clays and Clay Minerals* 46, 423–428.
- Undabeytia, T., Nir, S., Rytwo, G., Serban, C., Morillo, E., Maqueda, C., 2002. Modeling adsorption-desorption processes of Cu on edge and planar sites of montmorillonite. *Environmental Science and Technology* 36, 2677–2683.
- Vansant, E.F., Uytterhoeven, J.B., 1972. Thermodynamics of the exchange of *n*-alkylammonium ions on Na-montmorillonite. *Clays and Clay Minerals* 20, 47–54.
- Venaruzzo, J.L., Volzone, C., Rueda, M.L., Ortiga, J., 2002. Modified bentonitic clay minerals as adsorbents of CO, CO<sub>2</sub> and SO<sub>2</sub> gases. *Microporous and Mesoporous Materials* 56, 73–80.
- Vengris, T., Binkiene, R., Sveikauskaite, A., 2001. Nickel, copper and zinc removal from waste water by a modified clay sorbent. *Applied Clay Science* 18, 183–190.
- Violante, A., DeCristofaro, A., Rao, M.A., Gianfreda, L., 1995. Physicochemical properties of protein-smectite and protein-Al(OH)<sub>x</sub>-smectite complexes. *Clay Minerals* 30, 325–336.
- Volzone, C., Ortiga, J., 2000. O<sub>2</sub>, CH<sub>4</sub> and CO<sub>2</sub> gas retentions by acid smectites before and after thermal treatment. *Journal of Materials Science* 21, 5291–5294.
- Voudrias, E.A., 2002. The concept of a sorption chemical barrier for improving effectiveness of landfill liners. *Waste Management and Research* 20, 251–258.
- Wu, J., Laird, D.A., Thompson, M.L., 1999. Sorption and desorption of copper on soil clay components. *Journal of Environmental Quality* 28, 334–338.
- Xu, S., Boyd, S.A., 1995a. Cationic surfactant sorption to a vermiculite subsoil via hydrophobic bonding. *Environmental Science and Technology* 29, 312–320.
- Xu, S.H., Boyd, S.A., 1995b. Cationic surfactant adsorption by swelling and nonswelling layer silicates. *Langmuir* 1, 2508–2514.
- Xu, S.H., Boyd, S.A., 1995c. Alternative model for cationic surfactant adsorption by layer silicates. *Environmental Science and Technology* 29, 3022–3028.
- Xu, S., Sheng, G.Y., Boyd, S.A., 1997. Use of organoclays in pollution abatement. *Advances in Agronomy* 59, 25–62.
- Yariv, S., 2002. Introduction to organo-clay complexes and interactions. In: Yariv, S., Cross, H. (Eds.), *Organo-Clay Complexes and Interactions*. Marcel Dekker, New York, pp. 39–111.
- Yong, R.N., Warkentin, B.P., Phadungchewit, Y., Galvez, R., 1990. Buffer capacity and lead retention in some clay minerals. *Water, Air and Soil Pollution* 53, 53–67.
- Zhao, H.T., Jaynes, W.F., Vance, G.F., 1996. Sorption of the ionizable organic compound, dicamba (3,6-dichloro-2-methoxy benzoic acid), by organo-clays. *Chemosphere* 33, 2089–2100.
- Zhu, H.Y., Ding, Z., Lu, C.Q., Lu, G.Q., 2002a. Molecular engineered porous clays using surfactants. *Applied Clay Science* 20, 165–175.
- Zhu, H.Y., Li, J.-Y., Zhao, J.-C., Churchman, G.J., 2005. Photocatalysts prepared from layered clays and titanium hydrate for degradation of organic pollutants in water. *Applied Clay Science* 28, 79–88.
- Zhu, H.Y., Orthman, J.A., Li, J.Y., Churchman, G.J., Vansant, E.F., 2002b. Novel composites of TiO<sub>2</sub> (anatase) and silicate nanoparticles. *Chemistry of Materials* 14, 5037–5044.
- Zhu, L.Z., Su, Y.H., 2002. Benzene vapor sorption by organobentonites from ambient air. *Clays and Clay Minerals* 50, 421–427.
- Zielke, R.C., Pinnavaia, T.J., 1988. Modified clays for the adsorption of environmental toxicants: binding of chlorophenols to pillared, delaminated, and hydroxy-interlayered smectites. *Clays and Clay Minerals* 36, 403–408.

This page intentionally left blank

## *Chapter 11.2*

### **CLAYS AND PESTICIDES**

**S. NIR, Y. EL NAHHAL, T. UNDABEYTIA, G. RYTWO,  
T. POLUBESOVA, Y. MISHAEL, U. RABINOVITZ AND  
B. RUBIN**

*Faculty of Agricultural, Food and Environmental Quality Sciences, The Hebrew  
University of Jerusalem, PO Box 12, IL-76100 Rehovot, Israel*

This chapter describes clay-based formulations of pesticides, whose design was to solve environmental and economical problems, focusing on herbicides, which are the leading type of pesticide used.

Herbicides are applied to fields to impede the growth of weeds. However, only a part of the applied amount is bioactive, a certain part remains attached to the soil, and another part is leached out and migrates into ground water, or undergoes surface migration. Thus, application of herbicides to the field causes serious water contamination, and can hurt neighbouring crops. This problem is particularly serious with hydrophobic herbicides, such as acetochlor, and anionic herbicides, such as sulfometuron (Fig. 11.2.1a). Leaching of the herbicide requires higher amounts of the herbicides to be applied, which also enhances environmental problems. Additional threat to crop safety can occur if a persistent herbicide is leached, but because of fluctuation in localized water tables, can re-enter the rooting zone. As production and uses of herbicides are increasing, the serious health and environmental problems posed by these toxic compounds must be controlled to minimize the harmful effects of these products (Cohen et al., 1986; Koterba et al., 1993; Pasquarelly and Boyer, 1996; Ritter et al., 1996; Thurman et al., 1996; Carter, 2000). The EC Drinking Water Directive (80/778/EC) stipulates the requirement that no single pesticide should exceed 0.1 µg/L and total pesticides should not exceed five-fold of this level in drinking water from the tap.

Similar rules in states in North America resulted in prohibiting the use of certain herbicides, e.g., alachlor. However, the hydrophobic herbicide acetochlor designed to replace other herbicides, such as alachlor and metolachlor was already detected in many sites (Kolpin et al., 1996; Balinova, 1997).

Volatility of certain herbicides is another source of loss of their activity and a factor in polluting the atmosphere. Photodegradation of pesticides also brings about an increase in the applied amounts.



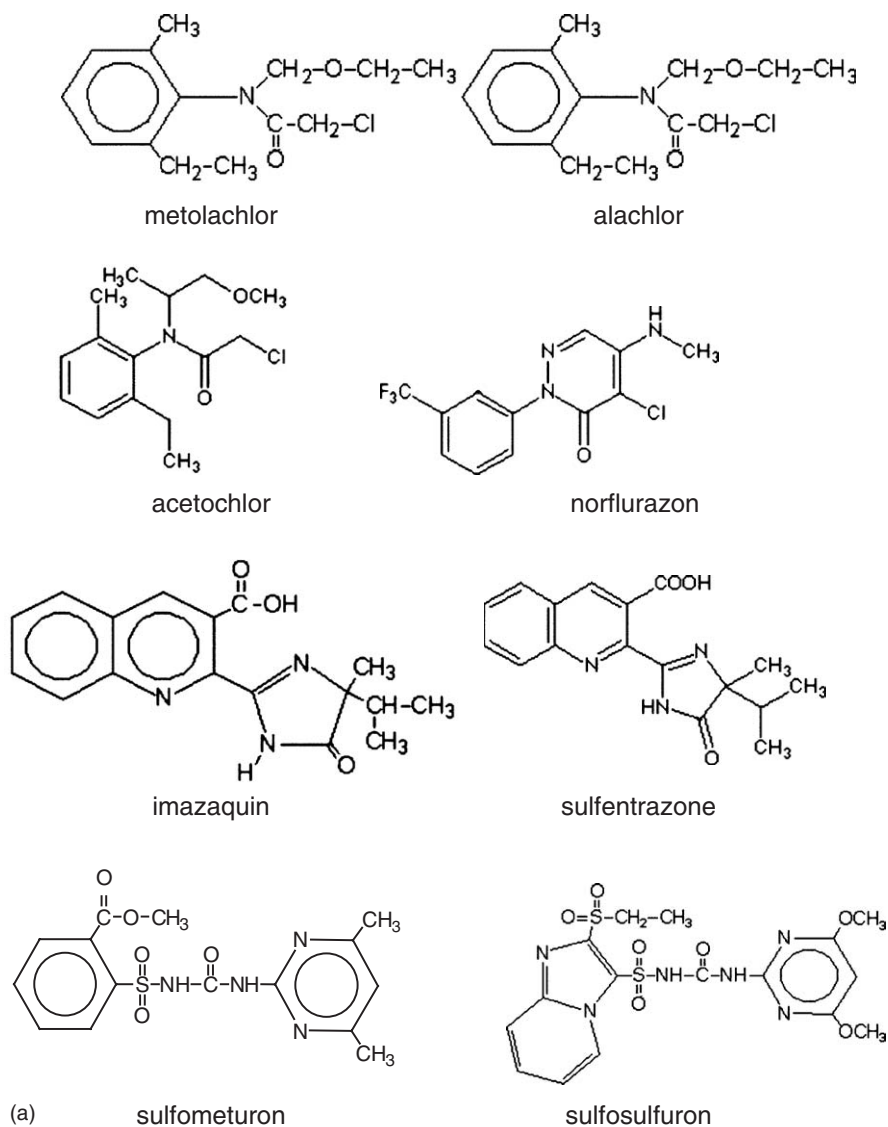


Fig. 11.2.1. (a) Molecular structures of the organic cations. (b) Molecular structures of the herbicides.

We will review developments in employing clay minerals, which are a natural and relatively cheap component of soils, in the design of clay-based formulations of pesticides for reducing their leaching, photodegradation and volatilization. We will also review an approach based on utilizing the interactions between organic cations

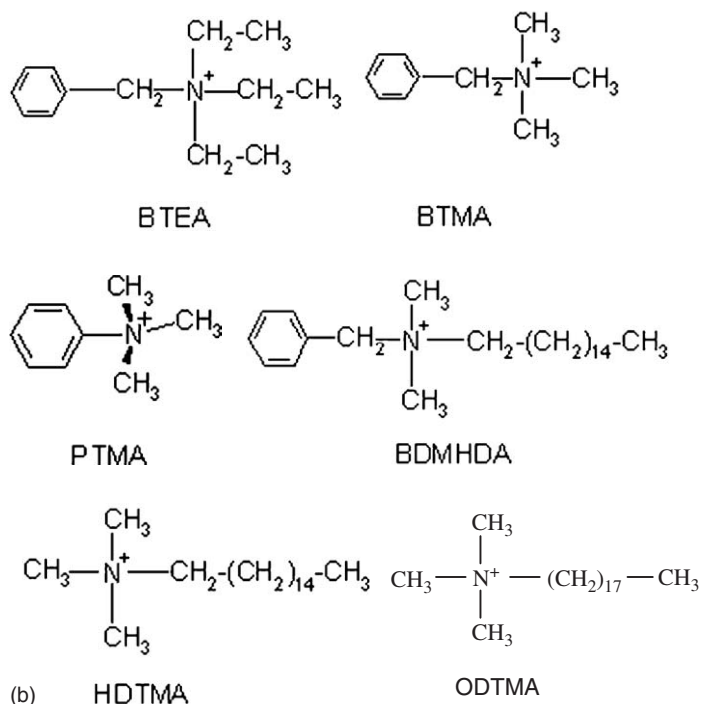


Fig. 11.2.1. (Continued)

and clay minerals for reducing the applied amounts of potent but dangerous divalent herbicides, such as paraquat and diquat.

We will elaborate on two general approaches for slow-release formulations of pesticides, whose aim was to reduce leaching, organo-clays and micelle-clays. Other approaches employing clays or a combination of clays and polymers were already described (Davis et al., 1996; Gerstl et al., 1998; Johnson and Pepperman, 1998; González-Pradas et al., 1999; Cox et al., 1999).

Insecticide formulations are often prepared from biodegradable materials. Materials used in insecticide formulations include synthetic polymers such as polyvinyl-alcohol, polypeptides, biopolymers from plants, animals and microorganisms, such as polysaccharides (e.g., starches, cellulose, chitins, gums, pectin), proteins, polyesters, lignins, shellack, sporopollenin, latex, resins; modified biopolymers. In these formulations, clays can be added to the matrix as modifiers for enhancing the slow release of the active ingredient. As an example, a number of alginate formulations of pesticides were described, but the release is rapid unless a sorptive phase is included in the granule (or bead) (Pepperman et al., 1991; Gerstl et al., 1998). The insecticide imidacloprid was incorporated into alginate granules using calcium chloride as gellant (González-Pradas et al., 1999). The addition of natural bentonite reduced its

rate of release and increased granule yields, thus producing a more efficient and cheaper formulation. These alginate–bentonite formulations also reduced the vertical mobility of imidacloprid in greenhouse soils (González-Pradas, 1999). Fernández-Pérez et al. (2000) also showed that alginate–bentonite formulations are efficient systems for reducing carbofuran leaching in clay soils. These authors indicated that the release mechanism of this insecticide was a diffusion-controlled process.

In some formulations of microbial insecticides currently in use, the granules, baits and dusts are simply clay-based carriers that deliver the toxin to the feeding site of the pest. Ignoffo and Garcia (1996) used a formulation composed of talc for better survival of the virus from *Heliothis/Helicoverpa*. Foliar application of formulations of the microbial insecticide *Bacillus thuringiensis* is of limited commercial use because of their rapid degradation by UV light, and considerable research attempted to improve its field persistence by several means, one of them consisting of addition of clay granules (White et al., 1999). In passing, published information regarding clay–insecticide formulations is scarce since many preparation processes were developed by companies (Sparks and Jacobs, 1999).

### 11.2.1. ORGANO-CLAY FORMULATIONS

Leaching of cationic pesticides is rarely a problem, since they have strong affinity of adsorption on clay minerals and soil colloids (Rytwo et al., 1996a, 1996b; Undabeytia et al., 1999; Polubesova et al., 2001). Organo-clays were mainly designed to promote the adsorption of neutral and hydrophobic pesticides and slow their release.

The adsorption of organic cations on clays modifies the nature of the clay mineral surface, transforming it from hydrophilic to hydrophobic. The modified clay mineral surface can enhanced affinity for sorbing neutral organic molecules of hydrophobic characteristics (Lagaly, 1995; Xu et al., 1997). In addition, organo-clays were frequently considered for removing organic pollutants from water. As reported for several hydrophobic molecules (Sheng et al., 1998), the enhancement of their adsorption by HDTMA-montmorillonite increases with the amount of HDTMA amount, being maximal at a loading corresponding to the CEC of montmorillonite, i.e., 80 cmol/kg.

However, another pattern was observed for the adsorption of many other hydrophobic molecules by organo-clays. The adsorption of the hydrophobic herbicides alachlor, metolachlor (El-Nahhal et al., 1998, 1999a, 1999b, 2000; Nir et al., 2000), norflurazon (Nir et al., 2000; Undabeytia et al., 2000a) and acetochlor (El-Nahhal et al., 2001), all of which contain a phenyl ring was maximal for montmorillonite preadsorbed by a small cation, e.g., phenyltrimethylammonium (PTMA) at a loading corresponding to 5/8 of the CEC (Fig. 11.2.1b). Nir et al. (2000) suggested that the enhanced adsorbed amounts of the above hydrophobic herbicides are mainly due to interactions between the phenyl rings of these molecules and the adsorbed organic cations, which are favoured with the smaller cation. Thus optimization of the

formulations of hydrophobic pesticides requires a selection of structurally compatible organic cations preadsorbed on the clay at optimal coverage.

Another type of an organo-clay arises when the loading of the organic cations exceeds the CEC of the clay mineral, which becomes positively charged and potentially suitable for the adsorption of anions, such as imazaquin (Polubesova et al., 2002). It should be emphasized that the binding coefficients for adsorption on montmorillonite of the cations ODTMA, HDTMA (Mishaal et al., 2002a), BTMA (Polubesova et al., 1997), or PTMA (El-Nahhal et al., 2000) are about three orders of magnitude above that of  $\text{Na}^+$ , whereas the binding coefficients of the monovalent organic dyes are even several orders of magnitude larger (Margulies et al., 1988a; Nir et al., 1994; Rytwo et al., 1995). At a loading corresponding to 5/8 of the CEC, or less, complete adsorption of the above cations occurred, whereas the dyes, such as crystal violet (CV) yielded complete adsorption even at 25% excess loading of montmorillonite above the CEC. Washing does not cause desorption of the above organic cations and the effect of the ionic strength is minimal.

Optimal organo-clay formulations yielded slow release in water, e.g., 2% release after two days for a 1% (w/w) suspension of a montmorillonite-PTMA formulation of acetochlor (El-Nahhal et al., 2001). Leaching of herbicides from the organo-clay and commercial formulations was tested by a bioassay using a column technique and test plants (Fig. 11.2.2).

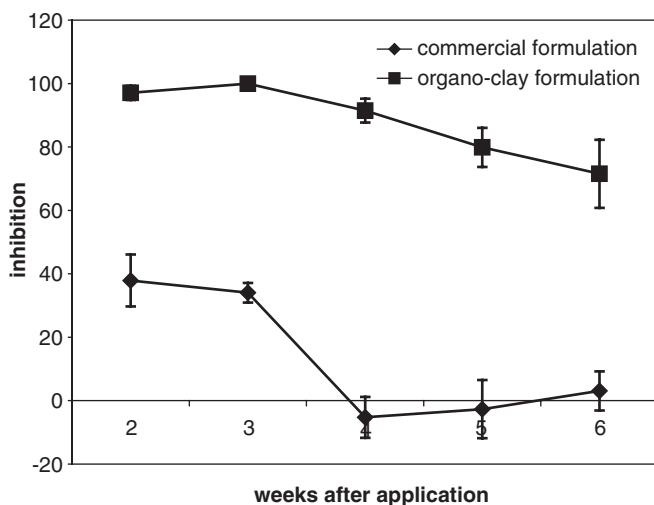


Fig. 11.2.2. Effect of acetochlor formulations applied in field study on green foxtail growth as determined 2–6 weeks after application. Soil samples were collected from field plots at a depth of 0–5 cm. Total irrigation (including rain) was equivalent to 60, 70, 92, 142, 146 mm after 2, 3, 4, 5, and 6 weeks, respectively. Acetochlor formulations were commercial formulation and acetochlor adsorbed on clay exchanged with PTMA at a loading of 0.5 mmol/g—(organo-clay formulation). The organo-clay-based formulation contained 7.5% acetochlor.

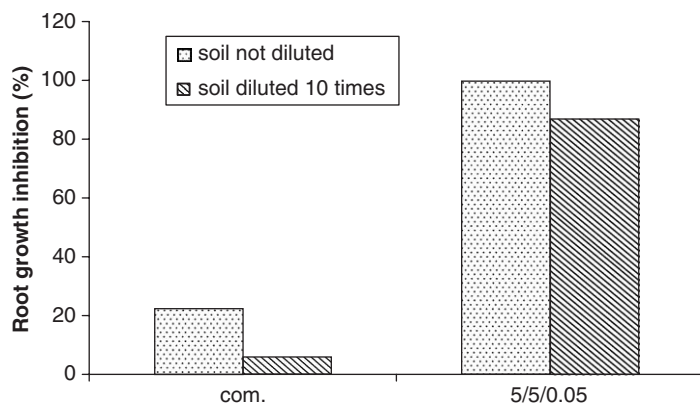


Fig. 11.2.3. Root growth inhibition of a test plant (sorghum) at a soil depth of 0–5 cm sprayed with the SFM commercial formulation and formulation 5/5/0.05 (5 g clay/L; 5 mM ODTMA; 0.05 mM SFM).

The organo-clay formulations exhibited a significant reduction in leaching, which implied maintaining high and relatively enhanced herbicidal activity in the topsoil, and little activity at larger soil depths. These tests included formulations of alachlor (El-Nahhal et al., 1997, 1998, 2000), metolachlor (El-Nahhal et al., 1999a, 2000; Nennemann et al., 2001), norflurazon (Undabeytia et al., 2000a), acetochlor (El-Nahhal et al., 2001) and fenuron (Hermosin et al., 2001). The studies on metolachlor (Nennemann et al., 2001) and norflurazon (Undabeytia et al., 2000b) achieved good slow release formulations by employing acid-activated pillared montmorillonite.

The organo-clay formulations of alachlor (El-Nahhal et al., 1998 and acetochlor (El-Nahhal et al., 2001) were also shown to reduce leaching and enhance and prolong herbicidal activity under field conditions. An illustration is given in Fig. 11.2.3.

### 11.2.2. REDUCTION OF VOLATILIZATION

Volatilization is a major factor limiting the lifetime of certain pesticides in the field, e.g., carbamothiate herbicides (Wilkinson, 1988). Margulies et al. (1994) succeeded in significantly reducing the volatility of the herbicide S-ethyl dipropylcarbamothiate (EPTC) by sorbing it on montmorillonite or sepiolite. At 30 °C, the half-life ( $T_{1/2}$ ) of the herbicide adsorbed on montmorillonite was extended to more than five days, in comparison to 10 h for the herbicide in its free form. Oat bioassays showed that the herbicidal activity of EPTC adsorbed on the clay mineral was extended by more than 1 week.

A reduction in volatilization was also observed for organo-clay formulations of alachlor and metolachlor (El-Nahhal et al., 1999b). We expect that, in general,

slowing the release of pesticides in water by employing organo-clay formulations will also reduce pesticide volatility, but more studies are needed to support this deduction.

### 11.2.3. CLAY-MICELLE FORMULATIONS

The starting point was a concentrated solution (several millimolar) of organic cations which include a large hydrophobic part and consequently have a very small critical micelle concentration (CMC), such as octadecyltrimethylammonium (ODTMA), whose CMC equals 0.3 mM. The anionic organic molecules are bound by the positively charged micelles whose interior also provides a hydrophobic environment for the hydrophobic moiety of the organic anion. The mixed micelles, which carry a net positive charge adsorb on negatively charged clay mineral particles such as montmorillonite.

The adsorption of hexadecyltrimethylammonium (HDTMA) and ODTMA (Fig. 11.2.1b) on montmorillonite was studied above and below their CMC (Mishael et al., 2002a). At added concentrations above the CMC, the loading exceeded the CEC of the clay mineral and indicated higher affinity of the cation with the longer alkyl chain. An adsorption model could adequately simulate adsorption at added concentrations below the CMC, and yielded fair predictions for the effect of ionic strength. The model indicated that above the CMC, adsorbed micelles contributed significantly to the amount of ODTMA adsorbed. Evidence for adsorption of ODTMA micelles on montmorillonite was provided by freeze-fracture electron microscopy, XRD and dialysis measurements. Electron microscopy showed a high concentration of micelles in the size range of about 7 to 17 nm. ODTMA added inside a dialysis bag to a clay suspension outside the dialysis bag gave similar features of the clay particles as observed for the clay alone. The freeze-fracture measurements confirmed the expected outcome that no micelles would be seen on the clay added outside the dialysis bag, since only monomers can pass through the bag and adsorb.

The basal spacing of the untreated montmorillonite was 1.48 nm. When adding ODTMA at 6 mM and 1.6 g/L clay inside a dialysis bag (where micelle adsorption was expected) a well-defined series of peaks, due to the micelles and an additional peak at 2.07 nm were observed. When the clay was added outside the dialysis bag and only monomer adsorption was expected, only one strong peak was observed at 1.83 nm. Such spacing might be ascribed to a bilayer of ODTMA cations lying parallel to the surface of the clay mineral.

It should be emphasized that the amount of ODTMA adsorbed was similar when the clay was added inside or outside the dialysis bag. However, in the presence of micelles (clay inside the dialysis bag) the basal spacing was 2.07 nm indicating a difference in the montmorillonite ODTMA structure.

When adding 5 mM of ODTMA to a concentrated clay suspension (10 g/L), we predicted that the monomers would adsorb and, due to the high clay concentration,

micelles would decompose to monomers. Indeed, this sample exhibited only a basal spacing of 1.48 nm without any additional peaks, indicating monomer adsorption.

In the presence of 5 mM ODTMA and 5 g/L clay, 95% of the anionic herbicide sulfometuron (SFM) adsorbed (Mishael et al., 2002b), whereas the anionic herbicide sulfosulfuron yielded 99% adsorption (Mishael et al., 2002c). A very small fraction of these herbicides adsorbed when ODTMA was inside a dialysis bag and the clay was outside, despite the similarity in the adsorbed amounts of ODTMA in both cases. Thus, the complex formed between ODTMA and montmorillonite in the presence of an excess of micelles is very different from the complex formed in the exclusive presence of ODTMA monomers, as shown by electron microscopy, XRD and adsorption measurements. Unlike the monomer–clay complex, which was not efficient for the adsorption of anionic organic molecules, such as SFM or SFS, the micelle–clay complex was highly efficient.

At a 1% (w/w) water suspension, only 0.5% of the adsorbed SFM was released at times varying from hours to nine days. An analytical test in Seville soil showed that under excessive irrigation (400 mm), 100% of the commercial formulation leached, whereas the micelle–clay formulations showed only 50–65% elution. A plant bioassay in Rehovot soil showed that the commercial dispersible granule formulation (Oust, 75% ai sulfometuron methyl) yielded only 23% root elongation inhibition at the top 5 cm of the soil, whereas complete inhibition was achieved with the micelle–clay formulation. The detected concentration of SFM for the micelle–clay formulation at a depth of 15–20 cm was half of that detected for the commercial one, indicating a reduction in leaching when applying the micelle–clay formulation. A 10-fold reduction in the applied dose of SFM in the micelle–clay formulations resulted in good herbicidal activity of 60–87% inhibition (Fig. 11.2.3).

The adsorbed amount of the anionic herbicide sulphentrazone on ODTMA-montmorillonite was 99% of added at 2.5 mM ODTMA and 0.2% clay; desorption of the herbicide was 0.3% after 24 h. After 10 washings in funnels with thin layer of soil only 2.6% of the herbicide was released from ODTMA-montmorillonite formulations versus 100% release from the commercial formulation. The ODTMA-clay formulations of sulfentrazone yield almost complete growth inhibition of green foxtail, at 700 ga.i./ha versus 40% inhibition by commercial formulations applied at the same rate. (Polubesova et al., 2003). Hence the slow release from micelle–clay formulations of sulfentrazone promotes its biological activity and reduces environmental contamination.

These characteristics make the new formulations promising from the environmental and economic points of view.

#### 11.2.4. PHOTOSTABILIZATION OF PESTICIDES BY ORGANO-CLAYS

An organic cation adsorbed on the clay mineral can act as an energy acceptor of the photo-excited molecule of the pesticide, which returns to its ground state before its photodecomposition occurs, thus becoming photostabilized.



Margulies et al. (1987) observed that the insecticide bioresmethrin adsorbed on montmorillonite at a load of 0.2 mmol/g of the dye methylgreen retained its activity after three days of exposure to sunlight whereas the commercial insecticide lost its activity after one day of irradiation. However, an increase in the loading of the dye for the same concentration of the insecticide (0.2 mmol/g) did not achieve any photostabilization. Similarly, Margulies et al. (1988b) obtained a high degree of photostabilization of the insecticide NMH by using the dye thioflavin-T (TFT). The highest photoprotection was obtained for samples containing 0.5 mmol TFT and 0.2 mmol NMH/g clay and again, an increase in the loading of the organic cation on the clay mineral surface abolished the photostabilization of the pesticide molecules.

These patterns indicate the role of specific molecular interactions between the organic cation and the pesticide molecules; evidence was obtained by infrared spectroscopy (Margulies et al., 1985). Because the efficiency of energy transfer processes depends on the matching of energy levels of donor and acceptor chromophores, the distance between them, and their relative orientations (Margulies et al., 1993), an excessive loading of the clay mineral surface would impair the molecular interactions between the pesticide and the organic cation, and less photostabilization would be obtained.

In these studies, the role of the clay mineral was to keep the organic cation and the pesticide molecules at an optimal distance and perhaps orientation as well for energy transfer processes. However, in certain cases (e.g., the herbicide trifluralin (Margulies et al., 1992)), the clay mineral itself could provide photostabilization. NMH adsorbed on montmorillonite and nontronite decomposed more slowly than that adsorbed on hectorite in line with their increasing iron content, which was attributed to charge transfer from the excited pesticide molecules to  $\text{Fe}^{3+}$  ions in the clay mineral structure (Rozen and Margulies, 1991). Banerjee and Dureja (1995) also found a slightly lower rate of photodegradation for quinalphos adsorbed on palygorskite than on kaolinite, in accord with the relatively low content of structural iron in kaolinite.

Undabeytia et al. (2000b) obtained a high degree of photostabilization of the herbicide norflurazon by preadsorbing TFT on montmorillonite. This was due to energy transfer involving  $\pi-\pi^*$  transitions between triplet states of the herbicide and the organic cation, but an additional mechanism was also reported. Unlike the insecticide NMH, the irradiation of norflurazon in the presence of montmorillonite enhanced its photolysis, which was explained by the reaction of the herbicide molecules with hydroxyl and hydroperoxyl radicals formed on the clay mineral by irradiation. Consequently, loading the clay mineral surface with the organic cation may lower the levels of production of these radicals, and yield photostabilization. The photostabilization of the insecticide quinalphos was also due to modification of the catalytic properties of the clay mineral surface when covered with the organic cation crystal violet (Banerjee and Dureja, 1995).

In other organo-clay complexes, the organic cation is not really involved in the photo-protection of the herbicide. For example, El-Nahhal et al. (1999b) observed



that the largest adsorption of the herbicides alachlor and metolachlor by montmorillonite, preadsorbed with the organic cation BTMA, correlated with an optimal reduction of photodecomposition. It appeared that the role of the organic cation was to enhance the adsorption of the non-polar herbicides to the organo-clay complex, whereas the photoprotection was provided by the clay mineral itself. Margulies et al. (1992) suggested that the mechanism operating for the photostabilization of trifluralin was steric hindrance by the clay mineral surface to the cyclization step of the photochemical reaction, which leads to one of its photoproducts. This mechanism could also occur for the photostabilization obtained for trifluralin by using sepiolite-TFT instead of montmorillonite-BTMA (Casal et al., 2001).

#### 11.2.5. EXPLOITING CLAY-ORGANIC INTERACTIONS TO ENHANCE THE EFFICACY OF BIPYRIDYL HERBICIDES

Paraquat (PQ) and diquat (DQ) are divalent organic bipyridyl herbicides, widely used for rapid post-emergence weed control. Both herbicides are highly toxic, and relatively expensive. Hence, it is advantageous to reduce their use rate and minimize their costs and health hazard. A decrease in efficacy of DQ and PQ is caused by dust particles on leaves of weeds (Wicks and Fenster, 1996), which adsorb the herbicide, reducing its amount available for biological activity, hence causing inactivation (Calderbank, 1968). The adsorbed herbicide molecules interact with the negatively charged sites on the surface of clay mineral particles, as was observed by several analytical techniques (Rytwo et al., 1996a, 2002). The herbicides also bind to soils by reaction with humic acids and organic matter (Wauchope et al., 1992).

Previous studies showed that certain monovalent organic cations can compete with the bipyridyl divalent herbicides for adsorption to montmorillonite (Rytwo et al., 1996a) or sepiolite (Rytwo et al., 2002). On this basis, Rytwo and Tropp (2001) proposed to add a monovalent organic cation to the herbicide formulation. The main idea was to utilize the strong interactions between certain monovalent organic cations and clay minerals in order to make more herbicide molecules available for acting on the plant cells, rather than being irreversibly adsorbed by dust.

Based on this hypothesis, Rytwo (2000) and Rytwo and Tropp (2001) observed that clay sprayed on plants reduced the herbicidal activity of bipyridyl herbicides. This reduction which was ascribed to the adsorption of the herbicide on clay mineral sites was larger in a high CEC clay mineral, such as montmorillonite, than in a low CEC clay mineral, such as sepiolite. Addition of monovalent cations, such as acriflavin or mepiquat (MQ) could overcome the influence of a clay dust. Such addition gave good herbicidal activity (Fig. 11.2.4) with less than 1/3 of the normally used amount of herbicide. MQ should be preferred, since it is a chemical allowed for agricultural use.

Rytwo and Tavasi (2003) showed a similar enhancing effect by using the monovalent herbicide difenzoquat (DZ). They observed a decrease in the efficacy of the



Fig. 11.2.4. Effect of addition of MQ on the efficacy of DQ/PQ herbicide. Pot (a) contains a control plant. Pots (b) and (c) show a clean and a clay-dusted plant, respectively, sprayed with 800 ml/ha of DQ/PQ herbicide. Plant (d) is clay-dusted, sprayed with 800 ml/ha DQ/PQ and 225 g/ha MQ.

herbicide when the plants were dusted with common soil either from mineral source (57% clay, 4.5% organic matter) or organic peat (6% clay, 20% organic matter). The proposed formulations exhibit both economic and environmental advantages.

## REFERENCES

- Balinova, M.A., 1997. Acetochlor—a comparative study on parameters governing the potential for water pollution. *Journal of Environmental Science and Health B* 32 (5), 645–658.
- Banerjee, K., Dureja, P., 1995. Photostabilization of quinalphos by crystal violet on the surface of kaolinite and palygorskite. *Pesticide Science* 43, 333–337.
- Calderbank, A., 1968. The bipyridylum herbicides. *Advances in Pest Control* 8, 127–190.
- Carter, D.A., 2000. Herbicide movement in soil: principles, pathways and processes. *Weed Research* 40, 113–122.
- Casal, B., Merino, J., Serratosa, J.M., Ruiz-Hitzky, E., 2001. Sepiolite-based materials for the photo- and thermal-stabilization of pesticides. *Applied Clay Science* 18, 245–254.
- Cohen, S.Z., Elden, C., Lorber, N.M., 1986. Monitoring ground water for pesticides. In: Garnar, R.C., Honeycure, R.C., Higgs, H.N. (Eds.), *Evaluation of Pesticides in Ground Water*. ACS Symposium Series 315. American Chemical Society, Washington, DC, pp. 170–196.
- Cox, L., Celis, R., Hermosin, M.C., Cornejo, J., 1999. Use of natural colloids to retard simazine and 2,4-D leaching in soil. *Journal of Agricultural and Food Chemistry* 48, 93–99.
- Davis, R.F., Wauchope, R.D., Johnson, A.W., Burgos, B., Pepperman, A.B., 1996. Release of fenamiphos, atrazine, and alachlor into flowing water from granules and spray deposits of conventional and controlled-release formulations. *Journal of Agricultural and Food Chemistry* 44, 2900–2907.
- El-Nahhal, Y., Nir, S., Polubesova, T., Margulies, L., Rubin, B., 1997. Organo-clay formulations of alachlor: reduced leaching and improved efficacy. Brighton Crop Protection Conference. *Weeds* 1, 21–26.

- El-Nahhal, Y., Nir, S., Polubesova, T., Margulies, L., Rubin, B., 1998. Leaching, phytotoxicity and weed control of new formulations of alachlor. *Journal of Agricultural and Food Chemistry* 46, 3305–3313.
- El-Nahhal, Y., Nir, S., Polubesova, T., Margulies, L., Rubin, B., 1999a. Movement of metolachlor in soil: effect of new organo-clay formulations. *Pesticide Science* 55, 857–864.
- El-Nahhal, Y., Nir, S., Margulies, L., Rubin, B., 1999b. Reduction of photodegradation and volatilization of herbicides in organo-clay formulations. *Applied Clay Science* 14, 105–119.
- El-Nahhal, Y., Nir, S., Serban, C., Rabinovitch, O., Rubin, B., 2000. Montmorillonite-phenyltrimethylammonium yields environmentally improved formulations of hydrophobic herbicides. *Journal of Agricultural and Food Chemistry* 48, 4791–4801.
- El-Nahhal, Y., Nir, S., Serban, C., Rabinovitz, O., Rubin, B., 2001. Organo-clay formulation of acetochlor for reduced movement in soil. *Journal of Agricultural and Food Chemistry* 49, 5364–5371.
- Fernández-Pérez, M., Villafranca-Sánchez, M., González-Pradas, E., Martínez-López, F., Flores-Céspedes, F., 2000. Controlled release of carbofuran from an alginate-bentonite formulation: water release kinetics and soil mobility. *Journal of Agricultural and Food Chemistry* 48, 938–943.
- Gerstl, Z., Nasser, A., Mingelgrin, A., 1998. Controlled release of pesticides in soils from clay-polymer formulations. *Journal of Agricultural and Food Chemistry* 46, 3797–3802.
- González-Pradas, E., 1999. Mobility of imidacloprid from alginate-bentonite controlled-release formulations in greenhouse soils. *Pesticide Science* 55, 1109–1115.
- González-Pradas, E., Fernandez-Perez, M., Villafranca-Sanchez, M., Martinez-Lopez, F., Flores-Céspedes, F., 1999. Use of bentonites and humic acids as modifying agents in alginate-based controlled-release formulations of imidacloprid. *Pesticide Science* 55, 546–552.
- Hermosin, M.C., Calderon, M.J., Aguer, J.P., Cornejo, J., 2001. Organoclays for controlled release of the herbicide fenuron. *Pest Management Science* 57, 803–809.
- Ignoffo, C.M., Garcia, C., 1996. Simulated sunlight-UV sensitivity of experimental dust formulations of the nuclear polyhedrosis virus of *Helicoverpa/Heliiothis*. *Journal of Invertebrate Pathology* 67, 192–194.
- Johnson, R.M., Pepperman, A.B., 1998. Release of atrazine and alachlor from clay-oxamide controlled-release formulations. *Pesticide Science* 53, 233–240.
- Kolpin, W.D., Nations, K.B., Goolsby, D., Thurman, M.E., 1996. Acetochlor in hydrologic system in the Midwestern United States, 1994. *Environmental Science and Technology* 30, 1459–1464.
- Koterba, M.T., Banks, W.S.L., Shedlock, R.J., 1993. Pesticides in shallow ground water in the Delmarva Peninsula. *Journal of Environmental Quality* 22, 500–518.
- Lagaly, G., 1995. Surface and interlayer reactions. In: Churchman, G.J., Fitzpatrick, R.W., Eggleton, R.A. (Eds.), *Clays: Controlling the Environment*. Proceedings of the 10th International Clay Conference, Adelaide, Australia. 1993 CSIRO Publishing, Melbourne, pp. 137–144.
- Margulies, L., Cohen, E., Rozen, H., 1987. Photostabilization of bioresmethrin by organic cations on a clay surface. *Pesticide Science* 18, 79–87.
- Margulies, L., Rozen, H., Cohen, E., 1985. Energy transfer at the surface of clays and protection of pesticides from photodegradation. *Nature* 315, 658–659.
- Margulies, L., Rozen, H., Nir, S., 1988a. Model for competitive adsorption of organic cations on clays. *Clays and Clay Minerals* 36, 270–276.

- Margulies, L., Rozen, H., Cohen, E., 1988b. Photostabilization of nitromethylene heterocycle insecticide on the surface on montmorillonite. *Clays and Clay Minerals* 36, 159–164.
- Margulies, L., Stern, T., Rubin, B., Ruzo, L., 1992. Photostabilization of trifluralin adsorbed on a clay matrix. *Journal of Agricultural and Food Chemistry* 40, 152–155.
- Margulies, L., Stern, T., Rubin, B., 1994. Slow release of *S*-ethyl dipropylcarbamothiate from clay surfaces. *Journal of Agricultural and Food Chemistry* 42, 1223–1227.
- Margulies, L., Rozen, H., Stern, T., Rytwo, G., Rubin, B., Ruzo, L., Nir, S., Cohen, E., 1993. Photostabilization of pesticides by clays and chromophores. *Archives of Insect Biochemistry and Physiology* 22, 467–486.
- Mishaël, Y.G., Undabeytia, T., Rytwo, G., Papahadjopoulos-Sternberg, B., Rubin, B., Nir, S., 2002a. Sulfometuron incorporation in cationic micelles adsorbed on montmorillonite. *Journal of Agricultural and Food Chemistry* 50, 2856–2863.
- Mishaël, Y.G., Undabeytia, T., Rabinovitz, O., Rubin, B., Nir, S., 2002b. Slow release formulations of sulfometuron incorporated in micelles adsorbed on montmorillonite. *Journal of Agricultural and Food Chemistry* 50, 2864–2869.
- Mishaël, Y.G., Undabeytia, T., Rabinovitz, O., Rubin, B., Nir, S., 2002. Sulfosulfuron incorporated in micelles adsorbed on montmorillonite for slow release formulations. *Journal of Agricultural and Food Chemistry* 51, 2253–2259.
- Nennemann, A., Mishaël, Y.G., Nir, S., Rubin, B., Polubesova, T., Bergaya, F., Van Damme, H., Lagaly, G., 2001. Clay-based formulations of metolachlor with reduced leaching. *Applied Clay Science* 18, 265–275.
- Nir, S., Rytwo, G., Yermiyahu, U., Margulies, L., 1994. A model for cation adsorption to clays and membranes. *Colloid and Polymer Science* 272, 619–632.
- Nir, S., Undabeytia, T., Yaron-Marcovich, D., El-Nahhal, Y., Polubesova, T., Serban, C., Rytwo, G., Lagaly, G., Rubin, B., 2000. Optimization of adsorption of hydrophobic herbicides on montmorillonite pre-adsorbed by monovalent organic cations: interaction between phenyl rings. *Environmental Science and Technology* 34, 1269–1274.
- Pasquarelly, G.C., Boyer, D.C., 1996. Herbicides in karst groundwater in Southeast West Virginia. *Journal of Environmental Quality* 25, 755–765.
- Pepperman, A.B., Kuan, J.-C.W., McCombs, C., 1991. Alginate controlled release formulations of metribuzin. *Journal of Controlled Release* 17, 105–112.
- Polubesova, T.A., Rytwo, G., Nir, S., Serban, C., Margulies, L., 1997. Adsorption of benzyltrimethylammonium and benzyltriethylammonium on montmorillonite: experimental studies and model calculations. *Clays and Clay Minerals* 45, 834–841.
- Polubesova, T., Nir, S., Gerstl, Z., Borisover, M., Rubin, B., 2002. Imazaquin adsorbed on pillared clay and crystal violet-montmorillonite complexes for reduced leaching in soil. *Journal of Environmental Quality* 31, 1657–1664.
- Polubesova, T., Nir, S., Rabinovitz, O., Rubin, B., 2001. Mepiquat-acetochlor formulations: sorption and leaching. *Applied Clay Science* 18, 299–307.
- Polubesova, T., Nir, S., Rabinovitz, O., Borisover, M., Rubin, B., 2003. Sulfentrazone adsorbed on micelle-montmorillonite complexes for slow release in soil. *Journal of Agricultural and Food Chemistry* 51, 3410–3414.
- Ritter, W.F., Chirnside, A.E.M., Scarborough, R.W., 1996. Movement and degradation of triazines, alachlor, and metolachlor in sandy soils. *Journal of Environmental Science and Health* 31, 2699–2721.

- Rozen, H., Margulies, L., 1991. Photostabilization of tetrahydro-2-(nitromethylene)-2*H*-1,3thiazine adsorbed on clays. *Journal of Agricultural and Food Chemistry* 39, 1320–1325.
- Rytwo, G., 2000. The use of clay-organic interactions to improve efficacy of contact herbicides: addition of monovalent organocations to divalent herbicides. In: *Proceedings of the 1st Latin-American Clay Conference "Clays in Volcanic Environments"*. Funchal, Madeira, 1, pp. 332–344.
- Rytwo, G., Nir, S., Margulies, L., 1995. Interaction of monovalent organic cations with montmorillonite: adsorption studies and model calculations. *Soil Science Society of America Journal* 59, 554–564.
- Rytwo, G., Nir, S., Margulies, L., 1996a. Adsorption and interaction studies of the divalent cationic herbicides diquat and paraquat with montmorillonite. *Soil Science Society of America Journal* 60, 601–610.
- Rytwo, G., Nir, S., Margulies, L., 1996b. A model for adsorption of divalent organic cations to montmorillonite. *Journal of Colloid and Interface Science* 181, 551–560.
- Rytwo, G., Serban, C., Tropp, D., 2002. Adsorption and interactions of diquat, paraquat and methyl green on sepiolite: experimental results and model calculations. *Applied Clay Science* 20, 273–282.
- Rytwo, G., Tavasi, M., 2003. Addition of a monovalent cationic pesticide to improve efficacy of bipyridyl herbicides in Hulah valley soils. *Pest Management Science* 59, 1265–1270.
- Rytwo, G., Tropp, D., 2001. The use of clay-organic interactions to improve efficacy of contact herbicides: addition of monovalent organocations to diquat. *Applied Clay Science* 18, 327–333.
- Sheng, G., Wang, X., Wu, S., Boyd, S.A., 1998. Enhanced sorption of organic contaminants by smectitic soils modified with a cationic surfactant. *Journal of Environmental Quality* 27, 806–814.
- Sparks, R.E., Jacobs, I.C., 1999. Selection of coating and microencapsulation processes. In: Scher, H.B. (Ed.), *Controlled-Release Delivery Systems for Pesticides*. Marcel Dekker, New York, pp. 3–29.
- Thurman, E.M., Goolsby, D.A., Aga, D.S., Pomes, M.L., Meyer, M.T., 1996. Occurrence of alachlor and its sulfonated metabolite in rivers and reservoirs of the Midwestern United States. The importance of sulfonation in transport of chloroacetanilide herbicides. *Environmental Science and Technology* 30, 569–574.
- Undabeytia, T., Nir, S., Polubesova, T., Rytwo, G., Morillo, E., Maqueda, C., 1999. Adsorption-desorption of chlordimeform on montmorillonite: effect of clay aggregation and competitive adsorption with cadmium. *Environmental Science and Technology* 33, 864–869.
- Undabeytia, T., Nir, S., Rubin, B., 2000a. Organo-clay formulations of the hydrophobic herbicide norflurazon yield reduced leaching. *Journal of Agricultural and Food Chemistry* 48, 4767–4773.
- Undabeytia, T., Nir, S., Tel-Or, E., Rubin, B., 2000b. Photostabilization of the herbicide norflurazon by using organoclays. *Journal of Agricultural and Food Chemistry* 48, 4774–4779.
- Wauchope, R.D., Buttler, T.M., Hornsby, A.G., Augustijn Beckers, P.W.M., Burt, J.P., 1992. SCS/ARS/CES Pesticide properties database for environmental decision making. *Reviews of Environmental Contamination and Toxicology* 123, 1–157.
- White, C.A., Leonard, B.R., Burris, E., Graves, J.B., 1999. Laboratory and field evaluations of *Bacillus thuringiensis* Berliner insecticides against tobacco budworm (Lepidoptera: noctuidae). *The Journal of Cotton Science* 3, 92–101.

- Wicks, G.A., Fenster, C.R., 1996. Ecofarming fallow aids in winter heat-fallow rotation (File G546 under: FIELD CROPS D-10, Small Grains Issued February 1981) published by Cooperative Extension, University of Nebraska, Institute of Agriculture and Natural Resources, <http://www.ianr.unl.edu/pubs/fieldcrops/g546.htm>.
- Wilkinson, R.E., 1988. Carbamothiates. In: Kearney, P.C., Kaufman, D.D. (Eds.), *Herbicides, Chemistry, Degradation and Mode of Action*. Marcel Dekker, New York, pp. 246–333.
- Xu, S., Sheng, G., Boyd, S.A., 1997. Use of organo-clays in pollution abatement. *Advances in Agronomy* 59, 25–62.

This page intentionally left blank

### *Chapter 11.3*

## **CLAY LINERS AND WASTE DISPOSAL**

**K. CZURDA**

*Angewandte Geologie, Universität Karlsruhe, D-76128 Karlsruhe, Germany*

As populations grow and technologies advance, the type and quantity of waste produced keeps on growing. As a result, waste disposal became a huge environmental problem. This chapter is concerned with waste encapsulation in relation to environmental clean-up and protection. The term ‘encapsulation’ refers to the sealing of waste body by geological and engineered liner systems. In most cases, such systems partly consist of clay liners with varied modifications. Thus, encapsulation systems are as varied as the environments in which they are built, and the components of an encapsulation system are as multiple and complex as the wastes themselves. For all waste types, encapsulation is the only option if the waste has to be permanently isolated from the accessible environment (Caldwell and Reith, 1993). The requirements for an encapsulation system are basically the same, whether the waste is municipal refuse in a landfill, hospital debris in a low-level waste dump, or mixed wastes of diverse industrial production/construction activities. This leads us to the need to classify wastes because encapsulation systems consist of engineered liner components according to the magnitude of the risks which are associated with the waste.

From the beginning, sophisticated engineered liners should meet two requirements: (i) to guarantee practical imperviousness so as to prevent leachates from infiltrating the environment and (ii) to possess retention or at least retardation properties preventing contaminant migration by convection and diffusion (Drescher, 1997). In many cases—but not absolutely—the surface barrier (layer) may be slightly permeable, allowing further decomposition of sanitary wastes by precipitation moisture. Because of the different functions of the surface and the base encapsulation barriers, different state-of-the-art systems were developed (Fig. 11.3.1). In practice, clay liners are designed so that most of the required properties are optimally expressed (Fig. 11.3.2).

### **11.3.1. WASTE CATEGORIES**

Different waste compositions require different sealing units. For example, it is not economical to use a multilayer system for inert construction wastes or to design an



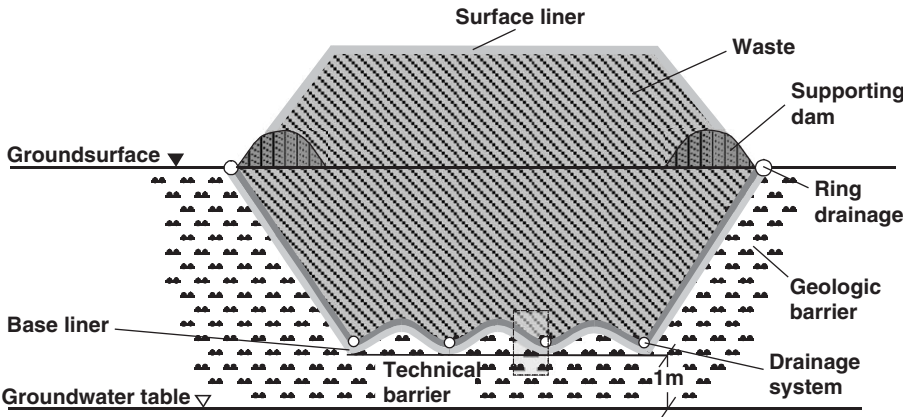


Fig. 11.3.1. Multibarrier system for waste encapsulation. Geologic in situ barriers and engineered technical barriers (compacted mineral layers and geomembranes) are the main parts of the system.

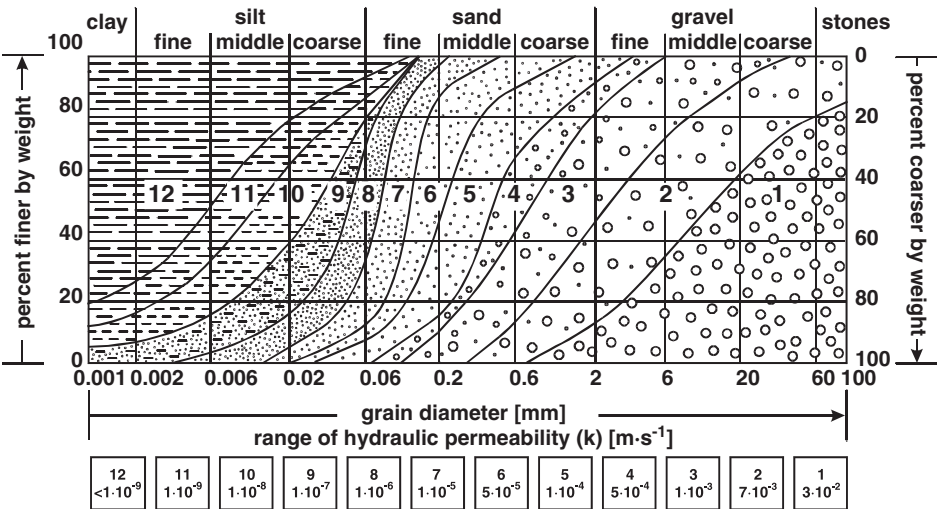


Fig. 11.3.2. Practical imperviousness is the main function of liner systems. Hydraulic permeabilities are expressed as  $k$  coefficients in  $\text{ms}^{-1}$ . The range of  $k \leq 10^{-7} \text{ms}^{-1}$  is considered as one of the most important barrier features of mineral sealing units in the national regulations. Grain size distribution areas 10, 11, and 12 refer to this.

identical system for sanitary landfills and toxic industrial wastes (Bradshaw et al., 1992). For this reason, all regional waste repository regulations have to categorise wastes not according to the input of waste components but mainly in terms of leaching the waste and quantifying the contaminant content (Czurda, 1992). The

European Union, most European countries, the USA, Canada, Japan, etc. follow this system, ending up with similar waste categories. Taking radioactive waste into account leads to the following classification scheme:

- inert construction and industrial waste,
- domestic waste,
- toxic industrial waste,
- incineration ashes and slags, and
- radioactive waste.

Nuclear waste repositories have to follow special national regulations and are not further treated in this chapter.

As an example for waste assignments, some threshold values according to German regulations (Gassner, 1991; TA Siedlungsabfall, 1993; Deponieverordnung, 2002) are shown in Table 11.3.1. They are close to European Union values (EU-Richtlinie, 1999).

### 11.3.2. MINERAL BARRIERS

Clay rocks, clay mineral admixtures, and zeolite admixtures are the most important and widely used natural materials for constructing mineral barriers within engineered sealing layers. These materials are also used as constituents of in situ geological barriers, i.e., waste deposit location. The use of alternative materials such as amorphous silica, fly ashes, fly ash zeolites, clay remnants from coal flotation, etc. is not discussed.

Table 11.3.1. Assignment criteria for waste categories according to the German regulations TA-A and TA-Si. Selected examples. Category I is inert waste, category II is domestic waste, and category III is toxic industrial waste. The leachable parts are listed as examples for very common toxic waste constituents

	I	II	III
Conductivity	$\leq 6000 \mu\text{S}/\text{cm}$	$\leq 50000 \mu\text{S}/\text{cm}$	$\leq 100000 \mu\text{S}/\text{cm}$
Uniaxial strength	$\geq 50 \text{ kN}/\text{m}^2$	$\geq 50 \text{ kN}/\text{m}^2$	$\geq 50 \text{ kN}/\text{m}^2$
TOC*	$\leq 20 \text{ mg}/\text{L}$	$\leq 100 \text{ mg}/\text{L}$	$\leq 200 \text{ mg}/\text{L}$
Phenols	$\leq 0.2 \text{ mg}/\text{L}$	$\leq 50 \text{ mg}/\text{L}$	$\leq 100 \text{ mg}/\text{L}$
Mercury	$\leq 0.005 \text{ mg}/\text{L}$	$\leq 0.020 \text{ mg}/\text{L}$	$\leq 0.100 \text{ mg}/\text{L}$
Cadmium	$\leq 0.050 \text{ mg}/\text{L}$	$\leq 0.100 \text{ mg}/\text{L}$	$\leq 0.500 \text{ mg}/\text{L}$
Lead	$\leq 0.200 \text{ mg}/\text{L}$	$\leq 1000 \text{ mg}/\text{L}$	$\leq 2000 \text{ mg}/\text{L}$
Sulphate	$\leq 500 \text{ mg}/\text{L}$	$\leq 1400 \text{ mg}/\text{L}$	$\leq 5000 \text{ mg}/\text{L}$
Soluble part	$\leq 3\%$	$\leq 6\%$	$\leq 10\%$

\*Total Organic Carbon

### A. Clay Rocks and Clay Minerals

In using clays and zeolites and other fine-grain material for sealing purposes, two main issues are relevant: (i) leachate retention due to low-hydraulic conductivities and (ii) toxic constituent retention or retardation due to adsorption, precipitation, redox processes, and other mechanisms. Soil barriers, containing enough clay minerals with adequate properties to provide low permeability, are used extensively to prevent rapid advective migration of various leachates from waste disposal sites (Hiltmann and Stribrny, 1998). The clayey barriers vary from thin geosynthetic clay liners (GCL) of 1–3 cm thickness, to compacted clay liners (CCL) up to 300 cm in thickness, to natural undisturbed clayey barriers up to 30 m or more in thickness. The hydraulic conductivity of undisturbed clayey deposits depends on the mineralogy, environment of deposition, and stress history of the deposits. The same holds true for GCL and CCL.

Clays attract water, other polar liquids, and cations. A dried-out clay will expand as it adsorbs water between its layers and particles when placed in an aqueous solution. If toxic ions are present in the solution, they can adsorb on the charged clay surface mineral by ion exchange. Thus, clays can accept or release ions depending on the concentration of the ions in solution relative to that on the surface. These ions, e.g., from the leachate, are not finally fixed but can participate in further exchange processes depending on the chemical environment.

The nature of the cations initially present at the clay mineral surface (derived, for example, from the marine environment) is of decisive influence on adsorption potentials. According to the diameter of hydrated cations and their valency they are differently adsorbed by the clay surface mineral and are therefore exchangeable in different quantities. For example,  $\text{Na}^+$ -bentonites are especially suitable for base liner construction. Because of their high-swelling potential and adsorption capacity, they fulfil the requirements for a high degree of imperviousness, and a high contaminant retention potential. Table 11.3.2 shows the cation exchange capacity (CEC) and specific surface areas of some clay minerals and other materials. The theoretical specific surface areas of smectites and vermiculites of 750–800 m<sup>2</sup>/g are only effective when the contaminants can fully penetrate the interlayer space. This may be the case for ion exchange with pure inorganic ions (see Chapter 12.10) and suitable organic cations (see Chapter 7.3) but does not often apply to the adsorption of neutral (non-ionic) compounds.

### B. Zeolites

Zeolites show a high potential as contaminant adsorbents due to their high exchange capacity and selectivity for certain cations, such as  $\text{NH}_4^+$ ,  $\text{Pb}^{2+}$ ,  $\text{Cd}^{2+}$ ,  $\text{Sr}^{2+}$ , and other metal ions, especially after ‘activation’ by sodium chloride. The selectivity of certain zeolites for specific chemicals is controlled by their pore size and charge

Table 11.3.2. Cation exchange capacity (CEC) and specific surface area of some clay minerals and other materials

Adsorbent	CEC (cmol(+)/kg)*	Specific surface area (m <sup>2</sup> /g)
Allophane	50–100	500–700
Kaolinite	3–15	10–20
Illite	10–40	50–100
Montmorillonite	70–120	10–800 <sup>†</sup>
Vermiculite	130–210	1–800 <sup>†</sup>
Fe- + Al-(hydr)oxides (pH 8.0)	3–25	25–40
Humic material	150–250	about 800

\* = meq/100 g.

<sup>†</sup>depending on the participation of internal surfaces; lowest value represents the external specific surface area.

properties. By analogy with clay minerals, the substitution of  $\text{Al}^{3+}$  for  $\text{Si}^{4+}$  in the structure leads to a net negative charge and a high CEC for most natural zeolites.

Natural zeolites occur in sediments, lava vesicles, deuteric-altered plutonic rocks, and hydrothermal systems associated with alkaline volcanic rocks. Since natural zeolites generally derive from volcanic glass, they are of widespread occurrence.

Fig. 11.3.3 shows the isotherms for the adsorption of  $\text{Cu}^{2+}$  from deionised water and a 0.01 M  $\text{CaCl}_2$  solution by clinoptilolite (a very common natural zeolite) and  $\text{Na}^+$ -clinoptilolite (Huttenloech et al., 2001). The isotherms are curvi-linear, and can be described by the Freundlich equation:  $c_s = K_f C_w^n$  where  $c_s$  denotes the amount of the solute adsorbed per unit mass of adsorbent,  $c_w$  is the equilibrium solute concentration,  $K_f$  and  $n$  are empirical parameters specific of the adsorbate-adsorbent interaction.

### 11.3.3. WASTE DEPOSIT MULTIBARRIER SYSTEMS

Waste deposits can in principle be constructed as underground storages and at the surface as slope storage, slope dump, or depression storage. Common domestic waste, incineration residues, inert construction wastes, etc. may be stored at the surface. Underground storage as a special deposition mode is not treated in this chapter.

#### A. Base Liners

Base liner systems must be able to prevent leakage of contaminants from the waste, and their infiltration into the subsoil. These systems have to prove a high potential for retaining toxic materials by adsorption, precipitation, and/or redox processes (Rowe et al., 1995). Adsorption on mineral surfaces mainly occurs by ion exchange. In many cases toxicants can be retarded during their migration through the sealing layers.

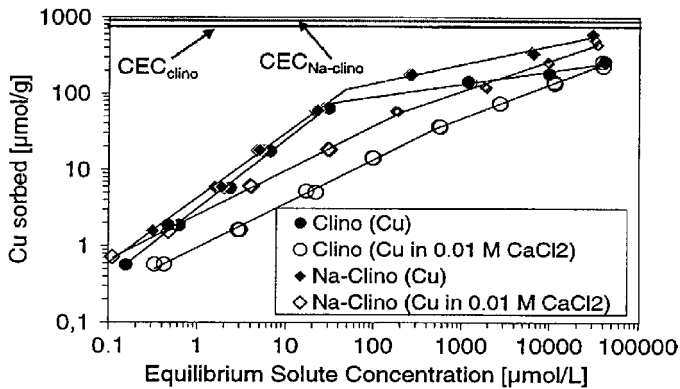


Fig. 11.3.3. Adsorption isotherms of  $\text{Cu}^{2+}$  on natural and  $\text{Na}^{+}$  clinoptilolite in deionised water and 0.01 M  $\text{CaCl}_2$  solution (1 g samples in 40 mL copper salt solutions, contact time 96 h, at  $20^\circ\text{C}$ ). The CEC of clinoptilolite is  $720 \mu\text{mol}(+)/\text{g}$  and of  $\text{Na}^{+}$ -clinoptilolite is  $900 \mu\text{mol}(+)/\text{g}$ .

Figs. 11.3.4a, b shows an example of a base liner constructed according to German regulations for inert and domestic wastes. The essential components are compacted clay layers, and in case of domestic wastes, a geomembrane in addition to the mineral layers and of course the geological barrier (Fig. 11.3.5). The basal system contains a leachate collecting layer, connected to a purification plant. There are different leakage detection systems on the market.

### B. Surface Liners

The exclusive function of the surface liner is to prevent precipitation water from infiltrating into the waste. In case of household wastes, the capping system has to have a gas drainage system. Capping layers for all types of waste are therefore constructed with a drainage layer (usually 16–32 mm gravel) in case of leaks in the system.

As in the case of basal systems, CCL and geomembranes are the prevailing sealing elements (Fig. 11.3.6a, b). But there is an important difference in the clay mineral composition of the CCLs. Whereas the base CCL-clay should contain 2:1 layer clay minerals (e.g., montmorillonite, vermiculite), the surface CCL-clay should contain 1:1 phyllosilicates (e.g., kaolinite) as index minerals. The 2:1 minerals enable retardation by adsorption and a high degree of impermeability to be obtained, while the 1:1 clays of the surface sealing unit, combined with a sand/silt matrix, are practically impermeable but have a low-adsorption potential. Because of the small particle size, a sand-silt-kaolinite admixture for the mineral surface sealing can have a very low permeability ( $k_f = 10^{-8} - 10^{-12} \text{ cm/s}$ ).

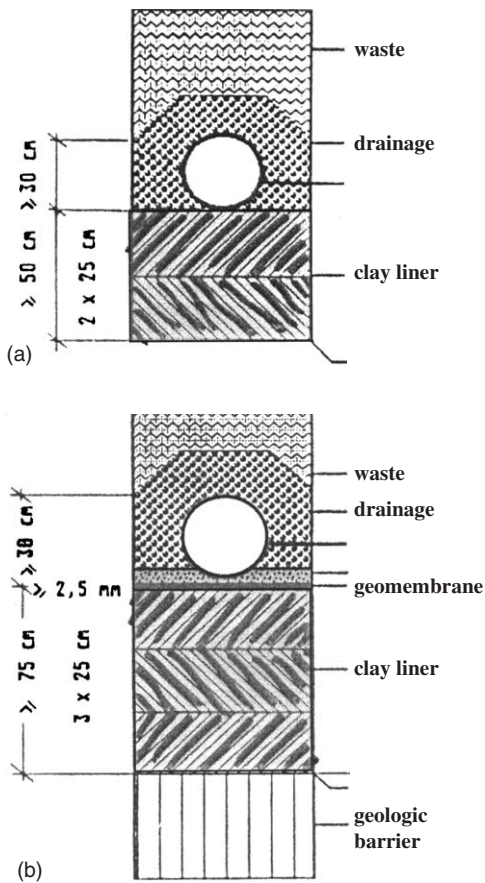


Fig. 11.3.4. (a) Base liner system for inert waste. Two CCL without geomembrane (b) Base liner system for domestic waste. Three CCL combined with a geomembrane.

#### 11.3.4. CONCLUSIONS

For hazardous industrial wastes and toxic sanitary landfills, we have to locate a site that functions primarily as a geologic barrier with  $k_f < 10^{-6}$  m/s and at least 3 m in thickness. In case of inert (non-toxic) wastes a geologic barrier is not necessary. It is essential, however, to follow the multibarrier concept and to add on top of the geologic barrier a system of engineered barriers and drainage layers. The engineered barriers comprise as a core unit the combined CCL and geomembrane double layer. A similar multibarrier system has to be constructed for the cover sealing. The difference is expressed in the type of GCL and the drainage layers. The GCL should not contain expanding 2:1 clay minerals, such as montmorillonite or vermiculite, because they tend to dry out and form desiccation cracks. Therefore non-swelling 1:1 clay

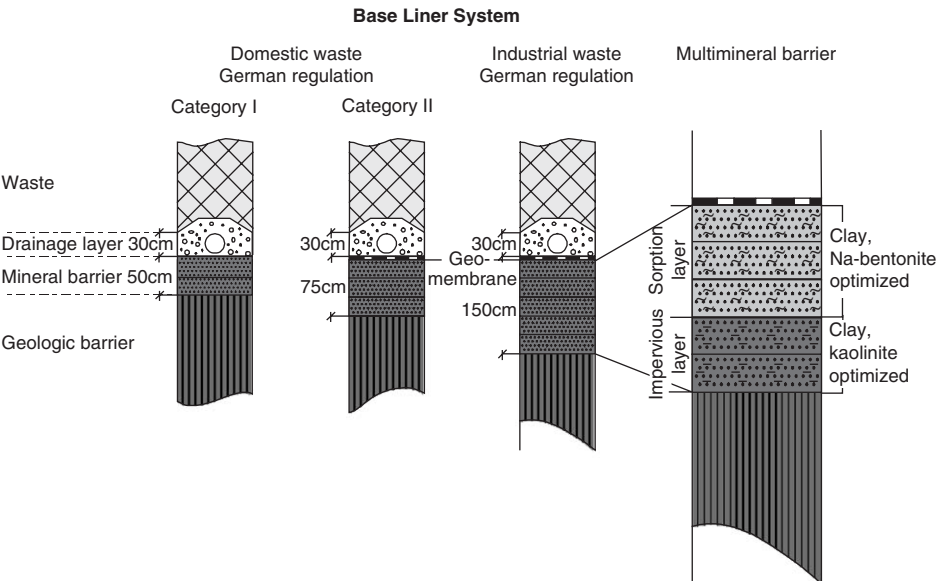


Fig. 11.3.5. Comparing different base liner systems. The multibarrier system consists of two clay units: an adsorbing bentonite unit and a sealing kaolinite unit.

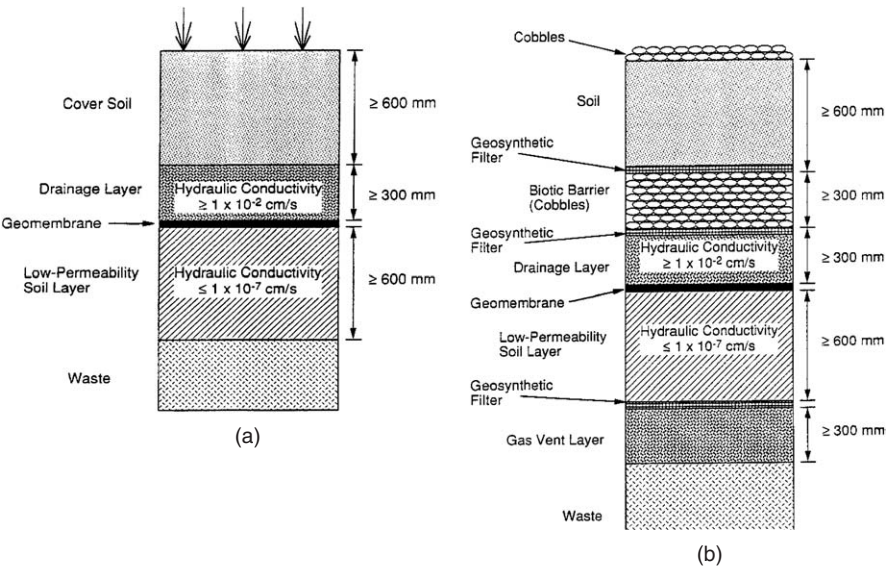


Fig. 11.3.6. Environmental Protection Agency (EPA) recommendation for surface liner systems in the USA. Clay barriers are combined with geomembranes (a) The optional system (b) comprises additional filler systems: a biotic filter on top of the sealing unit and a gas collection layer below.

minerals (e.g., kaolinite) or tectosilicates (e.g., zeolites) should be the index minerals for the sand–silt–clay surface GCL. In case of untreated household waste, a gas drainage layer has to be provided in order to divert the methanol that develops as the waste decomposes.

## REFERENCES

- Bradshaw, A.D., Southwood, R., Warner, F., 1992. *The Treatment and Handling of Wastes*. Chapman & Hall, London.
- Caldwell, J.A., Reith, C.C., 1993. *Principles and Practice of Waste Encapsulation*. Lewis Publishers, Boca Raton, FL.
- Czurda, K.A., 1992. *Deponie und Altlasten*. EF-Verlag für Energie- und Umwelttechnik GmbH, Berlin.
- Deponieverordnung, 2002. *Verordnung über Deponien und Langzeitlager*, Bundesministerium für Umwelt, Naturschutz und Reaktorsicherheit, Berlin.
- Drescher, J., 1997. *Deponiebau*. Alphabet KG, Berlin.
- EU-Richtlinie, 1999. *Richtlinie über Abfalldeponien*, Rat der Europäischen Union. Amtsblatt der Europäischen Union, Brüssel.
- Gassner, E., 1991. *Gesamtfassung der Zweiten allgemeinen Verwaltungsvorschrift zum Abfallgesetz 1. Teil*. Verlag Franz Rehm, München.
- Hiltmann, W., Stribrny, B., 1998. *Tonmineralogie und Bodenphysik*. Springer-Verlag, Berlin.
- Huttenloch, P., Roehl, K.E., Czurda, K.A., 2001. Sorption of nonpolar aromatic contaminants by chlorosilane surface-modified natural minerals. *Environmental Science and Technology* 35, 4260–4264.
- Rowe, R.K., Quigley, R.M., Booker, J.R., 1995. *Clayey Barrier Systems for Waste Disposal Facilities*. Chapman & Hall, London.
- TA Siedlungsabfall, 1993. *Technische Anleitung zur Verwertung, Behandlung und sonstigen Entsorgung von Siedlungsabfällen*, Ministerium für Umwelt, Rheinland-Pfalz. Bundesanzeiger, Köln.



This page intentionally left blank

## *Chapter 11.4*

# CLAYS AND NUCLEAR WASTE MANAGEMENT

R. PUSCH

*Geodevelopment AB, Ideon, S-22370 Lund, Sweden*

Eliminating the risk of transportation of radionuclides from radioactive waste stored underground to the biosphere is the goal set by all countries that make use of nuclear power. Different countries plan “geologic disposal” in rocks, salt and clay sediments. The design principle is that highly radioactive waste, like burnt-out fuel and products from processed waste, is enclosed in containers—canisters—isolated by smectitic (smectite-rich) clay. These canisters are placed in vertical boreholes or long horizontal bored or blasted tunnels at a depth of 300–800 m. Low- and medium-level waste has shorter lifetimes and can be stored at smaller depth with less effective isolation.

Selection of smectitic clays with suitable bulk density to embed the canisters, is based on the fact that this type of “clay buffer” has the following valuable properties: (i) very low hydraulic conductivity; (ii) very low anion diffusion capacity and fairly low transport capacity of positively charged radionuclides; (iii) a high swelling potential for self-sealing of gaps and openings in the buffer and its contacts with the rock and canisters; (iv) favourable rheological properties, such as sufficient bearing capacity to minimise settlement of the heavy canisters, and sufficient softness to avoid transfer of high tectonically induced shear stresses to the canisters; (v) sufficient thermal conductivity to transfer heat caused by the radioactive decay to the rock without being too hot; (vi) colloid filtering capacity; and (vii) capacity to filter microbes.

The optimum bulk density at fluid saturation should be in the region of 1900–2100 kg/m<sup>3</sup> to meet the criteria; this density cannot be achieved by on-site compaction. Instead, very dense blocks of highly compacted smectitic clay powder are placed around the canisters, embedding them tightly. The required tightness is attained when the clay material swells after taking up water from the surrounding rock. Suggested design principles for repositories are illustrated in [Fig. 11.4.1](#). The design of a repository for low- and medium-radioactive waste is illustrated in [Fig. 11.4.2](#). This type of repository is located about 150 km north of Stockholm and has been in operation for 15 years ([Pusch, 1994](#)).

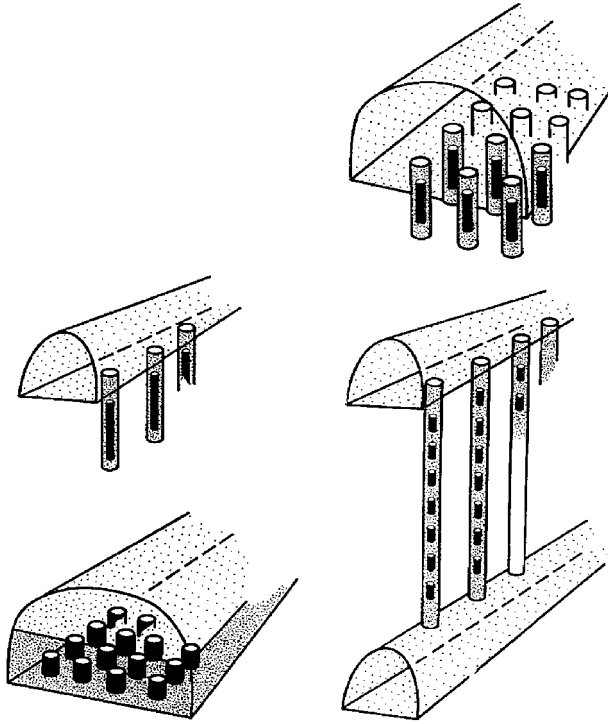


Fig. 11.4.1. Repository concepts, most of them implying that canisters with highly radioactive waste are surrounded by dense smectite clay and placed in holes or tunnels.

#### 11.4.1. BUFFER MATERIALS

Table 11.4.1 shows the candidate buffer-clay materials tested in international research work, and the major physical properties that have been determined. Typical hydraulic conductivity and swelling pressure data of tested buffer materials are collected in Tables 11.4.2 and 11.4.3 for different bulk densities.

In a few cases, the raw bentonite is so uniform and rich in smectite that only simple drying in the sun of the excavated material with subsequent grinding is required at the quarries and plants. However, in most cases the clay material must be dried in rotating kilns, and also transformed to a suitable  $\text{Na}^+$ -form.

The processed clay is commonly stored in silos or in stock piles protected from rain, and is packed in 25–50 kg paper bags or 1000 kg big bags for delivery. The preparation of buffer clay is made by compaction of dry clay powder to blocks with a high density. The blocks are then placed in the deposition holes to surround the canisters as illustrated in Fig. 11.4.3 for the Swedish KBS-3 concept. Fig. 11.4.4 shows a big ring-shaped block of bentonite for use in a KBS-3 repository (Johannesson et al., 1995).

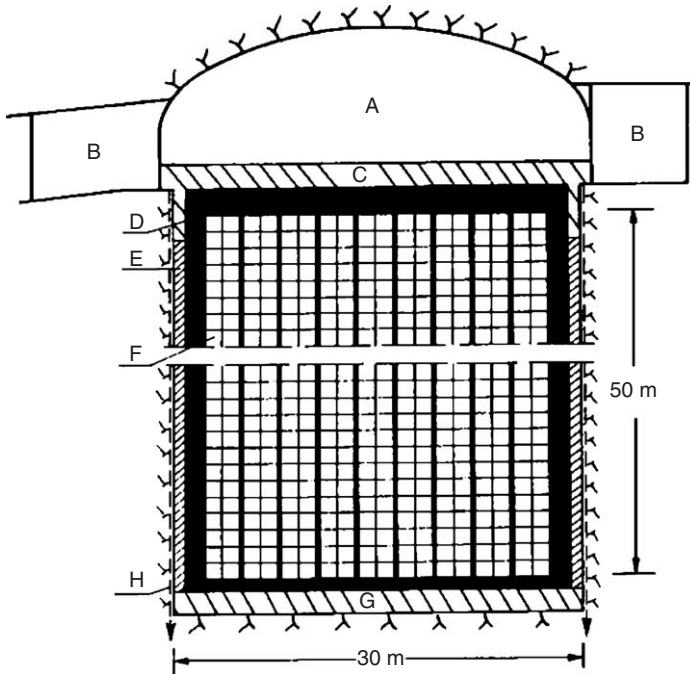


Fig. 11.4.2. Schematic section through a big concrete silo for final storage of low and intermediate radioactive waste in Sweden. (A) Cement-stabilised sand, (B) Concrete plugs, (C) Top cover of bentonite/sand mixture, (D) Concrete silo, (E) Fill of granulated bentonite, (F) Waste packages, (G) Bottom bed of bentonite/sand mixture (10/90) and (H) Rock drainage with discharge to a lower tunnels system until the repository is closed.

For isolation of less dangerous radioactive waste with a lifetime of less than about 500 years and causing almost no heat by radioactive decay, loosely filled granulates of smectite clay can be used as shown in Fig. 11.4.2.

#### 11.4.2. PREDICTED PERFORMANCE OF THE "CLAY BUFFER"

There are three major phases in the performance of the engineered buffer barrier: a first phase comprising application and evolution of the buffer including water uptake and swelling, leading to maturation (0–100 years); a second phase with the matured buffer exposed to a thermal gradient (100–1000 years); and a third phase with tectonic or glacial impact under ambient or reduced temperature (1000–1,000,000 years).

The first phase involves strong radiation and complex physico-chemical processes partly controlling the long-term performance of the buffer. This phase was regarded

Table 11.4.1. Physical properties of some buffer clay candidates. The first column indicates the major smectite mineral (Mt. means Montmorillonite) and the name of the commercial product

Clay	Manufacturing company	Smectite content	Properties <sup>1</sup>				
			$K$	$D$	$p_s$	$\lambda$	$(\phi, a, b)$
Mt. MX-80	American Colloid (USA)	75	*	*	*	*	*
Mt. Tixoton	Süd-Chemie (Germany)	90	*	—	*	—	—
Mt. Moosburg	Süd-Chemie (Germany)	65	*	—	*	—	*
Mt. IBECO Na	Silver & Baryte (Greece)	80	*	—	*	*	*
Mt. IBECO Ca	Silver & Baryte (Greece)	80	*	—	*	*	*
Saponite	(Geohellas, Greece)	80	*	—	*	—	—
Beidellite	(Through Enresa, Spain)	35	*	—	*	—	—
Kunigel	Kunimine Ind., Japan	50	*	—	*	—	—
Montm. RMN	Obrnice (Czech Republic)	90	*	—	*	*	—
Mixed-layer, Friedland	DURTEC (Germany)	45	*	—	*	—	—

\* = tests performed

<sup>1</sup> $K$  = Hydraulic conductivity,  $D$  = Diffusivity,  $p_s$  = Swelling pressure,  $\lambda$  = heat conductivity and capacity,  $(\phi, a, b)$  = rheological parameters.

Table 11.4.2. Hydraulic conductivity in m/s of SKB-tested potential buffer materials saturated and percolated with distilled water. Bulk densities 1800–2100 kg/m<sup>3</sup>

Density (kg/m <sup>3</sup> )	1800	1900	2000	2100
MX-80	$4 \cdot 10^{-13}$	$2 \cdot 10^{-13}$	$8 \cdot 10^{-14}$	$3 \cdot 10^{-14}$
IBECO, Na	$9 \cdot 10^{-13}$	—	$4 \cdot 10^{-13}$	—
IBECO, Ca	$2 \cdot 10^{-11}$	—	$2 \cdot 10^{-13}$	—
RMN	—	$4 \cdot 10^{-13}$	—	$8 \cdot 10^{-12a}$
Kunigel	$3 \cdot 10^{-12}$	—	$10^{-12}$	—
Beidellite	$5 \cdot 10^{-12}$	—	$5 \cdot 10^{-13}$	—
Saponite	$10^{-12}$	—	$5 \cdot 10^{-13}$	—

<sup>a</sup>With 5% graphite and 10% quartz powder.

as particularly important and has therefore been the focus of most of the international work up to now. If the hydraulic conductivity and swelling pressure are not significantly changed during this phase, the buffer will be practically impermeable. As such, it can serve as an excellent isolation of the waste in any time perspective. This applies if the canisters stay intact for the first few thousands of years, and significant mineral changes in the buffer do not occur in any of the phases. It is therefore of fundamental importance that the canister-embedding clay offers physical and

Table 11.4.3. Swelling pressure ( $p_s$ ) in MPa of a number of tested buffer materials saturated with distilled water

Density at saturation ( $\text{kg/m}^3$ )	1300	1500	1700	1800	1900	2000	2100
MX-80	0.06	0.2	0.4	0.8–0.9	1.4	4–5	10–12
IBECO, Na	—	—	—	0.6–1	—	4–5	—
IBECO, Ca	—	—	—	0.2	—	5	—
RMN	—	—	0.45	1.9 <sup>a</sup>	2.5 <sup>b</sup>	3.9 <sup>b</sup>	—
Beidellite	—	—	—	1.5	—	4.2	—
Saponite	—	—	—	2.5	—	8.8	—
Kunigel	—	—	—	0.2	—	0.9	—
Friedland	—	—	0.05	0.1	0.3	0.8–1	2–2.5

<sup>a</sup>Density at saturation 1850  $\text{kg/m}^3$ .

<sup>b</sup>Mixture with 5% graphite and 10% quartz powder. Density at saturation 1950  $\text{kg/m}^3$ .

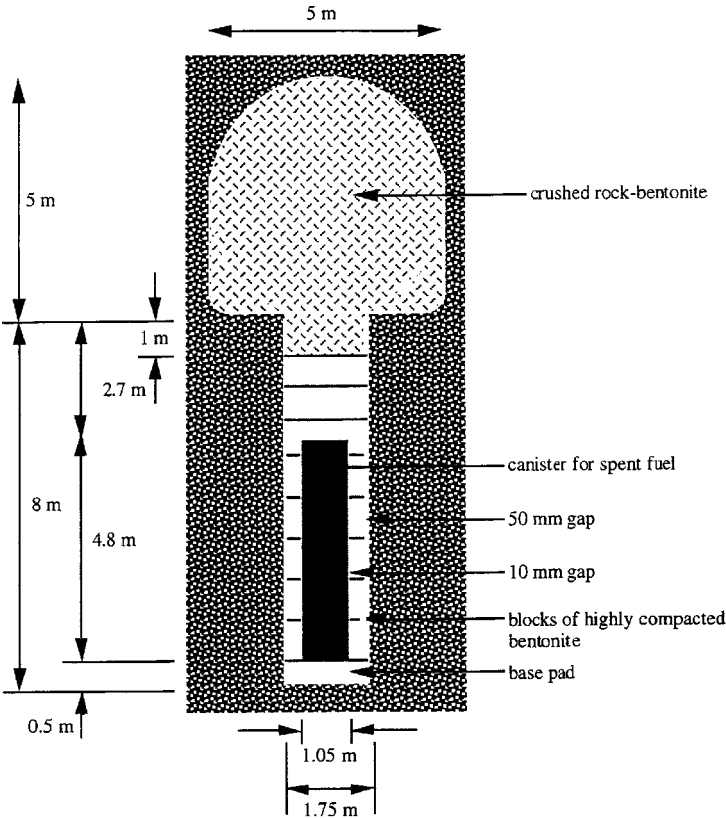


Fig. 11.4.3. Cross section of a deposition tunnel and hole for disposal of 20 ton canister of copper and steel containing used reactor fuel rods. KBS-3 concept.

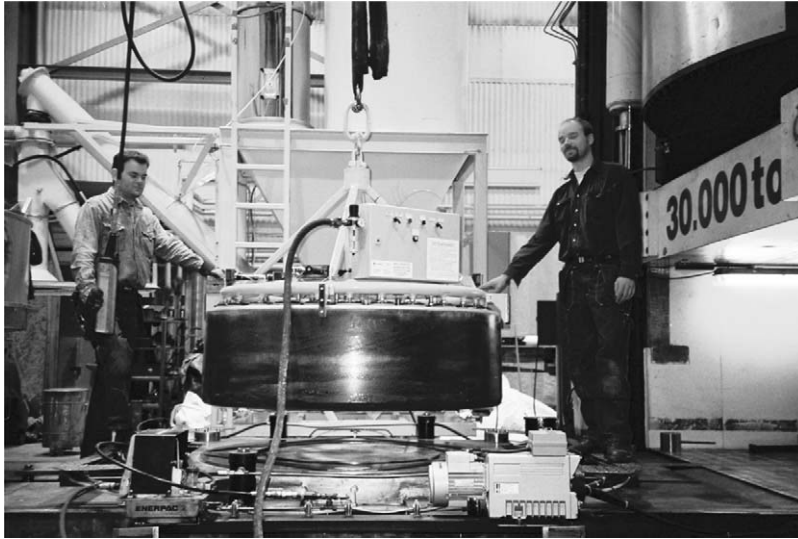


Fig. 11.4.4. Block of uniaxially compacted MX-80 clay powder using 100 MPa pressure. The diameter is 1.7 m and the height 0.5 m. The water content is about 12% and the density approximately  $2000 \text{ kg/m}^3$ .

chemical environments that preserve the tightness of the canisters for a long time, and delay the migration of radionuclides that may ultimately escape from them.

Taking the KBS-3 repository concept as a reference for isolation of highly radioactive waste by the use of compacted smectitic blocks a generalised conceptual model of the buffer has the following features:

1. Thermally induced redistribution of the initial pore-water in the clay
2. Uptake of water from the rock and backfill leading to hydration of the buffer
3. Expansion of the buffer yielding displacement of the canisters and overlying backfill
4. Dissolution of buffer minerals and precipitation of chemical compounds in the buffer.

Processes related to temperature are termed (T); those related to hydraulic processes (H); those dealing with mechanical, or rather rheological, behaviour (M); and mechanisms that have to do with chemical changes are termed (C).

#### *A. Thermally Induced Redistribution of the Initial Pore-Water and Maturation of the Pellet Fill (TH)*

Pore-water is transported in liquid and vapour form from the hotter to the colder parts of the buffer. This yields early saturation of the buffer close to the rock and desiccation close to the hot canister.

### *B. Uptake of Water from the Rock (THMC)*

Uptake of water from the rock and backfill is the process that ultimately yields complete water saturation and the final density distribution. If the rock gives off very little water to the clay, the backfill in the overlying tunnel may serve as the major water source. The water transport from the backfill to the buffer is controlled by the water pressure and by the suction of the buffer, as well as by the degree of water saturation of the backfill.

The wetting has a (C)-effect since  $\text{Ca}^{2+}$ ,  $\text{Mg}^{2+}$ ,  $\text{K}^{+}$ ,  $\text{SO}_4^{2-}$  and  $\text{Cl}^{-}$  ions will be precipitated at the wetting front which moves towards the canister. Thus, a rather large part of the buffer may contain such precipitates, which interact with the smectite minerals and the canisters. The temperature gradient has also a (C)-effect. This is because silicate minerals (including the smectite component) that are close to the heater will dissolve to a larger extent than those at the rock. The mechanism by which released silica migrates towards the rock and precipitates in the outer part of the bentonite is not well understood. Silicification causes some cementation and brittleness of the clay.

### 11.4.3. NUMERICAL MODELLING

The evolution of a detailed design of the buffer (the interacting components for the KBS-3 concept are defined in Fig. 11.4.5) has to be modelled with respect to maturation and homogenisation. Current co-operative international work, partly supported by the EU, deals with these issues. The conceptual model is the basis for the selection and development of numerical tools to predict and evaluate the T, H, M and C processes in the engineered barriers.

The proposed numerical formulations are exemplified by the EU-supported on-going work “Prototype Repository Project” by H.R Thomas and P.J Cleall (personal communication) at Cardiff University. The main features of their numerical model, code-named COMPASS, are

1. Moisture flow involves both liquid flow and vapour transfer. Liquid flow is assumed to follow a generalised Darcy’s law, while vapour transfer is represented by a modified Philip and de Vries approach.
2. Heat transfer includes conduction, convection and latent heat of vaporisation transfer in the vapour phase.
3. Flow of dry air due to the bulk flow of air and that of dissolved air in the liquid phase are considered. The bulk flow of air, induced by an air pressure gradient, is again represented by a generalised Darcy’s law. Henry’s law is employed to calculate the quantity of dissolved air and its flow is coupled to the flow of pore-liquid.
4. Deformation effects are included via either a non-linear elastic approach or an elastoplastic formulation. In both cases deformation is taken to be dependent on suction, stress and temperature changes.



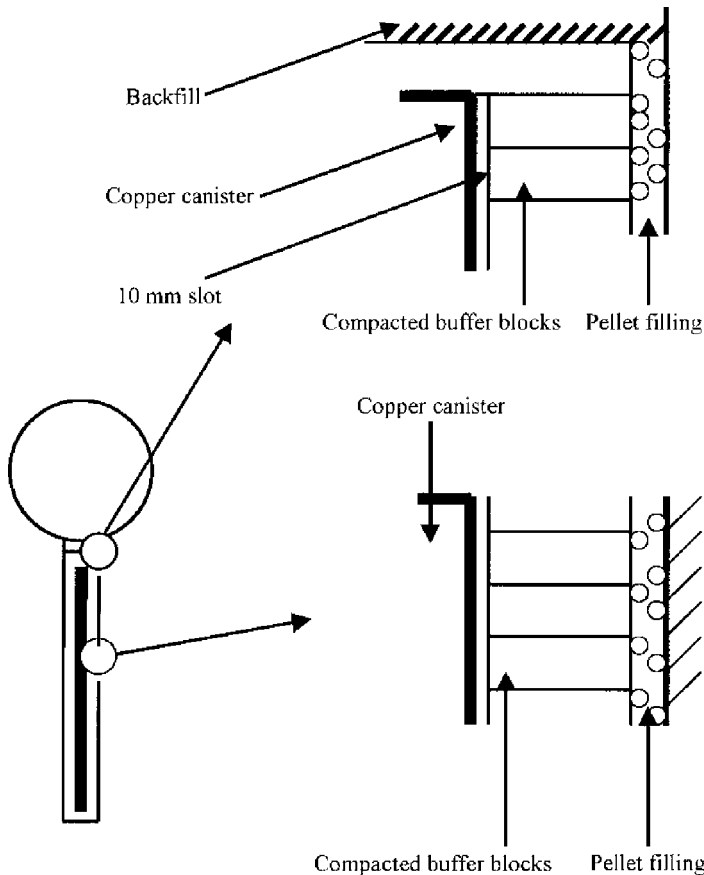


Fig. 11.4.5. Detail of KBS-3 deposition hole with copper-shielded canister embedded in compacted buffer blocks and bentonite pellet filling.

5. Chemical solute transport for multi-chemical species includes diffusion, dispersion and accumulation from reactions due to sorption.

The basis for formulation of governing equations is that heat conduction and flow are expressed using classical physics but is generalised by including the velocities of liquid, vapour and air. The velocities of pore-liquid and pore-air are calculated using a generalised Darcy's law with special respect to the chemical solute concentration gradient, the conductivity of the air phase and the pore-air pressure. Also, an osmotic flow term in the liquid velocity is included to represent liquid flow behaviour in some highly compacted clays. Air in partly saturated soil may exist in two forms: bulk air and dissolved air. In this approach, the proportion of dry air in the pore-liquid is defined using Henry's law.

When a chemical solute is non-reactive, its sorption on to the soil surface may be ignored. The governing equation for chemical transfer can then be expressed in terms of diffusion and dispersion. This equation, given in primary variable form, can be extended to a multi-chemical species form by introducing a sink term to account for mass accumulation from reactions due to sorption. This is then coupled to a geochemical model.

The total strain consists of components related to suction, temperature, chemical and stress changes. Formulations have been employed, taking into account both elasticity and elastoplasticity. The contribution of chemical solute to the stress-strain behaviour of the soil can, to a first approximation, be described by an elastic state surface concept based on osmotic potential.

A numerical solution of the governing differential equations is achieved by using the Galerkin weighted residual method to formulate the finite element discretisation. Shape functions are used to define approximation polynomials in the flow and stress/strain equations. The outcome of predictive modelling for the evolution of the “near-field” KBS-3 concept, made at Cardiff University, are shown in Figs. 11.4.6 (basic geometry), 11.4.7 (pore-water pressure in the buffer in contact with the canister) and 11.4.8 (temperature at the canister/buffer contact).

Both the theoretical model and the full-scale experiments actually show in-flow from the host rock overwhelming the predicted drying close to the hot canister, leading to eventual saturation (Fig. 11.4.7). The peak in temperature evolution (Fig. 11.4.8) represents the state when the buffer is at its driest. This demonstrates the effect of coupling between the hydraulic field and the temperature field, and that

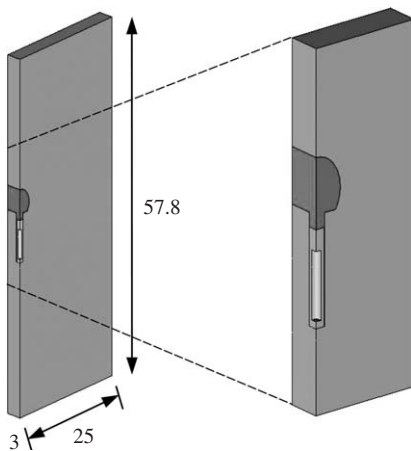


Fig. 11.4.6. Tunnel and rock section used for the thermal analysis and enlarged view of cross-section (ongoing modelling at Cardiff University for the EU-supported project “Prototype Repository Project”).

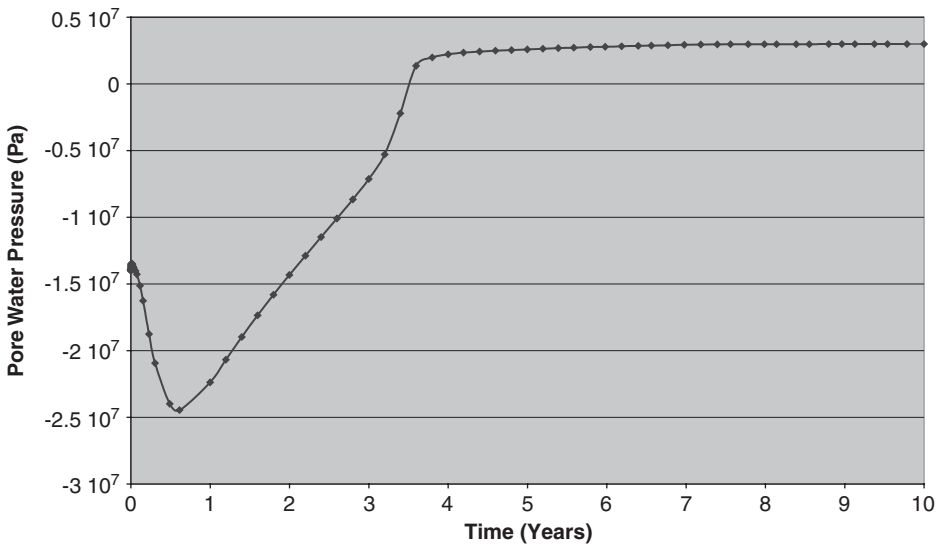


Fig. 11.4.7. Pore-water pressure plot at the heater/buffer interface at mid-heater height (ongoing modelling at Cardiff University for the EU-supported project “Prototype Repository Project”).

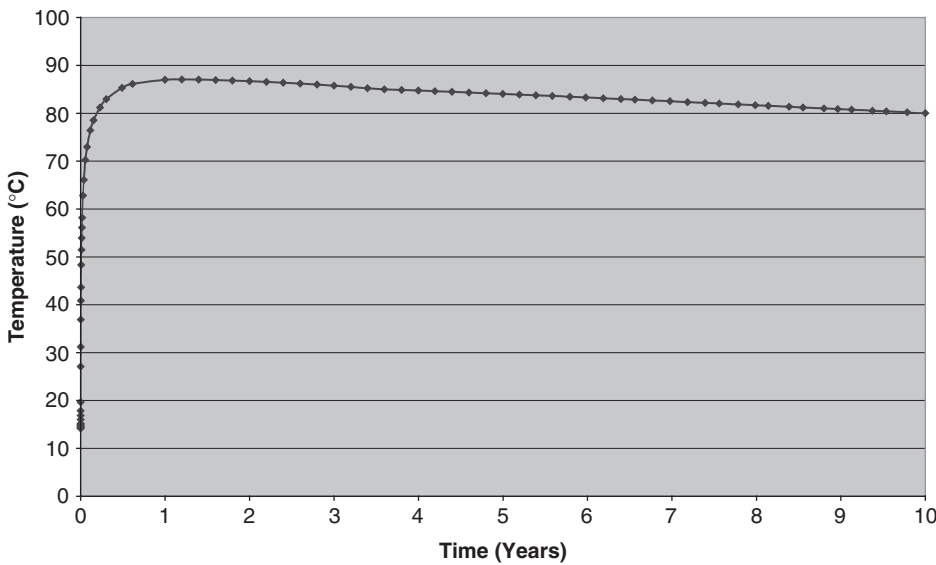


Fig. 11.4.8. Temperature plot at the heater/buffer interface at mid-height of the heater (ongoing modelling at Cardiff University for the EU-supported project “Prototype Repository Project”).

relevant numerical predictions should be based on coupled (THMC) models when possible.

#### 11.4.4. LONG-TERM PHYSICAL PERFORMANCE OF THE BUFFER

For physical stability of the buffer clay two major factors are identified: colloid transport and filtering, and microbiological filtering.

The issue of colloid transport through buffers was not examined in detail but some general conditions were defined. For example, by sorbing positively charged radionuclides and other cations, very small smectite particles can transport contaminants to the biosphere. Like many other constituents of colloidal size, such particles can form aggregates, gels and networks that easily link to the dense buffer clay (Pusch, 1999). Although smectite aggregates can be released if the pore-water flow is sufficiently high, this seems impossible under the local hydraulic gradients that prevail in the rock after closing the repository.

However, the buffer clay will tend to enter fractures in the rock although the front of fracture-penetrating clay may be very soft. Groundwater flowing in the fractures may, therefore, tear off small aggregates and transport them if the flow rate exceeds a few millimeters per second. Experiments as well as field observations demonstrate that the size of aggregates may range from 2 to 50  $\mu\text{m}$ . Because of their surface charge the aggregates can interact with, and attach to, the common fracture minerals, such as chlorite and micas. For this reason, the transport of smectite aggregates over long distances is not significant.

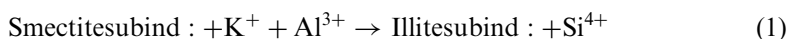
Bacteria may stay alive and develop in soft smectitic clay. Those that reduce sulphate are of particular importance to engineered barriers of the SKB-type as they usually carry a negative surface charge, and hence can move through clay like large organic polymers, such as humus colloids. However, such movement can be limited, at least partly, by hydration conditions and the very small pore space that exists in dense buffer clay (Pedersen, 1997). For MX-80 type clay with a density higher than 1800  $\text{kg/m}^3$ , the small size of interconnected voids and the limited access to free water prevent bacteria from moving and staying alive. Although spores may survive and be operative, the working hypothesis is that ultimately all life forms in the buffer will be eradicated.

#### 11.4.5. CHEMICAL STABILITY OF THE BUFFER

While gamma radiation has a small impact on the longevity of the buffer smectites (Pusch, 1994), dissolution and conversion to non-expanding clay minerals is a threat. The chemical integrity of smectites is determined by thermodynamically controlled reactions. Thus, mineral stability and transformations depend on the prevailing conditions of temperature and temperature gradient under which minerals and pore-water interact.

Three major types of processes take place in the water-saturated buffer: (i) dissolution/precipitation; (ii) conversion of smectite to non-expandable mineral forms; and (iii) cementation by neo-formed complexes.

Dissolution of buffer silicates with concomitant diffusion of released elements (primarily silicon) is negligible under normal pH conditions and ambient rock temperature, but it can be significant in hot repositories. Under temperature gradients  $\text{Si}^{4+}$  moves into relatively cold parts, and precipitates in the form of amorphous silica, cristobalite or quartz according to the generalised model given by Eq. (1)



The conversion of smectite to non-expandable minerals (“illitisation”) in buffer smectites is generally considered as the major threat. This process depends on the temperature and groundwater composition in a very complex way. Under commonly prevailing pH conditions, the most probable mechanism is the alteration of smectite (S) to non-expanding hydrous mica, i.e. “illite” (I). The structure of illite is similar to that of montmorillonite but illite has a higher layer charge arising from isomorphous substitution of  $\text{Al}^{3+}$  for  $\text{Si}^{4+}$  in the tetrahedral sheet. Illite does not expand because the interlayer space is occupied by non-hydrated  $\text{K}^+$  ions. The smectite-to-illite conversion is assumed to take place in two ways: (i) replacement of tetrahedral silicon by aluminium and uptake of external potassium, leading to mixed-layer (I/S) minerals where I becomes progressively dominant, and (ii) neo-formation of illite in the pore space of the smectite supplying silicon, aluminium or magnesium, while potassium enters from outside and triggers illite formation.

Irrespective of the mechanism involved, the rate of conversion of smectite to illite is assumed to be controlled by the access to potassium. Neo-formation of illite is expected to take place at certain concentrations of silicic acid ( $\text{H}_4\text{SiO}_4$ ), aluminium and potassium, yielding crystal nuclei in the form of laths. When precipitation takes place the potassium concentration drops locally and the concentration gradient thus formed brings in more potassium by which the process continues. Geochemical codes tend to indicate that illite should be formed from smectites in a certain “window” of phase diagrams of silica, aluminium and potassium, but they do not seem to be able to indicate whether the conversion takes place via mixed-layer mineral stages or by dissolution/neo-formation.

Natural analogues provide examples of the extent and rate of conversion from smectite to non-expandable minerals. The Ordovician Kinnekulle bentonite still contains about 25% smectite after a heating sequence very similar to that expected in a KBS-3 repository. The Silurian Hamra bentonite also has about the same smectite content after 10 million years of exposure to somewhat more than 100 °C (Pusch, 1994). Detailed descriptions of these two bentonites seem to validate the working model that is presently used in the Swedish R&D work on smectite conversion. It is based on the hypothesis that smectite alteration can take place either by successive transformation to mixed smectite/illite and further to pure illite or by dissolution of

smectite and neo-formation of illite. Both require sufficient energy and access to potassium. The model is based on Pytte's theory (Pytte, 1982) which has the following basic mathematical form:

$$-\frac{dS}{dt} = [Ae^{-U/RT(t)}] \left[ \left( \frac{K^+}{Na^+} \right) m S^n \right] \quad (2)$$

where:

$S$  = Mole fraction of smectite in  $I/S$  assemblages

$R$  = Universal gas constant

$T$  = Absolute temperature

$U$  = Activation energy, kcal/mol

$t$  = Time

$A$  = pre-exponential factor

$m, n$  = coefficients

The problem with this and similar theories is that the activation energy is not known with great certainty. It is assumed to be in the range of 26–28 kcal/mol for which calculations give reasonable agreement with natural analogues. The potassium content is the most important parameter for any temperature. Fig. 11.4.9 shows the temperature dependence of illitisation for an activation energy of 113 kJ/mol and a potassium concentration of 0.01 mol/L in the water, which is high. It implies that 90% of the smectite would remain after 1000 years at 100 °C temperature and 50% would still be intact after 10,000 years. Since the temperature will be down to

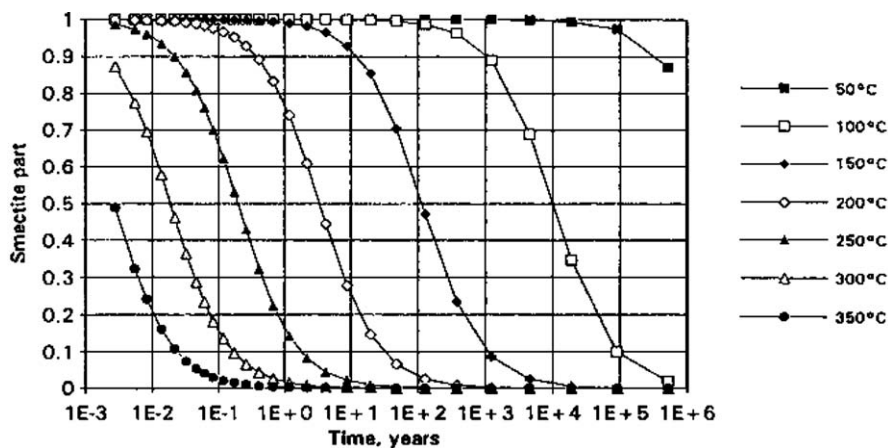


Fig. 11.4.9. Rate of conversion of smectite to illite according to the Pytte-based model for 27 kcal/mol activation energy and a potassium concentration of 0.01 mol/L (Pusch, 1994). The initial smectite content (smectite part) that is taken as 100% (unity) drops successively with time.

ambient already after a few thousand years, the large majority of the smectite minerals in the buffer will be preserved for hundreds of thousand of years provided that the temperature does not exceed 100–150 °C in any of the buffer evolution phases.

Cementation by precipitation of neo-formed substances can take place by release of silica in the hottest part of the buffer and migration of silica in hydrated form towards the colder part, where precipitation and cementation of smectite particles can take place (Pusch, 1998). In the Kinnekulle case, the application of solid-state smectite conversion models (using the activation energies 117 and 101 kJ/mol and chemical codes) described in the reference, has shown that the amount of dissolved smectite and released silica that can be precipitated are small. In good agreement with these results, shear tests indicate that silicification has only led to slight cementation, yielding a somewhat brittle behaviour and a shear strength that is slightly higher than the overburden pressure would produce.

## REFERENCES

- Johannesson, L-E., Börjesson, L., Sandén, T. 1995. Compaction of bentonite blocks. SKB Technical Report 95-19. SKB, Stockholm.
- Pedersen, K., 1997. Investigations of subterranean microorganisms and their importance for performance assessment of radioactive waste disposal. SKB Technical Report TR 97-22. SKB, Stockholm.
- Pusch, R., 1994. Waste Disposal in Rock. Developments in Geotechnical Engineering. Elsevier, Amsterdam, p. 76.
- Pusch, R., 1998. Chemical processes causing cementation in heat-affected smectite—the Kinnekulle bentonite. SKB Technical Report TR 98-25. SKB, Stockholm.
- Pusch, R., 1999. Clay colloid formation and release from MX-80 buffer. SKB Technical Report TR 99-31. SKB, Stockholm.
- Pytte, A.M., 1982. The Kinetics of the Smectite to Illite Reaction in Contact Metamorphic Shales. M.A. Thesis. Dartmouth College, Hanover, NH.

## Chapter 11.5

# CLAYS AND HUMAN HEALTH

M.I. CARRETERO<sup>a</sup>, C.S.F. GOMES<sup>b</sup> AND F. TATEO<sup>c</sup>

<sup>a</sup>*Departamento de Cristalografía, Mineralogía y Química Agrícola, Facultad de Química, Universidad de Sevilla, ES-41071 Sevilla, Spain*

<sup>b</sup>*Departamento de Geociências, Universidade de Aveiro, P-3810-193 Aveiro, Portugal*

<sup>c</sup>*Istituto di Ricerca sulle Argille, CNR, I-85050 Tito Scalo (PZ), Italy*

Clay minerals can be beneficial to human health by serving as active principles or excipients in pharmaceutical preparations, in spas, and in beauty therapy medicine. In some cases, however, these minerals can be harmful to human health. Both the beneficial and harmful effects of clay minerals are described in this chapter.

## 11.5.1. BENEFICIAL EFFECTS OF CLAYS AND CLAY MINERALS

### *A. Historical Background*

Since prehistoric times man used clay for therapeutic purposes. There are indications that *homo erectus* and *homo neanderthalensis* used ochres mixed with water and different types of mud to cure wounds, to soothe irritations, as a method of skin cleaning, etc. This might be due to their mimicking animals, many of which instinctively use minerals for such kind of purposes. The clay plates of Nippur, Mesopotamia, which date back to about 2500 BC, contain a reference to the use of clay for therapeutic purposes, including the treatment of wounds and the inhibition of haemorrhages. In ancient Egypt, Pharaoh's doctors used Nubian earth as an anti-inflammatory agent, and yellow ochre (a mixture of clay and iron oxy/hydroxides) as a cure for skin wounds and internal maladies and as a preservative in mummification. Likewise, Cleopatra (44–30 BC), Queen of Egypt, used muds from the Dead Sea for cosmetic purposes (Bech, 1987; Newton, 1991; Robertson, 1996; Veniale, 1997; Reinbacher, 1999).

In the Ancient Greek period, mud materials were used as antiseptic cataplasms to cure skin afflictions, as cicatrices, or as a cure for snakebites. *Bolus Armenus*, a red clay found in the mountain caves of Cappadocia, old Armenia, present-day Turkey, was famous as a medicinal clay, as were the so-called *terras* of the Greek islands Lemnos, Chios, Samos, Isola, Milos, and Kimolos. These *terras* were prepared and



shaped into disks (called “earth coins” and used until the 19th century) that were marked or stamped with different symbols, for example with the goat stamp, the mark of the goddess Diana/Artemis (Bech, 1987). Among these, the *terra sigillata* of Lemnos deserves particular mention, because of its astringent and absorbent properties. The clay from Kimolos was identified as  $\text{Ca}^{2+}$ -smectite (Robertson, 1986), and the *terra sigillata* of Samos as kaolinite or illite/smectite mixed-layer mineral (Giammatteo et al., 1997). Galeno (131–201 AD), a Greek doctor (born in Pergamo) described medicinal muds, and used clays to deal with malaria, and stomach and intestinal ailments.

In some civilisations, the use of clays was extended to ingesting clays for therapeutic purposes. Aristotle (384–322 BC) made the first reference to the deliberate eating of earth, soil, or clay by humans (for therapeutic and religious purposes). Later, Marco Polo described how in his travels he saw Muslim pilgrims cured fevers by ingesting “pink earth”. This practice is still followed in certain countries and communities for therapeutic purposes, or even to relieve famine (Mahaney et al., 2000). The rubbing of clays into the body for therapeutic purposes was known for a very long time. However, this custom (as practiced in contemporary spa centres) did not become widespread in Europe until Roman times when dedicated buildings, called “balnea”, were erected. Later, the use of spas declined. During the 19th century and the beginning of the 20th century spas reappeared, and were frequently visited. Many of them continue using muds for therapeutic purposes. Some examples are Centro Termal das Furnas in Vale das Furnas, on the island of São Miguel (Azores), Montecatini Terme, Ischia and Abano Terme in Italy, Karlovi Vary in the Czech Republic, and Archena and El Raposo in Spain.

The famous *Papyrus Ebers* (dated about 1600 BC, but a copy of a papyrus from 2500 BC) describes some diseases and their treatment using mineral- and, particularly, clay-based medicines. Other references to the curative powers of clays appear in *Pen Ts'ao Kang Mu*, a famous old catalogue about Chinese medicine. In Roman times similar references could be found in Dioscorides' *De Materia Medica* (60 BC). This book also has a section dealing with minerals and chemical substances used in pharmacy. In his *Natural History*, Pliny the Elder (23–79 AD) also described the use of clays, especially those found around Naples (volcanic muds), for curing stomach and intestinal ailments. In the 11th and 12th centuries Avicena (980–1037 AD) and Averroes (1126–1198 AD) classified and encouraged the use of medicinal muds (Bech, 1987; Veniale, 1999a). Later, *Lapidarios*, dealing partially with the use of minerals from a therapeutic perspective, would appear. Among these works is the famous *Lapidarios* of the Spanish King, Alfonso X the Wise (1221–1284 AD). The first extant *Lapidario* is a translation into Spanish by Yhuda Mosca and Garci Pérez of Abolays' book in Arabic that Abolays himself had previously translated from Chaldean, although its original source is not known (Brey Mariño, 1982). During the Renaissance *Pharmacopoeia* appeared. These were texts that, among other drugs, classify different minerals for medicinal uses. In addition, they described regulations concerning their uses, such as the official codes that must be followed to produce

medicines. Their appearance coincided with the first mineralogical classifications. In the 17th century the first scientific academies were founded, one aspect of whose work was to document the advances of mineralogy in medico-pharmaceutical matters, thus producing various entries in the pharmacopoeias. In the early 20th century the development of chemistry enabled numerous minerals to be obtained through synthesis. The use of synthetic minerals had a negative effect on the use of naturally occurring minerals for therapeutic uses and as excipients. However, given the difficulty and cost involved in synthesising minerals on an industrial scale, natural clay minerals are mainly used for such purposes at present. An exception is “Laponite S”, a synthetic hectorite made by the Laporte Company (NL), and used as a jellifying material in cosmetic formulations (Galán et al., 1985; Bech, 1987; Carretero, 2002).

### *B. Clay Minerals in Pharmaceutical Formulations*

The use of clay minerals in pharmaceutical formulations was described by many authors (Del Pozo 1978, 1979; Galán et al., 1985; Bech, 1987; Cornejo, 1990; Gámiz et al., 1992; Bolger, 1995; Veniale, 1992, 1997; Viseras and López-Galindo, 1999; López-Galindo and Viseras, 2000; Carretero, 2002), and collected in different pharmacopoeias (AA.VV., 1996, 1998, 2002a,b,c,d).

Kaolinite, talc, palygorskite, and smectites are used for therapeutic purposes in pharmaceutical formulations as active principles or excipients. The possible use of sepiolite as active principle or excipient in pharmaceutical formulations was also investigated (Hermosín et al., 1981; Cornejo et al., 1983; Forteza et al., 1988; Ueda and Hamayoshi, 1992; Del Hoyo et al., 1993, 1998; Viseras and López-Galindo, 1999; López-Galindo and Viseras, 2000; Cerezo et al., 2001) and there are commercial medicine that includes sepiolite in its composition (as active principle and excipient). The fundamental properties for which clay minerals are used in pharmaceutical formulations are high specific area and sorptive capacity, favourable rheological characteristics, chemical inertness, low or null toxicity for the patient, and low price.

#### *Use as Active Principles*

As gastrointestinal protectors, antacids, and antidiarrhoeaics, clay minerals can be administered to the patient orally in the form of pills, powders, suspensions, and emulsions. Clay minerals are also applied topically (to the body's exterior, or on a limited portion of the body) as dermatological protectors or for cosmetic reasons.

Kaolinite and palygorskite are used as gastrointestinal protectors. Their therapeutic action is based on their high specific area and sorption capacity. They adhere to the gastric and intestinal mucous membrane and protect them, and can absorb toxins, bacteria, and even viruses. However, since they also eliminate enzymes and other necessary nutritive elements, their prolonged use is inadvisable. Although smectites also have a large surface area and sorption capacity, they are not generally used as gastrointestinal protectors. This is because smectites tend to decompose

when they come into contact with the stomach's hydrochloric acid (pH 2), and probably also when they get to the bowel (pH 6).

Smectites and palygorskite are used as antacid due to their  $H^+$  neutralising capacity. They are indicated in the treatment of gastric and duodenal ulcers.

Kaolinite, smectites and palygorskite are also used as antidiarrhoeaics due to their high water adsorption capacity. By eliminating the excess water from faeces, the material becomes more compact. Calcium smectites are also used as antidiarrhoeaics due to the astringent action of the  $Ca^{2+}$  ion, which forms non-soluble, hydrated phosphates.

Kaolinite, talc, and smectites are used as dermatological protectors. These clay minerals can adhere to skin, forming a film that mechanically protects the skin against external physical or chemical agents. By absorbing the skin's secretions, and creating a large surface for their evaporation, they also have a refreshing action. Surface evaporation also promotes a gentle antiseptic action as it produces a water-poor medium that is unfavourable for the development of bacteria. This latter action is reinforced by the capacity of these minerals to sorb dissolved and suspended substances, such as greases, toxins, and even bacteria and viruses.

The use of these clay minerals as dermatological protectors should be preceded by a mineralogical study of the corresponding raw materials. This is because in many cases they contain mineral impurities such as quartz (in smectites), and chrysotile or tremolite (in talc) that are dangerous for inhalation. For example, [Bowes et al. \(1977\)](#) reported that of the 27 consumer talcum powders, purchased in the USA, 11 contained tremolite and/or anthophyllite in proportions ranging from 0.5 to over 14%. The use of palygorskite as a dermatological protector is not advisable. Nor does palygorskite appear in any pharmaceutical formulation as powder because of current doubts about its possible carcinogenic effect if inhaled (see below).

Kaolinite, smectite, talc, and palygorskite (the last one recommended only in liquid preparations such as creams, emulsions, etc.) are used as active principles in cosmetics. They feature in face masks because of their high capacity for adsorbing greases, toxins, etc. They are also used in creams, powders, and emulsions as antiperspirants, to give the skin opacity, remove shine, and cover blemishes. The 2002 market saw the appearance of a moisturising cream that contained very small particles of mica (possibly muscovite), producing a luminous, light reflective effect.

#### *Use as Excipients*

Kaolinite, talc, palygorskite, and smectites are used as excipients in cosmetics and pharmaceutical preparations. In the latter application, these minerals function as:

- (i) lubricants to ease the manufacture of pills (talc);
- (ii) agents to aid disintegration through their ability to swell in the presence of water (smectites), or through the dispersion of fibres (palygorskite), promoting release of the drug when it arrives in the stomach; and
- (iii) emulsifying, polar gels and thickening agents because of their colloidal characteristics (palygorskite, smectites, kaolinite) by avoiding segregation of the

pharmaceutical formulation's components and the formation of a sediment that is difficult to re-distribute.

Although all the excipients are considered to be inert, research carried out during the last 30 years showed that interaction may occur between the drug and the clay mineral used (White and Hem, 1983; Sánchez Martín et al., 1988; Cornejo, 1990). This process can influence two highly important aspects in the drug's bioavailability: its liberation and stability. With respect to the drug's liberation, the interaction between the drug and its excipient can retard the drug's release and therefore its absorption, lowering its levels in the blood. This phenomenon, detectable by *in vitro* studies, may produce undesirable effects on a patient's health if, for the drug to be effective, immediate therapeutic levels in the blood are required, as in the case of antihistamines (White and Hem, 1983). However, the slow, controlled desorption of the drug can have a positive effect on its therapeutic action, as in the case of amphetamines and antibiotics (Mc Ginity and Lach, 1977; Porubcan et al., 1978), or water-resistant sun screens (Vicente et al., 1989; Del Hoyo et al., 1998, 2001). Regarding the drug's stability, interaction between drug and mineral excipient can accelerate degradation of the drug with consequent loss of therapeutic activity and increased health risk (Porubcan et al., 1979; Hermosín et al., 1981; Cornejo et al., 1983; Forteza et al., 1988, 1989).

The interaction of drugs with clay mineral excipients used in pharmaceutical preparations should be studied on a drug-by-drug basis. Doctors must also keep this point in mind when they prescribe medication to patients. Given the high surface reactivity of clay minerals, this interaction can occur either in the pharmaceutical formulation itself or in the gastrointestinal tract, even though the drugs are administered in different pharmaceutical formulations. This interaction can be detrimental to human health and, in some cases, to human life. For example, montmorillonite can catalyse the acid hydrolysis of digoxin, a cardiovascular tonic (Porubcan et al., 1979). When digoxin is administered in liquid preparation (without clay minerals), it can come in contact with montmorillonite from another pharmaceutical preparation administered at the same time. The interaction between digoxin and montmorillonite in the stomach (pH 2) could cause degradation of the drug. As a result, the drug loses its therapeutic activity and the patient's life is endangered.

### *C. Clay Minerals in Spa and Beauty Therapy*

Kaolinite and smectites are used in spa and beauty therapy, as are illite, interstratified illite/smectite and chlorite, and, on occasion, sepiolite and palygorskite.

Common (polymineralic) clays are also used. Besides phyllosilicates, these minerals contain Fe-Mn-(hydr)oxides and other associated phases such as calcite, quartz, and feldspars. The presence of these phases should be controlled, because the final product applied to the patient should have only the required and appropriate mineral properties for their use.

The main properties of clay minerals determining their usefulness in spa and aesthetic medicine, are:

- (i) softness and small particle size since the application of the mud, particularly as face mask, can otherwise be unpleasant;
- (ii) appropriate rheological properties for the formation of a viscous and consistent paste, and good plastic properties for easy application, and adherence to the skin during treatment;
- (iii) similarity in pH to that of the skin so as to avoid irritation or other dermatological problems;
- (iv) high sorption capacity. Clays can eliminate excess grease and toxins from skin, and hence are very effective against dermatological diseases such as boils, acne, ulcers, abscess, and seborrhoea. An organic active principle can also be incorporated into the clay mineral before its application to the patient's skin for therapeutic purposes;
- (v) high CEC, enabling an exchange of nutrients ( $K^+$  or  $Na^+$ ) to take place while the clay mineral is in contact with the skin; and
- (vi) high heat-retention capacity. As heat is also a therapeutic agent, clay minerals are applied hot to treat chronic rheumatic inflammations, sport traumatism, and dermatological problems.

Smectites (bentonite clays) fulfil many of the requirements for usage in spa and beauty therapy.

#### *Types of Application and Therapeutic Activity*

The different types of application and therapeutic activity of clay minerals in spas and beauty therapy received much attention over the past 20 years (Messina and Grossi, 1983; Torrescani, 1990; Barbieri, 1996; De Bernardi and Pedrinazzi, 1996; Novelli, 1996; Martín Díaz, 1998; Benazzo and Todesca, 1999; Lotti and Ghersetich, 1999; Nappi, 2001; Carretero, 2002).

Clays can be used mixed with water (geotherapy), mixed with sea or salt lake water or minero-medicinal water, and then matured (pelotherapy), or mixed with paraffin (paramuds). These three methods are used in spas and in beauty therapy. In geotherapy and pelotherapy the application form can be as face masks, cataplasms, or mud baths, depending on the body area to be treated, although in some spas they are also used for corporal massages. Application temperature (hot or cold) depends on the therapeutic aims. The paramuds are applied only as cataplasms, and always hot.

Face masks are used mainly in beauty therapy. Cataplasms are used in spas and in beauty therapy, when the mud is applied to only a small area of the body. Mud baths are preferentially used in spas, as the area under treatment is extensive. Application is carried out by submerging part of the body (bathing the arms, hands, or feet) or the whole body in a bowl or bath filled with a mixture of clay and water. The application of face masks and cataplasms is carried out in layers of between 1 and 5 cm for 20–30 min. When applied hot (40–45 °C) cataplasms are covered with an

impermeable material to conserve the heat. In most cases the paste is recycled from one patient to another.

Hot application is recommended in geotherapy, pelotherapy or paramuds in beauty therapy for the following therapeutic purposes:

- (i) to moisturise the skin, since during application the perspiration produced cannot evaporate as the paste is covered with an impermeable material. This perspiration soaks into the upper layers of the epidermis, moisturising it from within. Moreover, after application, the skin is in a hyper-porous state, which means cosmetic substances will be easily absorbed by the corneous layer, reaching the deepest layers of the epidermis;
- (ii) to treat compact lipodystrophies in their initial evolution when they need preventive care but cannot be treated more aggressively, and before the application of cosmetics;
- (iii) to retard the development of cellulite, given that they stimulate venous and lymphatic circulation in the application area and that they act as anti-inflammatories; and
- (iv) for cutaneous cleaning and treating dermatological conditions such as black-heads, spots, acne, ulcers, abscess, and seborrhoea. Heat promotes perspiration and the flow of sebaceous secretions in a fluid state, and their sorption by the clay mineral. Heat also opens the pylosebaceous orifices, improving sorption of the cosmetic substances.

Hot clay application produces a sensation of heat in the area treated, as well as vasodilatation, perspiration, and the stimulation of cardiac and respiratory frequency. As this creates a stimulatory, antiphlogistic, and analgesic action, such applications are recommended in spas, for the two following diseases: (i) chronic rheumatic processes including degenerative osteoarthritis in any part of the body, dysendocrine arthropathies, spondilo-arthritis ankylopoietic, spondylosis, myalgias, neuralgias and (ii) sequelae of osteo-articular injuries, fractures, dislocations; disorders following vasculopathies.

We should note that hot application is contra-indicated in areas of the body with circulatory problems (e.g., varicose veins), and in the acute and sub-acute phases of rheumatic processes, discompensated cardiopathies, tuberculosis, and renal or hepatic deficiencies. In acute pathologies (inflamed or congested areas), the application temperature must be lower than body temperature (cold muds). Here the application produces a cooling of the area under treatment, and since the mixture is a good conductor of the heat given off by the inflammation, it acts as an anti-inflammatory agent. The mixtures can also be used cold in liquid-retention problems.

### *Pelotherapy*

Of the three types of application of clay minerals in spas and beauty therapy, pelotherapy is the most favoured, because the maturation process improves the therapeutic properties of the final product (peloid) applied to the patient.

The International Society of Medical Hydrology defines “peloid” as “... a natural product consisting of a mixture of sea, salt lake, or minero-medicinal water (liquid phase), with organic and inorganic material (solid phase) produced by biological action (humus) and geological action (clay minerals)”.

A comprehensive report on peloid preparation, particularly on the maturation process, is not available. However, much progress was made in this direction by the Gruppo Italiano of AIPEA who sponsored two meetings (Veniale, 1996, 1999b) and published a catalogue of Italian “clay geomaterials for peloids” (Veniale, 1999c). Since Italy has an exceptional tradition of thermal treatments, the catalogue and meetings provide a snapshot of pelotherapy, with about 30 spas collaborating to varied extents on compiling the catalogue. In recent years there were other important contributions to the knowledge of pelotherapy (Ferrand and Yvon, 1991; Veniale and Setti, 1996; Yvon and Ferrand, 1996; Veniale, 1997; Summa and Tateo, 1998; Bettero et al., 1999; Cara et al., 1999; Gorgoni et al., 1999; Jobstraibizer, 1999; Minguzzi et al., 1999; Summa and Tateo, 1999; Veniale et al., 1999; Cara et al., 2000a, 2000b; Sánchez et al., 2000a, 2000b; Gomes and Silva, 2001; Carretero, 2002; Sánchez et al., 2002).

Peloid preparation varies from place to place. Depending on the particular spa tradition, the maturation process ranges from a few months to two years. Some spas use naturally matured clays collected from a spring basin, others collect the peloid from saline pools. The majority of spas, however, use artificial ponds where the natural (“virgin”) clay is mixed with mineral, thermo-mineral, or sea water that issues in the vicinity of the spas or inside the spa buildings. The clay is placed in the ponds for some months, during which period it is periodically shaken. The water may be stagnant, periodically renewed, or, more rarely, continuously flowing through the ponds. Interestingly, many spas initially used local clays but when these ran low, switched to commercial clays, or a mixture of local and commercial materials. An alternative strategy, adopted by some spas, is to recycle the material (after use on a patient), that is, the “exhausted” peloid is again matured. It is assumed that all harmful and hazardous elements, taken up from the previous patient, are removed during re-maturation.

Maturation is a very complex process involving water and a multiplicity of materials, including minerals (the mud is usually not mono-mineralic), inorganic solutes, biogenic components, and organic molecules as well as different physico-chemical conditions, such as temperature, Eh, and pH. Furthermore, many of these parameters are modified during the maturation period (cycling of temperature, light, hydrologic regime, shaking time). This can influence the manner in which certain materials develop. The length of maturation is a key parameter. The three main factors controlling peloid properties are raw clay composition, water composition, and mixing mode (“maturation”). During maturation organic substances as well as macro- and micronutrient elements present in the water are taken up by the peloid and can be released during application to the human body.

The maturation process improves some physical properties of the clay minerals, such as heat retention capacity, rheology, and adhesion. At the same time, some



changes in mineralogy and organic matter take place. These modifications improve the therapeutic effect of clay in pelotherapy.

With regard to specific heat, Ferrand and Yvon (1991) published a report on mixtures of clays. The thermal behaviour of several mixtures of kaolinite, bentonite, silt, and sand was tested and the temperature was measured at an appropriate and constant viscosity. The authors propose a lineal equation for the calculation of the specific heat, in function of the current in water. Likewise, Cara et al. (2000a) propose a similar formula to that of Ferrand and Yvon (1991) to calculate the specific heat of (Sardinian) bentonites. In agreement with the previous work, the specific heat was dependent on the smectite content of the bentonite. Although this investigation was not yet carried out with peloids (only with mixed water-clay, without maturation), the findings are important. By extrapolating the results to pelotherapy, heat dissipation during peloid treatment could be predicted.

The rheological and adhesive properties of peloids are important since the surficial interactions of skin with peloid drive the mass and heat transfer between the two bodies. Obviously, the nature of the raw material, the minero-medicinal water, and the maturation process have a profound influence. A number of parameters were recently used to measure the characteristics of the muds and their affinity to the skin. Bettero et al. (1999) used the RTM<sup>®</sup> and TVS<sup>®</sup> indices. The RTM<sup>®</sup> index represents the evolution of the viscous, elastic, visco-elastic, and structural features of the mud, whereas the TVS<sup>®</sup> is a bioadhesive index, representing the affinity of different materials (mud, water, etc.) for the surface of the skin in question. Both indices can be used to predict peloid quality obtained through a given maturation process. Sánchez et al. (2000b) used the adherence index, a measure of the adhesiveness of the peloid to the skin, and found that this index did not vary with the maturation time (one clay, two different waters). However, these results cannot be extrapolated to all spas (with different composition of the waters and clay mineralogy), and further investigation in this field is necessary.

While the rheological properties of various clay minerals were long investigated in relation to different applications (Güven and Pollastro, 1993; Penner and Lagaly, 2001), not much research was carried out in terms of pelotherapy. It seems likely, however, that the rheological and adhesive properties of therapeutic clays can be “tuned” to their mineralogical composition and maturation conditions.

Little information is available about the clay mineral composition in peloids and the changes in mineralogy that occur during maturation. There are some pioneering papers on the topic, and others are concerned with spas that use fast methods of maturation, or those that are developed by the authors themselves. Since the number of publications dealing with clay mineralogy is limited, and the results are not always consistent, no general trends can be outlined, and more research is needed. Differences in results can be due to the different raw materials and water composition used in maturation. For example, in maturing an illitic-smectitic clay in a ferruginous-bicarbonate-sulphate water (pH 6.4), Sánchez et al. (2002) found that the content of smectite (and <2 µm fraction) decreased after three months. This finding was



explained in terms of degradation of the illite–smectite as indicated by a decrease in the mineral's crystallinity. An improvement in the quality of the muds was indicated by an increase of the plasticity index and a slowing of the cooling rate. Similarly, Veniale et al. (1999) observed an increase in the Atterberg plastic and liquid limits (the latter implying a decrease in cooling rate). On the other hand, the granulometric results showed the opposite trend to that reported by Sánchez et al. (2002). However, since different raw materials and maturation water were used by both groups, different mineralogical changes would occur. Thus, maturation with the water used by Sánchez et al. (2002) led to a reduction in the smectite content. Veniale et al. (1999) reported that sulphurous water degraded some constituents of the starting clayey admixture (chlorite, illite/smectite, and feldspars) into smectite, while bromic-iodic-salty water transformed smectite into an “intergrade” and/or chlorite. In investigating the composition of two matured muds from different spas, Summa and Tateo (1998) also found that maturation led to a decrease in grain size, while both mineralogy and chemistry were almost unchanged. In addition, these authors observed that some ultratrace elements could be leached by water after maturation but not before. Likewise, Minguzzi et al. (1999) detected little change in mineralogy and chemistry (two spas considered) although the thermal behaviour of carbonate minerals is greatly altered in one case. Therefore, until investigation advances in this field, it is advisable to study the effects of maturation in the raw material, using water specific to each spa.

The qualitative determination of organic substances in peloid is well documented (see Curini et al., 1990). Jobstraibizer (1999, 2002) observed an increase in the content of organic matter and diatoms as maturation progressed, but only in the case of virgin clays, whereas the recycled muds seemed already in equilibrium with the maturing environment. Galzigna et al. (1996) reported that sulphoglycolipid (a powerful anti-inflammatory agent produced by diatoms) developed immediately after the drop in chlorophyll  $\alpha$  concentration, at about one month of maturation in sulphate-Br-I waters. An increase in organic matter content following maturation was also observed by Curini et al. (1990), but only for two of the three spas investigated. On the other hand, the increase in diatoms and organic materials obtained by Jobstraibizer (2002) was accompanied by a rise in exchange capacity and plasticity although the peloid in question was low in clay minerals and contained little smectite.

Finally, it is always advisable to assess the potential risks to human health of the peloids applied in each spa, because they occasionally contain hazardous elements that may be released during application. These elements can occur in the clay (and associated phases in clay), or in the minero-medicinal water. For example, Summa and Tateo (1998) found that sweat, produced during typical pelotherapy, can extract trace amounts of hazardous chemical elements from matured peloids. Some of these elements (As, Se, Tl) probably come from the maturation water, rather than being intrinsic to the pristine clay. Obviously, the toxicological aspects of pelotherapy are the concern of specialists (as Bressa and Cima (1999) described in the case

of Italy) but clay scientists and geochemists must play an active role in assuring peloid quality.

The possibility that some peloids could be radioactive must also be borne in mind. The water of many spas (for example, more than 25 Spanish spas) is radioactive, and hence fundamentally useful for treating rheumatic problems. The radioactive elements of most therapeutic interest in minero-medicinal waters are isotopes of radio-uranium, uranium–actinium, and thorium. The radio-uranium isotopes,  $^{226}\text{Ra}$  and  $^{222}\text{Rn}$ , and their disintegration products are the most therapeutically important (San José Arango, 2001). Radioactive elements, incorporated in the peloid during maturation, can be beneficial to human health. In some cases, however, the quantity of radioactive elements absorbed by clay minerals could be so high as to be harmful to health, particularly if the material is recycled.

Gorgoni et al. (1999) pointed out that most spa centres are built in the vicinity of springs (or exactly over them), and hence are vulnerable to Rn contamination. The deeper the spring, the longer it takes for the water to reach the crust, and the higher is the probability of Rn accumulation (before emergence). At high concentrations radon is dangerous because it emits ionising radiation, is volatile, and can be inhaled (Committee on Health Risks of Exposure to Radon, 1999). Inside the lung radon quickly disintegrates, giving rise to a radioactive solid ( $^{218}\text{Po}$ ). This material remains permanently in the lung because it is not volatile as Rn is. The solid begins a disintegration cycle by emitting alpha and beta particles within minutes. The resultant damage to lung cells can cause lung cancer. Because the affinity of Rn for solid substances is very low, Rn hazard does not appear to be directly associated with peloids but with pelotherapy in a general sense. A different consideration applies to spas that recycle the peloid. In this case, the exhausted mud may retain some radioactive elements, the concentration of which would increase during repeated recycling.

## 11.5.2. HARMFUL EFFECTS OF CLAYS AND CLAY MINERALS

### A. Background Information

The harmful effects of some minerals on human health were known for centuries. In his medical writings Hippocrates (460–355 BC) referred to the metal digger as a man who breathed with difficulty. Later, Pliny the Elder (23–79 AD) described illnesses associated with exposure to Hg sulphide dust. By the Middle Ages, illness caused by mineral dust was sufficiently recognised to be mentioned by Agricola, in *De Re Metallica* (1556):

“... Some mines are so dry that they are entirely devoid of water and this dryness causes the workmen even greater harm, for the dust, which is stirred and beaten up by digging, penetrates into the windpipe and lungs and produces difficulty in breathing ... . It eats away the lungs and implants consumption in

the body ... In the mines of [the] Carpathian Mountains women are found who married seven husbands, all of whom this terrible consumption carried off to a premature death”.

Agricola also recorded that the miners at Joachimstal, Bohemia, used gauze masks in order to obtain some relief and protection. This report is certainly one of the earliest references to respiratory protection equipment (Chisholm, 1994).

Mineral dusts cause damage by inhalation, and rarely by ingestion, or ingress into the skin. In the lungs the minerals can produce diverse pathologies: (i) lung cancer; (ii) mesothelioma (mesothelial cancer); and (iii) pneumoconiosis (the lung becomes fibrous and loses its capacity to work). Mineral pathogenicity can be determined by epidemiological studies (evaluating the relationships between human exposure to a hazardous substance and the potential health effects), *in vivo* studies (animal models are used extensively to study the effects of exposure to mineral dusts), and *in vitro* studies (specific cells are used to determine a mineral's biological activity) (Guthrie, 1992).

In most biological experiments particle shape and particle-size distribution, together with mass concentration or dose employed, are generally controlled, since these parameters appear to relate to the material's biological activity. However, the exact mineral composition (type and content) of the dusts is rarely characterised. In other words, little attention is generally paid to the identification and quantification of contaminants in the dust sample. Instead, it is assumed that the mineral composition of the sample accords with the information provided by the supplier. However, samples obtained from most suppliers potentially contain a mixture of minerals. Another mineralogical problem in biological studies is that the surface properties of the samples are generally not adequately characterised, given that the toxicity of minerals relates to their surface state and surface area, which in turn can vary substantially between samples. These mineralogical deficiencies in biomedical research can be rectified through collaborative efforts between toxicologists, biomedical experts, chemists, geologists, and mineralogists (Guthrie, 1992; Santaren and Alvarez, 1994; Wagner et al., 1998).

Particle dimensions and surface properties, as well as mobility in the respiratory system determine the depth to which particles may penetrate the lung. In general, particles with aerodynamic diameters greater than about 10  $\mu\text{m}$  impact on the upper reaches of the respiratory tract, and are rapidly moved up the bronchioles by specially adapted cells that sweep the particles towards the throat. These particles are then cleared and expectorated or swallowed. Particles with equivalent spherical diameters of 1–2  $\mu\text{m}$  would deeply penetrate the alveolar regions of the lung. Since the body's natural clearance processes in the deep lung are not efficient, these particles tend to remain in the alveolar walls. As a result, gas exchange across the alveolar membrane is reduced.

Mineral dusts are cleared from the lung by several different mechanisms, including exhalation of suspended particles, sequestration of particles by macrophages, relocation via the mucocilliary escalator and the lymphatic system, *in situ* dissolution, or

a combination of these mechanisms (Brown et al., 1991; Lehnert, 1993). Since macrophages cannot completely engulf mineral fibres that are longer than the cells themselves, there is incomplete phagocytosis of fibres, and irreversible cell damage and death can occur (Kane, 1991). Stanton et al. (1981) established that the optimum dimensions for the induction of intrapleural tumours is a diameter  $\leq 0.25 \mu\text{m}$  and a length  $> 8 \mu\text{m}$ . However, Nolan and Langer (1993) showed that the “Stanton hypothesis”, relating a fibre’s morphology to its activity for the induction of tumours, has some limitations. Other studies defined the critical fibre dimensions for lung cancer and mesothelioma as  $< 0.3\text{--}0.8 \mu\text{m}$  in diameter and  $> 10\text{--}100 \mu\text{m}$  in length for lung cancer, and  $0.1 \mu\text{m}$  in diameter and  $> 5\text{--}10 \mu\text{m}$  in length for mesothelioma (Harington, 1981; Lippmann, 1988). Pott (1989) showed that fibre pathogenicity not only depends on the dimensions of the fibre, but also on its persistence in the lung.

Currently, the important factors influencing the health hazards of minerals are considered to be (i) site of ingress to body (skin, ingestion, inhalation); (ii) type of response (irritation, fibrosis, cancer); (iii) duration of exposure to the particles; (iv) particle size; (v) morphology of thin asymmetrical fibres with diameters  $< 0.25 \mu\text{m}$  and lengths  $> 8.0 \mu\text{m}$ ; (vi) composition, including high iron content; (vii) low solubility at low pH; (viii) value and sign of the surface potential; (ix) hydrophobicity vs. hydrophilicity; (x) *in vitro* activation of phagocytic leukocytes; and (xi) generation of hydroxyl radicals that can break the DNA strand which constitutes the initial step in genotoxicity and cancer (Gilson, 1977; Bates et al., 1989; Bignon, 1990; Brown et al., 1991; Guthrie, 1992; Guthrie and Mossman, 1993; van Oss et al., 1999). Using factors (v), (vii), and (x) van Oss et al. (1999) classified mineral particles as Category I (exceedingly dangerous), or Category II (dangerous after continuous and protracted exposure). For both categories, the onset of overt disease in humans usually occurs after one to several decades. It should also be noted here that the mineral dust risks are closely related to cigarette smoking. For the same period of mineral dust exposure, smokers are more likely to be affected than non-smokers.

The two main illnesses related to mineral dust exposure and inhalation that produced most human deaths in history are silicosis and asbestosis. Silicosis (a pneumoconiosis type), caused by exposure to quartz particles, was widespread during the Industrial Revolution as quartz was a major component of many raw materials used in many processes. Thus, the growth of the iron and steel industry led to increased use of sand for casting, and of sandstone for grinding edge tools and fettling metal casting (Winkler, 1975; Chisholm, 1994). Asbestosis is a serious illness caused by the inhalation of asbestos. “Asbesto” is a commercial name for fibrous minerals including (i) fibrous amphiboles such as actinolite, tremolite, crocidolite (blue asbesto), and amosite (brown asbesto) and (ii) serpentine species notably chrysotile (white asbesto). The dust of these minerals produces lung fibrosis that can develop into lung cancer or mesothelioma. Asbestos clothes were mentioned by Charlemagne (747–814 AD) and later by Marco Polo (1254–1324 AD). Having its beginnings in the 1850s, the asbestos industry grew rapidly from the 1890s onwards

in Europe and the USA (Bowes et al., 1977; Chisholm, 1994). As a result, asbestosis spread widely during the 20th century. References to the harmful effects of quartz and asbestos can be found in the papers by Bowes et al. (1977), Gilson (1977), Germine and Puffer (1989), Brown et al. (1991), Guthrie (1992), Hume and Rimstidt (1992), Guthrie and Mossman (1993), and Bérubé et al. (1998).

Although quartz and asbestos are the most harmful for human health, clay minerals could also be dangerous because of their limited solubility in the lung, reactivity, small particle size, and fibrous habit (as in the case of sepiolite and palygorskite).

### *B. Pathogenicity of Clay Minerals*

Although clay minerals could, in some cases, be dangerous when ingested (Mascolo et al., 1999; Tateo et al., 2001), the pathogenicity of clay minerals is mainly caused by inhalation. There are investigations about the pathogenicity of kaolinite, talc, sepiolite, palygorskite, illite, and smectites (montmorillonite). The possible pathogenicity of these clay minerals was reviewed by Bignon (1990), Hollinger (1990), Guthrie (1992), Davis (1993), Ross et al. (1993), Santaren and Alvarez (1994), Governa et al. (1995), Galán (1996), Wagner et al. (1998), and Jurinski and Rimstidt (2001).

The results of these investigations are contradictory. Most epidemiological studies indicate that clay minerals are only dangerous for human health when exposure time is very long, and toxicity is generally related to the presence of quartz or asbestos in mining. For example, chrysotile and tremolite are commonly associated with talc, quartz with kaolinite, quartz and amphiboles with illite and smectites, etc. *In vivo* and *in vitro* studies, however, indicate that these minerals can be harmful, although in many cases the initial sample was not pure but was contaminated with quartz or asbestos.

For example, Adamis and Timar (1980) reported that bentonite, illite, and three out of four kaolin samples were all cytotoxic *in vitro* but could not find a relationship between their quartz content and their harmful effect. Guthrie (1992) indicated in his review that most samples containing 1:1 clay minerals can produce fibrosis or tumours *in vivo* and can be highly active *in vitro*. Some samples with 2:1 clay minerals, can produce fibrosis *in vivo* and can be highly active *in vitro*. However, epidemiological data suggest fibrosis may not be a problem under modern mining conditions. Clay minerals can be cleared rapidly from the lung, and hence are not pathogenic in humans. Their activity may therefore provide clues to the mechanisms of mineral-induced pathogenesis. Wagner et al. (1998) suggested that changes to the lung only result from prolonged (in excess of 20 years) heavy exposures to clay minerals, since they are weakly fibrogenic. These workers are concerned only with inflammatory and fibrotic responses since exposures to clay minerals are not associated with the development of malignancies unless the samples are contaminated with such minerals as quartz and asbestos.

The pathogenicity of sepiolite and palygorskite is related to geological formation conditions since these determine fibre length and particle crystallinity.

The main harmful effects of different clay minerals are discussed below.

### *Kaolinite*

The harmful effect of kaolinite is mainly related to the presence of quartz since kaolinite-bearing rocks generally contain variable amounts of other minerals including quartz. Kaolinite workers who were heavily exposed to kaolinite dust may develop pneumoconiosis, often referred to as kaolinosis. An increased lung cancer risk was not reported in kaolinite workers (Ross et al., 1993).

Epidemiological studies, reviewed by Guthrie (1992), suggest that kaolinite-bearing dust is fibrogenic only under extraordinary conditions, notably high concentrations of dust or exposure combined with another respiratory disease, such as tuberculosis. Lapenas et al. (1984) found kaolinite in the pulmonary tissue of five kaolin workers who had pneumoconiosis but did not detect silica in the lung samples. Similar findings were reported by Davis (1993).

The results of *in vivo* experiments on the fibrogenic potential of kaolinite-bearing dusts are inconclusive. For example, Mossman and Craighead (1982) found that kaolinite (3–5 µm in diameter, Georgia Kaolin Company) does not induce tumours in golden Syrian hamsters following subcutaneous implantation of *in vitro*-exposed tracheas. Inhalation experiments by Wagner (1990) produced no lung tumours in 20 rats exposed over a period of 3–24 months although a slight fibrogenic response was observed. However, the samples contained 85–95% kaolinite, with the remainder consisting of mica, feldspar, and quartz. Davis (1993) has suggested that the differences in results between experimental inhalation studies with kaolin dusts are due to differences in the dosage used. Likewise, Wagner et al. (1998) indicated that kaolinite is mildly fibrogenic.

*In vitro* experiments show that some kaolinite-bearing samples are cytotoxic to most cell types. For example, kaolinite is cytotoxic to rabbit alveolar macrophages (Low et al., 1980) or mouse peritoneal macrophages (Davies, 1983), but is much less cytotoxic to guinea pig peritoneal macrophages than silica minerals (Marks and Nagelschmidt, 1959). The cell-damaging capacity of kaolins can vary markedly from sample to sample, presumably because of variations in mineralogical properties (such as crystallinity) among deposits, and the presence of varied quantities of other minerals, particularly types of silica. As a result, investigations carried out at about the same period of time can show different results. Thus, the pure kaolin samples studied by Robertson et al. (1982) were markedly cytotoxic whereas the two kaolin samples used by Gormley and Addison (1983) were essentially non-cytotoxic. Further, Daniel and Le Bouffant (1980) reported a low cytotoxicity for kaolin, while Low et al. (1980) suggested that kaolin is cytotoxic to alveolar macrophages by causing membrane damage, similar to that proposed for other silicates.

### *Talc*

Chronic exposures to high concentrations of talc were associated with the development of talcosis, a type of pneumoconiosis. There were numerous health studies of talc workers, but their results were often ambiguous.



In general, epidemiological studies suggest that exposure to talc-bearing dusts elicits a dose-dependent response. Serpentine minerals, including chrysotile, are commonly associated with talc in ultramaphic source rocks, while tremolite commonly occurs with talc in metamorphosed carbonate rocks (Bowes et al., 1977; Davis, 1993). Therefore, talc miners are exposed to dusts other than talc, and it is not possible to assign the results of epidemiological studies to talc exposure alone. Ross et al. (1993) indicated that talc workers exposed to talc dust may exhibit symptoms of talc pneumoconiosis. Several epidemiological studies of talc workers are in disagreement as to whether talc causes lung cancer. Excess cancer may be related to underestimation of smoking habits or to previous exposure to commercial asbestos. Epidemiological studies of talc workers have not provided conclusive evidence that talc is carcinogenic. This is because the number of workers studied was not large enough to produce statistically significant data, smoking habits were not well defined, and the workers were often exposed to other mineral dusts. There is no doubt, however, that heavy exposure to talc dust can cause non-malignant respiratory disease.

*In vivo* experiments on talc-bearing dusts suggest that talc is non-fibrogenic and non-carcinogenic. *In vitro* experiments are inconclusive about the cytotoxic activity of talc-bearing dusts (Guthrie, 1992). Talc is much less hemolytic than kaolinite or montmorillonite (Woodworth et al., 1982). Experimental studies by Davis (1993) demonstrated that talc dust possesses only a low level of pathogenicity but this result is not borne out by other studies. For example, Hollinger (1990) suggested that the pulmonary toxicity of talc for babies, who somehow inhale excessive amounts, can be severe and lasting. Talc, used inappropriately and intravenously, can produce microemboli in small pulmonary vessels, leading to various degrees of tissue granulation, compromise pulmonary function, or death. This fits well with the preferential transport by phagocytes of insoluble particles to the lungs. Talc, with low solubility, and a particle shape and dimension allowing for complete phagocytic engulfment, can produce leukocyte activation and would be more dangerous than silica (van Oss et al., 1999). However, industrial exposure to silica is typically much longer than exposure to talc. Jurinski and Rimstidt (2001) measured the dissolution rate of a well-characterised sample of powdered talc, and estimated a lifetime of about eight years for a 1- $\mu$ m talc particle under pulmonary conditions. Talc dissolves in the body considerably faster than quartz, but slower than chrysotile. These authors suggested that mineral durability does not seem to be a major factor in the development of pulmonary disease, since biodurability does not appear to correlate with the disease-causing potential of mineral dust exposures.

#### *Sepiolite and Palygorskite*

Epidemiological studies of sepiolite and palygorskite workers showed that exposure to sepiolite-bearing dust does not increase the risk of pulmonary disease. There is no evidence of pleural plaque and no reported mesothelioma. Therefore, exposure to these minerals does not present any risk (Baris et al., 1980; Guthrie, 1992; O'Driscoll, 1992; Mc Connochie et al., 1993; Ross et al., 1993; Santaren and Alvarez, 1994).

*In vivo* and *in vitro* studies indicated that, in some cases, sepiolite and palygorskite could be dangerous for human health. Health hazards depend mostly on the type of deposit and its geological formation conditions, which determine fibre length and particle crystallinity.

Wagner et al. (1987) carried out intrapleural tests with sepiolite in rats, and found no increased incidence of tumours. Similar results were obtained with rats inhaling sepiolite and palygorskite. These minerals did not produce fibrosis but only an interstitial reaction similar to that caused by nuisance dust.

*In vivo* studies of palygorskite suggested that most palygorskite-bearing dusts are mildly active in the lung, though some samples can be very active (Guthrie, 1992). *In vitro* experiments indicated palygorskite is as hemolytic as chrysotile, but in other non-erythrocyte cell types palygorskite is non-genotoxic and, at most, only slightly cytotoxic. The lysis of erythrocytes was studied by Oscarson et al. (1986) who found sepiolite and palygorskite to be lysing agents. The edge surfaces and silanol groups of the minerals are important to the lysing process, whereas their elongate particle morphology appears to be irrelevant.

However, Wagner et al. (1987) provided evidence to show that inhalation by rats of sepiolite and palygorskite, containing a significant number of fibres greater than 5–6  $\mu\text{m}$  in length, produces mesothelioma. Pott et al. (1990) carried out an intraperitoneal injection study with a sepiolite from a geological deposit in Finland. The mineral was formed under hydrothermal conditions, allowing for the development of a high degree of crystallinity. In causing a high incidence of tumours, this sample of sepiolite was classified by Pott (1989) as “probably carcinogenic”. Koshi et al. (1991) studied the biological activity of sedimentary and non-sedimentary sepiolites with different crystallisation grade and particle length. Well-crystallised sepiolite with long particles showed strong cytotoxic and genotoxic effects. Chamberlain et al. (1982) also found a relationship between fibre length and cytotoxicity for sepiolite and palygorskite. Nolan et al. (1991) reported that the *in vitro* activity of palygorskite varies between samples. Among nine palygorskites with varied surface characteristics they found a corresponding range in hemolytic activity. Davis (1993) suggested that samples with fibres > 5  $\mu\text{m}$  in length were harmful, whereas materials consisting entirely of short fibres were not. To determine the possible pathogenicity of sepiolite from Vallecas-Vicalvaro (Spain), Santaren and Alvarez (1994) reviewed the epidemiological data on both *in vivo* studies with different methods of administration (inhalation, intrapleural injection, and intraperitoneal inoculation) and *in vitro* studies. The results were consistently negative, showing a low intrinsic biological activity and an absence of exposure-related diseases. The conclusion is that sepiolite from Vallecas-Vicalvaro is not carcinogenic and the only effects that can be expected from this material are the same as for other non-fibrous nuisance dusts.

#### *Illite and Smectites*

Only a few epidemiological studies of respiratory disease resulting from exposure to dusts containing illite and smectites were published. Some studies suggested that



such samples can elicit a mild, dose-dependent fibrogenic response at high exposure levels. Generally, however, there is a concomitant exposure to other minerals (e.g., silica and amphiboles), and the response to these minerals complicates the interpretation of the data. For example, bentonite deposits generally contain other minerals, including very fine-grained quartz and amorphous silica. In the case of Wyoming bentonites, the silica content (which included both quartz and cristobalite) ranges from 0 to 24% (Ross et al., 1993).

*In vivo* experiments suggest that samples containing these minerals are slightly fibrogenic, and *in vitro* experiments indicate that they may be slightly cytotoxic (Guthrie, 1992). Gormley and Addison (1983) studied three different samples of montmorillonite. Although the materials show different cytotoxicities, much of the variability is apparently due to SiO<sub>2</sub> polymorphs. However, most other montmorillonite samples proved to be very cytotoxic *in vitro* (Daniel and Le Bouffant, 1980).

Lysis of bovine red blood cells (erythrocytes) by some silicate minerals was studied by Oscarson et al. (1986). The hemolytic activity of these minerals decreases in the order smectites > silica > palygorskite  $\approx$  sepiolite > chrysotile > kaolinite. These *in vitro* studies showed that the reaction is complete in less than 1 h when the mineral surfaces became saturated with cellular components and lost their lytic activity.

### 11.5.3. CONCLUDING REMARKS

In pharmaceutical formulations, spas and beauty therapy, clay minerals are used for therapeutic purposes and their beneficial effect on human health. In pharmaceutical formulations these minerals are used as active principles (gastrointestinal protectors, antacids antidiarrhoeaics, dermatological protectors, cosmetics) and excipients (inert bases, delivery systems, lubricants, emulsifiers). In spas and beauty therapy clay minerals are used in geotherapy, pelotherapy, and paramuds, to treat dermatological diseases, alleviate the pain of chronic rheumatic inflammations, moisturise the skin, and combat compact lipodystrophies and cellulite.

However, clay minerals can also have an adverse effect on human health when they are inhaled over a very long period. In the lung, clay minerals can cause diverse pathologies such as cancer, mesothelioma, or pneumoconiosis, but the toxicity of these minerals is generally related to the presence of quartz or asbestos from mining operations. The pathogenicity of fibrous clay minerals (sepiolite and palygorskite) is related to the geological conditions of formation.

### REFERENCES

- AA, V.V., 1996. Martindale. The Extra Pharmacopoeia, 31st edition. Royal Pharmaceutical Society, London.
- AA, V.V., 1998. Real Farmacopea Española. Primera Edición (Contiene íntegra la tercera edición de la Farmacopea Europea). Ministerio de Sanidad y Consumo, Madrid.

- AA, V.V., 2002a. The United States Pharmacopeia. The National Formulary. United States Pharmacopeial Convention, Inc., Washington, DC.
- AA, V.V., 2002b. Vademecum Internacional. Especialidades Farmacéuticas y Biológicas. Productos y Artículos de Parafarmacia. Métodos de diagnóstico, 43<sup>a</sup> edition. Medicom, S.A. Ediciones Médicas, Madrid.
- AA, V.V., 2002c. Suplemento 2.1 de la Real Farmacopea Española, 2<sup>a</sup> edition. Ministerio de Sanidad y Consumo, Madrid.
- AA, V.V., 2002d. British Pharmacopoeia, vols. I, II, III and IV. Stationery Office, Health Ministers, London.
- Adamis, Z., Timar, M., 1980. Investigations of the effects of quartz, aluminium silicates and colliery dusts on peritoneal macrophages *in vitro*. In: Brown, R.C., Gormley, I.P., Chamberlain, M., Davies, R. (Eds.), *The In vitro Effects of Mineral Dusts*. Academic Press, London, pp. 13–18.
- Barbieri, P., 1996. Validità terapeutica dei fanghi delle Terme di Salice. In: Veniale, F. (Ed.), *Atti Convegno "Argille Curative"*, Salice Terme/PV. Gruppo Italiano AIPEA., pp. 13–15.
- Baris, Y.I., Sahin, A.A., Erkan, M.L., 1980. Clinical and radiological study in sepiolite workers. *Archives of Environmental Health* 35, 343–346.
- Bates, D.V., Dungworth, D.L., Lee, P.N., McClellan, R.O., Roe, F.J.C. (Eds.), 1989. *Assessment of Inhalation Hazards*. Springer, Berlin.
- Bech, J., 1987. Les terres medicinales. Discurs per Reial Academia de Farmàcia de Barcelona. Reial Acadèmia de farmàcia de Barcelona-CIRIT (Generalitat de Catalunya), Barcelona.
- Benazzo, F., Todesca, A., 1999. Terapia termale nella riabilitazione dei traumi dello sportivo. In: *Abstracts Simposio "Argille per fanghi peloidi termali e per trattamenti dermatologici e cosmetici"*, Montecatini Terme. Gruppo Italiano AIPEA.
- BéruBé, K., Mossman, B., Quinlan, T., Taatjes, D., 1998. Diverse microscopy imaging techniques for studies of asbestos-induced lung disease. *European Microscopy and Analysis* (March), 21–23.
- Bettero, A., Marcazzan, M., Semenzato, A., 1999. Aspetti reologici e tensiometrici di matrici fangose di impiego termale e cosmetico. Proposta di un protocollo per la loro qualificazione. *Mineralogica et Petrographica Acta* XLII, 277–286.
- Bignon, J. (Ed.), 1990. *Health Related Effects of Phyllosilicates*. NATO ASI Series, vol. G 21. Springer, Berlin.
- Bolger, R., 1995. Industrial minerals in pharmaceuticals. *Industrial Minerals* (August), 52–63.
- Bowes, D.R., Langer, A.M., Rohl, A.N., 1977. Nature and range of mineral dusts in the environment. *Philosophical Transactions of the Royal Society of London A* 286, 593–610.
- Bressa, G., Cima, F., 1999. The risk from inorganic substances in Italy. ANPA (Agenzia Nazionale per la Protezione dell'Ambiente), Rome (in Italian).
- Brey Mariño, M., 1982. *Lapidario de Alfonso X Rey de Castilla*. Castalia, Madrid.
- Brown, R.C., Hoskins, J.A., Johnson, N.F. (Eds.), 1991. *Mechanisms in Fibre Carcinogenesis*. Plenum Press, New York.
- Cara, S., Carcangiu, G., Padalino, G., Palomba, M., Tamanini, M., 2000a. The bentonites in pelotherapy: chemical, mineralogical and technological properties of materials from Sardinia deposits (Italy). *Applied Clay Science* 16, 117–124.
- Cara, S., Carcangiu, G., Padalino, G., Palomba, M., Tamanini, M., 2000b. The bentonites in pelotherapy: thermal properties of clay pastes from Sardinia (Italy). *Applied Clay Science* 16, 125–132.

- Cara, S., Carcangiu, G., Tamanini, M., 1999. Proprietà termiche dei fanghi termali bentonitici: proposta di una metodologia speditiva per un controllo di qualità. In: Atti Simposio "Argille per fanghi peloidi termali e per trattamenti dermatologici e cosmetici", Montecatini Terme. Mineralogica et Petrographica Acta XLII, 299–305.
- Carretero, M.I., 2002. Clay minerals and their beneficial effects upon human health: a review. *Applied Clay Science* 21, 155–163.
- Cerezo, P., Viseras Iborra, C., López Galindo, A., Ferrari, F., Caramella, C., 2001. Use of water uptake and capillary suction time measures for evaluation of the anti-diarrhoeic properties of fibrous clays. *Applied Clay Science* 20, 81–86.
- Chamberlain, M., Davies, R., Brown, R.C., Griffiths, D.M., 1982. *In vitro* tests for the pathogenicity of mineral dusts. *Annals of Occupational Hygiene* 26, 583–592.
- Chisholm, J., 1994. Mineral dusts and occupational health. *Mineralogical Society Bulletin* 102, 3–7.
- Committee on Health Risks of Exposure to Radon, 1999. Health Effects of Exposure to Radon: BEIR VI. National Research Council, National Academy Press, Washington, DC.
- Cornejo, J., 1990. Las arcillas en formulaciones farmacéuticas. In: Galán, E., Ortega, M. (Eds.), Conferencias de IX y X Reuniones de la Sociedad Española de Arcillas, pp. 51–68.
- Cornejo, J., Hermosin, M.C., White, J.L., Barnes, J.R., Hem, S.L., 1983. Role of ferric iron in the oxidation of hydrocortisone by sepiolite and palygorskite. *Clays and Clay Minerals* 31, 109–112.
- Curini, R., D'Ascenzo, G., Fraioli, A., Lagana, A., Marino, A., Messina, B., 1990. Instrumental multiparametric study of the maturing of therapeutics muds of some italian spas. *Thermochimica Acta* 157, 377–393.
- Daniel, H., Le Bouffant, L., 1980. Study of quantitative scale for assessing the cytotoxicity of mineral dusts. In: Brown, R.C., Gormley, I.P., Chamberlain, M., Davies, R. (Eds.), *The In vitro Effects of Mineral Dusts*. Academic Press, London, pp. 33–39.
- Davies, R., 1983. Factors involved in the cytotoxicity of kaolinite towards macrophages *in vitro*. *Environmental Health Perspectives* 51, 249–252.
- Davis, J.M.G., 1993. *In vivo* assays to evaluate the pathogenic effects of minerals in rodents. In: Guthrie, G.D., Mossman, B.T. (Eds.), *Health Effects of Mineral Dusts*. Reviews in Mineralogy, vol. 28. Mineralogical Society of America, Washington, DC, pp. 471–487.
- De Bernardi, M., Pedrinazzi, G.M., 1996. Biological actions of themal peloids. In: Veniale, F. (Ed.), Atti Convegno "Argille Curative", Salice Terme/PV. Gruppo Italiano AIPEA, pp. 17–24 (in Italian).
- Del Hoyo, C., Rives, V., Vicente, M.A., 1993. Interaction of *N*-methyl-8-hydroxy quinoline methyl sulphate with sepiolite. *Applied Clay Science* 8, 37–51.
- Del Hoyo, C., Vicente, M.A., Rives, V., 1998. Application of phenyl salicylate-sepiolite systems as ultraviolet radiation filters. *Clay Minerals* 33, 467–474.
- Del Hoyo, C., Vicente, M.A., Rives, V., 2001. Preparation of drug-montmorillonite UV-radiation protection compounds by gas–solid adsorption. *Clay Minerals* 36, 541–546.
- Del Pozo, A., 1978. Farmacia Galénica Especial. Tomo 2°. Romargraf S.A., Barcelona.
- Del Pozo, A., 1979. Farmacia Galénica Especial. Tomo 3°. Romargraf S.A., Barcelona.
- Ferrand, T., Yvon, J., 1991. Thermal properties of clay pastes for pelotherapy. *Applied Clay Science* 6, 21–38.

- Forteza, M., Cornejo, J., Galán, E., 1988. Effects of fibrous clay minerals on dexamethasone stability. In: Konta, J. (Ed.), Proceedings of the 10th Conference on Clay Mineralogy and Petrology, Ostrava. Universitas Carolina, Prague, pp. 281–286.
- Forteza, M., Galán, E., Cornejo, J., 1989. Interaction of dexamethasone and montmorillonite. Adsorption-degradation process. Applied Clay Science 4, 437–448.
- Galán, E., 1996. Properties and applications of palygorskite-sepiolite clays. Clay Minerals 31, 443–453.
- Galán, E., Liso, M.J., Forteza, M., 1985. Minerales utilizados en la industria farmacéutica. Boletín de la Sociedad Española de Mineralogía 8, 369–378.
- Galzigna, L., Moretto, C., Lalli, A., 1996. Physical and biochemical changes of thermal mud after maturation. Biomedicine and Pharmacotherapy 50, 306–308.
- Gámiz, E., Linares, J., Delgado, R., 1992. Assessment of two Spanish bentonites for pharmaceutical uses. Applied Clay Science 6, 359–368.
- Germine, M., Puffer, J.H., 1989. Origin and development of flexibility in asbestiform fibres. Mineralogical Magazine 53, 327–335.
- Giammatteo, M., Cipriani, N., Corona, L., Magaldi, D., Pantaleoni, G., 1997. Osservazioni sull'origine e la composizione chimico-mineralogica delle terre sigillate dell'Isola di Samo. Mineralogia et Petrographica Acta XL, 327–337.
- Gilson, J.C., 1977. Environmental mineralogy. Medicine and mineralogy. Philosophical Transactions of the Royal Society of London A 286, 585–592.
- Gomes, C., Silva, J. (Eds.), 2001. Beach Sand and Bentonite of Porto Santo Island: Potentialities for Applications in Geomedicine. O Liberal, Câmara de Lobos, Madeira.
- Gorgoni, C., Bertolani, M., Loschi Ghittoni, A.G., Pallante, P., 1999. Composizione, radioattività, mineralogia e reologia dei fanghi delle Salse Emiliane. In: Abstracts Simposio “Argille per fanghi peloidi termali e per trattamenti dermatologici e cosmetici”, Montecatini Terme. Gruppo Italiano AIPEA.
- Gormley, I.P., Addison, J., 1983. The *in vitro* cytotoxicity of some standard clay mineral dusts of respirable size. Clay Minerals 18, 153–163.
- Governa, M., Valentino, M., Visonà, I., Monaco, F., Amati, M., Scancarello, G., Scansetti, G., 1995. *In vitro* biological effects of clay minerals advised as substitutes for asbestos. Cellular Biological Toxicity 11, 237–249.
- Guthrie, G.D., 1992. Biological effects of inhaled minerals. American Mineralogist 77, 225–243.
- Guthrie, G.D., Mossman, B.T. (Eds.), 1993. Health Effects of Mineral Dusts. Reviews in Mineralogy, vol. 28. Mineralogical Society of America, Washington, DC.
- Güven, N., Pollastro, R.M. (Eds.), 1993. Clay–Water Interface and its Rheological Implications, CMS Workshop Lectures, vol. 4. Clay Minerals Society, Boulder, CO.
- Harington, J.S., 1981. Fiber carcinogenesis: epidemiological observations and the Stanton hypothesis. Journal of the National Cancer Institute 67, 977–989.
- Hermoin, M.C., Cornejo, J., White, J.L., Hem, S.L., 1981. Sepiolite, a potential excipient for drugs subject to oxidative degradation. Journal of Pharmaceutical Sciences 70, 189–192.
- Hollinger, M.A., 1990. Pulmonary toxicity of inhaled and intravenous talc. Toxicology Letters 52, 121–127.
- Hume, L.A., Rimstidt, J.D., 1992. The biodurability of chrysotile asbestos. American Mineralogist 77, 1125–1128.

- Jobstraibizer, P., 1999. Definizione mineralogica e chimica del fango termali e per trattamenti dermatologici e cosmetici, Montecatini Terme. *Mineralogica et Petrographica Acta* XLII, 317–327.
- Jobstraibizer, P., 2002. Bioprecipitazione di silice e pirite nei fanghi termali euganei. *Plinius* 27, 189–194.
- Jurinski, J.B., Rimstidt, J.D., 2001. Biodurability of talc. *American Mineralogist* 86, 392–399.
- Kane, A.B., 1991. Fiber dimensions and mesothelioma, a reappraisal of the Stanton hypothesis. In: Brown, R.C., Hoskins, J.A., Johnson, N.F. (Eds.), *Mechanisms in Fibre Carcinogenesis*. Plenum Press, New York, pp. 131–141.
- Koshi, K., Kohyama, N., Myojo, T., Fukuda, K., 1991. Cell toxicity, haemolytic action and clastogenic activity of asbestos and its substitutes. *Industrial Health* 29, 37–56.
- Lapenas, D., Gale, P., Kennedy, T., Rawlings, W. Jr., Dietrich, P., 1984. Kaolin pneumoconiosis. *American Review of Respiratory Disease* 130, 282–288.
- Lehnert, B.E., 1993. Defense mechanisms against inhaled particles and associated particle–cell interactions. In: Guthrie, G.D., Mossman, B.T. (Eds.), *Health Effects of Mineral Dusts. Reviews in Mineralogy*, vol. 28. Mineralogical Society of America, Washington, DC, pp. 427–469.
- Lippmann, M., 1988. Asbestos exposure indices. *Environmental Research* 46, 86–106.
- López-Galindo, A., Viseras, C., 2000. Pharmaceutical applications of fibrous clays (sepiolite and palygorskite) from some circum-mediterranean deposits. In: Gomes, C.S.F. (Ed.), 1st Latin American Clay Conference, Funchal, Madeira, Associação Portuguesa de Argilas (APA), vol.1, pp. 258–270.
- Lotti, T., Ghersetich, I., 1999. Peolidi: trattamento dermato-cosmetologico termale emergente. In: Abstracts Simposio “Argille per fanghi peloidi termali e per trattamenti dermatologici e cosmetici”, Montecatini Terme. Gruppo Italiano AIPEA.
- Low, R.B., Leffingwell, C.M., Bulman, C.A., 1980. Effect of kaolinite on amino acid transport and incorporation into protein by rabbit pulmonary alveolar macrophages. *Archives of Environmental Health* 35, 217–223.
- Mahaney, W.C., Milner, M.W., Mulyono, Hs., Hancock, R.G.V., Aufreiter, S., Reich, M., Wink, M., 2000. Mineral and chemical analyses of soils eaten by humans in Indonesia. *International Journal of Environmental Health Research* 10, 93–109.
- Marks, J., Nagelschmidt, G., 1959. Study of the toxicity of dust with use of the *in vitro* dehydrogenase technique. *American Medical Association Archives of Industrial Health* 20, 37/383–43/389.
- Martín Díaz, L., 1998. Arcillas, peloides y parafangos en medicina estética. Tesis de Máster Universitario de Medicina Estética. Univ. Islas Baleares, 45pp.
- Mascolo, N., Summa, V., Tateo, F., 1999. Characterization of toxic elements in clays for human healing use. *Applied Clay Science* 15, 491–500.
- Mc Connochie, K., Bevan, C., Newcombe, R.G., Lyons, J.P., Skidmore, W.J., Wagner, J.C., 1993. A study of Spanish sepiolite workers. *Thorax* 48, 370–374.
- Mc Ginity, J.W., Lach, J.L., 1977. Sustained-release applications of montmorillonite interaction with amphetamine sulfate. *Journal of Pharmaceutical Science* 66, 63–66.
- Messina, B., Grossi, F., 1983. *Elements of Medical Hydrology*. S.E.U., Rome (in Italian).
- Minguzzi, V., Morandi, N., Tagnin, S., Tateo, F., 1999. Le argille curative in uso negli stabilimenti termali emiliano-romagnoli: verifica della composizione e delle proprietà.

- In: Atti Simposio "Argille per fanghi peloidi termali e per trattamenti dermatologici e cosmetici", Montecatini Terme. Mineralogica et Petrographica Acta XLII, 287–298.
- Mossman, B.T., Craighead, J.E., 1982. Comparative cocarcinogenic effects of crocidolite asbestos, hematite, kaolin and carbon in implanted tracheal organ cultures. *Annals of Occupational Hygiene* 26, 553–567.
- Nappi, G., 2001. *Medicine and Thermal Clinic*. Edizioni Selecta Medica, Pavia (in Italian).
- Newton, P., 1991. The use of medicinal plants by primates—a missing link. *Trends in Ecology & Evolution* 6, 297–299.
- Nolan, R.P., Langer, A.M., 1993. Limitations of the Stanton hypothesis. In: Guthrie, G.D., Mossman, B.T. (Eds.), *Health Effects of Mineral Dusts. Reviews in Mineralogy*, vol. 28. Mineralogical Society of America, Washington, DC, pp. 309–326.
- Nolan, R.P., Langer, A.M., Herson, G.B., 1991. Characterization of palygorskite specimens from different geological locales for health hazard evaluation. *British Journal of Industrial Medicine* 48, 463–475.
- Novelli, G., 1996. Applicazioni medicali e igieniche delle bentoniti. In: Veniale, F. (Ed.), *Atti Convegno "Argille Curative"*, Salice Terme/PV. Gruppo Italiano AIPEA, pp. 25–33.
- O'Driscoll, M., 1992. European cat litter. Absorbing market growth. *Industrial Minerals* (August), 46–65.
- Oscarson, D.W., Van Scoyoc, G.E., Ahlrichs, J.L., 1986. Lysis of erythrocytes by silicate minerals. *Clays and Clay Minerals* 34, 74–80.
- Penner, D., Lagaly, G., 2001. Influence of anions on the rheological properties of clay mineral dispersions. *Applied Clay Science* 19, 131–142.
- Porubcan, L.S., Born, G.S., White, J.L., Hem, S.L., 1979. Interaction of digoxin and montmorillonite: mechanism of adsorption and degradation. *Journal of Pharmaceutical Sciences* 68, 358–361.
- Porubcan, L.S., Serna, C.J., White, J.L., Hem, S.L., 1978. Mechanism of adsorption of clindamicine and tetracycline by montmorillonite. *Journal of Pharmaceutical Sciences* 67, 1081–1087.
- Pott, F., 1989. Carcinogenicity of fibers in experimental animals. Data and evaluation. In: Bates, D.V., Dungworth, D.L., Lee, P.N., McClellan, R.O., Roe, F.J.C. (Eds.), *Assessment of Inhalation Hazards*. Springer, Berlin, pp. 243–253.
- Pott, F., Bellmann, B., Muhle, H., Rödelberger, K., Rippe, R.M., Roller, M., Rosenbruch, M., 1990. Intraperitoneal injection studies for the evaluation of the carcinogenicity of fibrous phyllosilicates. In: Bignon, J. (Ed.), *Health Related Effects of Phyllosilicates*, NATO ASI Series, vol. G 21. Springer, Berlin, pp. 319–329.
- Reinbacher, W.R., 1999. A brief history of clay in medicine. *CMS News* 11 (1), 22–23.
- Robertson, A., Dodgson, J., Gormley, I.P., Collings, P., 1982. An investigation of the adsorption of oxides of nitrogen on respirable mineral dusts and the effects on their cytotoxicity. In: Walton, W.H. (Ed.), *Inhaled Particles V*. Pergamon Press, Oxford, pp. 607–622.
- Robertson, R.H.S., 1986. *Fuller's Earth: A History of Calcium Montmorillonite*. Volturna Press, Hythe, Kent, 421pp.
- Robertson, R.H.S., 1996. Cadavers, cholera and clays. *British Mineralogical Society Bulletin* 113, 3–7.
- Ross, M., Nolan, R.P., Langer, A.M., Cooper, W.C., 1993. Health effects of mineral dusts other than asbestos. In: Guthrie, G.D., Mossman, B.T. (Eds.), *Health Effects of Mineral*

- Dusts. Reviews in Mineralogy, vol. 28. Mineralogical Society of America, Washington, DC, pp. 361–409.
- Sánchez, C.J., Parras, J., Carretero, M.I., 2002. The effect of maturation upon the mineralogical and physicochemical properties of illitic-smectitic clays for pelotherapy. *Clay Minerals* 37, 457–464.
- Sánchez, C., Parras, J., Carretero, M.I., Barba, P., 2000a. Aplicaciones terapéuticas de las arcillas de Santa Cruz de Mudela (Ciudad Real). In: Pascual, J. (Ed.), *Integración Ciencia-Tecnología de las Arcillas en el Contexto Tecnológico-Social del Nuevo Milenio*. Sociedad Española de Arcillas, pp. 31–40.
- Sánchez, C., Parras, J., Carretero, M.I., Barba, P., 2000b. Behaviour of matured illitic-smectitic clays for pelotherapy. In: Gomes, C.S.F. (Ed.), *1st Latin American Clay Conference*, Funchal, Madeira, Associação Portuguesa de Argilas (APA), vol. 2, pp. 317–321.
- Sánchez Martín, M.J., Sánchez Camazano, M., Sayalero, M.L., Dominguez Gil, A., 1988. Physicochemical study of the interaction of montmorillonite with hydralazine hydrochloride, a cardiovascular drug. *Applied Clay Science* 3, 53–61.
- San José Arango, C., 2001. *Hidrología Médica y Terapias Complementarias*. Secretariado de Publicaciones de la Universidad de Sevilla.
- Santaren, J., Alvarez, A., 1994. Assessment of the health effects of mineral dusts. The sepiolite case. *Industrial Minerals* (April), 101–117.
- Stanton, M.F., Layard, M., Tegeris, A., Miller, E., May, M., Morgan, E., Smith, A., 1981. Relation of particle dimension to carcinogenicity of amphibole asbestoses and other fibrous minerals. *Journal of the National Cancer Institute* 67, 965–975.
- Summa, V., Tateo, F., 1998. The use of pelitic raw materials in thermal centres: mineralogy, geochemistry, grain size and leaching test: examples from the Lucania area (southern Italy). *Applied Clay Science* 12, 403–417.
- Summa, V., Tateo, F., 1999. Geochemistry of two peats suitable for medical uses and their behaviour during leaching. *Applied Clay Science* 15, 477–489.
- Tateo, F., Summa, V., Bonelli, C.G., Bentivenga, G., 2001. Mineralogy and geochemistry of herbalist's clays for internal use: simulation of the digestive process. *Applied Clay Science* 20, 97–109.
- Torrescani, C., 1990. Utilizzo del fango termale sulfureo nel trattamento della cute seborreica. *Cosmesi Dermatologica* 30, 59–71.
- Ueda, H., Hamayoshi, M., 1992. Sepiolite as a deodorant material: an ESR study of its properties. *Journal of Materials Science* 27, 4997–5002.
- van Oss, C.J., Naim, J.O., Costanzo, P.M., Giese, R.F. Jr., Wu, W., Sorling, A.F., 1999. Impact of different asbestos species and other mineral particles on pulmonary pathogenesis. *Clays and Clay Minerals* 47, 697–707.
- Veniale, F., 1992. Clay science: facts and perspectives. In: *Proceedings of the Mediterranean Clay Meeting*, Lipari, September 27–30. *Mineralogica et Petrographica Acta* XXXV-A, 13–44.
- Veniale, F. (Ed.), 1996. *Atti Convegno "Argille Curative"*, Salice Terme/PV. Gruppo Italiano AIPEA.
- Veniale, F., 1997. Applicazioni e utilizzazioni medico-sanitarie di materiali argillosi (naturali e modificati). In: Morandi, N., Dondi, M. (Eds.), *Argille e Minerali delle Argille. Guida alla Definizione di Caratteristiche e Proprietà per gli Usi Industriali*. Corso di Formazione, Gruppo Italiano AIPEA, Rimini, Italy, pp. 205–239.

- Veniale, F., 1999a. Le argille nelle terapie curative: dalla leggenda all'empirismo, fino ai tempi moderni. In: Atti Simposio "Argille per fanghi peloidi termali e per trattamenti dermatologici e cosmetici", Montecatini Terme. Mineralogica et Petrographica Acta XLII, 263–265.
- Veniale, F. (Ed.), 1999b. Simposio "Argille per fanghi peloidi termali e per trattamenti dermatologici e cosmetici". Montecatini Terme, May 14–15, 1999, Pisa, Italy. Gruppo Italiano AIPEA.
- Veniale, F. (Ed.), 1999c. Catalogue. Clay geomaterials for "peloids". Preliminary version. Symposium "Argille per fanghi peloidi termali e per trattamenti dermatologici e cosmetici". Montecatini Terme, May 14–15, 1999, Pisa, Italy. Gruppo Italiano AIPEA, 130pp.
- Veniale, F., Setti, M., 1996. L'argilla di Pontestura/Al. Potenzialità di impiego nella formulazione di fanghi "peloidi". In: Veniale, F. (Ed.), Atti Convegno "Argille Curative", Salice Terme/PV. Gruppo Italiano AIPEA, pp. 139–145.
- Veniale, F., Setti, M., Soggetti, F., Lofrano, M., Troilo, F., 1999. Esperimenti di "maturazione" di geomateriali argillosi con acqua sulfurea e salso-bromo-ionica per la preparazione di fanghi "peloidi" termali e per trattamenti dermatologici. In: Atti Simposio "Argille per fanghi peloidi termali e per trattamenti dermatologici e cosmetici", Montecatini Terme. Mineralogica et Petrographica Acta XLII, 267–275.
- Vicente, M.A., Sanchez-Camazano, M., Sanchez-Martin, M.J., Del Arco, M., Martin, C., Rives, V., Vicente-Hernandez, J., 1989. Adsorption and desorption of *N*-methyl-8-hydroxy quinoline methyl sulphate on smectite and the potential use of the clay-organic product as an ultraviolet radiation collector. Clays and Clay Minerals 37, 157–163.
- Viseras, C., López-Galindo, A., 1999. Pharmaceutical applications of some Spanish clays (sepiolite, palygorskite, bentonite): some preformulation studies. Applied Clay Science 14, 69–82.
- Wagner, J.C., 1990. Review on pulmonary effects of phyllosilicates after inhalation. In: Bignon, J. (Ed.), Health Related Effects of Phyllosilicates. NATO ASI Series, vol. G 21. Springer, Berlin, pp. 309–318.
- Wagner, J.C., Griffiths, D.M., Munday, D.E., 1987. Experimental studies with palygorskite dust. British Journal of Industrial Medicine 44, 749–763.
- Wagner, J.C., McConnochie, K., Gibbs, A.R., Pooley, F.D., 1998. Clay minerals and health. In: Parker, A., Rae, J.E. (Eds.), Environmental Interactions of Clays. Springer, Berlin, pp. 243–265.
- White, J.L., Hem, S.L., 1983. Pharmaceutical aspects of clay-organic interactions. Industrial Engineering Chemistry Product Research and Development 22, 665–671.
- Winkler, E.M., 1975. Silicosis. In: Winkler, E.M. (Ed.), Stone: Properties, Durability in Man's Environment. Springer, New York, pp. 182–186.
- Woodworth, C.D., Mossman, B.T., Craighead, J.E., 1982. Comparative effects of fibrous and nonfibrous minerals on cells and liposomes. Environmental Research 27, 190–205.
- Yvon, J., Ferrand, T., 1996. Preparation *ex-situ* de peloides. Propriétés thermiques, mécaniques et d'échange. In: Veniale, F. (Ed.), Atti Convegno "Argille Curative", Salice Terme/PV. Gruppo Italiano AIPEA, pp. 67–78.



This page intentionally left blank

*Chapter 11.6*

## CLAYS AND CLAY MINERALS AS DRUGS

M.T. DROY-LEFAIX<sup>a</sup> AND F. TATEO<sup>b</sup>

<sup>a</sup>*Beaufour-IPSEN, F-75016 Paris, France*

<sup>b</sup>*Istituto di Ricerca sulle Argille, CNR, I-85050 Tito Scalo (PZ), Italy*

Clay therapy is based on the ability of clays and clay minerals to adsorb and retain harmful and toxic substances. The beneficial effects of these materials to human health, notably in the treatment of gastrointestinal disorders, were recognized. Indeed, the eating of clay ('geophagy') was practiced since antiquity in all parts of the world. Among the variety of clays and clay minerals that were used by primitive tribes are bentonite, kaolinite, montmorillonite, smectite, and 'pascalite' (a Ca<sup>2+</sup>-montmorillonite from Wyoming, USA) (Eaton and Eaton, 1995).

Examination of the diets of certain tribes in the high Andes of South America and central Africa, and those of Australian aborigines, showed that these people use clay to avoid getting stomach-ache, dysentery, and food infections. Indeed, the Quetchus Indians of South America used to dip their potatoes into an aqueous suspension of clay, immediately before eating, in order to prevent the build-up of acidity in the stomach. This dietetic procedure is still being followed by some tribes of American Indians. A similar practice was traditionally carried out on board ships where sailors used clays not only to adsorb odours and moisture but also to treat dysentery, burns, boils, sore mouths, and other internal and external disorders.

Although recent research confirmed that clays and clay minerals possess general curative properties, it is the treatment of disorders that remains the focus of attention. By adsorbing 'aggressors' (infectious factors) of the gastrointestinal mucosa barrier, these materials can serve as both prophylactic and therapeutic agents.

### 11.6.1. INTERACTIONS OF CLAY MINERALS WITH GASTROINTESTINAL MUCUS

At the surface of the gut, a mucus gel adheres to the epithelial cells of the mucosa. This adherent mucus is dynamic, being continuously secreted by the caliciform cells and regularly eroded by environmental 'aggressors' present in the gut lumen.

The mucus gel is largely composed of glycoprotein polymers, lipids, and proteins, linked together by covalent bonds. As such, it acts as a physical barrier protecting

the mucosa against penetration by extraneous molecules and mechanical injury. By maintaining a pH gradient and competing with the epithelial surface for micro-organisms, the mucus gel also acts as a chemical barrier.

Thus, a weakening of the mucus gel barrier may be at the origin of disorders such as gastritis and colitis (Droy-Lefaix, 1987). Short-term treatment with clay minerals, such as smectites (Moré et al., 1987) and attapulgite (Moré et al., 1992) increases the thickness of the adherent mucus. This may be ascribed to interactions of mineral particles with mucus components (Leonard et al., 1994) by which the gastrointestinal glycoproteins are modified, and their polymerization is enhanced (Droy-Lefaix et al., 1986). Similarly, aluminium (hydr)oxides (e.g., boehmite) can reduce mucus degradation (Bouyssou et al., 1990). The beneficial effects of minerals are also associated with improvements in the rheological properties of the mucus gel, such as spinability. This reflects the increased extent of polymerization, and the improvement in quality, of the adherent mucus (Droy-Lefaix et al., 1985). Changes in the physico-chemical properties of the mucus, induced by the action of clay minerals, were confirmed by electron paramagnetic resonance and fluorescence spectroscopy. The results indicate that clay mineral ingestion decreases mucus solubility. At the same time, the viscosity and hydrophobicity of the mucus increases, enhancing its adhesion to epithelial cells.

#### 11.6.2. CLAY MINERALS, MUCOSAL BARRIER, AND GASTROINTESTINAL 'AGGRESSORS'

By acting directly on the mucus gel, clays and clay minerals exert a stabilizing effect on the mucosal barrier (Gwozdziński et al., 1997), providing protection against different 'aggressors' of the gastrointestinal mucosa.

Pepsin, a substance necessary for digestion, is a typical 'aggressor'. Experiments with rats showed that if pepsin secretion at the surface of the gastric mucosa is strongly increased (due to pathological dysregulation), the adherent mucus layer is progressively disrupted. At the same time haemorrhagic mucosal lesions appear, and significant bleeding occurs in the lumen as well as localized ulceration in an otherwise intact epithelium. By binding to the mucus components, smectite can completely inhibit the damage induced by pepsin (Leonard et al., 1994).

Samson et al. (1995), for example, showed that patients with ulcerative colitis show a six-fold greater mean total faecal proteinase activity (expressed in mmol terminal  $\text{NH}_2/\text{min/g}$  dry weight of faeces) than the control. Smectite totally inhibits this enzyme activity. The effects of smectite on mucus proteolysis are assessed using a model of mucolytic activity, assayed by the release of degraded colonic mucin from the adherent mucus gel of freshly prepared pig colonic bags in vitro. Similarly, trypsin (2 mg/mL) releases three times more soluble mucin per bag than the control. Smectite (100 mg/mL) inhibits trypsin activity, causing the level of degraded mucin to fall below the normal value. This is ascribed to the interaction of smectite

with the adherent mucus layer, and the binding of trypsin to the mineral (Samson et al., 1995).

Clay minerals can also provide protection against attack by bile acids that cause gastrointestinal ulceration. In rats, oral administration of sodium glycodeoxycholate or sodium taurocholate induces severe erosion of the jejunal mucosa. After treatment with smectite (which interacts closely with the mucus glycoproteins) the severity of surface erosion is greatly diminished (Fioramonti et al., 1990), while the rheological properties of the adherent mucus gel are maintained within normal limits (Droy-Lefaix et al., 1985).

Because of their strong bioadhesive properties, clay minerals also afford protection of the colon against damage from reactive oxygen species. Oxygenated free radicals, released by infiltration of white cells into the colonic mucosa barrier, are very unstable. Their presence can induce severe erosion of the colonic mucosa, leading to mucolysis. By maintaining the solution viscosity of the colonic mucin, and inhibiting the hypersecretion of mucus, smectite can prevent the onset of mucolysis (Pearson et al., 1996; Knight et al., 1998).

In many digestive diseases, the intestinal barrier is weakened by the release of pro-inflammatory cytokines, induced by abnormal activation of the epithelial cells and the underlying immune system. These cytokines include a tumour necrosis factor- $\alpha$  (TNF- $\alpha$ ) and an interferon- $\gamma$  factor (INF- $\gamma$ ). When intestinal cells (line HT 29-19 A) are incubated with TNF- $\alpha$  and INF- $\gamma$ , intestinal function (assessed in Ussing chambers by measuring ionic conductance, apicobasal fluxes of  $^{14}\text{C}$ -mannitol, and intact horseradish peroxidase) is altered, and the tight junction between cells is disrupted. In the presence of smectite (100 mg/mL) the values of these parameters are similar to those of the control (Mahraoui et al., 1997).

The cytoprotective effects of clay minerals can also account for their ability to prevent damage of the gastrointestinal mucosa caused by such 'aggressors' as ethanol and anti-inflammatory drugs. Ethanol, directly administered into the stomach, gives rise to severe gastric ulcerations and macroscopic necrosis of the gastric mucosa. These deleterious effects are accompanied by a decrease in the gastric transmural potential difference which serves as a criterion of the functional integrity of the mucosa (Fioramonti et al., 1990). Erosion of the mucus layer leads to a significant alteration of rheological properties (Droy-Lefaix et al., 1992; Slitine-Bonet et al., 1994). Smectite treatment for two days can significantly counteract the harmful effect of ethanol, reducing the irritative index (Fioramonti et al., 1990).

Clay minerals also provide protection against the action of anti-inflammatory drugs. For example, the oral administration of aspirin (2 g) to pigs, and phenylbutazone (200 mg/kg) to rats, decreases the gastric potential difference, and induces severe ulceration due to mucus alteration (Fioramonti et al., 1990; Droy-Lefaix et al., 1992). The extent of lesion and mucus degradation is significantly reduced after treatment with smectite. In humans the symptoms of gastropathies, induced by non-steroid anti-inflammatory drugs, can be successfully treated by ingestion of smectite (Peignot et al., 1997).

### 11.6.3. ADSORPTIVE PROPERTIES OF CLAYS AND CLAY MINERALS

The adsorptive properties of clay minerals provide the basis for the therapeutic uses of clays.

#### A. *Toxins*

Clays can adsorb a variety of toxic substances, such as strychnine (Droy-Lefaix, 1986), mycotoxins (e.g., T2 toxin) (Fioramonti et al., 1987b), aflatoxin (Schell et al., 1993), enterotoxins (Brouillard and Rateau, 1989), and toxins produced by *Vibrio cholerae*, *Escherichia coli* (Fioramonti et al., 1987b), and *Yersinia pseudotuberculosis* (Carnoy et al., 2000).

By doing so, clays can provide active protection against disturbances during gastrointestinal transit. In mice, for example, gastric emptying and small intestinal transit are significantly accelerated after oral administration (1 mg/kg for 4 days) of T2 toxin. However, if the toxin is incubated with smectite for 24 h beforehand, no increase in the rate of gastric emptying and small intestinal transit occurs (Fioramonti et al., 1987a).

In conscious dogs, intraduodenal administration of cholera toxin (200 mg) affects gastrointestinal transit, and disrupts the migrating motor complexes (MMCs) of the stomach and jejunum. According to the duration of treatment (at a dose of 100 mg/kg/day), smectite can effectively counteract the effects of cholera toxin (Fioramonti et al., 1987b).

Smectite can also adsorb the enterotoxin of *Clostridium difficile* (Martirosian et al., 1998). In rats, this toxin causes intestinal permeability to increase through hypersecretion of colonic water. Both these conditions can be alleviated by treatment with <sup>51</sup>Cr-EDTA in the presence of smectite (Fioramonti et al., 1994).

*E. coli* toxin is an infectious agent causing diarrhoea. Heat-stable toxin (ST) from *E. coli*, directly administered to New Zealand rabbits, induces a significant increase in intestinal permeability (as estimated by Evans Blue) and severe damage to ileal loops (as revealed by scanning electron microscopy). The presence of smectite in the ileal loops has a protective effect (Pons et al., 1997).

Similar results are obtained with the enterotoxin of *Bacteroides fragilis* administered to HT/29 C1 cells (human colon adenocarcinoma cell line). Prior incubation of this toxin with smectite suppresses its toxic effects (Martirosian et al., 1998).

#### B. *Pesticides*

Because of their high adsorptive capacity, clay minerals can also protect the digestive mucosa against pesticide damage. Diquat, a widely used non-selective desiccant herbicide, induces erosion of intestinal mucosa and fluid hypersecretion. In rats that were given diquat, treatment with smectite (500 mg/kg for 2 weeks) brings about a normalization of mucus rheological properties and intestinal permeability, as

indicated by urine analysis using  $^{51}\text{Cr}$ -EDTA (Theodorou et al., 1995). Similarly, montmorillonite and bentonite are good adsorbents, and may be recommended for the treatment of pesticide poisoning (Meredith and Vale, 1987).

### C. Microorganisms

Clay minerals are efficient drugs for treating disorders of the gastrointestinal mucosa, induced by microorganisms. Kaolinite and montmorillonite are capable of adsorbing viruses (Lipson and Stotzky, 1984). As such, these minerals can induce rapid recovery when administered to children suffering from gastroenteritis. Similarly, the strong adsorptive power of smectite lies behind its ability to aggregate bacteria, such as strains of *E. coli* with the plasmid P, carrying a virulence factor in the form of an external protein CS 31A (Girardeau, 1987).

In the stomach, *Helicobacter pylori* is associated with gastritis and gastroduodenal ulcers. This bacterium is also one of the most important ethiopathogenic factors causing peptic ulcer. Smectite, on HeLa cells infected by *H. pylori* isolated from human biopsies, significantly reduces adhesion of the bacteria to the surface of epithelial cells (Bonneville et al., 1990). This is why smectite is effective in treating the symptoms of people with non-ulcer dyspepsia who are infected by *H. pylori* (De Korwin et al., 1993).

In the intestine, smectite is effective against diarrhoea as shown by clinical data for new-born calves with neonatal gastroenteritis. Faeces analysis reveals the presence of rotavirus in 41.3% of the animals as well as that of *E. coli* K99, coronavirus, and Salmonella. Recovery is observed in 72% of calves after 2.8 and 2.2 days of receiving 250 and 500 mg/kg smectite, respectively, and after 4.2 days in calves which do not receive smectite. After 4 days of treatment, the consistency of the faeces is significantly better in calves receiving smectite than in the control animals (Espinasse et al., 1987).

### D. Gas

Clay minerals can serve as gas adsorbents in patients with symptoms of flatulence and abdominal distension. Thus, smectite can reduce the amount of hydrogen emitted during colonic fermentation (Frexinos et al., 1986; Arbeille et al., 1991).

### E. Alimentary Allergy

Food allergy is also responsible for disturbances in colonic transit, water absorption, and intestinal permeability. Guinea pigs that were sensitized by  $\beta$ -lactoglobulin from cow milk show colonic transit acceleration, a colonic hypersecretory response, a strong increase in intestinal permeability, and a decrease in faecal dry matter. These effects are not observed in animals that were treated with smectite. Clays can inhibit anaphylaxis probably by controlling the release of mediators at the origin of the degranulation of the mast cells (Theodorou et al., 1994).

#### 11.6.4. CLAY MINERALS AND CLINICAL APPLICATIONS

Being good adsorbents and mucostabilizers, clay minerals are efficacious against several aggressive agents causing severe intestinal disorders. Acute gastroenteritis is a major cause of morbidity and mortality among children worldwide (Madkour et al., 1993). By adsorbing viruses, bacteria, and other digestive irritants, clay minerals can shorten the course of acute diarrhoea, and reduce the occurrence of prolonged diarrhoea. Furthermore, these minerals do not interfere with the electrolyte balance, and are well tolerated by patients (Buttron, 1987; DuPont et al., 1990; Bauer and Hirschbrunn, 1992; Charritat et al., 1992; Dupont et al., 1992; Vivatvakin et al., 1992; Lexomboon et al., 1994; Karas, 1996; Milocco et al., 1999; Guarino et al., 2001; Narkeviciute et al., 2002).

Clay minerals also provide protection against diarrhoeas induced by antibiotics treatments (Benhamou et al., 1995), alleviate chronic diarrhoeas induced by chemotherapy and radiation (Hornbrink et al., 1995; Ippolite, 1998; Santantonio et al., 2000), enteral nutrition (Perrotin et al., 1990), and HIV infection (Phanuphak et al., 1992; Mastroianni et al., 1998).

Clay minerals are promising drugs in the treatment of irritable bowel syndrome (IBS), a rather frequent disease in adults with a complex pathogenic mechanism. By enhancing the thickness of the mucus barrier, both colon movement function and faeces consistency are restored, and the symptoms of IBS are alleviated (Opriu et al., 1996; Secondulfo et al., 2002). In parallel, clay minerals have a positive effect on flatulence and abdominal distension (Lukas and Lukas, 2000).

#### 11.6.5. CONCLUSIONS

Clay minerals protect and are efficient against several ‘aggressors’ that cause major disorders of the gut. These beneficial effects of clay minerals (on the gastrointestinal mucosa) are associated with two mechanisms of action: (1) adsorption of the ‘aggressors’ or their toxic secretions and (2) modification of the thickness and rheological properties of the adherent mucus, reinforcing the natural defenses of the gastrointestinal mucosa.

#### REFERENCES

- Arbeille, P.H., Schillio, Y., Bidard, S., 1991. Value of using a gas reductor (Diosmectite) for the preparation of patients prior to the echography of the epigastric area. *Gastroenterology* 100, Abstract 347.
- Bauer, C., Hirschbrunn, P., 1992. Treatment of acute diarrhea in infants. *Der Kinderarzt* 5, 878–884.
- Benhamou, P.H., Berlier, P., Longue, J., Dupont, C., 1995. Intestinal manifestation during antibiotics treatments in children: a prospective study. *Gastroenterology* 108, Abstract 273.

- Bonneville, F., Moyen, E.N., Droy-Lefaix, M.T., Fauchère, J.L., 1990. *In vitro* effect of smectite on *Campylobacter pylori* adhesion upon epithelial cells. Gastroentérologie Clinique et Biologique 14, Abstract 123.
- Bouyssou, T., Bioss, S., Cochat, C., Goudey, V., Doubovetzky, M., Poiret, M., 1990. Protective effect of an aluminium hydroxide, boehmite, on rat gastric mucus. Gastroenterology 98, Abstract 25.
- Brouillard, M.Y., Rateau, J.G., 1989. Adsorption potency of 2 clays, smectite and kaolin on bacterial endotoxin. *In vitro* study in cell culture and on the intestine of newborn mice. Gastroentérologie Clinique et Biologique 13, 18–24.
- Buttron, O., 1987. Treatment of chronic functional diarrheas. Therapiewoche 37, 2723–2726.
- Carnoy, C., Muller Alouf, H., Mullet, C., Droy-Lefaix, M.T., Simonet, M., 2000. Oral infection of mice with superantigenic toxic producing *Yersinia pseudotuberculosis*. Effect of diosmectite. International Journal of Medical Microbiology 290 (30), Abstract 83.
- Charritat, J.L., Corbineau, D., Guth, S., Meunier, M., Perrin, P., Pflieger, H., 1992. Therapeutic evaluation of Mormoiron attapulgit in acute diarrheas of infants and children. A multicenter study in controlled liberal practice versus placebo in 113 patients. Annales de Pédiatrie (Paris) 39, 326–332.
- De Korwin, J.D., Forestia, B., Plique, O., 1993. Symptomatic improvement of patients with non ulcer dyspepsia and *Helicobacter pylori* after treatment with diosmectite. Randomized double-blind study versus placebo. Acta Gastroenterologica Belgica 56, Abstract 149.
- Droy-Lefaix, M.T., 1986. Adsorption properties of clays. In Precepta Medica, Digestive Disease Week 4, 42–44.
- Droy-Lefaix, M.T., 1987. Intestinal mucosa barrier and smectite. Revue de Médecine Vétérinaire 138, 411–421.
- Droy-Lefaix, M.T., Drouet, Y., Schatz, B., 1985. Sodium glycodeoxycholate and spinability of gastrointestinal mucosa: protective effect of smectite. Digestive Disease Week 5, Abstract 1369.
- Droy-Lefaix, M.T., Plique, O., Géraud, G., Drouet, Y., 1992. Protective effect of diosmectite on the decrease of the adherent mucus gel thickness induced by phenylbutazone on rat stomach. Hellenic Journal of Gastroenterology 5 (70), Abstract 279.
- Droy-Lefaix, M.T., Schatz, B., Drouet, Y., 1986. Importance of viscoelasticity in the study of the adherent mucus gel. Digestive Disease Science 31, Abstract 1401.
- Dupont, C., Moreno, J.L., Barau, E., Bargaoui, K., Thian, E., Plique, O., 1992. Effect of diosmectite on intestinal permeability changes in acute diarrhea: a double blind placebo-controlled trial. Journal of Pediatric Gastroenterology and Nutrition 14, 413–419.
- DuPont, H.L., Ericsson, C.D., DuPont, M.W., Cruz Luna, A., Mattewson, J.J., 1990. A randomized, open-label comparison of loperamide and attapulgit in the symptomatic treatment of acute diarrhea. American Journal of Medicine 20, 20–23.
- Eaton, J.R., Eaton, T.M., 1995. Bentonite: Public Research Project: An Educational Compilation of Related Commentaries and Articles. <http://www.cytonsearth.org/bentonite.html>.
- Espinasse, J., Navetat, H., Droy-Lefaix, M.T., Roger, C., 1987. Treatment and prevention of diarrhea in young calves by a cytoprotector agent of intestinal mucus barrier: smectite. Bulletin de la Société Vétérinaire Pratique de France 71, 4–13.



- Fioramonti, J., Bouaouiche, F., Droy-Lefaix, M.T., Plique, O., Corthier, G., Bueno, L., 1994. Diosmectite treatment delays colonic water secretion and reduces increase in intestinal permeability by *Clostridium difficile* toxins in rats. *Gut* 35 (Suppl 4), A31–A32.
- Fioramonti, J., Droy-Lefaix, M.T., Bueno, L., 1987a. Changes in gastric-intestinal motility induced by cholera toxin and experimental osmotic diarrhoea in dogs: effects of treatment with an argillaceous compound. *Digestion* 36, 230–237.
- Fioramonti, J., Fargeas, M.J., Bueno, L., 1987b. Action of T-2 toxin on gastrointestinal transit in mice: protective effect of an argillaceous compound. *Toxicology Letters* 36, 227–232.
- Fioramonti, J., Navetat, H., Droy-Lefaix, M.T., Moré, J., Bueno, L., 1990. Antidiarrheal properties of clay minerals: pharmacological and clinical studies. In: Simon, F., Lees, P., Semjen, G. (Eds.), *Veterinary Pharmacology, Toxicology and Therapy in Food Producing Animals. Proceedings of the 4th Congress of Pharmacology and Toxicology*, Budapest, 1988. University of Veterinary Science, Budapest, pp. 245–251.
- Frexinos, J., Suduca, J.M., Schatz, B., 1986. Smectite and colic fermentation. *Semaine des Hôpitaux de Paris* 62, 2025–2028.
- Girardeau, J.P., 1987. *Escherichia coli* smectite aggregation. *Acta Gastroenterologica Belgica* 50, Abstract 85.
- Guarino, A., Bisceglia, M., Castellucci, G., Lacono, G., Bruzzese, E., Musetta, A., Greco, L., 2001. Smectite in the treatment of acute diarrhea: a nationwide randomized controlled study of the Italian Society of Pediatric Gastroenterology and Hepatology (SIGEP) in collaboration with primary care pediatricians. SOGEP study groups for smectite in acute diarrhea. *Journal of Pediatric Gastroenterology and Nutrition* 32, 71–75.
- Gwozdinski, K., Jedrzejewska, A., Janocka, M., Droy-Lefaix, M.T., 1997. Effect of diosmectite on the physico-chemical properties of gastric mucus *in vivo* and *in vitro*. *Gastroenterology* 12, Abstract 136.
- Hornbrink, J., Voss, A.C., Fröhlich, D., Glatzel, M., Krauns, A., Glaser, F.A., 1995. Therapy trends in the prevention of radiation induced diarrhea after pelvic and abdominal irradiation. Results of a tricenter study. *Strahlentherapie und Onkologie* 174, 49–53.
- Ippolite, C., 1998. Antidiarrheal agents for the management of treatment related diarrhea in cancer patients. *American Journal of Health System Pharmacy* 55, 1573–1580.
- Karas, J., 1996. Smecta and its place in the treatment of acute rotavirus gastroenteritis of neonates. *Cesko-Slovenska Pediatrie* 55, 85–90.
- Knight, J., Pearson, J.P., Droy-Lefaix, M.T., Allen, A., 1998. Could the discontinuous and structurally weaker colonic mucus gel in ulcerative colitis be a result of free radical damage? *Digestive Disease Week, 99th Annual Meeting of AGA*, New Orleans, LA.
- Leonard, A.J., Droy-Lefaix, M.T., Allen, A., 1994. Pepsin hydrolysis of the adherent mucus barrier and subsequent gastric mucosal damage in the rat: effect of diosmectite and 16,16 dimethyl prostaglandin E2. *Gastroentérologie Clinique et Biologique* 8, 609–616.
- Lexomboon, U., Harikul, S., Lortholary, O., 1994. Control randomized study of rehydration with dioctahedral smectite in ambulatory Thai infants with acute diarrhea. *Southeast Asian Journal of Tropical Medicine and Public Health* 25, 157–162.
- Lipson, S.M., Stotzky, G., 1984. Effect of proteins on reovirus adsorption to clay minerals. *Applied Environmental Microbiology* 8, 525–530.
- Lukas, K., Lukas, M., 2000. Dioctahedral smectite in the treatment of irritable colon. *Prakticky Lekar* 80, 27–29.

- Madkour, A.A., Madina, E.M.H., El Azzouni, O.E.Z., Amor, M.A., El Waliti, T.M.K., Abbass, T., 1993. Smectite in acute diarrhea in children: a double-blind study placebo-controlled clinical trial. *Journal of Pediatric Gastroenterology and Nutrition* 17, 176–181.
- Mahraoui, L., Heyman, M., Plique, O., Droy-Lefaix, M.T., Desjeux, J.F., 1997. Apical effect of diosmectite on damage to the intestinal barrier induced by basal tumour necrosis factor- $\alpha$ . *Gut* 40, 339–343.
- Martirosian, G., Rouyan, G., Zalewski, T., Meisel Mikolajczyk, F., 1998. Dioctahedral smectite neutralization activity of *Clostridium difficile* and *Bacteroides fragilis* toxins *in vitro*. *Acta Microbiologica Polonica* 47, 171–183.
- Mastroianni, A., Canallieri, C., Coronado, O., Manfred, R., Chiodo, F., Pignatari, S., 1998. Smectite in AIDS-associated chronic idiopathic diarrheas. *Minerva Gastroenterologica et Dietologica* 44, 231–234.
- Meredith, T.J., Vale, J.A., 1987. Treatment of paraquat poisoning in man. Methods to prevent absorption. *Human Toxicology* 6, 49–55.
- Milocco, C., Bolis, A., Rizzo, V., Suprani, T., Cerasoli, G., Marani, M., Pocecco, M., 1999. Evaluation of diosmectite in acute diarrhea in children. *Pediatrica Medica e Chirurgica* 21, 129–133.
- Moré, J., Benazet, F., Fioramonti, J., Droy-Lefaix, M.T., 1987. Effects of treatment with smectite on gastric and intestinal glycoproteins in the rat: a histochemical study. *Histochemical Journal* 19, 665–670.
- Moré, J., Fioramonti, J., Bueno, L., 1992. Changes in gastrointestinal mucins caused by attapulgit. Experimental study. *Gastroentérologie Clinique et Biologique* 16, 988–993.
- Narkeviciute, J., Rudzeviciene, O., Levinere, G., Mociskiene, K., Eidukevicius, R., 2002. Management of Lithuanian children's acute diarrheas with gastrolit solution and dioctahedral smectite. *European Journal of Gastroenterology and Hepatology* 14, 419–424.
- Opriu, A.L., Diclescu, M., Lov, A., Calin, S., Dumitrescu, A., Calin, G., Manuc, M., Pitigoi, D., 1996. Enterocyte covering agent versus intestinal motility inhibition in the irritable bowel. *Gut* 9, Abstract 34.
- Pearson, J.P., Ayre, D., Droy-lefaix, M.T., Allen, A., 1996. Mucolysis of the colonic mucus barrier by oxygen free radicals: implication for ulcerative colitis. *Gastroenterology* 110, Abstract 988.
- Peignot, J.F., Giral, P., Plique, O., 1997. A multicentric, double-blind, placebo controlled study of the efficacy of diosmectite in the treatment of secondary stomach pain due to administration of non steroid antiinflammatory agents. *Médecine et Chirurgie Digestive* 26, 233–241.
- Perrotin, D., Legras, A., Boulain, T., Ginies, G., 1990. Diarrhea under parenteral nutrition in reanimation. Prevention study using an adsorbent drug. In: *Réanimation et Appareil digestif*. Société de Réanimation de Langue française, Paris, pp. 49–53.
- Phanuphak, P., Hanvanick, M., Lortholary, O., 1992. Smectite in HIV-associated diarrheas: a preliminary study. *Journal of Acquired Immune Deficiency Syndrome* 5, 954–955.
- Pons, L., Droy-Lefaix, M.T., Leguere, N., Guillemain, J., 1997. Protective effects of diosmectite from alterations of mucosal permeability and morphology of rabbit ileal loops induced by *Escherichia coli* enterotoxin. *Gastroenterology* 112, Abstract 395.
- Samson, H.J., Pearson, J.P., Srivastava, E.D., Droy-Lefaix, M.T., Allen, A., 1995. Increased serine-dependent proteinases in ulcerative colitis: mucolysis and inhibition by diosmectite. *Gastroenterology* 108, Abstract 909.

- Santantonio, M., Colella, M., Fiorica, F., Aratisali, S., Stefanelli, A., Falchi, A.M., 2000. Diosmectite (diosmectal) prevention antidiarrheic therapy in patients submitted to pelvic radiation. *Minerva Gastroenterologica et Dietologica* 46, 225–230.
- Schell, T., Lindemann, M.D., Kornegay, E.T., Blodgett, D.L., Doerr, J.A., 1993. Effectiveness of different types of clay for reducing the detrimental effects of aflatoxin-contaminated diets on performance and serum profiles of weanling pigs. *Journal of Animal Science* 71, 1226–1231.
- Secondulfo, M., Mennella, R., Fenderico, C., 2002. Ruolo dei fattori psicologi nei pazienti affetti da sindrome dell'intestino irritabile. *Internista* 10, 169–173.
- Slitine-Bonet, F., Vatie, J., Droy-Lefaix, M.T., 1994. Structural study of rat's gastric adherent mucus: protective effect of diosmectite from alcohol injury. *Gut* 35, Abstract 210.
- Theodorou, V., Chrestian, B., Fioramonti, J., Droy-Lefaix, M.T., Bueno, L., 1995. Diosmectite treatment prevents intestinal permeability and mucus alterations induced by ingestion of a pesticide in rats. *Gut* 37, Abstract 148.
- Theodorou, V., Fioramonti, J., Droy-Lefaix, M.T., Plique, O., Bueno, L., 1994. Protective action of diosmectite treatment on digestive disturbances induced by intestinal anaphylaxis in the guinea pig. *Alimentary Pharmacology and Therapeutics* 8, 295–299.
- Vivatvakin, B., Jongpipatvanich, S., Harikul, S., Eksaengri, P., Lortholary, O., 1992. Control study of oral rehydration solution (ORS) + dioctahedral smectite in hospitalized Thai infants with acute secretory diarrhea. *Southeast Asian Journal of Tropical Medicine and Public Health* 23, 414–419.

## Chapter 12

## CRITICAL ASSESSMENT OF SOME ANALYTICAL TECHNIQUES

F. BERGAYA<sup>a</sup>, B.K.G. THENG<sup>b</sup> AND G. LAGALY<sup>c</sup><sup>a</sup>CRMD, CNRS-Université d'Orléans, F-45071 Orléans Cedex 2, France<sup>b</sup>Landcare Research, Palmerston North, New Zealand<sup>c</sup>Institut für Anorganische Chemie, Universität Kiel, D-24118 Kiel, Germany

This composite chapter consists of eleven parts. The first eight are concerned with spectroscopic and instrumental techniques that are more or less frequently used to characterize clays and clay minerals. These include, presented in the order of increasing wavelength, as shown by the 'panorama' (Fig. 12.1) of the various spectroscopic techniques: Mössbauer Spectroscopy (Chapter 12.1), Identification and Quantitative Analysis of Clay Minerals (Chapter 12.2). As X-ray diffraction is the most documented technique in the clay science literature, this instrumental method is described here mainly in terms of its use in identifying and quantifying clay minerals.

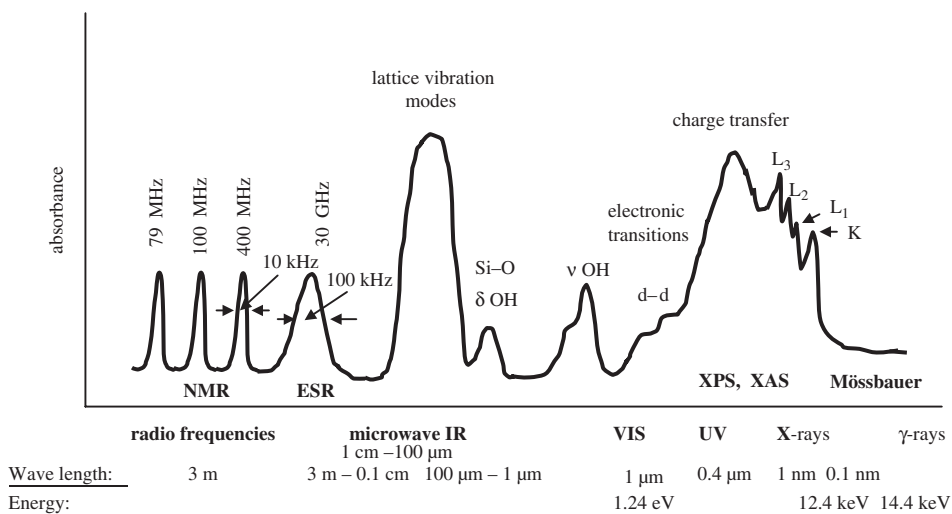


Fig. 12.1. A 'panorama' of the various spectroscopic techniques with their corresponding wavelengths.

X-ray Absorption Spectroscopy (Chapter 12.3), X-ray Photoelectron Spectroscopy (Chapter 12.4), Small-angle Scattering Techniques (Chapter 12.5), Fourier Transform Infrared Spectroscopy (Chapter 12.6), Nuclear Magnetic Resonance Spectroscopy (Chapter 12.7), and Transmission Electron Microscopy (Chapter 12.8) which is discussed in some details because this technique is not routinely applied to clay-mineral analysis. The results of spectroscopic analyses, however, have to be interpreted with due caution because of the finely divided, heterogeneous nature of clay materials, and the presence of associated minerals and phases.

Similarly, the measurement of important surface properties, notably surface area and porosity (Chapter 12.9), and ion exchange (Chapter 12.10) are critically assessed. Although the thermal analysis of clay minerals is also well documented because of its importance to ceramic research, Chapter 12.11 gives an updated account of thermal techniques.

Many new surface analytical methods, such as atomic force microscopy (AFM), are not included in this chapter because of space limitations. Other modern instrumental techniques, such as ion-beam analysis (IBA), particle-induced X-ray emission (PIXE), proton-induced  $\gamma$ -ray emission (PIGE), and Rutherford backscattering spectroscopy (RBS) were developed during the past decade and used in the analysis of paints, ceramics, pottery, and archaeological objects. However, these techniques were not so far widely applied to clay mineral analysis.

## Chapter 12.1

# MÖSSBAUER SPECTROSCOPY OF CLAYS AND CLAY MINERALS

E. MURAD

*Bayerisches Landesamt für Umwelt, D-95603 Marktredwitz, Germany*

### 12.1.1. HISTORICAL BACKGROUND

The earliest Mössbauer data on clay minerals *sensu stricto* (clay-size phyllosilicates) were published (Malden and Meads, 1967; Weaver et al., 1967) less than a decade after the appearance of the first report on the Mössbauer effect (Mössbauer, 1958a, 1958b). Since then Mössbauer spectroscopy was widely used to study and characterise clay-related materials. The *Mössbauer Mineral Handbook* (Stevens et al., 1998) lists 68 publications that refer to montmorillonite, 46 to chlorite, and 44 each to glauconite and nontronite. In addition, the handbook contains 132 references to hematite and 112 references to goethite, two of the most common accessory constituents of soils and raw clays. Almost all of these entries were concerned with  $^{57}\text{Fe}$ , and the present discussion will be confined to this nuclide.

Although there are still some discrepancies on specific details such as data evaluation, Mössbauer spectroscopy is now routinely used for the characterisation of the oxidation state of iron in clays and clay minerals. In favourable cases the coordination of iron can also be deduced and, where applicable, the magnetic properties induced by the presence of iron in the structure. For some minerals (including the majority of iron oxides), Mössbauer spectroscopy can also be used to identify the actual species.

### 12.1.2. BASIC PRINCIPLES

Mössbauer spectroscopy involves the recoil-free emission and absorption of gamma rays. A principal feature of the technique is that it only ‘sees’ the nuclide under survey. Thus the sole effects arising from the presence of other elements in samples of complex chemical composition are dilution and absorption. The vast majority of Mössbauer spectra are taken in the transmission mode. Here a source ( $^{57}\text{Co}$  for iron spectra) emitting gamma rays of the appropriate energy is periodically moved over a succession of velocities, and the radiation transmitted by the sample (‘absorber’) is registered as a function of the source velocity.

Mössbauer spectra result from the so-called hyperfine interactions between the resonant nuclei and their electric and magnetic environments. The principal hyperfine interactions are (1) the electric monopole interaction, giving rise to the isomer shift ( $\delta$ ); (2) the electric dipole interaction, leading to the quadrupole splitting ( $\Delta$ ); and (3) the magnetic hyperfine interaction when a magnetic hyperfine field ( $B_{\text{hf}}$ ) acts at the nuclei of the resonant atoms. The isomer shift is the shift of the centroid of the spectrum from zero velocity, and is given relative to either the source or some standard material—in the case of  $^{57}\text{Fe}$  usually metallic iron. The quadrupole splitting is the separation of the two lines of a  $^{57}\text{Fe}$  doublet. Both isomer shift and quadrupole splitting are customarily given in terms of the source velocity in mm/s. Isomer shifts are related to the oxidation state of iron and may provide information on iron coordination, whereas the quadrupole splitting provides a measure for  $\text{Fe}^{3+}$  site distortion. An intrinsic ('hyperfine') or extrinsic magnetic field splits an  $\text{Fe}^{3+}$  Mössbauer spectrum into a sextet, the spread of which is proportional to the field, and is usually expressed in kilooersteds or tesla (1 T = 10 kOe).

In complex spectra the relative intensities of individual components are often taken as proportional to the corresponding site population. This relationship, however, only applies as a first approximation; for example,  $\text{Fe}^{2+}$  exhibits a lower recoil-free fraction than  $\text{Fe}^{3+}$  (De Grave and Van Alboom, 1991). Additional information may be obtained from the widths and shapes of the lines. The ideal Mössbauer line shape is the Lorentzian, and experimental data are often computer-fitted on this basis. However, deviations from Lorentzian shape may occur because of variations of local environments or fluctuations of parameters, to name just two factors. In such cases, the data may have to be fitted using other functions, for example, the Voigtian (a convolution of Gaussian and Lorentzian functions) or distributions of Lorentzians.

Numerous textbooks on the Mössbauer effect and its applications were published (for example Gonser (1975) and Gibb (1976) to name two of the better known 'classics', and more recently a book by Murad and Cashion (2004) that focuses on the Mössbauer spectra of materials formed on the earth's surface), and for more information on the Mössbauer effect than can be included here, the reader is referred to these and similar sources.

Depending upon sample structure and composition,  $^{57}\text{Fe}$  Mössbauer spectra may consist of one or more singlet(s), quadrupole-split doublet(s), and magnetically split sextet(s). Singlets develop only in the case of cubic symmetry around  $\text{Fe}^{3+}$ , and hence are not observable in the spectra of phyllosilicates. Sextets, arising from iron in magnetically ordered materials, are only observed for extremely iron-rich phyllosilicates at low temperatures ( $\leq 10$  K), and for iron oxides of sufficiently good crystallinity and chemical purity. The Mössbauer spectra of phyllosilicates thus generally consist of one doublet for iron in each oxidation state on every structural site.

### 12.1.3. MÖSSBAUER SPECTRA OF SELECTED CLAY MINERALS

Both divalent and trivalent iron can substitute for aluminium and magnesium in the structures of phyllosilicates. The extent of substitution depends on both the availability

of iron during mineral formation and the specific mineral structure (i.e., the numbers and geometries of structural sites into which iron can be incorporated).

Although kaolinites, in general, show little variation of chemical composition, some substitution of iron for aluminium in octahedral sites can occur. As a result, the Mössbauer spectra of kaolinite are deceptively simple: a single  $\text{Fe}^{3+}$  doublet or, as observed in the early study by Malden and Meads (1967), each one  $\text{Fe}^{3+}$  and  $\text{Fe}^{2+}$  doublet. Besides confirming this observation, subsequent studies of kaolinite—the *Mössbauer Mineral Handbook* (Stevens et al., 1998) lists a total of 20 references—indicated that octahedral substitution by  $\text{Fe}^{3+}$  is more common than that by  $\text{Fe}^{2+}$ . A detailed investigation of 22 kaolinites from different genetic environments and with widely varying iron contents (Murad and Wagner, 1991), however, indicates that it is not uncommon to have  $\text{Fe}^{2+}$  substituting for  $\text{Al}^{3+}$ . Indeed, in one sample (KGa-1) the concentration of  $\text{Fe}^{2+}$  even exceeds that of  $\text{Fe}^{3+}$ . This study also confirms the work by Fysh et al. (1983) that slow paramagnetic relaxation can have a marked influence on the Mössbauer spectra of kaolinite as indicated by a non-specific broadening of the paramagnetic doublet at room temperature and the development of a magnetic component at 4.2 K (Fig. 12.1.1).

The 2:1 layer silicates offer a larger variety of possibilities for the incorporation of iron than their 1:1 counterparts. Not only can iron occupy two distinctly different octahedral sites (*cis*- and *trans*-OH) in 2:1 structures, but  $\text{Fe}^{3+}$  can sometimes also substitute for silicon in tetrahedral sites. The problem of distinguishing iron between *cis* and *trans* sites, and also between tetrahedral and octahedral  $\text{Fe}^{3+}$  by Mössbauer spectroscopy was hotly debated. In many instances, the spectra were fitted with an increasing number of doublets until the fitted and experimental data matched adequately well, after which the resulting spectral components were assigned to structural sites. High-quality spectra of well-crystallized phyllosilicates, however, showed that this procedure of assigning parameters to *cis* and *trans* sites is often untenable (Murad and Wagner, 1994; Rancourt, 1994). A debate between Dyar (1993) and Rancourt (1993) illustrates the problem of characterising tetrahedral  $\text{Fe}^{3+}$ . The isomer shift of tetrahedral  $\text{Fe}^{3+}$  is known to be lower than that of octahedral  $\text{Fe}^{3+}$  by about 0.1 mm/s. Using computer-fitted data, Dyar (1993) assigns doublets with a correspondingly low isomer shift to tetrahedrally coordinated  $\text{Fe}^{3+}$ . On the other hand, Rancourt (1993) contends that tetrahedral  $\text{Fe}^{3+}$  is not present unless the spectra show a visible shoulder from the high-velocity line of the tetrahedral  $\text{Fe}^{3+}$  doublet.

The iron contents of illites range from <1 to over 10 wt.% (Środoń and Eberl, 1984), and their Mössbauer spectra were reported in a number of papers. Unfortunately, data comparison is complicated by the large variation in chemical composition as well as a multiplicity of (often not comparable) models used to fit the spectra. In an attempt to rationalise the data, Murad and Wagner (1994) have taken the Mössbauer spectra of 8 illites with iron contents between 0.8 and 8.4 wt.% Fe. The main conclusions of this study are that tetrahedral  $\text{Fe}^{3+}$  is present only in the most iron-rich sample, and that many illites, like kaolinite, show distinct effects of paramagnetic relaxation at 4.2 K.



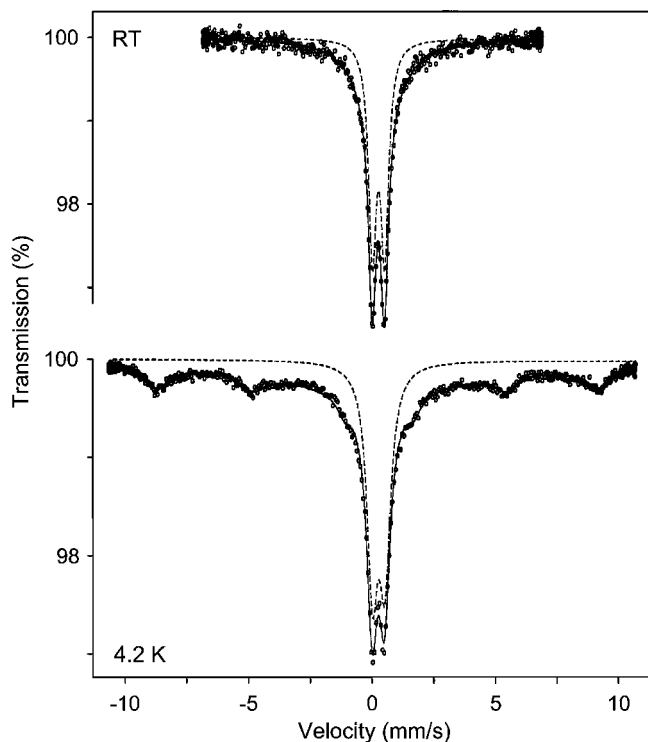


Fig. 12.1.1. Mössbauer spectra of a kaolinite (total Fe content 1.29 wt.%) from the Jari deposit in Brazil, taken at room temperature (RT) and 4.2 K. The effects of slow paramagnetic relaxation at these temperatures are evidently different. Nevertheless, the non-relaxing components resulting from  $\text{Fe}^{3+}$  in the octahedral sites, indicated by the broken subspectra, have identical parameters ( $\delta/\text{Fe} = 0.35$ ,  $\Delta = 0.51$  mm/s). Adapted from Murad and Wagner (1991).

Nontronite is the iron-rich end-member of the dioctahedral beidellite–nontronite smectite group. Nontronites contain much more iron than kaolinite and illite; in some instances, the iron content may exceed 24 wt.% (Köster et al., 1999). Room temperature Mössbauer spectra of nontronite show a rather small average quadrupole splitting ( $\sim 0.4$  mm/s), consistent with a moderate distortion of the octahedral sites. The broad  $\text{Fe}^{3+}$  resonance has to be fitted with at least two Lorentzian doublets of similar isomer shift but different quadrupole splittings. There was some controversy regarding the origin of these doublets. In early papers these are interpreted in terms of *cis* and *trans* octahedral site occupancies, although electron microscopy (e.g., Méring and Oberlin, 1967) indicates that iron occupies only the *cis* sites. The most probable cause for the line broadening is the existence of many different environments at the atomic scale, causing the Mössbauer parameters to

‘smear out’. Such cases are best accounted for by fitting the spectra with distributions of quadrupole splittings (Murad, 1987).

The ratios of tetrahedral  $\text{Fe}^{3+}$  to total iron, derived from Mössbauer spectra of selected nontronites (e.g., Garfield H33a), also showed a ‘disconcertingly’ large variation (Stucki, 1988). These variations may be due to differences between subsamples, incompatible fitting techniques (such as the use of different line profiles or constraint of parameters), and the presence of other minerals, in particular iron oxides. Indeed, the association of finely divided iron oxides with nontronites seems to be the rule rather than the exception (Murad, 1987). However, when spectra are taken at room temperature, the contributions of iron oxides (see next section) cannot be separated from the lines due to nontronite. Such a separation would require taking Mössbauer spectra at significantly lower temperatures (Fig. 12.1.2).

Variations in the  $\text{Fe}^{2+}/\text{Fe}^{3+}$  ratios of smectites as a result of chemical treatments can be readily monitored by Mössbauer spectroscopy. Mössbauer spectra can also provide evidence for non-reversible changes in mineralogy when some nontronites are reoxidised following reduction with sodium dithionite (e.g., Rozenson and Heller-Kallai, 1976; Russell et al., 1979), showing that problems can occur if such treatments are not carried out with sufficient care.

#### 12.1.4. MÖSSBAUER SPECTRA OF IRON (HYDR)OXIDES

Iron oxides and/or oxyhydroxides, collectively referred to as ‘iron (hydr)oxides’ (see Chapters 1 and 5), are common constituents of soils and clays. As already remarked on, these ‘associated minerals’ can have significant effects on the Mössbauer spectra of phyllosilicates.

Iron (hydr)oxides have relatively high magnetic ordering temperatures, ranging from 955 K for hematite and 400 K for goethite (both of which should therefore be magnetically ordered at room temperature) to 77 K for lepidocrocite. In practice, however, the Mössbauer spectra of iron (hydr)oxides, associated with soils and clays, frequently deviate from ideal behaviour. One reason for this is that other elements, notably aluminium, can substitute for iron in the iron (hydr)oxide structure. As a result, the magnetic ordering temperatures decrease and the magnetic hyperfine fields are reduced at all temperatures. Moreover, small-particle effects may cause fluctuations of the magnetic field (‘superparamagnetic relaxation’), leading to line broadening and hyperfine field reduction. In extreme cases, magnetic order can be completely suppressed. In order to differentiate iron (hydr)oxides from phyllosilicates, Mössbauer spectra must be taken at temperatures that are adequately low to minimise these effects and ensure the establishment of magnetic order in the iron (hydr)oxides, yet high enough to avoid magnetic order in the phyllosilicates (generally in the range 120–20 K).

Mössbauer spectroscopy is extremely sensitive to the presence of magnetically ordered phases in samples of complex composition. Murad and Wagner (1991, 1994), for example, showed that as little as 1% ferrihydrite associated with illite

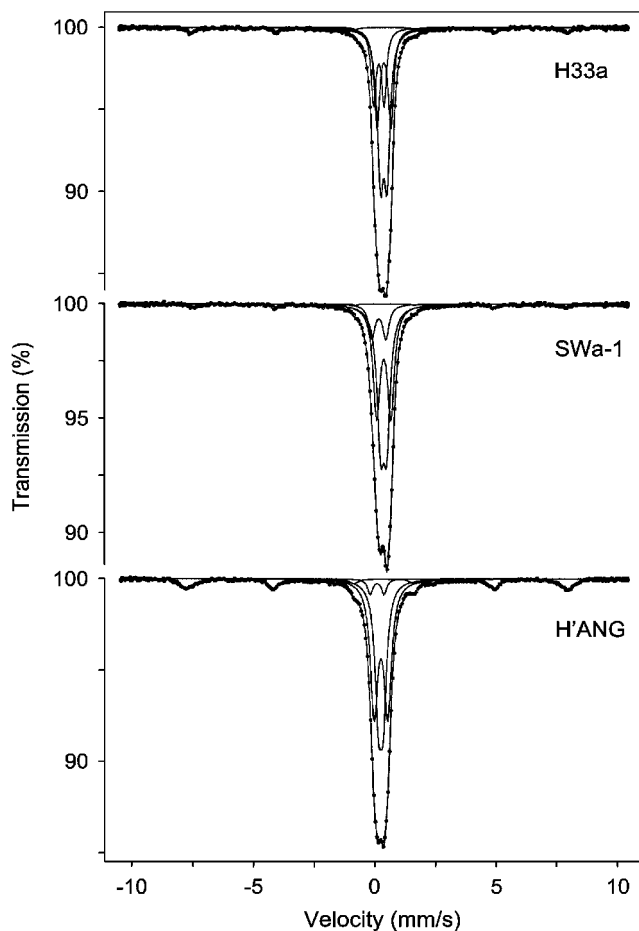


Fig. 12.1.2. Low-temperature Mössbauer spectra of three 'pure' nontronites: H33a and SWa-1 (taken at 77 K) and H'ANG (taken at 120 K). The central doublet is assigned to  $\text{Fe}^{3+}$  in the nontronite structure, whereas sextets are due to ancillary goethite. Analyses of the spectra indicate that goethite makes up 2.9% of the iron in H33a, 4.6% in SWa-1, and 13% in H'ANG. Adapted from Murad (1987).

(Fig. 12.1.3), and 0.1% goethite in association with kaolinite, can be clearly detected in Mössbauer spectra taken at 4.2 K.

### 12.1.5. MÖSSBAUER SPECTRA OF FIRED CLAY MINERALS

Mössbauer spectroscopy is ideally suited for monitoring the thermal reactions of clays and clay minerals because it can reveal variations in  $\text{Fe}^{2+}/\text{Fe}^{3+}$  ratios as well

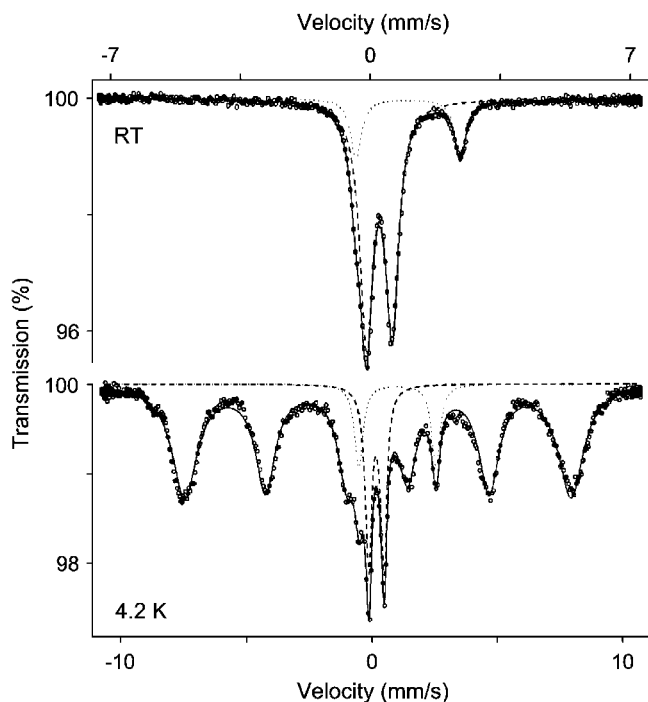


Fig. 12.1.3. Mössbauer spectra of an iron-poor illitic clay (total Fe content 0.80 wt.%) from Upper Silesia, Poland, taken at room temperature (RT) and 4.2 K. Doublets arising from  $\text{Fe}^{2+}$  and  $\text{Fe}^{3+}$  are indicated with dotted and broken lines, respectively. Note the different velocity ranges of the spectra. The sextet in the latter spectrum shows that the iron mineralogy of the sample is dominated by ferrihydrite (although this amounts to just 1% of the sample), whereas no more than 25% of the iron content are bound in the phyllosilicates. Adapted from Murad and Wagner (1994).

as changes in coordination polyhedron symmetry. The samples used in many published investigations, however, are not well characterised, and their mineralogical purity is open to question. Furthermore, the results are often difficult to compare because of variations in experimental conditions (specifically with respect to the duration of heating) and spectral fitting techniques. In an attempt to resolve this problem, Murad and Wagner (1991, 1996) recorded the Mössbauer spectra of a kaolinite from the Jari deposit in Brazil (see Fig. 12.1.1) and a reference illite (OECD #5) after heating the kaolinite in steps of 50 °C up to 1350 °C and the illite up to 1300 °C.

When the illite is heated under free access of air, the first change that occurs is a decrease in the proportion of  $\text{Fe}^{2+}$ , from an initial value of ~ 7% to essentially zero

at 300 °C (Fig. 12.1.4). However, the most striking result for both kaolinite and illite is the development of regions of high quadrupole splitting between  $\sim 450$  and 900 °C. In the case of kaolinite, the quadrupole splitting increases from 0.52 mm/s (for the unheated material) to a maximum of 1.63 mm/s, while the illite spectra show a less pronounced increase from 0.63 to 1.53 mm/s. This observation is indicative of an extensive  $\text{Fe}^{3+}$  site distortion in metakaolin. The average quadrupole splittings for the paramagnetic components decreases somewhat after firing to 900 °C and above, but the complex appearance of the spectra indicates the presence of iron in more than one (high-temperature) phase.

The room temperature spectra of the fired kaolinite show only minor indications of a magnetically ordered phase, whereas the corresponding illite spectra exhibit distinct hematite sextets after firing to temperatures between 950 and 1250 °C (Fig. 12.1.4). At 4.2 K, the spectra of the fired illite show poorly defined, broad magnetic components from 650 °C upwards, whereas a well-defined magnetic component that can be attributed to hematite first appears at 900 °C. It would therefore appear that the iron oxides initially formed are of small particle size, and their magnetisation is subject to superparamagnetic relaxation. As the firing temperature is raised, both the proportion and particle size of the hematite formed increase. The disappearance of hematite at  $\geq 1250$  °C coincides with the formation of glass, capable of incorporating more iron than the crystalline high-temperature phases.

Mössbauer spectroscopy was often used to characterise archaeological ceramics. Provided that the nature and origin of the clay material used for their manufacture are known, it is possible to reconstruct details of the processing technique, such as

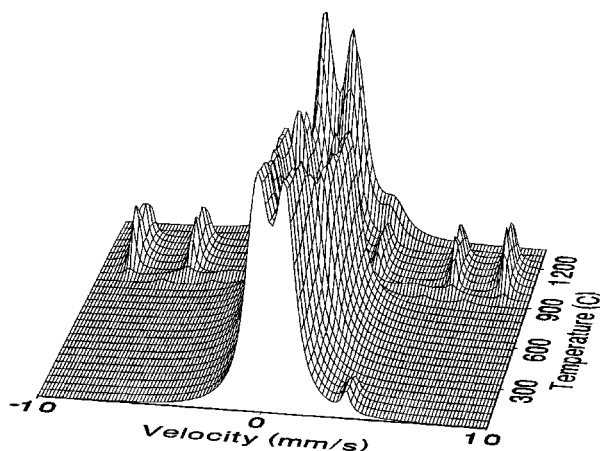


Fig. 12.1.4. Room temperature Mössbauer spectra of the OECD #5 illite (total Fe content 5.18 wt.%) fired in 50 °C steps for 48 h. Note the disappearance of  $\text{Fe}^{2+}$  at 300 °C, the appearance of a magnetically ordered component (hematite) at 950 °C, and its subsequent disappearance 1250 °C. From Murad and Wagner (1996).

the temperature and duration of firing, and whether oxidising or reducing conditions were used (Wagner et al., 1998). Given that such potsherds may be the sole remnants of some former civilisations, this information can be of inestimable value to archaeological research.

## REFERENCES

- De Grave, E., Van Alboom, A., 1991. Evaluation of ferrous and ferric Mössbauer fractions. *Physics and Chemistry of Minerals* 18, 337–342.
- Dyar, M.D., 1993. Mössbauer spectroscopy of tetrahedral  $\text{Fe}^{3+}$  in trioctahedral micas—Discussion. *American Mineralogist* 78, 665–668.
- Fysh, S.A., Cashion, J.D., Clark, P.E., 1983. Mössbauer effect studies of iron in kaolin. I. Structural iron. *Clays and Clay Minerals* 31, 285–292.
- Gibb, T.C., 1976. *Principles of Mössbauer Spectroscopy*. Chapman & Hall, London.
- Gonser, U. (Ed.), 1975. *Mössbauer Spectroscopy*. Springer-Verlag, Berlin.
- Köster, H.M., Ehrlicher, U., Gilg, H.A., Jordan, R., Murad, E., Onnich, K., 1999. Mineralogical and chemical characteristics of five nontronites and Fe-rich smectites. *Clay Minerals* 34, 579–599.
- Malden, P.J., Meads, R.E., 1967. Substitution by iron in kaolinite. *Nature* 215, 844–846.
- Méring, J., Oberlin, A., 1967. Electron-optical study of smectites. *Clays and Clay Minerals* 15, 3–25.
- Mössbauer, R.L., 1958a. Kernresonanzabsorption von Gammastrahlung in  $\text{Ir}^{191}$ . *Naturwissenschaften* 45, 538–539.
- Mössbauer, R.L., 1958b. Kernresonanzfluoreszenz von Gammastrahlung in  $\text{Ir}^{191}$ . *Zeitschrift für Physik* 151, 124–143.
- Murad, E., 1987. Mössbauer spectra of nontronites: structural implications and characterization of associated iron oxides. *Zeitschrift für Pflanzenernährung und Bodenkunde* 150, 279–285.
- Murad, E., Cashion, J., 2004. *Mössbauer Spectra of Environmental Materials and their Industrial Utilization*. Kluwer, Boston.
- Murad, E., Wagner, U., 1991. Mössbauer spectra of kaolinite, halloysite and the firing products of kaolinite: new results and a reappraisal of published work. *Neues Jahrbuch für Mineralogie, Abhandlungen* 162, 281–309.
- Murad, E., Wagner, U., 1994. The Mössbauer spectrum of illite. *Clay Minerals* 29, 1–10.
- Murad, E., Wagner, U., 1996. The thermal behaviour of an Fe-rich illite. *Clay Minerals* 31, 45–52.
- Rancourt, D.G., 1993. Mössbauer spectroscopy of tetrahedral  $\text{Fe}^{3+}$  in trioctahedral micas—Reply. *American Mineralogist* 78, 669–671.
- Rancourt, D.G., 1994. Mössbauer spectroscopy of minerals. II. Problem of resolving *cis* and *trans* octahedral  $\text{Fe}^{2+}$  sites. *Physics and Chemistry of Minerals* 21, 250–257.
- Rozenson, I., Heller-Kallai, L., 1976. Reduction and oxidation of  $\text{Fe}^{3+}$  in dioctahedral smectites – 1: reduction with hydrazine and dithionite. *Clays and Clay Minerals* 24, 271–282.
- Russell, J.D., Goodman, B.A., Fraser, A.R., 1979. Infrared and Mössbauer studies of reduced nontronites. *Clays and Clay Minerals* 27, 63–71.

- Środoń, J., Eberl, D.D., 1984. Illite. In: Bailey, S.W. (Ed.), *Micas. Reviews in Mineralogy*, vol. 13. Mineralogical Society of America, Washington, DC, pp. 495–544.
- Stevens, J.G., Khasanov, A.M., Miller, J.W., Pollak, H., Li, Z., 1998. Mössbauer Mineral Handbook. Mössbauer Effect Data Center, Asheville, N.C., p. 527.
- Stucki, J.W., 1988. Structural iron in smectites. In: Stucki, J.W., Goodman, B.A., Schwertmann, U. (Eds.), *Iron in Soils and Clay Minerals*. D. Reidel, Dordrecht, pp. 625–675.
- Wagner, U., Gebhard, R., Grosse, G., Hutzelmann, T., Murad, E., Riederer, J., Shimada, I., Wagner, F.E., 1998. Clay: an important material for prehistoric man. *Hyperfine Interactions* 117, 323–335.
- Weaver, C.E., Wampler, J.M., Pecuil, T.E., 1967. Mössbauer analysis of iron in clay minerals. *Science* 156, 504–508.

*Chapter 12.2*

## **IDENTIFICATION AND QUANTITATIVE ANALYSIS OF CLAY MINERALS**

**J. ŚRODOŃ**

*Institute of Geological Sciences, PAN, PL-31-002 Krakow, Poland*

Because of their great structural diversity, clay minerals are difficult to identify and quantify. Powder X-ray diffraction remains the standard technique of clay mineral identification although transmission electron microscopy (TEM) plays an increasingly important role in this regard during the last two decades.

The identification of clay minerals by X-ray diffraction (XRD) was described in a number of textbooks, three of which are of particular importance and relevance. The monograph edited by [Brindley and Brown \(1980\)](#) remains the most comprehensive data source, although the user-friendly textbook by [Moore and Reynolds \(1997\)](#) provides adequate information for routine analysis. Most students of clays or soils consult [Jackson's \(1975\)](#) book for chemical methods of treating clay prior to clay mineral separation and fractionation.

The Mineralogical Society (UK), the Mineralogical Society of America, and the Clay Minerals Society (USA) also published several monographs on techniques of clay mineral analysis and identification. The book edited by [Wilson \(1994\)](#) concentrates on spectroscopic methods of clay mineral analysis, while that by [Amonette and Zelazny \(1994\)](#) is dedicated to the quantitative analysis of soil clay minerals. The theoretical principles behind the identification of interstratified clay minerals were discussed by [Drits and Tchoubar \(1990\)](#).

[Środoń \(2002\)](#) reviewed the quantitative analysis of clay-rich rocks using a range of chemical and instrumental techniques. Simplified analytical methods have long been able to provide semi-quantitative data. Some techniques recently produced satisfactory quantitative results and further progress is expected in this field.

This chapter provides a brief introduction into the world of clay mineral identification and quantification, and is a guide to the corresponding literature.



### 12.2.1. IDENTIFICATION TECHNIQUES

#### *A. Sample Size*

If sufficient material is available, the best identification strategy is to start with XRD and apply other supplementary techniques as required. Such a course of action will be followed in this chapter. XRD allows for the most precise identification and provides very representative data, as each measurement represents an average over millions of clay mineral particles. If sample size is limited, however, the identification may have to be done by electron microscopy techniques, allowing observation and measurement to be made of individual particles. This investigative approach has many advantages, but special care must be taken to ensure that the observations are representative, even if the studied rock appears very homogeneous (Środoń et al., 1992).

#### *B. Clay Mineral Separation*

Clay minerals are most often identified by reflection powder XRD of both oriented and random preparations. Identification is greatly facilitated if the clay fraction is first separated from the rock (bulk sample) as this would minimize contamination by non-clay minerals.

It is common practice to separate and study either the  $<2$  or  $<0.2\ \mu\text{m}$  fractions or both. Besides being more representative of the clay minerals present in the rock, the  $<2\ \mu\text{m}$  fraction corresponds to the widely accepted granulometric definition of ‘clay’ (see Chapter 1). The  $<2\ \mu\text{m}$  fraction is also better suited for studying coarser-grained clay minerals such as kaolinite and chlorite. Being more abundant, this fraction is also generally easier to separate from the rock by gravitational settling in a column of water. The advantages of using  $<0.2\ \mu\text{m}$  fraction are two-fold (i) common mixed-layer clay minerals (in particular illite–smectite), making up the finest-grained components of rocks, are concentrated in this fraction and (ii) a superior orientation of particles can be achieved when preparing sedimented samples for XRD. As a result, series of 001 intensities are obtained with an order of magnitude stronger as compared with the  $<2\ \mu\text{m}$  material, and which are free of  $hk$  reflections. This effect is related to the nature of clay grains in the two fractions: the dominance of aggregates in the  $<2\ \mu\text{m}$  fraction, and the dominance of individual clay mineral particles in the  $<0.2\ \mu\text{m}$  fraction (see Chapter 1 for definitions of ‘aggregate’ and ‘particle’). Separation of the  $<0.2\ \mu\text{m}$  fraction is usually carried by centrifugation at a few thousand rpm (e.g. 3000 rpm for about 45 min) using large centrifuge bottles ( $\sim 1\ \text{L}$  capacity).

Two conditions must be met for a successful fractionation (i) the clay mineral particles have to be liberated from the rock and (ii) the clay dispersion has to be stable (no coagulation). To achieve these ends a variety of procedures are used, depending on the degree of consolidation of the rock, the presence of coagulating substances (e.g., salt or acid solutions, sulphates, and carbonates that dissolve easily

in distilled water), and that of cementing agents (e.g., carbonates, sulphates, Fe oxides, organic matter) (see Chapter 4).

If the rock is unconsolidated and free of coagulating and cementing agents, simple soaking in water and stirring, plus sonification with an ultrasonic probe may produce a stable dispersion. Some kaolins (weathering products), bentonites (sedimentary rocks), and many hydrothermally altered volcanic rocks fall into this category. On the other hand, if the rock contains electrolytes the dispersion will tend to coagulate. In that case the electrolytes must be removed (by repeated centrifugation in distilled water until the dispersion becomes stable). However, even such mild treatment (dispersion in a volume of distilled water) would change the composition of exchangeable cations (towards divalent species) because the exchange coefficients depend on solution concentration (Sayles and Mangelsdorf, 1977).

Sedimentary rocks commonly contain some carbonates. Besides acting as binding agents, carbonates dissolve during centrifugation causing clay mineral coagulation. Digestion in an acetic acid–sodium acetate buffer (pH = 5.5) is the most commonly used technique of carbonate removal (Jackson, 1975). The mild pH of this buffer causes only minimal damage to the clay minerals but the original exchangeable cations are replaced by  $\text{Na}^+$ . This is an added advantage, however, since  $\text{Na}^+$  promotes clay dispersion and the formation of a stable dispersion. For this reason, the acetate buffer treatment is routinely applied in the author's laboratory. However, the excess electrolyte has to be removed prior to separation because of its flocculating effect. The acetate treatment is effective even for carbonate-rich rocks (see Chapter 4).

If the rock is organic-rich, it can be reacted with hydrogen peroxide after treatment with acetate buffer. The removal of organic matter by  $\text{H}_2\text{O}_2$  is a standard procedure in studying soil clays (Jackson, 1975). The above order of treatment is important because a carbonate-free and slightly acidic environment is required for effective peroxide action without side effects (see Chapter 4).

If the colour of the rocks is reddish, brownish, or yellow after the buffer or peroxide treatment, free iron (hydr)oxide removal is required. This step is performed under slightly alkaline conditions using sodium dithionite as reductant (Jackson, 1975). The amount of dithionite used should be kept to a minimum if the presence of iron-rich clay minerals is suspected because the treatment may reduce some structural iron. On the other hand, dithionite treatment is often a key to success in clay mineral separation because iron oxides are very effective cement agents (see Chapter 4).

Soils often contain measurable amounts of X-ray amorphous Si and Al oxides that can be removed using various alkaline extraction techniques without damaging the clay minerals (Jackson, 1975; Smith, 1994). This issue is not important when dealing with common rocks.

Soaking in water is usually not sufficient to achieve disintegration of consolidated rocks. Crushing or even pulverising may have to be applied. However, pulverising should be avoided unless absolutely necessary (e.g., deep burial) since this treatment changes the particle size distribution, contaminating finer fractions with fragments of coarser minerals. Applying cycles of freeze-thaw is a safer technique by forcing a

rock to disintegrate along natural grain boundaries. A special instrument is needed, and the procedure is very time-consuming. It is only worth pursuing if required by the nature of the study (e.g., isotope dating, crystal thickness measurements, Liewig et al., 1987). In any case, a few minutes of sonification with an ultrasonic probe in a small volume of water should follow other procedures of disintegration before proper separation is performed. Ultrasonification is not harmful to clay minerals, helps break aggregates, and liberates clay mineral particles.

The separated clay fractions are voluminous dispersions and contain salts added during the pretreatments. The excess salt should be removed before drying. A practical way of achieving this goal involves three steps (i) coagulation with an appropriate 1 M chloride salt to introduce the required exchangeable cation, followed by at least two further washings (additions) to complete the exchange; (ii) removal of the excess electrolyte by washing with distilled water and centrifuging (2–3 times); and (iii) dialysis until all electrolyte is removed.

Dialysis is performed after dispersing the sediment (in the centrifuge bottle) into a small amount of water using an ultrasonic probe, and pouring the dispersion into a dialysis tube. The tube is closed and hung in a beaker filled with deionized water. By connecting a series of beakers and flowing deionized water through them the dialysis period can be greatly shortened. Dialysis is stopped when the conductivity of the water in the beakers approaches that of deionized water (the reference pure water should be in contact with atmospheric CO<sub>2</sub> as long as the water used for dialysis).

As some time can be saved if clays are in the Na<sup>+</sup> form, the final coagulation with NaCl has long been a standard practice in shale studies. From today's perspective, Ca<sup>2+</sup> saturation seems preferable if smectites or mixed-layer clay minerals involving smectite are studied. This is because at low humidity, typical of dry climates, illite–smectites in the Na<sup>+</sup> form may behave like illite-vermiculites during standard XRD tests, whereas illite–smectites in the Ca<sup>2+</sup> form preserve their characteristics (Eberl et al., 1987). Recent studies by Sakharov et al. (1999) indicated that this behaviour is also shown at high humidity. Mixed-layer clay minerals identified routinely as illite–smectite often display illite–smectite–vermiculite characteristics if studied more precisely in the Na<sup>+</sup> form. Yet these mixed-layer minerals can be modelled as a two component illite–smectite system in the Ca<sup>2+</sup> form. Since two-component systems are much easier to analyse, Ca<sup>2+</sup> is the exchange cation of choice.

The dialysed clay dispersion has to be dried. This is commonly done by placing the dispersion in a disposable plastic dish or a ceramic dish, covered with a plastic foil, and drying in an oven. The disadvantage of this technique is clay segregation during drying. Hand grinding has to be applied as a final step to homogenize the clay. Soft, homogeneous clay can be obtained by freeze-drying (see Chapter 4).

### C. Sample Preparation

Oriented preparations enable the 00 $l$  series of reflections to be obtained, providing information about mixed-layering, groups, chemistry (some species) and crystal

thickness distribution. There are numerous techniques for preparing oriented samples for XRD examination (Moore and Reynolds, 1997). Sedimentation onto a glass slide is commonly used for identifying clay minerals (from the 00 $l$  series of reflections) but this technique is inappropriate for quantitative analysis because of clay segregation during sedimentation on the slide. An ultrasonic probe should be used for a few seconds in order to completely disperse the clay, just before making the slide. Frosted glass offers better adhesion of the clay layer than a smooth glass surface, some disorientation may occur if the film is too thin. The clay layer should be sufficiently thick (10 mg/cm<sup>2</sup>) to ensure ‘infinite thickness’ for X-rays. When this condition is fulfilled, relative peak intensities become independent on the clay layer thickness and can be modelled using computer programmes (see below), in order to evaluate layer chemistry. If the clay layer is too thin, a broad band from glass, centered at about 0.34 nm becomes visible.

Random preparations provide hkl (h k) reflections, enabling di- and tri-octahedral minerals (subgroups) to be distinguished, polytypes to be identified, and stacking faults to be assessed. Side loading, described in detail by Moore and Reynolds (1997) is the most practical technique of making random preparation for identification purposes. From personal experience the author would recommend sieving the sample through a screen (ca. 0.4 mm) just before loading it into the holder, using frosted glass (never a plastic) in front of the holder opening, and tapping or vibrating in order to pack the powder (using a tamper to pack may produce orientation). Spray-drying is even more effective in producing reproducible, complete randomized clay samples (Hillier, 1999). This technique, however, is not very practical for routine identification work, unless precise computer modelling is attempted, as it is time-consuming and requires relatively large samples.

An alternative XRD strategy of studying hkl reflections is to use an oriented clay film in the transmission mode. The clay film is prepared by sedimenting a dispersion on a plastic foil, separating the material from the foil, and mounting in a transmission goniometer. In such a configuration, 00 $l$  reflections are eliminated from the XRD pattern, and hkl reflections are maximized (Wiewióra, 1985).

#### *D. Pure vs. Mixed-Layer Clay Minerals*

The official classification of sheet silicates by the International Mineralogical Association deals only with pure end-member minerals, dividing them into groups, subgroups, and species. In nature, however, pure species are rare, while interstratified clay minerals are common (Środoń, 1999). Thus, any scheme of clay mineral identification has to start by choosing between pure clay mineral and mixed-layer clay mineral. Only after doing this step, should the identification of group, subgroup, and species be attempted.

Pure clay minerals, like any other mineral, are characterized by one type of unit cell. They display an integral series of 00 $l$  reflections with similar broadening, controlled mostly by crystal thickness (Sherrer equation; see Drits et al. (1997) for

details). On the other hand, particles of mixed-layer clay minerals contain two or more types of layers (different unit cells), giving rise to a non-integral series of  $00l$  peaks (Bragg Law does not apply). The positions of the peaks are intermediate between those of the pure end-members, and peak broadening can be highly variable, depending on the distance between the corresponding end-member peaks (Méring rule see Fig. 8.1 in Moore and Reynolds (1997)). The so called 'regular mixed-layer clay minerals' are the exception to this rule. The particles of these minerals are composed of two alternating layer types (ABABAB ...), and hence may be considered to comprise AB unit cells. Such minerals are rare in nature, although seven species were identified and recognized as separate minerals, and given individual names (Środoń, 1999). They show integral series of  $00l$  reflections with similar broadening; including so-called superstructure  $001/001$  reflections that correspond to  $d_A + d_B$  spacings (where  $d_A$  and  $d_B$  are spacings of the component layers).

To summarize the identification criteria (1) integral series of  $00l$  peaks with similar broadening identifies pure clay minerals (or regular mixed-layer clay minerals if the superstructure reflection is present) and (2) non-integral series of peaks with variable broadening indicates an irregular mixed-layer clay mineral. These criteria also apply to electron diffraction studies.

In most cases, the distinction is straightforward. Doubts may arise as to whether a clay mineral is strictly pure or contains  $<5\%$  layers of a different type. In the latter instance, the peak displacements and broadening due to interstratification are so small that special care must be taken to distinguish them from minute irregularities related to other factors. This reservation also applies to regular interstratifications. Serpentine–chlorite interstratification is another special case. In this case the peaks are not displaced relative to the positions of pure chlorite because the  $001$  serpentine reflection (ca. 0.7 nm) is very close to the  $002$  chlorite reflection. Only peak broadening serves as an identification criterion. Both subjects will be described in the paragraph on identifying mixed-layer clay minerals.

### *E. Identification of Pure Clay Minerals*

#### *General Rules*

The criteria used to classify phyllosilicates (see Chapter 1) often are not very useful for their identification. In particular, groups are identified according to (though not exclusively by) their layer charge, a property that is directly measurable only in monomineralic samples. Operational definitions were therefore proposed. The books by Brindley and Brown (1980) and Moore and Reynolds (1997) should be consulted for more details.

Commonly used operational XRD definitions of clay mineral groups are based on the positions of  $00l$  reflections of samples in four different states: air-dry, saturated with ethylene glycol, and heated at 300 and 550 °C. Clay mineral groups are identified by applying one or any combination of these tests. Tri- and di-octahedral

subgroups are differentiated using the position of the 06 reflection (the  $b_0$  parameter is much larger for tri- than di-octahedral clay minerals and this difference manifests clearly at high  $2\theta$  angles) and/or the stretching region in the infrared spectrum ( $3500\text{--}3700\text{ cm}^{-1}$ ). Except for species in the serpentine–kaolin group (mostly representing different structural modifications) all other species are defined solely by their chemical compositions. In some cases, different tests based only on XRD can produce positive identification but often chemical methods have to be applied to identify clay mineral species.

If the concentration of clay minerals in the clay fraction is substantial ( $> 10\%$ ) identification can be made by XRD, at least to subgroup level, supported in some cases by IR spectroscopy. At lower concentrations, and in some particularly difficult cases, one has to resort to EM techniques.

#### *Serpentine–kaolin Group*

A  $\sim 0.7$  nm spacing in the air-dry state identifies kaolin-serpentine minerals with the exception of halloysite. If halloysite is a possibility, the preparations should first be recorded air-dry and then heated at  $350^\circ\text{C}$  for a few hours to ensure full dehydration of this mineral. Halloysite in its natural, fully hydrated state has a basal spacing of  $\sim 1$  nm, so it has occasionally been misidentified as illite. Halloysite that was partially dehydrated during sample preparation, or storage, exhibits spacings between 1 and 0.7 nm (see Fig. 5.2 in Moore and Reynolds (1997)), indicative of partial removal of one of two types of interlayer water. Sometimes it develops well-defined 0.86 nm spacing (complete removal of one type of water (Giese, 1988)). In such an intermediate state of hydration halloysite may resemble mixed-layer kaolinite-2:1 clay mineral, but the total dehydration test ( $350^\circ\text{C}$ ) distinguishes between the two, as the mixed layer material will not collapse to 0.7 nm.

Churchman et al. (1984) developed a simple test to differentiate halloysite from kaolinite in mixtures by intercalation of formamide. Intercalation into halloysite is rapid ( $< 1$  h) and complete whereas intercalation into kaolinite requires at least 4 h of contact with formamide, and even then the process is incomplete. The formamide test also allows the proportion of halloysite in the mixture to be estimated from changes in the intensity of the XRD peaks near 0.7 and 1.0 nm. However, formamide intercalation is influenced by particle size, crystallinity, and iron content. Prior air-drying and mild heating also tend to inhibit layer expansion. The quantitative analysis of kaolin minerals in mixtures would therefore require the application of a combination of chemical and instrumental techniques, such as XRD, differential thermal analysis, and electron microscopy (Joussain et al., 2005).

Kaolin and serpentine subgroups may be distinguished from their respective XRD peaks in the 06 region (0.149 nm for all kaolin minerals and 0.153–0.156 nm for serpentine). The Fourier transform infrared spectroscopy (FTIR) spectra of kaolins and serpentine are also clearly different (Russell and Fraser, 1994). If Mg serpentine are excluded, a strong and narrow band near  $3700\text{--}3697\text{ cm}^{-1}$  allows kaolin layers (both discrete and mixed-layered) to be detected at a level of 1–2% of the

sample mass. This is also the most effective technique of detecting small amounts of kaolin minerals in the dominant presence of chlorite. If kaolin minerals are abundant, a clear splitting of the 002 kaolin (0.354 nm) and 004 chlorite (0.356 nm) reflections is observable with narrow slits. The 06 region also differentiates the two minerals (0.154–0.155 nm for chlorites vs. 0.149 nm for kaolins). However, all these tests fail to detect serpentine when chlorite with a similar chemical composition is dominantly present in which case inspection of high resolution transmission electron microscopy (HRTEM) images may be the only reliable means of identification.

Identification of kaolin species is based on diagnostic reflections in random mounts (see Table 7.6 in the book by [Moore and Reynolds \(1997\)](#)). To detect halloysite in mixtures dominated by kaolinite (no separate 001 peak visible) intercalation tests are applied as described above (see also [Giese \(1988\)](#)). Careful comparison of peak profiles between air-dry and heated preparations is also helpful.

Mg-rich serpentine minerals (lizardite, chrysotile, antigorite), characteristic of metamorphic serpentinite rocks, are usually coarse-grained minerals (not clay-size). These species show different structural modifications and their XRD identification was described in detail by [Wicks and O'Hanley \(1988\)](#). Amesite and cronstedtite are an Al- and Fe-rich analogue of lizardite, respectively; both were characterized in detail by [Bailey \(1988\)](#).

Berthierine and odinite are two genuine clay-size serpentines, encountered with other clay minerals in sedimentary rocks. Their structures are so similar ([Bailey, 1988](#)) that they cannot be distinguished without chemical analysis (main difference in  $\text{Fe}^{2+}/\text{Fe}^{3+}$ ).

#### *Talc-pyrophyllite Group*

These coarse-crystalline minerals, characteristic of metamorphic environments, are identified in air-dry preparations by distinct 001 spacings (0.92 nm for pyrophyllite and 0.93 nm for talc) in combination with 060 (0.1493 nm for pyrophyllite and 0.1527 nm for talc). In surface environments (weathering of ultrabasic rocks, saline lakes) clay-size analogues of talc called kerolite or pimelite (Ni-rich species) can be found. Kerolites are characterized by a basal ( $d_{001}$ ) spacing of 0.96 nm, but the 001 reflection is displaced to 1.0–1.01 nm because the particles are very thin ([Evans and Guggenheim, 1988](#)). Thus, the distinction between kerolite and illite is based on higher order 001 reflections. The 06 reflection (0.1527 nm for talc vs. 0.150 nm for illite) or the vibration band in the FTIR spectrum ( $3676\text{ cm}^{-1}$  for talc vs.  $3620\text{ cm}^{-1}$  for illite) can provide further confirmation.

#### *Smectite Group*

Since smectites are expandable their 001 spacings depend on the interplay of several factors: layer charge, charge location, nature of interlayer cation, humidity, and type of polar molecules introduced between the layers. All known smectites, including Otay montmorillonite (with a layer charge of  $0.6/\text{O}_{10}(\text{OH})_2$ ) show a rational series of 001 reflections at medium relative humidities. Under these conditions, the basal



( $d_{001}$ ) spacing of the sodium form, after saturation with ethylene glycol, is 1.66–1.72 nm (Środoń, 1980). At low humidity, some  $\text{Na}^+$ -smectites may display characteristics of vermiculite ( $d_{001} \sim 1.45$  nm), while the  $\text{Ca}^{2+}$ -exchanged forms retain their smectitic character. Thus the operational definition of smectite, applicable to the full range of relative humidity, should include glycol saturation and  $\text{Ca}^{2+}$  as the exchangeable cation, except for glycol saturation. Using this test, smectite cannot be mistaken for any other mineral, provided that the 00/ series is rational. Rationality should be checked using higher order reflections because the positions of the 001 and 002 reflections are affected by small particle thickness. It should be stressed that the 001 reflection alone cannot be used as evidence for smectite, because randomly interstratified clay minerals such as illite–smectite or kaolinite–smectite have reflections at exactly the same position. If higher order reflections cannot be measured, the identification is less precise and mixed-layering is possible. In such a case, a narrow 001 peak is indicative of pure smectite as mixed-layer clay minerals have peaks at 1.7 nm that are substantially broader than those of pure smectite. After K-saturation followed by heating at 300 °C for 1 h, a pure smectite should produce an XRD pattern resembling that of illite (basal spacing  $\sim 1$  nm). If the 00/ reflections after heating correspond to a higher spacing, the presence of isolated brucite or gibbsite ‘islands’ in the smectitic interlayers is indicated. This ‘incipient chloritization’ (see below) does not inhibit swelling but can prevent full collapse of the interlayers on heating. Infrared analysis can be used to detect small amounts of kaolin layers in kaolin–smectite (Madejová et al., 2002).

The position of the 06 reflection uniquely distinguishes dioctahedral smectites (0.149–0.152 nm) from their trioctahedral counterparts (0.152–0.153 nm). The overlapping 0.152 nm value of dioctahedral clay minerals is characteristic of nontronite. This mineral is distinguishable from trioctahedral clay minerals by very weak 002 and 003 reflections, thermogravimetric analysis (nontronite dehydroxylates at 300–400 °C, while trioctahedral clay minerals require temperatures above 700 °C), FTIR (3556 vs. 3677  $\text{cm}^{-1}$ ), and of course, by chemical analysis. Most pure bentonitic smectites are low in Fe (0.149–0.150 nm), while Fe-rich smectites, characteristic of soil weathering, show intermediate 06 values. The Greene-Kelly test (saturation with Li and heating at 300 °C) can be used to distinguish beidellite from montmorillonite (montmorillonite does not re-expand and beidellite does (Moore and Reynolds, 1997)). Chemical analysis is always required to confirm the identity of trioctahedral species (saponite, stevensite, hectorite).

### *Vermiculite Group*

Like smectite, vermiculite is an expandable mineral. However, the expansion of vermiculite is more restricted because its layer charge is higher than that of smectite, and this charge is largely located in the tetrahedral sheet. The border separating vermiculite from smectite is arbitrary, based on a layer charge of 0.6 eq/ $\text{O}_{10}(\text{OH})_2$  (see Chapter 1). Some clay mineralogists argued that both groups of minerals should be treated as one continuous series. Extensive work was done on trioctahedral



vermiculites (de la Calle and Suquet, 1988) but data on the dioctahedral counterparts are very scarce (see for instance Malla and Douglas (1987)). The most widely accepted operational definition of vermiculite is based on its ca. 1.45 nm basal spacing for the  $\text{Mg}^{2+}$ -exchanged form after treatment with glycerol, and the collapse of the  $\text{K}^+$ -form to 1.0 nm on heating at 300 °C for 1 h. Of course, pure vermiculite should display a rational series of very narrow reflections, but such minerals are very rare. The glycerol test distinguishes vermiculite from smectite, and the heating test distinguishes vermiculite from chlorite (the 1.4 nm basal spacing of chlorite is not affected by heating). The heating test can be used to detect vermiculite in the presence of chlorite. The application of different tests to soil vermiculites was described in detail by Malla and Douglas (1987).

### *Illite Group*

The classification scheme (see Chapter 1) does not provide criteria for distinguishing illite from vermiculite. Indeed, illite is regarded as a species in the true (flexible) mica group. Both illite and vermiculite have a closely similar range of layer charge but illite is non-expandable and has fixed instead of exchangeable cations in the inter-layer space. In reality, illites are exclusively dioctahedral and clay-size, while vermiculites are most commonly trioctahedral and often mica-size. The charge of illite layers is  $0.9/\text{O}_{10}(\text{OH})_2$ , but the overall charge is often lower than this because illite particles are very thin (Środoń et al., 1992).

Operationally, illite can be defined as a clay-size material, exhibiting a rational series of reflections with a  $d_{001}$  spacing of about 1.0 nm that does not change on ethylene glycol saturation or heating to 300 °C. Swelling test detects mixed-layering with expandable layers, and heating discriminates between illite and hydrated halloysite. This definition includes micro-divided mica, if it is present in  $<2\ \mu\text{m}$  fraction. Short of calculating the structural formula from chemical analysis of uncontaminated specimens, there is no way to distinguish illite from dioctahedral mica.

The positions, shapes, and relative intensities of 00 $l$  reflections of an illitic material often change slightly after glycol treatment, indicating some mixed-layering. The most sensitive indicator of mixed-layering is based on the intensities, rather than the positions, of the 00 $l$  reflections (Środoń, 1984):

$$Ir = (001/003 \text{ air-dry})/(001/003 \text{ glycol})$$

where  $Ir$  denotes the intensity ratio of the 001 and 003 reflections from air-dry and glycolated samples. A value of  $Ir = 1 \pm 0.1$  is indicative of pure illite.

Common species of the illite group are illite proper, ferruginous illite, and glauconite ( $\text{K}^+$ -illites), brammalite ( $\text{Na}^+$ -illite), and tobellite ( $\text{NH}_4^+$ -illite). The first three all have  $d_{001} = 0.998\text{--}1.00\text{ nm}$ . The presence of some iron species should be suspected if the 002 reflection is clearly weaker than in typical  $\text{Al}^{3+}$ -illites and an admixture of trioctahedral micas can be ruled out. Such hypothesis can be verified in

the 06 region if smectites are absent: 0.150 nm reflection identifies  $\text{Al}^{3+}$ -illite, 0.151 nm reflection indicates ferruginous illite and glauconite, and 0.154 nm is typical for trioctahedral micas. The FTIR spectrum is equally conclusive:  $3630\text{ cm}^{-1}$  for  $\text{Al}^{3+}$ -illite,  $3530\text{--}3560\text{ cm}^{-1}$  for glauconite,  $3605\text{--}3580\text{ cm}^{-1}$  for ferruginous illite,  $3594\text{ cm}^{-1}$  for biotite, and  $3796\text{ cm}^{-1}$  for phlogopite. Only chemical analysis enables indisputable discrimination to be made between ferruginous illite and glauconite.

$\text{Na}^+$ -illite is not a well-documented species. Most non-expandable sodium phyllosilicates are coarse grained and correspond to sodium mica (paragonite) in composition. Only detail chemistry can differentiate the two. The data on rectorites (regular mixed-layer clay minerals) provided by [Brown and Weir \(1963\)](#) indicate that the illitic component of the interstratification is a genuine brammalite. Paragonite and brammalite can be easily distinguished from  $\text{K}^+$ -illites and micas as well as from pyrophyllite and talc, by the 001 series based on  $d_{001} = 0.96\text{ nm}$ . The 060 region is equally conclusive: 0.148 nm.

$\text{NH}_4^+$ -illite is a well-documented species ([Środoń and Eberl, 1984](#); [Šucha et al., 1994](#)). Distinction from  $\text{K}^+$ -illites is based on 001 series with  $d_{001} = 1.033\text{ nm}$ . Solid solution between  $\text{K}^+$  and  $\text{NH}_4^+$  forms occurs, and their ratio can be evaluated from the position of the 005 reflection ([Lindgreen et al., 2000](#)). FTIR can also be used to detect  $\text{NH}_4^+$  in illite ( $\text{NH}_4^+$  ions give rise to a band at  $1400\text{ cm}^{-1}$  ([Šucha et al., 1998](#))).

Polytypic varieties and types of structural defects in illite are well recognized. [Moore and Reynolds \(1997\)](#) gave a guide to their identification and quantification by means of computer modelling of XRD, the application of which was reviewed by [Środoń \(2002\)](#). *Cis-* vs. *trans*-vacant layers in illite can be quantified by thermal analysis ([Drits et al., 1998](#)).

### Chlorite Group

The unique dehydroxylation behaviour of chlorite allows this mineral to be indisputably identified in any clay mineral mixture. On heating at  $550^\circ\text{C}$  for 1 h, the  $d_{001}$  spacing of chlorite decreases from slightly above 1.4 nm to 1.38–1.39 nm. At the same time, the intensity of 001 reflection strongly increases, while the intensities of the higher-order reflections decrease. This test distinguishes chlorite from vermiculite and minerals with incomplete chlorite layers, all of which collapse to 1.0 nm. It also differentiates chlorite from mixed-layer minerals involving chlorite and incomplete chlorite layers, showing mixed-layer 1.4/1.0 nm reflections. Chlorite may also be distinguished from mixed-layer chlorite-serpentine since the even-numbered reflections of the latter are broader ([Reynolds et al., 1992](#)).

Common chlorites are trioctahedral minerals with  $d_{060} > 1.53\text{ nm}$ . This distinguishes them from di-trioctahedral and dioctahedral species, which can be discriminated among themselves only by chemical analysis.

Trioctahedral chlorites display a range of iron contents and also a variable distribution of iron between the octahedral sheet and the interlayer space. Both the iron content and its distribution can be quantified from the relative intensities of 001 peaks, using the technique of [Moore and Reynolds \(1997\)](#). In order to perform such

determination in mixtures, the overlapping vermiculite peaks have to be removed by heating at 300 °C, while the kaolinite peaks are shifted by intercalation (op. cit.). The measurement is not possible in the presence of serpentine without detailed computer modelling of the XRD pattern. The chemical composition of trioctahedral chlorites can also be evaluated from the  $d_{001}$  and 060 values (Wiewióra et al., 1998).

Moore and Reynolds (1997) described methods for identifying chlorite polytypes. This may be difficult in mixtures with other clay minerals, and magnetic separation of chlorite may be required (Amonette and Zelazny, 1994, p. 248).

#### *Sepiolite and Palygorskite Group*

These minerals have clay-size particles and a fibrous morphology. In oriented preparations, they do not display a series of 00 $l$  reflections. If present in quantity, their identification can be based on several XRD peaks (see Table 7.3 in Moore and Reynolds' (1997) book). A small admixture is marked only by the presence of strong 110 reflections at 1.20–1.29 nm (sepiolite) and 1.03–1.05 nm (palygorskite) that are insensitive to ethylene glycol or glycerol treatment. When sepiolite is heated at 300 °C, the reflection at 1.2 nm disappears and new peaks appear at 1.04 and 0.82 nm (these changes are reversible upon hydration). When palygorskite is heated the intensity of the 1.03 nm reflection decreases, and a new reflection at 0.92 nm appears (Jones and Galán, 1988). These tests distinguish sepiolite and palygorskite from mixed-layer clay minerals. IR spectroscopy (Russell and Fraser, 1994) may also aid identification, while the fibrous particle morphology can be observed by SEM and TEM.

### 12.2.2. IDENTIFICATION OF MIXED-LAYER CLAY MINERALS

#### *A. Peak Position Approach*

The identification of rare regular mixed-layer clay minerals involves recognizing the nature of the component layers. The same criteria, as used for pure minerals, are applied. For example, smectite layers are expected to swell to ~1.7 nm with ethylene glycol and to collapse to ~1.0 nm on heating, while illite layers remain stable. Thus rectorite, a regularly interstratified illite–smectite, should show a rational series of 00 $l$  reflections, based on a 2.7 nm spacing for a glycolated sample, and a 2.0 nm spacing when heated. Specified criteria of integrity (Bailey, 1982) have to be met in order to classify a clay mineral as a regularly interstratified species. The 06 reflections and IR spectra can be used to distinguish di- from tri-octahedral species.

An irrational series of 00 $l$  reflections indicates irregular mixed-layering. The nature of the component layers, their proportions, and the pattern of interstratification should be identified. A practical identification scheme starts from considering two-component systems, because they are the most common and easiest to recognize. First, the low angle region is inspected for the superstructure reflection

(corresponding to A + B spacing). This reflection appears if interstratification is ordered, that is, the layers are not arranged in a random array but the alternation of component layers (AB ... sequences) is favoured. It is relatively strong if the ratio of the component layers is close to 1:1. A lack of superstructure reflection indicates that the interstratification is either random or dominated by one type of layer. The presence of a superstructure reflection (spacing) and its behaviour following standard treatments may be very helpful in identifying the component layers.

In both ordered and random cases, the identification is based on Méring's rules, as explained in detail by Moore and Reynolds (1997). We recommend doing the glycolation and heating tests before identification is attempted, because these tests help narrow the range of possibilities (e.g., no change after glycolation eliminates smectite). If a chosen model is correct, all mixed layer reflections of a random clay mineral should be located between corresponding reflections of pure component minerals. In case of an ordered mineral, its regular version serves as one of the end-members (e.g., rectorite for ordered illite–smectites), and the dominant layer as the other end-member. Broadening of the mixed-layer reflections depends on the distance between the reflections of pure component layers, and may serve as an additional identification criterion. In extreme cases, when the distance is very large (as between the 001 reflection of glycolated smectite and the 001 reflection of illite), only broadening and decreased intensity of the 1.7 nm peak (smectite 001) are observed in randomly interstratified illite–smectite but the position of this peak does not change.

If several peaks of a sample were recorded, under test conditions appropriate for a given case, and all followed Méring's rules, the identification of a two-component mineral was achieved. Otherwise, an alternative model consisting of more than two components has to be investigated.

If the clay mineral was identified as a two-component system, either random or ordered, the layer ratio can be measured. Several techniques are in use, based on the positions of selected peaks, on their broadening or on the computer simulation of entire XRD patterns.

Drits et al. (1994) published an approximate but universal technique as an extension of the Méring approach. Layer ratios are calculated from peak positions on the assumption of their linear migration, from one end-member position to another, as a function of layer ratio.

Reynolds and Hower (1970) introduced a similar approach, but based instead on peak migration curves, constructed from computer-generated XRD patterns. They proposed measuring the layer ratio in illite–smectite from 002/003 peak positions in the glycolated state. Since then, numerous plots of this nature, dedicated to the identification of various mixed-layer minerals, were published (review in Środoń, 2002). The problems associated with identifying minerals involving chlorite were discussed by Reynolds (1988), while those related to the identification of all common mixed-layer minerals were reviewed by Moore and Reynolds (1997).

The identification techniques for illite–smectite are the most detailed because this mixed-layer clay mineral is the most frequently studied. It is also the most abundant

mineral, and useful for geological interpretations such as dating and deriving paleotemperatures. Środoń (1980) and Watanabe (1981) used pairs of reflections to minimize the effect of particle thickness and of variable thickness of the glycol–water interlayer complex, while Dudek and Środoń (1996) applied realistic (log-normal) distributions of the thickness of the mixed-layer particles. Special techniques were proposed for dealing with the most common case of illite-smectite in mixtures with discrete illite (Środoń, 1981, 1984). These allow the layer ratio to be measured until ca. 90% illite in the mixed-layer clay mineral if the latter is relatively abundant.

### *B. Peak Broadening Approach*

The techniques based on peak positions fail if

- (1) the admixture of another type of layer is very low (a few per cent);
- (2) the peak positions of the two components coincide (as in the case of serpentine-chlorite); and
- (3) a mixed-layer clay mineral having a composition dominated by one end-member is a minor component of a mixture with that end-member as a discrete phase.

In (1) the Q technique of Moore and Reynolds (1997) based on peak broadening can be applied. In (2) the serpentine/chlorite ratio can be measured from peak broadening of 004 vs. 005 peaks (Reynolds et al., 1992). A well-known example of (3) is the illitic fraction of clastic rocks from the zone of advanced diagenesis and anchimetamorphism. There is no simple technique of measuring the illite/smectite ratio in such materials. Instead, broadening of the 1.0 nm peak (overlapping illite and illite–smectite reflection) is used most often as the diagenetic/metamorphic grade indicator (Kübler index (Kish, 1987)).

The Kübler index is a complex function of the illite/swelling layer ratio in the mixed-layer clay mineral, the state (spacing) of the swelling layer (which itself depends on several factors), the ratio between mixed-layer clay mineral and discrete illite, and the particle size distribution of the two clay minerals. This measurement can be made more rigorous, if a modified Scherrer equation is applied to the 1.0 nm reflection of a  $K^+$ -exchanged and heated (dehydrated) sample (Drits et al., 1997). Under such experimental conditions, the 1.0 nm peak broadening becomes a function of crystal thickness distribution exclusively, and the mean crystal thickness of the mixture can be measured.

Another alternative to the Kubler index is the XRD measurement of crystal thickness distribution by the Bertaut–Warren–Averbach (BWA) method, adapted to clay minerals by Drits et al. (1998), using the MudMaster computer program. In this approach, information on crystal thickness distribution is extracted from the shape of the 1.0 nm peak. Pure non-swelling illite can be studied by this technique in its natural state. If swelling is detectable, its effect has to be eliminated before the measurement (peak broadening should not be affected by mixed-layering). It can be done either by  $K^+$  saturation and heating (collapsing swelling layers to 1.0 nm (Kotarba and Środoń, 2000)), or by dispersing the illite-smectite component of the

mixture into fundamental illite particles, using the poly(vinylpyrrolidone) (PVP) technique (Eberl et al., 1998). The PVP technique is potentially capable of providing a sensitive grade indicator of deep diagenesis and anchimetamorphism. The MudMaster program can also be used to study crystal thickness distributions of other clay minerals, such as smectites (Mystkowski et al., 2000).

### C. Expert Systems

A computer can guide the student of mixed-layer clay minerals through mineral identification procedures. Two such expert systems are available INTERSTRAT by Garvie (1994) and the program of Plançon and Drits (1994). In identifying mixed-layer clay minerals, INTERSTRAT relies on a series of patterns calculated with NEWMOD, whereas Plançon and Drits' program relies on published techniques based on selected peak characteristics.

### D. Integrated Approach: Computer Modelling

The identification based on peak position and broadening can be verified by direct modelling of the 001 XRD pattern, using existing computer programs (Środoń, 2002). Also, computer modelling is the only technique capable of identifying and quantifying mixed-layering, if more than two components are present. The most complete theoretical treatment of the statistical description of interstratification and the XRD analysis by disordered particles, underpinning computer modelling, were published by Drits and Tchoubar (1990). A practical guide for modelling two-component mixed-layer clay minerals, using the NEWMOD computer program, is also available (Moore and Reynolds, 1997).

Modelling is usually very time-consuming because it uses a trial-and-error approach: input data are adjusted manually, until a satisfactory fit of peak positions, shapes, and intensities in the entire XRD profile is reached. The use of a log-normal shape of crystal thickness distribution, discovered by Drits et al. (1997) for illites, simplifies modelling (Dudek and Środoń, 1996). Nevertheless, the number of variables is so large that solutions are often non-unique. For this reason, Sakharov et al. (1999)—who conducted an intensive study to model complex clay mineral mixtures involving mixed-layer clay minerals—proposed that the model should be judged reliable if it provided a satisfactory fit for at least two states of a sample (e.g., air-dry and glycolated for clay minerals involving a smectite layer). Unfortunately, no generally accepted strict criteria of 'satisfactory fit' exist. Sometimes, the least squares criterion of the quality of fit of the entire pattern is used. In the author's opinion, such a criterion is adequate if quantitative analysis of a mixture is the target of a fitting exercise (see below). If the layer ratio of a mixed-layer clay mineral is the main goal, the criterion of fit should be based in most cases on peak positions, as they are usually most sensitive to the layer ratio. As an example, a  $0.1^\circ$   $2\theta$  error in peak position changes the evaluation of illite layers in randomly interstratified illite-smectite by

about 15% (absolute values). It would be appropriate to specify the criterion of fit for a case under study.

The modelling procedure can be automated using available optimization techniques. At least two such approaches are in use, both of which are proprietary of oil companies. At Exxon, [Pevear and Schuette \(1993\)](#) used genetic algorithms and NEWMOD to model XRD patterns of clay mineral mixtures. The SYBILLA program, developed at ChevronTexaco ([Mystkowski and Sakharov](#), personal communication) applies evolutionary programming and the modelling program of [Drits and Sakharov \(1976\)](#). SYBILLA can handle not only two-component but also multi-component mixed-layering, and automatically models all clay mineral components of a mixture that were identified by the operator.

### 12.2.3. QUANTITATIVE ANALYSIS

Quantitative analysis is most often performed to obtain percentages of clay minerals either in the bulk rock or in the clay fraction. XRD is the most commonly used technique, but IR spectroscopy and major element analysis, combined with qualitative XRD, were also applied. All these methods were reviewed by [Środoń \(2002\)](#).

Clay minerals are very difficult to quantify, and large analytical errors have to be expected. This is because their particles have varied chemical compositions and structures, and tend to adopt a preferred orientation. In most cases the results are semi-quantitative. However, a recent worldwide contest in the quantitative analysis of artificial rocks containing clay minerals ([McCarty, 2002](#); [Kleeberg, 2005](#)) would indicate that some XRD techniques are capable of providing very accurate results (below 10% of cumulative error from actual values for samples composed of 13 minerals, including 4 clay minerals). It is not certain at present whether techniques other than XRD can achieve this level of accuracy. Further comments will be therefore restricted to XRD techniques.

The overall success of quantitative analysis strongly depends on sample preparation, data processing, and selection of standards. These aspects will be briefly characterized below, separating bulk rock from clay fraction analysis.

#### *A. Bulk Rock Quantitative Mineral Analysis*

##### *Sample Preparation*

Because of their platy habit, clay mineral particles have a strong tendency for orientation, enhancing the  $00l$  reflections and weakening the  $hk$  reflections as compared with a fully random preparation. Most XRD methods of quantitative analysis require perfectly random preparations. Methods based on Rietveld refinement can correct for orientation although this adds variables that have to be dealt with. Most techniques use an internal standard in order to avoid normalization to 100%. Thus, sample preparation generally aims at achieving three goals: randomness, homogenization



with a known amount of internal standard, and reduction in the size of coarse-grained minerals below ca. 20  $\mu\text{m}$ , in order to assure good reproducibility of peak intensities. Size reduction should not cause measurable damage to the layer structure.

The required reduction in size can be achieved by 5 min of wet grinding of 3 g sample in the McCrone Micronizing Mill. This particular grinding process produces narrow grain size distributions (O'Connor and Chang, 1986), without a coarse-grain 'tail', characteristic of other grinding techniques. Sample weight (3 g) assures that there is enough material between the corundum rollers, so the corundum contamination is negligible. Water, methanol, or hexane can be used as grinding fluids.

Wet grinding also assures perfect homogenization of the sample and the standard.  $\text{Al}_2\text{O}_3$ , advocated by Chung (1974), is the most commonly used internal standard. Środoń et al. (2001) introduced  $\text{ZnO}$ , which can be used in smaller quantities (10%), and which produces less peak coincidences with common rock forming minerals.

The techniques of producing random preparations from powders of samples containing clay minerals were described earlier (see Section 12.2.1.C). For quantitative analysis, care should be taken to produce, as much as possible, a similar degree of packing, which is important for the reproducibility of XRD patterns (peak displacement and broadening due to variations in sample density).

#### *Data Collection, Processing, and Selection of Standards*

The data collection procedure should ensure high peak/background ratios, low sensitivity to sample density variations, and good counting statistics, while the strongest peaks (e.g. 0.334 nm quartz) stay within the linearity range of the counter, and the beam stays entirely within the preparation for the lowest 2 theta angle, from which the analysis is performed.

Numerous strategies of data processing are in use. They all rely upon measuring the intensity of diffraction of a given mineral in the investigated sample and comparing it with the intensity of a pure standard of this mineral. The matrix effect on the intensity is taken into account by using an internal standard and experimentally established mineral/standard peak ratios (called RIR or MIF: Hubbard and Snyder, 1988; Reynolds, 1989) to calculate directly percentages of each crystalline phase (for details see e.g., Środoń et al. (2001)). Three main groups of techniques are currently in use. They differ by what they measure, how they do the measurement, and what they use for standards. All require a priori knowledge of the qualitative mineral composition of the sample. Thus detailed mineral identification is pre-requisite for a successful quantitative analysis.

The first group of techniques, which could be called single peak/natural standard, relies upon a selected individual peak as a measure of the mineral concentration, and upon natural specimens as standards (e.g., Hillier, 2000; Środoń et al., 2001). The second group (whole pattern/natural standard) obtains intensities of the components of a mixture by fitting the entire XRD pattern of a sample with patterns of pre-registered pure standards (e.g., Smith et al., 1987; Batchelder and Cressey, 1998). The third group (whole pattern/computed standard) fits the experimental pattern with



the patterns of pure components calculated from the crystallographic data. Elaborate procedures are used for refining line widths and shapes of the calculated patterns, correcting for absorption contrast, orientation, amorphous material content, several intensity aberrations, and the fit is maximized by the Rietveld technique (Taylor, 1991; Bergmann et al., 1998). All three types of techniques were used by top contestants during recent world competitions in quantitative analysis of rocks (Reynolds Cup organized at Clay Mineral Society conferences in 2002 and 2004). The main advantages of the Rietveld-based techniques are the calculation of standards and the correction for instrumental errors, which makes this technique easily transferable from one instrument to another, less dependent on the quality of sample preparation, and independent on the availability of pure standards. The first advantage does not apply to clay minerals at the present stage of the development of these techniques. Natural clay mineral standards are used instead, because of the complexity of clay mineral structures (mixed-layering, polytypes, tri-dimensional defects), making them not suitable for Rietveld refinement. Calcium dolomites, which are quite common components of sedimentary rocks, pose the same problem (V. Drits and D.K. McCarty, personal communication). For such variable minerals, the problem of possibly good correspondence between the standard and the analysed mineral remains very important. The error related to the selection of standards can be minimized in the single peak technique by choosing analytical peaks possibly insensitive to structural variations, but at the expense of the convenience of automated whole pattern fitting. A technique combining both advantages uses evolutionary programming to perform the fit with natural standard patterns, but assigns different weights to fitting different portions of the pattern (Mystkowski et al., 2002). Weights are radically increased for the portions containing selected analytical reflections. 06 reflections are used for the analysis, allowing the following clay minerals to be quantified: Fe-chlorite + berthierine, Mg-chlorite, trioctahedral 2:1 clay minerals, dioctahedral 2:1 Fe clay minerals (nontronite + glauconite), dioctahedral 2:1 Al-rich clay minerals (illite + smectite + illite-smectite + mica), and kaolinite. This is probably as good as anybody can do today in the field of clay analysis from random preparations. If more detailed quantification of clay mineral species is required, the analysis of oriented preparations has to follow.

Clay mineral peaks are relatively broad and weak. For this reason, the analysis of clay minerals in the bulk rock is feasible provided that the clay contents are not too low. If the clay content is low (e.g. relatively clean sandstones or carbonates), a better strategy is to remove quantitatively most of the dominant mineral (e.g. to dissolve carbonate) and to apply the random preparation analysis to the residue.

### *B. Quantitative Mineral Analysis of Clay Fraction*

#### *Sample Preparation*

The 001 series of reflections contains information on the clay mineral species present in a sample. The preparation technique for quantitative analysis should

ensure, as much as possible, good orientation in order to intensify these reflections and avoid segregation of clay particles during sample preparation. The sedimentation technique, commonly used in clay mineral identification, produces segregation with respect to grain size. Quantitative analysis of such preparations would therefore overestimate fine-grained clay minerals. The technique of smearing a clay paste on to a glass slide and the use of a 'Millipore' transfer filter are apparently well suited for quantitative analysis (Moore and Reynolds, 1997). Analysing a series of clay fractions is a very useful means of characterizing soil clays (Tributh, 1970, 1976).

#### *Data Processing*

Following Schultz (1964) and Biscaye (1965) simplified techniques, based on assigning 'weighting factors' to different clay mineral peaks, were commonly used until quite recently. The results generated by such techniques should be considered semi-quantitative. Moore and Reynolds (1997) proposed a more rigorous single-peak technique, based on the standard intensities calculated by NEWMOD. In assuming the same degree of orientation for all analysed clay minerals, this technique shares one short-coming with the old ones. In reality, the orientations may be different because of differences in the shape of clay mineral particles (in particular, curled shape of swelling clay mineral particles vs. flat shape of common non-swelling clay minerals).

Fitting the entire experimental patterns with computer-generated patterns of identified clay minerals offers the best chance of accurate quantification of clay mineral species. In this approach, the orientation of different clay minerals can be modelled individually. Manual fitting was performed (e.g., Sakharov et al., 1999; Lindgreen et al., 2000), but this approach is too time-consuming for routine applications. The future of quantitative clay analysis using oriented preparations lies with automated fitting techniques, the likes of which were described above.

#### REFERENCES

- Amonette, J.E., Zelazny, L.W. (Eds.), 1994. Quantitative Methods in Soil Mineralogy. Miscellaneous Publication. Soil Science Society of America, Madison, WI.
- Bailey, S.W., 1982. Nomenclature for regular interstratifications. *American Mineralogist* 67, 394–398.
- Bailey, S.W., 1988. Structures and compositions of other trioctahedral 1:1 phyllosilicates. In: Bailey, S.W. (Ed.), *Hydrous Phyllosilicates. Reviews in Mineralogy*, vol. 19. The Mineralogical Society of America, Washington, DC, pp. 169–188.
- Batchelder, M., Cressey, G., 1998. Rapid, accurate phase quantification of clay-bearing samples using a position-sensitive X-ray detector. *Clays and Clay Minerals* 46, 183–194.

- Bergmann, J., Friedel, P., Kleeberg, R., 1998. BGMN—a new fundamental parameter-based Rietveld program for laboratory X-ray sources, its use in quantitative analysis and structure investigations. *CPD Newsletter* No. 20, 5–8.
- Biscaye, P.E., 1965. Mineralogy and sedimentation of recent deep-sea clays in the Atlantic Ocean and the adjacent seas and oceans. *Geological Society of America Bulletin* 76, 803–832.
- Brindley, G.W., Brown, G. (Eds.), 1980. *Crystal Structures of Clay Minerals and their X-ray Identification*. Mineralogical Society, London.
- Brown, G., Weir, A.H., 1963. The identity of rectorite and alleverdite. *Proceedings of the International Clay Conference, Stockholm*, vol. 1, pp. 27–37.
- Chung, F.H., 1974. Quantitative interpretation of X-ray diffraction patterns of mixtures. I. Matrix flushing method for quantitative multicomponent analysis. *Journal of Applied Crystallography* 7, 519–525.
- Churchman, G.J., Whitton, J.S., Claridge, G.G.C., Theng, B.K.G., 1984. Intercalation method using formamide for differentiating halloysite from kaolinite. *Clays and Clay Minerals* 32, 241–248.
- de la Calle, C., Suquet, H., 1988. Vermiculite. In: Bailey, S.W. (Ed.), *Hydrous Phyllosilicates (Exclusive of Micas)*. Reviews in Mineralogy, vol. 19. Mineralogical Society of America, Washington, DC, pp. 455–496.
- Drits, V.A., Eberl, D.D., Środoń, J., 1998. XRD measurement of mean thickness, thickness distribution and strain for illite and illite/smectite crystallites by the Bertaut–Warren–Averbach technique. *Clays and Clay Minerals* 46, 38–50.
- Drits, V.A., Lindgreen, H., Salyn, A.L., Ylagan, B., McCarty, D.K., 1998. Semiquantitative determination of trans-vacant and cis-vacant 2:1 layers in illites and illite–smectites by thermal analysis and X-ray diffraction. *American Mineralogist* 83, 1188–1198.
- Drits, V.A., Sakharov, B.A., 1976. *X-ray Structural Analysis of Mixed-Layer Minerals*. Nauka, Moscow (in Russian).
- Drits, V.A., Środoń, J., Eberl, D.D., 1997. XRD measurement of mean crystal thickness of illite and illite/smectite: reappraisal of the Kübler index and the Scherrer equation. *Clays and Clay Minerals* 45, 461–475.
- Drits, V.A., Tchoubar, C., 1990. *X-ray Diffraction by Disordered Lamellar Structures: Theory and Applications to Microdivided Silicates and Carbons*. Springer-Verlag, New York.
- Drits, V.A., Varaxina, T.V., Sakharov, B.A., Plançon, A., 1994. A simple technique for identification of one-dimensional powder X-ray diffraction patterns for mixed-layer illite-smectites and other minerals. *Clays and Clay Minerals* 42, 383–390.
- Dudek, T., Środoń, J., 1996. Identification of illite/smectite by X-ray powder diffraction taking into account the lognormal distribution of crystal thickness. *Geologica Carpathica-Series Clays* 5, 21–32.
- Eberl, D.D., Nüesch, R., Šucha, V., Tsipursky, S., 1998. Measurement of fundamental particle thicknesses by X-ray diffraction using PVP-10 intercalation. *Clays and Clay Minerals* 46, 89–97.
- Eberl, D.D., Środoń, J., Lee, M., Nadeau, P.H., Northrop, H.R., 1987. Sericite from the Silverton caldera, Colorado: correlation among structure, composition, origin, and particle thickness. *American Mineralogist* 72, 914–934.
- Evans, B.W., Guggenheim, S., 1988. Talc, pyrophyllite, and related minerals. In: Bailey, S.W. (Ed.), *Hydrous Phyllosilicates (Exclusive of Micas)*. Reviews in Mineralogy, vol. 19. Society of America, Washington, DC, pp. 225–294.

- Garvie, L.A.J., 1994. INTERSTRAT—an expert system to help identify interstratified clay minerals from powder XRD data: II. Testing the program. *Clay Minerals* 29, 21–32.
- Giese, R.F. Jr., 1988. Kaolin minerals: structures and stabilities. In: Bailey, S.W. (Ed.), *Hydrous Phyllosilicates (Exclusive of Micas)*. Reviews in Mineralogy, vol. 19. Mineralogical Society of America, Washington, DC, pp. 29–66.
- Hillier, S., 1999. Use of an air-brush to spray-dry samples for X-ray powder diffraction. *Clay Minerals* 34, 127–135.
- Hillier, S., 2000. Accurate quantitative analysis of clay and other minerals in sandstones by XRD: comparison of a Rietveld and a reference intensity ratio (RIR) method and the importance of sample preparation. *Clay Minerals* 35, 291–302.
- Hubbard, C.R., Snyder, R.L., 1988. RIR—measurement and use in quantitative XRD. *Powder Diffraction* 3, 74–77.
- Jackson, M.L., 1975. *Soil Chemical Analysis—Advanced Course*, 2nd edition. Published by the author, Madison, WI.
- Jones, B.F., Galán, E., 1988. Sepiolite and palygorskite. In: Bailey, S.W. (Ed.), *Hydrous Phyllosilicates (Exclusive of Micas)*. Reviews in Mineralogy, vol. 19. Mineralogical Society of America, Washington, DC, pp. 631–674.
- Joussain, E., Petit, S., Churchman, G.J., Theng, B.K.G., Righi, D., Delvaux, B., 2005. Halloysite clay minerals: A review. *Clay Minerals* 40, 383–426.
- Kish, H.J., 1987. Correlation between indicators of very low-grade metamorphism. In: Frey, M. (Ed.), *Low Temperature Metamorphism*. Blackie, Glasgow, pp. 227–299.
- Kleeberg, R., 2005. Outcomes of the second Reynolds Cup in quantitative mineral analysis. In: Dohrmann, R., Kaufhold, S. (Eds.), *Contributions of the annual meeting DTTG*, vol 11. Celle, pp. 26–35.
- Kotarba, M., Środoń, J., 2000. Diagenetic evolution of crystallite thickness distribution of illitic material in Carpathian flysch shales studied by Bertaut–Warren–Averbach XRD method (MudMaster computer program). *Clay Minerals* 35, 387–395.
- Liewig, N., Clauer, N., Sommer, F., 1987. Rb–Sr and K–Ar dating of clay diagenesis in Jurassic sandstone oil reservoir, North Sea. *American Association Petroleum Geologists Bulletin* 71, 1467–1474.
- Lindgreen, H., Drits, V.A., Sakharov, B.A., Salyn, A.L., Dainyak, L.G., 2000. Illite–smectite structural changes during metamorphism in black Cambrian Alum Shales from the Baltic area. *American Mineralogist* 85, 153–172.
- Madejová, J., Kečkéš, J., Pálková, H., Komadel, P., 2002. Identification of components in smectite–kaolinite mixtures. *Clay Minerals* 37, 377–388.
- Malla, P.B., Douglas, L.A., 1987. Identification of expanding layer silicates: layer charge vs. expansion properties. In: Schultze, L.G., van Olphen, H., Mumpton, F.A. (Eds.), *Proceedings of the International Clay Conference*, Denver, 1985. The Clay Minerals Society, Bloomington, IN, pp. 277–283.
- McCarty, D.K., 2002. Quantitative mineral analysis of clay-bearing mixtures: the Reynolds Cup contest. *International Union of Crystallography, Commission on Powder Diffraction Newsletter* 27, 12–15.
- Moore, D.M., Reynolds, R.C. Jr., 1997. *X-ray Diffraction and the Identification and Analysis of Clay Minerals*. Oxford University Press, Oxford.
- Mystkowski, K., Środoń, J., Elsass, F., 2000. Mean thickness and thickness distribution of smectite crystallites. *Clay Minerals* 35, 545–557.

- Mystkowski, K., Środoń, J., McCarty, D.K., 2002. Application of evolutionary programming to automatic XRD quantitative analysis of clay-bearing rocks. The Clay Minerals Society 39th Annual Meeting, Boulder, CO, Abstracts with Programs.
- O'Connor, B.H., Chang, W.J., 1986. The amorphous character and particle size distribution of powders produced with the micronizing mill for quantitative X-ray powder diffractometry. *X-ray Spectrometry* 15, 267–270.
- Pevear, D.R., Schuette, C.M., 1993. Inverting the NEWMOD X-ray diffraction forward model for clay minerals using genetic algorithms. In: Reynolds, R.C. Jr., Walker, J.R. (Eds.), *Computer Applications in X-ray Powder Diffraction Analysis of Clay Minerals. CMS Workshop Lectures*, vol. 5. The Clay Minerals Society, Boulder, CO, pp. 20–41.
- Plançon, A., Drits, V.A., 1994. Expert system for structural characterization of phyllosilicates: I. Description of the expert system. *Clay Minerals* 29, 33–38.
- Reynolds, R.C., 1988. Mixed layer chlorite minerals. In: Bailey, S.W. (Ed.), *Hydrous Phyllosilicates (Exclusive of Micas). Reviews in Mineralogy*, vol. 19. Mineralogical Society of America, Washington, DC, pp. 601–630.
- Reynolds, R.C., 1989. Principles and techniques of quantitative analysis of clay minerals by X-ray powder diffraction. In: Pevear, D.R., Mumpton, F.A. (Eds.), *Quantitative Mineral Analysis of Clays. CMS Workshop Lectures*, vol. 1. Evergreen, CO, pp. 4–36.
- Reynolds, R.C., DiStefano, M.P., Lahann, R.W., 1992. Randomly interstratified serpentine/chlorite: its detection and quantification by powder X-ray diffraction methods. *Clays and Clay Minerals* 40, 262–267.
- Reynolds, R.C., Hower, J., 1970. The nature of interlayering in mixed-layer illite-montmorillonites. *Clays and Clay Minerals* 18, 25–36.
- Russell, J.D., Fraser, A.R., 1994. Infrared methods. In: Wilson, M.J. (Ed.), *Clay Mineralogy: Spectroscopic and Chemical Determinative Methods*. Chapman & Hall, London, pp. 11–67.
- Sakharov, B.A., Lindgreen, H., Salyn, A.L., Drits, V.A., 1999. Determination of illite-smectite structures using multispecimen X-ray diffraction profile fitting. *Clays and Clay Minerals* 47, 555–566.
- Sayles, F.L., Mangelsdorf, P.C., 1977. The equilibration of clay minerals with sea water: exchange reactions. *Geochimica et Cosmochimica Acta* 41, 951–960.
- Schultz, L.G., 1964. Quantitative interpretation of mineralogical composition from X-ray and chemical data for the Pierre Shale. *USGS Professional Paper*, 391-C.
- Smith, B.F.L., 1994. Characterization of poorly ordered minerals by selective chemical methods. In: Wilson, M.J. (Ed.), *Clay Mineralogy: Spectroscopic and Chemical Determinative Methods*. Chapman & Hall, London, pp. 333–358.
- Smith, D.K., Johnson, G.G. Jr., Scheible, W., Wims, A.M., Johnson, J.L., Ullmann, G., 1987. Quantitative X-ray powder diffraction method using the full diffraction pattern. *Powder Diffraction* 2, 73–77.
- Środoń, J., 1980. Precise identification of illite/smectite interstratifications by X-ray powder diffraction. *Clays and Clay Minerals* 28, 401–411.
- Środoń, J., 1981. X-ray identification of randomly interstratified illite/smectite in mixtures with discrete illite. *Clay Minerals* 16, 297–304.
- Środoń, J., 1984. X-ray powder diffraction identification of illitic materials. *Clays and Clay Minerals* 32, 337–349.
- Środoń, J., 1999. Nature of mixed-layer clays and mechanisms of their formation and alteration. *Annual Review of Earth and Planetary Sciences* 27, 19–53.

- Środoń, J., 2002. Quantitative mineralogy of sedimentary rocks with emphasis on clays and with applications to K–Ar dating. *Mineralogical Magazine* 66, 677–687.
- Środoń, J., Drits, V.A., McCarty, D.K., Hsieh, J.C.C., Eberl, D.D., 2001. Quantitative XRD analysis of clay-rich rocks from random preparations. *Clays and Clay Minerals* 49, 514–528.
- Środoń, J., Eberl, D.D., 1984. Illite. In: Bailey, S.W. (Ed.), *Micas. Reviews in Mineralogy*, vol. 13. Mineralogical Society of America, Washington, DC, pp. 495–544.
- Środoń, J., Elsass, F., McHardy, W.J., Morgan, D.J., 1992. Chemistry of illite/smectite inferred from TEM measurements of fundamental particles. *Clay Minerals* 27, 137–158.
- Šucha, V., Elsass, F., Eberl, D.D., Kuchta, L., Madejová, J., Gates, W.P., Komadel, P., 1998. Hydrothermal synthesis of ammonium illite. *American Mineralogist* 83, 58–67.
- Šucha, V., Kraus, I., Madejová, J., 1994. Ammonium illite from anchimetamorphic shales associated with anthracite in the Zemplinicum of the western Carpathians. *Clay Minerals* 29, 69–77.
- Taylor, J.C., 1991. Computer programs for standardless quantitative analysis of minerals using the full powder diffraction profile. *Powder Diffraction* 6, 2–9.
- Tributh, H., 1970. Die Bedeutung der erweiterten Tonfraktionierung für die genaue Kennzeichnung des Mineralbestandes und seiner Eigenschaften. *Zeitschrift für Pflanzenernährung und Bodenkunde* 126, 117–134.
- Tributh, H., 1976. Die Umwandlung der glimmerartigen Schichtsilicate zu aufweitbaren Dreischicht-Tonmineralen. *Zeitschrift für Pflanzenernährung und Bodenkunde* 139, 7–25.
- Watanabe, T., 1981. Identification of illite/smectite interstratification by X-ray powder diffraction. *Journal of Mineralogical Society of Japan, Special Issue* 15, 32–41 (in Japanese).
- Wicks, F.J., O'Hanley, D.S., 1988. Serpentine minerals: structures and petrology. In: Bailey, S.W. (Ed.), *Hydrous Phyllosilicates (Exclusive of Micas). Reviews in Mineralogy*, vol. 19. Mineralogical Society of America, Washington, DC, pp. 91–168.
- Wiewióra, A., 1985. X-ray powder transmission diffractometry determination of mica polytypes: method and application to natural samples. *Clay Minerals* 20, 231–248.
- Wiewióra, A., Wilamowski, A., Łacka, B., Kuźniarski, M., Grabska, D., 1998. Chamosite from oolitic ironstones: the necessity of a combined XRD–EDX approach. *Canadian Mineralogist* 36, 1547–1557.
- Wilson, M.J. (Ed.), 1994. *Clay Mineralogy: Spectroscopic and Chemical Determinative Methods*. Chapman & Hall, London.

This page intentionally left blank

### *Chapter 12.3*

## **X-RAY ABSORPTION SPECTROSCOPY**

**W.P. GATES**

*Centre for Green Chemistry, School of Chemistry, Monash University, Clayton, VIC 6800, Australia*

X-ray absorption spectroscopy (XAS) is used here as a general term denoting a range of X-ray spectroscopic techniques based on scattering, absorption and emission (fluorescence, auger) of X-rays by matter. Since many of these techniques are synchrotron-based, it is only in the past 20 years or so that they become generally available for investigating the crystal structures and surface chemistry of clays and clay minerals. Detailed information about synchrotrons and synchrotron radiation together with their applications in clay mineralogy, geochemistry and environmental science can be found in the books and reviews by Hodgson et al. (1984), Koningsberger and Prins (1988), Hawthorne (1988), Decarreau (1990), Mottana and Burrigato (1990), Amonette and Zelazny (1994), Schulze et al. (1999) and Fenter et al. (2002). The application of other X-ray techniques to mineral surface chemistry was described by Vaughan and Patrick (1995), Bertsch and Hunter (2001), de Groot (2001) and Fenter et al. (2002).

Synchrotron-based X-ray sources produce an intense X-ray emission with total fluxes and flux densities several orders of magnitude greater than conventional X-ray tubes. As a result, a nearly flat spectral distribution is produced over a large range of mineralogically important elements. This and recent advances in X-ray optics, detectors, insertion and focusing devices (Fenter et al., 2002) as well as modelling of scattering processes (e.g., Rehr et al., 1991, 1992; Rehr, 2003) made XAS a valuable tool for obtaining atomic-level information not previously attainable by conventional X-ray sources. In other words, synchrotron-based X-ray techniques extend diffraction methods beyond simply determining static atomic positions in minerals. Besides allowing detailed local structural information to be obtained, XAS is also more versatile than other bulk and surface analytical techniques, such as Mössbauer and NMR spectroscopies.

Here we review synchrotron-based studies of clays and clay minerals, focusing on the application of XAS to elucidating the structure and reactivity of 2:1 phyllosilicates, with particular emphasis on smectites. Reference to other clay minerals and to short-range order soil minerals will be made where appropriate.



### 12.3.1. SYNCHROTRON-BASED TECHNIQUES

Various synchrotron-based techniques are at the disposal of the modern clay mineralogists, including X-ray absorption/emission, X-ray scattering and X-ray microprobe techniques. The most important of these are absorption/emission methods, notably extended X-ray absorption fine structure (EXAFS), X-ray absorption near edge structure (XANES) or near edge absorption fine structure (NEXAFS) methods, X-ray fluorescence (XRF), X-ray photoelectron spectroscopy (XPS; see Chapter 12.4), photoelectron diffraction and the Auger effect. Scattering methods encompass X-ray diffraction (XRD), surface sensitive X-ray reflectivity and X-ray standing wave (XSW) techniques. Microprobe techniques enable X-ray absorption spectroscopic and diffraction techniques to be used for chemical mapping and imaging.

Synchrotron-based X-ray studies were largely concerned with determining the reactive sites on mineral surfaces that are involved in the sorption, dissolution and co-precipitation of metal hydroxides and the epitaxial growth of new phases. These studies provide new insights into the limits of low-temperature solid–solution and solid–solid transformations. Other significant areas of research include the interactions between metals, minerals and organisms. Likewise, advances in the development of specialised techniques (e.g., polarised EXAFS) permitted detailed structural studies of short-range order minerals. The capability of synchrotrons to deliver picosecond (ps) pulses of X-rays of nanosecond (ns) duration made possible kinetic methodologies which already contributed significantly to molecular-level understanding of reactions of clays and clay minerals.

White light-based techniques, including XRF elemental mapping using microprobes (Sutton and Rivers, 1999; Bertsch and Hunter, 2001), were prominent in soils and geochemical studies. However, they are generally restricted to high-energy synchrotron beamlines (hard X-rays,  $>4\text{--}4.5\text{ keV}$ , atomic number ( $Z$ )  $>20$ ). Photoelectron microprobe or electron microscope-based techniques are often more suitable for analysing elements of low  $Z$  (lighter than Ca) (Hochella, 1988), while X-ray absorption fine structure (XAFS) generally has greater sensitivity for elements of  $Z >20$ . Hard X-rays penetrate deeper into samples than soft X-rays, but are also attenuated less by air in the X-ray path. Recent advances in the development of ‘environmental cells’ open the possibility of analysing samples ( $Z <20$ ) under *in situ* conditions using soft X-rays (Meyer-Ilse and Attwood, 2000). Also, improvements in X-ray optics design and engineering of 3rd generation synchrotrons overcome many limitations for low  $Z$  elements (Brown and Sturchio, 2002).

Since the X-ray source can be “tuned” to energies specific to the absorption energies of many elements of interest, monochromatised X-rays are commonly applied to obtain information that is specific to the local environment of the targeted element. Element-specific analyses were often used in conjunction with microprobe techniques to study the relationships between minerals in aggregates, metals and mineral surfaces, soil contaminants and the potential efficacy of rehabilitation/remediation methods. Crystallographic studies employing XAFS concentrated on

local structural refinement of poorly crystalline nontronites, micas, chlorites, kaolins, phyllosulfates as well as (hydr)oxide and double hydroxide structures. The high intensity of monochromatic synchrotron light allows for *in situ* and element-specific analysis of samples for most elements heavier than carbon ( $Z = 6$ ). XAFS can be near-surface sensitive (to a depth of about 10 nm, depending on energy) if grazing incidence techniques are employed (Fenter, 2002; Waychunas, 2002). However, when transmission or fluorescence methods are used XAFS is a bulk technique, providing averaged local structural information around the target atom throughout the solid sample. Techniques that specifically probe surfaces independently of the bulk structure include standing wave (Bedzyk and Cheng, 2002) and grazing incidence (Waychunas, 2002) XAS.

#### A. X-ray Absorption and Scattering Processes

The energies of most X-rays are similar to core-electron-binding energies of atoms, which, in turn, are strongly dependent on atomic number ( $Z$ ) and less strongly on oxidation state and coordination environment. Electrons at core levels (e.g., 1s or 2p energy states) within atoms absorb energy from X-rays and are shifted to excited energy states. If the X-ray energy exceeds these electronic transition energies, the photoelectron is expelled from the atom into the surrounding atomic environment. Thus, X-ray absorption (or emission) by matter can be used to probe core-electron-binding energies of specific elements in substances with distinct chemistries and structure. Since X-ray wavelengths of about 10 pm (0.1 Å) are comparable to inter-atomic distances, X-ray scattering yields information about the surrounding local environment in short-range order materials. Of course, if long-range periodic order exists in a material, X-ray diffraction provides essential information on unit cell parameters (see Chapter 2).

X-ray spectroscopy is characterised by features corresponding to the absorption of an X-ray by an absorbing atom. The intensity,  $I$ , following an X-ray absorption event is given by

$$I = I_0 e^{-\mu t} \quad (1)$$

where  $I_0$  is the incident X-ray intensity,  $t$  the sample thickness and  $\mu$  the absorption coefficient. Eq. (1) indicates that the probability of X-rays being absorbed by matter is given by  $\mu$ . The value of  $\mu$  is averaged for all absorbing atoms, and is related to the properties of the sample by

$$\mu \cong \frac{\rho Z^4}{AE^3} \quad (2)$$

where  $\rho$  is the sample density,  $Z$  the atomic number,  $A$  the atomic mass and  $E$  the X-ray energy. Eq. (2) shows that X-ray absorption depends on the atomic make-up of matter (i.e., the type and number of atoms present) and the energy of the X-rays.

Generally, the magnitude of  $E$  is tuned such that a particular element is dominantly involved in absorption, while the surrounding elements in physical space are involved in scattering. When absorption processes are measured,  $\mu$  varies smoothly with the X-ray energy,  $\mu(E)$ , as the log of the ratio of measured to incident intensities

$$\mu(E) = \log \left( \frac{I}{I_0} \right) \quad (3)$$

but in fluorescence,  $\mu(E)$  becomes proportional to the ratio of the monitored intensity of the fluorescence line, ( $I_f$ ), to the incident intensity

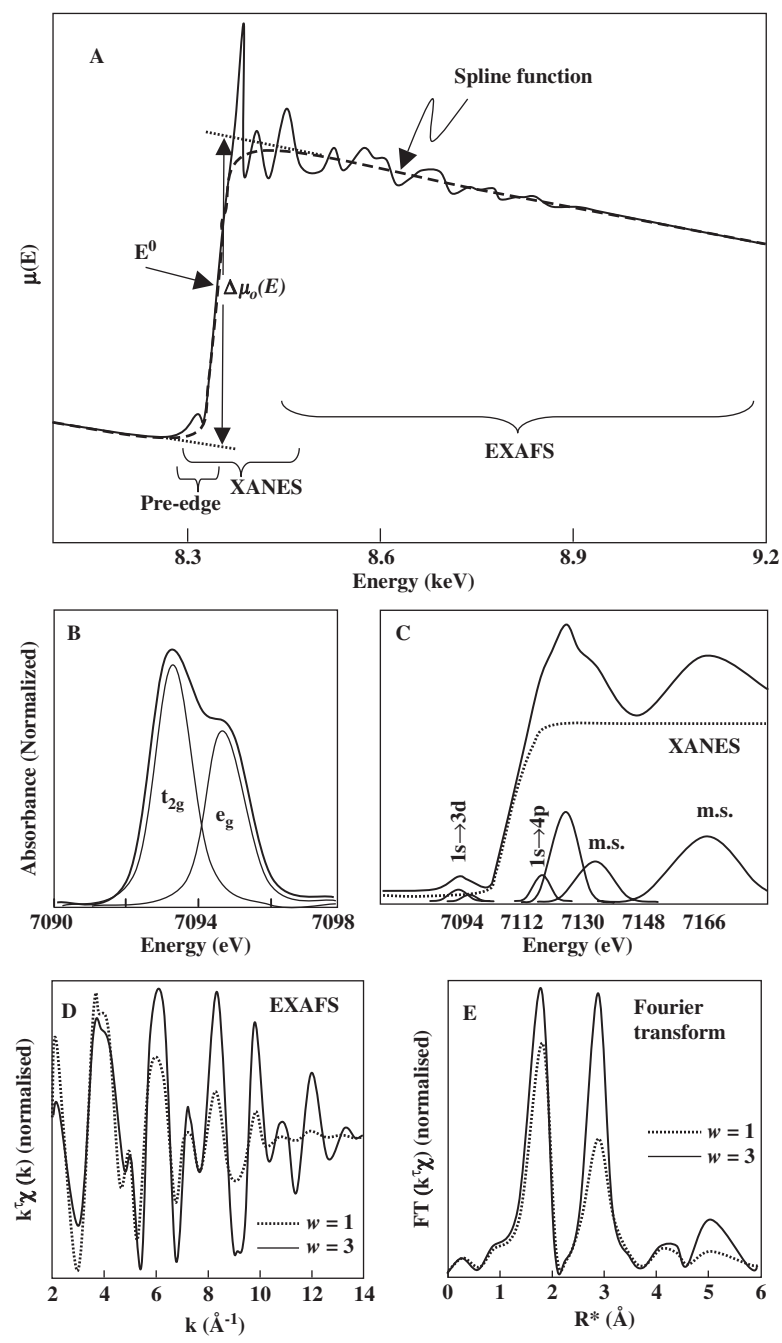
$$\mu(E) \propto \left( \frac{I_f}{I_0} \right) \quad (4)$$

X-ray absorption processes are the result of electronic transitions from core states to unoccupied electronic states. Since these transitions occur at discrete energies (quanta) unique to a particular element and its local environment, X-ray spectroscopy, especially pre-edge and XANES, can provide information about the electronic configuration of the absorbing atom (Bianconi et al., 1985; McKeown et al., 1985) in its local chemical and bonding environments.

The excitation of a core state electron having orbital angular momentum  $l$  enables one to probe the unfilled ( $l + 1$  and  $l - 1$ ) electronic states. The dipole selection rules state that  $s \rightarrow p$  and  $p \rightarrow d$  transitions are dipole-allowed, but  $s \rightarrow d$  transitions are dipole-forbidden. However, symmetry-enhanced orbital mixing can occur in crystal structures, and dipole-forbidden transitions are often observed (e.g., de Groot, 2001). The main absorption discontinuity of a 1st row transition metal K edge absorption spectrum (Fig. 12.3.1A) is due to  $1s \rightarrow 4p$  transitions and the edge features are related to unoccupied states having p-like character. The weak pre-edge feature of about 15 eV below the absorption jump arises from dipole-forbidden  $1s \rightarrow 3d$

---

Fig. 12.3.1. (A) Example of Ni K EXAFS spectra of Ni-kerolite (after Manceau and Calas, 1986) showing traditional divisions into pre-edge, XANES and EXAFS. Also depicted is an example of spline function used to background correct and normalise the XAFS spectrum so that direct comparisons with other XAFS spectra can be made.  $\Delta\mu_0(E)$  is defined as the difference between a point on the absorption edge extrapolated back from the EXAFS portion of the spectrum and the pre-edge background. (B) Example of Fe K pre-edge spectra showing  $1s \rightarrow 3d$   $t_{2g}$  and  $e_g$  transitions (after Manceau and Gates, 1997). (C) Typical Fe K XANES spectrum of montmorillonite and possible decomposition of  $1s \rightarrow 3d$ ,  $1s \rightarrow 4p$  transitions and multiple-scattering (m.s.) events. (D) Example of EXAFS spectra (Fe K of Garfield nontronite after Manceau et al. (1998)) showing the effects of  $k^{\omega=1}$  and  $k^{\omega=3}$  weighted Kaiser-Bessel functions on the EXAFS amplitude ( $\chi(k)$ ) as a function of reciprocal  $k$  space. (E) The resulting Fourier transforms of the  $k^{\omega=1}$  and  $k^{\omega=3}$  weighted EXAFS spectra displayed in (D), uncorrected for phase shift, showing the FT amplitude ( $\chi$ ) variation (position of atomic shells) as a function of distance from the target absorber.



transitions that are allowed due to p- and d-state mixing caused by distortion (flattening) of the octahedra (Calas and Petiau, 1983; Waychunas et al., 1983; Waychunas, 1987; Manceau and Gates, 1997). Thus, the excitation energy required for electronic transitions from core to excited states depends not only on the number of unoccupied states available, but also on the amount of symmetry mixing between the core and excited states.

The element-specific information regarding bound electronic states obtained from pre-edge and XANES spectra can be calculated using molecular-orbital and crystal-field stabilisation theories. For example, ‘density of states’ calculations of electrons in the metal–oxygen bonds of 1st row transition metal oxides were found to be in excellent agreement with the observed ligand (O) K XANES spectra (de Groot, 2001). For 2p elements (e.g., Al) the K-edge structure (amplitude and position) was shown to depend on site symmetry, bond angles, interatomic distances and the identity of nearest neighbours (Bianconi et al., 1985; McKeown et al., 1985; McKeown, 1989; Wu et al., 1996). All of these factors affect the crystal field strength and symmetry mixing within the bonding environment about the target atom, and thus the XAS spectra.

X-ray absorption spectroscopies (NEXAFS, EXAFS) also involve the release of photoelectrons into the ‘continuum’ (the surrounding atomic environment) and subsequent scattering of the photoelectron. The EXAFS process can be thought of as an *in situ* electron diffraction, in which the X-ray absorbing atom is the photoelectron source. When the kinetic energy of the ejected photoelectron is great enough to enable it to escape the bound state, it interacts with electrons in the bound states of other atoms within (about 600 pm) the local chemical environment surrounding the absorber. Energetically, the ‘continuum’ is up to several hundred electron volts above the absorption edge. Interactions between the ejected photoelectron and other electrons produce secondary sources of scattering and interference on return of the backscattering waves to the absorber (Fig. 12.3.2). Interferences between outgoing scattering and incoming backscattering waves result in low frequency oscillations between ~50 and ~1000 eV above the absorption edge.

These EXAFS oscillations are of interest as they contain structural and chemical information specific to the scattering atomic shells, including the number of coordinating atoms ( $N$ ), their distance from the absorber ( $R^*$ ), their identity ( $Z$ ) and the degree of disorder in the surrounding environment ( $\sigma$ ). An atomic shell is a group of atoms of the same species at the same distance ( $\pm$  a few picometer) from the absorbing atom. Qualitatively, the EXAFS oscillations are of higher frequency for long interatomic distances between the backscattering elements and the absorber, and of lower frequency for shorter interatomic distances (Brown et al., 1988). Quantitatively, the amplitudes of EXAFS oscillations can identify the type and number of backscattering atoms as well as the distribution of these atoms about a mean distance from the absorbing atom.

Single-scattering events generally probe shorter interatomic distances in crystals than do multiple-scattering events. Single-scattering events (Fig. 12.3.2a)

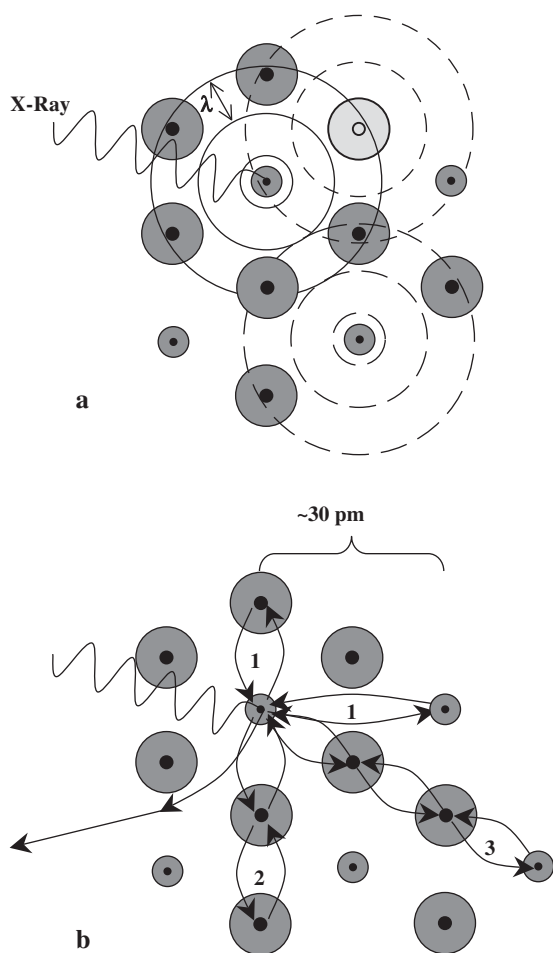


Fig. 12.3.2. Schematic of X-ray absorption processes in crystals. (a) Outgoing photoelectron wave (solid circles) from the absorbing (target) atom interferes with the photoelectron waves backscattered (dashed circles) from electron clouds of neighbouring atoms. Constructive (long-dashed circles) and destructive (short-dashed circles) interference results in oscillations in the absorption at energies above the absorption edge. (b) Single (1) and collinear (2, 3) multiple-scattering events are generally sufficient to depict EXAFS and XANES spectra in most minerals of interest to clay scientists.

predominate when the photoelectron wavelength is smaller than the interatomic distance between back-scatterer and absorber, and probe interatomic distances to about  $\sim 500$  pm from the absorber. When the photoelectron wavelength is greater than the interatomic distance, multiple-scattering events (Fig. 12.3.2b) predominate

and larger distances are probed. Because an XAFS spectrum is taken over a range of increasing X-ray energies, single- and multiple-scattering events dominate in different portions of the spectrum. The higher energy portions of EXAFS spectra are dominated by single-scattering events within only some tenth of nanometer (500–600 pm) from the absorber, and contain information specific to the local structure surrounding the absorber. On the other hand, XANES or NEXAFS spectra, being centred close to the absorption jump, are dominated by multiple-scattering events extending a few nm from the absorber.

Comparisons of experimental Fe K EXAFS spectra with those calculated for nontronites (derived from FEFF code (Rehr et al., 1991, 1992; Rehr, 2003)), indicate that multiple-scattering events can be important at  $R^* > \sim 450$  pm (Manceau et al., 1998), while co-linear multiple scattering events involving three or more high  $Z$  atoms can be considerable at shorter distances (Manceau et al., 2000a). Vantelon et al. (2003) observed important amplitude differences in calculated Fe K EXAFS spectra, incorporating multiple scattering, as compared with those that consider only single-scattering events, especially in the 300–500 pm range. In modelling Al K XANES spectra, Cabaret et al. (1996a) and Bugaev et al. (1998, 2000) found that single-scattering events were unimportant.

### B. XAFS Data Analysis

The procedures for XAS data processing (especially EXAFS) are standardised (Stern and Heald, 1983; Rehr et al., 1991) and there are simplified, user-friendly computer programs, such as IFEFFIT (Newville, 2003). Brown et al. (1988) and Fendorf (1999) described XAFS data analysis methods suitable for use in clay and soil sciences, while detailed information on more diverse techniques was given by Schulze et al. (1999), de Groot (2001), Bertsch and Hunter (2001) and Fenter et al. (2002).

Spectral processing requires background and levelling corrections and energy calibration. The amplitude of each spectrum must be normalised so that baseline values of the amplitude function ( $\mu(E)$ ) below the edge are near zero, and the averaged values of  $\mu(E)$  in the EXAFS portion are  $< 1$ . Typically, a spline function is applied to accomplish these steps (Fig. 12.3.1A). Energy and amplitude calibrations must be performed because of ‘drift’ that occurs during data collection due to differential heating of monochromators, beam instability and decay of the ring current. The importance of these standardised ‘pre-conditioning’ treatments, and their systematic and consistent application, cannot be stressed enough.

Analysis of XAFS spectra requires the extraction of data from the absorption experiment. Owing to scattering interference and the limited mean free path of the photoelectron, the magnitudes of X-ray scattering events typically decay rapidly with increasing energy above the absorption edge (Fig. 12.3.1A). Therefore the fine structure amplitude function,  $\chi(E)$ , of an EXAFS spectrum is isolated from

post-edge background,  $\mu_0(E)$ , using the relation (Teo, 1986)

$$\chi(E) = \frac{\mu(E) - \mu_0(E)}{\Delta\mu_0(E)} \quad (5)$$

where  $\mu(E)$  is the experimental absorbance as described above,  $\mu_0(E)$  the atomic contribution to the absorbance coefficient (X-ray absorption without the EXAFS oscillations),  $\Delta\mu_0(E)$  the measured absorption jump and  $E$  the kinetic energy of the photoelectron (the difference in the energies of the X-ray and that needed to eject the photoelectron into the continuum). Eq. (5) provides a means of normalising and correcting background for all portions of the XAFS spectra, whether one's interest is in the pre-edge, the XANES or the EXAFS regions (Fig. 12.3.1A).

Pre-edge and XANES spectral analyses often involve the decomposition and assignment of spectral features (Figs. 12.3.1B, C) and/or comparison with known reference spectra (Ildefonse et al., 1994, 1998). During decomposition of spectra, derivative curves can be used to locate abscissa where peaks occur. In common with other quantitative spectral analyses, decomposition generally incorporates Gaussian (normal) or Lorentzian (bell shaped) line shape functions, or Voigt (mixtures of Gaussian and Lorentzian).

For EXAFS (and NEXAFS) spectral analysis, the contributions of single- and multiple-scattering events need to be quantified since these events give rise to amplitude modulations in the spectra. The oscillations in the EXAFS spectra can be described quantitatively by

$$\chi(k) = \sum_j \frac{N_j f_j(k) e^{2k^2 \sigma_j^2}}{k R_j^2} \sin(2k R_j + \delta_j(k)) \quad (6)$$

Here  $N_j$  is the number of atoms making up the  $j$ th shell,  $f_j(k)$  the backscattering amplitude function corresponding to each atom within shell  $j$ ,  $\delta_j(k)$  the total phase shift function associated with the backscattering atom,  $\sigma_j^2$  the EXAFS Debye–Waller factor for thermal and static disorder, indicating the variance about the interatomic distances ( $R_j$ ) between the absorbing and backscattering atoms of the  $j$ th shell. The wavenumber of the wavevector,  $k$ , is given by

$$k = \sqrt{2m(E - E_0)/\hbar^2} \quad (7)$$

where  $E_0$  is now defined as the edge energy absorption threshold, usually located on the edge at one-half  $\Delta\mu_0(E)$  (Fig. 12.3.1A),  $m$  the electron mass and  $\hbar = h/2\pi$  ( $h$  is Planck's constant). The backscattering amplitude function is specific to the atoms involved in the backscattering process. The electronic terms,  $f_j(k)$  and  $\delta_j(k)$ , in Eq. (6) relate to the type of atom, while the terms  $N_j$ ,  $R_j$  and  $\sigma_j$  are associated with the local arrangement of other atoms surrounding the absorber. The EXAFS spectrum therefore contains information on the number, identity and distance ( $\pm 2$  pm) of



surrounding atoms as well as on the oxidation state and coordination number of the absorbing atom. The task is to quantitatively extract  $N$ ,  $R$  and  $\sigma$  from what is known about the scattering amplitude  $f(k)$  and phase-shift  $\delta(k)$  of a given absorber and its local chemical and structural environment.

The Fourier transform (FT) of Eq. (6) into ‘ $R$ ’ space is defined as

$$k^w(\chi R) = \frac{1}{2\pi} \int_{-\infty}^{\infty} dk \sin(2kR) k^w \chi(k) \Omega(k) \quad (8)$$

where  $\Omega(k)$  is a window function and  $w$  a  $k$  weighting factor. The  $\chi(k)$  wavevector spectrum is multiplied by the weighting factors,  $k^w$ , where  $w = 1, 2, 3, \dots$ , to enhance regions of high  $k$  (Fig. 12.3.1D). Sometimes the same data are analysed using different  $w$  weight factors (e.g.,  $w = 1$  and  $3$ ; Manceau et al., 2000a). Window functions, such as the ‘Hannell’ or ‘Kaiser-Bessel’ windows are applied to a selected  $k$  range to truncate the ends of the spectrum, thereby minimising ‘termination ripples’ in the FT (Waychunas et al., 1986). These mathematical functions influence the form of the EXAFS and ultimately the amplitude, phase and position of peaks in the resulting FT (Fig. 12.3.1E) (Teo, 1986). Their systematic application is thus important.

Peaks in the FT represent atomic shells, and are often complex combinations of several different atomic shells. Polarised EXAFS (Section 12.3.1F) can help differentiate between sub-shells making up particular peaks in the FT of layered materials, such as smectites. In powder EXAFS (Section 12.3.1E), however, entire peaks are used to determine the contributions of sub-shells to structural information. The papers by Teo (1986), Brown et al. (1988), Fendorf (1999) and Newville (2003) should be consulted for more detailed information on XAFS data processing.

The FT of an EXAFS spectrum (Fig. 12.3.1E) provides information on the distribution of atomic shells as a function of distance from the target absorber. By isolating shells of interest and back transforming the selected  $k$  region into ‘ $q$  space’, one creates a partial EXAFS spectrum that can then be compared to calculated scattering ( $f$ ) and phase ( $\delta$ ) functions in order to determine  $N$ ,  $R$  and  $\sigma$  associated with that particular shell. The FT is sometimes referred to as radial distribution (RDF) or radial structure (RSF) functions. Whatever the designation, they represent sums of all possible pair correlations involving the absorbing atom (Waychunas et al., 1986). Since phase corrections are usually not included in the FT, represented distances ( $R^*$ ) are generally 20–30 pm less than real interatomic distances ( $R$ ).

Care should be taken to ensure consistency during sample preparation because differences in sample thickness and density can have a profound impact on the XAFS amplitude,  $\Delta\mu_0(E)$  (Stern and Kim, 1981; Waychunas et al., 1983; Lu and Stern, 1993; Manceau and Gates, 1997). Disagreements over the interpretation of various XAFS spectra were documented, such as the structures of  $\text{Co}^{2+}$ -sepiolite (Fukushima and Okomoto, 1987; Fukushima, 1988; Manceau and Decarreau, 1988),

tetrahedral Fe in ferrihydrite (Eggleton and Fitzpatrick, 1988; Combes et al., 1989a; Manceau et al., 1990b; Drits et al., 1993; Manceau and Drits, 1993; Zhao et al., 1993, 1994; Manceau and Gates, 1997) and sorption complexes in oxides. These disagreements may partly arise from differences in sample preparation and presentation. In general, however, they can be attributed to variations in sample thickness and density, pre-analysis normalisation, data quality and the models used to interpret and quantify the spectra. Although interpretational disagreements are an important and necessary part of scientific research, they may cause considerable confusion for novice XAS experimentalists and those who are not well acquainted with the literature. The potential for further confusion still exists.

### C. Pre-Edge XAFS Spectroscopy

Features near the absorption edge are related to electronic transitions from core states to empty bonding states. Oxygen 1s (K) XANES experiments and calculations on transition metal dioxide (tetrahedral) structures showed that filling of empty 3d states in  $\text{TiO}_2$ ,  $\text{VO}_2$ ,  $\text{CrO}_2$  and  $\text{MnO}_2$ , are in agreement with experimental spectra (de Groot, 2001) and correspond to increased 3d  $t_{2g}$  state occupancies: 0 for Ti(IV), 1 for  $\text{VO}_2$ , 2 for  $\text{CrO}_2$  and 3 for Mn(IV). Pre-edge features are often observed in the XAFS spectra of transition metal absorbers (Figs. 12.3.1A, B). Sometimes these features represent intense dipole-allowed transitions, such as the 1s  $\rightarrow$  3d transition of tetrahedral Cr(VI) in  $\text{CrO}_4^{2-}$  (Sutton et al., 1993; Bertsch and Hunter, 2001) or of tetrahedral Fe (Waychunas et al., 1983), due to symmetry allowed p  $\rightarrow$  3d state mixing (de Groot, 2001). For octahedral symmetry, dipole (e.g., 1s  $\rightarrow$  3d) transitions are forbidden (Calas and Petiau, 1983) although pre-edge features can be observed because the octahedral sites in most minerals are distorted, allowing some p  $\rightarrow$  3d state mixing. Waychunas (1987) showed that the amount of distortion-induced p  $\rightarrow$  d mixing influences the amplitude and shape of the transition metal pre-edge features for many minerals. Manceau and Gates (1997) observed this also in the Fe K pre-edge spectra of nanocrystalline ferrihydrite.

Fig. 12.3.3A shows the effect of site distortions for the Fe K pre-edge XAFS spectra of goethite, hydrous ferric oxide and nontronite. Being a centrosymmetric, *trans*-vacant, dioctahedral smectite, nontronite has a relatively weak pre-edge structure, depending on tetrahedral Fe content. Furthermore, the octahedral sites in nontronite are only moderately distorted (Manceau et al., 1998) with a flattening angle,  $\beta_{\text{Fe}\dots\text{O}}$ , of about  $57^\circ$ . On the other hand, goethite ( $\alpha$ -FeOOH) and hydrous ferric oxide (HFO) can have appreciable octahedral distortion due to hydroxylation and hydration (Manceau and Gates, 1997; Ford and Bertsch, 1999). The increased distortion of Fe octahedra in these two hydrous oxides results in 30–40% amplitude enhancement compared with nontronite. Isomorphous substitutions of Al, Cr, Zn or Cu for Fe in the structure of (hydr)oxides can result in considerable enhancement of pre-edge amplitudes (Waychunas et al., 1986).

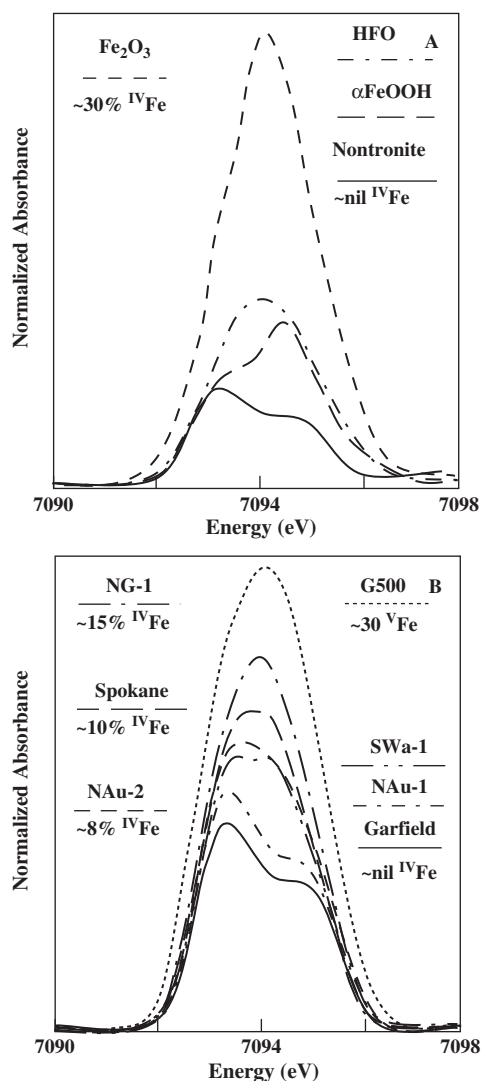


Fig. 12.3.3. Examples of Fe K pre-edge XAFS spectra showing differences in the  $1s \rightarrow 3d$  transition ( $t_{2g}$  and  $e_g$ ) amplitudes and shape as a function of coordination environment and site distortions. (A) Amplitude enhancement due to presence of tetrahedral coordination ( $\text{Fe}_2\text{O}_3$  and  $\text{FePO}_4$ ), broadening due to multiple sites ( $\text{Fe}_2\text{O}_3$ ) and amplitude enhancement due to dispersion of  $\text{Fe}\dots\text{O}$  distances and site distortion ( $\text{FeOOH}$ ,  $\text{HFO}$ ). (B) Amplitude enhancement due to incorporation of four-fold (NG-1) and five-fold (G500) Fe in the nontronite structure. Also depicted is broadening due to distortions in the local Fe environment (G500). G500 = Garfield nontronite heated to 500 °C for 3 h.  $\text{HFO}$  = hydrous ferric oxide, NG-1 Spokane, Nau-1 and Nau-2 are nontronite specimens with varying tetrahedral Fe content. Modified after Manceau and Gates (1997) and Gates et al. (2002).

*D. X-ray Near-Edge Spectroscopy (XANES or NEXAFS)*

The processes responsible for near-edge absorption structure are related to ejection of core electrons into ‘continuum states’, and involve single- and multiple-scattering events off the first atomic shell surrounding the absorber, as well as multiple-scattering events from more distant atomic shells (Fig. 12.3.1C). Edge features (position and shape) reflect oxidation states and coordination environments in the vicinity of the absorber (Waychunas et al., 1983; Waychunas, 1987; Cressey et al., 1993; Bajt et al., 1994, 1995; Ildefonse et al., 1994; Li et al., 1995; Delaney et al., 1996a, 1996b; Wu et al., 1996; Gates et al., 1997; Manceau and Gates, 1997; Delaney et al., 1998). This technique is now routinely applied to discern coordination and oxidation states of metals in minerals at  $\text{ng g}^{-1}$  concentrations (e.g., Bertsch and Hunter, 2001; Manceau et al., 2002a).

XANES spectra were traditionally interpreted by comparison with the spectra of reference materials (Waychunas et al., 1983; Waychunas, 1987; Bianconi, 1988; McKeown et al., 1989; Ildefonse et al., 1994; Ildefonse et al., 1998). Decomposition of the spectral components can indicate electron ‘density of states’ for the transition metals (de Groot, 2001) as well as differentiate between different site symmetries (Ildefonse et al., 1994, 1998; Bugaev et al., 1998, 2000) and assist in quantifying oxidation states in various mineral species (Fig. 12.3.4) (Waychunas, 1987; Bajt et al., 1995; Li et al., 1995; Delaney et al., 1996a, 1996b, 1998; Berry and O’Neill, 2004). Recent advances in multiple-scattering formalism, showed that XANES (NEXAFS) spectra can be treated like EXAFS spectra to gain element-specific information on bonding environment, such as coordination number and inter-atomic distances. Programs such as FEFF (Ankudinov et al., 1998; Rehr, 2003) or SELCOMP (Bugaev et al., 1998, 2000), using self-consistent full-potential multiple-scattering calculations, were instrumental in such advances. Simulations of multiple-scattering events reveal that XANES spectra are generally well characterised by nearest neighbour (single- and multiple-scattering events), next-nearest-neighbour (multiple-scattering events) and next-next-nearest-neighbour (multiple-scattering events) intervals from the absorber.

Calculations by Cabaret et al. (1996a) indicated that clusters with radii as large as 3 nm (30 Å or 3000 pm) are necessary to effectively model Al K-XANES spectra. Thus, even XANES spectra can provide short- to medium-range structural information. Although this finding has yet to be fully exploited in clay mineral studies, Bugaev et al. (2002) reported that Fourier filtering of XANES spectra can provide quantitative information of coordination number and bond distances for both crystalline and short-range order compounds. Thus, detailed study of NEXAFS spectra has the potential for more precise quantification than can be obtained from spectral comparison of target atoms for which the absorption edges of other elements overlap within the EXAFS region of the spectrum. Such situations disallow the collection of sufficient data in  $k$  space (e.g., K edges of many 1st row transition metals overlap with L edges of lanthanides) for satisfactory analysis to be carried out.

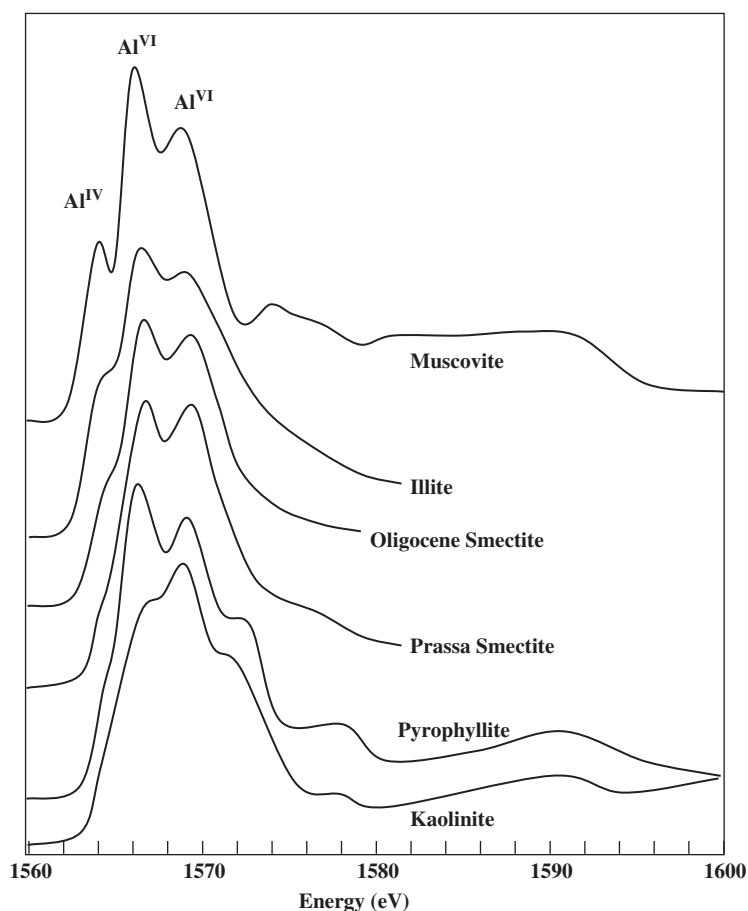


Fig. 12.3.4. Examples of Al K XANES (or NEXAFS) spectra of selected layer silicates. Decomposition of the first three peaks at  $\sim 1564$ ,  $1566\text{--}1567$  and  $1569\text{--}1570$  eV allows quantitative estimation of tetrahedral Al content. Adapted and redrawn from Ildefonse et al. (1994).

### E. Powder EXAFS Spectroscopy

As already mentioned, the oscillations of an EXAFS spectrum result from interference between the outgoing ejected photoelectron wavefront and the scattered wavefronts returning from near-neighbour environments. In clay structures, destructive interference occurs between waves backscattered from octahedral Fe and octahedral Al (Fig. 12.3.5), because a near  $\pi$ -difference in phase shift exists between 3d (e.g., Fe, Mn, Ni) and 3p (e.g., Si, Mg, Al) elements (Waychunas et al., 1986; Calas et al., 1990; Manceau, 1990). Similarly, a near  $\pi$ -difference in phase shift

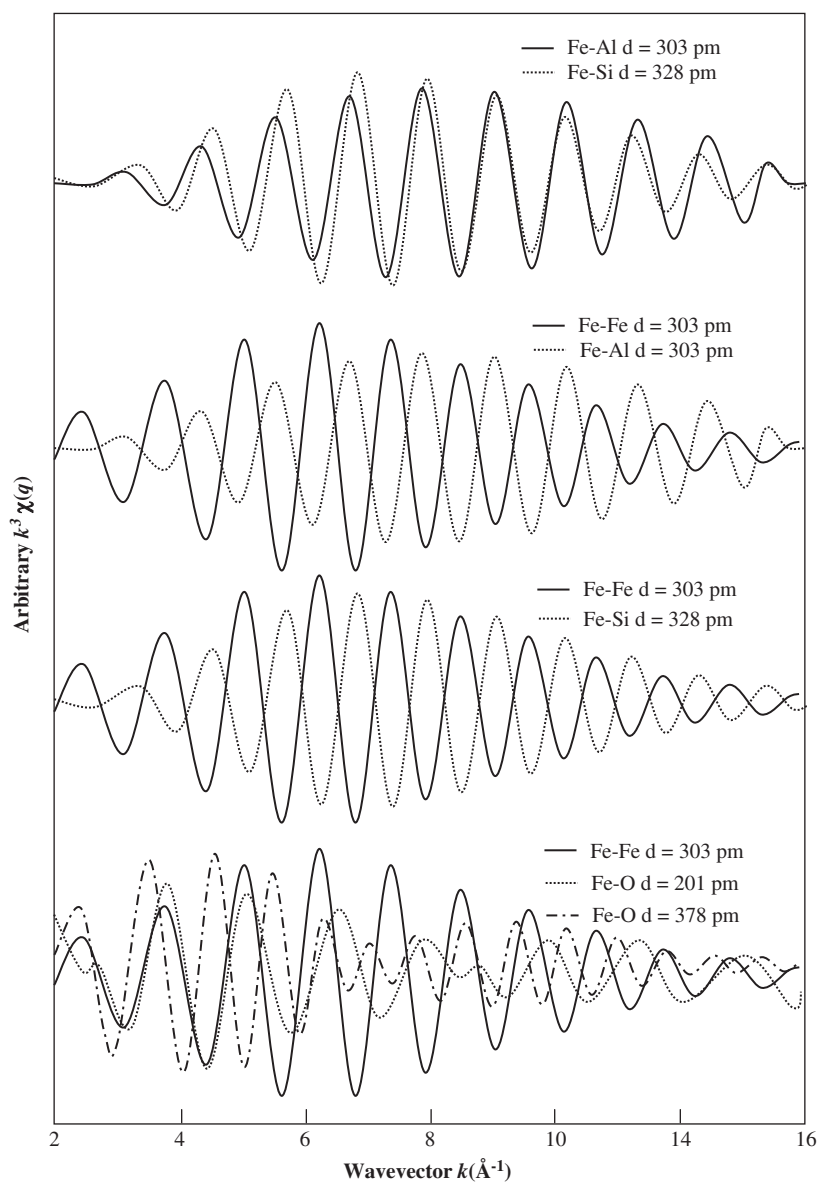


Fig. 12.3.5. Comparison of the calculated amplitudes and phases of nearest ligand (Fe...O) and cation (Fe...Fe, Fe...Si, Fe...Al) atomic shell contributions to Fe K EXAFS spectra of a typical smectite structure. Top panel: octahedral Al shell at  $d = 303$  pm and tetrahedral Si shell at  $d = 328$  pm. Upper middle panel: octahedral Fe shell at  $d = 303$  pm and octahedral Al shell at  $d = 303$  pm. Lower middle panel: octahedral Fe shell at  $d = 303$  pm and tetrahedral Si shell at  $d = 328$  pm. Bottom panel: octahedral Fe shell at  $d = 303$  and O shells at  $d = 201$  pm and  $d = 378$  pm. All waveform amplitudes were adjusted to differing degrees relative to the Fe...Fe signal.

occurs between waves that are backscattered from tetrahedral and octahedral cations of the same species, at least for the phyllosilicates (Manceau et al., 1998; Gates et al., 2002). These phenomena were exploited to study octahedral cation occupancies in Ni<sup>2+</sup>-smectite, Ni<sup>2+</sup>-sepiolite, montmorillonites, ferruginous smectites and nontronites and can be applied to kaolinite, pyrophyllite, allophane, imogolite and other important minerals.

Powder EXAFS spectroscopy of clays and clay minerals does suffer from rather severe limitations, however. One limitation is the difficulty in discriminating between atoms of similar atomic number (Z), due to the similarity of their backscattering wave functions (Fig. 12.3.5). While improvements were made in modelling these contributions, it is still not possible to unequivocally differentiate between Al, Si and Mg, or between Ni, Mn and Fe, as second cation-shell neighbours in a smectite structure. Another limitation is the existence and complexity of multiple sites occupied by a given absorbing species (Table 12.3.1). For example, in magnetite with an inverse spinel structure, Fe occupies both octahedral and tetrahedral sites, and has two different oxidation states. Strong overlap of the backscattering amplitudes of tetrahedral and octahedral cations (Fig. 12.3.5) adversely affects quantitative resolution between these two sites. Further, suitable reference materials with varied coordination sites are lacking. For example, the five-fold coordinated Fe(III), Fe(II) or Al in dehydroxylated structures of smectites is highly distorted (Rossman and Tarlan, 2001; see Fig. 12.3.3 for Fe(III)). Vacancies (e.g., goethite), defects (e.g., ferrihydrite) and poor order (e.g., octahedral sheet of dioctahedral smectites) in

Table 12.3.1. Scattering paths used in fit of powder (film at  $\alpha = 35^\circ$ ) Fe K EXAFS of SWa-1 displayed in Fig. 12.3.6. Single-scattering paths alone were found to enable a satisfactory fit\* to determine  $N$  and  $R_{\text{eff}}$  in IFEFFIT (Newville, 2003). Chemistry<sup>†</sup> and symmetry<sup>‡</sup> were input into TKATOMS (Ravel, 1999) to enable FEFF (Rehr, 2003) to determine scattering paths

Shell	Scattering atom	Path	$N$	$R_{\text{eff}}$ (pm)
Fe...O <sub>1</sub>	O	Fe→O→Fe	2	201
	O	Fe→O→Fe	4	203
Fe...M <sub>1</sub>	Oct Al	Fe→Al→Fe	0.7	301
	Oct Fe	Fe→Fe→Fe	2.3	307
	Tet Si	Fe→Si→Fe	4	337
Fe...O <sub>2</sub>	O	Fe→O→Fe	2	342
Fe...O <sub>3</sub>	O	Fe→O→Fe	2	371
	O	Fe→O→Fe	4	388
Fe...M <sub>2</sub>	Tet Si	Fe→Si→Fe	4	445
Fe...Int	Interlayer Na	Fe→Na→Fe	2	510
Fe...M <sub>3</sub>	Oct Fe	Fe→Fe→Fe	3	523

\*Fitting results:  $\text{So}^2 = 0.658$ ;  $\Delta E = -5.58 \text{ eV}$ ;  $\chi^2_v = 21$ .  $\sigma$  was held constant at 0.07.

<sup>†</sup>Chemistry from Gates (2004) or Gates et al. (2002).

<sup>‡</sup>c2/m.

mineral structures make unambiguous spectral interpretations the exception. In layered structures, any preferential orientation will also affect the resulting EXAFS amplitude, leading to misinterpretation. As already discussed, sample preparation, presentation and spectral processing issues can also impact on the quality of the XAFS spectrum and its interpretation.

EXAFS spectra can be quantified using IFEFFIT and associated program code (Ravel, 1999, 2003a, 2003b; Newville, 2003), while scattering paths can be calculated using TKATOMS (Ravel, 1999) and FEFF (Rehr, 2003). These programs incorporate the effects of curve waveforms and single- and multiple-scattering paths, providing improved data analysis. The contributions of each scattering path within a given distance from the absorber are calculated, and the resulting theoretical EXAFS spectrum represents a sum of all these contributions. A scattering path defines the atoms from which the photoelectron can scatter before returning to the absorber. As described in Section 12.3.1A, single- and multiple-scattering paths occur, and based on the crystallography of the mineral, calculated paths are used to deduce the atomic shells surrounding the absorber. These are then compared to the experimentally derived partial spectrum by applying least-squares analysis, which was back-transformed from a peak isolated in the FT. The IFEFFIT code was recently modified, allowing larger regions of the FT to be fit simultaneously. For such methodology to be used effectively in the analysis of disordered clay minerals, the user must have as much detailed knowledge as possible of the crystal chemistry of the specimen being studied, or be able to extract this information from known reference materials. Thus, EXAFS is rarely a suitable stand-alone technique for unknown samples. Most studies use a variety of other more conventional measurements into which EXAFS is incorporated as a secondary or supplementary technique.

The powder EXAFS spectrum of the ferruginous smectite, SWa-1 (Fig. 12.3.6) illustrates some of the pros and cons of fitting a large region (rather than isolated peaks) of the EXAFS spectrum using IFEFFIT. Some different fits are shown, while the results of one fit are displayed in Table 12.3.1. When the Fe...M<sub>1</sub> shell was isolated from the FT (Fig. 12.3.6, lower middle panel) fitting of the partial EXAFS spectrum resulted in two octahedral components consisting of 2.1Fe at  $d = 305$  pm, 0.9Al at  $d = 303$  pm, and one tetrahedral component of 4Si at  $d = 337$  pm. A fit of the entire FT from  $R^* = 0$ –600 pm results in 2.3Fe at  $d = 307$  pm, 0.7Al at  $d = 301$  pm and 4Si at  $d = 337$  pm. Contrast these results with those of Manceau et al. (2000a) and Vantelon et al. (2003) who studied the same mineral. The best fit of the Fe...M<sub>1</sub> shell in the latter study was 2.2Fe at  $d = 309$  pm and 0.8Al at  $d = 302$  pm, not too dissimilar from the results in Table 12.3.1 (Fig. 12.3.6, bottom panel). The best fit of the octahedral contributions to the Fe...M<sub>1</sub> shell by Manceau et al. (2000a) was 2Fe at  $d = 305$  pm and 1Al at  $d = 303$  pm, similar to those displayed in Fig. 12.3.6 (lower middle panel). Since the octahedral contributions were isolated using polarised EXAFS (P-EXAFS), the fits of Manceau et al. (2000a) should be considered superior. This example also illustrates the importance of collecting high  $k$  data for good accuracy on  $R_{\text{eff}}$ . While the  $N_{\text{eff}}$  determined by both



these studies is within error for coordination number determinations, the interatomic distances are different. Contributions from wave vectors at higher  $k$  influence the fit to wave vectors at lower  $k$ , resulting in different  $R_{\text{eff}}$ . Interestingly, incorporating more shells at higher  $R^*$ , and ignoring any contributions of multiple-scattering events, improve the fit on  $R_{\text{eff}}$ . This can be seen by comparing the results in Table 12.3.1 with those of Vantelon et al. (2003).

### F. Polarised EXAFS Spectroscopy

Application of P-EXAFS to layer silicates is unique in that it allows all out-of-plane contributions to the EXAFS spectrum to be systematically removed, and accurate structural information about the in-plane contributions only (and vice versa) to be obtained. A backscattering phase shift between a heavy (e.g., Fe, Mn, Ni, etc.) and a light (e.g., Al, Mg) atom enhances quantification of the heterogeneous nature of octahedral and tetrahedral cation occupancies in smectites and other layered minerals. P-EXAFS also has the inherent ability to increase spectral resolution enabling differentiation of atomic shells separated by only 10–20 pm (Manceau et al., 1998). In powder EXAFS, the resolution power in the  $R^*$  range is limited by low signal-to-noise ratios in the high  $k$  region. On the other hand, the P-EXAFS method increases the signal-to-noise ratio at high  $k$ , thereby improving the resolving power in  $R^*$ .

For powdered systems (random disorder of the particles) P-EXAFS spectra taken at several angles will show little, if any, variation in amplitude (Manceau, 1990). For self-supporting clay mineral films where the layers are aligned, changes in the film angle ( $\alpha$ ) with respect to the X-ray beam will alter the amplitude (pleochroism). Backscattering atoms situated out-of-plane (tetrahedral Si, Al or Fe, structural oxygen) from the target absorber (e.g., octahedral Fe) will contribute positive pleochroism (amplitude enhancement) and those atoms within the film plane (e.g., Al, Mg, Fe) will contribute negative pleochroism to the EXAFS amplitude with increasing  $\alpha$ .

Exactly how the P-EXAFS amplitude varies with  $\alpha$  for Garfield nontronite (Manceau et al., 1998) is shown in Table 12.3.2 and Fig. 12.3.7A. In Table 12.3.2, the term  $\beta$  is the average angle between the absorber and the backscattering atoms of a particular shell, with respect to the film plane normal, and  $N_{\text{cryst}}$  the number of

---

Fig. 12.3.6. Analysis of ligand (Fe...O<sub>1</sub>) and nearest cation (Fe...M<sub>1</sub>) contributions to the  $k^3$  weighted Fe K EXAFS spectra of ferruginous smectite SWa-1, collected on an oriented film at  $\alpha = 35^\circ$  (equivalent to a powder EXAFS). The Fe...O<sub>1</sub> and Fe...M<sub>1</sub> shells were isolated from the Fourier transform at  $R^*$  ranges of 0.8–2.05 Å and 2.05–3.2 Å, respectively, and back-transformed (top panel). The Fe...O<sub>1</sub> (upper middle panel) and Fe...M<sub>1</sub> (lower middle panel) shells were fit to the structural parameters displayed. A fit of the total contribution of the Fe...O<sub>1</sub> and Fe...M<sub>1</sub> shells, as well as higher  $R^*$  shells, to the EXAFS is shown in the bottom panel. See Table 12.3.1 for fitting parameters of this latter fit.

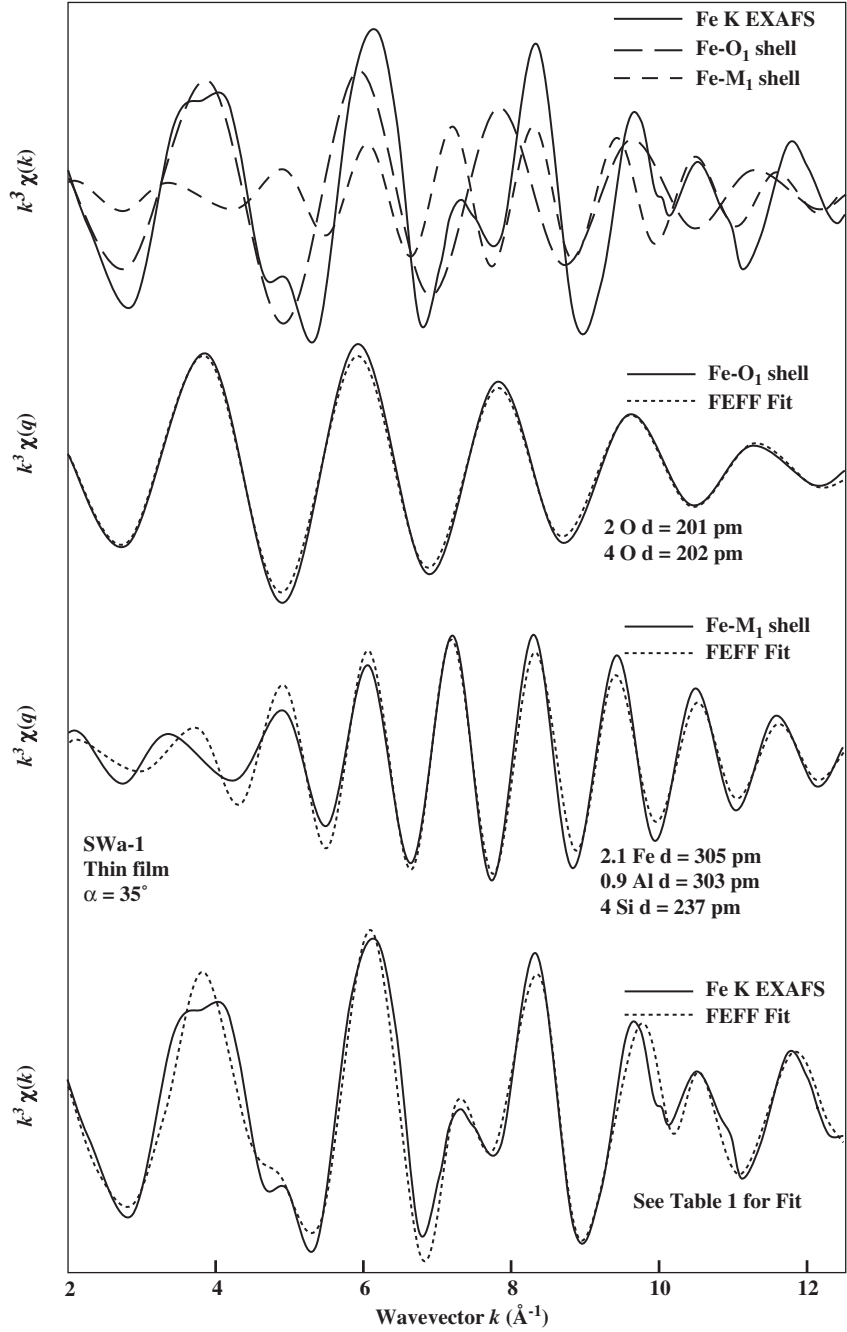


Table 12.3.2. Angular dependence of some atomic shell contributions to P-EXAFS spectra of Garfield nontronite. Modified after Manceau et al. (1999a), with  $R^*$  calculated using FEFF. The  $\beta$  angle is measured with respect to film normal. See text for definitions

Shell	$R^*$ (pm)	$\langle \beta \rangle$ (°)	$N_{\text{cryst}}$	$N_{\text{eff}}^0$	$N_{\text{eff}}^{20}$	$N_{\text{eff}}^{35}$	$N_{\text{eff}}^{60}$	$N_{\text{eff}}^{80}$	$N_{\text{eff}}^{90}$
Fe...O <sub>1</sub>	197, 204	57	6	6.3	6.2	6.0	5.6	5.4	5.3
Fe...Fe <sub>1</sub>	304	90	3	4.5	4.0	3.0	1.1	0.1	0
Fe...(Si,Al) <sub>1</sub>	326	32	4	1.7	2.5	4.0	7.3	8.4	8.6
Fe...O <sub>2</sub>	345	11	2	0.1	0.8	2.0	4.4	5.6	5.8
Fe...O <sub>3</sub>	374, 382	73	6	8.2	7.4	6.0	3.2	1.7	1.5
Fe...O <sub>4</sub>	402, 419	37	4	2.2	2.8	4.0	6.3	7.5	7.6
Fe...(Si,Al) <sub>2</sub>	449	52	4	3.7	3.8	4.0	4.3	4.5	4.5
Fe...Na	510	15	2	0.2	0.8	2.0	4.2	5.4	5.6
Fe...Fe <sub>2</sub>	528	90	6	9	7.9	6.0	2.3	0.3	0
Fe...Fe <sub>3</sub>	609	90	3	4.5	4.0	3.0	1.1	0.1	0

atoms of the shell of the idealised structure. The relationship between  $N_{\text{cryst}}$  and the effective number of neighbouring atoms ( $N_{\text{eff}}$ ) actually seen by P-EXAFS at a given film angle, is given by (Manceau et al., 1999)

$$\chi_{ij}(k, \alpha) = \frac{N_{\text{eff}}}{N_{\text{cryst}}} \chi_{ij}^{\text{iso}}(k) \quad (9)$$

In Eq. (9),  $\chi_{ij}(k, \alpha)$  is the amplitude determined by P-EXAFS for an atomic pair as a function of reciprocal  $k$ -space and film angle  $\alpha$  and  $\chi_{ij}^{\text{iso}}(k)$  the amplitude determined on perfectly random systems.  $N_{\text{eff}}$  for each film angle is given by

$$N_{\text{eff}}^{\alpha} = 3N_{\text{cryst}} \left[ \cos^2 \beta \sin^2 \alpha + \frac{(\sin^2 \beta \cos^2 \alpha)}{2} \right] \quad (10)$$

Note that at  $\alpha = 0^\circ$

$$N_{\text{eff}}^0 = \frac{3N_{\text{cryst}} \sin^2 \beta}{2} \quad (11)$$

and at  $\alpha = 90^\circ$

$$N_{\text{eff}}^{90} = 3N_{\text{cryst}} \cos^2 \beta \quad (12)$$

From knowledge of the crystallographic angle,  $\beta$ , between the absorbing and the backscattering atoms, as well as the idealised number of neighbours,  $N_{\text{cryst}}$ , it is possible to calculate the effective number of neighbours,  $N_{\text{eff}}^{\alpha}$ , observed at any angle in a P-EXAFS experiment. Alternatively,  $\beta$  can be calculated from knowledge of  $N_{\text{eff}}^{\alpha}$  determined from P-EXAFS spectra or from simulations. The ability to predict  $N_{\text{eff}}$

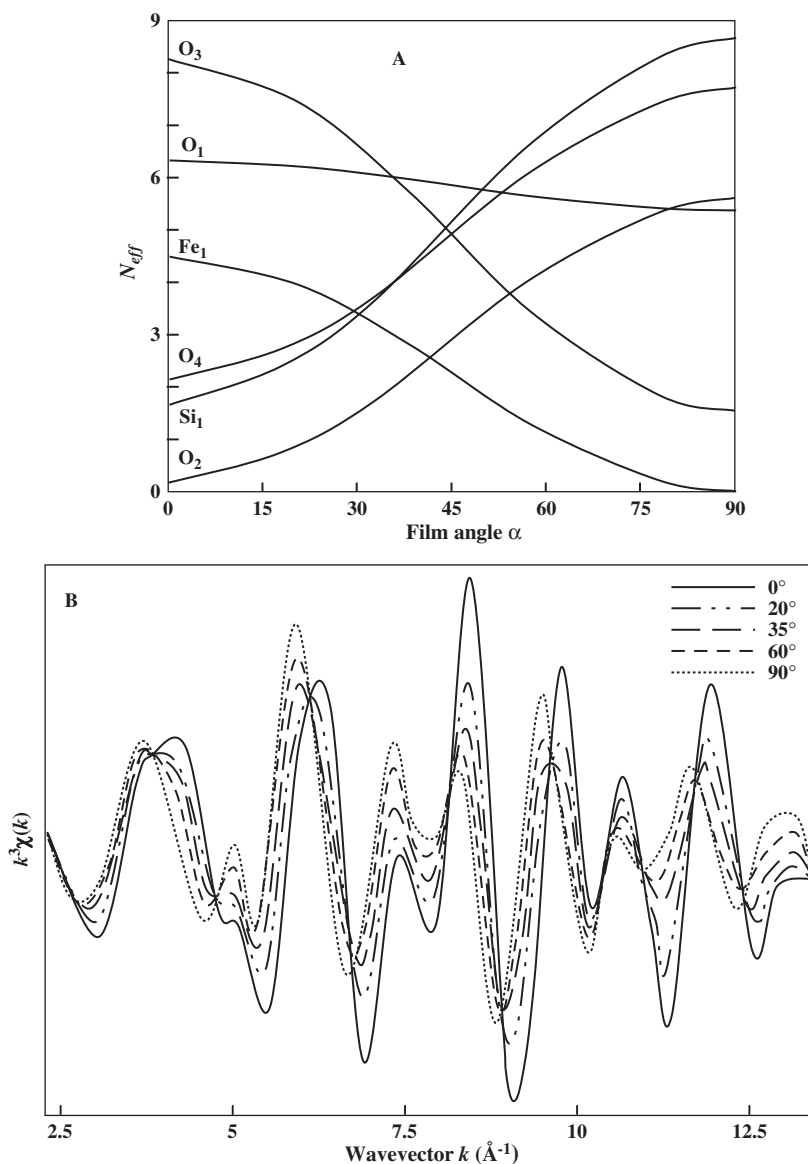


Fig. 12.3.7. (A) Variation of  $N_{\text{eff}}$  as a function of film angle  $\alpha$  for Fe K P-EXAFS spectra. (B) Polarised  $k^3$  weighted Fe K EXAFS spectra of ferruginous smectite SWa-1. The  $\alpha = 90^\circ$  spectrum was calculated from a linear extension of the experimental amplitude as a function of  $\cos^2\alpha$ . Isobestic points occur where the EXAFS amplitude ( $k^3\chi(k)$ ) is invariant regardless of  $\alpha$ , and separate in-plane contributions, where  $k^3\chi(k)$  increases with increasing  $\alpha$ , from out-of-plane contributions, where  $k^3\chi(k)$  decreases with increasing  $\alpha$ .

from structural information provides better fits of the spectra, as it decreases the number of fitting variables, or at least puts realistic limits upon them.

Table 12.3.2 shows that for shells whose atoms lie at shallow angles with respect to the film normal (e.g., Fe...O<sub>2</sub>, Fe...O<sub>4</sub> and Fe...(Si,Al)<sub>1</sub>), large increases in  $N_{\text{eff}}^z$  occur with increasing  $\alpha$ . For those shells having atoms residing at steep angles with respect to the film normal (e.g., Fe...Fe<sub>1</sub>, Fe...Fe<sub>2</sub>, Fe...Fe<sub>3</sub> and Fe...O<sub>3</sub>),  $N_{\text{eff}}^z$  decreases by differing amounts:  $N_{\text{eff}}^z$  diminishes to 0 for the Fe...Fe<sub>1</sub>, Fe...Fe<sub>2</sub> and Fe...Fe<sub>3</sub> shells at  $\alpha = 90^\circ$ , but to 1.5 for O<sub>3</sub>. For shells with atoms lying near  $\beta = 55^\circ$ , little change occurs in  $N_{\text{eff}}^z$  as a function of  $\alpha$ . Thus,  $\beta \approx 55^\circ$  is a critical angle where  $N_{\text{eff}}^z$  is invariant for all values of  $\alpha$ . At a film angle of  $\alpha \approx 35^\circ$ , the effective number of neighbours is approximately equal to the crystallographic number ( $N_{\text{eff}}^{35} \approx N_{\text{cryst}}$ ), a fact demonstrated by Manceau et al. (1988) for single crystal and powdered mica. Thus,  $\alpha \approx 35^\circ$  is another critical angle in that P-EXAFS spectra collected at  $\alpha \approx 35^\circ$  will be identical to powder EXAFS spectra.

The in-plane contributions can be completely removed from an  $\alpha = 90^\circ$  EXAFS spectrum, which can then be used to estimate the magnitude of out-of-plane contributions. This estimate is then used to remove any out-of-plane contributions from the  $\alpha = 0^\circ$  spectrum to obtain an estimate of in-plane contributions only. Transmission measurements at  $\alpha = 90^\circ$  are not easily obtained experimentally—it should be possible to use glancing angle or wide angle X-ray scattering (GAXS or WAXS) analyses—and P-EXAFS data are usually collected at several angles of the self-supporting film with respect to the X-ray beam (Figs. 12.3.7B and 12.3.8A). Processing P-EXAFS data requires careful amplitude normalisation because the amount of sample probed increases with increasing  $\alpha$  (it doubles from  $\alpha = 0^\circ$  to  $60^\circ$ ). The normalised  $\alpha = 0^\circ, 20^\circ, 35^\circ, \dots, 60^\circ$  spectra for a given sample are then used to calculate an  $\alpha = 90^\circ$  spectrum by linear regression of the  $k^3\chi(k)$  (or  $k^1\chi(k)$ ) amplitude against  $\cos^2\alpha$ , for all points in reciprocal ( $k$ ) space (Manceau et al., 1998). The resulting calculated  $\alpha = 90^\circ$  spectrum is then processed in the same way as for other EXAFS spectra, the difference being that the  $\alpha = 90^\circ$  contributions are isolated from the forward FTs and subtracted from those isolated from the  $\alpha = 0^\circ$  spectrum to obtain a partial EXAFS spectrum containing only in-plane contributions.

Recall that the Fe...M<sub>1</sub> shell in a powder EXAFS spectrum of a smectite is a composite of in-plane (octahedral cations) and out-of-plane (ligand and tetrahedral cations) contributions. The difference of the resulting in-plane Fe...M<sub>1</sub> partial P-EXAFS spectra from that obtained on powder samples where the out-of-plane scattering events contribute, is striking (Fig. 12.3.8B) and, as was shown above, influences the resulting analysis (Table 12.3.1 and discussion in Section 12.3.2D). As the subtraction process removes the out-of-plane contributions, a phase shift to lower wave vectors is observed in the partial Fe...M<sub>1</sub> P-EXAFS spectrum relative to the partial Fe...M<sub>1</sub> powder EXAFS spectrum.

The  $\alpha = 90^\circ$  contributions are normally only calculated for a limited  $k(q)$  range, but there is no reason, other than increased complexity, that the entire spectrum could not be processed and analysed in a similar fashion. Detailed analysis of highly

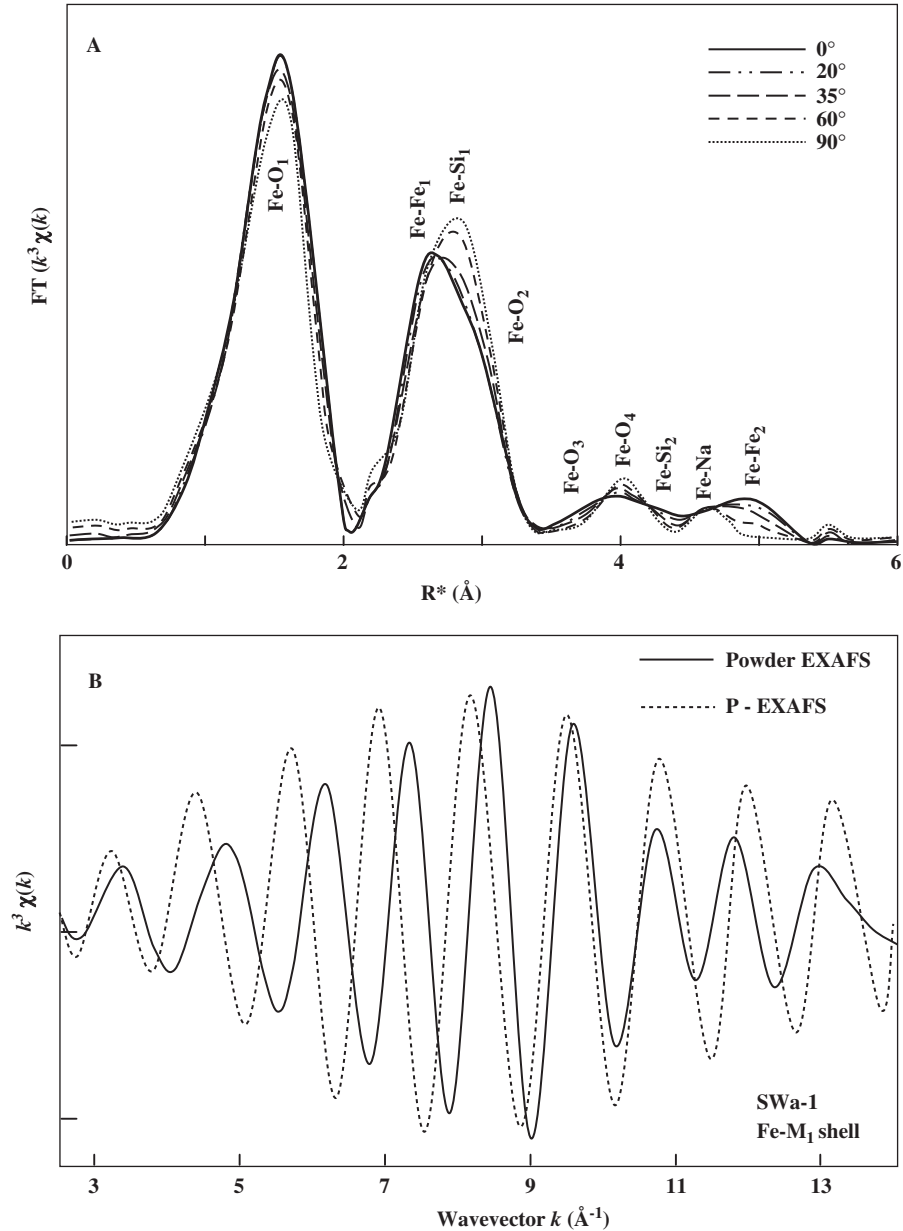


Fig. 12.3.8. (A) The resulting Fourier transforms of  $k^3$  weighted Fe K P-EXAFS in Fig. 12.3.7B. Assignments to shells based on Manceau et al. (2000a). (B) Comparison of the Fe...M<sub>1</sub> shell isolated from the  $\alpha = 35^\circ$  spectrum of ferruginous smectite SWa-1 before (powder EXAFS) and after (P-EXAFS) subtracting the tetrahedral contributions using the procedures described in Section 12.3.3.

textured self-supporting nontronite films (Manceau et al., 1998, 2000a, 2000b) indicates that P-EXAFS spectra returns the appropriate values calculated from theory. Interestingly, Schlegel et al. (1999a, 1999b, 2001a) and Dähn et al. (2002a, 2002b, 2003) recently collected P-EXAFS data at angles as high as  $\alpha = 80^\circ$ . Given the uncertainties associated with measurement and extraction of EXAFS amplitudes, as well as the dispersion inherent in self-supporting films (Manceau et al., 1998, 1999; Schlegel et al., 1999a, 1999b; Manceau et al., 2000a, 2000b; Schlegel et al., 2001a; Dähn et al., 2002a, 2002b, 2003) this measurement is essentially equivalent to one calculated from an  $\alpha = 90^\circ$  spectrum (compare the  $N_{\text{eff}}$  values at  $\alpha = 80^\circ$  and  $\alpha = 90^\circ$  in Fig. 12.3.7A).

For further information on experimental set-up, sample preparation and spectral analysis of P-EXAFS data, the reader is referred to the papers by Manceau et al. (1998, 1999, 2000a) and Manceau and Schlegel (2001). Poor alignment of individual particles within self-supporting films remains a potential limitation of P-EXAFS as this will result in dispersion, amplitude dampening for out-of-plane features, amplitude augmentation of in-plane features and loss of linearity in the pleochroic relation. However, for typical smectite self-supporting films, the error arising from this condition is either small enough to be neglected or can be corrected using charts prepared by Manceau and Schlegel (2001).

### 12.3.2. XAFS STUDIES ON SMECTITE STRUCTURE

#### *A. Structural Refinement by P-EXAFS*

It is only recently that P-EXAFS was applied to investigate the structures of fine-grained and poorly crystalline layer silicates (Manceau et al., 1998, 1999a; Schlegel et al., 1999a; Manceau et al., 2000a, 2000b; Schlegel et al., 2001a; Dähn et al., 2002a, 2002b, 2003), although it was earlier used to study the location of Fe in micas and chlorites (Manceau et al., 1988, 1990a; Manceau, 1990; Waychunas and Brown, 1990; Dyar et al., 2002) and to determine bond angles in graphite intercalates (Bonnin et al., 1986). Heald and Stern (1977) were the first to use anisotropic X-ray absorption to study single crystals. Manceau et al. (1988) applied P-EXAFS to examine Fe distribution in chlorite and biotite, observing that the second peak (Fe...M<sub>1</sub>) in the FT occurred at shorter  $R^*$  distance when the electric vector was in-plane with the octahedral sheet than when it was out-of-plane. Direct comparison of the back-transformed partial EXAFS spectra with that of biotite showed that about 25% of the total Fe was located in interlayer sites of the chlorite.

P-EXAFS was extended to structural refinements of nontronite (Manceau et al., 1998, 1999a, 2000a, 2000b) and phyllomanganates (Manceau et al., 1999a) and more recently to determine the location of adsorbed metals on hectorite (Schlegel et al., 1999a, 1999b, 2000) and montmorillonite (Dähn et al., 2002a, 2002b, 2003) surfaces. P-EXAFS improved our understanding of sorption sites (Hazemann et al., 1992;

O'Day et al., 1994a; Schlegel et al., 1999a, 1999b, 2001a, 2001b; Dähn et al., 2002a, 2002b, 2003). The technique is also potentially capable of assessing site occupancies of Al and Mg in Fe-poor beidellites, montmorillonites and saponites, where  $^{27}\text{Al}$  NMR fails (Muller et al., 1997; Manceau et al., 2000a; Vantelon et al., 2003). P-EXAFS has yet to be applied to obtain structural refinements of other layered minerals such as palygorskites, sepiolites and layered double hydroxides. In addition, P-EXAFS would be suitable for assessing trace metal substitution (e.g., Zn or Mn for Al) in smectites formed under various geochemical conditions or exposed to different weathering regimes.

The structures of some nontronites and ferruginous smectite were refined by Manceau et al. (1998, 1999a, 2000a) using a combination of P-EXAFS and modelling. Distance-valence least-squares (DVLS) modelling of the  $c2/m$  symmetry of nontronite enabled the contribution of atomic scattering paths (from FEFF) to partial EXAFS spectra to be determined (Manceau et al., 1998). The DVLS and FEFF method was found to produce calculated spectra in excellent agreement with experimental spectra. In addition, Manceau et al. (1999a) provided a method to determine crystallographic angles associated with the layered structure. Manceau et al. (2000a) found that Fe(III) predominantly occupies M2 (*cis*) octahedra in agreement with earlier electron diffraction studies (Tsipursky and Drits, 1984). For the Fe-poor smectites, Vantelon et al. (2003) recently observed that modelling powder EXAFS spectra in which Fe(III) cations occupied both M1 (*trans*) and M2 octahedra provided good agreement with experimental spectra, but attempts at further refinement of the montmorillonite structure using P-EXAFS have yet to be published.

### *B. Dioctahedral vs. Trioctahedral Structural Types*

Trioctahedral smectites may readily be distinguished from dioctahedral smectites by XRD (see Chapter 12.1) and IR spectroscopy (see Chapter 12.6). Since the *b* unit cell parameter is longer in trioctahedral smectites, the  $d(060)$  (or  $d(06\cdot33)$ ) line in the XRD pattern is close to 0.153 nm as compared with  $\approx 0.149$  nm for dioctahedral smectites (Brindley and Brown, 1980). The OH stretching region in the IR spectrum of trioctahedral smectites is shifted by about  $100\text{ cm}^{-1}$  to higher energies relative to dioctahedral smectites of similar composition, and also shows considerable pleochroism under plane polarisation (Farmer, 1974).

P-EXAFS is arguably the best XAFS technique for distinguishing tri- from dioctahedral smectites because the out-of-plane contributions from the tetrahedral sheet can be isolated and removed (Manceau et al., 1988, 1998; Manceau, 1990). In fact, if the tetrahedral Si and Al contributions are not accounted for in powder EXAFS analysis of smectites, the contribution from octahedral Al and Mg would be overestimated. This is due to overlap of the backscattering phases for these atoms at the two different interatomic distances typically associated with octahedra and tetrahedra (Fig. 12.3.5) (Manceau et al., 1988). As a result, the in-phase difference



between  $M\cdots Si_{(tet)}$  and  $M\cdots Al_{(oct)}$  shells due to differences in interatomic distances ( $M\cdots Si_{(tet)} \approx 316\text{--}328\text{ pm}$ ;  $M\cdots Al_{(oct)} \approx 300\text{--}310\text{ pm}$ ) is cancelled. If the octahedral sheet contains heavy atoms, these atoms would be underestimated if the tetrahedral contributions were not fully accounted for. The same would also occur if the contributions from lighter octahedral atoms are not taken into account, or the lighter atoms themselves are underestimated. As will be shown in Sections 12.3.1C and 12.3.1D, much progress was made in dealing with complex chemistries by combining P-EXAFS with other methods.

In powder EXAFS, trioctahedral character is indicated by the amplitude and position of the first cation shell (Muller et al., 1997). This shell could be used *a priori* (Manceau et al., 1998) to distinguish between the two groups of minerals since an absorber would be surrounded by six other octahedral cations in a trioctahedral structure, but only by three other cations in a dioctahedral structure. However, when Al, Mg and different oxidation states of Fe are present, misinterpretations can easily be made. Manceau (1990) therefore recommended that EXAFS be used in a supportive role for such studies. The first cation shell in the FT of the Fe K P-EXAFS spectra is shifted to slightly lower  $R^*$  ( $\sim 30\text{ pm}$ ) and is only 50–60% as intense for biotite (trioctahedral mica) compared with nontronite (dioctahedral smectite), despite there being only  $3Fe^{3+}$  nearest octahedral neighbours in nontronite compared with  $4Fe^{2+}$  and 2Al or Mg nearest octahedral neighbours in biotite (Manceau, 1990). The magnitude of amplitude change, as a function of film angle, is greater in biotite than in nontronite. Two strongly pleochroic shells, in the 380–620 pm  $R^*$  range are observed for biotite, but not for nontronite. This indicates increased coherence in both interatomic distances and crystallographic angles in the trioctahedral structure as compared with its dioctahedral counterpart. A third cation shell ( $Fe\cdots Fe_3$ ) at about 580 pm is observed for biotite (Manceau et al., 1998), the amplitude of which is increased by constructive interference between outgoing and incoming scattered waves in co-linear multiple-scattering events (O'Day et al., 1994c). These co-linear scattering paths do not exist to any great extent in dioctahedral structures (Manceau et al., 1998). In a dioctahedral structure, tetrahedral sheet rotation and tilting results in a splitting of  $Fe\cdots O_3$  and  $Fe\cdots O_4$  interatomic distances into two distinct ranges (Table 12.3.2), thus diminishing the overall signal of these ligand shells due to interference. These and additional ligand shells at  $R^*$  as high as  $\sim 600\text{ pm}$  also interfere with octahedral cation backscattering contributions (Fig. 12.3.5).

### C. Tetrahedral Cation Distributions in Smectites

#### EXAFS Spectroscopy

Since Bonnin et al. (1985) first applied Fe K pre-edge XAFS to determine the amount of tetrahedral Fe in Garfield nontronite, XAFS studies of site occupancy in smectites become more common. Bonnin et al. (1985) found that the amount of tetrahedral Fe in nontronites, if present, was less than about 5% of total Fe, in

accord with IR, Mössbauer (Bonnin et al., 1985) and P-EXAFS (Manceau et al., 1998) analyses. Using Fe K pre-edge and P-EXAFS analyses, Manceau et al. (2000a) assumed that the Garfield nontronite had nil tetrahedral Fe and used it as their reference octahedral Fe(III) mineral. They found that the Panamint Valley nontronite and the ferruginous smectite SWa-1 also contained nil tetrahedral Fe, but that the German nontronite NG-1 contained about 17% Fe in tetrahedral sites.

Given the uncertainties associated with pre-edge analyses (Manceau and Gates, 1997), Gates et al. (2002) applied Fe K powder EXAFS, in conjunction with IR and XRD methods, to two ferruginous smectites and 12 nontronites to determine the distribution of Fe in tetrahedral and octahedral sites. The first peak in the FT of Fe K EXAFS spectra contains all the contributions of the ligand first shell. A nearly  $\pi$ -difference in phase exists between the  $^{IV}\text{Fe}\dots\text{O}$  ( $d = 195$  pm) and  $^{VI}\text{Fe}\dots\text{O}$  ( $d = 202$  pm) waveforms (Manceau et al., 2000a) in the reverse transform of this peak. The  $\text{Fe}\dots\text{O}$  contributions to the EXAFS spectra associated with tetrahedral Fe interfere systematically with those contributions associated with octahedral Fe (Fig. 12.3.9). This finding was used by Gates et al. (2002) to estimate tetrahedral Fe in nontronites. For nontronites with significant Al ( $\text{Al}_2\text{O}_3 \geq 5$ –12% ignited basis), least-squares fitting of linear combinations of the  $^{IV}\text{Fe}\dots\text{O}$  ( $d = 195$  pm) and  $^{VI}\text{Fe}\dots\text{O}$  ( $d = 202$  pm) waveforms to experimental data yielded tetrahedral Fe contents within 3% of total Fe. However, the method was less sensitive ( $> 5\%$  of total Fe) for nontronites with very low total Al contents. For example, the Spokane nontronite with  $< 3\%$   $\text{Al}_2\text{O}_3$  (ignited basis) was estimated to have 12% of total Fe occupying tetrahedral sites (Fig. 12.3.9B) by this method. Although this value falls within the error of the method, it is unrealistically low because the tetrahedral cation composition would be unfilled. Near-IR or XRD analyses are more reliable over the entire composition range studied (Gates et al., 2002), but for the majority of samples, the XAS method would be highly useful. Obviously, refinements in  $d(^{VI}\text{Fe}\dots\text{O})$  and  $d(^{IV}\text{Fe}\dots\text{O})$  for each individual nontronite would improve the ability of this powder EXAFS technique in determining tetrahedral Fe.

#### *Pre-Edge Spectroscopy*

The effect of incorporating  $^{IV}\text{Fe}$  into the structure of nontronite is depicted in Fig. 12.3.3B (Manceau et al., 2000a; Gates et al., 2002). The German nontronite, NG-1, was found by other methods to have as much as 17% of total Fe in tetrahedral sites. As such, it displays considerably enhanced pre-edge amplitude compared to the Garfield nontronite, despite being chemically similar. The pre-edge amplitude is enhanced for the Spokane nontronite and the South Australian nontronite, NAu-2, as well. For all three nontronites, the resolution of the  $t_{2g} \rightarrow e_g$  splitting of energy states is lost relative to Garfield nontronite, suggesting that  $^{IV}\text{Fe}$  with a smaller  $t_{2g} \rightarrow e_g$  splitting is present in these samples.

The pre-edge amplitude for Spokane nontronite suggests an unrealistically low (Gates et al., 2002) estimate of  $^{IV}\text{Fe}$  ( $\sim 10\%$ ). The diminished amplitude of the Spokane nontronite is likely related to a high symmetry about the octahedral sites.

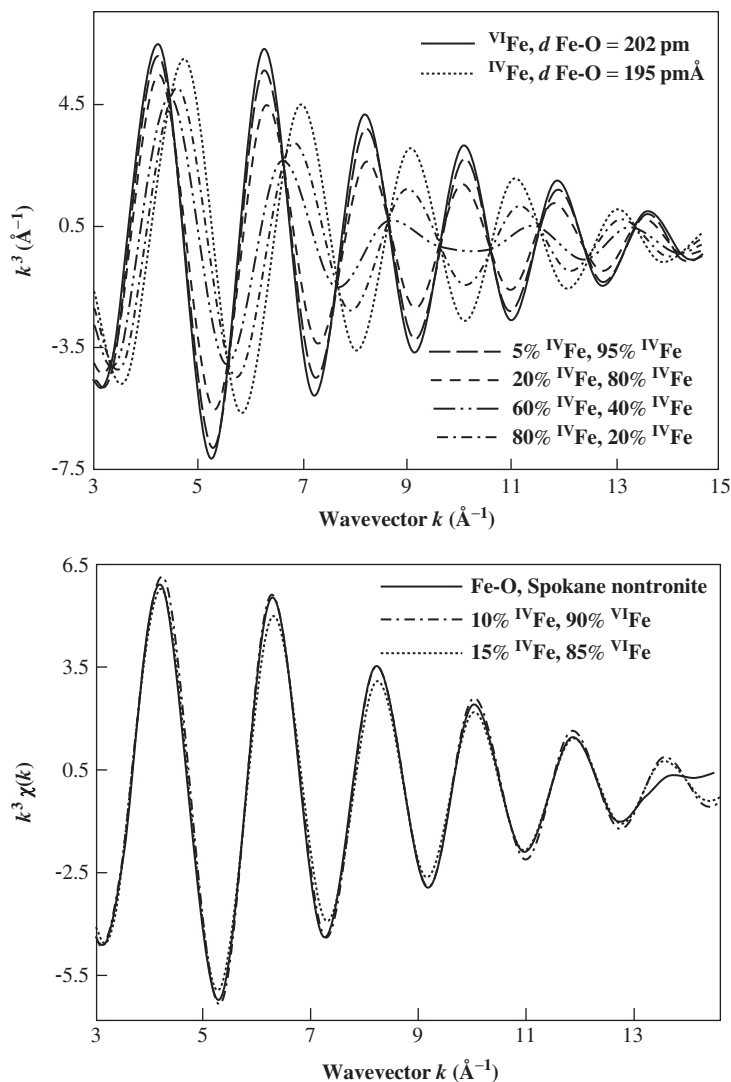


Fig. 12.3.9. Application of the Fe...O contributions of powder Fe K EXAFS in determining the tetrahedral Fe content of nontronites. (A) The amplitude and phase changes of the Fe...O wave vector as a function of mixing different amounts of  $^{IV}\text{Fe}$  at  $d = 195 \text{ pm}$  to  $^{VI}\text{Fe}$  at  $d = 202 \text{ pm}$ . (B) Example least squares fit for the Fe...O contribution of Spokane nontronite assuming  $d = 195 \text{ pm}$  for tetrahedral Fe and  $d = 202 \text{ pm}$  for octahedral Fe. Modified after Gates et al. (2002).

At the opposite extreme, the pre-edge amplitude of the ferruginous smectite SWa-1 is enhanced, yet the other methods indicated that SWa-1 has nil tetrahedral Fe(III). In this case, the enhanced amplitude is related to a high degree of distortion of Fe octahedra caused by the presence of neighbouring Al and Mg octahedra. The distortion is sufficient to decrease the  $t_{2g} \rightarrow e_g$  splitting, which is better resolved than for the NG-1, NAu-2 and Spokane nontronites (Fig. 12.3.3B). The South Australian nontronite, NAu-1, also has an enhanced pre-edge structure, but this enhancement seems to be primarily due to its increased Al content compared with the Garfield sample (Gates et al., 2002). Using other methods, Gates et al. (2002) found that the Garfield and NAu-1 nontronites may contain 2–3% of total Fe in tetrahedral coordination, essentially at the detection limit of pre-edge XAFS spectroscopy (Manceau and Gates, 1997).

Finally, the presence of different sites in layer structures affects the pre-edge XAFS spectra. The pre-edge spectra of heat-treated Garfield nontronite (G500) is shown in Fig. 12.3.3B. The pre-edge amplitude is enhanced, in this case due to the presence of ~30% five-fold coordinated Fe ( $^V\text{Fe}$ ) in G500. Additionally, the pre-edge peak of G500 is broadened by as much as 30% of the non-heated samples. Heat treatment causes dehydroxylation and migration of some M2 cations to M1 sites (Drits et al., 1998b). The M1 site is slightly larger than the M2 site, so distortion is introduced in a new average of interatomic angles and distances. The broadening of G500 is ~30% compared with that of the Spokane sample, reiterating just how uniform the Fe(III) octahedra are in the end member nontronite.

#### *XANES Spectroscopy*

Ildefonse et al. (1994, 1998) could estimate the amount of tetrahedral Al in layer silicates by decomposition of the Al K XANES spectra (Fig. 12.3.4). By comparison with a variety of reference minerals, they found that all Al-bearing layered structures had three amplitude maxima in the near-edge structure related to Al coordination environment. The first maxima near 1564 eV showed up as an inflection in the rising edge of references containing no  $^{\text{IV}}\text{Al}$ , but became well-resolved and quite pronounced for layer silicates containing appreciable  $^{\text{IV}}\text{Al}$ . The two peaks near 1566 and 1569 eV were related to  $^{\text{VI}}\text{Al}$ . By decomposing the three peaks in the Al K XANES, Ildefonse et al. (1994, 1998) estimated accurately the  $^{\text{IV}}\text{Al}$  content of several montmorillonites and illite–smectite interstratifications. Thus, Al K XANES can be used to determine tetrahedral Al content in smectites where such techniques as NMR fail due to the presence of too much Fe (Gates et al., 1996).

The substitution of Ga for Al in synthetic kaolins and smectites was investigated by Martin et al. (1998), using Ga K XANES, IR, electron microscopy and XRD analyses. They found that Ga substitution in kaolins was limited presumably because of the size difference between Ga and Al. When the ratio  $\text{Ga}/(\text{Ga} + \text{Al}) < 0.1$ , Ga incorporation into the kaolin structure was confirmed by an increase in the  $d(06\text{--}33)$  spacing. At  $\text{Ga}/(\text{Ga} + \text{Al}) > 0.1$ , kaolin-smectite and kaolin-oxide precipitates occurred, but Ga was predominately associated with the smectite phases as observed by

IR. Ga K XANES spectra of Ga-kaolin and Ga-smectite showed that Ga substituted for Al in the octahedral sheet of kaolin, but in both octahedral and tetrahedral sites in smectite, indicating the flexible nature of the 2:1 phyllosilicate structure.

For the Fe-bearing phyllosilicates, the form of the edge crest in the Fe K XANES spectra provides information on oxidation state and degree of crystallinity (Gates et al., 1997; Dyar et al., 2001). A shoulder within  $\sim 4$  eV above  $E_0$  in the edge crest is observed in reduced montmorillonite and nontronite, the resolution of which is improved with increasing levels of Fe(II) (Gates et al., 1997). Similar features were observed in the Fe K XANES spectra of biotite micas (Dyar et al., 2001) but here the edge crests are better resolved due to greater crystallinity, and are probably related to multiple-scattering contributions.

#### D. Octahedral Cation Distributions and Isomorphous Substitutions in Smectites

In dioctahedral smectite structures, two types of octahedral cation arrays are present. Most beidellites, ferruginous smectites, nontronites and illites are composed of *trans*-vacant (centrosymmetric) octahedra. Here each (mostly) divalent octahedral cation occupies M2 sites, shares its two hydroxyl anions with one adjacent cation in an M2 site along one edge (2OH edge), and two oxygen anions (2O edge) along edges with two other M2 cations at  $120^\circ$  (Fig. 12.3.10). Fe-poor smectites and montmorillonites have octahedral cations in both *cis* (M2) and *trans* (M1) sites (non-centrosymmetric structure) (Drits et al., 1998b; Sains-Diaz et al., 2001). In the latter structure, one M2 site is vacant, and any given octahedral cation (M1, M2) will share two edges containing both O and OH (O,OH edge) and a 2O edge with adjacent different (M2, M1) cations. In trioctahedral structures, where all octahedral sites are filled with divalent cations, each M1 cation shares four O,OH edges and two 2O edges with M2 cations. Each M2 cation shares one 2OH edge and two 2O edges with other M2 cations, but two O,OH edges and a 2O edge with M1 cations. Such distinctions are important as they affect the number of shells, and the number of atoms within shells that are calculated based on the symmetry of the octahedra sheet (Manceau et al., 1998; Dähn et al., 2003; Vantelon et al., 2003).

Table 12.3.3 displays the number of atoms in shells and the distances of the shells from the absorber (Al in this case) for a hypothetical Ni-saturated and Ni-substituted Texas montmorillonite STx-1, as calculated by TKATOMS (Ravel, 1999) in two different symmetries. Note that more oxygen atoms within particular shells are calculated for *c2/m* (*trans* vacant, centrosymmetric) symmetry than for the correct *cis*-vacant *c2* symmetry. Also, more atoms make up the tetrahedral shells, which show splitting due to the makeup of the octahedral sheet. Thus, while an apparently subtle difference exists between *cis*- and *trans*-vacant structures, it can have a large impact on the parameters used by EXAFS analysis programmes in calculating scattering paths.

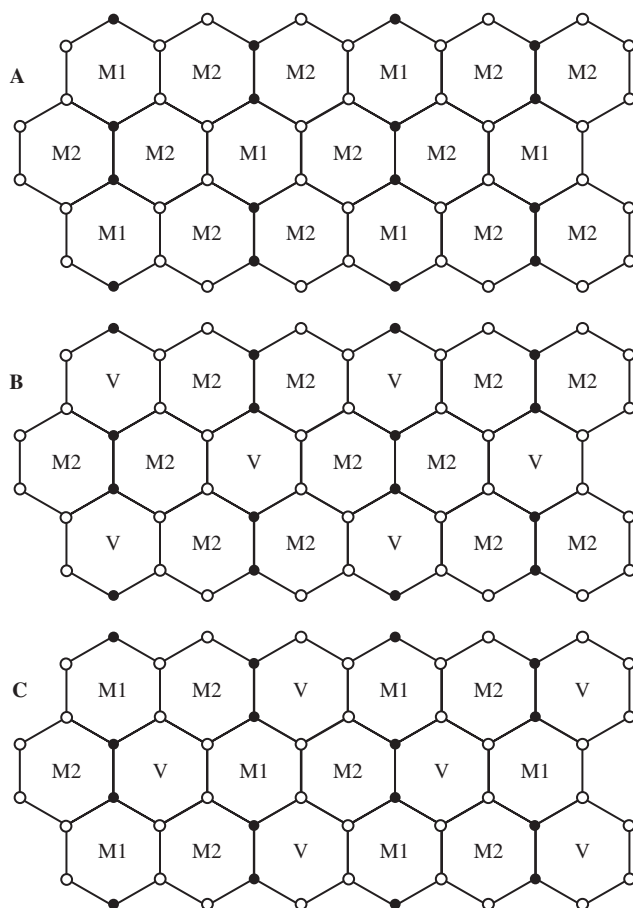


Fig. 12.3.10. Representation of different configurations of the octahedral sheets in dioctahedral smectites showing (A) the location of M1 and M2 sites in trioctahedral sheets and the location of vacancies (V) in (B) *trans* vacant and (C) *cis* vacant, dioctahedral sheets. Solid circles represent hydroxyls and hollow circles represent oxygens.

#### *Ni Bearing Layer Silicates and Minerals*

The occurrence of Ni in various layer silicates attracted considerable attention given the industrial importance of these minerals as Ni ore sources. Manceau and Calas (1985, 1986, 1987) and Decarreau et al. (1987) found that Ni associated with lateritic smectite and other layer silicate structures always occurs in Ni-enriched clusters of at least 2–3 nm diameter. Associated infrared studies (Gérard and Herbillon, 1983) indicated a predominance of NiNiMg-OH over NiMgMg-OH absorption stretching bands, suggesting that Ni substitutes within the octahedral layer near sites initially having charge deficit.

Table 12.3.3. Number of neighbours,  $N$ , and interatomic distances calculated for centrosymmetric and non-centrosymmetric structures of a hypothetical Ni-saturated, Ni-substituted montmorillonite using chemistry reported by Dähn et al. (2003) for the montmorillonite STx-1 and unit cell parameters (as determined by XRD) of  $a = 518$  pm,  $b = 989$  pm, and assuming  $c^* = 967$  pm (collapsed interlayer). Chemistry\* and symmetry† were input into TKATOMS (Ravel, 1999) enabling scattering paths to be determined by FEFF (Rehr, 2003). Only single scattering events were taken to determine  $R_{\text{eff}}$  in IFEFFIT (Newville, 2003)

	Centrosymmetric (c2/m)		Non-centrosymmetric (c2)	
	$N$	$R_{\text{eff}}$ (pm)	$N$	$R_{\text{eff}}$ (pm)
Ni...O <sub>1</sub>	6	201 (2), 204 (2), 213 (2)	6	185 (2), 198 (2), 226 (2)
Ni...Oct <sub>1</sub>	3	307 (2), 330 (1)	3	307 (2), 329 (1)
Ni...Tet <sub>1</sub>	4	324(2), 331 (2)	4	244 (2), 389 (2)
Ni...O <sub>2</sub>	4	346 (2), 368 (2)	2	325
Ni...O <sub>3</sub>	6	393 (2), 403 (2), 406 (2)	4	353 (2), 378 (2)
Ni...O <sub>4</sub>	8	4.21 (2), 457 (2), 462 (2), 463 (2)	6	396 (2), 426 (2), 467 (2)
Ni...Tet <sub>2</sub>	4	445 (2), 467 (2)	4	532 (4)
Ni...Int	2	516	2	534
Ni...Oct <sub>2</sub>	2	518	2	518
Ni...Tet <sub>3</sub>	8	534 (2), 557 (2), 569 (2), 578 (2)	4	532
Ni...Oct <sub>3</sub>	4	558	4	558

\*Al and Mg concentrations were combined for calculations. Ni was assumed to occupy 10% of M2 sites.

†Al was taken at the origin of an M2 site for both c2 and c2/m symmetry.

#### *Ni Substitution in Montmorillonite Using the Hofmann–Klemen Effect*

On heating Ni<sup>2+</sup>-saturated Camp Bertaux montmorillonite at 300 °C, Muller et al. (1997) observed changes in the Ni K EXAFS spectra consistent with the formation of Ni...M (M = Fe, Al, Mg) shells at ~290 pm from the absorber (Fig. 12.3.11A). Increases in the  $b$  parameter ( $d(06-33)$  diffraction peak) indicate that interlayer Ni<sup>2+</sup> migrates into vacant octahedral sites, presumably those closest to sites of Mg<sup>2+</sup> substitution where octahedral charge is located. The extraordinary amplitude of this new shell in the EXAFS spectra clearly relates to the close proximity of Fe<sup>3+</sup> to the substituted Ni<sup>2+</sup> (recall the  $\pi$ -difference in phase-shift between heavy and light atoms at similar interatomic distances). Muller et al. (1997) interpreted this finding in terms of the preferential migration of Ni<sup>2+</sup> into vacant M2 (*cis*) octahedra between Mg<sup>2+</sup> and pairs of Fe<sup>3+</sup> octahedra. From changes in the OH bending region of the IR spectrum they further deduced that Fe–Mg clustering (Fig. 12.3.11B) occurred within the octahedral sheet of the montmorillonite.

The IR spectrum of Camp Bertaux montmorillonite showed a band near 800 cm<sup>-1</sup>, assigned by Muller et al. (1997) to OH bending mode of pairs of OH-sharing octahedral Fe (FeFe-OH). However, Gates (2005) attributed bands at 790–800 cm<sup>-1</sup> in the IR spectra of 32 dioctahedral smectites (including Wyoming



montmorillonites) containing between 0 and 4  $^{56}\text{Fe}$  per unit cell, to FeMg-OH indicating that OH sharing between Fe-Mg pairs is common. Since the chemical composition and IR spectrum of Camp Bertaux montmorillonite are not dissimilar from those of Wyoming montmorillonite, the OH bending band near  $800\text{ cm}^{-1}$  in the IR spectrum of Muller et al. (1997) should probably be assigned to FeMg-OH. The octahedral cation distributions in Camp Bertaux montmorillonite is thus likely to look like that shown in Fig. 12.3.11C with Fe-Mg pairs as OH-sharing cations. This model is consistent with the EXAFS analysis of Muller et al. (1997), and similar to that proposed by Vantelon et al. (2003) for other comparable smectites.

The pioneering work by Muller et al. (1997) made available to clay science a valuable new approach to quantifying octahedral occupancies in smectites. Although limited to montmorillonites and those smectites where the layer charge is dominantly located in the octahedral sheet, this method serves as a model for future researchers who wish to improve their understanding of the distribution of octahedral cations in dioctahedral smectites.

#### *Octahedral Cation Distribution in Fe-rich Layer Silicates*

The P-EXAFS study by Manceau et al. (1990a) on the distribution of Fe and Mg in the octahedral sheet of biotite indicated that Fe-Mg clustering is also common among biotites, in agreement with NMR data (Sanz and Stone, 1983). However, P-EXAFS can provide additional information that is not attainable by NMR. The amplitudes and phases of the Fe...M<sub>1</sub> shell contribution in the reverse FT of Fe K EXAFS spectra are nearly identical for biotite minerals with widely differing octahedral Fe/Mg ratios. This would indicate that in biotites the local environment around Fe is the same regardless of chemical composition. In other words, Fe and Mg are not randomly distributed (Manceau, 1990; Dyar et al., 2001).

Using powder XRD, Manceau et al. (2000a) showed that the octahedral sheets of nontronite were *trans*-vacant (centrosymmetric) within 5% error. By assuming complete centrosymmetric layer structures, the calculated (DVLS-FEFF) partial P-EXAFS spectra were in excellent agreement with those extracted from experimental spectra. A recent EXAFS study also indicated that a centrosymmetric layer structure for the ferruginous smectite, SWa-1, was appropriate (Vantelon et al., 2003).

P-EXAFS spectra indicated that the distribution of octahedral cations in SWa-1 was random with respect to Fe...Fe and Fe...(Al,Mg) cation proximities (Manceau et al., 2000a). This contrasted with probability determinations by Madejová et al. (1994) using IR spectroscopy. They indicated that Fe...Fe and Al...Mg pairings were more likely at the expense of Fe...Al and Fe...Mg pairings than would be allowed by simple random distribution. In a centrosymmetric structure, the OH stretching and bending bands (in the IR spectra) preferentially probe octahedral cation pairing along the *b* cell dimension, whereas all directions within the octahedral plane are probed by EXAFS. The EXAFS data (Manceau et al. 2000a) can be reconciled with IR data (Madejová et al., 1994) by arranging the cations in such a



way that the octahedral chemical composition, IR absorbances and EXAFS data are satisfied (Fig. 12.3.12).

#### *Octahedral Cation Distributions in Fe-poor Smectites*

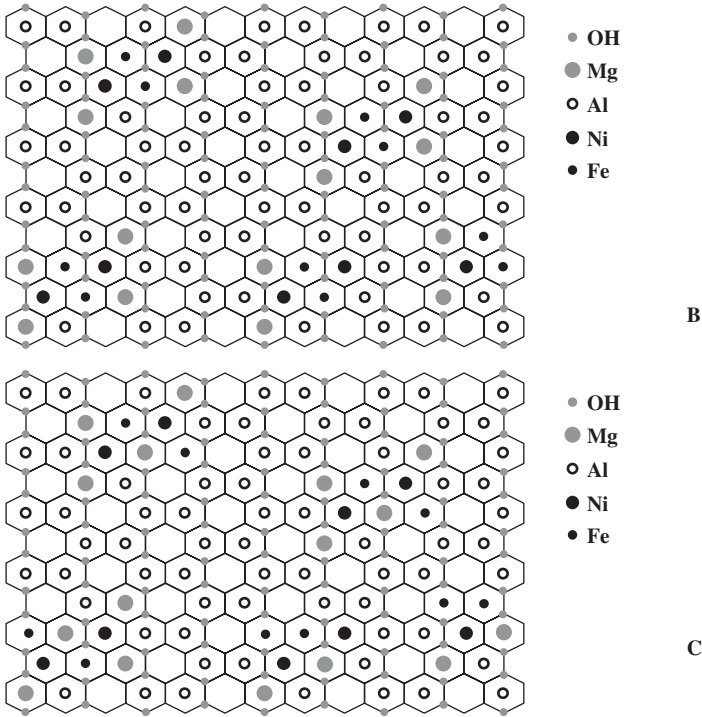
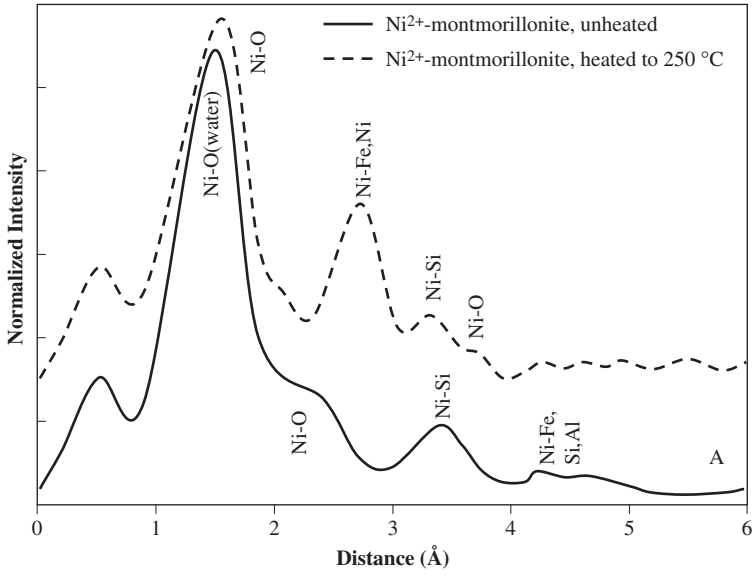
Vantelon et al. (2001, 2003) applied IR and powder Fe K EXAFS to the study of octahedral occupancy in smectites with Fe contents ranging from  $\sim 0.1$  to  $\sim 0.6$  atoms per  $\text{O}_2(\text{OH})_4$ . In order to acceptably fit their EXAFS data, they used *cis*-vacant (non-centrosymmetric) octahedral sheets for all Fe-poor smectite samples (Table 12.3.3).

The results (Vantelon et al., 2003) would suggest a strong departure from random distribution of cation ordering within the octahedral sheet. On the basis of their EXAFS spectra the smectites may be classified into four distinct groups in agreement with IR (Vantelon et al., 2001) and a host of previous analyses (e.g., Güven, 1988). For Wyoming montmorillonites (SWy-1 and SWy-2) the octahedral cation distribution indicated Fe–Fe avoidance. For the other smectites, the distribution indicated varying degrees of Fe clustering, but not necessarily as OH-sharing pairs (as inferred from IR). The FTs of the  $k^3$  weighted Fe K EXAFS spectra revealed a splitting of the second peak between 220 and 350 pm (Fig. 12.3.13). The FEFF-modelled EXAFS spectra (Vantelon et al., 2003) showed that splitting of the first cation shell was due to the presence of octahedral Al. Thus, splitting is strongly suppressed for octahedral arrays where each  $\text{Fe}^{3+}$  has as neighbours on average 2 other  $\text{Fe}^{3+}$  and 1  $\text{Al}^{3+}$  (or  $\text{Mg}^{2+}$ ) cations, as for the ferruginous smectite SWa-1. With increasing  $\text{Al}^{3+}$  and  $\text{Mg}^{2+}$  content the splitting increases, with a shoulder growing on the shorter  $R^*$  side of the  $\text{Fe}\dots\text{M}_1$  shell (Fig. 12.3.14). This splitting is a result of interference from the  $\pi$ -phase difference between light (Mg, Al) and heavy (Fe) backscattering atoms (Fig. 12.3.5 and Section 12.3.1E).

The models proposed by Vantelon et al. (2003) for the distribution of cations in the octahedral sheets of Fe-poor smectites, are in general agreement with previous studies indicating clustering of certain cations in smectites (Decarreau et al., 1987; Muller et al., 1997). However, since FeMg–OH bands occur in the IR spectra of many smectites, including Wyoming (SWy-2) (Madejová et al., 1994) and Arizona (SAz-1) (Gates, 2005) montmorillonites, the models of Vantelon et al. (2003) appear to neglect OH-sharing Fe–Mg octahedra. In Fig. 12.3.15, the octahedral cation

---

Fig. 12.3.11. (A) Powder Ni K EXAFS spectra of Ni-saturated Camp Bertaux montmorillonite before and after heating to 250 °C, redrawn from Muller et al. (1997). Labels for atomic shells from interlayer (unheated) or octahedral (heated) Ni derived from TkATOMS and FEFF scattering calculations of montmorillonite with chemistry reported by Muller et al. (1997). (B) Two-dimensional cation distribution in the octahedral sheet of Camp Bertaux montmorillonite based on Muller et al. (1997). (C) Rearrangement of the octahedral cation array based on re-assignment of the IR band near  $800\text{ cm}^{-1}$  as FeMg–OH bending (Gates, 2004).



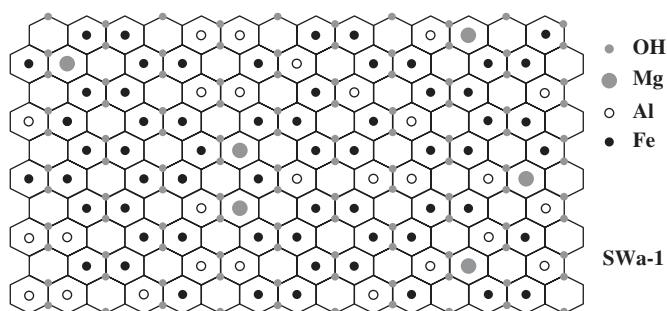


Fig. 12.3.12. Model for the two-dimensional cation distribution in the octahedral sheet of SWa-1, based on Manceau et al. (2000a), but modified using updated chemical and IR data (Gates et al., 2002; Gates, 2005).

distributions, deduced from EXAFS analysis (Vantelon et al., 2003), were modified by taking the IR data into account (Gates, 2004).

Insightful studies such as those by Vantelon et al. (2003) have the potential to provide important information on the variety of structures associated with smectites that may be used to advantage in nanotechnology or other industrial or environmental applications. An obvious and rich area of study is to extend such analyses (incorporating P-EXAFS techniques) to smectites with compositions intermediate between SWy-2 (~5% Fe<sub>2</sub>O<sub>3</sub>) and SWa-1 (~25% Fe<sub>2</sub>O<sub>3</sub>), and to correlate octahedral compositions with geochemical information on formation and weathering of smectites.

### 12.3.3. ORIENTATION OF INTERCALATED ORGANIC MOLECULES

Only limited use was made of synchrotron-based techniques to study the orientation of intercalated organic species in layer silicates, and all analyses were carried out with micas or related minerals (Hähner et al. 1996a, 1996b; Lin et al., 1997; Fischer et al., 1998; Brovelli et al., 1999; Fenter and Sturchio, 1999). In majority of the cases, the alkyl and aromatic groups of organic molecules are oriented at high angles with respect to the interlayer surface (Bedzyk and Cheng, 2002; Fenter, 2002). This is partly due to the high (negative) layer charge, and partly to co-sorption of the organic cation–inorganic anion (in the case of alkylammonium halides), giving rise to a high packing density (Slade and Gates, 2004a).

Brovelli et al. (1999) used polarised C K NEXAFS spectroscopy to determine the orientation of monolayers of octadecyltrimethylammonium (ODTMA) and dioctadecyldimethylammonium (DODMA) cations on the external surface of mica crystals (the layer charge,  $X$ , was unspecified but assumed to be  $2e^-$  per  $O_{20}(OH)_4$ ). For DODMA, a well-ordered self-assembled monolayer was observed with the alkyl

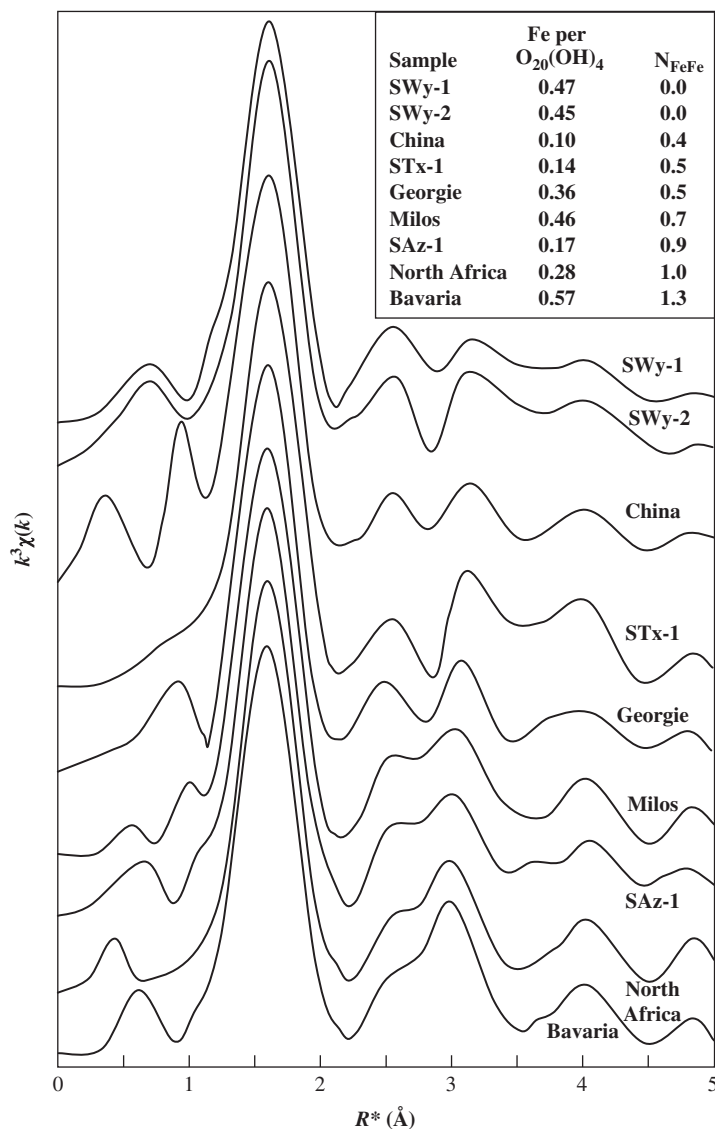


Fig. 12.3.13. Fourier transforms of  $k^3$  weighted Fe K EXAFS spectra of Fe-bearing dioctahedral smectites. Inset: the number of Fe atoms per  $\text{O}_{20}(\text{OH})_4$  reported by Vantelon et al. (2003) for each sample and the number of Fe neighbours in the Fe...M<sub>1</sub> shell ( $N_{\text{FeFe}}$ ) determined by least squares FEFF analysis. Modified and redrawn from Vantelon et al. (2003).

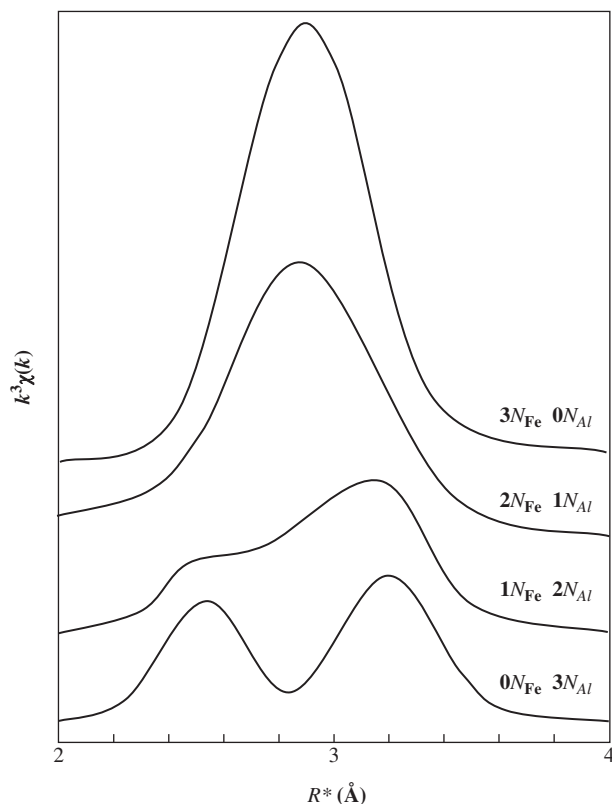


Fig. 12.3.14. Fourier transforms calculated from FEFF showing the Fe...M<sub>1</sub> shell of smectites in which the first cation shell is varied between Fe and Al. Non-centrosymmetric structure assumed for  $N_{\text{Fe}} = 0$ ,  $N_{\text{Al}} = 3$  and  $N_{\text{Fe}} = 1$ ,  $N_{\text{Al}} = 2$  shells; centrosymmetric structure assumed for  $N_{\text{Fe}} = 2$ ,  $N_{\text{Al}} = 1$  and  $N_{\text{Fe}} = 3$ ,  $N_{\text{Al}} = 0$  shells. Fe...Fe and Fe...Al interatomic distances were held constant at  $d = 307$  pm and  $d = 301$  pm, respectively.

chain standing at an average angle of  $52^\circ$  with respect to the layer plane. In the case of ODTMA, the invariance in NEXAFS amplitude with respect to measurement angle was interpreted in terms of complete disorder of the alkyl chain, although the opposite possibility of perfect order with a tilt angle at  $54.7^\circ$  could not be ruled out.

The difference in orientation between the di- and mono-alkyl ammonium ions was probably a result of the packing order and density of alkyl chains on the external mica surface with DODMA having twice the chain density per formula unit than ODTMA. Given that the layer charge of mica can be nearly twice that of low-charge vermiculites, these results are not surprising. In the case of intercalated hexadecyltrimethylammonium (HDTMA) in vermiculite ( $X = 1.23$  and  $1.5e^-$ ) the alkyl chains on

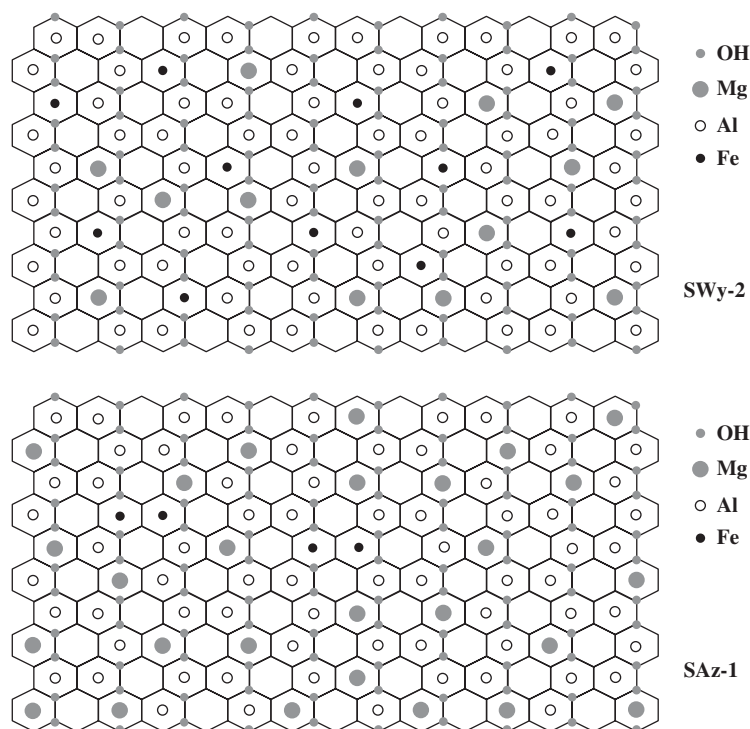


Fig. 12.3.15. Models for the two-dimensional distribution of cations in the octahedral sheet of montmorillonites SWy-2 and SAZ-1 based on the XAFS analyses of Vantelon et al. (2003), but modified using chemical and IR data (Gates et al., 2002; Gates, 2004).

opposing layers will protrude into the interlayer space, doubling the chain packing density as compared with a single surface (Slade and Gates, 2004b). Using scaled models of intercalated HDTMA-vermiculites based on powder and single-crystal X-ray transmission diffraction data, Slade and Gates (2004b) deduced an angle of repose of about  $50^\circ$ . By analogy the octadecyl chains (of ODTMA) on the external surfaces of mica (Brovelli et al., 1999) might have a highly close-packed two-dimensional order with the chains making an angle of  $54.7^\circ$  to the surface. Slade and Gates (2004b) also found that at loadings satisfying the vermiculite layer charge, HDTMA assembled into a  $3a \times b$  super cell commensurate with the dimensions of the silicate surface. When uptake of HDTMA-Br was in excess of the layer charge, the alkyl tails of the HDTMA-Br ion pairs caused closest packing and rotation, destroying the commensurate structure, although transmission diffraction still indicated a highly ordered organic interlayer structure. Obviously, this is a potentially fruitful area of research with implications for nanotechnology and self-assembly, and for which synchrotron-based techniques will be very useful.

Lin et al. (1997) studied the location of  $\text{Br}^-$  counterions sorbed during the self-assembly of organic mono- and multi-layers on Mo/Si surfaces, using X-ray standing wave techniques. The standing wave coherence indicated a narrow distribution of positions for the  $\text{Br}^-$  anions, located about 1 nm above the surface. These inner  $\text{Br}^-$  positions remained unchanged when multilayers of organic compounds were sorbed, and the distances from the surface of additional layers of  $\text{Br}^-$  were found to be consistent with the distances between positively charged nitro groups of the organic molecules (bromopropyl trichlorosilane derivatives). These results strongly suggest that self-assembly produces ordered superlattice structures, as Slade and Gates (2004b) observed for HDTMA-vermiculites. Sorption of the halide anion along with the organic cation within the structures of organo-clays clearly influence many of their practical applications, as shown by the thermal stability of organo-clay complexes (Davis et al., 2004).

Finally, the studies by Fisher et al. (1998) and Hähner et al. (1996b) provided information on the attachment of dye molecules to mineral surfaces. Using C and N K NEXAFS Hähner et al. (1996b) showed that the fused aromatic ring plane of methylene blue resides at steep angles ( $65^\circ$ – $70^\circ$ ) with respect to the mica surface. Fischer et al. (1998) observed similarly for crystal violet and malachite green. These results indicate that the specific surface areas of smectites, determined by sorption of methylene blue, are overestimated if the dye is assumed to lie with its aromatic rings flat to the silicate surface. The steep angle of inclination may be due to the high packing density of methylene blue on high-charge micas. Visible spectroscopic studies (Bujdák and Komadel, 1997; Bujdák et al., 2001) showed that the interaction of methylene blue molecules with reduced-charge smectites (with a layer charge  $<0.25$  that of micas) is more complex. When the layer charge is very low, methylene blue is intercalated as oligomers by van der Waals interactions with a residence time proportional to layer charge. Eventually these oligomers are protonated and degrade to isolated monomers at the surface. A steeply inclined orientation of the oligomers, with the aromatic rings lying parallel to one another, would favour dye–dye electron transfer.

#### 12.3.4. SPATIAL RESOLUTION WITH MICROPROBE XAFS

Micro-XAFS ( $\mu$ -XAFS, or specific applications such as  $\mu$ -XRF,  $\mu$ -EXAFS,  $\mu$ -XANES or  $\mu$ -XRD) can now achieve spatial resolution of  $<1\ \mu\text{m}^2$  with respect to chemical interactions between metal sorbates on minerals (Bajt et al., 1993, 1994, 1995; Hunter and Bertsch, 1998; Manceau et al., 2002a), plant material (Schulze et al., 1995a, 1995b; Punshon et al., 2003) and animal material (Hunter et al., 1997). Spatially resolved XRF studies showed that the distribution of trace metals at mineral surfaces influences their incorporation during crystallisation (Hunter and Bertsch, 1998; Bertsch and Hunter, 2001; Manceau et al., 2002a). Trace metals also influence mineral formation during pedogenesis (Manceau et al., 2002b;

Strawn et al., 2002). The reviews by Schulze et al. (1999), Bertsch and Hunter (2001), Fenter et al. (2002) and Hirshchmugl (2002) provide excellent background on the various applications, as well as the pros and cons, of synchrotron-based microprobe XAFS, X-ray and infrared spectromicroscopy.

### 12.3.5. XAFS STUDIES OF REACTIVITY OF CLAYS AND CLAY MINERALS

Synchrotron-based XAFS made an important contribution to environmental science in the past 20 years because of its ability to assess structural, compositional and reaction mechanisms under *in situ* conditions. Such applications include the study of phosphates (Hesterberg et al., 1999) or biogenic silica (Gehlen et al., 2002). Because the EXAFS phenomenon occurs at a much faster time-scale than many processes such as diffusion, exchange, sorption, precipitation and even electron transfer, EXAFS can provide nearly instantaneous ‘snapshots’ of these reactions, especially those involving chemically unstable intermediate minerals. Recent applications include assessing the structure of hydrated mineral surfaces (Eng et al., 2000), and that of the diffuse electric double layer (Sturchio et al., 1997). Studies of the sorption of heavy metals by phyllosilicates are summarised in Table 12.3.4. The interested reader is referred to Hayes and Katz (1991), Schulze et al. (1999) and Fenter et al. (2002) for comprehensive reviews on the application of various synchrotron-based techniques (fluorescence, reflectivity, etc.) to study the reactivity of minerals and mineral surfaces.

Table 12.3.4 shows that the application of P-EXAFS to the sorption of various metals by smectites provided an insight into the types of complexes formed. The examples described below illustrate that unambiguous interpretation of XAFS experiments is very difficult. They also show the importance of a solid understanding of the mineral phase involved.

#### *A. Exchange/Sorption Reactions at the Smectite–Water Interface*

The terms ‘outer-sphere’ (OS) and ‘inner-sphere’ (IS) are often used in the non-clay mineral literature to describe two distinctly different sorption mechanisms. OS implies an indirect electrostatic bonding where a coordination sphere surrounds the sorbed species that is not directly bound to the surface other than by hydrogen bonding or electrostatic attraction. Hydrated exchangeable cations occupying interlayer sites in smectites are examples of OS sorption complexes. Although the exchangeable cations have more affinity for the surface than the diffuse swarm of ions in the electric double layer, both are considered OS sorption complexes because the interaction is electrostatic. An IS sorption complex is one where direct coordination bonding exists between the sorbed species and the surface, usually but not necessarily through a surface ligand. The sorption of phosphate or citrate at the



Table 12.3.4. Summary of metals and metalloid ion sorption complexes at the phyllosilicate/solution interface studied by XAFS spectroscopy. Individual references should be consulted for exact conditions of pH, ionic strength, metal concentration, surface coverage and other experimental variables. See [Brown and Sturchio \(2002\)](#) for a more complete listing of sorption mechanisms involving related minerals

Metal	Layer silicate	Complex reported	Reference
Co(II)	Kaolinite	IS edge sites	<a href="#">Charlet and Manceau (1994)</a> <a href="#">O'Day et al. (1994a, 1994b)</a> <a href="#">Chen and Hayes (1999)</a>
		IS multinuclear, bidentate	
	Illite	OS low pH charge sites	<a href="#">Chen and Hayes (1999)</a> , <a href="#">Thompson et al. (1999, 2000)</a> <a href="#">Chen and Hayes (1999)</a>
		Co(II)Al LDH precipitate	
		OS low pH charge sites	
	Hectorite	Co(II)Al LDH precipitate	<a href="#">Papelis and Hayes (1996)</a> , <a href="#">Chen and Hayes (1999)</a> <a href="#">Chen and Hayes (1999)</a> <a href="#">Schlegel et al. (1998, 1999a, 1999b)</a>
		OS low pH charge sites	
Ni(II)	Montmorillonite	Co(II)Al LDH precipitate	<a href="#">Papelis and Hayes (1996)</a>
		IS edge sites	
	Sepiolite	OS low pH, charge sites	<a href="#">Fukushima and Okomoto (1987)</a> <a href="#">Manceau and Decarreau (1988)</a> , <a href="#">Charlet and Manceau (1994)</a>
		IS polynuclear (high pH)	
		Co(II)Al LDH precipitate	
Ni(II)	Kaolinite	IS exchange site	<a href="#">Eick and Fendorf (1998)</a> <a href="#">Scheidegger et al. (1996b, 1997, 1998)</a> , <a href="#">Elzinga and Sparks (1999)</a> , <a href="#">Ford et al. (1999b)</a> , <a href="#">Scheinost and Sparks (2000)</a> , <a href="#">Scheckel et al. (2000)</a>
		IS edge site	

(continued on next page)

Table 12.3.4. (*Continued*)

Metal	Layer silicate	Complex reported	Reference
	Montmorillonite	Ni(II)Al LDH precipitate	Scheidegger et al. (1996, 1997, 1998)
		IS edge sites	Elzinga and Sparks (1999), Dähn et al. (2001, 2002b, 2003)
	Pyrophyllite Smectite mix	Ni(II)Al LDH precipitate & IS edge sites	Elzinga and Sparks (1999)
	Talc	$\alpha$ -Ni(OH) <sub>2</sub> precipitate	Scheinost and Sparks (2000), Scheckel et al. (2000)
	Soil clay	Ni(II)Al LDH precipitate	Roberts et al. (1999)
Cu(II)	Muscovite	IS at defects	Farquhar et al. (1996, 1997)
	Biotite	OS and IS	Farquhar et al. (1997)
	Montmorillonite	OS & IS edge sites monodentate	Morton et al. (2001)
Zn(II)	Pyrophyllite	Zn(II)Al LDH precipitate	Ford and Sparks (2000)
	Hectorite	IS edge sites	Manceau et al. (2000c), Schlegel et al. (2001a, 2001b)
		OS exchange sites	Schlegel et al. (2001b)
As(III)	Kaolinite	Oxidation to As(V)	Foster et al. (1998b)
Sr(II)	Kaolinite	OS/IS edge sites (low concentration)	Chen et al. (1998), Sahai et al. (2000), O'Day et al. (2000b), Parkman et al. (1998)
	Illite	OS	Chen et al. (1998), Chen and Hayes (1999)
	Hectorite	OS	Chen et al. (1998), Chen and Hayes (1999)
	Montmorillonite	OS	Chen et al. (1998), Chen and Hayes (1999)

*(continued on next page)*

Table 12.3.4. (Continued)

Metal	Layer silicate	Complex reported	Reference
Cd(II)	Muscovite	OS	Farquhar et al. (1997)
	Biotite	OS, IS	Farquhar et al. (1997)
I(-I)	Biotite	IS ( $\text{IO}_3^-$ sorbed)	Fuhrmann et al. (1998)
Cs(I)	Montmorillonite	OS hydrated, interlayer	Kemner et al. (1997)
	Illite	OS dehydrated, interlayer	Kemner et al. (1997)
	Phlogopite	OS dehydrated, interlayer	Kemner et al. (1997)
Pb(II)	Montmorillonite	OS low I, pH < 6.5 OS/IS high I, pH > 6.5	Strawn and Sparks (1999)
Th(IV)	Montmorillonite	IS bidentate (low concentration) $\text{Th}(\text{OH})_2$ precipitate (high concentration)	Dähn et al. (2002a)
U(VI)	Kaolinite	IS multiple sites	Thompson et al. (1998)]
	Montmorillonite	OS interlayer (low pH) IS neutral pH	Sylwester et al. (2000a, 2000b)
	Hydrobiotite	OS interlayer, IS when dry	Hudson et al. (1999)
	Vermiculite	OS interlayer, IS when dry	Hudson et al. (1999)
	Muscovite	U(VI) hydroxide precipitate	Moyes et al. (2000)

broken edges of smectite particles would be an example of an IS sorption complex since the anion forms a coordination bond with one or more oxygen atoms exposed at the octahedral and tetrahedral edge site. IS sorption complexes can occur as isolated units (mononuclear) or in clusters (multinuclear) as with polymers. IS complexes can be mono-, bi-, tri-, tetra- or multidentate, implying the formation of 1, 2, 3, 4 or more bonds, respectively, connecting the sorbed species with the surface.

Two other variants of OS and IS exist (i) 'fixed' cations in the (collapsed) interlayers of illites, micas, and some smectites are considered to be OS as the forces holding the cation are electrostatic and physical in nature, and not covalent, even though the fixed cation lost its waters of hydration; and (ii) layer substituted cations which enter the structure either by exchange, diffusion or coprecipitation. Layer substitution is considered different from simple IS sorption as it generally involves multidentate bonding.

Table 12.3.4 illustrates that sorption complexes formed by transition metals at smectite surfaces are highly dependent on experimental conditions. Generalisations to conditions differing strongly from those reported should be made with care, but trends can be discerned. For example, monovalent (e.g.,  $\text{Cs}^+$ ) and certain divalent cations ( $\text{Co}^{2+}$ ,  $\text{Cd}^{2+}$ ,  $\text{Sr}^{2+}$ ) form OS complexes in the interlayers under low pH or low ionic strength (Papelis and Hayes, 1996; Farquhar et al., 1997; Kemner et al., 1997; Chen and Hayes, 1999; Strawn and Sparks, 1999). The same divalent cations may form IS sorption complexes at clay mineral edges under high pH or ionic strength conditions (Papelis and Hayes, 1996; Farquhar et al., 1997; Kemner et al., 1997; Schlegel et al., 1999a, 1999b; Strawn and Sparks, 1999). Other divalent cations, such as  $\text{Cu}^{2+}$  and  $\text{Zn}^{2+}$  appear to form mostly IS sorption complexes, but were shown to sorb as OS complexes for a short time (Farquhar et al., 1997; Morton et al., 2001; Schlegel et al., 2001a, 2001b). Still other divalent cations such as  $\text{Ni}^{2+}$  only appear to form IS sorption complexes, regardless of pH and ionic strength. Indeed, these metal ions also react strongly with layer silicates that have no permanent (pH-independent) charge (Scheidegger et al., 1996a, 1996b, 1997, 1998). Finally,  $\text{Th}^{2+}$  was shown to be IS at low electrolyte concentrations, but OS at high electrolyte concentrations (Dähn et al., 2002b).

Interestingly, these same metals and metaloids behave differently with respect to other mineral surfaces from what was described above for smectites. Thus, the following divalent metals generally form isolated IS complexes at low concentrations, but multinuclear IS complexes at higher sorption densities: Co(II) (Chisholm-Brause et al., 1989a, 1990a, 1991; Towle et al., 1995, 1999a, 1999b), Pb(II) (Chisholm-Brause et al., 1989b, 1990b; Roe et al., 1991; Trainor et al., 2002; Bargar et al., 2004), Cu(II) (Weesner and Bleam, 1997; Xia et al., 1997; Cheah et al., 1998, 1999, 2000; Bochatay et al., 1997) and Zn(II) (Trainor et al., 1999; Trivedi et al. 2001a, 2001b; Roberts et al., 2003). The reasons for these differences in sorption complexes are probably as varied as the number of studies. However, it appears that the greater the tendency for a metal or metaloid to undergo hydrolysis, the greater its tendency to form IS sorption complexes. Metal hydrolysis reactions are strongly dependent on pH, thus

the formation of sorption complexes is sensitive to pH. The following two examples of XAFS studies of hydrolysing and non-hydrolysing cations at the surfaces of smectite further illustrate the complexity of OS or IS sorption.

In an EXAFS study of Cs–Ca competition at exchange sites on montmorillonite (SWy-1), illite (Silver Hill) and phlogopite mica, [Kemner et al. \(1997\)](#) found that at Cs loadings of 100% of the cation exchange capacity (CEC), Cs L EXAFS spectra showed limited long-range order. On the other hand, at low Cs loadings (e.g., 10% CEC), the Cs environment showed strong long-range order up to 600 pm. The 10% CEC loadings gave similar FT amplitudes of the atomic shells for illite and mica, but 3–4 times less intense for montmorillonite. The Cs L EXAFS FT for montmorillonite with 10% CEC Cs also showed a shift of the FT peaks to higher  $R^*$ . These observations were interpreted in terms of Cs occupying interlayer sites for which the extent of interlayer collapse increases in the sequence montmorillonite > illite > mica. Although the authors did not venture beyond that explanation, it seems reasonable to suggest that Cs occupies hydrated OS coordination environments in the interlayers of hydrated montmorillonite, but dehydrated OS (or fixed interlayer) sites in illite and mica. (Note that [Brown and Sturchio \(2002\)](#) preferred to label fixed interlayer sorption as IS, but in reality, the attraction is electrostatic and the immobilisation of the cation between the smectitic layers is due primarily to steric hindrance.)

What else might the Cs L EXAFS data tell us? Recall that both illite and mica have a higher total layer charge as well as considerable  $\text{Al}^{3+}$  for  $\text{Si}^{4+}$  substitution in the tetrahedral sheets as compared with montmorillonite. Thus, the enhanced structural order of Cs at low CEC coverage, observed by Cs L EXAFS, is a function of the probability of exchangeable Cs occurring near sites of tetrahedral substitution, where a local site specificity may exist. Comparison of the layer charges (montmorillonite  $X \approx 0.75$  about 25% of which is in the tetrahedral sheet; illite  $X \approx 1.5$  of which 67% is tetrahedral; mica  $X \approx 2$  of which 67% is tetrahedral) indicates that tetrahedral-to-total charge ratios agree well with the reported amplitude differences in the Cs L EXAFS spectra ([Kemner et al., 1997](#)). The greater long-range order of Cs in illite and mica are due to Cs residing between two adjacent layers within a distinct site, probably above the ditrigonal cavity near sites of  $\text{Al}^{3+}$  substitution in the tetrahedral sheet. With an anhydrous radius of 196 pm, Cs can partially sit within the ditrigonal cavities of dioctahedral smectites ([Güven, 1988](#)). The high layer charge density, and hence the high field strength at the basal surfaces, of illite and mica cause dehydration of most monovalent cations occupying any interlayer exchange sites, and ultimately interlayer collapse. Thus, the Cs L EXAFS results of [Kemner et al. \(1997\)](#) clearly differentiate between a hydrated (in montmorillonite) and a dehydrated (in illite and mica) exchangeable cation at low CEC coverage. This interpretation is in agreement with previous NMR interpretations ([Weiss et al., 1990](#)). A worthwhile extension would be to study the interlayer structures of  $\text{La}^{3+}$ - or  $\text{Ba}^{2+}$ -smectites, the structures of which, at least for vermiculites, were well characterised by conventional powder X-ray transmission techniques ([Telleria et al., 1977](#); [Slade et al., 1998](#)).

As a second example, Dähn et al. (2002a) studied the sorption of Th by montmorillonite at under- ( $10^{-6}$ – $10^{-4}$  M, pH 2–3) and super-saturated ( $10^{-5}$ – $10^{-4}$  M, pH 5) conditions (with respect to  $\text{ThO}_2$ ). They precluded the formation of OS (exchange) complexes by including 0.1 M  $\text{NaClO}_4$ . The Th K EXAFS of the supersaturated Th-montmorillonite most resembled poorly crystalline  $\text{Th}(\text{OH})_4$ , but at under-saturated conditions, their spectral analysis was consistent with the formation of IS edge-sharing bidentate complexes. The analysis clearly showed that (i) IS complexes of Th formed at low electrolyte concentrations with Si making up the neighbouring cation shell at  $R^* \approx 380$ – $390$  pm, and (ii) the Th–Si interatomic distance was consistent with edge-sharing polyhedra. The results were also consistent with those reported by Östols et al. (1997) for the sorption of Th by poorly crystalline Si. The lack of pleochroism, however, implied that Th did not form IS complexes at the smectite surface, and they thus proposed that Th sorption complexes at Si/Al edges were disordered with respect to the montmorillonite surface. They discounted the possibility of Th sorbing to a poorly crystalline  $\text{SiO}_2$  phase because the measured Si release rates were not affected by the addition of Th. However, they did report that soluble Si increased continually throughout the experiment, whereas soluble Al remained constant. This was taken as an indication that silica precipitation was unlikely under the conditions of their study. One source of Si considered by Dähn et al. (2002a) was poorly crystalline  $\text{SiO}_2$ , but it escaped detection by XRD in the bulk montmorillonite (STx-1) used. Therefore, Dähn et al. (2002a) preferred the interpretation that Th formed bidentate, edge-sharing complexes with Si and Al at the edges of montmorillonite that underwent incongruent dissolution. Obviously, further work is required to decipher the ambiguities of Th sorption by montmorillonite.

Of the oxyanions (e.g., As(V), As(III), Se(VI), Se(IV) and U(VI)), only U(VI) sorption by smectite (Chisholm-Brause et al., 1992; Dent et al., 1992; Chisholm-Brause et al., 1994; Peterson et al., 1996; Giaquinta et al., 1997a, 1997b; Sylwester et al., 2000; Ritherdon et al., 2003), hydrobiotite and vermiculite (Hudson et al., 1999), muscovite mica (Moyes et al., 2000) and kaolin (Thompson et al., 1998) was studied. This is because swelling uranyl-clay complexes are potent photo-oxidisers (Suib and Carrado, 1985; Duff et al., 1999). The aqueous uranyl oxyanion ( $\text{UO}_2^{2+}$ ) forms OS complexes (exchangeable cation) at low pH. At pH 5–6, uranyl-hydroxide species begin to form (Toth and Begun, 1981). The hydrolysis of  $\text{UO}_2^{2+}$  at higher pH results in the formation of IS bidentate complexes in the presence of competing ions (Sylwester et al., 2000). At low pH the U L EXAFS spectra of U(VI)-montmorillonite resemble those of aqueous uranyl (Chisholm-Brause et al., 1994; Peterson et al., 1996; Giaquinta et al., 1997a, 1997b; Sylwester et al. 2000), but at higher pH (6.4) the spectra more closely resemble U(VI) sorption complexes on silica or alumina (IS bidentate complex) (Reich et al., 1998; Allard et al., 1999; Sylwester et al., 2000). The composite evidence indicates that U(VI)-surface complexes are commonly formed with montmorillonite and most minerals (Thompson et al., 1997), although Duff et al. (2002) showed that U(VI) sorption by goethite also involved layer substitution

(co-precipitation) as uranate. Uranium-bearing goethites can also be reduced by bacteria to form insoluble U(IV) complexes (Frederickson et al., 2000, 2002).

The general consensus is that oxyanions on oxides dominantly form IS complexes with the bidentate type being the most common (Hayes et al., 1987; Manceau et al., 1992a, 1992b, 1992c; Manceau and Charlet, 1992, 1994; Waychunas et al., 1993, 1995; Manceau, 1995; Foster et al., 1998a; Furrman et al., 1998; Reich et al., 1998; Moyes et al., 2000; Manning et al., 2002). However, the IR study by Peak et al. (1999) shows that sulphate sorption by goethite is OS when the ionic strength is low and the pH is above 6, but both OS and IS occur at higher ionic strengths and lower pH. The proportion of IS to OS complexes formed increases as pH falls and ionic strength rises. Peak et al. (1999) also noted that the spectra of sorbed  $\text{SO}_4^{2-}$  in goethite resemble those of schwertmannite, a ferric hydroxysulphate species, indicating that IS complexes probably predominate.

### *B. Mineral Neoformation Reactions: Smectites as Nucleation Templates*

In studying the kinetics of sorption and precipitation reactions of  $\text{Co}^{2+}$  on hectorite, Schlegel et al. (1998, 1999a, 1999b) found that at near neutral pH and low surface coverage, sorbed Co forms both OS and IS complexes at the edges of the mineral. The proportion of IS complexes increased with reaction time, suggesting that  $\text{Co}^{2+}$  migrated from exchange sites to edge sites during precipitation (Schlegel et al., 1999b). Precipitation of  $\text{Co}^{2+}$  as part of a layer double hydroxide epitaxial on to the edges was confirmed by P-EXAFS (Schlegel et al., 1999a, 1999b). Initially, sorbed IS Co had a greater proportion of Si and Mg neighbours in the first cation ( $\text{Co}\dots\text{M}_1$ ) shell but with time, the number of Co atoms in the  $\text{Co}\dots\text{M}_1$  shell increased. Sorption of Co was also accompanied by  $\text{Mg}^{2+}$  release. Since the reaction ceased when sufficient  $\text{Mg}^{2+}$  had been released, Schlegel et al. (1998, 1999b) proposed incongruent dissolution of the hectorite, at least initially, and that  $\text{Co}^{2+}$  replaced only the  $\text{Mg}^{2+}$  exposed at the edge surface.

A recent Ni K powder and P-EXAFS study of Ni sorption by montmorillonite indicated the neoformation of an Ni phyllosilicate without the addition of soluble Si (Dähn et al., 2002b, 2003). Other workers (d'Espinosa de la Caillerie et al., 1995a, 1995b; Scheidegger et al., 1996a, 1996b, 1997, 1998; Scheckel and Sparks, 2000) observed the formation of an Ni–Al layer double hydroxide during the sorption of  $\text{Ni}^{2+}$  by pyrophyllite, gibbsite and alumina. Recently, Galois et al. (2003) observed that Si was randomly grafted on to trioctahedral Ni clusters. The Ni K EXAFS spectra of montmorillonite, reacted with  $660\text{ }\mu\text{M}$   $\text{Ni}^{2+}$  at pH 8 and ionic strength of  $0.2\text{ M}$   $\text{Ca}(\text{NO}_3)_2$ , showed an Ni-rich precipitate in which Ni (on average) was surrounded by edge-sharing Ni ( $2.6\text{ Ni}$ ,  $d = 308\text{ pm}$ ) and corner-sharing Si ( $4.2\text{ Si}$ ,  $d = 326\text{ pm}$ ). This is consistent with Ni sorbing near edge-exposed Al octahedra (Dähn et al., 2002b). The kinetic study showed that Ni-enriched clusters formed within 1 day, with the high  $\text{Ca}^{2+}$  content ensuring negligible  $\text{Ni}^{2+}$  OS complex formation. The angular dependence of

the P-EXAFS amplitude indicated that the Ni...Al interatomic dimension was in-plane, and those of the Ni...Si were out-of-plane with respect to the smectite. Subsequent reactions with about 20  $\mu\text{M}$   $\text{Ni}^{2+}$  at pH 7.2 and ionic strength of 0.3 M  $\text{Ca}(\text{NO}_3)_2$ , indicated structural parameters of 2 edge-sharing Al ( $d = 300$  pm), 2 corner-sharing Si ( $d = 312$  pm) and 4 other corner-sharing Si ( $d = 326$  pm). The low values of  $N_{\text{Ni...Al}}$  may indicate the absence of octahedral substitution, even after 1 year. These results were consistent with the neoformation of a dioctahedral Ni phyllosilicate at the montmoillonite edges (Dähn et al., 2002b, 2003).

Dähn et al. (2002b, 2003) were unable to account for sufficient dissolved Si for precipitation of phyllosilicates. However, the STx-1 montmorillonite used was likely to contain opal CT (cristobalite–tridamite) as an impurity. Even in the  $<0.1$   $\mu\text{m}$  fraction of STx-1 sufficient opal CT remained as indicated by moderately broad XRD reflection at about 0.409 nm (Gates, 2004, unpublished data). Opal CT could well be the source of sufficient dissolved Si for the precipitation of Ni complexes on STx-1 just as it could be for Th...Si signals in the complexes described above. If so, the addition of Si would not be necessary as it was for hectorite (Schlegel et al., 1998) which is much more soluble than STx-1 under the conditions used. Similarly, Manceau et al. (1999b) showed that a  $\text{Co}^{2+}$  phyllosilicate is neoformed in the presence of quartz.

Research on the neoformation of minerals raises many questions. How does a stable mineral phase (e.g., pyrophyllite) generate sufficient soluble Si to react with sorbed metals? What takes the place of OS-sorbed metals on the exchange complex of smectite when they ‘switch’ to IS? Does the layer charge change? Why should sorption of divalent transition metals at the edges of phyllosilicates result in mineral dissolution? Montmorillonite is generally far more stable than hectorite at  $\text{pH} \leq 8$ . The ability of metals such as  $\text{Cu}^{2+}$ ,  $\text{Ni}^{2+}$ ,  $\text{Al}^{3+}$ , to undergo hydrolysis (Bargar et al., 1997a, 1997b, 1998, 2004) and release of  $\text{H}^+$  is well known. These reactions apparently occur even in well-buffered aqueous systems at pH 7–8 (Hayes and Katz, 1996; Dähn et al., 2002b, 2003; Galois et al., 2003). Protons ( $\text{H}_3\text{O}_{\text{aqueous}}^+$ ) can create an unstable  $\text{H}^+$ -smectite. That is, acid attack on sites of isomorphous substitution in the tetrahedral and octahedral sheets leads to the release of tetrahedral  $\text{Si}^{4+}$ ,  $\text{Al}^{3+}$  and octahedral  $\text{Fe}^{3+}$ ,  $\text{Fe}^{2+}$  and  $\text{Mg}^{2+}$  into solution (Janek and Komadel, 1993, 1998). These metal cations can then participate in precipitation reactions at nucleation sites, probably at the mineral edges (Scheidegger et al., 1996a, 1996b, 1997, 1998; Scheinost et al., 1999; Schlegel et al., 1999a, 1999b, 2001a, 2001b; Dähn et al., 2003). Eventually non-hydrolysable cations ( $\text{Mg}^{2+}$ ) released will replace  $\text{H}^+$ ,  $\text{Al}^{3+}$  or other metals on the exchange complex, and ‘auto-transformation’ ceases (Janek and Komadel, 1993). Thus, auto-transformation is initiated by sorbed hydrolysable metals such as  $\text{Ni}^{2+}$ ,  $\text{Zn}^{2+}$  or  $\text{Co}^{2+}$ . Through mineral dissolution, this reaction can supply both the cations necessary to satisfy the exchange complex as well as the soluble Si and other elements needed for the precipitation of the metals into new phases. Whether auto-transformation reactions are responsible for the precipitation of metal (hydr)oxide or phyllosilicate phases is another question altogether. EXAFS



studies would suggest that conventional concepts of low-temperature transformation of clays and clay minerals require rethinking.

### *C. Redox Reactions (Abiotic and Biotic) of Clays and Clay Minerals*

We already mentioned (Section 12.3.2) that the energies at which XAFS absorptions occur are sensitive to the oxidation state of the target element. A number of researchers (Bajt et al., 1994, 1995; Delaney et al., 1996a, 1996b, 1998; Berry et al., 2003; Berry and O'Neill, 2004) used this relationship to estimate the oxidation state of metals in a variety of mineral samples, including primary aluminosilicates and (secondary) clays and clay minerals in soils and sediments. For example, the XANES energies of the Cr K-edge are very sensitive to Cr oxidation state. Sutton et al. (1993) differentiated five valence states of Cr in lunar basalts: Cr[0], Cr[II], Cr[III], Cr[IV] and Cr[VI], using a microprobe. Olivine minerals were dominated by Cr[II] and pyroxenes by Cr[III]. The dominance of Cr(II) indicated that the basalt was crystallised under highly reducing conditions. For a wide range of primary minerals the Fe oxidation state could be reasonably calibrated using the centroid of the Fe pre-edge signal (Bajt et al., 1994). Variations of this technique were used to calibrate XANES spectra for biotite micas (Dyar et al., 2001), amphiboles (Delaney et al., 1996a, 1996b), and silicate glasses (Berry et al., 2003). Interestingly, the calibration curves developed by Dyar et al. (2001) were indistinguishable from those of Bajt et al. (1994) and Delaney et al. (1996a, 1996b), indicating the insensitivity of this technique to gross mineral differences. Gates et al. (1997) found that features of the edge crest were more useful for assessing Fe oxidation states of reduced smectites. Recently, Berry et al. (2003) and Berry and O'Neill (2004) used the derivative of the absorption edge to determine Cr(II)/total Cr ratios in silicate glasses. They indicate that local disorder effects should be considered when analysing a specific class of minerals.

The oxidation states of structural constituents in clays and clay minerals, or the reactions of clays and clay minerals with the surrounding environment, were rarely investigated by XAFS, primarily because of sample handling difficulties. For smectites, such studies were limited to Fe-rich species (Gates et al., 1997; Hunter et al., 1999; Manceau et al., 2000a) although Cr(VI) redox reactions at smectite surfaces were reported (Fendorf, 1995; Brigati et al., 2000; Taylor et al., 2000). Similar reactions of transition metals or metaloids at the surfaces of phyllosilicates (Charlet and Manceau, 1992; Silvester et al., 1995) and (hydr)oxides (Peterson et al., 1996, 1997; Drits et al., 1997, 1998a; Fitts et al., 2000; Kendelewicz et al., 2000; Foster et al., 2002; Tournassat et al., 2002) were also investigated (Table 12.3.4). Aspects of some of these studies will be detailed below.

#### *P-EXAFS Study of Reduced Nontronite Structure*

P-EXAFS analysis of the structures of reduced nontronite showed that in the  $R^*$  300–600 pm region the octahedral sheet differs dramatically from its oxidised or

unaltered counterpart (Manceau et al., 2000b). There was evidence to suggest that on reduction from Fe(III) to Fe(II), Fe atoms migrate from M2 to M1 sites, thereby forming clusters of vacancies and domains of trioctahedral character. The increase to 0.154 nm of the XRD  $d(06-33)$  reflection, and the appearance of an OH stretching vibration near  $3623\text{ cm}^{-1}$  on reduction of  $>90\%$  of the octahedral Fe, were consistent with the formation of trioctahedral domains. The migration of Fe(II) from *cis* to *trans* sites was probably accompanied by dehydroxylation and re-protonation/hydration (see Chapter 8), in a fashion similar to transitions during thermal dehydroxylation of smectite (Drits et al., 1998b).

Reduction of more than 90% of the octahedral Fe(III) resulted in decreased amplitude of the first two shells in the FTs of the Fe K P-EXAFS spectra. Fitting inferred a decrease in the number of oxygen ligands and an increase in the Fe...O<sub>1</sub> interatomic distances (6O at  $d = 201\text{ pm}$  for the oxidised Garfield nontronite as against 5.3O at  $d = 210\text{ pm}$  for the form). Likewise the Fe...Fe<sub>1</sub> parameters changed from 4.5Fe<sub>1</sub> at  $d = 303\text{ pm}$  for the oxidised nontronite to 4.9Fe<sub>1</sub> at  $d = 312\text{ pm}$  for the reduced form. The FT of the reduced nontronite further showed a loss of the Fe...Fe<sub>2</sub> shell near  $R^* \approx 500\text{ pm}$ , but an increase in the Fe...Fe<sub>3</sub> shell near  $R^* \approx 600\text{ pm}$ , compared to the oxidised nontronite. Recall that a focussing effect of co-linear multiple-scattering events can increase amplitudes in this region of the EXAFS spectra of trioctahedral structures. Manceau et al. (2002b) considered that these features were consistent with such an effect.

The reoxidation of reduced nontronites produced materials that were similar to, but not identical with, the unaltered nontronite, indicating that the reaction was not fully reversible, at least following complete reduction of the nontronite (Manceau et al., 2000b). Infrared studies of highly reduced nontronites and ferruginous smectites (Komadel et al., 1995; Fialips et al., 2002a, 2002b) support this conclusion, but other studies with slightly reduced montmorillonite, ferruginous smectite and nontronite (Gates et al., 1996, 1997; Hunter et al., 1999) indicated that the reduction–reoxidation reaction was reversible within the errors of the measurements. Both the total Fe content of the smectite and the absolute level of reduction are apparently important factors affecting the reversibility of the redox reaction (see Chapter 8).

#### *Redox Coupling between Octahedral Fe in Smectites and Sorbed TPB*

Gates et al. (1997) and Hunter et al. (1999) used Fe K XANES and Fe K EXAFS to follow the changes in oxidation state of octahedral Fe in montmorillonite, ferruginous smectite and nontronite during reaction with Na-tetraphenylboron (TPB). Abiotic oxidative degradation of TPB, occurring at Lewis sites within the interlayers, resulted in measurable shifts (1–2 eV) and changes to features in the X-ray absorption edge, indicative of electron transfer to octahedral Fe(III). Analysis of Fe K EXAFS spectra of the TPB-montmorillonite system revealed an increased spread in the Fe...O bond lengths, consistent with reduction of Fe(III) to Fe(II). Further, the kinetics of the  $2e^-$  transfer from TPB to octahedral Fe were closely similar to those determined using wet-chemical techniques to quantify TPB degradation (Hunter and

Bertsch, 1994; Gates et al., 1997; Hunter et al., 1999). Although the Fe(III) content of nontronite is an order of magnitude greater than that of montmorillonite, the total amount of Fe(III) reduced by reaction with TPB was nearly identical. It would therefore appear that the reaction was more efficient in montmorillonite than in nontronite, but this might be because the nontronite particles were dispersed within an Fe-free smectite medium (hectorite). The ordering of Fe(III) within the structure of Wyoming montmorillonite does not seem to limit electron transfer from the interlayer.

#### *Cr(VI) and Cr(III) Redox Reactions at Mineral Surfaces*

Brigatti et al. (2000) used Cr K XANES to show that Cr(VI) was reduced to Cr(III) by a natural Fe(II)-bearing chlorite. Another Cr K XANES study (Taylor et al., 2000) showed that when reduced with dithionite ferruginous smectite mediated the reduction of sorbed Cr(VI) to Cr(III) with a ratio of 3:1 of structural Fe(II) oxidation to sorbed Cr(VI) reduction. Furthermore, their evidence suggested that Cr(VI) probably sorbed within the interlayer of reduced smectite, as the reaction was greater for Na-exchanged than for K-exchanged reduced smectite. The oxidation of Cr(VI) at magnetite surfaces (Peterson et al., 1996, 1997; Kendelewicz et al., 2000) and iron sulphides (Patterson et al., 1997) results in the formation of immobile hydrous Cr(III)Fe oxide phases. An interesting reaction occurs for Cr(III) sorption onto birnessite (Charlet and Manceau, 1993; Silvester et al., 1995). The Cr(III) initially either migrates into the phyllomanganate structure (filling vacancies), or precipitates at the surface, but eventually electron transfer occurs, and the Cr(III) is oxidised to Cr(VI) by Mn(IV) reduction to Mn(II). The Cr(VI) forms  $\text{CrO}_4^{2-}$  at the surfaces, which ultimately is an undesirable product as Cr(VI) is more soluble, mobile and toxic than Cr(III).

#### *Redox Reactions at Oxide and Organic Surfaces*

Abiotic redox reactions of a variety of metals and metaloids on a variety of minerals, e.g., Se(VI) oxidation on Fe oxyhydroxides (Myneni et al., 1997), As(V) oxidation on birnessite (Foster et al., 2002; Manning et al., 2002; Tournessat et al., 2002) and anatase (Foster et al., 1998a), Tc(VII) oxidation on FeS and green rust (Wharton et al., 1999; Bunker et al., 2002) and U(VI) oxidation on FeS (Moyes et al., 2000) and goethite (Duff et al., 2002) were studied since synchrotron radiation became readily available to the geosciences. In nearly all these cases, the redox reaction is associated with the formation of a surface precipitate. The sole exception is U(VI) oxidation at goethite surfaces giving rise to layer substitution or co-precipitation (Duff et al., 2002).

Other electron transfers coupled with lattice substitutions of transition metals in oxides were observed. Sorbed Co(II) migrates into the octahedral vacancies within the structure of phyllomanganates and forms a redox couple with Mn(IV) (Charlet and Manceau, 1993; Manceau et al., 1997). When sufficient Mn(IV) was reduced to Mn(II), the latter is expelled from the crystal lattice. Similar reactions were reported

for Ce(III) and Tl(I) (Bidoglio et al., 1993) on phyllomanganate surfaces. In common with their Co(III) counterparts, complexes of Ce(IV) and Tl(III) are much less soluble and remain as part of the manganate structure.

Several studies were recently conducted on biological systems. Schulze et al. (1995a, 1995b) showed that reactions taking place in the rhizosphere of wheat roots, infected by the take-all fungus, result in the oxidation and precipitation of Mn(IV) at the plant root surfaces. Studies by Templeton et al. (1999, 2003a, 2003b) showed that Pb redox reactions at mineral surfaces can be mediated by microbial biofilms. Tokunaga et al. (1997, 1998) studied Se and Cr redox reactions in soil aggregates mediated by soil microorganisms.

### 12.3.6. XAFS STUDIES OF OTHER CLAY MINERALS

In order to gain a better understanding of the XAFS spectral features of smectites and oxyhydroxides, a host of reference minerals were studied in detail. The accumulated information was thoroughly reviewed elsewhere (Hodgson et al., 1984; Koningsberger and Prins, 1988; Hawthorne, 1988; Decarreau, 1990; Mottana and Burrigato, 1990; Schulze et al., 1999; Bertsch and Hunter, 2001; Fenter et al., 2002).

#### A. Other Layer Silicates

As shown in Table 12.3.4, most XAFS studies of layer silicates (e.g., kaolin, illite, sepiolite, pyrophyllite, talc, vermiculite/hydrobioite) were conducted in conjunction with sorption studies, either as sorbents or reaction products. However, Bugaev et al. (1998) showed that, for model Al-containing compounds having from 4-fold to 12-fold coordination, Al K XANES spectra could be reproduced considering single-, double- and triple-scattering processes on multi-atom chains. They reported that the Al K XANES spectrum of pyrophyllite could be reproduced with excellent agreement with single and linear multiple-scattering processes occurring between atoms of the first ligand shell:  $d(\text{Al}\dots\text{O}) = 2\text{O}$  at 188 pm and 4O at 192 pm. The maximum divergence angle for the multiple-scattering paths was  $\sim 14^\circ$  and the maximum total path length was  $\sim 1800$  pm. Spectral fitting of diasporite ( $\alpha\text{-AlOOH}$ ), gave a similar total path length, but a much smaller divergence angle from linear scattering paths ( $< 4^\circ$ ) with a greater degree of distortion about the Al octahedra ( $d(\text{Al}\dots\text{O}) = 2\text{O}$  at 185, 1O at 186 and 3O at  $\sim 198$  pm) (Bugaev et al., 1998). For kaolinite Bugaev et al. (1998) found an inversion of the amplitude of two peaks associated with octahedral Al compared with other Al-bearing layer silicates (Fig. 12.3.3). This was ascribed to the presence of two distorted Al octahedral sites: site 1  $d(\text{Al}\dots\text{O}) = 2\text{O}$  at 188, 4O at 194 pm and site 2  $d(\text{Al}\dots\text{O}) = 2\text{O}$  at 189 and 4O at 194 pm. The parameters for site 2 octahedra increased the amplitude of the second octahedral Al peak. This illustrates the potential usefulness of XANES (NEXAFS) in identifying and quantifying local structural information in a similar manner as EXAFS.

### *B. Oxides and Oxyhydroxides*

The structures and reactivity of Fe and Mn (hydr)oxides were studied in detail since the availability of synchrotron X-ray sources. Such studies provided tremendous insight into many low-temperature geochemical reactions that take place in soils and sediments. Synchrotron-based XAFS analyses, applied to the condensation of iron oxyhydroxide precipitates from gels (Combes et al., 1986, 1989a, 1990; Hazemann et al., 1992; Manceau and Drits, 1993; Bottero et al., 1994; Ford et al., 1999a), showed that the rate of hydrolysis controls the local structural order beyond the first ligand shell (Charlet and Manceau, 1993). The polymerisation of Fe into clusters is only observed by EXAFS as peaks in the FT near 305 and 345 pm, when the hydrolysis rate exceeds 1OH per 1Fe. The polymeric gels tend to be locally ordered with structures similar to  $\alpha$ -FeOOH (goethite) or  $\beta$ -FeOOH (akaganeite), respectively, if the products are prepared from Fe(III)-nitrate or Fe(III)-chlorite salts. Such local structural order is preserved during the crystallisation and dehydration of the gels (Combes et al., 1989b; Drits et al., 1993; Manceau and Drits, 1993). Synchrotron-based SAXS studies (Bottero et al., 1994) showed that the hydrolysis rates influence crystallite formation and aggregation in (hydr)oxide gels. When the fractal dimension exceeds  $\sim 2$ , aggregate flocculation leads to the formation of HFO or  $\delta$ -FeOOH (ferrioxhyte or 2-line ferrihydrite) precipitates. On further ageing, these precipitates convert into hematite. Similar reactions occur with the Mn (hydr)oxides, although these appear to be more complex (Charlet and Manceau, 1993) because of the existence of a wide variety of Mn oxide polymorphs. The precipitation of Fe gels in the presence of SiO<sub>2</sub> was studied by Waychunas et al. (1999), Doelsch et al. (2000, 2002) and Masion et al. (2001). The studies of Masion et al. (2001) showed that at low hydrolysis rates, Si can hinder the precipitation of Fe(II) gels, but not that of Fe(III) gels, indicating that hydrolysis reactions control both short- and long-range order formation.

XAFS studies of the sorption of metals and metaloids on surfaces of oxides, or their coprecipitation within the structure, provide information on the nature of the reactive sites (e.g., Combes et al., 1992; Bajt et al., 1993; Spadini et al., 1994; Waite et al., 1994; Bargar et al., 1996; Bochatay et al., 1997; Axe et al., 1998, 2000; Collins et al., 1998, 1999; Randal et al., 1998, 1999; Ford et al., 1999b; Manceau et al., 2000c, 2000d; Arai et al., 2001). It is commonly assumed that specific crystallographic faces have specific reactivities and are differentially responsive to sorbing metals/metaloids due to the dynamics of surface potential, metal hydrolysis, surface hydration and steric effects (e.g., Manceau, 1995; Ford et al., 1997a; Ford and Bertsch, 1999; Criscenti and Sverjensky, 2002).

The crystal dimensions of Fe(III) oxides formed in the presence of other metals are affected by the concentration and type of metal impurity (Ford et al., 1997b). However, Manceau et al. (2000c) showed that the bulk structures of two different FeOOH polymorphs strongly influence the types and amounts of sorption complexes formed, at least for weakly hydrolysing metals. The goethite ( $\alpha$ -FeOOH) structure is

composed of chains of double rows of Fe(III) octahedra, in which the octahedra share edges within the chains and corners between chains. The lepidocrocite ( $\gamma$ -FeOOH) structure is composed of chains of double edge-sharing octahedra, but the octahedra share edges between chains rather than corners, as in goethite. Cd K EXAFS clearly shows that at low surface coverage (11–13%) isolated Cd octahedra (Cd...O  $d = 224$ – $225$  pm) share corners (Cd...Fe  $d = 380$ – $390$  pm) and edges (Cd...Fe  $d = 329$  pm) with Fe octahedra in both goethite and lepidocrocite. At high surface coverage, only isolated edge-sharing Cd octahedra (bidentate) were observed in lepidocrocite, and only isolated corner-sharing Cd monodentate octahedra were detected in goethite. Manceau et al. (2000c) suggested that in addition to differences in bonding between chains in these structures, there are differences in the stacking sequences of the anion layers (hexagonal in goethite and cubic in lepidocrocite). The resultant morphological forms (prismatic to acicular in goethite and lath-like in lepidocrocite) influence the sorption complexes formed.

An ongoing controversy concerns the presence of tetrahedral Fe(III) in the structure of many iron (hydr)oxides. Manceau et al. (1990b), Manceau and Drits (1993) and Drits et al. (1993) proposed that the (hydr)oxides of iron, and presumably other metals, were structurally similar in that inter-conversion and mixing of polyhedra could adequately describe the EXAFS spectra. Thus, ferrihydrite was proposed to be a mixture of (i) defect-free goethite-like structure with double chains of edge-sharing octahedra; (ii) defective goethite-like structure, with the proportion of defect sites being higher for 2-line than 6-line ferrihydrite; and (iii) ultra-dispersed hematite grains with scattering domain sizes  $< 2$  nm (Drits et al., 1993). Others related the various features in the XAFS spectra and XRD patterns of ferrihydrite to tetrahedral Fe(III) (Eggleton and Fitzpatrick, 1988; Zhao et al., 1993, 1994).

Whether or not tetrahedrally coordinated Fe(III) exists in ferrihydrite is not simply an academic question. Ferrihydrite readily converts into maghemite when heated, and may constitute a major source of maghemite and goethite in soils (see the review by Jambor and Dutrizac, 1998). Ferrihydrite contains much structural (co-ordinated) water that is readily lost with common laboratory treatments. Such de-watering is important in the conversion of ferrihydrite into goethite or maghemite, and the formation of maghemite from ferrihydrite gives rise to tetrahedral Fe(III) sites. Thus the stoichiometries of ferrihydrite and other poorly crystalline hydr(oxides) are important, especially in determining the amount of 'crystalline' water (Mavrocordatos and Fortin, 2002). The accumulated evidence from XAFS (Calas and Petiau, 1983; Waychunas et al., 1983; Manceau and Combes, 1988; Combes et al., 1989a, 1989b, 1990; Manceau et al., 1990b; Drits et al., 1993; Manceau and Drits, 1993; Waychunas et al., 1993; Bottero et al., 1994; Galois et al., 2001a, 2001b) and photoelectron energy loss spectroscopy (TEM PEELS) (Mavrocordatos and Fortin, 2002) strongly indicate that for oxyhydroxides of Fe in soils and sediments, as well as in mineral and glass phases, tetrahedral coordination of  $\text{Fe}^{3+}$  is the exception rather than the rule.



In nano-size ferrihydrite particles, a significant proportion (up to 30%) of the Fe(III) at the crystallite edges could be coordination under-saturated (CUS) with respect to the oxygen and hydroxyl framework (Zhao et al., 1994). The occurrence of highly distorted octahedra would impact on the amplitude of the XAFS signal (Manceau and Gates, 1997). The bulk Fe atoms are coordinated to oxo (O) and hydroxyl (OH) bridging anions, whereas the edge Fe atoms have bridging OH anions to the bulk structure but non-bridging H<sub>2</sub>O ligands to satisfy the excess valence charge. Distortion effects of Fe octahedra (Fig. 12.3.3A) at the surfaces of nano-crystalline ferrihydrite (due to coordination with water molecules and hydroxyls) were shown by Manceau and Gates (1997) to be partly responsible for the enhanced Fe K pre-edge XAFS features observed by Zhao et al. (1993, 1994). Manceau and Gates (1997) further proposed that two types of H<sub>2</sub>O molecules were present in ferrihydrite nano-crystals: those directly coordinated to the surface Fe atoms, and those hydrogen-bonded to the coordination water. The doubly hydrogen-bonded water (forming two H-bonds with two other coordination waters) is more stable than the singly hydrogen-bonded water. That is, the latter can be removed at relatively moderate humidities or low temperatures. High-resolution thermogravimetry (Ford and Bertsch, 1999) lends considerable support to this hypothesis.

Finely divided goethite particles with varied morphologies were shown to have three reversible surface dehydration/dehydroxylation temperatures: near 195–215, 220–240 and 240–260 °C, probably representing H<sub>2</sub>O/OH bonded to 1 (S<sub>1</sub>-OH), 2 (S<sub>2</sub>-OH) and 3 (S<sub>3</sub>-OH) surface atoms, respectively. These three dehydration/dehydroxylation events preceded the bulk dehydroxylation temperature near 270–280 °C; their resolution from each other and from the bulk dehydroxylation appears to correspond to the degree of crystallinity of the goethite which, in turn, depends on the ferrihydrite-to-goethite transformation rate.

Similar surface-induced effects were shown to occur on other mineral surfaces, such as freshly cleaved  $\gamma$ -Al<sub>2</sub>O<sub>3</sub> in water (England et al., 1999; Eng et al., 2000) and when divalent heavy metals are substituted for Ca<sup>2+</sup> in calcite (Reeder et al., 1999). Changes in bond strength and residual charge on ligands, with changes in bond length, are the origin of the high capacity of ultra small particle surfaces to take up metals and metaloids from solution (Reeder et al., 1994, 2000, 2001; Lamble et al., 1995, 1997; Rakovan et al., 2002). Distortion of surface coordination environments undoubtedly plays a pivotal role in the formation of surface complexes and coprecipitates (Scheinost et al., 1999, 2001; Manceau et al., 2000d; Mavrocordatos and Fortin, 2002; Waychunas et al., 2002a, 2002b).

### 12.3.7. FUTURE OUTLOOK AND CONCLUDING REMARKS

Many questions often emerge from improved understanding of nature. Synchrotron-based studies on clays and clay minerals certainly raised their fair share of questions. For example, why is the M1 site more energetically favourable than the

M2 site for Fe(II)? Why are sorption sites at clay surfaces apparently more selective or site-specific at low concentrations of a particular electrolyte than at high concentrations? Is this really selectivity or simply a function of the number of “ideal” sites available at a surface? How exactly do dioctahedral smectites, or even minerals such as quartz, act as templates for neoformation of trioctahedral phyllosilicate species? How does the inherently flexible structure of the 2:1 layer maintain its crystalline integrity after such apparently destructive processes as redox or heat-induced dehydroxylation? Questions such as these still face researchers attempting to understand the nature and properties of smectites and related poorly crystalline minerals.

In recent years we entered a truly new age of scientific investigation, one where dynamic molecular modelling will progress to the forefront of improving our understanding of clay mineral structures and reactivity. But all models must be validated by experiment. Without experimental fact a model is nothing more than an opinion, and often an expensive one at that. In combination with other more conventional and routine techniques, synchrotron-based studies will continue to play an important part in gathering these experimental facts. As this review showed the increased application of synchrotron-based analyses over the last decade greatly improved our understanding of the structures and reactions of poorly crystalline clays and clay minerals. We should point out, however, that synchrotron-based studies by themselves could generally only provide a limited amount of new information. Only when combined with other spectroscopic and/or wet chemical methods, can synchrotron-based techniques provide a firm foundation for models to stand on.

## REFERENCES

- Allard, T., Ildefonse, P., Beaucaire, C., Calas, G., 1999. Structural chemistry of uranium associated with Si, Al, Fe gels in a granitic uranium mine. *Chemical Geology* 158, 81–103.
- Amonette, J.E., Zelazny, L.W. (Eds.), 1994. Quantitative methods in soil mineralogy. Proceedings of a Symposium Sponsored by Division S-9, San Antonio, TX, October, 1990. SSSA Miscellaneous Publication. Soil Science Society of America, Madison, WI, 462pp.
- Ankudinov, A.L., Ravel, B., Rehr, J.J., Conradson, S.D., 1998. Real-space multiple-scattering calculation and interpretation of X-ray absorption near-edge structure. *Physics Review B* 58, 7565–7576.
- Arai, Y., Elzinga, E.J., Sparks, D.L., 2001. X-ray absorption spectroscopic investigation of arsenite and arsenate adsorption at the aluminium oxide–water interface. *Journal of Colloid and Interface Science* 235, 80–88.
- Axe, L., Bunker, G.B., Anderson, P.R., Tyson, T.A., 1998. An XAFS analysis of strontium at the hydrous ferric oxide surface. *Journal of Colloid and Interface Science* 199, 44–52.
- Axe, L., Tyson, T.L., Trivedi, P., Morrison, T., 2000. Local structure analysis of strontium sorption to hydrous manganese oxide. *Journal of Colloid and Interface Science* 224, 408–416.



- Bajt, S., Clark, S.B., Sutton, S.R., Rivers, M.L., Smith, J.V., 1993. Synchrotron X-ray microprobe determination of chromate content using X-ray absorption near edge structure. *Analytical Chemistry* 65, 1800–1804.
- Bajt, S., Sutton, S.R., Delaney, J., 1994. X-ray microprobe analysis of iron oxidation states in silicates and oxides using X-ray absorption near edge structure (XANES). *Geochimica et Cosmochimica Acta* 58, 5209–5214.
- Bajt, S., Sutton, S.R., Delaney, J., 1995. Microanalysis of iron oxidation states in earth and planetary materials. *Physica B* 208, 209, 243–244.
- Bargar, J.R., Brown, G.E., Parks, G.A., 1997a. Surface complexation of Pb(II) at oxide/water interfaces: 1. XAFS and bond-valence determination of mononuclear and polynuclear Pb(II) sorption products on aluminium oxides. *Geochimica et Cosmochimica Acta* 61, 2617–2637.
- Bargar, J.R., Brown, G.E., Parks, G.A., 1997b. Surface complexation of Pb(II) at oxide/water interfaces: 2. XAFS and bond-valence determination of mononuclear Pb(II) sorption products and surface functional groups on iron oxides. *Geochimica et Cosmochimica Acta* 61, 2639–2652.
- Bargar, J.R., Brown, G.E., Parks, G.A., 1998. Surface complexation of Pb(II) at oxide/water interfaces: 3. XAFS determination of Pb(II) and Pb(II)-chloro adsorption complexes on goethite and alumina. *Geochimica et Cosmochimica Acta* 62, 193–207.
- Bargar, J.R., Towle, S.N., Brown, G.E., Parks, G.A., 1996. Outer-sphere lead(II) adsorbed at specific surface sites on single crystal  $\alpha$ -alumina. *Geochimica et Cosmochimica Acta* 60, 3541–3547.
- Bargar, J.R., Trainor, T.P., Fitts, J.P., Chambers, S.A., Brown, G.E., 2004. *In-situ* grazing incidence EXAFS study of Pb(II) chemisorption on hematite (0001) and (1-102). *Langmuir* 20, 1667–1673.
- Bedzyk, M.J., Cheng, L., 2002. X-ray standing wave studies of minerals and mineral surfaces: principles and applications. In: Fenter, P.A., Rivers, M.L., Sturchio, N.C., Sutton, S.R. (Eds.), *Applications of Synchrotron Radiation in Low-Temperature Geochemistry and Environmental Science. Reviews in Mineralogy and Geochemistry*, vol. 49. Mineralogical Society of America, Washington, DC, pp. 221–266.
- Berry, A.J., O'Neill, H.St.C., 2004. A XANES determination of the oxidation state of chromium in silicate glasses. *American Mineralogist* 89, 790–798.
- Berry, A.J., O'Neill, H.St.C., Jayasuriya, K.D., Cambell, S.J., Foran, G.J., 2003. XANES calibrations for the oxidation state of iron in a silicate glass. *American Mineralogist* 88, 867–977.
- Bertsch, P.M., Hunter, D.B., 2001. Applications of synchrotron-based X-ray microprobes. *Chemical Reviews* 101, 1809–1842.
- Bianconi, A., 1988. XANES spectroscopy. In: Koningsberger, D.C., Prins, R. (Eds.), *X-ray Absorption: Principles, Applications, Techniques of EXAFS, SEXAFS and XANES*. Wiley, New York, pp. 573–662.
- Bianconi, A., Fritsch, E., Calas, G., Petiau, J., 1985. X-ray absorption near-edge structure of 3d transition elements in tetrahedral coordination. The effect of bond length variation. *Physics Reviews B* 32, 4292–4295.
- Bidoglio, G., Gibson, P.N., O'Gorman, M., Robert, K.J., 1993. X-ray absorption spectroscopy investigation of surface redox transformations of thallium and chromium on colloidal mineral oxides. *Geochimica et Cosmochimica Acta* 57, 2389–2394.

- Bochatay, L., Persson, P., Lövgren, L., Brown, G.E., 1997. XAFS study of Cu(II) at the water-goethite ( $\alpha$ -FeOOH) interface. *Journal of Physique IV, France* 7, C2, 819–820.
- Bonnin, D., Bouat, J., Kaiser, P., Fréty, C., Béguin, F., 1986. Bond angle determination by angular EXAFS study and Debye–Waller anisotropy in 2D graphite intercalation compounds. In: Lagarde, P., Rouax, D., Petiau, J. (Eds.), *EXAFS and Near Edge Structure IV. Journal de Physique colloque*, C8, 865–868.
- Bonnin, D., Calas, G., Suquet, H., Pezerat, H., 1985. Sites occupancy of  $\text{Fe}^{3+}$  in Garfield nontronite: a spectroscopy study. *Physics and Chemistry of Minerals* 12, 55–64.
- Bottero, J.-Y., Manceau, A., Villiéras, F., Tchoubar, D., 1994. Structure and mechanism of nucleation of FeOOH(Cl) polymers. *Langmuir* 10, 316–319.
- Brigatti, M.F., Lugli, C., Cibir, G., Marcelli, A.G.G., Paris, E., Mottana, A., Wu, Z., 2000. Reduction and sorption of chromium by Fe(II)-bearing phyllosilicates: chemical treatments and X-ray absorption spectroscopy (XAS) studies. *Clays and Clay Minerals* 48, 272–281.
- Brindley, G.W., Brown, G., 1980. *Crystal Structures of Clay Minerals and their X-ray Identification*. Mineralogical Society, London.
- Brovelli, D., Caseri, W.R., Hähner, G., 1999. Self-assembled monolayers of alkylammonium ions on mica: direct determination of the orientation of the alkyl chains. *Journal of Colloid and Interface Science* 216, 418–423.
- Brown, G.E., Calas, C., Waychunas, G.A., Petiau, J., 1988. X-ray absorption spectroscopy and its application in mineralogy and geochemistry. In: Hawthorne, F.C. (Ed.), *Spectroscopic Methods in Mineralogy and Geology. Reviews in Mineralogy*, vol. 18. Mineralogical Society of America, Washington, DC, pp. 431–512.
- Brown, G.E., Sturchio, N.C., 2002. An overview of synchrotron radiation applications to low temperature geochemistry and environmental science. In: Fenter, P.A., Rivers, M.L., Sturchio, N.C., Sutton, S.R. (Eds.), *Applications of Synchrotron Radiation in Low-temperature Geochemistry and Environmental Science. Reviews in Mineralogy and Geochemistry*, vol. 49. Mineralogical Society of America, Washington, DC, pp. 1–115.
- Bugaev, L.A., Ildefonse, P., Flank, A.-M., Sokolenko, A.P., Dmitrienko, H.V., 1998. Aluminum K-XANES spectra in minerals as a source of information on their local atomic structure. *Journal of Physics: Condensed Matter* 10, 5463–5473.
- Bugaev, L.A., Ildefonse, P., Flank, A.-M., Sokolenko, A.P., Dmitrienko, H.V., 2000. Determination of interatomic distances and coordination numbers by K-XANES in crystalline minerals with distorted local structure. *Journal of Physics: Condensed Matter* 12, 1119–1131.
- Bugaev, L.A., Sokolenko, A.P., Dmitrienko, H.V., Flank, A.-M., 2002. Fourier filtration of XANES as a source of quantitative information of interatomic distances and coordination numbers in crystalline minerals and amorphous compounds. *Physics Reviews B* 65, 1–8.
- Bujdák, J., Janek, M., Madejová, J., Komadel, P., 2001. Methylene blue interactions with reduced-charge smectites. *Clays and Clay Minerals* 49, 244–254.
- Bujdák, J., Komadel, P., 1997. Interaction of methylene blue with reduced charge montmorillonite. *Journal of Physical Chemistry B* 101, 9065–9068.
- Bunker, D.J., Jones, M.J., Charnock, J.M., Livens, F.R., Patrick, R.A.D., Collinson, D., 2002. EXAFS studies of co-precipitation and adsorption reactions of  $\text{Tc}$ . *Proceedings of the Euroconference and NEA Workshop on Speciation, Techniques, and Facilities for Radioactive Materials at Synchrotron Light Sources*, Grenoble, France, 2000. Nuclear

- Energy Agency/Organisation for Economic Co-operation and Development, AEN/NEA, Paris, pp. 207–213.
- Cabaret, D., Saintavit, P., Ildefonse, P., Flank, A.-M., 1996. Full multiple-scattering calculations on silicates and oxides at the Al *K* edge. *Journal of Physics: Condensed Matter* 8, 3691–3704.
- Calas, G., Manceau, A., Combes, J.M., Farges, F., 1990. Application of EXAFS in mineralogy. In: Mottana, A., Burragato, F. (Eds.), *Absorption Spectroscopy in Mineralogy*. Elsevier, Amsterdam, pp. 171–204.
- Calas, G., Petiau, J., 1983. Coordination of iron in oxide glasses through high resolution *K*-edge spectra: information from the pre-edge. *Solid State Communications* 48, 625–629.
- Charlet, L., Manceau, A., 1992. X-ray absorption spectroscopy study of the sorption of Cr(III) at the oxide/water interface. 2. Adsorption, coprecipitation, and surface precipitation on ferric hydrous oxide. *Journal of Colloid and Interface Science* 148, 443–458.
- Charlet, L., Manceau, A., 1993. Structure, formation, and reactivity of hydrous oxide particles: Insight from X-ray absorption spectroscopy. In: Buffle, J., van Leeuwen, H.P. (Eds.), *Environmental Particles. Environmental Analytical and Physical Chemistry Series*, vol. 2. Lewis Publishers, Boca Raton, FL, pp. 117–164.
- Charlet, L., Manceau, A., 1994. Evidence for the neoformation of clays upon sorption of Co(II) and Ni(II) on silicates. *Geochimica et Cosmochimica Acta* 58, 2577–2582.
- Cheah, S.-F., Brown, G.E., Parks, G.A., 1998. XAFS spectroscopic study of Cu(II) sorption on amorphous SiO<sub>2</sub> and  $\gamma$ -Al<sub>2</sub>O<sub>3</sub>: effect of substrate and time on sorption complexes. *Journal of Colloid and Interface Science* 208, 110–128.
- Cheah, S.-F., Brown, G.E., Parks, G.A., 1999. Structure and composition of copper(II)-2,2'-bipyridine sorption complexes on amorphous SiO<sub>2</sub>. *Geochimica et Cosmochimica Acta* 63, 3229–3246.
- Cheah, S.-F., Brown, G.E., Parks, G.A., 2000. XAFS study of copper model compounds and copper(II) sorption on amorphous SiO<sub>2</sub>,  $\gamma$ -Al<sub>2</sub>O<sub>3</sub>, and anatase. *American Mineralogist* 85, 118–132.
- Chen, C.-C., Hapelis, C., Hayes, K.F., 1998. Extended X-ray absorption fine structure (EXAFS) analysis of aqueous Sr(II) ion sorption at clay–water interfaces. In: Jenne, E.A. (Ed.), *Adsorption of Metals by Geomedia: Variables, Mechanisms, and Model Applications*. Academic Press, New York, pp. 333–348.
- Chen, C.-C., Hayes, K.F., 1999. X-ray absorption spectroscopy investigation of aqueous Co(II) and Sr(II) sorption at clay–water interfaces. *Geochimica et Cosmochimica Acta* 63, 3205–3215.
- Chisholm-Brause, C.J., Brown, G.E., Parks, G.A., 1989a. EXAFS investigation of aqueous Co(II) sorbed on oxide surfaces *in situ*. *Physica B* 158, 646–648.
- Chisholm-Brause, C.J., Brown, G.E., Parks, G.A., 1991. *In situ* EXAFS study of changes in Co(II) sorption complexes on  $\alpha$ -Al<sub>2</sub>O<sub>3</sub> with increasing sorption densities. In: Hasnain, S. (Ed.), *XAFS VI, 6th International Conference on X-ray Absorption Fine Structure*. Ellis Horwood, Chichester, pp. 263–265.
- Chisholm-Brause, C.J., Conradson, S.D., Buscher, C.T., Eller, P.G., Morris, D.E., 1994. Speciation of uranyl sorbed at multiple sites on montmorillonite. *Geochimica et Cosmochimica Acta* 58, 3625–3631.

- Chisholm-Brause, C.J., Hayes, K.F., Roe, A.L., Brown, G.E., Parks, G.A., Leckie, J.O., 1990b. Spectroscopic investigation of Pb(II) complexes at the  $\gamma$ -Al<sub>2</sub>O<sub>3</sub>/water interface. *Geochimica et Cosmochimica Acta* 54, 1897–1909.
- Chisholm-Brause, C.J., Morris, D.E., Richard, R.E., 1992. Speciation of uranium(VI) sorption complexes on montmorillonite. In: Arehart, G.B., Hulston, J.R. (Eds.), *Proceedings of the 7th International Symposium on Water–Rock Interactions*, vol. 1, pp. 137–140.
- Chisholm-Brause, C.J., O'Day, P.A., Brown, G.E., Parks, G.A., 1990a. Evidence for multinuclear metal-ion complexes at solid/water interfaces from X-ray absorption spectroscopy. *Nature* 348, 528–531.
- Chisholm-Brause, C.J., Roe, A.I., Hayes, K.F., Brown, G.E., Parks, G.A., Leckie, J.O., 1989b. XANES and EXAFS study of aqueous Pb(II) sorbed on oxide surfaces. *Physica B* 158, 674–676.
- Collins, C.R., Sherman, D.M., Ragnarsdottir, K.V., 1998. The adsorption mechanism of Sr<sup>2+</sup> on the surface of goethite. *Radiochimica Acta* 81, 201–206.
- Collins, C.R., Sherman, D.M., Ragnarsdottir, K.V., 1999. Surface complexation of Hg<sup>2+</sup> on goethite: mechanism from EXAFS spectroscopy and density functional calculations. *Journal of Colloid and Interface Science* 219, 345–350.
- Combes, J.M., Chisholm-Brause, C.J., Brown, G.E., Parks, G.A., Conradson, S.D., Eller, P.G., Triay, I., Meier, A., 1992. EXAFS spectroscopic study of neptunium(V) sorbed at the  $\alpha$ -FeOOH/water interface. *Environmental Science and Technology* 26, 376–382.
- Combes, J.M., Manceau, A., Calas, G., 1986. Study of the local structure in poorly ordered precursors of iron oxyhydroxides. *Journal de Physique C* 8, 697–701.
- Combes, J.M., Manceau, A., Calas, G., 1989a. XAFS study of the evolution of local order around iron(III) in the solution to gel to iron oxide ( $\alpha$ -Fe<sub>2</sub>O<sub>3</sub>) transformation. *Physica B* 158, 419–420.
- Combes, J.M., Manceau, A., Calas, G., 1990. Formation of ferric oxides from aqueous solutions: a polyhedral approach by X-ray absorption spectroscopy. 2. Hematite formation from ferric gels. *Geochimica et Cosmochimica Acta* 54, 1083–1091.
- Combes, J.M., Manceau, A., Calas, G., Bottero, J.Y., 1989b. Formation of ferric oxides from aqueous solutions: a polyhedral approach by X-ray absorption spectroscopy. 1. Hydrolysis and formation of ferric gels. *Geochimica et Cosmochimica Acta* 53, 583–594.
- Cressey, G., Henderson, C.M.B., van der Laan, G., 1993. Use of *L*-edge X-ray absorption spectroscopy to characterize multiple valence states of 3d transition metals; a new probe for mineralogical and geochemical research. *Physics and Chemistry of Minerals* 20, 111–119.
- Criscenti, L.J., Sverjensky, D.A., 2002. A single-site model for divalent transition and heavy metal adsorption over a range of metal concentrations. *Journal of Colloid and Interface Science* 253, 339–352.
- Dähn, R., Scheidegger, A.M., Manceau, A., Curti, E., Baeyens, B., Bradbury, M.H., Chateigner, D., 2002a. Th uptake on montmorillonite: a powder and polarized extended X-ray absorption fine structure (EXAFS) study. *Journal of Colloid and Interface Science* 249, 8–21.
- Dähn, R., Scheidegger, A.M., Manceau, A., Schlegel, M.L., Baeyens, B., Bradbury, M.H., Chateigner, D., 2003. Structural evidence for the sorption of Ni(II) atoms on the edges of montmorillonite clay minerals: a polarized X-ray absorption fine structure study. *Geochimica et Cosmochimica Acta* 67, 1–15.

- Dähn, R., Scheidegger, A.M., Manceau, A., Schlegel, M.L., Baeyens, B., Bradbury, M.H., Morales, M., 2002b. Neoformation of Ni phyllosilicate upon Ni uptake on montmorillonite: a kinetics study by powder and polarized extended X-ray absorption fine structure spectroscopy. *Geochimica et Cosmochimica Acta* 66, 2335–2347.
- Dähn, R., Scheidegger, A.M., Manceau, A., Schlegel, M.L., Baeyens, B., Bradbury, M.H., 2001. Ni clay neoformation on montmorillonite surface. *Journal of Synchrotron Radiation* 8, 533–535.
- Davis, R.D., Gilman, J.W., Sutto, T.E., Callahan, J.H., Trulove, P.C., De Long, H.C., 2004. Improved thermal stability of organically modified layered silicates. *Clays and Clay Minerals* 52, 171–179.
- Decarreau, A., 1990. *Matériaux Argileux—Structure, propriétés et applications*. Ouvrage collectif sous la direction de A. Decarreau. Société Française de Minéralogie et de Cristallographie, Groupe Français des Argiles, Paris 586pp.
- Decarreau, A., Colin, F., Herbillon, A., Manceau, A., Nahon, D., Paquet, H., Trauth-Badaud, D., Trescases, J.J., 1987. Domains segregation in Ni–Fe–Mg-bearing smectites. *Clays and Clay Minerals* 35, 1–10.
- de Groot, F., 2001. High-resolution X-ray emission and X-ray absorption spectroscopy. *Chemical Reviews* 101, 1779–1808.
- Delaney, J.S., Bajt, S., Dyar, M.D., Sutton, S.R., McKay, G., Roeder, P., 1996a. Comparison of quantitative microXANES (SmX) FeIII/(FeII+FeIII) results for amphibole and silicate glass with independent measurements. *Lunar and Planetary Sciences XXVII*, 299–300.
- Delaney, J.S., Bajt, S., Sutton, S.R., Dyar, M.D., 1996b. *In situ* microanalysis of  $\text{Fe}^{3+}/\Sigma\text{Fe}$  ratios in amphibole by X-ray absorption near edge structure (XANES) spectroscopy. *Mineral Spectroscopy (R. Burns memorial volume)* 5, 165–171.
- Delaney, J.S., Dyar, M.D., Sutton, S.R., Bajt, S., 1998. Redox ratios with relevant resolution: solving an old problem by using the synchrotron microXANES probe. *Geology* 26, 139–142.
- Dent, A.J., Ramsay, J.D.F., Swanton, S.W., 1992. An EXAFS study of uranyl ions in solutions and sorbed onto silica and montmorillonite clay colloids. *Journal of Colloid and Interface Science* 150, 45–60.
- d'Espinosa de la Caillerie, J.-B., Bobbin, C., Rebours, B., Clause, O., 1995b. Alumina/water interfacial phenomena during impregnation. In: Delmon, B., Grange, P., Jacobs, P.A. (Eds.), *Preparation of Catalysts VI—Scientific Basis for the Preparation of Heterogeneous Catalysts*. Elsevier, New York, pp. 168–184.
- d'Espinosa de la Caillerie, J.-B., Kermarec, M., Clause, O., 1995a. Impregnation of  $\gamma$ -alumina with Co(II) and Ni(II) ions at neutral pH: hydrotalcite-type coprecipitate formation and characterisation. *Journal of the American Chemical Society* 117, 11471–11481.
- Doelsch, E., Rose, J., Masion, A., Bottero, J.Y., Nahon, D., Bertsch, P.M., 2000. Speciation and crystal chemistry of iron(III) chloride hydrolysed in the presence of  $\text{SiO}_4$  ligands. 1. An Fe K-edge EXAFS study. *Langmuir* 16, 4727–4731.
- Doelsch, E., Rose, J., Masion, A., Bottero, J.Y., Nahon, D., Bertsch, P.M., 2002. Hydrolysis of iron(II) chloride under anoxic conditions and influence of  $\text{SiO}_4$  ligands. *Langmuir* 18, 4292–4299.
- Drits, V.A., Lanson, B., Gorshkov, A.I., Manceau, A., 1998a. Substructure and superstructure of four-layer Ca-exchanged birnessite. *American Mineralogist* 83, 97–118.

- Drits, V.A., Lindgreen, H., Salyn, A.L., Ylagan, R., McCarty, D.K., 1998b. Semiquantitative determination of *trans*-vacant and *cis*-vacant 2:1 layers in illites and illite-smectites by thermal analysis and X-ray diffraction. *American Mineralogist* 83, 1188–1198.
- Drits, V.A., Sakharov, B.A., Salyn, A.L., Manceau, A., 1993. New structural model for ferrihydrite. *Clay Minerals* 28, 185–208.
- Drits, V.A., Silvester, E., Gorshkov, A.I., Manceau, A., 1997. Structure of synthetic monoclinic Na-rich birnessite and hexagonal birnessite. 1. Results from X-ray diffraction and selected-area electron diffraction. *American Mineralogist* 82, 946–961.
- Duff, M.C., Coughlin, J.U., Hunter, D.B., 2002. Uranium co-precipitation with iron oxide minerals. *Geochimica et Cosmochimica Acta* 66, 3533–3547.
- Duff, M.C., Hunter, D.B., Bertsch, P.M., Amrhein, C., 1999. Factors influencing uranium reduction and solubility in evaporation pond sediments. *Biogeochemistry* 45, 95–114.
- Dyar, M.D., Delaney, J.S., Sutton, S.R., 2001. Fe XANES spectra of iron-rich micas. *European Journal of Mineralogy* 13, 1079–1098.
- Dyar, M.D., Gunter, M., Delaney, J.S., Lanzarotti, A., Sutton, S.R., 2002. Systematics in the structure and XANES spectra of pyroxenes, amphiboles, and micas as derived from oriented single crystals. *Canadian Mineralogist* 40, 1375–1393.
- Eick, M.J., Fendorf, S.E., 1998. Reaction sequence of nickel(II) with kaolinite: mineral dissolution and surface complexation and precipitation. *Soil Science Society of America Journal* 62, 1257–1267.
- Eggleton, R.A., Fitzpatrick, R.W., 1988. New data and revised structural model for ferrihydrite. *Clays and Clay Minerals* 36, 111–124.
- Elzinga, E., Sparks, D.L., 1999. Nickel sorption mechanism in pyrophyllite-montmorillonite mixture. *Journal of Colloid and Interface Science* 213, 506–512.
- Eng, P.J., Trainor, T.P., Brown, G.E., Waychunas, G.A., Newville, M., Sutton, S.R., Rivers, M.L., 2000. Structure of the hydrated  $\alpha$ -Al<sub>2</sub>O<sub>3</sub> (0001) surface. *Science* 28, 1029–1033.
- England, K.E.R., Charnock, J.N., Patrick, R.A.D., Vaughan, D.J., 1999. Surface oxidation studies of chalcopyrite and pyrite by glancing-angle X-ray absorption spectroscopy (REFLEXAFS). *Mineralogical Magazine* 63, 559–566.
- Farmer, V.C., 1974. *The Infrared Spectra of Minerals*. Mineralogical Society, London.
- Farquhar, M.L., Charnock, J.N., England, K.E.R., Vaughan, D.J., 1996. Adsorption of Cu<sup>2+</sup> on the (0001) plane of mica. A REFLEXAFS and XPS study. *Journal of Colloid and Interface Science* 177, 561–567.
- Farquhar, M.L., Vaughan, D.J., Hughes, C.R., Charnock, J.N., England, K.E.R., 1997. Experimental studies of the interaction of aqueous metal cations with mineral substrates: lead, cadmium, copper with perthitic feldspar, muscovite and biotite. *Geochimica et Cosmochimica Acta* 61, 3051–3064.
- Fendorf, S.E., 1995. Surface reactions of chromium in soils and waters. *Geoderma* 67, 55–71.
- Fendorf, S., 1999. Fundamental aspects and applications of X-ray absorption spectroscopy in clay and soil science. In: Schulze, D.G., Stucki, J.W., Bertsch, P.M. (Eds.), *Synchrotron X-ray Methods in Clay Science*. CMS Workshop Lectures, vol. 9. The Clay Minerals Society, Boulder, CO, pp. 19–67.
- Fenter, P.A., 2002. X-ray reflectivity as a probe of mineral-fluid interfaces: a user guide. In: Fenter, P.A., Rivers, M.L., Sturchio, N.C., Sutton, S.R. (Eds.), *Applications of Synchrotron Radiation in Low-temperature Geochemistry and Environmental Science*. Reviews in Mineralogy and Geochemistry, vol. 49. Mineralogical Society of America, Washington, DC, pp. 149–220.

- Fenter, P.A., Rivers, M.L., Sturchio, N.C., Sutton, S.R. (Eds.), 2002. Applications of Synchrotron Radiation in Low-temperature Geochemistry and Environmental Science. Reviews in Mineralogy and Geochemistry, vol. 49. Mineralogical Society of America, Washington, DC.
- Fenter, P.A., Sturchio, N.C., 1999. Structure and growth of sterate monolayers on calcite: first results of an *in situ* X-ray reflectivity study. *Geochimica et Cosmochimica Acta* 63, 3145–3152.
- Fialips, C.-I., Huo, D., Yan, L., Wu, J., Stucki, J.W., 2002a. Infrared study of reduced and reduced–reoxidized ferruginous smectite. *Clays and Clay Minerals* 50, 455–469.
- Fialips, C.-I., Huo, D., Yan, L., Wu, J., Stucki, J.W., 2002b. Effect of iron oxidation state on the IR spectra of Garfield nontronite. *American Mineralogist* 87, 630–641.
- Fischer, D., Caseri, W.R., Hähner, G., 1998. Orientation and electronic structure of ion exchanged dye molecules on mica: an X-ray absorption study. *Journal of Colloid and Interface Science* 198, 337–346.
- Fitts, J.P., Brown, G.E., Parks, G.A., 2000. Structural evolution of Cr(III) polymeric species  $\gamma$ -Al<sub>2</sub>O<sub>3</sub>/water interface. *Environmental Science and Technology* 34, 5122–5128.
- Ford, R.G., Bertsch, P.M., 1999. Distinguishing between surface and bulk dehydration–dehydroxylation reactions in synthetic goethites by high resolution thermogravimetric analysis. *Clays and Clay Minerals* 47, 329–337.
- Ford, R.G., Sparks, D.L., 2000. The nature of Zn precipitates formed in the presence of pyrophyllite. *Environmental Science and Technology* 34, 2479–2483.
- Ford, R.G., Bertsch, P.M., Farley, K.J., 1997a. Changes in transition and heavy metal partitioning during hydrous iron oxide aging. *Environmental Science and Technology* 31, 2028–2033.
- Ford, R.G., Bertsch, P.M., Seaman, J.C., 1997b. Goethite morphologies investigated via X-ray diffraction of oriented samples. *Clays and Clay Minerals* 45, 769–772.
- Ford, R.G., Kemner, K.M., Bertsch, P.M., 1999a. Influence of sorbate–sorber interaction on the crystallization kinetics of nickel- and lead-ferrihydrite coprecipitates. *Geochimica et Cosmochimica Acta* 63, 39–48.
- Ford, R.G., Scheinost, A.C., Sheckel, K.G., Sparks, D.L., 1999b. The link between clay mineral weathering and the stabilisation of nickel surface precipitates. *Environmental Science and Technology* 33, 3140–3144.
- Foster, A.L., Brown, G.E., Parks, G.A., 1998a. XAFS study of photocatalyzed, heterogeneous As(III) oxidation on kaolin and anatase. *Environmental Science and Technology* 32, 1444–1452.
- Foster, A.L., Brown, G.E., Tingle, T.N., Parks, G.A., 1998b. Quantitative arsenic speciation in mine tailings using X-ray absorption spectroscopy. *American Mineralogist* 83, 553–568.
- Foster, A.L., Brown, G.E., Parks, G.A., 2002. EXAFS study of As(V) and Se(IV) sorption complexes on hydrous Mn oxides. *Geochimica et Cosmochimica Acta* 67, 1937–1953.
- Frederickson, J.K., Zachara, J.M., Kennedy, D.W., Duff, M.C., Gorby, Y.A., Li, S.-M.W., Krupka, K.M., 2000. Reduction of U(VI) in goethite ( $\alpha$ -FeOOH) suspensions by a dissimilatory metal-reducing bacterium. *Geochimica et Cosmochimica Acta* 64, 3085–3098.
- Frederickson, J.K., Zachara, J.M., Kennedy, D.W., Liu, C., Duff, M.C., Hunter, D.B., Dohnalkova, A., 2002. Influence of Mn oxides on the reduction of uranium(VI) by the metal-reducing bacterium *Shewanella putrifaciens*. *Geochimica et Cosmochimica Acta* 66, 3247–3262.

- Fukushima, Y., 1988. Extended X-ray absorption fine structure study of cobalt-exchanged sepiolite: reply. *Clays and Clay Minerals* 36, 384.
- Fukushima, Y., Okomoto, T., 1987. Extended X-ray absorption fine structure study of cobalt-exchanged sepiolite. In: Schultz, L.G., van Olphen, H., Mumpton, F.A. (Eds.), *Proceedings of the International Clay Conference*, Denver, 1985. The Clay Minerals Society, Bloomington, IN, pp. 9–16.
- Fuhrmann, M., Bajt, S., Schoonen, M.A.A., 1998. Sorption of iodine on minerals investigation by X-ray absorption near edge structure (XANES) and  $^{125}\text{I}$  tracer sorption experiments. *Applications in Geochemistry* 13, 127–141.
- Galoisy, L., Calas, G., Arrio, M.A., 2001a. High-resolution XANES spectra of iron in minerals and glasses: structural information from the pre-edge region. *Chemical Geology* 174, 307–319.
- Galoisy, L., Cormier, L., Calas, G., Briois, V., 2001b. Environment of Ni, Co and Zn in low alkali borate glasses: information from EXAFS and XANES spectra. *Journal of Non-Crystalline Solids* 293–295, 105–111.
- Gates, W.P., 2005. Infrared spectroscopy and the chemistry of dioctahedral smectites. In: Klopogge, J.T. (Ed.), *The Application of Vibrational Spectroscopy to Clay Minerals and Layered Double Hydroxides*. CMS Workshop Series, vol. 13. The Clay Minerals Society, Aurora, CO, pp. 125–168.
- Gates, W.P., Hunter, D.B., Nuessel, P.R., Bertsch, P.M., 1997. A time resolved XANES study of an organo-clay redox system. *Journal of Physique, IV France* 7, C2, 785–787.
- Gates, W.P., Slade, P.G., Manceau, A., Lanson, B., 2002. Site occupancy by Fe in nontronite. *Clays and Clay Minerals* 50, 223–239.
- Gates, W.P., Stucki, J.W., Kirkpatrick, R.J., 1996. Structural properties of reduced Upton montmorillonite. *Physics and Chemistry of Minerals* 23, 535–541.
- Gehlen, M., Beck, L., Calas, G., Flank, A.-M., van Bennekom, A.J., van Beusekom, J.E.E., 2002. Unravelling the atomic structure of biogenic silica: evidence of the structural association of Al and Si in diatom frustules. *Geochimica et Cosmochimica Acta* 66, 1601–1609.
- Gérard, P., Herbillon, A., 1983. Infrared studies of Ni-bearing clay minerals of the kero-lite–pimelite series. *Clays and Clay Minerals* 31, 143–151.
- Giaquinta, D.M., Soderholm, L., Yuchs, S.E., Wasserman, S.R., 1997a. The speciation of uranium in a smectite clay. Evidence for catalysed uranyl reaction. *Radiochemica Acta* 76, 113–121.
- Giaquinta, D.M., Soderholm, L., Yuchs, S.E., Wasserman, S.R., 1997b. Hydrolysis of uranium and thorium in surface-modified bentonite under hydrothermal conditions. *Journal of Alloys and Compounds* 249, 142–145.
- Güven, N., 1988. Smectites. In: Bailey, S.W. (Ed.), *Hydrous Phyllosilicates*. Exclusive of Micas. *Reviews in Mineralogy*, vol. 19. Mineralogical Society of America, Washington, DC, pp. 497–559.
- Hähner, G., Marti, A., Spencer, N.D., Brunner, S., Caseri, W.R., Suter, U.W., 1996a. Self-assembled layers of substituted poly(*p*-phenylene)s on gold and copper investigated by soft X-ray spectroscopy. *Langmuir* 12, 719–725.
- Hähner, G., Marti, A., Spencer, N.D., Caseri, W.R., 1996b. Orientation and electronic structure of methylene blue on mica: a near edge X-ray absorption fine structure spectroscopy study. *Journal of Chemical Physics* 104, 7749–7757.



- Hayes, K.F., Roe, A.L., Brown, G.E., Hodgson, K.O., Leckie, J.O., Parks, G.A., 1987. *In situ* X-ray absorption study of surface complexes at oxide/water interfaces: selenium oxyanions on  $\alpha$ -FeOOH. *Science* 238, 783–786.
- Hayes, K.O., Katz, L.E., 1996. Application of X-ray absorption spectroscopy for surface complexation modelling of metal ion sorption. In: Brady, P.V. (Ed.), *Physics and Chemistry of Mineral Surfaces*. CRC Press, Boca Raton, FL, pp. 147–223.
- Hawthorne, F.C. (Ed.), 1988. *Spectroscopic Methods in Mineralogy and Geology*. Reviews in Mineralogy, vol. 18. Mineralogical Society of America, Washington, DC.
- Hazemann, J.-L., Manceau, A., Saintavrit, P., Malgrange, C., 1992. Structure of the  $\alpha$ -Fe<sub>x</sub>Al<sub>1-x</sub>OOH solid solution. 1 Evidence by polarized EXAFS for epitaxial growth of hematite-like clusters in Fe-diaspore. *Physics and Chemistry of Minerals* 19, 25–38.
- Heald, S.M., Stern, E.A., 1977. Anisotropic X-ray absorption in layered compounds. *Physics Review B* 16, 5549–5559.
- Hesterberg, D., Zhau, W., Hutchinson, K.J., Beauchemin, S., Sayer, D.E., 1999. XAFS study of adsorbed and mineral forms of phosphate. *Journal of Synchrotron Radiation* 6, 636–638.
- Hirshchmugl, C.J., 2002. Applications of storage ring infrared spectromicroscopy and reflection–absorption spectroscopy to geochemistry and environmental science. In: Fenter, P.A., Rivers, M.L., Sturchio, N.C., Sutton, S.R. (Eds.), *Applications of Synchrotron Radiation in Low-Temperature Geochemistry and Environmental Science*. Reviews in Mineralogy and Geochemistry, vol. 49. Mineralogical Society of America, Washington, DC, pp. 317–339.
- Hochella, M.F., 1988. Auger electron and X-ray photoelectron spectroscopy. In: Hawthorne, F.C. (Ed.), *Spectroscopic Methods in Mineralogy and Geology*. Reviews in Mineralogy, vol. 18. Mineralogical Society of America, Washington, DC, pp. 573–637.
- Hodgson, K.O., Hedman, B., Penner-Hahn, J.E., 1984. EXAFS and near edge structure III. *Springer Proceedings in Physics*. Springer, Berlin.
- Hudson, E.A., Terminello, L.J., Viann, B.E., Denecke, M., Reich, T., Allen, P.G., Bucher, J.J., Shuh, D.K., Edelstein, N.M., 1999. The structure of uranium(VI) sorption complexes on vermiculite and hydrobiotite. *Clays and Clay Minerals* 47, 439–457.
- Hunter, D.B., Bertsch, P.M., 1994. *In situ* measurements of tetraphenylboron degradation kinetics on clay mineral surfaces by IR. *Environmental Science and Technology* 28, 686–691.
- Hunter, D.B., Bertsch, P.M., 1998. *In situ* examination of uranium contaminated soil particles by micro-X-ray absorption and micro-fluorescence spectroscopies. *Journal of Radioanalytical and Nuclear Chemistry* 234, 237–242.
- Hunter, D.B., Bertsch, P.M., Kemner, K.M., Clark, S.B., 1997. Distribution and chemical speciation of metals and metaloids in biota collected from contaminated environments by spatially resolved XRF, XANES, and EXAFS. *Journal of Physique IV, France* 7, C2, 767–771.
- Hunter, D.B., Gates, W.P., Bertsch, P.M., Kemner, K.M., 1999. Degradation of tetraphenyl boron at hydrated smectite surfaces by time-resolved IR and X-ray absorption spectroscopies. In: Sparks, D.L., Grundl, T.J. (Eds.), *Mineral–Water Interfacial Reactions: Kinetics and Mechanisms*. ACS Symposium Series, vol. 715. American Chemical Society, Washington, DC, pp. 282–330.

- Ildefonse, P., Kirkpatrick, R.J., Montez, B., Calas, G., Flank, A.-M., Lagarde, P., 1994.  $^{27}\text{Al}$  MAS NMR and aluminum X-ray absorption near edge structure study of imogolite and allophanes. *Clays and Clay Minerals* 42, 276–287.
- Ildefonse, P., Cabaret, D., Saintavit, P., Calas, G., Flank, A.M., Lagarde, P., 1998. Aluminium X-ray absorption near edge structure in model compounds and Earth's surface minerals. *Physics and Chemistry of Minerals* 25, 112–121.
- Jambor, J.L., Dutrizac, J.E., 1998. Occurrence and constitution of natural and synthetic ferrihydrite, a widespread iron oxyhydroxide. *Chemical Reviews* 98, 2549–2585.
- Janek, M., Komadel, P., 1993. Autotransformation of H-smectites in aqueous solution. The effect of octahedral iron content. *Geologica Carpathica, Series Clays* 44, 59–64.
- Janek, M., Komadel, P., 1998. Acidity of proton saturated and autotransformed smectites characterised with proton affinity distribution. *Geologica Carpathica, Series Clays* 50, 373–378.
- Kemner, K.M., Hunter, D.B., Bertsch, P.M., Kirkland, J.P., Elam, W.T., 1997. Determination of site specific binding environments of surface sorbed cesium on clay minerals by Cs-EXAFS. *Journal of Physique IV, France* 7, C2, 811–812.
- Kendelewicz, T., Liu, P., Doyle, C.S., Brown, G.E., 2000. Spectroscopic study of the reaction of  $\text{Cr(VI)}_{\text{aq}}$  with  $\text{Fe}_3\text{O}_4$  (III) surfaces. *Surface Science* 469, 144–163.
- Komadel, P., Madejová, J., Stucki, J.W., 1995. Reduction and reoxidation of nontronite: questions of reversibility. *Clays and Clay Minerals* 45, 105–110.
- Koningsberger, D.C., Prins, R., 1988. X-ray Absorption: Principles, Applications, Techniques of EXAFS, SEXAFS and XANES. Wiley, New York.
- Lamble, G.M., Lee, J.F., Staudt, W.J., Reeder, R.J., 1995. Structural studies of selenate incorporation into calcite crystals. *Physica B* 208, 209, 589–590.
- Lamble, G.M., Reeder, R.J., Northoup, P.A., 1997. Characterization of heavy metal incorporation in calcite by XAFS spectroscopy. *Journal of Physique IV, France* 7, C2, 793–797.
- Li, D., Bancroft, M., Fleet, M.E., Feng, X.H., Pan, Y., 1995. Al-K edge spectra of aluminosilicate minerals. *American Mineralogist* 80, 432–440.
- Lin, W., Lee, T.L., Lyman, P.F., Bedzyk, M.J., Marks, T.J., 1997. Atomic resolution X-ray standing wave microstructural characterisation of NLO-active self-assembled chromophoric superlattices. *Journal of the American Chemical Society* 119, 2205–2211.
- Lu, K., Stern, E.A., 1993. Size effect of powdered sample on EXAFS amplitude. *Nuclear Instruments and Methods* 212, 475–478.
- Madejová, J., Komadel, P., Čičel, B., 1994. Infrared study of octahedral site populations in smectites. *Clay Minerals* 29, 319–326.
- Manceau, A., 1990. Distribution of cations among the octahedra of phyllosilicates: insight from EXAFS. *Canadian Mineralogist* 28, 321–328.
- Manceau, A., 1995. The mechanism of anion adsorption on Fe oxides: evidence for the bonding of arsenate tetrahedral on free  $\text{Fe}(\text{O},\text{OH})_6$  edges. *Geochimica et Cosmochimica Acta* 59, 3647–3653.
- Manceau, A., Calas, G., 1985. Heterogeneous distribution of nickel in hydrous silicates from New Caledonia ore deposits. *American Mineralogist* 70, 549–558.
- Manceau, A., Calas, G., 1986. Nickel-bearing clay minerals: 2. Intracrystalline distribution of nickel: a K-ray absorption study. *Clay Minerals* 21, 341–360.
- Manceau, A., Calas, G., 1987. Absence of evidence for Ni/Si substitution in phyllosilicates. *Clay Minerals* 22, 357–362.

- Manceau, A., Charlet, L., 1992. X-ray adsorption spectroscopic study of Cr(III) at the oxide–water interface. I Molecular mechanisms of Cr(III) oxidation on Mg oxides. *Journal of Colloid and Interface Science* 148, 425–442.
- Manceau, A., Charlet, L., 1994. The mechanism of selenate adsorption on goethite and hydrous ferric oxide. *Journal of Colloid and Interface Science* 168, 87–94.
- Manceau, A., Combes, J.M., 1988. Structure of Mn and Fe oxides and oxyhydroxides: a topological approach by EXAFS. *Physics and Chemistry of Minerals* 15, 283–295.
- Manceau, A., Decarreau, A., 1988. Extended X-ray absorption fine-structure study of cobalt-exchanged sepiolite: comment on a paper by Y. Fukushima and T. Okamoto. *Clays and Clay Minerals* 36, 382–383.
- Manceau, A., Drits, V.A., 1993. Local structure of ferrihydrite and ferroxhyte by EXAFS spectroscopy. *Clay Minerals* 28, 165–185.
- Manceau, A., Gates, W.P., 1997. Surface structural model for ferrihydrite. *Clays and Clay Minerals* 45, 448–460.
- Manceau, A., Bonnin, D., Kasier, P., Fretigny, C., 1988. Polarized EXAFS spectra of biotite and chlorite. *Physics and Chemistry of Minerals* 16, 180–185.
- Manceau, A., Bonnin, D., Stone, W.E.E., Sanz, J., 1990a. Distribution of Fe in the octahedral sheet of trioctahedral micas by polarized EXAFS. Comparison with NMR results. *Physics and Chemistry of Minerals* 17, 363–370.
- Manceau, A., Combes, J.M., Calas, G., 1990b. New data and a revised model for ferrihydrite: comment on a paper by R.A. Eggleton and R.W. Fitzpatrick. *Clays and Clay Minerals* 38, 331–334.
- Manceau, A., Chateigner, D., Gates, W.P., 1998. Polarized EXAFS, distance-valence least-squares modelling (DLVS), and quantitative texture analysis approaches to the structural refinement of Garfield nontronite. *Physics and Chemistry of Minerals* 25, 347–365.
- Manceau, A., Charlet, L., Boisset, M.C., Didier, B., Spadini, L., 1992a. Sorption and speciation of heavy metals on hydrous Fe and Mn oxides. From microscopic to macroscopic. *Applied Clay Science* 7, 201–223.
- Manceau, A., Drits, V.A., Lanson, B., Chateigner, D., Wu, J., Huo, D., Gates, W.P., Stucki, J.W., 2000a. Oxidation–reduction mechanism of iron in dioctahedral smectites: 2. Crystal chemistry of reduced nontronites. *American Mineralogist* 85, 153–172.
- Manceau, A., Drits, V.A., Silvester, E., Bartoli, C., Lanson, B., 1997. Structural mechanism of  $\text{Co}^{2+}$  oxidation by the phyllo-manganate busenite. *American Mineralogist* 82, 1150–1175.
- Manceau, A., Gorshkov, A.I., Drits, V.A., 1992b. Structural chemistry of manganese, iron cobalt and nickel and manganese hydrous oxides: Part 1. Information from XANES spectroscopy. *American Mineralogist* 77, 1133–1143.
- Manceau, A., Gorshkov, A.I., Drits, V.A., 1992c. Structural chemistry of manganese, iron cobalt and nickel and manganese hydrous oxides: Part 2. Information from EXAFS spectroscopy. *American Mineralogist* 77, 1144–1157.
- Manceau, A., Lanson, B., Drits, V.A., Chateigner, D., Gates, W.P., Wu, J., Huo, D., Stucki, J.W., 2000a. Oxidation–reduction mechanism of iron in dioctahedral smectites: 1. Crystal chemistry of oxidized reference nontronites. *American Mineralogist* 85, 133–152.

- Manceau, A., Lanson, B., Schlegel, M.L., Harge, J.C., Musso, M., Eybert-Berard, L., Hazemann, J.-L., Chateigner, D., Lambie, G.M., 2000b. Quantitative Zn speciation in smelter-contaminated soils by EXAFS spectroscopy. *American Journal of Science* 300, 289–343.
- Manceau, A., Marcus, M.A., Tamura, N., 2002a. Quantitative speciation of heavy metals in soils and sediments by synchrotron X-ray techniques. In: Fenter, P.A., Rivers, M.L., Sturchio, N.C., Sutton, S.R. (Eds.), *Applications of Synchrotron Radiation in Low-Temperature Geochemistry and Environmental Science. Reviews in Mineralogy and Geochemistry*, vol. 49. Mineralogical Society of America, Washington, DC, pp. 341–428.
- Manceau, A., Nagy, K.L., Spadini, L., Ragnarsdottir, K.V., 2000c. Influence of anionic layer structure of Fe-oxyhydroxides on the structure of Cd surface complexes. *Journal of Colloid and Interface Science* 228, 306–316.
- Manceau, A., Schlegel, M., 2001. Texture effect on polarized EXAFS amplitude. *Physics and Chemistry of Minerals* 28, 52–56.
- Manceau, A., Schlegel, M.L., Chateigner, D., Lanson, B., Bartoli, C., Gates, W., 1999a. Application of polarised EXAFS to fine-grained layered minerals. In: Schulze, D.G., Stucki, J.W., Bertsch, P.M. (Eds.), *Synchrotron X-ray Methods in Clay Science. CMS Workshop Lectures*, vol. 9. The Clay Minerals Society, Boulder, CO, pp. 69–114.
- Manceau, A., Schlegel, M.L., Musso, M., Sole, V.A., Gauthier, C., Petit, P.E., Trolard, F., 2000d. Crystal chemistry of trace elements in natural and synthetic goethite. *Geochimica et Cosmochimica Acta* 64, 3643–3661.
- Manceau, A., Schlegel, M.L., Nagy, K.L., Charlet, L., 1999b. Evidence for the formation of trioctahedral clay upon sorption of  $\text{Co}^{2+}$  on quartz. *Journal of Colloid and Interface Science* 220, 181–197.
- Manceau, A., Tamura, N., Marcus, M.A., McDowell, A.A., Celestre, R.S., Sublett, R.E., Sposito, G., Padmore, H.A., 2002b. Deciphering Ni sequestration in soil ferromanganese nodules by combining X-ray fluorescence, absorption and diffraction at micrometer scales of resolution. *American Mineralogist* 87, 1494–1499.
- Manning, B.A., Fendorf, S.E., Bostick, B., Suarez, D.L., 2002. Arsenic(III) oxidation and arsenic(V) adsorption reactions on synthetic birnessite. *Environmental Science Technology* 36, 976–981.
- Martin, F., Petit, S., Decarreau, A., Ildefonse, P., Grauby, O., Beziat, D., de Parseval, P., Noack, Y., 1998. Ga/Al substitutions in synthetic kaolinites and smectites. *Clay Minerals* 33, 231–241.
- Masion, A., Doelsch, E., Rose, J., Moustier, S., Bottero, J.Y., Bertsch, P.M., 2001. Speciation and crystal chemistry of iron(III) chloride hydrolysed in the presence of  $\text{SiO}_4$  ligands. 3. Semilocal scale structure of the aggregates. *Langmuir* 17, 4753–4757.
- Mavrocordatos, D., Fortin, D., 2002. Quantitative characterization of biotic iron oxides by analytical electron microscopy. *American Mineralogist* 87, 940–946.
- McKeown, D.A., 1989. Aluminum X-ray absorption near edge structure of some oxide minerals: calculation versus experimental data. *Physics and Chemistry of Minerals* 16, 678–683.
- McKeown, D.A., Waychunas, G.A., Brown, G.E., 1985. EXAFS study of the coordination environment of aluminum in a series of silica-rich glasses and selected minerals within the  $\text{Na}_2\text{O}-\text{Al}_2\text{O}_3-\text{SiO}_2$  system. *Journal of Non-Crystalline Solids* 74, 349–371.
- Meyer-Ilse, W., Attwood, T.W., 2000. *X-ray Microscopy*, vol. 507. American Institute of Physics, Berkeley.

- Morton, J.D., Semrau, J.D., Hayes, K.F., 2001. An X-ray absorption spectroscopy study of the structure and reversibility of copper adsorbed to montmorillonite clay. *Geochimica et Cosmochimica Acta* 65, 2709–2722.
- Mottana, A., Burragato, F., 1990. *Absorption Spectroscopy in Mineralogy*. Elsevier, Amsterdam.
- Moyes, L.N., Parkman, R.H., Charnock, J.N., Vaughan, D.J., Livens, F.R., Hughes, C.R., Braithwaite, A., 2000. Uranium uptake from aqueous solution by interaction with goethite, lepidocrocite, muscovite, and mackinawite: an X-ray absorption spectroscopy study. *Environmental Science and Technology* 34, 1062–1068.
- Muller, F., Besson, G., Manceau, A., Drits, V.A., 1997. Distribution of isomorphous cations within octahedral sheets in montmorillonite from Camp Bertaux. *Physics and Chemistry of Minerals* 24, 159–166.
- Myneni, S.C.B., Tokunaga, T.K., Brown, G.E., 1997. Abiotic selenium redox transformations in the presence of Fe(II,III) hydroxides. *Science* 278, 1106–1109.
- Newville, M., 2003. IFEFFIT 1.2.5. Copyright 2003, M. Newville, University of Chicago, and documentation support. (<http://cars9.uchicago.edu/ifeffit>).
- O'Day, P.A., Brown, G.E., Parks, G.A., 1994a. X-ray absorption spectroscopy of cobalt(II) multinuclear surface complexes and surface precipitates on kaolinite. *Journal of Colloid and Interface Science* 165, 269–289.
- O'Day, P.A., Newville, M., Neuhoﬀ, P.S., Sahai, N., Carroll, S.A., 2000b. X-ray absorption spectroscopy of strontium(II) coordination. I. Static and thermal disorder in crystalline, hydrated, and precipitated solids and in aqueous solutions. *Journal of Colloid and Interface Science* 222, 184–197.
- O'Day, P.A., Parks, G.A., Brown, G.E., 1994b. Molecular structure and binding sites of cobalt(II) surface complexes on kaolinite from X-ray absorption spectroscopy. *Clays and Clay Minerals* 42, 337–355.
- O'Day, P.A., Rehr, J.J., Zabinsky, S.I., Brown, G.E., 1994c. Extended X-ray absorption fine structure (EXAFS) analysis of disorder and multiple-scattering in complex crystalline solids. *Journal of the American Chemical Society* 116, 2938–2949.
- Östols, E., Manceau, A., Farges, F., Charlet, L., 1997. Adsorption of thorium on amorphous silica: an EXAFS study. *Journal of Colloid and Interface Science* 194, 10–21.
- Papelis, C., Hayes, K.F., 1996. Distinguishing between interlayer and external sorption sites of clay minerals using X-ray absorption spectroscopy. *Colloids and Surfaces A* 107, 89–96.
- Parkman, R.H., Charnock, J.M., Livens, F.R., Vaughan, D.J., 1998. A study of the interaction of strontium ions in aqueous solutions with the surfaces of calcite and kaolinite. *Geochimica et Cosmochimica Acta* 62, 1481–1492.
- Patterson, R.R., Fendorf, S., Fendorf, M., 1997. Reduction of hexavalent chromium by amorphous iron sulphide. *Environmental Science and Technology* 31, 2039–2044.
- Peak, D., Ford, R.G., Sparks, D.L., 1999. An *in situ* ATR-FTIR investigation of sulfate bonding mechanisms on goethite. *Journal of Colloid and Interface Science* 218, 289–299.
- Peterson, M.L., Brown, G.E., Parks, G.A., Stein, C.L., 1997. Differential redox and sorption of Cr(III/VI) on natural silicate and oxide minerals: EXAFS and XANES results. *Geochimica et Cosmochimica Acta* 61, 3399–3412.
- Peterson, M.L., Parks, G.A., Brown, G.E., 1996. Direct XAFS evidence for heterogeneous redox at the aqueous/magnetite interface. *Colloids and Surfaces* 107, 77–88.

- Punshon, T., Bertsch, P.M., Lanziorotti, A., McLeod, K., Burger, J., 2003. Geochemical signature of contaminated sediment remobilization revealed by spatially resolved X-ray microanalysis of annual rings of *Salix nigra*. *Environmental Science and Technology* 37, 1766–1774.
- Rakovan, J., Reeder, R.J., Elzinga, E.J., Cerniak, D.J., Tait, C.D., Morris, D.E., 2002. Structural characterisation of U(VI) in apatite by X-ray absorption spectroscopy. *Environmental Science and Technology* 36, 3114–3117.
- Randal, S.R., Sherman, D.M., Ragnarsdottir, K.V., 1998. An extended X-ray absorption fine structure spectroscopy investigation of cadmium sorption on cryptomelane ( $\text{KMn}_{18}\text{O}_{16}$ ). *Chemical Geology* 151, 95–106.
- Randal, S.R., Sherman, D.M., Ragnarsdottir, K.V., Collins, C.R., 1999. The mechanism of cadmium surface complexation on iron oxyhydroxide minerals. *Geochimica et Cosmochimica Acta* 63, 2971–2987.
- Ravel, B., 1999. TKATOMS 3.0 beta7 (XAFS analysis software) Copyright, 1999, B. Ravel, University of Washington. (<http://feff.phys.washington.edu/~ravel/software/exafs>.)
- Ravel, B., 2003a. ATHENA 0.8.024 (XAFS analysis software). Copyright 2003, B. Ravel, University of Washington. (<http://feff.phys.washington.edu/~ravel/software/exafs>.)
- Ravel, B., 2003b. ARTEMIS 0.6.009 (XAFS analysis software). Copyright 2003, B. Ravel, University of Washington. (<http://feff.phys.washington.edu/~ravel/software/exafs>.)
- Reeder, R.J., Lamble, G.M., Lee, J.-F., Staudt, W.J., 1994. Mechanism of  $\text{SeO}_4^{2-}$  substitution in calcite: an XAFS study. *Geochimica et Cosmochimica Acta* 58, 5639–5646.
- Reeder, R.J., Lamble, G.M., Northrup, P.A., 1999. XAFS study of the coordination and local relaxation around  $\text{Co}^{2+}$ ,  $\text{Zn}^{2+}$ ,  $\text{Pb}^{2+}$ , and  $\text{Ba}^{2+}$  trace elements in calcite. *American Mineralogist* 84, 1049–1060.
- Reeder, R.J., Nugent, M., Lamble, G.M., Tait, C.D., Morris, D.E., 2000. Uranyl incorporation into calcite and aragonite: XAFS and luminescence studies. *Environmental Science and Technology* 34, 638–644.
- Reeder, R.J., Nugent, M., Tait, C.D., Morris, D.E., Heald, S.M., Beck, K.M., Hess, W.P., Lanziorotti, A., 2001. Coprecipitation of uranium(VI) with calcite: XAFS, micro-XAFS, and luminescence characterization. *Geochimica et Cosmochimica Acta* 65, 3491–3503.
- Rehr, J.J., 2003. FEFF software. Copyright 2003, J. Rehr, University of Washington. (<http://feff.phys.washington.edu/feff>.)
- Rehr, J.J., Mustre de Leon, J., Zabinsky, S.I., Albers, R.C., 1991. Theoretical X-ray absorption fine structure standards. *Journal of the American Chemical Society* 113, 5135–5145.
- Rehr, J.J., Zabinsky, S.I., Albers, R.C., 1992. High-order multiple-scattering calculations of X-ray absorption fine structure. *Physics Reviews Letters* 69, 3397.
- Reich, T., Moll, H., Arnold, T., Denecke, M.A., Hennig, C., Geipel, G., Bernhard, G., Nitsche, H., Allen, P.G., Bucher, J.J., Edelstein, N.M., Shuh, D.K., 1998. An EXAFS study of uranium(VI) sorption onto silica gel and ferrihydrite. *Journal of Electron Spectroscopy and Related Phenomena* 96, 237–243.
- Ritherdon, B., Hughes, C.R., Curtis, C.D., Livens, F.R., Mosselmans, J.F.W., Richardson, S., Braithwaite, A., 2003. Heat-induced changes in speciation and extraction of uranium associated with sheet silicate minerals. *Applied Geochemistry* 18, 1121–1135.
- Roberts, D.R., Ford, R.G., Sparks, D.L., 2003. Kinetics and mechanisms of Zn complexation on metal oxides using EXAFS spectroscopy. *Journal of Colloid and Interface Science* 263, 364–376.

- Roberts, D.R., Scheidegger, A.N., Sparks, D.L., 1999. Kinetics of mixed Ni–Al precipitate formation on a soil clay fraction. *Environmental Science and Technology* 33, 3749–3754.
- Roe, A.L., Hayes, K.F., Chisholm-Brause, C.J., Brown, G.E., Hodgson, K.O., Parks, G.A., Leckie, J.O., 1991. X-ray absorption study of lead complexes at  $\alpha$ -FeOOH/water interfaces. *Langmuir* 7, 367–373.
- Rossman, G.R., Tarlan, M.N., 2001. Spectroscopic standards for four- and five-fold coordinated  $\text{Fe}^{2+}$  in oxygen-based minerals. *American Mineralogist* 86, 896–903.
- Sahai, N., Carroll, S.A., Roberts, S., O'Day, P.A., 2000. X-ray absorption spectroscopy of strontium(II) coordination. 2. Sorption and precipitation at kaolin, amorphous silica and goethite surfaces. *Journal of Colloid and Interface Science* 222, 198–212.
- Sains-Diaz, C.I., Hernández-Laguna, A., Dove, M.T., 2001. Theoretical modelling of *cis*-vacant and *trans*-vacant configurations in the octahedral sheet of illites and smectites. *Physics and Chemistry of Minerals* 28, 322–331.
- Sanz, J., Stone, W.E.E., 1983. NMR study of minerals. III. The distribution of  $\text{Mg}^{2+}$  and  $\text{Fe}^{2+}$  around the OH groups in mica. *Journal of Physics C: Solid State Physics* 16, 1271–1281.
- Scheckel, K.G., Scheinost, A.C., Ford, R.G., Sparks, D.L., 2000. Stability of layered Ni hydroxide surface precipitates—a dissolution kinetics study. *Geochimica et Cosmochimica Acta* 64, 2727–2735.
- Scheckel, K.G., Sparks, D.L., 2000. Kinetics of the formation and dissolution of Ni precipitates in a gibbsite/amorphous silica mixture. *Journal of Colloid and Interface Science* 229, 222–229.
- Scheidegger, A.M., Lamble, G.M., Sparks, D.L., 1996a. Investigations of Ni adsorption on pyrophyllite. *Environmental Science and Technology* 30, 548–554.
- Scheidegger, A.M., Fendorf, M., Sparks, D.L., 1996b. Mechanisms of nickel sorption on pyrophyllite. Macroscopic and microscopic approaches. *Soil Science Society of America Journal* 60, 1763–1777.
- Scheidegger, A.M., Lamble, G.M., Sparks, D.L., 1997. Spectroscopic evidence for the formation of mixed-cation hydroxide phases upon metal sorption on clays and aluminum oxides. *Journal of Colloid and Interface Science* 186, 118–128.
- Scheidegger, A.M., Strawn, D.G., Lamble, G.M., Sparks, D.L., 1998. The kinetics of mixed Ni–Al hydroxide formation on clay and aluminum oxide minerals: a time resolved XAS study. *Geochimica et Cosmochimica Acta* 62, 2233–2245.
- Scheinost, A.C., Abend, S., Pandya, K.I., Sparks, D.L., 2001. Kinetic controls on Cu and lead sorption by ferrihydrite. *Environmental Science and Technology* 35, 1090–1096.
- Scheinost, A.C., Ford, R.G., Sparks, D.L., 1999. The role of Al in the formation of secondary Ni precipitates on pyrophyllite, gibbsite, talc, and amorphous silica: a DRS study. *Geochimica et Cosmochimica Acta* 63, 3193–3203.
- Scheinost, A.C., Sparks, D.L., 2000. Formation of layered single and double-metal hydroxide precipitates at the mineral/water interface: a multiple scattering XAFS analysis. *Journal of Colloid and Interface Science* 223, 1–12.
- Schlegel, M.L., Charlet, L., Manceau, A., 1998. Adsorption mechanism of Co(II) on hectorite and its consequence on the dissolution process: insight from EXAFS and kinetic chemical studies. *Mineralogical Magazine* 62A, 1337–1338.

- Schlegel, M.L., Manceau, A., Charlet, L., 1999a. Sorption of metal ions on clay minerals. 2. Mechanism of Co sorption on hectorite at high and low ionic strength and impact on the sorbent stability. *Journal of Colloid and Interface Science* 220, 392–405.
- Schlegel, M.L., Manceau, A., Charlet, L., Chateigner, D., Hazemann, J.-L., 2001a. Sorption of metal ions on clay minerals. 3. Nucleation and epitaxial growth of Zn phyllosilicate on edges of hectorite. *Geochimica et Cosmochimica Acta* 65, 4155–4170.
- Schlegel, M.L., Manceau, A., Chateigner, D.L., Charlet, L., 1999b. Sorption of metal ions on clay minerals. 1. Polarized EXAFS evidence for the adsorption of Co on the edges of hectorite particles. *Journal of Colloid and Interface Science* 215, 140–158.
- Schlegel, M.L., Manceau, A., Charlet, L., Hazemann, J.L., 2001b. Absorption mechanisms of Zn on hectorite as a function of time, pH and ionic strength. *American Journal of Science* 301, 798–830.
- Schulze, D.G., McCay-Buis, T., Sutton, S.R., Huber, D.M., 1995a. Manganese oxidation states in *Gaeumannomyces* infested wheat rhizospheres probed by micro XANES spectroscopy. *Phytopathology* 85, 990–994.
- Schulze, D.G., Stucki, J.W., Bertsch, P.M., 1999. Synchrotron X-ray Methods in Clays Science. CMS Workshop Lectures, vol. 9. The Clay Minerals Society, Boulder, CO.
- Schulze, D.G., Sutton, S.R., Bajt, S., 1995b. Determining Mn oxidation states in soils using X-ray absorption near-edge structure (XANES) spectroscopy. *Soil Science Society of America Journal* 59, 1540–1548.
- Silvester, E., Charlet, L., Manceau, A., 1995. Mechanism of Cr(III) oxidation by Na-birnesite. *Journal of Physical Chemistry* 99, 16662–16669.
- Slade, P.G., Gates, W.P., 2004a. The swelling of HDTMA smectites as influenced by their preparation and layer charges. *Applied Clay Science* 25, 93–101.
- Slade, P.G., Gates, W.P., 2004b. The ordering of HDTMA in the interlayers of vermiculite and the influence of solvents. *Clays and Clay Minerals* 52, 204–210.
- Slade, P.G., Self, P.G., Quirk, J.P., 1998. The interlayer structure of La-vermiculite. *Clays and Clay Minerals* 46, 629–635.
- Spadini, L., Manceau, A., Schindler, P.W., Charlet, L., 1994. Structure and stability of  $\text{Cd}^{2+}$  surface complexes on ferric oxides. 1. Results from EXAFS spectroscopy. *Journal of Colloid and Interface Science* 168, 73–86.
- Stern, E.A., Heald, S.M., 1983. Basic principles and applications of EXAFS. In: Koch, E.E. (Ed.), *Handbook of Synchrotron Science*. North-Holland, New York, pp. 955–1014.
- Stern, E.A., Kim, K., 1981. Thickness effect on the extended X-ray absorption fine structure amplitude. *Physics Reviews B* 23, 3781–3787.
- Strawn, D.G., Doner, H., Zavarin, M., McHugo, S., 2002. Microscale investigation into the geochemistry of arsenic, selenium and iron in soil developed in pyritic shale materials. *Geoderma* 108, 237–257.
- Strawn, D.G., Sparks, D.L., 1999. The use of XAFS to distinguish between inner- and outer-sphere lead adsorption complexes on montmorillonite. *Journal of Colloid and Interface Science* 216, 257–269.
- Sturchio, N.C., Chiarello, R.P., Cheng, L., Lyman, P.F., Bedzyk, M.J., Qian, Y., You, H., Yee, D., Geissbuhler, P., Liang, Y., Baer, D.R., 1997. Lead adsorption at the calcite–water interface: synchrotron X-ray standing wave and X-ray reflectivity studies. *Geochimica et Cosmochimica Acta* 61, 251–263.
- Suib, S.L., Carrado, K.A., 1985. Uranyl clay photocatalysts. *Inorganic Chemistry* 24, 863–867.



- Sutton, S., Rivers, M., 1999. Hard X-ray synchrotron microprobe techniques and applications. In: Schulze, D.G., Stucki, J.W., Berstch, P.M. (Eds.), *Synchrotron X-ray Methods in Clay Science*. CMC Workshop Lectures, vol. 9. The Clay Minerals Society, Boulder, CO, pp. 146–163.
- Sutton, S.R., Jones, K.W., Gordon, B., Rivers, M.L., Smith, J.V., 1993. Reduced chromium in olivine grains from lunar basalt 15555: X-ray absorption near edge structure (XANES). *Geochimica et Cosmochimica Acta* 57, 461–468.
- Sylwester, E.R., Hudson, E.A., Allen, P.G., 2000. The structure of uranium(VI) sorption complexes on silica, alumina, and montmorillonite. *Geochimica et Cosmochimica Acta* 64, 2431–2438.
- Taylor, R.W., Shen, S., Bleam, W.F., Tu, S.I., 2000. Chromate removal by dithionite-reduced clays: evidence from direct X-ray absorption near edge spectroscopy (XANES) of chromate reduction at clay surfaces. *Clays and Clay Minerals* 48, 648–654.
- Telleria, M.I., Slade, P.G., Radoslovich, E.W., 1977. X-ray study of the interlayer region of a barium-vermiculite. *Clays and Clay Minerals* 25, 119–125.
- Templeton, A.S., Ostergren, J.D., Trainor, T.P., Foster, A.L., Traina, S.J., Spormann, A.M., Brown, G.E., 1999. XAFS and XSW studies of the distribution and chemical speciation of Pb sorbed to biofilms on  $\alpha$ -Al<sub>2</sub>O<sub>3</sub> and  $\alpha$ -FeOOH surfaces. *Journal of Synchrotron Radiation* 6, 642–644.
- Templeton, A.S., Spormann, A.M., Brown, G.E., 2003b. Speciation of Pb(II) sorbed by *Burkholderia cepacia*/goethite composites. *Environmental Science and Technology* 37, 2166–2172.
- Templeton, A.S., Trainor, T.P., Spormann, A.M., Newville, M., Sutton, S., Dohnalkova, A., Gorby, Y., Brown, G.E., 2003a. Sorption vs biomineralisation of Pb(II) within *Burkholderia cepacia* biofilms on alumina. *Environmental Science and Technology* 37, 300–307.
- Teo, B.K., 1986. EXAFS: Basic Principles and Data Analysis. *Inorganic Chemistry Concepts* 9. Springer, New York.
- Thompson, H.A., Brown, G.E., Parks, G.E., 1997. XAFS study of uranyl coordination in solids and aqueous solution. *American Mineralogist* 82, 483–496.
- Thompson, H.A., Parks, G.A., Brown, G.E., 1998. Structure and composition of uranium(VI) sorption complexes at the kaolinite–water interface. In: Jenne, E.A. (Ed.), *Adsorption of Metals by Geomedia: Variables, Mechanisms, and Model Applications*. Academic Press, New York, pp. 349–370.
- Thompson, H.A., Parks, G.A., Brown, G.E., 1999. Dynamic interactions of dissolution, surface adsorption and precipitation in an aging cobalt(II)–clay–water system. *Geochimica et Cosmochimica Acta* 63, 1767–1779.
- Thompson, H.A., Parks, G.A., Brown, G.E., 2000. Formation and release of cobalt(II) sorption and precipitation products in aging kaoline–water slurries. *Journal of Colloid and Interface Science* 222, 241–253.
- Tokunaga, T.K., Brown, G.E., Pickering, I.J., Sutton, S.R., Bajt, S., 1997. Selenium redox reactions and transport between ponded waters and sediments. *Environmental Science and Technology* 31, 1419–1425.
- Tokunaga, T.K., Sutton, S.R., Bajt, S., Nuessle, P., Shea-McCarthy, G., 1998. Selenium diffusion and reduction at the water-sediment boundary: Micro XANES spectroscopy of reactive transport. *Environmental Science and Technology* 32, 1092–1098.
- Toth, L.M., Begun, G.M., 1981. Raman spectra of uranyl ion and its hydrolysis products in aqueous HNO<sub>3</sub>. *Journal of Physical Chemistry* 85, 547–549.

- Tournassat, C., Charlet, L., Bosbach, D., Manceau, A., 2002. Arsenic(III) oxidation by birnessite and precipitation of manganese(II) arsenate. *Environmental Science and Technology* 36, 493–500.
- Towle, S.N., Bargar, J.R., Brown, G.E., Parks, G.A., Barbee, T.W., 1995. Effect of surface structure of adsorption of Co(II) on  $\alpha$ -Al<sub>2</sub>O<sub>3</sub>: a glancing angle XAFS study. *Materials Research Society Symposium (Structure and Properties of Interfaces in Ceramics) Proceedings*, vol. 357, pp. 23–28.
- Towle, S.N., Bargar, J.R., Brown, G.E., Parks, G.A., 1999b. Sorption of Co(II) on metal oxide surfaces: 2. Identification of Co(II) (aq) adsorption sites on (1-102) and (0001) surfaces of  $\alpha$ -Al<sub>2</sub>O<sub>3</sub> by grazing-incidence XAFS spectroscopy. *Journal of Colloid and Interface Science* 217, 312–321.
- Towle, S.N., Brown, G.E., Parks, G.A., 1999a. Sorption of Co(II) on metal oxide surfaces: 1. Identification of specific binding sites of Co(II) on (110) and (001) spaces of TiO<sub>2</sub> (rutile) by grazing-incidence XAFS spectroscopy. *Journal of Colloid and Interface Science* 217, 299–311.
- Trainor, T.P., Fitts, J.P., Grochimund, D., Bargar, J.R., Brown, G.E., 1999. Grazing-incidence XAFS study of aqueous Zn(II) on sapphire single crystals. *Journal of Synchrotron Radiation* 6, 618–620.
- Trainor, T.P., Templeton, A.S., Brown, G.E., Parks, G.A., 2002. Application of the long-period X-ray standing wave technique to the analysis of surface reactivity: Pb(II) sorption at  $\alpha$ -Al<sub>2</sub>O<sub>3</sub>/aqueous solution interfaces in the presence and absence of Se(VI). *Langmuir* 18, 5782–5791.
- Trivedi, P., Axe, L., Tyson, T.A., 2001a. An analysis of Zn sorption to amorphous vs crystalline iron oxides using XAS. *Journal of Colloid and Interface Science* 244, 230–238.
- Trivedi, P., Axe, L., Tyson, T.A., 2001b. XAS studies of Ni and Zn sorbed to hydrous manganese oxide. *Environmental Science and Technology* 35, 4515–4521.
- Tsipursky, S.I., Drits, V.A., 1984. The distribution of cations in the 2:1 layers of dioctahedral smectites studied by oblique-texture electron diffraction. *Clay Minerals* 19, 177–193.
- Vantelon, D., Montarges-Pelletier, E., Michot, L.J., Briois, V., Pelletier, M., Thomas, F., 2003. Iron distribution in the octahedral sheet of dioctahedral smectites. An Fe K-edge X-ray absorption spectroscopy study. *Physical Chemistry of Minerals* 30, 44–53.
- Vantelon, D., Pelletier, M., Michot, L.J., Barres, O., Thomas, F., 2001. Fe, Mg, and Al distribution in the octahedral layer of montmorillonites. An infrared study in the OH bending region. *Clay Minerals* 36, 369–379.
- Vaughan, D.J., Patrick, R.A.D., 1995. *Mineral Surfaces*, vol. 5. The Mineralogical Society Series. Chapman & Hall, London.
- Waite, T.D., Davis, J.A., Payne, T.E., Waychunas, G.A., Xu, N., 1994. Uranium(VI) adsorption on ferrihydrite: application of a surface complexation model. *Geochimica et Cosmochimica Acta* 58, 5465–5478.
- Waychunas, G.A., 1987. Synchrotron radiation XANES spectroscopy of Ti in minerals: effects of Ti bonding distances, Ti valence and site geometry on absorption edge structure. *American Mineralogist* 72, 89–101.
- Waychunas, G.A., 2002. Grazing-incidence X-ray absorption and emission spectroscopy. In: Fenter, P.A., Rivers, M.L., Sturchio, N.C., Sutton, S.R. (Eds.), *Applications of Synchrotron Radiation in Low-Temperature Geochemistry and Environmental Science. Reviews in Mineralogy and Geochemistry*, vol. 49. Mineralogical Society of America, Washington, DC, pp. 267–311.

- Waychunas, G.A., Apte, M.J., Brown, G.E., 1983. X-ray absorption spectra of Fe minerals and model compounds. *Physics and Chemistry of Minerals* 10, 1–9.
- Waychunas, G.A., Brown, G.E., 1990. Polarized X-ray absorption spectroscopy of metal ions in minerals. *Physics and Chemistry of Minerals* 17, 420–430.
- Waychunas, G.A., Brown, G.E., Apte, M.J., 1986. X-ray K-edge absorption spectra of Fe minerals and model compounds: II EXAFS. *Physics and Chemistry of Minerals* 13, 31–47.
- Waychunas, G.A., Davis, J.A., Fuller, C.C., 1995. Geometry of sorbed arsenate on ferrihydrite and crystalline FeOOH: re-evaluation of EXAFS results and topological factors in predicting sorbate geometry, and evidence for monodentate complexes. *Geochimica et Cosmochimica Acta* 59, 3655–3661.
- Waychunas, G.A., Davis, J.A., Reitmeyer, R., 1999. GIXAFS study of Fe<sup>3+</sup> sorption and precipitation on natural quartz surfaces. *Journal of Synchrotron Radiation* 6, 615–617.
- Waychunas, G.A., Fuller, C.C., Davis, J.A., 2002a. Surface complexation and precipitate geometry for aqueous Zn(II) sorption on ferrihydrite: 1. X-ray absorption extended fine structure spectroscopy analysis. *Geochimica et Cosmochimica Acta* 66, 1119–1137.
- Waychunas, G.A., Fuller, C.C., Davis, J.A., Rehr, J.J., 2002b. Surface complexation and precipitate geometry for aqueous Zn(II) sorption of ferrihydrite: 2. XANES analysis. *Geochimica et Cosmochimica Acta* 67, 1031–1043.
- Waychunas, G.A., Rea, B.A., Fuller, C.C., Davis, J.A., 1993. Surface chemistry of ferrihydrite: Part 1. EXAFS studies of the geometry of coprecipitated and adsorbed arsenate. *Geochimica et Cosmochimica Acta* 57, 2251–2269.
- Weesner, F.J., Bleam, W.F., 1997. X-ray absorption and EPR spectroscopic characterization of adsorbed copper(II) complexed at the boehmite (AlOOH) surface. *Journal of Colloid and Interface Science* 196, 79–86.
- Weiss, C.A., Kirkpatrick, R.J., Altaner, S.P., 1990. Variations in interlayer cation sites of clay minerals as studied by <sup>133</sup>Cs MAS nuclear magnetic resonance spectroscopy. *American Mineralogist* 75, 970–982.
- Wharton, M.J., Atkins, B., Charnock, J.M., Livens, F.R., Patrick, R.A.D., Collison, D., 1999. An X-ray absorption spectroscopy study of the coprecipitation of Tc and Re with meekinsite (FeS). *Applied Geochemistry* 15, 347–354.
- Wu, Z., Marcelli, A., Mottana, A., Giulli, G., Paris, E., Seifert, F., 1996. Effects of higher-coordination shells in garnets detected by X-ray absorption spectroscopy at the Al K-edge. *Physics Reviews B* 54, 2976–2979.
- Xia, K., Mehadi, A., Taylor, R.W., Bleam, W.F., 1997. X-ray absorption and electron paramagnetic resonance studies of Cu(II) sorbed to silica: surface-induced precipitation at low surface coverages. *Journal of Colloid and Interface Science* 185, 252–257.
- Zhao, J., Huggins, F.E., Feng, Z., Huffman, G.P., 1994. Ferrihydrite: surface structure and its effects on phase transformation. *Clays and Clay Minerals* 42, 737–746.
- Zhao, J., Huggins, F.E., Feng, Z., Lu, F., Shah, N., Huffman, G.P., 1993. Structure of a nanophase iron oxide catalyst. *Journal of Catalysis* 143, 499–509.

*Chapter 12.4*

## X-RAY PHOTOELECTRON SPECTROSCOPY

H. SEYAMA<sup>a</sup>, M. SOMA<sup>b,1</sup> AND B. K.G. THENG<sup>c</sup>

<sup>a</sup>*Environmental Chemistry Division, National Institute for Environmental Studies, 16-2 Onogawa, Tsukuba, Ibaraki 305-8506, Japan*

<sup>b</sup>*Institute for Environmental Sciences, University of Shizuoka, 52-1 Yada, Shizuoka, Shizuoka 422-8526, Japan*

<sup>c</sup>*Landcare Research, Palmerston North, New Zealand*

The size of clay particles is in the micrometer range. As the specific surface area of a particulate assemblage is inversely proportional to the size of its constituent particles, clays make an important contribution to many processes that occur at the surface of soil particles. However, even for a particle of micrometer dimensions the number of atoms exposed at the surface is a small fraction of the total. For example, in a simple cubic lattice with a lattice constant of 0.2 nm, the fraction of surface-exposed atoms of a 1  $\mu\text{m}$  cube is only  $1.2 \times 10^{-3}$ . For this reason, surface-specific analytical techniques are required for assessing the chemical composition of clay particle surfaces. A general review of these techniques together with their mineralogical applications was provided by [Hochella \(1995\)](#).

X-ray photoelectron spectroscopy (XPS) is the single, most versatile technique for analysing the surface composition of clay mineral particles under different chemical conditions. XPS can detect almost all elements in the surface layer with sensitivities not varying by two orders of magnitude, and provide information on chemical bonding. An added advantage is that XPS is essentially non-destructive even for materials of high susceptibility. Thus XPS can reveal differences in chemical composition between the surface and the bulk, and assess changes in composition and chemical bonding as a result of surface interactions with other materials.

Here we focus on the application of XPS for characterizing clay and clay mineral surfaces. An advanced textbook on the principles and instrumentation of electron spectroscopy is that by [Briggs and Seah \(1990\)](#). The analysis of clay materials by XPS was earlier reviewed by [Cocke et al. \(1994\)](#) and [Paterson and Swaffield \(1994\)](#), while [Seyama and Soma \(2003\)](#) summarized the application of XPS and other surface-analytical techniques in the analysis of geological and environmental samples.

---

<sup>1</sup>Present Address: 6-8 Tsutsujigaoka, Aoba-ku, Yokohama, kanagawa 227-0055, Japan

## 12.4.1. PRINCIPLES OF X-RAY PHOTOELECTRON SPECTROSCOPY

XPS measures the kinetic-energy distribution of electrons (photoelectrons) emitted from core levels of the elements constituting a solid when the sample is irradiated by X-rays (Fig. 12.4.1). The measured core electron binding energy ( $BE_X$ ), defined as the difference between the energy of the primary photon ( $h\nu$ ) and the kinetic energy of the photoelectron ( $KE_P$ ), allows the element in question to be identified:

$$BE_X = h\nu - KE_P \quad (1)$$

In practice, Eq. (1) must be corrected for some experimental factors, as described below.

When an atom emits a photoelectron, it is left with a vacancy in its inner orbital, and becomes unstable. Auger transition is one of the processes by which the unstable, excited atom undergoes relaxation (Fig. 12.4.1). Here, an outer-orbital electron is transferred to the vacancy, and the excess energy is released through the emission of another outer-orbital electron (XYZ Auger electron). The Auger electron kinetic energy ( $KE_A$ ), given approximately by Eq. (2), is a characteristic of an Auger transition for a specific atom:

$$KE_A = BE_X - BE_Y - BE_Z \quad (2)$$

XPS measures both photoelectrons and Auger electrons.

The X-ray beam penetrates the sample to a depth of 1–100  $\mu\text{m}$ , causing the ejection of photoelectrons and Auger electrons. Electrons that escape to the surface from deeper parts of the sample may lose kinetic energy through inelastic scattering. It is such inelastically scattered electrons that give rise to the background in an XPS spectrum. The inelastic mean free-path of an electron in the solid depends on its

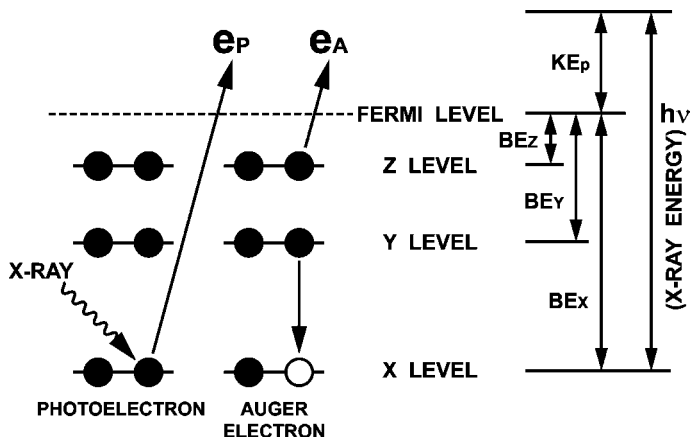


Fig. 12.4.1. Photoelectron ( $e_P$ ) and Auger electron ( $e_A$ ) emission processes induced by X-ray.

kinetic energy. Both photoelectron and Auger electron measured by conventional XPS have kinetic energy less than 1500 eV and their inelastic free-path is very short, typically of the order of nm. Therefore XPS is a surface-sensitive technique. All elements, other than H and He, are detectable by XPS when their concentrations exceed 0.1–1%. For samples with a flat surface, the spectral background can be reduced by using a total-reflection X-ray or a grazing-incidence X-ray because of its shallow depth of penetration (Kawai et al., 1995). Since XPS is non-destructive, the characteristic features of photoelectron and Auger electron spectra also provide information on the state of chemical bonding of the elements concerned.

Recent developments in XPS instrumentation enable photoelectron images with a lateral resolution in the micrometer to submicrometer range to be obtained through scanning or direct imaging techniques (Garwood, 1995). In particular, photoelectron emission microscopy (PEEM) is a promising technique for observing direct photoelectron images of surface chemical composition (Kordesch, 1995; De Stasio et al., 1998). A lateral resolution down to 20 nm was achieved using X-ray PEEM (X-PEEM) with a synchrotron-radiation photon source (De Stasio et al., 1999). The application of X-PEEM to the analysis of geological samples was reported by De Stasio et al. (2001).

## 12.4.2. EXPERIMENTAL TECHNIQUES

### *A. Instrumentation and Sample Handling*

XPS measurements are conducted under ultra-high vacuum ( $<10^{-8}$  Torr) so as to avoid collision between photoelectrons and gas molecules in the spectrometer, while surface contamination from residual gases is minimized. Fig. 12.4.2 shows a schematic diagram of a typical X-ray photoelectron spectrometer, consisting of an X-ray source, an electron energy analyzer, and a photoelectron detector. Common X-ray sources are Al K $\alpha$  (1486.6 eV) and Mg K $\alpha$  (1253.6 eV). By using monochromatized X-rays with a narrow line width, satellite spectra excited by K $\alpha_{3,4}$  and K $\beta$  lines can be eliminated, and the energy resolution of photoelectrons improved. The ejected photoelectrons are transferred to an electron energy analyzer, and separated according to their kinetic energy. Among the various types of analyzers (Briggs and Seah, 1990), the concentric hemispherical analyzer (CHA) and cylindrical mirror analyzer (CMA) are the most commonly employed. Following energy analysis, the photoelectrons are detected by electron multipliers.

Fig. 12.4.3 shows a wide-scan spectrum of Na<sup>+</sup>-montmorillonite excited by Al K $\alpha$ , demonstrating the multi-element detection capability of XPS. In this respect, it is comparable with X-ray fluorescence (XRF) spectrometry for bulk elemental analysis. The wide-scan XPS spectrum shows the photoelectron and Auger electron lines of the constituent elements, notably Si (2s, 2p), Al (2s, 2p), Mg (KLL Auger), Na (1s, KLL Auger), and O (2s, 1s, KLL Auger). The set of core photoelectron lines,

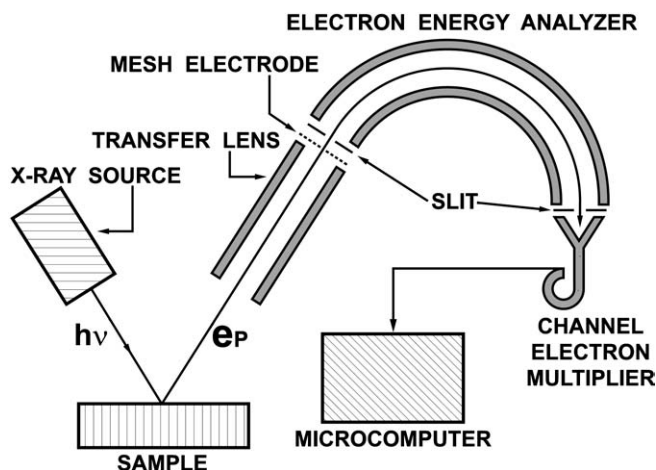


Fig. 12.4.2. Schematic diagram of XPS measurement system equipped with a concentric hemispherical analyzer (CHA).

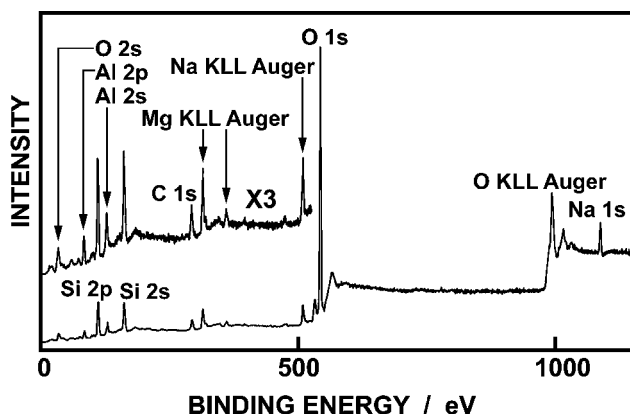


Fig. 12.4.3. Wide-scan X-ray photoelectron spectrum of Na-montmorillonite excited by Al  $K\alpha$  radiation.

together with the X-ray-induced Auger electron lines, are useful for element identification. At the same time, however, the probability of overlap with lines of different atoms increases. This can sometimes cause difficulties in identifying and quantifying minor constituents.

Because clays are electrical insulators, positive electrostatic charges can build up at the sample surface due to electron emission during measurement. In practice, the measured kinetic energy ( $KE_m$ ) differs from the ideal value ( $KE_i$ ), identifiable with

$KE_P$  in Eq. (1) or  $KE_A$  in Eq. (2). The relationship between  $KE_m$  and  $KE_i$  is given by:

$$KE_m = KE_i - \Phi_{sp} - E_c \quad (3)$$

where  $\Phi_{sp}$  is the work function of the spectrometer; that is, the energy required to bring the electron from its zero binding energy (or Fermi) level to that of the spectrometer.  $E_c$  is the additional retarding energy due to sample charging. In order to determine the photoelectron binding energy and Auger electron kinetic energy, the measured electron energy should be corrected for  $\Phi_{sp}$  and  $E_c$ .

The C 1s or Au 4f<sub>7/2</sub> line is widely used as a primary standard for the calibration of electron energies. It is often convenient to use the C 1s line (of hydrocarbons) for this purpose since this peak usually arises from adventitious surface contamination by vacuum pump oil. However, the C 1s binding energy depends on the nature of the carbon source, and hence is not an accurate binding energy standard. Further, differential charging of the sample and hydrocarbons (due to differences in electric non-conductance) may cause an unexpected error in binding energy determination. On the other hand, the Au 4f<sub>7/2</sub> line of a gold film, evaporated onto the sample, is a reliable standard since its binding energy (84.0 eV) was precisely measured (Ebel et al., 1983; Anthony and Seah, 1984). Thus, the electron binding energy of the constituent elements in a given sample is frequently determined relative to that of Au 4f<sub>7/2</sub> on the assumption that the Fermi level of the sample coincides with that of the evaporated gold.

Mineral samples for analysis by XPS usually come in the form of a powder or a thin section. Before being inserted into the apparatus, the sample is dried and attached to a metal sample holder by a double-sided sticky tape, an electrically conductive paste, or by other means. Samples may also be mounted by placing a suspension of the powder on the sample holder, and by allowing the dispersant to evaporate. Alternatively, the sample may be pressed into a soft metal, such as indium. Whatever method is adopted, due care should be taken to avoid or, at least, minimize surface contamination.

### B. Quantitative Analysis

The area under a given peak in a photoelectron spectrum is directly proportional to the concentration of the element in question, assuming that the element is homogeneously distributed in the analyzed volume. Since peak intensity increases as the effective surface area of the sample increases, it is difficult to estimate the absolute concentration of a given element. In practice, one derives the concentration of element A relative to that of a reference element B (atomic ratio,  $N_A/N_B$ ) from the measured photoelectron intensities ( $I_A$  for element A and  $I_B$  for element B):

$$\frac{N_A}{N_B} = \left( \frac{1}{S_{AB}} \right) \times \left( \frac{I_A}{I_B} \right) \quad (4)$$



where  $S_{AB}$  is the relative atomic sensitivity factor. Included in this factor are such parameters as the photoionization cross-section, anisotropy of photoelectron emission, detection efficiency of the spectrometer, and mean free-paths of photoelectrons. Relative atomic sensitivity factors are derived either theoretically (from calculated photoionization cross-sections and other parameters), or experimentally (from XPS measurements of reference compounds of known homogeneous chemical composition). Commercial XPS instruments are equipped with a microcomputer for instrument control, data acquisition, and data handling. Relative surface concentrations (elemental compositions) can be calculated by the computer using appropriate software (smoothing, background subtraction, peak deconvolution, peak area calculation, etc.).

The uncertainty in elemental quantification by XPS mainly arises from the application of the atomic sensitivity factor to samples with different matrices (Seah, 1980). In our experience, the relative surface concentration of an element can be obtained within an error of 10–20%, using experimentally determined relative atomic sensitivity factors. However, for photoelectrons with a low kinetic energy (i.e., a high binding energy) the values derived are less certain. This is because the mean free-path of the corresponding photoelectrons is shorter, and their intensity is more susceptible to surface contamination, than their high-energy counterparts.

The reproducibility in deriving relative surface concentrations from XPS spectra was checked by Seyama and Soma (1984, 1988). From measurement of the area intensity ratios of Si 2s to Al 2p of montmorillonite samples having different exchangeable cations, these workers concluded that the values are reproducible within  $\pm 10\%$ . On the surfaces of freshly prepared silicates (clay and related minerals), the relative abundances of major cations (Si, Al, Fe, Mg, Na, K, etc.) usually correspond to their bulk chemical compositions. However, the surface concentration of oxygen tends to exceed the bulk value because of the presence of  $\text{OH}^-$  ions and/or water molecules at the surface (Seyama and Soma, 1985, 1988).

### C. Chemical Information

Characteristic features of photoelectron and Auger electron spectra, such as peak position (electron binding or kinetic energy), satellite structure, and multiplet splitting, reflect the bonding state of elements. For some elements, it is possible to measure both photoelectron and Auger electron spectra. In such cases, it is especially informative to obtain a two-dimensional plot of both electron energies (Wagner et al., 1979). Such a 'chemical-state plot' was used to characterize the bonding state of some elements in clay minerals (Seyama and Soma, 1984, 1988; Dutta et al., 1999). Wagner et al. (1979) also measured the modified Auger parameter ( $\alpha'$ ), defined as the sum of the photoelectron binding energy and Auger electron kinetic energy of an element, and proposed that the value of  $\alpha'$  is unique to each chemical-bonding state.

For bonding state characterization it is customary to compare the photoelectron binding energy and/or Auger electron kinetic energy of an element in the sample

with that of a reference compound. The shift in peak (electron energy) position relative to that of the reference compound is called the chemical shift. The chemical shift in the photoelectron binding energy ( $\Delta BE_X$ ) is dependent on the state (chemical environment) of the atom, in particular its electron density (oxidation number). The lower the electron density, the higher the photoelectron binding energy. The Fe 2p photoelectron spectrum is a case in point. The Fe 2p<sub>3/2</sub> binding energy of Fe<sup>3+</sup> in silicate minerals (about 712 eV) is higher than that of Fe<sup>2+</sup> (710–711 eV). Further, the Fe 2p spectra of silicate minerals have satellite peaks characteristic of the oxidation state of the iron (Seyama and Soma, 1987). The nature of atoms surrounding the host atom, that is of nearest neighbours (and, in some cases, non-nearest neighbours), also influences the chemical shift. For example, for silicate minerals there is a positive correlation between the photoelectron binding energies of Si 2s (2p) and O 1s (Seyama and Soma, 1985, 1988). These values refer to the silicate framework (structure), and decrease as the negative charge on the silicate structure increases.

Fig. 12.4.4, showing the Mg 1s and Mg KL<sub>23</sub>L<sub>23</sub> Auger electron spectra of Mg<sup>2+</sup>-montmorillonite excited by Al K $\alpha$  radiation, gives another example of

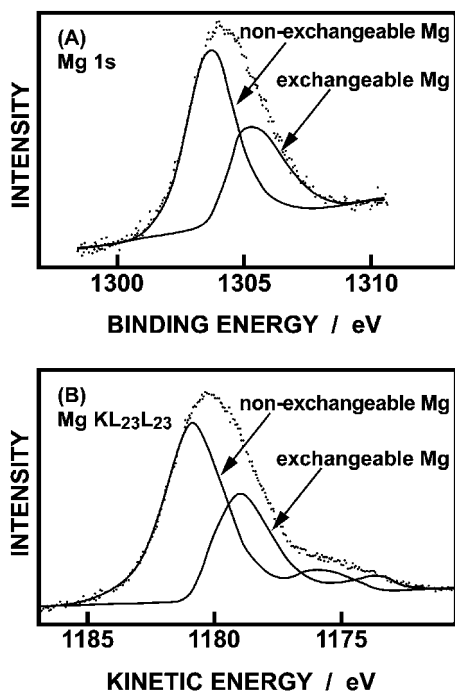


Fig. 12.4.4. (A) Mg 1s and (B) KL<sub>23</sub>L<sub>23</sub> Auger spectra of Mg-montmorillonite (Reproduced, by permission of The Royal Society of Chemistry, from Seyama and Soma, 1984).

deriving chemical information from XPS analysis (Seyama and Soma, 1984). For both electrons the spectra are broad, and each can be deconvoluted into two components corresponding to: (i) non-exchangeable  $\text{Mg}^{2+}$  ions occupying octahedral sites within the layer structure; and (ii) exchangeable  $\text{Mg}^{2+}$  ions occupying interlayer sites.

Fig. 12.4.5 shows a chemical-state plot for magnesium, comparing the relationship between Mg 1s binding energy and Mg  $\text{KL}_{23}\text{L}_{23}$  Auger kinetic energy for  $\text{Mg}^{2+}$ -montmorillonite with that of magnesium halides and magnesium oxide. The position of exchangeable (interlayer)  $\text{Mg}^{2+}$  ion falls between that of  $\text{MgCl}_2 \cdot 6\text{H}_2\text{O}$  and  $\text{MgF}_2$ . In contrast, the point for non-exchangeable (structural)  $\text{Mg}^{2+}$  ion is close to that for  $\text{MgO}$ . The Mg 1s binding energy for non-exchangeable  $\text{Mg}^{2+}$  ions is 1.5 eV lower, while the Mg  $\text{KL}_{23}\text{L}_{23}$  Auger kinetic energy is 2.0 eV higher, than the corresponding values for exchangeable  $\text{Mg}^{2+}$  ions. These large differences may be attributed to the effect of neighbouring atoms. Apparently, the flow of electronic charge to  $\text{Mg}^{2+}$  as well as the extra-atomic relaxation (a screening of the final-state ion in the Auger transition by electrons from neighbouring atoms) are larger for non-exchangeable  $\text{Mg}^{2+}$  ions because of its stronger interaction with  $\text{O}^{2-}$  and  $\text{OH}^-$  ions within the aluminosilicate layers.

Although XPS is essentially non-destructive, irradiation by X-rays can occasionally cause chemical damage (alteration) to the sample. For example, during XPS measurement  $\text{Cu}^{2+}$  ions (structural, adsorbed, or interlayer) in clay minerals can be converted into  $\text{Cu}^+$  through photoreduction (Mosser et al., 1992).

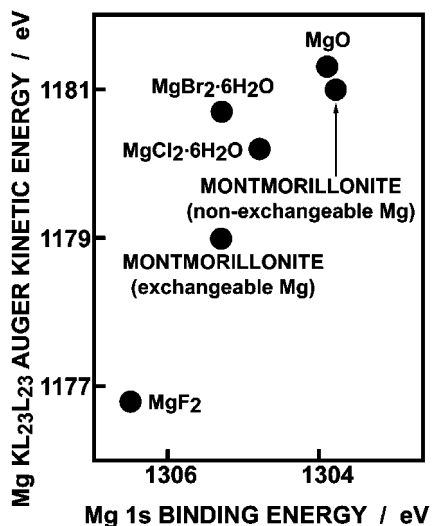


Fig. 12.4.5. Chemical-state plot for Mg (Reproduced, by permission of The Royal Society of Chemistry, from Seyama and Soma, 1984).

### 12.4.3. APPLICATIONS

Despite its limited sensitivity in terms of spatial and binding energy (chemical shift) resolution, XPS can provide valuable information on the surface composition of clays and clay minerals, and the chemical bonding of the constituent elements. The examples below illustrate this capability.

The particles of naturally occurring clay minerals (phyllosilicates) are often coated by ferric (hydr)oxides which, therefore, may significantly influence surface properties. Conventionally this (external) coating of iron can be extracted by treatment with sodium citrate–dithionite–bicarbonate (CDB), leaving the structural iron more or less intact. Using this approach, Soma et al. (1992) were able to characterize the surface chemical composition of five New Zealand halloysites with different particle morphologies by XPS. Except for the sample from Hamilton, most of the iron in the halloysites were structural, and hence not extractable with CDB. The Hamilton halloysite contained the highest amount of iron, of which about 80% was external and extractable by CDB. The Fe 2p<sub>3/2</sub> photoelectron binding energy (711.6 eV) of this sample was consistent with that of ferric (hydr)oxides, such as goethite (McIntyre and Zetaruk, 1977). Its iron-to-silicon (Fe/Si) atomic ratio, determined by XPS, was also significantly larger than the bulk value determined by X-ray fluorescence analysis. On the other hand, the Fe 2p<sub>3/2</sub> binding energy of the other halloysites (about 712.8 eV) was characteristic of ferric ion in silicate structures (Seyama and Soma, 1987). Their surface Fe/Si atomic ratio (by XPS) was close to, or less than, the bulk value, indicating that the surface layers of some halloysites were depleted in (structural) iron. This observation would have important implications for determining the surface charge characteristics and chemical reactivity. After CDB extraction, the surface Fe/Si atomic ratio of Hamilton halloysite was comparable with the corresponding bulk ratio, while the Fe 2p<sub>3/2</sub> binding energy shifted to 712.6 eV, close to the value for structural iron. This example clearly demonstrates the capability of XPS in providing information on the radial distribution and chemical-bonding state of an element (here iron) in minerals with a heterogeneous microstructure.

XPS analysis of siliceous ferrihydrites provides insight into the bonding state and localization of silicon (Soma et al., 1996). The surface Si/Fe atomic ratios of five natural siliceous ferrihydrites (determined by XPS) were close to, or slightly smaller than, their respective bulk values (0.18–0.43). This indicated that Si was well dispersed throughout the ferrihydrite matrix at the scale of the photoelectron mean free-path (of the order of several nm), with a tendency for depletion in the outer (surface) layers. The Si 2s binding energy of  $152.9 \pm 0.2$  eV for all five natural samples was close to that for olivine (152.9–153.0 eV) (Seyama et al., 1996), a nesosilicate with isolated SiO<sub>4</sub> tetrahedra. However, it was markedly lower than the value for quartz (154.4 eV) (Seyama et al., 1996), indicating the absence of a three-dimensional network of SiO<sub>4</sub> tetrahedra. Thus, both the surface Si/Fe atomic ratio and the Si 2s photoelectron binding energy of natural siliceous ferrihydrites were consistent with the model of Parfitt et al. (1992). These workers suggested that

silicate is bonded to, or forms a bridge between, the surfaces of 'micro-crystalline domains' making up a primary ferrihydrite particle of several nm in diameter.

The XPS results for a synthetic ferrihydrite with an Si/Fe atomic ratio of about 0.1 and a low Si 2s binding energy also suggest that Si is well dispersed in the matrix and, as such, would inhibit the conversion (of ferrihydrite) into hematite (Glasauer et al., 2000). On the other hand, for a synthetic precipitate of ferrihydrite with a relatively high-silicon content, the surface Si/Fe atomic ratio (0.48) was much larger than the bulk value (0.18), while the Si 2s binding energy (154.1 eV) was close to that of quartz (Soma et al., 1996). These observations indicate that silica layers with three-dimensionally polymerized SiO<sub>4</sub> units covered the outer particle surfaces of the precipitated ferrihydrite. In line with this postulate, the O 1s photoelectron spectrum showed two peaks of which the one with a higher binding energy was assigned to oxygen in a three-dimensional SiO<sub>4</sub> network (Seyama and Soma, 1985).

An important aspect of the surface chemistry of phyllosilicates (clay minerals) is related to their anisotropic layer structure, exposing basal-plane, and crystal-edge surfaces. The spatial resolution of conventional XPS is not sufficient to differentiate between these two surfaces of micrometer-size clay mineral particles. However, anisotropic surface reactivity may be assessed using macrocrystalline micas with a specimen surface area comparable to that of an X-ray beam. For example, Ilton et al. (1997) used XPS to investigate the interaction of chromate ions (CrO<sub>4</sub><sup>2-</sup>) with mica (biotite and phlogopite) crystals in aqueous solutions containing an alkaline salt. The study was undertaken because hexavalent chromium is toxic, and its fate in the environment is of great concern. The photoelectron spectra of the treated biotite showed the presence of chromium on the edge surface but none on the basal plane. In the case of phlogopite, however, no chromium was detected on either the edge or basal surface. The Cr 2p<sub>3/2</sub> binding energy indicated that chromium was bound as a trivalent species to the edge surface of biotite. This finding was explained in terms of the reduction of hexavalent chromate by ferrous cations, present in the layer structure, followed by adsorption (at the biotite edge surface) of the resultant trivalent chromium cation. The overall process was promoted by sodium and lithium salts whereas the presence of RbCl and CsCl in solution had an inhibiting effect. It is suggested that hydrated Na<sup>+</sup> and Li<sup>+</sup> ions could replace interlayer K<sup>+</sup> ions in biotite, and so facilitate the heterogeneous reduction of chromate at the edge/solution interface.

Both biotite and phlogopite were able to adsorb Cr<sup>3+</sup> cations from solutions containing NaCl and KCl (Ilton et al., 2000). However, adsorption was larger, and the photoelectron binding energies of Cr 2p<sub>3/2</sub> and 3p were higher for the NaCl than the KCl system. The adsorption of Cr<sup>3+</sup> ions from KCl solution was apparently confined to crystal-edge surfaces. In NaCl solution, on the other hand, Cr<sup>3+</sup> was adsorbed at both edge and interlayer sites since Cr<sup>3+</sup> and Na<sup>+</sup> could replace interlayer K<sup>+</sup> ions in mica.

The interactions of organic matter with clay minerals have important technical and environmental applications. As already remarked, the C 1s photoelectron line is

unsuitable for characterizing organic compounds adsorbed on mineral surfaces since this peak is affected by hydrocarbons from vacuum pump oil. On the other hand, the N 1s photoelectron line can often serve as a convenient marker of nitrogen-containing organic molecules, such as amines. The adsorption from aqueous solutions of partially hydrolyzed polyacrylamide (HPAM) by kaolinite, feldspar, and quartz illustrates this point (Graveling et al., 1997; Allen et al., 1998). Measurement of the N 1s and Si 2p lines in the XPS spectrum following adsorption (of HPAM) allowed the surface concentration of N to be normalized for surface Si sites. Among the three minerals investigated, kaolinite showed the highest adsorption of HPAM (pH 2–10), probably involving hydrogen bonding between basal oxygens of the clay mineral and amide groups of the polymer. The high reactivity of kaolinite was also demonstrated by imaging XPS of mixed kaolinite/quartz crystals after adsorption of HPAM (Allen et al., 1998). Using Si 2p, Al 2p, and N 1s photoelectron images with  $<10\text{ }\mu\text{m}$  spatial resolution it was possible to differentiate between domains in the kaolinite matrix containing more HPAM and quartz grains with fewer polymers. We would expect that further developments in XPS-associated microscopy techniques will extend the application of XPS to complex systems containing clays and clay minerals.

The magnitude and distribution of surface charge have a great influence on the charge characteristics of clay minerals. The application of XPS to assessing the surface charge of some micas (margarite, muscovite, and sericite) was reported by Gier and Johns (2000) and Johns and Gier (2001). After the replacement of surface cations by  $\text{Ba}^{2+}$  these workers determined the atomic ratios of surface  $\text{Ba}^{2+}$  to interlayer  $\text{Ca}^{2+}$  (for margarite),  $\text{K}^{+}$  (for muscovite and sericite), and  $\text{Na}^{+}$  (for margarite, muscovite, and sericite). These measured ratios were indicative of the relative layer charge on external surface and the uppermost interlayer. Assuming that the interlayer charge was equally divided between the two external cleavage surfaces, the  $\text{Ba}^{2+}$ /interlayer cation atomic ratio would indicate the occurrence of layer charge asymmetry. The O/Ba atomic ratio of mica, determined by XPS, could also be used to assess the magnitude and distribution of surface charge (Johns and Gier, 2001).

Photoelectron intensity from a single crystal surface as a function of electron take-off angle shows a characteristic fluctuating pattern. This phenomenon, known as ‘photoelectron diffraction’, is due to the elastic scattering of photoelectrons by neighbouring atoms. Since the X-ray photoelectron diffraction (XPD) pattern depends on crystal structure, it can yield information about the location of atoms within the crystal. Evans and co-workers (Evans and Raftery, 1980, 1982; Ash et al., 1987) measured the XPD patterns of mica single crystals, rotating at an angle about a specific crystallographic axis, and examined the location (sites) of minor elements in the minerals. They were able to show that in biotite Ti preferentially occupied octahedral sites whereas in lepidolite Rb and Mn, respectively, occupied sites that were essentially identical with those of K (interlayer) and Li (octahedral).

Aluminium in silicate minerals can occupy both tetrahedral and octahedral sites. The distribution of  $\text{Al}^{3+}$  ions between the two sites is important in determining the

magnitude of negative charge and the cation exchange capacity (CEC) of clay minerals. This is because the substitution of  $\text{Si}^{4+}$  for  $\text{Al}^{3+}$  in the tetrahedral sheet, and  $\text{Al}^{3+}$  for  $\text{Mg}^{2+}$ ,  $\text{Fe}^{2+}$ , etc. in the octahedral sheet, is at the origin of the (permanent) negative charge in the phyllosilicate structure. XPS is capable of distinguishing between four- and six-coordinated  $\text{Al}^{3+}$  ions. As [Wagner et al. \(1982\)](#) pointed out, the sum of the Al 2p binding energy and Al  $\text{KL}_{23}\text{L}_{23}$  Auger kinetic energy (modified Auger parameter for Al) for four-coordinated  $\text{Al}^{3+}$  in silicate minerals is smaller than that of six-coordinated  $\text{Al}^{3+}$ . In other words, the extra-atomic relaxation for four-coordinated  $\text{Al}^{3+}$  is smaller than that for six-coordinated  $\text{Al}^{3+}$ . Recently, [Evans and Hiorns \(1996\)](#) examined the cleaved surface of chlorite single crystals by angle-resolved XPS. From the magnitude of anisotropy in the XPD patterns they were able to estimate the content of tetrahedrally coordinated  $\text{Al}^{3+}$  as a percentage of total  $\text{Al}^{3+}$  ions.

## REFERENCES

- Allen, G.C., Hallam, K.R., Eastman, J.R., Graveling, G.J., Ragnarsdottir, V.K., Skuse, D.R., 1998. XPS analysis of polyacrylamide adsorption to kaolinite, quartz and feldspar. *Surface and Interface Analysis* 26, 518–523.
- Anthony, M.T., Seah, M.P., 1984. XPS: energy calibration of electron spectrometers. 1 – An absolute, traceable energy calibration and the provision of atomic reference line energies. *Surface and Interface Analysis* 6, 95–106.
- Ash, L.A., Evans, S., Hiorns, A.G., 1987. Cation ordering in lepidolite and biotite studied by X-ray photoelectron diffraction. *Clay Minerals* 22, 375–386.
- Briggs, D., Seah, M.P. (Eds.), 1990. *Particle Surface Analysis*, 2nd edition, vol. 1, Auger and X-ray Photoelectron Spectroscopy. Wiley, Chichester.
- Cocke, D.L., Vempati, R.K., Loeppert, R.H., 1994. Analysis of soil surfaces by X-ray photoelectron spectroscopy. In: Amonette, J.E., Zelazny, L.W. (Eds.), *Quantitative Methods in Soil Mineralogy*. Soil Science Society of America, Madison, WI, pp. 205–235.
- De Stasio, G., Capozzi, M., Lorusso, G.F., Baudat, P.A., Droubay, T.C., Perfetti, P., Margaritondo, G., Tonner, B.P., 1998. MEPHISTO: performance tests of a novel synchrotron imaging photoelectron spectromicroscope. *Review of Scientific Instruments* 69, 2062–2066.
- De Stasio, G., Gilbert, B., Frazer, B.H., Neilson, K.H., Conrad, P.G., Livi, V., Labrenz, M., Banfield, J.F., 2001. The multidisciplinary of spectromicroscopy: from geomicrobiology to archaeology. *Journal of Electron Spectroscopy and Related Phenomena* 114–116, 997–1003.
- De Stasio, G., Perfetti, L., Gilbert, B., Fauchoux, O., Capozzi, M., Perfetti, P., Margaritondo, G., Tonner, B.P., 1999. MEPHISTO spectromicroscope reaches 20 nm lateral resolution. *Review of Scientific Instruments* 70, 1740–1742.
- Dutta, N.C., Iwasaki, T., Ebina, T., Hayashi, H., 1999. A combined X-ray photoelectron and Auger electron spectroscopic study of cesium in variable-charge montmorillonites. *Journal of Colloid and Interface Science* 216, 161–166.
- Ebel, M.F., Ebel, H., Zuba, G., Wernisch, J., 1983. Calibration of an X-ray photoelectron spectrometer by means of noble metals. *Surface and Interface Analysis* 5, 170–172.

- Evans, S., Hiorns, A.G., 1996. Angle-resolved X-ray photoelectron studies of cleavage in chlorites. *Clays and Clay Minerals* 44, 398–407.
- Evans, S., Raftery, E., 1980. X-ray photoelectron studies of titanium in biotite and phlogopite. *Clay Minerals* 15, 209–218.
- Evans, S., Raftery, E., 1982. X-ray photoelectron diffraction studies of lepidolite. *Clay Minerals* 17, 443–452.
- Garwood, G.A. Jr., 1995. Scanning X-ray photoelectron microscopy (SXPEM). In: Hubbard, A.T. (Ed.), *The Handbook of Surface Imaging and Visualization*. CRC Press, Boca Raton, FL, pp. 687–704.
- Gier, S., Johns, W.D., 2000. Heavy metal-adsorption on micas and clay minerals studied by X-ray photoelectron spectroscopy. *Applied Clay Science* 16, 289–299.
- Glasauer, S.M., Hug, P., Weidler, P.G., Gehring, A.U., 2000. Inhibition of sintering by Si during the conversion of Si-rich ferrihydrite to hematite. *Clays and Clay Minerals* 48, 51–56.
- Graveling, G.J., Ragnarsdottir, V.K., Allen, G.C., Eastman, J.R., Brady, P.V., Balsley, S.D., Skuse, D.R., 1997. Controls on polyacrylamide adsorption to quartz, kaolinite, and feldspar. *Geochimica et Cosmochimica Acta* 61, 3515–3523.
- Hochella, M.F. Jr., 1995. Mineral surfaces: their characterization and their chemical, physical and reactive nature. In: Vaughan, D.J., Pattrick, R.A.D. (Eds.), *Mineral Surfaces. The Mineralogical Society Series 5*. Chapman & Hall, London, pp. 17–60.
- Ilton, E.S., Moses, C.O., Veblen, D.R., 2000. Using X-ray photoelectron spectroscopy to discriminate among different sorption sites of micas: with implications for heterogeneous reduction of chromate at the mica–water interface. *Geochimica et Cosmochimica Acta* 64, 1437–1450.
- Ilton, E.S., Veblen, D.R., Moses, C.O., Paeburn, S.P., 1997. The catalytic effect of sodium and lithium ions on coupled sorption–reduction of chromate at the biotite edge-fluid interface. *Geochimica et Cosmochimica Acta* 61, 3543–3563.
- Johns, W.D., Gier, S., 2001. X-ray photoelectron spectroscopic study of layer charge magnitude in micas and illite–smectite clays. *Clay Minerals* 36, 355–367.
- Kawai, J., Hayakawa, S., Kitajima, Y., Gohshi, Y., 1995. X-ray absorption and photoelectron spectroscopies using total reflection X-rays. *Analytical Sciences* 11, 519–524.
- Kordesch, M.E., 1995. Photoelectron emission microscopy. In: Hubbard, A.T. (Ed.), *The Handbook of Surface Imaging and Visualization*. CRC Press, Boca Raton, FL, pp. 581–596.
- McIntyre, N.S., Zetaruk, D.G., 1977. X-ray photoelectron spectroscopic studies of iron oxides. *Analytical Chemistry* 49, 1521–1529.
- Mosser, C., Mosser, A., Romeo, M., Petit, S., Decarreau, A., 1992. Natural and synthetic copper phyllosilicates studied by XPS. *Clays and Clay Minerals* 40, 593–599.
- Parfitt, R.L., Van der Gaast, S.J., Childs, C.W., 1992. A structural model for natural siliceous ferrihydrite. *Clays and Clay Minerals* 40, 675–681.
- Paterson, E., Swaffield, R., 1994. X-ray photoelectron spectroscopy. In: Wilson, M.J. (Ed.), *Clay Mineralogy: Spectroscopic and Chemical Determinative Methods*. Chapman & Hall, London, pp. 226–259.
- Seah, M.P., 1980. The quantitative analysis of surfaces by XPS: a review. *Surface and Interface Analysis* 2, 222–239.
- Seyama, H., Soma, M., 1984. X-ray photoelectron spectroscopic study of montmorillonite containing exchangeable divalent cations. *Journal of the Chemical Society, Faraday Transactions 1* (80), 237–248.



- Seyama, H., Soma, M., 1985. Bonding-state characterization of the constituent elements of silicate minerals by X-ray photoelectron spectroscopy. *Journal of the Chemical Society, Faraday Transactions 1* (81), 485–495.
- Seyama, H., Soma, M., 1987. Fe 2p spectra of silicate minerals. *Journal of Electron Spectroscopy and Related Phenomena* 42, 97–101.
- Seyama, H., Soma, M., 1988. Application of X-ray Photoelectron Spectroscopy to the Study of Silicate Minerals. Research Report from the National Institute for Environmental Studies, Japan, No. 111.
- Seyama, H., Soma, M., 2003. Surface-analytical studies on environmental and geochemical surface processes. *Analytical Sciences* 19, 487–497.
- Seyama, H., Soma, M., Tanaka, A., 1996. Surface characterization of acid-leached olivines by X-ray photoelectron spectroscopy. *Chemical Geology* 129, 209–216.
- Soma, M., Churchman, G.J., Theng, B.K.G., 1992. X-ray photoelectron spectroscopic analysis of halloysites with different composition and particle morphology. *Clay Minerals* 27, 413–421.
- Soma, M., Seyama, H., Yoshinaga, N., Theng, B.K.G., Childs, C.W., 1996. Bonding state of silicon in natural ferrihydrites by X-ray photoelectron spectroscopy. *Clay Science* 9, 385–391.
- Wagner, C.D., Gale, L.H., Raymond, R.H., 1979. Two-dimensional chemical state plots: a standardized data set for use in identifying chemical states by X-ray photoelectron spectroscopy. *Analytical Chemistry* 51, 466–482.
- Wagner, C.D., Passoja, D.E., Hillery, H.F., Kinisky, T.G., Six, H.A., Jansen, W.T., Taylor, J.A., 1982. Auger and photoelectron line energy relationships in aluminum–oxygen and silicon–oxygen compounds. *Journal of Vacuum Science & Technology* 21, 933–944.

*Chapter 12.5*

## SMALL-ANGLE SCATTERING TECHNIQUES

D. TCHOUBAR<sup>a</sup> AND N. COHAUT<sup>b</sup>

<sup>a</sup>*Expert CRT-Plasma Laser, Orléans, F-45160 Olivet, France*

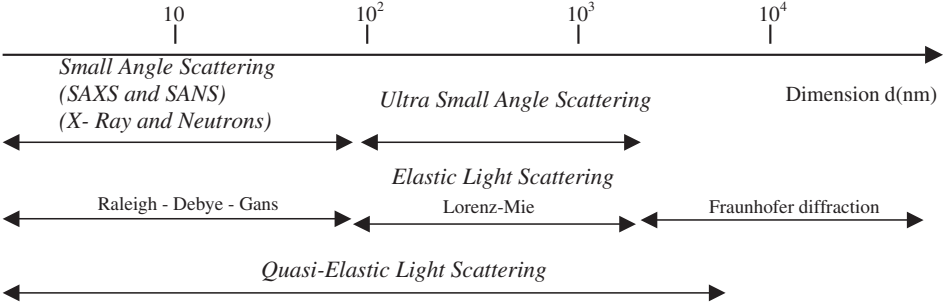
<sup>b</sup>*CRMD, CNRS-Université d'Orléans, F-45071 Orléans Cedex 2, France*

With the possible exception of those who live in very dry deserts, people can see small-angle scattering (SAS) by water droplets when they observe a moon halo predicting rain for the next day. Indeed, any medium showing matter density fluctuations can give rise to observable SAS when it is placed in the path of a radiation beam, provided the medium is adequately transparent and the fluctuations in matter density are at appropriate scales with respect to the radiation wavelengths. This chapter is concerned with scattering by a heterogeneous medium in the form of a colloidal dispersion of small particles in a solvent.

The last 50 years have seen the development of small-angle scattering by X-rays (SAXS), neutrons (SANS) and light (SALS), and the use of these techniques to investigate a large number and variety of media (Guinier and Fournet, 1955; Bacon, 1975; Glatter and Kratky, 1982). Light scattering by colloidal particles was studied for over a century, starting with the theoretical works by Lord Rayleigh (1842–1919). Bohren and Huffman (1998) published a relatively modern review of light scattering by small particles. SAS patterns are observable if the dimension of the dispersed particles is comparable with the radiation wavelength (Table 12.5.1).

The different techniques, shown in Table 12.5.1, are generally complementary, taking into account their respective wavelengths. For light scattering experiments, the choice of samples is more restricted by the necessity for transparency, and problems of turbidity and multiple scattering. In all cases involving elastic scattering (without changing the wavelength of the scattered beam), the experimental principles are approximately the same. A sample is placed on the path of a well-collimated beam of X-rays, neutrons or light. The special devices used are described in the references cited above. “Zooming” on the central part of the diffraction patterns enables a profile analysis to be made.

Table 12.5.1. Scattering techniques in relation to particle dimension (nm) (from Glatter, 1991)



12.5.1. PRINCIPLES

The physical principles of scattering are the same for both wide-angle diffraction (WAD) and SAS. The latter technique consists of analyzing only the 000 reflection profile. Being insensitive to atomic structure, this feature is not taken into account in the classical WAD studies. The principal difference between WAD and SAS lies in the extent to which structural details can be investigated. Therefore, the meaning of the scattering unit has to be explained.

The intensity of a scattered beam is recorded as a function of the scattering angle,  $2\theta$ . The modulus  $|q|$  of the scattering vector,  $\mathbf{q}$ , is related to the scattering angle by  $q = 4\pi\sin\theta/\lambda$  where  $\lambda$  is the radiation wavelength. Some papers use the parameter  $s = q/2\pi = 1/d$  (where  $d$  is the Bragg distance) in place of  $q$ . For particles in dispersion, the scattered intensity is expressed by

$$I(\mathbf{q}) = I_0 \Phi k^2 P(\mathbf{q}) \tag{1}$$

where  $I(\mathbf{q})$  is the number of photons (or neutrons) counted per unit of solid angle and time;  $I_0$  the intensity of the incident beam, i.e., the total number of photons (or neutrons) irradiating the sample per unit of time;  $\Phi$  the volume fraction of particles that are immersed in the incident beam; and  $k$  the scattering length contrast of the particle (see below). The interference function,  $P(\mathbf{q})$ , is the most important parameter of Eq. (1) because its profile depends on the size and shape of particles, on their interactions, and if the particles are heterogeneous, on their internal structure.

A. Scattering Length and Particle Scattering Length Contrast

It is generally assumed that the unit domain size (scattering unit) is large in comparison with the interatomic distances. On this assumption, the angular extension of

the SAS pattern is limited to a  $q_{\max}$  value much lower than the first diffraction peak position. In this case, the scattering unit is considered to be homogeneous and characterized by its mean scattering length,  $b_u$ . Depending on the interaction mode of the radiation with the material,  $b_u$  is specific to each technique.

### Neutron Scattering

The neutrons normally used (Cotton, 1991) have an energy of about  $10^3$  eV and their wavelengths are  $0.1 \text{ nm} < \lambda < 2 \text{ nm}$ . The neutrons interact with the nuclei of the atoms of the particles and the dispersion medium. For each nucleus, the scattering length,  $b$ , cannot yet be theoretically computed but only experimentally evaluated. The  $b$  values were tabulated (Bacon, 1975). The values can either be positive or negative, and differ from one isotope to another. The difference in value between hydrogen ( $-0.374 \times 10^{-12} \text{ cm}$ ) and deuterium ( $+0.667 \times 10^{-12} \text{ cm}$ ) is an important point.

Taking into account the atomic composition of the scattering unit,  $b_u$  may be computed from the relation:  $b_u = \sum_i n_i b_i$  where  $n_i$  indicates the number of atoms of type  $i$ , and  $b_i$  their scattering lengths. The summation ( $\sum_i$ ) is performed on all types of atoms constituting the scattering unit.

If the particles are homogeneous, the particle scattering length density,  $\rho_p$ , is defined as the ratio  $b_u/v_u$  where  $v_u$  is the scattering unit volume. For particles that are dispersed in a solvent, the solvent scattering length density,  $\rho_s$ , must also be computed.

The scattering length contrast,  $k$ , of the particle is defined by the difference ( $\rho_p - \rho_s$ ), while the scattering power of the dispersed particle is given by:

$$\Phi k^2 = \Phi(\rho_p - \rho_s)^2 \quad (2)$$

### X-ray Scattering

The X-ray photons have an energy of about  $10^4$  eV and their wavelengths,  $\lambda$ , are distributed about  $0.05 \text{ nm} < \lambda < 0.5 \text{ nm}$  (Guinier and Fournet, 1955). Their electromagnetic interactions with matter involve the  $Z$  electrons of the atom electronic shell. Therefore, the scattering length for one atom is  $b = Zb_e$ , where  $b_e$  ( $= +0.282 \times 10^{-12} \text{ cm}$ ) is the scattering power of an electron and can be computed theoretically. In that case, the scattering power of the dispersion only depends on the electron density of the particle and that of the solvent, and on the scattering power of free electron,  $I_e$  ( $= b_e^2$ ):

$$\Phi k^2 = \Phi I_e (\rho_p - \rho_s)^2 \quad (3)$$

where  $\rho_p$  and  $\rho_s$  are respectively the particle and the solvent electron density.

### Light Scattering

The visible light photons have an energy of about 10 eV. Their electromagnetic interaction with matter is macroscopic and induces an electrical field giving rise to electric dipoles in the medium. The scattering length is expressed as a function of the

polarizability,  $\alpha$ , of the medium, which, in turn, is related to the refraction indexes of the particles and the solvent. The theoretical expression of the scattering power of the dispersion depends on the size of the particles, in comparison with the wavelength of the light. This expression, therefore, depends on the approximations used in the theoretical treatment of the patterns. Table 12.5.1 illustrates the range of validity of the different methods of SALS. The corresponding theories were discussed by Hofer (1991).

### B. Quantitative Definitions of the Interference Function, $P(\mathbf{q})$

#### *Dilute Suspension of Homogeneous Particles without any Interactions*

In the case of a statistically isotropic dispersion, the particles can adopt all possible orientations. The interference function,  $P(\mathbf{q})$ , from Eq. (1), is expressed by the following Fourier transform:

$$P(q) = 4\pi \int_0^\infty p(r) \frac{\sin qr}{qr} dr \quad \text{with} \quad p(r) = r^2 V_p \gamma(r) \quad (4)$$

For monodisperse particles,  $V_p$  is the particle volume and  $\gamma(r)$ , the characteristic function of the particle (Porod, 1982). It is defined as the probability to find two points at the distance  $r$  within a particle.

The intensity  $i(q)$  scattered by only one particle is called the particle shape function:

$$i(q) = 4\pi \int_0^\infty r^2 \gamma(r) \frac{\sin qr}{qr} dr \quad (5)$$

One property is of interest: for  $q = 0$ ,  $i(0) = V_p$  and therefore  $P(0) = (V_p)^2$ . If the parameter  $k$  and the particle volume fraction,  $\Phi$ , is known, the particle mass can be determined from  $I(0)$  in the general expression of Eq. (1).

Scattering by dilute suspensions of monodisperse or weakly polydisperse particles may be analysed by comparing the experimental curve profiles with theoretical  $i(q)$ . Expressions for  $i(q)$  were determined for all geometrical shapes, including such complex configurations as polymer blobs (Guinier and Fournet, 1955; Glatter and Kratky, 1982).

#### *Properties of the Shape Function $i(q)$*

The  $i(q)$  profile for homogeneous particles is characterized by three ' $q$ -ranges' (Fig. 12.5.1). Range (1) depends only on particle size. As shown by Guinier and Fournet (1955),  $i(q)$  can be approximated by

$$i(q) \cong 1 - \frac{q^2 R_g^2}{3} + \dots \cong \exp\left(-\frac{q^2 R_g^2}{3}\right) \quad (6)$$

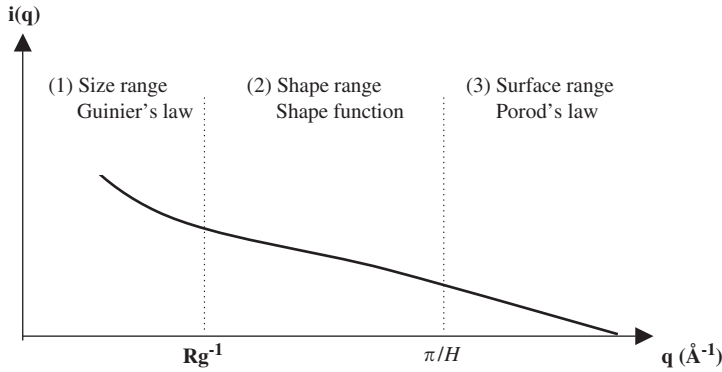


Fig. 12.5.1. The three ranges of the SAS scheme related to the geometrical properties of dilute particle dispersions.

where  $R_g$  is the gyration radius of the particle.  $q$ -range (1) is limited by the condition  $qR_g = 1$ . The corresponding Guinier plot  $\ln i(q)$  vs.  $q^2$  shows a linear decrease whose slope is equal to  $-R_g^2/3$ . Extrapolation to  $q = 0$  yields  $i(0)$ . The  $q$ -range (2) depends on particle shape. For a cylinder of diameter  $2R$  and height  $2H$ ,

$$i(q) = V \int_0^{\pi/2} \left[ \frac{\sin(qH \cos \varphi)}{qH \cos \varphi} \right] \left[ 4 \frac{J_1^2(qR \sin \varphi)}{(qR \sin \varphi)^2} \right] \sin \varphi \, d\varphi \quad (7)$$

where  $V$  is the volume of a particle,  $J_1$ , the first order Bessel function and the integration variable  $\varphi$ , the angle between the scattering vector  $\mathbf{q}$  and the cylinder axis. For very thin disks, Eq. (7) is approximated by

$$i_D(q) \cong \frac{2}{q^2 R^2} \exp \frac{q^2 H^2}{3} \quad (8a)$$

If the thickness of the disk is very small in comparison with its radius,

$$i_D(q) \cong \frac{K}{q^2 R^2} \quad (8b)$$

This applies to montmorillonite layers. If the clay mineral is totally dispersed, the plot of  $\log i(q)$  vs.  $\log q$  shows a linear decrease, with of slope of  $-2$  within the  $q$ -ranges (2) and (3) (Fig. 12.5.1).

Auvray and Auroy (1991) discussed the scattering by thin microemulsion layers. Their first conclusion is that layer curvature does not change the scattering behaviour and always decreases as  $q^{-2}$ .

The  $q$ -range (3) is essentially sensitive to the external surface of the particle, obeying Porod's (1982) law (Guinier and Fournet, 1955; Glatter and Kratky, 1982).

For compact particles, the external part of scattering,  $i(q)$ , varies as  $\sigma q^{-4}$ , where  $\sigma$  is the specific surface area.

### Particle Size Distribution

If the particles are not equal (polydisperse),  $i(q)$  is replaced by its average,  $\langle i(q) \rangle$ :

$$\langle i(q) \rangle = \sum \alpha_m i_m(q) \quad (9)$$

where  $\alpha_m$  is the particle weight fraction of size  $m$ , and  $i_m(q)$ , its respective scattering. The mean particle volume  $\langle V_p \rangle$  replaces  $V_p$  in Eq. (4).

This case is illustrated by the SANS study of Hall et al. (1985) on dilute suspensions (0.8%, w/v) of allophane particles. The spherical shape of these particles is particularly well suited for determining their size distribution by SAS techniques. The analysis was performed by comparing experimental SANS spectra with simulated ones.

### Heterogeneous Particles

The  $p(r)$  function not only depends on particle size and shape but also on its internal structure. In this case the product  $k^2 i(q)$ , indicating the scattering power of one particle, is replaced by the structure factor  $F(q)^2$ . If the particles are fractal clusters, their mass fractal dimension  $\alpha$  is generally a non-integer, varying within  $1 < \alpha < 3$  (Mandelbrot, 1967, 1977). The scattered intensity varies as the power law  $i(q) \approx q^{-\alpha}$  within the  $q$ -ranges (2) and (3) in Fig. 12.5.1 (Schaefer et al., 1985). The limit value of  $\alpha = 3$  for uncompacted particles, observed for some clay gels, is not yet clearly and quantitatively explained.

In case of homogeneous particles but with fractal surfaces, a generalized Porod's law was derived by Bale and Schmidt (1984), as by  $i(q) \approx q^{ds-6}$ , where  $ds$  is the fractal dimension of the surface. For a smooth surface,  $ds = 2$  and the classic Porod's law is recovered.

### Interacting Identical Particles

The function  $P(\mathbf{q})$  also takes into account interparticle interactions (Guinier and Fournet, 1955). In the simplest case of spherical particles  $P(\mathbf{q}) = F(q)^2 G(q)$  and the scattered intensity is expressed by

$$I(q) = I_0 \Phi F(q)^2 G(q) \quad (10)$$

where  $F(q)$  is the structure factor of one particle;  $G(q)$  the interparticle interference function that only depends on particle-particle interactions.

If  $F(q)$  is known,  $G(q)$  can be obtained from the relation

$$G(q) = I(q)/(I_0 \Phi F(q)^2) \quad (11)$$

$W(r)$ , the inverse Fourier transform of  $G(q)$ , is the radial function distribution giving the probability of finding a particle at a distance  $r$  from any other particle, taken as the origin. From  $W(r)$  it is also possible to compute  $g(r)$ , the first neighbour particle distance distribution. Such an operation is quite delicate because it can give rise to an “artefact” due to the limited extension of the scattering curves. It could be applied only if the external parts of the experimental scattering can be assimilated into an extrapolatable law such as Porod’s law for largest  $q$  values, or into the Guinier’s plot for the lowest ones. This allows the computation limits to be widened to such an extent that the cut-off effects do not influence the experimental results.

### C. Special Problems for Clay Minerals

For natural smectites the situation is not really simple, even when we deal with dilute dispersions.

- (1) Because of the layer structure of particles and their great anisotropy, the condition of statistical isotropy for the dispersions is not so evident and needs to be specified in each case. For locally oriented systems, Eqs. (10) and (11) have to be resolved taking into account the particle orientation.
- (2) Because of the small layer thickness, a continuum of scattering could exist between the 000 and the 001 reflections. The interlayer distances can be distributed within a wide range of dimensions from about a nanometer to several micrometers. Indeed, the limit between WAD and low-angle scattering is not well defined in some cases.
- (3) The particles in the same sample have different thicknesses.

In case of interacting anisotropic particles, the correlation of orientation with position cannot be directly determined from  $G(q)$ , except in special experiments with well-oriented samples. The best methods consist in simulating the  $G(q)$  functions.

### D. Definitions

The ‘basal spacing’,  $d$ , is the distance from the centre of the oxygen plane of one layer to the centre of the oxygen plane of an adjacent layer, as directly deduced from the position of the 001 reflection in the XRD spectrum.  $W(r)$  is the probability of finding a layer at a distance  $r$  from a layer taken as the origin.

The ‘interlayer spacing’,  $h$ , is the distance between two neighbouring parallel layers. Thus,  $h = d - e$ , where  $e$  is the layer thickness.

The interference function,  $G(q)$  is replaced by  $S(q)$ , the “structure factor of dispersions”, in many publications. Following Mering (1949), we prefer using the notation  $G(q)$ , the ‘interference function’; to avoid confusion with the “particle structure factor”  $F(q)$ .



### 12.5.2. SAS BY CLAY MINERALS

There are two sets of publications dealing with the characterization of clay dispersions using SAS techniques.

The first set focuses on the hydration mechanisms by which a powder of smectite is transformed into a concentrated gel or a paste. The SAS investigations consist of observing the shift in diffraction peaks that occurs during clay mineral hydration, i.e., monitoring the profile change of the (001) reflections from the dry state (corresponding to  $d \approx 1$  nm) to the gel state. During this process, the interlayer distances can increase to several tens or even several hundreds of nanometers. This evolution was followed as a function of various parameters such as clay concentration, nature of interlayer cation, ionic strength, external pressure or temperature. As already mentioned, most investigations are concerned with natural di- and tri-octahedral smectites and vermiculites.

The second set relates to the relatively recent development of powerful SAS devices, such as ultra SAS of neutrons and X-rays. These investigations focus on the sol-gel transition mechanisms, the relationship between gel structure and rheological behaviour and thermodynamic models of the swelling clay dispersions. In order to minimize experimental difficulties associated with earlier studies, most of the second-generation researchers used Laponite (synthetic hectorite) as the clay mineral. The small diameter of Laponite platelets, in comparison with natural smectites, allows interparticle interactions to be simplified. Laponite particles also have a narrow particle size distribution, and hence a 'mean' size may be used. The diameter of Laponite platelets is much smaller than the size that is accessible to SAS techniques. In case of Montmorillonite, even ultra SAS of X-rays or neutrons cannot include the whole range of Montmorillonite particle diameters. Unlike montmorillonite, the structure and behaviour of Laponite dispersions can be thoroughly studied. The light scattering scale could be suitable, even if it is generally available for highly dilute dispersions.

#### *A. Initial Hydration Stages and Osmotic Transition*

##### *SAS Analysis by Fourier Transform of Intensity*

Rausell-Colom and Norrish (1962) and Norrish and Rausell-Colom (1963) have used SAXS to investigate the swelling in salt-water solutions of orientated flakes of  $\text{Na}^+$ -montmorillonite (Wyoming) and single crystals of  $\text{Li}^+$ -vermiculite (Kenya). The increase in interlayer spacing was studied as a function of the ionic strength. The scattering intensity was recorded along the direction perpendicular to the flake (or single crystal) plane using a low-angle diffractometer and within an angular range that allows interlayer distances to be measured just after the transition to 'osmotic' swelling, that is, from 3 to 50 nm. The scattered intensity can be expressed by Eq. (10), in which the  $\mathbf{q}$  vector is replaced by its component  $q_z$  perpendicular to the flakes.

$$I(q_z) \propto F^2(q_z)G(q_z) \quad (12)$$

The one-dimensional Fourier transform of  $G(q_z)$  is given by:

$$W(r) - 1 = \frac{d_m}{\pi} \int_0^\infty G(q_z) \cos(rq_z) dq_z \quad (13)$$

In this case,  $W(r)$  is the one-dimensional distance distribution. The most probable basal distance  $d$  corresponds to the maximum of  $W(r)$ . Because the structure of these clay mineral-water systems is heterogeneous and disordered,  $W(r)$  gave poor information. Nevertheless, the following conclusions can be made. Interlayer ('crystalline') swelling occurs by a process that is highly dependent on the hydration energy of the interlayer cations. With some monovalent interlayer cations such as  $\text{Na}^+$  and  $\text{Li}^+$ , the interlayer distance 'jumps' at a high water content. Gel formation can be explained in terms of repulsive osmotic forces resulting from the entry of water into the interlayer space and the development of ionic double layers. After passing the osmotic transition threshold, the increase in interlayer distance is proportional to the water content, as is the case for swelling in pure water. In salt solutions, the interlayer distance increases linearly with  $C^{-1/2}$ , where  $C$  is the electrolyte concentration.

Andrews et al. (1967) carried out the same analysis with a SAS device that can extend to smaller scattering angles, i.e., much larger particle size than in the above experiment (about 100 nm). In agreement with Rausell-Colom and Norrish (1962) and Norrish and Rausell-Colom (1963), they point out the inaccuracy of using a direct Fourier transform for such samples.

### *Geometrical Simulation of SAS*

The description of the gel structure can be improved by simulation of the scattering curves. Experiments performed with standard laboratory SAS are not easy to model, because a punctual collimation of X-ray sources is impossible to realize while maintaining the intensity of scattering. It is then necessary to correct the experimental data by using a heavy desmearing method or to introduce a complex optical transfer function in the spectra simulation. This problem was overcome by using radiation supplied by a synchrotron, allowing pinpoint collimation with a high intensity to be achieved.

Pons et al. (1981, 1982a) performed small-angle X-ray experiments with a synchrotron beam of the Laboratoire d'Utilisation du Rayonnement Synchrotron (LURE, Orsay, France). They studied the swelling of Wyoming  $\text{Na}^+$ -montmorillonite and  $\text{Li}^+$ -saponite in pure water, starting from a gel containing 17%, (w/w) clay. The scattering evolution was observed in the course of alternate freezing at  $-70^\circ\text{C}$  followed by slow warming up to room temperature. The time-resolved diffraction patterns were recorded during temperature increase. The theoretical spectra were simulated using the methods previously elaborated for the simulation of 00l reflections from disordered or interstratified layer stacking systems (see Section 12.5.1). The simulation model of the dispersion consists of particles (layer stackings) that are

disoriented from each other. The intensity is given by:

$$I(q) = \frac{F_{00}^2(q)}{\Omega q^2} \sum_M \alpha(M) G(q, M, p_i, d_i) \quad (14)$$

where  $\Omega$  is the unit cell area,  $F_{00}(q)$  the structure factor of the unit layer along the 001 direction,  $q$  the vector modulus,  $M$ , the number of layers in a particle,  $\alpha(M)$ , the weight distribution of particles containing  $M$  layers, and  $G(q, M, p_i, d_i)$  is the interference function (or modulation function) that depends on  $M$  and on the interlayer distance,  $d_i$  with their respective probabilities,  $p_i$ .

The spectra confirmed the increase of basal spacing from 2 to more than 3 nm at the osmotic transition threshold, and the reversibility of this transition. But the primary aim of the study was to compare the scattering evolution between 0 °C and room temperature (Fig. 12.5.2).

The peak position was the same at both temperatures, but the narrow peak at 0 °C transformed into a diffuse modulation at room temperature, indicating that swelling

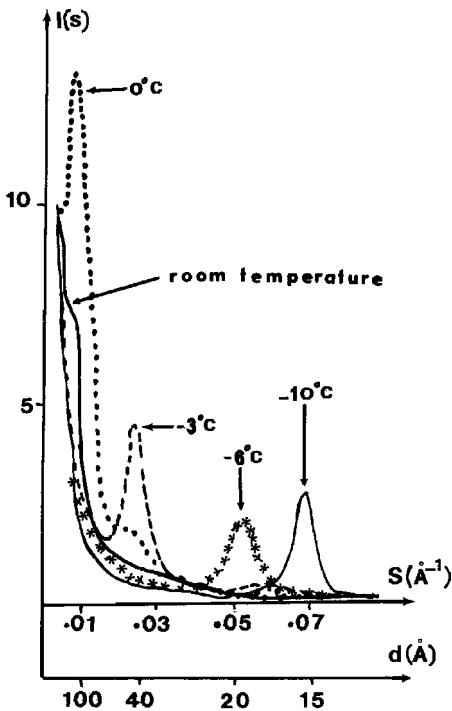


Fig. 12.5.2. Time-resolved experiments showing the evolution of experimental SAXS intensity  $I(s)$  vs. basal distance  $d$  or  $S = 1/d$ , of a gel after freezing at  $-70^\circ\text{C}$  and then slowly heated to room temperature. From Pons (1980) and Calas et al. (1984).

was not impeded at 0°C. At this temperature, the system was constrained by the presence of residual ice in equilibrium with water. At room temperature, a large disorder in layer stacking took place but with the same most probable basal distance. This would indicate that the energy spent in establishing a swelling equilibrium contains an entropy term inducing a dispersion of unit layers and the formation of smaller particles (stacked layers) that are disoriented from each other.

Comparison of experimental and theoretical scattering curves showed that the Na<sup>+</sup>-montmorillonite gel at 17% (w/w) formed at room temperature, consists of particles containing between 1 and 8 parallel layers with interlayer distances of 4–20 nm, giving an average value of ~10 nm. The particles themselves are completely disoriented from each other. The proposed structural model was checked by high resolution transmission electron microscopy (Pons et al., 1982b). Because of the high clay concentration, other explanations may be proposed such as the formation of nematic structures (see below).

The same simulation and fitting method was used by Rausell-Colom et al. (1989) to analyse the swelling of single crystals of Santa Olalla vermiculite in aqueous solutions of L-ornithine hydrochloride. They compared the basal spacing distributions obtained from SAS with those derived from the DLVO theory, taking into account a Boltzmann distance distribution and a layer of water molecule on the clay mineral surface (Cebula et al., 1980). Fig. 12.5.3 illustrates the fit between the two types of plots for different ionic concentrations of the swelling solution.

Following Callaghan and Ottewill (1974), Ben Rhaiem et al. (1987) studied the hydration–dehydration behaviour of Na<sup>+</sup>- and Ca<sup>2+</sup>-montmorillonite in 10<sup>−3</sup> M

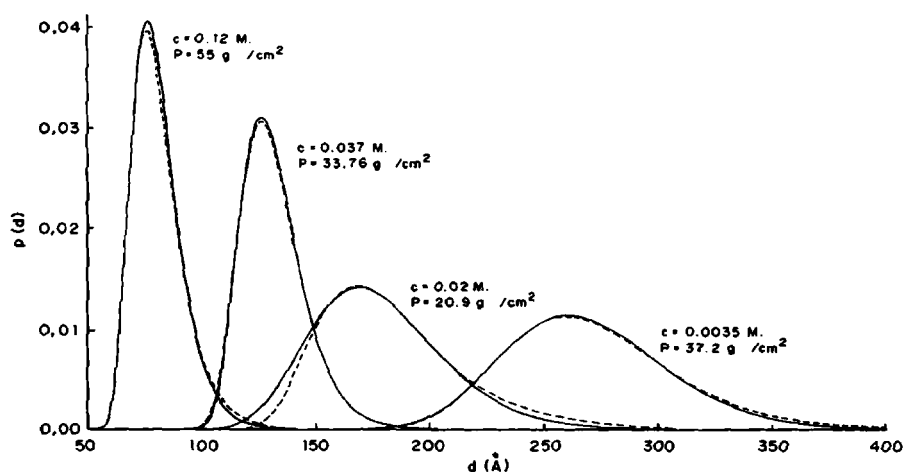


Fig. 12.5.3. Vermiculite wafer swelling. Comparison of basal spacing distributions computed from diffuse double-layer interaction (broken line) and inferred from XRD data (continuous line).  $c$ , ionic concentration of solvent;  $p$ , pressure applied on the wafer to balance the swelling pressure. From Rausell-Colom et al. (1989).

NaCl and CaCl<sub>2</sub> by synchrotron SAS. The samples were examined during drying and rewetting in an ultrafiltration cell by varying the suction. Their results again confirm an osmotic transition and its reversibility for Na<sup>+</sup>-montmorillonite but not for Ca<sup>2+</sup>-montmorillonite. They further show that the gel, at least at high clay contents, is formed by stackings of expanded layers as in nematic domains with variable interlayer distances that are disoriented from each other. These gel domains alternate with pores whose hierarchical size distribution can be determined by comparing SAS spectra and permeability results of pressure experiments.

Keren and Klein (1995) used SALS to determine the clay concentration in aqueous dispersions of bi-ionic Na<sup>+</sup>/Ca<sup>2+</sup>-montmorillonite. The samples were carefully prepared by selecting particle size and stirring the two homoionic clay mineral dispersions for long periods. From experiments with various Na<sup>+</sup>/Ca<sup>2+</sup> ratios and a 0.1% clay concentration, they concluded that the SALS technique is not appropriate for such systems because of the broad particle-size heterogeneity. A theory for mixtures is required to take into account the scattering of particles with different sizes (cf. the light scattering theories in Table 12.5.1).

Indeed, it is always perilous to analyse heterogeneous media without any possibility to perform contrast matching in SAS experiment. As described below, there are techniques that can be used for particular cases.

### B. Anomalous Small Angle X-ray Scattering

Anomalous small-angle X-ray scattering (ASAXS) refers to an extension of standard SAXS experiments in which the energy of the probing X-rays are tuned near the K, L or M absorption edges of an element in the sample. By performing SAXS experiments near one of the characteristic absorption edges of any given atom, it is possible to vary the scattering contrast of that atom. This systematic variation in contrast yields the partial scattering functions of the specific atomic species. In general, the atomic scattering can be expressed as

$$f(q, E) = f_0(q) + f'(q, E) + if''(q, E) \quad (15)$$

where  $E$  is the energy of the probing X-rays and  $f'$  and  $f''$  the real and imaginary parts of anomalous scattering. The variation of  $f'$  is responsible for the change in contrast seen in the ASAXS signals.

Near the absorption edge the scattering intensity is given by

$$I(q, \lambda) = I_n(q) + f'(\lambda)I_c(q, \lambda) + (f'^2(\lambda) + f''(\lambda))I_r(q) \quad (16)$$

Here  $I_n(q)$  is the normal non-resonant scattering,  $I_c$  is a cross term reflecting scattering between the specific element of interest and the remainder of material and  $I_r$  corresponds to the distance correlations of the resonant scattering centres.

This matching method is easily accessible to elements having  $Z$  values between 20 and 36 for K edges, and between 50 and 82 for L edges. Since  $f'$  and  $f''$  are sharply varying functions near the edge, these experiments require the highest possible energy resolution ( $\Delta\lambda/\lambda \approx 10^{-4}$ ). To resolve Eq. (16) it is necessary to perform several measurements with different wavelengths far and near the edge. Such a technique can reveal the distribution of specific species within a multicomponent matrix.

Carrado et al. (1998) exploited ASAXS to monitor the solvation behaviour of transition metal and lanthanide ions within the interlayer space of montmorillonite. The experiments were performed at the Stanford Synchrotron Radiation Laboratory (SSRL, USA). The variations of scattering intensities, as a function of the absorption energy were monitored for  $\text{Cu}^{2+}$ -,  $\text{Er}^{3+}$ - and  $\text{Yb}^{3+}$ - montmorillonites as a function of hydration.

### C. Gel Structure and Sol–Gel Transition

The second series of investigations, using an ultra-small-angle X-ray scattering (USAXS), neutrons and light scattering were devoted to study the structure of clay gels and the sol–gel transition.

#### *Gel Structure in Natural Smectite Dispersions*

Cebula et al. (1980) performed SANS experiments at the Institute Laue-Langevin (ILL) in Grenoble, France on aqueous dispersions, comparing the effect of exchangeable  $\text{Li}^+$ ,  $\text{K}^+$  and  $\text{Cs}^+$  cations on the structure of dilute montmorillonite sols (0.8%, w/w).

Fig. 12.5.4 illustrates the Guinier plots:  $\ln(q^2I)$  vs.  $q^2$ . The particle thickness may be derived from the slope of the linear part of each curve, using Eq. (8a). The extrapolation of these straight lines to  $q = 0$  gives  $(Iq^2)_0$ . This last value was used to control the exchange  $\text{H}_2\text{O} \rightarrow \text{D}_2\text{O}$ . By changing the relative proportions between  $\text{H}_2\text{O}$  and  $\text{D}_2\text{O}$ , it was possible to reach the condition  $(Iq^2)_0 = 0$  when the contrast disappears. Matching allows even a very low exchange between  $\text{D}_2\text{O}$  and  $\text{H}_2\text{O}$  layers at the clay mineral surface to be detected, and compared with the free  $\text{H}_2\text{O}$  molecules of the bulk solvent. Matching enhances the scattering contribution of these water layers and allows their thickness (of about two water layers) to be evaluated. The measurement of particle thickness, using the plots of Fig. 12.5.4, showed that  $\text{Li}^+$ -montmorillonite was completely delaminated with a layer thickness of ca. 1.10 nm including the water layers. In  $\text{K}^+$ -montmorillonite the average particle thickness was ca. 2.6 nm, corresponding to two parallel clay mineral layers. In  $\text{Cs}^+$ -montmorillonite aggregation was more pronounced with a broad distribution of particles around a thickness of about 4.2 nm corresponding to three associated layers with their hydration layers. Matching of the particle–solvent scattering length contrast was obtained with a solvent containing 65%  $\text{D}_2\text{O}$ . This experimental defined amount of  $\text{D}_2\text{O}$  cannot be obtained theoretically by only considering the scattering length of the clay mineral and of the solvent. This experimental value also depends on the very low

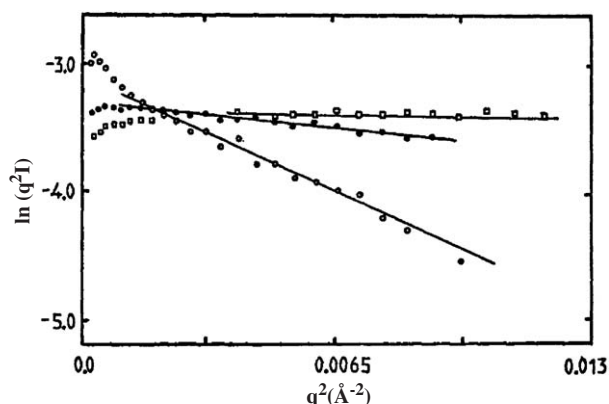


Fig. 12.5.4. Guinier plots obtained from SANS experiments for aqueous dispersions of  $\text{Li}^+$ -montmorillonite ( $\square$ ),  $\text{K}^+$ -montmorillonite ( $\bullet$ ) and  $\text{Cs}^+$ -montmorillonite ( $\circ$ ). Clay mineral concentration was 0.8% (w/w). From Cebula et al. (1980).

exchange rate between hydrogen and deuterium in water within the interlayer space, even if this water is very mobile (self-diffusion coefficient  $\approx 10^{-10} \text{ m}^2/\text{s}$ ).

Pinnavaia et al. (1984) used SANS (ILL, Grenoble) to study particle aggregation and particle-pore distribution of Spur homoionic montmorillonites (in the  $\text{Li}^+$ ,  $\text{Na}^+$ ,  $\text{K}^+$  or  $\text{Cs}^+$  forms). For 1% (w/w) dispersions,  $\text{Li}^+$ -montmorillonite obeyed Guinier's law, while  $\text{Cs}^+$ -montmorillonite followed Porod's law ( $I(q) \propto q^{-4}$ ), indicating particle aggregation in the presence of  $\text{Cs}^+$  ions.  $\text{Na}^+$ -montmorillonite dispersions showed some aggregation of clay minerals layers, while  $\text{K}^+$ -montmorillonite gave a pattern similar to  $\text{Cs}^+$ -montmorillonite. The dynamics of water and other intercalated molecules were also investigated by quasi-elastic neutron scattering.

#### Comparing Montmorillonite with Laponite

Morvan et al. (1994) performed USAXS and SAXS experiments (CEA, Saclay, France) on Laponite in pure water and in salt solutions. Fig. 12.5.5 shows the log-log plots of scattering curves at 1.8, 3.5 and 10% (w/w).

The 1.8 and 3.5% (w/w) samples give curves that are typical for ideally dispersed disk-like particles. Their profile was simulated using the  $i(q)$  intensity expression of Eq. (7) for randomly oriented cylinders of axial length  $2H$  and cross-sectional radius  $R$ , and Eq. (3) taking into account the scattering length contrast. A plateau is observed for the Guinier plot domain. Thus, the Laponite layers scatter independently without any interactions. For the 10% (w/w) concentration, the increase in intensity at small  $q$  values has an exponent  $\alpha = -3.1$  indicative of a heterogeneous medium.

Fig. 12.5.6 shows USAXS curves for a 4% (w/w) montmorillonite dispersions in 0.1 M NaCl. (Faisandier-Cauchois et al., 1995; Faisandier et al., 1998). Both plots

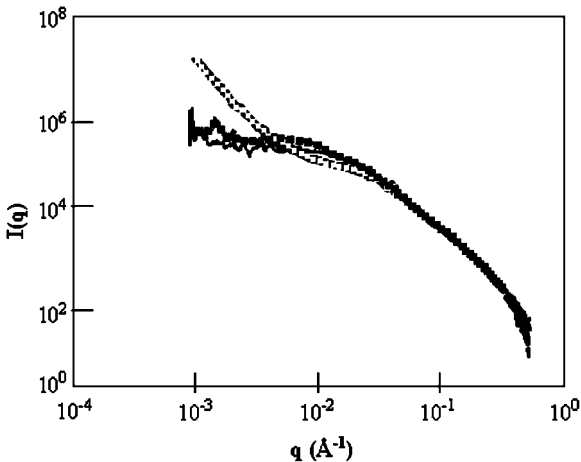


Fig. 12.5.5. Experimental USAXS intensity  $I(q)$  vs. the modulus of scattering vector  $q$  of aqueous Laponite dispersions, presented as a log–log plot. The corresponding clay concentrations were (■ ■ ■) 1.8% (w/w); (—) 3.5% (w/w) and (□ □ □) 10% (w/w). From Morvan et al. (1994).

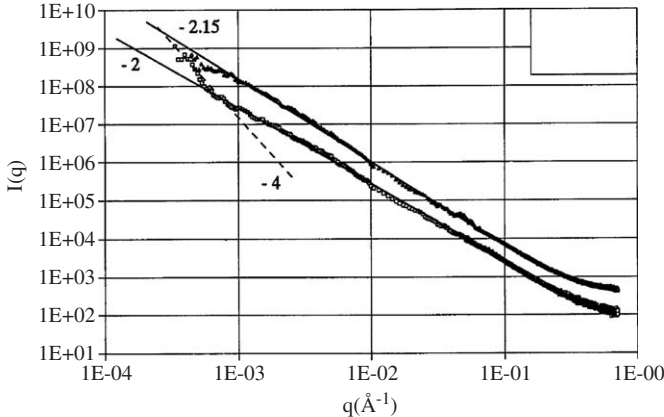


Fig. 12.5.6. Experimental USAXS intensity  $I(q)$  vs. the modulus of scattering vector  $q$  of aqueous montmorillonite dispersions in 0.1 M NaCl, presented as a log–log plot. Clay mineral concentration is 4% (w/w). From Faisandier-Cauchois et al. (1995). The slope values (–2.15, –2, –4) represent scale laws characteristic of the different structures.

are typical of well-dispersed montmorillonites obeying scaling laws over the whole  $q$ -range. Such behaviour is also typical of scattering by non-interfering very large membranes with a diameter  $D = \pi/q_m \approx 1 \mu\text{m}$  (where  $q_m$  is the lowest experimental  $q$  value), and a thickness of ca. 1 nm. This diameter is clearly larger than the usual



diameter of one montmorillonite unit layer. For the sample prepared at room temperature the exponent 2.15 indicates that some layers are parallel. For the sample under pressure (in sealed ampoules at 200 °C), the slope is  $-2$  as expected for ideally dispersed layers. These results show that at this clay concentration and ionic strength, the unit layers form large bands by edge-to-edge contacts, as mentioned by Low (1991).

Ramsay et al. (1990) compared neutron diffraction and SANS (PLUTO Harwell, UK) data for Laponite RD and Wyoming montmorillonite in  $D_2O$ . The structural changes investigated concerned samples in which the clay platelets were initially aligned in the dry state. The authors followed the development of orientational disorder and eventually a randomly oriented isotropic structure, over a wide range of  $D_2O$  concentration ( $D_2O$ /clay ratio.  $x = 0.2$  to 31 (w/w)).

The Porod's part of the SAS curves followed a  $Q^x$  law with same exponent for both clays. As the heavy water concentration increased, the exponent varied from  $-4$  in the compacted system to  $-2$  for the highly dilute dispersions.

Because of the small size of Laponite particles (in comparison with montmorillonite), the SAS in the lowest  $q$ -range allows particle diameters (25–30 nm) to be determined, using Eqs. (8a) and (8b).

#### *SANS Studies under Shear*

Using SANS (ILL, Grenoble), Ramsay and Lindner (1993) compared the *in situ* scattering of Laponite and montmorillonite dispersions under static conditions and during shearing in a Couette-type cell. The patterns were recorded with a 2D detector. The range of clay contents was chosen within 0.5–6.5% (w/w) where time-dependent gelation and thixotropic behaviour occur. Spatial and orientation correlations between the particles developed in dispersions of low ionic strength ( $<10^{-3}$  mol/L). Such self-organized structures are limited to domains of restricted size, as indicated by the anisotropic scattering behaviour, and are influenced by the clay mineral concentration, particle size and particle shape (Fig. 12.5.7).

Orientational correlations were more extensive for the relatively large montmorillonite particles. Some preferential alignment was observed at distances  $\geq 10^2$  nm under equilibrium conditions. The effect of shear on structures was indicated by the anisotropic SANS patterns. At low rates of shear, montmorillonite dispersions showed preferential alignment of particles in the direction of flow, but spatial correlations also persisted. At high shear rates (ca.  $10^4$  s $^{-1}$ ) the three-dimensional structure broke down and only the preferential alignment was observed. The time-resolved SANS studies of montmorillonite dispersions showed a high degree of thixotropy.

Similarly, Hanley et al. (1994) carried out a SANS study of a 1% (w/w) dispersion of  $Na^+$ -montmorillonite using the instrument at CNR (Cold Neutron Research) facility of the National Institute of Science and Technology (NIST), USA. The spectra were recorded on a two-dimensional detector. At equilibrium, the plot of  $\log I$  vs.  $\log q$  showed the classical scaling law with a slope of  $-2.2$  indicating a high degree of dispersion with scarcely detectable anisotropy. The behaviour of the

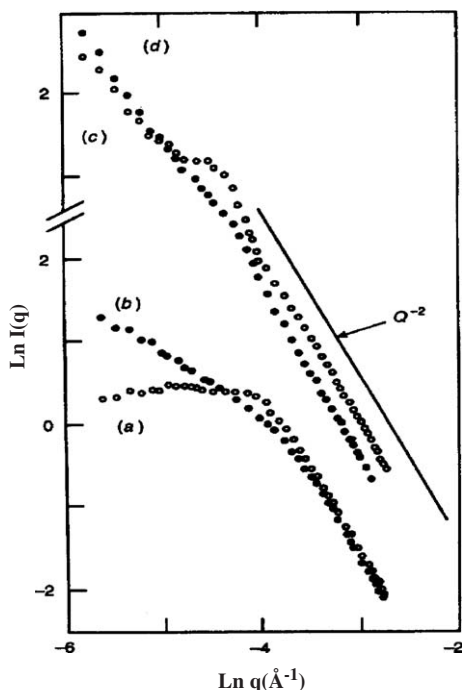


Fig. 12.5.7. SANS curves for aqueous Laponite dispersions: (a) static, (b) sheared. For montmorillonite dispersions: (c) static, (d) sheared. Clay mineral concentration,  $0.05 \text{ g/cm}^3$ ; shear rate,  $\dot{\gamma} = 1.2 \times 10^4 \text{ s}^{-1}$ . Data are radially averaged. From Ramsay and Lindner (1993).

dispersion under shear was as expected for disk-shaped particles. The disks aligned under shear with the normal parallel to the velocity gradient.

#### *Small-angle Light Scattering and Dynamic Light Scattering*

Avery and Ramsay (1986) investigated a  $\text{Na}^+$ -Laponite dispersion ( $\leq 10 \text{ g/L}$ ) at low ionic strength ( $[\text{Na}] \approx 10^{-3} \text{ mol/L}$ ) by static SALS, dynamic light scattering (DLS) and SANS (PLUTO, AERE, Harwell, UK). This will be discussed below.

**SALS.** The data were evaluated using the scattering equation based on the Rayleigh–Debye theory: because of the difficulty in measuring absolute intensities, the Rayleigh ratio,  $R_q$ , is generally used with  $R_q = I_q/I_0$ , where  $I_0$  and  $I_q$  are the intensity of the incident and scattered beam, respectively.

$$K^* \left( \frac{c}{R_q} \right) = [\langle M_w \rangle P(q)^{-1}] + 2Bc \quad (17)$$

Here  $c$  is the particle number density,  $q (= 4\pi \sin \theta / \tilde{n}\lambda)$  the scattering vector, and  $P(q)$  the particle scattering factor. Taking into account the size of the particle in

comparison with the radiation wavelength ( $\lambda = 546 \text{ nm}$ ),  $P(q)$  is a constant  $\approx 1$ ,  $B$  the second osmotic virial coefficient, and  $\langle M_w \rangle$  the weight-average molecular weight of the dispersed particles.  $K^*$  is the optical constant, equivalent to the scattering length for neutrons or X-rays and given by

$$K^* = 2\pi^2 \tilde{n}_0^2 \left( \frac{d\tilde{n}}{dc} \right)^2 \lambda^4 N^{-1} \quad (18)$$

where  $\tilde{n}_0$  is the refractive index of the solvent,  $d\tilde{n}/dc$  the refractive index increment, and  $N$  the Avogadro number. For interacting particles, the Rayleigh ratio can be expressed by

$$R(q, c) = K^* c M P(q) G(q, c) \quad (19)$$

where  $G(q)$  is the interference function which depends on particle concentration. For  $q \rightarrow 0$   $G(0, c)$  depends on the isothermal osmotic compressibility  $(dp/dc)_T$  by the relation:

$$G(0, c) = \frac{kT}{(dp/dc_n)_T} \quad (20)$$

where  $T$  is the absolute temperature,  $k$  the Boltzmann's constant and  $c_n$  the particle number density.  $R_q$  is plotted as a function of  $q$  for concentrations varying from 10 to 2.5 g/L. This method permits the molecular weight  $\langle M_w \rangle$  of Laponite particles to be determined, and their diameter (ca. 25 nm) and thickness (ca. 1 nm) to be evaluated. There is evidence to indicate that the particles are completely dispersed at these clay concentrations.

**DLS.** This technique provides information on the Brownian motion in a sample by analysing the fluctuation of the scattered light intensity (Berne and Pecora, 1990). The DLS data yield the autocorrelation function of intensity  $g(\tau)$  in a normalized form, given by

$$g(\tau) = \frac{\langle I(0)I(\tau) \rangle}{\langle I \rangle^2} \quad (21)$$

where  $I(0)$  is the intensity measured at some arbitrary time,  $I(\tau)$  that after a delay of  $\tau$  and  $\langle I \rangle$  the time-averaged intensity.  $I(\tau)$  is measured at a fixed angle.

$$g(\tau) - 1 = e^{-2Dq^2\tau} \quad (22)$$

In case of monodisperse or weakly polydisperse suspensions,  $g(\tau)$  is related to the translational diffusion  $D$  ( $= kT/f$ ) of the particles, where  $k$  is the Boltzmann constant and  $f$  ( $= 6\pi\eta R_H$ ) the collective friction factor.  $\eta$  is the solvent viscosity and  $R_H$  the hydrodynamic effective particle radius.

Experiments were performed by Avery and Ramsay (1986) for three clay contents (10, 15 and 30 g/L) and also at different times after preparation (2.5, 8 and 29 h). In order to extract the translational diffusion  $D$  from the correlation function,  $\ln g(\tau)$  is plotted vs.  $q^2\tau$ . If the particles move independently without any interaction, and without changing the dispersion viscosity, the decay is almost linear over the whole  $q$ -range. This was observed for the lowest clay content and after 2.5 h. For higher contents and at longer  $\tau$  values, a certain deviation from linearity indicated a progressive decrease of the effective translational coefficient  $D$ . These authors suggested that the particles became spatially constrained in an equilibrium structure due to the mutual interaction of their double layers.

**SANS.** Aqueous dispersions of Laponite containing increasing amounts of  $D_2O$  were studied by Avery and Ramsay (1986). The SANS spectra obtained at the lowest clay concentration (25 g/L) followed Guinier's law only for the smallest  $q$ , as predicted by Eq. (8a) for non-interacting particles. The gyration radius computed from the slope of Guinier's plot:  $\ln q^2 I(q)$  vs.  $q^2$ , corresponded to disks with a thickness of 1 nm. Thus, the Laponite particles were well dispersed. At all other concentrations, interaction effects were observed, confirming the beginning of gelation.

Similarly, Rosta and Von Gunten (1990) investigated aqueous dispersions of  $Na^+$ -Laponite RD in KCl solutions at different ionic strength in the concentration range of 0.025–5.0 g/L, using static and DLS. By combining these techniques with membrane filtration and electron microscopy, they observed that the majority of the sol particles occurred in the form of particles, composed of 2–4 parallel layers with a lateral extension of about 30 nm and an average molecular weight of  $3000 \pm 500$  kg/mol. The authors also found a large deviation of the interparticle interference function  $G(0,c)$  from 1, clearly indicating strong double-layer interactions between the particles. The hard body and electrostatic contributions to the collective friction factor were evaluated by first-order virial expressions. The electrostatic friction  $f_{E,0}$  at infinite dilution varied inversely with the concentration of an added electrolyte and was always larger than the usual Stokes friction factor,  $f_0$ , at the ionic strengths considered ( $<0.0025$  M). Electrostatic coupling between the colloidal particles contributes significantly to the collective friction.

Thompson and Butterworth (1992) investigated Laponite XLG by electron microscopy, electron diffraction, ultracentrifuge analysis and SAXS. Concerning the size and the dispersion state of the particles, they came to the same conclusions as Rosta and Von Gunten (1990). They emphasized the necessity of careful attention to the preparation of Laponite dispersions and the choice and control of pH.

This brief survey clearly indicates that for natural smectites (montmorillonites) the conditions for investigating sol–gel transition by SAS techniques are relatively restricted. Because of the high anisotropy of the clay mineral layers, the large size distribution of particles, the determination of the smallest  $q$  values (to derive the overall size of particles and their interaction distance range) involves making a series

of simplifications. The majority of studies on sol–gel transition mechanisms were therefore performed with Laponite dispersions.

#### *D. Modelling Sol–Gel Transition in Laponite Dispersions*

Mourchid et al. (1995) combined USAXS, SAXS (CEA, Saclay, France) and rheology experiments on Laponite dispersions with cryofracture and flow birefringence observations. The experimental SAS spectra were compared with spectra computed for hypothetical dispersion structures deduced from the equilibrium properties of dispersions modelled by Monte Carlo simulations. The general purpose of these numerical simulations was to evaluate the organization of clay particles induced by excluded volume effects and electrostatic repulsion between the diffuse double layers. The most interesting parts of this work are the phase diagram, (ionic strength vs. clay concentration), describing the sol–gel transition, and the state equations (Fig. 12.5.8).

The curves of osmotic pressure vs. Laponite concentration showed a break corresponding to the sol–gel transition followed by a pseudo-plateau separating the liquid and the gel phase. This was explained by an isotropic–nematic (I–N) transition

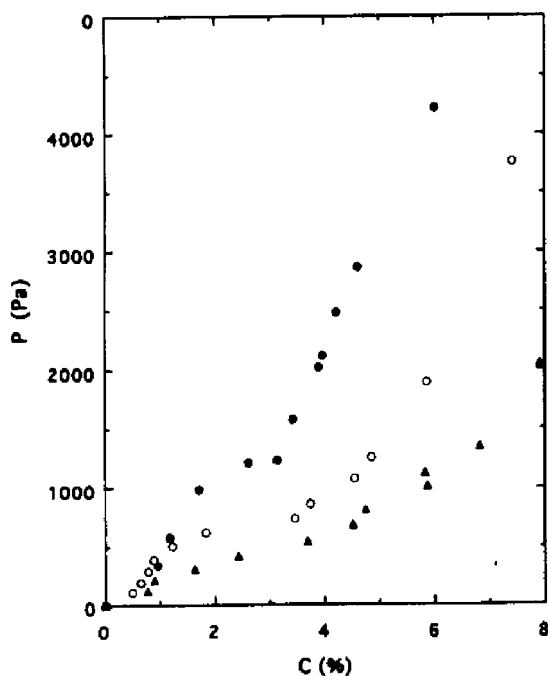


Fig. 12.5.8. Experimental equations of state for Laponite dispersions. The plots show variation of osmotic pressure  $P$  with clay concentration  $C$  at different ionic strengths  $I$  of NaCl: (●)  $I = 10^{-4}$  M; (○):  $I = 5 \times 10^{-3}$  M; (▲):  $I = 10^{-2}$  M. From Mourchid et al. (1995).

(Onsager transition). However, the phase separation as predicted by this theory was not observed along the short pseudo-plateaus of Fig. 12.5.8. In explanation, the authors admitted the possibility of a thermodynamic transition coinciding with a mechanical phase transition resulting in a frustrated I–N transition.

Another important result, deduced from the structure simulation, was that the most energetically favourable configuration between the two first neighbouring Laponite particles was the perpendicular orientation without any edge-to-face contact. This could be compatible with a certain number of like card-house structures (van Olphen, 1977) observed in flocculated dispersions by electron microscopy. The USAXS spectra indicate repulsive effects between particles and the absence of interparticle contacts. Dijkstra et al. (1997) also discussed a Monte Carlo model for the structure and gelation of smectite clay dispersions. They confirmed the edge-to-face particle configuration without any contacts.

Kroon et al. (1996) made a DLS study of sol–gel transition in Laponite dispersions at various clay mineral concentrations (1–3.5%), on both sides of the gelling time,  $T_g$ . Measurements of the static part of scattering combined with the DLS results showed the slowing down of the dynamics of a homogeneous sol until  $T_g$ . Thus, the sol–gel transition threshold was marked by a drastic change in the static part of the scattered intensity. In the gel phase, the function showed a power law decay, with a concentration-dependent scaling exponent. The authors showed the strong similarity with the scenarios predicted by the mode-coupling theory of the structural glass transition. However, transition should lead to a fragile glass and should not be far off an isotropic–nematic transition.

Using SANS (ILL, Grenoble), SALS and USAXS (CEA, Saclay), Pignon et al. (1997) showed that Laponite XLG dispersions have fractal structures over very large length scales when the gels are observed over time. Parallel rheometric measurements reveal two characteristic scale lengths in the gel behaviour. The authors suggested that the gel is composed of subunits measuring a few tens of nm. The subunits combine to form dense aggregates measuring ca. 1  $\mu\text{m}$ . At larger scale length, these micrometer-sized aggregates form isotropic fractal arrangements of dimension  $D$ , which increase with particle volume fraction. The isotropic fractal arrangement may control the macroscopic mechanical behaviour. Fig. 12.5.9 illustrates the structural evolution of a Laponite dispersion as a function of gelation time, derived from static light scattering patterns.

Mourchid and Levitz (1998) used SALS and USAXS to study long-term gelation of Laponite dispersions. A plot of  $\log I(q)$  vs.  $\log q$  showed a linear decrease with a slope  $2 < \alpha < 3$  for the smallest  $q$  values. The authors concluded that this phenomenon involved a long-term mechanism leading to the formation of glassy systems with a fractal structure. However, such structure is not observed if the starting chemical parameters are stable during the experiment. For example, a decrease in pH causes a release of divalent and trivalent cations, which in turn, promotes aggregation. Therefore, chemical modification of the colloid particles can play a central role in the evolution of the system.

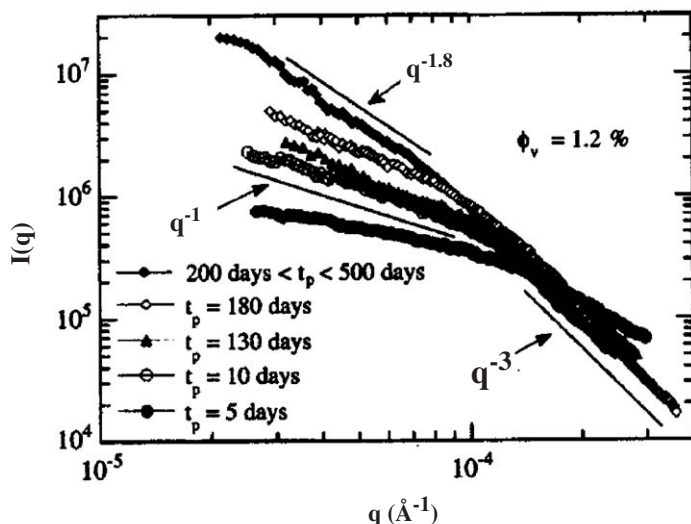


Fig. 12.5.9. Static light scattering for Laponite dispersions at different equilibrium gelation times. Volume fraction of clay, 1.2%; ionic strength,  $10^{-3}$  M NaCl; and pH = 9.5. From Pignon et al. (1997).

Pignon et al. (2000) investigated the structures of Laponite dispersions and the deposits that form during filtration at a transmembrane pressure of 0.5 bar using SANS (ILL, Grenoble) and SALS. They compared the gel structures to the respective fractal structures of the deposits.

Levitz et al. (2000) showed that at low ionic strength ( $I = 3.10^{-5}$  M) and low-clay contents (0.82, 1.02 and 1.85%), the Laponite dispersions gave USAXS spectra with correlation peaks that are compatible with long-range electrostatic stabilization. Close inspection of these correlation peaks indicate that the individual particles are not homogeneously dispersed in the space. Such results contrast strongly with the behaviour at high ionic strength ( $I > 10^{-4}$  M).

To evaluate the nematic order in dilute dispersions, Lemaire et al. (2002) performed SAXS experiments on oriented samples of Laponite gel, at the European Synchrotron Radiation Facilities (ESRF) in Grenoble. They used a 3%(w/w) dispersion, obtained by slow evaporation of a 1% dispersion. The spectra were recorded on a two-dimensional detector. The nematic order parameter,  $S$ , was derived from the scattered intensity of an oriented sample. At a clay content of 3%,  $S$  is similar to that found for classical liquid crystals.

Cousin et al. (2002) followed a new way to determine the gel structure of Laponite dispersions along the transition pseudo-plateau of Fig. 12.5.8. Magnetic spherical colloidal particles of maghemite were added to the Laponite dispersions for SANS

studies (ILL, Grenoble, France). The scattered intensity is given by

$$I_T(q) = I_L(q) + I_p(q) + I_{LP}(q) \quad (23)$$

where  $I_T(q)$  is the total scattering by the dispersion,  $I_L(q)$  the scattering by the Laponite particles,  $I_p(q)$  the scattering of the dispersed magnetic maghemite particles and  $I_{LP}(q)$  an intensity contribution due to the coupling between Laponite and maghemite particles.

By varying the ratio of D<sub>2</sub>O/water, the contrast between Laponite particles and the solvent was extinguished and  $I_T(q)$  was reduced to  $I_p(q)$ . As the maghemite particles are spherical, the interference function  $G(q)$  was obtained from Eqs. (11) and (12). Thus, the distributions of the maghemite particles in the gel could be determined for different Laponite contents. Concentrations and ionic strengths of dispersions were selected to follow the pseudo-plateau of sol–gel transition (Fig. 12.5.8). SANS and viscosity measurements showed that the magnetic probes were homogeneously dispersed in Laponite dispersions except in the region of the plateau where they were enriched in domains of low Laponite contents, indicating that the Laponite dispersions are microscopically biphasic. The authors concluded that this structure could be consistent with a frustrated I–N transition or a spinodal decomposition.

DLS and shear rejuvenation experiments on a dilute Laponite dispersion (3%, w/w) in pure water were performed by Bonn et al. (2002). Shear rejuvenation is given as the decay of the correlation function  $g(\tau)^{-1}$  vs. time (as measured by DLS), when different share rates are applied to a dispersion after ageing (e.g., 1 h) for different shearing times. The reversion of the dispersion state after shearing is compared to the dispersion states previously observed after different ageing times. The results suggest that the dynamic behaviour of such a colloid is very close to that of a glassy system.

The overall conclusion that can be drawn is that the sol–gel transition in Laponite dispersions may be explained in terms of a glassy transition with some specific characteristic probably due to particle anisotropy.

#### *Dispersions in Organic Solvents*

Ho et al. (2001) used WAXS and SANS to study the structure of organophilic clay minerals and their interaction with various organic solvents. Both types of experiments were performed at the NIST, NCNR (USA). Na<sup>+</sup>-montmorillonite was exchanged with ditallowl dimethylammonium ions, consisting of a mixture of long-chain alkylammonium ions (ca. 65% C<sub>18</sub>, 30% C<sub>16</sub> and 5% C<sub>14</sub>). The organic solvents chosen covered a range of solubility parameters. The organo-clay samples were used as received and after purification. In both cases, the layers were fully exfoliated in chloroform, while the particles retained their layer structure and expanded to a similar extent in benzene, toluene and *p*-xylene. However, the extracted (purified) material had a stronger tendency to gel. At the same clay concentration, the swollen particles of this



sample were also thinner, and therefore more numerous, than those of the unpurified counterpart. The SANS curves in the lowest  $q$ -range (from  $0.04 \text{ nm}^{-1}$ ) followed a type of scale law ( $q^{-\alpha}$ ), with  $\alpha$  depending on the degree of dispersion, very similar to that in aqueous dispersions. The lateral size of the organically modified montmorillonite particles, estimated by atomic force microscopy, is in the range of  $0.4\text{--}1.0 \mu\text{m}$ .

### 12.5.3. APPLICATION OF SAS TO PILLARED CLAYS AND CLAY-POLYMER NANOCOMPOSITES

Some examples of pillared clay minerals and clay-polymer nanocomposites are given, showing the different structural details that can be obtained by matching SANS spectra, modelling SAXS curve profiles and by measuring SANS under shear.

#### *A. Structure of Pillared Clay Minerals and Organo-Clays*

Pinnavaia et al. (1984) studied two samples of pillared montmorillonite by SANS (PLUTO, Harwell, UK). The samples were prepared by exchanging the interlayer  $\text{Na}^+$  ions with  $\text{Al}_{13}^{7+}$  (Keggin) cations at  $70^\circ\text{C}$ , and heating the product at  $350^\circ\text{C}$  (see Chapter 7.5). The problem was to measure the sizes of pores between the clay mineral particles, on the one hand, and pores between the  $\text{Al}_{13}$  cations or  $\text{Al}_2\text{O}_3$  pillars in the interlayer space, on the other. The scattering from spaces between particles was suppressed by contrast-matching with a mixture of  $\text{C}_6\text{H}_6$  and  $\text{C}_6\text{D}_6$ . The scattering from pillars could be completely suppressed by filling the interlayer space with  $\text{C}_6\text{D}_6$ . Although the SANS patterns were not thoroughly analysed, the authors clearly showed how the different pores types can be distinguished and how the pillars are distributed within the interlayer space.

Steriotis et al. (2002) used SANS contrast-matching to study montmorillonite and beidellite pillared with  $\text{Mg}^{2+}/\text{Al}^{3+}$ ,  $\text{Al}^{3+}$  or Keggin cations. They were able to determine the distances between pillars in the interlayer space.

Hanley et al. (1997) investigated the dispersion of Laponite in cetyl trimethylammonium bromide (CTAB) solution by SANS and DLS. The experiments were performed at NIST, NCNR (USA). The SANS patterns of the surfactant-free dispersion confirmed that the Laponite particles were scattered independently. After an addition of CTAB close to four times the cation exchange capacity (CEC) of the clay mineral, contrast matching by H-D exchange in the solvent indicated that the CTAB-Laponite complex retained a disk morphology, despite the large excess of CTAB. An analysis of the DLS correlation function revealed two configurations: (i) free clay mineral particles; and (ii) CTAB-exchanged particles containing surfactants in excess of the CEC, probably enough to form a stable bilayer. The effect of CTAB concentration on aggregation of clay mineral particles, and subsequent re-dispersion was also reported and the influence of clay minerals on possible CTAB micelle formation was briefly discussed.

Khatib et al. (1995) characterized dimethyl dioctadecylammonium (DDA)-exchanged montmorillonite by SAXS, and by adsorption of nitrogen and methanol. The SAXS patterns were analysed by comparison with simulated patterns for interstratification of reacted and unreacted layers. The interlayer DDA cations were assumed to be tilted at different angles to the silicate surface. Under methanol vapour pressures the mobility of the alkyl chains was enhanced. After dispersion in liquid methanol, the sample became homogeneous as indicated by a strong increase in structural order.

#### *B. Clay-polymer Nanocomposites*

Schmidt et al. (2002) studied the effect of shear on the viscoelastic behaviour of clay-polymer hybrids using Rheo-SANS. The sample was a 3% (w/w) dispersion of Laponite LRD in a 1.5% aqueous solution of polyethylene oxide (PEO). With an increasing shear rate an anisotropic scattering pattern was developed due to orientation of clay mineral particles in the shear field. Under shear, an unusual alignment of clay mineral particles was observed along the flow direction. The shear-induced orientation of the macromolecules and the particles were measured in D<sub>2</sub>O. SANS measurements of contrast-matched samples revealed the orientation of the polymer molecules alone. As the shear rate increased, the clay mineral particles orient first, and then the PEO chains become more and more stretched. The recovery from anisotropy is much faster than expected from simple Brownian motion of only the clay mineral particles in a medium of the same viscosity. This behaviour would indicate dynamic coupling of the polymer chains to the clay mineral.

#### 12.5.4. CONCLUSIONS

All scattering techniques are capable of making in situ observations of finely divided materials, in particular colloidal dispersions, without causing any damage to the samples.

**SAXS.** Many SAS studies were performed by X-rays because X-ray techniques preceded neutron scattering and the scattering contrast of clay mineral layers is high for X-rays. Unlike neutrons, X-rays do not give any background of inelastic scattering at small angles. The matching method based on the anomalous scattering near the absorption edges is a useful feature. A number of synchrotron-radiation centres with specially designed spectrometers were developed, making the technique available to non-specialists.

**SANS.** The primary advantage of neutrons is their very weak absorption by clay mineral dispersions and powders. The samples can be as thick as 1 cm whereas they cannot be thicker than 0.2–0.5 mm for SAXS. Thus, dry clay mineral samples can be

investigated by SANS, and particular SAS experiments such as Rheo-SANS, can be performed. The added advantage of using neutrons is the possibility to change the scattering contrast by varying the D:H ratio in water and organic molecules.

**SALS.** This technique can be used to investigate dispersions at a large length scale, and thus provide a relatively large overview of the samples than do other techniques. But the range of samples that can be studied by SALS is limited because dispersions have to be transparent to light. Nevertheless, the use of SALS was probed for clay colloid studies in combination with DLS and rheological measurements. The Fraunhofer scattering range (cf. Table 12.5.1) is interesting for granulometric measurements, which can be made in conjunction with sedimentation experiments, as illustrated by the work of Pabst et al. (2000) on kaolins.

SAXS, SANS and SALS, when used together, allow a multiscale sample exploration to be done (from nanometer to several tens of micrometers) under static and dynamic conditions. In many cases, the macroscopic behaviour of materials can be explained on the basis of the structure of the system in the nanometer dimension.

In this non-exhaustive review of SAS techniques we indicated the possibility and potential of using these methods to characterize clay mineral dispersions. The sol–gel transition in such systems, for example, is now reasonably well understood. Sample preparation, however, must be carefully controlled if consistent results are to be obtained, and valid data interpretation is to be achieved. SAS techniques were long used to study aqueous colloidal dispersions of “pure” clay minerals. It is only relatively recently that other clay mineral systems, notably organo-clays and smectite–polymer composites, were investigated by scattering methods.

## REFERENCES

- Andrews, D.E., Schmidt, P., van Olphen, H., 1967. X-ray studies of interactions between montmorillonite platelets. *Clays and Clay Minerals* 13, 321–330.
- Auvray, L., Auroy, P., 1991. Scattering by interfaces: variations on Porod’s law. In: Lindner, P., Zemb, T. (Eds.), *Neutron, X-ray and Light Scattering*. Elsevier, Amsterdam, pp. 199–221.
- Avery, R.G., Ramsay, J.D.F., 1986. Colloidal properties of synthetic hectorite clay dispersions. II. Light and small-angle neutron scattering. *Journal of Colloid and Interface Science* 109, 448–454.
- Bacon, G.E., 1975. *Neutron Diffraction*. Clarendon Press, Oxford.
- Bale, H.D., Schmidt, P.W., 1984. Small-angle X-ray scattering investigation of submicroscopic porosity with fractal properties. *Physical Review Letters* 53, 596–599.
- Ben Rhaïem, H., Pons, C.H., Tessier, D., 1987. Factors affecting the microstructure of smectites: role of cation and history of applied stresses. In: Schultz, L.G., van Olphen, H., Mumpton, F.A. (Eds.), *Proceedings of the International Clay Conference, Denver, 1985*. The Clay Minerals Society, Bloomington, IN, pp. 292–297.

- Berne, B.J., Pecora, R., 1990. *Dynamic Light Scattering: With Applications to Chemistry, Biology and Physics*, Reprint Edition. Krieger, Malabar, FL.
- Bohren, C.F., Huffman, D.R., 1998. *Absorption and Scattering of Light by Small Particles*. Wiley, New York.
- Bonn, D., Tanase, S., Abou, B., Tanaka, H., Meunier, J., 2002. Laponite: aging and shear rejuvenation of a colloidal glass. *Physical Review Letters* 89, 015701.
- Calas, G., Basset, W.A., Petiau, J., Steinberg, M., Tchoubar, D., Zarka, A., 1984. Some mineralogical applications of synchrotron radiation. *Physics and Chemistry of Minerals* 11, 17–36.
- Callaghan, I.C., Ottewill, R.H., 1974. Interparticle forces in montmorillonite gels. *Faraday Discussions of the Chemical Society* 57, 110–118.
- Carrado, K.A., Thiagarajan, P., Song, K., Winans, R.E., 1998. Anomalous small-angle X-ray scattering studies of interlayer heavy metal ions in clay minerals. *Chemistry of Materials* 10, 1130–1134.
- Cebula, D.J., Thomas, R.K., White, J.W., 1980. Small angle neutron scattering from dilute aqueous dispersions of clay. *Journal of the Chemical Society, Faraday Transactions 1* (76), 314–321.
- Cotton, J.P., 1991. Introduction to scattering experiments. part I. In: Lindner, P., Zemb, T. (Eds.), *Neutron, X-ray and Light Scattering*. Elsevier, Amsterdam, pp. 1–37.
- Cousin, F., Cabuil, V., Levitz, P., 2002. Magnetic colloidal particles as probes for the determination of the structure of Laponite dispersions. *Langmuir* 18, 1466–1473.
- Dijkstra, M., Hansen, J.P., Madden, P.A., 1997. Statistic model for the structure and gelation of smectite clay suspensions. *Physical Review E* 55, 3044–3053.
- Faisandier-Cauchois, K., Pons, D.H., Tchoubar, D., 1995. Analyse de la structure multi-échelle des dispersions de montmorillonite. PIRSEM Report, France, p. 10.
- Faisandier, K., Pons, D.H., Tchoubar, D., Thomas, F., 1998. Structural organization of Na- and K-montmorillonite suspensions in response to osmotic and thermal stresses. *Clays and Clay Minerals* 46, 636–648.
- Glatter, O., 1991. Small angle scattering and light scattering, part I. In: Lindner, P., Zemb, T. (Eds.), *Neutron, X-ray and Light Scattering*. Elsevier, Amsterdam, pp. 33–82.
- Glatter, O., Kratky, O. (Eds.), 1982. *Small Angle X-ray Scattering*. Academic Press, London.
- Guinier, A., Fournet, G. (Eds.), 1955. *Small-Angle Scattering of X-rays*. Wiley, New York.
- Hall, P.L., Churchman, G.J., Theng, B.K.G., 1985. Size distribution of allophane unit particles in aqueous suspensions. *Clays and Clay Minerals* 33, 345–349.
- Hanley, H.J.M., Muzny, C.D., Butler, B.D., 1997. Surfactant adsorption on a clay mineral: application of radiation scattering. *Langmuir* 13, 5276–5282.
- Hanley, H.J.M., Straty, G.C., Tsvetkov, F., 1994. A small-angle neutron scattering study of a clay suspension under shear. *Langmuir* 10, 3362–3364.
- Ho, D.L., Briber, R.M., Glinka, C.J., 2001. Characterisation of organically modified clays using scattering and microscopy techniques. *Chemistry of Materials* 13, 1923–1931.
- Hofer, M., 1991. Basic concepts in static and dynamic light scattering. Application to colloids and polymers, part VI. In: Lindner, P., Zemb, T. (Eds.), *Neutrons, X-ray and Light Scattering*. Elsevier, Amsterdam, pp. 301–324.
- Keren, R., Klein, E., 1995. Sodium/calcium-montmorillonite suspension and light scattering. *Soil Science Society of America Journal* 59, 1032–1035.

- Khatib, K., Pons, C.H., Bottero, J.Y., François, M., Baudin, I., 1995. Study of the structure of dimethyldioctadecylammonium-montmorillonite by small angle X-ray scattering. *Journal of Colloid and Interface Science* 172, 317–323.
- Kroon, M., Wegdam, G.H., Sprik, R., 1996. Dynamic light studies on the sol–gel transition of a suspension of anisotropic colloidal particles. *Physical Review E* 54, 6541–6550.
- Lemaire, B.J., Panine, P., Gabriel, J.C.P., Davidson, P., 2002. The measurements by SAXS of the nematic order parameter of Laponite gels. *Europhysics Letters* 59, 55–61.
- Levitz, P., Lecolier, E., Mourchid, A., Delville, A., Lyonnard, S., 2000. Liquid-solid transition of Laponite suspensions at very low ionic strength: long-range electrostatic stabilisation of anisotropic colloids. *Europhysics Letters* 49, 672–677.
- Low, P.F., 1991. Interparticle forces in clay suspensions flocculation, viscous flow and swelling. In: Guven, N., Pollastro, R.M. (Eds.), *Clay-Water Interface and its Rheological Implications*. CMS Workshop Lectures, vol. 4. The Clay Minerals Society, Boulder, CO, pp. 157–190.
- Mandelbrot, B.B., 1967. How long is the coast of Britain? Statistical self-similarity and fractional dimension. *Science* 155, 636–638.
- Mandelbrot, B.B., 1977. *Fractals: Form, Chance and Dimension*. W.H. Freeman, San Francisco.
- Mering, J., 1949. L'interprétation des rayons X dans les systèmes à stratification désordonnée. *Acta Crystallographica* 2, 371–377.
- Morvan, M., Espinat, D., Lambard, J., Zemb, T., 1994. Ultrasmall and small-angle X-ray scattering of smectite clay suspensions. *Colloids and Surfaces A* 82, 193–203.
- Mourchid, A., Delville, A., Lambard, J., Lécolier, E., Levitz, P., 1995. Phase diagram of colloidal dispersions of anisotropic charged particles: equilibrium properties, structure and rheology of Laponite suspensions. *Langmuir* 11, 1942–1950.
- Mourchid, A., Levitz, P., 1998. Long-term gelation of Laponite aqueous dispersions. *Physical Review E* 57, 4887–4890.
- Norrish, K., Rausell-Colom, J.A., 1963. Low-angle diffraction studies of the swelling of montmorillonite and vermiculite. *Clays and Clay Minerals* 10, 123–149.
- Pabst, W., Kunes, K., Havrda, J., Gregorova, E., 2000. A note on particle size analyses of kaolins and clays. *Journal of the European Ceramic Society* 20, 1429–1437.
- Pignon, F., Magnin, A., Piau, J.M., Cabane, B., Lindner, P., Diat, O., 1997. Yield stress thixotropic clay suspension: investigations of structure by light, neutron, and X-ray scattering. *Physical Review E* 56, 3281–3289.
- Pignon, F., Magnin, A., Piau, J.M., Cabane, B., Aimar, P., Meireles, M., Lindner, P., 2000. Structural characterisation of deposits formed during frontal filtration. *Journal of Membrane Science* 174, 189–204.
- Pinnavaia, T.J., Rainey, V., Ming-Shin, T., White, J.W., 1984. Characterisation of pillared clays by neutron scattering. *Journal of Molecular Catalysis* 27, 213–224.
- Pons, C.H., 1980. Mise en évidence des relations entre la texture et la structure dans les systèmes eau-smectites par diffusion aux petits angles du rayonnement synchrotron. Thèse, Université d'Orléans, France.
- Pons, C.H., Rousseaux, F., Tchoubar, D., 1981. Utilisation du rayonnement synchrotron en diffusion aux petits angles pour l'étude du gonflement des smectites: I. Etude du système eau-montmorillonite-Na en fonction de la température. *Clay Minerals* 16, 23–42.

- Pons, C.H., Rousseaux, F., Tchoubar, D., 1982a. Utilisation du rayonnement synchrotron pour l'étude du gonflement des smectites: II. Etude de différents systèmes eau-smectites en fonction de la température. *Clay Minerals* 17, 327–338.
- Pons, C.H., Tessier, D., Ben Rhaïem, H., Tchoubar, D., 1982b. A comparison between X-ray studies and electron microscopy observations of smectite fabric. In: van Olphen, H., Veniale, F. (Eds.), *International Clay Conference, 1981, Developments in Sedimentology* 35. Elsevier, Amsterdam, pp. 177–185.
- Porod, G., 1982. General theory. In: Glatter, O., Kratky, O. (Eds.), *Small-Angle X-ray Scattering*. Academic Press, London, pp. 17–51.
- Ramsay, J.D.F., Lindner, P., 1993. Small-angle neutron scattering investigations of the structure of thixotropic dispersions of smectite clay colloids. *Journal of the Chemical Society, Faraday Transactions* 89, 4207–4214.
- Ramsay, J.D.F., Swanton, S.W., Bunce, J., 1990. Swelling and dispersion of smectite clay colloids: determination of structure by neutron diffraction and small angle neutron scattering. *Journal of the Chemical Society, Faraday Transactions* 86, 3919–3926.
- Rausell-Colom, J.A., Norrish, K., 1962. Low-angle diffractometer for studying the swelling of clay minerals. *Journal of Scientific Instruments* 39, 156–159.
- Rausell-Colom, J.A., Saez-Auñon, J., Pons, C.H., 1989. Vermiculite gelation: structural and textural evolution. *Clay Minerals* 24, 459–478.
- Rosta, L., Von Gunten, H.R., 1990. Light scattering characterisation of laponite sols. *Journal of Colloid and Interface Science* 134, 397–406.
- Schaefer, D.W., Martin, J.E., Hurd, A.J., Keefer, K.D., 1985. Structure of random materials. In: Boccara, N., Daoud, M. (Eds.), *Physics of Finely Divided Matter. Proceedings of the Winter School. Les Houches, France*. Springer, Berlin, pp. 31–45.
- Schmidt, G., Nakatani, A.I., Butler, P.D., Han, C.C., 2002. Small angle neutron scattering from viscoelastic polymer-clay solutions. *Macromolecules* 35, 4725–4732.
- Steriotis, T.A., Stefanopoulos, K.L., Keiderling, U., De Stefanis, A., Tomlinson, A.A.G., 2002. Characterisation of pillared clays by contrast-matching small-angle neutron scattering. *Chemical Communications* 20, 2396–2397.
- Thompson, D.W., Butterworth, J.T., 1992. The nature of Laponite and its aqueous dispersions. *Journal of Colloid and Interface Science* 151, 236–243.
- van Olphen, H., 1977. *An Introduction to Clay Colloid Chemistry*, 2nd edition. Wiley, New York.

This page intentionally left blank

## *Chapter 12.6*

# FOURIER TRANSFORM INFRARED SPECTROSCOPY

S. PETIT

*UMR 6532, HydrASA, F-86022 Poitiers Cédex, France*

Infrared (IR) spectroscopy is a technique based on vibrations of atoms in a molecule. The IR spectrum of a clay mineral is sensitive to its chemical composition, isomorphous substitution and layer stacking order. This makes Fourier Transform Infrared (FTIR) spectroscopy, the most informative single technique for assessing the mineralogy and crystal-chemistry of a clay mineral sample. This chapter summarizes the potential of FTIR for clay mineral studies.

## 12.6.1. PRINCIPLE AND METHODS

The absorption of IR radiation by clay minerals depends critically on atomic mass, and the length, strength and force constants of interatomic bonds in the structures of these minerals. Absorption is also influenced by the overall symmetry of the unit cell, and the local site symmetry of each atom within the unit cell. Since theory alone gives only limited crystallo-chemical information, the interpretation of IR spectra is generally done by empirically assigning the observed signals to vibrational modes. Structural investigations of well-characterized families of natural and synthetic clay minerals played an essential role in relating spectral features to mineral structures. The monograph by [Farmer \(1974\)](#), provides one of the most useful texts on the IR spectra of clay minerals. Since then, however, many spectra were modeled using increasingly complex calculations. The recent modeling study by [Balan et al. \(2001\)](#) showed that the major features in the IR spectrum of kaolinite can be correctly reproduced.

The detector in FTIR spectrometers continuously monitors the full wavenumber range of radiation emitted by the IR source. A computer is needed to transform this information into an absorption spectrum. FTIR spectrometers may be either single beam (where the background must be subtracted to the sample) or double beam (where the background is continuously subtracted from the sample) producing a transmittance spectrum. Most systems multiply the transmittance value by 100, to give percent transmittance ( $T$ ). However, the absorbance ( $A$ ) scale, where



$A = -\ln(T/100)$ , is more and more used for quantitative analysis, following Beer's law that there is a linear relationship between absorbance and sample concentration.

So far, FTIR spectroscopy was mainly used in the middle infrared (MIR) region ( $4000\text{--}300\text{ cm}^{-1}$ ) where the fundamental vibrational modes appear. The pressed discs technique is most used for routine studies in this region. Here the sample is dispersed, (usually) in KBr, at a sample/KBr ratio of about 1% and pressed into a disc. Discs may be heated at  $120^\circ\text{C}$  overnight to remove absorbed water, whose IR bands can overlap with those of the sample.

The near infrared (NIR) region ( $11,000\text{--}4000\text{ cm}^{-1}$ ), showing the first overtone ( $2\nu$ ) and combination ( $\nu + \delta$ ) vibrations of the OH groups, is useful for the study of OH vibrations. The diffuse reflectance technique (DRIFT) is especially appropriate in the NIR region. In contrast to the MIR region, this technique does not require dilution of the sample. Thus, the IR analysis can be done very quickly and non-destructively. It is worth noting that remote-sensing and field spectrometers work exclusively in the NIR (and visible) region. [Hunt and Salisbury \(1970\)](#) and [Hunt et al. \(1973\)](#) compiled the NIR spectra of some clay minerals.

Appropriate methods of sample preparation, such as sedimentation and precipitation are used for specific investigations. For example, microscopy allows IR spectra to be obtained from samples as small as  $12\text{ }\mu\text{m}$  in diameter.

## 12.6.2. MINERALOGICAL APPLICATIONS

The application of IR spectroscopy to the identification of clay minerals was reviewed by [Russell and Fraser \(1994\)](#) who presented spectra of many types of clay and associated minerals. They also included some representative soil clays, indicating how IR spectra may be used to assess the constituent minerals in a given sample. Other useful compilations of IR spectra are those by [van der Marel and Beutelspacher \(1976\)](#), [Moenke \(1962, 1966\)](#) and [Ferraro \(1982\)](#), but these are less focused and detailed than the review by [Russell and Fraser \(1994\)](#). IR spectroscopy is a useful supplement to XRD for detecting mineral impurities, notably the presence of kaolinite, calcite and quartz in bentonite ([Madejová and Komadel, 2005](#)), and for distinguishing between X-ray amorphous and poorly crystallized clay minerals. This capability is very useful in following clay mineral crystallization during clay mineral syntheses ([Decarreau, 1980](#)). IR spectroscopy is also a powerful technique for discriminating between different kaolinite polymorphs ([Prost et al., 1989](#)).

## 12.6.3. CRYSTALLO-CHEMICAL APPLICATIONS

The vibrations of layer silicates can be more or less separated into those of the constituent units: the OH groups, the silicate anion, the octahedral cations and the interlayer cations if any. Of these, the vibrations of the OH groups are very slightly

dependent on the vibrations of the rest of the structure. However, they are markedly influenced by the ions to which the OH groups are coordinated.

The vibrations of the OH groups are the most fully understood and studied because they are very sensitive indicators of their environment. In published quantitative results, the absorption coefficients of the OH stretching ( $\nu\text{OH}$ ) vibration bands are assumed to be constant, whatever the local chemistry around OH groups within dioctahedral (Slonimskaya et al., 1986; Madejová et al., 1994; Besson and Drits, 1997) and trioctahedral clay minerals (Papin et al., 1997; Petit et al., 2004b). The absorbance of each OH band is then proportional to the number of absorbing centres of each type. When all the OH vibration bands occurring in the FTIR spectra are correctly assigned, the FTIR spectra can be quantitatively used. Using an environmental IR microbalance cell, Xu et al. (2000) found that the molar absorptivity of the OH bending vibrations ( $\delta\text{OH}$ ) varies with the  $\text{H}_2\text{O}$  content. A number of reviews about the factors affecting the OH vibrations in clay minerals were published (Vedder, 1964; Velde, 1983; Robert and Kodama, 1988; Petit et al., 1995; Besson and Drits, 1997; Gates, 2005). The OH vibrations are affected by the octahedral cations to which the OH group is coordinated, and to a lesser degree, by the tetrahedral, and interlayer environments.

#### A. The Octahedral Environment

In the simple case of talc where there are neither multivalent substitutions nor vacant sites, the OH groups point perpendicularly toward the hole of the hexagonal cavity. The  $\nu\text{OH}$  wavenumber of the  $\text{Mg}_3\text{OH}$  group remains almost constant at  $3677\text{ cm}^{-1}$  even when other divalent cations such as  $\text{Ni}^{2+}$ ,  $\text{Co}^{2+}$ ,  $\text{Zn}^{2+}$  are present in the octahedral sheet. Solid-solutions between end-members can be easily obtained by hydrothermal syntheses (Petit, 2005). When  $\text{Mg}^{2+}$  is replaced by another cation, the difference in properties (electronegativity, atomic mass and cation size) between  $\text{Mg}^{2+}$  and the substituted ion changes the wavenumber of the  $\nu\text{OH}$  (Table 12.6.1). Up to four OH vibration bands can be distinguished when  $\text{Mg}^{2+}$  is partially replaced by another divalent cation. These bands correspond to the four possible combinations of the two different cations within three octahedral sites that are directly linked to an OH group (Fig. 12.6.1). The content of each octahedral cation can be obtained as a sum of the absorbances of the bands of those OH groups to which the cation is coordinated.

As low as  $<0.01\text{ Fe}^{2+}$  or  $\text{Al}^{3+}$  ions per half-unit cell can be detected in natural talcs from the NIR region ( $2\nu\text{OH}$  bands), while the sensitivity is almost half that in the MIR region ( $\nu\text{OH}$  bands) (Petit et al., 2004b). Using  $\nu\text{OH}$  bands, Madejová et al. (1994) and Besson and Drits (1997) were able to estimate the populations of octahedral cations for dioctahedral smectites and fine-grained micaceous clay minerals, respectively. Cuadros and Altaner (1998) also obtained good agreement between the IR and chemical data of mixed-layer illite-smectite in bentonites, using the  $\delta\text{OH}$  bands ( $960\text{--}750\text{ cm}^{-1}$ ). Gates et al. (2002) determined the  $\text{Al}^{3+}$  and  $\text{Fe}^{3+}$  site

Table 12.6.1. Wave numbers of the  $\nu R_3OH$  bands for synthetic talcs

$M^{IV}$	R	$\nu R_3OH$ ( $cm^{-1}$ )
Si	Mg	3677*
Si	Ni	3627*
Si	$Fe^{2+}$	3624†
Si	Co	3631*
Si	Zn	3641*
Si	Cu	3656†
Ge	Mg	3635*
Ge	Ni	3584*
Ge	Co	3586*

\*From [Petit et al. \(2004a\)](#)

†For partially substituted samples from [Wilkins and Ito \(1967\)](#).

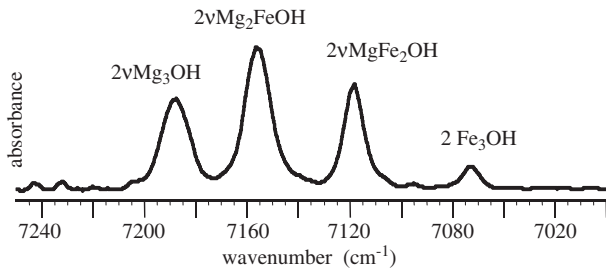


Fig. 12.6.1. First overtone  $R_3OH$  vibration bands in the FTIR spectrum of a natural unusually iron-rich talc from the Sterling mine, Antwerp, USA.

occupancies in ferruginous smectites and nontronites from the octahedral  $Al^{3+}$  content of the samples, using the OH combination bands in NIR. After ensuring that the octahedral chemical composition agrees with chemical analyses, the order–disorder cationic distribution can also be quantified. This was done by [Wilkins and Ito \(1967\)](#) and [Petit et al. \(2004b\)](#) for talc; by [Madejová et al. \(1994\)](#) for smectite; and by [Besson and Drits \(1997\)](#) for celadonite-glaucanite.

*B. The Tetrahedral Environment*

Synthetic talcs with substitution of  $Ge^{4+}$  for  $Si^{4+}$  show a shift of the  $\nu R_3OH$  bands of almost  $40\,cm^{-1}$  toward lower wavenumbers ([Table 12.6.1](#)), indicating the strong influence of the tetrahedral environment on the  $\nu OH$  bands.

In natural clay minerals, the major changes in tetrahedral environment are due to multivalent substitutions of  $Al^{3+}$  and  $Fe^{3+}$  for  $Si^{4+}$ . Even if the sensitivity is less than for the octahedral environment, several features in the IR spectra are observed

that are related to the degree of tetrahedral substitution such as the appearance of the Si-O-Al<sup>IV</sup> band and the shift of  $\nu$ OH and  $\delta$ OH bands (Russell and Fraser, 1994).

### C. Interlayer Cations

Vibrational modes of the interlayer cation are typically very low in frequency and occur in the far IR region ( $50\text{--}150\text{ cm}^{-1}$ ). This region is suitable for studying the interlayer environment of clay minerals, using the interlayer cations as probes. However, only cations with low hydration energies in anhydrous clay minerals can be studied (Fripiat, 1981; Prost and Laperche, 1990; Laperche and Prost, 1991; Schroeder, 1992; Diaz et al., 2002).

Especially for relatively high-charge clay minerals, the spectra in the  $\nu$ OH region may change with the interlayer composition due to repulsion between the charge-balancing cation and the protons of the OH groups. For example, in K<sup>+</sup>-saturated synthetic saponites (Fig. 12.6.2), two bands are observed at 3712 and 3677 cm<sup>-1</sup>. Both are  $\nu$ Mg<sub>3</sub>OH bands, the latter being due to unperturbed Mg<sub>3</sub>OH groups as in talc, and the former to Mg<sub>3</sub>OH groups perturbed by K<sup>+</sup> (Pelletier et al., 1999). The position of the perturbed OH varies with the cation, revealing the strength of repulsion (Diaz et al., 2002).

One interesting inorganic interlayer cation that can be studied in the MIR region is ammonium. This cation shows two main absorption bands near 1400 and 3200 cm<sup>-1</sup> due to the N $\leftrightarrow$ H vibrations. The band near 1400 cm<sup>-1</sup> can be used to measure the concentration of ammonium in clay minerals (Petit et al., 1998). The only limitation is that the sample has to be free of carbonate because of band overlap. The position and the shape of the band near 1400 cm<sup>-1</sup> depend on the symmetry of the NH<sub>4</sub><sup>+</sup> ion, and is indicative of where isomorphous substitution occurs (Chourabi and Fripiat, 1981; Pironon et al., 2003). Using the pellet technique, this band can also

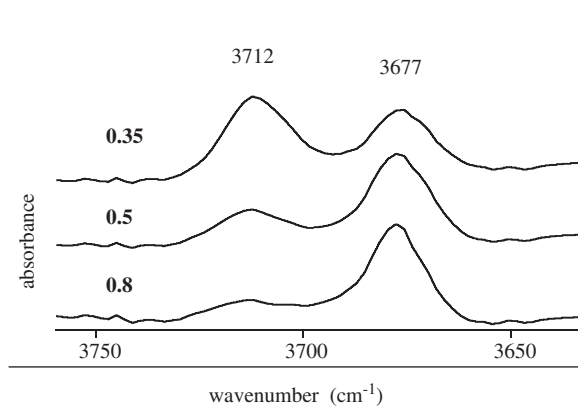


Fig. 12.6.2. FTIR spectra in the  $\nu$ OH region of K<sup>+</sup>-saturated saponites (synthesized by J.L. Robert, Orléans, France). The bold numbers denote the layer charge per half unit cell.

indicate the exchangeability of  $\text{NH}_4^+$  by other cations (Petit et al., 1999). This allows the amount and the origin of the layer charge (compensated by  $\text{NH}_4^+$ ) to be quantified. Similarly the proportion of different clay minerals in mixtures such as  $\text{NH}_4^+$ -illite/smectite (Lindgreen, 1994), gel/illite crystallization ratio in syntheses experiments (Šucha et al., 1998) can be assessed by this method. Using the ammonium signal, Mortland and Raman (1968) studied the surface acidity of smectites, while Joussein et al. (2001) used this signal to measure the molar absorption coefficient ratio between kaolinite and smectite. They found a value of about 5, which accords with the value deduced by Madejová et al. (2002) from spectral decompositions.

#### 12.6.4. ADSORPTION PHENOMENA

##### *A. Clay–Water Interactions*

Water molecules that are strongly hydrogen-bonded exhibit different vibrational properties from those that are weakly bonded to the oxygen atoms of the silicate anions. This offers a good opportunity for IR studies. The interactions of water with smectites were extensively investigated (e.g. Prost, 1976; Farmer, 1978; Poinsignon et al., 1978; Sposito and Prost, 1982; Johnston et al., 1992; Xu et al., 2000).

Two distinct environments of sorbed water can be shown: (i) water molecules directly coordinated to exchangeable cations; and (ii) those occupying the pores. When the water content is low, the water molecules strongly coordinated to the exchangeable cations are polarized, the more so when the cation has a high hydration energy.

One point to emphasize for quantitative studies is that the absorption coefficient for the  $\nu_2$  band of water (near  $1630\text{ cm}^{-1}$ ) varies with the water content of the clay mineral (Johnston et al., 1992). In the overtone range (NIR region), the extinction coefficient of OH involved in strong hydrogen bonding is much smaller than that in the fundamental range (MIR region). This facilitates the study of water molecules that interact with clay minerals (Prost, 1975; Cariati et al., 1981, 1983; Bishop et al., 1994).

##### *B. Clay–Organic Interactions*

IR spectroscopy is extensively used to study the clay–organic intercalation. An abundant literature exists on the use of IR to study pesticides adsorption by clay minerals (Cox et al., 1994; Pusino et al., 2003) and organo-clays (Hermosín and Cornejo, 1993; Cox et al., 2001). Dichroism measurements are often used to study the orientation of the functional groups of the organic species (Serratos, 1966; Vimond-Laboudigue and Prost, 1995; Sheng et al., 2002).

The surface acidity of pillared clay minerals is commonly measured by pyridine adsorption followed by IR spectroscopy. Besides being able to identify the type of acid sites present, this method can provide a semi-quantitative evaluation of acid strength (Carvalho et al., 2003).

IR spectroscopy was often used to show the intercalation and solvation of organic molecules into kaolinite. Upon intercalation, the hydrogen bonds between the inner surface hydroxyls and the siloxane of the next adjacent layer is replaced by those between the kaolinite and the intercalated molecules.

IR spectroscopy was used to calculate the contribution of hydrogen bonding to the intercalation process. A recent review of IR (and Raman) studies dealing with the intercalation of organic compounds (formamide, hydrazine, dimethyl sulphoxide (DMSO), potassium and cesium acetates) is that by [Frost and Martens \(2005\)](#). [Yariv et al. \(2000\)](#) used IR spectroscopy to study the intercalation of potassium halides by DMSO-kaolinite. Only in the case of KCl does a new band appear at  $3652\text{ cm}^{-1}$  due to the inner OH groups. They suggested that the  $\text{Cl}^-$  ions penetrate into the ditrigonal holes forming hydrogen bonds with the inner OH groups. On the other hand,  $\text{Br}^-$  and  $\text{I}^-$  ions are too large to enter the ditrigonal cavities.

## 12.6.5. CONCLUSIONS

FTIR spectroscopy is a rapid, economical, easy and non-destructive technique deserving of being used more widely in clay mineral investigations. The development in FTIR spectrometers greatly enhanced the field of applications. Modern instruments high sensitivity, speedy data collection, enhanced spectral precision and reproducibility. Efficient computers enable routine transmission methods to be improved. They also allow the use of different reflectance techniques that are difficult to implement with classical dispersive instruments.

## REFERENCES

- Balan, E., Saitta, A.M., Mauri, F., 2001. First-principles modeling of the infrared spectrum of kaolinite. *American Mineralogist* 86, 1321–1330.
- Besson, G., Drits, V.A., 1997. Refined relationships between chemical composition of dioctahedral fine-dispersed mica minerals and their infrared spectra in the OH stretching region. Part I: identification of the stretching band. *Clays and Clay Minerals* 45, 158–169.
- Bishop, J.L., Pieters, C.M., Edwards, J.O., 1994. Infrared spectroscopic analyses on the nature of water in montmorillonite. *Clays and Clay Minerals* 42, 702–716.
- Cariati, F., Erre, L., Micera, G., Piu, P., Gessa, C., 1981. Water molecules and hydroxyl groups in montmorillonites as studied by near infrared spectroscopy. *Clays and Clay Minerals* 29, 157–159.
- Cariati, F., Erre, L., Micera, G., Piu, P., Gessa, C., 1983. Polarization of water molecules in phyllosilicates in relation to exchange cations as studied by near infrared spectroscopy. *Clays and Clay Minerals* 31, 155–157.
- Carvalho, A.P., Martins, A., Silva, J.M., Pires, J., Vasques, H., Brotas de Carvalho, M., 2003. Characterization of the acidity of Al- and Zr-pillared clays. *Clays and Clay Minerals* 51, 340–349.

- Chourabi, B., Fripiat, J.J., 1981. Determination of tetrahedral substitutions and interlayer surface heterogeneity from vibrational spectra of ammonium in smectites. *Clays and Clay Minerals* 29, 260–268.
- Cox, L., Hermosín, M.C., Cornejo, J., 1994. Interactions of methomyl with montmorillonites. *Clay Minerals* 29, 767–774.
- Cox, L., Hermosín, M.C., Koskinen, W.C., Cornejo, J., 2001. Interactions of imidacloprid with organic- and inorganic-exchanged smectites. *Clay Minerals* 36, 267–274.
- Cuadros, J., Altaner, S.P., 1998. Compositional and structural features of the octahedral sheet in mixed-layer illite/smectite from bentonites. *European Journal of Mineralogy* 10, 111–124.
- Decarreau, A., 1980. Cristallogénèse expérimentale des smectites magnésiennes : hectorite, stévensite. *Bulletin de Minéralogie* 103, 579–590.
- Díaz, M., Huard, E., Prost, R., 2002. Far infrared analysis of the structural environment of interlayer  $K^+$ ,  $NH_4^+$ ,  $Rb^+$  and  $Cs^+$  selectively retained by vermiculite. *Clays and Clay Minerals* 50, 284–293.
- Farmer, V.C., 1974. The layer silicates. In: Farmer, V.C. (Ed.), *The Infrared Spectra of Minerals*. Mineralogical Society, London, pp. 331–365.
- Farmer, V.C., 1978. Water on particle surfaces. In: Greenland, D.J., Hayes, M.H.B. (Eds.), *Chemistry of Soil Constituents*. Wiley, Chichester, pp. 405–448.
- Ferraro, J.R., 1982. *The Sadtler Infrared Spectra Handbook of Minerals and Clays*. Sadtler/Heyden, London.
- Fripiat, J.J., 1981. Application of far infrared spectroscopy to the study of clay minerals and zeolites. In: Fripiat, J.J. (Ed.), *Advanced Techniques for Clay Minerals Analysis*. Elsevier, Amsterdam, pp. 191–210.
- Frost, R.L., Martens, W.N., 2005. Raman spectroscopy of kaolinite and selected intercalates. In: Kloppege, J.T. (Ed.), *The Application of Vibrational Spectroscopy to Clay Minerals and Layered Double Hydroxides*, CMS Workshop Lectures, vol. 13, The Clay Minerals Society, Aurora, CO, pp. 9–40.
- Gates, W.P., 2005. Infrared spectroscopy and the chemistry of dioctahedral smectites. In: Kloppege, J.T. (Ed.), *The Application of Vibrational Spectroscopy to Clay Minerals and Layered Double Hydroxides*, CMS Workshop Lectures, vol. 13, The Clay Minerals Society, Aurora, CO, pp. 125–168.
- Gates, W.P., Slade, P.G., Manceau, A., Lanson, B., 2002. Site occupancies by iron in nontronites. *Clays and Clay Minerals* 50, 223–239.
- Hermosín, M.C., Cornejo, J., 1993. Binding mechanism of 2,4-dichlorophenoxyacetic acid by organoclays. *Journal of Environmental Quality* 22, 325–331.
- Hunt, G.R., Salisbury, J.W., 1970. Visible and infrared spectra of minerals and rocks: I Silicate minerals. *Modern Geology* 1, 283–300.
- Hunt, G.R., Salisbury, J.W., Lenhoff, C.J., 1973. Visible and infrared spectra of minerals and rocks: VI Additional silicate. *Modern Geology* 4, 85–106.
- Johnston, C.T., Sposito, G., Erickson, C., 1992. Vibrational probe studies of water interactions with montmorillonite. *Clays and Clay Minerals* 40, 722–730.
- Joussein, E., Petit, S., Decarreau, A., 2001. Une nouvelle méthode de dosage des minéraux argileux en mélange par spectroscopie IR. *Comptes Rendus de l'Académie des Sciences*, Paris 332, 83–89.

- Laperche, V., Prost, R., 1991. Assignment of the far-infrared absorption bands of K in micas. *Clays and Clay Minerals* 39, 281–289.
- Lindgreen, H., 1994. Ammonium fixation during illite-smectite diagenesis in Upper Jurassic shale, North Sea. *Clay Minerals* 29, 527–537.
- Madejová, J., Kečkéš, J., Komadel, P., Pálková, H., Komadel, P., 2002. Identification of components in smectite/kaolinite mixtures. *Clay Minerals*, 377–388.
- Madejová, J., Komadel, P., 2005. Information available from infrared spectra of the fine fraction of bentonites. In: Kloppege, J.T. (Ed.), *The Application of Vibrational Spectroscopy to Clay Minerals and Layered Double Hydroxides*, CMS Workshop Lectures, vol. 13, The Clay Minerals Society, Aurora, CO, pp. 65–98.
- Madejová, J., Komadel, P., Čičel, B., 1994. Infrared study of octahedral site populations in smectites. *Clay Minerals* 29, 319–326.
- Moenke, H., 1962. *Mineralspektren I*. Akademie-Verlag, Berlin.
- Moenke, H., 1966. *Mineralspektren II*. Akademie-Verlag, Berlin.
- Mortland, M.M., Raman, K.V., 1968. Surface acidity of smectites in relation to hydration, exchangeable cation, and structure. *Clays and Clay Minerals* 16, 393–398.
- Papin, A., Sergeant, J., Robert, J.L., 1997. Intersite OH-F distribution in an Al-rich synthetic phlogopite. *European Journal of Mineralogy* 9, 501–508.
- Pelletier, M., Michot, L.J., Barrès, O., Humbert, B., Petit, S., Robert, J.L., 1999. Influence of KBr conditioning on the infrared hydroxyl-stretching region of saponites. *Clay Minerals* 34, 439–445.
- Petit, S., 2005. Crystal-chemistry of talcs: A NIR and MIR spectroscopic approach. In: Kloppege, J.T. (Ed.), *The Application of Vibrational Spectroscopy to Clay Minerals and Layered Double Hydroxides*, CMS Workshop Lectures, vol. 13, The Clay Minerals Society, Aurora, CO, pp. 41–64.
- Petit, S., Decarreau, A., Martin, F., Buchet, R., 2004a. Refined relationship between the position of the fundamental OH stretching and the first overtones for clays. *Physics and Chemistry of Minerals* 31, 585–592.
- Petit, S., Martin, F., Wiewiora, A., De Parseval, Ph., Decarreau, A., 2004b. Crystal-chemistry of talc: a near infrared (NIR) spectroscopy study. *American Mineralogist* 89, 319–326.
- Petit, S., Righi, D., Madejová, J., Decarreau, A., 1998. Layer charge estimation of smectites using infrared spectroscopy. *Clay Minerals* 33, 579–591.
- Petit, S., Righi, D., Madejová, J., Decarreau, A., 1999. Interpretation of the infrared  $\text{NH}_4^+$  spectrum of the  $\text{NH}_4^+$ -clays: application to the evaluation of the layer charge. *Clay Minerals* 34, 543–549.
- Petit, S., Robert, J.L., Decarreau, A., Besson, G., Grauby, O., Martin, F., 1995. Apport des méthodes spectroscopiques à l'étude des argiles. *Bulletin des Centres de Recherches Exploration-Production elf aquitaine* 19, 119–147.
- Pironon, J., Pelletier, M., De Donato, P., Mosser-Ruck, R., 2003. Characterization of smectite and illite by FTIR spectroscopy of interlayer  $\text{NH}_4^+$  cations. *Clay Minerals* 38, 201–211.
- Poinsignon, C., Cases, J.M., Fripiat, J.J., 1978. Electrical-polarization of water molecules adsorbed by smectites. An infrared study. *Journal of Physical Chemistry* 82, 1855–1860.
- Prost, R., 1976. Interactions between adsorbed water molecules and the structure of clay minerals: hydration mechanism of smectites. In: Bailey, S.W. (Ed.), *Proceedings of the International Clay Conference 1975*. Applied Publishing, Wilmette, IL, pp. 351–359.



- Prost, R., Dameme, A., Huard, E., Driard, J., Leydecker, J.P., 1989. Infrared study of structural OH in kaolinite, dickite, nacrite, and poorly crystalline kaolinite at 5 to 600 K. *Clays and Clay Minerals* 37, 464–468.
- Prost, R., Laperche, V., 1990. Far-infrared study of potassium micas. *Clays and Clay Minerals* 38, 351–355.
- Pusino, A., Gelsomino, A., Fiori, M.G., Gessa, C., 2003. Adsorption of two quinolinecarboxylic acid herbicides on homoionic montmorillonites. *Clays and Clay Minerals* 51, 143–149.
- Robert, J.L., Kodama, H., 1988. Generalization of the correlations between hydroxyl-stretching wavenumbers and composition of micas in the system  $K_2O$ - $MgO$ - $Al_2O_3$ - $SiO_2$ - $H_2O$ . A single model for trioctahedral and dioctahedral micas. *American Journal of Science* 288A, 196–212.
- Russell, J.D., Fraser, A.R., 1994. Infrared methods. In: Wilson, M.J. (Ed.), *Clay mineralogy: Spectroscopic and Chemical Determinative Methods*. Chapman & Hall, London, pp. 11–67.
- Schroeder, P.A., 1992. Far infrared study of the interlayer torsional–vibrational mode of mixed-layer illite smectites. *Clays and Clay Minerals* 40, 81–91.
- Serratos, J.M., 1966. Infrared analysis of the orientation of pyridine molecules in clay complexes. *Clays and Clay Minerals*, 385–391.
- Sheng, G., Johnston, C.T., Teppen, B.J., Boyd, S.A., 2002. Adsorption of dinitrophenol herbicides from water by montmorillonites. *Clays and Clay Minerals* 50, 25–34.
- Slonimskaya, M.V., Besson, G., Dainyak, L.G., Tchoubar, C., Drits, V.A., 1986. Interpretation of the IR spectra of celadonites and glauconites in the region of OH-stretching frequencies. *Clay Minerals* 21, 377–388.
- Sposito, G., Prost, R., 1982. Structure of water adsorbed on smectites. *Chemical Reviews* 82, 553–573.
- Šucha, V., Elsass, F., Eberl, D.D., Kuchta, L., Madejová, J., Gates, W.P., Komadel, P., 1998. Hydrothermal synthesis of ammonium illite. *American Mineralogist* 83, 58–67.
- van der Marel, H.W., Beutelspacher, H., 1976. *Atlas of Infrared Spectroscopy of Clay Minerals and their Admixtures*. Elsevier, Amsterdam.
- Vedder, W., 1964. Correlations between infrared spectrum and chemical composition in mica. *American Mineralogist* 49, 736–768.
- Velde, B., 1983. Infrared OH-stretching bands in potassic micas, talc and saponite. Influence of electronic configuration and site of charge compensation. *American Mineralogist* 68, 1169–1173.
- Vimond-Laboudigue, A., Prost, R., 1995. Etude comparée des complexes hectorite- et vermiculite-decylammonium à l'aide des spectrométries infrarouge et Raman. *Clay Minerals* 30, 337–352.
- Wilkins, R.W.T., Ito, J., 1967. Infrared spectra of some synthetic talcs. *American Mineralogist* 52, 1649–1660.
- Xu, W., Johnston, C.T., Parker, P., Agnew, S.F., 2000. Infrared study of water sorption on Na-, Li-, Ca-, and Mg-exchanged (Swy-1 and SAz-1) montmorillonite. *Clays and Clay Minerals* 48, 120–131.
- Yariv, S., Lapides, I., Nasser, A., Lahav, N., Brodsky, I., Michaelian, K.H., 2000. Infrared study of the intercalation of potassium halides in kaolinite. *Clays and Clay Minerals* 48, 10–18.

Chapter 12.7

## NUCLEAR MAGNETIC RESONANCE SPECTROSCOPY

J. SANZ

*Instituto de Ciencia de Materiales de Madrid, CSIC, Campus de Cantoblanco, ES-28049 Madrid, Spain*

Nuclear magnetic resonance (NMR) spectroscopy provides information on both the structural and dynamic aspects of solids, including clay minerals. In NMR spectroscopy, the interaction of nuclear magnetic moments,  $\mu_n = (h/2\pi) \gamma_n I$ , with an external magnetic field,  $B_0$ , induces the splitting of the  $2I+1$  energy levels of the nuclear spin  $I$  (Zeeman interaction). In the last expression,  $\gamma_n$  stands for the magnetogyric ratio of nuclei and  $h$  for the Planck constant. Irradiation of the sample with the radio frequency,  $\omega_0 (= \gamma_n B_0)$ , produces the absorption of the resonant energy between adjacent energy levels (detection of NMR experiment) (Fig. 12.7.1a).

NMR spectroscopy is sensitive to the local environment of atoms. Nuclei in different structural environments ‘see’ slightly different magnetic fields and consequently absorb photons of different frequencies. Since these magnetic fields are generally dependent on the crystal orientation with respect to  $B_0$ , the NMR spectra of powder samples show low resolution. Besides chemical shift, there are other anisotropic interactions that reduce spectral resolution: (i) dipolar interactions,  $H_D$ , between magnetic moments of nuclei; (ii) paramagnetic interactions,  $H_P$ , between magnetic moments of nuclei and paramagnetic centers; and (iii) quadrupolar interactions,  $H_Q$ , between quadrupolar moments of nuclei and electric field gradients at occupied sites (Slichter, 1990).

The spectral resolution of solids can be improved by: (1) rotating the sample around an axis inclined at  $54^\circ 44'$  with respect to the magnetic field  $B_0$ ; this ‘magic-angle spinning’ (MAS) technique averages the angular dependence, and (2) applying decoupling techniques that reduce the spin term of hamiltonians describing magnetic interactions.

In MAS experiments, (Fig. 12.7.1b) the spinning frequency must be larger than the width of the NMR signal expressed in cycles per second (cps). If this is smaller, side bands spaced by the same quantity (spinning rate) are detected in spectra. The analysis of spinning side band patterns provides useful information about sites occupied by nuclei, distortions of polyhedra, and local symmetry of occupied sites. The

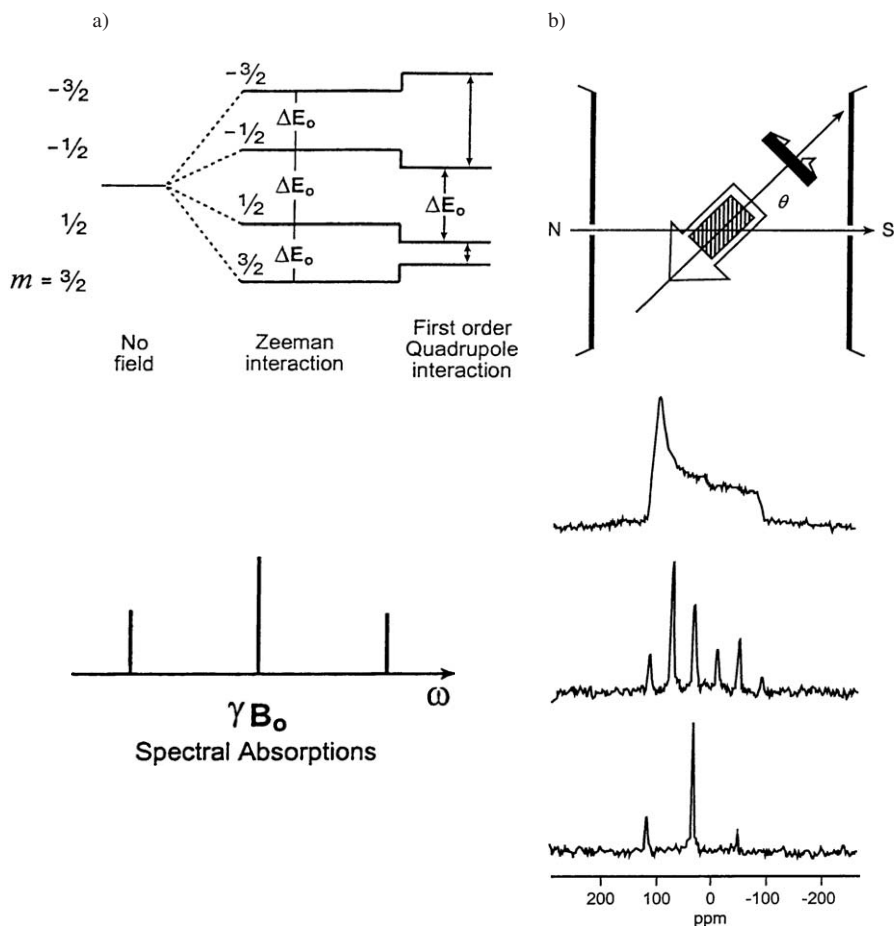


Fig. 12.7.1. (a) Energy levels for a nucleus with  $I = 3/2$  in a magnetic field  $B_0$  with the allowed transitions. The figure shows the effect of the first-order quadrupolar interactions. (b) Experimental arrangement of samples in MAS-NMR experiments (spinning around  $\theta = 54^\circ 44'$ ). Influence of increasing spinning rates on the  $^{31}\text{P}$  CP-MAS spectra of triphenylphosphine oxide. From Wasylshen and Fyfe (1982).

position of the central peak of these patterns (isotropic chemical shift) is indicative of the chemical environment of nuclei.

Chemical shift anisotropies and first-order quadrupolar interactions ( $I > 1/2$ ) decrease with the MAS technique. However, for systems in which second-order quadrupolar interactions are important, the position and shape of the central components can be seriously affected (Samoson and Lippmaa, 1983). In this case, second-order quadrupolar effects can be attenuated by using higher magnetic fields ( $B_0$ ) or double

rotation (DOR, DAS) techniques. Further, a separated evaluation of chemical shift and quadrupole contributions was achieved by the application of two-dimensional multi-quantum techniques (Massiot et al., 1996). As a result, the spectral features of individual sites can now be determined. However, in very anisotropic environments signals can be strongly broadened, making quantitative analysis difficult (Alma et al., 1984; Massiot et al., 1990).

On the other hand, decoupling techniques can average spin terms of heteronuclear dipolar interactions, giving improved spectral resolution (Duer, 2002). Spectral broadening is often caused by  $^1\text{H}$  atoms. In such cases, irradiation of protons at the Larmor frequency during recording of the NMR signal can reduce linewidth of components. If the sample is rotated during decoupling, the spectral resolution can be further improved (DR-MAS technique). A modified form of this technique is termed 'cross-polarization (CP)-MAS'. Its application can improve the detection of atoms located near OH/H<sub>2</sub>O groups through transfer of polarization from hydrogen atoms to analysed nuclei (Pines et al., 1973).

### 12.7.1. NMR SPECTROSCOPY OF CLAY MINERALS

In the following sections, several examples were chosen to illustrate the applicability of the NMR technique to investigating the structural and dynamic aspects of clay minerals (Sanz and Serratos, 2002).

#### *A. Structural Characterization*

##### *Cation Coordination*

For some phyllosilicates the location of Al is difficult to assess from chemical or structural analyses. In particular, the distinction of Al and Si in tetrahedral sites by X-ray diffraction (XRD) is problematic because of the similarity of their atomic scattering factors. In this case,  $^{27}\text{Al}$  MAS-NMR spectroscopy can provide direct information on Al coordination, as the signals corresponding to octahedral ( $\sim 0$  ppm) and tetrahedral ( $\sim 70$  ppm) Al are well resolved. Fig. 12.7.2a shows the  $^{27}\text{Al}$ -NMR spectra of three representative phyllosilicates: pyrophyllite, muscovite, and phlogopite (Sanz and Serratos, 1984). The spectra consist of one or two principal components and a series of small side bands associated with the spinning of the sample. Pyrophyllite contains only  $\text{Al}^{\text{VI}}$ , while muscovite has both  $\text{Al}^{\text{VI}}$  and  $\text{Al}^{\text{IV}}$ . Although the ideal composition of phlogopite contains only  $\text{Al}^{\text{IV}}$ , the sample analysed contains a small amount of  $\text{Al}^{\text{VI}}$  (substituting for Mg) in the octahedral sheet (see Chapter 1).

In these spectra the resolution is very good and, in principle, a quantitative determination of site occupancy is feasible. To this end, side bands of all nuclear transitions should be considered (Alma et al., 1984; Massiot et al., 1990). Also, small flip angles, strong magnetic fields, and high-rotation frequencies must be used (Samoson and Lippmaa, 1983). The  $^{27}\text{Al}$  MAS-NMR spectra can also be used to

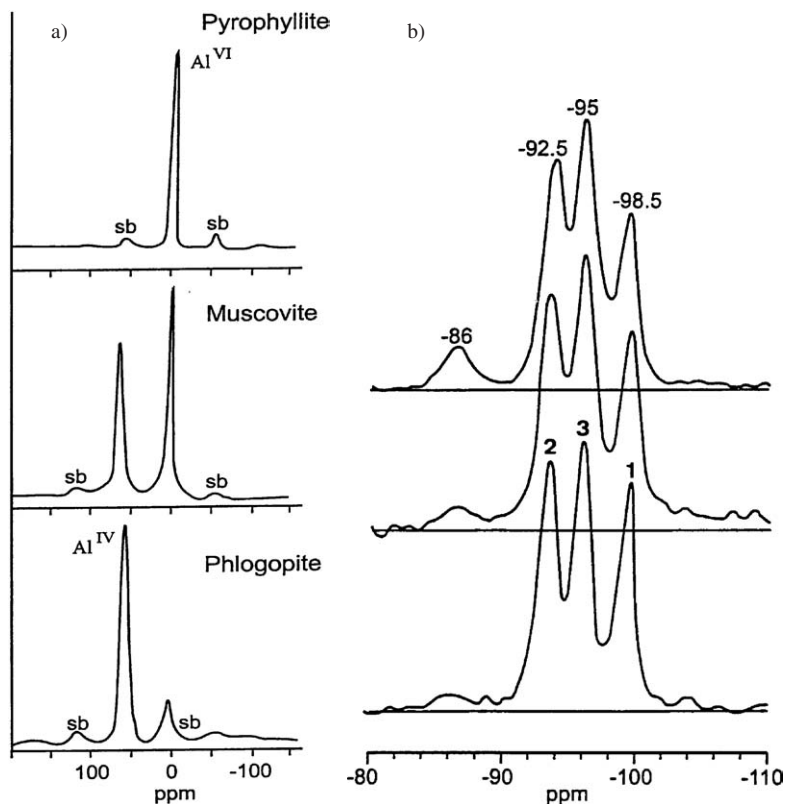


Fig. 12.7.2. (a)  $^{27}\text{Al}$  MAS-NMR spectra of pyrophyllite, muscovite, and phlogopite showing the signals corresponding to tetrahedral and octahedral Al. Spinning side bands are labelled as sb. From Sanz and Serratosa (1984). (b)  $^{29}\text{Si}$  MAS-NMR spectra of three samples of sepiolite with different degree of crystallinity. In this mineral, three different crystallographic sites are detected. From Sanz (1990).

analyse distortions on Al polyhedra. To accomplish this, spinning side band patterns must be analysed in terms of anisotropy and asymmetry parameters that describe quadrupolar interactions.

### Crystallographic Sites

The  $^{29}\text{Si}$  MAS-NMR spectra of sepiolite,  $\text{Mg}_8\text{Si}_{12}\text{O}_{30}\text{OH}_4(\text{H}_2\text{O})_4(\text{H}_2\text{O})_m$ , show three resonances at -92.5, -95.0, and -98.5 ppm, associated with the three crystallographic sites of this mineral (Fig. 12.7.2b). The resonance at -98.5 ppm decreases when a new component at -86 ppm is detected. This led Barron and Frost (1985) to assign both components to Si atoms in Si-O-Si and Si-O-H groups at the edges of individual ribbons. The two remaining signals at -92.5 and -95.0 ppm may be

identified by cross-polarization and two-dimensional techniques. However, the assignment of the three signals is not yet definitive (Barron and Frost, 1985; Sanz, 1990; d'Espinose de la Caillerie and Fripiat, 1994; Weir et al., 2002).

In the case of kaolinite,  $\text{Si}_2\text{Al}_2\text{O}_5(\text{OH})_4$ , the  $^{29}\text{Si}$ -NMR spectrum displays two components, associated with Si tetrahedra interacting in a different way with contiguous layers (Thompson, 1985; Thompson and Barron, 1987). The two components in the  $^{27}\text{Al}$  MAS-NMR spectrum of kaolinite were also interpreted in terms of the presence of two octahedral aluminium sites (Rocha and Pedrosa de Jesús, 1994).

### Cation Distribution

In examining a series of aluminosilicates with well-defined structures, Lippmaa et al. (1980) found that the chemical shift of the  $^{29}\text{Si}$  MAS-NMR signal depends on the degree of tetrahedral polymerization. In the tetrahedral sheet of 2:1 phyllosilicates, substitution of  $\text{Al}^3$  for  $\text{Si}^{4+}$  in neighbouring tetrahedra causes the  $^{29}\text{Si}$  line to shift to a lower field. This allows the Si atoms that are surrounded by 3Si, 2Si1Al, 1Si2Al, and 3Al to be identified (Sanz and Serratosa, 1984) (Fig. 12.7.3).

The chemical shift of the Si signal is sensitive to layer distortion arising from matching of tetrahedral and octahedral sheets (see Chapter 2). In particular, the chemical shifts of the four Si components of  $\text{Na}^+$ -saponites and micas change with respect to the twisting angle,  $\alpha$ , between contiguous tetrahedra (Sanz and Robert, 1992). A parallel analysis of chemical shift values versus TOT angles shown that, in agreement with other silicates, these values become more negative when TOT angles increase (Engelhardt and Mitchell, 1987).

Analysis of the  $^{29}\text{Si}$  MAS-NMR spectra of phyllosilicates enables the tetrahedral composition ( $\text{Si}_{4-x}\text{Al}_x$ ) of samples with  $\text{Si} > \text{Al}$  to be estimated. When Loewenstein's rule ( $\text{Al}_\text{T}-\text{O}-\text{Al}_\text{T}$  avoidance (Loewenstein, 1954) is satisfied, the tetrahedral Si/Al ratio can be derived from the expression (Sanz and Serratosa, 1984):

$$\frac{\text{Si}}{\text{Al}} = \frac{\sum I_n}{(1/3) \sum nI_n} = \frac{1 - x_1}{x_1}$$

where  $I_n$  stands for relative intensity of Si-NMR components associated with  $n\text{Al}$  and  $(3-n)\text{Si}$ .

The distribution of Si and Al in the tetrahedral sheets of 2:1 phyllosilicates may be estimated from the intensity of the four Si-NMR components. In particular, the dispersion of Al and Si is shown to favour the existence of  $\text{Al}-\text{O}-\text{Si}$  at the expense of  $\text{Al}-\text{O}-\text{Al}$  and  $\text{Si}-\text{O}-\text{Si}$  associations (Herrero et al., 1985, 1987, 1989). Monte Carlo simulations indicated that Al dispersion is intermediate between that deduced from the Loewenstein and MDC (maximum dispersion of charges) models. The  $^{29}\text{Si}$ -NMR spectra of a large number of samples are reproducible when the number of Al in hexagonal rings of the tetrahedral sheet is assumed to be as close as possible to the average value deduced for each composition from the HDC (homogeneous dispersion of charges) model (Herrero et al., 1987, 1989). In the case of

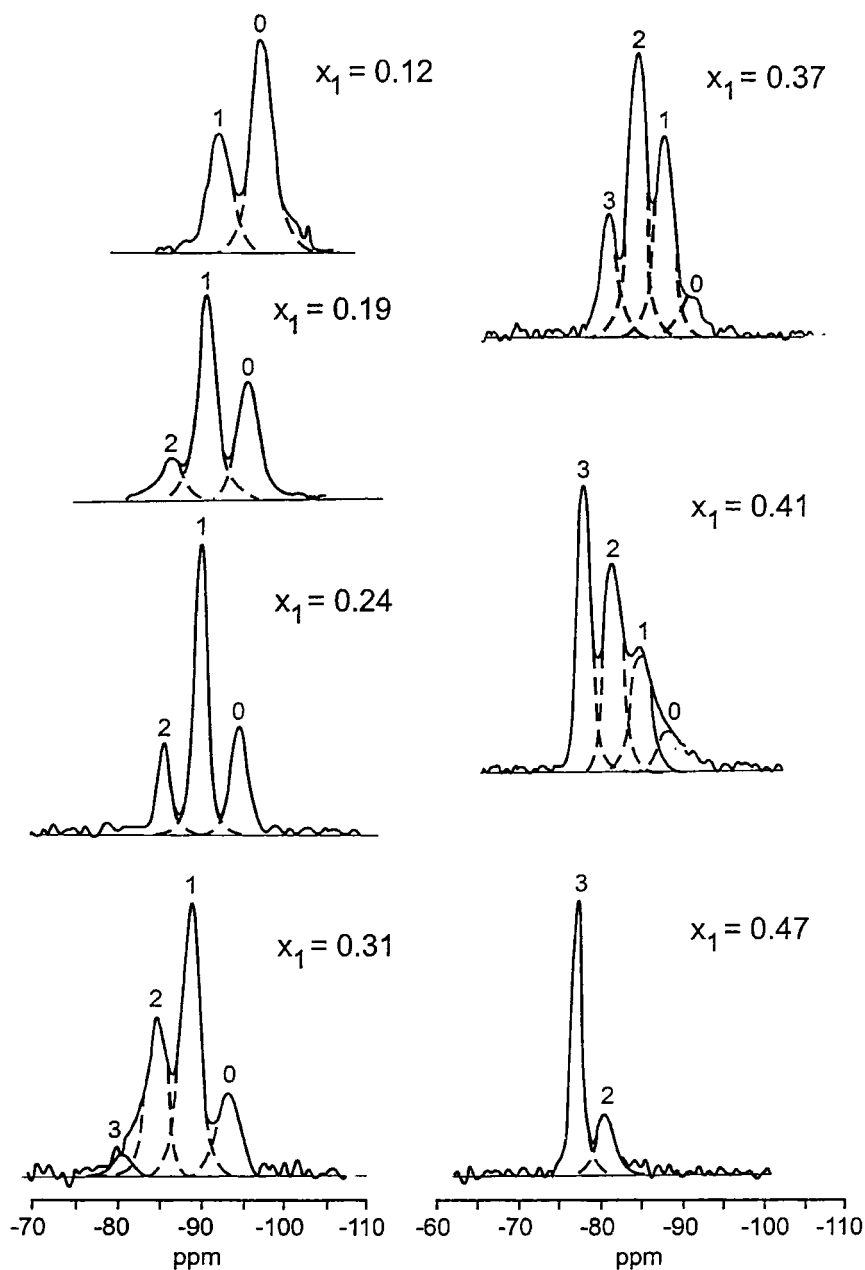


Fig. 12.7.3.  $^{29}\text{Si}$  MAS-NMR spectra of phyllosilicates 2:1 as a function of tetrahedral Al fractional content,  $x_1 = \text{Al}/(\text{Si} + \text{Al})$ . The number that identifies each component represents the number of Al, which surround a given Si tetrahedron. From [Sanz and Robert \(1992\)](#).

phyllosilicates with  $\text{Al} > \text{Si}$ , Loewenstein's rule is not obeyed but the HDC model remains valid (Sanz et al., 2003).

A parallel study was carried out with respect to the octahedral sheet of trioctahedral micas. In this case, the distribution of  $\text{Mg}^{2+}$  and  $\text{Fe}^{2+}$  around  $\text{OH}^-$  and  $\text{F}^-$  ions is undertaken on monocrystalline samples formed by superposition of platelets with axes  $a$  and  $b$  disposed in the same way. By recording the  $^1\text{H}$  and  $^{19}\text{F}$ -NMR spectra as a function of sample orientation, four possible associations  $\text{Mg}_3$ ,  $\text{Mg}_2\text{Fe}$ ,  $\text{MgFe}_2$ , and  $\text{Fe}_3$  around the OH groups can be identified (Sanz and Stone, 1983a). On the contrary, a direct coordination of  $\text{F}^-$  ions to Fe is not found (Sanz and Stone, 1979). Quantitative analysis of the spectra indicates that  $\text{F}^-$  ions are preferentially coordinated to  $\text{Mg}^{2+}$ , while  $\text{OH}^-$  groups coordinate to the remaining  $\text{Mg}^{2+}$  and  $\text{Fe}^{2+}$  cations. As a result, the Mg/Fe ratio (deduced from the  $^1\text{H}$  signal) decreases as the  $\text{F}^-$  content increases. It is concluded that fluoro-magnesium and hydroxyl domains are locally segregated in the octahedral sheet of micas (Sanz and Stone, 1983b).

### B. Adsorption Phenomena

#### Clay–Water Interactions

In hydrated Cs-Vermiculites, residual motions are cancelled out at low temperatures. This allows the following two peaks to be resolved: (i) associated with  $\text{Cs}^+$  in the Stern layer near the basal oxygen planes of the layers ( $-29$  ppm); and (ii) associated with  $\text{Cs}^+$  ions in the Gouy diffuse layer surrounded by their hydration shells ( $-8$  ppm) (Weiss et al., 1990; Sullivan et al., 1998). Laperche et al. (1990) studied the NMR signals of  $^{23}\text{Na}$ ,  $^{111}\text{Cd}$ , and  $^{133}\text{Cs}$  in the interlayer space of Llano vermiculite as a function of water content. Each hydration state, corresponding to two, one, or zero water layers, is characterized by one specific value of the isotropic chemical shift of cations. As the number of water molecules coordinated to the cations increases, the lines shift downfield (Fig. 12.7.4a).

The  $^1\text{H}$ -NMR spectrum of hydrated 2:1 layer clay minerals consists of a central line due to structural OH groups, and a doublet due to sorbed water (Hougardy et al., 1976). By changing the angle between the magnetic field ( $B_0$ ) and the  $c$ -axis of the clay mineral aggregate, a dependence ( $3\cos^2\theta - 1$ ) is obtained for the doublet separation. This indicates that the water molecules maintain a preferential orientation with respect to the clay mineral layers (Fig. 12.7.4b). The NMR spectra of the two-layer hydrate of Na-vermiculite suggest that water molecules rotate around their  $c_2$  symmetry axis, while the hydration shells rotate around the  $c^*$ -axis of the phyllosilicate (Fig. 12.7.4c). The angle deduced between the  $c_2$  and  $c^*$ -axes is close to  $65^\circ$ . According to this model, the two minima in the  $T_1$  curves at 225 and 360 K are associated with the rotation of  $\text{H}_2\text{O}$  molecules around their  $c_2$  axis, and the rotation/diffusion of  $[\text{Na}^+(\text{H}_2\text{O})_6]$  hydration shells (Hougardy et al., 1976). In both cases, the values deduced for the activation energy are between 25 and 35 KJ/mol. A similar model was proposed for the one-layer hydrate of Li-hectorite (basal spacing = 1.26 nm).



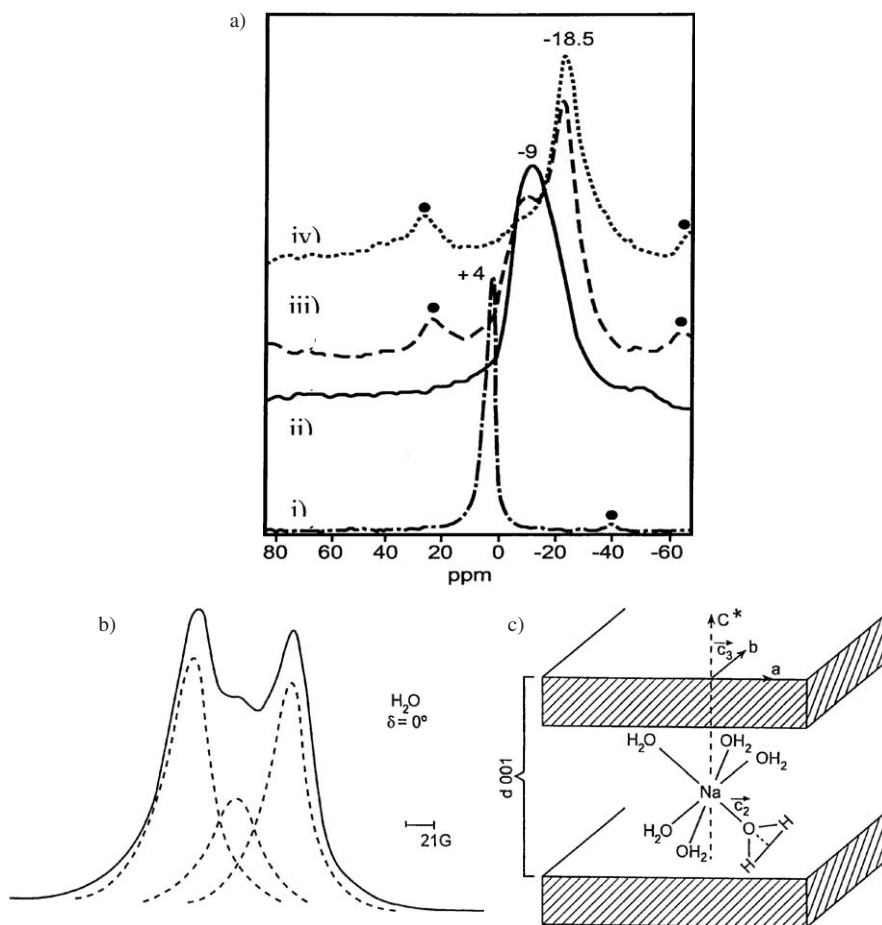


Fig. 12.7.4. (a)  $^{23}\text{Na}^+$  MAS-NMR spectra of Na-vermiculite at different hydration levels: (i) two layers (1.475 nm); (ii) one layer (1.175 nm); (iii) biphasic, one, and zero layer, and (iv) dehydrated. Spinning sidebands are indicated by (●). From Laperche et al. (1990). (b)  $^1\text{H}$  spectrum of the two-layers hydrate of  $\text{Na}^+$ -vermiculite at room temperature showing the doublet and the central line. (c) Octahedral arrangement of water molecules around the  $\text{Na}^+$  ions. From Hougardy et al. (1976).

Fripiat et al. (1980) suggested that each  $\text{Li}^+$  is coordinated to three water molecules arranged in a dynamic pyramidal configuration showing two rotational motions (around the  $c_2$  and  $c^*$  axes) similar to those found for the two-layer hydrate of  $\text{Na}^+$ -vermiculite (Hougardy et al., 1976).

Hofmann and Klemen (1950) proposed that when a  $\text{Li}^+$ -montmorillonite is heated at  $300^\circ\text{C}$  the exchangeable  $\text{Li}^+$  ions move irreversibly into the layer structure.

However, NMR spectroscopy provided evidence that these ions do not migrate into vacant octahedral positions but occupy very distorted sites at the bottom of the ditrigonal cavities (Luca et al., 1989; Alvero et al., 1994; Theng et al., 1997). At high water vapour pressure, the  $\text{Li}^+$  ions can return to their original positions in the interlayer space.

### *Pillared Clays*

Pillaring of smectites by intercalation of aluminium oligomers and subsequent heating at high temperatures, makes a large fraction of the clay interlayer surface (up to 400–500 m<sup>2</sup>/g) available for adsorption of extraneous molecules (see Chapter 7.5). <sup>27</sup>Al and <sup>29</sup>Si MAS-NMR spectroscopy provides useful information on the mechanism of pillaring. In pillared hectorite and laponite, the layers retain their structural integrity even after heating at 350 °C, while in pillared beidellite the intercalated polyoxyaluminium cations react with the tetrahedral sheet of the mineral, forming links through the inversion of some aluminium tetrahedra (Plee et al., 1985; Schultz et al., 1987). A similar structural arrangement (i.e., inversion of tetrahedra) was reported by Pinnavaia et al. (1985) and Tennakoon et al. (1986a) for pillared fluoro-hectorite and hectorite.

### *Clay–Organic Interactions*

NMR studies on clay–organic complexes were carried out to elucidate the orientation and mobility (rotational or translational) of the sorbed organic species. These studies are restricted to synthetic or natural clay minerals with low iron content (notably hectorite).

Pratum (1992) used solid-state <sup>13</sup>C MAS-NMR spectroscopy to assess the mobility of tetramethylammonium (TMA) and hexadecyl trimethylammonium (HDTMA) ions in montmorillonite. These organic cations show rapid motions with average of <sup>1</sup>H–<sup>13</sup>C dipolar interactions. This motion appears to be isotropic for TMA and anisotropic in the case of HDTMA.

### *Adsorption by 2:1 Clay Minerals*

Multinuclear NMR spectroscopy was used to investigate the interactions of hex-1-ene with Na<sup>+</sup>- and Al<sup>3+</sup>-exchanged laponites (Tennakoon et al., 1986b), and of triethylphosphate (TEP) with Mg<sup>2+</sup>-, Al<sup>3+</sup>-, or tetrabutylammonium (Bu<sub>4</sub>N<sup>+</sup>)-exchanged smectites (O'Brien et al., 1991).

The intercalation of macrocyclic compounds (crown ethers and cryptands) into montmorillonite and hectorite results in the formation of interlayer 1:1 and 2:1 ligand/cation complexes. In Na<sup>+</sup>-hectorite, the chemical shift of the <sup>23</sup>Na-NMR signal varies according to the sodium–macrocyclic interaction (Aranda and Ruiz-Hitzky, 1992; Casal et al., 1994). The <sup>13</sup>C CP-MAS spectra of complexes of Na<sup>+</sup>-, K<sup>+</sup>-, or Ba<sup>2+</sup>-hectorite with polyethylene oxide (PEO) consist of a single signal at about 70 ppm, assigned to the gauche conformation of the methylene groups in PEO. The <sup>23</sup>Na MAS-NMR spectrum of the PEO/Na<sup>+</sup>-hectorite complex shows a single

peak at 10.8 ppm, indicating that the  $\text{Na}^+$  ions are directly coordinated to the oxyethylene units of the polymer (Aranda and Ruiz-Hitzky, 1992).

The arrangement of molecules in the interlayer space may be determined using samples (clay aggregates) that can be oriented in the magnetic field. One interesting study of this kind is that of benzene intercalated into  $\text{Ag}^+$ -exchanged hectorite (Resing et al., 1980) (Fig. 12.7.5). The  $^{13}\text{C}$ -NMR spectrum, recorded at ambient temperature, shows a single line whose position depends on the orientation of the benzene–hectorite complex (upper left in Fig. 12.7.5). When  $B_0$  is perpendicular to the sample ( $\theta = 0$ ), the observed shift at 182 ppm corresponds to an orientation in which the plane of the benzene ring is parallel to the magnetic field. From the small linewidth of the signal, it is inferred that the benzene molecules execute some fast motion (right in Fig. 12.7.5). When mobility decreases, linewidth increases and for complexes disposed parallel to the magnetic field ( $\theta = 90^\circ$ ), a two-dimensional anisotropy pattern is detected around the central peak at 251 K (Fig. 12.7.5). This pattern is exactly what is expected for benzene standing on its edge between the silicate layers. Accordingly, the most realistic model is one in which benzene molecules are subject to two different rotations: (i) about the hexagonal molecular axis and (ii) about the normal to the silicate layers. The latter motion is quenched at 77 K (Fig. 12.7.5;  $\theta = 0$ ).

#### *Intercalation of Kaolin Minerals*

Intercalation complexes of kaolin minerals were the subject of numerous NMR studies. Thompson (1985) used  $^{29}\text{Si}$  and  $^{13}\text{C}$ -NMR spectroscopy to study the disposition and bonding of formamide, hydrazine, dimethylsulphoxide (DMSO) and pyridine-*N*-oxide (PNO) intercalated into kaolinite. The  $^{29}\text{Si}$ -NMR spectra of the untreated kaolinite show two  $^{29}\text{Si}$  resonances (at  $-91.9$  and  $-91.5$  ppm), which converge into a single signal in the intercalate (interlayer complex). In the  $^{13}\text{C}$ -NMR spectra, the  $^{13}\text{C}$  resonances of the intercalated molecules are shifted downfield as a result of increased hydrogen bonding. The  $^{13}\text{C}$ -NMR spectrum of the kaolinite–DMSO complex shows two equally intense methyl carbon signals (Fig. 12.7.6a). The interpretation of this doublet, however, was controversial. Hayashi (1997) and Hayashi and Akiba (1994) proposed that below 300 K, all interlayer DMSO molecules are equivalent. One of the methyl groups of DMSO is keyed into the ditrigonal holes of the silicate sheet, and these groups can rotate freely about their  $\text{C}_3$  axis. At low temperatures (about 160 K) this axis is blocked but at high temperatures, the methyl groups initiate a wobbling motion whose amplitude increases with temperature. Above 320 K, the keyed methyl groups are released from the ditrigonal holes, and the intercalated DMSO molecules undergo anisotropic rotations (Fig. 12.7.6b).

Kaolinite-polymer nanocomposites also attracted considerable attention. Sugahara et al. (1990) obtained a kaolinite–polyacrylamide composite by intercalating acrylamide (basal spacing = 1.13 nm), heating the clay–monomer complex at increasing

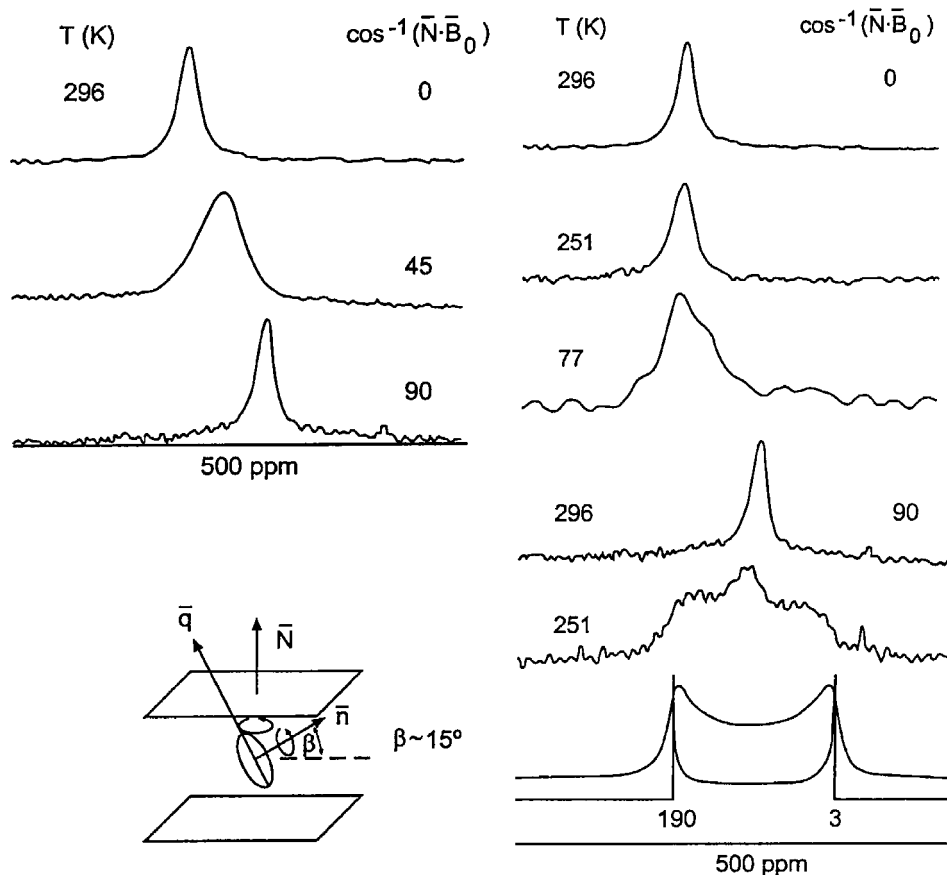


Fig. 12.7.5.  $^{13}\text{C}$ -NMR spectra of benzene sorbed on an oriented aggregate of Ag-hectorite taken at various temperatures and for several orientations of the platelet director  $N$  in the magnetic field  $B_0$ . The lower-bottom left figure shows the model deduced for the average orientation of the benzene molecules between the clay layers. The lower-bottom right figure is the calculated anisotropy patterns for  $T = 251\text{ K}$  when  $B_0$  is disposed parallel to the layers. From Resing et al. (1980).

temperatures to induce polymerization, and following the process with  $^{13}\text{C}$  CP/MAS-NMR spectroscopy. Polymerization of ethylene glycol (EG) did not occur with the kaolinite-EG intercalate (basal spacing = 0.94 nm). However, complexes of kaolinite with poly(ethylene glycol) (PEG) can be obtained by direct displacement of intercalated DMSO with PEG 3400 and PEG 1000 from their melts at 150–200 °C (Tunney and Detellier, 1996).

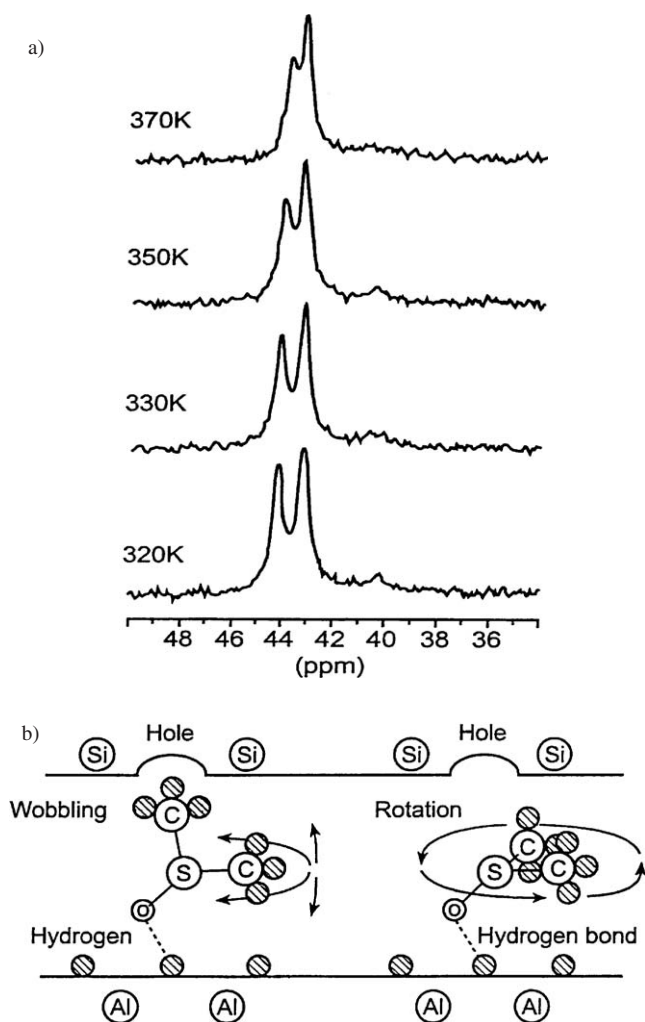


Fig. 12.7.6. (a)  $^{13}\text{C}$  CP/MAS-NMR spectra of kaolinite-DMSO intercalate at different temperatures. (b) Schematic diagram showing the disposition and motion of DMSO in the interlayer space of kaolinite. From Hayashi (1997).

## 12.7.2. REACTIVITY OF CLAY MINERALS

### A. Alkaline Activation of Kaolinites

Sanz et al. (1988) investigated the thermal decomposition of kaolinite by  $^{29}\text{Si}$  and  $^{27}\text{Al}$  MAS-NMR spectroscopy. They show that kaolinite is completely dehydroxylated at

750 °C, forming tetra- and penta-coordinated aluminium (Fig. 12.7.7b). The partial breaking of the tetrahedral sheet takes place at 850 °C and the segregation of amorphous silica occurs at 980 °C (Fig. 12.7.7a). The exothermic peak at 980 °C in the DTA pattern is due to transformation of  $\text{Al}^{\text{V}}$  into the more stable  $\text{Al}^{\text{VI}}$ . Above 980 °C, characteristic peaks at 42 and 60 ppm of mullite 3:2 intensify, while the peak due to octahedrally coordinated Al narrows (Fig. 12.7.7b). Similar results have also been reported by Lambert et al. (1989), Rocha and Klinowski (1990) and Massiot et al. (1995).

NMR spectroscopy shows that alkali treatment of kaolinites that were heated between 400 and 1000 °C causes dissolution of the mineral with the formation of  $\text{Al}(\text{OH})_4^-$  and  $\text{SiO}_4^{4-}$  species (Madani et al., 1990). These species constitute the base for zeolite formation (Fig. 12.7.8b). The nature of the zeolites (hydroxysodalite, Na-A, and tetragonal  $\text{P}_1$  phillipsite) varies with thermal activation of the starting silicates. Prolonged leaching of the samples favours formation of the more stable  $\text{P}_1$  zeolite at the expense of hydroxysodalite and Na-A zeolites (Fig. 12.7.8a). As the Si/Al ratio of the  $\text{P}_1$  zeolite is  $> 1$ , its formation requires the release of aluminium from the zeolites initially formed (Si/Al = 1). This process is accompanied by the appearance of five signals in the  $^{29}\text{Si}$  MAS-NMR spectra, associated with  $\text{Si}_4$ ,  $\text{Si}_3\text{Al}$ ,  $\text{Si}_2\text{Al}_2$ ,  $\text{SiAl}_3$ , and  $\text{Al}_4$  environments (Fig. 12.7.8a).

### B. Heterogeneous Catalysis

NMR spectroscopy is an important technique for studying ‘in situ’ transformations of adsorbed species at solid surfaces (heterogeneous catalysis). For example, Tennakoon et al. (1983) used  $^{13}\text{C}$ -NMR to follow the catalytic conversion of 2-methyl-propene (isobutene) into *t*-butanol in the interlayer space of a synthetic  $\text{Al}^{3+}$ -hectorite. The  $^{13}\text{C}$ -NMR spectrum of the end product shows two peaks at 35 and 75 ppm corresponding to the two types of carbon atoms in *t*-butanol,  $(\text{CH}_3)_3\text{-COH}$ . On the other hand, the intercalation of methanol into  $\text{Al}^{3+}$ -hectorite, followed by adsorption of isobutene, gives rise to methyl-*t*-butyl ether as shown by the presence of three peaks in the  $^{13}\text{C}$ -NMR spectrum.

Carrado et al. (1990) investigated the cleavage of the oxygen-methyl bond in *m*-methylanisole, guaiacol, 4-hydroxy-3-methoxytoluene, and 4-phenoxy-3-methoxytoluene adsorbed on clay and pillared clay surfaces. All four molecules have some similarity to the monomeric unit of lignin and can serve as model compounds in the formation of coal. NMR spectroscopy shows that the mobility of these compounds is markedly reduced on adsorption.

### C. Grafting of Organic Species

The grafting of organic molecules to mineral substrates through the formation of true covalent bonds is well documented in the literature (Iler, 1979; Sherrington, 1980; Rosset, 1985; Ruiz-Hitzky, 1988). Most of these reactions take place through Si-OH groups present at the edges of mineral particles with the formation of

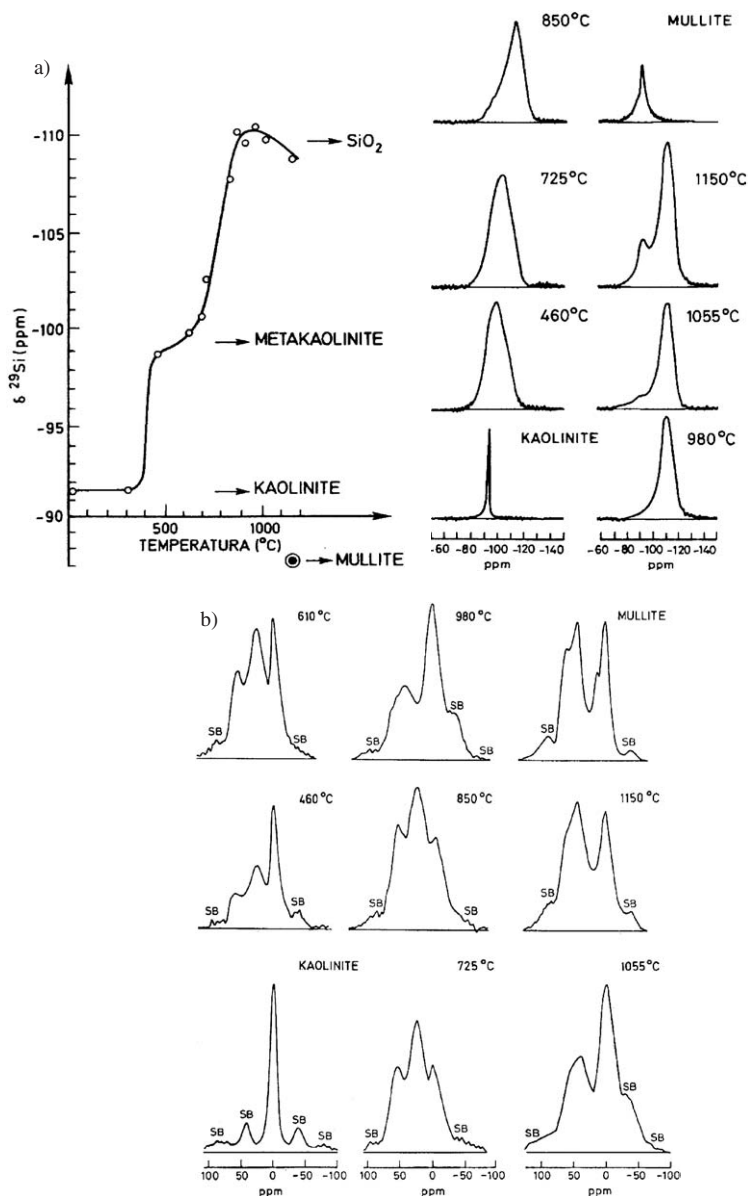


Fig. 12.7.7. (a)  $^{29}\text{Si}$  and (b)  $^{27}\text{Al}$  MAS-NMR spectra of kaolinite samples heated at different temperatures. For comparison, the spectrum of a pure 3:2 mullite is given. Variation of the  $^{29}\text{Si}$  chemical shift versus the temperature of treatment is also given. From Sanz et al. (1988).

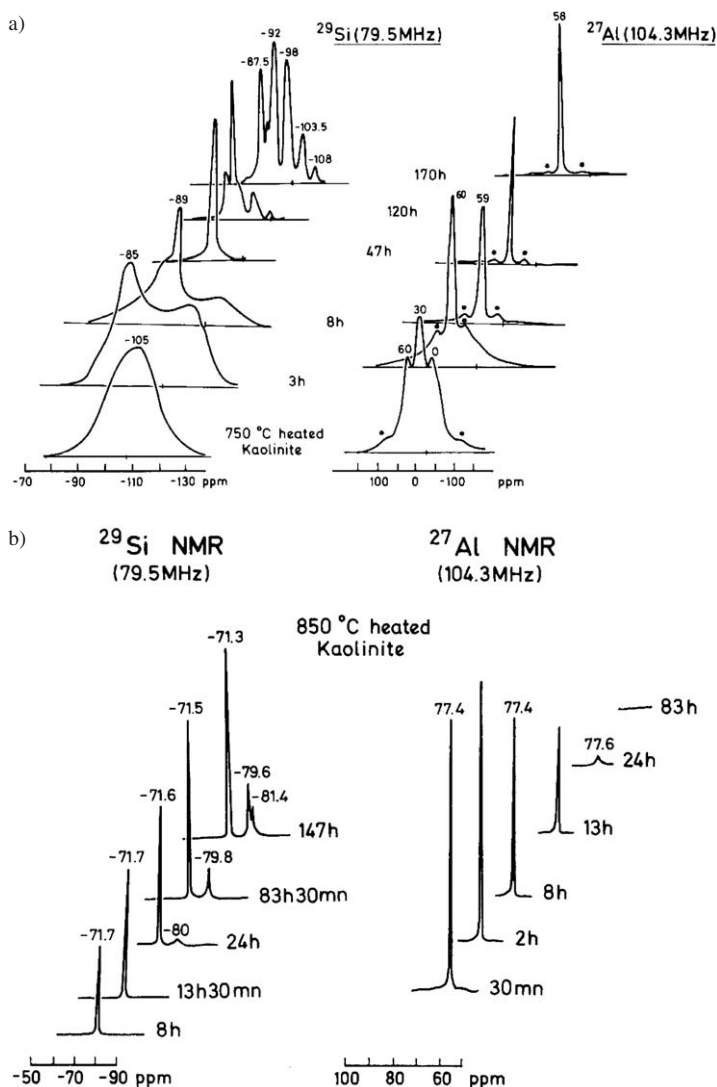


Fig. 12.7.8. The upper figures correspond to  $^{29}\text{Si}$  and  $^{27}\text{Al}$  MAS-NMR spectra of kaolinite samples heated at 850 °C, after different NaOH treatments. (a) The lower figures correspond to  $^{29}\text{Si}$  and  $^{27}\text{Al}$  NMR spectra of the liquid phase for the same treatments (b) From Madani et al. (1990).

Si–O–Si– or –Si–O–C–bonds, although reactions of organic molecules with –Al–OH of gibbsite or kaolinite were also reported.

The content of reactive Si–OH groups in fibrous clays (sepiolite and palygorskite) is much larger than in plate-like clays. The former minerals can therefore serve as suitable substrates for direct grafting reactions. Aznar and Ruiz-Hitzky (1988) and



Aznar et al. (1992) studied the grafting of phenyl-organosilanes ( $\text{Si}-\text{C}_6\text{H}_5$ ,  $\text{Si}-(\text{C}_6\text{H}_5)_2$  and  $\text{Si}-(\text{CH}_2)_n-\text{C}_6\text{H}_5$ ) on sepiolite. In general, the process leads to a simultaneous extraction of Mg, implying an alteration of the mineral substrate. The  $^{29}\text{Si}$ -NMR spectrum of the amorphous silica produced shows new signals at  $-110$ ,  $-102$ , and  $-92$  ppm, attributed to Si surrounded by (4Si), (3Si, 1OH), and (2Si, 2OH) ( $\text{Q}^4$ ,  $\text{Q}^3$ , and  $\text{Q}^2$  in Lippmaa's notation). The  $^{13}\text{C}$  CP-MAS spectra of the phenyl derivatives give information on the nature of the grafted groups in the solid substrate (Aznar et al., 1992). The preparation of sulpho or nitro derivatives, with  $-\text{SO}_3\text{H}$  or  $-\text{NO}_2$  radicals attached to the aromatic rings of the grafted species, was reported by Aznar and Ruiz-Hitzky (1988). These derivatives exhibit properties that make them useful for some industrial applications.

Grafting reactions in the interlayer space of kaolinite were reported by Tunney and Detellier (1993). The kaolinite was first expanded by intercalation of DMSO or *N*-methylformamide (NMF), and then refluxed with alcohols (e.g., EG, propane-1,2-diol). This produces organo derivatives in which the alcohol molecules are grafted to the interlayer surface of the mineral through Al-O-C bonds.

### 12.7.3. CONCLUDING REMARKS

The application of multinuclear high-resolution NMR spectroscopy over the last two decades provided valuable information on the structures of phyllosilicates, such as crystallographic sites, cation coordination, silicate network distortion, and cation distributions. However, conventional low-resolution NMR spectroscopy is still useful for investigating the surface orientation of adsorbed molecules and their mobility.

In situ reactions between co-adsorbed molecules or between adsorbed species and clay mineral surfaces can now be studied by high-resolution NMR (MAS and CP-MAS) techniques. In particular, the formation of pillared clays was extensively studied by multinuclear NMR spectroscopy. The same can be said for zeolite formation by alkali treatment of clay minerals. These developments have important implications for the industrial applications of clays and clay minerals.

### REFERENCES

- Alma, N.C.M., Hays, G.R., Samoson, A., Lippmaa, E., 1984. Characterization of synthetic dioctahedral clays by solid-state silicon-29 and aluminium-27 nuclear magnetic resonance. *Analytical Chemistry* 56, 729–733.
- Alvero, R., Alba, M.D., Castro, M.A., Trillo, S.M., 1994. Reversible migration of lithium in montmorillonite. *Journal of Physical Chemistry* 98, 7848–7853.
- Aranda, P., Ruiz-Hitzky, E., 1992. Poly(ethylene oxide)-silicate intercalation materials. *Chemistry of Materials* 4, 1395–1403.
- Aznar, A.J., Ruiz-Hitzky, E., 1988. Arylsulphonic resins based on organic/inorganic macromolecular systems. *Molecular Crystals, Liquid Crystals Including Nonlinear Optics* 161, 459–469.

- Aznar, A.J., Sanz, J., Ruiz-Hitzky, E., 1992. Mechanism of the grafting of organosilanes on mineral surfaces. IV. Phenyl derivatives of sepiolite and poly(organosilanes). *Colloid and Polymer Science* 270, 165–176.
- Barron, P.F., Frost, R.L., 1985. Solid state  $^{29}\text{Si}$  NMR examination of the 2:1 ribbon magnesium silicates, sepiolite and palygorskite. *American Mineralogist* 70, 758–766.
- Carrado, K.A., Hayatsu, R., Botto, R.E., Winans, R.E., 1990. Reactivity of anisoles on clay and pillared clay surfaces. *Clays and Clay Minerals* 38, 250–256.
- Casal, B., Aranda, P., Sanz, J., Ruiz-Hitzky, E., 1994. Interlayer adsorption of macrocyclic compounds (crown-ethers and cryptands) in 2:1 phyllosilicates: structural features. *Clay Minerals* 29, 191–203.
- Duer, M.J., 2002. Solid-state NMR spectroscopy. Principles and Applications. Blackwell Science, Oxford.
- Engelhardt, G., Mitchell, D., 1987. High Resolution Solid-State NMR of Silicates and Zeolites. Wiley, New York.
- d'Espinose de la Caillerie, J.B., Fripiat, J.J., 1994. A reassessment of the  $^{29}\text{Si}$  MAS-NMR spectra of sepiolite and aluminated sepiolite. *Clay Minerals* 29, 313–318.
- Fripiat, J.J., Kadi-Hanifi, M., Conard, J., Stone, W.E.E., 1980. NMR study of adsorbed water, III molecular orientation and protonic motions in the one-layer of a Li-hectorite. In: Fraissard, J.P., Resing, H.A. (Eds.), *Magnetic Resonance in Colloid and Interface Science. Proceedings of NATO Advanced Study Institute, Menton, France, 1979*. D. Reidel, Dordrecht, pp. 529–535.
- Hayashi, S., 1997. NMR study of dynamics and evolution of guest molecules in kaolinite/dimethylsulfoxide intercalation compounds. *Clays and Clay Minerals* 45, 724–732.
- Hayashi, S., Akiba, E., 1994. Interatomic distances in layered silicates and their intercalation compounds as studied by cross polarization NMR. *Chemical Physics Letters* 226, 495–500.
- Herrero, C.P., Gregorkiewitz, M., Sanz, J., Serratos, J.M., 1987.  $^{29}\text{Si}$  MAS-NMR spectroscopy of mica-type silicates. Observed and predicted distribution of tetrahedral Al–Si. *Physics and Chemistry of Minerals* 15, 84–90.
- Herrero, C.P., Sanz, J., Serratos, J.M., 1985. Tetrahedral cation ordering in layer silicates by  $^{29}\text{Si}$  NMR spectroscopy. *Solid State Communications* 53, 151–154.
- Herrero, C.P., Sanz, J., Serratos, J.M., 1989. The dispersion of charge deficit in the tetrahedral sheet of phyllosilicates. Analysis from  $^{29}\text{Si}$  NMR spectra. *Journal of Physical Chemistry* 93, 4311–4315.
- Hofmann, U., Klemen, R., 1950. Verlust der Austauschfähigkeit von Lithiumionen an Bentonit durch Erhitzung. *Zeitschrift für Anorganische und Allgemeine Chemie* 262, 95–99.
- Hougardy, J., Stone, W.E.E., Fripiat, J.J., 1976. NMR study of adsorbed water. I. Molecular orientation and protonic motions in the two-layer hydrate of a Na-vermiculite. *Journal of Physical Chemistry* 64, 3840–3851.
- Iler, R.K., 1979. *The Chemistry of Silica*. Wiley Interscience, New York.
- Lambert, J.F., Millman, W.S., Fripiat, J.J., 1989. Revisiting Kaolinite dehydroxylation. A  $^{29}\text{Si}$  and  $^{27}\text{Al}$  MAS-NMR study. *Journal of the American Chemical Society* 111, 3517–3522.
- Laperche, V., Lambert, J.F., Prost, R., Fripiat, J.J., 1990. High-resolution solid state NMR of exchangeable cations in the interlayer surface of a swelling mica:  $^{23}\text{Na}$ ,  $^{111}\text{Cd}$  and  $^{138}\text{Cs}$  vermiculites. *Journal of Physical Chemistry* 94, 8821–8831.

- Lippmaa, E., Magi, M., Samoson, A., Engelhardt, G., Grimmer, A.R., 1980. Structural studies of silicates by solid-state high-resolution  $^{29}\text{Si}$  NMR. *Journal of the American Chemical Society* 102, 4489–4893.
- Loewenstein, W., 1954. The distribution of aluminum in the tetrahedra of silicates and aluminates. *American Mineralogist* 39, 92–96.
- Luca, V., Cardile, C.M., Meinhold, R.H., 1989. High resolution multinuclear NMR study of cation migration in montmorillonite. *Clay Minerals* 24, 115–119.
- Madani, A., Aznar, A., Sanz, J., Serratosa, J.M., 1990.  $^{29}\text{Si}$  and  $^{27}\text{Al}$  NMR study of zeolite formation from alkali-leached kaolinites. Influence of thermal activation. *Journal of Physical Chemistry* 94, 760–765.
- Massiot, D., Bessada, C., Coutures, J.P., Taulelle, F., 1990. A quantitative study of  $^{27}\text{Al}$  MAS NMR in crystalline YAG. *Journal of Magnetic Resonance* 90, 231–242.
- Massiot, D., Dion, P., Alcover, J.F., Bergaya, F., 1995.  $^{27}\text{Al}$  and  $^{29}\text{Si}$  MAS NMR Study of Kaolinite Thermal Decomposition by Controlled Rate Thermal Analysis. *Journal of the American Ceramic Society* 78, 2940–2944.
- Massiot, D., Touzo, B., Trumeau, D., Coutures, J.P., Virlet, J., Florian, P., Grandinetti, P.J., 1996. Two-dimensional magic-angle spinning isotropic reconstruction sequences for quadrupolar nuclei. *Solid State NMR* 6, 73–83.
- O'Brien, P., Williamson, C.J., Groombridge, C.J., 1991. Multinuclear solid-state MAS and CP-MAS NMR study of the binding of triethylphosphate to a montmorillonite. *Chemistry of Materials* 3, 276–280.
- Pines, A., Gibby, M.G., Waugh, J.S., 1973. Proton enhanced NMR of diluted ions in solids. *Journal of Chemical Physics* 59, 569–590.
- Pinnavaia, T.J., London, S.D., Tzou, M.S., Johnson, I.D., Lipsicas, M., 1985. Layer cross-linking in pillared clays. *Journal of the American Chemical Society* 107, 722–724.
- Plee, D., Borg, F., Gatineau, L., Fripiat, J.J., 1985. High resolution solid-state  $^{27}\text{Al}$  and  $^{29}\text{Si}$  nuclear magnetic resonance study of pillared clays. *Journal of the American Chemical Society* 107, 2362–2369.
- Pratum, T.K., 1992. A solid-state  $^{13}\text{C}$  NMR study of tetraalkylammonium/clay complexes. *Journal of Physical Chemistry* 96, 4567–4571.
- Resing, H.A., Slotfeldt-Ellingsen, D., Garroway, A.N., Weber, D.C., Pinnavaia, T.J., Unger, K., 1980.  $^{13}\text{C}$  chemical shifts in adsorption systems: molecular motions, molecular orientations, qualitative and quantitative analysis. In: Fraissard, J.P., Resing, M.A. (Eds.), *Magnetic Resonance in Colloid and Interface Science. Proceedings of NATO Advanced Study Institute, Menton, France, 1979*. D. Reidel, Dordrecht, pp. 239–258.
- Rocha, J., Klinowski, J., 1990.  $^{29}\text{Si}$  and  $^{27}\text{Al}$  magic-angle-spinning NMR studies of the thermal transformation of kaolinite. *Physical Chemistry of Minerals* 17, 179–186.
- Rocha, J., Pedrosa de Jesús, J.D., 1994.  $^{27}\text{Al}$  satellite transition MAS-NMR spectroscopy of kaolinite. *Clay Minerals* 29, 287–291.
- Rosset, R., 1985. Connaissance chimique et structurale de quelques gels de silice greffés et confrontation avec la chromatographie en phase liquide. *Bulletin de la Société Chimique de France*, 1128–1138.
- Ruiz-Hitzky, E., 1988. Génie cristallin dans les solides organo-minéraux. *Molecular Crystals, Liquid Crystals Including Nonlinear Optics* 161, 459–469.
- Samoson, A., Lippmaa, E., 1983. Excitation phenomena and line intensities in high-resolution NMR powder spectra of half integer quadrupolar nuclei. *Physical Review B* 28, 6567–6570.

- Sanz, J., 1990. Distribution of ions in phyllosilicates by NMR spectroscopy. In: Mottana, A., Burrigato, F. (Eds.), *Absorption Spectroscopy in Mineralogy*. Elsevier, Amsterdam, pp. 103–144.
- Sanz, J., Herrero, C.P., Robert, J.L., 2003. Distribution of Si and Al in clintonites: a combined MMR and Monte Carlo study. *The Journal of Physical Chemistry* 107, 8337–8342.
- Sanz, J., Madani, A., Serratos, J.M., Moya, J.S., Aza, S., 1988. Aluminum-27 and silicon-29 magic-angle spinning nuclear magnetic resonance study of the kaolinite-mullite transformation. *Journal of the American Ceramic Society* 71, C-418–C-421.
- Sanz, J., Robert, J.L., 1992. Influence of structural factors on  $^{29}\text{Si}$  and  $^{27}\text{Al}$  NMR chemical shifts of phyllosilicates 2:1. *Physics and Chemistry of Minerals* 19, 39–45.
- Sanz, J., Serratos, J.M., 1984.  $^{29}\text{Si}$  and  $^{27}\text{Al}$  high resolution MAS-NMR spectra of phyllosilicates. *Journal of the American Chemical Society* 106, 4790–4793.
- Sanz, J., Serratos, J.M., 2002. Nuclear magnetic resonance spectroscopy of organo-clay complexes. In: Yariv, S., Cross, H. (Eds.), *Organo-Clay Complexes and Interactions*. Marcel Dekker, New York, pp. 221–272.
- Sanz, J., Stone, W.E.E., 1979. NMR study of micas. II. Distribution of  $\text{Fe}^{2+}$ ,  $\text{F}^-$  and  $\text{OH}^-$  in the octahedral sheet of phlogopites. *American Mineralogist* 64, 119–126.
- Sanz, J., Stone, W.E.E., 1983a. NMR study of micas. III. The distribution of  $\text{Mg}^{2+}$  and  $\text{Fe}^{2+}$  around the  $\text{OH}^-$  groups in micas. *Journal of Physical Chemistry Solid State Physics* 16, 1271–1281.
- Sanz, J., Stone, W.E.E., 1983b. NMR applied to minerals: IV. Local order in the octahedral sheet of micas: Fe-F avoidance. *Clay Minerals* 18, 187–192.
- Schultz, A., Stone, W.E.E., Poncelet, G., Fripiat, J.J., 1987. Preparation and characterization of bidimensional zeolitic structures obtained from synthetic beidellite and hydroxy-aluminium solutions. *Clays and Clay Minerals* 35, 251–261.
- Sherrington, D.C., 1980. Preparation, functionalization, and characteristics of polymer supports. In: Hodge, P., Sherrington, D.C. (Eds.), *Polymer-supported Reactions in Organic Synthesis*. Wiley, Chichester, pp. 1–80.
- Slichter, C.P., 1990. *Principles of Magnetic Resonance*, 3rd edition. Springer, Berlin.
- Sugahara, Y., Satokawa, S., Kuroda, K., Kato, C., 1990. Preparation of a kaolinite-polyacrylamide intercalation compound. *Clays and Clay Minerals* 38, 137–143.
- Sullivan, D.J., Shore, J.S., Rice, J.A., 1998. Assessment of cation binding to clay minerals using solid state NMR. *Clays and Clay Mineral* 46, 349–354.
- Tennakoon, D.T.B., Jones, W., Thomas, J.M., 1986a. Structural aspects of metal-oxide-pillared sheet silicates. *Journal of the Chemical Society, Faraday Transactions I* 82, 3081–3095.
- Tennakoon, D.T.B., Schlögl, R., Rayment, T., Klinowski, J., Jones, W., Thomas, J.M., 1983. The characterization of clay-organic systems. *Clays and Clay Minerals* 31, 357–371.
- Tennakoon, D.T.B., Thomas, J.M., Jones, W., Carpenter, T.A., Ramdas, S., 1986b. Characterization of clays and clay-organic systems. Cation diffusion and dehydroxylation. *Journal of the Chemical Society, Faraday Transactions I* 82, 545–562.
- Theng, B.K.G., Hayashi, S., Soma, M., Seyama, H., 1997. Nuclear magnetic resonance and X-ray photoelectron spectroscopic investigation of lithium migration in montmorillonite. *Clays and Clay Minerals* 45, 718–723.
- Thompson, J.G., 1985. Interpretation of solid-state  $^{13}\text{C}$  and  $^{29}\text{Si}$  nuclear magnetic resonance spectra of kaolinite intercalates. *Clays and Clay Minerals* 33, 173–180.

- Thompson, J.G., Barron, P.F., 1987. Further consideration of  $^{29}\text{Si}$  nuclear magnetic resonance spectrum of kaolinite. *Clays and Clay Minerals* 35, 38–42.
- Tunney, J.J., Detellier, C., 1993. Interlaminar covalent grafting of organic units on kaolinite. *Chemistry of Materials* 5, 747–748.
- Tunney, J.J., Detellier, C., 1996. Aluminosilicate nanocomposite materials. Poly(ethyleneglycol)-kaolinite intercalates. *Chemistry of Materials* 8, 927–935.
- Wasylishen, R.E., Fyfe, C.A., 1982. High resolution NMR of solids. In: Webb, G.A. (Ed.), *Annual Report on NMR Spectroscopy*. Academic Press, New York.
- Weir, M.R., Kuang, W., Facey, G.A., Detellier, C., 2002. Solid-state nuclear magnetic resonance study of sepiolite and partially dehydrated sepiolite. *Clays and Clay Minerals* 50, 240–247.
- Weiss, C.A., Kirkpatrick, R.J., Altaner, S.P., 1990. Variations in interlayer cation sites of clay minerals as studied by  $^{133}\text{Cs}$  MAS nuclear magnetic resonance spectroscopy. *American Mineralogist* 75, 970–982.

*Chapter 12.8*

## TRANSMISSION ELECTRON MICROSCOPY

F. ELSASS<sup>a</sup>

*INRA, Unité de Science du Sol, Centre Versailles-Grignon, F-78026 Versailles, France*

Transmission electron microscopy (TEM) techniques allow the following properties of clay minerals to be determined in a non-destructive way: (i) morphology; (ii) structure (by selected area electron diffraction, SAED); (iii) lattice imaging (by high-resolution transmission electron microscopy, HRTEM); and (iv) chemical composition (by energy dispersive X-ray fluorescence, EDXRF). The above information may be obtained on individual particles, domains of a selected area, or aggregates depending on the nature of the material studied and the aim of the investigation.

X-ray diffraction (XRD) was extensively used in the study of phyllosilicates with a particle size of less than 2 µm (Decarreau, 1990; Drits and Tchoubar, 1990; Moore and Reynolds, 1997; Parker and Rae, 1998; see also Chapter 12.2). Information about clay mineral structures, provided by XRD, serves as a basis for the interpretation of data obtained by TEM.

In surveying the literature using only ‘electron microscopy’ as the keyword, the scientist can overlook a large number of articles where the fundamental properties of clay minerals were interpreted on the basis of TEM data. Many case studies would indicate that TEM can provide insight into weathering and diagenetic phenomena. In particular, SAED, HRTEM, and EDXRF, either singly or combined, can support hypotheses concerning processes and mechanisms that occur in clay-rich materials, such as soils or rocks.

This short review summarizes electron microscopy techniques that are most commonly used in clay science, gives an update on operating modes, and presents some major results. The aim here is to guide new users into following validated approaches for sample preparation and data collection. This would help avoid creating artefacts that can lead to biased interpretation.

---

<sup>a</sup>Present address: CNRS, Centre de Géochimie de la Surface, 1 rue Blessig, F-67084 Strasbourg, France.

### 12.8.1. TEM TECHNIQUES

A detailed description of the theoretical physics underlying TEM was given by [Drits \(1987\)](#), [Eberhart \(1989\)](#), [Buseck \(1992\)](#), [Reimer \(1997\)](#), and [Kogure \(2002\)](#).

TEM methods are based on selected interaction phenomena occurring between matter and the electron beam. Information about unit cells and cell dimensions may be derived from images and diffraction diagrams arising from the diffraction and diffraction of electron beams. Data on chemical composition may be extracted from the X-ray fluorescence spectrum of the sample irradiated by the electron beam. Here we outline the basic principles of electron beam-matter interactions to help users obtain images of clay minerals, and make an intuitive interpretation of these images. Guidelines are given for setting operating conditions that are appropriate to the study of clay minerals. However, the most appropriate settings do not necessarily, or even rarely, correspond to the maximum capability of the apparatus.

#### *A. Formation of Images*

The image projected on the screen is produced in two steps. First, an image of the sample is formed in the plane of the objective lens of the microscope, at low magnification (around 30x). Second, this (first) image is enlarged through a sequence of magnifying lenses, involving magnifications of  $10^3$ – $10^6$ . As a result, micrometric to nanometric objects become visible to the human eye. Since images recorded on microscope plates or as raster images can be further enlarged using common printers or scanners, the level of magnification rarely needs to exceed  $10^5$ . Most routine work is performed at magnifications ranging between  $10^4$  and  $5 \times 10^4$ . The imaging of a wide window may be preferred to the imaging of a small detail as the former would be more representative of the sample under investigation.

#### *B. Principles*

The basic principle of quantum physics, describing the propagation of an electron in the microscope column, and its interaction with the sample, is the particle/wave dualism ([Willaime, 1987](#)). It is expressed by a relation between the energy of the electron and the associated wavelength of a ray. The kinetic energy,  $E$ , of an electron having a charge,  $e$ , and submitted to an accelerating potential,  $V$ , is:

$$E = eV$$

$E$  can also be expressed in terms of the mass,  $m$ , and velocity,  $v$ , of the electron:

$$E = \frac{1}{2}mv^2$$

The wavelength,  $\lambda$ , associated to the electron ray is expressed by:

$$\lambda = \frac{h}{mv}$$

where  $h$  is Planck's constant. Under an accelerating potential of 100 kV, the energy  $E$  of an electron is 100 keV, and the wavelength  $\lambda$  is equal to 0.00387 nm. For  $E = 120$  keV,  $\lambda = 0.0037$  nm.

A plane wave is associated with a moving group of electrons. The wave function is the amplitude of the wave. The square of the wave function is the intensity of light at a point. For an isolated electron, it represents the probability that the electron is present at this point.

An electron passing in the neighbourhood of an atom (atomic number,  $Z$ ) is repelled by the negative electronic potential of the electron cloud of the atom. As the electron is deviated without loss of energy, the process is referred to as elastic scattering or diffusion. The scattering factor for the elastic diffusion of an electron (with an energy  $eV$ ) is proportional to  $Z^2/V^2$ . As a result, clay minerals containing heavy elements (high  $Z$  value) will produce diffraction patterns (and images) of relatively high contrast. This is illustrated by comparing the patterns of Fe-rich clays with those of their Mg- or Al-rich counterparts, irrespective of crystal structure. This observation applies to micas as well as smectites.

The electron carries its energy in the form of a non-quantized kinetic energy. The electron will lose this energy in random quantities during successive interactions (inelastic scattering or diffusion). The scattering factor is markedly increased with respect to X-rays that lose all their energy in one single interaction. Since the scattering factor for inelastic diffusion is proportional to  $Z/V^2$ , this parameter is less sensitive to the atomic number ( $Z$ ) than elastic diffusion is.

We should also mention that the probability of diffusion (both elastic and inelastic) decreases as the accelerating voltage of the electron beam increases. Similarly, the probability of diffusion increases progressively with the loss of energy of the electron as it travels through matter. In other words, increasing the microscope voltage is not an appropriate option for observing 'light' structures, such as layer silicates.

### *Wave Transfer in the Microscope*

The power of resolution is the smallest distance between two objects giving a separate image in the apparatus. One can distinguish between point-to-point resolution and line-to-line resolution, the latter being easier to obtain in the image.

The wave issued from the object is affected by all interactions that happen between the electrons and the sample; i.e., it carries all the information about the solid crossed by the electron beam (Fig. 12.8.1).

The transfer function of the apparatus, used to define the power of resolution, is the highest spatial frequency transmitted by the microscope. In other words, the transfer function defines the bandwidth of the microscope (Fig. 12.8.2).



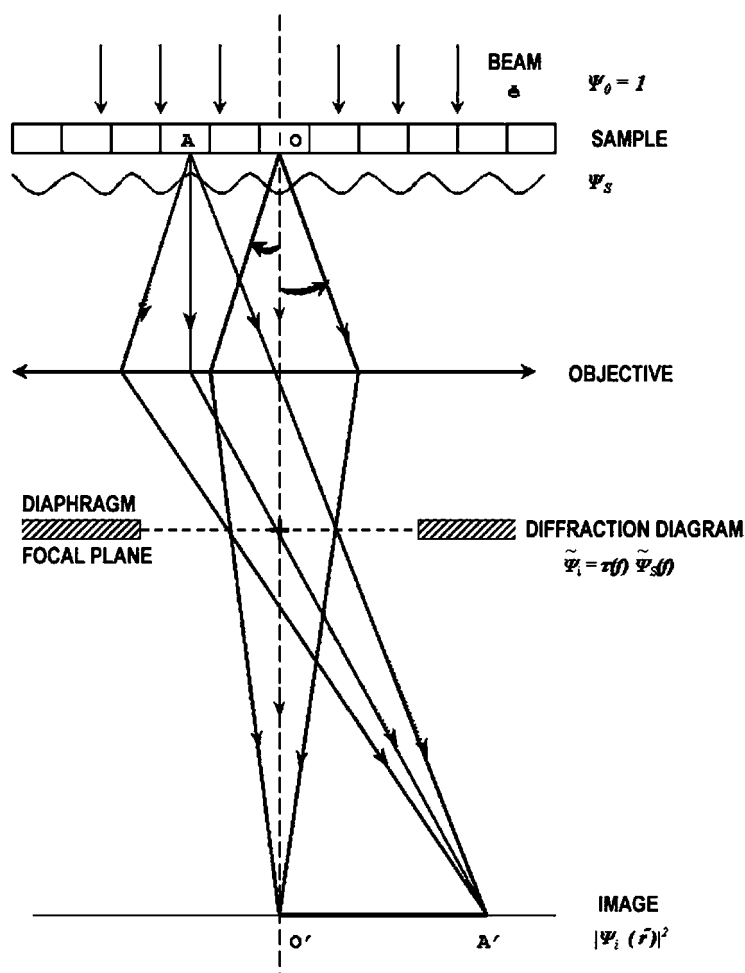


Fig. 12.8.1. Image formation in HRTEM. The wave function  $\Psi_s$  of the electrons after crossing the object is transferred to the objective lens. The Fourier transform  $\tilde{\Psi}_s(f)$  of the sample is corrected by the transfer function of the microscope  $T(f)$ . The wave function in the focal plane  $\tilde{\Psi}_i(f)$  forms the diffraction diagram. The intensity in the image is given by  $|\Psi_i|^2$ .

A weak-phase object has a weak scattering power either because it is extremely thin, poorly ordered, or its atomic density is low. This applies to clays and clay minerals with a particle size of  $< 2 \mu\text{m}$ .

Using a high-energy electron beam and weak-phase objects, the intensity (i.e., the square of the wave function) of the transmitted beam gives a good representation of the atomic structure as projected along the optic axis.

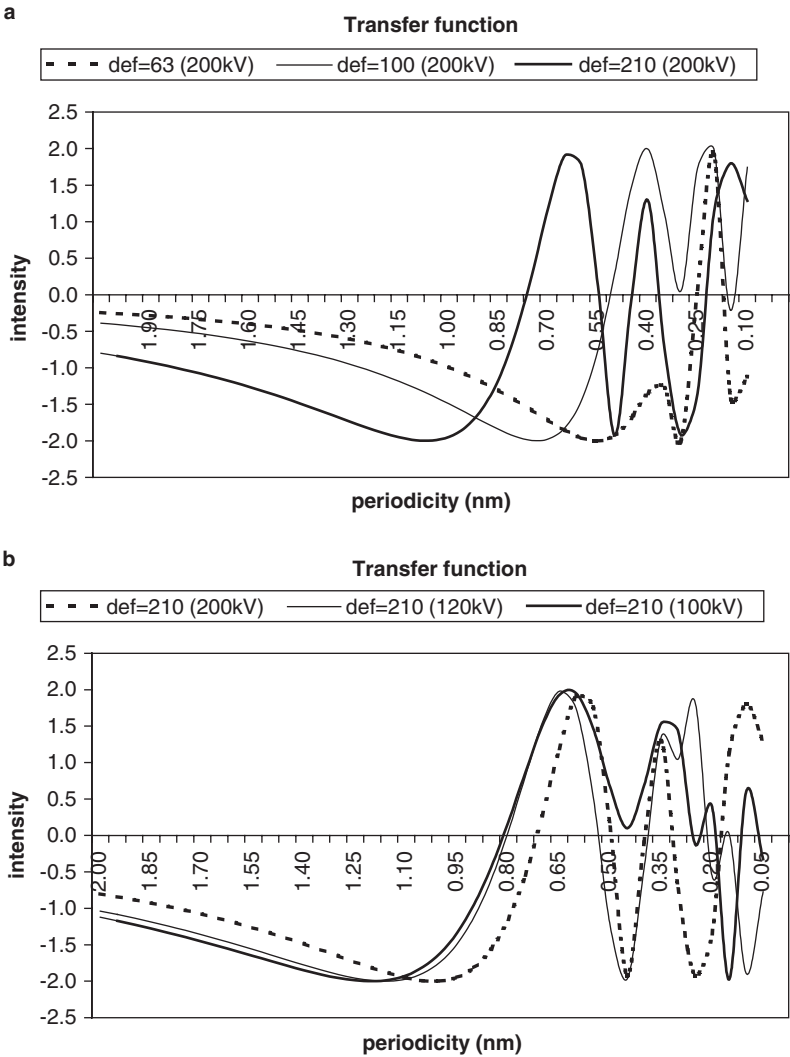


Fig. 12.8.2. Simulation of the transfer function in periodicity: (a) for different defocus in a 200 kV microscope and (b) for a 210 nm defocus in microscopes operated at 200, 120, and 100 kV.

C. Transfer in the Real Microscope

*Optical Settings of the Illumination Stage*

If microscopes were perfect and without focusing faults, the wave function of the image would perfectly reproduce the wave function of the object. If the films and

cameras were perfect, the registered intensity would accurately reproduce the distribution of electrons exiting the object. But microscopes are far from perfect. Aberrations of the lenses strongly disturb the transfer of the wave function. The spherical and chromatic aberrations are the most important. These can be minimized by selecting the appropriate operating conditions.

The spherical aberration of the objective lens is inherent to the geometry of lens construction. Beams issued from a same point of the sample and diffracted at different angles do not converge to the same point in the focal plane of the lens. The manufacturer gives a value of the spherical aberration coefficient ( $C_s$ ) for the objective lens. The more elevated the spatial frequency relative to the image (small distances), the more important is the influence of the aberration. In some microscopes, the spherical aberration is reduced by inserting a diaphragm between the objective lens and the focal plane, thus limiting the divergence angle,  $\alpha$ , of the electron beam trajectory. The radius,  $r$ , of the spherical aberration circle is given by  $2r_s = 1/2C_s\alpha^3$ .

Chromatic aberration is due to the instability of the power supply, giving rise to a spotty image and a loss of spatial resolution. Chromatic aberration can be reduced by improving the stability ( $\Delta V/V$ ) of the accelerating voltage. The coefficient of chromatic aberration ( $C_c$ ) can also be minimized by using parallel illumination, e.g., by increasing the intensity of the magnetic field in the last condenser lens. The radius,  $r$ , of the chromatic aberration circle is given by  $2r_c = C_c\alpha\Delta E/E$ .

A small part of the axial astigmatism is due to imperfections of the objective lens. More common and damaging is the presence of dirt on the beam trajectory. Regular cleaning of the diaphragms, or preferably replacement with new ones, is recommended.

### *Optical Settings of the Objective Stage*

A diaphragm is placed in the focal plane of the objective so as to limit the number of waves available to form the image. Although the information contained in this image will be reduced, the structural information selected by the operator will be enhanced. This selection can be done by observing the diffraction diagram and choosing a diaphragm of the proper size which lets through only the main beams and discards the superfluous diffracted beams. The first order of diffraction is very important as it shows the structure (stacking periodicity of the layers in the case of cross-sections of layer silicates), and should always pass through the diaphragm. Higher orders of diffraction, indicative of long-range order, are only important to keep when dealing with micaceous samples. As a simple rule, only diffracted beams displaying clear spots or circles in the diffraction diagram should be kept for image formation. Diffused diffraction will only add 'noise' to the image.

### *D. High Resolution Imaging*

High-resolution electron microscopy defines the operating conditions to be used in order to obtain images of spatial frequencies ( $f$ ) of atomic planes for weak-phase objects without major distortion.

The transfer function of frequencies is used to characterize the power of the microscope in high-resolution imaging. It is used to define the defocus settings required to optimize the intensity in the transferred image.  $T(f)$  is proportional to  $2 \sin \gamma(f)$  with:

$$\gamma(f) = 2\pi \left( Cs\lambda^3 \frac{f^4}{4} + \Delta z\lambda \frac{f^2}{2} \right)$$

As an illustration, the term  $2 \sin \gamma(f)$  was calculated for three microscopes, having different spherical aberration coefficients and operated at different acceleration voltages (Fig. 12.8.2). The assumed conditions correspond to the most common microscopes currently used in laboratories. The right transfer corresponds to negative values of  $2 \sin \gamma(f)$ . It enables a direct interpretation of the position of atoms. The positive values of  $2 \sin \gamma(f)$  result in reversed intensities in images. Objective diaphragms must be adapted to the transfer curve in order to eliminate improper transfer.

## 12.8.2. ENERGY DISPERSIVE X-RAY FLUORESCENCE (EDXRF)

### A. Chemical Analysis by EDXRF

Clay mineral layers, particles, and aggregates have specific chemical compositions that can be established using the characteristic X-ray fluorescence of the constituting ions under the electron beam. The energy of the emitted X-rays is characteristic of the ions in question. Since the intensity of the peaks is proportional to the emission by the atoms, the intensity of the emitted X-rays reflects the concentration of ions in the irradiated domain, according to the Cliff-Lorimer law (Cliff and Lorimer, 1972, 1975). Quantitative X-ray microanalysis can be performed if the specimen satisfies the thin-film criterion (Metha et al., 1979). This means that the emitted X-rays are neither absorbed by interaction with neighbouring atoms nor cause X-ray fluorescence. The ratio technique uses the expression:

$$\frac{C_A}{C_B} = k_{AB} \frac{I_A}{I_B}$$

where  $I_A$  and  $I_B$  are the simultaneously measured characteristic X-ray intensities, and  $C_A$  and  $C_B$  are the fractions of two elements A and B in the thin film. The constant  $k_{AB}$  is independent of sample thickness and composition as long as the thin-film criterion is satisfied (Goldstein, 1979). However,  $k_{AB}$  varies with operating voltage and is sensitive to absorption by (i) the window of the EDS detector; (ii) the carbon that builds up on the window; and (iii) the carbon-contaminated surface layer. It is therefore recommended that  $k$  values be calibrated for a specific instrument and

under specific operating conditions. Different instruments may therefore yield different values of  $k_{AB}$ . The effect of absorption is especially important for X-ray energies of  $<1.6$  keV, such as the characteristic emissions of Na, Mg, and Al (Lorimer et al., 1977).

The detector is a Si/Li diode mono-crystal maintained under vacuum and at a low temperature (using liquid nitrogen). The complete emission spectrum is analysed by energy dispersion, the detected X-rays being stored in a multi-channel analyser (Adda et al., 1993). An energy spectrum is displayed on the screen. The detector is sensitive to X-rays with an energy between 1 and 20 keV. This allows almost all elements to be detected by at least one of their characteristic X-rays (K, L, M series). However, light elements with  $Z < 11$  (e.g., sodium) may be difficult to detect using standard detectors with a beryllium window, while elements with  $Z < 6$  (e.g., carbon) require detectors with an ultra-thin window. The current energy resolution is around 133 eV, permitting all characteristic X-rays of the  $K\alpha$  series to be separated. X-rays of the L and M series are more difficult to separate. As the concentrations of the detected elements are normalized to 100, the procedure is semi-quantitative. The structural formulae of minerals can be derived but not the complete OH and  $H_2O$  contents.

### *B. Calibration for Quantitative Chemical Analyses of Clay Minerals*

The calibration factors, also called 'k-ratios', are given in the software package of modern analytical systems. They are set for a given configuration of detection, the type of detector, and the accelerating voltage. The calibration factors must be checked experimentally by the analyst using his/her own standards and corrected in the software when necessary (and if possible). Analysis of clay minerals requires the use of clay mineral standards and the same operating conditions. This is because irradiation damage, leading to a loss of matter, is unavoidable. The level of damage is strongly related to (i) the structure of the matter and (ii) the operating conditions, notably beam intensity. Hydroxyl groups are decomposed by heating under the electron beam, and atoms are volatilized in the microscope column (Eberhardt, 1989). Ahn et al. (1986) observed numerous lenticular fissures in electron micrographs of paragonite, due to irradiation damage. AEM analysis shows a significant loss of sodium from the beam-damaged paragonite, the degree of damage being a function of exposure to the beam. The authors suggested that the fissures are directly associated with the interlayer  $Na^+$  ion, and that beam damage effects in micas are related to interlayer cations. The less well crystallized the material, the greater is the loss of matter. Clay minerals with weakly bound interlayer cations, as is the case for hydrated cations, are dramatically sensitive to volatilization in the microscope column.

Since clay minerals can easily be damaged by irradiation, mild analytical conditions should be used to limit mass loss. Scanning transmission electron microscopy (STEM), using a small probe and intense electron flux, is known to be highly damaging to structures such as plagioclase and kaolinite (Mackinnon et al., 1986;

Mackinnon and Kaser, 1987). Romero et al. (1992a) tested different analytical conditions (time, count rate) on reference kaolinite samples. As TEM conditions with weak electron beam definitely appear to induce only limited mass loss, elemental microanalysis under these conditions is recommended. Elemental microanalysis of rather large domains (at least 100 nm in diameter) under low electron dose provides sufficient count rates for satisfactory statistical analysis to be performed, and even permits the transformation of gels into clay precursors and halloysite to be followed (Romero et al., 1992b).

Recent improvements in signal treatment, leading to higher count rates, can reduce counting time down to 10–30 s. By limiting the exposure of the clay mineral sample to the electron beam, irradiation damage is minimized.

### *C. Data Treatment and Interpretation*

When dealing with layer silicates, the acquisition and treatment of EDXRF data are based on the quantification of the concentration of structural cations relative to that of silicon. As oxygen and hydrogen are generally not quantified, such analyses are semi-quantitative, i.e., OH and H<sub>2</sub>O contents are not quantifiable using this technique. Irrespective of irradiation damage, all major and minor elements (Na, Mg, Al, K, Ca, Ti, Fe) can be detected and quantified. The analytical error and detection limits can be evaluated by classical methods as done for any other analytical measurement.

## 12.8.3. PREPARATION TECHNIQUES

Sample preparation is critical to investigating clay minerals by electron microscopy. As clay minerals are commonly hydrated, it is important to preserve their natural layer arrangement. Drying should be avoided because it causes severe modifications in texture and irreversible layer collapse (Tessier, 1987, 1991). The samples processed by the embedding techniques are concentrates of clay fractions. Concentrates must be in a gel or paste state for proper curing.

### *A. Agar Coating*

Agar was first used by Shomer and Mingelgrin (1978) to determine the number of layers in smectite tactoids by TEM. To this end, several drops of a 2% aqueous solution of agar was poured on a drop of clay suspension mounted on a glass slide in order to fix the organization of the clay mineral layers. A 2 mm<sup>3</sup> portion of the boundary region of the solidified agar in which the clay particles were fixed was transferred for embedment in resin. Similarly, Chenu and Jaunet (1990) prepared a suspension of smectite in agar to study textural modifications following the adsorption of agar. However, they did not give the concentration of the agar in the mixture.

In the following procedure, agar is used as an external coater for hydrated pellets of clay gels or pastes. Agar powder is placed in a container and dissolved in pure water to

give a 5% concentration. The container is put in a water bath, heating the agar suspension close to the boiling point for 1 h. Glass cups are filled with liquid agar. After a few minutes the clay samples are dropped in the liquid. At this stage the agar is about to gellify, the solidification point being around 40 °C. It is recommended to limit the size of the clay pellets to 1 mm<sup>3</sup> in order to ensure further rapid and complete dehydration-impregnation of the sample as it becomes embedded. Such a size is also suitable for optimal slicing with a diamond knife to give ultra-thin sections.

### *B. Water Potential Control*

The apparatus used for controlling the water potential of clays was first described by Tessier and Berrier (1979). The filtration cells are plunged in a beaker containing a solution in contact with the sample through a membrane filter. This allows the samples to be submitted to a range of gas pressures between 3.2 and 100 kPa corresponding to the range between the gel and paste states.

The agar cakes are put in filtration cells under a selected gas pressure to equilibrate the water potential at a constant suction. Equilibrium is reached overnight when the samples are in a state close to saturation. The agar coating ensures perfect contact with the porous membrane of the filtration cell, and homogeneous hydration of the clay pellet. The agar coating also protects the clay against dehydration by direct contact with dry air, and preserves the clay organization from mechanical stress when handled with tweezers. After equilibration at the selected water potential, the agar cakes are reduced to cubes of 2 mm<sup>3</sup>, thus keeping the clay pellet coated with a thin shell of agar for embedding.

The filtration cells can also be used to concentrate clay suspensions into gels or pastes, following the same law of correspondence between water potential and applied gas pressure.

### *C. Resin Embedding*

Foster and De (1971) were the first to investigate in detail the techniques for impregnating hydrated mineral samples, using a series of liquids to replace the water initially present. The embedding technique, originally developed by Spurr (1969) for curing biological specimens, was modified by Tessier (1984) who studied changes in the organization of clay minerals that had been submitted to desiccation–rehydration cycles. As the microstructure of the clay is preserved (Tessier and Pedro, 1982; Tessier, 1987), the modified method was extensively used by clay mineralogists. Further modifications and refinements were introduced by soil scientists who use the method for curing soil samples that are more difficult to handle than pure smectites (Środoń et al., 1990; Robert et al., 1991; Kim et al., 1995). Using a transmission XRD device, Elsass et al. (1998) were able to follow the change in interlayer distance during the replacement of the saturating liquid by solvent, and resin. Na<sup>+</sup>- and Ca<sup>2+</sup>-exchanged smectite samples were equilibrated at 3.2 kPa ( $pF = 1$ ) and 100 kPa

( $pF = 3$ ) gas pressures. Intercalation of alcohol and resin is pervasive, and XRD indicates a significant collapse of basal spacings (1.9 nm in water to 1.7 nm in resin).

The embedding process consists of 10 successive exchanges (Table 12.8.1). For samples of <1 mm in diameter, and pastes equilibrated under a low gas pressure (3.2 kPa), the time for exchanges can be reduced down to 10 min if leaching of adsorbed elements or mobilization of colloids is suspected. For compact samples with fine pores, such as rock chips of argillites, micro drill cores of clayey matrix in thin sections, and clays equilibrated under a relatively high gas pressure (> 100 kPa), the time for exchange must be at least 20 min. This can be extended to one hour with no major risk of dispersion since the sample is moulded in agar.

The cubes of agar containing clay pellets saturated with water must be embedded in resin, thus maintaining liquid saturation throughout the whole procedure. Samples containing organic matter that is soluble in solvents must be treated so as to fix the organic components before embedding (Thierry, 1967; Glauert, 1975). Further staining using contrast enhancers for organic matter is carried out on the ultra-thin sections obtained by slicing the hardened blocks of polymerized resin.

D. Ultra Thin Sectioning

The hardened blocks of resin are allowed to cool at room temperature overnight before ultra-thin sectioning. The blocks are then sliced up at the appropriate thickness (McKee and Brown, 1977).

Table 12.8.1. Procedure of impregnation in Spurr resin

Exchange step	Water (%)	Methanol (%)	Epoxy-propane (%)	Resin (%)	Time	Temperature (°C)
Initial state	100					25
Exch. 1	75	25			10–60 min	25
Exch. 2	50	50			10–60 min	25
Exch. 3	25	75			10–60 min	25
Exch. 4		100			10–60 min	25
Exch. 5		75	25		10–60 min	25
Exch. 6		50	50		10–60 min	25
Exch. 7		25	75		10–60 min	25
Exch. 8			100		10–60 min	25
Exch. 9			50	50	16 h	25
Exch. 10				100	3 h	25
Polymerization				100	20 h	70
Cooling				100	24 h	25



#### 12.8.4. CHARACTERIZATION OF CLAY PHASES

The concepts of ‘layer’, ‘particle’, ‘aggregate’, and ‘association’ in clay material (see Chapter 1) are based upon criteria of unit-cell size, 3-dimensional arrangement, and chemical composition.

##### *A. Morphological Criteria and Crystal Size Measurement*

Lateral extensions in the (a, b) plane are measured on images obtained for objects lying normal to the optic axis (with care to eucentric condition for magnification calibration; see Section 12.8.1). The thickness, perpendicular to the (a, b) plane, is measured on images obtained for objects oriented parallel to the optic axis of the microscope (for orientation of strongly anisomorphic objects, see Section 12.8.3).

The layer thickness is characteristic of the type of clay mineral (kaolinite, mica, smectite, chlorite). HRTEM images can give basal spacings (Środoń et al., 1990) corresponding to the stacking periodicity measured by XRD (0.7 nm for 1:1 phyllosilicates, 1.0 nm for 2:1 non-swelling phyllosilicates and up to 1.4 nm for 2:1 swelling phyllosilicates and chlorite). Intermediate values are obtained for mixed-layer clay minerals (Środoń et al., 1990, 1992; Veblen et al., 1990; Veblen, 1992).

The aggregate thickness is best expressed by the total thickness, indicating the number of particles superimposed in the aggregate normal to their (a, b) plane.

##### *B. Structural Criteria and Lattice Parameter Calculation*

Structural criteria imply three characteristics that must be verified together: crystallinity, stacking orientation, and stacking periodicity.

##### *Crystalline Versus Amorphous*

The crystalline status of an object can be assessed when the diffraction plane is normal to the optical axis of the microscope. This configuration is easily obtainable by placing a suspension of the clay mineral on the microscope grid, and allowing the water to evaporate, inducing the clay mineral particles to lie with their (a, b) plane horizontal.

To verify the crystalline status of an object, a dotted diffraction diagram must be obtained, at least for one orientation of the sample. For clay minerals a single silicate layer, made up of ordered tetrahedral and octahedral sheets, is sufficient for obtaining a symmetrical diffraction diagram. This allows the *a* and *b* parameters to be derived from the six dots of the (a, b) plane.

##### *Ordered Versus Disordered Stacking Orientation in the (a, b) Plane*

When several layers are stacked on top of each other, the electron diffraction shows the classic symmetrical diffraction diagram of six dots when all layers are oriented in the (a, b) plane in exactly the same way (coherent orientation of the *a* and *b* axes).

The stacking of layers is then called 'ordered'. A similar diffraction diagram is obtained for layers parallelly stacked with rotation angles of  $60^\circ$  modulo  $n$  in the (a, b) plane ('semi-ordered stacking'). When rings are obtained instead of dots, the layers are disordered in the (a, b) plane with respect to the  $a$  and  $b$  axes. The stacking is then referred to as 'disordered'.

#### *Regular Versus Random Periodicity along the Stacking Direction*

Particles that are oriented with their layers parallel to the optic axis can show either regular or random stacking periodicity. In the case of regular stacking periodicity along the  $c$  axis, the electron diffraction pattern shows a single line of dots corresponding to basal reflections  $d(00l)$ . In the case of random stacking periodicity, no dot is clearly visible but only a blurry line is seen along the  $(00l)$  direction. When several particles are superposed, and all of them are oriented with their layers parallel to the optic axis but with angular disorientation between particles, the diffraction diagram is composed of several lines of dots, each particle producing one single line of dots.

### *C. Chemical Criteria and Structural Formulae*

#### *Derivation of Structural Formulae*

The chemical composition of a sample can be used to derive its structural formula. Once a structural model was determined, the last step is the identification of the mineral according to the international nomenclature. The structural model is generic and defines the group of phyllosilicates such as kaolinite, mica, chlorite, smectite (see Chapter 1). The chemical composition determines the species of clay mineral. Chemical data can sometimes complicate the identification of minerals that are commonly found in the earth crust, because their compositions differ from those of the pure end-members used for classification (Caillère and Henin, 1963; Deer et al., 1965; Velde, 1977).

Structural hypotheses have to be used in interpreting the physical chemistry of clay minerals that occur either as pure phyllosilicate phases, or mixed with other non-phyllosilicate minerals. The non-phyllosilicate minerals such as metal (hydr)oxides, phosphates, sulphates, and carbonates are then considered as impurities. In order to avoid confusion and misunderstanding, it is necessary to define the basic layer structures of common phyllosilicates, 1:1 (TO) or 2:1 (TOT) (2:1) (see Chapter 2), and the chemical occupancies of the different layers. Each chemical analysis has then to be transformed into a structural formula. The classical method, proposed by Foster (1953, 1962, 1963) and Köster (1977), is still applicable. The negative charges of the oxygen and hydroxyl ions balance the positive charges of the structural cations. The cation content is then normalized to a number of oxygen ions of the corresponding hypothetical structure. Hypotheses on pure phyllosilicate phases are restricted to three main structural models:  $O_5(OH)_4 \rightarrow 7O$  for a 1:1 kaolinite/serpentine

structure;  $\text{O}_{10}(\text{OH})_2 \rightarrow 22\text{O}$  for a 2:1 mica/illite/smectite structure;  $\text{O}_{10}(\text{OH})_8 \rightarrow 14\text{O}$  for a chlorite structure.

An initial difficulty arises from the fact that EDXRF can measure the concentration of atoms but not their oxidation state. This may be a real problem in the case of iron. The possibility of significant mineral oxidation has to be considered and evaluated in relation with other bulk measurements and considerations. Mössbauer (see Chapter 12.1) and IR spectroscopy (see Chapter 12.6) can be used to assess the oxidation state and structural location of iron (Petit et al., 2002, see also Chapter 8).

Another limitation is that the proposed structural scheme for establishing structural formula is not usable when non-detectable cations, such as  $\text{H}^+$  or  $\text{NH}_4^+$ , are present as is common in natural environments.

### *Representation of Chemical Compositions*

Different basic representations of clay mineral compositions can be chosen to interpret chemical analysis obtained by EDXRF (Velde, 1977; Peacor, 1992). Despite the problem (and limitation) of determining the structural formula of phyllosilicates, semi-quantitative analyses can be directly treated using the relative cation content of the clay minerals. Ternary diagrams can be constructed showing domains distinguishable by the amount of layer charge deficit, charge location in the structure, the di-trioctahedral character, and the composition of the interlayer cations. One can select any of the constituting cations of the phyllosilicate layer ( $\text{Si}^{4+}$ ,  $\text{Al}^{3+}$ ,  $\text{Fe}^{2+}$ ,  $\text{Fe}^{3+}$ ,  $\text{Mg}^{2+}$ ,  $\text{Mn}^{2+}$ ,  $\text{Ti}^{4+}$ ) and the interlayer cations ( $\text{K}^+$ ,  $\text{Na}^+$ ,  $\text{Ca}^{2+}$ ), or combinations of them ( $\text{M}^+ = \text{K}^+ + \text{Na}^+ + \frac{1}{2}\text{Ca}^{2+}$ ;  $\text{R}^{2+} = \text{Mg}^{2+} + \text{Fe}^{2+} + \text{Mn}^{2+}$ ;  $\text{R}^{3+} = \text{Al}^{3+} + \text{Fe}^{3+}$ ) to plot the chemical data. Ternary diagrams can display the derived chemical composition of individual particles, the composition of selected groups of them, or the mean composition of a given population. Reference compositions of pure end-members may be plotted together with experimental data to assist the determination of clay minerals based on chemical analyses obtained by EDXRF in TEM.

## 12.8.5. CHARACTERIZATION OF CLAY MATERIAL AT DIFFERENT STATES

### *A. Gel State: Highly Hydrated Smectites*

Smectite reaches its highest hydration state when fully saturated with water under low partial pressure. Observation by HRTEM of ultra-thin sections after resin impregnation displays loose individual layers or groups of 2–3 layers intercalated with resin. This state and the measured interlayer distances are characteristic of a gel. Chenu and Jaunet (1990) reported interlayer distances of  $\geq 2$  nm, while Al-Mukhtar et al. (1996) studied the fabric of clay gels under controlled mechanical and hydraulic stress.

### *B. Paste State: Pillared Clays, Organo-Clays, Mixed-Layer Clay Minerals*

#### *Pillared Clays*

When smectite is pillared with aluminium polycations, it forms particles of 20–30 layers with basal spacings of 1.75 nm (Suquet et al., 1994, see also Chapter 7.5). When local concentrations of excess Al occurs, this excess can be observed on particle edges as wedge-shaped fillings in the interlayer spaces or as thick coatings on planar surfaces.

#### *Organo-Clays*

Vali and Köster (1986) were the first to present TEM images of clay minerals after intercalation of alkylammonium ions. TEM is a valuable technique for investigating such (intercalated) organo-clays which were widely used in the synthesis of clay mineral-polymer nanocomposites (see Chapters 7.3 and 10.3)

#### *Mixed-Layer Clay Minerals*

The smectite content of mixed-layer clay minerals can be evaluated by measuring the thickness of fundamental particles (Chapters 5 and 12.2), expressed as the number of collapsed layers per particle, and calculating the overall particle thickness distribution and mean number of collapsed layers in the sample (Środoń et al., 1990, 1992; Veblen et al., 1990; Mystkowski et al., 2000).

Sucha et al. (1996) used this calculation method after embedment of the water-saturated clay fraction. Even though the number of measured particles is low (< 50), the deduced expandability results are consistent with those obtained by other methods (XRD, Pt-shadowing, K content).

By dispersing Na<sup>+</sup>-saturated mixed-layer illite-smectite in polyvinylpyrrolidone (PVP-10), Uhlik et al. (2000) were able to increase the interlayer distance between expanded layers, and hence count the number of collapsed layers. They found good agreement between Pt-shadowing and HRTEM for PVP-10-intercalated illite-smectite in terms of the thickness distribution of illite particles, calculated mean crystal thickness, and total expandability of the material. The bimodal thickness distribution of illite particles suggests two origins: (i) coarse illite of detrital micromica type and (ii) authigenic (diagenetic) illite from burial of shales and clay stones. The thickness distribution of authigenic illite particles has a characteristic log-normal shape.

Dudek et al. (2002) applied the same protocol of preparation, measurement, and calculation in comparing TEM with XRD data. Their aim was to interpret crystal thickness distributions in terms of illitization mechanisms in shales.

Since its introduction by Eberl et al. (1998), using 33 illite samples, the PVP-10 dispersion method was extensively used and documented. Measurements by various techniques, including the Bertaut-Waren-Averbach and integral peak width by XRD, fixed cation content by chemical analysis, and Pt-shadowing (in TEM) give comparable results on fundamental illite particle thicknesses. To assess the size of fundamental particles by TEM and XRD swelling effects must first be eliminated. As these techniques reflect interparticle diffraction by aggregates of fundamental

particles (Nadeau et al., 1984; Uhlik et al., 2000), the aggregation of particles and their ability to form mixed-layer clay minerals can be evaluated (Robert et al., 1991).

Righi and Elsass (1996) characterized multi-phase clay mineral assemblages, using a curve decomposition program of XRD patterns and direct measurements on HRTEM photographs obtained after impregnation of moist or wet samples. When performed on  $K^+$ -saturated samples that had been subjected to wetting–drying cycles, HRTEM observations were consistent with XRD results. Vermiculite and high-charge smectite preserve their initial hydration state on impregnation but with low-charge smectites the resin molecules can penetrate into the interlayer space.

### *C. Dry State: Strongly Indurated Materials; Bricks of Consolidated Clay*

Deep diagenesis and low-grade metamorphism give rise to samples containing non-dispersible clays. Because of their low porosity and strong hardness, ion-milling is the only way to obtain samples suitable for TEM examination. Most bricks of consolidated clay, especially after heating at temperatures  $> 150^\circ\text{C}$  are irreversibly dehydrated and must be treated like solids of low porosity. Increasing metamorphic grade leads to the formation of thick particles ( $N > 20$ ) as Warr and Nieto (1998) observed with strongly indurated materials, using the same method of measuring particle thickness distributions.

## 12.8.6. IMAGE ANALYSIS

### *A. Morphometry*

Morphometry involves measuring an object in the image, which thus becomes a source of quantitative data. The quantitative aspect of microscope images is often neglected when they are used to illustrate a talk. The real power of electron microscopy lies in its capability of allowing scale changes over at least 4 orders of magnitude to be followed. To perform image analysis, while ensuring representativeness, it is important to go from a general scale (large area at small magnification) to a detail scale (small area at high magnification). Data must be recorded at progressive scales without forgetting intermediate scales. The sampling of data on a microscope grid must be done as for any other sampling method where data on a set of aliquots are acquired. Several distinct areas (3 is minimum, 10 is now normally required for publications) must be visited all over the grid in order to avoid bias due to sample heterogeneity, segregation effects, or locally produced artefacts.

The measured parameters generally qualify the size (diameter, area) of layers, particles or aggregates and are equivalent to laser granulometry (Dur et al., 2004). Image analysis is also concerned with the organization of the material in the wide sense, such as distances between objects, arrangement of organo-mineral associations, and density of objects, as a function of physical or chemical variables. The

measurement of parameters that refer to individual objects may allow objects to be separated into classes (e.g., grain size) or selection criteria (e.g., loose or aggregated).

#### *Measuring Size*

For particles having a regular shape (circle, square, rectangle), size parameters such as length and width are easily measured. The particles of many clay minerals, however, are non-rigid, and hence their linear (size) dimensions can only be roughly characterized. Nevertheless, size measurements give a fair approximation of the clay mineral surface. Moreover, this is the only way to estimate the real geometrical surface the reactivity of which is affected by association with other compounds. This information is important for complex materials such as soils and industrial clays.

#### *Measuring Shape*

Shape parameters are non-dimensional, and derive from size parameters (Coster and Chermant, 1989; Paciornik, 2000; Paciornik and Mauricio, 2004). For clay minerals with layer structures the most important parameters are the aspect (length/width) ratio, the form (area/perimeter<sup>2</sup>) factor, and convexity (convex perimeter/external perimeter). These parameters are very sensitive to the aggregation mode of fundamental units and reflect the texture of polydisperse objects.

#### *B. Quantitative Analysis*

The quantity of a given object in TEM images may be expressed by its frequency of occurrence or relative surface. In combination with size and shape measurements, quantity is of great interest for the practitioner who is concerned with the frequency of a phenomenon or the relative abundance of different objects.

Many additional features and parameters set up for image analysis were described by Russ (1991, 1995), Gonzalez and Woods (1992), and Castleman (1996). The Journal of Computer Assisted Microscopy should be consulted for advanced analysis. Numerous softwares are available on the international market; some of which offer a free-share version having already the basic functions to perform measurements and classifications.

By linking morphometry with chemical element analysis and additional features (e.g., certain types of defects), a physical specification for the elements or group of elements can be obtained. The use of cross-linked data opens the possibility of establishing a quantitative typology of the studied objects.

### 12.8.7. CLAYS IN PEDOGENETIC ALTERATION

The combination of TEM with analytical electron microscopy can be used to assess the processes involved in the formation of clays in weathering profiles, and the underlying mechanisms.

Soils develop from all types of rocks that occur at the earth surface, and almost always contain clay minerals. The genetic printout of the clay is the key to tracing its origin, the physicochemical factors affecting its formation, and the progressive alteration with time (Šucha et al., 2001).

When the age of soils in a chronosequence is approximately known, the clay mineral transformations can be used to evaluate the effect of time on the genesis of expandable clays as in podzolization (Gillot et al., 2000). Such transformations can also support the results of geological studies on tectonic movements and paleo-weathering at a large regional scale. For example, the Alpine orogeny of the Iberian Hercynian Massif is associated with general deep weathering before fossilization occurs under a sedimentary cover (Vicente et al., 1997).

Wilson (1987) described a podzol smectite that is morphologically similar to vermiculite, yielding a 'single spot' type of electron diffraction pattern. Based on these assessments, Gillot et al. (2000) ascribed the production of clay particles of various shape and size to dissolution and physical breakdown. The processes of dissolution and fragmentation induce modulated structural changes.

According to Aoudjit et al. (1996) and Hardy et al. (1999) physical breakdown, i.e., fragmentation and exfoliation without major chemical alteration, typically produce short and thick particles (of biotite and chlorite). Being less susceptible to weathering than biotite and chlorite, phengitic mica gives rise to relatively thin and flexible particles (Gillot et al., 2000). The signature of the parent material indicates evolution of phengite into beidellite through an alteration process which can be described as a 2:1 solid-phase transformation without extensive dissolution or chemical modification of the original structure (Vicente et al., 1997). The distinction between beidellite and montmorillonite is based on the structural formula, using the chemical composition deduced from AEM. The beidellite, formed by transformation of phengite, is characterized by: (i) replacement of Al by Fe–Mg from the octahedral phengitic sheet; (ii) a high layer charge, still partially saturated by  $K^+$  from the mica structure; and (iii) a specific arrangement of dense and rigid particles inherited from the typical morphology of micas.

The smectite in close proximity to muscovite particles was classified as neoformed (Vicente et al., 1997) but it could also arise from a similar transformation process, involving only slight local structural reorganization of the 2:1 network. Smectite is also found in microsites, formed by precipitation of dissolution products of aluminosilicates such as plagioclase (Aoudjit et al., 1995).

In studying buried paleosols, Elsass et al. (1997) observed aggregates of illite–smectite particles with two distinct morphologies, containing different proportions of illite layers. HRTEM observations are not decisive regarding the origin of variation within the illitic material. This may arise from burial diagenetic illitization of smectitic material, or represent telogenic alteration of illitic clay by acid waters penetrating down from the coal bed. In either case, it is an aggregate-by-aggregate and not a fundamental particle-by-particle process, and cannot be explained by a simple opening or collapse of interlayer spaces.



The alteration of biotite into kaolinite represents an extreme example of compositional change. Nevertheless, the process occurs frequently, especially under a tropical climate (White et al., 1998). An understanding of the mechanisms at the atomic scale is critical for constructing a chemical mass balance (Murphy et al., 1998). Metastable, moderately altered biotite, and halloysite are formed at low temperatures when reactions are sluggish, consistent with the Ostwald step rule (Dong et al., 1998). By contrast, the reaction kinetics at high temperatures (Ahn and Peacor, 1987) favour a direct alteration of the reactant (biotite) to the product (kaolinite).

Although there are no consistent differences in the chemical and mineralogical composition of the original materials, the alteration of pyroclastic deposits over large areas leads to a great diversity of 1:1 minerals and allophanic phases. Different parts of the deposits are characterized by a particular particle morphology of kaolinite (platy, wavy, degree of automorphy) or halloysite (tabular, tubular, spheroidal). These particles are most often associated with relict minerals (sanidine, plagioclase, micas), an amorphous Si-rich phase, and/or poorly crystallized silicates (opal, cristobalite, tridymite). The morphological and mineralogical differences suggest changes in physico-chemical conditions and/or preferential percolations (Adamo et al., 2001). Delvaux et al. (1992) related the morphology of halloysite in the clay fractions of soil pedons to weathering stage and the nature of the exchangeable cation. They suggested a weathering sequence for similar volcanic parent materials. Similar differentiation between 1:1 clay minerals are also common in soil profiles (Robain et al., 1990; Romero et al., 1992b) and toposequences (Hidalgo et al., 1998; Elsass et al., 2000).

#### 12.8.8. CLAYS IN DIAGENETIC ALTERATION

Diagenetic transformations can very often be assessed by HRTEM observations. The smectite-to-illite transition was extensively studied by XRD. The development of HRTEM and AEM techniques enabled this transformation to be followed. These techniques were also used to provide information about the mechanism of illitization in deep burial diagenesis (Lee et al., 1985; Ahn and Peacor, 1986). Similarly, Klimentidis and Mackinnon (1986) combined XRD with TEM to study well-known mixed-layer clay minerals with the aim of verifying current mixed-layer stacking models. They and others (Eberhart and Triki, 1972; Tchoubar et al., 1973; Brown and Jackson, 1973; McKee and Brown, 1977) used several methods of sample preparation, and avoided collapse of smectitic interlayer spaces.

Different preparation methods give different results, while the apparent discrepancy between XRD and HRTEM results is difficult to reconcile. Nevertheless experimentally observed layer sequences (illite/smectite and corrensite) agree well with the illite/smectite layer sequences calculated using the Monte Carlo model for illitization. Clusters of segregated illite and/or smectite layers tend to develop as well as mixed-layer structures.

Disordered mica structures (Iijima and Buseck, 1978) and perfect mica polytypes (Amouric et al., 1981) were used to interpret HRTEM images.



## REFERENCES

- Adamo, P., Violante, P., Wilson, M.J., 2001. Tubular and spheroidal halloysite in pyroclastic deposits in area of the Roccamonfina volcano (Southern Italy). *Geoderma* 99, 295–316.
- Adda, Y., Dupouy, J.M., Philibert, J., Quéré, Y., 1993. In: INSTN (Ed.), *Techniques du laboratoire de science des matériaux*. Tome 2, Commissariat à l'Energie Atomique, Gif-sur-Yvette, France, pp. 399–750.
- Ahn, J.H., Peacor, D.R., 1986. Transmission and analytical electron microscopy of the smectite-to-illite transition. *Clays and Clay Minerals* 34, 165–179.
- Ahn, J.H., Peacor, D.R., 1987. Kaolinitization of biotite: TEM data and implications for an alteration mechanism. *American Mineralogist* 72, 353–356.
- Ahn, J.H., Peacor, D.R., Essene, E.J., 1986. Cation-diffusion-induced characteristic beam damage in transmission electron microscope images of micas. *Ultramicroscopy* 19, 375–381.
- Al-Mukhtar, M., Belanteur, N., Tessier, D., Vanapalli, S.K., 1996. The fabric of a clay soil under controlled mechanical and hydraulic stress states. *Applied Clay Science* 11, 99–115.
- Amouric, M., Mercuriot, G., Baronnet, A., 1981. On computed and observed HRTEM images of perfect mica polytypes. *Bulletin de Minéralogie* 104, 298–313.
- Aoudjit, H., Elsass, F., Righi, D., Robert, M., 1996. Mica weathering in acidic soils by analytical electron microscopy. *Clay Minerals* 31, 319–322.
- Aoudjit, H., Robert, M., Elsass, F., Curmi, P., 1995. Detailed study of smectite genesis in granite saprolites by analytical electron microscopy. *Clay Minerals* 30, 135–148.
- Brown, J.L., Jackson, M.L., 1973. Chlorite examination by ultramicrotomy and high resolution electron microscopy. *Clays and Clay Minerals* 21, 1–7.
- Buseck, P.R. (Ed.), 1992. *Minerals and reactions at the atomic scale: transmission electron microscopy*. Reviews in Mineralogy, Vol. 27. Mineralogical Society of America, Washington, DC.
- Caillère, S., Henin, S., 1963. *Minéralogie des Argiles*. Masson, Paris.
- Castleman, K.R., 1996. *Digital Image Processing*, 2nd edition. Prentice-Hall, Englewood Cliffs, NJ.
- Chenu, C., Jaunet, A.M., 1990. Modifications in the textural organization of a calcium montmorillonite following the adsorption of a polysaccharide. *Comptes Rendus de l'Académie des Sciences (Paris)* 310, 975–980.
- Cliff, G., Lorimer, G.W., 1972. Quantitative analysis of thin metal foil using EMMA-4. The ratio technique. *Proceedings of the 5th European Congress on Electron Microscopy*. The Institute of Physics, Bristol and London.
- Cliff, G., Lorimer, G.W., 1975. The quantitative analysis of thin specimens. *Journal of Microscopy* 103, 203.
- Coster, M., Chermant, J.L., 1989. *Précis d'Analyse d'Images*. Presses du CNRS, Paris.
- Decarreau, A., 1990. *Matériaux argileux. Structure, Propriétés et Applications*. Société Française de Minéralogie et Cristallographie, Paris.
- Deer, W.A., Howie, R.A., Zussman, J., 1965. *Rock forming minerals. Sheet Silicates*, Vol. 3. Longmans, London.
- Delvaux, B., Tessier, D., Herbillon, A.J., Burtin, G., Jaunet, A.M., Vielvoye, L., 1992. Morphology, texture, and microstructure of halloysitic soil clays as related to weathering and exchangeable cation. *Clays and Clay Minerals* 4, 446–456.

- Dong, H., Peacor, D.R., Murphy, S.F., 1998. TEM study of progressive alteration of igneous biotite to kaolinite throughout a weathered soil profile. *Geochimica et Cosmochimica Acta* 62, 1881–1887.
- Drits, V.A., 1987. *Electron Diffraction and High Resolution Electron Microscopy*. Springer, Berlin.
- Drits, V.A., Tchoubar, C., 1990. X-ray diffraction by disordered lamellar structures. Theory and Application to Microdivided Silicates and Carbons. Springer, Berlin.
- Dudek, T., Środoń, J., Eberl, D.D., Elsass, F., Uhlik, P., 2002. Thickness distribution of illite crystals in shales. I: X-ray diffraction vs. high-resolution transmission electron microscopy measurements. *Clays and Clay Minerals* 50, 562–577.
- Dur, J.C., Elsass, F., Chaplain, V., Tessier, D., 2004. The relationship between particle-size distribution by laser granulometry and image analysis by transmission electron microscopy in a soil clay fraction. *European Journal of Soil Science* 55, 265–270.
- Eberhardt, J.P., 1989. *Analyse Structurale et Chimique des Matériaux. Diffraction des Rayons X, Électrons et Neutrons. Spectrométrie des Rayons X, Électrons et Ions. Microscopie Électronique*. Dunod, Paris.
- Eberhart, J.P., Triki, R., 1972. Description d'une technique permettant d'obtenir des coupes minces de minéraux argileux par ultramicrotomie. Application à l'étude des minéraux argileux interstratifiés. *Journal of Microscopy* 15, 111–120.
- Eberl, D.D., Nüesch, R., Šucha, V., Tshipursky, S., 1998. Measurement of fundamental illite particle thicknesses by X-ray diffraction using PVP-10 intercalation. *Clays and Clay Minerals* 46, 89–97.
- Elsass, F., Beaumont, A., Pernes, M., Jaunet, A.M., Tessier, D., 1998. Changes in layer organization of Na- and Ca-exchanged smectite materials during solvent exchanges for embedment resin. *Canadian Mineralogist* 36, 1475–1483.
- Elsass, F., Dubroeuq, D., Thiry, M., 2000. Diagenesis of silica minerals from clay minerals in volcanic soils of Mexico. *Clay Minerals* 35, 477–489.
- Elsass, F., Środoń, J., Robert, M., 1997. Illite-smectite alteration and accompanying reactions in a pennsylvanian underclay studied by HRTEM. *Clays and Clay Minerals* 45, 390–403.
- Foster, M.D., 1953. Geochemical studies of clay minerals: II relation between substitution and swelling in montmorillonite. *American Mineralogist* 38, 994–1006.
- Foster, M.D., 1962. Interpretation of the composition and classification of chlorites. *US Geological Survey Professional Papers* 414-A, 1–33.
- Foster, M.D., 1963. The composition of vermiculites and hydrobiotites. *Clays and Clay Minerals* 10, 70–89.
- Foster, R.H., De, P.K., 1971. Optical and electron microscopic investigation of shear induced structures in lightly consolidated (soft) and heavily consolidated (hard) kaolinite. *Clays and Clay Minerals* 19, 31–47.
- Gillot, F., Righi, D., Elsass, F., 2000. Pedogenic smectites in podzols from central Finland: an analytical electron microscopic study. *Clays and Clay Minerals* 48, 655–664.
- Glauert, A.M. (Ed.), 1975. Fixation, dehydration and embedding of biological specimens, Vol. III. Part I. In: *Practical Methods in Electron Microscopy*. North-Holland, Amsterdam, pp. 1–207.
- Goldstein, J.I., 1979. Principles of thin film X-ray analysis. In: Hren, J.J., Goldstein, J.I., Joy, D.C. (Eds.), *Introduction to Analytical Electron Microscopy*. Plenum Press, New York, pp. 83–120.

- Gonzalez, R.C., Woods, R., 1992. Digital Image Processing. Addison-Wesley, Reading, MA.
- Hardy, M., Jamagne, M., Elsass, F., Robert, M., Chesneau, D., 1999. Mineralogical development of the silt fractions of a podzoluvisol on loess in the Paris Basin (France). *European Journal of Soil Science* 50, 443–456.
- Hidalgo, C., Thiry, M., Elsass, F., Quantin, P., 1998. Caractérisation minéralogique des argiles des sols volcaniques indurés de la vallée de Mexico. 16th World Congress of Soil Science, Montpellier, France, pp. 20–26.
- Iijima, S., Buseck, P.R., 1978. Experimental study of disordered mica structures by high-resolution electron microscopy. *Acta Crystallographica A* 34, 709–719.
- Kim, J.W., Peacor, R., Tessier, D., Elsass, F., 1995. A technique for maintaining texture and permanent expansion of smectite interlayers for TEM observations. *Clays and Clay Minerals* 43, 51–57.
- Klimentidis, R.E., Mackinnon, I.D.R., 1986. High-resolution imaging of ordered mixed-layer clays. *Clays and Clay Minerals* 34, 155–164.
- Kogure, T., 2002. Investigations of micas using advanced transmission electron microscopy. In: Mottana, A., Sassi, F.P., Thompson, J.B. Jr., Guggenheim, S. (Eds.), *Micas: Crystal Chemistry & Metamorphic Petrology. Reviews in Mineralogy*, Vol. 46. Mineralogical Society of America, Washington, DC, pp. 281–312.
- Köster, H.M., 1977. Die Berechnung kristallchemischer Strukturformeln von 2:1 Schichtsilicaten. *Clay Minerals* 12, 45–54.
- Lee, J.H., Ahn, J.H., Peacor, D.R., 1985. Textures in layered silicates: progressive changes through diagenesis and low temperature metamorphism. *Journal of Sedimentology and Petrology* 55, 532–590.
- Lorimer, G.W., Al-Salman, S.A., Cliff, G., 1977. The quantitative analysis in thin specimen: Effects of absorption, fluorescence, and beam spreading. In: Misell, D.L. (Ed.), *Developments in Electron Microscopy and Analysis*. Institute of Physics Conference Series 36. The Institute of Physics, Bristol and London, 369 pp.
- Mackinnon, I.D.R., Kaser, S.A., 1987. Microanalysis of clays at low temperature. *Microbeam Analysis* 22, 332–334.
- Mackinnon, I.D.R., Lumpkin, G.R., van Deusen, S.B., 1986. Thin-film analyses of silicate standards at 200 kV: the effect of temperature on element loss. *Microbeam Analysis* 24, 451–454.
- McKee, T.R., Brown, J.L., 1977. Preparation of specimens for electron microscopic examination. In: Dixon, J.B., Weed, S.B. (Eds.), *Minerals in Soil Environments*. Soil Science Society of America, Madison, WI, pp. 809–841.
- Metha, S., Goldstein, J.I., Williams, D.B., Romig, A.D. Jr., 1979. Determination of Cliff-Lorimer k calibration factors for thin-foil X-ray microanalysis of Na, Mg, and Al in the STEM. *Microbeam Analysis* 14, 119–123.
- Moore, D.M., Reynolds, R.C. Jr., 1997. *X-ray Diffraction and the Identification and Analysis of Clay Minerals*. Oxford University Press, Oxford.
- Murphy, S.F., Brandtley, S.L., Blum, A.E., White, A.F., Dong, H., 1998. Chemical weathering in a tropical watershed, Luquillo Mountains, Puerto Rico: II the rate and mechanism of biotite weathering. *Geochimica et Cosmochimica Acta* 62, 227–243.
- Mystkowski, K., Środoń, J., Elsass, F., 2000. Mean thickness and thickness distribution of smectite crystallites. *Clay Minerals* 35, 545–557.

- Nadeau, P.H., Wilson, M.J., McHardy, W.J., Tait, J.M., 1984. Interstratified clays as fundamental particles. *Science* 225, 923–925.
- Paciornik, S., 2000. Image Processing and Analysis for Microscopy. Website created 2000, Access still valid in 2006. [www.dcm.puc-rio.br/courses/Imaging/](http://www.dcm.puc-rio.br/courses/Imaging/).
- Paciornik, S., Mauricio, M.H.P., 2004. Digital imaging. In: Van der Voort, G. (Ed.), *Metallography and Microstructures*. ASM Handbook, Vol. 9. ASM International, Materials Park, OH, pp. 368–402.
- Parker, A., Rae, J.E., 1998. *Environmental Interactions of Clays*. Clays and the Environment. Springer, New York.
- Peacor, D.C., 1992. Analytical electron microscopy: X-ray analysis. In: Buseck, P.R. (Ed.), *Minerals and Reactions at the Atomic Scale: Transmission Electron Microscopy. Reviews in Mineralogy*, Vol. 27. Mineralogical Society of America, Washington, DC, pp. 113–140.
- Petit, S., Caillaud, J., Righi, D., Madejova, J., Elsass, F., Köster, H.M., 2002. Characterization and crystal chemistry of an Fe-rich montmorillonite from Ölberg, Germany. *Clay Minerals* 37, 283–297.
- Reimer, L., 1997. *Transmission Electron Microscopy: Physics of Image Formation and Microanalysis*. Springer, Berlin.
- Righi, D., Elsass, F., 1996. Characterization of soil clay minerals: decomposition of X-ray diffraction diagrams and high resolution electron microscopy. *Clays and Clay Minerals* 44, 791–800.
- Robain, H., Tessier, D., Grimaldi, M., Elsass, F., 1990. Importance de la texture des kaolinites dans la caractérisation des couvertures ferrallitiques. Conséquences sur l'organisation et la stabilité physique des sols. *Comptes Rendus de l'Académie des Sciences (Paris)* 311, 239–246.
- Robert, M., Hardy, M., Elsass, F., 1991. Crystallochemistry, properties and organization of soil clays derived from major sedimentary rocks in France. *Clay Minerals* 26, 409–420.
- Romero, R., Robert, M., Elsass, F., Garcia, C., 1992a. Evidence by transmission electron microscopy of weathering microsystems in soils developed from crystalline rocks. *Clay Minerals* 27, 21–33.
- Romero, R., Robert, M., Elsass, F., Garcia, C., 1992b. Abundance of halloysite neoformation in soils developed from crystalline rocks. Contribution of transmission electron microscopy. *Clay Minerals* 27, 35–46.
- Russ, J.C., 1991. *Computer-assisted Microscopy*. Plenum Press, New York.
- Russ, J.C., 1995. *The Image Processing Handbook*, 2nd edition. CRC Press, Boca Raton, FL.
- Shomer, I., Mingelgrin, U., 1978. A direct procedure for determining the number of plates in tactoids of smectites: the Na/Ca- montmorillonite case. *Clays and Clay Minerals* 26, 135–138.
- Spurr, A.R., 1969. A low viscosity epoxy resin embedding medium for electron microscopy. *Journal of Ultrastructural Research* 26, 31–43.
- Środoń, J., Andreoli, C., Elsass, F., Robert, M., 1990. Direct high-resolution electron microscopic measurement of expandability of mixed-layer illite/smectite in bentonite rock. *Clays and Clay Minerals* 38, 373–379.
- Środoń, J., Elsass, F., McHardy, W.J., Morgan, D.J., 1992. Chemistry of illite-smectite inferred from TEM measurements of fundamental particles. *Clay Minerals* 27, 137–158.

- Šucha, V., Šrodoň, J., Clauer, N., Elsass, F., Eberl, D.D., Kraus, I., Madejová, J., 2001. Weathering of smectite and illite-smectite under temperate climatic conditions. *Clay Minerals* 36, 403–419.
- Šucha, V., Šrodoň, J., Elsass, F., McHardy, J.M., 1996. Particle shape versus coherent scattering domain of illite/smectite: evidence from HRTEM of Dolna Ves. *Clays and Clay Minerals* 44, 665–671.
- Suquet, H., Franck, R., Lambert, J.F., Elsass, F., Marcilly, C., Chevalier, S., 1994. Catalytic properties of two pre-cracking matrices: a leached vermiculite and Al-pillared saponite. *Applied Clay Science* 8, 349–364.
- Tchoubar, C., Rautureau, M., Clinard, C., Ragot, J.P., 1973. Technique d'inclusion appliquée à l'étude des silicates lamellaires et fibreux. *Journal of Microscopy* 18, 147–154.
- Tessier, D., 1984. Etude expérimentale de l'organisation des matériaux argileux. Thèse de doctorat d'État, Université de Paris VII. Institut National de la Recherche Agronomique, Paris.
- Tessier, D., 1987. Validité des techniques de déshydratation pour l'étude de la micro-organisation des sols. Apport des matériaux argileux purs. In: Fedoroff, N., Bresson, L.M., Courty, M.A. (Eds.), *Soil Micromorphology*. Association Française pour l'Étude des Sols, Plaisir, pp. 23–29.
- Tessier, D., 1991. Behaviour and microstructure of clay minerals. In: de Boedt, M.F., Hayes, M.H.B., Herbillon, A. (Eds.), *Soil Colloids and their Associations in Aggregates*. NATO ASI Series, Series B: Physics, Vol. 215. Plenum Press, New York, pp. 387–415.
- Tessier, D., Berrier, J., 1979. The use of scanning electron microscopy in soil studies. Observation of soils equilibrated with different pF. *Science du Sol* 1, 67–82.
- Tessier, D., Pedro, G., 1982. Electron microscopy study of Na smectite fabric—role of layer charge, salt concentration and suction parameters. In: van Olphen, H., Veniale, F. (Eds.), *International Clay Conference 1981. Developments in Sedimentology* 35. Elsevier, Amsterdam, pp. 165–176.
- Thierry, J.P., 1967. Mise en évidence de polysaccharides sur coupes fines en microscopie électronique. *Journal of Microscopy* 6, 987–1017.
- Uhlik, P., Šucha, V., Elsass, F., Caplovicova, M., 2000. High resolution transmission electron microscopy of mixed-layer clays dispersed in PVP-10: a new technique to distinguish detrital and authigenic illitic material. *Clay Minerals* 35, 781–789.
- Vali, H., Köster, H.M., 1986. Expanding behaviour, structural disorder, regular and random irregular interstratification of 2:1 layer-silicates studied by high-resolution images of transmission electron microscopy. *Clay Minerals* 21, 827–859.
- Veblen, D.R., Guthrie, G.D., Livi, K.J.T., Reynolds, R.C.J., 1990. High-resolution transmission electron microscopy and electron diffraction of mixed-layer illite/smectite: experimental results. *Clays and Clay Minerals* 38, 1–13.
- Veblen, D.R., 1992. Electron microscopy applied to nonstoichiometry, polysomatism, and replacement reactions in minerals. In: Buseck, P. (Ed.), *Minerals and Reactions at the Atomic Scale: Transmission Electron Microscopy*. Reviews in Mineralogy, Vol. 27. Mineralogical Society of America, Washington, DC, pp. 181–229.
- Velde, B., 1977. *Clays and Clay Minerals in Natural and Synthetic Systems*. Developments in Sedimentology 21. Elsevier, Amsterdam.
- Vicente, M.A., Elsass, F., Molina, E., Robert, M., 1997. Paleoweathering in slates from the Iberian Hercynian massif (Spain): investigation by TEM of clay mineral signatures. *Clay Minerals* 32, 435–451.

- Warr, L., Nieto, F., 1998. Crystallite thickness and defect density of phyllosilicates in low-temperature metamorphic pelites: a TEM and XRD study of clay mineral crystallinity-index standards. *Canadian Mineralogist* 36, 1453–1474.
- White, A.F., Blum, A.E., Schulz, M.S., Vivit, D.V., Stonestrom, D.A., Larsen, M., Murphy, S.F., Eberl, D., 1998. Chemical weathering in a tropical watershed, Luquillo Mountains, Puerto Rico: I. Long-term vs. short-term weathering fluxes. *Geochimica et Cosmochimica Acta* 62, 209–226.
- Willaime, C., 1987. *Initiation à la Microscopie Électronique*. Société Française de Minéralogie et Cristallographie, Paris.
- Wilson, M.J., 1987. Soil smectites and related interstratified minerals: recent developments. In: Schultz, L.G., van Olphen, H., Mumpton, F.A. (Eds.), *Proceedings of the International Clay Conference, Denver 1985*. The Clay Minerals Society, Bloomington, IN, pp. 167–173.

This page intentionally left blank

*Chapter 12.9*

## **SURFACE AREA AND POROSITY**

**L.J. MICHOT AND F. VILLIÉRAS**

*Laboratoire Environnement et Minéralurgie, BP 40, F-54501 Vandoeuvre Cedex, France*

The specific surface area (SSA) of clay minerals and related materials is one of their most important properties controlling surface phenomena. The SSA of non-swelling and non-microporous phyllosilicates ranges from a fraction to more than one hundred square meters per gram. Higher values are obtained with microporous clay minerals, such as sepiolite and palygorskite, and swelling (expanding) clay minerals.

Clay minerals play an important role in natural and industrial processes as they can take up organic and inorganic molecules at solid–liquid or solid–gas interfaces. The surface properties of these minerals have to be precisely determined if we are to gain insight into the underlying mechanisms. The present chapter has two parts; the first is concerned with the determination of the SSA of clay minerals, in general, and related topics, while the second part is specific to swelling clay minerals.

### **12.9.1. THE SPECIFIC SURFACE AREA OF CLAY MINERALS**

In the case of non-swelling clay minerals, the most widely used technique for determining SSA is based on gas adsorption, notably of nitrogen gas at 77 K. Adsorption isotherms, describing the amount of gas adsorbed as a function of relative pressure ( $P/P_0$ ) can exhibit different features depending on the size of particles, the presence of organized pores (between 0.5 and 50 nm), and the energetic properties of the mineral surface (Sing et al., 1985).

Fig. 12.9.1 shows the classical shape of a gas adsorption isotherm. In the low-pressure region, from  $P/P_0 = 0$  to  $\simeq 0.2$ , adsorption occurs on the external surface of the particles and the surface of micropores, if such pores (diameter 0–2 nm) exist. At larger relative pressures ( $0.4 < P/P_0 < 0.95$ ), adsorption of the second and third layers occurs, accompanied by condensation into mesopores (4–40 nm). Finally, at relative pressures  $> 0.95$ , condensation into macropores ( $> 40$  nm) takes place.



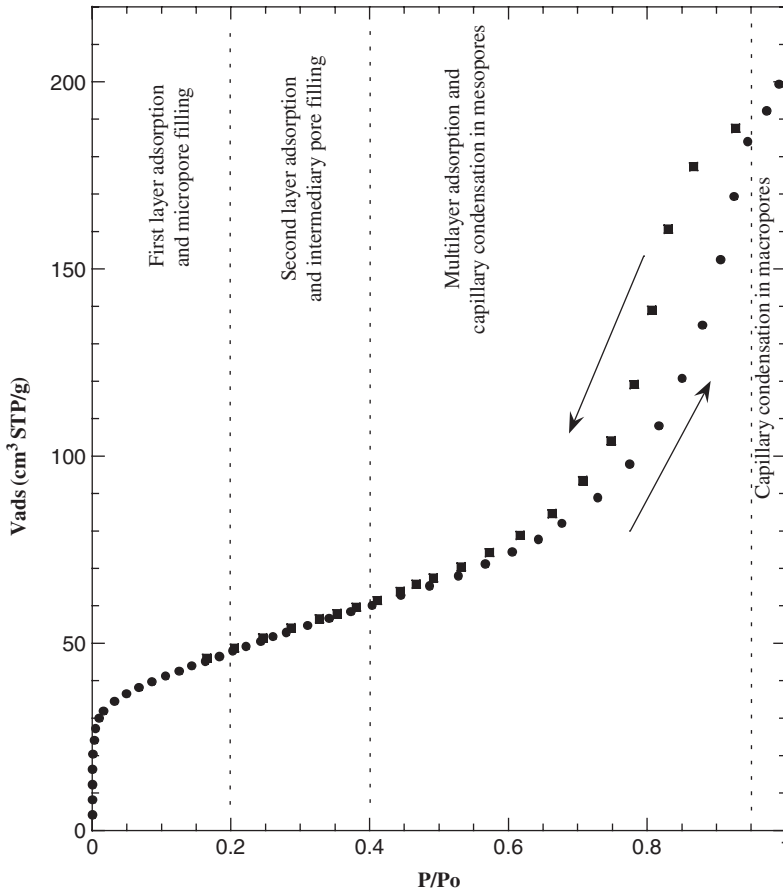


Fig. 12.9.1. Adsorption isotherm, general feature and corresponding phenomena.

Different methods of data analysis are used to derive quantitative information from experimental adsorption curves of which the Brunauer Emmett and Teller (BET) analysis is the most common. This is based on the equation proposed by Brunauer et al. (1938), describing multilayer adsorption. From the linearised form, expressed by Eq. (1), it is possible to derive the amount of gas required to cover the surface of the particles by a single statistical layer,  $Q_{\text{mono}}$ . (Gregg and Sing, 1982).

$$\frac{x}{Q_{\text{ads.}}(1-x)} = \frac{C-1}{Q_{\text{mono.}}C}x + \frac{1}{Q_{\text{mono.}}C} \quad (1)$$

Here  $x$  is the relative pressure ( $P/P_0$ ),  $Q_{\text{ads.}}$  the adsorbed amount at  $P/P_0$ , and  $C$  a constant related to the interactions between the adsorbed species and the surface.

The SSA, also called the 'BET surface area', can be derived from the monolayer capacity ( $Q_{\text{mono.}}$ ) and the cross-sectional area of the gas used. In the case of microporous materials, the measured BET surface area describes the combination of surface phenomena such as adsorption on external particle surfaces, and spatial phenomena such as condensation into micropores.

A different method should then be used to derive the external surface area and micropore volume, based on comparing the experimental adsorption isotherm with a reference isotherm obtained on a non-porous sample. In the case of nitrogen, the most commonly used is the 't-plot method' (de Boer et al., 1966). For other gases, the ' $\alpha_s$  method' can be used (Gregg and Sing, 1982).

Information on mesoporosity can also be obtained from the gas adsorption isotherm in the medium and high relative pressure ranges. Several methods were developed to describe simultaneous multilayer adsorption and capillary condensation. The most common is the 'BJH method' proposed by Barrett et al. (1951).

Although, techniques for gas adsorption and their analysis have long been established and tested, the results should always be treated with caution when accurate values are required. The lack of accuracy of the BET method for microporous samples has already been remarked. In this instance, the measured adsorption isotherms are also strongly dependent on outgassing conditions as illustrated by the behaviour of fibrous clay minerals such as sepiolite (Grillet et al., 1988) and palygorskite (Cases et al., 1991). The proper outgassing conditions under which all weakly adsorbed (zeolitic) water is removed, while structural water molecules are not affected, cover a narrow temperature range (25–100 °C for palygorskite and 25–200 °C for sepiolite). In that context, sample-controlled thermal analysis techniques, such as controlled rate thermal analysis (CRTA) (Rouquerol, 1970, 1989; Rouquerol et al., 1992) should be implemented before gas adsorption isotherms are determined.

Furthermore, the volume of very narrow micropores may not be totally filled by the gas, especially when conventional step-by-step adsorption is used. The only way to assess the total micropore volume of sepiolite, for example, is to use a quasi-equilibrium adsorption set-up with carbon dioxide gas as a probe (Michot et al., 1990). In the case of  $\text{Al}_{13}$ -pillared clay minerals with varied layer charges, the following paradox is observed (Bergaoui et al., 1995): the higher the layer charge the higher the nitrogen BET surface area. Here again, accurate micropore volumes and expected changes with layer charge are obtained from quasi-equilibrium carbon dioxide adsorption. The above paradox arises because gases such as argon and nitrogen, are adsorbed around the pillars, and do not condense into micropores (Michot et al., 1998).

For non-microporous clay minerals, other problems arise when the results for the adsorption of different gases are compared. For instance, the SSA of kaolinites measured by argon adsorption is generally lower than that obtained using nitrogen (Cases et al., 1986). The cross-sectional area of water adsorbed on non-swelling minerals depends on the crystallo-chemical properties of the minerals and the nature

of the exchangeable cation (van Olphen, 1970). The explanation seems to lie in the surface heterogeneity of phyllosilicates. These minerals have at least two types of surfaces, basal, and edge, with different chemistry and properties. In kaolinite, the reactive surfaces are mainly located on particle edges (Cases et al., 1986, 2000). The effect of surface heterogeneity on gas adsorption should be assessed from adsorption in the very low-pressure region, during the formation of the first monolayer on the surface. This kind of information may be obtained from quasi-equilibrium set-ups equipped with accurate pressure sensors (Michot et al., 1990; Villieras et al., 1992, 1997b, 2002a). The experimental data are plotted as the derivative of the amount adsorbed versus the logarithm of the relative pressure as shown in Fig. 12.9.2.

The importance of the derivative plot is that the abscissa is proportional to the free energy of adsorption. Thus, the derivative curve can be considered as a fingerprint of the adsorption energy distribution of the gas probe. Such a curve can be further analysed on a quantitative basis using the ‘derivative isotherm summation’ (DIS) method developed by Villieras et al. (1992, 1997a, 1997b).

Argon can be used to obtain information on the shape of clay mineral particles. The derivative curves are always similar in shape to that shown in Fig. 12.9.2 for talc (layer charge =  $\sim 0$ ). The DIS method allows the SSA of the basal (low-energy adsorption) and edge/lateral (medium-energy adsorption) surface to be calculated (Villieras et al., 1992, 1997a, 1997b, 2002a; Michot et al., 1994; Bardot, 1998; Cases et al., 2000; Michot and Villieras, 2002). For clay minerals with a layer charge  $> 0$ ,

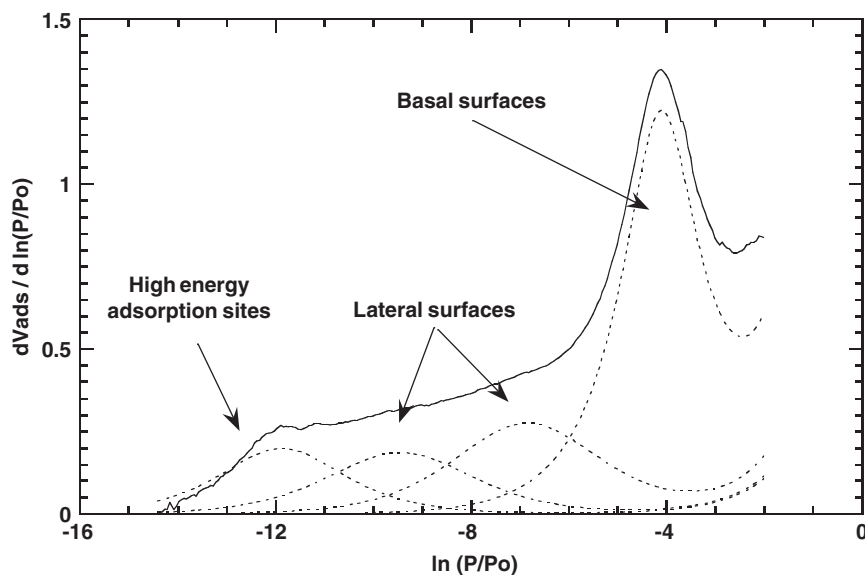


Fig. 12.9.2. Example of derivative adsorption isotherm obtained in the case of talc/argon at 77 K. From Michot et al. (1994).

such a procedure yields correct basal and lateral surface areas only with small monovalent exchangeable cations, such as lithium and sodium since larger cations interfere with the formation of an adsorbed film (Bardot, 1998).

Low-pressure adsorption and derivative plots also give information on specific adsorption sites. In the case of talc, additional high-energy adsorption sites are observed with argon (Fig. 12.9.2). Quantitative DIS analysis indicates that these sites are identifiable with the ditrigonal holes in the tetrahedral sheet (Michot et al., 1994). Such sites are also present in low-charge synthetic saponites (Michot and Villieras, 2002) and layered silicas (Eypert-Blaison et al., 2002) but not in high-charge saponites, kaolinites, or illites.

When nitrogen is used, specific interactions can take place between the probe molecules and the polar surface sites (Villieras et al., 1997b, 2002a, 2002b). As a consequence, the shape of the nitrogen derivative plots differs from that of argon, and the plots are less easy to interpret. High-energy sites, identifiable with empty ditrigonal holes, are present on basal surfaces of clay minerals whatever the layer charge. Additional sites, corresponding to interaction between nitrogen and surface cations were identified in synthetic saponites (Michot and Villieras, 2002) and probably exist in other charged minerals.

In conclusion, the accurate determination of the SSA of clay minerals is not straightforward and nitrogen may not be the best probe to use for this purpose. Nevertheless, the BET-N<sub>2</sub> SSA commonly serves as a reference as nitrogen is the most widely used gas for the BET analysis (van Olphen, 1970). As described below, other techniques for measuring the SSA of clay minerals were proposed. A promising method is atomic force microscopy (AFM) (Bickmore et al., 2002) as it can provide important complementary information.

## 12.9.2. SWELLING CLAY MINERALS

The determination of the SSA of swelling clay minerals is rather complicated since the measured value depends on sample preparation, the adsorbate used, and the nature of the exchangeable cation. In principle, the total specific surface area of swelling clay minerals can be deduced from the unit cell parameters:  $a$ ,  $b$ , and  $c$ . Indeed, for isolated clay mineral layers considered as infinite bi-dimensional platelets, the surface area can be written as

$$2ab/(dabc) = 2/cd$$

where  $d$  is the solid density.

Depending on the values for  $c$  and  $d$ , the surface area thus determined varies between 700 and 850 m<sup>2</sup>/g. This is the maximum surface area available for the adsorption of any compound. Since the SSA deduced from adsorption experiments depends on whether or not the adsorbed species can induce swelling (and gain access

to the internal/interlayer surface), the SSA values for a given sample can be highly variable (van Olphen, 1970). It is useful, therefore, to make a distinction between adsorbates that induce swelling and those that do not.

A. Adsorbates that Induce Swelling

For swelling (expanding) clay minerals, the adsorbates that can induce swelling are polar molecules such as water, alcohols, etc. Thus the first problem of surface area determination is to define the initial state that is reached after outgassing the sample, prior to its analysis. Similar outgassing conditions (e.g., 110 °C and a residual vacuum of 0.1 Pa) can result in different initial states due to variable water contents. This is well illustrated by CRTA (Rouquerol, 1970, 1989; Rouquerol et al., 1992) measurements on Wyoming montmorillonite exchanged with different cations (Table 12.9.1) (Berend et al., 1995; Cases et al., 1997).

At a given outgassing temperature, the residual water content strongly depends on the nature of the cation. In terms of water molecules per cation, the number varies between 1.0 for  $K^+$  and 4.4 for  $Ca^{2+}$ . As a result, the number of sites available for adsorption will be variable. Furthermore, when adsorbates can access the interlayer space and induce swelling, the situation is rather complicated. This is because the number of sites available for adsorption changes along the adsorption isotherm in a way that strongly depends on the nature of the interlayer cation. This feature can clearly be observed when comparing the adsorption isotherms for water on Wyoming montmorillonite exchanged with various interlayer cations (Fig. 12.9.3) (Berend et al., 1995; Cases et al., 1997). It must also be noted that the reproducibility of these isotherms for divalent-exchanged montmorillonites is not perfect because of small differences in sample preparation and pretreatment conditions. In that case, a direct application of the BET treatment in the classical range of relative pressure 0.05–0.25 would lead to the values listed in Table 12.9.2.

The monolayer volume thus determined strongly depends on the nature of the interlayer cation. Indeed, the BET equation cannot be applied to montmorillonites exchanged with rubidium and cesium ions because there is no relative pressure region where the BET transform (Eq. (1)) displays a linear behaviour. Even if the problems associated with the choice of the cross-sectional area for water molecules (van Olphen, 1970) are disregarded, no true SSA value can be derived. Such isotherms can

Table 12.9.1. Number of water molecules coordinated to the exchangeable cations after outgassing different homoionic Wyoming montmorillonites at 110 °C under a residual pressure of 0.1 Pa

Exchangeable cation	$Li^+$	$Na^+$	$K^+$	$Rb^+$	$Cs^+$	$Mg^{2+}$	$Ca^{2+}$	$Sr^{2+}$	$Ba^{2+}$
Water molecules per exchangeable cation	1.54	1.36	1.0	1.18	1.02	4.2	4.4	3.2	1.8

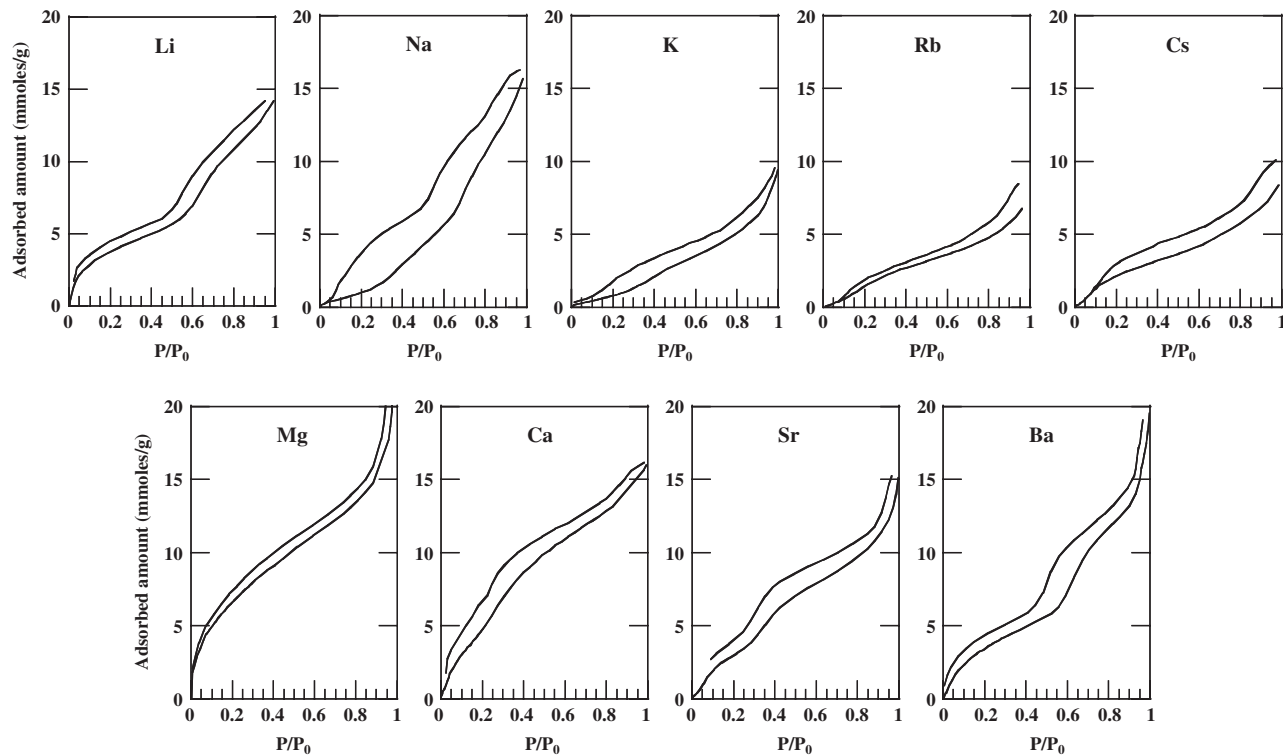


Fig. 12.9.3. Water adsorption-desorption isotherms obtained at 303 K for different homoionic Wyoming montmorillonites.

Table 12.9.2. Monolayer volumes and C constants determined by application of the BET equation at relative pressures 0.05–0.25 for different homoionic Wyoming montmorillonites

Interlayer cation	C constant	Monolayer volume ( $\text{cm}^3 \text{g}^{-1}$ )
$\text{Li}^+$	30	76.1
$\text{Na}^+$	6.3	28.7
$\text{K}^+$	5.1	25.0
$\text{Rb}^+$	n.d.	n.d.
$\text{Cs}^+$	n.d.	n.d.
$\text{Mg}^{2+}$	25	136.6
$\text{Ca}^{2+}$	9.2	120.3
$\text{Sr}^{2+}$	11	80.4
$\text{Ba}^{2+}$	12.5	80.4

n.d. = not determined.

only be interpreted in terms of the evolution of interlayer distances with water relative pressure together with spectroscopic information about the status of adsorbed water molecules.

Fig. 12.9.4 shows the changes of interlayer spacing with water relative pressure for the same sample as that described in Fig. 12.9.3. The curves are similar in shape to the adsorption isotherms and provide some insights into water adsorption mechanisms. For samples exchanged with divalent cations and lithium, water molecules can enter the interlayer space at the lowest relative pressures investigated. However, this is not the case for the other monovalent cation-exchanged montmorillonites. On the basis of these data and using different assumptions about the energetics of the clay mineral surface, it is possible to derive adsorption isotherms for water on the external and internal surfaces of swelling clay minerals. This improves understanding of adsorption mechanisms.

In the case of other swelling-inducing adsorbates such as methanol and isopropanol (Annabi-Bergaya et al., 1979, 1980a, 1980b, 1981), the nature of the interlayer cation also has a strong influence on adsorption features. Here, too, it is not possible to derive surface areas from such experiments. A detailed knowledge of the structural evolution of the particles along the adsorption isotherm is required to unravel the complex behaviour of swelling clay minerals. Spectroscopic information on the status of adsorbate molecules may also be needed.

Other swelling-inducing adsorbates such as ethylene glycol monoethyl ether (EGME), methylene blue (MB), and para-nitrophenol (*p*NP) were used for determining the SSA of clay minerals and soils (Theng, 1995; Helmy et al., 1999; Kozaki et al., 1999; Hedley et al., 2000; Parfitt et al., 2001). For non-swelling clay minerals and metal (hydr)oxides, the SSA values derived from adsorption of *p*NP are within 10% of the corresponding BET- $\text{N}_2$  areas (Theng, 1995). Since EGME, MB, and *p*NP can penetrate the interlayer space of swelling clay minerals, the SSA values derived

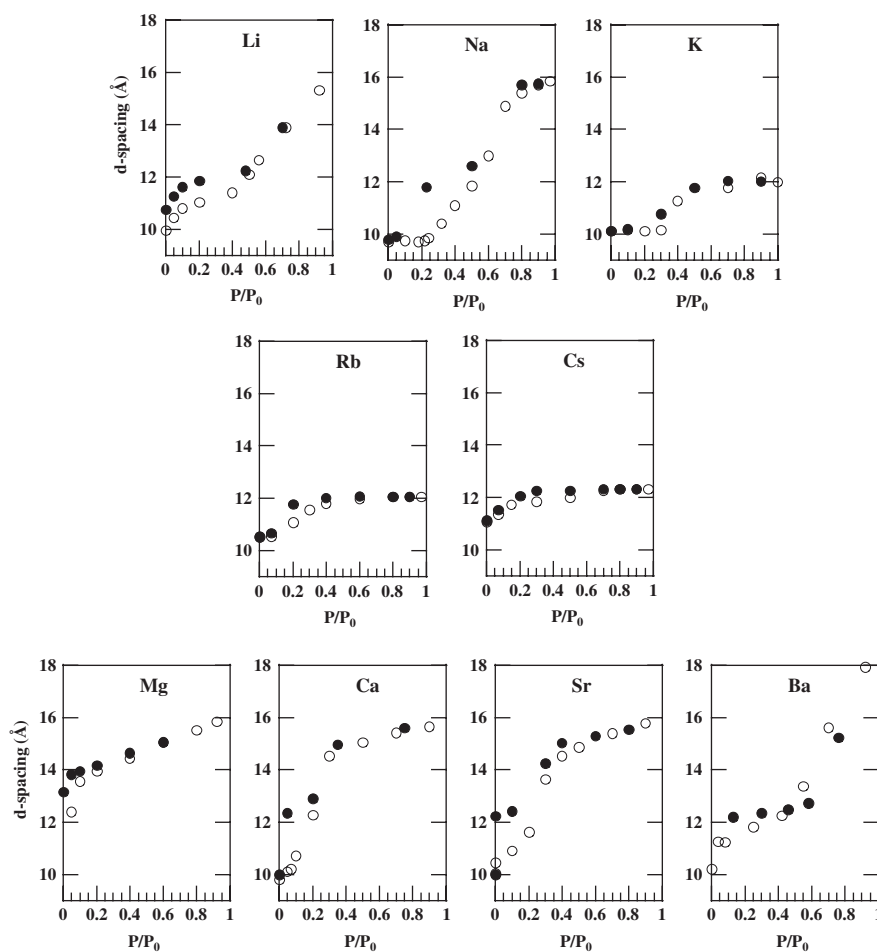


Fig. 12.9.4. Basal spacing of homoionic Wyoming montmorillonites as a function of the relative pressure of water.

from their adsorption are assumed to include the internal surface area of the mineral, that is, the total accessible surface area.

However, experimental conditions, layer charge, and the nature of the exchangeable cations significantly affect the results. For instance, [Kahr and Madsen \(1995\)](#) show that reliable surface areas can only be obtained by adsorption of MB when the layer charge is compatible with the size of adsorbed MB. This corresponds to a layer charge between 0.28 and 0.33 per half unit cell.

In the case of EGME, both the nature of the exchangeable cation and the magnitude of layer charge modify the apparent cross-sectional area of the adsorbed



molecule (Kellomäki et al., 1987, 1989; Chiou and Rutherford, 1993, 1997). This leads to the conclusion that reliable surface areas cannot be measured using this method. Nevertheless the EGME retention method can provide useful comparative data for soils and soil clays (Tiller and Smith, 1990; Churchman et al., 1991). Moreover, recent measurements show that the SSA derived from EGME retention is correlated with the cation exchange capacity (Abdullah et al., 1999; Bigorre et al., 2000), rendering the use of this technique even more dubious.

### *B. Adsorbates that do not Induce Swelling*

When the adsorbate does not induce swelling, the nitrogen or argon adsorption isotherm characterises the dry state, and can provide some information about the size, structure, the different porosities (Chapter 1) and sometimes shape of clay mineral particles and aggregates. The analysis of the hierarchical porosity (see Chapter 1) of swelling clay minerals is somewhat problematic. Indeed, the organization of the particles and aggregates strongly depends on preparation conditions that, in turn, can influence the determination of surface areas, micropore volumes, and mesopore size distributions.

For instance, the  $N_2$  SSA of a freeze-dried powder of Wyoming  $Na^+$ -montmorillonite is close to  $45\text{ m}^2/\text{g}$  whereas a film of the same sample has a surface area of about  $35\text{ m}^2/\text{g}$  (Bihannic, 1998). In terms of clay mineral characteristics, the nature of the exchangeable cation strongly modifies the SSA and pore volumes of dried samples as illustrated by measurements on cation exchanged Wyoming montmorillonites (Berend et al., 1995; Cases et al., 1997; Rutherford et al., 1997) and Arizona montmorillonites (Rutherford et al., 1997). For Wyoming montmorillonites, the measured  $N_2$  surface areas range from  $30\text{ m}^2/\text{g}$  for the calcium- to  $130\text{ m}^2/\text{g}$  for the cesium-exchanged form. The microporosity of the  $Cs^+$ -montmorillonite, deduced from the  $t$ -plot, is also much higher than for the other cation-exchanged samples. This finding may be ascribed to the large ionic radius of the  $Cs^+$  ion (also indicated by the basal spacing of 1.12 nm for dry samples), allowing access of some nitrogen molecules to the interlayer space (Aylmore et al., 1970; Berend et al., 1995; Rutherford et al., 1997). Such an explanation can only be proposed for bulky interlayer cations. In all other cases, the investigated samples almost always have some micropores. Their presence is due to (i) the turbostratic arrangement of clay mineral layers giving rise to slit-shaped micropores at particle edges, the extent of which is strongly dependent on both the crystal-chemistry of the clay mineral (size of elementary layers, charge, nature of the cation) and preparation conditions; and (ii) the presence of high-energy adsorption sites on the basal (planar) surfaces that are considered as micropores when using classical procedures such as  $t$ -plots or  $\alpha_s$  plots.

The adsorption isotherms of gases that do not induce swelling indicate the presence of mesopores between particles. Some of these pores, especially the lenticular type (Touret et al., 1990; Bihannic, 1998) are not accessible to such gases. The amount adsorbed strongly depends on the nature of the exchangeable cation and

sample preparation. Accessible pores generally exhibit a wide-size distribution that is not easy to characterise by classical gas adsorption techniques. Likewise, the pore-size distribution is strongly influenced by the nature of the exchangeable cation and preparation conditions. Because of problems associated with the connectivity of the pore network, the pore size distributions measured by gas adsorption and mercury porosimetry are often affected by artefacts. Thus, these measurements reflect the accessible porosity rather than the true porosity (Sauzéat et al., 2001).

## REFERENCES

- Abdullah, W.S., Alshibli, K.A., Al-Zou'bi, M.S., 1999. Influence of pore water chemistry on the swelling behavior of compacted clays. *Applied Clay Science* 15, 447–462.
- Annabi-Bergaya, F., Cruz, M.I., Gatinéau, L., Fripiat, J.J., 1979. Adsorption of alcohols by smectites: I. Distinction between internal and external surfaces. *Clay Minerals* 14, 249–258.
- Annabi-Bergaya, F., Cruz, M.I., Gatinéau, L., Fripiat, J.J., 1980a. Adsorption of alcohols by smectites: II. Role of the exchangeable cations. *Clay Minerals* 15, 219–223.
- Annabi-Bergaya, F., Cruz, M.I., Gatinéau, L., Fripiat, J.J., 1980b. Adsorption of alcohols by smectites: III. Nature of the bonds. *Clay Minerals* 15, 225–237.
- Annabi-Bergaya, F., Cruz, M.I., Gatinéau, L., Fripiat, J.J., 1981. Adsorption of alcohols by smectites: IV. Models. *Clay Minerals* 16, 115–122.
- Aylmore, L.A.G., Sills, I.D., Quirk, J.P., 1970. Surface area of homoionic illite and montmorillonite clay minerals as measured by the sorption of nitrogen and carbon dioxide. *Clays and Clay Minerals* 18, 91–96.
- Bardot, F., 1998. Les Minéraux Argileux et leur Hétérogénéité Superficielle: Influence de la Nature des Cations Compensateurs Superficiels de l'Illite sur les Mécanismes d'Adsorption de Gaz. Ph.D. thesis. INPL Nancy.
- Barrett, E.P., Joyner, L.G., Halenda, P.H., 1951. Determination of pore volumes and area distributions in porous substances. I. Computation from nitrogen isotherms. *Journal of the American Chemical Society* 73, 373–380.
- Berend, I., Cases, J.M., François, M., Uriot, J-P., Michot, L.J., Masion, A., Thomas, F., 1995. Mechanism of adsorption of water vapor by homoionic montmorillonite. 2. The  $\text{Li}^+$ ,  $\text{Na}^+$ ,  $\text{K}^+$ ,  $\text{Rb}^+$  and  $\text{Cs}^+$  exchanged forms. *Clays and Clay Minerals* 43, 324–336.
- Bergaoui, L., Lambert, J.F., Vicente-Rodriguez, M.A., Michot, L.J., Villieras, F., 1995. Porosity of synthetic saponites with variable layer charge pillared by  $\text{Al}_{13}$  polycations. *Langmuir* 11, 2849–2852.
- Bickmore, B.R., Nagy, K.L., Sandlin, P.E., Crater, T.S., 2002. Quantifying surface areas of clays by atomic force microscopy. *American Mineralogist* 87, 780–783.
- Bigorre, F., Tessier, D., Pedro, G., 2000. Contribution des argiles et des matières organiques à la rétention de l'eau dans les sols. Signification et rôle fondamental de la capacité d'échange en cations. *Comptes Rendus de l'Académie des Sciences, Paris, Sciences de la Terre et des Planètes* 330, 245–250.
- Bihannic, I., 1998. Structure et Microtexture du Gonflement Cristallin de la Montmorillonite. Thèse. Université d'Orléans.
- Brunauer, S., Emmett, P.H., Teller, E., 1938. Adsorption of gases in multimolecular layers. *Journal of the American Chemical Society* 60, 309–319.

- Cases, J.M., Berend, I., François, M., Uriot, J-P., Michot, L.J., Thomas, F., 1997. Mechanism of adsorption of water vapor by homoionic montmorillonite. 3. The  $\text{Mg}^{2+}$ ,  $\text{Ca}^{2+}$ ,  $\text{Sr}^{2+}$  and  $\text{Ba}^{2+}$  exchanged forms. *Clays and Clay Minerals* 45, 8–22.
- Cases, J.M., Cunin, P., Grillet, Y., Poinssignon, C., Yvon, J., 1986. Method of analysing morphology of kaolinites: relations between crystallographic and morphological properties. *Clay Minerals* 21, 55–68.
- Cases, J.M., Grillet, Y., François, M., Michot, L., Villieras, F., Yvon, J., 1991. Evolution of porous structure and surface area of palygorskite under vacuum thermal treatment. *Clays and Clay Minerals* 39, 191–201.
- Cases, J.M., Villieras, F., Michot, L.J., 2000. Le Point Sur: Les phénomènes d'adsorption, d'échange ou de rétention à l'interface solide-solution aqueuse: 1 Connaissance des propriétés structurales, texturales et superficielles des solides. *Comptes Rendus de l'Académie des Sciences, Paris, Sciences de la Terre et des Planètes* 331, 1–11.
- Chiou, C.T., Rutherford, D.W., 1993. Sorption of  $\text{N}_2$  and EGME on some soils, clays and mineral oxides and determination of sample surface area by use of sorption data. *Environmental Science and Technology* 27, 1587–1594.
- Chiou, C.T., Rutherford, D.W., 1997. Effects of exchanged cation and layer charge on the sorption of water and EGME vapors on montmorillonite clays. *Clays and Clay Minerals* 45, 867–880.
- Churchman, G.J., Burke, C.M., Parfitt, R.L., 1991. Comparison of various methods for the determination of specific surfaces of subsoils. *Journal of Soil Science* 42, 449–461.
- de Boer, J.H., Lippens, B.C., Linsen, B.G., Broekhoff, J.C.P., van der Heuvel, A., Osinga, Th.J., 1966. The  $t$ -curve of multiplayer  $\text{N}_2$ -adsorption. *Journal of Colloid and Interface Science* 21, 405–414.
- Eypert-Blaison, C., Villieras, F., Michot, L.J., Pelletier, M., Humbert, B., Ghanbaja, J., Yvon, J., 2002. Surface heterogeneity of kanemite, magadiite and kenyaite: a high resolution gas adsorption study. *Clay Minerals* 37, 531–542.
- Gregg, S.J., Sing, K.S.W., 1982. *Adsorption, Surface Area and Porosity*, 2nd edition. Academic Press, London.
- Grillet, Y., Cases, J.M., François, M., Rouquerol, J., Poirier, J.E., 1988. Modification of the porous structure and surface area of sepiolite under vacuum thermal treatment. *Clays and Clay Minerals* 36, 233–242.
- Hedley, C.B., Sagggar, S., Theng, B.K.G., Whitton, J.S., 2000. Surface area of soils of contrasting mineralogies using para-nitrophenol adsorption and its relation to air-dry moisture content of soils. *Australian Journal of Soil Research* 38, 155–167.
- Helmy, A.K., Ferreira, E.A., Bussetti, S.G., 1999. Surface area evaluation of montmorillonite. *Journal of Colloid and Interface Science* 210, 167–171.
- Kahr, G., Madsen, F.T., 1995. Determination of the cation exchange capacity and the surface area of bentonite, illite and kaolinite by methylene blue adsorption. *Applied Clay Science* 9, 327–336.
- Kellomäki, A., Kuula-Väisänen, P., Nieminen, P., 1989. Sorption and retention of ethylene glycol monoethyl ether (EGME) on silicas. *Journal of Colloid and Interface Science* 129, 373–378.
- Kellomäki, A., Nieminen, P., Ritamäki, L., 1987. Sorption of ethylene glycol monoethyl ether (EGME) on homoionic montmorillonites. *Clay Minerals* 22, 297–303.

- Kozaki, T., Sato, Y., Nakajima, M., Kato, H., Sato, S., Ohashi, H., 1999. Effect of particle size on the diffusion behavior of some radionuclides in compacted bentonite. *Journal of Nuclear Materials* 270, 265–272.
- Michot, L., François, M., Cases, J.M., 1990. Surface heterogeneity studied by quasi-equilibrium gas adsorption procedure. *Langmuir* 6, 677–681.
- Michot, L.J., Villieras, F., 2002. Assessment of surface energetic heterogeneity of synthetic Na-saponites. The role of layer charge. *Clay Minerals* 37, 39–57.
- Michot, L.J., Villieras, F., François, M., Yvon, J., Le Dred, R., Cases, J.M., 1994. The structural microscopic hydrophobicity of talc. *Langmuir* 10, 3765–3773.
- Michot, L.J., Villieras, F., Lambert, J.F., Bergaoui, L., Grillet, Y., Robert, J.L., 1998. Surface heterogeneity in micropores of pillared clays: the limits of classical pore-filling mechanisms. *Journal of Physical Chemistry B* 102, 3466–3476.
- Parfitt, R.L., Whitton, J.S., Theng, B.K.G., 2001. Surface reactivity of A horizons towards polar compounds estimated from water adsorption and water content. *Australian Journal of Soil Research* 39, 1105–1110.
- Rouquerol, J., 1970. L'analyse thermique à vitesse de décomposition constante. *Journal of Thermal Analysis* 2, 123–140.
- Rouquerol, J., 1989. Controlled transformation rate thermal analysis: the hidden face of thermal analysis. *Thermochimica Acta* 144, 209–224.
- Rouquerol, J., Bordère, S., Rouquerol, F., 1992. Controlled rate evolved gas analysis: recent experimental set-up and typical results. *Thermochimica Acta* 203, 193–202.
- Rutherford, D.W., Chiou, C.T., Eberl, D.D., 1997. Effects of exchanged cation on the microporosity of montmorillonite. *Clays and Clay Minerals* 45, 534–543.
- Sauzéat, E., Guillaume, D., Villieras, F., Dubessy, J., François, M., Pfeiffert, C., Pelletier, M., Ruck, R., Barrès, O., Yvon, J., Cathelineau, M., 2001. Caractérisation minéralogique, cristallographique et texturale de l'argile MX-80. Rapport ANDRA n° C RP 0ENG 01-001.
- Sing, K.S.W., Everett, D.H., Haul, R.A.W., Moscou, L., Pierotti, R.A., Rouquerol, J., Siemieniowska, T., 1985. Reporting physisorption data for gas/solid systems with special reference to the determination of surface area and porosity. *Pure and Applied Chemistry* 57, 603–619.
- Theng, B.K.G., 1995. On measuring the specific surface area of clays and soils by adsorption of para-nitrophenol: use and limitations. In: Churchman, G.J., Fitzpatrick, R.W., Eggleton, R.A. (Eds.), *Clays: Controlling the Environment. Proceedings of the 10th International Clay Conference, Adelaide, Australia, 1993*. CSIRO Publishing, Melbourne, pp. 304–310.
- Tiller, K.G., Smith, L.H., 1990. Limitations of EGME retention to estimate the surface area of soils. *Australian Journal of Soil Research* 28, 1–26.
- Touret, O., Pons, C.H., Tessier, D., Tardy, Y., 1990. Etude de la répartition de l'eau dans des argiles saturées  $Mg^{2+}$  aux fortes teneurs en eau. *Clay Minerals* 25, 217–233.
- van Olphen, H., 1970. Determination of surface areas of clays—evaluation of methods. In: *IUPAC Supplement to Pure and Applied Chemistry, Surface Area Determination*, Butterworths, London, 255–271.
- Villieras, F., Cases, J.M., François, M., Michot, L., Thomas, F., 1992. Texture and surface energetic heterogeneity of solids from modelling of low pressure gas adsorption isotherms. *Langmuir* 8, 1789–1795.

- Villieras, F., Chamerois, M., Bardot, F., Michot, L.J., 2002b. Evaluation of wetting properties of powders from gas adsorption experiments. In: Mittal, K.L. (Ed.), *Contact Angle, Wettability and Adhesion*, vol. 2. VSP, Utrecht, pp. 435–447.
- Villieras, F., Michot, L.J., Bardot, F., Cases, J.M., François, M., Rudzinski, W., 1997a. An improved derivative isotherm summation method to study surface heterogeneity of clay minerals. *Langmuir* 13, 1104–1117.
- Villieras, F., Michot, L.J., Bardot, F., Chamerois, M., Eypert-Blaison, C., François, M., Gérard, G., Cases, J.M., 2002a. Surface heterogeneity of minerals. *Comptes Rendus Geosciences* 334, 597–609.
- Villieras, F., Michot, L.J., Cases, J.M., Berend, I., Bardot, F., François, M., Gérard, G., Yvon, J., 1997b. Static and dynamic studies of the energetic surface heterogeneity of clay minerals. In: Rudzinski, W., Steele, W.A., Zgrablich, G. (Eds.), *Equilibria and Dynamics of Gas Adsorption on Heterogeneous Solid Surfaces*. Elsevier, Amsterdam, pp. 573–623.

Chapter 12.10

## CATION AND ANION EXCHANGE

F. BERGAYA<sup>a</sup>, G. LAGALY<sup>b</sup> AND M. VAYER<sup>a</sup>

<sup>a</sup>CRMD, CNRS-Université d'Orléans, F-45071 Orléans Cedex 2, France

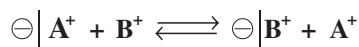
<sup>b</sup>Institut für Anorganische Chemie, Universität Kiel, D-24118 Kiel, Germany

Thomson (1850), Way (1852), Johnson (1859), and van Bemmelen (1888) pioneered the study of cation exchange in soils. Since that time much progress was made in our understanding of this phenomenon. The upsurge of interest in such issues as fertilizer efficiency or contaminant mobility in the environment contributed to the large increase in publications on cation exchange in soils, particularly with respect to the clay fraction of soils. Ion exchange is of fundamental and practical importance to soil studies and all fields in which clay materials feature. Indeed, the ability of colloidal particles (including clay minerals) to retain and exchange positively charged ions is 'perhaps the most important chemical property of natural porous media' (Verburg and Baveye, 1994). This property has a controlling influence on the mobility of positively charged chemical species in soil, such as potassium (from fertilizers) and heavy metal ions (see Chapter 11.1) as well as on the geochemical cycling of cations in general.

This chapter gives a brief survey of cation and anion exchange, with particular reference to the definition and determination of the cation exchange capacity (CEC) of clay minerals. The main questions are concerned with (i) the best method to measure CEC and (ii) the real meaning of the measured CEC under specified conditions.

### 12.10.1. ION EXCHANGE REACTIONS

#### A. Cation Exchange Equilibria



Cation exchange equilibria are often illustrated in diagrams by plotting the concentration ( $\bar{c}_{A^+}$ ) or equivalent fraction ( $\bar{\chi}_{A^+}$ ) of  $A^+$  at the surface vs. the concentration ( $c_{A^+}$ ) or equivalent fraction ( $\chi_{A^+}$ ) of this ion in the equilibrium solution. For monovalent cations the equivalent fractions are given by

$$\begin{aligned}\bar{\chi}_{A^+} &= \bar{m}_{A^+} / (\bar{m}_{A^+} + \bar{m}_{B^+}) \\ \chi_{A^+} &= m_{A^+} / (m_{A^+} + m_{B^+})\end{aligned}\quad (1)$$

where  $m$  denotes the concentration (in mol per volume or area unit) of the specified cations at the surface and in solution. Fig. 12.10.1 shows the exchange of ammonium ions on montmorillonite by sodium, potassium, rubidium, and caesium ions (Martin and Laudelout, 1963). The diagonal of the 'square plot' (broken line) indicates no preference for either cation. In practice, the exchange shows a certain preference of one cation over another as indicated by the deviation of the curve from the diagonal. Thus, in contact with sodium ions the equivalent fraction of ammonium ions at the surface is distinctly higher than that in solution, i.e.,  $\text{NH}_4^+$  ions are preferentially adsorbed over  $\text{Na}^+$  ions. By contrast,  $\text{Cs}^+$  ions are preferred to  $\text{NH}_4^+$  ions.

Cation exchange reactions may be described by the law of mass action using the activities of the ions, rather than their concentrations

$$K = \frac{\bar{a}_{B^+} a_{A^+}}{\bar{a}_{A^+} a_{B^+}} \quad (2)$$

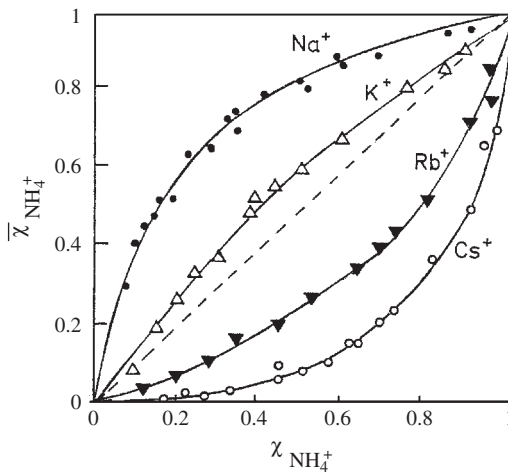


Fig. 12.10.1. Exchange of ammonium ions by alkali ions on montmorillonite (Camp Berteau) in 0.05 M solutions at 25 °C.  $\bar{\chi}_{\text{NH}_4^+}$  and  $\chi_{\text{NH}_4^+}$  are the molar fractions (Eq. 1) of ammonium ions at the surface and in the equilibrium solution (Martin and Laudelout, 1963). From Jasmund and Lagaly (1993).

where  $a_{A^+}$  and  $a_{B^+}$  are the activities of ions  $A^+$  or  $B^+$  in solution,  $\bar{a}_{A^+}$  and  $\bar{a}_{B^+}$  the activities of these ions at the surface of the exchanger, and  $\gamma$  is the activity coefficient. That is,  $a_{A^+} = c_{A^+}\gamma_{A^+}$  and  $\bar{a}_{A^+} = \bar{c}_{A^+}\bar{\gamma}_{A^+}$ .  $K$  represents the thermodynamic equilibrium constant. If the cation exchange is performed in sufficiently dilute solution, the activity coefficients of the ions in solution  $\gamma_i$  approach unity but this does not apply to the activity coefficients of the ions at the surface ( $\bar{\gamma}_i$ ). This is because the concentration of all ions at the surface (i.e.,  $\bar{c} = \bar{c}_{A^+} + \bar{c}_{B^+}$ ) does not decrease when the solution is diluted.

Using concentrations and activity coefficients, Eq. (2) becomes

$$K = \frac{\bar{c}_{B^+}\bar{\gamma}_{B^+}}{\bar{c}_{A^+}\bar{\gamma}_{A^+}} \frac{c_{A^+}\gamma_{A^+}}{c_{B^+}\gamma_{B^+}} = K_S \frac{\bar{\gamma}_{B^+}}{\bar{\gamma}_{A^+}} \quad (3)$$

where  $K_S$  is the selectivity coefficient. This coefficient is often used instead of the true equilibrium constant,  $K$ , because all parameters in  $K_S$  can be directly measured. As mentioned above,  $\gamma_{A^+}$  and  $\gamma_{B^+}$  but not  $\bar{\gamma}_{A^+}$  and  $\bar{\gamma}_{B^+}$  approach unity in dilute solutions. It is noteworthy that  $K_S$  is not constant but changes as the exchange reaction progresses, i.e., with the ratio  $\bar{c}_{B^+}/\bar{c}_{A^+}$ . When  $B^+$  approaches the surface that is mainly occupied by  $A^+$ , steric effects and the free energy of exchange can be different from the situation when  $B^+$  approaches a surface with  $B^+$  cations occupying most exchange positions. Fig. 12.10.2 illustrates the variation of  $K_S$  as the amount of sodium ions on the surface increases for a vermiculite and a montmorillonite (Gast and Klobe, 1971; Gast, 1972).

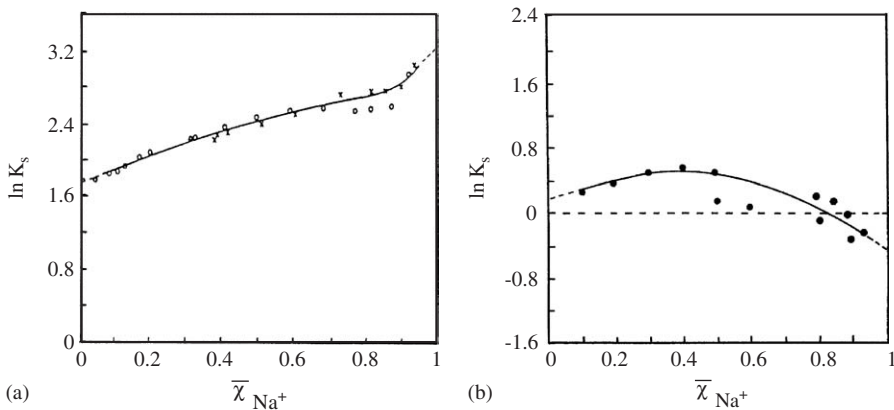
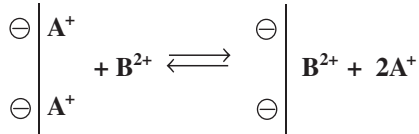


Fig. 12.10.2. Variation of the selectivity coefficient  $K_S$  with the molar fraction of sodium ions,  $\bar{\chi}_{Na^+}$ , on the clay mineral when the  $Li^+$  cations are exchanged by  $Na^+$  at 25 °C (Gast and Klobe, 1971; Gast, 1972). From Jasmund and Lagaly (1993). (a) Vermiculite (Transvaal, South Africa), total electrolyte concentration 0.01 M. (b) Montmorillonite (Chambers; Arizona, API No. 23), total electrolyte concentration 0.001 M.



To obtain the true equilibrium constant,  $K$ , the activity coefficients of the cations on the surface have to be determined. This procedure and the evaluation of the free enthalpy of exchange (by integrating the function  $\ln K_S$ ) were described by [Gast and Klobe \(1971\)](#). The same principles earlier used by [Theng et al. \(1967\)](#) to describe the exchange of alkylammonium ions with sodium and calcium ions on montmorillonite.

For the heterovalent exchange



the thermodynamic equilibrium constant is

$$K = \frac{\bar{a}_{\text{B}^{2+}} a_{\text{A}^+}^2}{\bar{a}_{\text{A}^+}^2 a_{\text{B}^{2+}}} \quad (4)$$

Often the equivalent fractions of the ions on the surface were introduced

$$\begin{aligned} \bar{\chi}_{\text{A}^+} &= \bar{m}_{\text{A}^+} / (\bar{m}_{\text{A}^+} + 2\bar{m}_{\text{B}^{2+}}) \\ \bar{\chi}_{\text{B}^{2+}} &= 2\bar{m}_{\text{B}^{2+}} / (\bar{m}_{\text{A}^+} + 2\bar{m}_{\text{B}^{2+}}) \end{aligned} \quad (5)$$

where  $m$  is expressed in mol per volume or area. The (Gaines–Thomas) selectivity coefficient is given by

$$K_s = \frac{\bar{\chi}_{\text{B}^{2+}} a_{\text{A}^+}^2}{\bar{\chi}_{\text{A}^+}^2 a_{\text{B}^{2+}}} \quad (6)$$

Soil scientists often use other coefficients such as the Vanselow selectivity coefficient,  $K_{S,V}$  ([Anderson and Sposito, 1991](#)), or the Gapon coefficient,  $K_{S,G}$

$$K_{S,V} = \frac{\bar{\chi}_{\text{B}^{2+}} a_{\text{A}^+}^2}{\bar{\chi}_{\text{A}^+} a_{\text{B}^{2+}}} \quad (7)$$

$$K_{S,G} = \frac{\bar{\chi}_{\text{B}^{2+}} a_{\text{A}^+}}{\bar{\chi}_{\text{A}^+} \sqrt{a_{\text{B}^{2+}}}} \quad (8)$$

The separation factor,  $\alpha$ , only considers concentrations

$$\alpha = \frac{\bar{c}_{\text{B}^{2+}} c_{\text{A}^+}}{\bar{c}_{\text{A}^+} c_{\text{B}^{2+}}} \quad (9)$$

The Vanselow and Gapon coefficients are introduced because in some particular cases (Shainberg et al., 1987) their values show little change with the degree of exchange.

In heterovalent exchange reactions, the more highly charged cations are preferred over monovalent ions, as indicated by Eq. (4) (Laudelout et al., 1968). This is illustrated by Fig. 12.10.3 showing the equilibrium ( $\bar{\chi}_{K^+}$  vs.  $\chi_{K^+}$ ) and selectivity coefficient for the  $K^+/Ca^{2+}$  exchange on montmorillonite (Inoue and Minato, 1979).

Nir and co-workers (Nir et al., 1986, 1994; Margulies et al., 1988; Hirsch et al., 1989; Rytwo et al., 1996) evaluated the cation-binding coefficients from the exchange isotherms (Table 12.10.1). The procedure consists in solving the electrostatic Gouy–Chapman equations and calculating the amounts of cations adsorbed as the sum of the cations residing in the double-layer region and those bound to the surface. The model also accounts explicitly for cation complexation in solution. By taking into account the adsorption of  $CaCl^+$  and  $MgCl^+$ , the apparent increase in CEC with divalent cation concentration is eliminated.

An alternative thermodynamic model was developed by Kraepiel et al. (1999) who consider the clay mineral particles as a porous solid bearing permanent charges. In this model, the Gouy–Chapman diffuse ionic layer is extended to the interlayer space, while the high concentration of cations and their (different) distribution in the interlayer space (Kjellander, 1996; Quirk, 2001) are ignored.

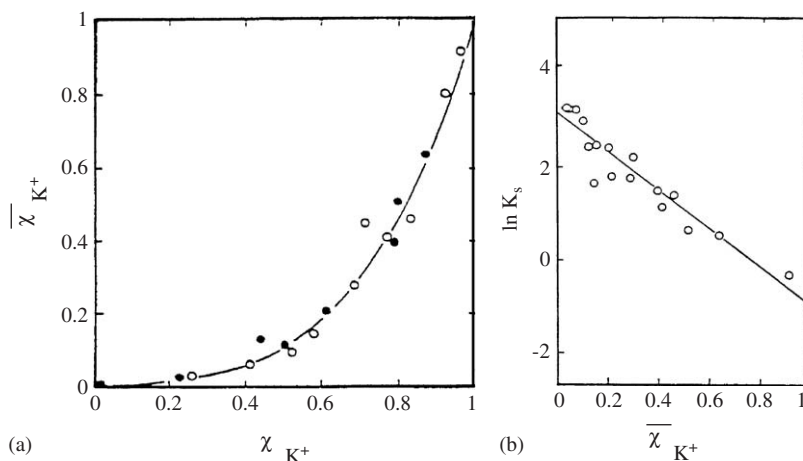


Fig. 12.10.3. Exchange of  $Ca^{2+}$  ions by  $K^+$  ions ( $\circ$ ) and of  $K^+$  ions by  $Ca^{2+}$  ions ( $\bullet$ ) at 35 °C. Montmorillonite Aterazawa (Yamagata Pref., Japan) (Inoue and Minato, 1979). From Jasmund and Lagaly (1993). (a) Equivalent fractions of  $K^+$  ions on montmorillonite,  $\bar{\chi}_{K^+}$ , vs. the equivalent fraction of  $K^+$  ions in the equilibrium solution,  $\chi_{K^+}$ . (b) Variation of the selectivity coefficient with  $\bar{\chi}_{K^+}$ .

Table 12.10.1. Binding coefficients for different cations on montmorillonite (in  $M^{-1}$ )

$Li^+$	$Na^+$	$K^+$	$Cs^+$	$Mg^{2+}$	$Ca^{2+}$	$Sr^{2+}$	$Cd^{2+}$	$MB^+$	$TFT^+$
0.6*	1*	2*	200*	2 <sup>†</sup>	4–40 <sup>†</sup>	5*	10 <sup>‡</sup>	10 <sup>8§</sup>	10 <sup>9§</sup>

$MB^+$  = methylene blue;  $TFT^+$  = thioflavin.

\*Nir et al. (1986).

<sup>†</sup>Rytwo et al. (1996).

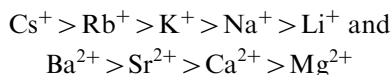
<sup>‡</sup>Hirsch et al. (1989).

<sup>§</sup>Margulies et al. (1988).

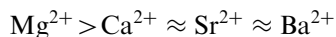
The exchangeable cations occupy sites of different energy in the interlayer space (Goulding and Talibudeen, 1980; Brouwer et al., 1983). The formation of ion-exchange sites with very high selectivity for caesium ions, induced by (i) repeated wetting–drying cycles of potassium montmorillonite and (ii) layer charge reduction using the Hofmann–Klemen effect, was described by Maes et al. (1985).

### B. Selectivity

Clay minerals show a preference for larger over smaller inorganic cations. This tendency, referred to as ‘fixation’ in the soil science literature, becomes more pronounced as layer charge increases (Klobe and Gast, 1967; Laudelout et al., 1968; Gast and Klobe, 1971; Sawhney, 1972; Maes and Cremers, 1977; Jasmund and Lagaly, 1993). For smectites, this preference (for larger cations) follows the order:



At higher layer charge (vermiculites) the preference is



As a consequence of the particular interaction between the large alkali ions and the siloxane surface, these surface sites show the preference for caesium ions over lithium ions whereas the ionizable surface groups at the edges have a much lower selectivity for caesium ions (Anderson and Sposito, 1991).

The selectivity of the preferentially adsorbed cations decreases with increasing degree of coverage by this cation (Gast and Klobe, 1971; Sawhney, 1972; Inoue and Minato, 1979; McBride, 1979; Bergseth, 1980; Maes et al., 1985; Siantar and Fripiat, 1995; Staunton and Roubaud, 1997).

The increased preference of clay minerals for potassium (and also rubidium and caesium) ions as layer charge increases (Schwertmann, 1962) is related not only to the decrease in hydration energy ( $K^+ = -314 \text{ kJ/mol}$ ;  $Li^+ = -508 \text{ kJ/mol}$ ) but also

to the strongly enhanced van der Waals energy because  $K^+$  can fit closely into the ditrigonal cavity of the silicate layer. When  $Li^+$  is displaced by  $K^+$  in Wyoming montmorillonite, the entropy change is negative ( $\Delta S^\circ = -3.12 \text{ J/K}$ ), the (decisive) value of  $\Delta H^\circ$  is  $-2.98 \text{ kJ/mol}$  and  $\Delta G^\circ$  is  $-2.05 \text{ kJ/mol}$  (Gast and Klobe, 1971; Gast, 1972; Maes and Cremers, 1977; Eberl, 1980; Goulding and Talibudeen, 1980).

The preference of clay minerals for certain cations is caused by several effects. These include hydration of the cations at the surface and in solution (entropy!), electrostatic cation–surface and cation–cation interactions, interaction between the water molecules and the surface, and the polarizability or hard and soft acid–base (HSAB) character of the cations (Xu and Harsh, 1992; Auboiroux et al., 1998). Entropic effects are also often decisive (Laudelout et al., 1968; Gast and Klobe, 1971; Gast, 1972; Maes and Cremers, 1977; Inoue and Minato, 1979; McBride, 1979; Jasmund and Lagaly, 1993). An influence of the oxidation state of the structural iron was also observed (see Chapter 8).

The structure of the silicate layers (localization of charges, orientation of OH dipoles, rotation of tetrahedra) should have a strong effect when the layer separation is small as in the case of micas (Kodama et al., 1974). Potassium ions in micas can be exchanged by other cations only under particular conditions, e.g., by complexing the displaced  $K^+$  in very dilute solutions (Scott et al., 1973), or reacting with barium ions at  $80\text{--}120^\circ\text{C}$  (Reichenbach and Rich, 1969; Reichenbach, 1973). The latter process is accompanied by a decrease in layer charge (Beneke and Lagaly, 1982). The cation exchange reaction in micas often proceeds as a co-operative process (Reichenbach and Rich, 1969; Reichenbach, 1973).

### C. Hysteresis

Exchange reactions on clay minerals typically show hysteresis effects. This is illustrated in Fig. 12.10.4 for the  $K^+/Ca^{2+}$  exchange on montmorillonite induced by drying. The curves A, B, and C (dotted) represent the exchange of  $Ca^{2+}$  by  $K^+$  at three different total concentrations. For  $K^+$ -montmorillonite that was dried at  $80^\circ\text{C}$ , the exchange of  $K^+$  by  $Ca^{2+}$  follows the solid curves indicating that the  $K^+/Ca^{2+}$  ratios on the surface are higher than those obtained during the exchange of  $Ca^{2+}$  by  $K^+$  (Inoue and Minato, 1979).

The thermodynamics of binary exchange of cations on clay minerals and soils was reviewed by Verburg and Baveye (1994). The model proposed takes into account the clay mineral type, state of hydration, and electrolyte concentration, at least qualitatively. The exchangeable cations are classified into three groups (Table 12.10.2). If exchange occurs between cations of different groups, hysteresis appears due to one of several mechanisms: heterogeneous distribution of charges or surface sites, site inaccessibility caused by coagulation or flocculation (formation of aggregates), clay mineral dehydration, differences in cation hydration, and osmotic or extensive interlayer swelling (see Chapters 5 and 13.2). A satisfactory explanation of hysteresis effects is still lacking.

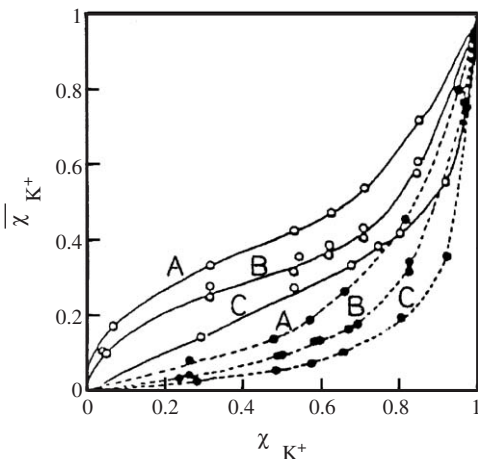


Fig. 12.10.4. Hysteresis of the  $\text{Ca}^{2+}/\text{K}^{+}$  exchange on montmorillonite after drying at  $80^{\circ}\text{C}$ . Dotted curves denote exchange of  $\text{Ca}^{2+}$  by  $\text{K}^{+}$ , while full curves describe exchange of  $\text{K}^{+}$  by  $\text{Ca}^{2+}$ . Total electrolyte concentrations (eq/L): A, 0.1; B, 0.05; C, 0.01. Montmorillonite as in Fig. 3 (Inoue and Minato, 1979). From Jasmund and Lagaly (1993).

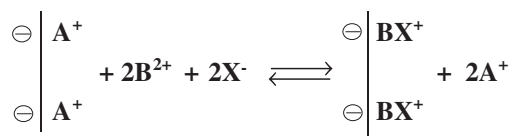
Table 12.10.2. Classification of cations in three groups. Hysteresis was documented for binary reactions involving cations from different groups (Verburg and Baveye, 1994)

Group 1	Group 2	Group 3
$\text{Na}^{+}$	$\text{K}^{+}$	$\text{Ca}^{2+}$
$\text{Li}^{+}$	$\text{Rb}^{+}$	$\text{Ba}^{2+}$
	$\text{Cs}^{+}$	$\text{Sr}^{2+}$
	$\text{NH}_4^{+}$	$\text{Mg}^{2+}$
		$\text{Mn}^{2+}$
		$\text{Cu}^{2+}$
		$\text{Ni}^{2+}$

D. Heavy Metal Ion Adsorption

The exchange adsorption of heavy metal cations by clay minerals was widely studied because of environmental concerns about heavy metal pollution (see Chapter 11.1) (Nagy and Kónya, 1988; Siantar and Fripiat, 1995; Altin et al., 1998; Bereket et al., 1997; Kodama and Komarneni, 1999; Schlegel et al., 1999a, 1999b; Strawn and Sparks, 1999; Abollino et al., 2003). The amount of multivalent heavy metal cations adsorbed often exceeds the CEC of the clay mineral. One reason is that multivalent cations can be bound by equimolar, rather than equivalent, exchange (Weiss, 1958c;

Rytwo et al., 1996; Tournassat et al., 2004.):



In addition, the heavy metal ions can be precipitated at the surface in the form of (hydr)oxides, hydroxy carbonates, or other basic salts (Siantar and Fripiat, 1995) (for surface precipitation see Chapter 5). In analysing cation exchange data it is therefore important to separate the exchange reaction from accompanying processes such as adsorption, surface precipitation, and dissolution (Nagy and Kónya, 1988; Schlegel et al., 1999b; Tournassat et al., 2004).

The presence of complexing compounds promotes the exchange of interlayer cations in clay minerals (Köster et al., 1973; Maes et al., 1982; Rytwo et al., 1996; Kónya and Nagy, 1998; Kónya et al., 1998; Abollino et al., 2003). The influence of solvents on the exchange process was investigated by Hanna et al. (1995) and El-Batouti et al. (2003).

### E. Anion Exchange

Clay minerals also have a certain capacity for anion exchange. For anions, such as chloride and nitrate, the anion exchange capacity amounts to a few cmol(–)/kg. By contrast, up to 20–30 cmol(–)/kg of phosphate and arsenate can be adsorbed by kaolinite and montmorillonite (Muljadi et al., 1966a, 1966b, 1966c; Grim, 1968; Parfitt, 1978; Bergseth, 1985; Violante and Pigna, 2002) and distinctly more by allophanes (Theng et al., 1982). Kaolinite and montmorillonite can also adsorb 10–20 and 20–30 cmol(–)/kg of fluoride ions, respectively (Weiss et al., 1956).

Clay minerals can adsorb anions by three different mechanisms:

- (1) By electrostatic interaction with particle edges when these are positively charged (see Chapter 5) (van Olphen, 1951b; Schofield and Samson, 1954; Ferris and Jepson, 1975).
- (2) By exchanging structural OH groups at the edges, and also on basal (planar) surfaces of kaolinite (Muljadi et al., 1966a, 1966b, 1966c; Parfitt, 1978; Theng et al., 1982). This process is referred to as ‘ligand exchange’ or ‘specific adsorption’ although the latter term is outmoded (see Fig. 5.2 in Chapter 5).
- (3) By accompanying multivalent cations at exchange positions (see Section D).

In mechanism (1) the extent of anion exchange decreases with increasing pH and approaches zero at the point of zero net proton charge, p.z.n.p.c. (see Chapter 5). The amount of anions bound by ligand exchange should increase to a maximum around the p.z.n.p.c. However, the adsorption of anions as counterions in an acidic medium may decrease with increasing pH as it is generally observed for phosphate

(Ioannou and Dimirkou, 1997). Anions can be adsorbed in larger amounts by ligand exchange than by counterion binding because ligand exchange also operates when the surface is uncharged or even negatively charged.

In the case of multivalent anions, the dominance of a certain species in solution at a distinct range of pH values does not imply that this species is the major surface species. The presence of the differently charged anions in the aqueous solution is determined by the dissociation constants ( $pK_a$  values), whereas the formation of the surface species also depends on the surface complexing constants. The constant capacitance model, one of the models used to describe surface complexation (Goldberg, 1992), indicates that the proportion of neutral species  $[SH_2PO_4]$  ( $S$  = surface) decreases to zero at pH 7, while the proportion of  $[SHPO_4^-]$  species increases to a maximum at pH  $\sim 5.5$ , and  $[SPO_4^{2-}]$  is the sole species at pH  $> 8$  (Ioannou and Dimirkou, 1997). Arsenate adsorption showed a maximum around pH  $\sim 6$  (Manning and Goldberg, 1996).

Multivalent cations may form insoluble salts with anions, making it uncertain whether the adsorption of the anions proceeds as a true anion exchange or by precipitation (Rao and Murti, 1987).

Weiss et al. (1956) found that the anion exchange capacity depends on the diameter of the montmorillonite particles if their shape is assumed to be almost regular. This would be expected if the anion exchange occurs on the edges. From the adsorption of fluoride ions, the authors derived average diameters of montmorillonite particles of 300–450  $\mu m$ . By contrast, most of the fluoride ions are adsorbed at the basal (planar) surface of kaolinite particles, and the anion exchange capacity depends on the thickness of these particles.

Although the anion exchange capacity of clay minerals is small compared to their CEC, the adsorption of anions is of great importance to soil fertility and plant nutrition. The adsorption of phosphate by soil and soil minerals received particular attention (Parfitt, 1978; Bowden et al., 1980; Fox, 1980; Theng et al., 1982). Wendelbo and Rosenqvist (1987) observed that sulphate can exert a dispersive effect on clay soils, intermediate between chloride and phosphate. Phosphate, oligophosphates, polyphosphates, and many other polyanions are capable of stabilising clay mineral dispersions against coagulation and flocculation (see Chapters 5 and 10.1).

Methods for determining the adsorption of phosphate and chloride were described by Bain and Smith (1987).

## 12.10.2. DEFINITION OF CEC AND FACTORS INFLUENCING ITS MEASUREMENT

The CEC of clays and clay minerals may be defined as the quantity of cations available for exchange at a given pH (Table 12.10.3), and is traditionally expressed in milliequivalents (meq)/100 g of calcined clay (Bergaya and Vayer, 1997). Thus, the

Table 12.10.3. CEC of clay minerals in cmol(+)/kg( = meq/100 g) (Weiss, 1958b; Grim, 1968)

Kaolinite	3–15
Halloysite · 2H <sub>2</sub> O	5–10
Halloysite · 4H <sub>2</sub> O	40–50
Montmorillonite	70–120
Vermiculite	130–210
Illite	10–40
Micas (biotite, muscovite)	up to 5
Chlorite	10–40
Sepiolite, palygorskite	20–30

pH value during the exchange reaction has to be specified. Various units were used in the literature to express CEC. Although CEC values are often given in terms of dried clay, the drying conditions (105, 110, 140 °C, or higher temperature) are not always specified (van Olphen, 1951a, 1977; van Olphen and Fripiat, 1979). The unit of CEC recommended by the IUPAC is cmol(+)/kg, which is numerically equivalent to meq/100 g. Only a few papers mention the pH during the exchange reaction.

The exchange capacity is usually determined at neutrality (pH = 7). Table 12.10.3 lists the CEC of some clay minerals, showing the broad range of values. This is because cation exchange is influenced by many factors, such as the nature of the exchangeable cations, particle size (grinding can change the CEC), temperature, and phase conditions (dilute or concentrated aqueous solutions, organic solvents, solid-state reactions). As a result, CEC is difficult to determine accurately. In any case, CEC determination requires the complete replacement of all exchangeable cations by ‘index’ cations that are not present in the clay mineral sample.

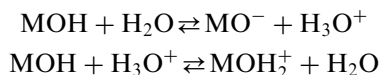
### 12.10.3. ORIGIN OF CEC

The CEC of clay minerals is generally related to the layer charge. The measured CEC is equivalent to the layer charge only when all the charge-compensating cations are exchangeable. The CEC corresponds to the summation of two types of charges arising from

- (i) Layer (isomorphous) substitution if the compensating cations are not fixed on the clay mineral and are exchangeable by other cations. This structural charge is also called constant or permanent and is generated by ion substitutions or site vacancies in the octahedral and/or tetrahedral sheets (Gast, 1977) (see Chapter 2). In most cases, the compensating cations are exchangeable. Specific interactions with the silicate layers can impede quantitative exchange of the compensating cations. An example is potassium ions in illites and micas, which are ‘fixed’ in the ditrigonal cavities (Verburg and Baveye, 1994). Some cations undergo chemical reactions altering the expected classical exchange behaviour (see Chapter 5).



- (ii) Coordination of the cations at the edges of the silicate layers is, depending on the pH, completed by  $\text{H}_3\text{O}^+$ ,  $\text{H}_2\text{O}$ , or  $\text{OH}^-$  (see Chapter 5). This pH-dependent charge varies with the nature of the solution (ionic strength, pH) due to the reactions:



with  $\text{M} = \text{Si}^{4+}$ ,  $\text{Al}^{3+}$ , or  $\text{Mg}^{2+}$ . For other possible reactions, see [Tournassat et al. \(2004\)](#). The contribution of the variable charge to the total charge depends on particle morphology and the ratio of the edge/basal surface area. In case of smectites, the pH-dependent charge varies between 10 and 20% of the total charge ([Anderson and Sposito, 1991](#)). In kaolinites, the layers are aggregated to larger particles, and the edges represent a larger fraction of the total surface area (see Chapter 12.9). As kaolinites have little layer substitution, their structural charge is relatively low, and the CEC is mainly attributed to the edge charges ([Gast, 1977](#)).

#### 12.10.4. CEC MEASUREMENTS

The CEC of clay minerals can be determined by a variety of established methods ([Van Olphen, 1951a](#), [Weiss, 1958a, 1958b](#); [Grim, 1968](#); [Bain and Smith, 1987](#)). The choice of technique depends on the magnitude of the expected CEC, the nature of the charge-compensating cations, and the available quantity of the sample. Some methods are tedious and entail theoretical uncertainties and practical difficulties. It is difficult to recommend a universal method for different clays and clay minerals.

The most widely used methods involve the displacement of the interlayer cations with the index cations in a known volume of solution and the analytical determination of the cations by standard techniques such as atomic absorption, spectrophotometry, or titration.

##### *A. Classical Methods*

These methods are based on the exchange between the cations at the clay mineral surface and the index cations in solution. The measurements are influenced by a number of experimental variables, including pH, temperature, solution ionic strength, and nature of the index cation as well as by factors relating to the clay mineral such as nature of the compensating cations, particle morphology and size, and surface area/volume ratio of the particles ([Grim, 1968](#)). The two last factors are important when the pH-dependent charge is high compared with the permanent charge.

### *B. Influence of Exchangeable and Index Cations*

The exchange reaction of clay minerals is stoichiometric in relation to the charges. As discussed above, the different cations have neither the same replaceability nor the same replacing power. For measuring CEC, it is important to use cations that are preferred or held more tightly on the surface than the cations being replaced. In some cases, the cations are fixed on the clay mineral and are not displaced by other cations even when an excess of highly preferred cations is added. Typical examples are potassium ions in micas (see Section 12.10.1) and many organic cations.

Clay minerals show a strong preference for organic cations (Theng et al., 1967). Several authors (see Section 12.10.5) used organic cations such as methylene blue and crystal violet as index cations. Such cations are strongly adsorbed by clay minerals, their binding coefficients (Nir et al., 1986) are very high compared with alkali or alkali-earth cations (Table 12.10.1).

When exchanging cations such as  $\text{NH}_4^+$  or  $\text{Ba}^{2+}$  are used, the procedure needs several incubation and separation cycles. In this case the CEC measurements are also influenced by further factors like the number of washings and the nature of the washing solvent.

### *C. Influence of pH*

The pH of the solution has two impacts:

- (i) The pH at which the exchange reaction takes place as well as the nature of the unbuffered or buffered solution determine the type of measured charge: permanent or pH dependant charge. Thus, the pH during the exchange has to be carefully measured and controlled. Grim (1968) proposed to determine the CEC at  $\text{pH} = 7$  assuming that only the exchangeable cations on permanent sites will participate in the exchange reaction. Amacher et al. (1990) proposed to determine the CEC in soils at different conditions in order to determine not only the exchangeable cations but also the exchangeable cations at acidic sites.
- (ii) The pH determines also the form of the ions present in solution. Depending on pH, many multivalent cations form oligomeric and polymeric hydroxo metal ions (see Chapter 5) and also at  $\text{pH} = 7$  the cations form different complexes. The estimation of CEC from analytically determined amounts of cations presupposes that the charge of these cations is known. If different forms of cations are bound, the numerical value of the CEC is not correct (Bache, 1976).

## 12.10.5. ANALYTICAL TECHNIQUES

The basic steps of CEC determination starting from an X-clay are illustrated in Fig. 12.10.5. We distinguish two kinds of determinations: the first is based on quantitative analysis (E) after the replacement of exchangeable cations X by the index cation A or B; the second consists of titrations (T) performed during the

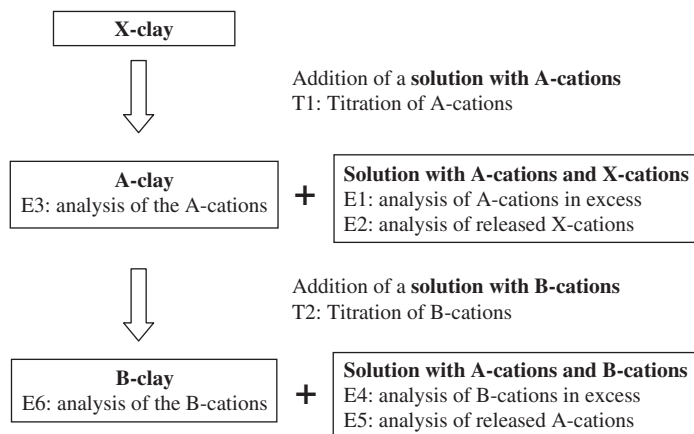


Fig. 12.10.5. Basic steps of CEC determinations.

addition of the index cation A or B and supposes that the replacement of the initial exchangeable cations X by the index cations A or B occurs immediately.

The first step is the replacement of all cations X on the clay mineral by the index cations A when the solution containing cations A is added to the clay mineral. During this step, the CEC is evaluated (T1) by following some physical properties of the dispersion or the supernatant solution (after sedimentation) such as conductivity (Dakshinamurti and Bhavanarayana, 1982), surface tension when a cationic surfactant is the index cation (Burrafato and Miano, 1993), or the appearance of flocculation (Pleysier et al., 1986).

When all cations X are replaced (in some cases, total exchange needs several cycles and thus is very time consuming), the CEC is derived by analysing either the excess of cations A in solution (E1), the released cations X in solution (E2), or the index cations A retained by the clay mineral (E3). E1 and E2 are complementary methods. If E2 is used, the total volume of washing solution must be collected and considered. Generally, it is the same for E1; in this case we consider the quantity and not the concentration. Method E3 needs the complete removal of the non-adsorbed index cations A by washing. The samples are generally washed with organic solvents. Small amounts of salts can be retained if the organic solvent is not carefully chosen, in which case the CEC is not correctly measured (Francis and Grigal, 1971). All E3 methods cited in the literature require sophisticated instruments such as radioactivity counters or microwave equipment, or are completely destructive.

Other methods are based on the replacement of the cations A by the index cations B in a second step. During this step, the CEC can be evaluated (T2) in the same way as by T1. Either the excess of cations B remaining in solution (E4) is measured, or the amount of the index cations A released into the solution is determined (E5). CEC determination by measuring the amount of index cations B fixed on the clay mineral (E6) was never reported. For both steps, classical analytical techniques such as

volumetry, atomic absorption spectrometry, inductively coupled plasma emission spectrometry (ICPES), etc. are used.

The selection of a particular method is determined (i) by the choice of the index cations and (ii) more simply, by the techniques available in the laboratory. CEC determinations using different index cations are described below.

#### *A. Exchange with Protons*

Hissink (1924) measured the acidity of soils, and derived their CEC from titration. Later, Glaeser (1946) and Grim (1968) proposed methods based on the acid–base titration of  $H^+$ -exchanged clay minerals. These methods are no longer in use because the preparation of  $H^+$ -clay minerals needs special care. Further, it is impossible to reach constant pH because the presence of protons leads to autotransformation of the minerals (see Chapter 5).

#### *B. Exchange with Organic Cations*

Since organic cations are preferentially exchanged over inorganic cations, they (especially methylene blue) were widely used for determining CEC as well as specific surface areas (Brindley and Thompson, 1970; Hang and Brindley, 1970; API, 1990; Rytwo et al., 1991; Kahr and Madsen, 1995) (see Chapter 7.3). Although total exchange of the inorganic cations needs only one incubation cycle, the determination of CEC by adsorption of methylene blue (MB) seems questionable because the adsorbed MB cations can assume more than one orientation at the clay mineral surface (Hang and Brindley, 1970). The surface area of the flat-lying monovalent MB cation is about  $1.32\text{ nm}^2$ . For highly charged clay minerals, the interlayer area per charge can be smaller than the area occupied by MB, and hence the amount adsorbed may no longer be equal to the CEC.

Brindley and Thompson (1970) and Hang and Brindley (1970) derived the CEC of clay minerals from saturation adsorption of MB but this is only valid for the  $Li^+$ - and  $Na^+$ -exchanged forms. Rytwo et al. (1991) and Kahr and Madsen (1995) showed that clay minerals adsorb MB in excess of the CEC. Accordingly, Rytwo et al. (1991) proposed to determine the CEC from the amount of cations released into solution, while Kahr and Madsen (1995) used the point where the MB added to the clay dispersion is no longer adsorbed. This method requires the clay minerals to be in the  $Na^+$  form.

#### *C. Exchange with Ammonium Ions*

Several methods use  $NH_4^+$  as the index cation. The method involving leaching with ammonium acetate and subsequent replacement of the  $NH_4^+$  ions from exchange sites is widely used, and often serves as a standard or reference procedure (Peech, 1945; Mackenzie, 1951; Fraser and Russell, 1969; Busenberg and Clemency, 1973; Greenhill and Peverill, 1977; Gillmann et al., 1983). However, the method is

time-consuming because the exchange with  $\text{NH}_4^+$  involves five to six steps. In addition, the CEC is generally determined by analysing the washed clay using techniques that are sometimes laborious. However, the method has the following advantages: (i) the exchange can be accomplished at a well-defined pH using buffered solutions (pH 7 for  $\text{NH}_4\text{OAc}$  and pH 8.5 for  $\text{NH}_4\text{Cl}/\text{NH}_3$ ) and (ii) several techniques can be used to determine the nitrogen content (Kjeldahl titration, acidimetry, ammonium sensitive electrodes, colorimetry).

#### *D. Exchange with Alkali or Alkaline-Earth Cations*

The use of alkali or alkaline earth cations such as  $\text{Cs}^+$  (Hillier and Clayton, 1992),  $\text{Ba}^{2+}$  (Bache, 1970),  $\text{Ca}^{2+}$ ,  $\text{Na}^+$ ,  $\text{K}^+$ , and  $\text{Sr}^{2+}$  as index cations A or B is also very time-consuming as several cycles are needed to reach complete exchange. Different analytical techniques are used such as conductivity (Mortland and Mellor, 1954), electrochemical measurements with specific electrodes (Malcolm and Kennedy, 1969; Chiu et al., 1990), nephelometry for small quantities (Adams and Evans, 1979), or isotopic techniques (Bache, 1970; Francis and Grigal, 1971; Brouwer et al., 1983; Maes et al., 1985) all of which are not commonly available in laboratories.

#### *E. Exchange with Transition Metal Ions or Organo-Metal Complexes*

The last group of methods used hydrates or complexes of transition metal cations as index cations, such as  $[\text{Co}(\text{H}_2\text{O})_6]^{2+}$  (Rhodes and Brown, 1994) or  $[\text{Co}(\text{NH}_3)_6]^{3+}$  (Mantin and Glaeser, 1960), silver thiourea cations (Chhabra et al., 1976; Pleysier and Juo, 1980; Pleysier et al., 1986; Searle, 1986) and  $[\text{Ni}(\text{en})_n]^{2+}$  (en = ethylene diamine) (Cornell and Aksoyoglu, 1991).

Mantin (1969) proposed a novel method to determine the CEC of clay minerals. It consists of saturating the samples with metal cations ( $\text{Cu}^{2+}$ ,  $\text{Ni}^{2+}$ ,  $\text{Zn}^{2+}$ ,  $\text{Mn}^{2+}$ ,  $\text{Al}^{3+}$ ,  $\text{Fe}^{3+}$ ), and then adding varied quantities of ethylene diamine to the clay mineral dispersion. As a result, the complex  $[\text{M}(\text{en})_n]^{p+}$  is formed in the interlayer space. The CEC is derived from the quantity of ethylene diamine required for transforming the metal cation completely into the complex. Mantin further suggested the use of  $[\text{M}(\text{en})_n]^{p+}$  complexes such as  $[\text{Ni}(\text{en})_n]^{2+}$  for CEC determinations. The method based on  $[\text{Cu}(\text{en})_2]^{2+}$  was developed by Bergaya and Vayer (1997), while Meier and Kahr (1999) proposed the use of  $[\text{Cu}(\text{trien})_3]^{2+}$  complex to determine CEC. Ammann et al. (2005) found good agreement between the two methods if the pH-dependence of the photometric determinations is taken into account.

### 12.10.6. OTHER TECHNIQUES

The CEC of smectites and vermiculites can be calculated from the layer charge determined by the alkylammonium method (Lagaly, 1994). The CEC values so

derived correspond to the permanent negative layer charge that in the case of smectites, are 10–20% smaller than the (total) exchange capacity (Lagaly, 1981, 1994). The CEC can also be estimated from the colloidal properties and the sediment values of clay dispersions in the presence of surfactants (Janek and Lagaly, 2003). On the rare occasion when the clay mineral sample is non-interstratified and very pure, or when its mineralogical composition is exactly known, the CEC may be deduced from chemical analysis.

### 12.10.7. CONCLUSIONS

The determination of CEC of clay minerals, using  $[\text{Cu}(\text{en})_2]^{2+}$  and  $[\text{Cu}(\text{trien})]^{2+}$  complexes, is presently the most versatile method.

- (1) The procedure is very simple and well suited for routine analysis. No sophisticated chemicals and materials are required. Only glass vessels, stirring devices, a centrifuge, and possibly a photometer are needed.
- (2) The exchange reaction is fast.
- (3) The  $\text{Cu}^{2+}$  complexes can displace all kinds of cations from exchange sites on the clay minerals, including heavy metal cations. Full quantitative exchange can be obtained with  $\text{Na}^+$ - and  $\text{Ca}^{2+}$ -montmorillonites (Bergaya and Vayer, 1997; Ammann et al., 2005). This accords with the high equilibrium constant of the  $\text{Cu}^{2+}/\text{Na}^+$  exchange reaction, indicative of ideal ion-exchange behaviour (Fletcher and Sposito, 1989).
- (4) The results are reproducible over a wide range of CEC values, and good accuracy may be obtained even with small amounts of samples or clays with low CEC.
- (5) The measurement is not restricted to a particular pH (Ammann et al., 2005).

Although the use of metal complexes as index cations may not be universally applicable, the method allows the CEC of many types of clays and clay minerals to be determined simply and reliably.

### REFERENCES

- Abollino, O., Aceto, M., Malandrino, M., Sarzanini, C., Mentasti, E., 2003. Adsorption of heavy metals on Na-montmorillonite. Effect of pH and organic substances. *Water Research* 37, 1619–1627.
- Adams, J.M., Evans, S., 1979. Determination of the cation-exchange capacity (layer charge) of small quantities of clays minerals by nephelometry. *Clays and Clay Minerals* 27, 137–139.
- Altin, O., Özbelge, H.Ö., Doğu, T., 1998. Use of general purpose adsorption isotherms for heavy metal–clay mineral interactions. *Journal of Colloid and Interface Science* 198, 130–140.
- Amacher, M.C., Henderson, R.E., Breithaupt, M.D., Seale, C.L., Labauve, J.M., 1990. Unbuffered and buffered salt methods for exchangeable cations and effective cation exchange capacity by potentiometric titration using divalent cation electrodes. *Soil Science Society of America Journal* 54, 1036–1042.

- Ammann, L., Bergaya, F., Lagaly, G., 2005. Determination of the cation exchange capacity of clays with copper complexes revisited. *Clay Minerals* 40, 441–453.
- Anderson, S.J., Sposito, G., 1991. Cesium-adsorption method for measuring accessible structural surface charge. *Soil Science Society of America Journal* 55, 1569–1576.
- API, 1990. Recommended practice standard procedure for laboratory testing drilling fluids. API Recommended Practice 13, 1.
- Auboiroux, M., Melou, F., Bergaya, F., Touray, J.C., 1998. Hard and soft acid–base model applied to bivalent cation selectivity on a 2:1 clay mineral. *Clays and Clay Minerals* 46, 546–555.
- Bache, B.W., 1970. Barium isotope method for measuring cation-exchange capacity of soils and clays. *Journal of the Science of Food and Agriculture* 21, 169–171.
- Bache, B.W., 1976. The measurement of cation exchange capacity of soils. *Journal of the Science of Food and Agriculture* 27, 273–280.
- Bain, D.C., Smith, B.F.L., 1987. Chemical analysis. In: Wilson, M.J. (Ed.), *A Handbook of Determinative Methods in Clay Mineralogy*. Blackie, Glasgow, pp. 248–274.
- Beneke, K., Lagaly, G., 1982. The brittle mica-like  $\text{KNiAsO}_4$  and its organic derivatives. *Clay Minerals* 17, 175–183.
- Bereket, G., Aroğuz, A.Z., Özel, M.Z., 1997. Removal of  $\text{Pb(II)}$ ,  $\text{Cd(II)}$ ,  $\text{Cu(II)}$ , and  $\text{Zn(II)}$  from aqueous solutions by adsorption on bentonite. *Journal of Colloid and Interface Science* 187, 338–343.
- Bergaya, F., Vayer, M., 1997. CEC of clays: measurement by adsorption of a copper ethylenediamine complex. *Applied Clay Science* 12, 275–280.
- Bergseth, H., 1980. Selektivität von Illit, Vermiculit und Smectit gegenüber  $\text{Cu}^{2+}$ ,  $\text{Pb}^{2+}$ ,  $\text{Zn}^{2+}$ ,  $\text{Cd}^{2+}$  und  $\text{Mn}^{2+}$ . *Acta Agricultura Scandinavica* 30, 460–468.
- Bergseth, H., 1985. Selektierungsvermögen eines Eisenoxidhydroxids und einiger Tonminerale gegenüber Phosphat und Sulfationen. *Acta Agricultura Scandinavica* 35, 375–388.
- Bowden, J.W., Posner, A.M., Quirk, J.P., 1980. Adsorption and charging phenomena in variable charge soils. In: Theng, B.K.G. (Ed.), *Soils with Variable Charge*. New Zealand Society of Soil Science, Lower Hutt, pp. 147–166.
- Brindley, G.W., Thompson, T.D., 1970. Methylene blue adsorption by montmorillonite: determination of surface areas and exchange capacity with different initial cation saturations. *Israel Journal of Chemistry* 8, 409–415.
- Brouwer, E., Baeyens, B., Maes, A., Cremers, A., 1983. Cesium and rubidium ion equilibria in illite clay. *Journal of Physical Chemistry* 87, 1213–1219.
- Burrafato, G., Miano, F., 1993. Determination of the cation exchange of clays by surface tension measurements. *Clay Minerals* 28, 475–481.
- Busenberg, E., Clemency, C.V., 1973. Determination of the cation exchange capacity of clays and soils using an ammonia electrode. *Clays and Clay Minerals* 21, 213–218.
- Chhabra, R., Pleysier, J., Cremers, A., 1976. The measurement of CEC and exchangeable cations in soils: a new method. In: Bailey, S.W. (Ed.), *Proceedings of the International Clay Conference 1975*. Applied Publishing, Wilmette, IL, pp. 439–449.
- Chiu, Y.C., Huang, N.L., Uang, C.M., Huang, J.F., 1990. Determination of cation exchange capacity of clays minerals. *Colloids and Surfaces* 46, 327–337.
- Cornell, R.M., Aksoyoglu, E.S., 1991. Simultaneous determination of the cation exchange capacity and the exchangeable cations on marl. *Clay Minerals* 26, 567–570.

- Dakshinamurti, C., Bhavanarayana, M., 1982. An isoconductivity method for determining the cation exchange capacity of soils and clays. *Catena* 9, 175–179.
- Eberl, D.D., 1980. Alkali cation selectivity and fixation by clay minerals. *Clays and Clay Minerals* 28, 161–172.
- El-Batouti, M., Sadek, O.M., Assaad, F.F., 2003. Kinetics and thermodynamic studies of copper exchange on Na-montmorillonite clay mineral. *Journal of Colloid and Interface Science* 259, 223–227.
- Ferris, A.P., Jepson, W.B., 1975. The exchange capacities of kaolinite and the preparation of homoionic clays. *Journal of Colloid and Interface Science* 51, 245–259.
- Fletcher, P., Sposito, G., 1989. The chemical modelling of clay–electrolyte interactions for montmorillonite. *Clay Minerals* 24, 375–391.
- Fox, R.L., 1980. Soils with variable charge: agronomic and fertility aspects. In: Theng, B.K.G. (Ed.), *Soils with Variable Charge*. New Zealand Society of Soil Science, Lower Hutt, pp. 195–224.
- Francis, C.W., Grigal, D.F., 1971. A rapid and simple procedure using Sr 85 for determining cation exchange capacities of soils and clays. *Soil Science* 112, 17–21.
- Fraser, A.R., Russell, J.D., 1969. A spectrophotometric method for determination of cation exchange capacity of clay minerals. *Clay Minerals* 8, 229–230.
- Gast, R.G., 1972. Alkali metal exchange on Chambers montmorillonite. *Soil Science Society of America Proceedings* 36, 14–19.
- Gast, R.G., 1977. Surface and colloid chemistry. In: Dixon, J.B., Weed, S.B. (Eds.), *Minerals in Soil Environments*. Soil Science Society of America, Madison, WI, pp. 27–73.
- Gast, R.G., Klobe, D., 1971. Sodium–lithium exchange equilibria on vermiculite at 25 °C and 50 °C. *Clays and Clay Minerals* 19, 311–319.
- Gillmann, G.P., Bruce, R.C., Davey, B.G., Kimble, J.M., Searle, P.L., Skjemstad, J.O., 1983. A comparison of methods used for determination of cation exchange capacity. *Communications in Soil Science and Plant Analysis* 14, 1005–1014.
- Glaeser, R., 1946. Détermination de la capacité d'échange de base dans la montmorillonite. *Comptes Rendus de l'Académie des Sciences, Paris*, vol. 222, pp. 1179–1181.
- Goldberg, S., 1992. Use of surface complexation models in soil chemical systems. *Advances in Agronomy* 47, 233–329.
- Goulding, K.W.T., Talibudeen, O., 1980. Heterogeneity of cation-exchange sites for K–Ca exchange in aluminosilicates. *Journal of Colloid and Interface Science* 78, 15–24.
- Greenhill, N.B., Peverill, K.I., 1977. Determination of cation exchange capacity of soils using ammonia and chloride electrodes. *Communications in Soil Science and Plant Analysis* 8, 579–589.
- Grim, R.E., 1968. *Clay Mineralogy*, 2nd edition. McGraw-Hill, New York.
- Hang, P.T., Brindley, G.W., 1970. Methylene blue adsorption by clay minerals. Determination of surface areas and cation exchange capacities (Clay—organic studies XVIII). *Clays and Clay Minerals* 18, 203–212.
- Hanna, M.T., Zaghloul, A.A., El-Batouti, M., El-Shazly, S.A., 1995. Solvent effect on the kinetics of the exchange of copper ions on Na-montmorillonite. *Journal of Colloid and Interface Science* 176, 418–421.
- Hillier, S., Clayton, T., 1992. Cation exchange ‘staining’ of clay minerals in thin-section for electron microscopy. *Clay Minerals* 27, 379–384.
- Hirsch, D., Nir, S., Banin, A., 1989. Prediction of cadmium complexation in solution and adsorption to montmorillonite. *Soil Science Society of America Journal* 53, 716–721.



- Hissink, D.J., 1924. Base exchange in soils. *Transactions of the Faraday Society* 20, 550–566.
- Inoue, A., Minato, H., 1979. Ca–K exchange reaction and interstratification in montmorillonite. *Clays and Clay Minerals* 27, 393–401.
- Ioannou, A., Dimirkou, A., 1997. Phosphate adsorption on hematite, kaolinite, and kaolinite-hematite systems as described by a constant capacitance model. *Journal of Colloid and Interface Science* 192, 119–128.
- Janek, M., Lagaly, G., 2003. Interaction of a cationic surfactant with bentonite: a colloid chemistry study. *Colloid and Polymer Science* 281, 293–301.
- Jasmund, K., Lagaly, G. (Eds.), 1993, *Tonminerale und Tone. Struktur, Eigenschaften, Anwendung und Einsatz in Industrie und Umwelt*. Steinkopff Verlag, Darmstadt.
- Johnson, S.W., 1859. On some points of agricultural science. *American Journal of Science and Arts, Series 2* 28, 71–85.
- Kahr, G., Madsen, F.T., 1995. Determination of the cation exchange capacity and the surface area of bentonite, illite and kaolinite by methylene blue adsorption. *Applied Clay Science* 9, 327–336.
- Kjellander, R., 1996. Ion–ion correlations and effective charges in electrolyte and macroion systems. *Berichte der Bunsengesellschaft für Physikalische Chemie* 100, 894–904.
- Klobe, W.D., Gast, R.G., 1967. Reactions affecting cation exchange kinetics in vermiculite. *Soil Science Society of America Proceedings* 31, 744–749.
- Kodama, H., Ross, G.J., Toshimichi, J., Robert, J.W., 1974. Effect of layer charge location on potassium exchange and hydration of mica. *American Mineralogist* 59, 491–495.
- Kodama, T., Komarneni, S., 1999. Na-4-mica:  $\text{Cd}^{2+}$ ,  $\text{Ni}^{2+}$ ,  $\text{Co}^{2+}$ ,  $\text{Mn}^{2+}$ , and  $\text{Zn}^{2+}$  ion exchange. *Journal of Materials Chemistry* 9, 533–539.
- Kónya, J., Nagy, N.M., 1998. The effect of complexing-forming agent (EDTA) on the exchange of manganese ions on calcium-montmorillonite I. Reaction scheme and calcium–montmorillonite– $\text{Na}_2\text{EDTA}$  system. *Colloids and Surfaces A* 136, 299–310.
- Kónya, J., Nagy, N.M., Király, R., Gelencsér, J., 1998. The effect of complexing-forming agent (EDTA) on the exchange of manganese ions on calcium-montmorillonite II. Calcium–montmorillonite– $\text{Mn}(\text{ClO}_4)_2$ – $\text{Na}_2\text{EDTA}$  system. *Colloids and Surfaces* 136, 311–319.
- Köster, H.M., Kohler, E.E., Krahel, J., Kröger, J., Vogt, K., 1973. Veränderungen am Montmorillonit durch Einwirkung von 0,1 m  $\text{AeDTE}$ -Lösungen, 1 n  $\text{NaCl}$ -Lösung und 0.1 n Salzsäure. *Neues Jahrbuch Mineralogische Abhandlungen* 119, 83–100.
- Kraepiel, A.M.L., Keller, K., Morel, F.M.M., 1999. A model for metal ion adsorption on montmorillonite. *Journal of Colloid and Interface Science* 210, 43–54.
- Lagaly, G., 1981. Characterization of clays by organic compounds. *Clay Minerals* 16, 1–21.
- Lagaly, G., 1994. Layer charge determination by alkylammonium ions. In: Mermut, A.R. (Ed.), *Layer Charge Characteristics of 2:1 Silicate Clay Minerals. CMS Workshop Lectures*, vol. 6. The Clay Minerals Society, Boulder, CO, pp. 1–46.
- Laudelout, H., van Bladel, R., Bolt, G.H., Page, A.L., 1968. Thermodynamics of heterovalent cation exchange reactions in a montmorillonite clay. *Transactions of the Faraday Society* 64, 1477–1488.
- Mackenzie, R.C., 1951. A micromethod for determination of cation exchange capacity of clay. *Journal of Colloid Science* 6, 219–221.
- Maes, A., Cremers, A., 1977. Charge density effects in ion exchange, part I—heterovalent exchange equilibria. *Journal of the Chemical Society, Faraday Transactions I* 73, 1807–1814.

- Maes, A., Rasquin, E., Cremers, A., 1982. Thermodynamic study of the influence of complexation on exchange equilibria in Wyoming bentonite clay. *Journal of the Chemical Society, Faraday Transactions I* 78, 2041–2049.
- Maes, A., Verheyden, D., Cremers, A., 1985. Formation of highly selective cesium-exchange sites in montmorillonite. *Clays and Clay Minerals* 33, 251–257.
- Malcolm, R.L., Kennedy, V.C., 1969. Rate of cation exchange on clay minerals as determined by specific ion electrode techniques. *Soil Science Society of America Proceedings* 33, 247–253.
- Manning, B.A., Goldberg, S., 1996. Modeling arsenate competitive adsorption on kaolinite, montmorillonite and illite. *Clays and Clay Minerals* 44, 609–623.
- Martin, I., 1969. Mesure des capacités d'échange par l'éthylène diamine et les ions complexes de l'éthylène. *Comptes Rendus de l'Académie des Sciences, Paris*, vol. 269, pp. 815–818.
- Martin, I., Glaeser, R., 1960. Fixation des ions cobaltihexamines par les montmorillonites acides. *Bulletin du Groupe Français des Argiles* 12, 83–88.
- Margulies, L., Rozen, H., Nir, S., 1988. Model for competitive adsorption of organic cations on clays. *Clays and Clay Minerals* 36, b270–b276.
- Martin, H., Laudelout, H., 1963. Thermodynamique de l'échange des cations alcalins dans les argiles. *Journal de Chimie Physique*, 1086–1099.
- McBride, M., 1979. An interpretation of cation selectivity variations in  $M^+ - M^+$  exchange on clays. *Clays and Clay Minerals* 27, 417–422.
- Meier, L., Kahr, G., 1999. Determination of cation exchange capacity (CEC) of clay minerals using the complexes of copper (II) ion with triethylenetetramine and tetraethylenepentamine. *Clays and Clay Minerals* 47, 386–388.
- Mortland, M.M., Mellor, J.L., 1954. Conductimetric titration of soils for cation exchange capacity. *Soil Science Society of America Proceedings* 18, 363–364.
- Muljadi, D., Posner, A.M., Quirk, J.P., 1966a. The mechanism of phosphate adsorption by kaolinite, gibbsite, and pseudoboehmite. Part I. The isotherms and the effect of pH on adsorption. *Journal of Soil Science* 17, 212–229.
- Muljadi, D., Posner, A.M., Quirk, J.P., 1966b. The mechanism of phosphate adsorption by kaolinite, gibbsite, and pseudoboehmite. Part II. The location of the adsorption sites. *Journal of Soil Science* 17, 230–237.
- Muljadi, D., Posner, A.M., Quirk, J.P., 1966c. The mechanism of phosphate adsorption by kaolinite, gibbsite, and pseudoboehmite. Part III. The effect of temperature on adsorption. *Journal of Soil Science* 17, 238–247.
- Nagy, N.M., Kónya, J., 1988. The interfacial processes between calcium-bentonite and zinc ion. *Colloids and Surfaces* 32, 223–235.
- Nir, S., Hirsch, D., Navrot, J., Banin, A., 1986. Specific adsorption of lithium, sodium, potassium, and strontium to montmorillonite: observations and predictions. *Soil Science Society of America Journal* 50, 40–45.
- Nir, S., Rytwo, G., Yermiyahu, U., Margulies, L., 1994. A model for cation adsorption to clays and membranes. *Colloid and Polymer Science* 272, 619–632.
- Parfitt, R.L., 1978. Anion adsorption by soils and soil materials. *Advances in Agronomy* 30, 1–50.
- Peech, M., 1945. Determination of exchangeable cations and exchange capacity of soils. *Soil Science* 59, 25.
- Pleysier, J., Janssens, J., Cremers, A., 1986. A clay suspension stability end point titration method for measuring cation exchange capacity of soils. *Soil Science Society of America Journal* 50, 887–891.

- Pleysier, J., Juo, A.S.R., 1980. A single extraction method using silver-thiourea for measuring exchangeable cations and effective CEC in soils with variable charges. *Soil Science* 129, 205–211.
- Quirk, J.P., 2001. The significance of the threshold and turbidity concentrations in relation to sodicity and microstructure. *Australian Journal of Soil Research* 39, 1185–1217.
- Rao, K.P.C., Krishna Murti, G.S.R., 1987. Influence of noncrystalline material on phosphate adsorption by kaolin and bentonite clays. In: Schultz, L.G., van Olphen, H., Mumpton, F.A. (Eds.), *Proceedings of the International Clay Conference, Denver 1985*. The Clay Minerals Society, Bloomington, IN, pp. 179–185.
- Reichenbach, H., Graf von, 1973. Exchange equilibria of interlayer cations in different particle size fractions of biotite and phlogopite. In: Serratos, J.M. (Ed.), *Proceedings of the International Clay Conference, Madrid 1972*. Division de Ciencias, CSIC, Madrid, pp. 457–466.
- Reichenbach, H., Graf von, Rich, C.I., 1969. Potassium release from muscovite as influenced by particle size. *Clays and Clay Minerals* 17, 23–29.
- Rhodes, C.N., Brown, D.R., 1994. Rapid determination of the cation exchange capacity of clays using Co(II). *Clay Minerals* 29, 799–801.
- Rytwo, G., Banin, A., Nir, S., 1996. Exchange reactions in the Ca–Mg–Na–montmorillonite system. *Clays and Clay Minerals* 44, 276–285.
- Rytwo, G., Serban, C., Nir, S., Margulies, L., 1991. Use of methylene blue and crystal violet for the determination of exchangeable cations in montmorillonite. *Clays and Clay Minerals* 39, 551–555.
- Sawhney, B.L., 1972. Selective sorption and fixation of cations by clay minerals: a review. *Clays and Clay Minerals* 20, 93–100.
- Schlegel, M.L., Charlet, L., Manceau, A., 1999b. Sorption of metal ions on clay minerals II. Mechanism of Co sorption on hectorite at high and low ionic strength and impact on the sorbent stability. *Journal of Colloid and Interface Science* 220, 392–405.
- Schlegel, M.L., Manceau, A., Chateigner, D., Charlet, L., 1999a. Sorption of metal ions on clay minerals I. Polarized EXAFS evidence for the adsorption of Co on the edges of hectorite particles. *Journal of Colloid and Interface Science* 215, 140–158.
- Schofield, R.K., Samson, H.R., 1954. Flocculation of kaolinite due to the attraction of oppositely charge crystal faces. *Discussions of the Faraday Society* 18, 135–145.
- Schwertmann, U., 1962. Die selektive Kationenadsorption der Tonfraktion einiger Böden aus Sedimenten. *Zeitschrift für Pflanzenernährung und Bodenkunde* 97, 9–25.
- Scott, A.D., Ismail, F.T., Locaties, R.R., 1973. Changes in interlayer potassium exchangeability induced by heating micas. In: Serratos, J.M. (Ed.), *Proceedings of the International Clay Conference, Madrid, 1972*. Division de Ciencias, CSIC, Madrid, pp. 467–479.
- Searle, P.L., 1986. The measurement of soil cation exchange properties using the single extraction, silver thiourea method: an evaluation using a range of New Zealand soils. *Australian Journal of Soil Research* 24, 193–200.
- Shainberg, I., Alperovitch, N.I., Keren, R., 1987. Charge density and Na–K–Ca exchange on smectites. *Clays and Clay Minerals* 35, 68–73.
- Siantar, D., Fripiat, J.J., 1995. Lead retention and complexation in a magnesium smectite (hectorite). *Journal of Colloid and Interface Science* 169, 400–407.
- Staunton, S., Rouboud, M., 1997. Adsorption of  $^{137}\text{Cs}$  on montmorillonite and illite: effect of charge compensating cation, ionic strength, concentration of Cs, K and fulvic acid. *Clays and Clay Minerals* 45, 251–260.

- Strawn, D., Sparks, D.L., 1999. The use of XAFS to distinguish between inner- and outer-sphere lead adsorption complexes on montmorillonite. *Journal of Colloid and Interface Science* 216, 257–269.
- Theng, B.K.G., Greenland, D.J., Quirk, J.P., 1967. Adsorption of alkylammonium cations by montmorillonite. *Clay Minerals* 7, 1–17.
- Theng, B.K.G., Russell, M., Churchman, G.J., Parfitt, R.L., 1982. Surface properties of allophane, halloysite, and imogolite. *Clays and Clay Minerals* 30, 143–149.
- Thomson, H.S., 1850. On the adsorbent power of soils. *Journal of the Royal Agricultural Society of England* 11, 68–74.
- Tournassat, C., Ferrage, E., Poinçon, C., Charlet, L., 2004. The titration of clay minerals II. Structure-based model and implications for clay reactivity. *Journal of Colloid and Interface Science* 273, 234–246.
- van Bemmelen, J.M., 1888. Über die Absorptionsverbindungen und das Absorptionsvermögen der Ackererde. *Landwirtschaftliche Versuchsstation* 35, 69–136.
- van Olphen, H., 1951a. A tentative method for determination of the base exchange capacity of small samples of clay minerals. *Clay Minerals Bulletin* 1, 169–170.
- van Olphen, H., 1951b. Rheological phenomena of clay sols in connection with the charge distribution on the micelles (sic!). *Discussions of the Faraday Society* 11, 82–84.
- van Olphen, H., 1977. *An Introduction to Clay Colloid Chemistry*, 2nd edition. Wiley, New York.
- van Olphen, H., Fripiat, J.J., 1979. *Data Handbook for Clay Materials and other Non-metallic Minerals*. Pergamon Press, Oxford.
- Verburg, K., Baveye, P., 1994. Hysteresis in the binary exchange of cations on 2:1 clay minerals: a critical review. *Clays and Clay Minerals* 42, 207–220.
- Violante, A., Pigna, M., 2002. Competitive sorption of arsenate and phosphate on different clay minerals and soils. *Soil Science Society of America Journal* 66, 1788–1796.
- Way, J.T., 1852. On the power of soils to absorb (sic!) manure. *Journal of the Royal Agricultural Society of England* 13, 123–143.
- Weiss, A., 1958a. Über das Kationenaustauschvermögen der Tonminerale. I. Vergleich der Untersuchungsmethoden. *Zeitschrift für Anorganische und Allgemeine Chemie* 297, 232–256.
- Weiss, A., 1958b. Über das Kationenaustauschvermögen der Tonminerale. II. Kationenaustausch bei den Mineralen der Glimmer-, Vermiculit- und Montmorillonitgruppe. *Zeitschrift für Anorganische und Allgemeine Chemie* 297, 257–286.
- Weiss, A., 1958c. Über äquimolaren Kationenaustausch bei niedrig geladenen Ionenaustauschern. *Kolloid-Zeitschrift* 158, 22–28.
- Weiss, A., Mehler, A., Koch, G., Hofmann, U., 1956. Über das Anionenaustauschvermögen der Tonminerale. *Zeitschrift für Anorganische und Allgemeine Chemie* 284, 247–271.
- Wendelbo, R., Rosenqvist, I.T., 1987. Effects of anion adsorption on mechanical properties of clay–water systems. In: Schultz, L.G., van Olphen, H., Mumpton, F.A. (Eds.), *Proceedings of the International Clay Conference, Denver 1985*. The Clay Minerals Society, Bloomington, IN, pp. 422–426.
- Xu, S., Harsh, J.B., 1992. Alkali cation selectivity and surface charge of 2:1 clay minerals. *Clays and Clay Minerals* 40, 567–574.

This page intentionally left blank

*Chapter 12.11*

## THERMAL ANALYSIS

F. ROUQUEROL, J. ROUQUEROL AND P.L. LLEWELLYN

*Laboratoire MADIREL, UMR CNRS-Université de Provence Centre de St Jérôme,  
13397 Marseille Cedex 20, France*

### 12.11.1. BACKGROUND AND DEVELOPMENT

Clays were among the first materials to be studied by thermal analysis following the development of this technique toward the end of the 19th century ([Le Chatelier, 1887](#)). In general terms, thermal analysis embraces any technique where a physical property of the material in question is assessed as a function of temperature. This is illustrated in [Fig. 12.11.1](#) where property “X” (e.g., mass, temperature difference, length, flow of evolved gas) is plotted against temperature.

In his famous work, entitled “About the action of heat on clays”, Henri [Le Chatelier \(1887\)](#), a professor at the School of Mines in Paris, applied two of his newly invented thermal analytical methods to the study of clays. The first invention was the Pt/(Pt,10%Rh) thermocouple (still a standard, more than a century later), while the second was a special photographic recording method. In this method the temperature reached by the sample (proportional to the distance from the origin of the recording) and the actual rate of heating (as influenced by self-cooling of the sample) are simultaneously recorded. This is deduced from the appearance of a spark, at 2-second intervals, in the form of a small bar on a photographic plate ([Fig. 12.11.2](#)). When an endothermic phenomenon occurs, the actual heating rate of the sample decreases causing the density of the bars to increase. Thus, the physical property assessed by [Le Chatelier \(1887\)](#) was the self-cooling of the sample vs its temperature. This was the first automatic recording of a thermal analysis experiment on clays.

Equally interesting were the reasons that Le Chatelier put forward to justify his choice of clays for the experiment: “the hydrated aluminium silicates (clays, kaolins, etc ...) ... generally form mixtures too complex for chemical analysis to furnish any precise data on their structure. I have thought that in studying the temperature of dehydration of these substances, one could perhaps begin to characterise a small number of chemical species and to distinguish the presence of each of these in various mixtures. If one rapidly heats a small quantity of clay, there is produced, at

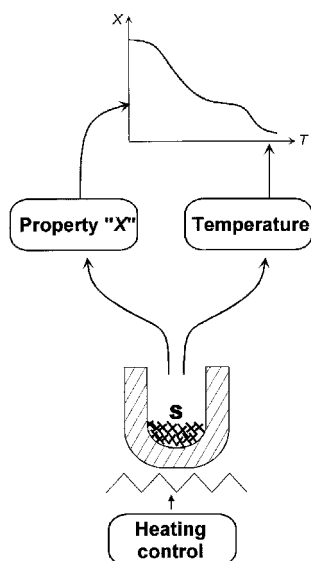


Fig. 12.11.1. Principle of thermal analysis in general (Rouquerol, 2003).

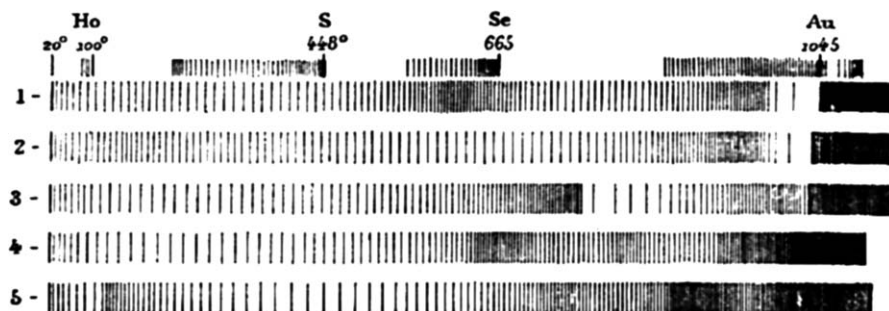


Fig. 12.11.2. Original thermal analysis traces of Le Chatelier for (1) halloysite, (2) allophane, (3) kaolin, (4) pyrophyllite, (5) montmorillonite. The short traces on top were used for temperature calibration after the boiling point of water (Ho), sulphur (S) or selenium (Se) or after the melting point of gold (Au).

the moment of dehydration, a deceleration in the temperature rise (elevation); this point of arrest can be used to establish a distinction among the various hydrated aluminium silicates. The comparison of observations carried out on a very large number of clays, shows that the complexity of these substances is much less than one would have originally been led to believe" (quoted from the full English translation by Wendlandt and Collins (1976). From these very first experiments Le Chatelier (1887) concluded: "The clays could now be classified, according to their pyrogenous decomposition, in five distinct categories".

The next step, taken at a much later date, was to relate the thermal behaviour of clays to their crystalline structure. [Caillère and Hénin \(1948\)](#) discussed the temperatures of dehydration (an endothermic phenomenon), dehydroxylation (also endothermic) and recrystallisation (exothermic) in relation to the structures and chemical compositions of a large set of phyllosilicates and fibrous clay minerals. Given the marked effect of impurities on the differential thermal analysis (DTA) patterns, [Caillère and Hénin \(1948\)](#) further suggested that DTA may provide a simple means of tracing the origin of a natural sample. It was not until the late 1950s, however, that DTA became an important tool for clay mineral identification. Structural studies, indicating the location of water and hydroxyls (as described below for simple phyllosilicates) provided insight into the dehydration behaviour of clay minerals ([Mackenzie, 1970](#)).

[Földvari \(1991\)](#) gave a comprehensive description of all types of water in minerals (and especially clay minerals) that can be assessed by thermal analysis. A first great distinction can be made between the water that occurs (i) as molecular water, and (ii) as hydroxyls capable of condensing into water during thermal analysis. ‘Molecular water’ can exist as interlayer water (in smectites, this water is stabilized by the presence of exchangeable cations), as zeolitic water (in mordenite and sepiolite) in cavities or channels, as water adsorbed on the external surface of clay minerals, or as water formed by capillary condensation in large pores (in chrysotile). Most of these types of water can be removed by heating at temperatures  $< 100^{\circ}\text{C}$  and the initial amount largely depends on ambient conditions of humidity and temperature. Hydroxyls are part of the clay structure and cannot be released without causing more or less irreversible structural modifications. Hydroxyls make up what is often called ‘constitutional water’. This term, however, may lead to misunderstanding because hydroxyls can only become water through condensation. In phyllosilicates, these hydroxyls are usually bound to the structure by ionic or covalent bonds. Since hydroxyls have a broad bond energy distribution (due to the different locations in the structure), and their diffusion between sheets or in channels can be hindered in different ways, hydroxyls are liberated over a very broad temperature range (between  $150$  and  $1000^{\circ}\text{C}$ ). This phenomenon is precisely what makes the thermal analysis of clay minerals so interesting. At the same time, water and hydroxyls can serve as probes to differentiate clay minerals.

Before discussing some results on the thermal analysis of clay minerals, we will briefly describe the main techniques available and the two basic modes of operation, namely, ‘temperature-controlled thermal analysis’ and ‘sample-controlled thermal analysis’.

## 12.11.2. TEMPERATURE-CONTROLLED (CONVENTIONAL) THERMAL ANALYSIS

More than 95% of the thermal analysis work on clay minerals is carried out using techniques where the temperature programme of the furnace (or, sometimes, the sample) is selected and imposed by the experimenter. This ‘temperature-controlled’ or



'conventional' thermal analysis is schematically shown in Fig. 12.11.3. Here the heating control loop makes use of the temperature of the sample or furnace (together with the measurement of elapsed time, in order to get a temperature programme). More often than not the programme is linear, that is, a constant heating rate is imposed.

In the case of clay minerals, the property "X" refers, first of all, to the temperature difference ( $\Delta T$ ) between one point in/close to the sample and another point in/close to an inert reference (Fig. 12.11.4).

Following Le Chatelier (1887), such an experiment measures the self-cooling or self-heating of the sample but with the added benefit of having a permanent comparison

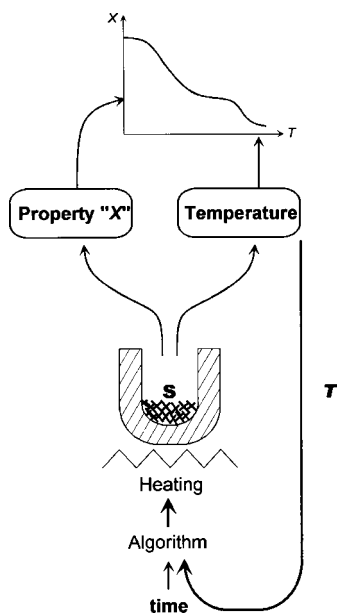


Fig. 12.11.3. Principle of conventional or "temperature-controlled" thermal analysis (Rouquerol, 2003).

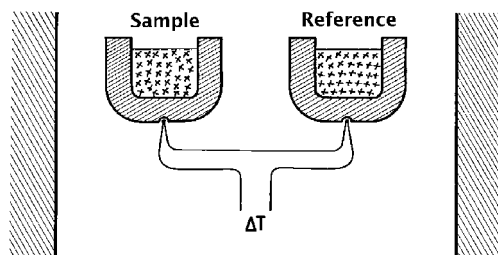


Fig. 12.11.4. Principle of DTA.

between the 'sample temperature' and the 'reference temperature'. This arrangement was due to [Roberts-Austen \(1899\)](#), a chemist at the Royal Mint, London, and later named 'Differential Thermal Analysis' (DTA). The reference temperature would be similar to that of the sample if it did not undergo any thermal transformation. Since the temperature difference is usually smaller than 10 K, this can be the full scale of the recorder and small thermal events may be detected with great sensitivity. These events can be endothermic (usually corresponding to water losses) or exothermic (usually reflecting structural rearrangements). Let us stress that maximum sensitivity, in DTA, is obtained at maximum heating rates (typically between 5 and 20 K/min).

For quantitative thermal analysis, 'Differential Scanning Calorimetry' (DSC) is by principle superior to DTA since the former method not only determines the temperature of transformation but also the corresponding heat. Nevertheless, DSC has two drawbacks: (i) the upper temperature (typically between 600 and 850 °C) is lower than that obtainable by DTA ( $\geq 1000$  °C); and (ii) the energy of dehydroxylation is not a constant (being dependent on the type of bond), and hence, no simple relationship exists between the amount of heat absorbed and the amount of water released.

The latter limitation is overcome by 'Thermogravimetry' (TG) where the quantity measured is the sample mass. Here the mass of water evolved and thus its amount is precisely measured irrespective of bonding mode. TG also allows slow heating rates to be selected but unlike the situation with DTA or DSC, these conditions do not diminish the sensitivity or accuracy of the experiment.

At first sight the combination of DTA with TG, available in a number of modern instruments, is attractive. However, good critical judgment is required for interpreting the results. This is because, the two techniques may not reveal the same thing although the measurements are done simultaneously. For example, a mass loss (due to the release of water vapour from the upper part of the sample) can be detected few minutes before the self-cooling wave reached the DTA thermocouple in the bottom of the crucible. Further, the best sample arrangement for thermogravimetry is a thin layer of powder, whereas the best one for DTA is a heap around or above the thermocouple. Thus, both experiments cannot simultaneously be at their best.

A fourth thermal analysis technique, called 'Thermodilatometry', is well suited for investigating the sintering and firing behaviour of clay minerals. Here the quantity "X" refers to the length or volume of the sample. Indeed, thermogravimetry is not very useful above 800 °C because the residual water constitutes only a few per cent of the initial quantity. On the other hand, thermodilatometry can readily detect the dimensional changes due to sintering that occur at these temperatures.

For a given sample the temperature at which specific thermal phenomena occur (as detected by DTA, DSC or TG) is well defined and reproducible, provided the experimental procedure is very carefully defined. This means that any change in sample mass/shape/size, crucible cover, location of the two thermocouples, atmosphere (sample preconditioning), or heating rate is able to modify the resulting DTA, DSC or TG curve. For this reason, one cannot speak of 'standard' temperatures for the various DTA peaks or TG steps. Nor can a DTA or TG curve be

reproduced by someone else if the above experimental variables are not specified. On the other hand, highly reproducible and well-resolved DTA or TG patterns, can be obtained speedily (often within <1 h) if the same experimental procedure is always used. The latter point is sufficient reason for using these thermal analytical techniques to compare, screen, and check natural clays and clay minerals. We should also add that although the peak/step temperatures are strongly dependent on heating rate (temperature shifts as high as 100 K are observed when the heating rate drops from 10 to 0.5 K/min), the general shape of a DTA or TG curve, with its peaks or steps, is quite specific to, and hence, can serve as a fingerprint of a given clay. Another noteworthy feature of thermal analysis is that it provides a continuous trace of the temperature-induced transformation. By contrast, spectroscopic techniques commonly used to assess and interpret structural and surface modifications provide a discontinuous analysis of selected states of the sample.

### 12.11.3. SAMPLE-CONTROLLED THERMAL ANALYSIS

The limitations of DTA, DSC and TG, arising from the large dependence of the recordings on experimental details, also apply to most other conventional, temperature-controlled thermal analysis techniques. The main problem stems from the existence of (i) temperature gradients enhanced by the self-cooling of the sample on dehydration, and (ii) pressure gradients produced within the sample by the release of water vapour. Since these two types of gradients are directly related to the rate of thermolysis, it is desirable to control and limit this rate.

The left-hand scheme in Fig. 12.11.5 shows the simplest and most straightforward manner to achieve this end. By exclusively using the physical quantity “X” (sample mass, length, enthalpy, gas evolved etc.), which is directly related to the rate or extent of thermal transformation, heating of the sample is controlled in such a way as to keep the reaction rate at the desired level. The procedure is therefore, referred to as ‘Controlled transformation Rate Thermal Analysis’ (CRTA).

The right-hand scheme in Fig. 12.11.5 represents the generalised principle of what is now called ‘Sample-Controlled Thermal Analysis’ (SCTA) which includes CRTA, the most ancient and most developed form. SCTA also opens the possibility of using a more complex heating control device, where the temperature (T) of the sample can play a part. In any SCTA experiment, the ‘X loop’ (i.e., the use of a feedback from the sample) is compulsory whereas the ‘T-loop’ is only supplementary and optional.

As we shall illustrate by a few examples later on, the SCTA approach proved to be extremely rewarding for analytical purposes (enhanced resolution and separation due to the control of temperature and pressure gradients), preparative purposes (homogeneity of the final product) and kinetic purposes (sample temperature and its rate of transformation can be accurately measured, while the latter parameter can be modulated).

This principle of SCTA was successfully applied to ‘Evolved Gas Detection’ (Rouquerol, 1964), ‘Thermogravimetry’ (Erdey et al., 1965) and ‘Thermodilatometry’

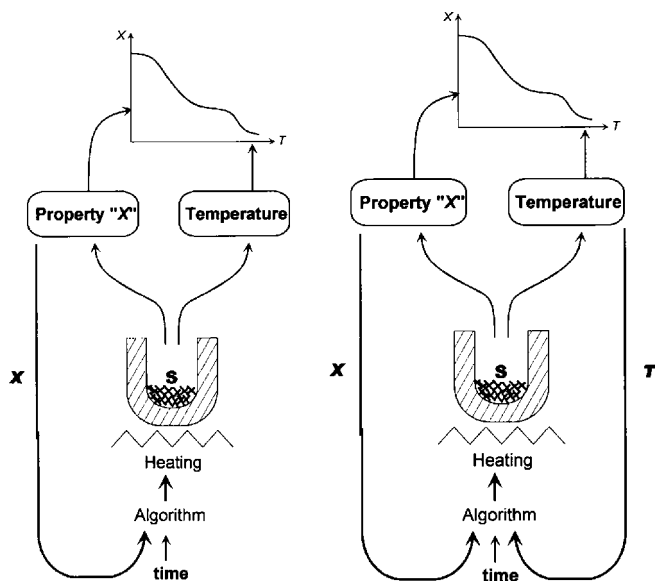


Fig. 12.11.5. Principle of Controlled Rate Thermal Analysis (CRTA, left), a part of the more general method of Sample-Controlled Thermal Analysis (SCTA, right) where, nevertheless, only the “X loop” is compulsory, not the “T loop” (Rouquerol, 2003).

(Palmour and Johnson, 1967). The latter two approaches were subsequently developed by Sørensen (1978) who devised a special heating procedure called ‘Stepwise Isothermal Analysis’ (SIA). Here isothermal sections are combined with constant heating rate sections in such a way as to keep the rate of mass loss or of sintering between two pre-determined values. This is to combine the interest of an approximately controlled rate of dehydration or sintering and that of an easy kinetic processing of the isothermal steps by relatively standard equations.

Fig. 12.11.6 shows the principle by which the thermal behaviour of clay minerals may be studied incorporating the three improvements indicated above (analytical, preparative and kinetic) (Rouquerol, 1970), using the technique of ‘Controlled Rate Evolved Gas Detection’ (CR-EGD).

Here, the clay mineral sample is placed on the bottom of a fused silica bulb and is permanently evacuated through a diaphragm, D. Any water vapour released by sample causes an increase in the residual pressure (or “vacuum”) above the sample, and therefore, a small pressure drop through the diaphragm. The heating control is set so as to maintain a constant rate of water vapour release from the clay mineral; this is obtained by keeping the pressure drop through the diaphragm constant, and therefore, by simply keeping constant the residual pressure above the sample (since vacuum is constant downstream). The residual pressure is measured by a vacuum gauge, G (Pirani, thermocouple or Penning gauge, or capacitance manometer) whose

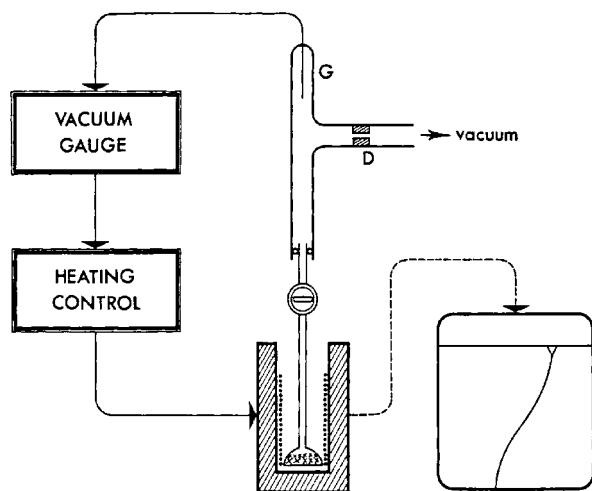


Fig. 12.11.6. Principle of a simple set-up of Controlled Rate Evolved Gas Detection (CR-EGD) operating with continuous evacuation (Rouquerol, 1970).

signal directly feeds the heating control of the furnace (instead of the usual temperature signal provided by a thermocouple or a resistance thermometer). As it will be seen, this set up is used by several authors for the study of clay minerals.

Another set-up is that of the Constant Rate Thermogravimetry (CR-TG) proposed by Paulik and Paulik (1971) under the name of “Quasi-Isothermal, Quasi-Isobaric Derivatography” and specially used by Földvari (1991) for the studies of clay minerals. The set-up consists of a thermobalance operating at atmospheric pressure, and controlled in the CRTA mode by feeding the heating control of the furnace with the derivative  $dm/dt$  of the mass signal.

#### 12.11.4. APPLICATION OF THERMAL ANALYSIS TO CLAYS

Our aim is not to provide a comprehensive summary of the literature on the thermal analysis of clay minerals; rather, we will describe the most promising techniques and approaches for future work in this field. In particular, we will show what can be obtained with careful control of the experimental conditions, i.e., with Sample-Controlled Thermal Analysis. With the help of microprocessors and microcomputers, SCTA now reached an interesting state of maturity.

##### *A. Analytical Aspects*

The first objective of a good thermal analysis experiment is of course to separate as much as possible the successive steps of any thermal reaction. In the case of clay

minerals, this means separating as much as possible the steps of water evolution, i.e., separating the various types of water initially present. The improvement brought by the SCTA approach is illustrated in Fig. 12.11.7 for a natural sepiolite from Vallecas (Spain).

The dashed curve corresponds to a conventional TG experiment (Rautureau and Mifsud, 1977) whereas, the solid curve was obtained by Controlled Transformation Rate Evolved Gas Detection. The four steps are more clearly separated on the CR-EGD than the TG curve (Grillet et al., 1988). Step I corresponds to the desorption of zeolitic water. This is followed by the release of water molecules bound to Mg atoms exposed at layer edges in two successive steps (II and III), before final dehydroxylation of the mineral occurs (step IV).

The successive steps of the dehydroxylation of montmorillonite are also easily seen on the CR-EGD trace in Fig. 12.11.8. (Laureiro et al., 1996). The first step up to ca. 350 °C is due to water desorption from the surface of the mineral (BET surface area = 78 m<sup>2</sup>/g. The second step up to ca. 650 °C is due to dehydroxylation limited by a two-dimensional diffusion mechanism, while the last step corresponds to sintering.

The separation power of SCTA is also illustrated in Fig. 12.11.9 (Villieras et al., 1992) showing the CR-EGD curve obtained for a mixture of talc and chlorite. The dehydroxylation of chlorite apparently occurs in two separate steps (1 and 2), while talc dehydroxylates in a single step (between 800 and 1000 °C). The SCTA curve can be used to determine the proportion of chlorite and talc in the sample.

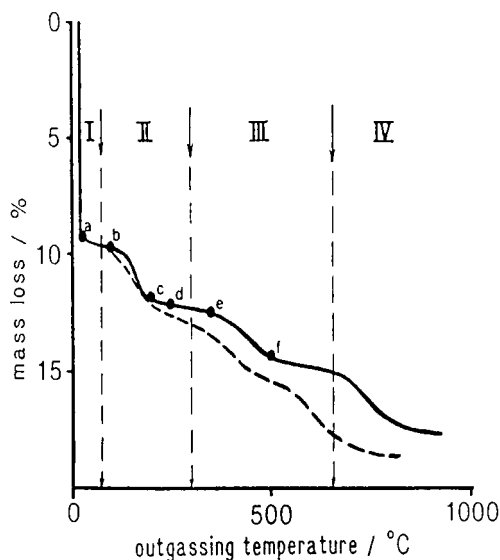


Fig. 12.11.7. CR-EGD curve of a sepiolite from Vallecas (solid curve) and corresponding conventional TG curve (dashed curve) (Grillet et al., 1988).

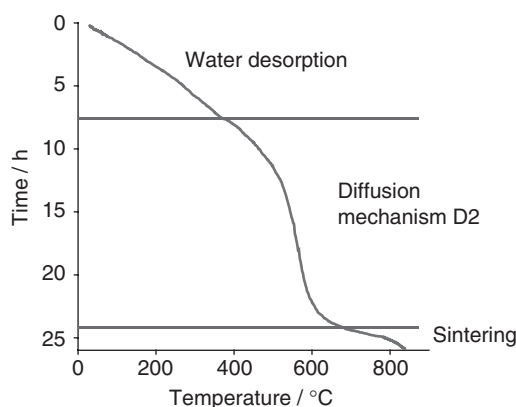


Fig. 12.11.8. CR-EGD trace for the thermolysis of montmorillonite (Laureiro et al., 1996).

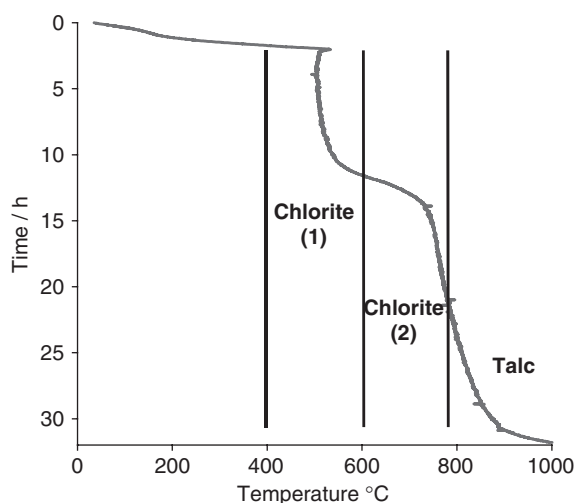


Fig. 12.11.9. CR-EGD traces for a mixture of talc with chlorite (Villieras et al., 1992).

SCTA can also be used to characterise the initial state of clay minerals and, more particularly, to distinguish between similar mineral species.

This is illustrated in Fig. 12.11.10 for two kaolinites of different origin (Dion et al., 1998). Both samples (one from Charentes, France, the other from Keokuk, UK) have the same grain size and are submitted to the same conditions of thermolysis (same rate of dehydration of  $4.5 \text{ mg h}^{-1} \text{ g}^{-1}$ , and the same residual water vapour pressure of 0.45 mbar). The large displacement of one curve from the other may be ascribed to the larger proportion of defects in the Charentes sample as compared

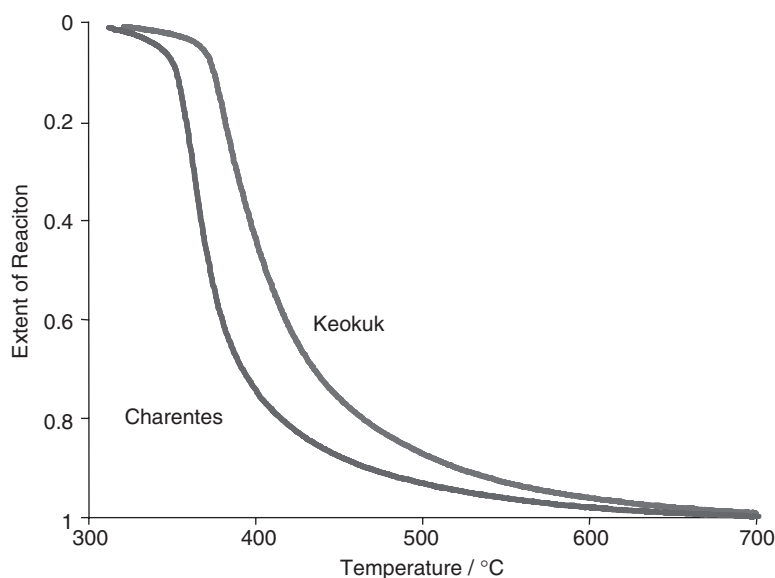


Fig. 12.11.10. CR-EGD traces for two kaolinites of different origin (Dion et al., 1998).

with the Keokuk material. These structural defects are responsible for lowering the dehydroxylation temperature.

The high resolution obtainable from a Sample-Controlled experiment allows impurities or very weak phenomena to be detected. Fig. 12.11.11 shows how the recrystallisation of metakaolinite can be detected, in a CR-EGD experiment. This event is indicated by the simple perturbation of the pressure signal. This perturbation is directly due to structural reorganisation allowing a very small amount (less than 0.1% of the initial water content) of weakly bound water to escape at that instant.

### B. Preparative Aspects

Sample-Controlled Thermal Analysis allows samples of much greater homogeneity to be prepared than is possible with standard temperature-programmed heating. This is because the rate of dehydration can be controlled at a sufficiently low level for low temperature and pressure gradients to be obtained. These conditions are required for homogeneity of the final product. This approach is indeed shown to be most efficient to control the thermal transformation corresponding to the heating of kaolinite (Dion, 1994; Massiot et al., 1995).

It is worth stressing that this SCTA approach lends itself to industrial application simply by making use of the SCTA results recorded in the laboratory with a test sample. One simply needs indeed to reproduce, in the industrial furnace, the same  $T=f(t)$  profile to ensure a controlled rate of dehydration up to the selected temperature.



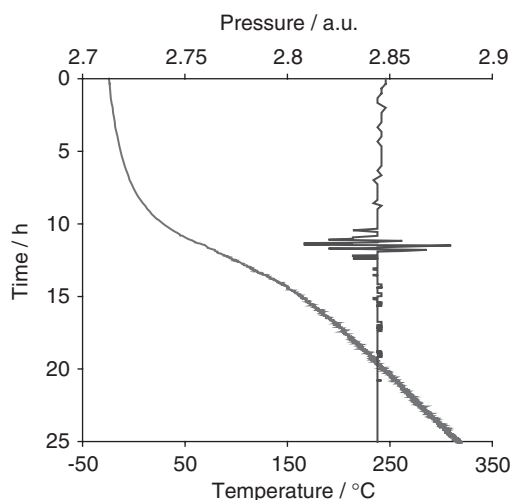


Fig. 12.11.11. CR-EGD traces (temperature trace and pressure trace with perturbations) showing transformation from kaolinite to metakaolinite (Dion, 1994).

### C. Kinetic Aspects

The major advantages of using SCTA to study the kinetics of thermolysis for a solid like a clay mineral are as follows:

- (i) the temperature gradients can be reduced at will; the single temperature sensor in good contact with the sample therefore measures a 'meaningful temperature'. This is far from being the case in conventional (constant heating rate) thermal analysis where temperature differences from 5 to 50 K are observed between different points of the sample in obtaining a DTA signal (Liptay, 1973);
- (ii) at any time during dehydration the energy of activation may be determined by the 'rate-jump method' (Rouquerol and Rouquerol, 1972). In this method, the rate of dehydration is made to swing between two values (say, in the ratio 1/3 or 1/4) and the resulting modulated  $T = f(t)$  curve is recorded (Fig. 12.11.12). Each modulation of the experiment provides a set of 2 rates of dehydration,  $r_1$  and  $r_2$  (imposed) and 2 sample temperatures,  $T_1$  and  $T_2$  (measured). During the 'rate-jump' from one temperature to the next, the state of the sample is virtually unchanged, since the experiment is usually carried out in such a way as to increase the extent of dehydration by less than 0.1%. This allows Arrhenius' law to be applied while the dependence of the rate of reaction on its extent is ignored, i.e., without assuming any  $f(x)$  law. Under these conditions, the method can be called either 'isoconversional' or 'assumptionless';
- (iii) provided the rate of dehydration is kept constant throughout the experiment, each dehydration mechanism gives rise to a specific shape of the CRTA curve, as shown in Fig. 12.11.13 (Criado et al., 1990). These curves allow the major

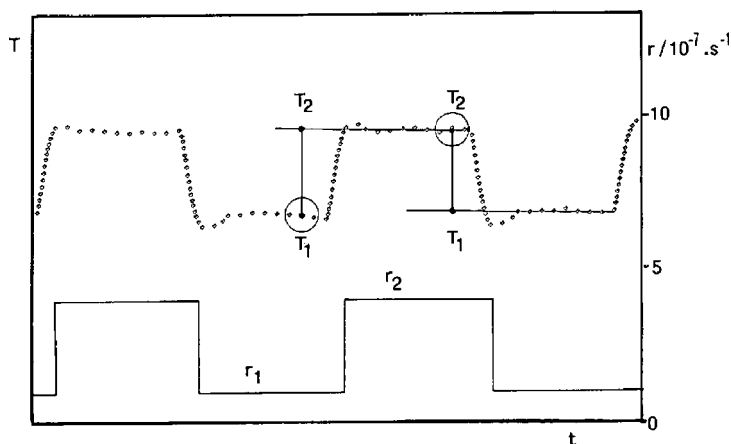


Fig. 12.11.12. Modulated  $T = f(t)$  curve as recorded when applying the rate-jump procedure to determine the activation energy.

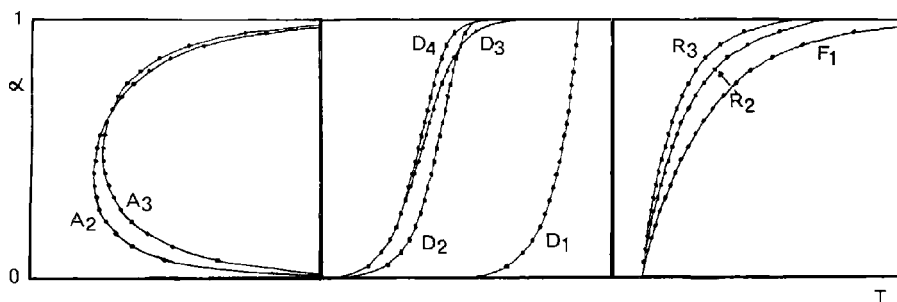


Fig. 12.11.13. Three main shapes of isokinetic curves, corresponding to different basic mechanisms (Criado et al., 1990).

mechanisms to be differentiated; that is, where the rate of the dehydration is controlled either by germination and growth of nuclei (saddle shaped, with minimum), or by diffusion (S-shaped) or by interfacial advancement (no minimum, no inflexion);

- (iv) as reaction rates can be closely controlled CRTA uniquely provides a means of passing progressively from a 'thermodynamic regime' (at very low rate of dehydration, under quasi-equilibrium conditions) to a 'kinetic regime' (at a higher rate which is controlled by heat and/or mass transport phenomena);
- (v) as CRTA can separate the successive steps in thermolysis and control the process from beginning to end, rate laws within the entire reaction domain may be established as was done for kaolinite (Nahdi et al., 2002a). This contrasts with isothermal kinetics where either the first or the final part of the reaction, or both, is skipped.

- (vi) finally, the reaction mechanism may be modelled for application to industrial heating conditions as Nahdi et al. (2002b) done for kaolinite dehydroxylation.

## REFERENCES

- Caillère, S., Hénin, S., 1948. L'analyse thermique et son interprétation. Proceedings of the International Congress on Ceramics, Paris, pp. 137–151.
- Criado, J.M., Ortega, A., Gotor, F., 1990. Correlation between the shape of controlled rate thermal analysis curves and the kinetics of solid state reactions. *Thermochimica Acta* 157, 171–179.
- Dion, P., 1994. Déshydroxylation de la kaolinite par analyse thermique à vitesse de transformation contrôlée. Etude de la métakaolinite. Ph.D. thesis. Université d'Orléans, France.
- Dion, P., Alcover, J.F., Bergaya, F., Ortega, A., Llewellyn, P., Rouquerol, F., 1998. Kinetic study by controlled transformation rate thermal analysis of the dehydroxylation of kaolinite. *Clay Minerals* 33, 269–276.
- Erdey, L., Paulik, F., Paulik, J., 1965. Device for automatic heating control of thermobalances, in the case of stepwise isothermal heating. Hungarian Patent N° 152197, registered 31 October 1962, published 1 December 1965.
- Földvari, M., 1991. Measurement of different water species in minerals by means of thermal derivatography. In: Smykatz-Kloss, W., Warne, S.St.J. (Eds.), *Thermal Analysis in the Geosciences*. Springer, Berlin, pp. 84–100.
- Grillet, Y., Cases, J.M., François, M., Rouquerol, J., Poirier, J.E., 1988. Modification of the porous structure and surface area of sepiolite under vacuum thermal treatment. *Clays and Clay Minerals* 36, 233–242.
- Laureiro, Y., Jerez, A., Rouquerol, F., Rouquerol, J., 1996. Dehydration kinetics of Wyoming montmorillonite studied by controlled transformation rate thermal analysis. *Thermochimica Acta* 278, 165–173.
- Le Chatelier, H., 1887. De l'action de la chaleur sur les argiles. *Bulletin de la Société Française de Minéralogie* 10, 204–211.
- Liptay, G., 1973. Atlas of thermoanalytical curves. Akademia Kiado, Budapest.
- Mackenzie, R.C., 1970. *Differential Thermal Analysis, Volume 1*. Academic Press, London and New York.
- Massiot, D., Dion, P., Alcover, J.F., Bergaya, F., 1995.  $^{27}\text{Al}$  and  $^{29}\text{Si}$  MAS NMR study of kaolinite thermal decomposition by controlled rate thermal analysis. *Journal American Chemical Society* 78, 2940–2944.
- Nahdi, K., Perrin, S., Pijolat, M., Rouquerol, F., Ariguib, N., Ayadi, M., 2002a. Nucleation and anisotropic growth model for isothermal kaolinite dehydroxylation under controlled water vapour pressure. *Physical Chemistry and Chemical Physics* 4, 1972–1977.
- Nahdi, K., Llewellyn, P., Rouquerol, F., Rouquerol, J., Ariguib, N.K., Ayadi, M.T., 2002b. Controlled rate thermal analysis of kaolinite dehydroxylation: effect of water vapour pressure on the mechanism. *Thermochimica Acta* 390, 123–132.
- Palmour, H., Johnson, D.R., 1967. Phenomenological model for rate-controlled sintering. In: Kuczynski, G.C., Hooton, N.A., Gibbon, C.F. (Eds.), *Sintering and Related Phenomena*. Gordon and Breach, New York, p. 779.

- Paulik, J., Paulik, F., 1971. Quasi-isothermal thermogravimetry. *Analytica Chimica Acta* 56, 328–331.
- Rautureau, M., Mifsud, A., 1977. Étude par microscopie électronique des différents états d'hydratation de la sépiolite. *Clay Minerals* 12, 309–318.
- Roberts-Austen, W.C., 1899. *Proceedings of the Institute of Mechanical Engineering* (London), 1, 35–102.
- Rouquerol, J., 1964. Méthode d'analyse thermique sous faible pression et à vitesse de décomposition constante. *Bulletin de la Société Chimique de France* 31–32.
- Rouquerol, J., 1970. L'analyse thermique à vitesse de décomposition constante. *Journal of Thermal Analysis* 2, 123–140.
- Rouquerol, F., Rouquerol, J., 1972. Activation energy of a thermolysis: conditions for a significant measurement under very low pressures. In: *Thermal Analysis. Proceedings of the 3rd International Conference on Thermal Analysis, Davos, Switzerland, Vol. 1*, Birkhauser, Basel-Stuttgart, pp. 373–377.
- Rouquerol, J., 2003. A general introduction to SCTA and to rate-controlled SCTA. *Journal of Thermoanalysis* 72, 1081–1086.
- Sörensen, O.T., 1978. Thermogravimetric studies of non-stoichiometric cerium oxides under isothermal and quasi-isothermal conditions. *Journal of Thermoanalysis* 13, 429–437.
- Villieras, F., Yvon, J., Cases, J.M., Zimmermann, J.L., Baeza, R., 1992. Dosage et localisation du fer 11 dans le talc et la chlorite par analyse spectrométrique du gaz de thermolyse. *CR Acad. Sci, Paris* 315, 121–1206.
- Wendlandt, W.W., Collins, L.W., 1976. *Thermal Analysis. Benchmark Papers in Analytical Chemistry, Volume 2*. Dowden, Hutchinson & Ross, Stroudsburg, PA, p. 13.

This page intentionally left blank

*Chapter 13*

## **SOME OTHER MATERIALS RELATED TO CLAYS**

**F. BERGAYA<sup>a</sup>, B.K.G. THENG<sup>b</sup> AND G. LAGALY<sup>c</sup>**

<sup>a</sup>*CRMD, CNRS-Université d'Orléans, F-45071 Orléans Cedex 2, France*

<sup>b</sup>*Landcare Research, Palmerston North, New Zealand*

<sup>c</sup>*Institut für Anorganische Chemie, Universität Kiel, D-24118 Kiel, Germany*

In this chapter the layered double hydroxides (LDH) called anionic clays (Chapter 13.1), three-dimensional zeolites (Chapter 13.2), which share several common properties with two-dimensional phyllosilicates, and finally the hydrated cement phases that benefit from the knowledge of clay mineral properties are discussed (Chapter 13.3). Many other layer silicates and a large diversity of non-silicate layered materials are not discussed even if the properties are sometimes quite similar (Schwieger and Lagaly, 2004).

### **REFERENCE**

Schwieger, W., Lagaly, G., 2004. Alkali silicates and crystalline silicic acids. In: Auerbach, S.M., Carrado, K.A., Dutta, P.K. (Eds.), *Handbook of Layered Materials*. Marcel Dekker, New York, pp. 541–629.

This page intentionally left blank

## Chapter 13.1

# LAYERED DOUBLE HYDROXIDES

C. FORANO<sup>a</sup>, T. HIBINO<sup>b</sup>, F. LEROUX<sup>a</sup> AND  
C. TAVIOT-GUÉHO<sup>a</sup>

<sup>a</sup>Laboratoire de Matériaux Inorganiques, CNRS UMR 6002, Université Blaise Pascal, F-63177 Aubière Cedex, France

<sup>b</sup>Ecological Materials Group, AIST, 16-1 Onogawa, Tsukuba 305-8569, Japan

## 13.1.1. DEFINITIONS

*Among the group of minerals referred to as 'Non-Silicate Oxides and Hydroxides' (Newman, 1987), the 'layered double hydroxides' (LDH) have many physical and chemical properties that are surprisingly similar to those of clay minerals. Their layered structure, wide chemical compositions (due to variable isomorphous substitution of metallic cations), variable layer charge density, ion-exchange properties, reactive interlayer space, swelling in water, and rheological and colloidal properties make LDH clay-like. But because of their anion-exchange properties, LDH were referred to as 'anionic clays'.*

As hydrotalcite is one of the most representative mineral of the group, LDH were also called 'hydrotalcite-like compounds' (HTlc). The structure of hydrotalcite is related to that of brucite,  $\text{Mg}(\text{OH})_2$  in which some of the  $\text{Mg}^{2+}$  cations in the layer structure were replaced by  $\text{Al}^{3+}$ . Carbonate anions are intercalated between the layers to maintain electroneutrality. The chemical formula of hydrotalcite may therefore be given as  $\text{Mg}_{0.75}\text{Al}_{0.25}(\text{OH})_2(\text{CO}_3)_{0.5} \cdot 0.5\text{H}_2\text{O}$ , and abbreviated to  $[\text{Mg}-\text{Al}-\text{CO}_3]$  or  $[\text{Mg}-\text{Al}]$ .

The general formulae for other members of the family, based on a combination of divalent and trivalent metal cations, can be written as  $[\text{M}^{\text{II}}_{1-x}\text{M}^{\text{III}}_x(\text{OH})_2][\text{X}^{q-}_{x/q} \cdot n\text{H}_2\text{O}]$  or  $[\text{M}^{\text{II}}-\text{M}^{\text{III}}-\text{X}]$  or  $[\text{M}^{\text{II}}-\text{M}^{\text{III}}]$ , where  $[\text{M}^{\text{II}}_{1-x}\text{M}^{\text{III}}_x(\text{OH})_2]$  ( $[\text{M}^{\text{II}}-\text{M}^{\text{III}}]$ ) represents the layer, and  $[\text{X}^{q-}_{x/q} \cdot n\text{H}_2\text{O}]$  the interlayer composition (Figs. 13.1.1 and 13.1.2). Extension to multicomponent systems may be expressed as  $[\text{M}^{\text{II}}-\text{M}'^{\text{II}}-\text{M}^{\text{III}}-\text{M}''^{\text{III}}-\text{X}-\text{Y}]$ . Tetravalent cations such as  $\text{Zr}^{4+}$  and  $\text{Sn}^{4+}$  can also be incorporated (Velu et al., 1999a). Cation radius (size) is an important parameter in LDH formation. The LDH structure is not stable when the ionic radius of  $\text{M}(\text{II})$  is  $<0.06$  nm. With large cations such as  $\text{Ca}^{2+}$ , the hydrotalcite-type structure transforms into that of hydrocalumite.



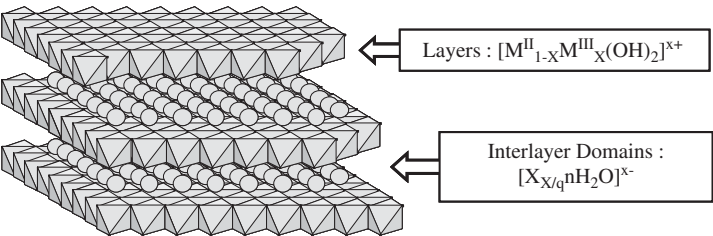


Fig. 13.1.1. Structure of layered double hydroxides.

Layers : $[M^{II}_{1-x}M^{III}_x(OH)_2]^{x+}$																		He					
H																							
Li	Be																	B	C	N	O	F	Ne
Na	Mg																	Al	Si	P	S	Cl	Ar
K	Ca	Sc	Ti	V	Cr	Mn	Fe	Co	Ni	Cu	Zn	Ga	Ge	As	Se	Br	Kr						
Rb	Sr	Y	Zr	Nb	Mo	Tc	Ru	Rh	Pd	Ag	Cd	In	Sn	Sb	Te	I	Xe						
Cs	Ba	La	Hf	Ta	W	Re	Os	Ir	Pt	Au	Hg	Tl	Pb	Bi	Po	At	Rn						
Fr	Ra	Ac																					
			Ce	Pr	Nd	Pm	Sm	Eu	Gd	Tb	Dy	Ho	Er	Tm	Yb	Lu							
			Th	Pa	U	Np	Pu	Am	Cm	Bk	Cf	Es	Fm	Md	No	Lr							

Interlayers : $[X^{q-}_{x/q}.nH_2O]^{x-}$																		He					
H																							
Li	Be																	B	C	N	O	F	Ne
Na	Mg																	Al	Si	P	S	Cl	Ar
K	Ca	Sc	Ti	V	Cr	Mn	Fe	Co	Ni	Cu	Zn	Ga	Ge	As	Se	Br	Kr						
Rb	Sr	Y	Zr	Nb	Mo	Tc	Ru	Rh	Pd	Ag	Cd	In	Sn	Sb	Te	I	Xe						
Cs	Ba	La	Hf	Ta	W	Re	Os	Ir	Pt	Au	Hg	Tl	Pb	Bi	Po	At	Rn						
Fr	Ra	Ac																					
			Ce	Pr	Nd	Pm	Sm	Eu	Gd	Tb	Dy	Ho	Er	Tm	Yb	Lu							
			Th	Pa	U	Np	Pu	Am	Cm	Bk	Cf	Es	Fm	Md	No	Lr							

Fig. 13.1.2. Elements entering in the composition of natural and synthetic anionic clays.

13.1.2. NATURAL OCCURRENCE

Hydrotalcite,  $Mg_6Al_2(OH)_{16}(CO_3) \cdot 4H_2O$ , is a white hydrous mineral with a rhombohedral crystalline system, a low hardness (2.00), and a low density (2.06). Snarum, Norway, is the original site of occurrence but the mineral was found in New

South Wales and Tasmania, Australia. HTlc are rare in nature, and are often associated with serpentine and calcite. The principal minerals belonging to the hydrotalcite and manasseite groups are presented in Table 13.1.1.

Although natural stocks of hydrotalcite are limited, the formation in soils of mixed metal-Al hydroxide phases on the surface of phyllosilicates and gibbsite crystallites was shown by XAFS (Scheidegger et al., 1997, 1998). Most metals in the first transition series can be incorporated into the hydroxyl sheet of the hydrotalcite-like structure. Thus, the formation of mixed metal-Al secondary precipitates may be a general reaction mechanism for transition metal adsorption to clay minerals.

LDH with the general chemical formula  $[\text{Fe}_{(1-x)}^{\text{II}}\text{Fe}_x^{\text{III}}(\text{OH})_2]^{x+} [\text{X}^{q-}]_{x/q} \cdot n\text{H}_2\text{O}$  ( $\text{X}^{q-} = \text{SO}_4^{2-}$ ,  $\text{CO}_3^{2-}$  or  $\text{Cl}^-$ ) constitute the green rust family. Their occurrence in hydromorphic soils was shown by Mössbauer and Raman spectroscopy (Trolard et al., 1997). These minerals play a central role in controlling the solubility and transport of iron in soil solutions and aquifers (Génin et al., 1988, 1998) and more generally in the biogeochemistry of Fe. They may also control some redox processes in aquifers and participate in the transformation of various pollutants (Génin et al., 2001).

Another subgroup related to hydrotalcite is the hydrocalumite group whose representative is  $\text{Ca}_2\text{Al}(\text{OH})_6\text{Cl} \cdot 3\text{H}_2\text{O}$  and more generally for other members of the group  $[\text{Ca}_2\text{M}^{\text{III}}(\text{OH})_6]^{x+} [\text{X}^{q-}]_{x/q} \cdot n\text{H}_2\text{O}$  with  $\text{M}^{3+} = \text{Al}^{3+}$ ,  $\text{Fe}^{3+}$ ,  $\text{Cr}^{3+}$ ,  $\text{Ga}^{3+}$ , and  $\text{X}^{q-} = \text{SO}_4^{2-}$ ,  $\text{CO}_3^{2-}$ , or  $\text{Cl}^-$ . Hydrocalumite is a rare, hydrated  $\text{Ca}^{2+}$  aluminate,

Table 13.1.1. Minerals of the manasseite and hydrotalcite group

Mineral	Formula					Space group
	Layer composition			Interlayer composition		
	M <sup>II</sup>	M <sup>III</sup>	(OH)	X	· nH <sub>2</sub> O	
Hydrotalcite	Mg <sub>6</sub>	Al <sub>2</sub>	(OH) <sub>16</sub>	(CO <sub>3</sub> )	· 4(H <sub>2</sub> O)	R-3m (-3 2/m)
Stichtite	Mg <sub>6</sub>	Cr <sub>2</sub>	(OH) <sub>16</sub>	(CO <sub>3</sub> )	· 4(H <sub>2</sub> O)	R-3m (-3 2/m)
Desautelsite	Mg <sub>6</sub>	Mn <sub>2</sub>	(OH) <sub>16</sub>	(CO <sub>3</sub> )	· 4(H <sub>2</sub> O)	R3m or R-3m Trig
Pyroaurite	Mg <sub>6</sub>	Fe <sub>2</sub>	(OH) <sub>16</sub>	(CO <sub>3</sub> )	· 4(H <sub>2</sub> O)	R-3m (-3 2/m)
Takovite	Ni <sub>6</sub>	Al <sub>2</sub>	(OH) <sub>16</sub>	(CO <sub>3</sub> ,OH)	· 4(H <sub>2</sub> O)	R-3m (-3 2/m)
Reevesite	Ni <sub>6</sub>	Fe <sub>2</sub>	(OH) <sub>16</sub>	(CO <sub>3</sub> )	· 4(H <sub>2</sub> O)	R-3m (-3 2/m)
Comblainite	Ni <sub>x</sub>	Co <sub>1-x</sub>	(OH) <sub>2</sub>	(CO <sub>3</sub> ) <sub>(1-x)/2</sub>	· n(H <sub>2</sub> O)	R-3m (-3 2/m)
Sergeevite	Ca <sub>2</sub>	Mg <sub>11</sub>	(OH) <sub>4</sub>	(CO <sub>3</sub> ) <sub>9</sub> (HCO <sub>3</sub> ) <sub>4</sub>	· 6(H <sub>2</sub> O)	R32 3 2
Honessite	Ni <sub>6</sub>	Fe <sub>2</sub>	(OH) <sub>16</sub>	(SO <sub>4</sub> )	· 4H <sub>2</sub> O	R-3m (-3 2/m)
Caresite	(Fe,Mg) <sub>4</sub>	Al <sub>2</sub>	(OH) <sub>12</sub>	(CO <sub>3</sub> )	· 3H <sub>2</sub> O	P3112 or P321(2 3 2)
Charmarite	Mn <sub>4</sub> <sup>2+</sup>	Al <sub>2</sub>	(OH) <sub>12</sub>	(CO <sub>3</sub> )	· 3H <sub>2</sub> O	P6322 (6 2 2)
Iowaite	Mg <sub>6</sub>	Fe <sub>2</sub>	(OH) <sub>16</sub>	Cl <sub>2</sub>	· 4H <sub>2</sub> O	R-3m (-3 2/m)
Meixnerite	Mg <sub>6</sub>	Al <sub>2</sub>	(OH) <sub>16</sub>	(OH) <sub>2</sub>	· 4H <sub>2</sub> O	R-3m (-3 2/m)
Wermlandite	(Ca,Mg) <sub>7</sub>	(Al,Fe) <sub>2</sub>	(OH) <sub>18</sub>	(SO <sub>4</sub> ) <sub>2</sub>	· 12H <sub>2</sub> O	P-3c1 (-3 2/m)
Woodallite	Mg <sub>6</sub>	(Cr,Fe) <sub>2</sub>	(OH) <sub>16</sub>	Cl <sub>2</sub>	· 4H <sub>2</sub> O	R-3m (-3 2/m)
Zincowoodwardite	Zn <sub>1-x</sub>	Al <sub>x</sub>	(OH) <sub>2</sub>	(SO <sub>4</sub> ) <sub>x/2</sub>	· n(H <sub>2</sub> O)	P3- or R-3m (-3z)

occurring as bladed crystals in a wide cavity of a phonolitic rock at Montalto di Castro, Italy (Passaglia and Sacerdoti, 1988) or in limestone inclusions in basalt from Bellerberg, near Ettringen (Germany), and from Boissejour (France) (Fischer et al., 1980). The structure of hydrocalumite is based on an ordered arrangement of  $\text{Ca}^{2+}$  and  $\text{M}^{3+}$  ions, in the corrugated brucite-like layers leading to a monoclinic crystal lattice (Rousselot et al., 2002). These compounds can form during hydration of cement compounds (Kuzel and Baier, 1996). They are being intensively investigated for the immobilization of toxic cations or the optimization of concrete properties.

13.1.3. SYNTHETIC LDH

A. Chemical Composition of the Layers

A wide range of  $\text{M}^{2+}/\text{M}^{3+}$  combinations of the layers was found (Fig. 13.1.2; Tables 13.1.2 and 13.1.3). Only one example is known with a monovalent cation,  $\text{LiAl}_2(\text{OH})_6\text{X} \cdot n\text{H}_2\text{O}$ . Velu et al. (1997a, 1999a, 1999b, 2000a) and Tichit et al. (2002a) showed that tetravalent metal cations can be incorporated to some extent. LDH are not limited to binary combinations of metal cations; ternary, quaternary, and multicomponent LDH can also be synthesized. Multicomponent LDH are interesting precursors for the preparation of finely divided mixed oxides with an homogeneous distribution of metal (Jiratova et al., 2002). Partial substitution of metal can be used to tune the catalytic properties of the material. When Mg is partially replaced by Cu or Fe in the hydrotalcite-like layer, using the coprecipitation method, the LDH display a selective effect on the synthesis of methylamines (Carja et al., 2002).

B.  $\text{M}^{2+}/\text{M}^{3+}$  Ratio Variation

LDH with Variable  $\text{M}^{2+}/\text{M}^{3+}$  Ratios

In many cases, the M(II)/M(III) ratio may vary according to the coprecipitation conditions and initial concentration of the salts (Table 13.1.3). In the general

Table 13.1.2. Chemical compositions of LDH and optimal pH of coprecipitation

$\text{M}^{\text{II}}\text{--M}^{\text{III}}\text{--X}$	$\text{pH}_{\text{form}}$	$\text{M}^{\text{II}}/\text{M}^{\text{III}}$ (R) range	$\text{M}^{\text{II}}\text{--M}^{\text{III}}\text{--X}$	$\text{pH}_{\text{form}}$	$\text{M}^{\text{II}}/\text{M}^{\text{III}}$ (R) range
[Zn–Al–Cl]	7.0	$1.0 \leq R \leq 5.0$	[Zn–Cr–Cl]	4.5	$R \approx 2.0$
[Zn–Al–Cl]	10.0	$1.0 \leq R \leq 3.0$	[Zn–Cr–Cl]	10.0	$2.0 \leq R \leq 3.0$
[Ni–Cr–Cl]	11.5	$1.0 \leq R \leq 3.0$	[Mg–Fe–CO <sub>3</sub> ]	—	$2.7 \leq R \leq 5.6$
[Ni–Cr–CO <sub>3</sub> ]	13.0	$1.0 \leq R \leq 2.0$	[Ni–Al–ClO <sub>4</sub> ]	10.0	$1.0 \leq R \leq 3.0$
[Cu–Cr–Cl]	5.5	$1.6 \leq R \leq 2.3$	[Co–Fe–Cl]	9.0	$1.8 \leq R \leq 4.0$
[Zn–Al–CO <sub>3</sub> ]	9.0	$1.7 \leq R \leq 2.3$	[Co–Fe–CO <sub>3</sub> ]	9.0	$1.0 \leq R \leq 3.0$
[Mg–Al–CO <sub>3</sub> ]	8.0	$1.0 \leq R \leq 3.0$			

Table 13.1.3. Some references for the preparation of LDH

LDH	Anions	References
[Mg–Al]	$\text{CO}_3^{2-}, \text{NO}_3^-, \text{Cl}^-$	Miyata (1980)
[Mg–Fe]	$\text{CO}_3^{2-}$	Fernandez et al. (1998)
[Mg–Ga]	$\text{CO}_3^{2-}, \text{NO}_3^-, \text{terephthalate}$	Aramendia et al. (2002), Lopez-Salinas et al. (1996)
[Mg–Cr]	$\text{Cl}^-$	Bocclair et al. (1999)
[Mg–In]	$\text{NO}_3^-$	Aramendia et al. (2002, 2000)
[Mg–CoII–CoIII]	$\text{NO}_3^-$	Zeng et al. (1998)
[Mg–ScIII], [Mg–MnIII]	$\text{Cl}^-$	Rousselot et al. (1999)
Co/Mg/Al	$\text{CO}_3^{2-}, \text{NO}_3^-$	Tichit et al. (1998)
[Mg–Y]	$\text{CO}_3^{2-}$	Fernández et al. (1997)
[Co–Ni–Mg–Al]	$\text{CO}_3^{2-}, \text{NO}_3^-$	Tichit et al. (2001)
[Mg–Al–Sn], [Ni–Al–Sn], [Co–Al–Sn]	$\text{CO}_3^{2-}, \text{NO}_3^-, \text{Cl}^-$	Velu et al. (2000a)
[Mg–Al–Zr], [Ni–Al–Zr], [Zn–Al–Zr]	$\text{CO}_3^{2-}$	Tichit et al. (2002a)
[Zn–Al]	$\text{CO}_3^{2-}$	Thevenot et al. (1989)
[Zn–Cr]	$\text{Cl}^-, \text{SO}_4^{2-}$	Martin and Pinnavaia (1986), Khaldi et al. (1997)
[Ni–Al]	$\text{Cl}^-$	Kwon et al. (1988)
[Cu–Al]	$\text{CO}_3^{2-}, \text{NO}_3^-$	Lwin et al. (2001)
[Mn–Al]	$\text{Cl}^-, \text{NO}_3^-, \text{dicarboxylic acids}$	Aisawa et al. (2002)
[Li–Al]	$\text{CO}_3^{2-}$	Ulibarri et al. (1987)
[Ca–Al], [Ca–Ga], [Ca–Fe], [Ca–Sc]	$\text{Cl}^-$	Rousselot et al. (2002)
[Cd–Al]	$\text{CO}_3^{2-}, \text{NO}_3^-$	Vichi and Alves (1997)
[Ba–Al]	$\text{Cl}^-$	Don Wang et al. (1995)
[Ni–V <sup>III</sup> ]	$\text{Cl}^-$	Caravaggio et al. (2001)
[Ni–Fe]	$\text{CO}_3^{2-}$	del Arco et al. (1999)
[Co–Fe]	$\text{Fe}(\text{CN})_6^{4-}$	Bender (2001)
[CoII–CoIII]	$\text{NO}_3^-$	Zapata et al. (2002)

formula of  $[\text{M}_{1-x}^{\text{II}}\text{M}_x^{\text{III}}(\text{OH})_2][\text{X}^{q-}_{x/q} \cdot n\text{H}_2\text{O}]$ ,  $x$  gives the molar fraction of M(III) per total metal

$$x = \frac{\sum M^{3+}}{\sum M_i}$$

Some natural and synthetic minerals exist with a fixed  $x$  value of  $1/3$ . In the majority of cases  $x$  varies in the range  $0.10 \leq x \leq 0.33$ .

Large cations such as  $Y^{3+}$  may destabilize the LDH structure (Fernandez et al., 1997), or even impede its formation. Electrostatic  $M^{3+}-M^{3+}$  and  $M^{3+}-M^{2+}$  interactions appear to be a limiting factor for the preparation of LDH with  $M^{3+}$  substitution rates  $> 0.33$ . Some exceptions remain: [Li–Al] and some Al-rich [Zn–Al] HTlc with  $x = 0.44$ , obtained by coprecipitation (Thevenot et al., 1989). Also  $[Mg_{1-x}Ga_x(OH)_2] (CO_3)_{x/2} \cdot nH_2O$  with  $x = 0.072-0.35$  ( $Mg/Ga = 12.9-1.8$ ) by coprecipitation (Lopez-Salinas et al., 1996). Attempts to obtain Ga-rich hydrotalcites ( $Mg/Ga < 1.8$ ) resulted in solids with a constant  $Mg/Ga$  ratio of 1.8, which appears to be the maximum Ga content. During  $Mg^{2+}-Co^{2+}$  precipitation nearly 23% of the  $Co^{2+}$  ions are oxidized to  $Co^{3+}$  (Zeng et al., 1998).

#### *LDH with Fixed $M^{2+}/M^{3+}$ Ratios*

The cation layer composition is fixed for some  $M^{II}/M^{III}$  combinations. In the  $LiAl_2(OH)_6X_{1/3} \cdot nH_2O$  phase, the  $Li^+/Al^{3+}$  ratio is fixed at 0.5 caused by ordering of the cations (Serna et al., 1982; Fogg and O' Hare, 1999). In hydrocalumite-like compounds, the large difference in ionic radii ( $Ca^{2+}$ , 99 pm;  $Al^{3+}$ , 56 pm;  $Fe^{3+}$ , 64 pm) leads to a strong distortion of the local  $Ca^{2+}$  environment from a regular octahedron to a heptavalent coordination and gives rise to an ordering of the divalent and trivalent cations in a corrugated brucite-like layer.  $Cr^{3+}$ -containing LDH with  $Mg^{2+}$ ,  $Zn^{2+}$ ,  $Co^{2+}$ ,  $Ni^{2+}$ , or  $Mn^{2+}$  exist preferentially with  $M^{2+}/Cr^{3+} = 2$  (Bocclair et al., 1999; Roussel et al., 2000, 2001). A structural pathway involving direct condensation of hexaaquo zinc(II) complexes with deprotonated  $Cr^{3+}$  monomeric aquo complexes is proposed to explain the formation of LDH with a fixed  $Zn/Cr$  ratio of 2. The structural pathway strongly supports the concept of cationic order in the [Zn–Cr–Cl] LDH sheets. Using a combination of powder XRD and X-ray absorption (XAS), Vucelic et al. (1997) demonstrated that in synthetic pyroaurite there is no correlation between Fe(III) cation positions over distances of a few tens of Angstroms. This signifies a very high level of local ordering, avoiding the existence of Fe(III)–Fe(III) neighbours. The same situation may apply to other  $M(II)/M(III)$  LDH. On the other hand, Li/Al LDH show long-range cation ordering.

#### *C. Interlayer Anion Composition*

A priori, there is no theoretical limit to the intercalation of all types of anions into the LDH structure. Fig. 13.1.2 shows the large number of elements that can be intercalated in anionic form. Neutral molecules can also be intercalated together with these anions, giving rise to a very wide range of compositions for the interlayer domains. The following families of anions can be found:

- halides ( $F^-$ ,  $Cl^-$ ,  $Br^-$ ,  $I^-$ ),
- non-metal oxoanions ( $BO_3^{3-}$ ,  $CO_3^{2-}$ ,  $NO_3^-$ ,  $Si_2O_5^{2-}$ ,  $HPO_4^{2-}$ ,  $SO_4^{2-}$ ,  $ClO_4^-$ ,  $AsO_4^{3-}$ ,  $SeO_4^{2-}$ ,  $BrO_4^-$ , etc.),

- oxometallate anions ( $\text{VO}_4^{3-}$ ,  $\text{CrO}_4^{2-}$ ,  $\text{MnO}_4^-$ ,  $\text{V}_{10}\text{O}_{28}^{6-}$ ,  $\text{Cr}_2\text{O}_7^{2-}$ ,  $\text{Mo}_7\text{O}_{24}^{6-}$ ,  $\text{PW}_{12}\text{O}_{40}^{3-}$ , etc.),
- anionic complexes of transition metals ( $\text{Fe}(\text{CN})_6^{2-}$ , etc.),
- volatile organic anions ( $\text{CH}_3\text{COO}^-$ ,  $\text{C}_6\text{H}_5\text{COO}^-$ ,  $\text{C}_{12}\text{H}_{25}\text{COO}^-$ ,  $\text{C}_2\text{O}_4^{2-}$ ,  $\text{C}_6\text{H}_5\text{SO}_3^-$ , etc.),
- anionic polymers (PSS, PVS, etc.).

#### 13.1.4. SYNTHESIS

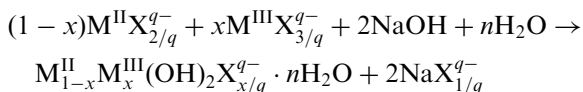
LDH are simple and inexpensive to synthesize on laboratory and industrial scales (Trifiro and Vaccari, 1996). Many methods allow the preparation of materials with tailored physical and chemical properties suitable for many applications. For a catalytic system, whose activity results from a cooperative effect between the active phase and mixed oxides support, a precursor containing all the components homogeneously distributed in the same phase may be a suitable choice. LDH are such types of precursors. The metal cations are homogeneously distributed inside the brucite sheets; calcination and reduction yield well-dispersed, small and stable metal particles on mixed oxides support (Das and Srivastava, 2002). As an example, the reduction of Pd-containing Mg–Al LDH leads to Pd/MgAl oxide bifunctional catalysts. Another way to introduce Pd in the LDH structure is anion exchange with the  $[\text{PdCl}_2(\text{OH})_2]^{2-}$  complex (Carpentier et al., 2002). These two methods appear quite different in terms of Pd loading or structural changes in the reduction step. Table 13.1.2 shows the large number of elements that can be incorporated into the LDH structure.

The preparation, properties, and applications of LDH were well documented (Cavani et al., 1991; Miyata, 1991; de Roy et al., 1992; Mascolo, 1995; Trifiro and Vaccari, 1996; Rives and Ulibarri, 1999; Hibino et al., 1999; Vaccari, 1999a; Sels et al., 2001; Rives, 2001; Newman and Jones, 2002). Here we give a general overview of typical methods of synthesis.

##### A. Coprecipitation

LDH are readily prepared by the addition of a base to solutions containing a mixture of M(II) and M(III). In this titration or variable-pH coprecipitation method, M(III) hydroxides or hydrous oxides are initially formed, and further addition of base results in coprecipitation or conversion into LDH. Bocclair et al. (1999) reported a well-defined transition step between constant-pH precipitation of the M(III) hydroxides ( $\text{M} = \text{Al}, \text{Fe}$ ) and the mixed  $[\text{M}(\text{II})\text{--M}(\text{III})]$  precipitates where  $\text{M}(\text{II}) = \text{Mg}^{2+}$ ,  $\text{Zn}^{2+}$ ,  $\text{Co}^{2+}$ ,  $\text{Ni}^{2+}$ ,  $\text{Mn}^{2+}$ . The conversion of  $\text{M}(\text{OH})_3$  (or  $\text{MO}(\text{OH})$ ) to LDH proceeds by a dissolution/precipitation mechanism. In  $[\text{M}(\text{II})\text{--Cr}^{3+}]$  systems ( $\text{M}(\text{II}) = \text{Zn}^{2+}$ ,  $\text{Co}^{2+}$ , and  $\text{Ni}^{2+}$ ), the absence of pH transition is indicative of the preferential precipitation of LDH over  $\text{Cr}(\text{OH})_3$  (Bocclair et al., 1999).

To obtain LDH with high chemical homogeneity, coprecipitation at constant pH is recommended. It allows the preparation of a great number of LDH with  $\text{CO}_3^{2-}$ ,  $\text{Cl}^-$ , or  $\text{NO}_3^-$  anions as precursors for subsequent reactions (anion-exchange reactions, thermal decomposition, noble metal impregnations, etc.). The pH is kept constant during the reaction by the simultaneous addition of a base solution (NaOH, KOH, and  $\text{NH}_4\text{OH}$ ) and a mixed metal salt solution:



Crepaldi et al. (2000a) demonstrated that materials prepared by this method show interesting properties for technological applications, including high crystallinity, small particle size, high specific surface area, and high average pore diameter.

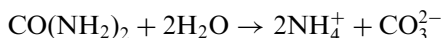
The pH of coprecipitation has a crucial effect on the chemical, structural, and textural properties of the phases. For instance, powder XRD of the [Zn–Al–Cl] samples with variable Zn/Al ratio shows that only the LDH phase crystallizes at neutral pH. The X-ray pattern shows good resolution when  $\text{Zn}^{2+}/\text{Al}^{3+} \approx 3$ . At pH 10.0 and for a  $\text{Zn}^{2+}/\text{Al}^{3+}$  ratio  $\geq 3$ , Zn–Al–Cl coexists with  $\text{Zn}(\text{OH})_2$ , while for a  $\text{Zn}^{2+}/\text{Al}^{3+}$  ratio  $\leq 1$ , the excess  $\text{Al}^{3+}$  ions crystallize as bayerite ( $\text{Al}(\text{OH})_3$ ). The best crystalline phase is obtained for  $\text{Zn}^{2+}/\text{Al}^{3+} \leq 3$ , whatever the pH. In the case of pure [Ni–Cr–Cl] and [Ni–Cr– $\text{CO}_3$ ] phases, LDH with a  $\text{M}^{\text{II}}/\text{M}^{\text{III}}$  ratio changing from 1.0 to 3.0 and 1.0 to 2.0, respectively, were obtained only after subsequent hydrothermal treatment.

The coprecipitation method is sometimes limited by competitive reactions such as precipitation of metal salts in the case of oxoanions with high metal ion affinity (e.g., phosphate and oxometallates). Anion exchange of the  $\text{Cl}^-$  or  $\text{NO}_3^-$  LDH precursor then appears to be an alternative method.

### B. The Urea Method

During the standard coprecipitation, supersaturation of the precipitating agent ( $\text{OH}^-$ ) is reached rapidly and maintained throughout the reaction. This leads to the continuous nucleation of mixed hydroxides simultaneous with the growing and Oswald ageing (aggregation) of the particles, resulting in a wide particle size distribution. By using a base retardant as precipitating agent, the nucleation step can be separated from particle growth, and ageing is prevented from the beginning. Coprecipitation using urea as the base was developed to prepare monodisperse particles. Urea is a very weak Brønsted base ( $\text{p}K_b = 13.8$ ), is highly soluble in water.

According to Shaw and Bordeaux (1955), hydrolysis of urea proceeds in two steps: (i) formation of ammonium cyanate ( $\text{NH}_4\text{CNO}$ ) as the rate-determining step; and (ii) fast hydrolysis of the cyanate into ammonium carbonate:



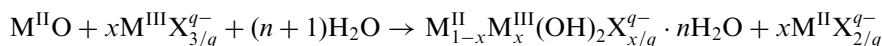


The hydrolysis rate of urea can be controlled by temperature. The rate constant increases about 200 times when the temperature is increased from 60 to 100 °C.

Large platelets of well-crystallized hydrotalcite with hexagonal shape are obtained by this method (Oh, et al., 2002; Ogawa and Kaiho, et al., 2002; Adachi-Pagano et al., 2003). The reaction temperature and the concentration of reactants control the particle size. Monodisperse particles between 1 and 5 μm, and up to 20 μm are obtained.  $M_3^{2+}Al(OH)_8(CO_3)_{0.5} \cdot nH_2O$  ( $M^{2+} = Mg^{2+}, Ni^{2+}, Zn^{2+}$ ) LDH were synthesized by Costantino et al. (1998).

### C. Induced Hydrolysis

When oxides such as ZnO, NiO, and CuO are contacted dropwise with acidic solutions of trivalent metal salts such as  $AlCl_3$  or  $CrCl_3$ , the oxides are progressively dissolved, and LDH are precipitated provided the pH is buffered by the oxide and/or hydroxide suspension (de Roy et al., 1992):



This synthesis was first used to prepare [Zn–Cr–Cl] LDH but was then extended to other systems, in particular [Zn–Cr–Cl], [Zn–Cr–NO<sub>3</sub>], [Zn–Al–Cl], and [Zn–Al–NO<sub>3</sub>] (Boehm et al., 1977). More recently, a new [Zn–Cr] LDH,  $[Zn_7Cr_4(OH)_{22}(CO_3)_2 \cdot 5H_2O]$ , was prepared by reaction of a perchlorate solution of the hydrolytic dimer  $[(H_2O)_4Cr(\mu-OH)_2Cr(H_2O)_4]^{4+}$  with ZnO and subsequent anion exchange with  $Na_2CO_3$  (Gutmann and Mueller, 1996).

Induced hydrolysis is not limited to reactions between di- and trivalent cations but can involve divalent–divalent, divalent–tetraivalent and trivalent–trivalent species (Taylor, 1984).

### D. Reconstruction

Miyata (1980) was the first to describe the reconstruction of the original LDH structure by hydration of the calcined LDH. This unique property, ascribable to a structural memory effect, can be used as a general preparation method of LDH. In the first step the LDH containing a volatile anion is calcined into a mixture of oxides and then to rehydrated in an aqueous solution containing the anion to be intercalated. The method was used for the preparation of several LDH (Kooli et al., 1994, 1995, 1997b) and the intercalation of several oxoanions ( $CrO_4^{2-}$ ,  $HPO_4^{2-}$ ,  $HVO_4^{2-}$ ,  $SiO_3^{2-}$ ,  $HGaO_3^{2-}$ , and  $SO_4^{2-}$ ) into [Mg–Al] (Tsugio et al., 1986).

The calcination conditions (temperature, rate, and duration) are important parameters determining structure recovery. The hydrotalcite structure is reconstructed at controlled water vapour pressure by 24 h rehydration, provided that the thermal treatment of the precursors does not exceed 600 °C (Rocha et al., 1999). Samples calcined at 750 °C recover their original structure if they are equilibrated for 3 days.



Tetrahedral Al generated by the decomposition of the parent mineral is converted again into octahedral Al in the brucite layer. Kinetic data (Millange et al., 2000), using the Avrami–Erofe’ev nucleation-growth model, are consistent with dissolution of the mixed oxide and crystallization of the LDH from solution. Using SEM and XRD techniques, Stanimirova et al. (2001) confirmed the dissolution/reconstruction process. This mechanism is not related to a memory effect as assumed previously.

Nevertheless, some limits of reversibility were observed. Repeated calcination/hydration cycles with hydrotalcite decrease the content of interlayer carbonate anions and increasing extraction of  $\text{Al}^{3+}$  from the brucite layers. There is also progressive segregation of the  $\text{MgAl}_2\text{O}_4$  spinel phase the formation of which is unusual at these soft conditions of calcination (Hibino and Tsunashima, 1998). Nor can the reconstruction method be used for all  $\text{M}^{\text{II}}\text{--M}^{\text{III}}$  combinations. Reconstruction of  $\text{Fe}^{3+}$ -containing hydrotalcites is limited by the formation of  $\text{MgFe}_2\text{O}_4$  spinel, which appears even at low content of  $\text{Fe}^{3+}$ . In the case of  $[\text{Mg--Al--Y}]$ , reconstruction leads to segregation of  $\text{Y}^{3+}$ -containing oxides and  $[\text{Mg--Al}]$  LDH (Fernandez et al., 1997). In the case of  $[\text{Zn--Al}]$  LDH, restoration of the hydrotalcite-like structure is independent of the Zn/Al ratios for samples calcined between 300 and 400 °C; however, a second phase, Al hydroxide or Zn oxide, is detected. At temperatures above 600 °C, the formation of the spinel  $\text{ZnAl}_2\text{O}_4$  prevents any reconstruction. The rehydrated phases have Zn/Al ratios close to 2, irrespective of the composition of the starting material (Kooli et al., 1997a).

This method is suitable for the preparation of hybrid LDH with large organic anions such as dyes. For instance, phenolphthalein was intercalated into Zn–Al LDH (Latterini et al., 2002).

### *E. Sol-Gel Technique*

The sol-gel process was first explored by Lopez et al. (1996) in the preparation of Mg–Al type samples. The sol-gel hydrotalcites show thermal stability up to 550 °C (Lopez et al., 1997). However, LDH samples prepared by coprecipitation are more crystalline than those prepared by the sol-gel method. The marked increase in specific surface area is ascribed to the increase in mesopore volume. The textural properties of the calcined samples are not appreciably influenced by the method of synthesis (Aramendia et al., 2002).

As an example,  $\text{Mg/M(III)}$  ( $\text{M} = \text{Al, Ga, In}$ ) LDH were prepared from magnesium ethoxide and the acetylacetonates of the trivalent metals. However, the method usually described is not exactly a sol-gel approach, since the alkoxide is first dissolved in an alcohol/acid mixed solution ( $\text{EtOH/HCl}$ , 35% in aqueous solution). A solution containing acetone and the acetylacetonate of  $\text{M(III)}$  is then added, and the pH is adjusted to 10 with aqueous ammonia (Prinnetto et al., 2000b).

Similar conditions were used for the preparation of Mg/Al (hydrotalcite) and Ni/Al (takovite). The nature of the acid used during the first step, either  $\text{HNO}_3$  or  $\text{HCl}$ , is of great importance (Prinnetto et al., 2000a). With the sol-gel method samples with

larger  $\text{Mg}^{2+}/\text{Al}^{3+}$  ratios (2.47–4.29) and up to 10–25% higher specific surface areas are obtained as compared with samples prepared by classical coprecipitation (Aramendia et al., 2002). Sol-gel materials are also more basic due to different textural and morphological features (Prinnetto et al., 2000a).

For NiAl using Ni acetylacetonate and aluminium isopropylate, the oxidic forms ( $\text{NiO-Al}_2\text{O}_3$ ) with a high reducibility were obtained (Jitianu et al., 2000a). The sol-gel approach was extended to the preparation of Mg/Cr and Ni/Cr LDH. In the latter case, some organic groups are retained on the surface (Jitianu et al., 2003).

#### *F. Hydrothermal, Microwave, and Ultrasound Treatments*

Different in situ or post-synthesis treatments were applied to the ‘as-prepared’ samples in order to control structural and textural properties. Microwaves were used during synthesis in order to accelerate both the growing and ageing steps. Short microwave irradiation results in a well-crystallized material compared to conventional coprecipitation (Kannan and Vir Jasra, 2000; Mohmel et al., 2002). The extent of enhancement in crystallinity depends on the nature of the trivalent metal ion (Kannan and Vir Jasra, 2000). An increase of the specific surface area from 40 up to  $240\text{ m}^2/\text{g}$  is observed for synthetic hydrotalcite coprecipitated under 360 W microwave irradiation (Fetter et al., 2001). In general, the surface area and porosity of the synthetic materials are increased with the duration of microwave exposure. For  $\text{Co}_6^{2+}\text{Co}_2^{3+}(\text{OH})_{16}(\text{NO}_3)_2 \cdot n\text{H}_2\text{O}$  microwave-treated samples exhibit higher thermal stability, and formation of the spinel  $\text{Co}_3\text{O}_4$  is delayed up to  $200^\circ\text{C}$  (Zapata et al., 2002). Charge distribution, nature of the hydrotalcite network, and the presence of water molecules in the interlayer space lead to effective absorption of microwaves, favouring long-range ordering.

Crystallinity of the phases can also be improved by ultrasound irradiation. Larger LDH crystallites are observed while adsorption capacities are enhanced (Seida et al., 2002).

Hydrothermal treatment is also used to improve the crystallinity of the compounds or to increase the anion-exchange rate of low-affinity anions such as alkyl carboxylates. Hydrothermal treatment has a strong effect on the chemical composition ( $\text{Mg}^{2+}/\text{Al}^{3+}$ ) of synthetic hydrotalcite (Labajos et al., 1992).

#### *G. Anion-Exchange Reactions*

The anion-exchange capacity (AEC) is dependent on  $x$ . For the ideal composition of  $\text{M}_{1-x}^{\text{II}}\text{M}_x^{\text{III}}(\text{OH})_2\text{X} \cdot 0.66\text{H}_2\text{O}$ , it can be calculated as

$$\text{AEC} = \frac{x10^5}{\text{FW}} \quad (\text{cmol/kg})$$

where the formula weight  $FW = (M_{MII} + 46) + x(M_{MIII} + M_X - M_{MII})$ , and  $0.66H_2O$  accounts for the total occupancy of interlayer vacant sites by water.

FW relates to full occupancy (2/3) of the interlayer crystallographic sites by water molecules ( $0.66H_2O/metal$ ). Since AEC is dependent on  $x$ , it is constant for some LDH materials such as  $LiAl_2$ ,  $Zn_2Cr$ , and  $Cu_2Cr$ , and highly tunable for some others like  $Zn_xAl$  ( $1 < x < 4$ ) or  $Ga_xAl$  ( $1 < x < 7.5$ ) (Lopez-Salinas et al., 1997b). Table 13.1.4 gives the calculated AECs, the layer charge densities (c.d. =  $(a^2\sqrt{3}/2x)^{-1}$ ) and the free cross sectional area ( $S_{free} = 1/c.d.$  ( $nm^2/charge$ )) per layer for a series of LDH. The usual values range from 200 to 400 cmol/kg (= meq/100 g) and show the higher AEC of LDH in comparison to clay minerals (Parker et al., 1995; Inacio et al., 2001; Ulibarri et al., 2001). For Mg–Al LDH with Mg/Al = 3 and containing simple anions, the AEC value is 320–360 cmol/kg. However, measured AEC values for LDHs are often less than the values calculated from the structural formula, due to contamination by carbonate anions, which have a strong affinity for LDHs. The charge densities for LDHs range from 0.25 to 0.40  $nm^2/charge$  (Leroux and Besse, 2001).

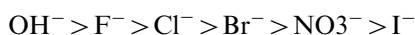
Miyata (1983) reported the ion-exchange isotherms at 25 °C of [Mg–Al] for a series of monovalent and divalent anions. All isotherms display a sigmoid shape arising from a continuous mixing of the anions in the LDH.

The powder XRD study during exchange of various systems  $[M^{II}-M^{III}-X/Y]$  (Miyata, 1983), and more particularly of  $[Zn-Cr-Cl/X]$  and  $[Zn-Al-Cl/X]$  ( $X = F^-$ ,  $Br^-$ ,  $I^-$ ), does not show a continuous variation of basal spacings with increasing molar fraction of the index anion. Non-miscibility of the different anions in LDH and the short-lived coexistence of two LDH phases are observed. Only a few examples are known of  $CO_3^{2-}/NO_3^-$  and  $CO_3^{2-}/SO_4^{2-}$  mixed intercalates in synthetic hydrotalcites, while mixed anion compositions are found in natural minerals. Preferential anion intercalation is often observed because of the co-intercalation process is thermodynamically unfavourable.

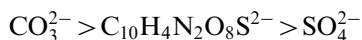
Table 13.1.4. Anion-exchange capacity values for some synthetic LDH

$[M^{II}-M^{III}]$	$x$	Formula weight	AEC (cmol/kg)	$a$ (nm)	Charge density (charge/ $nm^2$ )	Equivalent surface area ( $nm^2/charge$ )
[Mg–Al–Cl]	0.20	77.92	256.7	0.3060	2.47	0.405
	0.25	79.83	313.2	0.3054	3.09	0.323
	0.33	82.88	398.2	0.3042	4.24	0.236
[Zn–Al–Cl]	0.20	110.80	180.5	0.309	2.49	0.401
	0.25	110.65	225.9	0.308	3.13	0.319
	0.33	110.41	298.9	0.307	4.16	0.240
[Mg–Al–CO <sub>3</sub> ]	0.33	81.08	407.0	0.3042	4.24	0.236
[Mg–Al–NO <sub>3</sub> ]	0.33	91.64	360.1	0.3042	4.24	0.236
[Li–Al–Cl]	0.33	78.12	422.4	0.3070	4.16	0.240

From a thermodynamic point of view, exchange in LDH depends mainly on the electrostatic interactions between positively charged hydroxylated sheets and the exchanging anions, and to a small extent on the free energy involved in the changes of hydration (Israeli et al., 2000). Another important feature is that the equilibrium constant increases when the radius of the bare anion decreases. Exchange is therefore favoured for ingoing anions with a high charge density. By calculating the equilibrium constant of various exchange reactions, Miyata (1983) were able to list the order of affinity of LDH for monovalent anions



and divalent anions

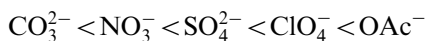


These results confirm the strong affinity for carbonate anions and underline the strong need to prepare these compounds under a  $\text{CO}_2$ -free atmosphere. For [Cu–Al–X/Y] systems, Yamaoka et al. (1998) determined a similar selectivity sequence for monovalent anions, while for divalent oxoanions the following order was proposed:

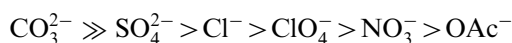


The selectivity for divalent anions is higher than for monovalent anions. According to these results, nitrate- and chloride-containing LDHs appear to be among the best precursors for exchange reactions.

For  $\text{Ni}_{1-x}\text{M}_x(\text{OH})_2(\text{CO}_3)_{x/2} \cdot n(\text{H}_2\text{O})$  ( $\text{M} = \text{Co}, \text{Fe}$ ), a strong dependence of basal spacings on the size and charge of the intercalated ions is observed. The spacing increases in the following order:



These hydroxides exhibit a selectivity for the anions in the sequence



Recent interest in using anionic clays for environmental remediation led to the re-investigation of their anion-exchange properties. Examining these properties over a wide concentration range of the incoming anions allows surface and bulk processes to be differentiated, and the rate of exchange at surface sites to be quantified. Inacio et al. (2001) and Ulibarri et al. (2001) showed that both the type of interlayer anion and the crystallinity of the LDH strongly affect AEC. In adsorption experiments conducted under identical conditions [Mg–Al– $\text{CO}_3$ ] does not adsorb dodecylsulphate whereas, [Mg–Al–Cl] adsorbs it completely. Molecular dynamics and ion

diffusion studies at surfaces and interfaces (Kalinichev et al., 2002) show that the structure and surface composition of LDH control the fluid structure in the interlayer space, as well as the effective diffusion coefficients of surface-adsorbed species, their surface lifetimes, and their rotational and translational dynamics.

Experimental adsorption isotherms, usually interpreted in terms of the classical Langmuir or Freundlich models (Inacio et al., 2000), can yield adsorption capacity coefficients. For amphoteric anions such as glyphosate (*N*-(phosphonomethyl)glycine) two different adsorbent/adsorbate interactions are identified: electrostatic adsorption and ligand exchange. Adsorption is limited to the external surface, and the distribution coefficients ( $K_d$ ) depend on the pH of the solution (Sanchez Martin et al., 1999). In a study of internal versus external uptake of anions, Bocclair et al. (2001) showed ferrocyanide does not displace interlayer carbonate from synthetic hydrotalcite but is adsorbed on the outside of the particles. Anion uptake here is controlled by specific hydrogen bonding requirements and not by charge density alone, a feature that can be used to control whether uptake will be both internal and external, or only external.

#### *H. Synthesis of Polyoxometallate-LDH*

Direct methods are not suitable for the preparation of oxoanion- and polyoxometallate (POM)-containing LDH because of their ability to incorporate or precipitate metal cations. Anion-exchange reactions are alternatively employed, requiring tight control of solution pH (Don Wang et al., 1995; Rives and Ulibarri., 1999). Indeed, the pH of exchange must be compatible with the domain of stability of the hydroxy layer and the anion to be intercalated. For example, complete exchange of chloride by  $V_{10}O_{28}^{6-}$  in [Zn–Al–Cl], [Zn–Cr–Cl], and [Ni–Al–Cl] using  $[NH_4]_6[V_{10}O_{28}^{6-}] \cdot 6H_2O$  must be carried out at pH = 4.5 (Kwon et al., 1988; Doeuff et al., 1989; Malherbe et al., 1997). At higher pH, carbonate intercalation may occur preventing complete exchange. Direct exchange of decavanadate in [Zn<sub>2</sub>–Al] can be facilitated by ultrasound treatment (Kooli et al., 1997b). It is noteworthy that such pH conditions are not compatible with the existence of the basic LDH matrix ([Mg–Al], [Ca–Al]). Silicate species in [Zn–Cr] and [Zn–Al] are intercalated either by anion exchange or coprecipitation (Schütz and Biloen, 1987; Depège et al., 1996). The pH of the solution must then be higher than 9.0 in order to prevent precipitation of undesirable amorphous silicates and metal hydroxides.

Pillaring ions may also be intercalated through a reconstruction process (Miyata and Hirose, 1978; Drezdon, 1988; Chibwe and Jones, 1989b; Dimotakis and Pinnavaia, 1990; Ulibarri et al., 1994; Pinnavaia, 1995; Hibino and Tsunashima, 1997; Nijs et al., 1999).

An alternative method involves exchange in expanded, organic anion-containing LDH (Drezdon, 1988; Dimotakis and Pinnavaia, 1990; Malherbe et al., 1997, 1998). Drezdon et al. (1988) were able to exchange decavanadate in [Mg–Al-terephthalate]. Terephthalate anions were previously introduced in the structure in order

to increase the basal spacing up to 1.4 nm and facilitate the diffusion of  $V_{10}O_{28}^{6-}$  under acidification (pH = 5.0). LDH with nonanoic, adipic, *p*-toluenesulphonic, and squaric acids in their anionic forms were also used as intermediate exchangers (Dimotakis and Pinnavaia, 1990). References to POM intercalation in LDH are given in Table 13.1.5.

Pillaring is also accomplished by the grafting of ethylene glycol or anions (chromate, dichromate, phosphate, phosphonate, or sulphonate) to the hydroxide layers (Depège et al., 1994; Costantino et al., 1997; Khaldi et al., 1998; Guimarães et al., 2000; Malherbe and Besse, 2000; Prévot et al., 2001). Grafting reduces the basal spacing.

Owing to the relatively high-layer charge density of LDH, the intercalated anions are sometimes close packed in the interlayer space.

### I. Synthesis of Organo-LDH

Both direct precipitation and anion-exchange reactions were extensively used for the intercalation of organic anions in LDH (Meyn et al., 1990; Bonnet et al., 1997; Nijss et al., 1998; Prévot et al., 1998). Urea hydrolysis appears to be a good method to prepare organo-LDH of good crystallinity (Trujillano et al., 2002).

Amino acid-intercalated LDH were obtained by coprecipitation (Aisawa et al., 2001). The degree of intercalation is strongly dependent on pH due to the amphoteric character of amino acids. Recently, anion-exchange reaction as a soft chemistry process was intensively studied for intercalation of anions of pharmaceutical interest such as salicylate, citrate, glutamate, and aspartate (Tronto et al., 2001).

The preferential intercalation of organic anions in [Zn–Al] (in the order naphthalene-2,6-disulphonate > terephthalate ≫ anthraquinone-2,6-disulphonate) was interpreted in terms of the molecular recognition ability of the LDH structure (Kuk and Huh, 1998).

Table 13.1.5. References for POM–LDH

LDH	POM anions	References
[Mg <sub>2</sub> –Al]	$V_{10}O_{28}^{6-}$	Drezdon (1988)
[Mg <sub>2</sub> –Al]	$V_{10}O_{28}^{6-}$	Dimotakis and Pinnavaia (1990)
[Mg <sub>2</sub> –Al]	$SiW_9V_3O_{40}^{7-}$	Weber et al. (1993)
[Zn <sub>2</sub> –Al]	$V_{10}O_{28}^{6-}$	Kooli and Jones (1995)
[Zn <sub>2</sub> –Al]	$SiW_{11}O_{39}Co(H_2O)^{6-}$	Hu et al. (1997)
[Zn <sub>2</sub> –Al]	$\alpha-[SiV_3W_9O_{40}]^{7-}$	Kwon and Pinnavaia (1992)
	$\alpha-[BV(IV)W_{11}O_{40}]^{7-}$	
	$\alpha-[PV_3W_9O_{40}]^{6-}$	
	$\alpha-[H_2W_{12}O_{40}]^{6-}$	
[Zn <sub>2</sub> –Al]	$SiW_{11}O_{39}$ , $SiW_{11}O_{39}Mn(H_2O)$	Guo et al. (2002)

When direct intercalation and standard exchange reactions are unsuccessful, alternative methods can be used. For instance, Dimotakis et al. (1990) reacted synthetic meixnerite,  $[\text{Mg}_3\text{Al}(\text{OH})_8]\text{OH} \cdot 2\text{H}_2\text{O}$ , with the free acid form of the desired anion in the presence of glycerol as a swelling agent. Reaction with nonanoic, adipic, *p*-toluenesulphonic, and squaric acids gives the corresponding intercalates in quantitative yield as single crystalline phases with basal spacings of 2.02, 1.44, 1.74, and 1.01 nm. The reaction of the basic Mg–Al mixed oxides obtained by calcination of the hydrotalcite with molten organic acids leads to the reconstruction of the LDH with intercalated organic anions (Carlino et al., 1996).

A new method of anion exchange was proposed by Crepaldi et al. (2000b). An anionic surfactant intercalated LDH is contacted with a solution containing the anion to be exchanged and a cationic surfactant. The anion exchange is favoured by the formation of a salt between the anionic and cationic surfactants, which are easily separated from the clay aqueous suspension with an organic solvent.

### *J. Synthesis of LDH-Based Nanocomposites*

There are several possible strategies to incorporate a polymer into LDH (Schöllhorn, 1996) (see also Chapter 10.3): (i) intercalation of the monomer and subsequent in situ polymerization, (ii) direct intercalation of extended polymer chains via exchange reactions (in the case of low molecular-weight species) or via coprecipitation, (iii) transformation of the host material into a colloidal dispersion and subsequent re-stacking in presence of the polymer, and (iv) reconstruction of the LDH structure in the presence of the polymer (Table 13.1.6).

In situ polymerization is highly suitable and was achieved by incorporation of various monomers, such as aniline, aminocaproic acid, or styrene sulphonate. The process is limited by two factors (Leroux and Besse, 2001; Leroux et al., 2001b): (i) monomer-to-monomer distance when the monomer is strongly anchored (or grafted) to the host matrix, i.e., its degree of freedom must somehow be in agreement with the layer charge; and (ii) the polymerization conditions (temperature, pH, or redox reaction) must leave the layer structure intact.

Acrylate- $[\text{Mg}_2\text{Al}]$  LDH hybrid material, obtained by exchange of  $\text{Cl}^-$  or  $\text{NO}_3^-$  can be polymerized at 80 °C (Tanaka et al., 1989). Carbonate LDH phase does not react with acrylate anions. Acrylic acid, intercalated into an iron-substituted nickel LDH material, can be polymerized by potassium persulphate (Rey et al., 1999).

Challier and Slade (1994) were the first to intercalate conjugated polymers into the LDH framework. Terephthalate and hexacyanoferrate-exchanged  $[\text{Cu}_2\text{Cr}]$  LDH phases are used as host matrices for the oxidative polymerization of aniline. An alternative method consists of intercalation of a soluble anionic monomer such as aniline-2-sulphonate or metanilic acid (3-aminobenzene sulphonate— $\text{H}_2\text{NC}_6\text{H}_4\text{SO}_3\text{H}$ ). These monomers can polymerize under less drastic conditions than aniline, giving rise to a relatively well-ordered system (Moujahid et al., 2002b). Poly( $\alpha,\beta$  aspartate) was intercalated into  $[\text{Mg}_3\text{Al}]$  LDH by in situ thermal



Table 13.1.6. LDH-polymer nanocomposites

LDH-polymer	Pathway	References
LiAl-PANI	a	Isupov et al. (2001)
CuCr-PANI	a	Moujahid et al. (2002b)
CuAl-PANI	a	Challier and Slade (1994)
CaAl-PVA	a	Messersmith and Stupp (1995)
MgAl-poly( $\alpha,\beta$ -aspartate)	a, b1	Whilton et al. (1997)
MgAl-PSS	b2	Oriakhi et al. (1997)
ZnAl-PSS	b2	Oriakhi et al. (1997)
	a, b2	Moujahid et al. (2002a)
MgAl-PS	a	Shouldice et al. (1995)
MgAl-PA, PVS	b2	Wilson et al. (1999)
ZnAl-PA, PVS	b2	Oriakhi et al. (1996)
CoAl-PVS	b2	Oriakhi et al. (1996)
CaAl-PA, PVS, PSS	b2	Oriakhi et al. (1996)
MgAl-PA	a	Tanaka et al. (1989)
NiFe-PA	b1	Rey et al. (1999)
ZnAl-PSS	a, b1, c	Leroux and Besse (2001)

*Note:* PANI, poly(aniline); PVA, poly(vinylalcohol); PSS, poly(styrene sulphonate); PVS, poly(vinyl sulphonate); PA, poly(acrylic acid). Pathways: a, in situ polymerization; b1, polymer incorporation; b2, polymer coprecipitation; c, restacking.

polycondensation or by direct intercalation as a co-solute in the basic reaction solution (Whilton et al., 1997).

Generally, the presence of polymer not only affects the crystallinity but also the dimension and morphology of the host material but enhances the thermal stability of the LDH.

#### K. LDH with Intercalated Nanoparticles

In order to prepare mesoporous materials or multifunctional catalysts, intercalation of oxide nanoparticles was performed in different ways. Manganese oxide nanoparticles were intercalated into Mg-Al LDH by ion exchange of interlayer nitrate with permanganate anion, followed by reduction with organic reagents (D(+)glucose, ethanol, L(+)ascorbic acid) or by photodecomposition (Villegas et al., 2002).

The requirement by industry for materials with a high surface area stimulated research into developing of nano-sized LDH. Nano-size  $\text{Co}^{\text{II}}$ Al-hydrotalcite-like particles (5–7 nm) on  $\gamma\text{-Al}_2\text{O}_3$  as support were synthesized by Xu et al. (2001) and Trainor et al. (2000).  $\gamma\text{-Al}_2\text{O}_3$  also acts as the source of  $\text{Al}^{3+}$  ions. Zhao et al. (2002) synthesized LDH  $[\text{Mg}_{1-x}\text{Al}_x(\text{OH})_2](\text{CO}_3)_{x/2} \cdot y\text{H}_2\text{O}$  ( $x = 1.7\text{--}3.3$ ) by separating the nucleation and ageing steps. The key features of this method are a very rapid mixing



and nucleation process in a colloid mill followed by separated ageing. Uniform crystals with a narrow range of diameters are obtained.

### *L. Grafting Reactions*

After grafting, the interlayer anions are not exchanged with other anions, and are then stabilized in the interlayer space (Costantino et al., 1997). Grafting also occurs in other combinations of LDH and guest anions, such as Cu–Cr LDH/ $\text{CrO}_4^{2-}$  and  $\text{Cr}_2\text{O}_7^{2-}$ , Zn–Al LDH/ethylene glycol, and Zn–Al and Cu–Cr LDH/organic anion (Depège et al., 1994; Costantino and Pinnavaia, 1995; Khaldi et al., 1998; Prévot et al., 1998; Guimarães et al., 2000; Malherbe and Besse, 2000; Prévot et al., 2001).

## 13.1.5. STRUCTURE

### *A. General*

The first structural studies were performed by Allmann (1968) and Ingram and Taylor (1967), using monocrystals of sjögrenite and pyroaurite. The former mineral crystallizes in a hexagonal symmetry with the space group  $\text{P6}_3/\text{mmc}$  with lattice parameters  $a = 0.316 \text{ nm}$  and  $c = 1.566 \text{ nm}$  (twice the basal spacing). The stacking sequence of the layers is of the type 2H (–AB–BA–AB–). The cell has  $Z = 1/4$  and the formula is  $\text{Mg}_6\text{Fe}_2(\text{OH})_{16}\text{CO}_3 \cdot 4\text{H}_2\text{O}$ . The pyroaurite crystallizes in rhombohedral symmetry, space group  $\text{R-3m}$ , with the cell parameters  $a = 0.311 \text{ nm}$  and  $c = 2.341 \text{ nm}$ . The stacking sequence is of the 3R type (–AB–BC–CA–AB–). The crystal structure of shigaite  $[\text{Mn}_2\text{Al}(\text{OH})_6]_3(\text{SO}_4)_2\text{Na}(\text{H}_2\text{O})_6 \cdot 6\text{H}_2\text{O}$  is rhombohedral, space group  $\text{R-3}$ , with cell parameters  $a = 0.9512 \text{ nm}$  and  $c = 3.3.74 \text{ nm}$  (Cooper and Hawthorne, 1996).

The stacking sequences 3R and 2H are often found. Natural  $\text{Mg}_6\text{Al}_2(\text{OH})_{16}\text{CO}_3 \cdot 4\text{H}_2\text{O}$  may crystallize in  $2\text{H}_1$  (manasseite) or  $3\text{R}_1$  (hydrotalcite) structural polytypes.  $1\text{H}$  is observed for the hydrated sulphate phase (Ennadi et al., 1994). Recently, a polytype  $3\text{R}_2$  (–AB–CA–BC–AB–) is reported for a MgAl LDH prepared by hydrothermal treatment of aluminium oxide and magnesium oxide (Newman and Jones, 2002). Many synthetic LDH such as  $\text{Zn}_2\text{Al}(\text{OH})_6\text{Cl} \cdot 2\text{H}_2\text{O}$  (Fig. 13.1.3) crystallize in the 3R structural polytype.

More complexed stacking is observed in  $\text{LiAl}_2(\text{OH})_7 \cdot 2\text{H}_2\text{O}$  (Thiel et al., 1993). On the basis of a Rietveld refinement, the authors showed that the cations within each  $[\text{LiAl}_2(\text{OH})_6]^+$  layer are ordered but their relative positions in successive layers are random. Indexing in a hexagonal cell indicates a C-centred monoclinic cell with  $b = a\sqrt{3}$  and  $\cos \beta = -a/3c$ . A 12-layer model (with up to 54 layers) is also proposed.

In the case of hydrocalumite types (Taylor, 1973; Kirkpatrick et al., 1999; Kalinichev et al., 2000), the highest symmetry of the layers  $[\text{Ca}_2\text{Al}(\text{OH})_6]^+$  is P-3, the

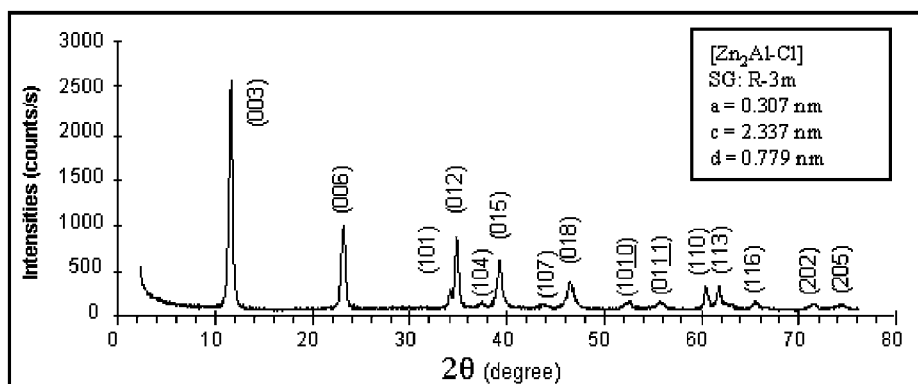


Fig. 13.1.3. X-ray diffraction pattern of  $\text{Zn}_2\text{Al}(\text{OH})_6\text{Cl} \cdot 2\text{H}_2\text{O}$ .

water molecules being linked to  $\text{Ca}^{2+}$  ions. The nature of the interlayer anions determines the space group. For large anions, the space group is R-3, while for small anions (such as  $\text{Cl}^-$ ) it is C2/c.  $\text{Ca}_2\text{Al}(\text{OH})_6\text{NO}_3 \cdot 2\text{H}_2\text{O}$  shows a structural transition from P-3c1 to R-3c induced by grafting of  $\text{NO}_3^-$  anions (Meyn et al., 1990).

### B. Cation and Anion Ordering

The question of order within the LDH sheets (Vucelic et al., 1995, 1997) is important for catalytic applications where large surface areas combined with a high degree of metal dispersion are required.

Structural cation ordering is indicated by the presence of additional diffraction peaks related to superlattices as observed in pyroaurite ( $\text{Mg}_{2,3}\text{Fe}-\text{NO}_3$ ) (Vucelic et al., 1997), and ( $\text{LiAl}_2-\text{OH}$ ) (Thiel et al., 1993; Besserguenev et al., 1997). For the latter compound, the ordering of the cations is explained by migration of  $\text{Li}^+$  ions into the empty octahedra sites. Apart from these few cases, there is a general lack of cation ordering because of the large difference in size between  $\text{M}^{\text{II}}$  and  $\text{M}^{\text{III}}$  cations (Bellotto et al., 1996). This applies to many LDH with  $\text{Al}^{3+}$  as trivalent cations. Yet, despite the lack of long-range ordering, local ordering is generally observed by XAS spectroscopy (see below and also Chapter 12.3). Cation ordering requires particular structural conditions. Thus, a M(II)/M(III) ratio of 2 implies that each divalent cation is surrounded by 3 M(II) and 3 M(III) and that the trivalent cations are surrounded by 6 M(II) (Hofmeister and von Platen, 1992). A change in this ratio also induces a change in the theoretical local order.

The interlayer anions may also show a regular distribution, exemplified by the highly ordered two-dimensional superlattice present in ( $\text{Zn}_2\text{Al}-\text{SO}_4^{2-}$ ) (Bookin et al., 1993).

### C. Stacking Phenomena

#### *Staging*

Most of the articles on the intercalation chemistry of LDH describe the fully exchanged materials, while only a few report on mixed ion-exchanged forms. Mendiboure and Schöllhorn (1987) investigated the competitive intercalation of  $\text{ClO}_4^-$  and  $\text{NO}_3^-$  into  $[\text{ZnCr}]$  LDH. The two phases coexist, implying that the formation of phases with mixed anions in the interlayer space is energetically unfavourable. Theoretical models would suggest that regular stacking, referred to as 'staging', as commonly observed in graphite, does not occur in LDH due to the rigidity of the layers (Schon et al., 1988). However, using in situ time-resolved XRD, Fogg et al. (1998) demonstrated that  $[\text{LiAl}_2(\text{OH})_6\text{Cl} \cdot 2\text{H}_2\text{O}]$  can form second-stage intermediates, i.e., every second layer is filled by dicarboxylate anions (succinate, tartrate, adipate, fumarate, maleate, L-malate, phthalate, and terephthalate). This technique was also used by O'Hare et al. (2000) to investigate the intercalation chemistry of layer materials. Kaneyoshi and Jones (1998) observed layer interstratification during the interlayer exchange of terephthalate with chloride and nitrate anions. This is ascribed to two orientations of terephthalate anions, vertical and horizontal, which can be controlled by varying the layer charge density and the extent of drying. On the other hand, Iyi et al. (2002), studying the direct synthesis of mixed hydroxide/azobenzene intercalates, assume a segregation of the hydrophobic organic anions and the hydrophilic inorganic anions, similar to that reported for staged fluorohectorites (Ijdo and Pannavaia, 1998). Colloidal layered nanoparticles are formed in solution that subsequently transform into staging structures when dried. These few cases show that staging in LDH can occur either during the exchange process, or by direct synthesis, and is associated with different interlayer contents or different orientations of the same molecule.

#### *Random Stacking*

Synthetic LDH commonly show faults in the stacking of successive layers as a result of fine intergrowth of the rhombohedral with hexagonal polytypes. This random stacking sequence is expected on the basis of the equal layer–interlayer topology of the two polytypes. In a turbostratically disordered phase, the layers are randomly orientated about the  $c$ -axis, thus eliminating all  $(hkl)$  reflections. The only reflections seen are the  $(00l)$  and the two-dimensional  $(hk)$  bands. In particular, stacking faults are indicated by the broadness and the asymmetry of the  $(01l)$  reflections. Although routinely observed in synthetic materials, only a few studies refer to the influence of preparation techniques, composition, and nature of the layer–interlayer bonds, on layer-stacking faults (Pausch et al., 1986; Clause et al., 1992). XRD measurements on a series of  $\text{NiAl}-\text{CO}_3^{2-}$  LDH powder samples by Solin et al. (1996) and Hines et al. (1997) provided evidence for a  $(\sqrt{3} \times \sqrt{3})R30^\circ$  honeycomb superlattice ordering in the octahedral sheet only for  $x = 0.33$  but not for other compositions. The anionic layer also forms a commensurable in-plane structure  $(\sqrt{13} \times \sqrt{13})R13.9^\circ$  at  $x = 0.33$

but is laterally uncorrelated despite the highly ordered stacking of the layers (3R). This random anionic layer stacking was attributed to the high degree of degeneracy (26-fold) of carbonate ion sites. Bellotto et al. (1996a) examined the layer stacking arrangement of MgAl, MgGa, and NiAl by XRD analysis with the DIFFAX program. The occurrence of faults is quantified by a 'fault probability', describing the probability for a specific layer sequence to be arranged in rhombohedral or hexagonal stacking. The stacking arrangement is random for the solids investigated, except for MgAl–CO<sub>3</sub><sup>2–</sup>, which shows a preference for the rhombohedral polytype. This feature is assigned to a predominantly Coulombic layer–interlayer bonding. The stacking sequence is not affected by hydrothermal treatments at 470 K, which only increased crystallinity. The higher entropy of random sequences can account for their thermal stability.

#### D. Guest–Host Interactions

Interactions between guests (anions) and host (the brucite-like layer) are controlled by electrostatic interactions and hydrogen bonding between the hydroxyl surface groups and the anions. The interaction depends on the ordering of the metal cations in the layer, and the chemical nature of the anion. For ordered LDH structures such as [Li–Al], the anions are aligned perpendicular to the Li<sup>+</sup>–Li<sup>+</sup> axis (Fogg and O' Hare, 1999), showing the key role of electrostatic interactions in this structure.

Generally, oxoanions strongly interact with the hydroxyl surface groups and a dense packing of the anions is often achieved. This can be explained in terms of symmetry compatibility between the oxoanions polyhedra and the octahedral layers of the host structure. The various hexagonal or rhomboedrical stacking of the LDH layers define octahedral, prismatic, and tetrahedral interlayer crystallographic sites, which can ideally accommodate monomeric oxoanions. Optimal hydrogen bonds are formed when the Td or Oh units are arranged face to face or corner to corner. As an example, the structure of the [Zn–Cr–SO<sub>4</sub>] interlayer domains is described as an ordered arrangement of alternate inverse interlayer SO<sub>4</sub> tetrahedra. The tetrahedra retain their C<sub>3</sub>-axis perpendicular to the layer, with one oxygen pointing to a metal cation of the octahedral layer and the other three oxygens facing three OH groups of the opposite layer. The short hydrogen bond lengths of 0.293 and 0.271 nm indicate strong interactions between the layers and sulphate anions, resulting in a 0.892 nm basal spacing (Khaldi et al., 1997). The structural series of XO<sub>4</sub>-containing LDH ([Zn–Cr–SO<sub>4</sub>], [Zn–Al–SO<sub>4</sub>], [Cu–Cr–SO<sub>4</sub>], [Zn–Al–CrO<sub>4</sub>], [Cu–Cr–CrO<sub>4</sub>], [Zn–Cr–Cr<sub>2</sub>O<sub>7</sub>], and [Cu–Cr–Cr<sub>2</sub>O<sub>7</sub>]) shows basal spacings close to the *d* value of [Zn–Cr–SO<sub>4</sub>]. In all these phases, the oxoanions are orientated similar to the SO<sub>4</sub><sup>2–</sup> ions in the reference material. Similar *d* values obtain even with the more flexible Cr<sub>2</sub>O<sub>7</sub> because the anions can lie flat and parallel to the layers (Bigey et al., 1997).

When interlayer anions strongly interact with the layers, modification of molecular dynamic is expected. Intercalation of CO<sub>3</sub><sup>2–</sup>, SO<sub>4</sub><sup>2–</sup>, and ClO<sub>4</sub><sup>–</sup> into [Mg–Al] LDH lowers the symmetry of the anions due to hydrogen bonding with intercalated

water molecules and OH groups as shown by Fourier transform infrared (FTIR) and Raman spectroscopy (Kloprogge et al., 2002). On the other hand, the  $\text{NO}_3^-$  anions seem to be randomly distributed in the interlayer space because their vibration bands remain unaffected during intercalation.

Cell parameter refinement for intercalated silicate anions  $[\text{Zn-Cr-SiO}_4]$  gives the typical hexagonal 3R lattice as for  $[\text{Zn-Cr-Cl}]$  (Schütz and Biloen, 1987; Depège et al., 1996). Additional reflections of the  $[\text{Zn-Al-SiO}_4]$  phase are attributed to a superstructural arrangement of the silicate species in the LDH interlayer space. The XRD pattern can be indexed in the 1H stacking hexagonal mode with a unit cell parameter  $a = a_0\sqrt{3}$ . The  $^{29}\text{Si}$  NMR chemical shifts are similar to those in phyllosilicates, suggesting that the  $\text{SiO}_4^{4-}$  groups in the LDH phases are arranged similarly, and that the silicon environment is either of type  $\text{Si}(\text{OSi})_{3-y}(\text{OM})_y(\text{OH})$  or  $\text{Si}(\text{OSi})_{3-y}(\text{OM})_y(\text{OM}')$  (with typically  $\text{M} = \text{Al}$  and  $\text{M}'$  in octahedral site) (Fig. 13.1.4).

Very short basal spacings are obtained with voluminous anions such as  $\text{V}_{10}\text{O}_{28}^{6-}$  because of a flat orientation of the decaoctahedra building block of  $\text{V}_{10}\text{O}_{28}^{6-}$ . The limited size of the oxometallate anions and their low charge density do not allow the formation of interlayer microporosity. Indeed, the basal spacing of LDH containing oxopolyanions never surpasses 1.4 nm, whereas intercalation of  $\text{Al}_{13}$  hydroxocations into clay minerals yields a distinctly greater interlayer expansion (Pinnavaia, 1987).

Organic anions always interact with their anionic groups ( $-\text{CO}_2^-$ ,  $-\text{SO}_3^-$ ,  $-\text{PO}_3^{2-}$ ,  $-\text{OSO}_3^-$ ,  $-\text{OPO}_3^{2-}$ ) being strongly hydrogen bonded to the surface hydroxyl groups, while their hydrophobic hydrocarbon chains are pushed far away from the hydrophilic layer surface, and adopt the lowest energy conformation (Meyn et al., 1990).  $\alpha$ ,  $\omega$ -Dianionic molecules can bridge two adjacent layers, giving a basal spacing proportional to the length of the hydrocarbon chain. With monovalent long-chain anions, either a bilayer or an interdigitated arrangement is formed. As a result, the basal spacing is usually greater than 1.5 nm (Sanz and Serratosa, 1984; Meyn et al., 1990; Bonnet et al., 1996; Prévot et al., 1998; Costantino et al., 1999).

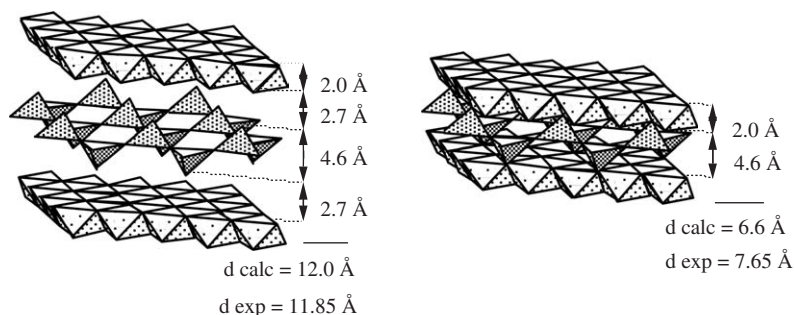


Fig. 13.1.4. Polycondensation of silicate layers in double layered hydroxides.

In particular, the interlayer packing depends on the relation between the charge and size of the organic anions and the equivalent area of the layer. When the cross-sectional area of the anions is similar to the equivalent area, optimal packing is obtained. This is the case for dodecylsulphate-containing  $[\text{Zn}_2\text{Al}]$  LDH. The anions adopt the same packing as in their sodium salt, with electrostatic and hydrogen bonding between anionic head groups and the surface OH groups and van der Waals bonding between lateral hydrocarbon chains. Guest–guest interactions are then determined by the layer charge density, which is a determining factor in the adsorption of neutral molecules (alkyl amines and alcohols) in alkylsulphate-containing LDH (Boehm et al., 1977; Kopka et al., 1988; Meyn et al., 1990, 1993), catalysis reactions, and in situ polymerization (Leroux and Besse, 2001).

### *E. Analytical Methods*

Since synthetic LDH are commonly not highly crystalline, various and complementary techniques are needed to get structural information.

#### *XRD*

Diffraction peaks for synthetic LDH are usually refined in R-3m space group in rhomboedral symmetry, and the parameters calculated according to the equation  $1/d^2 = [4(h^2 + hk + k^2)/3a^2] + l^2/c^2$ . The basal spacing is expected to decrease with increasing layer charge density (and vice versa) due to enhanced electrostatic attraction between hydroxide layers and interlayer anions. For an ideal in-plane octahedral assembly, the size of the octahedra sharing edges is related to the metal–oxygen distance ( $d$ ) by the relation  $a = \sqrt{2}d(\text{M–O})$  and the latter to the ionic radius ( $r$ ) by the relation  $d(\text{M–O}) = (1-x)r(\text{M}^{2+}) + xr(\text{M}^{3+})$ . The variation of the lattice parameter  $a$  with the M(III) content is given by  $\delta a/\delta x = -\sqrt{2}[r(\text{M}^{2+}) - r(\text{M}^{3+})]$ . This relation is often used to assess the cation substitution in LDH.

The coherence length along the stacking direction may be estimated from the (001) FWHM using the Scherrer formula  $D_{hkl} = K\lambda/\beta_{1/2}\cos\theta$ , where  $\lambda$  is the X-ray wavelength,  $\theta$  the diffraction angle;  $\beta_{1/2}$  the full-width at half-maximum intensity; and  $K$  is a constant usually taken to be equal to 0.9 ( $\text{CuK}_\alpha$  radiation). The values are highly dependent on the LDH composition. For synthetic hydrotalcite ( $\text{Mg}_2\text{Al}$ ) a value of 90 nm is calculated, corresponding roughly to 100 layers (Oriakhi et al., 1997), 37 nm for  $\text{Zn}_3\text{Al}$  (Prévot et al., 1998), and 18 nm for  $\text{Ni}_2\text{Al}$  (Oriakhi et al., 1997).

EDX is useful for studying the kinetics of formation or exchange reaction. When time resolved, it allows staging phenomena in some LDH to be observed (Khan and O'Hare, 2002).

#### *Neutron Diffraction*

Structures of  $\text{LiAl}_2(\text{OH})_6\text{X}$  ( $\text{X} = \text{Cl}, \text{Br}, \text{NO}_3$ ) dehydrated phases may be determined by neutron powder diffraction technique (Besserguenev et al., 1997). These phases are isomorphous and crystallize in the  $\text{P6}_3/\text{mcm}$  space group. This technique is also

applied to improve understanding of the thermal evolution of the Pd/Mg/Al system (segregation and oxide formation) (Basile et al., 2000).

Inelastic neutron scattering was used to study the interlayer water (Kagunya et al., 1998). Quasi-elastic neutron scattering showed previously that the water molecules are not fixed in one location, but exhibit translational diffusion as well as reorientation motions. The basal spacing of the LDH influences water mobility (Kagunya, 1996).

### XAS

Because of the poorly crystalline nature of LDH, XAS was widely used to investigate LDH formation (Roussel et al., 2001; Yamaguchi et al., 2002). XAS indicates local ordering for pyroaurite (Vucelic et al., 1997) and other synthetic LDH such as  $\text{Co}_2\text{Fe}_y\text{Al}_{1-y}(\text{OH})_6\text{Cl} \cdot n\text{H}_2\text{O}$  (Intissar et al., 2002).

EXAFS shows structural changes arising from substitutions as in  $(\text{Co}_{1-y}\text{Cu}_y)_2\text{Al}(\text{OH})_6\text{Cl} \cdot n\text{H}_2\text{O}$ , where for  $y = 1$  the local structure is similar to that of bottallackite (Leroux et al., 2002). When the M(II)/M(III) ratio is greatly changed as in  $\text{Co}_x\text{Al}(\text{OH})_{2(1+x)}\text{Cl} \cdot n\text{H}_2\text{O}$ , the decrease of layer charge density is compensated by oxidation Co(II) to Co(III) (Leroux et al., 2001a) (Fig. 13.1.5).

EXAFS is also used to determine the interlayer structure and possible grafting reactions. For example, the W LIII-edge and Nb K-edge absorption shows that hexametallate anions,  $\text{Nb}_x\text{W}_{6-x}\text{O}_{19}^{(x+2)-}$ , orient with their  $C_3$ -axis perpendicular to the host layers (Evans et al., 1996). For  $\text{CrO}_4^{2-}$  and  $\text{Cr}_2\text{O}_7^{2-}$ , Cr-K edge absorption

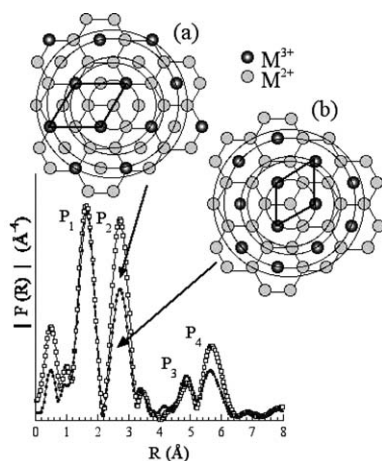


Fig. 13.1.5. Moduli of the Fourier transform for  $\text{Co}_n\text{Al}(\text{OH})_{2(n+1)}\text{Cl} \cdot n\text{H}_2\text{O}$ : (a)  $n = 3$  and (b)  $n = 2$ . The distances are not corrected from atomic phases. The ideal cation intralamellar arrangement is displayed. Co K-edge EXAFS spectra were recorded at the beam line D44 (LURE, Orsay).



shows that the decrease in basal spacing is related to grafting of these oxoanions to the surface OH groups (Malherbe et al., 1999).

Sulphur K-edge absorption was used to determine the degree of interaction of styrene sulphonate with the ZnAl LDH surface. To illustrate the high selectivity of the XAS technique, an ill-defined ZnS-like phase was detected after heating to 600 °C under nitrogen (Moujahid et al., 2003).

#### *Raman and FTIR*

The application of both Raman and FTIR spectroscopy to the characterization of LDH has been reviewed by Klopogge and Frost (2001).

FTIR and Raman spectroscopy were used to investigate the local structures of LDH such as  $M_6Al_2(OH)_{13}CO_3 \cdot nH_2O$  ( $M = Mg, Ni, Co$ ) (Klopogge and Frost, 1999) and  $Mg_xZn_{6-x}Al_2(OH)_{16}(CO_3) \cdot 4H_2O$  (Johnson et al., 2002). Raman microspectroscopy of hydrocalumites reveal the dynamic disorder resulting from the free rotation of the nitrate groups around the [001] axis, and from the half-bonded and half-free  $H_2O$  molecules (Renaudin and François, 1999). The orientation of  $Co^{2+}$  and  $Ni^{2+}$  phthalocyanine in the interlayer space was also studied by the Raman spectroscopy. The results indicate interactions of the  $\pi$  electrons with the surface, causing the organic molecules to adopt a flat orientation with respect to the surface (De Fria et al., 1998).

Raman spectroscopy was also used to investigate the kinetics and mechanisms of catalytic activity, including the decomposition of  $H_2O_2$  by a molybdate-exchanged LDH (Sels et al., 2001), and the epoxidation of geraniol by a vanadium-pillared LDH (Villa et al., 2001).

FTIR spectroscopy is largely used to follow the alteration of the vibration bands after intercalation and/or thermal treatment (Rives, 2002; Guo et al., 2002; Villegas et al., 2002). This technique is also useful for assessing catalytic activity (e.g., catalytic oxidation of sulphides (Choudary et al., 2002) and wet air oxidation of phenol (Alejandre et al., 2001)), as well as surface acid–base properties. In the latter case, the shift of a particular vibration band of a probe molecule, such as  $CDCl_3$  or  $CO_2$ , is used to scale the interactions with basic surface sites, while the absorption bands for pyridine and  $NH_3$  provide an estimate of Brønsted and Lewis surface acidity (Lopez-Salinas et al., 1997a, Chisem et al., 1998; Kooli et al., 1997c; Prinetto et al., 2000a).

#### *Solid-State NMR*

Different nuclei located either in the inorganic layers or the interlayer space may be investigated by solid-state NMR spectroscopy.  $^{27}Al$  NMR is commonly used to determine the degree of conversion of  $Al^{3+}$  from octahedral to tetrahedral environment during the thermal decomposition or reconstruction of LDH phases (Rocha et al., 1999).  $^{27}Al$  and  $^{71}Ga$  MAS NMR were used to investigate the thermal decomposition of Mg/Al and Mg/Ga LDH (Aramendia et al., 1999).

Characterization of the interlayer species and their interactions with the host structure are the subject of numerous NMR studies. The ordering of interlayer water



and carbonate was studied using  $^1\text{H}$  and  $^{13}\text{C}$  NMR techniques (van der Pol et al., 1994).

Incorporation of  $\text{C}_{60}$  into LDH was established by measuring the spin-lattice relaxation time ( $T_1$ ) by  $^{13}\text{C}$  NMR. The  $\text{C}_{60}$  guest molecule does not freely rotate as in the pure solid form (Tseng et al., 1996).

Other notable NMR studies are concerned with intercalated silicates by  $^{29}\text{Si}$  (Depège et al., 1996), phenylphosphonic acid by  $^{31}\text{P}$  (Carlino et al., 1996), styrene sulphonate and poly(styrene) sulphonate by  $^{13}\text{C}$  CP MAS (Moujahid et al., 2002a), and borate by  $^{11}\text{B}$  (del Arco et al., 2000). Static  $^{51}\text{V}$  NMR spectra indicate hyperfine magnetic interaction exerted by unpaired electrons of  $\text{Ni}^{2+}$  on the inserted vanadium nuclei in NiCo LDH (Ménétrier et al., 1997).

NMR experiments on uncommon nuclei were also reported. For example, Hou and Kirkpatrick (2000) investigated the structures and dynamics of seleno-oxoanions in LDH phases by solid-state  $^{77}\text{Se}$  NMR. Although selenate is a tetrahedral anion, the observed  $^{77}\text{Se}$  chemical shift anisotropy is uniaxial when the anion is incorporated between the LDH layers. Static  $^{35}\text{Cl}$  NMR spectroscopy was performed on hydrotalcite and hydrocalumite samples (Hou et al., 2002). The collected data indicate that the chlorine environment varies significantly with the hydration state.  $^{27}\text{Al}$ ,  $^{35}\text{Cl}$ , and  $^6,^7\text{Li}$  nuclei in  $\text{LiAl}_2\text{-Cl}$  LDH phases were studied by Hou and Kirkpatrick (2001).

Further developments in this area would be expected with the application of two-dimensional heteronuclear-correlated MAS NMR spectroscopy, e.g.,  $^1\text{H}$ - $^{27}\text{Al}$  and  $^{27}\text{Al}$ - $^{31}\text{P}$  correlations (Fernandez et al., 2001; Alba et al., 2001).

### *$^{57}\text{Fe}$ Mössbauer Spectroscopy*

This technique provided information on the mechanisms of oxidation of Ni(II)-Fe(II) hydroxides in chloride-containing aqueous media leading to a Ni-Fe pyroaurite-type material (Refait and Génin, 1997).  $^{57}\text{Fe}$  Mössbauer spectroscopy was also used to study the in situ behaviour of a hydrated iron-substituted nickel hydroxide in a Ni/Cd electrochemical cell (Guerlou-Demourgues et al., 1996).

### *Computer Modeling*

By comparison with clay minerals, only a few computer-modelling studies on LDH materials were reported so far (Newman et al., 2001).

Molecular dynamics computer simulations of Mg/Al hydrotalcite containing  $\text{Cl}^-$  were performed to improve understanding of the structure, hydration, and swelling behaviour of LDH (Wang et al., 2001; Hou et al., 2002). Similar approaches were used by Kalinichev and Kirkpatrick (2002) on Friedel salt ( $\text{Ca}_2\text{Al}(\text{OH})_6\text{Cl}\cdot 2\text{H}_2\text{O}$ , hydrocalumite) and ettringite to model some components of crystalline cement phases. Bonapasta et al. (2001, 2002) modelled the cross-linking of polyacrylate and poly(vinyl alcohol) with Ca or Al atoms via the carboxylate or OH groups. This reaction may be a key factor determining the filling of large voids in macro defect-free cements.

The surface adsorption and intercalation of fluorescein anions into ZnAl hydrotalcite were computed based on the structure of the host and the dimensions of the guest compound (Costantino et al., 2000).

Other models were used to estimate the relative layer rigidity of LDH materials in comparison to other 2D structures. The dependence on composition of the basal spacing, determined by XRD, was simulated using an extended version of the discrete finite-layer rigidity model including both intralayer and interlayer rigidity effects (Solin et al., 1995).

### 13.1.6. MORPHOLOGY

#### *A. Size and Shape*

The shape of LDH particles is obviously dependent on the method of preparation. In the standard coprecipitation method both nucleation and growth steps occur simultaneously during synthesis. Particles are obtained with a high degree of crystallinity leading to well-resolved XRD patterns but with a wide range of sizes. The control of particle size is more effective by hydrothermal treatment or homogeneous precipitation using urea hydrolysis. Well-defined plate-like hydrotalcite particles with regular hexagonal shape and sizes between 2 and 20  $\mu\text{m}$  were prepared (Ogawa and Kaiho, 2002; Oh et al., 2002). The urea method always gives rise to larger particles.

Yun and Pinnavaia (1995) compared the effect of coprecipitation conditions on particle morphology and porosity. Fine-grained particles with rough surfaces, relatively high surface areas, and mesopores of size in the range 5–30 nm in size are obtained by coprecipitation at variable pH. On the other hand, at constant pH, larger, well-formed hexagonal particles with a narrower mesopore size distribution (about 2 nm radius) are obtained. Edge-face particle aggregation and co-facial layer stacking create interparticle mesopores. Structural defects in [Mg–Ga] were observed by TEM (Lopez-Salinas et al., 1998). Layers located near the edges of the particles are more loosely held together than those in the bulk of the particles. Adachi-Pagano et al. (2003) studied the effect of preparation procedure on particle size and aggregation of  $\text{Cu}_2\text{Cr}(\text{OH})_6\text{Cl}\cdot 2\text{H}_2\text{O}$  and  $\text{Mg}_2\text{Al}(\text{OH})_6(\text{CO}_3)_{0.5}\cdot 2\text{H}_2\text{O}$  (Fig. 13.1.6). Coprecipitation with long ageing time often favours a sand-rose morphology.

Morphology is also affected by chemical composition. Partial substitution of  $\text{Fe}^{2+}$  or  $\text{Cu}^{2+}$  for  $\text{Mg}^{2+}$  in synthetic hydrotalcite leads to a distinct change in textural properties (Carja et al., 2001). The  $\text{Cu}^{2+}$ -substituted LDH displays a relatively uniform porous structure with enlarged mesopores and decreased specific surface area compared with the unsubstituted  $\text{Mg}^{2+}$  compound. The  $\text{Fe}^{2+}$ -substituted LDH develops microporosity, non-uniform particles, decreased pore sizes, and increased specific surface area.

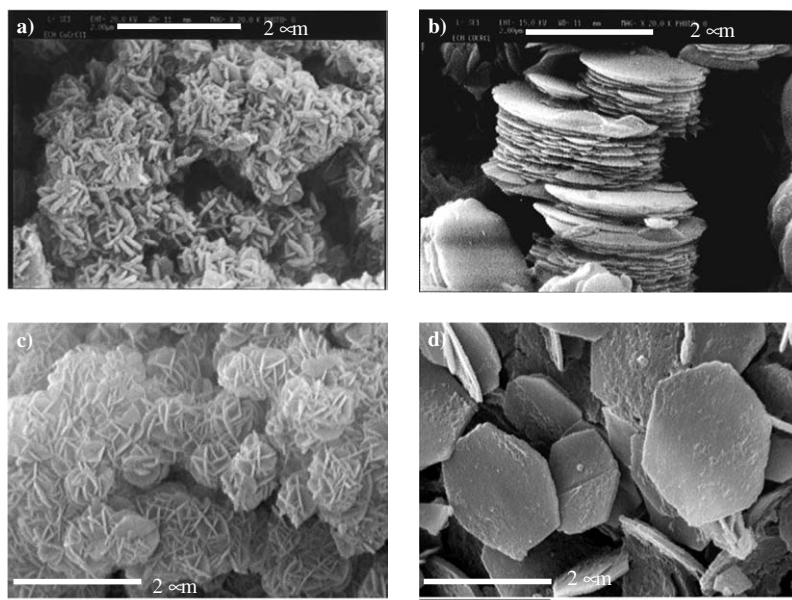


Fig. 13.1.6. SEM of  $\text{Cu}_2\text{Cr}(\text{OH})_6\text{Cl}\cdot 2\text{H}_2\text{O}$  prepared by (a)  $\text{CuO}/\text{CrCl}_3$ -induced hydrolysis and (b) coprecipitation (V. Prévot, unpublished results) and  $\text{Mg}_2\text{Al}(\text{OH})_6(\text{CO}_3)_{0.5}\cdot 2\text{H}_2\text{O}$  prepared by (c) coprecipitation and (d) urea method (Adashi-Pagano, et al., 2003).

Hydrotalcite-like materials with a unique sheet-like morphology and a diameter/thickness ratios  $> 100$  were prepared by reacting  $\text{MgO}$ ,  $\text{AlOOH}$ , and a monocarboxylic acid in aqueous media at  $80\text{--}90^\circ\text{C}$  for 6 h at  $\text{pH} > 7$  (Kelkar and Schutz, 1997a; Kelkar, et al., 1997b). In contrast to conventional hydrotalcites with hexagonal particle morphology, these materials have high mechanical strength making them useful industrially. Acicular particles of  $[\text{Mg}\text{--Al}]$  hydrotalcite were prepared by coprecipitation, and they show a high endothermic DSC peak and a wide temperature range of decomposition (Ren et al., 2002).

### B. Specific Surface Area and Porosity

The specific surface area of a single LDH layer with known composition and structure may be derived from the formula

$$S = a^2 \sqrt{3} \cdot 10^{-18} N / M$$

where  $N$  is the Avogadro's number ( $= 6.022 \times 10^{23}$ ),  $a$  the cell parameter (nm), and  $M$  the molecular weight of the unit formula. For  $\text{Zn}_2\text{Cr}(\text{OH})_6\text{Cl}\cdot 2\text{H}_2\text{O}$  and  $\text{Mg}_3\text{Al}(\text{OH})_8(\text{CO}_3)_{0.5}\cdot 2\text{H}_2\text{O}$ , the calculated  $S$  values are 817 and  $1285\text{ m}^2/\text{g}$ , respectively. Such high values are not measured because the internal surfaces are often

inaccessible. Typical values of the specific surface area measured by the BET technique range from 20 to 85 m<sup>2</sup>/g (del Arco et al., 1994). For Mg–Al LDH containing simple anions such as carbonate, chloride, and nitrate, the surface area is mostly less than 100 m<sup>2</sup>/g (Pesic et al., 1992; Di Cosimo et al., 1998; Hussein et al., 2001; Inacio et al., 2001). Hydrothermal crystallization decreases the surface area (Labajos et al., 1992). Synthesis by coprecipitation in mixed solutions of water and organic solvents increases the surface area (Malherbe et al., 1997; Inacio et al., 2001).

Nitrogen adsorption–desorption isotherms (type II with a narrow hysteresis) indicate that LDH-containing simple anions are mesoporous with no microporosity even when large POM pillars are intercalated (Labajos et al., 1992; Pesic et al., 1992; Inacio et al., 2001). However, [Mg–Al] LDH intercalated by [Fe(CN)<sub>6</sub>] complexes have an exceptionally high specific surface area of 499 m<sup>2</sup>/g (Nijs et al., 1999) and a narrow pore size distribution with the majority of pores <0.71 nm. A correlation is found between the Mg<sup>2+</sup>/Al<sup>3+</sup> ratio and the resulting microporosity after pillaring. The optimal ratio is about 3.3, resulting in a pillared [Fe(CN)<sub>6</sub>]–MgAl–LDH with a specific Langmuir surface area of 499 m<sup>2</sup>/g and a micropore volume between 0.158 and 0.177 mL/g.

### 13.1.7. FUNDAMENTAL PROPERTIES

#### A. Chemical Stability

Chemical stability is of importance to many practical applications in which LDH feature. For example, this parameter needs to be assessed when LDH are used as a sink of radioactive metal ions from nuclear waste repositories (Allda et al., 2002). In geochemical assessments, the stability of LDH is evaluated in terms of its solubility in water (Ford et al., 1999; Scheckel et al., 2000). Solubility data for metal hydroxides and LDH were derived from pH titration (Bocclair and Braterman, 1998, 1999; Bocclair et al., 1999). The stability of LDH increases in the order Mg<sup>2+</sup> < Mn<sup>2+</sup> < Co<sup>2+</sup> ≈ Ni<sup>2+</sup> < Zn<sup>2+</sup> for divalent cations, and Al<sup>3+</sup> < Fe<sup>3+</sup> for trivalent cations (Bocclair and Braterman, 1999). This trend accords with the pK<sub>sp</sub> values of the corresponding metal hydroxides (K<sub>sp</sub> is the solubility product). Because the pK<sub>sp</sub> of Mg(OH)<sub>2</sub> is smaller than that of Zn(OH)<sub>2</sub>, Mg-based LDH are more soluble. Thus, the aqueous solution of a Mg-based LDH is more basic than the corresponding aqueous solution of a Zn-based LDH. Saturated aqueous solutions of Mg–Al–Cl LDH and Zn–Al–Cl LDH, deaerated with Ar, have pH values of 8.91 and 6.97, respectively (Shaw et al., 1990).

In addition to direct measurements of solubility, Allda et al. (2002) calculated the aqueous solubility of an LDH from thermochemical data. The heat of formation and the free energy of formation of the carbonate form of an LDH are equal to the values for a physical mixture of the binary compounds, i.e., the metal hydroxides and carbonates. Their simple physical mixture model indicates that the aqueous

solubilities of LDH are affected by the interlayer anions. Relative to carbonate, silicate and borate decrease solubility, while nitrate and sulphate increase it.

### B. Thermal Stability

The thermal stability of LDH was intensely investigated because the thermal decomposition products are interesting as catalysts. Despite the diversity in composition most LDH exhibit a similar thermal decomposition behaviour. When heated, LDH release interlayer water up to ca. 250 °C, followed by dehydroxylation of the hydroxide layers, and decomposition of the interlayer anions at higher temperatures. The differential thermal analysis (DTA) curves of Mg–Al–CO<sub>3</sub> LDH show two major endothermic peaks (Fig. 13.1.7). The first peak (150–250 °C) corresponds to the loss of interlayer water, while the second (250–450 °C) arises from the decomposition of the hydroxide layers and carbonate anions. In some cases, the second peak splits into two peaks, the first of which corresponds to the loss of hydroxyl groups bound to Al, while the second of the split peaks represents the loss of hydroxyl groups bound to Mg together with decomposition of carbonate anions (Miyata, 1980). These weight-loss steps are observed in the corresponding TG curve. The XRD patterns indicate that the layer structure does not collapse with the loss of interlayer water (Fig. 13.1.8). Valente et al. (2000) measured the decomposition temperatures of carbonate forms of LDH containing various metal cations under the same experimental conditions. They found that the thermal stability increases in the order Co–Al < Zn–Al  $\approx$  Cu–Al < Mg–Fe  $\approx$  Ni–Al < Mg–Al  $\approx$  Mg–Cr. The highest decomposition temperature is ca. 400 °C for Mg–Al LDH and Mg–Cr LDH, and the lowest decomposition temperature is 220 °C for Co–Al LDH.

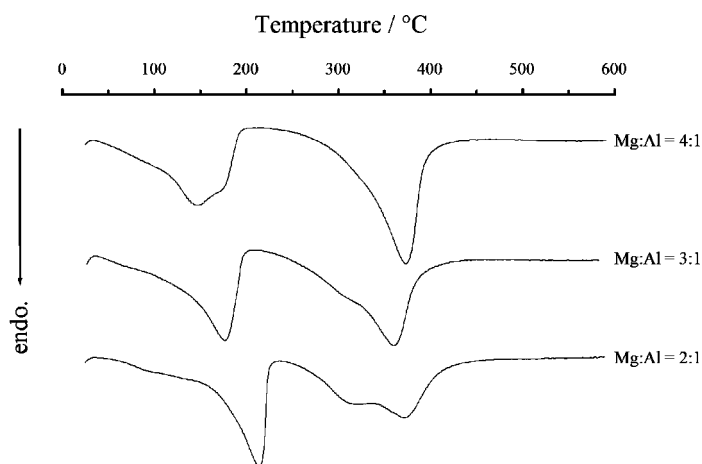


Fig. 13.1.7. DTA curves of Mg–Al–CO<sub>3</sub> LDHs having various Mg/Al atomic ratios. The Mg/Al ratio is indicated on each curve.

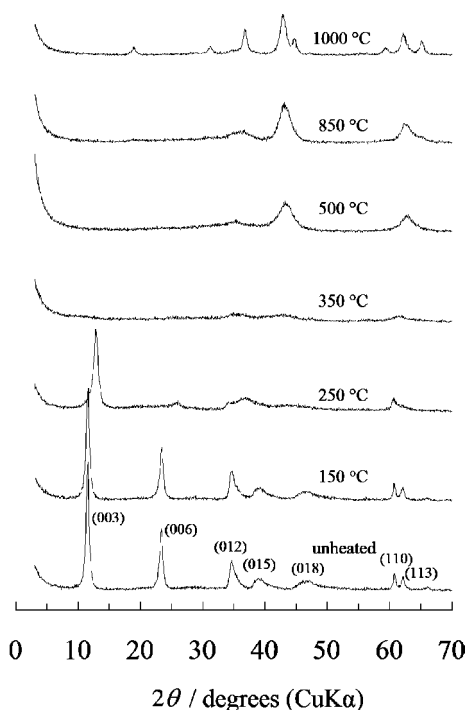


Fig. 13.1.8. Changes in the XRD pattern when Mg–Al–CO<sub>3</sub> LDH with Mg/Al = 2:1 is heated at various temperatures. The calcinations temperatures and Miller indices are indicated in the figure.

The thermal decomposition sequence of Mg-based LDH, as typified by Mg–Al–CO<sub>3</sub> LDH, is well documented. The MgO phase is observed between ca. 400 and 850 °C, and has a smaller lattice constant  $a$  than pure MgO due to the incorporation of Al<sup>3+</sup> ions. Above 900 °C, Al ions are released and the spinel (MgAl<sub>2</sub>O<sub>4</sub>) is formed. Pure MgO and MgAl<sub>2</sub>O<sub>4</sub> are obtained at 1000 °C (Fig. 13.1.8) (Miyata, 1980; Hibino et al., 1995). Mg–Ga–CO<sub>3</sub> LDH behave in a similar way (Lopez-Salinas et al., 1997c). In the case of Mg–Fe–CO<sub>3</sub> LDH, MgFe<sub>2</sub>O<sub>4</sub> spinel forms together with a MgO phase at 350 °C (Rouxhet and Taylor, 1969; Fernández et al., 1998; Hibino and Tsunashima, 2000).

Mg-based LDH-containing oxidizable trivalent metal ions yield oxides where the metals occur in varied states of oxidation (Fernández et al., 1994; Labajos et al., 1996; Labajos and Rives, 1996; Bahranowski et al., 1999). For LDH with tetravalent metal ions, all the constituent metal ions are homogeneously dispersed in the oxides that form after calcination (Velu et al., 1997a, 1999a).

Zinc-based LDH are generally less thermally stable than their Mg-based counterparts (Bertoldi et al., 1988; Fuda et al., 1993a, 1993b; Hussein et al., 1995;

del Arco et al., 1996; Kooli et al., 1997a; Velu et al., 1997b; Prévot et al., 1998; Ennadi et al., 2000; Crespo et al., 2001). Nickel-based LDH have thermal stabilities intermediate between those of Mg- and Zn-based LDH (Clause, 1991, 1992; Trifirò et al., 1994; Barriga et al., 1996; Kannan et al., 1996; Labajos and Rives, 1996; del Arco et al., 1999; Jitianu et al., 2000b). Cobalt-based LDH decompose at lower temperatures than other LDH (Kannan and Swamy, 1992; Kannan et al., 1995; Xu and Zeng, 1998, 2001a; del Arco et al., 1998; Zeng and Lim, 2000; Pérez-Ramírez et al., 2001a, 2001b, 2001c, 2001d).

Other forms of LDH such as calcium-based LDH (Messersmith and Stupp, 1995), Li–Al LDH (Hernández et al., 1985; Hou and Kirkpatrick, 2001), and multicomponent LDH (Morpurgo et al., 1996; Velu and Swamy, 1996; Alejandre et al., 1999; Castiglioni et al., 2000; Tichit et al., 2001) show their own distinguishing phases during thermal decomposition.

#### *Effect of Interlayer Anions*

The thermal decomposition of LDH into the corresponding oxides is moderately affected by the nature of the interlayer anions. For example, DTA indicates that the nitrate forms of Mg–Al LDH are thermally more stable when the layer charge  $x$  ( $= \text{Al}/(\text{Mg} + \text{Al})$ ) increases (Xu and Zeng, 2001b). By contrast, the carbonate forms show a decrease in decomposition temperature when  $x$  increases. The thermal behaviour of the nitrate forms is attributed to the arrangement of the interlayer nitrate ions which changes from ‘flat-lying’ to ‘stick-lying’ as the number of nitrate anions increases (Xu and Zeng, 2001c). Dehydroxylation is apparently retarded when the nitrate group adopts the ‘stick-lying’ conformation, being alternately attached to top and bottom hydroxyl sheets of contiguous layers.

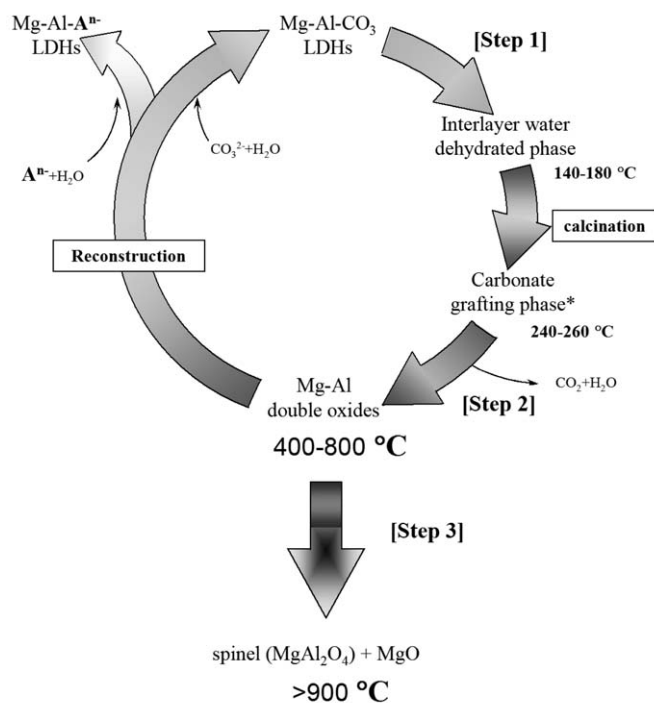
LDH, containing certain organic anions, can change their basal spacings on mild heating. Expansion or contraction may occur during loss of interlayer water. Thus, the basal spacing of Li–Al LDH with intercalated long-chain fatty acids ( $\text{CH}_3(\text{CH}_2)_n\text{COOH}$ ,  $n = 10, 12$ , and  $14$ ) expands on heating to  $100^\circ\text{C}$ , whereas that of the analogous Mg–Al forms contracts (Borja and Dutta, 1992). Terephthalate and benzoate intercalates of Mg–Al LDH also show changes in basal spacing due to a change in orientation of the anions from vertical to horizontal or to interstratification (Vucelic et al., 1995; Kooli et al., 1996).

Contraction of basal spacings also occurs when anions are grafted to the hydroxide layers. Grafting can enhance thermal stability (Prévot et al., 1998). The higher thermal stability of LDH sulphate relative to the carbonate and hydroxide forms may be explained in terms of the grafting of sulphate anions to the hydroxide layers (Constantino and Pinnavaia, 1995).

#### *Calcination/Hydration Cycles and Reconstruction*

The thermal behaviour of Mg–Al– $\text{CO}_3$  LDH is characterized by three major steps (Fig. 13.1.9) (Miyata, 1980; Sato et al., 1986a, Labajos et al., 1992; Pesic et al., 1992; Rey et al., 1992; MacKenzie et al., 1993; Hibino et al., 1995; Hudson et al., 1995;





\*: Suggested in Stanimirova et al. [1999].

Fig. 13.1.9. Decomposition of Mg–Al–CO<sub>3</sub> LDHs by calcinations and reconstruction from calcined LDHs in aqueous solutions.

Tichit et al., 1998). Up to 250 °C, interlayer water is lost (step 1). At 250–500 °C, the layer structure collapses, and the LDH converts into a mixed-oxide MgO-like phase (step 2). The mixed oxide can reconstruct into the (original) LDH by exposure to an aqueous solution (see Section 13.1.4.D). At ca. 900 °C the mixed oxide decomposes to MgO and MgAl<sub>2</sub>O<sub>4</sub> spinel (step 3). The foregoing is a simplified outline of the thermal behaviour of LDH.

In reality, the processes involved in steps 1–3 are more complicated than described. Loss of interlayer water in step 1 is concomitant with the appearance of tetrahedrally coordinated Al (Bellotto et al., 1996b). The metaphases that form are characterized by a slight contraction of basal spacing, the absence of (006) reflection (see Fig. 13.1.8), and the splitting of the carbonate  $\nu_3$  band (at 1360 cm<sup>-1</sup>) into two bands at 1330 and 1540 cm<sup>-1</sup> (see Fig. 13.1.10) (Rey et al., 1992; Hibino et al., 1995; Bellotto et al., 1996b; Kanazaki, 1998a, 1998b, 1998c; Tichit et al., 1998; Rocha et al., 1999; Millange et al., 2000; Pérez-Ramírez et al., 2001d), due probably to grafting of carbonate anions to the hydroxide layers (Stanimirova et al., 1999). Formation of tetrahedrally coordinated Al was also observed during step 2 (MacKenzie et al., 1993;



Béres et al., 1997; Tichit et al., 1998; Rocha et al., 1999). However, the local location of Al(IV) is uncertain (Rebours et al., 1994; Shen et al., 1998), and this Al(IV) disappears after reconstruction (Rey et al., 1992; Parker et al., 1995). A variety of anions can be intercalated following calcination at ca. 500 °C (step 2) and subsequent reconstruction (Fig. 13.1.9), (Chibwe and Jones, 1989a, 1989b; Dimotakis and Pinnaia, 1990; Cavani et al., 1991; Narita et al., 1991; Newman et al., 1998, 2001) although some carbonate anions remain in the calcined materials (e.g., Clause, 1991; Hibino et al., 1995; Klopogge et al., 2001). A decrease in anion sorption capacity (Parker et al., 1995) or a change in crystal symmetry (Stanimirova et al., 2001) may also occur in the first calcination/reconstruction cycle, while a  $\text{MgAl}_2\text{O}_4$  spinel phase may appear in further cycles (see Fig. 13.1.11) (Hibino and Tsunashima, 1998).

Mixed oxides obtained from LDH often serve as catalysts. Reconstruction leads to a reduction in catalytic activity. In addition, undesirable oxide phases can appear upon repeated cycles of calcination and reconstruction (Alcaraz et al., 1998; Hibino and Tsunashima, 1998; Marchi and Apesteguía, 1998; Pérez-Ramírez et al., 2001a). The ease of reconstruction depends on the nature of the constituent metal cations

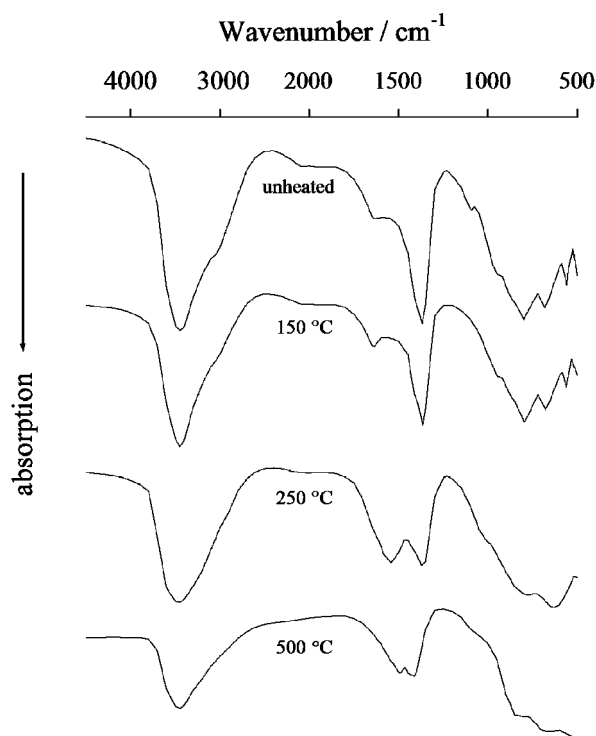


Fig. 13.1.10. Changes in the IR spectrum when  $\text{Mg-Al-CO}_3$  LDH with  $\text{Mg/Al} = 2:1$  is heated at various temperatures. The calcinations temperatures are indicated on the spectra.

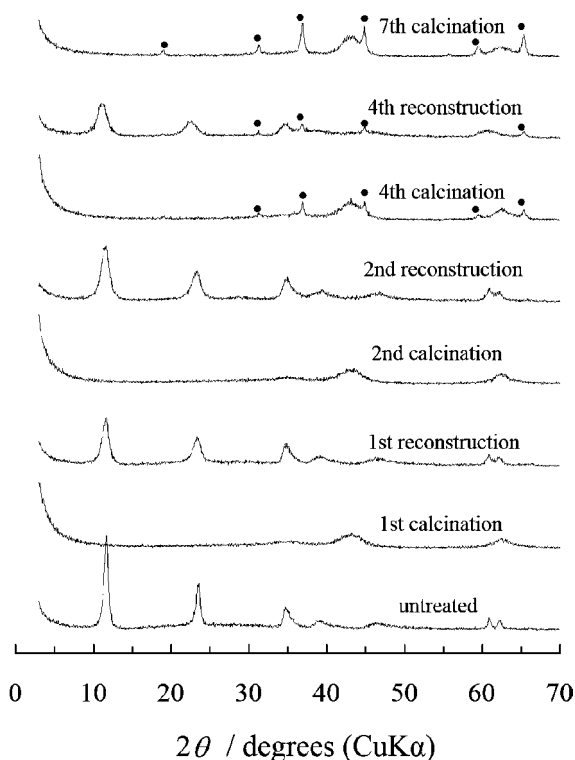


Fig. 13.1.11. Changes in the XRD pattern when Mg–Al–CO<sub>3</sub> LDH with Mg/Al = 2:1 is subjected to repeated calcinations/reconstruction. Diffraction peaks corresponding to spinel are labeled with a solid circle.

(Sato et al., 1988; Kooli et al., 1997a; Tichit et al., 2002a). For example, mixed oxides from Ni-based LDH are much more difficult to reconstruct than those from Mg- or Zn-based LDHs. Mixed oxides from Mg-based LDH can be reconstructed in an aqueous solution at room temperature. With Zn-based LDH, some ZnO-like phase remains under the same mild conditions. Ni-based LDH require hydrothermal treatment for reconstruction, whereas thermal treatment gives rise to crystalline ZnO in the case of Zn-based LDH.

An excellent example of a metal cation-dependent reconstruction was reported by Alcaraz et al. (1998), who were able to solve the problem of deactivation (induced by rehydration of the oxide catalysts back to LDH) by using Ni<sup>2+</sup> instead of Mg<sup>2+</sup> for the synthesis of the LDH precursor.

#### *Layered Double Oxides and Pre-spinel Phases*

Oxides obtained by decomposition of LDH form a single-phase rock salt-type solid solution before segregating into M(II)O and spinel phases when the temperature is

further increased. There is no doubt that the mixed oxides retain some structural homogeneity. Models for local ordering or local segregation in the calcined materials were proposed. One such model involves formation of a layered double oxide (LDO) (Hudson et al., 1995; Carlino et al., 1996; Carlino, 1997). Like LDH, LDO can intercalate guest anions.

Another model involves formation of a pre-spinel or quasi-amorphous spinel-type phase. Calcination of Ni–Al LDH between 350 and 800 °C gives rise to the following local phases: (i) a NiO phase; (ii) a spinel-type phase; and (iii) an alumina-type phase (Clause et al., 1992; Trifirò et al., 1994; Jitianu et al., 2000b; Pérez-Ramírez et al., 2001d).

When Ni–Fe LDH are calcined at 450 °C, an amorphous phase forms with a structure related to inverse spinels such as NiFe<sub>2</sub>O<sub>4</sub> or  $\gamma$ -Fe<sub>2</sub>O<sub>3</sub> (del Arco et al., 1999).

### C. Surface and Colloidal Properties

#### Surface Characterization

The surface properties of LDH influence catalytic reactivity, colloidal stability, adsorption, and intercalation. The specific surface area and AEC of LDH were described in Sections 13.1.6.B and 13.1.4.G, respectively.

Zeta potentials were measured for Mg–Al–CO<sub>3</sub>/NO<sub>3</sub> LDH as a function of pH or electrolyte concentration (Table 13.1.7). At a fixed salt concentration the isoelectric point (IEP) decreases sharply for divalent anion (Châtelet et al., 1996). Divalent anions also reduce particle mobility (Lagaly et al., 2001a). These results show that divalent anions are more strongly adsorbed by LDH than monovalent anions.

The zero point of charge (z.p.c.) (see Chapter 5) ranges from 12.0 to 12.3 for Mg–Al LDH and from 10.3 to 10.8 for Mg–Fe LDH (Han et al., 1998; Hou et al., 2001). The amount of charge may be calculated from potentiometric titration.

Table 13.1.7. Isoelectric point for LDH in various electrolytes

Electrolyte	IEP	
	pH at 0.01 M salt concentration <sup>a</sup>	Salt concentration (mmol/L) at pH 7 <sup>b</sup>
Water	11.1	—
NaCl	> 11.1	> 100
NaSCN	—	87
Na <sub>2</sub> SO <sub>4</sub>	7.6	3
Na <sub>2</sub> CO <sub>3</sub>	7.8	3
Na <sub>2</sub> CrO <sub>4</sub>	6.7	—
Na <sub>2</sub> HPO <sub>4</sub>	—	0.7

<sup>a</sup>Values from Châtelet et al. (1996).

<sup>b</sup>Values from Lagaly et al. (2001a).

However, the separate contribution of surface adsorption and ion exchange to z.p.c. values is difficult to assess.

#### *Surface Modification*

Hydrophobization of LDH by exchange with organic anions (surfactants) is an important procedure for obtaining new types of adsorbents. Thus, intercalation of dodecyl sulphate or dodecyl benzenesulphonate into Ca–Al LDH yields hydrophobic LDH capable of adsorbing organic solvents, such as *n*-heptane, benzene, toluene, and *n*-propanol. These surfactant-modified LDH show interlayer swelling in *n*-heptane (Dékány et al., 1997). Hydrophobic LDH can also be obtained by intercalation of myristic acid, or esterification of sebacoyl chloride with surface hydroxyl groups on the interlayer surface (Jakupca and Dutta, 1995; Morioka et al., 1995; Esumi and Yamamoto, 1998). In studying the adsorption of surfactants, Pavan et al. (1998–2000) found that the interlayer carbonate anions of LDH are not replaced by surfactants through simple ion exchange. However, some carbonate anions can be exchanged by organic acids from the melt (Carlino and Hudson, 1994, 1995; Carlino et al., 1996; Carlino, 1997).

Extraction of interlayer dodecyl sulphate by a cationic surfactant (*N*-cetyl-*N,N,N*-trimethylammonium bromide) leads to fast anion exchange, the amount of dodecyl sulphate exchanged being proportional to the amount of cationic surfactant added (Crepaldi et al., 1999, 2000b). New hybrid films of LDH and surfactants were prepared by the Langmuir–Blodgett (LB) method to obtain electrodes for sensors (He et al., 2001). Finally, modification of the interlayer surface with polymerized silicate was reported, offering a way of synthesizing new catalysts (Yun et al., 1995; Depège et al., 1996).

#### *Colloidal Dispersions and Delamination*

The term ‘colloidal solution of LDH’ is somewhat ambiguous since it can be interpreted in two ways: a suspension of LDH particles, or a dispersion of exfoliated single layers of LDH (i.e., delaminated LDH). For example, the turbid supernatant after intense washing with water, or treatment with ultrasound, consists of a suspension of LDH particles. Such suspensions were used to measure electrophoretic mobility (Lagaly et al., 2001a) and rheological properties (Albiston et al., 1996). Colloidal suspensions of LDH were also used as solid emulsion stabilizers (Abend et al., 1998; Neuhausler et al., 1999; Thieme et al., 1999; Lagaly et al., 2001b). Oil–water emulsions, stabilized by heterocoagulates of bentonite and LDH, are useful for cosmetic or pharmaceutical formulations.

A dispersion of delaminated LDH is totally different from a suspension of particles. Delamination, which can be thought of as infinite swelling, results in colloidal solutions that are very stable. Several methods for delaminating LDH were reported: treatment of Zn–Al–dodecyl sulphate LDH in alcohols under reflux at 120 °C (Adachi-Pagano et al., 2000), simple mixing of Mg–Al–glycine LDH and formamide (Hibino and Jones, 2001), mixing water and Mg–Al–alkoxide LDH prepared in

alcohols (Gardner et al., 2001), and mixing Mg–Al–dodecyl sulphate LDH and acrylate monomers at 70 °C (O’Leary et al., 2002). When colloidal dispersions of delaminated LDH are gently dried, well-ordered LDH are recovered (Hibino and Jones, 2001; Leroux et al., 2001a). On the other hand, when such dispersions are freeze-dried, the recovered materials are X-ray amorphous (Leroux et al., 2001a). Nanocomposites of LDH and polymers were obtained from colloidal dispersions of delaminated LDH and polymers (Leroux and Besse, 2001).

#### *Surface Properties of Calcined Materials*

Thermal decomposition of the LDH structure increases the specific surface area (Table 13.1.8) (Kannan and Swamy, 1992; Labajos et al., 1992; Barriga et al., 1996; Kannan et al., 1996; Marchi and Apesteguía, 1998; Shen et al., 1998; Hussein et al., 2001; Tichit et al., 2001; Olsbye et al., 2002). Formation of oxide phases and sintering of particles at high temperature cause a marked decrease in specific surface area. Nitrogen adsorption–desorption isotherms of the calcined materials are classified as type IIb rather than type IV. Type IIb isotherms are characteristic of aggregates of plate-like particles, classically found with clay minerals (Tichit et al., 2001).

The acidity and basicity of calcined Mg–Al–CO<sub>3</sub> LDH were evaluated by microcalorimetric adsorption of NH<sub>3</sub> and CO<sub>2</sub>. Acidity decreases in the order  $\gamma$ -Al<sub>2</sub>O<sub>3</sub> > LDH calcined at 400 °C > LDH calcined at 600 °C  $\approx$  LDH calcined at 800 °C, while basicity follows the order MgO > LDH calcined at 600 °C > LDH calcined at 800 °C > LDH calcined at 400 °C. IR spectroscopy indicates that the acid/base sites on the surface of calcined LDH are mainly of the Lewis type (Shen et al., 1998). Weak Lewis acid sites appear to be associated with Al<sup>3+</sup> ions, while basicity is related to isolated surface hydroxyl groups (del Arco et al., 1993). Calcined Mg–Al LDH contain surface sites of low (OH<sup>−</sup> group), medium (Mg–O pairs), and strong (O<sup>2−</sup> anions) basicity. The relative contribution of low- and medium-strength basic sites to the total basicity increases with increasing Al<sup>3+</sup> content (Di Cosimo et al., 1998).

### 13.1.8. INDUSTRIAL AND ENVIRONMENTAL APPLICATIONS: CONVENTIONAL AND NOVEL

#### *A. Catalytic Applications*

Mixed oxides obtained by calcination of LDH can serve as solid-base catalysts for (i) polymerization of alkene oxides; (ii) aldol condensation of aldehydes and ketones; (iii) methane or hydrocarbon steam reforming; (iv) methanation; (v) synthesis of methanol and higher alcohols; (vi) hydrocarbon (Fischer–Tropsch) synthesis; and (vii) hydrolysis of nitriles (Cavani et al., 1991; Vaccari, 1998, 1999b). The thermal decomposition of LDH, containing transition metal ions, was intensively studied

Table 13.1.8. Specific surface area of calcined LDH

Composition <sup>a</sup>	Treatment for original LDH	Degassing temperature (°C)	Calcination temperature (°C)	Specific surface area (m <sup>2</sup> /g)	References
Co/Al = 2/1	Aging, 65 °C, 24 h	120	Not calcined	47	Kannan and Swamy (1992)
			200	270	
Mg/Al = 2/1	None	Not described	750	ca. 200	
			1100	ca. 50	
Ni/Mn = 2/1	None	Not described	Not calcined	70	Barriga et al. (1996)
			125	80	
			450	58	
			700	15	
			1000	< 1	
Ni/Mn = 3/1			Not calcined	70	
			125	72	
			450	56	
			700	17	
			1000	4	
Ni/Al = 2/1	Aging, 65 °C, 24 h	Not described	Not calcined	92	Kannan et al. (1996)
			450	170	
Ni/Al = 2.5/1			Not calcined	124	
			450	146	
Ni/Al = 3/1			Not calcined	83	
			450	137	
Ni/Al = 3.5/1			Not calcined	121	
			450	92	
(Cu + Co + Zn)/Al = 3/1	60 °C during coprecipitation	400	400	203	Marchi and Apesteguía (1998)
			500	163	
			600	79	
Mg/Al = 3/1	None	Not described	400	195	Shen et al. (1998)
			600	132	
			800	114	
Mg/Al = 4/1	Aging, 70 °C, 18 h	Not described	Not calcined	68.0	Hussein et al. (2001)
			500	201.9	
Co/Al = 3/1	None	200	Not calcined	—	Tichit et al. (2001)
			300	166	
			500	145	
Co/Mg/Al = 2/1/1			Not calcined	174	
			300	230	
			500	149	
Co/Ni/Mg/Al = 1.5/0.5/1/1			Not calcined	17	
			300	209	
			500	163	
Co/Ni/Mg/Al = 1/1/1/1			Not calcined	20	
			300	235	
			500	199	
Co/Ni/Mg/Al = 0.5/1.5/1/1			Not calcined	30	
			300	254	
			500	204	
Ni/Mg/Al = 2/1/1	None	200	Not calcined	20	Tichit et al. (2001)
			300	251	

(continued on next page)

Table 13.1.8 (Continued)

Composition <sup>a</sup>	Treatment for original LDH	Degassing temperature (°C)	Calcination temperature (°C)	Specific surface area (m <sup>2</sup> /g)	References
Co/Ni/Al = 1.5/1.5/1			500	192	Olsbye et al. (2002)
			Not calcined	13	
			300	201	
			500	144	
Co/Ni/Mg/Al = 1.2/1.2/0.6/1			Not calcined	15	
			300	234	
			500	127	
			Not calcined	96	
Co/Ni/Mg/Al = 0.8/10.8/1.4/1			300	296	
			500	270	
	60 °C during coprecipitation	Not described	800	162	

<sup>a</sup>Compensating anions are carbonate or nitrate.

because the products are potentially useful as catalyst precursors. The transition metals include nickel (Clause, 1991, 1992; Trifirò et al., 1994; Alcaraz et al., 1998; del Arco et al., 1999; Jitianu et al., 2000b), cobalt (del Arco et al., 1998; Pérez-Ramírez et al., 2001a, 2001d; Tichit et al., 2001), iron (Raja and Santhanalakshmi, 1996; Ge et al., 2001), and copper (Morpurgo et al., 1996; Velu and Swamy, 1996; Marchi and Apesteguía, 1998; Castiglioni et al., 2000). The reactivity of LDH itself (as a solid-base catalyst) was investigated using 2-methyl-3-butyn-2-ol as a probe (Constantino and Pinnavaia, 1995).

An emerging trend is the application of LDH-derived catalysts in green chemistry. Solid-base catalysts are environment friendly, as compared with their liquid counterparts, because their waste products are easier to dispose than the huge volumes of liquid alkali waste (Ono and Baba, 1997). Solid bases from LDH were used in mercaptan oxidation for sweetening (Alcaraz et al., 1998), formation of C–C bonds (Choudary et al., 2000, 2001b), and condensation of citral and ketones (Roelofs et al., 2001). Environment friendly technologies using LDH were also developed for the production of hydrogen from vegetable oils (Marquevich et al., 2001), the simultaneous production of hydrogen and nanocarbon by decomposition of methane (Li et al., 2000), and the high-rate synthesis of amine N-oxides (Choudary et al., 2001a). Velu et al. (1999b, 2000b) investigated Cu–Zn–Al–Zr LDH as precursors of catalysts for steam reforming of methanol to produce CO-free hydrogen for fuel cells.

Another environmental application of LDH-derived catalysts involves decomposing gaseous air pollutants and greenhouse gases. The performance of Cu–Mg–Al mixed oxides (obtained by calcination of LDH) in the selective catalytic reduction of NO by NH<sub>3</sub> is comparable to that of a commercial V<sub>2</sub>O<sub>5</sub>–WO<sub>3</sub>/TiO<sub>2</sub> catalyst

(Montanari et al., 1997). Calcined Co–Mg–Al LDH are equally active in both NO and SO<sub>2</sub> removal but doping with cerium oxide is required (Palomares et al., 1999). Calcined LDH are superior to zeolites, spinels, perovskite-type oxides, and supported metals as catalysts for the decomposition of N<sub>2</sub>O (Kapteijn et al., 1996). N<sub>2</sub>O is a greenhouse gas, contributing to the destruction of stratospheric ozone. The main anthropogenic sources of N<sub>2</sub>O emission are cultivated soils, biomass burning, combustion processes, and the chemical industry, especially plants manufacturing adipic acid or nitric acid. A wide range of LDH, including Co–Al, Ni–Al, Cu–Al, Co–Pd–Al, Co–Rh–Al, Co–Mg–Al, Co–La–Al, and Co(II)–Co(III) LDH, are precursors of catalysts for N<sub>2</sub>O decomposition (Kannan and Swamy, 1994; Armor et al., 1996; Xu and Zeng, 1998; Pérez-Ramírez et al., 1999). The removal of NO<sub>x</sub> and N<sub>2</sub>O by LDH derivatives was reviewed by Serwicka (2001).

Pillaring of LDH is a new trend in catalyst synthesis. Various bulky POMs and Fe(CN)<sub>6</sub><sup>3–</sup> ions were intercalated into LDH to obtain microporous materials. Like zeolites, such pillared LDH can serve as shape-selective catalysts (see Section 13.1.4.H).

Incorporation of tetravalent metal cations such as Zr<sup>4+</sup> and Sn<sup>4+</sup> into the LDH structure results in unusual acid–base properties after calcination, or yields novel materials having catalytic properties similar to those of zeolites containing Zr<sup>4+</sup> or Sn<sup>4+</sup> (Velu et al., 1997a, 1999a; Tichit et al., 2002a).

### *B. Medical Applications*

Since LDH have a prolonged buffering effect and bile-binding activity, they can act as antacids for the treatment of gastric or duodenal ulcers. In experimental studies with rats and dogs, Mg–Al–CO<sub>3</sub> LDH inhibit significantly gastric lesions induced by stress and aspirin (Ishihara and Okabe, 1981). The effectiveness of LDH was confirmed in patients having gastric or duodenal ulcers. Unlike sodium bicarbonate, LDH are effective in treating ulcerative gastritis (Barlattani et al., 1982). The effectiveness of LDH in healing gastric ulcers is comparable to that of ranitidine; the respective healing rates are 81% for LDH and 79% for ranitidine (Holtermüller et al., 1993). As to duodenal ulcers, endoscopy performed at the end of 4 weeks of treatment shows healing in 68.2% of patients. Side effects associated with aluminium and magnesium hydroxides are well known. These are constipation, phosphate depletion, malaise, and anorexia for aluminium hydroxide; and diarrhea and hypomagnesaemia, leading to renal malfunction for magnesium hydroxide. On the other hand, no side effects were observed during treatment with LDH (Bhanumathi et al., 1993).

Apart from their use as antacids, LDH were evaluated as phosphate binders. Hyperphosphataemia in patients with end-stage renal failure may lead to secondary hyperparathyroidism and renal osteodystrophy. Absorption of inorganic phosphate may be prevented by administering compounds that form insoluble phosphate complexes in the gastrointestinal tract. Rankin et al. (2001) studied phosphate



precipitation at different pH values in aqueous solution and in various food mixtures in the presence of LDH,  $\text{Al}(\text{OH})_3$ ,  $\text{CaCO}_3$ , and  $\text{Mg}(\text{OH})_2$ , with LDH showing considerable promise as phosphate binders.

### C. Additives for Polymers

Synthetic LDH are commercially used as acid neutralizers or HCl scavengers in stabilizer packages for poly(vinyl chloride) (PVC). PVC undergoes autocatalytic dehydrochlorination when exposed to heat or UV light, becoming brittle and changing colour. Mori et al. (1981) reported that adding LDH to PVC in the presence of 6-anilino-1,3,5-triazine-2,4-dithiol and zinc stearate, jointly used as a stabilizer, reduces the rate of PVC discolouration. Van der Ven et al. (2000) investigated the mechanism of stabilization by LDH by measuring the thermal stability and HCl adsorption capacity. Thermal stability is determined by monitoring the time required to effect a change in colour of PVC/LDH compounds on heating at 200 °C. There is a linear relationship between thermal stability and HCl adsorption capacity. The reaction between HCl and LDH occurs in two steps: (i) interlayer anions react with HCl; and (ii) the LDH decompose, giving rise to metal chlorides.

LDH are also used as flame retardants in polymers. From an environmental standpoint, LDH-based flame retardants are preferable to their halogen-based counterparts. In flame-retardancy tests, LDH are superior to other inorganic hydroxides, such as magnesium and aluminium hydroxides (Camino et al., 2001). In mass-loss calorimetric analyses, an ethylene vinyl acetate (EVA) polymer, filled with 50 wt% of Mg–Al– $\text{CO}_3$  LDH, shows the lowest rate of heat release and the lowest temperature for gas evolution. The modified EVA polymer has the longest ignition time. The high performance of LDH is ascribed to heat absorption due to loss of water over a wide temperature range (200–500 °C).

The composites of polymers and additives are not homogeneously mixed at the microscopic level. In order to achieve intimate mixing, the majority of LDH/polymer nanocomposite materials are synthesized either by templating or in situ polymerization. Template synthesis is carried out by coprecipitating LDH in solution in the presence of soluble polymers, such as poly(styrene sulphonate), poly( $\alpha,\beta$ -aspartate), poly(vinyl sulphonate), poly(vinyl alcohol), and polyacrylate (Messersmith and Stupp, 1995; Oriakhi et al., 1996, 1997; Whilton et al., 1997; Wilson et al., 1999). Formation of LDH and the incorporation of the polymer occur simultaneously. LDH are ideal materials for templating because they can be synthesized at room temperature or under mild conditions that do not cause polymer decomposition. In situ polymerization consists of intercalating monomer anions or polar monomer molecules, and subsequent or concomitant polymerization (Tanaka et al., 1989; Challier and Slade, 1994; Whilton et al., 1997; Rey et al., 1999; Isupov et al., 2001; O'Leary et al., 2002). This method requires appropriate monomers. To date, intercalation of polyacrylate, polyaniline, poly(aminobenzoate) and poly( $\alpha,\beta$ -aspartate)

was reported. LDH-polymer nanocomposites were also obtained by intercalating the polymer through the delamination state (Leroux and Besse, 2001).

The above-mentioned LDH-polymer nanocomposites and their basal spacings are summarized in Table 13.1.9. Although the properties of LDH-polymer nanocomposites were not fully investigated, LDH-polymer and smectite-polymer nanocomposites are expected to have similar properties. That is, LDH-polymer nanocomposites containing small amounts of LDH would be expected to show improved mechanical strength, reduced permeability toward gases and liquids, and self-extinguishing characteristics (Giannelis, 1996) (see Chapter 10.3).

#### D. Environmental Applications

##### Adsorption of Pollutants

LDH can take up a variety of contaminants and toxic substances directly from the environment through anion-exchange, reconstruction, and adsorption (Fig. 13.1.12). Capturing target anions can be attained by simple anion exchange in solution or by reconstruction of calcined LDH. Hermosín et al. (1996) demonstrated that Mg-Al-CO<sub>3</sub> LDH adsorbs 2,4,6-trinitrophenol (TNP) by anion exchange up to 20% of its AEC when the initial pH was 2. For Mg-Al-CO<sub>3</sub> LDH calcined at 500 °C, the amount of TNP adsorbed was 40% of the AEC. Similarly, calcined LDH can adsorb dodecyl benzenesulphonate (Ulibarri et al., 2001), and Zn-Al-Cl LDH can remove the pesticide 2,4-dichlorophenoxyacetic acid from aqueous solution by anion exchange (Lakraimi et al., 1999).

Phosphate, a causative factor in surface water eutrophication, can be captured by the chloride or nitrate forms of LDH through anion exchange (Shin et al., 1996; Legrouri et al., 1999). Competing anions affect phosphate uptake. For example, nitrate causes only a slight decrease in phosphate removal whereas sulphate causes a 12–13%, and carbonate a 33%, reduction. Toxic inorganic anions such as

Table 13.1.9. Polymer-intercalated LDH

Polymer	Basal spacing (nm)	References
Polyacrylate	1.20–1.34	Tanaka et al. (1989), Oriakhi et al. (1996), Rey et al. (1999), Oleary et al. (2002)
Poly(styrenesulphonate)	1.96–2.16	Oriakhi et al. (1996, 1997), Wilson et al. (1999), Leroux and Besse (2001a)
Poly(vinylsulphonate)	1.27–1.33	Oriakhi et al. (1996), Wilson et al. (1999)
Polyaniline	1.33–1.35	Challier and Slade (1994)
Poly(vinyl alcohol)	18.0	Messersmith and Stupp (1995)
Poly(α,β-aspartate)	0.90–1.51	Whilton et al. (1997)
Poly(aminobenzoate)	1.55	Isupov et al. (2001)

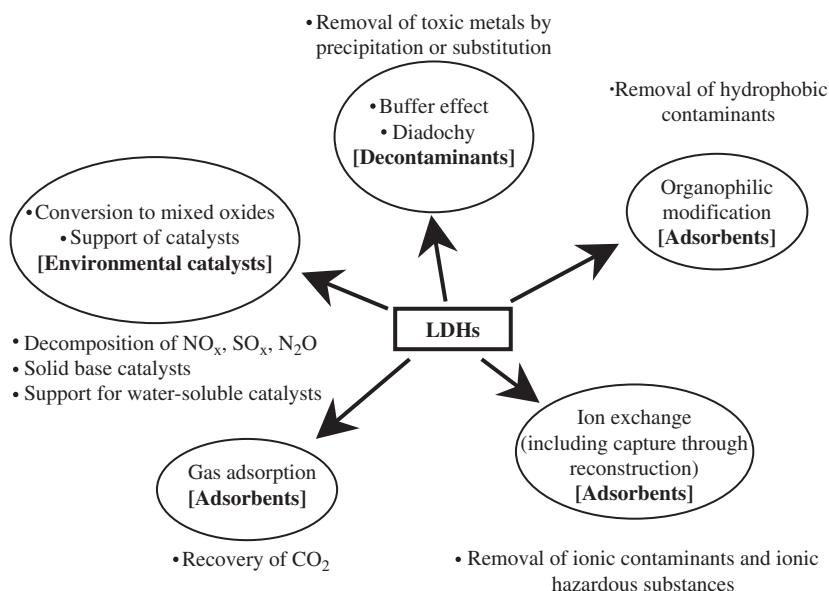


Fig. 13.1.12. Environmental applications of LDHs. (Environmental catalysts are described in Sections 4.1 and 4.5)

$\text{SeO}_3^{2-}$ ,  $\text{SeO}_4^{2-}$ , and  $\text{Cr}_2\text{O}_7^{2-}$  may be removed by anion exchange or the reconstruction process (Goswamee et al., 1998; You et al., 2001). Again, competing anions in solution strongly decrease the adsorption of  $\text{SeO}_3^{2-}$  and  $\text{Cr}_2\text{O}_7^{2-}$ . Adsorbed  $\text{SeO}_3^{2-}$  or  $\text{Cr}_2\text{O}_7^{2-}$  can be released from LDH by ion exchange with  $\text{CO}_3^{2-}$ . Kameda et al. (2000) investigated the treatment of waste acid solution with calcined LDH. Almost 100% of the chloride ions in hydrochloric acid can be removed.

The hydrophobic environment induced by intercalation of surfactants permits adsorption of nonanionic and hydrophobic organic contaminants. Organo-LDH modified with dodecyl sulphate are as good as organo-montmorillonites in adsorbing hydrophobic pesticides (Villa et al., 1999). Similarly, Dutta and Robins (1994) showed that pyrene can intercalate from methanol–water mixtures into Li–Al LDH-containing interlayer myristic and hexanoic acids.

LDH and calcined LDH can also remove humic substances from water but it is uncertain whether intercalation of humic substances occurs (Amin and Jayson, 1996; Seida and Nakano, 2000; Hussein et al., 2001).

LDH can also be used to remove metal cations from aqueous solutions. In the case of transition metal cations, such as  $\text{Cu}^{2+}$ ,  $\text{Ni}^{2+}$ ,  $\text{Co}^{2+}$ , and  $\text{Zn}^{2+}$ , the process is one of substitution, mainly for  $\text{Mg}^{2+}$  in the structure (Komarneni et al., 1998). This can be achieved by shaking a mixture of an aqueous solution of the appropriate salt (pH 4–5) and Mg–Al–CO<sub>3</sub> LDH or Mg–Al–NO<sub>3</sub> LDH at room temperature for 1 day. A second method for removing metal cations from solutions is based on the

buffer effect (Lehmann et al., 1999; Seida et al., 2001). Adding Mg-based LDH to aqueous solutions leads to an increase in pH, which causes metal cations in the solution to precipitate as metal hydroxides. This process was used to remove toxic  $\text{Pb}^{2+}$  and  $\text{Zn}^{2+}$  cations. These two methods are more straightforward than using a combination of LDH and metal ion-chelating compounds (Tsyganok et al., 2001).

Adsorption of carbon dioxide onto LDH was investigated as a possible method for recovery of  $\text{CO}_2$  from hot gas streams (Yamamoto et al., 1995; Ding and Alpay, 2001; Yong et al., 2001). The recovery of  $\text{CO}_2$  from power-plant flue gases is considered to be the first step in reducing total  $\text{CO}_2$  emission. The carbon dioxide adsorption capacity of LDH, ranging from 10 to  $33 \text{ cm}^3$  (STM)/g, is dependent on the micropore volume, interlayer spacing, and layer charge density of the material.

#### *Waste Barriers*

Containers of cementitious materials and glasses are commonly used in immobilization strategies for the disposal of hazardous and radioactive waste. To predict the safety of these containers, changes in the composition and structure of the container material during degradation, cement or glass is subjected to hydrothermal treatment at 80–200 °C, or to continuous leaching in salt solutions (Abdelouas et al., 1994; Wang and Scrivener, 1995; Faucon et al., 1996; Paul and Glasser, 2000; Scheidegger et al., 2001). LDH were found to be one of corrosion products of cement or glass.

It is impossible to ensure the integrity of cementitious or glass vaults over the hundreds of years required for the decay of radioactive waste. Therefore, backfills that can absorb and retain radionuclides were investigated. Among the radionuclides present in nuclear fuel waste,  $^{129}\text{I}^-$  is especially problematic. It has a long half-life, and does not interact strongly with most geological materials such as clay, sand, and rock.  $^{129}\text{I}^-$  may reach the biosphere before it decays to insignificant levels. Organic materials are not practical for use as adsorbents in backfills, because they are not stable over long periods. Corrosion products of cement such as ettringite and LDH (Altenhein-Haese et al., 1994) are potential inorganic candidates for scavenging  $^{129}\text{I}^-$ . Other inorganic materials such as imogolite, metal sulphides, copper oxides, and coals were also investigated. Optimal scavenging of  $^{129}\text{I}^-$  depends on environmental conditions. Near-neutral pH seems optimal for LDH (Balsley et al., 1998). However, only a small fraction of the exchange sites are occupied by  $\text{I}^-$  ions, indicating that anion exchange takes place only on the external surface (Olguín et al., 1998; Fetter et al., 1999).

#### *E. Future Developments*

##### *Drug Delivery and Controlled-Release Formulations*

Controlled-release drug delivery is ideal for drug therapy. Ideally, the correct dosage of drug is transported to, and absorbed by, the target, without delivery of the drug to other tissues. Drug delivery systems are complex and difficult to design. Currently, controlled-release drugs are being used to reduce the number of doses and side

effects that are associated with frequent administration. Usually, polymer-encapsulated drugs are used for this purpose (Khan et al., 2001). Developing suitable materials for the capsule is a key step in the design of a controlled-release drug delivery system. LDH are being studied as potential reservoirs or delivery carriers of biomolecules. Choy et al. (2000) demonstrated that the DNA of herring tests and methotrexate (an anticancer drug) can intercalate into Mg–Al LDH by ion exchange. They also intercalated nucleoside mono- and triphosphate. Adsorption by LDH of adenosine 5'-triphosphate (ATP) increases the efficiency of ATP transfer into cells. This is attributed to alleviation of the electric repulsion at the cell wall when the negative charge on the phosphate groups is neutralized by the positive hydroxide layers (Choy et al., 2001).

A variety of pharmaceutical anionic materials were intercalated into LDH (Table 13.1.10) (Ambrogi et al., 2001; Hwang et al., 2001; Khan et al., 2001). An example is ibuprofen [ $\alpha$ -methyl-4-(2-methylpropyl)benzeneacetic acid], a nonsteroidal anti-inflammatory drug used to relieve symptoms of rheumatoid arthritis and osteoarthritis. The in vitro release of this drug from ibuprofen-LDH is much slower than from a commercial formulation in phosphate buffer at pH 7.5 (Ambrogi et al., 2001).

#### *Biosensors, Biomimetic Catalysts, and Biological Reactions*

He et al. (2001) prepared hybrid thin films of Ni–Al–Cl LDH and an amphiphilic anionic Ru(II) complex ( $[\text{Ru}(\text{CN})_4\text{L}]^{2-}$ , where  $\text{L} = 4,4'$ -di-*n*-dodecylaminoyl-2,2'-bipyridyl), using the LB technique. Ni cations in the hydroxide layers mediate the oxidation of  $[\text{Ru}(\text{CN})_4\text{L}]^{2-}$  to  $[\text{Ru}(\text{CN})_4\text{L}]^-$ . Ru(II) cyano complexes are known to function as a redox mediator in reactions such as the oxidation of glucose by glucose oxidase. In this context, the LB hybrid films are potentially useful for electrochemical sensing of biomolecular materials.

Table 13.1.10. LDH intercalated with pharmaceutical materials

Guest	Basal spacing (nm)	Host LDH	References
Ibuprofen	2.17	Mg/Al = 2/1	Ambrogi et al. (2001)
Citric acid	1.21		
Ascorbic acid	1.05		
Retinoic acid	3.78		
Indoleacetic acid	not given		
4-Biphenylacetic acid	2.04	Zn/Al = 2/1	Hwang et al. (2001)
Diclofenac	2.23		
Gemfibrozil	2.32		
Ibuprofen	2.27	Li/Al = 1/2	Khan et al. (2001)
Naproxen	2.15		
2-Propylpentanoic acid	1.87		
Tolfenamic acid	2.19		

LDH can also be used as supports for biomimetic metallomacrocylic catalysts. Anionic metalloporphyrins and metallophthalocyanines were intercalated into LDH (Ukrainczyk et al., 1995; Bonnet et al., 1996; Chibwe et al., 1996). As these intercalates lack microporosity, the reactants might only be able to access the metallo-macrocyces located at the edges and external surfaces. Nevertheless, catalytic activity for reductive dehalogenation of  $\text{CCl}_4$  and for oxidation of 2,6-di-*tert*-butylphenol by oxygen was confirmed. Biomimetic catalysts consisting of tungstate intercalated into LDH were also reported (Sels et al., 1999). These materials can selectively catalyse oxidative bromination and bromide-assisted epoxidation reactions.

Lotsch et al. (2001) reported the selective intercalation of nucleoside monophosphates into LDH, suggesting that LDH are useful for the purification and separation of complex biomolecules. LDH were also investigated as supports for enzymes. The enzyme penicillin G acylase is immobilized by LDH (Ren et al., 2001). Finally, two biopoesis-relevant biological reactions induced by LDH were reported: the al-domerization of glycolaldehyde phosphates to sugar phosphates (Pitsch et al., 1995) and the self-addition of cyanide (Bocclair et al., 2001).

#### *Electrochemical Applications*

The electrochemical response of redox species intercalated into LDH was studied by cyclic voltametry. Electrodes modified with LDH were prepared by casting an LDH suspension onto an electrode or by mixing LDH with a carbon paste. Some electroactive responses were observed for these modified electrodes (Itaya et al., 1987; Mousty et al., 1994; Ballarin et al., 1998; Therias et al., 1998). A variety of electroactive anions were intercalated into LDHs (Table 13.1.11). In most cases, a large portion of the intercalated redox species are electrochemically silent. Anions involved in the redox reaction at the electrodes are apparently located on particle edges and near the electrodes (Therias et al., 1996; Doménech et al., 1998). Qiu and Villemure (1995) calculated that only 3.5–6.8% of the anions in  $\text{Mg-Al-}[\text{Fe}(\text{CN})_6]$  LDH are involved in the redox reaction. However, a way to improve electron transfer efficiency was found. In Ni-based LDH, the Ni mediates the transfer of electrons to electroactive anions. In this case, the amount of electrochemically active anions increases in the range 17.4–27%. With  $\text{Zn-Al-}[\text{Fe}(\text{CN})_6]$  LDH, the redox reaction proceeds by a different mechanism, and a Prussian blue-like film forms on the surface of the LDH (Shaw et al., 1990).

A quartz crystal microbalance (QCM) was used to investigate the mass transfer in the redox reaction of the electroactive interlayer anions in LDH-modified electrodes (Yao et al., 1998a). Electrochemical QCM measurements on an electrode modified with  $\text{Mg-Al-}[\text{Fe}(\text{CN})_6]$  LDH indicate reversible changes in mass: mass increases on oxidation and decreases on reduction. Adsorption and desorption studies, using a QCM and UV-visible spectroscopy, show that the excess charge generated in the film by reduction is compensated by the leaching out of ion-paired species; in this case  $\text{Na}_2[\text{Fe}(\text{CN})_6]^-$  or  $\text{Na}[\text{Fe}(\text{CN})_6]^{2-}$ . Electrochemical scanning tunneling microscopy

Table 13.1.11. LDH intercalated with electroactive anions

Anion	Basal spacing (nm)	Host LDH	Reference
Mo(CN) <sub>8</sub> <sup>4-</sup>	1.12	Mg/Al = 3/1	Itaya et al. (1987)
Fe(CN) <sub>6</sub> <sup>3-</sup>	1.12		
IrCl <sub>6</sub> <sup>2-</sup>	1.08		
Fe(CN) <sub>6</sub> <sup>3-</sup>	1.064	Zn/Al (ratio is not given)	Shaw et al. (1990)1.08
<i>m</i> -Nitrobenzenesulphonate	1.562	Zn/Cr = 2/1	Mousty et al. (1994)
2-Anthraquinonesulphonate (AQS-2)	1.99		
2,6-Anthraquinonedisulphonate (AQDS-2,6)	1.89		
1,5-Anthraquinonedisulphonate	1.592		
2,2'-Azinobis(3-ethylbenzothiazoline-6-sulphonate)	1.95		
	2.08	Zn/Al = 1.8–2.6	Therias et al. (1996)
AQS-2	2.03	Mg/Al = 2.5/1	Ballarin et al. (1998)
AQDS-2,6	1.87		
<i>p</i> -Toluenesulphonate	1.7.2–1.73	Zn/Cr = 2.5/1	Doménech et al. (1998)
	1.73		
Bis(2-mercapto-2,2-diphenylethanoate) dioxomolybdate(VI) complex	not given	Zn/Al = 3/1	
Ferrocene monosulphonate	2.00	Zn/Cr = 2/1	
Ferrocene disulphonate	1.50		Therias et al. (1998)
2,2,6,6-Tetramethyl-1-oxylpiperidylidene succinate	1.67	Zn/Al = 2/1	

(ECSTM) indicates that the distance between [Fe(CN)<sub>6</sub>] ions, adsorbed on the external surface, changes after redox reaction. This distance increases when the anions are reduced, and decreases when the anions are oxidized (Yao et al., 1998b).

Various types of electrodes modified with LDH show electrocatalytic activity. Phenol was oxidized at electrodes modified with Mg–Al–Cl LDH (Shaw et al., 1990), and alcohols at electrodes modified with Ni–Al–Cl LDH (Ballarin et al., 1999). Electrodes modified with Mg–Al–SO<sub>4</sub> LDH are potentially useful as sulphate sensors in the analysis of industrial and environmental water samples (Morigi et al., 2001). Electrodes modified with Ni–Al–Cl LDH were tested as sensors for methanol, mannitol, and glucose (Scavetta et al., 2001). The reactants were detected through electrocatalytic oxidation. SEM further shows that very few LDH particles are strictly in



contact with the electrode, that is, only a very small portion of the LDH is involved in the electrocatalytic process. It seems, therefore, desirable to increase the contact between the LDH and electrode (Scavetta et al., 2001).

LDH-modified electrodes were also used in applications involving alkaline secondary cells. During charge-discharge cycles,  $\alpha$ -Ni(OH)<sub>2</sub> is preferable to  $\beta$ -Ni(OH)<sub>2</sub> for efficiency. However,  $\alpha$ -Ni(OH)<sub>2</sub> is unstable in an alkaline medium and transforms to  $\beta$ -Ni(OH)<sub>2</sub>. Kamath et al. (1994) synthesized a Ni–Al LDH having the same structure as that of  $\alpha$ -Ni(OH)<sub>2</sub>. They found that the LDH has a prolonged stability under strongly basic conditions, and a discharge capacity value of 240 mAh/g. Ni–Al LDH is therefore attractive for application in an alkaline secondary battery. In an attempt at making modified electrodes, Indira and Kamath (1994) cathodically reduced metal salt solutions. Mg, Al, Mn, Cr, Ni, Co, La, Nd, and Pr are deposited in the hydroxide or LDH forms, but Zn, Cd, Cu, Bi, and Pb form metallic deposits. Finally, Moneyron et al. (1990, 1991a, 1991b, 1991c) prepared a humidity sensor based on LDH deposited as a thick film by screen printing. This application is based on the ability of LDH to act as protonic conductors (de Roy et al., 1985; de Roy and Besse, 1991; Ducos et al., 2001).

#### *Novel Functional Materials*

The synthesis and development of novel functional materials containing LDH received much attention. Immobilization of functional materials by intercalation into LDH is the main route. Two fluorescent anions (methyl orange and xanthene dye) and a luminescent anion (Ru(BPS)<sub>3</sub><sup>4-</sup>; where BPS = 4,7-diphenyl-1,10-phenanthrolinedisulphonate] were intercalated into LDH (Giannelis et al., 1987; Costantino et al., 1999, 2000). The photoluminescence is affected by the environment around the anions. Especially for the xanthene dye, the absorption and emission spectra of the interlayer dye anions are similar to those of the crystalline dye, whereas the spectra of the dye adsorbed onto the external surface are similar to those of the dye in solution.

Intercalation of C<sub>60</sub> was accomplished by co-intercalation with toluene or hexane into organo-LDH (Tseng et al., 1996), or by using a negatively charged C<sub>60</sub> through reduction (Ding et al., 1996). Intercalated C<sub>60</sub> exhibits enhanced photoluminescence.

Tagaya et al. (1994) prepared a photochromic LDH complex by intercalating sulphonated indolinespirobenzopyran in the presence of *p*-toluenesulphonic acid. The colour of the composite changed from red to yellow when irradiated with visible light. Photocatalysts were also immobilized in LDH. Semiconductor particles of TiO<sub>2</sub>, CdS, and ZnS were incorporated into the interlayer spaces, using the corresponding precursors (titanium butoxide for TiO<sub>2</sub>, and anionic chelate compounds of Cd and Zn for CdS and ZnS, respectively) (Sato et al., 1993; Robins and Dutta, 1996). A POM intercalate of LDH can decompose pesticides by a photocatalytic reaction (Guo et al., 2001). The water-soluble POM can be recycled by immobilization on the LDH.



Porous carbon was obtained from LDH-containing organic anions (Putyera et al., 1996; Xu et al., 2001). On calcination, the organic moieties in the interlayer space convert into a carbonaceous residue, forming a microporous carbon-like material.

## REFERENCES

- Abdelouas, A., Crovisier, J.L., Lutze, W., Fritz, B., Mosser, A., Müller, R., 1994. Formation of hydrotalcite-like compounds during R7T7 nuclear waste glass and basaltic glass alteration. *Clays and Clay Minerals* 42, 526–533.
- Abend, S., Bonnke, N., Gutschner, U., Lagaly, G., 1998. Stabilization of emulsions by heterocoagulation of clay minerals and layered double hydroxides. *Colloid and Polymer Science* 276, 730–737.
- Adachi-Pagano, M., Forano, C., Besse, J.-P., 2000. Delamination of layered double hydroxides by use of surfactants. *Chemical Communications*, 91–92.
- Adachi-Pagano, M., Forano, C., Besse, J.P., 2003. Synthesis of Al-rich hydrotalcite-like compounds by using urea hydrolysis reaction—control of size & morphology. *Journal of Materials Chemistry* 13, 1988–1993.
- Aisawa, S., Hirahara, H., Uchiyama, H., Takahashi, S., Narita, E., 2002. Synthesis and thermal decomposition of Mn–Al layered double hydroxides. *Journal of Solid State Chemistry* 167, 152–159.
- Aisawa, S., Takahashi, S., Ogasawara, W., Umetsu, Y., Narita, E., 2001. Direct intercalation of amino acids into layered double hydroxides by coprecipitation. *Journal of Solid State Chemistry* 162, 52–62.
- Alba, M.D., Becerro, A.I., Castro, M.A., Perdigon, A.C., 2001. Two-dimensional heteronuclear  $^1\text{H} \leftarrow \rightarrow ^{27}\text{Al}$ -correlated MAS NMR spectra of layered silicates. *Chemical Communications*, 249–250.
- Albiston, L., Franklin, K.R., Lee, E., Smeulders, J.B.A.F., 1996. Rheology and microstructure of aqueous layered double hydroxide dispersions. *Journal of Materials Chemistry* 6, 871–877.
- Alcaraz, J.J., Arena, B.J., Gillespie, R.D., Holmgren, J.S., 1998. Solid base catalysts for mercaptan oxidation. *Catalysis Today* 43, 89–99.
- Alejandre, A., Medina, F., Rodriguez, X., Salagre, P., Cesteros, Y., Sueiras, J.E., 2001. Cu/Ni/Al layered double hydroxides as precursors of catalysts for the wet air oxidation of phenol aqueous solutions. *Applied Catalysis B: Environmental* 30, 195.
- Alejandre, A., Medina, F., Salagre, P., Correig, X., Sueiras, J.E., 1999. Preparation and study of Cu–Al mixed oxides via hydrotalcite-like precursors. *Chemistry of Materials* 11, 939–948.
- Allda, R.K., Navrotsky, A., Berbeco, H.T., Casey, W.H., 2002. Thermochemistry and aqueous solubilities of hydrotalcite-like solids. *Science* 296, 721–723.
- Allmann, R., 1968. The crystal structure of pyroaurite. *Acta Crystallographica Section B* 24, 972.
- Altenhein-Haese, C., Bischoff, H., Fu, L., Mao, J., Marx, G., 1994. Adsorption of actinides on cement compounds. *Journal of Alloys and Compounds* 213–214, 554–556.
- Ambroggi, V., Fardella, G., Grandolini, G., Perioli, L., 2001. Intercalation compounds of hydrotalcite-like anionic clays with antiinflammatory agents. I. Intercalation and in vitro release of ibuprofen. *International Journal of Pharmaceutics* 220, 23–32.

- Amin, S., Jayson, G.G., 1996. Humic substance uptake by hydrotalcites and PILCS. *Water Resources* 30, 299–306.
- Aramendia, M.A., Aviles, Y., Boreau, V., Luque, J.M., Marinas, J.M., Ruiz, J.R., Urbano, F.J., 1999. Thermal decomposition of Mg/Al and Mg/Ga layered-double hydroxides: a spectroscopic study. *Journal of Materials Chemistry* 9, 1603–1608.
- Aramendia, M.A., Boreau, V., Jimenez, C., Marinas, J.M., Luque, J.M., Ruiz, J.R., Urbano, F.J., 2000. Synthesis and characterization of a novel Mg/In hydrotalcite-like compound. *Materials Letters* 43, 118–121.
- Aramendia, M.A., Boreau, V., Jimenez, C., Marinas, J.M., Ruiz, J.R., Urbano, F.J., 2002. Comparative study of Mg/M(III) (M = Al, Ga, In) layered double hydroxides obtained by coprecipitation and the sol-gel method. *Journal of Solid State Chemistry* 168, 156–161.
- Armor, J.N., Braymer, T.A., Farris, T.S., Li, Y., Petrocelli, F.P., Weist, E.L., Kannan, S., Swamy, C.S., 1996. Calcined hydrotalcites for the catalytic decomposition of N<sub>2</sub>O in simulated process streams. *Applied Catalysis B: Environmental* 7, 397–406.
- Bahranowski, K., Dula, R., Kooli, F., Serwicka, E.M., 1999. ESR study of the thermal decomposition of V-containing layered double hydroxides. *Colloids and Surfaces A: Physicochemical and Engineering Aspects* 158, 129–136.
- Ballarin, B., Gazzano, M., Seeber, R., Tonelli, D., Vaccari, A., 1998. Electrodes coated by hydrotalcite-like clays: effect of the metals and the intercalated anions on ion accumulation and retention capability. *Journal of Electroanalytical Chemistry* 445, 27–37.
- Ballarin, B., Seeber, R., Tonelli, D., Vaccari, A., 1999. Electrocatalytic properties of nickel(II) hydrotalcite-type anionic clay: application to methanol and ethanol oxidation. *Journal of Electroanalytical Chemistry* 463, 123–127.
- Balsley, S.D., Brady, P.V., Krumhansl, J.L., Anderson, H.L., 1998. Anion scavengers for low-level radioactive waste repository backfills. *Journal of Soil Contamination* 7, 125–141.
- Barlattani, M., Mantera, G., Fasani, R., Carosi, M., 1982. Efficacy of antacid treatment in peptic ulcerative patients: therapeutic value of synthetic hydrotalcite (Talcid). *Clinical Trials Journal* 19, 359–367.
- Barriga, C., Fernández, J.M., Ulibarri, M.A., Labajos, F.M., Rives, V., 1996. Synthesis and characterization of new hydrotalcite-like compounds containing Ni(II) and Mn(III) in the hydroxide layers and of their calcination products. *Journal of Solid State Chemistry* 124, 205–213.
- Basile, F., Fornasari, G., Gazzano, M., Vaccari, A., 2000. Synthesis and thermal evolution of hydrotalcite-type compounds containing noble metals. *Applied Clay Science* 16, 185–200.
- Bellotto, M., Rebours, B., Clause, O., Lynch, J., Bazin, D., Elkaïm, E., 1996a. A reexamination of hydrotalcite crystal chemistry. *Journal of Physical Chemistry* 100, 8527–8534.
- Bellotto, M., Rebours, B., Clause, O., Lynch, J., Bazin, D., Elkaïm, E., 1996b. Hydrotalcite decomposition mechanism: a clue to the structure and reactivity of spinel-like mixed oxides. *Journal of Physical Chemistry* 100, 8535–8542.
- Bender, K.C., 2001. Investigating layered double hydroxides by Mössbauer spectroscopy. In: Rives, V. (Ed.), *Layered Double Hydroxides*. Nova Science Publishers, Huntington, pp. 215–228.
- Béres, A., Pálinkó, I., Bertrand, J.-C., Nagy, J.B., Kiricsi, I., 1997. Dehydration–rehydration behaviour of layered double hydroxides: a study by X-ray diffractometry and MAS NMR spectroscopy. *Journal of Molecular Structure* 410–411, 13–16.

- Bertoldi, M., Fubini, B., Giamello, E., Busca, G., Trifirò, F., Vaccari, A., 1988. Structure and reactivity of zinc–chromium mixed oxides. Part 1. The role of non-stoichiometry on bulk and surface properties. *Journal of the Chemical Society, Faraday Transactions 1* (84), 1405–1421.
- Besserguenev, A.V., Fogg, A.M., Francis, R.J., Price, S.J., O'Hare, D., 1997. Synthesis and structure of the Gibbsite intercalation compounds  $[\text{LiAl}_2(\text{OH})_6 \{X=\text{Cl, Br, NO}_3\}]$  and  $[\text{LiAl}_2(\text{OH})_6\text{Cl} \cdot \text{H}_2\text{O}]$  using synchrotron X-ray and neutron powder diffraction. *Chemistry of Materials* 9, 241–247.
- Bhanumathi, S., Kar, P., Acharya, N.R., Gupta, S., 1993. Hydrotalcite in the management of duodenal ulcer. *Advances in Therapy* 10, 9–11.
- Bigey, L., Depège, C., de Roy, A., Besse, J.P., 1997. EXAFS and XANES study of layered double hydroxides. *Journal de Physique IV* 7, 949–950.
- Bocclair, J.W., Braterman, P.S., 1998. One-step formation and characterization of Zn(II)–Cr(III) layered double hydroxides,  $\text{Zn}_2\text{Cr}(\text{OH})_6\text{X}$  ( $X=\text{Cl, } 1/2\text{SO}_4$ ). *Chemistry of Materials* 10, 2050–2052.
- Bocclair, J.W., Braterman, P.S., 1999. Layered double hydroxide stability. 1. Relative stabilities of layered double hydroxides and their simple counterparts. *Chemistry of Materials* 11, 298–302.
- Bocclair, J.W., Braterman, P.S., Brister, B.D., Jiang, J., Lou, S., Wang, Z., Yarberry, F., 2001. Cyanide self-addition, controlled adsorption, and other processes at layered double hydroxides. *Origin of Life and Evolution of the Biosphere* 31, 53–69.
- Bocclair, J.W., Braterman, P.S., Jiang, J., Lou, S., Yarberry, F., 1999. Layered double hydroxide stability. 2. Formation of Cr(III)-containing layered double hydroxides directly from solution. *Chemistry of Materials* 11, 303–307.
- Boehm, H.P., Steinle, J., Wieweger, C., 1977.  $[\text{Zn}_2\text{Cr}(\text{OH})_6]\text{X} \cdot 2\text{H}_2\text{O}$ , new layer compounds capable of anion exchange and intracrystalline swelling. *Angewandte Chemie, International Edition in English* 16, 265.
- Bonapasta, A.A., Buda, F., Colombet, P., 2001. Interaction between Ca ions and poly(acrylic acid) chains in macro-defect-free cements: a theoretical study. *Chemistry of Materials* 13, 64–70.
- Bonapasta, A., Buda, F., Colombet, P., Guerrini, G., 2002. Cross-linking of poly(vinyl alcohol) chains by Ca ions in macro-defect-free cements. *Chemistry of Materials* 14, 1016–1022.
- Bonnet, S., Bigey, L., Forano, C., de Roy, A., Besse, J.-P., Maillard, P., Momenteau, M., 1997. Intercalation of porphyrin in Zn–Al layered double hydroxides. *Chemical Industries (Dekker)*, 69 (*Synthesis of Porous Materials*), 627–640.
- Bonnet, S., Forano, C., de Roy, A., Besse, J.P., Maillard, P., Momenteau, M., 1996. Synthesis of hybrid organo-mineral materials: anionic tetraphenylporphyrins in layered double hydroxides. *Chemistry of Materials* 8, 1962–1968.
- Bookin, A.S., Cherkashin, V.I., Drits, J.A., 1993. Polytype diversity of the hydrotalcite-like minerals. II. Determination of the polytypes of experimentally studied varieties. *Clays and Clay Minerals* 41, 558–564.
- Borja, M., Dutta, P.K., 1992. Fatty acids in layered metal hydroxides: membrane-like structure and dynamics. *Journal of Physical Chemistry* 96, 5434–5444.
- Camino, G., Maffezzoli, A., Braglia, M., de Lazzaro, M., Zammarano, M., 2001. Effect of hydroxides and hydroxycarbonate structure on fire retardant effectiveness and mechanical

- properties in ethylene–vinyl acetate copolymer. *Polymer Degradation and Stability* 74, 457–464.
- Caravaggio, G.A., Detellier, C., Wronski, Z., 2001. Synthesis, stability and electrochemical properties of NiAl and NiV layered double hydroxides. *Journal of Materials Chemistry* 11, 912–921.
- Carja, G., Nakamura, R., Aida, T., Niiyama, H., 2001. Textural properties of layered double hydroxides: effect of magnesium substitution by copper or iron. *Microporous and Mesoporous Materials* 47, 275–284.
- Carja, G., Nakamura, R., Niiyama, H., 2002. Copper and iron substituted hydrotalcites: properties and catalyst precursors for methylamine synthesis. *Applied Catalysis, A: General* 236, 91–102.
- Carlino, S., 1997. The intercalation of carboxylic acids into layered double hydroxides: a critical evaluation and review of the different methods. *Solid State Ionics* 98, 73–84.
- Carlino, S., Hudson, M.J., 1994. Reaction of molten sebacic acid with a layered (Mg/Al) double hydroxide. *Journal of Materials Chemistry* 4, 99–104.
- Carlino, S., Hudson, M.J., 1995. Thermal intercalation of layered double hydroxides: capric acid into an Mg–Al LDH. *Journal of Materials Chemistry* 5, 1433–1442.
- Carlino, S., Hudson, M.J., Husain, W.S., Knowles, J.A., 1996. The reaction of molten phenylphosphonic acid with a layered double hydroxide and its calcined oxide. *Solid State Ionics* 84, 117–129.
- Carpentier, J., Lamonier, J.F., Siffert, S., Zhilinskaya, E.A., Aboukais, A., 2002. Characterisation of Mg/Al hydrotalcite with interlayer palladium complex for catalytic oxidation of toluene. *Applied Catalysis, A: General* 234, 91–101.
- Castiglioni, G.L., Minelli, G., Porta, P., Vaccari, A., 2000. Synthesis and properties of spinel-type Co–Cu–Mg–Zn–Cr mixed oxides. *Journal of Solid State Chemistry* 152, 526–532.
- Cavani, F., Trifirò, F., Vaccari, A., 1991. Hydrotalcite-type anionic clays: preparation, properties and applications. *Catalysis Today* 11, 173–301.
- Challier, T., Slade, R.C.T., 1994. Nanocomposite materials: polyaniline-intercalated layered double hydroxides. *Journal of Materials Chemistry* 4, 367–371.
- Châtelet, L., Bottero, J.Y., Yvon, J., Bouchelaghem, A., 1996. Competition between monovalent and divalent anions for calcined and uncalcined hydrotalcite: anion exchange and adsorption sites. *Colloids and Surfaces A: Physicochemical and Engineering Aspects* 111, 167–175.
- Chibwe, K., Jones, W., 1989a. Intercalation of organic and inorganic anions into layered double hydroxides. *Journal of the Chemical Society: Chemical Communications*, 926–927.
- Chibwe, K., Jones, W., 1989b. Synthesis of polyoxometalate-pillared layered double hydroxides via calcined precursors. *Chemistry of Materials* 1, 489–490.
- Chibwe, M., Ukrainczyk, L., Boyd, S.A., Pinnavaia, T.J., 1996. Catalytic properties of biomimetic metallomacrocycles intercalated in layered double hydroxides and smectite clay: the importance of edge-site access. *Journal of Molecular Catalysis A: Chemical* 113, 249–256.
- Chisem, I.C., Jones, W., Martin, I., Martin, C., Rives, V., 1998. Probing the surface acidity of lithium aluminum and magnesium aluminum layered double hydroxides. *Journal of Materials Chemistry* 8, 1917–1926.
- Choudary, B., Bharathi, B., Reddy, Ch., Kantam, M.L., 2002. Tungstate-exchanged Mg–Al–LDH catalyst: an eco-compatible route for the oxidation of sulfides in aqueous medium. *Journal of the Chemical Society, Perkin Transactions* 18, 2069–2074.

- Choudary, B.M., Bharathi, B., Reddy, C.V., Kantam, M.L., Raghavan, K.V., 2001a. The first example of catalytic *N*-oxidation of tertiary amines by tungstate-exchanged Mg–Al layered double hydroxide in water: a green protocol. *Chemical Communications*, 1736–1737.
- Choudary, B.M., Kantam, M.L., Kavita, B., Reddy, C.V., Figueras, F., 2000. Catalytic C–C bond formation promoted by Mg–Al–O-*t*-Bu hydrotalcite. *Tetrahedron* 56, 9357–9364.
- Choudary, B.M., Kantam, M.L., Neeraja, V., Rao, K.K., Figueras, F., Delmotte, L., 2001b. Layered double hydroxide fluoride: a novel solid base catalyst for C–C bond formation. *Green Chemistry* 3, 257–260.
- Choy, J.-H., Kwak, S.-Y., Park, J.-S., Jeong, Y.-J., 2001. Cellular uptake behavior of [ $\gamma$ - $^{32}$ P] labeled ATP–LDH nanohybrids. *Journal of Materials Chemistry* 11, 1671–1674.
- Choy, J.-H., Park, J.-S., Kwak, S.-Y., Jeong, Y.-J., Han, Y.-S., 2000. Layered double hydroxide as gene reservoir. *Molecular Crystals and Liquid Crystals* 341, 425–429.
- Clause, O., Gazzano, M., Trifiró, F., Vaccari, A., Zatorski, L., 1991. Preparation and thermal reactivity of nickel/chromium and nickel/aluminium hydrotalcite-type precursors. *Applied Catalysis* 73, 217–236.
- Clause, O., Rebours, B., Merlen, E., Trifiró, F., Vaccari, A., 1992. Preparation and characterization of nickel–aluminum mixed oxides obtained by thermal decomposition of hydrotalcite-type precursors. *Journal of Catalysis* 133, 231–246.
- Constantino, V.R.L., Pinnavaia, T.J., 1995. Basic properties of  $\text{Mg}_{1-x}^{2+}\text{Al}_x^{3+}$  layered double hydroxides intercalated by carbonate, hydroxide, chloride, and sulfate anions. *Inorganic Chemistry* 34, 883–892.
- Cooper, M.A., Hawthorne, F.C., 1996. The crystal structure of Shigaite,  $[\text{AlMn}_2^{2+}(\text{OH})_6]_3(\text{SO}_4)_2\text{Na}(\text{H}_2\text{O})_6\{\text{H}_2\text{O}\}_6$ , a hydrotalcite-group mineral. *Canadian Mineralogist* 34, 91–97.
- Costantino, U., Casciola, M., Massinelli, L., Nocchetti, M., Vivani, R., 1997. Intercalation and grafting of hydrogen phosphates and phosphonates into synthetic hydrotalcites and a.c.-conductivity of the compounds thereby obtained. *Solid State Ionics* 97, 203–212.
- Costantino, U., Coletti, N., Nocchetti, M., 1999. Anion exchange of methyl orange into Zn–Al synthetic hydrotalcite and photophysical characterization of the intercalates obtained. *Langmuir* 15, 4454–4460.
- Costantino, U., Coletti, N., Nocchetti, M., Aloisi, G.G., Elisei, F., Latterini, L., 2000. Surface uptake and intercalation of fluorescein anions into Zn–Al-hydrotalcite: photophysical characterization of materials obtained. *Langmuir* 16, 10351–10358.
- Costantino, U., Marmottini, F., Nocchetti, M., Vivani, R., 1998. New synthetic routes to hydrotalcite-like compounds. Characterization and properties of the obtained materials. *European Journal of Inorganic Chemistry* 10, 1439–1446.
- Crepaldi, E.L., Pavan, P.C., Valim, J.B., 1999. A new method of intercalation by anion exchange in layered double hydroxides. *Chemical Communications*, 155–156.
- Crepaldi, E.L., Pavan, P.C., Valim, J.B., 2000a. Comparative study of the coprecipitation methods for the preparation of layered double hydroxides. *Journal of the Brazilian Chemical Society* 11, 64–70.
- Crepaldi, E.L., Pavan, P.C., Valim, J.B., 2000b. Anion exchange in layered double hydroxides by surfactant salt formation. *Journal of Materials Chemistry* 10, 1337–1343.
- Crespo, I., Barriga, C., Ulibarri, M.A., González-Bandera, G., Malet, P., Rives, V., 2001. An X-ray diffraction and absorption study of the phases formed upon calcination of Zn–Al–Fe hydrotalcites. *Chemistry of Materials* 13, 1518–1527.

- Das, N.N., Srivastava, S.C., 2002. Catalytic characterization of bi-functional catalysts derived from Pd–Mg–Al layered double hydroxides. *Bulletin of Materials Science* 25, 283–289.
- De Fria, D.L., Al Costantino, V.R.L., Baldwin, K.J., Batchelder, D.N., Pinnavaia, T.J., Chibwe, M., 1998. Raman microspectroscopy of phthalocyanine intercalates: tetrasulphonated cobalt and nickel phthalocyanines in layered double hydroxide. *Journal of Raman Spectroscopy* 29, 103–108.
- Dékány, I., Berger, F., Imrik, K., Lagaly, G., 1997. Hydrophobic layered double hydroxides (LDHs): selective adsorbents for liquid mixtures. *Colloid and Polymer Science* 275, 681–688.
- del Arco, M., Gutiérrez, S., Martin, C., Rives, V., Rocha, J., 2000. Effect of the Mg:Al ratio on borate (or silicate)/nitrate exchange in hydrotalcite. *Journal of Solid State Chemistry* 151, 272–280.
- del Arco, M., Malet, P., Trujillano, R., Rives, V., 1999. Synthesis and characterization of hydrotalcites containing Ni(II) and Fe(III) and their calcination products. *Chemistry of Materials* 11, 624–633.
- del Arco, M., Martin, C., Martin, I., Rives, V., Trujillano, R., 1993. A FTIR spectroscopic study of surface acidity and basicity of mixed Mg,Al-oxides obtained by thermal decomposition of hydrotalcite. *Spectrochimica Acta* 49A, 1575–1582.
- del Arco, M., Rives, V., Trujillano, R., 1994. Surface and textural properties of hydrotalcite-like materials and their decomposition products. *Studies in Surface Science and Catalysis*, 87 (Characterization of Porous Solids III), 507–515.
- del Arco, M., Rives, V., Trujillano, R., Malet, P., 1996. Thermal behavior of Zn–Cr layered double hydroxides with hydrotalcite-like structures containing carbonate or decavanadate. *Journal of Materials Chemistry* 6, 1419–1428.
- del Arco, M., Trujillano, R., Rives, V., 1998. Cobalt–iron hydroxycarbonates and their evolution to mixed oxides with spinel structure. *Journal of Materials Chemistry* 8, 761–767.
- Depège, C., El Metoui, F.-Z., Forano, C., de Roy, A., Dupuis, J., Besse, J.-P., 1996. Polymerization of silicates in layered double hydroxides. *Chemistry of Materials* 8, 952–960.
- Depège, C., Forano, C., de Roy, A., Besse, J.-P., 1994. [Cu–Cr] layered double hydroxides pillared by  $\text{CrO}_4^{2-}$  and  $\text{Cr}_2\text{O}_7^{2-}$  oxometalates. *Molecular Crystals and Liquid Crystals* 244, 161–166.
- de Roy, A., Besse, J.-P., 1991. Evolution of protonic conduction in some synthetic clays. *Solid State Ionics* 46, 95–101.
- de Roy, A., Besse, J.-P., Bondot, P., 1985. Structural approach and conductivity of lamellar hydroxides  $\text{Zn}_2\text{Cr}(\text{OH})_6\text{X} \cdot n\text{H}_2\text{O}$  (X = anion) by XANES, EXAFS and X-ray diffraction. *Materials Research Bulletin* 20, 1091–1098.
- de Roy, A., Forano, C., El Malki, M., Besse, J.-P., 1992. Anionic clays: trends in pillaring chemistry. In: Ocelli, M.L., Robson, H.E. (Eds.), *Synthesis of Microporous Materials, Expanded Clays and Other Microporous Solids*. Van Nostrand Reinhold, New York, pp. 108–170.
- Di Cosimo, J.I., Diez, V.K., Xu, M., Iglesia, E., Apesteguía, C.R., 1998. Structure and surface and catalytic properties of Mg–Al basic oxides. *Journal of Catalysis* 178, 499–510.
- Dimotakis, E.D., Pinnavaia, T.J., 1990. New route to layered double hydroxides intercalated by organic anions: precursors to polyoxometalate-pillared derivatives. *Inorganic Chemistry* 29, 2393–2394.
- Ding, W., Gu, G., Zhong, W., Zang, W.-C., Du, Y., 1996. Enhanced photoluminescence of  $\text{C}_{60}$  incorporated into interlayers of hydrotalcite. *Chemical Physics Letters* 262, 259–262.

- Ding, Y., Alpay, E., 2001. High temperature recovery of CO<sub>2</sub> from flue gases using hydrotalcite adsorbent. *Process Safety and Environmental Protection* 79, 45–51.
- Doeuff, M., Kwon, T., Pinnavaia, T.J., 1989. Layered double hydroxides pillared by polyoxometalate anions: EXAFS studies and chemical synthesis. *Synthetic Metals* 34, 609–615.
- Doménech, A., Ribera, A., Cervilla, A., Llopis, E., 1998. Electrochemistry of hydrotalcite-supported bis(2-mercapto-2,2-diphenyl-ethanoate) dioxomolybdate complexes. *Journal of Electroanalytical Chemistry* 458, 31–41.
- Don Wang, J., Serrette, G., Tian, Y., Clearfield, A., 1995. Synthetic and catalytic studies of inorganically pillared and organically pillared layered double hydroxides. *Applied Clay Science* 10 (1–2), 103–115.
- Drezdon, M.A., 1988. Synthesis of isopolymetalate-pillared hydrotalcite via organic-anion-pillared precursors. *Inorganic Chemistry* 27, 4628–4632.
- Ducos, V., de Roy, A., Besse, J.P., 2001. Evolution of protonic conduction in [Zn–Al–Cl] lamellar double hydroxide phases with temperature and trivalent metal content. *Solid State Ionics* 145, 399–405.
- Dutta, P.K., Robins, D.S., 1994. Pyrene sorption in organic-layered double-metal hydroxides. *Langmuir* 10, 1851–1856.
- Ennadi, A., Khaldi, M., de Roy, A., Besse, J.-P., 1994. Structural results about localization of tetrahedral oxo-anions intercalated in lamellar double hydroxides. *Molecular Crystals and Liquid Crystals* 244, 373–378.
- Ennadi, A., Legrouiri, A., de Roy, A., Besse, J.P., 2000. X-ray diffraction pattern simulation for thermally treated [Zn–Al–Cl] layered double hydroxide. *Journal of Solid State Chemistry* 152, 568–572.
- Esumi, K., Yamamoto, S., 1998. Adsorption of sodium dodecyl sulfate on hydrotalcite and adsolubilization of 2-naphthol. *Colloids and Surfaces A: Physicochemical and Engineering Aspects* 137, 385–388.
- Evans, J., Pillinger, M., Zhang, J., 1996. Structural studies of polyoxometalate-anion-pillared layered double hydroxides. *Journal of the Chemical Society, Dalton Transactions* 14, 2963–2974.
- Faucon, P., le Bescop, P., Adenot, F., Bonville, P., Jacquinet, J.F., Pineau, F., Felix, B., 1996. Leaching of cement: study of the surface layer. *Cement and Concrete Research* 26, 1707–1715.
- Fernandez, C., Morais, C., Pruski, M., 2001. Comment on “<sup>27</sup>Al → <sup>31</sup>P 3QMAS/HETCOR experiment in aluminophosphate molecular sieves” by G. Mali, J.-P. Amoureux and V. Kaučič. *Physical Chemistry Chemical Physics* 3, 2552–2553.
- Fernandez, J.M., Barriga, C., Ulibarri, M.A., Labajos, F.M., Rives, V., 1997. New hydrotalcite-like compounds containing Yttrium. *Chemistry of Materials* 9, 312–318.
- Fernández, J.M., Barriga, C., Ulibarri, M.-A., Labajos, F.M., Rives, V., 1994. Preparation and thermal stability of manganese-containing hydrotalcite, [Mg<sub>0.75</sub>Mn<sub>0.04</sub>Mn<sup>III</sup><sub>0.21</sub>(OH)<sub>2</sub>](CO<sub>3</sub>)<sub>0.11</sub> · nH<sub>2</sub>O. *Journal of Materials Chemistry* 4, 1117–1121.
- Fernández, J.M., Ulibarri, M.A., Labajos, F.M., Rives, V., 1998. The effect of iron on the crystalline phases formed upon thermal decomposition of Mg–Al–Fe hydrotalcites. *Journal of Materials Chemistry* 8, 2507–2514.
- Fetter, G., Botello, A., Lara, V.H., Bosch, P., 2001. Detrital Mg(OH)<sub>2</sub> and Al(OH)<sub>3</sub> in microwave hydrotalcites. *Journal of Porous Materials* 8, 227–232.

- Fetter, G., Olguín, M.T., Bosch, P., Lara, V.H., Bulbulian, S., 1999.  $^{131}\text{I}^-$  sorption from aqueous solutions by nitrated hydrotalcites. *Journal of Radioanalytical and Nuclear Chemistry* 241, 595–599.
- Fischer, R., Kuzel, H.J., Schellhorn, H., 1980. Hydrocalumite: solid solution of “Friedel salt”  $3\text{CaO} \cdot \text{Al}_2\text{O}_3 \cdot \text{CaCl}_2 \cdot 10\text{H}_2\text{O}$  and tetracalcium aluminate hydrate  $3\text{CaO} \cdot \text{Al}_2\text{O}_3 \cdot \text{Ca}(\text{OH})_2 \cdot 12\text{H}_2\text{O}$ . *Neues Jahrbuch fuer Mineralogie, Monatshefte* (7), 322–334.
- Fogg, A., Dunn, M., O'Hare, J.S.D., 1998. Formation of second stage intermediates in anion exchange intercalation reactions of the layered double hydroxide  $[\text{LiAl}_2(\text{OH})_6]\text{Cl} \cdot \text{H}_2\text{O}$  as observed by time resolved, in situ X-ray diffraction. *Chemistry of Materials* 10, 356–360.
- Fogg, A.M., O'Hare, D., 1999. Study of the intercalation of lithium salt in gibbsite using time-resolved in situ X-ray diffraction. *Chemistry of Materials* 11 (7), 1771–1775.
- Ford, R.G., Scheinost, A.C., Scheckel, K.G., Sparks, D.L., 1999. The link between clay mineral weathering and the stabilization of Ni surface precipitates. *Environmental Science and Technology* 33, 3140–3144.
- Fuda, K., Kudo, N., Kawai, S., Matsunaga, T., 1993a. Preparation of Zn/Ga-layered double hydroxide and its thermal decomposition behavior. *Chemistry Letters*, 777–780.
- Fuda, K., Suda, K., Matsunaga, T., 1993b. Oxidation of Cr(III) to Cr(VI) species during the thermal decomposition process of Zn/Cr-layered double hydroxide carbonate. *Chemistry Letters*, 1479–1482.
- Gardner, E., Huntoon, K.M., Pinnavaia, T.J., 2001. Direct synthesis of alkoxide-intercalated derivatives of hydrotalcite-like layered double hydroxides: precursors for the formation of colloidal layered double hydroxide suspensions and transparent thin films. *Advanced Materials* 13, 1263–1266.
- Ge, X., Li, M., Shen, J., 2001. The reduction of Mg–Fe–O and Mg–Fe–Al–O complex oxides studied by temperature-programmed reduction combined with in situ Mössbauer spectroscopy. *Journal of Solid State Chemistry* 161, 38–44.
- Génin, J.-M.R., Bourrié, G., Trolard, F., Abdelmoula, M., Jaffrezic, A., Refait, Ph., Maître, V., Humbert, B., Herbillon, A., 1988. Thermodynamic equilibria in aqueous suspensions of synthetic and natural Fe(II)–Fe(III) green rusts: occurrences of the mineral in hydromorphic soils. *Environmental Science and Technology* 32, 1058–1064.
- Génin, J.-M.R., Refait, Ph., Bourrié, G., Abdelmoula, M., Trolard, F., 2001. Structure and stability of the Fe(II)–Fe(III) green rust “fougerite” mineral and its potential for reducing pollutants in soil solutions. *Applied Geochemistry* 16 (5), 559–570.
- Giannelis, E.P., 1996. Polymer layered silicate nanocomposites. *Advanced Materials* 8, 29–35.
- Giannelis, E.P., Nocera, D.G., Pinnavaia, T.J., 1987. Anionic photocatalysts supported in layered double hydroxides: intercalation and photophysical properties of a ruthenium complex anion in synthetic hydrotalcite. *Inorganic Chemistry* 26, 203–205.
- Goswamee, R.L., Sengupta, P., Bhattacharyya, K.G., Dutta, D.K., 1998. Adsorption of Cr(VI) in layered double hydroxides. *Applied Clay Science* 13, 21–34.
- Guerlou-Demourgues, L., Fournès, L., Delmas, C., 1996. In situ  $^{57}\text{Fe}$  Mossbauer spectroscopy study of the electrochemical behavior of an iron-substituted nickel hydroxide electrode. *Journal of the Electrochemical Society* 143, 3083–3087.
- Guimarães, J.L., Marangoni, R., Ramos, L.P., Wypych, F., 2000. Covalent grafting of ethylene glycol into the Zn–Al– $\text{CO}_3$  layered double hydroxide. *Journal of Colloid and Interface Science* 227, 445–451.



- Guo, Y., Li, D., Hu, C., Wang, E., Zou, Y., Ding, H., Feng, S., 2002. Preparation and photocatalytic behavior of Zn/Al/W(Mn) mixed oxides via polyoxometalates intercalated layered double hydroxides. *Microporous and Mesoporous Materials* 56, 153–162.
- Guo, Y., Li, D., Hu, C., Wang, Y., Wang, E., Zhou, Y., Feng, S., 2001. Photocatalytic degradation of aqueous organochlorine pesticide on the layered double hydroxide pillared by paratungstate A ion,  $\text{Mg}_{12}\text{Al}_6(\text{OH})_{36}(\text{W}_7\text{O}_{24}) \cdot 4\text{H}_2\text{O}$ . *Applied Catalysis B: Environmental* 30, 337–349.
- Gutmann, N., Mueller, B., 1996. Insertion of the dinuclear dihydroxo-bridged Cr(III) aquo complex into the layered double hydroxides of hydrotalcite-type. *Journal of Solid State Chemistry* 122, 214–220.
- Han, S., Hou, W., Zhang, C., Sun, D., Huang, X., Wang, G., 1998. Structure and the point of zero charge of magnesium aluminium hydroxide. *Journal of the Chemical Society, Faraday Transactions* 94, 915–918.
- He, J.X., Kobayashi, K., Takahashi, M., Villemure, G., Yamagishi, A., 2001. Preparation of hybrid films of an anionic Ru(II) cyanide polypyridyl complex with layered double hydroxides by the Langmuir–Blodgett method and their use as electrode modifiers. *Thin Solid Films* 397, 255–265.
- Hermosín, M.C., Pavlovic, I., Ulibarri, M.A., Cornejo, J., 1996. Hydrotalcite as sorbent for trinitrophenol: sorption capacity and mechanism. *Water Resources* 30, 171–177.
- Hernández, M.J., Ulibarri, M.A., Cornejo, J., Peña, M.J., Serna, C.J., 1985. Thermal stability of aluminium hydroxycarbonates with monovalent cations. *Thermochimica Acta* 94, 257–266.
- Hibino, T., Jones, W., 2001. New approach to the delamination of layered double hydroxides. *Journal of Materials Chemistry* 11, 1321–1323.
- Hibino, T., Tsunashima, A., 1997. Synthesis of paramolybdate intercalates of hydrotalcite-like compounds by ion exchange in ethanol/water solution. *Chemistry of Materials* 9, 2082–2089.
- Hibino, T., Tsunashima, A., 1998. Characterization of repeatedly reconstructed Mg–Al hydrotalcite-like compounds: gradual segregation of aluminum from the structure. *Chemistry of Materials* 10, 4055–4061.
- Hibino, T., Tsunashima, A., 2000. Calcination and rehydration behavior of Mg–Fe– $\text{CO}_3$  hydrotalcite-like compounds. *Journal of Materials Science Letters* 19, 1403–1405.
- Hibino, T., Uchisawa, J., Tsunashima, A., 1999. Synthesis and applications of hydrotalcite-type anionic clays. *Shigen Kankyo Gijutsu Sogo Kenkyusho Hokoku* 28, 1–61 i–iv.
- Hibino, T., Yamashita, Y., Kosuge, K., Tsunashima, A., 1995. Decarbonation behavior of Mg–Al– $\text{CO}_3$  hydrotalcite-like compounds during heat treatment. *Clays and Clay Minerals* 43, 427–432.
- Hines, D.R., Seidler, G.T., Treacy, M.M.J., Solin, S.A., 1997. Random stacking of a commensurate guest layer in an ordered host: of Ni/Al layer-double-hydroxides. *Solid State Communications* 101, 835–839.
- Hofmeister, W., von Platen, H., 1992. Crystal chemistry and atomic order in brucite-related double-layer structures. *Crystallography Reviews* 3, 3–29.
- Holtermüller, K.H., Liskay, M., Bernard, I., Haase, W., Eisold, H., Fischner, C., Fürer, M., Fumagalli, J., Hebbeln, H., Hennig, H., Martens, K., Panijel, M., Pelloni, S., Pelz, W., Plancherel, P., Rosprich, G., Schenk, J., Schütz, E., Seiler, P., 1993. Treatment for benign gastric ulcers with low-dose antacid versus ranitidine: Results of a double-blind, randomly

- allocated, multicentre trial. *European Journal of Gastroenterology and Hepatology* 5, S139–S144.
- Hou, W.-G., Su, Y.-L., Sun, D.-J., Zhang, C.-G., 2001. Studies on zero point of charge and permanent charge density of Mg–Fe hydrotalcite-like compounds. *Langmuir* 17, 1885–1888.
- Hou, X., Kalinichev, A.G., Kirkpatrick, R.J., 2002. Interlayer structure and dynamics of  $\text{Cl}^-$ – $\text{LiAl}_2$ -layered double hydroxide:  $^{35}\text{Cl}$  NMR observations and molecular dynamics modeling. *Chemistry of Materials* 14, 2078–2085.
- Hou, X., Kirkpatrick, R.J., 2000. Solid-state  $^{77}\text{Se}$  NMR and XRD study of the structure and dynamics of seleno-oxyanions in hydrotalcite-like compounds. *Chemistry of Materials* 12, 1890–1897.
- Hou, X., Kirkpatrick, R.J., 2001. Thermal evolution of the  $\text{Cl}(-)$ – $\text{LiAl}_2$  layered double hydroxide: a multinuclear MAS NMR and XRD perspective. *Inorganic Chemistry* 40, 6397–6404.
- Hu, C., Zhang, X., He, Q., Wang, E., Wang, S., Guo, Q., 1997. The rapid synthesis of the heteropolyoxometalate-pillared layered double hydroxide  $\text{Zn}_2\text{Al}(\text{OH})_6$   $[\text{SiW}_{11}\text{O}_{39}\text{Co}(\text{H}_2\text{O})]_{1/6} \cdot 4\text{H}_2\text{O}$  by the action of ultrasound. *Transition Metal Chemistry (London)* 22, 197–199.
- Hudson, M.J., Carlino, S., Apperley, D.C., 1995. Thermal conversion of a layered (Mg/Al) double hydroxide to the oxide. *Journal of Materials Chemistry* 5, 323–329.
- Hussein, M.Z.B., Zainal, Z., Choong, E.M., 2001. Structure and surface transformations of humic-adsorbed synthetic hydrotalcite-like materials. *Journal of Porous Materials* 8, 219–226.
- Hussein, M.Z., Zainal, Z., Swee, H.H., 1995. Scanning electron microscopy and surface area studies of calcined  $\text{ZnCrCl}$  layered double hydroxides. *Journal of Materials Science Letters* 14, 1747–1750.
- Hwang, S.-H., Han, Y.-S., Choy, J.-H., 2001. Intercalation of functional organic molecules with pharmaceutical, cosmeceutical and nutraceutical functions into layered double hydroxides and zinc basic salts. *Bulletin of the Korean Chemical Society* 22, 1019–1022.
- Ijdo, W.L., Pinnavaia, T.J., 1998. Staging of organic and inorganic gallery cations in layered silicate heterostructures. *Journal of Solid State Chemistry* 139, 281–289.
- Inacio, J., Taviot-Guého, C., Forano, C., Besse, J.-P., 2001. Adsorption of MCPA pesticide by  $\text{MgAl}$ -layered double hydroxides. *Applied Clay Science* 18, 255–264.
- Indira, L., Kamath, P.V., 1994. Electrogeneration of base by cathodic reduction of anions: novel one-step route to unary and layered double hydroxides (LDHs). *Journal of Materials Chemistry* 4, 1487–1490.
- Ingram, L., Taylor, H.F.W., 1967. Crystal structures of sjogrenite and pyroaurite. *Mineralogical Magazine and Journal of the Mineralogical Society* 36 (280), 465–479.
- Intissar, M., Segni, R., Payen, C., Besse, J.-P., Leroux, F., 2002. Trivalent cation substitution effect into layered double hydroxides  $(\text{Co}_2\text{Fe}_y\text{Al}_{1-y})(\text{OH})_6\text{Cl} \cdot n\text{H}_2\text{O}$ : study of the local order. Ionic conductivity and magnetic properties. *Journal of Solid State Chemistry* 167, 508–516.
- Ishihara, Y., Okabe, S., 1981. Effects of cholestyramine and synthetic hydrotalcite on acute gastric or intestinal lesion formation in rats and dogs. *Digestive Diseases and Sciences* 26, 553–560.
- Israeli, Y., Taviot-Gueho, C., Besse, J.-P., Morel, J.-P., Morel-Desrosiers, N., 2000. Thermodynamics of anion exchange on a chloride-intercalated zinc-aluminum layered double

- hydroxide: a microcalorimetric study. *Journal of the Chemical Society, Dalton Transactions* 5, 791–796.
- Isupov, V.P., Chupakhina, L.E., Ozerova, M.A., Kostrovsky, V.G., Poluboyarov, V.A., 2001. Polymerization of  $m\text{-NH}_2\text{C}_6\text{H}_4\text{COO}$  anions in the intercalation compounds of aluminium hydroxide  $[\text{LiAl}_2(\text{OH})_6][m\text{-NH}_2\text{C}_6\text{H}_4\text{COO}] \cdot n\text{H}_2\text{O}$ . *Solid State Ionics* 141–142, 231–236.
- Itaya, K., Chang, H.-C., Uchida, I., 1987. Anion-exchanged hydrotalcite-like-clay-modified electrodes. *Inorganic Chemistry* 26, 624–626.
- Iyi, N., Kurashima, K., Fujita, T., 2002. Orientation of an organic anion and second-staging structure in layered double-hydroxide intercalates. *Chemistry of Materials* 14, 583–589.
- Jakupca, M., Dutta, P.K., 1995. Thermal and spectroscopic analysis of a fatty acid-layered double-metal hydroxide and its application as a chromatographic stationary phase. *Chemistry of Materials* 7, 989–994.
- Jiratova, K., Cuba, P., Kovanda, F., Hilaire, L., Pitchon, V., 2002. Preparation and characterisation of activated Ni (Mn)/Mg/Al hydrotalcites for combustion catalysis. *Catalysis Today* 76, 43–53.
- Jitianu, M., Balasoïu, M., Zaharescu, M., Jitianu, A., Ivanov, A., 2000a. Comparative study of sol-gel and coprecipitated Ni–Al hydrotalcites. *Journal of Sol-Gel Science and Technology* 19, 453–457.
- Jitianu, M., Jitianu, A., Zaharescu, M., Crisan, D., Marchidan, R., 2000b. IR structural evidence of hydrotalcites derived oxidic forms. *Vibrational Spectroscopy* 22, 75–86.
- Jitianu, M., Zaharescu, M., Balasoïu, M., Jitianu, A., 2003. The sol-gel route in synthesis of Cr(III)-containing clays. Comparison between Mg–Cr and Ni–Cr anionic clays. *Journal of Sol-Gel Science and Technology* 26, 217–221.
- Johnson, T.E., Martens, W., Frost, R.L., Ding, Z., Klopogge, J.T., 2002. Structured water in hydrotalcites of formula  $\text{Mg}_x\text{Zn}_{6-x}\text{Al}_2(\text{OH})_{16}(\text{CO}_3) \cdot 4\text{H}_2\text{O}$ : a Raman microscopic study. *Journal of Raman Spectroscopy* 33, 604–609.
- Kagunya, W., Baddour-Hadjean, R., Kooli, F., Jones, W., 1998. Vibrational modes in layered double hydroxides and their calcined derivatives. *Chemical Physics* 236, 225–234.
- Kagunya, W.W., 1996. Properties of water adsorbed in anionic clays: a neutron scattering study. *Journal of Physical Chemistry* 100, 327–330.
- Kalinichev, A.G., Kirkpatrick, R.J., 2002. Molecular dynamics modeling of chloride binding to the surfaces of calcium hydroxide, hydrated calcium aluminate, and calcium silicate phases. *Chemistry of Materials* 14, 3539–3549.
- Kalinichev, A.G., Kirkpatrick, R.J., Cygan, R.T., 2000. Molecular modeling of the structure and dynamics of the interlayer and surface species of mixed-metal layered hydroxides: chloride and water in hydrocalumite (Friedel's salt). *American Mineralogist* 85, 1046–1052.
- Kalinichev, A.G., Kirkpatrick, R.J., Wang, J., 2002. Molecular dynamics simulation of ionic sorption and diffusion on surfaces and interfaces of layered double hydroxides. Abstracts of Papers, 223rd ACS National Meeting, Orlando, FL, April 7–11, 2002, GE0C-070. American Chemical Society, Washington, DC.
- Kamath, P.V., Dixit, M., Indira, L., Shukla, A.K., Kumar, V.G., Munichandraiah, N., 1994. Stabilized  $\alpha\text{-Ni}(\text{OH})_2$  as electrode material for alkaline secondary cells. *Journal of the Electrochemical Society* 141, 2956–2959.
- Kameda, T., Miyano, Y., Yoshioka, T., Uchida, M., Okuwaki, A., 2000. New treatment methods for waste water containing chloride ion using magnesium–aluminum oxide. *Chemistry Letters*, 1136–1137.

- Kaneyoshi, M., Jones, W., 1998. Exchange of interlayer terephthalate anions from a Mg–Al layered double hydroxide: formation of intermediate interstratified phases. *Chemical Physics Letters* 296, 183–186.
- Kanezaki, E., 1998a. A thermally induced metastable solid phase of Mg/Al-layered double hydroxides by means of in situ high temperature powder X-ray diffraction. *Journal of Materials Science Letters* 17, 371–374.
- Kanezaki, E., 1998b. Effect of atomic ratio Mg/Al in layers of Mg and Al layered double hydroxide on thermal stability of hydrotalcite-like layered structure by means of in situ high temperature powder X-ray diffraction. *Materials Research Bulletin* 33, 773–778.
- Kanezaki, E., 1998c. Thermal behavior of the hydrotalcite-like layered structure of Mg and Al-layered double hydroxides with interlayer carbonate by means of in situ powder HTXRD and DTA/TG. *Solid State Ionics* 106, 279–284.
- Kannan, S., Narayanan, A., Swamy, C.S., 1996. Effect of composition on the physicochemical properties of nickel aluminium hydrotalcites. *Journal of Materials Science* 31, 2353–2360.
- Kannan, S., Swamy, C.S., 1992. Synthesis and physicochemical characterization of cobalt aluminium hydrotalcite. *Journal of Materials Science Letters* 11, 1585–1587.
- Kannan, S., Swamy, C.S., 1994. Catalytic decomposition of nitrous oxide on “in situ” generated thermally calcined hydrotalcites. *Applied Catalysis B: Environmental* 3, 109–116.
- Kannan, S., Velu, S., Ramkumar, V., Swamy, C.S., 1995. Synthesis and physicochemical properties of cobalt aluminium hydrotalcites. *Journal of Materials Science* 30, 1462–1468.
- Kannan, S., Vir Jasra, R., 2000. Microwave assisted rapid crystallization of Mg–M(III) hydrotalcite where M(III) = Al, Fe or Cr. *Journal of Materials Chemistry* 10, 2311–2314.
- Kapteijn, F., Rodriguez-Mirasol, J., Moulijn, J.A., 1996. Heterogeneous catalytic decomposition of nitrous oxide. *Applied Catalysis B: Environmental* 9, 25–64.
- Kelkar, C.P., Schutz, A.A., 1997a. Ni-, Mg- and Co-containing hydrotalcite-like materials with a sheet-like morphology: synthesis and characterization. *Microporous Materials* 10, 163–172.
- Kelkar, C.P., Schutz, A.A., Cullo, L.A., 1997b. Synthesis of hydrotalcite-like materials with a sheet-like morphology. *Chemical Industries (Dekker)* 69(Synthesis of Porous Materials), 691–703.
- Khalidi, M., Badreddine, M., Legroui, A., Chaouch, M., Barroug, A., de Roy, A., Besse, J.-P., 1998. Preparation of a well-ordered layered nanocomposite from zinc–aluminium–chloride layered double hydroxide and hydrogenophosphate by ion exchange. *Materials Research Bulletin* 33, 1835–1843.
- Khalidi, M., de Roy, A., Chaouch, M., Besse, J.-P., 1997. New varieties of zinc–chromium–sulfate lamellar double hydroxides. *Journal of Solid State Chemistry* 130, 66–73.
- Khan, A.I., Lei, L., Norquist, A.J., O'Hare, D., 2001. Intercalation and controlled release of pharmaceutically active compounds from a layered double hydroxide. *Chemical Communications*, 2342–2343.
- Khan, A.I., O'Hare, D., 2002. Intercalation chemistry of layered double hydroxides: recent developments and applications. *Journal of Materials Chemistry* 12, 3191–3198.
- Kirkpatrick, R.J., Yu, P., Hou, X., Kim, Y., 1999. Interlayer structure, anion dynamics, and phase transitions in mixed-metal layered hydroxides: variable temperature  $^{35}\text{Cl}$  NMR spectroscopy of hydrotalcite and Ca-aluminate hydrate (hydrocalumite). *American Mineralogist* 84, 1186–1190.

- Kloprogge, J.T., Frost, R.L., 1999. Fourier transform infrared and Raman spectroscopic study of the local structure of Mg-, Ni-, and Co-hydrotalcites. *Journal of Solid State Chemistry* 146, 506–515.
- Kloprogge, J.T., Frost, R.L., 2001. Infrared and Raman spectroscopic studies of layered double hydroxides (LDHs). In: Rives, V. (Ed.), *Layered Double Hydroxides*. Nova Science Publishers, Huntington, pp. 139–192.
- Kloprogge, J.T., Hickey, L., Frost, R.L., 2001. Heating stage Raman and infrared emission spectroscopic study of the dehydroxylation of synthetic Mg-hydrotalcite. *Applied Clay Science* 18, 37–49.
- Kloprogge, J.T., Wharton, D., Hickey, L., Frost, R.L., 2002. Infrared and Raman study of interlayer anions  $\text{CO}_3^{2-}$ ,  $\text{NO}_3^-$ ,  $\text{SO}_4^{2-}$  and  $\text{ClO}_4^-$  in Mg/Al-hydrotalcite. *American Mineralogist* 87, 623–629.
- Komarneni, S., Kozai, N., Roy, R., 1998. Novel function for anionic clays: selective transition metal cation uptake by diadochy. *Journal of Materials Chemistry* 8, 1329–1331.
- Kooli, F., Chisem, I.C., Vucelic, M., Jones, W., 1996. Synthesis and properties of terephthalate and benzoate intercalates of Mg–Al layered double hydroxides possessing varying layer charge. *Chemistry of Materials* 8, 1969–1977.
- Kooli, F., Depège, C., Ennaqadi, A., de Roy, A., Besse, J.-P., 1997a. Rehydration of Zn–Al layered double hydroxides. *Clays and Clay Minerals* 45, 92–98.
- Kooli, F., Jones, W., 1995. Direct synthesis of polyoxovanadate-pillared layered double hydroxides. *Inorganic Chemistry* 34, 6237–6238.
- Kooli, F., Jones, W., Rives, V., Ulibarri, M.A., 1997b. An alternative route to polyoxometalate-exchanged layered double hydroxides: the use of ultrasound. *Journal of Materials Science Letters* 16, 27–29.
- Kooli, F., Martin, C., Rives, V., 1997c. FT-IR spectroscopy study of surface acidity and isopropanol decomposition on mixed oxides obtained upon calcination of layered double hydroxides. *Langmuir* 13, 2303–2306.
- Kooli, F., Rives, V., Ulibarri, M.A., 1994. Vanadate-pillared hydrotalcite containing transition metal cations. *Materials Science Forum*, 152–153 (Soft Chemistry Routes to New Materials), 375–378.
- Kooli, F., Rives, V., Ulibarri, M.A., 1995. Preparation and study of decavanadate-pillared hydrotalcite-like anionic clays containing transition metal cations in the layers. 1. Samples containing nickel-aluminum prepared by anionic exchange and reconstruction. *Inorganic Chemistry* 34, 5114–5121.
- Kopka, H., Beneke, K., Lagaly, G., 1988. Anionic surfactants between double metal hydroxide layers. *Journal of Colloid and Interface Science* 123, 427–436.
- Kuk, W.-K., Huh, Y.-D., 1998. Preferential intercalation of organic anions into layered double hydroxide. *Bulletin of the Korean Chemical Society* 19, 1032–1036.
- Kuzel, H.J., Baier, H., 1996. Hydration of calcium aluminate cements in the presence of calcium carbonate. *European Journal of Mineralogy* 8, 129–141.
- Kwon, T., Pinnavaia, T.J., 1992. Synthesis and properties of anionic clays pillared by  $[\text{XM}_{12}\text{O}_{40}]^{n-}$  Keggin ions. *Journal of Molecular Catalysis* 74, 23–33.
- Kwon, T., Tsigdinos, G.A., Pinnavaia, T.J., 1988. Pillaring of layered double hydroxides (LDHs) by polyoxometalate anions. *Journal of the American Chemical Society* 110, 3653–3654.

- Labajos, F.M., Rives, V., 1996. Thermal evolution of chromium(III) ions in hydrotalcite-like compounds. *Inorganic Chemistry* 35, 5313–5318.
- Labajos, F.M., Rives, V., Malet, P., Centeno, M.A., Ulibarri, M.A., 1996. Synthesis and characterization of hydrotalcite-like compounds containing  $V^{3+}$  in the layers and of their calcination products. *Inorganic Chemistry* 35, 1154–1160.
- Labajos, F.M., Rives, V., Ulibarri, M.A., 1992. Effect of hydrothermal and thermal treatments on the physicochemical properties of Mg–Al hydrotalcite-like materials. *Journal of Materials Science* 27, 1546–1552.
- Lagaly, G., Mecking, O., Penner, D., 2001a. Colloidal magnesium aluminum hydroxide and heterocoagulation with a clay mineral. I. Properties of colloidal magnesium aluminum hydroxide. *Colloid and Polymer Science* 279, 1090–1096.
- Lagaly, G., Mecking, O., Penner, D., 2001b. Colloidal magnesium aluminum hydroxide and heterocoagulation with a clay mineral. II. Heterocoagulation with sodium montmorillonite. *Colloid and Polymer Science* 279, 1097–1103.
- Lakrismi, M., Legrouri, A., Barroug, A., de Roy, A., Besse, J.-P., 1999. Removal of pesticides from water by anionic clays. *Journal de Chimie Physique et de Physico-Chimie Biologique* 96, 470–478.
- Latterini, L., Elisei, F., Aloisi, G.G., Costantino, U., Nocchetti, M., 2002. Space-resolved fluorescence properties of phenolphthalein-hydrotalcite nanocomposites. *Physical Chemistry Chemical Physics* 4, 2792–2798.
- Legrouri, A., Badreddine, M., Barroug, A., de Roy, A., Besse, J.-P., 1999. Influence of pH on the synthesis of the Zn–Al–nitrate layered double hydroxide and the exchange of nitrate by phosphate ions. *Journal of Materials Science Letters* 18, 1077–1079.
- Lehmann, M., Zouboulis, A.I., Matis, K.A., 1999. Removal of metal ions from dilute aqueous solutions: a comparative study of inorganic sorbent materials. *Chemosphere* 39, 881–892.
- Leroux, F., Adachi-Pagano, M., Intissar, M., Chauvière, S., Forano, C., Besse, J.-P., 2001a. Delamination and restacking of layered double hydroxides. *Journal of Materials Chemistry* 11, 105–112.
- Leroux, F., Besse, J.-P., 2001. Polymer interleaved layered double hydroxide: a new emerging class of nanocomposites. *Chemistry of Materials* 13, 3507–3515.
- Leroux, F., Moujahid, M., Roussel, H., Flank, A.-M., Briois, V., Besse, J.-P., 2002. Local order of the transition metals for the substitution  $(Co_{1-y}Cu_y)_2Al(OH)_6Cl \cdot nH_2O$  ( $0 < y < 1$ ) in a copper–aluminium layered double hydroxide-like phase. *Clays and Clay Minerals* 50, 260–270.
- Leroux, F., Moujahid, M., Taviot-Guého, C., Besse, J.-P., 2001b. Effect of layer charge modification for Co–Al layered double hydroxides: study by X-ray absorption spectroscopy. *Solid State Science* 3, 81–92.
- Li, Y., Chen, J., Qin, Y., Chang, L., 2000. Simultaneous production of hydrogen and nanocarbon from decomposition of methane on a nickel-based catalyst. *Energy and Fuels* 14, 1188–1194.
- Lopez, T., Bosh, P., Ramos, E., Gomez, R., Novaro, O., Acosta, D., Figueras, F., 1996. Synthesis and characterization of sol-gel hydrotalcites. Structure and texture. *Langmuir* 12, 189–192.
- Lopez, T., Ramos, E., Bosh, P., Asomoza, M., Gomez, R., 1997. DTA and TGA characterization of sol-gel hydrotalcites. *Materials Letters* 30, 279–282.

- Lopez-Salinas, E., Abasolo, J.A., Acosta, D.R., 1998. Electron microscopy studies of a gallium substituted synthetic hydrotalcite-like-compound. In: Benavides, C., Hector, A., Yacamán, J., M. (Eds.), *Electron Microscopy 1998, Proceedings of the 14th International Congress on Electron Microscopy*, Cancun, Mexico, vol. 3. Institute of Physics Publishing, Bristol, pp. 339–340.
- Lopez-Salinas, E., Garcia-Sanchez, M., Llanos-Serrano, M., Navarrete-Bolano, J., 1997a. Formation of base sites on calcined Mg–Ga hydrotalcite-like  $[\text{Mg}_{1-x}\text{Ga}_x(\text{OH})_2](\text{CO}_3)_{x/2} \cdot \text{H}_2\text{O}$ . *Journal of Physical Chemistry*, B 101, 5112–5117.
- Lopez-Salinas, E., Garcia-Sanchez, M., Montoya, J.A., Acosta, D.R., Abasolo, J.A., Schifter, I., 1997b. Structural characterization of synthetic hydrotalcite-like  $[\text{Mg}_{1-x}\text{Ga}_x(\text{OH})_2](\text{CO}_3)_{x/2} \cdot \text{H}_2\text{O}$ . *Langmuir* 13, 4748–4753.
- Lopez-Salinas, E., Garcia-Sanchez, M., Ramon-Garcia, M.L., Schifter, I., 1996. New gallium-substituted hydrotalcites:  $[\text{Mg}_{1-x}\text{Ga}_x(\text{OH})_2](\text{CO}_3)_{x/2} \cdot m\text{H}_2\text{O}$ . *Journal of Porous Materials* 3, 169–174.
- Lopez-Salinas, E., Torres-García, E., García-Sánchez, M., 1997c. Thermal behavior of hydrotalcite-like  $[\text{Mg}_{1-x}\text{Ga}_x(\text{OH})_2](\text{CO}_3)_{x/2} \cdot m\text{H}_2\text{O}$  as a function of gallium content. *Journal of Physics and Chemistry of Solids* 58, 919–925.
- Lotsch, B., Millange, F., Walton, R.I., O'Hare, D., 2001. Separation of nucleoside monophosphates using preferential anion exchange intercalation in layered double hydroxides. *Solid State Sciences* 3, 883–886.
- Lwin, Y., Yarmo, M.A., Yaakob, Z., Mohamad, A.B., Ramli Wan Daud, W., 2001. Synthesis and characterization of Cu–Al layered double hydroxides. *Materials Research Bulletin* 36, 193–198.
- MacKenzie, K.J.D., Meinhold, R.H., Sherriff, B.L., Xu, Z., 1993.  $^{27}\text{Al}$  and  $^{25}\text{Mg}$  solid-state magic-angle spinning nuclear magnetic resonance study of hydrotalcite and its thermal decomposition sequence. *Journal of Materials Chemistry* 3, 1263–1269.
- Malherbe, F., Besse, J.-P., 2000. Investigating the effects of guest–host interactions on the properties of anion-exchanged Mg–Al hydrotalcites. *Journal of Solid State Chemistry* 155, 332–341.
- Malherbe, F., Bigey, L., Forano, C., de Roy, A., Besse, J.-P., 1999. Structural aspects and thermal properties of takovite-like layered double hydroxides pillared with chromium oxoanions. *Journal of the Chemical Society, Dalton Transactions* 21, 3831–3839.
- Malherbe, F., Depège, C., Forano, C., Besse, J.-P., Atkins, M.P., Sharma, B., Wade, S.R., 1998. Alkoxylation reaction catalyzed by layered double hydroxides. *Applied Clay Science* 13, 451–466.
- Malherbe, F., Forano, C., Besse, J.-P., 1997. Use of organic media to modify the surface and porosity properties of hydrotalcite-like compounds. *Microporous Materials* 10, 67–84.
- Marchi, A.J., Apesteguía, C.R., 1998. Impregnation-induced memory effect of thermally activated layered double hydroxides. *Applied Clay Science* 13, 35–48.
- Marquevich, M., Farriol, X., Medina, F., Montané, D., 2001. Hydrogen production by steam reforming of vegetable oils using nickel-based catalysts. *Industrial and Engineering Chemistry Research* 40, 4757–4766.
- Martin, K.J., Pinnavaia, T.J., 1986. Layered double hydroxides as supported anionic reagents. Halide-ion reactivity in zinc chromium hexahydroxide halide hydrates  $[\text{Zn}_2\text{Cr}(\text{OH})_6 \cdot n\text{H}_2\text{O}]$  ( $X = \text{Cl}, \text{I}$ ). *Journal of the American Chemical Society* 108, 541–542.
- Mascolo, G., 1995. Synthesis of anionic clays by hydrothermal crystallization of amorphous precursors. *Applied Clay Science* 10, 21–30.

- Mendiboure, A., Schöllhorn, R., 1987. Formation and anion exchange reactions of layered transition metal hydroxides  $[\text{Ni}_{1-x}\text{M}_x](\text{OH})_2(\text{CO}_3)_{x/2}(\text{H}_2\text{O})_z$  ( $\text{M}$  = iron, cobalt). *Revue de Chimie Minérale* 23, 819–827.
- Ménétrier, M., Han, K.S., Guerlou-Delourgues, L., Delmas, C., 1997. Vanadate-inserted layered double hydroxides: A (51)V NMR investigation of the grafting process. *Inorganic Chemistry* 36, 2441–2445.
- Messersmith, P.B., Stupp, S.I., 1995. High-temperature chemical and microstructural transformations of a nanocomposite organoceramic. *Chemistry of Materials* 7, 454–460.
- Meyn, M., Beneke, K., Lagaly, G., 1990. Anion-exchange reactions of layered double hydroxides. *Inorganic Chemistry* 29, 5201–5207.
- Meyn, M., Beneke, K., Lagaly, G., 1993. Anion-exchange reactions of layered double salts. *Inorganic Chemistry* 32, 1209–1215.
- Millange, F., Walton, R.I., O'Hare, D., 2000. Time-resolved in situ X-ray diffraction study of the liquid-phase reconstruction of Mg–Al–carbonate hydrotalcite-like compounds. *Journal of Materials Chemistry* 10, 1713–1720.
- Miyata, S., 1983. Anion-exchange properties of hydrotalcite-like compounds. *Clays and Clay Minerals* 31, 305–311.
- Miyata, S., 1991. Properties and applications of hydrotalcite-type minerals. *Zeoraito* 8, 7–16.
- Miyata, S., 1980. Physico-chemical properties of synthetic hydrotalcites in relation to composition. *Clays and Clay Minerals* 28, 50–56.
- Miyata, S., Hirose, T., 1978. Adsorption of  $\text{N}_2$ ,  $\text{O}_2$ ,  $\text{CO}_2$ , and  $\text{H}_2$  on hydrotalcite-like system:  $\text{Mg}^{2+}\text{--Al}^{3+}\text{--}(\text{Fe}(\text{CN})_6)^{4-}$ . *Clays and Clay Minerals* 26, 441–447.
- Mohmel, S., Kurzawski, I., Uecker, D., Muller, D., Gessner, W., 2002. The influence of a hydrothermal treatment using microwave heating on the crystallinity of layered double hydroxides. *Crystal Research and Technology* 37, 359–369.
- Moneyron, J.E., de Roy, A., Besse, J.-P., 1990. Realisation of hydrotalcite-type protonic conductor thick films by the screen-printing technique. *Hybrid Circuits* 22, 25–28.
- Moneyron, J.E., de Roy, A., Besse, J.-P., 1991a. Protonic conductivity of hydrotalcite-type compound thick films: application to a humidity sensor. *Solid State Ionics* 46, 175–181.
- Moneyron, J.E., de Roy, A., Besse, J.-P., 1991b. Realisation of a humidity sensor based on the protonic conductor  $\text{Zn}_2\text{Al}(\text{OH})_6\text{Cl} \cdot n\text{H}_2\text{O}$ . *Hybrid Circuits* 24, 26–31.
- Moneyron, J.E., De Roy, A., Besse, J.-P., 1991c. Realization of a humidity sensor. *Sensors and Actuators B* 4, 189–194.
- Montanari, B., Vaccari, A., Gazzano, M., Käbner, P., Papp, H., Pasel, J., Dziembaj, R., Makowski, W., Lojewski, T., 1997. Characterization and activity of novel copper-containing catalysts for selective catalytic reduction of NO with  $\text{NH}_3$ . *Applied Catalysis B: Environmental* 13, 205–217.
- Morigi, M., Scavetta, E., Berrettoni, M., Giorgetti, M., Tonelli, D., 2001. Sulfate-selective electrodes based on hydrotalcites. *Analytica Chimica Acta* 439, 265–272.
- Mori, K., Nakamura, Y., Kikuchi, I., 1981. Modification of poly(vinyl chloride): XLI. Effect of hydrotalcite on the stabilization of poly(vinyl chloride) by 6-anilino-1,3,5-triazine-2,4-dithiol and zinc stearate. *Journal of Polymer Science: Polymer Letters Edition* 19, 623–628.
- Morioka, H., Tagaya, H., Karasu, M., Kadokawa, J., Chiba, K., 1995. Preparation of new useful materials by surface modification of inorganic layered compound. *Journal of Solid State Chemistry* 117, 337–342.



- Morpurgo, S., Jacono, M.L., Porta, P., 1996. Copper–zinc–cobalt–aluminium–chromium hydroxycarbonates and mixed oxides. *Journal of Solid State Chemistry* 122, 324–332.
- Moujahid, M., Besse, J.-P., Leroux, F., 2002a. Synthesis and characterization of polystyrene sulfonate layered double hydroxide nanocomposite. In-situ polymerization versus polymer incorporation. *Journal of Materials Chemistry* 12, 3324–3330.
- Moujahid, M., Besse, J.-P., Leroux, F., 2003. Polystyrene sulfonate layered double hydroxide nanocomposites. Stability and subsequent structural transformation in temperature. *Journal of Materials Chemistry* 13, 258–264.
- Moujahid, M.E., Dubois, M., Besse, J.-P., Leroux, F., 2002b. The role of atmospheric oxygen for the polymerization of interleaved aniline sulfonic in LDH. *Chemistry of Materials* 14, 3799–3807.
- Mousty, C., Therias, S., Forano, C., Besse, J.-P., 1994. Anion-exchanging clay-modified electrodes: synthetic layered double hydroxides intercalated with electroactive organic anions. *Journal of Electroanalytical Chemistry* 374, 63–69.
- Narita, E., Kaviratna, P., Pinnavaia, T.J., 1991. Synthesis of heteropolyoxometalate pillared layered double hydroxides via calcined zinc–aluminium oxide precursors. *Chemistry Letters* 805–808.
- Neuhäusler, U., Abend, S., Jacobsen, C., Lagaly, G., 1999. Soft X-ray spectromicroscopy on solid-stabilized emulsions. *Colloid and Polymer Science* 277, 719–726.
- Newman, A.C.D., 1987. *Chemistry of Clays and Clay Minerals*. Wiley-Interscience, New York.
- Newman, S.P., Greewell, H.C., Coveny, P.V., Jones, W., 2001. Computer modelling of layered double hydroxides. In: Rives, V. (Ed.), *Layered Double Hydroxides*. Nova Science Publishers, Huntington, pp. 93–114.
- Newman, S.P., Jones, W., 1998. Synthesis, characterization and applications of layered double hydroxides containing organic guests. *New Journal of Chemistry* 22, 105–115.
- Newman, S.P., Jones, W., 2002. Layered double hydroxides as templates for the formation of supramolecular structures. In: Jones, W., Rao, C.N.R. (Eds.), *Supramolecular Organization and Materials Design*. Cambridge University Press, Cambridge.
- Newman, S.P., Jones, W., O'Connor, P., Stamires, D.N., 2002b. Synthesis of the 3R<sub>2</sub> polytype of a hydrotalcite-like mineral. *Journal of Materials Chemistry* 12, 153–155.
- Nijs, H., Clearfield, A., Vansant, E.F., 1998. The intercalation of phenylphosphonic acid in layered double hydroxides. *Microporous and Mesoporous Materials* 23, 97–108.
- Nijs, H., De Bock, M., Vansant, E.F., 1999. Evaluation of the microporosity of pillared [Fe(CN)<sub>6</sub>]-MgAl-LDHs. *Microporous and Mesoporous Materials* 30, 243–253.
- Ogawa, M., Kaiho, H., 2002. Homogeneous precipitation of uniform hydrotalcite particles. *Langmuir* 18, 4240–4242.
- O'Hare, D., Evans, J.S.O., Fogg, A.M., O'Brien, S., 2000. Time-resolved, in situ X-ray diffraction studies of intercalation in lamellar hosts. *Polyhedron* 19, 297–305.
- Oh, J.-M., Hwang, S.-H., Choy, J.-H., 2002. The effect of synthetic conditions on tailoring the size of hydrotalcite particles. *Solid State Ionics* 151, 285–291.
- O'Leary, S., O'Hare, D., Seeley, G., 2002. Delamination of layered double hydroxides in polar monomers: new LDH–acrylate nanocomposites. *Chemical Communications*, 1506–1507.
- Olguín, M.T., Bosch, P., Acosta, D., Bulbulian, S., 1998. <sup>131</sup>I<sup>−</sup> sorption by thermally treated hydrotalcites. *Clays and Clay Minerals* 46, 567–573.

- Olsbye, U., Akporiaye, D., Rytter, E., Rønnekleiv, M., Tangstad, E., 2002. On the stability of mixed  $M^{2+}/M^{3+}$  oxides. *Applied Catalysis A: General* 224, 39–49.
- Ono, Y., Baba, T., 1997. Selective reactions over solid base catalysts. *Catalysis Today* 38, 321–337.
- Oriakhi, C.O., Faar, I.V., Lerner, M.M., 1996. Incorporation of poly(acrylic acid), poly(vinylsulfonate) and poly(styrenesulfonate) within layered double hydroxides. *Journal of Materials Chemistry* 6, 103–107.
- Oriakhi, C.O., Faar, I.V., Lerner, M.M., 1997. Thermal characterization of poly(styrene sulfonate)/layered double hydroxide nanocomposites. *Clays and Clay Minerals* 45, 194–202.
- Palomares, A.E., López-Nieto, J.M., Lázaro, F.J., López, A., Corma, A., 1999. Reactivity in the removal of  $SO_2$  and  $NO_x$  on Co/Mg/Al mixed oxides derived from hydrotalcites. *Applied Catalysis B: Environmental* 20, 257–266.
- Parker, L.M., Milestone, N.B., Newman, R.H., 1995. The use of hydrotalcite as an anion absorbent. *Industrial and Engineering Chemistry Research* 34, 1196–1202.
- Passaglia, E., Sacerdoti, M., 1988. Hydrocalumite from Montalto di Castro, Viterbo, Italy. *Neues Jahrbuch fuer Mineralogie, Monatshefte* (10), 454–461.
- Paul, M., Glasser, F.P., 2000. Impact of prolonged warm (85 °C) moist cure on Portland cement paste. *Cement and Concrete Research* 30, 1869–1877.
- Pausch, I., Lohse, H.H., Schürmann, K., Allmann, R., 1986. Syntheses of disordered and Al-rich hydrotalcite-like compounds. *Clays and Clay Minerals* 34, 507–510.
- Pavan, P.C., Crepaldi, E.L., Gomes, G.deA., Valim, J.B., 1999. Adsorption of sodium dodecylsulfate on a hydrotalcite-like compound: effect of temperature, pH and ionic strength. *Colloids and Surfaces A: Physicochemical and Engineering Aspects* 154, 399–410.
- Pavan, P.C., Crepaldi, E.L., Valim, J.B., 2000. Sorption of anionic surfactants on layered double hydroxides. *Journal of Colloid and Interface Science* 229, 346–352.
- Pavan, P.C., Gomes, G.deA., Valim, J.B., 1998. Adsorption of sodium dodecyl sulfate on layered double hydroxides. *Microporous and Mesoporous Materials* 21, 659–665.
- Pérez-Ramírez, J., Mul, G., Kapteijn, F., Moulijn, J.A., 2001a. On the stability of the thermally decomposed Co–Al hydrotalcite against retrotopotactic transformation. *Materials Research Bulletin* 36, 1767–1775.
- Pérez-Ramírez, J., Mul, G., Kapteijn, F., Moulijn, J.A., 2001b. A spectroscopic study of the effect of the trivalent cation on the thermal decomposition behaviour of Co-based hydrotalcites. *Journal of Materials Chemistry* 11, 2529–2536.
- Pérez-Ramírez, J., Mul, G., Kapteijn, F., Moulijn, J.A., 2001c. In situ investigation of the thermal decomposition of Co–Al hydrotalcite in different atmospheres. *Journal of Materials Chemistry* 11, 821–830.
- Pérez-Ramírez, J., Mul, G., Moulijn, J.A., 2001d. In situ Fourier transform infrared and laser Raman spectroscopic study of the thermal decomposition of Co–Al and Ni–Al hydrotalcites. *Vibrational Spectroscopy* 27, 75–88.
- Pérez-Ramírez, J., Overijnder, J., Kapteijn, F., Moulijn, J.A., 1999. Structural promotion and stabilizing effect of Mg in the catalytic decomposition of nitrous oxide over calcined hydrotalcite-like compounds. *Applied Catalysis B: Environmental* 23, 59–72.
- Pesic, L., Salipurovic, S., Markovic, V., Vucelic, D., Kagunya, W., Jones, W., 1992. Thermal characteristics of a synthetic hydrotalcite-like material. *Journal of Materials Chemistry* 2, 1069–1073.

- Pinnavaia, T.J., 1987. Swelling clays and related complex layered oxides. NATO ASI, Ser. B 172, 233–252.
- Pinnavaia, T.J., 1995. Nanoporous layered materials. *Materials Chemistry: Advances in Chemistry Series* 245, 283–300.
- Pitsch, S., Eschenmoser, A., Gedulin, B., Hui, S., Arrhenius, G., 1995. Mineral induced formation of sugar phosphates. *Origin of Life and Evolution of the Biosphere* 25, 297–334.
- Prévo, V., Forano, C., Besse, J.-P., 2001. Hybrid derivatives of layered double hydroxides. *Applied Clay Science* 18, 3–15.
- Prévo, V., Forano, C., Besse, J.-P., Abraham, F., 1998. Syntheses and thermal and chemical behaviors of tartrate and succinate intercalated  $\text{Zn}_3\text{Al}$  and  $\text{Zn}_2\text{Cr}$  layered double hydroxides. *Inorganic Chemistry* 37, 4293–4301.
- Prinetto, F., Ghiotti, G., Durand, R., Tichit, D., 2000a. Investigation of acid-base properties of catalysts obtained from layered double hydroxides. *Journal of Physical Chemistry B* 104, 11117–11126.
- Prinetto, F., Ghiotti, G., Graffin, P., Tichit, D., 2000b. Synthesis and characterization of sol-gel  $\text{Mg}/\text{Al}$  and  $\text{Ni}/\text{Al}$  layered double hydroxides and comparison with co-precipitated samples. *Microporous and Mesoporous Materials* 39, 229–247.
- Putyera, K., Bandosz, T.J., Jagieo, J., Schwarz, J.A., 1996. Effect of template constraints on adsorption properties of synthetic carbons prepared within the gallery of layered double hydroxides. *Carbon* 34, 1559–1567.
- Qiu, J., Villemure, G., 1995. Anionic clay modified electrodes: electrochemical activity of nickel(II) sites in layered double hydroxide films. *Journal of Electroanalytical Chemistry* 395, 159–166.
- Raja, T., Santhanalakshmi, J., 1996. Physico-chemical studies on synthetic disordered  $\text{Ni-Fe}$  layered double hydroxides. *Journal of Materials Science Letters* 15, 718–720.
- Rankin, B.J., Zhu, H., Webb, M., Roberts, N.B., 2001. The development and in-vitro evaluation of novel mixed metal hydroxy-carbonate compounds as phosphate binders. *Journal of Pharmacy and Pharmacology* 53, 361–369.
- Rebours, B., de la Caillerie, J.-B.D., Clause, O., 1994. Decoration of nickel and magnesium oxide crystallites with spinel-type phases. *Journal of the American Chemical Society* 116, 1707–1717.
- Refait, Ph., Génin, J.-M.R., 1997. Mechanisms of oxidation of  $\text{Ni(II)-Fe(II)}$  hydroxides in chloride-containing aqueous media: role of the pyroaurite-type  $\text{Ni-Fe}$  hydroxychlorides. *Clay Minerals* 32, 597–613.
- Renaudin, G., François, M., 1999. The lamellar double-hydroxide (LDH) compound with composition  $3\text{CaO} \cdot \text{Al}_2\text{O}_3 \cdot \text{Ca}(\text{NO}_3)_2 \cdot 10\text{H}_2\text{O}$ . *Acta Crystallographica Section C* 55, 835–841.
- Ren, L., He, J., Evans, D.G., Duan, X., Ma, R., 2001. Some factors affecting the immobilization of penicillin G acylase on calcined layered double hydroxides. *Journal of Molecular Catalysis B: Enzymatic* 16, 65–71.
- Ren, Q., Luo, Q., Wu, H., Chen, S., 2002. Preparation and thermal property of the acicular  $\text{Mg,Al}$ -hydrotalcite. *Key Engineering Materials*, 224–226 (*High-Performance Ceramics* 2001), 237–242.
- Rey, F., Fornés, V., Rojo, J.M., 1992. Thermal decomposition of hydrotalcites: an infrared and nuclear magnetic resonance spectroscopic study. *Journal of the Chemical Society, Faraday Transactions* 88, 2233–2238.

- Rey, S., Mérida-Robles, J., Han, K.-S., Guerlou-Demourgues, L., Delmas, C., Duguet, E., 1999. Acrylate intercalation and in situ polymerization in iron substituted nickel hydroxides. *Polymer International* 48, 277–282.
- Rives, V. (Ed.), 2001. *Layered Double Hydroxides*. Nova Science Publishers, Huntington.
- Rives, V., 2002. Characterisation of layered double hydroxides and their decomposition products. *Materials Chemistry and Physics* 75, 19–25.
- Rives, V., Ulibarri, M.A., 1999. Layered double hydroxides intercalated with metal coordination compounds and oxometalates. *Coordination Chemistry Reviews* 181, 61–120.
- Robins, D.S., Dutta, P.K., 1996. Examination of fatty acid exchanged layered double hydroxides as supports for photochemical assemblies. *Langmuir* 12, 402–408.
- Rocha, J., del Arco, M., Rives, V., Ulibarri, M.A., 1999. Reconstruction of layered double hydroxides from calcined precursors: a powder XRD and  $^{27}\text{Al}$  MAS NMR study. *Journal of Materials Chemistry* 9, 2499–2503.
- Roelofs, J.C.A.A., van Dillen, A.J., de Jong, K.P., 2001. Condensation of citral and ketones using activated hydrotalcite catalysts. *Catalysis Letters* 74, 91–94.
- Roussel, H., Briois, V., Elkaim, E., de Roy, A., Besse, J.-P., 2000. Cationic order and structure of  $[\text{Zn}-\text{Cr}-\text{Cl}]$  and  $[\text{Cu}-\text{Cr}-\text{Cl}]$  layered double hydroxides: a XRD and EXAFS study. *Journal of Physical Chemistry, B* 104, 5915–5923.
- Roussel, H., Briois, V., Elkaim, E., de Roy, A., Besse, J.-P., Jolivet, J.-P., 2001. Study of the formation of the layered double hydroxide  $[\text{Zn}-\text{Cr}-\text{Cl}]$ . *Chemistry of Materials* 13, 329–337.
- Rousselot, I., Taviot-Gueho, C., Besse, J.-P., 1999. Synthesis and characterization of mixed Ga/Al-containing layered double hydroxides: study of their basic properties through the Knoevenagel condensation of benzaldehyde and ethyl cyanoacetate, and comparison to other LDHs. *International Journal of Inorganic Materials* 1, 165–174.
- Rousselot, I., Taviot-Gueho, C., Leroux, F., Leone, P., Palvadeau, P., Besse, J.-P., 2002. Insights on the structural chemistry of hydrocalumite and hydrotalcite-like materials: investigation of the series  $\text{Ca}_2\text{M}_3+(\text{OH})_6\text{Cl}\cdot 2\text{H}_2\text{O}$  ( $\text{M}_3^+:$   $\text{Al}^{3+}$ ,  $\text{Ga}^{3+}$ ,  $\text{Fe}^{3+}$  and  $\text{Sc}^{3+}$ ) by X-ray Powder Diffraction. *Journal of Solid State Chemistry* 167, 137–144.
- Rouxhet, P.G., Taylor, H.F.W., 1969. Thermal decomposition of sjögrenite and pyroaurite. *Chimia* 23, 480–485.
- Sanchez Martin, M.J., Villa, M.V., Sanchez-Camazano, M., 1999. Glyphosate-hydrotalcite interaction as influenced by pH. *Clays and Clay Minerals* 47, 777–783.
- Sanz, J., Serratos, J.M., 1984. Silicon-29 and aluminum-27 high-resolution MAS-NMR spectra of phyllosilicates. *Journal of the American Chemical Society* 106, 4790–4793.
- Sato, T., Fujita, H., Endo, T., Shimada, M., Tsunashima, A., 1988. Synthesis of hydrotalcite-like compounds and their physico-chemical properties. *Reactivity of Solids* 5, 219–228.
- Sato, T., Kato, K., Endo, T., Shimada, M., 1986a. Preparation and chemical properties of magnesium aluminium oxide solid solutions. *Reactivity of Solids* 2, 253–260.
- Sato, T., Masaki, K., Yoshioka, T., Okuwaki, A., 1993. Photocatalytic properties of CdS and CdS–ZnS mixtures incorporated into the interlayer of layered compounds. *Journal of Chemical Technology and Biotechnology* 58, 315–319.
- Scavetta, E., Berrettoni, M., Seeber, R., Tonelli, D., 2001.  $[\text{Ni}/\text{Al}-\text{Cl}]$ -based hydrotalcite electrodes as amperometric sensors: preparation and electrochemical study. *Electrochimica Acta* 46, 2681–2692.

- Scheckel, K.G., Scheinost, A.C., Ford, R.G., Sparks, D.L., 2000. Stability of layered Ni hydroxide surface precipitates: a dissolution kinetics study. *Geochimica et Cosmochimica Acta* 64, 2727–2735.
- Scheidegger, A.M., Lamble, G.M., Sparks, D.L., 1997. Spectroscopic evidence for the formation of mixed-cation hydroxide phases upon metal sorption on clays and aluminum oxides. *Journal of Colloid and Interface Science* 186, 118–128.
- Scheidegger, A.M., Wieland, E., Scheinost, A.C., Dähn, R., Tits, J., Spieler, P., 2001. Ni phases formed in cement and cement systems under highly alkaline conditions: an XAFS study. *Journal of Synchrotron Radiation* 8, 916–918.
- Schöllhorn, R., 1996. Intercalation systems as nanostructured functional materials. *Chemistry of Materials* 8, 1747–1752.
- Schon, J.C., Alder, D., Dresselhaus, G., 1988. Theory of staging in intercalation compounds. *Journal of Physics C: Solid State Physics* 21, 5595–5614.
- Schütz, A., Biloën, P., 1987. Interlamellar chemistry of hydrotalcites. I. Polymerization of silicate anions. *Journal of Solid State Chemistry* 68, 360–368.
- Seida, Y., Nakano, Y., 2000. Removal of humic substances by layered double hydroxide containing iron. *Water Resources* 34, 1487–1494.
- Seida, Y., Nakano, Y., Nakamura, Y., 2001. Rapid removal of dilute lead from water by pyroaurite-like compound. *Water Resources* 35, 2341–2346.
- Seida, Y., Nakano, Y., Nakamura, Y., 2002. Crystallization of layered double hydroxides by ultrasound and the effect of crystal quality on their surface properties. *Clays and Clay Minerals* 50, 525–532.
- Sels, B., de Vos, D., Buntinx, M., Pierard, F., Kirsch-de Mesmaeker, A., Jacobs, P., 1999. Layered double hydroxides exchanged with tungstate as biomimetic catalysts for mild oxidative bromination. *Nature* 400, 855–857.
- Sels, B.F., De Vos, D.E., Jacobs, P.A., 2001. Hydrotalcite-like anionic clays in catalytic organic reactions. *Catalysis Reviews—Science and Engineering* 43, 443–488.
- Serna Carlos, J., Rendon, J.L., Iglesias, J.E., 1982. Crystal-chemical study of layered  $[Al_2Li(OH)_6] + X \cdot nH_2O$ . *Clays and Clay Minerals* 30, 180–184.
- Serwicka, E.M., 2001. Clays as catalysts for removal of nitrogen oxides. *Polish Journal of Chemistry* 75, 307–328.
- Scheidegger, A.M., Strawn, D.G., Geraldine, M., Lamble, G.M., Sparks, D.L., 1998. The kinetics of mixed Ni–Al hydroxide formation on clay and aluminum oxide minerals: a time-resolved XAFS study. *Geochimica et Cosmochimica Acta* 62, 2233–2245.
- Shaw, B.R., Deng, Y., Strillacci, F.E., Carrado, K.A., Fessehaie, M.G., 1990. Electrochemical surface analysis of nonconducting solids: ferricyanide and phenol as electrochemical probes of the surfaces of layered double hydroxide anion-exchanging clays. *Journal of the Electrochemical Society* 137, 3136–3143.
- Shaw, W.H.R., Bordeaux, J.J., 1955. The decomposition of urea in aqueous media. *Journal of the American Chemical Society* 77, 4729–4733.
- Shen, J., Tu, M., Hu, C., 1998. Structural and surface acid/base properties of hydrotalcite-derived MgAlO oxides calcined at varying temperatures. *Journal of Solid State Chemistry* 137, 295–301.
- Shin, H.-S., Kim, M.-J., Nam, S.-Y., Moon, H.-C., 1996. Phosphorus removal by hydrotalcite-like compounds (HTLcs). *Water Science and Technology* 34, 161–168.

- Shouldice, G.T.D., Choi, P.Y., Koene, B.E., Nazar, L.F., Rudin, A., 1995. A novel way to study the initial stages of soap-free emulsion polymerizations: the intercalation of polystyrene oligomers into hydrotalcite. *Journal of Polymer Science* 33, 1409–1417.
- Solin, S.A., Hines, D.R., Seidler, G.T., Treacy, M.M.J., 1996. Novel structural properties of  $\text{Ni}_{1-x}\text{Al}_x$  layer double hydroxides. *Journal of Physics and Chemistry of Solids* 57, 1043–1048.
- Solin, S.A., Hines, D., Yun, S.K., Pinnavaia, T.J., Thorpe, M.F., 1995. Layer rigidity in 2D disorder Ni–Al layer double hydroxides. *Journal of Non-Crystalline Solids* 182, 212–220.
- Stanimirova, T.S., Kirov, G., Dinolova, E., 2001. Mechanism of hydrotalcite regeneration. *Journal of Materials Science Letters* 20, 453–455.
- Stanimirova, T.S., Vergilov, I., Kirov, G., Petrova, N., 1999. Thermal decomposition products of hydrotalcite-like compounds: low-temperature metaphases. *Journal of Materials Science* 34, 4153–4161.
- Tagaya, H., Sato, S., Kuwahara, T., Kadokawa, J., Masa, K., Chiba, K., 1994. Photo-isomerization of indolinespirobenzopyran in anionic clay matrices of layered double hydroxides. *Journal of Materials Chemistry* 4, 1907–1912.
- Tanaka, M., Park, I.Y., Kuroda, K., Kato, C., 1989. Formation of hydrotalcite–acrylate intercalation compounds and their heat-treated products. *Bulletin of the Chemical Society of Japan* 62, 3442–3445.
- Taylor, H.F.W., 1973. Crystal structures of some double hydroxide minerals. *Mineralogical Magazine* 39, 377–389.
- Taylor, R.M., 1984. The rapid formation of crystalline double hydroxy salts and other compounds by controlled hydrolysis. *Clay Minerals* 19, 591–603.
- Therias, S., Lacroix, B., Schöllhorn, B., Mousty, C., Palvadeau, P., 1998. Electrochemical study of ferrocene and nitroxide derivatives intercalated in Zn–Cr and Zn–Al layered double hydroxides. *Journal of Electroanalytical Chemistry* 454, 91–97.
- Therias, S., Mousty, C., Forano, C., Besse, J.P., 1996. Electrochemical transfer at anionic clay modified electrodes: case of 2,2′-azinobis(3-ethylbenzothiazoline-6-sulfonate). *Langmuir* 12, 4914–4920.
- Thevenot, F., Szymanski, R., Chaumette, P., 1989. Preparation and characterization of aluminum-rich zinc-aluminum hydrotalcite-like compounds. *Clays and Clay Minerals* 37, 396–402.
- Thiel, J.P., Chiang, C.K., Poeppelmeier, K.R., 1993. Structure of  $\text{LiAl}_2(\text{OH})_7 \cdot 2\text{H}_2\text{O}$ . *Chemistry of Materials* 5, 297–304.
- Thieme, J., Abend, S., Lagaly, G., 1999. Aggregation in pickering emulsions. *Colloid and Polymer Science* 277, 257–260.
- Tichit, D., Bennani, M.N., Figueras, F., Ruiz, J.R., 1998. Decomposition processes and characterization of the surface basicity of  $\text{Cl}^-$  and  $\text{CO}_3^{2-}$ –hydrotalcites. *Langmuir* 14, 2086–2091.
- Tichit, D., Das, N., Coq, B., Durand, R., 2002a. Preparation of Zr-containing layered double hydroxides and characterization of the acido-basic properties of their mixed oxides. *Chemistry of Materials* 14, 1530–1538.
- Tichit, D., Ribet, S., Coq, B., 2001. Characterization of calcined and reduced multi-component Co–Ni–Mg–Al-layered double hydroxides. *European Journal of Inorganic Chemistry* 2, 539–546.

- Trainor, T.P., Brown, G.E. Jr., Parks, G.A., 2000. Adsorption and precipitation of aqueous Zn(II) on alumina powders. *Journal of Colloid and Interface Science* 231, 359–372.
- Trifiro, F., Vaccari, A., 1996. Hydrotalcite-like anionic clays (layered double hydroxides). In: Alberti, G., Bein, T. (Eds.), *Comprehensive Supramolecular Chemistry*, vol. 7. Elsevier, Oxford, pp. 251–291.
- Trifirò, F., Vaccari, A., Clause, O., 1994. Nature and properties of nickel-containing mixed oxides obtained from hydrotalcite-type anionic clays. *Catalysis Today* 21, 185–195.
- Trolard, F., Génin, J.-M.R., Abdelmoula, M., Bourrié, G., Humbert, B., Herbillon, A., 1997. Identification of a green rust mineral in a reductomorphic soil by Mössbauer and Raman spectroscopies. *Geochimica et Cosmochimica Acta* 61, 1107–1111.
- Tronto, J., Crepaldi, E.L., Pavan, P.C., De Paula, C.C., Valim, J.B., 2001. Organic anions of pharmaceutical interest intercalated in magnesium aluminum LDHs by two different methods. *Molecular Crystals and Liquid Crystals Science and Technology, Section A: Molecular Crystals and Liquid Crystals* 356, 227–237.
- Trujillano, R., Holgado, M.J., Rives, V., 2002. Alternative synthetic routes for NiAl layered double hydroxides with alkyl and alkylbenzene sulfonates. *Studies in Surface Science and Catalysis*, 142B (Impact of Zeolites and Other Porous Materials on the New Technologies at the Beginning of the New Millennium), 1387–1394.
- Tseng, W.-Y., Lin, J.-T., Mou, C.-Y., Cheng, S., Liu, S.-B., Chu, P.P., Liu, H.-W., 1996. Incorporation of C60 in layered double hydroxide. *Journal of the American Chemical Society* 118, 4411–4418.
- Tsyganok, A.I., Suzuki, K., Hamakawa, S., Takehira, K., Hayakawa, T., 2001. Alternative approach to incorporation of nickel into layered structure of Mg–Al double hydroxides: intercalation with [Ni(edta)]<sup>2–</sup> species. *Chemistry Letters* (1), 24–25.
- Ukrainczyk, L., Chibwe, M., Pinnavaia, T.J., Boyd, S.A., 1995. Reductive dechlorination of carbon tetrachloride in water catalyzed by mineral-supported biomimetic cobalt macrocycles. *Environmental Science and Technology* 29, 439–445.
- Ulibarri, M.A., Cornejo, J., Hernandez, M.J., 1987. Effects of hydrothermal treatment on textural properties of aluminum lithium hydroxide carbonate hydrate ([Al<sub>2</sub>Li(OH)<sub>6</sub>] 2CO<sub>3</sub> · *n*H<sub>2</sub>O). *Journal of Materials Science* 22, 1168–1172.
- Ulibarri, M.A., Labajos, F.M., Rives, V., Trujillano, R., Kagunya, W., Jones, W., 1994. Comparative study of the synthesis and properties of vanadate-exchanged layered double hydroxides. *Inorganic Chemistry* 33, 2592–2599.
- Ulibarri, M.A., Pavlovic, I., Barriga, C., Hermosín, M.C., Cornejo, J., 2001. Adsorption of anionic species on hydrotalcite-like compounds: effect of interlayer anion and crystallinity. *Applied Clay Science* 18, 17–27.
- Vaccari, A., 1998. Preparation and catalytic properties of cationic and anionic clays. *Catalysis Today* 41, 53–71.
- Vaccari, A., 1999a. Hydrotalcite-type anionic clays (layer double hydroxides) as precursors of both catalysts and catalyst supports. *Advances in Science and Technology* (Faenza, Italy), 16 (Ceramics: Getting into the 000's, Pt. D), 571–584.
- Vaccari, A., 1999b. Clays and catalysis: a promising future. *Applied Clay Science* 14, 161–198.
- Valente, J.S., Figueras, F., Gravelle, M., Kumbhar, P., Lopez, J., Besse, J.-P., 2000. Basic properties of the mixed oxides obtained by thermal decomposition of hydrotalcites containing different metallic compositions. *Journal of Catalysis* 189, 370–381.

- Van der Pol, A., Mojet, B.L., Van de Ven, E., de Boer, E., 1994. Ordering of intercalated water and carbonate anions in hydrotalcite. An NMR study. *Journal of Physical Chemistry* 98, 4050–4054.
- Van der Ven, L., van Gemert, M.L.M., Batenburg, L.F., Keern, J.J., Gielgens, L.H., Koster, T.P.M., Fischer, H.R., 2000. On the action of hydrotalcite-like clay materials as stabilizer in polyvinylchloride. *Applied Clay Science* 17, 25–34.
- Velu, S., Ramaswamy, V., Ramani, A., Chanda, B.M., Sivasanker, S., 1997a. New hydrotalcite-like anionic clays containing  $Zr^{4+}$  in the layers. *Chemical Communications*, 2107–2108.
- Velu, S., Ramkumar, V., Narayanan, A., Swamy, C.S., 1997b. Effect of interlayer anions on the physicochemical properties of zinc–aluminium hydrotalcite-like compounds. *Journal of Materials Science* 32, 957–964.
- Velu, S., Suzuki, K., Kapoor, M.P., Tomura, S., Ohashi, F., Osaki, T., 2000a. Effect of Sn incorporation on the thermal transformation and reducibility of M(II)Al-layered double hydroxides [M(II) = Ni or Co]. *Chemistry of Materials* 12, 719–730.
- Velu, S., Suzuki, K., Okazaki, M., Kapoor, M.P., Osaki, T., Ohashi, F., 2000b. Oxidative steam reforming of methanol over CuZnAl(Zr)-oxide catalysts for the selective production of hydrogen for fuel cells: catalyst characterization and performance evaluation. *Journal of Catalysis* 194, 373–384.
- Velu, S., Suzuki, K., Okazaki, M., Osaki, T., Tomura, S., Ohashi, F., 1999a. Synthesis of new Sn-incorporated layered double hydroxides and their thermal evolution to mixed oxides. *Chemistry of Materials* 11, 2163–2172.
- Velu, S., Suzuki, K., Osaki, T., 1999b. Oxidative steam reforming of methanol over CuZnAl(Zr)-oxide catalysts: a new and efficient method for the production of CO-free hydrogen for fuel cells. *Chemical Communications* 2341–2342.
- Velu, S., Swamy, C.S., 1996. Synthesis and physicochemical properties of a new copper–manganese–aluminium ternary hydrotalcite-like compound. *Journal of Materials Science Letters* 15, 1674–1677.
- Vichi, F.M., Alves, O.L., 1997. Preparation of Cd/Al layered double hydroxides and their intercalation reactions with phosphonic acids. *Journal of Materials Chemistry* 7, 1631–1634.
- Villa, A.L., De Vos, D.E., Verpoort, F., Sels, B.F., Jacobs, P.A., 2001. Study of V-pillared layered double hydroxides as catalysts for the epoxidation of terpenic unsaturated alcohols. *Journal of Catalysis* 198, 223–231.
- Villa, M.V., Sánchez-Martín, M.J., Sánchez-Camazano, M., 1999. Hydrotalcites and organo-hydrotalcites as sorbents for removing pesticides from water. *Journal of Environmental Science and Health B34*, 509–525.
- Villegas, J.C., Giraldo, O.H., Suib, S.L., 2002. New-layered double hydroxides containing intercalated manganese oxide nanoparticles: synthesis and characterization. Abstracts of Papers, 224th ACS National Meeting, Boston, MA, INOR-508. American Chemical Society, Washington, DC.
- Vucelic, M., Jones, W., Moggridge, G.D., 1997. Cation ordering in synthetic layered double hydroxides. *Clays and Clay Minerals* 45, 803–813.
- Vucelic, M., Moggridge, G.D., Jones, W., 1995. Thermal properties of terephthalate- and benzoate-intercalated LDH. *Journal of Physical Chemistry* 99, 8328–8337.
- Wang, J., Kalinichev, A.G., Kirkpatrick, R.J., Hou, X., 2001. Molecular modeling of the structure and energetics of hydrotalcite hydration. *Chemistry of Materials* 13, 145–150.



- Wang, S.-D., Scrivener, K.L., 1995. Hydration products of alkali activated slag cement. *Cement and Concrete Research* 25, 561–571.
- Weber, R.S., Gallezot, P., Lefebvre, F., Suib, S.L., 1993. Partial pillaring of layered double hydroxides by  $[\text{SiW}_9\text{V}_3\text{O}_{40}]^{7-}$ . *Microporous Materials* 1, 223–227.
- Whilton, N.T., Vickers, P.J., Mann, S., 1997. Bioinorganic clays: synthesis and characterization of amino- and polyamino acid intercalated layered double hydroxides. *Journal of Materials Chemistry* 7, 1623–1629.
- Wilson, O.C. Jr., Olorunyolemi, T., Jaworski, A., Borum, L., Young, D., Siriawat, A., Dickens, E., Oriakhi, C., Lerner, M., 1999. Surface and interfacial properties of polymer-intercalated layered double hydroxide nanocomposites. *Applied Clay Science* 15, 265–279.
- Xu, R., Zeng, H.C., 2001a. Synthesis of nanosize supported hydrotalcite-like compounds  $\text{CoAl}_x(\text{OH})_2 + 2x(\text{CO}_3)_y(\text{NO}_3)_x - 2y \cdot n\text{H}_2\text{O}$  on  $\gamma\text{-Al}_2\text{O}_3$ . *Chemistry of Materials* 13, 297–303.
- Xu, Z.P., Xu, R., Zeng, H.C., 2001. Sulfate-functionalized carbon/metal-oxide nanocomposites from hydrotalcite-like compounds. *Nano Letters* 1, 703–706.
- Xu, Z.P., Zeng, H.C., 1998. Thermal evolution of cobalt hydroxides: a comparative study of their various structural phases. *Journal of Materials Chemistry* 8, 2499–2506.
- Xu, Z.P., Zeng, H.C., 2001b. Decomposition pathways of hydrotalcite-like compounds  $\text{Mg}_{1-x}\text{Al}_x(\text{OH})_2(\text{NO}_3)_x \cdot n\text{H}_2\text{O}$  as a continuous function of nitrate anions. *Chemistry of Materials* 13, 4564–4572.
- Xu, Z.P., Zeng, H.C., 2001c. Abrupt structural transformation in hydrotalcite-like compounds  $\text{Mg}_{1-x}\text{Al}_x(\text{OH})_2(\text{NO}_3)_x \cdot n\text{H}_2\text{O}$  as a continuous function of nitrate anions. *Journal of Physical Chemistry B* 105, 1743–1749.
- Yamaguchi, N.U., Schinost, A.C., Sparks, D.L., 2002. Influence of gibbsite surface area and citrate on Ni sorption mechanisms at pH 7.5. *Clays and Clay Minerals* 50, 784–790.
- Yamamoto, T., Kodama, T., Hasegawa, N., Tsuji, M., Tamaura, Y., 1995. Synthesis of hydrotalcite with high layer charge for  $\text{CO}_2$  adsorbent. *Energy Conversion and Management* 36, 637–640.
- Yao, K., Taniguchi, M., Nakata, M., Shimazu, K., Takahashi, M., Yamagishi, A., 1998a. Mass transport on an anionic clay-modified electrode as studied by a quartz crystal microbalance. *Journal of Electroanalytical Chemistry* 457, 119–128.
- Yao, K., Taniguchi, M., Nakata, M., Yamagishi, A., 1998b. Electrochemical STM observation of  $[\text{Fe}(\text{CN})_6]^{3-}$  ions adsorbed on a hydrotalcite crystal surface. *Journal of Electroanalytical Chemistry* 458, 249–252.
- Yong, Z., Mata, V., Rodrigues, A.E., 2001. Adsorption of carbon dioxide onto hydrotalcite-like compounds (HTlcs) at high temperatures. *Industrial and Engineering Chemistry Research* 40, 204–209.
- You, Y., Vance, G.F., Zhao, H., 2001. Selenium adsorption on Mg–Al and Zn–Al layered double hydroxides. *Applied Clay Science* 20, 13–25.
- Yun, S.K., Constantino, V.R.L., Pinnavaia, T.J., 1995. Synthesis and catalytic properties of silicate-intercalated layered double hydroxides formed by intragallery hydrolysis of tetraethylorthosilicate. *Clays and Clay Minerals* 43, 503–510.
- Yun, S.K., Pinnavaia, T.J., 1995. Water content and particle texture of synthetic hydrotalcite-like layered double hydroxides. *Chemistry of Materials* 7, 348–354.
- Zapata, B., Bosch, P., Valenzuela, M.A., Fetter, G., Flores, S.O., Cordova, I.R., 2002. Thermal stability of monometallic Co-hydrotalcite. *Materials Letters* 57, 679–683.

- Zeng, H.C., Lim, Y.Y., 2000. Synthesis of  $\text{Co}_3\text{O}_4$  spinel at ambient conditions. *Journal of Materials Research* 15, 1250–1253.
- Zeng, H.C., Xu, Z.P., Qian, M., 1998. Synthesis of non-Al-containing hydrotalcite-like compound  $\text{Mg}_0.3\text{CoII}_0.6\text{CoIII}_0.2(\text{OH})_2(\text{NO}_3)_0.2\cdot 2\text{H}_2\text{O}$ . *Chemistry of Materials* 10, 2277–2283.
- Zhao, Y., Li, F., Zhang, R., Evans, D.G., Duan, X., 2002. Preparation of layered double-hydroxide nanomaterials with a uniform crystallite size using a new method involving separate nucleation and aging steps. *Chemistry of Materials* 14, 4286–4291.

This page intentionally left blank

*Chapter 13.2*

## **PARALLELS AND DISTINCTIONS BETWEEN CLAY MINERALS AND ZEOLITES**

**D.L. BISH**

*Department of Geological Science, Indiana University, Bloomington,  
IN 47405-1405, USA*

Clay minerals and zeolites are among the most hydrated minerals on the Earth's surface and are found in a myriad of environments, including soils, seafloor deposits, hydrothermal alteration products, altered volcanic deposits, sediments, etc. Although they often occur together and have many similar attributes, many of the properties of clay minerals and zeolites are distinctive due to important differences in their crystal structures. The similarities and distinctions hold true for a variety of clay minerals and zeolites, but for the purpose of this discussion, I will compare and contrast smectites and natural zeolites.

### **13.2.1. SMECTITES AND ZEOLITES: SIMILARITIES**

It is well known that smectites and zeolites both often occur as fine-grained, authigenic phases, and they are good records of low-temperature secondary alteration. Smectites and zeolites also have open structures, containing exchangeable cations and water molecules. Both classes of minerals have very high cation exchange capacities (CEC) and exhibit useful cation selectivities. Smectite CEC are approximately 90–130 cmol(+) /kg (e.g., [Weaver and Pollard, 1973](#)), and the exchange capacity results from substitutions in both the tetrahedral and octahedral sheets of the 2:1 layers (Chapter 12.10). Theoretical exchange capacities for zeolites (calculated based on structural formulae) are higher and exhibit wider variation, 180–300 for clinoptilolite and mordenite (two of the most common natural zeolites), and from 300 to 400 meq/100 g for other common zeolites such as chabazite, stilbite, phillipsite, erionite, and laumontite ([Barrer, 1978](#); [Colella, 1996](#)). Zeolite cation exchange capacity originates solely from substitutions in the tetrahedral framework. Both smectites and zeolites are generally selective for large, univalent ions (e.g.,  $\text{Cs}^+$ ) over smaller, more hydrated cations such as  $\text{Li}^+$  or  $\text{Mg}^{2+}$  (Chapter 12.10.), and this

selectivity has been exploited in removing contaminants from natural and process waters (Chapter 11.1).

As emphasised above, smectites and zeolites are some of the most hydrated minerals. Both smectites and zeolites can contain large amounts of water, up to ~20% in zeolites and in excess of 30% in some smectites (at 100% relative humidity (RH), not in liquid water, where smectites osmotically swell). Note that measurements of maximum water content of both sets of minerals cannot be made reliable by simply drying a sample at high temperature and recording the weight loss. Such a measurement would only provide information on the hydration state of the mineral under room conditions of humidity. Both zeolites and smectites continue to take up water as the partial pressure of water (RH) is increased, up to a point in zeolites that is structurally constrained. The water in zeolites and smectites can reversibly leave and re-enter the structures, giving rise to anomalous thermal behaviour unlike that of most silicates. Unlike most solids, smectites and zeolites contract on heating (and/or dehydration) and expand on cooling and/or hydration. It is seldom that the effects of thermal expansion are seen with zeolites below about 300 °C, as they are overshadowed by the larger effects of dehydration-induced contraction.

### 13.2.2. SMECTITES AND ZEOLITES: DISTINCTIONS

In spite of the many similarities between smectites and zeolites, many of their properties are distinctive due to major differences in their crystal structures. Smectites and phyllosilicates in general have layer structures, with exchangeable cations and variable amounts of water molecules in the interlayer region. In clay minerals with lower layer charges, such as smectites, the attractive forces between the individual layers are approximately balanced by expansive forces due to hydration of interlayer cations. As a result of the weak layer–layer bonding, there is often little or no crystallographic order from layer to layer. Water enters the interlayer region to interact with the interlayer surface and hydrate the interlayer cations. Water molecules can only enter the interlayer region in integral amounts, that is, one at a time and not in fractional amounts. Thus, smectites hydrate in a layer-by-layer manner, going from a zero-water layer structure to a four-water-layer structure (Chapter 5). These structures have basal spacings of approximately 1.0, 1.25, 1.5, 1.7, and 2.0 nm. The measured smectite basal spacings often only approximately reflect such a stepwise increase in layer repeat distances due to the existence of interstratifications of adjacent hydrates. As a result of this stepwise hydration, many smectite phenomena, specifically those related to interlayer hydration, are quantised.

In contrast to the two-dimensional layer structures of smectites, zeolites have three-dimensionally connected aluminosilicate framework structures, and their frameworks are negatively charged due primarily to  $\text{Al}^{3+}$  - for  $\text{Si}^{4+}$  substitutions. Unlike smectite structures, zeolite structures are typically ordered in three dimensions although stacking faults are known to occur in some zeolites like mordenite (Campbell

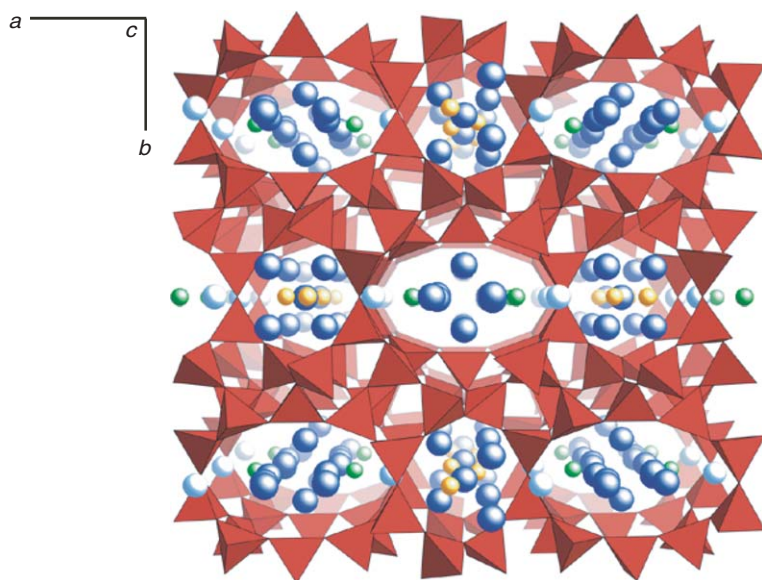


Fig. 13.2.1. Clinoptililite structure,  $(\text{Na}, \text{K}, 1/2\text{Ca})_6[\text{Al}_6\text{Si}_{30}\text{O}_{72}] \bullet 20\text{H}_2\text{O}$ , down  $c$ , showing extraframework cations in the large structural cavities.

and Cheetham, 2002). These aluminosilicate frameworks form large structural cavities known as extraframework sites in which exchangeable cations and  $\text{H}_2\text{O}$  molecules occur (Fig. 13.2.1). Structural studies have shown that  $\text{H}_2\text{O}$  interacts with both the framework and exchangeable cations, and  $\text{H}_2\text{O}$  commonly enters the extraframework sites progressively as the partial pressure of water is increased (increase in RH). There is also evidence for a more or less continuous rearrangement of extraframework cations and  $\text{H}_2\text{O}$  molecules and concomitant structural relaxation as hydration or dehydration proceed. As a result of this progressive hydration (or dehydration), associated phenomena are considerably less quantised than with smectites. However, structural studies have also shown that  $\text{H}_2\text{O}$  molecules occur in multiple sites with potentially very different attraction energies, see review by Bish and Carey (2001). Indeed, if interaction energies for distinct  $\text{H}_2\text{O}$  molecules are significantly different, or if hydration/dehydration-induced structural changes are large, stepwise hydration/dehydration reactions may occur, as in the zeolite laumontite,  $\text{Ca}_4[\text{Al}_8\text{Si}_{16}\text{O}_{48}] \bullet 16\text{H}_2\text{O}$  (Fig. 13.2.2).

### 13.2.3. CRYSTAL STRUCTURAL TRANSITIONS

As a result of the layer-by-layer hydration/dehydration behaviour of smectites, their T- or P( $\text{H}_2\text{O}$ )-induced structural transitions are typically quantised, that is, they

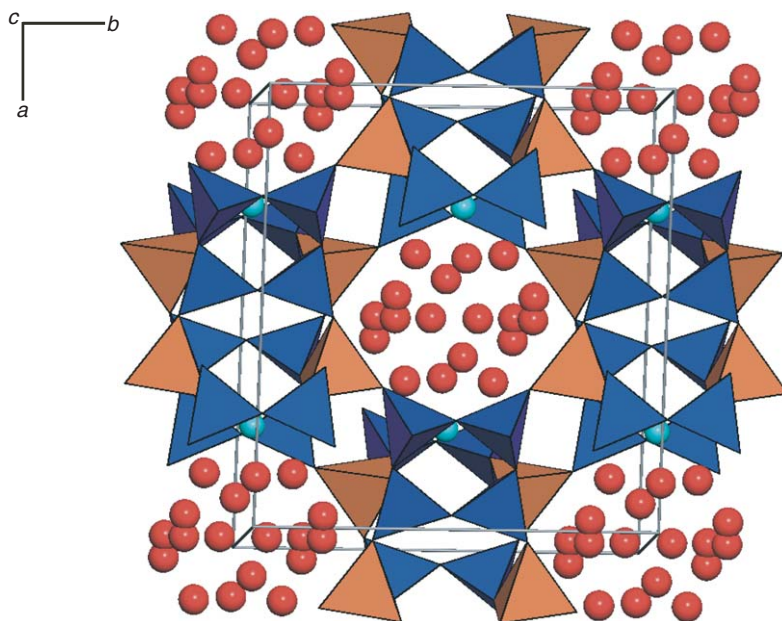


Fig. 13.2.2. Laumontite structure,  $\sim$  down  $c$ , showing the positions of extraframework  $\text{Ca}^{2+}$  ions and water molecules.

occur in a stepwise fashion. As  $\text{H}_2\text{O}$  molecules enter or leave the interlayer region, large structural transitions occur, as illustrated in Fig. 13.2.3 for a  $\text{Na}^+$ -exchanged nontronite. This figure illustrates several important aspects of smectite hydration and dehydration. First, the stepwise expansion of the smectite layers as RH increases is apparent, with “steps” centred around 1.0,  $\sim 1.2$ , and  $\sim 1.5$  nm. Equally noteworthy is the hysteresis between the hydration and dehydration branches; note that the increasing-RH path is distinct from the decreasing-RH path. Although this feature has not yet been quantitatively explained, it is a result of the large structural changes associated with hydration and dehydration, namely expansion/contraction on the order of 0.25 nm. Hysteretic hydration/dehydration behaviour is generally the rule for smectites. The accompanying X-ray diffraction data in Fig. 13.2.3 illustrate the changes in patterns throughout the hydration/dehydration reaction. Important points to note from these data include the increasing breadth of the (001) reflections between “steps” and the large changes in intensity that occur with changes in hydration state. The increased reflection breadth between “steps” results from the existence of interstratifications of adjacent hydrates.

Similar data are shown in Fig. 13.2.4 for three cation-exchanged varieties of the Clay Minerals Society source SAz-1 smectite. The data for the  $\text{Na}^+$ -exchanged variety illustrate the stepwise hydration/dehydration reaction very well, with distinct steps near basal spacings of 1.25 nm and 1.5 nm. This figure also shows that the

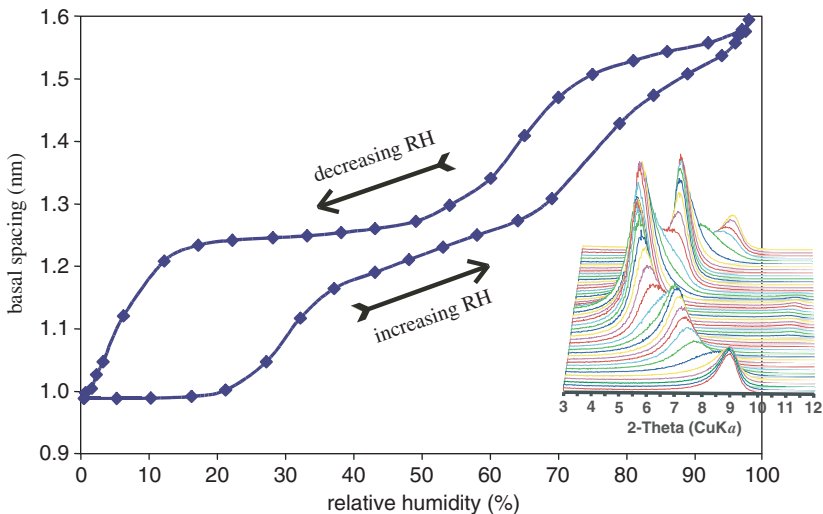


Fig. 13.2.3. Basal spacing for  $\text{Na}^+$ -exchanged NG-1 nontronite as a function of relative humidity. Data are shown for both increasing-RH and decreasing-RH directions. Also shown are the X-ray powder diffraction patterns, taken with Cu  $\text{K}\alpha$  radiation, beginning with an RH of 0% at the bottom, progressing through an RH of 100% in the middle, and ending with an RH of 0% at the top.

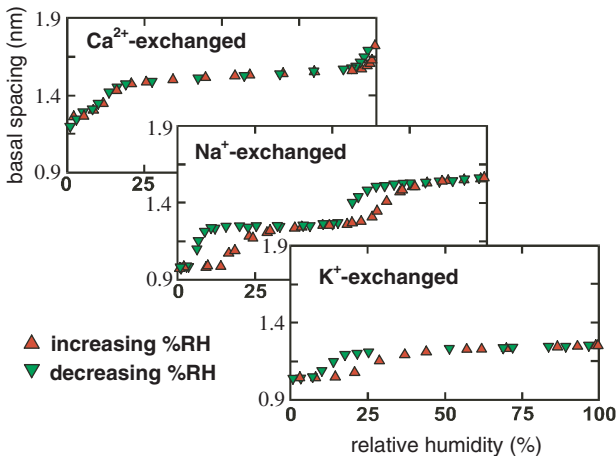


Fig. 13.2.4. Basal spacing for cation-exchanged SAz-1 smectite as a function of relative humidity. Data are shown for both increasing-RH (triangles pointing up) and decreasing-RH (triangles pointing down) directions.



hydration/dehydration behaviour is a function of the interlayer cation, with both the nature of the “steps” and the hysteresis changing as the interlayer cation changes.

At higher water contents, smectites continue to expand, transforming from a region where approximately integral layers of  $\text{H}_2\text{O}$  occupy the interlayer space to the so-called osmotic swelling region (Fig. 13.2.5) (Chapter 5.2). This behaviour stands in stark contrast to the behaviour exhibited by zeolites, whose structural expansion is limited by their three-dimensional framework structure. The low-layer charge and weak interlayer bonding in smectites make it possible for the material to delaminate completely. Both the layer-by-layer expansion and osmotic swelling of smectites are very important in numerous applications.

The T- or P( $\text{H}_2\text{O}$ )-induced structural transitions in zeolites are generally regular and reversible as a result of the more homogeneous distribution of  $\text{H}_2\text{O}$  molecule attraction energies. Although these transitions in zeolites generally do not display stepwise behaviour, cation–water interactions and migrations during changes in hydration state can give rise to quantised behaviour. Fortunately, because zeolites are three-dimensionally ordered, it has been possible to obtain detailed crystal structure information that is generally not available for smectites. Such structural studies show that  $\text{H}_2\text{O}$  molecules in extraframework cavities are bonded to each other, to extra-framework cations, and/or to the framework, depending on the degree of hydration.

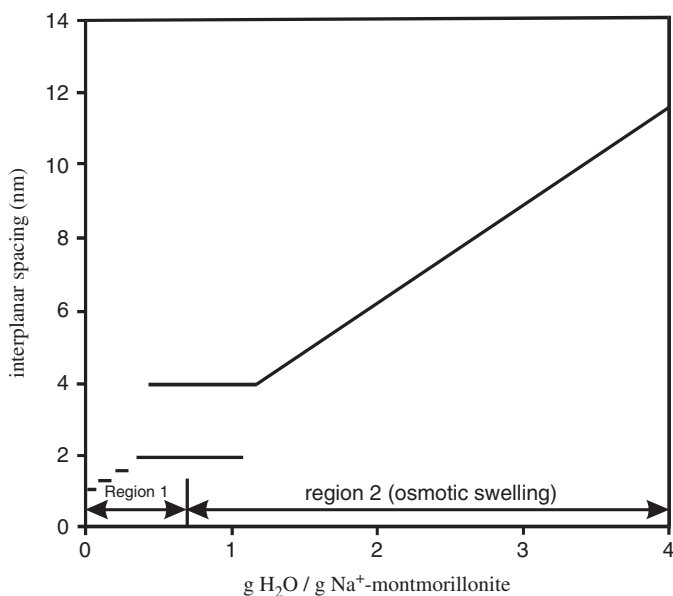


Fig. 13.2.5. Interplanar spacing of Na-montmorillonite as a function of water content (modified from Norrish (1972)).

T- or P(H<sub>2</sub>O)-induced structural transitions result from a gain or loss of water, but are also affected by migration of H<sub>2</sub>O molecules (Armbruster and Gunter, 2001). These transitions are generally reversible (except at high temperatures where irreversible structural changes take place), and hysteretic behaviour is rare.

The structural effects of zeolite hydration and dehydration are easily studied using powder or single-crystal X-ray diffraction, and the unit-cell parameters often provide useful insight into the hydration/dehydration process. Such X-ray diffraction data, combined with thermal analytical data, have shown that the most important variable controlling the reaction is the vapour pressure of water. Fig. 13.2.6 illustrates the behaviour of the clinoptilolite unit-cell volume as a function of RH, going from water-saturated conditions to 0% RH, and back to 100% RH. These data show the large volumetric changes occurring simply by changing the vapour pressure of water. They also demonstrate that the dehydration reaction, evidenced in the reduction of unit-cell volume as the RH goes to zero, is reversible as the RH is returned to 100%.

Although seemingly of only academic interest, this P(H<sub>2</sub>O)-induced structural transition in clinoptilolite is of importance in a variety of applications, including in the proposed high-level radioactive waste repository at Yucca Mountain, Nevada, USA. The rocks near the proposed waste repository level consist of both devitrified volcanic tuff (Topopah Spring Member, primarily alkali feldspar and silica minerals

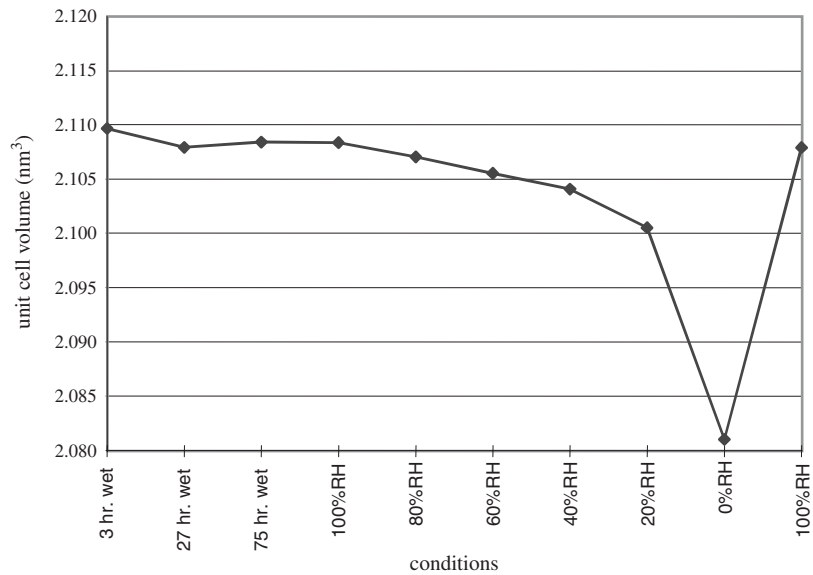


Fig. 13.2.6. Unit-cell volume of Ca-exchanged clinoptilolite from Fish Creek Mountains, Nevada, USA, as a function of humidity (from Bish and Carey, 2000). “3 hr wet” and “27 hr wet” samples were wet with liquid water, and the “75 hr wet” contained little, if any, liquid water.

with minor smectite) and zeolitised volcanic tuff (Calico Hills Tuff, primarily clinoptilolite with lesser amounts of feldspar and silica minerals). Fig. 13.2.7 illustrates the axial stress generated by expansion of 2.54 cm diameter cores of these two rock types. The cores had been previously vacuum dried, without heating, and were immersed in liquid water for this experiment. The contrast in behaviour of the devitrified tuff (Topopah Spring) and the zeolite-bearing tuff (Calico Hills) is remarkable. The Topopah Spring tuff generated a small ( $< 1$  MPa) stress, likely due to hydration of the small amount of smectite in the rock. However, the clinoptilolite-rich Calico Hills tuff generated an axial stress  $> 10$  MPa. One need only consider that the tensile strength of the Calico Hills Tuff is 5–7 MPa to conclude that dehydration-induced tensile cracking is possible (as the hydration-induced volumetric-expansion stress is greater than the strength of the rocks).

Similar X-ray diffraction experiments on clinoptilolite, mordenite, and erionite, among others, have shown no evidence of hysteresis in the T- or  $P(H_2O)$ -induced structural transitions. However, some zeolites show an intriguing mixture of different T- and  $P(H_2O)$ -induced structural transitions. Fridriksson et al. (2003) showed that the zeolite laumontite,  $Ca_4[Al_8Si_{16}O_{48}] \cdot 16H_2O$ , experiences structural changes at partial pressures of water below  $\sim 22$  mbar that are similar to those exhibited by most other zeolites. This behaviour is illustrated in Fig. 13.2.8, where the unit-cell volumes measured from near 0 to  $\sim 22$  mbar  $P(H_2O)$  are reversible and no hysteresis is evident. However, Fridriksson et al. (2003a, 2003b) noted an abrupt change in unit-cell volume between  $\sim 24$  and 29 mbar, followed by gradual and continuous behaviour above this water vapour pressure. Both the abrupt nature of this change, and the hysteresis obvious between the hydration and dehydration data are exciting

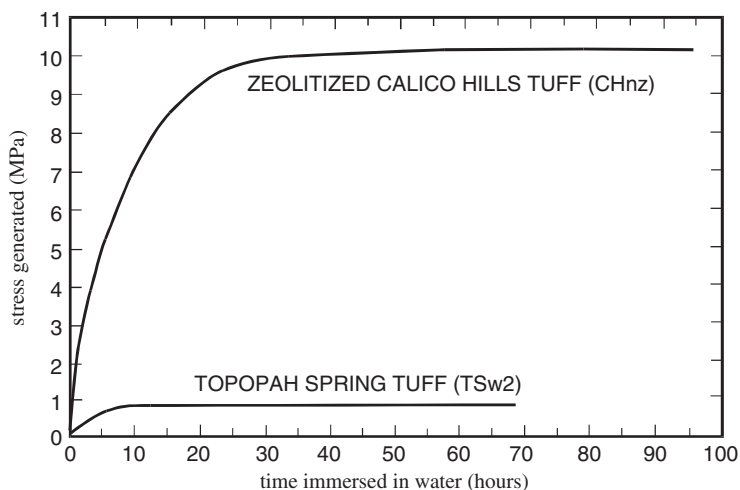


Fig. 13.2.7. Axial stress generated against fixed platens (axially confined) in unjacketed cylindrical samples after vacuum drying and immersion in water (Kranz et al., 1989).

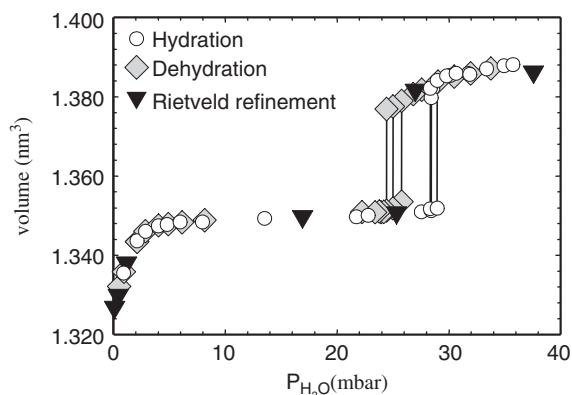


Fig. 13.2.8. Laumontite unit-cell volume as a function of  $P(\text{H}_2\text{O})$  at 27.0°–29.3 °C. Triangles represent data from Rietveld refinements, and circles and diamonds represent data from hydration and dehydration experiments, respectively. Solid lines connect coexisting laumontite phases during hydration (28–29 mbar) and dehydration (24–25 mbar). From (Fridriksson et al., 2003).

evidence of a first-order phase transition in laumontite. These data illustrate that cation– $\text{H}_2\text{O}$  interactions in zeolite extraframework sites are dynamic, even under room conditions of temperature and RH.

#### 13.2.4. DEHYDRATION PHENOMENA

For the most part, smectite hydration and dehydration mirror the structural transitions documented above. Gravimetric experiments are the most common method of studying hydration and dehydration, and they usually show pronounced hysteresis between the hydration and dehydration loops. Interestingly, the quantised behaviour apparent in structural transitions is less pronounced in gravimetric results (Fig. 13.2.9), but hysteresis is obvious. The gravimetric data in Fig. 13.2.9 show that the hydration reactions are reversible, and the amount of water taken up by the smectite depends on the nature of the interlayer cation.  $\text{Ca}^{2+}$ , with its high hydration energy, takes up the most interlayer water whereas  $\text{K}^+$  with its low hydration energy takes up the least of the three. Note also that at close to 0% RH both  $\text{K}^+$ - and  $\text{Na}^+$ -smectites contain a small but finite amount of water whereas the  $\text{Ca}^{2+}$ -smectite contains  $\sim 6.5\%$   $\text{H}_2\text{O}$ . The fact that all of these smectites retain measurable  $\text{H}_2\text{O}$  under low- $P(\text{H}_2\text{O})$  conditions is a reflection of the fact that much of the  $\text{H}_2\text{O}$  in these minerals is held with energies higher than in liquid water. Analysis of the data of Dios Cancela et al. (1997) allows derivation of the partial molar enthalpies of hydration for  $\text{Na}^+$ - and  $\text{Ca}^{2+}$ -smectites, shown in Fig. 13.2.10. This figure shows the stepwise hydration behaviour noted above and demonstrates that  $\text{H}_2\text{O}$  in smectite is

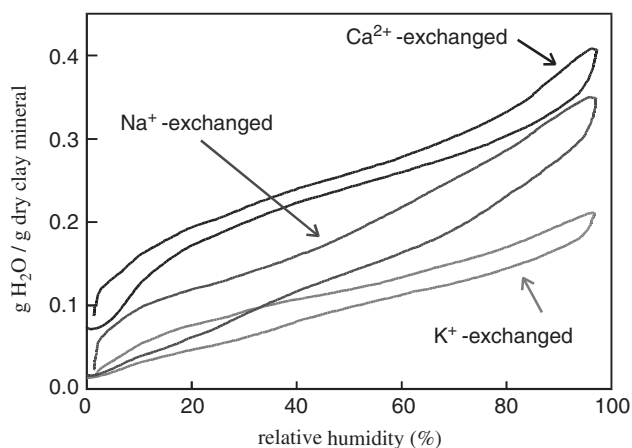


Fig. 13.2.9. Gravimetric water vapour adsorption isotherms (22 °C) measured for Na<sup>+</sup>-, Ca<sup>2+</sup>-, and K<sup>+</sup>-exchanged SAz-1 smectite.

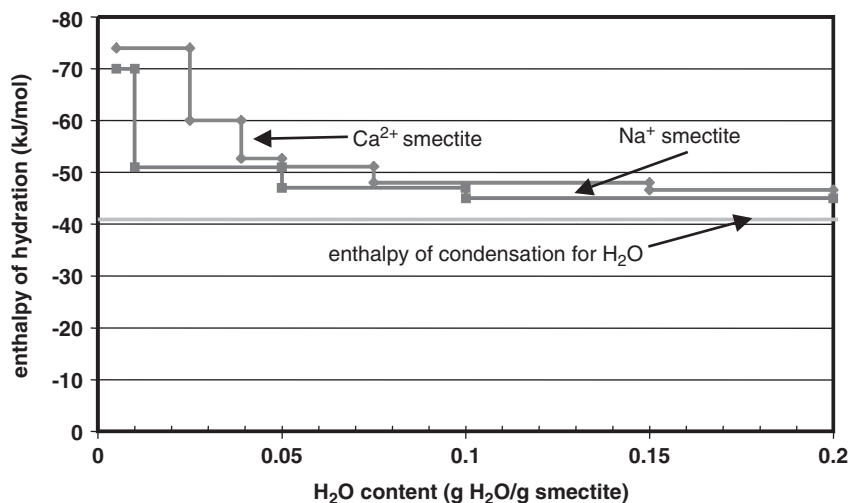


Fig. 13.2.10. Partial molar enthalpies of hydration for Na<sup>+</sup>- and Ca<sup>2+</sup>-smectite, derived from data of [Dios Cancela et al. \(1997\)](#).

held increasingly strongly as the amount of interlayer H<sub>2</sub>O decreases. Note that interlayer H<sub>2</sub>O in partially dehydrated smectite has a hydration enthalpy approaching twice that of liquid water. I will discuss the implications of these significant energetic differences below.

As with smectites, zeolite hydration and dehydration mirror the structural transitions observed with diffraction methods. Zeolite hydration/dehydration reactions are typically continuous and reversible, usually with no obvious hysteresis (as long as the zeolite is not heated to temperatures at which it undergoes irreversible phase transitions). Fig. 13.2.11 shows thermogravimetric analysis data for the zeolite chabazite,  $\text{Ca}_2[\text{Al}_4\text{Si}_8\text{O}_{24}]\bullet 12\text{H}_2\text{O}$ , illustrating the gradual, multistage loss of weight that is common for zeolites. The multiple weight-loss events (note inflection points near  $150^\circ\text{C}$  and  $270^\circ\text{C}$ ) are a reflection of the existence of  $\text{H}_2\text{O}$  in more than one distinct type of crystallographic site. Also note that chabazite continues to undergo weight loss at temperatures above  $300^\circ\text{C}$  indicating that  $\text{H}_2\text{O}$  is held quite strongly. As a result of the strong  $\text{H}_2\text{O}$ –cation and  $\text{H}_2\text{O}$ –framework interactions that occur in zeolite extraframework sites, this appears to be the rule for many zeolites. It is possible to quantify the energetics of hydration/dehydration reactions by measuring the response of a zeolite to changing  $\text{H}_2\text{O}$  vapour pressure at a given temperature. These data, known as water vapour adsorption isotherms, measured at a series of temperatures can provide quantitative information on the nature of the  $\text{H}_2\text{O}$  molecule(s) in a zeolite. The data in Fig. 13.2.12 illustrate such adsorption isotherms for  $\text{Na}^+$ -clinoptilolite, measured from 25 to  $218^\circ\text{C}$ . Carey and Bish (1996) used these data, and similar data for  $\text{K}^+$ - and  $\text{Ca}^{2+}$ -clinoptilolite, to determine the partial molar enthalpies of hydration shown in Fig. 13.2.13. They were able to fit these data assuming a single energetically distinct  $\text{H}_2\text{O}$  site, but experiments on other zeolites (e.g., chabazite) show clear evidence for multiple  $\text{H}_2\text{O}$  sites that must be considered

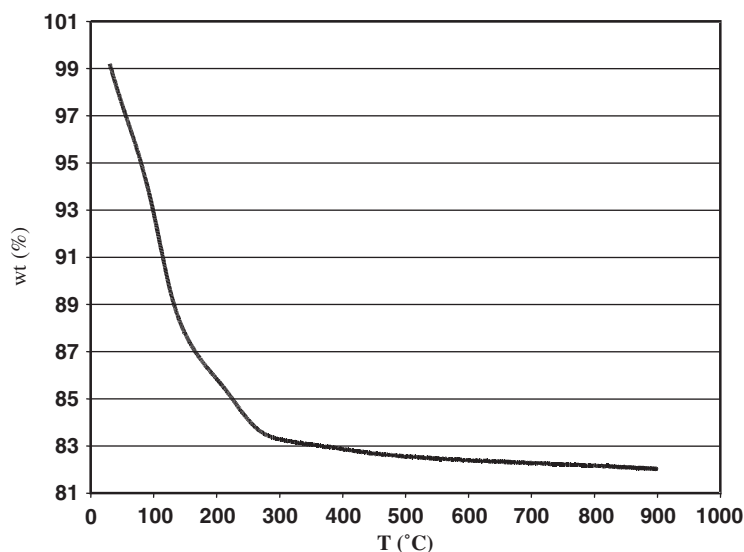


Fig. 13.2.11. Thermogravimetric analysis data for chabazite measured at a heating rate of  $2^\circ\text{C}/\text{min}$  in a  $\text{N}_2$  atmosphere.

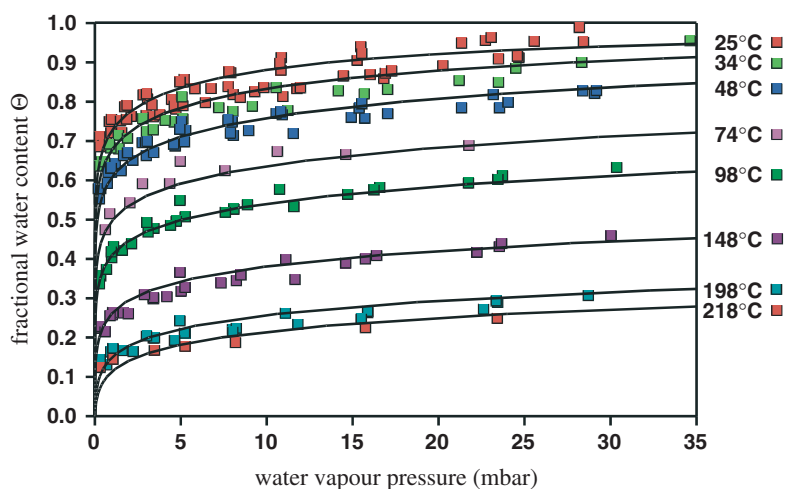


Fig. 13.2.12. Experimental (symbols) and calculated (solid line)  $\text{H}_2\text{O}$ -vapour adsorption isotherms for  $\text{Na}^+$ -clinoptilolite measured at the indicated temperatures.  $\theta$  is the fractional water content, where a  $\theta$  value of 1 indicates full  $\text{H}_2\text{O}$  occupancy and a  $\theta$  value of 0 indicates complete dehydration.

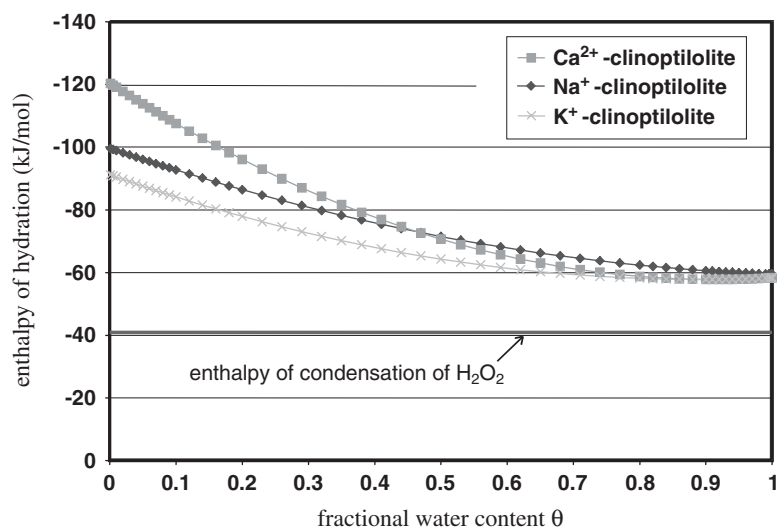


Fig. 13.2.13. Calculated curves of the partial molar enthalpies of hydration for  $\text{Na}^+$ -,  $\text{K}^+$ -, and  $\text{Ca}^{2+}$ -clinoptilolite at 25°C.

when fitting experimental isotherm data (Bish et al., 2003b). Fig. 13.2.13 shows that the energy required to remove H<sub>2</sub>O molecules from clinoptilolite (or the energy gained on hydration) is significantly greater than the energy required to evaporate liquid H<sub>2</sub>O, up to almost three times the enthalpy of vapourisation of liquid water in a largely dehydrated Ca-clinoptilolite. This figure also shows, once again, the large effect of exchangeable cation on hydration behaviour.

Although zeolite hydration/dehydration is typically continuous and non-hysteretic, some zeolites exhibit discontinuous and hysteretic behaviour, notably laumontite. The unit-cell volume data in Fig. 13.2.8 are mirrored well in Fig. 13.2.14, showing the results of gravimetric H<sub>2</sub>O isotherm measurements on laumontite. Most interestingly, the discontinuous and hysteretic behaviour shown in Fig. 13.2.8 is evidenced here only in the 23.4 °C data, and this discontinuous hydration/dehydration reaction does not appear at higher temperatures.

The dehydration and hydration behaviour of smectites and zeolites, and their associated structural effects, are very important in a wide variety of applications, both environmental and technological. The importance of these properties possibly extends beyond Earth, to the surface of Mars. Great excitement was generated with the recent discovery by the Mars Odyssey spacecraft of heterogeneously distributed hydrogen at Martian mid-latitudes, suggesting that large areas of the near-equatorial highlands contain near-surface deposits of “chemically and/or physically bound H<sub>2</sub>O and/or OH” in amounts up to  $8.5 \pm 1.3\%$  water-equivalent hydrogen (Feldman, Mars conference). Bish et al. (2003a, 2003b) used quantitative data on the hydration

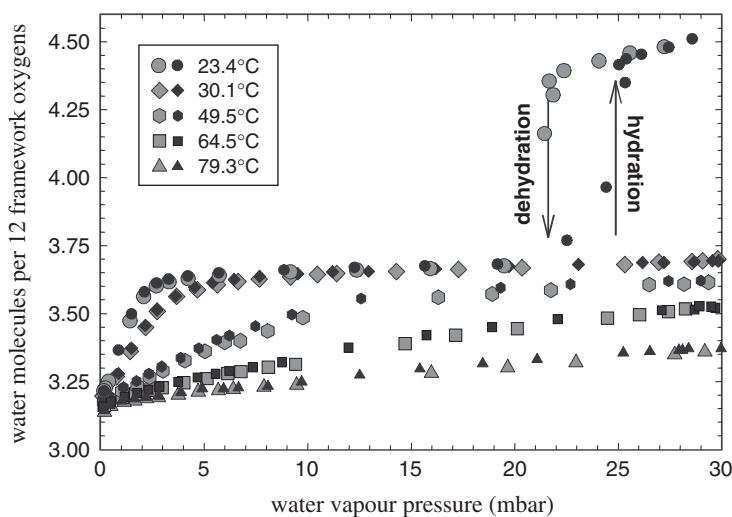


Fig. 13.2.14. Gravimetric H<sub>2</sub>O adsorption isotherm measurements for laumontite made at the indicated temperatures. Solid symbols represent data obtained during hydration, and shaded symbols represent data obtained during dehydration. From Fridriksson et al. (2003).



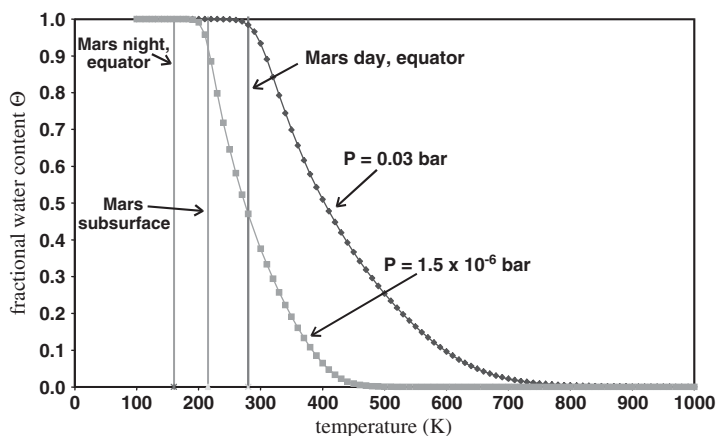


Fig. 13.2.15. Equilibrium hydration state of  $\text{Na}^+$ -clinoptilolite as a function of temperature at a  $P(\text{H}_2\text{O})$  of  $1.5 \times 10^{-6}$  and 0.03 bar. Mars equatorial night, day, and subsurface temperatures are indicated. Data were calculated from the equilibrium isothermal data of Carey and Bish (1996).

and dehydration of smectites, clinoptilolite, and chabazite, to determine whether or not these minerals could exist in a hydrated state on the surface of Mars, a cold and very dry environment (equatorial surface temperatures range from 160 to 280 K,  $P(\text{H}_2\text{O})$  on the surface is  $\sim 1.5 \times 10^{-6}$  bar). Fig. 13.2.15 summarises the calculated behaviour for  $\text{Na}^+$ -clinoptilolite. Not surprisingly, the curve for 0.03 bars, typical of a humid day on Earth, shows that  $\text{Na}^+$ -clinoptilolite is largely hydrated. However, the curve calculated for Martian  $P(\text{H}_2\text{O})$  shows the unexpected result that  $\text{Na}^+$ -clinoptilolite is at least 50% hydrated under Martian surface conditions! The apparent ability of clinoptilolite, and of smectite and other zeolites, to retain  $\text{H}_2\text{O}$  even under conditions of very low partial pressure of  $\text{H}_2\text{O}$  is a direct result of the large energies of attraction that the minerals have for water molecules.

### 13.2.5. SUMMARY AND CONCLUSIONS

The data presented here illustrate the important interplay between crystal structure and hydration/dehydration behaviour for both smectites and zeolites. In spite of the fact that smectites and zeolites have many similar properties, their very distinct crystal structures often give rise to very different properties. As a result of their layer structure, smectite structural transitions are quantised and hysteretic, and they generally approximate first-order transitions. This stepwise behaviour is mirrored in the hydration/dehydration behaviour. Quantitative analysis of  $\text{H}_2\text{O}$ -vapour adsorption isotherms shows that the first few layers of  $\text{H}_2\text{O}$  molecules entering the interlayer region are held very strongly.

Zeolites rarely show the hysteretic behaviour that is so common with smectites, and structural transitions are usually gradual, reversible, and second order. Accurate crystal structure information has shown that many natural zeolites have multiple H<sub>2</sub>O sites, and zeolite hydration and dehydration often reflect this, with multiple weight-loss events often occurring up to temperatures > 250 °C. However, the complex interactions between H<sub>2</sub>O molecules and exchangeable cations in the zeolite extraframework sites can give rise to hysteretic stepwise transitions when the cations and H<sub>2</sub>O molecules migrate during hydration or dehydration. As with smectites, analysis of adsorption data shows that H<sub>2</sub>O molecules in zeolite extraframework sites is held very strongly, up to three times the enthalpies for liquid water. Such high vapourisation enthalpies have important implications in a variety of areas and mean that zeolites and smectites can contain H<sub>2</sub>O molecules under very dry conditions. They are also further reflection of the importance of H<sub>2</sub>O in these minerals; water is not a passive occupant in zeolite and smectite structures. Perhaps the future will bring more quantitative information on smectite structures similar to those existing for zeolites.

## REFERENCES

- Armbruster, T., Gunter, M.E., 2001. Crystal structures of natural zeolites. In: Bish, D.L., Ming, D.W. (Eds.), *Natural Zeolites: Occurrence, Properties, Applications*. MSA Reviews in Mineralogy and Geochemistry, vol. 45. Mineralogical Society of America, Washington, DC, pp. 1–67.
- Barrer, R.M., 1978. Cation-exchange equilibria in zeolites and feldspathoids. In: Sand, L.B., Mumpton, F.A. (Eds.), *Natural Zeolites: Occurrence, Properties, Use*. Pergamon Press, Oxford, England, pp. 385–395.
- Bish, D.L., Carey, J.W., 2000. Coupled X-ray powder diffraction and thermogravimetric analysis of clinoptilolite dehydration behavior. In: Colella, C., Mumpton, F.A. (Eds.), *Natural Zeolites for the Third Millennium*. De Frede Editore, Naples, pp. 249–257.
- Bish, D.L., Carey, J.W., 2001. Thermal behavior of natural zeolites. In: Bish, D.L., Ming, D.W. (Eds.), *Natural Zeolites: Occurrence, Properties, Applications*. MSA Reviews in Mineralogy and Geochemistry, vol. 45. Mineralogical Society of America, Washington, DC, pp. 403–452.
- Bish, D.L., Carey, J.W., Vaniman, D.T., Chipera, S.J., 2003a. Stability of hydrous minerals on the martian surface. *Icarus* 164, 96–103.
- Bish, D.L., Vaniman, D.T., Fialips, C., Carey, J.W., Feldman, W.C., 2003b. Can hydrous minerals account for the observed Mid-Latitude water on Mars? 6th International Conference on Mars, July 20–25, 2003.
- Campbell, B.J., Cheetham, A.K., 2002. Linear framework defects in zeolite mordenite. *The Journal of Physical Chemistry B* 106, 57–62.
- Carey, J.W., Bish, D.L., 1996. Equilibrium in the clinoptilolite-H<sub>2</sub>O system. *American Mineralogist* 81, 952–962.
- Colella, C., 1996. Ion exchange equilibria in zeolite minerals. *Mineral Deposits* 31, 554–562.

- Dios Cancela, G., Huertas, F.J., Romero Taboada, E., Sanchez-Rasero, F., Hernandez Laguna, A., 1997. Adsorption of water vapor by homoionic montmorillonites: heats of adsorption and desorption. *Journal of Colloid and Interface Science* 185, 343–354.
- Fridriksson, T., Bish, D.L., Bird, D.K., 2003a. Hydrogen-bonded water in laumontite I: X-ray powder diffraction study of water site occupancy and structural changes in laumontite during room-temperature isothermal hydration/dehydration. *American Mineralogist* 88, 277–287.
- Fridriksson, T., Carey, J.W., Bish, D.L., Bird, D., Neuhoﬀ, P.S., 2003b. Hydrogen-bonded water in laumontite II: Experimental determination of site-specific thermodynamic properties of hydration of the W1 and W5 sites. *American Mineralogist* 88, 1060–1072.
- Kranz, R.L., Bish, D.L., Blacic, J.D., 1989. Hydration and dehydration of zeolitic tuff from Yucca Mountain, Nevada. *Geophysical Research Letters* 16, 1113–1116.
- Norrish, K., 1972. Forces between clay particles. *International Clay Conference Preprints* 2, 3–14.
- Weaver, C.E., Pollard, L.D., 1973. *The Chemistry of Clay Minerals*. Elsevier, Amsterdam.

*Chapter 13.3*

## CEMENT HYDRATES

H. VAN DAMME<sup>a</sup> AND A. GMIRA<sup>b</sup>

<sup>a</sup>*Ecole Supérieure de de Physique et de Chimie Industrielle (ESPCI-PPMD), F-75231 Paris Cedex, France*

<sup>b</sup>*CRMD, CNRS-Université d'Orléans, F-45071 Orléans Cedex 2, France*

Concrete is, by volume, the most widely used industrial material in the world: about two tons per year and per person. An artificial rock that is one of the bases of developed societies, concrete is basically a structural material (Neville, 1963). It owes its cohesion to cement or, more exactly, to the reaction products of cement with water, called 'hydrates' (Taylor, 1997). Cement and its hydrates have special relationships with clays. The first one is that Portland cement—discovered in the 19th century by Aspdin and by far the most common type of cement—is essentially the high-temperature reaction product of limestone with clay. The second relationship, discussed in this short chapter, is that the most important cement hydrates share two essential properties with smectites and layered double hydroxides (LDHs), namely, a layered structure and an electrically charged surface. In calcium silicate hydrates, the layers are negatively charged as in smectites, while in the calcium aluminate hydrates, they are positively charged as in LDHs.

Yet, there are also dramatic differences. Dipping a clayey rock in water may lead to swelling and possibly to complete colloidal dispersion, whereas the same treatment applied to hardened cement leaves it basically unchanged. Cement is even able to set and harden under water. Current theories on the origin of this difference will be briefly reviewed.

### 13.3.1. PORTLAND CEMENT AND ITS HYDRATION

Portland cement is the ground form of clinker, the artificial rock obtained from the non-equilibrium cooling of a sintered mass in the system  $\text{CaO-SiO}_2\text{-Al}_2\text{O}_3$ , with magnesium and iron impurities, starting from a mixture of clay and limestone as raw material. Each grain is a polycrystal containing several mineral phases, the most abundant being impure tricalcium silicate,  $\text{Ca}_3\text{SiO}_5$  (alite,  $\text{C}_3\text{S}$  in short) and dicalcium silicate,  $\text{Ca}_2\text{SiO}_4$  (belite,  $\text{C}_2\text{S}$  in short) (Taylor, 1997).<sup>1</sup> The other phases, which

<sup>1</sup>We will use the cementitious nomenclature throughout: C for  $\text{CaO}$ ; S for  $\text{SiO}_2$ ; A for  $\text{Al}_2\text{O}_3$ ; H for  $\text{H}_2\text{O}$ ; and  $\bar{\text{S}}$  for  $\text{SO}_3$ .

are liquid during the synthesis at  $1450^{\circ}\text{C}$ , are a tricalcium aluminate,  $\text{Ca}_3\text{Al}_2\text{O}_6$  ( $\text{C}_3\text{A}$  in short) and a calcium aluminoferrite,  $\text{Ca}_4\text{Al}_2\text{Fe}_2\text{O}_{10}$  (celite,  $\text{C}_4\text{AF}$  in short). Gypsum,  $\text{CaSO}_4 \cdot 2\text{H}_2\text{O}$ , ( $\text{C}\bar{\text{S}}\text{H}_2$  in short) is added to ground clinker in order to regulate the reactivity of the aluminate phases.

When cement is mixed with water, it undergoes a dissolution reaction, generating calcium, silicate and aluminate ions, among others, in the interstitial solution. Very soon new products precipitate, the most important of which are calcium silicate hydrate (CSH) and calcium hydroxide (portlandite, CH). The aluminate ions react with calcium and sulphate ions to form first calcium trisulphato aluminate hydrate (ettringite) initially. When all the gypsum was consumed, calcium monosulphato aluminate hydrate is formed as a result of the reaction of ettringite with residual tricalcium aluminate. As the hydration reaction proceeds, more and more anhydrous material is converted into hydrates. This leads to an overall decrease in porosity since the molar volume of hydrates is much larger than that of the anhydrous phases (more than twice in the case of tricalcium silicate (Powers, 1958)). The remaining porosity, the residue of the incomplete filling of the initial intergranular porosity, is referred to as the ‘capillary porosity’ (Fig. 13.3.1).

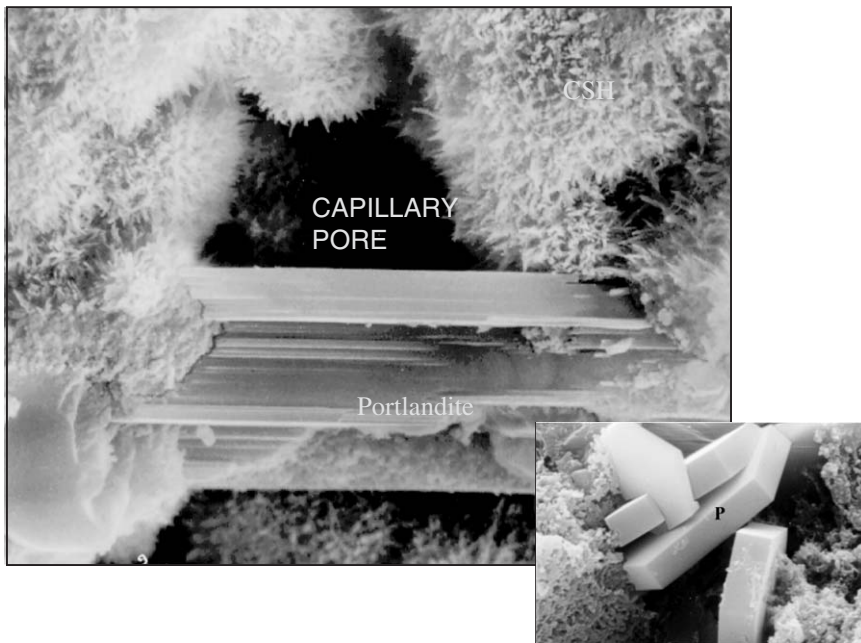


Fig. 13.3.1. SEM micrograph of a hardened cement paste showing urchin-like CSH, a portlandite crystal and, in the middle, a residual capillary pore. Inset: well-crystallized hexagonal portlandite crystals (courtesy Moranville).

The crystal habits developed by the hydrates are strongly dependent on hydration conditions such as temperature, water/cement ratio and organic additives. Nevertheless, typical shapes may be recognized. For instance, CSH often grows as fine urchin needles around the parent cement particle (Fig. 13.3.1). Portlandite crystals may easily be recognized by their well-defined hexagonal shape and large size (Fig. 13.3.1). Ettringite grows as stiff but fragile needles that may restrict the ability of the fresh paste to flow. Finally, the crystals of monosulphato aluminate grow as hexagonal platelets, like portlandite, but much smaller. All those shapes are well developed when crystal growth takes place in dilute conditions, but they may hardly be recognizable in dense pastes.

### 13.3.2. STRUCTURE AND SURFACE PROPERTIES OF CEMENT HYDRATES

The hydrates are minerals that give cohesion to hardened cement. All the hydrates play a role in this cohesion, but in Portland cement, the most important is undoubtedly CSH. Unfortunately, the structure of this hydrate is still imperfectly resolved.

CSH is basically a non-stoichiometric compound (Taylor, 1997). The average Ca/Si ratio in ordinary hardened cement paste is around 1.7. Local values fluctuate between 0.6 and 2 or more (Viehland et al., 1996; Zhang et al., 2000; Gatty et al., 2001). Pure CSH may also be synthesized directly from the oxides or hydroxides—lime, silica and water—in dilute suspension and under mild thermal conditions. This is the so-called pozzuolanic synthesis route, similar to what was in Roman times the common way of preparing binders from natural lime and silica-rich volcanic ashes ('pozzuolanas', from the name of the city of Pozzuoli, near Naples). The pozzuolanic method provides greater flexibility in the control of the Ca/Si ratio than the simple mixing of cement and water. This is because the Ca/Si ratio in CSH is thermodynamically controlled by the calcium ions activity in solution and this activity is much easier to control in the pozzuolanic method. Thus, CSH with a Ca/Si ratio varying from 0.66 to 1.5 may be prepared in this way. To prepare CSH with higher and well-controlled Ca/Si ratios, tricalcium silicate has to be hydrated in lime solutions supersaturated with respect to portlandite (Damidot et al., 1995).

Though CSH is generally poorly organized (hence the widespread use of the expression 'CSH gel'), it is widely recognized as having a layered crystal structure similar to tobermorite (Fig. 13.3.2) or jennite, with a layer thickness in the nanometer range (Taylor, 1986; Henderson and Bailey, 1988; Richardson and Groves, 1992; Taylor, 1993; Richardson, 1999). This morphology is hardly recognizable in real hardened cement paste but becomes evident from XRD and direct TEM observations of pozzuolanic CSH (Fig. 13.3.2).

Tobermorite exists in two forms, with basal distances of 1.1 and 1.4 nm, respectively. The difference corresponds to one layer of water molecules. Only the structure

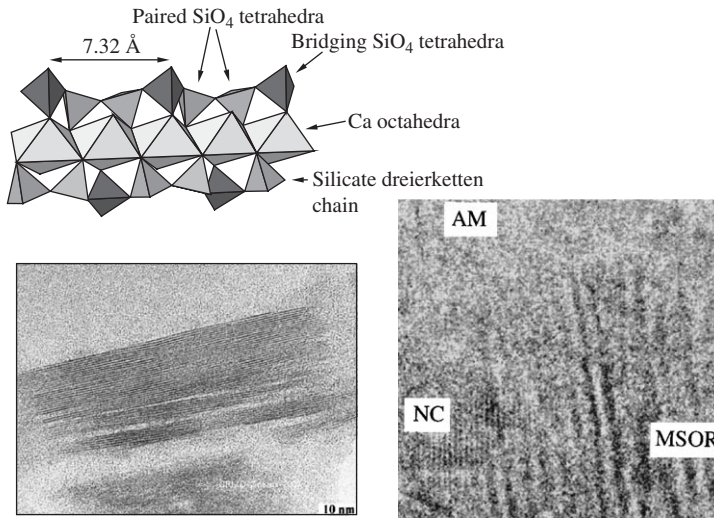


Fig. 13.3.2. Upper left: model of CSH at  $\text{Ca/Si} = 0.66$ , with the central double layer of calcium ions, connected on each side to chains of silica tetrahedra. Lower left: TEM micrograph of CSH prepared by reaction of lime with amorphous silica at  $\text{Ca/Si} = 1$  (Gmira et al., 2004); Lower right: HRTEM micrograph of the hydrated region in a real, dense, CSH (Gatty et al., 2001). AM, NC and MSOR indicate amorphous, nanocrystalline and mesoscopically ordered regions, respectively.

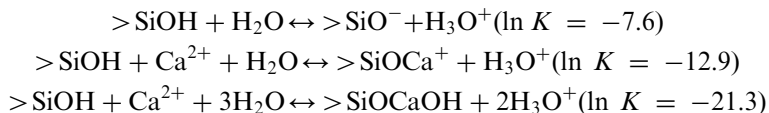
of the 1.1 nm form was resolved. Two models were proposed, that by Hamid (1981) and a more recent one by Merlino et al. (2001). The two models share in common a central double plane of calcium ions 6- or 7-coordinated by oxygen ions, to which silicate chains are grafted on each side. These composite layers, stacked along the 001 direction, are separated by  $\text{Ca}^{2+}$  ions and water molecules.

The difference between Hamid's model and that of Merlino et al. lies in the structure and bonding of the silicate chains. In Hamid's (1981) structure the repeating units along the chains are so-called 'dreierketten' (Liebau, 1985), with two pairing tetrahedra linked to the CaO polyhedra by sharing edges with them, and one bridging tetrahedron pointing away from the CaO polyhedra sheet (Fig. 13.3.2). In perfect tobermorite, with  $\text{Ca/Si} = 0.66$ , the chains are infinite and run parallel to the  $b$  axis. All the oxygen atoms involved in the dangling bonds of the silicate chain are protonated as hydroxyl groups, so that the structure is neutral. The interlayer space is occupied only by water molecules. No chemical bonds exist between adjacent layers. On the contrary, in the structure proposed by Merlino et al. (2001) the layers are linked by bridging Si–O–Si bonds, generating cavities analogous to those found in zeolites. Recent *ab initio* calculations showed that Hamid's structure is significantly more stable ( $\sim 8\%$ ) than that of Merlino et al. (Gmira, 2003; Gmira et al., 2004).

Due to its ill-organized structure, no direct structural determinations can be performed on CSH. Nevertheless, high-resolution  $^{29}\text{Si}$ ,  $^1\text{H}$  and  $^{17}\text{O}$  NMR, X-ray absorption spectroscopy, IR and Raman spectroscopy (Colombet et al., 1998) provided a great deal of information on the structure of the layers. Up to  $\text{Ca/Si} = 1.5$ , CSH may be considered as a defect tobermorite structure (Fig. 13.3.5). A crucial point is that the solution in equilibrium with CSH is always at very high pH. For  $\text{Ca/Si} = 1$ , the pH is already beyond 10. In the low  $\text{Ca/Si}$  regime, the structural evolution involves the progressive replacement of the protons of the initially doubly protonated bridging tetrahedra by  $\text{Ca}^{2+}$  ions that go into the hydrated interlayer space.

At  $\text{Ca/Si} = 1$ , a first-phase transition occurs and a new type of CSH forms with a lower degree of polymerization of the chains. The main defects are missing bridging tetrahedra. The higher the  $\text{Ca/Si}$  ratio the larger the number of missing bridging tetrahedra and the shorter the average chain length. This length goes from average pentameric units at  $\text{Ca/Si} = 1$  to dimeric units at  $\text{Ca/Si} = 1.5$ . Ionization of the hydroxyl groups of the dangling bonds, generated by this chain shortening, maintains the negative charge of the layers and the number of  $\text{Ca}^{2+}$  ions in the interlayer space. At  $\text{Ca/Si} = 1.5$ , a second-phase transition seems to take place. The structure of CSH in this high  $\text{Ca/Si}$  ( $> 1.5$ ) regime remains very controversial. Three main models were proposed. In the solid-solution model, the CSH is considered to be a solid solution of CSH with  $\text{Ca/Si} < 1.5$  and portlandite,  $\text{Ca}(\text{OH})_2$  (Richardson and Groves, 1992; Cong and Kirkpatrick, 1996). In the nanophase model, CSH is believed to be a nanophasic mixture of tobermorite- and jennite-related units, at nanometer scale (Taylor, 1986, 1993; Viehland et al., 1996). In the third model, the increase of  $\text{Ca/Si}$  above 1.5 is achieved by replacement of  $\text{SiO}_2$  units by  $\text{Ca}(\text{OH})_2$  (Nonat and Lecoq, 1998).

As far as surface properties are concerned, the CSH layers should bear a mixture of  $\equiv\text{Si}-\text{OH}$  and  $\equiv\text{Si}-\text{O}^-$  groups. The proportion of  $\equiv\text{Si}-\text{O}^-$  groups increases as the  $\text{Ca/Si}$  ratio and the pH increase (the equilibrium pH of a Portland cement slurry is close to 13). This is confirmed by the decrease of the  $\text{Si}-\text{OH}$  stretching band at  $3740\text{ cm}^{-1}$  in the IR spectrum when the  $\text{Ca/Si}$  ratio increases (Yu et al., 1999). Thus, the CSH layers are intrinsically negatively charged colloids. However, due to the strong affinity of the  $\text{Ca}^{2+}$  ions for the  $\equiv\text{Si}-\text{O}^-$  groups, charge reversal may occur. Modelling of the titration curves of CSH with lime indicates the existence of three acid-base equilibria (Pointeau, 2000):



Thus, as the  $\text{Ca}^{2+}$  concentration and pH increase, four types of surface groups are successively formed:  $>\text{SiOH}$ ,  $>\text{SiO}^-$ ,  $>\text{SiOCa}^+$  and finally  $>\text{SiOCaOH}$ . The



existence of CaOH sites at the highest Ca/Si ratios and pH is confirmed by the appearance of a band at  $3600\text{ cm}^{-1}$  in the IR spectrum (Yu et al., 1999).

Electrophoretic measurements show that the zeta potential of CSH increases with the Ca/Si ratio (which is itself determined by the calcium concentration and pH in the solution in equilibrium with the solid). It becomes positive as soon as the Ca/Si ratio is larger than 0.8 (the equilibrium calcium ions concentration is then 2 mmol/L), indicating that the calcium ions compensating the layer charge are potential-determining (Nachbaur et al., 1998; Terrasse-Viallis et al., 2001). At an equilibrium calcium concentration of 20–30 mmol/L (reached in the interstitial solution of ordinary Portland cement), corresponding to CSH with the highest Ca/Si ratios, the zeta potential ranges from +10 to +20 mV. This shows that not all the surface groups are in the neutral  $\equiv\text{SiOCaOH}$  form. A significant proportion of  $\equiv\text{SiOCa}^+$  sites still exist.

Sulphate ions also play a particularly important role in the surface properties of CSH. Addition of an alkaline sulphate to the equilibrium solution of CSH shifts the point of zero charge to higher calcium concentrations and decreases the zeta potential. The latter may even become negative at low Ca/Si ratio (Nachbaur et al., 1998).

The other important hydrate in a mature cement paste is the tetracalcium monosulphato aluminate hydrate or CmSAH, with a general formula  $[\text{Ca}_4\text{Al}_2(\text{OH})_{12}](\text{SO}_4) \cdot 15\text{H}_2\text{O}$ . Like portlandite, CmSAH crystallizes in the form of thin hexagonal platelets (Taylor, 1997). Its structure is that of an LDH (see Chapter 13.1) consisting of a calcium hydroxide sheet in which 1/3 of the  $\text{Ca}^{2+}$  ions are replaced by  $\text{Al}^{3+}$  or  $\text{Fe}^{3+}$  ions, with charge-balancing sulphate anions and water molecules in the interlayer space. In ordinary Portland cement, part of the  $\text{Al}^{3+}$  ions are replaced by  $\text{Fe}^{3+}$  ions, as a result of isomorphous substitution in the raw clay mineral used for clinker synthesis.

Due to substitution of  $\text{Al}^{3+}$  (or  $\text{Fe}^{3+}$ ) for  $\text{Ca}^{2+}$  in their structures, aluminate hydrates carry an intrinsic positive charge. To what extent this positive charge is screened, or even reversed, by adsorbed anions such as sulphate or carbonate ions, is not known.

### 13.3.3. THE MESO- AND MICRO-STRUCTURE OF CSH

The widespread use of the term ‘CSH gel’ indicates our inability to qualify the way the individual layers and their aggregates fill space. XRD techniques are of little help as both the in-plane extension and stacking order of the layers are very limited. High resolution transmission electron microscopy (HRTEM) shows very little local order in ordinary cement at early stages; even in well-cured high-density samples the coherence lengths remain small (Viehland et al., 1996; Zhang et al., 2000; Gatty et al., 2001).

Direct observation by atomic force microscopy (AFM) of the growth of CSH on smooth silica surfaces at the solid/lime solution interface reveals the formation of discrete, elongated 5 nm thick, disk-shaped aggregates with a long axis of the order of 60 nm (Gauffinet et al., 1998). Each aggregate consists of a few CSH layers. Globular units of similar size (~60 nm) are observed by bright field TEM observation of ultrathin sections of mature hydrated calcium silicate pastes (Maggion et al., 1996; Van Damme, 2002). Although it is not known if these features are universal, the observed size seems typical of locally compact aggregates of CSH layers.

The microstructure at larger length scales is also controversial. AFM observations show that on silica substrates, large assemblies of the basic units form as CSH nucleation and growth proceed (Gauffinet et al., 2000). These assemblies grow laterally, parallel to the substrate surface, or axially, perpendicular to the surface.

Such detailed observations cannot be performed on real dense pastes, but numerous models were proposed on the basis of indirect data such as surface area and porosity determinations (Jennings et al., 1996). The most recent model (Jennings, 2000) assumes the existence of two types of aggregates, compact and loose. On the other hand, small angle X-ray and neutron scattering (SAXS and SANS) (Craievich, 1987; Adenot et al., 1993; Winslow et al., 1995; Maggion et al., 1996), mercury intrusion (Maggion et al., 1996), image analysis (Maggion et al., 1996) and NMR relaxometry (Plassais, et al., 2005) provided evidence to indicate that at high degrees of hydration the texture exhibits scale invariant (fractal) properties on scale lengths from at least the nm to the  $\mu\text{m}$  scale. This does not contradict the existence of two types of CSH aggregates. Disordered growth processes may lead either to surface or to mass fractal structures, depending on the rate-limiting step and confinement conditions (Van Damme, 2002). A conjectural cartoon, inspired by the pioneering work of Powers (1958) and TEM micrographs (Maggion et al., 1996), is shown in Fig. 13.3.3.

#### 13.3.4. CSH AND SMECTITES

It will not escape readers of this book that CSH and smectites share a number of features:

- (i) elementary particles with a 2D structure and a layer morphology with a thickness of the order of 1 nm. The lateral extension of the layers is more limited in CSH than in natural smectites but close to the layer size in synthetic smectite (Laponite). As a result, the deformability of the layers, and more so of the particles (stacked layers), in CSH is much less than in montmorillonite for instance. Likewise, the surface of the layers, at the atomic scale, is much rougher than the oxygen planes in clay minerals (Fig. 13.3.2). Infinite chains of dreierketten units are already very rough and their roughness may be further amplified by defects that appear as the Ca/Si ratio increases (see Section 13.3.2). This would introduce a strong stacking disorder, accounting for the quasi-amorphous character of CSH in hardened cement;

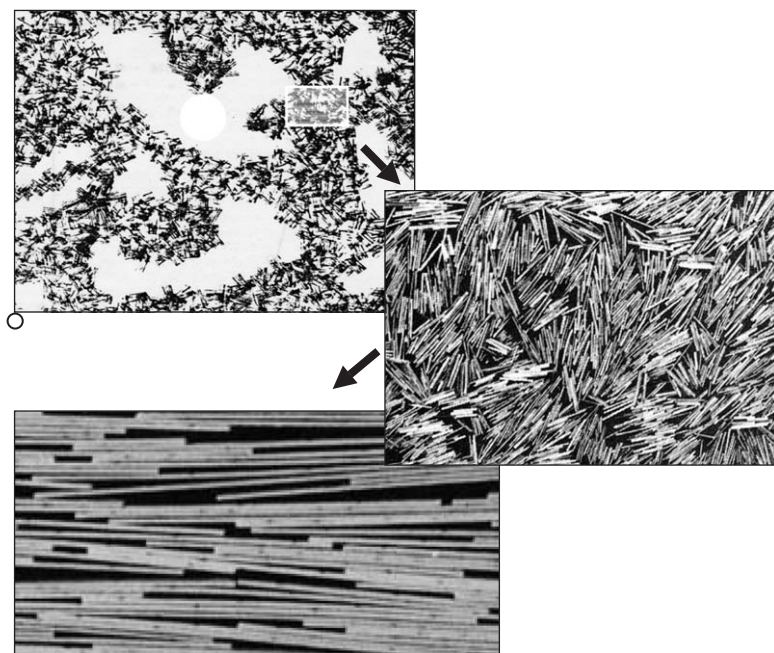


Fig. 13.3.3. Cartoon illustrating the possible structure of CSH at increasing magnifications from top to bottom, from the scale of the capillary voids to that of the elementary layers. The last cartoon (bottom) illustrates the two length scales that have to be considered for understanding the cohesion of cement: the scale of the nanoparticles (light grey) where calcium ions form inner sphere complexes with surface oxygen atoms, and the meso scale of the larger pores (black areas) where fully hydrated and mobile calcium ions generate ion–ion correlation forces (first cartoon adapted from Powers, 1958).

- (ii) a negative charge and
- (iii) a hydrated interlayer space.

At the same time, CSH and smectites differ as to the localization and density of electric charge. In CSH, the charge is not due to ionic substitution in the structure but to ionization of surface groups and to specific adsorption of calcium ions that, as pointed out above, induce charge reversal in zeta potential measurements at high Ca/Si ratio. It is also noteworthy that the calcium ions in CSH are essentially non-exchangeable.

The surface charge density,  $\sigma$ , of the layers, without adsorbed ions, is also vastly different. No direct measurements were reported but  $\sigma$  may be estimated from the structure of the reference mineral tobermorite. Assuming that all surface OH groups are ionized, one obtains  $\sigma \cong 3e^-/\text{nm}^2$ . This is about four times larger than in typical montmorillonites. Interestingly, this value is of the same order of magnitude as the surface charge density in LDHs and in the other important hydrate, CmSAH.

### 13.3.5. COHESION VS. SWELLING

Bearing in mind these similarities and differences, how might we account for the remarkable cohesion of CSH? The question may be made more general by asking how charge density and the nature of the interlayer ions affect swelling and cohesion of any charged layered material, including clay minerals and LDHs. We will only consider the case of saturated systems, i.e., materials in which the void space is totally filled with water and ions.

As in clay minerals, the problem should be considered at two different length scales. One is the sub-nano scale of interlayer distances within the dense CSH particles and interparticle 'contact' points. The other is the meso scale of inter-wall distances in the particle fabric (Fig. 13.3.3). A similar distinction is made in smectite/water systems where the small-scale interlayer ('crystalline') swelling is usually distinguished from the larger scale 'osmotic' swelling. In thermodynamic terms, the driving force for interlayer swelling is essentially the hydration enthalpy of the interlayer ions and the surface oxygen atoms. The driving force for osmotic swelling is the entropy gain of the mobile hydrated ions when their confinement space expands (as in a perfect gas). Thus, the ideal conditions for swelling are small, very mobile, fully hydrated and homogeneously distributed ions in the interlayer space. Any factor that restricts the hydration and/or the mobility of the interlayer ions and/or their homogeneous distribution in the interlayer space will also restrict swelling.

Complementary to the driving forces for swelling, consideration must be given to the attractive forces that need to be overcome (by the repulsive forces). Non-retarded van der Waals interactions belong to this category. Their magnitude may be estimated from the continuum theory and the Hamaker constants. A system composed of two charged particles with like charges, separated by charge-balancing ions in water, would also generate strongly attractive configurations due to purely electrostatic interactions (Kjellander and Marcelja, 1984, 1986; Ennis et al., 1996; Belloni and Spalla, 1997; Gronbech-Jensen et al., 1997; Larsen and Grier, 1997). At interlayer distances in the nm range, these attractive forces may be considerably stronger than the van der Waals interactions.

A clear example is the restricted swelling (in water) of  $\text{Ca}^{2+}$ -montmorillonite as compared with the extensive swelling of the  $\text{Na}^+$ -exchanged form. As Kjellander et al. (1988a, 1988b) showed, the swelling behaviour of  $\text{Ca}^{2+}$ -montmorillonite is due to the so-called ionic 'correlation forces' (see Chapter 5). In the Poisson–Boltzmann treatment of two identically charged surfaces with an intervening electrolyte solution, the two halves of the cell are symmetrical and neutral. Thus, no electric field is induced by one cell onto the other. In a real system, the overwhelming majority of instantaneous ionic configurations do not achieve this ideal situation (Fig. 13.3.4). On average, the electric field generated by one half of the layer system is still zero in the other half, but for every configuration there is a spatially varying field. The charges of the second half respond to this instantaneous field by adopting configurations of lower energy, different from the mean field configuration. These

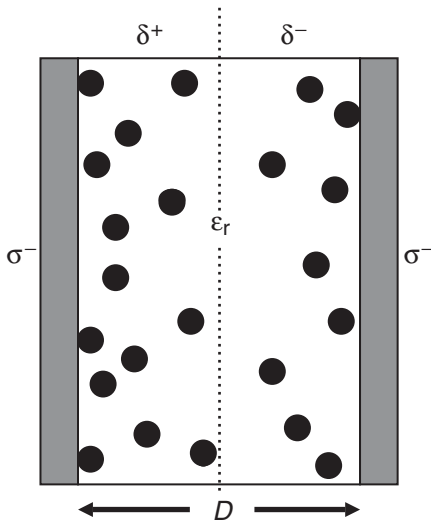


Fig. 13.3.4. Two uniformly charged walls separated by a dielectric continuum in which hydrated ions are free to move. In the overwhelming majority of instantaneous configurations, the distribution is neither symmetrical with respect to the mid-plane nor homogeneous along the vertical axis. An excess density of ions in some place leads to a deficit in other places. This generates strongly attractive electrostatic forces that may overcome the osmotic repulsion and are not taken into account in traditional double-layer theories.

correlated polarizations of the ionic clouds give rise to an ionic van der Waals type force, much in the same way as correlations between fluctuating electronic dipoles give rise to the London dispersion force. These attractive forces are not taken into account in the DLVO theory of colloid stability.

Ionic correlation forces increase as the surface charge density of the layers, and the charge of the interlayer ions, increase. Using Monte Carlo simulations, Pellenq and co-workers (Pellenq et al., 1997a, 1997b; Delville and Pellenq, 2000) carried out a systematic study of correlation forces in water between surfaces with a broad range of charge densities, within the framework of the so-called ‘primitive model’ (smooth surfaces separated by ions in a dielectric continuum). As expected, the attractive ion correlation forces are particularly strong when the CSH layers are fully ionized and separated by hydrated and mobile calcium ions. Attractive pressures as strong as 60 atm are obtained at an interlayer distance of 0.7 nm.

A different kind of attractive electrostatic interaction may appear when the ionic mobility vanishes. Just as the distribution of cations and anions in a NaCl crystal gives rise to a strong Madelung cohesive energy, the distribution of adsorbed, translationally immobile, charge-balancing ions in a narrow interlayer space may lead to a strong cohesive energy. A covalent contribution may also appear at small

counterion-surface distances. A correct modelling of this requires atomic level simulations, using either potential energy minimization or direct quantum methods.

The case of tobermorite-like CSH was recently considered (Gmira, 2003; Gmira et al., 2004). The *ab initio* quantum approach indicates that the attractive contribution of electronic dispersion interactions (van der Waals forces) is about 20% of the cohesion energy. Since the partial electronic charge on the atoms is independent of interlayer distance, the nature of the bonds between and within the layers remains unchanged. The ionic character of the bonds in the layers is close to 60%. The charge on the interlayer calcium ions is +1.38, which is slightly higher than for ions within the layers (+1.29), but still much lower than the value expected for a purely ionic bond. If the ions were totally hydrated and free to diffuse in an electric double layer, they would have a charge of +2. Furthermore, the distance between the interlayer calcium ions and the oxygen atoms of the layers is very close to the Ca–O distance within the layers (Fig. 13.3.5). This indicates that the interlayer calcium ions are linked to the layers by a strong ionic bond, with a significant covalent character.<sup>2</sup>

The potential energy (at 0 K), the free energy (at 300 K) and the derived interlayer pressure of the structure were also calculated as a function of the interlayer distance. A strongly cohesive behaviour is obtained with attractive pressures even higher than in the primitive model.

### 13.3.6. SUMMARY AND CONCLUSIONS

The results summarized here show that there is probably a conceptual continuity between the limited swelling of Ca-smectites and the strongly cohesive behaviour of hardened cement with particular reference to calcium silicate hydrate.

For cohesive forces at very short length scales, the hydration state of the interlayer cations and the possible specific interaction of these cations with surface sites are the key parameters. In equilibrium with humid air, the calcium ions in the interlayer space of smectites have a complete hydration shell and do not interact specifically with some surface sites of the clay mineral. In CSH, on the other hand, the interlayer calcium ions are partially dehydrated and interact specifically with  $\equiv\text{Si}-\text{O}^-$  groups of the short silica chains. This confers a partially covalent character to the bonding between the surface and the interlayer cation. In addition, it allows for a much stronger ‘surface–cation–surface’ ionic–covalent interaction.

As far as cohesive forces at somewhat larger (but still sub-nanometer) length scales are concerned, the ion correlation forces are the best candidates, both in clay minerals and in cement. However, they require mobile (i.e., exchangeable) cations.

---

<sup>2</sup>Calcium may be involved in partially covalent bonds. Even in CaO the bonding scheme is not 100% ionic. Pauling’s rule predicts that the Ca–O bond has 21% covalent character, which is not far from our estimate (30%). The electron density, calculated by Gmira, is too high for a purely ionic bond because of the inner-sphere character of the configuration. All inner-sphere complexes have a partially covalent character.

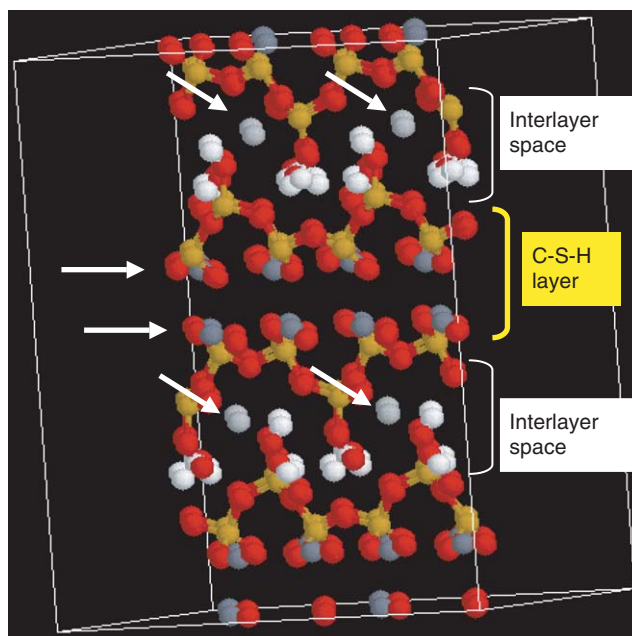


Fig. 13.3.5. A relaxed configuration of tobermorite-like CSH (Hamid's structure) after potential energy minimization, at  $\text{Ca/Si} = 0.83$  and four water molecules per unit cell in the interlayer space. The double plane of calcium ions in the central CSH layer is indicated by horizontal arrows. The hydrogen atoms of the water molecules, on each side of this layer, are in white. The interlayer calcium ions are in light grey and indicated by tilted arrows. Note the short distance between the interlayer calcium ions and the closest oxygen atom from the neighbouring layer, showing that the calcium ions form an inner sphere complex with the surface.

This requirement is clearly met by smectites but not by CSH. To be significant, ion correlation forces also require a high surface charge density. From that point of view, CSH is *a priori* favoured with respect to smectites. However, the extensive screening of surface charge by the specifically adsorbed cations may well reduce the effective surface charge of CSH to values that are not much larger than those of smectites.

A surprising feature is that, in spite of strong differences in cohesion, especially as far as short range cohesive forces are concerned, smectites and synthetic CSH (Fig. 13.3.2) form particles not vastly different from each other in thickness (typically from a few layers to a few tens). The lack of explanation for this observation in terms of surface forces (Sposito, 1992) shows that we are still largely disarmed by something as widespread and as apparently simple as the self-associating properties of layered minerals in water.

The relationship between local order and local cohesion, on the one hand, and macroscopic strength, on the other, is an open question. The lateral extension of



particles is definitely much larger in natural smectites than in the CSH of hardened cement. The connectivity between locally ordered regions is also much better in smectites. This is due to the large size and flexibility of individual smectite layers, allowing a single layer to participate in several particles. Yet, in spite of poorer order and poorer single layer connectivity, hardened cement has a tensile and compressive strength higher than that of clay minerals (at comparable porosity). What this observation suggests is that a quantitative description of defects is probably as important as the knowledge of order. This is not only valid for the comparison between cement and smectites, but also applies to comparing smectites exchanged with different cations (Zabat et al., 1997).

## REFERENCES

- Adenot, F., Auvray, L., Touray, J.C., 1993. Determination of the fractal dimension of CSH aggregates of different origins and compositions. *Comptes Rendus de l'Académie des Sciences*, Paris 317 series II, 185–189.
- Belloni, L., Spalla, O., 1997. Attraction of electrostatic origin between colloids. *Journal of Chemical Physics* 107, 465–480.
- Colombet, P., Grimmer, A.R., Zanni, H., Sozzani, P., 1998. Nuclear Magnetic Resonance Spectroscopy of Cement-Based Materials, Part II. Springer, Berlin, pp. 117–234.
- Cong, X., Kirkpatrick, R.J., 1996.  $^{29}\text{Si}$  MAS NMR study of the structure of calcium silicate hydrate. *Advanced Cement-based Materials* 3, 144–156.
- Craievich, A.F., 1987. SAXS study of the porous fractal structure of tricalcium silicate dry gels. *Journal of Applied Crystallography* 20, 327–329.
- Damidot, D., Nonat, A., Barret, P., Bertrandie, D., Zanni, H., Rassem, R., 1995.  $\text{C}_3\text{S}$  hydration in diluted and stirred suspensions. *Advances in Cement Research* 7, 1–8.
- Delville, A., Pellenq, R.J.M., 2000. Electrostatic attraction and/or repulsion between charged colloids. *Molecular Simulations* 24, 1–24.
- Ennis, J., Marcelja, S., Kjellander, R., 1996. Effective surface charge for symmetric electrolytes in the primitive model double layer. *Electrochimica Acta* 41, 2115–2124.
- Gatty, L., Bonnamy, S., Clinard, C., Feylessoufi, A., Richard, P., Van Damme, H., 2001. A transmission electron microscopy study of interfaces and matrix homogeneity in ultra-high-performance cement-based materials. *Journal of Materials Science* 36, 4013–4026.
- Gauffinet, S., Finot, E., Lesniewska, E., Nonat, A., 1998. Direct observation of the growth of calcium silicate hydrate on alite and silica surfaces by atomic force microscopy. *Comptes Rendus de l'Académie des Sciences*, Paris, Earth & Planetary Sciences 327, 231–236.
- Gauffinet, S., Finot, E., Nonat, A., 2000. Experimental study and simulation of CSH nucleation and growth. In: Nonat, A. (Ed.), *Hydration and Setting*. RILEM Publications S.A.R.L., Cachan, pp. 199–214.
- Gmira, A., 2003. Etude Texturale et Thermodynamique d'Hydrates Modèles du Ciment. Ph.D. thesis, University of Orléans, Orléans, France.
- Gmira, A., Zabat, M., Pellenq, R.J.-M., Van Damme, H., 2004. Microscopic physical basis of the poromechanical behavior of cement-based materials. *Materials and Structures/Concrete Science and Engineering* 37, 3–14.



- Gronbech-Jensen, N., Mashl, R.J., Bruisma, R.F., Gelbart, W.M., 1997. Counterion-induced attraction between rigid polyelectrolytes. *Physical Review Letters* 78, 2477–2480.
- Hamid, S.A., 1981. The crystal structure of the 11 Ångström natural tobermorite. *Zeitschrift für Kristallografie* 154, 189–198.
- Henderson, E., Bailey, J.E., 1988. Sheet-like structure of calcium silicate hydrate. *Journal of Materials Science* 23, 501–508.
- Jennings, H.M., 2000. A model for the microstructure of calcium silicate hydrate in cement paste. *Cement and Concrete Research* 30, 101–116.
- Jennings, H.M., Hsieh, J., Srinivasan, R., Jaiswal, S., Garci, M., Sohn, D., Hinnners, C., Heppner, S., Neubauer, C., 1996. Modelling and materials science of cement-based materials. In: Jennings, H., Kropp, J., Scrivener, K. (Eds.), *The Modeling of Microstructure and its Potential for Studying Transport Properties and Durability*. NATO ASI Series E: Applied Sciences, vol. 304. Kluwer Academic Publishers, Dordrecht, pp. 29–62.
- Kjellander, R., Marcelja, S., 1984. Correlation and image charge effects in electric double layers. *Chemical Physics Letters* 112, 49–53.
- Kjellander, R., Marcelja, S., 1986. Double-layer interaction in the primitive model and the corresponding Poisson-Boltzmann description. *Journal of Physical Chemistry* 90, 1230–1232.
- Kjellander, R., Marcelja, S., Pashley, R.M., Quirk, J.P., 1988a. Double-layer ion correlation forces restrict calcium-clay swelling. *Journal of Physical Chemistry* 92, 6489–6492.
- Kjellander, R., Marcelja, S., Quirk, J.P., 1988b. Attractive double-layer interactions between calcium clay particles. *Journal of Colloid and Interface Science* 126, 194–211.
- Larsen, A.E., Grier, D.G., 1997. Like-charge attractions in metastable colloidal crystallites. *Nature* 385, 230–233.
- Liebau, F., 1985. *Structural Chemistry of Silicates: Structure, Bonding, and Classification*. Springer, Berlin.
- Maggion, R., Bonnamy, S., Levitz, P., Van Damme, H., 1996. A scaling model of the microstructural evolution in  $C_3S/C-S-H$  pastes. In: Jennings, H., Kropp, J., Scrivener, K. (Eds.), *The Modeling of Microstructure and its Potential for Studying Transport Properties and Durability*. NATO ASI Series E: Applied Sciences, vol. 304. Kluwer Academic Publishers, Dordrecht, pp. 137–155.
- Merlino, S., Bonaccorsi, E., Armbrumster, T., 2001. The real structure of tobermorite 11 Å: normal and anomalous forms. *European Journal of Mineralogy* 13, 577–590.
- Nachbaur, L., Nkinamubanzi, P.C., Nonat, A., Mutin, J.C., 1998. Electrokinetic properties which control the coagulation of silicate cement suspensions during early age hydration. *Journal of Colloid and Interface Science* 202, 261–268.
- Neville, A.M., 1963. *Properties of Concrete*. Pitman, London.
- Nonat, A., Lecoq, X., 1998. The structure, stoichiometry and properties of C–S–H prepared by  $C_3S$  hydration under controlled conditions. In: Colombet, P., Grimmer, A.R., Zanni, H., Sozzani, P. (Eds.), *Nuclear Magnetic Resonance Spectroscopy of Cement-Based Materials*. Springer, Berlin, pp. 197–207.
- Pellenq, R.J.-M., Caillol, J.M., Delville, A., 1997b. Electrostatic attraction between two charged surfaces: a (N,V,T) Monte Carlo simulation. *Journal of Physical Chemistry* 101, 8584–8594.
- Pellenq, R.J.-M., Delville, A., Van Damme, H., 1997a. Cohesive and swelling behaviour of charged interfaces: a (N,V,T) Monte-Carlo study. In: McEnaney, B., Mays, T.J., Rouquerol, J., Rodriguez-Reinoso, F., Sing, K.S.W., Unger, K.K. (Eds.), *Characterization of Porous Solids IV*. The Royal Society of Chemistry, Cambridge, pp. 596–603.

- Plassais, A., Pomiès, M.P., Lequeux, N., Korb, J.P., Petit, D., Barberon, F., Bresson, B., 2005. Microstructure evolution of hydrate cement pastes. *Phys. Rev. E*, 041041.
- Pointeau, I., 2000. Etude mécanistique et modélisation de la rétention de radionucléides par les CSH des ciments. Ph.D. thesis, University of Reims-Champagne-Ardenne, Reims, France.
- Powers, T.C., 1958. Structure and physical properties of hardened Portland cement paste. *Journal of the American Ceramic Society* 41, 1–6.
- Richardson, I.G., 1999. The nature of C–S–H in hardened cements. *Cement and Concrete Research* 29, 1131–1147.
- Richardson, I., Groves, G.W., 1992. Models for the composition and structure of calcium silicate hydrate (CSH) gel in hardened tricalcium silicate pastes. *Cement and Concrete Research* 22, 1001–1010.
- Sposito, G., 1992. The diffuse-ion swarm near smectite particles suspended in 1:1 electrolyte solutions: modified Gouy-Chapman theory and quasicrystal formation. In: Güven, N., Pollastro, R.M. (Eds.), *Clay-Water Interface and its Rheological Implications. CMS Workshop Lectures*, vol. 4. The Clay Minerals Society, Boulder, CO, pp. 127–155.
- Taylor, H.F.W., 1986. Proposed structure for calcium silicate hydrate gel. *Journal of the American Ceramic Society* 69, 464–467.
- Taylor, H.F.W., 1993. Nanostructure of CSH: current status. *Advanced Cement-Based Materials* 1, 38–46.
- Taylor, H.F.W., 1997. *Cement Chemistry*, 2nd edition. Thomas Telford Publishing, London.
- Terrasse-Viallis, H., Nonat, A., Petit, J.C., 2001. Zeta potential study of calcium silicate hydrate interacting with alkaline cations. *Journal of Colloid and Interface Science* 244, 58–65.
- Van Damme, H., 2002. Colloidal chemo-mechanics of cement hydrates and smectite clays: cohesion vs swelling. In: Hubbard, A. (Ed.), *Encyclopedia of Surface and Colloid Science*. Marcel Dekker, New York, pp. 1087–1103.
- Viehland, D., Li, J.-F., Yuan, L.-J., Xu, Z., 1996. Mesostructure of calcium silicate hydrate (CSH) gels in Portland cement paste: short-range ordering, nanocrystallinity, and local compositional order. *Journal of the American Ceramic Society* 79, 1731–1744.
- Winslow, D., Bubowski, J., Young, J.F., 1995. The fractal arrangement of hydrated cement paste. *Cement and Concrete Research* 25, 147–156.
- Yu, P., Kirkpatrick, R.J., Poe, B., McMillan, P.F., 1999. Structure of calcium silicate hydrate (CSH): near-, mid- and far-infrared spectroscopy. *Journal of the American Ceramic Society* 82, 742–748.
- Zabat, M., Vayer, M., Harba, R., Bonnamy, S., Van Damme, H., 1997. Surface topography and mechanical properties of smectite films. *Progress in Colloid and Polymer Science* 105, 96–102.
- Zhang, X., Chang, W., Zhang, T., Ong, C.K., 2000. Nanostructure of calcium silicate hydrate gels in cement paste. *Journal of the American Ceramic Society* 83, 2600–2604.

This page intentionally left blank

## *Chapter 14*

# GENESIS OF CLAY MINERALS

E. GALÁN

*Departamento de Cristalografía, Mineralogía y Química Agrícola, Facultad de Química, Universidad de Sevilla, ES-41071 Sevilla, Spain*

The origin of clay minerals is an important topic for applied clay scientists to consider. Clay minerals formed in diverse environments under varying temperature and pressure conditions may exhibit different properties. The crystallochemical make up, the physical and physico-chemical properties, and the technical behaviour of a kaolin formed in one environment, for example, may be considerably different from a kaolin formed in another. The special properties of clays are origin dependent. Knowledge of clay genesis can also contribute to the exploration and selective mining of the clay materials most appropriate for specific industrial requirements.

Clays occur in many different geological environments: weathering crusts and soils, continental and marine sediments, volcanic deposits, geothermal fields, wall-rock alteration produced by intrusion of plutonic rocks and hydrothermal fluids, and very low-grade metamorphic rocks. Clay minerals mostly form from pre-existing minerals, primarily from rock-forming silicates by transformation, and/or neof ormation, where rocks are in contact with water, air, or steam.

As Konta (1992) stated ‘everything starts in weathering crust’. While many common igneous and metamorphic rock-forming silicates are destroyed by weathering processes, phyllosilicates, quartz, and some heavy minerals are highly resistant, and in this environment the crystallization and growth of clay minerals are favourable. Erosion, transportation, and deposition of these weathering crusts in lakes, seas, and oceans, lead to sedimentary sequences where clay-sized material, composed mainly of phyllosilicates and Fe-hydr(oxides), makes up about 50% of the volume of sedimentary rocks (Taylor, 1952). The phyllosilicates are mostly composed of clastic (inherited) muscovite, biotite, and chlorite, with small amounts of kaolinite, smectites, and vermiculite produced in soils and weathering crusts, or after deposition in the new environment.

The clay minerals formed in the weathering crust should be considered stable under supergene conditions. In many cases, however, they are metastable needing more time to reach equilibrium with ambient conditions; in other cases, their transformation into stable forms is not thermodynamically and/or kinetically possible.

If these new clay minerals can be reasonably considered stable in the supergene environment, and erosion, transportation, and post-depositional processes have not basically modified them, then sedimentary records can be used for paleoclimatic interpretations (Millot, 1964; Singer, 1979–1980, 1984; Galán, 1986; López Aguayo, 1990).

However, transportation, deposition, burial, and diagenesis of the weathered materials usually change the physico-chemical properties of clay minerals, and even influence their transformation into other clay minerals.

Clay formation and evolution are distinctive events in the geological history of a basin. Source area, transport, depositional environment of clays, and the transformation and diagenetic changes are fundamental for analysis of sedimentary basins (Chamley, 1989; Merriman, 2002, 2003). Clay minerals are particularly sensitive to pressure and temperature variations and to the chemical environment. This sensitivity is expressed in terms of their chemistry and mineralogy. The study of clay minerals can therefore provide information about the processes that occur during the evolution of the series of which they form a part. Following Millot (1964) clay minerals in a sedimentary basin can be neoformed (i.e., by direct precipitation or via the ageing of X-ray amorphous materials), inherited from the source area and transported with little modification, or transformed (i.e., derived from inherited clay minerals in response to environmental reactions).

During transformation, the essential silicate structure of the clay mineral is largely maintained although the interlayer space can be greatly modified due to changing composition of the tetrahedral and octahedral sheets. Millot (1964) distinguished between ‘degradation’ and ‘aggradation’ in the transformation process. The conversion of illite to smectite (illite → vermiculite → smectite) is an example of degradation since it involves a depletion of K and other elements, while the reverse transformation is one of aggradation because it involves the addition of various elements. Degradation is characteristic of rocks and soils weathering, while aggradation is very rare in such environments although it probably occurs in burial diagenesis.

Hydrothermal alteration of some volcanic and plutonic rocks can also give rise to massive accumulation of clays. The intrusion of plutonic rocks, on the other hand, leads to wall-rock alteration and transformation of some rock-forming minerals into clayey material, along with the neoformation of many other minerals, including phyllosilicates. As the transformed and neoformed minerals occur sequentially from the contact towards the coldest part of the host rock in different assemblages, they can be used as geological thermometers. Their geochemistry can be a good indicator of the composition of the intrusive material and associated ores.

In summary, clays can be used in interpreting and understanding geological processes, such as environmental conditions of sedimentary facies, zonation, stratigraphic correlations, source area of sediments, weathering and hydrothermal alterations, diagenesis, and low-grade metamorphism (i.e., Weaver, 1960; Keller, 1970; Singer, 1979–1980; Galán, 1982, 1986; Henley, 1985; Ortega-Huertas et al., 1991;

Konta, 1992; Chamley, 1993; Essene and Peacor, 1995; Hillier, 1995; Pletsch et al., 1996; Gutierrez-Mas et al., 1997; Środoń, 1999; Carretero et al., 2002; Merriman, 2002).

## 14.1. GEOLOGICAL ENVIRONMENTS FOR CLAY FORMATION

### 14.1.1. Weathering

The weathering environment is usually subaerial. It involves physical disaggregation and chemical decomposition, leading to the transformation of original minerals into clay minerals. The factors controlling rock weathering include: rock type, climate (rainfall: a chemical factor, and temperature: a physical factor), time (the age of the weathering profile), topography (affecting the ratio of water to rock through drainage), and the presence of organisms and organic matter. The chemical composition of the weathered rock and the water/rock ratio are the principal factors determining the type of clay minerals formed (Fig. 14.1), while temperature and time influence the rate of chemical processes (Velde, 1992; Foley, 1999).

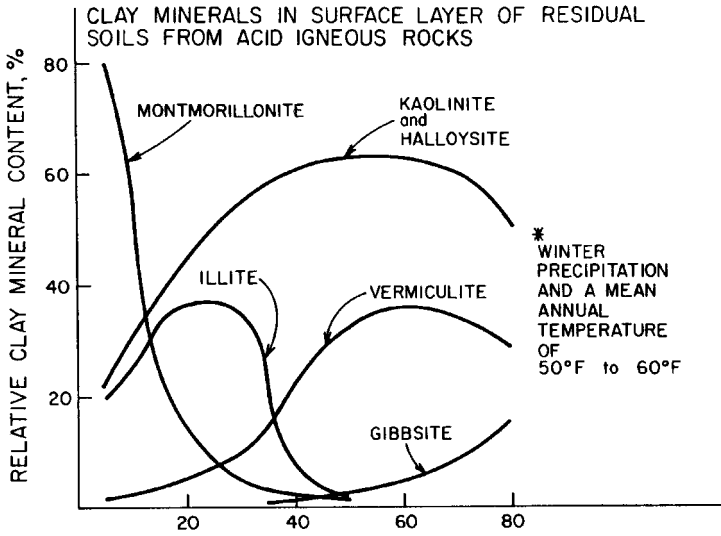
Weathering of non-sedimentary rocks commonly produces either of two clay minerals: kaolinite and dioctahedral smectite. These species are thermodynamically stable with respect to the chemical composition of near-surface pore waters. The chemical composition of this water is determined by the interplay between rainfall, drainage rate, chemical composition, and dissolution rate of the parent rock. These clay minerals and the degradation products of the micaceous rock-forming minerals (i.e., illite) constitute the bulk of the weathering products by volume (Velde, 1992).

On a global scale the clay distribution depends on the prevailing climatic conditions, because these determine the weathering intensity (Millot, 1979). In cold (polar) climates illite and chlorite are favoured, while in mild climates vermiculite and mixed-layer structures are the most frequently formed clay minerals. In tropical zones and Mediterranean climates with seasonal contrast, smectites are favoured, and finally under wet tropical and equatorial climatic conditions kaolinite and Al-Fe (hydr)oxides are the main clay mineral components of soils. This simple and attractive zonation scheme based on the present-day clay mineral distribution is not true in detail, because the other factors cited above have an influence that often disturb this generalized distribution of clay minerals.

In fact, stable isotope studies on kaolinites from weathering profiles in Australia, India, and South America shown that kaolinite is formed under cold climates. Chivas and Bird (1995) suggested that Permian kaolins of Australia are formed from glacial melt waters. Thus, the presence of a kaolinite weathering crust by itself can no longer be interpreted as being indicative of tropical weathering.

Velde (2001) shown that the clay minerals formed from different starting mineral assemblages (fine-grained phyllosilicates) in the uppermost horizons of agricultural soils, under similar geomorphologic and climatic conditions, consist of two

A)



B)

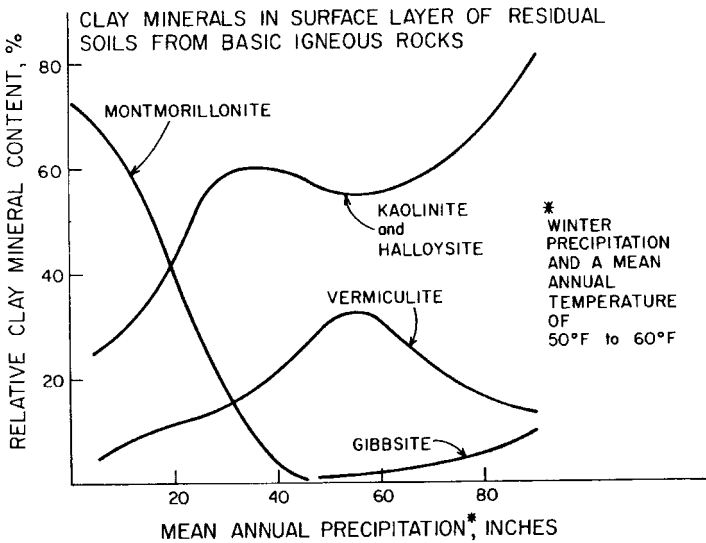


Fig. 14.1. The effect of mean annual precipitation (1 inch = 25.4mm) on the frequency distribution of clay minerals and gibbsite in the surface layer of residuals soils from acid (A) and basic (B) igneous rocks in California. After Barshad (1966).

disordered illite–smectite minerals. One of these has about 50% smectite layers; the other has 20% smectite and is less abundant. Both types co-exist in the same horizon, with beidellite and montmorillonite as the expanding layers. Smaller amounts of illite, kaolinite, and vermiculite are also present, but rarely chlorite. Irrespective of climate (continental) and parent material, a convergence in mineralogy towards mixed-layer phases seems to occur. That is, there is a tendency towards the same chemical and mineralogical equilibrium, be it metastable or not. Nevertheless, the clay minerals along a soil profile often show great diversity because of the complex transformation and reaction processes that operate with increasing depth.

In the weathering environment, most clays are formed by incongruent dissolution of unstable silicates. Reaction of the unstable mineral with less soluble compounds can produce new clay minerals. Direct precipitation from solution can also give rise to neoformed clay minerals with compositions that are very different from those of the (dissolved) parent minerals. Eventually, a clay mineral can become unstable because of intense drainage, forming oxides and liberating most ions.

Hydrolysis generally involves the exchange of protons from the solution for soluble mono- and divalent cations in the minerals. Thus, the flow rate and acidity of water play a key role in the formation of clay minerals. In a soil profile developed under high rainfall, kaolinite is found in the upper part, while montmorillonite commonly occurs in the lower part of the weathering profile, and closer to the rock where the accumulation of leached ions can produce more chemically complex clay minerals. Leaching is stronger when the topography is smooth or plain, and kaolinite can predominate in soils of slight slope, while smectites are dominant in soils formed in depressions (Kantor and Schwertmann, 1974).

In the classic example of granite weathering, a large part of the soils consists of metastable muscovite, biotite, and chlorite. These minerals alter progressively into clay minerals. Muscovite is degraded into illite, and both minerals can transform into regular or random illite–smectite (I/S) mixed-layer minerals. Biotite and chlorite transform into smectite through the formation of a regular mixed-layer phase containing biotite and smectite, or chlorite and smectite. Corrensite, a 1:1 chlorite–saponite mixed-layer mineral, is very common in soils. In many cases all these primary minerals (muscovite, biotite, chlorite) can be transformed into vermiculite. When rainfall is high, muscovite and biotite eventually transform into kaolinite in the upper part of the profile. Like the micas, plagioclase and orthoclase are also destabilized and transform into kaolinite and some illite. Kaolinite decreases towards the lower part of the alteration profile, while illite, I/S mixed-layer minerals, vermiculite, and neoformed clay minerals (smectites) tend to increase with depth. This evolution pathway also typifies the weathering of gneisses, and other types of aluminous pelitic rocks.

In basic rocks, smectites (Fe-beidellite, nontronite) and vermiculite can form from Ca-plagioclases, amphiboles, and pyroxenes. Depending on the Al content, minor amounts of kaolinite may be formed. On ultrabasic rocks, saponite, serpentine, chlorite, and talc are the most frequent phyllosilicates derived from pyroxenes and



olivine. Nevertheless, under a tropical climate, kaolinite can be the major clay mineral formed from basalt (Siefferman and Millot, 1969), anorthosites (Gomes et al., 1994), or gabbros (Galán et al., 1996) by hydrothermal or weathering alteration.

The weathering of quartz–chlorite schists can produce a complex sequence of clay minerals starting from chlorite and finishing with kaolinite. In the host rock of uranium ore deposit at Koongarra, Australia, Murakami et al. (1996) observed the following weathering sequence: (i) chlorite; (ii) chlorite–vermiculite intergrade; (iii) interstratified chlorite and vermiculite; (iv) vermiculite; and (v) kaolinite.

A special case of weathering takes place when eruptive rocks react with sea water in a deep ocean environment. Basalt, the most frequent rocks found in ocean floors, are hydrolyzed to form clays on the floor surface. These clays contain much Fe, and become progressively enriched in alkaline elements at lower temperatures. Clay mineral formation begins below 30 °C, with saponite forming at high, and Fe-rich beidellite and celadonites at intermediate temperatures.

The genesis of the various clay minerals found in specific weathering profiles remains to be resolved in detail. The multitude of factors involved in this environment are responsible for many variations in weathering sequence and the crystallochemical properties of the intermediate and end member products. However, some generalization is possible.

Illite and other micaceous minerals are inherited from parent rocks or other materials, where they form under different P–T conditions from those existing at the earth's surface (Fanning et al., 1989). The formation of illite by a pedogenic process is possible but it is very rare (Wilson, 1999). The formation of illite from micaceous minerals involves cleavage of the relatively thick, micro-size mica particles with a full content of K into very thin particles depleted in K (illite) (Roberts et al., 1991; Romero et al., 1992). The majority of micaceous soil clays are dioctahedral and aluminous, although some rare trioctahedral illites, derived from biotite, do exist.

Smectite formation in soils takes place when the following factors come together: base-rich parent rocks, poor drainage, low-lying topography, high pH, high silica activity, and abundance of basic cations (Table 14.1) (Keller, 1970; Borchardt, 1989). These conditions can occur under very different climates (temperate, cold, or even tropical) when leaching is limited. Soil smectites consist principally of dioctahedral montmorillonite and beidellite that are somewhat enriched in Fe as compared with their ideal compositions (Wilson, 1987a). They are also somewhat different from the smectites in bentonite deposits. This might be because the chemical variability is higher in the weathering environment than during bentonization since the smectites in most soils can be inherited, transformed, and neoformed (Table 14.2). Smectites of different composition may crystallize locally in microenvironments from different parent materials (Aoudjit et al., 1995). The illite-to-smectite transformation seems to be a simple degradation process but illitization of smectite ('aggradation') in weathering environments is not fully understood.

Vermiculite is very common in soils and weathering profiles developed on acidic and basic rocks. Vermiculite seems to be formed by the weathering of micas, mainly

Table 14.1. Geological environment of primary-stage montmorillonitization (Keller, 1970)

A. Retention of $Mg^{2+}$ , $Ca^{2+}$ , $Fe^{2+}$ , $Na^{+}$			
a. Evaporation exceeds precipitation, as semi-arid climate			
b. Ineffective leaching			
Stagnant water and water logging			
Ash in lakes and marine basins			
Low effective permeability of rocks			
c. Alkalinity			
d. $Fe^{2+}$ not combined with $O^{2-}$ or $S^{2-}$			
e. Silicates characterized by			
High specific surface, as for volcanic ash			
High susceptibility to hydrolysis			
B. Retention of silica			
a. Flocculated by $Ca^{2+}$ , $Mg^{2+}$ , and other cations			
Rock rich in $Ca^{2+}$ , $Mg^{2+}$ , and $Fe^{2+}$			
b. Ineffective leaching			
c. Clay-size cristobalite			
C. Retention of parent texture and mineralogy			
a. Shards or flow			
b. Igneous-type minerals			

Table 14.2. Abundance of smectites in soils as assessed from the literature (Wilson, 1999)

Soils	Inheritance	Neoformation	Transformation
Entisols	+++	+++	+
Aridisols	+++	+++	—
Inceptisols	+++	+++	+++
Vertisols	+++	+++	+
Mollisols	+	++	++
Alfisols	+	+++	++
Spodosols	—	+	+++
Ultisols	+++	+	—
Oxisols	—	—	—

+++ major importance, ++ moderate importance, + minor importance, — no importance.

from biotite (trioctahedral vermiculite), involving the release of interlayer  $K^+$ , and the oxidation of structural  $Fe^{2+}$  (Vicente-Hernández et al., 1983). Soil vermiculite may also derive from muscovite (dioctahedral vermiculite) but this transformation was not well understood until the application of high-resolution transmission electron microscopy (HRTEM). Aoudjit et al. (1996) presented HTREM images of the vermiculitization of muscovite in an acidic soil, showing particles with a muscovite core and a vermiculite rim consisting of about 15 layers. Very fine-grained muscovite particles of high specific surface area and reactivity seem necessary for transformation into vermiculite in soil. The degradation of chlorite by decomposition of the interlayer hydroxide sheet is another means of obtaining vermiculite (Makumbi and Herbillon, 1972; Ross and Kodama, 1976).

Chlorite is an inherited clay mineral in soils and weathering crusts. This layer silicate is easily weatherable and transformable into regularly interstratified chlorite-vermiculite and vermiculite (Proust, 1982; Buurman et al., 1988). Chlorite can also be formed pedogenically by the intercalation of Al (hydr)oxides into pre-existing smectite, vermiculite, or interstratified expansible minerals. The source of the interlayer Al is the degradation of both the tetrahedral and octahedral sheets of layer silicates, weathering of Al-minerals (i.e., feldspars), or decomposition of organic matter containing adsorbed Al. Like smectite and illite, chlorite is very sensitive to acidification. In soils affected by 'acid rain' or acidified surface water, trioctahedral chlorite is destroyed in the E horizons, illite transforms into vermiculite via regularly interstratified illite-vermiculite, interlayer hydroxy-Al sheets are liberated (particularly in B horizons), and poorly ordered material (probably allophane) is precipitated in B horizons (Wilson, 1987b). Galán et al. (1999) shown that acid mine drainage is responsible for the progressive degradation of chlorite in the basin of the Tinto River (Spain).

Kaolinite can be a neoformed, transformed, or inherited mineral in soils. As already mentioned, high rainfall and a temperate climate can transform muscovite and biotite into kaolinite together with some illite. Al-(hydr)oxides liberated by extensive leaching can react with silica to produce kaolinite under slightly acidic conditions ( $pH \approx 5$ ), and when silica activity is moderate and the concentration of basic cations is low. Keller (1970) summarized the general conditions for the weathering formation of kaolinite (Table 14.3). Like kaolinite that derives from weathering, soil kaolinite is usually highly disordered and may contain  $Fe^{3+}$  from isomorphous substitution. In some cases, it is also interstratified with smectites (Linares and Huertas, 1971; La Iglesia and Van Oosterwyck-Gastuche, 1978; Herbillon et al., 1981; Dixon, 1989).

Halloysite occurs frequently as a neoformed mineral in weathering crusts developed on acidic volcanic rocks (Siefferman and Millot, 1969). Under supergene conditions halloysite can transform into kaolinite according to the sequence: disordered halloysite  $\rightarrow$  ordered halloysite  $\rightarrow$  metahalloysite  $\rightarrow$  disordered kaolinite  $\rightarrow$  ordered kaolinite (Ponder and Keller, 1960; Chem, 1969). As La Iglesia and Galán (1975) shown, this process is one of recrystallization, requiring the presence of organic

Table 14.3. Geological environment for primary kaolinitization (Keller, 1970)

A. Removal of $\text{Ca}^{2+}$ , $\text{Mg}^{2+}$ , $\text{Fe}^{2+}$ , $\text{Na}^{+}$ , $\text{K}^{+}$	
a.	Precipitation exceeds evaporation
b.	Permeable rocks
c.	Percolating water
d.	Oxidation of $\text{Fe}^{2+}$ to $\text{Fe}_2\text{O}_3$ or $\text{FeS}_2$
B. Addition of $\text{H}^{+}$	
a.	Fresh water
b.	Acids
	Sulphur compounds
	Carbonic, air and soil atmosphere
	Organic, living and dead organisms
C. High Al:Si ratio	
a.	Removal of silica
	Na and K silicates
	Organic complexes
b.	High concentration of Al
	$\text{Al}^{3+}$ in acid solution
	Al–OH polymers

acids. Kaolinite can also transform into halloysite (Singh and Mackinnon, 1996; Bobos et al., 2001).

Palygorskite and sepiolite, the fibrous clay minerals in soils and paleosols, are generally neoformed (Singer, 1979). The instability of these minerals in wet climates favours their presence in soils under dry or semi-dry climates. The occurrence of palygorskite in soils is associated with one of the following conditions: (i) in modern soils that, at present or in the past, were affected by rising ground water of pH 7–8 and abundant salinity; (ii) in soils with distinct and sharp textural transitions because these minerals accumulate in the coarse fraction (this group includes many paleosols); and (iii) in calcretes, caliches (Singer, 1984). In all these cases, palygorskite (and very rarely sepiolite, when Al is absent or immobilized (Jones and Weir, 1983)) is precipitated by evaporation of the vadose water. Cemented soils (duricrusts) can be caused by palygorskite (palycretes), or by silica (silcretes) and calcite (calcretes) (Rodas et al., 1994). The transformation of smectite into palygorskite was described in terms of a dissolution–precipitation process (Jones and Galán, 1988), or

transformation through kerolite–smectite mixed-layer minerals (Eberl et al., 1982). The transformation of smectite and illite to palygorskite was verified by Suarez et al. (1995), López Galindo et al. (1996), and Sánchez and Galán (1995). Palygorskite is more easily formed in weathering environments than sepiolite, or else sepiolite is less stable under supergene conditions, and hence is rarer. Traces of palygorskite found in some arid soils are considered as inherited (Shadfan and Dixon, 1984; Mackenzie et al., 1984).

In summary, we can say that under weathering conditions most common rock-forming silicates (except quartz) are destroyed, and practically all clay minerals can form. Illite derives from micaceous minerals and feldspars, chlorite can be inherited or formed from biotite. Kaolinite can be neoformed, or derived from muscovite and feldspars, and more rarely from smectite or vermiculite. Vermiculite comes from muscovite/biotite and chlorite through interstratified structures. Smectite can form directly by alteration of basic silicates (pyroxenes, amphiboles), or from illite and/or vermiculite. Palygorskite can be directly precipitated under certain climatic conditions, or formed from smectite and illite. Sepiolite seldom forms in soils. The complexity of the systems is very large and not all the possibilities were yet demonstrated. Some of the most frequent pathways are illustrated in Fig. 14.2.

#### 14.1.2. Sedimentation

Ancient sedimentary rocks are composed of about 70% mudstones (containing about 50% clay-size particles) and shales (Blatt et al., 1980). Presently, sedimentary environments that contain muds cover about 60% of marine continental shelves and 40% of deep ocean basins (Hillier, 1995). Continental aquatic environments such as lakes, rivers, estuaries, and deltas also contain high proportions of clays. The amounts and varieties of clay minerals found in sediments and sedimentary rocks are a direct result of source area differences, changes occurring during transport and deposition, and changes taking place after sedimentation (diagenesis).

The erosion of soils is governed by the profile structure, the humidity, the clay content, the slope, and the climatic conditions. A well-developed soil is more sensitive to erosion, because it shows a thick upper zone where clays predominate and which can be easily removed. The finest particles of the profile (mostly clay minerals) are most easily transportable. On the other hand, clays can contain significant amounts of adsorbed water, providing protection against erosion by sudden abundant rainfall, which is the principal erosion factor.

Clay transportation mainly occurs by water flow (stream, river), but the timespan of this transport is very short and has practically no influence on clay alteration. The deposition zone spreads from the mouth of rivers to lagoons, lakes, seas, and oceans, producing a particle-size fractionation from the mouth to the interior, together with different mineral settings. According to Parham (1966), the order of the first appearance of major clay mineral groups from shoreward to basinward areas is as follows: kaolinite, illite, chlorite, palygorskite, and sepiolite. Montmorillonite and

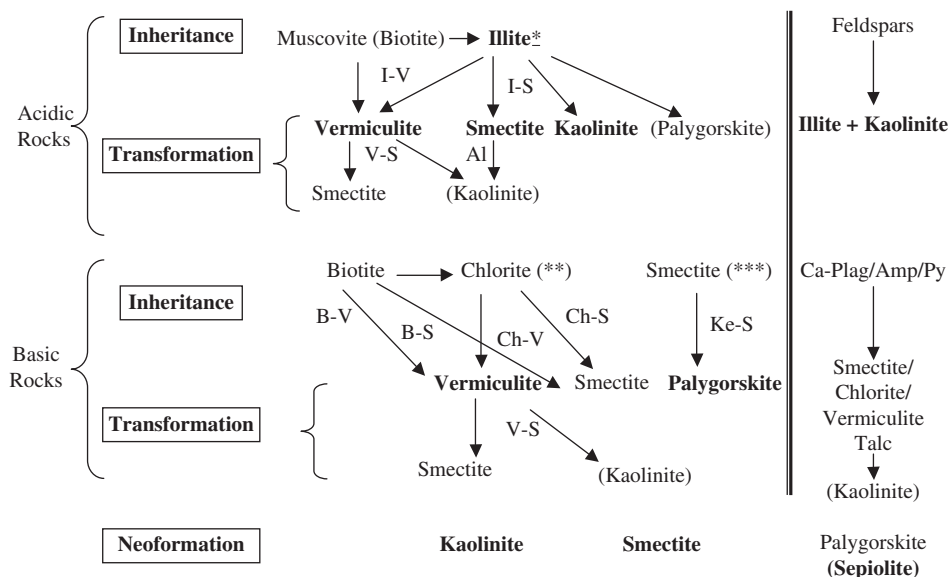


Fig. 14.2. Pathways for the formation of clay minerals in weathering environment from different starting materials. Minerals in bold type indicate the most probable end products. In brackets are minerals that do not form easily according to that pathway, or are rare. Clay minerals derived from other rock-forming silicates could be formed by transformation and/or neoformation. (\*) Illite can be considered inherited in soils, and as the first degradation product of muscovite, (\*\*) Chlorite may be inherited or transformed from biotite, (\*\*\*) Smectite may be inherited in soils. Also some palygorskite may be inherited in soils.

I/S mixed layered minerals are present over the entire range. This approach continues to be true in the most cases, except for the fibrous clay minerals (specially sepiolite). On the other hand, salinity changes can also produce coagulation processes affecting some clay minerals. A typical clay mineral distribution found from the coastline to the open sea is: kaolinite → illite → smectite.

After deposition the interstitial water solution in the sediment has a higher ionic concentration than that in the weathering profile, leading to a change in chemical equilibrium. The chemical potential of the elements in solution is different from that for clay formation in the continent, and clays react with the environment solution. The time of connection between the sediment pore water and water reservoir can be very long or very short depending on sediment accumulation rates. Typical reactions are clay-clay, and clay-(hydr)oxide transformations with chemical contribution from the sedimentary solution. The new phases formed depend on the redox potential of the ambient solution which is partly controlled by organic matter, and partly by living organisms at the water/sediment interface. For example, microbial action can change the oxidation state of Fe, or stabilize sulphides, and hence control the

availability of certain elements that clays can fix. This early post-deposition changes are usually termed 'early diagenesis'.

In general, clay minerals of sedimentary sequences (in areas not subject to tectonic activity) mainly reflects the climate, relief, and lithology of source areas. However, in zones of intense tectonic activity (flysch) the clay mineral assemblages in sediments can reflect the composition of the parent rocks because tectonic activity prevents the formation of soils in the continent. The rapid transport of material by turbidity currents with high solid concentrations does not produce well-sorted sediments; rather, the sediments usually have a grain-size distribution similar to that of the parent suspensions (Ruiz Cruz, 1999). The mineralogy of recent sediments in coastal shelves and estuaries is generally consistent with terrigenous origin, that is, from soils and weathered rocks of the hinterland (Chamley, 1989). Sometimes a particular mineral can be an indicator of continental origin. For example, sediments from the Galician Coast of Spain contain significant amounts of gibbsite, a common constituent of soils found in weathering profiles of this region (Belzunce-Segarra et al., 2002).

In continental-shelf and deep-sea sediments the bulk of the clay fraction is detrital (Kastner, 1981; Chamley, 1993) but some of the smectites, I/S mixed-layer minerals, glauconite, and berthierine are neoformed by alteration of volcanic material, and by low-temperature interaction between X-ray amorphous hydr(oxides) and biogenic silica.

Certain clay minerals formed in marine environments can serve as paleoenvironmental indicators. For example, both glauconite and berthierine are typical marine clay minerals formed from pre-existing clays (kaolinite, smectite, and iron oxides, at temperature around 4 °C) by diffusion of ions in the solid state and then recrystallization. Berthierine does not incorporate  $K^+$  as does glauconite, but takes up large amounts of  $Fe^{2+}$  and  $Fe^{3+}$ . The geological environment of both minerals seems to be different. Glauconite occurs in a calmer ambient situation (shallow shores of oceanic platforms) than berthierine.

Glauconization is analogous to illitization. It involves a gradual alteration of neoformed Fe-rich smectite into Fe-illite, similar to celadonite, through intermediate mixed-layer structures. Glauconitization is complete when the layers no longer expand and the  $K_2O$  content increases to 9%, which requires about 1 Ma (Odin, 1988).

Transformations of detrital clay minerals at the bottom of seas and oceans include the formation of Al-smectites, showing that these minerals can be stable in this environment. In addition, devitrification of volcanic materials in the deep ocean environment yields new crystalline phases, such as smectites and zeolites.

Palygorskite of detrital origin can also be found in oceans, having come from the continent, as in the case of deep-sea Atlantic palygorskite close to Morocco, which was transported by SW winds from near-shore shallow African basins into the ocean (Pletsch et al., 1996). Palygorskite can also be derived from smectite by diagenetic transformation in the marine environment (López Galindo, 1986), sometimes associated with marine phosphorites (Chahi et al., 1999). Sepiolite can also be of

diagenetic origin through the transformation of magnesite at pH 10.5–11.5 in silica-rich lake waters (Ece, 1998). However, most of the palygorskite and sepiolite in the world are neoformed (precipitated) in lacustrine and peri-marine environments. Although these minerals can be derived from other clay minerals, the most common mechanism is crystallization from solution, promoted by the presence of amorphous silica. Experiments by Birsoy (2002) indicated that low aqueous Al-activities favour sepiolite and kerolite relative to palygorskite and saponite.

In some shallow restricted basins with evaporitic conditions fibrous clay minerals and  $\text{Mg}^{2+}$ -rich smectites (saponite, stevensite, kerolite) can form authigenic minerals, usually together with sulphate and carbonate minerals. In this environment smectite can also be transformed into palygorskite (Sánchez and Galán, 1995). In a typical playa-lake sequence, from the basin edge to the centre, detrital minerals (illite, kaolinite, smectite) dominate at the lake edge, palygorskite with some  $\text{Al}^{3+}$ -smectite near the shore, while sepiolite and other  $\text{Mg}^{2+}$ -clay minerals abound towards the centre.

In summary, we can say that sedimentary basins are repositories of clay minerals, forming part of the clay cycle (weathering → deposition → diagenesis/metamorphism → magmagenesis). The clay minerals can be formed by neoformation (i.e., direct precipitation from solution or through ageing of amorphous materials, such as glassy volcanic ash), inheritance (i.e., transported from the source to the basin with little modification), and transformation (i.e., when neoformed and inherited clays in the basin react by diagenesis and low-grade metamorphism). Basins formed at active plate tectonic margins tend to have a greater diversity of clay origins than at passive margins or within-plate basins (Fig. 14.3).

#### 14.1.3. Burial Diagenesis and Low-Grade Metamorphism

When sedimentary clays are buried, free or weakly bonded water is eliminated. As a result, the porosity decreases from 80% to about 20% at the first kilometer of burial. As depth increases, sediments tend to reach a global chemical equilibrium and new phases can form under the new environmental conditions. The unstable phases tend to disappear and the number of species diminishes. The reactions are mostly of the clay–clay and clay–solution types with time and temperature being the principal factors governing the transformations. The new minerals are more highly ordered and of large size than their original minerals.

After the disappearance of most inherited soil clay minerals, new clay minerals are formed: I/S- and chlorite–smectite mixed-layer minerals, chlorite, kaolinite together with zeolite, some quartz, and feldspars. In general, illite is the most common diagenetic product, and I/S mixed-layer minerals are the main indicator of diagenetic evolution of a sedimentary basin (Dudek and Środoń, 2003).

The last stage of diagenesis is the beginning of metamorphism (anchimetamorphism) when most of the interstratified clay minerals and kaolinite are destroyed, resulting in an illite–chlorite facies with pyrophyllite, biotite, and paragonite.



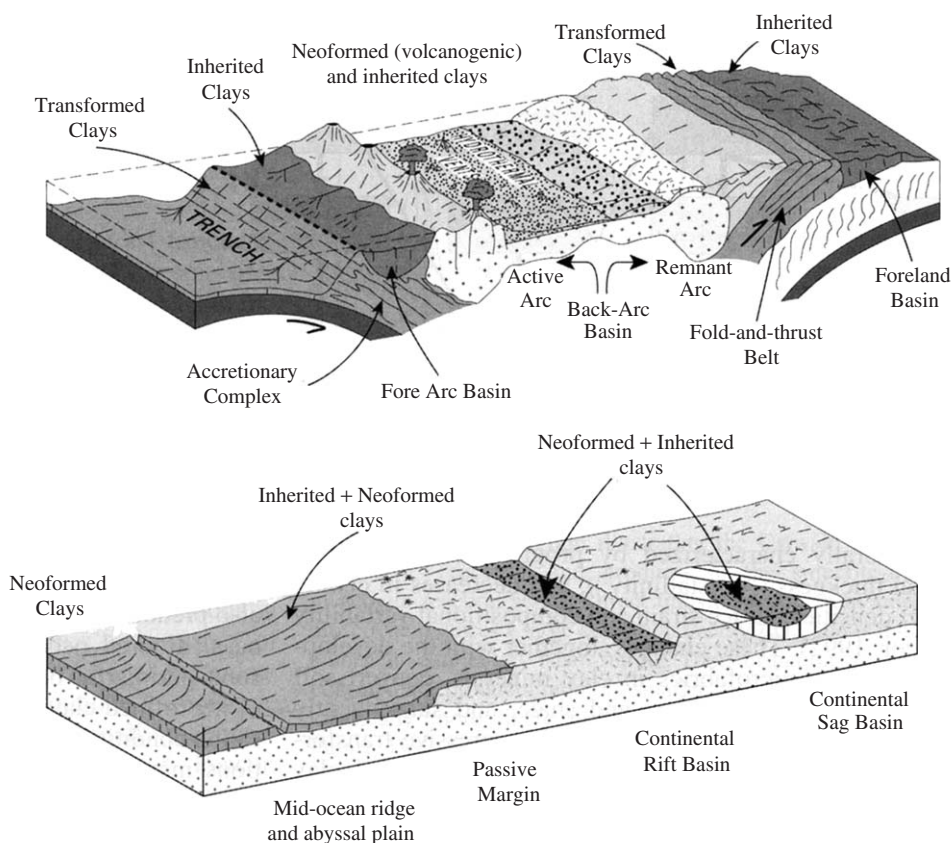


Fig. 14.3. Characteristic modes of origin of clays in sedimentary basins at an active plate margin (above), and a passive margin and within-plate setting (below). From Merriman (2003).

Typical low-grade metamorphic rocks derived from the clay sediments are pelitic rocks (slates), mainly composed of mica (or illite), chlorite, alkali feldspar and quartz, with some pyrophyllite, and/or paragonite. Shales are gradually transformed into phyllites, and with increasing metamorphism, into schists. Phyllosilicate particles become too large to be considered clay minerals, although they can be similar crystallochemically.

Perhaps the most significant mineral change on burial diagenesis is the gradual loss of expandable minerals, mainly the transformation of  $\text{Al}^{3+}$ -smectite into illite through I/S mixed-layered structures. The change occurs step-by-step. The first one is the random interstratification of smectite with illite (Reichweite,  $R = 0$ ), and composition ranging from pure to 50% smectite. The 50% I/S mixed-layer structure is a regular interstratification of good stability. The last stage is the formation of illite

showing a gradual increase of particle thickness, and a decrease in particle defect density, lattice strain, and compositional variability (Peacor, 1992). The evolution of dioctahedral clay minerals during diagenesis is smectite  $\rightarrow$  random I/S  $\rightarrow$  ordered I/S  $\rightarrow$   $1M_d$  illite  $\rightarrow$   $2M_1$  muscovite.

The transformation of smectite to illite ('illitization') occurs when the sediment containing I/S mixed-layer minerals is progressively buried in the basin, and the proportion of illite layers increases. Potassium ions required for the illitization are supplied mainly from the alteration of  $K^+$ -feldspar within the sandstones, and from mica within the shales (Furlan et al., 1996). In this sense the transformation of smectite to illite seems to occur through a continuous series of interstratified I/S minerals. However, in the Nankai Trough, Site 808 (an accretionary wedge where the Philippine plate subducts the Eurasian plate) Masuda et al. (2001) observed that (i) authigenic  $K^+$ -rich smectite of high Fe-content forms directly as an alteration product of volcanic glass at a depth of  $\approx 500$  m below the seafloor with no intermediate precursor; (ii) smectite is largely replaced by I/S minerals with Reichweite  $R = 1$  and minor illite and chlorite over a depth of 500–700 m below the seafloor. Most smectite and I/S minerals are derived from glass alteration, rather than detrital as usually assumed; and (iii) I/S minerals with discrete layer sequences ( $R = 1$ ) and illite co-exist, indicating discontinuities of the transformation from smectite to illite. This observation is similar to that of Dong et al. (1997), who observed packets from Gulf Coast and other shales dominated by smectite, I/S minerals with  $R = 1$  ( $\approx 50\%$  illite), or illite. Thus, the smectite to illite transformation is not simple and several mechanisms are possible.

On the other hand, Środoń (1999) used the concept of 'fundamental particles' to interpret illitization. This concept was first proposed by McHardy et al. (1982) and further developed by Nadeau et al. (1984). Środoń suggested that the entities that evolve during illitization are not mixed-layer crystals but fundamental particles.

The existence of interstratified I/S minerals in the diagenetic environment was demonstrated by TEM, in apparent opposition to the 'fundamental particle' theory. Thus, Nieto et al. (1996) were able to show by TEM the co-existence of chlorite, calcite, and two I/S mixed-layer minerals ( $R = 1$  with 50% of illite layers and  $R > 3$  with more than 90% illite), both thermodynamically incompatible, over distances of  $< 100$  nm (Fig. 14.4). This assemblage suggests that the evolution of smectite to illite is an Ostwald-type ripening process (Morse and Casey, 1988) in which phases reach equilibrium through progressive steps, with less heterogeneity and closer to the stable phases.

Therefore, two mechanisms of smectite-to-illite transformation are possible (i) through dissolution-recrystallization without involving mixed-layer minerals (Inoue and Kitagawa, 1994; Clauer et al., 1997; Środoń, 1999; Środoń et al., 2000) mostly applicable to bentonite transformation and (ii) through I/S mixed-layer phases (Eberl and Środoń, 1988; Inoue et al., 1988; Christidis, 1995; Nieto et al., 1996), applicable to shales and some hydrothermally altered bentonites. Mechanism (ii) involves solid-state layer-by-layer transformation, including random interstratification, transition to ordered mixed-layer minerals, and development of long-range order (Bethke and Altaner, 1986).

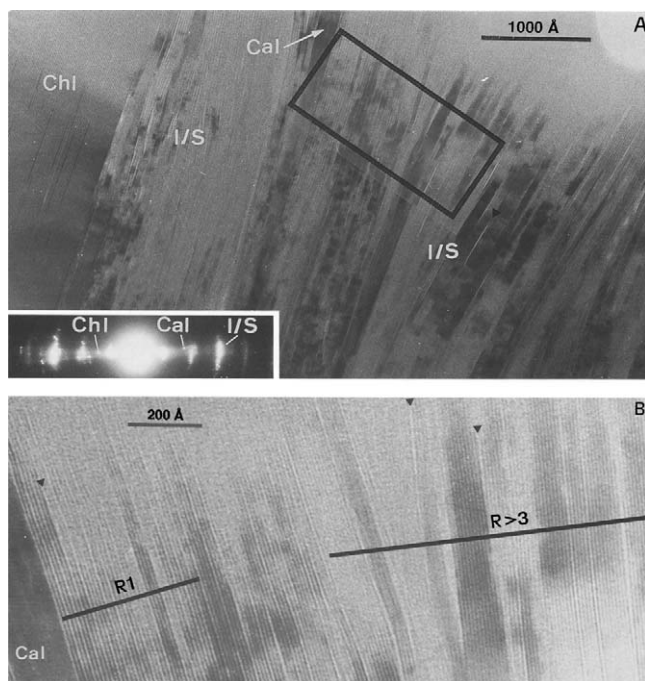


Fig. 14.4. (A) TEM image of a sample UG-17 including chlorite, I/S mixed-layer minerals with  $R = 1$  and  $R > 3$ , and calcite. (B) lattice fringe image of the area marked in (A) showing well-defined individual packets of I/S minerals with  $R = 1$  and  $R > 3$ . From Nieto et al. (1996).

Another interesting finding, illustrating the structural and chemical heterogeneity of these I/S mixed-layer minerals, and their evolution in a basin, was described by Drits et al. (2002). In oil-source shales from the North Sea (Upper Jurassic), oil generation takes place simultaneously with diagenetic transformation of I/S. A link between these two reactions can be the following:  $\text{NH}_3$  released during maximum oil generation is fixed as  $\text{NH}_4^+$  cations in the  $\text{NH}_4^+$ -bearing mica (tobelite) layers formed from smectite or vermiculite layers of I/S minerals. This process leads to the formation of four-component illite–tobelite–smectite–vermiculite (I-T-S-V) minerals in a diagenetic interval, called ‘tobelitization window’. Drits et al. (2002) also found that the amount of tobelite layers and fixed  $\text{NH}_4^+$  increased with diagenesis, while the amount of  $\text{K}^+$  fixed in the I/S mixed-layer minerals as well as the proportion of  $\text{K}^+$ -bearing illite layers remained constant, irrespective of sample location and depth and degree of diagenetic transformation. They concluded that in these oil-source shales, diagenesis is accompanied not by smectite illitization, as is generally the case, but by smectite (or vermiculite) tobelitization. The constant proportion of illite layers and the constant number of cations are considered as evidence of solid-phase transformation of the I-T-S-V because any other mechanism would destroy this

constancy. Tobelization of smectite in I/S minerals is probably typical of all oil-source shales.

Contemporaneous with the smectite-to-illite transformation, significant chlorite is formed from smectite (through loss of  $\text{Fe}^{3+}$  and  $\text{Mg}^{2+}$ ) or kaolinite (by diffusion of  $\text{Fe}^{3+}$  and  $\text{Mg}^{2+}$  in the structure). The change of trioctahedral smectite to chlorite in a Mg-rich environment can give a mixed-layer structure of the corrensite type.

During burial diagenetic I/S transformation,  $\text{Mg}^{2+}$  cations can also be fixed in the smectite layers. The formation of brucite-like sheets can give rise to an I/S-dioctahedral chlorite structure (tosudite) (Lindgreen et al., 2002). Later diagenesis may lead to neoformation of tosudite and trioctahedral chlorite-berthierine.

Diagenetic changes convert muds into lithified mudrocks, that is, mudstone  $\rightarrow$  shale  $\rightarrow$  slate. The clay mineral reactions approach chemical equilibrium through intermediate metastable products. Reactions rates in clays heated by igneous intrusion temperatures are many orders of magnitude faster and promote direct transformation of smectite to muscovite without intermediate phases (Merriman, 2002).

Clay mineral reactions require relatively small activation energies because the new minerals formed have similar compositions and structures to the reactants. As a result, they can form sequences of reactants and products or reaction series (Merriman and Peacor, 1999). Fig. 14.5 shows the reaction series recognized in British Lower Paleozoic mudrocks (Merriman and Roberts, 1985, 2001; Fortey, 1989; Roberts et al., 1990, 1991), according to the basic phyllosilicate structure and

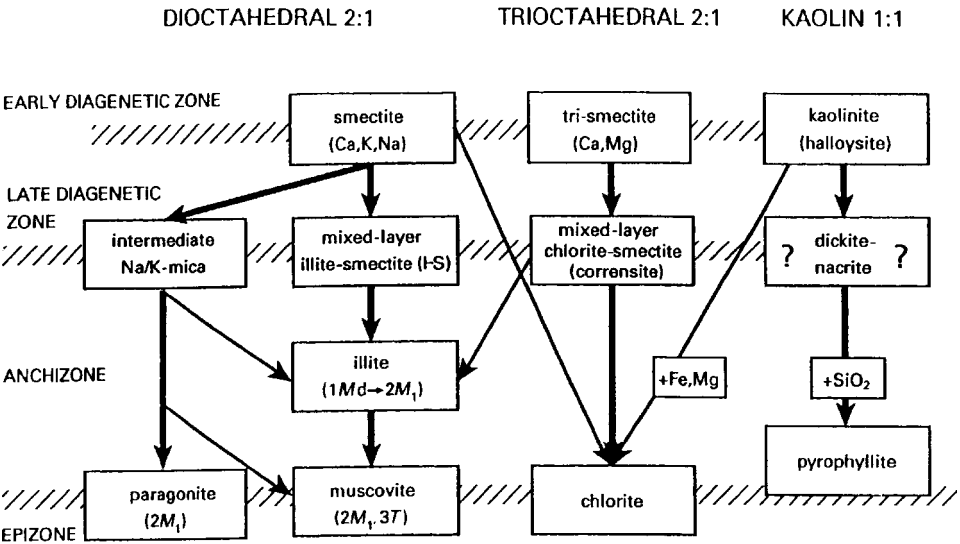


Fig. 14.5. Clay mineral reaction series observed in British Lower Paleozoic slate belts. Reaction proceeds from top to bottom, indicated by heavy arrows. Diagonal arrows indicate products contributed from one series to another. From Merriman (2002).

increasing diagenetic-metamorphic conditions. For 2:1 dioctahedral clay minerals, the series includes basically the smectite illitization, and considering the Na/K ratio, this series evolves to muscovite ( $K^+$ ) or paragonite ( $Na^+$ ). For the 2:1 trioctahedral clay minerals ( $Ca^{2+}$ ,  $Mg^{2+}$  smectites), the smectite chloritization is the fundamental transformation, usually through corrensite. Finally, for the most simple clay minerals, 1:1 dioctahedral ones (kaolinite), the basic transformation is the formation of more ordered polytypes (mainly dickite), and the possibility of pyrophyllite formation in the anchizone–epizone conditions. These series described for the British Lower Paleozoic were also recognized in other belts, that is, in the Cantabrian Cordillera (Spain) (Galán and Aparicio, 1980).

Clay mineral assemblages found in slates can also be related to the geotectonic setting and thermal history of the basin (Merriman, 2002). Extensional basins are characterized by high-heat flow ( $> 35^\circ C/km$ ) and hydrothermal activity, and tend to have a greater diversity of transformed clay minerals containing both  $K^+$ - and  $Na^+$ -rich products of the 2:1 dioctahedral reaction series. Pyrophyllite, rectorite, corrensite, and paragonite can be recognized but kaolinite is rare. In contrast, clay assemblages that evolve in convergent low-heat flow basins generally contain fewer mineral species, simply  $K^+$ -white mica and chlorite, and  $Na^+$ -mica and pyrophyllite are rare or absent. In extensional basins  $Na^+$  ions may come from low-temperature mixing of hydrothermal fluids and sea water. Such fluids are unavailable in convergent basins because of a lack of volcanic activity.

Over the last few decades, clay mineral assemblages and some parameters, such as the Kübler index for illite, smectite–illite reactions, chlorite composition, and the Arkay index for chlorite, were used as geothermometers and geobarometers for assessing the conditions in basins that were submitted to burial diagenesis and very low-grade metamorphism. However, as Essene and Peacor (1995) pointed out, the use of such systems and parameters does not provide accurate geothermometers because most of them are not based on equilibrium reactions.

Recent research demonstrated that most clay minerals are out of equilibrium with their environment. Clay mineral transformations are equivalent to Ostwald-ripening steps, driven by the potential for minimum free energy, and clay minerals may reach equilibrium only in very low or low-grade metamorphism. The application of clay mineral assemblages is based on physical calibration as observed for natural clay-bearing systems. The repeatability of clay mineral assemblages in space and time, as a function of increasing P–T conditions, is often assumed to imply equilibrium. However, this observation is not evidence for equilibrium although it is a necessary condition (Essene and Peacor, 1995). Most clay mineral associations are metastable, and the chemical reaction kinetics depend on a great variety of parameters and circumstances, such as time, fluid/rock ratio, tectonic history (deformation), starting material, pressure, and temperature.

On the other hand, ‘retrograde’ reactions can occur where I/S mixed-layer minerals form by replacement of metamorphic illite (Jiang et al., 1990), smectite derives from chlorite (Nieto et al., 1994), or smectite and highly expandable I/S minerals from illite (Zhao et al., 1999).

Another interesting formation of clay minerals in this environment is due to the devitrification of volcanic ash, leading to the formation of massive smectite (bentonite). The process seems to consist of slow ionic diffusion caused by a slow burial rate, and hence a low compaction rate in an open chemical system. In many bentonite beds I/S mixed-layer minerals with high  $K^+$  content are found in contact with the enclosing sedimentary rock, indicating that the diffusion process gradually transforms smectite into I/S mixed-layer minerals over a long period of time.

A special case of great practical interest is the formation by diagenesis of clay minerals in sandstone pores. Connected pores in sandstone create permeability. Since sandstones can serve as possible hydrocarbon reservoirs, porosity and permeability are two important factors. Both parameters can decrease due to the diagenetic formation and growth of clays in pores and in the passages connecting them, hindering the passage of fluids and reducing the economic value of the reservoir. Kaolinite is the most frequent clay mineral formed, often as vermicular 'books' of stacked layers but I/S interstratified clay minerals, berthierine, and lath-shaped illite are also common.

Diagenetic kaolinite can form by flushing sandstones with meteoric water. Kaolinite-feldspar assemblages are stable until 120–140 °C and react to form illite. Huang et al. (1986) confirmed the role of fluid/rock ratio in altering feldspars into kaolinite or illite. Ehrenberg et al. (1993) and Ruiz Cruz and Andreo (1996) documented the kaolinite→dickite transition at  $\approx 120^\circ\text{C}$ .

According to Beaufort et al. (1998) the kaolinite-to-dickite reaction proceeds by gradual structural changes concomitant with crystal coarsening and a change from booklet to blocky morphology (Fig. 14.6). The crystallization of dickite follows two different pathways: (i) accretion of new material from the dissolution of unstable kaolinite particles and/or detrital minerals, or coarser metastable kaolinite and (ii) neoformation of ordered dickite by dissolution–crystallization process. They suggest that the kaolinite-to-dickite reaction has a petrogenetic significance, useful for reconstructing the burial diagenesis of sedimentary basins, and for petroleum and gas exploration.

Lanson et al. (2002) reviewed the authigenic minerals formed in sandstones during burial diagenesis. While early precipitation of kaolinite is generally related to flushing by meteoric waters and as a consequence of feldspar dissolution in an open system, subsequent diagenetic kaolinite-to-dickite transformation probably results from invasion by acidic fluids of organic origin. This conversion is kinetically controlled and dickite is the most stable polytype in sandstone. However, dickite is not formed exclusively by diagenetic transformation of kaolinite. It can also form from dissolution of  $K^+$ -feldspars and other Al-rich silicates with increasing temperature, probably in the presence of organic acids. On the other hand, illite crystallization at the expense of kaolinite implies that an energy barrier is overcome either by an increase in  $K^+/H^+$  activity ratio in solution or by a temperature increase. Illitization of kaolinite is not necessarily coupled to dissolution of K-feldspars as usually described, but a potassium source is required.



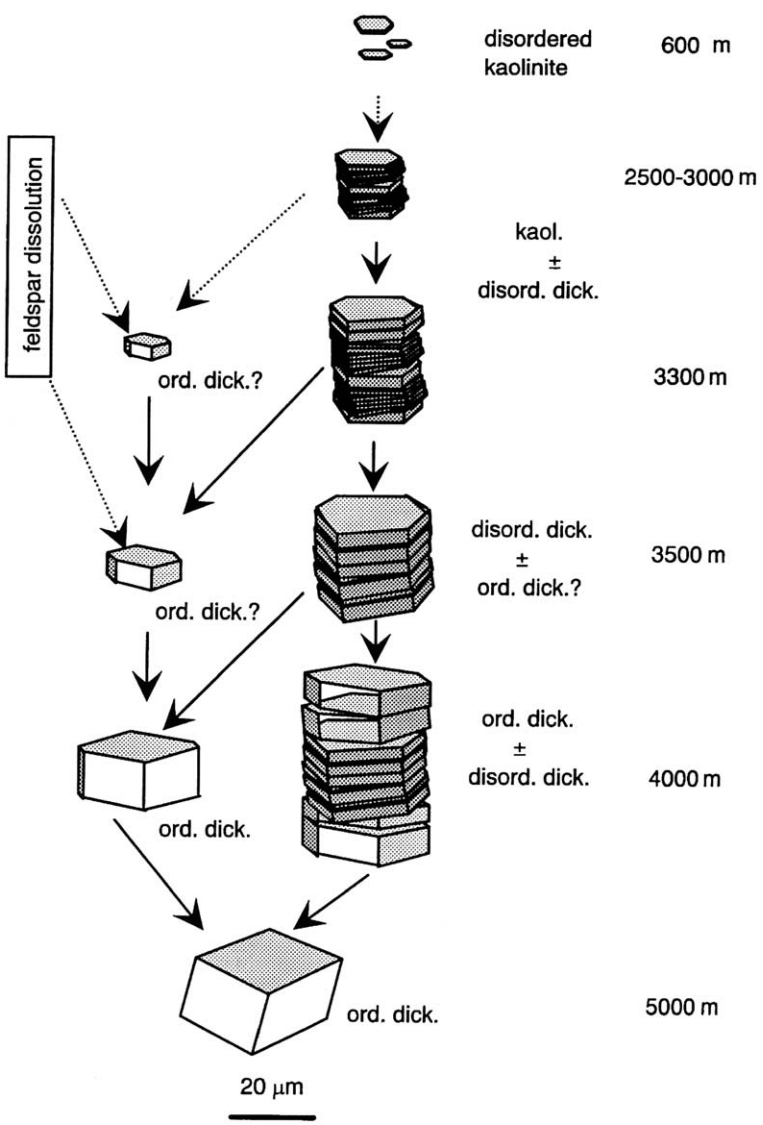


Fig. 14.6. Schematic model of the kaolinite-to-dickite reaction involving both morphological and structural changes as a result of water-rock interaction for increasing burial depths in sandstone reservoirs. Arrows indicate the transfer of matter due to material redistribution involved in the dissolution-crystallization processes. After Beaufort et al. (1998).

In summary, we can say that early burial diagenesis and the passage to low-grade metamorphism (anchimetamorphism) transform clay minerals into other minerals until environmental equilibrium is reached. Typical clay minerals formed during diagenesis are the I/S interstratified minerals, which are intermediate phases in smectite illitization. This transformation was studied in much detail, because the reaction can induce petroleum migration and build up geopressures by liberating water from smectite interlayers. Soluble  $\text{SiO}_2$ ,  $\text{Fe}^{3+}$ , and  $\text{Mg}^{2+}$  liberated during illitization may cause cementation in the pores of sedimentary rocks (see [Altaner and Bethke \(1988\)](#) and references therein). With increasing burial other phyllosilicates can be formed, such as pyrophyllite and paragonite. These minerals are in metastable equilibrium with I/S mixed-layer minerals in the anchimetamorphism zone. Chlorite can also be formed from smectite or kaolinite. The first stage of transformation can give rise to corrensite. On the other hand, massive smectite can be formed from the devitrification of volcanic ash.

Kaolinite is a typical clay mineral formed in sandstone pores by direct precipitation. At 120–140 °C it can transform into illite (by reaction with feldspars) or dickite. Dickite can also form directly from dissolution of feldspars ([Lanson et al., 2002](#)).

XRD was fundamental to following the evolution of clay minerals in a basin as a function of depth, time, and tectonics. The application of other instrumental techniques, notably HRTEM, provided much valuable information, and novel insights into clay mineral formation and transformation. More studies are still necessary, in particular, on the relationship between these processes and their geotectonic setting ([Merriman, 2002](#)).

#### 14.1.4. Hydrothermal Alteration

As mentioned before, intrusion of plutonic rocks and the deposition of volcanic events lead to wall-rock alteration and transformation of some rock-forming minerals into clayey materials. Clays can be genetically associated with late-stage deposits (chloritization), pegmatites, albitite-greissen deposits (muscovitization, chloritization), and hydrothermal veins. The veins are most important because crystal-chemical variations of clay minerals are particularly related to the fluid composition and controlled by the type of altered rock.

Hydrothermal alteration involves water–rock interaction at temperature above  $\approx 50^\circ\text{C}$ . In general, the altered material forms at higher temperatures than those of the hydrothermal fluids, hence the minerals are unstable in the presence of water at the temperatures considered. The fluids are aqueous and contain gaseous components and dissolved materials.

Hydrothermal systems are open to components where convecting fluids produce maximum water/rock ratios, and depths may be shallow ([Henley, 1985](#)). Very different clay minerals may form at the same time, but at different temperatures. At 300–400 °C the clay alteration facies include sericite or mica, potassium feldspars and



chlorite, very similar to that of the greissen deposits. As temperature decreases illite and kaolinite predominate with some I/S mixed-layer minerals. At still lower temperatures smectite or kaolinite can be the most important clay minerals. The most striking examples of hydrothermal alteration are the production of pure kaolin and silica. These minerals can occur on the scale of kilometers, and are of economical interest.

In epithermal ore deposits, found in the upper ( $<1\text{--}2\text{ km}$ ) geothermal systems where predominantly meteoric fluids convect, interaction with the host rock takes place at temperatures of  $200\text{--}300^\circ\text{C}$ . In general, these systems are relatively short-lived, remaining active over periods of hundreds of thousands of years or less (Henley and Ellis, 1983). Nonetheless, interesting clay (e.g., kaolin) deposits can be produced.

The following three cases illustrate the diversity of clay minerals formed in this environment under the influence of altered rock type, P and T, and fluid chemistry.

In the Golden Cross epithermal Au–Ag deposit at Waihi, New Zealand hosted by andesitic and dacitic lavas, hydrothermal alteration of the rocks gives rise to quartz, adularia, calcite, clay minerals (chlorite, illite, kaolinite, I/S mixed-layer minerals, and smectite), and others. According to Tillick et al. (2001) all phyllosilicates are neoformed directly from the fluids. I/S mixed-layer minerals ( $R = 1$ ) and micas form simultaneously without intermediate series, as Masuda et al. (2001) observed for the burial diagenesis of mudstones. The illite content in the I/S minerals increases with depth and proximity to the central vein system. Smectites co-exist with ( $R = 1$ ), rather than ( $R = 0$ ), I/S minerals.

The second case is the hydrothermal alteration of bentonites of the Tsantili deposit in Milos Island, Greece. The original Wyoming-type montmorillonite was illitized along a 40 m vertical profile, forming I/S mixed-layer minerals with different proportions of expandable layers and different ordering (Fig. 14.7). The alteration is characterized by a massive incorporation of  $\text{K}^+$  and removal of  $\text{Si}^{4+}$ ,  $\text{Na}^+$ ,  $\text{Ca}^{2+}$ ,  $\text{Mg}^{2+}$ , and  $\text{Fe}^{3+}$  from the rock. The hydrothermal alteration is probably associated with the emplacement close to the parent bentonite of barite veins at  $<200^\circ\text{C}$ . Illitization is controlled by temperature,  $\text{K}^+$  availability, and fluid/rock ratio. It can be considered to be the result of  $\text{K}^+$ -metasomatism. As the potassium is derived from the dissolution of authigenic  $\text{K}^+$ -feldspar, the I/S mineral particles are apparently formed by solid-state transformation. According to Christidis (1995), the illitization and spatial distribution of expandable minerals could be used as a guide for the exploration of mineral deposits.

The third case concerns the intrusion of a magmatic rock in a sedimentary series, leading to contact metamorphism in the host rock. Subsequent hydrothermal alteration usually yields clayey materials. For instance, in the Priego de Córdoba area (Subbetic zone of the Betic Cordilleras, Spain), a lacolith of stratiform dolerite intruded marly sediments at quite shallow depths below the ocean floor during the intracontinental rifting phase. In the first stage, contact metamorphism caused crystallization of  $\text{Ca}^{2+}$ -silicates at about  $500^\circ\text{C}$ . During a process of hydrothermal alteration superimposed on the contact aureole, chlorite was formed in the area

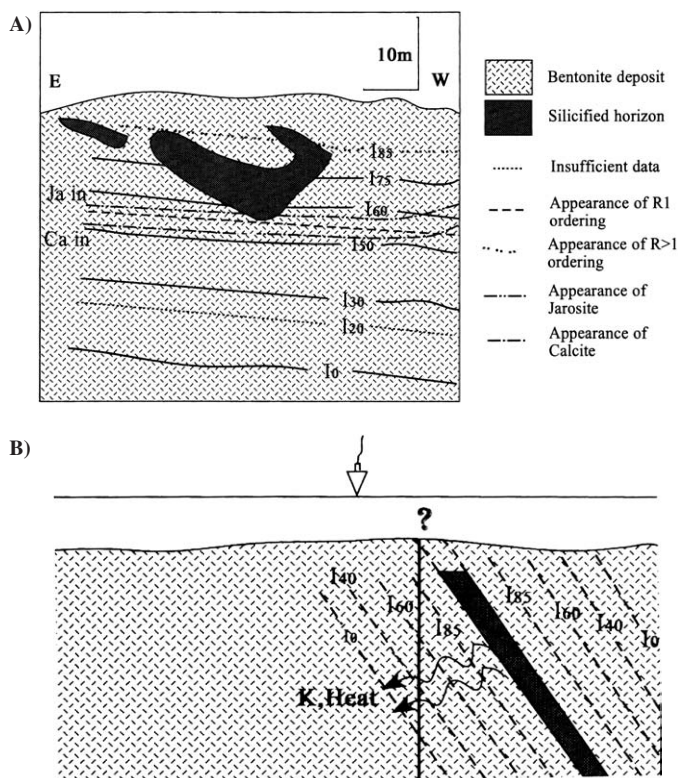


Fig. 14.7. (A) Schematic cross-section of the south sector of the Tsantili bentonite deposit (Greece). Ii ( $i = 0 - 85$ ) is the illite content of the I/S mixed-layer minerals. Ca in = presence of calcite incompatible with jarosite; Ja in = presence of jarosite incompatible with calcite; (B) Simplified model proposed for the illitization of Wyoming-type montmorillonite in the Tsantili deposit in relation to barite vein (vertical line represents the cross-section of (A)). K, Heat =  $K^+$  availability and temperature are decreasing from the deposit. After Christidis (1995).

closest to the volcanic rocks in a first step. In the zone farthest from the contact area corrensite was formed, but a later cooling phase led to crystallization of saponite in the host rock, and di- and trioctahedral smectites inside the volcanic rock (Abad et al., 2003). Temperature can decrease from  $\approx 300^\circ\text{C}$  (chlorite) to  $270\text{--}200^\circ\text{C}$  (chlorite-smectite interstratifications) in the prograde phase, and to  $180\text{--}130^\circ\text{C}$  (saponite) in the retrograde phase (Stakes and O'Neil, 1982; Dudoignon et al., 1997).

Deep-sea hydrothermal alteration is rather different from the alteration described above. Hydrothermal alteration in basic and acidic rocks tends to produce Mg- and Fe-free clay mineral assemblages, whereas alteration of deep-sea basalts at very low temperatures yields Fe-rich clays. With decreasing temperatures from  $\approx 300^\circ\text{C}$  the

sequence of clay minerals in the altered basalts is serpentine→saponite→celadonite→nontronite. The last mineral is found in the ‘weathering’ zone on basalts, that is, at the sea water–rock interface.

In summary, clay minerals formed by hydrothermal activity are not related to sedimentary layers or weathering crusts. In contrast with the other environment described, zonation from the heat source is a characteristic of this complex environment, which can be very variable over short distances. Clay minerals formed can have an economic interest, and a detailed study can provide information about their use as indicators for exploring ore deposits.

## 14.2. ORIGIN OF CLAY DEPOSITS OF ECONOMIC INTEREST

Commercial clays, that is, clays used as raw material in industry rank as the leading industrial rocks in both tonnages and total value. Clay is a rock historically linked to humans in their agricultural, industrial, and cultural development. It is a relatively abundant raw material with many different applications, encompassing a wide spectrum of products. These range from low-value materials, produced with a minimal degree of processing (e.g., certain plastic clays for bricks) to high added-value materials (e.g., refined kaolins for paper coating) (see Chapter 10.1). About 90% of production comprises building clays, or miscellaneous clays for structural products. Only 10% of deposits are largely composed of a clay mineral (kaolin, bentonite, fuller’s earths, etc.); these are generally referred to as ‘special clays’.

The origin of commercial clays is of great basic interest because the uncommonly massive concentrations of very pure clay material are produced under special conditions. Geological criteria shown by genetic studies can be used for the exploration and mining of new deposits.

Here we give a brief overview of the genesis of the principal clay deposits, other than structural clays. The latter are sedimentary formations (marine and continental) abundantly distributed throughout the world from the Carboniferous to the Cenozoic.

### 14.2.1. Kaolins

Kaolinite can be formed by weathering (residual kaolins) and hydrothermal activity (hydrothermal kaolin), or occur as an authigenic sedimentary mineral. Residual and hydrothermal kaolins, called primary kaolins, are formed *in situ* by surface and underground waters or hydrothermal fluids. Sedimentary kaolins, called secondary kaolins, are composed of kaolinized material from a source area that was eroded, transported, and deposited in a continental or coastal environment. Most kaolinites in sedimentary kaolins are formed before deposition, in a primary environment, but some can be authigenic after the deposition of the arkosic or sandy material, usually by the action of underground water.

Kaolinization by weathering involves an aqueous environment with pH between 6 and 4, annual temperatures between 15 and 20 °C, and precipitation > 1000 mm (climate close to the subtropical and tropical forested zones). Geomorphological conditions must be favourable for the permanent removal of  $K^+$ ,  $Na^+$ ,  $Ca^{2+}$ ,  $Mg^{2+}$ , and partly  $SiO_2$  by leaching. Deferration can also occur at about pH 3 or at higher pH if organic matter is present (Kuzvart, 1977).

The energetic conditions for kaolinization are satisfied either by long-term action of exogenous agents or by a fast action of low-temperature acidic hydrothermal fluids. The latter conditions are associated with post-magmatic processes, giving rise to ore-deposits. The two models of hydrothermal kaolin deposits are the Cornwall type and the arc-island type (Harvey and Murray, 1997). In the latter case, heating comes from cooling of a deep pluton, or from a magmatic source close to the surface (kaolin deposits of Japan and of Mexico). When the hydrothermal activity originates from convective circulation of underground water (heated by radioactive disintegration in granite), the kaolin formed follows the Cornwall pattern (Dewu and Durrance, 1993). Temperature is higher in the arc-island than in the Cornwall pattern, and fluids can be more acidic.

#### 14.2.2. Bentonite

Smectites form in very different environments (soils, weathering crusts, oceans, hydrothermal activity) independent of geological age. However, bentonite deposits are mainly formed by alteration of volcanic rock or by direct precipitation (authigenesis) in alkaline continental basins.

In the first case, smectite can be formed by supergene or hydrothermal activity, most likely by a dissolution–precipitation mechanism with volcanic glass playing an important role (Caballero et al., 1992). In general, temperature and time enhances the formation of smectite, while  $Mg^{2+}$  controls its growth. In the absence of  $Mg^{2+}$ , smectite can form from glass by solid-state reaction; dioctahedral smectites, firstly  $Fe^{3+}$ -rich (nontronite) and subsequently  $Al^{3+}$ -rich (montmorillonite–beidellite) minerals are formed. In the presence of  $Mg^{2+}$  direct precipitation of saponite is more probable (Fiore et al., 2000).

Wyoming, Montana, and Arizona (Cheto) bentonites are produced by transformation of volcanic material (ashes, tuffs) to smectites. In the case of Wyoming bentonite, the alteration occurred in a Cretaceous marine environment practically contemporaneously with the deposition of rhyolitic material. Cheto bentonite also formed by transformation of a vitric ash of quartz–latitic composition deposited in ponds, in a non-marine Pliocene series (Bidahochi formation) (Grim and Güven, 1978; Moll, 1979).

Other deposits of bentonites are hydrothermally formed (Milos, Greece; Ponza and Sardinia, Italy; Oran, Algeria; Yamagata and Kitambuza, Japan). Bentonites from Cabo de Gata, Spain were produced by devitrification of Neogene andesites and rhyodacites through the action of hydrothermal fluids (75–100 °C), followed by the action of weathering water ( $\approx 40$  °C) (Leone et al., 1983; Caballero et al., 1985).

Grim and Güven (1978) also described bentonites formed from igneous rocks by 'deuteric alteration'. This process involves a reaction between primary magmatic minerals and water-saturated solutions that separate from the same magma body at a late stage of cooling. This bentonisation is difficult to differentiate from the hydrothermal process.

The direct precipitation of smectites in essentially continental basins is not very frequent. Saponite is formed, usually together with other  $Mg^{2+}$ -rich clay minerals (sepiolite, stevensite, palygorskite), as in the case of the Madrid basin bentonite (Pozo and Casas, 1999).

#### 14.2.3. *Palygorskite and Sepiolite*

The principal palygorskite deposits of Georgia and Florida, USA, formed in a Miocene peri-marine environment under shallow waters, mostly by smectite–palygorskite transformation, but detrital palygorskite from the continent is also present (Weaver and Beck, 1977).

In other cases, palygorskite is formed by transformation of basalts in an alkaline restricted marine environment (Dakar, Senegal) (Wirth, 1968) or by weathering (Decan, India) (Siddiqui, 1984).

Sepiolite is mainly formed by direct precipitation in saline lacustrine environments with other  $Mg^{2+}$ -rich clay minerals. The sepiolite deposits of the Madrid basin, the most economically important in the world, are of this type. Massive concentrations appear in several facies of the continental basin. In the arkosic facies (fringing alluvial fan areas) sepiolite occurs both in calcrete with the alluvium and in marginal ponds at the leading edges of alluvial fans. In the transition facies (mud flat-marginal lake complex) sepiolite occurs together with smectites, stevensite, and kerolite (Jones and Galán, 1988).

Other deposits, including those of Amargosa (Nevada) (Hay et al., 1986), Eskişehir (Ece and Çoban, 1994) and Denizli (Turkey) (Akbulut and Kadir, 2003), El Bur (Somalia) (Singer et al., 1998), Amboseli (Tanzania-Kenya) (Hay et al., 1995) were also formed in lacustrine environments (playa-lake type).

#### 14.2.4. *Summary*

Deposits of industrial clays may have complex origins. One deposit is not like another of the same material, but genetic integrative models can produce useful patterns for exploration purposes.

## REFERENCES

- Abad, I., Jimenez Millán, J., Molina, J.M., Nieto, F., Vera, J.A., 2003. Anomalous reverse zoning of saponite and corrensite caused by contact metamorphism and hydrothermal alteration of marly rocks associated with subvolcanic bodies. *Clays and Clay Minerals* 51, 543–554.

- Akbulut, A., Kadir, S., 2003. The geology and origin of sepiolite, palygorskite and saponite in the Neogene lacustrine sediments of the Serinhisar-Acipayam basin, Denizli, SW Turkey. *Clays and Clay Minerals* 51, 279–292.
- Altaner, S.P., Bethke, C.M., 1988. Interlayer order in illite/smectite. *American Mineralogist* 73, 766–774.
- Aoudjit, H., Elsass, F., Righi, D., Robert, M., 1996. Mica weathering in acidic soils by analytical electron microscopy. *Clay Minerals* 31, 319–332.
- Aoudjit, H., Robert, M., Elsass, F., Curmi, P., 1995. Detailed study of smectite genesis in granitic saprolites by analytical electron microscopy. *Clay Minerals* 30, 135–148.
- Barshad, I., 1966. Effect of a variation in precipitation on the nature of clay mineral formation in soils from acid and basic igneous rocks. In: Heller, L., Weiss, A. (Eds.), *Proceedings of the International Clay Conference, Jerusalem*, vol. 1. Israel Program for Scientific Translation, pp. 167–173.
- Beaufort, D., Cassagnabere, A., Petit, S., Son, B., Berger, G., Lacharpagne, J.C., Johansen, H., 1998. Kaolinite-to-dickite reaction in sandstone reservoirs. *Clay Minerals* 33, 297–316.
- Belzunce-Segarra, M.J., Wilson, M.J., Fraser, A.R., Lachowski, E., Duthie, D.M.L., 2002. Clay mineralogy of Galician coastal and oceanic surface sediments: contributions from terrigenous and authigenic sources. *Clay Minerals* 37, 23–37.
- Bethke, C.M., Altaner, S.P., 1986. Layer-by-layer mechanism of smectite illitization and application to a new rate law. *Clays and Clay Minerals* 34, 136–145.
- Birsoy, R., 2002. Formation of sepiolite-palygorskite and related minerals from solution. *Clays and Clay Minerals* 50, 736–745.
- Blatt, H., Middleton, G., Murray, R., 1980. *Origin of Sedimentary Rocks*, 2nd edition. Prentice-Hall, Englewood Cliffs.
- Bobos, I., Duplay, J., Rocha, F., Gomes, C., 2001. Kaolinite to halloysite-7 Å transformation in the kaolin deposit of São Vicente de Pereira, Portugal. *Clays and Clay Minerals* 49, 596–607.
- Borchardt, G., 1989. Smectites. In: Dixon, J.B., Weed, S.B. (Eds.), *Minerals in Soil Environments*, 2nd edition. Soil Science Society of America, pp. 675–727.
- Buurman, P., Meyer, E.L., van Wijk, J.H., 1988. Weathering of chlorite and vermiculite in ultramafic rocks of Cabo Ortegal, northwest Spain. *Clays and Clay Minerals* 36, 263–269.
- Caballero, E., Reyes, E., Delgado, A., Huertas, F., Linares, J., 1992. The formation of bentonite: mass balance effects. *Applied Clay Science* 6, 265–276.
- Caballero, E., Reyes, E., Huertas, F., Linares, J., 1985. Hydrothermal solutions related to bentonite genesis, Almería, SE Spain. First Italian-Spanish Congress, Seians di Vico Equene, Italia. *Mineralogica Petrographica Acta* 29A, 187–196.
- Carretero, M.I., Ruiz, F., Rodríguez Ramírez, A., Cáceres, L., Rodríguez Vidal, J., González Regalado, M.L., 2002. The use of clay minerals and microfossils in paleoenvironmental reconstructions: the Holocene littoral of Las Nuevas (Doñana National Park, SW Spain). *Clay Minerals* 37, 93–103.
- Chahi, A., Clauer, N., Toulkeridis, T., Bouabdelli, M., 1999. Rare-earth elements as tracers of the genetic relationship between smectite and palygorskite in marine phosphorites. *Clay Minerals* 34, 419–427.
- Chamley, H., 1989. *Clay Sedimentology*. Springer, Berlin.

- Chamley, H., 1993. Le sédimentation marine des minéraux argileux. In: Paquet, H., Clauer, N. (Eds.), *Sédimentologie et Géochimie de la Surface. Colloque à la mémoire de George Millot Les Colloques de l'Académie des Sciences et du Cadast, Institute de France*, pp. 217–241.
- Chem, P., 1969. Occurrence and genesis of kaolin minerals from Taiwan. Part I: Kaolinite, halloysite and allophane. *Proceedings of the Geological Society of China* 12, 30–48.
- Chivas, A.R., Bird, M.I., 1995. Paleoclimate from Gondwanaland clays. In: Churchman, G.J., Fitzpatrick, R.W., Eggleton, R.A. (Eds.), *Clays: Controlling the Environment. Proceedings of the 10th International Clay Conference, Adelaide, Australia, 1993*. CSIRO Publishing, Melbourne, pp. 333–338.
- Christidis, G.E., 1995. Mechanism of illitization of bentonites in the geothermal field of Milos Island, Greece. Evidence based on mineralogy, chemistry, particle thickness and morphology. *Clays and Clay Minerals* 43, 569–585.
- Clauer, N., Środoń, J., Francu, J., Sucha, V., 1997. K–Ar dating of illite fundamental particles separated from illite-smectite. *Clay Minerals* 32, 181–196.
- Dewu, B.B.M., Durrance, E.M., 1993. Mobility of U and granite kaolinization in southwest England. In: Murray, H.H., Bundy, W.H., Harvey, C.C. (Eds.), *Kaolin Genesis and Utilization. Clay Minerals Society Special Publications* 1, 75–97.
- Dixon, J.B., 1989. Kaolin and serpentine group minerals. In: Dixon, J.B., Weed, S.B. (Eds.), *Minerals in Soil Environments*, 2nd edition. Soil Science Society of America, Madison, WI, pp. 467–525.
- Dong, H., Peacor, D.R., Freed, R.L., 1997. Phase relations among smectite, R1 illite-smectite, and illite. *American Mineralogist* 82, 379–391.
- Drits, V.A., Lindgreen, H., Sakhavov, B.A., Jakobsen, H.J., Salyn, A.L., Duinyak, L.G., 2002. Tobelitization of smectite during oil generation in oil-source shales. Application to North Sea illite-tobelite-smectite-vermiculite. *Clays and Clay Minerals* 50, 82–98.
- Dudek, T., Środoń, J., 2003. Thickness distribution of illite crystals in shales. II Origin of the distribution and the mechanism of smectite illitization in shales. *Clays and Clay Minerals* 51, 529–542.
- Dudoignon, P., Proust, D., Gachon, A., 1997. Hydrothermal alteration associated with rift zones at Fangataufa Atoll (French Polynesia). *Bulletin of Volcanology* 58, 583–596.
- Eberl, D.D., Środoń, J., 1988. Ostwald ripening and interparticle diffraction effects for illite crystals. *American Mineralogist* 73, 1335–1345.
- Eberl, D.D., Jones, B.F., Khoury, H.N., 1982. Mixed-layer kerolite/stevensite from the Amargosa Desert, Nevada. *Clays and Clay Minerals* 30, 321–326.
- Ece, O.I., 1998. Diagenetic transformation of magnesite pebbles and cobbles to sepiolite (Meerschaum) in the Miocene Eskişehir lacustrine basin, Turkey. *Clays and Clay Minerals* 46, 436–445.
- Ece, O.I., Çoban, F., 1994. Geology, occurrences and genesis of Eskişehir sepiolites, Turkey. *Clays and Clay Minerals* 42, 81–92.
- Ehrenberg, S.N., Aagaard, P., Wilson, M.J., Fraser, A.R., Duthie, D.M.L., 1993. Depth dependent transformation of kaolinite to dickite in sandstones of the Norwegian continental shelf. *Clay Minerals* 28, 325–352.
- Essene, E.J., Peacor, D.R., 1995. Clay mineral thermometry. A critical perspective. *Clays and Clay Minerals* 43, 540–553.

- Fanning, D.S., Keramidas, V.Z., El-Desoky, M.A., 1989. Micas. In: Dixon, J.B., Weed, S.B. (Eds.), *Minerals in Soil Environments*, 2nd edition. Soil Science Society of America, Madison, WI, pp. 551–634.
- Fiore, S., Huertas, F.J., Huertas, F., Linares, J., 2000. Smectite formation in rhyolitic obsidian as inferred by microscopic (SEM-TEM-AEM) investigation. *Clay Minerals* 36, 489–500.
- Foley, N.K., 1999. Environmental characteristics of clays and clay mineral deposits. USGS Information Handout, 4pp.
- Fortey, N.J., 1989. Low grade metamorphism in the Lower Ordovician Skiddaw Group of the Lake District, England. *Proceedings of the Yorkshire Geological Society* 47, 325–337.
- Furlan, S., Clauer, N., Chaudhuri, S., Sommer, F., 1996. K transfer during burial diagenesis in the Mahakam delta basin (Kalimantan, Indonesia). *Clays and Clay Minerals* 44, 157–169.
- Galán, E., 1982. Geology of clays. In: van Olphen, H., Veniale, F. (Eds.), *International Clay Conference, 1981. Developments in Sedimentology* 35. Elsevier, Amsterdam, pp. 273–277.
- Galán, E., 1986. Las arcillas como indicadores paleoambientales. *Boletín de la Sociedad Española de Mineralogía* 9, 11–22.
- Galán, E., Aparicio, A., 1980. Las características del metamorfismo de bajo y muy bajo grado en el sector oriental del Sistema Central (Guadalajara). *Estudios Geológicos* 36, 75–84.
- Galán, E., Aparicio, P., Miras, A., Michailidis, K., Tsirambidis, A., 1996. Technical properties of compounded kaolin sample from Griva (Macedonia, Greece). *Applied Clay Science* 10, 477–490.
- Galán, E., Carretero, M.I., Fernández Caliani, J.C., 1999. Effects of acid mine drainage on clay minerals suspended in the Tinto River (Rio Tinto, Spain). An experimental approach. *Clay Minerals* 34, 99–108.
- Gomes, C., Velho, J., Guimavaes, F., 1994. Kaolin deposit of Mevaiela (Angola) alteration product of anorthosite: assessment of kaolin potentialities for application in paper. *Applied Clay Science* 9, 97–106.
- Grim, R.E., Güven, N., 1978. *Bentonites. Geology, Mineralogy, Properties and Uses*. Elsevier, Amsterdam.
- Gutierrez-Mas, J.M., López Galindo, A., López Aguayo, F., 1997. Clay minerals of Miocene–Pliocene materials at the Vera basin, Almería, Spain. Geological interpretation. *Mineralogica et Petrographica Acta* 29A, 259–266.
- Harvey, C.C., Murray, H.H., 1997. Industrial clays in the 21st century: a perspective of exploration, technology and utilization. *Applied Clay Science* 11, 305–310.
- Hay, R.E., Hughes, R.E., Kyser, T.K., Glass, H.D., Lin, J., 1995. Magnesium-rich clay of the meerschaum mines in the Amboseli Basin, Tanzania and Kenya. *Clays and Clay Minerals* 43, 455–466.
- Hay, R.E., Pexton, R.E., Teague, T.T., Kyser, T.K., 1986. Spring-related carbonate rocks, Mg clays, and associated minerals in Pliocene deposits of the Amargosa Desert, Nevada and California. *Geological Society of America Bulletin* 97, 1488–1503.
- Henley, R.W., 1985. The geothermal framework for epithermal systems. In: Berger, B.R., Bethle, P.M. (Eds.), *Reviews on Economic Geology*, vol. 2. *Geology and Geochemistry of Epithermal Systems*. Society of Economic Geologists, Chelsea, MI, pp. 1–24.
- Henley, R.W., Ellis, A.J., 1983. Geothermal systems ancient and modern: a geochemical review. *Earth Science Reviews* 19, 1–50.
- Herbillon, A.J., Frankort, R., Vielvoye, L., 1981. An occurrence of interstratified kaolinite-smectite minerals in a red-black soil toposequence. *Clay Minerals* 16, 195–201.



- Hillier, S., 1995. Erosion, sedimentation and sedimentary origin of clays. In: Velde, B. (Ed.), *Origin and Mineralogy of Clays*. Springer, Berlin, pp. 162–219.
- Huang, W.L., Bishop, A.M., Brown, R.W., 1986. The effect of fluid/rock ratio on feldspar dissolution and illite formation under reservoir conditions. *Clay Minerals* 21, 585–601.
- Inoue, A., Kitagawa, R., 1994. Morphological characteristics of illitic clay minerals from a hydrothermal system. *American Mineralogist* 79, 700–711.
- Inoue, A., Velde, B., Meunier, A., Touchard, G., 1988. Mechanism of illite formation during smectite to illite conversion in a hydrothermal system. *American Mineralogist* 73, 1325–1334.
- Jiang, W.T., Peacor, D.R., Merriman, R.J., Roberts, B., 1990. Transmission and analytical electron microscopic study of mixed-layer illite-smectite formed as an apparent replacement product of diagenetic illite. *Clays and Clay Minerals* 38, 449–468.
- Jones, B.F., Galán, E., 1988. Sepiolite and palygorskite. In: Bailey, S.W. (Ed.), *Hydrous Phyllosilicates (Exclusive of Micas)*. Reviews in Mineralogy, vol. 19. Mineralogical Society of America, Washington, DC, pp. 631–674.
- Jones, B.F., Weir, A.H., 1983. Clay minerals of lake Albert, an alkaline saline lake. *Clays and Clay Minerals* 31, 161–172.
- Kantor, W., Schwertmann, U., 1974. Mineralogy and genesis of clays in red black soil toposequences on basic rocks in Kenya. *Journal of Soil Science* 25, 67–68.
- Kastner, M., 1981. Authigenic silicates in deep-sea sediments: formation and diagenesis. In: Emiliani, E. (Ed.), *The Sea*. Wiley, New York, pp. 915–988.
- Keller, W.D., 1970. Environmental aspects of clay minerals. *Journal of Sedimentary Petrology* 40, 798–813.
- Konta, J., 1992. Phyllosilicates in rivers: result of weathering, erosion, transportation and deposition. In: Galán, E., Ortega-Huertas, M. (Eds.), *XI Reunión Científica Sociedad Española de Arcillas*. University of Granada, Spain, pp. 23–44.
- Kuzvart, M., 1977. Aspects of kaolin genesis. In: Galán, E. (Ed.), *Proceedings of the 8th International Kaolin Symposium and Meeting on Alunite*, Madrid-Rome. Ministerio de Industria y Energía, Madrid, K 12.
- La Iglesia, A., Galán, E., 1975. Halloysite-kaolinite transformation at room temperature. *Clays and Clay Minerals* 23, 109–113.
- La Iglesia, A., Van Oosterwyck-Gastuche, M.C., 1978. Kaolinite synthesis I. Crystallization conditions at low temperatures and calculation of thermodynamic equilibria. Applications to laboratory and field observations. *Clays and Clay Minerals* 26, 397–408.
- Lanson, B., Beaufort, D., Berger, G., Bauer, A., Cassagnabère, A., Meunier, A., 2002. Authigenic kaolin and illitic minerals during burial diagenesis of sandstones: a review. *Clay Minerals* 37, 1–22.
- Leone, G., Reyes, E., Cortecchi, G., Pochini, A., Linares, J., 1983. Genesis of bentonites from Cabo de Gata, Almería, Spain: a stable isotope study. *Clay Minerals* 18, 227–238.
- Linares, J., Huertas, F., 1971. Kaolinite synthesis at room temperature. *Science* 171, 896–897.
- Lindgreen, H., Drits, V.A., Sakharov, B.A., Jakobsen, H.J., Salyn, A.L., Dainyak, L.G., Kroyer, H., 2002. The structure and diagenetic transformation of illite-smectite and chlorite-smectite from North Sea Cretaceous-Tertiary chalk. *American Mineralogist* 87, 429–450.

- López Aguayo, F., 1990. Aplicación de la mineralogía de arcillas al análisis de cuencas. In: Galán, E., Ortega Huertas, M. (Eds.), IX y X Reuniones Científicas. Sociedad Española de Arcillas. Universidad de Granada, Spain, pp. 69–86.
- López Galindo, A., 1986. Las facies oscuras del Cretácico medio en la zona de la Subbética. Mineralogía y Sedimentación. Ph.D thesis. Servicio de Publicaciones Universidad de Granada, 227 pp.
- López Galindo, A., Ben Aboud, A., Fenoll Hach-Ali, P., Casas Ruiz, J., 1996. Mineralogical and geochemical characterization of palygorskite from Gabasa (NE, Spain). Evidence of a detrital precursor. *Clay Minerals* 31, 33–44.
- McHardy, W.J., Wilson, M.J., Tait, J.M., 1982. Electron microscope and X-ray diffraction studies of filamentous illitic clay from sandstones of the Magnus field. *Clay Minerals* 17, 23–39.
- Mackenzie, R.C., Wilson, M.J., Mashhady, A.S., 1984. Origin of palygorskite in some soils of the Arabian Peninsula. In: Singer, A., Galán, E. (Eds.), Palygorskite-Sepiolite. Occurrences, Genesis and Uses. *Developments in Sedimentology* 37. Elsevier, Amsterdam, pp. 177–186.
- Makumbi, M.N., Herbillon, A.J., 1972. Vermiculitisation expérimentale d'une chlorite. *Bulletin du Groupe Français des Argiles* 24, 153–164.
- Masuda, H., Peacor, D.R., Dong, H., 2001. Transmission electron microscopy study of conversion of smectite to illite in mudstones of the Nankai Trough: contrast with coeval bentonites. *Clays and Clay Minerals* 49, 109–118.
- Merriman, R.J., 2002. Contrasting clay mineral assemblages in British Lower Paleozoic slate belts: the influence of geotectonic setting. *Clay Minerals* 37, 207–219.
- Merriman, R.J., 2003. Clay minerals and sedimentary basin history. Euroclay'03, Modena. Book of Abstracts, pp. 188–190.
- Merriman, R.J., Peacor, D.R., 1999. Very low-grade metapelites; mineralogy, microtextures and measuring reaction progress. In: Frey, M., Robinson, D. (Eds.), *Low-Grade Metamorphism*. Blackwell Science, Oxford, pp. 10–60.
- Merriman, R.J., Roberts, B., 1985. A survey of white mica crystallinity and polytypes in pelitic rocks of Snowdonia and Llyn, N. Wales. *Mineralogical Magazine* 49, 305–319.
- Merriman, R.J., Roberts, B., 2001. Low-grade metamorphism in the Scottish Southern Uplands terrane: deciphering the patterns of accretionary burial, shearing and crystic aureoles. *Transactions of the Royal Society of Edinburgh, Earth Sciences* 91, 521–537.
- Millot, G., 1964. *Geologie des Argiles*. Masson et cie, Paris.
- Millot, G., 1979. La arcilla. *Investigación y Ciencia* 33, 47–57.
- Moll, W.F., 1979. Origin of CMS samples. In: van Olphen, H., Fripiat, J.J. (Eds.), *Data Handbook for Clay Materials and Other Non-metallic Minerals*. Pergamon Press, Oxford, pp. 69–125.
- Morse, J.W., Casey, W.H., 1988. Ostwald processes and mineral paragenesis in sediments. *American Journal of Science* 288, 537–560.
- Murakami, T., Isobe, H., Sato, T., Ohnuki, T., 1996. Weathering of chlorite in a quartz–chlorite schist: 1 mineralogical and chemical changes. *Clays and Clay Minerals* 44, 244–256.
- Nadeau, P.H., Wilson, M.J., McHardy, W.J., Tait, J.M., 1984. Interstratified clays as fundamental particles. *Science* 225, 923–925.
- Nieto, F., Ortega-Huertas, M., Peacor, D., Arostegui, J., 1996. Evolution of illite-smectite from early diagenesis through incipient metamorphism in sediments of the Basque-Cantabrian basin. *Clays and Clay Minerals* 44, 304–323.

- Nieto, F., Velilla, N., Peacor, D.R., Ortega-Huertas, M., 1994. Regional retrograde alteration of sub-green schist facies chlorite to smectite. *Contributions to Mineralogy and Petrology* 115, 243–253.
- Odin, G.S. (Ed.), 1988. *Green Marine Clays*. Elsevier, Amsterdam.
- Ortega-Huertas, M., Palomo, I., Moresi, M., Oddone, M., 1991. A mineralogical and geochemical approach to establish a sedimentary model in a passive continental margin (Subbetic Zone, Betic Cordilleras, SE Spain). *Clay Minerals* 26, 389–407.
- Parham, W.E., 1966. Lateral variations of clay mineral assemblages in modern and ancient sediments. In: Heller, L., Weiss, A. (Eds.), *Proceedings of the International Clay Conference, Jerusalem*, vol. 1. Israel Program for Scientific Translation, pp. 135–145.
- Peacor, D.R., 1992. Diagenesis and low-grade metamorphism of shales and slates. In: Buseck, P.R. (Ed.), *Minerals and Reactions at the Atomic Scale: Transmission Electron Microscopy*. Reviews in Mineralogy, vol. 27. Mineralogical Society of America, Washington, DC, pp. 335–380.
- Pletsch, T., Daoudi, L., Chamley, H., Deconinck, J.F., Charroud, M., 1996. Paleogeographic controls on palygorskite occurrence in mid-Cretaceous sediments of Morocco and adjacent basins. *Clay Minerals* 31, 403–416.
- Ponder, H., Keller, W.D., 1960. Geology, mineralogy and genesis of selected fire-clays from Latah Country, Idaho. 8th National Conference. Pergamon Press, New York, *Clays and Clay Minerals* 8, 44–63.
- Pozo, M., Casas, J., 1999. Origin of kerolite and associated Mg-clays in palustrine environments. The Esquivas deposit (Neogene, Madrid Basin, Spain). *Clay Minerals* 34, 395–418.
- Proust, D., 1982. Supergene alteration of metamorphic chlorite in an amphibolite from the Massif Central, France. *Clay Minerals* 17, 159–173.
- Roberts, B., Merriman, R.J., Pratt, W., 1991. The relative influences of strain, lithology and stratigraphical depth on white mica (illite) crystallinity in mudrocks from the district centred on the Corris Slate Belt, Gwynedd-Powys. *Geological Magazine* 128, 633–645.
- Roberts, B., Morrison, C., Hirons, S., 1990. Low grade metamorphism of the Manx Group, Isle of Man: a comparative study of white mica crystallinity techniques. *Journal of the Geological Society, London* 147, 271–277.
- Rodas, M., Luque, F.J., Mas, R., Garzón, G., 1994. Calcretes, palcretes and silcretes in the Paleogene detrital sediments of the Duero and Tajo Basins. *Clay Minerals* 29, 273–285.
- Romero, R., Robert, M., Elsass, F., Garcia, C., 1992. Evidence by transmission electron microscopy of weathering microsystems in soils developed from crystalline rocks. *Clay Minerals* 27, 21–34.
- Ross, G.J., Kodama, H., 1976. Experimental alteration of chlorite into a regularly interstratified chlorite-vermiculite by chemical oxidation. *Clays and Clay Minerals* 24, 183–190.
- Ruiz Cruz, M.D., 1999. Clay mineral assemblages in flysch from the Campo de Gibraltar area (Spain). *Clay Minerals* 34, 345–364.
- Ruiz Cruz, M.D., Andreo, B., 1996. Genesis and transformation of dickite in Permo-Triassic sediments (Betic Cordilleras, Spain). *Clay Minerals* 31, 133–152.
- Sánchez, C., Galán, E., 1995. An approach to the genesis of palygorskite in a Neogene-Quaternary continental basin using principal factor analysis. *Clay Minerals* 30, 225–238.
- Shadfan, H., Dixon, J.B., 1984. Occurrence of palygorskite in the soils and rocks of the Jordan Valley. In: Singer, A., Galán, E. (Eds.), *Palygorskite-Sepiolite. Occurrences, Genesis and Uses*. Developments in Sedimentology 37. Elsevier, Amsterdam, pp. 187–198.

- Siddiqui, M.H.K., 1984. Occurrence of palygorskite in the Deccan Trap Formation in India. In: Singer, A., Galán, E. (Eds.), *Palygorskite-Sepiolite. Occurrences, Genesis and Uses. Developments in Sedimentology* 37. Elsevier, Amsterdam, pp. 243–250.
- Siefferman, G., Millot, G., 1969. Equatorial and tropical weathering of recent basalts from Cameroon: allophane, halloysite, metahalloysite, kaolinite and gibbsite. In: Heller, L. (Ed.), *Proceedings of the International Clay Conference, Tokyo*, vol. 1, pp. 417–430.
- Singer, A., 1979. Palygorskite in sediments: detrital, diagenetic or neoformed. A critical review. *Geologische Rundschau* 68, 996–1008.
- Singer, A., 1979–1980. The paleoclimatic interpretation of clay minerals in soils and weathering profiles. *Earth-Science Reviews* 15, 303–326.
- Singer, A., 1984. Pedogenic palygorskite in the arid environment. In: Singer, A., Galán, E. (Eds.), *Palygorskite-Sepiolite. Occurrences, Genesis and Uses. Developments in Sedimentology* 37. Elsevier, Amsterdam, pp. 169–177.
- Singer, A., Stahr, K., Zarei, M., 1998. Characteristics and origins of sepiolite (Meerschaum) from Somalia. *Clay Minerals* 33, 349–362.
- Singh, B., Mackinnon, D.R., 1996. Experimental transformation of kaolinite to halloysite. *Clays and Clay Minerals* 44, 825–834.
- Środoń, J., 1999. Use of clay minerals in reconstructing geological processes: recent advances and some perspectives. *Clay Minerals* 34, 27–37.
- Środoń, J., Eberl, D.D., Drits, V.A., 2000. Evolution of fundamental particle size during reaction of smectite and implications for the illitization mechanism. *Clays and Clay Minerals* 48, 446–458.
- Stakes, D.S., O'Neil, J.R., 1982. Mineralogy and stable isotope geochemistry of hydrothermally altered oceanic rocks. *Earth and Planetary Science Letters* 57, 285–304.
- Suarez, M., Robert, M., Elssass, F., Pozas, J.M.M., 1995. Evidence of a precursor in the neoformation of palygorskite. New data by analytical electron microscopy. *Clay Minerals* 29, 255–264.
- Taylor, J.H., 1952. Clay minerals and the evolution of sedimentary rocks. *Clay Minerals Bulletin* 1, 238–243.
- Tillick, D., Peacor, D.R., Mauk, J.L., 2001. Genesis of dioctahedral phyllosilicates during hydrothermal alteration of volcanic rocks: 1 The Golden Cross epithermal ore deposit, New Zealand. *Clays and Clay Minerals* 49, 126–140.
- Velde, B., 1992. *Introduction to Clay Minerals*. Chapman & Hall, London.
- Velde, B., 2001. Clay minerals in the agricultural surface soils in the Central United States. *Clay Minerals* 36, 277–294.
- Vicente-Hernández, J., Vicente, M.A., Robert, M., Goodman, B.A., 1983. Evolution des biotites en fonction des conditions d'oxydo-reduction du milieu. *Clay Minerals* 18, 267–275.
- Weaver, C.E., 1960. Possible uses of clay minerals in the search for oil. *Clays and Clay Minerals*, 8th National Conference. Pergamon Press, New York, pp. 214–227.
- Weaver, C.E., Beck, K.C., 1977. Miocene of the SE United States: a model for chemical sedimentation in a peri-marine environment. *Sedimentary Geology* 17, 1–234.
- Wilson, M.J., 1987a. Soil smectites and related interstratified minerals: recent developments. In: Schultz, L.G., van Olphen, H., Mumpton, F.A. (Eds.), *Proceedings of the International Clay Conference, Denver, 1985*. The Clay Minerals Society, Bloomington, IN, pp. 167–173.

- Wilson, M.J., 1987b. Clay mineralogy and mineral weathering; their significance in acid rain and catchment studies. In: Pérez-Rodríguez, J.L., Galán, E. (Eds.), *Lectures 6th Meeting of the European Clay Groups*. Sociedad Española de Arcillas, Sevilla, pp. 167–184.
- Wilson, M.J., 1999. The origin and formation of clay minerals in soils: past, present and future perspectives. *Clay Minerals* 34, 7–25.
- Wirth, L., 1968. Attapulgites du Sénégal occidental. Rapport 26, Laboratoire de Géologie. Faculté des Sciences. Université de Dakar.
- Zhao, G., Peacor, D.R., McDowell, S.D., 1999. Retrograde diagenesis of clay minerals in the Precambrian Freda sandstone, Wisconsin. *Clays and Clay Minerals* 47, 119–130.

*Chapter 15*

## **HISTORY OF CLAY SCIENCE: A YOUNG DISCIPLINE**

**F. BERGAYA<sup>a</sup>, G. LAGALY<sup>b</sup> AND K. BENEKE<sup>b</sup>**

<sup>a</sup>*CRMD, CNRS-Université d'Orléans, F-45071 Orléans Cedex 2, France*

<sup>b</sup>*Institut für Anorganische Chemie, Universität Kiel, D-24118 Kiel, Germany*

The contents of this handbook attest to the great diversity of clays and clay minerals in terms of their structures, properties, and practical applications. Clays were known and used since antiquity but yet remain essential to the synthesis and development of modern materials, such as clay-polymer nanocomposites (see Chapter 10.3). However, clay science (i.e., the scientific study of clay) is a relatively young discipline, having begun only about a century ago. Many factors contribute to the rapid development of clay science over the past 100 years. Among these are the development of analytical and instrumental techniques, enhanced clay production, and increased industrial applications (Grim, 1988; Konta, 1995, 2000; Bergaya et al., 2001).

### **15.1. DEVELOPMENT OF CLAY SCIENCE**

#### *15.1.1. Early Studies*

Geologists were the first to refer to the finely divided particles in sediments as clay although the true nature and properties of this material were largely unknown. For instance, Jean Jacques Théophile Schlösing (1824–1919) fractionated clay by sedimentation and described the properties of the various fractions (Schlösing, 1874). He also showed that nitrification was a biological process because the production of nitrate was inhibited by chloroform vapour. One of the important applications of this finding was the treatment of sewage. The Swedish chemist and soil scientist Albert Mauritz Atterberg (1846–1916) studied the flocculation behaviour of different soil fractions obtained by sedimentation (Atterberg, 1905, 1910). The Atterberg technique is still widely used for separating clays and clay minerals into particle size fractions (see Chapter 5).

Agronomists also used particle size as a criterion for clay identification although the chemical and structural properties of the material were not well understood.

Until the middle of the 19th century the only tools available for the study of clays were the optical microscopy and chemical analysis. Clays were considered to be ‘colloidal complexes’ of amorphous materials with properties that were typical of colloidal substances (Jasmund, 1991). Interestingly, the first publication by Robert Wilhelm Bunsen (1811–1899) was concerned with the occurrence of allophane in a plastic clay (Bunsen, 1834). Jakob Maarten van Bemmelen (1830–1911) considered clays to be mixtures of aluminium and silicon oxides (van Bemmelen, 1877, 1878, 1888). The idea of chemical bonding between these oxides was not developed until the following decades when crystalline particles were observed by microscopy. The amorphous fraction soluble in hydrochloric acid was referred to as *Allophanton* (from German *ton*, clay), while the crystalline fraction was called *Kaolinton* (Jasmund, 1991). Henri Louis Le Châtelier (1850–1936) used thermal dehydration to study clays, observing that water was desorbed at distinct temperatures, typical of crystalline materials (Le Châtelier, 1887) (see Chapter 12.10). Advances in optical microscopy enabled an increasing number of clay minerals to be identified (Ross and Shannon, 1925, 1926; Ross and Kerr, 1931a, 1931b, 1934).

The electrophoretic mobility of clay particles (Reuss, 1809) was first described by Ferdinand Fiodorovich Reuss (1778–1852). In his 35th letter, describing the relation between chemistry and agriculture, Justus von Liebig (1803–1873) stressed the role of clay minerals in providing soils with essential nutrients for plant growth, especially following lime addition. He also described the ‘thickening’ of common clays (*Töpferton* and *Pfeifererde*) by addition of calcium carbonate and the gradual replacement of the alkali ions from the clay (von Liebig, 1858, 1865; Lagaly, 2002).<sup>1</sup> Later, Atterberg (1910, 1911) described the plasticity of clays (see Chapter 5). In explanation, Le Châtelier suggested that the plate-like particles of clay adhered like cards when thrown on a table, and thus was the first to have used the term ‘house-of-cards’ (Salmang, 1927). In this connection, we should also mention that Schalek and Szegvary (1923a, 1923b) were the first to describe thixotropy (see Chapter 5), an important phenomenon in clay application (Reitstötter, 1954).

In 1852 John Thomas Way (1820–1883) described the base exchange capacity of soils which, at that time, was considered to be related to the presence of amorphous materials (Way, 1852). Even Lemberg (1876), more than 20 years later, assumed that this capacity arose from newly formed very finely divided zeolitic complexes. The interpretation of base exchange as a cation exchange process, as we now know, goes back to van Bemmelen. Besides recognising many important properties of clays, van Bemmelen (1877, 1878, 1888, 1910) determined the adsorption capacity of many agricultural soils, and gave the first description of cation exchange. He was also the founder of the theory of solute-solid adsorption.

The first report on clay resources was that by Ries (1920) who used a petrographic microscope to identify some physical properties of clays, such as plasticity, shrinkage, and firing behaviour. After 1920, several groups in Sweden (Hadding, 1923),

<sup>1</sup>We thank Ewa Serwicka and Krzysztof Bahranowski (Krakow) for this reference.

Germany (Rinne, 1924), and the USA (Ross and Shannon, 1925, 1926; Ross and Kerr, 1931a, 1931b, 1934) investigated clays and clay minerals using chemical analysis, optical microscopy, and X-ray diffraction (XRD). In Germany, Correns (1929, 1933, 1936) studied clay minerals in sediments.

Only a few textbooks on clay science were published up to the middle of the 20th century. The first German text, entitled *Die Tone* (“Clays”) by Paul Rohland (1866–1916) was published in 1909 (Rohland, 1909). The textbook on soil colloids by Ehrenberg (1915) also contained a section on clays. The second textbook in German by Karl Jasmund (1913–2003) was published in 1951 (Jasmund 1951). In 1953, Ralph E. Grim published his famous book *Clay Mineralogy*, followed by *Applied Clay Mineralogy* in 1962 (Grim, 1953, 1962). The first edition of *An Introduction to Clay Colloid Chemistry* by H. van Olphen came out in 1963 (Van Olphen, 1963).

### 15.1.2. XRD: An Essential Tool for Clay Mineral Research

Three Nobel prizes were awarded in relation to the discovery of X-ray radiation and its application to elucidating clay mineral structures. In 1901 Wilhelm Conrad Röntgen (1845–1923) received the physics Nobel prize for the discovery of X-rays (*Röntgenstrahlen* in German) (Röntgen, 1895), followed in 1914 by Max von Laue (1879–1960) for XRD (Friedrich et al., 1912), and by Linus Pauling (1901–1994) who won the Nobel prize for chemistry in 1954, and for peace in 1962 (Pauling, 1930a, 1930b). The first X-ray powder diffraction data on clay minerals, obtained with the Debye–Scherrer technique, were published by Assar Robert Hadding (1886–1962) in 1923 and Friedrich Rinne (1863–1933) in 1924. In 1956, Karl Jasmund developed a special camera (*Texturkamera*) for the rapid investigation of clay minerals based on the intensity enhancement of the basal reflections by texture.

Pauling (1930a, 1930b) was the first to determine the structure of micas and related materials, providing the basis for the elaboration of many other phyllosilicate structures. In 1932 John Walter Gruner (1890–1981) proposed the structure of kaolinite (Gruner, 1932). A year later, Ulrich Hofmann (1903–1986), Kurd Endell (1887–1945) and Diederich Wilm elucidated the atomic arrangement, interlayer expansion (*innerkristalline Quellung*), and swelling properties, of montmorillonite (Endell et al., 1933; Hofmann et al., 1933). Hofmann et al. (1934) also studied a montmorillonite sample from Montmorillon (France) together with many other clay mineral species. Mehmel (1935) investigated the structure of halloysite and meta-halloysite. Later Hendricks and Teller (1942) elaborated the theory of XRD for interstratified minerals.

### 15.1.3. Other Useful Tools for Clay Mineral Research

Other instrumental techniques, besides optical microscopy and XRD, were developed in the 1930s. One of these was differential thermal analysis (DTA), providing insight into the physical and chemical changes that occurred during heating. The



changes observed by ceramists were especially useful to understanding clay mineral structures. The new phases developed during heating were further identified by XRD. Another powerful tool was electron microscopy, revealing the shape and morphology of clay mineral particles. [von Ardenne et al. \(1940\)](#) obtained the first electron micrographs of clay minerals.

#### *15.1.4. Importance of Commercial Bentonite Production*

The commercial production of bentonite played a major role in the growth of clay science. It was [Knight \(1898\)](#) who suggested the name ‘bentonite’ for a clay-like material with soapy properties from Fort Benton, Montana, USA. [Hewett \(1917\)](#) showed that this clay was formed by in-situ alteration of volcanic ash. The commercial production of the Wyoming deposits in the USA began in the 1920s and in Europe about 10 years later, first in Bavaria (Germany), and then in many other countries. An important step was the modification of bentonites with soda to give alkali- or soda-activated bentonites ([Hofmann and Endell, German Patent 1934, British Patent 1935; Hofmann, 1976](#)). Soda-activation, introduced by Hofmann, transforms German bentonites into materials similar to their Wyoming counterparts ([Beneke and Lagaly, 2002a](#)). The industrial production of bentonites in raw or modified form is still very important (see Chapter 10.3).

#### *15.1.5. Clay Research and Applications*

Basic research into the atomic structures and surface properties of clay minerals together with improvements in instrumental techniques (e.g., XRD, infrared spectroscopy, DTA), and modification of raw clays (by acid-, soda-, and organo-activation) greatly advanced clay science and clay mineral technology. Increased bentonite production and several particular applications also led to a flood of clay research since the beginning of the 20th century.

##### *A. Bleaching Earth*

Natural bleaching earth (fuller’s earth) was used since antiquity for degreasing and thickening of cloth ([Siddiqui, 1968; Robertson, 1986; Novelli, 2000; Beneke and Lagaly, 2002b](#)). Bleaching earth is usually produced by reacting bentonites with hydrochloric acid (see Chapters 7.1 and 10.1). The first industrial plant for the production of bleaching earth (Pfirsinger Mineralwerke) was erected in 1906 at Kitzingen, Germany. Not long afterward Tonwerke Moosburg (now Süd-Chemie), Germany, produced a similar product. This was marketed as ‘Tonsil’, a name that is still being used ([Beneke and Lagaly, 2002b](#)).

##### *B. Clays as Catalysts*

Until the 1920s, crude oils were refined by distillation. Catalytic conversion, using acid-activated bentonite (‘Houdry process’) was introduced in 1937 ([Hettinger, 1991](#)).

A few years later this catalyst was replaced by acid-activated kaolinite, and in the 1950s by 'base-activated kaolinite' (i.e., zeolites A and/or X). The advent of synthetic zeolites spelt the demise of clays for petroleum refining. Renewed interest in clay catalysis emerged in the 1970s due to the development of pillared clays (see Chapter 7.5). The accumulated information and knowledge about zeolites advanced our understanding of clay mineral properties but the reverse is also true (Fripiat, 1995).

Clays (raw, activated, and pillared) are being used as heterogeneous catalysts in many organic reactions (see Chapter 10.2). Clays might also served as catalysts in processes related to the origin and development of life on earth (see Chapter 7.4).

### *C. Clays in Engineering*

Geotechnical problems encountered during construction of the Chicago subway (in 1940) convinced engineers—who performed many tests but could not predict the outcome—that basic knowledge of clay properties was essential to understanding the clay behaviour. Similar problems arose in other large cities like London, Paris, San Paulo, and Mexico City that are built on soft soil materials. The relevance of clay science to civil engineering is further discussed in Chapter 10.1.

### *D. Organoclays*

The importance of interdisciplinary research was emphasised during the meeting celebrating the 5th anniversary of the foundation of Chicago University in 1942. Symposia on various frontiers of science were organised. The department of geology held a symposium on clay mineralogy, pointing out the significance of this discipline to geology. The meeting also showed the broad utility of bentonites, and a technical guidance committee was established. John W. Jordan (1912–2001), who pioneered research into organophilic bentonites, became the first fellow of this committee (Jordan, 1949a, 1949b; Jordan et al., 1950; Jordan and Williams, 1954).

#### *15.1.6. Clay Research after World War II*

The development of clay science since 1930 was described in detail by Köster (1994) and Konta (1995, 2000). The five aspects that contributed to the advancement of clay science and the practical applications of clays are as follows:

- (i) Progress in analytical and instrumental techniques. These techniques are constantly being improved, and often revisited. New techniques are developed and/or applied, including NMR, Raman, Neutron, and Mössbauer spectroscopy, SEM, ESEM, AFM, controlled rate thermal analysis (CRTA), plasma and laser techniques, and finally computer modelling. Very useful information is gained from the simultaneous application of different techniques on the same sample and under the same conditions (Annabi-Bergaya, 1978, 1982).
- (ii) Coupling the macroscopic behaviour of clay minerals to their nano-, micro-, and mesoscopic properties as already remarked on in previous chapters of this

- handbook. Nevertheless, more attention should be paid to this aspect than was the case, particularly in civil engineering.
- (iii) Development of novel clay-based materials, such as pillared clays, special porous clays, inorganic/organic clay hybrids, clay-polymer nanocomposites, and clay films (using layer-by-layer deposition and Langmuir–Blodgett techniques). These materials are the basis for a great diversity of modern applications as well as optical and electronic devices (see Chapters 3, 5, 7.3, 7.5, 10.3, 11.1). Other, yet unknown, clay-based materials are likely to emerge, given the inventiveness of man. Thus, the scope of clay science is very wide, if not unlimited.
  - (iv) Development of new layered materials, such as LDH (see Chapter 13.1), alkali silicates, crystalline silicic acids, M(IV)-phosphates, niobates, titanates, etc. (Lagaly and Beneke, 1991; Schwieger and Lagaly, 2004).
  - (v) Interdisciplinary approach and collaboration. Although not new, this concept is gaining ground and acceptance. For example, the biological sciences become an important part of clay research (Theng and Orchard, 1995) (see also Chapter 9).

## 15.2. NAMES, FIRST LOCALITY, AND STRUCTURAL IDENTIFICATION

*Allophane* (Hausmann and Stromeyer, 1816): The name ‘allophane’ was first applied by Hausmann and Stromeyer (1816) to material lining cavities in marl near Balingen, Germany. The term derives from Greek *allos* (different, other) and *phanēs* (appear, appearance), and alludes to the ability of allophane to change from a glassy material to one with an earthy appearance as water is lost on standing. Since the work of Hausmann and Stromeyer, a variety of materials were described or classified as allophane. Because these materials were generally amorphous, allophane came to be identified with the (X-ray) amorphous constituents of clay (Grim, 1968). Structural identification: (Ross and Kerr, 1934).

*Attapulgit* (de Lapparent, 1936): The name ‘attapulgit’ was first applied by Molière Jacques de Lapparent (1883–1948) to the clay that he found in fuller’s earth from Attapulgis, Georgia (USA); Quincy, Florida (USA); and Mormoiron (France) (de Lapparent, 1936). Although ‘attapulgit’ still appears in the literature, the name ‘palygorskite’ should be used in preference. Structural identification: (de Lapparent, 1938; Bradley, 1940).

*Batavite* (Weinschenk, 1897): Ernst Weinschenk (1897) was the first to use ‘batavite’ for colourless nacrite-like crystals. The name derives from Castra Batava, the locality near Passau, Germany. The structure of this mineral is very similar to vermiculite. Structural identification: (Weiss and Hofmann, 1951).

*Beidellite* (Larson and Wherry, 1917, 1925; Ross and Shannon, 1925): ‘Beidellite’ was first used by Larson and Wherry (1925) for a clay mineral found in a gouge clay in a mine at Beidell, Colorado, USA. The mineral was initially (in 1917) referred to as leverrierite but Larson and Wherry (1925) later suggested that it was a distinct

species. The name ‘leverrierite’, after Le Verrier (a mining engineer), was first used by Termier (1890) for a material occurring in black carbonaceous shale near St. Etienne, France (Grim, 1968). Excellent specimens of beidellite (often showing a weak pink colour) were found in phonolite quarries near Unterrupsroth, Germany (Heide, 1928). Structural identification: (Ross and Hendricks, 1945; Nadeau et al., 1985).

**Bentonite** (Knight, 1897, 1898): This clay material was initially called ‘taylorite’ in honour of William Taylor who first drew attention to the corresponding deposits in the USA. The name ‘bentonite’ was given by Knight (1898) after the site near Fort Benton, Montana, USA where the deposit was first discovered. Hewett (1917) showed that this clay was formed by in-situ alteration of volcanic ash. Structural identification: (Hofmann et al., 1933).

**Brammallite** (Bannister, 1943; also structural identification): Named after A. Brammall, a British geologist and mineralogist.

**Celadonite** (Glocker, 1847): Named after the grey-green dress of the shepherd Céladon in the novel *L’Astrée* by H. D’Urfé (1568–1625). Celadonite is a soft grey-green hydrous silicate of iron, magnesium, and potassium (Glocker, 1847). Similar materials were earlier referred to as *terra verti* by de Lish (1783) and *Grünerde* by Hofmann (1788). Hendricks and Ross (1941) showed that celadonite and glauconite were similar in structure. The original celadonite came from amygdaloidal fillings. Kerr and Hamilton (1948) suggested that the name ‘celadonite’ be retained because it had a different origin from that of glauconite (Grim, 1968). Structural identification: (Hendricks and Ross, 1941).

**Chlorites** (Werner, 1789a): Abraham Gottlob Werner (1749–1817) was apparently the first to use the name ‘chlorite’ (Werner, 1789a) for a group of green hydrous silicates, closely related to the micas, and containing much ferrous iron. A large variety of materials were described as chlorites, and there was much confusion regarding the identity and validity of species belonging to the group (Grim, 1968). Structural identification: (Pauling, 1930b).

**Corrensite** (Lippmann, 1954): The mineral was named in honour of Carl Wilhelm Correns (1893–1980) (Lippmann, 1960). Structural identification: (Stephen and MacEwan, 1950).

**Dickite** (Dick, 1908): Allan Brugh Dick (1833–1926), a Scottish metallurgical chemist, described a mineral from the island of Anglesey, Wales, UK. He did not give a specific name, referring to it as a ‘mineral of kaolin’ (Dick, 1908). Ross and Kerr (1931a) showed that the ‘Dick mineral’ was a distinct species, and were the first to use the name ‘dickite’ (Grim, 1968). Structural identification: (Ross and Kerr, 1930, 1931a).

**Fuller’s earth** (before 3000 BC in Mesopotamia, Egypt and Greece (Beneké and Lagaly, 2002b)): The word ‘fuller’ (French *foulon*; Italian *fullone*) derives from the Latin *fullo*, denoting a person whose job was that of degreasing and felting cloth. In Roman times, pieces of cloth were first steeped into old urine (very rich in ammonia) or other alkaline solutions, then heavily trod on in a trough or basin containing a slurry of ‘fuller’s earth’ (Latin *creta fullonia*). Fresh water was used to rinse off the

fuller's earth, and remove a large part of the grease and dirt from the fleece (Robertson, 1986). This method was also used by the Greeks and Egyptians.

*Glauconite* (Keferstein, 1827): From Greek *glaukos* (bluish shining). Structural identification: (Gruner, 1935a; Kohler and Köster, 1976).

*Halloysite* (Berthier, 1826): The name 'halloysite' was given by Pierre Berthier (1782–1861) to a material found in pockets of carboniferous limestone in a district of old zinc and iron mines near Liège, Belgium (Berthier, 1826). It was named in honour of Omalius d'Halloy, a Belgian geologist (1707–1789) who had observed the mineral several years previously. Prior to the development of X-ray-diffractometry many materials were described as halloysite. Thus, under halloysite James Dwight Dana (1813–1895) listed 16 names of minerals that he considered to be synonymous with it (Dana, 1914). Ross and Kerr (1934) studied a number of halloysites by modern methods, obtaining samples from the mineralogical collection of the University of Liège. These were probably as nearly representative of the type material available at the time. They showed that halloysite was crystalline and closely related to, but distinct from, kaolinite (Grim, 1968). Structural identification: (Hofmann et al., 1934; Mehmel, 1935).

*Hectorite* (Strese and Hofmann, 1941): The name 'hectorite' was given to a material from Hector, San Bernadino, California, USA. Structural identification: (Strese and Hofmann, 1941).

*Illite* (Grim et al., 1937): The term 'illite' was proposed by Grim et al. (1937) as a general term for the "mica occurring in argillaceous sediments". The name derives from the abbreviation (IL) for the state of Illinois, USA. Prior to 1937 the widespread occurrence of a mica-like, potash-bearing clay mineral, similar to 'sericite' and *Glimmerton*, had been suggested. Grim et al. (1937) voiced objections to these earlier names, and the term illite was now widely accepted for a mica-type clay mineral with a 1.0 nm *c*-axis spacing that shows essentially no interlayer expansion (in water). Hofmann et al. (1943) suggested 'sarospatite' as a substitute for illite. However, the same objection can be raised, namely, that the type material from Sárospatak, Hungary, is a mixture of clay materials. It seems advisable to use a new name for this group of clay minerals, rather than redefine an old name, particularly if the old name originally describes a mixture of minerals (Grim, 1968). Structural identification: (Grim, 1939).

The name 'sarospatite' was initially used by Maegdefrau (1941), and the mineral was first described by Maegdefrau and Hofmann (1937) (Viczián, 2000, 2002).

*Imogolite* (Yoshinaga and Aomine, 1962a): The name 'imogolite' was first used by Yoshinaga and Aomine (1962a, 1962b) for a component present in the clay fraction of the "imogo" soil, derived from glassy volcanic ash, near Hitoyoshi, Komamoto Prefecture, Japan. Structural identification: (Wada and Yoshinaga, 1969).

*Kaolinite* (Johnson and Blake, 1867): The name 'kaolin' is a corruption of the Chinese *kauling* (high ridge), referring to a hill near Jauchau Fu, China, where the material was obtained centuries ago. Occurrences of kaolinite in many parts of the world were well documented (see Chapter 10.1). Johnson and Blake (1867) were

apparently the first to use the name kaolinite for the ‘mineral of kaolin’. [Ross and Kerr \(1931a\)](#) showed that the kaolin minerals were not composed of a single mineral species. Rather, there are three distinct species of kaolin: kaolinite, nacrite, and dickite ([Grim, 1968](#)). Structural identification: ([Ross and Kerr, 1931a](#)).

*Montmorillonite* ([Cronstedt, 1758](#); [Damour and Salvétat, 1847](#)): [Mauduyt \(1847\)](#) named ‘montmorilloniste’ after the town of Montmorillon, France. Likewise, [Damour and Salvétat \(1847\)](#) proposed this name for a mineral from Montmorillon. [Correns \(1950\)](#) suggested ‘montmorin’ as the group name. One year later, the term ‘montmorillonoid’ was suggested as a group name so as to avoid confusion with montmorillonite as a specific mineral name (see [MacEwan, 1961](#)). Neither of these names found favour. ‘Smectite’ as a group name was proposed by the Clay Minerals Group of the Mineralogical Society of Great Britain. From the outset this proposal met strong opposition, particularly from many American mineralogists, but it is becoming widely accepted ([Grim, 1968](#)). Structural identification: ([Hofmann et al., 1933](#)).

*Morencite* ([Lindgren and Hillebrand, 1904](#)): Morencite from Morenci, Arizona, USA was first described by [Lindgren and Hillebrand \(1904\)](#) as a brownish-yellow hydrous silicate of ferric iron with magnesium, calcium, and aluminium. [Gruner \(1935b\)](#) showed the mineral to be structurally the same as nontronite ([Grim, 1968](#)). Structural identification: ([Gruner, 1935b](#)).

*Nacrite* ([Brongniart, 1807](#)): From French *nacre* (mother-of-pearl). The name ‘nacrite’ was proposed by Brongniart in 1807. Later [Des Cloizeaux \(1862\)](#), and much later [Dick \(1908\)](#), described a nacrite from mines (Einigkeit Mine, Brand-Erbisdorf, Freiberg) in Saxony, Germany. Dick also provided sufficient analytical data to differentiate it from the ‘Dick material’ but not from the ‘mineral of kaolin’. [Mellor \(1916\)](#) accepted nacrite as a distinct mineral, and [Ross and Kerr \(1931a\)](#) finally established its identity ([Grim, 1968](#)). Structural identification: ([Ross and Kerr, 1931a](#)).

*Nontronite* ([Berthier, 1827](#)): Berthier proposed the name ‘nontronite’ for a material associated with manganese ore in the arrondissement of Nontron near the village of Saint Pardoux, France. Chemical analysis showed the mineral to be a hydrous ferric iron silicate ([Berthier, 1827](#)). [Collins \(1877\)](#) appeared to have been the first to recognise the association between nontronite and montmorillonite. The similarity of nontronite to montmorillonite was established by [Larson and Steiger \(1928\)](#), [Ross and Kerr \(1931b\)](#), and [Gruner \(1935b\)](#). Nontronite is now generally applied to the iron-rich end-member of the montmorillonite group of minerals ([Grim, 1968](#)). Structural identification: ([Nagelschmidt, 1938](#)).

*Palygorskite* ([Ssaftschenskow, 1862](#)): ‘Palygorskite’ is named after the town of Palygorsk in the Ural Mountains, Russia. Palygorskite and attapulgite are mineralogically indistinguishable but the name ‘palygorskite’ has priority. Structural identification: ([Bradley, 1940](#)).

*Pyrophyllite* ([Hermann, 1829](#)): From Greek *pýr* (fire), *phýllon* (leaf), and *lithos* (stone). Structural identification: ([Ross and Hendricks, 1945](#)).



*Saponite* (Svanberg, 1840): The earliest use of the name ‘saponite’ is difficult to establish. Svanberg (1840) used this name, derived from Latin *sapo* (soap). Chemical analysis showed the material to be essentially a hydrous magnesium silicate. Like many other clay minerals, this mineral could not be well characterised prior to the development of modern analytical techniques, and a wide variety of materials were included under this name. Ross and Kerr (1931b) identified saponite as a member of the montmorillonite group with a high content of MgO. Ross and Hendricks (1945) defined saponite as a member of the montmorillonite group for which the replacement of  $\text{Al}^{3+}$  by  $\text{Mg}^{2+}$  in the octahedral sheet was essentially complete, while some replacement of  $\text{Si}^{4+}$  by  $\text{Al}^{3+}$  occurred in tetrahedral positions (Grim, 1968). Structural identification: (Ross and Hendricks, 1945).

*Sauconite* (Roeppe, 1875): Sauconite is named after the locality: Ueberroth mine, Saucon Valley, near Friedensville, Lehigh County, Pennsylvania, USA. (Roeppe, 1875). Structural identification: (Ross, 1946).

*Sepiolite* (Glocker, 1847): The name ‘sepiolite’ is derived from Greek *sepion* (squid, cuttlefish) and *lithos* (stone). First locality: Baldissero Canavese, Piedmont, Italy. ‘Sepiolite’ and ‘Meerschaum’ were long considered as synonymous. Werner (1789b) was apparently the first to use the name *Meerschaum* (German, meaning sea froth) in allusion to the lightness and colour of the material. The term ‘sepiolite’ was first used in 1847 by Ernst Friedrich Glocker (1793–1858) because the mineral was light and porous like the bone of cuttlefish. Structural identification: (Migeon, 1936; Nagy and Bradley, 1955).

*Smectite*: ‘Smectite’ is a group name, derived from Greek *smectis* (fuller’s earth) and *smechein* (wipe off, clean) (see montmorillonite).

*Stevensite* (Leeds, 1873): Named after E.A. Stevens, founder of the Stevens Institute of Technology, Hoboken, New Jersey, USA. First locality: the railway tunnel at Bergen Hill, Hudson County, New Jersey, USA. Structural identification: (Faust and Murata, 1953).

*Vermiculite* (Webb, 1824): The name ‘vermiculite’ derives from Latin *vermiculari* (full of worms). It was first used by Webb (1824) for a platy mineral from Millbury near Worcester, Massachusetts, USA as the (hydrated) mineral exfoliates when heated and wriggles like a worm (see Chapters 7.2 and 10.1). Structural identification: (Gruner, 1934, 1939).

*Volkonskoite* (Anonymous, 1830): This mineral was discovered on a certain estate in the Province of Perm (Perm Basin, Ural Mountains, Russia) and named in honour of the Minister of the Imperial Court, Prince Volkonskoi (Anonymous, 1830; Mackenzie, 1984). Structural identification: (Ross and Hendricks, 1945; Weiss et al., 1954).

### 15.3. HISTORY OF CLAY MEETINGS

In 1948 the first international clay committee under the presidency of Ralph Grim decided to promote cooperation between clay scientists from different countries. To

that end, the 'Comité International pour l'Étude des Argiles' (CIPEA) was formed under the auspices of the International Geologic Congress (IGC). In 1960, it was proposed that CIPEA should become independent of IGC and organise its own meetings. The first International Clay Conference (ICC) was held in 1963. In 1966 CIPEA became effectively independent of IGC, and was renamed 'Association Internationale pour l'Étude des Argiles' (AIPEA).

The first European Clay Groups (ECG) meeting was held in Madrid in 1972, following on an informal bilateral meeting between the Spanish and Belgium clay groups, held in Madrid two years previously, initiated by J.M. Serratosa and J.J. Fripiat. During the 6th ECG meeting in 1987 in Seville, European scientists established the 'European Clay Groups Association' (ECGA) in order to stimulate clay science and technology. As a result, the term 'ECG' was changed to 'Euroclay'.

In 1983 the decision was made to hold all Euroclay and ICC meetings every four years but with a two-year stagger so as to avoid overlap. In addition, other multi-national clay meetings were convened since 1984 (Table 15.1). Participation in clay conferences is an important feature in the career of any clay scientist. Nevertheless, it seems advisable to halt further proliferation of clay meetings.

At the inception (in 1966) the AIPEA decided to produce an international newsletter with the aim of promoting worldwide cooperation between clay scientists. This newsletter was since published annually. Likewise, the ECGA published a newsletter but on an annual basis. The first issue came out in 1997, a decade after its founding; the latest issue (No. 5) was published in 2002 (Lagaly, 2002).

## 15.4. DEFINITION OF 'CLAY SCIENTIST'

This definition was given in three languages in the first AIPEA Newsletter (1966).

*English version:* "The term 'clay scientist' is used in its widest sense as it covers a very large and varied group, with representatives in the cement industry, ceramics industry, civil engineering, cosmetic industry, crystallography, foundry technology, geology, geotechnics, medicine, mineralogy, paint industry, paper industry, pedology, petroleum industry, rubber industry, et cetera".

*French version:* "Le terme 'spécialiste qui s'intéresse aux argiles' est employé dans sa signification la plus vaste et couvre un groupe très varié et grand, qui a des représentants dans l'industrie de la céramique, l'industrie du ciment, l'industrie du caoutchouc, l'industrie de la cosmétique, la cristallographie, la technologie des fonderies, la géologie, la géotechnique, les ingénieurs civils, la médecine, la minéralogie, l'industrie du papier, la pédologie, l'industrie de la peinture, l'industrie du pétrole, et cetera".

*German version:* "Der Term 'Tonspezialist' wird hier sehr weit gefaßt und deckt eine große und vielfältige Gruppe, deren Repräsentanten in vielen verschiedenen Zweigen der Forschung und Industrie tätig sind: Bauingenieur, Wissenschaft, Bodenkunde, Farbindustrie, Geologie, Geotechnik, Gießereitechnik, Gummiindustrie,



Table 15.1. Clay meetings and conferences

1948	International Geological Congress (IGC) The first international committee for the study of clay (CIPEA) was established under the auspices of IGC with Ralph Grim as president (Grim held this function until 1960)	London
1950	CIPEA/IGC	Amsterdam
1952	CIPEA/IGC	Algiers
1954	CIPEA/IGC	Paris
1956	CIPEA/IGC	Mexico City
1958	CIPEA/IGC	Brussels
1960	CIPEA/IGC CIPEA to become independent of IGC, and organise own meetings	Copenhagen
1963	1st ICC CIPEA decided to establish an international association for the study of clay (AIPEA), affiliated to UISG. This decision was ratified during the 22nd IGC (India, 1966) In 1966 the UISG executive committee accepted this affiliation.	Stockholm
1966	2nd ICC General Assembly: AIPEA became independent of geology First AIPEA newsletter published	Jerusalem
1969	3rd ICC	Tokyo
1970	First Spanish-Belgian preparative meeting initiated by J.M. Serratosa and J.J. Fripiat	Madrid
1971	informal colloquium Spain-Belgium (including France and Great Britain)	Leuven
1972	4th ICC First meeting of 12 European national clay groups (including clay scientists from Switzerland), considered as	Madrid
	1st ECG	Madrid
1974	2nd ECG	Strasbourg
1975	5th ICC	Mexico City
1977	3rd ECG	Oslo
1978	6th ICC	Oxford
1980	4th ECG	Freising
1981	7th ICC	Bologna/Pavia
1983	5th ECG	Prague
1984	First Italo-Spanish congress was held (in Italy)	Seiano di Vico Equense and Amalfi
1985	8th ICC	Denver
1987	6th Euroclay	Sevilla

Table 15.1 (*Continued*)

	Founding of ECGA to stimulate clay science and technology among European scientists; ECG became Euroclay	
	First ECGA newsletter was published in 1997	
1989	9th ICC	Strasbourg
1991	7th Euroclay	Dresden
1993	10th ICC	Adelaide
1995	8th Euroclay	Leuven
1996	Second Italo-Spanish meeting (including France, Great Britain, Norway, Switzerland, USA), considered as	
	1st MCM	Granada
1997	11th ICC	Ottawa
1998	2nd MCM	Aveiro
1999	9th Euroclay	Krakow
2000	1st LACC	Madeira
2001	12th ICC	Bahia Blanca
	1st MECC	Stará Lesná
2002	3rd MCM	Jerusalem
2003	10th Euroclay	Modena
2004	2nd MECC	Miskolc
2005	13th ICC	Tokyo
2007	11th Euroclay	Aveiro

AIPEA, Association Internationale pour l'Étude des Argiles; CIPEA, Comité International pour l'Étude des Argiles; ECG, European Clay Groups; ECGA, European Clay Groups Association; ICC, International Clay Conference; IGC, International Geological Congress; LACC, Latin-American Clay Conference; MCM, Mediterranean Clay Meeting; MECC, Mid-European Clay Conference; UISG, Union Internationale des Sciences Géologiques.

Keramische Industrie, Kosmetikindustrie, Kristallographie, Medizin, Mineralogie, Papierindustrie, Petroleumindustrie u. a. m".

## REFERENCES

- Annabi-Bergaya, F., 1978. Organisation de molécules polaires adsorbées par la montmorillonite. Thèse de Doctorat d'Etat ès Sciences Physiques. Université d'Orléans.
- Annabi-Bergaya, F., 1982. Adsorption du méthanol par la montmorillonite. *Agronomie* 2, 947–950.
- Anonymous, 1830. Description of the occurrence of a green-coloured mineral discovered on a certain estate in the Province of Perm and named in honour of Mr. Minister of the Imperial Court Volkonskoite (i. e. Prince Volkonskoï). *Gorn Zhurnal Moskov* Part IV, 261–267.
- Atterberg, A., 1905. Die rationelle Klassifikation der Sande und Kiese. *Chemiker Zeitung* 29, 195–198.

- Atterberg, A., 1910. Die Plastizität und Kohärenz der Tone und Lehme. *Chemiker Zeitung* 42, 369–371 379–380.
- Atterberg, A., 1911. Die Plastizität der Tone. *Internationale Mitteilungen der Bodenkunde* I, 4–37.
- Bannister, F.A., 1943. Brammallite (sodium illite), a new mineral from Llandebie, South Wales. *Mineralogical Magazine* 26, 304–307.
- Beneke, K., Lagaly, G., 2002a. Curriculum vitae and scientific research of Ulrich Hofmann (1903–1986). In: Lagaly, G. (Ed.), *ECGA Newsletter* 5. Verlag Reinhard Knof, Nehnten, pp. 13–23.
- Beneke, K., Lagaly, G., 2002b. From fuller's earth to bleaching earth. A historical note. In: Lagaly, G. (Ed.), *ECGA Newsletter* 5. Verlag Reinhard Knof, Nehnten, pp. 57–78.
- Bergaya, F., Beneke, K., Lagaly, G., 2001. History and perspectives of clay science. *ECGA Newsletter* 4. pp. 5–41.
- Berthier, P., 1826. Analyse de l'halloysite. *Annales de Chimie et Physique* 32, 332–335.
- Berthier, P., 1827. Nontronite, nouveau minéral, découvert dans le département de la Dordogne. *Annales de Chimie et de Physique Série* 2, 36, 22–27.
- Bradley, W.F., 1940. The structure scheme of attapulgite. *American Mineralogist* 25, 405–410.
- Brongniart, A., 1807. *Traité élémentaire de minéralogie, avec des applications aux arts, etc.* Paris (2 volumes), vol. 1, p. 505.
- Bunsen, R., 1834. Über ein neues Vorkommen des Allophans in der Formation des plastischen Thons. *Annalen der Physik und Chemie* 2. Folge (Poggendorffs Annalen) 31, 53–59.
- Collins, J.H., 1877. Remarks on gramenite from Smallcombe, and the chloropal group of minerals. *Mineralogical Magazine* 1, 67–82.
- Correns, C.W., 1929. Bestimmung der Brechungsexponenten in Gemengen feinkörniger Minerale und von Kolloiden. *Zentralblatt der Mineralogie, Abteilung A* 11, 408–411.
- Correns, C.W., 1933. Über die Bestandteile der Tone. *Zeitschrift der Deutschen Geologischen Gesellschaft* 85, 706–712.
- Correns, C.W., 1936. Petrographie der Tone. *Naturwissenschaften* 24, 117–124.
- Correns, C.W., 1950. Objection to the name Montmorillonoid. *Clay Minerals Bulletin* 1, 194–195.
- Cronstedt, A., 1758. *Försök til mineralogie, eller mineralrikets upställning*, Stockholm. (English translation: Magellan, John Hyacinth. *An essay towards a system of mineralogy.*) London (1788).
- Damour, A., Salvetat, D., 1847. Analyses sur un hydrosilicate d'alumine trouvé à Montmorillon. *Annales de Chimie et Physique, Série* 3, 21, 376–383.
- Dana, J.D., 1914. *System of Mineralogy*, 6th edition. Wiley, New York.
- de Lapparent, J., 1936. Formula and structure of attapulgite. *Comptes Rendus de l'Académie des Sciences, Paris* 202, 1728–1731.
- de Lapparent, J., 1938. Défense de l'attapulgite. *Bulletin de la Société Française de Minéralogie* 61, 253–283.
- de Lish, R., 1783. *Cristallographie ou description des formes propres à tous les corps du règne minéral*. vol. 2, Paris, p. 502.
- Des Cloizeaux, A., 1862. Supplement to manual of mineralogy. vol. 1, Paris, pp. 548–549.
- Dick, A.B., 1908. Supplementary notes on the mineral kaolinite. *Mineralogical Magazine* 15, 124–127.
- Ehrenberg, P., 1915. *Die Bodenkolloide*. Verlag von Theodor Steinkopff, Dresden und Leipzig. (The 3rd edition appeared 1922).

- Endell, K., Hofmann, U., Wilm, D., 1933. Über die Natur der keramischen Tone. *Berichte der Deutschen Keramischen Gesellschaft* 14, 407–438.
- Faust, G.T., Murata, K.J., 1953. Stevensite redefined as a member of the montmorillonite group. *American Mineralogist* 38, 973–987.
- Friedrich, W., Knipping, P., von Laue, M., 1912. Interferenzerscheinungen bei Röntgenstrahlen. *Sitzungsberichte der königlichen Bayerischen Akademie der Wissenschaften, Mathematisch-Physikalische Klasse*, pp. 303–322.
- Fripiat, J.J., 1995. From clay to zeolites and back. In: Elsen, A., Grobet, P., Keung, M., Leemann, H., Schoonheydt, R., Toufar, H. (Eds.), *Book of Abstracts, Euroclay'95*, Leuven, p. 5.
- Glocker, E.F., 1847. *Generum et Specierum Mineralium Secundum ordines Naturales Digestorium Synopsis*. Halle, p. 195.
- Grim, R.E., 1939. Relation of the composition to the properties of clay. *Journal of the American Ceramic Society* 22, 141–151.
- Grim, R.E., 1953. *Clay Mineralogy*. McGraw-Hill, New York.
- Grim, R.E., 1968. *Clay Mineralogy*, 2nd Edition. McGraw-Hill, New York.
- Grim, R.E., 1962. *Applied Clay Mineralogy*. McGraw-Hill, New York.
- Grim, R.E., 1988. The history of the development of clay mineralogy. *Clays and Clay Minerals* 36, 97–101.
- Grim, R.E., Bray, R.H., Bradley, W.F., 1937. The mica in argillaceous sediments. *American Mineralogist* 22, 813–829.
- Gruner, J.W., 1932. The crystal structure of kaolinite. *Zeitschrift für Kristallographie* 83, 74–88.
- Gruner, J.W., 1934. The structures of vermiculite and their collapse by dehydration. *American Mineralogist* 19, 557–575.
- Gruner, J.W., 1935a. The structural relationship of glauconite and mica. *American Mineralogist* 20, 699–714.
- Gruner, J.W., 1935b. Structural relations of nontronites and montmorillonites. *American Mineralogist* 20, 475–483.
- Gruner, J.W., 1939. Water layers in vermiculite. *American Mineralogist* 24, 428–433.
- Hadding, A., 1923. Eine röntgenographische Methode, kristalline und kryptokristalline Substanzen zu identifizieren. *Zeitschrift für Kristallographie* 58, 108–112.
- Hausmann, J.F.L., Stromeyer, F., 1816. (“Allophan”, named and analyzed by Stromeyer but reported by Hausmann, J.F.L.). *Göttingische Gelehrte Anzeigen* 2, 1251–1253.
- Heide, F., 1928. Beiträge zur Mineralogie und Petrographie der Rhön. *Chemie der Erde* 3, 91–97.
- Hendricks, S.B., Ross, C.S., 1941. The chemical composition and genesis of glauconite and celadonite. *American Mineralogist* 26, 708–863.
- Hendricks, S.B., Teller, E., 1942. X-ray interference in partially ordered layer lattices. *The Journal of Physical Chemistry* 10, 147–167.
- Hermann, R., 1829. Zerlegung des Pyrophyllits, eines neuen Minerals. *Annalen der Physik und Chemie (Poggendorfs Annalen)*, 2. Folge 15, 592.
- Hettinger, W.P., 1991. Contribution to catalytic cracking in the petroleum industry. *Applied Clay Science* 5, 445–468.
- Hewett, D.F., 1917. The origin of bentonite. *Journal of the Washington Academy of Sciences* 7, 196–198.
- Hoffmann, C., 1788. *Bergmännisches Jahrbuch*, p. 519.
- Hofmann, U., 1976. Anfänge der Silicatiforschung in den dreissiger Jahren. *Tonindustrie Zeitung* 100, 314.

- Hofmann, U., Endell, K., Maegdefrau, E., 1943. Die Einheitlichkeit des glimmerartigen Tonminerals Sárospatit. *Berichte der Deutschen Keramischen Gesellschaft* 24, 339–344.
- Hofmann, U., Endell, K., Wilm, D., 1933. Kristallstruktur und Quellung von Montmorillonit (Das Tonmineral der Bentonittone). *Zeitschrift für Kristallographie* 86, 340–348.
- Hofmann, U., Endell, K., Wilm, D., 1934. Röntgenographische und kolloidchemische Untersuchungen über Ton. *Angewandte Chemie* 47, 539–547.
- Jasmund, K., 1951. *Die Silikatischen Tonminerale*. Verlag Chemie, Weinheim. (The 2nd edition appeared in 1955.)
- Jasmund, K., 1991. Von den Tonkolloiden zu den Tonmineralen. In: Tributh, H., Lagaly, G., (Eds.), *Berichte der Deutschen Ton- und Tonmineralgruppe, DTTG*, Gießen, pp. 11–20.
- Johnson, S.W., Blake, J.M., 1867. On kaolinite and pholerite. *American Journal of Science* (2nd series) 43, 351–361.
- Jordan, J.W., 1949a. Alteration of the properties of bentonite by reaction with amines. *Mineralogical Magazine* 28, 598–605.
- Jordan, J.W., 1949b. Organophilic bentonites. I. Swelling in organic liquids. *Journal of Physical and Colloid Chemistry* 53, 294–306.
- Jordan, J.W., Hook, B.W., Finlayson, C.M., 1950. Organophilic bentonites. II. *Journal of Physical and Colloid Chemistry* 54, 1196–1208.
- Jordan, J.W., Williams, F.J., 1954. Organophilic bentonites. III. Inherent properties. *Kolloid-Zeitschrift* 137, 40–48.
- Keferstein, C., 1827. (Glaukonit) Teutschland geognostisch-geologisch dargestellt und mit Charten und Durchschnittszeichnungen erläutert. Im Verlage des Landes-Industrie-Comptoirs, Veimar 5, 508–511.
- Kerr, P.F., Hamilton, P.K., 1948. Glossary of clay minerals names. Report 1, American Petroleum Institute Project 49. Columbia University, New York.
- Knight, W.C., 1897. Mineral soap. *Engineering and Mining Journal* 63, 600–601.
- Knight, W.C., 1898. Bentonite. *Engineering and Mining Journal* 66, 491.
- Köster, H.M., 1994. Gedanken zur Erforschung der Tonminerale und Tone. In: Kohler, E.E. (Ed.), *Berichte der Deutschen Ton- und Tonmineralgruppe (DTTG)*. Beiträge zur Jahrestagung Regensburg, DTTG, pp. 1–9.
- Kohler, E.E., Köster, H.M., 1976. Zur Mineralogie, Kristallchemie und Geochemie kretazischer Glaukonite. *Clay Minerals* 11, 273–302.
- Konta, J., 1995. Clay and man: clay raw materials in the service of man. *Applied Clay Science* 10, 275–335.
- Konta, J., 2000. Clay science at the threshold of the new millennium: a look at the history and present trends. *Acta Universitatis Carolinae—Geologica* 44, 11–48.
- Lagaly, G. (Ed.), 2002. *ECGA Newsletter* 5. Verlag Reinhard Knof, Nehnten.
- Lagaly, G., Beneke, K., 1991. Intercalation and exchange reactions of clay minerals and non-clay layer compounds. *Colloid and Polymer Science* 269, 1198–1211.
- Larson, E.S., Steiger, G., 1928. Dehydration and optical studies of Alunogen, Nontronite, and Griffithite. *American Journal of Science Series* 5, 15, 1.
- Larson, E.S., Wherry, E.T., 1917. Leverrierite from Colorado. *Journal of the Washington Academy of Sciences* 7, 208–217.
- Larson, E.S., Wherry, E.T., 1925. Beidellite—a new mineral name. *Journal of the Washington Academy of Sciences* 15, 465–466.

- Le Châtelier, H., 1887. De l'action de la chaleur sur les argiles. *Bulletin de la Société Française de Minéralogie* 10, 204–207.
- Leeds, A.R., 1873. A hydrous unisilicate approaching pyrosclerite. *American Journal of Science* 6, 22–24.
- Lemberg, J., 1876. Über Silicatumwandlungen. *Zeitschrift der Deutschen Geologischen Gesellschaft* 28, 519–526.
- Lindgren, W., Hillebrand, W.F., 1904. Minerals from the Clifton, Morenci district, Arizona. *American Journal of Science Series* 4, 18, 448–460.
- Lippmann, F., 1954. Keuper Ton von Zaiserweiher. *Heidelberger Beiträge zur Mineralogie und Petrographie* 4, 130–134.
- Lippmann, F., 1960. Corrensit. In: Hintze, C., (Ed.), *Handbuch der Mineralogie*. Chudoba, K.F., (Ed.) *Ergänzungsband II. Neue Mineralien und Mineralnamen*, Teil III, pp. 688–691.
- MacEwan, D.M.C., 1961. The montmorillonite minerals. In: Brown, G. (Ed.), *X-ray Identification and Crystal Structures of Clay Minerals*. Mineralogical Society (Clay Minerals Group), London, pp. 86–107.
- Mackenzie, R.C., 1984. Discovery of volkonskoite. *Mineralogical Magazine* 48, 297–298.
- Maegdefrau, E., 1941. Die Gruppe der glimmerartigen Tonmineralien. *Sprechsaal für Keramik-Glas-Email* 74, 369–372 381–383, 393–396, 399–401.
- Maegdefrau, E., Hofmann, U., 1937. Glimmerartige Mineralien als Tonsubstanzen. *Zeitschrift für Kristallographie* 98, 31–59.
- Mauduyt, 1847. Un mot sur un morceau de quartz d'une variété particulière, ainsi que sur une substance minérale trouvée dans le département de la Vienne. *Bulletin de la Société Géologique de France Série* 2 (4), 168–170.
- Mehmel, M., 1935. Über die Struktur von Halloysite und Metahalloysite. *Zeitschrift für Kristallographie* 90, 35–43.
- Mellor, J.W., 1916. Do fireclays contain halloysite or clayite? *Transactions of the Ceramic Society (England)* 16, 83.
- Migeon, G., 1936. Contribution à l'étude de la définition des sépiolites. *Bulletin de la Société Française de Minéralogie* 59, 6–133.
- Nadeau, P.H., Farmer, V.C., McHardy, W.J., Bain, D.C., 1985. Compositional variations of the Unterrupsroth beidellite. *American Mineralogist* 70, 1004–1010.
- Nagelschmidt, G., 1938. On the atomic arrangement and variability of the members of montmorillonite group. *Mineralogical Magazine* 25, 140–155.
- Nagy, B., Bradley, W.F., 1955. Structure of sepiolite. *American Mineralogist* 40, 885–892.
- Novelli, G., 2000. La bentonite—una argilla nei secoli. (Also in English: Bentonite—a clay over centuries. Lecture presented 1999 during the institution of the prize “Giovanni Novelli” on industrial applications of smectitic clays. *Incontri Scientifici*, Volume II. Fiore, H.S. (Ed.) Istituto di Ricerca sulle Argille, pp. 207–304.
- Pauling, L., 1930a. The structure of mica and related materials. *Proceedings of the National Academy of Sciences, USA* 16, 123–129.
- Pauling, L., 1930b. The structure of chlorites. *Proceedings of the National Academy of Sciences, USA* 16, 578–582.
- Reitstötter, J., 1954. Herbert Freundlich. *Kolloid-Zeitschrift* 139, 1–11.
- Reuss, F.F., 1809. Sur un nouvel effet de l'électricité galvanique. *Mémoires de la Société Impériale des Naturalistes de Moscou* 2, 327–337.

- Ries, H., 1920. Clays and shales of Virginia, west of the Blue Ridge. Virginia Geological Survey Bulletin 20, 118.
- Rinne, F., 1924. Röntgenographische Untersuchungen an einigen feinzerteilten Mineralien, Kunstprodukten und dichten Gesteinen. *Zeitschrift für Kristallographie* 60, 55–69.
- Robertson, R.S.H., 1986. Fuller's Earth. A History. Volturra Press, Hythe, Kent, UK.
- Roepper, W.T., 1875. In: Genth, F.A. (Ed.), Preliminary Report on the Mineralogy of Pennsylvania, 1874. 2nd Geological Survey, Harrisburg, 120B–121B.
- Rohland, P., 1909. Die Tone. A. Hartleben's Verlag, Wien und Leipzig.
- Röntgen, W.C., 1895. Über eine neue Art von Strahlen (Vorläufige Mitteilung). *Sitzungsberichte der physikalisch-medizinischen Gesellschaft Würzburg*, pp. 137–141.
- Ross, C.S., 1946. Sauconite—a clay mineral of the montmorillonite group. *American Mineralogist* 31, 411–424.
- Ross, C.S., Hendricks, S.B., 1945. Minerals of the montmorillonite group. U.S. Geological Survey, Professional Paper 205B, 23–79.
- Ross, C.S., Kerr, P.F., 1930. Dickite, a kaolin mineral. *American Mineralogist* 15, 34–39.
- Ross, C.S., Kerr, P.F., 1931a. The kaolin minerals. U.S. Geological Survey Professional Paper 165-E, 151–176.
- Ross, C.S., Kerr, P.F., 1931b. The clay minerals and their identity. *Journal of Sedimentary Petrology* 1, 55–65.
- Ross, C.S., Kerr, P.F., 1934. Halloysite and allophane. U.S. Geological Survey, Professional Paper 185G, 135–148.
- Ross, C.S., Shannon, E.V., 1925. The chemical and optical properties of beidellite. *Journal of the Washington Academy of Sciences* 15, 467–468.
- Ross, C.S., Shannon, E.V., 1926. Minerals of bentonite and related clays and their properties. *Journal of the American Ceramics Society* 9, 77–96.
- Salmang, H., 1927. Die Ursachen der Bildsamkeit der Tone. *Zeitschrift für Anorganische und Allgemeine Chemie* 162, 115–126.
- Schalek, E., Szegvary, A., 1923a. Über Eisenoxidgallerten. *Kolloid-Zeitschrift* 32, 318–319.
- Schalek, E., Szegvary, A., 1923b. Die langsame Koagulation konzentrierter Eisenoxydsole zu reversiblen Gallerten. *Kolloid-Zeitschrift* 32, 326–334.
- Schlösing, T., 1874. Sur la constitution des argiles: kaolins. *Comptes Rendus de l'Académie des Sciences, Paris* 79, 473–477.
- Schwieger, W., Lagaly, G., 2004. Alkali silicates and crystalline silicic acids. In: Auerbach, S.M., Carrado, K.A., Dutta, P.K. (Eds.), *Handbook of Layered Materials*. Marcel Dekker, New York, pp. 541–629.
- Siddiqui, M.K., 1968. Bleaching Earths. Pergamon Press, Oxford.
- Ssaftschenskow (also: Savchenkov), T.V., 1862. Palygorskit. *Verhandlungen der Russisch Kaiserlichen Gesellschaft für Mineralogie, Sankt Petersburg*, pp. 102–104.
- Stephen, I., MacEwan, D.M.C., 1950. Swelling chlorite. *Géotechnique* 2, 82–83.
- Strese, H., Hofmann, U., 1941. Synthese von Magnesiumsilikat-Gelen mit zweidimensional regelmäßiger Struktur. *Zeitschrift für Anorganische und Allgemeine Chemie* 247, 65–95.
- Svanberg, L.F., 1840. Saponit och Rosit, tvenne nya mineralier. *Kungliga Vetenskap Akademien Stockholm Handlingar*, 153–166; see also *Annalen der Physik und Chemie (Poggendorfs Annalen)*, 2. Folge, 57 (1842), 165–170.
- Termier, P., 1890. Étude sur la leverrierite. *Annales des Mines* 17, 372–398.

- Theng, B.K.G., Orchard, V.A., 1995. Interactions of clays with microorganisms and bacterial survival in soil: A physicochemical perspective. In: Huang, P.M., Berthelin, J., Bollag, J.-M., McGill, W.B., Page, A.L. (Eds.), *Environmental Impact of Soil Component Interactions*. Lewis Publishers, Boca Raton, FL, pp. 123–143.
- van Bemmelen, J.M., 1877. Das Adsorptionsvermögen der Ackererde. *Landwirtschaftliche Versuchsstation* 21, 135–191.
- van Bemmelen, J.M., 1878. Das Adsorptionsvermögen der Ackererde. *Berichte der Deutschen Chemischen Gesellschaft* 11, 2228–2233.
- van Bemmelen, J.M., 1888. Über die Adsorptionsverbindungen und das Adsorptionsvermögen der Ackererde. *Landwirtschaftliche Versuchsstation* 35, 69–136.
- van Bemmelen, J.M., 1910. Die Adsorption, *Gesammelte Abhandlungen über Kolloide und Adsorption*. Mit Unterstützung des Verfassers neu herausgegeben von Dr. Wo. Ostwald. Verlag von Theodor Steinkopff, Dresden.
- van Olphen, H., 1963. *An Introduction to Clay Colloid Chemistry*. Wiley, New York (The 2nd edition appeared in 1977.).
- Viczán, I., 2000. History of mineralogical investigations of the Füžerradvány “illite” near Sárospatak, Hungary. *Acta Geologica Hungarica* 43, 493–500.
- Viczán, I., 2002. Sarospatite: two years earlier. In: Lagaly, G. (Ed.), *ECGA Newsletter* 5. Verlag Reinhard Knof, Nehnten, p. 56.
- von Ardenne, M., Endell, K., Hofmann, U., 1940. Untersuchungen feinsten Fraktionen von Bentoniten und Tonböden mit dem Universal-Elektronenmikroskop. *Berichte der Deutschen Keramischen Gesellschaft* 21, 209–227.
- von Liebig, J., 1858. Über einige Eigenschaften der Ackerkrume. *Annalen der Chemie und Pharmazie* 105, 109–144.
- von Liebig, J., 1865. *Chemische Briefe*, 35. Brief, C.F. Winter’sche Verlagshandlung, Heidelberg.
- Wada, K., Yoshinaga, N., 1969. The structure of imogolite. *American Mineralogist* 54, 50–71.
- Way, J.T., 1852. On the power of soils to absorb manure. *Journal of the Royal Agronomical Society of England* 13, 123–143.
- Webb, T.H., 1824. New localities of tourmalines and talc [vermiculites]. *American Journal of Science* 7, 55.
- Weinschenk, E., 1897. Beiträge zur Mineralogie Bayerns. I. Vorkommnisse aus den Graphitlagerstätten nördlich von Passau. II. Der sogenannte Anthophyllit von Bodenmais. III. Spessartin von Aschaffenburg. *Zeitschrift für Kristallographie* 28, 157–164.
- Weiss, A., Koch, G., Hofmann, U., 1954. Zur Kenntnis von Wolchonskoit. *Berichte der Deutschen Keramischen Gesellschaft* 31, 301–305.
- Weiss, A., Hofmann, U., 1951. Batavit. *Zeitschrift für Naturforschung* 6b, 405–409.
- Werner, A.G., 1789a. Chlorit (als Gruppenname). Im *Mineralsystem des Herrn Inspektor Werner mit dessen Erlaubnis herausgegeben von C.A.S. Hoffmann*. *Bergmännisches Journal* 2, 376, 391.
- Werner, G., 1789b. *Letztes Mineral System*. Herausgegeben von C. Hoffmann. *Bergmännisches Journal* 1, 377.
- Yoshinaga, N., Aomine, S., 1962a. Imogolite in some Ando soils. *Soil Science and Plant Nutrition (Tokyo)* 8, 22–29.
- Yoshinaga, N., Aomine, S., 1962b. Allophane in some Ando soils. *Soil Science and Plant Nutrition (Tokyo)* 8, 6–13.



This page intentionally left blank

*Chapter 16*

## TEACHING CLAY SCIENCE: A GREAT PERSPECTIVE

R.W. BERRY<sup>a</sup>, F. BERGAYA<sup>b</sup> AND G. LAGALY<sup>c</sup>

<sup>a</sup>*Department of Geological Sciences, San Diego State University, San Diego, CA 92182-1020, USA*

<sup>b</sup>*CRMD, CNRS-Université d'Orléans, Orléans Cedex 2, France*

<sup>c</sup>*Institut für Anorganische Chemie, Universität Kiel, D-24118 Kiel, Germany*

The complex nature of clay (different species, different properties, and different modifications of natural clays) as well as the innumerable uses and applications of clays demand that clay scientists from different universities and countries establish educational subjects and techniques that are at least minimally standardized. This interest in clay science is extended to undeveloped countries because naturally occurring cheap clay materials may be found in all countries and are used in many parts of our daily life.

Clay science is an extraordinarily complex, heterogeneous, and multi-faceted discipline, because the clay mineral properties are very complex and are dependent on environmental conditions. The techniques for characterization of clay minerals are very delicate, because of fine grain-size of clay materials. Analyses are made even more difficult because clay minerals are in perpetual thermodynamic interaction with a changing environment (Millot, 1989). For example, the question of where adsorption (e.g., pollutants) by clay particles occurs, in interlayer or interparticle spaces, is difficult to determine because the particles are not inert and consequently the size and the shapes of the pores are varying continually with the environment (see Chapter 1).

Even though scientific knowledge of clay mineral properties progressed greatly during the last century, many people continue to use clays without knowing the cause of the clay mineral's usefulness. For instance, some cheap clay incubators are still used to protect premature babies from the cold. In many parts of the world drinking water is cooled by evaporative processes in porous clay pots or jugs. Properties of clay minerals lend themselves well to serving as dispensers of chemicals in the pharmaceutical, crop fertilization, and insecticide industries as well as for animal waste and industrial waste adsorption. Wines, vegetable oil, and crankcase oil are all subject to clarification and purification by filtering them through beds of clay minerals. The ceramics and nanocomposite industries are also sub-sets of the

field of clay science. Each of these disparate sub-sets requires unique education and training regimens for development of practitioners who are capable of contributing to their particular fields. Some of the sub-sets of clay science require use of equipment about which researchers in other sub-sets have no expertise.

However, there is a commonality that crosses the disciplinary boundaries between all sub-sets of clay science. It takes the form of classic clay mineralogy including X-ray diffraction (XRD) analysis. Both of which existed for nearly a century being inspired by, and following in part, the content of the textbook by Grim (1953). XRD is the universal technique for studying clay minerals that is taught in various academic departments and at different levels at universities around the world.

Teachers, researchers, engineers, users of clay materials (bentonite, kaolin, talc), and politicians responsible for establishing education curricula in each country, need to recognize the importance of multidisciplinary education in clay science. Homogeneous education curricula and teaching techniques do not exist across the full spectrum of clay science. Each sub-set of clay science is sufficiently complex and detailed that no university can afford professors and equipment to establish programs for all sub-sets. On the other hand, those aspects of clay science (e.g., clay mineralogy and XRD techniques) that are common to all sub-sets of clay science are being ignored by increasing numbers of universities that have either marginalized them or dropped them from their curricula altogether. As a result, clay mineralogy and XRD techniques are too often taught in scattered snatches delivered in geology, mineralogy, crystallography, colloid chemistry, and soil science courses.

Serious investigation is needed concerning what is considered fundamental in the clay science curricula of all universities in all countries. It seems timely to identify the programmatic commonalities across all sub-sets of the discipline. Inter- and intra-university communication between teachers and researchers will be facilitated when knowledge of course content and level of teaching is shared. The factors and reasoning that control or dictate clay science curricula at various universities should be documented in order to assist the establishment of commonalities in clay science curricula. Ultimately, students will be the beneficiaries.

The importance of clay mineralogy and XRD techniques is recognized universally across all sub-sets of clay science. Can this common subject matter be enlarged to encompass information or techniques that were not yet included in classes on clays and clay minerals? What subject matter will not yet been be of maximum benefit to the greatest number of students as they seek employment? Aside from the basic concepts of physics, chemistry, and mathematics, what other subjects and techniques should be added to the core curriculum for all aspects of clay science? The breadth of teaching within the sub-sets of clay science will correspond approximately to the topics listed in the Table of Contents of this handbook.

In general, these following fundamental questions must be answered:

- **Why** must clay science be taught?
- **What** has to be taught?
- At **Which** grade of education must clay science teaching be delivered?

Recently, [Rule and Guggenheim \(2002\)](#) answered the last question. They declared that “Teaching Clay Science is often thought of as forming the curriculum of upper-level for juniors. Although clays and clay minerals are complex subjects often requiring extensive background to understand in detail, introducing topics related to clays does not require such specialization.” These authors further add that “It does not seem reasonable to wait until a student reaches the upper-college level to introduce the subject, although the introduction of clay science must be approached at levels appropriate to the student’s development and background.”

The sooner basic clay mineralogy is introduced into a university curriculum, the better students will be able to understand the properties of these unique materials and the reasons behind many applications such as the medicinal value of some clays, even for trees protection against specific illness ([Sarrazin, 2004](#)), or cosmetic effectiveness of other clays (such as North African ‘ghassoul,’ used in spas or for hair washing). Studying clay science can avoid potential dangers that may accompany the use of clay minerals as reported in Chapter 11.

There is actually little educational homogeneity regarding clay science as it is taught in different countries. Clay science university curricula were controlled to a significant extent by needs and interests at the local, provincial, or state levels.

In the USA the Clay Minerals Society is attempting to have a positive influence on teaching clay science at the university level across state boundaries. The results of these efforts may be of value to universities outside North America. The remainder of the chapter is devoted to presenting the current status of clay science education in North America (principally the USA), in Europe (mainly in Germany), and also in New Zealand and Australia.

## 16.1. TEACHING CLAY SCIENCE IN THE USA

Clay science education is changing throughout the world, in general, and in the United States of America, in particular. The number of universities that offer programs in classical clay mineralogy, usually associated with departments of geology or earth sciences, is diminishing for several reasons. Clay mineralogy plays a lesser role in the petroleum industry, thereby diminishing employment opportunities for classically trained clay scientists. Government research laboratories such as the United States Geological Survey (USGS) and the Commonwealth Scientific and Industrial Research Organization (CSIRO) in Australia are focusing less on projects related to clay mineralogy and in some cases are cutting clay science programs completely ([Churchman, 2002](#)). These cut backs also contribute to diminishing employment opportunities. Many professors who once carried the load of supervising graduate students in traditional clay science programs are retiring without being replaced by others of a similar background, owing to what university administrations perceive as lessened scientific importance of the field and diminished employment opportunities.

In the USA, fewer degrees (BS, MS, and PhD) in all areas of geosciences, including clay science, were granted in 2001 than in 1973 (Ridky, 2002).

However, clay science in the United States and elsewhere remains strong at universities with soils programs, particularly where associated with schools of agriculture. Here, students are taught clay mineralogy applied to the processes of soil formation and maturation, as well as how clay science may be applied to the solution of pedologic problems. To a much lesser degree, departments of civil engineering support programs in clay mineralogy that are narrowly focused on foundation problems related to construction of dams, highways, and large office or housing structures. University departments of environmental studies, ground water hydrology or hydrogeology recognize the importance of clays and clay minerals as they relate to permeability, water quality, and remediation of pollution problems (such as spills of environmentally damaging and carcinogenic substances) but rarely teach clay mineralogy courses. Companies that manufacture absorbent substances from clay minerals (for control of pet wastes, and environmental spills) generally depend upon departments of chemistry to provide employees who are trained in this area of clay science.

Kaolinite and bentonite mining industries remain strong, worldwide. Research scientist vacancies are filled from academic departments that continue to graduate persons trained in classical clay mineralogy or from departments of agriculture. Some private industrial research laboratories support highly focused in-house clay mineralogical training programs in support of company goals and objectives. Such programs rarely have an impact outside individual companies.

An entirely new field grown (and continues to grow) out of clay mineralogy; the modification of clay minerals or outright synthesis of clay mineral-like substances called pillared clays, micro-composites, and ceramics. In the 1950s a few clay scientists became involved with a new field of ceramic engineering applied to electronics. The piezoelectric ceramic phonograph cartridge was one of the first products to emerge from this field of endeavor. In fact, the piezoelectric and modest semiconductor properties of ceramics fired from clay minerals contributed to a field that revolutionized electronics. As research progressed, “ceramic” materials were synthesized from substances unrelated to clay minerals. The term ceramic remains in use in semi-conductor and nanocomposite fields of research but is rarely recognized as related to clay science. The task of educating future scientists for this field of research now resides primarily in departments of physics and occasionally in departments of chemistry that support strong programs in surface chemistry, crystallography, and atomic structure. Pillared clay research continues mostly in departments of chemistry and engineering. New materials with exceptionally small pore diameters (micro sieves) were developed in academic departments and private research labs but these applications are concerned with clay-sized material and may be more closely related to zeolite than clay mineralogy.

Although clay science remains widely recognized for its importance in a variety of disciplines and fields of research, it is clear that future professors of clay science

necessarily are being educated differently now than they were decades ago. Rarely are they the products of classic clay mineral programs housed in geology or earth sciences programs. With the possible exception of soil sciences, the curricula that served as cores of university programs in the 1960s and 1970s are no longer adequate. Professors must now be prepared to teach within much narrower disciplines, preparing their students to work successfully in such widely divergent fields as soil and earth sciences, nanocomposites, engineering geology, environmental science, molecular sieves, and the pharmaceutical industry. This does not mean that clays are no longer important in the geological sciences but it does mean that clay science is more commonly combined with geochemistry and geophysics in sophisticated ways. As geologists attempt to solve highly complex problems related, for example, to ancient climates, plate tectonics, early composition and evolution of the lithosphere, they find it increasingly helpful to use the sensitivity of clays to environmental changes to provide chemical and physical information that helps solve their earth science problems.

#### *16.1.1. Teaching Clay Science at the University Level*

##### *Teaching Practices*

The trend toward using authentic or at least realistic, experiential techniques (Thomas, 2002) in undergraduate science education applies to teaching clay science. In the United States of America the phrase “hands-on education” is now being used in undergraduate education in the same way as it was used for many years in primary and secondary public schools. Students are being introduced to sophisticated analytical techniques at increasingly earlier stages of their undergraduate education. Theoretical courses in basic clay mineralogy will never be displaced from modern curricula, but these courses are now being infused with opportunities to apply what was learned to the solution of realistic problems.

Some professors use their own consulting and research experiences when constructing classroom, field, or laboratory exercises that enable students to learn techniques of problem solving. Undergraduate students are increasingly being included in the professional research projects of their professors. “Teaching Clay Science,” edited by Rule and Guggenheim (2002) contains examples of ways to incorporate practical problem-solving activities in clay science classrooms. “Teaching Mineralogy,” edited by Brady et al. (1997) is focused on classroom experiments and activities related to mineralogy in general. However, many of these experiments and activities can be used in clay mineralogy classes with minimal modification. Papers that describe experiments and other hands-on classroom activities are listed in Table 16.1.

Teaching methods in undergraduate and to some extent in graduate classes undergone scrutiny and are changing. Methodologies that were once used almost exclusively at the primary and secondary school levels are becoming increasingly common in university classrooms. Cooperative learning techniques (Srogi and

Table 16.1. Sources of classroom activities and experiments in clay science

1. *Teaching mineralogy*

Brady, J.B., Mogk, D.W., Perkins II, D. (Eds.), 1997. Mineralogical Society of America, Washington, DC., 406pp. (papers devoted to teaching general mineralogy, and applicable to teaching clay science include this list in the order in which they appear in the volume.)

“Introduction to properties of clay minerals”, by *S. Guggenheim*.

“From 2D to 3D: I. Escher drawings, crystallography, crystal chemistry, and crystal defects”, by *P.R. Buseck*

“A fun and effective exercise for understanding lattices and space groups”, by *D. Perkins*.

“Building crystal structure ball models using pre-drilled templates: Sheet structures, tridymite, and cristobalite”, by *K. Hollocher*.

“Directed-discovery of crystal structures using ball and stick models”, by *D.W. Mogk*. (includes biotite as the only phyllosilicate example)

2. *A Laboratory manual for X-ray powder diffraction*

Poppe, L.J., Paskevich, V.F., Hathaway, J.C., Blackwood, D.S., 2001. U.S. Geological Survey Open-File Report 01-041, CD-ROM.

3. *Teaching clay science*

Rule, A.C., Guggenheim, S. (Eds.), 2002. CMS Workshop Lectures, Volume 11. The Clay Minerals Society, Aurora, CO, 223pp. (papers listed in the order in which they appear in the volume.)

“Using a discrepant event to teach the coagulation and flocculation of colloids”, by *S.B. Parekh and A.C. Rule*.

“Rubrics in teaching assessment”, by *R.W. Berry* (classroom activities about interpretation of clay mineral XRD data and their application).

“An introduction to the analysis of clay minerals by laser and X-ray diffraction techniques”, by *S. Guggenheim*.

“Interlayer reactions in expandable clays: Exchange, solvation, and intercalation experiments”, by *B. Ross and S. Guggenheim*.

“Infrared spectroscopy in clay science”, by *P.A. Schroeder*.

“Structure and chemistry of clay minerals: Learning through application”, by *J.H. Laukant*

4. *Resources on the Internet*

U.S. Geological Survey publications: <<http://pubs.usgs.gov/>>

Proceedings from and information about workshops in Clay Mineralogy at the research center in Karlsruhe and the university in Jena: <<http://141.35.2.84/chemie/geowiss/tagungen/clay2002/clay2002.html>>

“Demonstrations in Soil Science” from Purdue University: <<http://www.agry.purdue.edu/courses/agry255/brochure/brochure.PDF>>

Baloche, 1997; Guggenheim and Kane, 2002), teaching by analogy (Rule, 2002a), differentiated teaching techniques (California Department of Education and the California Association for the Gifted, 1994), differentiation in classrooms (Tomlinson, 1995) and other creative educational techniques invaded university teaching in the USA. The once widely accepted practice for university students to sit in class and listen to whatever the professor felt like talking about is being subjected to critical scrutiny. More and more frequently, professors are asked to consider what a student

should know and be able to do when he or she completes the course. Departmental colleagues now exert more influence on what is taught in each other's classes, leading to formal or informal sets of course standards. Course standards become small subsets of a larger set of standards that guide departmental curricula. Departmental and university curricula in the USA are being adjusted to align with state and national content standards (Rule, 2002b).

### *Assessment*

Something else invaded university education. Assessment as it was used in primary and secondary educational systems in the USA is becoming more widespread in colleges and universities. Assessment tools grown to be much more than a few quizzes and exams, supplemented by lab reports and term papers. Once standards were established for what a student should know or be able to do on completion of the course, assessment must determine how successfully the course (or curriculum of courses) met the standards. Portfolios, journals, and scoring rubrics are assessment tools that, although new to many university professors, are becoming more common at the university level. An outline of the history of the introduction of statewide standards and assessment at the California State University since 1988 is presented by Berry (2002). The subject is discussed for Texas by Cawelti (2000), for Virginia by Thayer (2000), and for Massachusetts by Noyce et al. (2000).

Students benefit when university professors pay close attention to what they teach and how they teach it. Appropriately applied standards help improve the focus of a course and assessment provides professors with information about teaching effectiveness (Berry, 2002). Students will also benefit if they adjust their study techniques in the light of assessment results.

It is important to realize that assessment and evaluation are significantly different even though they may overlap each other. Assessment does not necessarily include grade consequences whereas evaluation almost always does. Evaluation (generally the assignment of grades) focuses on teaching and learning that has already taken place. At best, evaluation can no more than incidentally help students improve their study skills and learning strategies. Professors are seldom motivated to make changes in a course solely as a result of the assignment of grades. On the other hand, assessment helps students and professors alike measure the effectiveness of both the teaching and learning processes. If assessment is begun early, teaching methodologies, learning strategies, and subject matter content may be adjusted and improved before completion of a course. Performance assessment and authentic assessment are both helpful. Performance assessment encourages students to construct responses that illustrate how they might apply the knowledge they acquired. Authentic assessment encourages students to construct responses that demonstrate an actual application of knowledge, often in "real life" situations. More may be learned about performance and authentic assessments from Marzano and Kendall (1996).



### 16.1.2. Clay Science in the Public Schools

A neglected aspect of teaching clay science is the preparation of primary and secondary (public school) students for a successful experience at colleges and universities. Clay science professionals, particularly university professors, have a vested interest in the quality of education received by students before they enter institutions of higher education and ultimately enter the professional work force. Most public school teachers are open to if not enthusiastically supportive of cooperation with subject matter experts, especially in science.

The generally low levels of scientific expertise held by primary school teachers provide clay scientists with an opportunity to serve as subject matter consultants or resource persons. Primary school students' keen interest in soil provides an *entrée* for a team of classroom teachers and clay science professionals to introduce age-appropriate information about soils as they relate to clays and clay minerals. Similarly, strong interest in the physical environment in which they live provides opportunities for teacher and clay scientist to promote study and experimentation about the environment and preservation of its quality. Here again, clays play an important role.

Secondary school teachers usually have strong backgrounds in the subject matter of the courses they teach. However, they too usually welcome opportunities to interact with clay science professionals who may be in a position to help construct experimental protocols and supply access to equipment that otherwise would be unavailable to secondary school students. Assistance with planning and carrying out honors activities or science fair projects is highly valued by secondary students and teachers, alike.

There is great satisfaction in taking part in the intellectual growth of children and youths, and clay science professionals may find it very fulfilling to contribute to the teaching and learning processes of primary and secondary school student. There are additional rewards for university professors that result from interaction with public school teachers. Public school teachers are experienced in standards-based education methods and assessment tools, the same things that are relatively new on college and university campuses. They may serve as a significant resource for the university professor who is struggling with understanding and implementing new teaching methodologies.

### 16.1.3. Concluding Comments on the Scene in the USA and Other Industrialized Nations

Changes are taking place in the teaching of science in general and clay science in particular. Fundamentally, these changes are driven by changes in society on the one hand and increased complexity of modern science on the other hand. A strong impetus for implementation of standards-based science education (and attendant

assessment programs) is a societal focus on accountability. In the USA as well as in other industrialized nations, when measures of student success in learning show a decline society wants to know who is responsible for the decline and how the trend can be reversed. One way to hold schools, teachers, and students accountable is to establish subject matter standards and assess the success of students in meeting these standards.

Perhaps not the best, but certainly one of the easiest assessment tools to use is a standardized test. This is true for all educational levels from primary schools to universities. There is much to recommend standardized testing at universities. University administrators, professors, and students are provided, in this way, with a measure of teaching and learning effectiveness. Students, departments, and universities can be compared on the basis of test results. Standardized testing is most beneficial when analyses of test scores result in programs that improve teaching methods, subject matter selection, and student learning strategies.

Standardized tests may become punitive when evaluation rather than assessment is emphasized. Under these circumstances, when test scores are judged to be too low, there is a risk that students may be held back from graduation, and campus and departmental funding may be curtailed or faculty remuneration affected. Under these conditions the tests are called “High Stakes Tests.” At first it may seem like a good thing to use high stakes tests to hold campuses, faculty, and students accountable for poor educational outcomes. However, educational problems arise when emphasis is placed on passing the test rather than on improving teaching and learning. Although the research results are not consistent, high stakes testing may well increase student dropout rates. Another potential outcome is that teaching and learning may be unduly controlled by the person(s) who construct the tests rather than by university faculty and administration. In the USA, “teaching to the test” describes when professors focus too much on their students’ ability to pass the test rather than learn the subject matter.

A disturbing trend in the USA and a few other industrialized nations is to apply a business model to higher education. In this model, students are viewed as customers, and knowledge is a product with tuition as the product’s price. This places university faculty in the position of being salespersons and casts administration in a management role. The model mandates that faculty salaries be influenced by incentive increases that are primarily controlled by results of high stakes tests and faculty evaluation surveys completed by students. At universities that emphasize funded research, a professor’s salary and teaching load may be influenced by how much extramural funding he or she can attract, without regard to the quality and quantity of student involvement.

Some private universities, based entirely on a business model, are financially successful. Most of these private universities focus on continuing education for those who are already employed in local businesses. The financial success of these universities suggests that the business model of higher education has something to recommend it. Students believe they are getting something of value or they would not pay the tuition, but are they really getting as much of value as they could?

The previously mentioned downside of a broad application of the business model to institutions of higher education must not be ignored. Educational quality suffers when professors teach to the high stakes tests and inflate grades. These actions may cause the professor to look good when incentive pay raises are awarded but do little to forward teaching excellence. Patronizing students to acquire high evaluation scores (sometimes called “student satisfaction scores”) may be financially rewarding but may cause traditional and usually beneficial student–faculty relationships to suffer.

If the business model of higher education is allowed to exert inappropriate control of colleges and universities, curriculum decisions will be made by default by whom-ever boards of trustees or legislative committees assign the responsibility for writing high stakes tests. Clearly this not yet happened widely. If university faculty and administration reject the business model of higher education, control over curriculum and teaching excellence will not be abdicated to those least qualified to exert control.

Teaching clay science in the next decade will be in a state of change, driven by changes in the clay minerals marketplace. University curricula will change to reflect the universal move away from traditional clay mineralogy and toward more highly specialized and complex topics. Physics, chemistry, and computer modeling will play ever-greater roles in clay science. There is no doubt that the discipline of clay science and the teaching of clay science will survive, but the giants of the clay mineralogical past might not recognize them as part of the same profession they once served.

## 16.2. TEACHING CLAY SCIENCE IN GERMANY AND OTHER EUROPEAN COUNTRIES

In Germany and probably most European countries the same trend is observed as in the USA, perhaps even more pronounced. The need for clay mineralogists and geologists is decreasing and vacancies are seldom filled by clay scientists. Now, at the beginning of 21st century, even responsible people do not recognize the change of clay mineralogy into clay science. They are not aware of the need for well-trained clay scientists. They do not or cannot recognize that clay is a highly complex material which usually needs marked chemical or physical modification in order to meet application requirements. The rapid development in the use of clays and clay minerals in the production of enhanced materials (see Chapters 10 and 11) and the need for optimization of clays for hundreds of uses, including the area of health protection, require clay scientists to be well trained in chemistry, surface and colloid science, physics, and more and more in biological science. It often happens that open positions in industry, environmental technology, and administration that should have been occupied by modern clay scientists have been given to chemists and physicists who are not acquainted with clay science. The lack of basic knowledge in clay science is reflected in many publications!

The second important point is that teaching about clays and clay minerals at universities (teaching is almost absent in schools) strongly decreased. Typically,

knowledge about clays and clay minerals was imparted in mineralogy and geology courses. The number of students decreased with the number of positions for mineralogists and geologists, a welcome process at universities under the influence of the government to reduce the chairs in these disciplines. The decreasing interest in clay science is also observed in agronomy, in spite of the importance of clay minerals in soils. The alternative of teaching clay science in chemistry departments is urgently needed but is seldom implemented. Even the optimal combination of clay and colloid science is taught only at a few places in the world, ignoring that well-trained students will have the best chances to find industrial positions.

That clay science is seldom imparted in faculties other than geological science, is the consequence of too strict and too many regulations at universities. This is at least true for Germany although the situation in other European countries might be expected to be similar. Most governments and responsible politicians consider it important that the residence time of students at universities is as short as possible. Nor is great importance placed on students receiving a broad, all-embracing education. Students have little time to follow special interests, in great contrast to real needs in our high-tech world, and no longer possess the required degrees of freedom. The development of science is impeded by administrative and bureaucratic regulations for all disciplines, and clay science, in particular.

The transition of clay mineralogy into clay science, followed closely by a movement toward material science is a great change, even if it does not have much impact on teaching activities. It is a challenge for the National Clay Groups to fill the gap by increasing the number of courses that they offer. Success in the future depends on people recognizing the transformation of traditional clay mineralogy and geology into modern clay and material science. We should never forget that the pathway from ideas to technical realization can be long. Nor should we forget that future developments derive from present ideas and knowledge. For example, the term ‘nanotechnology,’ introduced some 30 years ago by [Taniguchi \(1974\)](#), is only now universally in vogue.

### 16.3. TEACHING CLAY SCIENCE IN NEW ZEALAND AND AUSTRALIA

The situation in New Zealand and Australia as regards teaching clay science is similar to that in Germany (and probably most countries in the European Union). Clay research, in general, diminished greatly in both New Zealand and Australia ([Churchman and Theng, 2002](#)). A small amount of clay mineralogy is taught as an adjunct to soil science which itself is in decline because of cut backs in funding and competition between research agencies for the available funds. However, countries like New Zealand that earn much of their living from agriculture must sooner or later “wake up” to the fact that soils and the clay minerals they contain are a key to economic prosperity.

## 16.4. CONCLUSIONS

Descriptions of the status of clay mineral and clay science education in the USA, European countries and in New Zealand and Australia are not sufficient to allow extrapolations about the global state-of-the-art regarding clay science teaching. The incompleteness is regrettable but the lack of data may inspire mobilization of the international clay community to seek an improved international understanding of clay science education.

It would be a service to the discipline of clay science if AIPEA took the initiative to:

1. Consult with national clay groups about the need to survey each country about its national teaching system.
2. Name a small group of experts (about 5 members) to synthesize and homogenize all the materials furnished by each national group. The experts could be asked to give their own recommendations on this subject. A financial donation from each national clay group could be used to cover expenses related to meetings and to the publishing of a final report on teaching clay science at an international scale.

### The word of the end



Teaching clay science must become as universal as teaching music. We have the same universal notes and the final musical sound is almost universal, although characteristic of each country.

Learning about clay structure and properties allow to play with the fundamental notes to create new properties, new applications which improve the quality of our life.

## REFERENCES

- Berry, R.W., 2002. Rubrics in teaching assessment. In: Rule, A.C., Guggenheim, S. (Eds.), *Teaching Clay Science. CMS Workshop Lectures*, vol. 11. The Clay Minerals Society.
- Brady, J.B., Mogk, D.W., Perkins, II, D. (Eds.), 1997. *Teaching Mineralogy*. Mineralogical Society.
- California Department of Education and the California Association for the Gifted, 1994. *Differentiating the core curriculum and instruction to provide advanced learning opportunities. A position paper*. California Department of Education, Sacramento, CA.
- Cawelti, G., 2000. Portrait of a benchmark school. *Educational Leadership* 57, 42–44.
- Churchman, G.J., 2002. R.I.P. another clay research group. *New Zealand Soil News* 50, 118–119.
- Churchman, G.J., Theng, B.K.G., 2002. Clay research in Australia and New Zealand. *Applied Clay Science* 20, 153–156.

- Grim, R.E., 1953. *Clay Mineralogy*. McGraw-Hill, New York.
- Guggenheim, S., Kane, S., 2002. Cooperative learning techniques: applications to clay science. In: Rule, A.C., Guggenheim, S. (Eds.), *Teaching Clay Science*. CMS Workshop Lectures, vol. 11. The Clay Minerals Society.
- Marzano, R.J., Kendall, J.S., 1996. *A Comprehensive Guide to Designing Standards-based Districts, Schools, and Classrooms*. Association for Supervision and Curriculum.
- Millot, G., 1989. Opening lecture. 9th International Clay Conference, Strasbourg, personal communication.
- Noyce, P., Persa, D., Traver, R., 2000. Creating data-driven schools. *Educational Leadership* 57, 52–56.
- Ridky, R., 2002. Why we need a corps of earth science educators. *Geotimes* 47 (9), 16–19.
- Rule, A.C., 2002a. Using analogies to enhance learning in clay science. In: Rule, A.C., Guggenheim, S. (Eds.), *Teaching Clay Science*. CMS Workshop Lectures, vol. 11. The Clay Minerals Society.
- Rule, A.C., 2002b. Learning theory and national standards applied to teaching clay science. In: Rule, A.C., Guggenheim, S. (Eds.), *Teaching Clay Science*. CMS workshop lectures, vol. 11. The Clay Minerals Society.
- Rule, A.C., Guggenheim, S. (Eds.), 2002. *Teaching Clay Science*. CMS Workshop Lectures, vol. 11. The Clay Minerals Society.
- Sarrazin, C., 2004. Lutte contre le psylle, protéger le poirier avec l'argile blanche. *La France Agricole*, p. 43.
- Srogi, L.A., Baloch, L., 1997. Using cooperative learning to teach mineralogy (and other courses, too!). In: Brady, J.B., Mogk, D.W., Perkins II, D. (Eds.), *Teaching Mineralogy*, 406. Mineralogical Society.
- Taniguchi, N., 1974. On the basic concept of 'nano-technology.' *Proceedings of the International Conference of Product Engineering, Tokyo, Part II*. Japan Society of Precision Engineering, Tokyo.
- Thayer, Y., 2000. Virginia's standards make all students stars. *Educational Leadership* 57, 70–72.
- Thomas, R.C., 2002. DIALOGUE: Overcoming obstacles to incorporating experiential learning into the geology curriculum. *GSA Today* 12, 8, 11.
- Tomlinson, C.A., 1995. *How to differentiate instruction in mixed-ability classrooms*. Association for Supervision and Curriculum Development, Alexandria, VA.

This page intentionally left blank

## SUBJECT INDEX

### A

- $\alpha$ - and  $t$ -plots, 395
- abattoirs, 634
- ab-initio calculations, 31, 37, 1116
- ab-initio energy minimization, 27
- ab-initio molecular dynamic simulation, 29
- absorptivity, 98, 911
- academic departments, 1184, 1186
- accessory minerals, 9
- acetals, 557
- acetate, 124, 127, 128, 220, 221, 224, 225, 311, 315, 316, 658, 767, 993, 1062
- acetone clay mineral dispersion, 404
- acid activation, 263–281
- acid attack, 263, 265, 266, 268, 270, 277, 279, 292, 299, 596, 837
- acid cracked wasted liquor, 660
- acid dissolution, 267–272
- acid treatment, 264–267, 271, 274, 277–280, 292, 545, *see also* acid activation
- acid-activated clay, 274, 278, 557, 561, 633
- acid-activated kaolinite, 1167
- acid-activation, 263–281
- acid-base character, 985
- acid-base pairs, 324
- acid-base reaction, 318
- acidic site, 101, 264, 265, 274, 276–280, 295–297, 407, 590, 591, 914
- acidity of soils, 993
- acrylic acid, 193, 599, 634, 1036
- acrylic amide, 634
- actinium (Ac), 727
- actinolite, 729
- activated carbon, 401, 641, 653, 655
- activation energy, 124, 715, 1015
- active principles, 623, 717, 719, 720, 734
- acridine orange, 479
- acylating, 560
- adamantine, 647
- adenosine phosphate, 327
- adhesion, 724, 744, 747, 769
- administration, 733, 745, 746, 1066, 1191, 1192
- adsorbent, 718, 1186
- adsorption capacity, 516
- adsorption excess, 340, 342
- adsorption excess isotherm, 340–342
- adsorption isotherm, 639, 965, 967, 970, 972, 974
- adsorptive properties, 336, 401, 746
- AEC (anion exchange capacity), 656, 657, 1031–1033, 1056
- AES (Auger electron spectroscopy), 631
- aesthetic, 623, 722
- aesthetic medicine, 623, 722
- AFM (atomic force microscopy), 104, 161, 192, 223, 270, 486, 754, 969, 1119
- ageing time, 402, 1047
- aggradation, 1130, 1134
- aggregate, 11, 102, 125, 141, 142, 212, 351, 517, 662, 747, 925, 950, 1119
- agriculture, 3, 460, 1164, 1186, 1193
- AIPEA (Association Internationale pour l'Etude des Argiles), 4, 25, 33, 724, 1173, 1194
- AIPEA Nomenclature Committee, 25, 33
- akaganeite, 181, 210, 842
- Al (five-coordinated), 37, 55
- Al (four-coordinated), 876
- Al (six-coordinated), 876
- <sup>27</sup>Al chemical shifts, *see* chemical shift
- <sup>27</sup>Al NMR spectroscopy, 55, 397
- Al chlorohydrate, 398
- Al Keggin cations, 397, 406
- Al Keggin ions, 397
- Al oxocations, 408
- Al oxyhydroxide, 612, *see also* aluminium hydr(oxide)
- Al<sub>13</sub>, 397–399, 401, 404, 407–409, 902, 1042
- Al<sub>13</sub> dimer (Al<sub>24</sub>O<sub>72</sub>), 397
- Al<sub>13</sub> precursor, 398
- (Al<sub>13</sub>)<sup>7+</sup> pillaring agent, 397
- Al<sub>26</sub>, 397
- Al-Fe PILC, *see* PILC
- alcohol, 175, 177, 221, 310, 321, 327, 346, 934, 949, 1030
- aldehydes, 318, 556, 557, 1058
- aldol, 556, 1058
- aldoximes, 563
- aliettite, 25
- aliphatic, 322, 610



- alkali silicates, 10, 1168
- alkali-activation, 518, 930, *see also* soda activation
- alkaline earth, 21, 95, 505, 628, 630, 994
- alkene, 445, 1058
- alkene isomerisation, 1058
- alkenylammonium, 593
- alkoxysilane, 592
- alkylammonium cations, 108, 595, 633, 635, 642
- alkylammonium method, 172, 322, 994
- alkylammonium salts, 327, 523–525
- alkylating, 280, 560, 561
- allergy, 747
- allophane Al-rich, 303
- allophane Al/Si ratio(s), 51, 54, 55
- allophane defect-kaolin, 54
- allophane ferric, 33
- allophane halloysite-like, 54
- allophane imogolite-like, 51, 52, 54
- allophane-like constituents, 49
- allophane silica springs/stream deposit, 54, 55
- allophane Si-rich, 54, 55
- allophanton, 1164
- AlMPILC, 400
- Al-oxide, 394
- Al-pillared clay mineral, 181, 396
- Al-Si pillaring agent, 401
- alumina cluster, 408
- $\gamma$ -alumina structure, 408
- aluminium five-fold coordination, 37
- aluminium 4-coordinate, 55
- aluminium 5-coordinate, 55
- aluminium (hydr)oxide, 195, 632, 635, 655, 1061
- aluminium sulphate, 508, 634, 659
- aluminosilicate layer, 650, 656, 854
- aluminosilicate short-range order, 48
- amesite, 33, 34, 772
- amide, 195, 310, 315, 634, 875
- amines, 43, 318, 319, 322, 325, 327, 557, 633, 654, 845, 1043
- amino acid, 326, 382, 386, 387, 1035
- aminoacyladenylates, 386
- asymmetric polymerisation, 382
- ammonia, 277, 278, 382, 546, 552, 636, 1030
- amorphous material, 782
- amphiphilic cation, 106, 107
- amphoteric, 635, 661
- anandite, 38
- anhydride, 386, 561, 599
- aniline, 445, 590, 608, 1036
- anilinium, 44, 555, 608
- animal husbandry, 510
- anion exchange capacity (AEC), 9, 352, 353, 609, 656, 987, 988, 1031
- anionic clay, 11
- anisotropy, 8, 219, 332, 870, 876, 885, 894, 897, 901, 903, 922, 928, 1046
- anomalous small angle X-ray scattering, *see* ASAXS
- antacid, 720
- antibiotic, 635, 721, 748
- anticaking, 516
- antifriction agent, 503
- antigorite, 33, 34, 772
- anti-Markovnikov addition, 555
- anti-settling, 516
- antithixotropic, antithixotropy, 219, 222
- anti-transpirants, 181
- antique vases, 518
- Aparicio-Galán-Ferrell index, 30
- application of knowledge, 1189
- applied clay mineralogy, 2, 625, 1165
- applied research, 16, 281
- aqueous clay mineral dispersion, 104, 396
- aquifer, 641
- argillology, 2
- argon, 967–969, 974
- aromatic substitution, 551, 554
- aromaticity, 650
- arsenic (As), 726, 831, 835, 840
- ASAXS (anomalous small angle X-ray scattering), 890–891
- asbestos, 729, 730, 732, 734
- asbestosis, 729, 730
- aspect ratio, 153, 161, 441
- asphalt, 509
- associated mineral(s), 9, 10, 66, 501, 517, 754, 759, 910
- associated phase(s), 9, 10, 721, 726
- Association Internationale pour l'Etude des Argiles, *see* AIPEA
- atomic arrangement, 51, 1165
- atomic force microscopy, *see* AFM
- atomic number, 790, 791, 804, 941
- atomic shell, 794, 801
- atomic structure, 880, 942, 1186
- atrazine, 95, 96, 442, 653, 655
- attapulgit, 69, 393, 564, 631, 637, 744, 1168, 1171
- attenuated total reflection (ATR), 107
- Atterberg limit, 206, 207, 726
- Atterberg method, 206
- attractive gel, 216

Auger electron spectroscopy, *see* AES

Auger parameter, 870, 876

auromycin, 635

autotransformation, 265, 993

Avrami-Erofeev equation, 313

axial stress, 1104

azide, 561, 562

## B

$\pi$ -bonds, 649

bacitracin, 635

backfill, 708, 709

backscattering, 754, 794, 797, 804, 806, 808, 813, 814, 822

bacterial reduction, 433, 501

baileychlore, 6, 45

ball clay, 8, 659

balnea, 718

band-type arrangement, 207

barasym, 101

barium (Ba), 511, 985

barrier, 383, 409, 610, 653, 693, 698, 699, 705, 743–745, 748, 1147

basal ( $d_{001}$ ) spacing, 98, 394

base exchange capacity, 1164

base pairing, 327

base-activated kaolinite, 1167

basic dyes, 660, *see also* dye

basic site, 1058

basicity, 103, 149, 397, 436, 1058

bata vite, 1168

Beckman rearrangement, 562

beidellite, 42, 43, 89, 121, 122, 142, 172, 173, 215, 279, 396, 408, 409, 552, 758, 773, 902, 927, 956, 1133, 1134, 1153, 1168, 1169

bemenite, 7, 33

beneficial effects, 717, 743, 744, 748

Bentone<sup>®</sup>, 593

bentonite, 8, 48, 106, 145, 152, 157, 159, 199, 205, 219, 220–222, 249, 253, 257, 263, 279, 387, 444, 493, 494, 501, 503, 506, 508, 509, 511, 512, 514, 517, 518, 521, 523, 525, 531, 545, 625, 631–634, 637, 639, 642, 647, 653, 659, 660, 662, 663, 679, 680, 704, 709, 714, 722, 725, 730, 734, 743, 747, 910, 1057, 1134, 1143, 1147, 1150, 1152–1154, 1166, 1169, 1184, 1186

bentonites Cheto type, 1153

bentonites Wyoming type, 106, 734, 1153

benzene, 280, 319, 320, 339, 342, 355, 399, 590, 640, 651, 653, 901, 928, 1057

benzo(a)pyrene, 655

benzoyl peroxide, 355, 594

Bertaut-Warren-Averbach procedure, 161, 778

berthierine, 33, 772, 1140, 1145, 1147

BET (Brunauer Emmett and Teller), 272, 277, 281, 290, 294, 966, 967, 969, 970, 1049

betaines, 175, 176, 220

bidentate, 835, 836, 843

bilayer, 146, 322, 327, 328, 333, 336–338, 347, 588, 648, 683, 902

binding agent, 508, 514, 767, 1061, 1062, 1115

binding coefficient, 681, 983, 991

binding site, 631

bioavailability, 721

biochemical oxygen demand (BOD), 634

bio-clays, 477, 478, 480

biodegradation, 642

biological cations, 633–636, 661

biological science, 1192

biology, 2

biomimetic catalyst, 1066, 1067

biomineralisation, 3, 477, 478, 486, 496

biopoiesis, 1067

biopyrroles, 60

biosensor, 105

biotite, 60, 156, 454, 775, 812, 814, 818, 821, 838, 874, 875, 956, 957, 1129, 1133, 1134, 1136, 1138, 1141

bipyridinium halides, 635

bitumen, 511

bityite, 38

bleaching earth, 8, 662, 1166

blue asbestos, 729

blue-green algae, 641

boehmite, 120, 182, 214, 744

bonding, *see* hydrogen bonding

bonding energies, 630

bone china, 505

boromuscovite, 38

bovine serum albumin, 354, 635

brammallite, 1169

bricks, 1, 502, 518, 954, 1152

bridging, 87, 184, 192, 195–199, 844, 1116, 1117

brindleyite, 33

brinrobertsite, 37

brittle mica, 38

broken edge, 91, 270, 271, 833

bromination, 560, 1067

Brønsted acid, 264, 274, 278, 296, 300, 547, 590, 591  
 brown asbestos, 729  
 brown-tide, 660  
 Brunauer Emmett and Teller, *see* BET  
 BTEA (benzyltriethylammonium), 647, 653  
 BTMA (benzyltrimethylammonium), 593, 647, 681, 686  
 buffering, 1065  
 building industry, 516  
 bulk technique, 791  
 burial diagenesis, 957, 1130, 1141, 1142, 1146, 1147, 1149, 1150  
 butachlor, 642  
 butylacrylate, 596

## C

C<sub>60</sub>, 1046, 1069  
 cadmium (Cd), 628, 695  
 cadmium-cysteine, 311  
 calcium (Ca), 126, 128, 146, 148, 149, 154, 170, 188, 189, 199, 204, 205, 263, 301, 321, 323, 326, 327, 506, 508, 511, 512, 518, 637, 659, 679, 720, 782, 974, 982, 1052, 1113, 1114, 1115, 1116, 1118, 1119, 1120, 1122, 1123, 1164, 1171  
 calcium carbonate, 199, 518, 1164  
 calcium hydroxide, 659, 1114, 1118  
 capillary porosity, 1114, *see also* porosity  
 car washes, 508, 662  
 carbene, 557  
 carbocations, 547  
 carbon tetrachloride, 649, 650  
 carbonaceous clays, 594, 609  
 carbonate decomposition, 1050  
 carbonless copying papers, 263, 358, 514, 654  
 carbonyl, 310, 386, 387, 557, 598  
 carbonylation, 547, 560  
 carboxylic acid, 386  
 card-house, *see* house of cards  
 carlosturanite, 35  
 caryopillite, 33  
 $\beta$ -carotene, 273, 654  
 carotenoids, 654  
 carrier, 506  
 carriers for catalysts, 503, 516  
 casting, 104, 357, 358, 502, 506, 508, 729, 1067  
 casting sand, *see* moulding sand  
 cat litter, 510

catalysis, 2, 3, 10, 96, 105, 261, 384, 385, 393, 399, 499, 501, 512, 537, 542, 545–547, 552, 557, 558, 931, 1043, 1167  
 catalyst, 277, 278, 279, 292, 684, 452, 499, 508, 513, 541, 542, 545, 546, 547, 552, 557, 560, 561, 562, 564, 656, 1060, 1061, 1167  
 catalytic activity, 123, 274, 278–281, 354, 355, 384, 501, 547, 556, 560, 598, 636, 1045, 1054, 1067  
 catalytic applications, 123, 407, 1039, 1058–1061  
 catalytic cracking, 553  
 catalytic properties, 43, 277, 281, 399, 544, 560, 562, 685, 1024, 1061  
 cataplasma, 717, 722  
 cation distribution, 34, 39, 302, 821, 822, 923  
 cation exchange, 9, 42, 99, 109, 127, 141, 145, 222, 264, 314, 319, 325, 327, 330, 333–335, 352, 358, 396, 446, 524, 525, 542, 545, 547, 588, 593, 626, 628, 630, 663, 696, 834, 876, 902, 974, 979, 980, 981, 985, 987, 989, 1097, 1164  
 cation exchange capacity, *see* CEC  
 cation fixation capacity, 460  
 cation order-disorder, 912  
 cation size, 911  
 cationic clays, 10  
 cationic dyes, 99, 100, 309, 330, 357, 358, 653, *see also* dye  
 cationic exchange, 96  
 cationic pillar, 395  
 cationic polyelectrolytes, 197, 653  
 cationic polymers, 104, 196, 352, 657  
 CEC (cation exchange capacity), 42, 99, 127, 264, 446, 524, 593, 628, 696, 697, 876, 902, 979  
 CEC measurements, 980–991  
 celadonite, 38, 48, 302, 912, 1140, 1169  
 celadonite-nontronite, 48  
 cement, 3, 10, 300, 301, 506, 767, 1019, 1024, 1046, 1065, 1113–1115, 1117–1119, 1123, 1125, 1173  
 cement hydrates, 3, 1113–1125  
 centrifugation, 129, 130, 155, 327, 386, 403, 517, 766, 767  
 centrosymmetric, 108, 427, 428, 799, 818, 821  
 ceramic mass, 206, 506  
 ceramic materials, 1186  
 ceramics, 1, 499, 505, 506, 509, 518, 531, 625, 754, 762, 1183, 1186  
 ceramics industry, 5, 1173  
 ceramists, 158, 505, 518, 1166  
 cesium (Cs), 915, 970

- cetyl pyridinium, 175  
chabazite, 1097, 1107, 1110  
chamosite, 45, 46  
charge density, 11, 42, 94–96, 127, 128, 143–146, 153, 166, 168–172, 174, 176, 180, 184–189, 191, 192, 195, 264, 298, 329, 381, 429, 448, 504, 511, 834, 1033, 1034, 1040, 1042–1044, 1065, 1120–1122, 1124  
charge ratio, 834  
charge reversal, 153, 154, 182, 662, 1117, 1120  
charge transfer, 318, 320, 334, 355, 460, 609, 635, 685  
cheap clay materials, 1183  
chemical analysis, 66, 265, 266, 268, 598, 772–775, 945, 951, 952, 954, 995, 1003, 1164, 1171, 1172  
chemical bonding, 395, 865, 867, 870, 873, 1164  
chemical bonds, 266, 1116  
chemical shift,  $^{27}\text{Al}$ , 54  
chemical shift,  $^{29}\text{Si}$ , 923, 932  
chemical stability, 713, 1049–1050  
chemical-bonding state, 870, 873  
chemical-state plot, 870, 872  
chemisorption, 629  
chiral, 27, 108, 335, 380, 381, 383, 552, 560  
chiral recognition, 335  
chlorinated aliphatic, 433, 442, 443, 445  
chlorite dioctahedral, 25, 1145  
chlorite interlayer octahedral sheet, 45  
chlorite trioctahedral, 45, 775, 776  
chloritization, 773, 1146, 1149  
chloroalkane, 548  
chlorobenzene, 632, 649  
chloroform, 105, 106, 108, 223, 901, 1163  
chlorohydrocarbons, 649, 653  
chlorophyll, 479, 486, 494, 654, 726  
chlorhydrol, 403, 404, 405  
chromate, 657, 874, 1035  
chromate ion, *see*  $\text{CrO}_4^{2-}$   
chromium (Cr), 42, 45, 451, 545, 657, 874  
chrysotile, 33, 34, 119, 301–303, 596, 720, 729, 730, 732, 733  
 $\alpha$ -chymotrypsin, 635  
CIPEA (Comité International pour l'Etude des Argiles), 1173  
cis-coordinated, 39  
cis-orientation, 19  
cis-site, 39, 40, 302, 428, 456, 459, 757  
cis-trans isomerisation, 333, 559  
cis-vacant (sites), 26, 39, 40, 818  
civil engineering, 247, 511, 512, 1167, 1168 1173, 1186  
classical oxides, 408  
classroom field, 1187  
clays as drugs, 3  
clay catalyst, 278, 545  
clay colour, 298  
claycop, 514, 543, 545, 559, 562  
clay cycle, 1141  
clay deposits, 3, 9, 1152  
clay dispersion, 128, 155, 187, 196, 396, 403, 766–768, 993  
clay-environment interaction, 11  
clayfen, 514, 543, 545, 559, 562  
clay film, 769  
clay identification, 1163  
clays in industry, 3, 499  
clays in sedimentary basins, 1142  
clay incubators, 1183  
clay liners, 650, 693, 696  
clay mineral structure, 97, 266, 1005, 1194  
clay mineralogy, 2, 625, 725, 789, 1165, 1167, 1184, 1185, 1186, 1187, 1192, 1193  
clay-modified electrodes, 264, 274, 335, 459, 556  
clay-organic interaction, 3, 310  
clay organisation, 104  
clay-polymer nanocomposites, 338, 354, 499, 562, 586, 587, 592, 599, 600, 611, 902, 903, 1163, 1168  
clay powder, 404, 703, 704  
clay processing, 704  
clay purification, 2, 115, 612  
clay science, 1–3, 16, 141, 247, 281, 461, 754, 821, 939, 1163, 1165–1168, 1173, 1183–1187, 1190, 1192–1194  
clay science education, 1185, 1194  
clay science professionals, 1190  
clay scientists, 2, 11, 16, 141, 147, 150, 247, 583, 584, 612, 727, 1129, 1172, 1173, 1183, 1185, 1186, 1190, 1192  
clay separation, 1164  
clay therapy, 743  
clay transportation, 1138  
claystone, 314  
Clayzic, 543  
cleaning agents, 510  
clinochlore, 45, 47  
clinoenstatite, 65  
clinoptilolite, 697, 698, 1097, 1103, 1104, 1107, 1109, 1110  
clintonite, 38

- Cloisite<sup>®</sup>, 602  
 CLS (cross-linked smectites), 395  
 clusters of SiO<sub>2</sub>, 401  
 CO<sub>2</sub>, 108, 128, 211, 381, 768, 1033, 1045, 1065  
 co-adsorption, 327, 333, 357, 608, 649  
 coagulation, *see* fast coagulation  
 coagulating agent, 181, 660  
 coating, 104, 222, 290, 317, 459, 478, 479, 499, 502, 503, 504, 514, 873, 947, 948  
 coating clay, 358, 556  
 cobalt (Co), 556, 560, 1052, 1060  
 coefficient of variability, 25  
 co-hydrolysis, 124, 596, 612  
 co-ion exclusion, 161  
 cohesion, 37, 207, 1113, 1115, 1121, 1123, 1124  
 colleges, 1189, 1190, 1192  
 colloid chemistry, 2, 1184  
 colloid filtration, 703  
 colloid science, 5, 16, 154, 222, 1192, 1193  
 colloidal complexes, 1164  
 colloidal dispersion, 146, 150–152, 154, 155, 158, 161, 162, 172, 173, 175, 189, 192, 220, 314, 506, 509, 903, 904, 1057, 1058  
 colloidal solution, *see* colloidal dispersion  
 colour, 273, 290, 298, 319–321, 330, 358, 478, 502, 504, 514, 767, 1062  
 Comité International pour l'Etude des Argiles, *see* CIPEA  
 commercial clays, 724, 1152  
 commercial users of clays, 3  
 common clays, 5, 160, 501, 502, 518, 1164  
 Commonwealth Scientific and Industrial Research Organization, *see* CSIRO  
 competitive adsorption, 327, 646  
 competitive exchange, 407  
 complexation, 275, 276, 325, 326, 334, 628–630, 632, 661, 983, 988  
 complexes inner-sphere, 41, 149  
 complexes outer-sphere, 41, 149, 629  
 compliance, 214  
 composting, 510  
 compressibility, 247, 896  
 compressive strength, 257, 1125  
 computer modelling, 769, 775, 776, 779, 1046, 1167  
 computer program (FEFF), 801  
 computer program (IFEFFIT), 796  
 computer program (TKATOMS), 805  
 concentrated clay slurry, *see* slurry  
 concentrated clay suspension, 404, 683  
 concentrated clay dispersion, 154, 404, 683  
 concentrated medium, 403  
 concept, 1, 146, 189, 322, 393, 699, 704, 708, 709, 711, 1143  
 concepts of chemistry, 1184  
 concepts of mathematics, 1184  
 concepts of physics, 1184  
 concrete, 10, 301, 511, 1024, 1113  
 condensation, 41, 157, 556, 557, 562, 842, 965, 967, 1005, 1026, 1058, 1060  
 conducting polymer, 555, 608  
 conductivity, 129, 131, 247, 250, 251, 278, 441, 442, 477, 584, 591, 607–609, 696, 703, 704, 706, 710, 768, 992, 994  
 conformational, 193, 344, 346–348, 354, 635  
 consultants, 537, 1190  
 contact angle, 90, 149  
 containment, 502, 641  
 contaminant, 382, 640, 693, 694, 696, 979  
 contaminated land, 641  
 contraction, 1052, 1053, 1098, 1100  
 contrast matching, 890, 902  
 controlled rate thermal analysis, *see* CRYTA  
 controlled-release, 1065, 1066  
 conventional applications, 3, 499, 501, 537  
 convergent basins, 1146  
 co-operative, co-operativity, 219, 313, 314, 709, 985  
 cookeite, 45  
 coordination compounds, 400  
 coordination environment, 91, 791, 817  
 co-polymer, 634  
 copper (Cu), 319, 320, 323, 559, 560, 628, 1060, 1065  
 cordierite, 303  
 core electron transition, 792, 794, 799  
 core sand, *see* moulding sand  
 correlation distance, 407  
 corrensite, 25, 452, 1133, 1145, 1146, 1151  
 corrosion, 516, 1065  
 cosmetics, 1, 501, 516, 517, 720, 734  
 cosorption, 327, 333, 357, 608, 649, 824, *see also* co-adsorption  
 cost, 530, 537, 599, 653, 661, 662  
 Coulombic attraction, 186, 220  
 coupling agents, 595  
 coupling macroscopic behaviour to the nano-, micro-, and mesoscopic structure, 1167  
 coupling reaction, 598  
 course standards, 1189  
 covalent bond, 309, 316, 628, 743, 931, 1005  
 covalent bonding, 546

covalent Si-(OH)-Al pillar bond, 409  
CP-MAS (cross polarisation magic angle spinning), 927, 934, 921  
cracking catalysts, 393  
cream, 720  
creative educational techniques, 1189  
creeping measurement, 213  
Creta fullonia, 1169  
cristobalite, 37, 299, 303, 714, 734  
criteria of pillaring, 395  
critical assessment of spectroscopic and analytical techniques, 3  
critical coagulation concentration, 147, 162, 163, 168–170, 174, 182, 184, 200, 216  
 $\text{CrO}_4^{2-}$  (chromate ion), 799, 840, 874  
crocidolite, 729  
cronstedtite, 33, 772  
cross-linked smectites, *see* CLS  
cross-linked structure, 272, 409  
cross polarisation magic angle spinning, *see* CP-MAS  
crown ether, 324, 927  
CRTA (controlled rate thermal analysis), 967, 970, 1008, 1010, 1014, 1015, 1167  
crystal chemistry, 121, 805, 909, 974  
crystal growth, 48, 117–120, 1115  
crystal size, 48, 120  
crystal size measurement, 950  
crystal structure, 27, 28, 31, 32, 36, 38, 48, 60, 182, 315, 875, 941, 1038, 1102, 1110, 1111, 1116  
crystal violet, 178, 180, 331, 514, 636, 653, 658, 681, 685, 828, 991  
crystalline materials, 1164  
crystalline physiology, 380  
crystalline silica, 835  
crystalline silicic acid 1019, 1168  
crystallinity, 119–121, 124, 125, 275, 610, 611, 726, 730, 731, 733, 756, 771, 818, 844, 950, 1028, 1031, 1033, 1035, 1037, 1041, 1047  
crystallisation, 48, 117, 119, 123–125, 275, 380, 477, 492, 914, 1129, 1141, 1147, 1151  
crystallisation of gels, 591  
crystallisation of polymers, 611  
crystallite, 842, 844  
crystallographic angles, 813, 814  
crystallography, 121, 397, 805, 1173, 1184, 1186  
C-S-H, 1114, 1115, 1117–1125  
CSIRO (Commonwealth Scientific and Industrial Research Organization), 1185  
curriculum, 2, 1184, 1185, 1192

cyanide, 382, 1067  
cyanobacteria, 486, 641  
cyclic, 387, 552  
cyclic heptapeptide, 634  
cyclic voltammetry, 459, 1067  
cyclododecyltrimethyl, 648  
cysteine, 311, 326, 632

## D

daily life, 3, 1183  
DAM (dry as moulded), 602  
DCB (dichlorobenzene), 651  
DDDMA (didodecyl dimethylammonium), 649  
decarboxylation, 562  
Debye-Scherrer, 1165  
decolouration, 510, 654  
decoration, 518  
decoupled rotation MAS, *see* DR-MAS  
deflocculating agent, 155  
deflocculation, 199  
deformation band, 99  
degradable, 642  
degree of hydrolysis (OH/Al ratio), 398  
de-inking, 510  
delamination, 9, 157, 160, 175, 407, 605  
delaminated clay, 605  
delaminated pillared Laponite, 407  
delamination, 106, 126, 150, 152, 153, 155, 159, 173, 198, 202, 220, 314, 338, 351, 356, 505, 521, 584, 1057, 1063  
departments of chemistry, 1185, 1186  
departments of physics, 1186  
depolluting agent, 1  
deposition, 104–106, 108, 184, 199, 696, 704, 1138, 1149  
detrital palygorskite, 1154  
devitrification, 1140, 1147, 1149, 1153  
dewatering, 504, 843  
diagenesis, 40, 778, 1130, 1138, 1140, 1146, 1150  
diagenetic alteration, 957  
dialysis, 129–131, 157, 404, 768  
dialysis bag, 129, 404, 683, 684  
diaphragma walling, 512  
diarrheas, 1061  
diaspore, 181, 842  
diatoms, 493, 726  
diazoalkanes, 558  
3,5-dichlorophenol, 655  
dichroism, 333

- dickite, 26, 27, 30, 31, 275, 299, 309, 311, 1147, 1169  
 dielectric relaxation, 97  
 Diels-Alder, 542, 557, 558  
 diethyl ketone, 632  
 differential scanning calorimetry, *see* DSC  
 differential thermal analysis, *see* DTA  
 differential thermogravimetry, *see* DTG  
 diluent, 503  
 dilute dispersion, 130, 404  
 dilute pillaring solution, 404  
 dimers, 100, 101, 332, 333, 384, 385, 397  
 DIMOS (direct intercalation of metal oxide sols), 401  
 dinitrophenol, 638  
 diol, 549, 551  
 dioxin, 655  
 dipole moment, 94, 100, 313  
 diquat, 178, 633, 634, 637, 679, 686, 746  
 direct intercalation of metal oxide sols, *see* DIMOS  
 dirt, 2, 944, 1170  
 disciplinary boundaries, 1184  
 discipline, 1, 2, 1163  
 dispersant, *see* peptisation  
 dispersion forces, 1122  
 displacement reaction, 316  
 dissolution, 48, 117, 125–127, 129, 145, 146, 184, 263, 265, 267–272, 274–277, 398, 425, 429, 433, 434, 447, 632, 708, 713, 714, 728, 732, 790, 835–837, 931, 956, 987, 1027, 1030, 1114, 1131, 1133, 1137, 1143, 1147–1150, 1153  
 dissolution of Al metal, 398  
 dissolved natural organic matter, 659  
 distance of closest approach, 146, 147, 189  
 dithionite, 127, 128, 427, 430–432, 435, 441, 444–447, 452, 455, 460, 759, 767, 873, 740  
 ditrigonal, 32, 34, 43, 44, 98, 99, 316, 915, 928, 969  
 diuron, 647  
 divalent cation, 911, 983, 1039  
 DLS (dynamic light scattering), 161, 163, 201, 895–897, 899, 901, 902, 904  
 DLVO theory, 168, 180, 186, 189, 220, 889, 1122  
 DMBL (dimethyl benzyl lauryl), 637  
 DMDO (dimethyl dioctadecyl), 637  
 DMDOA (dimethyl dioctadecyl ammonium), 632, 639  
 DMSO (dimethylsulphoxide), 158, 226, 311, 315–317, 337, 589, 915, 928  
 DODMA (dioctadecyl trimethylammonium), 49, 824, 826  
 donbassite, 45  
 double layer, 149, 166, 177, 188, 189, 213, 250, 699, 829, 983  
 DR-MAS (decoupled rotation MAS), 921  
 drilling mud, 200, 211, 509  
 drinking water, 659, 677, 1183  
 drug delivery, 1065, 1066  
 dry cleaning, 654  
 drying at low temperature, 402  
 drying at room temperature, 402  
 drying by freeze-drying, 402  
 drying in an oven, 768  
 DSC (differential scanning calorimetry), 349, 352, 1007, 1008, 1048  
 DTA (Differential thermal analysis), 302, 440, 1005, 1007, 1050, 1165  
 DTG (differential thermogravimetry), 323  
 DTMA (dodecyl trimethylammonium), 649  
 dye, 99, 100, 309, 330, 357, 358, 653, 660  
 dye-sensitisers, 660  
 dynamic light scattering, *see* DLS  
 dynamic mobility, 154  
  
 E  
 early diagenesis, 1140  
 earth sciences, 1185, 1187  
 earthenware, 502, 505  
 ECG (European Clay Groups), 1173  
 ECGA (European Clay Groups Association), 1173  
 economic benefits, 16  
 edge site, 833  
 educational subjects, 1183  
 educational techniques, 1188  
 EDX (energy dispersive X-ray), 67, 68, 480, 481, 1043  
 EDXRF (energy dispersive X-ray fluorescence), 939, 945, 947, 952  
 effect pigment, *see* nacreous pigment  
 effluent, 170, 659  
 egg-shell porcelain, 314, 505  
 EGME (ethylene glycol monoethyl ether), 972–974  
 Eh (redox potential), 477  
 elastic and dynamic light scattering, 875, 879, 941, *see also* ELS and DLS  
 elastic and inelastic neutron scattering, 1044  
 elastic modulus, 600, 601



- electrical conductivity, 477, 591, 608, 609
- electroacoustic, 154
- electrochemical devices, 591, 608, 609
- electrochemical properties, 607
- electrokinetic mobility, 152, 183
- electrolysis of  $\text{AlCl}_3$  solution, 398
- electron acceptor, 433
- electron diffraction, 32, 441, 480, 486, 491, 794, 950, 951, 956
- electron microscope, 141, 162, 450, 790
- electron spin resonance, *see* ESR
- electronegative, electronegativity, 88, 89, 409, 911
- electronegativity equalization method (EEM), 89
- electronic conducting polymers, 608
- electronic devices, 1168
- electronic transition, 100, 101, 430, 791
- electrophoretic mobility, 152, 153, 657, 1057, 1164
- electrophoretic mobility, *see* electrokinetic mobility
- electrostatic forces, 148, 179, 190, 195, 203, 650, 655
- electroviscous effect, 202–204, 214
- element specific analyses, 790
- ELS (elastic light scattering) and QELS (quasi-elastic light scattering), 880
- ELS (expanded layered structures), 395
- emeraldine, 608
- employment opportunities, 1185
- emulsion, 162, 511, 1057
- emulsion stabilizer, 517, 1057
- enamine, 557
- enantiomer, 381, 382, 385
- encapsulation systems, 693
- energy dispersive X-ray, *see* EDX
- energy dispersive X-ray fluorescence, *see* EDXRF
- energy storage, 295
- engineered barriers, 699, 709, 713
- engineering geology, 255, 1187
- engineers, 565, 584, 1167, 1184
- enstatite, 301, 303
- enthalpies, 90, 97, 341, 638, 1105, 1107, 1111
- enthalpy, 95, 336, 340–342, 344, 356, 599, 982, 1106, 1109, 1121
- entraining reaction, 311, 316
- entropy effects, 344, 635
- environmental applications, 1, 261, 409, 660, 824, 874, 1058, 1063–1065
- environmental cells, 790
- environmental engineering, 3
- environmental protection, 10, 394, 496, 625, 626, 661
- environmental scanning electron microscopy, *see* ESEM
- environmental technology, 1192
- enzyme, 354, 355, 384, 636, 1067
- ephesite, 38
- epidemiological studies, 728, 730–733
- epitaxial growth, 790
- epithermal ore deposits, 1150
- epizone, 40, 1146
- epoxidation, 555, 1045, 1067
- epoxides, 596, 598
- epoxy functions, 598
- epoxy resins, 600
- epoxy rings, 598
- equivalent area, 328, 1043
- equivalent coagulation, 180
- ESEM (environmental scanning electron microscopy), 162, 1167
- ESR (electron spin resonance), 96, 631
- ester, esterification, 108, 562, 1057
- ethanol, 174, 224, 319, 561, 640, 745
- ether, 278, 279, 298, 598, 972
- ethylbenzene, 560, 640
- Euroclay, 1173
- European clay groups, *see* ECG
- European clay groups association, *see* ECGA
- eutrophication, 634, 1063
- Everett-Schay method, 340
- evolved gas detection, 1008, 1009, 1011
- EXAFS (extended X-ray absorption fine structure), 40, 121, 428, 429, 456, 459, 629, 790, 794, 796–798, 801, 802, 804–806, 808, 810, 812–815, 818, 820–822, 824, 828, 829, 834–839, 841–843, 1044
- EXAFS oscillations, 794, 797
- excipients, 623, 717, 719, 721, 734
- exchange reactions, 96, 276, 319, 327, 980, 983, 985, 1031, 1036
- exchangeable cation, 87, 89, 94, 96–98, 102, 153, 250, 255, 403, 545, 588, 589, 768, 834, 957, 968, 969, 973
- exfoliated clays or clay minerals, 584
- exfoliated layers, 407
- exfoliation, 294, 356, 584, 585, 592, 600, 603, 607, 610, 956
- exhausted peloid, 724
- expandible clays, 652
- expansive clays, 648
- expert system, 30
- ex-situ pillaring, 404



extended X-ray absorption fine structure, *see*  
EXAFS  
extensional basins, 1146  
external surface, 145, 148, 314, 326, 330, 587, 591,  
595, 875, 1005, 1065, 1069  
extinction, 99, 914

## F

face mask, 722  
falcondoite, 687  
fast coagulation, 163  
fat, 513  
fatty acids, 311, 319, 321, 654, 1052  
feldspar(s), 9, 55, 66, 116, 158, 721, 726, 1136,  
1138, 1141, 1147, 1149  
fenamiphos, 642  
ferric (hydr)oxide, 873  
ferric chloride, 659  
ferrihydrite, 185, 759, 799, 804, 842–844, 873, 874  
ferropyrosmalite, 33  
fertiliser, 447, 448  
fibre glass, 510  
fibres, 11, 58, 153, 292, 303, 503, 505, 583, 594,  
606, 720, 729  
filler, 502, 503, 505, 516, 531, 583, 584, 587, 611  
filter cake, 212, 506, 509, 511  
filter press, 404  
filtration, 129, 207, 213, 272, 327, 403, 659, 897,  
900, 948  
fines, 660  
fire clay, 8  
fire resistance, 606  
fire retardancy, 605–607  
firing, 5, 7, 502, 763, 1007, 1164  
firing behaviour, 1007, 1164  
first-order, 897, 920, 1105, 1110  
flame-retardant, 1062  
flint clay, 4, 13  
flocculant, 626, 659, 660  
flocculation, 146, 192, 194–197, 199, 213, 508,  
518, 659, 660, 662, 663, 842, 985, 988, 992,  
1163  
flocculating agents, 194, 508  
flotation, 90, 518, 659, 695  
fluctuating cycles, 387, 875, 1122  
fluorohectorite, 409, 591, 605, 927  
fluoro-organoclay, 603  
fluxing agent, 509  
flysch, 1140  
foam, 634

food processing, 634  
food stuff industry, 510  
forsterite, 301, 303  
Fort Benton, 1166, 1169  
fouling, 662  
foundation problems, 1186  
foundry, 207, 506, 508, 509, 625  
Fourier transform analysis, 406  
Fourier transform infrared spectroscopy, *see*  
FTIR  
fractionation, 125, 126, 129, 154–157, 159, 161,  
208, 505, 517, 518, 634, 765, 766, 1138  
fraipontite, 6, 33  
framework structures, 1098  
franklinfurnaceite, 45  
free energy, 342, 383, 384, 438, 968, 981, 1033,  
1049, 1123, 1146  
free height, 395  
freeze-drying, 130, 195, 290, 402, 480, 768  
freezing, 162, 289–291, 887  
Freundlich isotherm, 697, 1034  
Friedel-Crafts, 263, 278, 564  
friedelite, 7, 33  
F-tetrasilic mica, 396  
FTIR (Fourier transform infrared spectroscopy),  
754, 771, 909–915  
fuel oils, 640  
fuller, 1169  
fuller's earth, 8, 69, 512, 513, 526, 637, 1166,  
1168–1170, 1172  
fulling, 514, 637  
fullo, *see* fuller  
fullone, *see* fuller  
fundamental particle, 956, 1143  
fundamental research, 406  
fundamental structure, 1, 276  
fungicides, 503, 654  
fuzzy assembly, 223

## G

Ga<sub>13</sub> ion, 399  
galvanic water, 632  
Gapon coefficient, 982  
gas barrier, 610  
gas conductivity, 247, 251  
gas permeability, 599, 610  
gas permeation, 610  
gases, 251, 279, 280, 294, 599, 638–640, 642, 867,  
1060, 1065  
gastroenteritis, 747, 748

gastrointestinal disorders, 743  
gauche-block, 345, 346, 348  
gauche-bond, 329  
gel structure, 124, 886, 887, 891, 900  
gelation, 201, 203, 219, 220, 894, 897, 899, 900  
gellant, 512, *see also* gellation  
genesis, 3, 956, 1129, 1134, 1152  
genetic takeover, 380  
geobarometers, 1146  
geochemistry, 789, 1130, 1187  
geological environment for kaolinization, 1137  
geological environment of montmorillonite, 1135  
geological liner systems, 693  
geological sciences, 1187, 1193  
geologists, 115, 728, 1163, 1187, 1192, 1193  
geology, 2, 3, 5, 25, 478, 533, 1167, 1173, 1174, 1184, 1185, 1187, 1193  
geophagy, 743  
geophysics, 1187  
geosciences, 840, 1186  
geotectonic setting, 1146, 1149  
geotherapy, 722, 723, 734  
geothermometers, 1146  
germination, 117, 118, 1015  
ghassoul, 1185  
gibbsite, 51, 52, 91, 93, 96, 116, 122, 184, 201, 425, 773, 836, 933, 1023, 1132, 1140  
Glanzton technique, 518  
glauconite, 6, 48, 302, 755, 774, 775, 782, 912, 1140, 1169, 1170  
glauconite-nontronite, 48  
goethite, 91, 210, 269, 755, 759, 760, 799, 804, 835, 836, 840, 842–844, 873  
gossypol, 654  
Gouy-Chapman layer, 983, *see also* “double layer”  
government research laboratories, *see* politician governments, 1193  
grain size, 6, 7, 694, 726, 781, 783, 955, 1012, 1140, 1183  
granite weathering, 1133  
gravimetric, 39, 119, 271, 336, 1105, 1106, 1109  
grease, 506, 637, 641, 722, 1170  
green chemistry, 561, 656, 1060  
greenalite, 7, 33, 35  
grinding, 36, 316, 317, 519, 545, 704, 729, 768, 781, 989  
ground water, 511, 641, 677, 1137, 1186

## H

H-type aggregate, 102, 357  
half-time of dissolution, 268, 269  
halloysite-(7 Å), 32  
halloysite-(10 Å), 32  
halloysite ‘associated’ water, 32  
halloysite dehydration, 32, 33  
halloysite ‘hole’ water, 32, 33  
halloysite in weathering crusts, 1137  
halloysite unit cell parameters, 33  
Hamaker constant, 176, 188  
hard and soft acids and bases (HSAB), 985  
hardening, 5, 8, 663  
harmful effects, 677, 717, 727, 730  
HDPY (hexadecylpyridinium), 593, 656  
HDTMA (hexadecyl trimethylammonium), 593, 632, 639, 640, 642, 643, 647–651, 653, 659, 680, 681, 683, 826–828, 927  
HDTMA vermiculite, 827, 828  
health protection, 3, 1192  
health risks, 721, 731, 732  
heat deformation temperature, 612  
heat insulation, 503, 516  
heat of immersion, *see* heat of wetting  
heat of wetting, 341  
heat-expanded vermiculite, 514, 515  
heat retention capacity, 722, 724  
heavy metal, 334, 339, 626–633, 660, 661, 979, 986, 987, 995  
Heck reaction, 559  
hectorite, 24, 43, 105, 122, 123, 215, 219, 270–272, 279, 302, 319, 331, 332, 335, 387, 396, 445, 501, 531, 560, 586, 647, 685, 719, 773, 812, 836, 837, 840, 886, 925, 927, 928, 931, 1170  
Helmholtz-Smoluchowski equation, 152  
hematite, 40, 116, 120, 181, 755, 759, 762, 842, 843, 874  
Henry equation, 152  
herbicide, 640, 642, 653, 658, 677, 682, 684–687, 746  
herbicide formulations, 686  
heterocoagulation, 180, 183, 201  
heterocyclic, 562, 564  
heterogeneity, 141, 159, 169, 172, 250, 251, 265, 631, 890, 954, 968, 1143, 1144  
heterogeneous catalysis, 2, 542, 931  
heterogenisation, 541, 546, 547  
heteropolyacids, 545  
hexachlorocyclohexane, 640  
hexagonal symmetry, 19, 23, 1038

- hexamethylene diamine, 604  
 hexamethylene di-isocyanate, 597, 598  
 high performance liquid chromatography, *see* HPLC  
 high resolution transmission electron microscopy, *see* HRTEM  
 high stakes tests, 1191, 1192  
 high-level radioactive waste, 1103  
 Hinckley index, 29, 30  
 hisingerite, 33  
 history, 2, 3, 393, 513, 610, 696, 718, 729, 1130, 1146, 1163, 1172, 1189  
 Hofmann-Klemen effect, 121, 269, 298, 820, 984  
 horticulture, 509, 510  
 host-rock, 711, 1130, 1134, 1150, 1151  
 Houdry process, 1166  
 house of cards, 201  
 HPLC (high performance liquid chromatography), 442  
 HRTEM (high resolution transmission electron microscopy), 26, 35, 48–50, 266, 269, 629, 631, 772, 939, 942, 950, 952–954, 956, 957, 1116, 1118, 1136, 1149  
 HSAB, *see* hard and soft acids and bases  
 human health, 3, 623, 638, 653, 717, 721, 726, 727, 730, 733, 734, 743  
 human health protection, 3  
 humic acid, 52, 146, 201, 659  
 humic substance, 201, 506, 1064  
 hybrid, 107, 108, 123, 222, 223, 280, 309, 460, 499, 583, 591, 1030, 1036, 1057, 1066  
 hybrid thin film, 1066  
 (hydr)oxide dissolution, 126–128  
 (hydr)oxides of aluminium, 128, 632, 744  
 (hydr)oxides of iron and aluminium, 9  
 (hydr)oxides of magnesium, 12, 591, 606, 1061, 1062  
 (hydr)oxides of metal ions, 12  
 (hydr)oxides of silicon, 12  
 hydr(oxide), 42, 517, 627, 628, 662, 843, 1140  
 hydration force, 188  
 hydraulic conductivity, 247, 250–253, 441, 442, 696, 703, 704, 706  
 hydrazine, 98, 225, 310, 312, 314–317, 430, 431, 555, 915  
 hydrazones, 563  
 hydrocarbons, 95, 96, 263, 280, 331, 339, 547, 553, 554, 556, 639, 640, 646, 649, 869, 875  
 hydrocycloning, 518  
 hydrogel, 220, 326, 338, 352  
 hydrogen bond, 148, 195, 321, 1041  
 hydrogen bonding, 28, 34, 195, 221, 315, 588, 591, 635, 654, 839, 875, 914, 915, 928, 1034, 1041, 1043  
 hydrogenase, 105  
 hydrogeology, 1186  
 hydrology, 478, 724, 1186  
 hydrolysis behaviour of metal cations, 396  
 hydrolysis constants, 630  
 hydrophilic, hydrophilicity, 89, 90, 94, 96–98, 106, 108, 149, 280, 292, 336, 339, 341, 342, 502, 591, 592, 595, 637, 646, 654, 662, 680, 729, 1040, 1042  
 hydrophobic, hydrophobicity, hydrophobisation, 95, 180, 219, 280, 342, 477, 638, 654, 729, 1057  
 hydrotalcite, 10, 1021–1024, 1029–1031, 1034, 1036–1038, 1043, 1046–1048  
 hydrotalcite-like compounds, 10, 1021  
 hydrothermal alteration, 116, 531, 1097, 1130, 1149–1152  
 hydrothermal treatment, 117, 118, 123–125, 552, 1028, 1031, 1038, 1047, 1055, 1065  
 hydrous aluminium oxide, 633  
 hydrous ferric oxide (HFO), 799, 800  
 hydrous oxide, 799, 1027  
 hydroxo-cations, 404  
 hydroxo-ion, 629  
 hydroxo-Ni, 630  
 hydroxy cations, 630, 632, 633, 658  
 hydroxy interlayering, 632  
 hydroxy-Al, 658, 1136  
 hydroxy-cations, 632  
 hydroxy-Zr, 633, 655  
 hydroxyl (OH), 844  
 hydroxyl inner, 31  
 hydroxyl inner-surface, 31, 315  
 hydroxyl surface, 91, 1041  
 hyperfine interaction, 756  
 hysteresis, 97, 219, 256, 292, 521, 628, 985–986, 1100, 1102, 1104, 1105, 1107, 1049
- I
- ICC (International Clay Conference), 1173–1175  
 ICG (International Clay Groups), 1173, 1174  
 illite, 21, 30, 35, 66, 123, 129, 163, 197, 206, 249, 256, 257, 265, 269, 291, 342, 386, 387, 449, 450, 481, 518, 552, 630, 640, 641, 650, 651, 657, 659, 721, 758, 759, 761, 762, 771, 772, 834, 841, 1131, 1138, 1170

- i.e.p. (isoelectric point), 146, 152, 154, 325, 326, 354, 355, 635, 1056
- illite *cis*-vacant, 26, 39, 40, 818
- illite-chlorite, 26, 1141
- illite-chlorite facies, 1141
- illite formation, 714
- illite group, 15, 774
- illite-smectite, 26, 47, 48, 272, 726, 766, 768, 773, 776–779, 782, 817, 911, 953, 956, 1133, 1139
- illite/smectite mixed-layer minerals, 4, 5, 330, 768, 1133, 1140, 1141, 1143, 1144, 1146, 1147, 1149–1151
- illite *trans*-vacant, 26, 39, 40, 775, 818
- illite-vermiculite, 26, 1130, 1136
- illitization, 48, 953, 956, 957, 1134, 1140, 1143, 1144, 1146, 1147, 1149–1151
- image analysis, 407, 954–955, 1119
- image formation, 942, 944
- imaging XPS, 875
- imazaquin, 658, 678, 681
- immobilization, 1024, 1065, 1069
- imogolite, 10, 48–52, 54, 153, 295, 401, 481, 486, 491, 1170, 1065
- Imperm<sup>TM</sup>, 610
- impregnation, 397, 400, 948, 949, 952, 954
- index Aparicio-Galán-Ferrell, 29, 30
- index Flehmig, 40
- index Hinckley, 29, 30, 119
- index Kübler, 40, 778, 1146
- index Liétard, 30
- index Range-Weiss, 30
- index Stoch, 29
- index Watanabe, 40
- index Weaver, 40
- index Weber, 40
- infrared spectroscopy, *see* IR
- in plane contribution, 806, 809, 810
- in-situ method, 402, 403, 452
- in vitro studies, 721, 728, 730, 733, 734
- in vivo studies, 728, 733
- index cations, 989–995
- indicators (paleoenvironmental, continental origin, diagenetic evolution), 1140
- industrial applications, 5, 309, 348, 499, 501, 505, 583, 593, 598, 934, 1163
- industrial chemists, 3
- industrial clays, 502, 517, 528, 530, 532, 955, 1154
- inheritance, 303, 1135, 1139, 1141
- ink speck formation, 663
- inner hydrogen, 89
- inner-sphere, 41, 149, 829
- inorganic cation, 399
- inorganic polymers, 14
- inorganic/organic clay hybrids, 1168
- inorgano-organo pillaring agents, 400
- inorgano-organo-clays, 655, 659
- insecticide, 679, 680, 685, 1183
- insulation, 503, 516
- interaggregate, 11, 12, 97
- interatomic distance, 795, 835
- intercalation, 10, 41, 44, 158, 215, 225, 261, 273, 309–319, 322, 326, 331, 333, 337, 348, 349, 354, 356–358, 394–396, 399, 401, 403, 404, 407, 544, 547, 586, 588–590, 593, 594, 599, 603, 608, 609, 639, 646, 649, 651, 661, 771, 772, 776, 915, 927, 928, 931, 934, 949, 953, 1026, 1029, 1032, 1034–1037, 1040–1042, 1045, 1047, 1056, 1057, 1064, 1069
- intercalation of polymers in clays, 348
- intercalative polymerisation, 590
- interfaces, 108, 119, 631, 965, 1034
- interference, 479, 794–796, 802, 814, 822, 880, 882, 884, 885, 888, 896, 897, 901
- interlamellar water mobility, 323, 324
- interlayer exchangeable cations, 394
- interlayer H-bonding, 31
- interlayer hydration, 41, 1098
- interlayer OH vectors, 28
- interlayer region, 96–98, 330, 395, 543, 1098, 1100, 1110
- interlayer sites, 556, 628, 812, 829, 834, 872, 874
- interlayer space, 21, 24, 32, 35–37, 41, 43, 97–99, 144, 148–150, 159, 172, 187, 189, 197, 205, 206, 215, 220, 224, 226, 249, 253, 254, 265, 277, 298, 309, 311, 313, 315, 316, 318, 319, 321, 323, 326, 329, 331–335, 337, 344, 349, 351, 352, 354–356, 394, 395, 403, 408, 450, 509, 543, 547, 559, 585, 586, 589–591, 593, 602, 608, 639, 643, 696, 714, 774, 775, 827, 887, 891, 892, 902, 925, 927, 928, 931, 934, 935, 970, 972, 974, 983, 984, 1031, 1034, 1035, 1038, 1040, 1042, 1045, 1102, 1116–1118, 1121–1123, 1130
- interlayer surface, 309, 409, 444, 639, 648, 824, 927, 934, 970, 1057, 1098
- interlayer thickness, 34
- interlayer translations, 30
- interlayer water, 32, 44, 148, 149, 195, 248–250, 294, 295, 319, 320, 323, 326, 355, 543, 546, 547, 771, 1005, 1044, 1045, 1050, 1052, 1053, 1105
- intermediate phase, 120, 123, 124

internal surface, 8, 352, 973  
 International Clay Conference, *see* ICC  
 International Clay Groups, *see* ICG  
 International Union of Pure Applied Chemistry,  
*see* IUPAC  
 interparticle, 11, 12, 66, 97, 150, 197, 208, 214,  
 292, 294, 884, 886, 897, 899, 953, 1047,  
 1121, 1183  
 interstratification, 24, 25, 48, 161, 313, 314, 318, 770,  
 775–777, 779, 903, 1040, 1052, 1142, 1143  
 interstratified clay mineral, 48, 1149, 1165  
 interstratified pyrophyllite-beidellite, 396  
 inverted Si tetrahedra, 409  
 iodine (I), 608  
 iodide, 145, 337, 656  
 ion correlation forces, 168, 1120, 1122–1124  
 ion diffusion, 247, 253  
 ion exchange, 8, 10, 106, 253, 264, 274, 276, 325,  
 407, 525, 545, 560, 561, 594, 599, 612, 626,  
 628, 629, 696, 697, 754, 979–988, 995, 1032,  
 1037, 1057, 1064, 1066  
 ion exchange process, 635, 1164  
 ion-dipole, 318, 319, 321, 588, 590  
 ionic bonds, 323  
 ionic conductivity, 607, 608  
 ionic radius, 90, 428, 974, 1021, 1043  
 ionic strength, 11, 163, 326, 355, 628, 633, 681,  
 683, 833, 836, 837, 886, 894, 895, 897, 898,  
 900, 990  
 ion-ion correlation, 168, 189, 1120  
 IR (infrared) spectroscopy, 125, 149, 266, 269,  
 296, 299, 560, 596, 598, 771, 776, 780, 813,  
 821, 909, 910, 914, 915, 952, 1058  
 iron gels, 30  
 iron (hydr)oxide, 184, 210, 425, 491, 759, 767  
 iron complexes, 401  
 iron site migration, 455, 456, 459  
 iron site occupancy, 457, 459  
 irradiation damage, 946, 947  
 irreversibility, 628  
 isocyanates, 596–598  
 isoelectric point, *see* i.e.p.  
 isomerisation, 280, 333, 348, 546, 553, 559, 561  
 isoprene, 558, 591  
 isostructural, 399  
 isotherm, 340, 639, 646, 649, 651, 965–968, 970,  
 972, 974, 1109  
 IUPAC (International Union of Pure and  
 Applied Chemistry), 394, 395, 989  
 IUPAC definition, 394  
 izod impact, 604

## J

J-type aggregate, 357  
 jet-freezing, 162  
 Joint Nomenclature Committees (JNCs), 4–11  
 Juice, 510

## K

'k' space, 801, 808, 810  
 kanamycin, 635  
 kaolin, 29, 30, 54, 123, 155, 219, 275, 279, 309,  
 310, 314, 317, 501, 503, 505, 518, 532, 533,  
 536, 537, 634, 730, 731, 772, 773, 817, 818,  
 835, 841, 928, 1129, 1150, 1152, 1169–1171,  
 1184  
 kaolin arc-island type, 1153  
 kaolin Cornwall-type, 1153  
 kaolin group, 15, 26, 90, 91, 98, 771  
 kaolin residual, 4  
 kaolin sedimentary, 504, 531  
 kaolinite, 5, 20, 55, 87, 89, 91, 94, 96, 98, 118,  
 120, 122, 123, 129, 145, 146, 152, 154, 158,  
 161–163, 170, 171, 182–184, 197, 201, 206,  
 210, 211, 224, 226, 248, 249, 265, 269, 275,  
 276, 280, 289, 309–318, 326, 355, 380, 382,  
 387, 409, 423, 481, 491, 501–503, 506, 516,  
 518, 552, 557, 587, 589, 590, 612, 631, 632,  
 634, 636, 640, 650, 654, 657, 659, 685, 698,  
 718–721, 725, 730–732, 734, 743, 747, 757,  
 758, 761, 762, 766, 771, 772, 804, 875, 909,  
 910, 914, 915, 923, 928–930, 933, 934, 946,  
 947, 950, 951, 957, 968, 987, 988, 1013,  
 1015, 1016, 1129, 1134, 1139–1141, 1145,  
 1146, 1149, 1150, 1165, 1167, 1170, 1171,  
 1186  
 kaolinite deuterated, 28  
 kaolinite hydrothermal formation, 124  
 kaolinite inherited, 1136, 1138  
 kaolinite interlayer H bonding, 31  
 kaolinite neoformed, 1133, 1136–1138  
 kaolinite order-disorder, 30  
 kaolinite polytypes, 26, 27, 29  
 kaolinite transformed, 299, 301  
 kaolinite weathering crust, 1131  
 kaolinite weathering formation, 1136  
 kaolinite-dickite transformation, 1147  
 kaolinite-serpentine group, 33  
 kaolinite-smectite, 26, 125, 773  
 Kaolinton, 1164  
 Keggin cation, 181, 398, 403, 407

Keggin structure, 397  
 kellyite, 6, 33  
 kerolite, 6, 37, 120, 772, 1138, 1141, 1154  
 ketene, 557  
 ketones, 318, 549, 550, 555–557, 559, 1058, 1060  
 kink, kink block, 345–347  
 kinoshitalite, 6, 38  
 Knoevenagel reaction, 557  
 $K_{OM}$  (organic matter-normalised adsorption coefficients), 643  
 $K_{OW}$  (octanol-water partition coefficient), 643  
 Kübler index, 778

## L

laboratory exercises, 1187  
 lactone, 514, 548  
 landfill, 641, 693  
 Langmuir-Blodgett films, 104, 223, 358, 1057, 1168  
 lanthanum (La), 397, 400, 401  
 Laponite, 100, 105, 163, 168, 217, 219, 327, 396, 560, 586, 719, 886, 892, 894, 896–903, 927, 1119  
 laser techniques, 1167  
 laths, 11, 14, 32, 714  
 lattice expansion, 317  
 lattice fringes, 1144  
 lattice hydroxyls, 409  
 laumontite, 1097, 1099, 1100, 1104, 1105, 1109  
 layer charge, 11, 24, 35, 37, 39–43, 87, 95, 101, 127, 128, 143, 146, 153, 159, 169, 215, 264, 265, 269, 295, 298, 322, 326–329, 331, 332, 409, 446, 447, 456–458, 460, 502, 558, 623, 635, 638, 639, 642, 648, 657, 714, 770, 772–774, 821, 824, 826–828, 834, 837, 875, 914, 952, 956, 967, 973, 984, 985, 989, 994, 995, 1032, 1035, 1036, 1040, 1043, 1052, 1065, 1102, 1118  
 layer silicate, 328, 481, 589, 608, 819, 830–832, 1136  
 layer stacking disorder, 9  
 layer-by-layer deposition, 104, 105, 1168  
 layer-by-layer technique, 223  
 layered material, 2, 556, 1121  
 layer structure, 8, 10, 19, 23, 27, 33, 35, 36, 52, 54, 276, 289, 292, 298, 299, 302, 395, 525, 781, 821, 872, 874, 885, 901, 926, 1021, 1036, 1050, 1053, 1098, 1110, 1142, 1145  
 LDH (layered double hydroxides), 3, 1019, 1021  
 LDH-polymer nanocomposite, 1062

LDO (layered double oxide), 1056  
 leachates, 627, 633, 693, 696  
 lead (Pb), 695, 630, 632, 832, 833, 841, 1069  
 lees, 637  
 Lemnian earth, 625  
 lepidocrocite, 759, 843  
 leuco dyes, 514, 654  
 leucophyllite-smectite, 48  
 leverrierite, 1168  
 Lewis acid, 264, 280, 295–297, 320, 324, 355, 546, 552, 553, 560, 1058  
 Lewis base, 42, 90  
 $Li^+$ -fixation, *see* Hofmann-Klemen effect  
 Liétard index, 30  
 ligand exchange, 144, 169, 170, 547, 987, 988, 1034  
 light scattering, 161–163, 201, 397, 879–881, 886, 890, 891, 895, 899  
 lindane, 640, 641  
 liners, 623, 626, 627, 641, 650, 693, 696–698  
 liquefaction, 219, 506, 507  
 liquefying, *see* liquefaction  
 liquid adsorption, 340, 341  
 liquid limit, 206, 207  
 liver toxins, 634  
 lizardite, 6, 33, 34, 120, 772  
 local structure of phyllosilicates, 11, 756, 934  
 Locron, 404, 405  
 loops, 154, 349, 352, 657, 746, 1105  
 loughlinitite, 7, 36, 68  
 low-grade metamorphism, 121, 954, 1130, 1141, 1146, 1149  
 lubricant, 222, 509, 513  
 luminescence, 330–332, 334, 348, 349

## M

macrocrystalline, 8, 874  
 macromolecule, 9, 154, 192, 193–195, 199, 339, 348, 349, 351, 354, 504, 635, 903  
 macropore, 290, 407, 965  
 macroscopic, 6, 11, 96, 117, 150, 160, 247, 631, 745, 881, 899, 904, 1124, 1167  
 magic angle spinning nuclear magnetic resonance, *see* MAS-NMR  
 magnesium (Mg), 12, 117, 118, 121, 122, 125, 126, 149, 154, 263, 279, 323, 512, 531, 591, 606, 714, 756, 872, 925, 1030, 1038, 1061, 1062, 1113, 1169, 1171, 1172  
 malonate, 548, 557, 563

- manganese (Mn), 127, 393, 491, 559, 560, 1037, 1171  
 manganese (hydr)oxide, 127  
 manganese oxide, 393, 491, 1037  
 manganpyrosmalite, 7, 33  
 manufacturing of clay barriers, *see* barriers  
 manure treatment, 510  
 margarite, 6, 15, 38, 875  
 marine organisms, 660  
 Mars, 1109, 1110  
 MAS-NMR (magic angle spinning nuclear magnetic resonance), 37, 266, 273, 921–923, 927, 929–931  
 MAS (magic angle spinning) and CP-MAS (cross polarisation MAS) techniques, 934  
 materials science, 16, 222  
 maturation, 530, 705, 708, 709, 723–727, 1186  
 maya blue, 320, 321  
 mcgillite, 7, 33  
 mechanical properties, 3, 36, 127, 247, 291, 503, 584, 586, 594–596, 600–602, 606, 610, 612  
 mechanical treatment, 518  
 Meerschau, 66, 516, 1172  
 MELS (molecularly engineered layered structures), 395  
 melt intercalation, 589, 603  
 melted-state science, 14  
 membranes, 131, 322, 347, 383, 441, 461, 481, 484, 542, 564, 662, 719, 728, 731, 893, 897, 948  
 mercury (Hg), 630, 659, 975, 1119  
 mesopore, 546, 974, 1030, 1047  
 mesoporosity, 123, 292, 293, 967  
 mesoporous silica, 560  
 mesothelioma, 728, 729, 732–734  
 metachromasy, 330  
 metahalloysite, 1136, 1165  
 metakaolin, 762  
 metakaolinite, 124, 125, 275, 277, 279–280, 298–301, 632, 1013  
 metal hydr(oxide), 184, 401, 546, 594, 606, 629, 790, 794, 1034, 1049, 1065  
 metamorphism, 40, 121, 778, 779, 954, 1130, 1141, 1142, 1146, 1149, 1150  
 metaphase, 1053  
 methylene blue (MB), 43, 101, 298, 330, 331, 514, 636, 653, 660, 828, 972, 991, 993  
 methyl green, 178, 180, 636, 653  
 methylacrylate, 596  
 methylmethacrylate, 596  
 mica, 6, 21, 25, 35, 38, 39, 104, 121, 122, 158, 294, 396, 423, 502, 516, 555, 714, 720, 731, 774, 775, 782, 874, 875, 950, 951, 956, 957, 1134, 1142–1144, 1146, 1149, 1170  
 micelle-clay formulations, 684  
 Michael addition, 557, 558  
 micro-composites, 585, 587, 590, 595, 1186  
 micro-wave irradiation, 403, 404, 562, 1031  
 microanalysis, 945, 947  
 microbalance, 911, 1067  
 microbial agent, 637  
 microbial mats, 477–481, 485, 486, 496  
 microbiology, 478  
 microcalorimetry, 340, 341, 408  
 microorganisms, 477, 486, 679, 744, 663  
 micropore, *see* microporosity  
 microporosity, 271, 277, 291, 292, 294, 300, 974, 1042, 1047, 1049, 1067  
 microporous materials, 393, 394, 967, 1061  
 microporous solid, 2, 300  
 microprobe, 67, 790, 828, 829, 838  
 microscopic, 11, 161, 162, 584, 631, 643, 1062  
 microstructure, 250, 258, 259, 873, 948, 1119  
 microwave, 403, 404, 433, 561–564, 589, 992, 1031  
 mid infrared, *see* MIR  
 mineral barriers, *see* barrier  
 mineral surfaces, 94, 97, 100, 109, 168, 289, 290, 295, 325, 330, 339, 381, 388, 425, 435, 442, 443, 445, 452, 543, 561, 595, 598, 629, 631, 635, 697, 734, 790, 828, 829, 833, 840, 841, 844, 865, 875, 934  
 mineral term, 8  
 minnesotaite, 7, 36, 37  
 MIR (mid infrared) spectroscopy, 910, 911, 913, 914  
 mixed-layer clay mineral identification, 768, 770, 776–780  
 mixed-layer structures, 24–26, 957, 1131, 1140, 1142, 1145  
 mixed-layer structures disordered (regular), 24  
 mixed-layer structures ordered (irregular), 25  
 mixed-layer structures randomly stacked, 26  
 mixed oxide, 184, 1024, 1027, 1030, 1036, 1053–1056, 1058, 1060  
 mixed pillaring agents  
 mixed Al-Ce agent, 400  
 mixed Al-Cr agent, 399  
 mixed Al-Cu agent, 400  
 mixed Al-Fe agent, 399, 407, 1131  
 mixed Al-Ga agent, 399



- mixed Al-Ge agent, 399
  - mixed Al-La agent, 400
  - mixed Al-Mo agent, 400, 554
  - mixed Al-Ru agent, 400
  - mixed Cr-Fe-Zr agent, 400
  - mixed Cr-Zr agent, 400
  - mixed Fe-Cr agent, 400
  - mixed inorganic/organic, 653
  - mixed pillaring solution, 400
  - medications, 632
  - modified electrode, 264, 274, 335, 459, 556, 1067, 1069
  - molar absorptivity, 98, 911
  - molecular dynamics, 31, 90, 91, 149, 352, 1033, 1046
  - molecular sieves, 394, 1187
  - molecular weight, 129, 154, 195, 351, 600, 607, 648, 657, 896, 897, 1036, 1048
  - monodentate, 831, 843
  - monolayer, 98, 104, 106–108, 142, 146, 147, 321, 327–329, 331, 336, 349, 351, 585, 588, 589, 645, 648, 824, 967, 968, 970, 972
  - mononuclear, 833
  - monovalent cations, 99, 149, 153, 253, 546, 636, 686, 834, 972, 980, 1024
  - Monte Carlo simulation, 42, 149, 898, 924, 1122
  - montmorillon, 1165, 1171
  - montmorillonite, 5, 24, 42, 89, 98, 121, 122, 126, 129, 141, 143–145, 148–150, 154, 157, 159, 162, 163, 166, 169–172, 174–176
  - montmorillonoid, 1171
  - montmorin, 1171
  - morenite, 1171
  - mortar, 301, 327, 506, 512
  - Mössbauer, 426, 753, 755–762
  - moulding sand, 207, 208, 508, 509, 625
  - mucus gel, 743–745
  - mud, 2, 717, 722, 724, 725, 727, 1154
  - mullite, 37, 299, 303, 931, 932
  - multidentate, 833
  - multi-disciplinary, 2, 16, 478
  - multidisciplinary education, 1184
  - multilayer, 106, 693, 828, 966, 967
  - multibarrier systems, 694, 697, 699, 700
  - multinuclear, 37, 830, 833, 927, 934
  - multiple scattering events, 794–797, 801, 806, 814, 839
  - multiscale approach, 904
  - muscovite, 37–40, 121, 122, 156, 188, 720, 835, 875, 921, 956, 1129, 1133, 1136, 1138, 1145, 1146
  - muscovitization, 1149
  - mycotoxin, 510, 513, 746
  - mycrocystin, 634, 641
- N
- N<sub>2</sub> adsorption-desorption isotherms, 395
  - nacreous pigment, 503, 516
  - nacrite, 26, 27, 31, 32, 275, 299, 309, 311, 1168, 1171
  - nanoclay, 599, 4
  - nanocomposite, 1, 401, 583–586, 589, 590, 592, 594, 595, 598, 600, 604–607, 609–612, 1062, 1183, 1186
  - Nanocor, 599, 606
  - nanofillers, , 583, 586, 604
  - nanometer-size unit particles, 1
  - nanoparticle, 105, 223–226, 321, 560, 603, 604, 1037, 1040, 1120
  - nanotechnology, 2, 824, 827, 1193
  - naphthalene, 642, 647, 651
  - near edge X-ray absorption fine structure, *see* NEXAFS
  - nelenite, 7, 33
  - neof ormation, 115, 836, 837, 845, 1129, 1130, 1139, 1141, 1145, 1147
  - neof ormed clay minerals, 1133
  - neof ormed palygorskite, 1141
  - neomycin, 635
  - nepouite, 6, 33
  - neutron, 27, 28, 41, 97, 150, 313, 315, 380, 879, 880, 881, 886, 891, 892, 894, 896, 903, 904, 1043, 1044, 1119, 1167,
  - newspaper recycling, 508, 662
  - NEXAFS (near edge X-ray absorption fine structure), 790, 794, 796, 797, 801, 824, 826, 828, 841
  - nickel (Ni), 383, 459, 460, 1036, 1046, 1052, 1060
  - Nile river, 634
  - nimite, 6, 45
  - niobates, 10, 229, 1168
  - NIR (near infrared) spectroscopy, 428, 429, 910
  - nitriles, 318, 588, 1058
  - nitroarenes, 555
  - nitroaromatic, 432, 442, 444, 445
  - nitrobenzene, 338, 445, 649
  - nitrogen, 265, 323, 325, 588, 635, 875, 903, 946, 965, 967, 969, 974, 994, 1045, 1049, 1058
  - NMR (nuclear magnetic resonance) spectroscopy, 96, 97, 329, 631, 753, 754, 919
  - NO<sub>x</sub>, 560, 1061, 1064



–NO<sub>2</sub> groups, 443, 638  
 Nobel prizes, 1165  
 nomenclature, 3, 25, 33, 45, 142, 951, 1113  
 non-centrosymmetric, 108, 427, 818, 820, 822, 826  
 non-coulombic, 460  
 non-crystalline, 9, 33, 50  
 non-exchangeable, 298, 446, 633, 872, 1120  
 non-ionic, 43, 194, 349, 351, 401, 637, 638, 640, 652, 654, 655, 660, 661, 696  
 non-ionic surfactants, 401, 654, 655  
 nonlinear optics, 223  
 non-plastic clays, 5  
 nontron, 1171  
 nontronite, 33, 122, 268, 270, 271, 424, 427–429, 446, 455, 456, 491, 492, 556, 685, 755, 758, 759, 773, 782, 799, 806, 812–815, 817, 821, 838–840, 1100, 1133, 1152, 1153, 1171  
 norrishite, 38  
 nucleation, 117, 303, 313, 314, 346, 347, 381, 611, 629, 836, 837, 660, 1028, 1030, 1037, 1038, 1047, 1119  
 nuclear magnetic resonance, *see* NMR  
 nuclein base, 326  
 nucleoproteins, 634  
 nucleotides, 383–385, 552  
 nylon, 594, 595, 599–607, 610–612

## O

occupancies, 758, 912, 951, 799, 804, 806, 813, 821  
 octadecylammonium, 107, 345, 602, 632, 903  
 octadecyl trimethylammonium, 683, 824  
 octahedral cation, 36, 38, 41, 43, 46, 60, 804, 814, 818, 821, 822, 911  
 octahedral (O) sheet, 11  
 octahedral sites, 19, 24, 26, 31, 35, 39, 41, 45, 58, 298, 427, 453, 456, 757, 758, 799, 815, 818, 820, 841, 872, 875, 911  
 octanol-water partition coefficients, *see* K<sub>OW</sub>  
*o*-DCB (ortho-dichlorobenzene), 651  
 odour control, 510  
 oil industry, 47, 508–510, 662  
 ointment, 503, 509, 516  
 oligomeric (hydr)oxy aluminium cations, 265, 325  
 oligomeric ion, 409  
 Oppenauer oxidation, 557  
 optical devices, 394

optical microscopy, 352, 478–480, 485, 486, 1164, 1165  
 optical setting, 943, 944  
 optimization of clays, 1192  
 organic carbon, 400, 695  
 organic matter, 9, 379, 477, 481, 612, 627, 628, 635, 638, 639, 643, 651, 653, 663, 686, 687, 725, 726, 767, 874, 949, 1131, 1136, 1139, 1153,  
 organic matter-normalised adsorption coefficients, *see* K<sub>OM</sub>  
 organic pillared clay minerals, 394  
 organic/inorganic molecule, 11  
 organo-activation, *see* organo-clay  
 organoclay, 583, 585, 594, 599, 600, 602, 604–607, 610–612  
 organo-inorgano clay mineral, 401  
 organo-inorgano oxobridged Fe complexes, 401  
 organo-metal complex, 994, 401  
 organometallic complexes, 334, 400  
 organo-modified clay, 657, 600  
 organophilic, 105, 221, 224, 336, 344, 593, 595, 638, 650, 654, 661, 662, 901, 1167, *see also* hydrophobic  
 organophilic bentonites, 221, 1167  
 organophosphate, 317  
 organo-pillared smectites, 408, 409, 655, 934  
 organo-salts, 657  
 organosilanes, 595, 596  
 organo-smectite, 594, 647,  
 origin of life, 379, 383  
 orthoester, 551, 564  
 osmium (Os), 397, 556  
 osmotic swelling, 150, 886, 1102, 1121  
 osmotic transition, 886–888, 890  
 OsO<sub>4</sub>, 596  
 Ostwald-de-Izaguirre equation, 340  
 Ostwald ripening, 48, 1146  
 outer-sphere complex, 149, 628, 629, 829  
 oxide sol particles, 401  
 oxide pillars, 401, 408, 546  
 oxihydroxide, *see* hydr(oxide)

## P

package industry, 503  
 packing, 44, 211, 326, 329, 334, 336, 504, 648, 781, 826, 827, 1043  
 paint, 503, 593, 1173  
 palladium (Pd), 224, 559, 560, 561

- palygorskite, 5, 36, 56, 59, 63, 65, 66, 69, 125, 162, 170, 171, 213, 266, 272, 277, 289, 292, 320, 393, 501, 503, 513, 516, 631, 637, 659, 685, 719–721, 730, 732–734, 776, 933, 965, 967, 1137, 1138, 1140, 1141, 1154, 1168, 1171
- palygorskite EDX analysis, 68
- palygorskite formula, 67
- palygorskite structural changes on heating, 60
- palygorskite structure, 60, 58
- palygorskite trace elements, 68
- palygorskite XRD patterns, 60
- PAN (polyacrylonitrile), 590, 591, 594, 606, 609
- PANI (polyaniline), 590, 591, 608
- paper recycling, 510
- paraffin-like, 648
- paraffin-type arrangement, 330, 357
- paraffin-type structure, 321, 645
- paragonite, 121, 775, 946, 1141, 1146, 1149
- paraquat, 178, 633–637, 662, 679, 686
- parent-rock, 121, 1131
- particle aggregation, 5, 892, 1047
- particle density, 155, 156
- particles of colloidal size, 9
- partition, 187, 643–647, 654, 655
- partitioning, 339, 639, 640, 646, 648
- passive margins, 1141
- paste, 886, 947
- patch-charge interaction, 192, 193, 197, 198
- patches, 192, 657
- pathogenic organisms, 659, 660
- pathogenicity, 728–730, 732–734
- PCBs (polychlorinated biphenyls), 655
- PCDD (polychlorinated dibenzo dioxins), 655
- PCP (pentachlorophenol), 640, 654, 655
- PCS (photon correlation spectroscopy), 161
- p*-DCB (para-dichlorobenzene), 651
- PDDA (poly(dimethyldiallyl)), 105
- PE (polyethylene), 279, 591, 606, 611
- Pechmann condensation, 550
- pedogenetic alteration, 955
- PEEM (photoelectron emission microscopy), 867
- PEG (poly(ethylene glycol)), 588–590, 929
- pelletising, pelletisation, 506, 508, 564
- peloid, 723–727
- pelotherapy, 722–727, 734
- pennantite, 45
- PEO (poly(ethylene oxide)), 656 903, 927
- pepsin, 637, 744
- peptides, 633, 635
- peptisation, 154, 159, 189, 199
- performance assessment, 1189
- periodic table of elements, 396
- periodicity, 21, 24–26, 32, 33, 944, 950, 951
- permanent dipole, 94
- permanent porosity, 394, 406
- permeability, 48, 186, 213, 599, 607, 610, 642, 653, 696, 698, 746, 747, 890, 1063, 1147, 1186
- pertechnetate, 656
- pesticides, 433, 442, 443, 446, 451, 460, 503, 552, 623, 626, 633, 638, 641, 642, 662, 677–679, 680–684, 746–747, 914, 1064, 1069
- pesticide degradation, 434
- pesticide formulations, 356
- pet litter, 506, 626, 636
- petrochemicals, 541
- petrographic microscope, 1164
- petroleum cracking, 394
- petroleum industry, 1173, 1185
- petroleum storage, 641
- pfeifenerde, 1164
- pH, 9, 42, 52, 87, 91, 118, 120, 123, 124, 127, 143–145, 152, 153, 163, 170, 181, 182, 184, 185
- pharmaceutical formulations, 623, 719, 721, 734, 1057
- pharmaceutical industry, 1187
- phase-transfer catalyst, 561
- phase transitions, 42, 344–348, 1107
- phenol, 338, 555, 561, 632, 639, 653, 654, 662, 663, 1045, 1068
- phenoxyalkanoic, 641
- pheophytin, 654
- phlogopite, 38, 39, 122, 273, 396, 775, 834, 874, 921
- phonolite, 1169
- phosphate binder, 1061, 1062
- phospholipids, 654
- photo stabilization, 684
- photon correlation spectroscopy, *see* PCS
- photocatalyst, 1069
- photochromism, 348, 357, 358
- photocycloaddition, 333
- photodegradation, 656
- photoelectron wavelength, 795
- photoluminescence, 331, 1069
- photo-oxidative methods, 637
- photoreactivity, 333
- phthalocyanine, 1045
- phyllosilicate, 9, 423, 425, 452, 454, 836, 837, 876, 925, 951, 952, 1142, 1145, 1165
- phyllosilicate 1:1, 24, 35, 91, 698, 950

- phyllosilicate 2:1, 39, 56, 818
- phyllosilicate chain, 56
- phyllosilicate mixed-layer, 24
- physical environment, 16, 1190
- physils, 7
- physiology, 380
- PI (plasticity index), 5, 634, 635
- PILC (pillared interlayered clay), 274, 280, 281, 393–396, 401, 403, 404, 406–410, 546, 552, 555, 564
- PILC Al-Fe, 407
- PILCM (pillared interlayered clay minerals), 393
- pillared beidellite, 408, 927
- pillared bentonites, 407
- pillared clays, 42, 281, 393–395, 410, 544, 633, 654, 655, 902, 927, 934, 953, 1167, 1168, 1186
- pillared interlayered clay, *see* PILC
- pillared interlayered clay minerals, *see* PILCM
- pillared layered structures, *see* PLS
- pillared smectites, 408, 409, 655
- pillaring concept, 393
- pillaring species, 394, 396–401, 403, 409
- pilot scale level production, 403
- PLS (pillared layered structures), 395
- pinacol to pinacolone rearrangement, 562
- pinene, 278, 280, 281, 296, 393, 546
- pipe jacking, 509
- pipette method, 161
- plasma, 11, 481, 993, 1167
- plasma-state science, 11
- plastering, 211, 212, 511, 512
- plastic, 4, 206, 508, 600
- plastic clay, *see* plasticity
- plastic limit, 5, 206
- plasticity, 5, 7, 9, 10, 96, 206–207, 291, 502, 511, 512, 516, 526, 726, 1164
- plasticity index, 5, 206, 726
- plastics, 1, 206, 280, 502
- plate tectonic, 1141
- plates, 11, 32, 186, 192, 212, 223, 717, 940
- PNVC (poly(N-vinyl carbazole)), 590, 609
- PNVP (poly(N-vinyl pyrrolidone)), 588
- point of zero charge, *see* p.z.c.
- point of zero net proton charge, *see* p.z.n.p.c.
- Poisson-Boltzmann equation, 188, 189
- polarised EXAFS, 429, 456, 459, 790, 798, 805, 806
- polarizing power, 398
- polarity, 331, 341, 342, 591, 592, 594, 595, 599, 650, 651
- polishing, 510
- politicians, 1184, 1193
- politics, 16
- pollution control, 3, 309, 625, 626
- polyacrylate, 195, 506, 1046, 1062, 1063
- poly(acrylic acid), 1037, 634
- poly(hydroxo aluminium) cation, 181, 655
- poly(hydroxo metal) cation, 181, 182, 394
- polyacrylamide, 146, 194, 195, 196, 199, 213, 315, 875, 928
- polyacrylate, 195, 506, 1046, 1062, 1063
- polyaluminium chloride, 660
- polyamine, 632
- polyanion, 195, 200, 201
- polyaromatic leuco compounds, 654
- polycation, 198, 280, 653, 657, 659
- polycation-modified clays, 633, 658
- polycondensation, 181, 182, 315, 326, 355, 356, 1037
- poly-DADMAC  
(poly(diallyldimethylammonium chloride))  
653, 657, 658
- polyether, 322, 598
- poly(ethylene oxide), *see* PEO
- polymer, 1, 105, 154, 182, 192, 193, 195–198, 213, 223, 309, 338, 349, 351, 352
- polymer-clay nanocomposites, 584
- polymeric, 42, 182, 261, 659, 842, 991
- polymeric (hydr)oxymetal cations, 394, *see also*  
poly(hydroxo metal) cation
- polymerisation, 263, 326, 355, 356, 586, 587, 590, 591, 594, 595, 608, 842
- polypeptide, 383, 386, 387
- polyphenol oxidase, 105
- polyphosphates, 155, 380, 504, 511, 632, 988
- polypyrrole, 608
- polyolithionite, 38, 39
- polytypes, 24, 26, 27, 33, 35–37, 47, 275, 310, 769, 776, 957, 1038, 1040, 1146
- polytypes disordered, 29
- polytypes 1M structure, 27
- polytypes ordered, 1146
- polytypic series, 24
- polytypism, *see* polytypes
- poorly crystalline, 50, 427, 791, 812, 835, 843, 845
- porcelain, 1, 158, 314, 501, 505, 506
- pores, 11, 41, 97, 141, 142, 152, 212, 249, 257, 278, 291, 293, 294, 299, 336, 395, 407, 541, 552, 587, 637, 639, 646, 650, 890, 902, 914, 949, 965, 975, 1005, 1147, 1149, 1183

porosity, 43, 253, 263, 272, 292, 294, 300, 301,  
     394, 395, 403, 406, 407, 502, 546, 655, 754,  
     954, 965, 974, 975, 1031, 1047, 1048, 1114,  
     1119, 1141, 1147  
 porosity measurement, 395  
 porous carbon, 1070  
 porous clay heterostructures, 274, 655  
 porous clay pots (or jugs), 1183  
 porous clays, 1168  
 porous layered (hydr)oxides, 14  
 porous materials, 292, 393, 592  
 porphin, 331  
 porphyrine, 331–333  
 portlandite, 1114, 1115, 1117, 1118  
 positive charge, 41, 42, 45, 92, 185, 275, 355, 633,  
     635, 657, 683, 1118  
 postgraduate students, 3  
 potable water, 641, 653  
 potassium (K), 146, 148, 191, 311, 316, 317, 337,  
     447, 714, 715, 979, 991, 1143, 1147, 1149,  
     1150, 1169  
 potential energy, 1123, 1124  
 powder EXAFS, 798, 802, 804–806, 810, 813–815  
 PP (polypropylene), 560, 561  
 pre-exchange, 403  
 prebiotic, 380–382, 384, 386–388  
 prebiotic synthesis, 1, 384, 552  
 prebiotic catalyst, 383  
 pre-edge XAFS spectroscopy, 799, 817  
 preiswerkite, 38  
 pre-spinel phase, 1055  
 primary and secondary public schools, 1187  
 primary school teachers, 1190  
 primitive model, 1122, 1123  
 pristine clay, 406, 590, 592, 726  
 private universities, 1191  
 professional research projects, 1187  
 prograde phase/reactions, 1151  
 propping open, 319, 352  
 protection, 3, 10, 394, 496, 516, 625, 626, 661,  
     685, 693, 728, 744, 748, 1138, 1185, 1192  
 proto-allophane, 51  
 proto-imogolite, 48, 49, 54  
 proton adsorption, 275, 458  
 proton affinity distribution, 265  
 protons released, 409  
 PS (polystyrene), 354, 594, 599, 600  
 pseudo-hexagonal symmetry, 19  
 pseudotrimolecular, 328  
 pseudotrimolecular arrangement, 329, 593  
 public school, 1190

pulp, 660  
 pure clay minerals, 9, 155, 639, 769, 770, 904  
 pyridine, 276, 280, 296, 311, 323, 552, 591, 914  
 pyridinium, 174, 323, 357  
 pyrite, 38, 425  
 pyrophyllite, 35–37, 40, 90, 94, 145, 166, 269, 302,  
     303, 502, 516, 630, 631, 772, 775, 804, 836,  
     921, 1141, 1142, 1146, 1149, 1171  
 pyrophyllite dehydroxylation, 37  
 pyrophyllite substitution, 37  
 pyrophyllite thermal transformation, 37  
 pyrosmalite, 33  
 pyrrole, 331, 590, 591, 608  
 p.z.c., 42, 92, 118, 145  
 p.z.n.p.c., 145, 987

## Q

QACs (quaternary ammonium compounds), 593,  
     637–643, 645–648, 650, 651, 653, 656, 657  
 QELS (quasi-elastic light scattering), 880  
 quality of life, 16  
 quantized, 941  
 quartz, 9, 30, 66, 125, 155–158, 207, 267, 269,  
     427, 714, 720, 721, 729–731, 734, 837, 874,  
     875, 910, 1129, 1134, 1141, 1142  
 quasi-elastic light scattering, *see* QELS  
 quasi-reversible, 394  
 quaternary ammonium, 175, 439, 560, 561, 593,  
     604, 637, 639, 652, 653, 661, 663

## R

‘R’ space, 798  
 racemic adsorption, 335  
 radioactive species, 631  
 radioactive waste, 253, 625, 627, 656, 695,  
     703–705, 708, 1065, 1103  
 radioactivity, 382, 992  
 radium (Ra), 631  
 radon (Rn), 727  
 Raman spectroscopy, 96, 397, 1023, 1042, 1045,  
     1117  
 range-Weiss index, 30  
 rate-jump method, 1014  
 raw clays, 9, 130, 592, 755, 1166  
 reaction product, 272, 1113  
 rearrangement reactions, 551  
 reconstruction, 1029–1030, 1034, 1036, 1045,  
     1052, 1054, 1055, 1063  
 recovery of CO<sub>2</sub>, 1064, 1065

rectorite, 6, 25, 48, 396, 776, 777, 1146  
 recycle, 637, 724, 727  
 redox coupling, 839  
 redox reaction, 452, 1036, 1067  
 red-tide, 660  
 reduced nontronite, 456, 838, 839  
 reduced-charge montmorillonite, 298  
 reduction potential, 445, 446, 451, 460  
 refining, 507, 510, 513, 625, 782, 1167  
 refractories, 4, 503  
 refractory industry, 503  
 regioselectivity, 547  
 regolith, 641  
 rehydration, 66, 948, 1029, 1055  
 related materials, 755, 965, 1165  
 relative humidity, 43, 157, 546, 773, 1098, 1101, 1106  
 relaxation, 36, 92, 97, 152, 757–759, 762, 866, 872, 876, 1046, 1099  
 remediation of pollution problems, 1186  
 repositories, 627, 695, 703, 714, 1049, 1141  
 repulsive gel, 213, 214, 216, 217  
 research scientists, 3  
 researchers, 16, 47, 330, 593, 595, 821, 838, 845, 886, 1184  
 residual cation, 407  
 residual treatment chemicals, 627, 659, 660  
 resin embedding, 948–949  
 responsible politicians, *see* politician  
 restoration, 642, 1030  
 retardation, 152, 642, 693, 696, 698  
 retention aid, 198, 354  
 retrograde phase/reactions, 1146, 1151  
 reversible, 42, 194, 214, 215, 219, 256, 276, 293, 331, 394, 432, 628, 629, 759, 776, 839, 844, 1067, 1102–1105, 1107  
 rewetting, 890  
 rheological properties, 127, 131, 204, 247, 257–259, 291, 501, 504, 508, 509, 523, 525, 703, 722, 725, 744–746, 748, 1057  
 rheology, 2, 504, 724, 898  
 rhodamine-B, 100, 653  
 rhodamine 6G, 100, 358  
 ribose, 384  
 RNA (ribonucleic acid), 381, 384, 385, 388, 479, 552  
 rock weathering, 380, 1131  
 RTM<sup>®</sup>, 725  
 rubber, 1, 502, 503, 516, 603, 604, 1173  
 ruthenium (Ru), 224, 334, 335, 479, 486, 487

## S

SAED (selected area electron diffraction), 939  
 saline pools, 724  
 salts, 14, 116, 124, 129, 130, 146, 150, 162, 166–168, 180, 181, 189, 213, 220, 224, 295, 301, 311, 314, 316, 326, 327, 337, 338, 397, 398, 447, 506, 511, 523–526, 560, 562, 593, 640, 657, 768, 842, 874, 987, 988, 992, 1024, 1028, 1029  
 sample-controlled thermal analysis, *see* SCTA  
 sandstones, 782, 1143, 1147  
 sanitaryware, 1, 505, 506  
 saponite, 6, 15, 25, 41, 43, 95, 106, 107, 122, 215, 226, 271, 272, 303, 333, 334, 357, 358, 396, 405, 409, 456, 546, 586, 706, 707, 773, 887, 1133, 1134, 1141, 1151–1154, 1172  
 sauconite, 122, 1172, 43  
 SALS (small angle light scattering), 879, 882, 890, 895, 896, 899, 900, 904  
 SANS (small angle neutron scattering), 150, 152, 879, 880, 884, 892–894, 896, 897, 899, 900, 902–904, 1119  
 SAS (small angle scattering), 150, 215, 351, 754, 879–881, 883, 884, 886–890, 894, 897, 898, 902, 904  
 SAXS (small angle X-ray scattering), 142, 161, 215, 397, 586, 842, 879, 886, 890, 892, 897, 898, 902, 903, 1119  
 scanning electron microscopy, *see* SEM  
 scanning force microscopy, *see* SFM  
 scattering events, 794–797, 801, 806, 810, 814, 839  
 scattering process, 789, 791, 841  
 scavenger, 660, 1062  
 schallerite, 33  
 scientific expertise, 1190  
 SCTA (sample-controlled thermal analysis), 1008, 1010, 1011, 1012, 1013  
 sealing, 211, 251, 511, 693, 695, 698, 700, 703  
 secondary ion mass spectroscopy (SIMS), 631  
 secondary public schools, 1187  
 secondary school teachers, 1190  
 second-order, 920  
 sedimentation, 126, 154–159, 161, 162, 196, 207–211, 213, 517, 518, 545, 769, 783, 904, 910, 992, 1138, 1163  
 sediments, 5, 9, 33, 35, 122, 130, 207, 211, 212, 219, 423, 425, 450, 451, 460, 478, 480, 486, 491, 625, 641, 656, 697, 703, 838, 842, 1097, 1129, 1130, 1138, 1140, 1141, 1142, 1150, 1163

- selected area electron diffraction, *see* SAED  
selective adsorbents, 394  
selective coagulation, 171, 172, 183, 184  
selectivity, 42, 279, 280, 327, 393, 541, 543, 544, 546, 547, 561, 562, 630, 631, 639, 640, 646, 647, 654, 696, 981–984, 1033, 1045, 1098  
selectivity coefficient, 981, 982, 983  
selenium (Se), 1004  
self assembling, 104–105  
self-reproduction, 379  
SEM (scanning electron microscopy), 162, 211, 275, 397, 480, 481, 776, 1167, 1030, 1068  
SEM-EDX (SEM-energy dispersive X-ray spectrometry), 491, 493–495  
semicarbazones, 549, 563  
sensor, 1014, 1069  
separation factor, 982  
sepiolite, 4, 5, 7, 36, 56–60, 63–69, 125, 266, 272, 277, 292–295, 320, 409, 501, 503, 508, 510, 513, 516, 587, 589, 591, 593, 595–598, 612, 636, 641, 798, 804, 841, 682, 686, 719, 730, 732–734, 776, 922, 933, 934, 965, 967, 1005, 1011, 1137–1141, 1154, 1172  
sepiolite cation exchange capacity, 593  
sepiolite chemical analysis, 66  
sepiolite DTA/TG curves, 65  
sepiolite EDX analysis, 68  
sepiolite space group, 58  
sepiolite structural changes on heating, 65  
sepiolite structure, 57, 60, 68  
sepiolite trace elements, 68  
sepiolite unit cell parameters, 58  
sepiolite XRD pattern, 60  
sepiolite-palygorskite group, 125  
sericite, 875, 1149, 1170  
serpentine, 7, 15, 20, 22, 26, 33, 87, 91, 729, 732, 770–772, 775, 776, 778, 951, 1023, 1133, 1152  
sewage, 511, 634, 637, 660, 1163  
sewage sludge, 510  
sewer pipe, 502, 508  
SFM (scanning force microscopy), 631  
shaft sinking, 509  
shampoo, 517  
SHG (second harmonic generation), 108, 315  
shield tunnelling, 509  
shock-proof filling material, 516  
short-chain, 108, 311, 336, 639, 640, 642, 643, 645, 646, 662  
shrinkage, 502, 1164  
siderophyllite, 38, 39  
silanes, *see* alkoxysilane and organosilanes  
silanol group, 195, 316, 320, 324, 409, 595, 596, 598, 733  
silica dissolution, 129  
silica gels, 30, 66  
silica pillars, 401  
silicate minerals, 8, 379, 709, 734, 871, 875, 876  
silicon, 12, 44, 423, 447, 714, 757, 873, 874, 947, 1164, 1042  
silicosis, 729  
siloxanes, 87, 89–91, 94–96, 98, 99, 101, 104, 109, 149, 276, 339, 588, 595, 596, 646, 647, 915, 984  
simple cations, 626, 660  
SIMS (secondary ion mass spectroscopy), 631  
simultaneous application of different techniques on the same sample, 1167  
single scattering events, 794, 796, 820  
single layer, 157, 1125  
slow release formulations, 679, 682  
sludge, 660, *see also* slurry  
slurry, 404, *see also* sludge  
small angle light scattering, *see* SALS  
small angle neutron scattering, *see* SANS  
small angle scattering, *see* SAS  
small angle X-ray scattering, *see* SAXS  
smectite, 3, 5, 21, 25, 26, 30, 35, 42, 43, 48, 66, 102, 104, 105, 120, 122, 123, 128, 141, 152, 153, 158, 159, 161, 186, 249, 250, 251, 256, 257, 263, 267, 290, 295, 298, 330, 394, 406, 427, 430, 433, 439, 441, 444, 446, 447, 509, 516, 545, 590, 704, 709, 713, 716  
smectite cation exchange capacity, 99  
smectite chloritization, 1146  
smectite formation, 1134  
smectite group, 758, 772–773  
smectite illitisation, 714  
smectite interlayer hydration, 41  
smectite layer charge, 642  
smectite-palygorskite transformation, 1154  
smectite swelling, 434  
Sn PILC, 408  
SO<sub>2</sub>, 654, 1061  
soda-activated bentonites, 523, 1166  
soda-activation, 152, 518, 523, 930, 1166  
sodium (Na), 117, 127–129, 150, 166, 168, 169, 172, 174, 182  
sodium metasilicate, 117  
soil colloids, 680, 1165  
soil fractions, 1163  
soil improvement, 509, 510

- soil injection, 511
- soil organic matter, 638, 651, 653
- soil science courses, 1184
- soil scientist, 115, 1163
- soil vermiculite, 1163
- soils programs, 1186
- sol, 49, 123, 213, 216, 401, 897, 899
- sol-gel transition, 213–220, 886, 891, 897–899, 901, 904
- solid-base catalyst, 1058, 1060
- solidification, 948, 663
- solid-solid reaction, 319, 406
- solid-solid state reaction, 410
- solid-state reaction, 320, 1153
- solid-state transformation, 48, 1150
- solubility, 163, 184, 251, 298, 301, 546, 650, 730, 744, 901, 1049
- solubility product, 117, 118, 1049
- solute-solid adsorption, 1164
- solvation, 97, 318, 321, 344, 891, 915, 646, 649, 651
- solvent, 97, 98, 100, 101, 105, 192–194, 219, 318, 327, 337–339, 395, 541, 546, 547, 557, 603, 633, 650, 881, 901, 948, 991, 1036
- sorbate, 828
- sorption, 95–98, 253, 340, 442, 546, 710, 711, 719, 790, 799, 828, 829, 833, 835, 841, 843, 1054
- sound dissipation, 516
- spa, 718, 721, 722, 724, 726, 727
- spatial resolution, 874, 875, 944, 828
- special clays, 1152
- specific surface area, 9, 161, 224, 263, 271, 273, 276, 277, 280, 322, 330, 341, 406, 460, 525, 623, 865, 884, 965, 969, 1028, 1030, 1031, 1047, 1048, 1136
- spent bleaching earths, 661
- spillover, spill over, 153
- spills, 166, 1186, 641
- spin coating, 104, 222
- spinel, 298, 804, 1030, 1031, 1051, 1053, 1055, 1056
- stability (thermal), 274, 293, 356, 395, 401, 408, 409, 546, 607, 828, 1030, 1031, 1041, 1050–1056, 1062
- stability factor, 163, 183
- stabilizer, 1062
- stacking sequence, 24, 26, 27, 31, 38, 1038, 1040, 1041
- standardized, 1183
- standardized test, 1191
- starch, 504, 517, 659
- states (solid, melted solid, liquid, gas and plasma), 11
- statistics, 501, 781
- stereoselective adsorption, 326
- stereoselectivity, 547, 558
- steric, 346, 353, 355, 511, 641, 686, 834
- steric exclusion, 641
- steric stabilisation, 176, 193–196, 200, 201, 504, 506, 511
- Stern layer, 153, 168, 174, 186, 188, 216, 925
- stevensite, 122, 773, 1141, 1154, 1172
- Stoch index, 30
- Stokes' equation, 155
- Stokes' equivalent spherical diameter, 155, 159, 161
- Stokes' law, 130, 207
- stoneware, 502, 508
- straight-chain, 649
- streptomycin, 635
- strontium (Sr), 323
- structural formula, 19, 36, 98, 774, 951, 952, 956, 1032
- structural models, 59, 952
- structural order-disorder, 29
- structure, 3, 11, 26, 27, 31–34, 36, 38, 44, 52, 60, 65, 66, 68, 88
- structure breaking, 148, 149, 168, 337, 338
- structure of the intercalated species, 410
- styrene, 355, 560, 590, 591, 594, 596, 1036, 1045, 1062
- substitution, 24, 26, 37, 38, 41, 42, 87, 122, 149, 264, 269, 429, 560, 602, 756, 757, 909, 913, 989
- sub-surface, 432, 452
- Sudanese clay, 625
- sudoite, 45
- sulfometron, 658
- sulphate, 124, 408
- sulphite liquor, 660
- sulphur production, 510
- superacids, 300, 545, 561
- support programs, 1186
- supported reagents, 514, 546, 549, 559, 562
- surface adsorption, 1047, 1057
- surface charge, 42, 91, 94–96, 144, 153, 184, 187, 189, 265, 446, 713, 873, 875
- surface complexation, 275, 276, 988, 628, 629, 630, 633
- surface conductance, 154
- surface coverage, 105, 151, 278, 352, 598, 657, 830, 836, 843



surface hydrogen, 89  
 surface hydroxyls, 31, 915  
 surface metabolism, 381  
 surface oxygen, 87–89, 91, 100, 103, 104, 148,  
 149, 326, 336, 344, 349, 435, 1120, 1121  
 surface potential, 41, 42, 143, 153, 169, 186, 188,  
 201, 729, 842  
 surface precipitation, 184, 987, 628, 629  
 surface pressure, 106, 107  
 surface properties, 1, 2, 87, 89, 90, 180, 261, 292,  
 436, 501, 594, 623, 728, 754, 873, 965, 1056,  
 1115, 1118, 1166  
 surface reaction, 48, 118  
 surface reactivity, 721, 874  
 surface-analytical technique, 865, 631, 661, 789  
 surface-chemical properties, 2  
 surfactant, 174, 196, 218, 219, 222, 223, 327–329,  
 331, 401, 555, 593, 604, 655, 902, 992, 1036  
 swelling clay minerals, 396, 783, 965, 969–970,  
 972, 974  
 swelling pressure, 186–188, 213, 248, 250, 251,  
 255, 256, 315, 438, 439, 704, 706  
 swelling potential, 247, 696, 701  
 swelling properties, 1165  
 swinefordite, 6, 43  
 symmetry forbidden transitions, 792  
 synchrotron, 27, 215, 630, 789–791, 824, 827, 829,  
 842, 845, 867, 887, 890, 891, 903  
 syn-gas, 553  
 synergism, 300, 327  
 synthesis, 1, 115–118, 121, 226, 271, 301, 380,  
 383, 393, 394, 396, 460, 552, 557, 587, 588,  
 591, 719, 953, 1115  
 synthetic clay minerals, 2, 115, 120, 396, 612, 626,  
 909  
 synthetic kaolinite, 119  
 synthetic mica, 38, 121, 555  
 synthetic smectite, 396, 459, 1119  
 synthetic zeolite(s), 393, 1167  
 syrup, 510

## T

*t*- and  $\alpha$ -plots, 395  
 tails, 352, 657, 827  
 tainiolite, 38  
 talc, 21, 25, 36, 89, 94, 98, 122, 123, 302, 303, 396,  
 502, 516, 517, 611, 719, 720, 730–732, 772,  
 911, 1011, 1133, 1184  
 talc-pyrophyllite group, 15, 772  
 talcum, 503, 720

tanneries, 641  
 tar, 509  
 taylorite, 1169  
 TCE (trichloroethylene), 649–651  
 TCM (tetrachloromethane), 444, 651, 653  
 TEA (tetraethylammonium), 638, 647  
 teachers, 3, 1184, 1190, 1191  
 teaching techniques, 1184, 1188  
 TEM (transmission electron microscopy), 266,  
 330, 479, 480, 585, 754, 765, 772, 889, 939,  
 1118  
 TEM image analysis, 407  
 template synthesis, 587, 591, 592, 1062  
 tensile modulus, 601, 602  
 tensile properties, 600, 602  
 tensile strength, 508, 600, 602, 1104  
 TEOS (tetraethoxysilane =  
 tetraethylorthosilicate), 116, 123, 401  
 terminology, 3, 50, 247  
 terracotta, 502  
 terra verti, 1169  
 terramycin, 635  
 tertiary amines, 654  
 tetraalkylammonium ions, 145, 394, 611  
 tetra-ferriphlogopite, 38, 39  
 tetrahedral (T) sheet, 14  
 tetrahedral iron, 428–430  
 tetrahedral site, 19, 24, 38, 41, 43, 54, 427, 429,  
 757, 804, 815, 818, 921  
 tetrahedral symmetrical structure, 397  
 TGA (thermal gravimetric analysis), *see*  
 thermogravimetry  
 thawing, 291  
 thermal decomposition, 278, 279, 325, 930, 1028,  
 1045, 1050–1052, 1058  
 thermal dehydration, 1164  
 thermal expansion, 1098  
 thermal gravimetric analysis (TGA), 39  
 thermal insulators, *see* heat insulation  
 thermal properties, 605  
 thermal protection, 503, 516  
 thermal stability, 274, 293, 356, 395, 401, 408,  
 409, 546, 607, 828, 1030, 1031, 1037, 1041,  
 1050, 1052, 1062  
 thermal treatment, 3, 124, 261, 277, 290, 298, 594,  
 1029, 1045, 1055  
 thermodynamic conditions, 11, 14, 249, 586  
 thermogravimetry, 1007, 1008, 1010, 844  
 thermo-XRD study, 408  
 thickening, thickeners, 220, 356, 504, 512, 516,  
 593, 720, 1164, 1166



thin film, 174, 332, 358, 945, 1066  
thioacetals, 549, 563  
thiocyanide, 560  
thioesters, 387  
thioflavin-T, 653, 685  
thioketals, 549, 563  
thioketones, 559, 563  
thionine, 100  
thixotropic, thixotropy, 219, 222, 356, 504, 511, 512, 514, 516, 520, 521, 524, 525, 593, 894, 1164  
thorium (Th), 727, 832, 833, 835  
Ti PILC, 406, 407, 409  
tiles, 1, 502, 505, 518  
titanates, 10, 329, 1168  
titanium dioxide, 656  
TMA (tetramethylammonium), 44, 177, 280, 281, 339, 357, 358, 638, 927  
TMP (trimethylphosphonium), 647  
TMPA (trimethyl phenylammonium), 95, 439, 440, 644, 646, 647, 650, 651  
TO layer, 8  
tobelite, 1144  
tobermorite, 1115–1117, 1120, 1123, 1124  
tocopherols, 654  
toluene, 224, 226, 280, 344, 345, 594, 640, 658, 901, 1057, 1069  
Tonsil, 550, 1166  
Tonstein, 314  
Töpferton, 1164  
tosudite, 6, 25, 1145  
total pore volume, 407  
TOT layer, 8, 11  
toxic materials, 625, 697  
toxic pollutants, 401, 640  
toxins, 634, 641, 661, 719, 720, 722, 746  
Toyota, 594, 595, 599, 602  
TPD (temperature programme desorption), 546  
trace metals, 654, 828  
train, 352, 657  
trans-coordinated, 38  
transition metals, 400, 547, 552, 557, 591, 612, 801, 833, 837, 840, 1060  
transmission electron microscopy, *see* TEM  
trans-orientation, 19  
trans-site, 20  
trans-vacant (sites), 26, 39, 427, 775, 799, 818, 821  
tremolite, 720  
tricalcium aluminate, 1114  
tricalcium silicate, 1113–1115  
trichlorophenol, 338, 339, 640

tridecamers, 397  
trihalomethanes, 641, 659  
trioctahedral sheet, 21, 35, 819  
true micas, 35, 38  
TSLS (tubular silicate layered silicate) nanocomposite, 401  
tubules, 11, 50  
tuperssuatsiaite, 69  
turbidity, 161, 879, 1140, 659, 662  
TVS<sup>®</sup>, 725  
two-dimensional zeolite-like materials, 393  
TX100, 636

## U

ultrafiltration, 890, 662  
ultrasmall angle X-ray scattering, *see* USAXS  
ultrasound, 403, 445, 491, 494, 495, 555, 594, 637, 767–769  
undeveloped countries, 1183  
unit-cell volume, 1103–1105, 1109  
United States Geological Survey, *see* USGS  
universities, 1183–1186, 1189–1193  
university departments, 1186  
university professors, 1189, 1190  
university teachers, 3  
uranium (U), 346, 727, 1134, 836  
uranyl-clay, 835  
urea, 310, 312, 314, 315, 317, 597, 598, 636, 1028, 1029, 1035, 1047  
urease, 105, 636  
USAXS (ultrasmall angle X-ray scattering), 891–893, 898–900  
users of clay materials, 1184  
USGS (United States Geological Survey), 1185, 1188  
UV-visible spectroscopy, 1067

## V

V<sub>2</sub>O<sub>5</sub>, 656, 1060  
van der Waals interactions, 36, 37, 176, 177, 179, 180, 182, 190, 195, 204, 216, 310, 318, 321, 327, 333, 336–338, 349, 354, 355, 543, 635, 637, 650, 828, 985, 1121–1123  
Vanselow selectivity coefficient, 982  
vapour, 146, 292, 295, 318, 319, 326, 336, 518, 598, 610, 708–710, 903, 927, 1007–1009, 1012, 1103, 1104, 1107–1110, 1163, 638, 1029

vapour pressure, 146, 292, 326, 903, 927, 1012, 1103, 1104, 1107–1109, 1029  
 variability, 24, 25, 533, 542, 734, 1134, 1143, 631  
 variable charge, 42, 990  
 varnish, 509  
 vermiculite, 6, 25, 35, 43–44, 98, 160, 220, 269, 294, 322, 326, 396, 503, 514, 516, 552, 594, 697, 773, 889, 925, 954, 956, 989, 1129, 1134, 1172  
 vermiculite group, 15, 773–774  
 vermiculite layer charge, 827  
 vinylacetate, 596  
 vinylcarbazole, 590  
 vinylsilanes, 596  
 virgin clay, 724, 726  
 virus, 680, 719, 720, 747, 748, 626, 634, 661  
 viscoelastic behaviour, 214, 903  
 viscosity, 145, 155, 156, 169, 175, 203, 204, 219, 265, 291, 504, 511, 512, 531, 606, 607, 725, 744, 745, 896, 897, 901, 903  
 volatilization, 678, 682, 946  
 volkonskoite, 6, 43, 1172

## W

wacker, 560  
 WAD (wide angle diffraction), 880, 885  
 wall-rock alteration, 1130, 1149  
 washing (filtration and/or by dialysis), 402  
 waste barrier, 1065  
 waste disposal, 3, 506, 623, 693, 696, 625, 626  
 waste repositories, 695, 627, 1049  
 waste water, 508, 511, 526  
 wastes, 693, 694, 697–699, 1186, 631, 634, 650, 653, 661  
 waste types, 693  
 wastewaters, 633, 635, 637, 659, 660, 662  
 Watanabe index, 40  
 water, 4, 11, 21, 32, 33, 41–43, 50, 56, 87, 90, 91, 95–100, 104, 129, 130  
 water quality, 1186  
 water vapour, 146, 295, 518, 927, 1007, 1008, 1009, 1012, 1104, 1106, 1107, 1029  
 wave transfer, 941  
 wax, 509, 510  
 WAXS (wide angle X-ray scattering), 810, 901  
 weathering alteration, 1134  
 weathering crusts, 1129, 1131, 1136, 1152, 1153

weathering profile, 955, 1131, 1133, 1134, 1139, 1140  
 Weaver index, 40  
 Weber index, 40  
 wide angle diffraction, *see* WAD  
 wide angle X-ray scattering, *see* WAXS  
 willemseite, 37  
 white asbestos, 729  
 wine, 510, 634  
 wool scouring, 660  
 Wyoming deposits, 1166

## X

XAFS (X-ray absorption fine structure), 37, 40, 790  
 XANES (X-ray absorption near edge structure), 122, 429, 790, 817  
 xanthophylls, 654  
 XAS (X-ray absorption spectroscopy), 631, 753, 1026, 1044–1045, 789, 791, 794, 796, 799, 815  
 XPD (X-ray photoelectron diffraction), 875, 876  
 X-PEEM (X-ray photoelectron emission microscopy), 867  
 XPS (X-ray photoelectron spectroscopy), 55, 631, 790, 865–878  
 X-ray absorption fine structure, *see* XAFS  
 X-ray absorption near edge structure, *see* XANES  
 X-ray absorption spectroscopy, *see* XAS  
 X-ray amorphous materials, 9, 483, 484, 1130  
 X-ray crystallography, 121, 397  
 X-ray diffraction, *see* XRD  
 X-ray fluorescence, *see* XRF  
 X-ray photoelectron diffraction, *see* XPD  
 X-ray photoelectron emission microscopy, *see* X-PEEM  
 X-ray photoelectron spectroscopy, *see* XPS  
 X-ray wave spectroscopy, *see* XWS  
 XRD (X-ray diffraction), 479, 585, 765, 921, 939, 1184  
 XRD preparations, 766, 769  
 XRF (X-ray fluorescence), 299, 480, 790, 867  
 XWS (X-ray wave spectroscopy), 828  
 xylene, 222, 280, 901, 639, 640

## Y

yofortierite, 7, 69  
 Yucca Mountain, 1103

## Z

- zeolite, 118, 295, 300, 301, 386, 393, 401, 552, 695, 697, 931, 934, 1098, 1099, 1103–1105, 1107, 1109, 1111, 1141, 1186, 639
- zeolite-like, 393, 401, 639
- zeolitic complexes, 1164
- zeolitic water, 56, 58, 64, 65, 292, 294, 591, 967, 1005, 1011
- zero point of charge, *see* p.z.c.
- zeta potential, 152, 153, 1118, 1120, 657, 658, 1056
- zinc (Zn), 42, 560, 606, 1170, 632, 1026, 1051, 1062
- zinc selenide (ZnSe), 106, 107, 108
- zinnwaldite, 39
- zirconia-pillared, 555
- zirconium (Zr), 560, 561, 562, 633

This page intentionally left blank